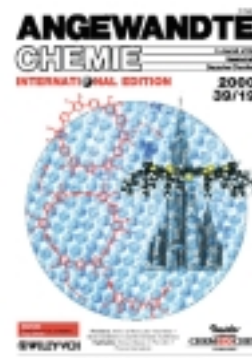
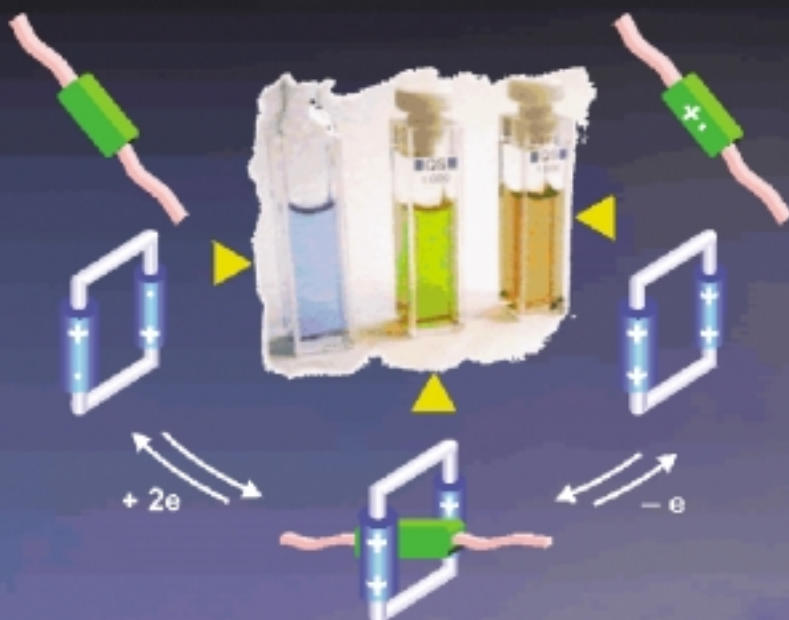
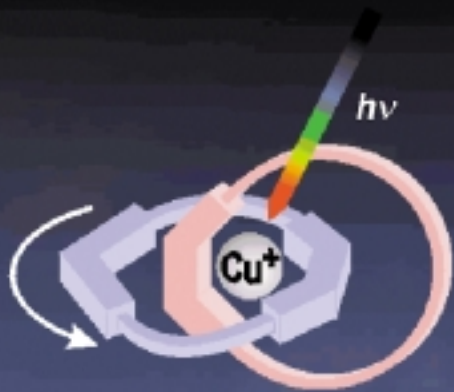


Cover Picture

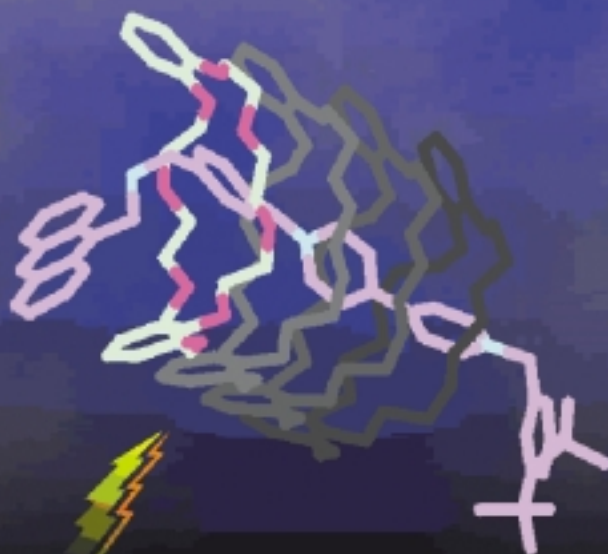
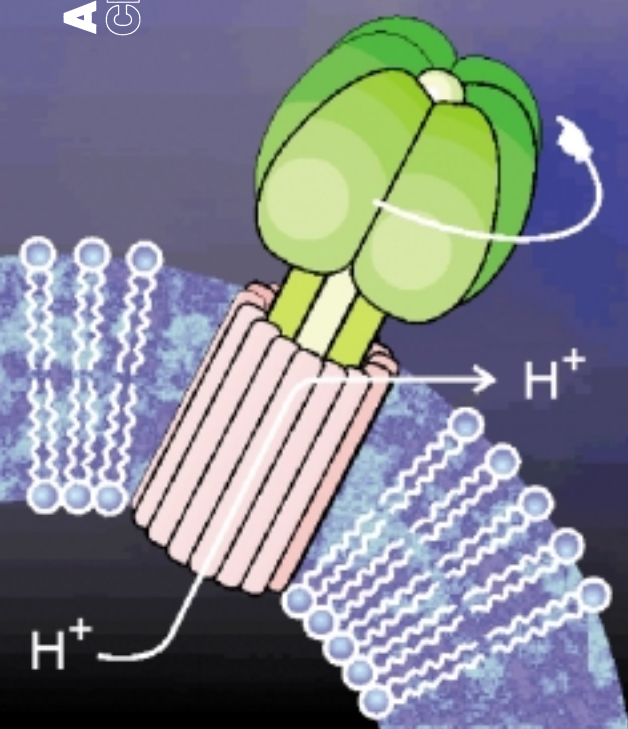
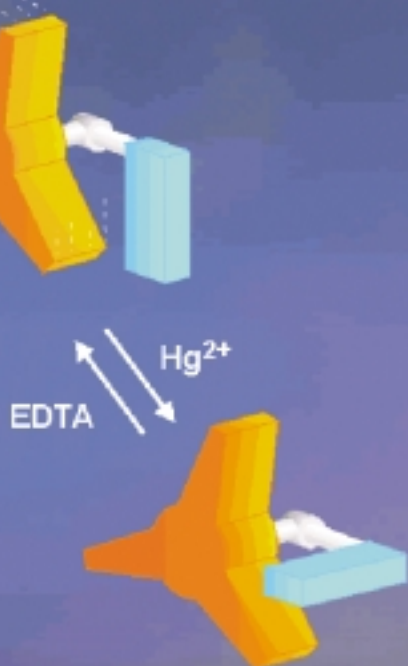
**Jens Krömer, Idoia Rios-Carreras, Gerda Fuhrmann,
Christiane Musch, Markus Wunderlin, Tony Debaerdemaeker,
Elena Mena-Osteritz and Peter Bäuerle**

The cover picture shows the synthesis of novel conjugated macrocycles assembled from oligothiophenes bearing terminal acetylene groups. Under pseudo-high-dilution conditions the oxidative cyclooligomerization first gives the oligothiophenediynes, the precursors to the new class of α -cyclo[n]thiophenes. The detailed structure of macrocycles with up to 76 ring members and cavities of up to 3 nm could be investigated by means of X-ray structure analysis, scanning tunneling microscopy, and quantum chemical calculations (see the molecular model top right). The novel rings combine the excellent electronic properties of the corresponding linearly conjugated oligomers with the possibility of complexing large organic guest molecules or other objects (the tower of the Cathedral at Ulm represents a nanometer-sized, rodlike entity), which should have new fundamental properties and applications. The background shows the image obtained by scanning electron microscopy of a self-assembled and perfectly ordered monolayer of macrocycles on a graphite surface. More on these fascinating nanometer-sized rings can be found in the communication by P. Bäuerle et al. on p. 3481 ff.





Machines at the Molecular Level



Artificial Molecular Machines

Vincenzo Balzani,* Alberto Credi, Francisco M. Raymo, and J. Fraser Stoddart*

The miniaturization of components used in the construction of working devices is being pursued currently by the large-downward (top-down) fabrication. This approach, however, which obliges solid-state physicists and electronic engineers to manipulate progressively smaller and smaller pieces of matter, has its intrinsic limitations. An alternative approach is a small-upward (bottom-up) one, starting from the smallest compositions of matter that have distinct shapes and unique properties—namely molecules. In the context of this particular challenge, chemists have been extending the concept of a macroscopic machine to the molecular level. A *molecular-level machine* can be defined as an assembly of a distinct number of molecular components that are designed to perform machinelike movements (output) as a result of an appropriate external stimulation (input). In common with their macroscopic counterparts, a molecular machine is characterized by 1) the kind of energy input supplied to make it work, 2) the nature of the movements of its component parts, 3) the way in

which its operation can be monitored and controlled, 4) the ability to make it repeat its operation in a cyclic fashion, 5) the timescale needed to complete a full cycle of movements, and 6) the purpose of its operation. Undoubtedly, the best energy inputs to make molecular machines work are *photons* or *electrons*. Indeed, with appropriately chosen photochemically and electrochemically driven reactions, it is possible to design and synthesize molecular machines that do work. Moreover, the dramatic increase in our fundamental understanding of self-assembly and self-organizational processes in chemical synthesis has aided and abetted the construction of artificial molecular machines through the development of new methods of *noncovalent synthesis* and the emergence of *supramolecular assistance to covalent synthesis* as a uniquely powerful synthetic tool. The aim of this review is to present a unified view of the field of molecular machines by focusing on past achievements, present limitations, and future perspectives. After analyzing a few important examples of natural molec-

ular machines, the most significant developments in the field of artificial molecular machines are highlighted. The systems reviewed include 1) chemical rotors, 2) photochemically and electrochemically induced molecular (conformational) rearrangements, and 3) chemically, photochemically, and electrochemically controllable (co-conformational) motions in interlocked molecules (catenanes and rotaxanes), as well as in coordination and supramolecular complexes, including pseudorotaxanes. Artificial molecular machines based on biomolecules and interfacing artificial molecular machines with surfaces and solid supports are amongst some of the cutting-edge topics featured in this review. The extension of the concept of a machine to the molecular level is of interest not only for the sake of basic research, but also for the growth of nanoscience and the subsequent development of nanotechnology.

Keywords: catenanes • molecular machines • nanodevices • photochemistry • rotaxanes • supramolecular chemistry

[*] Prof. V. Balzani, Dr. A. Credi

Dipartimento di Chimica "G. Ciamician"

Università di Bologna

via Selmi 2, 40126 Bologna (Italy)

Fax: (+39)051-2099456

E-mail: vbalzani@ciam.unibo.it

Prof. J. F. Stoddart

Department of Chemistry and Biochemistry

University of California, Los Angeles

405 Hilgard Avenue, Los Angeles, CA 90095-1569 (USA)

Fax: (+1)310-206-1843

E-mail: stoddart@chem.ucla.edu

Prof. F. M. Raymo

Center for Supramolecular Science

Department of Chemistry, University of Miami

1301 Memorial Drive, Coral Gables, FL 33146-0431 (USA)

E-mail: fraymo@miami.edu

1. Molecular-Scale Machines

What would be the utility of such machines? Who knows? I cannot see exactly what would happen, but I can hardly doubt that when we have some control of the arrangement of things on a molecular scale we will get an enormously greater range of possible properties that substances can have, and of the different things we can do.

Richard P. Feynman^[1] (1959)

1.1. The Concept of a Machine at the Molecular Level

In everyday life we make extensive use of (macroscopic) machines. A machine is^[2] "an apparatus for applying mechanical power, having several parts each with a definite function".



V. Balzani



A. Credi



F. M. Raymo



J. F. Stoddart

Vincenzo Balzani was born in Forlimpopoli (Italy) in 1936. He received his “Laurea” in Chemistry at the University of Bologna in 1960. After a few years as Assistant Professor at the University of Ferrara, he joined the Faculty of Science of the University of Bologna in 1969, where he has remained to this day. He was Director of the Photochemistry and Radiation Chemistry Institute of the Italian National Research Council (1977–1988) and Chairman of the European Photochemistry Association (1988–1992). He has obtained several awards, including the Ziegler–Natta Lectureship of the Gesellschaft Deutscher Chemiker (1994), the Italgas European Prize for Research and Innovation (1994), the Centenary Lectureship of the Royal Chemical Society (1996), and the Porter Medal for Photochemistry (2000). He is the author of two monographs and of more than 400 scientific papers. His research interests include photochemistry, electron-transfer reactions, supramolecular chemistry, dendrimer chemistry, and molecular-level devices and machines.

Alberto Credi was born in Bologna (Italy) in 1970. After receiving a “Laurea” in Chemistry from the University of Bologna (1994), he spent one more year in the same University as a research fellow (Ciba-Geigy), and six months as a visiting scientist (NATO) at the University of Virginia with Professor F. S. Richardson. In early 1999 he obtained his Ph.D. in Chemical Sciences from the University of Bologna under the supervision of Professor V. Balzani. He was selected, as a graduate student, to attend the meeting *Scientia Europaea*, and invited to illustrate his research at the University of Zurich, Switzerland. His dissertation, entitled “Molecular-level Machines and Logic Gates”, received the annual award of the Italian Chemical Society and, very recently, the 2000 IUPAC Prize for young Chemists. After a short period as a research assistant, he is presently researcher at “G. Ciamician” Department of Chemistry of the University of Bologna. His research interests, which include photophysics, photochemistry and electrochemistry of metal complexes, supramolecular systems, and dendrimers, are mainly focused on the development of molecular-level devices and machines. He is the author of about 60 publications in the field of molecular and supramolecular photochemistry and electrochemistry.

Francisco M. Raymo was born (1969) and educated in Messina (Italy). He obtained a “Laurea in Chimica” (1992) from the University of Messina and a “Ph.D. in Chemistry” (1996) from the University of Birmingham. As a graduate student, he developed numerous approaches to the template-directed syntheses of catenanes and rotaxanes under the supervision of Professor J. F. Stoddart. Thereafter, he was a Postdoctoral Research Fellow at the University of Birmingham (1996–1997) and, later, at UCLA (1997–1999) working, in collaboration with Professors K. N. Houk and J. F. Stoddart, on the design, synthesis, and computational investigation of molecular machines incorporating interlocked components. Currently, he is an Assistant Professor in the Center for Supramolecular Science at the Department of Chemistry of the University of Miami. In 1998, he was selected as the “Marie Curie Success Story” for Chemistry by the European Commission and also received a “Chancellor’s Award for Postdoctoral Research” at UCLA. His research interests range from the design and synthesis of artificial self-assembling systems, molecule-based materials, and mechanically interlocked molecules to crystal engineering, template-directed syntheses, and the computational investigation of recognition phenomena. He is the author of more than 90 publications in the areas of computational chemistry, chemical synthesis, materials science, and supramolecular chemistry.

J. Fraser Stoddart was born in Edinburgh, Scotland in 1942. He received all of his degrees (B.Sc., 1964; Ph.D., 1966; D.Sc., 1980) from the University of Edinburgh. He carried out postdoctoral work at Queen’s University in Canada before joining the academic staff at the University of Sheffield in 1970. After a seven-year spell as the Professor of Organic Chemistry at the University of Birmingham, he moved, in 1997, to the Saul Winstein Chair of Organic Chemistry at UCLA. Much of his research effort over the last 15 years has been channeled into the design and construction of molecular machinery based on switchable catenanes and rotaxanes obtained by both noncovalent synthesis and supramolecular assistance to covalent synthesis. Present and future research goals include the interfacing of artificial molecular machines with the macroscopic world by applying self-assembly protocols to the fabrication of molecular devices.

When a machine is working, at least some of its components display changes in their relative positions. A machine is characterized by 1) the kind of energy input supplied to make it work, 2) the type of movements performed by its components, 3) the manner in which its operation can be monitored and controlled, 4) the possibility to repeat the operation at will and establish a cyclic process, 5) the timescale needed to complete a cycle of operation, and 6) the function performed by the machine.

The concept of a machine can be extended to the molecular level. A *molecular-level machine* can be defined as an assembly of a discrete number of molecular components designed to perform mechanical-like movements (output) as a consequence of appropriate external stimuli (input). Although there are many chemical compounds whose constitutions and/or shapes can be modified by an external stimulus—for example, molecules capable of undergoing photoinduced *cis/trans* isomerizations of their C=C, C=N, or N=N bonds—the term molecular-level machine will only be used for systems whose component parts undergo movement with relatively large amplitudes. Furthermore, systems in which the molecular movements are not controlled by some easily identifiable and well-characterized external stimulus will not be considered to be molecular-level machines. The extension of the concept of a machine to the molecular level is of interest not only for the sake of basic research, but also for the growth of nanoscience and the subsequent development of nanotechnology.

The concept of a machine at the molecular level is not a new one. Our bodies can be viewed as very complex ensembles of molecular-level machines that power our physical motions in a multitude of different guises, repair tissue damage in a wide spectrum of situations and circumstances, as well as preside over our innermost worlds where we are preoccupied by our sensory perceptions, emotional states, and thought processes. The idea of constructing artificial molecular-level machines, however, is quite a recent one. The first time the topic was seriously contemplated was in 1959 by Richard Feynman,^[1] Nobel Laureate in Physics, in his historic address “There is Plenty of Room at the Bottom” to the American Physical Society in December of that year. The earliest examples of synthetic molecular-level machines, based on the photoisomerization of azobenzene, were reported^[3] in the early 1980s. In the last 15 years research in the field of artificial molecular-level machines has been stimulated by several major scientific breakthroughs and paradigm shifts: they include 1) the rapid development of probe microscopies^[4] following the award of the Nobel Prize in Physics to Binnig and Rohrer in 1986; 2) a growing interest in supramolecular chemistry^[5] after the award of the 1987 Nobel Prize in Chemistry to Pedersen, Cram, and Lehn; 3) the elucidation and unraveling of the working mechanisms of some key biological devices and machines,^[6, 7] such as those involved in photosynthesis (Deisenhofer, Huber, and Michel recognized by the 1988 Nobel Prize in Chemistry) and in the ATP synthesis (leading to the 1997 Nobel Prize in Chemistry to Boyer, Skou, and Walker); 4) the great progress in understanding the mechanisms of the homogeneous and heterogeneous thermal and photoinduced electron-transfer reactions^[8] provided by Marcus who was

awarded the Nobel Prize in Chemistry in 1992; and 5) the realization that the (physical) top-down approach to miniaturization in the electronics industry, for example, has intrinsic limitations and the increasing confidence that it can be replaced profitably by a (chemical) bottom-up approach.^[9]

In the past few years interest in artificial molecular machinery has grown exponentially and several short reviews covering specific aspects of the field are now available.^[10] The aim of this article is to present a unified view of the field by focusing in on past achievements, present limitations, and future perspectives.

1.2. Defining Molecular-Level Machines

We have already identified the features and characteristics of macroscopic machines in Section 1.1, and have also established that one of the operational requirements of a molecular machine will be that the movement of its component parts will have relatively large amplitudes—a property which implies the occurrence of chemical reactions. In his 1959 address to the American Physical Society, Feynman^[1] noted that “An internal combustion engine of molecular size is impossible. Other chemical reactions, liberating energy when cold, can be used instead.” Even relatively “cold” chemical reactions, however, can destroy the molecules constituting a machine. Since such a machine works by repeating cycles (Point 4), an important requirement is that any chemical change or reaction taking place in the system has to be reversible. Within this constraint, any kind of chemical process that causes motions of a machine’s component parts—for example, isomerizations, acid/base reactions, oxidation/reduction processes, complexation/decomplexation equilibria involving, for example, the making and breaking of hydrogen bonds—can be useful. Most chemical reactions occur as a result of thermal activation on mixing the reactants. If a molecular-level machine has to work by thermal activation it will need the addition of reagents at all steps in its working cycle, since the added reagents play the role (Point 1) of chemical energy inputs. Although such kinds of input can be useful, clearly the repeated addition of reagents will result in the accumulation of by-products that, after a relatively small number of cycles, will compromise the operation of the machine unless the products can be removed from the system, which is not an easy task to perform. In principle, the best energy inputs to make a molecular machine work (Point 1) are photons and electrons (or holes). Indeed, with appropriately chosen photochemically or electrochemically driven reactions, it is possible to design interesting and intriguing molecular machines.

The motions performed by the component parts of a molecular-level machine (Point 2) depend to some extent on whether the machine is molecular or supramolecular in nature.^[11] Movements of component parts within classical molecules will necessarily involve changes in their conformations and/or configurations around covalent bonds that are formally single or double, respectively, in their orders, although these changes in molecular structure are accompanied by the making and breaking of *intramolecular non-covalent bonds*. Movements of the component parts within

supermolecules (complexes) may be accompanied by conformational and/or configurational changes within their covalently linked molecular components; however, it will be largely the reorganization of *intermolecular noncovalent bonds* between the molecules that will usually reflect and constitute the movements within these kinds of molecular-level machines. In nonclassical so-called interlocked molecules the mechanical bonds that link the component parts together offer the close to unique opportunity, within relatively small molecules at least, to effect movements with large amplitudes upon their components, mainly as a result of the making and breaking of *intercomponent noncovalent bonds*.

In order to monitor and control the operation (Point 3) of a molecular machine the motions of the component parts should bring about readable changes in some properties of the system. Any kind of chemical or physical probe can be useful in providing read-outs, particularly the various different types of spectroscopies that are currently available to us. In this regard, it should be pointed out that photochemistry and electrochemistry are often very useful since both photons and electrons can play the dual role of “writing”, that is, causing the change in the system, and “reading”, that is, reporting the resulting state of the system. The operating timescale (Point 5) of molecular machines is that of nuclear motions, which can range from nanoseconds to seconds depending on the nature of the components involved and the type of motions that are happening. We would like to point out that the description of a motion implies the definition of a fixed reference system. In the case of molecular machines, this matter is not so trivial (see Section 4.2). Finally, the functions that can be performed by exploiting the movements of the components in artificial machines (Point 6) are largely unpredictable. Some comments on this topic will be presented later on in Section 5.

1.3. Natural Molecular Machines

Before reviewing artificial molecular machines, we will discuss a few examples of natural molecular machines. Since the molecular machines produced by nature are extremely complicated systems, there is little hope of reproducing them artificially, at least in the short term. The functions of living organisms involve free energy differences caused by 1) changes in chemical potential, mechanical forces, temperature, extent of order, pressure, etc., or by 2) changes arising from absorption of light or other electromagnetic radiations. The task of biological molecular machines, which are assemblies of proteins, is to convert energy from one form or location into another.^[12] When energy in one of the above forms is available to the correct protein construct, that is, a specific molecular machine, it can be converted or transduced by the appropriate protein into any one of the other forms of energy. Living organisms represent the synergistic integration of functionally diverse molecular machines.^[13]

In the last few years the outstanding development of single molecule manipulation and observation, particularly by fluorescence spectroscopy,^[14, 15] has thrown light on the operational mechanism of several biological machines.

1.3.1. A Rotary Motor: F_1 -ATPase

Mitochondria, bacteria, and chloroplasts use the free energy stored in transmembrane ion gradients to manufacture adenosine triphosphate (ATP) from adenosine diphosphate (ADP) and inorganic phosphate (P_i) by the action of ATP synthase. This enzyme consists^[16] of two principal domains (Figure 1). The asymmetric membrane-spanning F_0 portion

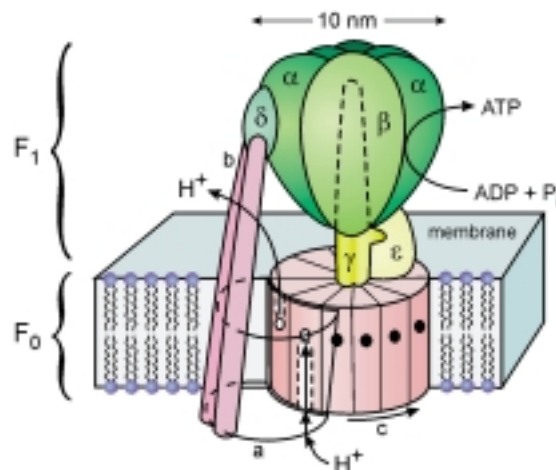


Figure 1. The structure of F_0F_1 ATP synthase.^[16] The catalytic region is composed of the subunits α – ϵ . The proton channels lie at the interface between the subunits a and c (dashed lines indicate the putative inlet and outlet channels). Proton flow through the channels develops torque between the a and c subunits. This torque is transmitted to F_1 via the γ shaft and the ϵ subunit, where it is used to release ATP sequentially from the catalytic sites in F_1 . The c subunit consists of 9–12 twin α -helices arranged in a central membrane-spanning array. The a subunit consists of 5–7 membrane-spanning α -helices and is connected to F_1 by the b and δ subunits. Reprinted by permission from ref. [16f] (Copyright© Macmillan Magazines Ltd 1998).

contains a proton channel, and the soluble F_1 portion contains three catalytic sites which cooperate in the synthetic reactions. The catalytic region is made up of nine protein subunits in the stoichiometry $\alpha:\beta:\gamma:\delta:\epsilon = 3:3:1:1:1$ and approximates to a flattened sphere, 10 nm across and 8 nm high. The flow of protons through F_0 is thought to generate a torque which is transmitted to F_1 by an asymmetric shaft, the coiled-coil γ -subunit. This subunit acts as a rotating “cam” within F_1 , sequentially releasing ATP molecules from the three active sites. The free-energy difference across the inner membrane of mitochondria and bacteria is sufficient to produce three ATP molecules per twelve protons that pass through the motor. The F_0F_1 -ATP synthase is reversible, that is, the full enzyme can synthesize or hydrolyze ATP; F_1 in isolation, however, can only hydrolyze it. The spinning of F_1 -ATPase, namely, the rotary motor nature of this enzyme, was first proposed by Boyer.^[16b] Recently, the rotation of F_1 -ATPase has been directly observed^[17] during ATP hydrolysis by attaching a fluorescent actin filament as a marker to the γ subunit. In other experiments^[18] performed with actin filaments of variable length, discrete 120° rotations have been observed, as expected from the threefold rotational symmetry of γF_1 . A rather puzzling result is that F_1 -ATPase is reported to convert chemical into mechanical energy with near 100% efficiency.

1.3.2. Linear Motor Proteins: Myosin

Enzymes such as myosin, kinesin, dynein, and their relatives are linear motors which convert the energy of ATP hydrolysis into mechanical work along polymer substrates—myosin along actin filaments in muscle and other cells, and kinesin and dynein along microtubules.^[13] Motion derives from a mechano-chemical cycle during which the motor protein binds to successive sites along the substrate in such a way as to move forward on average.

Myosin provides the power for all of our voluntary motions (running, walking, lifting, etc.) as well as for involuntary muscles (for example, beating heart). Myosin is composed of two large heads connected to a long, thin tail. In the muscle cells, many myosin molecules combine by aligning their tails, staggered one relative to the next. Muscle cells are also filled with cables of actin, which are used as a ladder on which myosin climbs. The head groups of myosin extend from the surface of the resulting filament like bristles in a bottle brush. The bristling head groups provide the power to contract muscles. They reach from the myosin filament to a neighboring actin filament and attach to it. Breakage of an ATP molecule then forces the myosin head into a radically different shape. It bends near the center and drags the myosin filament along the actin filament. This is the power stroke of muscle contraction. In a rapidly contracting muscle, each myosin head may stroke five times a second, each stroke moving the filament about 10 nm.

The term myosin refers to at least 14 classes of proteins, each containing actin-based motors. For myosin II (skeletal muscle myosin), the working stroke has been observed^[19] by optical methods in the following way (Figure 2): An actin

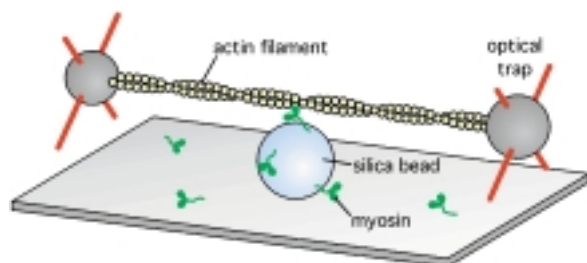


Figure 2. Experimental geometry used^[19] to observe single myosin molecules binding and pulling an actin filament. The filament was attached at either end to a trapped bead. These beads were used to stretch the filament taut and move it near surface-bound silica beads that were decorated sparsely with myosin molecules. Adapted with permission from ref. [19] (Copyright© Macmillan Magazines Ltd 1994).

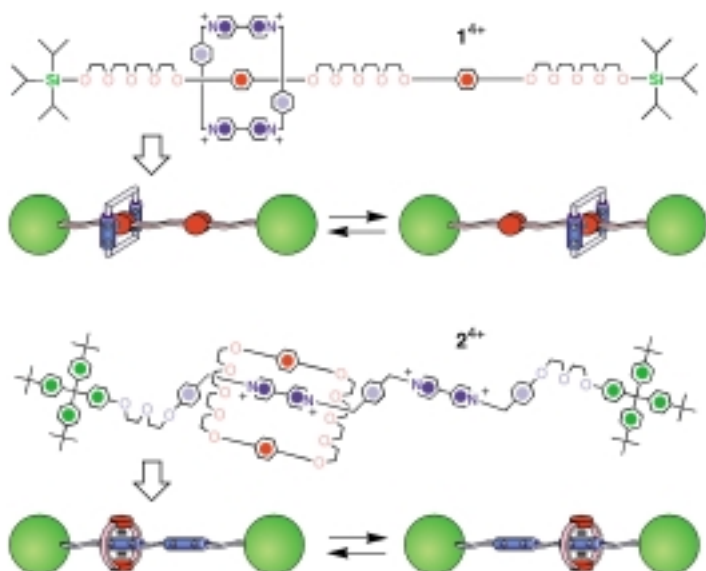
filament was bound at either end to a polystyrene bead to form a dumbbell structure. Both beads were then optically trapped, and the filament was pulled taut and moved near surface-bound silica spheres that were decorated sparsely with myosin molecules. Transient bead deflections parallel to the long filament axis were observed and interpreted as reflecting myosin binding and the pulling of the filament. These experiments, however, could not resolve a number of issues—such as the motor mechanism—which are still the subject of extensive investigation.^[20] Several other biological processes are based on motions. For example, RNA polymer-

ase moves along DNA while carrying out transcriptions, thus it acts as a molecular motor. The force and velocity of single molecules of RNA polymerase have recently been measured.^[21] Evidence of concerted operation of kinesin and myosin motors has also been reported.^[22]

1.4. Interlocked Molecules as Prototypes of Artificial Molecular Machines

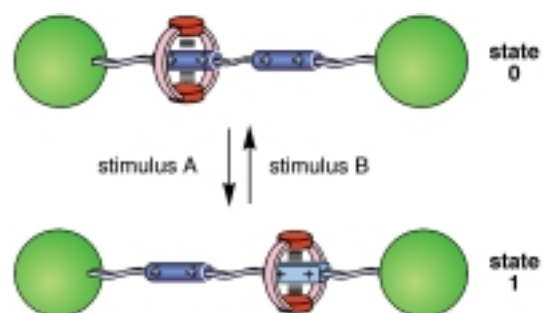
One of the goals of supramolecular chemistry^[5, 11] is to create organized, functioning molecular-scale devices which are able to interpret, store, process, and dispatch information just like the sophisticated machines found in natural systems. Arguably, the most profound influence upon the art of chemical synthesis in recent times has been a supramolecular one, in which intermolecular noncovalent bonding interactions play a prominent role in templating reactions.^[23, 24] While *supramolecular synthesis* has led to the creation of the so-called *rotaxanes*^[25, 26] under thermodynamic control, *supramolecular assistance to molecular synthesis*, under both kinetic and thermodynamic control,^[27] has led to the construction of the so-called *catenanes*,^[25, 26] as well as of the rotaxanes. As observed in natural systems, *self-assembly*^[28] in its strictest sense, and also with covalent modification, has provided the impetus for the development of *synthetic supramolecular chemistry*^[29] to a point where synthesizing catenanes and rotaxanes is quite routine.

A [2]rotaxane^[25, 26] is a molecule composed of a macrocyclic and a dumbbell-shaped component. The macrocycle encircles the linear rodlike portion of the dumbbell-shaped component and is trapped mechanically around it by two bulky stoppers. Thus, the two components cannot dissociate from one another, even although they are not linked covalently to each other. If it can be arranged, during the template-directed synthesis^[23, 24] of a [2]rotaxane, to locate two identical recognition sites within its dumbbell component, then the result is a degenerate, co-conformational^[30] equilibrium state in which the macrocyclic component can shuttle back and forth along the linear portion of the dumbbell. Such a molecule constitutes a *molecular shuttle*.^[31, 32] Two examples^[31, 33] of [2]rotaxanes that behave as degenerate molecular shuttles are shown in Scheme 1. When the two recognition sites in the dumbbell component differ in their constitutions, then the [2]rotaxane can exist as two different equilibrating co-conformations,^[30] whose populations reflect their relative free energies as determined primarily by the strengths of the two different sets of noncovalent bonding interactions in the molecule. In the schematic representation shown in Scheme 2, it has been assumed that the molecular shuttle resides preferentially in “state 0” until a stimulus is applied that switches off the stronger of the two recognition sites, thus inducing the macrocycle to move to the second weaker recognition site, “state 1”. In appropriately designed [2]rotaxanes, this nondegenerate process can be controlled^[10p,q,t,v,y, 34] reversibly using stimuli that are either chemical, electrochemical, or photochemical. Protonation/deprotonation as well as oxidation/reduction processes can all be exploited to alter reversibly the stereoelectronic properties

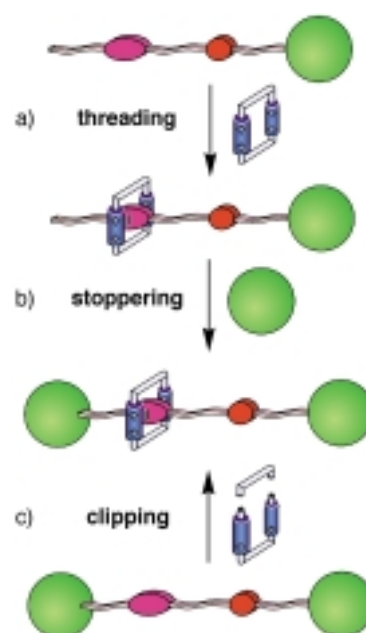


Scheme 1. In the [2]rotaxane 1^{4+} , the bipyridinium-based cyclophane shuttles^[31] from one 1,4-dioxybenzene recognition site to the other at a rate of about 2000 s^{-1} in $(\text{CD}_3)_2\text{CO}$ at ambient temperature. In the [2]rotaxane 2^{4+} , the 1,4-dioxybenzene-based macrocyclic polyether shuttles^[33] from one bipyridinium recognition site to the other one at a rate of about $300\,000\text{ s}^{-1}$ under the same conditions.

of one of the two recognition sites, thus affecting their relative abilities to sustain noncovalent bonds. By switching the recognition properties of one of the two recognition sites off and on again, the relative proportions of the two species can be controlled reversibly. These kinds of controllable molecular shuttles can be self-assembled using one of a number of different template-directed synthetic strategies.^[23, 24] In one instance, a linear half-dumbbell-shaped compound is threaded (Scheme 3; step a) through the cavity of a preformed macrocycle with the assistance of noncovalent bonding interactions and then the so-called *pseudorotaxane*^[35] is stoppered (step b) by the covalent attachment of a bulky group. In another instance, the macrocycle is clipped (step c) around the preformed dumbbell, again with the help of noncovalent bonding interactions. Both the threading followed by stoppering and the clipping approaches to synthesizing controllable molecular shuttles are examples of supramolecular assistance to molecular synthesis. An alternative approach is provided by slippage,^[36] which is an example of supramolecular (noncovalent) synthesis.^[29] In this approach



Scheme 2. The two co-conformations associated with a [2]rotaxane incorporating two different recognitions sites within its dumbbell-shaped component^[31] can be interchanged by appropriate stimuli.



Scheme 3. The a) threading followed by b) stoppering and the c) clipping strategies^[28c] for the template-directed synthesis of a [2]rotaxane.

the macrocyclic and the dumbbell-shaped components are synthesized separately. When the two species are heated together in solution the macrocycle “slips” over the dumbbell’s stoppers to form a molecular shuttle. Upon cooling the reaction mixture, the macrocycle is obliged to remain threaded on the dumbbell as a result of the thermodynamic trap (Figure 3) provided by the stabilizing noncovalent bonding interactions.

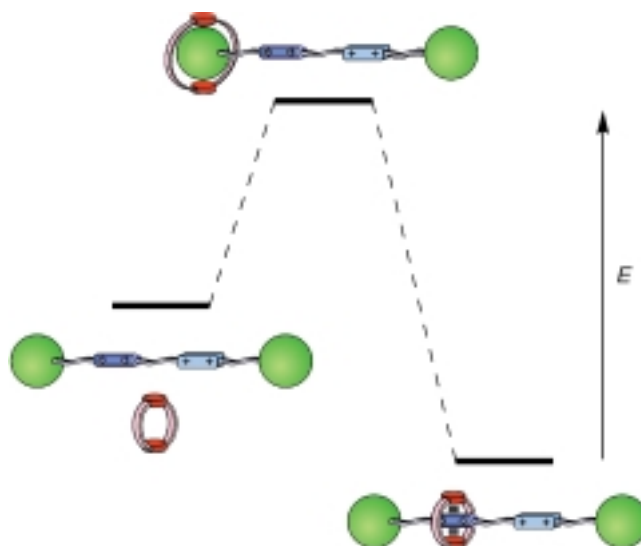
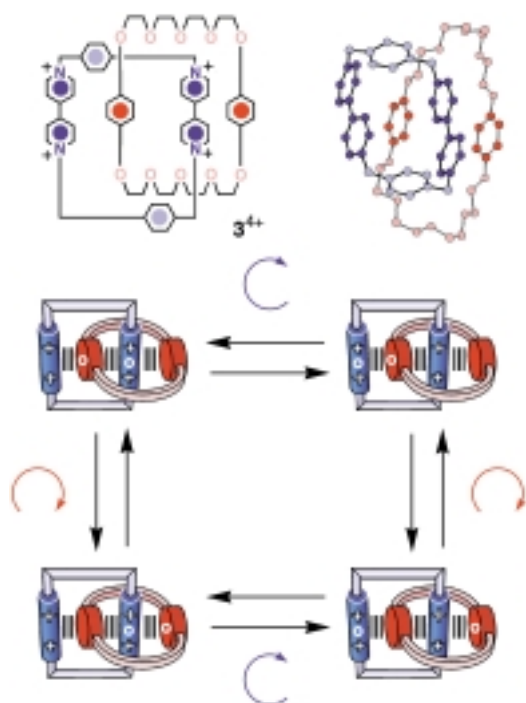


Figure 3. The change in energy associated with the slippage^[36] of a macrocycle over one of the stoppers of a dumbbell-shaped compound.

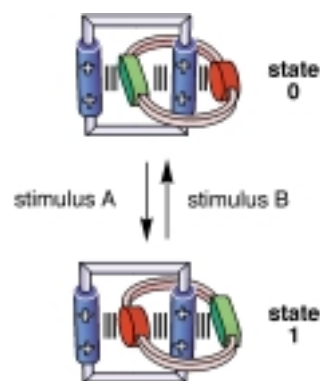
A [2]catenane^[25, 26] is a molecule composed of two interlocked macrocyclic components. The two macrocycles are not linked covalently to each other: rather, a mechanical bond holds them together, and prevents their dissociation. If it is arranged during the template-directed synthesis^[23, 24] to have

two identical recognition sites located within two different macrocycles, then the [2]catenane that results is one that undergoes a degenerate co-conformational^[30] change when one of the macrocycles circumrotates^[37] through the cavity of the other and vice versa. An example^[38] of a degenerate [2]catenane is shown in Scheme 4 wherein the dynamic



Scheme 4. The solid-state structure of the [2]catenane 3^{4+} and the dynamic processes associated^[38] with this molecule in solution which involve the circumrotations of the macrocyclic components through each other's cavities.^[26h]

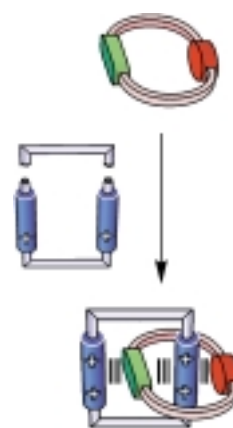
processes in solution are illustrated together with its solid-state structure. When one of the two macrocyclic rings carries two different recognition sites then the opportunity exists to control^[10p,q,v,y, 39, 40] the dynamic processes in these switchable [2]catenanes (Scheme 5) in a manner reminiscent of the controllable molecular shuttles. In essence, the requirement for being able to switch between “state 0” and “state 1” in



Scheme 5. The two co-conformations associated with a [2]catenane that incorporates two different recognition sites within one of its two macrocyclic components can be interchanged by appropriate stimuli.

such a [2]catenane is that the “symmetric” macrocyclic component resides preferentially around one of the two different recognition sites incorporated within the “asymmetric” macrocycle. The two associated co-conformations^[30] are stabilized by intercomponent noncovalent bonding interactions and their interconversion requires the circumrotation of the “asymmetric” macrocycle through the cavity of the “symmetric” one. In solution, the equilibrium between the two co-conformations is governed by the relative magnitudes of the intercomponent noncovalent bonding interactions. By switching off and on again the recognition properties of one of the two recognition sites of the “asymmetric” macrocycle, the relative populations of the two species can be controlled reversibly. Complexation/decomplexation of metal ions or of neutral organic molecules as well as protonation/deprotonation and oxidation/reduction processes can all be exploited to alter reversibly the stereoelectronic properties of one of the two recognition sites, thus affecting its ability to sustain noncovalent bonds. These kinds of switchable [2]catenanes can be prepared following the template-directed synthetic strategy^[23, 24] illustrated in Scheme 6 wherein one of the two macrocyclic components is preformed and then the other one is clipped around it with the help of noncovalent bonding interactions in what amounts to supramolecular assistance to molecular synthesis.

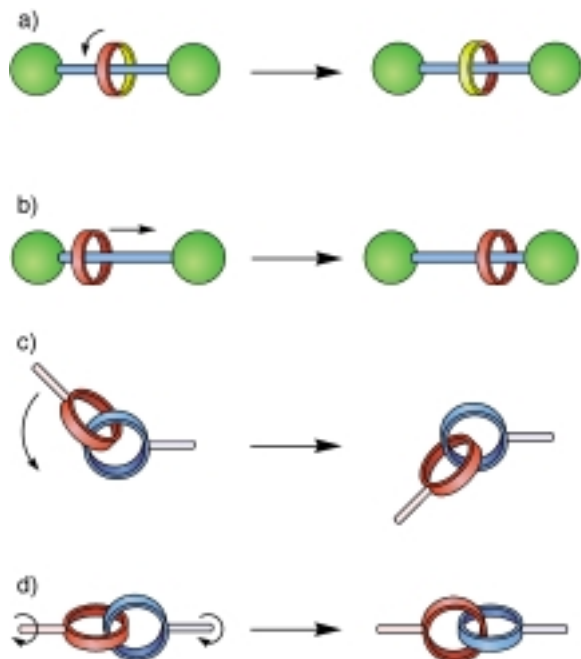
A large variety of recognition sites and noncovalent bonding interactions have been employed^[25, 26] to assist in the covalent syntheses of rotaxanes and catenanes. For example, the ability of 1) cyclodextrins to bind organic molecules in aqueous solution, 2) crown ethers to bind metal cations or secondary dialkylammonium recognition sites, and 3) amide groups to sustain hydrogen-bonding interactions have all been exploited to template the formation of these interlocked molecules. However, rotaxanes and catenanes which are particularly attractive for the generation of molecular machines are those incorporating redox- and/or photo-active units in one or both or all of their interlocked components.^[10p,q,t,v,y] Thus, the most promising synthetic strategies for the generation of molecular machines incorporating interlocked components are those relying on the use of transition metal templates or of complementary π -electron-rich and π -electron-deficient recognition sites. Indeed, the ability of transition metals to coordinate organic ligands with specific geometries has been exploited^[25b, 26b–d] to template the formation of rotaxanes and catenanes incorporating phenanthroline ligands. The redox- and photo-active metal centers embedded in the resulting interlocked molecules provide the means to address them electrochemically and photochemically.^[10q,r,x] Similarly, the ability of bipyridinium recognition sites to sustain π - π and C-H \cdots O interactions with polyethers incorporating π -electron-rich recognition sites has been employed^[25b, 26g,h,j–l,n,o] to



Scheme 6. The clipping strategy^[28c] for the template-directed synthesis of a [2]catenane.

self-assemble, under kinetic or thermodynamic control,^[27] rotaxanes and catenanes. The presence of the redox-active π -electron-rich and π -electron-deficient units makes these interlocked molecules perfect candidates for building molecular machines.^[10a,b,h,i,p,y]

The co-conformational changes associated with rotaxanes and catenanes are reminiscent^[10p,q] of the mechanical motions associated with some macroscopic machines. In a [2]rotaxane, the “wheel” component can rotate around or shuttle along (Scheme 7a and b, respectively) the “axis” component. The



Scheme 7. Some of the dynamic processes^[10q] associated with (a and b) a [2]rotaxane and (c and d) a [2]catenane.

movement of one ring relative to the other in a [2]catenane is reminiscent of a “ball and socket joint”, as illustrated in Scheme 7c. Similarly, the twisting of one ring around the main axis of the [2]catenane forces (Scheme 7d) the other ring to rotate in the same direction in a manner reminiscent of a “universal joint”.^[41]

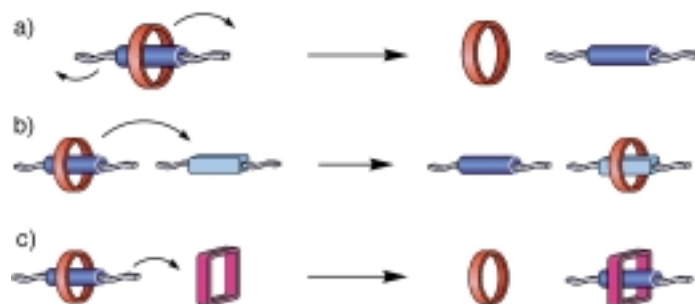
1.5. Pseudorotaxanes as Prototypes of Artificial Molecular Machines

Supramolecular complexes are appealing systems for the construction of simple molecular-level machines since they can be obliged to undergo dissociation into their free molecular components and eventually assemble again upon appropriate counter-stimulations. They are an attractive proposition and of considerable interest because they can be prepared under thermodynamic control simply by mixing the molecular components in solution. The challenge for chemists engaged in this particular approach to building molecular-level machines resides in the “programming” of the system, that is, in the design and synthesis of components, which carry

within their structures the pieces of information necessary for the construction of the desired supramolecular architecture.^[5, 11]

From the viewpoint of molecular machines, the most interesting complexes are the pseudorotaxanes.^[35] The reason is that they can be reversibly dissociated into a free ring-type host and a free thread-type guest, which gives rise to dethreading/rethreading motions. Some of the molecular motions that can be obtained with pseudorotaxanes are represented pictorially in Scheme 8. Starting from the simple dethreading/rethreading motion (Scheme 8a), more complex processes can be devised. In a chemical system composed of a macrocycle and two threadlike species one can select (Scheme 8b), by means of a suitable input, which thread enters the ring’s cavity. Analogously, a suitable stimulus can be employed to choose which one of the two macrocycles surrounds (Scheme 8c) a particular threadlike species. The investigation of such systems is of interest not only for its own sake, but also for the design of more complex molecular machines based on rotaxanes and catenanes (see Section 3).

The external stimulus employed to operate such rudimentary molecular machines must be able to weaken the non-covalent bonding forces that stabilize the initial supramolecular complex. Therefore, the type of stimulus that is used depends on the nature of such forces. The majority of complexes studied so far rely on $^+N-H\cdots O$ and $C-H\cdots O$ hydrogen-bonding or on a combination of $C-H\cdots O$ hydrogen-bonding and π -electron donor/acceptor (charge-transfer) interactions.^[10a,b,h,i,p,y] $^+N-H\cdots O$ Hydrogen-bonding interactions can be easily destroyed by addition of a base capable of deprotonating an ammonium center, and can be restored by addition of an acid capable of reprotonating an amine function. Thus, in supramolecular complexes based on hydrogen-bonding interactions, mechanical motions can be driven by means of chemical (acid/base) stimulation. When the interactions responsible for complexation are donor/acceptor in nature, they can be weakened by oxidation of the electron-donor unit or by reduction of the electron-acceptor one. The reduction of the electron-acceptor unit also weakens the $C-H\cdots O$ hydrogen bonds which accompany the donor/acceptor interactions in most of these supramolecular complexes. In most cases, the donor/acceptor interaction can be restored by means of the reverse redox process. The oxidation



Scheme 8. a) The dissociation of a pseudorotaxane and the interchange of b) a macrocycle between two threads and of c) a thread between two macrocycles.^[10y]

and reduction processes needed to dissociate/associate a supramolecular complex can be achieved by means of chemical, photochemical, or electrochemical stimulation.

1.6. Types of Molecular Machines

Some structure and order is required in any meaningful discussion. This task is never an easy one when discussing chemical systems. The reason relates to their complexity which, in turn, results from their multi-dimensional character. Artificial molecular machines are no exception. Nonetheless, one clear-cut distinction that can be made between different types of artificial molecular machines is according to 1) whether the component parts involved only rotate about covalent, usually single or partial double, bonds in conventional molecules or 2) whether the component parts are associated with topological or other geometrically related changes occurring within interlocked molecules, for example, catenanes and rotaxanes. The terms conformation and co-conformation are employed in this review in order to distinguish between these two types of fundamentally different motions that can take place within molecules. Some kind of mechanical bonding within a molecule is required, on top of the normal range of covalent and noncovalent bonds, to permit changes in the relative positionings of components that are co-conformational in nature. It is convenient to extend this terminology from the molecular world into the supramolecular domain, such that pseudorotaxanes, for example, may be considered to undergo co-conformational changes between their complexed and uncomplexed states. The other clear-cut distinction that can be made in discussing the abilities of molecules and supramolecules to behave as switches is how they are stimulated to perform their internal movements. In this review, it has been found convenient to discuss the addressing issue under the headings of chemical, electrochemical, and photochemical, depending on the nature of the fuel. In this ad hoc manner, we have been able to introduce some semblance of structure and order into our discussion of artificial molecular machines.

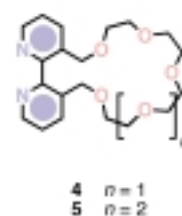
2. Artificial Molecular Machines Based on Conformational Motions

2.1. Chemically Induced Conformational Motion

2.1.1. On/Off Switches Based on Allosteric Effects

In enzymology, conformational changes induced by binding give rise to interactions between remote sites (allosteric effects) and provide a means by which the activity of enzymes can be regulated. Amongst the earliest examples of artificial chemically induced conformational motions are those^[42] related to the construction of molecules, such as **4** and **5**, which are capable of allosteric behavior (Scheme 9). Such molecules are characterized by 1) an active site, 2) an allosteric or remote site, and 3) a conformational mechanism which transmits binding information from one site to the

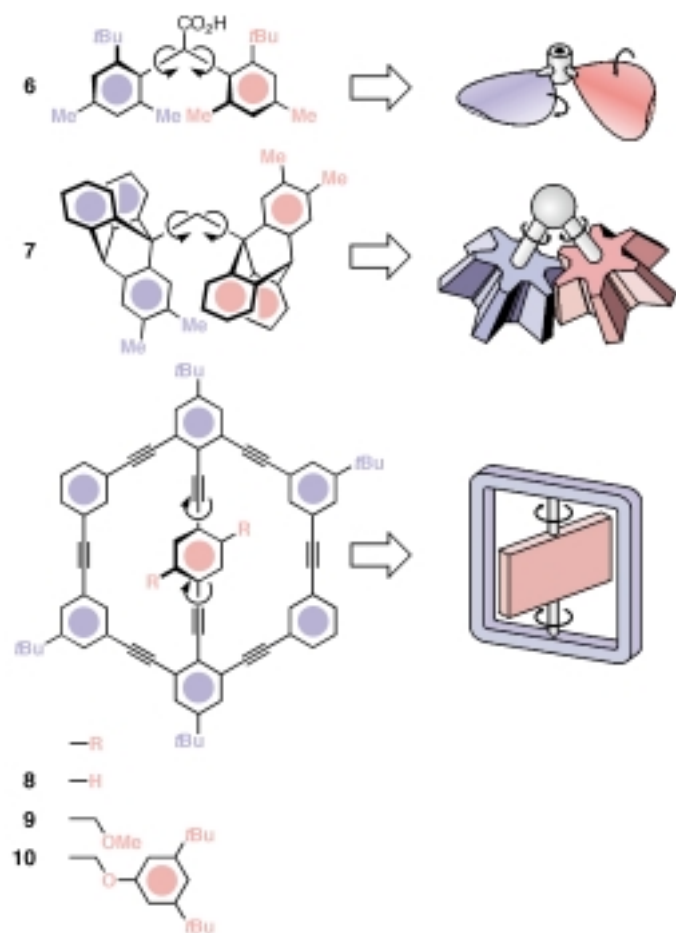
other. In the ditopic receptors **4** and **5**, the 2,2'-bipyridine and crown ether binding sites, although separated and electronically insulated, cannot behave independently. Chelation of metals with the 2,2'-bipyridine unit forces the aromatic rings toward coplanarity and brings the groups in the 3- and 3'-positions of the bipyridyl unit close together. This binding restricts the conformational freedom of the crown ether and thereby alters its receptivity toward metal ions. In the case of compound **4**, the change in selectivity is small (a factor of four for K^+).^[42b] However, in the case of compound **5**, which contains a larger crown ether macrocycle, it has been found^[42c] that the capability of the macrocycle to coordinate $Hg(CF_3)_2$ in a pseudorotaxanelike manner is drastically affected by coordination of Pd^{2+} at the bipyridyl site (on/off behavior).



Scheme 9. The ditopic receptors **4** and **5**,^[42] in which conformational changes induced by metal binding at one site alter the receptivity of a remote binding site.

2.1.2. Chemical Rotors

The correlated rotation of bulky groups in crowded molecules has presaged^[43] the design of molecular-sized propellers and gears. A molecule composed of two bulky aryl rings attached to a “focal” atom can be regarded as the molecular equivalent of a macroscopic two-bladed propeller. The diarylacetic acid derivative **6** (Scheme 10) incorporates^[44] two identical aryl rings linked to the same atom. Rotation of one ring in one direction about the single bond linking it to the “focal” methine carbon atom forces^[44, 45] the other ring to rotate in the opposite direction. Thus, when one ring rotates clockwise, the other must rotate anticlockwise, and vice versa. The mechanism for this coupled conformational motion, which involves a concerted disrotation, has been termed “cogwheeling”.^[46] The coupled motions of two chemical rotors have also been exploited^[47, 48] in the design of *molecular gears* incorporating triptycyl ring systems. For example, the molecular gear **7** (Scheme 10) incorporates^[47c] two 9-triptycyl ring systems bridged by a methylene group. The aryl rings of the two 9-triptycyl ring systems interdigitate in a manner reminiscent of the notches of a pair of meshed bevel gears. As a result, the rotations of the two 9-triptycyl ring systems about the single bonds linking them to the “focal” methylene group are coupled. When one 9-triptycyl ring system rotates clockwise, the other one rotates anticlockwise, and vice versa. Another interesting class of chemical rotors are the macrobicyclic molecules^[49] **8–10** illustrated in Scheme 10. The central phenyl ring of **8** can rotate about its axis. This conformational motion is reminiscent of the movement of the spindle of a turnstile^[50] and, as a result, this compound has been called a *molecular turnstile*. The dynamic process associated with the molecular turnstile is affected considerably by the size of the R groups attached to the central *p*-phenylene ring. Indeed, two degenerate conformations can be identified in the case of **9** by low temperature 1H NMR spectroscopy. At ambient temperature, however, the rotation about the axis of the central ring of **9** is fast on the 1H NMR



Scheme 10. The molecular propeller **6**,^[44] the molecular gear **7**,^[47c] and the molecular turnstiles **8**–**10**.^[49]

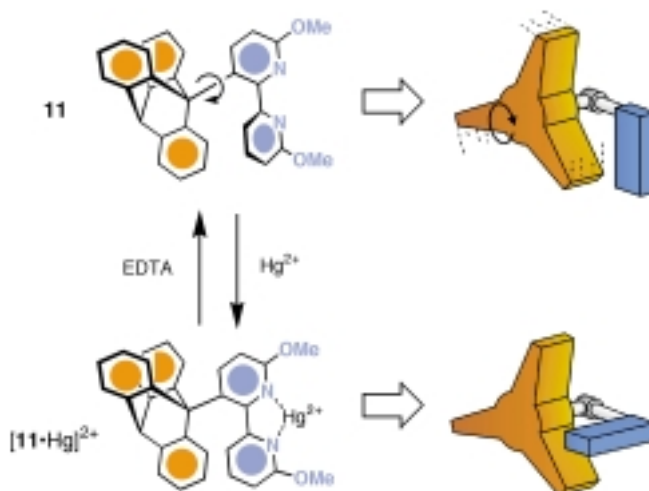
timescale and a free energy barrier of $13.4 \text{ kcal mol}^{-1}$ is associated with this dynamic process. By contrast, this rotation does not occur in **10**, even when a solution of this compound is heated up to high temperatures. In this instance, the substituents attached to the central p -phenylene ring are far too bulky to be able to pass through the cavities of the macrobicyclic ring system.

The rotations associated with the chemical rotors **6**–**9** are spontaneous, in common with the conformational motions observed in most organic molecules possessing single bonds.^[51] By contrast, the large amplitude motion associated with a real molecular machine has to be controllable.

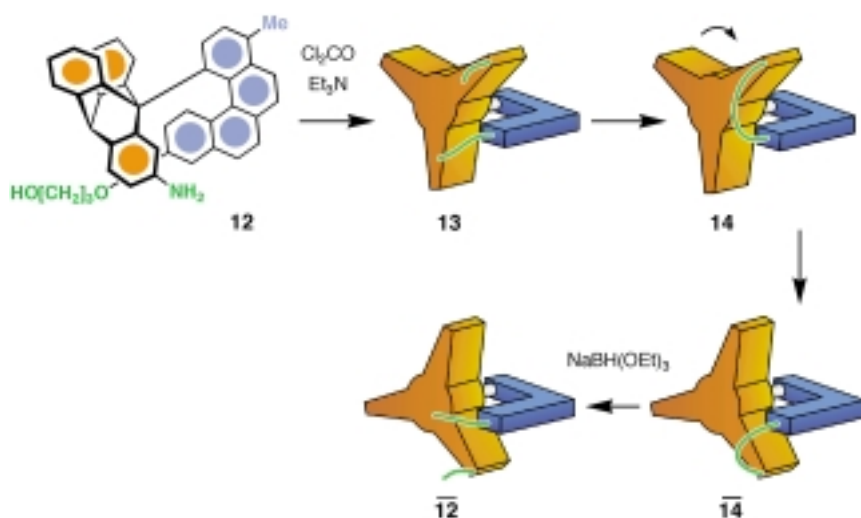
An example of a chemically controllable rotor^[52] is the compound shown in Scheme 11 which incorporates a 9-triptycyl ring system attached to a 2,2'-bipyridine unit. The rotation about the single bond connecting these two units in $(\text{CD}_3)_2\text{CO}$ at 303 K is fast on the ^1H NMR timescale. As a result, only four sets of resonances are observed in the ^1H NMR spectrum for the aromatic protons of the 9-triptycyl ring system. The solution has to be cooled down to 193 K to slow down this dynamic process. Under these conditions the twelve aromatic protons of the 9-triptycyl unit became nonequivalent. Upon addition of $\text{Hg}(\text{O}_2\text{CCF}_3)_2$ to a solution of **11** in $(\text{CD}_3)_2\text{CO}$, the metal ion is coordinated by the 2,2'-bipyridine ligand. As a result, the conformation of this unit is

locked and the ^1H NMR spectra (303 K) recorded before and after the addition of the metal ion are markedly different. Upon chelation, the singlet associated with the protons of the methoxy group attached to the disubstituted pyridine ring is shifted downfield by $+2.02 \text{ ppm}$. Furthermore, the resonances of the aromatic protons of the 9-triptycyl ring system broaden significantly. At 243 K, rotation about the single bond connecting the 9-triptycyl ring system to the 2,2'-bipyridine unit is already slow enough to render some of the aromatic protons of the 9-triptycyl ring system nonequivalent. These observations indicate that the locked conformation of the 2,2'-bipyridine unit brakes the rotation of the 9-triptycyl ring system. The *molecular brake* can be released by adding EDTA to the solution of $[\mathbf{11} \cdot \text{Hg}]^{2+}$ in $(\text{CD}_3)_2\text{CO}$. Indeed, removal of the coordinated metal unlocks the conformation of the 2,2'-bipyridine unit, thus disengaging the brake.

In order to generate a chemical rotor which undergoes unidirectional^[53] motion, the design of the molecular brake **11** was modified. The 2,2'-bipyridine unit was replaced^[54] by helicenes of appropriate lengths and the unidirectional, ratchet-type rotation about the single bond connecting the 9-triptycyl ring system to a [4]helicene has now been achieved.^[55] The steric hindrance associated with the [4]helicene group of **12** (Scheme 12) inhibits the rotation about the single bond connecting this unit to the 9-triptycyl ring system. Treatment of **12** with Cl_2CO and Et_3N gives the isocyanate **13**. The intramolecular reaction of the hydroxyl and isocyanate groups affords the urethane **14** in a highly strained conformation. The strain is released by the clockwise rotation of the 9-triptycyl ring system about the single bond connecting it to the [4]helicene. Cleavage of the urethane linkage regenerates compound **12** in a conformation that is different from the original one. This new conformation is obtained as a result of a unidirectional 120° rotation induced by the formation of a covalent bond. The process can be followed by ^1H NMR spectroscopy using the bridgehead proton of the 9-triptycyl ring system as a probe. The rapid transformation of **12** into **14** is accompanied by a shift of the singlet associated with the



Scheme 11. The molecular brake **11** is engaged^[52] upon chelation of a Hg^{II} ion by the 2,2'-bipyridine ligand and it is released upon addition of EDTA which captures the metal ion ($(\text{CD}_3)_2\text{CO}$, 303 K).

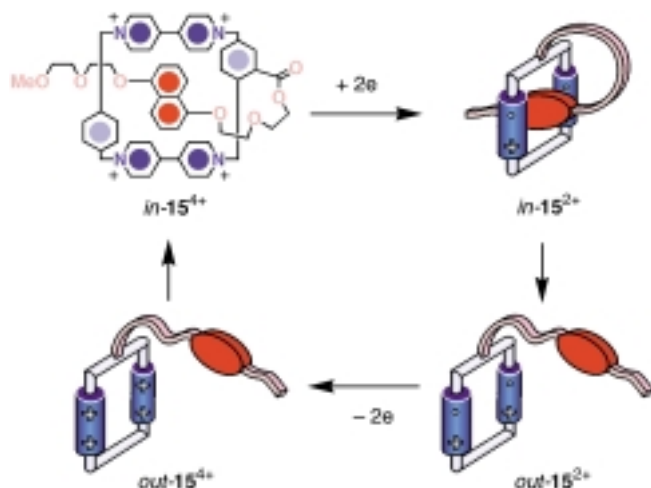


Scheme 12. The rotation about the single bond connecting the 9-triptycyl ring system to the [4]helicene group in chemical rotor **12** (CDCl_3 , 295 K) is assisted^[55] by the formation of a covalent bond and occurs in one direction only.

probe proton to low field and is followed by the unidirectional rotation which causes a decrease in the intensity of this signal and the concomitant growth of another singlet. After about 6 h, the conformational change is almost complete.

2.2. Electrochemically Induced Conformational Motion

Conformational changes can be induced electrochemically^[56] in appropriately designed self-complexing molecules. An example is compound *in-15*⁴⁺ (Scheme 13), which incorporates^[57, 58] a π -electron-deficient head and a π -electron-rich



Scheme 13. The motion of the π -electron-rich tail of the self-complexing compound **15**⁴⁺ can be induced^[57] electrochemically in MeCN solution at 298 K by reducing/oxidizing the bipyridinium units of the π -electron-deficient head.

tail. The tail threads through the cavity of its own head in solution, which results in the positioning the 1,5-dioxynaphthalene ring system between the two bipyridinium units. This conformation is stabilized by π - π stacking interactions

between the complementary π -electron-rich and π -electron-deficient aromatic units, as well as by C-H...O hydrogen bonds between the α -bipyridinium hydrogen atoms and the polyether oxygen atoms. Consistently, the absorption spectrum of *in-15*⁴⁺ recorded in MeCN at 298 K shows a band in the visible region at 515 nm, which arises from charge-transfer interactions between the 1,5-dioxynaphthalene ring system and the sandwiching bipyridinium units. The absorbance of the charge-transfer band increases linearly with the concentration. This behavior is remarkably similar to that of a model self-complexed system^[57] bearing a bulky stopper at the end of the tail. The stopper prevents dethreading of the tail and so this model compound can exist only in a self-complexed conformation. The similarities between the absorption spectra of *in-15*⁴⁺

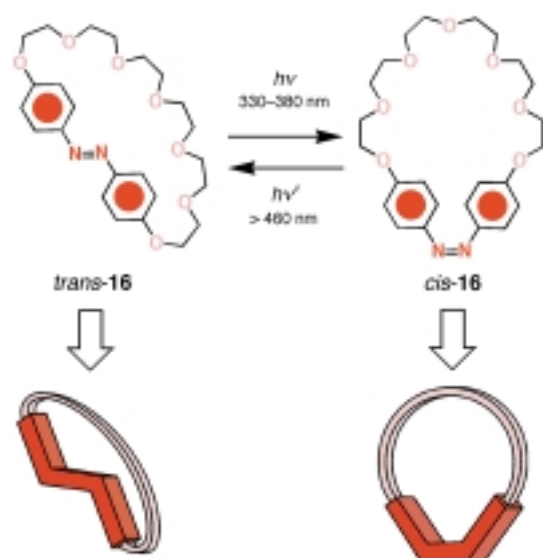
and of this model compound indicate that *in-15*⁴⁺ also exists completely in its self-complexed conformation in solution. The cyclic voltammogram of *in-15*⁴⁺ shows two reversible two-electron reduction waves. The first one (-0.35 V versus the saturated calomel electrode (SCE)) corresponds to the simultaneous addition of one electron to each of the two bipyridinium units. The second one (-0.71 V) corresponds to the simultaneous addition of a second electron to each of the two bipyridinium units. A model tetracationic cyclophane that does not incorporate the 1,5-dioxynaphthalene tail undergoes two consecutive two-electron reduction processes at -0.29 and -0.70 V. Thus, the first reduction process occurs at a more negative potential in the case of *in-15*⁴⁺, while the second reduction process occurs at the same potential in both compounds. These observations indicate that the 1,5-dioxynaphthalene unit of *in-15*⁴⁺ is sandwiched (Scheme 13) initially between the two bipyridinium units, which makes their first reduction more difficult. However, after the addition of one electron to each of the two bipyridinium units, the 1,5-dioxynaphthalene unit is expelled from the cavity of the tetracationic cyclophane^[59] and the second reduction process is not affected by the presence of the π -electron-rich unit. Subsequent removal of the electrons previously added to the bipyridinium units leads back to the insertion of the tail into the cyclophane. This is an example of an artificial molecular machine where both the input and the output are electrochemical.

2.3. Photochemically Induced Conformational Motion

Suitable donor-bridge-acceptor compounds have been shown^[60] to undergo conformational folding in nonpolar solvents upon excitation with light. Excitation of such compounds with light leads to the formation of an excited state, localized on the acceptor subunit, which then decays to a charge-separated state. In this state, the donor and the acceptor subunits carry a positive and a negative charge,

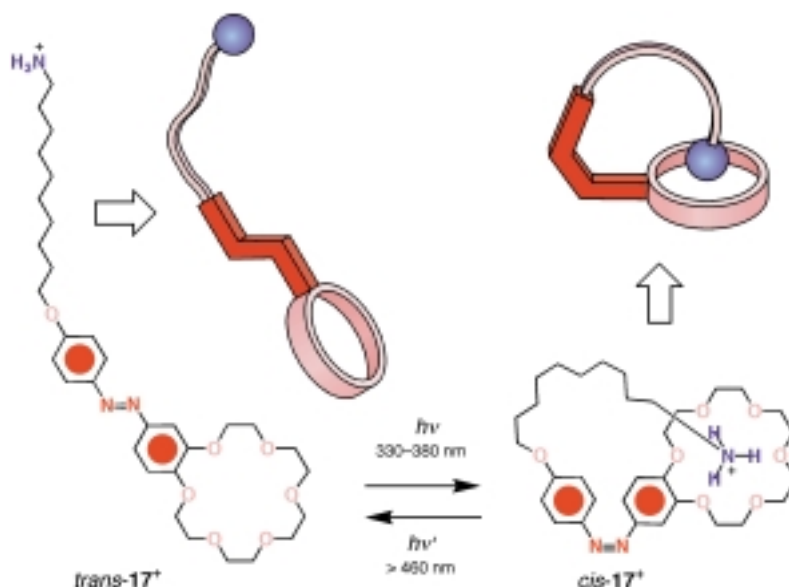
respectively, and are well separated in space. However, electrostatic attractions bring the subunits close together, thereby making the molecule fold over on itself. Crucial for the observation of this “harpooning” motion is the fact that both the extended and folded charge-separated states show a characteristic fluorescence. This is an excellent example of a system in which photons are employed as both a stimulation and a read-out signal.

The N=N bond of azobenzene (1,2-diphenyldiazene) can adopt *cis* and *trans* configurations. Their interconversion can be induced by irradiation at appropriate wavelengths. Thus, the geometries of molecules incorporating one or more azobenzene units can be altered reversibly by the controlled isomerization of these photoactive sites. In turn, these structural changes can be exploited to modulate the physico-chemical properties of such molecules and/or of their surrounding environment. Indeed, this strategy has been employed extensively to control the geometries and functions of biomolecules,^[61] of organic materials,^[62] and of supramolecular complexes.^[3, 63, 64] For example, the photoresponsive crown ether *trans*-**16** (Scheme 14) incorporates a *trans*-azobenzene unit.^[65, 66] Upon irradiation of a solution of *trans*-**16** in *o*-dichlorobenzene at 330–380 nm a *trans* → *cis* isomerization of the photoactive unit occurs. The photoinduced configurational change about the N=N bond is accompanied by pronounced conformational changes of the polyether linkages. The overall effect is an expansion of the macrocyclic cavity upon *trans* → *cis* isomerization. The *cis* → *trans* reversion can be induced by irradiating at a different wavelength (>460 nm). Thus, the macrocyclic cavity associated with **16** can be expanded and contracted reversibly by irradiating this compound at appropriate wavelengths. In turn, these con-



Scheme 14. The photoinduced *cis/trans* isomerization of the azobenzene unit of **16** (*o*-dichlorobenzene, 303 K) is accompanied^[65] by the expansion/contraction of the macrocyclic cavity of this molecule.

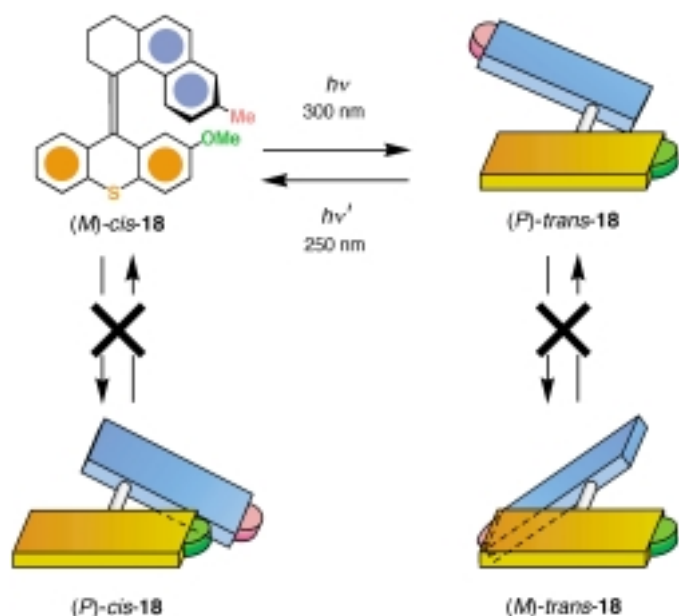
trolled configurational and conformational changes affect the binding ability of **16**. Thus, while the “expanded” macrocycle *cis*-**16** binds alkali metal cations, the “contracted” one *trans*-**16** does not. In a similar fashion, the photoinduced *cis/trans* isomerization of azobenzene was exploited to shrink and enlarge the cavities of cyclophanes,^[67] to shorten and elongate the distance between the recognition sites of ditopic receptors,^[64, 68, 69] and to induce (Scheme 15) intramolecular complexation in self-complementary molecules^[70, 71] such as **17**⁺. This compound incorporates a macrocyclic polyether head



Scheme 15. The photoinduced *cis/trans* isomerization of the azobenzene unit of **17**⁺ (*o*-dichlorobenzene, 303 K) is accompanied^[70] by the motion of the cationic tail which can only interact with its macrocyclic head in the *cis* isomer.

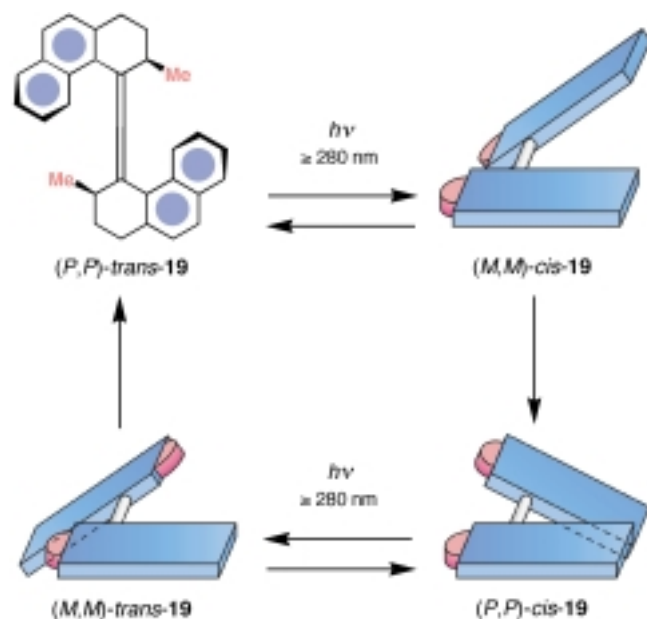
bridged by a photoactive azobenzene unit to a linear tail bearing a terminal ammonium group. The ammonium recognition site in the *trans* isomer is positioned away from the complementary macrocyclic head. Upon irradiation (*o*-dichlorobenzene, 330–380 nm), however, *trans* → *cis* isomerization occurs, which brings the ammonium recognition site in closer to the crown ether head and allows their intramolecular association. Thus, while the *trans* isomer of **17**⁺ has a strong affinity for metal cations, the binding ability of the *cis* isomer toward metal cations is almost completely suppressed by the photoinduced self-complexation.

Two pairs of enantiomers (Scheme 16) are associated^[72, 73] with the helical compound **18**. Polarimetry, ¹H NMR spectroscopy, and high performance liquid chromatography (HPLC) revealed that no racemization and no *cis/trans* isomerization occur under ambient conditions. The bulky and flexible tetrahydrophenanthrene unit prevents racemization without producing an excessive distortion of the central double bond. Upon continuous irradiation of a solution of pure (*M*)-*cis*-**18** at either 250 or 300 nm, *cis/trans* isomerization occurs to afford mixtures of (*M*)-*cis*-**18** and (*P*)-*trans*-**18** in ratios of 68:32 or 64:36, respectively. The same results were obtained when (*P*)-*trans*-**18** was irradiated. In all instances, however, no racemization occurred. Interconversion between the two photostationary states associated with this chiroptical molec-



Scheme 16. The photoinduced *cis/trans* isomerization of the chiroptical molecular switch **18** (*n*-hexane/*i*PrOH 9/1, 298 K) is not accompanied^[72] by any racemization.

ular switch can be achieved by the consecutive irradiation at 250 and 300 nm. The periodical change in the ratio of the isomers (*M*)-*cis*-**18** and (*P*)-*trans*-**18** produced by the alternating irradiation can be followed by monitoring the intensities of the absorption bands at 232 and 262 nm in the circular dichroism (CD) trace. In order to generate a light-driven unidirectional molecular rotor, the design of this molecular switch was modified^[74] (Scheme 17) by replacing the thioxanthylidene ring system with another tetrahydrophenanthrene unit. Each of the two helical subunits of the resulting compound **19** can adopt a right-handed (*P*) or a left-handed



Scheme 17. The light-fueled rotary motor **19** undergoes^[74] unidirectional rotation in *n*-hexane at 333 K upon irradiation at appropriate wavelengths.

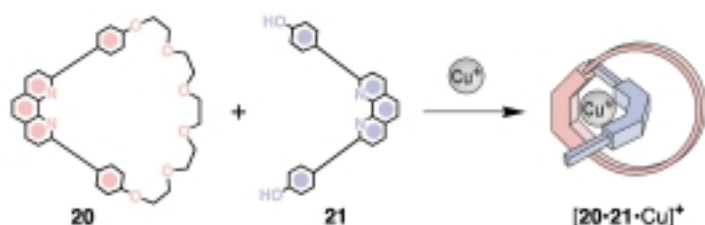
(*M*) helicity. As a result, a total of four stereoisomers (Scheme 17) are possible for this compound. However, the *cis/trans* isomerizations are reversible and occur upon irradiation at appropriate wavelengths. By contrast, the inversions of helicities, while maintaining a *cis* or a *trans* configuration, occur irreversibly under the influence of thermal energy. Upon irradiation (≥ 280 nm, 218 K) of a solution of (*P,P*)-*trans*-**19**, a mixture of (*P,P*)-*trans*-**19** and (*M,M*)-*cis*-**19** is obtained in a ratio of 5:95. By warming the solution up to 293 K, (*M,M*)-*cis*-**19** interconverts irreversibly to (*P,P*)-*cis*-**19**. Subsequent irradiation (≥ 280 nm) of the solution produces a mixture of (*P,P*)-*cis*-**19** and (*M,M*)-*trans*-**19** in a ratio of 10:90. Upon increasing the temperature further (333 K), (*M,M*)-*trans*-**19** interconverts irreversibly to the original isomer (*P,P*)-*trans*-**19**. Thus, a sequence of light- and temperature-induced isomerizations can be exploited to move this molecular rotor in one direction only. Indeed, when (*P,P*)-*trans*-**19** is irradiated (≥ 280 nm) at a high temperature (293 K), a clockwise 360° rotation occurs spontaneously. The overall process can be followed by monitoring the change in the intensity of the absorption band at 217 nm in the CD trace. The unidirectional motion in this system is dictated by the stereogenic centers associated with the two methyl substituents. As a result of a *trans* \rightarrow *cis* isomerization, the axial methyl substituents of (*P,P*)-*trans*-**19** are forced to adopt a less favorable equatorial orientation in (*M,M*)-*cis*-**19**. However, the strain associated with the equatorial methyl substituents is released upon thermal interconversion of (*M,M*)-*cis*-**19** to the more stable isomer (*P,P*)-*cis*-**19**. The subsequent *cis* \rightarrow *trans* isomerization forces the methyl groups to adopt, once again, equatorial orientations in the isomer (*M,M*)-*trans*-**19**. Finally, the thermal interconversion of (*M,M*)-*trans*-**19** to the original isomer (*P,P*)-*trans*-**19** is accompanied by a change from the equatorial to the more stable axial orientations for the methyl substituents.

3. Artificial Molecular Machines Based on Co-Conformational Motions

3.1. Supramolecular Complexes

3.1.1. Chemically Controllable Complexes

Coordination around a metal center was the first kind of interaction exploited^[75] in order to organize molecular components in a pseudorotaxane fashion.^[35] Suitably designed macrocyclic and threadlike species containing phenanthroline ligands, such as **20** and **21**, self-assemble (Scheme 18) upon addition of Cu^I ions to yield a pseudorotaxane. Such a complex was used as an intermediate in the template-directed synthesis of metal-containing catenanes^[25b, 26b-d] and could therefore also be called a precatenane.^[25a] The formation of this complex can be followed easily by ¹H NMR spectroscopy as well as visually, since it is accompanied by a change in the color of the solution.^[75] Cu^I-containing pseudorotaxane complexes are very stable and therefore difficult to dethread: the copper ion can only be removed^[76] upon treatment of the complexes with an excess of highly nucleophilic ligands, such



Scheme 18. The gathering ability of a Cu^+ ion induces^[75] the threading of the phenanthroline-based macrocycle **20** onto the phenanthroline-based ligand **21** (MeCN, ambient temperature).

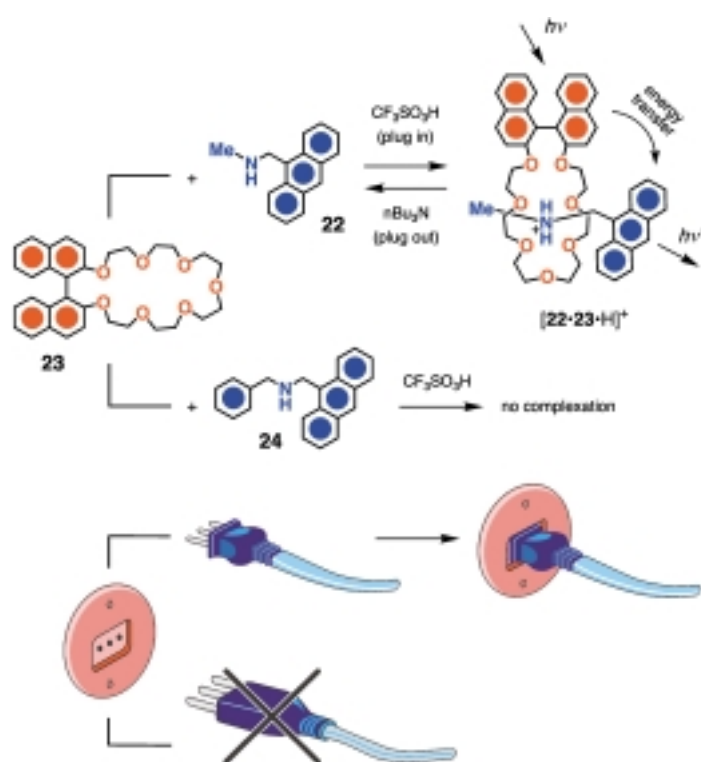
as cyanide ions. For this reason, metal complexation has not been used to develop prototypes of molecular machines based on chemically stimulated threading/dethreading movements. Nonetheless, it is a very convenient way^[25b, 26b–d, 75, 76] to promote the threading of pseudorotaxanes using suitably designed threadlike and macrocyclic ligands. The versatility and the properties of metal complexes have been exploited to design and construct elegant examples of catenane- and rotaxane-based molecular machines (see Sections 3.2 and 3.3).

An interesting example^[77] of redox-induced ion translocation^[78] is that which occurs in triple-stranded helical ligands that contain internal, “hard” hydroxamate and external, “soft” bipyridyl binding sites. When the metal ion is Fe^{III} , it is accommodated in the hard coordination environment. The metal ion translocates to the external soft bipyridyl sites upon chemical reduction to the Fe^{II} state. The translocation is reversible and takes place with a change in color.

Complexes which are good candidates for chemical switching include those that rely upon hydrogen-bonding interactions between ammonium ions and crown ethers. It has long been known that organic ammonium ions can form adducts with crown ethers.^[25b, 26h,j,l,n] More recently, it has been found^[79] that suitable threadlike dialkylammonium ions, for example, the dibenzylammonium cation, can interpenetrate suitably sized crown ethers, for example, dibenzo[24]crown-8, in nonpolar solvents to form pseudorotaxanes.^[35] These complexes, whose formation can be demonstrated by ^1H NMR spectroscopy in solution and by X-ray crystallography in the solid state, are stabilized by $^+\text{N}-\text{H} \cdots \text{O}$ and, to a lesser extent, by $\text{C}-\text{H} \cdots \text{O}$ hydrogen bonds and sometimes also by $\pi-\pi$ stacking interactions. Once the pseudorotaxane has been obtained, it can be easily dethreaded^[80] by adding a base that is able to destroy the hydrogen bonds by deprotonating the $^+\text{NH}_2$ center. Suitable bases are bulky, non-nucleophilic amines such as $i\text{Pr}_2\text{NEt}$ and $n\text{Bu}_3\text{N}$. The pseudorotaxanes can also be prepared from a mixture of the crown ether and a threadlike dialkylamine by addition of an acid (typically, $\text{CF}_3\text{SO}_3\text{H}$ or $\text{CF}_3\text{CO}_2\text{H}$) which protonates the amine function: the threading process can again be reversed upon addition of a base.^[81] The acid has to be selected so that it does not give insoluble ammonium salts and such that its anion does promote ion-pairing.^[82]

Recently, chromophoric and/or luminescent units such as dioxybenzene,^[83] dioxynaphthalene,^[83b,c] binaphthyl,^[84] anthracene,^[83a,b] as well as fullerenes,^[85] have been incorporated

into crown ethers or ammonium ions in order to study the photoinduced processes that take place within pseudorotaxanes. In all these cases, the goal is to design chemically (acid/base) controllable molecular machines that are able to give a light signal as a readout. For instance, the absorption and fluorescence spectra of a solution of amine **22** and crown ether **23** in CH_2Cl_2 (Scheme 19) indicate^[84a] the absence of any interaction between the two compounds. Addition of a stoichiometric amount of acid with respect to the amine causes profound changes in the fluorescence spectrum of the solution. These changes arise particularly from the result of the quenching of the luminescence of **23** and the sensitization of the luminescence of **22** upon excitation with light that is absorbed exclusively by the crown ether. These observations are consistent with the formation of a pseudorotaxane-type adduct wherein very efficient energy transfer takes place from the binaphthyl unit of the crown ether to the anthracenyl group incorporated within the dialkylammonium ion. Such a pseudorotaxane can be disassembled by the subsequent addition of a stoichiometric amount of base, thereby interrupting the photoinduced energy flow, as indicated by the fact that the initial absorption and fluorescence spectra are restored. Besides the machine aspect, such systems can be viewed (Scheme 19) as molecular-level plug-in-socket devices since they are characterized by 1) chemically controlled, reversible “plug in”/“plug out” behavior and 2) photoinduced energy transfer in the “plug in” state. Interestingly, the “plug in” process does not take place when a plug component that is



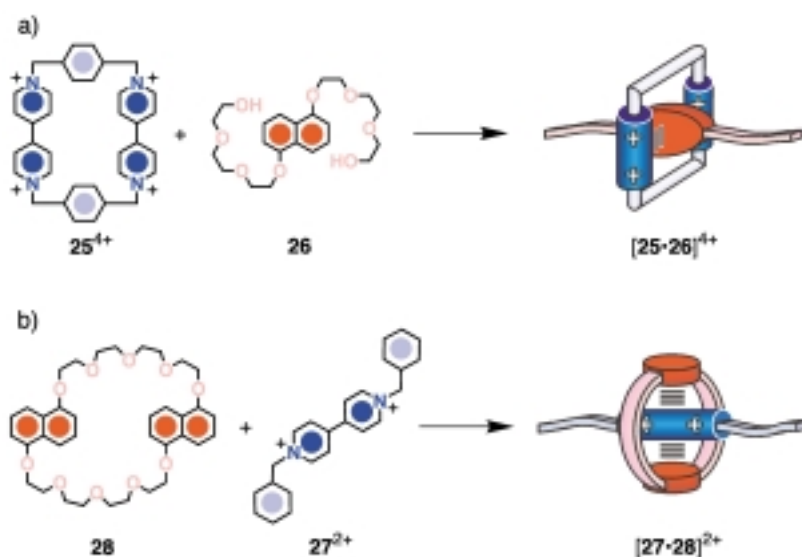
Scheme 19. A molecular-level plug/socket system based^[84a] on the reversible acid/base-driven threading/dethreading motions in the hydrogen-bonded pseudorotaxane $[22 \cdot 23 \cdot \text{H}]^+$ (CH_2Cl_2 , 298 K). The acid-driven threading of the compound **24**, which incorporates a bulky benzyl group, through the macrocyclic cavity of **23** does not occur.

incompatible with the size of the socket, such as the benzyl-substituted amine **24**, is employed.

A similar system has been reported^[86] where the chemical stimuli provided by counterions are employed to achieve switching. In keeping with detailed results from previous investigations,^[83a,b] the (9-anthrylmethyl)methylammonium cation [**22**·H]⁺ dissolves in CH₂Cl₂ as its hexafluorophosphate salt and threads through the cavity of dibenzo[24]crown-8 to form a pseudorotaxane. Such a pseudorotaxane can be dethreaded by the addition of one equivalent of *n*Bu₄NCl as a result of the formation of an ion pair between the chloride ions and the ⁺NH₂ center incorporated in [**22**·H]⁺. Rethreading of the molecular components can be performed by the further addition of one equivalent of *n*Bu₃NH⁺ ions (as the hexafluorophosphate salt) which compete with [**22**·H]⁺ for the binding of chloride ions. All the processes can be followed by changes in the luminescence properties of the solution and the cycle can be repeated several times on the same system, as tertiary and quaternary ammonium ions do not compete with [**22**·H]⁺ in its association with dibenzo[24]crown-8. Such a chemical system can also be viewed as a fluorescent chemosensor^[10k] for species as different as protons, amines, and chloride ions. These kinds of multimode molecular devices,^[10y] which can be operated by either acid/base or anionic stimuli, are expected to prove useful for information processing, for example, for the construction of molecular-level logic gates (see below and Section 3.1.2).

Threadlike dimeric pyridylpyridinium dication, in which the aromatic units are linked by a long alkyl chain, have been used^[87] as guests for α -cyclodextrin. In this system the formation of a pseudorotaxane in aqueous solution is driven by hydrophobic interactions between the aliphatic chain and the lipophilic cavity of α -cyclodextrin. It has been shown that the pseudorotaxane can be partially dethreaded by protonating the two basic nitrogen atoms of the terminal pyridyl units of the thread. This response can be explained by the decrease in the hydrophobic character associated with the alkyl chain in the protonated guest.

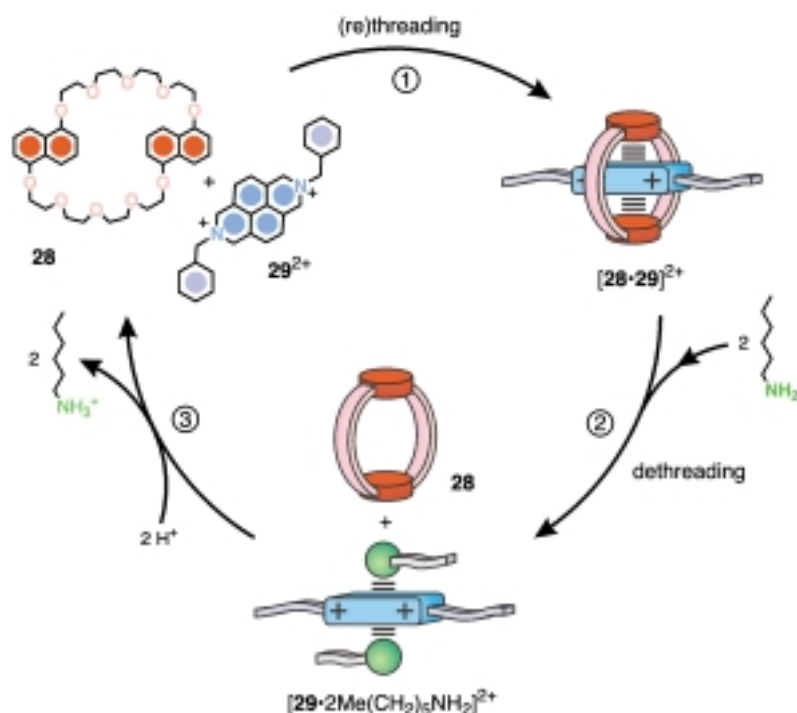
As an alternative to metal coordination and ⁺N–H···O hydrogen-bonding interactions, the stabilization that exists between π -electron-donor and π -electron-acceptor species, aided and abetted often by C–H···O hydrogen-bonding interactions, is a means of template direction which has been used^[25b, 26g,h,j–l,n,o] extensively to produce threaded superstructures. In the last few years, a number of complexes with pseudorotaxane geometries have been prepared from the self-assembly (Scheme 20 a) of a π -electron-rich threadlike component, such as **26**, and a π -electron-deficient macrocycle,^[25b, 26g,h,j–l,n,o] such as the tetracationic cyclophane cyclobis(paraquat-*p*-phenylene) (**25**⁴⁺). Similarly, pseudorotaxanes, in which a linear π -electron-deficient species, such as the 1,1'-dibenzyl-4,4'-bipyridinium dication **27**²⁺, threads (Scheme 20 b) through the cavity of a π -electron-rich macro-



Scheme 20. The formation of the pseudorotaxanes [**25**·**26**]⁴⁺ and [**27**·**28**]²⁺ incorporating π -electron-rich and π -electron-deficient components.^[26h]

cycle such as 1,5-dinaphtho[38]crown-10 (**28**), have been characterized.^[25b, 26g,h,j–l,n,o] These complexes^[88] are stabilized by a combination of electrostatic and dispersive forces, in particular 1) π – π stacking^[89] (including charge-transfer) interactions, 2) C–H···O hydrogen bonds^[90] between the hydrogen atoms located in the α -positions, with respect to the nitrogen atoms, of the bipyridinium unit and some of the polyether oxygen atoms, and 3) C–H··· π interactions.^[91] For instance, the 2,7-dibenzylidiazapyrenium dication **29**²⁺ self-assembles (Scheme 21) in solution with crown ethers, such as **28**, to give pseudorotaxanes (process 1), as shown by a variety of techniques, including absorption, luminescence, and ¹H NMR spectroscopies.^[92] The dication **29**²⁺ forms^[92] adducts with aliphatic amines, presumably as a result of charge-transfer interactions and, possibly, also because of hydrogen bonding to the acidic α -protons of the dication. Such an affinity has been exploited chemically to drive the dethreading of its pseudorotaxane with **28**. In fact, upon addition of 20 molar excess of *n*-hexylamine to a solution of the pseudorotaxane in MeCN, profound absorption and luminescence spectral changes are observed, which indicates that the free crown ether and the adduct between **29**²⁺ and the amine are formed (process 2). The dethreading can be reversed quantitatively (process 3) by the addition of a stoichiometric amount of CF₃CO₂H (with respect to the added amine) to the solution. Despite its structural similarity to the dication **29**²⁺, the 1,1'-dibenzyl-4,4'-bipyridinium dication **27**²⁺ (Scheme 20 b) does not interact with amines. This observation has led^[93] to the above system being extended to one in which the amine/acid chemical inputs select which one of two threadlike species enters the cavity of the macrocycle, which can cause a reversible interchange to occur between the threads.

The ability of pseudorotaxanes composed of **29**²⁺ and aromatic crown ethers to be disassembled by aliphatic amines has been coupled with the possibility of dethreading the same systems by protonation of the crown ether in nonpolar solvents. It has been shown^[94] that the pseudorotaxane formed



Scheme 21. Schematic representation of the amine/acid-controlled dethreading/rethreading cycle^[92] of the pseudorotaxane $[28 \cdot 29]^{2+}$ (MeCN, 298 K).

by 29^{2+} and 2,3-dinaphtho[30]crown-10 in CH_2Cl_2 can be dethreaded upon addition of $n\text{Bu}_3\text{N}$ and assembled again by adding protons. The same result can be obtained by reversing the order of the two chemical inputs, that is, dethreading can be achieved by the protonation of the crown ether's cavity and rethreading can be obtained by the addition of $n\text{Bu}_3\text{N}$. All these processes are accompanied by on/off switching of easily monitorable changes in the absorption and luminescence spectra, particularly of an intense fluorescence band, characteristic of the aromatic crown ether, with a maximum at 343 nm. It is worth emphasizing that these results contrast with the usual behavior of chemical systems that either remain unchanged or undergo very different changes upon addition of reactants of opposite chemical types such as amines and acids. An important consequence of this behavior is that the input/output relationships of the system correspond to those of the XOR (eXclusive OR) logic operation.^[95] This development shows^[10y] that carefully designed dual-mode chemically driven molecular machines are potentially useful for information processing.

The assembly of complexes based on electron donor/acceptor interactions can be controlled by means of redox stimuli, which can be provided by the addition of oxidants and reductants. The inclusion complex^[96] formed between the electron-acceptor cyclophane 25^{4+} and the well-known electron donor tetrathiafulvalene (TTF, **30**), as well as pseudorotaxanes^[97] composed of 25^{4+} and threadlike species containing a tetrathiafulvalene unit, can be disassembled^[93, 97] into their free components by oxidation of the tetrathiafulvalene unit to its radical cation with one equivalent of $\text{Fe}(\text{ClO}_4)_3$ in MeCN or aqueous solution. The one-electron-oxidized form of the TTF unit is stable in such conditions and can be reduced back to its neutral form by adding a stoichiometric amount of

ascorbic acid. The reduction results in the insertion of the tetrathiafulvalene unit into the tetracationic cyclophane. Dethreading can also be achieved by adding *o*-chloroanil, which forms an adduct with the TTF unit. The addition of $\text{Na}_2\text{S}_2\text{O}_5$ in the presence of water results in the reduction of *o*-chloroanil and the generation of the original pseudorotaxane.^[97c] Such dethreading/rethreading processes can be easily monitored by UV/Vis absorption spectroscopy, since 1) the complex shows a broad absorption band with a maximum around 850 nm, which is ascribed to the charge-transfer interaction between the electron-rich tetrathiafulvalene unit and the electron-poor bipyridinium units of 25^{4+} , and 2) the neutral and cationic forms of the tetrathiafulvalene unit exhibit very different absorption features. Moreover, a system of this kind can serve as a basis for the construction of a supramolecular device in which it is possible—by means of chemical stimuli—to select which one of two guests enters (Figure 4) a macrocycle's cavity and to interchange reversibly the two guests.^[93] Addition of the threadlike compound **26**, which contains a π -electron-rich

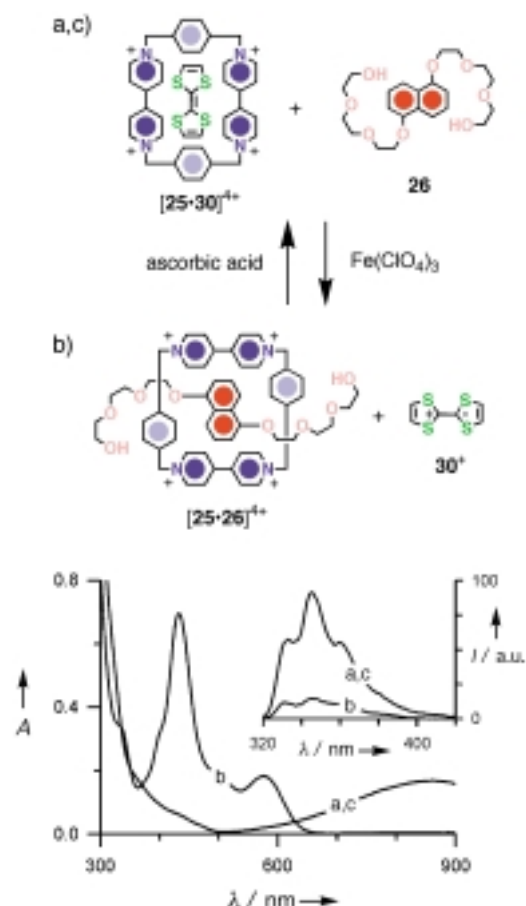
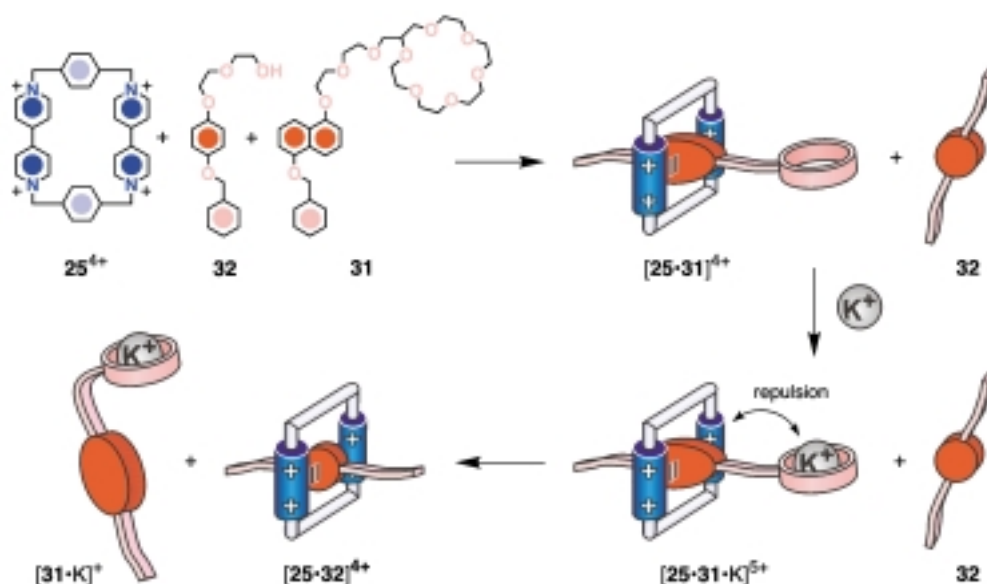


Figure 4. Top: the chemically induced interchange of guests **26** and **30** into the cavity of cyclophane 25^{4+} .^[93] Bottom: absorption and (inset) fluorescence ($\lambda_{\text{exc}} = 295 \text{ nm}$) spectra of a) a $5 \times 10^{-5} \text{ M}$ aqueous solution (298 K) of $[25 \cdot 30]^{4+}$ and **26**; b) the same solution after addition of one equivalent of $\text{Fe}(\text{ClO}_4)_3$; c) solution b) after addition of one equivalent of ascorbic acid.

dioxynaphthalene unit, to an aqueous solution of the $[25 \cdot 30]^{4+}$ complex affects neither the charge-transfer absorption band characteristic of the complex nor the strong fluorescence band of the dioxynaphthalene-based thread (Figure 4, curves a), which indicate that this thread does not displace **30** from inside the macrocyclic host. On addition of a stoichiometric amount of $\text{Fe}(\text{ClO}_4)_3$ (with respect to **30**), the absorption bands of the radical cation 30^+ are formed, and the charge-transfer band of $[25 \cdot 30]^{4+}$ disappears, while the fluorescence band of the dioxynaphthalene-based species is substantially quenched (curves b). These results show that oxidation causes expulsion of 30^+ from 25^{4+} and its replacement by the dioxynaphthalene-based thread. On subsequent addition of ascorbic acid, the system returns to its initial state (curves c).

Recently, threadlike species containing both π -electron-acceptor and hydrogen-bonding recognition sites have been prepared and employed to generate^[83c] multicomponent pseudorotaxanes of various stoichiometries that, in their turn, can be used to construct acid/base-controlled molecular machines that exhibit a complex pattern of dethreading/rethreading motions. Another way of controlling the association between the 25^{4+} cyclophane and threadlike guests containing electron-donor units takes advantage of allosteric effects, that is, of the electrostatic repulsion that arises when a positive charge is created in the vicinity of the tetracationic cyclophane. For example, the pseudorotaxane composed of 25^{4+} and a molecular thread which incorporates a dioxynaphthalene unit in its middle and is terminated at each end by [12]crown-4 rings is dethreaded^[98] readily in MeCN upon addition of an excess of alkali metal salts, such as NaPF_6 or LiPF_6 . These changes are a response to the electrostatic repulsion between the alkali metal cation within the [12]crown-4 macrocycles and the tetracationic cyclophane. The dethreading of the pseudorotaxane can be followed visually by the decrease in the intensity of the characteristic charge-transfer absorption band of the pseudorotaxane.

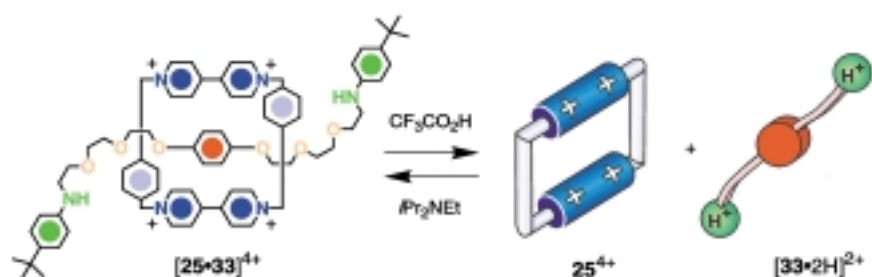
Such a strategy can be employed to design even more complex devices, where, not only the dethreading of the system, but also the replacement of a thread with another one can be controlled by chemical stimuli provided in the form of alkali metal cations. The [18]crown-6 derivative **31**, which carries a 1,5-dioxynaphthalene moiety, is a ditopic compound that can act (Scheme 22) as a host for alkali metal cations and as a guest for 25^{4+} , in this latter case, with the formation of a pseudorotaxane.^[99] In MeCN, the $[25 \cdot 31]^{4+}$ species is not affected by the presence of the 1,4-dioxynaphthalene-containing



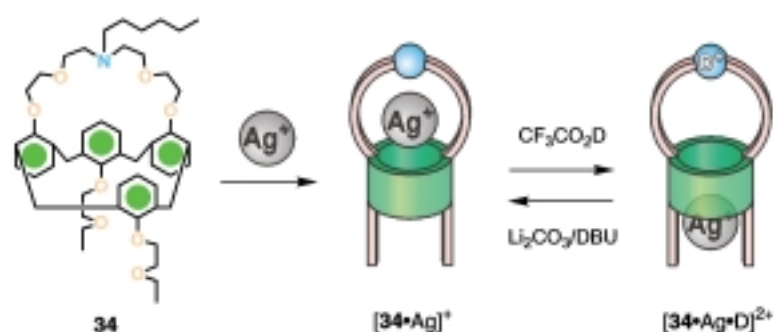
Scheme 22. The chemically controlled competition^[99] in MeCN at 298 K between the two threadlike species **31** and **32** for the cavity of a tetracationic cyclophane 25^{4+} .

thread **32**, while it dethreads upon addition of K^+ ions because of the electrostatic repulsions between the bound potassium cation and the 25^{4+} tetracation and is then free to host the neutral thread **32** within its cavity, thus forming the pseudorotaxane $[25 \cdot 32]^{4+}$. Since the exchange of guests causes the color of the solution to change from purple to red-orange, this molecular machine can also be regarded as a metal-controlled chromophoric molecular switch. The exchange processes occurring in these supramolecular systems can also be monitored by ^1H NMR spectroscopy.

Although the exploitation of electrostatic repulsion exerted by positive charges to dethread pseudorotaxanes is a promising strategy, if metal cations are used to provide such positive charges, then problems can be anticipated as far as the reversibility of the system is concerned because of the difficulty of removing the bound metal cations to achieve rethreading. For this reason, acid/base reactions are preferred because of their reversibility and simplicity. Quite recently,^[100] the pseudorotaxane $[25 \cdot 33]^{4+}$, which comprises a dioxynaphthalene-containing thread **33** terminated by *tert*-butylaniline groups, has been self-assembled (Scheme 23) in solution. In this supramolecular system, protonation of the nitrogen atoms of the thread with $\text{CF}_3\text{CO}_2\text{H}$ results in the complete dethreading of the pseudorotaxane, as evidenced in both the absorption and ^1H NMR spectra. Addition of $i\text{Pr}_2\text{NEt}$, which acts as a base, restores (Scheme 23) the original equilibrium and regenerates the pseudorotaxane. The acid-driven dethreading and base-induced rethreading processes can be repeated on the same solution without risk of degrading the participating species. Other intriguing acid/base switchable systems have been described in the recent literature. An interesting example^[101] is the ingeniously designed prototype of the so-called “molecular syringe” **34** (Scheme 24), which uses a 1,3-alternate calix[4]arene as a π -basic tube that carries a nitrogen-containing crown cap on one side of the calixarene and two ethoxyethoxy groups on the other side. An Ag^+ ion,



Scheme 23. The base/acid-controlled dethreading/rethreading motions^[100] of the pseudorotaxane [25·33]⁴⁺ in MeCN at 298 K.



Scheme 24. The reversible acid/base-controlled metal pumping in a "molecular syringe" 34,^[101] designed from a 1,3-alternate calix[4]arene (CD₂Cl₂/CD₃OD 4/1, 303 K). Conditions: protonation with CF₃CO₂D; deprotonation with Li₂CO₃/1,8-diazabicyclo[5.4.0]undec-7-ene (DBU).

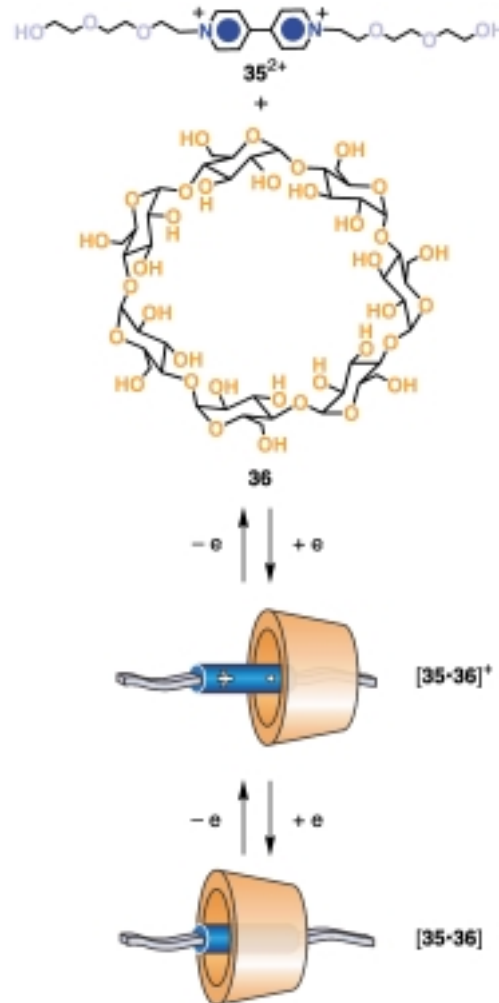
which is coordinated to the azacrown ether, is pushed through the tube to the side carrying the twin ethoxyethoxy groups when the nitrogen atom in the azacrown ether is protonated. On deprotonation of the nitrogen atom, the Ag^I ion is sucked back through the middle of the calixarene once again.

3.1.2. Electrochemically Controllable Complexes

Redox processes have been used extensively to control molecular recognition.^[10s,t, 11f,g, 102] Indeed, electrochemical stimulation represents a valuable tool for triggering host–guest interactions. Electrochemical techniques can be employed, not only to induce chemical or (co-)conformational changes in supramolecular systems, but also to probe their superstructures and organization. In other words, electrochemistry gives us a handle on both the input stimuli and the readout signals that are necessary for the operation of molecular machines.

A large number of inclusion complexes in which the association/dissociation of the components can be triggered by changing the oxidation state of the guest or the host have been investigated.^[10s,t, 11f,g, 102] Some of the key features of such systems are 1) the presence of an electroactive unit in one component which exhibits reversible redox processes and 2) the effect of the other component on the electrochemical behavior of the component containing the electroactive unit. This second property allows the investigation of the complexation/decomplexation process by, for example, voltammetric techniques. Cyclodextrins are a class of hosts that are inactive electrochemically yet can form stable inclusion complexes with a variety of electroactive guests.^[103] For example, it has

been found^[104] that, while bipyridinium-containing compounds in the dicationic forms (for example, 35²⁺; Scheme 25) are not bound by β -cyclodextrin (36), they interact weakly with the cavity of this host when reduced to their monocationic forms, and give fairly stable pseudorotaxane complexes with 36 when they are finally reduced to their uncharged forms. Similar results have been found^[105] for cobaltocenium derivatives, that do not

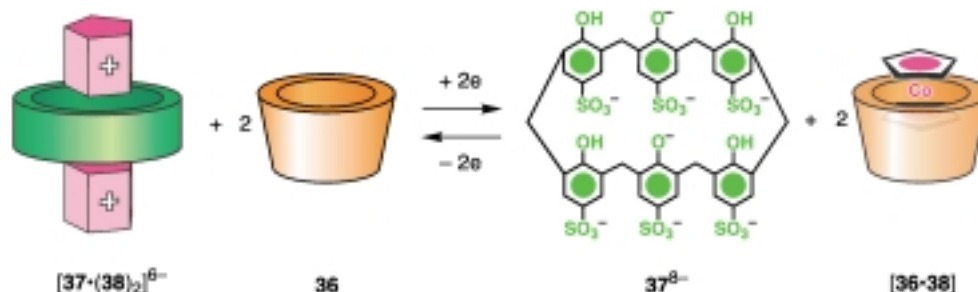


Scheme 25. The electrochemically induced threading/dethreading processes (H₂O, pH 7, 298 K)^[104a] associated with the pseudorotaxane [35·36]²⁺.

interact with cyclodextrins, yet become good guests for inclusion in 36 upon one-electron reduction to yield the neutral cobaltocene. Ferrocene and its derivatives exhibit^[106] the opposite behavior, that is, they are strongly bound in their most stable oxidation states, which correspond to uncharged species. When they are oxidized, they are not bound. These features have been exploited recently to construct dendrimers that display redox-controllable multisite complexation of 36, since the dendrimers contain up to 16 ferrocene units^[107] or up to 32 cobaltocenium units^[108] on their peripheries. Such

dendrimers form very large supramolecular architectures that can be either broken apart or assembled upon oxidation of the ferrocene units^[107] or upon reduction of the cobaltocenium units,^[108] respectively.

Similar investigations have been carried out on calixarenes, another important class of redox-inactive receptors. It has been found^[109] that the water-soluble calixarene hexasulfonate **37**⁸⁻ forms (Scheme 26) stable complexes with ferrocene



Scheme 26. Redox switching (H₂O, pH 7, 298 K)^[109] between the complexes [37·(38)₂]⁶⁻, which incorporate two cobaltocenium cations (38⁺) and one octaanionic calixarene **37**⁸⁻, and [36·38], which is composed of cobaltocene (38) and β-cyclodextrin (36).

and cobaltocene derivatives,^[110] as well as with bipyridinium-based compounds.^[111] However, in contrast with cyclodextrins, the binding to calixarenes such as **37**⁸⁻ becomes stronger on increasing the charge on the guest. This result has been exploited^[110] to design a three-component supramolecular system where an electroactive guest can choose reversibly between two macrocyclic hosts, depending on its oxidation state.^[112] The cobaltocenium cation (38⁺) gives a strong 2:1 complex with **37**⁸⁻, even in the presence of an excess of **36**. However, reduction of the cobaltocenium guests leads (Scheme 26) to their inclusion in **36** and subsequent oxidation back to the monocation affords the initial complex.

Unlike cyclodextrins and calixarenes, the cyclophane **39**²⁻ is electroactive^[113] and was one of the early examples (Scheme 27) of redox-switchable macrocyclic receptors. In-



Scheme 27. Redox switching (H₂O, pH 10, 298 K)^[113] between the complexes [39·40]²⁻ and [39·40]³⁻ in which the naphthalene ring system (40) is located "alongside" the macrocyclic cavity of **39**²⁻ and "inside" that of **39**³⁻, respectively.

terestingly, this host in its oxidized form interacts with naphthalene (**40**) in an "alongside" fashion: however, upon two-electron reduction of its isoalloxazine moiety, the binding

mode of naphthalene changes and an inclusion complex is formed.

Inorganic systems capable of exhibiting a redox-driven linkage isomerism resulting in molecular hysteresis are known.^[114] Electrochemically driven cation^[115] and anion^[116] translocations have also been reported. Translocation of Cl⁻ or NCO⁻ ions has been achieved^[116a] in a system consisting of a tripodal tetramine subunit (tris(2-aminoethyl)amine, tren)

and a tetramine macrocyclic ring (1,4,8,11-tetraazacyclotetradecane, cyclam), covalently linked by a 1,4-xylyl spacer. When Cu^{II} occupies the tren center and Ni^{II} the cyclam ring, the X⁻ anion is coordinated to the Cu^{II} center. However, upon oxidation of Ni^{II} to Ni^{III}, the X⁻ anion moves to the Ni^{III} coordinating center. This redox-driven anion translocation, which is intramolecular in nature, is fast and fully reversible.

One of the most extensively studied receptors in recent years has been the cyclophane **25**⁴⁺. It constitutes^[26h] a very efficient host for a wide variety of π-electron-donating guests. Since it is redox active,^[117] its binding ability can be subjected to electrochemical control. The tetracationic cyclophane **25**⁴⁺ shows two bielectronic reduction processes, the first one corresponding to the uptake of the first electron by each of the equivalent bipyridinium units and the second one to the subsequent reduction of radical cations to neutral units. In general, when an electron-donor unit is located inside the cavity of the cyclophane, the half-wave potential associated with the first reduction process is shifted to more negative values, as a consequence of the charge-transfer interactions with the two bipyridinium groups of **25**⁴⁺ which stabilize^[11g, 97, 117, 118] the complex. The fact that this cyclophane exhibits another reduction process at more negative potentials is very important since it can be used to monitor the occurrence of decomplexation induced^[10t, 11g] by the first two-electron reduction. For example, in the presence of an excess of a threadlike compound composed of a polyether chain containing one 1,4-dioxybenzene ring the potential value for the first bielectronic reduction of **25**⁴⁺ is shifted cathodically, while the second reduction process is practically unaffected.^[117] This observation is consistent with 1) formation of a [2]pseudorotaxane between the cyclophane and the thread and 2) dethreading of the [2]pseudorotaxane upon two-electron reduction of the **25**⁴⁺ host, so that the second two-electron reduction process reflects that of the free host. The occurrence of the dethreading process is not surprising because reduction of the electron-acceptor component weakens the charge-transfer interaction that helps to hold the components of the supramolecular architecture together. Since all these processes are reversible, oxidation of **25** back to the tetracationic form affords the original [2]pseudorotaxane. In principle, it should be possible to obtain useful information on the occurrence of dethreading/

rethreading processes from the electrochemical behavior of the guest; however, the poor reversibility of the oxidation process associated with a 1,4-dioxybenzene ring prevents the use of this type of control. More interesting are [2]pseudorotaxanes wherein both the cyclophane and thread components exhibit chemically reversible redox processes, as in the case of the complex $[25 \cdot 30]^{4+}$ of tetrathiafulvalene (**30**) with **25**⁴⁺ [97a, 118b] and related [2]pseudorotaxanes.^[97] This improvement in design not only permits the monitoring of the formation of the supramolecular species, by studying both the reduction of the electron-acceptor component and the oxidation of the electron-donor one, but it also provides a dual mode (reductive and oxidative) of control on the dethreading/rethreading process. The molecular thread **41**, obtained by adorning a tetrathiafulvalene unit with two polyether chains (Figure 5), forms^[97a] a very stable ($K_a = 5 \times 10^5 \text{ M}^{-1}$ in MeCN) [2]pseudorotaxane with **25**⁴⁺. Although the TTF unit in **41** retains the same electron-donor power of free tetrathiafulvalene, as revealed by comparing their voltammograms, the K_a value for the complex $[25 \cdot 41]^{4+}$ is 50 times higher than that for the complex $[25 \cdot 30]^{4+}$, which indicates that the presence of the polyether chains strengthens the association because of the hydrogen bonding between the oxygen atoms in the chain and the hydrogen atoms in the α -positions with respect to the nitrogen atoms of the bipyridinium units. This cooperative interaction is extremely important in improving the on/off switching. It has been shown^[97a] that reversible dethreading/rethreading cycles of the complex $[25 \cdot 41]^{4+}$ (as well as of $[25 \cdot 30]^{4+}$) can be performed either 1) by oxidation and successive reduction of the electron-donating thread or 2) by reduction and successive oxidation of the electron-accepting cyclophane. Such processes are accompanied by pronounced spectral differences (Figure 5) that

can be followed easily by the naked eye since the solution changes color from the emerald green typical of the pseudorotaxane to either brown or deep blue upon oxidative or reductive dethreading, respectively. This unique behavior makes this system appealing for the construction of electrochromic display devices and, since its input(electrochemical)/output(color) characteristics correspond to those of the XNOR (eXclusive NOR) logic operation,^[97a] for the design of molecular-level logic gates.^[94, 95] Moreover, the voltammetric behavior on oxidation of this system is scan-rate dependent,^[119] which indicates that the dethreading/rethreading processes (Figure 5) associated with the redox steps take place on the timescale of the electrochemical experiment.^[120]

The supramolecular complex composed (Scheme 28) of the enlarged tetracationic cyclophane **42**⁴⁺ and the ferrocene-based thread **43** has been studied^[121] recently with the aim of developing new dual-mode switchable systems. This tetracation is an electron-acceptor cyclophane related to **25**⁴⁺; however, while the cavity of **25**⁴⁺ is ideal for accommodating aromatic rings, that of **42**⁴⁺ is perfect^[122] for hosting ferrocene as a guest. It has been found^[121] by means of absorption and electrochemical experiments that the $[42 \cdot 43]^{4+}$ complex, which interestingly does not adopt a pseudorotaxane geometry, can be dethreaded reversibly (Scheme 28) either by oxidation/reduction of the ferrocene unit of **43** or by reduction/oxidation of the bipyridinium units of **42**⁴⁺.

Very recently, a three-component supramolecular system composed (Scheme 29) of tetrathiafulvalene (**30**), which can exist in three stable forms—namely, **30**, **30**⁺, and **30**²⁺—and two hosts, specifically the π -electron-accepting cyclophane (**25**⁴⁺) and the π -electron-donating crown ether **28**, has been investigated.^[123] In its role as an electron donor, **30** forms a 1:1 inclusion complex with **25**⁴⁺ which can be dissociated/reasso-

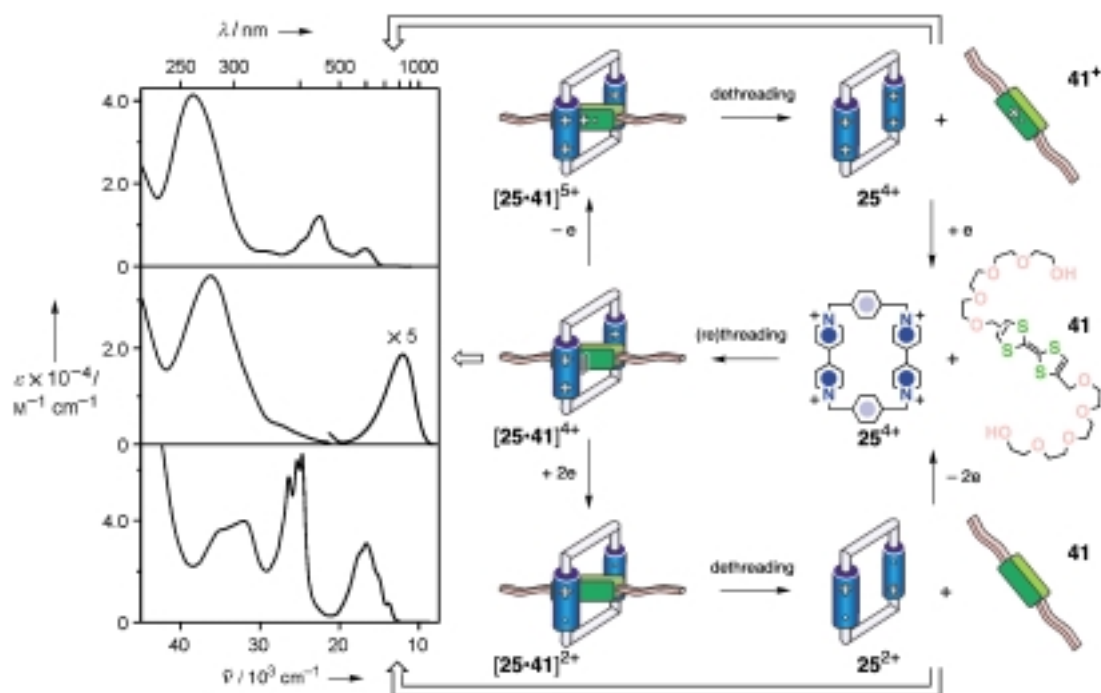
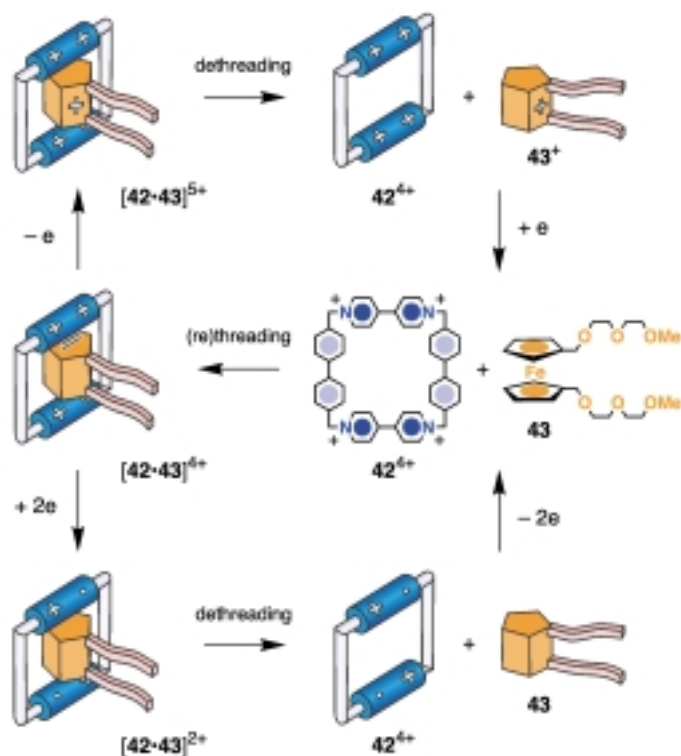
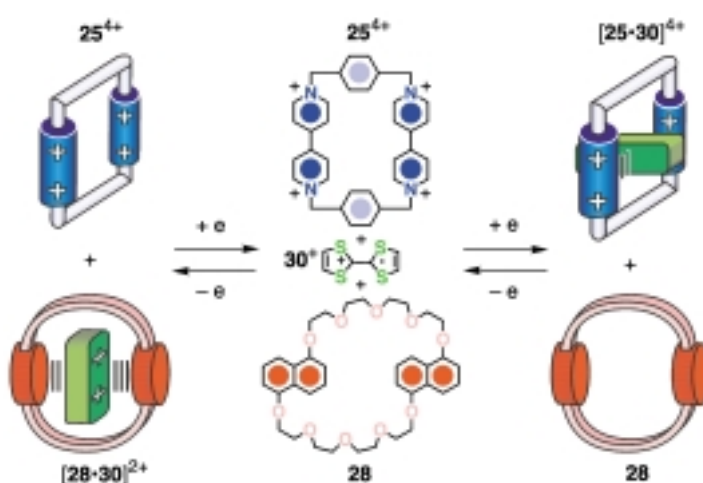


Figure 5. The electrochemically induced dethreading/rethreading processes^[97a] associated with the pseudorotaxane $[25 \cdot 41]^{4+}$ and the absorption spectra recorded (MeCN, 298 K) before (center) and after oxidation (top) or reduction (bottom).



Scheme 28. The decomplexation/recomplexation of the inclusion complex $[42 \cdot 43]^{4+}$ upon electrochemical reduction or oxidation (MeCN, 298 K).^[121]

ciated reversibly by cyclic oxidation/reduction of **30**,^[97a, 118b] while 30^{2+} acts^[123] as a π -electron acceptor to give a 1:1 inclusion complex ($K_a = 4 \times 10^3 \text{ M}^{-1}$ in MeCN at 298 K) with **28**. By contrast, 30^+ is not bound by either of the two hosts. When the electrochemical potential applied to the solution becomes more positive than about +0.4 V versus SCE **30** is oxidized to the radical cation and the $[25 \cdot 30]^{5+}$ complex disassembles, to give three essentially noninteracting species. Further one-electron oxidation of 30^+ to 30^{2+} at potentials more positive than about +0.7 V versus SCE leads to the insertion of the dication into the cavity of **28**. Since both

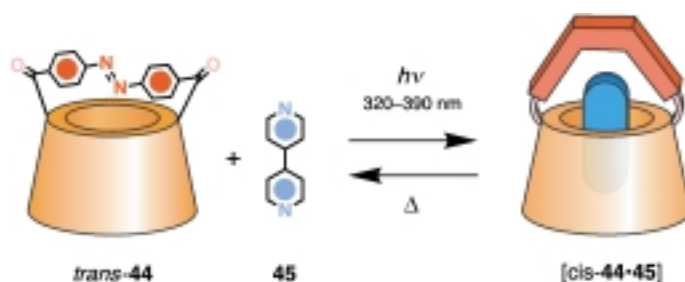


Scheme 29. Redox switching (MeCN, 298 K)^[123] between the complexes $[28 \cdot 30]^{2+}$, which incorporates the macrocyclic polyether **28** and the dication 30^{2+} , and $[25 \cdot 30]^{4+}$, which is composed of the tetracationic cyclophane 25^{4+} and tetrathiafulvalene (**30**).

oxidized forms of **30** are stable, the initial state can be restored by subsequent reduction. This system can therefore be switched^[124] reversibly between three distinct states by exercising electrochemical control over the guest behavior of **30**. The fact that the three states have different colors, coupled with the ease of their electrochemical interconversion, renders this supramolecular system suitable for electrochromic applications; moreover, the system could form the basis for the construction of molecular devices in which energy- or electron-transfer processes between selected components can be controlled.^[123] This investigation, along with others discussed in this review, suggests that carefully designed molecular machines could be employed to perform^[10y] a variety of valuable functions that go far beyond the molecular motions they display.

3.1.3. Photochemically Controllable Complexes

Stimulation by light is arguably the most interesting and promising way to control the formation/disruption of supramolecular complexes in a machinelike fashion. Photons, like electrons, can be exploited,^[11d,e] both for causing the changes (“writing”) in chemical systems and for monitoring (“reading”) their states. In general, the systems of this type that have been reported so far can be subdivided into those based on photoisomerizations, and those relying on photoinduced electron-transfer processes.



Scheme 30. The photoinduced inclusion^[128] of 4,4'-bipyridine (**45**) inside the cavity of the azobenzene-capped β -cyclodextrin derivative **44** (H_2O , pH 7.2, 298 K). The 4,4'-dicarbonylazobenzene unit is attached to two of the primary oxygen atoms of the β -cyclodextrin derivative.

Photoisomerizations, particularly the well-known^[125] reversible *cis/trans* photoisomerization of the azobenzene group, have long been used^[3, 62–74, 126, 127] to exert photocontrol on chemical systems. The azobenzene-capped β -cyclodextrin **44** (Scheme 30) cannot bind^[128] 4,4'-bipyridine (**45**) at all when the azobenzene group is in the *trans* form: its conversion to the *cis* isomer, upon irradiation with UV light, leads to the inclusion ($K_a \approx 500 \text{ M}^{-1}$ in aqueous solution at 298 K) of **45** into the expanded cavity of *cis-44*, as indicated by circular dichroism studies. The reversion to the *trans* isomer, with subsequent ejection of the guest, takes place (Scheme 30) in the dark. Azobenzene-containing compounds can also act as photocontrollable guests. For example, the *trans* form of *p*-(phenylazo)benzoate is bound^[129] by β -cyclodextrin (**36**) more strongly than the *cis* isomer in aqueous solution. The different affinity has been ascribed to the fact that the “stretched”,

threadlike structure of the *trans*-azobenzene group fits the cavity of **36** better than the elbow-shaped *cis* isomer. This observation has been exploited to trigger the catalytic activity of **36** in ester hydrolysis, since the cavity of **36** can be made available to the substrate upon light-driven expulsion of the azobenzene guest.

Threadlike species containing a π -electron-rich azobiphen-oxo unit have been used^[130] (Figure 6), in conjunction with electron-accepting hosts such as **25**⁴⁺ or **46**⁴⁺, to obtain charge-

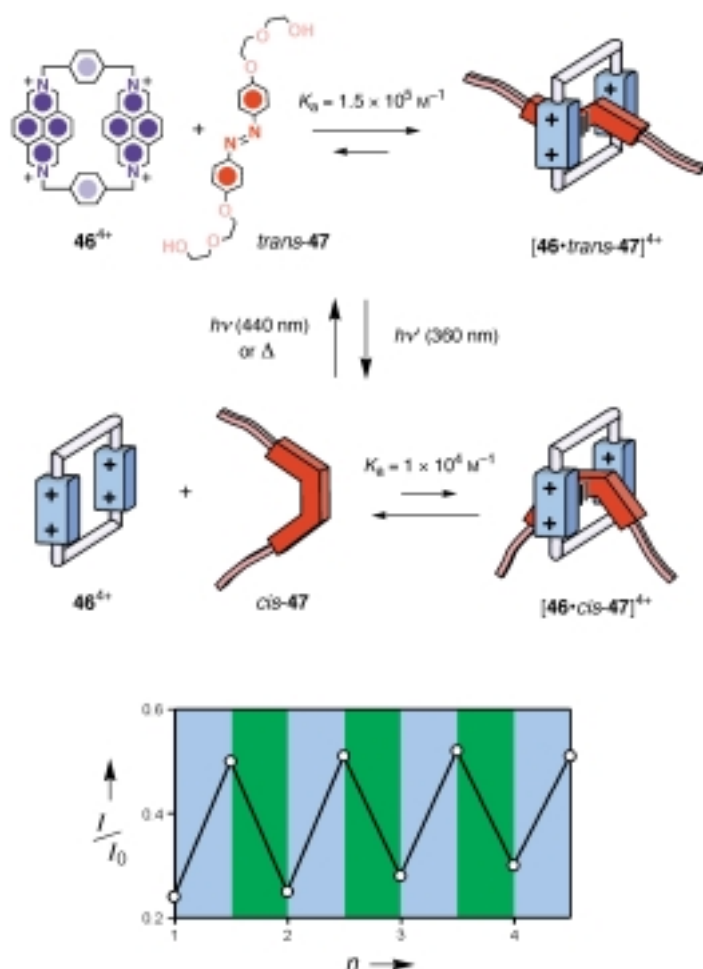


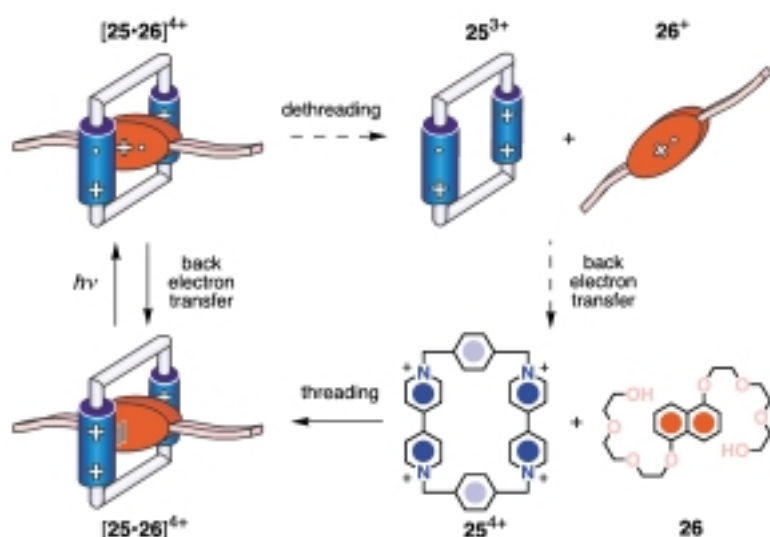
Figure 6. The change in intensity of the luminescence ($\lambda_{\text{exc}} = 411 \text{ nm}$) associated^[133] with the tetracationic cyclophane **46**⁴⁺ for an equimolar solution ($1 \times 10^{-4} \text{ M}$, MeCN, 298 K) of **46**⁴⁺ and **47** upon consecutive *trans* \rightarrow *cis* (irradiation at 365 nm, cyan areas) and *cis* \rightarrow *trans* (irradiation at 436 nm and rest in the dark, green areas) isomerization cycles. I_0 is the luminescence intensity of the tetracationic cyclophane **46**⁴⁺ in the absence of the guest under otherwise identical experimental conditions.

transfer complexes with pseudorotaxane geometries. Indeed, the compound *trans*-**47** self-assembles with **25**⁴⁺ to give^[130] a pseudorotaxane ($K_a = 470 \text{ M}^{-1}$ in MeCN at 298 K) both in solution and in the solid state, as shown by ¹H NMR spectroscopy and X-ray crystallography, respectively. On irradiation at 360 nm of an equimolar MeCN solution of **25**⁴⁺ and *trans*-**47**, which are in part associated to give a pseudorotaxane superstructure, the N=N bond isomerizes to the *cis* form and the pseudorotaxane dethreads. The *trans* isomer of the guest can be reformed and, as a result, rethreads

inside the cyclophane either on irradiation at 440 nm or by warming the solution in the dark. These photoinduced dethreading/rethreading motions have been monitored by ¹H NMR spectroscopy and by careful photochemical studies, which have also shown that the photoisomerization efficiency of *trans*-**47** is reduced considerably when it is encircled by the tetracationic cyclophane. It is not clear^[131] whether such a decreased photoreactivity, as well as the lower affinity of *cis*-**47** for **25**⁴⁺, is a consequence of steric or electronic effects. Because of its excellent reversibility, a system of this type is of considerable potential interest for the development of molecular machines featuring photoinduced dethreading/rethreading motions. However, the efficiency of the self-assembly of the molecular components needs to be improved. For this purpose, the cyclophane **46**⁴⁺, in which the bipyridinium units have been replaced (Figure 6) by the more effective^[93, 94, 132] π -electron-accepting 2,7-diazapyrenium units, has been used instead of **25**⁴⁺ as a host for *trans*-**47**. Moreover, since the 2,7-diazapyrenium unit shows highly characteristic absorption and luminescence bands, **46**⁴⁺ provides additional readout signals for the system. In fact, **46**⁴⁺ self-assembles^[133] very efficiently ($K_a = 1.5 \times 10^5 \text{ M}^{-1}$ in MeCN at 298 K) with the *trans* isomer of **47**, but it also interacts with the *cis* form ($K_a = 1 \times 10^6 \text{ M}^{-1}$ under the same conditions). The photochemical and chemical processes occurring in this system are schematized in Figure 6. Although it is clear that irradiation with light does not lead to 100% dethreading, these photocontrolled dethreading/rethreading motions can be followed easily by absorption and luminescence spectroscopy: the diagram in Figure 6 shows the changes in the fluorescence intensity characteristic of the uncomplexed macrocycle **46**⁴⁺ upon repeated *trans* \rightarrow *cis* and *cis* \rightarrow *trans* isomerization cycles of the thread **47**.

We now focus on complexes, such as [**25**·**26**]⁴⁺ (Scheme 31), which are primarily stabilized by π -electron-donor/acceptor interactions. In most cases, these interactions introduce new energy levels that cause^[57, 92–94, 97–100, 117a, 123] the appearance of charge-transfer absorption bands, often in the visible region of the spectrum. Excitation in these bands leads formally to the transfer of an electron from the donor to the acceptor component and is therefore expected to destabilize the charge-transfer interaction responsible for self-assembly. Furthermore, in some cases, the photoinduced electron transfer leads to the formation of charges of the same sign that repel each other and so contribute to forcing the molecular components apart. This simple approach, however, is precluded by the fact that the back electron transfer, that is, the deactivation of the charge-transfer excited state to the ground state, is much faster than the separation of the molecular components, a process which requires^[134] extended nuclear motions and solvation processes. In some particular cases,^[135] laser flash photolysis experiments have been interpreted as indicating the dissociation of a small fraction of the irradiated complex.

In order to achieve light-induced dethreading of the [**25**·**26**]⁴⁺ complex, a different approach was devised^[57, 134a] which was based on the use (Scheme 32) of an external electron-transfer photosensitizer (P) and a reductant scavenger (red.) species. The photosensitizer must be able to 1) absorb light



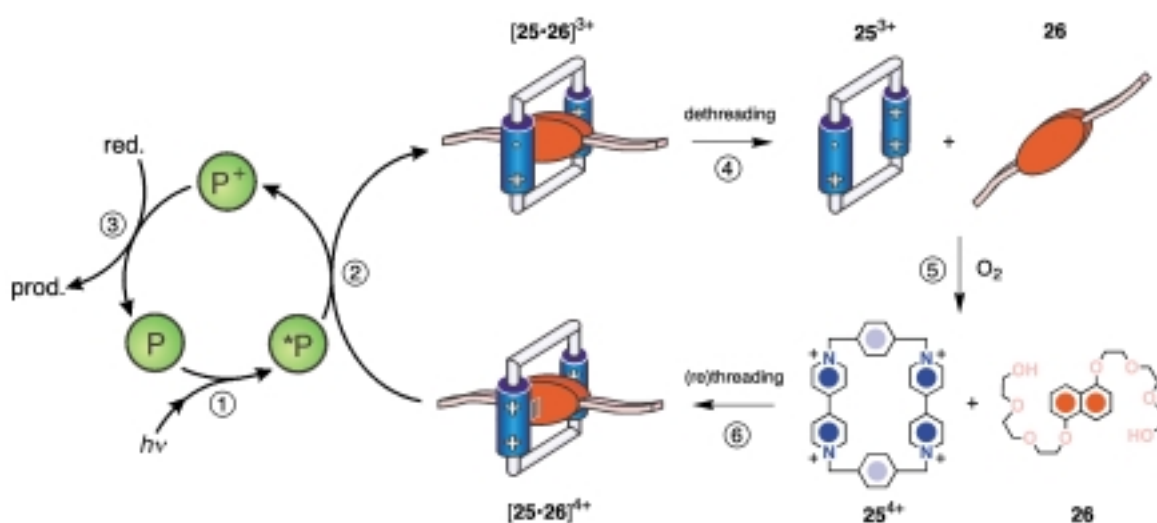
Scheme 31. The photochemical processes associated with the pseudorotaxane $[25 \cdot 26]^{4+}$ upon excitation in its charge-transfer absorption band.^[57, 134a] The processes indicated by dashed arrows are unlikely to occur (see text).

efficiently and 2) have a sufficiently long-lived and reductant excited state so that its irradiation by light (process 1) in the presence of the pseudorotaxane will lead (process 2) to the transfer of an electron to a bipyridinium unit of the cyclophane. The relatively fast back electron transfer from the reduced cyclophane component to the oxidized photosensitizer is prevented by the reductant which, if present in a sufficient amount ($> 10^{-2}$ M), intercepts the oxidized photosensitizer and regenerates (process 3) the original photosensitizer. Good candidates for the role of photosensitizer are 9-anthracenecarboxylic acid^[136] and metal complexes^[137] such as $[\text{Ru}(\text{bpy})_3]^{2+}$ (bpy = 2,2'-bipyridine), while efficient reductant scavengers are triethanolamine and polycarboxylate anions (for example, oxalate).^[138] Under these conditions, the persistent reduction of a bipyridinium unit of 25^{4+} is

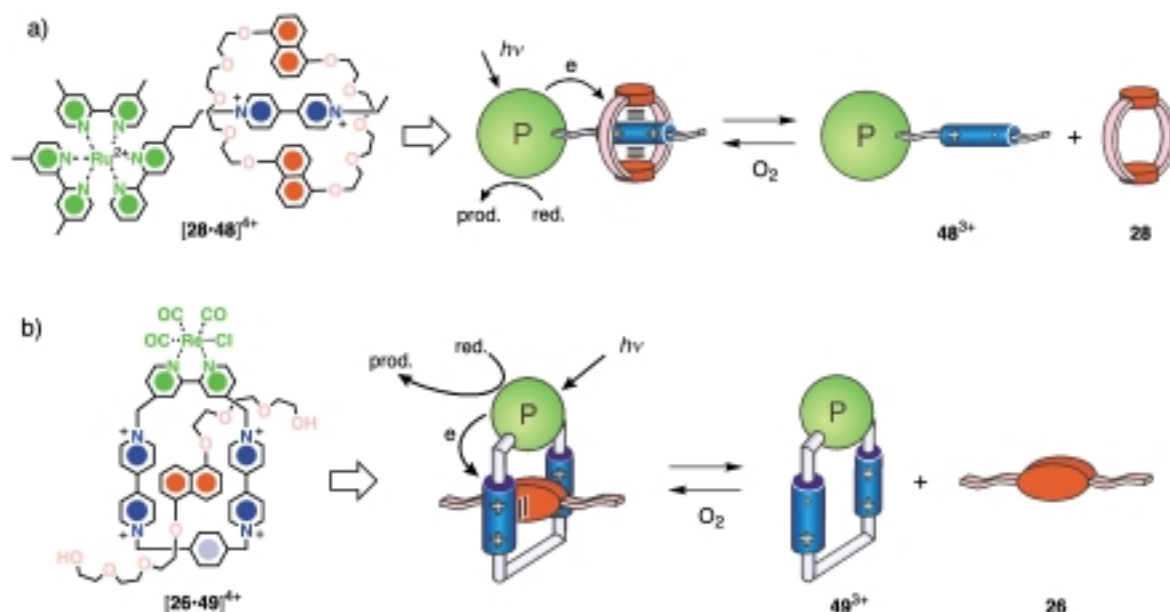
achieved and the pseudorotaxane dethreads (process 4), as evidenced by absorption spectral changes and, more importantly, by the increase in the intensity of the 1,5-dioxynaphthalene fluorescence, which can only originate from free **26**. Oxygenation of the solution—from which O_2 was initially removed—reoxidizes the cyclophane back (process 5) to the tetracationic form, thereby promoting rethreading (process 6) with **26** as shown by the absorption and luminescence spectra.

This strategy has been extended recently to second-generation pseudorotaxanes in which the metal-complex photosensitizer, which can also be called a “light-fueled” motor, has been incorporated (Scheme 33) either into the thread^[139] or into the ring^[140] component.^[141] The construction of these “integrated” pseudorotaxanes is not an easy task and so careful design is of paramount importance before embarking on sometimes time-consuming and demanding synthetic work.

The successful operation of such a molecular machine is the result of 1) the appropriate choice of the functional units and 2) their covalent linking into the thread and ring components in order to achieve the correct integration of functions—for example, receptor ability, redox features, photophysical properties—and sequence of processes—for example, electron-transfer processes—as well as the lack of interference between the units. As in the case of the molecular machine shown in Scheme 32, the dethreading and rethreading motions of the pseudorotaxanes represented in Scheme 33 can be triggered by irradiation with visible light and oxygenation of the solution, respectively. The motions can also be easily monitored by means of UV/Vis absorption and luminescence spectroscopy. Once again, the most important readout signal is the intensity of the 1,5-dioxynaphthalene fluorescence associated with the free ring **28** (Scheme 33 a) or



Scheme 32. The photochemically induced dethreading (MeCN or H_2O , room temperature) of the pseudorotaxane $[25 \cdot 26]^{4+}$, based on the use of the external photosensitizer P (9-anthracenecarboxylic acid) and the reductant scavenger (red. = triethanolamine). Rethreading occurs upon oxygenation of the solution.^[57, 134a]



Scheme 33. Photocontrollable molecular machines based on pseudorotaxanes.^[139, 140] In these second-generation systems the “light-fueled” motor (namely, the photosensitizer) is part of the acyclic and of the macrocyclic components of $[28 \cdot 48]^{4+}$ and $[26 \cdot 49]^{4+}$, respectively. Triethanolamine (red.) is the reductant scavenger. Conditions: a) EtOH, 298 K; b) H_2O , 298 K.

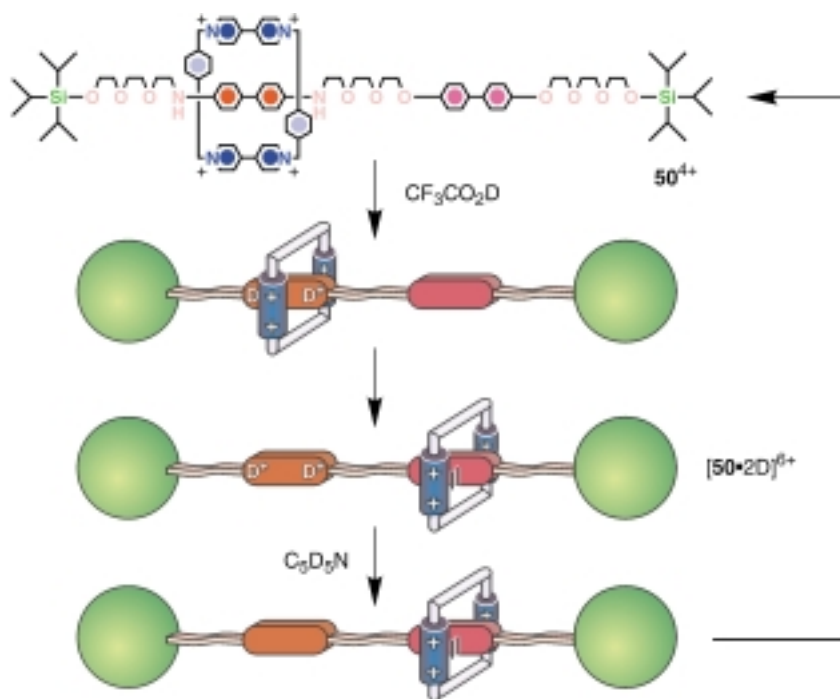
free thread **26** (Scheme 33b) components. It is worth noting that through a repeated sequence of deoxygenation and irradiation followed by oxygenation many dethreading/rethreading cycles can be performed on the same solution without any appreciable loss of signal until most of the reductant scavenger is consumed. It should also be stressed that systems which rely on this photosensitizer-scavenger strategy produce “waste” species from the decomposition of the reductant scavenger. In this regard, the search for efficient molecular machines exploiting “clean”, reversible photochemical reactions—in other words, machines which use only light as an energy supply—is of fundamental importance.

3.2. Molecular Shuttles

3.2.1. Chemically Controllable Molecular Shuttles

The [2]rotaxane **50**⁴⁺ incorporates (Scheme 34) a π -electron-deficient macrocycle and a π -electron-rich dumbbell.^[142] In solution the macrocycle resides around the benzidine or the biphenol recognition site. The two co-conformations are stabilized by π – π stacking interactions between the bipyridinium units of the macrocycle and the sandwiched π -electron-rich recognition site of the dumbbell, as well as by C–H \cdots O interactions between the α -bipyridinium hydrogen atoms and the polyether oxygen atoms. The ^1H NMR spectrum (CD_3CN ,

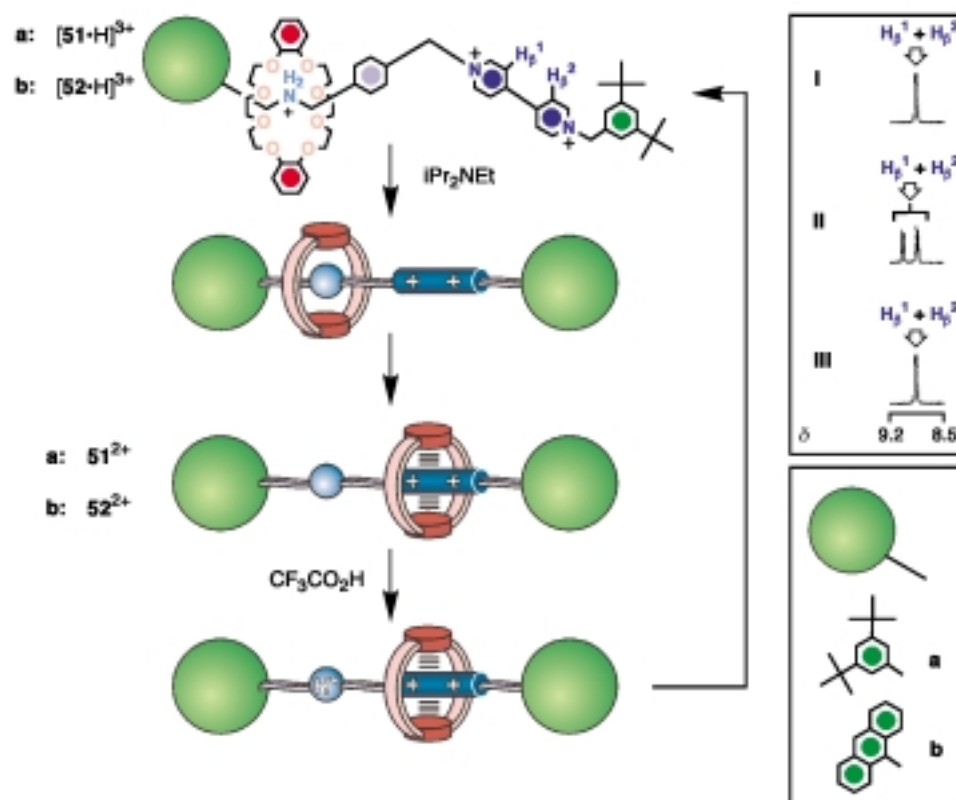
229 K) of this [2]rotaxane shows distinct signals for the two co-conformations. The ratio between them is 84:16 in favor of the isomer having the benzidine unit inside the cavity of the macrocycle. This selectivity is a result of the relative binding affinity^[118a] of the tetracationic cyclophane for the two π -electron-rich recognition sites. The association constant for a complex formed between the tetracationic cyclophane and a model benzidine guest is one order of magnitude higher than



Scheme 34. The shuttling of the macrocyclic component of **50**⁴⁺ along its dumbbell-shaped component can be controlled^[142] chemically or electrochemically in CD_3CN at 229 K by protonating/deprotonating or oxidizing/reducing the benzidine unit.

that for an equivalent complex incorporating a biphenol guest. The addition (Scheme 34) of $\text{CF}_3\text{CO}_2\text{D}$ to a solution of the [2]rotaxane in CD_3CN results in protonation of the benzidine unit. As a result, the tetracationic cyclophane shuttles away from the newly formed dicationic unit to encircle exclusively the biphenol recognition site in $[\mathbf{50} \cdot 2\text{D}]^{6+}$. Consistently, the ^1H NMR spectrum shows only the signals of the isomer having the biphenol recognition site inside the cavity of the tetracationic cyclophane. Upon addition of $\text{C}_5\text{D}_5\text{N}$, the benzidine recognition is deprotonated and the original equilibrium between the two co-conformations is restored.

The [2]rotaxanes $[\mathbf{51} \cdot \text{H}]^{3+}$ and $[\mathbf{52} \cdot \text{H}]^{3+}$ incorporate (Scheme 35) a dialkylammonium and a bipyridinium recognition site in their dumbbell-shaped components.^[143] Gradi-



Scheme 35. The chemically controllable^[143] molecular shuttles $[\mathbf{51} \cdot \text{H}]^{3+}$ and $[\mathbf{52} \cdot \text{H}]^{3+}$ and the ^1H NMR spectra ($(\text{CD}_3)_2\text{CO}$, 298 K) of $[\mathbf{51} \cdot \text{H}]^{3+}$ recorded before (I) and after the addition of $i\text{Pr}_2\text{NEt}$ (II), and after the addition of $\text{CF}_3\text{CO}_2\text{H}$ (III).

ent-enhanced NOE spectroscopy demonstrated that the macrocycle resides exclusively around the ammonium recognition site in $(\text{CD}_3)_2\text{CO}$ at 298 K. Indeed, irradiation of the *p*-phenylene protons adjacent to the ammonium recognition site showed NOEs for some of the CH_2O protons of the macrocycle. Similar effects were observed when the protons of the stopper adjacent to the ammonium recognition site were irradiated. The preference of the macrocycle for the ammonium recognition site is a result of a combination of $^+\text{N}-\text{H} \cdots \text{O}$ and $\text{C}-\text{H} \cdots \text{O}$ interactions between the CH_2NH_2^+ hydrogen atoms of the dumbbell and the oxygen atoms of the macrocycle. Upon addition (Scheme 35) of an excess of

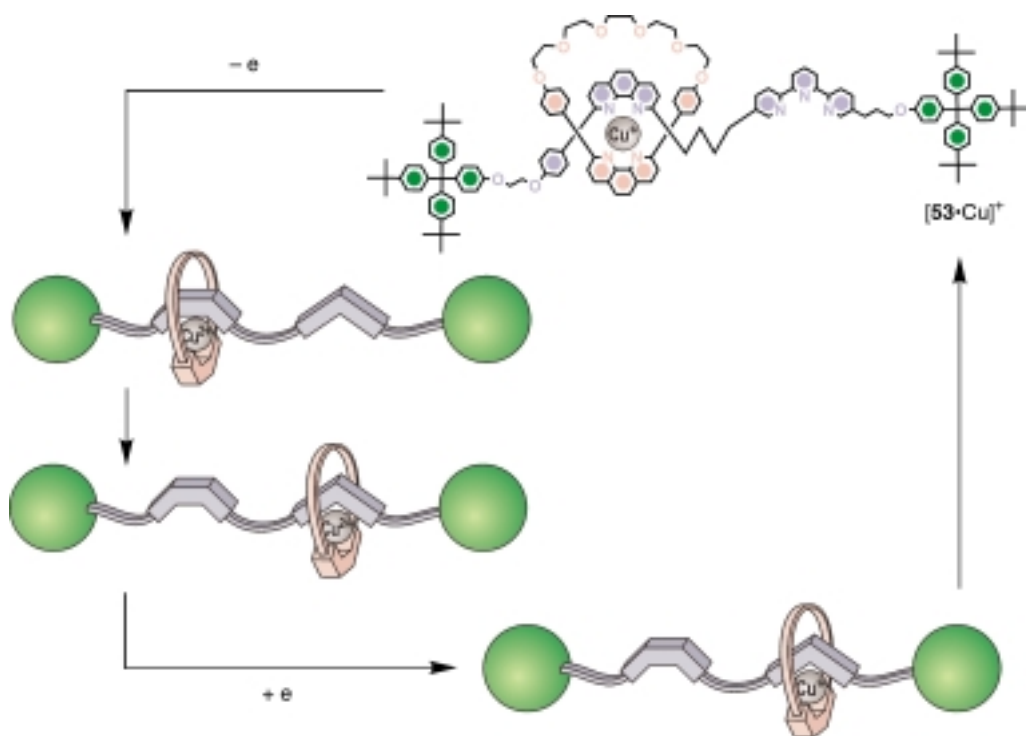
$i\text{Pr}_2\text{NEt}$ to a solution of one of these [2]rotaxanes in $(\text{CD}_3)_2\text{CO}$, deprotonation of the ammonium recognition site occurs. As a result, the intercomponent hydrogen bonds are destroyed and the macrocycle shuttles to the bipyridinium recognition site in $\mathbf{51}^{2+}$ and $\mathbf{52}^{2+}$. However, the original co-conformation is restored after the addition of $\text{CF}_3\text{CO}_2\text{H}$, since the protonation of the ammonium recognition site is followed by the shuttling of the macrocycle back to encircle the NH_2^+ center. The shuttling process can be followed by ^1H NMR spectroscopy by employing the bipyridinium protons H_β^1 and H_β^2 as probes. The ^1H NMR spectrum ($(\text{CD}_3)_2\text{CO}$, 298 K) of $[\mathbf{51} \cdot \text{H}]^{3+}$ shows (signal I in Scheme 35) a single resonance for the protons H_β^1 and H_β^2 . After deprotonation of the ammonium recognition site, the macrocycle shuttles to the bipyridinium recognition site and two distinct resonances can be

observed (signal II) for the protons H_β^1 and H_β^2 . Once the ammonium group is regenerated after protonation, the macrocycle shuttles back to encircle this recognition site and the original signal for the protons H_β^1 and H_β^2 is restored (signal III). The movement of the ring can be also monitored by electrochemical techniques.

3.2.2. Electrochemically Controllable Molecular Shuttles

The shuttling of the macrocyclic component of [2]rotaxane $\mathbf{50}^{4+}$ along the linear portion of its dumbbell-shaped component can be also controlled^[142, 144] (Scheme 34) electrochemically. Indeed, the benzidine recognition site undergoes two consecutive one-electron oxidations.^[118a] Comparison of the half-wave potentials of the [2]rotaxane with those of a model compound incorporating a benzidine unit not encircled

by the tetracationic cyclophane shows that the potential for the first oxidation is more positive in the [2]rotaxane while that for the second oxidation is the same in both compounds. These observations indicate that the tetracationic cyclophane makes the first one-electron oxidation of the encircled benzidine unit more difficult. However, once this unit is oxidized to the corresponding radical cation, the tetracationic cyclophane moves away from it to encircle the biphenol unit and so does not influence the second one-electron oxidation. Upon reduction of the benzidine unit back to its neutral state, the original equilibrium between the two co-conformations associated with the [2]rotaxane is restored.

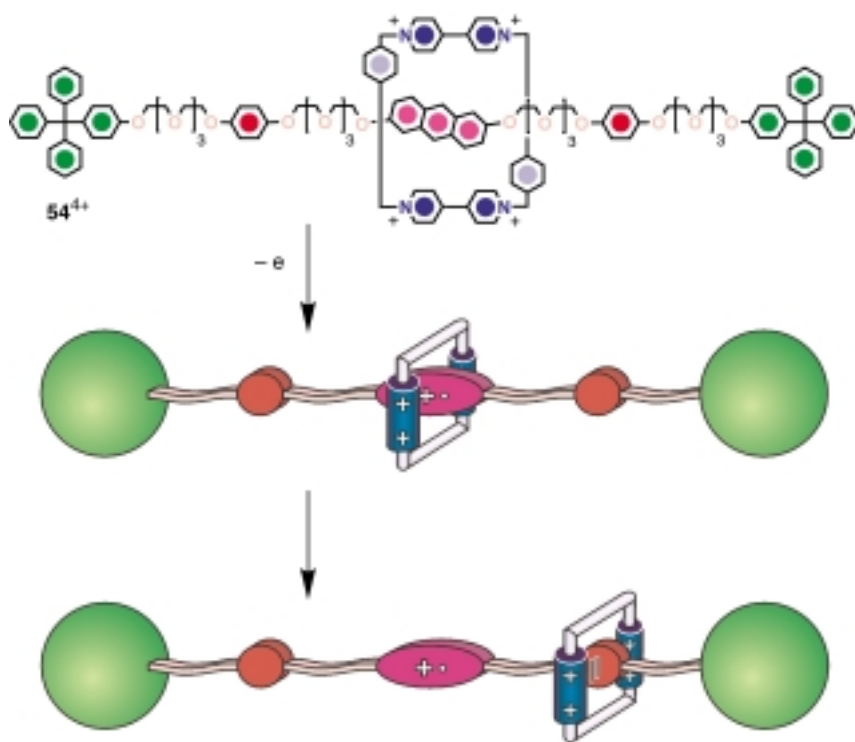


Scheme 36. The shuttling of the macrocyclic component of $[53 \cdot \text{Cu}]^+$ along its dumbbell-shaped component can be controlled^[145] electrochemically by oxidizing/reducing the metal center (MeCN, 298 K).

The [2]rotaxane $[53 \cdot \text{Cu}]^+$ has (Scheme 36) a phenanthroline and a terpyridine unit in its dumbbell-shaped component.^[145] It also incorporates a Cu^{I} center coordinated tetrahedrally by the phenanthroline ligand of the dumbbell together with the phenanthroline ligand of the macrocycle. Oxidation of the tetracoordinated Cu^{I} center of $[53 \cdot \text{Cu}]^+$ to a tetracoordinated Cu^{II} ion occurs^[145b, 146] upon electrolysis (+1.0 V versus SCE) of a solution of the [2]rotaxane in MeCN. In response to the preference of Cu^{II} for a pentacoordination geometry, the macrocycle shuttles away from the bidentate phenanthroline ligand of the dumbbell and encircles the terdentate terpyridine ligand instead. In this co-conformation, the Cu^{II} center adopts a pentacoordination geometry that is significantly more stable than the tetracoordination one associated with the original co-conformation. Consistently, the cyclic voltammogram shows the disappearance of the reversible wave (+0.68 V) associated with the tetracoordinated $\text{Cu}^{\text{II}}/\text{Cu}^{\text{I}}$ redox couple and the concomitant appearance of a reversible wave (−0.03 V) corresponding to the pentacoordinated $\text{Cu}^{\text{II}}/\text{Cu}^{\text{I}}$ redox couple. A second electrolysis (−0.03 V) of the solution of the [2]rotaxane in MeCN reduces the pentacoordinated Cu^{II} center back to a pentacoordinated Cu^{I} ion. In response to the preference of Cu^{I} for a tetracoordination geometry, the macrocycle moves away from the terdentate terpyridine ligand and encircles the bidentate phenanthroline ligand. The cyclic voltammogram recorded after the second electrolysis shows the original redox wave (+0.68 V) corresponding to the tetracoordinated $\text{Cu}^{\text{II}}/\text{Cu}^{\text{I}}$ redox couple.

The [2]rotaxane 54^{4+} incorporates (Scheme 37) a π -electron-deficient macrocycle and a π -electron-rich dumbbell.^[147] The macrocycle resides around the 2,6-dioxyanthracene recognition site in solution. This co-conformation is stabilized

by π – π stacking interactions between the bipyridium units of the macrocycle and the sandwiched 2,6-dioxyanthracene recognition site of the dumbbell, as well as by C–H \cdots O interactions between the α -bipyridinium hydrogen atoms and the polyether oxygen atoms. The ^1H NMR spectrum ($(\text{CD}_3)_2\text{CO}$, 298 K) of this [2]rotaxane shows a singlet at $\delta = 4.30$ for the protons in positions 9 and 10 of the 2,6-dioxyanthracene ring system. By contrast, these protons resonate at $\delta = 8.16$ in the ^1H NMR spectrum of the “free” dumbbell. The dramatic chemical shift change ($\Delta\delta = -3.86$) experienced by the resonances associated with these protons is a result of shielding effects exerted on them by the sandwiching bipyridinium units. The cyclic voltammogram of a solution of this [2]rotaxane in MeCN shows a first oxidation wave (+1.03 V versus SCE) that corresponds to the oxidation of the 2,6-dioxyanthracene recognition site. This oxidation occurs at a potential that is more positive than that of a model compound incorporating this unit. As far as the oxidation of the two 1,4-dioxybenzene rings is concerned, two waves (+1.29 and +1.59 V versus SCE) are observed. The oxidation of the first 1,4-dioxybenzene ring of the [2]rotaxane occurs at a potential that is almost identical to that of a model compound incorporating this unit. The oxidation of the second 1,4-dioxybenzene ring of the [2]rotaxane occurs at a potential that is almost identical to that of a model [2]rotaxane incorporating this unit that is encircled by the tetracationic cyclophane. These observations suggest that the tetracationic cyclophane resides (Scheme 37) initially around the 2,6-dioxyanthracene recognition site making its oxidation more difficult. However, once this recognition site is oxidized, the tetracationic cyclophane moves away from it and encircles one of the two 1,4-dioxybenzene rings.



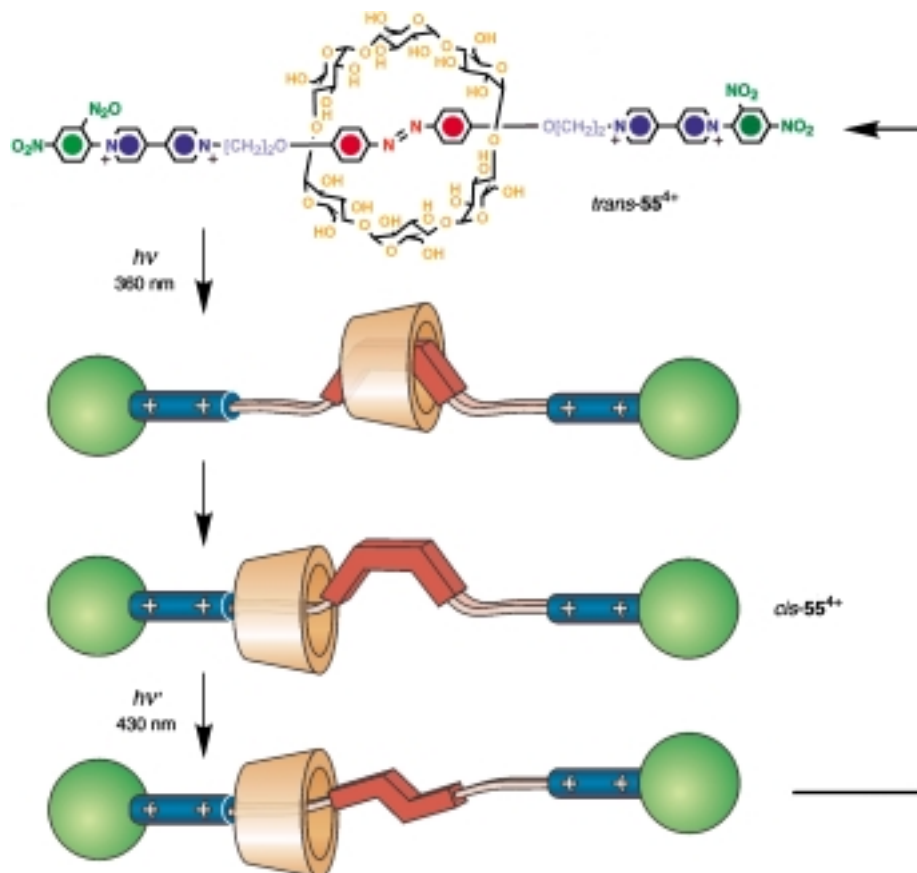
Scheme 37. The shuttling of the macrocyclic component of 54^{4+} along its dumbbell-shaped component can be induced^[147] by oxidizing electrochemically the anthracene ring system (MeCN, 298 K).

3.2.3. Photochemically Controllable Molecular Shuttles

The shuttling of the macrocyclic component of the [2]rotaxane $[53 \cdot \text{Cu}]^+$ (Scheme 36) along the linear portion of its dumbbell-shaped component can also be induced photochemically.^[145b, 148] Upon irradiation (464 nm) of a solution of the [2]rotaxane in MeCN, in the presence of *p*-nitrobenzylbromide, the Cu^{I} -based chromophoric unit is excited to a metal-to-ligand charge-transfer excited state. Electron transfer from the photoexcited [2]rotaxane to *p*-nitrobenzylbromide follows, which generates a tetracoordinated Cu^{II} center. In response to the preference of the Cu^{II} ion for a pentacoordination geometry, the macrocycle shuttles away from the bidentate phenanthroline ligand of the dumbbell and encircles the terdentate terpyridine ligand instead. Upon addition of ascorbic acid, the pentacoordinated Cu^{II} center is reduced to a pentacoordinated Cu^{I} ion. In response to the preference of Cu^{I} for a tetracoordination geometry, the

macrocycle moves away from the terdentate terpyridine ligand and encircles the bidentate phenanthroline ligand to restore the original co-conformation.

The [2]rotaxane 55^{4+} incorporates (Scheme 38) an α -cyclodextrin torus and a *trans*-azobiphenoxy-containing dumbbell.^[149] Comparison of the ^1H NMR spectra (D_2O , 303 K) of the [2]rotaxane and of its “free” dumbbell-shaped component indicates that the cyclodextrin resides exclusively around the *trans*-azobiphenoxy recognition site. While only two sets of signals are observed for the *trans*-azobiphenoxy protons of the “free” dumbbell, four sets of resonances are associated with the same protons in the [2]rotaxane. In the [2]rotaxane, the local C_2 symmetry of the *trans*-azobiphenoxy unit is lost, as a result of the toroidal shape of the α -cyclodextrin component, and the two *p*-phenylene rings are no longer equivalent. Also, the circular dichroism spectrum (H_2O , 278 K) of the [2]rotaxane shows a positive band (360 nm) corresponding to $\pi \rightarrow \pi^*$ transitions of the azobiphenoxy unit. This observation indicates that this unit is encircled by the α -



Scheme 38. The shuttling of the macrocyclic component of 55^{4+} along its dumbbell-shaped component can be controlled^[149] reversibly by photoisomerizing the azobenzene unit (H_2O , 278 K).

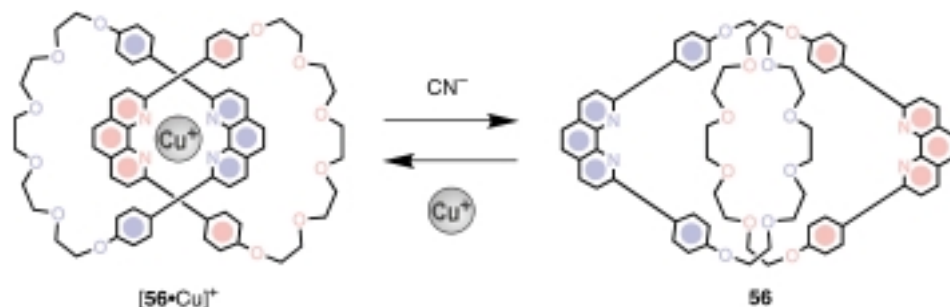
cyclodextrin component, since long-axis-polarized transitions of aromatic guests inserted through the cavity of α -cyclodextrin hosts produce positive bands. Upon irradiation (360 nm), the azobiphenoxy unit isomerizes^[150] (Scheme 38) from *trans* to *cis* “pushing” the α -cyclodextrin component away to encircle one of the $(\text{CH}_2)_2\text{O}$ chains. As a result, the intensity of the positive band decreases. Upon further irradiation (430 nm), the azobiphenoxy unit isomerizes from *cis* back to *trans*. This process is accompanied by the shuttling of the α -cyclodextrin component back to encircle the *trans*-azobiphenoxy recognition site and, consequently, by an increase in intensity of the positive band at 360 nm.

3.3. Catenanes

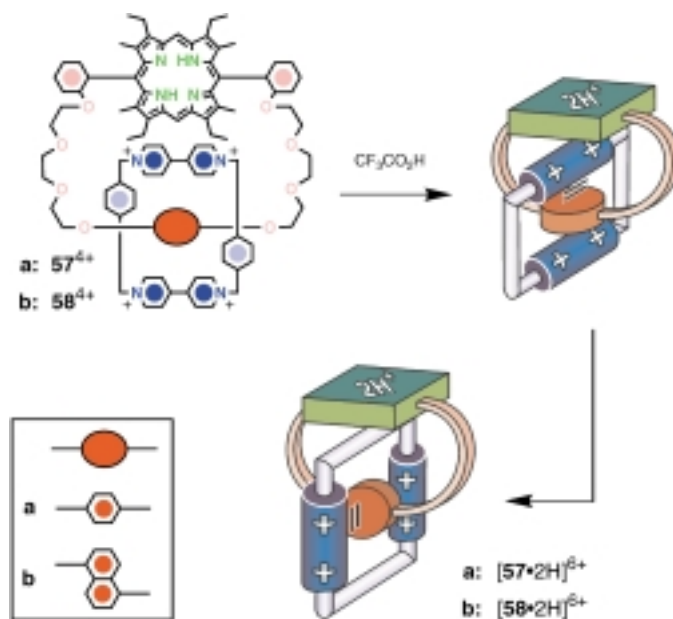
3.3.1. Chemically Controllable Catenanes

The [2]catenane $[\mathbf{56} \cdot \text{Cu}]^+$ incorporates (Scheme 39) two identical macrocyclic components.^[75, 151] They possess a phenanthroline unit and a polyether chain connected by two *p*-phenylene rings. The X-ray crystallographic analysis of $[\mathbf{56} \cdot \text{Cu}]^+$ revealed^[152] that the two phenanthroline ligands embrace the “central” Cu^+ ion, while the two polyether chains are located away from each other. However, a co-conformational change, which involves the circumrotation of both macrocycles through the cavity of each other, occurs (Scheme 39) upon demetalation. Indeed, the [2]catenand $\mathbf{56}$ is obtained^[151, 153] quantitatively upon treating a solution of the [2]catenane $[\mathbf{56} \cdot \text{Cu}]^+$ with KCN. The X-ray analysis of $\mathbf{56}$ revealed^[152] a co-conformation that is markedly different from the one adopted by $[\mathbf{56} \cdot \text{Cu}]^+$. In the [2]catenand $\mathbf{56}$, the phenanthroline ligands are positioned away from each other, while the entangled polyether chains are located at the “center” of the molecule. Complete rearrangement of $\mathbf{56}$ occurs^[154, 155] when $[\text{Cu}(\text{MeCN})_4]\text{BF}_4$ is added to a solution of this [2]catenand. The two macrocyclic components circumrotate through the cavity of each other to allow the coordination of the Cu^+ ion by the two phenanthroline ligands and yield back the [2]catenane $[\mathbf{56} \cdot \text{Cu}]^+$. A similar co-conformational change was observed^[156, 157] upon metalation of the [2]catenand with a variety of metal ions or upon protonation of one of the phenanthroline nitrogen atoms.

The [2]catenanes $\mathbf{57}^{4+}$ and $\mathbf{58}^{4+}$ incorporate (Scheme 40) a bipyridinium-based tetracationic cyclophane and a π -elec-



Scheme 39. Demetalation of the [2]catenane $[\mathbf{56} \cdot \text{Cu}]^+$ and the reverse reaction, metalation of catenand $\mathbf{56}$, is accompanied^[151] by co-conformational changes involving the circumrotation of the macrocyclic components through each other's cavity. Conditions: demetalation: KCN/ H_2O , MeCN/ CH_2Cl_2 , 298 K; metalation: $[\text{Cu}(\text{MeCN})_4]\text{BF}_4/\text{MeCN}/\text{CH}_2\text{Cl}_2$, H_2O , 298 K.

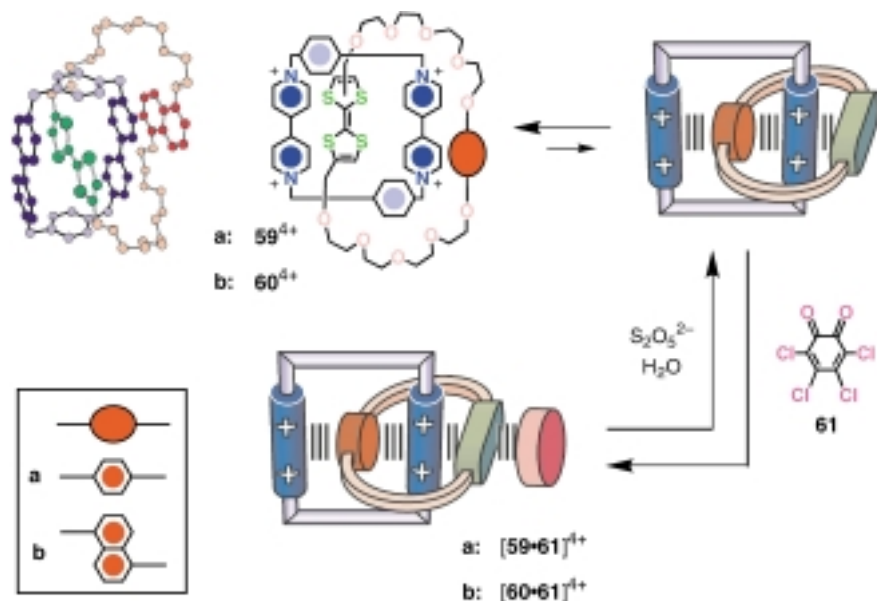


Scheme 40. The circumrotation of the tetracationic cyclophane component of the [2]catenanes $\mathbf{57}^{4+}$ and $\mathbf{58}^{4+}$ occurs^[159] upon protonation of the porphyrin unit ($(\text{CD}_3)_2\text{CO}$, 238 K).

tron-rich macrocyclic polyether comprising a porphyrin ring system and either a 1,4-dioxybenzene or a 1,5-dioxynaphthalene unit.^[158] The tetracationic cyclophane encircles exclusively the dioxyarene unit as a result of π - π stacking interactions between this recognition site and the sandwiching bipyridinium units. The protons of the 1,4-dioxybenzene ring of the [2]catenane of $\mathbf{57}^{4+}$ resonate at $\delta = 2.62$ in the ^1H NMR spectrum (CD_3CN , 343 K). Similarly, the protons in positions 4 and 8 of the 1,5-dioxynaphthalene ring system in the [2]catenane $\mathbf{58}^{4+}$ resonate at $\delta = 1.47$ in the ^1H NMR spectrum ($(\text{CD}_3)_2\text{SO}$, 378 K). These “unusual” chemical shift values for the dioxyarene protons are a result of shielding effects exerted upon them by the sandwiching bipyridinium units. The porphyrin ring system is also engaged in π - π stacking interactions with the bipyridinium unit located inside the cavity of the macrocyclic polyether. However, the tetracationic cyclophane circumrotates through the cavity of the macrocyclic polyether exchanging the “inside” and “alongside” bipyridinium units and, in the case of $\mathbf{57}^{4+}$, the rate of circumrotation is about 1500 times per second (CD_3CN , 298 K). This dynamic process is slow on the ^1H NMR timescale at 238 K in $(\text{CD}_3)_2\text{CO}$ and signals for the “inside” and “alongside” bipyridinium units can be distinguished. Upon addition (Scheme 40) of $\text{CF}_3\text{CO}_2\text{H}$, the porphyrin ring system is protonated.^[159] As a result of electrostatic repulsion, the tetracationic cyclophane circumrotates to move the “inside” dicationic bipyridinium unit away from the now dicationic porphyrin ring system. As a consequence, the

^1H NMR spectra ($(\text{CD}_3)_2\text{CO}$, 238 K) of the protonated [2]catenanes $[\mathbf{57} \cdot 2\text{H}]^{6+}$ and $[\mathbf{58} \cdot 2\text{H}]^{6+}$ show two distinct environments for the two *p*-phenylene rings of the tetracationic cyclophane. In the co-conformation obtained after protonation, one of the *p*-phenylene rings is located inside the cavity of the macrocyclic polyether, while the other is positioned alongside. Chemical-shift differences of $\Delta\delta = -0.39$ and -0.50 are observed between the resonances for the protons of the “inside” and “alongside” *p*-phenylene rings of $[\mathbf{57} \cdot 2\text{H}]^{6+}$ and $[\mathbf{58} \cdot 2\text{H}]^{6+}$, respectively.

The [2]catenanes $\mathbf{59}^{4+}$ and $\mathbf{60}^{4+}$ incorporate (Scheme 41) a bipyridinium-based tetracationic cyclophane and a π -electron-rich macrocyclic polyether comprising a tetrathiafulva-



Scheme 41. The circumrotation of the macrocyclic polyether component of the [2]catenanes $\mathbf{59}^{4+}$ and $\mathbf{60}^{4+}$ can be controlled^[97c, 160] reversibly in MeCN at 298 K by adding *o*-chloroanil (**61**), which forms a charge-transfer adduct with the tetrathiafulvalene unit of these [2]catenanes. The adduct can be disrupted by reducing *o*-chloroanil with $\text{S}_2\text{O}_5^{2-}$ ions. The geometry adopted in the solid state by $\mathbf{60}^{4+}$ is also shown.

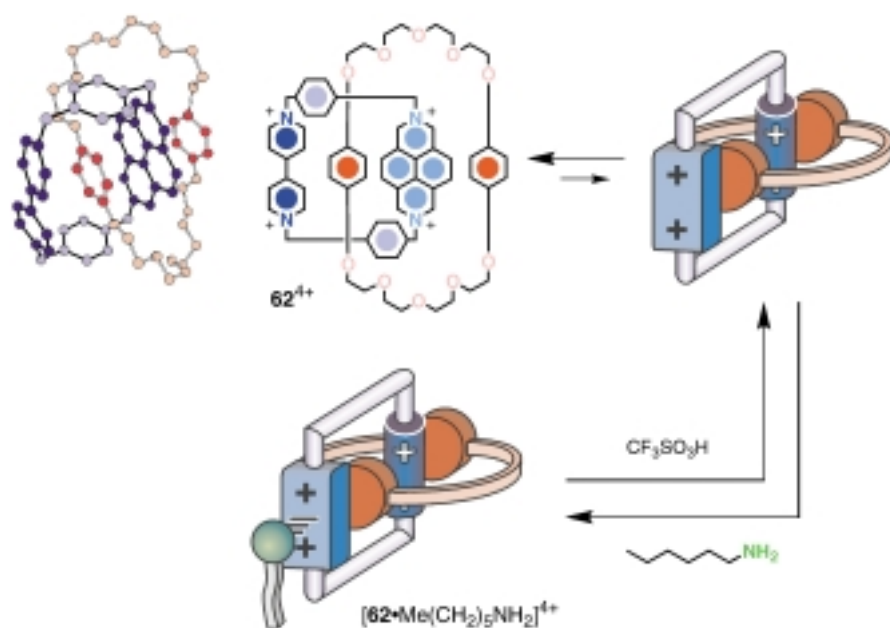
lene ring system and either a 1,4-dioxybenzene or a 1,5-dioxynaphthalene unit.^[97c, 160] The X-ray crystallographic analysis of the [2]catenane $\mathbf{60}^{4+}$ revealed (Scheme 41) that the tetracationic cyclophane encircles exclusively the tetrathiafulvalene ring system in the solid state. Also, the ^1H NMR spectra (CD_3CN , 298 K) of $\mathbf{59}^{4+}$ and $\mathbf{60}^{4+}$ indicate that the tetrathiafulvalene unit resides preferentially inside the cavity of the tetracationic cyclophane in solution, while the dioxyarene unit is positioned alongside. For example, the characteristic^[117a, 161] upfield shifts for resonances associated with protons in the dioxyarene units that are encircled by the tetracationic cyclophane are not observed in these [2]catenanes. The 1,4-dioxybenzene protons of $\mathbf{59}^{4+}$ and the 1,5-dioxynaphthalene protons of $\mathbf{60}^{4+}$ resonate at chemical shift values downfield from $\delta = 6.4$. Thus, if the co-conformation having a dioxyarene ring inside the cavity of the tetracationic cyclophane is present at all in solution, its concentration must be below the limit of detection by ^1H NMR spectroscopy. Nonetheless, the ability of *o*-chloroanil (**61**) to stack (Scheme 41) against a tetrathiafulvalene ring system can be

exploited^[97c, 160] to “lock” this unit alongside the cavity of the tetracationic cyclophane. Indeed, comparison of the ^1H NMR spectra, recorded at 298 K before and after the addition of **61** to a CD_3CN solution of either $\mathbf{59}^{4+}$ or $\mathbf{60}^{4+}$, shows significant upfield chemical shifts for the resonances associated with the 1,4-dioxybenzene protons of $\mathbf{59}^{4+}$ ($\Delta\delta \approx -3$) and the protons in positions 4 and 8 of the 1,5-dioxynaphthalene ring system of $\mathbf{60}^{4+}$ ($\Delta\delta \approx -5$). These observations indicate that, after the addition of **61**, the dioxyarene rings become encircled by the tetracationic cyclophane and their protons suffer pronounced shielding effects from the sandwiching bipyridinium units. Upon addition of a mixture of $\text{Na}_2\text{S}_2\text{O}_5$ and NH_4PF_6 in H_2O , the adduct formed between the tetrathiafulvalene ring system

and *o*-chloroanil is destroyed, and the original co-conformation with the tetrathiafulvalene unit inside the cavity of the tetracationic cyclophane is restored. Consistently, the original resonances for the protons of the “alongside” dioxyarene rings are observed again in the ^1H NMR spectra of both [2]catenanes.

The [2]catenane $\mathbf{62}^{4+}$ incorporates (Scheme 42) a 1,4-dioxybenzene-based macrocyclic polyether and a tetracationic cyclophane comprising a bipyridinium and a diazapyrenium unit.^[132] Its X-ray crystallographic analysis revealed that the macrocyclic polyether encircles exclusively the diazapyrenium ring system in the solid state. The ^1H NMR spectrum ($(\text{CD}_3)_2\text{CO}$, 193 K) of $\mathbf{62}^{4+}$ shows the signals for two distinct co-conformations in a ratio of 96:4. In the major isomer, the diazapyrenium ring system is located inside the cavity of the macrocyclic polyether and the bipyridinium unit is positioned “alongside”. In the minor isomer, the bipyridinium unit is located inside the cavity of the macrocyclic

polyether and the diazapyrenium ring system is positioned “alongside”. The ability of *n*-hexylamine to form^[92–94] adducts with diazapyrenium ring systems can be exploited^[162] to displace the equilibrium between the two co-conformations in favor of the isomer having the diazapyrenium ring system alongside the cavity of the macrocyclic polyether. The differential pulse voltammogram (MeCN, 298 K) of $\mathbf{62}^{4+}$ shows two peaks at -0.31 and -0.57 V versus SCE for the monoelectronic reductions of the “alongside” bipyridinium unit and of the “inside” diazapyrenium ring system, respectively. After the addition of *n*-hexylamine, the first peak shifts by -60 mV to a potential that corresponds to the monoelectronic reduction of a bipyridinium unit encircled by the 1,4-dioxybenzene macrocyclic polyether. Similarly, the second peak shifts by -20 mV to a potential that is associated with the monoelectronic reduction of a diazapyrenium ring system interacting with *n*-hexylamine. Protonation of *n*-hexylamine occurs upon addition of $\text{CF}_3\text{SO}_2\text{H}$. As a result the adduct formed between *n*-hexylamine and the diazapyrenium unit of the [2]catenane is destroyed and the original equilibrium



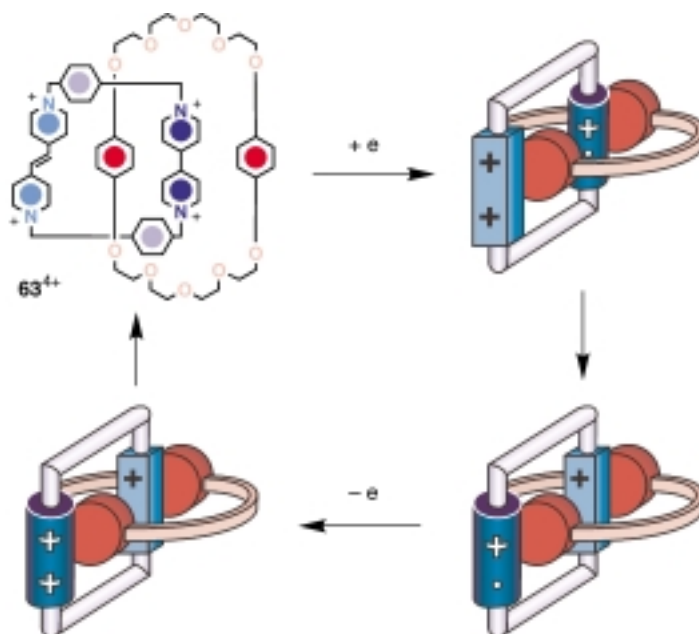
Scheme 42. The circumrotation of the tetracationic cyclophane component of the [2]catenane 62^{4+} can be controlled^[162] reversibly in MeCN at 298 K by adding *n*-hexylamine, which forms a charge-transfer adduct with the diazapyrenium unit of this [2]catenane. The adduct can be disrupted by protonating *n*-hexylamine with $\text{CF}_3\text{SO}_3\text{H}$. The geometry adopted in the solid state by the [2]catenane 62^{4+} is also shown.

between the two co-conformations associated with 62^{4+} is restored. The differential pulse voltammogram recorded after the addition of $\text{CF}_3\text{SO}_3\text{H}$ is identical with that recorded before the addition of *n*-hexylamine.

3.3.2. Electrochemically Controllable Catenanes

The co-conformational motion associated with the [2]catenanes 59^{4+} and 60^{4+} (Scheme 41) can also be controlled^[160, 163, 164] electrochemically by the reversible oxidation/reduction of the tetrathiafulvalene ring system. The cyclic voltammograms of the “free” macrocyclic polyethers show a reversible wave (ca. +0.3 V versus SCE) for the monoelectronic oxidation of the tetrathiafulvalene unit. In the [2]catenanes, the tetrathiafulvalene ring system is located inside the cavity of the tetracationic cyclophane and its monoelectronic oxidation occurs at more positive potentials. Furthermore, a large separation between the anodic and cathodic peaks associated with this process is observed. This separation varies as the scan rate is changed. Upon increasing the scan rate, the anodic peak moves to more positive potentials, while the cathodic one shifts to less positive values. These observations indicate that the oxidation/reduction of the tetrathiafulvalene unit is accompanied by circumrotation of the macrocyclic polyether through the cavity of the tetracationic cyclophane and that this co-conformational change is occurring on the timescale of the electrochemical experiment. Indeed, after oxidation, the newly formed monocationic tetrathiafulvalene unit is expelled from the cavity of the tetracationic cyclophane and is replaced by the neutral dioxyarene unit. After reduction, the original co-conformation is restored as the neutral tetrathiafulvalene unit replaces the dioxyarene unit inside the cavity of the tetracationic cyclophane.

The [2]catenane 63^{4+} incorporates (Scheme 43) a 1,4-dioxybenzene-based macrocyclic polyether and a tetracationic cyclophane comprising a bipyridinium and a *trans*-bis(pyridinium)-ethylene unit.^[165] The ^1H NMR spectrum ($(\text{CD}_3)_2\text{CO}$, 213 K) of 63^{4+} shows the signals for two distinct co-conformations in a ratio of 92:8. In the major isomer, the bipyridinium unit is located inside the cavity of the macrocyclic polyether and the *trans*-bis(pyridinium)-ethylene unit is positioned “along-side”. The first two reduction waves in the cyclic voltammogram (MeCN, 298 K) of the “free” tetracationic cyclophane occur at –0.31 and –0.43 V versus SCE. They correspond to the first monoelectronic reductions of the bipyridinium and of the *trans*-bis(pyridinium)ethylene unit, respectively. In the case of the [2]catenane, these two waves are shifted to more negative potentials and occur at –0.39 and

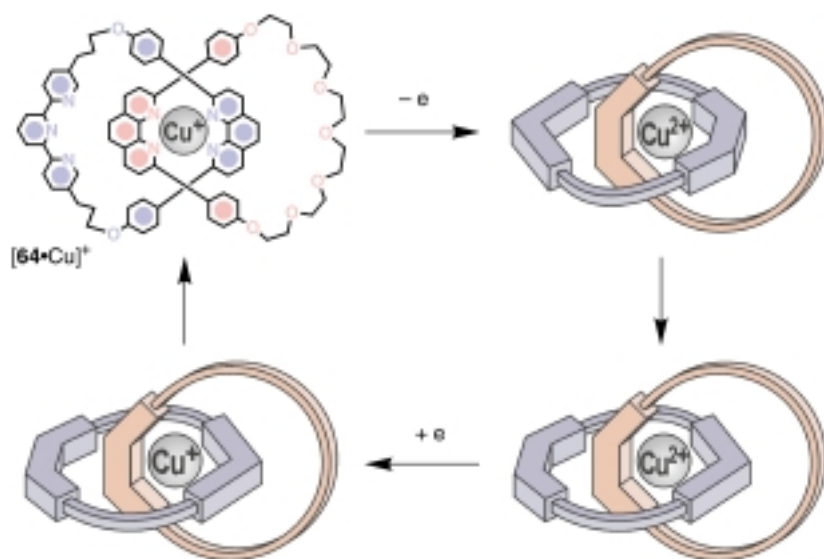


Scheme 43. The circumrotation of the tetracationic cyclophane component of the [2]catenane 63^{4+} can be controlled^[165] reversibly in MeCN at 298 K by oxidizing/reducing electrochemically its bipyridinium unit.

–0.49 V. These observations indicate that the bipyridinium unit is preferentially located (Scheme 43) “inside” the cavity of the macrocyclic polyether and its reduction is more difficult than in the case of the “free” tetracationic cyclophane. However, once this unit is reduced, the tetracationic cyclophane circumrotates through the cavity of the macrocyclic polyether moving the *trans*-bis(pyridinium)ethylene unit “inside”, as shown by comparison of its reduction potential with that of a catenane model compound.^[165b] The original

equilibrium between the two co-conformations associated with the [2]catenane **63**⁴⁺ is restored upon oxidation of both units back to their dicationic states.

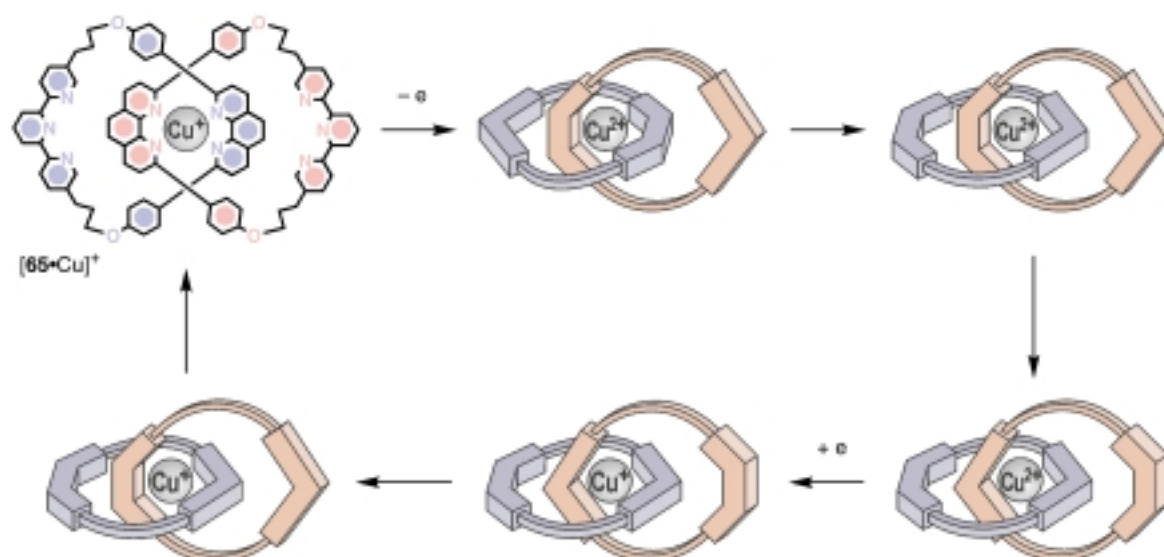
The [2]catenane **[64·Cu]**⁺ incorporates (Scheme 44) a terpyridine ligand in one of its two macrocyclic components and a phenanthroline ligand in both.^[166] Oxidation of the tetracoordinated Cu^I center of **[64·Cu]**⁺ to a tetracoordinated Cu^{II} ion occurs^[166, 167] upon electrolysis (+0.8 V versus SCE) of a solution of the [2]catenane in MeCN. In response to the preference of Cu^{II} for a pentacoordination geometry, the terpyridine-containing macrocycle circumrotates through the cavity of the other one. In the resulting co-conformation, the Cu^{II} center adopts a pentacoordination geometry that is significantly more stable than the original tetracoordinated one. The cyclic voltammogram shows the disappearance of



Scheme 44. The circumrotation of the terpyridine-containing macrocyclic component of the [2]catenane **[64·Cu]**⁺ can be controlled^[166] reversibly in MeCN at 298 K by oxidizing/reducing the metal center.

the reversible wave (+0.63 V) associated with the tetracoordinated Cu^{II}/Cu^I redox couple and the concomitant appearance of a reversible wave (−0.07 V) corresponding to the pentacoordinated Cu^{II}/Cu^I redox couple. A second electrolysis (−0.4 V) of the solution of the [2]catenane in MeCN reduces the pentacoordinated Cu^{II} center back to a pentacoordinated Cu^I ion. In response to the preference of Cu^I for a tetracoordination geometry, the terpyridine-containing macrocycle circumrotates through the cavity of the other one affording back the original co-conformation. The cyclic voltammogram recorded after the second electrolysis shows the original redox wave (+0.63 V) corresponding to the tetracoordinated Cu^{II}/Cu^I redox couple.

The [2]catenane **[65·Cu]**⁺ incorporates (Scheme 45) two identical macrocyclic components comprising a terpyridine and a phenanthroline ligand.^[168] The Cu^I ion is coordinated tetrahedrally by the two phenanthroline ligands, while the two terpyridine ligands are located well away from each other. The cyclic voltammogram of **[65·Cu]**⁺ shows a reversible wave at +0.63 V versus SCE which is associated with the tetracoordinated Cu^{II}/Cu^I redox couple. The visible absorption spectrum of the [2]catenane reveals a metal-to-ligand charge-transfer band at 439 nm for the tetracoordinated Cu^I chromophore. Upon electrochemical oxidation of **[65·Cu]**⁺ or upon treatment with NOBF₄, the tetracoordinated Cu^I center is converted into a tetracoordinated Cu^{II} ion. As a result, the visible absorption spectrum reveals a band at 670 nm for the tetracoordinated Cu^{II} chromophore. However, the intensity of this band decreases with time. Indeed, in response to the preference of the Cu^{II} ion for a coordination number higher than four, one of the two macrocycles circumrotates through the cavity of the other



Scheme 45. The circumrotation of the macrocyclic components of the [2]catenane **[65·Cu]**⁺ can be controlled^[168] reversibly in MeCN at 298 K by oxidizing/reducing the metal center.

to afford a pentacoordinated Cu^{II} ion. Subsequently, the other macrocycle undergoes a similar circumrotational process to yield a hexacoordinated Cu^{II} ion which shows instead a weak absorption band at 687 nm. Electrolysis (-1.0 V) of the solution of the [2]catenane in MeCN reduces the hexacoordinated Cu^{II} center back to a hexacoordinated Cu^{I} ion. In response to the preference of Cu^{I} for a tetracoordination geometry, the two macrocycles circumrotate through the cavity of each other in turn to afford the original co-conformation quantitatively.

3.3.3. Photochemically Controllable Catenanes

The co-conformational motion associated with the [2]catenane $[\mathbf{64} \cdot \text{Cu}]^+$ (Scheme 44) can be also induced photochemically.^[166b, 169] Upon irradiation (464 nm) of a solution of the [2]catenane in MeCN, in the presence of *p*-nitrobenzylbromide, the Cu^{I} -based chromophoric unit is excited to a metal-to-ligand charge-transfer excited state. Electron transfer from the photoexcited [2]catenane to *p*-nitrobenzylbromide follows, which generates a tetraordinated Cu^{II} center. In response to the preference of the Cu^{II} ion for a pentacoordination geometry, the terpyridine-containing macrocycle circumrotates through the cavity of the other affording a pentacoordinated Cu^{II} center. Upon addition of ascorbic acid, the pentacoordinated Cu^{II} center is reduced to a pentacoordinated Cu^{I} ion. In response to the preference of Cu^{I} for a tetracoordination geometry, the terpyridine-containing macrocycle circumrotates through the cavity of the other, which restores the original co-conformation.

4. Perspectives

With an eye to the future, there are two prominent emerging perspectives concerning molecular machines, namely, the development of artificial molecular machines based on biomolecules and the interfacing of artificial molecular machines with solid supports, which we would now like to highlight.

4.1. Artificial Molecular Machines Based on Biomolecules

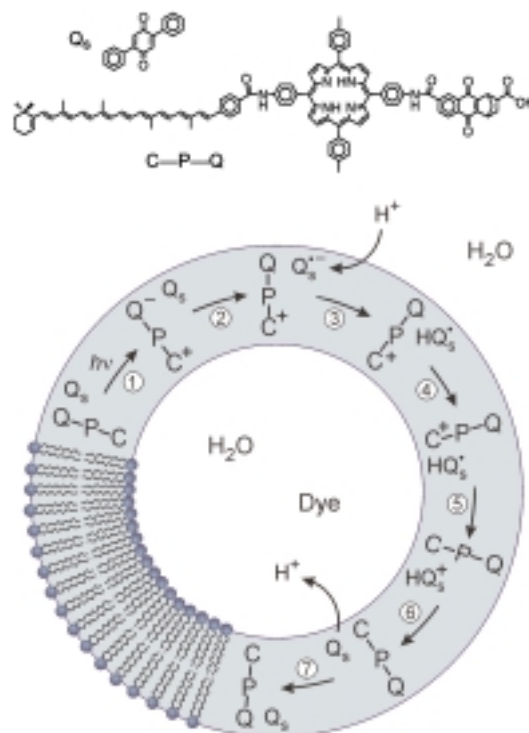
4.1.1. A Power Plant and Motor

Recent scientific advances in both molecular biology and nanofabrication technology have opened up the possibility of building functional hybrid organic and inorganic devices on a nanometer scale. One long-term objective is to utilize the finest attributes associated with the worlds of both organic and inorganic materials for the creation of nanomechanical systems that are powered by biological motors.

At present, the best characterized biological motor is ATP synthase. The synthesis of ATP by this enzyme is based (see Section 1.3.1) on a proton pump across a membrane. Perhaps, the most spectacular molecular-scale machine constructed in

recent years is a biomimetic, photon-driven proton pump which is able to power ATP synthase to produce ATP.

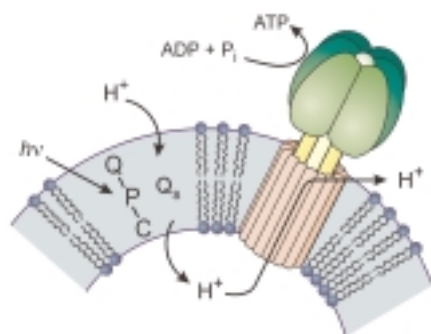
The first step in this research was the design of multi-component systems capable of performing photoinduced charge-separation reactions.^[170] Later on, a so-called C-P-Q triad for photoinduced charge separation that was composed of a naphthoquinone Q as the electron acceptor, free-base porphyrin P as the primary electron donor, and carotene C as the final electron donor^[171] was implanted (Scheme 46) into



Scheme 46. Schematic representation of the liposome-based proton pump powered by a photoinduced charge-separation process.^[172]

the lipid bilayer of a reconstituted liposome.^[172] Photoinduced electron transfer in the triad molecule spanning the wall of the vesicle sets up an electrochemical potential difference between the interior and the exterior of the liposome and leads to directional proton transfer. The preference for the orientation of the triad within the layer is in part thermodynamic (the bulky porphyrin and quinone remain in the less densely packed outer layer) and in part kinetic (the activation barrier for the insertion of lipophilic carotenoid into the bilayer is much lower than those for the polar quinone and carboxylic group). Photoexcitation of the porphyrin moiety of C-P-Q with visible light generates, with a quantum yield of 0.1, the $\text{C}^+-\text{P}-\text{Q}^-$ charge-separated state (Scheme 46, step 1), which can be detected by monitoring the transient absorbance of the carotenoid radical. Electron transfer from Q^- to the lipid-soluble 2,5-diphenylbenzoquinone (Q_s), with a reduction potential 0.6 V more positive than that of Q, results (step 2) in the formation of the radical anion $\text{Q}_\text{s}^{\bullet-}$. The reduced form of Q_s accepts a proton from the external aqueous solution to form the corresponding uncharged semiquinone $\text{HQ}_\text{s}^{\bullet}$, which diffuses through the membrane and performs the crucial

function of a proton shuttle (steps 3 and 4). Upon reaching the interior layer of the membrane, HQ_s^- encounters the carotenoid radical cation, undergoes (step 5) oxidation to HQ_s^\bullet , and releases (step 6) the proton into the aqueous medium inside the vesicle. Random diffusion of the regenerated Q_s closes (step 7) the cycle. The pH-dependent fluorescent excitation spectrum of a water-soluble dye was used to monitor changes in the proton concentration inside liposomes. The efficiency of the system can be increased if an ionophore, such as valinomycin, is added in order to relax the membrane potential. The pH gradient thus established across the bilayer membrane gives rise to a proton-motive force, that is, the biological analogue of the electromotive force. In principle, such a force can be utilized to perform work.^[173] F_0F_1 -ATP Synthase has been incorporated (Scheme 47) into liposomes



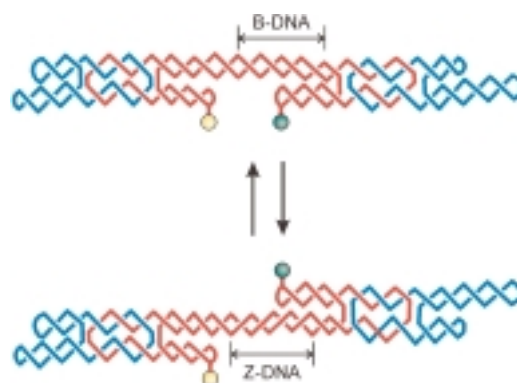
Scheme 47. Schematic representation of a liposome-based artificial photosynthetic membrane.^[173]

containing the components of the proton-pumping photocycle. Irradiation of this artificial membrane with visible light leads to the charge-separation process that causes proton translocation and generation of a proton-motive force. When sufficient proton-motive force has accumulated protons flow through the F_0F_1 -ATP synthase, with the concomitant formation of ATP from ADP and P_i . The functioning of the system was monitored by the luciferin–luciferase fluorescence assay. The results show that the synthesis of ATP occurs against an ATP chemical potential of approximately 12 kcal mol^{-1} and with a quantum yield of more than 7%. One molecule of ATP is synthesized per 14 absorbed photons of light with a wavelength of 633 nm, an observation which means that up to 4% of the initial energy incident on the sample is stored by the system. The photocyclic system operates efficiently over a timescale of hours with a turnover number of seven ATP molecules per F_0F_1 per second. This system is the first complete biomimetic one which effectively couples electrical potential, derived from photoinduced electron transfer, to the chemical potential associated with the ADP-ATP conversion, thereby mimicking the entire process of bacterial photosynthesis. It constitutes a synthetic biological motor that, in principle, can be used to power anything which requires a proton gradient or ATP to work, for example, enzymatic systems that catalyze important reactions or even future nanomachines. Recently, a recombinant expression system has been established for the large-scale production of F_1 -ATPase that has been modified to

contain chemically active “handles”.^[174] Further performance data on motor rotation have also been obtained through the attachment of fluorescent microspheres to the tip of the γ subunit.^[174] Hybrid systems exploiting the motor protein kinesin^[175] and dynein^[176] to transport nonbiological molecules are under investigation. It is clear that this field is going to be an expansionary one in the near future.

4.1.2. A DNA-Based Mechanical Device

An interesting DNA-based artificial machine has recently been reported.^[177] In DNA double-crossover (DX) molecules, two DNA double helices are joined to each other twice to yield rigid molecules. By attaching two DX molecules to one end of a longer DNA strand, a structure (Scheme 48)



Scheme 48. Schematic representation of a DNA-based mechanical device.^[177] The two circles represent dyes whose separation distance changes upon the change in conformation of the middle DNA segment. The change in distance is measured by the change in resonance-energy transfer. Adapted by permission of the authors from ref. [199].

consisting of two short double helices anchored to a longer double helix has been obtained. The segment separating the two DX units consists of a special sequence which can switch conformation. Depending on the solution conditions, this segment can assume either the B conformation, in which DNA twists to the right, or the Z conformation, which has a left-handed twist. The two DX molecules lie on the same side of the longer DNA strand when the middle segment is in the B form and on opposite sides when that segment assumes the Z form. The B–Z transition results in a rotary displacement of up to 6 nm as well as a 0.6-nm lengthening of the segment. The motion (Scheme 48) is monitored through changes in the fluorescence of dyes attached to the free ends of the DX molecules. When the segment is in the B form, the two dyes are on the same side and closer to each other than when the segment is in the Z form. Thus, energy transfer is higher in the B form than in the Z form.

4.1.3. Machines Based on Protein Folding/Unfolding

The specific function of a protein is determined by its three-dimensional structure and the ability of this tertiary structure to evolve with time. The functional conformation of a protein is determined by its amino acid sequence, and understanding

how the one-dimensional primary sequence folds into the functional three-dimensional tertiary structure is a central problem in structural biology.^[178] The folding of a protein is a complex molecular motion which results from a sequence of simple processes and starts from rotations about single bonds. In the search for kinetic methods of experimental investigation, ways of triggering the folding and unfolding processes have been developed. One particular approach consists of the reduction or oxidation of a component of the protein so as to shift the folded/unfolded equilibrium. Examples of proteins in which large-amplitude motions can be controlled by light, through a photoinduced electron-transfer reaction on the heme group of cytochrome *c*,^[179] or by redox stimulation of methionine units^[180] in the amino acid chain, have been reported. Such systems could serve as a basis for the construction of controllable nanomechanical motors based on proteins.

4.2. Interfacing Artificial Molecular Machines with Surfaces and Solid Supports

The investigation of supramolecular systems in solution is not only of fundamental importance to an understanding of their complex behavior, it also represents a starting point for the construction of molecular-level machines. A solution, however, contains a huge number of molecules which behave incoherently since they cannot be addressed individually and hence controlled.^[181] It seems reasonable therefore that before functional supramolecular assemblies can be employed in a machinelike manner they have to be interfaced with the macroscopic world by ordering them in some way. The next generation of molecular machines will need to be organized at interfaces^[182] or deposited on surfaces^[183] so that they can behave coherently—either in parallel or in series—and can also be addressed on the nanometer scale.^[184] We will now discuss an experiment in which the rotation of single molecules on a surface has been observed by scanning tunneling microscopy (STM), and some recent examples of interlocked molecular systems supported on solid electrodes.

4.2.1. Rotation of a Single Molecule within a Supramolecular Bearing on a Solid Surface

Nowadays experimental techniques involving various kinds of probe microscopies allow^[4, 14, 15] the visualization and manipulation of single molecules. Single molecule rotors surrounded by like molecules that form a supramolecular bearing on a surface have been studied^[185] recently by STM in ultrahigh vacuum. The molecular rotors are propeller-shaped hexa-*tert*-butyldecacyclene molecules of approximately 1.5 nm diameter, which were deposited onto an atomically clean Cu(100) surface. At surface coverages of just less than one monolayer, a close-packed supramolecular layer with nanometer-sized holes is formed by the molecules. As a result of robust intermolecular interactions, the packed molecules cannot rotate on the Cu(100) surface and they appear in the STM images (Figure 7a) as six-lobed objects. However, some

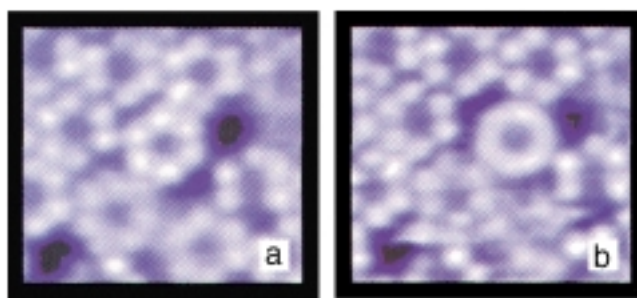
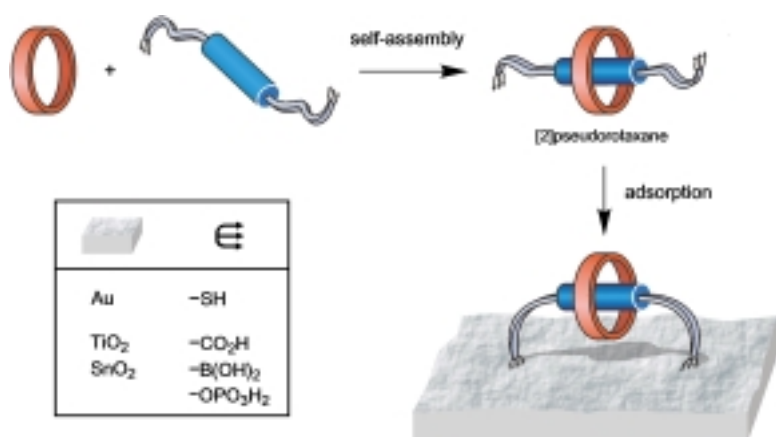


Figure 7. Ultrahigh-vacuum STM images of an atomically clean Cu(100) surface covered with hexa-*tert*-butyldecacyclene molecules.^[185] In a) the molecule appears as a six-lobed object since it is immobilized by the surrounding molecules. In b) the same molecule rotates rapidly on the metal surface and it appears as a torus. Reprinted by permission from ref. [185].

of these molecules can dissociate from the supramolecular assembly to enter one of the nanometer-sized voids in which they are free to rotate. The rate of rotation is greater than the scan rate of imaging at ambient temperature and, as a result, the molecules in motion appear (Figure 7b) as toroidal objects. Interestingly, a single rotating molecule can be translated, with the aid of the STM tip, to a position where it is immobilized by the surrounding molecular layer. Although this system represents an impressive example of real-space observation of molecular motions, it should be noted that molecular machines powered by ambient (thermal) energy cannot be used to do work, unless they are driven by some kind of “asymmetric” stimulus.^[53–55, 74, 186]

4.2.2. Modified Electrodes

With the aim of constructing electrochemical sensors, the affinity of thiol groups for gold surfaces has been exploited to develop electrodes modified with self-assembled monolayers containing receptors^[187, 188] derived from both **25**⁴⁺ and **36**. The self-assembly of molecular components in solution can be coupled (Scheme 49) to deposition techniques for obtaining surface-attached supramolecular and interlocked molecular systems. Amongst the most interesting examples are a monolayer constituted of macrocycles **25**⁴⁺ or **20** catenated onto a gold surface by means of a molecular thread bearing thiol groups at both ends^[189] and a polyrotaxane deposited as a film onto an electrode by electropolymerization.^[190] In the latter case, the rotation of the ring component around the polymer-derivatized thread, confined to the film, can be electrochemically triggered. Another interesting approach is provided by the emerging field of heterosupramolecular chemistry.^[191] Heterosupramolecular systems, that is, supramolecular systems in which one or more components are in the condensed phase (for example, nanocrystals), are expected to offer considerable advantages from the viewpoints of molecular organization and addressability. Following the strategy outlined in Scheme 49, hetero[2]catenanes in which nanosized particles of TiO₂ or SnO₂ are incorporated as a part of one of the ring components have been prepared and are currently the subject of photochemical and electrochemical investigations.^[192]



Scheme 49. Pictorial representation of the preparation of a surface-attached catenane by coupling self-assembly in solution with chemisorption onto a solid support.^[189, 192]

5. Reflections

Miniaturization of the components for the construction of useful devices is currently pursued by the large-downward (top-down) approach. This approach, however, which leads solid-state physicists and electronic engineers to manipulate progressively smaller pieces of matter, has intrinsic limitations. An alternative approach to the construction of nano-scale-sized components and devices is the small-upward (bottom-up) approach. Chemists, by the nature of their discipline, are in an ideal position to develop bottom-up strategies since they are able to manipulate molecules, that is, the smallest entities of matter that have distinct shapes and properties. Although the first steps have been taken along the path to constructing simple artificial molecular machines, it is very early days yet and much progress remains to be made at a fundamental level before the knowledge base reaches that critical threshold which will allow it to be exploited to the full in a technological context. The majority of the systems discussed in this review relate to investigations carried out in solution where incoherence remains a major impediment when it comes to designing and realizing molecular-level devices with machinelike characteristics that perform useful functions. To date, however, the research that has been conducted on artificial molecular machines reveals a number of positive features, a few of which we would like to highlight 40 years since Feynman^[1] laid down the gauntlet. Let us reflect, for example, on the fact that:

- chemical synthesis is a massive parallel manufacturing process: for example, 100 milligrams of a machinelike compound with a molecular weight of 1000 Daltons correspond to 6×10^{19} molecular-level machines;
- for some applications such as drug delivery, artificial molecular machines need to be able to work in solution;^[126c]
- the use of molecular machines for the homogeneous catalysis of chemical reactions has already been demonstrated;^[64, 129]
- natural molecular machines work in solution with the help of membranes and artificial analogues working under very similar conditions have already been constructed;^[172–174]

- with the aim of achieving interfacing with the macroscopic world, artificial molecular machines can be organized in the form of monolayers and as Langmuir–Blodgett films^[182] or congregated on surfaces^[183] on and between electrodes;^[184, 187–192]
- artificial molecular machines are able to perform logic operations^[94, 97a] and, as such, constitute the forerunners of chemical computers;^[184, 193–196]
- “when we have some control of the arrangement of things on a molecular scale, we will get an enormously greater range of possible properties that substances can have”,^[1] and that these new properties will lead most certainly to a wide variety of applications which we cannot even begin to envisage today;^[197]
- last, but by no means least, the current high level of research activity surrounding artificial molecular machines demonstrates how new concepts continue to instill new life into Chemistry as a scientific discipline.^[198]

6. Addendum

Since this review article was accepted for publication—aside from references to communications, papers, and reviews that could be inserted within the original bibliography—some announcements in the literature have been sufficiently important and novel to merit special mention in an addendum. In the area of programmed chemical systems, Lehn^[199] has published an interesting article on multiple processing and expression of molecular information. Intriguing examples^[200, 201] of molecular machines based on metal-induced conformational changes have been described. Bermudez et al.^[202] have shown that the hydrogen-bonded components of amide-based rotaxanes can be induced to move under the influence of oscillating electric fields. In a process which is reminiscent of those operating in natural muscles, a linear rotaxane-like dimer capable of undergoing contraction and stretching motions under the action of a chemical stimulus has been described by Sauvage et al.^[203] The very important achievement of STM-controlled reversible shuttling of α -cyclodextrin beads within a polyrotaxane has been reported.^[204] Research on multiwalled carbon nanotubes has led^[205] to the construction of low-friction nanoscale linear bearings. A DNA-fueled molecular machine has been described^[206] and interest in the development of molecular computers has been highlighted yet again^[207] and again.^[208]

We thank our many colleagues and co-workers, whose names appear beside ours in some of the references, with whom we had the distinct pleasure, in Sheffield, Birmingham, Bologna, and Los Angeles, to develop many of the concepts highlighted in this review. Their intellectual inputs and practical outputs gave the science done in our own research laboratories its direction and its substance. The research was supported in Birmingham by the University of Birmingham and the Engineering and Physical Sciences Research Council, in

Bologna by the European Union (TMR grants FMRX-CT96-0031 and FMRX-CT96-0076), the University of Bologna (Funds for Selected Research Topics), and MURST (Supramolecular Devices Project), and in Los Angeles by the American Chemical Society, the Defense Advanced Research Project Agency, Dupont Pharmaceuticals, the National Science Foundation, the Petroleum Research Fund, and the University of California, Los Angeles.

Received: December 14, 1999 [A375]

- [1] a) R. P. Feynman, *Eng. Sci.* **1960**, 23, 22–36; b) R. P. Feynman, *Saturday Rev.* **1960**, 43, 45–47.
- [2] J. M. Hawkins, *The Oxford Paperback Dictionary*, Oxford University Press, Oxford, **1979**.
- [3] S. Shinkai, O. Manabe, *Top. Curr. Chem.* **1984**, 121, 76–104.
- [4] G. Binnig, H. Rohrer, *Angew. Chem.* **1987**, 99, 622–631; *Angew. Chem. Int. Ed. Engl.* **1987**, 26, 606–614.
- [5] a) J.-M. Lehn, *Angew. Chem.* **1988**, 100, 91–116; *Angew. Chem. Int. Ed. Engl.* **1988**, 27, 89–112; b) D. J. Cram, *Angew. Chem.* **1988**, 100, 1041–1052; *Angew. Chem. Int. Ed. Engl.* **1988**, 27, 1009–1020; c) C. J. Pedersen, *Angew. Chem.* **1988**, 100, 1053–1059; *Angew. Chem. Int. Ed. Engl.* **1988**, 27, 1021–1027.
- [6] a) J. Deisenhofer, H. Michel, *Angew. Chem.* **1989**, 101, 872–892; *Angew. Chem. Int. Ed. Engl.* **1989**, 28, 829–847; b) R. Huber, *Angew. Chem.* **1989**, 101, 849–871; *Angew. Chem. Int. Ed. Engl.* **1989**, 28, 848–869.
- [7] a) P. D. Boyer, *Angew. Chem.* **1998**, 110, 2424–2436; *Angew. Chem. Int. Ed.* **1998**, 37, 2296–2307; b) J. E. Walker, *Angew. Chem.* **1998**, 110, 2438–2450; *Angew. Chem. Int. Ed.* **1998**, 37, 2308–2319; c) J. C. Skou, *Angew. Chem.* **1998**, 110, 2452–2461; *Angew. Chem. Int. Ed.* **1998**, 37, 2320–2328.
- [8] R. A. Marcus, *Angew. Chem.* **1993**, 105, 1161–1172; *Angew. Chem. Int. Ed. Engl.* **1993**, 32, 1111–1121.
- [9] a) *Molecular Electronic Devices* (Ed.: F. L. Carter), Dekker, New York, **1982**; b) *Molecular Electronic Devices* (Ed.: F. L. Carter), Dekker, New York, **1987**; c) *Molecular Electronic Devices* (Eds.: F. L. Carter, R. E. Siatkowski, H. Wohltjen), Elsevier, Amsterdam, **1988**; d) *Molecular Electronics—Science and Technology* (Ed.: A. Aviram), Engineering Foundation, New York, **1989**; e) *Molecular Electronics: Materials and Methods* (Ed.: P. I. Lazarev), Kluwer Academic Publishers, Dordrecht, **1991**; f) *Molecular Electronics—Science and Technology* (Ed.: A. Aviram), American Institute of Physics, Washington, **1992**; g) *Molecular Electronics* (Ed.: G. J. Ashwell), Wiley, New York, **1992**; h) *Molecular Electronics and Molecular Electronic Devices* (Ed.: K. Sienicki), CRC, Boca Raton, FL, **1993**; i) *Molecular and Biomolecular Electronics* (Ed.: R. R. Birge), American Chemical Society, Washington, **1994**; j) *Introduction to Molecular Electronic Devices* (Eds.: M. C. Petty, M. R. Bryce, D. Bloor), Oxford University Press, New York, **1995**; k) *Molecular Electronics* (Eds.: J. Jortner, M. Ratner), Blackwell Science, Oxford, **1997**; l) *Molecular Electronics: Science and Technology* (Eds.: A. Aviram, M. Ratner), New York Academy of Sciences, New York, **1998**; m) *Chem. Rev.* **1999**, 99, 1641–1990 (special issue on nanostructures); n) *Acc. Chem. Res.* **1999**, 32, 387–454 (special issue on nanoscale materials); o) *Handbook of Nanostructured Materials and Nanotechnology* (Ed.: H. S. Nalwa), Academic Press, New York, **2000**.
- [10] a) J. F. Stoddart, *Chem. Aust.* **1992**, 59, 576–577 and 581; b) V. Balzani, *Tetrahedron* **1992**, 48, 10443–10514; c) R. A. Bissell, A. P. de Silva, H. Q. N. Gunaratne, P. L. M. Lynch, G. E. M. Maguire, C. P. McCoy, K. R. A. S. Sandanayake, *Top. Curr. Chem.* **1993**, 168, 223–264; d) A. P. de Silva, C. P. McCoy, *Chem. Ind.* **1994**, 992–996; e) J. A. Preece, J. F. Stoddart, *Nanobiology* **1994**, 3, 149–166; f) L. Fabbri, A. Poggi, *Chem. Soc. Rev.* **1995**, 24, 197–202; g) J. A. Preece, J. F. Stoddart in *Ultimate Limits of Fabrication and Measurements* (Eds.: M. E. Welland, J. K. Gimzewski), Kluwer Academic, Dordrecht, **1996**, pp. 1–8; J. A. Preece, J. F. Stoddart in *Ultimate Limits of Fabrication and Measurements* (Eds.: M. E. Welland, J. K. Gimzewski), Kluwer Academic, Dordrecht, **1996**, pp. 225–228; h) A. C. Benniston, *Chem. Soc. Rev.* **1996**, 25, 427–435; i) M. Gómez-López, J. A. Preece, J. F. Stoddart, *Nanotechnology* **1996**, 7, 183–192; j) F. M. Raymo, J. F. Stoddart in *Magnetism: A Supramolecular Function* (Ed.: O. Kahn), Kluwer Academic, Dordrecht, **1996**, pp. 33–51; k) A. P. de Silva, H. Q. N. Gunaratne, T. Gunlaugsson, A. J. M. Huxley, C. P. McCoy, J. T. Rademacher, T. E. Rice, *Chem. Rev.* **1997**, 97, 1515–1566; l) M. D. Ward, *Chem. Ind.* **1997**, 640–645; m) M. Gómez-López, J. F. Stoddart, *Bull. Soc. Chim. Belg.* **1997**, 106, 491–500; n) P. D. Beer, *Acc. Chem. Res.* **1998**, 31, 71–80; o) T. M. Swager, *Acc. Chem. Res.* **1998**, 31, 201–207; p) V. Balzani, M. Gómez-López, J. F. Stoddart, *Acc. Chem. Res.* **1998**, 31, 405–414; q) J.-P. Sauvage, *Acc. Chem. Res.* **1998**, 31, 611–619; r) J.-C. Chambron, J.-P. Sauvage, *Chem. Eur. J.* **1998**, 4, 1362–1366; s) A. Niemz, V. M. Rotello, *Acc. Chem. Res.* **1999**, 32, 42–52; t) A. E. Kaifer, *Acc. Chem. Res.* **1999**, 32, 62–71; u) L. Fabbri, M. Licchelli, P. Pallavicini, *Acc. Chem. Res.* **1999**, 32, 846–853; v) D. A. Leigh, A. Murphy, *Chem. Ind.* **1999**, 178–183; w) P. Piotrowski, *Chem. Soc. Rev.* **1999**, 28, 143–150; x) M.-J. Blanco, M. C. Jiménez, J.-C. Chambron, V. Heitz, M. Linke, J.-P. Sauvage, *Chem. Soc. Rev.* **1999**, 28, 293–305; y) V. Balzani, A. Credi, M. Venturi in *Supramolecular Science: Where It Is and Where It Is Going* (Eds.: R. Ungaro, E. Dalcanele), Kluwer Academic, Dordrecht, **1999**, pp. 1–22; z) *Supramolecular Materials Design* (Eds.: W. Jones, C. N. R. Rao), Cambridge University Press, Cambridge, **2000**; aa) *Molecular Switches* (Ed.: B. L. Feringa), Wiley-VCH, Weinheim, **2000**; ab) M. D. Ward, *Chem. Ind.* **2000**, 22–26; ac) V. Balzani, A. Credi, M. Venturi in *Stimulating Concepts in Chemistry* (Eds.: M. Shibasaki, J. F. Stoddart, F. Vögtle), Wiley-VCH, Weinheim, **2000**, pp. 255–266. See also: “Molecular-Level Machines and Logic Gates”: A. Credi, Ph.D. thesis, Università di Bologna, **1998** (this dissertation can be downloaded from the internet at <http://www.ciam.unibo.it/photochem.html>).
- [11] The most authoritative and widely accepted definition (see ref. [5a] and J.-M. Lehn, *Angew. Chem.* **1990**, 102, 1347–1362; *Angew. Chem. Int. Ed. Engl.* **1990**, 29, 1304–1319) of supramolecular chemistry is “the chemistry beyond the molecule, bearing on the organized entities of higher complexity that result from the association of two or more chemical species held together by intermolecular forces.” On the basis of this definition, it is tempting to classify molecular machines as either molecular or supramolecular. However, it is not as simple and straightforward as one might think and so we avoid this classification. The fundamental nature of all the systems we discuss is their multicomponent nature. For any kind of device—be it macroscopic or otherwise—the observed function results from the cooperative interactions between the various component parts. See: a) V. Balzani, F. Scandola, *Supramolecular Photochemistry*, Horwood, Chichester, **1991**; b) J.-M. Lehn in *Organic Chemistry: Its Language and Its State of the Art* (Ed.: M. V. Kisakürek), VCH, Weinheim, **1993**, pp. 77–89; c) J.-M. Lehn, *Supramolecular Chemistry: Concepts and Perspectives*, VCH, Weinheim, **1995**; d) V. Balzani, A. Credi, F. Scandola in *Transition Metals in Supramolecular Chemistry* (Eds.: L. Fabbri, A. Poggi), Kluwer Academic Publishers, Dordrecht, **1994**, pp. 1–32; e) V. Balzani, F. Scandola, in *Comprehensive Supramolecular Chemistry, Vol. 10* (Eds.: J.-M. Lehn, J. L. Atwood, J. E. D. Davies, D. D. Macnicol, F. Vögtle), Pergamon, Oxford, **1996**, pp. 687–746; f) P. L. Bolas, M. Gómez-Kaifer, L. Echegoyen, *Angew. Chem.* **1998**, 110, 226–258; *Angew. Chem. Int. Ed.* **1998**, 37, 216–247; g) M. Venturi, A. Credi, V. Balzani, *Coord. Chem. Rev.* **1999**, 185/186, 233–256.
- [12] a) D. W. Urry, *Angew. Chem.* **1993**, 105, 859–883; *Angew. Chem. Int. Ed. Engl.* **1993**, 32, 819–841; b) J. Howard, *Nature* **1997**, 389, 561–567.
- [13] a) D. S. Goodsell, *Our Molecular Nature: The Body's Motors, Machines, and Messages*, Copernicus, New York, **1996**; b) R. D. Vall, R. A. Milligan, *Science* **2000**, 288, 88–95.
- [14] *Acc. Chem. Res.* **1996**, 29, 561–613 (special issue on single molecules and atoms).
- [15] a) W. E. Moerner, T. Basché, *Angew. Chem.* **1993**, 105, 537–557; *Angew. Chem. Int. Ed. Engl.* **1993**, 32, 457–476; b) W. E. Moerner, M. Orrit, *Science* **1999**, 283, 1670–1676; c) J. K. Gimzewski, C. Joachim, *Science* **1999**, 283, 1683–1688; d) S. Weiss, *Science* **1999**,

- 283, 1676–1683; e) P. Tamarat, A. Maali, B. Lounis, M. Orrit, *J. Phys. Chem. A* **2000**, *104*, 1–16.
- [16] a) R. Cross, T. Duncan, *J. Bioenerg. Biomem.* **1996**, *28*, 403–408; b) P. Boyer, *Biochim. Biophys. Acta*, **1993**, *1140*, 215–250; c) S. M. Block, *Nature* **1997**, *386*, 317–319; d) S. Engelbrecht, W. Junge, *FEBS Lett.* **1997**, *414*, 485–491; e) W. S. Allison, *Acc. Chem. Res.* **1998**, *31*, 819–826; f) T. Elston, H. Wang, G. Oster, *Nature* **1998**, *391*, 510–513; g) R. H. Fillingame, *Science* **1999**, *286*, 1687–1688; h) D. Stock, A. G. W. Leslie, J. E. Walker, *Science* **1999**, *286*, 1700–1704.
- [17] a) H. Noji, R. Yasuda, M. Yoshida, K. Kinoshita, Jr., *Nature* **1997**, *386*, 299–302; b) A. D. Mehta, M. Rief, J. A. Spudich, D. A. Smith, R. M. Simmons, *Science* **1999**, *283*, 1689–1695; c) Y. Sambongi, Y. Iko, M. Tanabe, H. Omote, A. Iwamoto-Kihara, I. Ueda, T. Yanagida, Y. Wada, M. Futai, *Science* **1999**, *286*, 1722–1724.
- [18] R. Yasuda, H. Noji, K. Kinoshita, Jr., M. Yoshida, *Cell* **1998**, *93*, 1117–1124.
- [19] J. T. Finer, R. M. Simmons, J. A. Spudich, *Nature* **1994**, *368*, 113–115.
- [20] a) K. Kitamura, M. Tokunaga, A. H. Iwane, T. Yanagida, *Nature* **1999**, *397*, 129–134; b) C. Veigel, L. M. Coluccio, J. D. Jontes, J. C. Sparrow, R. A. Milligan, J. E. Molloy, *Nature* **1999**, *398*, 530–533; c) A. L. Wells, A. W. Lin, L. Q. Chen, D. Safer, S. M. Chain, T. Hasson, B. I. Carragher, R. A. Milligan, H. L. Sweeney, *Nature* **1999**, *401*, 505–508; d) M. L. Walker, S. A. Burgess, J. R. Sellers, F. Wang, J. A. Hammiller III, J. Trinick, P. J. Knight, *Nature* **2000**, *405*, 804–807; e) S. A. Endow, H. Higuchi, *Nature* **2000**, *406*, 913–916.
- [21] M. D. Wang, M. J. Schnitzer, H. Yin, R. Landick, J. Gelles, S. M. Block, *Science* **1998**, *282*, 902–907.
- [22] J.-D. Huang, S. T. Brady, B. W. Richards, D. Stenoien, J. H. Resau, N. G. Copeland, N. A. Jenkins, *Nature* **1999**, *397*, 267–270.
- [23] For some excellent articles on the role of templating in reactions, see *Templated Organic Synthesis* (Eds.: F. Diederich, P. J. Stang), Wiley-VCH, Weinheim, **1999**.
- [24] a) D. H. Busch, N. A. Stephenson, *Coord. Chem. Rev.* **1990**, *100*, 119–154; b) D. H. Busch, *J. Inclusion Phenom. Mol. Recognit. Chem.* **1992**, *12*, 389–395; c) S. Anderson, H. L. Anderson, J. K. M. Sanders, *Acc. Chem. Res.* **1993**, *26*, 469–475; d) R. Cacciapaglia, L. Mandolini, *Chem. Soc. Rev.* **1993**, *22*, 221–231; e) R. Hoss, F. Vögtle, *Angew. Chem.* **1994**, *106*, 389–398; *Angew. Chem. Int. Ed. Engl.* **1994**, *33*, 375–384; f) J. P. Schneider, J. W. Kelly, *Chem. Rev.* **1995**, *95*, 2169–2187; g) F. M. Raymo, J. F. Stoddart, *Pure Appl. Chem.* **1996**, *68*, 313–322; h) T. J. Hubin, A. G. Kolchinski, A. L. Vance, D. L. Busch, *Adv. Supramol. Chem.* **1999**, *5*, 237–357.
- [25] a) G. Schill, *Catenanes, Rotaxanes and Knots*, Academic Press, New York, **1971**; b) *Molecular Catenanes, Rotaxanes and Knots* (Eds.: J.-P. Sauvage, C. O. Dietrich-Buchecker), Wiley-VCH, Weinheim, **1999**.
- [26] a) D. M. Walba, *Tetrahedron* **1985**, *41*, 3161–3212; b) C. O. Dietrich-Buchecker, J.-P. Sauvage, *Chem. Rev.* **1987**, *87*, 795–810; c) C. O. Dietrich-Buchecker, J.-P. Sauvage, *Bioorg. Chem. Front.* **1991**, *2*, 195–248; d) J.-C. Chambron, C. O. Dietrich-Buchecker, J.-P. Sauvage, *Top. Curr. Chem.* **1993**, *165*, 131–162; e) H. W. Gibson, H. Marand, *Adv. Mater.* **1993**, *5*, 11–21; f) H. W. Gibson, M. C. Bheda, P. T. Engen, *Prog. Polym. Sci.* **1994**, *19*, 843–945; g) D. B. Amabilino, I. W. Parsons, J. F. Stoddart, *Trends Polym. Sci.* **1994**, *2*, 146–152; h) D. B. Amabilino, J. F. Stoddart, *Chem. Rev.* **1995**, *95*, 2725–2828; i) H. W. Gibson in *Large Ring Molecules* (Ed.: J. A. Semlyen), Wiley, New York, **1996**, pp. 191–202; j) M. Belohradsky, F. M. Raymo, J. F. Stoddart, *Collect. Czech. Chem. Commun.* **1996**, *61*, 1–43; k) F. M. Raymo, J. F. Stoddart, *Trends Polym. Sci.* **1996**, *4*, 208–211; l) M. Belohradsky, F. M. Raymo, J. F. Stoddart, *Collect. Czech. Chem. Commun.* **1997**, *62*, 527–557; m) R. Jäger, F. Vögtle, *Angew. Chem.* **1997**, *109*, 966–980; *Angew. Chem. Int. Ed. Engl.* **1997**, *36*, 930–944; n) F. M. Raymo, J. F. Stoddart, *CHEMTRACTS: Org. Chem.* **1998**, *11*, 491–511; o) F. M. Raymo, J. F. Stoddart, *Chem. Rev.* **1999**, *99*, 1643–1664; p) G. A. Breault, C. A. Hunter, P. C. Mayers, *Tetrahedron* **1999**, *55*, 5265–5293; q) C. Seel, F. Vögtle, *Chem. Eur. J.* **2000**, *6*, 21–24; r) M. B. Nielsen, C. Lombolt, J. Becher, *Chem. Soc. Rev.* **2000**, *29*, 153–164.
- [27] a) D. B. Amabilino, P. R. Ashton, L. Pérez-García, J. F. Stoddart, *Angew. Chem.* **1995**, *107*, 2659–2572; *Angew. Chem. Int. Ed. Engl.* **1995**, *34*, 2378–2380; b) R. E. Gillard, F. M. Raymo, J. F. Stoddart, *Chem. Eur. J.* **1997**, *3*, 1933–1940; c) D. B. Amabilino, P. R. Ashton, J. F. Stoddart, A. J. P. White, D. J. Williams, *Chem. Eur. J.* **1998**, *4*, 460–468; d) S. J. Cantrill, S. J. Rowan, J. F. Stoddart, *Org. Lett.* **1999**, *1*, 1363–1366; e) S. J. Rowan, J. F. Stoddart, *Org. Lett.* **1999**, *1*, 1913–1916; f) M. Fujita, F. Ibukuro, H. Hagihara, K. Ogura, *Nature* **1994**, *367*, 720–723; g) B. Mohr, M. Weck, J.-P. Sauvage, R. H. Grubbs, *Angew. Chem.* **1997**, *109*, 1362–1365; *Angew. Chem. Int. Ed. Engl.* **1997**, *36*, 1301–1308; h) M. Weck, B. Mohr, J.-P. Sauvage, R. H. Grubbs, *J. Org. Chem.* **1999**, *64*, 5463–5471; i) M. Fujita, *Acc. Chem. Res.* **1999**, *32*, 53–61; j) F. Ibukuro, M. Fujita, K. Yamaguchi, J.-P. Sauvage, *J. Am. Chem. Soc.* **1999**, *121*, 11014–11015; k) A. C. Try, M. M. Harding, D. G. Hamilton, J. K. M. Sanders, *Chem. Commun.* **1998**, 723–724; l) T. J. Kidd, D. A. Leigh, A. J. Wilson, *J. Am. Chem. Soc.* **1999**, *121*, 1599–1600; m) A. J. Baer, D. H. Macartney, *Inorg. Chem.* **2000**, *39*, 1410–1517; n) K. Chichak, M. C. Walsh, N. R. Branda, *Chem. Commun.* **2000**, 847–848; o) K.-S. Jeong, J. S. Choi, S.-Y. Chang, H.-Y. Chang, *Angew. Chem.* **2000**, *112*, 1758–1761; *Angew. Chem. Int. Ed.* **2000**, *39*, 1692–1695.
- [28] a) J. S. Lindsey, *New J. Chem.* **1991**, *15*, 153–180; b) G. M. Whitesides, J. P. Mathias, C. T. Seto, *Science* **1991**, *254*, 1312–1319; c) D. Philp, J. F. Stoddart, *Synlett* **1991**, 445–458; d) G. M. Whitesides, E. E. Simanek, J. P. Mathias, C. T. Seto, D. N. Chin, M. Mammen, D. M. Gordon, *Acc. Chem. Res.* **1995**, *28*, 37–44; e) D. Philp, J. F. Stoddart, *Angew. Chem.* **1996**, *108*, 1242–1286; *Angew. Chem. Int. Ed. Engl.* **1996**, *35*, 1155–1196; f) J. Rebek, Jr., *Chem. Soc. Rev.* **1996**, *25*, 255–264; g) M. M. Conn, J. Rebek, Jr., *Chem. Rev.* **1997**, *97*, 1647–1668; h) J. Rebek, Jr., *Acc. Chem. Res.* **1999**, *32*, 278–286; i) M. C. T. Fyfe, J. F. Stoddart, *Adv. Supramol. Chem.* **1999**, *5*, 1–53; j) M. C. T. Fyfe, J. F. Stoddart, *Coord. Chem. Rev.* **1999**, *183*, 139–155; k) D. H. Gracias, J. Tien, T. L. Breen, C. Hsu, G. M. Whitesides, *Science* **2000**, *289*, 1170–1172.
- [29] M. C. T. Fyfe, J. F. Stoddart, *Acc. Chem. Res.* **1997**, *30*, 393–401.
- [30] In the context of classical stereochemical nomenclature (*Pure Appl. Chem.* **1976**, *45*, 13–30), the term “conformation” relates strictly to molecules. Thus, it describes “the different spatial arrangements of atoms in molecules that result solely from torsions (rotations) around single and/or partial double bonds”. This definition allows the liberal extension of the use of this term to describe isomerizations that occur on the excitation of formal double bonds, since, as a result of such activations, they assume considerable single bond character. Thus, the movements we will observe between the component parts of “traditional” molecules fall comfortably under the umbrella of conformational motions. However, when we enter the realm of supermolecules (complexes) and interlocked molecules with mechanical bonds, alterations in their shapes result, not so often from conformational changes within their covalently linked component parts, but more often than not from differences in the relative dispositions and orientations of the component parts that are also, to varying degrees, noncovalently bound to each other. Thus, we have advocated (M. C. T. Fyfe, P. T. Glink, S. Menzer, J. F. Stoddart, A. J. P. White, D. J. Williams, *Angew. Chem.* **1997**, *109*, 2158–2160; *Angew. Chem. Int. Ed. Engl.* **1997**, *36*, 2068–2070) the use of the term *co-conformation* to designate the different three-dimensional spatial arrangements of a) the constituent parts (for example, host and guest) in supramolecular systems and of b) the components of interlocked molecular systems. With few exceptions, the co-conformational changes observed in catenanes and rotaxanes are associated with very much larger amplitude motions than result from conformational changes, at least within relatively small molecules. Indeed, it is the co-conformational motions that can be induced in interlocked molecules that helps to make catenanes and rotaxanes such attractive molecules with which to design and construct molecular machinery.
- [31] a) P.-L. Anelli, N. Spencer, J. F. Stoddart, *J. Am. Chem. Soc.* **1991**, *113*, 5131–5133; b) P. L. Anelli, M. Asakawa, P. R. Ashton, R. A. Bissell, G. Clavier, R. Górski, A. E. Kaifer, S. J. Langford, G. Mattersteig, S. Menzer, D. Philp, A. M. Z. Slawin, N. Spencer, J. F. Stoddart, M. S. Tolley, D. J. Williams, *Chem. Eur. J.* **1997**, *3*, 1113–1135.
- [32] For an interesting quantum-mechanical description of the shuttling process associated with a [2]rotaxane, see D. A. Leigh, A. Troisi, F. Zerbetto, *Angew. Chem.* **2000**, *112*, 358–361; *Angew. Chem. Int. Ed.* **2000**, *39*, 350–353.
- [33] P. R. Ashton, D. Philp, N. Spencer, J. F. Stoddart, *J. Chem. Soc. Chem. Commun.* **1992**, 1124–1128.

- [34] For examples of solvent-induced co-conformational changes in [2]rotaxanes, see a) C. Gong, H. W. Gibson, *Angew. Chem.* **1997**, *109*, 2426–2428; *Angew. Chem. Int. Ed. Engl.* **1997**, *36*, 2331–2333; b) A. X. Lane, D. A. Leigh, A. Murphy, *J. Am. Chem. Soc.* **1997**, *119*, 11092–11093; c) W. Clegg, C. Gimenez-Saiz, D. A. Leigh, A. Murphy, A. M. Z. Slawin, S. J. Teat, *J. Am. Chem. Soc.* **1999**, *121*, 4124–4129.
- [35] A pseudorotaxane (P. R. Ashton, D. Philp, N. Spencer, J. F. Stoddart, *J. Chem. Soc. Chem. Commun.* **1991**, 1677–1679) is an interwoven inclusion complex in which a molecular thread is encircled by one or more beads (macrorings) so that the thread's extremities are directed away from the bead's center. At least one of the thread's extremities does not possess a bulky stopper group. Hence, the constituents of the assemblage, like any complex, are at liberty to dissociate into separate molecular species. In contrast with rotaxanes, there is no attendant mechanical bond to maintain the system's integrity.
- [36] a) P. R. Ashton, M. Belohradsky, D. Philp, J. F. Stoddart, *J. Chem. Soc. Chem. Commun.* **1993**, 1269–1274; b) P. R. Ashton, R. Ballardini, V. Balzani, M. Belohradsky, M. T. Gandolfi, D. Philp, L. Prodi, F. M. Raymo, M. V. Reddington, N. Spencer, J. F. Stoddart, M. Venturi, D. J. Williams, *J. Am. Chem. Soc.* **1996**, *118*, 4931–4951; c) M. Asakawa, P. R. Ashton, R. Ballardini, V. Balzani, M. Belohradsky, M. T. Gandolfi, O. Kocian, L. Prodi, F. M. Raymo, J. F. Stoddart, M. Venturi, *J. Am. Chem. Soc.* **1997**, *119*, 302–310; d) F. M. Raymo, J. F. Stoddart, *Pure Appl. Chem.* **1997**, *69*, 1987–1997; e) P. R. Ashton, I. Baxter, M. C. T. Fyfe, F. M. Raymo, N. Spencer, J. F. Stoddart, A. J. P. White, D. J. Williams, *J. Am. Chem. Soc.* **1998**, *120*, 2297–2307; f) F. M. Raymo, K. N. Houk, J. F. Stoddart, *J. Am. Chem. Soc.* **1998**, *120*, 9318–9322; g) M. C. T. Fyfe, F. M. Raymo, J. F. Stoddart, in *Stimulating Concepts in Chemistry* (Eds.: M. Shibasaki, J. F. Stoddart, F. Vögtle), Wiley-VCH, Weinheim, **2000**, pp. 211–220.
- [37] For computational analyses of the circumrotational processes associated with some catenanes, see a) D. A. Leigh, A. Murphy, J. P. Smart, M. S. Deleuze, F. Zerbetto, *J. Am. Chem. Soc.* **1998**, *120*, 6458–6467; b) F. M. Raymo, K. N. Houk, J. F. Stoddart, *J. Org. Chem.* **1998**, *63*, 6523–6528; c) M. S. Deleuze, D. A. Leigh, F. Zerbetto, *J. Am. Chem. Soc.* **1999**, *121*, 2364–2379; d) M. S. Deleuze, *J. Am. Chem. Soc.* **2000**, *122*, 1130–1143.
- [38] P. R. Ashton, T. T. Goodnow, A. E. Kaifer, M. V. Reddington, A. M. Z. Slawin, N. Spencer, J. F. Stoddart, C. Vicent, D. J. Williams, *Angew. Chem.* **1989**, *101*, 1404–1408; *Angew. Chem. Int. Ed. Engl.* **1989**, *28*, 1396–1399.
- [39] For an example of a [2]catenane that can exist in four different states, see P. R. Ashton, L. Pérez-García, J. F. Stoddart, A. J. P. White, D. J. Williams, *Angew. Chem.* **1995**, *107*, 607–610; *Angew. Chem. Int. Ed. Engl.* **1995**, *34*, 571–574.
- [40] For examples of solvent-induced co-conformational changes in [2]catenanes, see a) P. R. Ashton, M. Blower, D. Philp, N. Spencer, J. F. Stoddart, M. S. Tolley, *New J. Chem.* **1993**, *17*, 689–695; b) D. A. Leigh, K. Moody, J. P. Smart, K. J. Watson, A. M. Z. Slawin, *Angew. Chem.* **1996**, *108*, 326–331; *Angew. Chem. Int. Ed. Engl.* **1996**, *35*, 306–310; c) M. Asakawa, P. R. Ashton, W. Dehaen, G. L'abbé, S. Menzer, J. Nouwen, F. M. Raymo, J. F. Stoddart, M. S. Tolley, S. Toppet, A. J. P. White, D. J. Williams, *Chem. Eur. J.* **1997**, *3*, 772–787; d) R. Ballardini, V. Balzani, M. T. Gandolfi, R. E. Gillard, J. F. Stoddart, E. Tabellini, *Chem. Eur. J.* **1998**, *4*, 449–459.
- [41] M. R. Johnston, M. J. Gunter, R. Warrener, *Chem. Commun.* **1998**, 2739–2740.
- [42] a) J. Rebek, Jr., J. E. Trend, R. V. Wattle, S. Chakravorti, *J. Am. Chem. Soc.* **1979**, *101*, 4333–4337; b) J. Rebek, Jr., R. V. Wattle, *J. Am. Chem. Soc.* **1980**, *102*, 4853–4854; c) J. Rebek, Jr., L. Marshall, *J. Am. Chem. Soc.* **1983**, *105*, 6668–6670; d) J. Rebek, Jr., *Acc. Chem. Res.* **1984**, *17*, 258–264.
- [43] a) K. Mislow, *CHEMTRACTS: Org. Chem.* **1989**, *2*, 151–174; b) J. Vacek, J. Michl, *New J. Chem.* **1997**, *21*, 1259–1268.
- [44] a) O. S. Akkerman, J. Coops, *Rec. Trav. Chim. Pays-Bas* **1967**, *86*, 755–761; b) O. S. Akkerman, J. Coops, *Rec. Trav. Chim. Pays-Bas* **1970**, *89*, 673–679.
- [45] For other examples of two- and three-bladed molecular propellers, see a) M. Allen, R. Y. Moir, *Can. J. Chem.* **1959**, *37*, 1799–1809; b) D. Gust, K. Mislow, *J. Am. Chem. Soc.* **1973**, *95*, 1535–1547; c) P. Finocchiaro, D. Gust, K. Mislow, *J. Am. Chem. Soc.* **1974**, *96*, 3198–3205; d) K. Mislow, D. Gust, P. Finocchiaro, R. J. Boettcher, *Top. Curr. Chem.* **1974**, *47*, 1–28; e) P. Finocchiaro, *Gazz. Chim. Ital.* **1975**, *105*, 149–163; f) K. Mislow, *Acc. Chem. Res.* **1976**, *9*, 26–33; g) R. Glaser, J. F. Blount, K. Mislow, *J. Am. Chem. Soc.* **1980**, *102*, 2777–2786; h) W. Y. Lam, J. C. Martin, *J. Org. Chem.* **1981**, *46*, 4458–4462; i) W. Y. Lam, J. C. Martin, *J. Org. Chem.* **1981**, *46*, 4462–4468; j) R. William, M. Gielen, C. Hoogzand, H. Pepermans in *Advances in Dynamic Stereochemistry, Vol. 1* (Ed.: M. F. Gielen), Freund Publishing House, London, **1985**, chap. 5; k) W. Weissensteiner, J. Scharf, K. Schlögl, *J. Org. Chem.* **1987**, *52*, 1210–1215; l) S. E. Biali, D. A. Nugiel, Z. Rappoport, *J. Am. Chem. Soc.* **1989**, *111*, 846–852.
- [46] a) J. J. Bergman, W. D. Chandler, *Can. J. Chem.* **1972**, *50*, 353–363; b) H. Kwart, S. Alekman, *J. Am. Chem. Soc.* **1968**, *90*, 4482–4483.
- [47] a) Y. Kawada, H. Iwamura, *J. Org. Chem.* **1980**, *45*, 2547–2548; b) W. D. Hounshell, C. A. Johnson, A. Guenzi, F. Cozzi, K. Mislow, *Proc. Natl. Acad. Sci. USA* **1980**, *77*, 6961–6964; c) F. Cozzi, A. Guenzi, C. A. Johnson, K. Mislow, W. D. Hounshell, J. F. Blount, *J. Am. Chem. Soc.* **1981**, *103*, 957–958; d) Y. Kawada, H. Iwamura, *J. Am. Chem. Soc.* **1981**, *103*, 958–960; e) C. A. Johnson, A. Guenzi, K. Mislow, *J. Am. Chem. Soc.* **1981**, *103*, 6240–6242; f) Y. Kawada, H. Iwamura, *Tetrahedron Lett.* **1981**, *22*, 1533–1536; g) C. A. Johnson, A. Guenzi, R. B. Nachbar, Jr., J. F. Blount, O. Wennerström, K. Mislow, *J. Am. Chem. Soc.* **1982**, *104*, 5163–5168; h) H.-B. Bürgi, W. D. Hounshell, R. B. Nachbar, Jr., K. Mislow, *J. Am. Chem. Soc.* **1983**, *105*, 1427–1438; i) A. Guenzi, C. A. Johnson, F. Cozzi, K. Mislow, *J. Am. Chem. Soc.* **1983**, *105*, 1438–1448; j) Y. Kawada, H. Iwamura, *J. Am. Chem. Soc.* **1983**, *105*, 1449–1459; k) N. Koga, Y. Kawada, H. Iwamura, *J. Am. Chem. Soc.* **1983**, *105*, 5498–5499; l) Y. Kawada, Y. Okamoto, H. Iwamura, *Tetrahedron Lett.* **1983**, *24*, 5359–5362; m) H. Iwamura, T. Ito, H. Ito, K. Toriumi, Y. Kawada, E. Osawa, T. Fujiyoshi, C. Jaime, *J. Am. Chem. Soc.* **1984**, *106*, 4712–4717; n) N. Koga, H. Iwamura, *J. Am. Chem. Soc.* **1985**, *107*, 1426–1427; o) H. Iwamura, *J. Mol. Struct.* **1985**, *126*, 401–412; p) N. Koga, Y. Kawada, H. Iwamura, *Tetrahedron* **1986**, *42*, 1679–1686; q) Y. Kawada, H. Yamazaki, G. Koga, S. Murata, H. Iwamura, *J. Org. Chem.* **1986**, *51*, 1472–1477; r) N. Koga, H. Iwamura, *Chem. Lett.* **1986**, 247–250; s) Y. Kawada, J. Ishikawa, H. Yamazaki, G. Koga, S. Murata, H. Iwamura, *Tetrahedron Lett.* **1987**, *28*, 445–448; t) H. Iwamura, K. Mislow, *Acc. Chem. Res.* **1988**, *21*, 175–182.
- [48] For related examples, see a) M. Oki, *The Chemistry of Rotational Isomers*, Springer, Berlin, **1993**; b) P. Beak, S. T. Kerrick, D. J. Gallagher, *J. Am. Chem. Soc.* **1993**, *115*, 10628–10636; c) P. Bowles, J. Clayden, M. Tomkinson, *Tetrahedron Lett.* **1995**, *36*, 9219–9222; d) P. Bowles, J. Clayden, M. Helliwell, C. McCarthy, M. Tomkinson, N. Westlund, *J. Chem. Soc. Perkin Trans. 1* **1997**, 2607–2616; e) A. M. Stevens, C. J. Richards, *Tetrahedron Lett.* **1997**, *38*, 7805–7808; f) J. Clayden, J. H. Pink, S. A. Yasin, *Tetrahedron Lett.* **1998**, *39*, 105–108; g) J. Clayden, J. H. Pink, *Angew. Chem.* **1998**, *110*, 2040–2043; *Angew. Chem. Int. Ed.* **1998**, *37*, 1937–1939.
- [49] T. C. Bedard, J. S. Moore, *J. Am. Chem. Soc.* **1995**, *117*, 10662–10671.
- [50] For a discussion of the “turnstile mechanism”, see I. Ugi, D. Marquarding, H. Klusacek, P. Gillespie, F. Ramirez, *Acc. Chem. Res.* **1971**, *4*, 288–296.
- [51] For an example of the oscillation of two porphyrin ligands around a metal center, see K. Tashiro, T. Fujiwara, K. Konishi, T. Aida, *Chem. Commun.* **1998**, 1121–1222.
- [52] T. R. Kelly, M. C. Bowyer, K. V. Bhaskar, D. Bebbington, A. Garcia, F. Lang, M. H. Kim, M. P. Jette, *J. Am. Chem. Soc.* **1994**, *116*, 3657–3658.
- [53] a) A. P. Davis, *Angew. Chem.* **1998**, *110*, 953–954; *Angew. Chem. Int. Ed.* **1998**, *37*, 909–910; b) A. P. Davis, *Nature* **1999**, *401*, 120–121.
- [54] a) T. R. Kelly, I. Tellitu, J. P. Sestelo, *Angew. Chem.* **1997**, *109*, 1969–1972; *Angew. Chem. Int. Ed. Engl.* **1997**, *36*, 1866–1868; b) T. R. Kelly, J. P. Sestelo, I. Tellitu, *J. Org. Chem.* **1998**, *63*, 3655–3665.
- [55] a) T. R. Kelly, H. De Silva, R. A. Silva, *Nature* **1999**, *401*, 150–152; b) T. R. Kelly, R. A. Silva, H. De Silva, S. Jasmin, Y. Zhao, *J. Am. Chem. Soc.* **2000**, *122*, 6935–6949.
- [56] An example of electrochemically controlled assembly/disassembly processes with copper ions and a polytopic ligand has been recently reported. See V. Amendola, L. Fabbri, L. Linati, C. Mangano, P.

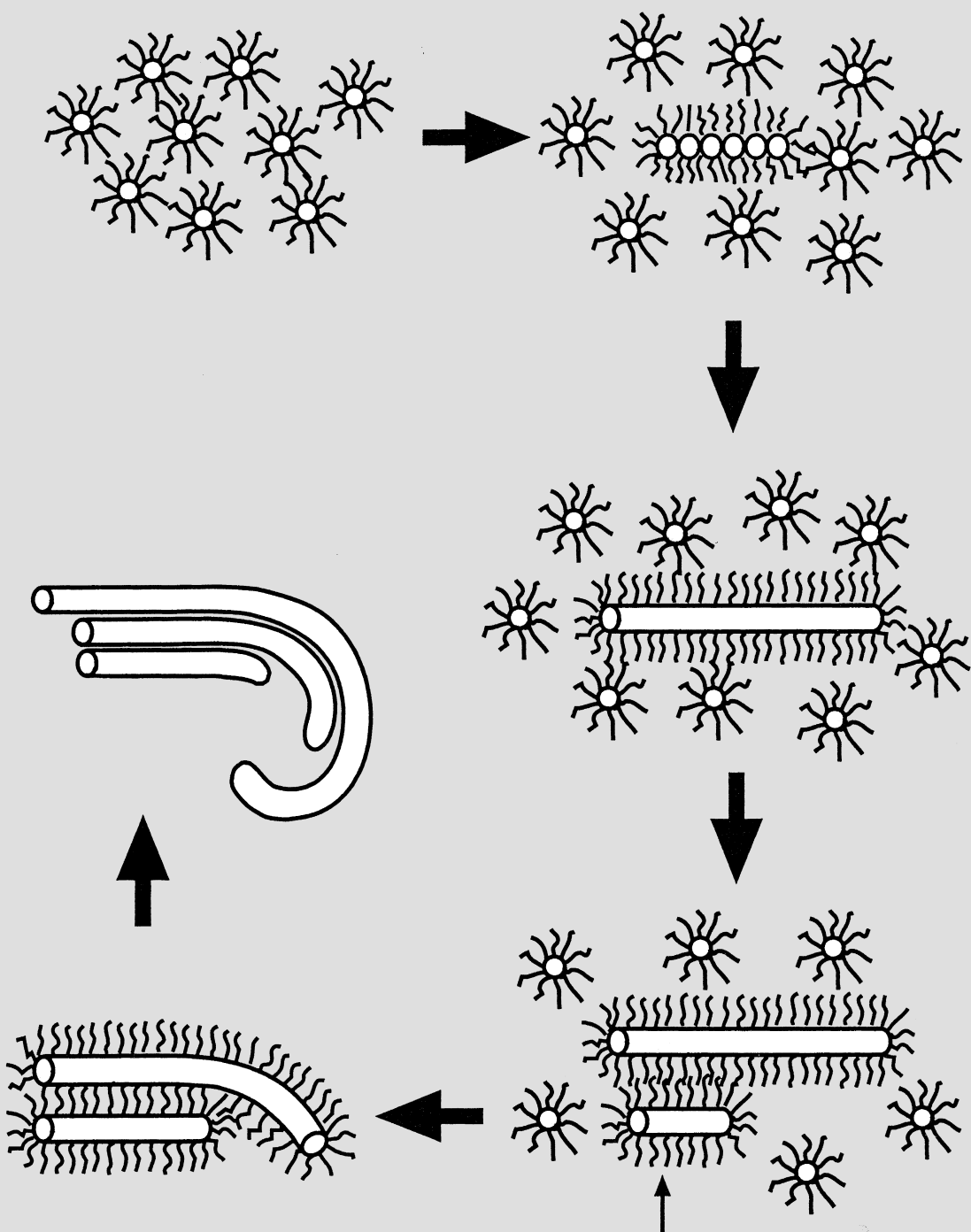
- Pallavicini, V. Pedrazzini, M. Zema, *Chem. Eur. J.* **1999**, *5*, 3679–3688.
- [57] P. R. Ashton, R. Ballardini, V. Balzani, S. E. Boyd, A. Credi, M. T. Gandolfi, M. Gómez-López, S. Iqbal, D. Philp, J. A. Preece, L. Prodi, H. G. Ricketts, J. F. Stoddart, M. S. Tolley, M. Venturi, A. J. P. White, D. J. Williams, *Chem. Eur. J.* **1997**, *3*, 152–170.
- [58] For related self-complexing compounds, see a) P. R. Ashton, M. Gómez-López, S. Iqbal, J. A. Preece, J. F. Stoddart, *Tetrahedron Lett.* **1997**, *38*, 3635–3638; b) M. B. Nielsen, S. B. Nielsen, J. Becher, *Chem. Commun.* **1998**, 475–476; c) M. B. Nielsen, J. G. Hansen, J. Becher, *Eur. J. Org. Chem.* **1999**, 2807–2815.
- [59] For a system showing a similar conformational change, see L. Fabbri, M. Licchelli, P. Pallavicini, L. Parodi, *Angew. Chem.* **1998**, *110*, 838–841; *Angew. Chem. Int. Ed.* **1998**, *37*, 800–802.
- [60] a) B. Wegewijs, R. M. Hermant, J. W. Verhoeven, A. G. M. Kunst, R. P. H. Rettschnick, *Chem. Phys. Lett.* **1987**, *140*, 587–590; b) X. Y. Lauteslager, M. J. Bartels, J. J. Pier, J. M. Warman, J. W. Verhoeven, A. M. Brouwer, *Eur. J. Org. Chem.* **1998**, 2467–2481; c) X. Y. Lauteslager, I. H. M. van Stokkum, H. J. van Ramesdonk, A. M. Brouwer, J. W. Verhoeven, *J. Phys. Chem. A* **1999**, *103*, 653–659.
- [61] a) I. Willner, S. Rubin, *Angew. Chem.* **1996**, *108*, 419–439; *Angew. Chem. Int. Ed. Engl.* **1996**, *35*, 367–385; b) I. Willner, *Acc. Chem. Res.* **1997**, *30*, 347–356; c) H. Asanuma, X. Liang, T. Yoshida, A. Yamazawa, M. Komiyama, *Angew. Chem.* **2000**, *112*, 1372–1374; *Angew. Chem. Int. Ed.* **2000**, *39*, 1316–1318.
- [62] a) M. Irie, *Adv. Polym. Sci.* **1990**, *94*, 27–67; b) B. L. Feringa, W. F. Jager, B. de Lange, *Tetrahedron* **1993**, *49*, 8267–8310; c) J. I. Anzai, T. Osa, *Tetrahedron* **1994**, *50*, 4039–4070.
- [63] a) F. Vögtle, *Supramolecular Chemistry*, Wiley, New York, **1991**, chap. 7; b) S. Shinkai in *Comprehensive Supramolecular Chemistry*, Vol. 1 (Eds.: J.-M. Lehn, J. L. Atwood, J. E. D. Davies, D. D. MacNicol, F. Vögtle), Pergamon, Oxford, **1996**, pp. 671–700.
- [64] For the photochemical control of the catalytic activity of a synthetic receptor, see F. Würthner, J. Rebek, Jr., *J. Chem. Soc. Perkin Trans. 2* **1995**, 1727–1734.
- [65] S. Shinkai, T. Minami, Y. Kusano, O. Manabe, *J. Am. Chem. Soc.* **1983**, *105*, 1851–1856.
- [66] For related examples, see a) M. Shiga, M. Takagi, K. Ueno, *Chem. Lett.* **1980**, 1021–1022; b) J. F. Biernat, E. Luboch, A. Cygan, Y. A. Simonov, A. A. Dvornik, E. Muszalska, R. Bilewicz, *Tetrahedron* **1992**, *48*, 4399–4406.
- [67] a) K. H. Neumann, F. Vögtle, *J. Chem. Soc. Chem. Commun.* **1988**, 520–522; b) S. Shinkai, A. Yoshioka, H. Nakayama, O. Manabe, *J. Chem. Soc. Perkin Trans. 2* **1990**, 1905–1909; c) N. Tamaoki, K. Koseki, T. Yamaoka, *Angew. Chem.* **1990**, *102*, 66–67; *Angew. Chem. Int. Ed. Engl.* **1990**, *29*, 105–106; d) N. Tamaoki, K. Koseki, T. Yamaoka, *Tetrahedron Lett.* **1990**, *31*, 3309–3312.
- [68] a) S. Shinkai, T. Ogawa, Y. Kusano, O. Manabe, *Chem. Lett.* **1980**, 283–286; b) S. Shinkai, T. Nakai, T. Ogawa, K. Shigematsu, O. Manabe, *J. Am. Chem. Soc.* **1981**, *103*, 111–115; c) S. Shinkai, K. Shigematsu, Y. Kusano, O. Manabe, *J. Chem. Soc. Perkin Trans. 1* **1981**, 3279–3283; d) S. Shinkai, T. Ogawa, Y. Kusano, O. Manabe, K. Kikukawa, T. Goto, T. Masuda, *J. Am. Chem. Soc.* **1982**, *104*, 1960–1967; e) S. Shinkai, Y. Honda, Y. Kusano, O. Manabe, *J. Chem. Soc. Chem. Commun.* **1982**, 848–850; f) S. Shinkai, Y. Honda, T. Minami, K. Ueda, O. Manabe, M. Tashiro *Bull. Chem. Soc. Jpn.* **1983**, *56*, 1700–1704; g) S. Shinkai, Y. Honda, K. Ueda, O. Manabe, *Isr. J. Chem.* **1984**, *24*, 302–306; h) S. Shinkai, T. Yoshida, O. Manabe, F. Fuchita, *J. Chem. Soc. Perkin Trans. 1* **1988**, 1431–1437; i) H. Shinmori, M. Takeuchi, S. Shinkai, *J. Chem. Soc. Perkin Trans. 2* **1998**, 847–852.
- [69] For phototweezers based on the photoisomerization of diarylethene compounds, see a) M. Takeshita, K. Uchida, M. Irie, *Chem. Commun.* **1996**, 1807–1808; b) M. Takeshita, M. Irie, *J. Org. Chem.* **1998**, *63*, 6643–6649; c) M. Takeshita, M. Irie, *Tetrahedron Lett.* **1998**, *39*, 613–616.
- [70] S. Shinkai, M. Ishihara, K. Ueda, O. Manabe, *J. Chem. Soc. Perkin Trans. 2* **1985**, 511–518.
- [71] For a related example, see S. Shinkai, T. Minami, Y. Kusano, O. Manabe, *J. Am. Chem. Soc.* **1982**, *104*, 1967–1972.
- [72] B. L. Feringa, W. F. Jager, B. de Lange, A. W. Meijer, *J. Am. Chem. Soc.* **1991**, *113*, 5468–5470.
- [73] For related examples, see a) W. F. Jager, J. C. de Jong, B. de Lange, N. P. M. Huck, A. Meetsma, B. L. Feringa, *Angew. Chem.* **1995**, *107*, 346–349; *Angew. Chem. Int. Ed. Engl.* **1995**, *34*, 348–350; b) B. L. Feringa, N. P. M. Huck, H. A. van Doren, *J. Am. Chem. Soc.* **1995**, *117*, 9929–9930; c) B. L. Feringa, N. P. M. Huck, A. M. Schoevaars, *Adv. Mater.* **1996**, *8*, 681–684; d) N. P. M. Huck, W. F. Jager, B. de Lange, B. L. Feringa, *Science* **1996**, *273*, 1686–1688; e) A. M. Schoevaars, W. Kruizinga, R. W. J. Zijlstra, N. Veldman, A. L. Spek, B. L. Feringa, *J. Org. Chem.* **1997**, *62*, 4943–4948.
- [74] a) N. Koumura, R. W. J. Zijlstra, R. A. van Delden, N. Harada, B. L. Feringa, *Nature* **1999**, *401*, 152–155; b) B. L. Feringa, R. A. van Delden, N. Koumura, E. M. Geertsema, *Chem. Rev.* **2000**, *100*, 1789–1816.
- [75] C. O. Dietrich-Buchecker, J.-P. Sauvage, J.-P. Kintzinger, *Tetrahedron Lett.* **1983**, *24*, 5095–5098.
- [76] J.-C. Chambrun, C. O. Dietrich-Buchecker, J.-F. Nierengarten, J.-P. Sauvage, N. Soolladić, A. M. Albrecht-Gary, M. Meyer, *New J. Chem.* **1995**, *19*, 409–426.
- [77] a) L. Zelikovich, J. Libman, A. Shanzer, *Nature* **1995**, *374*, 790–792; b) T. R. Ward, A. Lutz, S. P. Parel, J. Ensling, P. Gütlisch, P. Buglyó, C. Orvig, *Inorg. Chem.* **1999**, *38*, 5007–5017.
- [78] For an example of pH-controlled cation translocation, see V. Amendola, L. Fabbri, C. Mangano, P. Pallavicini, A. Perotti, A. Taglietti, *J. Chem. Soc. Dalton Trans.* **2000**, 185–186. Another novel strategy, using redox-switched, exciton-coupled circular dichroism, has been employed with a Cu⁺/Cu^{II} complex system to develop a binary molecular device. See: S. Zahn, J. W. Canary, *Angew. Chem.* **1998**, *110*, 321–323; *Angew. Chem. Int. Ed.* **1998**, *37*, 305–307.
- [79] a) A. G. Kolchinski, D. H. Busch, N. W. Alcock, *J. Chem. Soc. Chem. Commun.* **1995**, 1289–1291; b) P. R. Ashton, P. J. Campbell, E. J. T. Chrystal, P. T. Glink, S. Menzer, D. Philp, N. Spencer, J. F. Stoddart, P. A. Tasker, D. J. Williams, *Angew. Chem.* **1995**, *107*, 1997–2001; *Angew. Chem. Int. Ed. Engl.* **1995**, *34*, 1865–1869; c) P. R. Ashton, E. J. T. Chrystal, P. T. Glink, S. Menzer, C. Schiavo, N. Spencer, J. F. Stoddart, P. A. Tasker, A. J. P. White, D. J. Williams, *Chem. Eur. J.* **1996**, *2*, 709–728; d) P. T. Glink, C. Schiavo, J. F. Stoddart, D. J. Williams, *Chem. Commun.* **1996**, 1483–1490.
- [80] Very recently, the thermoregulated threading/dethreading of a diammonium guest into crown ethers appended to peptides has been exploited to change the optical properties of the peptide chain. See: J.-C. Meillon, N. Voyer, E. Biron, F. Sanschagrin, J. F. Stoddart, *Angew. Chem.* **2000**, *112*, 147–149; *Angew. Chem. Int. Ed.* **2000**, *39*, 143–145.
- [81] For other examples of acid/base-switchable supramolecular complexes, see a) F. Ibukuro, T. Kusukawa, M. Fujita, *J. Am. Chem. Soc.* **1998**, *120*, 856–8562; b) D. Whang, J. Heo, J. H. Park, K. Kim, *Angew. Chem.* **1998**, *110*, 83–85; *Angew. Chem. Int. Ed.* **1998**, *37*, 78–80; c) G. Pistolis, A. Malliaris, D. Tsiourvas, C. M. Paleos, *Chem. Eur. J.* **1999**, *5*, 1440–1444.
- [82] The ability of some anions to form ion pairs with ammonium cations in nonpolar solvents can be exploited (see below in this section) to drive the dethreading of pseudorotaxanes.
- [83] a) M. Montalti, R. Ballardini, L. Prodi, V. Balzani, *Chem. Commun.* **1996**, 2011–2012; b) P. R. Ashton, R. Ballardini, V. Balzani, M. Gómez-López, S. E. Lawrence, M.-V. Martínez-Díaz, M. Montalti, A. Piersanti, L. Prodi, J. F. Stoddart, D. J. Williams, *J. Am. Chem. Soc.* **1997**, *119*, 10641–10651; c) P. R. Ashton, R. Ballardini, V. Balzani, M. C. T. Fyfe, M. T. Gandolfi, M. V. Martínez-Díaz, M. Morosini, C. Schiavo, K. Shibata, J. F. Stoddart, A. J. P. White, D. J. Williams, *Chem. Eur. J.* **1998**, *4*, 2332–2341.
- [84] a) E. Ishow, A. Credi, V. Balzani, F. Spadola, L. Mandolini, *Chem. Eur. J.* **1999**, *5*, 984–989; b) S. J. Cantrill, M. C. T. Fyfe, A. M. Heiss, J. F. Stoddart, A. J. P. White, D. J. Williams, *Chem. Commun.* **1999**, 1251–1252.
- [85] F. Diederich, L. Echegoyen, M. Gómez-López, R. Kessinger, J. F. Stoddart, *J. Chem. Soc. Perkin Trans. 2* **1999**, 1577–1586.
- [86] M. Montalti, L. Prodi, *Chem. Commun.* **1998**, 1461–1462.
- [87] R. Castro, L. A. Godínez, C. M. Criss, A. E. Kaifer, *J. Org. Chem.* **1997**, *62*, 4928–4935.
- [88] For computational modeling of host–guest complexes of 25⁴⁺ with aromatic π -electron-rich species, see G. A. Kaminski, W. L. Jorgensen, *J. Chem. Soc. Perkin Trans. 2* **1999**, 2365–2375.

- [89] a) C. A. Hunter, J. K. M. Sanders, *J. Am. Chem. Soc.* **1990**, *112*, 5525–5534; b) M. H. Schwartz, *J. Inclusion Phenom. Mol. Recognit. Chem.* **1990**, *9*, 1–35; c) J. H. Williams, *Acc. Chem. Res.* **1993**, *26*, 593–598; d) C. A. Hunter, *Angew. Chem.* **1993**, *105*, 1653–1655; *Angew. Chem. Int. Ed. Engl.* **1993**, *32*, 1584–1586; e) C. A. Hunter, *J. Mol. Biol.* **1993**, *230*, 1025–1054; f) T. Dahl, *Acta Chem. Scand.* **1994**, *48*, 95–116; g) F. Cozzi, J. S. Siegel, *Pure Appl. Chem.* **1995**, *67*, 683–689; h) C. G. Claessens, J. F. Stoddart, *J. Phys. Org. Chem.* **1997**, *10*, 254–272.
- [90] a) G. R. Desiraju, *Acc. Chem. Res.* **1991**, *24*, 290–296; b) G. R. Desiraju, *Acc. Chem. Res.* **1996**, *29*, 441–449; c) T. Steiner, *Chem. Commun.* **1997**, 727–734; d) I. Berger, M. Egli, *Chem. Eur. J.* **1997**, *3*, 1400–1404.
- [91] a) M. Oki, *Acc. Chem. Res.* **1990**, *23*, 351–356; b) M. C. Etter, *J. Phys. Chem.* **1991**, *95*, 4601–4610; c) M. J. Zaworotko, *Chem. Soc. Rev.* **1994**, *23*, 283–288; d) M. Nishio, Y. Umezawa, M. Hirota, Y. Takeuchi, *Tetrahedron* **1995**, *51*, 8665–8701; e) M. Nishio, Y. Umezawa, M. Hirota, *The C–H... π Interaction*, Wiley-VCH, New York, **1998**; f) Y. Umezawa, S. Tsuboyama, H. Takahashi, J. Uzawa, M. Nishio, *Tetrahedron* **1999**, *55*, 10047–10056; g) H. Takahashi, S. Tsuboyama, Y. Umezawa, K. Honda, M. Nishio, *Tetrahedron* **2000**, *56*, 6185–6191.
- [92] R. Ballardini, V. Balzani, A. Credi, M. T. Gandolfi, S. J. Langford, S. Menzer, L. Prodi, J. F. Stoddart, M. Venturi, D. J. Williams, *Angew. Chem.* **1996**, *108*, 1056–1059; *Angew. Chem. Int. Ed. Engl.* **1996**, *35*, 978–981.
- [93] A. Credi, M. Montalti, V. Balzani, S. J. Langford, F. M. Raymo, J. F. Stoddart, *New J. Chem.* **1998**, *22*, 1061–1065.
- [94] A. Credi, V. Balzani, S. J. Langford, J. F. Stoddart, *J. Am. Chem. Soc.* **1997**, *119*, 2679–2681.
- [95] For other recent examples of the implementation of logic functions with molecular systems, see a) A. P. de Silva, H. Q. N. Gunaratne, C. P. McCoy, *J. Am. Chem. Soc.* **1997**, *119*, 7891–7892; b) A. P. de Silva, I. M. Dixon, H. Q. N. Gunaratne, T. Gunnlaugsson, P. R. S. Maxwell, T. E. Rice, *J. Am. Chem. Soc.* **1999**, *121*, 1393–1394; c) F. Pina, M. Maestri, V. Balzani, *Chem. Commun.* **1999**, 107–114; d) T. Gunnlaugsson, D. A. Mac Dónail, D. Parker, *Chem. Commun.* **2000**, 93–94; e) A. P. de Silva, N. D. McClenaghan, *J. Am. Chem. Soc.* **2000**, *122*, 3965–3966; f) A. P. de Silva, D. B. Fox, T. S. Moody in *Stimulating Concepts in Chemistry* (Eds.: M. Shibasaki, J. F. Stoddart, F. Vögtle), Wiley-VCH, Weinheim, **2000**, pp. 307–315.
- [96] D. Philp, A. M. Z. Slawin, N. Spencer, J. F. Stoddart, D. J. Williams, *J. Chem. Soc. Chem. Commun.* **1991**, 1584–1586.
- [97] a) M. Asakawa, P. R. Ashton, V. Balzani, A. Credi, G. Mattersteig, O. A. Matthews, M. Montalti, N. Spencer, J. F. Stoddart, M. Venturi, *Chem. Eur. J.* **1997**, *3*, 1992–1996; b) M. Asakawa, P. R. Ashton, V. Balzani, S. E. Boyd, A. Credi, G. Mattersteig, S. Menzer, M. Montalti, F. M. Raymo, C. Ruffilli, J. F. Stoddart, M. Venturi, D. J. Williams, *Eur. J. Org. Chem.* **1999**, 985–994; c) V. Balzani, A. Credi, G. Mattersteig, O. A. Matthews, F. M. Raymo, J. F. Stoddart, M. Venturi, A. J. P. White, D. J. Williams, *J. Org. Chem.* **2000**, *65*, 1924–1936.
- [98] P. R. Ashton, S. Iqbal, J. F. Stoddart, N. D. Tinker, *Chem. Commun.* **1996**, 479–481.
- [99] M. Asakawa, S. Iqbal, J. F. Stoddart, N. D. Tinker, *Angew. Chem.* **1996**, *108*, 1054–1056; *Angew. Chem. Int. Ed. Engl.* **1996**, *35*, 976–978.
- [100] O. A. Matthews, F. M. Raymo, J. F. Stoddart, A. J. P. White, D. J. Williams, *New J. Chem.* **1998**, *22*, 1131–1134.
- [101] Y.-A. Ikeda, T. Tsudera, S. Shinkai, *J. Org. Chem.* **1997**, *62*, 3568–3574.
- [102] A. E. Kaifer, *Supramolecular Electrochemistry*, Wiley-VCH, Weinheim, **1999**.
- [103] a) K. A. Connors, *Chem. Rev.* **1997**, *97*, 1325–1357; b) *Comprehensive Supramolecular Chemistry, Vol. 3* (Eds.: J.-M. Lehn, J. L. Atwood, J. E. D. Davies, D. D. Macnicol, F. Vögtle), Pergamon, Oxford, **1996**.
- [104] a) A. Mirzoian, A. E. Kaifer, *Chem. Eur. J.* **1997**, *3*, 1052–1057; b) A. Mirzoian, A. E. Kaifer, *Chem. Commun.* **1999**, 1603–1604.
- [105] Y. Wang, S. Mendoza, A. E. Kaifer, *Inorg. Chem.* **1998**, *37*, 317–320.
- [106] a) B. Siegel, R. Breslow, *J. Am. Chem. Soc.* **1975**, *97*, 6869–6870; b) R. Breslow, M. F. Czarniecki, J. Emert, H. Hamaguchi, *J. Am. Chem. Soc.* **1980**, *102*, 762–770; c) H.-J. Thiem, M. Brandl, R. Breslow, *J. Am. Chem. Soc.* **1988**, *110*, 8612–8616; d) A. Harada, S. Takahashi, *J. Chem. Soc. Chem. Commun.* **1984**, 645–646; e) A. Harada, S. Takahashi, *J. Inclusion Phenom. Mol. Recognit. Chem.* **1984**, *2*, 791–798; f) T. Matsue, T. Osa, D. H. Evans, *J. Inclusion Phenom. Mol. Recognit. Chem.* **1984**, *2*, 547–554; g) T. Matsue, D. H. Evans, T. Osa, N. Kobayashi, *J. Am. Chem. Soc.* **1985**, *107*, 3411–3417; h) A. Ueno, F. Moriwaki, T. Osa, F. Hamada, K. Murai, *Tetrahedron Lett.* **1985**, *26*, 899–902; i) T. Matsue, T. Kato, U. Akiba, T. Osa, *Chem. Lett.* **1986**, 843–846; j) T. Osa, N. Kobayashi, *Chem. Lett.* **1986**, 421–424; k) A. Ueno, I. Suzuki, T. Osa, *Makromol. Chem. Rapid Commun.* **1987**, *8*, 131–134; l) F. M. Menger, M. J. Sherrod, *J. Am. Chem. Soc.* **1988**, *110*, 8606–8611; m) R. Isnin, C. Salam, A. E. Kaifer, *J. Org. Chem.* **1991**, *56*, 35–41; n) R. Isnin, A. E. Kaifer, *J. Am. Chem. Soc.* **1991**, *113*, 8188–8190; o) L. A. Godínez, S. Patel, C. M. Criss, A. E. Kaifer, *J. Phys. Chem.* **1995**, *99*, 17449–17455; p) R. M. Nielson, L. A. Lyon, J. T. Hupp, *Inorg. Chem.* **1996**, *35*, 970–973; q) Y. M. Li, X. J. Yao, X. Feng, X. M. Wang, J. T. Wang, *J. Organomet. Chem.* **1996**, *509*, 221–224; r) J. S. Wu, K. Toda, A. Tanaka, I. Sanemasa, *Bull. Chem. Soc. Jpn.* **1998**, 1615–1618; s) R. C. Sabapathy, S. Bhattacharyya, W. E. Cleland, C. L. Hussey, *Langmuir* **1998**, *14*, 3797–3807; t) H. X. Ju, D. Leech, *Langmuir* **1998**, *14*, 300–306.
- [107] R. Castro, I. Cuadrado, B. Alonso, C. M. Casado, M. Mórán, A. E. Kaifer, *J. Am. Chem. Soc.* **1997**, *119*, 5760–5761.
- [108] B. González, C. M. Casado, B. Alonso, I. Cuadrado, M. Mórán, Y. Wang, A. E. Kaifer, *Chem. Commun.* **1998**, 2569–2570.
- [109] L. Zhang, A. Macías, T. Lu, J. I. Gordon, G. W. Gokel, A. E. Kaifer, *J. Chem. Soc. Chem. Commun.* **1993**, 1017–1019.
- [110] Y. Wang, J. Alvarez, A. E. Kaifer, *Chem. Commun.* **1998**, 1457–1458.
- [111] A. R. Bernardo, T. Lu, E. Córdova, L. Zhang, G. W. Gokel, A. E. Kaifer, *J. Chem. Soc. Chem. Commun.* **1994**, 529–530.
- [112] For a related redox-switchable three-component system, see R. Deans, A. Niemz, E. C. Breinlinger, V. M. Rotello, *J. Am. Chem. Soc.* **1997**, *119*, 10863–10864.
- [113] E. M. Seward, R. B. Hopkins, W. Sauerer, S.-W. Tam, F. Diederich, *J. Am. Chem. Soc.* **1990**, *112*, 1783–1790.
- [114] a) M. Sano, H. Taube, *J. Am. Chem. Soc.* **1991**, *113*, 2327–2328; b) M. Sano, H. Taube, *Inorg. Chem.* **1994**, *33*, 705–709; c) J. A. Wytko, C. Boudon, J. Weiss, M. Gross, *Inorg. Chem.* **1996**, *35*, 4469–4477; d) A. Tomita, M. Sano, *Inorg. Chem.* **2000**, *39*, 200–205.
- [115] C. Belle, J.-L. Pierre, E. Saint-Aman, *New J. Chem.* **1998**, *22*, 1399–1402.
- [116] a) L. Fabbri, F. Gatti, P. Pallavicini, E. Zambbarbieri, *Chem. Eur. J.* **1999**, *5*, 682–690; b) G. De Santis, L. Fabbri, D. Iacopino, P. Pallavicini, A. Perotti, A. Poggi, *Inorg. Chem.* **1997**, *36*, 827–832.
- [117] a) P.-L. Anelli, P. R. Ashton, R. Ballardini, V. Balzani, M. Delgado, M. T. Gandolfi, T. T. Goodnow, A. E. Kaifer, D. Philp, M. Pietraszkiewicz, L. Prodi, M. V. Reddington, A. M. Z. Slawin, N. Spencer, J. F. Stoddart, C. Vicent, D. J. Williams, *J. Am. Chem. Soc.* **1992**, *114*, 193–218; b) E. A. Smith, R. R. Lilienthal, R. J. Fonseca, D. K. Smith, *Anal. Chem.* **1994**, *66*, 3013–3020.
- [118] a) E. Córdova, R. A. Bissell, N. Spencer, P. R. Ashton, J. F. Stoddart, A. E. Kaifer, *J. Org. Chem.* **1993**, *58*, 6550–6552; b) W. Devonport, M. A. Blower, M. R. Bryce, L. M. Goldenberg, *J. Org. Chem.* **1997**, *62*, 885–887.
- [119] D. H. Evans, *Chem. Rev.* **1990**, *90*, 739–751.
- [120] The rate constants of such motions can be obtained by digital simulation of the experimental voltammetric patterns. See, for example, ref. [104a].
- [121] V. Balzani, J. Becher, A. Credi, M. B. Nielsen, F. M. Raymo, J. F. Stoddart, A. M. Talarico, M. Venturi, *J. Org. Chem.* **2000**, *65*, 1947–1956.
- [122] a) P. R. Ashton, S. Menzer, F. M. Raymo, G. K. H. Shimizu, J. F. Stoddart, D. J. Williams, *Chem. Commun.* **1996**, 487–490; b) M. Asakawa, P. R. Ashton, S. Menzer, F. M. Raymo, J. F. Stoddart, A. J. P. White, D. J. Williams, *Chem. Eur. J.* **1996**, *2*, 877–893.
- [123] P. R. Ashton, V. Balzani, J. Becher, A. Credi, M. C. T. Fyfe, G. Mattersteig, S. Menzer, M. B. Nielsen, F. M. Raymo, J. F. Stoddart, M. Venturi, D. J. Williams, *J. Am. Chem. Soc.* **1999**, *121*, 3951–3957.
- [124] The three-pole nature of this system is clearly apparent if compared to the two-pole nature of other three-component systems.^[11g, 93, 110, 112]

- [125] a) G. S. Kumar, D. C. Neckers, *Chem. Rev.* **1989**, 89, 1915–1925; b) H. Rau in *Photochromism: Molecules and Systems* (Eds.: H. Dürr, H. Bouas-Laurent), Elsevier, Amsterdam, **1990**, chap. 4.
- [126] For recent examples of photoswitchable supramolecular systems based on azobenzene, see a) A. Archut, F. Vögtle, L. De Cola, G. C. Azzellini, V. Balzani, P. S. Ramanujam, R. H. Berg, *Chem. Eur. J.* **1998**, 4, 699–706; b) A. Bencini, M. A. Bernardo, A. Bianchi, M. Ciampolini, V. Fusi, N. Nardi, A. J. Parola, F. Pina, B. Valtancoli, *J. Chem. Soc. Perkin Trans. 2* **1998**, 413–418; c) A. Archut, G. C. Azzellini, V. Balzani, L. De Cola, F. Vögtle, *J. Am. Chem. Soc.* **1998**, 120, 12187–12191; d) D. G. Walter, D. J. Campbell, C. A. Mirkin, *J. Phys. Chem. B* **1999**, 103, 402–405; e) M. S. Vollmer, T. D. Clark, C. Steinem, M. R. Ghadiri, *Angew. Chem.* **1999**, 111, 1703–1706; *Angew. Chem. Int. Ed.* **1999**, 38, 1598–1601; f) H. Asanuma, T. Ito, T. Yoshida, X. Liang, M. Komiyama, *Angew. Chem.* **1999**, 111, 2547–2549; *Angew. Chem. Int. Ed.* **1999**, 38, 2393–2395; g) D. M. Junge, D. V. McGrath, *J. Am. Chem. Soc.* **1999**, 121, 4912–4913; h) S. Li, D. V. McGrath, *J. Am. Chem. Soc.* **2000**, 122, 6795–6796.
- [127] For examples in which photochemical reactions other than isomerization processes are utilized to exert photocontrol on chemical systems, see a) S. R. Adams, J. P. Y. Kao, G. Grynkiewicz, A. Minta, R. Y. Tsien, *J. Am. Chem. Soc.* **1988**, 110, 3212–3220; b) S. R. Adams, J. P. Y. Kao, R. Y. Tsien, *J. Am. Chem. Soc.* **1989**, 111, 7957–7968; c) R. Arad-Yellin, B. S. Green, *Nature* **1994**, 371, 320–322; d) M. T. Stauffer, D. B. Knowles, C. Brennan, L. Funderburk, F.-T. Lin, S. G. Weber, *Chem. Commun.* **1997**, 287–288; e) E. L. Piatnitski, K. D. Deshayes, *Angew. Chem.* **1998**, 110, 1022–1024; *Angew. Chem. Int. Ed.* **1998**, 37, 970–972.
- [128] A. Ueno, H. Yoshimura, R. Saka, T. Osa, *J. Am. Chem. Soc.* **1979**, 101, 2779–2780.
- [129] A. Ueno, K. Takahashi, T. Osa, *J. Chem. Soc. Chem. Commun.* **1980**, 837–838.
- [130] M. Asakawa, P. R. Ashton, V. Balzani, C. L. Brown, A. Credi, O. A. Matthews, S. P. Newton, F. M. Raymo, A. N. Shipway, N. Spencer, A. Quick, J. F. Stoddart, A. J. P. White, D. J. Williams, *Chem. Eur. J.* **1999**, 5, 860–875.
- [131] A photoswitchable complex composed of a bipyridinium–azobenzene diad and eosin has been reported in which the effect of the azobenzene photoisomerization on the stability of the complex was ascribed mainly to dipole-moment changes associated with the *trans*→*cis* isomerization. See: I. Willner, Y. Eichen, A. Doron, S. Marx, *Isr. J. Chem.* **1992**, 32, 53–59.
- [132] P. R. Ashton, S. E. Boyd, A. Brindle, S. J. Langford, S. Menzer, L. Pérez-García, J. A. Preece, F. M. Raymo, N. Spencer, J. F. Stoddart, A. J. P. White, D. J. Williams, *New J. Chem.* **1999**, 23, 587–602.
- [133] V. Balzani, J. F. Stoddart, unpublished results.
- [134] a) R. Ballardini, V. Balzani, M. T. Gandolfi, L. Prodi, M. Venturi, D. Philp, H. G. Ricketts, J. F. Stoddart, *Angew. Chem.* **1993**, 105, 1362–1364; *Angew. Chem. Int. Ed. Engl.* **1993**, 32, 1301–1303; b) M. Seiler, H. Dürr, I. Willner, E. Joselevich, A. Doron, J. F. Stoddart, *J. Am. Chem. Soc.* **1994**, 116, 3399–3404; c) M. Kropf, E. Joselevich, H. Dürr, I. Willner, *J. Am. Chem. Soc.* **1996**, 118, 655–665; d) A. C. Benniston, A. Harriman, V. M. Lynch, *J. Am. Chem. Soc.* **1997**, 117, 5275–5291; e) E. David, R. Born, E. Kaganer, E. Joselevich, H. Dürr, I. Willner, *J. Am. Chem. Soc.* **1997**, 119, 7778–7790.
- [135] a) A. C. Benniston, A. Harriman, D. Philp, J. F. Stoddart, *J. Am. Chem. Soc.* **1993**, 115, 5298–5299; b) A. C. Benniston, A. Harriman, D. S. Yufit, *Angew. Chem.* **1997**, 109, 2451–2454; *Angew. Chem. Int. Ed. Engl.* **1997**, 36, 2356–2358.
- [136] O. Johansen, A. W. H. Mau, W. H. F. Sasse, *Chem. Phys. Lett.* **1983**, 94, 107–112.
- [137] A. Juris, V. Balzani, F. Barigelletti, S. Campagna, P. Belser, A. von Zelewsky, *Coord. Chem. Rev.* **1988**, 84, 85–277.
- [138] E. Amouyal, *Sol. Energy Mater. Sol. Cells* **1995**, 38, 249–276.
- [139] P. R. Ashton, R. Ballardini, V. Balzani, E. C. Constable, A. Credi, O. Kocian, S. J. Langford, J. A. Preece, L. Prodi, E. R. Schofield, N. Spencer, J. F. Stoddart, S. Wenger, *Chem. Eur. J.* **1998**, 4, 2413–2422.
- [140] P. R. Ashton, V. Balzani, O. Kocian, L. Prodi, N. Spencer, J. F. Stoddart, *J. Am. Chem. Soc.* **1998**, 120, 11190–11191.
- [141] For related covalently linked metal complex (photosensitizer) and bipyridinium (acceptor) diads, see a) E. H. Yonemoto, R. L. Riley, Y. L. Kim, S. J. Atherton, R. H. Schmehl, T. E. Mallouk, *J. Am. Chem. Soc.* **1992**, 114, 8081–8087; b) E. H. Yonemoto, G. B. Saupe, R. H. Schmehl, S. M. Hubig, R. L. Riley, B. L. Iverson, T. E. Mallouk, *J. Am. Chem. Soc.* **1994**, 116, 4786–4795; c) L. A. Kelly, M. A. J. Rodgers, *J. Phys. Chem.* **1995**, 99, 13132–13140; d) P. R. Ashton, V. Balzani, A. Credi, O. Kocian, D. Pasini, L. Prodi, N. Spencer, J. F. Stoddart, M. S. Tolley, A. J. P. White, D. J. Williams, *Chem. Eur. J.* **1998**, 4, 590–607.
- [142] R. A. Bissell, E. Córdova, A. E. Kaifer, J. F. Stoddart, *Nature* **1994**, 369, 133–137.
- [143] a) M.-V. Martínez-Díaz, N. Spencer, J. F. Stoddart, *Angew. Chem.* **1997**, 109, 1991–1994; *Angew. Chem. Int. Ed. Engl.* **1997**, 36, 1904–1907; b) P. R. Ashton, R. Ballardini, V. Balzani, I. Baxter, A. Credi, M. C. T. Fyfe, M. T. Gandolfi, M. Gómez-López, M.-V. Martínez-Díaz, A. Piersanti, N. Spencer, J. F. Stoddart, M. Venturi, A. J. P. White, D. J. Williams, *J. Am. Chem. Soc.* **1998**, 120, 11932–11942.
- [144] For a discussion of the electrochemically controlled pirouetting motion of the macrocyclic component of a [2]rotaxane around the linear portion of its dumbbell-shaped component, see L. Raehm, J.-M. Kern, J.-M. Sauvage, *Chem. Eur. J.* **1999**, 5, 3310–3317.
- [145] a) P. Gaviña, J.-P. Sauvage, *Tetrahedron Lett.* **1997**, 38, 3521–3524; b) N. Armaroli, V. Balzani, J.-P. Collin, P. Gaviña, J.-P. Sauvage, B. Ventura, *J. Am. Chem. Soc.* **1999**, 121, 4397–4408.
- [146] J.-P. Collin, P. Gaviña, J.-P. Sauvage, *New J. Chem.* **1999**, 21, 525–528.
- [147] R. Ballardini, V. Balzani, W. Dehaen, A. E. Dell’Erbà, F. M. Raymo, J. F. Stoddart, M. Venturi, *Eur. J. Org. Chem.* **1999**, 591–602.
- [148] For other examples of photoactive [2]rotaxanes, see ref.[134d] and a) A. C. Benniston, A. Harriman, *Angew. Chem.* **1993**, 105, 1553–1555; *Angew. Chem. Int. Ed. Engl.* **1993**, 32, 1459–1461; b) A. C. Benniston, A. Harriman, V. M. Lynch, *Tetrahedron Lett.* **1994**, 35, 1473–1476; c) P. R. Ashton, R. Ballardini, V. Balzani, A. Credi, R. Dress, E. Ishow, C. J. Kleverlaan, O. Kocian, J. A. Preece, N. Spencer, J. F. Stoddart, M. Venturi, S. Wenger, *Chem. Eur. J.* **2000**, 6, 3558–3574.
- [149] H. Murakami, A. Kawabuchi, K. Kotoo, M. Kunitake, N. Nakashima, *J. Am. Chem. Soc.* **1997**, 119, 7605–7606.
- [150] The interesting possibility of exploiting the *trans*→*cis* photoisomerization of an azobenzene unit located in the middle of the dumbbell component to generate a stopperlike barrier for the ring component in a [2]rotaxane has recently been proposed. This would correspond to a “mechanical frequency doubling” of the shuttling process since, at a given temperature, the effective length for this motion would be cut in half. See: C. Kaufmann, W. M. Müller, F. Vögtle, S. Weinman, S. Abramson, B. Fuchs, *Synthesis* **1999**, 849–853.
- [151] a) C. O. Dietrich-Buchecker, J.-P. Sauvage, J.-M. Kern, *J. Am. Chem. Soc.* **1984**, 106, 3043–3045; b) C. O. Dietrich-Buchecker, J.-P. Sauvage, *Tetrahedron* **1990**, 46, 503–512.
- [152] M. Cesario, C. O. Dietrich-Buchecker, J. Guilhem, C. Pascard, J.-P. Sauvage, *J. Chem. Soc. Chem. Commun.* **1985**, 244–247.
- [153] A.-M. Albrecht-Gary, Z. Saad, C. O. Dietrich-Buchecker, J.-P. Sauvage, *J. Am. Chem. Soc.* **1985**, 107, 3205–3209.
- [154] A.-M. Albrecht-Gary, C. O. Dietrich-Buchecker, Z. Saad, J.-P. Sauvage, *J. Am. Chem. Soc.* **1988**, 110, 1467–1472.
- [155] For the chemical control of the co-conformational behavior associated with [2]catenane as a result of anion chelation, see A. Andrievsky, F. Ahuis, J. L. Sessler, F. Vögtle, D. Gudat, M. Moini, *J. Am. Chem. Soc.* **1998**, 120, 9712–9713.
- [156] a) M. Cesario, C. O. Dietrich-Buchecker, A. Edel, J. Guilhem, J.-P. Kintzinger, C. Pascard, J.-P. Sauvage, *J. Am. Chem. Soc.* **1986**, 108, 6250–6254; b) A.-M. Albrecht-Gary, C. O. Dietrich-Buchecker, Z. Saad, J.-P. Sauvage, *J. Chem. Soc. Chem. Commun.* **1992**, 280–282; c) N. Armaroli, L. De Cola, V. Balzani, J.-P. Sauvage, C. O. Dietrich-Buchecker, J.-M. Kern, A. Bailal, *J. Chem. Soc. Dalton Trans.* **1993**, 3241–3246.
- [157] Similar co-conformational changes were observed 1) upon demetalation/metalation and upon demetalation/protonation of analogous phenanthroline-containing [3]catenanes, and 2) upon demetalation/metalation of a phenanthroline-containing [2]catenane incorporating π -electron-rich and π -electron-deficient recognition sites, as well as 3) upon demetalation/metalation of a phenanthroline-containing multi-porphyrinic rotaxane. See a) J.-P. Sauvage, J. Weiss, *J. Am. Chem. Soc.* **1985**, 107, 6108–6110; b) C. O. Dietrich-Buchecker, A. Khemiss, J.-P. Sauvage, *J. Chem. Soc. Chem. Commun.* **1986**, 1376–

- 1378; c) N. Armaroli, V. Balzani, L. De Cola, C. Hemmert, J.-P. Sauvage, *New J. Chem.* **1994**, 18, 775–782; d) D. B. Amabilino, C. O. Dietrich-Buchecker, A. Livoreil, L. Pérez-García, J.-P. Sauvage, J. F. Stoddart, *J. Am. Chem. Soc.* **1996**, 118, 3905–3913; e) M. Linke, J.-C. Chambron, V. Heitz, J.-P. Sauvage, V. Semetey, *Chem. Commun.* **1998**, 2469–2470.
- [158] a) M. J. Gunter, M. R. Johnston, *J. Chem. Soc. Chem. Commun.* **1992**, 1163–1165; b) M. J. Gunter, D. C. R. Hockless, M. R. Johnston, B. W. Skelton, A. H. White, *J. Am. Chem. Soc.* **1994**, 116, 4810–4823.
- [159] M. J. Gunter, M. R. Johnston, *J. Chem. Soc. Chem. Commun.* **1994**, 829–830.
- [160] M. Asakawa, P. R. Ashton, V. Balzani, A. Credi, C. Hamers, G. Mattersteig, M. Montalti, A. N. Shipway, N. Spencer, J. F. Stoddart, M. S. Tolley, M. Venturi, A. J. P. White, D. J. Williams, *Angew. Chem.* **1998**, 110, 357–361; *Angew. Chem. Int. Ed.* **1998**, 37, 333–337.
- [161] M. Asakawa, P. R. Ashton, S. E. Boyd, C. L. Brown, R. E. Gillard, O. Kocian, F. M. Raymo, J. F. Stoddart, M. S. Tolley, A. J. P. White, D. J. Williams, *J. Org. Chem.* **1997**, 62, 26–37.
- [162] V. Balzani, A. Credi, S. J. Langford, F. M. Raymo, J. F. Stoddart, M. Venturi, *J. Am. Chem. Soc.* **2000**, 122, 3542–3543.
- [163] For the electrochemically controlled suppression of the circumrotation of the macrocyclic components of a [2]catenane, see P. Ceroni, D. A. Leigh, L. Mottier, F. Paolucci, S. Roffia, D. Tetard, F. Zerbetto, *J. Phys. Chem. B* **1999**, 103, 10171–10179.
- [164] For the electrochemical characterization of a neutral [2]catenane incorporating π -electron-rich and π -electron-deficient components, see D. G. Hamilton, M. Montalti, L. Prodi, M. Fontani, P. Zanello, J. K. M. Sanders, *Chem. Eur. J.* **2000**, 6, 608–617.
- [165] a) P. R. Ashton, R. Ballardini, V. Balzani, M. T. Gandolfi, D. J.-F. Marquis, L. Pérez-García, L. Prodi, J. F. Stoddart, M. Venturi, *J. Chem. Soc. Chem. Commun.* **1994**, 177–180; b) P. R. Ashton, R. Ballardini, V. Balzani, A. Credi, M. T. Gandolfi, S. Menzer, L. Pérez-García, L. Prodi, J. F. Stoddart, M. Venturi, A. J. P. White, D. J. Williams, *J. Am. Chem. Soc.* **1995**, 117, 11171–11197.
- [166] a) A. Livoreil, C. O. Dietrich-Buchecker, J.-P. Sauvage, *J. Am. Chem. Soc.* **1994**, 116, 9399–9400; b) A. Livoreil, J.-P. Sauvage, N. Armaroli, V. Balzani, L. Flamigni, B. Ventura, *J. Am. Chem. Soc.* **1997**, 119, 12114–12124.
- [167] F. Baumann, A. Livoreil, W. Kaim, J.-P. Sauvage, *Chem. Commun.* **1997**, 35–36.
- [168] D. J. Cárdenas, A. Livoreil, J.-P. Sauvage, *J. Am. Chem. Soc.* **1996**, 118, 11980–11981.
- [169] For a discussion of the photochemical control of the rate of circumrotation of the macrocyclic components of a [2]catenane (namely, a molecular brake operated by light), see a) F. Vögtle, W. M. Müller, U. Müller, M. Bauer, K. Rissanen, *Angew. Chem.* **1993**, 105, 1356–1358; *Angew. Chem. Int. Ed. Engl.* **1993**, 32, 1295–1297; b) M. Bauer, W. M. Müller, U. Müller, K. Rissanen, F. Vögtle, *Liebigs Ann.* **1995**, 649–656.
- [170] D. Gust, T. A. Moore, A. L. Moore, *Acc. Chem. Res.* **1993**, 26, 198–205.
- [171] S.-C. Hung, A. N. Macpherson, S. Lin, P. A. Liddell, G. R. Seely, A. L. Moore, T. A. Moore, D. Gust, *J. Am. Chem. Soc.* **1995**, 117, 1657–1658.
- [172] G. Steinberg-Yfrach, P. A. Liddell, S.-C. Hung, A. L. Moore, D. Gust, T. A. Moore, *Nature* **1997**, 385, 239–241.
- [173] G. Steinberg-Yfrach, J.-L. Rigaud, E. N. Durantini, A. L. Moore, D. Gust, T. A. Moore, *Nature* **1998**, 392, 479–482.
- [174] C. Montemagno, G. Bachand, *Nanotechnology* **1999**, 10, 225–231.
- [175] See, for example: a) J. R. Dennis, J. Howard, V. Vogel, *Nanotechnology* **1999**, 10, 232–236; b) L. Limberis, R. J. Stewart, *Nanotechnology* **2000**, 11, 47–51.
- [176] H. C. Taylor, M. E. J. Holwill, *Nanotechnology* **1999**, 10, 237–243.
- [177] C. Mao, W. Sun, Z. Shen, N. C. Seeman, *Nature* **1999**, 397, 144–146.
- [178] a) C. M. Dobson, A. Sali, M. Karplus, *Angew. Chem.* **1998**, 110, 908–935; *Angew. Chem. Int. Ed.* **1998**, 37, 868–893; b) *Acc. Chem. Res.* **1998**, 31, 697–780 (special issue on protein folding); c) D. Baker, *Nature* **2000**, 405, 39–42.
- [179] a) T. Pascher, J. P. Chesick, J. R. Winkler, H. B. Gray, *Science* **1996**, 271, 1558–1560; b) E. Chen, P. Wittung-Stafshede, D. S. Kliger, *J. Am. Chem. Soc.* **1999**, 121, 3811–3817.
- [180] G. P. Dado, S. H. Gellman, *J. Am. Chem. Soc.* **1993**, 115, 12609–12610.
- [181] An intriguing problem with molecular machines is to establish which components are moving and which are not. Since, in solution, the motions of the molecular components cannot be referred to a fixed reference point, the question cannot even be addressed. One answer to this question is the immobilization of one or more components to a fixed frame such as a surface.
- [182] For recent examples of Langmuir films composed of molecular and supramolecular systems incorporating interlocked components, see a) R. C. Ahuja, P.-L. Caruso, D. Möbius, G. Wildburg, H. Ringsdorf, D. Philp, J. A. Preece, J. F. Stoddart, *Langmuir* **1993**, 9, 1534–1544; b) R. C. Ahuja, P.-L. Caruso, D. Möbius, D. Philp, J. A. Preece, H. Ringsdorf, J. F. Stoddart, G. Wildburg, *Thin Solid Films* **1996**, 284/285, 671–677; c) D. B. Amabilino, M. Asakawa, P. R. Ashton, R. Ballardini, V. Balzani, M. Belohradsky, A. Credi, M. Higuchi, F. M. Raymo, T. Shimizu, J. F. Stoddart, M. Venturi, K. Yase, *New J. Chem.* **1998**, 959–972; d) D. E. Lynch, D. G. Hamilton, N. J. Calos, B. Wood, J. K. M. Sanders, *Langmuir* **1999**, 15, 5600–5605; e) C. L. Brown, U. Jonas, J. A. Preece, H. Ringsdorf, M. Seitz, J. F. Stoddart, *Langmuir* **2000**, 16, 1924–1930.
- [183] For recent examples of supramolecular systems deposited on surfaces, see a) P. Laitenberger, C. G. Claessens, L. Kuipers, F. M. Raymo, R. E. Palmer, J. F. Stoddart, *Chem. Phys. Lett.* **1997**, 279, 209–214; b) G. Ashkenasy, G. Kalyuzhny, J. Libman, I. Rubinstein, A. Shazer, *Angew. Chem.* **1999**, 111, 1333–1336; *Angew. Chem. Int. Ed.* **1999**, 38, 1257–1261; c) M. Lahav, L. Leiserowitz, *Angew. Chem.* **1999**, 111, 2691–2694; *Angew. Chem. Int. Ed.* **1999**, 38, 2533–2536; d) Semenov, J. P. Spatz, M. Möller, J.-M. Lehn, B. Sell, D. Schubert, C. H. Weidl, U. S. Schubert, *Angew. Chem.* **1999**, 111, 2701–2705; *Angew. Chem. Int. Ed.* **1999**, 38, 2547–2550; e) N. Bampos, C. N. Woodburn, M. E. Welland, J. K. M. Sanders, *Angew. Chem.* **1999**, 111, 2949–2953; *Angew. Chem. Int. Ed.* **1999**, 38, 2780–2783; f) H. Imahori, H. Yamada, S. Ozawa, K. Ushida, Y. Sakata, *Chem. Commun.* **1999**, 1165–1166; g) M. Asakawa, M. Higuchi, G. Mattersteig, T. Nakamura, A. R. Pease, F. M. Raymo, T. Shimizu, J. F. Stoddart, *Adv. Mater.* **2000**, 12, 1089–1102.
- [184] An amphiphilic dumbbell-shaped compound incorporating two redox-active bipyridinium units in its middle hydrophilic portion with two redox-active hydrophobic stoppers situated at each of its termini, together with both [2]- and [3]-rotaxane derivatives obtained therefrom by slippage, have all been employed in the fabrication of single molecule thick electrochemical junctions. Although, in these three compounds, the two bipyridinium units can be reduced reversibly, redox active phenoxy rings present in their two stoppers can only be oxidized. On the basis of these solution-state electrochemical properties, logic gates have been fabricated from an array of configurable solid-state switches, which consist of a Langmuir-type monolayer of one or other of these redox-active molecules sandwiched between two electrodes. The switches were read by monitoring the current flow at reducing voltages. In their “closed” state, current flow was dominated by resonance tunneling through the electronic states associated with the bipyridinium units in the molecules. Upon application of an oxidizing voltage, the molecules are oxidized irreversibly and the solid-state switches are “opened” permanently. Several devices were configured together to produce AND and OR logic gates. For more details, see a) C. P. Collier, E. W. Wong, M. Belohradsky, F. M. Raymo, J. F. Stoddart, P. J. Kuekes, R. S. Williams, J. R. Heath, *Science* **1999**, 285, 391–394; b) E. W. Wong, C. P. Collier, M. Belohradsky, F. M. Raymo, J. F. Stoddart, J. R. Heath, *J. Am. Chem. Soc.* **2000**, 122, 5831–5840.
- [185] J. K. Gimzewski, C. Joachim, R. R. Schlittler, V. Langlais, H. Tang, I. Johansson, *Science* **1998**, 281, 531–533.
- [186] R. D. Astumian, *Science* **1997**, 276, 917–922.
- [187] a) M. T. Rojas, A. E. Kaifer, *J. Am. Chem. Soc.* **1995**, 117, 5883–5884; b) M. T. Rojas, R. Königer, J. F. Stoddart, A. E. Kaifer, *J. Am. Chem. Soc.* **1995**, 117, 336–343.
- [188] An electrode covered with a superstructure made of Au nanoparticles cross-linked by 25^{++} molecules has been recently developed for sensoric applications. See: a) M. Lahav, A. N. Shipway, I. Willner, *J. Chem. Soc. Perkin Trans. 2* **1999**, 1925–1931; b) A. N. Shipway, M.

- Lahav, I. Willner, *Adv. Mater.* **2000**, *12*, 993–998; c) A. N. Shipway, E. Katz, I. Willner, *ChemPhysChem* **2000**, *1*, 18–52.
- [189] a) T. Lu, L. Zhang, G. W. Gokel, A. E. Kaifer, *J. Am. Chem. Soc.* **1993**, *115*, 2542–2543; b) J.-M. Kern, L. Raehm, J.-P. Sauvage, *C. R. Acad. Sci. Paris* **1999**, *2*, 41–47.
- [190] G. Bidan, M. Billon, B. Divisia-Blohorn, J.-M. Kern, L. Raehm, J.-P. Sauvage, *New J. Chem.* **1998**, 1139–1141. For a related recent example, see J. Buey, T. M. Swager, *Angew. Chem.* **2000**, *112*, 622–626; *Angew. Chem. Int. Ed.* **2000**, *39*, 608–612.
- [191] a) X. Marguerettaz, G. Redmond, S. N. Rao, D. Fitzmaurice, *Chem. Eur. J.* **1996**, *2*, 420–428; b) L. Cusack, S. N. Rao, D. Fitzmaurice, *Chem. Eur. J.* **1997**, *3*, 202–207; c) G. Will, G. Boschloo, R. Hoyle, S. N. Rao, D. Fitzmaurice, *J. Phys. Chem. B* **1998**, *102*, 10272–10278.
- [192] R. Argazzi, C. A. Bignozzi, V. Balzani, J. Cao, A. Credi, G. Mattersteig, F. M. Raymo, J. F. Stoddart, M. Venturi, unpublished results.
- [193] Recently, a solid-state, electronically addressable, bi-stable [2]catenane-based molecular switching device has been fabricated from a single monolayer of the [2]catenane **60**⁴⁺ (see Scheme 41), anchored with phospholipid counterions, and sandwiched between an n-type polysilicon bottom electrode with a titanium/aluminum top electrode. The device exhibits hysteretic current/voltage characteristics. The switch can be opened at +2 V, closed at –2 V, read at ~0.2 V, and may be recycled many times under ambient conditions. A mechanism for the action of the switch, which is molecular and mechanical in nature, has been presented. The mechanism is consistent with temperature-dependent measurements, which indicate that the overall cycling of the switches has at least one thermally activated stage and another thermally and voltage-activated stage and is quenched at about 200 K. The devices are robust under ambient conditions and could be cycled many times. The change in the junction resistance between the closed and open states of the device is approximately a factor of 1.8, which implies that they may be useful as memory devices, but are unlikely to be important for logic. For more details, see C. P. Collier, G. Mattersteig, E. W. Wong, K. Beverly, J. Sampaio, F. M. Raymo, J. F. Stoddart, J. R. Heath, *Science* **2000**, *289*, 1172–1175.
- [194] It has been pointed out that most of the components of a chemical computer, such as quantum wires and molecular switches, are already in existence. According to one prediction the chemical computer is likely to have replaced our present technology by the year 2025 (D. H. Rouvray, *Chem. Br.* **1998**, *34*(2), 26–29). In 1965, Moore predicted that every three years 1) device size would reduce by 33 %, 2) chip size would increase by 50 %, and 3) the number of components on a chip would quadruple (G. E. Moore, *Electronics* **1965**, April 19, 114–117). It is becoming increasingly apparent that today's computer technology, which relies on silicon-based chips, is rapidly approaching the upper-limits of its physical capabilities. In a recent letter (D. A. Muller, T. Sorsch, S. Moccio, F. H. Baumann, K. Evans-Lutterodt, G. Timp, *Nature* **1999**, *399*, 758–761), researchers at Bell Laboratories in New Jersey predict that silicon-based chips will reach their physical limit by the year 2012. The reason is their discovery that a layer of silicon dioxide must be at least four or five atoms thick to function as an insulator. To quote Max Schultz in the same issue of *Nature* (M. Schultz, *Nature* **1999**, *399*, 729–730), “science and industry will have to find new ways to build faster and larger computers.”
- [195] Watson–Crick hybridization of pairs of complementary DNA strands makes possible a representation of highly parallel selective operations that could allow computations to be done using molecules, see a) L. M. Adleman, *Science* **1994**, *266*, 1021–1024; b) L. M. Adleman, *DIMACS Series on Discrete Mathematics and Theoretical Computer Science* **1996**, *27*, 1–21. For a recent discussion of the prospects for large-scale neural network computation using DNA molecules, see A. P. Mills, Jr., B. Yurke, *Proceedings of the International Symposium on Cluster and Nanostructure Interfaces* (Richmond, VA, USA) **1999**, pp. 1–6.
- [196] The term “molecular computer” is still an emotive one among chemists in spite of the continuous advances in the field of molecular electronics (see ref. [9] and *Acc. Chem. Res.* **1999**, *32*, 191–275 (special issue on molecular materials in electronic and optoelectronic devices)) and the forecast contained in the Pimentel report (*Opportunities in Chemistry*, National Academy of Sciences, National Academy Press, Washington, DC, **1985**), which stated some 15 years ago now that “There are those who dismiss as far-fetched the idea of man-made molecular scale computers. Only a few decades ago, however, these same individuals might have classified as science fiction a proposal that someday there would be a man on the Moon, that fertility could be controlled by taking a pill, or that we could learn the structure of DNA. But since we know that molecular computers are routine accessories of all animals from ants to zebras, it would be prudent to change the question from whether there will be man-made counterparts to questions concerning when they will come into existence and who will be leading in their development. The when question will be answered on the basis of fundamental research in chemistry; the who question will depend on which countries commit the required resource and creativity to the search”.
- [197] Some people have envisaged that nanoscale devices will be used for repairing and manufacturing—thereby remodeling engineering, chemistry, and medicine, as well as computer technology. See, for example: a) K. E. Drexler, *Nanosystems: Molecular Machinery, Manufacturing, and Computation*, Wiley, New York, **1992**; b) T. D. Schneider, *Nanotechnology* **1994**, *5*, 1–18; c) R. C. Merkle, *Nanotechnology* **1997**, *8*, 23–28; d) S. Becker, K. Müllen in *Stimulating Concepts in Chemistry* (Eds.: M. Shibasaki, J. F. Stoddart, F. Vögtle), Wiley-VCH, Weinheim, **2000**, pp. 317–337.
- [198] In a recent editorial (A. J. Bard, *Chem. Eng. News* **1999**, *77*(36), 5) stigmatizing hype in chemistry, the use of terms employed in the macroscopic world to discuss the behavior of chemical systems has also been criticized. While we would agree wholeheartedly that the properties of chemical systems at the molecular and supramolecular levels should not be described in inappropriate ways, we do believe that looking at interwoven supramolecular and interlocked molecular systems from the viewpoint of their functions and with some judicious mentioning of devices in the macroscopic world is a highly stimulating exercise that helps the development of Chemistry as a scientific discipline by introducing new concepts onto the scene. There are some people who share our philosophy: aside from another editorial (R. M. Baum, *Chem. Eng. News* **1999**, *77*(31), 3) entitled “In Defense of Hype” (!), in the final chapter of a monograph (P. M. S. Monk, *The Viologens: Physicochemical Properties, Synthesis and Applications of the Salts of 4,4'-Bipyridine*, Wiley-VCH, New York, **1998**, chap. 14) devoted to the viologens, the author seems to despair that “so much jargon is introduced”, yet refers to the fact that “an almost infectious enthusiasm permeates the reports of viologen self-assembly” at the beginning of the chapter and then concludes, at the end of the chapter, that “an understanding of physicochemical properties of the viologens allows for the construction of chemical species which are novel and exciting, but which can also show great beauty.” We would not disagree—and would add that fresh fields of science have always generated their own vocabulary.^[11b,c]
- [199] J.-M. Lehn, *Chem. Eur. J.* **2000**, *6*, 2097–2102.
- [200] M. H. Al-Sayah, N. R. Branda, *Angew. Chem.* **2000**, *112*, 975–977; *Angew. Chem. Int. Ed.* **2000**, *39*, 945–947.
- [201] R. Krauss, H.-G. Weinig, M. Seydack, J. Bendig, U. Koert, *Angew. Chem.* **2000**, *112*, 1905–1908; *Angew. Chem. Int. Ed.* **2000**, *39*, 1835–1837.
- [202] V. Bermudez, N. Capron, T. Gase, F. G. Gatti, F. Kajzar, D. A. Leigh, F. Zerbetto, S. Zhang, *Nature* **2000**, *406*, 608–611.
- [203] M. Consuelo Jiménez, C. Dietrich-Buchecker, J.-P. Sauvage, *Angew. Chem.* **2000**, *112*, 3422–3425; *Angew. Chem. Int. Ed.* **2000**, *39*, 3284–3287.
- [204] H. Shigekawa, K. Miyake, J. Sumaoka, A. Harada, M. Komiyama, *J. Am. Chem. Soc.* **2000**, *122*, 5411–5412.
- [205] J. Cummings, A. Zettl, *Science* **2000**, *289*, 602–604.
- [206] B. Yurke, A. J. Turberfield, A. P. Mills, Jr., F. C. Simmel, J. L. Neumann, *Nature* **2000**, *406*, 605–608.
- [207] M. A. Reed, J. M. Tour, *Sci. Am.* **2000**, *282*(6), 86–93.
- [208] P. Ball, *Nature* **2000**, *406*, 118–120.



**Synthesis of barium sulfate
from surfactant – inorganic
nanoparticles**

The Chemistry of Form

Stephen Mann*

The emergence of complex form in living and nonliving systems remains a deep question for scientists attempting to understand the origins and development of shape and structure. In recent years, biologists and physicists have made significant advances in explaining fundamental problems in fields such as morphogenesis and pattern formation. Chemists, on the other hand, are only just beginning to contemplate the possibility of preparing manmade materials with lifelike form. This review traces a route to the direct synthesis of inorganic structures with biomimetic form, beginning from an understanding of crystal morphology

and biomineralization. The equilibrium form of crystals can be modified by surface-active additives but only within limits dictated by the symmetry of the unit cell. In contrast, biological minerals, such as shells, bones, and teeth, are distinguished by a complexity of form that bears little resemblance to the underlying order of their inorganic crystals. By understanding the constructional processes that give rise to the inorganic structures of life it should be possible to develop a chemistry of form in the laboratory. For example, complex small-scale inorganic architectures are produced at room temperature by undertaking precipitation re-

actions in self-assembled organic media, such as surfactant micelles, block copolymer aggregates and microemulsion droplets. Unusual inorganic forms emerge when these reaction fields are subjected to instability thresholds and synthesis and self-assembly can be coupled to produce materials with higher-order organization. Like their biological counterparts, these hard inorganic structures represent new forms of organized matter which originate from soft chemistry.

Keywords: biomimetics • biomineralization • crystal growth • inorganic materials • morphology

1. Introduction

The notion of *form* has intrigued and inspired artists and philosophers since antiquity. In sculpture and architecture, form is more than spatial structure. It embodies aesthetics and metaphysical ideas such as the classical proportions of Greek and Roman architecture, humanism in Renaissance sculpture, and fluidity of shape in modern art. In sculpture, form emerges from the formless by the exclusion of matter—the carving of stone and wood, for example. Through this process, sculptors seek to release latent qualities of the material; a craft not dissimilar from that of the modern-day scientist who carves out nanofabricated patterns in the featureless terrain of a silicon wafer. Architecture in contrast is a bottom-up approach, in which building blocks are integrated into a spatial structure that has functional, aesthetic, and societal value. What sculpture is to physics, architecture is to chemistry.

Nature, however, is indifferent to aesthetics, and survival of the genes through functional adaptation becomes an overriding principle in the appearance of biological form. What is so striking about the natural world is the remarkable level of morphological diversity and complexity, the seemingly endless variation of form in association with common functions. Trying to make sense of this is no easy task even though it is a central objective of palaeontology, and evolutionary and developmental biology. Prior to Darwin, natural form was studied with a metaphysical vigor to match the pursuit of sculpture and architecture. For example, German Naturphilosophie, as espoused by Ernst Haeckel (1834–1919), promulgated the coexistence of matter and spirit, and nowhere was this more exemplified than in the tiny ornate shells of single-celled organisms such as diatoms, coccoliths, and radiolarians (Figure 1).^[1] This was contested by D'Arcy Thompson, whose book *On Growth and Form*^[2] provided a compelling argument that natural form was simply the result of known physical and engineering principles applied to biological growth and development. In this paradigm, the inevitability of physical principles, such as space-filling and surface tension, could account for the general appearance of biological form, and geometric and topological perturbations to this blueprint paved the way to diversity. This view was also an affront to the

[*] Prof. S. Mann
School of Chemistry
University of Bristol
Bristol BS8 1TS (UK)
Fax: (+44) 117-929-0509
E-mail: s.mann@bris.ac.uk

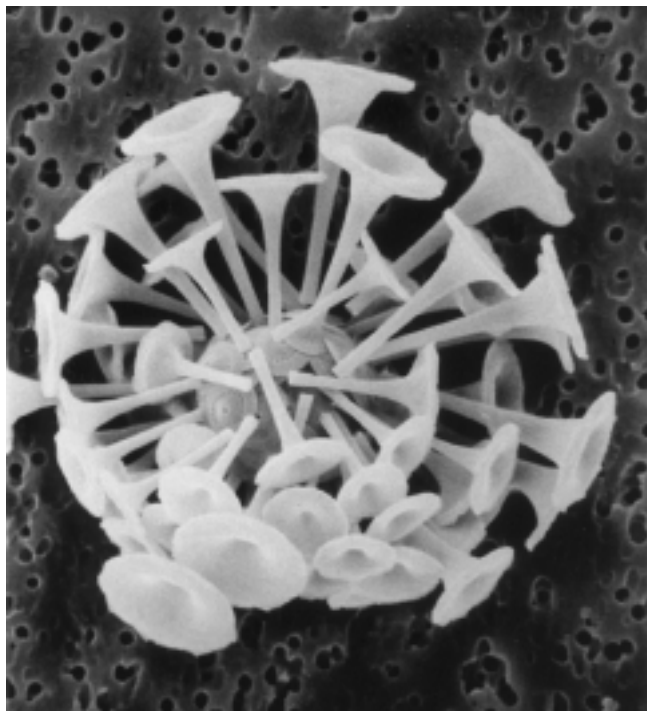


Figure 1. Natural form as expressed in the calcium carbonate exoskeleton of a marine coccolith (algae; diameter ca. 13 μm). (Photography courtesy of J. M. Young, Natural History Museum, London).

Darwinian theory of adaptation and natural selection, and although influential fell out of fashion as the culture of molecular biology developed in the late twentieth century.

The contention that biology is really just complicated physics is being currently reasserted as mathematical descriptions of self-organization become increasingly accessible. A wide range of natural patterns and forms—zebra stripes, butterfly wings, the structures of trees and lungs—can now be simulated and described by models based on fractal geometry and Turing waves.^[3] What emerges is a view of form as a spatio-temporal process written in genetic code and subjected in part to the push-and-shove of physical contingency. The interplay and correlation of these factors produce a large

gallery of potential forms that together describe the phylogenetic landscape of organisms.

The integration of mathematical (physical) and genetic (Darwinian) descriptions of natural form ultimately rests on an understanding of the mechanisms that transform the information coded in DNA into the expression of shape and pattern in time and space. The missing ingredient in this description is chemistry! For example, our knowledge of morphogenesis has increased rapidly in recent years because the activators and inhibitors have been identified at the molecular level and the processes that account for their secretion and spatial differentiation elucidated. Indeed, it is the patterning of chemical reactivity in localized space that appears to be central to the development of form.

If natural form is an emergent property of molecular processes then it should be possible for chemists to develop synthetic strategies that loosely mimic these processes. This review attempts to identify some ground rules for such an endeavor. We begin with the problem of form as described by structure, and then develop the notion of the equilibrium form of crystals and how geometric shapes are modified in the presence of surface-active molecules. Because the structural basis for crystal morphology contrasts markedly with the nonregularity but recognizable natural form of biominerals, the general principles of shape control in biomineralization are outlined. This leads to the question: how can an understanding of pattern formation in biomineral morphogenesis be integrated within a synthetic approach to inorganic materials with complex form? In response to this challenge, and as a starting point for future development, a conceptual framework for morphosynthesis is developed by using examples from recent investigations into the synthesis of inorganic materials in self-assembled reaction media.

2. Form as Description in Structure

Chemists on the whole focus on internal periodic order, and thus tend to neglect the richness and importance of external morphological form, even though soft matter and the natural world are replete in complex systems exhibiting aperiodicity,



Stephen Mann, born in 1955, is Professor in the School of Chemistry and Director of the Centre for Organized Matter Chemistry at the University of Bristol. He received his BSc. degree in chemistry from the University of Manchester Institute of Science and Technology (UMIST) in 1976, and was awarded a D.Phil. in 1982 from the University of Oxford for his work on biomineralization and bioinorganic materials chemistry. In 1981, he was elected to a Junior Research Fellowship at Keble College, Oxford, and took up a lectureship at the University of Bath in 1984 where he was promoted to reader in 1988, and appointed to a full professorship in 1990. His current research is concerned with biomimetic synthesis, as well as the characterization and emergence of complex forms of organized matter across extended length scales. He has obtained awards from the Royal Society of Chemistry (Corday-Morgan Medal in 1993, and RSC Interdisciplinary Award in 1999), is a recipient of the Max-Planck Research Prize for International Cooperation, awarded in 1998, and currently on the editorial and advisory board

of numerous journals including Advanced Materials, Angewandte Chemie, and Chemistry of Materials. He was admitted as a Fellow of the Royal Society of Chemistry in 1996.

curvature, and hierarchy. However, there is a sense of wonder to be found in structural chemistry with its crystallographic databanks teeming with exquisite molecular contortions. But the nature of crystallinity forces us to reduce the breadth of form to a special subset concerned solely with the periodicity of unit cells. And in so doing, synthetic chemistry has effectively become trapped within the symmetry limitations of 230 space groups. The recent discovery of quasi-crystals with nonequivalent units represents a first step away from orthodox crystallography.^[4] Ultimately this leads to a generalized study of order in soft matter^[5]—vesicles, micelles, lipid tubules etc.—and an attempt to systematically describe the complexity of natural forms, such as trees, termite nests, human anatomy, etc., expressed in aperiodic hierarchical systems. Of course, it is not surprising that chemists remain enchanted with periodic order since it is so readily and elegantly elucidated by X-ray diffraction methods. And many structural challenges remain unresolved. For example, even simple crystal structures, such as calcium carbonate, have several polymorphic forms that are not readily predicted by *ab initio* methods. Indeed, it is debatable whether thermodynamics is the appropriate tool to extend the range of structure description, as local energy minima, activation energies, and reaction landscapes are likely to be responsible for the selection between polymorphs, particularly where differences in global energies at equilibrium are marginal. For instance, the vast number of zeolite structures of comparable free energies of formation can be attributed to kinetic selectivity induced by template-directed mechanisms during crystallization.^[6]

The situation becomes even more complicated with the structural description of natural forms. Although these structures clearly retain a recognizable and reproducible pattern of order at the level of visual perception, they do not fit the crystallographers' *Weltanschauung* for several reasons. First, they are ordered but nonperiodic. Second, curvature is an integral aspect of this order. Third, the architecture is constructed hierarchically on length scales from the nanometer to millimeter level. Fourth, the expressed form evolves not only over long periods of time but in some cases over individual lifespans (metamorphosis). These features suggest that the formation of complex form is connected with patterning processes which arise from dynamic interactions and information transfer present within multicomponent systems, rather than intrinsic structural parameters. Nevertheless, without an understanding of the structural basis of morphology it is difficult to progress to a process-based description of form. For this reason, we now discuss the classical approaches used to describe the equilibrium form and habit modification of inorganic crystals.

3. Growth and Form of Crystals

The geometric shape (habit) of a crystal is determined by the external expression of a selected set of symmetry-related faces. Although the unit cell symmetry governs the spatial relations between the faces, their selection is mechanistically determined by the relative rates of growth along different crystallographic directions. In general, faces perpendicular to

the fast directions of growth have smaller surface areas and slow growing faces therefore dominate the morphology. A needle-shaped crystal therefore corresponds to fast growth along one specific axis, whereas preferential growth along two directions produces a platelike morphology. In each case, the relative rates of growth reflect differences in the interplay between the internal lattice structure and external environment of the crystallization system.

3.1. Equilibrium Morphology

Under equilibrium conditions, the morphology of a crystal is determined solely by intrinsic factors. The faces comprising the crystal habit correspond directly with the most energetically stable atomic planes in the lattice. These planes have low Miller indices (*hkl*) so they usually correspond to the symmetry of the Bravais lattice and the crystal shape is a macroscopic expression of the unit cell (Figure 2). Low index

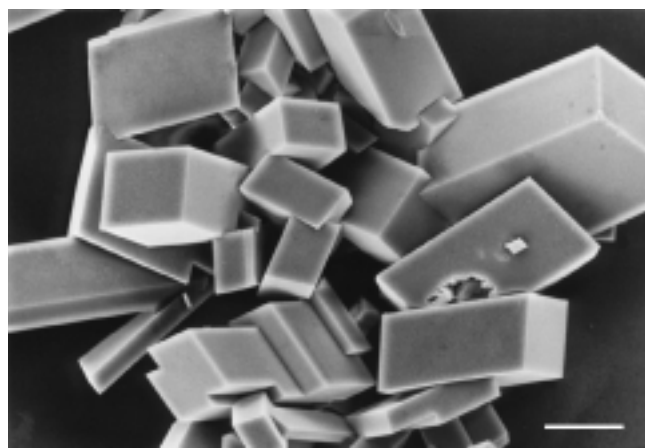


Figure 2. Scanning electron microscopy (SEM) image illustrating the correspondence between space symmetry and morphological form for calcite (CaCO_3) crystals grown under equilibrium conditions. The rhombohedral shape consists of six $\{10\cdot4\}$ faces and is a macroscopic expression of the $R\bar{3}c$ space symmetry of the unit cell. Scale bar = 10 μm .

faces are often relatively stable because they contain densely packed arrays of strongly bonded atoms. However, this simple structural approach does not always apply and a more complete description, involving knowledge of the surface energies ($\sigma_{s(hkl)}$) for all the crystal planes is required, where $\sigma_{s(hkl)}$ is defined as the excess energy per unit area of the surface lattice layer compared with the same plane in the bulk lattice. If the values for these energies can be obtained, either experimentally or from calculations, then the equilibrium crystal morphology possesses the Gibbs' condition for minimum total surface energy for a given volume [Eq. (1)],^[7] where $A_{(hkl)}$ is the surface area of the (*hkl*) crystallographic face.

$$\sum_{hkl} \sigma_{s(hkl)} A_{(hkl)} = \text{minimum} \quad (1)$$

Wulff proposed in 1901^[8] that the shape of a crystal can be defined by vectors of length $l_{(hkl)}$, each of which is drawn

normal to the corresponding (*hkl*) face. Thus, according to the Gibbs' condition for minimum surface energy, these vectors have a length that is directly proportional to $\sigma_{s(hkl)}$. So if the surface energies of various planes are known then it is relatively simple to use a computer program to draw out the morphology from a set of vectors of known lengths and angular intercepts.

On this basis, there are several methods available for predicting the equilibrium form. Because a full treatment requires knowledge of the surface structure and a detailed description of the bonding between atoms in the surface layers and bulk lattice, the models have until recently been semiquantitative. Significant progress has been made by considering the number and types of periodic bond chains that exist in the plane of different crystal faces.^[9] This relates to a value called the "attachment energy" which is the energy per molecule released when one slice of thickness $d_{(hkl)}$ is added onto the existing crystal face. If this value is low then the out-of-plane bonding is weak and the face is relatively stable because of the significant number of in-plane bond chains.

More recently, an atomistic simulation approach has been developed to predict inorganic crystal morphology.^[10] For this, one needs to have a detailed understanding of the force field that describes the bonding in the crystal structure. In practice this means that the calculation of the lattice energy has to take into account not only the Born–Mayer electrostatic interactions between all the ions but the second-order short-range repulsive and attractive forces described by the Buckingham potential. Terms for bending and torsional potentials may also be required. To test the validity of the model and the corresponding interatomic potentials, calculations of the lattice energy and elastic constants are made and checked against reputable experimental values. Then the surface energies can be calculated by theoretically cleaving the crystal structure along a specific direction and allowing atoms on the new (*hkl*) surfaces to relax until they achieve a minimum energy configuration. The energy for the surface lattice is then calculated by using the interatomic potentials derived for the bulk lattice along with the structural details obtained by energy minimization. The surface excess energy is then given by the difference between the values calculated for the surface and bulk lattice structures.

3.2. Habit Modification

In practice, most inorganic crystals grow under nonequilibrium conditions and habits are strongly influenced by changes in supersaturation and ionic strength (Figure 3).^[11] This raises the important question whether the rate of growth of a face is directly related to its intrinsic surface energy under nonequilibrium conditions, or arises as a consequence of mechanistic processes and interactions with the external

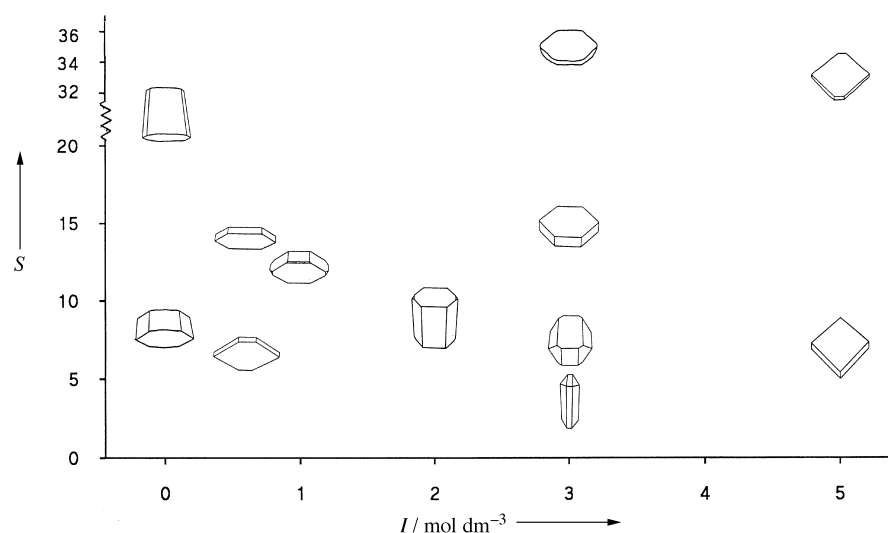


Figure 3. Plot of the morphological forms for BaSO₄ crystals grown under different conditions of supersaturation (*S*) and ionic strength (*I*). The crystals are drawn with their unit cell axes oriented in the same direction (the [001] axis is projected out of the page).^[11]

environment. It seems reasonable that the rate of growth of a face that is relatively stable (low surface energy) will be mechanistically slow. Moreover, because different crystal faces have different surface energies, the relative rates of growth should be proportional to the energy differences provided that the growth mechanism is the same on each face. Under these conditions, faces with high surface energies grow fast and become eliminated in the final morphology.

The relative order of crystal surface energies, as well as the mechanistic processes of growth, can be dramatically changed by the preferential adsorption of soluble additives to specific faces. Systematic modifications in morphology can occur. For example, the rhombohedral habit of calcite (CaCO₃) crystals shown above in Figure 2 changes to a tabular form in the presence of Li⁺ ions (Figure 4), which adsorb specifically on to

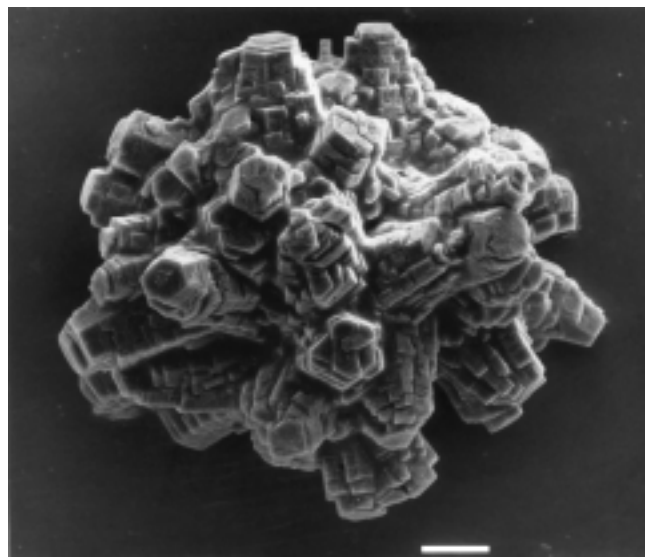


Figure 4. SEM image of a polycrystalline aggregate of calcite grown from supersaturated calcium bicarbonate solution in the presence of Li⁺ ions. The tabular outgrowths originate from the preferential interaction of the additive with the {001} faces that lie perpendicular to the crystallographic *c* axis. Scale bar = 10 μm.

the {001} planes and inhibit growth of these faces.^[12] It is generally true (but not always) that the crystal face perpendicular to the direction of growth that is inhibited by the additive increases in surface area. This means that it is often easy to read out from the changes in the relative areas of the faces in the modified morphology which crystallographic planes specifically interact with the soluble additive.

If the rate of crystal growth can be equated with the surface energies of particular crystal faces then it should be possible to accommodate the thermodynamic principles described above within a kinetic approach to crystal morphology. We would then be able to calculate the relative changes in surface energies of particular faces resulting from their interactions with additive molecules and predict the resulting habit modifications. For example, the surface energies for various calcite crystal faces with 50 to 100 % coverage of Mg^{2+} , Li^+ , or HPO_4^{2-} ions have been calculated and the resulting morphologies predicted are in agreement with calcite crystallization experiments.^[10] The results predict the rhombohedral equilibrium form and show how it is modified by preferential lowering of certain faces ({1 $\bar{1}$.0} for Mg^{2+} and HPO_4^{2-} , {001} surface for Li^+) to produce crystals with prismatic or tabular habits (Figure 5).

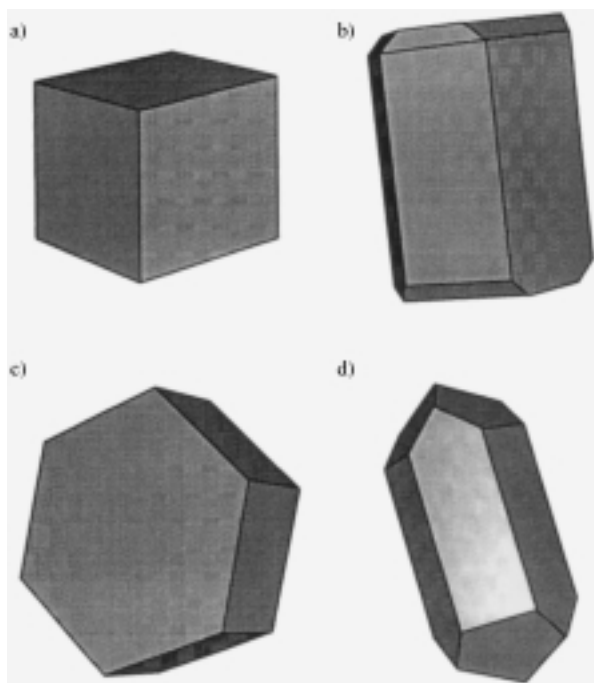


Figure 5. Predicted morphologies based on atomistic simulation of calcite surfaces in the presence of various additives. a) {10.4} rhombohedral (no additives), b) {1 $\bar{1}$.0} prismatic, stabilized by Mg^{2+} , c) {001} tabular, stabilized with Li^+ , d) prismatic-rhomb {1 $\bar{1}$.0}/{10.4}, stabilized with HPO_4^{2-} .

How successful this approach will be as a general method for predicting habit modification awaits further research. Besides the intrinsic problems of determining accurate interatomic potentials that can realistically describe the force fields of the modified inorganic surfaces, there are major reservations about the absence of mechanistic features—kinks, steps, screw dislocations etc—that underpin the kinetic theories of crystal growth. It seems clear from atomic force

microscopy (AFM) studies that morphological changes can accompany the preferential interaction of additives with step and kink sites present on low-energy surfaces that changes the growth kinetics along certain directions.^[13] Even though these mechanistic effects result in changes in the localized surface energies, they are too transient to be described by an atomistic simulation model which considers only equilibrium states on modified surfaces.

One central problem of the kinetic description of morphology is that the kink/step sites are treated as abstract geometric entities in theories of inorganic crystal growth. In reality, these sites have a molecular structure and shape derived from a localized perturbation in the relaxed surface lattice. If we could model the structure and dynamics of these sites then we might be able to simulate how they interact electronically and stereochemically with particular additive molecules. It is conceivable that these crystal surface interactions exhibit levels of molecular recognition analogous to biochemical processes such as antibody–antigen, and enzyme–substrate binding.

3.3. Molecular Recognition

Although no high-resolution structural details are currently available, there is circumstantial evidence that strongly suggests that molecular recognition in the form of charge, stereochemical, and structural matching of anion binding with packing motifs in crystal surfaces is an important factor in controlling the habit modification of inorganic crystals. The specificity of the interactions between additive and crystal surface growth sites are concentration dependent and can be dramatically changed through small modifications in the molecular structure of the soluble molecule.

Low molecular weight additives that have molecular structures with variable conformational states interact with inorganic crystal surfaces principally through electrostatic and stereochemical processes. For example, α - ω -dicarboxylic acids $[(\text{CH}_2)_n(\text{CO}_2\text{H})_2]$ are effective at stabilizing faces essentially parallel to the {1 $\bar{1}$.0} surface of calcite provided that both carboxylate groups are ionized and $n < 3$ (Figure 6).^[14] These faces contain both Ca^{2+} and CO_3^{2-} ions with the latter oriented such that the plane of the triangular anion is perpendicular to the surface. Thus incorporation of carbonate anions into the {1 $\bar{1}$.0} face during growth occurs through bidentate binding of two of the three oxygen atoms to Ca^{2+} ions in the surface. This stereochemical arrangement can also be adopted by binding of the dicarboxylate to the crystal surface (Figure 7). Moreover, both carboxylates in the additive molecule can bind simultaneously to two different calcium ions if the spacing between the CO_2^- groups is close to 0.4 nm. Both malonate ($n = 1$) and the unsaturated diacid, maleate ($\text{cis-}^- \text{O}_2\text{CCH=CHCO}_2^-$) fit this criterion but the increased rigidity of the latter reduces the binding affinity. The *trans* isomer, fumarate, has no morphological effect because cooperative binding can not take place.

It is important to note that the potency and morphological specificity of these dicarboxylate additives are lost at high concentrations where nonspecific binding becomes para-

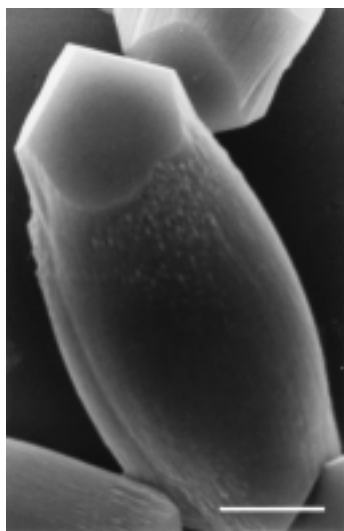


Figure 6. SEM micrograph of a spindle-shaped calcite crystal grown from supersaturated calcium bicarbonate solution in the presence of malonate at $[\text{Ca}^{2+}]:[\text{malonate}] = 3.16$. Crystal faces approximately parallel to the c axis are severely inhibited by the additive. Scale bar = 5 μm .

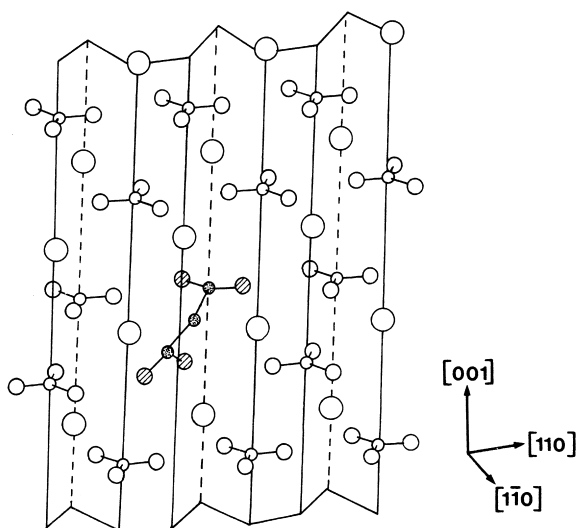


Figure 7. Perspective drawing of the calcite $\{1\bar{1}.0\}$ face showing a possible binding site for malonate anion.

mount. On the other hand, they can be increased by additional charge functionalization in the molecule. For example, both α -aminosuccinate (aspartate) and γ -carboxyglutamate show more effective stabilization of the prismatic calcite $\{1\bar{1}.0\}$ faces than succinate or glutamate.^[14]

There are also a growing number of examples where macromolecular additives can have specific effects on crystal habit. For example, polysaccharides such as sodium alginate and various carrageenans, when added to supersaturated solutions of sodium chloride, inhibit surface nucleation by adsorption onto edge sites allowing dislocation growth to dominate over edge nucleation.^[15] The resulting crystals have a well-defined cubic habit compared with the control crystals prepared in the absence of the inhibitors. Clearly, when one begins to consider the stereochemical possibilities of macromolecular interactions with inorganic crystal faces, then the recognition processes can become extremely complex and

subtle. Studies have shown that acidic macromolecules extracted from the Mg-calcite biominerals of adult sea urchins interact specifically with calcite prismatic faces lying almost parallel to the $\{1\bar{1}.0\}$ surface.^[16] These molecules have high levels of aspartic and glutamic acid residues that can stereochemically mimic the coordination environment of ions in the $\{1\bar{1}.0\}$ face by bidentate binding to the surface growth sites.

Understanding the molecular-specific interactions between surface-active molecules and selected crystal faces offers the potential to design additives for specific morphological changes. This has been achieved for example through the molecular synthesis of certain diphosphonate additives that interact specifically with BaSO_4 crystals grown from aqueous solution.^[17]

4. Growth and Form of Biominerals

The majority of biominerals, such as bones, shells, and teeth, have complex morphologies that bear little resemblance to the same minerals formed in chemical or geological systems (Figure 1). Indeed, the shape of biominerals challenges the structural view of morphology presented above because there appears to be no direct relationship between the unit cell and the macroscopic form. Thus, ideas about the systematic habit modification of equilibrium shapes offer little help in explaining the complex spiral forms of calcium carbonate seashells or lacelike porous silica skeletons of diatoms. However, an understanding of biomineral morphogenesis might provide new concepts and insights for the chemical synthesis of complex form.

As a general principle, we can consider biomineralized structures to originate from the vectorial regulation of crystal growth and patterning in or between organic assemblies such as vesicles and polymeric frameworks.^[18] The elaborate inorganic shapes arise from replication of the associated organic matrix through processes that are analogous to a cast produced in a mould. Metaphorically, the process of biomineralization acts as a “chemical medusa” that transforms soft organized matter into hard stonelike structures. In some systems, inorganic deposition and vesicle shaping proceed in concert, with the mineralization front remaining some distance behind the developing organic structure. Under these circumstances, synergistic interactions between the mineral and vesicle induce changes in the patterning process through coupling of the inorganic and organic processes. In particular, as the mineral begins to dominate the replicated organic morphology and the shape rigidifies, there is no longer any requirement for the vesicle to be held in place by associated biological structures, such as microtubules, and the patterning process becomes modified.

The general features of pattern formation in biomineralization^[19] are illustrated in Figure 8 in which the dynamic shaping of vesicles takes place by anchoring the lipid membrane through the use of microtubule-based directing agents to an underlying scaffold like the cell wall. Intracellular space is criss-crossed with microskeletal networks and associated stress fields, so the equilibrium spherical shape of a

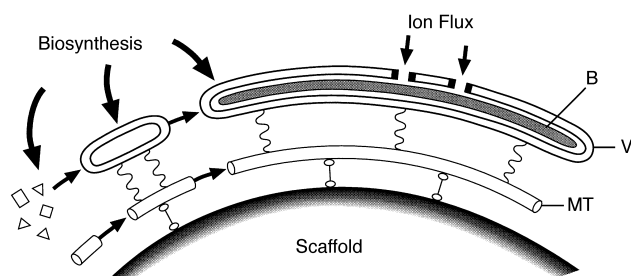


Figure 8. Illustration of the general features of programmed assembly in biomineralization. Cell walls, intracellular organelles and cellular assemblages can act as scaffolds for the assembly of microtubules (MT) which in turn are used as directing agents for the patterning of vesicles (V) involved in biomineralization (B).

vesicle membrane can be readily distorted by mechanical and structural forces operating locally and at a distance. Empirically, it appears that the shaping of a vesicle can be directed by two perturbing force fields acting either tangentially along the surface of the cell wall or an internal organelle (for example the endoplasmic reticulum and nuclear envelope), or radially along structural filaments such as those based on the protein, tubulin. Very complex morphologies are produced if the radial and tangential growth of vesicles and their associated biominerals are coupled in a programmed sequence. For example, many radiolarian microskeletons exhibit several concentric shells of reticulated silica that are structurally connected by radiating arrays of small silica spicules.^[20]

Assemblies of close-packed vesicles are used as patterning templates for the construction of the porous silica shells of radiolarians and diatoms (Figure 9). The complexity of the shell (frustule) can be rationalized on the basis of geometric packing of large “areolar” vesicles (AV) that are secreted and attached to the membrane wall (plasmalemma, PL) of the cell prior to mineralization (Figure 10). The vesicles are arranged into a thin polygonal foam with organized interstitial spaces that become mineralized in the form of a continuous silica framework. The vesicles remain unmineralized and are therefore used to pattern the void spaces in the silica skeleton. Thus, the diversity of patterns observed in diatom shells can be explained by geometrical deviations in the close packing of the areolar vesicles against the curved cell surface. However, this is not controlled primarily by surface tension but is the consequence of programmed cellular organization within the interstitial spaces that results in the secretion and assembly of

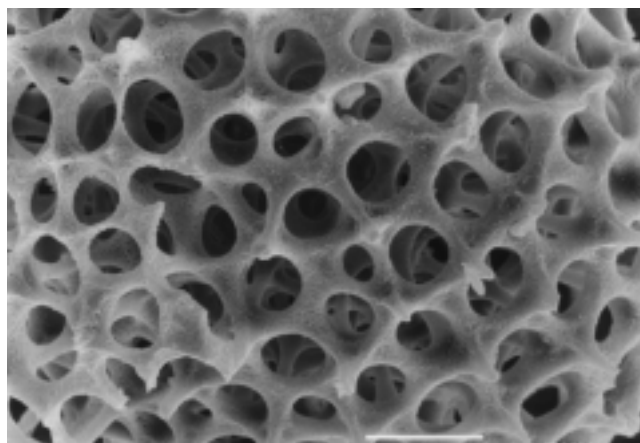


Figure 9. High-magnification SEM image of a radiolarian shell showing the void space patterning and continuous silica wall structure formed by mineralization in an organized “vesicle foam”. Scale bar = 10 μm .

tubular vesicles and associated microtubules in the gaps between the large areolar vesicles (Figure 10).^[21] Silica deposition is confined tangentially to the tubular system such that an open geometric mesh of mesopores is established. The areolar vesicles subsequently detach and withdraw from the plasmalemma, and the resulting space is infiltrated with smaller vesicles that produce a thin patterned shell of silica across the top of the void spaces.

The sculpting of biomineral form represents a compromise between the force fields of inorganic crystallization and biological organization. In some systems, the intrinsic crystallographic anisotropy of a mineral such as calcite (CaCO_3) is exploited in the biomineralization of elongated spicules by aligning the direction of fast crystal growth (c axis) with the morphological long axis defined by the underlying stress filaments of the vesicle system. In others, the genetic patterning of vesicle morphogenesis offsets the intrinsic crystallographic symmetry to produce complex shapes (e.g. coccoliths) that bear no resemblance to the underlying crystal structure. In both cases, the high fidelity of mineral replication arises from patterning processes that are ultimately programmed by genetic information. However, on close inspection it becomes clear that even between individual organisms of the same species, the complex biomineral forms are similar but not identical. That is, they are reproducibly recognizable but not perfect copies. This morphological similarity (equiva-

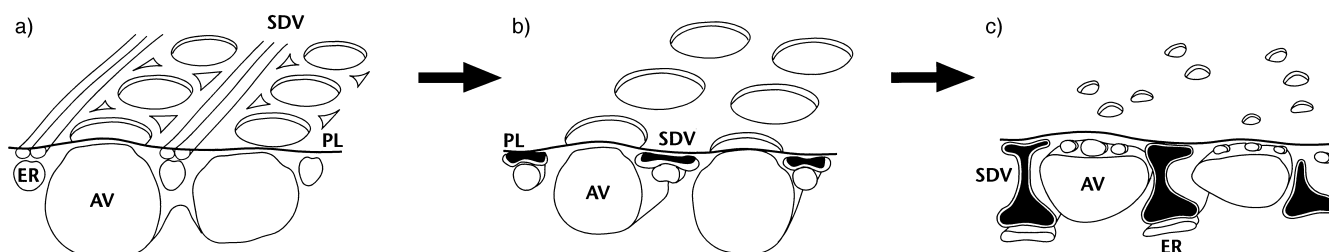


Figure 10. Illustration of the key stages in the formation of the siliceous diatom exoskeleton. a) Silica deposition vesicles (SDV) are preorganized with microtubules around the boundary spaces of large areolar vesicles (AR) attached to the plasmalemma (PL). b) The SDVs are mineralized with amorphous silica to give a patterned porous wall. c) The mineralized wall is thickened by extension of each SDV in association with the endoplasmic reticulum (ER). In some diatoms, detachment and retraction of the areolar vesicles from the plasmalemma results in infiltration with new SDVs and further mineralization of the pore spaces. Adapted from reference [21].

lence) reflects the tension between predetermined genetic mechanisms involved with the formation of the organic matrix, and the indeterminacy of fluctuations in the surrounding chemical and physical environment during the lifetime of the organism. Biomineral assembly is therefore determined by the complex interplay between the chemistry and geometry of the biological environment, both of which vary with time.

5. Morphosynthesis of Biomimetic Form

The vectorial regulation of the shaping and patterning of vesicles associated with the morphogenesis of biominerals such as coccoliths and diatom shells is inspiring new synthetic approaches to inorganic materials with complex form. The aim of *morphosynthesis* is to prepare inorganic materials with biomimetic form by direct chemical routes.^[19, 22] In this section we highlight how the coupling of inorganic mineralization and instability thresholds in the surrounding reaction environment is a central feature of morphosynthesis. For example, complex inorganic morphologies can be produced by fluctuations in chemical processes that cause local perturbations in the stability of fluid–solid interfaces during mineralization. Similarly, the confinement of inorganic deposition within organized reaction environments (reaction fields) formed from compartmentalized fluids, such as microemulsions and biliquid foams, can result in complex forms, particularly when the reaction fields become unstable by in situ mineralization. And in the special case of mineral–surfactant mesostructures, structural modulations during growth can lead to curved forms through the interplay of bending, twisting, and compaction forces.

We now discuss some of the main chemical principles of morphosynthesis. A summary of the various approaches and typical materials produced is given in Table 1.

5.1. Fluid–Solid Instabilities

The fluid–solid interface of a growing crystal is susceptible to extrinsic factors that induce local instabilities and produce complex shapes and patterns. For example, unusual inorganic morphologies can be prepared from crystallization reactions in viscous solutions or gels in which nonlinear processes arising from chaotic mixing, vortex formation, diffusion and

chemical gradients, and instabilities in hydrodynamic flow give rise to spatial and temporal patterns in mineral deposition at the fluid–solid interface. Banded inorganic structures (Liesegang's rings) are observed in silica and agar gels, and calcium phosphate precipitation in collagen gels gives rise to branched fractal structures.^[23] In most cases, the periodicity and patterning of precipitation arises from diffusion-limited and mass transport processes in the fluid, and can be mathematically modeled.^[24]

More complex inorganic forms are produced if the chemical reactivity of a viscous phase such as a silica gel is increased. For example, helical ribbons and spiral foils of calcium carbonate are obtained when solutions containing Ca^{2+} or HCO_3^- ions are allowed to counter-diffuse through a silica gel raised to pH values above 8.^[25] These shapes are the result of the interplay between localized growth and inhibition at the fluid–solid interface which arises from the indeterminate formation and rupture of a semi-impermeable calcium silicate membrane around the developing crystals—a phenomenon commonly observed in “crystal gardens”. A similar mechanism is responsible for the formation of distorted spirals of calcium carbonate (vaterite) in aqueous solutions of polyaspartate.^[26] Similar experiments with polyacrylate induce the formation of elaborate cone-shaped assemblies of BaSO_4 filamentous crystals that are hierarchically organized into complex architectures (Figure 11).^[11]

The ability of soluble polymers to induce complex shapes in inorganic materials may be widespread and deserves further investigation. Usually, the main problem concerns finding the appropriate window of activity, which often corresponds to a very limited set of reaction conditions among many permutations (ionic concentrations, molar ratios, polymer molecular weights etc). However, when appropriate conditions are found, wonderful structures can arise from this purely empirical approach.

5.2. Reaction Field Replication

The simplest synthetic representation of a typical membrane vesicle used in biomineral morphogenesis is a super-saturated microemulsion water droplet stabilized in oil by the segregation of surfactant molecules, such as sodium dodecyl-sulfate, at the oil–water interface. These droplets can be used to prepare hollow mineralized shells by specific nucleation and growth of the inorganic phase at the surfactant head-

Table 1. Current strategies in morphosynthesis.

Strategy	Product	Systems	Materials
fluid–solid patterning	banded aggregates, helicoids filaments, cones banded shells spirals, helicoids	SiO_2/OH^- gel polyacrylate hydroxyethyl cellulose polyaspartate	CaCO_3 BaSO_4 CaCO_3 CaCO_3
reaction field replication	hollow microshells cellular thin films, porous microshells	emulsion droplets microemulsion foams + latex beads	CaCO_3 CaCO_3 , Fe oxides, MnOOH
adaptive construction	microskeletal frameworks mesoskeletons, nested filaments	bicontinuous microemulsions block copolymer micelles	$\text{Ca}_{10}(\text{OH})_2(\text{PO}_4)_6$ SiO_2 Ca phosphate
structural modulation	twisted ribbons/cones helicoids discoids, gyroids, helicoids	reverse micelles/ microemulsions surfactant–silicate liquid crystals	BaSO_4 , BaCrO_4 mesostructured SiO_2

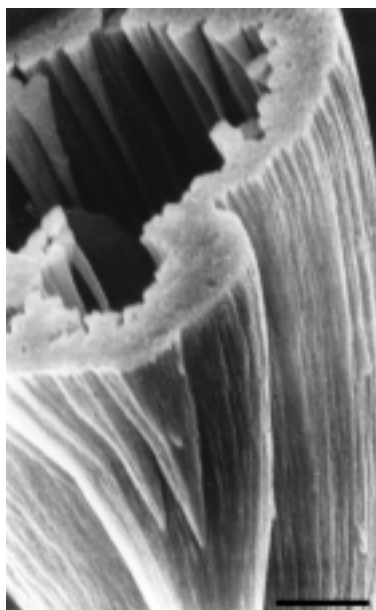


Figure 11. Hierarchical structure of BaSO_4 cones formed in the presence of a 0.5 mM aqueous solution of polyacrylate ($M_n = 5100$). The hollow cone consists of myriad smaller BaSO_4 cones that assembly from the close packing of nanofilaments. Scale bar = 1 μm .

groups. Moreover, if the droplets are stable during inorganic precipitation, the shell diameter can be controlled through adjustments in the amount of water in the microemulsion. For example, microemulsions containing micrometre-sized water droplets prepared from a supersaturated calcium bicarbonate solution have been used to prepare calcium carbonate (vaterite) hollow microspheres (Figure 12).^[27] The droplets only become supersaturated when CO_2 is degassed from the solution. This occurs by nucleation of microbubbles of CO_2 at the oil–water interface of each droplet so that the vaterite crystals in the shell structure are “patterned” by the entrapped gas bubbles. Thus, each droplet becomes preserved in the form of a micrometer-size vaterite hollow spheroid with an unusual surface texture consisting of pores and indentations, 0.3 to 1 μm in size.

This strategy can be extended to the synthesis of inorganic materials exhibiting three-dimensional (3D) micrometer-scale frameworks if we reverse the phase structure to produce a biliquid foam consisting of high concentrations of oil droplets stabilized by a thin soapy aqueous film and a continuous phase of a supersaturated solution. The organized structure can be used as a biomimetic representation of the patterning of the silica shell of diatoms by the space-filling aerolar vesicles that we discussed previously. For example, stabilized foams of freon (fluorotrichloromethane) droplets dispersed in water have been used to prepare honeycomb silica morphologies by in situ gelation of a silica sol within the boundary and interstitial spaces of the organized fluid.^[28]

Another strategy is to produce transitory foams by spreading a thin film of a supersaturated microemulsion onto a metal substrate and partially removing the oil phase by washing with hot hexane. This destabilizes the microemulsion film and causes microphase separation of the remaining oil and supersaturated aqueous solution into a self-organized foam-

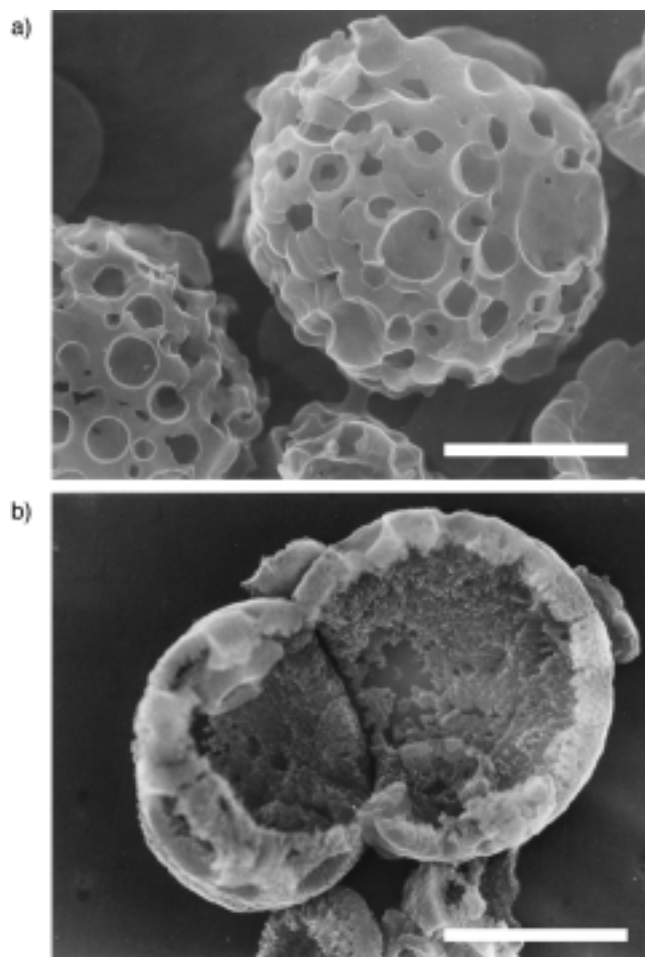


Figure 12. SEM images showing sponglike vaterite spheroids prepared from water-in-oil supersaturated microemulsions (octane:sodium dodecylsulfate: $\text{CaHCO}_3 = 71:4:25$ wt %). a) Individual vaterite spheroid showing complex surface patterning, b) broken spheroid showing hollow internal space. Scale bar = 10 μm , for both micrographs

like array of submicrometer-size oil droplets surrounded by supersaturated aqueous fluid. Growth of inorganic crystals then occurs in the interstitial spaces and boundary edges between the oil droplets to produce a mineralized imprint of the cellular structure. This approach has been used to prepare disordered frameworks of calcium carbonate (aragonite) and transition metal oxides (FeOOH , MnOOH) (Figure 13).^[29] Typically, the cellular films have continuous, branched mineral walls 20 to 100 nm in width, and enclosed cells of average size, 45 to 300 nm, depending on the size of the oil droplets, which in turn are controlled by the reaction conditions. Because the foam is a transitory structure, mineralization and oil droplet self-assembly must occur almost simultaneously if the interstitial spaces are to be filled with a continuous inorganic framework of calcium carbonate or metal oxide. This is achieved, respectively, by outgassing of CO_2 from or O_2 diffusion into the microemulsion. Both these processes are accelerated as the air–water interfacial area increases during foam formation, and give rise to rapid increases in supersaturation in the interstitial spaces by shifting the carbonate–bicarbonate and $\text{Fe}^{\text{II}}/\text{Fe}^{\text{III}}$ redox/hydrolysis equilibria, respectively.

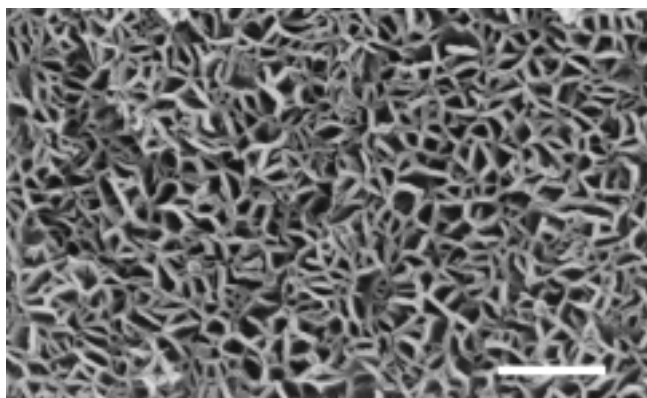


Figure 13. SEM image of a cellular film of CaCO_3 (aragonite) synthesized by reaction field replication in a transitory oil droplet biliquid foam. Scale bar = 1 μm .

Sculpting these cellular films into closed microshells produces structures that can be loosely described as biomimetic coccoliths (Figure 14).^[29] This is achieved by spreading the microemulsion film over micrometer-sized polystyrene beads and washing in hot hexane. Hexane is a suitable solvent

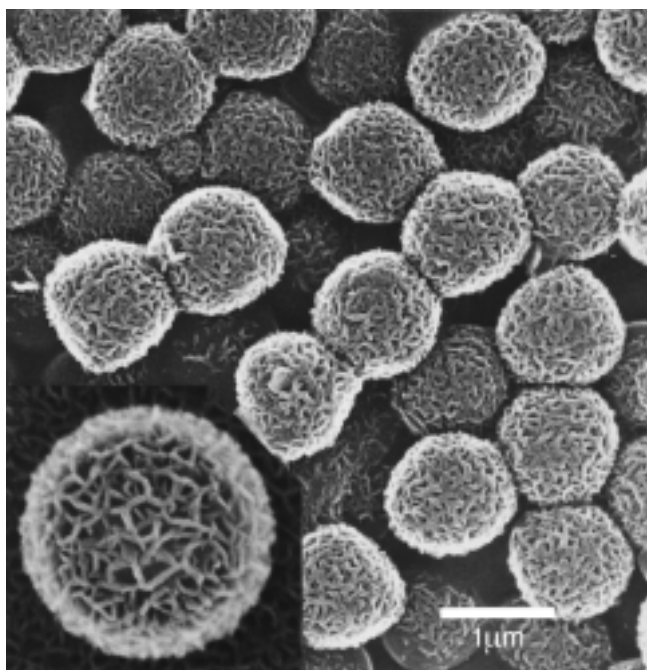


Figure 14. SEM image of intact hollow shells of mesoporous aragonite. Inset shows a high-magnification SEM image of an intact shell with well-defined cellular substructure. Scale bar = 1 μm .

because it does not dissolve the polymer template but induces demixing and mineralization of the transient cellular structure. The beads are then dissolved in chloroform or destroyed by heating to give porous hollow shells of cellular calcium carbonate or Fe oxide.

5.3. Adaptive Construction

The basic principle of reaction field materials replication rests on the assumption that there is a direct correspondence between the original shape and size of the fluid-filled

environments and that of the final mineral phase. Clearly, in many cases this is not true because the development of the inorganic structure perturbs the local environment in which it grows. As the reaction field adjusts to the presence of the incipient mineral then this in turn influences the new growth directions and a feedback loop is established. Thus, the inorganic morphology becomes dependent on the interplay of these processes, their synergism, and how they change with time. Form is therefore an emergent property established by a process of adaptive construction.

An interesting aspect of these interactive systems is that the mineral morphology often superficially resembles the reaction field but is different when compared in terms of scale. For example, bicontinuous microemulsions assembled from mixtures of tetradecane, water and the cationic surfactant didodecyltrimethylammonium bromide (DDAB) are structured as compartmentalized liquids in which the oil and water components are separated into highly branched and interconnected conduits, approximately 2 nm wide. By using a supersaturated calcium phosphate solution in place of water, and freezing the oil channels at temperatures above 0 °C, one might expect to replicate the reaction field as a nano-textured calcium phosphate phase. Instead, a remarkable microskeletal architecture, with micrometer-size pores in the interconnected framework, is deposited.^[30] The scale is over two orders of magnitude greater in length than the channel-like nanoscopic reaction environments. Similar micron-scale structures are obtained for silica polymerization in oil-frozen bicontinuous microemulsions.^[31] In this case, the reaction proceeds by partitioning the alkoxide precursor, tetraethoxysilane (TEOS), in the oil channels and allowing the TEOS molecules to slowly hydrolyze at the oil–water interface. The silicate species then migrate into the water channels where they undergo condensation reactions to produce amorphous silica.

Analogous processes of adaptive construction are observed when the precipitation of calcium phosphate is carried out in soft colloidal aggregates formed from block copolymers consisting of a long poly(ethylene oxide) block and a short poly(methacrylic acid) domain that is partially alkylated with a long-chain amine group.^[32] The polymer molecules are sufficiently hydrophobic that they self-assemble into 130 nm-size aggregates of entangled micelles to produce a colloid that is stable across a pH range of 3 to 9. Although the block-copolymer aggregates are polydisperse and disordered on the mesoscale, they are effective reaction fields for the sequestration of aqueous Ca^{2+} . At polymer to Ca^{2+} mole ratio of 4:1, nearly all the Ca^{2+} ions are associated with the acrylate and ethylene oxide groups so that the addition of phosphate ions at pH values between 3.5 and 5 increases the local supersaturation and results in the nucleation of calcium phosphate within the dispersed aggregates rather than in bulk solution. However, instead of the formation of small clusters of calcium phosphate embedded within the disordered polymer chains, a delicate mesoskeleton of interconnected inorganic needles evolves from the calcium-loaded aggregates. At pH = 3.5, the initial structures are 200 nm in size, with a starlike morphology consisting of a small number of 17 nm-thick inorganic filaments that are longer than the average diameter of the aggregate (130 nm) (Figure 15a). With time, the number of

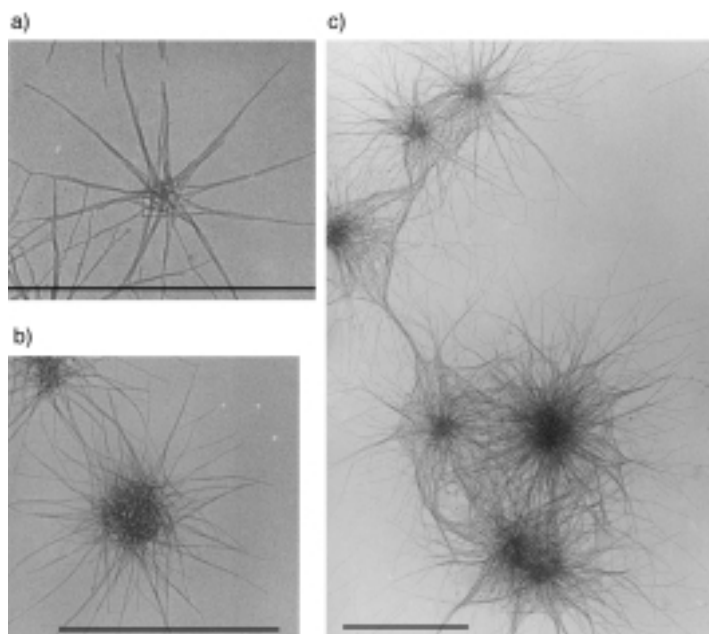


Figure 15. TEM images of calcium phosphate block copolymer nested colloids. a) Starlike form at early stage at pH 3.5, b) later stage showing complex central core, c) neuron-like tangles produced at pH 5. Scale bar = 0.5 μm .

filaments in each structure increases to produce a complex nested form (Figure 15b). After 100 h, the architecture becomes destabilized and the filaments reduce in length as the central core densifies to produce a mesostructured mineral-polymer colloid of similar diameter to the reaction field of the unmineralized aggregates. In contrast, the nested forms produced at pH 5 are stable and do not transform into the densified aggregate. Instead, the nanofilaments are thinner (3 nm) and longer (500 nm) than those initially formed at lower pH, and highly entangled to give neuron-like structures with a dense 120 nm-wide core (Figure 15c).

These complex forms represent higher-order coupling of the inorganic growth processes with changes in the organization and stability of the polymer aggregates. The concomitant changes in morphology represent adaptations to modifications in the structural, interfacial, and energetic properties of the coupled system. The supersaturation in the Ca^{2+} -loaded polymer aggregate is not particularly high at pH 3 because most of the phosphate anions are protonated. This means that interfacial factors, present solely within the reaction field of the polymer aggregate, promote the nucleation of calcium phosphate within these environments rather than in bulk solution. (At pH 7, no complex forms are observed because the rate of precipitation is fast due to the higher supersaturation and deposition in the bulk solution occurs). Once the inorganic clusters begin to grow within the colloidal aggregates competing force fields are set up as the particles push aside the entangled polymer chains. An instability threshold is reached when the polymer–mineral interactions become strong enough to disrupt the organic mesostructure and produce a cooperative growth process.

The exceedingly high anisotropy of the nanofilaments suggests that the polymer chains are strongly associated with

all the inorganic surfaces except the tip, which is not blocked from further growth because these are the only sites exposed to phosphate anions diffusing from the bulk phase into the Ca^{2+} -loaded aggregates. In the early stages of growth only a few nucleation sites occur in the aggregates and these are propagated through and outside of the disordered polymer matrix to produce the delicate nanoskeletal forms. As the filaments extend beyond the aggregate, polymer molecules must be drawn out along the sides of the inorganic needles. This depletes the core of the aggregate, which reconstructs and becomes progressively unstable as the number of filaments increase. However, the metastability is maintained at pH 5 because the polymer-coated inorganic filaments, even though they are only 3 nm wide, are stable with respect to dissolution. In contrast, calcium phosphate is relatively soluble at pH 3 so the filaments start to dissolve as the supersaturation reduces with time. This allows the polymer aggregates to be reestablished along with a secondary calcium phosphate phase.

5.4. Structural Modulation

Morphological transitions similar to those described in the previous section are particularly prominent for ordered hybrid mesophases in which the inorganic and organic components are regularly arranged over distances of 3 to 5 nm. This arrangement is particularly susceptible to structural modulation because inefficient space-filling and mismatching in interfacial structure and charge readily lead to metastability and in situ changes in form. A similar process occurs for the calcium phosphate block copolymer nested colloids described above except that there is no intrinsic long-range ordering in the intermediate structures. When there is periodic ordering, local deviations in structure (density, defects) and surface energy (charge, hydrophobicity) can produce morphological curvature through processes of bending, folding, twisting, and elastic deformation. For example, such processes account for the growth and form of micrometer-long twisted bundles of BaSO_4 and BaCrO_4 nanofilaments in water-in-oil microemulsions prepared from the anionic surfactant, sodium bis(2-ethylhexyl)sulfosuccinate (commonly called, AOT) (Figure 16a).^[33] The reaction occurs at room temperature in unstirred isooctane containing a mixture of $\text{Ba}(\text{AOT})_2$ reverse micelles and NaAOT microemulsions with encapsulated sulfate (or chromate) anions. The reverse micelles are about 2 nm in diameter and consist of a spherical cluster of about 10 Ba^{2+} ions strongly associated with the sulfonic acid headgroups of the surfactant, along with water of hydration. In contrast, the microemulsions are larger (4.5 nm across) because they contain bulk water (aqueous Na_2SO_4 or Na_2CrO_4) at a water to surfactant molar ratio, $w = 10$. When mixed together, the two reaction fields interact so that the constituents are slowly exchanged and BaSO_4 or BaCrO_4 nanoparticles nucleate and grow within the delineated space.

Discrete nanoparticles, 11 nm in size, are only formed in this system if the anion concentration is two to five times that of the Ba^{2+} ions.^[34] Under these conditions, the surface charge

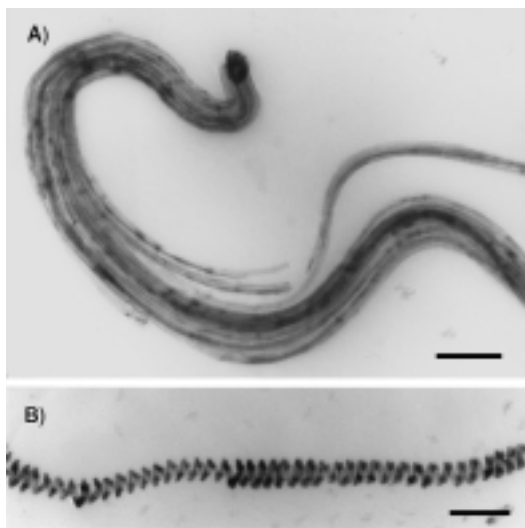


Figure 16. TEM images of BaSO_4 complex fibers showing; a) closely packed bundle of nanofilaments and coiled terminus, b) helical filament with 40 nm pitch. Scale bars = 200 nm.

on the BaSO_4 or BaCrO_4 crystals is negative (a surface excess of anions) and there is therefore minimal interaction with the anionic headgroups of the AOT molecules. On the other hand, if there is a stoichiometric excess of Ba^{2+} ions the nanoparticles are positively charged and the AOT molecules are strongly adsorbed onto the inorganic surfaces and growth is terminated by the time the clusters reach 5 nm in size. Furthermore, the pinning of the AOT molecules onto the surface induces aggregation of the clusters by inter-particle interdigitation of the immobilized surfactant chains. The clusters aggregate into a linear array that fuses together to give a single 5 nm-wide crystallographically aligned inorganic filament. The structural reconstruction originates from the strong coupling between the increase in inorganic lattice energy and reduction in membrane curvature that specifically accompanies linear association. Moreover, the structure propagates along one direction because surfactant molecules at the tips are readily displaced compared with those assembled along the filament edges.

With time, other filaments are formed parallel to the original thread to produce a small bundle of coaligned inorganic nanofilaments held together by surfactant bilayers. The locking in of new filaments by surfactant interdigitation generates a bending force in the nonattached segment of the longer primary thread. This results in the coiling of the bundle into a characteristic spiral-shaped structure several hundred nanometers in size that becomes self-terminating at one end because further addition of the primary nanoparticles is prevented by spatial closure. The final angle of rotation is dependent on the number of secondary nucleation events that occur on the internal edge of the primary filament. Since the number of coaligned filaments increases as the structures grow away from the terminus, the bending energy decreases and the bundle becomes straight. However, two further structural modulations can occur as the bundles extend in length. First, dissipation of strain energy arising from lateral packing pressure causes some bundles to splay outwards into

cone-shaped growth ends. Second, if the strain energy is low and the bundle is relatively thin, then differences in rigidity along the bundle can induce twisting of the filaments. This can arise from the lateral fusion and compaction of filaments by displacement of the AOT bilayers, and takes place initially in the older coiled end of the bundle. Because the twisting is not associated with any stress field or elastic deformation, it can propagate throughout the length of the bundle as the filaments coalesce to produce a single-crystal helicoid (Figure 16b).

Similar explanations account for the remarkable morphologies observed for surfactant–silica hexagonal mesophases formed in quiescent acidic medium.^[35] These materials consist of closely packed silica-coated rodlike micelles that can easily bend through 180° if the surface charge is not too high to produce topological defects that generate curved gyroids and discoids. Moreover, the low surface charge favors a growth model in which the curved micelles are added side-on to the existing structure. In contrast, a straight fiberlike morphology is produced under very acidic conditions because the highly protonated surfaces maintain a rigid-rod conformation that sustains an end-on growth mechanism.

The liquid crystalline nature of these mesophases makes them susceptible to elastic deformations that become manifest in regular radial patterns at the surface of the discoid form. Moreover, the polymerization of silica between the micelle rods is a slow process so that the initially formed regions, such as the center of the discoids, are more densely compacted than those at the edges. This differential contraction parallel and perpendicular to the rods leads to folding of strips of the structure into an open-ended microscopic helical tube. When the twisting is combined with differences in polymerization (contraction) along the tube, wonderful archimedean screwlike shapes are produced.^[36]

6. Higher-Order Assembly

Many biominerals exhibit complex forms that arise from the organized assembly of preformed mineral building blocks. These structures are associated with a variety of constructional processes involving the cellular processing of shaped and patterned biominerals into higher-order assemblies with micro- or macroscopic architecture. For example, magnetite crystals in magnetotactic bacteria are sequentially synthesized along a linear chain of vesicles so that the cells contain a permanent magnetic dipole for navigation in the geomagnetic field.^[37] In certain protozoa, curved silica rods are transported sideways through the cell membrane and out into the extracellular space, where they act as building blocks for the construction of an open-ended basketlike framework (lorica).^[38]

These biomineralization processes are inspiring new ideas in *crystal tectonics*, which can be defined as the chemical construction of higher-order structures from solid-state building blocks, such as inorganic nanoparticles. To achieve this, there has to be sufficient informational content in the preformed inorganic surfaces to control long-range ordering through interactive self-assembly. A relatively simple level of

communication is achieved by the interdigitation of surfactant chains attached to nanoparticle surfaces. The hydrophobic driving force for assembly gives rise to a bilayer between adjacent particles and this becomes directional if the organic molecules are located on specific crystal faces. For example, we described above how it was possible to chemically synthesize complex filamentous structures by a process that involved surfactant-induced linear coalescence of BaSO_4 or BaCrO_4 nanoparticles. Clearly, by preventing the fusion of the nanoparticles whilst maintaining a degree of micellar aggregation, it should be possible to synthesize a linear array of discrete spatially separated inorganic crystals. This has been achieved by increasing the stability of the individual nanoparticles without compromising the aggregation process. These criteria are met when the surface charge of the crystals is close to neutral, that is when the $[\text{Ba}^{2+}]:[\text{SO}_4^{2-}]$ (or $[\text{Ba}^{2+}]:[\text{CrO}_4^{2-}]$) molar ratio is equal to 1.0. Under these conditions, remarkable linear chains of individual BaSO_4 or BaCrO_4 nanoparticles are formed in a single step from the microemulsion reaction media (Figure 17).^[34] The colloidal

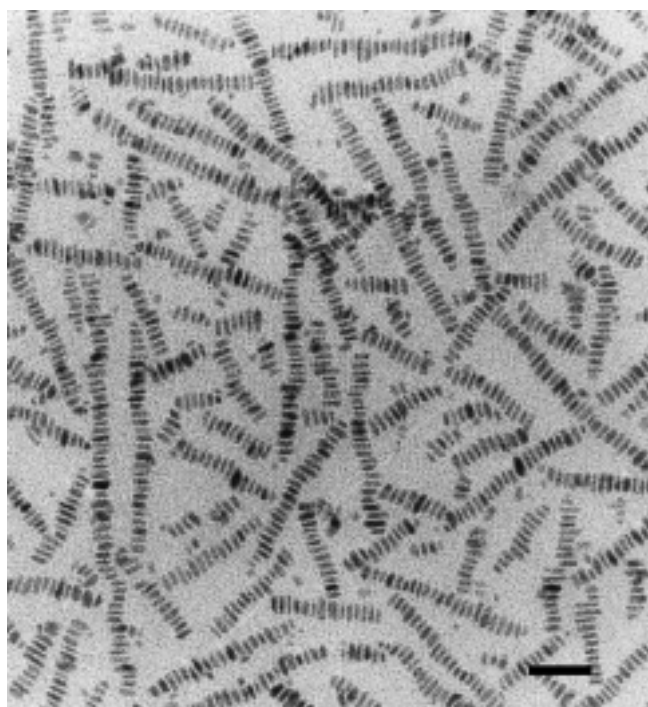


Figure 17. TEM image showing ordered chains of prismatic BaSO_4 nanoparticles prepared in AOT microemulsions at $[\text{Ba}^{2+}]:[\text{SO}_4^{2-}]$ molar ratio = 1 and $w = 10$. Scale bar = 50 nm.

chains are 50 to 500 nm in length and assembled directly in solution. Each chain consists of discrete rectangular prismatic crystals that are uniform in size ($16 \times 6.8 \times 6$ nm at $w = 10$) and preferentially aligned with the long axis of each particle perpendicular to the chain direction. Significantly, a regular spacing of 2 nm, corresponding to an interdigitated bilayer of surfactant molecules, separates each crystal in the chain so that they look like a biomimetic counterpart of the linear chains of discrete membrane-bounded magnetite chains synthesized in magnetotactic bacteria.^[37]

The linear arrays spontaneously form in the microemulsion fluid so nanoparticle synthesis and self-assembly are intimately coupled. The ordered assembly is determined by the uniformity in particle size in combination with crystal faces of regular shape and size. Together these facilitate crystal face-specific interactions between the hydrophobic tails of AOT molecules adsorbed onto the flat side faces of the BaSO_4 or BaCrO_4 prismatic crystallites. This process occurs specifically along one direction because there are two sets of side faces that differ in surface area. Aggregation is therefore directed along the axis perpendicular to the larger faces because this maximises the hydrophobic–hydrophobic interactions between the crystals and lowers the free energy of the surfactant–nanoparticle biphasic.

7. Summary and Outlook

Natural form is a spatio-temporal representation of chemical processes that are programmed by genetic information. The study of such processes, for example in biomineralization, should lead to similar emergent properties in chemical systems. As a first step towards the chemistry of form, this article has traced a route from the equilibrium form of crystals to the synthesis of complex shapes by reactions in organized fluids. In general, crystal morphology is determined by the relative rates of growth of different crystal faces, with the slow growing surfaces dominating the final form. The equilibrium shape therefore consists of the set of symmetry-related faces that give the minimum total surface energy, and can be predicted from knowledge of the surface structures and bonding interactions. Low and high molecular weight additives can stabilize nonequilibrium morphologies by changing the relative growth rates of different crystal faces through molecular-specific interactions with certain surfaces that modify the surface energy or growth mechanism, or both.

The vectorial regulation of the shaping and patterning of vesicles associated with the morphogenesis of biominerals such as coccoliths and diatom shells is inspiring new synthetic approaches to inorganic materials with complex form. The aim of morphosynthesis is to prepare inorganic materials with biomimetic form by direct chemical routes and central to this process is the coupling of inorganic precipitation and instability thresholds in the surrounding reaction environment. A number of systems have been discussed in this review. For example, the fluid–solid interface of a growing crystal is susceptible to extrinsic factors that induce local instabilities and produce complex shapes and patterns. And porous inorganic shells and membranes can be synthesized by materials replication of stable or transitory reaction fields established in microemulsion droplets and bilyquid foams. Significantly, mineral-induced instabilities in channellike microemulsions and block-copolymer aggregates give rise to the emergence of complex three-dimensional inorganic morphologies through time-dependent correlations and adaptations. Curved morphologies are also produced in ordered inorganic–organic mesophases by structural modulations that give rise to bending, twisting, folding, and elastic deformation. Finally, nanoparticle synthesis and self-assembly can be

coupled by the interfacial activity of reverse micelles and microemulsions to produce higher-order forms such as linear chains.

In biology, the general features of form are clearly connected to function—bone shape to movement, for example. But the elaboration of fine structure may be redundant. For example, whilst it is important to pattern voids in the exoskeleton of a diatom for chemical communication with the external environment, the exact shape of the pores may be functionally irrelevant. Thus a wide range of species-specific pore shapes appear to have evolved from subtle changes in processing rather than functional advantage. This fluidity of form in function raises important issues for a chemical approach to morphology with technological exploitation as an immediate goal. It is well known that the shape and texture of materials determine properties such as the long-term stability of products, flow and transport behavior, catalytic activity, separation efficiency, and adhesion. Synthesizing inorganic materials with complex patterns will therefore be relevant to the design of new types of catalyst supports, membranes for the separation of large polymers, colloids and cells, biomedical implants with macroporosity, drug carriers, and vectors for delivery and release of viruses and DNA in transfection procedures. At the current time, however, we have few ideas about the level of precision required to match form to function in synthetic applications.

I am indebted to many scientists for their contributions to the work described in this review. In particular, I wish to express my thanks to; Professor Steve Parker and Dr. James Titloye (University of Bath, UK) who pioneered the atomistic simulation of calcite surfaces and habit modification; Dr. Jon Didymus for his insightful studies on the growth and form of calcite in the presence of dicarboxylic acids; Dr. Dominic Walsh for his pioneering contributions in the study of calcium carbonate and calcium phosphate crystallization in microemulsions; Dr. Jeremy Hopwood for his discovery of BaSO₄ filaments and helicoids from microemulsion-based reactions; and Mei Li for her remarkable breakthrough in the higher-order synthesis and self-assembly of BaSO₄ and BaCrO₄ nanoparticles. I am also greatly indebted to Professor Markus Antonietti and Dr. Christine Goeltner and Dr. Helmut Cölfen (Max-Planck-Institut für Kolloid- und Grenzflächenforschung, Golm, Germany) for their frontier research on calcium phosphate-block copolymer micelles, and the many insights, technical skills, and creative ideas that they have shared throughout a long-standing and most enjoyable collaboration.

Received: February 17, 1999 [A398]

- [1] A. L. Mackay, *Forma* **1999**, 14, 11.
- [2] D. W. Thompson, *On Growth and Form*, Cambridge University Press, Cambridge, **1942**.
- [3] P. Ball, *The Self-made Tapestry: Pattern Formation in Nature*, Oxford University Press, Oxford, **1999**.
- [4] A. L. Mackay, *Mater. Sci. Forum* **1994**, 150, 1.
- [5] A. L. Mackay, *Theochem* **1995**, 336, 293.
- [6] M. M. Helmkamp, M. E. Davis, *Annu. Rev. Mater. Sci.* **1995**, 25, 161.
- [7] J. W. Gibbs, *Collected Works*, Longman, New York, **1928**.
- [8] G. Wulff, *Z. Krist. Kristallgeom.* **1901**, 949.
- [9] P. Hartmann, P. Bennema, *J. Cryst. Growth* **1980**, 49, 145.
- [10] J. O. Titloye, S. C. Parker, D. J. Osguthorpe, S. Mann, *J. Chem. Soc. Chem. Commun.* **1991**, 1494; J. O. Titloye, S. C. Parker, S. Mann, *J. Cryst. Growth* **1993**, 131, 533.
- [11] J. D. Hopwood, Ph.D. thesis, University of Bath, **1996**.
- [12] S. Rajam, S. Mann, *J. Chem. Soc. Chem. Commun.* **1990**, 1789.
- [13] A. J. Gratz, P. E. Hillner, *J. Cryst. Growth* **1993**, 129, 789; P. M. Dove, M. F. Hochella, *Geochim. Cosmochim. Acta* **1993**, 57, 705.
- [14] S. Mann, J. M. Didymus, N. P. Sanderson, E. J. Aso-Samper, B. R. Heywood, *J. Chem. Soc. Faraday Trans. 1* **1990**, 86, 1873.
- [15] J. D. Birchall, R. J. Davey, *J. Cryst. Growth* **1981**, 54, 323.
- [16] A. Berman, L. Addadi, S. Weiner, *Nature* **1988**, 331, 546.
- [17] R. J. Davey, S. N. Black, L. A. Bromley, D. Cottier, B. Dobbs, J. E. Rout, *Nature* **1991**, 353, 549.
- [18] S. Mann, *J. Mater. Chem.* **1995**, 5, 935.
- [19] S. Mann, G. A. Ozin, *Nature* **1996**, 382, 313; S. Mann, *J. Chem. Soc. Dalton Trans* **1997**, 3953.
- [20] O. R. Anderson, *Biom mineralization in Lower Plants and Animals*, Vol. 30 (Eds.: B. S. C. Leadbeater, R. Riding), Oxford University Press, Oxford, **1986**, pp. 375–391 (Systematics Association).
- [21] R. M. Crawford, A.-M. M. Schmid *Biom mineralization in Lower Plants and Animals*, Vol. 30 (Eds.: B. S. C. Leadbeater, R. Riding), Oxford University Press, Oxford, **1986**, pp. 290–314 (Systematics Association).
- [22] S. Mann, S. L. Burkett, S. A. Davis, C. E. Fowler, N. H. Mendelson, S. D. Sims, D. Walsh, N. T. Whilton, *Chem. Mater.* **1997**, 9, 2300; G. A. Ozin, *Acc. Chem. Res.* **1997**, 30, 17.
- [23] R. Kniep, S. Busch, *Angew. Chem.* **1996**, 108, 2787; *Angew. Chem. Int. Ed. Engl.* **1996**, 35, 2624.
- [24] H. K. Henisch, J. M. Garcia-Ruiz, *J. Cryst. Growth* **1986**, 75, 195.
- [25] J. M. Garcia-Ruiz, *J. Cryst. Growth* **1985**, 73, 251.
- [26] S. D. Sims, J. M. Didymus, S. Mann, *J. Chem. Soc. Chem. Commun.* **1995**, 1031; L. A. Gower, D. A. Tirrell, *J. Cryst. Growth*, **1998**, 191, 153.
- [27] D. Walsh, B. Lebeau, S. Mann, *Adv. Mater.* **1999**, 11, 324.
- [28] M. Wu, T. Fujii, G. L. Messing, *J. Non-Cryst. Solids* **1990**, 121, 407.
- [29] D. Walsh, S. Mann, *Nature* **1995**, 377, 320; D. Walsh, S. Mann, *Adv. Mater.* **1997**, 9, 658.
- [30] D. Walsh, J. D. Hopwood, S. Mann, *Science* **1994**, 264, 1576; D. Walsh, S. Mann, *Chem. Mater.* **1996**, 8, 1944.
- [31] S. D. Sims, D. Walsh, S. Mann, *Adv. Mater.* **1998**, 10, 151.
- [32] M. Antonietti, M. Breulmann, C. G. Goltner, H. Cölfen, K. K. W. Wong, D. Walsh, S. Mann, *Chem. Eur. J.* **1998**, 4, 2491.
- [33] J. D. Hopwood, S. Mann, *Chem. Mater.* **1997**, 9, 1819; M. Li, S. Mann, *Langmuir* **2000**, 16, 7088.
- [34] M. Li, H. Schnablegger, S. Mann, *Nature* **1999**, 402, 393.
- [35] S. Oliver, A. Kuperman, N. Coombs, A. Lough, G. A. Ozin, *Nature* **1995**, 378, 47; G. A. Ozin, *Can. J. Chem.* **1999**, 77, 2001.
- [36] S. M. Yang, I. Sokolov, N. Combs, C. T. Kresge, G. A. Ozin, *Adv. Mater.* **1999**, 11, 1427.
- [37] S. Mann, N. H. C. Sparks, R. G. Board, *Adv. Microbial. Phys.* **1990**, 31, 125.
- [38] B. S. C. Leadbeater, *Proc. R. Soc. London B* **1984**, 304, 529.

“Condensative Chain Polymerization”—A Way Towards “Living” Polycondensation?

Brigitte Voit*

A significant portion of the commercial polymers is prepared by polycondensation techniques. In particular the synthesis of polyesters and polyamides is based on melt condensation which has been a well established technical process since the 1930s.^[1] However, even today the problem of how to reach the high conversions which are required for high molar mass polycondensates is not fully solved. In contrast to chain-growth processes, a significant increase in molar mass can be achieved only at conversions above 90 % in the step-growth process of the polycondensation reaction. The theoretical degree of polycondensation at 90 % conversion is only 10, at 99 % it reaches 100. Growth does not occur specifically at the chain end but instead occurs as a result of reactions between monomers, dimers, and already formed oligomers. In general equilibrium reactions are involved in polycondensation. Thus, the products of polycondensation reactions usually have a molar mass distribution \bar{M}_w/\bar{M}_n of 2. Molar mass and polydispersity is controlled by statistics and the degree of conversion; the end groups of the polymer can be controlled to some extent by the choice of monomers and the reaction stoichiometry. Chain-growth polymerization processes allow the formation of high molar mass products even at low monomer conversion, which means that high molar mass polymer chains and a significant amount of monomer can be present at the same time. The molar mass is controlled by the monomer/initiator ratio, and functional end groups can be introduced through the initiator or by a terminating agent.

There are numerous methods for controlled polymerization—ionic and radical—available which allow the formation of polymers with a molar mass distribution \bar{M}_w/\bar{M}_n of less than 1.1. Attempts are being made in academic circles to synthesize polycondensates in a controlled manner, that is, with control over the structure and molar mass. Examples of this work are the perfectly branched dendrimer species^[2] which have been studied intensively over the last 10 years, and also the synthesis of well-defined oligomers. However, the transfer of these repetitive synthetic approaches into an industrial

process is problematic because of the high costs and scale-up problems.

In recent years, however, a high level of control over molar mass, polydispersity, end groups, and architecture has also become a high priority for commercial polymers. Thus, it should be possible to generate new polymer property profiles from known monomers and established techniques. This trend can be seen in the field of chain-growth polymerization with the rapid development of the metallocene polymerization of olefins^[3] and controlled radical polymerization.^[4]

Yokozawa and Suzuki^[5] of the Kanagawa University have presented a new technique which should allow a level of control over molar mass and polydispersity in polycondensation reactions that up to now was only possible in controlled chain-growth processes. When analyzed in detail the new technique actually represents a conversion of the polycondensation reaction into a chain-growth reaction; this is done by promoting growth only at the “reactive” end of the polymer chains through the use of suitable monomers, initiators, and special reaction conditions. The authors call this process “condensative chain polymerization” in accord with the more specified classification of polymerization reactions by the IUPAC commission in 1994.^[6] This term was given to chain-growth reactions which involve the typical initiating and growth steps but also the elimination of low molar mass species.

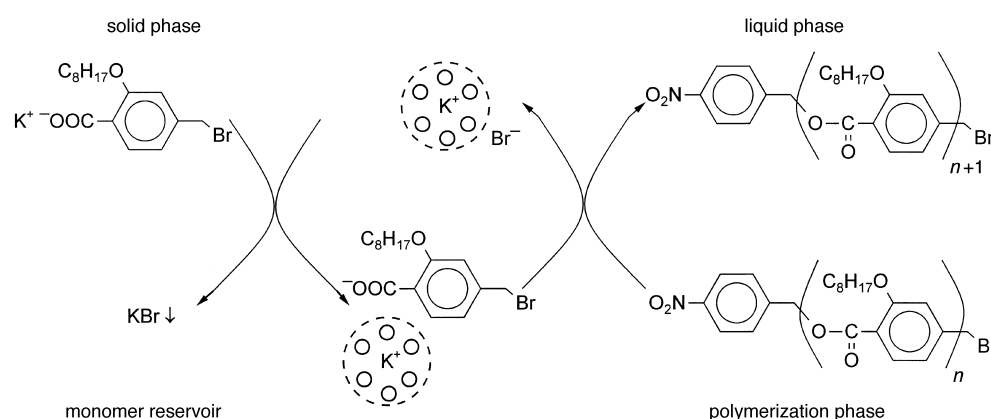
The first investigations were reported by Lenz^[7] in the 1960s. Later, Robello et al.^[8] used the “self condensation” of 4-halobenzenesulfonate for the preparation of poly(p-phenylene sulfone); for this reaction they discussed a chain-growth mechanism which had some of the features of a living process. The important features of the reaction were the formation of high molar mass products even at low monomer conversion and the absence of oligomers in the final product, something which can not be avoided in a classical step-growth process. However, the synthesis of polyesters with acyclic monomers and full control over molar mass, polydispersity, and end groups could not be achieved.

In model studies, Yokozawa and Shimura^[9] demonstrated that some monomers suitable for polyester synthesis, for example 4-(trimethylsilyloxy)benzoyl chloride or the combination of 4-bromophenol and carbon monoxide, have the potential to let the condensation reaction run by a chain-

[*] Prof. Dr. B. Voit
Institut für Polymerforschung Dresden e.V.
Hohe Strasse 6, 01069 Dresden (Germany)
Fax: (+49) 351-4658565
E-mail: voit@ipfdd.de

growth mechanism. Here, in a monomer A-B, the reactivity of the functionality B towards A is increased by the reaction of an "initiator" with the functionality A, for example an electron donating substituent is converted in an electron withdrawing group. However, this method must still be converted into a working polymerization process.

It is essential for good control that the reaction occurs exclusively at the end of the growing chain, this means the monomers must not react with each other. To meet this condition Yokozawa and Suzuki took advantage of a heterogeneous reaction, with a phase transfer catalyst as outlined in Scheme 1. In principle, the use of phase-transfer catalysis in polycondensation processes is not new,^[10] but up to now it has not been used to control the products in this way.



Scheme 1. Mechanism of the controlled polycondensation according to Yokozawa and Suzuki.^[5]

Yokozawa and Suzuki first dispersed the solid monomer, potassium-4-bromomethyl-2-*n*-octyloxybenzoate, in a nonsolvent (acetone). The addition of [18]crown-6 allows a small amount of the monomer to be solubilized. In solution, the monomer can react with the initiator, 4-nitrobenzyl bromide, to form a *para*-nitrobenzyl ester. The best results were obtained when initiator and crown ether were used in equimolar amounts, for example, 10 mol % of each, with respect to the monomer. After initiation, the chain growth starts, potassium bromide precipitates, and a small amount of [18]crown-6 is liberated. This leads again to the solubilization of a small amount of monomer which can add to the ends of the oligomers in the reaction solution. By this mechanism, the amount of free monomer in solution is always very small and therefore the self condensation of monomer molecules can be suppressed.

The important criteria in this reaction are the solubility of monomer, initiator, and growing polymer chain. If the solubility of the monomer in the reaction medium is too high, then a parallel step-growth reaction can take place. If the amount of crown ether is too low, too little monomer enters the reaction mixture and so homogeneous growth starting from all initiator molecules can not take place. The growing polymers chains naturally have to be soluble in the reaction media even at higher molar mass. Therefore, transfer of this polymerization process to other monomer systems is not simple and only a selected number of monomers will fulfill all the necessary criteria.

The system described, in which an alkoxy-substituted poly(benzyl ester) is formed, demonstrates that the detailed analysis of the reaction development and of the properties of the reagents is required for the success of the reaction. Polymerization in acetone at 25 °C with 7 mol % of initiator and [18]crown-6 leads to a linear increase of molar mass with conversion, the polydispersity \bar{M}_w/\bar{M}_n for all the samples is below 1.3, and the ratio of end groups (after the reaction of the benzyl bromide end groups with potassium 4-methoxyphenolate) to initiator groups is very close to 1 even at low conversion. Therefore, one can assume a chain-growth mechanism with almost exclusive growth at the chain end.

A further experiment was carried out to investigate whether the molar mass can be controlled by the monomer/initiator ratio. For this, the amount of initiator was varied from 100 to 7 mol %, with respect to the monomer, and the polymerization reaction was driven to complete conversion. A linear relationship between molar mass and the monomer/initiator ratio was found. In addition, the molar masses of the products agreed well with values calculated on the basis of the monomer/initiator ratio, which indicates a high initiator efficiency. The \bar{M}_w/\bar{M}_n was again below 1.3. The reaction exhibits the fea-

tures comparable to those of a controlled polymerization of vinyl or cyclic monomers. To be able to transfer these results into a commercially viable process it is necessary to reduce the initiator concentration further so that products can be prepared that have molar masses above 5000 g mol⁻¹ and thus have interesting materials properties.

Yokozawa and Suzuki demonstrated convincingly that control of molar mass, polydispersity, and end groups can be achieved in polycondensates if the step-growth process is converted into a controlled chain-growth reaction. Logically, the kinetics follow those of a chain-growth mechanism when termination and side reactions are suppressed. Since a heterogeneous, phase transfer catalyzed process is involved, which has already been introduced successfully in industrial polycondensation processes, a transfer to commercial use seems possible. If this method can be applied successfully to other monomers one can imagine that the presented concept might have the same importance for polymer synthesis as the recent developments in controlled radical polymerization. Certainly, the area of classical polycondensation will not be revolutionized tomorrow, but one can expect many new ideas to be initiated by this work from Yokozawa and Suzuki.

[1] A. Echte, *Handbuch der Technischen Polymerchemie*, VCH, Weinheim, 1993.

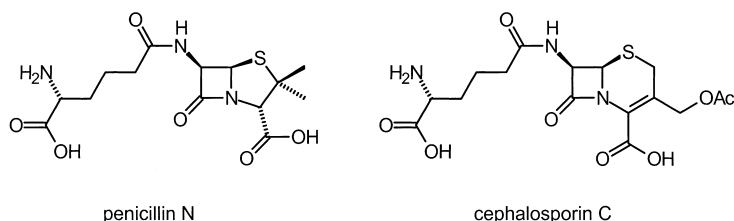
[2] D. A. Tomalia, A. M. Taylor, W. A. Goddard III, *Angew. Chem.* **1990**, 2, 119–238; *Angew. Chem. Int. Ed. Engl.* **1990**, 29, 138; M. Fischer, F.

- Vögtle, *Angew. Chem.* **1999**, *111*, 934–955; *Angew. Chem. Int. Ed.* **1999**, *38*, 884–905, and references therein.
- [3] For example, H.-H. Brinzing, D. Fischer, R. Mülhaupt, B. Rieger, R. Waymouth, *Angew. Chem.* **1995**, *107*, 1255; *Angew. Chem. Int. Ed. Engl.* **1995**, *34*, 1143.
- [4] For example, D. Colombani, *Prog. Polym. Sci.* **1997**, *22*, 1649; E. E. Malmström, C. J. Hawker, *Macromol. Chem. Phys.* **1998**, *199*, 923; T. E. Patten, K. Matyjaszewski, *Adv. Mater.* **1998**, *10*, 901, and references therein.
- [5] T. Yokozawa, H. Suzuki, *J. Am. Chem. Soc.* **1999**, *121*, 11573.
- [6] I. Mita, R. F. T. Stepto, U. W. Suter, *Pure Appl. Chem.* **1994**, *66*, 2483.
- [7] R. W. Lenz, C. E. Handlovitis, H. A. Smith, *J. Polym. Sci.* **1962**, *58*, 351.
- [8] D. R. Robello, A. Ulman, E. J. Uranka, *Macromolecules* **1993**, *26*, 6718.
- [9] T. Yokozawa, H. Shimura, *J. Polym. Sci. Part A* **1999**, *37*, 2607.
- [10] For example, L. H. Tagle in *Handbook of Phase Transfer Catalysis* (Eds.: Y. Sasson, R. Neuman), Blackie Academic & Professional, London, **1997**, p. 200.

Isopenicillin N Synthase: An Enzyme at Work

Wolfdieter A. Schenk*

The discovery of penicillin in 1929^[1] has revolutionized medicine.^[2] Many of the potentially lethal bacterial infections lost their specter as life threatening diseases—a situation which could change again soon.^[3] The penicillins (Scheme 1)



Scheme 1. Structures of a typical penicillin and a typical cephalosporin. Ac = acetyl.

were the first antibiotics, and for a long time the term “penicillin” was used by the general public as a synonym for “antibiotic”.

Further milestones were set with the determination of the structure of penicillin^[4] and the first total synthesis of a naturally occurring penicillin.^[5] The laboratory synthesis of penicillin and its derivatives turned out to be quite a challenge because of its bicyclic structure, which makes the β -lactam ring particularly labile.^[6] It is not surprising then that the question, “how does nature do it?” attracted the attention of the scientific community.

Most of the early information came from fairly indirect evidence.^[7] The immediate precursor, the linear tripeptide L- α -amino adipoyl-L-cysteinyl-D-valine (LLD-ACV), is first assembled from its component amino acids by the action of ACV synthase, which also mediates the necessary epimerization of valine. The key step, the stoichiometrically simple oxidative cyclization [Eq. (1)], is brought about by a single,



non-heme iron-containing enzyme dubbed isopenicillin N synthase (IPNS). Further enzymes are then responsible for the epimerization of isopenicillin N to penicillin N, the derivatization to other penicillins, and the ring expansion that eventually leads to the various cephalosporins.

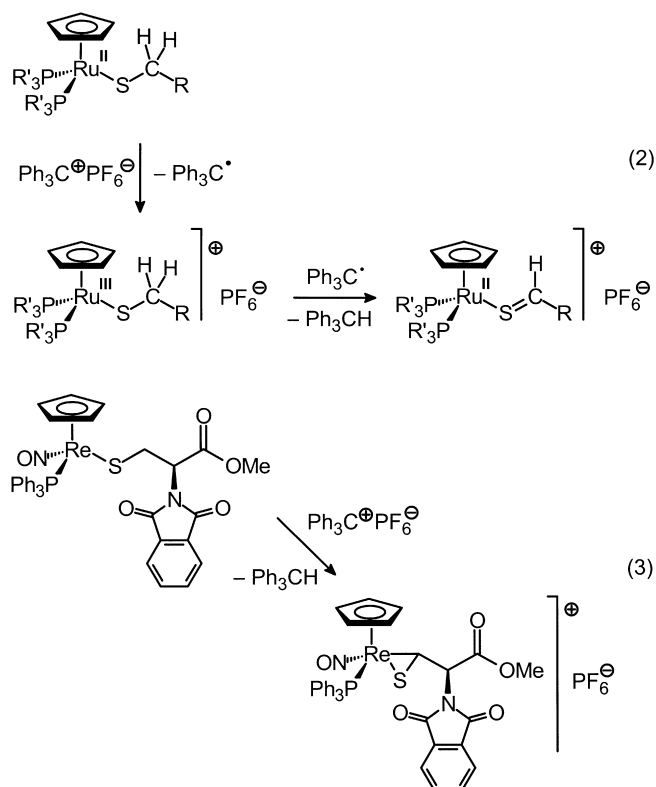
Despite considerable effort enzyme-free intermediates of this process have never been found. This indicates that both rings are formed within the same enzyme–substrate complex. Studies with modified substrates served to define the properties of the active site. A surprising range of variations of both the amino adipoyl and the valinyl termini of ACV are tolerated, which helped the gathering of mechanistic information. Thus, if D-valine was replaced by other amino acids containing allyl or cyclopropylmethyl groups as “radical clocks”, the appearance of the typical rearrangement products indicated that an (perhaps conformationally restrained) isopropyl radical intermediate is presumably involved in the formation of the thiazolidine ring.^[8] The L-amino adipoyl terminus may be replaced by a range of nonpolar substituents of similar size that are not necessarily terminated by a carboxylic group. This is good evidence that the corresponding part of the binding region of IPNS is nonpolar but contains a hydrogen-bonding site at the end of the pocket.^[7] The central cysteine unit, however, is essentially inviolate. This is

[*] Prof. Dr. W. A. Schenk
Institut für Anorganische Chemie
Universität Würzburg, Am Hubland, 97074 Würzburg (Germany)
Fax: (+49) 931-8884605
E-mail: wolfdieter.schenk@mail.uni-wuerzburg.de

understandable in view of the constraints imposed by the formation of the strained β -lactam ring.

Further insight into the details of the mechanism came from a series of ingeniously planned deuteration experiments. For example, a large kinetic isotope effect was found when IPNS was fed a mixture of ACV doubly labeled in the 3-position of cysteine, and unlabeled ACV. On the other hand, IPNS does not discriminate between unlabeled ACV and ACV labeled in the 3-position of valine. This was taken as compelling evidence that the formation of the β -lactam ring is rate-limiting and precedes the closure of the thiazolidine ring.^[9] Furthermore, through the use of ACV containing stereo-specifically deuterated cysteine it was demonstrated that the hydrogen abstraction and ring-closure sequence occurs with retention of configuration, perhaps via an enzyme-bound thioaldehyde.^[7a]

Transition metal complexes of thioaldehydes are well known since 1977.^[10] A synthesis of metal-bound thioaldehydes by hydrogen abstraction from thiolate complexes was reported in 1992^[11] [Eq. (2)] and recently extended to a range of aliphatic thioaldehydes, and includes an example of a side-on coordinated thioaldehyde derived from cysteine [Eq. (3)].^[12]

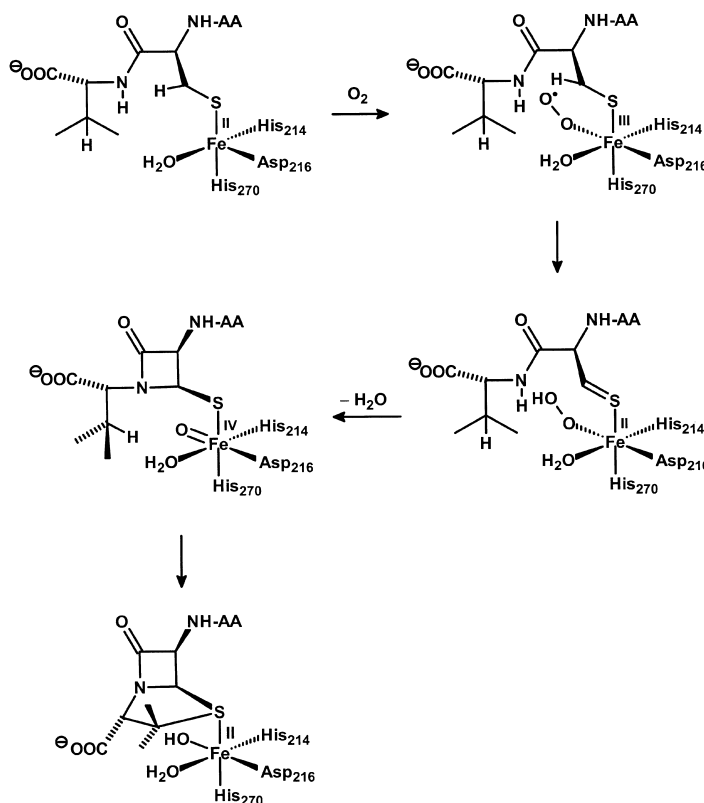


These reactions, which even show a comparably high kinetic isotope effect,^[11] may be taken as organometallic analogues of the hydride abstraction step of the penicillin biosynthesis. Furthermore, the addition of nucleophiles to metal-bound thioaldehydes is well documented,^[13] lending further support to the proposed mechanism.

A major breakthrough in this field came again from the group of J. E. Baldwin with the successful determination of the structure of IPNS.^[14] The crystals were grown under

anaerobic conditions so that the enzyme lacked the oxygen necessary for the reaction. By using this trick it was even possible to study the intact enzyme–substrate complex. Furthermore, after treatment with nitric oxide the corresponding nitrosyl complex was obtained which can serve as an unreactive structural model of the O₂-addition intermediate. In both cases the carboxylate groups at the ends of ACV are anchored through hydrogen bridges to the surrounding protein. This forces the substrate into an extended conformation which facilitates the closure of the β -lactam ring.

Based on this wealth of information a detailed mechanism of the action of IPNS could be formulated (Scheme 2). After binding the substrate ACV through the deprotonated thiol

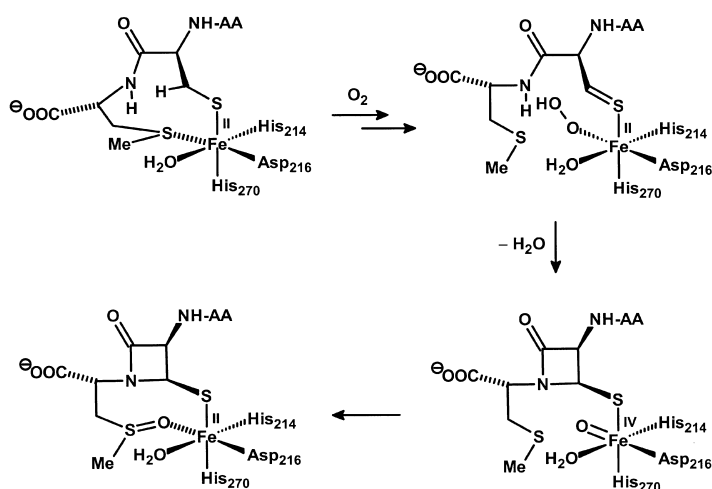


Scheme 2. Mechanism of the biosynthesis of isopenicillin N. AA = aminoadipoyl.

group of the cysteine, the iron center takes up an oxygen molecule and changes oxidation state. Intramolecular transfer of a hydrogen atom from C-3 of the cysteine unit takes the iron back to the +II state and produces a thioaldehyde as well as a hydroperoxy ligand. The latter serves to deprotonate the amide function, which then closes the β -lactam ring by nucleophilic attack at the thioaldehyde carbon atom. With this the hydrogen atom at C-3 of valine comes in closer proximity to the highly electrophilic iron(IV) oxo ligand. A second hydrogen transfer follows, presumably producing an isopropyl radical which attacks the thiolate sulfur atom and thus closes the thiazolidine ring.

This already conclusive work has now been topped, again by the group around J. E. Baldwin, with a series of experiments which make IPNS now one of the best understood

enzymes.^[15] A crystal of the IPNS-ACV complex has been incubated with oxygen at 4 MPa for 320 min and the structure of the complex determined. It turned out that the substrate ACV had been transformed to isopenicillin N (IPN) which remained bound to the active site (some residual electron density indicated that under these conditions ca. 30 % of the substrate remain unchanged). In a separate set of experiments IPNS was complexed with a modified substrate (ACmC) in which valine had been replaced by (*S*)-methylcysteine. The structure of the active site of IPNS-ACmC is very similar to that of IPNS-ACV, except that the (*S*)-methyl group now occupies the sixth iron coordination site. Treatment of this crystal with oxygen (2 MPa, 10 min) gave a monocyclic β -lactam product complexed to the active site through the cysteinyl sulfur atom and a methylsulfenyl group, which may have originated from an interception reaction at the proposed Fe^{IV} oxo intermediate (Scheme 3).



Scheme 3. IPNS-mediated oxidative cyclization of ACmC.

This product is a good model of the monocyclic β -lactam intermediate of the IPN synthesis, whose transient existence had been inferred previously (see above). An overlay of the four structures is shown in Figure 1. Note in particular the

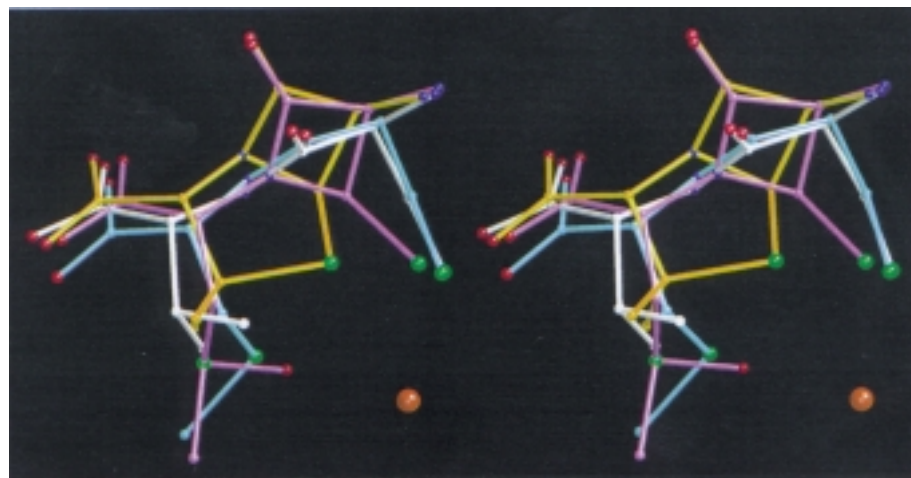
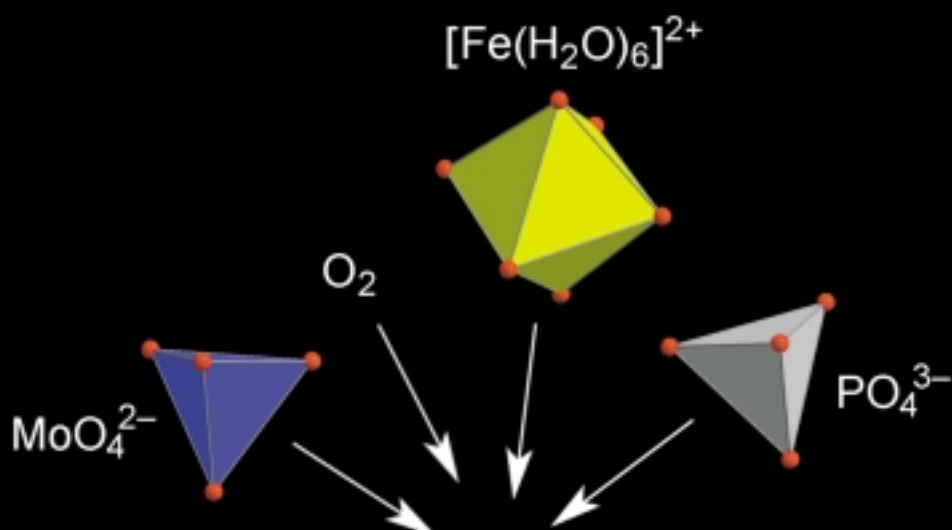


Figure 1. Stereoview of overlaid structures of the active site of IPNS complexed with ACV (white), ACmC (blue), oxidized ACmC (pink), and IPN (yellow). Reprinted with permission from *Nature* (*Nature* **1999**, 401, 721–724), Copyright **1999**, Macmillan Magazines Ltd.

extension of the Fe–S bond of the final product which anticipates the release of IPN from the active site.

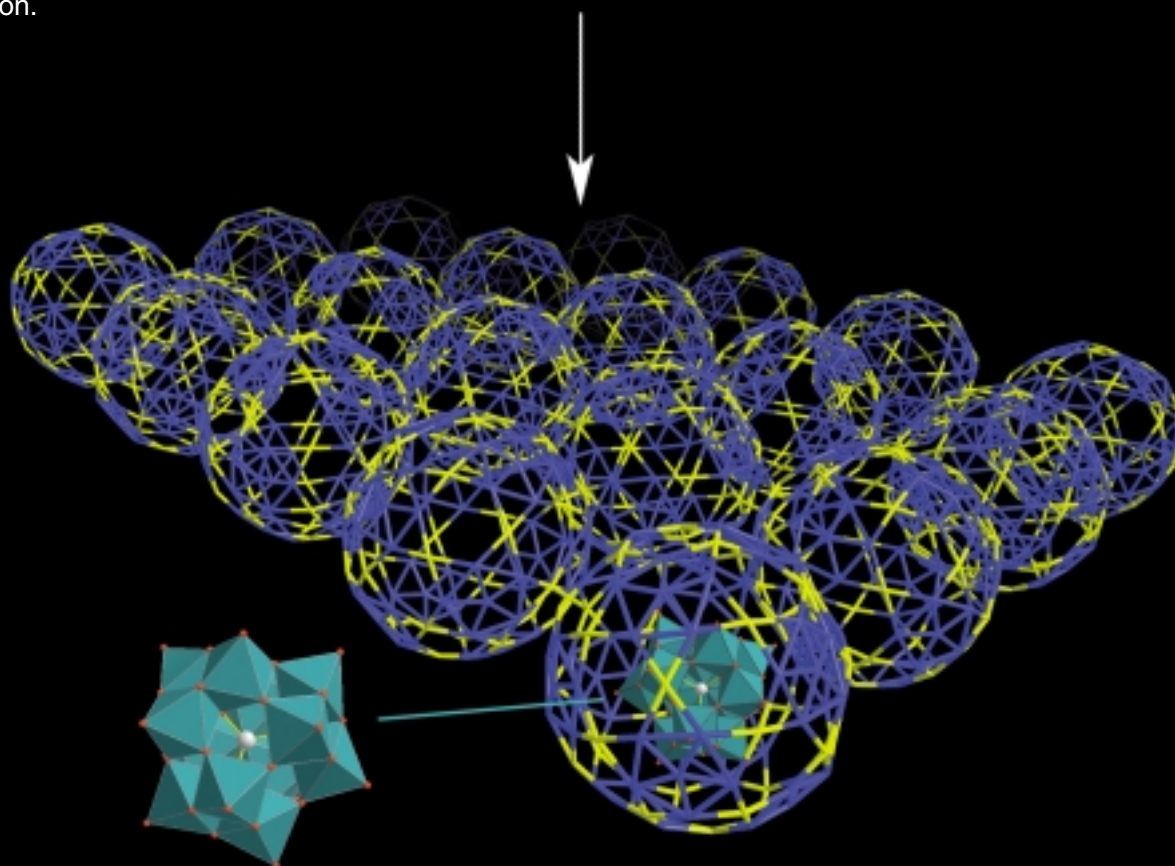
With the oxidized ACmC taken as a model of the β -lactam intermediate, this series of structures provides a kind of animated cartoon of the details of the function of an enzyme. The rapid development of crystallographic instrumentation and methods may soon make investigations such as this a routine part of the elucidation of enzymatic reactions.

- [1] A. Fleming, *Brit. J. Exp. Path.* **1929**, 10, 226.
- [2] E. Chain, H. W. Florey, A. D. Gardner, N. G. Heatley, M. A. Jennings, J. Orr-Ewing, A. G. Sanders, *Lancet* **1940**, 226–228.
- [3] D. Niccolai, L. Tarsi, R. J. Thomas, *Chem. Commun.* **1997**, 2333–2342.
- [4] D. Crowfoot, C. W. Bunn, B. W. Rogers-Low, A. Turner-Jones in *The Chemistry of Penicillin* (Eds.: H. T. Clarke, J. R. Johnson, R. Robinson), Princeton University Press, Princeton, **1949**, chap. 11.
- [5] a) J. C. Sheehan, K. R. Henery-Logan, *J. Am. Chem. Soc.* **1957**, 79, 1262–1263; b) J. C. Sheehan, K. R. Henery-Logan, *J. Am. Chem. Soc.* **1959**, 81, 3089–3094.
- [6] K. C. Nicolaou, E. J. Sorensen, *Classics in Total Synthesis*, VCH, Weinheim, **1996**, chap. 3.
- [7] a) J. E. Baldwin, M. Bradley, *Chem. Rev.* **1990**, 90, 1079–1088; b) J. E. Baldwin, C. J. Schofield in *The Chemistry of β -Lactams* (Ed.: M. I. Page), Chapman and Hall, London, **1992**, chap. 1.
- [8] a) J. E. Baldwin, R. M. Adlington, B. P. Domayne-Hayman, G. Knight, H.-H. Ting, *J. Chem. Soc. Chem. Commun.* **1987**, 1661–1663; b) J. E. Baldwin, M. Bradley, N. J. Turner, R. M. Adlington, A. R. Pitt, H. Sheridan, *Tetrahedron* **1991**, 47, 8203–8222; c) J. E. Baldwin, M. Bradley, N. J. Turner, R. M. Adlington, A. R. Pitt, A. E. Derome, *Tetrahedron* **1991**, 47, 8223–8242.
- [9] J. E. Baldwin, R. M. Adlington, S. E. Moroney, L. D. Field, H.-H. Ting, *J. Chem. Soc. Chem. Commun.* **1984**, 984–986.
- [10] a) T. J. Collins, W. R. Roper, *J. Chem. Soc. Chem. Commun.* **1977**, 901–902; b) R. G. W. Gingerich, R. J. Angelici, *J. Am. Chem. Soc.* **1979**, 101, 5604–5608; c) R. D. Adams, N. M. Golembeski, J. P. Selegue, *Organometallics* **1982**, 1, 240–245; d) M. Herberhold, W. Ehrenreich, W. Bühlmeier, *Angew. Chem.* **1983**, 95, 332–333; *Angew. Chem. Int. Ed. Engl.* **1983**, 22, 315–316; e) W. Paul, H. Werner, *Angew. Chem.* **1983**, 95, 333–334; *Angew. Chem. Int. Ed. Engl.* **1983**, 22, 316–317; f) W. E. Buhro, A. T. Patton, C. E. Strouse, J. A. Gladysz, F. B. McCormick, M. C. Etter, *J. Am. Chem. Soc.* **1983**, 105, 1056–1058.
- [11] a) W. A. Schenk, T. Stur, E. Dombrowski, *Inorg. Chem.* **1992**, 31, 723–727; b) W. A. Schenk, T. Stur, E. Dombrowski, *J. Organomet. Chem.* **1994**, 472, 257–273.
- [12] N. Burzlaff, W. A. Schenk, *Eur. J. Inorg. Chem.* **1999**, 1435–1443.
- [13] H. Fischer, R. Stumpf, G. Roth, *Adv. Organomet. Chem.* **1999**, 43, 125–196.
- [14] P. L. Roach, I. J. Clifton, C. M. H. Hensgens, N. Shibata, C. J. Shofield, J. Hajdu, J. E. Baldwin, *Nature* **1997**, 387, 827–830.
- [15] N. I. Burzlaff, P. J. Rutledge, I. J. Clifton, C. M. H. Hensgens, M. Pickford, R. M. Adlington, P. L. Roach, J. E. Baldwin, *Nature* **1999**, 401, 721–724.



The route to a *novel supramolecular compound* in a cascade reaction: Molybdenum-iron-oxide based composites, each consisting of a magnetic capsule with 150 unpaired electrons and an encapsulated noncovalently bonded electron reservoir Keggin-ion nucleus, can get cross-linked according to a well-defined simple inorganic condensation reaction.

Interestingly, the Keggin ion which acts as template for the formation of the capsule can either be generated in the reaction mixture or can—in the absence of phosphate—be added to it. Find out more on the following pages.



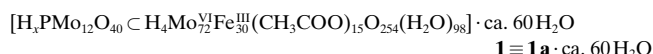
A New Type of Supramolecular Compound: Molybdenum-Oxide-Based Composites Consisting of Magnetic Nanocapsules with Encapsulated Keggin-Ion Electron Reservoirs Cross-Linked to a Two-Dimensional Network**

Achim Müller,* Samar K. Das, Paul Kögerler, Hartmut Bögge, Marc Schmidtman, Alfred X. Trautwein, Volker Schünemann, Erich Krickemeyer, and Wilhelm Preetz

Dedicated to Professor Gérard Férey on the occasion of his 60th birthday

The fabrication of ordered arrays of well-defined nanoparticles or clusters is of fundamental and technological interest. As this is a difficult task, different techniques have been employed.^[1] An elegant approach would be to link well-defined building blocks in a chemically straightforward procedure yielding a monodisperse or a completely homogeneous material. We have succeeded now even to cross-link assembled nanosized metal-oxide-based composites—novel supramolecular entities—under one-pot conditions. The supramolecular metal-oxide-based entity, we are dealing with, consists of an oxidized icosahedral capsule as host (internal cavity diameter ~ 16 Å) corresponding to a paramagnet of the type $\{\text{Mo}_{72}^{\text{VI}}\text{Fe}_{30}^{\text{III}}\}$ and the reduced Keggin cluster $[\text{H}_x\text{PMo}_{12}\text{O}_{40}]^{3-}$ ($x=1$ or 2 ; diameter of the Keggin anion ~ 14 Å) as nucleus (guest). Interestingly, the linking is based on a well known inorganic condensation process and the guest (nucleus) acts as a template for the generation of the host (capsule). This was our prior assumption, as according to a modeling investigation it turned out that the Keggin anion just fits exactly into the capsule.

In an acidified aqueous solution (pH 2) containing only polymolybdate, iron(II) chloride, and acetic acid as well as a relatively small amount of phosphate in the presence of air, a stepwise assembly process takes place leading to a new type of material, that is the neutral layer compound **1**. Compound **1**



[*] Prof. Dr. A. Müller, Dr. S. K. Das, Dipl.-Chem. P. Kögerler, Dr. H. Bögge, M. Schmidtman, E. Krickemeyer
Lehrstuhl für Anorganische Chemie I
Fakultät für Chemie der Universität
Postfach 100 131, 33501 Bielefeld (Germany)
Fax: (+49) 521-106-6003
E-mail: a.mueller@uni-bielefeld.de

Prof. Dr. A. X. Trautwein, V. Schünemann
Institut für Physik, Medizinische Universität
Ratzeburger Allee 160, 23562 Lübeck (Germany)
Prof. Dr. W. Preetz
Institut für Anorganische Chemie
Christian-Albrechts-Universität zu Kiel
Olshausenstrasse 40, 24098 Kiel (Germany)

[**] We thank Prof. Dr. H. U. Güdel (Bern), Dr. L. Cronin (Birmingham), and Dr. E. Diemann (Bielefeld) for helpful discussions.

was characterized by elemental analyses, thermogravimetry (to determine the crystal water content), single-crystal X-ray structure analysis^[2] (including the calculation of bond valence sums^[3] in order to distinguish between (terminal) O and OH_2 ligands), and spectroscopic methods (IR, resonance-Raman, UV/Vis, NIR, ^{57}Fe Mössbauer) as well as magnetic measurements (Table 1).

As **1** can also be assembled by adding the normal Keggin anion $[\text{PMo}_{12}\text{O}_{40}]^{3-}$ directly to the aqueous reaction mixture containing no phosphate according to our first approach, the other reaction (see Experimental Section, method 1) corresponds to a molecular cascade with the formation of the Keggin ion as the initial step. Correspondingly, the reaction takes a different route (with no formation of **1**!) in the presence of larger amounts of phosphate, while adding the Keggin unit seems to accelerate the capsule formation as a template. It is important to start from Fe^{II} (which gets gradually oxidized) rather than from Fe^{III} , as the latter starting material immediately results in a not well-defined precipitate.

The building block of each layer of **1** is the spherical icosahedral giant oxidized cluster cage of the $\{(\text{Mo}^{\text{VI}})\text{Mo}_5^{\text{VI}}\}_{12}\text{Fe}_{30}^{\text{III}}$ type, comparable to that reported^[4] earlier, but which now has a reduced metal-oxide-based cluster—the tetrahedral reduced Keggin $[\text{H}_x\text{PMo}_{12}\text{O}_{40}]^{3-}$ ion^[2]—as nucleus (Figure 1). Each of the cluster–cluster composites is linked

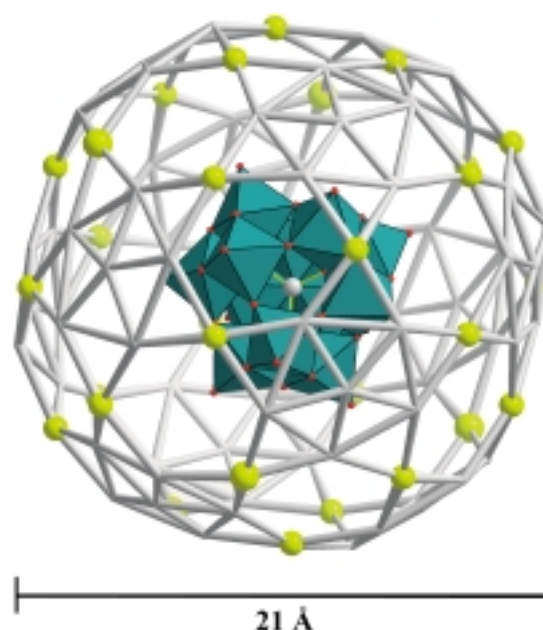


Figure 1. Demonstration of the structure of the building block of **1** with the capsule (host) and encapsulated Keggin-type cluster nucleus (guest idealized): the metal $\{\text{Mo}_{72}\text{Fe}_{30}\}$ capsule in wire frame representation—with 30 Fe^{III} centers (highlighted as yellow spheres) linking the 12 $\{(\text{Mo}^{\text{VI}})\text{Mo}_5^{\text{VI}}\}$ pentagons—and the Keggin nucleus in polyhedral representation.

to four others through Fe–O–Fe bonds to form a layer structure (Figure 2). The spherical capsule comprises 12 pentagonal fragments of the type $\{(\text{Mo})\text{Mo}_5\text{O}_{21}\}$ (built up by a central bipyramidal MoO_7 group linked by edge-sharing to five MoO_6 octahedra) which are connected by 30 $\{(\text{Fe}^{\text{III}}(\text{H}_2\text{O})_2)^{3+}\}$ linkers. The (disordered) acetate ligands, which make the assembly neutral in result, are located inside

Table 1. Characteristics of the two-dimensional layer structure formed by cross linking novel supramolecular-type (composite) building blocks: $\{\text{Mo}_{12}\subset\text{Mo}_{72}\text{Fe}_{30}\}$ (spherical icosahedral capsule and an encapsulated nucleus of tetrahedral symmetry).

	capsule (host)	Building block (capsule and nucleus) Keggin nucleus (guest)	Interaction characteristics
imposed Platonic/ Archimedean solids	icosidodecahedron (Fe_{30}) icosahedron ($\{(\text{Mo})\text{Mo}_5\}_{12}$)	cubeoctahedron (Mo_{12}) rhombicuboctahedron (O_{24})	topological host–guest complementarity
symmetry	icosahedral metal framework (I_h)	tetrahedral (T_d)	
geometrical data	diameter: ca. 2.5 nm		min. O(shell) ... O(nucleus) = ca. 2.6 Å
building units	90 octahedra ($\text{Fe}^{\text{III}}\text{O}_4(\text{H}_2\text{O})_2$, $\text{Mo}^{\text{VI}}\text{O}_6$) 12 pentagonal bipyramids ($\text{Mo}^{\text{VI}}\text{O}_7$)	1 tetrahedron ($\text{P}^{\text{V}}\text{O}_4$) 12 octahedra ($\text{Mo}^{\text{VI}}\text{O}_6$)	
electronic transitions [cm^{-1}]	$\text{O}\rightarrow\text{Mo}^{\text{VI}}$ charge transfer: ~ 27000	intervalence charge transfer ($\text{Mo}^{\text{V}}\rightarrow\text{Mo}^{\text{VI}}$): $\sim 11\,600/\sim 9500$ [a]	nucleus \rightarrow shell charge transfer: $\sim 18\,100$
vibrations [cm^{-1}] ^[b]	$\nu(\text{MoO}_4)$ (IR): 960	$\nu(\text{O}_{\text{br}})$ -breathing(resonance Raman) ^[c] : 830 $\nu_{\text{as}}(\text{PO}_4)$ (IR): 1068	
redox state ^[d]	oxidized (72 Mo^{VI} and 30 Fe^{III})	reduced (electron reservoir)	
magnetism	strong paramagnet corresponding to 26 antiferro- magnetically coupled Fe^{III} ($S=5/2$) centers (at RT, $\chi_{\text{mol}}T=114\text{ emu K mol}^{-1}$) ^[e]		
nuclei properties [mm s^{-1}]	^{57}Fe Mössbauer isomer shift/quadrupole splitting (180 K): $\delta=0.48/\Delta E_{\text{Q}}=0.70$ (characteristic for $\text{Fe}^{\text{III}}\text{O}_6$)		

[a] Solid, transmission of a film obtained from the pure substance by pressure (10 kbar) between saphir pistils (the electronic spectra of reduced Keggin ions strongly depend on their environment, for example the type of solvent). [b] KBr pellet (the band at 1068 cm^{-1} supports the presence of a Keggin ion^[2]). [c] $\lambda_{\text{e}}=1064\text{ nm}$. [d] Potentiometric titration using $\text{Ce}(\text{SO}_4)_2$. [e] Whereas the susceptibility of discrete $\{\text{Mo}_{72}\text{Fe}_{30}\}$ units which exist in the wet crystals (measured directly after filtration) at room temperature corresponds to 30 nearly uncorrelated Fe^{III} centers, due to the linking of the building blocks through four $\text{Fe}^{\text{III}}\text{--O--Fe}^{\text{III}}$ bonds (see also ref. [4] for a related problem) the magnetic moment corresponds effectively to only 26 uncorrelated Fe^{III} centers at room temperature.

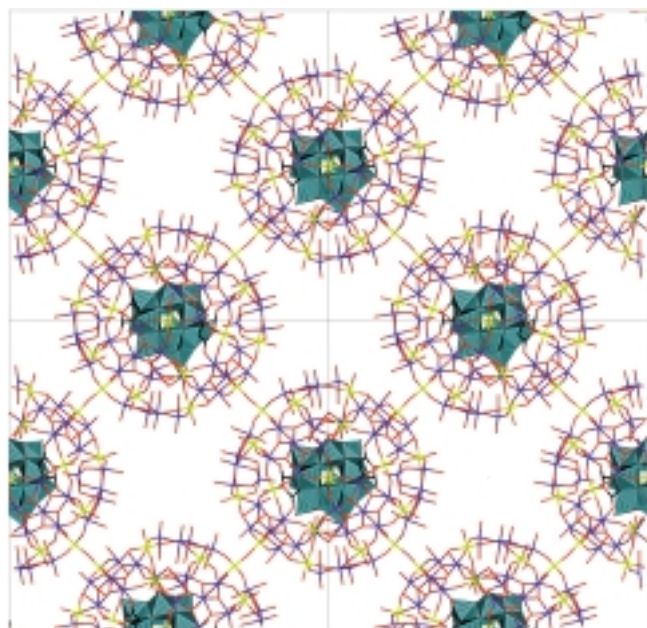


Figure 2. Schematic structural depiction of a layer segment in crystals of **1** with the capsules (including O atoms in contrast to Figure 1) in wire frame (O: red; Fe: yellow; Mo: blue) and the Keggin ions (idealized) in polyhedral representation.

the sphere and coordinate as bidentate ligands to the metal centers, preferably bridging Fe and Mo sites.

Selected physical properties of **1** are summarized in Table 1 and displayed in Figure 3. They not only prove the existence

of the two separate, noncovalently bonded parts of each supramolecular entity (the capsule and its nucleus), but show also its interesting topological, spectroscopic, electronic, and magnetic properties. The reduced Keggin cluster can be identified nicely by means of the resonance-Raman effect (Figure 3d) showing only the vibrational bands of this unit. The nanocapsules of the type $\{(\text{Mo}^{\text{VI}})\text{Mo}_5^{\text{VI}}\}_{12}\text{Fe}_{30}^{\text{III}}$, which form a system of magnetic dots (each individual discrete dot represents as yet the strongest known molecular paramagnet due to the presence of 30 Fe^{III} centers with 150 (!) unpaired electrons, that is, $S=150/2$ at room temperature), encapsulate the reduced nuclei (quantum dots) as guests which can be regarded as potential electron-storage elements. Notably, the free Keggin cluster can be reduced in several steps in association with concomitant protonation thus keeping its charge constant.^[5]

The noncovalent host–guest interactions are worthy of consideration as the reduced electron reservoir-type Keggin ion fits exactly into the capsule cavity (the shortest $\text{O}_{\text{host}}\cdots\text{O}_{\text{guest}}$ bond lengths, typical for hydrogen bonding, are of the order of 2.6 Å). This type of composite/supramolecular entity with a reduced nucleus in an oxidized shell is unprecedented. The band observed at $\sim 550\text{ nm}$ ($\sim 18.1\times 10^3\text{ cm}^{-1}$; Figure 3b) which contributes to the color can tentatively be assigned to a novel charge transfer transition of the type *reduced nucleus* \rightarrow *oxidized shell*.^[6]

The knowledge of the chemistry of nanocapsules which are variable in size^[4a] and linkable^[4b] allows us the synthesis of new types of materials. It is even possible to open the capsules, exchange their contents, and close them again^[7] which allows

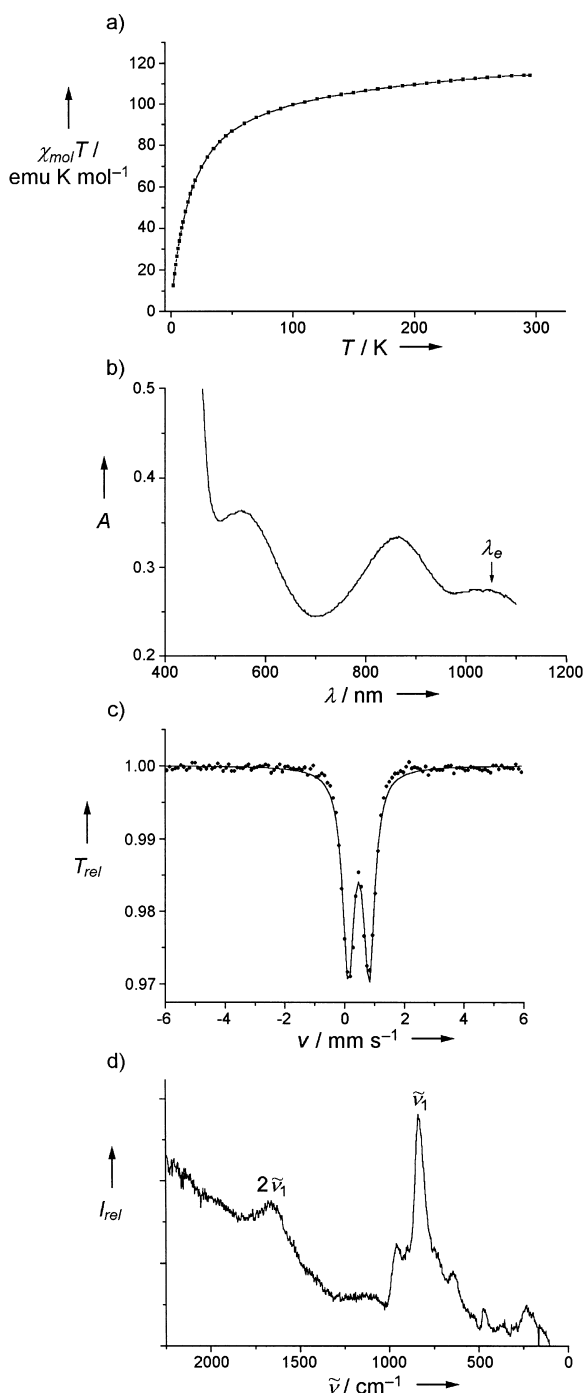


Figure 3. Physical/spectroscopic data of **1** that characterize the capsule and encapsulated nucleus: a) magnetic susceptibility as function of temperature, b) electronic absorption with λ_e for the resonance Raman spectrum, c) ^{57}Fe Mössbauer, and d) resonance-Raman spectra (for details see Table 1).

the fabrication of different types of cross-linked composites. We refer to a new class of novel composite (a cluster encapsulated in a cluster) type materials, in which the electronic/magnetic structure of the composite (quantum/magnetic dot) can, in principle, be tuned by changing the relevant properties of the constituents, for instance by changing the electron population of the nucleus (Keggin anion).

Experimental Section

1: Method 1: $\text{NaH}_2\text{PO}_4 \cdot 2\text{H}_2\text{O}$ (0.21 g, 1.35 mmol) was added to a solution obtained by treating a mixture of H_2O (75 mL), $\text{FeCl}_2 \cdot 4\text{H}_2\text{O}$ (1.0 g, 5.03 mmol), and $\text{Na}_2\text{MoO}_4 \cdot 2\text{H}_2\text{O}$ (5.0 g, 20.66 mmol) with CH_3COOH (100%, 10 mL). After acidification with about 3 mL of 32% hydrochloric acid (pH of the reaction mixture ~ 2.0), the solution was stirred for 15 min at room temperature and filtered. The filtrate was kept for seven days at 20°C in an open 250 mL beaker for crystallization. The greenish crystals (thin plates) were filtered, washed with water, and dried at room temperature. Yield: 0.45 g (14.8% based on Fe) (correct analysis).

Method 2: $\text{H}_3[\text{P}(\text{Mo}_3\text{O}_{10})_4]$ (2.5 g, 1.37 mmol) was added to a solution obtained by treating a mixture of H_2O (75 mL), $\text{FeCl}_2 \cdot 4\text{H}_2\text{O}$ (1.0 g, 5.03 mmol), and $\text{Na}_2\text{MoO}_4 \cdot 2\text{H}_2\text{O}$ (2.0 g, 8.27 mmol) with CH_3COOH (100%, 10 mL). After acidification with about 0.5 mL 32% HCl acid (pH of the reaction mixture ~ 2.0), the solution was stirred for 45 min at room temperature and filtered. The filtrate was kept in an open 250 mL beaker for crystallization for five days. The crystals were filtered, washed with water, and dried at room temperature. Yield: 0.5 g (correct analysis).

Received: June 19, 2000 [Z15279]

- [1] a) C. P. Collier, R. J. Saykally, J. J. Shiang, S. E. Henrichs, J. R. Heath, *Science* **1997**, 277, 1978–1981; b) G. Schmid, M. Bäumle, N. Beyer, *Angew. Chem.* **2000**, 112, 187–189; *Angew. Chem. Int. Ed.* **2000**, 39, 181–183; c) S. Chen, *Adv. Mater.* **2000**, 12, 186–189; d) S. Sun, C. B. Murray, D. Weller, L. Folks, A. Moser, *Science* **2000**, 287, 1989–1992.
- [2] Crystal structure analysis of **1**: Space group *Cmca*, $a = 36.621(2)$, $b = 34.778(2)$, $c = 34.824(2)$ Å, $V = 44351(4)$ Å³, $Z = 4$, $\rho = 2.727$ g cm⁻³, $\mu = 3.367$ mm⁻¹, $F(000) = 34904$, crystal dimensions $0.36 \times 0.18 \times 0.02$ mm³. Dry crystals were cooled to 183(2) K on a Bruker axis SMART diffractometer (MoK α , graphite monochromator). A total of 112330 reflections ($1.50 < \theta < 25.06^\circ$) was collected, of which 19640 unique reflections ($R_{\text{int}} = 0.1328$) were used. The structure was solved by using the program SHELXS-97 and refined (1423 parameters) by using the program SHELXL-93 to $R = 0.073$ for 11094 reflections with $I > 2\sigma(I)$ (both programs from G. M. Sheldrick, University of Göttingen, 1993/1997, respectively). Several molecules of water of crystallization could not be located due to their disorder. For the encapsulated Keggin ion only the central P atom and partly disordered Mo atoms (but not the O atoms because of the disorder) could be detected for which the occupancy factors, however, add up to 12. This together with the analysis, the vibrational spectrum (for related IR $\nu(\text{PO})$ bands see C. Rocchiccioli-Deltcheff, R. Thouvenot, *J. Chem. Res. (S)* **1977**, 46–47; C. Rocchiccioli-Deltcheff, R. Thouvenot, *J. Chem. Res. (M)* **1977**, 549–571) and the used pH value supports the presence of a complete Keggin ion rather than a lacunary type one. Due to the disorder and related basic analytical problems in connection with the error limit of the number of acetate ligands differently protonated and reduced (singly/doubly) Keggin ions cannot be completely excluded (see also L. A. Combs-Walker and C. L. Hill, *Inorg. Chem.* **1991**, 30, 4016–4026. Crystallographic data (excluding structure factors) for the structure reported in this paper have been deposited with the Cambridge Crystallographic Data Centre as supplementary publication no. CCDC-140422 (**1**). Copies of the data can be obtained free of charge on application to CCDC, 12 Union Road, Cambridge CB21EZ, UK (fax: (+44) 1223-336-033; e-mail: deposit@ccdc.cam.ac.uk).
- [3] I. D. Brown in *Structure and Bonding in Crystals, Vol. II* (Eds.: M. O'Keeffe, A. Navrotsky), Academic Press, New York, **1981**, pp. 1–30.
- [4] a) A. Müller, S. Sarkar, S. Q. N. Shah, H. Bögge, M. Schmidtman, Sh. Sarkar, P. Kögerler, B. Hauptfleisch, A. X. Trautwein, V. Schünemann, *Angew. Chem.* **1999**, 111, 3435–3439; *Angew. Chem. Int. Ed.* **1999**, 38, 3238–3241; b) A. Müller, E. Krickemeyer, S. K. Das, P. Kögerler, S. Sarkar, H. Bögge, M. Schmidtman, Sh. Sarkar, *Angew. Chem.* **2000**, 112, 1674–1676; *Angew. Chem. Int. Ed.* **2000**, 39, 1612–1614.
- [5] a) M. T. Pope, *Heteropoly and Isopoly Oxometalates*, Springer, Berlin, **1983**; b) M. T. Pope, A. Müller, *Angew. Chem.* **1991**, 103, 56–70; *Angew. Chem. Int. Ed.* **1991**, 30, 34–48; c) J. N. Barrows, M. T. Pope, *Adv. Chem. Ser.* **1990**, 226, 403–417; d) A. Müller, E. Krickemeyer, M. Penk, V. Wittneben, J. Döring, *Angew. Chem.* **1990**, 102, 85–87; *Angew.*

Chem. Int. Ed. **1990**, 29, 88–90; e) M. T. Pope in *Mixed-Valence Compounds* (Ed.: D. B. Brown), Reidel, Dordrecht, **1980**, pp. 365–386; f) J. N. Barrows, G. B. Jameson, M. T. Pope, *J. Am. Chem. Soc.* **1985**, 107, 1771–1773.

[6] Neither a relevant reduced Keggin ion $[H_2PMo_{12}O_{40}]^{3-}$ nor the $[Mo_{72}Fe_{30}]$ -type compounds containing only Mo^{VI} and Fe^{III} centers without an encapsulated Keggin ion (see ref. [4]) taken separately show this electronic absorption band at 550 nm. Using blue or green excitation lines give Raman spectra of the capsule with changing intensity only of the 830 cm^{-1} band.

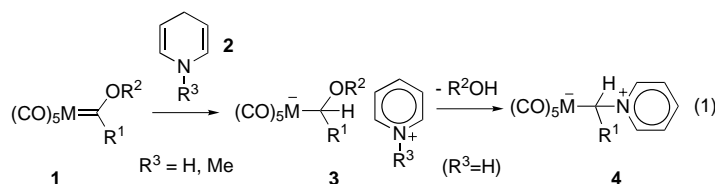
[7] A. Müller, S. Polarz, S. K. Das, E. Krickemeyer, H. Bögge, M. Schmidtman, B. Hauptfleisch, *Angew. Chem.* **1999**, 111, 3439–3443; *Angew. Chem. Int. Ed.* **1999**, 38, 3241–3245.

Linear Coupling of Three CO Ligands of Chromium Hexacarbonyl Leading to Functionalized Butenolides via Fischer Carbene Complexes

Henri Rudler,* Andrée Parlier, Victor Certal, and Jacqueline Vaissermann

Fischer carbene complexes have been widely used for the synthesis of a broad spectrum of organic compounds.^[1, 2] By far the best known applications are the formation of cyclopropanes and phenols by reaction with olefins and alkynes, respectively. Whereas in the former, besides the olefin, one CO ligand of $[Cr(CO)_6]$ is incorporated as a carbene group, in the latter, besides the alkyne, two CO ligands are included in the final product, the first one again as a carbene group. Here we describe the first general synthesis of functionalized polycyclic butenolides by incorporation of three CO groups of $[Cr(CO)_6]$, besides an alkyne. This reaction involves successive insertion reactions of a carbene complex of chromium, an alkyl chromate, an acylium chromate, and a ketene complex of chromium.

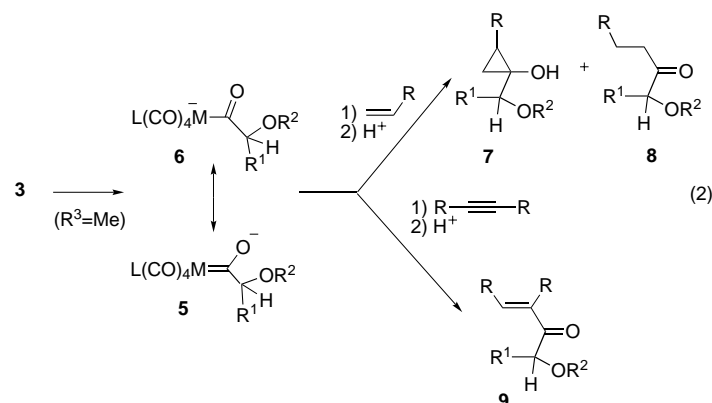
In previous papers, we have described a general dihydropyridine-induced reduction of alkoxy carbene complexes of chromium and tungsten to pyridinium metalates **3** [Eq. (1)].^[3–5] When $R^3 = H$, isolable pyridinium ylide complexes **4** were formed in high yield; for $R^3 = Me$, unstable *N*-methylpyridi-



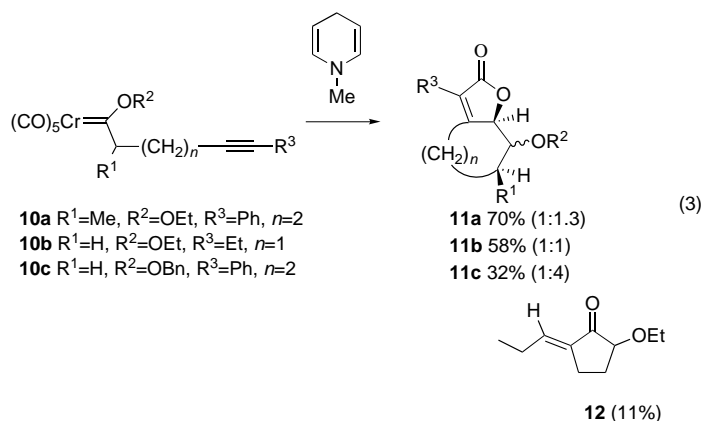
[*] Dr. H. Rudler, Dr. A. Parlier, V. Certal

Laboratoire de Chimie Organique et Organométallique, UMR 7611
 Université Pierre et Marie Curie T44-45
 4 place Jussieu 75252, Paris Cedex 5 (France)
 Fax: (+33) 1-4427-5504
 E-mail: rudler@ccr.jussieu.fr
 Dr. J. Vaissermann
 Laboratoire de Chimie Inorganique et
 Matériaux Moléculaires, UA 7071,
 Université Pierre et Marie Curie T44-45
 4 place Jussieu 75252, Paris Cedex 5 (France)

nium metalates **3** could be characterized by NMR spectroscopy. Interestingly, the latter complexes underwent a CO insertion reaction, akin to that observed for other (carbonyl)-metalates,^[6–12] to give oxycarbene complexes **5**, a resonance form of the acylium metalates **6**. These complexes gave hydroxycyclopropanes **7** and/or ketones **8** with alkenes, whereas reaction with alkynes gave α,β -unsaturated ketones **9** [Eq. (2)].

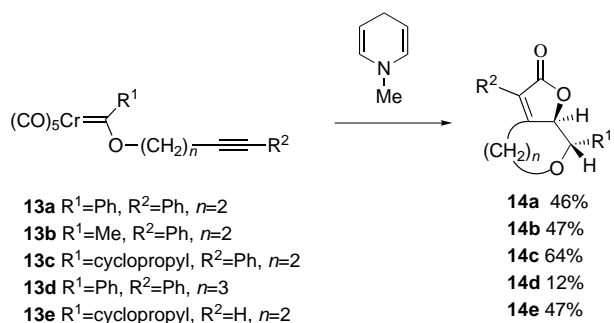


However the most gratifying transformation occurred in the case of alkynylalkoxycarbene complexes of chromium. When complex **10a** was treated with a twofold excess of *N*-methyl dihydropyridine at -10°C and the reaction mixture warmed to room temperature overnight, the bicyclic butenolide **11a** was obtained in 70% yield as a 1/1.3 mixture of *cis/trans* isomers which differ in the relative configuration of the hydrogen atoms at the ring junction and on the carbon atom bearing the ethoxyl group [Eq. (3)]. Their structures were established by NMR spectroscopy.



Changing the nature of the substituents on the triple bond and the number of methylene groups in the alkynyl chain did not affect the course of the reaction: complex **10b** gave **11b** in 58% yield as a 1/1 mixture of isomers together with 11% of **12**. The alkoxy group was modified by a known procedure, which in the case of benzyl alcohol led to **10c**.^[13, 14] Reaction of **10c** with *N*-methyl dihydropyridine gave the butenolide **11c**, again as a mixture of isomers (1:4), in 32% yield.

Similarly, the introduction of alkynyloxy groups led to the carbene complexes **13a–e**. In all the cases examined so far, clean conversion to the expected butenolides **14a–e**, as single isomers, was observed. Lengthening of the alkynyl chain led to the expected product **14d** containing a seven-membered ring, albeit in a much lower yield (12%) [Eq. (4)].



The structure of compound **14a** was confirmed by X-ray crystallography, and a Cameron projection appears in Figure 1. It clearly shows the *trans* stereochemistry of the

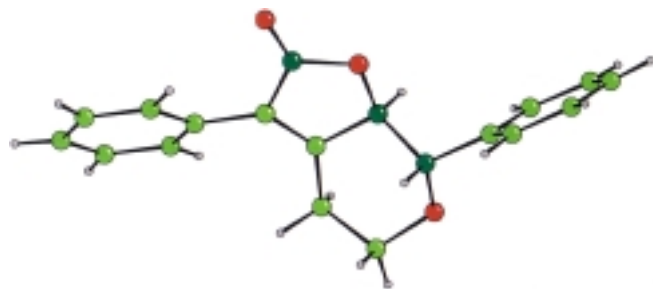
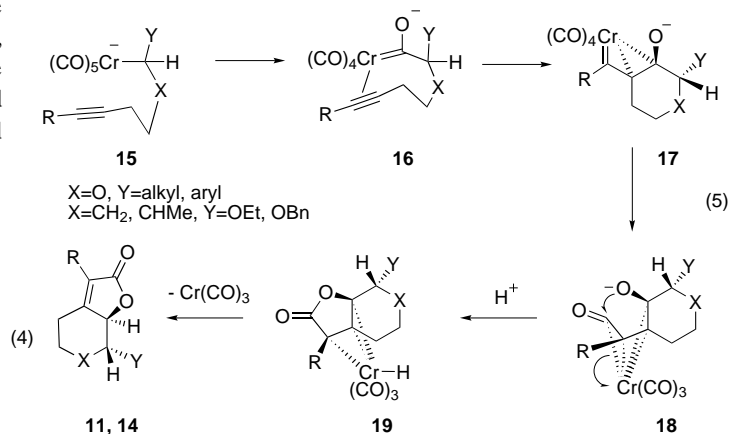


Figure 1. Molecular projection of the butenolide **14a** showing the carbon and the oxygen atoms of the incorporated carbonyl groups. Color code: C green, O red, H grey.

carbon–oxygen single bond of the lactone with respect to the phenyl group, and more importantly, the presence of the coupled three former CO groups.

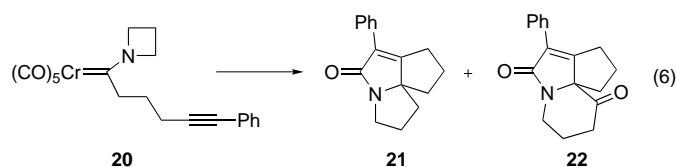
Although the exact structures of the intermediates are unknown as yet, a mechanism can be suggested on the basis of previous observations. The reduction of the starting carbene complexes with *N*-methyl-2-pyrrolidone leads first to the chromate **15** [Eq. (5)]. A straightforward transformation into an oxycarbene complex **16** by migration of the (alkoxy)alkyl group to an adjacent CO ligand then occurs with concomitant coordination of the triple bond. A classical transformation of **16** leads to **17**, a new carbene complex, then to ketene complex **18**. The close proximity of a nucleophile to the central carbon atom of the ketene, a situation which was already encountered in the insertion of alkynes into alkoxy- and aminocarbene complexes of chromium, promotes the formation of an oxygen–carbon bond, the last step of a linear oligomerization of three CO groups of [Cr(CO)₆].^[15, 17, 18]

The general stereochemical outcome of these cascade insertions is linked to two determining steps: the transfer of a hydride to the carbene carbon atom and the addition of a proton to the carbon atom α to the former carbene carbon



atom in the ketene complex **18**. The exact mechanism of these processes is still a matter of speculation. Three cases must be considered: first, when the alkynyl chain is linked to the oxygen atom as in **15** (X=O, Y=alkyl or aryl), then the reaction led specifically to a single isomer in which Y is *trans* with respect to the carbon–oxygen single bond of the lactone. This might be indicative of a metal-assisted stereospecific protonation:^[16] for steric reasons, the cycloaddition between the triple bond and the carbene moiety in **16** is likely to lead to **17** and then to **18**, in which the alkoxide is *trans* to Y and to the metal center. Protonation at the metal atom would then lead to **19**, which might deliver hydride *cis* to Y and give **14**. For less bulky substituents, as in **15** (Y=OEt, X=CH₂), the selectivity of the protonation step is obviously less marked, and both the *cis* and *trans* isomers are formed. The behavior of complexes of the type **15** (Y=OEt, OBn, X=CHMe) was peculiar, since only two isomers, in which the carbon–oxygen single bond of the lactone and the methyl groups adopt a *cis* configuration, were detected. Three contiguous asymmetric carbon centers are present in **11a**, two of which are formed during the insertion reactions. In these cases, the lack of complete diastereoselectivity may be due to a lack of stereoselectivity in the hydride-transfer step.

Although we had already observed during the thermolysis of aminocarbene complexes of the type **20**, besides the expected product **21**, a product of structure **22**, in which three CO groups have been incorporated, its structure, and thus the mode of its formation is fundamentally different, since the CO groups are not linearly coupled in the tricyclic nitrogen-containing compound.^[17, 18] [Eq. (6)]



Taken together, the transformations described here lead to butenolides in which three former CO ligands of [Cr(CO)₆] are linked together by carbon–carbon or carbon–oxygen bonds.

Experimental Section

Reaction of *N*-methylidihydropyridine with carbene complexes (general procedure): A solution of *N*-methylidihydropyridine (3 equiv) in CH₂Cl₂ (0.5 mL per mmol of amine) was added dropwise to a solution of carbene complex (1 equiv) in CH₂Cl₂ (25 mL per mmol of carbene) at -10 °C under argon. After 15 min, the ice bath was removed and the mixture was stirred at room temperature for 24 h. The solution slowly turned dark red. The solvent was evaporated under vacuum, and the residue purified by chromatography on silica gel with petroleum ether (PE)/Et₂O as eluent.

The general procedure was followed with carbene complex **10a** (2.03 g, 5 mmol). Elution with PE/Et₂O (70/30) gave a 4:3 mixture of two isomers (0.953 g, 70 %). **11a** (*trans*): ¹H NMR (200 MHz, CDCl₃): δ = 7.49–7.24 (m, 5H; ArH), 4.74 (d, ³J(H,H) = 8.4 Hz, 1H; H^{7a}), 4.06 (m, 1H; OCH₂), 3.60 (m, 1H; OCH₂), 2.81 (dd, ³J(H,H) = 10.2, 8.4 Hz, 1H; H⁷), 2.32 (m, 1H; H⁴), 1.90 (m, 1H; H⁴), 1.56 (m, 1H; H⁵), 1.75 (m, 1H; H⁶), 1.24 (t, ³J(H,H) = 7 Hz, 3H; CH₃), 1.08 (d, ³J(H,H) = 6.3 Hz, 1H; H⁸), 0.84 (m, 1H; H⁵); ¹³C NMR (100 MHz, CDCl₃): δ = 172.6 (CO), 161.2 (C³), 129.5, 128.8, 128.5, 128.3, 128.1 (Ar), 124.4 (C^{3a}), 87.8 (C^{7a}), 85.9 (C⁷), 67.9 (OCH₂), 35.9 (C⁶), 32.3 (C⁴), 25.7 (C⁵), 17.4 (C⁸), 15.5 (CH₃). **11a** (*cis*): ¹H NMR (200 MHz, CDCl₃): δ = 7.49–7.24 (m, 5H; ArH), 4.82 (d, ³J(H,H) = 3.4 Hz, 1H; H^{7a}), 3.82 (brs, 1H; H⁷), 3.72 (m, 1H; OCH₂), 3.57 (m, 1H; OCH₂), 3.01 (m, 1H; H⁴), 2.30 (m, 1H; H⁴), 1.80 (m, 1H; H⁵), 1.58 (m, 2H; H⁵), 1.08 (d, ³J(H,H) = 6.3 Hz, 3H; H⁸), 1.05 (t, 3H; ³J(H,H) = 9 Hz, 3H; CH₃); ¹³C NMR (100 MHz, CDCl₃): δ = 173.3 (CO), 161.0 (C³), 130.5, 129.2, 128.9, 128.8, 128.6 (Ar), 125.7 (C^{3a}), 83.0 (C^{7a}), 80.9 (C⁷), 69.8 (OCH₂), 34.5 (C⁶), 26.7 (C⁴), 26.1 (C⁵), 17.8 (C⁸), 15.9 (CH₃); HR-MS (positive EI) calcd. for C₁₇H₂₁O₃: 273.1491; found: 273.1495.

The general procedure was followed with carbene complex **13a** (2 g, 4.69 mmol). Elution with PE/Et₂O (80/20) gave **14a** as a white solid (0.631 g, 46 %), m.p. 59 °C. ¹H NMR (200 MHz, CDCl₃): δ = 7.58–7.35 (m, 10H; ArH), 4.75 (d, ³J(H,H) = 8.8 Hz, 1H; H^{7a}), 4.38 (dd, ³J(H,H) = 11.4 Hz, 1H; H⁵), 4.15 (d, 1H; ³J(H,H) = 8.8 Hz, 1H; H⁷), 3.52 (td, 1H; ³J(H,H) = 11.4, 3 Hz, 1H; H⁵), 3.15 (dd, 1H; ³J(H,H) = 2.5, 14 Hz, H⁴), 2.91 (ddd, ³J(H,H) = 14, 11.8, 6 Hz, 1H; H⁴); ¹³C NMR (50 MHz, CDCl₃): δ = 171.9 (CO), 159.4 (C³), 138.0 (C^{3a}), 129.3, 128.9, 128.8, 128.6, 126.3, 124.8 (Ar), 85.0 (C⁷), 81.1 (C^{7a}), 67.8 (C⁵), 29.3 (C⁴); elemental analysis calcd for C₁₉H₁₆O₃: C 78.08, H 5.49; found: C 77.93, H 5.49. HR-MS (positive EI) calcd for C₁₉H₁₆O₃: 293.1178; found: 293.1174.

Crystallographic data (excluding structure factors) for the structure reported in this paper have been deposited with the Cambridge Crystallographic Data Centre as supplementary publication no. CCDC-137062. Copies of the data can be obtained free of charge on application to CCDC, 12 Union Road, Cambridge CB21EZ, UK (fax: (+44)1223-336-033; e-mail: deposit@ccdc.cam.ac.uk).

Received: March 31, 2000

Revised: June 15, 2000 [Z14934]

- [1] a) E. O. Fischer, K. H. Dötz, *Chem. Ber.* **1970**, *103*, 1273; b) K. H. Dötz, *Angew. Chem.* **1975**, *87*, 672; *Angew. Chem. Int. Ed. Engl.* **1975**, *14*, 644.
- [2] Reviews: a) K. H. Dötz, P. Tomuschat, *Chem. Soc. Rev.* **1999**, *28*, 187–198; b) W. D. Wulff, *Organometallics* **1998**, *17*, 3116–3134; c) D. F. Harvey, D. M. Sigano, *Chem. Rev.* **1996**, *96*, 271–288; d) R. Aumann, H. Nienaber, *Adv. Organometal. Chem.* **1997**, *41*, 163–242; e) L. S. Hegedus, *Tetrahedron* **1997**, *53*, 4105–4128; f) W. D. Wulff in *Comprehensive Organic Synthesis*, Vol. 5 (Eds.: B. Trost, I. Fleming, L. A. Paquette), Pergamon, Oxford, **1991**, pp. 1065–1113; g) M. S. Brookhart, W. B. Studebaker, *Chem. Rev.* **1987**, *87*, 411–432.
- [3] H. Rudler, M. Audouin, A. Parlier, B. Martin-Vaca, R. Goumont, T. Durand-Réville, *J. Am. Chem. Soc.* **1996**, *118*, 12045–12058.
- [4] B. Martin-Vaca, H. Rudler, M. Audouin, M. Nicolas, T. Durand-Réville, B. Vissière, *J. Organomet. Chem.* **1998**, *567*, 119–126.
- [5] H. Rudler, A. Parlier, B. Martin-Vaca, E. Garrier, J. Vaissermann, *Chem. Commun.* **1999**, 1439–1440.
- [6] E. J. Corey, L. S. Hegedus, *J. Am. Chem. Soc.* **1969**, *91*, 4926.
- [7] J. Y. Merour, J. L. Roustan, C. Charrier, J. Collin, J. Benaim, *J. Organomet. Chem.* **1973**, *51*, C24.

- [8] J. P. Collman, *Acc. Chem. Res.* **1975**, *8*, 342.
- [9] P. DeShong, D. R. Sidler, P. J. Rybczynski, G. A. Slough, A. L. Rheingold, *J. Am. Chem. Soc.* **1988**, *110*, 2575.
- [10] T. R. Hoye, G. M. Rehberg, *J. Am. Chem. Soc.* **1990**, *112*, 2841.
- [11] H. Alper, J. K. Currie, H. Desabbayes, *J. Chem. Soc. Chem. Commun.* **1978**, 311.
- [12] B. C. Soderberg, D. C. York, *Organometallics* **1994**, *13*, 4501.
- [13] M. F. Semmelhack, J. J. Bozell, *Tetrahedron Lett.* **1982**, *23*, 2931.
- [14] B. C. Soderberg, L. S. Hegedus, *Organometallics* **1990**, *9*, 3113.
- [15] K. H. Dötz, W. Sturm, *J. Organomet. Chem.* **1985**, *285*, 205.
- [16] That the metal atom remains bound to the ligand until the end of the reaction is in agreement with previous reports^[2, 10, 18] and was also suggested by a referee, whom the authors acknowledge.
- [17] E. Chelain, R. Goumont, L. Hamon, A. Parlier, M. Rudler, H. Rudler, J. C. Daran, J. Vaissermann, *J. Am. Chem. Soc.* **1992**, *114*, 8088–8098.
- [18] E. Chelain, A. Parlier, M. Audouin, H. Rudler, J. C. Daran, J. Vaissermann, *J. Am. Chem. Soc.* **1993**, *115*, 10568.

Spectroscopy of the Formation of Microporous Transition Metal Ion Containing Aluminophosphates under Hydrothermal Conditions**

Bert M. Weckhuysen,* David Baetens, and Robert A. Schoonheydt

One of the greatest challenges of experimentalists working in the field of molecular sieve science is the understanding of the principles that determine how porous crystalline materials are formed starting from a precursor gel under hydrothermal conditions.^[1] This is far from easy because hydrothermal crystallizations take place in a closed vessel, where many interactions, equilibria, and chemical processes continuously change with crystallization time.^[2] The lack of knowledge about these phenomena means that a rational a priori design of novel molecular sieves is still impossible and, consequently to date, the synthesis of such materials requires a systematic and intelligent screening of the *n*-dimensional reaction. Recently, the concepts of combinatorial chemistry^[3] and experimental design^[4] have been successfully explored in order to speed up this screening process. Clearly, a more detailed understanding of the processes occurring during the synthesis of these materials is required, which can lead to a more rational approach towards zeolite syntheses.

[*] Dr. ir. B. M. Weckhuysen, ir. D. Baetens, Prof. Dr. ir. R. A. Schoonheydt
Centrum voor Oppervlaktechemie en Katalyse, K.U.Leuven
Kardinaal Mercierlaan 92, 3001 Heverlee-Leuven (Belgium)
Fax: (+32)16-321998
E-mail: Bert.Weckhuysen@agr.kuleuven.ac.be.

[**] This work was supported by the Fonds voor Wetenschappelijk Onderzoek-Vlaanderen (F.W.O.) and the Geconcerteerde Onderzoeksactie (G.O.A.) of the Flemish Government. B.M.W. thanks the FWO for a postdoctoral fellowship at K.U.Leuven. The authors also thank Dr. F. E. Mabbs and Dr. D. Collison of the EPSRC c.w. EPR Service Centre of the University of Manchester (UK) for using their ESR spectrometer equipped with liquid He cryostat.

A very attractive but almost unexplored way of probing the hydrothermal crystallization process is to do in situ studies in real time and under realistic laboratory conditions; that is, at high temperatures and pressures. To the best of our knowledge, only IR,^[5] NMR,^[6] X-ray diffraction,^[7] extended X-ray absorption fine structure (EXAFS),^[8] and small-angle/wide-angle X-ray scattering (SAXS-WAXS)^[9] have been used up to now for performing such in situ studies. Herein, we present a novel methodology based on diffuse reflectance spectroscopy (DRS) in the UV/Vis region and electron spin resonance (ESR) for probing the changes in coordination of transition metal ions during the hydrothermal crystallization of molecular sieves. The method is generally applicable to metal ions that are paramagnetic and possess d–d transitions. Its application not only requires the use of specially designed autoclaves, which allow one to perform such spectroscopic measurements, but also the development of procedures for performing hydrothermal synthesis of molecular sieves in these spectroscopic cells.

Figure 1 (see also the illustration in the table of contents) shows the specially developed in situ DRS cell, which consists of a small container with an internal volume of 12.66 cm³

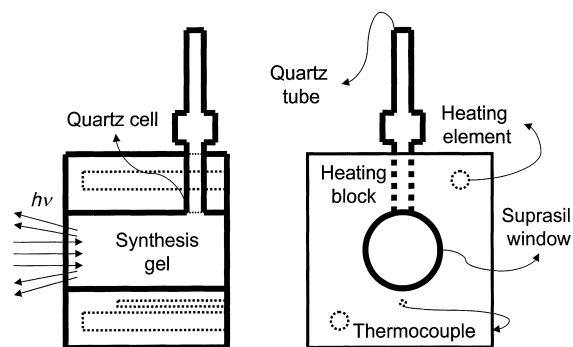


Figure 1. In situ DRS cell for monitoring the coordination environment of transition metal ions during the synthesis of molecular sieves at high temperatures and pressures. See text for details.

consisting of walls of high-purity quartz (thickness: 0.5 cm). The synthesis cell could be filled with the precursor gel through a 10 cm long quartz tube, which was equipped with an expansion volume for safety reasons. The quartz tube was sealed after filling the cell, and the cell was placed in a heating mantle, which was controlled with a Eurotherm thermoregulator. The flat front window of the synthesis cell allowed in situ spectra to be recorded with the diffuse reflectance attachment of the diffuse reflectance spectrometer. Important operational conditions for obtaining high-quality microporous materials in this in situ cell are the initial heating rate and the filling factor. High-purity quartz tubes with an internal volume of 0.47 cm³ were used for performing ESR measurements on the synthesis gels. These quartz tubes were filled with the precursor gel and after sealing were placed either directly in the ESR cavity or in a separate furnace. The synthesis process was quenched by bringing the ESR tube immediately to liquid nitrogen or helium temperatures. This allowed reliable ESR measurements to be conducted. Slowly reheating the sample in the ESR tube to the actual synthesis

temperature did not significantly affect the synthesis process of the molecular sieves.

Herein, we present as an example the hydrothermal crystallization of CoAPO-5 molecular sieves in the DRS and ESR cells at 175 °C under autogeneous pressure and static conditions. Crystallizations of other molecular sieves, such as VAPO-5, CrAPO-5, and NiAPO-5, were equally successful. All these materials are known to be promising catalysts for various oxidation reactions and therefore the isomorphous substitution of transition metal ions in microporous aluminophosphates is an important topic in the literature.^[10]

The in situ DRS spectra of the CoAPO-5 gel as a function of the synthesis time are given in Figure 2. The DRS spectrum of the initial pink CoAPO-5 gel is characterized by absorption

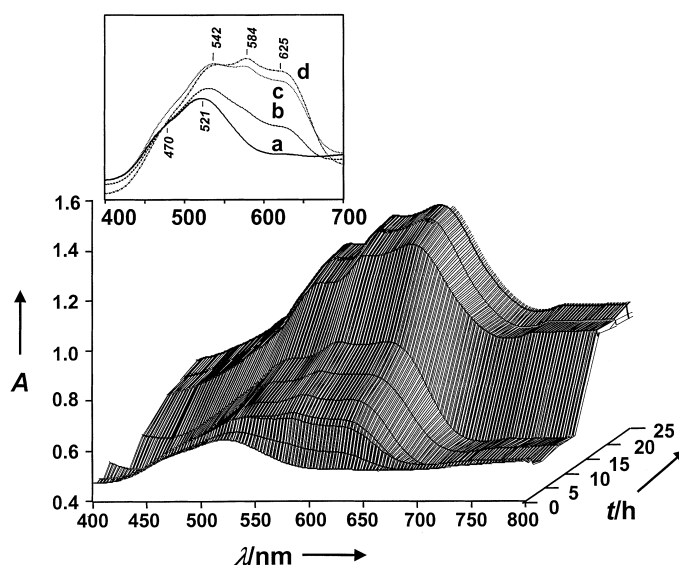


Figure 2. In situ DRS spectra of the CoAPO-5 gel as a function of the synthesis time. The insert shows some DRS spectra as a function of the heating temperature in the initial stages of the hydrothermal synthesis; a) room temperature, b) 60 °C, c) 100 °C, and d) 175 °C.

bands at 521 and 470 nm. The gel was heated up to 175 °C and an isosbestic point became clearly visible in the DRS spectra (see spectra a–d in Figure 2), indicating the presence of two distinct Co²⁺ species. The absorption band at 521 nm is due to the ⁴T_{1g}(F) → ⁴T_{1g}(P) transition (ν_3 band) of high-spin [Co(H₂O)₆]²⁺^[11] present in the synthesis gel, while the shoulder at 470 nm can be assigned to the ⁴T_{1g}(F) → ⁴A_{2g}(P) transition (ν_3 band) of a tetragonally coordinated high-spin Co²⁺ species, most probably of the type [CoO₄(H₂O)₂] (with O, an oxygen atom-bound to phosphorus).^[12] Heating the synthesis gel to 175 °C also results in a gradual change of the color from pink to light blue, and a triplet with absorption bands at 542, 584, and 625 nm is observed in the DRS spectrum. This triplet, which is assigned to the ⁴A_{2g}(F) → ⁴T_{1g}(P) transition (ν_3 band) of high-spin pseudo-tetrahedral Co²⁺,^[11, 13] strongly increases in intensity with increasing synthesis time and becomes the most intense after 26 h. The sample was intense blue and about 1.5 g of highly crystalline single-phase CoAPO-5 material could be recovered from the cell. Importantly, no crystalline phase was formed during the first

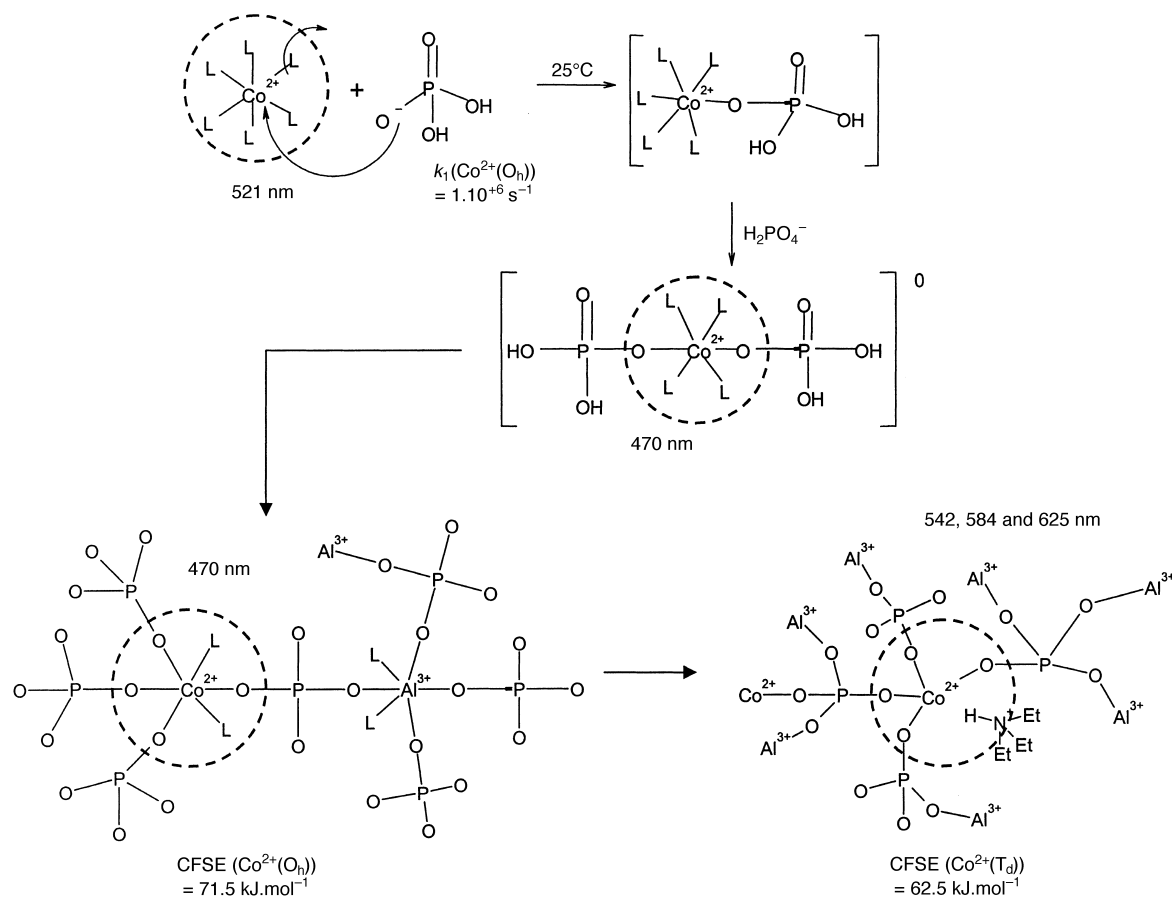
hours of the synthesis process, whereas synthesis times higher than 26 h led to the formation of less crystalline and even other crystalline phases (e.g., CoAPO-C).

The ESR spectrum of the initial CoAPO-5 gel quenched in liquid nitrogen and cooled down to $-263\text{ }^{\circ}\text{C}$ indicated the presence of one broad axial signal with $g_{xx}=g_{yy}=2.643$, $g_{zz}=2.020$, and $D=25\text{ cm}^{-1}$, which is typical for the presence of pseudo-octahedral Co^{2+} .^[14] The ESR spectra gradually changed with synthesis time and after 24 h one single axial Co^{2+} signal with $g_{xx}=g_{yy}=2.643$, $g_{zz}=2.020$ and $D=3.5\text{ cm}^{-1}$ was observed. These ESR parameters, obtained by spectrum simulation, are typical for the presence of pseudo-tetrahedral Co^{2+} ;^[14] about 0.05 g of highly crystalline single-phase CoAPO-5 could be recovered from the ESR cell.

Thus, both DRS and ESR spectroscopies, together with X-ray diffraction, indicate that the formation of CoAPO-5 molecular sieves is accompanied by the presence of a pseudo-octahedral $[\text{CoO}_4(\text{H}_2\text{O})_2]$ intermediate in the initial synthesis stages and a gradual transformation of this intermediate species into a pseudo-tetrahedral framework Co^{2+} species. A possible reaction mechanism for the formation of CoAPO-5 molecular sieves can be proposed on the basis of these spectroscopic data, and this is illustrated in Scheme 1. $[\text{Co}(\text{H}_2\text{O})_6]^{2+}$, which is present in the initial gel at pH 2, is a kinetic labile species ($k_1(\text{Co}(\text{O}_n))=10^6\text{ s}^{-1}$ for the exchange of water ligands) and will readily undergo nucleophilic attack by H_2PO_4^- .^[15] The reaction between $[\text{Co}(\text{H}_2\text{O})_6]^{2+}$ and H_2PO_4^- results in the formation of the $[\text{CoO}_4(\text{H}_2\text{O})_2]$ intermediate.

This species can be envisaged as Co^{2+} linked to four phosphorus atoms through oxygen bridges, after a nucleophilic attack of four H_2PO_4^- species onto one $[\text{Co}(\text{H}_2\text{O})_6]^{2+}$ complex.^[16] The entities formed after these initial reactions can be further condensed to an aluminophosphate gel, in which both Co^{2+} and Al^{3+} are present as octahedral species with two extra-lattice water ligands. Heating of the gel results in the expulsion of these water ligands from the first coordination sphere of Al^{3+} and Co^{2+} . Co^{2+} is thus gradually transformed from a species with pseudo-octahedral coordination into a tetrahedral framework species. Because of the small differences in crystal field stabilization energy (CFSE) between the octahedral (71.5 kJ mol^{-1}) and tetrahedral coordination (62.5 kJ mol^{-1}) of Co^{2+} (d^7),^[17] this transformation process must be favorable and is indeed experimentally observed. The positively charged $(\text{CH}_3\text{CH}_2)_3\text{NH}^+$ template molecules will then compensate the negative charge, which results from the isomorphous substitution of Al^{3+} for Co^{2+} in the CoAPO-5 molecular sieves.

In summary, we have developed and explored the possibilities of combined DRS–ESR spectroscopies for monitoring the changes in the coordination environment of transition metal ions during the hydrothermal crystallization of molecular sieves at high temperatures and pressures. The spectroscopic data obtained allow a better understanding of the hydrothermal crystallization process of CoAPO-5 molecular sieves in terms of the coordination chemistry of Co^{2+} in the synthesis gel.



Scheme 1. Proposed mechanism for the processes taking place in the synthesis gel during the hydrothermal synthesis of CoAPO-5 molecular sieves.

Experimental Section

CoAPO-5 was prepared according to a standard recipe procedure^[13] starting from the following gel composition: 0.75R[Co_{0.02}Al_{0.98}P₁]O₄ · 20H₂O with R, the template molecule triethylamine (Janssen Chimica, 99 %), and with Co(CH₃CO₂)₂ · 4H₂O (Acros, p.a.). Pseudo-boehmite from Vista (Capatal Alumina 70 % Al₂O₃) was used as the Al source, and H₃PO₄ (Janssen Chimica, 85 % in H₂O) as the P source. Diffuse reflectance spectra in the UV/Vis–NIR region were measured by using a Varian Cary 5 spectrometer equipped with a diffuse reflectance attachment with integration sphere. The spectra were recorded against a halon white reflectance standard in the range 2500–200 nm. ESR measurements were recorded on a Bruker ESP300E spectrometer with an Oxford Instruments liquid helium cryostat at –263 °C. Simulations of the ESR spectra were performed by simulation programs developed by Mabbs and Collison.^[18] Powder X-ray diffraction patterns of the obtained solids were recorded on a Siemens D5000 diffractometer by using CuK_α radiation.

Received: December 21, 1999

Revised: April 26, 2000 [Z14435]

- [1] B. M. Lok, T. R. Cannon, C. A. Messina, *Zeolites* **1983**, 3, 282.
- [2] M. E. Davis, R. F. Lobo, *Chem. Mater.* **1992**, 4, 756.
- [3] D. E. Akporiaye, I. M. Dahl, A. Karlsson, R. Wendelbo, *Angew. Chem.* **1998**, 110, 629; *Angew. Chem. Int. Ed.* **1998**, 37, 609; J. Klein, C. W. Lehmann, H.-W. Schmidt, W. F. Maier, *Angew. Chem.* **1998**, 110, 3557; *Angew. Chem. Int. Ed.* **1998**, 37, 3369; K. Choi, D. Gardner, N. Hilbrandt, T. Bein, *Angew. Chem.* **1999**, 111, 3070; *Angew. Chem. Int. Ed.* **1999**, 38, 2891.
- [4] X. Gao, B. M. Weckhuysen, R. A. Schoonheydt, *Microporous Mesoporous Mater.* **1999**, 27, 75; L. Frunza, P. Van Der Voort, E. F. Vansant, R. A. Schoonheydt, B. M. Weckhuysen, *Microporous Mesoporous Mater.*, accepted.
- [5] W. R. Moser, J. E. Cossen, A. W. Wang, S. A. Krouse, *J. Catal.* **1985**, 95, 21.
- [6] M. Haouas, C. Gerardin, F. Taulelle, C. Estournes, T. Loiseau, G. Férey, *J. Chim. Phys.* **1998**, 95, 302; F. Taulelle, M. Haouas, C. Gerardin, C. Estournes, T. Loiseau, G. Férey, *Colloids and Surfaces A* **1999**, 158, 299.
- [7] P. Norby, A. N. Christensen, J. C. Hanson, *Stud. Surf. Sci. Catal.* **1994**, 84, 179; G. Sankar, J. M. Thomas, F. Rey, G. N. Greaves, *Chem. Commun.* **1995**, 2549; A. T. Davies, G. Sankar, C. R. Catlow, S. M. Clark, *J. Phys. Chem. B* **1997**, 101, 10115; A. N. Christensen, T. R. Jensen, P. Norby, J. C. Hanson, *Chem. Mater.* **1998**, 10, 1688; C. L. Cahill, Y. Ko, J. C. Hanson, K. Tan, J. B. Parise, *Chem. Mater.* **1998**, 10, 1453; M. Lindén, S. A. Schunk, F. Schüth, *Angew. Chem.* **1998**, 110, 871; *Angew. Chem. Int. Ed.* **1998**, 37, 821; A. R. Overweg, J. W. de Haan, P. C. M. M. Magusin, R. A. van Santen, G. Sankar, J. M. Thomas, *Chem. Mater.* **1999**, 11, 1680; R. J. Francis, S. O'Brien, A. M. Fogg, P. S. Halasyamani, D. O'Hare, T. Loiseau, G. Férey, *J. Am. Chem. Soc.* **1999**, 121, 1002.
- [8] G. Sankar, J. M. Thomas, F. Rey, G. N. Greaves, *Chem. Commun.* **1995**, 2549; F. Rey, G. Sankar, J. M. Thomas, P. A. Barret, D. W. Lewis, C. R. A. Catlow, G. N. Greaves, S. M. Clark, *Chem. Mater.* **1995**, 7, 1435; A. R. Overweg, J. W. de Haan, P. C. M. M. Magusin, R. A. van Santen, G. Sankar, J. M. Thomas, *Chem. Mater.* **1999**, 11, 1680.
- [9] P. P. E. A. de Moor, T. P. M. Beelen, R. A. van Santen, K. Tsuji, M. E. Davis, *Chem. Mater.* **1999**, 11, 36; P. P. E. A. de Moor, T. P. M. Beelen, R. A. van Santen, *J. Phys. Chem. B* **1999**, 103, 1639; P. P. E. A. de Moor, T. P. M. Beelen, B. U. Komanschek, L. W. Beck, P. Wagner, M. E. Davis, R. A. van Santen, *Chem. Eur. J.* **1999**, 5, 2083.
- [10] Recent reviews on this subject: I. W. C. E. Arends, R. A. Scheldon, M. Wallau, U. Schuchardt, *Angew. Chem.* **1997**, 109, 1190; *Angew. Chem. Int. Ed.* **1997**, 36, 1144; B. M. Weckhuysen, R. Ramachandra Rao, J. A. Martens, R. A. Schoonheydt, *Eur. J. Inorg. Chem.* **1999**, 565; M. Hartmann, L. Kevan, *Chem. Rev.* **1999**, 99, 635.
- [11] A. B. P. Lever, *Inorganic Electronic Spectroscopy*, Elsevier, Amsterdam, **1984**.
- [12] A tetragonal distortion of an octahedral complex leads to the splitting of the ⁴T_{1g}(P) level in a ⁴A_{2g} and ⁴E_g level. This splitting gives rise to

two transitions, ⁴T_{1g}(F) → ⁴A_{2g}(P) and ⁴T_{1g}(F) → ⁴E_g(P), which are located at 450 and 538 nm, respectively, for, for example, [Co(H₂O)₄Cl₂] (see ref. [11]). We are only able to observe the ⁴T_{1g}(F) → ⁴A_{2g}(P) transition of the [CoO₄(H₂O)₂] species as a shoulder at 470 nm and the ⁴T_{1g}(F) → ⁴E_g(P) transition must be overshadowed by the ⁴T_{1g}(F) → ⁴E_g(P) transition at 521 nm of the more abundant [Co(H₂O)₆]²⁺ species in the synthesis gel. Although [CoO_x(H₂O)_{6-x}] (with x = 1–3) intermediates can also be formed, only the most stable tetragonally coordinated Co²⁺ species is experimentally observed.

- [13] R. A. Schoonheydt, R. De Vos, J. Pelgrims, H. Leeman in *Zeolites: Facts, Figures, Future* (Eds.: P. A. Jacobs, R. A. van Santen), Elsevier, Amsterdam, **1989**, p. 559; A. A. Verberckmoes, B. M. Weckhuysen, R. A. Schoonheydt, *Microporous Mesoporous Mater.* **1998**, 22, 165.
- [14] M. W. Makinen, L. C. Kuo, M. B. Yim, G. B. Wells, J. M. Fukujama, J. E. Kim, *J. Am. Chem. Soc.* **1985**, 107, 5245; M. W. Makinen, L. C. Kuo, M. B. Yim, G. B. Wells, J. M. Fukujama, J. E. Kim, *J. Am. Chem. Soc.* **1985**, 107, 5245.
- [15] B. M. Weckhuysen, A. A. Verberckmoes, M. G. Uytterhoeven, F. E. Mabbs, D. Collison, E. de Boer, R. A. Schoonheydt, *J. Phys. Chem. B* **2000**, 104, 37.
- [16] F. Basolo, R. G. Pearson, *Mechanisms of Inorganic Reactions, A study of metal complexes in solution*, 2nd ed., Wiley, New York, **1967**.
- [17] The pH of the initial gel at 25 °C, as measured with a Consort P514 pH meter, was equal to 2 and this value increased to around 3.5 after heating the synthesis gel to 175 °C. After synthesis the pH was around 7. In this pH range, the dominant species in aqueous solutions are [Co(H₂O)₆]²⁺ and H₂PO₄[–] (N. N. Greenwood, A. Earnshaw, *Chemistry of the Elements*, Pergamon, Oxford, **1984**). Importantly, in view of the work of Gerardin et al. (C. Gerardin, M. In, L. Allouche, M. Haouas, F. Taulelle, *Chem. Mater.* **1999**, 11, 1285) the reported pH values have to be taken with caution.
- [18] F. E. Mabbs, D. Collison, *Electron Paramagnetic Resonance of d Transition Metal Compounds*, Elsevier, Amsterdam, **1992**.

First Catalytic Aldol-Transfer Reaction via Aluminum Enolates: A New Way To Generate Aldol Adducts of Aldehydes from Aldol Adducts of Ketones**

Ilkka Simpura and Vesa Nevalainen*

The addition of nucleophiles to carbonyl compounds has been under investigation for decades.^[1] Examples include the addition of enolates to aldehydes and the Meerwein–Ponndorf–Verley (MPV) reduction of ketones^[2] (hydride as the nucleophile, Figure 1, (a)). Amongst recent achievements in this area are: alkynyl transfer reactions reported by Maruoka and co-workers^[3] (Figure 1 (b)), allyl-transfer reactions reported by Nokami et al.^[4] (Figure 1, (c)), which as the reaction is proposed to occur by a stepwise ionic mechanism^[4] is only formally analogous to the MPV reaction, and cyanide-transfer reactions reported by Inoue and co-workers^[5] (Figure 1, (d)). The major advantage of these nucleophile-transfer reactions

[*] Dr. V. Nevalainen, I. Simpura
Department of Chemistry
University of Helsinki
P.O. Box 55 (A.I. Virtasen aukio 1), 00014 Helsinki (Finland)
Fax: (+358) 9-191-40466
E-mail: vesa.nevalainen@helsinki.fi

[**] This work was partially supported by the TEKES research foundation.

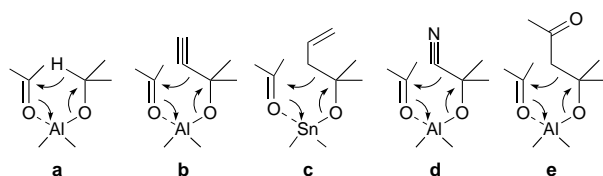
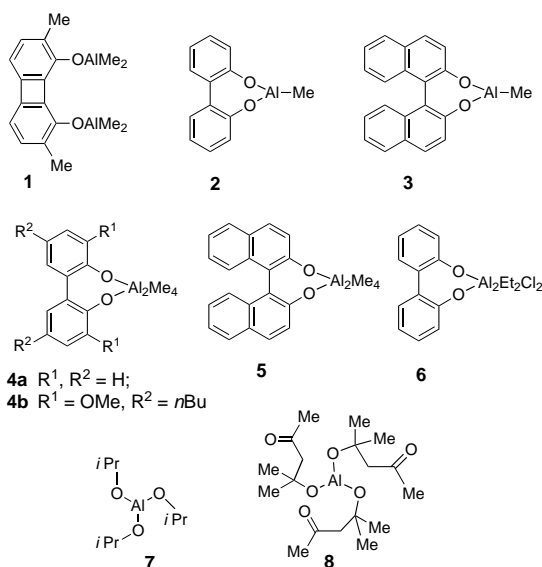


Figure 1. Formal flow of electrons in the six-membered cyclic transition states (**a–d**) of the MPV-type nucleophile-transfer reactions described in the literature. The related hypothetical mechanism of the aluminum-catalyzed aldol-transfer reaction is illustrated by **e**. Despite of formal analogy of **a–e**, the reactions depicted by **c** (ref. [4]) and **e** (Scheme 2) are proposed to take place by a stepwise ionic mechanism.

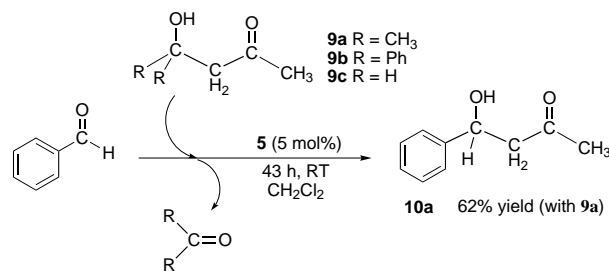
is the utilization of cheap and simple propargyl alcohols (e.g. 2-methyl-3-propyn-2-ol)^[3] or allyl alcohols (e.g. 2-methyl-3-propen-2-ol)^[4] as starting materials for the construction of more complicated alcohols under mild reaction conditions.

Herein we report the first catalytic aldol-transfer reaction (Figure 1, (**e**)) for various aldehydes in which diacetone alcohol (**9a**) was used as an aldol source (see Scheme 1). Other methods for the synthesis of aldols have been reported by the groups of Lerner^[6] (enzymatic and biomimetic), Yamamoto^[7] (using hindered aluminum bisphenoxides), and Morken^[8] (using the reduction of α,β -unsaturated esters).

The present work was inspired by the pioneering studies of Maruoka et al.^[9] who reported that the bis(dialkylaluminum) reagent **1** accelerated the addition of nucleophiles to carbonyl compounds. Thus, for the aldol-transfer reaction we considered using the aluminum chelates **2** and **3**, their bisaluminum analogues **4–6**, and simple alkoxides **7** and **8**.^[10]



A typical procedure is shown in Scheme 1: the aldol-transfer reaction of the alcohol **9a** with benzaldehyde catalyzed by **5**, gave the aldol adduct **10a** in 62% yield (after flash chromatography). The generality of this aldol-transfer method was confirmed by the synthesis of aldol adducts **10a–j** (Table 1). A possible mechanism to rationalize the aldol-transfer reaction is illustrated in Scheme 2.

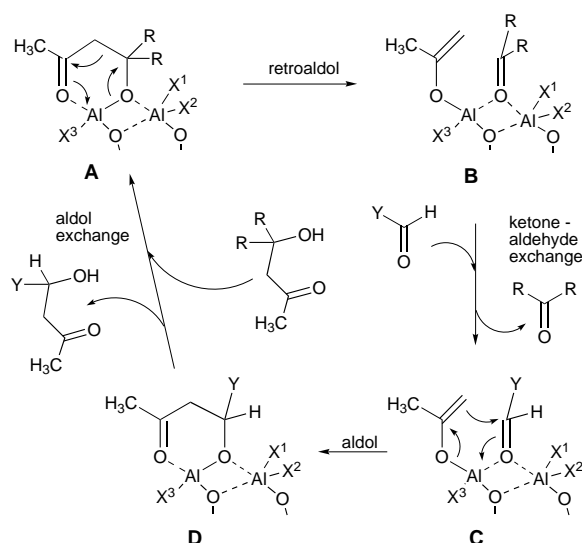


Scheme 1. The catalytic aldol-transfer reaction of benzaldehyde utilizing β -hydroxy ketones (**9a–c**) as starting material.

Table 1. The catalytic aldol-transfer reaction of aldehydes

Entry	R^2	Catalyst	Aldol source	Run time [h]	mol % of catalyst	<i>trans</i> -aldol	Yield [%]
1	C_6H_5	5	9a	43	5	10a	62
2	C_6H_5	5	9a	22	5	10a	43
3	C_6H_5	4a	9a	22	5	10a	39
4	C_6H_5	4a	9a	22	10	10a	53
5	C_6H_5	4a	9b	21	5	10a	49
6	C_6H_5	7	9a	22	10	10a	28
7	C_6H_5	8	9a	22	10	10a	43
8	C_6H_5	4b	9a	22	5	10a	36
9	$4-O_2N-C_6H_4$	4a	9a	22	10	10b	58
10	$4-Cl-C_6H_4$	4a	9a	22	10	10c	56
11	$4-H_3CO-C_6H_4$	4a	9a	22	10	10d	47
12	hept-3-yl	5	9a	26	5	10e	73
13	$(CH_3)_3C$	5	9a	40	5	10f	72
14	1-phenylethyl	4a	9a	22	10	10g	63
15	$H_2C(CH_2)_2$	5	9a	40	5	10h	26
16	$H_3C(CH_2)_2$ ^[a]	4a	9a	48	5	10h	47
17	prop-2-yl	5	9a	22	5	10i	24
18	$C_6H_5-CH=CH$	5	9a	22	5	10j	11

[a] Two equivalents of **9a** were used.



Scheme 2. The proposed mechanism of the aldol-transfer reaction described in Scheme 1. X^1 , X^2 , and X^3 = alkyl, alkoxy, and aryloxy, respectively. R = alkyl. Y = aryl.

The results indicate that the aldol-transfer reaction of **9a** with benzaldehyde can be induced by any of the compounds **4–8**^[10] (entries 1–8, Table 1; data for compound **6** is not listed in the Table because it gave only trace amounts of **10a**). With compound **3** as the catalyst the yield of **10a** was only 7 %. If **3** is allowed to react^[10] with one more equivalent of Me₃Al then complex **5** is generated. With **5** as the catalyst the yield of **10a** increased substantially (43 %, entry 2). The related reaction with **4a** gave a slightly lower yield of **10a** (39 %, entry 3). The yield of **10a**, however, increased to 53 % (entry 4) when 10 mol % of **4a** was used (instead 5 mol %) indicating the importance of the amount of the catalyst added. The reaction of benzaldehyde with **9a** catalyzed by **8**^[10] gave **10a** in 43 % yield (entry 7). Surprisingly, the yield of **10a** decreased to a trace amount when **8**^[10] was used as a reagent and not as the catalyst. The reaction with **7** as the catalyst gave **10a** in only 28 % yield (entry 6). These results indicate that the aryloxy groups of **4a** improve the yield of **10a** obtained only by about 10 % over that obtained from comparable reactions with **8** which contains β -alkyloxy groups. The performance of **7** containing simple alkoxy groups is clearly inferior to that of **4a** and **8**.

Enhancing the electron richness of the aromatic ligand in the catalyst did not provide any advantages: Aldol **10a** was obtained in 36 % yield (entry 8, Table 1) with catalyst **4b**, whereas with **4a** the yield was 39 % (entry 3). Altering the electron richness of the aluminum center of the catalyst was not beneficial. When Et₂AlCl was used to prepare the catalyst (in situ formation of **6**^[10]), product **10a** was detected only in trace amounts.

A comparison of the reactivity of the precursor aldols **9a–c** (Scheme 1) reveals factors that support the retro-aldol–aldol mechanism (Scheme 2) of the aldol-transfer reaction (Scheme 1). The aluminum chelate **A** (Scheme 2) undergoes a retro-aldol reaction to give **B**, the stability of which is dependent on the electron-donating effects of the R groups. Because the intermediate **B** (R=Ph) generated from **9b** should be more stable than **B** (R=CH₃) generated from **9a**, the retro-aldol step (**A**→**B**) should be easier for **9b** than for **9a**. Indeed, aldol **10a** was produced from **9b** in a higher yield than from **9a** (entries 5 and 3, respectively, Table 1). On the other hand, as the stability of **B** should decrease with the decreasing electron-donating effects of the R group, the aldol-transfer reaction of **9c** should give much lower yields than that of **9a**. This trend was confirmed experimentally; the aldol-transfer reactions of **9c** (both with butanal and *o*-phthalic aldehyde, catalyzed by **4a** (5 mol %)) failed.

Although the aldol-transfer reactions utilizing **9a** and **9b** (Scheme 1) as starting materials gave aldols in modest yields, the related reactions of β -hydroxy esters (benzaldehyde with ethyl 3-hydroxy-butanoate or ethyl 3-methyl-3-hydroxybutanoate catalyzed by **4a** (10 mol %)) and β -hydroxyaldehydes (benzaldehyde with 2-ethyl-3-ethoxycarbonyl-3-hydroxy butanal catalyzed by **4a** (10 mol %)) failed. Further limitations of the aldol-transfer reaction were found with ketones as reactants instead of aldehydes. Because the aldol-transfer reaction of **9a, b** produces a sacrificial ketone (that is R₂C=O, Scheme 1) the ketone that reacts in place of the aldehyde should have properties that differ from those of the sacrificial one. However, an aldol-transfer reaction of **9a** with aceto-

phenone catalyzed by **5** (5 mol %) gave the product aldol in only 6 % yield.

Aldol-transfer reactions of **9a** with benzaldehyde catalyzed by **4a** or **5** give yields in the range of 50 ± 14 % (entries 1–5 and 8, Table 1). Slightly better yields are obtained with electron-poor benzaldehydes than with benzaldehyde (cf. entries 4 with 9 and 10). This suggests that electron-donating substituents on the aldehyde moiety decrease the yield and electron -withdrawing substituents on the aldehyde moiety increase the yield. For instance with respect to that obtained for benzaldehyde the aldol-transfer reaction of 4-methoxy benzaldehyde with **9a** gave aldol **10d** in 47 % yield (entry 11) which is lower than the yields of reactions of related more electron -poor aldehydes (cf. entries 4, 9, and 10).

The best yields (Table 1) were achieved with α -substituted alkanals. When compared with the yield of **10a** derived from benzaldehyde, yields of **10e**, **10f**, and **10g** derived from 2-ethylhexanal (compare entries 2 and 12), 2,2-dimethylpropanal (cf. entries 1 and 13) and 2-phenylpropanal (cf. entries 4 and 14), respectively, were clearly higher. These results indicate that the aldol-transfer reaction favors sterically crowded or electron-poor aldehydes. This conclusion is supported by results obtained with *n*-butanal and 2-methylpropanal. In the former the case aldol **10h** was obtained in 26 % yield and in the latter case **10i** in 24 % yield (entries 15 and 17, respectively, Table 1). This is substantially less than the yield obtained for the aldol **10e** from 2-ethylhexanal (73 %, entry 12). However, when two equivalents of **9a** were used (instead of one equivalent) with *n*-butanal the yield of **10h** was 47 % (entry 16). A comparison of the yields (entries 15 and 16, Table 1) indicates that excess of **9a** could enhance the yield of **10a** (although the catalytic performance of **4a** and **5** is very similar only a rough comparison is possible).

The aldol-transfer reaction is favored by a bulky aldehyde moiety, this was confirmed by the reaction of **9a** with the sterically undemanding aldehyde 3-phenylpropenal. This reaction was catalyzed by **5** (5 mol %, entry 18) and gave the aldol **10j** in only 11 % yield. Although the low yield obtained with *n*-butanal and 2-methylpropanal (entries 16 and 17) can be explained by the lower stability of aldehyde complex **C** (relative to ketone complex **B**, Scheme 2) it does not explain the poor yield of 11 % obtained from 3-phenylpropenal. This result could be attributable to the higher stabilization of **D** (R=CH=CH-Ph; Scheme 2) by conjugation. If **D** is significantly more stable than **A** the aldol-transfer reaction cannot be catalytic (that is the regeneration step **D**→**A** hardly occurs).

In conclusion, we have shown that it is possible to utilize simple and cheap aldol adducts of ketones (such as **9a**) as starting materials for the construction of aldol adducts of aldehydes. Further studies on the synthetic utility, choice of metals (related [Ti(OiPr)₄][–] (3 equivalents) promoted reactions of rapamycin and one related compound with two aldehydes have been recently reported^[12]) and the mechanism of this aldol-transfer reaction are in progress.

Experimental Section

Typical procedure for the MPV transfer of the CH₃-CO-CH₃ unit of diacetone alcohol to aldehydes: A suspension of bi-2-naphthol (23.2 mg,

80 μmol) in dry CH_2Cl_2 (1 mL) was degassed, and a 2 M solution of Me_3Al (80 μL , 0.16 mmol in toluene/heptane, Aldrich) was added at room temperature under argon and the mixture was then stirred for 60 min. Immediately after evolution of gas had stopped the solution obtained (containing **5**) was cooled to 0°C , equal amounts of benzaldehyde (0.16 mL, 1.6 mmol) and diacetone alcohol (0.20 mL, 1.6 mmol) were added simultaneously to the solution. After evolution of gas ceased the clear light yellow solution obtained was allowed to warm up to room temperature. The mixture was stirred for 43 h then poured into a 0.5 M HCl solution (5 mL) and extracted with diethyl ether. The combined extracts were dried over MgSO_4 . Evaporation of solvents and purification of the residual oil by flash chromatography (silica gel, hexane/ethyl acetate, 1/5) gave 3-oxo-1-phenyl-butan-1-ol (**10a**, 164 mg, 1.0 mmol) as a colorless oil (62% yield). ^1H NMR (200 MHz, CDCl_3 , 20°C , CHCl_3 ref. $\delta = 7.27$): $\delta = 7.4\text{--}7.2$ (m, 5H, Ph), 5.1 (m $J = 3.3$ Hz, $J' = 3.7$ Hz, $J'' = 8.1$ Hz, 1H; CH), 3.3 (d, $J = 3.3$ Hz, 1H; OH), 2.83 (dd, $J = 8.1$ Hz, $J' = 17.6$ Hz, 1H; CH_2), 2.79 (dd, $J = 3.7$ Hz, $J' = 17.6$ Hz, 1H; CH_2), 2.1 (s, 3H; CH_3).

Received: February 10, 2000

Revised: April 27, 2000 [Z14681]

Applications of a Nonlinear Organic Reaction of Carbamates To Proliferate Aliphatic Amines

Koji Arimitsu, Mana Miyamoto, and Kunihiro Ichimura*

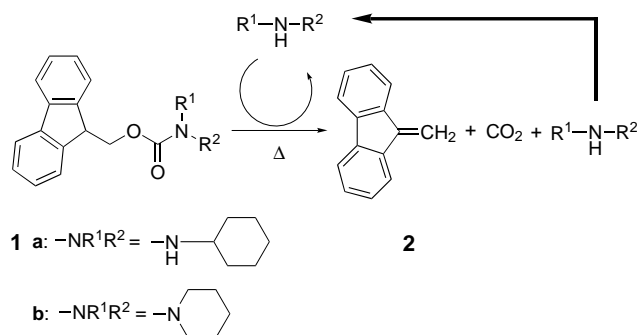
We recently proposed the concept of acid proliferations in which acid-sensitive compounds (referred to as acid amplifiers) generate strong acids in a nonlinear manner.^[1] The compounds developed so far undergo fragmentations to form sulfonic acids which are acidic enough to lead to autocatalytic decomposition. The addition of the acid amplifiers to chemically amplified photoresists (composed of photoacid generators and acid-sensitive polymers^[2]) enhances the photosensitivity and improves resist performance.^[3] This happens because the number of photogenerated acid molecules increases markedly as a result of the acid proliferation of the doped acid amplifiers. On the other hand, despite the widespread use of base catalysis in organic chemistry, analogous chemically amplified resist systems relying on the photochemical liberation of a basic species^[4] has received far less attention. This may be because of relatively low quantum yields for photobase photogeneration, which leads to low photosensitivity. If base molecules could be produced, for example, by the base-catalyzed transformation of a precursor, to increase the amount of basic species in a geometric progression, the rates of subsequent base-catalyzed reactions should be enhanced considerably, in a manner similar to that of systems involving acid proliferation. This idea led us to the molecular design and synthesis of base precursors which can be termed "base amplifiers"; this name is appropriate because the compounds generate more base molecules than they react with. Base proliferation processes can be coupled with versatile base-catalyzed reactions to develop various types of nonlinear chemical transformation. We were particularly interested in combining a base amplifier with a photobase generator because a tiny amount of a photogenerated base may enhance rates of subsequent base-catalyzed reactions owing to the autocatalytic decomposition of the base amplifier. This process leads to the improvement of photosensitivity of base-sensitive photopolymer systems. Herein we describe novel base-sensitive compounds as base amplifiers that improve the efficiency of the photoinduced insolubilization of poly(glycidyl methacrylate) (PGMA) as a base-sensitive polymer.^[5]

Our efforts have focused on the development of base amplifiers which should fulfill the following requirements: first, a base amplifier should undergo a base-catalyzed decomposition to liberate a base, thus leading to autocatalytic decomposition; second, a base amplifier should be thermally stable in the absence of a base under reaction conditions that advance both the autocatalytic decomposition and the subsequent base-catalyzed reaction; third, the liberated base

- [1] T. A. Nielsen, W. J. Houlihan, *Org. React. N. Y.* **1968**, 16, 1.
- [2] H. Meerwein, R. Schmidt, *Liebigs Ann. Chem.* **1925**, 444, 221.
- [3] T. Ooi, T. Miura, K. Maruoka, *J. Am. Chem. Soc.* **1998**, 120, 10790.
- [4] a) J. Nokami, K. Yoshizane, H. Matsuura, S-i. Sumida, *J. Am. Chem. Soc.* **1998**, 120, 6609; b) S. Sumida, M. Ohga, J. Mitani, J. Nokami, *J. Am. Chem. Soc.* **2000**, 122, 1310.
- [5] A. Mori, K. Kinoshita, M. Osaka, S. Inoue, *Chem. Lett.* **1990**, 1171.
- [6] a) G. Zhong, R. A. Lerner, C. F. Barbas III, *Angew. Chem.* **1999**, 111, 3957; *Angew. Chem. Int. Ed.* **1999**, 38, 3738; b) B. List, R. A. Lerner, C. F. Barbas III, *J. Am. Chem. Soc.* **2000**, 122, 2395.
- [7] A. Marx, H. Yamamoto, *Angew. Chem.* **2000**, 112, 182; *Angew. Chem. Int. Ed.* **2000**, 39, 178.
- [8] S. J. Taylor, J. P. Morken, *J. Am. Chem. Soc.* **1999**, 121, 12202.
- [9] T. Ooi, M. Takahashi, K. Maruoka, *Angew. Chem.* **1998**, 110, 875; *Angew. Chem. Int. Ed.* **1998**, 37, 835.
- [10] Aluminum complexes used as catalysts: a) complex **3** was generated by treatment of binaphthol with one equivalent of Me_3Al (in toluene/heptane, Aldrich); b) complexes **4a**, **4b**, and **5** were generated by the treatment of the corresponding biphenols of binaphthol with two equivalents of Me_3Al ; c) complex **6** was generated by treatment of biphenol with two equivalents of Et_2AlCl (in hexane, Aldrich); d) isopropoxide **7** was from Fluka and was used as supplied; e) alkoxide **8** was formed in situ by treatment of Me_3Al by 20 equivalents of diacetone alcohol; f) for use as a reagent the alkoxide **8** was formed by treatment of Me_3Al with three equivalents of diacetone alcohol.
- [11] The reaction of **9b** (entry 5, Table 1) produced benzophenone as a side product, which was detected while monitoring the reaction by thin-layer chromatography.
- [12] W. Yang, C. A. Digits, M. Hatada, S. Narula, L. W. Rozamus, C. M. Huestis, J. Wong, D. Dalgarno, D. A. Holt *Org. Lett.* **1999**, 1, 2033.

[*] Prof. Dr. K. Ichimura, K. Arimitsu, M. Miyamoto
Chemical Resources Laboratory
Tokyo Institute of Technology
4259 Nagatsuta, Midori-ku, Yokohama 226-8503 (Japan)
Fax: (+81)45-924-5276
E-mail: kichimur@res.titech.ac.jp

should be strong enough to catalyze subsequent chemical reactions and thus cause a nonlinear chemical transformation. Consequently, we designed 1-(9-fluorenylmethoxycarbonyl)-cyclohexylamine (**1a**) and 1-(9-fluorenylmethoxycarbonyl)piperidine (**1b**) as base amplifiers, taking note that the 9-fluorenylmethoxycarbonyl group is a useful protective groups for amino groups in peptide synthesis.^[6] Although the carbamate compound **1a** was reported^[6] as a demonstration of the utility of the 9-fluorenylmethoxycarbonyl group in peptide synthesis, information on the decomposition kinetics of **1a** with reference to the potential to proliferate amines has not been described. The carbamate compounds **1a** and **1b** were isolated as thermally stable crystals from the reaction of 9-fluorenylmethyl chloroformate with cyclohexylamine and piperidine, respectively. The base-catalyzed decomposition of **1a** and **1b** probably represents an E1cB-elimination to release the corresponding amines, cyclohexylamine and piperidine, respectively, which are sufficiently basic to lead to the decomposition of parent molecules (Scheme 1).^[6]



Scheme 1. Autocatalytic fragmentation of **1**.

The thermal behavior of **1a** in 1,4-[D₈]dioxane at 100 °C was monitored by ¹H NMR spectroscopy. Figure 1 shows both the consumption of **1a** and the formation of dibenzofulvene (**2**) in

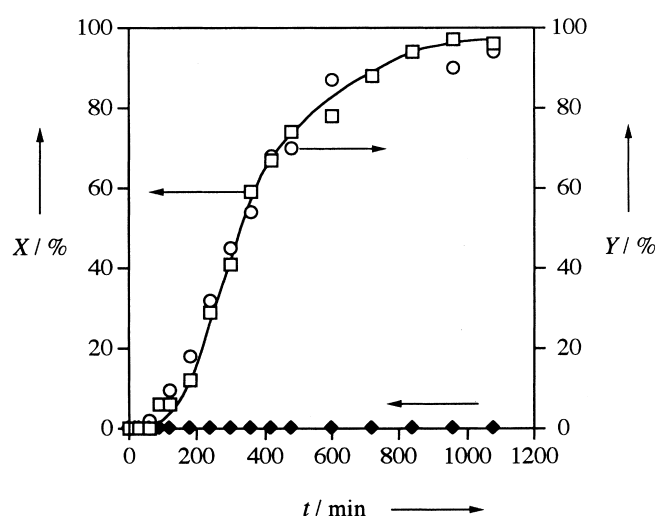
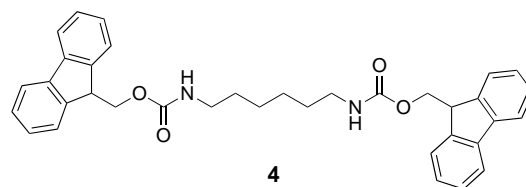
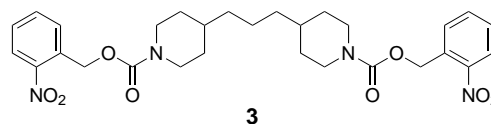
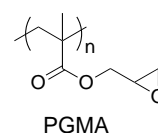


Figure 1. The consumption (*X*) of **1a** (70 mmol dm⁻³) (□) and the formation (*Y*) of dibenzofulvene (**2**) (○) as a function of heating time (*t*) in the presence of cyclohexylamine (11 mmol dm⁻³), as well as the conversion of **1a** in the absence of cyclohexylamine (♦) in 1,4-[D₈]dioxane at 100 °C.

the presence and absence of a catalytic amount of cyclohexylamine. The carbamate **1a** disappeared immediately, with a sigmoidal time conversion curve, in the presence of cyclohexylamine to form **2**. This reaction is quantitative (complete decomposition of **1a**) which indicates that the fragmentation of **1a** is autocatalytic leading to the proliferation of amines (Scheme 1). On the other hand, the carbamate **1a** was thermally stable in the absence of cyclohexylamine under the conditions that advance the autocatalytic decomposition reaction. The carbamate **1b** also showed the autocatalytic behavior in 1,4-[D₈]dioxane at 100 °C in a similar manner to **1a** except that the decomposition rate of **1b** is faster than that of **1a**. The difference in decomposition rates results from the basicity of the amines proliferated from the base amplifiers, **1a** and **1b**; the *pK_a* values of the conjugated acids of cyclohexylamine and piperidine are 10.64^[7] and 11.22,^[7] respectively.

PGMA becomes insoluble in the presence of a photobase generator upon UV irradiation and after post-exposure baking, owing to the crosslinking reaction of epoxy groups with a photogenerated amine, which functions as a negative-tone photoresist.^[8] Therefore, to examine the enhancement effect of **1a** and **1b** on the photoin-solubilization of the



polymer, a thin film of PGMA, doped with either the carbamate compound **1a** or **1b**, and 1,3-bis[(2-nitrobenzyl)oxycarbonyl-4-piperidyl]propane (**3**)^[4c] as a photobase generator was exposed to UV light, followed by heating. However, no enhancement of the photoin-solubilization was observed in the presence of **1a** or **1b**, probably because of the volatility of cyclohexylamine and piperidine generated from the base amplifiers during the post-exposure baking. These facts led us to generate 1,6-diaminohexane (**5**) that has a higher molecular weight which should reduce its volatility; compound **5** was generated from bis[(9-fluorenylmethoxy)carbonyl]hexane-1,6-diamine (**4**). In addition, the liberated **5** was expected to be an efficient crosslinker of epoxy polymers because of the double reactivity of each terminal primary

amino group towards epoxy residues. A spin-cast film of PGMA doped with **3** and **4** was exposed to UV light, then heated at 110 °C for 15 min. This was followed by solvent development to obtain photosensitivity curves. As shown in Figure 2 the exposure time required for the insolubilization is considerably reduced in the presence of **4**. The sensitivity,

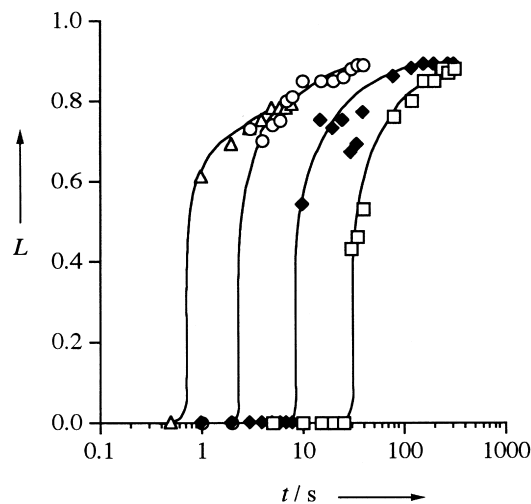


Figure 2. Photosensitivity curves of PGMA films containing 10 wt % of the photobase generator **3** in the absence of (□) and in the presence of 2 wt % (◆), 4 wt % (○), and 9 wt % of **4** (△), respectively. *L* and *t* denote normalized film thickness and irradiation time, respectively.

which is defined here as the irradiation time required for the reduction of normalized film thickness by half, is much improved by factors of 4, 20, and 50 by the addition of 2, 4, and 9 wt % of **4**, respectively. These results indicate that the photosensitivity enhancement arises from the proliferation reaction of **4** that generates the diamine **5** in a nonlinear manner, which by crosslinking contributes to the insolubilization of the polymer. In this way, the marked sensitivity enhancement of a polymer curing system, sensitized with a photobase generator, was achieved by the addition of the base amplifier **4**. Base proliferation may lead to marked improvements in other UV curing systems. Finally, it is anticipated that other types of base-sensitive polymers, irrespective of whether they are of negative-working or positive-working photoresists, would display photosensitivity enhancement on the addition of base amplifiers; thus base amplifiers could be applicable to microlithographic patterning, though optimization is needed.

In conclusion, we propose the concept of base proliferation reactions to improve performances of photopolymer systems based on base-catalyzed transformations. The base proliferation was demonstrated by a base-catalyzed decomposition of carbamate compounds **1a** and **1b** in solution, which resulted in a nonlinear fragmentation to produce aliphatic amine molecules. The carbamate compound **4**, termed a base amplifier, generated the diamine **5**, which improved the photosensitivity of a negative-working photoresist based on PGMA sensitized with a photobase generator.

Experimental Section

1b: Piperidine (1.31 g, 15.4 mmol) in diethyl ether (20 mL) was added slowly to an ice-cooled solution of 9-fluorenylmethyl chloroformate (2.00 g, 7.72 mmol) in diethyl ether (50 mL), and the mixture was stirred under cooling for 20 min and at room temperature for 1.5 h. The solution was washed successively with water, 5% hydrochloric acid solution, and saturated sodium chloride solution, dried over anhydrous magnesium sulfate, and evaporated to dryness. The solid residue was recrystallized from ethanol to give colorless crystals (0.98 g; 41%), m.p. 102–105 °C. ¹H NMR (90 MHz, CDCl₃): δ = 1.55 (br s, 6H; CH₂), 3.3–3.6 (m, 4H; CH₂), 4.1–4.5 (m, 3H; CH, CH₂), 7.1–7.7 (m, 8H; Ar-H); IR (KBr): $\tilde{\nu}$ = 2936, 1686, 1437, 1259, 1232, 1151, 1106, 762, 739 cm⁻¹; elemental analysis calcd for C₂₀H₂₁NO₂ (%): C 78.14, H 6.89, N 4.56; found: C 77.90, H 6.72, N 4.41.

4: A solution of 9-fluorenylmethanol (7.84 g, 40.0 mmol) in dry benzene (60 mL) containing a catalytic amount of di-*n*-butyltin dilaurate (0.1 g) was brought to reflux and treated dropwise with a solution of hexamethylene diisocyanate (3.36 g, 20.0 mmol) in dry benzene (20 mL) under nitrogen. Once the addition was complete, the solution was heated at reflux for 2 h and then cooled to room temperature. The resulting solid precipitate was filtered off and dried in vacuo to give the crude product as a creamy solid. The product was recrystallized from cyclohexanone and washed with acetone to give colorless crystals (10.0 g; 89.3%), m.p. 175 °C (decomp). ¹H NMR (90 MHz, CDCl₃): δ = 1.0–1.7 (m, 8H; CH₂), 2.9–3.4 (m, 4H; CH₂NH), 4.0–4.9 (m, 8H; CH, CH₂, NH), 7.1–7.9 (m, 16H; Ar-H); IR (KBr): $\tilde{\nu}$ = 3336, 2943, 1685, 1529, 1450, 1259, 1139, 1004, 758, 737 cm⁻¹; elemental analysis calcd for C₃₆H₃₆N₂O₄ (%): C 77.12, H 6.47, N 5.00; found: C 77.20, H 6.44, N 4.94.

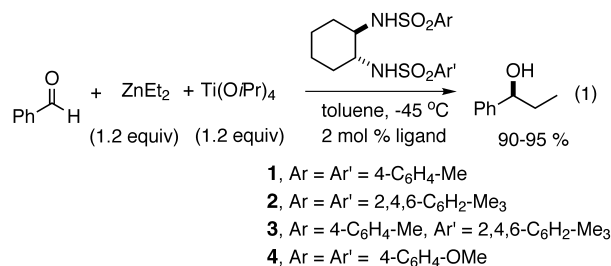
Base proliferation in solution: The carbamate **1a** (70 mmol dm⁻³), cyclohexylamine (11 mmol dm⁻³), and mesitylene as an internal standard were dissolved in 1,4-[D₈]dioxane containing a small amount of tetramethylsilane. The solution was placed in a sealed NMR tube and heated at 100 °C in an oven. The base-catalyzed decomposition of the carbamate compound was monitored by intermittent NMR measurements. The consumption of the carbamate compound was followed by monitoring the decrease of proton signals of the methine and methylene groups, while the formation of dibenzofulvene **2** was followed by monitoring the proton signal of the vinyl group; mesitylene was used as an internal standard.

Sensitivity determination: Photoresist solutions were prepared by dissolving PGMA (0.08 g/mL), the photobase generator **3** (10 wt % relative to the polymer), and the base amplifier **4** (2, 4, or 9 wt % relative to the polymer) in 1,1,1,3,3,3-hexafluoro-2-propanol. The solutions were spin-coated on silicon wafers and heated at 110 °C for 60 s to give thin films of 1.1 μm thickness. The thin films were exposed to UV light by using a Hg-Xe lamp without a glass filter, then heated at 110 °C on a hot stage for 15 min. The films were developed with 2-methoxyethyl acetate and the rinse with ethanol. The thickness of residual films was measured to evaluate photosensitivity.

Received: March 3, 2000 [Z14804]

- a) K. Ichimura, K. Arimitsu, K. Kudo, *Chem. Lett.* **1995**, 551–552; b) K. Ichimura, K. Arimitsu, S. Noguchi, K. Kudo, *ACS Symp. Ser.* **1998**, 706, 161–171.
- S. A. MacDonald, C. G. Willson, J. M. J. Fréchet, *Acc. Chem. Res.* **1994**, 27, 151–158.
- a) K. Arimitsu, K. Kudo, K. Ichimura, *J. Am. Chem. Soc.* **1998**, 120, 37–45; b) T. Ohfuji, M. Takahashi, K. Kuhara, T. Ogawa, H. Ohtsuka, M. Sasago, K. Ichimura, *Proc. SPIE Int. Soc. Opt. Eng.* **1997**, 3049, 76–82; c) K. Arimitsu, K. Ichimura, *Chem. Lett.* **1998**, 823–824; d) K. Kudo, K. Arimitsu, H. Ohmori, H. Ito, K. Ichimura, *Chem. Mater.* **1999**, 11, 2119–2125; e) H. Ito, K. Ichimura, *Macromol. Chem. Phys.* **2000**, 201, 132–138.
- a) E. J. Urankar, J. M. J. Fréchet, *Chem. Mater.* **1997**, 9, 2861–2868; b) J. M. J. Fréchet, M.-k. Leung, E. J. Urankar, C. G. Willson, J. F. Cameron, S. A. MacDonald, C. P. Niesert, *Chem. Mater.* **1997**, 9, 2887–2893; c) E. J. Urankar, I. Brehm, Q. J. Niu, J. M. J. Fréchet, *Macromolecules* **1997**, 30, 1304–1310; d) A. Mejiritski, A. M. Sarker, B. Wheaton, D. C. Neckers, *Chem. Mater.* **1997**, 9, 1488–1494.

- [5] K. Arimitsu, M. Miyamoto, K. Ichimura, *Proc. Am. Chem. Soc. Polym. Mater. Sci. Eng.* **1999**, *81*, 93–94.
 [6] L. A. Carpino, G. Y. Han, *J. Org. Chem.* **1972**, *22*, 3404–3409.
 [7] H. K. Hall, Jr., *J. Am. Chem. Soc.* **1957**, *79*, 5441–5444.
 [8] K. Ito, M. Nishimura, M. Sashio, M. Tsunooka, *Chem. Lett.* **1992**, 1153–1156.



Probing the Conformation of Flexible Catalysts in Solution**

Jaume Balsells, Juan M. Betancort, and Patrick J. Walsh*

Understanding the origins of enantioselectivity in catalytic asymmetric reactions is of special interest because of the magnitude of the impact of enantioselective synthesis on the pharmaceutical industry.^[1] However, before delineating the subtle interactions between catalyst and substrate that are responsible for the degree of enantiofacial differentiation, more fundamental questions concerning the operation of the catalyst must be addressed.^[2] Knowledge of the parameters which govern the reactivity of the catalyst including the order in the catalyst and reagents, the location of the catalytically active binding site, and the shape of the chiral pocket are essential to relate enantioselectivity data to catalyst–substrate interactions. In catalysts with rigid, well-defined structures possessing limited conformational freedom, such studies are less complicated. However, in many highly enantioselective processes, the chiral environment of the catalyst is dynamic and the enantioselectivities are dependent on the complex interplay of conformational mobility and catalyst–substrate interactions.^[2] Herein we examine one such system, the asymmetric addition of alkyl groups to aldehydes with bis(sulfonamide) ligands [Eq. (1)]. We present evidence that indicates that the bis(sulfonamido) ligand adopts a C₂-symmetric conformation in the active form of the catalyst.

The asymmetric addition reaction [Eq. (1)] was developed by Ohno, Kobayashi, and co-workers.^[3, 4] Its broad utility and excellent enantioselectivities with a wide range of aldehydes

and organozinc reagents were demonstrated by Knochel and co-workers.^[5–10] The mechanism of this efficient process was proposed to involve the in situ formation of bis(sulfonamido)titanium complexes.^[3, 4, 11, 12] We subsequently reported the synthesis and structures of these species and determined that they perform analogously to the catalyst generated in situ [Eq. (1)].^[12] In the solid-state structures of bis(sulfonamido)titanium complexes (Figure 1), we found that one oxygen atom from each sulfonyl group was coordinated to the titanium center. Coordination of the sulfonyl oxygen atoms to the titanium center could serve to define a more rigid

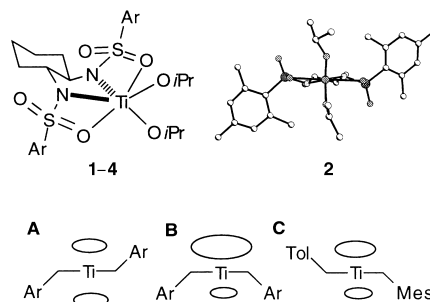


Figure 1. Drawing of the titanium complexes with ligands **1–4** (left); the molecular structure with ligand **2** (right) and representations of the titanium complexes with ligands **1–4** in the C₂-symmetric *anti* conformation (**A**) and the *syn* conformation (**B**); the pseudo C₂-symmetric conformation with ligand **3** (**C**).

asymmetric environment and may be important in the transfer of asymmetry in the transition state of the asymmetric addition reaction. To explore this possibility, it is necessary to determine the conformation of the bis(sulfonamido) ligand in the active catalyst. Two independent approaches based on structure–enantioselectivity studies were devised to accomplish this goal.

Two limiting conformations of the bis(sulfonamido) ligand bound to titanium can be envisioned. The first is the C₂-symmetric conformation seen in the crystal structures, where the aryl groups are positioned *anti* to each other (Figure 1, **A**). In the second limiting conformation, the aryl groups are *syn* to each other (Figure 1, **B**, to simplify the discussion, the conformations are abbreviated with line structures). The C₂-symmetric conformation (**A**) has two equivalent binding sites on the titanium center, which are represented by the ovals in Figure 1. In the catalyst formed from ditolyl ligand **1** [Eq. (1)], we would expect these binding sites to be more accessible

[*] Prof. P. J. Walsh, Dr. J. Balsells, Dr. J. M. Betancort
 P. Roy and Diane T. Vagelos Laboratories
 University of Pennsylvania
 Department of Chemistry
 231 South 34th Street, Philadelphia, PA 19104-6323 (USA)
 Fax: (+1) 215-571-6743
 E-mail: pwalsh@sas.upenn.edu

[**] This research was supported by the National Science Foundation in the form of a Career Award to P.J.W. (CHE-9733274) and by the National Institute of Health (GM58101). J.M.B. thanks Ministerio de Educación y Cultura of Spain for a fellowship. We also thank David Woodmansee for initial experiments.

Supporting information for this article is available on the WWW under <http://www.wiley-vch.de/home/angewandte/> or from the author.

than those of the dimesityl ligand **2** since the mesityl groups are larger. In the *syn* conformation of the ligand (Figure 1, **B**), the two binding sites are inequivalent with the binding site opposite the aryl rings being more available.

We have examined the enantioselectivity and reactivity of catalysts derived from ligands **1** and **2** [Eq. (1)]. The ditolyl ligand **1** has a high turnover frequency (TOF) and exhibits excellent enantioselectivity. By using the conditions outlined [Eq. (1)], the reaction with **1** was complete in 15 min and produced the alcohol in 97% enantiomeric excess (*ee*). Under identical conditions, the reaction catalyzed with the dimesityl ligand **2** was 84% complete after 8 h and generated the alcohol in 3% *ee*. The disparity in enantioselectivity and efficiency between these two similar ligands is remarkable.

In an effort to differentiate between conformations **A** and **B**, we prepared an unsymmetrical ligand which contains tolyl and mesityl groups [**3**, Eq. (1)]. If the ligand adopts a pseudo C_2 -symmetric conformation (Figure 1C) the two binding sites on this complex will be inequivalent and operate independently. Therefore, in the tolyl–mesityl ligand **3**, the binding site next to the tolyl group is expected to behave like the ditolyl ligand. Likewise, it is anticipated that the binding site near the mesityl group would react like the dimesityl catalyst **2**. Thus, the reaction at the site near the mesityl group should give low enantioselectivity and be slow, while the reaction at the site proximal to the tolyl group should give high enantioselectivity and be fast. If the catalyst adopts a pseudo C_2 -symmetric conformation (**C**) the reactivity of the tolyl–mesityl ligand is expected to be dominated by the site near the tolyl group and the enantioselectivity should be similar to ditolyl ligand **1**. If the conformation of the bound ligand is *syn* (**B**) in the active catalyst, it is anticipated that the enantioselectivity of the catalyst derived from **3** would lie between the ditolyl and dimesityl ligands. In the asymmetric addition reaction [Eq. (1)] the tolyl–mesityl ligand **3** gave 1-phenyl-1-propanol in 91% *ee*. The high enantioselectivity of the catalyst formed from **3** suggests that the catalysts derived from **1** and **3** are similar. It is also likely that the two binding sites operate independently and the aromatic groups are oriented in a C_2 -symmetric fashion in the transition state.

The second set of experiments involved the synthesis and evaluation of conformationally constrained cyclic bis(sulfonamide) ligands (Scheme 1). By linking the aryl groups together with a short tether, the conformation of the bound

ligand is restricted to **B** (see Figure 1). If the ligand in the nontethered catalyst were to assume conformation **B** in the transition state, ligands with short tethers would show similar reactivity and enantioselectivity profiles to ligands with longer chains and to open-chain ligands. If the C_2 -symmetric conformation is preferred by the nontethered ligands, ligands with short tethers would exhibit markedly different behavior to those with longer chains.

We have synthesized a series of macrocyclic ligands with carbon-based tethers consisting of 6, 9, 10, 12, 18, and 22 methylene units by two synthetic approaches (Scheme 1). The preparation of the ligands **5** ($n=6$), **6** ($n=9$), **7** ($n=10$), and **8** ($n=12$) was accomplished by high-dilution techniques. The longer chain analogues **9** ($n=18$) and **10** ($n=22$) were prepared by ring-closing metathesis with the Grubbs catalyst,^[13] which proved to be superior (22–35% yield) to the high-dilution approach.

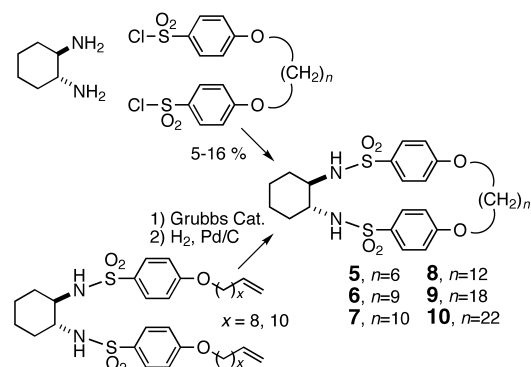
The reactivity and enantioselectivity of the tethered ligands was compared to the non-tethered ligands (Table 1). The use of the 4-methoxybenzene derivative **4** [Eq. (1)] gave fast reactions and high enantioselectivity (98% *ee*), which indicates that electronic effects caused by electron-donating OR groups are small.

Table 1. Enantioselectivities and percent conversions with ligands **1** and **4–10** (2 mol %) with the *R,R* configuration in Equation (1).

Ligand	1	4	5 $n=6$	6 $n=9$	7 $n=10$	8 $n=12$	9 $n=18$	10 $n=22$
conv. [%] $t=1$ h	100	100	21.6	32.1	39.8	61.3	73.7	97.4
conv. [%] $t=3$ h			57.3	66.6	70.8	80.0	100	100
<i>ee</i>	97	98	–10	25	19	38	76	89
(config)	(<i>S</i>)	(<i>S</i>)	(<i>R</i>)	(<i>S</i>)	(<i>S</i>)	(<i>S</i>)	(<i>S</i>)	(<i>S</i>)

The results of the asymmetric addition clearly indicate that when the tether is short, the resultant catalysts exhibit low enantioselectivity and significantly lower TOFs than their nontethered counterparts (Table 1). In the most extreme case, where the catalyst is strictly constrained to the *syn* conformation (**5**, $n=6$), the sense of enantioselectivity was reversed and the *R* enantiomer of the alcohol narrowly predominated. As the length of the tether is extended, the catalyst reactivity approaches that of the acyclic ligands in both enantioselectivity and TOF. A slightly anomalous, but reproducible behavior in the enantioselectivities of **6** and **7** was noted.

The data in Table 1, together with the enantioselectivity of the unsymmetrical ligand **3**, suggest that bis(sulfonamido) ligands that are highly enantioselective are bound to the catalyst in a C_2 -symmetric conformation in the transition state of the asymmetric addition reaction. It is then likely that the ligand is maintained in this conformation by the coordination of one of the diastereotopic oxygen atoms of each sulfonyl group to the titanium center. The resulting seven-coordinate titanium is bonded to the bis(sulfonamido) ligand, two alkoxide groups, and the substrate aldehyde. Although titanium species with coordination numbers above six are less common, we have recently isolated and characterized four eight-coordinate complexes of titanium bearing bis(sulfonamido) ligands.^[14] It is also conceivable that the catalyst



Scheme 1.

derived from ligand **2**, with its bulky mesityl groups, cannot achieve a C_2 -symmetric conformation in the enantioselectivity-determining step. Thus, a possible explanation for the low enantioselectivity of **2** might be that it adopts a *syn* conformation (Figure 1B).

The use of asymmetric Lewis acid catalysts bearing sulfonamido-based ligands is becoming more prevalent. In several of these systems, it is likely that the coordination of the sulfonyl oxygen atoms to the metal center plays an important role in defining the chiral environment of the catalyst,^[15–17] as it does with the titanium bis(sulfonamide) system. The experiments outlined here will be useful in understanding transfer of asymmetry in these, and other, systems (full experimental details can be found in the Supporting Information).

Received: March 10, 2000 [Z14835]

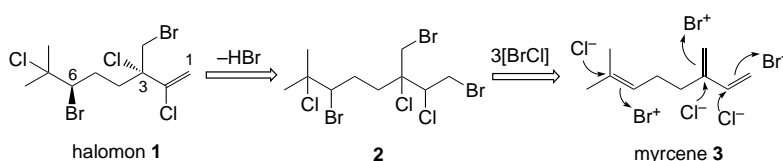
- [1] S. Stinson, *Chem. Eng. News* **1999**, 77(41), 101–120.
- [2] *Catalytic Asymmetric Synthesis* (Ed.: I. Ojima), VCH, New York, **1993**.
- [3] H. Takahashi, T. Kawakita, M. Yoshioka, S. Kobayashi, M. Ohno, *Tetrahedron Lett.* **1989**, 30, 7095–7098.
- [4] H. Takahashi, T. Kawakita, M. Ohno, M. Yoshioka, S. Kobayashi, *Tetrahedron* **1992**, 48, 5691–5700.
- [5] S. Berger, F. Langer, C. Lutz, P. Knochel, T. A. Mobley, C. K. Reddy, *Angew. Chem.* **1997**, 109, 1603–1605; *Angew. Chem. Int. Ed. Engl.* **1997**, 36, 1496–1498.
- [6] P. Knochel, *Chemtracts: Org. Chem.* **1995**, 8, 205–221.
- [7] C. Lutz, P. Knochel, *J. Org. Chem.* **1997**, 62, 7895–7898.
- [8] H. Lütjens, S. Nowotny, P. Knochel, *Tetrahedron: Asymmetry* **1995**, 6, 2675–2678.
- [9] S. Nowotny, S. Vettel, P. Knochel, *Tetrahedron Lett.* **1994**, 35, 4539–4540.
- [10] S. Vettel, C. Lutz, A. Diefenbach, G. Harderlein, S. Hammerschmidt, K. Kühling, M.-R. Mofid, T. Zimmermann, P. Knochel, *Tetrahedron: Asymmetry* **1997**, 8, 779–800.
- [11] R. Ostwald, P.-Y. Chavant, H. Stadtmüller, P. Knochel, *J. Org. Chem.* **1994**, 59, 4143–4153.
- [12] S. Pritchett, D. H. Woodmansee, P. Gantzel, P. J. Walsh, *J. Am. Chem. Soc.* **1998**, 120, 6423–6424.
- [13] R. H. Grubbs, S. Chang, *Tetrahedron* **1998**, 54, 4413–4450.
- [14] E. Royo, J. M. Betancort, T. J. Davis, P. Carroll, P. J. Walsh, *Organometallics*, in press.
- [15] T. Ichiiyanagi, M. Shimizu, T. Fujisawa, *J. Org. Chem.* **1997**, 62, 7937–7941.
- [16] D. A. Evans, S. G. Nelson, *J. Am. Chem. Soc.* **1997**, 119, 6452–6453.
- [17] J. Balsells, P. J. Walsh, *J. Am. Chem. Soc.* **2000**, 122, 1802–1803.

A Three-Step Synthesis of Halomon

Takayuki Sotokawa, Takeshi Noda, Sun Pi, and Masahiro Hirama*

Halomon (**1**), which was isolated from the red algae *Portieria hornemannii*,^[1] is a member of a novel class of antitumor agents with selective cytotoxicity against various tumor cell lines (see Scheme 1).^[2] Detailed studies on the biological activity of **1** have been hampered due to its limited accessibility. Halomon (**1**) is a small molecule that can be easily synthesized; however, the presence of five halogen atoms on the acyclic carbon chain has created a number of difficulties for regio- and stereocontrolled synthesis.^[3, 4] We report herein a very short and straightforward synthesis of **1**.

A close inspection of the structural features of **1** indicates a Markovnikov-type arrangement of Cl^- and Br^+ on the myrcene skeleton.^[1] We expected that **1** could be synthesized by three successive Markovnikov-type bromochlorinations of myrcene (**3**) followed by elimination of hydrogen bromide from the intermediate **2** (Scheme 1). Tetraalkylammonium dichlorobromate (R_4NBrCl_2) should be the reagent of choice for this halogenation.^[5] Myrcene (**3**) was first treated with excess $\text{Bu}_4\text{NBrCl}_2$ to obtain **2**, but this resulted in formation of a complex mixture. A stepwise bromochlorination reaction was then investigated. When **3** was treated with one equivalent of $\text{Bu}_4\text{NBrCl}_2$ in CH_2Cl_2 at 0°C , the trisubstituted double bond of **3** instead of the conjugate diene was bromochlorinated to yield **4** (Table 1) in an excellent example of Markovnikov selectivity ($>43:1$) (Scheme 2).^[6, 7] This exclusive formation of **4** is remarkable because 2-methyl-2-butene was reported to give a 2.4:1 mixture of regioisomers under similar reaction conditions.^[5b] It is likely that in the present case the attack of chloride ion on the less substituted C6 center of a bromonium-like intermediate could be hindered by the long and branched alkenyl substituent at C6. Therefore, the electronically favored attack of chloride ion on the more substituted C7 would become overwhelming. The regioselectivity of reactions of alkenes with $\text{Bu}_4\text{NBrCl}_2$ was found to be sensitive to the steric effect of the alkyl substituents.^[5b] The high selectivity for **3** was not affected by temperature (-78°C or 0°C) nor by alkyl substituents on



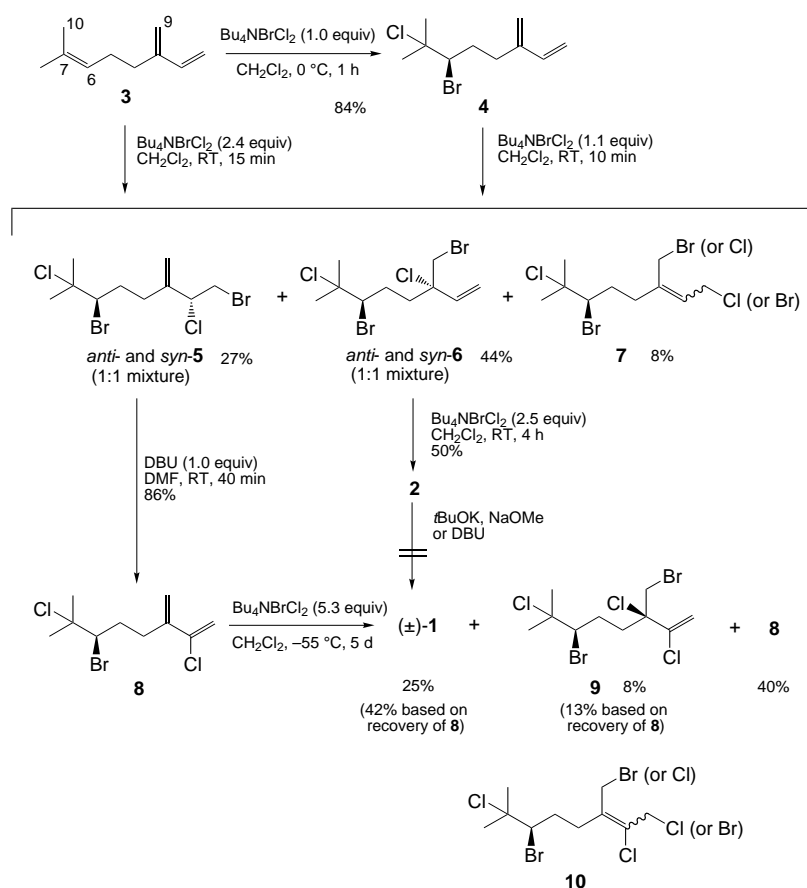
Scheme 1. Retrosynthetic scheme for the synthesis of halomon (**1**) from myrcene (**3**).

[*] Prof. M. Hirama, T. Sotokawa, Dr. T. Noda, S. Pi
Department of Chemistry
Graduate School of Science
Tohoku University, and CREST, Japan Science and Technology
Corporation (JST)
Sendai 980-8578 (Japan)
Fax: (+81)22-217-6566
E-mail: hirama@ykbcs.chem.tohoku.ac.jp

Table 1. 500 MHz ^1H NMR data of intermediates (**4–6**, and **8**) in CDCl_3 .^[a]

Carbon	4	5 ^[b]	<i>anti</i> - 6	<i>syn</i> - 6	8 ^[c]
1	5.29 (br d, $J = 17.3$ Hz, 1 H) 5.08–5.12 (m, 1 H)	3.71 (dd, $J = 10.0, 6.0$ Hz, 1 H) 4.61 (dd, $J = 10.0, 6.0$ Hz, 1 H)	5.35 (d, $J = 10.5$ Hz, 1 H) 5.49 (d, $J = 17.3$ Hz, 1 H)	5.36 (d, $J = 11.0$ Hz, 1 H) 5.49 (d, $J = 16.5$ Hz, 1 H)	5.26 (br s, 1 H) 5.45 (br s, 1 H)
2	6.38 (dd, $J = 17.3, 10.5$ Hz, 1 H)	3.66 (t, $J = 6.0$ Hz, 1 H)	5.98 (dd, $J = 17.3, 10.5$ Hz, 1 H)	5.98 (dd, $J = 17.5, 11.0$ Hz, 1 H)	
4, 5	1.89–1.98 (m, 1 H) 2.33 (qd, $J = 8.5, 7.5$ Hz, 1 H) 2.49 (qdd, $J = 9.0, 7.5, 1.5$ Hz, 1 H) 2.67 (ddd, $J = 13.5, 9.3, 4.6$ Hz, 1 H)	1.94–2.25 (m, 1 H) 2.28–2.36 (m, 1 H) 2.46–2.54 (m, 1 H) 2.56–2.63 (m, 1 H)	1.86–2.10 (m, 2 H) 2.44–2.56 (m, 2 H)	1.86–2.10 (m, 2 H) 2.44–2.56 (m, 2 H)	1.90–2.02 (m, 1 H) 2.34–2.62 (m, 2 H) 2.62–2.84 (m, 1 H)
6	4.07 (dd, $J = 11.0, 1.5$ Hz, 1 H)	4.11 (dd, $J = 11.5, 1.5$ Hz, 1 H)	4.05 (dd, $J = 11.0, 1.0$ Hz, 1 H)	4.01 (dd, $J = 11.3, 1.8$ Hz, 1 H)	4.04 (dd, $J = 11.0, 1.2$ Hz, 1 H)
8, 10	1.67 (s, 3 H) 1.78 (s, 3 H)	1.70 (s, 3 H) 1.81 (s, 3 H)	1.69 (s, 3 H) 1.80 (s, 3 H)	1.69 (s, 3 H) 1.80 (s, 3 H)	1.66 (s, 3 H) 1.78 (s, 3 H)
9	5.08–5.12 (m, 2 H)	5.19 (br s, 1 H) 5.30 (br s, 1 H)	3.68 (d, $J = 10.5$ Hz, 1 H) 3.72 (d, $J = 10.5$ Hz, 1 H)	3.68 (d, $J = 10.5$ Hz, 1 H) 3.72 (d, $J = 10.5$ Hz, 1 H)	5.53 (br s, 1 H) 5.66 (br s, 1 H)

[a] Chemical shifts referenced to tetramethylsilane. [b] Signals of *anti* and *syn* diastereomers are not separated. [c] Measured by 200 MHz ^1H NMR spectroscopy.



Scheme 2. Synthesis of halomon ((±)-1) and its congener 9 from myrcene (3).

ammonium salt reagents such as $\text{Me}_4\text{NBrCl}_2$ and $(\text{ocetyl})_4\text{NBrCl}_2$.

Bromochlorination of the conjugate diene **4** using 1.1 equivalents of $\text{Bu}_4\text{NBrCl}_2$ proceeded smoothly at room temperature and yielded the 1,2-adducts **5** and **6** in 27 and 44% yields, respectively, which were separable by HPLC.^[6] In addition, a small amount (8%) of the 1,4-adduct **7**^[8] was

produced (Scheme 2). Both **5** and **6** are 1:1 diastereomeric mixtures based on NMR spectral data (Table 1). The NMR spectrum of the *anti* diastereomer in **6** was identical with that of the natural product.^[1, 2b] We then attempted a bis-bromochlorination of **3** using 2.4 equivalents of $\text{Bu}_4\text{NBrCl}_2$ at room temperature. The mixture of **5** (21%), **6** (42%), and **7** (9%) was obtained in a one-pot reaction from **3**.

The terminal vinyl compound **6** was bromochlorinated regioselectively with $\text{Bu}_4\text{NBrCl}_2$ in CH_2Cl_2 at room temperature to yield **2** in 50% yield (Scheme 2).^[9] The planned regioselective elimination of hydrogen bromide from **2**, however, was not successful under any conditions investigated.

We next focused our attention on the *exo*-methylene compound **5**, which was expected to undergo the dehydrobromination more readily at the C1–C2 position because of the presence of an allylic hydrogen atom at C2. Treatment of **5** with 1,8-diazabicyclo[5.4.0]undec-7-ene (DBU) at room temperature yielded **8** (Table 1) in good yield, while elimination with $t\text{BuOK}$ produced a mixture (Scheme 2).^[10] Since the diene **8** is not stable, like 2-chloromyrcene,^[11] it was subjected to a final bromochlorination immediately after flash chromatography. Excess $\text{Bu}_4\text{NBrCl}_2$ was necessary to completely consume **8**, because **8** was less reactive than **4**, as expected.

A mixture of **1** and **9** was produced in 20% combined yield, when two equivalents of $\text{Bu}_4\text{NBrCl}_2$ were used at room temperature for 10 min. However, 1,4-adduct **10**^[8] was simultaneously formed (24%), and the total material balance was low probably because of the instability of **8** under the reaction conditions. After a considerable number of trials, we established optimal conditions to suppress the formation of **10**. The

reaction with 5.3 equivalents of $\text{Bu}_4\text{NBrCl}_2$ at -55°C under an argon atmosphere gave halomon (**1**: 25%; 42% based on recovery of **8**) and the diastereomer (**9**: 8%) together with recovered **8** (40%). The racemic halomon ((\pm)-**1**) was separated by reversed-phase HPLC (Cosmosil 5PYE; $\text{CH}_3\text{CN}/\text{water}$ 60/40); its ^1H and ^{13}C NMR spectra^[2a] are identical with those of natural halomon.^[12] Furthermore, pure natural enantiomer (+)-**1** was isolated by HPLC using DAICEL CHIRALPAK AD-RH ($\text{CH}_3\text{CN}/\text{water}$ 54/46) as colorless needles (from EtOH): m.p. $56.0\text{--}57.2^\circ\text{C}$; $[\alpha]_{\text{D}}^{25} = +42.6$ ($c = 1.0$, CH_2Cl_2); ref.^[2a] m.p. $49\text{--}50^\circ\text{C}$; $[\alpha]_{\text{D}}^{25} +206$ ($c = 1.08$, CH_2Cl_2). The structure of synthetic (+)-**1** was unambiguously confirmed by X-ray crystallographic analysis. Optically pure synthetic (–)-**1**, which was also isolated, exhibited $[\alpha]_{\text{D}}^{25} = -40.2$ ($c = 0.75$, CH_2Cl_2). Therefore, the reported large value of $[\alpha]_{\text{D}}^{25}$ for natural halomon^[2a] appears to arise from some impurity.

Thus, we have achieved the total synthesis of halomon (**1**) in only three steps from myrcene. This synthesis indicates the possible biosynthesis pathway of **1**.^[1] Further research directed towards a stereocontrolled and enantioselective total synthesis of halomon and its congeners is currently under way in our laboratory.

Experimental Section

5, 6, 7: $\text{Bu}_4\text{NBrCl}_2$ (0.94 g, 2.4 mmol) was added to a solution of **3** (0.17 mL, 1.0 mmol) in CH_2Cl_2 (10 mL) and the mixture was stirred at room temperature for 15 min. The reaction mixture was diluted with diethyl ether (10 mL), washed with water and brine, dried over Na_2SO_4 , and concentrated in vacuo. The residue was subjected to chromatography on silica gel (hexane) to yield an approximate 1:2 mixture of **5** and **6** (0.23 g, 0.63 mmol, 63%) together with **7** (34 mg, 0.090 mmol, 8%).

8: DBU (75 μL , 0.50 mmol) was added to a solution of a 0.6:1 mixture of **5** and **6** (0.59 g, 1.6 mmol) in DMF (15 mL), and the mixture was stirred at room temperature for 1.2 h. The reaction mixture was poured into a vigorously stirred mixture of ice–water (30 mL) and hexane (30 mL). The aqueous layer was extracted with diethyl ether. The combined organic layers were washed with water and brine, dried over Na_2SO_4 , and concentrated in vacuo. Flash column chromatography (SiO_2 , hexane) of the products gave **8** (0.11 g, 0.39 mmol, 78% from **5**) and the recovered **6** (0.36 g, 97% recovery).

1: $\text{Bu}_4\text{NBrCl}_2$ (14 g, 36 mmol) was added to a solution of **8** (1.95 g, 6.8 mmol) in CH_2Cl_2 (60 mL) under an argon atmosphere at -55°C , and the solution was allowed to stir at -55°C for five days. 2-Methyl-2-butene (7.8 mL, 74 mmol) was added to the reaction mixture at -55°C until the yellow color faded. The reaction mixture was diluted with hexane (60 mL), washed with water and brine, dried over Na_2SO_4 , and the solvent was removed in vacuo. The product was purified by flash column chromatography (SiO_2 , hexane) to yield a 3:1 mixture of **1** and **9** (0.93 g, 2.3 mmol, 33%) and the recovered **8** (0.79 g, 2.8 mmol, 40%). Compound **1** was separated from **9** by HPLC (Cosmosil 5PYE; $\text{CH}_3\text{CN}/\text{water}$ 60/40); **9** eluted as a shoulder on the front-side of the peak of **1**. HPLC of (\pm)-**1** using DAICEL CHIRALPAK AD-RH ($\text{CH}_3\text{CN}/\text{water}$ 54/46) gave the enantiomers; (–)-**1** was eluted prior to natural (+)-**1**.

Received: March 17, 2000 [Z14864]

- [1] B. J. Bureson, F. X. Wollard, R. E. Moore, *Chem. Lett.* **1975**, 1111.
[2] a) R. W. Fuller, J. H. Cardellina II, Y. Kato, L. S. Brinen, J. Clardy, K. M. Snader, M. R. Boyd, *J. Med. Chem.* **1992**, 35, 3007; b) R. W. Fuller, J. H. Cardellina II, J. Jurek, P. J. Scheuer, B. Alvarado-Lindner, M. McGuire, G. N. Gray, J. R. Steiner, J. Clardy, E. Menez, R. H.

Shoemaker, D. J. Newman, K. M. Snader, M. R. Boyd, *J. Med. Chem.* **1994**, 37, 4407.

- [3] For synthetic studies of the congeners and related compounds, see: a) M. E. Jung, M. H. Parker, *J. Org. Chem.* **1997**, 62, 7094; b) A. L. Boyes, M. Wild, *Tetrahedron Lett.* **1998**, 39, 6725.
[4] For the first synthesis of **1**, see: T. Schlama, R. Baati, V. Gouverneur, A. Valleix, J. R. Falck, C. Mioskowski, *Angew. Chem.* **1998**, 110, 2226; *Angew. Chem. Int. Ed.* **1998**, 37, 2085.
[5] a) T. Negoro, Y. Ikeda, *Bull. Chem. Soc. Jpn.* **1984**, 57, 2111; b) T. Negoro, Y. Ikeda, *Bull. Chem. Soc. Jpn.* **1986**, 59, 2547.
[6] The ratio was determined by HPLC analysis (Cosmosil 5C18-MS 4.6×150 mm, $\text{MeOH}/\text{H}_2\text{O}$ 80/20, 1 mL min^{-1}).
[7] Acetonitrile was also usable, while the reaction became too sluggish in hexane, and side reactions occurred in DMF.
[8] Neither the positions of the added bromine and chlorine atoms nor the geometry of the double bond were determined.
[9] The presence of four diastereomers was revealed by NMR spectroscopy.
[10] Separation of **5** and **6** by HPLC was inconvenient. Therefore, the mixture of **5** and **6** was treated with DBU without separation to yield the diene **8** and the recovered **6**, which were easily separated by flash chromatography (see Experimental Section).
[11] N. Ichikawa, Y. Naya, S. Enomoto, *Chem. Lett.* **1974**, 1333.
[12] We are grateful to Dr. Michael R. Boyd and Prof. C. Mioskowski for providing a ^1H NMR spectrum of (+)-**1** and ^1H NMR data for racemic **1** and **9**.

Synthesis of a Triazatriangulenium Salt

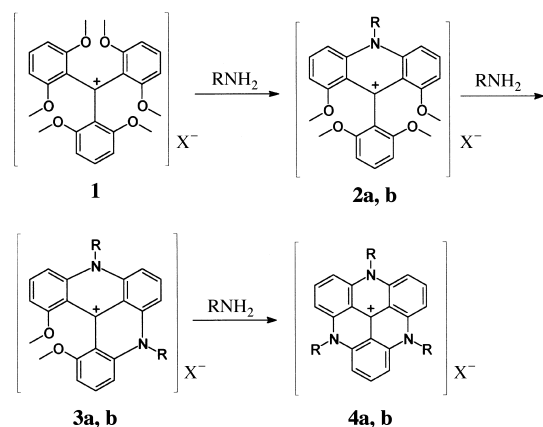
Bo W. Laursen* and Frederik C. Krebs

Stabilized carbenium ions such as the triarylmethyl, xanthyl, and acridinium cations are organic compounds of great scientific and commercial importance. Many of them are used as textile and laser dyes, as well as in various fluorescent probes and cellular stains for biological and diagnostic purposes.^[1–3] Consequently, their thermodynamic and photo-physical properties have been extensively studied, and great effort has been put into clarifying the relationship between structure and stability^[4, 5] as well as into synthesizing new carbenium ions with very high stability.^[6, 7] Aromatic nucleophilic substitution ($\text{S}_{\text{N}}\text{Ar}$) with amines on *para*-methoxy- or *para*-chloro-substituted carbenium ions has proven a powerful tool in the preparation of a variety of new triaryl carbenium ions.^[8–10] Until now no substitution of *ortho* groups in these ions has been described. Herein we report the synthesis of a novel and extremely stable trimethyl triaza-

[*] M. Sc. B. W. Laursen
The Macromolecular Chemistry Group
Condensed Matter Physics and Chemistry Department
Risø National Laboratory
4000 Roskilde (Denmark)
Fax: (+45) 4677-4791
E-mail: bo.laursen@risoe.dk
Dr. F. C. Krebs
Department of Chemistry
Technical University of Denmark
2800 Lyngby (Denmark)

triangulenium salt formed from the known carbenium salt **1** (see Scheme 1) through three consecutive *ortho* S_NAr reactions in a one-pot procedure.

The tetrafluoroborate salt of carbenium ion **1** was obtained in excellent yield (97 %) from the corresponding carbinol,^[11] by treatment with HBF₄. This carbenium ion has the necessary structural features to serve as a precursor to a variety of novel heterocyclic carbenium ions. Hence, the six *ortho* methoxy groups may serve as leaving groups in one, two, or three double S_NAr reactions with primary amines which would lead to the formation of nitrogen bridges (Scheme 1).



Scheme 1. S_NAr reaction of **1**-BF₄ with excess of primary amines; **a**: R = methyl, X⁻ = PF₆⁻; **b**: R = *n*-propyl, X⁻ = BF₄⁻.

At the same time the steric bulk of the methoxy groups protects the central carbon atom in cation **1** from nucleophilic addition, which otherwise would lead to the unreactive leuco adduct. Thus, we expected **1** to be an ideal starting material for exploring the *ortho* S_NAr reactions of triaryl carbenium ions. We found that the *ortho* methoxy groups in carbenium ion **1** do undergo substitution upon treatment with primary amines, as outlined in Scheme 1.

The reaction proceeds in a stepwise manner, thus we could isolate the partially substituted compounds **2a**-PF₆ and **3b**-BF₄ (in good yields) when the reaction was performed overnight at room temperature and at 100 °C for 45 min, respectively. The hexafluorophosphate salt of the 4,8,12-trimethyl-4,8,12-triazatriangulenium ion **4a** was obtained in 59 % yield after heating a solution **1** with excess methylamine to reflux in *N*-methylpyrrolidine (NMP) for 10 h; benzoic acid was added to raise the reflux temperature of the reaction mixture.

Several attempts were made to collect X-ray diffraction data on the very thin needlelike orange-red crystals of **4a**-PF₆; unfortunately the crystals scattered the X-rays very poorly and no true Bragg peaks were observed. However, on Weissenberg-oscillation films^[12] scattered intensity was observed in bands which correspond to a direct lattice translation of 3.5 Å, and could result from a stacked formation of **4a**. Whereas our structural studies of the pure oxygen analogues (trioxatriangulenium salts, TOTA) showed that these cations never stack in the solid state,^[13] there is one example of an amino-substituted triangulene that forms

cationic stacks.^[8] Thus, it is likely that **4a**, because of its pronounced charge delocalization, has the ability to form cationic stacks in the crystalline state. We showed that the disc-shaped cations in TOTA might rotate in the solid state at elevated temperature.^[13] In **4a** the methyl substituents make the structure more disclike than for TOTA (see Figure 1), thus molecular rotation (dynamic or static) in the solid state may explain the disorder in the crystals of **4a**.

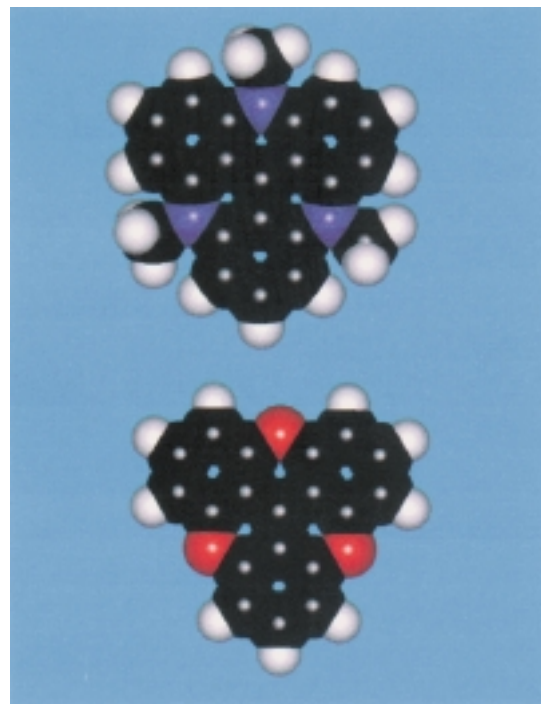


Figure 1. Space-filling models of the cations **4a** (top) and TOTA (below). The models were generated by AM1 calculations, the structure of the TOTA cation is in good agreement with the X-ray structure.

As a measure of the thermodynamic stability of the triazatriangulenium system, the p*K*_{R+} value of compound **4a** was determined by use of the C₋ acidity function;^[14] measurements were made by UV/Vis spectroscopy in a DMSO/water/tetramethylammonium hydroxide solvent system. Although the titration displayed nonideal behavior, the p*K*_{R+} value was estimated at 23.7(±0.2).^[15] This result indicates that the introduction of three nitrogen bridges into the triangulenium skeleton raises the stability by 14 orders of magnitude relative to the known oxygen analogue TOTA (p*K*_{R+} = 9.1),^[11] and underlines the unique stabilizing power of nitrogen bridges in heterocyclic carbenium salts. The extremely high stability of **4a** places this triazatriangulenium cation among the most stable carbenium ions.^[7]

Significant changes in the electronic absorption spectra of the cationic chromophores follows each substitution. The absorption spectra of the three new nitrogen-bridged heterocycles **2a**, **3b**, and **4a** are shown in Figure 2. The first ring closure converts a triaryl methane dye **1**^[16] into an acridinium system **2** (Scheme 1) which has a broad and structured low-intensity absorption in the visible region of the UV/Vis spectrum. Formation of the second nitrogen bridge causes a red shift of this band by almost 100 nm and a threefold

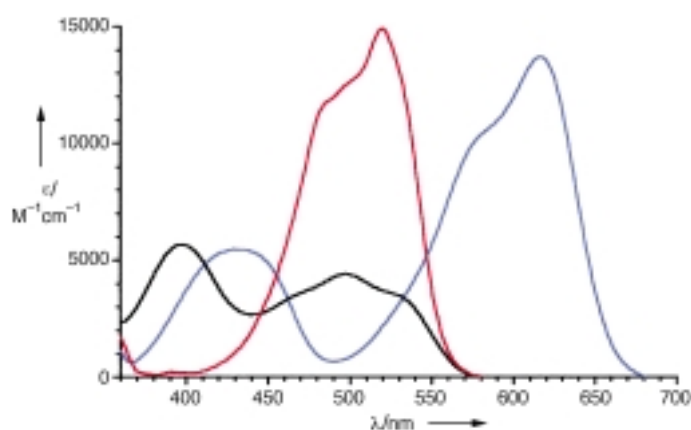


Figure 2. Absorption spectra of **2a**-PF₆ (black), **3b**-BF₄ (blue), and **4a**-PF₆ (red) in acetonitrile.

increase in the extinction coefficient. These effects can be attributed to the enlargement and twisting^[17] of the chromophoric system.^[18] The formation of the last nitrogen bridge gives the triazatriangulenium system **4**; the increased symmetry and planarity of this system results in a significant blue shift and narrowing of the low-energy absorption band.

In conclusion, the synthetic strategy based on the S_NAr reaction of **1**-BF₄ with primary amines provides a facile tool for the construction of new extended heterocyclic carbenium ions.

Experimental Section

2a-PF₆: Methylamine (5 mmol) in NMP (1 mL) was added to compound **1**-BF₄ (1.0 g, 2 mmol) dissolved in NMP (20 mL). After 20 h at room temperature the reaction mixture was poured into an aqueous KPF₆ solution (100 mL, 0.2 M), acidified with HPF₆ (60%, 1 g, 4 mmol), the precipitate was collected by filtration and washed thoroughly with water. Recrystallization from methanol gave **2a**-PF₆ as dark red needles (0.82 g, 78%). ¹H NMR ([D₃]MeCN): δ = 8.23 (dd, *J* = 8.1, 9.1 Hz, 2H), 7.96 (d, *J* = 9.1 Hz, 2H), 7.47 (t, *J* = 8.4 Hz, 1H), 7.12 (d, *J* = 8.0 Hz, 2H), 6.81 (d, *J* = 8.4 Hz, 2H), 4.64 (s, 3H), 3.58 (s, 6H), 3.57 (s, 6H); ¹³C NMR ([D₃]MeCN): δ = 160.80, 157.52, 156.17, 142.92, 140.05, 129.83, 120.15, 119.90, 109.98, 106.87, 104.11, 57.17, 56.04, 40.82; MS (MALDI-TOF): *m/z*: 390 [*M*⁺]; UV/Vis (MeCN), λ_{max} (nm, (lg ε)) = 525sh (3.56), 497 (3.65), 395 (3.75), 358 (3.37), 340 (3.06), 285 (4.86); elemental analysis calcd for C₂₄H₂₄N₄O₄PF₆ (%): C 53.83, H 4.48, N 2.61; found: C 53.83, H 4.33, N 2.59.

3b-BF₄: *n*-Propylamine (5.0 g, 85 mmol) was added to a solution of compound **1**-BF₄ (1.75 g, 3.4 mmol) in NMP (30 mL). The reaction mixture was heated to reflux (100–110 °C) for 45 min. The crude product precipitated on addition of water. Recrystallization from acetonitrile/ethanol gave **3b**-BF₄ as dark blue crystals (1.31 g, 77%). ¹H NMR ([D₃]MeCN): δ = 8.20 (t, *J* = 8.6 Hz, 1H), 7.93 (t, *J* = 8.5 Hz, 2H), 7.57 (d, *J* = 8.6 Hz, 2H), 7.52 (d, *J* = 8.9 Hz, 2H), 6.95 (d, *J* = 8.0 Hz, 2H), 4.66 (m, 2H), 4.42 (m, 2H), 3.76 (s, 6H), 2.10 (m, 4H), 1.23 (t, *J* = 7.4 Hz, 6H); ¹³C NMR ([D₃]MeCN): δ = 159.51, 142.39, 141.91, 138.76, 136.82, 136.27, 119.21, 112.79, 107.40, 104.81, 102.81, 55.37, 51.12, 19.34, 10.07; MS (MALDI-TOF): *m/z*: 413 [*M*⁺]; UV/Vis (MeCN), λ_{max} (nm, (lg ε)) = 616, (4.14), 582sh (4.02), 429 (3.74), 350sh (3.44), 334 (3.71), 310 (4.65); elemental analysis calcd for C₂₇H₂₉N₂O₂BF₄ (%): C 64.82, H 5.80, N 5.60; found: C 64.83, H 5.77, N 5.55.

4a-PF₆: Benzoic acid (6.2 g, 51 mmol) and methylamine (50 mmol) in NMP (10 mL) were added to a solution of compound **1**-BF₄ (1.0 g, 2.0 mmol) in NMP (12 mL). The reaction flask was fitted with a dry ice condenser and heated to reflux under argon for 10 h. Twice during the reaction extra methylamine (2 × 5 mmol) was added. Workup as for **2**-PF₆ followed by recrystallization from acetonitrile and pyridine gave **4a**-PF₆ as red needles (0.56 g, 59%). ¹H NMR ([D₃]MeCN): δ = 7.74 (t, *J* = 8.6 Hz, 3H), 6.75

(d, *J* = 8.6 Hz, 6H), 3.21 (s, 9H); ¹³C NMR ([D₃]MeCN): δ = 139.61, 138.02, 137.27, 108.32, 104.96, 34.67; MS (MALDI-TOF): *m/z*: 324 [*M*⁺]; UV/Vis (MeCN), λ_{max} (nm, (lg ε)) = 519 (4.17), 498sh (4.10), 487sh (4.07), 350 (3.80), 290sh (4.32), 272 (5.05); elemental analysis calcd for C₂₂H₁₈N₃PF₆ (%): C 56.29, H 3.84, N 8.95; found: C 56.56, H 3.91, N 8.97.

Received: March 20, 2000

Revised: June 13, 2000 [Z14873]

- [1] D. F. Duxbury, *Chem. Rev.* **1993**, 93, 381–433.
- [2] K. H. Drexhage in *Dye Lasers* (Ed.: F. P. Schäfer), Springer, **1990**, pp. 155–200.
- [3] R. P. Haugland, *Handbook of Fluorescent Probes and Research Chemicals*, 6th ed., Molecular Probes, Eugene, **1996**.
- [4] H. H. Freeman in *Carbonium Ions* (Eds.: G. A. Olah, P. v. R. Schleyer), Wiley-Interscience, New York, **1973**, Chap. 28.
- [5] E. M. Arnett, R. A. Flowers II in *Stable Carbocation Chemistry* (Eds.: G. K. Surya Prakash, P. von R. Schleyer), Wiley, Chichester, **1997**, pp. 265–296.
- [6] K. Komatsu, H. Akamatsu, Y. Jinbu, K. Okamoto, *J. Am. Chem. Soc.* **1988**, 110, 633–634.
- [7] S. Ito, S. Kikuchi, N. Morita, T. Asao, *J. Org. Chem.* **1999**, 64, 5815–5821.
- [8] B. W. Laursen, F. C. Krebs, M. F. Nielsen, K. Bechgaard, J. B. Christensen, N. Harrit, *J. Am. Chem. Soc.* **1998**, 120, 12255–12263.
- [9] M. Wada, T. Watanabe, S. Natsume, H. Mishima, K. Kirishima, T. Erabi, *Bull. Chem. Soc. Jpn.* **1995**, 68, 3233–3240.
- [10] L. Teruel, L. Viadel, J. Carilla, L. Fajari, E. Brillas, J. Sane, J. Rius, L. Juliá, *J. Org. Chem.* **1996**, 61, 6063–6066.
- [11] J. C. Martin, R. G. Smith, *J. Am. Chem. Soc.* **1964**, 86, 2252–2256.
- [12] Crystals were mounted and aligned optically along the longest axis of the crystal. Weissenberg-oscillation photographs were recorded by using filtered CuK_α radiation with rotation through ±100° and an exposure time of 24 h. This resulted in darkened films but the bands of scattered intensity were clearly visible.
- [13] F. C. Krebs, B. W. Laursen, I. Johansen, A. Faldt, K. Bechgaard, C. S. Jacobsen, N. Thorup, K. Boubekeur, *Acta Crystallogr. Sect. B* **1999**, 55, 410–423.
- [14] The procedure used was analogous to that reported in ref. [8] except for fitting of the C₊ and H₊ scales, where 7th order polynomials was used instead of 3rd order polynomials. The acidity functions C₊ and H₊ express the change in activity of OH[−] towards carbenium ions and the change in activity of OH[−] towards acidic protons, respectively.
- [15] The slope of lg([ROH]/[R⁺]) versus C₊ was found to be 0.85 and not the ideal value of 1.0; however, even if this change in the C₊ function begins just above the previous calibrated region (below 70 mol % DMSO, ref. [8]) a maximum decrease in the pK_R⁺ value of 0.5 pK_R⁺ units, relative to the measured value of 23.9, is obtained.
- [16] A discussion of a very different type of triaryl methane chromophore is found in ref. [11].
- [17] NMR spectra and molecular modeling of **3b** suggests that because of the steric repulsion between the two methoxy groups it exists in a twisted helical conformation.
- [18] J. Griffiths, *Colour and Constitution of Organic Molecules*, Academic Press, London, **1976**.

Octahedral Grignard Reagents Can Be Chiral at Magnesium**

Marcus Vestergren, Björn Gustafsson, Öjvind Davidsson, and Mikael Håkansson*

The typical Grignard reagent is four-coordinate in the solid state.^[1–6] That $[\text{CH}_3\text{MgBr}(\text{thf})_3]$ is five-coordinate^[7] can be rationalized by the small size of the methyl group.^[8–10] Higher coordination numbers in RMgX and MgR_2 reagents normally require R groups with substituents that can form intramolecular coordinate bonds.^[2, 3] We were thus surprised to find that *trans*- $[\text{Mg}(\text{thienyl})_2(\text{thf})_4]$ (**1**) is six-coordinate in the solid state (Figure 1). The possibility of preparing octahedral

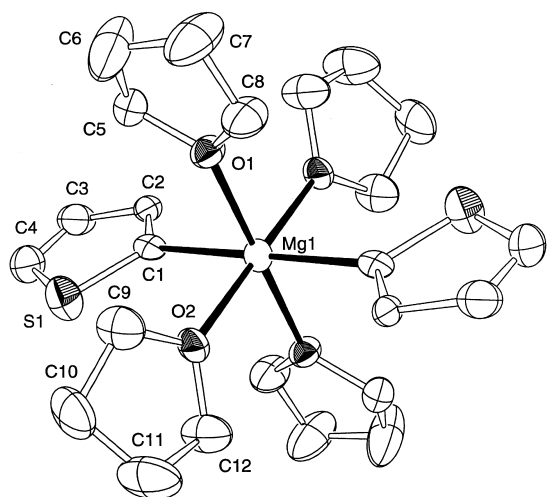


Figure 1. Magnesium is six-coordinate in *trans*- $[\text{Mg}(\text{thienyl})_2(\text{thf})_4]$ (**1**). Selected bond lengths [Å] and angles [°]: Mg1–O1 2.228(4), Mg1–O2 2.178(4), Mg1–C1 2.290(6), S1–C1 1.695(5), S1–C4 1.705(7), C1–C2 1.364(8), C2–C3 1.469(8), C3–C4 1.329(9); O1–Mg1–C1 89.90(17), O2–Mg1–C1 90.99(17), O2–Mg1–O1 89.53(14), C1–S1–C4 93.7(3).

Grignard reagents with stereogenic magnesium by using bidentate neutral ligands now seemed worth investigating. Since it is advantageous if the ligands can be identical to the solvent, dimethoxyethane (DME) was the obvious first ligand/solvent choice, and we prepared and structurally characterized the octahedral enantiomers Δ - and Λ -*cis*- $[(\text{thienyl})\text{MgBr}(\text{dme})_2]$ (**2**; Figure 2) as well as Δ - and Λ -*cis*- $[(\text{vinyl})\text{MgBr}(\text{dme})_2]$ (**3**; Figure 3). Both complexes were prepared and crystallized from neat DME.

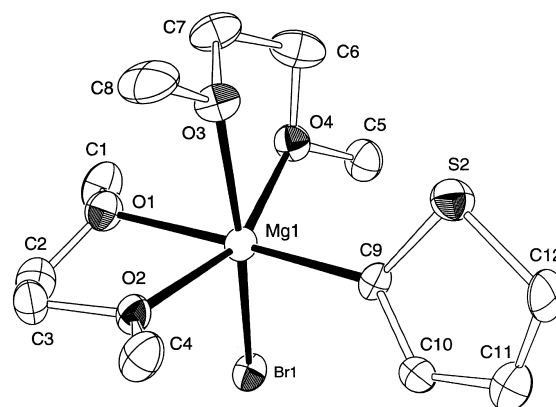


Figure 2. Molecular structure of Δ -**2**. Both enantiomers of the *cis* isomer are present in crystals of **2**. Selected bond lengths [Å] and angles [°]: Mg1–Br1 2.634(2), Mg1–O1 2.218(5), Mg1–O2 2.107(5), Mg1–O3 2.244(5), Mg1–O4 2.132(5), Mg1–C9 2.171(7), C9–C10 1.376(8), C9–S2 1.728(6), C10–C11 1.419(9), C11–C12 1.334(10), C12–S2 1.734(8); O1–Mg1–Br1 86.80(14), O2–Mg1–Br1 95.50(14), O3–Mg1–Br1 167.39(15), O4–Mg1–Br1 96.59(14), C9–Mg1–Br1 97.52(19), C9–Mg1–O1 172.0(2), C9–Mg1–O2 98.1(2), C9–Mg1–O3 93.1(2), C9–Mg1–O4 100.7(2), O2–Mg1–O4 156.09(19), O2–Mg1–O1 74.68(18), O4–Mg1–O1 85.48(18), O2–Mg1–O3 89.65(18), O4–Mg1–O3 74.71(17), O1–Mg1–O3 83.47(18).

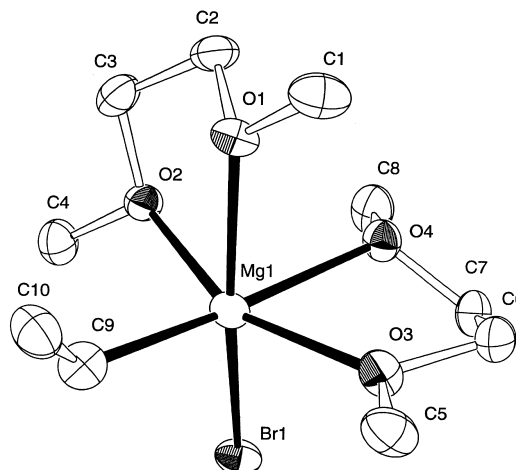


Figure 3. The Δ -enantiomer of **3**. The *cis* geometry is clearly preferred. Selected bond lengths [Å] and angles [°]: Br1–Mg1 2.6479(16), Mg1–O1 2.221(3), Mg1–O2 2.151(3), Mg1–O3 2.137(3), Mg1–O4 2.271(3), Mg1–C9 2.125(11), C9–C10 1.32(2); O1–Mg1–Br1 163.49(10), O2–Mg1–Br1 93.48(9), O3–Mg1–Br1 95.82(10), O4–Mg1–Br1 86.85(9), C9–Mg1–Br1 103.8(6), C9–Mg1–O1 89.6(6), C9–Mg1–O2 99.5(6), C9–Mg1–O3 99.8(6), C9–Mg1–O4 168.1(6), O3–Mg1–O2 155.88(13), O3–Mg1–O1 91.25(12), O2–Mg1–O1 74.56(11), O3–Mg1–O4 73.52(12), O2–Mg1–O4 84.86(12), O1–Mg1–O4 80.86(12), Mg1–C9–C10 132.0(12).

[*] Dr. M. Håkansson, M. Vestergren, B. Gustafsson
Department of Inorganic Chemistry
Chalmers University of Technology
41296 Göteborg (Sweden)
Fax: (+46) 31-772-2846
E-mail: hson@inoc.chalmers.se

Dr. Ö. Davidsson
Organic Chemistry
Department of Chemistry
Göteborg University
41296 Göteborg (Sweden)

[**] This work was supported by the Swedish Natural Science Research Council (NFR). We thank Karin Bengtsson, Fredrik Blomgren, Henrik Glänneskog, and Dan Lundberg for preparative assistance.

Octahedral RMgX and MgR_2 reagents are attractive, since they can be made configurationally chiral by simple solvation if the solvent is bidentate, such as DME. They are also likely to retain their solid-state structure in DME or THF solutions, since extended X-ray absorption fine structure spectroscopic (EXAFS) and large-angle X-ray scattering (LAXS) measurements^[11–15] have shown that octahedral monomers, at least when the R group is vinyl, dominate in THF. Indeed, ^1H NMR data show that *cis*-octahedral **2** seems to retain its solid-state structure in toluene solution^[16] (Figure 4). From $+50^\circ\text{C}$ to

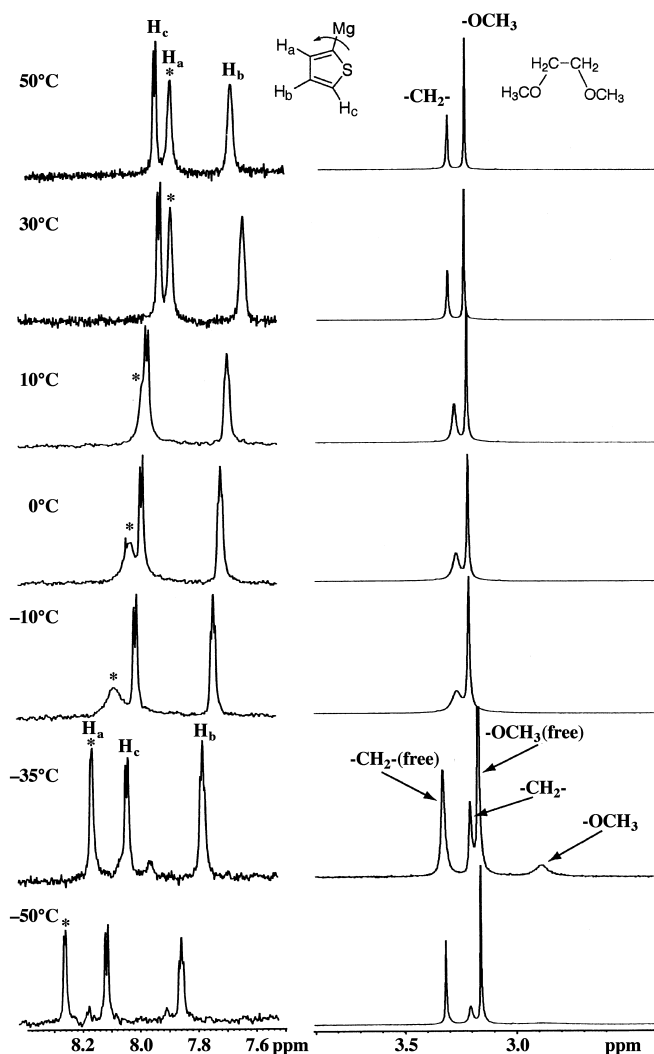


Figure 4. ^1H NMR spectra of **2** in $[\text{D}_8]\text{toluene}$ at selected temperatures with extracts between $\delta = 7.5$ to 8.4 (the chemical shift region for the thienyl protons) and between $\delta = 3.0$ to 3.5 (DME protons). The thienyl proton H_a (marked with an asterisk) shows chemical shift and lineshape changes due to restricted rotation around the Mg1-C9 bond. An additional set of DME proton signals appear at low temperatures due to freezing of the exchange between free and coordinated DME.

At -50°C , there is only one set of thienyl proton resonances, which makes it unlikely that the octahedral *trans* isomer is present in appreciable concentration. The thienyl proton closest to the magnesium atom, H_a , exhibits a broadening that can be explained by hindered rotation of the thienyl group around the Mg-C bond rather than inter- or intramolecular exchange. At -20°C , the broadening effect vanishes, which indicates that the thienyl group is locked into the solid-state position, where S-Br interactions are minimized (Figure 2). At -35°C , the CH_2 and CH_3 resonances from complexed DME appear upfield from the free DME signal and indicates that exchange processes with uncomplexed DME now are slow on the NMR time scale. Integrated proton intensities at -35°C show that the stoichiometry thienyl:DME is 1:2, which rules out both the presence of $[\text{Mg}(\text{thienyl})_2]$ complexes (from the Schlenk equilibrium) and tetrahedral complexes that would result from loss of one DME ligand.^[17] The formation

of soluble larger aggregates with this stoichiometry is also unlikely.

The crystal structure of **1** (Figure 1) exhibits magnesium in an octahedral geometry with thienyl groups in the *trans* positions. Octahedral *trans* coordination has previously been reported^[18–20] in the N,N,N',N' -tetramethyl-1,2-ethanediamine (TMEDA) complexes of bis(phenylethynyl)magnesium and bis(*tert*-butylethynyl)magnesium, which led to the assumption that *sp*-hybridization is necessary for sixfold coordination.^[3] The crystal structures of **2** and **3** (Figures 2 and 3) show that they are both octahedral *cis* isomers and, thus, chiral. This geometry has also been found in *cis*- $[\text{MgCl}_2(\text{dme})_2]$.^[21] The Mg-C distances in **1** (2.29 Å) are long, which could indicate a larger polarization of the Mg-C bond as a result of the coordination of the four Lewis basic THF ligands. The Mg-C distances in **2** (2.17 Å) and **3** (2.13 Å) are normal, despite the high coordination number, while the Mg-Br distances of 2.65 and 2.64 Å are significantly longer than the typical (2.4–2.5 Å) values for four-coordinate RMgBr complexes.^[3] Judging from the angles O-Mg-C9 (mean in **2**: 97° ; in **3**: 96°) and O-Mg-Br (mean in **2**: 93° ; in **3**: 92°), it seems as if the steric requirements are larger for both the thienyl and the vinyl group as compared to the bromide. It is noteworthy that the $\text{Br-Mg-C9}_{\text{vinyl}}$ angle in **3** is significantly larger (104°) than the $\text{Br-Mg-C9}_{\text{thienyl}}$ angle (98°) in **2**. Although there are short intermolecular C-H-Br' contacts in both **2** (2.64 Å) and **3** (2.74 Å), they can hardly be considered as classical hydrogen bonds.

Crystals of **2** and **3** are racemic. If octahedral Grignard reagents are to be useful in stereoselective synthesis, the Δ - and Λ -enantiomers have to be resolved. In some cases, spontaneous resolution may occur directly at crystallization^[22] but conventional resolution methods can, of course, also be utilized. We are presently trying to predetermine^[23] the chirality by the use of chiral ligands. For $[\text{RMgX}(\text{LL})_2]$ species, introduction of chirality into one or both of the bidentate neutral ligands (LL) is the apparent choice but using chiral anions is also viable.

In conclusion, and contrary to previous belief, six-coordinate Grignard reagents can be easily prepared in high yield by using appropriate R groups and bidentate neutral ligands. Such octahedral Grignard reagents have been found to be configurationally chiral and stereochemically rigid in toluene solution. Grignard reagents, which are chiral at the magnesium atom, should give strong asymmetric induction and if their chirality can be controlled or predetermined, they have a promising potential in stereoselective syntheses.

Experimental Section

All operations were carried out under argon using Schlenk, glove box, or low temperature^[24] techniques.

$[\text{Mg}(\text{thienyl})_2(\text{thf})_4]$ (**1**): Magnesium turnings (0.270 g, 11.1 mmol) and 2-bromothiophene (1.00 mL, 10.3 mmol) were stirred for 1 h at 50°C in THF (10 mL). Dioxane (3.0 mL, 35.4 mmol) was added and the resulting suspension was centrifuged and the clear brown solution was transferred by syringe to another Schlenk vessel. The solution was evaporated to dryness in order to remove residual dioxane, and THF (10 mL) was added. After 12 h at -80°C , colorless crystals of **1**, which lose THF rapidly when isolated at ambient temperature, had formed. Approximate yield: 1.0 g, 20%. Crystal structure data for $\text{MgS}_2\text{O}_4\text{C}_{24}\text{H}_{38}$ (**1**): crystal size $0.25 \times 0.20 \times 0.15$ mm,

monoclinic, space group $P2_1/c$ (no. 14), $a = 8.508(4)$, $b = 13.892(4)$, $c = 10.900(4)$ Å, $\beta = 92.70(3)^\circ$, $V = 1286.9(8)$ Å³, $Z = 2$, $\rho_{\text{calc}} = 1.236$ g cm⁻³, $2\theta_{\text{max}} = 50.0^\circ$, MoK α radiation, $\omega/2\theta$ scan mode, $T = -120^\circ\text{C}$, psi-scan corrections (abs. range 0.936–0.999), $\mu = 0.258$ mm⁻¹. Refinement on F^2 for 2256 reflections and 142 parameters gave $R1 = 0.057$ and $wR2 = 0.137$ for $I > 2\sigma(I)$. Residual electron density $-0.29 < \Delta\rho < 0.36$ e Å⁻³. Mg, S, O, and C atoms were refined anisotropically and the H atoms with a riding model.

[(thienyl)MgBr(dme)₂] (**2**): Magnesium turnings (0.360 g, 14.8 mmol) and 2-bromothiophene (1.00 mL, 10.3 mmol) were stirred for 1 h at 50°C in DME (20 mL). The reaction mixture was allowed to settle (by centrifugation, if necessary) and the clear brown solution was transferred by syringe to another Schlenk vessel. After a few hours at ambient temperature, large amounts of light brown crystals of **1** had formed. After recrystallization from DME, the crystals were washed with cold DME (2×2 mL) and dried briefly under vacuum. When treated in this way, solid **2** does not lose any DME. Yield: 1.80 g, 95%. Solubility: 0.01 M in DME at 20°C (2 M at 50°C); sparingly in toluene. IR (Nujol, Fluorolube): $\tilde{\nu} = 3072$ m, 3046 m, 3013 m, 2934 s, 2883 s, 2854 s, 2833 s, 2804 m, 2764 m, 2058 w, 1964 w, 1927 w, 1851 w, 1808 w, 1738 w, 1627 m, 1462 s, 1408 m, 1378 s, 1299 m, 1285 m, 1275 m, 1249 m, 1192 m, 1114 m, 1081 m, 1029 m, 982 m, 942 m, 866 m, 836 m, 820 m, 771 m, 712 m cm⁻¹. Crystal structure data for MgBrSO₄C₁₂H₂₃ (**2**): crystal size $0.20 \times 0.15 \times 0.15$ mm, monoclinic, space group $P2_1/c$ (no. 14), $a = 7.417(4)$, $b = 17.528(3)$, $c = 13.062(15)$ Å, $\beta = 95.85(3)^\circ$, $V = 1689.3(11)$ Å³, $Z = 4$, $\rho_{\text{calc}} = 1.445$ g cm⁻³, $2\theta_{\text{max}} = 50.0^\circ$, MoK α radiation, $\omega/2\theta$ scan mode, $T = -120^\circ\text{C}$, psi-scan corrections (abs. range 0.971–0.995), $\mu = 2600$ mm⁻¹. Refinement on F^2 for 2965 reflections and 264 parameters gave $R1 = 0.040$ and $wR2 = 0.068$ for $I > 2\sigma(I)$. Residual electron density $-0.66 < \Delta\rho < 0.46$ e Å⁻³. Mg, Br, S, O, and C atoms were refined with anisotropic thermal displacement parameters and the H atoms with isotropic parameters.

[(vinyl)MgBr(dme)₂] (**3**): The solvent was evaporated from a commercial solution of vinylmagnesium bromide in THF (10 mL, 10 mmol). The oily solids were dried briefly under vacuum and redissolved in DME (10 mL). From the resulting dark red solution, light brown crystals of **3** formed after a few hours at ambient temperature. Yield (not optimized): 1.07 g, 34%. IR (Nujol, Fluorolube): $\tilde{\nu} = 3072$ m, 3046 m, 3013 m, 2934 s, 2883 s, 2854 s, 2833 s, 2804 m, 2764 m, 2061 w, 1965 w, 1920 w, 1620 w, 1464 s, 1377 s, 1365 s, 1294 m, 1277 m, 1243 m, 1212 w, 1190 m, 1114 m, 1098 m, 1052 m, 1025 m, 867 m, 833 m, 771 w, 722 m cm⁻¹. Crystal structure data for MgBrO₄C₁₀H₂₃ (**3**): crystal size $0.30 \times 0.20 \times 0.10$ mm, monoclinic, space group $P2_1/n$ (No. 14), $a = 7.3311(18)$, $b = 15.353(2)$, $c = 12.9726(19)$ Å, $\beta = 90.986(17)^\circ$, $V = 1459.9(5)$ Å³, $Z = 4$, $\rho_{\text{calc}} = 1.417$ g cm⁻³, $2\theta_{\text{max}} = 50.0^\circ$, MoK α radiation, $\omega/2\theta$ scan mode, $T = -120^\circ\text{C}$, psi-scan corrections (abs. range 0.666–0.999), $\mu = 2856$ mm⁻¹. Refinement on F^2 for 2564 reflections and 255 parameters gave $R1 = 0.033$ and $wR2 = 0.066$ for $I > 2\sigma(I)$. Residual electron density $-0.37 < \Delta\rho < 0.33$ e Å⁻³. Mg, Br, O, and C atoms were refined with anisotropic thermal displacement parameters and the H atoms with isotropic parameters. The vinyl groups and bromide atoms are all disordered on double sites, to the effect that the ligands are interchanged. The site occupancy factor for the atoms shown in Figure 3, refined to 0.904.

All three structures were solved and refined using SHELX-97.^[25] Figures 1–3 were represented using ORTEP3.^[26] Crystallographic data (excluding structure factors) for the structures reported in this paper have been deposited with the Cambridge Crystallographic Data Centre as supplementary publication no. CCDC-140697, CCDC-140698, and CCDC-140699. Copies of the data can be obtained free of charge on application to CCDC, 12 Union Road, Cambridge CB2 1EZ, UK (fax: (+44) 1223-336-033; e-mail: deposit@ccdc.cam.ac.uk).

Received: March 23, 2000
Revised: July 4, 2000 [Z14888]

- [1] P. R. Markies, O. S. Akkerman, F. Bickelhaupt, W. J. J. Smeets, A. L. Spek, *Adv. Organomet. Chem.* **1991**, 32, 147.
- [2] P. R. Markies, G. Schat, S. Griffioen, A. Villena, O. S. Akkerman, F. Bickelhaupt, *Organometallics* **1991**, 10, 1531.
- [3] F. Bickelhaupt in *Grignard Reagents—New Developments* (Ed.: H. G. Richey), Wiley, Chichester, **2000**, p. 318.
- [4] F. Bickelhaupt, *J. Organomet. Chem.* **1994**, 475, 1.

- [5] C. E. Holloway, M. Melnik, *J. Organomet. Chem.* **1994**, 465, 1.
- [6] E. Weiss, *Angew. Chem.* **1993**, 105, 1565; *Angew. Chem. Int. Ed. Engl.* **1993**, 32, 1501.
- [7] M. Vallino, *J. Organomet. Chem.* **1969**, 20, 1.
- [8] J. Toney, G. D. Stucky, *J. Organomet. Chem.* **1971**, 28, 5.
- [9] H. Viebrock, E. Weiss, *J. Organomet. Chem.* **1994**, 464, 121.
- [10] D. Steinborn, T. Ruffer, C. Bruhn, F. W. Heinemann, *Polyhedron* **1998**, 17, 3275.
- [11] A. Wellmar, I. Persson, *J. Organomet. Chem.* **1991**, 415, 155.
- [12] A. Wellmar, A. Hallberg, I. Persson, *J. Organomet. Chem.* **1991**, 415, 167.
- [13] T. S. Ertel, H. Bertagnolli, *Polyhedron* **1993**, 12, 2175.
- [14] I. Abraham, W. Horner, T. S. Ertel, H. Bertagnolli, *Polyhedron* **1996**, 15, 3993.
- [15] T. S. Ertel, H. Bertagnolli in *Grignard Reagents—New Developments* (Ed.: H. G. Richey), Wiley, Chichester, **2000**, p. 364.
- [16] A small amount of extra DME was added (free:complexed = 60:40) during dissolution of **2** in toluene.
- [17] Above -30°C it is no longer possible to estimate the thienyl:DME ratio due to signal coalescence and one referee correctly pointed out that the possibility of tetrahedral species at ambient temperature has to be considered. The existence of two complexes (octahedral and tetrahedral) but only one set of thienyl signals could then be explained by assuming an equilibrium that is strongly shifted towards an octahedral complex at -50°C and towards a tetrahedral complex at 50°C . The broadening of the H_a signal would be interpreted as coalescence of resonances from tetra- and octahedral complexes, instead of restricted rotation around the Mg–C bond. The fact that there is no coalescence for the H_b and H_c resonances has to be explained by chemical shift equivalency. In our opinion, this is unlikely since the electronic effects in the thienyl group should be considerable on going from four- to six-fold coordination.
- [18] M. Perucaud, J. Ducom, M. Vallino, *C. R. Acad. Sci. Paris C* **1967**, 264, 571.
- [19] B. Schubert, U. Behrens, E. Weiss, *Chem. Ber.* **1981**, 114, 2640.
- [20] M. Geissler, J. Kopf, E. Weiss, *Chem. Ber.* **1989**, 122, 1395.
- [21] B. Neumuller, G. Stieglitz, K. Dehnicke, *Z. Naturforsch. B.* **1993**, 48, 1151.
- [22] M. Håkansson, M. Vestergren, B. Gustafsson, G. Hilmersson, *Angew. Chem.* **1999**, 111, 2336; *Angew. Chem. Int. Ed.* **1999**, 38, 2199.
- [23] U. Knof, A. von Zelewsky, *Angew. Chem.* **1999**, 111, 312; *Angew. Chem. Int. Ed.* **1999**, 38, 303.
- [24] M. Håkansson, *Inorg. Synth.* **1998**, 32, 222.
- [25] G. M. Sheldrick, University of Göttingen, Göttingen (Germany), **1998**.
- [26] L. J. Farrugia, *J. Appl. Crystallogr.* **1997**, 30, 565.

Design and Synthesis of Intramolecular Resonance-Energy Transfer Probes for Use in Ratiometric Measurements in Aqueous Solution

Yasutomo Kawanishi, Kazuya Kikuchi, Hideo Takakusa, Shin Mizukami, Yasuteru Urano, Tsunehiko Higuchi, and Tetsuo Nagano*

In recent years, many fluorescent probes have been developed to study biological phenomena in living cells. By using fluorescent probes, it is possible to follow a phenomenon in real time with high sensitivity. However, the fluorescence intensity of the probes is influenced by many factors, such as changes of environment around the probe (pH, polarity, temperature, and so forth), changes in the probe concentration, and changes in the excitation intensity. To reduce the influence of such factors, ratiometric measurements are utilized,^[1] namely, observation of changes in the ratio of the fluorescence intensities at two wavelengths. This technique allows more precise measurement and, with some probes, quantitative detection is possible. Many probes have been developed for ratiometric measurements,^[1] such as the calcium indicator Fura-2^[2] and the pH indicator SNARF-1.^[3] To carry out ratiometric measurements, the probe must exhibit a large shift in its emission or excitation spectrum after it reacts (or binds) with the target molecule. Resonance-energy transfer (RET) is one mechanism used to obtain a large shift in the spectral peak.

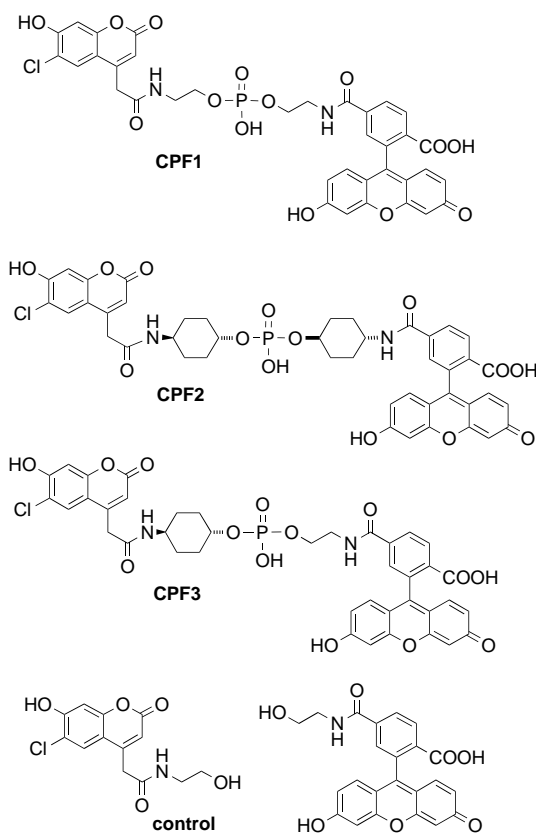
RET is a radiationless transmission of an energy quantum between two fluorophores in close proximity.^[4] If the bond between two linked fluorophores, which have an overlap in their spectra, is cleaved, we observe the emission of the acceptor, due to RET, before the cleavage and the emission of the donor after. This results in a large shift in the emission peak, which can be used for ratiometric measurements.

Little work has been done on chemically synthesized intramolecular RET probes except for the probe for detecting β -lactamase activity^[5] reported by Tsien and co-workers. This is because, even if two fluorophores are located in close proximity, self-quenching occurs due to the close contact of the two hydrophobic fluorophores in an aqueous solution.^[6] If we could observe the emission of the acceptor in chemically synthesized RET probes, we would be able to design probes for ratiometric measurements of many enzymes, by binding two fluorophores at the ends of a peptide substrate (or another cleavable linker), which could be cleaved selectively by the enzyme.

Herein, we present a method to observe the emission of the acceptor caused by intramolecular RET, applicable for ratiometric measurements in aqueous solution. This method is based upon the idea that self-quenching between the two

fluorophores can be blocked and the emission of the acceptor can be observed by restricting the flexibility of the linker between the two fluorophores, so that they can not readily come into close contact.

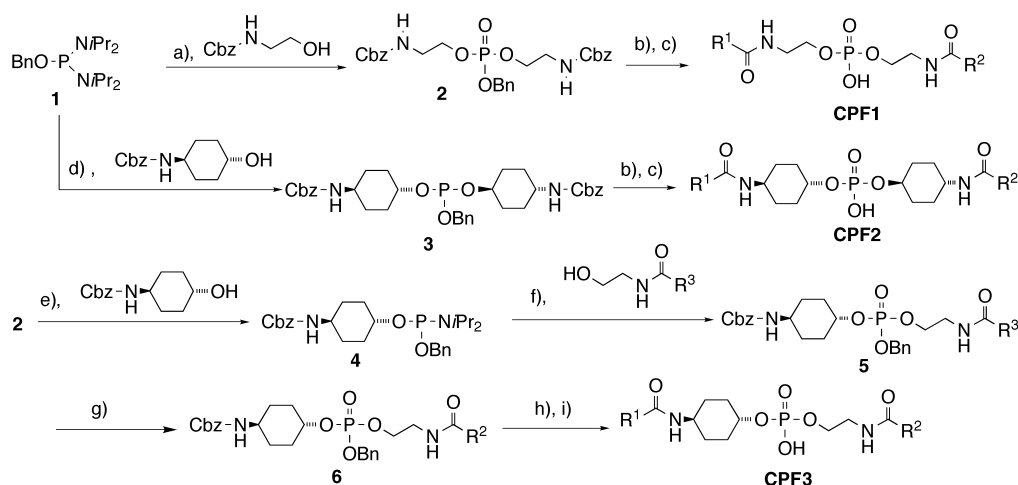
To investigate the relation between the flexibility of the linker and the emission spectrum, we designed and synthesized coumarin phosphodiester-linked fluoresceins (CPFs). CPFs have two fluorophores, coumarin as a donor and fluorescein as an acceptor. These two fluorophores are known to have a large overlap in their spectra and exhibit efficient emission in an aqueous solution. The phosphodiester moiety was introduced to enhance the aqueous solubility of the probe and was placed as a linker between the two fluorophores. Ethylene was chosen as a linker extension with high flexibility and cyclohexane as one with low flexibility. Three molecules with different linkers were synthesized; CPF1 with two



ethylene linkers, CPF2 with two cyclohexane linkers, and CPF3 with one ethylene and one cyclohexane linker. We used a mixture of the amide form of coumarin and fluorescein as the control. CPFs were synthesized as shown in Scheme 1.

The emission spectra of CPFs in an aqueous buffer excited at 370 nm (the excitation wavelength, λ_{ex} , of the coumarin moiety) are shown in Figure 1a. Efficient RET was observed with all CPFs, as more than 90 % of the emission of the coumarin donor ($\lambda_{\text{em}} = 450$ nm) was quenched. A strong emission of the fluorescein acceptor ($\lambda_{\text{em}} = 515$ nm) was observed only in CPF2. The fluorescein acceptor of CPF2 emitted 54 % of the photons that excited the donor. CPF1 and CPF3 had only weak emission and showed self-quenching.

[*] Prof. T. Nagano, Y. Kawanishi, Dr. K. Kikuchi, H. Takakusa, S. Mizukami, Dr. Y. Urano, Dr. T. Higuchi
Graduate School of Pharmaceutical Sciences
The University of Tokyo
7-3-1 Hongo, Bunkyo-ku, Tokyo 113-0033 (Japan)
Fax: (+81) 3-5841-4855
E-mail: tlong@mol.f.u-tokyo.ac.jp



Scheme 1. Synthesis of CPFs. Compound **1** was synthesized as previously reported.^[7] Fluorophores: R^1 = coumarin, R^2 = fluorescein, R^3 = fluorescein dipivaloate. Synthesis: a) 1) Tetrazole, CH_2Cl_2 , RT, Ar atmosphere; 2) 3-chloroperoxybenzoic acid (*m*-CPBA), -40°C . b) 10% Pd/C, 95% aq. EtOH, 1 atm H_2 . c) 1) Coumarin succinimide ester, MeOH, RT; 2) carboxyfluorescein succinimide ester, 100 mM aq. NaHCO_3 , RT. d) 1) Tetrazole, CH_2Cl_2 , 30°C , Ar atmosphere; 2) *m*-CPBA, -40°C . e) Diisopropylammonium tetrazolide, CH_2Cl_2 , 30°C . f) 1) Tetrazole, CH_2Cl_2 , 0°C , Ar atmosphere; 2) *m*-CPBA, -40°C . g) MeOH, 2N aq. NaOH. h) 2% Pd/C, 95% aq. EtOH, 1 atm H_2 . i) Coumarin succinimide ester, dimethylformamide, triethylamine. All CPFs were purified by reverse-phase HPLC. Bn = benzyl; Cbz = carbobenzoxy.

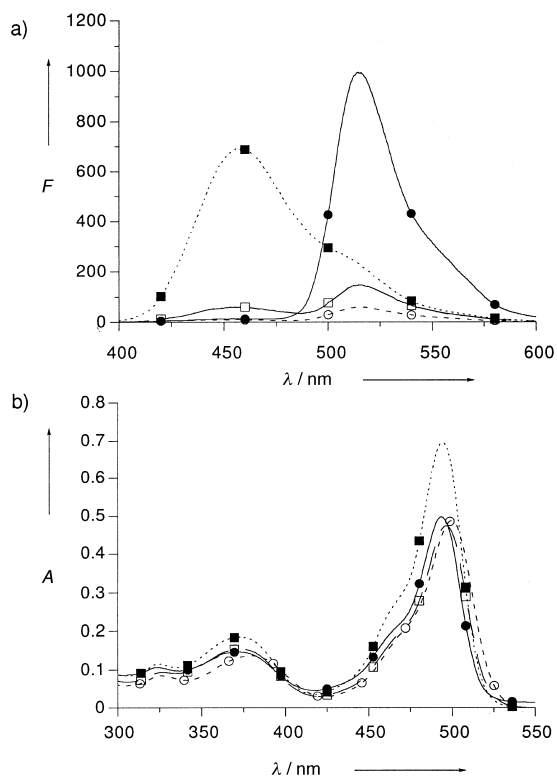


Figure 1. a) Emission ($\lambda_{\text{ex}} = 370$ nm) and b) absorption spectra of CPFs (CPF1 \circ , CPF2 \bullet , CPF3 \square , control \blacksquare ; all $1\ \mu\text{M}$). These spectra were measured in 100 mM sodium phosphate buffer (pH 7.4). F = fluorescence intensity (in arbitrary units), A = absorbance.

The control mixture showed a strong emission of the coumarin acceptor, which was not quenched intermolecularly. The quantum yields of CPFs, when the fluorescein acceptor was directly excited ($\lambda_{\text{ex}} = 492$ nm, conditions as per Figure 1), were 0.10 for CPF1, 0.83 for CPF2, and 0.27 for CPF3. These results correlate well with the intensity of the emission of the fluorescein acceptor in CPFs and indicate that the emission

intensity of the acceptor depends largely on the extent of self-quenching instead of the efficiency of RET.

CPF2 showed a large shift in its emission spectrum after the bond between the fluorophores was cleaved by treatment with base (Figure 2). This large shift of the emission spectrum indicates that the probe is suitable for ratiometric measurements.

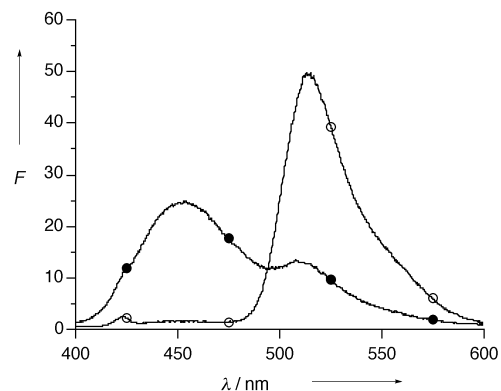


Figure 2. Emission spectra of CPF2 before and after cleavage in base (before cleavage \circ , after cleavage \bullet). F = fluorescence intensity (in arbitrary units). CPF2 was cleaved in 0.1 N aq. NaOH at 50°C . After cleavage, the solution was neutralized with 0.1 N aq. HCl and diluted with 100 mM sodium phosphate buffer (pH 7.4). The concentration of CPF2 was $0.1\ \mu\text{M}$.

The absorption spectra of CPFs in aqueous buffer are shown in Figure 1b. We observed a large red shift in the absorption spectra of CPF1 ($\lambda_{\text{max}} = 380$ nm, 500 nm), a small shift for CPF3 ($\lambda_{\text{max}} = 373$ nm, 497 nm), and no shift for CPF2 ($\lambda_{\text{max}} = 372$ nm, 494 nm), compared to the control ($\lambda_{\text{max}} = 373$ nm, 494 nm). This shift in the absorption spectra was supposed to be due to the close contact of two fluorophores. CPF1, which had the weakest emission, had the largest shift and CPF3, which had a weak emission, had a small shift. CPF2, which had a strong emission of the acceptor, showed no shift because the two fluorophores cannot interact with each other.

When the emission spectra of the CPFs in methanol (10% sodium phosphate buffer) excited at 370 nm were detected, the emission of the fluorescein acceptor could be observed in all CPFs. The hydrophobic interaction between the fluorophores would be weaker in methanol than in aqueous solution and the fluorophores may not come into close contact in organic solvents. When the absorption spectra of CPFs in methanol were detected, the red shift of the absorption spectra observed in aqueous solution was not observed, indicating that the two fluorophores did not come into close contact. This result indicates that, in methanol, the hydrophobic interaction between the fluorophores is weakened and the emission of the acceptor caused by RET can be observed.

In conclusion, we have shown that in designing a RET probe for ratiometric measurements, it is possible to observe the emission of the acceptor if the structure of the probe is such as to prevent close contact of the two fluorophores.

Received: April 11, 2000 [Z14974]

- [1] W. T. Mason in *Fluorescent and Luminescent Probes for Biological Activity*, 2nd ed. (Ed.: W. T. Mason), Academic Press, London, **1999**, pp. 175–195.
- [2] G. Grynkiewicz, M. Poenie, R. Y. Tsien, *J. Biol. Chem.* **1985**, *260*, 3440–3450.
- [3] J. E. Whitaker, R. P. Haugland, F. G. Frendergast, *Anal. Biochem.* **1991**, *194*, 330–344.
- [4] B. W. Van der Meer, G. Coker III, S.-Y. Chen, *Resonance Energy Transfer*, Wiley-VCH, New York, **1991**, pp. 1–33.
- [5] G. Zlokarnik, P. A. Negulescu, T. E. Knapp, L. Mere, N. Burres, L. Feng, M. Whitney, K. Roemer, R. Y. Tsien, *Science* **1998**, *279*, 84–88.
- [6] S. Mizukami, K. Kikuchi, T. Higuchi, Y. Urano, T. Mashima, T. Tsuruo, T. Nagano, *FEBS Lett.* **1999**, *453*, 356–360.
- [7] W. Bannwarth, A. Trzeciak, *Helv. Chim. Acta.* **1987**, *70*, 175–186.

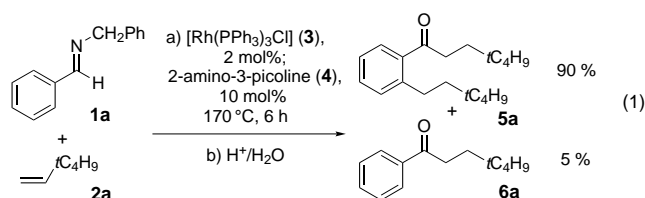
The Catalytic Alkylation of Aromatic Imines by Wilkinson's Complex: The Domino Reaction of Hydroacylation and *ortho*-Alkylation**

Chul-Ho Jun,* Jun-Bae Hong, Yeon-Hee Kim, and Kwan-Yong Chung

Transition metal catalyzed C–H bond activation and the subsequent coupling of the organic fragment to an olefin is a promising area in which to find a convenient method for the construction of a carbon skeleton.^[1] We have studied C–H bond activation through the hydroacylation of olefins using

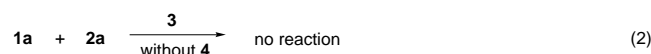
aldehydes, alcohols, and aldimines.^[2, 3] Unexpectedly during our experiments on transimination-assisted hydroacylation with aldimines,^[3] *ortho*-alkylation was observed. Alkylation of aromatic ketones at the *ortho* position in a ruthenium(II)-catalyzed reaction has been reported by Murai and co-workers, this is an outstanding example of sp²-CH/olefin coupling and a decisive breakthrough in efficiency and selectivity.^[4] However, while the reaction shows a high efficiency for vinyl silane or vinyl siloxane, it exhibits limitations for other olefins, for example low reactivity for 1-alkenes bearing allylic protons, probably because of facile double bond isomerization, and no reactivity for internal olefins and α,ω -dienes.^[5] Herein, we report an efficient *ortho*-alkylation of aromatic imines with various olefins by using Wilkinson's complex ([Rh(PPh₃)₃Cl] (**3**)) and hydroacylation. This *ortho*-alkylation is chelation-assisted and shows generality as well as regioselectivity, and high efficiency.

Treatment of the aldimine **1a** [Eq. (1)] with *tert*-butylethylene (**2a**) at 170 °C for 6 h with **3** (2 mol % based upon **1a**)

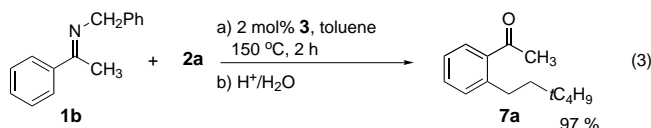


and 2-amino-3-picoline (**4**; 10 mol % based upon **1a**) as a cocatalytic system gave, after hydrolysis, compound **5a** in 90% yield along with a small amount of **6a** (5%). Compound **6a** is a hydroacylated product of **1a** and is formed by a transimination reaction, while **5a** is both a hydroacylated and an *ortho*-alkylated product. Of the various aldimines employed **1a**, prepared from benzylamine and benzaldehyde, showed the best reactivity for this simultaneous hydroacylation and *ortho*-alkylation.^[3]

Compound **1a** did not react with **2a** without the cocatalyst **4** [Eq. (2)],^[2] whereas, the ketimine **1b** (which is the benzylimine of acetophenone) was *ortho*-alkylated by **2a** in the



presence of **3** alone, to give **7a** in 97% yield [Eq. (3)]. These results show that the rhodium(I)-catalyzed *ortho*-alkylation takes place in ketimines, not in aldimines and that there is no *ortho*-alkylation without hydroacylation.



Ketimine **1b** was very reactive in the *ortho*-alkylation reaction with **3**; thus, various olefins were tested in reactions with this ketimine **1b** and **3** as catalyst (Table 1). In contrast to

[*] Prof. C.-H. Jun, J.-B. Hong, Y.-H. Kim, K.-Y. Chung
Department of Chemistry
Yonsei University, Seoul, 120-749 (Korea)
Fax: (+82) 2-364-7050
E-mail: junch@alchemy.yonsei.ac.kr

[**] This work was supported by the Brain Korea 21 Project, the Yonsei University Faculty Research Grant (1999), and the KOSEF (No. 97-05-01-01-3).

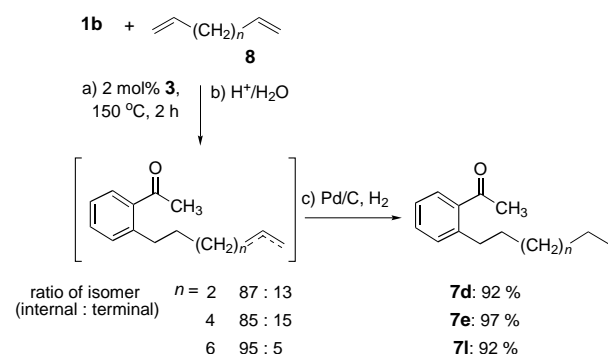
Supporting information for this article is available on the WWW under <http://www.wiley-vch.de/home/angewandte/> or from the author.

Table 1. The Rh^I-catalyzed *ortho*-alkylation of various ketimines and olefins [Eq. (4)].

Entry	R ¹	Ketimine	R ²	Olefin	Product	Yield [%] ^[b]
1	CH ₃	(1b)	<i>i</i> -C ₄ H ₉	(2a)	7a	97 (100)
2	CH ₃	(1b)	C ₆ F ₅	(2b)	7b	91 (100)
3	CH ₃	(1b)	Cy	(2c)	7c	65 (68)
4	CH ₃	(1b)	<i>n</i> -C ₄ H ₉	(2d)	7c	94 (97) ^[c]
5	CH ₃	(1b)	<i>n</i> -C ₆ H ₁₃	(2e)	7e	71 (78) ^[d]
6	CH ₃	(1b)	<i>n</i> -C ₁₀ H ₂₅	(2f)	7f	82 (92) ^[d]
7	CH ₃	(1b)	(CH ₃) ₃ Si	(2g)	7g	92 (96)
8	CH ₃	(1b)		(2h)	7h	95 (96)
9	CH ₃	(1b)		(2i)	7d	42 (47) ^[d]
10	CH ₃	(1b)		(2j)	7i	35 ^[d]
11	CH ₃ CH ₂	(1c)	(2g)		7j	93 (100) ^[e]
12	<i>n</i> -C ₅ H ₁₁	(1d)	(2g)		7k	73 (80) ^[f]

[a] Reactants: **1** (0.324 mmol), **2** (0.324 mmol), **3** (0.00649 mmol), toluene (0.1 g) and molecular sieves. [b] GC yields are given in parentheses. [c] 1.62 mmol of **2d** was used. Reaction time was 6 h. [d] 0.972 mmol of **2** was used. Reaction time was 6 h. [e] Included 12% of the di-*ortho*-alkylation product. [f] Included 16% of the di-*ortho*-alkylation product.

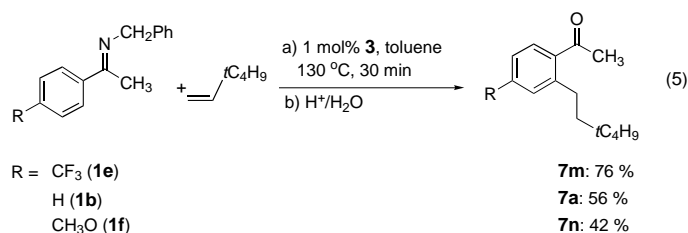
Murai's ruthenium(II)-catalyzed *ortho*-alkylation,^[4, 5] with our rhodium(I) system various 1-alkenes with or without allylic protons were used successfully in the *ortho*-alkylation of ketimines (Table 1, entries 1–6). Even α,ω -dienes (**8**; Scheme 1), which did not react in Murai's system, underwent



Scheme 1. The *ortho*-alkylation of α,ω -dienes and subsequent reduction.

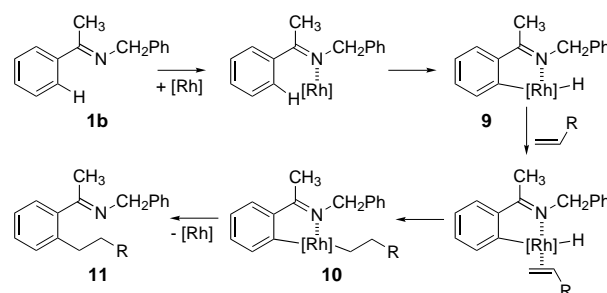
high-yielding *ortho*-alkylation reactions with our system. However, the *ortho*-alkylation only occurred at one end of the diene, not at both ends.^[6] Remarkably, the internal olefin **2h** reacted (via isomerization to the terminal olefin 1-pentene), with **1b** to yield the linear alkylated product **7h** in high yield (Table 1, entry 8). Even sterically hindered dialkyl-substituted olefin **2j** underwent a moderately successful *ortho*-alkylation reaction (entry 10).

With *para*-substituted ketimines [Eq. (5)] electron-withdrawing substituents gave much better reactivity than electron-donating ones; this is in contrast to the *ortho*-alkylation



of aromatic ketones, reported by Murai and co-workers, in which electron-withdrawing substituents retarded the reaction, whereas electron-donating ones accelerated it.^[7]

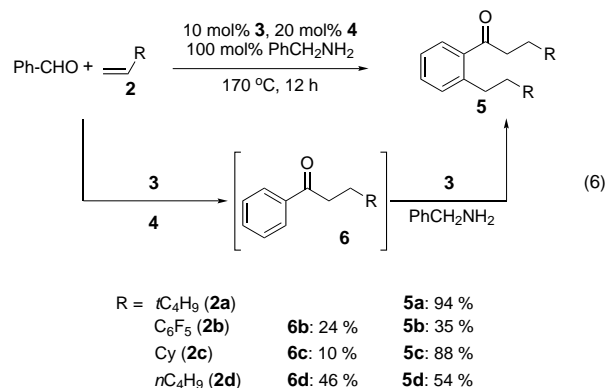
Our Rh^I-catalyzed *ortho*-alkylation is believed to occur by the mechanism shown in Scheme 2; the precoordination of the imine nitrogen atom to the Rh^I center assists in the



Scheme 2. The postulated mechanism for *ortho*-alkylation. [Rh] = [Rh(PPh₃)₃Cl].

activation of an aromatic C–H bond, this in turn leads to the formation of the metallacycle **9**.^[8] The C–H activation reaction proceeds by the oxidative addition of the *ortho*-C–H bond to the electron-rich [Rh(PPh₃)₃Cl] unit;^[9] olefin coordination and hydride insertion follow to give **10**. Finally, a reductive elimination produces the *ortho*-alkylated ketimine **11**.

In chelation-assisted hydroacylation,^[2, 3] **4** was used as a chelation-assistance tool; in our Rh^I-catalyzed reaction, benzylamine could also be used as a chelation-assistance tool. The reaction shown in Equation (6) consists of chelation-



assisted hydroacylation induced by **4** followed by imine-assisted *ortho*-alkylation effected by benzylamine. In this reaction benzaldehyde reacted with the olefins **2b–d**, **3**, **4**,

and benzylamine to yield a mixture of the ketones **6** and **5**.^[10, 11] In the case of *tert*-butylethylene (**2a**), only **5a** was isolated (94 % yield).

In conclusion, we identified a chelation-assisted, Rh^I-catalyzed *ortho*-alkylation reaction of ketimines with olefins. This type of *ortho*-alkylation shows generality as well as efficiency; the reactions of various olefins (including 1-alkenes, α,ω -dienes, and even internal olefins) with ketimines result in high yields of the corresponding *ortho*-alkylated products. In addition, successive Rh^I-catalyzed hydroacylation and *ortho*-alkylation of an aldehyde gave a product that has been alkylated at two sites.

Experimental Section

Full experimental details can be found in the Supporting Information.

A typical procedure for the preparation of **5a** [Eq. (6)]: A screw-capped pressure vial (1 mL) was charged with freshly purified benzaldehyde (0.216 mmol), 2-amino-3-picoline (**4**, 0.0432 mmol), benzylamine (0.216 mmol), [Rh(PPh₃)₃Cl] (**3**, 0.0216 mmol), and *tert*-butylethylene (**2a**, 1.08 mmol), the mixture was then stirred in an oil bath at 170 °C for 12 h. Purification by column chromatography (SiO₂, *n*-hexane/ethyl acetate = 5/2) gave pure 1-[2-(3,3-dimethyl-butyl)-phenyl]-4,4-dimethyl-pentan-1-one (**5a**) (0.203 mmol, 94 % yield).

Received: April 11, 2000 [Z14976]

Microreactors for Dynamic, High Throughput Screening of Fluid/Liquid Molecular Catalysis**

Claude de Bellefon*, Nathalie Tanchoux, Sylvain Caravieilhès, Pierre Grenouillet, and Volker Hessel

Today, high-throughput synthesis methodologies, such as combinatorial techniques, are applied to the discovery of pharmaceuticals, catalysts, and many other new materials.^[1, 2] In the near future, huge libraries of ligands, and hence of homogeneous catalyst precursors, will be accessible. Recent reports have demonstrated the effectiveness of this approach for restricted libraries and in the case of catalysis in a single liquid phase.^[2] High-throughput screening in one liquid phase should not represent a problem as long as the reactions are not too fast compared with micromixing rates. The micro-titration-based apparatus (combinatorial chemistry (CC) factory)^[2a] fulfils the requirement of ensuring reproducible tests on microquantities of samples,^[2] despite uncertainties attributed to the agitation process.^[2b] However, numerous reactions of interest, such as hydrogenation, carbonylation, and hydroformylation, operate in gas/liquid or gas/liquid/liquid systems.^[3] Inadequate control of phase and catalyst presentation, a result from nonoptimized agitation, may dramatically affect the estimation of selectivity and reactivity. Many enantio- and regioselective-catalyzed reactions, susceptible to mass transport effects, are known.^[4, 5] That may well be the explanation for the deceptively low enantiomeric excess (*ee* < 20 %) obtained in the screening of a 63-member library of rhodium/phosphane catalysts for asymmetric hydrogenation.^[2a] Thus, a major challenge is to develop special reactors^[1b] for rapid catalyst screening, that would ensure good mass and heat transport in a small volume.^[6]

Herein we describe a new concept to achieve high-throughput screening (HTS) of polyphasic fluid reactions. Two test reactions, a liquid/liquid isomerization and a gas/liquid asymmetric hydrogenation, have been chosen to validate our approach to HTS experiments.


As a liquid/liquid test reaction, the isomerization of allylic alcohols, a process currently of industrial interest in the field of geraniol chemistry^[7] was targeted [Eq. (1)].

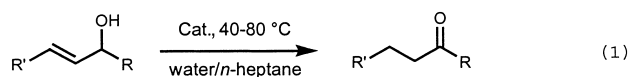
- [1] a) A. D. Ryabov, *Chem. Rev.* **1990**, 90, 403–424; b) A. E. Shilov, G. B. Shul'pin, *Chem. Rev.* **1997**, 97, 2879–2932; c) G. Dyker, *Angew. Chem.* **1999**, 111, 1808–1822; *Angew. Chem. Int. Ed.* **1999**, 38, 1698–1712.
- [2] a) C.-H. Jun, H. Lee, J.-B. Hong, *J. Org. Chem.* **1997**, 62, 1200–1201; b) C.-H. Jun, D.-Y. Lee, J.-B. Hong, *Tetrahedron Lett.* **1998**, 38, 6673–6676; c) C.-H. Jun, C.-W. Huh, S.-J. Na, *Angew. Chem.* **1998**, 110, 150–152; *Angew. Chem. Int. Ed.* **1998**, 37, 145–147; d) C.-H. Jun, H.-S. Hong, C.-W. Huh, *Tetrahedron Lett.* **1999**, 40, 8897–8900; e) C.-H. Jun, J.-B. Hong, D.-Y. Lee, *Synlett* **1999**, 1–12.
- [3] C.-H. Jun, J.-B. Hong, *Org. Lett.* **1999**, 1, 887–889.
- [4] a) S. Murai, F. Kakiuchi, S. Sekine, Y. Tanaka, A. Kamatani, M. Sonoda, N. Chatani, *Nature* **1993**, 366, 529–531; b) F. Kakiuchi, Y. Tanaka, T. Sato, N. Chatani, S. Murai, *Chem. Lett.* **1995**, 679–680; c) F. Kakiuchi, Y. Yamamoto, N. Chatani, S. Murai, *Chem. Lett.* **1995**, 681–682; d) M. Sonoda, F. Kakiuchi, A. Kamatani, N. Chatani, S. Murai, *Chem. Lett.* **1996**, 109–110; see also e) C. P. Lenges, M. Brookhart, *J. Am. Chem. Soc.* **1999**, 121, 6616–6623.
- [5] a) F. Kakiuchi, S. Sekine, T. Tanaka, A. Kamatani, M. Sonoda, N. Chatani, S. Murai, *Bull. Chem. Soc. Jpn.* **1995**, 68, 62–83; b) S. Murai, N. Chatani, F. Kakiuchi, *Pure Appl. Chem.* **1997**, 69, 589–594.
- [6] In *ortho*-alkylated ketones, because the unreacted double bond from the α,ω -diene isomerized into an internal olefin, we reduced the double bond to aid isolation and characterization.
- [7] M. Sonoda, F. Kakiuchi, N. Chatani, S. Murai, *Bull. Chem. Soc. Jpn.* **1997**, 70, 3117–3128.
- [8] a) Y.-G. Lim, Y. H. Kim, J.-B. Kang, *J. Chem. Soc. Chem. Commun.* **1994**, 2267–2268; b) Y.-G. Lim, J.-B. Kang, Y. H. Kim, *J. Chem. Soc. Perkin Trans 1* **1996**, 2201–2206.
- [9] N. A. Williams, Y. Uchimaru, M. Tanaka, *J. Chem. Soc. Chem. Commun.* **1995**, 1129–1130.
- [10] Recently, we have developed an efficient catalytic system for intermolecular transimination-assisted hydroacylation with aldehydes: C.-H. Jun, D.-Y. Lee, H. Lee, J.-B. Hong, *Angew. Chem.* **2000**, 112, 3214–3216; *Angew. Chem. Int. Ed.* **2000**, 39, 3070–3072.
- [11] Without benzylamine, only hydroacylation occurred. The ketimine of 2-amino-3-picoline did not show any *ortho*-alkylation, probably because of the coordination of the Rh^I catalyst to the pyridine moiety.

[*] Dr. C. de Bellefon, Dr. N. Tanchoux,^[+] S. Caravieilhès, Dr. P. Grenouillet
Laboratoire Génie des Procédés Catalytiques
CNRS/ESCE Lyon, 69100 Villeurbanne (France)
Fax : (+33)4-72-43-16-73
E-mail: cdb@lgpc.cpe.fr

[+] Present address: Max-Planck-Institut für Kohlenforschung
Kaiser-Wilhelm-Platz 1, 45470 Mülheim a. d. Ruhr (Germany)
Dr. V. Hessel
Institut für Mikrotechnik Mainz
Carl-Zeiss-Strasse 18–20, 55129 Mainz (Germany)

[**] This research was funded by the Région Rhône-Alpes, the CNRS, and the Ecole Supérieure de Chimie Physique Electronique de Lyon. S.C. is supported by a grant of the French Ministry of Education. Many thanks to Prof. D. Sinou for a gift of CBDTS.

 Supporting information for this article is available on the WWW under <http://www.wiley-vch.de/home/angewandte/> or from the author.



Biphasic catalytic systems involving organic and aqueous (catalytic) phases, are well known and used in industry.^[8] However, whereas numerous reports describe the monophasic isomerization of allylic alcohol,^[9] examples of efficient catalysis in biphasic media are scarce.^[10] In order to extend the scope of this isomerization to a liquid/liquid system, a restricted library composed of eight catalytic systems was constructed from four transition metal precursors (Rh, Ru, Pd, Ni),^[9, 10] and four sulfonated phosphane or diphosphane ligands.

A liquid/liquid HTS test reactor was then designed. Such an apparatus must be able to mix the two liquids with a low to very low inventory of catalytic material while still offering reasonably long residence times.^[11] The principle used is a combination of pulse injections of the catalyst and the substrate, a micromixer with negligible volume, and a tubular reactor (Figure 1).

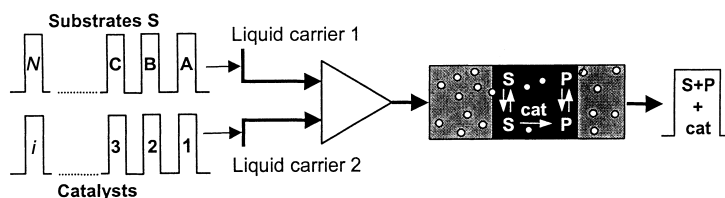


Figure 1. Schematic of the principle used for high-throughput sequential screening of *i* catalysts and *N* substrates. The substrate *S* is thus treated to form the product *P*.

During operation, the two carrier liquid phases, namely *n*-heptane and water, flow continuously through the apparatus. For a test, both the substrate and the catalyst are injected simultaneously. The pulses mix perfectly in the micromixer with a residence time less than 10^{-2} s. The liquids thereby emulsify and behave as a reacting segment, which then travels along the tubular reactor. Collection at the outlet of the reactor and analysis affords the conversion and selectivity data.

Application of this principle has been possible by using a static micromixer^[12] mounted in a dynamic microactivity test (Figure 2). The *n*-heptane/water emulsion was stable for more than 10 minutes without noticeable separation.

The catalyst library was then screened (Table 1). Palladium complexes were inactive when associated with monophosphane ligands and displayed a low activity with diphosphane (entries 7 and 8). The use of nickel resulted in a 1,3-transposition of the hydroxy group (entry 9). Ruthenium and rhodium gave comparable conversions. However, the ruthenium catalyst yields some hydrogenated side product due to hydride transfer from the alcohol (entry 6). Different precursors of rhodium(I) were active (entries 1 and 2) and comparable conversions were measured with mono- and diphosphane ligands (entries 1–5). These results led to the selection of Rh/TPPTS as the best catalyst.

This selected RhCl₃/TPPTS catalyst showed activity towards a large class of allylic alcohols (Figure 3).

That similar results were obtained in the microreactor and in a traditional well mixed batch reactor (40 cm³) proves the

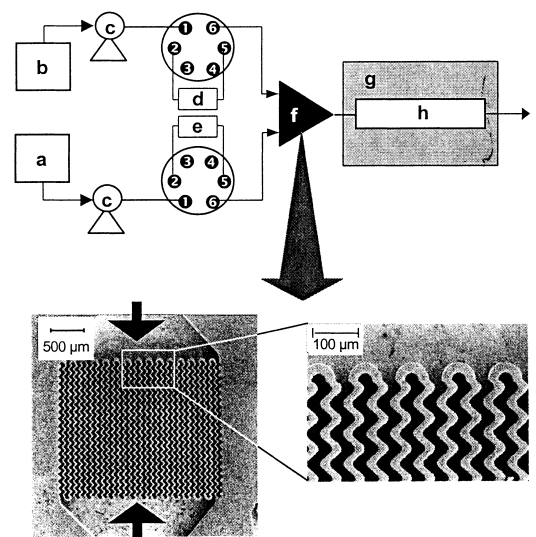
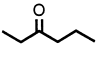
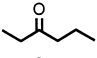
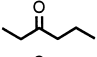
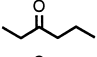
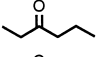
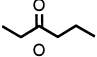
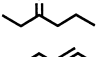
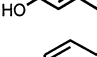
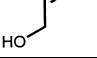


Figure 2. Apparatus: a) water reservoir; b) *n*-heptane reservoir; c) high-pressure liquid pumps; d) injection valve with a 200 µL loop; e) injection valve with a 1 mL loop; f) micromixer; g) thermoregulated bath; h) tubular stainless-steel reactor (0.4 cm i.d., 80 cm long); i) outlet to detectors. The two scanning electron microscopy (SEM) images show the micromixer, in which the 2 × 15 interdigitated microchannels (25 µm width) with corrugated walls are clear.

Table 1. Screening of catalysts for the isomerization of 1-hexene-3-ol.

Entry	Catalyst ^[a]	Ligand:metal	Product	Conv. [%] ^[b]
1	RhCl ₃ /TPPTS	4.6:1		53
2	Rh ₂ SO ₄ /TPPTS	4.1:1		34
3	[Rh(cod)Cl] ₂ /DPPBTS	1.1:1		36
4	[Rh(cod)Cl] ₂ /BDPPTS	1.1:1		1.5
5	[Rh(cod)Cl] ₂ /CBDTS	1.3:1		1
6	RuCl ₃ /TPPTS	4:1		61
7	PdCl ₂ /DPPBTS	2.6:1		3.5
				9
8	Ni(cod) ₂ /TPPTS	4:1		3

[a] All catalysts were prepared separately beforehand and stored under argon at 4 °C.^[10c] [b] Gas chromatography analysis. TPPTS = tris(*m*-sulphophenyl)phosphane, cod = cycloocta-1,4-diene, DPPBTS = di(sulphophenyl)phosphane, BDPPTS = sulfonated (2*S*,4*S*)-(–)-2,4-bis(diphenylphosphanyl)pentane, CBDTS = sulfonated (S,S)-1,2-bis(diphenylphosphanyl)methylcyclobutane.

validity of the concept. Differences observed between the substrates are explained by both their different solubilities in the catalytic layer and by their different intrinsic reactivities. Thus, substrates 1–4, which are likely to possess similar reactivities, displayed a decreasing conversions with an increasing hydrocarbon chain length. The molecular structure of the substrate is also of importance: For similar solubilities, 1 is more reactive than 5, 2 more than 6, and 3 more than 7 and 8 for the C₄, C₅, and C₆ compounds, respectively. This pairwise

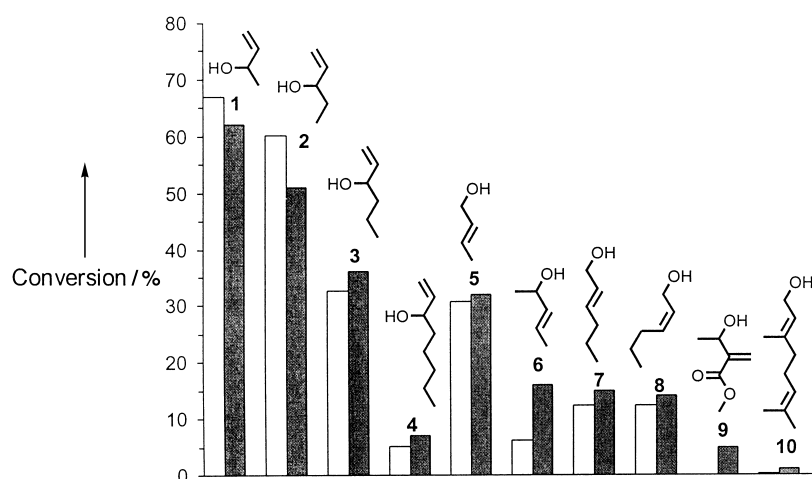


Figure 3. Comparison between the results of the screening of substrates **1–10** against one catalyst in a traditional batch reactor (white columns) and in the micro-dynamic test (gray columns). The catalyst pulse was 200 μL and $[\text{Rh}] = 4 \text{ mM}$, other conditions are given in the Experimental Section.

comparison leads to the known conclusion that secondary alcohols with terminal olefins are more reactive than other configurations.^[9a] All these results are in good agreement with those reported for monophasic systems and further validates the use of the microapparatus for chemical investigations.

The concept has been extended to gas/liquid catalysis with some modification to the experimental setup. Thus, hydrogen is introduced at one of the inlet of the micromixer and the liquid carrier phase is pumped into the other. The liquid, ethylene glycol/water (60/40 wt %) and sodium dodecyl sulfate (SDS) surfactant, is thus composed to ensure a stable foam (no coalescence was noticed for residence times up to 6 min at 60 °C) with small gas bubbles (about 200 μm average diameter) with a liquid volume of 20%. A pulse containing the substrate *Z*-(α)-acetamidocinamic methyl ester (MAC; 0.05–0.10 M) and the Rh/diphos catalyst (diphos ligands are *S,S*-CBDTS and *S,S*-BDPPTS) dissolved in the liquid mixture is injected. Using this procedure, we have found that the rate of reaction is proportional to the catalyst concentration and that the rate decreases with increasing SDS concentration, but no change in the *ee* was noticed (see Supporting Information for details). These results indicate strongly that the micro-reactor is working under a chemical regime. A further argument comes from the comparison of the enantioselectivities obtained in the microreactor and those previously reported for the catalysts Rh/*S,S*-CBDTS (*ee* 6% versus 20% (*S*)) and Rh/(*S,S*)-BDPPTS (*ee* 47% versus 45% (*R*)) under similar conditions.^[13]

In terms of catalyst and time consumption per test, the 18 tests for the liquid/liquid isomerization (Table 1 and Figure 3) were performed twice, to test for reproducibility, using one to two micromoles of metal and over a total screening time of one hour. The test for the the gas/liquid asymmetric hydrogenation showed similar features (down to 0.2 μmol Rh, 3–5 min per test). Throughput testing frequencies (TTFs) of more than 500 d^{-1} are thus achievable, albeit with computer control of the apparatus.

Such TTFs impose a characteristic time of about only 3 min for necessary online operations, such as injection, collection,

and analysis. The latter operation is often the rate-limiting step in combinatorial and related techniques. With the dynamic sequential method proposed here, any detectors that were originally designed for HPLC or GC analysis may be used, which includes mass detection, UV, IR, CD, and so forth. Fast chromatography with microcapillary columns is also possible (see the Supporting Information).

In summary, we propose a new concept for high-throughput experiments based on dynamic sequential operations with a combination of pulse injections and micromachined elements. Some advantages over traditional parallel batch operations are reduced sample amounts (to μg levels), a larger range of operating conditions (pressure, temperature), and fewer, simpler electro-mechanical moving parts.

Experimental Section

Liquid/liquid isomerization: Aqueous catalyst solution pulses (200 μL), which contain about 1–2 μmol (about 100 μg) of metal, and organic substrate pulses (1 mL), as *n*-heptane solutions (0.1 mol L^{-1}), were used for each test. Flow rates were 5 (aqueous phase) and 1 mL min^{-1} (organic phase), which corresponded to a residence time of 100 s in the stainless-steel tubular reactor (0.4 \times 80 cm) that was maintained at 80 °C.

Gas/liquid asymmetric hydrogenation: Aqueous catalyst solution pulses (200 μL), which contain about 1–4 mm of the catalyst, and organic substrate pulses of MAC (0.05–0.10 M) were used for each test. Flow rates were 1–4 mL min^{-1} (gas phase) and 0.3–1.0 mL min^{-1} (liquid phase), which corresponded to a residence time of 3–6 min in the tubular glass reactor (0.285 \times 156 cm), that was maintained at atmospheric pressure and at 40–60 °C.

Received: April 12, 2000
Revised: June 9, 2000 [Z14979]

- a) B. Jandeleit, D. J. Schaefer, T. S. Powers, H. W. Turner, W. H. Weinberg, *Angew. Chem.* **1999**, *111*, 2648; *Angew. Chem. Int. Ed.* **1999**, *38*, 2494; b) R. H. Crabtree, *CHEMTECH* **1999**, *29* (4), 21; c) T. Bein, *Angew. Chem.* **1999**, *111*, 335; *Angew. Chem. Int. Ed.* **1999**, *38*, 323; d) D. R. Liu, P. G. Schultz, *Angew. Chem.* **1999**, *111*, 36; *Angew. Chem. Int. Ed.* **1999**, *38*, 36.
- a) S. R. Gilbertson, X. Wang, *Tetrahedron Lett.* **1996**, *36*, 6475; b) K. Burgess, H.-J. Lim, A. M. Porte, G. A. Sulikowski, *Angew. Chem.* **1996**, *108*, 192; *Angew. Chem. Int. Ed. Engl.* **1996**, *35*, 220; c) M. B. Francis, N. S. Finney, E. N. Jacobsen, *J. Am. Chem. Soc.* **1996**, *118*, 8983; d) K. D. Shimizu, M. L. Snapper, A. H. Hoveyda, *Chem. Eur. J.* **1998**, *4*, 1885; e) D. A. Annis, O. Helluin, E. N. Jacobsen, *Angew. Chem.* **1998**, *110*, 2010; *Angew. Chem. Int. Ed.* **1998**, *37*, 1907; f) M. T. Reetz, M. H. Becker, K. M. Kühling, A. Holzwarth, *Angew. Chem.* **1998**, *110*, 2792; *Angew. Chem. Int. Ed.* **1998**, *37*, 2647; g) K. Ding, A. Ishii, K. Mikami, *Angew. Chem.* **1999**, *111*, 2268; *Angew. Chem. Int. Ed.* **1999**, *38*, 497; h) M. B. Francis, E. N. Jacobsen, *Angew. Chem.* **1999**, *111*, 987; *Angew. Chem. Int. Ed.* **1999**, *38*, 937; i) O. Lavastre, J. P. Morken, *Angew. Chem.* **1999**, *111*, 3357; *Angew. Chem. Int. Ed.* **1999**, *38*, 3163.
- B. Cornils, W. A. Herrmann, *Applied Homogeneous Catalysis with Organometallic Compounds*, VCH, Weinheim, **1996**.
- a) C. R. Landis, J. Halpern, *J. Am. Chem. Soc.* **1987**, *109*, 1746; b) R. V. Gholap, O. M. Kut, J. R. Bourne, *Ind. Eng. Chem. Res.* **1992**, *31*, 2446; c) N. Tanchoux, C. de Bellefon, *Tetrahedron: Asymmetry* **1998**, *9*, 3677.
- Y. Sun, R. N. Landau, J. Wang, C. Le Blond, D. G. Blackmond, *J. Am. Chem. Soc.* **1996**, *118*, 1348.

- [6] Computer-controlled apparatus with mixing and pressure handling capabilities are known. They are based on the concept of operating of traditional laboratory "glassware" procedures in parallel at a miniature scale and function batchwise with throughput testing frequencies (TTFs) of 10–40 day⁻¹. Mechanical mixing is the bottleneck for further miniaturization. Some information is available at www.ttpmyriad.co.uk, www.argotech.com, www.peptide.com, and www.gilson.com.
- [7] S. Otsuka, T. Kazuhide, *Synthesis* **1991**, 9, 665.
- [8] B. Cornils, E. G. Kuntz in *Aqueous-Phase Organometallic Catalysis* (Eds.: B. Cornils, W. A. Herrmann), Wiley-VCH, Weinheim, **1998**, p. 271.
- [9] a) Y. Sasson, G. L. Rempel, *Tetrahedron Lett.* **1974**, 47, 4133; b) K. Felföldi, M. Bartók, *J. Organomet. Chem.* **1985**, 297, 37; c) B. M. Trost, R. J. Kulawiec, *Tetrahedron Lett.* **1991**, 32, 3039; d) I. E. Marko, A. E. Gautier, M. Tsukazaki, A. Llobet, E. Plantalech-Mir, C. J. Urch, S. M. Brown, *Angew. Chem.* **1999**, 111, 2126; *Angew. Chem. Int. Ed.* **1999**, 38, 1960.
- [10] a) H. Schumann, V. Ravindar, L. Meltser, W. Baidossi, Y. Sasson, J. Blum, *J. Mol. Catal. A* **1997**, 118, 55; b) H. Bricout, E. Monflier, J. F. Carpentier, A. Mortreux, *Eur. J. Inorg. Chem.* **1998**, 1739; c) C. de Bellefon, S. Caravieilh, E. G. Kuntz, *C. R. Acad. Sci. Ser. 2*, in press.
- [11] C. de Bellefon, S. Caravieilh, N. Tanchoux *J. Organomet. Chem.* **1998**, 567, 143.
- [12] a) W. Ehrfeld, K. Golbig, V. Hessel, H. Löwe, T. Richter, *Ind. Eng. Chem. Res.* **1999**, 38, 1075; b) H. Löwe, W. Ehrfeld, V. Hessel, T. Richter, J. Schiewe, *Proc. 4th Int. Conf. Microreaction Technology* (Atlanta, GA, USA) **2000**.
- [13] Y. Amrani, L. Lecomte, D. Sinou, J. Bakos, I. Toth, B. Heil, *Organometallics* **1989**, 8, 542.

Macromolecular-Multisite Catalysts Obtained by Grafting Diaminoaryl Palladium(II) Complexes onto a Hyperbranched-Polytrialkylsilane Support**

Christian Schlenk, Arjan W. Kleij, Holger Frey,* and Gerard van Koten*

At present, dendrimers^[1] are widely investigated as supports for catalytically active transition metal fragments.^[2] Carbosilane dendrimers^[3] are well-suited for this purpose,

because they are relatively inert to common organometallic reagents and their structures can be easily modified. The main advantage of this type of nanosized, macromolecular catalyst is their convenient removal from product streams as realized recently in a continuously operating membrane reactor.^[4] However, the synthesis of dendrimers, that is monodisperse, well-defined molecules, involves expensive, labor-intensive multistep procedures that also limit the amount of available material. In contrast, hyperbranched polymers^[5] can be prepared in a single-step, one-pot procedure, from AB_m type monomers. This greatly facilitates their synthesis and allows the production of large quantities of material. However, as a consequence of the uncontrolled synthesis of such polymers, materials with high polydispersity are obtained. Furthermore, the reactive sites introduced by functionalization will be distributed throughout the molecules.

Recently, we reported carbosilane molecules functionalized with NCN [C₆H₃(CH₂NMe₂)₂-2,6]⁻ ligands^[6, 7] which could then be selectively lithiated without any decomposition of the carbosilane backbone.^[8] This lithiation enabled the subsequent incorporation of transition metals by means of transmetalation with suitable Group 8 metal salts.^[2a, 8b] Herein, we present the synthesis of a hyperbranched carbosilane (HCS), its functionalization with NCN moieties, and the introduction of palladium(II) sites into the structure. Furthermore, we show that this system can be conveniently converted into an effective catalyst system that can compete with metallodendritic catalysts.


To obtain hyperbranched HCS supports, neat triallylsilane^[9] was polymerized with platinum catalysis by polyaddition (Scheme 1).^[10] To keep the isomerization of the double bonds to a minimum, the reaction temperature was kept low (40 °C). This, however, led to prolonged reaction times (4 d in the case of **1**). The internal to external double-bond ratio could not be suppressed below 7.6 %. The presence of internal double bonds was indicated in the ¹H NMR spectrum of the isolated HCS material which showed the presence of extra multiplets at δ = 6.09 (SiCH=CH-CH₃) and 5.58 (SiCH=CH-CH₃). The polytrialkylsilane (PTAS) **1**, was obtained as a translucent, viscous oil, soluble in solvents such as diethyl ether and chloroform. The molecular weight (size exclusion chromatography (SEC), polystyrene (PS) standards) was 5500 g mol⁻¹ which corresponds to an apparent degree of polymerization of 36 (that is 72 allyl groups per molecule). As expected for a bulk polymerization of an AB_m monomer, the molecular-weight distribution was broad (*M_w*/*M_n* = 5.2).^[11] This polydispersity is also influenced by an intramolecular reaction, of the Si–H groups with allyl end groups. This side reaction consumes Si–H groups without enhancement of the molecular weight, resulting in the formation of core-type molecules.

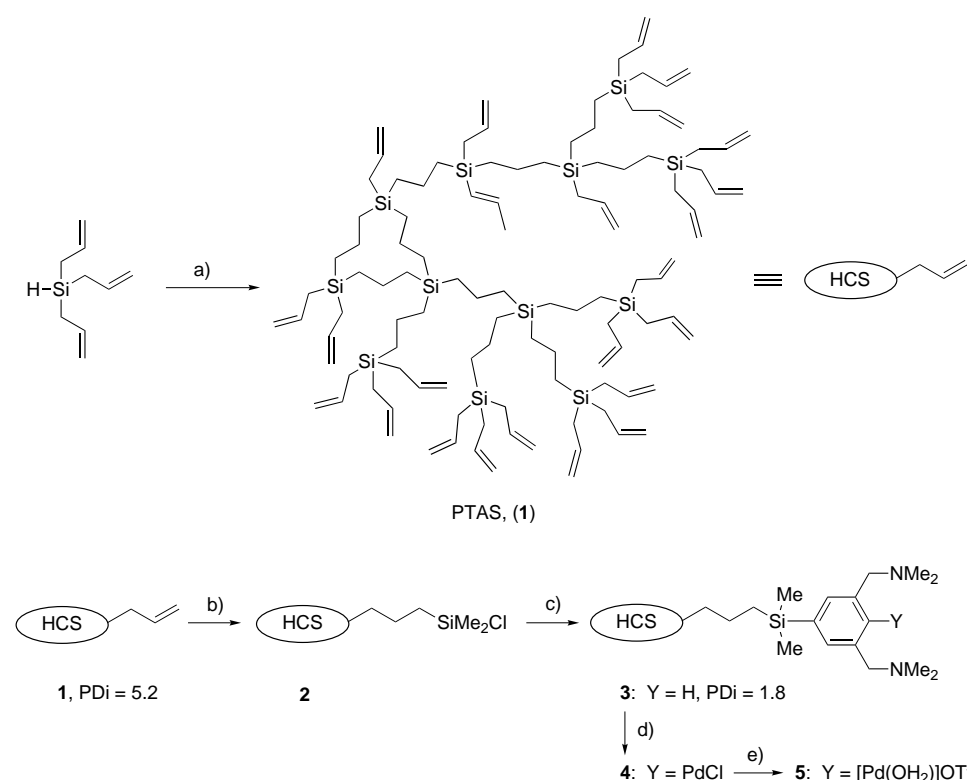
Polymer **1** was hydrosilylated with HSiMe₂Cl by platinum catalysis (Scheme 1) in neat HSiMe₂Cl at ambient temperature. After removal of the excess HSiMe₂Cl, the functionalized polymer HCS-SiMe₂Cl (**2**) was dissolved in diethyl ether. This solution was added to 3,5-bis[(dimethylamino)-methyl] phenyllithium (Li-NCN)^[8a] at –78 °C in diethyl ether (Scheme 2). Hydrolysis followed by extraction gave the crude HCS-SiMe₂-NC(H)N product. This diaminoaryl-functional-

[*] Prof. Dr. G. van Koten, A. W. Kleij
Debye Institute
Department of Metal-Mediated Synthesis
Utrecht University
Padualaan 8, 3584 CH, Utrecht (The Netherlands)
Fax: (+31) 30-252-3615
E-mail: g.vankoten@chem.uu.nl

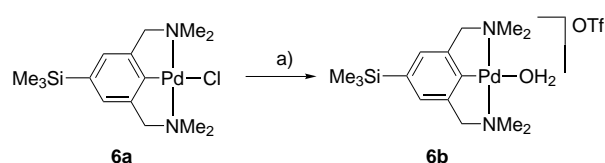
PD Dr. H. Frey, C. Schlenk
Freiburger Materialforschungszentrum und Institut für
Makromolekulare Chemie
Albert-Ludwigs-Universität, Freiburg
Stefan-Meier-Strasse 21/31, 79104 Freiburg (Germany)
Fax: (+49) 761-203-6319;
E-mail: holfrey@mfz.uni-freiburg.de

[**] We thank the Council for Chemical Sciences (CW) of the Netherlands Organization of Scientific Research (NWO) for financial support, Dr. R. Hanselmann for the size exclusion chromatography (SEC) measurements, and Dr. J. Boersma for critical reading of the manuscript.

 Supporting information for this article is available on the WWW under <http://www.wiley-vch.de/home/angewandte/> or from the author.



Scheme 1. Synthesis of the hyperbranched support **1** and its conversion into the (pre)catalytic hyperbranched Pd^{II} complex **5**. Reagents and Conditions: a) [(COD)PtCl₂], 40 °C, 4 d; b) excess HSiMe₂Cl, RT, [Pt(Bu₄N)₂PtCl₆], 12 h; c) excess Li-NCN, Et₂O, -78 °C → RT 16 h, *t*BuLi, pentane, dialysis; d) *t*BuLi, pentane, RT, 3 h; excess [PdCl₂(SMe₂)₂], THF, RT, 16 h; e) AgOTf, wet acetone, 16 h, RT, in the dark. PDI = polydispersity index.



Scheme 2. Synthesis of the model compound **6b**. Reagents and conditions: a) AgOTf, wet acetone, RT, 5 min.

ized HCS polymer was purified by dialysis in diethyl ether with a benzoylated cellulose nanofiltration membrane with a cut off mass of 1000 g mol⁻¹ to remove the excess NC(H)N ligand and the lower molecular weight fractions of the product. The polydispersity index dropped from 5.2 to 1.8 as monitored by SEC. This result shows that these polymers are good candidates for catalytic application in continuous membrane reactions.^[4] The HCS-SiMe₂-NC(H)N material **3**, was obtained as clear yellow, viscous oil (72 %).

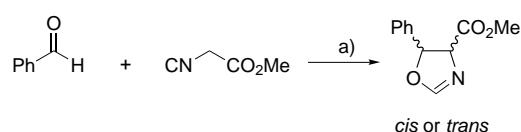
Lithiation^[8] of **3** with an excess of *tert*-butyllithium in pentane at room temperature followed by transmetalation of HCS-SiMe₂-NCN-Li with an excess of [PdCl₂(SMe₂)₂] in THF gave the Pd^{II} complex HCS-SiMe₂-NCN-PdCl (**4**) (Scheme 1).^[12] This reaction sequence illustrates one major advantage of the carbosilane backbone, that is the inertness to common organometallic reagents. Dialysis in CH₂Cl₂ with a membrane equivalent to that used for the purification of **3**, afforded **4** as a light brown solid in 71 % yield. The reaction was monitored by ¹H NMR spectroscopy and signals with the

diagnostic shifts for the N(CH₃)₂ and CH₂N groups of the NCN ligand were observed.^[11] The ¹H NMR spectrum showed signals that indicated the complete lithiation of all the NC(H)N groups in **3** and their quantitative conversion into NCN-PdCl groups. Subsequent treatment of **4** with AgOTf in wet acetone gave the cationic derivative [HCS-SiMe₂-NCN-Pd(OH₂)]OTf (**5**) (Scheme 1).

The mononuclear, cationic, precatalyst compound **6b** was prepared to model the catalytic activity of diaminoaryl palladium cations bound to a HCS support; **6b** was obtained by treatment of **6a**^[8b] with AgOTf in wet acetone (Scheme 2 and Supporting Information). As the electronic environment of the metal center in model compound **6b** is similar to that of the catalytic sites distributed throughout the hyperbranched support, differences in catalytic performance of **6b** and the HCS catalysts give an indication of the influence of the HCS support on the accessibility of the Pd^{II} sites in these hyperbranched materials.

Polymer **5** was used as a soluble catalyst in the aldol condensation of benzaldehyde and methyl isocyanoacetate,^[13] to give oxazolines (Scheme 3, Table 1, and Experimental Section). For comparison, model compound **6b** was used as a catalyst and both systems were compared with the uncata-

tion of the influence of the HCS support on the accessibility of the Pd^{II} sites in these hyperbranched materials.



Scheme 3. Catalytic aldol condensation of benzaldehyde and methyl isocyanoacetate in the presence of **5** or **6b**. Reagents and conditions: a) 1 mol % **5** or **6b**, CH₂Cl₂, EtN(*i*Pr)₂, mesitylene, RT.

Table 1. Aldol condensation catalysis with **5** and **6b** using benzaldehyde and methyl isocyanoacetate as substrates.

Catalyst	mol %	<i>trans/cis</i> ^[a]	Yield [%] ^[a]	TOF ^[b]	TTN/Pd site ^[a]
–	–	n.d. ^[c]	< 5	–	–
6b	0.99	1.88	99	37	100
5	0.79 ^[d]	2.00	> 5	19 ^[d]	78 ^[d]

[a] After 24 h obtained by specific signal integration using ¹H NMR spectroscopy and mesitylene as an internal standard (duplo experiment); TTN = total turnover number. [b] Turnover frequency per Pd center per hour; during the first hour. [c] Not determined. [d] Corrected values, see ref. [12].

lyzed reaction. Table 1 shows that **5** is indeed an active catalyst for this reaction. Although the initial activity of **5** expressed in TOF per Pd site per h is somewhat lower than that of **6b**, the total turnover number (TTN)/Pd site for both **6b** and **5** are similar.

In summary, we have established a general route to nanosize, hyperbranched-polycarbosilane compounds that are functionalized with arylidiamine metal complexes using a lithiation/transmetalation procedure. The Pd^{II} centers in the soluble, macromolecular catalyst **5** function as independent catalytic sites in a standard aldol condensation reaction and their activity is similar to that of the single-site Pd catalyst **6b**. To our knowledge, this is the first example of the use of hyperbranched polymers as soluble macromolecular supports for homogeneous catalysis. Moreover, the catalyst support properties of hyperbranched polymers are very similar to those of analogous dendrimers; thus, structural perfection is not always required. Purification of the polymers **3** and **4** by means of dialysis shows that **5** is suitable for continuous membrane applications.

Experimental Section

Standard protocol for the catalytic aldol condensation reaction: 1 mol % of Pd catalyst was added to a mixture of benzaldehyde (2.4 mmol), methyl isocyanacetate (1.6 mmol), mesitylene (1.6 mmol, internal standard), and EtN(iPr)₂ (10 mol %) in CH₂Cl₂ (10 mL). Samples were taken from the reaction mixture at regular time intervals, after careful removal of the solvent ¹H NMR spectra of these samples were recorded.

Received: April 17, 2000 [Z15003]

- [1] Reviews of dendrimers: a) A. W. Bosman, H. M. Janssen, E. W. Meijer, *Chem. Rev.* **1999**, 99, 1665–1688; b) G. Newkome, E. He, C. N. Moorefield, *Chem. Rev.* **1999**, 99, 1689–1746; c) M. Fischer, F. Vögtle, *Angew. Chem.* **1999**, 111, 934–955; *Angew. Chem. Int. Ed.* **1999**, 38, 884–905; d) J. M. J. Fréchet, C. J. Hawker, I. Gitsov, J. W. Leon, *J. Macromol. Sci. Pure Appl. Chem. A* **1996**, 33, 1399–1425; e) D. A. Tomalia, H. D. Durst, *Top. Curr. Chem.* **1993**, 165, 193–313.
- [2] For example: a) A. W. Kleij, R. A. Gossage, J. T. B. H. Jastrzebski, J. Boersma, G. van Koten, *Angew. Chem.* **2000**, 112, 179–182; *Angew. Chem. Int. Ed.* **2000**, 39, 176–178; b) M. T. Reetz, G. Lohmer, R. Schwickardi, *Angew. Chem.* **1997**, 109, 1559–1562; *Angew. Chem. Int. Ed. Engl.* **1997**, 36, 1526–1529; c) J. W. J. Knapen, A. W. van der Made, J. C. De Wilde, P. W. M. N. van Leeuwen, P. Wijkens, D. M. Grove, G. van Koten, *Nature* **1994**, 372, 659–663.
- [3] C. Schlenk, H. Frey, *Top. Curr. Chem.* **2000**, 210, 69–129.
- [4] a) N. J. Hovestad, E. B. Eggeling, H. J. Heidebüchel, J. T. B. H. Jastrzebski, U. Kragl, W. Keim, D. Vogt, G. van Koten, *Angew. Chem.* **1999**, 111, 1763–1765; *Angew. Chem. Int. Ed.* **1999**, 38, 1655–1658; b) N. Brinkmann, D. Giebel, G. Lohmer, M. T. Reetz, U. Kragl, *J. Catal.* **1999**, 183, 163–168; c) G. Giffels, J. Beliczey, M. Felder, U. Kragl, *Tetrahedron: Asymmetry* **1998**, 9, 691–696.
- [5] a) Y. H. Kim, *J. Polym. Sci. Polym. Chem. Ed.* **1998**, 36, 1685–1698; b) A. Sunder, R. Hanselmann, H. Frey, R. Mülhaupt, *Macromolecules* **1999**, 32, 4240–4246; c) A. Sunder, J. Heinemann, H. Frey, *Chem. Eur. J.* **2000**, 6, 2499–2506.
- [6] a) M. P. H. Rietveld, D. M. Grove, G. van Koten, *New J. Chem.* **1997**, 21, 751–771; b) G. van Koten, *Pure Appl. Chem.* **1989**, 61, 1681–1693.
- [7] L. van de Kuil, J. Luitjes, D. M. Grove, J. W. Zwikker, J. M. G. van der Linden, A. M. Roelofsen, L. W. Jenneskens, W. Drenth, G. van Koten, *Organometallics* **1994**, 13, 468–477.
- [8] a) A. W. Kleij, H. Klein, J. T. B. H. Jastrzebski, W. J. J. Smeets, A. L. Spek, G. van Koten, *Organometallics* **1999**, 18, 268–276; b) A. W.

Kleij, H. Kleijn, J. T. B. H. Jastrzebski, A. L. Spek, G. van Koten, *Organometallics* **1999**, 18, 277–285.

- [9] J. W. Jenkins, N. L. Lavery, P. R. Guenther, H. W. Post, *J. Org. Chem.* **1948**, 13, 862–895.
- [10] Similar hyperbranched polycarbosilanes: C. Lach, P. Müller, H. Frey, R. Mülhaupt, *Macromol. Rapid Commun.* **1997**, 18, 253–260.
- [11] See Supporting Information for more details about the obtained hyperbranched polymers.
- [12] The theoretical mass of the repeat unit of the HCS polymer **4** is 934.96 and contains two NCN-PdCl groups. However, the undesired double bond isomerization process (see main text) lowers the average molecular weight of a repeat unit to 875.4 g mol⁻¹.
- [13] See for instance: a) R. Kuwano, H. Miyazaki, Y. Ito, *Chem. Commun.* **1998**, 71–72; b) M. A. Stark, C. Richards, *Tetrahedron Lett.* **1997**, 38, 5881–5884; c) F. Gorla, A. Togni, L. M. Venanzi, A. Albinati, F. Lianza, *Organometallics* **1994**, 13, 1607–1616.

Effective Gelation of Water Using a Series of Bis-urea Dicarboxylic Acids**

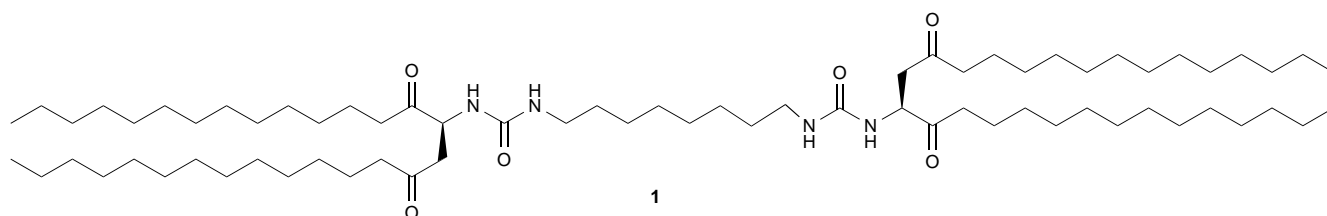
Lara A. Estroff and Andrew D. Hamilton*

A wide range of small organic molecules has been found, either through design or serendipity, to gel a variety of organic solvents.^[1] The property of gelation is thought to arise from the self-assembly of these small molecules into fibers, which, like polymer gels, become entangled and trap solvent.^[2] The formation of fibers requires a stabilizing intermolecular interaction and represents a balance between the tendency of the molecules to dissolve or to aggregate in a given solvent.

Organogelators often have hydrogen-bond donors and acceptors that promote aggregation and subsequent fiber formation. The attachment of long alkyl chains onto the hydrogen-bonded core enhances its solubility in organic solvents but also promotes association among the fibers, through van der Waals forces, and eventual gel formation. One effective class of organogelators exploits bis-urea derivatives to form a central, hydrogen-bonded stack to which long chain alkyl groups are attached. We^[3] and others have shown that bis-ureas such as **1** are able to gel a variety of nonpolar organic solvents (including supercritical carbon dioxide)^[3d] at concentrations less than 4 wt %. Recent crystal structures of these derivatives^[3b,c] have confirmed the importance of

[*] Dr. A. D. Hamilton, L. A. Estroff
Department of Chemistry
Yale University
P.O. Box 208107, New Haven, CT 06520-8107 (USA)
Fax: (+1) 203-432-3221
E-mail: andrew.hamilton@yale.edu

[**] We thank the National Science Foundation (CHE9817240) for financial support of this work and Dr. James Eckert (Department of Geology, Yale University) for assistance with the electron microscopy. We also thank R. E. Meléndez for compound **1**.

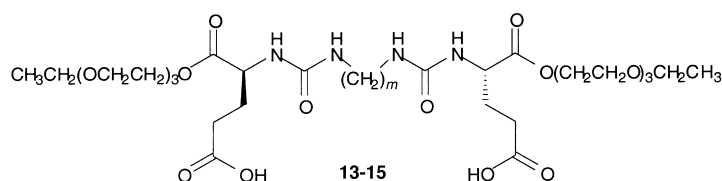
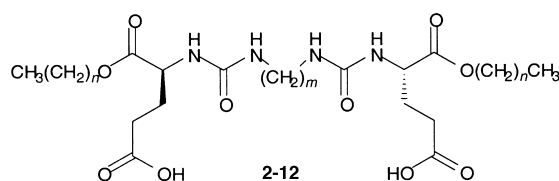


bidentate hydrogen-bonding interactions between urea groups in neighboring molecules and an intertwining of alkyl groups.

As part of an effort to use these aggregates as porous reaction vessels we were interested in extending the gelation properties into hydroxylic solvents, such as water. The design challenge was to modify the character of **1** to cause an already proven self-aggregating subunit to function in more polar solvent systems. Fiber formation by amphiphilic organic molecules in water is well documented,^[4] however, these fibers generally precipitate without forming a gel or display viscoelastic behavior at concentrations above the critical micelle concentration.^[5] There are only a few examples of nonpolymeric hydrogels formed by the self-assembly of small molecules.^[6]

Here we report the rational design of a novel family of hydrogelators (**2–15**) and the characterization of their aggregation properties in water. In the design, the self-assembling bis-urea motif of **1** was retained and free carboxylic acids were added for both solubility in water and pH control. We also anticipated that the long alkyl chains would promote aggregation in an aqueous environment. This series of compounds shows aggregation in aqueous bases that displays a strong pH and ionic strength dependence. Of particular interest is the gelation of water by these molecules at concentrations less than 0.3 wt % (>17000 molecules of water per gelator molecule) over a narrow pH range that varies depending on the total number of carbon atoms (*M*) in the spacer and alkyl esters ($M = 2n + m + 2$; see Table 1).

To test gelation ability, compounds **2–15** were dissolved in a series of hot phosphate buffers (0.2 M; pH 5.2, 5.9, 6.7, 7.9, and 10.7) with high ionic strength ($I = 1 \text{ mol kg}^{-1}$ from added



- | | |
|--------------------------|----------------------------|
| 2 $n = 0, m = 8$ | 9 $n = 11, m = 6$ |
| 3 $n = 3, m = 8$ | 10 $n = 11, m = 8$ |
| 4 $n = 5, m = 8$ | 11 $n = 11, m = 12$ |
| 5 $n = 3, m = 12$ | 12 $n = 14, m = 8$ |
| 6 $n = 7, m = 8$ | 13 $m = 4$ |
| 7 $n = 11, m = 4$ | 14 $m = 6$ |
| 8 $n = 7, m = 12$ | 15 $m = 8$ |

NaCl). Upon cooling, one of several types of aggregates (gel, vesicles, sheets, fibers, or crystallites) was formed depending on the chemical characteristics of the molecule and the pH of the solution (Table 1). These aggregates were examined by both polarizing light microscopy and scanning electron microscopy (SEM).

Giant vesicles (10–150 μm in diameter) were observed at pH values below the gelation pH by polarizing light microscopy (Figure 1 a). Often these vesicles were weakly birefringent and cracked when gentle pressure was applied. Fibers

Table 1. Aggregation of 0.3 wt % (2 mg in 0.75 mL of water) of bis-urea dicarboxylic acids **2–12**.^[a]

	M ^[b]	Water	pH 5.2 ^[c]	pH 5.9 ^[c]	pH 6.7 ^[c]	pH 7.9 ^[c]	pH 7.9 ^[d]	pH 10.7 ^[c]
2	10	C	S	S	S	S	S	N/A
3	16	F	V	V	AP	AP	S	N/A
4	20	Sh	V	OPG	C	F	S	S
5	20	Sh	V	LG	G	S	S	N/A
6	24	I	I	V	G	S	S	N/A
7	28	I	BP	V	LG	F	N/A	Sh
8	28	I	N/A	V	G	F	F	S/F ^[e]
9	30	I	I	V	G	OPG	S	Sh
10	32	I	I	V	V	G	LG	F
11	36	I	N/A	N/A	V	OPG	G	C
12	38	I	N/A	N/A	V	G	LG	F

[a] I: insoluble, AP: precipitate with no definite structure under the microscope, LG: loose gel that forms AP upon mechanical disruption (shaking), BP: strongly birefringent precipitate, F: fibrous aggregates, weakly birefringent, Sh: sheets, V: giant vesicles (10–150 μm), G: clear gel, S: homogeneous solution, OPG: opaque gel, C: fibrous crystallites, strongly birefringent. [b] $M = 2n + m + 2$. [c] 0.2 M phosphate buffer, $I = 1 \text{ mol kg}^{-1}$ from NaCl. [d] 0.2 M phosphate buffer, $I = 0.4 \text{ mol kg}^{-1}$. [e] **8** gave a turbid solution at pH 10.7 with no visible precipitate, however, small bundles of fibers were observed at 220X magnification. The solid line outlines the conditions under which gelation is observed.

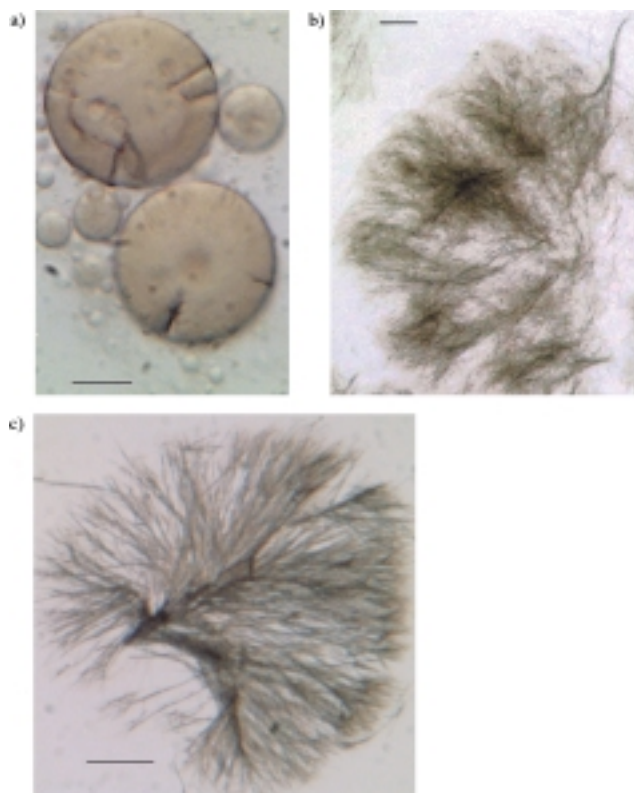


Figure 1. Optical micrographs of the precipitate formed by a) **12** in pH 6.7 phosphate buffer, b) **4** in pH 7.9 phosphate buffer and c) **3** in water. Scale bars: 50 μm .

were the predominant aggregate at higher pH values, as observed by both light microscopy (Figure 1 b, c) and electron microscopy. These fibers precipitated above the gelation pH and were birefringent as observed by polarizing light microscopy. The SEM images further revealed that the fibers themselves were composed of tightly intertwined and thinner fibers (ca. 500 nm in diameter; Figure 2 a). Although the gels appeared amorphous when viewed by polarizing light microscopy, observation by SEM showed them to be composed of fibers (Figure 2 c, d). In contrast to the fibrous aggregates of

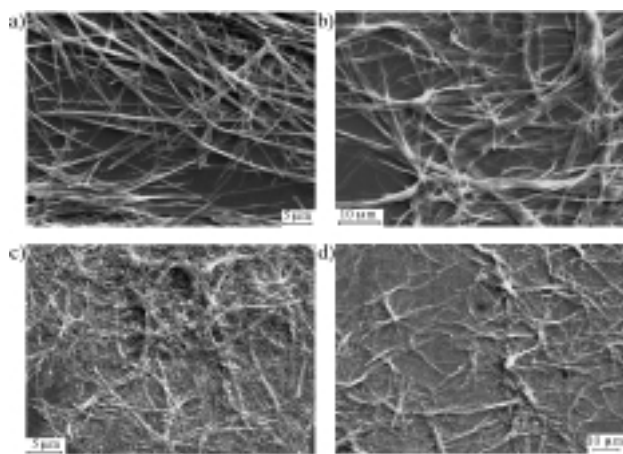


Figure 2. Scanning electron micrographs of a) the precipitate formed by **3** in water, b) the precipitate formed by **4** in pH 7.9 phosphate buffer, c) the dried hydrogel formed by **10** in pH 7.9 phosphate buffer, and d) the dried hydrogel formed by **7** in pH 6.7 phosphate buffer.

3 and **4**, these fibers are entangled and less densely packed, which is in agreement with their formation of a gel.^[7]

The circular dichroism spectra of **4–12** and the water-soluble derivatives **13–15** have minima at wavelengths similar to that observed for the corresponding organogelator **1** in hexanes (Figure 3). The similarity between the CD spectra of

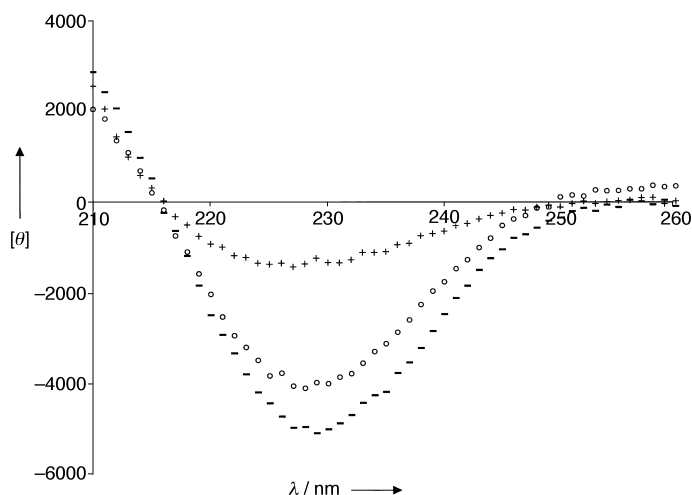


Figure 3. Circular dichroism spectra of **1** in hexanes (+), **15** in 0.2 M ($I = 1.0 \text{ mol kg}^{-1}$) pH 7.9 phosphate buffer (–), and **10** in 0.2 M ($I = 1.0 \text{ mol kg}^{-1}$) pH 7.9 phosphate buffer (o). All spectra were recorded at 55 °C.^[8]

the alkyl and dicarboxylic acid derivatives suggests a related mode of aggregation (hydrogen-bonded stacks of bis-ureas)^[3c] for the two families of gelators. Therefore, it appears that the carboxylic acids do not significantly influence the structure of the aggregates formed by **2–15**.

Potentiometric titrations of water-soluble derivatives **13–15** were performed to further investigate the dependence of gelation on the pH of the solution.^[4b–d, 6c, 9] Bis-ureas **13–15** displayed pK_a values in the expected range for free carboxylic acids ($pK_a \approx 4.3$) and the pK_a values did not vary significantly with the linker length. This result suggests that the carboxylic acids do not play a vital role in the aggregation of this family of hydrogelators.

The relationship between the number of methylene units (molecular weight) and the pH value at which gelation occurs (Table 1), indicates that a) hydrophobic interactions play an important role in promoting gelation and b) the primary function of the carboxylic acids is to modulate the solubility in water.^[6d] By controlling both the degree of ionization of the carboxylic acids and the hydrophobic surface area (molecular weight) of the molecule, control over the pH of gelation can be exercised. At lower pH values, where the carboxylates are partially protonated, the bolaform molecules assemble into vesicles.^[4c, 6c,d, 10, 11] As the pH is raised the solubility increases as a result of the increasing negative charge on the molecules. Aggregation now leads to the formation of fibers that can become entangled through the hydrophobic alkyl esters, thus trapping solvent and forming a gel. Above the pH of gelation, the bis-ureas precipitate from solution as either fibers or sheets. As the molecular weight decreases, the pH at which each of the aggregates forms is lowered until the aggregates

become too soluble and gelation does not occur at any pH. This trend can be explained by the reduction in the hydrophobic surface area and the accompanying increase in the solubility of the compounds and their aggregates in aqueous environments.^[6d, 12]

The dependence of aggregation on the ionic strength was shown to be directly related to the length of the alkyl linker (Table 1). Bis-ureas **9**, **10**, and **12** require 0.2 M phosphate buffers with $I = 1 \text{ mol kg}^{-1}$ to form a stable gel or other aggregate. However, bis-ureas **8** and **11**, which have the longest linkers (12 methylene groups), form stable aggregates in 25 mM phosphate buffer ($I = 0.2 \text{ mol kg}^{-1}$). This result suggests that the role of the cation is primarily to reduce the electrostatic repulsion between the carboxylate groups, which allows the molecule to assume the conformation required to form gelating fibers. As the linker length increases the distance between carboxylates increases, which decreases the concentration of the cation required to shield them from each other.

In summary, we have developed a novel series of molecules that can gel water. The presence of carboxylate groups in the design imparts a pH and ionic-strength dependence on the gelation process. We are currently investigating the use of these hydrogels to control reactions and crystal growth within the matrix.

Experimental Section

Synthesis: The bis-urea dicarboxylic acids (**2–15**) were accessible by a four step synthesis (45–70% overall yields). The commercially available *N*-*t*Boc-glutamic acid γ -benzyl ester (*t*Boc = *tert*-butoxycarbonyl) was first coupled (3-(3-dimethylaminopropyl)-1-ethylcarbodiimide (EDCI), 4-dimethylaminopyridine (DMAP)) to the long-chain alcohol. Treatment with trifluoroacetic acid (TFA) removed the Boc group. The bis-ureas were synthesized by the reaction of the TFA salts with bisocyanates in the presence of triethylamine. Finally, the benzyl ester was cleaved by hydrogenation (1 atm) using palladium on carbon.

Gelation: A weighed amount (ca. 1–2 mg mL⁻¹) of the bis-urea dicarboxylic acid (**2–13**) was dissolved in hot buffer and cooled to room temperature in a test tube fitted with a septum. The aggregation state was observed every ten minutes. The test tube was inverted to check for gelation. If no flow was observed and the resulting substance was homogeneous, the compound was said to have successfully gelled the solution. The solutions were allowed to set and the resulting gels/aggregates were transferred to glass slides, covered, and observed by a polarizing light microscope (Olympus SZH12, 7X-225X).

Electron microscopy: Samples were prepared by evaporation onto glass slides followed by multiple rinses with water to remove excess salts. The surfaces of the slides were then coated with carbon and imaged by a JEOL JXA-8600 electron microprobe with an accelerating voltage of 15 kV and an emission current of 2–10 nA.

pH titrations: Aqueous solutions of **13–15** (10 mM) were prepared and stirred overnight to allow equilibration to occur. They were then titrated with 0.1 M NaOH using a Corning semi-micro combo pH probe. The degree of ionization (α) was calculated by using Equation (1), where $C_{\text{H}^+, \text{total}}$ and $C_{\text{H}^+, \text{free}}$ are the total and free molar amounts of protons, respectively, and C is the molar concentration of bis-urea. The $\text{p}K_a$ value was determined from a graph of α versus pH as the pH value at $\alpha = 0.5$.^[6c]

$$\alpha = 1 - \frac{C_{\text{H}^+, \text{total}} - C_{\text{H}^+, \text{free}}}{2C} \quad (1)$$

CD spectroscopy: A hot solution of gelator was prepared as described above and transferred to a quartz CD cell (0.1-cm path length). The

solutions were then equilibrated at 55 °C for 30 minutes after which time wavelength scans from 210–260 nm were recorded on a Model 202 Aviv CD spectrometer equipped with a temperature control unit.

Received: May 5, 2000 [Z15086]

- [1] P. Terech, R. G. Weiss, *Chem. Rev.* **1997**, 97, 3133–3159.
- [2] P. J. Flory, *Discuss. Faraday Soc.* **1974**, 57, 7–18.
- [3] a) K. Hanabusa, M. Yamada, M. Kimura, H. Shirai, *Angew. Chem.* **1996**, 108, 2086–2088; *Angew. Chem. Int. Ed. Engl.* **1996**, 35, 1949–1951; b) J. van Esch, R. Schoonbeek, M. de Loos, H. Kooijman, A. L. Spek, R. M. Kellogg, B. L. Feringa, *Chem. Eur. J.* **1999**, 5, 937–950; c) A. J. Carr, R. Melendez, S. J. Geib, A. D. Hamilton, *Tetrahedron Lett.* **1998**, 39, 7447–7450; d) C. Shi, Z. Huang, S. Kilic, J. Xu, R. M. Enick, E. J. Beckman, A. J. Carr, R. E. Melendez, A. D. Hamilton, *Science* **1999**, 286, 1540–1543.
- [4] a) T. Shimizu, M. Masuda, *J. Am. Chem. Soc.* **1997**, 119, 2812–2818; b) T. Shimizu, M. Kogiso, M. Masuda, *J. Am. Chem. Soc.* **1997**, 119, 6209–6210; c) T. Imae, Y. Takahashi, H. Muramatsu, *J. Am. Chem. Soc.* **1992**, 114, 3414–3419; d) O. Trager, S. Sowade, C. Bottcher, J. H. Fuhrhop, *J. Am. Chem. Soc.* **1997**, 119, 9120–9124; e) J. H. Fuhrhop, W. Helfrich, *Chem. Rev.* **1993**, 93, 1565–1582; f) J. H. Fuhrhop, J. Koning, *Membranes and Molecular Assemblies: The Synergetic Approach*, Royal Society of Chemistry, Cambridge, **1994**.
- [5] H. Hoffmann, H. Rehage, W. Schorr, H. Thurn in *Surfactants in Solution*, Vol. 1 (Eds.: K. L. Mittal, B. Lindman), Plenum, New York, **1984**, pp. 425–454.
- [6] a) S. Bhattacharya, S. N. G. Acharya, *Chem. Mater.* **1999**, 11, 3504–3511; b) R. Oda, I. Huc, S. J. Candau, *Angew. Chem.* **1998**, 110, 2835–2838; *Angew. Chem. Int. Ed.* **1998**, 37, 2689–2691; c) M. Kogiso, S. Ohnishi, K. Yase, M. Masuda, T. Shimizu, *Langmuir* **1998**, 14, 4978–4986; d) S. Franceschi, N. de Viguier, M. Riviere, A. Lattes, *New J. Chem.* **1999**, 23, 447–452; e) M. Jokic, J. Makarevic, M. Zinic, *J. Chem. Soc. Chem. Commun.* **1995**, 1723–1724; f) G. R. Newkome, G. R. Baker, S. Arai, M. J. Saunders, P. S. Russo, K. J. Theriot, C. N. Moorefield, L. E. Rogers, J. E. Miller, T. R. Lieux, M. E. Murray, B. Phillips, L. Pascal, *J. Am. Chem. Soc.* **1990**, 112, 8458–8465.
- [7] The large dimensions and high degree of entanglement of these fibers are in contrast to rodlike micelles that are normally smaller (in terms of molecular dimensions).^[5]
- [8] Compounds **10** and **1** (but not **15**) exhibit linear dichroism at temperatures below 40 °C and 50 °C, respectively. This effect leads to a bathochromic shift and an increase in intensity in the circular dichroism spectra. These changes are presumably the result of further aggregation of the fibers upon gel formation.
- [9] D. Cistola, J. A. Hamilton, D. Jackson, D. A. Small, *Biochemistry* **1988**, 27, 1881–1888.
- [10] A. V. Peresykin, F. M. Menger, *Org. Lett.* **1999**, 1, 1347–1350.
- [11] T. Imae, B. Trend, *Langmuir* **1991**, 7, 643–646.
- [12] R. Smith, C. Tanford, *Proc. Natl. Acad. Sci. US* **1973**, 70, 289–293.

Ruthenium-Based Four-Coordinate Olefin Metathesis Catalysts**

Melanie S. Sanford, Lawrence M. Henling,
Michael W. Day, and Robert H. Grubbs*

Recent work has shown that the ruthenium alkylidene complex $[(PCy_3)_2Cl_2Ru=CHPh]$ (**1**) is a highly efficient catalyst for metathesis of olefins containing most common functional groups, and, as such, this complex has found extensive application in both organic and polymer chemistry.^[1] Detailed experimental^[2] and theoretical^[3] studies have been carried out to elucidate the mechanism of activity of catalyst **1**, and these investigations implicate a 14-electron, mono-phosphane alkylidene, $[(PCy_3)Cl_2Ru=CHR]$ (**2**) as a probable intermediate both on the metathesis reaction coordinate and in the decomposition of **1**. Complex **2** is remarkable both for its unusual coordinatively unsaturated structure and for its similarity to the four-coordinate Mo and W olefin metathesis catalysts, $[(ArN)(OR)_2M=CHR]$, developed by Schrock (Figure 1).^[4] Unfortunately, the short

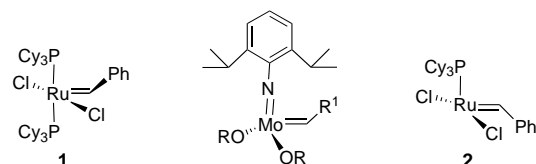
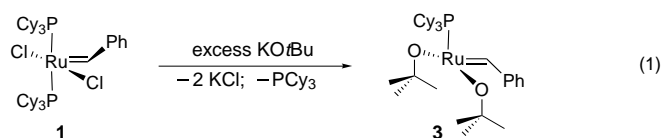


Figure 1. Olefin metathesis catalysts and the proposed intermediate **2**.

lifetime of this proposed intermediate **2** has rendered it elusive to isolation or even observation by spectroscopic methods, presumably a result of its high reactivity in solution with olefinic substrates,^[2a] coordinating solvents,^[5] and/or a second equivalent of **2**.^[2b] Prompted by considerable interest in the nature and structure of this intermediate, we have pursued the preparation of isolable analogues of **2**. We reasoned that complexes such as **2** should be stabilized by more π -donating ligands, which would increase the electron density at the coordinatively unsaturated Ru^{II} center, and by larger ligands, which would drive the equilibrium towards phosphane dissociation and alleviate potential bimolecular decomposition pathways. Herein we report that the replacement of the two halide ligands of **1** with tertiary alkoxides, which possess both π -donor abilities^[6] and steric parameters that can be easily modulated, has enabled the first four-coordinate, 14-electron ruthenium alkylidenes $[(PCy_3)(RO)_2Ru=CHPh]$ to be isolated.

The reaction of **1** with an excess of $KOtBu$ under rigorously anhydrous and air-free conditions proceeds cleanly to form $[(PCy_3)(tBuO)_2Ru=CHPh]$ (**3**) and one equivalent of PCy_3 [Eq. (1)]. Both of these products are extremely soluble in



pentane and common organic solvents; however, the two can be separated by the addition of $CuCl$, which reacts with the free phosphane to form an insoluble polymeric material.^[2a] The alkylidene product **3** is diamagnetic in solution and the NMR spectrum shows a single resonance signal for the carbene (doublet, $\delta = 15.5$) and alkoxide ($\delta = 1.29$) protons and a single ^{31}P resonance signal for the complex ($\delta = 83.5$). Although it is coordinatively unsaturated, complex **3** is remarkably stable, and solutions of **3** in C_6D_6 can be heated at $75^\circ C$ under an inert atmosphere for more than 24 h without significant decomposition (as observed by 1H NMR spectroscopy).

Single crystals of **3** were grown from a concentrated pentane solution at $-30^\circ C$ and its highly unusual solid-state structure is shown in Figure 2. Despite the expected steric

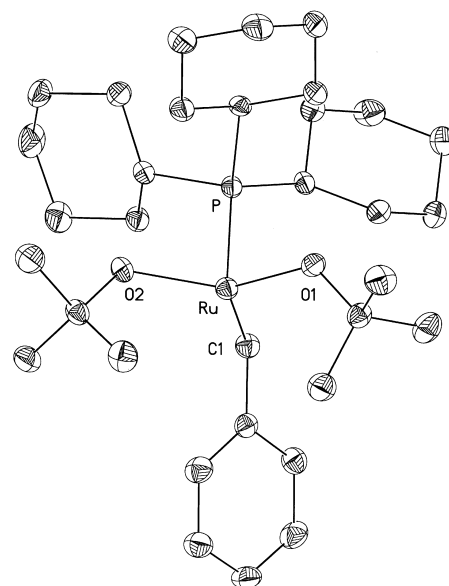


Figure 2. ORTEP plot of complex **3** (50% probability ellipsoids). Selected bond lengths [Å] and bond angles [$^\circ$]: $Ru-C1$ 1.850(2), $Ru-O1$ 1.9412(15), $Ru-O2$ 1.9558(15), $Ru-P$ 2.2232(7); $C1-Ru-O1$ 112.17(8), $C1-Ru-O2$ 114.47(9), $O1-Ru-O2$ 133.19(6), $C1-Ru-P$ 92.49(8), $O1-Ru-P$ 93.49(5), $O2-Ru-P$ 88.36(5).

preference for the four-coordinate Ru^{II} center to adopt a tetrahedral geometry (as is observed in Schrock's Mo and W systems),^[4] this complex crystallizes with a slightly distorted trigonal pyramidal ligand array. The phosphane ligand is at the vertex of the pyramid and the angles from the phosphane to the three other ligands are close to 90° . The angles within the trigonal plane are $133.19(6)$ ($O1-Ru-O2$), $114.47(9)$ ($O2-Ru-C1$), and $112.17(8)^\circ$ ($O1-Ru-C1$), which suggests that this geometry may be a sterically induced distortion of the square-pyramidal structure adopted by the ruthenium alkylidene complex **1**.^[7] In complex **3** the phenyl substituent of the carbene ligand is rotated away from the bulky phosphane and

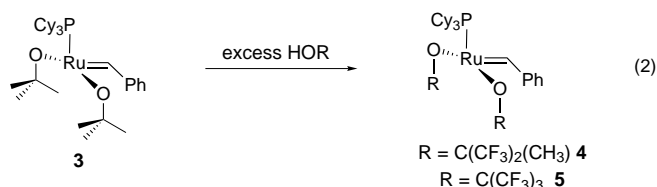
[*] Prof. R. H. Grubbs, M. S. Sanford, L. M. Henling, Dr. M. W. Day
Arnold and Mabel Laboratories of Chemical Synthesis
California Institute of Technology
Division of Chemistry and Chemical Engineering
Mail Code 164-30, Pasadena, CA 91125 (USA)
Fax: (+1) 626-564-9297
E-mail: rhg@its.caltech.edu

[**] The authors thank the NSF for generous support of this research.

into the space below the trigonal plane which results in a P-Ru-C_α-H_α dihedral angle of 12.2 (14)°. Similar angles have been observed in 16-electron Ru^{II} alkylidene complexes that contain relatively small ligands (e.g. PPh₃);^[8] however, complex **1** and its analogues which contain bulky PCy₃ ligands typically have P-Ru-C_α-H_α angles of close to 90°.^[7] Notably, mechanistic studies of catalytic reactions with **1** suggest that the rotation of the carbene moiety to the conformation observed in complex **3** may be a crucial step on the pathway to the formation of the metallacyclobutane intermediate.^[2a]

Another interesting feature of the structure of complex **3** is that despite the numerous accessible C-H bonds in the empty coordination site below the trigonal plane, the ruthenium center does not appear to be stabilized by agostic interactions. The closest Ru...C distance (other than C_α) is 3.091 Å and the closest Ru...H distance (other than H_α) is 2.75 Å, which are both long for agostic contacts.^[9, 10] Furthermore, an overlay of the two *t*Bu groups shows that they are identical, which indicates that neither of these ligands is sufficiently distorted so as to interact with the metal center. Both IR spectroscopy and variable temperature ¹H NMR spectroscopy studies (which shows that the resonance signals of the *t*Bu groups are equivalent to -120 °C in C₃D₁₂) suggest that **3** is free of agostic interactions in solution. Only three other four-coordinate 14-electron Ru^{II} complexes have been structurally characterized^[10] and all of these are formally 18-electron octahedral species with two agostic CH interactions occupying the two open coordination sites.

Complex **3** reacts readily with Brønsted acids including acidic alcohols and phenols. For example, the combination of **3** with an excess of HOC(CH₃)(CF₃)₂ or HOC(CF₃)₃ results in the rapid liberation of *t*BuOH and the formation of [(PCy₃)(CH₃(CF₃)₂CO)₂Ru=CHPh] (**4**) and [(PCy₃)((CF₃)₃CO)₂Ru=CHPh] (**5**), respectively [Eq. (2)].^[11] Preliminary



(NMR) experiments show that this reaction is equally facile for *ortho*-substituted phenols (e.g. 2,6-diphenylphenol and 2-phenylphenol); however, phenols without *ortho* substitution (e.g. *p*-nitrophenol) do not yield stable products. This is likely because the unsubstituted phenols lack the steric bulk to protect the metal center from bimolecular decomposition.^[2b] The use of acidic 1° or 2° alcohols leads to a mixture of ruthenium hydrides, presumably through β-hydrogen elimination from the coordinated alkoxide.

The olefin metathesis activities of complexes **3–5** for the ring-closing metathesis (RCM) of diethyl diallylmalonate were compared, and the results are summarized in Table 1. Although all of these four-coordinate alkylidene complexes are essentially inactive for RCM at room temperature, **4** and **5** exhibit moderate catalytic activity at 60 °C. However, the

Table 1. Ring-closing metathesis reactions of diethyl diallylmalonate with complexes **1** and **3–5**.^[a]

Catalyst	Additive	<i>T</i> [°C]	<i>t</i> [h]	Yield [%]
3	none	60	96	< 5
4	none	60	96	70
5	none	60	12	40
4	HCl ^[b]	25	0.65	> 96
1	none	25	1.5	> 96 ^[c]

[a] Reactions of five equivalents of substrate in C₆D₆; [catalyst] = 0.01 – 0.02 M; yields were estimated by integration of the ¹H NMR spectrum; unless indicated catalyst decomposition terminated the reaction. [b] Two equivalents of HCl were added as a 2 M solution in diethyl ether. [c] Catalyst remains at the end of the reaction.

activity of these complexes, particularly **5**, is limited by their low thermal stability in the presence of the olefinic substrate, and both decompose before the metathesis reaction reaches completion. Notably no propagating species (which is expected to be a ruthenium methylidene complex) is observed by ¹H NMR spectroscopy in any of these reactions. The results described here are qualitatively similar to earlier studies of complex **1** and its analogues in which it was found that more electron withdrawing ligands afford more active olefin metathesis catalysts.^[2a] These results are also consistent with Schrock's early transition metal systems in which catalytic activity increases with the acidity of the parent alcohol.^[4] The relatively low reactivities of **3–5** for the RCM reaction are likely due to of the same factors which render these species sufficiently stable to be isolated: the large steric bulk of the alkoxides effectively shields the metal from the incoming substrate,^[12] while π donation by these ligands discourages olefin binding by decreasing the electrophilicity of the Ru^{II} center.^[6]

However, complexes **3–5** become excellent catalysts for RCM when activated with HCl, and the representative example of the **4**/HCl system is shown in Table 1. The addition of two equivalents of HCl to a solution of complex **4** in C₆D₆ results in an instantaneous color change from red to brown. Although no new carbene resonance signals can be observed by ¹H NMR spectroscopy, a small amount of a highly metathesis active species is generated. In fact, under otherwise identical conditions, the RCM of diethyl diallylmalonate proceeds *at least twice as fast* with **4**/HCl than with catalyst **1** alone, despite the undetectably small amounts of active catalyst present in the **4**/HCl reaction mixture. By analogy to the ligand exchange reaction of **2** with acidic alcohols, we believe that the HCl serves to protonate the alkoxide ligands of **4**, to generate free HOC(CF₃)₂CH₃ (which is the sole species observed by ¹⁹F NMR spectroscopy) and the elusive four-coordinate species [(PCy₃)Cl₂Ru=CHR] (**2**). Evidence for this proposal is provided by the reaction of **4** with HCl in the presence of one equivalent of PCy₃; this reaction results in the regeneration of catalyst **1**.

In conclusion, a series of four-coordinate ruthenium alkylidene complexes with highly unusual trigonal pyramidal geometries has been prepared as analogues of the proposed olefin metathesis intermediate **2**. The new complexes show moderate activity as single component catalysts for ring-

closing metathesis. The RCM reactions can be greatly accelerated by the addition of HCl which is believed to generate the highly reactive complex **2** in solution.

Experimental Section

3: Complex **1** (0.91 mmol) and KOtBu (3.2 mmol) were combined in C₆H₆ (30 mL). The reaction mixture was stirred for 24 h during which time it changed color from purple to brownish red. The solvent was frozen and removed by sublimation under vacuum. The resulting solids were suspended in a mixture of C₆H₆ (0.5 mL) and pentane (50 mL). CuCl (9.1 mmol) was added, and the suspension was stirred for 20 min, and then cooled at –30 °C for 24 h. The supernatant solution was decanted and the solvent removed under vacuum to give **3** as a dark brown foamy solid (52 % yield). This solid is typically about 95 % pure (by ³¹P NMR), and contains traces of CuCl(PCy₃) polymer. ¹H NMR (400 MHz, C₆D₆): δ = 15.5 (d, ³J_{PH} = 4.4 Hz, 1 H, Ru=CH), 7.88 (d, ²J_{H,H} = 7.3 Hz, 2 H, *ortho*-H), 7.27 (t, ²J_{H,H} = 7.3 Hz, 1 H, *meta*-H), 7.17 (s, 2 H, *para*-H), 2.4–1.1 (m, 33 H, PCy₃), 1.29 (s, 9 H, *t*Bu); ³¹P{¹H} NMR (162 MHz, C₆D₆): δ = 83.5 (s); ¹³C{¹H} NMR (75 MHz, C₆D₆): δ = 230.5 (d, ²J_{PC} = 15.2 Hz, Ru=C), 152.1, 129.9, 125.3, 124.6, 74.50, 36.69, 34.57, 34.48, 34.14, 33.68, 33.44, 31.52, 29.61, 28.84, 28.70, 28.51, 28.37, 27.48.

4: Hexafluoro-*tert*-butanol (0.5 mL) was added to a solution of complex **3** (0.41 mmol) in pentane (25 mL). The reaction was stirred for 30 min then cooled to –30 °C for 24 h. The supernatant solution was decanted and the solvents were removed under vacuum to give an oily dark brown solid. The product was recrystallized from a minimum volume of pentane to afford reddish crystals of **4** (40 % yield). ¹H NMR (400 MHz, C₆D₆): δ = 17.5 (s, 1 H, Ru=CH), 7.88 (d, ²J_{H,H} = 5.9 Hz, 2 H, *ortho*-H), 7.14 (m, 3 H, *meta*-H and *para*-H), 2.4–1.1 (m, 33 H, PCy₃); ³¹P{¹H} NMR (162 MHz, C₆D₆): δ = 80.1 (s); ¹⁹F NMR (283 MHz, C₆D₆): δ = –77.93 (s), –79.27 (s); ¹³C{¹H} NMR (75 MHz, C₆D₆): δ = 262.6 (d, ²J_{PC} = 18 Hz, Ru=C), 150.6, 131.0, 130.4, 126.1 (q, ¹J_{FC} = 288 Hz), 125.4 (q, ¹J_{FC} = 288 Hz), 124.5, 34.33, 34.00, 29.49, 28.40, 28.26, 27.02, 20.46; elemental analysis calcd (%) for C₃₃H₄₅F₁₂O₂PRu: C 47.54, H 5.44; found: C 47.19, H 5.41.

5: The same procedure as for complex **4**, but using perfluoro-*tert*-butanol, afforded **5** as a reddish microcrystalline solid (37 % yield). ¹H NMR (400 MHz, C₆D₆): 19.2 (s, 1 H, Ru=CH), 7.72 (d, ²J_{H,H} = 7.34 Hz, 2 H, *ortho*-H), 7.14 (m, 3 H, *meta*-H and *para*-H), 2.1–0.8 (m, 33 H, PCy₃); ³¹P{¹H} NMR (162 MHz, C₆D₆): δ = 75.1 (s); ¹⁹F NMR (283 MHz, C₆D₆): δ = –73.55 (s); ¹³C{¹H} NMR (75 MHz, C₆D₆): δ = 286.5 (d, ²J_{PC} = 15.2 Hz, Ru=C), 151.4, 130.0, 129.6, 125.6, 123.0 (q, ¹J_{FC} = 292 Hz), 35.20, 34.90, 32.23, 31.91, 31.66, 31.63, 29.91, 28.34, 28.21, 27.95, 27.80, 26.94, 26.75; elemental analysis calcd (%) for C₃₃H₃₉F₁₈O₂PRu: C 42.09, H 4.17; found: C 41.60, H 4.18.

Crystal Structure of 3: Dark red-brown blades were grown from pentane: C₃₃H₅₇O₂PRu (617.83), crystal dimensions: 0.21 × 0.16 × 0.03 mm³, monoclinic, space group *P*2₁/*n* (no. 14), *a* = 10.0120(7), *b* = 20.5338(14), *c* = 15.7802(11) Å, β = 92.1300(10)°, *Z* = 4, *V* = 3241.9(4) Å³, ρ_{calc} = 1.266 mg m^{–3}, *T* = 93 K, 2θ = 57.5°, 29820 reflections were measured, 7759 independent reflections were obtained (*R*_{int} = 0.0683) on a Bruker SMART diffractometer with MoK_α radiation (λ = 0.71073 Å). The structure was solved by direct methods,^[13a] with refinement by full-matrix least squares of *F*² [^{13b}]; *R*₁ = 0.0328, *wR*₂ = 0.0527 (for *I* > 2σ(*I*)), *R*₁ = 0.0611, *wR*₂ = 0.0569 (for all data), residual electron density : +0.632/–0.510 e Å^{–3}. Crystallographic data (excluding structure factors) for the structure reported in this paper have been deposited with the Cambridge Crystallographic Data Centre as supplementary publication no. CCDC-140726. Copies of the data can be obtained free of charge on application to CCDC, 12 Union Road, Cambridge CB2 1EZ, UK (fax: (+44) 1223-336-033; e-mail: deposit@ccdc.cam.ac.uk), and structure factors are available on request from xray@caltech.edu.

Received: May 16 2000 [Z15131]

- [1] K. J. Ivin, J. C. Mol, *Olefin Metathesis and Metathesis Polymerization*, Academic Press, New York, 1997.
[2] a) E. L. Dias, S. T. Nguyen, R. H. Grubbs, *J. Am. Chem. Soc.* **1997**, *119*, 3887–3897; b) M. Ulman, R. H. Grubbs, *J. Org. Chem.* **1999**, *64*, 7202–7207.

- [3] O. M. Aagaard, R. J. Meier, F. Buda, *J. Am. Chem. Soc.* **1998**, *120*, 7174–7182.
[4] a) R. R. Schrock, *Polyhedron* **1995**, *14*, 3177–3195; b) R. R. Schrock, *Tetrahedron* **1999**, *55*, 8141–8153.
[5] D. M. Lynn, B. Mohr, R. H. Grubbs, *J. Am. Chem. Soc.* **1998**, *120*, 1627–1628.
[6] For a comprehensive review see: K. G. Caulton, *New J. Chem.* **1994**, *18*, 25–41.
[7] P. Schwab, J. Ziller, R. H. Grubbs, *J. Am. Chem. Soc.* **1996**, *118*, 100–110.
[8] For example, see: S. T. Nguyen, L. K. Johnson, R. H. Grubbs, J. W. Ziller, *J. Am. Chem. Soc.* **1992**, *114*, 3974–3975.
[9] Representative examples of Ru···CH agostic interactions include: a) S. Takahashi, S. Hikichi, M. Akita, Y. Moro-oka, *Organometallics* **1999**, *18*, 2571–2573; b) M. A. Bennett, S. Pelling, G. B. Robertson, W. A. Wickramasinghe, *Organometallics* **1991**, *10*, 2166–2172.
[10] a) D. J. Huang, K. Folting, K. G. Caulton, *J. Am. Chem. Soc.* **1999**, *121*, 10318–10322; b) D. J. Huang, W. E. Streib, J. C. Bollinger, K. G. Caulton, R. F. Winter, T. Scheiring, *J. Am. Chem. Soc.* **1999**, *121*, 8087–8097; c) W. Baratta, E. Herdtweck, P. Rigo, *Angew. Chem.* **1999**, *111*, 1733–1735; *Angew. Chem. Int. Ed.* **1999**, *38*, 1629–1631.
[11] Complexes **4** and **5** have also been characterized by X-ray crystallography, and their structures are qualitatively similar to that of **3**. However, reliable bond lengths and angles could not be determined because of the extreme disorder of the CF₃ groups in both molecules.
[12] We have attempted to study the binding of other ligands (including THF, PMe₃, and CH₃CN) to these complexes. Complexes **2–4** do not appear to bind THF, while the other ligands lead to decomposition or to a mixture of products.
[13] a) G. M. Sheldrick, *Acta Crystallogr. Sect. A* **1968**, *46*, 467–473; b) G. M. Sheldrick, SHELXL-97: Program for Structures Refinement, University of Gottingen, Germany, 1997.

Calix[6]arene as a Wheel for Rotaxane Synthesis**

Arturo Arduini, Riccardo Ferdani, Andrea Pochini,*
Andrea Secchi, and Franco Ugozzoli

Rotaxanes and catenanes^[1] are interesting supermolecules that have been extensively studied for their use in the preparation of molecular switches. A possible approach to their synthesis is based on the formation of an axial complex between a molecular wheel that is used as the host and a specific guest that is employed as the axle.

- [*] Prof. A. Pochini, Prof. A. Arduini, Dr. R. Ferdani, Dr. A. Secchi
Dip.to di Chimica Organica e Industriale dell'Università
Parco Area delle Scienze
17/A, 43100, Parma, (Italy)
Fax: (+39) 0521-905472
E-mail: pochini@unipr.it
Prof. F. Ugozzoli
Dip.to di Chimica Generale e Inorganica Chimica Analitica Chimica Fisica
Università di Parma and Centro di Studio per la Strutturistica Diffraattometrica del C.N.R.
Parco Area delle Scienze, 17/A, 43100 Parma (Italy)
[**] We thank MURST for financial support within the “Supramolecular Devices” project and C.I.M. of the University of Parma for mass and NMR measurements.

In this context calixarenes, which are versatile and potent receptors, have never been used as molecular wheels and, in spite of their similarity to cyclodextrins,^[2] no examples of axial complexation where all their inner binding sites are simultaneously involved in the binding of the guest have been reported. In fact the two rims in these macrocycles have usually been considered as distinct and separate domains.^[3] Examples exist in which the two calixarene rims have been shown to act in a combined manner, for example, in the recognition of both cations and anions^[4] or to exchange information between them.^[5] A rational approach to the synthesis of a calixarene-based rotaxane was thus undertaken to explore the possibility of utilizing a calixarene receptor as a molecular wheel.

The calix[6]arene platform was chosen on the basis of its ring size and because it possesses an annulus large enough to allow a sufficiently bulky and elongated guest to cross the two rims. On the basis of our previous studies on the binding ability of calix[6]arene derivatives^[6] compound **1**,^[7] which is "preorganized" by the presence of 1,3,5-trimethoxy-2,4,6-trioctyloxy groups on the lower rim^[8] and bears three phenylureido groups which extend the apolar cavity, was chosen as the wheel and the dioctylviologen dication was selected as the axle (Scheme 1).

Direct experimental evidence of complex formation and consequently of the passage of the guest through the macrocycle annulus was obtained by extraction experiments and ¹H NMR studies on the complex formed. The triphenylureidocalix[6]arene derivative **1** is able to dissolve the colorless crystals of dioctylviologen ditsylate (**2a**) in chloroform to afford a deep purple solution. Similar results were obtained by using the dioctylviologen diiodide.^[9] The ¹H NMR spectrum of the solution obtained by equilibrating a suspension of dioctylviologen diiodide (**2b**) in CDCl₃ with a solution of **1** showed the formation of a 1:1 adduct. The main features of the NMR spectrum (Figure 1) are the extensive upfield shift (1 to 3 ppm) of the signals corresponding to the aromatic CH and NCH₂ hydrogen atoms of the guest, which indicates that it is included inside the calix[6]arene cavity. The six protons of the host ureido groups suffer a downfield shift from δ = 6.7 and 7.1 to δ = 8.00 and 8.33, respectively, which suggests their participation in hydrogen-bonding interactions with the two iodine anions. Particularly informative was the observation that the protons of the methoxy groups present at the lower rim of **1**, which resonate at δ = 2.82 in the free calixarene because they are oriented into the calixarene cavity, are shifted downfield ($\Delta\delta$ = 1.12) in the complex. This observation indicates that their orientation has changed to a situation where they are no longer affected by the shielding effect of the aromatic cavity.

These data, together with 2D NMR experiments, could be rationalized with the hypothesis that a pseudorotaxane^[1] **3** was formed (Scheme 1). Evidence for the stability of this complex came from

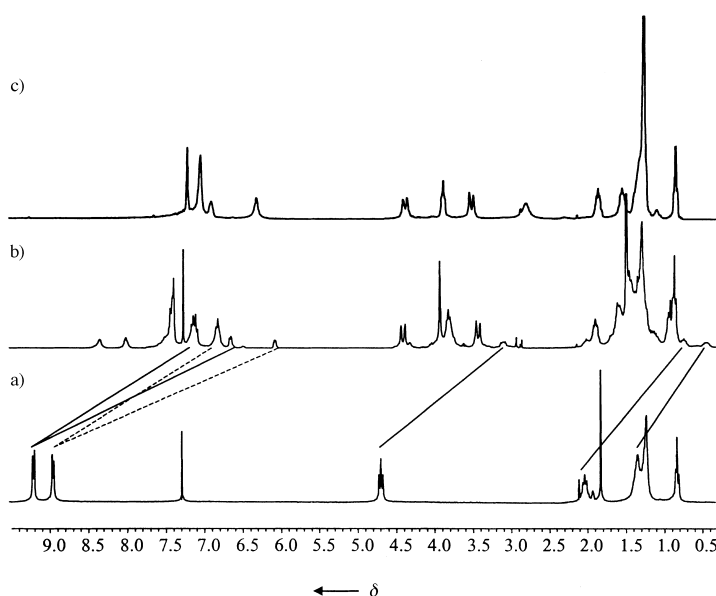
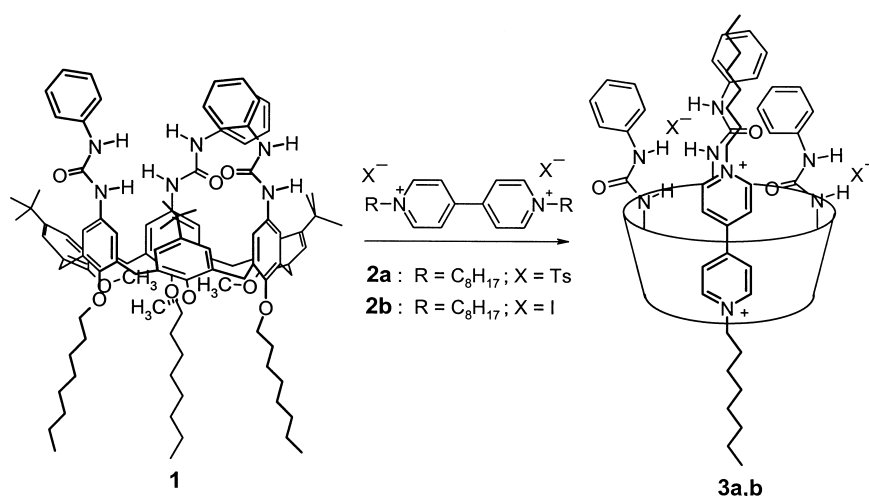


Figure 1. ¹H NMR spectra (300 MHz, 300 K) of: a) dioctylviologen diiodide (**2b**) in 10% CD₃CN/CDCl₃; b) pseudorotaxane **3b** in CDCl₃; c) triphenylureidocalix[6]arene (**1**) in CDCl₃.

thin layer chromatography which showed that it was possible to separate the complex in aprotic solvents without competitive decomplexation processes occurring. The slow evaporation of the solution containing host **1** and **2b** gave red crystals of **3b** that were suitable for X-ray analysis (Figure 2).^[10] Analysis of the structure shows that all the binding sites present in the host are involved in the stabilization of the supramolecular structure (Figure 3). The N1 atom is located 0.399(6) Å above the least-squares plane through the bridging methylene groups of the calixarene and points its attached octyl chain across the lower annulus of the macrocycle, thus expelling the three methoxy groups from the aromatic cavity. The lower pyridinium ring of the guest is sandwiched and stacked by rings F and B of the host (the distance between the centroids of these rings is 6.810(8) Å) and is almost perpendicular to rings A and D of the host. The two hydrogen atoms on C1 and C5 of the guest and the two hydrogen atoms of the octyl chain (C11) are involved in hydrogen-bonding inter-



Scheme 1. Synthesis of pseudorotaxanes **3a,b**.

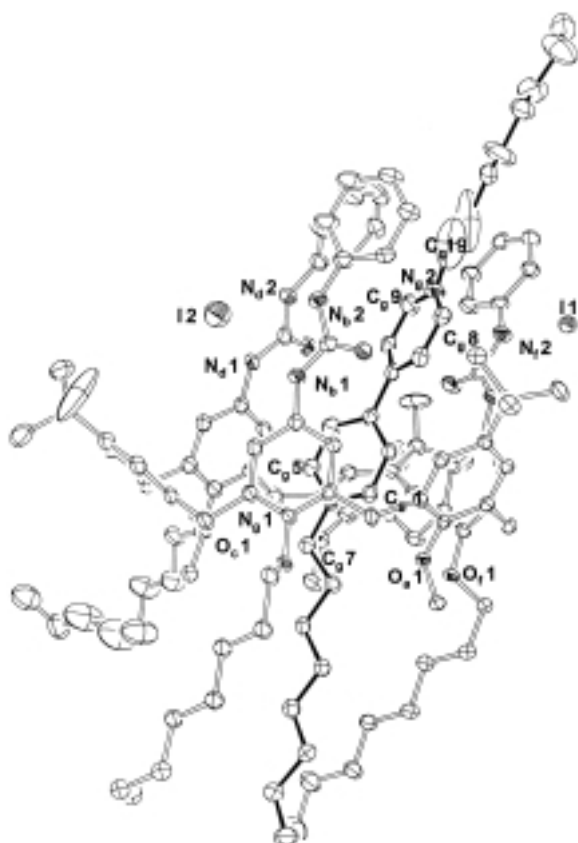
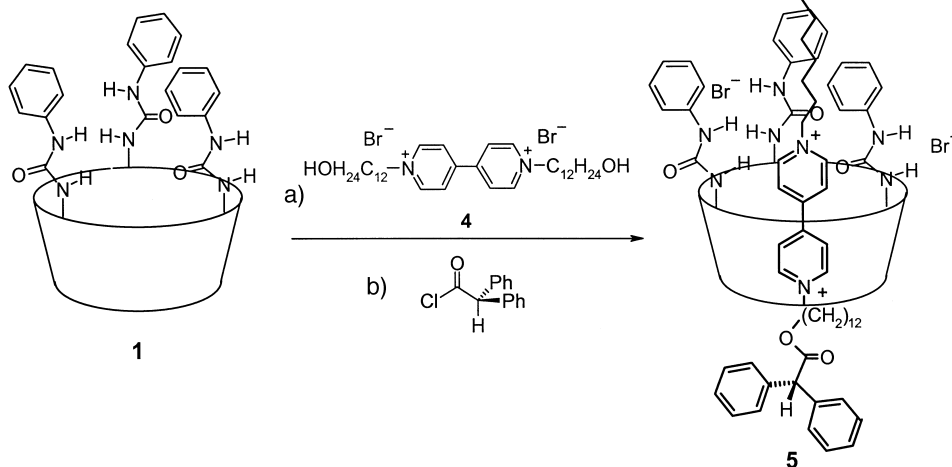


Figure 2. X-ray crystal structure of pseudorotaxane **3b** at 173 K. The hydrogen atoms are omitted for clarity, and the bonds of the guest are darkened for clarity.

actions with the three oxygen atoms of the host methoxy groups. The hydrogen atoms on C8 of the upper ring of the guest as well as one of those belonging to C19 form CH- π interactions with the phenyl groups D' (2.639(8) Å) and B' (2.641(8) Å), respectively. The two iodide ions also participate in the assembly process through hydrogen-bonding interactions with the NH ureido groups of the host.

The formation of the pseudorotaxane was then exploited to synthesize a rotaxane.^[11] Refluxing the diol axle **4** and wheel **1** in toluene gave an homogeneous deep red solution. This solution was then treated with diphenylacetyl chloride, which acted as the stopper (Scheme 2). Purification of the reaction mixture gave the rotaxane **5** in 25% yield. The ¹H NMR spectrum of **5** was very similar to that of the pseudorotaxane. The presence of a singlet at δ =5.05, a multiplet at δ =7.29, and a triplet at δ =4.17 for the ω CH₂



Scheme 2. Synthesis of rotaxane **5**. a) toluene, reflux, 24 h; b) toluene, reflux, 72 h.

protons are indicative of the introduction of the two stoppers

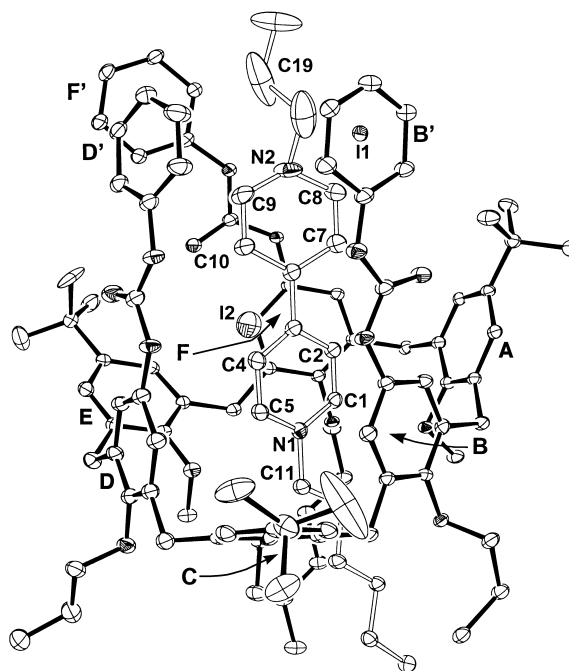


Figure 3. Structure of **3b** showing the numbering of the atoms and groups; part of the host structure is omitted for clarity.

at the ends of the axle. The ESI-MS spectrum and the elemental analysis of **5** are in agreement with the proposed structure.

Further studies to understand the role of the single interactions which stabilize and drive the formation of these unprecedented calixarene complexes and to extend the field of application to other calixarenes and ammonium salts to the preparation of molecular switching systems are in progress in our laboratories.

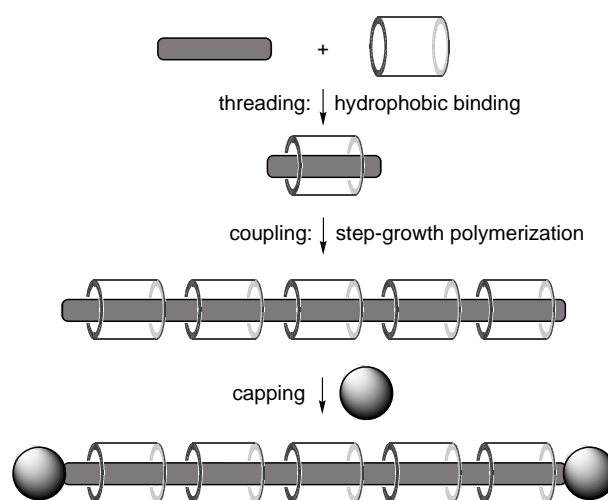
Received: April 25, 2000 [Z 15026]

- [1] See, for example, a) F. M. Raymo, J. F. Stoddart, *Chem. Rev.* **1999**, 99, 1643; b) C. Seel, F. Vögtle, *Chem. Eur. J.* **2000**, 6, 21, and references therein.
- [2] a) *Comprehensive Supramolecular Chemistry*, Vol. 3 (Eds.: J. Szejtli, T. Osa), Pergamon, Oxford, **1996**; b) S. A. Nepogodiev, J. F. Stoddart, *Chem. Rev.* **1998**, 98, 1959.
- [3] C. D. Gutsche *Calixarenes Revisited—Monograph in Supramolecular Chemistry* (Ed.: J. F. Stoddart), The Royal Society of Chemistry, Cambridge, **1998**.
- [4] See, for example, a) J. Scheerder, J. P. M. van Duynhoven, J. F. J. Egbersen, D. N. Reinhoudt, *Angew. Chem.* **1996**, 108, 1172; *Angew. Chem. Int. Ed. Engl.* **1996**, 35, 1090; b) N. Pelizzi, A. Casnati, A. Friggeri, R. Ungaro, *J. Chem. Soc. Perkin Trans. 2* **1998**, 1307.
- [5] See, for example, a) R. Castro, L. A. Godínez, M. C. Criss, A. E. Kaifer, *J. Org. Chem.* **1997**, 62, 4928; b) A. Mirzozian, A. E. Kaifer, *Chem. Eur. J.* **1997**, 3, 1052; c) A. Ikeda, S. Shinkai, *J. Am. Chem. Soc.* **1994**, 116, 3102; d) K. N. Koh, K. Araki, S. Shinkai, Z. Asfari, J. Vicens, *Tetrahedron Lett.* **1995**, 36, 6095; e) A. Ikeda, T. Tsudera, S. Shinkai, *J. Org. Chem.* **1997**, 62, 3568.
- [6] See, for example, A. Arduini, L. Domiano, L. Oglioni, A. Pochini, A. Secchi, R. Ungaro, *J. Org. Chem.* **1997**, 62, 7866.
- [7] Triureidocalix[6]arene (**1**) was synthesized as described in J. J. González, R. Ferdani, E. Albertini, J. M. Blasco, A. Arduini, A. Pochini, P. Prados, J. de Mendoza, *Chem. Eur. J.* **2000**, 6, 73.
- [8] J. P. M. van Duynhoven, R. G. Janssen, W. Verboom, S. M. Franken, A. Casnati, A. Pochini, R. Ungaro, J. de Mendoza, P. M. Nieto, P. Prados, D. N. Reinhoudt, *J. Am. Chem. Soc.* **1994**, 116, 5814.
- [9] The ditosylate of dioctylviologen is a colorless solid which is very insoluble in CDCl_3 . As a result its diiodide, which is a deep purple solid, was used because of its better solubility and sharper NMR spectra.
- [10] X-ray structural analysis was performed on an Enraf Nonius CAD4 diffractometer with graphite monochromated $\text{CuK}\alpha$ radiation ($\lambda = 0.71073 \text{ \AA}$). Data collection and refinement for $\text{C}_{128}\text{H}_{174}\text{I}_2\text{N}_4\text{O}_9$ at 173 K: transparent plate $0.20 \times 0.40 \times 0.5 \text{ mm}^3$, triclinic, space group $P\bar{1}$ no. 2, $a = 15.407(5)$, $b = 27.122(5)$, $c = 14.688(5) \text{ \AA}$, $\alpha = 94.65(2)$, $\beta = 90.83(2)$, $\gamma = 75.88(2)^\circ$, $V = 5933(3) \text{ \AA}^3$, $Z = 2$, $M_r = 2222.64$, $\rho_{\text{calcd}} = 1.244 \text{ g cm}^{-3}$, $\mu = 5.9 \text{ cm}^{-1}$, $\theta_{\text{max}} = 65$, 21077 reflections were collected ($\pm h, \pm k, \pm l$), of which 20151 were unique ($R_{\text{int}} = 0.06$) and 11677 observed ($F_o > 4\sigma(F_o)$). The structure was solved by direct methods using SIR92 (A. Altomare, M. C. Burla, M. Camalli, G. Casciarano, C. Giacovazzo, A. Guagliardi, G. Polidori, *J. Appl. Crystallogr.* **1994**, 27, 435) and refined on F using SHELXL-96 software (G. M. Sheldrick, *SHELXL-96*, University of Göttingen, Germany, **1996**). Data were corrected for Lorentz and polarization effects. Absorption correction was applied by Ψ scan measurements (min/max transmission factor = 0.75). The terminal aliphatic chains on the phenol oxygen atoms were affected by severe static disorder arising from several slightly different orientations. It proved impossible to rationalize the disorder in terms of different orientations with different site occupancy factors and the refinement was carried out with geometrical constraints on the chains. All non-hydrogen atoms were refined with anisotropic temperature factors and the hydrogen atoms were taken in their calculated positions "riding" on their parent atoms (1346 parameters, 30 constraints). Final $R_1 = 0.092$ and $wR_2 = 0.294$ with GOF = 0.984. Largest difference peak and hole 1.77 and -2.92 e \AA^{-3} , respectively. Geometrical calculations were obtained by PARST95 (M. Nardelli, *J. Appl. Crystallogr.* **1995**, 28, 659). Crystallographic data (excluding structure factors) for the structures reported in this paper have been deposited with the Cambridge Crystallographic Data Centre as supplementary publication no. CCDC-141315. Copies of the data can be obtained free of charge on application to CCDC, 12 Union Road, Cambridge CB21EZ, UK (fax: (+44) 1223-336-033; e-mail: deposit@ccdc.cam.ac.uk).
- [11] Calix[4]arene has been used as a stopper for rotaxane synthesis: C. Fischer, M. Nieger, O. Mogck, V. Böhmer, R. Ungaro, F. Vögtle, *Eur. J. Org. Chem.* **1998**, 155.

Insulated Molecular Wires: Synthesis of Conjugated Polyrotaxanes by Suzuki Coupling in Water**

Peter N. Taylor, Michael J. O'Connell, Luke A. McNeill, Michael J. Hall, Robin T. Aplin, and Harry L. Anderson*

The semiconductivity and fluorescence of conjugated polymers result in potential applications, particularly in the area of electroluminescent display devices.^[1] We are interested in enhancing the luminescence, stability, and processability of these polymers by threading them through macrocycles to form conjugated polyrotaxanes, as a type of "insulated molecular wire".^[2,3] Recently we proposed the general route to conjugated polyrotaxanes outlined in Scheme 1. Hydrophobic binding fixes the monomer inside



Scheme 1. Hydrophobic binding directs the synthesis of an insulated molecular wire.

the cavity of a macrocycle, this 1:1 pseudorotaxane complex is then polymerized to form a conjugated polypseudorotaxane, which is coupled to bulky end groups to give the polyrotaxane. Our initial attempts at realizing this scheme used a cationic cyclophane as the macrocycle and Glaser coupling as the polymerization reaction. This failed to give polyrotaxanes higher than the [3]rotaxanes, due to problems of unthreading, aggregation, and precipitation of the growing polymer

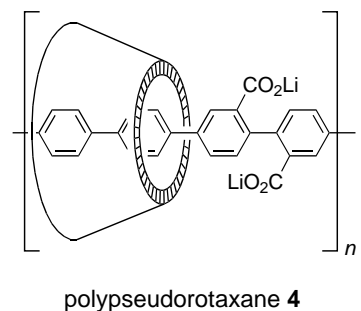
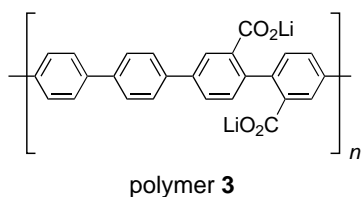
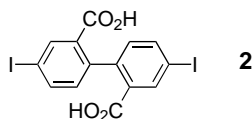
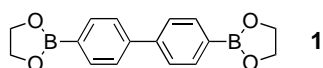
[*] Dr. H. L. Anderson, Dr. P. N. Taylor, M. J. O'Connell, Dr. L. A. McNeill, M. J. Hall, Dr. R. T. Aplin
University of Oxford
Department of Chemistry, Dyson Perrins Laboratory
South Parks Road, Oxford OX1 3QY (UK)
Fax: (+44) 1865-275674
E-mail: harry.anderson@chem.ox.ac.uk

[**] We are grateful to Carol A. Stanier for valuable discussion and to Professor Christopher J. Schofield for providing facilities for gel electrophoresis. Disodium 1-aminonaphthalene-3,6-disulfonate was generously provided by Dr. M. G. Hutchings of BASF plc (Cheadle Hulme, UK). This project is funded by the Engineering and Physical Sciences Research Council (UK).

Supporting information for this article is available on the WWW under <http://www.wiley-vch.de/home/angewandte/> or from the author.

chains.^[2b] Here we present a completely new way of implementing Scheme 1, using β -cyclodextrin (β -CD) as the macrocycle and Suzuki coupling^[4] as the polymerization reaction. Suzuki coupling works well in water,^[5] and has been used to prepare water-soluble conjugated polymers,^[5c,d] but it has not previously been used to make rotaxanes. Our new approach to polyrotaxane synthesis is remarkably successful, giving a highly threaded poly-*para*-phenylene (PPP). Insulation of the PPP backbone inside the cyclodextrins increases its fluorescence efficiency and increases its solubility (processability), suggesting that these polyrotaxanes may have real advantages over unencapsulated PPPs.

When 4,4'-biphenyldiboronic ester **1**^[6] and 4,4'-diiodobiphenyl-2,2'-dicarboxylic acid **2**^[7] are coupled (using phosphane-free aqueous $\text{Pd}(\text{OAc})_2$ catalyst,^[5] in the mole ratio



1:2:Pd of 1.00:0.91:0.09^[8] the product polymer **3** is mostly insoluble, as reported previously,^[9] although a fraction of the polymer is soluble enough in water, as the lithium salt, for spectroscopic characterization. When this reaction is carried out in the presence of three equivalents of β -cyclodextrin per 4,4'-biphenyldiboronic acid, a soluble polypseudorotaxane **4** is formed. This PPP complex was isolated in 71 % yield (calculated assuming one cyclodextrin per repeat unit), after precipitating with acid, dissolving in aqueous LiOH, and dialyzing^[10] to remove excess cyclodextrin, salts, and small oligomers.^[11] Integration of the aromatic and cyclodextrin regions of the ^1H NMR spectrum of this polypseudorotaxane in D_2O (Figure 1 a) indicates that there are 1.2 ± 0.3 macro-

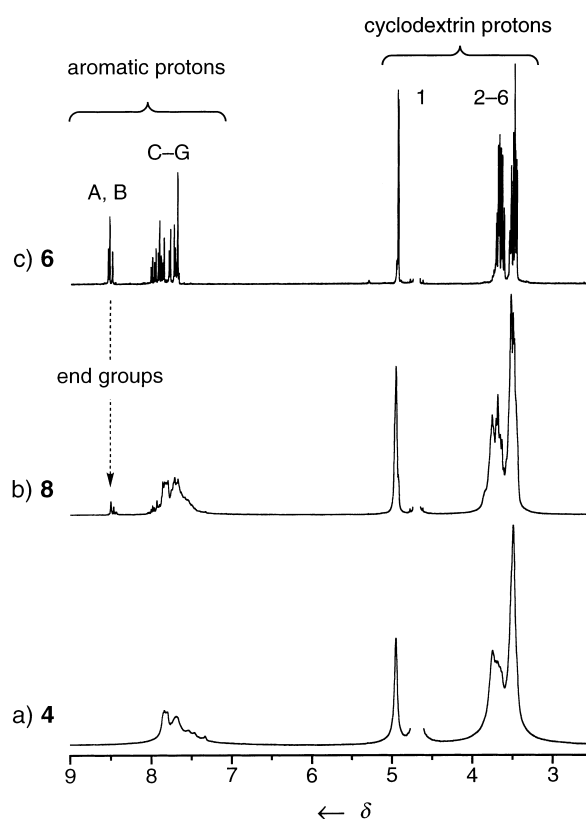
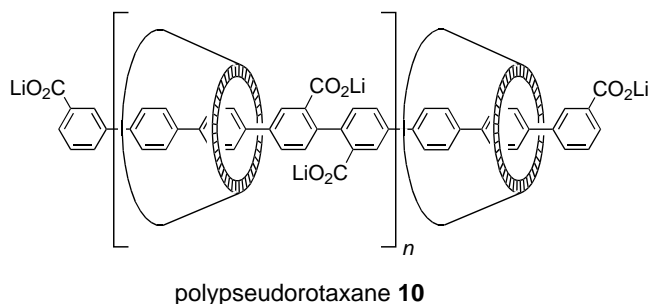
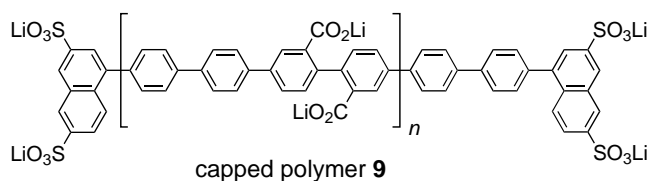
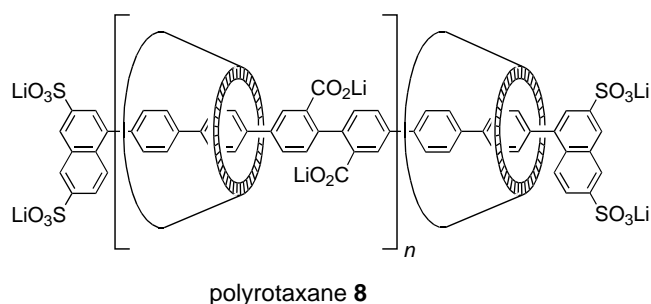
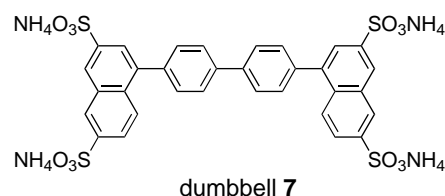
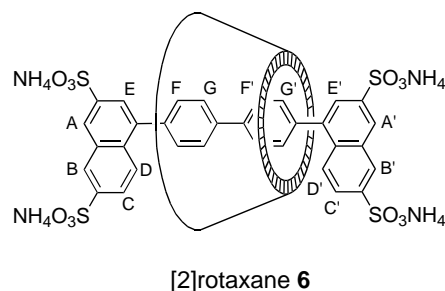
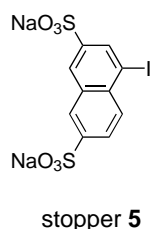


Figure 1. ^1H NMR spectra of a) polypseudorotaxane **4**, b) polyrotaxane **8**, and c) [2]rotaxane **6** (500 Hz in D_2O , with HOD peak truncated).

cycles per repeat unit. This threading ratio cannot be determined accurately because it gradually decreases during dialysis. As the cyclodextrins slip off the polymer chain it becomes increasingly gelatinous and insoluble.

The formation of genuine rotaxanes, rather than pseudorotaxanes, was achieved by reacting 4,4'-biphenyldiboronic ester **1** with disodium 1-iodonaphthalene-3,6-disulfonate (**5**)^[12] in the presence of β -cyclodextrin under identical aqueous Suzuki coupling conditions. This gave the [2]rotaxane **6**, together with the dumbbell **7**. ^1H NMR spectroscopy of crude reaction mixtures, after removing all free cyclodextrin by ion-exchange chromatography, showed that the ratio of **6:7** is about 1:2, which indicates that the naphthalene end groups significantly hinder cyclodextrin binding. It proved difficult to separate the [2]rotaxane **6** from dumbbell **7**, but **6** was isolated in 4 % yield by repeated recrystallization from aqueous methanol/ethanol. The ^1H NMR spectrum of **6** (Figure 1 c) shows that the symmetry of the cyclodextrin is imposed on the encapsulated dumbbell, doubling the number of aromatic signals.

This reaction was extended to synthesize polyrotaxane **8** by coupling a mixture of **1**, **2**, **5**, and β -cyclodextrin (mole ratio **1:2:5:Pd:β-CD** of 1.00:0.74:0.37:0.07:3.0).^[8] The PPP polyrotaxane **8** was isolated in 45 % yield, after precipitation and extensive dialysis.^[10] Although the ^1H NMR spectrum of **8** in D_2O is poorly resolved, it closely resembles those of **4** and **6** (as shown in Figure 1) and the resonance signals of the terminal naphthalene protons (A and B) are well separated from the other aromatic peaks. Integration of these end group



signals shows that the average degree of polymerization n is about 8 ± 2 . (This is higher than the value expected from the polymerization stoichiometry, perhaps because short oligomers are lost during purification). Integration of the cyclodextrin resonance signals shows that there are 1.1 ± 0.1 macrocycles per unsubstituted biphenyl unit. No change in this threading ratio occurred during dialysis.

The matrix-assisted laser desorption time-of-flight (MALDI-TOF) mass spectrum of polyrotaxane **8** (Figure 2) provides excellent evidence for its structural authenticity. All the observed peaks correspond to expected singly charged molecular ions, with up to six repeat units ($n = 3-6$) and up to nine threaded cyclodextrins ($x = 4-9$). No signals are detected for oligomers lacking naphthalene end groups. This mass spectrum confirms that some chains have more than one cyclodextrin per repeat unit, as indicated by NMR spectroscopy. The threading ratio [$y = x/(n + 1)$] ranges from 1 to 1.3, and is highest for the longest oligomers, which reflects weaker binding near the naphthalene sulfonate end groups (as deduced from the low yield of **6**). Polyacrylamide gel electrophoresis (PAGE)^[13] of **8** shows a broad band at 36–50 kDa, relative to denatured protein markers. Gel permeation chromatography (GPC) on a S200 Sephadex column gives a similar molecular weight, with a broad peak at 50 ± 4 kDa.^[14] This is higher than the molecular weight predicted from the NMR spectroscopy and MALDI TOF MS results, which may indicate that the polyrotaxane self-associates in solution.

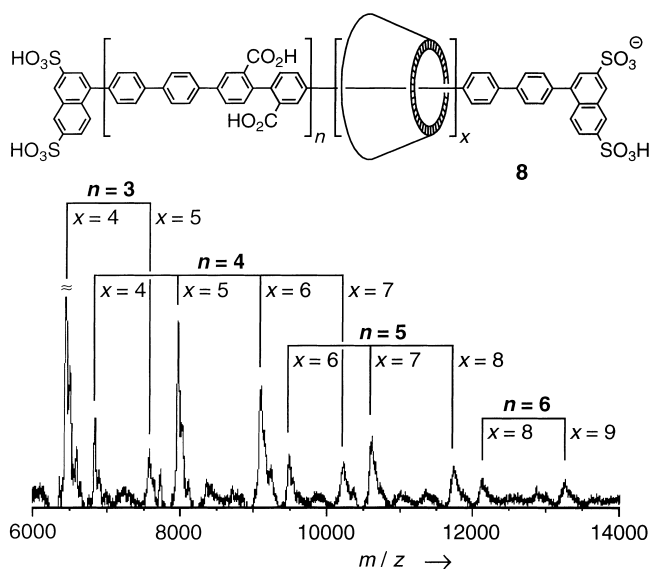


Figure 2. Negative-ion MALDI-TOF mass spectrum of the ammonium salt of polyrotaxane **8**, from a 2,5-dihydroxybenzoic acid matrix.

We have compared the polyrotaxane **8** with several model compounds. The uninsulated capped PPP **9** was prepared under identical conditions to **8**, except omitting the β -cyclodextrin. We also prepared a capped pseudorotaxane **10**, using identical conditions to the synthesis of **8**, except replacing the

end group **5** with 3-iodobenzoic acid. These end groups are too small to prevent unthreading, so the threading ratio in **10** gradually decreases during dialysis until all the cyclodextrin has been removed, leaving capped PPP **11**. This control experiment proves that **8**, which exhibits no unthreading, is a genuine polyrotaxane. The ^1H NMR spectra of the unencapsulated polymers **3**, **9**, and **11** are much broader than those of their encapsulated analogues **4**, **8**, and **10**, because encapsulation hinders aggregation.

The absorption and emission spectra of **4**, **6**, and **8** are compared in Figure 3, and the electronic spectra and fluorescence quantum yields of **3**, **4**, and **6–9** are summarized in Table 1. The peak at around 236 nm in the absorption spectra

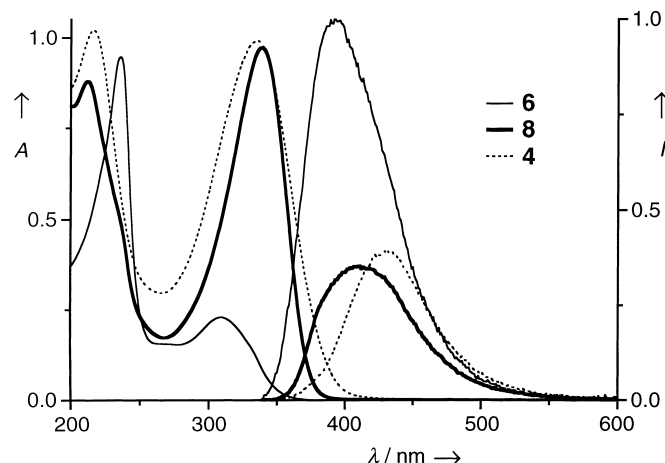


Figure 3. Absorption spectra (left) and emission spectra (right, arbitrary units) of [2]rotaxane **6** (solid), polyrotaxane **8** (bold) and polypseudorotaxane **4** (dashed), in aqueous solution. The concentrations of **6**, **8**, and **4** for the absorption spectra are 12, 26, and 25 mg L⁻¹, respectively.

Table 1. Electronic spectra and fluorescence quantum yields.^[a]

Compound	λ_{max} abs [nm]	λ_{max} em [nm]	Φ_f
PPP 3	215, 335	430	0.18
polypseudorotaxane 4	216, 332	432	0.19
[2]rotaxane 6	236, 310	393	0.95
dumbbell 7	235, 309	415	0.64
polyrotaxane 8	216, 338	410	0.29
capped PPP 9	212, 331	429	0.21

[a] Spectra were recorded in water. Quantum yields were measured relative to anthracene in cyclohexane ($\Phi_f = 0.36$).

of **6** and **7** is due to the naphthalene end group; a small shoulder at this wavelength is also apparent in the absorption spectra of **8** and **9**. Apart from this feature, the spectra of **8** and **9** resemble those of the **3** and **4**. Comparison of the emission spectra and quantum yield of **6** with **7**, and **8** with **9**, shows that encapsulation of the chromophore results in a blue shift of about 20 nm. There is also a significant fluorescence enhancement in **8**. Several other conjugated polypseudorotaxanes have been reported,^[3f–h] but this work represents the first synthesis of conjugated polyrotaxanes. Experiments are in progress towards exploring the behavior of these new materials in electroluminescent light-emitting diodes.

Experimental Section

6: 1-Iodonaphthalene-3,6-disulfonate disodium salt **5** (183 mg, 0.40 mmol), biphenyl-4,4'-diboronic acid diethylene glycol ester **1** (65 mg, 0.22 mmol), β -cyclodextrin (1.0 g, 0.88 mmol), and Pd(OAc)₂ (4.5 mg, 0.02 mmol) were dissolved in O₂-free Na₂CO₃ aq (3 mL, 0.2 M), and stirred at 85 °C for 20 h then cooled and acidified with acetic acid. The [2]rotaxane was purified by ion-exchange chromatography (Bio-Rad AG 4-X4 resin, 1 % NH₃ aq) and recrystallized three times from H₂O/MeOH and EtOH to give pure **6** as a white solid (15 mg, 4 %).

8: 1-Iodonaphthalene-3,6-disulfonate disodium salt **5** (45.8 mg, 0.10 mmol), biphenyl-4,4'-diboronic acid diethylene glycol ester **1** (79.4 mg, 0.27 mmol), 4,4'-diiodobiphenyl-2,2'-dicarboxylic acid **2** (98.8 mg, 0.20 mmol), Pd(OAc)₂ (4.5 mg, 0.02 mmol), and β -cyclodextrin (920 mg, 0.81 mmol) were dissolved in O₂-free Li₂CO₃ aq (6 mL, 0.2 M) and heated to 85 °C for under nitrogen for 20 h. Excess β -cyclodextrin was removed by precipitating the product with HCl aq (to pH 1). The resulting solid was redissolved in Li₂CO₃ aq and dialyzed.^[10] Removal of the solvent gave **8** as a glassy film (159 mg, 45 %).

Received: May 18, 2000 [Z15146]

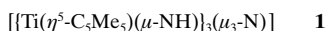
- [1] A. Kraft, A. C. Grimsdale, A. B. Holmes, *Angew. Chem.* **1998**, *110*, 416–443; *Angew. Chem. Int. Ed.* **1998**, *37*, 402–428.
- [2] a) S. Anderson, H. L. Anderson, *Angew. Chem.* **1996**, *108*, 2075–2078; *Angew. Chem. Int. Ed. Engl.* **1996**, *35*, 1956–1959; b) S. Anderson, R. T. Aplin, T. D. W. Claridge, T. Goodson III, A. C. Maciel, G. Rumbles, J. F. Ryan, H. L. Anderson, *J. Chem. Soc. Perkin Trans. 1* **1998**, 2383–2397.
- [3] For recent polyrotaxane and polypseudorotaxane syntheses see: a) F. M. Raymo, J. F. Stoddart, *Chem. Rev.* **1999**, *99*, 1643–1663; b) S. A. Nepogodiev, J. F. Stoddart, *Chem. Rev.* **1998**, *98*, 1959–1976; c) C. Gong, H. W. Gibson, *Molecular Catenanes, Rotaxanes and Knots* (Eds.: J.-P. Sauvage, C. Dietrich-Buchecker), Wiley-VCH, Weinheim, **1999**, pp. 277–321; d) D. Tuncel, J. H. G. Steinke, *Chem. Commun.* **1999**, 1509–1510; e) W. Herrmann, M. Schneider, G. Wenz, *Angew. Chem.* **1997**, *109*, 2618–2621; *Angew. Chem. Int. Ed. Engl.* **1997**, *36*, 2511–2514; f) P. L. Vidal, M. Billon, B. Divisia-Blohorn, G. Bidan, J. M. Kern, J. P. Sauvage, *Chem. Commun.* **1998**, 629–630; g) J. Buey, T. M. Swager, *Angew. Chem.* **2000**, *112*, 622–626; *Angew. Chem. Int. Ed. Engl.* **2000**, *39*, 608–612; h) C. Lagrost, K. I. C. Ching, J.-C. Lacroix, S. Aeiya, M. Jouini, P.-C. Lacaze, J. Tanguy, *J. Mater. Chem.* **1999**, *9*, 2351–2358.
- [4] A. Suzuki, *J. Organomet. Chem.* **1999**, *576*, 147–168; A. D. Schlüter, J. P. Rabe, *Angew. Chem.* **2000**, *112*, 860–880; *Angew. Chem. Int. Ed.* **2000**, *39*, 864–883; M. B. Goldfinger, K. B. Crawford, T. M. Swager, *J. Am. Chem. Soc.* **1997**, *119*, 4578–4593; C. Kowitz, G. Wegner, *Tetrahedron* **1997**, *53*, 15553–15574.
- [5] a) N. A. Bumagin, V. V. Bykov, *Tetrahedron* **1997**, *53*, 14437–14450; b) T. I. Wallow, B. M. Novak, *J. Org. Chem.* **1994**, *59*, 5034–5037; c) A. D. Child, J. R. Reynolds, *Macromolecules* **1994**, *27*, 1975–1977; d) S. Kim, J. Jackiw, E. Robinson, K. S. Schanze, J. R. Reynolds, J. Baur, M. F. Rubner, D. Boils, *Macromolecules* **1998**, *31*, 964–974.
- [6] I. G. C. Coutts, H. R. Goldschmid, O. C. Musgrave, *J. Chem. Soc. C* **1970**, 488–493.
- [7] 4,4'-Diiodobiphenyl-2,2'-dicarboxylic acid **2** was prepared by iodination of 2,2'-biphenyldicarboxylic acid by using HOAc/H₂SO₄/NaIO₃/NaI (R. S. Ajemian, A. J. Boyle, *J. Org. Chem.* **1959**, *24*, 1818–1819); we found this gave better results than the method of V. K. Chaikovskii, A. N. Novikov, N. M. Dubovitskaya, *Khim. Khim. Tekhnol. Geol. Mater. Reg. Nauchno-Prakt. Konf. Molodye. Uch. Spets.* **1980**, 67–69 [*Chem. Abs.* **1982**, *97*, 162475p].
- [8] These mole ratios were calculated on the assumption that the Pd(OAc)₂ is reduced to Pd⁰ by coupling boronic acid units in a reaction of the stoichiometry Pd(OAc)₂ + 2ArB(OH)₂ → Pd⁰ + Ar₂; M. Moreno-Mañas, M. Pérez, R. Pleixats, *J. Org. Chem.* **1996**, *61*, 2346–2351; K. A. Smith, E. M. Campi, W. R. Jackson, S. Marcuccio, C. G. M. Naeslund, G. B. Deacon, *Synlett* **1997**, 131–132.

- [9] F. E. Goodson, T. I. Wallow, B. M. Novak, *Macromolecules* **1998**, *31*, 2047–2056.
- [10] Dialysis was carried out in a stirred cell with a 5000 nominal molecular weight limit polyethersulfone ultrafiltration membrane, using a pressure of 5 atm to force over 1 L of water through the sample. Low-molecular-weight compounds such as free cyclodextrin and **7** are rapidly removed by this procedure.
- [11] We have no information on the relative orientation of the cyclodextrin units in **4**, **8**, and **11**; our schematic representation is not intended to imply that all the macrocycles point the same way.
- [12] Disodium 1-iodonaphthalene-3,6-disulfonate (**5**) was prepared in 86 % yield by treatment of the diazonium salt of disodium 1-aminonaphthalene-3,6-disulfonate with KI.
- [13] Electrophoresis was performed in 12 % urea-PAGE gels, using the Bio-Rad minigel system, with 5 M urea in the separating gel at pH 8.8, at 100 V.
- [14] GPC solvent: aqueous 100 mM Tris/HCl, 100 mM NaCl, pH 8; molecular weight markers: 12.4–67 kDa from Sigma.

[[Ti(η^5 -C₅Me₅)(μ -NH)]₃(μ_3 -N)]: An Efficient Entry to Single and Double Cube-Type Nitrido Complexes**

Angel Abarca, Avelino Martín, Miguel Mena,* and Carlos Yélamos

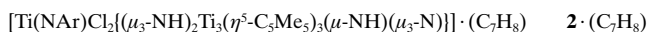
Group 4 tetrametallic derivatives of the formula [(ML_n)₄(μ_3 -E)₄] with cube-type cores remain extremely rare and are limited to halide-bridged [[TiL]₄(μ_3 -Cl)₄] (L = η^8 -C₈H₈,^[1] Me₃^[2]), chalcogenide-bridged [[Ti(η^5 -C₅H₅R)]₄(μ_3 -S)₄],^[3] and imido-bridged [[Ti(η^5 -C₅H₅)]₄(μ_3 -NSnMe₃)₄] complexes.^[4] Our first contributions in this field were the preparation of the singular nitrido and alkylidyne complexes [[Ti(η^5 -C₅Me₅)(μ_3 -E)]₄ (E = N^[5], CH^[6]), which contained an almost perfect Ti₄E₄ cube. A possible synthetic strategy to access this type of compounds would involve the incorporation of different metal complex fragments in a cuboidal core such as [Ti₃(μ -NH)₃(μ_3 -N)]₂,^[7] in a similar way to that reported for [M₃(μ -S)₃(μ_3 -S)] species.^[8–10] In this context, we have recently determined that the preorganized^[11] “organometallic ligand” **1** is able to displace mesitylene or carbonyl ligands in



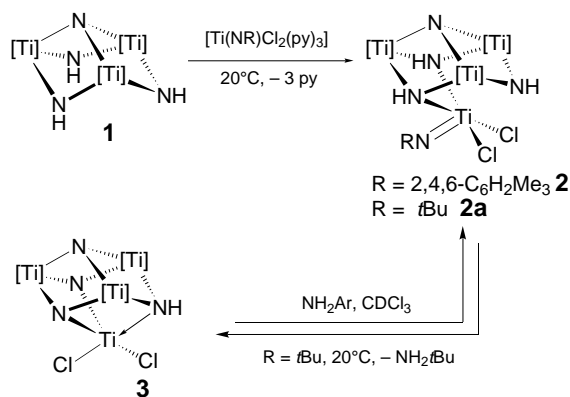
[Mo(CO)₃(1,3,5-Me₃C₆H₃)] or [M(CO)₆], respectively,^[12] and also reacts, by N–H activation, with tris(dimethylamido)cyclopentadienyltitanium(IV) compounds^[13] to give azametallocubane complexes. Herein we describe the reactions of **1** with several d⁰ imido- and amidotitanium and -zirconium com-

plexes that yield new cube-type derivatives and, for the first time, metal corner-shared double cube nitrido complexes. This synthetic method should be generally applicable and thus make the Ti₃N₄ core a very versatile building block for heterometal cluster chemistry and for molecular precursors of new ternary nitrides MTi_xN_y.

Reaction of complex **1** with [Ti(NAr)Cl₂(py)₃] (Ar = 2,4,6-C₆H₂Me₃)^[14] in toluene at room temperature results in displacement of the pyridine (py) ligands and formation of **2**·(C₇H₈) in 51 % yield (Scheme 1). Analogous treatment of **1** with the *tert*-butylimido derivative [Ti(N^tBu)Cl₂(py)₃]^[14] in toluene afforded the complex **3** as a green precipitate in 82 %



yield.^[15] The addition of 2,4,6-trimethylaniline (1 equiv) to a solution of **3** in CDCl₃ at room temperature gave **2** within several days. Complexes **2** and **3** were characterized by spectral and analytical methods, as well as by an X-ray structure determination in the case of **2** (vide infra).

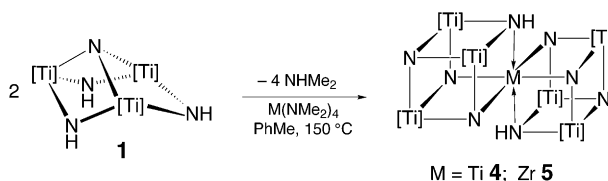


Scheme 1. Synthesis of **2** and **3** from **1**. [Ti] = Ti(η^5 -C₅Me₅).

Treatment of **1** with tetrakis(dimethylamido)titanium(IV) or -zirconium(IV) in toluene at 150 °C afforded the corner-shared double cube complexes **4**·2 C₇H₈ and **5**·1.5 C₇H₈, respectively,



as dark green crystals in 69 and 60 % yield, respectively (Scheme 2). Complex **5**·1.5 C₇H₈ was also prepared in 53 % yield through the reaction of **1** with the imido derivative [Zr(NAr')(NHAr')₂(py)₂] (Ar' = 2,6-C₆H₃iPr₂)^[16] in toluene at 90 °C. Once isolated complexes **4** and **5** are not soluble in



Scheme 2. Synthesis of **4** and **5** from **1**. [Ti] = Ti(η^5 -C₅Me₅).

[*] Dr. M. Mena, A. Abarca, Dr. A. Martín, Dr. C. Yélamos
Departamento de Química Inorgánica
Universidad de Alcalá
Campus Universitario, 28871 Alcalá de Henares-Madrid (Spain)
Fax: (+34) 1-8854683
E-mail: miguel.mena@uah.es

[**] This work was supported by the Spanish DGES (PB96-0672), and the Universidad de Alcalá (E027/99). C.Y. also thanks the CAM for a postdoctoral grant.

common solvents, precluding their characterization by NMR spectroscopy. Their IR spectra showed ν_{NH} vibrations at 3353 and 3345 cm^{-1} , respectively.

The X-ray crystal structures of **2**, **4**, and **5** were determined in order to establish the geometry around the metal centers and the bonding modes of the imido and nitrido ligands.^[17] Crystals of **2** bear one toluene molecule per titanium compound. The molecular structure of **2** consists of a distorted cube core (Figure 1).^[18] The incorporated titanium atom Ti4

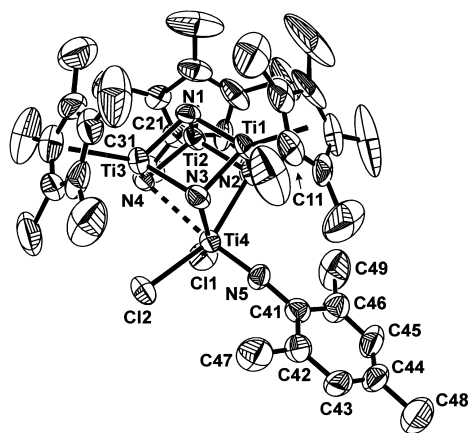


Figure 1. Structure of complex **2** (thermal ellipsoids at the 50% probability level). The C_7H_8 solvent molecule has been omitted for clarity. Selected lengths [Å] and angles [°]: Ti4–N2 2.263(8), Ti4–N3 2.304(9), Ti4...N4 2.602(7), Ti4–N5 1.695(8), Ti4–Cl1 2.365(3), Ti4–Cl2 2.373(3), Ti4...Ti(av) 3.143(3); Ti4–N5–C41 171.6(7), Cl1–Ti4–Cl2 98.3(1), N2–Ti4–N3 76.5(3), N2–Ti4–Cl1 92.4(2), N2–Ti4–Cl2 155.9(2), N2–Ti4–N4 75.3(3), N2–Ti4–N5 98.2(3), N3–Ti4–N4 75.2(3), N3–Ti4–N5 103.6(3), N3–Ti4–Cl1 155.8(2), N3–Ti4–Cl2 85.2(2), N4–Ti4–N5 173.6(3).

exhibits an apparent octahedral geometry with a “missing vertex”; the Ti4...N4 distance is 2.602(7) Å. Ti4 is bound to two chlorine, one linear arylimido ligand, and two imido groups of the incomplete cube core [$\text{Ti}_3(\mu\text{-NH})_3(\mu_3\text{-N})$]. The angle subtended at the arylimido nitrogen atom (Ti4–N5–C41 171.6(7)°) and the Ti4–N5 bond length (1.695(8) Å) are in the normal range for other imidotitanium complexes,^[19, 20] in which the ArN^{2-} ligand acts as a six-electron donor. The extremely strong *trans* influence of the arylimido group rationalizes the noncoordination of the third imido group of the cuboidal system (N5–Ti4–N4 173.6(3)°). The bond lengths between Ti4 and the nitrogen atoms of the NH groups are similar (Ti4–N2 2.263(8) and Ti4–N3 2.304(9)) and analogous to values for Ti–N distances in other titanium(IV) complexes with amino ligands.^[13, 21–23] Analogous Ti–N bond lengths and a similar *trans* influence of the imido ligands have been reported for a family of macrocyclic d^0 imidotitanium complexes [$\text{Ti}(\text{NtBu})\text{Cl}_2(\text{L})$] ($\text{L} = [9]\text{aneN}_3$, $\text{Me}_3[9]\text{aneN}_3$, and $\text{Me}_2[9]\text{aneN}_2\text{S}$).^[24]

Complex **4** crystallizes with two toluene molecules. The structure shows two cubes with a common titanium vertex (Figure 2). This titanium center exhibits a six-coordinate geometry, in which the nitrogen atoms lie at the vertices of a trigonal antiprism. The two “[$(\mu_3\text{-N})_3(\mu_3\text{-NH})\text{Ti}_3(\eta^5\text{-C}_5\text{Me}_5)_3$]” ligands adopt a mutually staggered conformation which may correspond to the minimization of the steric repulsion of the bulky pentamethylcyclopentadienyl ligands. The N–Ti–N an-

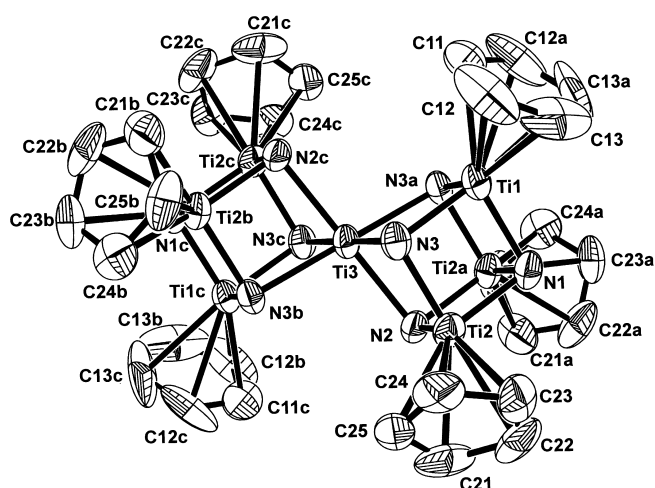


Figure 2. Structure of complex **4** (thermal ellipsoids at the 50% probability level). The methyl groups of the pentamethylcyclopentadienyl ligands as well as the C_7H_8 solvent molecules have been omitted for clarity. Selected lengths [Å] and angles [°]: Ti3–N2 2.125(9), Ti3–N3 2.122(6), Ti1–N1 1.931(7), Ti3–Ti 2.948(2), Ti1...Ti1 2.800(2); N1–Ti3–N1 81.1(3), N1–Ti3–N2 99.0(3). Subscript 1 means an atom of the same Ti_3N_4 unit, and subscript 2 means an atom of a second Ti_3N_4 unit, average values.

gles between the central atom and each tridentate ligand are 81.1(3)°, while the N–Ti–N *cis* angles between the two ligands span 99.0(3)°. The Ti3–N bond lengths are the same within the experimental error (2.122(6) and 2.125(9) Å), and range between those in amido-^[25–27] and aminotitanium(IV) complexes.^[13, 21–23] The tridentate ligands display similar Ti–N (av 1.931(7) Å) and Ti–Ti (2.800(2) Å) lengths to those determined for **1**.^[7]

Complex **5** (Figure 3) shows a similar geometry to that of **4** with a more elongated trigonal antiprism environment for the central zirconium atom due to the different atomic radii. Thus, the Zr–N bonds in complex **5** are longer than the Ti3–N bond in **4** (≈ 0.1 Å), the angles between zirconium and the nitrogen

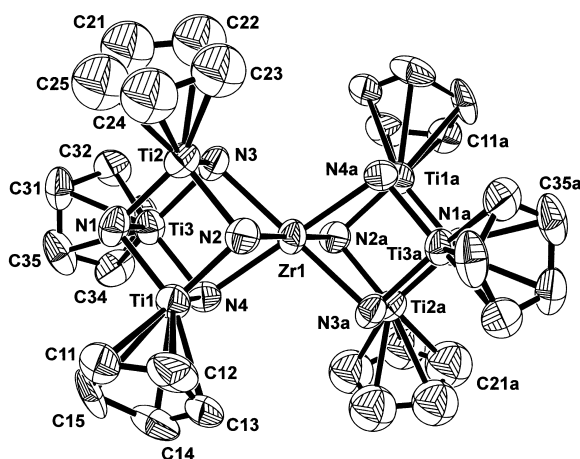


Figure 3. Structure of complex **5** (thermal ellipsoids at the 50% probability level). The methyl groups of the pentamethylcyclopentadienyl ligands as well as the C_7H_8 solvent molecules have been omitted for clarity. Selected lengths [Å] and angles [°]: Zr1–N2 2.233(11), Zr1–N3 2.234(11), Zr1–N4 2.237(11), Ti1–N1 1.94(1), Ti1...Ti1 2.802(4), Zr1...Ti1 3.072(3); N1–Zr1–N1 77.8(4), N1–Zr1–N2 102.2(4). Subscript 1 means an atom of the same Ti_3N_4 unit, and subscript 2 means an atom of a second Ti_3N_4 unit, average values.

atoms of the same tridentate ligand ($\approx 3.3^\circ$ less in **5**) are narrower, and the angles between the *cis* nitrogen atoms of the two ligands and zirconium ($\approx 3.2^\circ$ more in **5**) are wider.

In summary, we have examined the reactions of the incomplete cube compound **1** with a variety of titanium and zirconium d^0 complexes. The results indicate that the $[\text{Ti}_3\text{N}_4]$ core of **1** is capable of displacing labile ligands bound to inorganic derivatives by coordination of the NH groups as in the formation of complex **2**. However, the stability of the resulting adducts depends on the other ligands linked to the incorporated metal. If the N–H bonds of the organometallic ligand **1** are activated by metal–imido or metal–amido linkages, the elimination of organic molecules and formation of nitrido groups bridging the metal centers takes place.

Experimental Section

2· C_7H_8 : A 100-mL Schlenk flask was charged with **1** (0.50 g, 0.82 mmol), $[\text{Ti}(\text{NC}_6\text{H}_4\text{Me}_3)_2(\text{py})_3]$ (0.40 g, 0.82 mmol), and toluene (50 mL). The reaction mixture was stirred at room temperature for 24 h, then the resultant brown solution was concentrated to about 25 mL under reduced pressure. The solution was filtered and cooled to -10°C for 20 h to afford brown crystals of **2**· C_7H_8 (0.40 g, 51 %). IR (KBr): $\tilde{\nu} = 3343$ (s) cm^{-1} $\nu(\text{NH})$; ^1H NMR (300 MHz, C_6D_6 , 20°C): $\delta = 11.90$ (s br., 3H; NH), 6.66 (s, 2H; $\text{C}_6\text{H}_2\text{Me}_2\text{Me}$), 2.86 (s, 6H; $\text{C}_6\text{H}_2\text{Me}_2\text{Me}$), 2.16 (s, 3H; $\text{C}_6\text{H}_2\text{Me}_2\text{Me}$), 1.93 (s, 45H; C_5Me_5); $^{13}\text{C}\{^1\text{H}\}$ NMR (75 MHz, CDCl_3 , 20°C): $\delta = 156.6$, 133.2, 129.1, 127.3 ($\text{C}_6\text{H}_2\text{Me}_2\text{Me}$), 123.5 (C_5Me_5), 20.9 ($\text{C}_6\text{H}_2\text{Me}_2\text{Me}$), 19.4 ($\text{C}_6\text{H}_2\text{Me}_2\text{Me}$), 12.4 (C_5Me_5); elemental analysis calcd for $\text{C}_{46}\text{H}_{67}\text{N}_3\text{Cl}_2\text{Ti}_4$ (%): C 58.01, H 7.09, N 7.35; found: C 58.16, H 7.21, N 7.06.

3: A 100-mL Schlenk flask was charged with **1** (1.00 g, 1.64 mmol), $[\text{Ti}(\text{NBu})\text{Cl}_2(\text{py})_3]$ (0.70 g, 1.64 mmol), and toluene (50 mL). After the mixture had been stirred at room temperature for 48 h, the brown solution was separated from a fine green powder. The powder was washed with hexane (40 mL) and vacuum-dried for 3 h to afford **3** (0.98 g, 82 %). IR (KBr): $\tilde{\nu} = 3240$ (s) cm^{-1} $\nu(\text{NH})$; ^1H NMR (300 MHz, CDCl_3 , 20°C): $\delta = 13.46$ (s br., 1H; NH), 2.15 (s, 15H; C_5Me_5), 2.07 (s, 30H; C_5Me_5); $^{13}\text{C}\{^1\text{H}\}$ NMR (75 MHz, CDCl_3 , 20°C): $\delta = 123.3$ (C_5Me_5), 12.3 (C_5Me_5), 12.0 (C_5Me_5) (one C_5Me_5 resonance signal was not found due to the low solubility or to the coincidence with that at $\delta = 123.3$); elemental analysis calcd for $\text{C}_{30}\text{H}_{46}\text{N}_4\text{Cl}_2\text{Ti}_4$ (%): C 49.69, H 6.39, N 7.73; found: C 49.70, H 6.53, N 7.30.

4· $2\text{C}_7\text{H}_8$: A 200-mL Carius tube was charged with **1** (0.50 g, 0.82 mmol), $[\text{Ti}(\text{NMe}_2)_4]$ (0.09 g, 0.41 mmol), and toluene (60 mL). The tube was flame-sealed and heated at 150°C for 30 h. The reaction mixture was allowed to cool to room temperature overnight to afford green crystals of **4**· $2\text{C}_7\text{H}_8$ (0.41 g, 69 %). IR (KBr): $\tilde{\nu} = 3353$ (m), 2972 (m), 2906 (s), 2855 (s), 2719 (w), 1604 (w), 1494 (m), 1436 (s), 1373 (s), 1156 (w), 1079 (w), 1023 (m), 803 (s), 730 (s), 703 (vs), 687 (vs), 668 (vs), 612 (vs), 522 (w), 475 (m), 445 (s), 435 (s) cm^{-1} ; elemental analysis calcd for $\text{C}_{74}\text{H}_{108}\text{N}_8\text{Ti}_7$ (%): C 61.51, H 7.53, N 7.76; found: C 61.71, H 7.53, N 7.96.

5· $1.5\text{C}_7\text{H}_8$: Method A: In a similar way to the preparation of **4**, **1** (0.40 g, 0.66 mmol) and $[\text{Zr}(\text{NMe}_2)_4]$ (0.09 g, 0.34 mmol) were heated at 150°C to afford green crystals of **5**· $1.5\text{C}_7\text{H}_8$ (0.28 g, 60 %). Elemental analysis calcd for $\text{C}_{70.5}\text{H}_{104}\text{N}_8\text{Ti}_6\text{Zr}$ (%): C 58.72, H 7.27, N 7.77; found: C 58.98, H 7.39, N 7.47. Method B: A 100-mL ampoule (Teflon stopcock) was charged with **1** (0.30 g, 0.49 mmol), $[\text{Zr}(\text{NAr})(\text{NHAr})_2(\text{py})_2]$ ($\text{Ar} = 2,6\text{-C}_6\text{H}_3\text{Pr}_2$) (0.19 g, 0.24 mmol), and toluene (25 mL). After heating at 90°C for 2 d, the green solution was allowed to cool to room temperature overnight to afford green crystals of **5**· $1.5\text{C}_7\text{H}_8$ (0.19 g, 53 %). IR (KBr): $\tilde{\nu} = 3345$ (m), 2908 (s), 2855 (s), 1604 (w), 1495 (m), 1436 (s), 1374 (s), 1024 (m), 804 (vs), 729 (s), 694 (vs), 662 (vs), 647 (s), 611 (vs), 531 (w), 486 (s), 470 (m), 447 (s), 431 (s) cm^{-1} ; elemental analysis calcd for $\text{C}_{70.5}\text{H}_{104}\text{N}_8\text{Ti}_6\text{Zr}$ (%): C 58.72, H 7.27, N 7.77; found: C 58.35, H 7.26, N 7.72.

Received: May 19, 2000 [Z15148]

- [1] H. R. Van der Wal, F. Overzet, H. O. Van Oven, J. L. De Boer, H. J. De Liefde Meijer, F. Jellinek, *J. Organomet. Chem.* **1975**, 92, 329–340.
- [2] S. Kleinhenz, K. Seppelt, *Chem. Eur. J.* **1999**, 5, 3573–3580.
- [3] J. Darkwa, J. R. Lockmeyer, P. D. W. Boyd, T. B. Rauchfuss, A. L. Rheingold, *J. Am. Chem. Soc.* **1988**, 110, 141–149.
- [4] A. Decker, D. Fenske, K. Maczek, *Angew. Chem.* **1996**, 108, 3025–3028; *Angew. Chem. Int. Ed. Engl.* **1996**, 35, 2863–2866.
- [5] P. Gómez-Sal, A. Martín, M. Mena, C. Yélamos, *J. Chem. Soc. Chem. Commun.* **1995**, 2185–2186.
- [6] R. Andrés, P. Gómez-Sal, E. de Jesús, A. Martín, M. Mena, C. Yélamos, *Angew. Chem.* **1997**, 109, 72–74; *Angew. Chem. Int. Ed. Engl.* **1997**, 36, 115–117.
- [7] H. W. Roesky, Y. Bai, M. Noltemeyer, *Angew. Chem.* **1989**, 101, 788–789; *Angew. Chem. Int. Ed. Engl.* **1989**, 28, 754–755.
- [8] R. H. Holm, *Adv. Inorg. Chem.* **1992**, 38, 1–71.
- [9] J. Zhou, J. W. Raebiger, C. A. Crawford, R. H. Holm, *J. Am. Chem. Soc.* **1997**, 119, 6242–6250.
- [10] R. Hernández-Molina, A. G. Sykes, *J. Chem. Soc. Dalton Trans.* **1999**, 3137–3148, and references therein.
- [11] K. J. Haack, R. Goddard, K. R. Pörschke, *J. Am. Chem. Soc.* **1997**, 119, 7992–7999.
- [12] A. Abarca, M. Galakhov, P. Gómez-Sal, A. Martín, M. Mena, J. M. Poblet, C. Santamaría, *Angew. Chem.* **2000**, 112, 544–547; *Angew. Chem. Int. Ed.* **2000**, 39, 534–537.
- [13] A. Abarca, P. Gómez-Sal, A. Martín, M. Mena, J. M. Poblet, C. Yélamos, *Inorg. Chem.* **2000**, 39, 642–651.
- [14] A. J. Blake, P. E. Collier, S. C. Dunn, W.-S. Li, P. Mountford, O. V. Shishkin, *J. Chem. Soc. Dalton Trans.* **1997**, 1549–1558.
- [15] A complex analogous to **2** was characterized following this reaction by NMR spectroscopy in $[\text{D}_2]$ dichloromethane. The ^1H and $^{13}\text{C}\{^1\text{H}\}$ NMR spectra after 10 min showed complete reaction and formation of $[\text{Ti}(\text{NBu})\text{Cl}_2\{(\mu_3\text{-NH})_2\text{Ti}_3(\eta^5\text{-C}_5\text{Me}_5)_3(\mu\text{-NH})(\mu_3\text{-N})\}]$ (**2a**). This complex decomposed within hours to give **3** and *tert*-butylamine elimination. NMR data for **2a**: ^1H NMR (300 MHz, CD_2Cl_2 , 20°C): $\delta = 11.95$ (s br., 3H; NH), 2.14 (s, 45H; C_5Me_5), 1.02 (s, 9H; CMe_3); $^{13}\text{C}\{^1\text{H}\}$ NMR (75 MHz, CD_2Cl_2 , 20°C): $\delta = 123.4$ (C_5Me_5), 69.2 (CMe_3), 31.3 (CMe_3), 12.7 (C_5Me_5).
- [16] D. J. Arney, M. A. Bruck, S. R. Huber, D. E. Wigley, *Inorg. Chem.* **1992**, 31, 3749–3755.
- [17] X-ray crystal structure determinations of complexes **2**, **4**, and **5**: Brown crystals of compound **2** and green crystals of **4** and **5** were obtained from toluene solutions. All data were collected on an Enraf Nonius CAD4 diffractometer at room temperature, $\text{MoK}\alpha = 0.71073 \text{ \AA}$. All the structures were solved by using the WINGX^[28] package by direct methods (SHELXS-97), and refined by least-squares against F^2 (SHELXL-97).^[29] X-ray crystal structure data for $\text{C}_{46}\text{H}_{67}\text{Cl}_2\text{N}_3\text{Ti}_4$ (**2**· C_7H_8): $0.40 \times 0.35 \times 0.32 \text{ mm}^3$, triclinic, $P\bar{1}$, $a = 11.065(2)$, $b = 14.598(2)$, $c = 16.530(3) \text{ \AA}$, $\alpha = 71.45(1)$, $\beta = 78.33(1)$, $\gamma = 80.59(1)^\circ$, $V = 2464.8(6) \text{ \AA}^3$, $\rho_{\text{calcd}} = 1.283 \text{ Mg m}^{-3}$. Intensity measurements were performed by ω - 2θ scans in the range $4^\circ < 2\theta < 44^\circ$ for **2**; of the 6247 measured reflections, 5957 were independent; $R1 = 0.073$ and $wR2 = 0.194$ (for 3168 reflections with $F > 4\sigma(F)$). The values of $R1$ and $wR2$ are defined as $R1 = \Sigma ||F_o| - |F_c|| / \Sigma |F_o|$ and $wR2 = \{[\Sigma w(F_o^2 - F_c^2)^2] / [\Sigma w(F_o^2)^2]\}^{1/2}$. Largest difference peak and hole 1.037 and $-0.486 \text{ e \AA}^{-3}$, respectively. All non-hydrogen atoms, except those of the solvent, were anisotropically refined. X-ray crystal structure data for $\text{C}_{74}\text{H}_{108}\text{N}_8\text{Ti}_7$ (**4**· $2\text{C}_7\text{H}_8$): $0.35 \times 0.33 \times 0.30 \text{ mm}^3$, orthorhombic, $Pnmm$, $a = 14.389(1)$, $b = 15.405(1)$, $c = 16.550(1) \text{ \AA}$, $V = 3668.5(4) \text{ \AA}^3$, $\rho_{\text{calcd}} = 1.308 \text{ Mg m}^{-3}$. Intensity measurements were performed by ω - 2θ scans in the range $4^\circ < 2\theta < 44^\circ$ for **4**; of the 4565 measured reflections, 2340 were independent; $R1 = 0.090$ and $wR2 = 0.270$ (for 1478 reflections with $F > 4\sigma(F)$). Largest difference peak and hole 1.138 and $-0.648 \text{ e \AA}^{-3}$, respectively. All non-hydrogen atoms, except those of the solvent and C14, C15, and C16 (carbon atoms of methyl groups of one pentamethylcyclopentadienyl ring), were anisotropically refined. X-ray crystal structure data for $\text{C}_{70.5}\text{H}_{104}\text{N}_8\text{Ti}_6\text{Zr}$ (**5**· $1.5\text{C}_7\text{H}_8$): $0.43 \times 0.38 \times 0.32 \text{ mm}^3$, monoclinic, $P2_1/n$, $a = 14.480(1)$, $b = 15.408(1)$, $c = 16.579(1) \text{ \AA}$, $\beta = 90.12(1)^\circ$, $V = 3698.9(4) \text{ \AA}^3$, $\rho_{\text{calcd}} = 1.295 \text{ Mg m}^{-3}$. Intensity measurements were performed by ω scans in the range $5^\circ < 2\theta < 43^\circ$; of the 4532 measured reflections, 4327 were independent; $R1 = 0.107$ and $wR2 = 0.283$ (for 2253 reflections with $F > 4\sigma(F)$). All non-hydrogen atoms, except

those of the solvent and the carbon atoms of the C21–C30 pentamethylcyclopentadienyl ring, were anisotropically refined. Crystallographic data (excluding structure factors) for the structures reported in this paper have been deposited with the Cambridge Crystallographic Data Centre as supplementary publication nos. CCDC-144326, CCDC-144327, and CCDC-144328. Copies of the data can be obtained free of charge on application to CCDC, 12 Union Road, Cambridge CB21EZ, UK (fax: (+44) 1223-336-033; e-mail: deposit@ccdc.cam.ac.uk).

- [18] The ^1H NMR spectrum of **2** in $[\text{D}_8]\text{toluene}$ at -70°C showed two types of $\eta^5\text{-C}_5\text{Me}_5$ and NH ligands (2:1 ratio), consistent with the solid-state structure.
- [19] For a review of early transition metal imido complexes, see: D. E. Wigley, *Progr. Inorg. Chem.* **1994**, 42, 239–482.
- [20] P. Mountford, *Chem. Commun.* **1997**, 2127–2134.
- [21] T. S. Lewkebandara, P. H. Sheridan, M. J. Heeg, A. L. Rheingold, C. H. Winter, *Inorg. Chem.* **1994**, 33, 5879–5889.
- [22] R. Duchateau, A. J. Williams, S. Gambarotta, M. Y. Chiang, *Inorg. Chem.* **1991**, 30, 4863–4866.
- [23] H. Fuhrmann, S. Brenner, P. Arndt, R. Kempe, *Inorg. Chem.* **1996**, 35, 6742–6745.
- [24] P. J. Wilson, A. J. Blake, P. Mountford, M. Schröder, *Chem. Commun.* **1998**, 1007–1008.
- [25] D. W. Carpenetti, L. Kloppenburg, J. T. Kupec, J. L. Petersen, *Organometallics* **1996**, 15, 1572–1581.
- [26] A. Martín, M. Mena, C. Yélamos, R. Serrano, P. R. Raithby, *J. Organomet. Chem.* **1994**, 467, 79–84.
- [27] M. V. Galakhov, A. Martín, M. Mena, F. Palacios, C. Yélamos, P. R. Raithby, *Organometallics* **1995**, 14, 131–136.
- [28] WinGX L. J. Farrugia, *J. Appl. Crystallogr.* **1999**, 32, 837–838.
- [29] SHELX97: G. M. Sheldrick, **1997**. Program for crystal structure analysis (Release 97–2), Universität Göttingen, Germany.

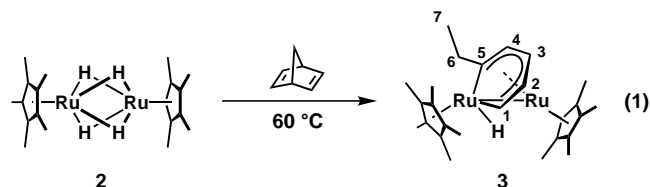
Novel Mode of C–C Bond Cleavage of Norbornadiene on a Dinuclear Ruthenium Complex**

Yasuhiro Ohki and Hiroharu Suzuki*

The activation of C–C bonds by transition metal complexes has attracted considerable attention in the field of organometallic chemistry due to its applicability to industrial processes such as petroleum refining and cracking. Most of the reported examples of C–C bond activation by transition metal complexes involve highly strained systems, pre-aromatic organic substrates such as alkylated cyclopentadienes,^[1] or intramolecular ligand activation in which the C–C bond is favorably oriented towards the metal center.^[2] In the last ten

years, we have intensively studied substrate activation on a multimetallic site and reported a novel selective C–C bond cleavage of cyclopentadiene on a trinuclear ruthenium pentahydride complex $[(\eta^5\text{-C}_5\text{Me}_5)\text{Ru}]_3(\mu\text{-H})_3(\mu_3\text{-H})_2$ (**1**).^[3] As well as this triruthenium cluster, the dinuclear ruthenium tetrahydride $[(\eta^5\text{-C}_5\text{Me}_5)\text{Ru}]_2(\mu\text{-H})_4$ (**2**) has been shown to provide an active species for multimetallic activation and to undergo cleavage of various types of bonds such as $\text{C}(\text{sp}^2)\text{-H}$, Si-H , and $\text{P-C}(\text{aryl})$ bonds under mild conditions.^[4] We have now focussed our attention on the activation of C–C bonds by a dinuclear complex and have examined the reaction of **2** with a variety of 1,3- and 1,4-cyclic dienes because these dienes have geometries suitable for coordination to a dimetallic site. We report herein an unprecedented type of selective carbon–carbon bond cleavage of norbornadiene by the dinuclear ruthenium tetrahydride complex **2**.

Treatment of **2** with three equivalents of norbornadiene in toluene at 60°C resulted in the formation of the dinuclear 2-ethylruthenacyclohexadienyl complex $[(\eta^5\text{-C}_5\text{Me}_5)\text{Ru}]_2(\mu\text{-}\eta^5\text{:}\eta^1\text{:}\eta^1\text{-C}_5\text{H}_4\text{C}_2\text{H}_5)(\text{H})$ (**3**) as the result of a C–C bond cleavage [Eq. (1)] (yield ca. 65 % from ^1H NMR data). The

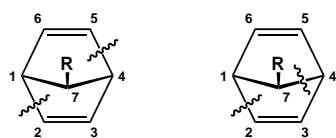


new complex **3** was isolated as a red crystalline solid in 44 % yield by column chromatography on neutral alumina, and identified on the basis of the ^1H and ^{13}C NMR, and $^{13}\text{C}\text{-}^1\text{H}$ HETCOR spectra. The ^{13}C NMR spectrum exhibited two characteristic signals for bridging alkenyl carbons, C1 and C5, at $\delta = 168.1$ ($J_{\text{CH}} = 141.9$ Hz) and $\delta = 186.2$, respectively. The gated ^{13}C NMR spectrum showed three doublets at $\delta = 91.1$ ($J_{\text{CH}} = 156.3$ Hz, C2), $\delta = 85.8$ ($J_{\text{CH}} = 159.5$ Hz, C3), and $\delta = 90.2$ ($J_{\text{CH}} = 151.0$ Hz, C4) for the carbon atoms of the ruthenacycle, and the chemical shifts were comparable to those observed in the related η^5 -cyclohexadienylruthenium complexes.^[5] A resonance signal due to the hydrogen atom attached to the α -carbon (C1) appeared at $\delta = 9.33$ in the ^1H NMR spectrum. The two hydrogen atoms on C6 are diastereotopic and their resonance signals appeared at $\delta = 2.38$ and $\delta = 3.18$.

There are two possible modes of C–C bond cleavage that account for the formation of the ruthenacycle **3**. One involves C–C bond cleavage at C1–C2 and C4–C5 of norbornadiene. The other pathway involves the C1–C2 and C4–C7 bond cleavage (Scheme 1). The latter mode of C–C bond cleavage is observed in the protonation of $[(\eta^5\text{-C}_5\text{R}_5)\text{Co}(\eta^4\text{-norbornadiene})]$.^[6] To elucidate the reaction pathway to **3**, complex **2** was allowed to react with 7-methylnorbornadiene^[7] under similar conditions to those with norbornadiene. This reaction generated the analogous ruthenacycle $[(\eta^5\text{-C}_5\text{Me}_5)\text{Ru}]_2(\mu\text{-}\eta^5\text{:}\eta^1\text{:}\eta^1\text{-C}_5\text{H}_3\text{CH}_3\text{C}_2\text{H}_5)(\text{H})$ (**4**) in which a methyl group was bound to C4 [Eq. (2)]. Complex **4** was isolated as a red

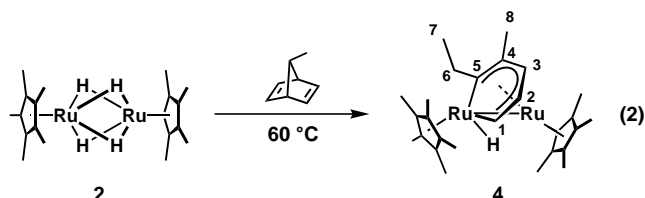
[*] Prof. H. Suzuki, Y. Ohki
Department of Applied Chemistry
Graduate School of Science and Engineering
Tokyo Institute of Technology and CREST, Japan Science and Technology Corporation (JST)
O-okayama, Meguro-ku, Tokyo 152-8552 (Japan)
Fax: (+81) 3-5734-3913
E-mail: hiroharu@n.cc.titech.ac.jp

[**] We are grateful to the Kanto Chemical Co., Inc., for a generous gift of pentamethylcyclopentadiene.



C–C cleavage at C1–C2 and C4–C5
C–C cleavage at C1–C2 and C4–C7

Scheme 1. The two possible modes of C–C bond cleavage in norbornadiene that can account for the formation of **3**.



crystalline solid in 24% yield, and assigned as a dinuclear ruthenacycle analogous to **3** on the basis of the similarity of the ^1H and ^{13}C NMR chemical shifts and the coupling pattern. The observation of methyl resonance signals at $\delta_{\text{H}} = 1.80$ and $\delta_{\text{C}} = 18.7$ and the disappearance of the proton signal at $\delta = 4.69$ (dd) for H4 proved that the methyl group was substituted at C4.

The structure of **4** was confirmed by X-ray crystallography (Figure 1) by using single crystals obtained from cold pentane.^[8] The structure clearly depicts the formation of a six-

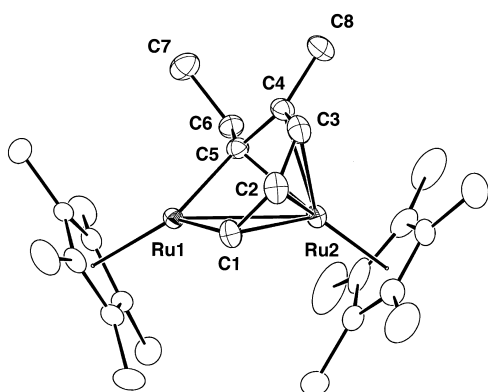


Figure 1. Molecular structure of **4** (with thermal ellipsoids at 30% probability level). Selected bond lengths [Å] and angles [°]: Ru1–Ru2 2.8496(6), Ru1–C1 1.946(6), Ru1–C5 1.999(5), Ru2–C1 2.219(5), Ru2–C2 2.179(6), Ru2–C3 2.176(6), Ru2–C4 2.222(6), Ru2–C5 2.227(5), C1–C2 1.399(8), C2–C3 1.402(9), C3–C4 1.429(8), C4–C5 1.432(7), C1–Ru1–C5 90.0(2), Ru1–C1–Ru2 86.1(2), Ru1–C1–C2 127.1(5), C1–C2–C3 123.5(5), C2–C3–C4 126.3(5), C3–C4–C5 120.9(5), C4–C5–Ru1 125.9(4), Ru1–C5–Ru2 84.6(2).

membered ruthenacycle. The Ru1–C1 and Ru1–C5 distances of 1.946(6) and 1.999(5) Å, respectively, correspond to those of a Ru–C σ bond. The Ru–C distances between Ru2 and the ruthenacycle (2.176(6)–2.227(5) Å) are within the range of those for a Ru–C π bond and are comparable to those observed in η^5 -cyclohexadienylruthenium complexes.^[5] The Ru–Ru distance of 2.8496(6) Å is indicative of a metal–metal single bond as anticipated from the 18-electron formalism applied to **4**.

The methyl group on C4 of the ruthenacycle **4** is derived from that attached to C7 of norbornadiene, and this evidently shows that the C1–C2 and C4–C5 bonds of norbornadiene were cleaved in the reaction with the dinuclear ruthenium tetrahydride complex **2**. The C–C bond cleavage probably took place to relieve the ring strain.

The reaction proceeds most likely by way of an intermediary μ -endo, η^2 : η^2 -norbornadiene complex, since the reactions of **2** with acyclic and cyclic 1,3-dienes afford the corresponding μ - η^2 : η^2 -diene complexes.^[9] Furthermore, a dinuclear ruthenium complex having a μ -endo, η^2 : η^2 -norbornadiene ligand was isolated by introducing a μ -PR₂ ligand into the diruthenium core.^[10]

Thus, we have discovered an unprecedented mode of C–C bond cleavage of norbornadiene on a dimetallic site due to the cooperative action of the two adjacent ruthenium centers. To our knowledge, this is the first selective and consecutive activation of two C–C bonds of norbornadiene.

Experimental Section

3: Norbornadiene (157 μL , 1.45 mmol) was added to a solution of $[(\eta^5\text{-C}_5\text{Me}_5)\text{Ru}]_2(\mu\text{-H})_4$ (230.6 mg, 0.484 mmol) in toluene. The reaction mixture was warmed at 60 °C and allowed to stir for 36 h. After removal of the volatile compounds under reduced pressure, the product was purified by column chromatography on neutral alumina with pentane–tetrahydrofuran (200:1) as the eluent. The product was obtained as a bright pink eluate. Removal of the solvent under reduced pressure afforded **3** (120.7 mg) as a red solid (44% yield). ^1H NMR (400 MHz, $[\text{D}_6]\text{benzene}$, RT, TMS): $\delta = 9.33$ (ddd, $J = 6.8, 2.0, 1.2$ Hz, 1 H; H1), 5.03 (ddd, $J = 6.8, 5.6, 1.2$ Hz, 1 H; H2), 4.69 (dd, $J = 6.0, 1.2$ Hz, 1 H; H4), 4.18 (ddd, $J = 6.0, 5.6, 1.2$ Hz, 1 H; H3), 3.18 (dq, $J = 12.0, 7.2$ Hz, 1 H; H6-a), 2.38 (dq, $J = 12.0, 7.6$ Hz, 1 H; H6-b), 1.98 (s, 15 H; C₅Me₅), 1.56 (s, 15 H; C₅Me₅), 1.51 (dd, $J = 7.6, 7.2$ Hz, 3 H; H7), -20.76 (d, $J = 2.0$ Hz, 1 H; Ru–H); ^{13}C NMR (100 MHz, $[\text{D}_6]\text{benzene}$, RT, TMS): $\delta = 186.2$ (s; C5), 168.1 (d, $J(\text{C},\text{H}) = 141.9$ Hz; C1), 97.4 (s; C₅Me₅), 91.1 (d, $J(\text{C},\text{H}) = 156.3$ Hz; C2), 90.2 (d, $J(\text{C},\text{H}) = 151.0$ Hz; C4), 89.0 (s; C₅Me₅), 85.8 (d, $J(\text{C},\text{H}) = 159.5$ Hz; C3), 43.6 (t, $J(\text{C},\text{H}) = 125.1$ Hz; C6), 18.1 (q, $J(\text{C},\text{H}) = 125.5$ Hz; C7), 11.9 (q, $J(\text{C},\text{H}) = 125.9$ Hz; C₅Me₅), 11.0 (q, $J(\text{C},\text{H}) = 126.4$ Hz; C₅Me₅).

Received: May 24, 2000 [Z15166]

- [1] a) R. Noyori, Y. Kumagai, I. Umeda, H. Takaya, *J. Am. Chem. Soc.* **1972**, *94*, 4018; b) D. Rondon, B. Chaudret, X.-D. He, D. Labroue, *J. Am. Chem. Soc.* **1991**, *113*, 5671; c) T. Fujimura, S. Aoki, E. Nakamura, *J. Org. Chem.* **1991**, *56*, 2809; d) C. Perthuisot, W. D. Jones, *J. Am. Chem. Soc.* **1994**, *116*, 3647; e) M. Lautens, Y. Ren, *J. Am. Chem. Soc.* **1996**, *118*, 10668; f) C. Perthuisot, B. L. Edelbach, D. L. Zubris, W. D. Jones, *Organometallics* **1997**, *16*, 2013; g) B. L. Edelbach, R. J. Lachicotte, W. D. Jones, *J. Am. Chem. Soc.* **1998**, *120*, 2843; h) M. Hayashi, T. Ohmatsu, Y.-P. Meng, K. Saigo, *Angew. Chem.* **1998**, *110*, 877; *Angew. Chem. Int. Ed.* **1998**, *37*, 837.
- [2] a) K. Kaneda, H. Azuma, M. Wayaku, S. Teranisi, *Chem. Lett.* **1974**, 215; b) J. W. Suggs, C. -H. Jun, *J. Chem. Soc. Chem. Commun.* **1985**, 92; c) M. Gozin, A. Weisman, Y. Ben-David, D. Milstein, *Nature* **1993**, *364*, 699; d) H. Harayama, T. Kuroki, M. Kimura, S. Tanaka, Y. Tamaru, *Angew. Chem.* **1997**, *109*, 2449; *Angew. Chem. Int. Ed. Engl.* **1997**, *36*, 2352; e) P. Steenwinkel, R. A. Gossage, G. van Koten, *Chem. Eur. J.* **1998**, *4*, 759.
- [3] H. Suzuki, Y. Takaya, T. Takemori, M. Tanaka, *J. Am. Chem. Soc.* **1994**, *116*, 10779.
- [4] a) H. Suzuki, H. Omori, Y. Moro-oka, *Organometallics* **1988**, *7*, 2579; b) H. Omori, H. Suzuki, Y. Take, Y. Moro-oka, *Organometallics* **1989**, *8*, 2270; c) H. Omori, H. Suzuki, Y. Moro-oka, *Organometallics* **1989**, *8*, 1576; d) H. Suzuki, T. Takao, M. Tanaka, Y. Moro-oka, *J. Chem. Soc. Chem. Commun.* **1992**, 476; e) H. Suzuki, H. Omori, D. H. Lee, Y.

Yoshida, M. Fukushima, M. Tanaka, Y. Moro-oka, *Organometallics* **1994**, *13*, 1129; f) T. Takao, H. Suzuki, M. Tanaka, *Organometallics* **1994**, *13*, 2554; g) T. Takao, S. Yoshida, H. Suzuki, M. Tanaka, *Organometallics* **1995**, *14*, 3855.

- [5] a) R. T. Swann, A. W. Hanson, V. Boekelheide, *J. Am. Chem. Soc.* **1984**, *106*, 818; b) S. C. Hockett, R. J. Angelici, *Organometallics* **1988**, *7*, 1491; c) M. I. Bruce, A. Catlow, M. P. Cifuentes, M. R. Snow, E. R. T. Tiekink, *J. Organomet. Chem.* **1990**, *397*, 187; d) H. Werner, G. Brauers, O. Nurnberg, *J. Organomet. Chem.* **1993**, *454*, 187; e) F. Urbanos, M. A. Halcrow, J. Fernandez-Baeza, F. Dahan, D. Labroue, B. Chaudret, *J. Am. Chem. Soc.* **1993**, *115*, 3484; f) C. M. Casado, T. Wagner, D. Astruc, *J. Organomet. Chem.* **1995**, *502*, 143; g) Y. Ishii, M. Kawaguchi, M. Hidai, *Chem. Lett.* **1995**, 983; h) Z. Shirin, A. Pramanik, P. Ghosh, R. Mukherjee, *Inorg. Chem.* **1996**, *35*, 3431; i) S. Bhambri, D. A. Tocher, *J. Organomet. Chem.* **1996**, *507*, 291; j) S. Bhambri, A. Bishop, N. Kaltsoyannis, D. A. Tocher, *J. Chem. Soc. Dalton Trans.* **1998**, 3379; k) S.-M. Yang, M. C.-W. Chan, S.-M. Peng, C.-M. Che, *Organometallics* **1998**, *17*, 151; l) X. Zhang, C. A. Dullaghan, E. J. Watson, G. B. Carpenter, D. A. Sweigart, *Organometallics* **1998**, *17*, 2067.
- [6] M. A. Bennett, J. C. Nicholls, A. K. F. Rahman, A. D. Redhouse, J. L. Spencer, A. C. Willis, *J. Chem. Soc. Chem. Commun.* **1989**, 1328; J. C. Nicholls, J. L. Spencer, *Organometallics* **1994**, *13*, 1781.
- [7] P. R. Story, S. R. Fahrenholtz, *J. Org. Chem.* **1963**, *28*, 1716.
- [8] X-ray structural determination of **4**: Crystals of **4** were grown at -20°C from a solution of the compound in pentane. Data were collected at -50°C on an AFC-7R diffractometer equipped with graphite-monochromated $\text{MoK}\alpha$ radiation. The compound crystallizes in space group $P2_1/a$, with $a = 15.264(1)$, $b = 14.446(2)$, $c = 11.618(2)$ Å, $\beta = 96.391(10)^{\circ}$, $V = 2546.0(5)$ Å³, $Z = 4$, $\rho_{\text{calc}} = 1.515$ g cm⁻³. A total of 6079 unique reflections were recorded in the range $6^{\circ} \leq 2\theta \leq 55^{\circ}$, of which 3387 were used ($F > 3\sigma(F)$) for solution and refinement. In the reduction of the data, Lorentz/polarization corrections and empirical absorption corrections based on azimuthal scans were applied to the data. The structure was solved by the Patterson method (DIRDIF92 PATTY), and all non-hydrogen atoms were refined anisotropically by using full-matrix least-squares techniques on F . The final structure of **4** was refined to $R = 0.034$, $R_w = 0.032$, and $\text{GOF} = 1.31$ for 286 parameters. Crystallographic data (excluding structure factors) for the structure reported in this paper have been deposited with the Cambridge Crystallographic Data Centre as supplementary publication no. CCDC-142799. Copies of the data can be obtained free of charge on application to CCDC, 12 Union Road, Cambridge CB2 1EZ, UK (fax: (+44) 1223-336-033; e-mail: deposit@ccdc.cam.ac.uk).
- [9] H. Suzuki, H. Omori, Y. Takahashi, M. Tanaka, unpublished results.
- [10] Y. Ohki, H. Suzuki, unpublished results.

Asymmetric, Catalytic Phenyl Transfer to Aldehydes: Enantioselective Synthesis of Diarylmethanols**

Carsten Bolm,* Nina Hermanns, Jens P. Hildebrand, and Kilian Muñiz

Chiral diarylmethanols are important intermediates for the synthesis of biologically and pharmaceutically active substances.^[1] Two major approaches exist for their enantioselective synthesis: the asymmetric reduction of unsymmetrical diaryl ketones and the enantioselective aryl transfer to benzaldehydes. The most prominent examples of the former are based on Corey's CBS reduction methodology^[2] and Noyori's enantioselective ketone hydrogenation catalyzed by 2,2'-bis(diphenylphosphanyl)-1,1'-binaphthyl (BINAP)/diamine ruthenium complexes.^[3] Both reactions work well but also require certain substrate attributes such as electronically very different aryls or *ortho*-substitution of one of the aryl groups. Successful examples of the second strategy have only recently been described.^[4] In organozinc chemistry,^[5] enantioselective phenyl transfers to aldehydes were first reported by Soai and co-workers who employed a zinc reagent prepared in situ from ZnCl_2 and phenylmagnesium bromide and stoichiometric amounts of *N,N*-dibutylnorephedrine as chiral ligand (up to 82% *ee*).^[5b, 6] Interestingly, salt-free diphenylzinc behaved differently and gave unsatisfactory results. The first successful application of isolated diphenylzinc in this reaction was described by Fu and co-workers in 1997 who demonstrated that a chiral azaferrocene catalyzed its addition to 4-chlorobenzaldehyde affording the corresponding diarylmethanol with 57% *ee*.^[7] Soon after, Pu and co-workers^[8] and Bolm and Muñiz^[9] independently developed other catalysts for the asymmetric phenylation of aldehydes based on 2,2'-dihydroxy-1,1'-biphenyl (BINOL) derivatives and planar-chiral ferrocenyl oxazoline **3**,^[10] respectively. Here we report on an improvement of the existing methodology which allows the catalytic synthesis of a wide range of arylphenylmethanols **2** from benzaldehydes **1** with very high enantioselectivities.


A major difficulty in the development of an efficient asymmetric phenyl transfer from diphenylzinc to aldehydes **1** is the rapid competitive uncatalyzed pathway, which diminishes the enantioselectivity. To compensate this effect some

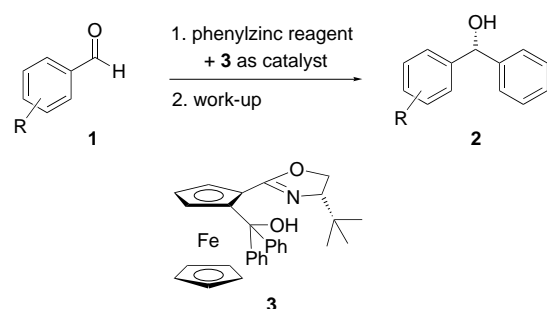
[*] Prof. Dr. C. Bolm, Dipl.-Chem. N. Hermanns, Dr. J. P. Hildebrand,^[+] Dr. K. Muñiz^[++]
Institut für Organische Chemie der RWTH Aachen
Professor-Pirlet-Strasse 1, 52056 Aachen (Germany)
Fax: (+49) 241-8888-391
E-mail: carsten.bolm@oc.rwth-aachen.de

[+] Current address: Department of Chemistry
Massachusetts Institute of Technology, Cambridge, MA 02139 (USA)

[++] Current address: Department of Chemistry
Nagoya University, Chikusa, Nagoya 464-8602 (Japan)

[**] We are grateful to the Fonds der Chemischen Industrie and to the Deutsche Forschungsgemeinschaft (DFG) within the Collaborative Research Center (SFB) 380 "Asymmetric Synthesis by Chemical and Biological Methods" for financial support. We thank Dr. John Blacker from AVECIA for an inspiring discussion.

 Supporting information for this article is available on the WWW under <http://www.wiley-vch.de/home/angewandte/> or from the author.



known catalytic systems rely on the use of high catalyst loadings or high dilution conditions. Furthermore, the loss of one phenyl as nontransferable aryl group on zinc has to be accepted. Based on literature data^[11, 12] we reasoned that the use of a modified phenylzinc reagent might help to suppress the undesired background reaction and even allow transfer of both phenyl groups.^[13] To our delight and supporting our hypothesis we found that employing an organozinc species formed in situ by mixing diphenylzinc and diethylzinc (in a ratio of 1:2)^[14] led to a dramatic increase in enantioselectivity. Thus, with 10 mol % of **3** the phenylation of 4-chlorobenzaldehyde now afforded the product alcohol with 97% *ee* compared to 88% *ee* with the original system^[9] employing diphenylzinc only (Table 1, entry 4). Under these conditions the catalyst loading could even be reduced to 2.5 mol % giving the product with 93% *ee* (Table 1, entry 2).

Table 1. Phenyl transfer to 4-chlorobenzaldehyde (**1a**) in the presence of catalytic amounts of ferrocene **3**.^[a]

Entry	3 [mol %]	ZnPh ₂ /ZnEt ₂ [equiv]	Yield [%] ^[b]	<i>ee</i> of 2a [%] ^[c,d]	Absolute config. ^[e]
1	1	0.65/1.3	84	79	<i>R</i>
2	2.5	0.65/1.3	86	93	<i>R</i>
3	5	0.65/1.3	92	95 (82)	<i>R</i>
4	10	0.65/1.3	89	97 (88)	<i>R</i>
5	15	0.7/1.4	68	97	<i>R</i>
6	40	1.0/2.0	94	99 (90)	<i>R</i>
7	100	1.5/3.0	81	99 (94)	<i>R</i>

[a] Reactions were carried out in toluene at 0 °C. [b] After column chromatography. [c] Determined by HPLC using a chiral stationary phase. [d] Values in parentheses refer to the results of reactions with pure ZnPh₂. [e] Determined by comparison of the order of peak elution during HPLC with literature values.

Further optimization was accomplished by varying the reaction temperature, solvent, and the amount and ratio of zinc reagents: toluene was found to be the solvent of choice and the temperature could be raised to 10 °C without loss of selectivity. As hoped for, use of the ZnPh₂/ZnEt₂ mixture had the additional benefit that the amount of diphenylzinc could be reduced, and even with only 0.65 equivalents of this zinc reagent high conversion of the aldehyde was achieved. For maximum selectivity a twofold excess of ZnEt₂ was essential, presumably to shift the equilibrium towards a mixed zinc

species.^[14] Under the optimized conditions several aldehydes were submitted to the aryl transfer reaction (Table 2).

Table 2 shows that for a wide range of aromatic aldehydes the addition proceeds with excellent enantioselectivities of up

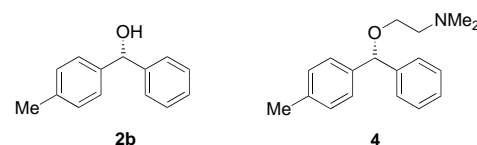
Table 2. Catalyzed phenyl transfer to various aldehydes.^[a]

Entry	R in RCHO	Yield [%] ^[b]	<i>ee</i> of 2 [%] ^[c,d]	Absolute config. ^[e]
1	4-Cl-C ₆ H ₄	86	97 (88)	<i>R</i>
2	4-H ₃ CO-C ₆ H ₄	82	98 (87)	<i>R</i>
3	3-H ₃ CO-C ₆ H ₄	99	96	<i>R</i>
4	4-H ₃ C-C ₆ H ₄	86	98 (85)	<i>R</i>
5	4-C ₆ H ₅ -C ₆ H ₄	98	97 (91)	<i>R</i>
6	2-C ₁₀ H ₉	70	96 (89)	<i>R</i>
7	2-Br-C ₆ H ₄	64	91 (73)	<i>R</i>
8	2-Furyl	99	95 (80)	<i>R</i>
9	<i>E</i> -C ₆ H ₅ CH=CH	97	90 (73)	<i>S</i>
10	C(CH ₃) ₃	68	94 (56)	<i>S</i>
11	C ₆ H ₅ -CH ₂	82	83	<i>S</i>
12	CH(CH ₃) ₂	75	91	<i>S</i>

[a] Reactions were carried out in toluene at 10 °C in the presence of 10 mol % of ferrocene **3** using a mixture of 0.65 equivalents of ZnPh₂ and 1.3 equivalents of ZnEt₂. [b] After column chromatography or purification using preparative HPLC. [c] Determined by HPLC using a chiral stationary phase. [d] Enantiomeric excess in parentheses refers to the reaction performed with 1.5 equivalents of ZnPh₂ instead of the ZnPh₂/ZnEt₂ combination (for entries 1–7: 10 mol % of **3**; for entries 8–10: 5 mol % of **3**). [e] Determined by comparison of the order of peak elution during HPLC with literature values, or tentatively assigned by assumption of an identical reaction pathway (entries 3–5, 11, 12)

to 98% *ee*. It should also be emphasized that with the new protocol the range of substrates is no longer limited to *para*-substituted aromatic aldehydes; *meta*- and even *ortho*-substitutions which have so far resulted in only moderate enantioselectivities^[9] are well tolerated and the corresponding chiral diarylmethanols are formed with high enantioselectivities (Table 2, entries 3 and 7). Furyl carbaldehyde and cinnamyl aldehyde also react highly selectively and give the corresponding alcohols with 95% *ee* and 90% *ee*, respectively (Table 2, entries 8 and 9).

Noteworthy is that product **2b**, which is obtained in a single step from 4-methylbenzaldehyde with 98% *ee*, is the direct precursor of antihistaminic (*R*)-neobenodine **4**.^[15] By reduction of the corresponding unsymmetrical diketone this compound is not directly available with high enantioselectivity.^[3]



The addition of diphenylzinc to aliphatic aldehydes was also briefly examined. For selected examples good to excellent enantioselectivities have been obtained (Table 2, entries 10–12). Compared to the previous results the new protocol proved superior again, giving, for example, the addition product of pivalaldehyde with 94% *ee*.

Experimental Section

In a glovebox a well-dried Schlenk flask was charged with diphenylzinc (36 mg, 0.16 mmol). The flask was sealed and removed from the glovebox. Freshly distilled toluene (3 mL) was added followed by diethylzinc (33 μL,

0.33 mmol). After the mixture had been stirred for 30 min at room temperature, ferrocene **3** (12 mg, 0.025 mmol) was added, and the resulting solution was then cooled to 10 °C. Stirring was continued for an additional 10 min at this temperature, and the aldehyde (0.25 mmol) was then added directly in one portion. The Schlenk flask was sealed, and the reaction mixture was stirred at 10 °C overnight. Quenching with water followed by extracting with dichloromethane, drying of the combined organic phase over MgSO₄, and evaporating the solvent under reduced pressure gave the crude product. Column chromatography (silica gel; eluents: hexanes/diethyl ether) afforded the pure secondary alcohol (for *ee* analyses by HPLC see Supporting Information).

Received: May 29, 2000 [Z15183]

- [1] For examples see: a) K. Meguro, M. Aizawa, T. Sohma, Y. Kawamatsu, A. Nagaoka, *Chem. Pharm. Bull.* **1985**, *33*, 3787; b) F. Toda, K. Tanaka, K. Koshiro, *Tetrahedron: Asymmetry* **1991**, *2*, 873; c) M. Botta, V. Summa, F. Corelli, G. Di Pietro, P. Lombardi, *Tetrahedron: Asymmetry* **1996**, *7*, 1263; d) S. Stanchev, R. Rakovska, N. Berova, G. Snatzke, *Tetrahedron: Asymmetry* **1995**, *6*, 183.
- [2] a) E. J. Corey, C. J. Helal, *Tetrahedron Lett.* **1995**, *36*, 9153; b) E. J. Corey, C. J. Helal, *Tetrahedron Lett.* **1996**, *37*, 4837; c) E. J. Corey, C. J. Helal, *Tetrahedron Lett.* **1996**, *37*, 5675; d) general review: E. J. Corey, C. J. Helal, *Angew. Chem.* **1998**, *110*, 2092; *Angew. Chem. Int. Ed.* **1998**, *37*, 1986.
- [3] a) T. Ohkuma, M. Koizumi, H. Ikehira, T. Yokozawa, R. Noyori, *Org. Lett.* **2000**, *2*, 659; b) general review: R. Noyori, T. Ohkuma, *Pure Appl. Chem.* **1999**, *71*, 1493.
- [4] For catalyses of this type involving metals other than zinc, see: a) Ti: B. Weber, D. Seebach, *Tetrahedron* **1994**, *50*, 7473; b) Rh/B: M. Sakai, M. Ueda, N. Miyaura, *Angew. Chem.* **1998**, *110*, 3475; *Angew. Chem. Int. Ed.* **1998**, *37*, 3475. For early studies of enantioselective versions involving stoichiometric amounts or excess of organometallic reagents, see: c) D. Seebach, A. K. Beck, S. Roggo, A. Wonnacott, *Chem. Ber.* **1985**, *118*, 3673; d) R. Noyori, S. Suga, K. Kawai, S. Okada, M. Kitamura, *Pure Appl. Chem.* **1988**, *60*, 1597; e) K. Tomioka, M. Nakajima, K. Koga, *Chem. Lett.* **1987**, *65*; f) M. Kaino, K. Ishihara, H. Yamamoto, *Bull. Chem. Soc. Jpn.* **1989**, *62*, 3736; g) J.-T. Wang, X. Fan, X. Feng, Y.-M. Qian, *Synthesis* **1989**, 291; h) M. Nakajima, K. Tomioka, K. Koga, *Tetrahedron* **1993**, *49*, 9751.
- [5] Reviews on diorganozinc additions to aldehydes: a) R. Noyori, M. Kitamura, *Angew. Chem.* **1991**, *103*, 34; *Angew. Chem. Int. Ed. Engl.* **1991**, *30*, 49; b) K. Soai, S. Niwa, *Chem. Rev.* **1992**, *92*, 833; c) K. Soai, T. Shibata in *Comprehensive Asymmetric Catalysis*, Vol. 2 (Eds.: E. N. Jacobsen, A. Pfaltz, H. Yamamoto), Springer, Berlin, **1999**, p. 911.
- [6] a) K. Soai, Y. Kawase, A. Oshio, *J. Chem. Soc. Perkin Trans. 1* **1991**, 1613; b) for a diastereoselective version, see: J. Hübscher, R. Barner, *Helv. Chim. Acta* **1990**, *73*, 1068.
- [7] a) P. I. Dosa, J. C. Ruble, G. C. Fu, *J. Org. Chem.* **1997**, *62*, 444; b) for a 3-*exo*-(dimethylamino)isoborneol (DAIB)-catalyzed asymmetric addition of ZnPh₂ to ketones, see: P. I. Dosa, G. C. Fu, *J. Am. Chem. Soc.* **1998**, *120*, 445.
- [8] a) W.-S. Huang, L. Pu, *J. Org. Chem.* **1999**, *64*, 4222; b) W.-S. Huang, Q.-S. Hu, L. Pu, *J. Org. Chem.* **1999**, *64*, 7940; c) W.-S. Huang, L. Pu, *Tetrahedron Lett.* **2000**, *41*, 145.
- [9] C. Bolm, K. Muñiz, *Chem. Commun.* **1999**, 1295.
- [10] For the use of ferrocene **3** in dialkylzinc additions, see: a) C. Bolm, K. Muñiz-Fernández, A. Seger, G. Raabe, *Synlett* **1997**, 1051; b) C. Bolm, K. Muñiz-Fernández, A. Seger, G. Raabe, K. Günther, *J. Org. Chem.* **1998**, *63*, 7860; c) C. Bolm, K. Muñiz, J. P. Hildebrand, *Org. Lett.* **1999**, *1*, 491.
- [11] For selected reports on other mixed zinc species, see: a) H. Nehl, W. R. Scheidt, *J. Organomet. Chem.* **1985**, *289*, 1; b) W. Oppolzer, R. N. Radinov, *Helv. Chim. Acta* **1992**, *75*, 170; c) S. Berger, F. Langer, C. Lutz, P. Knochel, T. A. Mobley, C. K. Reddy, *Angew. Chem.* **1997**, *109*, 1603; *Angew. Chem. Int. Ed. Engl.* **1997**, *36*, 1454; d) C. Lutz, P. Knochel, *J. Org. Chem.* **1997**, *62*, 7895; e) P. Wipf, S. Ribe, *J. Org. Chem.* **1998**, *63*, 6454; f) L. Tan, C. y. Chen, R. D. Tillyer, E. J. J. Grabowski, P. J. Reider, *Angew. Chem.* **1999**, *111*, 724; *Angew. Chem. Int. Ed.* **1999**, *38*, 711.
- [12] An example of the use of a combination of ZnPh₂ and ZnMe₂ in this reaction has been described before: Phenyl transfer to nicotinalde-

hyde catalyzed by *N,N*-diethylnorephedrine resulted in phenyl transfer with 20:1 selectivity to give 3-phenylpyridylmethanol in 70% *ee*, while the addition of ZnPh₂ only afforded the product alcohol in 73% *ee*; J. Blacker in *Third International Conference on the Scale Up of Chemical Processes* (Conference Proceedings) (Ed.: T. Laird), Scientific Update, UK, **1998**, p. 74.

- [13] In this study only isolated diphenylzinc (purchased from Strem) was used. For the preparation of other salt-free diarylzinc compounds and their subsequent catalyzed asymmetric addition to aldehydes, see: A. J. Blacker, J. M. Fielden (Zeneca), WO 98/28306, **1998**.
- [14] We presume that ethylphenylzinc is formed in an equilibrium with diethylzinc and diphenylzinc. Apparently, the ethyl group then behaves as a nontransferable moiety on zinc, while phenyl is transferred to the aldehyde with complete selectivity (no ethyl addition product was found). In order to reveal the nature of the zinc species, we used low-temperature ¹H NMR techniques. In a mixture of ZnEt₂ and ZnPh₂ (2:1 ratio) in [D₈]toluene only one set of ethyl group signals was observed at almost the same position as the ones of ZnEt₂ ($\Delta\delta(\text{CH}_2) = 0.03$ ppm). In [D₈]THF at –80 °C additional sets of ethyl and phenyl group protons were detected belonging to a new, albeit not yet identified species. Further studies are in progress to characterize the most relevant intermediates in this catalysis.
- [15] a) C. van der Stelt, W. J. Heus, W. T. Nauta, *Arzneim. Forsch.* **1969**, *19*, 2010; b) R. F. Rekker, H. Timmerman, A. F. Harms, W. T. Nauta, *Arzneim. Forsch.* **1971**, *21*, 688; c) A. F. Casy, A. F. Drake, C. R. Ganellin, A. D. Mercer, C. Upton, *Chirality* **1992**, *4*, 356.

A Synthetic Azinomycin Analogue with Demonstrated DNA Cross-Linking Activity: Insights into the Mechanism of Action of this Class of Antitumor Agent**

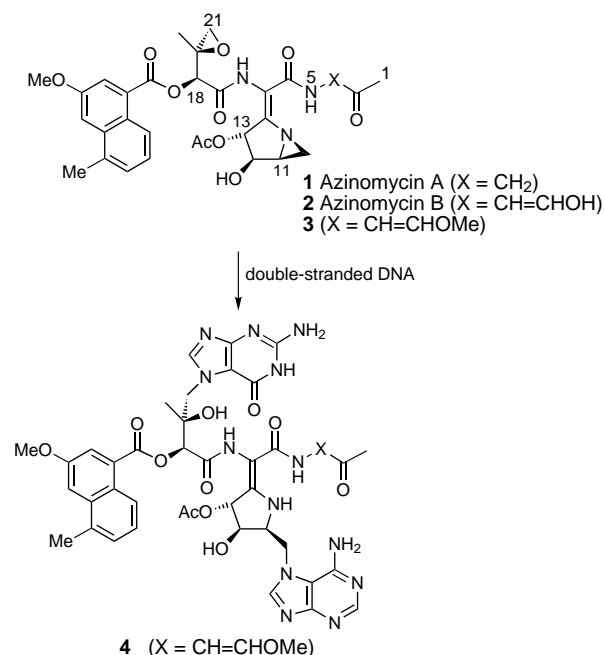
John A. Hartley,* Ali Hazrati, Lloyd R. Kelland,* Ruzwana Khanim, Michael Shipman,* Franck Suzenet, and Louise F. Walker

Chemical agents capable of inducing DNA interstrand cross-links (ISCs) comprise an extremely important class of clinical cancer chemotherapeutic agents.^[2] The azinomycins (**1**

- [*] Prof. J. A. Hartley, A. Hazrati, R. Khanim
CRC Drug-DNA Interactions Research Group
Department of Oncology
Royal Free & University College Medical School
University College London
91 Riding House Street, London W1P 8BT (UK)
Fax: (+44) 20-7436-2956
E-mail: john.hartley@ucl.ac.uk
- Dr. L. R. Kelland
CRC Centre for Cancer Therapeutics
Institute of Cancer Research
Sutton, Surrey, SM2 2NG (UK)
Fax: (+44) 181-7224101
E-mail: lloyd@icr.ac.uk
- Dr. M. Shipman, Dr. F. Suzenet, Dr. L. F. Walker
School of Chemistry
University of Exeter
Stocker Road, Exeter, EX4 4QD (UK)
Fax: (+44) 1392-263434
E-mail: m.shipman@exeter.ac.uk

[**] The authors gratefully acknowledge the financial support provided by the CRC and the EPSRC. We are indebted to the EPSRC National Mass Spectrometry Centre for performing mass spectral measurements, and the EPSRC Chemical Database Service at Daresbury.^[1]

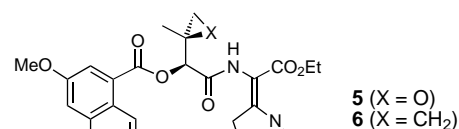
and **2**, Scheme 1) are a unique class of antibiotic which possess potent in vitro cytotoxic activity, significant in vivo antitumor activity, and which appear to act by ISC formation.^[3] Two reports have been published which provide insights into how



Scheme 1. Mechanism of action of the azinomycins, the azinomycins bind to two purine residues.

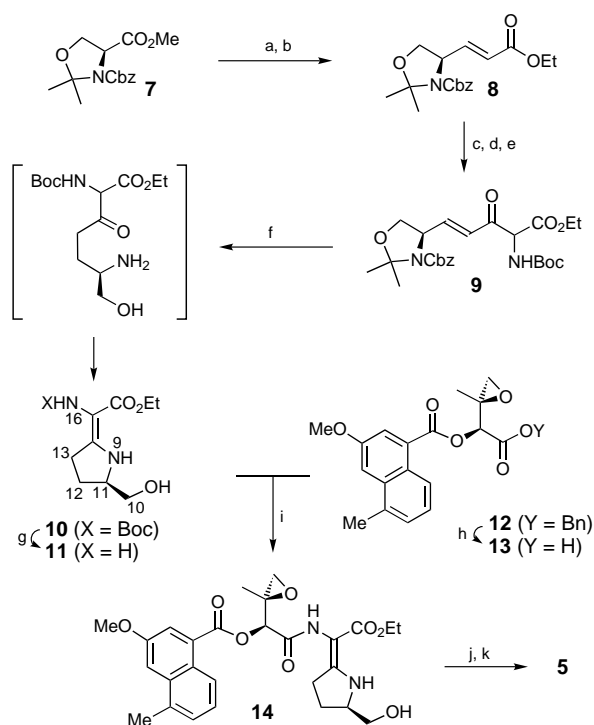
these natural products induce ISCs in double-stranded DNA. By using synthetic oligonucleotide duplexes, Armstrong et al. demonstrated that azinomycin B causes ISCs in the major groove of DNA by alkylation at N-7 of guanine (G) and reaction with another purine residue (A or G) two bases along on the complementary DNA strand.^[4] Recently, Fujiwara et al. isolated and partially characterized adduct **4**, produced upon treatment of the 4-methyl azinomycin B derivative **3** with the self-complementary oligodeoxynucleotide [d(TAGC-TA)₂], work which provided the first direct evidence of the involvement of the electrophilic epoxide and aziridine moieties in the DNA cross-linking event (Scheme 1).^[5]

To fully elucidate the mechanism of action of the azinomycins, work which might ultimately lead to the development of new clinically useful ISC agents, further studies are needed to determine the timing of the alkylation events that lead to ISC formation and to ascertain the role of other functional groups within the azinomycins (e.g. naphthyl residue, C-12/C-13 hydroxy groups) in DNA sequence recognition. One powerful way to address these issues would be to make simplified yet mechanistically fully functional analogues of the natural products. Surprisingly, despite the large volume of work that has been directed towards realizing the first total synthesis of the azinomycins,^[6] no reports have appeared on the ISC activity of any synthetic azinomycin derivatives. Herein we describe a flexible and efficient approach for the assembly of the basic C-6 to C-21 carbon skeleton of the azinomycins and demonstrate that this approach can be used to prepare simplified azinomycin analogues such as epoxy aziridine **5** and cyclopropyl aziridine **6**. Furthermore the analogue **5** is an ISC



agent and acts by a similar mechanism to that of the natural products.

Our synthesis of epoxy aziridine **5** is depicted in Scheme 2. Homochiral ester **7**,^[7] readily obtained from L-serine in three steps, was transformed into α,β -unsaturated ester **8** by DIBAL

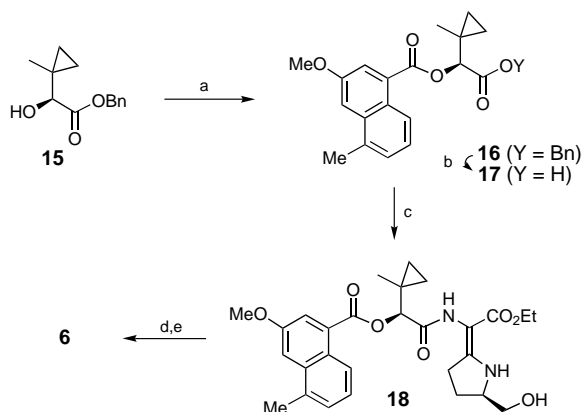


Scheme 2. Synthesis of the azinomycin analogue **5**. a) DIBAL, toluene, -78°C , 95%; b) $\text{Ph}_3\text{P}=\text{CHCO}_2\text{Et}$, toluene, 77%; c) NaOH, THF, H_2O ; d) $(\text{COCl})_2$, DMF (catalyst), CH_2Cl_2 ; e) $\text{EtO}_2\text{CCH}(\text{CO}_2\text{H})(\text{NHBoc})$, $\text{Mg}(\text{OEt})_2$, CCl_4 , 54% from **8**; f) H_2 , Pd/C, EtOH, HCl(aq), 68%; g) TFA, CH_2Cl_2 ; h) H_2 , Pd/C, MeOH; i) PyBOP, HOBT, Et_3N , DMF, 67% from **12**; j) MsCl, Et_3N , -78°C , CH_2Cl_2 , 91%; k) TBAF, 4 Å sieves, THF, 15 min, TLC, 45%. PyBOP = benzotriazol-1-yloxytripyrrolidino-phosphonium hexafluorophosphate, HOBT = 1-hydroxy-1H-benzotriazole, TBAF = tetrabutylammonium fluoride, MsCl = methanesulfonyl chloride, TFA = trifluoroacetic acid, Boc = *tert*-butoxycarbonyl, DIBAL = diisobutylaluminum hydride.

reduction and subsequent olefination by using (carboethoxymethylene)triphenylphosphorane. Further homologation of ethyl ester **8** to α -amino- β -ketoester **9** was accomplished by conversion to the acid chloride and coupling with $\text{EtO}_2\text{CCH}(\text{CO}_2\text{H})(\text{NHBoc})$ in the presence of magnesium ethoxide.^[8] Then, a pivotal step in the synthesis was executed by the hydrogenation of **9** in EtOH in the presence of aqueous hydrochloric acid to give dehydroamino acid **10** in 68% yield. We suggest that these reaction conditions produce the γ -amino ketone which undergoes spontaneous cyclization to the corresponding cyclic imine which then tautomerizes to the

thermodynamically more stable **10**. Dehydroamino acid **10** is produced as a variable mixture of geometric isomers in favor of the desired *E* isomer (*E*:*Z*; 10:1 to 6:1 (in CDCl₃)) as determined by NOE measurements,^[9] and in reproducibly high enantiomeric excess (*E* isomer = 90 % *ee*; *Z* isomer = 89 % *ee*) as established by chiral HPLC analysis.^[10] As yet, we have been unable to ascertain the source of the small amount of racemization observed in the conversion of **8** into **10**. Coupling of carboxylic acid **13**, produced by hydrogenation of benzyl ester **12**,^[6b] with 1.5 equivalents of amine **11** (formed by removal of the *N*-Boc group from **10**) yielded **14** in 67 % yield, as a mixture of geometric isomers (9:1 (in CDCl₃)). Finally, ring closure to give 1-azabicyclo[3.1.0]hexane **5** was accomplished via the corresponding mesylate according to methodology originally devised by Terashima and co-workers.^[11] In our hands, this ring closure was best performed with TBAF^[6c] which provides the bicyclic compound **5** in 45 % yield after rapid preparative thin-layer chromatography (TLC) on plates pretreated with triethylamine.

To study the mechanism of DNA cross-link formation by using simplified azinomycin analogues, we have also prepared **6**, containing a “left-hand” domain in which the electrophilic epoxide moiety has been replaced by the chemically inert cyclopropane ring. This was achieved by esterification of homochiral alcohol **15**^[12] with 5-methyl-3-methoxy-1-naphthoyl chloride to give benzyl ester **16** (Scheme 3). Subsequent



Scheme 3. Synthesis of the azinomycin analogue **6**. a) 5-Methyl-3-methoxy-1-naphthoyl chloride, DMAP (catalyst), Et₃N, CH₂Cl₂, 85 %; b) H₂, Pd/C, MeOH; c) PyBOP, HOBT, Et₃N, DMF, **11**, 65 % from **16**; d) MsCl, Et₃N, –78 °C, CH₂Cl₂, 80 %; e) TBAF, 4 Å molecular sieves, THF, 15 min, TLC, 34 %. DMAP = 4-dimethylaminopyridine

hydrogenolysis of this ester gave the corresponding acid **17**, which was coupled with amine **11** and further converted into **6** via **18** as described above for **5**. Whilst the gross structure of the bicyclic compounds **5** and **6** have been established unambiguously, the stereochemical assignment about the tetrasubstituted double bond can only be tentatively assigned as *trans*, based on comparisons with the earlier synthetic intermediates (e.g. **10**, Scheme 2).^[13]

By using an agarose gel assay,^[14] we have studied the interstrand cross-linking activity of three of our synthetic azinomycin compounds (**5**, **6**, **14**). We have determined that

epoxy aziridine **5** produces DNA cross-links (100 % cross-link formation at 100 μM after 1.5 h), whereas **6** and **14**, devoid of the epoxide or the aziridine, respectively, show little more than background-level activity (Figure 1). Thus, the presence

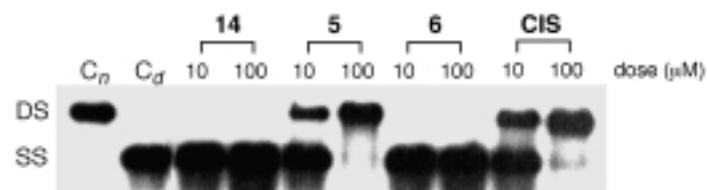


Figure 1. Agarose cross-linking gel for the synthetic azinomycin analogues (**5**, **6**, **14**). Plasmid DNA was treated with the agents at two separate concentrations (10 and 100 μM) for 1.5 h prior to denaturation and gel electrophoresis. CIS is the cross-linking drug cisplatin which was used for comparative purposes. C_n and C_d are control non-denatured and denatured samples, respectively. DS and SS indicate the positions of double- and single-stranded DNA, respectively.

of both functional groups is essential for ISC formation and indicates that **5** is acting on DNA in a similar manner to the natural products (see above). In an effort to elucidate the sequence specificity of these agents, we have evaluated them in a Taq DNA polymerase stop assay.^[15] All three analogues (**5**, **6**, **14**) induce Taq stops preferentially at G residues indicating alkylation at these bases, an observation which lends further credence to the idea that these compounds mimic the azinomycins (data not shown).^[4, 5]

The cytotoxicity of derivatives (**5**, **6**, **14**) was determined against a small panel of human tumor cell lines (SKOV-3, CH1, A2780 (all ovarian), HT-29 (colon), K-562 (leukemia)) using the SRB^[16] or MTT^[17] assay (Table 1). Significantly,

Table 1. Cytotoxicity data for **5**, **6**, and **14**.

Human tumor cell lines	14	5	6
A2780	0.06	0.076	5.2
A2780cisR ^[b]	0.14	0.28	10
CH1	0.058	0.078	8.6
CH1cisR ^[b]	0.035	0.087	5.8
SKOV-3	0.56	2.1	29
HT29	0.55	0.52	10
K562	0.52	0.143	1.9

[a] Dose of drug inhibiting growth by 50 % following a 96 h exposure (1 h in the case of K562) as determined by the SRB assay^[16] (MTT assay^[17] in the case of K562). [b] Cell line with acquired resistance to cisplatin. SRB = sulforhodamine blue, 3-(4,5-dimethylthiazol-2-yl)-2,5-diphenyltetrazolium bromide.

epoxide **5** displayed markedly greater potency (13–110 times) than the corresponding cyclopropane analogue **6**. Intriguingly, epoxide analogue **14**, devoid of the aziridine ring, showed potency comparable to that of **5**. These observations suggest that the epoxide moiety is largely responsible for the cytotoxic activity of these agents. This could indicate that whilst DNA cross-link formation has been demonstrated for both the azinomycins and the synthetic analogue **5**, in whole cells cytotoxicity may be induced by simple DNA alkylation

brought about by reaction with the epoxide center. Such a hypothesis would be consistent with earlier observations that simple azinomycin analogues based upon just the “left-hand” domain of the azinomycins are highly cytotoxic.^[12, 18] Additionally, it is notable that the synthetic agents **5**, and **6** retained activity in the two cell lines possessing acquired resistance to the widely used drug cisplatin, which forms a variety of intrastrand and interstrand bifunctional crosslinks on DNA.

In summary, our results suggest that synthetic azinomycin analogues such as **5** can be readily assembled, and induce ISC in double-stranded DNA along similar lines to the natural products. In view of the limited availability of the azinomycins, we believe that these and other analogues will prove useful in further addressing the molecular mechanism of action of this class of antitumor agent.

Received: June 6, 2000 [Z15232]

- [1] D. A. Fletcher, R. F. McMeeking, D. Parkin, *J. Chem. Inf. Comput. Sci.* **1996**, *36*, 746.
- [2] S. R. Rajski, R. M. Williams, *Chem. Rev.* **1998**, *98*, 2723.
- [3] a) K. Nagaoka, M. Matsumoto, J. Onoo, K. Yokoi, S. Ishizeki, T. Nakashima, *J. Antibiot.* **1986**, *39*, 1527; b) K. Yokoi, K. Nagaoka, T. Nakashima, *Chem. Pharm. Bull.* **1986**, *34*, 4554; c) S. Ishizeki, M. Ohtsuka, K. Irinoda, K.-I. Kukita, K. Nagaoka, T. Nakashima, *J. Antibiot.* **1987**, *40*, 60.
- [4] R. W. Armstrong, M. E. Salvati, M. Nguyen, *J. Am. Chem. Soc.* **1992**, *114*, 3144.
- [5] T. Fujiwara, I. Saito, H. Sugiyama, *Tetrahedron Lett.* **1999**, *40*, 315.
- [6] a) R. W. Armstrong, J. E. Tellew, E. J. Moran, *Tetrahedron Lett.* **1996**, *37*, 447; b) H. J. Bryant, C. Y. Dardonville, T. J. Hodgkinson, M. B. Hursthouse, K. M. A. Malik, M. Shipman, *J. Chem. Soc. Perkin Trans. I* **1998**, 1249; c) M. Hashimoto, S. Terashima, *Heterocycles* **1998**, *59*; d) R. S. Coleman, J.-S. Kong, T. E. Richardson, *J. Am. Chem. Soc.* **1999**, *121*, 9088; e) Y. Konda, T. Sato, K. Tsushima, M. Dodo, A. Kusunoki, M. Sakayanagi, N. Sato, K. Takeda, Y. Harigaya, *Tetrahedron* **1999**, *55*, 12723, and references therein.
- [7] P. L. Beaulieu, P. W. Schiller, *Tetrahedron Lett.* **1988**, *29*, 2019.
- [8] These reaction conditions were more effective than published methods (e.g. D. J. Krysan, *Tetrahedron Lett.* **1996**, *37*, 3303).
- [9] Selected NOE data for major (*E*)-**10** (simultaneous irradiation of H-13 and H-13' enhances N-16 (2.0%), H-12 (3.3%), and H-12' (4.2%); irradiation of N-9 enhances H-11 (6.2%), H-10 (1.5%), and H-10' (1.0%)).
- [10] HPLC retention times (Chiralpak AD column): (*E*)-**8** (98% *ee*, 5% isopropyl alcohol (IPA)/hexanes, 1.0 mL min⁻¹) = 14.27 min (*S*), 13.43 min (*R*); **10** (18% IPA/hexanes, 1.0 mL min⁻¹): *E* isomer (90% *ee*) = 8.35 min (*S*), 10.98 min (*R*); *Z* isomer (89% *ee*) = 7.74 min (*S*), 7.34 min (*R*). Racemic materials were prepared and used for comparison purposes.
- [11] Terashima and co-workers have previously reported a synthesis of **5** and demonstrated that it possesses cytotoxic activity (P388 leukemia: IC₅₀ 0.0023 µg mL⁻¹); however, no DNA affinity studies were reported by this group, see M. Hashimoto, M. Matsumoto, K. Yamada, S. Terashima, *Tetrahedron Lett.* **1994**, *35*, 2207.
- [12] T. J. Hodgkinson, L. R. Kelland, M. Shipman, F. Suzenet, *Biorg. Med. Chem. Lett.* **2000**, *10*, 239.
- [13] For bicyclic compounds **5** and **6**, no NOE enhancements on which a stereochemical assignment could be made were observed across the double bond. Significantly, no NOEs were observed across the double bond in the natural products. The double-bond geometry in the natural products was assigned solely on the basis of the surprisingly high chemical shift (δ = 10.8) of the amide hydrogen at N-5 (see ref. [3b]).
- [14] J. A. Hartley, M. D. Berardini, R. L. Souhami, *Anal. Biochem.* **1991**, *193*, 131.
- [15] M. Pontii, S. M. Forrow, R. L. Souhami, M. D'Incalci, J. A. Hartley, *Nucl. Acid Res.* **1991**, *19*, 2929.

- [16] P. Skehan, R. Storeng, D. Scudiero, A. Monks, J. McMahon, D. Vistica, J. Warren, H. Bokesch, S. Kenney, M. R. Boyd, *J. Nat. Cancer Inst.* **1990**, *82*, 1107.
- [17] J. Carmichael, W. G. DeGraff, P. F. Gazdar, J. D. Minna, J. B. Mitchell, *Cancer Res.* **1987**, *47*, 936.
- [18] K. S. Gates, H. Zang, *Abstr. Pap. Am. Chem. Soc.* **1999**, *218*, 368.

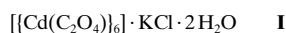
Fascinating Alkali Halide Structures of Different Dimensionalities Incorporated in Host Lattices

R. Vaidhyanathan, S. Neeraj, P.A. Prasad, Srinivasan Natarajan, and C.N.R. Rao*

Design and synthesis of supramolecular inorganic structures exhibiting novel host–guest interactions and molecular recognition have provided exciting new possibilities.^[1, 2] Some of these materials contain cages for ions or cation–anion aggregates, polyoxometalates with cages containing ions such as Cl⁻ and NO₃⁻, and ion-pairs such as NH₄⁺Cl⁻, being good examples.^[3] Several classes of inorganic–organic hybrid materials wherein the organic molecules subtly determine the structures of metal oxide lattices have also been prepared in recent years.^[4] Amongst these, metal–organic networks described in the recent literature^[5–7] are noteworthy, besides the large variety of inorganic open-framework structures, such as the metal phosphates^[8] and oxalates^[9] synthesized hydrothermally in the presence of organic amines. However, there is no report of materials to date, wherein extended structures of ionic compounds are incorporated in host lattices. Herein we report for the first time novel oxalate materials containing alkali halides with entirely new structures. The structures described include, a three-dimensional expanded KCl, a two-dimensional layered RbCl, and a one-dimensional KBr chain. The study makes an important addition to the chemistry of inorganic host–guest materials and suggests that many more such structures can indeed be synthesized.

To prepare materials incorporating new alkali halide structures, we have employed the hydrothermal method of synthesis, which is known to yield materials not obtained ordinarily.^[4, 10] The basic reaction employed is the simple exchange reaction between a cadmium halide and an alkali metal oxalate, carried out in the presence of an amine. The three new Cd oxalates containing alkali halides obtained by this means have the compositions **I–III**.

[*] Prof. Dr. C.N.R. Rao, R. Vaidhyanathan, S. Neeraj, P.A. Prasad, Dr. S. Natarajan
Chemistry and Physics of Materials Unit
and CSIR Centre of Excellence in Chemistry
Jawaharlal Nehru Centre for Advanced Scientific Research
Jakkur P.O., Bangalore 560 064 (India)
Fax: (+91)80-846-2766
E-mail: cnrrao@jncasr.ac.in



The structure of **I** (Figure 1 a) contains some extraordinary features.^[11] First, it has a cadmium oxide cluster of the composition $[\text{Cd}_6\text{O}_{24}]$, containing Cl^- ions in the center and

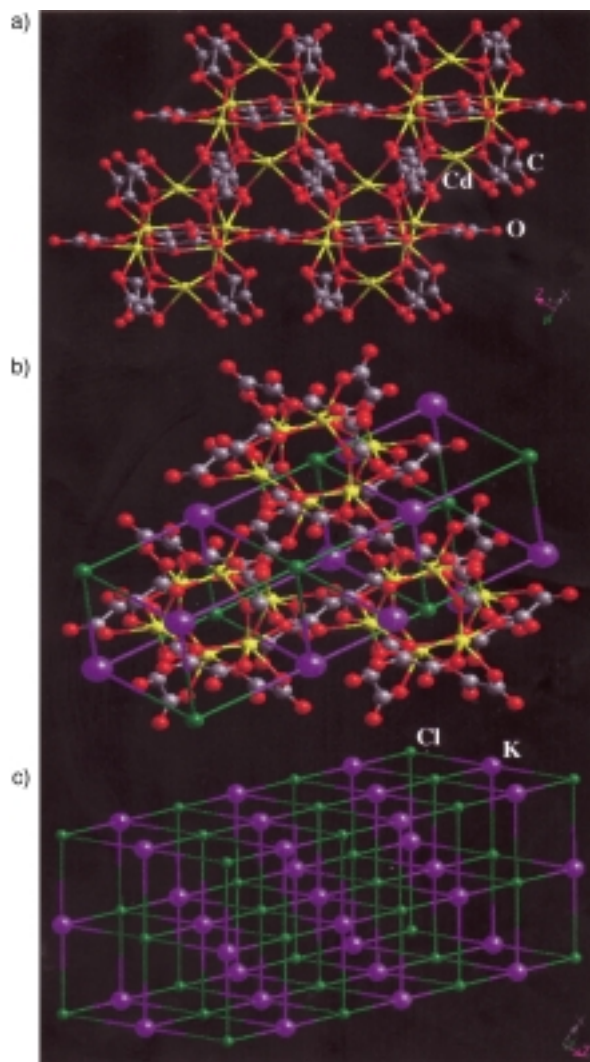


Figure 1. a) The structure of $[\text{Cd}(\text{C}_2\text{O}_4)_6] \cdot \text{KCl} \cdot 2\text{H}_2\text{O}$ (**I**) without the KCl guest. b) Structure of **I**, showing the host and the guest species, along the [001] direction. The KCl lattice can also be visualized. c) Expanded cubic structure of KCl. Note that the [100] KCl is along the [111] direction of the cadmium oxalate **I**.

with Cd in triangular prismatic coordination (Figure 1 b). To our knowledge, this is the first example of such Cd–O clusters. The $[\text{Cd}_6\text{O}_{24}]$ clusters are connected to each other through the oxalate units. Charge compensation for the Cl^- ions in the cluster is provided by the K^+ ions, located outside the clusters (Figure 1 b). Remarkably, the relative positions of the K^+ and Cl^- ions are perfectly ordered in three-dimensions forming an independent rock-salt structure with interpenetrating

FCC lattices (Figure 1 c). The cubic unit cell parameter of KCl is 13.4 Å, which is double that of ordinary KCl (6.7 Å). The [100] KCl planes run along the [111] direction of **I**. The K^+ ions are coordinated by 12 oxygen atoms at a distance of ~3 Å, and the Cl^- ions are coordinated by six cadmium ions at ~2.9 Å. We consider the incorporation of the KCl structure with an expanded unit cell in a host matrix to be noteworthy. An alternate way to describe the structure of **I** would be as follows: The Cl^- ion is at the center of a cluster of six Cd trigonal prisms, arranged in such a manner that the nearest neighbors are six Cd ions at the vertices of an octahedron, the next nearest neighbors being oxygen atoms of the six trigonal prisms, reminiscent of Chevrel phases. Thus, we could consider **I** as a rock salt arrangement of the two clusters, $[\text{ClCd}_6(\text{C}_2\text{O}_4)_3]^{5+}$ and $[\text{K}(\text{H}_2\text{O})_2(\text{C}_2\text{O}_4)_3]^{5-}$. This is indeed an illustration of “scale chemistry”, of the type proposed recently by Férey.^[12]

Encouraged by the above finding, we attempted to synthesize the rubidium halide analogue by carrying out the reaction of a 2:1 mixture of RbCO_3 and oxalic acid with other reactants. We, however, obtained a product with the composition **II**, with an entirely different structure.^[11b, 13] Compound **II** has a layer oxalate structure (Figure 2), with two closely spaced hexagonal RbCl layers separated by 3.3 Å. The RbCl layers are made of hexagonal Rb_3Cl_3 units (see inset of Figure 2) with an average Rb–Cl distance of ~3.6 Å (compared to 3.3 Å in solid RbCl of rock-salt structure). The hexagon has the chair conformation of cyclohexane. The RbCl layers are stabilized by the oxalate layer, present after every two RbCl layers, by providing the additional coordination required by the Rb^+ and Cl^- ions. The Cd ions are coordinated by four oxygen atoms at an average distance of 2.29 Å and by two chlorine atoms at 2.57 Å.

By the reaction of CdBr_2 with $\text{K}_2\text{C}_2\text{O}_4$, we have obtained a material of the composition **III**.^[11b, 14] Compound **III** is a three-dimensional Cd oxalate, with oxalate layers similar to that in **II**, but linked by oxalate bridges.^[9] This is also evident from the lattice parameters of **II** and **III**. One of the lattice parameters of **III** is ~5 Å larger than that in **II**, indicating that the *out-of plane* oxalate bridges the cadmium oxalate layers along that axis to form channels. Accordingly, one of the axes differs significantly in **II** compared to **III**. The K^+ ions located in the channels of **III** form linear KBr chains (Figure 3), with K–Br distances in the range 3.36–3.50 Å. The interchain Br–Br distance is 3.76 Å and the K^+ ions are coordinated by the oxalate oxygen atoms and the Br atoms.

The expanded KCl, the layered RbCl , and KBr chain reported here are most unusual in the sense that such structures were hitherto unknown. It has been possible to form these structures because of host–guest interactions, the host providing the additional coordination necessary to stabilize the structures. The guest species, involving extended ionic lattices, reported here are distinctly different from those resulting from ion-exchange in layered solids, such as the metal–anion arrays in oxide hosts,^[15] and somewhat comparable to the KCl/CsCl lattice in a phosphate framework obtained in a molten salt medium.^[16]

The present study demonstrates that it should be possible to isolate many more such materials containing extended alkali

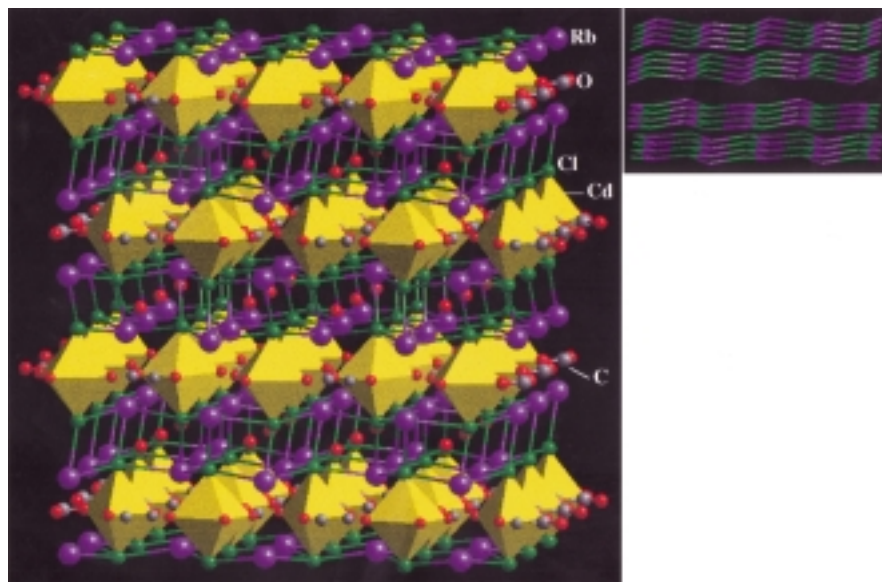


Figure 2. Structure of $[\text{Cd}(\text{C}_2\text{O}_4)] \cdot 2\text{RbCl} \cdot \text{H}_2\text{O}$ (**II**), showing the $\text{Cd}(\text{C}_2\text{O}_4)_2\text{Cl}_2$ layers with CdO_4Cl_2 octahedra (in yellow) along the $[100]$ direction. Layered RbCl can be seen in between the Cd oxalate layers. Note that the Cl^- ions are bonded to the Cd center and point into the interlamellar space. Inset: Arrangement of RbCl layers.

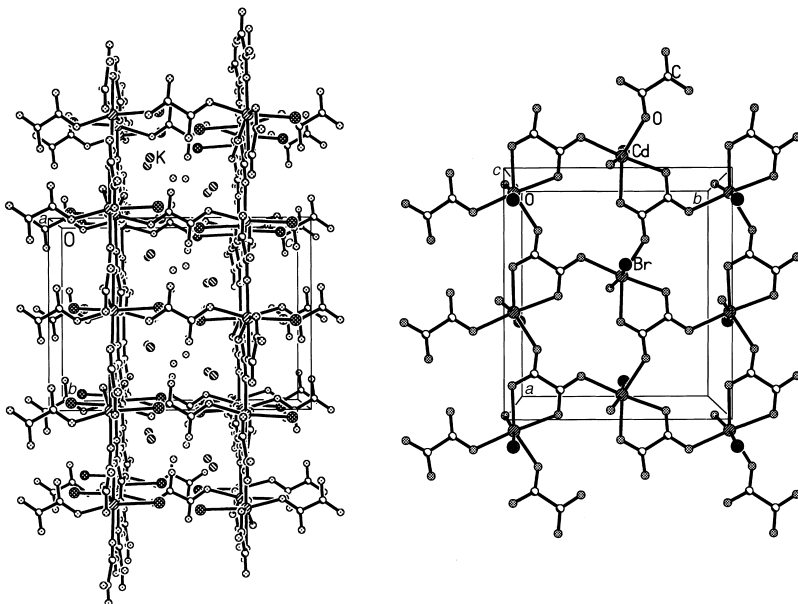
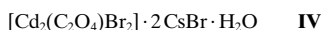


Figure 3. Left) Structure of $[\text{K}_2\text{Cd}_2(\text{C}_2\text{O}_4)_3] \cdot 2\text{KBr} \cdot 2\text{H}_2\text{O}$ (**III**) along the $[100]$ direction. Note that the oxalate group connects the two layers. K and water molecules are situated inside the channels. One-dimensional KBr chains can be seen. Right) Structure of the layer in **III**.

halide structures. In fact, we have just isolated a new compound of the formula **IV**, in which CsBr has a layer structure. It appears that the lower dimensional alkali halide structures are favored by larger alkali and halide ions as well as by a low oxalate:alkali halide ratio.



Experimental Section

I: $\text{K}_2\text{C}_2\text{O}_4$ (0.229 g) was added to a butan-2-ol/water mixture (2.3 mL, 0.6 mL) and stirred for 20 min. CdCl_2 (0.25 g) and glacial acetic acid

(0.28 g) were added to this solution under constant stirring. Finally, imidazole (0.127 g) was added and the mixture was homogenized for 2 h. The reaction mixture with the composition $\text{CdCl}_2:\text{K}_2\text{C}_2\text{O}_4:\text{CH}_3\text{COOH}:\text{C}_4\text{H}_9\text{OH}:\text{H}_2\text{O}$: 100(4):100(4):100(4):100(4):100(4), was sealed in a PTFE-lined stainless-steel autoclave and heated at 165°C for 55 h. The product containing crystals of **I** with a rodlike morphology was filtered, washed with deionized water, and dried under ambient conditions.

II: Rb_2CO_3 (0.287 g) and $\text{H}_2\text{C}_2\text{O}_4$ (0.157 g) were added to a butan-2-ol/water mixture (2.3 mL, 0.6 mL) and stirred for 20 min. CdCl_2 (0.25 g) and CH_3COOH (0.28 g) were added to this solution under constant stirring. Finally, imidazole (0.128 g) was added and the mixture was homogenized for 90 min. The gel was sealed in a PTFE-lined stainless-steel Parr autoclave and heated at 165°C for 55 h. Platelike crystals of **II** which resulted from this reaction were filtered, washed with deionized water, and dried under ambient conditions.

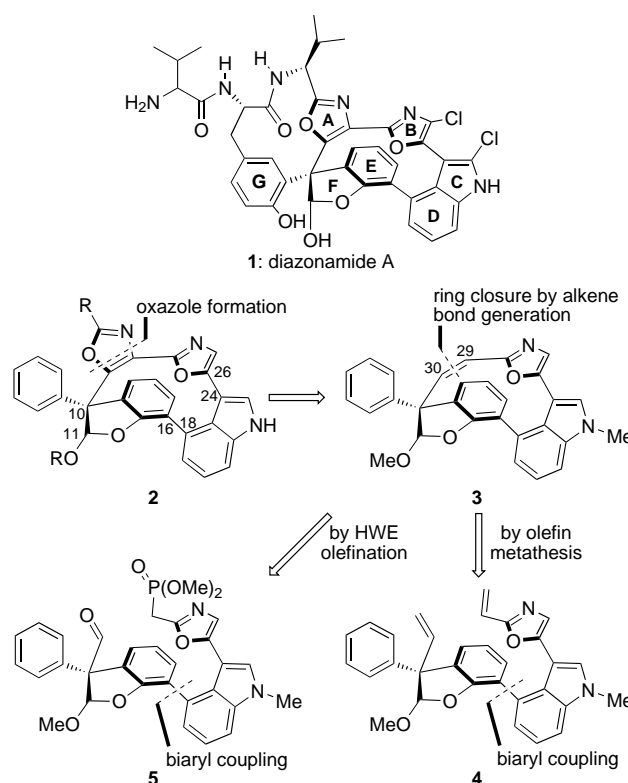
III: K_2CO_3 (0.102 g) and $\text{H}_2\text{C}_2\text{O}_4$ (0.125 g) were added to a butan-2-ol-water mixture (1.8 mL, 0.5 mL) and stirred for 5 min. CdBr_2 (0.2 g) and CH_3COOH (0.11 g) was added under constant stirring and the mixture was homogenized for 90 min. The gel with a composition $\text{CdBr}_2:\text{K}_2\text{CO}_3:1.35\text{H}_2\text{C}_2\text{O}_4:2.5\text{CH}_3\text{COOH}:27\text{C}_4\text{H}_9\text{OH}:38\text{H}_2\text{O}$ was sealed in a PTFE-lined stainless-steel Parr autoclave and heated at 150°C for 80 h. Rodlike crystals of **III** which resulted from this reaction were filtered, washed with deionized water, and dried under ambient conditions.

Received: June 13, 2000 [Z15255]

- [1] J.-M. Lehn, *Supramolecular Chemistry: Concepts and Perspectives*, VCH, New York, **1995**.
- [2] S. R. Batten, R. Robson, *Angew. Chem.* **1998**, *110*, 1558; *Angew. Chem. Int. Ed.* **1998**, *37*, 1460, and references therein.
- [3] A. Müller, H. Reuter, S. Dillinger, *Angew. Chem.* **1995**, *107*, 2505; *Angew. Chem. Int. Ed. Engl.* **1995**, *34*, 2328.
- [4] J. T. Rijssenbeek, D. J. Rose, R. C. Haushalter, J. Zubieta, *Angew. Chem.* **1997**, *109*, 1049; *Angew. Chem. Int. Ed. Engl.* **1997**, *36*, 1008, and references therein.
- [5] G. B. Gardener, D. Venkataraman, J. S. Moore, S. Lee, *Nature* **1995**, *374*, 792.
- [6] O. M. Yaghi, G. Li, H. Li, *Nature* **1995**, *378*, 703.
- [7] H. Li, M. Eddaoudi, M. O'Keeffe, O. M. Yaghi, *Nature* **1999**, *402*, 276, and references therein.
- [8] A. K. Cheetham, G. Férey, T. Loiseau, *Angew. Chem.* **1999**, *111*, 3466; *Angew. Chem. Int. Ed.* **1999**, *38*, 3268.
- [9] R. Vaidyanathan, S. Natarajan, A. K. Cheetham, C. N. R. Rao, *Chem. Mater.* **1999**, *11*, 3636.
- [10] A. Ranganathan, V. R. Pedireddi, C. N. R. Rao, *J. Am. Chem. Soc.* **1999**, *121*, 1752.
- [11] a) Crystal data for **I**: $[\{\text{Cd}(\text{C}_2\text{O}_4)_6\}] \cdot \text{KCl} \cdot 2\text{H}_2\text{O}$, $M_r = 656.6$, crystal dimensions $0.1 \times 0.1 \times 0.12$ mm, trigonal, space group $R\bar{3}$, $a = 9.346(1)$, $b = 9.346(1)$, $c = 23.961(1)$ Å, $V = 1812.6(3)$ Å³, $Z = 6$, $\rho_{\text{calcd}} = 3.614$ g cm⁻³, $\mu(\text{MoK}\alpha) = 5.593$ mm⁻¹, $\lambda = 0.71073$ Å. The structure was solved by direct methods (SHELXTL-PLUS), 2537 reflections, 590 independent reflections. Full-matrix least-squares on $|F^2|$ (SHELXS-93, G. M. Sheldrick, Gottingen, **1993**) to $R_1 = 0.06$ and $wR_2 = 0.13$. Residual density, min./max.: $-2.87/1.536$ e Å⁻³. b) Structure determinations were carried out using a Siemens SMART-CCD

diffractometer. Crystallographic data (excluding structure factors) for the structures reported in this paper have been deposited with the Cambridge Crystallographic Data Centre as supplementary publication no. CCDC-145227 (**I**), CCDC-145228 (**II**), and CCDC-145229 (**III**). Copies of the data can be obtained free of charge on application to CCDC, 12 Union Road, Cambridge CB21EZ, UK (fax: (+44) 1223-336-033; e-mail: deposit@ccdc.cam.ac.uk).

- [12] G. Fèrey, *J. Solid. State Chem.* **2000**, *152*, 37.
- [13] Crystal data for **II**: $[\text{Cd}(\text{C}_2\text{O}_4)_2] \cdot 2\text{RbCl} \cdot \text{H}_2\text{O}$, $M_r = 460.3$, crystal dimensions $0.06 \times 0.14 \times 0.18\text{ mm}$, orthorhombic, space group, *Pbcm*, $a = 6.018(2)$, $b = 10.861(2)$, $c = 15.503(4)\text{ Å}$, $V = 1013.4(5)\text{ Å}^3$, $Z = 4$, $\rho_{\text{calcd}} = 3.004\text{ g cm}^{-3}$, $\mu(\text{Mo K}\alpha) = 12.21\text{ mm}^{-1}$, $\lambda = 0.71073\text{ Å}$. The structure was solved by direct methods (SHELXTL-PLUS), 3866 reflections, 758 independent reflections. Full-matrix least-squares on $|F^2|$ (SHELXS-93, G. M. Sheldrick, Gottingen, **1993**) to $R_1 = 0.08$ and $wR_2 = 0.17$. Residual density, min./max.: $-2.72/2.03\text{ e Å}^{-3}$.^[11b]
- [14] Crystal data for **III**: $\text{K}_2\text{Cd}(\text{C}_2\text{O}_4)_3 \cdot 2\text{KBr} \cdot 2\text{H}_2\text{O}$, $M_r = 841.12$, crystal dimensions $0.12 \times 0.12 \times 0.24\text{ mm}$, orthorhombic, space group, *Pbca*, $a = 11.898(6)$, $b = 10.963(1)$, $c = 15.203(6)\text{ Å}$, $V = 1983.2(2)\text{ Å}^3$, $Z = 4$, $\rho_{\text{calcd}} = 2.817\text{ g cm}^{-3}$, $\mu(\text{Mo K}\alpha) = 7.077\text{ mm}^{-1}$, $\lambda = 0.71073\text{ Å}$. The structure was solved by direct methods (SHELXTL-PLUS), 7521 reflections, 1428 independent reflections. Full-matrix least-squares on $|F^2|$ (SHELXS-93, G. M. Sheldrick, Gottingen, **1993**) to $R_1 = 0.03$ and $wR_2 = 0.05$. Residual density, min./max.: $-0.593/0.369\text{ e Å}^{-3}$.^[11b]
- [15] T. A. Kodenkandath, J. N. Lalena, W. I. Zhou, E. E. Carpenter, C. Sangregorio, A. U. Falster, J. R. Simmons, C. J. O'Connor, J. B. Wiley, *J. Am. Chem. Soc.* **1999**, *121*, 10743.
- [16] Q. Huang, M. Ulutagay, P. A. Michener, S.-J. Hwu, *J. Am. Chem. Soc.* **1999**, *121*, 10323.



Scheme 1. Structure of diazonamide A (**1**) and retrosynthetic analysis of model system **2**.

Model Studies towards Diazonamide A: Synthesis of the Heterocyclic Core**

K. C. Nicolaou,* Scott A. Snyder, Klaus B. Simonsen, and Alexandros E. Koumbis

Diazonamide A (**1**, Scheme 1), a secondary metabolite isolated from the colonial ascidian *Diazona chinensis*, exemplifies an unprecedented molecular architecture encompassing a cyclic polypeptide backbone as well as an admirably

complex and strained halogenated heterocyclic core trapped as a single atropisomer harboring a quaternary center at the epicenter.^[1] Beyond the formidable synthetic challenge posed by such a daunting molecular framework, diazonamide A possesses potent in vitro cytotoxicity against human colon carcinoma and B-16 murine melanoma cell lines with IC_{50} values in the nanomolar range. These biological actions, however, are exerted through an unknown mode of action. Unfortunately, more extensive bioassays have been hampered by an inability to harvest additional material from the original source. As such, diazonamide A represents one of the most enticing natural products isolated in recent years and a serious challenge to synthetic chemists. Although several groups have reported progress on particular structural subunits of diazonamide A,^[2] no one has yet successfully prepared the fully unsaturated 12-membered polycycle. Herein we report the first synthesis of this heteroaromatic macrocyclic core by a concise and novel strategy which proceeds to provide atropisomerically pure product.

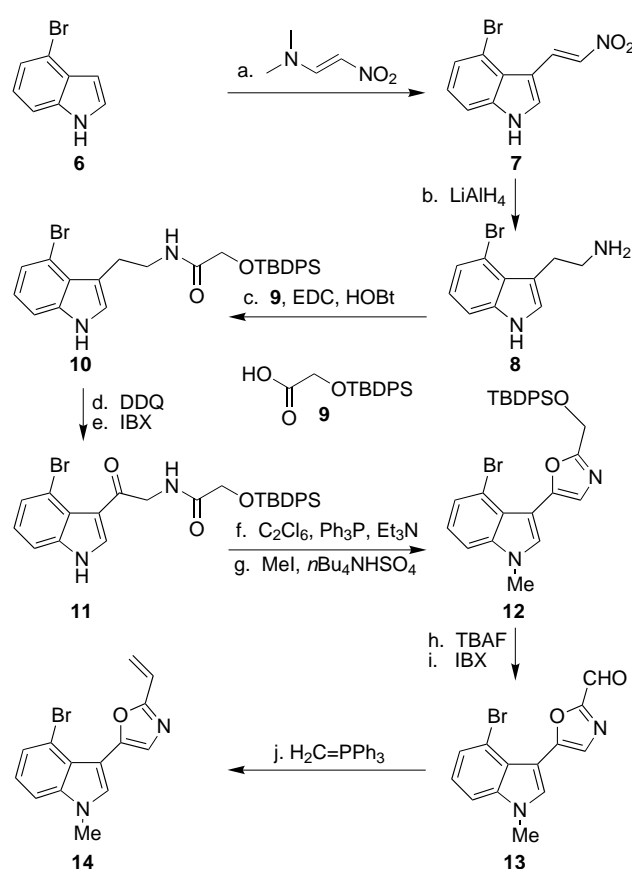
Since we envisioned from the outset that the heterocyclic core would pose the greatest synthetic challenge for a total synthesis of diazonamide A, we focused our efforts primarily on the preparation of model system **3** (Scheme 1) as a means to address key synthetic issues such as potential atropisomerism along the $\text{C}_{16}-\text{C}_{18}$ and $\text{C}_{24}-\text{C}_{26}$ biaryl linkages. As shown in Scheme 1, our synthetic rationale was based on two fairly obvious but strategic bond disconnections. Because numerous methods are currently available to generate macrocycles by alkene bond formation, we felt that disconnection of the $\text{C}_{29}-\text{C}_{30}$ alkene would be prudent and could potentially arise in the

[*] Prof. Dr. K. C. Nicolaou, S. A. Snyder, Dr. K. B. Simonsen, Dr. A. E. Koumbis
Department of Chemistry
and The Skaggs Institute for Chemical Biology
The Scripps Research Institute
10550 North Torrey Pines Road, La Jolla, CA 92037 (USA)
and
Department of Chemistry and Biochemistry
University of California San Diego
9500 Gilman Drive, La Jolla, CA 92093 (USA)
Fax: (+1) 858-784-2469
E-mail: kcn@scripps.edu

[**] We thank Dr. D. H. Huang, Dr. G. Suizdak, and Dr. R. Chadha for NMR spectroscopic, mass spectrometric, and X-ray crystallographic assistance, respectively. We also thank Professor R. H. Grubbs for a generous gift of catalyst **30**. Financial support for this work was provided by The Skaggs Institute for Chemical Biology, the National Institutes of Health (USA), a predoctoral fellowship from the National Science Foundation (S.A.S.), postdoctoral fellowships from the Alfred Benzon Foundation and the Danish Natural Science Research Council (K.B.S.), and grants from Abbott, Amgen, Array-Biopharma, Boehringer-Ingelheim, GlaxoWellcome, Hoffmann-LaRoche, DuPont, Merck, Novartis, Pfizer, and Schering Plough.

forward direction either by metathesis of the olefinic groups in **4** or by an intramolecular Horner–Wadsworth–Emmons (HWE) reaction between the phosphonate and aldehyde residues in **5**; the resultant C₂₉–C₃₀ alkene could then serve as a scaffold upon which to construct the A-ring oxazole, thereby completing the ABCDEF polycycle **2**. From either **4** or **5**, our second key disconnection rupturing the C₁₆–C₁₈ biaryl linkage revealed, by a retro Suzuki or Stille type coupling, two fragments of roughly equal molecular complexity, thereby affording a highly convergent retrosynthetic blueprint.

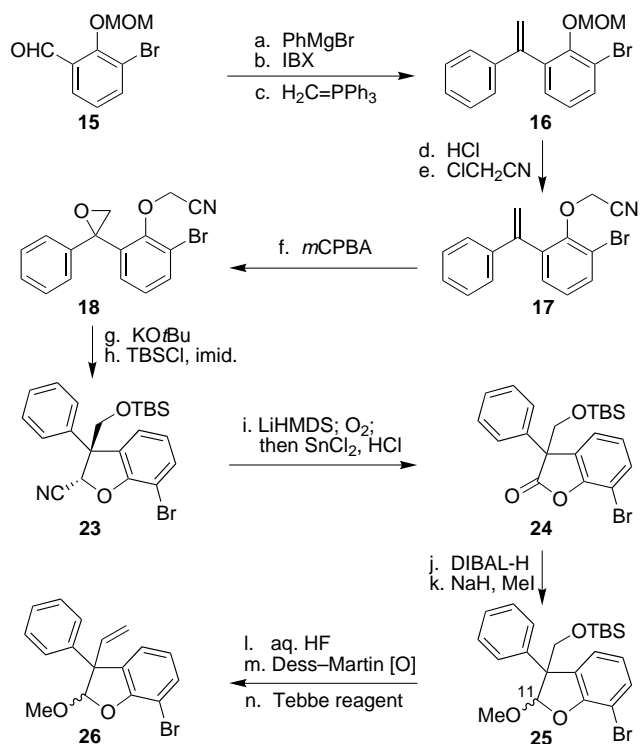
Due to the power of the olefin metathesis reaction in macrocycle formation, particularly with regard to complex natural product total synthesis,^[3] we initially sought to test this method as a means to generate the C₂₉–C₃₀ alkene. Toward this end, our synthetic endeavors commenced with preparation of the BCD indole–oxazole fragment **14** as shown in Scheme 2. Starting from 4-bromoindole (**6**),^[4] condensation



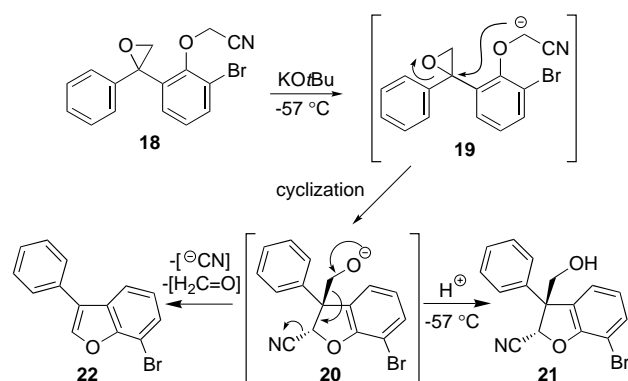
Scheme 2. Preparation of indole–oxazole fragment **14**: a) Dimethylamino-2-nitroethylene (1.1 equiv), TFA, 25 °C, 30 min; b) LiAlH₄ (1.0 M in THF, 6.0 equiv), THF, 25 °C → 65 °C, 4 h, 87% over two steps; c) **9** (1.0 equiv), EDC (1.0 equiv), HOBT (1.0 equiv), CH₂Cl₂, 25 °C, 2 h, 79%; d) DDQ (3.0 equiv), THF/H₂O (9/1), 0 °C, 3 h; e) IBX (3.0 equiv), THF/DMSO (1/1), 25 °C, 3 h, 90% over two steps; f) Cl₃CCl₃ (2.0 equiv), Ph₃P (2.0 equiv), Et₃N (4.0 equiv), 25 °C, 15 min; g) MeI (4.0 equiv), *n*Bu₄NH·SO₄ (1.1 equiv), C₆H₆, 10% aq. NaOH, 25 °C, 20 min, 88% over two steps; h) TBAF (1.0 M in THF, 1.5 equiv), THF, 25 °C, 15 min, 92%; i) IBX (3.0 equiv), THF/DMSO (1/1), 25 °C, 3 h, 90%; j) methylene triphenylphosphonium bromide (1.5 equiv), *n*BuLi (1.6 M in hexanes, 1.3 equiv), THF, 0 → 25 °C, 15 min, 89%. TFA = trifluoroacetic acid, EDC = 3-(3-dimethylaminopropyl)-1-ethylcarbodiimide, TBDPS = *tert*-butyldiphenylsilyl, HOBT = 1-hydroxy-1*H*-benzotriazole, DDQ = 2,3-dichloro-5,6-dicyano-1,4-benzoquinone, TBAF = tetrabutylammonium fluoride, IBX = 1-hydroxy-1,2-benziodoxol-3(1*H*)-one 1-oxide.

with dimethylamino-2-nitroethylene^[5] followed by LiAlH₄-mediated reduction readily afforded 4-bromotryptamine (**8**) in 87% overall yield. Subsequent coupling of **8** with TBDPS-protected glycolic acid derivative **9**^[6] in the presence of EDC and HOBT smoothly provided intermediate **10** (for abbreviations of reagents and protecting groups, see legends in schemes). Although the conversion of **10** to **11** upon treatment with DDQ is known,^[7] we found that far superior yields of **11** could be obtained by reverting to a two-step procedure in which initial exposure of **10** to DDQ in THF/H₂O (9/1) at 0 °C resulted in formation of the desired benzylic hydroxy group which was then readily oxidized by using IBX (90% overall yield).^[8] Notably, protection of the indole nitrogen was unnecessary during this synthetic sequence and exposure to IBX did not afford any N-oxidized products. The synthesis of **14** was then completed through the following five-step protocol: 1) formation of the oxazole ring using a modified variant of the Gabriel–Robinson cyclodehydration reaction;^[9] 2) *N*-methyl protection of the indole nucleus employing phase-transfer conditions (88% over two steps); 3) TBAF-mediated cleavage of the terminal TBDPS group (92%); 4) oxidation of the resultant hydroxyl group with IBX (90%); and 5) generation of the desired alkene upon Wittig reaction of **13** with Ph₃P=CH₂ (89%).

Our next task was to synthesize the requisite EFG fragment **26**, as delineated in Scheme 3. Although numerous methods to access such benzofuranone fragments in racemic form are known, we sought to develop a novel route to this type of system with the hope of generating the C₁₀ quaternary center of diazonamide A stereoselectively. As such, our approach began with aldehyde **15**.^[10] After initial treatment of **15** with PhMgBr, the hydroxy group of the resultant bisbenzylic compound was smoothly oxidized by utilizing IBX, and the newly generated ketone was treated with Ph₃P=CH₂ to afford olefin **16** in 80% overall yield over these three steps. Acid-catalyzed removal of the methoxymethyl (MOM) protecting group was then followed by alkylation of the resultant phenolic residue with chloroacetonitrile in acetone to afford **17** in 75% yield. Subsequent *m*CPBA-mediated epoxidation of the olefin provided key intermediate **18**. As shown in Scheme 4, we envisaged that upon exposure of **18** to base, deprotonation of the methylene group adjacent to the cyanide followed by selective 5-*exo*-tet opening of the epoxide ring would lead to the desired quaternary system **21** via intermediate **20**.^[11] Gratifyingly, treatment of **18** with KOtBu in DMF at –57 °C followed by immediate quenching with 10% aqueous HCl at that temperature afforded **21** in 54% yield. The only other product observed in this novel cyclization step was 3-phenylbenzofuran **22**, which resulted from a previously reported cyclofragmentation reaction.^[12] With **21** in hand, subsequent TBS protection afforded crystalline intermediate **23**, which when subjected to X-ray analysis^[13] revealed that the cyclization reaction proceeded to give a racemic mixture of compounds possessing only the relative *trans* stereochemistry as indicated for **21** and **23**. As such, stereoselective generation of the epoxide in **18** followed by our cyclization protocol would provide an enantioselective route to the C₁₀ quaternary center of diazonamide A.



Scheme 3. Preparation of quaternary center fragment **26**: a) PhMgBr (1.0 M in THF, 1.3 equiv), THF, $-78 \rightarrow 25^\circ\text{C}$, 2 h, 100%; b) IBX (2.0 equiv), THF/DMSO (1/1), 25°C , 1 h, 93%; c) methylene triphenylphosphonium bromide (1.4 equiv), *n*BuLi (1.6 M in hexanes, 1.2 equiv), THF, 0°C , 12 h, 86%; d) conc. HCl, EtOH/ CH_2Cl_2 (2/1), 40°C , 12 h, 100%; e) ClCH_2CN (3.0 equiv), K_2CO_3 (2.0 equiv), acetone, 56°C , 2 h, 75%; f) *m*CPBA (3.0 equiv), CH_2Cl_2 , 25°C , 6 h, 91%; g) KOtBu (1.0 M in THF, 1.5 equiv), DMF, -57°C , 2 min; then 10% HCl (excess), -57°C , 54%; h) TBSCl (1.5 equiv), imidazole (2.0 equiv), DMF, 25°C , 12 h, 99%; i) LiHMDS (1.0 M in THF, 2.0 equiv), THF, -78°C , 15 min; O_2 , 15 min, -78°C ; 1 M SnCl_2 in 10% aq. HCl, $-78 \rightarrow 0^\circ\text{C}$, 30 min, 94%; j) DIBAL-H (1.0 M in toluene, 1.5 equiv), toluene, -78°C , 1 h, 92%; k) NaH (60% dispersion in mineral oil, 3.0 equiv), MeI (5.0 equiv), THF, 25°C , 24 h, 91%; l) aq. HF, MeCN, 0°C , 1 h, 99%; m) Dess–Martin periodinane (1.2 equiv), CH_2Cl_2 , $0 \rightarrow 25^\circ\text{C}$, 2 h, 96%; n) Tebbe reagent (0.5 M in toluene, 1.5 equiv), THF, 0°C , 10 min, 74%. MOM = methoxymethyl, imid. = imidazole, *m*CPBA = *m*-chloroperoxybenzoic acid, TBS = *tert*-butyldimethylsilyl, LiHMDS = lithium salt of 1,1,1,3,3,3-hexamethyldisilazane, DIBAL-H = diisobutylaluminum hydride.

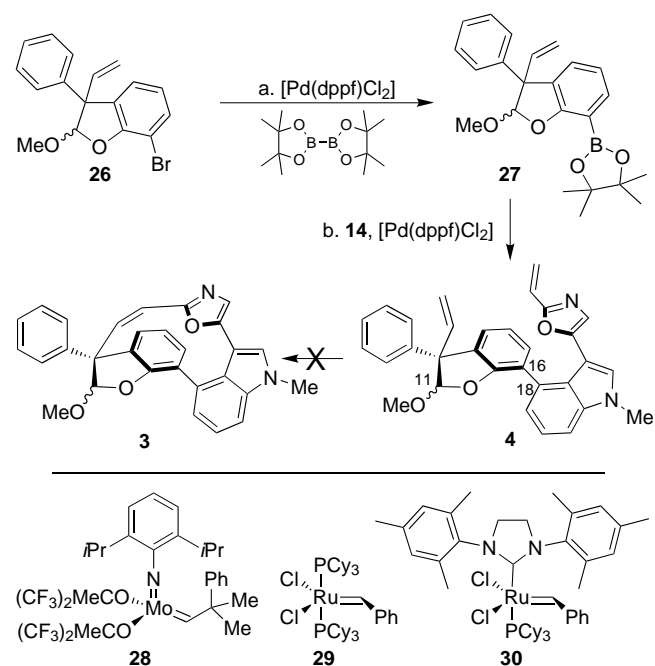


Scheme 4. Novel cyclization reaction to generate **21**.

The synthesis of **26** from **23** was then completed in six additional transformations. First, **23** was readily converted to benzofuranone **24** upon treatment with LiHMDS followed by

exposure to O_2 and SnCl_2 .^[14] Next, the lactone moiety was partially reduced with DIBAL-H to the corresponding lactol with subsequent protection of the hydroxy group as a methyl ether using NaH and MeI to afford **25** in 79% overall yield from **23**. Although the reduction proceeded stereoselectively, the methylation step resulted in epimerization of the C_{11} center. The TBS ether was then easily cleaved upon exposure to aqueous HF in MeCN, and the resultant primary alcohol was oxidized to the corresponding aldehyde using Dess–Martin periodinane. Finally, the desired terminal alkene group of **26** was generated upon treatment with Tebbe reagent (70% yield from **25**). Significantly, attempts to synthesize the final alkene through Wittig homologation utilizing $\text{Ph}_3\text{P}=\text{CH}_2$ led solely to 3-phenylbenzofuran **22** (Scheme 4). We postulate that a betaine intermediate (unobserved in the reaction with Tebbe reagent presumably due to the high oxophilicity of titanium) potentially provides a species capable of undergoing a cyclofragmentation reaction to **22**.

With **14** and **26** in hand, the stage was now set to attempt biaryl coupling of the two fragments and, subsequently, the key olefin metathesis-based macrocyclization. Efforts to prepare the boronic acid of either **14** or **26** under standard conditions (*n*BuLi, $\text{B}(\text{OMe})_3$) failed in numerous attempts. However, as shown in Scheme 5, the boronate ester of **26** was

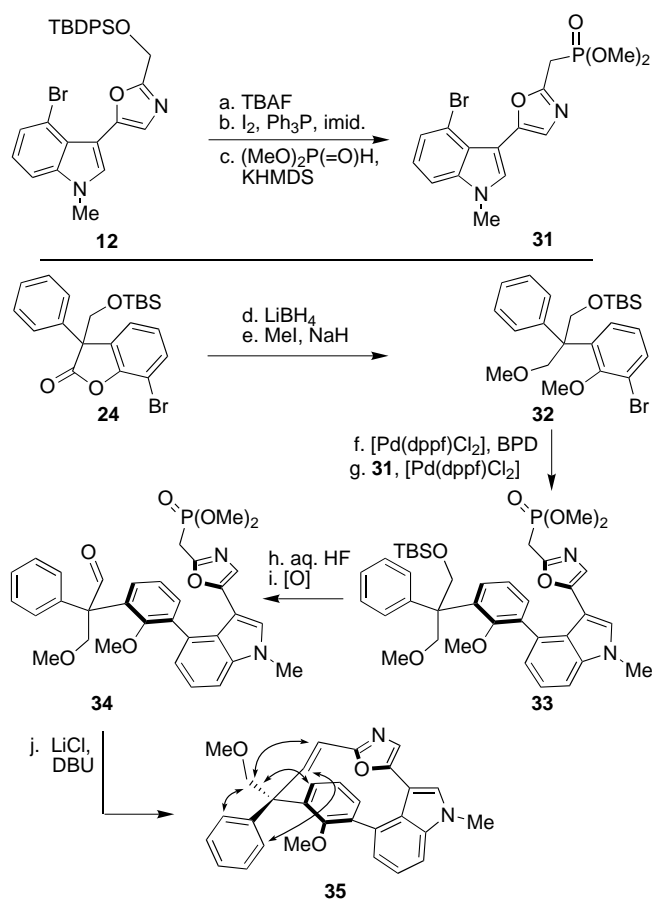


Scheme 5. Biaryl coupling to generate **4** and attempted olefin metatheses with catalysts **28**–**30** to provide **3**: a) Bis(pinacolato)diboron (1.2 equiv), $[\text{Pd}(\text{dppf})\text{Cl}_2] \cdot \text{CH}_2\text{Cl}_2$ (0.15 equiv), KOAc (3.0 equiv), DMSO, 90°C , 6 h, 42%; b) **14** (1.0 equiv), $[\text{Pd}(\text{dppf})\text{Cl}_2] \cdot \text{CH}_2\text{Cl}_2$ (0.15 equiv), K_2CO_3 (5.0 equiv), DME, 85°C , 2 h, 62%. dppf = diphenylphosphanylferrocene, Cy = cyclohexyl.

generated in modest yield (42%) using the conditions described by Ishiyama et al.^[15] and, gratifyingly, **27** could readily be coupled with **14** using $[\text{Pd}(\text{dppf})\text{Cl}_2]$ and K_2CO_3 in DME at 85°C to afford **4** in 62% yield. As expected, ^1H NMR analysis of **4** indicated a diastereomeric mixture of four compounds due to the mixture of C_{11} epimers and atropisom-

ers around the newly formed C₁₆–C₁₈ biaryl linkage, confirming a result observed earlier in a related system.^[2c] Unfortunately, although we were extremely pleased to have prepared **4** in only 16 linear steps from known starting materials, our excitement was quickly dashed when attempted olefin metatheses (toluene, 70 °C, several days) in the presence of catalysts **28**, **29**, or **30**^[16] failed to result in **3** and led only to recovered starting material or decomposition. Although we recognized from the outset that olefin metathesis in this system would prove challenging, with potential difficulties arising from the presence of heterocycles containing basic nitrogen atoms and the fact that styrene derivatives are less favorable substrates for the reaction,^[17] we believe that steric hindrance close to the double bonds is the overriding factor which prevents successful formation of **3**.^[18]

Despite these discouraging results, we felt that our overall synthetic plan could be resurrected, with little alteration of the previously developed chemistry, by utilizing an intramolecular variant of the HWE reaction, an extremely powerful and mild C–C bond-forming process which has been widely employed in organic synthesis.^[19] Although we desired to construct an intermediate such as **5** (see Scheme 1) possessing the requisite aldehyde and phosphonate functionalities necessary for condensation, based on our failure to generate alkene **26** from **25** using Ph₃P=CH₂ we felt that the carefully constructed lactol system would have to be opened prior to the key HWE reaction to prevent similar formation of a 3-arylbzofuran product. As such, we initiated efforts to prepare key intermediate **34**, as delineated in Scheme 6. The indole phosphonate **31** was readily generated in 74% overall yield from the previously synthesized indole–oxazole **12** by initial removal of the TBDPS group upon exposure to TBAF, halogen exchange of the resultant hydroxy group, and mild formation of the phosphonate residue by S_N2 displacement of the primary iodide using the anion generated from dimethyl phosphite. The other key building block, compound **32**, was synthesized in two steps from **24** in 63% overall yield utilizing LiBH₄ to fully reduce the lactone, followed by methylation of both the phenolic and the primary hydroxy groups. As before, the boronate ester of **32** was synthesized in 49% yield using bis(pinacolato)diboron in the presence of [Pd(dppf)Cl₂] and KOAc, and this intermediate could then be directly coupled to phosphonate **31** in 52% yield utilizing the Suzuki reaction protocol employed earlier.^[20] Subsequent cleavage of the TBS ether followed by Dess–Martin oxidation provided the key aldehyde phosphonate **34** in 85% yield over the two steps. Despite the failure of initial attempts to effect macrocyclization under mildly basic conditions (K₂CO₃, [18]crown-6),^[19b,c] use of LiCl and DBU^[21] smoothly led to the formation of a



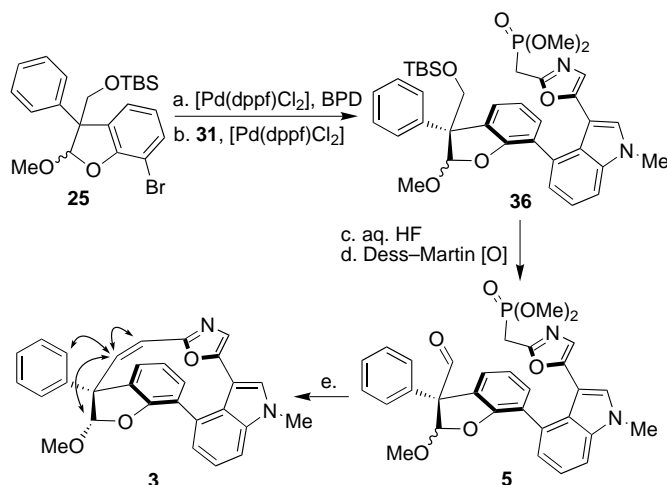
Scheme 6. Formation of macrocyclic alkene **35**: a) TBAF (1.0 M in THF, 1.5 equiv), THF, 25 °C, 15 min, 92%; b) Ph₃P (1.7 equiv), imidazole (2.0 equiv), I₂ (1.5 equiv), CH₂Cl₂, 0 °C, 10 min, 94%; c) (MeO)₂P(=O)H (2.0 equiv), KHMDS (0.5 M in toluene, 1.5 equiv), THF, 0 °C, 10 min, 86%; d) LiBH₄ (2.0 M in THF, 2.0 equiv), Et₂O, 0 °C, 2 h, 90%; e) NaH (60% dispersion in mineral oil, 5.0 equiv), MeI (10.0 equiv), THF, 25 °C, 12 h, 70%; f) bis(pinacolato)diboron (1.2 equiv), [Pd(dppf)Cl₂]·CH₂Cl₂ (0.15 equiv), KOAc (3.0 equiv), DMSO, 90 °C, 4 h, 49%; g) **31** (1.0 equiv), [Pd(dppf)Cl₂]·CH₂Cl₂ (0.30 equiv), K₂CO₃ (5.0 equiv), DME, 85 °C, 2 h, 52%; h) aq. HF, MeCN, 0 °C, 15 min; i) Dess–Martin periodinane (2.0 equiv), NaHCO₃ (2.0 equiv), CH₂Cl₂, 0–25 °C, 1 h, 85% over two steps; j) DBU (5.0 equiv), LiCl (5.0 equiv), MeCN, 25 °C, 6 h, 45%. BPD = bis(pinacolato)diboron, DBU = 1,8-diazabicyclo[5.4.0]undec-7-ene, KHMDS = potassium salt of 1,1,1,3,3,3-hexamethyldisilazane. Selected NOE interactions shown for **35** confirm the indicated stereochemistry.

new product in just 6 h at ambient temperature in 45% yield. Although NMR analysis of this HWE product confirmed that macrocyclization did indeed occur, NOE studies verified that only a single diastereomer of **34** reacted, providing **35** with the indicated undesired stereochemistry. As such, this particular pathway does not represent a viable method to prepare model system **3** since the previously opened F ring is inaccessible from **35**. However, the power of the HWE reaction to effect macrocyclization and install such a *trans* alkene in this highly strained system was encouraging. As such, we felt that we had to test whether our earlier reservations about employing aldehyde phosphonate **5** for an intramolecular HWE reaction were warranted.

Towards this end, **5** (see Scheme 7) was easily synthesized in four steps from **25** and **31** utilizing chemistry described earlier and, most gratifyingly, subsequent treatment of **5** with NaH in THF at 0 °C resulted in the formation of macrocycle **3** in 25% yield with none of the previously feared cyclofragmentation observed. Although NMR analysis of all intermediates from

Table 1. Selected physical properties for compounds **35** and **3**.

<p>35: R_f = 0.12 (silica gel, ethyl acetate/hexane 1/1); IR (film): $\tilde{\nu}_{\max}$ = 2912, 2851, 1590, 1487, 1451, 1410, 1371, 1226, 1108, 1010, 795, 703 cm^{-1}; ^1H NMR (600 MHz, CD_3CN): δ = 7.98 (d, J = 17.5 Hz, 1H), 7.46 (s, 1H), 7.44 (dd, J = 8.3, 0.8 Hz, 1H), 7.42 (dd, J = 8.3, 1.3 Hz, 1H), 7.36 (t, J = 7.9 Hz, 1H), 7.25–7.23 (m, 2H), 7.15 (dd, J = 8.1, 1.5 Hz, 1H), 6.98 (t, J = 7.7 Hz, 1H), 6.98 (dd, J = 7.4, 0.9 Hz, 1H), 6.85 (s, 1H), 6.82 (dd, J = 7.4, 1.7 Hz, 1H), 5.87 (d, J = 17.5 Hz, 1H), 4.26 (AB, J = 9.2 Hz, ν_{ab} = 64.7 Hz, 2H), 3.81 (s, 3H), 3.31 (s, 3H), 2.53 (s, 3H); ^{13}C NMR (150 MHz, CD_3CN): δ = 162.0, 157.6, 149.3, 148.2, 146.1, 141.1, 139.4, 139.2, 134.0, 130.4, 130.3, 129.0, 128.8, 127.1, 125.5, 125.4, 123.9, 122.3, 122.3, 117.9, 114.5, 110.8, 104.3, 75.3, 60.3, 60.2, 59.5, 33.7; HR-MS (matrix-assisted laser desorption/ionization) for $\text{C}_{30}\text{H}_{27}\text{N}_2\text{O}_3^+$ [$M+H^+$]: calcd: 463.2016, found: 463.2005.</p> <p>3: R_f = 0.18 (silica gel, ethyl acetate/hexane 1/1); IR (film): $\tilde{\nu}_{\max}$ = 2925, 1591, 1492, 1446, 1373, 1225, 1190, 1115, 928, 747 cm^{-1}; ^1H NMR (600 MHz, CD_3CN): δ = 7.53 (dd, J = 8.3, 0.8 Hz, 1H), 7.46 (s, 1H), 7.42–7.38 (m, 5H), 7.33–7.29 (m, 1H), 7.20 (dd, J = 7.0, 0.9 Hz, 1H), 6.97 (dd, J = 8.5, 1.3 Hz, 1H), 6.95 (dd, J = 8.3, 1.3 Hz, 1H), 6.90 (d, J = 12.7 Hz, 1H), 6.86 (s, 1H), 6.81 (t, J = 7.4 Hz, 1H), 6.46 (d, J = 12.7 Hz, 1H), 5.99 (s, 1H), 3.88 (s, 3H), 3.17 (s, 3H); ^{13}C NMR (150 MHz, CD_3CN): δ = 159.0, 146.0, 143.0, 138.5, 132.5, 131.9, 131.0, 130.9, 130.2, 129.4, 128.7, 127.9, 127.8, 126.4, 126.3, 124.5, 124.0, 123.3, 123.0, 122.0, 121.6, 119.1, 116.7, 110.9, 61.0, 57.9, 33.7; HR-MS (matrix-assisted laser desorption/ionization) for $\text{C}_{29}\text{H}_{23}\text{N}_2\text{O}_3^+$ [$M+H^+$]: calcd: 447.1703, found: 447.1707.</p>



Scheme 7. Synthesis of heterocyclic macrocycle **3**: a) Bis(pinacolato)diboron (1.2 equiv), $[\text{Pd}(\text{dppf})\text{Cl}_2] \cdot \text{CH}_2\text{Cl}_2$ (0.15 equiv), KOAc (3.0 equiv), DMSO, 90 °C, 4 h, 50%; b) **31** (1.0 equiv), $[\text{Pd}(\text{dppf})\text{Cl}_2] \cdot \text{CH}_2\text{Cl}_2$ (0.30 equiv), K_2CO_3 (3.0 equiv), DME, 85 °C, 2 h, 60%; c) aq. HF, MeCN, 0 °C, 15 min; d) Dess–Martin periodinane (2.0 equiv), NaHCO_3 (2.0 equiv), CH_2Cl_2 , 25 °C, 8 h, 85% over two steps; e) NaH (2.0 equiv), THF, 0 °C, 1 h, 25%. Selected NOE interactions shown for **3** confirm the indicated stereochemistry.

36 onward indicated a diastereomeric mixture of four compounds (due to a mixture of C_{11} epimers and atropisomerism around the C_{16} – C_{18} linkage), similar examination of **3** indicated that only a single diastereomer, which possesses the stereochemistry shown, resulted from this final transformation. Theoretically, one would expect a 50% yield from this HWE reaction since the atropisomers cannot interconvert at the reaction temperatures employed and only half of the material would have both the aldehyde and phosphonate groups on the same side of the molecule. Although this expectation was met, surprisingly only one of the C_{11} epimers

underwent the condensation reaction. Despite this unexpected outcome, the HWE reaction still served as an excellent means by which to separate the C_{16} – C_{18} atropisomers which resulted from the Suzuki coupling, providing **3** in atropisomerically pure form.

In conclusion, although the synthesis of the heterocyclic core of diazonamide A initially seemed elusive after numerous failed approaches, both as illustrated here as well as in several attempts whose description will have to await the full account of this work, the power of the Suzuki and HWE reactions to effect C–C bond formation has ultimately provided a highly convergent solution for the preparation of model system **3** in just 17 linear steps from known starting materials. As such, multigram quantities of both **25** and **31** are available, and analogues of both fragments for future biological studies can readily be incorporated into the existing synthetic pathway. Additionally, the chemistry described for the preparation of **25** has already been employed^[22] to synthesize a tyrosine-derived benzofuranone fragment possessing the requisite functionality necessary to complete diazonamide A. Continuing studies aim at the total synthesis of diazonamide A and further investigations of the chemical biology of this important new class of antitumor agents.

Received: August 2, 2000 [Z15571]

- N. Lindquist, W. Fenical, G. D. Van Duyne, J. Clardy, *J. Am. Chem. Soc.* **1991**, *113*, 2303–2304.
- For other approaches towards the synthesis of diazonamide A, see: a) X. Chen, L. Esser, P. G. Harran, *Angew. Chem.* **2000**, *112*, 967–970; *Angew. Chem. Int. Ed.* **2000**, *39*, 937–940; b) E. Vedejs, J. Wang, *Org. Lett.* **2000**, *2*, 1031–1032; c) E. Vedejs, D. A. Barba, *Org. Lett.* **2000**, *2*, 1033–1035; d) P. Magnus, E. G. McIver, *Tetrahedron Lett.* **2000**, *41*, 831–834; e) F. Chan, P. Magnus, E. G. McIver, *Tetrahedron Lett.* **2000**, *41*, 835–838; f) F. Lach, C. J. Moody, *Tetrahedron Lett.* **2000**, *41*, 6893–6896; g) M. C. Bagley, S. L. Hind, C. J. Moody, *Tetrahedron Lett.* **2000**, *41*, 6897–6900; h) M. C. Bagley, C. J. Moody, A. G. Pepper, *Tetrahedron Lett.* **2000**, *41*, 6901–6904; i) H. C. Hang, E. Drotleff, G. I. Elliott, T. A. Ritsema, J. P. Konopelski, *Synthesis* **1999**, 398–400; j) P. Magnus, J. D. Kreisberg, *Tetrahedron Lett.* **1999**, *40*, 451–454; k) A. Boto, M. Ling, G. Meek, G. Pattenden, *Tetrahedron Lett.* **1998**, *39*, 8167–8170; l) P. Wipf, F. Yokokawa, *Tetrahedron Lett.* **1998**, *39*, 2223–2226; m) S. Jeong, X. Chen, P. G. Harran, *J. Org. Chem.* **1998**, *63*, 8640–8641; n) C. J. Moody, K. J. Doyle, M. C. Elliott, T. J. Mowlem, *J. Chem. Soc. Perkin Trans. 1* **1997**, 2413–2419; o) J. P. Konopelski, J. M. Hottenroth, H. M. Oltra, E. A. Véliz, Z. C. Yang, *Synlett* **1996**, 609–611; p) C. J. Moody, K. J. Doyle, M. C. Elliott, T. J. Mowlem, *Pure Appl. Chem.* **1994**, *66*, 2107–2110.
- Recent examples of macrocyclization resulting from olefin metathesis include applications to the total synthesis of Sch 38516: Z. Xu, C. W. Johannes, S. S. Salman, A. H. Hoveyda, *J. Am. Chem. Soc.* **1996**, *118*, 10926–10927; epothilone A: K. C. Nicolaou, N. Winssinger, J. Pastor, S. Ninkovic, F. Sarabia, Y. He, D. Vourloumis, Z. Yang, T. Li, P. Giannakakou, E. Hamel, *Nature* **1997**, *387*, 268–272; and manzamine A: S. F. Martin, J. M. Humphrey, A. Ali, M. C. Hillier, *J. Am. Chem. Soc.* **1999**, *121*, 866–867.
- P. J. Harrington, L. S. Hegedus, *J. Org. Chem.* **1984**, *49*, 2657–2662.
- T. Severin, H.-J. Böhm, *Chem. Ber.* **1968**, *101*, 2925–2930.
- G. A. Roth, E. L. McClymont, *Synth. Commun.* **1992**, *22*, 411–420.
- See: Ref. [21] and Y. Oikawa, T. Toshioka, K. Mohri, O. Yonemitsu, *Heterocycles* **1979**, *12*, 1457–1462.
- IBX can readily be prepared from 2-iodobenzoic acid and oxone following the method of Santagostino et al. see: M. Frigerio, M. Santagostino, S. Sputore, *J. Org. Chem.* **1999**, *64*, 4537–4538.
- P. Wipf, C. P. Miller, *J. Org. Chem.* **1993**, *58*, 3604–3606.

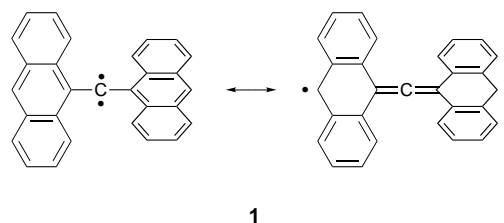
- [10] T. Mizuno, M. Takeuchi, S. Shinkai, *Tetrahedron* **1999**, *55*, 9455–9468.
- [11] In general, Lewis acid catalysts are required to direct the attack of nucleophiles towards the more substituted carbon of an epoxide (see: A. Mordini, S. Bindi, S. Pecchi, A. Capperucci, A. Degl'Innocenti, G. Reginato, *J. Org. Chem.* **1996**, *61*, 4466–4468). However, based on Baldwin's rules, we felt that the greater favorability of 5-*exo*-tet cyclization compared to the competing 6-*endo*-tet reaction would afford the desired product **21** in this case.
- [12] K. C. Nicolaou, S. A. Snyder, A. Bigot, J. A. Pfefferkorn, *Angew. Chem.* **2000**, *112*, 1135–1138; *Angew. Chem. Int. Ed.* **2000**, *39*, 1093–1096.
- [13] Crystallographic data (excluding structure factors) for structure **23** reported in this paper have been deposited with the Cambridge Crystallographic Data Centre as supplementary publication no. CCDC-147867. Copies of the data can be obtained free of charge on application to CCDC, 12 Union Road, Cambridge CB21EZ, UK (fax: (+44) 1223-336-033; e-mail: deposit@ccdc.cam.ac.uk).
- [14] Although the conversion of secondary nitriles into ketones is known (see: R. W. Freerksen, S. J. Selikson, R. W. Wroble, K. S. Kyler, D. S. Watt, *J. Org. Chem.* **1983**, *48*, 4087–4096), this represents the first reported application of this methodology for the generation of lactones.
- [15] T. Ishiyama, M. Murata, N. Miyaara, *J. Org. Chem.* **1995**, *60*, 7508–7510.
- [16] M. Scholl, S. Ding, C. W. Lee, R. H. Grubbs, *Org. Lett.* **1999**, *1*, 953–956.
- [17] For an example of a ring-closing metathesis (RCM) in the presence of an N atom, see: A. Fürstner, J. Grabowski, C. W. Lehmann, *J. Org. Chem.* **1999**, *64*, 8275–8280. In our case, however, the chelating ability of the nitrogens in the indole and oxazole rings is likely to be poor and is not an overriding concern for RCM. For an example of RCM involving an oxazole, see: K. C. Nicolaou, H. Vallberg, N. P. King, F. Roschangar, Y. He, D. Vourloumis, C. G. Nicolaou, *Chem. Eur. J.* **1997**, *3*, 1957–1970.
- [18] For pertinent discussion on the role of sterics in metathesis reactions, see: a) R. H. Grubbs, S. Chang, *Tetrahedron* **1998**, *54*, 4413–4450; b) R. H. Grubbs, S. J. Miller, G. C. Fu, *Acc. Chem. Res.* **1995**, *28*, 446–452.
- [19] For representative examples of the power of Wittig and Horner–Wadsworth–Emmons reactions to induce intramolecular macrocyclizations of complex substrates, see: a) I. Ernest, J. Gosteli, C. W. Greengrass, W. Holick, D. E. Jackman, H. R. Pfaendler, R. B. Woodward, *J. Am. Chem. Soc.* **1978**, *100*, 8214–8222; b) K. C. Nicolaou, S. P. Seitz, M. R. Pavia, N. A. Petasis, *J. Org. Chem.* **1979**, *44*, 4011–4013; c) K. C. Nicolaou, R. A. Daines, T. K. Chakraborty, Y. Ogawa, *J. Am. Chem. Soc.* **1988**, *110*, 4685–4696. For a recent review on the Wittig and HWE reactions in total synthesis, see: K. C. Nicolaou, M. W. Härter, J. L. Gunzner, A. Nadin, *Liebigs Ann.* **1997**, 1283–1301.
- [20] To the best of our knowledge, this represents the first example of a phosphonate being successfully employed in a Suzuki-type coupling reaction.
- [21] M. A. Blanchette, W. Choy, J. T. Davis, A. P. Essensfeld, S. Masamune, W. R. Roush, T. Sakai, *Tetrahedron Lett.* **1984**, *25*, 2183–2186.
- [22] K. C. Nicolaou, A. E. Koumbis, S. A. Snyder, K. B. Simonsen, *Angew. Chem.* **2000**, *112*, 2629–2633; *Angew. Chem. Int. Ed.* **2000**, *39*, 2529–2533.

Triplet Di(9-anthryl)carbene Undergoes Trimerization**

Yasutake Takahashi, Masaaki Tomura, Ken-ichi Yoshida, Shigeru Murata, and Hideo Tomioka*

A large number of triplet carbenes have been characterized by electron paramagnetic resonance (EPR) spectroscopy.^[1, 2] The principal information extracted from EPR spectra of triplet carbenes in randomly oriented matrices are the zero-field splitting (ZFS) parameters *D* and *E*, where *D* is a measure of the number of the unpaired electrons and thus allows the amount of delocalization in a carbene with conjugated π systems to be determined, while *E* measures the difference in the magnetic dipole interaction and, when weighted by *D*, allows one to estimate the bond angle at the carbene center.

Among the many triplet carbenes known, triplet di(9-anthryl)carbene (**1**) is unique as it shows the smallest *D* (0.113 cm⁻¹) and *E* (0.0011 cm⁻¹) values ever reported. This



means that the carbene has almost linear and perpendicular geometry with extensive delocalization of the unpaired electrons into the anthryl portions of the molecule.^[3]

Although these spectroscopic results suggest that the carbene should exhibit a reactivity that is substantially different from that observed for other diarylcarbenes, its chemistry has not been studied extensively. Herein we report that the carbene undergoes an unusual trimerization reaction, one that has never been observed before for any other carbenes.^[4]

[*] Prof. Dr. H. Tomioka, Prof. Dr. Y. Takahashi, K.-i. Yoshida
Chemistry Department for Materials
Faculty of Engineering, Mie University
Tsu, Mie 514-8507 (Japan)
Fax: (+81) 59-231-9416
E-mail: tomioka@chem.mie-u.ac.jp

Dr. M. Tomura
Research Center for Molecular Materials
Institute for Molecular Science
Okazaki, Aichi 444-8585 (Japan)

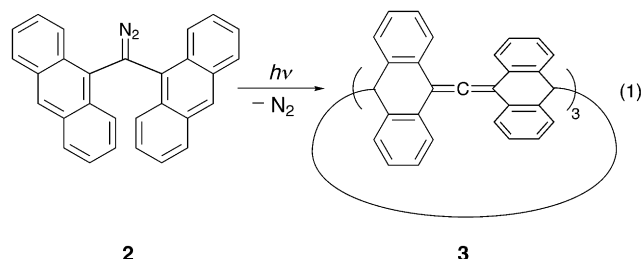
Prof. Dr. S. Murata
Department of Basic Science
Graduate School of Arts and Sciences, The University of Tokyo
Meguro, Tokyo 153-8902 (Japan)

[**] This work was supported by a Grant-in-Aid for Scientific Research from the Ministry of Education, Science, Sports, and Culture of Japan. We thank Prof. Dr. K. Tsujimoto (Japan Advanced Institute of Science and Technology, Hokuriku) for the FAB-MS measurement.



Supporting information for this article is available on the WWW under <http://www.wiley-vch.de/home/angewandte/> or from the author.

Irradiation ($\lambda > 300$ nm) of di(9-anthryl)diazomethane (**2**, 5×10^{-3} M) in degassed benzene caused rapid fading of the original orange diazo color with evolution of copious amounts of nitrogen gas to give a pale yellow solution [Eq. (1)]. After evaporation of the solvent, the resulting mixture was subjected to repeated gel-permeation chromatography, which eventually resulted in the isolation of white crystals



(m.p. 332–333 °C) in 50% yield. The mass spectrum (FAB-MS) of the product showed a signal at 1099.1 (19.1%), which corresponds to the $M + 1$ ion calculated for three di(anthryl)-carbene units. Additional peaks were observed at 732.1 (19.6%) and 366 (100%), which correspond to the fragment formed as a result of the successive loss of the carbene unit from the trimer. Thus, the data clearly suggest that the main product is the trimer of di(anthryl)carbene, rather than a dimer as had been suspected earlier.^[3b]

The structure of the trimer which best explains the NMR data is the one (**3**) formed as a result of a threefold coupling at positions 10 of the di(anthryl)carbenes. Thus, the ^1H NMR spectrum (500 MHz) showed the presence of eight aromatic proton signals ranging from $\delta = 7.79$ to 5.91 plus one signal at $\delta = 4.82$, which corresponds to a proton at a benzylic carbon atom.^[5] The ^{13}C NMR spectrum (126 MHz), on the other hand, displayed a total of twelve aromatic sp^2 signals between $\delta = 136.42$ and 125.46. In addition, two signals were observed at $\delta = 208.34$ and 111.10, which can most probably be assigned as the central and terminal carbon atoms of the allenic subunit, respectively, and one sp^3 carbon atom at $\delta = 55.06$. The assignments are fully supported by two-dimensional NMR measurements (see the Supporting Information).

The molecular structure of the trimer was unambiguously characterized by an X-ray crystallographic study. The analysis of **3** revealed that the compound has a complicated structure and contains a 27-membered ring with six fused benzo groups, which are oriented equatorially, and six bridging benzene subunits, three of which protrude axially on either side of the basic ring (Figure 1).^[6,7] The crystal lattice contains one crystallographically independent molecule of **3** and a solvent molecule (CH_2Cl_2) with 0.477 occupancy. No crystallographic symmetry element lies on **3**. The bond lengths in the allene moieties are normal,^[8] but the allene moieties bend slightly (177.2°).^[9] The 9-hydroanthracene moieties around the allene bonds are almost perpendicular to each other. The average value of the angles between the least-squares planes of the central six-membered rings at both ends of the allene bonds is 87.3° .

In spite of its sterically highly congested structure, trimer **3** exhibited surprising stability. It remained unchanged either upon heating in degassed benzene at 140°C for 2 h or by irradiating it in degassed benzene with light ($\lambda > 300$ nm) for

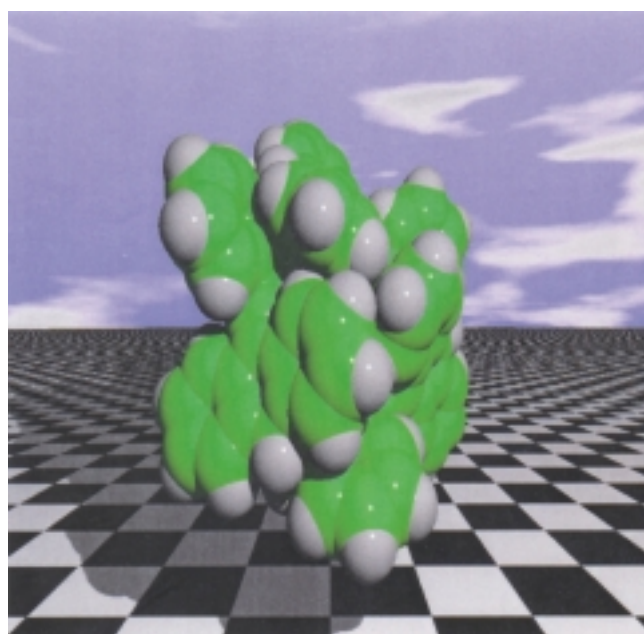
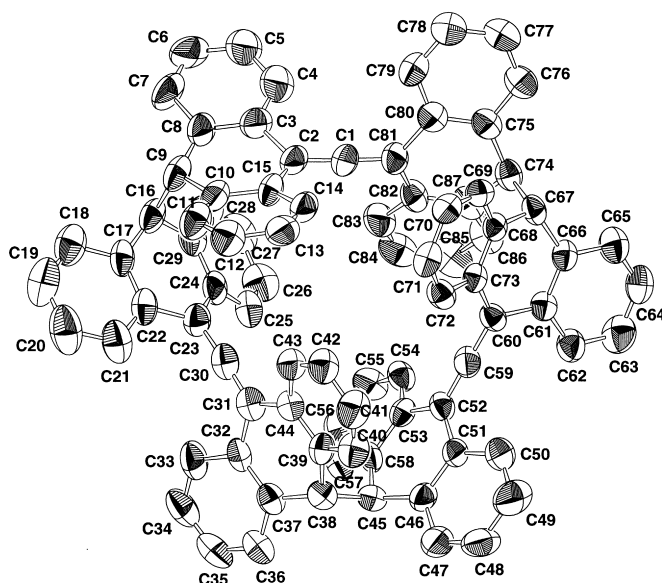


Figure 1. The X-ray crystallographic structure of the trimer **3**. Top: ORTEP drawing of **3** showing the labeling scheme; the solvent molecule (CH_2Cl_2) and the hydrogen atoms are omitted for clarity. Selected bond lengths [\AA] and angles [$^\circ$]: C1–C2 1.320(12), C1–C81 1.322(12), C23–C30 1.331(12), C30–C31 1.307(12), C52–C59 1.320(10), C59–C60 1.322(11); C2–C1–C81 $175.9(10)$, C23–C30–C31 $176.4(10)$, C52–C59–C60 $179.4(9)$. Bottom: Space-filling presentation of the structure.

2 h. However, it decomposed in air both thermally and photochemically to give anthraquinone as the main product.

Triplet carbenes, like radicals, can dimerize in a very fast and exothermic reaction. The efficiency of this process clearly depends on the concentration of the carbene. However, carbene dimers are usually not produced as major products in the reactions where “normal” carbenes are generated at room temperature by the steady-state photolysis of diazo precursors in solution. The probable reason for this is that nacsent and hence singlet carbenes react very efficiently with external reagents before they undergo intersystem crossing to form the triplet. Dimers may be formed instead by the attack of the

singlet carbene on the precursor, whose concentration is much higher, and usually occurs in concomitance with the formation of a large amount of azine.^[4] The formation of dimers as main products is observed only in the reaction of relatively stable triplet carbenes.^[10] For example, di(2,4,6-trimethylphenyl)carbene (dimesitylcarbene) and hexachlorodiphenylcarbene produce the corresponding tetraarylethenes in high yield without any sign of the formation of azine even in a steady-state photolysis in solution at room temperature.^[11, 12]

The trimerization of a carbene is completely unprecedented. The structure of trimer **3** clearly indicates that simple coupling at the carbenic carbon atom is not favored, as can be easily expected from the steric hindrance around the carbene center of **1**. Thus, **3****1** is forced to undergo self-reaction at positions 10 where some spin density is localized.

A similar coupling reaction at an aromatic carbon atom is also suggested as a decaying pathway for sterically congested diarylcarbenes, as deduced from the rather dramatic effects of *para* substituents on the lifetime of the triplet carbenes.^[13] For example, the lifetime of triplet diphenylcarbenes protected by four *ortho*-bromine groups is shown to increase by some two orders of magnitude when *para*-methyl substituents are replaced by *tert*-butyl groups. However, no products resulting from such a coupling have been isolated in this case.

The unusual formation of the product as a trimer in a significant amount as a result of such coupling at the aromatic moiety is rather unusual and clearly ascribable to its unique electronic and steric features. First, extensive delocalization of the unpaired electrons into the anthryl rings in **3****1** is more prominent than that into phenyl rings in diphenylcarbenes. Second, 10,10'-diradical forms are clearly stabilized by the conjugation of each electron with the two fused aromatic rings and therefore have a sufficiently long lifetime to encounter each other in solution, even at room temperature. Inspection of the molecular structure of the trimer **3** suggests that the trimerization may take place in a way so as to avoid the congestion as much as possible. Thus, two "anthryl" groups in a diradical unit are connected by the allenic bond and hence situated perpendicular each other. Each coupling of the diradical unit at the 10 and 10' positions takes place in a staggered fashion. In this way, three diradical units are suitably folded to eventually form the intricate cyclic compound. Intramolecular coupling of both ends at the dimer stage is clearly not favored, most probably because of a rather high activation barrier to ring closure that results from the very large distance between the radical centers. In a tetramer, on the other hand, steric repulsion arises between the "blades" as a consequence of a perturbation of the delicate balance between the linkers and blades.

These considerations explain, at least in part, the reason for this unusual trimerization process of **3****1**. It is clear that further research, including the kinetics of the process, is necessary. For this reason, studies are now in progress in our laboratory to fully understand this interesting behavior of **3****1**.

Experimental Section

Crystal data for **3**: Trimer **3** was dissolved in CH₂Cl₂ and the solvent was evaporated slowly at ambient temperature for 5 d to give a single crystal of

3 that was suitable for X-ray crystallographic analysis. Crystal data for C₈₇H₅₄(CH₂Cl₂)_{0.477}: colorless plate, crystal dimensions 0.40 × 0.10 × 0.05 mm³, triclinic, space group *P*1, *a* = 12.378(1), *b* = 13.271(2), *c* = 19.308(1) Å, α = 90.20(1), β = 104.73(1), γ = 100.30(1)°, *V* = 3014.0(6) Å³, *Z* = 2, ρ_{calc} = 1.305 Mg m⁻³, Cu α radiation (λ = 1.54178 Å), 2 θ_{max} = 148°. The data were collected on an Enraf-Nonius CAD4 diffractometer at 296 K. An absorption correction and a decay correction were not applied. The structure was solved by direct methods with SHELXS-86^[6] and refined by full-matrix least-squares analysis on *F*² with SHELXL-93.^[7] A total of 8513 reflections were collected, 8220 independent reflections were included in the refinement, 812 parameters, *R*₁ = 0.0726 and *wR*₂ = 0.1695 for data with *I* > 2 σ (*I*), GOF = 0.967, max. residual electron density 0.55 e Å⁻³. All non-hydrogen atoms were refined anisotropically. Hydrogen atoms were placed geometrically and refined by using a riding model. Crystallographic data (excluding structure factors) for the structure reported in this paper have been deposited with the Cambridge Crystallographic Data Centre as supplementary publication no. CCDC-124125. Copies of the data can be obtained free of charge on application to CCDC, 12 Union Road, Cambridge CB21EZ, UK (fax: (+44)1223-336-033; e-mail: deposit@ccdc.cam.ac.uk).

Received: April 25, 2000 [Z15031]

- [1] A large number of triplet carbenes have been characterized by EPR spectroscopy since the pioneering work by Wasserman et al.: H. Wasserman, L. C. Snyder, W. A. Yager, *J. Chem. Phys.* **1964**, *41*, 1763; E. Wasserman, R. S. Hutton, *Acc. Chem. Res.* **1977**, *10*, 27.
- [2] For reviews see: a) W. Sander, G. Bucher, S. Wierlacher, *Chem. Rev.* **1993**, *93*, 1583; b) H. Tomioka in *Advances in Strained and Interesting Molecules*, Vol. 8 (Ed.: B. Halton), JAI, Stamford, **2000**, p. 83; c) A. M. Trozzolo, E. Wasserman in *Carbenes*, Vol. 2 (Eds.: M. Jones, Jr., R. A. Moss), Wiley, New York, **1975**, p. 185.
- [3] a) E. Wasserman, V. J. Kuck, W. A. Yager, R. S. Hutton, F. D. Greene, V. P. Abegg, N. M. Weinshenker, *J. Am. Chem. Soc.* **1971**, *93*, 6355; b) D. J. Astles, M. Girard, D. Griller, R.-J. Kolt, D. D. M. Wayner, *J. Org. Chem.* **1988**, *53*, 6053.
- [4] a) W. Kirmse, *Carbene Chemistry*, Academic Press, New York, **1971**; b) R. A. Moss, M. Jones, Jr., *Carbenes*, Vol. 1 and 2, Wiley, New York, **1973** and **1975**; c) M. Regitz, *Carbene (oide)*, Carbine, Houben – Weyl, Thieme, Stuttgart, **1989**.
- [5] The chemical shift is compatible with the benzylic position of 9,10,9',10'-tetrahydro-[9,9']-bianthryl: W. Huber, K. Müllen, *J. Chem. Soc. Chem. Commun.* **1980**, 698; C. M. Berk, A. Streitwieser, *J. Organomet. Chem.* **1980**, *197*, 123.
- [6] G. M. Sheldrick, *Acta Crystallogr. Sect. A* **1990**, *46*, 467.
- [7] G. M. Sheldrick, SHELXL-93, Program for refinement of crystal structures, University of Göttingen, Germany, **1993**.
- [8] a) S. R. Landor, *The Chemistry of the Allenes*, Vols. 1–3, Academic Press, London, **1982**; b) H. Irngartinger, E. Kurda, H. Rodewald, A. Berndt, R. Bolze, K. Schlüter, *Chem. Ber.* **1982**, *115*, 967; c) M. Iyoda, Y. Kuwatani, M. Oda, Y. Kai, N. Kaneshta, N. Kasai, *Angew. Chem.* **1990**, *102*, 1077; *Angew. Chem. Int. Ed. Engl.* **1990**, *29*, 1062.
- [9] Bis(biphenyl-2,2'-diyl)allene has been shown to have a bent allene bond (170.1°): E. Weber, W. Seichter, B. Hess, G. Will, H.-J. Dasting, *J. Phys. Org. Chem.* **1995**, *8*, 94.
- [10] a) H. Tomioka, *Acc. Chem. Res.* **1997**, *30*, 315; b) H. Tomioka in *Advances in Carbene Chemistry*, Vol. 2 (Ed.: U. Brinker), JAI, Stamford, **1998**, p. 175.
- [11] a) H. E. Zimmerman, D. H. Paskovich, *J. Am. Chem. Soc.* **1964**, *86*, 2149; b) H. Tomioka, K. Hirai, T. Nakayama, *J. Am. Chem. Soc.* **1993**, *115*, 1285; c) H. Tomioka, H. Okada, T. Watanabe, K. Banno, K. Komatsu, K. Hirai, *J. Am. Chem. Soc.* **1997**, *119*, 1582.
- [12] A referee suggested that the trimer **3** could also be formed by the reaction of carbene **1** with the precursor diazomethane **2** as a result of **1** attacking **2** at position 10 and that this could be checked by examining the effect of the concentration of **2** on the rate of light-induced decay of **2**. We irradiated two samples containing different concentrations of **2** under identical conditions and found essentially no dependence of the rate on the concentration of **2**. We wish to thank the referee for the suggestion.
- [13] H. Tomioka, M. Hattori, K. Hirai, S. Murata, *J. Am. Chem. Soc.* **1996**, *118*, 8723.

Synthesis of the First Fully α -Conjugated Macrocyclic Oligothiophenes: Cyclo[n]thiophenes with Tunable Cavities in the Nanometer Regime**

Jens Krömer, Idoia Rios-Carreras, Gerda Fuhrmann, Christiane Musch, Markus Wunderlin, Tony Debaerdemaeker, Elena Mena-Osteritz, and Peter Bäuerle*

Polythiophenes and their corresponding finite model oligomers, α -conjugated oligothiophenes, belong to the most frequently investigated conjugated systems as a consequence of their chemical stability in various redox states, their outstanding electronic properties, the widespread possibilities of functionalization, and consequently their potential applicability in (molecular) electronic devices, such as organic light emitting diodes, lasers, or transistors.^[1] In various series of monodisperse linear oligothiophenes with controllable and defined structure the physical properties correlate well with the (conjugated) chain length and thus valuable structure–property relationships become available.^[2] In scanning probe studies on self-assembled monolayers of regioregular poly(3-alkylthiophene)s we observed that polymer folding occurs and seven or eight *syn*-arranged thiophene units form a “hair-pin” or 180° semicircle,^[3] hence our goal was the design and preparation of novel fully (macro)cyclic α -conjugated oligothiophenes. If these systems were sufficiently stable and large, in comparison to usual linear conjugated oligomers and polymers, completely novel perspectives and properties could arise. Cyclic derivatives could represent a model system which ideally combines an infinite π -conjugated chain of an idealized polymer with the advantages of a structurally well-defined oligomer but without any perturbing end-effects.^[4] As a consequence of the resulting cavities the recognition and selective complexation of guest molecules, which may depend on the redox state of the cyclic host, additionally come into play. On the other hand, macrocyclic systems such as cyclic oligopeptides can self-assemble to form nanotubes which enables their application in biological as well as materials

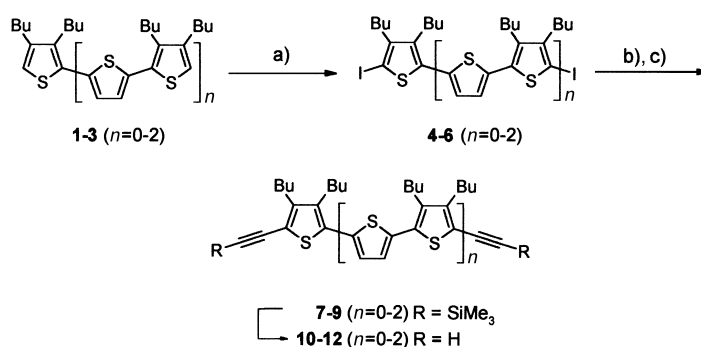
science.^[5] Herein we now report the successful synthesis and self-organization properties of a new class of conjugated macrocycles which we designate as α -cyclo[n]thiophenes (α -C[n]T).

In the 1970s Kauffmann et al. synthesized cross-conjugated cyclo[4]- and cyclo[6]thiophene from bithiophene precursors. However, these systems are only very weakly conjugated because of α,β - or β,β -linkages of the thiophene units.^[6] Thiophene-derived annulenes consisting of thiophene units and *cis* double bonds are also only partially conjugated.^[7] Quantum chemical calculations on α -conjugated cyclo[12]-thiophene result in a nearly nonstrained and coplanar conformation in which all 12 thiophene rings are arranged in a *syn* fashion, which demonstrates the importance and the feasibility of such macrocycles.^[8]

Typically, *m*-phenylene units or other electronically weak coupling units are used as angular building blocks to favor the formation of macrocycles.^[9] The largest ring so far, a 90-membered cyclic oligophenylene synthesized by repetitive Suzuki cross-coupling reactions by Schlüter et al., contains 24 phenylene rings and an estimated cavity of 3–3.5 nm, but lacks overall conjugation because of the electronic interruption by the angular corner units.^[10]

Our synthetic strategy relied on the common method to prepare macrocycles which involves oligomerization and cyclization at the same time. Since various products are generated in a single step, the yields are typically low and critically depend on the building blocks, the ring size, and the feasibility of separating the mixtures.^[11] Since attempts to use transition metal catalyzed cross-coupling reactions for the synthesis of the envisaged α -C[n]Ts completely failed,^[12] the intramolecular oxidative coupling of novel α,α' -difunctionalized thiophenediynes was used. The subsequent reaction of the products with sulfide anions should then result in the desired macrocycles.

The butylated thiophenes **1–3** were chosen as the starting materials for the synthesis of the required building blocks (Scheme 1). These thiophenes were synthesized as part of a



Scheme 1. Synthesis of thiophenediynes **10–12** as modular building blocks for the macrocyclization reactions. a) 2 I₂, Hg(OAc)₂, CHCl₃, 0–20 °C, 2 h; b) TMSA, [Pd(PPh₃)₂Cl₂], CuI, NEt₃, pyridine, 60 °C, 12 h; c) KOH, MeOH, THF, RT, 1 h.

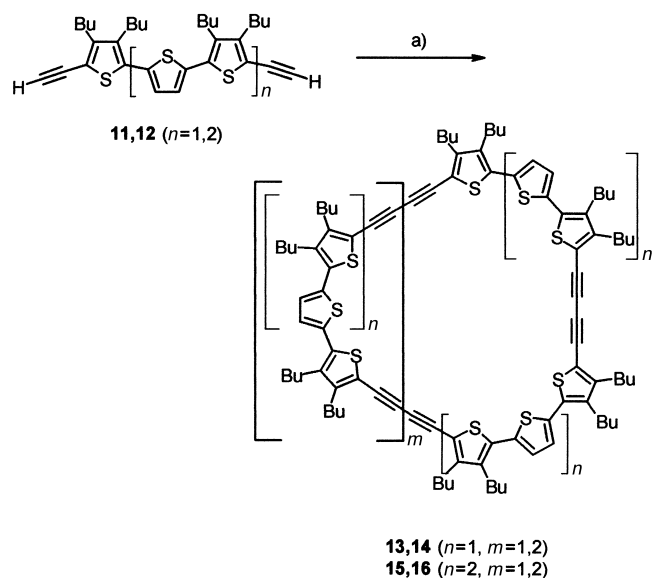
homologous series of linear oligothiophenes containing parent oligomers up to a 19-mer.^[13] Symmetrical substitution of thiophene units with butyl groups proved to be ideal for

[*] Prof. Dr. P. Bäuerle, Dr. J. Krömer, Dipl.-Chem. I. Rios-Carreras, Dipl.-Chem. G. Fuhrmann, Dr. C. Musch, Dr. M. Wunderlin, Dr. E. Mena-Osteritz
Abteilung Organische Chemie II
(Organic Materials and Combinatorial Chemistry)
Sektion Massenspektrometrie
Universität Ulm
Albert-Einstein-Allee 11, 89081 Ulm (Germany)
Fax: (+49) 731-502-2840
E-mail: peter.baeuerle@chemie.uni-ulm.de
Prof. Dr. T. Debaerdemaeker
Sektion Röntgen- und Elektronenbeugung
Universität Ulm
Albert-Einstein-Allee 11, 89081 Ulm (Germany)

[**] This work was supported by Fonds der Chemischen Industrie. We gratefully acknowledge helpful discussions with Priv.-Doz. Dr. S. Höger (MPI Mainz) and Dr. M. Mayor (Forschungszentrum Karlsruhe). We also would like to thank Dr. W. Amrein (ETH Zürich) for the initial measurement of MALDI-TOF mass spectra and Dr. R. Azumi (NIMCR, Tsukuba, Japan) for her help in crystallization experiments.

maintaining sufficient solubility and avoiding problems of regioisomer formation. In the first step, thiophenes **1–3** were selectively iodinated at the α -positions by elemental iodine and mercury(II) acetate in chloroform to yield diiodothiophenes **4–6** in 94, 85, and 87 %, respectively. The introduction of the terminal acetylenic groups was achieved by palladium-catalyzed Sonogashira–Hagihara coupling^[14] of diiodothiophenes **4–6** and trimethylsilylacetylene (TMSA). The TMS-protected thiophenes **7–9** were isolated in 69, 76, and 70 %, respectively, and deprotected nearly quantitatively under mild basic conditions to yield the thiophenediynes **10–12**. They were immediately used for subsequent coupling reactions after chromatographic work-up because of their inherent instability and tendency to polymerize.

Oxidative coupling of the smallest building block, 3,4-dibutyl-2,5-diethynylthiophene (**10**), was performed under various high-dilution conditions (Glaser: CuCl/CuCl₂/pyridine;^[15] Eglinton: Cu(OAc)₂/pyridine/MeOH;^[16] Hay: CuCl/O₂/TMEDA/CHCl₃^[17] (TMEDA = *N,N,N',N'*-tetramethylethylenediamine)). An immediate reaction was observed in each case and complex, nonseparable mixtures of linear and cyclic structures with 3–12 repeating units were obtained, as indicated by the ¹H NMR, IR, and matrix-assisted laser desorption/ionization time-of-flight (MALDI-TOF) mass spectra.^[18] Much better results were obtained by a modified Eglinton–Glaser coupling^[9c, 19] of the higher homologues, terthiophenediyne **11** and quinquethiophenediyne **12**, under pseudo-high-dilution conditions (Scheme 2). Pyridine solu-



Scheme 2. Macrocyclization of thiophenediynes **11** and **12** under modified Eglinton–Glaser conditions to the mixed cyclooligothiophenediacetylenes **13–16**. a) CuCl, CuCl₂, pyridine, RT, 44 + 48 h.

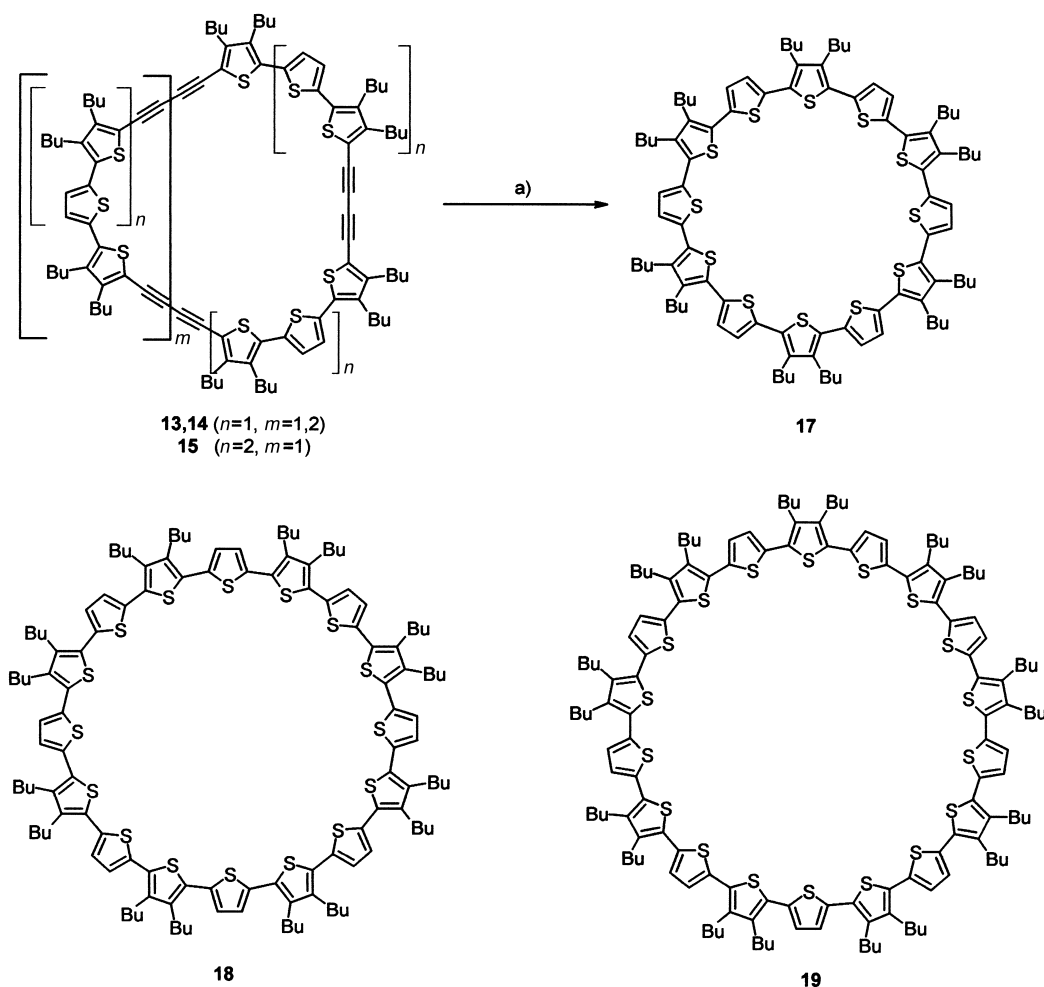
tions of the oligothiophenes were added by means of a syringe-pump over 3 days to a slurry of anhydrous CuCl and CuCl₂ in pyridine at room temperature. Characterization of the crude product mixtures by ¹H NMR spectroscopy and MALDI-TOF mass spectrometry indicated that cyclic products had already been formed. Separation of the mixtures by preparative HPLC resulted in the isolation of analytically

pure macrocyclic oligothiophenediacetylenes **13–16** as stable, bright yellow to red microcrystalline solids which have high solubility in most common organic solvents. In both cases the cyclotrimers **13** and **15** ($m=1$) and the cyclotetramers **14** and **16** ($m=2$) were isolated as the main products (yields 2–12 %).^[20]

A cyclodimer ($n=2, m=0$) and higher homologues ($n=1, m=3–7$; $n=2, m=3–6$) could also be detected by HPLC and assigned by MALDI-TOF-MS. ¹H, ¹³C NMR, and MALDI-TOF MS characterization of the isolated macrocycles **13–16** are in full accordance with the proposed structures. The high symmetry of the molecules made assignment of all the signals in the the NMR spectra possible. In each case, unambiguous structural proof came from MALDI-TOF mass spectrometry exhibiting exclusively one intense signal which corresponds to the theoretical mass of the macrocycle. Finally, we obtained macrocycles **13–16** with 39, 52, 57, and 76 chain members, respectively. Semiempirical calculations at the AM1 level showed the macrocycles have cavities with internal diameters of 1.37, 1.99, 2.14, and 3.07 nm, respectively (largest non-bonding S...S distance).^[21]

Dithienylbutadiynes react with sulfur nucleophiles in methanol to give the corresponding terthiophenes in excellent yields.^[22] We optimized this protocol for the synthesis of the linear parent compounds, and found that the butyl side chains exert sterical constraints on adjacent diyne units so that the reaction temperature had to be raised.^[13] Analogous reactions of macrocycles **13–15** with sodium sulfide gave the fully α -conjugated cyclo[*n*]thiophenes **17–19** (Scheme 3). Transformation of three diyne units in compounds **13** and **15** resulted in analytically pure cyclo[12]thiophene **17** and cyclo[18]thiophene **19** in 23 % and 27 % yield, respectively, after purification. Cyclo[16]thiophene **18** was isolated in 7 % yield after the reaction of the four diyne moieties in macrocycle **15**. These values correspond to 52–64 % per cyclization step and are in good agreement with the reactions of linear derivatives. The three macrocycles **17–19** are stable, bright yellow to red microcrystalline solids which are highly soluble in most common organic solvents. Characterization of the cyclo[*n*]thiophenes from their ¹H, ¹³C NMR, and MALDI-TOF mass spectra unequivocally proved the proposed structures.^[23] Although the novel macrocycles could be considered as $(4n)\pi$ antiaromatics, no obvious ring current shifts are observed, which indicates they have a benzenoid rather than annulenoid character. Cyclo[*n*]thiophenes **17–19** comprise 36, 48, and 54 chain members, respectively, and according to semiempirical calculations form cavities with inner diameters of 1.28, 1.81, and 2.00 nm, respectively (largest nonbonding S...S distance). The calculated strain energies of the cycles is rather low (0.0–1.8 kcal mol^{−1}).

Investigations of the optical and electrochemical properties of the new macrocycles and their correlation to structural and conformational features revealed rather surprising results and will be reported in detail elsewhere. The detailed structure of the macrocycles and their intermolecular interactions in the solid state are important features with respect to their use as large molecular building blocks to assemble new materials in a controlled manner. X-ray structure analysis of ring-shaped structures, however, are inherently difficult since the large



Scheme 3. Reaction of the mixed cyclooligothiophenediacetylenes **13–15** to the fully α -conjugated cyclo[n]thiophenes **17–19**. a) $\text{Na}_2\text{S} \cdot 9\text{H}_2\text{O}$, 2-methoxyethanol, *p*-xylene, 4 h reflux.

cavities in the crystal are typically filled by solvent molecules and cause structural disorder or destruction of the crystal when the solvent is lost.^[9c, 24] Both series of thiophene-containing macrocycles exhibited relatively high melting points which indicate strong π – π interactions between the molecules in the solid state. Oligothiophenediacetylene **14** crystallizes from toluene in orange prisms suitable for X-ray structure analysis.^[25] Their investigation gave unambiguous proof of the macrocyclic structure of **14** although the disorder of some of the butyl side chains made the refinement very difficult (R value after anisotropic refinement 0.145). The top view of an individual molecule (including atomic labeling), views of the unit cell, and the structure along various axes are given in Figure 1. The macrocycle forms a nearly planar rounded rectangle comprising all-*syn*-oriented terthiophene units at the edges which are connected by moderately strained diacetylene units (Figure 1a). Their angles are typical for distorted dehydroannulenes^[26] and cyclophanes^[27] and are convexly bowed at the longer side of the rectangle (C13–C15–C17 176°; C15–C17–C19 174°) and concavely at the smaller side (C33–C35–C37 173°; C35–C37–C39 173°). The alternating carbon–carbon bond lengths of the diyne units fall within the normal range. The central rings of the terthiophene moieties are distorted by 23–40° as a result of the steric constraints of

the butyl side chains. The nonbonding distances S5...S5' (1.94 nm), S2...S5 (1.48 nm), and S2...S5' (1.34 nm) reflect the size of the interior cavity of the 52-membered ring, which is good agreement with semiempirical calculations (S5...S5': 1.99 nm).

The side-view projection, which corresponds to a view along the molecular plane of the unit cell, shows that the single molecules are oriented parallel to each other and clearly form dimers. The molecules are slightly laterally displaced in the dimers and show a stacking distance of 4.27 Å between the planes, the distance between dimers is 7.64 Å (Figure 1b). Although the top-view projection along the a -axis reveals some overlaps of the macrocycles, most interestingly, channels with diameters of about 1 nm are formed (Figure 1c), which compare well with those of self-assembled peptide nanotubes.^[5] The closest intermolecular S...S distances of 3.5 Å (S1...S1') are slightly smaller than the sum of the van der Waals radii (sulfur 1.8 Å^[28]), which indicates intermolecular interactions occur.

Scanning tunneling microscopy (STM) offers an excellent and alternative way to directly investigate ordered structures in situ on the relevant length scales. Depending on the substitution pattern, linear oligothiophenes physisorb from solution to the basal plane of highly oriented pyrolytic

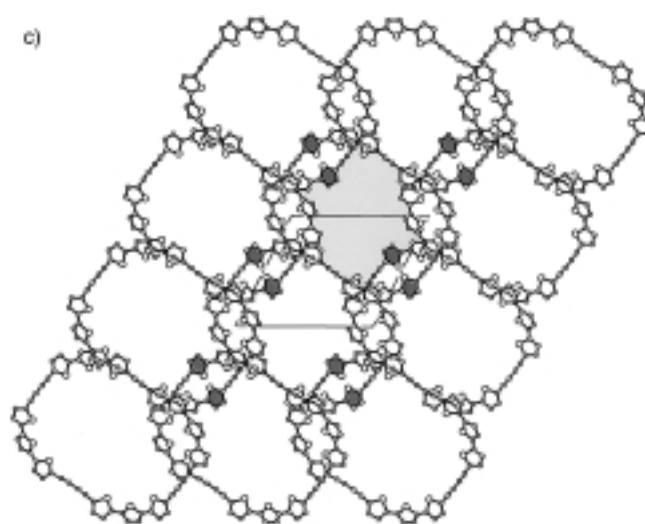
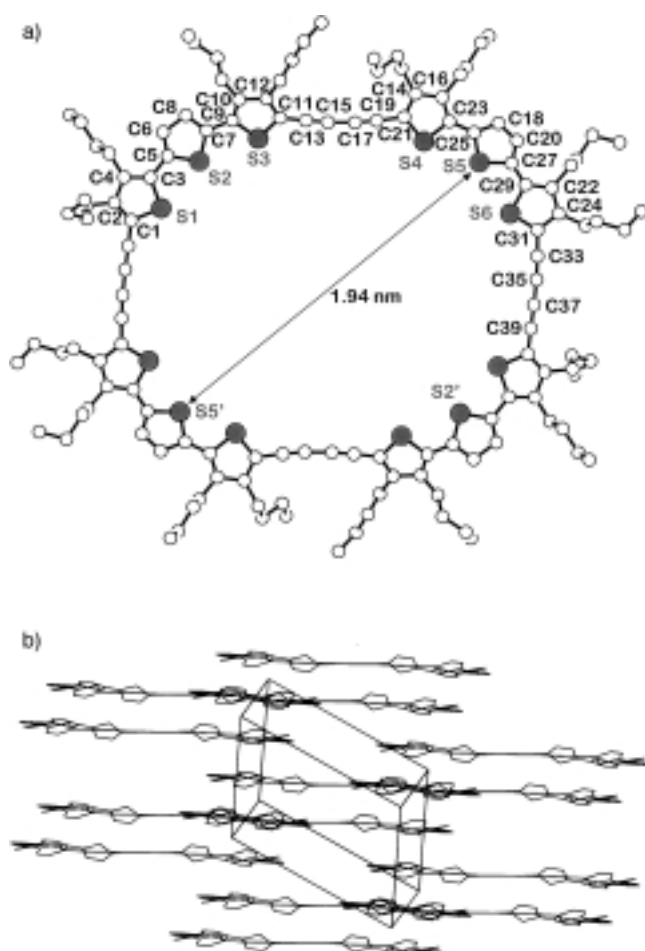


Figure 1. a) Molecular structure (top-view) of oligothiophenediacetylene **14** in the crystal (hydrogens have been removed for clarity). Selected interatomic distances [Å] and angles [°]: S1–C1 1.76(2), S1–C3 1.74(2), C1–C2 1.32(2), C2–C4 1.45(2), C4–C3 1.42(2), C3–C5 1.50(2), S2–C5 1.74(2), S2–C7 1.72(2), C5–C6 1.33(2), C6–C8 1.50(2), C8–C7 1.41(2), C7–C9 1.48(2), S3–C9 1.73(2), S3–C11 1.76(2), C9–C10 1.38(2), C10–C12 1.47(2), C12–C11 1.38(2), C11–C13 1.39(2), C13–C15 1.17(2), C15–C17 1.43(2), C17–C19 1.17(2), C19–C21 1.46(2); C9–S3–C11 92.9(9), S3–C9–C10 112.6(12), C9–C10–C12 110.4(14), C10–C12–C11 114.6(16), C12–C11–S3 109.3(13), S3–C11–C13 123.2(15), C12–C11–C13 127.4(18), C11–C13–C15 177(2), C13–C15–C17 176(2), C15–C17–C19 174(2), C17–C19–C21 176(2); b) packing (side) view of oligothiophenediacetylene **14** along the molecular plane in the unit cell; c) packing (top) view of oligothiophenediacetylene **14** along the *a*-axis. The dark gray underlayed rings are the thiophene rings which give the closest intermolecular S⋯S distances (S1⋯S1'), the light gray underlayed area represents an open channel along the *a*-axis.

graphite (HOPG) and form highly ordered two-dimensional (2D) crystalline monolayers which can be imaged by STM.^[29] Furthermore, in some cases the 2D ordering at the HOPG surface is most notably coincident with the molecular packing in the 3D crystal and gives valuable information about intermolecular and molecule–substrate interactions, which are important for the application of these materials in thin-film electronic devices.^[29a] We find spontaneous ordering at the solution/HOPG interface with the novel macrocyclic systems **13**–**19**. In Figure 2a (top) representative and characteristic STM images of well-ordered and very stable 2D crystalline monolayers of cyclo[12]thiophene **17** are shown.^[30] The images are typically found on larger areas ($\geq 1 \times 1 \mu\text{m}^2$) and display a long-range ordering of molecularly resolved individual macrocycles. A perfect hexagonal “honeycomb” pattern of the cycles with an optimal packing density and consequently only one persistent domain is observed. The lattice constants are 2.39, 2.36, and 2.28 nm and the molecules are oriented in the directions of the three main crystallographic axes of the underlying substrate. A height profile along one of these directions (cross-section) clearly reveals a perfect and regular alignment of the individual molecules. We can also observe submolecular resolution in this diagram: each molecule gives two separated signals with a peak-to-peak separation of 1.13 nm, which agrees well with the inner aromatic borders of the toroidal structure (Figure 2a, bot-

tom). This is in good agreement to calculated nonbonding S⋯S van der Waals distances. Semiempirical calculations and simulations confirm the arrangement and dimensions of the individual macrocycles (Figure 2b, top). The energy minimum of α -C[12]T does not correspond to a fully planar molecule (diameter 2.68 nm), but rather to a “spiderlike” conformation in which the butyl side chains are bent downwards (diameter 2.34 nm; diameter of the conjugated π system 1.83 nm) as a consequence of the uniform distortion of each second thiophene ring. The height of the molecule (0.48 nm) is in full accordance with the STM measurements, which indicates that a monolayer has been formed at the solution/HOPG interface (Figure 2b, bottom).

Large conjugated macrocycles **13**–**19** comprising up to 76 chain members and cavities up to 3 nm have been synthesized and their self-assembling properties investigated. We are currently optimizing the synthesis and broadening the scope of both macrocyclic series and we are most interested in the possible formation of channels or nanotubes from these conjugated materials. For the first time, these circular structures combine the excellent electronic properties of corresponding conjugated oligomers with complexation sites for larger organic guest molecules, and we anticipate novel fundamental properties and applications. Recognition experiments are currently under way in our laboratory. Calculations predict, for example, that fullerene C_{60} could be recognized by

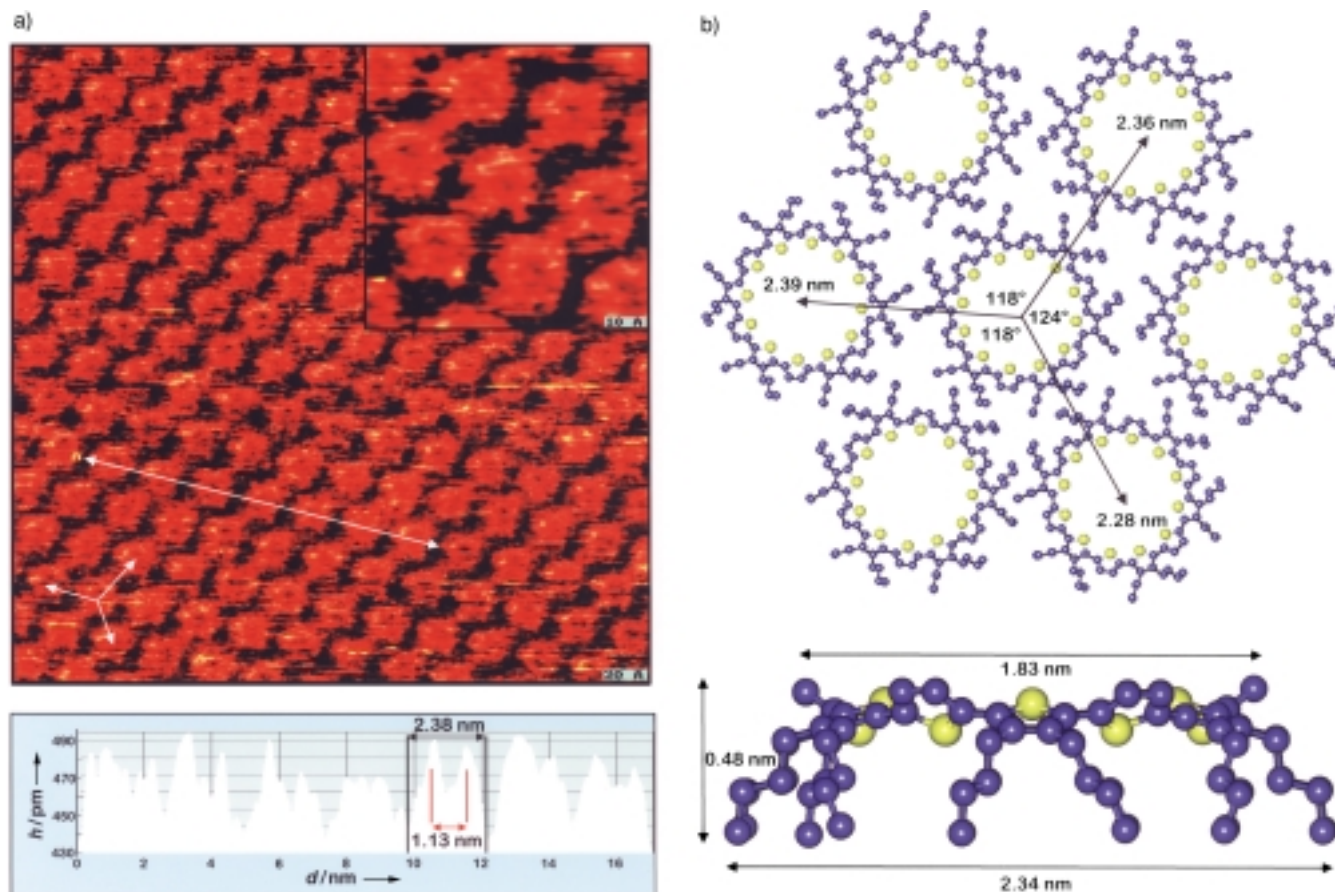


Figure 2. a) Top: STM image ($280 \times 280 \text{ Å}^2$) viewing the long-range ordering and 2D crystal of cyclo[12]thiophene **17** adsorbed on graphite. The inset shows the short-range ordering ($67 \times 67 \text{ Å}^2$). Both images were obtained with bias voltage of -430 mV (the sample is positive) and a tunnel current of 24 pA . Bottom: Height profile and cross-section along eight macrocycles (the white line is ca. 17 nm long). b) Schematic representation of the molecular arrangement of cyclo[12]thiophene **17**: hexagonal cluster consisting of seven molecules (top) and the calculated energy-minimum conformation of an individual macrocycle (bottom).

α -cyclo[12]thiophene and form a ring/sphere-shaped donor–acceptor complex.

Received: March 22, 2000 [Z14882]

- [1] *Handbook of Oligo- and Polythiophenes* (Ed.: D. Fichou), Wiley-VCH, Weinheim, **1999**.
- [2] a) "Oligothiophenes", P. Bäuerle in *Electronic Materials: The Oligomer Approach* (Eds.: K. Müllen, G. Wegner), Wiley-VCH, Weinheim, **1998**, pp. 105–197; b) R. E. Martin, F. Diederich, *Angew. Chem.* **1999**, *111*, 1440–1469; *Angew. Chem. Int. Ed.* **1999**, *38*, 1350–1377; c) J. Roncali, *Chem. Rev.* **1997**, *97*, 173–205; d) J. M. Tour, *Chem. Rev.* **1996**, *96*, 537–553.
- [3] E. Mena-Osteritz, A. Meyer, B. M. W. Langeveld-Voss, R. A. J. Janssen, E. W. Meijer, P. Bäuerle, *Angew. Chem.* **2000**, *112*, 2791–2796; *Angew. Chem. Int. Ed.* **2000**, *39*, 2679–2684.
- [4] P. Bäuerle, *Adv. Mater.* **1992**, *4*, 102–107.
- [5] J. D. Hartgerink, T. D. Clark, M. R. Ghadiri, *Chem. Eur. J.* **1998**, *4*, 1367–1372.
- [6] T. Kauffmann, *Angew. Chem.* **1979**, *91*, 1–19; *Angew. Chem. Int. Ed. Engl.* **1979**, *18*, 1–19.
- [7] Z. Hu, J. L. Atwood, M. P. Cava, *J. Org. Chem.* **1994**, *69*, 8071–8075.
- [8] A. J. W. Tol, *Synth. Met.* **1995**, *74*, 95–98.
- [9] a) M. Mayor, J.-M. Lehn, *J. Am. Chem. Soc.* **1999**, *121*, 11231–11232; b) U. H. F. Bunz, *Top. Curr. Chem.* **1999**, *201*, 131–161; c) S. Höger, S. Müller, L. Karcher, *Am. Chem. Soc. Div. Polym. Chem. Prepr.* **1997**, *38*, 72; d) S. Höger, V. Enkelmann, *Angew. Chem.* **1995**, *107*, 2917–2919; *Angew. Chem. Int. Ed. Engl.* **1995**, *34*, 2713–2716; e) D. W. J. McCallien, J. K. M. Sanders, *J. Am. Chem. Soc.* **1995**, *117*, 6611–6612; f) A. de Meijere, S. Kozhushkov, C. Puls, T. Haumann, R. Boese, M. J. Cooney, L. T. Scott, *Angew. Chem.* **1994**, *106*, 934–936; *Angew. Chem. Int. Ed. Engl.* **1994**, *33*, 869–871; g) J. S. Moore, J. Zhang, *Angew. Chem.* **1992**, *104*, 873–874; *Angew. Chem. Int. Ed. Engl.* **1992**, *31*, 922–924.
- [10] a) V. Hensel, A. D. Schlüter, *Chem. Eur. J.* **1999**, *5*, 421–429; b) V. Hensel, K. Lütow, J. Jakob, K. Gessler, W. Saenger, A. D. Schlüter, *Angew. Chem.* **1997**, *109*, 2768–2770; *Angew. Chem. Int. Ed. Engl.* **1997**, *36*, 2654–2656.
- [11] a) L. Rossa, F. Vögtle, *Top. Curr. Chem.* **1983**, *113*, 1–86; b) L. Mandolini, *Adv. Phys. Org. Chem.* **1986**, *22*, 1–110.
- [12] T. Fischer, Dissertation, University of Würzburg, **1998**.
- [13] J. Krömer, Dissertation, University of Ulm, **2000**. 3,4-Dibutylthiophene (**1**) was synthesized according to the literature: K. Tamao, K. Sumitani, Y. Kiso, M. Zembayasi, A. Fujikoa, I. Nakajama, A. Minato, M. Kumada, *Bull. Chem. Soc. Jpn.* **1976**, *49*, 1958–1969. 3,3',4,4'-Tetrabutyl-2,2':5',2''-terthiophene (**2**) was obtained in 82 % yield by a nickel-catalyzed cross-coupling of the Grignard reagent of 2-bromo-3,4-dibutylthiophene and 2,5-dibromothiophene; 3,3'',3''',4,4''''-tetrabutyl-2,2':5',2''':5''',2''''-quinquethiophene (**3**) was synthesized by a nickel-catalyzed coupling of the Grignard reagent of 2-bromo-3,4-dibutylthiophene with 5,5''-dibromo-3',4'-dibutyl-2,2':5',2''-terthiophene in 76 % yield.
- [14] a) K. Sonogashira, Y. Tohada, N. Hagihara, *Tetrahedron Lett.* **1975**, 4467–4470; b) S. Thorand, N. Krause, *J. Org. Chem.* **1998**, *63*, 8551–8553.
- [15] a) C. Glaser, *Chem. Ber.* **1869**, *2*, 422–424; b) U. Fritzsche, S. Hünig, *Tetrahedron Lett.* **1972**, 4831–4834; c) A. Vaitiekunas, F. F. Nord, *J. Am. Chem. Soc.* **1954**, *76*, 2733–2736.

- [16] G. Eglinton, A. R. Galbraith, *J. Chem. Soc.* **1959**, 889–896.
- [17] a) A. S. Hay, *J. Org. Chem.* **1962**, 27, 3320–3321; b) K. Okuhara, *Bull. Chem. Soc. Jpn.* **1981**, 54, 2045–2052.
- [18] C. Heim, Diploma thesis, University of Würzburg, **1995**. Typically, ^1H NMR spectra showed small signals at $\delta = 3.0$ – 3.5 , and the IR spectra weak absorptions at $\tilde{\nu} = 3300$ – 3350 cm^{-1} which indicate the presence of terminal acetylenic units. MALDI-TOF mass spectra revealed various peak pairs with a mass difference of m/z 2 corresponding to linear and cyclic oligomers of the same number of repeating units.
- [19] D. O’Krongly, S. R. Denmade, M. Y. Chiang, R. Breslow, *J. Am. Chem. Soc.* **1985**, 107, 5544–5545.
- [20] Representative physical data of the oligothiophenediynes macrocycles: **13**: ^1H NMR (CDCl_3): $\delta = 7.07$ (s, 6H, thiophene (Th)-H), 2.66 (m, 24H, $\alpha\text{-CH}_2$), 1.49 (m, 48H, $\beta,\gamma\text{-CH}_2$), 0.97 (m, 36H, CH_3); ^{13}C NMR (CDCl_3): $\delta = 149.63$, 138.32, 136.71, 133.73, 124.87 ($\alpha,\beta\text{-Th-C}$), 117.12 ($\alpha\text{-Th-C}$), 81.92 ($\text{C}\equiv\text{C}$), 78.63 ($\text{C}\equiv\text{C}$), 32.66, 32.38 ($\beta\text{-CH}_2$), 28.74, 27.64 ($\alpha\text{-CH}_2$), 22.96, 22.69 ($\gamma\text{-CH}_2$), 13.88 (CH_3); m.p. $> 300^\circ\text{C}$; MALDI-TOF-MS: m/z : 1554.8 [M^+]. **15**: ^1H NMR (CDCl_3): $\delta = 7.10$ (d, 6H, Th-H), 7.09 (d, 6H, Th-H), 2.71 (m, 36H, $\alpha\text{-CH}_2$), 1.54 (m, 72H, $\beta,\gamma\text{-CH}_2$), 0.99 (m, 54H, CH_3); ^{13}C NMR (CDCl_3): $\delta = 150.99$, 140.35, 138.50, 136.84, 135.71, 133.59, 129.96, 126.24, 125.71 ($\alpha,\beta\text{-Th-C}$), 116.62 ($\alpha\text{-Th-C}$), 81.44, 78.01 ($\text{C}\equiv\text{C}$), 32.82, 32.63, 31.58 ($\beta\text{-CH}_2$), 28.69, 27.90, 27.69 ($\alpha\text{-CH}_2$), 23.03, 22.94, 22.71 ($\gamma\text{-CH}_2$), 13.87 (CH_3); m.p. 203–204 $^\circ\text{C}$; MALDI-TOF-MS: m/z : 2386 [M^+].
- [21] J. J. P. Stewart, MOPAC Program Package, QCPE 455, Indiana University.
- [22] a) A. Carpita, R. Rossi, C. A. Veracini, *Tetrahedron* **1985**, 41, 1919–1929; b) D. M. Perrine, J. Kagan, *Heterocycles* **1986**, 24, 365–368.
- [23] Representative physical data of the cyclo[n]thiophenes **17**–**19**: **17**: ^1H NMR (CDCl_3): $\delta = 7.06$ (s, 12H, Th-H), 2.70 (t, 24H, $\alpha\text{-CH}_2$), 1.42 (m, 48H, $\beta,\gamma\text{-CH}_2$), 0.95 (t, 36H, CH_3); ^{13}C NMR (CDCl_3): $\delta = 140.31$ ($\beta\text{-Th-C}$), 136.55, 130.07 ($\alpha\text{-Th-C}$), 125.43 ($\beta\text{-Th-C}$), 32.80 ($\beta\text{-CH}_2$), 27.80 ($\alpha\text{-CH}_2$), 23.01 ($\gamma\text{-CH}_2$), 13.88 (CH_3); m.p. $> 250^\circ\text{C}$; MALDI-TOF-MS: m/z : 1656.80 [M^+]. **18**: ^1H NMR (CDCl_3): $\delta = 7.09$ (s, 16H, Th-H), 2.69 (t, 32H, $\alpha\text{-CH}_2$), 1.45 (m, 64H, $\beta,\gamma\text{-CH}_2$), 0.97 (t, 48H, CH_3); m.p. $> 250^\circ\text{C}$; MALDI-TOF-MS: m/z : 2210.81 [M^+]. **19**: ^1H NMR (CDCl_3): $\delta = 7.10$ (s, 18H, Th-H), 2.75 (t, 36H, $\alpha\text{-CH}_2$), 1.54 (m, 36H, $\beta\text{-CH}_2$), 1.47 (m, 36H, $\gamma\text{-CH}_2$), 0.99 (t, 54H, CH_3); ^{13}C NMR (CDCl_3): $\delta = 140.11$ ($\beta\text{-Th-C}$), 136.18, 129.98 ($\alpha\text{-Th-C}$), 125.72 ($\beta\text{-Th-C}$), 32.86 ($\beta\text{-CH}_2$), 27.94 ($\alpha\text{-CH}_2$), 23.06 ($\gamma\text{-CH}_2$), 13.90 (CH_3); m.p. 210 $^\circ\text{C}$; MALDI-TOF-MS: m/z : 2486 [M^+].
- [24] H. Plenio, *Angew. Chem.* **1997**, 109, 358–360; *Angew. Chem. Int. Ed. Engl.* **1997**, 36, 348–350.
- [25] Crystal data: $\text{C}_{128}\text{H}_{82}\text{S}_{12}$, $M_r = 2004.66$, triclinic, space group $P\bar{1}$, $a = 11.914(3)$, $b = 16.444(3)$, $c = 17.749(4)$ Å, $\alpha = 113.17(2)$, $\beta = 98.40(3)$, $\gamma = 104.63(3)^\circ$, $V = 2973.0$ Å 3 , $Z = 1$, $\rho_{\text{calc}} = 1.120\text{ g cm}^{-3}$, crystal dimensions $0.11 \times 0.22 \times 0.53\text{ mm}$, $T = 293(2)\text{ K}$, $\mu = 0.266\text{ mm}^{-1}$. Intensity data were collected on a STOE-IPDS image-plate diffractometer ($\text{MoK}\alpha$ radiation ($\lambda = 0.71073$ Å), graphite monochromator) in the φ rotation scan mode, $\theta_{\text{max}} = 26^\circ$, 23195 reflections measured, 10776 unique reflections were measured and used in the refinement. Lorentz and polarization correction. The structure was solved by direct methods (XMY93 program system: T. Debaerdemaeker, *Z. Kristallogr.* **1993**, 206, 173–182). The molecule is located on a crystallographic inversion centre. Refinement (SHELXL97; G. M. Sheldrick, University of Göttingen, **1993**) of positional and anisotropic thermal parameters for all non-hydrogen atoms converged to $R1 = 0.1446$ ($wR2 = 0.3344$) for 1483 reflections with $I \geq 2\sigma(I)$. No attempt was made to locate the hydrogen atoms. The relatively poor R value is probably a result of the large disorder in some of the butyl chains. Unfortunately, no suitable crystals were available for data collection at low-temperature. Crystallographic data (excluding structure factors) for the structures reported in this paper have been deposited with the Cambridge Crystallographic Data Centre as supplementary publication no. CCDC-142083. Copies of the data can be obtained free of charge on application to CCDC, 12 Union Road, Cambridge CB21EZ, UK (fax: (+44) 1223-336-033; e-mail: deposit@ccdc.cam.ac.uk).
- [26] F. Diederich, Y. Rubin, *Angew. Chem.* **1992**, 104, 1123–1146; *Angew. Chem. Int. Ed. Engl.* **1992**, 31, 1101–1123.
- [27] H. Ueda, C. Katayama, J. Tanaka, *Bull. Chem. Soc. Jpn.* **1981**, 54, 891–896.
- [28] A. Bondi, *J. Phys. Chem.* **1964**, 68, 441.
- [29] a) R. Azumi, G. Götz, T. Debaerdemaeker, P. Bäuerle, *Chem. Eur. J.* **2000**, 6, 735–744; b) T. Kirschbaum, R. Azumi, E. Mena-Osteritz, P. Bäuerle, *New J. Chem.* **1999**, 23, 241–251; c) M. S. Vollmer, F. Effenberger, R. Stecher, B. Gompf, W. Eisenmenger, *Chem. Eur. J.* **1999**, 5, 96–101; d) H. Müller, J. Petersen, R. Strohmaier, B. Gompf, W. Eisenmenger, M. S. Vollmer, F. Effenberger, *Adv. Mater.* **1996**, 8, 733–737; e) P. Bäuerle, T. Fischer, B. Bidlingmeier, A. Stabel, J. P. Rabe, *Angew. Chem.* **1995**, 34, 335–339; *Angew. Chem. Int. Ed. Engl.* **1995**, 34, 303–307; f) A. Stabel, J. P. Rabe, *Synth. Met.* **1994**, 67, 47–53.
- [30] The STM images were recorded at ambient temperature with the aid of low-current STM (RHK) regulated by a RHK STM-1000 control system equipped with a mechanically cut Pt/Ir tip. All of the images presented were obtained at quasi-constant height in the variable current mode without further manipulation or using a voltage pulse in order to induce the ordering, and without digital image processing. The bias voltages were typically around -400 to -450 mV and the setpoint currents around 0.3 – 0.5 nA . A freshly cleaved surface of HOPG was first carefully characterized under ambient conditions, then solutions of the macrocycles in 1,2,4-trichlorobenzene were deposited onto the substrate. In situ STM imaging of the self-assembled 2D monolayers was performed at the interface between HOPG and concentrated solutions of the macrocycles.

Investigating the Surface Morphology of Triacetyl Phases with Spin-Diffusion Solid-State NMR Spectroscopy**

Martin Raitza, Jürgen Wegmann, Stefan Bachmann, and Klaus Albert*

The detailed characterization of molecular recognition structures is one of the essential prerequisites for the development of new materials for specific applications in catalysis, sensor technology, and for the analysis of mixtures of compounds.

Highly selective stationary phases are needed for the efficient separation of complex mixtures of compounds in high-performance liquid chromatography (HPLC).^[1] The tailored synthesis of these phases is impossible without any detailed knowledge of the surface structure of the materials and a detailed understanding of the structural and dynamic properties of the separation phase. Routine applications in HPLC can be successfully performed with reversed-phase materials,^[2] which are prepared by modifying silica gel with n -alkylsilanes (for example, n -octadecylsilane). Reversed phas-

[*] Prof. Dr. K. Albert, Dr. M. Raitza, Dipl.-Chem. J. Wegmann, Dipl.-Chem. S. Bachmann
Institut für Organische Chemie der Universität Tübingen
Auf der Morgenstelle 18, 72076 Tübingen (Germany)
Fax: (+49) 7071-295875
E-mail: klaus.albert@uni-tuebingen.de

[**] This work was funded by the Deutsche Forschungsgemeinschaft (FOR 184/3-1) and the Fonds der Chemischen Industrie. We thank Bischoff Analysentechnik und -geräte GmbH, Leonberg, Germany for providing ProntoSIL silica gel.

es with triacontyl chains show an extremely high shape selectivity for the separation of stereoisomers (for example, β -carotene stereoisomers).^[3–5] Solid-state NMR spectroscopy is of great importance for the characterization of these amorphous compounds and through the many experiments possible delivers valuable information on the structural and dynamic behavior.

Reversed phases with high shape selectivity can be prepared by the solution polymerization procedure, in which a defined quantity of water is added during the modification reaction of silica gel with *n*-alkylsilanes. Solid-state ^{13}C NMR investigations of these materials reveal two signals for the methylene groups of the alkyl chain which can be assigned to one domain with preferentially all *trans* and the other one with mainly *gauche* conformations. Many investigations performed with “self-assembled monolayers” (SAMs) reveal that the observed signal splitting also takes place in diverse *n*-alkyl-modified inorganic oxides (Al_2O_3 , SiO_2 , TiO_2 , and ZrO_2).^[6–9] No information could be gained up to now upon the size, extension, and alignment of these domains, even though these parameters are responsible for the selectivity of the chromatographic separation.^[4, 10–16] The main question which still remains is what is the alignment of the domains: there could be a lateral alignment with the island structures at the silica surface or a mobility gradient along the alkyl chains with layers parallel to the silica surface.

The answer to this question can be found by employing spin-diffusion solid-state NMR investigations. These experiments have large practical applications for the determination of the homogeneity of polymers and have been mainly conducted to determine the phase structure of organic polymers.^[17–19] Moreover, the alignment and size of domains of different mobility can be determined in the range of 5 to 2000 Å. The basic principle of the method is outlined in Figure 1.^[18] The magnetization of the sample is shown in the

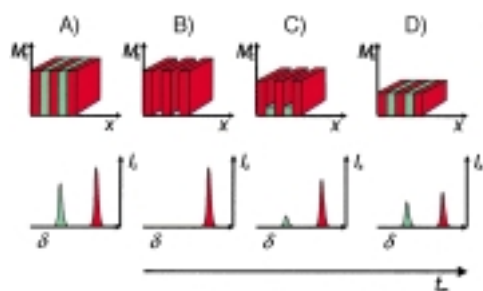


Figure 1. Schematic representation of the principle of spin-diffusion experiments. Top: sample magnetization, bottom: NMR spectra; red: mobile, green: rigid; A – B: selection, B – D: spin diffusion, t_m : mixing time.

upper part of Figure 1, while the lower part depicts the resulting NMR spectra. The sample under investigation consists of two domains with different mobility, which are indicated by different colors (red: mobile, green: rigid).

At the start of the NMR experiment the sample is in state A where the magnetization is distributed in both domains, and results in NMR signals of both domains. In a second step a selection process is performed by making use of the different relaxation times.^[20, 21] Thus in state B only one component of

the sample contains a significant magnetization, which is registered in the NMR spectrum. Spin diffusion starts at state B, that is, magnetization is transferred to neighboring nuclei by dipolar interactions and thus starts to diffuse. During this diffusion mixing time t_m the magnetization of mobile compounds decreases while the magnetization of rigid nonselected components increases again. Thus, the intensity of the signal corresponding to the mobile species in the NMR spectrum decreases while the second signal increases in intensity (state C). Finally the magnetization in the equilibrium state D is distributed on both components and the NMR spectra are similar to those of state A but show less signal intensity.

The reduction in the magnetization during the spin-diffusion mixing time t_m can be used to understand the distribution, that is, the size of areas of equal mobility. If the distribution of both components at the silica surface is very homogeneous, then a large number of border areas exist between domains with different mobility. Interactions between both components take place at these border areas and the equilibrium state can be reached very fast. A more uneven distribution with big domains of equal mobility results in less border areas and the adjustment of the magnetization takes more time.

Figure 2 shows the pulse sequence of the spin-diffusion experiment together with the application of the dipolar filter. First a 12 pulse block consisting of 90° pulses in the proton

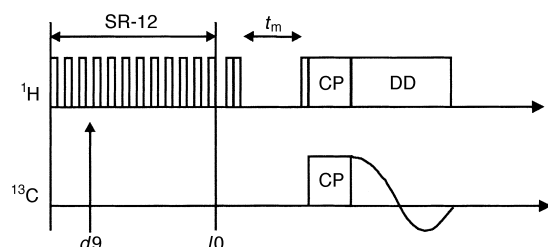


Figure 2. Schematic representation of the pulse sequence for the spin-diffusion experiment with a dipolar filter and ^{13}C detection. I_0 : number of repetitions of the 12 pulse sequence, d_9 : delay time between two 90° pulses, t_m : variable mixing time.

channel is applied, which eliminates the dipolar couplings of the protons in the mobile component. Thus, there is only a very small dephasing of the magnetization of the mobile components, while a fast dephasing of the magnetization of the rigid components takes place because of the strong dipole interactions. The delay times d_9 between the single pulses and the number of repetitions of the pulse block I_0 are parameters which can be varied for an optimal selection according to the nature of the investigated sample. Two 90° pulses follow, which alternately align the magnetization to the $+z$ or $-z$ axis of the corresponding phase cycles, in order to correct for T_1 effects. Spin diffusion takes place following the mixing time t_m , and is followed by the cross-polarization pulse sequence, and detection in the ^{13}C channel. Rows of spectra are registered by incrementing the mixing time t_m , which enables the time dependence of the diffusion to be studied by observing changes in the signal intensity.

Figure 3 shows the ^{13}C CP/MAS NMR spectra of a triacontyl separation phase recorded with mixing times t_m of the spin-diffusions experiment varied between 1 μs and

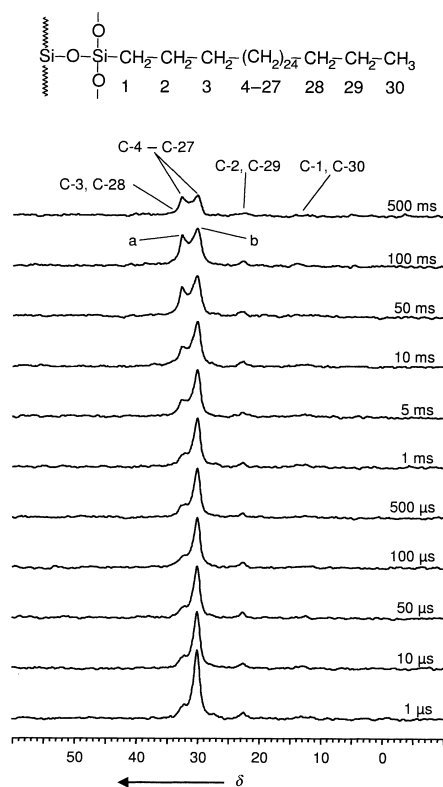


Figure 3. Spin-diffusion NMR experiment with ^{13}C detection of a C_{30} phase (ProntoSIL 3 μm , 200 \AA , surface coverage $3.5 \mu\text{mol m}^{-2}$) with a variable mixing time t_m and a temperature of 312 K ($t_0 = 6$, $d_9 = 10 \mu\text{s}$); a: rigid, b: mobile.

500 ms. Two resonances at $\delta = 32.8$ and 30.0 are observed for the carbon atoms of the methylene chain. These signals can be assigned to rigid all-*trans* and mobile *gauche* conformations, respectively, of the alkyl chain.^[14] The spectrum with the smallest mixing time t_m of 1 μs clearly depicts that only mobile domains exhibit a reasonable magnetization at the start of the spin-diffusion experiment, since only the high-field-shifted signal $\delta = 30.0$ is visible. Spin diffusion becomes more effective with increasing mixing time, and magnetization is transferred from the mobile to rigid domains. Thus the signal at $\delta = 30.0$ decreases in intensity whereas the signal at $\delta = 32.8$ increases in intensity. At the largest employed mixing time t_m of 500 ms both signals show comparable intensity. The decrease in the intensity of the signals of the carbon atoms of the mobile alkyl chains together with the increase in intensity of signals for the carbon atoms of the rigid alkyl chains corresponds to the transfer of magnetization from the mobile to the rigid alkyl-chain domains.

This phenomenon is direct proof for the existence of alkyl-chain domains of different mobility at the silica surface of C_{30} reversed phases, which are prepared under the special solution polymerization procedure. The distribution of the domains can be derived from the time dependence of the signal decay of the methylene chains recorded during the spin-

diffusion experiment. Domains parallel to the silica surface, which result from a mobility gradient from the silica surface to the end of the alkyl chain, should exhibit a very fast spin diffusion. This effect is in accordance with the hypothesis of a lateral distribution of domains, that is, island structures are formed at the silica surface. These different regions are caused by the different cross-linking of the silanes employed during the synthetic procedure. Thus clusters are formed from an array of closely packed C_{30} alkyl chains which bind to the silica surface and are organized in rigid domains.

The size of the domains can be estimated by comparing the decrease of the signal at $\delta = 30.0$ with the signal progression derived from a simulated spin-diffusion experiment. Here the whole sample is represented by a periodic array of quadratic single cells which exhibit different mobility and are mixed together (core/shell model; Figure 4, top). The system is

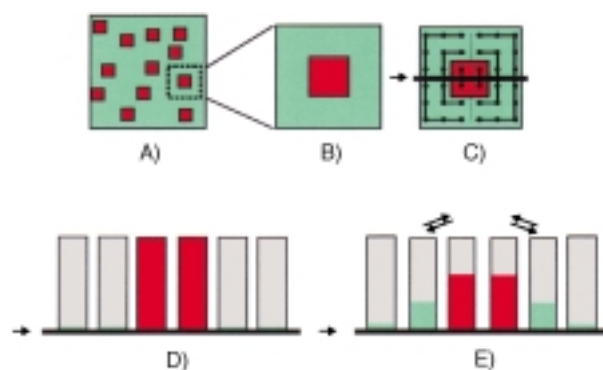


Figure 4. Schematic representation of the sample model (A). It was hypothesized that the sample consists of a periodic array of unit cells (B). The two-dimensional spin lattice (C) is projected into one dimension (D, E).

projected with respect to symmetry considerations into one dimension by summation of the lattice points that are able to receive magnetization. Thus the one-dimensional display contains marked lattice points at regular distances which are able to take up magnetization and to exchange with their neighbors (Figure 4, bottom). The whole system reaches the equilibrium state as a result of the different sizes of the two domains.

The size of the diffusion constant is important for the simulation of the spin-diffusion process. In earlier publications this process has been independently addressed and a diffusion constant in the range of $20\text{--}100 \text{\AA}^2 \text{ms}^{-1}$ was determined.^[17, 21–24] A diffusion constant $D_m = 30 \text{\AA}^2 \text{ms}^{-1}$ for the mobile component and of $D_r = 80 \text{\AA}^2 \text{ms}^{-1}$ for the rigid component was used for the interpretation of the current system. Figure 5 shows the comparison of the experimental data together with the simulated reduction. The signals (Figure 3) were simulated by peak deconvolution by employing Lorentian peak shapes. The intensity of the signal of the mobile component is related to the integral value of both signals, which corresponds to 100. A good fit with the experimental data is obtained with values of 112\AA for the core of the single cell (mobile component $D_m = 30 \text{\AA}^2 \text{ms}^{-1}$) and 16\AA for the shell of the unit cell (rigid component, $D_m = 80 \text{\AA}^2 \text{ms}^{-1}$). A calculation of the relative areas of both

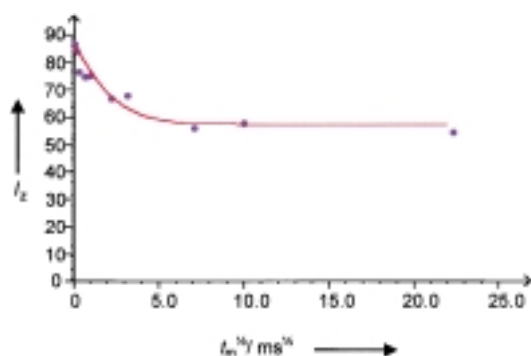


Figure 5. Comparison of the experimental decrease in the signal of the mobile component and the simulated curve with respect to the mixing time (ProntoSIL 3 μm , 200 \AA , surface coverage 3.5 $\mu\text{mol m}^{-2}$).

components for one unit cell is possible from the proposed structure and arrangement of unit cells (Figure 4). An area of $(112 \text{ \AA})^2 \approx 12500 \text{ \AA}^2$ (red area) results for the mobile component and an area of $(16 \text{ \AA} + 112 \text{ \AA} + 16 \text{ \AA})^2 - (112 \text{ \AA})^2 \approx 8200 \text{ \AA}^2$ (green area) for the rigid component. Thus the ratio of the mobile:rigid area is 60:40.

Thus it is clear that two domains exist with different densities of alkyl chains and their sizes can be evaluated. The model depicted in Figure 6 results from the described

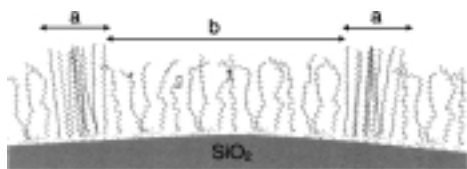


Figure 6. Model of the silica surface of a C_{30} phase chemically modified with trichlorotriacontylsilane. Region a: rigid, 32 \AA ; region b: mobile, 112 \AA .

measurements together with the computer simulation. Thus an average domain size of 8200 \AA^2 for the rigid all-*trans* alkyl-chain conformations (average alkyl-chain length 43 \AA) and of 12500 \AA^2 for the *gauche* alkyl-chain domains (average alkyl-chain length 31 \AA) can be concluded. Thus it was possible to derive insight into the spatial distribution of alkyl chains at the silica surface by employing the outlined solid-state NMR experiments. Direct proof of the existence of C_{30} alkyl chain domains with different mobility at the silica surface was obtained in the case of the investigated C_{30} reversed-phase spin-diffusion measurements.

Experimental Section

The investigated C_{30} phase was synthesized according to the solution polymerization procedure^[14]. Silica gel (ProntoSIL, particle size 3 μm , pore size 200 \AA , Bischoff Analysentechnik und -geräte GmbH, Leonberg, Germany) was dried under vacuum conditions at 180° for 4 h, suspended in xylene, and treated with a threefold excess of triacontyltrichlorosilane. The polymerization was started by the addition of a defined amount of water and the reaction mixture was heated at reflux overnight. A white powder was obtained after purification of the product.

NMR parameters: The NMR spectra were recorded on a Bruker ASX 300 spectrometer. ^{13}C CP/MAS NMR measurements were performed with a 7-mm probe at a spinning rate of 4000 Hz and a sample temperature of 312 K (90° pulse angle 6.5 μs , 2048 transients, contact time 6 ms, delay time

1 s, time domain 2 K data points with a spectral width (SW) of 23 kHz, acquisition time 45 ms).

Spin-diffusion MAS NMR measurements were recorded with the dipolar filter with six repetition cycles (*f0*) and a delay time of 10 μs (*d9*) between the ^1H pulses. A 7-mm probe was employed at a spinning rate of 4000 Hz and a sample temperature of 312 K (90° pulse angle 6.9 μs , 12288 transients, contact time 6 ms, delay time 1 s, time domain 2 K data points with a spectral width (SW) of 23 kHz, acquisition time 45 ms).

The simulation of the spin diffusion was performed with a self-developed computer program (MR-SpinDiff) on a PC (Pentium, 200 MHz).

Received: April 4, 2000 [Z14941]

- [1] K. K. Unger in *Packings and Stationary Phases in Chromatographic Techniques*, Vol. 47 (Ed.: K. K. Unger), Marcel Dekker, New York, **1990**.
- [2] W. R. Melander, C. Horvath, *High Performance Liquid Chromatography*, Vol. 2, Academic Press, New York, **1980**, p. 113.
- [3] L. C. Sander, K. Epler Sharpless, N. E. Craft, S. A. Wise, *Anal. Chem.* **1994**, *66*, 1667–1674.
- [4] M. Pursch, S. Strohschein, H. Händel, K. Albert, *Anal. Chem.* **1996**, *68*, 386–393.
- [5] S. Strohschein, M. Pursch, H. Händel, K. Albert, *Fresenius J. Anal. Chem.* **1997**, *357*, 498–502.
- [6] W. Gao, L. Reven, *Langmuir* **1995**, *11*, 1860–1863.
- [7] W. Gao, L. Dickinson, C. Grozinger, F. G. Morin, L. Reven, *Langmuir* **1996**, *12*, 6429–6435.
- [8] W. Gao, L. Dickinson, C. Grozinger, F. G. Morin, L. Reven, *Langmuir* **1997**, *13*, 115–118.
- [9] M. Pursch, L. C. Sander, K. Albert, *Anal. Chem.* **1996**, *68*, 4107–4113.
- [10] K. Albert, B. Evers, E. Bayer, *J. Magn. Reson.* **1985**, *62*, 428–436.
- [11] M. Pursch, R. Brindle, A. Ellwanger, L. C. Sander, C. M. Bell, H. Händel, K. Albert, *Solid-State NMR* **1997**, *9*, 191–201.
- [12] M. Pursch, L. C. Sander, H.-J. Egelhaaf, M. Raitza, S. A. Wise, D. Oelkrug, K. Albert, *J. Am. Chem. Soc.* **1999**, *121*, 3201–3213.
- [13] K. Albert, A. Ellwanger, M. Dachtler, T. Lacker, S. Strohschein, J. Wegmann, M. Pursch, M. Raitza in *Fundamentals and Applied Aspects of Chemically Modified Surfaces*, Vol. 7 (Eds.: J. Bliz, C. Little), The Royal Society of Chemistry, Cambridge, **1999**, pp. 111–128.
- [14] K. Albert, T. Lacker, M. Raitza, M. Pursch, H.-J. Egelhaaf, D. Oelkrug, *Angew. Chem.* **1998**, *110*, 809–812; *Angew. Chem. Int. Ed.* **1998**, *37*, 777–780.
- [15] K. Albert, *Trends Anal. Chem.* **1998**, *17*, 648–658.
- [16] M. Raitza, M. Pursch, S. Strohschein, L. C. Sander, K. Albert, *GIT Lab. J.* **1998**, *4*, 237–241.
- [17] J. Clauss, K. Schmidt-Rohr, A. Adam, C. Boeffel, H. W. Spiess, *Macromolecules* **1992**, *25*, 5208–5214.
- [18] K. Schmidt-Rohr, H. W. Spiess, *Multidimensional Solid State NMR and Polymers*, Academic Press, San Diego, **1994**, pp. 402–439.
- [19] F. Mellinger, M. Wilhelm, K. Landfester, H. W. Spiess, A. Haunschild, J. Packusch, *Acta Polym.* **1998**, *49*, 108–115.
- [20] M. Goldman, L. Shen, *Phys. Rev.* **1961**, *144*, 321–328.
- [21] J. Clauss, K. Schmidt-Rohr, H. W. Spiess, *Acta Polym.* **1993**, *44*, 1–17.
- [22] T. Kimura, K. Neki, N. Tamura, F. Horii, M. Nakagawa, H. Odani, *Polymer* **1992**, *33*, 493–497.
- [23] M. Ishida, K. Yoshinaga, F. Horii, *Macromolecules* **1996**, *29*, 8824–8829.
- [24] R. R. Eckman, P. M. Henrichs, A. J. Peacock, *Macromolecules* **1997**, *30*, 2474–2481.

The Influence of Mismatches on Long-Distance Charge Transport through DNA**

Bernd Giese* and Stefan Wessely

Studies by Barton et al.,^[1] Schuster,^[2] and our group^[3] have shown that double-stranded deoxyribonucleic acids (DNA) are able to transport a positive charge over long distances (>50 Å).^[4] We have described this long-range charge transport as a multistep reaction, in which the positive charge migrates by reversible tunneling reaction steps between neighboring guanine bases (G).^[3,5] Thus, guanines lying between the charge donor and the charge acceptor serve as relay stations for the positive charge (hopping mechanism).^[6] Since guanines play a central role in this hopping mechanism, mismatches of the guanine:cytosine (G:C) base pair should influence dramatically the efficiency of the charge transport. Indeed, we have now observed a strong decrease of the charge transport in DNA double strands, in which a mismatch was introduced at a G:C base pair. The studies were performed with double strands **1** that contained a 4'-acylated nucleotide (Scheme 1).



Scheme 1. Generation of a guanine radical cation $G^{+\bullet}$ in the ^{32}P -labeled strand **3** by photolysis of the acyl-substituted strand **1**.

Norrish-I photocleavage of **1** and subsequent heterolysis generated radical cation **2** that selectively oxidized a neighboring guanine to its radical cation ($G^{+\bullet}$).^[7] For analytical reasons we used double strands in which the charge was transferred to a G of the ^{32}P -labeled complementary strand (**2**→**3**). This $G^{+\bullet}$ initiates the charge transport through DNA towards the GGG sequence, a thermodynamic sink for the positive charge.^[8] At the positions where the guanine radical cation was trapped by H_2O , treatment with piperidine led to DNA cleavage products P_G that were separated and quantified by gel electrophoresis (Figure 1).^[5]

The kinetic analysis^[9] of the charge transport from the donor $G_1^{+\bullet}$ over the bridge to the acceptor GGG in double strand **4**^[10] (Figure 1) showed that tunneling steps of 10 Å

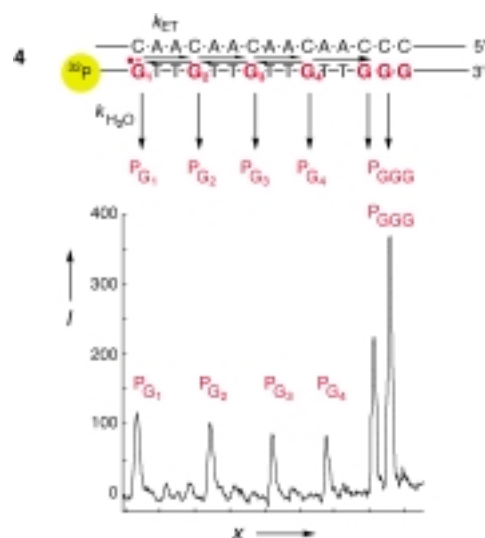


Figure 1. Charge transport from charge donor $G_1^{+\bullet}$ to charge acceptor GGG in the 54-mer **4**, from which only the decisive sequence segment is depicted.^[9] Bottom: A histogram of the cleavage products P_G and P_{GGG} , which were separated by gel electrophoresis (x = position).

between the guanines (k_{ET}) are considerably faster than the H_2O -trapping of the charge ($k_{\text{H}_2\text{O}}$). Therefore, the positive charge in double strand **4** should be distributed over the single guanines G_1 to G_4 before it is trapped by H_2O . This is indeed the case as the appearance of cleavage products P_G in Figure 1 shows. The intensities $\text{P}_G/\text{P}_{G_1}$ slowly decrease from G_1 over G_2 and G_3 to G_4 from 1.0 over 0.83 and 0.66 to 0.57. This slow decrease of the H_2O -trapping products with increasing distance from the charge injection site must not be interpreted as a weak distance dependence of the charge transfer rate k_{ET} described in the Marcus–Levich–Jortner Equation (a).^[11]

$$\ln k_{\text{ET}} \propto -\beta \Delta r \quad (\text{a})$$

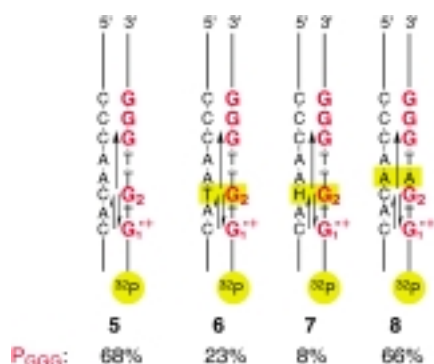
For the decrease of product yields, competition between the charge transfer (k_{ET}) and the H_2O -trapping reactions ($k_{\text{H}_2\text{O}}$) is decisive. Since in DNA strand **4** the charge transfer between the single guanines is considerably faster than the H_2O -trapping reaction,^[9] the charge decreases only slowly during its migration through the DNA strands.^[12] This reversible tunneling between the relay stations^[13] of DNA **4** can be compared with a multistep chemical reaction in which the intermediates interconvert faster into each other than they react irreversibly yielding the products. Such a reaction is well described by the Curtin–Hammett principle that takes into account the rate of the reversible steps (k_{ET}), the equilibrium constants (ionization potentials of the relay stations), and the irreversible reactions leading to the products ($k_{\text{H}_2\text{O}}$).^[14] In the extreme case, the yields of products P_G are nearly independent of the position of the DNA relay stations. Of course, this cannot be explained by a disappearance of the distance influence on the charge transfer rate (k_{ET}).

Further evidence that the charge in our assay is centered predominantly at the guanines was provided by experiments with DNA double strands containing mismatches. Thus, the efficiency of the charge transport from the donor $G_1^{+\bullet}$ to the acceptor GGG in oligomers **5**–**7** dropped from 68% for the

[*] Prof. Dr. B. Giese, Dipl.-Chem. S. Wessely
Department of Chemistry, University of Basel
St. Johannis-Ring 19, 4056 Basel (Switzerland)
Fax: (+41) 61-267-1105
E-mail: bernd.giese@unibas.ch

[**] This work was supported by the Swiss National Science Foundation and the Volkswagen Foundation.

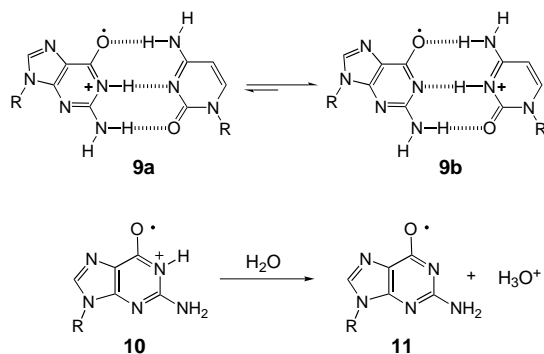
mismatch-free double strand **5** to 23 % (**6**) and 8 % (**7**), when a T or the abasic monomer H^[15], respectively, was introduced opposite to G₂ (Scheme 2).^[16] On the other hand, the



Scheme 2. Charge transport from the charge donor G₁⁺⁺ through double strands **5**–**8** towards the charge acceptor GGG. The efficiency of the charge transport was measured by the yield of the cleavage products P_{GGG} at the GGG sequence.^[12] As double strands 31-mers having G₂ in the middle of the strand were used.

efficiency of the charge transport remained almost unchanged when a mismatch at adenine (A) was introduced by an A in the complementary strand (**8**).

We assume that these effects are induced by a weakening of the hydrogen bonds in the mismatched guanine radical cations G₂⁺⁺ (Scheme 2). Steenken^[17] has shown that G⁺⁺ has a pK_a of 3.9. In a mismatch-free DNA the positive charge is distributed over both bases (**9a** ⇌ **9b**) of the G:C base pair **9**. If the hydrogen bonds are weakened, however, the probability of proton transfer to the surrounding water increases (**10** → **11**) and this retards the charge transport through DNA (Scheme 3).^[18]



Scheme 3. Transfer of a proton from the guanine radical cation G⁺⁺ to the paired cytosine (**9a** ⇌ **9b**) and to the surrounding water (**10** → **11**).

Thus, proton transfer from a G⁺⁺ to water could explain why mismatches of G:C pairs strongly diminish the efficiency of the charge transfer to the GGG acceptor (strands **6**, **7**).^[19] This interpretation is supported by another experiment in which we have generated a G⁺⁺ at the end of a double strand. This G⁺⁺ was unable to inject a positive charge into DNA because the base pair at the end of the double strand is so exposed to the surrounding water that a fast deprotonation of G⁺⁺ (**10** → **11**) occurs and the charge transport is suppressed.

Conclusion: A positive charge injected into DNA, is spread over the relay stations that are positioned between the charge donor and the charge acceptor. A slow decrease in the intensity of the H₂O-trapping products is not an indication for a weak distance dependence of the charge transfer rates (k_{ET}). It is the rate ratio between H₂O-trapping (k_{H_2O}) and charge transfer (k_{ET}) that plays the decisive role. Mismatched guanines suppress the charge transfer because of proton transfer from G⁺⁺ to the surrounding water.

Received: June 26, 2000 [Z15325]

- [1] M. E. Nunez, D. B. Hall, J. K. Barton, *Chem. Biol.* **1999**, *6*, 85.
- [2] G. B. Schuster, *Acc. Chem. Res.* **2000**, *33*, 253.
- [3] B. Giese, *Acc. Chem. Res.* **2000**, *33*, web release date June 20, 2000.
- [4] Commentaries on charge transfer in DNA: a) U. Diederichsen, *Angew. Chem.* **1997**, *107*, 2411; *Angew. Chem. Int. Ed.* **1997**, *36*, 2317; b) E. K. Wilson, *Chem. Eng. News* **1999**, *77*(34), 43; c) M. Ratner, *Nature* **1999**, *397*, 480; e) M. W. Grinstaff, *Angew. Chem.* **1999**, *111*, 3845; *Angew. Chem. Int. Ed.* **1999**, *38*, 3629.
- [5] E. Meggers, M. E. Michel-Beyerle, B. Giese, *J. Am. Chem. Soc.* **1998**, *120*, 12950.
- [6] Guanine is the DNA base with the lowest ionization potential: S. Steenken, S. V. Jovanovic, *J. Am. Chem. Soc.* **1997**, *119*, 617.
- [7] E. Meggers, A. Dussy, T. Schäfer, B. Giese, *Chem. Eur. J.* **2000**, *6*, 485.
- [8] a) H. Sugiyama, I. Saito, *J. Am. Chem. Soc.* **1996**, *118*, 7073; b) F. Prat, K. N. Houk, C. S. Foote, *J. Am. Chem. Soc.* **1998**, *120*, 845.
- [9] M. Bixon, B. Giese, S. Wessely, T. Langenbacher, M. E. Michel-Beyerle, J. Jortner, *Proc. Natl. Acad. Sci. USA* **1999**, *96*, 11713.
- [10] The experimental conditions and the sequence of double strand **4** are described in: B. Giese, S. Wessely, M. Spormann, U. Lindemann, E. Meggers, M. E. Michel-Beyerle, *Angew. Chem.* **1999**, *111*, 1050; *Angew. Chem. Int. Ed.* **1999**, *38*, 996.
- [11] Introducing the intensities (P_G/P_G) in Equation (a) results in a proportionality factor (apparent β-value) of 0.02.
- [12] The rate of charge transfer from a G⁺⁺ to a G 10 Å away (two A:T base pairs as bridge) is about 2.5 × 10⁶ s⁻¹: F. D. Lewis, X. Liu, J. Liu, S. E. Miller, R. T. Hayes, M. R. Wasielewski, *Nature* **2000**, *406*, 51. This rate and the product yields lead to a pseudo-first-order rate coefficient $k_{H_2O} = 6 \times 10^{-4}$ s⁻¹.
- [13] If charge transport occurs over long A:T sequences also adenine radical cation, formed in a thermally activated charge equilibration, might act as charge carrier.
- [14] The Curtin–Hammett principle can also explain long-range charge transport experiments of Schuster^[2] and Barton et al.^[1] In these studies, the relay stations consist of single Gs and of GG sequences. Since GG units have a lower ionization potential than single Gs,^[8] most of the charge is located at the GG sequence. Therefore, the H₂O-trapping products are observed mainly at the GG units. See also: S. M. Gasper, B. Armitage, X. Shui, G. G. Hu, C. Ya, G. B. Schuster, L. D. Williams, *J. Am. Chem. Soc.* **1988**, *110*, 12402.
- [15] In the abasic monomer H, a hydrogen atom replaces the nucleobase.
- [16] The sum of the cleavage products P_{G1} + P_{G2} + P_{GGG} was set to 100 %.
- [17] a) S. Steenken, *Free Radical Res. Commun.* **1992**, *16*, 349; b) S. Steenken, *Biol. Chem.* **1997**, *378*, 1293.
- [18] Another reason for the inefficient charge transport could be the increase of the ionization potential of G because of the weakening of the hydrogen bonds in the mismatched pair: M. Huter, T. Clark, *J. Am. Chem. Soc.* **1996**, *118*, 7574.
- [19] A decrease of the charge transport in G:T and G:A mismatches was also observed in electrochemical experiments with thin DNA-films: G. Hartwich, D. J. Caruana, T. de Lumley-Woodyear, Y. Wu, C. N. Campbell, A. Heller, *J. Am. Chem. Soc.* **1999**, *121*, 10803.

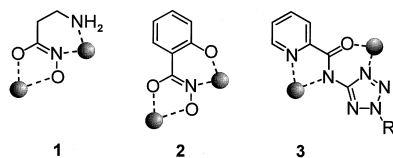
A Rectangular Zinc Cluster and a Rectangular Nickel Cluster That Exhibits Ferromagnetic Coupling**

Rolf W. Saalfrank,* Stefan Trummer, Uwe Reimann, Mubarik M. Chowdhry, Frank Hampel, and Oliver Waldmann*

Dedicated to Professor Siegfried Schneider on the occasion of his 60th birthday

In the last few years the development of new concepts for the rational design of polynuclear clusters has led to considerable progress in supramolecular chemistry.^[1] The use of carefully selected ligands and metal ions has allowed the construction of clusters with defined geometry and special properties. Particular interest has focused on the development of so-called single-molecule magnets.^[2]

β -Alaninehydroxamic acid and salicylhydroxamic acid react with appropriate metal ions to give tetranuclear metal-lacoronates.^[3] The cyclic linkage of the four metal ions is based on the building blocks **1** and **2**, which as a common feature exhibit a five- and a six-membered chelate ring (Scheme 1). Likewise, picoline-tetrazolylamides of the type

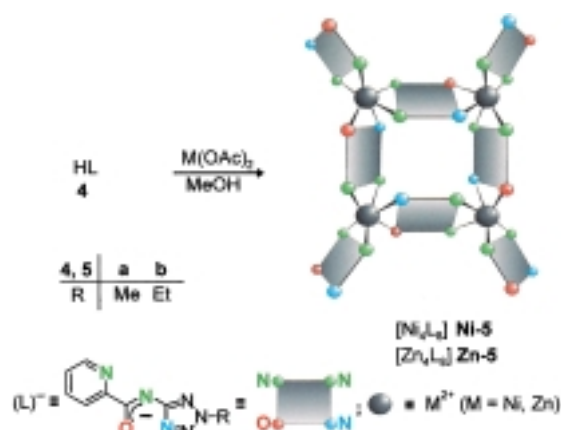


Scheme 1. Schematic representation of the commensurate building blocks **1**–**3** suitable for the construction of cyclic tetranuclear clusters.

HL **4** should also be suitable for the formation of four-membered metallacycles, provided, deprotonated **4** also fits the geometric conditions necessary to form the bischelate **3**, a structurally analogous module of **1** and **2**.

In order to confirm this hypothesis, we treated **4b** with nickel(II) acetate in methanol. After work-up a violet solid was isolated. Based on the elemental analysis and FAB-MS spectrum, **Ni-5b** (m/z 1972) is a tetranuclear metal chelate complex of the composition $[\text{Ni}_4\text{L}_8]^{4+}$ (Scheme 2).

For unequivocal characterization of $[\text{Ni}_4\text{L}_8]^{4+}$ **Ni-5b** we carried out an X-ray crystallographic structure analysis.^[4] According to this study, **Ni-5b** is present in the crystal as a



Scheme 2. Synthesis of the tetranuclear nickel and zinc clusters $[\text{M}_4\text{L}_8] \text{ 5}$.

square $[2 \times 2]$ grid ($d_{\text{Ni-Ni}} = 5.567 \text{ \AA}$, angle $_{\text{Ni-Ni-Ni}} = 84.40^\circ$). One of the main structural characteristics of **Ni-5b** is the two different sets of bonding modes observed for (L^-) . A set of four tetradentate ligands links two nickel ions each through a five-membered chelate ring and a six-membered chelate ring leading to the construction of the $[\text{Ni}_4\text{L}_8]^{4+}$ core. In this case (L^-) coordinates to one nickel ion through the pyridine and the amide nitrogen donors and to the neighboring nickel ion through the nitrogen donor of the tetrazolyl group and the oxygen donor of the amide function. In contrast, the four ligands (L^-) of the second set exhibit a bidentate bonding mode. These ligands coordinate across the pyridine and the amide nitrogen donors only and complete the slightly distorted octahedral coordination sphere at the nickel vertices (Figure 1).

Two enantiomeric pairs ((Δ)-, (Δ)-*fac*, and (Δ)-, (Δ)-*mer*) are principally possible for octahedral complexes of the type MA_3B_3 (with bidentate ligands $\text{M}(\text{AB})_3$).^[7] The cluster $[\text{Ni}_4\text{L}_8] \text{ Ni-5b}$ has idealized S_4 molecular symmetry and is thus achiral ((Δ), (Δ), (Δ), (Δ)-*fac,meso* form).

The zinc complex **Zn-5a** was obtained as a white solid in a similar manner to **Ni-5b**. Likewise, $[\text{Zn}_4\text{L}_8] \text{ Zn-5a}$ is present in the crystal as a square $[2 \times 2]$ grid ($d_{\text{Zn-Zn}} = 5.657 \text{ \AA}$, angle $_{\text{Zn-Zn-Zn}} = 81.04^\circ$) and is isostructural^[8] with $[\text{Ni}_4\text{L}_8] \text{ Ni-5b}$. Additional characterization of **Zn-5a** by NMR spectroscopy was hindered by its poor solubility.

The temperature dependence of the magnetic susceptibility of powder samples of **Ni-5b** is shown as χT in Figure 2. With decreasing temperature χT increases. It is well known that for Ni^{II} ions ligand-field interactions lead to a zero-field splitting (ZFS) and thereby to a deviation from the Curie-law ($\chi T = \text{constant}$) at low temperatures.^[9, 10] However, regardless of the sign of the ZFS a decrease of χT is always expected (see Figure 2).^[10] Therefore, the increase of χT can only be explained by an intramolecular ferromagnetic coupling of the Ni ions.

For a quantitative analysis of the magnetic properties of **Ni-5b** measurements at fields of 3, 10, 30, and 55 kG were all at once fitted to a model spin-Hamiltonian. The spin-Hamiltonian $H_{\text{ex}} = -J(S_1 S_2 + S_2 S_3 + S_3 S_4 + S_4 S_1)$, which solely takes into account a magnetic coupling, reproduced the data roughly. The additional inclusion of a ligand-field

[*] Prof. Dr. R. W. Saalfrank, Dr. S. Trummer, Dipl.-Chem. U. Reimann, Dr. M. M. Chowdhry, Dr. F. Hampel
 Institut für Organische Chemie der Universität Erlangen-Nürnberg
 Henkestrasse 42, 91054 Erlangen (Germany)
 Fax: (+49)9131-852-1165
 E-mail: saalfrank@organik.uni-erlangen.de

Dr. O. Waldmann
 Physikalisches Institut III der Universität Erlangen-Nürnberg
 Erwin-Rommel-Strasse 1, 91058 Erlangen (Germany)
 Fax: (+49)9131-15249
 E-mail: Waldmann@physik.uni-erlangen.de

[**] Chelate Complexes, Part 13. This work was supported by the Deutsche Forschungsgemeinschaft, Bayerisches Langzeitprogramm "Neue Werkstoffe" and the Fonds der Chemischen Industrie. Part 12: ref. [14].

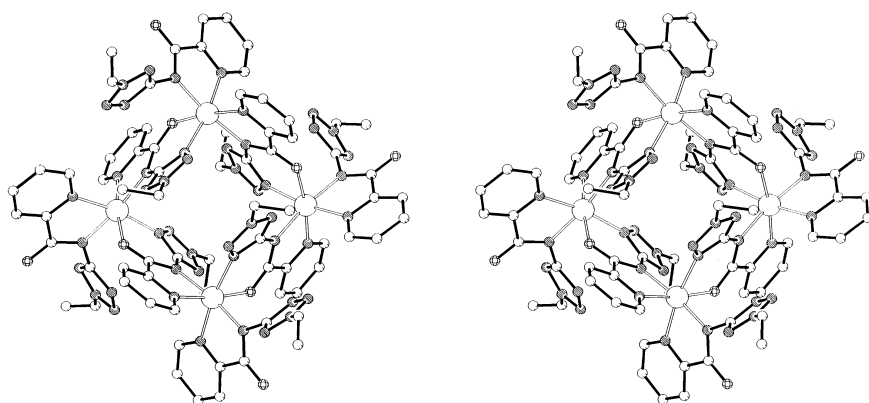


Figure 1. Molecular structure of **Ni-5b** in the crystal (PLUTON presentation). Stereoview perpendicular to the Ni_4 plane (along the S_4 axis); H atoms omitted for clarity. Carbon shaded, nitrogen hatched, oxygen chequered, nickel transparent. Selected bond lengths [Å] and angles [°] of tetradentate (L^b): N(pyridine)-Ni 2.111(3), N(amide)-Ni 2.065(3), N(tetrazole)-Ni 2.062(3), O-Ni 2.032(2); N(pyridine)-Ni-N(amide) 79.26, N(tetrazole)-Ni-O 131.00.

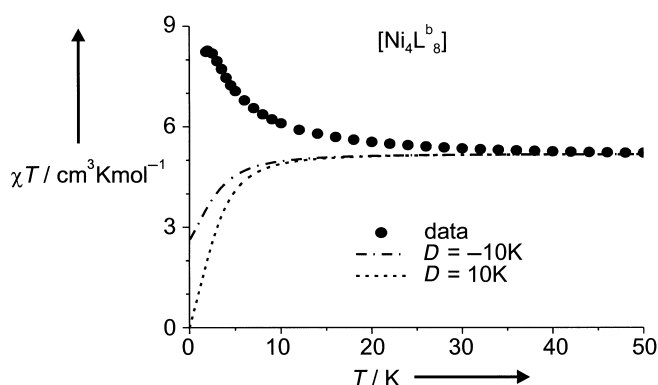


Figure 2. Temperature dependence of the magnetic susceptibility of **Ni-5b** as measured at a field of 3 kG. Dashed curves were calculated with the spin-Hamiltonian $H_{\text{ex}} + H_{\text{ZFS}}$ for $J = 0$ and $D = \pm 10$ K ($g = 2.24$).

interaction in the form of a uniaxial ZFS, $H_{\text{NFA}} = D \sum_i \left(S_{i,z}^2 - \frac{2}{3} \right)$, led to excellent fits of the data with $|D| \approx 3$ K and $g = 2.24$. The sign of D could not be determined unambiguously from the powder measurements. However, regardless of the sign of D , we obtained ferromagnetic values for the coupling J ($J \approx 1.5$ K), in agreement with the above qualitative consideration.

Experimental Section

Ligand **HL 4** was synthesized from 2-picolinyl chloride^[11] and 2-alkyl-5-aminotetrazole^[12] according to reference [13].

Ni-5b and **Zn-5a**: General procedure: A solution of **HL 4** (1.0 mmol) in methanol (20 mL) was added to a solution of nickel(II) or zinc(II) acetate (0.5 mmol) in methanol (30 mL). The reaction mixture was stirred at 20 °C for 2 h, concentrated to 20 mL, and layered with diethyl ether (10 mL). The precipitate was collected, dried under reduced pressure, and crystallized.

Ni-5b: Yield: 210 mg (85%) violet tetrahedrons (methanol/dichloromethane/diethyl ether 1:1:1); correct elemental analysis; decomp > 250 °C; IR (CHBr₃): $\tilde{\nu} = 1620$ cm⁻¹ (C=O), 1558 (C=C); FAB-MS (3-nitrobenzyl alcohol (3-NBA)): m/z (%): 1972 (6) [$Ni_4L^b_8$]⁺.

Zn-5a: Yield: 193 mg (86%) colorless tetrahedrons (methanol/diethyl ether 1:1); correct elemental analysis; decomp > 250 °C; IR (CHBr₃): $\tilde{\nu} = 1610$ cm⁻¹ (C=O), 1560 (C=C); FAB-MS (3-NBA): m/z (%): 741 (100) [$Zn_2L^a_3$]⁺.

The magnetic moment of a powder sample of **Ni-5b** was measured with a commercial SQUID magnetometer (Quantum Design). Data were corrected for diamagnetic contributions and temperature independent paramagnetism (TIP).

Received: April 7, 2000 [Z14952]

- [1] J.-M. Lehn, *Supramolecular Chemistry: Concepts and Perspectives*, VCH, Weinheim, **1995**; D. L. Caulder, K. N. Raymond, *Acc. Chem. Res.* **1999**, *32*, 975–982; P. J. Stang, *Chem. Eur. J.* **1998**, *4*, 19–27; M. Fujita, *Chem. Soc. Rev.* **1998**, *27*, 417–425; S. L. James, M. P. Mingos, A. J. P. White, D. J. Williams, *Chem. Commun.* **1998**, *21*, 2323–2324; C. J. Jones, *Chem. Soc. Rev.* **1998**, *27*, 289–299; “Transition Metals in Supramolecular Chemistry”: R. W. Saalfrank, B. Demleitner in *Perspectives in Supramolecular Chemistry*, Vol. 5 (Ed.: J. P. Sauvage), Wiley-VCH, Weinheim, **1999**, pp. 1–51; E. Uller, B. Demleitner, I. Bernt, R. W. Saalfrank, in *Structure and Bonding*, Vol. 96 (Ed.: M. Fujita), Springer, Berlin, **2000**, pp. 149–175; S. Leininger, B. Olenyuk, P. J. Stang, *Chem. Rev.* **2000**, *100*, 853–908.
- [2] D. Gatteschi, R. Sessoli, A. Cornia, *Chem. Commun.* **2000**, 725–732; Z. Zhao, C. J. Matthews, L. K. Thompson, S. L. Heath, *Chem. Commun.* **2000**, 265–266; M. A. Bolcar, S. M. J. Aubin, K. Folting, D. N. Hendrickson, G. Christou, *Chem. Commun.* **1997**, 1485–1486; C. Benelli, A. J. Blake, E. K. Brechin, S. J. Coles, A. Graham, S. G. Harris, S. Meier, A. Parkin, S. Parson, A. M. Seddon, R. E. P. Winpenny, *Chem. Eur. J.* **2000**, *5*, 883–896; C. J. Matthews, K. Avery, Z. Xu, L. K. Thompson, L. Zhao, D. O. Miller, K. Biradha, K. Poirier, M. J. Zaworotko, C. Wilson, A. E. Goeta, J. A. K. Howard, *Inorg. Chem.* **1999**, *38*, 5266–5276; C. S. Campos-Fernández, R. Clérac, K. R. Dunbar, *Angew. Chem.* **1999**, *111*, 3685–3688; *Angew. Chem. Int. Ed.* **1999**, *38*, 3477–3479; M. Monfort, I. Resino, J. Ribas, H. Stoeckli-Evans, *Angew. Chem.* **2000**, *112*, 197–199; *Angew. Chem. Int. Ed.* **2000**, *39*, 191–193; Z. E. Serna, L. Lezama, M. K. Urtiaga, M. I. Arriortua, M. G. Barandica, R. Cortés, T. Rojo, *Angew. Chem.* **2000**, *112*, 352–355; *Angew. Chem. Int. Ed.* **2000**, *39*, 344–347; A. J. Amoroso, J. C. Jeffery, P. L. Jones, J. A. McCleverty, P. Thornton, M. D. Ward, *Angew. Chem.* **1995**, *107*, 1577–1580; *Angew. Chem. Int. Ed. Engl.* **1995**, *34*, 1443–1446; J. Rojo, J.-M. Lehn, G. Baum, D. Fenske, O. Waldmann, P. Müller, *Eur. J. Inorg. Chem.* **1999**, 517–522; O. Waldmann, J. Schülein, R. Koch, P. Müller, I. Bernt, R. W. Saalfrank, H. P. Andres, H. U. Güdel, P. Allenspach, *Inorg. Chem.* **1999**, *38*, 5879–5886; O. Waldmann, J. Hassmann, P. Müller, G. S. Hanan, D. Volkmer, U. S. Schubert, J.-M. Lehn, *Phys. Rev. Lett.* **1997**, *78*, 3390–3393.
- [3] V. L. Pecoraro, A. J. Stemmler, B. R. Gibney, J. J. Bodwin, H. Wang, J. W. Kampf, A. Barwinski, *Prog. Inorg. Chem.* **1997**, *45*, 83–177.
- [4] Crystal structure analysis data for [$Ni_4L^b_8$] **Ni-5b**: $C_{72}H_{72}N_{48}O_8Ni_4 \cdot 4CH_2Cl_2$, $M_r = 2312.32$; crystal dimensions: $0.30 \times 0.30 \times 0.20$ mm, tetragonal; space group $I4(1)/a$; $a = b = 22.8466(6)$, $c = 20.1411(1)$ Å, $V = 10513.0(5)$ Å³; $Z = 8$; $F(000) = 4736$, $\rho_{\text{calcd}} = 1.461$ Mg m⁻³; diffractometer: Nonius KappaCCD; MoK_{α} radiation ($\lambda = 0.71073$ Å); $T = 173(2)$ K; graphite monochromator; measurement range: $6.95 \leq \theta \leq 24.98$; section of the reciprocal lattice: $-27 \leq h \leq 27$, $-19 \leq k \leq 19$, $-23 \leq l \leq 23$; of 8260 measured reflections, 4509 were independent, and 3436 with $I > 2\sigma(I)$; linear absorption coefficient 0.983 mm⁻¹. The structure was solved by direct methods using SHELXS-97 and refined with all data (326 parameters) by full-matrix least-squares on F^2 using SHELXL97;^[5] all non-hydrogen atoms were refined anisotropically; $R_1 = 0.0533$ (observed reflections); $wR_2 = 0.1552$ (all data); max./min. residual electron density $0.758/-0.403$ e Å⁻³.^[6]
- [5] SHELXS-86: G. M. Sheldrick, C. Krüger, P. Goddard, *Crystallographic Computing 3*, Oxford University Press, Oxford, **1985**, p. 175; G. M. Sheldrick, SHELXL-97, Program for Crystal Structure Refinement, University of Göttingen, **1997**.

- [6] Crystallographic data (excluding structure factors) for the structures reported in this paper have been deposited with the Cambridge Crystallographic Data Centre as supplementary publication nos. CCDC-140701 (**Ni-5b**), and CCDC-140702 (**Zn-5a**). Copies of the data can be obtained free of charge on application to CCDC, 12 Union Road, Cambridge CB2 1EZ, UK (fax: (+44) 1223-336-033; e-mail: deposit@ccdc.cam.ac.uk).
- [7] R. W. Saalfrank, B. Hörner, D. Stalke, J. Salbeck, *Angew. Chem.* **1993**, *105*, 1223–1225; *Angew. Chem. Int. Ed. Engl.* **1993**, *32*, 1179–1182.
- [8] Crystal structure analysis data for **Zn-5a**: $C_{64}H_{56}N_{48}O_8Zn_4 \cdot 4CH_3OH$, $M_r = 2011.20$; crystal dimensions: $0.30 \times 0.30 \times 0.15$ mm, tetragonal, space group $I\bar{4}$, $a = b = 14.251(2)$, $c = 21.302(2)$ Å, $V = 4326.3(9)$ Å³, $Z = 8$, $F(000) = 2056$, $\rho_{\text{calc}} = 1.544$ Mg m⁻³; diffractometer: Nonius Mach3; $MoK\alpha$ radiation ($\lambda = 0.71073$ Å); $T = 193(2)$ K; graphite monochromator; data collection mode ω scans; measurement range: $2.78 \leq \theta \leq 26.27$; section of the reciprocal lattice: $-17 \leq h \leq 0$, $-0 \leq k \leq 17$, $-0 \leq l \leq 26$; of 2441 measured reflections, 2433 were independent, and 1907 with $I > 2\sigma(I)$; linear absorption coefficient 1.183 mm⁻¹; absorption correction ψ scans. The structure was solved by direct methods using SHELXS-86 and refined with all data (298 parameters) by full-matrix least-squares on F^2 using SHELXL93;^[5] all non-hydrogen atoms were refined anisotropically; $R_1 = 0.0391$ (observed reflections); $wR_2 = 0.0987$ (all data); max./min residual electron density $0.514/-0.421$ e nm⁻³.^[5]
- [9] O. Waldmann, J. Hassmann, P. Müller, D. Volkmer, U. S. Schubert, J.-M. Lehn, *Phys. Rev. B* **1998**, *58*, 3277–3281.
- [10] O. Kahn, *Molecular Magnetism*, VCH, Weinheim, **1993**.
- [11] H. Brunner, G. Spettel, *J. Organomet. Chem.* **1978**, *160*, 149–158.
- [12] R. A. Henry, W. G. Finnegan, *J. Am. Chem. Soc.* **1954**, *76*, 923–926.
- [13] A. G. Oertli, W. R. Meyer, U. W. Suter, F. B. Joho, V. Gramlich, W. Petter, *Helv. Chim. Acta* **1992**, *75*, 184–189.
- [14] R. W. Saalfrank, N. Löw, B. Demleitner, D. Stalke, M. Teichert, *Chem. Eur. J.* **1998**, *4*, 1305–1311.

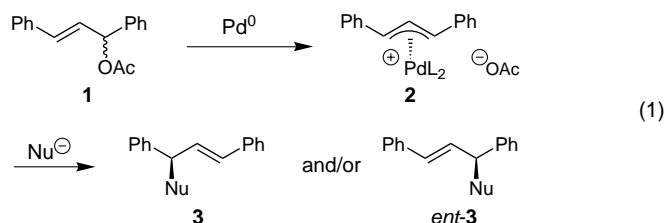
Diastereoselective and Enantioselective Palladium-Catalyzed Allylic Substitution with Nonstabilized Ketone Enolates**

Manfred Braun,* Frank Laicher, and Thorsten Meier

*Dedicated to Professor Rolf Huisgen
on the occasion of his 80th birthday*

The utility of transition metal mediated allylic substitutions in organic syntheses has been proven by numerous applications in the past three decades. A particularly efficient way of carbon–carbon bond formation was opened up by the reaction of carbon nucleophiles with allylpalladium complexes, the generation of which is accomplished in situ and requires only catalytic amounts of the transition metal.^[1] After mechanistic studies had treated the problem of stereochemistry,^[2] considerable efforts were directed towards enan-

tioselective variants,^[3] most of this work focussed on symmetrically substituted racemic allyl compounds such as **1**. The attack of a nucleophile on the palladium complex **2**, formed from **1**, can be directed in an enantioselective way by means of chiral ligands (L^*) so that either one of the substitution products, **3** or *ent*-**3**, can be prepared in a controlled manner [Eq. (1)].^[4]



Despite this impressive progress, the main limitation of this concept is that the carbon nucleophiles used so far have been almost exclusively “soft”, stabilized carbanions.^[3] Although the chemistry of “preformed” enolates^[5] evolved at the same time as that of allylpalladium chemistry, attempts to combine both concepts have been very rare, and their success rather limited. An early report on palladium-catalyzed reactions of ketone enolates with cyclic allyl acetates^[6] was questioned later.^[7] Furthermore, these attempts were plagued by the inevitable double allylations, low reactivities, and moderate yields.^[8a] These difficulties were partly overcome by the employment of enol stannanes instead of lithium enolates,^[8] an approach which led to the first enantioselective variant.^[9]

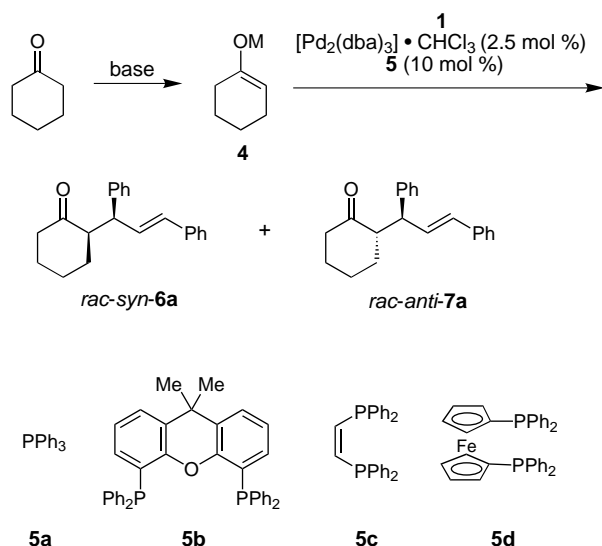
Recently, stereoselectivity was obtained in the reaction of an enantiopure allyl acetate with a chelated zinc enolate.^[10] However, the problem of producing a palladium-mediated allylation of enolates which provides both diastereoselectivity and catalyst-induced enantioselectivity has so far not been solved. Herein we report, as a solution to this problem, a method that is applicable to cyclic and acyclic ketone enolates.

Two adjacent stereogenic centers are created in the reaction of an α -substituted enolate and the meso complex **2**, which is formed in situ from the racemic acetate **1** [Eq. (1)]. Thus, we decided to tackle the problem of diastereoselectivity first. For this purpose, cyclohexanone was deprotonated with various bases in tetrahydrofuran to generate the enolate **4**; the advantage of this intermediate is its fixed enolate geometry (*E*, Scheme 1). The enolate **4** was allowed to react with the acetate **1** in the presence of 5 mol % of the palladium catalyst generated in situ from tris(dibenzylideneacetone)dipalladium–chloroform ($[Pd_2(dba)_3] \cdot CHCl_3$)^[11] and the corresponding phosphane ligands **5**. In all the cases that are listed in Table 1 there was smooth and quantitative conversion into the diastereomeric ketones **6a** and **7a**, which can clearly be distinguished from one another by the chemical shifts of their allylic protons (3.88 and 3.98 ppm, respectively) in the ¹H NMR spectra.

The diastereoselectivity was influenced not only by the ligands **5a–d**^[12] on the transition metal but also by the enolate counterion and the base used for the deprotonation. For the lithium enolate, substantial diastereoselectivity resulted from the use of chelating phosphane ligands (Table 1, entries 1

[*] Prof. Dr. M. Braun, Dr. F. Laicher, Dipl.-Chem. T. Meier
Institut für Organische und Makromolekulare Chemie
Universität Düsseldorf
40225 Düsseldorf (Germany)
Fax: (+49) 221-81-15079
E-mail: braunm@uni-duesseldorf.de

[**] This work was supported by the Deutsche Forschungsgemeinschaft and the Fonds der Chemischen Industrie. We thank Dipl.-Chem. Daniel Ridder for carrying out the crystal structure analyses.



Scheme 1. Palladium-catalyzed diastereoselective allyl substitution with cyclohexanone.

Table 1. Diastereoselective palladium-catalyzed reaction of ketones with allylic acetate **1**.

Entry	Ketone	Base	Ligand 5	<i>syn-6:anti-7</i>
1	(CH ₂) ₅ CO	LiN <i>i</i> Pr	5a ^[a]	6a:7a 57:43
2	(CH ₂) ₅ CO	LiN <i>i</i> Pr	5b ^[b]	6a:7a 81:19
3	(CH ₂) ₅ CO	LiN <i>i</i> Pr	5c ^[b]	6a:7a 83:17
4	(CH ₂) ₅ CO	LiN <i>i</i> Pr	5d ^[b]	6a:7a 87:13
5	(CH ₂) ₅ CO	LiN <i>i</i> Pr/LiCl	5d ^[b]	6a:7a 92:8
6	(CH ₂) ₅ CO	LiN(SiMe ₃) ₂	5d ^[b]	6a:7a 90:10
7	(CH ₂) ₅ CO	KN(SiMe ₃) ₂	5d ^[b]	6a:7a 60:40
8	(CH ₂) ₅ CO	ClMgN <i>i</i> Pr	5d ^[b]	6a:7a 97:3
9	Me ₃ C ₆ H ₂ COEt	LiN(SiMe ₃) ₂	5d ^[b]	6b:7b 33:67
10	Me ₃ C ₆ H ₂ COEt	LiN(<i>i</i> Pr) ₂	5d ^[b]	6b:7b 10:90

[a] 20 mol %. [b] 10 mol %.

versus 2–6), with the ferrocene derivative **5d** being the most efficient (entries 4–6). Disaggregation of the enolate by addition of one equivalent of lithium chloride^[13] led to a small but clear enhancement of the diastereomeric ratio (entry 5), whereas no further improvement came from the use of lithium hexamethyldisilazide (LiN(SiMe₃)₂; entry 6). Since the use of the supposedly more polar potassium enolate led to a considerable decrease in stereoselectivity (entry 7), the next logical step was a change to magnesium. Indeed, the product **6a** was obtained from the magnesium enolate in high diastereoselectivity (entry 8). The *syn* configuration of the main product **6a**, obtained as a diastereomerically pure racemic compound after recrystallization, was unambiguously determined by a crystal structure analysis (Figure 1).^[14] In contrast to the normally favored equatorial conformation of 2-methylcyclohexanone, the side chain of the ketone **6a** occupies the axial position, thus avoiding steric interaction of the bulky diphenylpropene substituent and the carbonyl oxygen atom.^[15]

To test the versatility of our method it was applied to an open-chained ketone. Mesityl ethyl ketone was chosen (mesityl ethyl ketone = 1-(2,4,6-trimethylphenyl)propan-1-one), which, depending on the deprotonation conditions used,

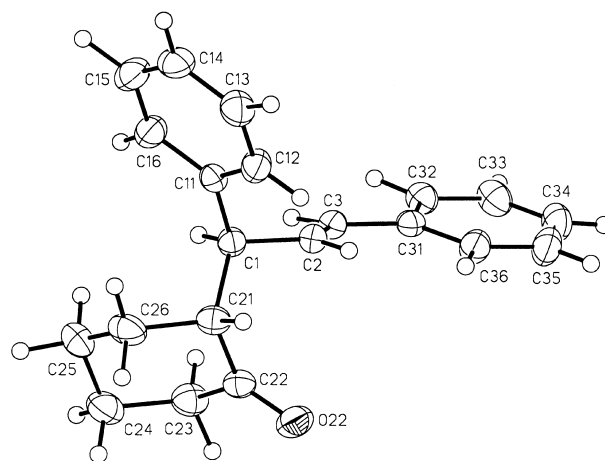
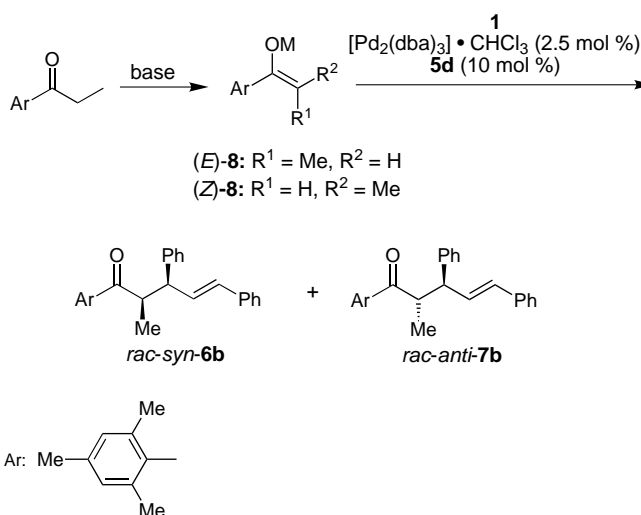


Figure 1. Crystal structure of *syn-6a* (SHELXTL-Plus; 25 % probability displacement ellipsoids).

can give either of the stereoisomers of the enolate **8**.^[5] When LiN(SiMe₃)₂ was used for deprotonation, predominantly (*Z*)-**8** was formed (Scheme 2).^[16a] The subsequent palladium-catalyzed allylation was controlled by the chelating ligand **5d** and afforded the stereoisomers **6b** and **7b** with only moderate



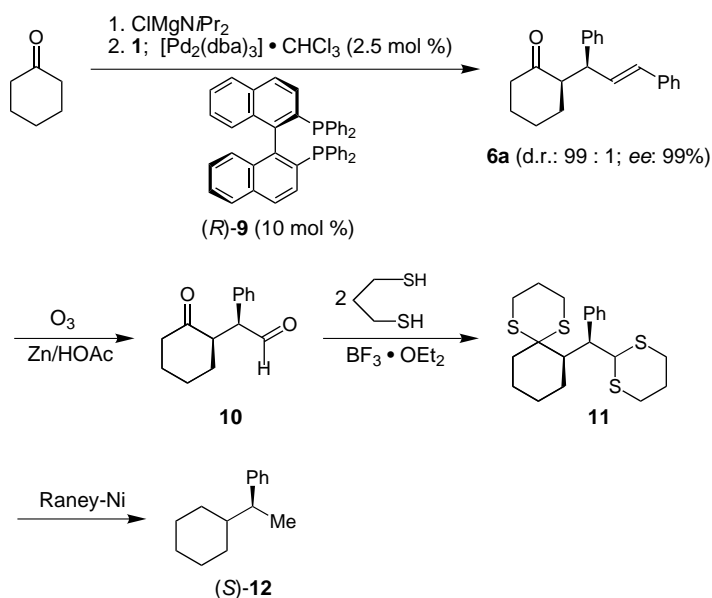
Scheme 2. Palladium-catalyzed diastereoselective allyl substitution with an acyclic ketone.

diastereoselectivity (entry 9). On the other hand, use of the *E*-configured enolate **8**,^[16b] which is generated by metalation of mesityl ethyl ketone with lithium diisopropylamide, enhanced the *syn:anti* ratio of the products **6b:7b** to 10:90 (entry 10). Thus unexpectedly, despite having the opposite configuration of the enolate **8**, the same stereoisomeric product **7b** was formed in excess (entries 9, 10). A possible explanation could come from the observation that, under the conditions of the allylic substitution reaction (that is, [Pd₂(dba)₃]·CHCl₃; ligand **5d**, without **1**; THF; 0 °C), a slow conversion of (*Z*)-**8** into the thermodynamically more stable (*E*)-**8** occurs,^[17] as shown by the formation of the corresponding enolsilanes ((*Z*)-**8**/(*E*)-**8**, M = SiMe₃). In contrast, the configuration of the *E* enolate **8** remains unchanged under

these conditions. Thus, the low diastereoselectivity obtained from the use of $\text{LiN}(\text{SiMe}_3)_2$ might stem from competing allylic substitution pathways of the *E* and *Z* enolates **8**, each of which lead to the other diastereomer of **6b** and **7b**.

The configuration of the major stereoisomer **7b** was determined by a crystal structure analysis, which unambiguously revealed it to be that of the *anti*-diastereomer. The major products **6a** and **7b**, formed from cyclohexanone and mesityl ethyl ketone, respectively, have opposite relative configurations, which is surprising in view of the identical enolate geometries in both enolates (*E*)-**4** and (*E*)-**8**. A possible explanation is the existence of two different types of transition state (closed versus open) for the two different types of ketone, this has yet to be confirmed experimentally.

Finally, we addressed the problem of enantioselectivity. For this purpose, the magnesium enolate **4** of cyclohexanone was allowed to react with the acetate **1** in the presence of the palladium-(*R*)-BINAP complex (BINAP = 2,2'-bis(diphenylphosphanyl)-1,1'-binaphthyl) generated in situ from $[\text{Pd}_2(\text{dba})_3] \cdot \text{CHCl}_3$ (2.5 mol %) and the chiral (*R*)-BINAP ligand (*R*)-**9** (10 mol %) as shown in Scheme 3. The reaction



Scheme 3. Palladium-catalyzed enantioselective allyl substitution with cyclohexanone.

turned out to be very efficient in three respects. First, quantitative conversion of the starting material **1** was observed; second the diastereoselectivity was enhanced even compared to that obtained with the achiral ligand **5d** (Table 1, entry 8); third, exceptional enantioselectivity was reached. Thus, the enantiomeric excess of the major diastereomer **6a** was determined to be 99% *ee* by HPLC on a chiralcel OJ column. The diastereomeric ratio of **6a**:**7a** was 99:1.

The absolute configuration of the ketone **6a** was elucidated by correlation with the hydrocarbon **12** as follows: The keto aldehyde **10** was generated in 72% yield by ozonolysis of the alkene **6a**. Subsequent thioacetalization provided the bis-dithiane **11**, which was isolated after (a material consuming) column chromatography in 13% yield. Finally, (*S*)-**12** was

obtained in 94% crude yield by desulfurization with Raney-nickel. Since the optical rotation of (*R*)-**12** was known,^[18] a comparison permitted us to assign the *S* configuration to the hydrocarbon **12** obtained from ketone **6a**.

A brief investigation revealed that by using the method described above open-chained ketones can react enantioselectively too. Thus, the reaction of the lithium enolate (*E*)-**8** with the acetate **1** was mediated by the palladium-(*R*)-BINAP catalyst. Again, the diastereomeric ratio was maintained (10:90). Furthermore the main diastereomer **7b** was formed in 88% *ee*, as determined by ^1H NMR spectroscopy in the presence of the chiral shift-reagent $[\text{Eu}(\text{hfc})_3]$.^[19]

To conclude palladium-catalyzed allylic substitution is feasible with nonstabilized preformed lithium and magnesium enolates of cyclic and open-chained ketones. For the first time, this reaction could be performed in such a way that the chiral ligand of the transition metal induced not only a high degree of diastereoselectivity but also enantioselectivity.

Experimental Section

Typical procedure: Methylmagnesium chloride (1.1 mmol, 0.37 mL; 3 M solution in THF) was added dropwise to diisopropylamine (0.15 mL, 1.1 mmol) dissolved in dry THF (1 mL) at -16°C under nitrogen. After 30 min, cyclohexanone (0.11 mL, 1.1 mmol) dissolved in THF (1 mL) was added dropwise, and stirring was continued for 30 min at -16°C . The enolate thus generated was injected into a solution of **1** (252 mg, 1 mmol), $[\text{Pd}_2(\text{dba})_3] \cdot \text{CHCl}_3$ (26 mg, 25 μmol), and (*R*)-BINAP (62 mg, 100 μmol) in dry THF (2 mL). After stirring the mixture for 16 h at 0°C it was hydrolyzed by addition of a phosphate-buffer (pH 7) and extracted with CH_2Cl_2 (3×50 mL). The combined organic layers were washed with brine, dried with MgSO_4 and concentrated in vacuo. The residue was dissolved in *n*-hexane and filtered through celite 557 in a suction filter. Evaporation of the solvent led to the crude product. NMR spectroscopy revealed signals corresponding to the clean and quantitative conversion of the substrate **1**. An analytically pure sample of **6a** (195 mg, 67%) was obtained by flash chromatography on silica gel (*n*-hexane:ethyl acetate, 10:1). The enantiomeric excess was determined by HPLC on a chiralcel OJ column (*n*-hexane:isopropanol, 96:4).

Selected physical and spectroscopic data: **6a**: m.p. 93°C ; ^1H NMR (500 MHz, CDCl_3): δ = 2.87 (ddd, J = 9.5, 9.5, 4.9 Hz, 1H, 2-H), 3.88 (dd, J = 9.5, 7.6 Hz, 1H, 1'-H), 6.33 (d, J = 15.8 Hz, 1H, 3'-H), 6.44 (dd, J = 15.8, 7.6 Hz, 1H, 2'-H); ^{13}C NMR (125 MHz, CDCl_3): δ = 23.93, 28.52, 32.17, 42.42, 48.39, 55.82, 126.45, 126.55, 127.14, 128.51, 128.60, 128.83, 130.46, 131.91, 137.33, 141.88, 212.46; elemental analysis calcd for $\text{C}_{21}\text{H}_{22}\text{O}$ (%): C 86.85, H 7.64; found: C 86.91, H 7.62. The minor diastereomer **7a** differs in: ^1H NMR (500 MHz, CDCl_3): δ = 3.98 (dd, J = 9.0, 9.0 Hz, 1H), 6.26 (dd, J = 15.7, 9.0 Hz, 1H), 6.45 (d, J = 15.7 Hz, 1H); ^{13}C NMR (125 MHz, CDCl_3): δ = 24.42, 28.30, 31.84, 42.15, 48.32, 55.55, 130.97, 131.21, 137.16, 143.24, 211.43. (1*S*,2*R*)-**6a**: $[\alpha]_D^{25}$ = 68.5 (c = 0.2 in CHCl_3); **7b**: m.p. 110.3°C ; ^1H NMR (500 MHz, CDCl_3): δ = 1.22 (d, J = 7.3 Hz, 3H, CH-CH_3), 1.99 (s, 6H, Ar-CH_3), 2.24 (s, 3H, Ar-CH_3), 3.40 (dq, J = 7.3, 7.8 Hz, 1H, 2-H), 4.10 (dd, J = 8.2, 7.8 Hz, 1H, 3-H), 6.43 (dd, J = 15.7, 8.2 Hz, 1H, 4-H), 6.48 (d, J = 15.7 Hz, 1H, 5-H); elemental analysis calcd for $\text{C}_{27}\text{H}_{28}\text{O}$ (%): C 88.00, H 7.66; found: C 87.89, H 7.76. The minor diastereomer **6b** differs in: ^1H NMR (500 MHz, CDCl_3): δ = 0.95 (d, J = 7.0 Hz, 3H), 2.21 (s, 3H), 3.49 (dq, J = 9.7, 7.0 Hz, 1H), 3.99 (dd, J = 9.7, 6.4 Hz, 1H), 6.34 (dd, J = 16.0, 6.4 Hz, 1H), 6.63 (d, J = 16.0 Hz, 1H).

Received: December 28, 1999
Revised: June 20, 2000 [Z14478]

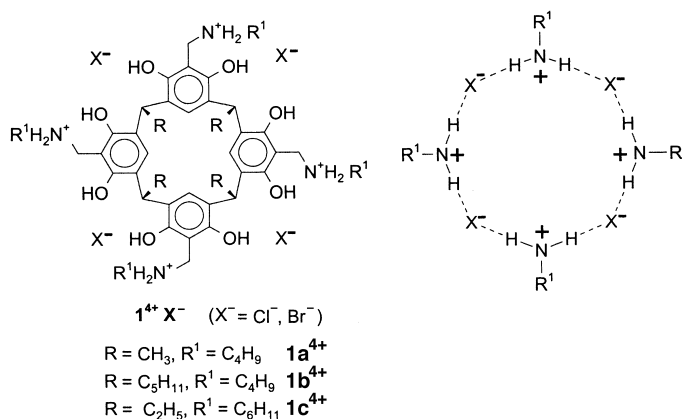
- [1] Reviews: a) B. M. Trost, *Tetrahedron* **1977**, 33, 2615–2649; b) J. Tsuji, *Organic Synthesis with Palladium Compounds*, Springer, New York, **1980**; c) B. M. Trost, *Acc. Chem. Res.* **1980**, 13, 385–393; d) B. M.

Hydrogen-Bonded Analogues of Cavitands**

Alexander Shivanyuk,* Thomas P. Spaniol,
Kari Rissanen, Erkki Kolehmainen, and
Volker Böhmer

Multiple hydrogen-bonding interactions are widely used for the design of hollow self-assembled structures capable of molecular encapsulation.^[1] In particular, intermolecular hydrogen bonds between urea functions are responsible for the stability of dimeric calixarene capsules,^[2] while the slow exchange of guests in self-folded cavitplexes is caused by a seam of intramolecular hydrogen bonds between amide groups.^[3]

Herein we describe a novel type of self-assembled concave structures $1^{4+} \cdot 4X^-$ in which the shallow socket of a resorcarenene is extended by a cyclic hydrogen-bonded array of four halide ions and four ammonium ions attached to the wide rim of the macrocycle. We demonstrate also that $1^{4+} \cdot 4Cl^-$, but not $1^{4+} \cdot 4Br^-$, is able to complex certain alcohols in $CDCl_3$ through the formation of hydrogen bonds and inclusion into the π -basic resorcarenene cavity.



Condensation of resorcarenenes^[4] with primary amines and formaldehyde readily gives the corresponding tetrabenzoxazine derivatives.^[5] The subsequent cleavage of the benzoxazine rings with HCl or HBr (*n*-butanol, 80 °C) yields the tetraammonium salts $1^{4+} \cdot 4X^-$ ($X^{-} = Cl^{-}$,^[6] Br^{-}) in 80–90 % yield.

[*] Dr. A. Shivanyuk, Prof. Dr. K. Rissanen, Dr. E. Kolehmainen
Department of Chemistry
University of Jyväskylä
P.O. Box 35, 40351, Jyväskylä (Finland)
Fax: (+358) 14 2602-501
E-mail: shivan@jyu.fi

Dr. T. P. Spaniol
Institut für Anorganische Chemie und Analytische Chemie
Fachbereich Chemie und Pharmazie
Johannes Gutenberg-Universität
Duesbergweg 10–14, 55099 Mainz (Germany)

Dr. V. Böhmer
Abteilung Lehramt Chemie
Fachbereich Chemie und Pharmazie, Johannes Gutenberg-Universität
Duesbergweg 10–14, 55099 Mainz (Germany)

[**] We are grateful to Mr. R. Kauppinen for his assistance with NMR measurements. This work was supported by the Finnish Academy.

- Trost, *Pure Appl. Chem.* **1981**, *53*, 2357–2370; e) J. Tsuji, *Pure Appl. Chem.* **1982**, *54*, 197–206; f) S. A. Godleski in *Comprehensive Organic Synthesis*, Vol. 4 (Ed.: B. M. Trost), Pergamon, Oxford, **1991**, pp. 585–661.
- [2] B. M. Trost, T. R. Verhoeven, *J. Org. Chem.* **1976**, *41*, 3215–3216; T. Hayashi, A. Yamamoto, T. Hagihara, *J. Org. Chem.* **1986**, *51*, 723–727; T. Hayashi, M. Kawatsura, Y. Uozumi, *J. Am. Chem. Soc.* **1998**, *120*, 1681–1687; M. Braun, C. Unger, K. Opdenbusch, *Eur. J. Org. Chem.* **1998**, 2389–2396; for a review, see C. G. Frost, J. Howarth, J. M. J. Williams, *Tetrahedron: Asymmetry* **1992**, *3*, 1089–1122.
- [3] Reviews: a) O. Reiser, *Angew. Chem.* **1993**, *105*, 576–578; *Angew. Chem. Int. Ed. Engl.* **1993**, *32*, 547–549; b) J. M. J. Williams, *Synlett* **1996**, 705–710; c) B. M. Trost, D. L. Van Vranken, *Chem. Rev.* **1996**, *96*, 395–422; d) G. Helmchen, *J. Organomet. Chem.* **1999**, *576*, 203–214.
- [4] B. M. Trost, D. L. Van Vranken, C. Bingel, *J. Am. Chem. Soc.* **1992**, *114*, 9327–9343; P. von Matt, A. Pfaltz, *Angew. Chem.* **1993**, *105*, 614–615; *Angew. Chem. Int. Ed. Engl.* **1993**, *32*, 566–568; J. Sprinz, G. Helmchen, *Tetrahedron Lett.* **1993**, *34*, 1769–1772; G. J. Dawson, C. G. Frost, J. M. J. Williams, S. J. Coote, *Tetrahedron Lett.* **1993**, *34*, 3149–3150; G. C. Lloyd-Jones, A. Pfaltz, *Angew. Chem.* **1995**, *107*, 534–536; *Angew. Chem. Int. Ed. Engl.* **1995**, *34*, 462–464; G. J. Dawson, J. M. J. Williams, S. J. Coote, *Tetrahedron: Asymmetry* **1995**, *6*, 2535–2546; H. Steinhausen, M. Reggelin, G. Helmchen, *Angew. Chem.* **1997**, *109*, 2199–2202; *Angew. Chem. Int. Ed. Engl.* **1997**, *36*, 2108–2110; R. Prétôt, A. Pfaltz, *Angew. Chem.* **1998**, *110*, 337–339; *Angew. Chem. Int. Ed.* **1998**, *37*, 323–325; D. S. Clyne, Y. C. Mermut-Bouvier, N. Nomura, T. V. RajanBabu, *J. Org. Chem.* **1999**, *64*, 7601–7611; D. Enders, R. Peters, J. Runsink, J. W. Bats, *Org. Lett.* **1999**, *1*, 1863–1866.
- [5] C. H. Heathcock in *Modern Synthetic Methods 1992* (Ed.: R. Scheffold), VCH/VCH, Basel/Weinheim, **1992**, pp. 1–102, and references therein.
- [6] J.-C. Fiaud, J.-L. Malleron, *J. Chem. Soc. Chem. Commun.* **1981**, 1159–1160; B. Åkermark, A. Jutand, *J. Organomet. Chem.* **1981**, *217*, C41–C43.
- [7] E. Negishi, H. Matsushita, S. Chatterjee, R. A. John, *J. Org. Chem.* **1982**, *47*, 3188–3190.
- [8] a) B. M. Trost, E. Keinan, *Tetrahedron Lett.* **1980**, *21*, 2591–2594; b) B. M. Trost, C. R. Self, *J. Org. Chem.* **1984**, *49*, 468–473.
- [9] B. M. Trost, G. M. Schroeder, *J. Am. Chem. Soc.* **1999**, *121*, 6759–6760.
- [10] U. Kazmaier, F. L. Zumpfe, *Angew. Chem.* **1999**, *111*, 1572–1574; *Angew. Chem. Int. Ed.* **1999**, *38*, 1468–1470.
- [11] T. Ukai, H. Kawazura, Y. Ishii, J. J. Bonnet, J. A. Ibers, *J. Organomet. Chem.* **1974**, *65*, 253–266.
- [12] The phosphanes **5a**, **5c**, **5d**, and **9** are commercially available. For the preparation of **5b**, see S. Hillebrand, J. Bruckmann, C. Krüger, M. W. Haenel, *Tetrahedron Lett.* **1995**, *36*, 75–78.
- [13] D. Seebach, *Angew. Chem.* **1988**, *100*, 1685–1715; *Angew. Chem. Int. Ed. Engl.* **1988**, *27*, 1624–1654.
- [14] Crystallographic data (excluding structure factors) for the structure reported in this paper have been deposited with the Cambridge Crystallographic Data Centre as supplementary publication no. CCDC-138291. Copies of the data can be obtained free of charge on application to CCDC, 12 Union Road, Cambridge CB21EZ, UK (fax: (+44) 1223-336-033; e-mail: deposit@ccdc.cam.ac.uk).
- [15] E. Eliel, S. H. Wilen, L. N. Mander, *Stereochemistry of Organic Compounds*, Wiley, New York, **1994**, pp. 731–737.
- [16] The ratio of (*E*)-**8**:(*Z*)-**8** was determined by conversion into the enolsilanes at –78 °C. a) 7:93; b) 96:4.
- [17] Starting from an *E*:*Z* mixture of 7:93, the ratio changed to 55:45.
- [18] S. J. Blarer, W. B. Schweizer, D. Seebach, *Helv. Chim. Acta* **1982**, *65*, 1637–1654; (*R*)-**12**: $[\alpha]_D^{20} = -8.6$; crude (*S*)-**12**, obtained from **6a**: $[\alpha]_D^{20} = 6.8$.
- [19] $[Eu(hfc)_3] = \text{tris}[3-(2,2,3,3,4,4,4\text{-heptafluoro-1-hydroxybutylidene})\text{-}D\text{-camphorato}]europium$ (Aldrich).

Single crystals of $\mathbf{1a}^{4+} \cdot 4\text{Cl}^-$ were obtained from MeCN/ CH_2Cl_2 .^[7] In the crystalline state $\mathbf{1a}^{4+}$ adopts a slightly distorted cone conformation (Figure 1) which is stabilized

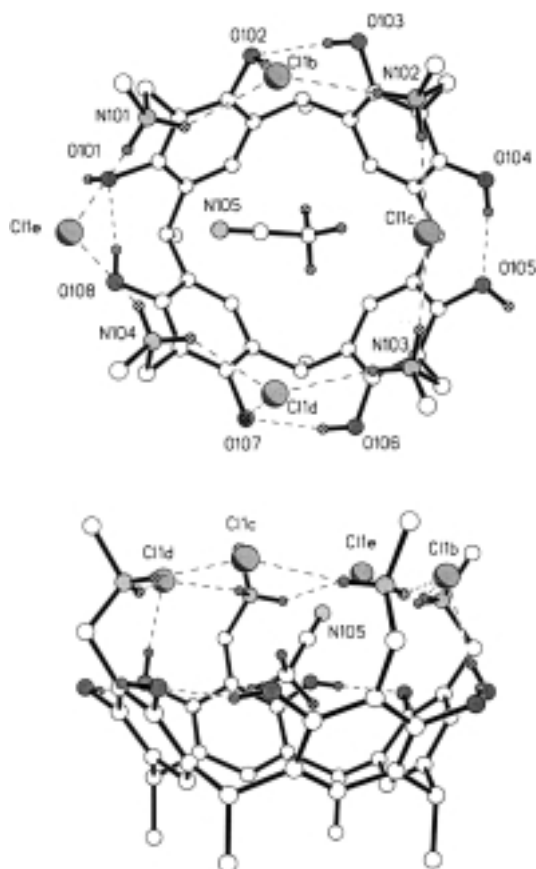


Figure 1. One of the two crystallographically independent $\mathbf{1a}^{4+} \cdot 4\text{Cl}^-$ complexes. Only the first carbon atoms of pendant butyl groups are shown, and the C-bound hydrogen atoms of the resorcarene molecule are omitted for clarity. Hydrogen bonds are indicated as dotted lines and heteroatoms are darkened. Top: top view; bottom: side view. Selected distances [Å]: N104-Cl1d 3.098(2), N104-Cl1e 3.211(2), N102-Cl1c 3.193(2), N102-Cl1b 3.230(2), N103-Cl1d 3.181(2), N103-Cl1c 3.227(2), N101-Cl1b 3.205(2), N101-Cl1e 3.277(2), O107-Cl1d 2.976(2), O106-O107 2.722(2), O104-O105 2.639(2), O103-O102 2.674(2), O108-O101 2.646(2), N101-N105 3.149(4), N104-N105 3.088(3).

by four intramolecular O—H...O—H hydrogen bonds. Each ammonium nitrogen atom forms two hydrogen bonds with two neighboring anions which results in a 16-membered $\text{Cl}^- \cdots \text{H}-\text{N}^+-\text{H} \cdots \text{Cl}^-$ array above the wide rim of the resorcarene molecule. In addition, two hydrogen bonds are found between the chloride ions and the resorcinol hydroxyl groups within the same $\mathbf{1a}^{4+} \cdot 4\text{Cl}^-$ unit while two other hydroxy groups form hydrogen bonds with chloride ions of the neighboring $\mathbf{1a}^{4+} \cdot 4\text{Cl}^-$ complexes. The structure of $\mathbf{1a}^{4+} \cdot 4\text{Cl}^-$ possesses a cavity of $8.4 \times 8.3 \times 5.3 \text{ Å}^3$ in which one acetonitrile molecule is included. The distances between the nitrogen atom of the acetonitrile molecule (N105) and two neighboring ammonium nitrogen atoms (N101, N104) are rather short (Figure 1), probably because of ion–dipole and/or weak hydrogen-bonding interactions between the host and the guest. Thus, the shallow cavity of the resorcarene is

significantly extended^[8] by the cyclic hydrogen-bonded array of ammonium and chloride ions.

The ^1H NMR spectra of $\mathbf{1}^{4+} \cdot 4\text{Cl}^-$ (500 MHz, 303 K) in CDCl_3 show one set of sharp signals for the protons of the resorcarene skeleton, which is in accordance with a C_{4v} -symmetric structure. NOE and ^1H - ^{15}N GHSQC experiments prove that the sharp singlet at $\delta = 9.5$ and the broadened resonance at $\delta = 7.8$ (Figure 2 a) correspond to the protons of

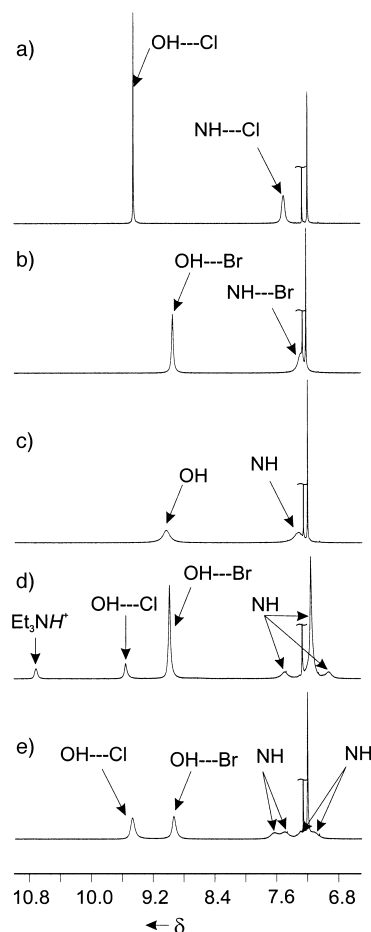


Figure 2. The lowfield region of the ^1H NMR spectra ($[\mathbf{1c}^{4+} \cdot 4\text{Cl}^-] = [\mathbf{1c}^{4+} \cdot 4\text{Br}^-] = 10^{-2} \text{ M}$, CDCl_3 , 500 MHz). The residual signal of CHCl_3 is shortened: a) $\mathbf{1c}^{4+} \cdot 4\text{Cl}^-$ at 303 K; b) $\mathbf{1a}^{4+} \cdot 4\text{Br}^-$ at 303 K; c) $\mathbf{1a}^{4+} \cdot 4\text{Br}^- + \text{Et}_3\text{NH}^+\text{Cl}^-$ at 303 K; d) $\mathbf{1a}^{4+} \cdot 4\text{Br}^- + \text{Et}_3\text{NH}^+\text{Cl}^-$ at 223 K; e) $\mathbf{1c}^{4+} \cdot 4\text{Cl}^- + \mathbf{1c}^{4+} \cdot 4\text{Br}^-$ at 303 K.

OH and NH_2^+ groups, respectively. The unusually high chemical shift for the OH protons can be explained by the hydrogen bonds to the Cl^- ions which are also observed in the crystalline state. The ^1H NMR spectra of $\mathbf{1}^{4+} \cdot 4\text{Br}^-$ are similar to those of the chloride analogues (Figure 2 b), which suggests that the two complexes have the same structure. The OH resonance of $\mathbf{1c}^{4+} \cdot 4\text{Br}^-$ is shifted upfield by $\Delta\delta = 0.5$ relative to the corresponding signal in $\mathbf{1c}^{4+} \cdot 4\text{Cl}^-$. This shift is probably a consequence of the weaker basicity (and hence the lower hydrogen-bonding ability) of the bromide ion. The ^1H NMR spectra of $\mathbf{1c}^{4+} \cdot 4\text{X}^-$ do not change considerably upon cooling the solution to 223 K. Thus, the O—H...O and O—H... X^- hydrogen bonds present in the crystalline state cannot be distinguished. In general, however, the structure in

solution is in agreement with the cavitand-like structure found in the crystal, and represents a rare example of the binding of four anions^[9] by a single receptor molecule.^[10]

Addition of $\text{Et}_3\text{NH}^+\text{Cl}^-$ to the solution of $\mathbf{1c}^{4+} \cdot 4\text{Br}^-$ in CDCl_3 at 303 K results in fast anion exchange and broad average NH and OH signals (Figure 2c). At 223 K the exchange becomes slow and the OH resonance splits into two singlets corresponding to the hydroxyl groups hydrogen bonded to Cl^- and Br^- ions (Figure 2d). The ratio between these signals is close to 1:4, which is in accord with the $\text{Cl}:\text{Br}$ ratio.^[11] The signal of the NH protons splits into three broadened peaks presumably because of the formation of heterocomplexes in which both anions are bound to the same tetracation. Anion exchange between $\mathbf{1c}^{4+} \cdot 4\text{Cl}^-$ and $\mathbf{1c}^{4+} \cdot 4\text{Br}^-$ is slow on the NMR timescale, even at 303 K (Figure 2e). This result reflects the high stability of the hydrogen-bonded array in $\mathbf{1c}^{4+} \cdot 4\text{X}^-$ which must be broken twice to exchange one anion. Although the chemical shifts of the OH signals are the same as in pure $\mathbf{1c}^{4+} \cdot 4\text{Cl}^-$ and $\mathbf{1c}^{4+} \cdot 4\text{Br}^-$, the four broadened resonances of the NH_2^+ protons suggest that the equilibrium involves heterocomplexes. Essentially the same ^1H NMR spectroscopic results were obtained for $\mathbf{1a}^{4+} \cdot 4\text{X}^-$ and $\mathbf{1b}^{4+} \cdot 4\text{X}^-$.

The ^1H NMR spectroscopic studies of $\mathbf{1a}^{4+} \cdot 4\text{Cl}^-$ in combination with the crystal structure strongly suggest that the complexes $\mathbf{1}^{4+} \cdot 4\text{X}^-$ ($\text{X}^- = \text{Cl}^-$, Br^-) keep a firm cavitand-like structure in CDCl_3 in which each anion is hydrogen bonded to two ammonium ions and two neighboring hydroxyl groups of the resorcinol rings. Therefore, we expected that small molecules fitting into the resorcarenene cavity and capable of hydrogen bonding with halogen ions and/or NH_2^+ groups could be included by $\mathbf{1}^{4+} \cdot 4\text{X}^-$ in apolar solvents.

Indeed, $\mathbf{1}^{4+} \cdot 4\text{Cl}^-$ binds several aliphatic alcohols in CDCl_3 . The guest exchange, for example, in the system $\mathbf{1c}^{4+} \cdot 4\text{Cl}^- / n\text{BuOH}$, is slow on the NMR time scale at 223 K (500 MHz). The ^1H NMR spectrum contains three broadened signals for the complexed butanol molecule at $\delta = 0.36$ (CH_2) – 0.89 (CH_2), and – 2.29 (CH_3 , $\Delta\delta = -3.1$), which is clearly a result of its inclusion into the π -basic resorcarenene cavity (Figure 3a).

The OH and NH signals of $\mathbf{1c}^{4+} \cdot 4\text{Cl}^-$ shift to higher and lower field, respectively, upon complexation (Figure 3b). This effect can be explained by the formation of hydrogen bonds between the OH group of *n*-butanol and the polar wide rim of $\mathbf{1c}^{4+} \cdot 4\text{Cl}^-$.^[12] In principle, this could include both $\text{O}-\text{H} \cdots \text{Cl}$ and $\text{HO} \cdots \text{H}_2\text{N}^+$ interactions, however, definite conclusions cannot be drawn from the NMR data.

The signals of the complex grow with increasing amounts of *n*BuOH, and at a ratio of $[\text{nBuOH}]:[\mathbf{1c}^{4+} \cdot 4\text{Cl}^-] = 10:1$ no free $\mathbf{1c}^{4+} \cdot 4\text{Cl}^-$ is detected (Figure 3b). Integration of appropriate signals shows that the inclusion complex has a 1:1 stoichiometry and leads to stability constants of $47 \pm 5 \text{ M}^{-1}$ at 213 K and $29 \pm 5 \text{ M}^{-1}$ at 223 K.

A similar complexation was also observed with *n*-propanol, 2-butanol, 2-methyl-2-propanol (*t*BuOH), and cyclopentanol. In the presence of a 1:1 mixture of *n*BuOH and *t*BuOH both complexes are formed in a 1:1 ratio, which shows there is no selectivity for their inclusion into the cavity of $\mathbf{1}^{4+} \cdot 4\text{Cl}^-$. For ethanol, 2-propanol, *n*-pentanol, *n*-hexanol, and cyclohexanol only the characteristic changes of the NH and OH signals

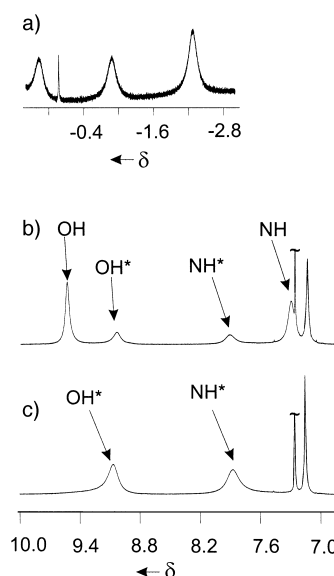


Figure 3. Sections of the ^1H NMR spectrum of $\mathbf{1c}^{4+} \cdot 4\text{Cl}^-$ in CDCl_3 in the presence of *n*BuOH at 223 K ($[\mathbf{1c}^{4+} \cdot 4\text{Cl}^-] = 10^{-2} \text{ M}$, CDCl_3 , 500 MHz): a) the signals of the shielded butyl chain; b) the aromatic region when $[\text{nBuOH}]:[\mathbf{1c}^{4+} \cdot 4\text{Cl}^-] = 1:1$; c) the aromatic region when $[\text{nBuOH}]:[\mathbf{1c}^{4+} \cdot 4\text{Cl}^-] = 10:1$. The NH and OH signals of the complex with *n*BuOH are marked with an asterisk. The assignment of the signals is based on ^1H - ^{15}N HMQC experiments.

were detected, while no strong upfield shifts could be observed for the CH protons of the guests. These results can be explained by an imperfect fit of the alkyl groups into the cavity of $\mathbf{1c}^{4+} \cdot 4\text{Cl}^-$; while the Et and *i*Pr groups are too small, the *n*-pentyl, *n*-hexyl, and cyclohexyl units are too big to be efficiently included.

The complexation of alcohols is anion dependent and no interaction occurs between $\mathbf{1c}^{4+} \cdot 4\text{Br}^-$ and ROH in CDCl_3 . This result could be a consequence of the weaker $\text{O}-\text{H} \cdots \text{X}^-$ hydrogen bonds and/or to a smaller size of the intramolecular cavity produced through blocking by bulky bromide ions.

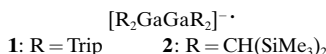
In conclusion, the attachment of four ammonium groups to the wide rim of resorcarenene leads to an effective complexation of four anions within a remarkably stable hydrogen-bonded cyclic array. The complexes $\mathbf{1}^{4+} \cdot 4\text{X}^-$ can be considered as hydrogen-bonded analogues of cavitands^[13] which are capable of anion-dependent complexation of certain alcohols in CDCl_3 . The almost unlimited structural diversity, the possible chirality,^[5] and the simple synthesis of $\mathbf{1}^{4+} \cdot 4\text{X}^-$ make these systems a promising new family of self-assembled receptors.

Received: April 3, 2000 [Z14935]

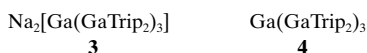
- [1] M. M. Conn, J. Rebek, Jr., *Chem. Rev.* **1997**, 97, 1647–1668.
- [2] a) B. C. Hamman, K. D. Shimizu, J. Rebek, Jr., *Angew. Chem.* **1996**, 108, 1425–1427; *Angew. Chem. Int. Ed. Engl.* **1996**, 35, 1326–1329; b) O. Mogck, E. F. Paulus, V. Böhmer, I. Thondorf, W. Vogt, *Chem. Commun.* **1996**, 2533–2534.
- [3] D. M. Rudkevich, G. Hilmersson, J. Rebek, Jr., *J. Am. Chem. Soc.* **1998**, 120, 12216–12225.
- [4] For a review on resorcarenene, see P. Timmerman, W. Verboom, D. N. Reinhoudt, *Tetrahedron* **1996**, 52, 2663–2704.

Brendan Twamley and Philip P. Power*

Electron-precise one- or two-dimensional, molecular gallium clusters can in principle be reduced to afford species which may contain Ga–Ga multiple bonds. For example, reduction of tetraorganodigallanes yields the radical anions $[\text{R}_2\text{GaGaR}_2]^- \cdot \mathbf{1}^{[1]}$ and $\mathbf{2}^{[2]}$



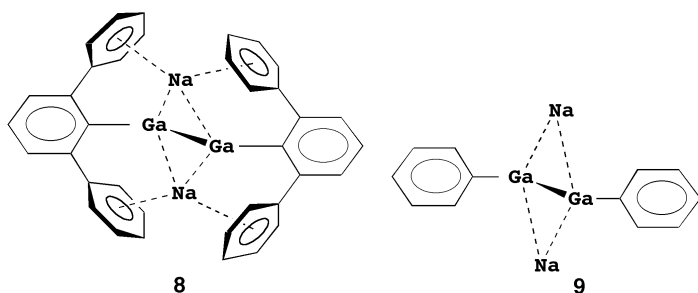
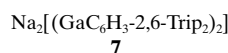
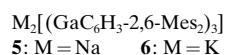
The Ga–Ga distances in **1** and **2** are 0.14–0.17 Å shorter than those in the neutral R₂GaGaR₂ precursors, and EPR data show that the unpaired electron resides in a π orbital to give a formal Ga–Ga bond order of 1.5. However, the attempted addition of a second electron to **1** results in rearrangement to the tetrametallic trigallylgallane salt **3**, which has shorter Ga–Ga bonds (av 2.39 Å) than the unreduced species **4** (Ga–Ga, av 2.47 Å) consistent with a formal Ga–Ga bond order of 1.33.^[3]



An important aspect of the structure of **3** is that the shortest of the three Ga–Ga bonds corresponds to the complexation of the two Na⁺ ions between the Trip substituents spanning the bond. Parallel work involving direct reduction of terphenylgallium dihalides has afforded the unprecedented cyclic trigallyl compounds **5**^[4a] and **6**^[4b] (Mes = C₆H₂-2,4,6-Me₃), or the dimeric **7**^[5] which also involve similar interactions between the alkali metal the aryl group across the Ga–Ga bond(s). However, the description of **7** as a “gallyne” on the basis of its short Ga–Ga bond (2.319(3) Å) has generated controversy,^[6] since the Na⁺–aryl interactions could also have caused the shortened Ga–Ga distance.^[7] Density functional theory (DFT) calculations^[8] on the model compounds for **7**–**9**, Na₂[(GaC₆H₃-2,6-Ph₂)₂] (**8**), and Na₂[(GaPh)₂] (**9**), suggest that such effects are structurally important since the Ga–Ga distance in **8** (2.362 Å), which has Na⁺–aryl interactions, is about 0.1 Å shorter than that in **9** (2.461 Å) which has no Na⁺–aryl contacts.

[*] Prof. P. P. Power, Dr. B. Twamley
Department of Chemistry, University of California
Davis, CA 95616 (USA)
Fax: (+1) 530-752-8995
E-mail: pppower@ucdavis.edu

[**] This work was supported by the National Science Foundation. The Bruker SMART 1000 diffractometer was funded in part by NSF Instrumentation Grant CHE-9808259.



In an earlier publication^[9] it was suggested that the structural effects of the Na⁺ ions in **7** could be investigated by synthesizing a solvent-separated species of the type $[\text{NaL}_n]_2[(\text{GaC}_6\text{H}_3\text{-2,6-Trip}_2)_2]$ (L = complexing ligand; e.g., crown ether or cryptand) with no Na⁺–aryl interactions. Unfortunately, no species of this type are known. An alternative investigative approach involves varying the alkali metal cations themselves. In essence, if the Ga–Ga moiety observed in **7** is a stable one, changing or removing the alkali metal counteranions should afford a similar structure. The observation of essentially identical structures for **5** and **6** which have Na⁺–aryl or K⁺–aryl interactions similar to those in **7** lends further support to this hypothesis. Accordingly, the reduction of $\text{Ga}(\text{C}_6\text{H}_3\text{-2,6-Trip}_2)\text{Cl}_2$ ^[10] with several alkali metals has been undertaken and our initial results are given herein.

Reduction of $\text{Ga}(\text{C}_6\text{H}_3\text{-2,6-Trip}_2)\text{Cl}_2$ in diethyl ether by Li, Na, K, or Cs initially afforded a green solution. For Li, the green color was persistent but with the other metals the color changed to dark red. These solutions possessed considerable stability in the case of those from Na and K but that from the Cs reduction rapidly (2 h) changed to brown. To date, X-ray quality crystals have only been obtained from the reactions with Na or K. The crystals from the Na reduction afforded X-ray data to high 2 θ angles which resulted in a refinement to a relatively low residual value.^[11] The structural parameters derived from this data set (Ga–Ga 2.324(1), Ga–C(av) 2.041(5) Å) were similar to those already reported for **7** (Ga–Ga 2.319(3), Ga–C(av) 2.04(2) Å)^[5] although it was found that the two Ga–Ga–C angles differ by over 8° which suggests considerable flexibility in the C–Ga–Ga–C array.^[12]

In contrast to these findings, the reduction of $\text{Ga}(\text{C}_6\text{H}_3\text{-2,6-Trip}_2)\text{Cl}_2$ with K did not yield $\text{K}_2[(\text{GaC}_6\text{H}_3\text{-2,6-Trip}_2)_2]$ ^[13] but the new tetragallium species **10** (Figure 1). The structure of **10** is centrosymmetric with a planar, almost square, Ga₄ core. The Ga–Ga distances are 2.4624(4) and 2.4685(3) Å and the internal angles are 87.228(11)° at Ga(1) and 92.772(11)° at Ga(2). The Ga(1) and Ga(1A) atoms are each substituted by a C₆H₃-2,6-Trip₂ group which has a Ga–C bond length of 2.006(2) Å. Although Ga(1) and Ga(1A) are planar coordinated, the external C(1)–Ga(1)–Ga(2) and C(1)–Ga(1)–Ga(2A) angles differ by almost 6°. The structure is completed by two K⁺ ions on either side of the Ga₄ plane. They do not lie directly above the center of the Ga₄ array, however, but are displaced such that the K(1)–Ga(1) and K(1)–Ga(2) distances (ca. 3.82 Å) are somewhat longer than the K(1)–Ga(1A)

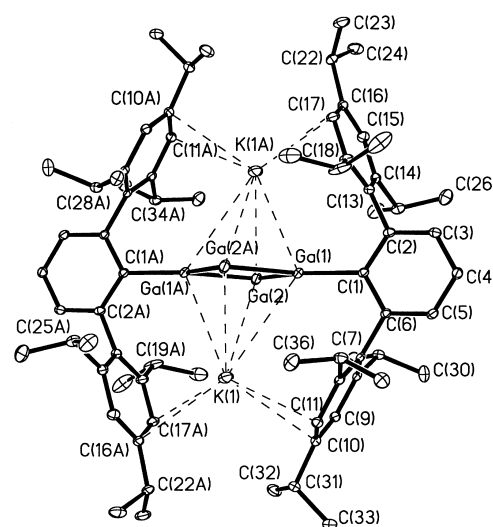
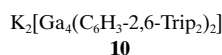


Figure 1. Structure of **10** (H atoms are not shown). Selected interatomic distances [Å] and angles [°]: Ga(1)–Ga(2) 2.4623(4), Ga(1)–Ga(2A) 2.4685(3), Ga(1)–C(1) 2.0058(19), Ga(1)–K(1) 3.8017(6), Ga(2)–K(1) 3.8330(6), Ga(1)–K(1A) 3.5883(6), Ga(2)–K(1A) 3.4710(6), K(1)–C(10) 3.2636(19), K(1)–C(11) 3.323(2), K(1)–C(16A) 3.327(2), K(1)–C(17A) 3.268(2), C(1)–Ga(1)–Ga(2) 139.33(6), C(1)–Ga(1)–Ga(2A) 133.44(6), Ga(2)–Ga(1)–Ga(2A) 87.222(11), Ga(1)–Ga(2)–Ga(1A) 92.778(11), C(6)–C(1)–C(2) 117.82(17).

and K(1)–Ga(2A) distances (ca. 3.53 Å). The K⁺ ions interact almost equally strongly with the two Trip rings to which they are coordinated and the closest distances involve C(10), C(11) (ca. 3.29 Å) and C(16A), C(17A) (ca. 3.30 Å).



Compound **10** differs from the known Ga₄ clusters which feature either a tetrahedral Ga₄ array in electron-deficient (GaR)₄ species,^[14] a trigonal-planar Ga(Ga)₃ framework as in **4**,^[3] or a pyramidal arrangement as in the ion $[\text{RGa}(\text{GaR})_3\text{I}_3]^-$ (R = Si(SiMe₃)₃).^[15] The Ga–Ga distances in **10** are consistent with single bonding and are very close to the Ga–Ga bond length of about 2.47 Å in **4**.^[3] Apparently, Ga(1) and Ga(1A) use their three valence electrons to bond a carbon and two other gallium atoms. Similarly, Ga(2) and Ga(2A) each employ an electron to bond to Ga(1) and Ga(1A) and their remaining coordination site is occupied by a lone pair—the extra electrons being provided by the 2 – charge.

The different structures of **10** and **7** are in sharp contrast to previous results for Na⁺ and K⁺ salts of related dianions with bulky terphenyl substituents. That work has shown that there are no stoichiometric and relatively minor structural differences between salts of these two alkali metals. Examples include the dianionic trigallium Na⁺ and K⁺ species, **5** and **6**^[4] (see above), the compounds $\text{M}_2[(\text{M}'\text{C}_6\text{H}_3\text{-2,6-Trip}_2)_2]$ (M = Na or K; M' = Ge or Sn),^[16] which are stoichiometrically and structurally very similar to **7**, and the salts $\text{M}_2(\text{SC}_6\text{H}_3\text{-2,6-Trip}_2)_2$ (M = Na or K).^[17] Part of the explanation for the differences between **10** and **7** may lie in the geometric constraints caused by the unequal sizes of the Na⁺ and K⁺ ions and the probable weakness of the Ga–Ga bond in **7**.

Theoretical opinion^[8, 18] on the nature of this bond is sharply divided but it is noteworthy that, apart from the DFT work on **8** and **9**,^[8] no other calculations address the role of interactions between the alkali metal and aryl group in **7** or related species, and there are no calculations on the strength of the Ga–Ga interactions in such compounds. It is likely, however, that the Ga–Ga bonding in **7** is weakened owing to Coulombic and steric repulsions. This is consistent with the above-mentioned attempts^[3] to synthesize $[\text{R}_2\text{GaGaR}_2]^{2-}$ (also involving significant Coulombic interactions) which afforded a rearrangement to the tetrametallic **3** where, presumably, Coulombic effects are dispersed over four metals as they are in **10**. Steric effects are also significant since a reduction in the size of the terphenyl group from $\text{C}_6\text{H}_3\text{-2,6-Trip}_2$ to $\text{C}_6\text{H}_3\text{-2,6-Mes}_2$ results in the trimeric structures in **5** and **6**^[4] instead of the dimeric **7**.^[5] The use of the ligand $\text{C}_6\text{H}_3\text{-2,6-Ph}_2$ in calculations on model compounds such as **8**^[8, 18a] does not provide a sufficiently accurate estimate of the steric effects of the *i*Pr substituents. However, its use is clearly superior to the ligands H or Me which neglect the aryl–alkali metal interactions entirely.

In summary it is probable that the alkali metal–aryl interactions in **7** and **10** play a unique and crucial role in their stabilization. Theoretical data^[19] have shown that interactions between alkali metals and aryl rings involve considerable binding energies (e.g., M–benzene: M = Li, 37.9 kcal mol^{−1}; M = Na, 28 kcal mol^{−1}; M = K, 18.3 kcal mol^{−1}) which supports their potential stabilizing effect.^[20] The seemingly integral role of the Na⁺ ions in the stabilization of **7** raises the question of the stability of the solvent-separated dianion $[(\text{GaC}_6\text{H}_3\text{-2,6-Trip}_2)_2]^{2-}$ in the absence of the sodium cations. Interestingly, perhaps, there do not appear to be any stable species known that involve multiple bonding between two negatively charged atoms without contact-solvated counter cations. Clearly, further experimental data on a range of main group dianionic species will be required to resolve such questions.

Experimental Section

All work was carried out under anaerobic and anhydrous conditions. Et₂O (60 mL) was added to a mixture of freshly cut potassium (1.75 g, 44.8 mmol) and Ga($\text{C}_6\text{H}_3\text{-2,6-Trip}_2$)Cl₂ (3.83 g, 6.15 mmol) with rapid stirring. After 10–12 h the suspension underwent a color change from gray to green, and after a further 1–2 h the green color became red-brown. Stirring was continued for 36 h at which point the stirrer was switched off and all precipitates were allowed to settle overnight. The supernatant liquid was decanted, and the red-brown solution was concentrated to about 25 mL and cooled at about 4 °C overnight to afford red-brown crystals of **10**. Yield 0.65 g, 32% (based on Ga). M.p. 226 °C (decomp). ¹H NMR (400 MHz, C₆D₆): δ = 0.96 (d, ³J_{H,H} = 6.8 Hz, 12H; *o*-CH(CH₃)₂), 1.19 (d, ³J_{H,H} = 6.8 Hz, 12H; *o*-CH(CH₃)₂), 1.52 (d, ³J_{H,H} = 6.8 Hz, 12H; *p*-CH(CH₃)₂), 2.41 (sept, ³J_{H,H} = 6.8 Hz, 4H; *o*-CH(CH₃)₂), 3.87 (sept, ³J_{H,H} = 6.8 Hz, 2H; *p*-CH(CH₃)₂), 6.71 (s, 4H; *m*-Trip), 7.22 (d, ³J_{H,H} = 6.8 Hz, 2H; *m*-C₆H₃), 7.33 (t, ³J_{H,H} = 6.8 Hz, 1H; *p*-C₆H₃); ¹³C{¹H} NMR (100 MHz): δ = 24.65 (*p*-CH(CH₃)₂), 25.43 (*o*-CH(CH₃)₂), 25.98 (*o*-CH(CH₃)₂), 30.75 (*o*-CH(CH₃)₂), 34.12 (*p*-CH(CH₃)₂), 119.46 (*m*-Trip), 127.885 (*m*-C₆H₃), 128.15 (*p*-C₆H₃), 142.91 (*o*-C₆H₃), 144.12 (*ipso*-Trip), 146.28 (*p*-Trip), 150.24 (*o*-Trip), 172.54 (*ipso*-C₆H₃); UV/Vis: λ (ε) = 435 (5200), 705 (270). The compound **7**·Et₂O was synthesized in about 35% yield under very similar conditions.

Received: April 25, 2000 [Z15036]

- [1] X. He, R. A. Bartlett, M. M. Olmstead, P. P. Power, *Angew. Chem.* **1993**, 105, 761; *Angew. Chem. Int. Ed. Engl.* **1993**, 32, 717.
- [2] W. Uhl, U. Schutz, W. Kaim, E. Waldhör, *J. Organomet. Chem.* **1995**, 501, 79.
- [3] R. J. Wehmschulte, P. P. Power, *Angew. Chem.* **1998**, 110, 3344; *Angew. Chem. Int. Ed.* **1998**, 37, 3154. Monomeric [GaR₂][−] ions have been stabilized as the species [(*t*BuN₃C₂)Ga][−]: S. Schmid, A. Jockisch, H. Schmidbauer, *J. Am. Chem. Soc.* **1999**, 121, 9758.
- [4] a) X.-W. Li, W. T. Pennington, G. H. Robinson, *J. Am. Chem. Soc.* **1995**, 117, 7578; b) X.-W. Li, Y. Xie, P. R. Schreiner, K. D. Gripper, R. C. Crittendon, C. F. Campana, H. F. Schaefer, G. H. Robinson, *Organometallics* **1996**, 15, 3798.
- [5] J. Su, X.-W. Li, R. C. Crittendon, G. H. Robinson, *J. Am. Chem. Soc.* **1997**, 119, 5471.
- [6] For a recent critical review of this controversy see: A. J. Downs, *Coord. Chem. Rev.* **1999**, 189, 59.
- [7] In addition, the C–Ga–Ga–C skeleton in **7** has a *trans*-bent rather than linear geometry (C–Ga–Ga = ca. 130°) which suggests lone-pair character at the gallium centers and reduced electron density in the Ga–Ga bond.
- [8] F. A. Cotton, A. H. Cowley, X. Feng, *J. Am. Chem. Soc.* **1998**, 120, 1795.
- [9] P. P. Power, *Dalton Trans.* **1998**, 2939.
- [10] B. Twamley, P. P. Power, *Chem. Commun.* **1999**, 1805.
- [11] Crystal structure analysis data for **7**·Et₂O (90 K) with MoK_α (λ = 0.71073 Å) radiation: *a* = 14.6020(8), *b* = 18.2193(10), *c* = 26.8103(15) Å, β = 97.662(1)°, *Z* = 4, space group *P*₂₁/*c*, *R*₁ = 0.0586 for 11 757 (*I* > 2σ(*I*)) data. Important interatomic distances [Å] and angles [°]: Ga(1)–Ga(2) 2.324(1), Ga(1)–C(1) 2.045(6), Ga(2)–C(37) 2.036(6), Ga(1)–Na(1) 3.103(3), Ga(1)–Na(2) 3.065(3), Ga(1)–Na(2) 3.065(3), Ga(2)–Na(2) 3.102(3), Na–C 2.847(6)–3.105(6); C(1)–Ga(1)–Ga(2) 125.93(17), C(37)–Ga(2)–Ga(1) 136.20(7). Crystal structure analysis data for **10** (90 K) with MoK_α (λ = 0.71073 Å) radiation: *a* = 12.7152(7), *b* = 17.1567(9), *c* = 16.9160(9) Å, *Z* = 2, space group *P*₂₁/*c*, *R*₁ = 0.0359 for 11 255 (*I* > 2σ(*I*)) data. Crystallographic data (excluding structure factors) for the structures reported in this paper have been deposited with the Cambridge Crystallographic Data Centre as supplementary publication nos. CCDC-143883 (**7**) and CCDC-144502 (**10**). Copies of the data can be obtained free of charge on application to CCDC, 12 Union Road, Cambridge CB21EZ, UK (fax: (+44) 1223-336-033; e-mail: deposit@ccdc.cam.ac.uk).
- [12] Also, H atoms bound to Ga in either a terminal or bridging manner (a possibility which was not completely excluded by previous data)^[5, 8] could not be located on a difference map. In view of the increased accuracy of the present data set, and the lack of Ga–H stretching bands in the IR spectrum, Ga–H bonds can be deemed absent.
- [13] It could be argued that K₂[(GaC₆H₃-2,6-Trip₂)₂] is present in solution but it does not crystallize. This possibility cannot be ruled out completely, but it is unlikely in view of the ease with which both Na⁺ and K⁺ salts of related terphenyl anions crystallize. Also the fact that **10** is present in significant quantities suggests that, at the minimum, it has comparable stability to the putative K₂[(GaC₆H₃-2,6-Trip₂)₂] species which indicates weak multiple Ga–Ga bonding in the latter.
- [14] a) W. Uhl, W. Hiller, M. Layh, W. Schwarz, *Angew. Chem.* **1992**, 104, 1378; *Angew. Chem. Int. Ed. Engl.* **1992**, 31, 1364; b) G. Linti, *J. Organomet. Chem.* **1996**, 520, 107; W. Uhl, A. Jantschak, *J. Organomet. Chem.* **1998**, 555, 263; c) G. Linti, A. Rodig, *Chem. Commun.* **2000**, 127.
- [15] W. Köstler, G. Linti, *Angew. Chem.* **1997**, 109, 2758; *Angew. Chem. Int. Ed. Engl.* **1997**, 36, 2644.
- [16] a) L. Pu, M. O. Senge, M. M. Olmstead, P. P. Power, *J. Am. Chem. Soc.* **1998**, 120, 12682; b) L. Pu, M. M. Olmstead, S. T. Haubrich, P. P. Power, unpublished results.
- [17] M. Niemeyer, P. P. Power, *Inorg. Chem.* **1996**, 35, 7264.
- [18] a) Y. Xie, R. S. Grev, J. Gu, H. F. Schaefer III, P. von R. Schleyer, J. Su, X.-W. Li, G. H. Robinson, *J. Am. Chem. Soc.* **1998**, 120, 3773; b) K. W. Klinkhammer, *Angew. Chem.* **1997**, 109, 2414; *Angew. Chem. Int. Ed. Engl.* **1997**, 36, 2320; c) I. Bytheway, Z. Lin, *J. Am. Chem. Soc.* **1998**, 120, 12133; d) Y. Xie, H. F. Schaefer III, G. H. Robinson, *Chem. Phys. Lett.* **2000**, 317, 174; e) T. L. Allen, W. H. Fink, P. P. Power, *J. Chem. Soc. Dalton Trans.* **2000**, 407; f) R. Köppe, H. Schnöckel, *Z. Anorg. Allg. Chem.* **2000**, 626, 1095; g) H. Grützmacher, T. F. Fässler, *Chem. Eur. J.* **2000**, 6, 2317.

- [19] a) R. L. Woodin, J. L. Beauchamp, *J. Am. Chem. Soc.* **1978**, *100*, 501; b) B. C. Guo, J. W. Purnell, A. W. Castelman, *Chem. Phys. Lett.* **1990**, *168*, 155; c) J. Sunder, K. Nishizawa, P. Kebarle, *J. Phys. Chem.* **1981**, *85*, 1814; d) M. Tacke, *Eur. J. Inorg. Chem.* **1998**, 537.
- [20] Recent calculations on related species such as $[R_2MMR_2]^{2-}$ ($M = Al, Ga, In, Tl$) indicate strong solvation of the counteranion is the key to their stabilization. A. J. Bridgeman, N. A. Nielsen, *Inorg. Chim. Acta* **2000**, *303*, 107.

Light-Driven Microfabrication: Assembly of Multicomponent, Three-Dimensional Structures by Using Optical Tweezers**

R. Erik Holmlin, Michele Schiavoni, Clifford Y. Chen, Stephen P. Smith, Mara G. Prentiss, and George M. Whitesides*

Methods to generate well-defined structures composed of cells have the potential to be useful in areas where aggregates of cells are relevant: a) analytical systems that use cells as sensors; b) systems for fundamental studies of metabolism, signaling, toxicology, cellular ecology, and the biophysics of cell–cell interactions; and c) systems that investigate relationships between cell attachment, development, and growth. Here, we have used optical tweezers to fabricate ordered, two-dimensional (2D) and three-dimensional (3D), composite microstructures in which the components are biological cells (erythrocytes and lymphocytes) and polystyrene microspheres. This method of fabrication, light-driven microfabrication, provides a method of generating a range of structurally well-defined arrays of cells in the form of composites incorporating cells and microspheres.

Figure 1 illustrates the important elements of light-driven microfabrication. We used erythrocytes, disk-shaped cells approximately 12 μm in width, and lymphocytes, roughly spherical cells approximately 5 μm in diameter, as model components with which to explore microassembly. The surfaces of these cells present multiple oligosaccharides that terminate in *N*-acetyl glucosamine (GlcNAc) and *N*-acetyl neuraminic acid (NeuAc);^[1] these sugars provide well-defined ligands when biospecific adhesion is required. There are three potential mechanisms for the attachment of cells to surfaces: nonbiospecific interactions (e.g. hydrogen bonds,^[2] hydrophobic interactions,^[2] or electrostatic interactions);^[3] biospe-

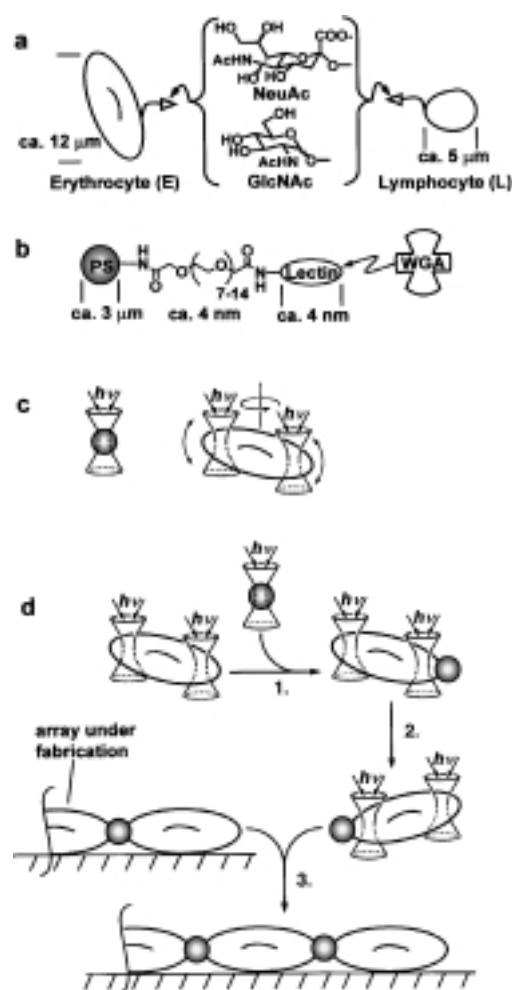


Figure 1. Fabrication of composite structures of cells and polymer microspheres by using optical tweezers. a) The oligosaccharides on surfaces of a chicken erythrocyte and chicken lymphocyte terminate in *N*-acetyl neuraminic acid (NeuAc) and *N*-acetyl glucosamine (GlcNAc). b) A polystyrene microsphere (3 μm in diameter) is linked with WGA, a lectin that binds to NeuAc and GlcNAc. c) One optical trap is used to support a WGA-linked microsphere, and two optical trapping beams orient and transport an erythrocyte. d) Light-driven microfabrication has three steps: The sequence begins with a cell supported in two traps. 1.) We use a third trap to bring a microsphere into contact with the surface of the cell. The sphere adheres to the cell by polyvalent, biospecific interactions between WGA and the NeuAc and GlcNAc groups. 2.) The two traps focused on the erythrocyte (with the attached microsphere) move the aggregate of microsphere and cell into the orientation desired for further steps in fabrication. 3.) The multiple traps are translated to bring the microsphere that is attached to the cell into contact with an assembly that is resting on the glass floor of the sample container. Repetition of this procedure generates the desired structure.

[*] Prof. G. M. Whitesides, Dr. R. E. Holmlin
Department of Chemistry and Chemical Biology
Harvard University, 12 Oxford Street
Cambridge, MA 02138 (USA)
Fax: (+1) 617-495-9857
E-mail: gwhitesides@gmwgroup.harvard.edu

M. Schiavoni, C. Y. Chen, S. P. Smith, Prof. M. G. Prentiss
Department of Physics, Harvard University
17 Oxford Street, Cambridge, MA 02138 (USA)

[**] This work was supported by DARPA (G.M.W.), the NIH (G.M.W.), and MRSEC (G.M.W., M.G.P.). R.E.H. thanks the NIH for a postdoctoral fellowship. We thank Emanuele Ostuni and Dr. Shuichi Takayama for helpful discussions.

cific interactions that are exclusively adhesive (for example, lectins binding to sugars);^[4] and biospecific interactions that are both adhesive and functional (for example, integrins binding to RGD (peptide sequence Arg–Gly–Asp) or fibronectin;^[5] selectins binding to cadherins).^[6] To connect cells biospecifically, we used polystyrene microspheres linked covalently to wheat germ agglutinin (WGA), a well-characterized dimeric lectin that recognizes NeuAc and GlcNAc;^[7, 8] to connect cells nonbiospecifically, we used unmodified polystyrene microspheres. It should also be possible to use

functional biospecific interactions between cell-adhesion molecules on the surface of microspheres and receptors on the surface of mammalian cells; we believe that this mode of attachment will provide a way to examine the influence of cell-surface interactions within structured aggregates of anchorage-dependent cells.^[9]

The essential feature of light-driven microfabrication is the application of optical tweezers, focused beams of light that can be used to hold, orient, and move transparent objects that have a refractive index greater than that of the surrounding medium.^[10] These optical tweezers are used to bring cells and microspheres into contact,^[11] and to control the geometry of the resulting assemblies (Figure 1 c). We used a single beam to support the polystyrene microsphere. By training two beams on different parts of the erythrocyte, we are able to control both its position and orientation. Lymphocytes are roughly spherical, and settle into the focal region of a single laser beam. Figure 1 d outlines the procedure for light-driven microfabrication.

Figure 2 shows several 2D structures. In each of these images, the structures rest on the surface of the glass microscope slide immersed in buffer. The erythrocytes are lying on the surface with their flat face facing into the line of sight. The different shadings of the polystyrene microspheres reflect the fact that they lie in slightly different positions relative to the focal planes in each structure; the brighter the sphere, the closer it is to the focal plane of the camera.

In structures 2a–2c and 2e, the cells are connected by biospecific interactions between WGA on the surface of the microspheres and NeuAc or GlcNAc on the surface of the erythrocytes. On basis of five observations we inferred that this adhesion was biospecific: a) upon contact, the WGA-linked microspheres adhered to the surface of the erythrocytes and could not be detached with optical forces over the range of 0.1–10 pN. b) Soluble carbohydrates that bind to WGA inhibited the adhesion: 15 mM GlcNAc, 0.05 mM *N,N'*-diacetylchitobiose (GlcNAc₂), or 0.01 mM tetra-*N*-acetylchitotetraose (GlcNAc₄) reduced the probability of adhesion (P^{ADH} between the sphere and the cell to approximately 0.5 (P^{ADH} is the ratio of the number of times a sphere adhered to the surface of a cell to the total number of collisions between cell and sphere); increasing the concentration of the inhibitor by a factor of approximately 10 blocked the adhesion completely ($P^{\text{ADH}} = 0$). c) Glucose (200 mM), which does not bind to WGA,^[7, 8] had no detectable effect on the adhesion. d) Microspheres to which oligomers of ethylene glycol were attached instead of WGA did not adhere to the cells.^[11] e) Individual WGA-linked microspheres did not adhere to each other.

Although the interactions between the individual binding sites of WGA and carbohydrates are relatively weak (dissociation constant $K_d^{\text{GlcNAc}} = 5 \text{ mM}$;^[4] $K_d^{\text{NeuAc}} = 2 \text{ mM}$ ^[12]), the spheres adhered strongly to the erythrocytes. We believe the strength of this adhesion reflects polyvalency^[13] in the interactions between multiple WGA molecules on the surface of the microsphere and multiple copies of sugar groups on the cell surface. The observation that these polyvalent interactions can be antagonized biospecifically at values of concentrations of sugars close to their values of K_d for WGA is also

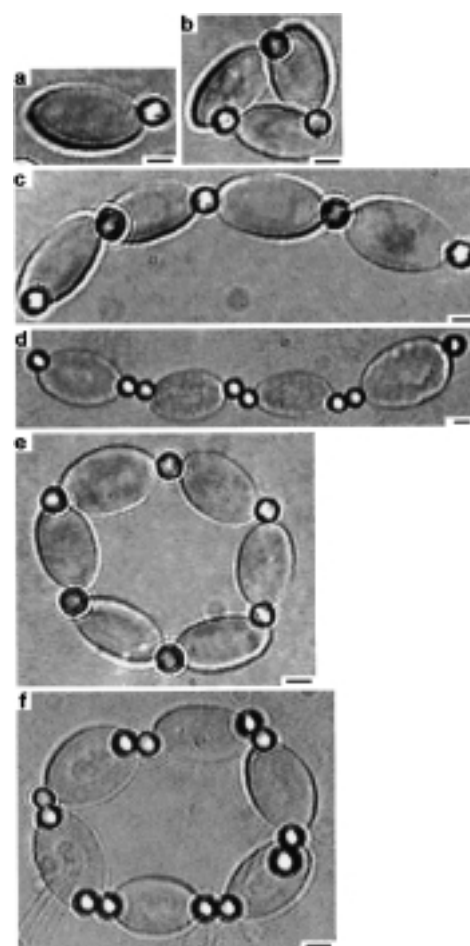


Figure 2. Optical micrographs of 2D microstructures fabricated by light-driven microfabrication. The structures in a)–c) and e) are connected by biospecific interactions between lectin-coated microspheres and sugars on the cell surfaces; structures d) and f) are connected by nonbiospecific interactions in which bare polystyrene microspheres adhere both to the cells and to one another. a) One microsphere coated with WGA attached to the surface of a single erythrocyte. b) Triangular network of three erythrocytes connected by three microspheres. c) Linear array of four erythrocytes with three bridging microspheres and two terminal microspheres. d) Linear array of four erythrocytes connected by nonbiospecific interactions. e) Hexagonal microstructure of six erythrocytes and six microspheres. f) Hexagonal structure of six erythrocytes joined by nonbiospecific interactions. We refer to these arrays as 2D because that is an approximate description of their shape, they do not, however, have an essential characteristic of 2D assemblies: that is, that one or more nodes connect to three (rather than two) other nodes. The bar in each image represents 3 μm .

compatible with polyvalency being the source of the strong binding between the microspheres and the cells.^[14, 15] Polyvalency makes it possible to use relatively weak interactions to design biospecific interactions to connect micron-scaled objects; a precondition is that the surface densities of receptors and ligands are sufficiently large.

By using reversible biospecific interactions to connect the cells and microspheres enables these structures to be disassembled biospecifically. After generating 2D arrays of erythrocytes, we introduced a solution of fetuin (ca. 10 mg mL^{-1})—a glycosylated protein bearing oligosaccharides that terminate in NeuAc—into the sample suspension. The connections between cells and spheres dissociated over

periods of about 45 min to 2 h, and the arrays disassembled. We believe this disassembly reflects competition of the sugar groups on fetuin with oligosaccharides on the cell surface for binding sites of WGA on the microspheres. The use of biospecific interactions to assemble these structures, and the consequent ability to disassemble them through competing interactions, distinguishes this method of fabrication with optical tweezers from methods that have used optical tweezers to align microspheres or colloids in 2D arrays and have frozen the resulting structures by photopolymerizing the solution that surrounded the particles.^[16, 17]

Structures 2d and 2f are held together by nonbiospecific interactions. In these assemblies, we used unmodified polystyrene microspheres, which also adhere to the surface of erythrocytes. We connected the cells together by first attaching a sphere to each cell and then bringing the two spheres together. In contrast to the WGA-linked microspheres, the bare polystyrene spheres adhere to one another. The soluble carbohydrates that inhibited adhesion of WGA-linked spheres to erythrocytes did not block adhesion of bare polystyrene spheres. Suspending the polystyrene sphere in a solution of bovine serum albumin (BSA, 1 mg mL⁻¹) prior to bringing it into contact with the cell or with another sphere did prevent adhesion. These observations are consistent with the idea that adhesion with unmodified polystyrene spheres results from nonspecific (probably hydrophobic) interactions.

Figure 3 shows a microstructure built with two types of cells—erythrocytes and lymphocytes—connected by WGA-coated microspheres. Erythrocytes are characterized by their

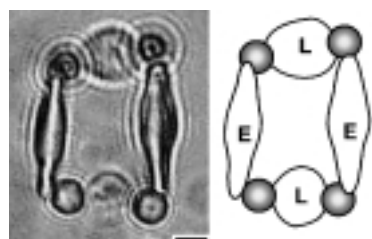


Figure 3. Optical micrograph and explanatory illustration of a composite structure with two cell types: erythrocytes and lymphocytes. The cells are connected by biospecific interactions between WGA-linked microspheres (gray spheres) and sugars on the surfaces of the cells. The erythrocytes are oriented perpendicularly to the cells in Figure 2. The bar in the micrograph represents 3 μ m.

disk shape and by the rigidity and elasticity of their membranes; lymphocytes are globular, and their membranes tend to deform more easily.^[18] In this structure, the erythrocytes were rotated by 90° with respect to the cells pictured in Figure 2, so their narrow edge is directed into the line of sight. We believe that the ability to incorporate several different cell types into one structure will be important in assays that require interactions among cells mediated by diffusible signaling molecules, and that address differences in response of different cell types to drugs, toxins, and environmental factors.

Fabrication of 3D microstructures is difficult. Optical tweezers should make it possible to assemble a range of structures. We illustrate this capability by the assembly of two 3D arrays of erythrocytes (Figure 4). The procedure for 3D

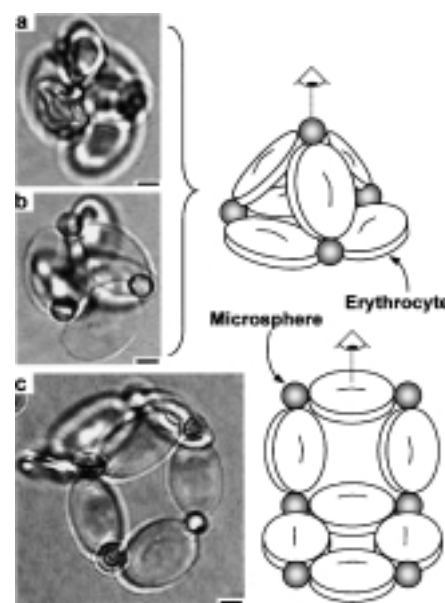


Figure 4. Optical micrographs and schematic illustrations of 3D arrays of erythrocytes. The micrographs in a) and b) are of the same tetrahedron imaged at two different focal planes: the image in a) was recorded with the focal plane near the apex of the assembly and the image in b) was recorded with the focal plane near the base of the assembly. In a) the apical microsphere is roughly in focus and in b) the cells and microspheres that make up the base are roughly in focus. The image in c) is that of two square planes joined perpendicularly along one edge. In the schematic drawings, the eye and the dotted line establish the line-of-sight used in generating the micrographs. The bar in each image represents 3 μ m.

fabrication is analogous to that described for 2D structures.

The 3D microassembly by using light tweezers is, of course, not limited to biological components.^[19–23] The application of optical tweezers in the fabrication of 2D and 3D structures should be generalizable to the assembly of a wide variety of objects with dimensions that range in size from μ m to a few hundred nm; the practical size limitation is set by the size of the focal region of the laser beam, approximately $\lambda/2\pi$ (where λ is the wavelength of the light) or about 150 nm at the wavelength we have used.^[24] The principal restrictions to the process are that the objects must have an index of refraction greater than that of the surrounding medium and that they must be transparent to the wavelength of the optical beam.^[24] In addition, a wide variety of recognition systems can be exploited for attachment: examples include protein–ligand interactions,^[4–6, 9] interactions between complementary strands of DNA,^[25–27] capillary forces,^[28] electrostatic forces,^[3] and hydrophobic interactions.^[2] The scope of the different shapes that can be exploited in fabrication has not been established. Optical tweezers have been employed to trap a variety of spherical and nonspherical objects, although theory that describes trapping nonspherical objects is not well established.^[29, 30] A limitation of the procedure that we have described is that it is a serial method. We believe that the application of acousto-optic devices to generate arrays of optical traps from a single laser beam is one strategy that offers the potential to extend light-driven microfabrication into a parallel method.^[16]

The 2D and 3D structures shown in Figures 2–4 would be difficult to fabricate by other methods. The ability both to position and to orient nonspherical objects in 3D by using multiple light beams is a valuable characteristic of optical tweezers. We believe that light-driven microfabrication is an adaptable method that provides a broadly applicable solution to the problem of assembling micron-sized, optically transparent components into structured arrays. Its use with biological cells illustrates its capability in manipulating both nonspherical and fragile components.

Experimental Section

To prepare WGA-linked microspheres, spheres presenting primary amino groups (0.001 g mL^{-1} ; polysciences) were suspended in a phosphate-buffered solution (ca. pH 6) of a dicarboxylic acid linker ($\text{HO}_2\text{C}-(\text{CH}_2\text{CH}_2\text{O})_n\text{CO}_2\text{H}$; $n = 7-14$; 0.05 g mL^{-1} ; Fluka), 1-[3-(dimethylamino)-propyl]-3-ethylcarbodiimide hydrochloride (EDC; 0.4 M), and *N*-hydroxy succinimide (NHS; 0.1 M). The suspension was agitated gently at room temperature for 8 h to couple the linker to the sphere. The beads were separated from the solution of reactants by centrifugation and resuspended in deionized water. This procedure was repeated three times. The beads were resuspended in a solution of EDC (0.4 M) and NHS (0.1 M) and agitated gently for 15 min. The beads were isolated by centrifugation and resuspended in a solution of WGA (0.5 mg mL^{-1}) in phosphate buffer (0.1 M , pH 8.1); the suspension was agitated gently for 4 h to couple WGA to active esters on the beads. The beads were isolated from the solution of WGA and stored in phosphate buffered saline.

The glass cover slips used to support the sample suspension were treated with tridecafluoro-1,1,2,2-tetrahydrooctyl-1-methyldichlorosilane (United Chemical Technologies) under vacuum for 3 h and then soaked the silanized slide in a solution of BSA (0.05 g mL^{-1}). This procedure introduced a monolayer of BSA that blocks nonspecific adsorption to the glass.

We used three optical traps (optical tweezers) that could be manipulated independently. One trap was created by using a collimated beam from a Helium-Neon (HeNe) laser (power = 22 mW). The beam was expanded in stages by two telescopes; a steering mirror was placed between these telescopes to allow us to adjust the position of the optical trap within the sample. A high power ($100\times$, numerical aperture = 1.2) oil immersion microscope objective focused the beam into the sample. A lens placed before the objective converted the collimated telescope output into a beam with the appropriate size and curvature. A dichroic mirror that transmits most visible light but reflects the light produced by the HeNe laser (632 nm) was used to direct the beam into the objective while allowing us to image the sample with a CCD video camera. The remaining two traps were generated by two linearly polarized diode lasers (852 nm) whose powers could be adjusted from 0 to about 100 mW . Each beam was collimated and passed through an anamorphic prism so that they were both roughly circular. Telescopes expanded each beam as necessary. We placed mirrors before each telescope to be used to steer the beams. The polarization of each beam was adjusted so the beams could be passed through a polarizing beam splitter. The resulting output was directed through a lens to adjust the radius of curvature and the size of the beams, then directed through a dichroic mirror to adjust the wavelength of the beams, and finally directed

through the microscope objective and into the sample. This arrangement produced three optical traps within the sample. We used the near-infrared (852 nm) beams to trap the cells and the visible (632 nm) beam to trap the polystyrene microspheres.

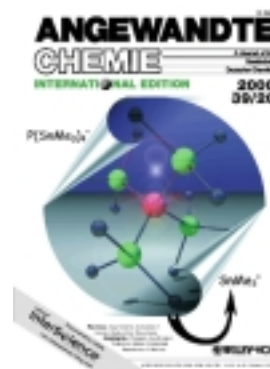
Received: May 2, 2000 [Z15062]

- [1] T. L. Steck, *J. Cell Biol.* **1974**, *62*, 1–19.
- [2] G. M. Whitesides, E. E. Simanek, J. P. Mathias, C. T. Seto, D. N. Chin, M. Mammen, D. M. Gordon, *Acc. Chem. Res.* **1995**, *28*, 37–44.
- [3] J. Tien, A. Terfort, G. M. Whitesides, *Langmuir* **1997**, *13*, 5349–5355.
- [4] H. Lis, N. Sharon, *Chem. Rev.* **1998**, *98*, 637–674.
- [5] *Extracellular Matrix* (Eds.: M. A. Zern, L. M. Reid), Marcel Dekker, New York, **1993**.
- [6] T. Feizi, P. R. Crocker, *Curr. Opin. Struct. Biol.* **1996**, *6*, 679–691.
- [7] Y. Nagata, M. M. Burger, *J. Biol. Chem.* **1974**, *249*, 3116–3122.
- [8] B. P. Peters, S. Ebisu, I. J. Goldstein, M. Flashner, *Biochemistry* **1979**, *18*, 5505–5511.
- [9] C. S. Chen, M. Mrksich, S. Huang, G. M. Whitesides, D. E. Ingber, *Science* **1997**, *276*, 1425–1428.
- [10] A. Ashkin, J. M. Dziedzic, J. E. Bjorkholm, S. Chu, *Opt. Lett.* **1986**, *11*, 288–291.
- [11] M. Mammen, K. Helmersson, R. Kishore, S. K. Choi, W. D. Phillips, G. M. Whitesides, *Chem. Biol.* **1996**, *3*, 757–763.
- [12] F. Jordan, E. Bassett, W. R. Redwood, *Biochem. Biophys. Res. Commun.* **1977**, *4*, 1015–1021.
- [13] M. Mammen, S. K. Choi, G. M. Whitesides, *Angew. Chem.* **1998**, *110*, 2908–2953; *Angew. Chem. Int. Ed.* **1998**, *37*, 2755–2794.
- [14] J. Rao, J. Lahiri, L. Isaacs, R. M. Weis, G. M. Whitesides, *Science* **1998**, *280*, 708–711.
- [15] J. Rao, J. Lahiri, R. M. Weis, G. M. Whitesides, *J. Am. Chem. Soc.* **2000**, *122*, 2968–2710.
- [16] D. W. M. Marr, C. Mio, *Langmuir* **1999**, *15*, 8565–8568.
- [17] H. Misawa, K. Sasaki, M. Koshioka, N. Kitamura, H. Masuhara, *Appl. Phys. Lett.* **1992**, *60*, 310–312.
- [18] *Hematology* (Eds.: W. J. Williams, E. Beutler, A. J. Erslev, R. W. Rundles), McGraw Hill, New York, **1972**.
- [19] E. R. Dufresne, D. G. Grier, *Rev. Sci. Instrum.* **1998**, *69*, 1974–1977.
- [20] A. Ashkin, J. M. Dziedzic, T. Yamane, *Nature* **1987**, *330*, 769–771.
- [21] A. Ashkin, J. M. Dziedzic, *Science* **1987**, *235*, 1517–1520.
- [22] K. Svoboda, S. M. Block, *Ann. Rev. Biophys. Biomol. Struct.* **1994**, *23*, 247–285.
- [23] K. Svoboda, S. M. Block, *Opt. Lett.* **1994**, *19*, 930–932.
- [24] S. P. Smith, S. R. Bhalotra, A. L. Brody, B. L. Brown, E. K. Boyda, M. Prentiss, *Am. J. Phys.* **1999**, *67*, 26–35.
- [25] C. A. Mirkin, R. L. Letsinger, R. C. Mucic, J. J. Storhoff, *Nature* **1996**, *382*, 607–609.
- [26] G. P. Mitchell, C. A. Mirkin, R. L. Letsinger, *J. Am. Chem. Soc.* **1999**, *121*, 8122–8123.
- [27] C. J. Loweth, W. B. Caldwell, X. G. Peng, A. P. Alivisatos, P. G. Schultz, *Angew. Chem.* **1999**, *111*, 1925–1929; *Angew. Chem. Int. Ed.* **1999**, *38*, 1808–1812.
- [28] N. Bowden, I. S. Choi, B. A. Grzybowski, G. M. Whitesides, *J. Am. Chem. Soc.* **1999**, *121*, 5373–5391.
- [29] A. L. Stout, W. W. Webb, *Meth. Cell Biol.* **1998**, *55*, 99–116.
- [30] A. Rosin, T. Wohland, E. Stelzer, *Zool. Stud.* **1995**, *34*, 167–169.

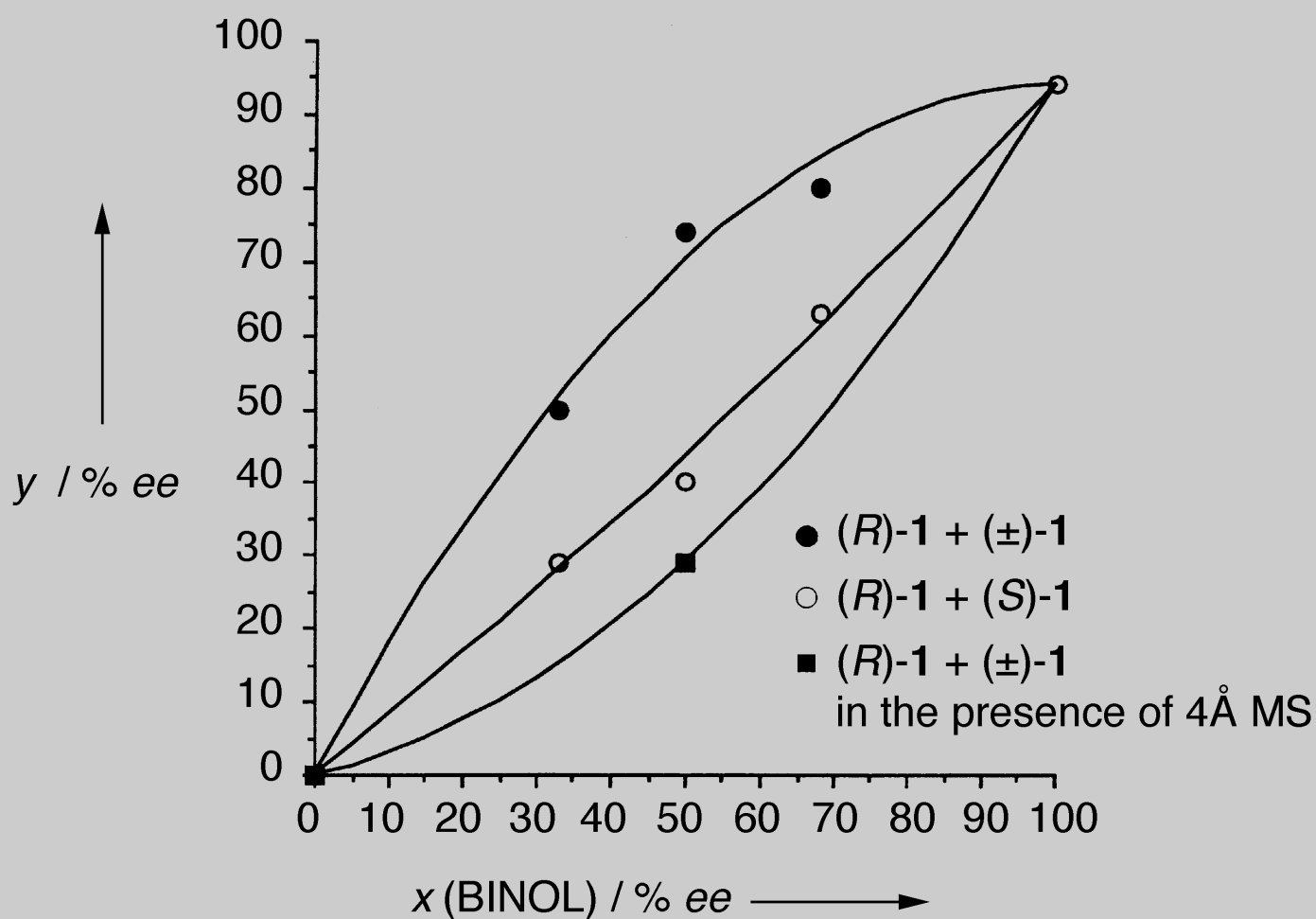
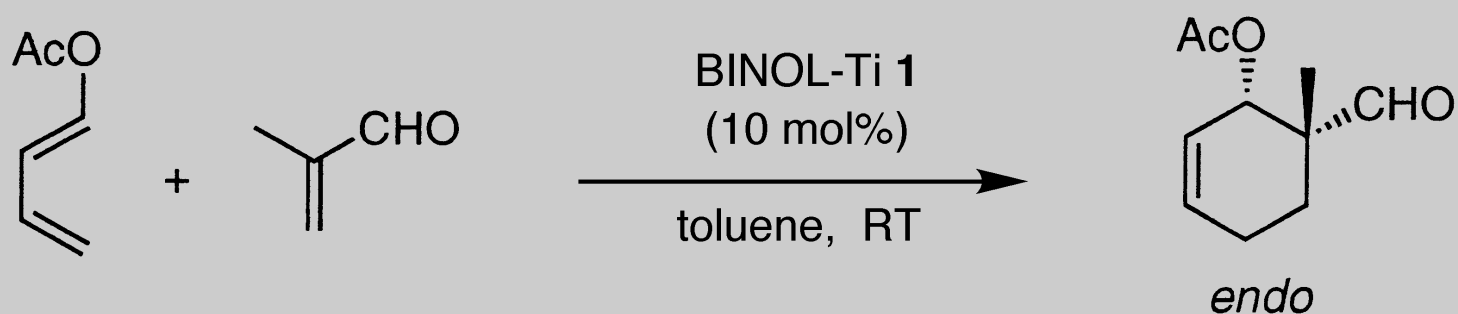
Cover Picture

Matthias Driess,* Christian Monsé, Klaus Merz and Christoph van Wüllen

The cover picture shows the structure, determined crystallographically, of the tetrakis(trimethylstannyl)phosphonium cation that is formed with surprising ease from the reaction of $\text{P}(\text{SnMe}_3)_3$ with Me_3SnOTf ($\text{OTf} = \text{OSO}_2\text{CF}_3$) and is isolated as the OTf salt. It is the first completely substituted main group organometallic phosphonium derivative, and, in contrast to the more common tetraorganic-substituted phosphonium cations is only stable in the solid state; in solution it functions as a masked Me_3Sn^+ reagent. More about this chameleonlike ion and the $\text{N}(\text{SnMe}_3)_4$ cation homologue, which is equally dynamic in solution and has unusual long Sn–N bond lengths, is reported by M. Driess et al. on p. 3684 ff.



Positive and negative nonlinear effects, as well as linear relationships, between the *ee* values of catalyst components and products can be observed by varying the method of catalyst preparation.



Asymmetric Activation

Koichi Mikami,* Masahiro Terada, Toshinobu Korenaga, Yousuke Matsumoto, Makoto Ueki, and Rémy Angelaud

While nonracemic catalysts can generate nonracemic products with or without the nonlinear relationship in enantiomeric excesses between catalysts and products, racemic catalysts inherently give only a racemic mixture of chiral products. Asymmetric catalysts, either in nonracemic or racemic form, can be further evolved into highly activated catalysts with association of chiral activators. This asymmetric activation process is particularly useful in racemic catalysis through selective activation of one enantiomer of the

racemic catalyst. Recently, a strategy whereby a racemic catalyst is selectively deactivated by a chiral additive has been reported to yield nonracemic products. However, reported herein is an alternative and conceptually opposite strategy in which a chiral activator selectively activates, rather than deactivates, one enantiomer of a racemic chiral catalyst. The advantage of this activation strategy over the deactivation counterpart is that the activated catalyst can produce a greater enantiomeric excess in the products—even

with the use of a catalytic amount of activator relative to chiral catalyst—than that attained by the enantiomerically pure catalyst on its own. Therefore, asymmetric activation could provide a general and powerful strategy for not only the use of atropisomeric, racemic ligands but also chirally flexible and proatropisomeric ligands without enantiomeric resolution!

Keywords: asymmetric catalysis • chiral poisoning • high-throughput screening • nonlinear effects

1. Introduction

Asymmetric catalysis of organic reactions which provide enantiomerically enriched products is of central importance in modern synthetic and pharmaceutical chemistry.^[1] Particularly, enantioselective catalysis is one of the most efficient processes in terms of chirality economy and environmental benignity. This technique affords a high proportion of the enantioenriched product and a small amount of waste material by taking advantage of a chiral catalyst. Therefore, the development of enantioselective catalysts is one of the most challenging and formidable endeavors in modern science and technology. Highly promising candidates for such enantioselective catalysts are metal complexes bearing chiral and nonracemic organic ligands, often in enantiopure form.

In the preparation of homogeneous asymmetric catalysts, Sharpless and co-workers emphasized the significance of “ligand-accelerated catalysis”^[2] through the construction of an asymmetric catalyst from an achiral precatalyst by ligand

exchange with a chiral ligand L* (Figure 1a). In heterogeneous asymmetric catalysis, the term “chiral modification”^[3] is coined instead for the process of modifying an achiral heterogeneous catalyst, particularly on a surface, with a chiral modifier, called the chiral ligand in homogeneous systems (Figure 1a). However, in some cases the modifier is reported to interact preferentially with a substrate (Figure 1b)^[4] rather than the achiral heterogeneous catalyst surface (Figure 1c).^[5]

The chiral homo- or heterogeneous catalysts prepared through chiral-ligand acceleration or chiral modification can be further evolved into highly activated catalysts through addition of chiral activators (Figure 1a). The term “asymmetric activation” may be proposed for this process, in close analogy to the activation process of an achiral reagent or catalyst to provide an activated but achiral one, for example an activated zinc reagent.^[6] This asymmetric activation process is particularly useful through selective activation of one enantiomer of a racemic catalyst (Scheme 1, Part 2).

While nonracemic catalysts thus developed can generate nonracemic products with or without the nonlinear relationship in enantiomeric excesses between catalysts and products,^[7] racemic catalysts inherently give only a racemic mixture of chiral products. Recently, a strategy relying on one enantiomer of a racemic catalyst, whereby a chiral molecule selectively deactivates a racemic catalyst, has been

[*] Prof. K. Mikami, Dr. M. Terada, Dr. T. Korenaga, Y. Matsumoto, M. Ueki, Dr. R. Angelaud
Department of Chemical Technology
Tokyo Institute of Technology
Meguro-ku, Tokyo 152-8552 (Japan)
Fax: (+81) 3-5734-2776
E-mail: kmikami@o.cc.titech.ac.jp

reported to yield nonracemic products (Scheme 1, Part 1). However, the level of asymmetric induction does not exceed that attained by enantiopure catalysts, wherein selective complexation and deactivation with a chiral poison is indispensable (Scheme 1, Part 1a and 1b).^[8,9] We have reported an alternative but conceptually opposite strategy to asymmetric catalysts in which a chiral activator selectively activates one enantiomer of a racemic catalyst (Scheme 1, Part 2).^[10] The advantage of this activation strategy over the deactivation counterpart is that the activated catalyst can produce a greater

enantiomeric excess ($X_{\text{act}}\% ee$) in the products, even with catalytic use of the activator, than the enantiomerically pure catalyst on its own ($X\% ee$). A chiral activator may selectively complex and activate one enantiomer of a racemic catalyst, to attain an enantioselectivity higher than that achieved with enantiopure catalysts ($\% ee_{\text{act}} \gg \% ee$), in addition to a higher level of catalytic efficiency ($k_{\text{act}} \gg k$; Scheme 1, Part 2a). Asymmetric activation can also be established even by nonpreferential complexation, to give activated diastereomeric catalysts (Scheme 1, Part 2b), based on the turnover

Koichi Mikami was born in 1953 in Bousou, Chiba, Japan. He received his PhD in 1982 under the supervision of Prof. Takeshi Nakai and Prof. Nobuo Ishikawa at the Tokyo Institute of Technology. He was a postdoctoral fellow at Yale University with Professor Frederic E. Ziegler (1982–1983) and then he returned to the Tokyo Institute of Technology to become an Assistant Professor. He became an Associate Professor in 1987. He has received the Teijima award for stereocontrol based on [2,3]-sigmatropic rearrangements, the Chemical Society of Japan Award (Shinpo-Sho) for asymmetric transmission and asymmetric synthesis based on [2,3]-Wittig rearrangements, the Society of Synthetic Organic Chemistry Japan Award (Asahi-Kasei Award) for asymmetric synthesis based on carbonyl-ene reactions, and the IBM award for highly efficient asymmetric catalysis. He was the Bristol-Myers-Squibb Lecturer at Colorado State University, and has held Visiting Professorships at the Université Paris-sud and in Taiwan.



K. Mikami



M. Terada



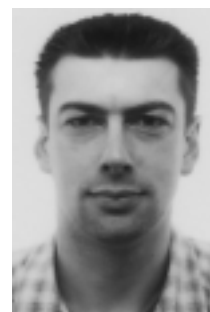
T. Korenaga



Y. Matsumoto



M. Ueki



R. Angelaud

Masahiro Terada was born in 1964 in Tokyo, Japan, and became a research associate in the Department of Chemical Technology at the Tokyo Institute of Technology in 1989. He received his PhD in 1993 from this university under the direction of Prof. Koichi Mikami. He was given awards for his PhD thesis from the Inoue and Teijima foundations in 1995. He has now joined the group of Prof. M. D. Shair at Harvard University as a postdoctoral worker.

Toshinobu Korenaga was born in 1969 in Niigata, Japan. He received his BSc in chemistry from the Science University of Tokyo in 1993 and his MSc in pharmacy from Kyoritsu College of Pharmacy in 1995. After two years of research as a synthetic chemist in industry, he recently received a PhD degree from the Tokyo Institute of Technology under the direction of Prof. Koichi Mikami. He is currently a JSPS postdoctoral fellow.

Yousuke Matsumoto was born in 1974 in Kanagawa, Japan. He received his BSc and then MSc from the Tokyo Institute of Technology under the supervision of Prof. Koichi Mikami. He is currently a JSPS graduate student working on the synthesis and structure analysis of chiral titanium complexes.

Makoto Ueki was born in 1975 in Tokyo, Japan. He received his BSc from the Tokyo Institute of Technology in 1998 under the direction of Prof. Koichi Mikami. He is currently working on chiral Lewis acid clusters.

Rémy Angelaud was born in 1967 in Bordeaux, France. He graduated from the Université d'Aix-Marseille-II in 1992. He then moved to the Faculté des Sciences de l'Université de Lausanne (Switzerland) where he obtained his PhD degree in 1997, under the supervision of Prof. Y. Landais and Prof. P. Vogel. During 1998–99, he joined Prof. V. K. Aggarwal's group at the University of Sheffield (UK) as a postdoctoral fellow (TMR Marie-Curie). He is currently a JSPS postdoctoral fellow at the Tokyo Institute of Technology (Japan) under the supervision of Prof. Koichi Mikami.

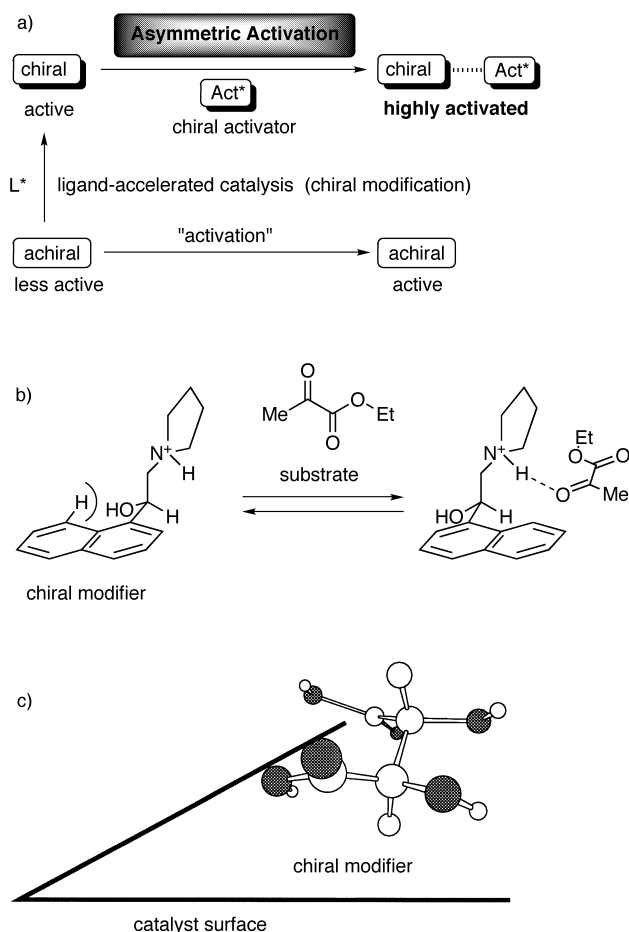


Figure 1. a) The principle of asymmetric activation. b), c) Interaction between a chiral modifier and a substrate or catalyst surface.

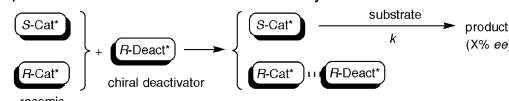
frequencies (catalytic activities) between the diastereomers ($k_{\text{act}} > k'_{\text{act}}$), which depend on substrates.^[11] Furthermore, an asymmetric activation/deactivation protocol can achieve higher enantioselectivity regardless of the substrates (Scheme 1, Part 3), by maximizing the difference in catalytic activity between enantiomeric catalysts. The positive nonlinear effect ((+)-NLE) or asymmetric amplification (see below) is an important phenomenon in asymmetric catalytic process, in which very high enantioselectivity of the product can be achieved even if a low enantiopurity chiral ligand is employed in the catalyst. Therefore, an enantiomerically pure ligand is not necessarily utilized for getting a high level of enantioselectivity. Even so, one has to perform a partial resolution of the racemic catalysts. Asymmetric catalysis can be carried out with racemic catalysts through in-situ and partial activation (/deactivation) of the racemic catalysts by adding easily prepared enantiopure additives (Scheme 1, Part 4).

2. Positive Nonlinear Effect of Nonracemic Catalysts

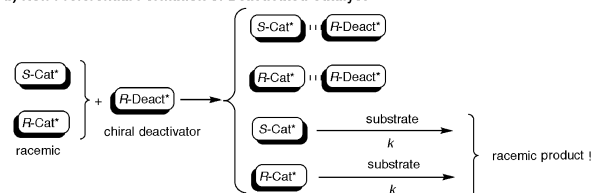
A chiral catalyst is not necessarily prepared from an enantiopure ligand because deviation from the linear relationship between the enantiomeric purity of chiral catalysts and

1) Asymmetric Deactivation

a) Preferential Formation of Deactivated Catalyst

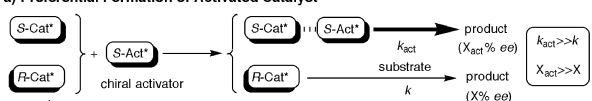


b) Non-Preferential Formation of Deactivated Catalyst

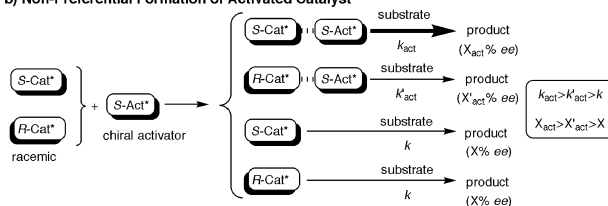


2) Asymmetric Activation

a) Preferential Formation of Activated Catalyst

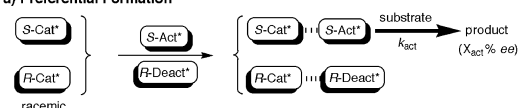


b) Non-Preferential Formation of Activated Catalyst

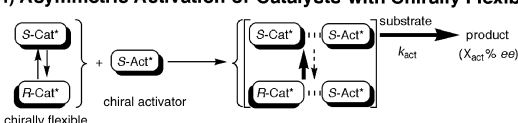


3) Asymmetric Activation / Deactivation

a) Preferential Formation



4) Asymmetric Activation of Catalysts with Chirally Flexible Ligands



Scheme 1. Asymmetric activation and deactivation..

the optical yields of the products, namely the nonlinear effect (NLE), is sometimes observed (Figure 2).^[7, 12–14, 16, 17, 19–29] The convex deviation, which Kagan and co-workers^[12] and Mikami and co-workers^[13] independently referred to as positive nonlinear effect (abbreviated as (+)-NLE), has attracted attention and a higher level of asymmetric induction than the enantiopurity of the nonracemic (partially resolved) catalysts has now been achieved.^[14]

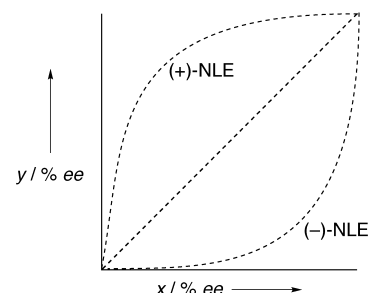
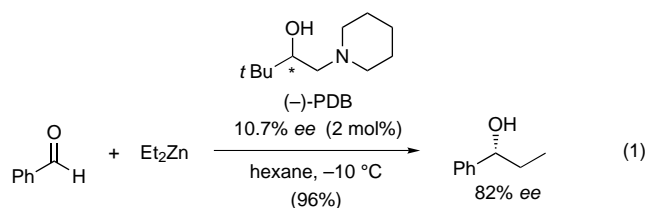
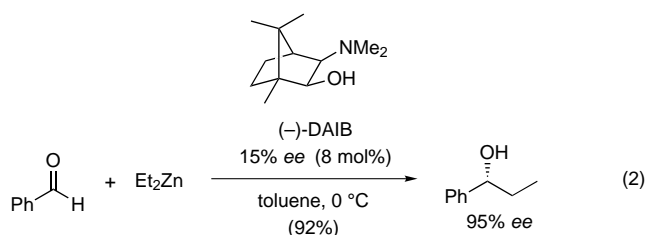


Figure 2. Possible relationships ((+)-NLE, linear, and (-)-NLE) between the enantiomeric purity of chiral ligands (x) and the optical yield of products (y).

Oguni et al. independently coined the term asymmetric amplification^[15] for (+)-NLE in an asymmetric carbonyl addition reaction of dialkylzinc reagents catalyzed by chiral amino alcohols, such as 1-piperidino-3,3-dimethyl-2-butanol (PDB) [Eq. (1)].^[16] In the same asymmetric carbonyl addition



reaction, Noyori and co-workers reported the use of a highly efficient amino alcohol catalyst, (2*S*)-3-*exo*-(dimethylamino)-isoborneol (DAIB) [Eq. (2)].^[17] They reported a beautiful



mechanistic investigation on the asymmetric amplification in view of the stability of the heterochiral dimer of the zinc amino alcohol compared to the homochiral dimer (Figure 3). We also reported a positive nonlinear effect in a carbonyl-ene reaction^[18] with glyoxylate catalyzed by a binaphthol (BINOL) derived chiral titanium complex [Eq. (3)].^[13] Bolm reported (+)-NLE in the 1,4-addition reaction of diethylzinc with catalysis by a nickel complex and a pyridyl alcohol [Eq. (4)].^[19]

Significant levels of (+)-NLE are also observed in the asymmetric catalysis by cationic complexes bearing *trans*-chelating tridentate ligands. Kanemasa et al. reported an aqua complex that exhibited a remarkable (+)-NLE; it was prepared from Ni(ClO₄)₂·6H₂O with 4,6-dibenzofurandiyl-2,2'-bis(4-phenyloxazoline) (DBFOX/Ph) as a tridentate ligand (Scheme 2 top).^[20] Two mechanisms were involved in the (+)-NLE: the irreversible formation of heterochiral [(*R,R*),(*S,S*)] 2:1 ligand:metal complexes and the heterochiral oligomerization of 1:1 ligand:metal complexes with the help of water bridging (Scheme 2 below).

Evans studied the asymmetric catalysis of carbon–carbon bond forming reactions with C₂-symmetric bisoxazoline–Cu^{II} complexes.^[21, 22] In an asymmetric aldol reaction catalyzed by a bis(oxazolonyl)pyridine (PYBOX)–Cu complex [Eq. (5)],^[22] the (+)-NLE observed was explained as a result of the relative stabilities of the heterochiral [(*S,S*),(*R,R*)] and homochiral [(*S,S*),(*S,S*)] 2:1 ligand–metal complexes.

Negative nonlinear effect (abbreviated as (–)-NLE)^[12, 13] stands, in turn, for the opposite phenomenon of concave deviation (Figure 2).^[14], m, n, z, ad, ag, ah, 23] The partially resolved catalyst provides the product in lower enantiomeric excess than calculated by linearity. In a conjugate addition reaction

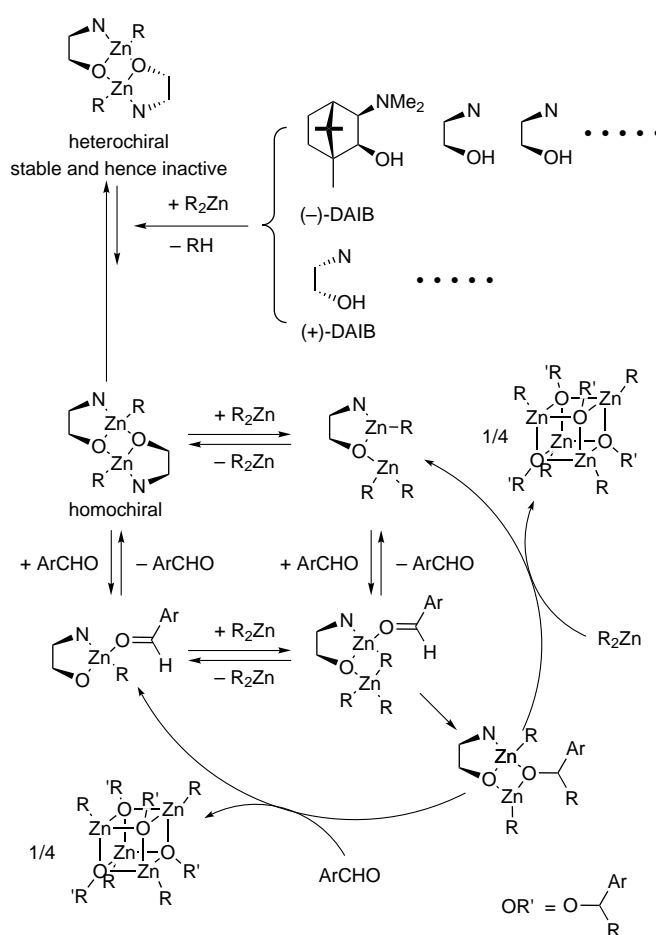
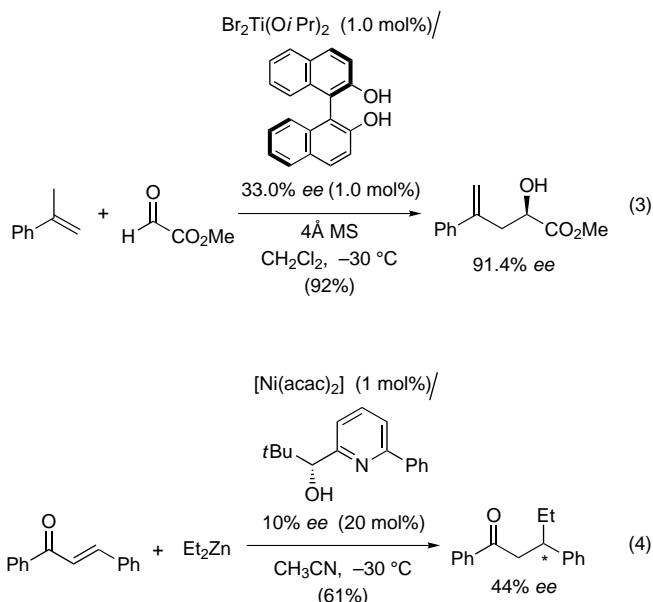
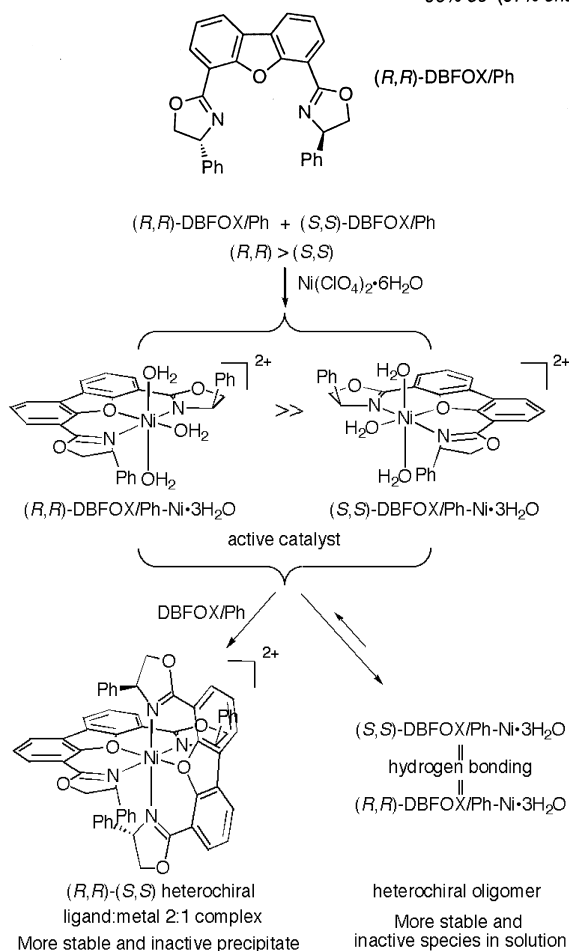
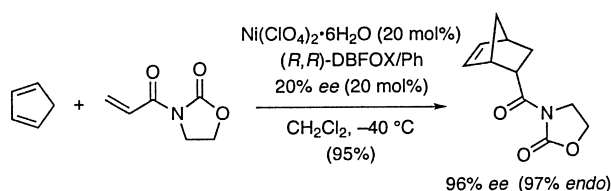


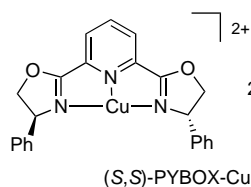
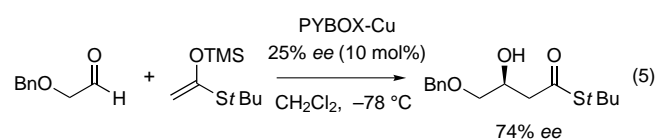
Figure 3. Mechanism of asymmetric amplification shown by Noyori et al.



with an organocopper reagent, an interesting shape of NLE was found. The (+)-NLE was observed with a more enantiopure chiral ligand, whilst a less enantiopure ligand led to (–)-NLE (Scheme 3).^[24] Kagan and co-workers suggested a tetrameric complex was the reactive species, by simulation of a mathematical model system of four chiral ligands.^[12a] We

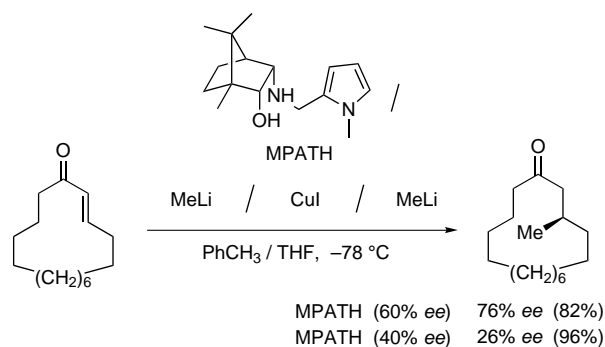


Scheme 2. Above: An asymmetric Diels–Alder reaction catalyzed by a DBFOX/Ph–Ni complex. Below: Mechanisms for the observed (+)-NLE.



could also reproduce the intriguing shape of the nonlinear curve on the basis of Kagan's equation for a tetrameric catalyst species (Figure 4).

Significantly, the mode of preparation of a catalyst sometimes determines not only the presence of a nonlinear effect (NLE) but also the direction (positive or negative) thereof.^[14], af, ag, 23, 25, 26] The BINOL–Ti catalyst **1** is prepared from partially resolved BINOL and $\text{Cl}_2\text{Ti}(\text{O}i\text{Pr})_2$ in the presence of



Scheme 3. Influence of ligand enantiopurity on the NLE during conjugated addition with organocopper compounds. The reagents were added in the following quantities: 367 mol % MPATH, 734 mol % MeLi, and 183 mol % CuI.

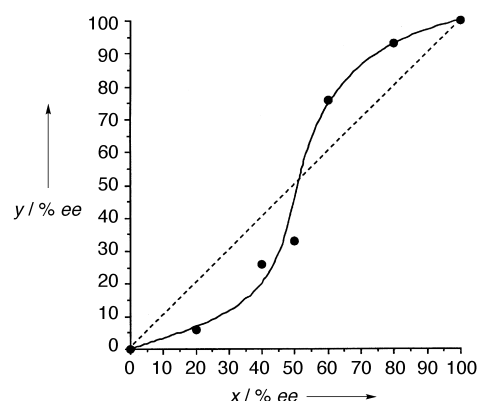


Figure 4. Relationship between the ee values of the ligand (x) and the product (y) for the reaction shown in Scheme 3. The complete line was calculated according to the method of Kagan and the experimental data are shown as points. The dotted line shows the expected result for a linear relationship.

4 Å molecular sieves, which are filtered off prior to the reaction;^[25] when this catalyst is utilized in the asymmetric Diels–Alder reaction shown in Figure 5, a (+)-NLE is observed (Table 1, entry 1). The combined use of enantiopure (R)-**1** and racemic (\pm)-**1** catalysts in a ratio of 1:1 results in a

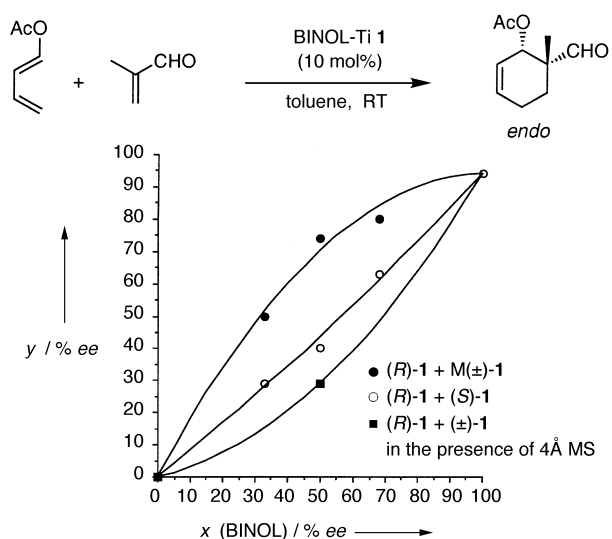


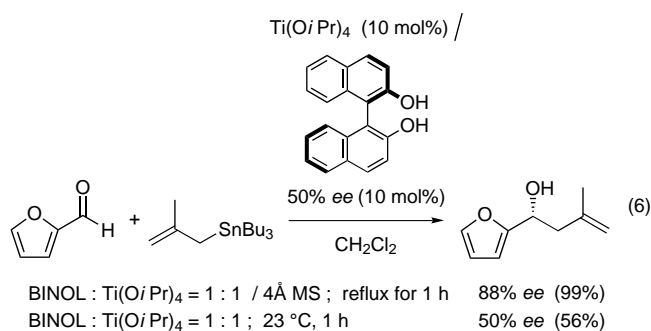
Figure 5. The graph shows the relationship of the NLE to the catalyst system for the asymmetric Diels–Alder reaction shown at the top. $y = ee$ value of the product.

Table 1. Dependence of the NLE on the catalyst system used for the asymmetric Diels–Alder reaction shown in Figure 5.

Entry	Preparation of the catalyst system	ee [%] of the catalyst system	Yield [%]	endo [%]	ee [%]
1	partially resolved BINOL (52% ee) and $\text{Cl}_2\text{Ti}(\text{OiPr})_2$	52	41	98	76
2	(<i>R</i>)- 1 + (±)- 1 (1:1)	50	50	99	74
3	(<i>R</i>)- 1 + (<i>S</i>)- 1 (3:1)	50	62	99	40
4	(<i>R</i>)- 1 + (<i>S</i>)- 1 (3:1)+4 Å molecular sieves (removed prior to the reaction)	50	67	99	60
5	(<i>R</i>)- 1 + (±)- 1 (1:1)+4 Å molecular sieves	50	62	95	29
6	only 4 Å molecular sieves	–	20	–	–
7	(<i>R</i>)- 1 + (<i>S</i>)- 1 (3:1) in CH_2Cl_2	50	52	99	53

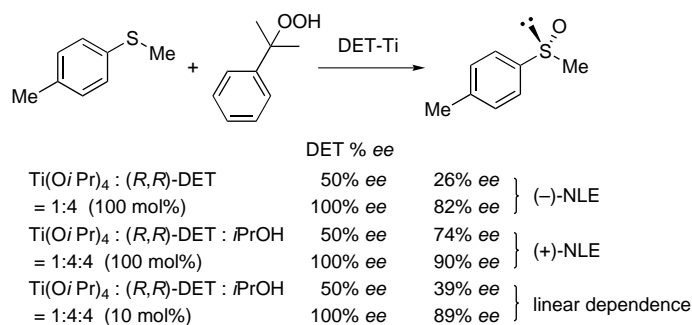
similar (+)-NLE (entry 2). By contrast, mixing enantiopure BINOL–Ti catalysts, (*R*)- and (*S*)-**1** in a ratio of 3:1 leads to a linearity (entry 3; no NLE!). However, when (*R*)- and (*S*)-**1** catalysts are mixed in the same ratio of 3:1, but in the presence of molecular sieves, which are then filtered off prior to the reaction, a (+)-NLE was observed (entry 4). Moreover, in dichloromethane, the combined use of (*R*)- and (*S*)-**1** catalysts (3:1), even without prior treatment with molecular sieves, exhibits a (+)-NLE (entry 7). These experimental results can be explained by the fact that the complex consists of oligomers, which do not interconvert in the absence of molecular sieves in toluene but do interconvert in dichloromethane (compare entries 3, 4, and 7). When the reaction is carried out in the presence of molecular sieves, however, a (–)-NLE is observed (entry 5), because the sieves act as an achiral catalyst for the Diels–Alder reaction (entry 6).

Keck et al. reported that BINOL-derived titanium catalysts prepared in the presence or absence of 4 Å molecular sieves showed a (+)-NLE or a linearity, respectively [Eq. (6)].^[26] In the presence of 4 Å sieves, the enantiopurity of the allylated product exceeded that of the BINOL used.



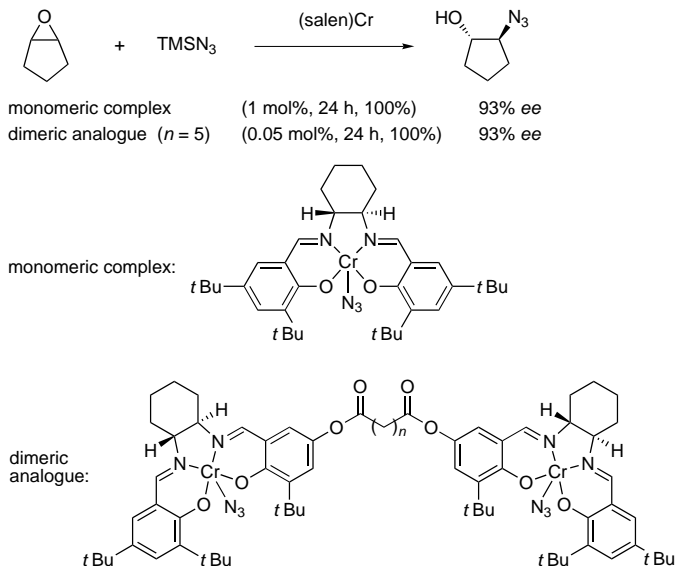
Kagan et al. pointed out the NLE as an indicator for distinction of closely related chiral catalysts (Scheme 4).^[23] In the asymmetric oxidation of sulfides with hydroperoxides promoted by chiral diethyl tartrate (DET)–Ti complexes, a wide diversity of titanium species was observed by minor modifications in the catalyst preparation step. Stoichiometric use of a 1:4 mixture of $\text{Ti}(\text{OiPr})_4$ and DET exhibited a (–)-NLE. Addition of *i*PrOH to this mixture (1:4:4 mixture of $\text{Ti}(\text{OiPr})_4$, DET, and *i*PrOH) provided a (+)-NLE, while catalytic use of this ternary system led to the disappearance of the NLE.

The study of the NLE in asymmetric catalysis can be useful for getting mechanistic insight and information about the



Scheme 4. (+)-NLE, (–)-NLE, and linear relationships can be obtained by variation of the catalyst preparation.

active species involved in the catalytic cycle, and their behavior in solution.^[27] Jacobsen and co-workers used the NLE as a mechanistic probe for the asymmetric ring opening of epoxides with trimethylsilyl azide catalyzed by a chiral Cr(salen)-type complex (Scheme 5).^[28] The observation of

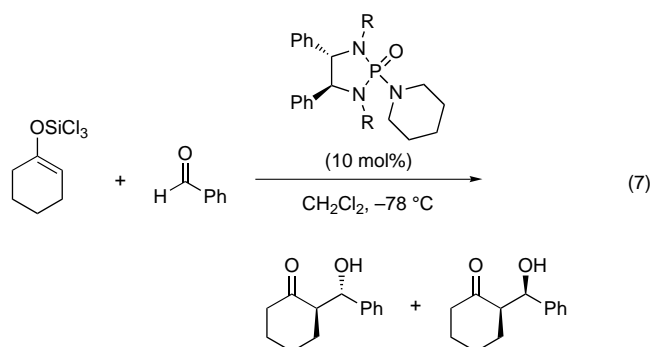


Scheme 5. The NLE as a mechanistic technique.

significant (+)-NLE coupled with a second-order kinetic dependence on the Cr(salen) catalyst led to a mechanistic proposal for simultaneous activation of both the epoxide and the azide by two different Cr(salen) complexes. On the basis of this cooperative mechanism they designed dimeric analogues of the Cr(salen) complex. Covalent linkage of the Cr(salen) complex unit with a suitable tether length and

position resulted in catalysts between one and two orders of magnitude more reactive than the monomeric analogues without any loss of enantioselectivity (Scheme 5).

On the basis of NLE studies coupled with kinetic analyses, Denmark et al. disclosed that the mechanism of rate acceleration by chiral phosphoramides in asymmetric aldol reactions of trichlorosilyl enolates with aldehydes stemmed from the ionization of the enolate by the phosphoramides [Eq. 7].^[29] Sterically demanding phosphoramides ($R = \text{Ph}$),



which exhibit a linear relationship, bind to the enolate in a 1:1 fashion. The resulting pentacoordinated cationic siliconate favors a boatlike transition state. In contrast, sterically less demanding phosphoramides ($R = \text{Me}$) with a (+)-NLE can bind in a 2:1 fashion. The resulting hexacoordinated cationic siliconate favors a chairlike arrangement.

Recently Blackmond demonstrated^[30] a detailed analysis of the experimental reaction rate in these nonlinear catalytic systems; this analysis can give an independent confirmation of the mathematical models developed by Kagan and co-workers.^[12a] Consideration of the kinetic behavior of nonlinear catalytic reactions can provide valuable mechanistic insights into the NLE by comparison of the predictions of the models.

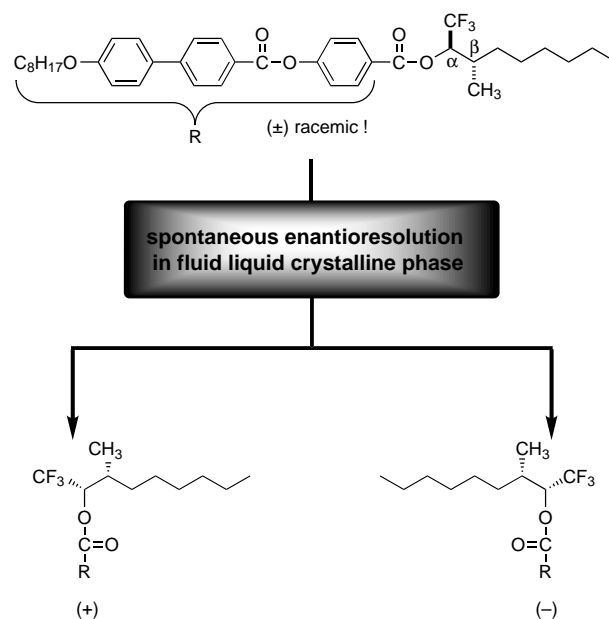
3. Autocatalysis

Another aspect of NLE is asymmetric autocatalysis as an event following symmetry breaking in nature. On the origin of chirality in nature, two major mechanisms have been proposed:^[31] 1) A chance mechanism to generate an optically active molecule followed by self-replication; 2) a determining mechanism to favor one enantiomer. Some physicochemical elements are determining factors which provide a nonequivalence of enantiomers. Nonconservation of the parity of weak interactions may lead to small differences in energy between two enantiomeric forms.^[32] A solid chiral adsorbent, such as quartz, can be another factor.^[33, 34] Circular polarized light^[35] and geophysical fields, such as the rotation of the earth and magnetic fields,^[36] have long been proposed as determining factors.

Pasteur showed an autocatalytic crystallization process (“spontaneous enantioresolution”) from a racemic mixture of the double salt sodium ammonium tartrate to give a conglomerate of one enantiomer.^[37] Later, Havinga reported dynamic crystallization of one enantiomer from an interconverting mixture of antipodes^[38] under two “bistable” states.^[39] A racemic chiral compound can crystallize in three different forms: As a racemic

compound, a pseudoracemate (solid solution), or, preferably, as a conglomerate.^[40] In the crystallization of a pseudoracemate, preferential enrichment^[41] of one enantiomer may occur in the mother liquid. However, spontaneous enantioresolution to give a conglomerate is rather difficult in fluid systems, such as liquid crystals, due to thermal fluctuations and/or molecular diffusion. Indeed, no one has succeeded in observing the same phenomenon in a fluid phase rather than in a static crystalline phase or on a surface; a monolayer film on a mica plate has shown two-dimensional conglomeration.^[42] A similar two-dimensional conglomerate has been observed from a racemic liquid-crystalline molecule, however, on a crystalline graphite surface, rather than in a fluid smectic phase.^[43] We have reported spontaneous enantioresolution (Scheme 6) of racemic CF_3 -containing liquid crystalline molecules with large spontaneous polarization (P_s) into a three-dimensional conglomerate, which exhibits an electrooptic response.^[44] This success is the result of accurate discrimination between the enantiomers of the racemate through the double stereogenic part of the molecule, even in the fluid condensed matter!

The nonequivalence of enantiomers through the spontaneous breaking of mirror symmetry in nature is amplified with asymmetric autocatalytic reactions^[45] (Frank’s spontaneous asymmetric synthesis;^[46, 47] see Figure 6). Alberts and Wynberg reported an enantioselective autoinduction in which a chiral lithium alkoxide product might be involved with the reactant to increase the enantioselectivity [Eq. (8)].^[48] The enantiomeric excess of the product, however, did not exceed the *ee* value of the catalyst. In the asymmetric hydrocyanation catalyzed by cyclic dipeptides, the *S*-cyanohydrin product made a complex with the cyclic peptide which increased the enantioselectivity in the *S*-cyanohydrin product in the course of the reaction up to 95.8% *ee* (Scheme 7).^[49] In the presence of an achiral amine, (*R*)-1-phenylpropan-1-ol catalyzed the carbonyl-addition reaction of diethylzinc to benzaldehyde, with the product showing a lower *ee* value than that of the catalyst employed.^[50]



Scheme 6. Spontaneous enantioresolution in the fluid liquid crystalline phase.

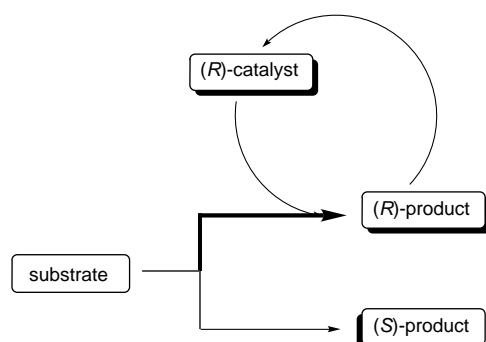
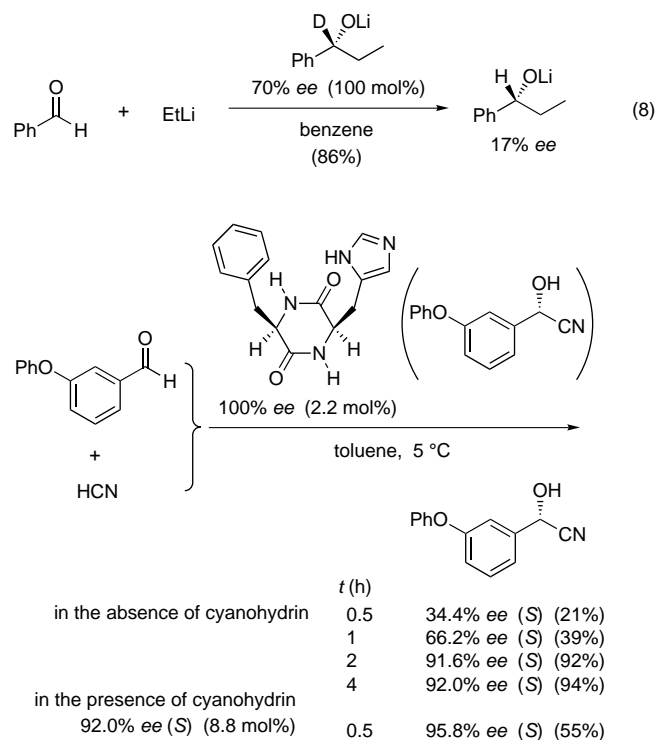
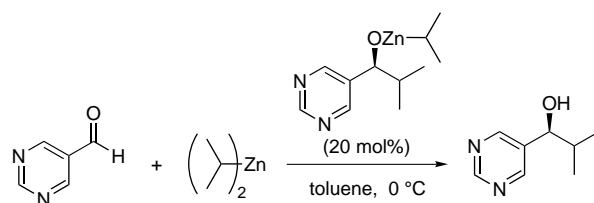


Figure 6. Spontaneous asymmetric synthesis.



Scheme 7. Autocatalysis in the asymmetric hydrocyanation catalysed by cyclic dipeptides.

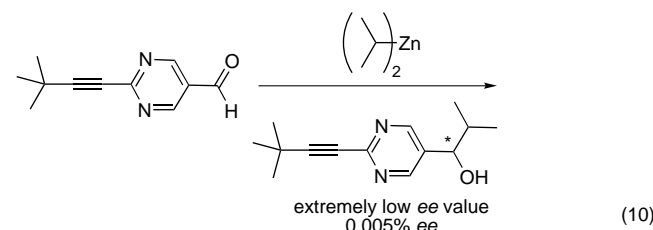
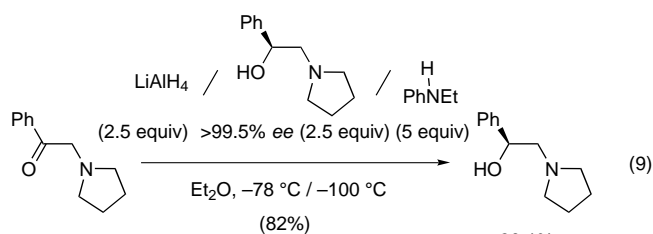
Soai et al. have reported the remarkable example of asymmetric autocatalysis in carbonyl-addition reactions of diisopropylzinc.^[51–56] Usually, zinc alkoxide forms an inactive tetramer. However, the use of pyridyl aldehyde as a substrate, to give a pyridyl alcohol product, can loop the catalytic cycle without formation of the inactive tetramer.^[51] In this autocatalytic system the *ee* value of the product does not exceed the level of the catalyst *ee* value,^[52] while the use of a chiral quinolyl alcohol as the catalyst, instead of the pyridyl counterpart, gives the product without any loss of enantiopurity.^[53a] A (+)-NLE is also observed when the quinolyl alcohol is used as the catalyst.^[53b] A significant improvement of (+)-NLE is achieved, however, by Soai in a similar carbonyl-addition reaction to pyrimidylcarbaldehyde.^[54] Starting from the *S* alcohol in 2% *ee* (20 mol%), the first reaction provides the *S* alcohol in 10% *ee* and after the fourth reaction the value is 88% *ee* (by way of 57 and 81% *ee*, Scheme 8).^[54a] Soai and co-workers have also investigated an enantioselective autoinduction in the reduction of α -amino



	catalyst	mixture of catalyst and product	product
1st	2% ee	10% ee (46%)	16% ee (26%)
2nd	10% ee	57% ee (75%)	74% ee (55%)
3rd	57% ee	81% ee (80%)	89% ee (60%)
4th	81% ee	88% ee (75%)	90% ee (55%)
5th	88% ee	88% ee (79%)	88% ee (59%)

Scheme 8. Autocatalysis in the addition of diisopropylzinc to pyrimidylcarbaldehyde.

ketones with lithium aluminum hydride modified with a chiral 1,2-amino alcohol and an achiral amine [Eq. (9)].^[55] Recently, they demonstrated amplification of a quite small nonequivalence of enantiomers on the basis of asymmetric autocatalysis [Eq. (10)].^[56] Thus, a small nonequivalence of enantiomers

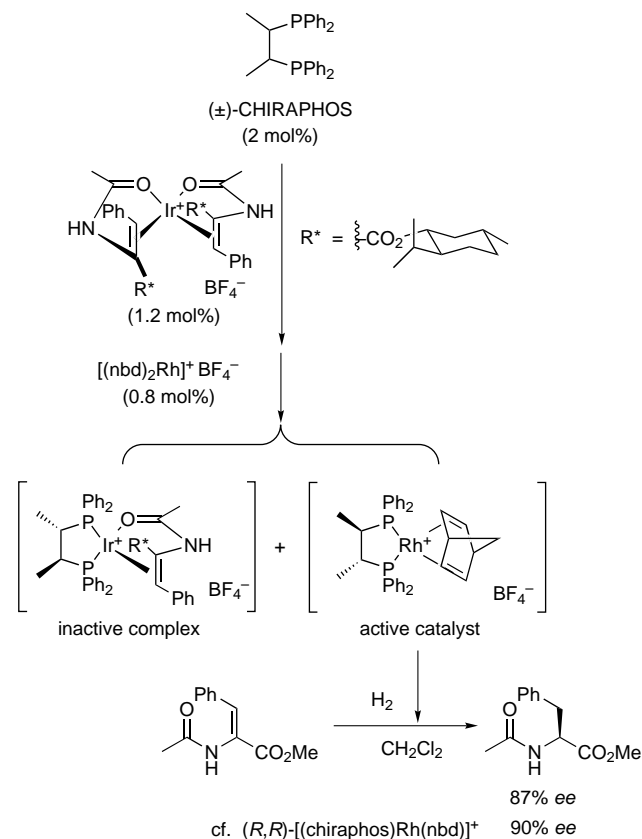


caused by symmetry breaking can be amplified through asymmetric autocatalysis to a large enantiomeric nonequivalence in molecules, as found in nature.

4. Asymmetric Deactivation of Racemic Catalysts

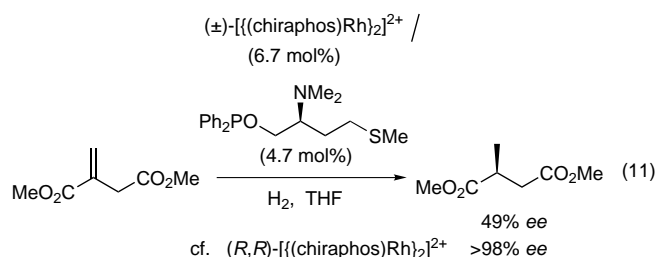
Whilst nonracemic catalysts can generate nonracemic products, with or without the NLE or asymmetric autocatalysis, racemic catalysts (0% *ee*) inherently produce only racemic (0% *ee*) products. A strategy whereby a racemic catalyst is enantioselectively deactivated by a chiral molecule

acting as a catalyst poison has recently been shown to yield nonracemic products (Scheme 1, Part 1 a).^[8] A unique resolution of racemic CHIRAPHOS has been attained with a chiral iridium complex to give a deactivated form, which leads to a chiral rhodium complex in association with the remaining enantiomer of CHIRAPHOS.^[8a] This process eventually results in a nonracemic hydrogenation product (Scheme 9).

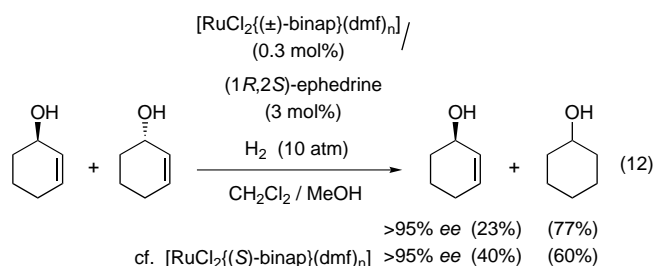


Scheme 9. Asymmetric deactivation by a chiral iridium complex.

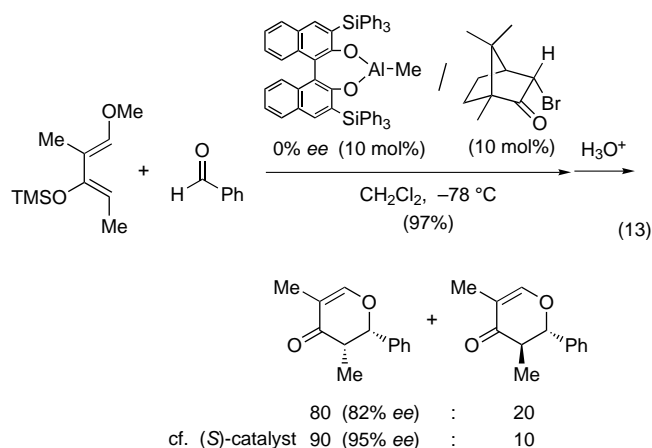
More recently, chiral poisoning,^[9, 57] in such a deactivating strategy, has been named as a factor in the context of hydrogenation by asymmetric catalysis with a similar CHIRAPHOS–Rh complex [Eq. (11)].^[9a,b] A chiral amino alcohol,



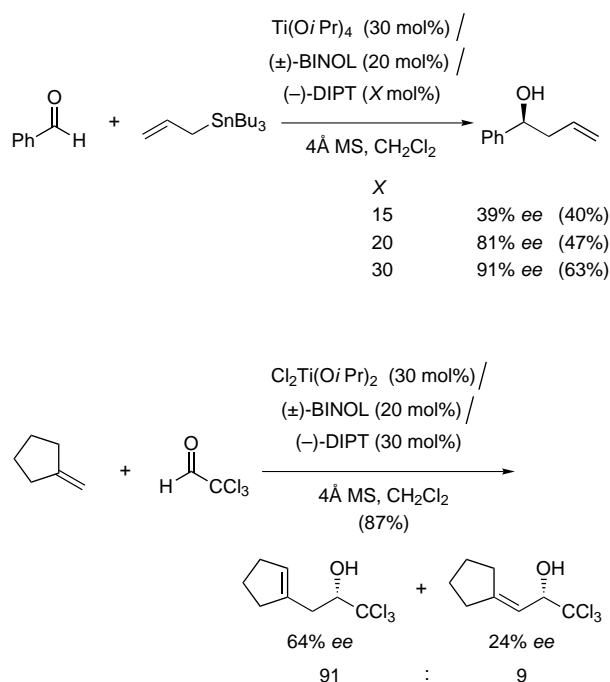
(1*R*,2*S*)-ephedrine, is also employable as a poison in the kinetic resolution of cyclic allylic alcohols using racemic BINAP [Eq. (12)].^[9b,c] However, the level of asymmetric induction does not exceed the level attained by the enantiopure catalyst (see Scheme 1, Part 1 a). A racemic aluminum reagent has been discriminated using chiral unreactive



ketones to yield hetero Diels–Alder products in a reaction catalyzed by the remaining enantiomer of the aluminum reagent [Eq. (13)].^[8c]



Enantiomerically pure diisopropoxytitanium tartrate (DIPT) can also be used as a poison for racemic binaphthol–titanium complexes (Scheme 10).^[9d,e] The *ee* value of the product increases with an increase in the amount of DIPT employed.



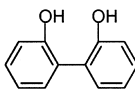
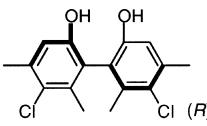
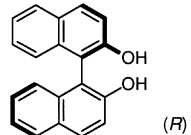
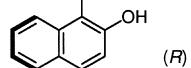
Scheme 10. DIPT as a poison for racemic binaphthol–titanium complexes.

5. Asymmetric Activation of Racemic Catalysts

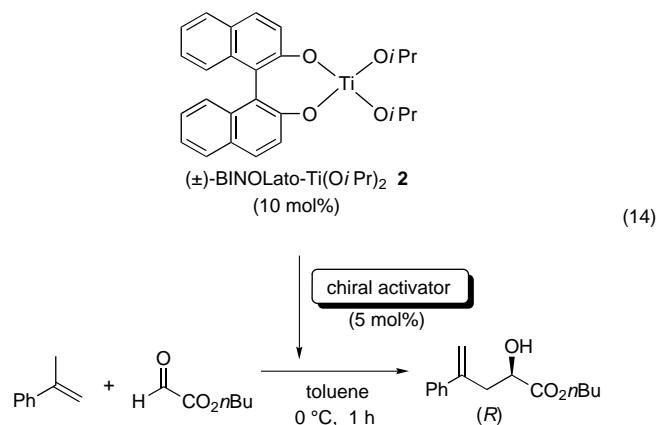
We have reported an alternative but conceptually opposite strategy to asymmetric catalysis by racemic catalysts: a chiral activator selectively activates one enantiomer of a racemic catalyst. A higher level of catalytic efficiency by more than two order of magnitude ($k_{\text{act}} > k \times 10^2$), in addition to a higher enantioselectivity, than that achieved by an enantiopure catalyst might be attained ($X_{\text{act}} \% ee > X \% ee$; Scheme 1, Part 2).

The ene reaction is one of the simplest methods for C–C bond formation; it converts readily available olefins, with C–H bond activation at an allylic site and allylic transposition of the C=C bond, into more functionalized products. The ene reaction encompasses a vast number of variants in terms of the enophile used.^[18b, 58] Amongst these, the ene reactions of carbonyl enophiles, aldehydes in particular, which we refer to as carbonyl-ene reactions,^[18] should in principle constitute a more efficient alternative to the carbonyl-addition reaction of allylmetals for stereocontrol.^[59] Catalysis of carbonyl-ene reactions with racemic BINOLato–Ti(OiPr)₂ (**2**) achieves extremely high enantioselectivity by adding another enantiopure diol for the enantioselective activation [Eq. (14)] (Table 2).^[10b] Significantly, a remarkably high enantioselectivity (89.8% *ee*, *R* isomer) was achieved adding (*R*)-BINOL activator to the racemic (\pm)-BINOLato–Ti(OiPr)₂ complex (**2**).

Table 2. Enantioselective activation of racemic (\pm)-**2** [Eq. (14)].

Entry	Chiral activator	Yield [%]	<i>ee</i> [%]
1	–	5.9	0
2		20	0
3		38	80.8
4		52	89.8
5 ^[a]		35	80.0

[a] Only 2.5 mol% of (*R*)-BINOL was used as a chiral activator.

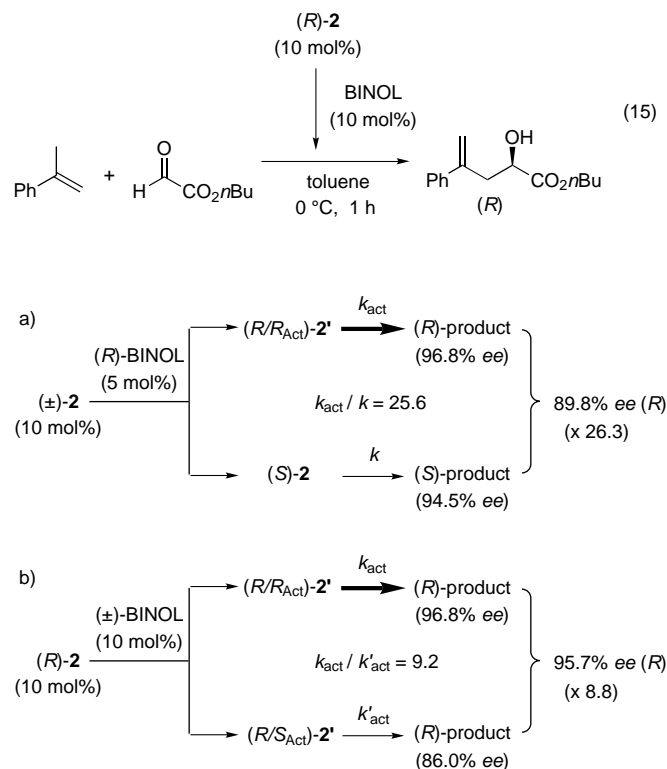


The activation of the enantiopure (*R*)-**2** catalyst can also be synthetically useful, by further addition of (*R*)-BINOL [Eq. (15)] (Table 3). The reaction proceeded quite smoothly to provide the carbonyl-ene product in higher chemical yield (82.1%) and enantioselectivity than without additional BINOL (entries 2 and 1, respectively). Comparing the results of enantioselective activation of the racemic catalyst (Table 2, entry 4) with those of the enantiopure catalyst with or without activator (entries 2 and 1), the reaction catalyzed by the (*R*)-BINOLato–Ti(OiPr)₂/(*R*)-BINOL complex (*R/R*_{Act})-**2'** was calculated to be 26.3 times faster than that catalyzed by the (*S*)-**2** in the racemic case (Scheme 11a). Indeed, kinetic studies showed that the reaction catalyzed by the (*R*)-**2**/(*R*)-BINOL complex (*R/R*_{Act})-**2'** was 25.6 times ($=k_{\text{act}}/k$) faster than that catalyzed by (*R*)-**2**. These results imply that the racemic (\pm)-(**2**) and half-molar amount of (*R*)-BINOL assemble preferentially into the (*R/R*_{Act})-**2'** and the (*S*)-**2** remains unchanged. In contrast, the enantiomeric form of the additional chiral ligand ((*S*)-BINOL) activates the (*R*)-**2** to a smaller degree, which provides the carbonyl-ene product in lower optical and chemical yields than (*R*)-BINOL does (Table 3, entry 3).

Another possibility was explored using racemic BINOL as an activator. Racemic BINOL was added to (*R*)-**2**, giving higher yield and enantioselectivity than that obtained without

Table 3. Asymmetric activation of enantiopure (*R*)-**2** [Eq. (15)].

Entry	BINOL	Yield [%]	<i>ee</i> [%]
1	–	19.8	94.5
2	<i>R</i>	82.1	96.8
3	<i>S</i>	48.0	86.0
4	\pm	69.2	95.7



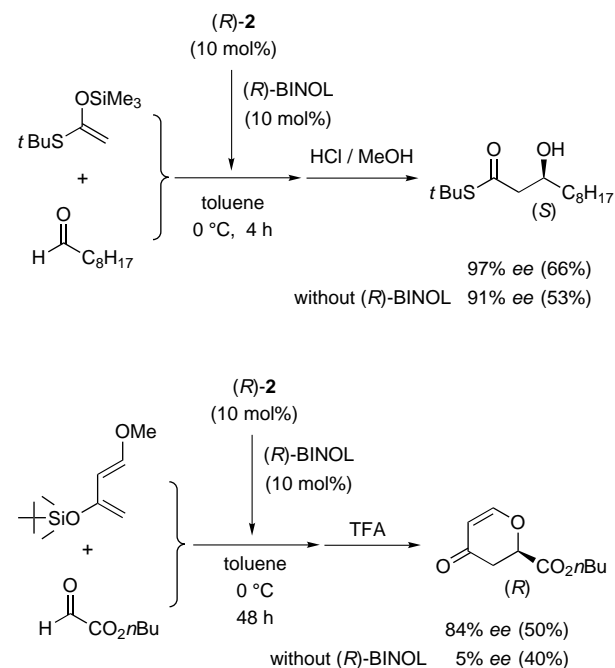
Scheme 11. Kinetic features of the asymmetric activation of BINOLato–Ti(OiPr)₂.

additional BINOL (compare entries 4 and 1 in Table 3). Comparison of the results from the racemic activator with those of enantiopure catalysts (R/R_{Act})-**2'** or (R/S_{Act})-**2'** (entry 4 compared with entries 2 and 3) shows that the reaction catalyzed by the (R/R_{Act})-**2'** complex is 8.8 times faster than that catalyzed by (R/S_{Act})-**2'** (Scheme 11 b). Kinetic studies also showed the reaction catalyzed by (R/R_{Act})-**2'** to be 9.2 ($=k_{\text{act}}/k'_{\text{act}}$) times faster than that catalyzed by (R/S_{Act})-**2'**.

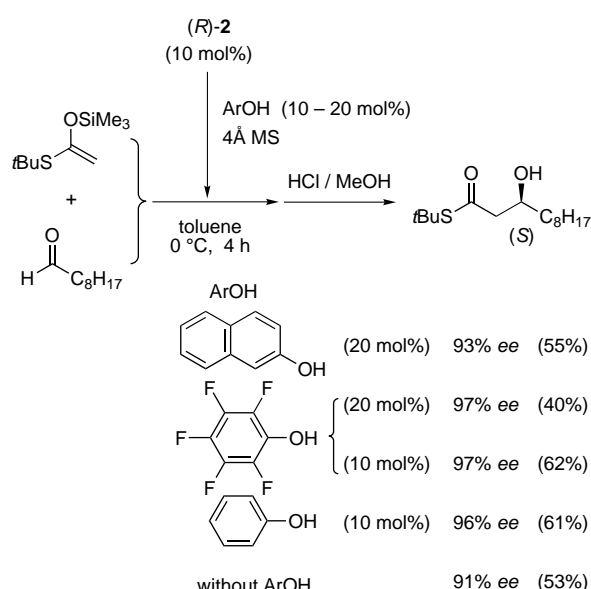
The great advantage of asymmetric activation with the racemic complex **2** is highlighted in a catalytic version (Table 2, entry 5). High enantioselectivity (80.0% *ee*) is obtained by adding less than the stoichiometric amount (0.25 mol% based on (\pm)-**2**) of additional (R)-BINOL. A similar phenomenon of enantioselective activation has been observed in aldol^[10a] and hetero Diels–Alder reactions,^[10c] catalyzed not only by a racemic but also by an enantiomerically pure BINOLato–Ti(O i Pr)₂ catalyst **2** (Scheme 12). Asymmetric activation of (R)-**2** by (R)-BINOL is essential to provide higher levels of enantioselectivity than those attained by the enantiopure catalyst **2** (84 instead of 5% *ee*) in the hetero Diels–Alder reaction of glyoxylates with the Danishefsky diene (Scheme 12 bottom).

Activation of **2** by phenolic alcohols as achiral rather than chiral activators^[10a, b] is also effective for providing higher levels of enantioselectivity than those attained by the parent enantiopure catalyst **2** in the Mukaiyama aldol reaction of silyl enol ethers (Scheme 13).^[60]

Catalytic asymmetric hydrogenation has been shown to be one of the most efficient processes for the asymmetric functional group transformation of organic molecules. Noyori and co-workers have reported a remarkable example of enantioselective catalysis by the enantiopure [RuCl₂(bi-*nap*)(dmf)_n] complex **3c** together with an enantiopure diamine and KOH to provide hydrogenation products of

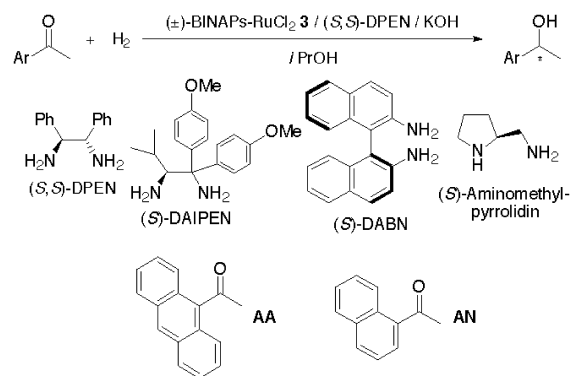


Scheme 12. Enantioselective activation of aldol and hetero Diels–Alder reactions.



Scheme 13. Enantioselectivity in the Mukaiyama aldol reaction of silyl enol ethers is improved by achiral activation.

carbonyl compounds with high enantioselectivity.^[11] We examined a variety of amines for asymmetric activation of a racemic BINAPs–RuCl₂ catalyst (**3**) for the enantioselective catalysis of the carbonyl hydrogenation (Scheme 14).^[61] The hydrogenation was performed in a mixture of racemic **3a**^[63] or **3b**,^[64] an enantiopure diamine, such as (S,S)- or (R,R)-1,2-diphenylethylenediamine (DPEN),^[65] and KOH in a ratio of 1:1:2, in a modification of the reported procedure with the enantiopure **3c** (Table 4^[62] and Scheme 14^[61]).



Scheme 14. Asymmetric activation of the racemic BINAPs–RuCl₂ catalyst **3** in the hydrogenation of carbonyl compounds. **a**: Ar = 4-methylphenyl (ligand = TolBINAP).^[63] **b**: Ar = 3,5-dimethylphenyl (ligand = Xylyl- or DM-BINAP).^[64] **c**: Ar = phenyl (ligand = BINAP). **AA** and **AN** are the ketones used in the asymmetric hydrogenation (see Tables 4 and 6).

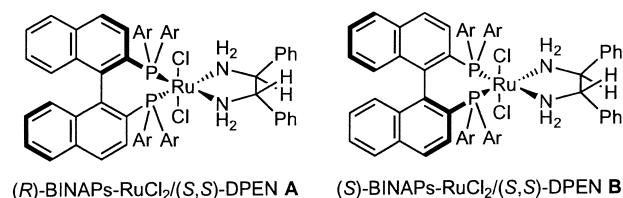
A chiral diamine leads to a nonracemic hydrogenation product, supporting the importance of chirality in the diamine activator for selective activation of one enantiomer of (\pm)-**3a** (compare entries 2 and 3). Thus, even the asymmetric activation of the racemic catalysts (\pm)-**3a** by the chiral diamine affords higher levels of asymmetric induction and catalytic activity than those attained by the enantiopure catalyst (+)-**3a** alone (compare entries 1 and 3). The enan-

Table 4. Asymmetric activation of racemic BINAPs-RuCl₂ catalyst **3** by enantiopure DPEN (Scheme 14).^[a]

Entry	3	<i>T</i> [°C]	<i>t</i> [h]	Yield [%]	<i>ee</i> [%]
1 ^[b]	(<i>R</i>)- 3a	28	18	2	29 (<i>S</i>)
2 ^[b]	(±)- 3a	28	18	< 1	0
3	(±)- 3a	28	18	28	80 (<i>R</i>)
4	(±)- 3a	80	10	99	80 (<i>R</i>)
5	(<i>R</i>)- 3a	80	10	99	81 (<i>R</i>)
6	(<i>S</i>)- 3a	80	10	91	40 (<i>R</i>)
7	(±)- 3b	28	4	99	80 (<i>R</i>)
8	(±)- 3b	−35	7	95	90 (<i>R</i>)
9 ^[c]	(±)- 3b	−35	7	90	90 (<i>R</i>)
10	(<i>S</i>)- 3b	28	4	99	> 99 (<i>R</i>)
11	(<i>R</i>)- 3b	28	4	99	56 (<i>S</i>)

[a] Under an H₂ atmosphere (8 atm). Catalyst **3a** was used in reactions with ketone **AA**, catalyst **3b** was used in reactions with ketone **AN** (see Scheme 14). Ketone:**3**:(*S,S*)-DPEN:KOH = 250:1:1:2. [b] In the absence of (*S,S*)-DPEN. [c] 0.5 mol % of (*S,S*)-DPEN was used based on the quantity of (±)-**3b**. **AN**:**3b**:DPEN:KOH = 250:1:0.5:2.

tioselectivity obtained by the (±)-**3a** and (*S,S*)-DPEN is very close to that obtained by the matched pair^[66] of (*R*)-**3**/(*S,S*)-DPEN complex (**A**; compare entry 4 with 5 and 6). However,

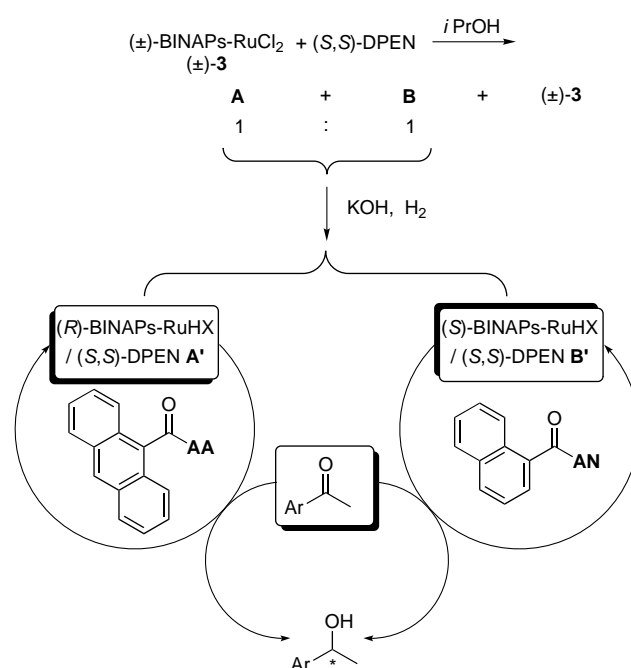


the matched pair is dramatically changed over on going from 9-acetylanthracene (**AA**) to 1'-acetonaphthone (**AN**; entries 7–11); in the latter case, the (*S*)-**3**/(*S,S*)-DPEN complex **B** is the more enantioselective combination (entries 10 and 11).

The dichotomous sense in enantioselectivity is determined by the ratio (which is 1:1 in this case though) and catalytic activity (turnover frequency) of mono- or dihydrido complexes^[67] **A'** and **B'**, which are derived from diastereomeric complexes **A** and **B**, respectively, under hydrogenation conditions (Scheme 15). It should be noted here that the catalytic activity critically depends on the nature of the carbonyl substrates. Interestingly, the use of a catalytic amount of diamine affords an equally high level of enantioselectivity to that obtained by an equimolar amount of diamine (Table 4, compare entries 9 and 8). Indeed, the ³¹P NMR spectrum of a mixture of (±)-**3a** and a catalytic amount of (*S,S*)-DPEN (0.5 mol % based on Ru) is identical to that of the 1:1 mixture, except for the remaining (±)-**3a** (entry 2).

6. The Continuum from Preferential Activation to Substrate Dependence

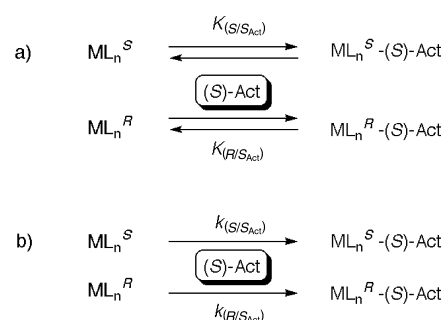
The asymmetric activation can be interpreted through a continuum from the preferential complexation with one enantiomer of the catalyst selectively giving the single, activated diastereomer, to the 1:1 complexation giving the



Scheme 15. Dichotomy in enantioselectivity shown by the diastereomeric BINAPs-RuHX/(*S,S*)-DPEN complexes **A'** and **B'** (X = H, Cl) for the conversions shown in Table 4.

activated diastereomeric mixture (1:1) of which the catalyst efficiency (turnover frequency) depends critically on the substrates employed.

For the sake of simplicity, the formation of the activated complexes can be discussed starting from the complexation of the chiral activator with racemic parent catalyst in monomeric form; this follows the thermodynamic and/or kinetic features (Scheme 16). 1) Under equilibrium conditions between the



Scheme 16. Formation of activated diastereomeric catalysts under thermodynamically (a) or kinetically (b) controlled conditions.

activated catalyst and the parent catalyst (Scheme 16a), the ratio of the activated diastereomeric catalysts depends on the thermodynamic stability. 2) Under nonequilibrium conditions, the ratio reflects the relative rate of the reaction of the enantiomeric catalyst with the chiral activator (Scheme 16b). Of course, the use of 1.0 equivalent of the activator per parent catalyst leads to a 1:1 mixture of the diastereomeric complexes. The kinetic or thermodynamic features described above are more apparent after treatment with less than 1.0 equivalent of the activator. Even with

0.5 equivalents of the activator, once a 1:1 mixture is formed, the relative activity of these activated diastereomeric catalysts to the substrate is the factor which determines the outcome, in terms of enantioselectivity, of the asymmetric reaction. In other words, the turnover efficiency of these activated diastereomers should be dependent on the complex with the substrate used.

Figure 7, for example, shows the variation of the relative rate $K_{\text{rel-act}}$ (logarithms from 0.01 to 100). In the case where

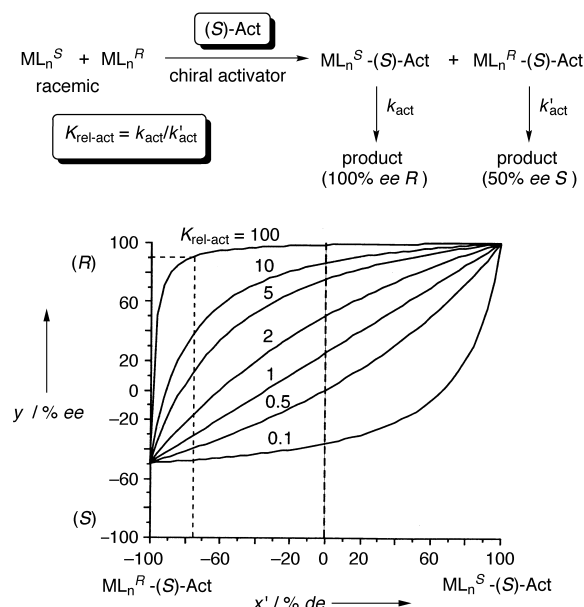


Figure 7. Influence of the *de* value of an activated diastereomeric catalyst (x') on the *ee* value y of the products in an asymmetric reaction with dependence upon $K_{\text{rel-act}}$.

one activated diastereomeric complex provides the product in 100% *ee* (*R*) and the other diastereomer provides the opposite enantiomeric product in 50% *ee* (*S*), if the relative rate of the two activated diastereomers is 100 ($\log K_{\text{rel-act}} = 2$), the product with more than 98% *ee* can be attained even when two activated diastereomer complexes are formed in 1:1 ratio (dotted line at 0% *de*). In a similar case, $K_{\text{rel-act}} = 100$, the product in more than 90% *ee* can be attained even in the presence of only 12.5% of the favorable diastereomer (dotted line at -75% *de*). Thermodynamically unstable and, hence, catalytically more active complexes may often be found.^[68] An alternative representation of a similar phenomenon can be drawn for the 1:1 formation of diastereomers. A relative rate of 14 ($\log K_{\text{rel-act}} = 1.15$) is sufficiently high to provide the desired product in more than 90% *ee* (Figure 8).

7. Asymmetric Activation/Deactivation of Racemic Catalysts

In an asymmetric deactivation strategy for racemic catalysis (Scheme 1, Part 1), enantioselective complexation and deactivation of a racemic catalyst with a chiral poison is indispensable (Scheme 1, Part 1a). Asymmetric activation is an alternative but conceptually opposite strategy to racemic catalysis, in which a chiral activator selectively activates one

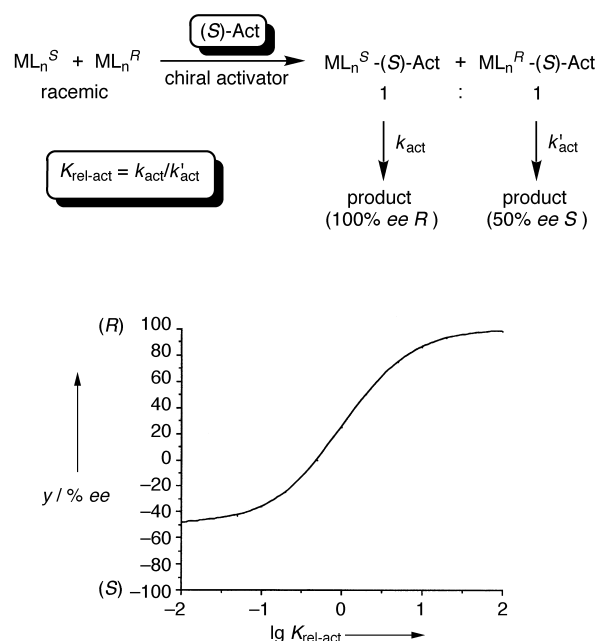


Figure 8. Influence of the relative rate $K_{\text{rel-act}}$ on the *ee* values of the products for an asymmetric reaction (shown above) catalyzed by an activated 1:1 diastereomeric mixture.

enantiomer of a racemic chiral catalyst (Scheme 1, Part 2). Significantly, asymmetric activation can also be established by nonpreferential complexation, to give activated diastereomeric catalysts (Scheme 1, Part 2b), when the turnover frequencies (catalytic activities) between the diastereomers ($k_{\text{act}} > k'_{\text{act}}$) are critically dependent on the substrates. In combination, an asymmetric activation/deactivation protocol can achieve higher enantioselectivity, regardless of the substrates (Scheme 1, Part 3), by maximizing the difference in catalytic activity between enantiomeric catalysts.^[69]

In Ru-catalyzed hydrogenation, the preferential complexation of (*S*)-BINAP-RuCl₂ with (*S*)-3,3'-dimethyl-2,2'-diamino-1,1'-binaphthyl (DM-DABN) was highly predictable by a modeling study (Figure 9a); the structure was confirmed by

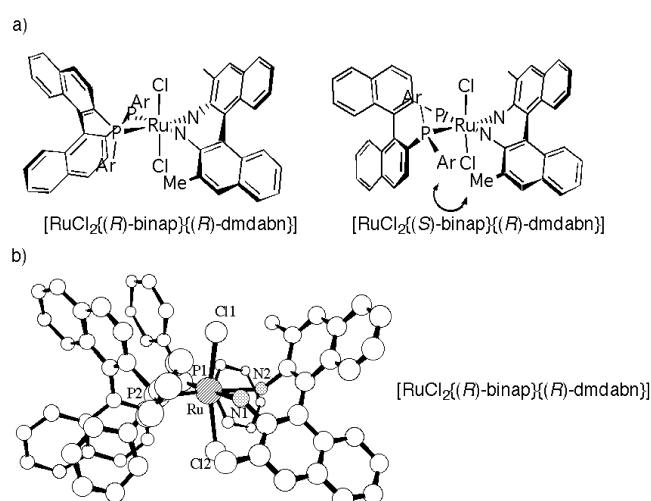
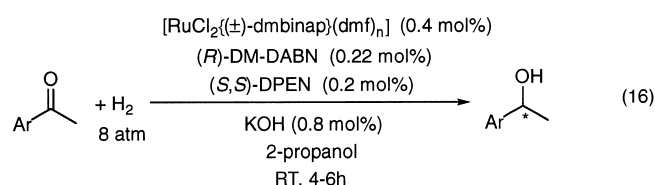


Figure 9. a) Model studies of the relative stability of diastereomeric $[\text{RuCl}_2(\text{binap})]\{(\text{S})\text{-dmdabn}\}$ complexes. The (*R*)-BINAP isomer is favored over the (*S*)-BINAP isomer. b) X-ray crystal structure analysis of $[\text{RuCl}_2(\text{binap})]\{(\text{R})\text{-dmdabn}\}$.

single-crystal X-ray analysis (Figure 9b). The addition of a racemic DM-BINAP-RuCl₂ species to one equivalent of (*R*)-DM-DABN resulted in preferential complexation into the single diastereomeric (*R*)-DM-BINAP-RuCl₂/(*R*)-DM-DABN complex. The remaining (*S*)-DM-BINAP-RuCl₂ enantiomer gave a different complex with the sequential addition of enantiopure (*S,S*)-DPEN. The two dichloro complexes with DM-DABN and DPEN may be further converted into mono- or dihydrido Ru species under hydrogenation conditions, while the DM-DABN complex is far less catalytically active under such conditions.

A racemic BINAP–Ru catalyst achieves higher enantioselectivity in carbonyl hydrogenation [Eq. (16)] using an activation/deactivation protocol (sequential addition of two different types of chiral diamines) than is attained by simple activation. The resultant (*R*)-DM-BINAP-RuCl₂/(*R*)-DM-DABN and (*S*)-DM-BINAP-RuCl₂/(*S,S*)-DPEN complexes give higher chiral efficiency than the racemic (±)-BINAP-



RuCl₂/(*S,S*)-DPEN (diastereomeric (*S*)-DM-BINAP-RuCl₂/(*S,S*)-DPEN and (*R*)-DM-BINAP-RuCl₂/(*S,S*)-DPEN) mixture. This asymmetric activation/deactivation strategy is also better than the simple asymmetric activation of the racemic BINAP–Ru catalyst, in terms of the wide scope of the ketonic substrates which can be accommodated by tuning the chirality of the activator employed. The enantioselectivity is higher than that obtained using the (±)-DM-BINAP-RuCl₂/(*S,S*)-DPEN complex at the same temperature and pressure (Table 5). Thus, the present asymmetric activation/deactivation protocol can be regarded as a paradigm shift in racemic catalysis by maximizing the difference in catalytic activity between enantiomeric catalysts.

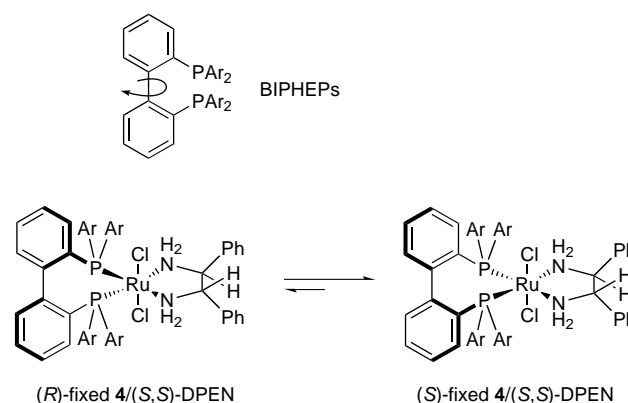
8. Asymmetric Activation of Catalyst with Chirally Flexible Ligands^[70]

An advanced strategy for asymmetric activation can be seen in using chirally flexible ligands that achieve higher enantioselectivity than that attained by chirally rigid and, hence, racemic ligands. As described in Section 5, combination of a racemic BINAPs–RuCl₂ **3** species with even half an equimolar amount of an enantiomerically pure diamine gives a 1:1 mixture of two diastereomeric **3**/DPEN complexes. When the chirally rigid BINAPs is replaced by a flexible^[71] and proatropisomeric BIPHEPs ligand (to form complex **4**),^[72] the diastereomeric complexes are formed, in principle, in unequal amounts (Scheme 17).^[73] When the major diastereomer shows higher chiral efficiency than the minor isomer, this strategy becomes more effective than the use of similar, but chirally rigid, analogues. The initially formed mixture of (*S*)- and (*R*)-**4b**/(*S,S*)-DPEN in [D₈]2-propanol (CDCl₃:

Table 5. Asymmetric activation/deactivation of DM-BINAP-RuCl₂ complex in Equation (16).

Entry	Ar	ee [%] ^[a]
1	1-naphthyl	96 (<i>R</i>) , 80 (<i>R</i>)
2	2-naphthyl	91 (<i>R</i>) , 45 (<i>R</i>)
3	phenyl	95 (<i>R</i>) , 70 (<i>R</i>)
4	2-tolyl	95 (<i>R</i>) , 82 (<i>R</i>)
5	3-tolyl	95 (<i>R</i>) , 60 (<i>R</i>)
6	4-tolyl	93 (<i>R</i>) , 60 (<i>R</i>)

[a] The ee values printed in bold were obtained with (*R*)-DM-DABN and those in normal type were obtained without. The yields for all the reactions were over 99 %.



Scheme 17. Stereomutation of BIPHEPs-RuCl₂/DPEN complexes **4**. **a**: Ar = phenyl (ligand = BIPHEP), **b**: Ar = 3,5-dimethylphenyl (ligand = Xylyl- or DM-BIPHEP).

(CD₃)₂CDOD = 1:2), when allowed to stand at room temperature (or at 80 °C), was found to give a 1:3 mixture of diastereomers, with (*S*)-**4b**/(*S,S*)-DPEN as the major component (Scheme 17). The equilibration occurred readily due to the conformational flexibility of the **4**/diamine complexes. The dichloro complexes may further be converted into active mono- or dihydrido Ru species under hydrogenation conditions.^[67]

The significant effect of the chirally flexible **4**/diamine complexes, in comparison with the enantioselectivity obtained using the **3b** catalyst, can be seen in the hydrogenation of 1'-acetonaphthone (**AN**; see Scheme 14). The enantioselectivity obtained with **4b** is higher than with the analogous **3b** (Table 6, compare entries 1 and 2). Further increase in enantioselectivity was attained at a lower reaction temperature (entry 3). The enantioselectivity attained with **4b**/(*S,S*)-DPEN was higher than with **3b**/(*S,S*)-DPEN complex at the same low temperature and high pressure (entry 4). Thus, (*R*)-1-(1-naphthyl)ethanol was obtained in quantitative yield with

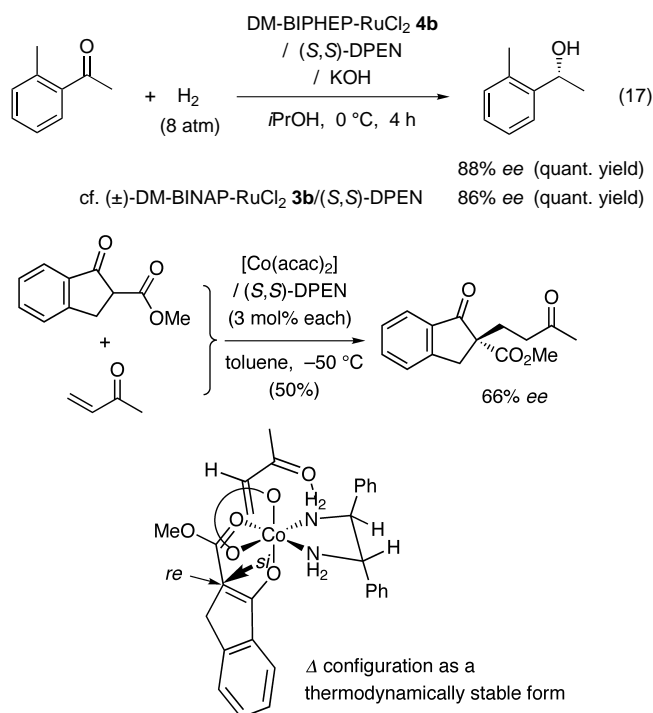
Table 6. BIPHEP ligand for enantioselective hydrogenation of **AN**.^[a]

Entry	Ligand	H ₂ [atm]	T [°C]	t [h]	ee [%]
1	4b	8	28	4	84
2 ^[b]	(±)- 3b	8	28	4	80
3	4b	40	–35	12	92
4 ^[b]	(±)- 3b	40	–35	7	

[a] **4**/(*S,S*)-DPEN in 2-propanol was preheated at 80 °C for 30 min; **3** was used without preheating. Ketone:ligand:(*S,S*)-DPEN:KOH = 250:1:1:2. Yields were greater than 99 % in all cases.

a 92% *ee* value. **4b**/(*S,S*)-DPEN was also useful in the reduction of *ortho*-methylacetophenone [Eq. (17)].

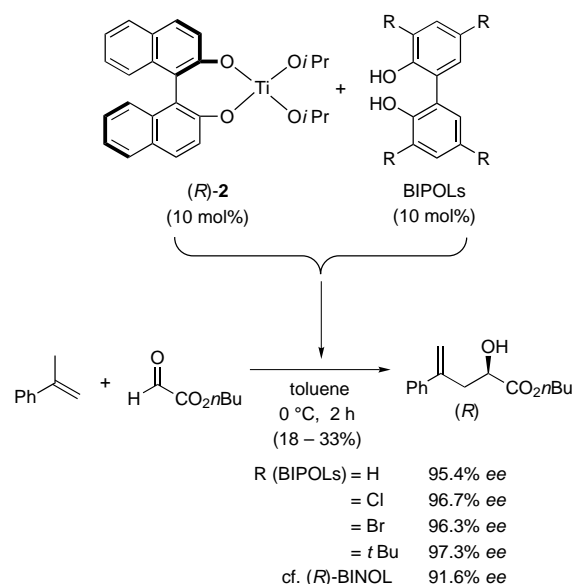
Brunner and Hammer have already reported the use of (*S,S*)-DPEN to control the chirality of the octahedral [Co^{II}(acac)₂]/diamine complex.^[70] This chiral complex [Co(acac)₂]{(*S,S*)-dpn} catalyzes the Michael addition reaction at –50 °C to give the product in up to 66% *ee* (Scheme 18).^[74] The *S,S* configuration of the DPEN ligand means the Δ conformation of the cobalt complex is thermodynamically more stable than the Λ conformation.^[70,75] Thus, the formation of *R* product is rationalized on the assumptions that the ketone group occupies an axial position and the ester group an equatorial one, and that methyl vinyl ketone is directed to the *Si* face of the ketoester complex by hydrogen bonding of the vinyl ketone oxygen to one of the NH groups (Scheme 18).



Scheme 18. Function of (*S,S*)-DPEN in the asymmetric Michael addition catalysed by [Co^{II}(acac)₂].

Self-organization of ligands in multicomponent titanium catalysts^[76] with conformationally flexible biphenols (BIPOLs) is also found in the enantioselective glyoxylate-ene reaction^[10b] to give significantly higher enantioselectivity (Scheme 19).^[77] Some molecular modeling studies reported that the hexacoordination of the titanium atom would make the central titanium atom a center of chirality and that the Λ isomer was more favorable than the Δ isomer (Figure 10).

Katsuki and co-workers extensively studied the asymmetric epoxidation of nonfunctionalized olefins catalyzed by chiral Mn(salen) complexes. Recently they proposed that the ligands of Mn(salen) complexes take a nonplanar, stepped conformation and the direction of the folding ligands is strongly related to the sense of chirality in the asymmetric epoxidation.^[78] On the basis of this proposal for conformational control by the achiral Mn(salen) complex, two enantio-



Scheme 19. Influence of the conformationally flexible biphenol BIPOLs on the enantioselectivity of the glyoxylate-ene reaction.

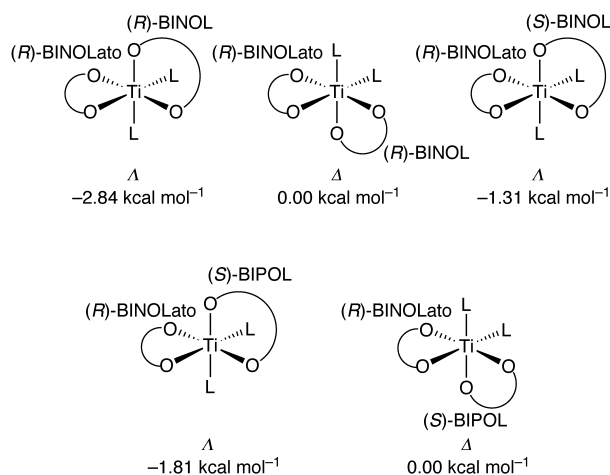
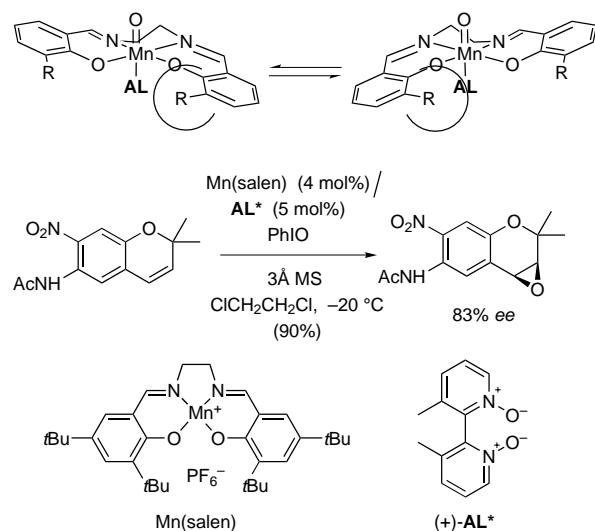


Figure 10. Relative energies of the Λ and Δ isomers of the complexes of (*R*)-BINOLato-Ti(O*i*Pr)₂ with BINOL or BIPOL (R = *t*Bu), L = O*i*Pr.

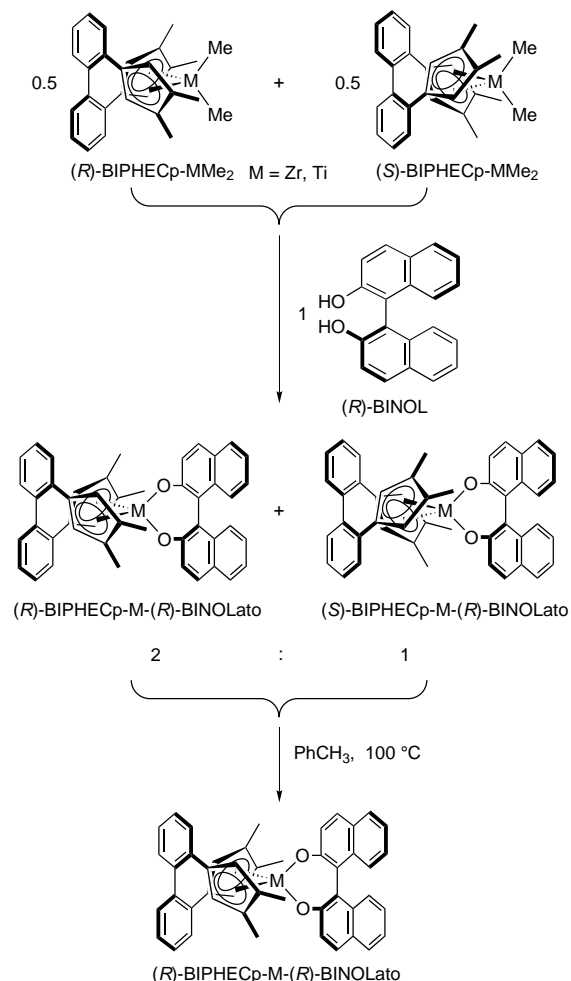
meric forms can be obtained by the use of chiral axial ligands AL*.^[79] In actual fact, the achiral Mn(salen) complex gave the epoxides in high enantiopurity in the presence of chiral bipyridine *N,N'*-dioxide which acts as an axial ligand (Scheme 20).

Chiral *ansa*-metallocene complexes have become useful catalysts in asymmetric polymerization reactions.^[80] While enantioresolution of *ansa*-metallocene racemates cannot yield more than 50% of a particular enantiomer, the readily accessible racemate of a biphenyl-bridged metallocene BIPHECp-M (M = Ti, Zr) has quite recently been reported to give enantiopure *ansa*-titanocene and -zirconocene complexes through BINOL-induced asymmetric transformation (Scheme 21).^[81] In the presence of *n*BuLi, the (*R*)-BIPHECp-TiCl₂ complex obtained was an efficient asymmetric catalyst of imine hydrogenation (Scheme 22).

Thus, the chirally rigid ligands can be replaced by flexible and, hence, proatropisomeric ligands to give preferentially the

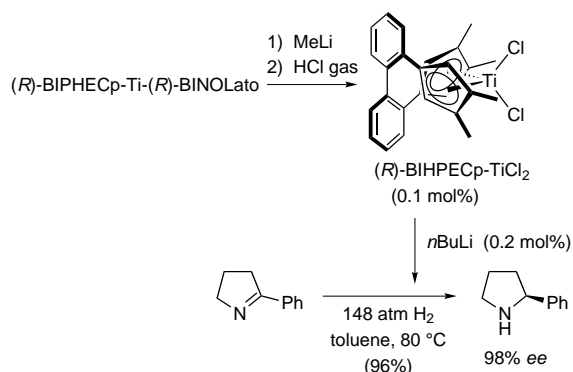


Scheme 20. Asymmetric activation of achiral Mn(salen) complexes.



Scheme 21. BINOL-induced asymmetric transformations of biphenyl-bridged metallocene complexes.

favorable diastereomer with higher chiral efficiency than the minor isomer. This strategy with flexible and proatropisomeric ligands becomes more beneficial than the use of structurally similar, but chirally rigid, ligands.

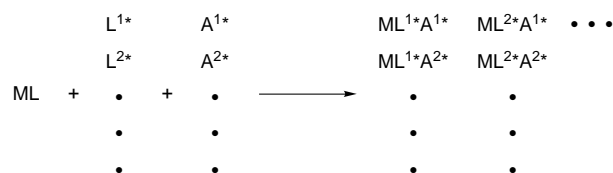


Scheme 22. Hydrogenation of imines with the titanium complex formed in Scheme 21 as a catalyst precursor.

9. High-Throughput Screening of Chiral Ligands and Activators

Combinatorial chemistry has been well recognized as a useful strategy for the discovery and optimization of bioactive drugs, coordination complexes, and solid-state materials.^[82] Between the split-and-mix and parallel-matrix methodologies for combinatorial chemistry, the latter is more employable for lead optimization, wherein the high-throughput screening (HTS) is an essential technique for tuning a variety of modulation.^[83] However, only a limited number of investigations has so far been reported, even on chiral ligand optimization for coordination complexes,^[84] due to the lack of HTS methods. In particular reactions, UV/Vis spectroscopy can be used; however, this gives only a rough estimation of hits.^[85] IR thermography can also be used for qualitative analysis.^[86] Quite recently, mass spectroscopy has been used to determine the enantiomeric excesses of limited types of samples.^[87] In the quantitative determination of *ee* values, high-performance liquid chromatography (HPLC) has long been used in combination with chirally modified columns to separate enantiomers. If the *ee* value can be determined using achiral columns, the separation of enantiomers using chiral columns would no longer be necessary. A circular dichroism method can be applied in the combinatorial search for enantioselective catalysts through asymmetric activation, using a JASCO-CD-995 (1595) instrument with achiral columns.^[88] This method involves the simultaneous monitoring of the CD signal ($\Delta\epsilon$), the absorption (ϵ), and their ratio to each other, called the dissymmetric or anisotropy factor g ($=\Delta\epsilon/\epsilon$), at a fixed wavelength in a flow system. The g -factor was introduced by Kuhn^[89] in 1930, refined by Mason and co-workers^[90] in 1980, and further developed by Salvadori et al.^[91] and Mannschreck.^[92] The g -factor is independent of concentration and is linearly related to the enantiomeric excess.^[93] With this technique, the *ee* value of the product could be determined within a minute on achiral stationary phases without separation of the enantiomeric products. Therefore, application of HPLC-CD provides a “super high throughput screening” (SHTS) system for finding the most effective catalyst through asymmetric activation.^[88] Chiral catalysts obtained by ligand exchange with chiral ligands (L^{1*} , L^{2*} , etc.) may be further developed, in parallel combination

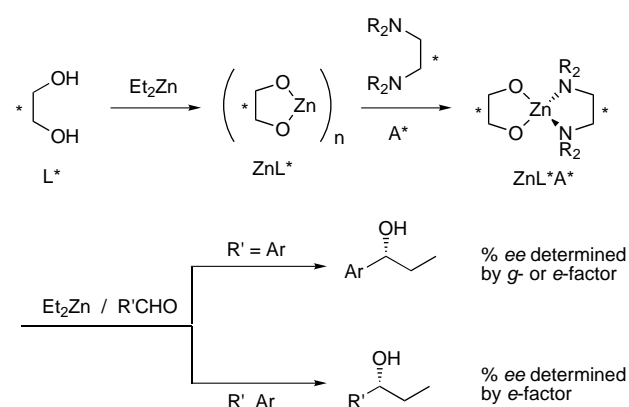
with chiral activators (A^{1*} , A^{2*} , etc.), to form the most catalytically active and enantioselectively activated catalyst (Scheme 23).



Scheme 23. General principle for the creation of a catalyst library of asymmetric activation catalysts.

The super high throughput screening (SHTS) of parallel solution libraries of activated catalysts by HPLC-CD is demonstrated for diol–Zn catalysts in the addition of diethylzinc to aldehydes. Amongst asymmetric catalysis of C–C bond forming reactions, enantioselective addition of diorganozinc reagents to aldehydes constitutes one of the most important and fundamental asymmetric reactions.^[11c, 7e, 94] Since the initial report by Oguni,^[95] various chiral ligands, including β -amino alcohols, have been used for this type of reaction. However, less attention has been paid to C_2 -symmetric binaphthol (BINOL) derivatives,^[96] despite their wide application as chiral ligands for B,^[97] Al,^[98] Ti,^[99] Zr,^[100] and Ln^[101] catalysts in, for example, enantioselective aldol and ene reactions. This is due to their lower catalytic activity and enantioselectivity for the organozinc addition reaction.^[102] Only very recently, some modified BINOLs^[103] were reported to be effective but the simple BINOL itself is less effective in the reaction.^[102]

It is reasonable to assume that the active catalyst species is a monomeric zinc alkoxide in the addition of diethylzinc to aldehydes; the cleavage of the higher aggregates could result in activation of the overall catalyst system (Scheme 24).^[14p, 104]

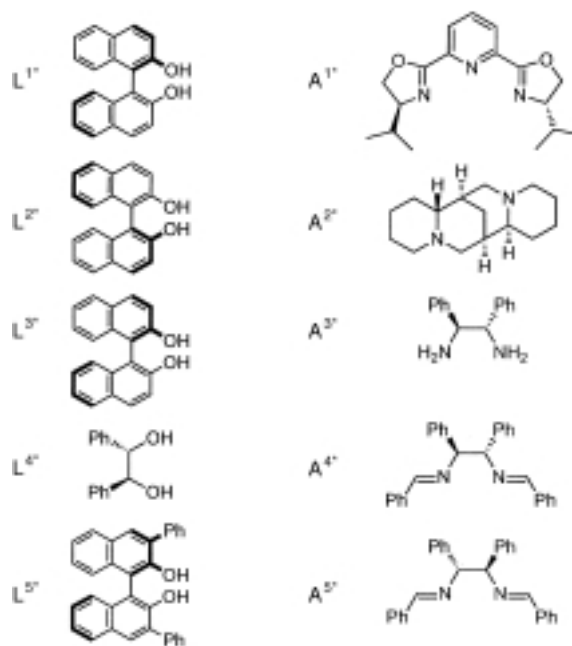


Scheme 24. Asymmetric activation of chiral diol–zinc catalysts by chiral nitrogen ligands.

The addition of chiral nitrogen activators should be one of the most efficient ways for activation of the BINOL–zinc catalyst system because of the strong coordinating ability of the nitrogen towards the zinc cation; this would facilitate the alkyl transfer. As a result, a monomeric zinc complex is expected to be formed in a similar manner to that of chiral salen–zinc

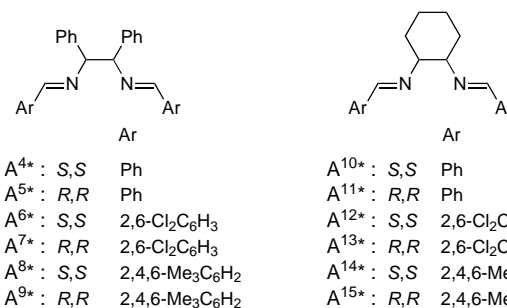
complexes.^[105] Furthermore, bimolecular combination of chiral activators with the diol–zinc complexes should be more convenient than the unimolecular combination. Thus, the primary combinatorial library of chiral ligands L^{1*} – L^{5*} and chiral activators A^{1*} – A^{5*} was initially examined, from which the leads can be further optimized for the next generation of the chiral ligands and activators.

An activation effect was actually observed in the random screening of chiral ligand/activator combinations. Enantioselectivity of the reaction is also increased by matched combinations of diol ligands and nitrogen activators. Substitution at the 3 and 3' positions with bulky phenyl groups, such as 3,3'-diphenyl-1,1'-bi-2-naphthol (L^{5*}), may further



prevent the aggregation of BINOLato–Zn because of their steric demands and may increase the enantioselectivity; (*S*)-1-phenylpropanol was obtained in quantitative yields with up to 65 % *ee*.

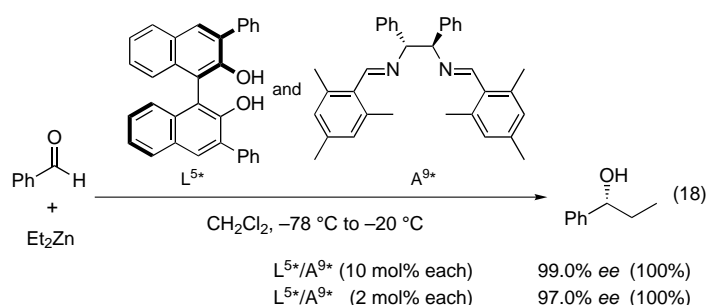
On the basis of the results collected from the primary combinatorial library, we then created the next generation library of diimine activators with twelve members A^{4*} – A^{15*} . All library members significantly activate the L^{5*} –Zn



complex and produce 1-phenylpropanol in higher yields and with higher enantioselectivities than those obtained by only using the ligand. The steric hindrance of the chiral activators is

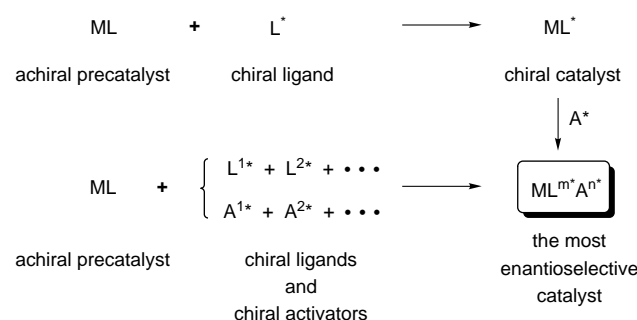
crucial, and hence the activator A^{9*} provides the best results. The reaction catalyzed by the best combination L^{5*}/A^{9*} is further optimized by lowering the reaction temperature. (*S*)-1-Phenylpropanol is obtained in quantitative yield and with 99% *ee* [Eq. (18)]. Even if only 2 mol % of L^{5*}/A^{9*} is used in the reaction, (*S*)-phenylpropanol can be obtained in quantitative yield and with 97% *ee*.

The best combination of chiral ligands and activators can easily be found in an efficient way by super high throughput screening (SHTS). The dissymmetry or anisotropy factor (*g*-factor) can be employed for UV-active aromatic compounds,^[88] and the optical rotation per refractive index unit or the enantiomeric factor (*e*-factor)^[106] can be used not only for UV-inactive aliphatic compounds or carbohydrates but also for UV-active aromatic compounds.



10. Smart Self-Assembly into the Most Enantioselective Catalyst

Sharpless and co-workers demonstrated the significance of ligand accelerated catalysis^[2] through the construction of an asymmetric catalyst from an achiral precatalyst by ligand exchange with a chiral ligand. By contrast, an achiral precatalyst combined with several chiral ligand components (L^{1*} , L^{2*} , etc.) may selectively assemble into the most catalytically active and enantioselectively activated catalyst ($ML^{m*}A^{n*}$) possible from the combinatorial library by association with chiral activators (A^{1*} , A^{2*} , etc.; Scheme 25).^[75]

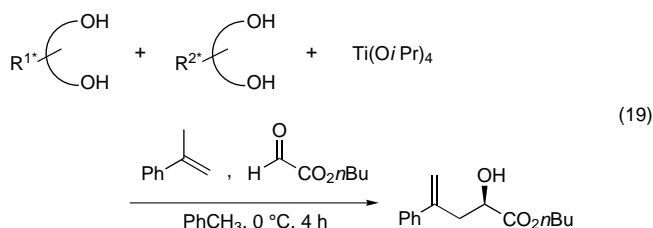


Scheme 25. General principle of ligand exchange based on smart self-assembly.

Two patterns of self-assembly are conceivable for an achiral precatalyst $Ti(OiPr)_4$ and couples of chiral diol components to form a single chiral titanium complex. In one case (Scheme 26a), a combination of acidic (*R*)-BINOL and a relatively basic diol, such as TADDOL,^[107] in a molar ratio of

1:1:1 suggests a push-pull assembly into a single (*R*)-BINO-Lato-Ti-(*R*)-TADDOLato complex **6a**; no isopropanol was observed after azeotropic removal with toluene. This complex **6a**, in the case of matched chirality, is obtained from (*R*)-TADDOLato-Ti(*OiPr*)₂ **5a** with (*R*)-BINOL or from (*R*)-BINOLato-Ti(*OiPr*)₂ **2** with (*R*)-TADDOL. In the other pattern (Scheme 26b), upon addition of (*R*)-BINOL and a more acidic diol (*R*)-5-Cl-BIPOL to $Ti(OiPr)_4$, the (*R*)-2/(*R*)-BIPOL complex **6b** is obtained. This complex is derived not only from **2**^[108] with 5-Cl-BIPOL^[10b] but also from 5-Cl-BIPOLato-Ti(*OiPr*)₂ **5b** with BINOL.

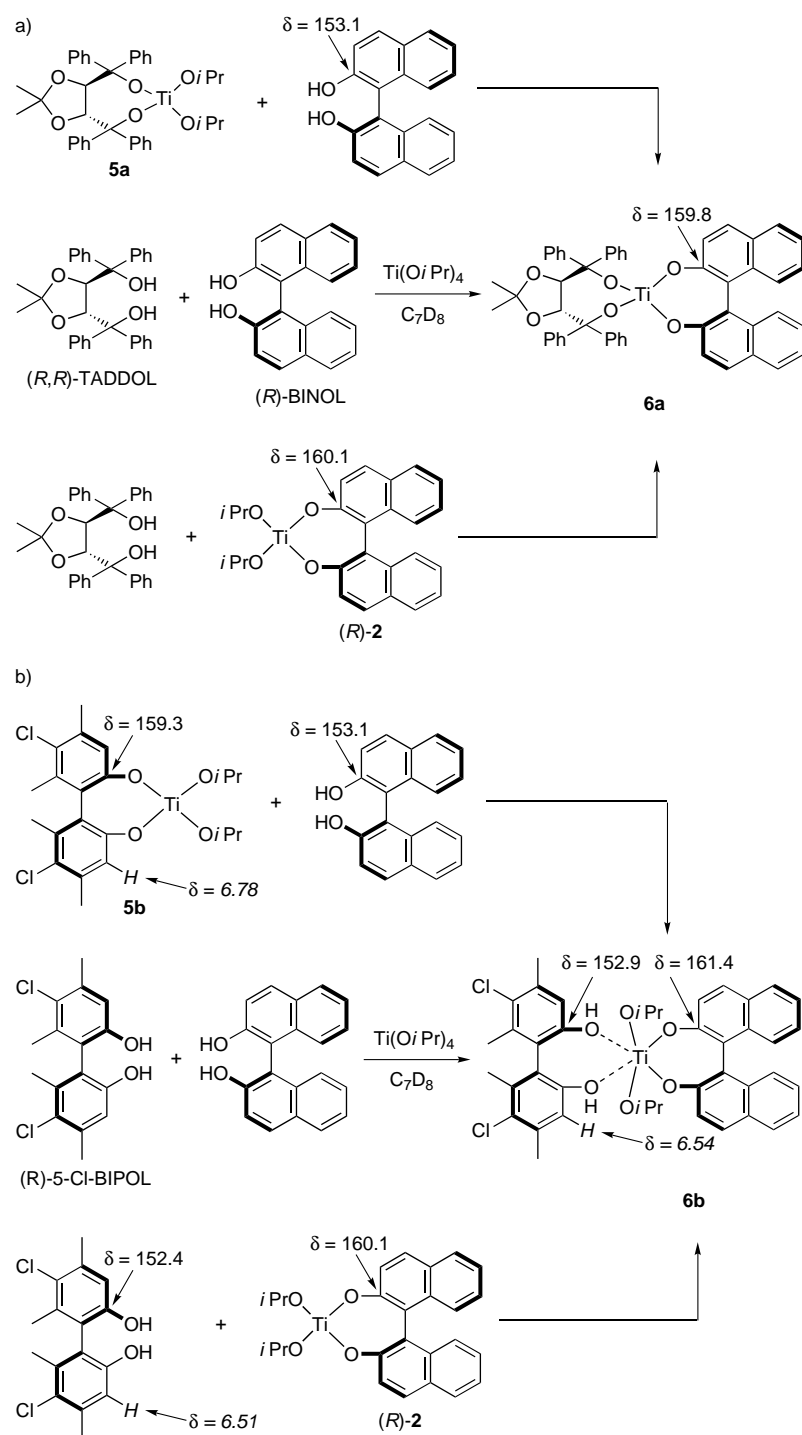
The role of multicomponent ligand assembly to form a highly enantioselective catalyst was exemplified in the investigation of enantioselective catalysis of the carbonyl-ene reaction [Eq. (19)]. The catalyst was prepared by mixing an



achiral precatalyst $Ti(OiPr)_4$ with a combination of BINOL and various chiral diols, such as TADDOL and 5-Cl-BIPOL, in a molar ratio of 1:1:1 (10 mol % with respect to the olefin and glyoxylate) in toluene (Table 7). A quantum jump in

Table 7. Asymmetric catalysis by multicomponent ligand-cooperation in the reaction shown in Equation (19).

Entry	$R^{1*}(\text{OH})_2$	$R^{2*}(\text{OH})_2$	Yield [%]	<i>ee</i> [%]
1			50	91
2		—	0	—
3			66	97
4		—	13	75
5		—	20	95



Scheme 26. Smart self-assembly of the highly activated Ti catalysts **6a** (a) and **6b** (b). The δ values refer to the ^{13}C (normal text) and ^1H (italicized text) NMR spectra. It is important in the characterization of **6a** that the *i*PrO signals are absent from the NMR spectra.

chemical yield from 0% to 50% was attained, in addition to a high enantioselectivity (91.0% *ee*, *R*), when a combination of (*R*)-TADDOL and (*R*)-BINOL was employed (compare entries 1 and 2). With a combination of (*R*)-BIPOL and (*R*)-BINOL, the reaction proceeded quite smoothly to produce the carbonyl-ene product in the highest chemical yield and with the highest enantioselectivity (entry 3). This finding is in direct contrast to the lower enantiomeric excesses and

chemical yields obtained with (*R*)-**5b** or (*R*)-**2** (entries 4 and 5, respectively).

Hill and Zhang reported the results of an elegant study in which smart self-assembly resulted in the creation of an achiral, “immortal” catalyst.^[109] We have reported an example of asymmetric catalysis through smart self-assembly into the most enantioselective chiral catalyst by virtue of multicomponent ligand cooperation. Thus, the present work represents chiral evolution from the studies of Hill and Zhang on an achiral catalyst.

11. Future Perspectives

Molecular chirality (handedness) is a principal element in nature that plays a key role in science and technology. Among various approaches to generate optically active molecules, asymmetric catalysis of organic reactions is the most efficient process. The candidates for such enantioselective catalysts are metal complexes bearing chiral and nonracemic organic ligands, often in enantiopure form. Therefore, tuning the catalysts to achieve the perfect match among chiral ligand, metallic ion, substrate, and chiral activator is the key for achieving the maximum chiral discrimination.

Catalytic systems that permit precise recognition among enantiotopic atoms, groups, or faces in prochiral substrates must be created efficiently by employment of chiral activators. Kagan stated that one must no more ignore the modern methods of combinatorial chemistry and high-throughput screening for finding the new catalyst or best catalyst tuned for asymmetric reactions.^[110]

Asymmetric activation (Scheme 1) will provide a general effective strategy for asymmetric catalysis involving even racemic or chirally flexible ligands without optical resolution. Not only chiral organic molecules but also chiral metal complexes can be used as chiral activators through heteromultimetallic activation. Asymmetric activation will be further employed as a new chiral doping technique in liquid crystalline material science. Furthermore, a chiral command surface might be built up as an alignment layer in the interface

between liquid crystalline and solid phases. Asymmetric activation may also be extended to solid-state processes or cluster chemistry. For example, the spontaneous crystallization (spontaneous resolution) of racemic mixtures could be facilitated by seeding with the crystals of one enantiomer. This could be done by a different but enantiopure molecule in the same, or a similar, crystalline structure as the seed. Asymmetric activation will be effective in molecular biology

processes. External chiral molecules may accelerate signal-transduction processes^[11] through association with a ligand/receptor complex. In the model system with the mutants of human growth hormone (hGH) and the hGH receptor, achiral indole analogues were employed as exogenous small molecules to activate growth hormone signaling.^[12]

We are grateful to Professor Ryoji Noyori and Professor Takeshi Ohkuma of Nagoya University for their generous collaboration on the BINAP–Ru catalyzed hydrogenation. We also thank our past and present students and co-workers listed in the references, particularly Dr. Satoru Matsukawa, now a research associate with Professor Tsuneo Imamoto at Chiba University, and Dr. Yukihiro Motoyama, now a research associate with Professor Hisao Nishiyama at the Toyohashi University of Technology & Science, for their contributions at the earliest stage of our research project on asymmetric activation.

Received: August 17, 1999 [A357]

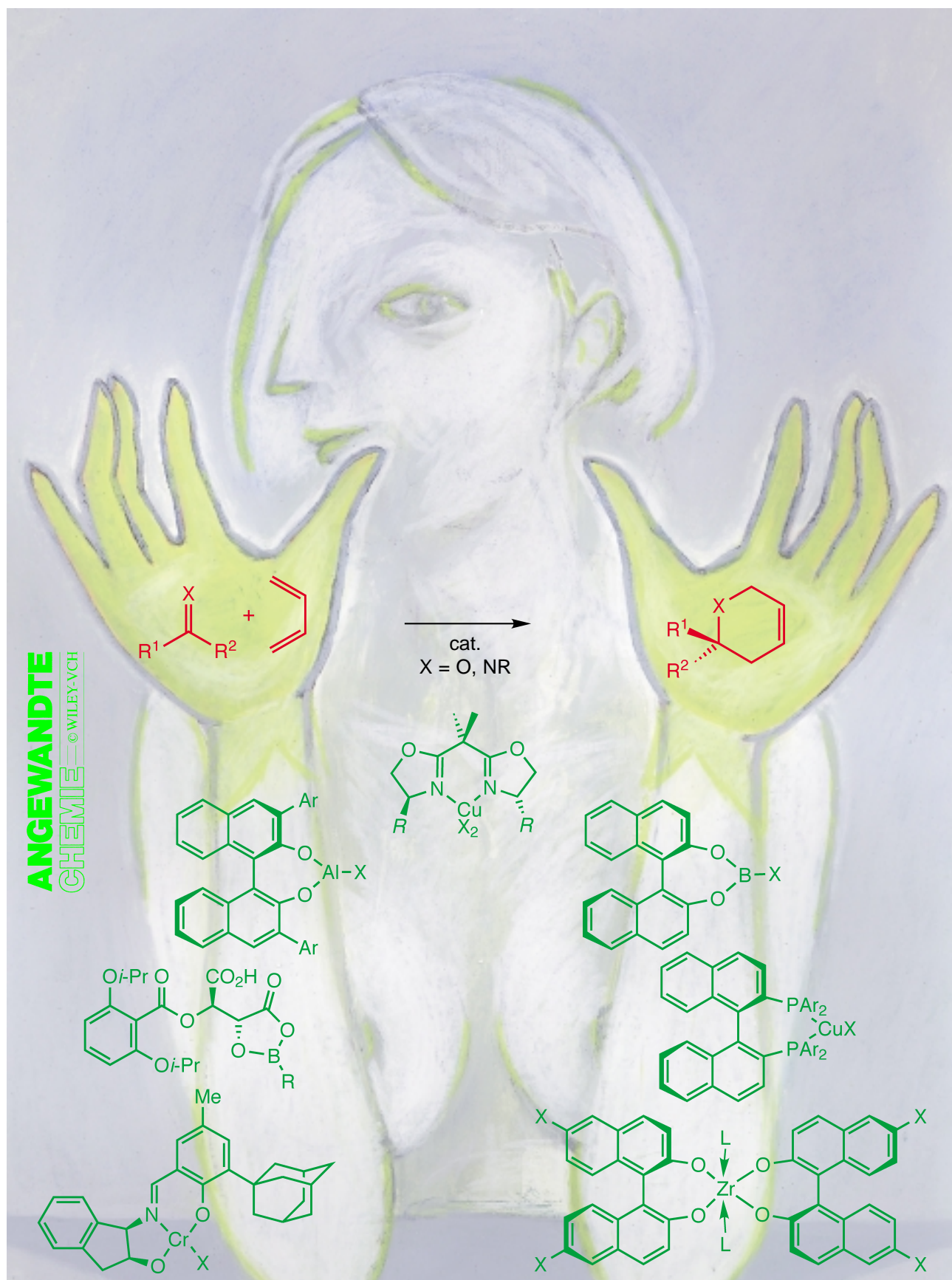
- [1] a) E. N. Jacobsen, A. Pfaltz, H. Yamamoto, *Comprehensive Asymmetric Catalysis*, Vol. 1–3, Springer, Berlin, **1999**; b) R. E. Gawley, J. Aube, *Principles of Asymmetric Synthesis*, Pergamon, London, **1996**; c) *Advances in Catalytic Processes*, Vol. 1 (Ed.: M. P. Doyle), JAI, London, **1995**; d) R. Noyori, *Asymmetric Catalysis in Organic Synthesis*, Wiley, New York, **1994**; e) H. Brunner, W. Zettlmeier, *Handbook of Enantioselective Catalysis*, VCH, Weinheim, **1993**; f) *Catalytic Asymmetric Synthesis* (Ed.: I. Ojima), VCH, New York, **1993**; g) H. B. Kagan, *Comprehensive Organic Chemistry*, Vol. 8, Pergamon, Oxford, **1992**; h) *Asymmetric Catalysis* (Ed.: B. Bosnich), Martinus Nijhoff, Dordrecht, **1986**.
- [2] D. J. Berrisford, C. Bolm, K. B. Sharpless, *Angew. Chem.* **1995**, *107*, 1159–1171; *Angew. Chem. Int. Ed. Engl.* **1995**, *34*, 1059–1070.
- [3] a) H.-U. Blaser, M. Müller, *Enantioselective Catalysis by Chiral Solids: Approaches and Results in Heterogeneous Catalysis and Fine Chemicals II* (Eds.: M. Guisnet, J. Barrault, C. Bouchoule, D. Duprez, G. Perot, M. Maurel, C. Montassier), Elsevier, Amsterdam, **1991**; b) H.-U. Blaser, *Tetrahedron: Asymmetry* **1991**, *2*, 843–866; c) M. Garland, H. U. Blaser, *J. Am. Chem. Soc.* **1990**, *112*, 7048–7050; d) J. L. Margitfalvi, P. Marti, A. Baiker, L. Botz, O. Sticher, *Catal. Lett.* **1990**, *6*, 281–288.
- [4] a) A. Pfaltz, T. Heinz, *Top. Catal.* **1997**, *4*, 229–239; b) M. Schurch, T. Heinz, R. Aeschimann, T. Mallat, A. Pfaltz, A. Baiker, *J. Catal.* **1998**, *173*, 187–195.
- [5] a) S. Akabori, S. Sakurai, Y. Izumi, Y. Fujii, *Nature* **1956**, *178*, 323–324; b) A. Akamatsu, Y. Izumi, S. Akabori, *Bull. Chem. Soc. Jpn.* **1962**, *35*, 1706–1711; c) Y. Izumi, M. Imaida, H. Fukawa, S. Akabori, *Bull. Chem. Soc. Jpn.* **1963**, *36*, 21–25; d) Y. Izumi, *Angew. Chem.* **1971**, *83*, 956–966; *Angew. Chem. Int. Ed. Engl.* **1971**, *10*, 871–881; e) A. Tai, T. Kikukawa, T. Sugimura, Y. Inoue, S. Abe, T. Osawa, T. Harada, *Bull. Chem. Soc. Jpn.* **1994**, *67*, 2473–2477; f) T. Sugimura, *Catal. Surf. Jpn.* **1999**, *3*, 37–42.
- [6] Reviews: a) R. D. Rieke, *Top. Curr. Chem.* **1975**, *59*, 1–31; b) E. Erdik, *Tetrahedron* **1987**, *43*, 2203–2212; c) P. Knochel, R. D. Singer, *Chem. Rev.* **1993**, *93*, 2117–2188; d) M. Nakamura, E. Nakamura, *J. Synth. Org. Chem. Jpn.* **1998**, *56*, 632–644. See, also: e) K. Takai, T. Kakiuchi, K. Uchimoto, *J. Org. Chem.* **1994**, *59*, 2668–2670; K. Takai, T. Kakiuchi, K. Uchimoto, *J. Org. Chem.* **1994**, *59*, 2671–2673.
- [7] Excellent reviews: a) C. Girard, H. B. Kagan, *Angew. Chem.* **1998**, *110*, 3088–3127; *Angew. Chem. Int. Ed.* **1998**, *37*, 2923–2959; b) M. Avalos, R. Babiano, P. Cintas, J. L. Jimenez, J. C. Palacios, *Tetrahedron: Asymmetry* **1997**, *8*, 2997–3017; c) H. B. Kagan, C. Girard, D. Guillaenoux, D. Rainford, O. Samuel, S. Y. Zhang, S. H. Zhao, *Acta Chem. Scand.* **1996**, *50*, 345–352; d) C. Bolm in *Advanced Asymmetric Synthesis* (Ed.: G. R. Stephenson), Blackie Academic, New York, **1996**, pp. 9–26; e) R. Noyori, M. Kitamura, *Angew. Chem.* **1991**, *103*, 34–55; *Angew. Chem. Int. Ed. Engl.* **1991**, *30*, 49–69.
- [8] a) N. W. Alcock, J. M. Brown, P. J. Maddox, *J. Chem. Soc. Chem. Commun.* **1986**, 1532–1534; b) J. M. Brown, P. J. Maddox, *Chirality* **1991**, *3*, 345–354; c) K. Maruoka, H. Yamamoto, *J. Am. Chem. Soc.* **1989**, *111*, 789–790. See also: K. Maruoka, T. Itoh, T. Shirasaka, H. Yamamoto, *J. Am. Chem. Soc.* **1988**, *110*, 310–312.
- [9] a) J. W. Faller, J. Parr, *J. Am. Chem. Soc.* **1993**, *115*, 804–805; b) J. W. Faller, M. R. Mazzieri, J. T. Nguyen, J. Parr, M. Tokunaga, *Pure Appl. Chem.* **1994**, *66*, 1463–1469; c) J. W. Faller, M. Tokunaga, *Tetrahedron Lett.* **1993**, *34*, 7359–7362; d) J. W. Faller, D. W. I. Sams, X. Liu, *J. Am. Chem. Soc.* **1996**, *118*, 1217–1218; e) J. W. Faller, X. Liu, *Tetrahedron Lett.* **1996**, *37*, 3449–3452; f) R. Sablong, J. A. Osborn, J. W. Faller, *J. Organomet. Chem.* **1997**, *527*, 65–70.
- [10] a) S. Matsukawa, K. Mikami, *Enantiomer* **1996**, *1*, 69–73; b) K. Mikami, S. Matsukawa, *Nature* **1997**, *385*, 613–615; c) S. Matsukawa, K. Mikami, *Tetrahedron: Asymmetry* **1997**, *8*, 815–816; d) T. Ohkuma, H. Doucet, T. Pham, K. Mikami, T. Korenaga, M. Terada, R. Noyori, *J. Am. Chem. Soc.* **1998**, *120*, 1086–1087.
- [11] a) T. Ohkuma, H. Ooka, S. Hashiguchi, T. Ikariya, R. Noyori, *J. Am. Chem. Soc.* **1995**, *117*, 2675–2676; b) T. Ohkuma, H. Ooka, T. Ikariya, R. Noyori, *J. Am. Chem. Soc.* **1995**, *117*, 10417–10418; c) T. Ohkuma, H. Ooka, M. Yamakawa, T. Ikariya, R. Noyori, *J. Org. Chem.* **1996**, *61*, 4872–4873; d) T. Ohkuma, H. Ikehira, T. Ikariya, R. Noyori, *Synlett* **1997**, 467–468; e) H. Doucet, T. Ohkuma, K. Murata, T. Yokozawa, M. Kozawa, E. Katayama, A. F. England, T. Ikariya, R. Noyori, *Angew. Chem.* **1998**, *110*, 1792–1796; *Angew. Chem. Int. Ed.* **1998**, *37*, 1703–1707.
- [12] a) D. Guillaenoux, S. H. Zhao, O. Samuel, D. Rainford, H. B. Kagan, *J. Am. Chem. Soc.* **1994**, *116*, 9430–9439; b) C. Puchot, O. Samuel, E. Duñach, S. Zhao, C. Agami, H. B. Kagan, *J. Am. Chem. Soc.* **1986**, *108*, 2353–2357.
- [13] a) M. Terada, K. Mikami, T. Nakai, *J. Chem. Soc. Chem. Commun.* **1990**, 1623–1624; b) K. Mikami, M. Terada, *Tetrahedron* **1992**, *48*, 5671–5680; c) M. Terada, K. Mikami, *J. Chem. Soc. Chem. Commun.* **1994**, 833–834; d) K. Mikami, Y. Motoyama, M. Terada, *Inorg. Chim. Acta* **1994**, *222*, 71–75.
- [14] See Ref. [12], [13], [16], [17], and [19–29]. Some other precedent examples involving negative nonlinear effects [(–)NLE]: Titanium: a) N. Iwasawa, Y. Hayashi, H. Sakurai, K. Narasaka, *Chem. Lett.* **1989**, 1581–1584; b) M. Hayashi, T. Matsuda, N. Oguni, *J. Chem. Soc. Chem. Commun.* **1990**, 1364–1365; M. Hayashi, T. Matsuda, N. Oguni, *J. Chem. Soc. Perkin Trans. 1* **1992**, 3135–3140; c) N. Komatsu, M. Hashizume, T. Sugita, S. Uemura, *J. Org. Chem.* **1993**, *58*, 4529–4533; N. Komatsu, M. Hashizume, T. Sugita, S. Uemura, *J. Org. Chem.* **1993**, *58*, 7624–7626; d) D. Seebach, R. Dahinden, R. E. Marti, A. K. Beck, D. A. Plattner, F. N. M. Kuhnle, *J. Org. Chem.* **1995**, *60*, 1788–1799; D. Seebach, R. E. Marti, T. Hintermann, *Helv. Chim. Acta* **1996**, *79*, 1710–1740; e) D. Kitamoto, H. Imma, T. Nakai, *Tetrahedron Lett.* **1995**, *36*, 1861–1864; f) P. Bedeschi, S. Casolari, A. L. Costa, E. Tagliavini, A. Umani-Ronchi, *Tetrahedron Lett.* **1995**, *36*, 7897–7900; g) D. R. Gauthier, Jr., E. M. Carreira, *Angew. Chem.* **1996**, *108*, 2521–2523; *Angew. Chem. Int. Ed. Engl.* **1996**, *35*, 2363–2365; zirconium: h) B. W. McClelland, W. A. Nugent, M. G. Finn, *J. Org. Chem.* **1998**, *63*, 6656–6666; nickel: i) A. H. M. de Vries, J. F. G. A. Jansen, B. L. Feringa, *Tetrahedron* **1994**, *50*, 4479–4491; j) U. Nagel, H. G. Nedden, *Chem. Ber.* **1997**, *130*, 535–542; copper: k) B. E. Rossiter, G. Miao, N. M. Swingle, M. Eguchi, A. E. Hernández, R. G. Patterson, *Tetrahedron: Asymmetry* **1992**, *3*, 231–234; B. E. Rossiter, M. Eguchi, G. Miao, N. M. Swingle, A. E. Hernández, D. Vickers, E. Flückiger, R. G. Patterson, K. V. Reddy, *Tetrahedron* **1993**, *49*, 965–986; l) G. van Koten, *Pure Appl. Chem.* **1994**, *66*, 1455–1462; m) Q.-L. Zhou, A. Pfaltz, *Tetrahedron* **1994**, *50*, 4467–4478; n) C. Zondervan, B. L. Feringa, *Tetrahedron: Asymmetry* **1996**, *7*, 1895–1898; zinc: o) C. Bolm, G. Schlingloff, K. Harms, *Chem. Ber.* **1992**, *125*, 1191–1203; p) C. Bolm, J. Müller, G. Schlingloff, M. Zehnder, M. Neuburger, *J. Chem. Soc. Chem. Commun.* **1993**, 182–183; C. Bolm, J. Müller, *Tetrahedron* **1994**, *50*, 4355–4362; q) K. Fitzpatrick, R. Hulst, R. M. Kellogg, *Tetrahedron: Asymmetry* **1995**, *6*, 1861–1864; r) T. Wirth, K. J. Kulicke, G. Fragale, *Helv. Chim. Acta* **1996**, *79*, 1957–1966; s) M. Shimizu, Y. Ukaji, K. Inomata, *Chem. Lett.* **1996**, 455–456; t) J. Kang, J. B. Kim, J. W. Kim,

- D. Lee, *J. Chem. Soc. Perkin Trans. 2* **1997**, 189–194; u) E. Rijnberg, N. J. Hovestad, A. W. Kleij, J. T. B. H. Jastrzebski, J. Boersma, M. D. Janssen, A. L. Spek, G. van Koten, *Organometallics* **1997**, *16*, 2847–2857; v) P. I. Dosa, G. C. Fu, *J. Am. Chem. Soc.* **1998**, *120*, 445–446; w) Y.-J. Cherng, J.-M. Fang, T.-J. Lu, *J. Org. Chem.* **1999**, *64*, 3207–3212; lanthanides: x) D. A. Evans, S. G. Nelson, M. R. Gagne, A. R. Muci, *J. Am. Chem. Soc.* **1993**, *115*, 9800–9801; y) H. Sasai, T. Suzuki, N. Itoh, M. Shibasaki, *Tetrahedron Lett.* **1993**, *34*, 851–854; z) S. Kobayashi, H. Ishitani, M. Araki, I. Hachiya, *Tetrahedron Lett.* **1994**, *35*, 6325–6328; S. Kobayashi, H. Ishitani, I. Hachiya, M. Araki, *Tetrahedron* **1994**, *50*, 11623–11636; aa) M. Bougauchi, S. Watanabe, T. Arai, H. Sasai, M. Shibasaki, *J. Am. Chem. Soc.* **1997**, *119*, 2329–2330; ab) V. K. Aggarwal, A. Mereu, G. J. Tarver, R. McCague, *J. Org. Chem.* **1998**, *63*, 7183–7189; osmium: ac) S. Y. Zhang, C. Girard, H. B. Kagan, *Tetrahedron: Asymmetry* **1995**, *6*, 2637–2640; lithium: ad) M. J. Sodergren, P. G. Andersson, *J. Am. Chem. Soc.* **1998**, *120*, 10760–10761; boron: ae) P. Simpson, D. Tschaen, T. R. Verhoeven, *Synth. Commun.* **1991**, *21*, 1705–1714; A. O. King, E. G. Corley, R. K. Anderson, R. D. Larsen, T. R. Verhoeven, P. J. Reider, Y. B. Xiang, M. Belley, Y. Leblanc, M. Labelle, P. Prasit, R. J. Zamboni, *J. Org. Chem.* **1993**, *58*, 3731–3735; I. Shinkai, A. O. King, R. D. Larsen, *Pure Appl. Chem.* **1994**, *66*, 1551–1556; M. Zhao, A. O. King, R. D. Larsen, T. R. Verhoeven, P. J. Reider, *Tetrahedron Lett.* **1997**, *38*, 2641–2644; af) C. Girard, H. B. Kagan, *Tetrahedron: Asymmetry* **1995**, *6*, 1881–1884; C. Girard, H. B. Kagan, *Tetrahedron: Asymmetry* **1997**, *8*, 3851–3854; aluminum: ag) G. Naraku, K. Hori, Y. N. Ito, T. Katsuki, *Tetrahedron Lett.* **1997**, *38*, 8231–8232; proline: ah) C. Agami, C. Puchot, *J. Mol. Catal.* **1986**, *38*, 341–343; C. Agami, *Bull. Soc. Chim. Fr.* **1988**, 499–507.
- [15] Chirality amplification has been used in chiroptical methods: E. L. Eliel, S. H. Wilen, L. N. Mander, *Stereochemistry of Organic Compounds*, Wiley, New York, **1994**, Chap. 13, p. 1057–1059.
- [16] N. Oguni, Y. Matsuda, T. Kaneko, *J. Am. Chem. Soc.* **1988**, *110*, 7877–7877.
- [17] a) M. Kitamura, S. Okada, S. Suga, R. Noyori, *J. Am. Chem. Soc.* **1989**, *111*, 4028–4036; b) M. Kitamura, S. Suga, M. Niwa, R. Noyori, *J. Am. Chem. Soc.* **1995**, *117*, 4832–4842; c) M. Kitamura, M. Yamakawa, H. Oka, S. Suga, R. Noyori, *Chem. Eur. J.* **1996**, *2*, 1173–1181; d) M. Kitamura, S. Suga, H. Oka, R. Noyori, *J. Am. Chem. Soc.* **1998**, *120*, 9800–9809; e) M. Kitamura, H. Oka, R. Noyori, *Tetrahedron* **1999**, *55*, 3605–3614.
- [18] Reviews: a) K. Mikami, T. Nakai in *Catalytic Asymmetric Synthesis*, 2nd ed. (Ed.: I. Ojima), Wiley-VCH, Weinheim, **2000**, pp. 543–569; b) K. Mikami, M. Terada in *Comprehensive Asymmetric Catalysis*, Vol. 3 (Eds.: E. N. Jacobsen, A. Pfaltz, H. Yamamoto), Springer, Heidelberg, **1999**, pp. 1143–1174; c) K. Mikami, M. Shimizu, *Chem. Rev.* **1992**, *92*, 1021–1050; d) B. B. Snider, *Comprehensive Organic Synthesis*, Vol. 2 (Eds.: B. M. Trost, I. Fleming), Pergamon, London, **1991**, pp. 527–561; e) K. Mikami, M. Terada, M. Shimizu, T. Nakai, *J. Synth. Org. Chem. Jpn.* **1990**, *48*, 292–303.
- [19] C. Bolm, *Tetrahedron: Asymmetry* **1991**, *2*, 701–704; C. Bolm, M. Ewald, M. Felder, *Chem. Ber.* **1992**, *125*, 1205–1215; C. Bolm, M. Felder, J. Müller, *Synlett* **1992**, 439–441.
- [20] S. Kanemasa, Y. Oderaotoshi, S. Sakaguchi, H. Yamamoto, J. Tanaka, E. Wada, D. P. Curran, *J. Am. Chem. Soc.* **1998**, *120*, 3074–3088.
- [21] Diels–Alder: a) D. A. Evans, S. J. Miller, T. Lectka, *J. Am. Chem. Soc.* **1993**, *115*, 6460–6461; b) D. A. Evans, J. A. Murry, P. von Matt, R. D. Norcross, S. J. Miller, *Angew. Chem.* **1995**, *107*, 864–866; *Angew. Chem. Int. Ed. Engl.* **1995**, *34*, 798–800; aldol: c) D. A. Evans, J. A. Murry, *J. Am. Chem. Soc.* **1996**, *118*, 5814–5815; d) D. A. Evans, M. C. Kozlowski, C. S. Burgey, D. W. C. MacMillan, *J. Am. Chem. Soc.* **1997**, *119*, 7893–7894; e) D. A. Evans, C. S. Burgey, M. C. Kozlowski, S. W. Tregay, *J. Am. Chem. Soc.* **1999**, *121*, 686–699; hetero Diels–Alder: f) D. A. Evans, E. J. Olhava, J. S. Johnson, J. M. Janey, *Angew. Chem.* **1998**, *110*, 3554–3557; *Angew. Chem. Int. Ed.* **1998**, *37*, 3372–3375; g) D. A. Evans, J. S. Johnson, *J. Am. Chem. Soc.* **1998**, *120*, 4895–4896; ene: h) D. A. Evans, C. S. Burgey, N. A. Paras, T. Vojkovsky, S. W. Tregay, *J. Am. Chem. Soc.* **1998**, *120*, 5824–5825; Michael: i) D. A. Evans, T. Rovis, M. C. Kozlowski, J. S. Tedrow, *J. Am. Chem. Soc.* **1999**, *121*, 1994–1995.
- [22] D. A. Evans, M. C. Kozlowski, J. A. Murry, C. S. Burgey, K. R. Campos, B. T. Connell, R. J. Staples, *J. Am. Chem. Soc.* **1999**, *121*, 669–685. See also: D. A. Evans, T. Lectka, S. J. Miller, *Tetrahedron Lett.* **1993**, *34*, 7027–7030.
- [23] J.-M. Brunel, T. O. Luukas, H. B. Kagan, *Tetrahedron: Asymmetry* **1998**, *9*, 1941–1946.
- [24] a) K. Tanaka, J. Matsui, Y. Kawabata, H. Suzuki, A. Watanabe, *J. Chem. Soc. Chem. Commun.* **1991**, 1632–1634; b) K. Tanaka, J. Matsui, H. Suzuki, *J. Chem. Soc. Perkin Trans. 1* **1993**, 153–157.
- [25] K. Mikami, Y. Motoyama, M. Terada, *J. Am. Chem. Soc.* **1994**, *116*, 2812–2820.
- [26] a) G. E. Keck, D. Krishnamurthy, M. C. Grier, *J. Org. Chem.* **1993**, *58*, 6543–6544; b) G. E. Keck, D. Krishnamurthy, *J. Am. Chem. Soc.* **1995**, *117*, 2363–2364.
- [27] Linear relationship as a probe for the stereodetermining step: a) B. Schmidt, D. Seebach, *Angew. Chem.* **1991**, *103*, 1383–1385; *Angew. Chem. Int. Ed. Engl.* **1991**, *30*, 1321–1323; b) T. Schwenkreis, A. Berkessel, *Tetrahedron Lett.* **1993**, *34*, 4785–4788; c) M. A. Giardello, V. P. Conticello, L. Bard, M. R. Gagne, T. J. Marks, *J. Am. Chem. Soc.* **1994**, *116*, 10241–10254; d) C. Bolm, F. Bienewald, *Angew. Chem.* **1995**, *107*, 2883–2885; *Angew. Chem. Int. Ed. Engl.* **1995**, *34*, 2640–2642; e) D. J. Ramon, G. Guillena, D. Seebach, *Helv. Chim. Acta* **1996**, *79*, 875–894; f) M. Yamaguchi, T. Shiraishi, M. Hiram, *J. Org. Chem.* **1996**, *61*, 3520–3530; g) S. E. Denmark, B. L. Christenson, S. P. O'Connor, *Tetrahedron Lett.* **1995**, *36*, 2219–2222; h) P. I. Dosa, J. C. Ruble, G. C. Fu, *J. Org. Chem.* **1997**, *62*, 444–445; i) M. Mori, T. Nakai, *Tetrahedron Lett.* **1997**, *38*, 6233–6236; j) C. Guo, J. Qiu, X. Zhang, D. Verdugo, M. L. Larter, R. Christie, P. Kenney, P. J. Walsh, *Tetrahedron* **1997**, *53*, 4145–4158; k) D. J. Ramon, M. Yus, *Tetrahedron* **1998**, *54*, 5651–5666; l) S. Pritchett, D. H. Woodmansee, P. Gantzel, P. J. Walsh, *J. Am. Chem. Soc.* **1998**, *120*, 6423–6424; m) A. Ford, S. Woodward, *Angew. Chem.* **1999**, *111*, 347–349; *Angew. Chem. Int. Ed.* **1999**, *38*, 335–336; n) K. B. Simonsen, P. Bayon, R. G. Hazell, K. V. Gothelf, K. A. Jorgensen, *J. Am. Chem. Soc.* **1999**, *121*, 3845–3853; o) D. A. Evans, J. S. Johnson, C. S. Burgey, K. R. Campos, *Tetrahedron Lett.* **1999**, *40*, 2879–2882.
- [28] a) K. B. Hansen, J. L. Leighton, E. N. Jacobsen, *J. Am. Chem. Soc.* **1996**, *118*, 10924–10925; b) R. G. Konsler, J. Karl, E. N. Jacobsen, *J. Am. Chem. Soc.* **1998**, *120*, 10780–10781.
- [29] S. E. Denmark, X. Su, Y. Nishigaichi, *J. Am. Chem. Soc.* **1998**, *120*, 12990–12991.
- [30] a) D. G. Blackmond, *J. Am. Chem. Soc.* **1997**, *119*, 12934–12939; b) D. G. Blackmond, *J. Am. Chem. Soc.* **1998**, *120*, 13349–13353; c) D. G. Blackmond, *Acc. Chem. Res.* **2000**, *33*, 402–411.
- [31] Comprehensive reviews: a) W. A. Bonner in *Topics in Stereochemistry*, Vol. 18 (Eds.: E. L. Eliel, S. H. Wilen), Wiley, New York, **1988**, pp. 1–96; b) M. Calvin, *Chemical Evolution*, Oxford University Press, Oxford, **1969**, pp. 149–152; c) P. Decker in *Origins of Optical Activity in Nature* (Ed.: D. C. Walker), Elsevier, New York, **1977**, pp. 109–124.
- [32] a) M. Avalos, R. Babiano, P. Cintas, J. L. Jimenez, J. C. Palacios, L. D. Barron, *Chem. Rev.* **1998**, *98*, 2391–2404; b) S. F. Mason, G. E. Tranter, *Chem. Phys. Lett.* **1983**, *94*, 34–37; c) S. F. Mason, G. E. Tranter, *J. Chem. Soc. Chem. Commun.* **1983**, 117–119.
- [33] In quartz, selective adsorption of one enantiomer has been reported: P. R. Kavasmaneck, W. A. Bonner, *J. Am. Chem. Soc.* **1977**, *99*, 44–50. Quartz-promoted highly enantioselective synthesis of a chiral organic compound: K. Soai, S. Osanai, K. Kadowaki, S. Yonekubo, T. Shibata, I. Sato, *J. Am. Chem. Soc.* **1999**, *121*, 11235–11236.
- [34] Interestingly, the slight natural predominance (50.69%) is favored for the L crystalline form of quartz: S. F. Mason, *Int. Rev. Phys. Chem.* **1983**, 217–241.
- [35] a) Reviews: O. Buchardt, *Angew. Chem.* **1974**, *86*, 222–228; *Angew. Chem. Int. Ed. Engl.* **1974**, *13*, 179–185; H. Rau, *Chem. Rev.* **1983**, *83*, 535–547; b) N. P. M. Huck, W. F. Jager, B. de Lange, B. L. Feringa, *Science* **1996**, *273*, 1686–1688; J. Bailey, A. Chrysostomou, J. H. Hough, T. M. Gledhill, A. McCall, S. Clark, F. Menard, M. Tamura, *Science* **1998**, *281*, 672–674.
- [36] a) G. Zadel, C. Eisenbaun, G.-J. Wolff, E. Breitmaier, *Angew. Chem.* **1994**, *106*, 460–462; *Angew. Chem. Int. Ed. Engl.* **1994**, *33*, 454–456. See also: b) B. L. Feringa, R. M. Kellogg, R. Hulst, C. Zondervan, W. H. Kruijzinga, *Angew. Chem.* **1994**, *106*, 1527–1528; *Angew. Chem. Int. Ed. Engl.* **1994**, *33*, 1458–1459; G. Kaupp, T. Marquardt,

- Angew. Chem.* **1994**, *106*, 1528–1530; *Angew. Chem. Int. Ed. Engl.* **1994**, *33*, 1459–1461.
- [37] L. Pasteur, *C. R. Hebd. Seances Acad. Sci.* **1848**, *26*, 535.
- [38] Reviews on dynamic kinetic resolution: a) R. Noyori, M. Tokunaga, M. Kitamura, *Bull. Chem. Soc. Jpn.* **1995**, *68*, 36–56; b) R. S. Ward, *Tetrahedron: Asymmetry* **1995**, *6*, 1475–1490.
- [39] E. Havinga, *Biochim. Biophys. Acta* **1954**, *13*, 171–174. The experiments described in this reference were performed, for the main part, in the Laboratory for Organic Chemistry, University of Utrecht, in 1938–1939 (Director: Prof. Dr. F. Kogl). A few later experiments were carried out in the Laboratory for Veterinary Biochemistry, University of Utrecht, (Director: Prof. Dr. L. Seekles) and in the Laboratory for Organic Chemistry, University of Leyden.
- [40] Leading references on spontaneous separation of enantiomers in crystals: a) J. Jacques, A. Collet, S. H. Wilen, *Enantiomers, Racemates, and Resolutions*, Wiley, New York, **1981**; b) I. Kuzmenko, I. Weissbuch, E. Gurovich, L. Leiserowitz, M. Lahav, *Chirality* **1998**, *10*, 415–424; c) I. Weissbuch, M. Berfeld, W. Bouwman, K. Kjaer, J. Als-Nielsen, M. Lahav, L. Leiserowitz, *J. Am. Chem. Soc.* **1997**, *119*, 933–942. Amplification of chirality by crystallization with chiral additives: d) L. Addadi, Z. B. Yellin, I. Weissbuch, J. van Mil, L. J. W. Shimon, M. Lahav, L. Leiserowitz, *Angew. Chem.* **1985**, *97*, 476–496; *Angew. Chem. Int. Ed. Engl.* **1985**, *24*, 466–485.
- [41] a) H. Takahashi, R. Tamura, T. Ushio, Y. Nakajima, K. Hirotsu, *Chirality* **1998**, *10*, 705–710; b) T. Ushio, R. Tamura, H. Takahashi, N. Azuma, K. Yamamoto, *Angew. Chem.* **1996**, *108*, 2544–2546; *Angew. Chem. Int. Ed. Engl.* **1996**, *35*, 2372–2374.
- [42] a) C. J. Ehardt, N. M. Peachy, D. R. Swanson, J. M. Takacs, M. A. Khan, X. Gong, J.-H. Kim, J. Wang, R. A. Uphaus, *Nature* **1993**, *362*, 614–616; b) P. Nassoy, M. Goldmann, O. Bouloussa, F. Rondelez, *Phys. Rev. Lett.* **1995**, *75*, 457–460; c) H. Mohwald, A. Dietrich, C. Bohm, G. Brezenski, *Mol. Membr. Biol.* **1995**, *12*, 29–38; d) E. M. Landau, S. G. Wolf, M. Levanon, L. Leiserowitz, M. Lahav, J. Sagiv, *J. Am. Chem. Soc.* **1989**, *111*, 1436–1445.
- [43] F. Stevens, D. J. Dyer, D. M. Walba, *Angew. Chem.* **1996**, *108*, 955–957; *Angew. Chem. Int. Ed. Engl.* **1996**, *35*, 900–901. S. De Feyter, A. Gesquière, P. C. M. Grim, F. C. S. Valiyaveetil, C. Meiners, M. Sieffert, K. Müller, *Langmuir* **1999**, *15*, 2817; S. De Feyter, P. C. M. Grim, M. Rücker, P. Vanoppen, C. Meiners, M. Sieffert, S. Valiyaveetil, K. Müller, F. C. De Schryver, *Angew. Chem.* **1998**, *110*, 1281–1284; *Angew. Chem. Int. Ed.* **1998**, *37*, 1223–1226.
- [44] Y. Takanishi, H. Takezoe, Y. Suzuki, I. Kobayashi, T. Yajima, M. Terada, K. Mikami, *Angew. Chem.* **1999**, *111*, 2502–2504; *Angew. Chem. Int. Ed.* **1999**, *38*, 2354–2357.
- [45] H. Wynberg, *Chimia* **1989**, *43*, 150–152; H. Wynberg, *J. Macromol. Sci. Chem. A* **1989**, *26*, 1033–1041; C. Bolm, F. Bienewald, A. Seger, *Angew. Chem.* **1996**, *108*, 1767–1769; *Angew. Chem. Int. Ed. Engl.* **1996**, *35*, 1657–1659.
- [46] F. C. Frank, *Biochim. Biophys. Acta* **1953**, *11*, 459–463.
- [47] V. I. Goldanskii, V. V. Kuz'min, *Z. Phys. Chem. Leipzig* **1988**, *269*, 216.
- [48] A. H. Alberts, H. Wynberg, *J. Am. Chem. Soc.* **1989**, *111*, 7265–7266; A. H. Alberts, H. Wynberg, *J. Chem. Soc. Chem. Commun.* **1990**, 453–454;
- [49] H. Danda, H. Nishikawa, K. Otake, *J. Org. Chem.* **1991**, *56*, 6740–6741. See also: Y. Shvo, M. Gal, Y. Becker, A. Elgavi, *Tetrahedron: Asymmetry* **1996**, *7*, 911–924.
- [50] L. ShengJian, J. Yaozhong, M. Aiqiao, Y. Guishu, *J. Chem. Soc. Perkin Trans. 1* **1993**, 885–886.
- [51] K. Soai, S. Niwa, H. Hori, *J. Chem. Soc. Chem. Commun.* **1990**, 982–983.
- [52] a) K. Soai, T. Hayase, C. Shimada, K. Isobe, *Tetrahedron: Asymmetry* **1994**, *5*, 789–792; b) K. Soai, T. Hayase, K. Takai, *Tetrahedron: Asymmetry* **1995**, *6*, 637–638; c) K. Soai, Y. Inoue, T. Takahashi, T. Shibata, *Tetrahedron* **1996**, *52*, 13355–13362; d) T. Shibata, H. Morioka, S. Tanji, T. Hayase, Y. Kodaka, K. Soai, *Tetrahedron Lett.* **1996**, *37*, 8783–8786.
- [53] a) T. Shibata, K. Choji, H. Morioa, T. Hayase, K. Soai, *Chem. Commun.* **1996**, 751–752; b) T. Shibata, K. Choji, T. Hayase, Y. Aizu, K. Soai, *Chem. Commun.* **1996**, 1235–1236.
- [54] a) K. Soai, T. Shibata, H. Morioka, K. Choji, *Nature* **1995**, *378*, 767–768; b) T. Shibata, H. Morioka, T. Hayase, K. Choji, K. Soai, *J. Am. Chem. Soc.* **1996**, *118*, 471–472; c) T. Shibata, T. Hayase, J. Yamamoto, K. Soai, *Tetrahedron: Asymmetry* **1997**, *8*, 1717–1719; d) T. Shibata, S. Yonekubo, K. Soai, *Angew. Chem.* **1999**, *111*, 749–751; *Angew. Chem. Int. Ed.* **1999**, *38*, 659–661.
- [55] T. Shibata, T. Takahashi, T. Konishi, K. Soai, *Angew. Chem.* **1997**, *109*, 2560–2562; *Angew. Chem. Int. Ed. Engl.* **1997**, *36*, 2458–2460.
- [56] a) T. Shibata, J. Yamamoto, N. Matsumoto, S. Yonekubo, S. Osanai, K. Soai, *J. Am. Chem. Soc.* **1998**, *120*, 12157–12158; b) T. Shibata, S. Yonekubo, K. Soai, *Angew. Chem.* **1999**, *111*, 746–748; *Angew. Chem. Int. Ed.* **1999**, *38*, 659–661.
- [57] An excellent review has just reported on achiral additives as poisons to kill undesired catalyst species and/or to deoligomerize less-active catalysts: E. M. Vogl, H. Groger, M. Shibasaki, *Angew. Chem.* **1999**, *111*, 1671–1680; *Angew. Chem. Int. Ed.* **1999**, *38*, 1570–1577.
- [58] Reviews: a) H. M. R. Hoffmann, *Angew. Chem.* **1969**, *81*, 597–618; *Angew. Chem. Int. Ed. Engl.* **1969**, *8*, 556–577; b) B. B. Snider in *Comprehensive Organic Synthesis*, Vol. 5 (Eds.: B. M. Trost, I. Fleming), Pergamon, London, **1991**, pp. 1–27; ref. [18c].
- [59] Reviews: a) B. Weidmann, D. Seebach, *Angew. Chem.* **1983**, *95*, 12–26; *Angew. Chem. Int. Ed. Engl.* **1983**, *22*, 31–45; b) Y. Yamamoto, *Acc. Chem. Res.* **1987**, *20*, 243–249; c) R. W. Hoffmann, *Angew. Chem.* **1987**, *99*, 503–517; *Angew. Chem. Int. Ed. Engl.* **1987**, *26*, 489–503; d) W. R. Roush in *Comprehensive Organic Synthesis*, Vol. 2 (Eds.: B. M. Trost, I. Fleming), Pergamon, London, **1991**, pp. 1–53; e) J. A. Marshall, *Chemtracts: Org. Chem.* **1992**, *5*, 75–98; f) Y. Yamamoto, N. Asao, *Chem. Rev.* **1993**, *93*, 2207–2293.
- [60] S. Matsukawa, K. Mikami, *Tetrahedron: Asymmetry* **1995**, *6*, 2571–2574. Prof. Murahashi and co-workers also reported the use of a BINOL–Ti naphthoxide catalyst in the reaction with nitrones: T. Kawakami, K. Harada, I. Imada, S. Murahashi, *Abstr. Pap. Annual Meeting of the Chemical Society of Japan (Kyoto)* **1995**, No. 2H105.
- [61] K. Mikami, T. Korenaga, Y. Matsumoto, M. Ueki, M. Terada, S. Matsukawa, *Pure Appl. Chem.*, in Press (19th IUPAC Meeting on Organometallic Chemistry).
- [62] T. Ohkuma, H. Doucet, T. Pham, K. Mikami, T. Korenaga, M. Terada, R. Noyori, *J. Am. Chem. Soc.* **1998**, *120*, 1086–1087.
- [63] TolBINAP = 2,2'-bis(di-*p*-tolylphosphanyl)-1,1'-binaphthyl: a) H. Takaya, K. Mashima, K. Koyano, M. Yagi, H. Kumobayashi, T. Taketomi, S. Akutagawa, R. Noyori, *J. Org. Chem.* **1986**, *51*, 629–635; b) M. Kitamura, M. Tokunaga, T. Ohkuma, R. Noyori, *Org. Synth.* **1992**, *71*, 1–13.
- [64] DM-BINAP = XylylBINAP = 2,2'-bis(di-3,5-xylylphosphanyl)-1,1'-binaphthyl: a) K. Mashima, Y. Matsumura, K. Kusano, H. Kumobayashi, N. Sayo, Y. Hori, T. Ishizaki, S. Akutagawa, H. Takaya, *J. Chem. Soc. Chem. Commun.* **1991**, 609–610; b) T. Ohkuma, M. Koizumi, H. Doucet, T. Pham, M. Kozawa, K. Murata, E. Katayama, T. Yokozawa, T. Ikariya, R. Noyori, *J. Am. Chem. Soc.* **1998**, *120*, 13529–13530.
- [65] a) P. Mangeney, T. Tejero, A. Alexakis, F. Grosjean, J. Normant, *Synthesis* **1988**, 255–257; b) S. Pikul, E. J. Corey, *Org. Synth.* **1992**, *71*, 22–29.
- [66] Review on matched and mismatched pairing in double asymmetric synthesis: S. Masamune, W. Choy, J. S. Petersen, L. R. Sita, *Angew. Chem.* **1985**, *97*, 1–31; *Angew. Chem. Int. Ed. Engl.* **1985**, *24*, 1–30.
- [67] The active species has been suggested to be a mono- or dihydride species (X = H or Cl): a) R. L. Chowdhury, J.-E. Bäckvall, *J. Chem. Soc. Chem. Commun.* **1991**, 1063–1064; b) K.-J. Haack, S. Hashiguchi, A. Fujii, T. Ikariya, R. Noyori, *Angew. Chem.* **1997**, *109*, 297–300; *Angew. Chem. Int. Ed. Engl.* **1997**, *36*, 285–288; c) R. Noyori, S. Hashiguchi, *Acc. Chem. Res.* **1997**, *30*, 97–102.
- [68] J. Halpern in *Asymmetric Synthesis*, Vol. 5 (Ed.: J. D. Morrison), Academic Press, New York, **1985**, pp. 41–69.
- [69] K. Mikami, T. Korenaga, T. Ohkuma, R. Noyori, *Angew. Chem.* **2000**, *112*, 3854–3857; *Angew. Chem. Int. Ed.* **2000**, *39*, 3707–3710.
- [70] In this section we will discuss the equilibrium phenomena between two enantiomeric forms of flexible ligand chiralities, rather than of metal-centered chiralities in which the Pfeiffer effects are operative. K. M. is grateful to Professor Jay Siegel for his useful comments on the Pfeiffer effects at the Bärnstock meeting 2000. See also: P. Pfeiffer, K. Quehl, *Ber. Dtsch. Chem. Ges.* **1931**, *64*, 2667–2671. For a clever application of DNA as the perturbation agent, see: B. Norden, F. Tjernereld, *FEBS Lett.* **1976**, *67*, 368–370.

- [71] Excellent reviews on atropisomerism: a) M. Oki, *Top. Stereochem.* **1983**, 14, 1–81; b) M. Oki, *The Chemistry of Rotational Isomers*, Springer, New York, **1993**; c) E. L. Eliel, *Stereochemistry of Carbon Compounds*, McGraw-Hill, New York, **1962**, Chap. 6, pp. 156–179; d) E. L. Eliel, S. H. Wilen, L. N. Mander, *Stereochemistry of Organic Compounds*, Wiley, New York, **1994**, Chap. 14, pp. 1142–1190.
- [72] a) The bisphosphane ligand **4a** was also named BPBP (2,2'-bis(diphenylphosphanyl)-1,1'-biphenyl) but only the monophosphane was successfully synthesized: A. Uehara, J. C. Bailar, Jr., *J. Organomet. Chem.* **1982**, 239, 1–10; use of the monophosphane as a ligand: b) M. A. Bennett, S. K. Bhargava, K. D. Griffiths, G. B. Robertson, *Angew. Chem.* **1987**, 99, 261–262; *Angew. Chem. Int. Ed. Engl.* **1987**, 26, 260–261; c) O. Desponds, M. Schlosser, *J. Organomet. Chem.* **1996**, 507, 257–261; d) O. Desponds, M. Schlosser, *Tetrahedron Lett.* **1996**, 37, 47–48; e) D. W. Allen, I. T. Millar, *J. Chem. Soc. C* **1968**, 2406–2408; f) T. Costa, H. Schmidbaur, *Chem. Ber.* **1982**, 115, 1367–1373; see also the 6,6'-substituted analogues: g) BIPHEMP (2,2'-bis(diphenylphosphanyl)-6,6'-dimethyl-1,1'-biphenyl): G. Svensson, J. Albertsson, T. Frejd, T. Klingstedt, *Acta Crystallogr. Sect. C* **1986**, 42, 1324–1327; R. Schmid, M. Cereghetti, B. Heiser, P. Schonholzer, H.-J. Hansen, *Helv. Chim. Acta* **1988**, 71, 897–929; h) BICHEPs (2,2'-bis(dicyclohexylphosphanyl)-6,6'-dimethyl-1,1'-biphenyl): T. Chiba, A. Miyashita, H. Nohira, *Tetrahedron Lett.* **1991**, 32, 4745–4748; i) MeO-BIPHEP (2,2'-bis(diphenylphosphanyl)-6,6'-dimethoxy-1,1'-biphenyl): R. Schmid, J. Foricher, M. Cereghetti, P. Schönholzer, *Helv. Chim. Acta* **1991**, 74, 370–389; R. Schmid, E. A. Broger, M. Cereghetti, Y. Cramer, J. Foricher, M. Lalonde, R. K. Müller, M. Scalone, G. Schoettl, U. Zutter, *Pure Appl. Chem.* **1996**, 68, 131–138; G. Trabesinger, A. Albinati, N. Feiken, R. W. Kunz, P. S. Pregosin, M. Tschöner, *J. Am. Chem. Soc.* **1997**, 119, 6315–6323; j) 2,2'-bis(diphenylphosphanyl)-6,6'-difluoro-1,1'-biphenyl: H. Jendralla, C.-H. Li, E. Paulus, *Tetrahedron: Asymmetry* **1994**, 5, 1297–1320.
- [73] K. Mikami, T. Korenaga, M. Terada, T. Ohkuma, T. Pham, R. Noyori, *Angew. Chem.* **1999**, 111, 517–519; *Angew. Chem. Int. Ed.* **1999**, 38, 495–497.
- [74] H. Brunner, B. Hammer, *Angew. Chem.* **1984**, 96, 305–307; *Angew. Chem. Int. Ed. Engl.* **1984**, 23, 312–313.
- [75] Review on center of chirality in metallic complexes: a) H. Brunner, *Adv. Organomet. Chem.* **1980**, 18, 151–206; b) A. von Zelewsky, *Stereochemistry of Coordination Compounds*, Wiley, New York, **1996**; c) U. Knof, A. von Zelewsky, *Angew. Chem.* **1999**, 111, 312–333; *Angew. Chem. Int. Ed.* **1999**, 38, 302–322.
- [76] K. Mikami, S. Matsukawa, T. Volk, M. Terada, *Angew. Chem.* **1997**, 109, 2936–2939; *Angew. Chem. Int. Ed. Engl.* **1997**, 36, 2768–2771.
- [77] M. Chavarot, J. J. Byrne, P. Y. Chavant, J. Pardillos-Guindet, Y. Vallee, *Tetrahedron: Asymmetry* **1998**, 9, 3889–3894.
- [78] a) T. Hamada, T. Fukuda, H. Imanishi, T. Katsuki, *Tetrahedron* **1996**, 52, 515–530; b) Y. Noguchi, R. Irie, T. Fukuda, T. Katsuki, *Tetrahedron Lett.* **1996**, 37, 4533–4536; c) Y. N. Ito, T. Katsuki, *Tetrahedron Lett.* **1998**, 39, 4325–4328; d) R. Irie, T. Hashihayata, T. Katsuki, M. Akita, Y. Moro-oka, *Chem. Lett.* **1998**, 1041–1042.
- [79] K. Miura, T. Katsuki, *Synlett* **1999**, 783–785.
- [80] Reviews: a) Y. Okamoto, T. Nakano, *Chem. Rev.* **1994**, 94, 349–372; b) H.-H. Brintzinger, D. Fischer, R. Mulhaupt, B. Rieger, R. M. Waymouth, *Angew. Chem.* **1995**, 107, 1255–1283; *Angew. Chem. Int. Ed. Engl.* **1995**, 34, 1143–1170; c) A. H. Hoveyda, J. P. Morken, *Angew. Chem.* **1996**, 108, 1378–1401; *Angew. Chem. Int. Ed. Engl.* **1996**, 35, 1262–1284; d) K. Mikami, M. Terada, A. Osawa, *Kobunshi/High Polym.* **1997**, 46, 72–76.
- [81] M. Ringwald, R. Stürmer, H. H. Brintzinger, *J. Am. Chem. Soc.* **1999**, 121, 1524–1527.
- [82] Special issues on combinatorial libraries: a) *Acc. Chem. Res.* **1996**, 29(3); b) *Chem. Eng. News* **1996**, 74(4); reviews: c) F. Balkenhohl, C. B. Hunnefeld, A. Lansky, C. Zechel, *Angew. Chem.* **1996**, 108, 2437–2476; *Angew. Chem. Int. Ed. Engl.* **1996**, 35, 2288–2337; d) C. Gennari, H. P. Nestler, U. Piarulli, B. Salom, *Liebigs Ann.* **1997**, 637–647; e) *Combinatorial Chemistry: Synthesis and Application* (Eds.: S. R. Wilson, A. W. Czarink), Wiley, New York, **1997**. f) *Combinatorial Chemistry = Synthesis, Analysis, Screening* (Ed.: G. Jung), Wiley-VCH, Weinheim, **1999**.
- [83] *High Throughput Screening* (Ed.: J. P. Devlin), Marcel Dekker, New York, **1997**.
- [84] a) K. Burgess, H.-J. Lim, A. M. Porte, G. A. Sulikowski, *Angew. Chem.* **1996**, 108, 192–194; *Angew. Chem. Int. Ed. Engl.* **1996**, 35, 220–222; A. M. Porte, J. Reibenspies, K. Burgess, *J. Am. Chem. Soc.* **1998**, 120, 9180–9187; b) B. M. Cole, K. D. Shimizu, C. A. Krueger, J. P. A. Harrity, M. L. Snapper, A. H. Hoveyda, *Angew. Chem.* **1996**, 108, 1776–1779; *Angew. Chem. Int. Ed. Engl.* **1996**, 35, 1668–1671; K. D. Shimizu, B. M. Cole, C. A. Krueger, K. W. Kuntz, M. L. Snapper, A. H. Hoveyda, *Angew. Chem.* **1997**, 109, 1781–1785; *Angew. Chem. Int. Ed. Engl.* **1997**, 36, 1703–1707; c) M. S. Sigman, E. N. Jacobsen, *J. Am. Chem. Soc.* **1998**, 120, 4901–4902; M. B. Francis, E. N. Jacobsen, *Angew. Chem.* **1999**, 111, 987–991; *Angew. Chem. Int. Ed.* **1999**, 38, 937–941; d) G. Liu, J. A. Ellman, *J. Org. Chem.* **1995**, 60, 7712–7713.
- [85] a) M. T. Reetz, A. Zonta, K. Schimossek, K. Liebeton, K.-E. Jaeger, *Angew. Chem. Int. Ed. Engl.* **1997**, 36, 2830–2832; b) G. Klein, J.-L. Reymond, *Helv. Chim. Acta* **1999**, 82, 400–406.
- [86] In homogeneous catalysis: M. T. Reetz, M. H. Becker, K. M. Kuhling, A. Holzwarth, *Angew. Chem.* **1998**, 110, 2792–2795; *Angew. Chem. Int. Ed.* **1998**, 37, 2647–2650.
- [87] a) J. Guo, J. Wu, G. Siuzdak, M. G. Finn, *Angew. Chem.* **1999**, 111, 1868–1871; *Angew. Chem. Int. Ed.* **1999**, 38, 1755–1758; b) M. T. Reetz, M. H. Becker, H.-W. Klein, D. A. Steckigt, *Angew. Chem.* **1999**, 111, 1872–1875; *Angew. Chem. Int. Ed.* **1999**, 38, 1758–1761.
- [88] K. Ding, A. Ishii, K. Mikami, *Angew. Chem.* **1999**, 111, 519–523; *Angew. Chem. Int. Ed.* **1999**, 38, 497–501. The structures of A4* and A5* shown in Scheme 3 of that paper are exchanged herein.
- [89] a) W. Kuhn, *Trans Faraday Soc.* **1930**, 26, 293–308; b) T. M. Lowry, H. S. French, *J. Chem. Soc.* **1932**, 2654–2656.
- [90] A. F. Drake, J. M. Gould, S. F. Mason, *J. Chromatogr.* **1980**, 202, 239–245.
- [91] a) P. Salvadori, C. Bertucci, C. Rosini, *Chirality* **1991**, 3, 376–385; b) P. Salvadori, C. Bertucci, C. Rosini in *Circular Dichroism. Principles and Application* (Eds.: K. Nakanishi, N. Berova, R. W. Woody), VCH, Weinheim, **1994**, pp. 541–560.
- [92] A. Mannschreck, *Trends Anal. Chem.* **1993**, 12, 220–225.
- [93] For the application of a CD detection system to measure optical purity by HPLC on nonchiral stationary phase, see: a) C. Bertucci, P. Salvadori, L. F. L. Guimaraes, *J. Chromatogr.* **1994**, 666, 535–539; b) P. Salvadori, C. Bertucci, C. Rosini, *Chirality* **1991**, 3, 376–385; c) A. F. Drake, J. M. Gould, S. F. Mason, *J. Chromatogr.* **1980**, 202, 239–245.
- [94] K. Soai, S. Niwa, *Chem. Rev.* **1992**, 92, 833–856.
- [95] N. Oguni, T. Omi, *Tetrahedron Lett.* **1984**, 25, 2823–2824.
- [96] Reviews: a) J. K. Whitesell, *Chem. Rev.* **1989**, 89, 1581–1590; b) C. Rosini, L. Franzini, A. Raffaelli, P. Salvadori, *Synthesis* **1992**, 503–517; c) K. Mikami, Y. Motoyama, *Encyclopedia of Reagents for Organic Synthesis, Vol. 1* (Ed.: L. A. Paquette), Wiley, New York, **1995**.
- [97] a) Kaufmann, R. Boese, *Angew. Chem.* **1990**, 102, 568–569; *Angew. Chem. Int. Ed. Engl.* **1990**, 29, 545–546; b) K. Hattori, H. Yamamoto, *J. Org. Chem.* **1992**, 57, 3264–3265; c) K. Ishihara, H. Kurihara, M. Matsumoto, H. Yamamoto, *J. Am. Chem. Soc.* **1998**, 120, 6920–6930.
- [98] a) K. Maruoka, T. Itoh, T. Shirasaka, H. Yamamoto, *J. Am. Chem. Soc.* **1988**, 110, 310–312; b) J. Bao, W. D. Wulff, A. L. Rheingold, *J. Am. Chem. Soc.* **1993**, 115, 3814–3815; c) D. P. Heller, D. R. Goldberg, W. D. Wulff, *J. Am. Chem. Soc.* **1997**, 119, 10551–10552; d) A. Graven, M. Johannsen, K. A. Jorgensen, *Chem. Commun.* **1996**, 2373–2374.
- [99] Reviews: K. Mikami, *Encyclopedia of Reagents for Organic Synthesis, Vol. 1* (Ed.: L. A. Paquette), Wiley, New York, **1995**, pp. 397–407; a) M. T. Reetz, S. H. Kyung, C. Bolm, T. Zierke, *Chem. Ind.* **1986**, 824–824; b) D. Seebach, A. K. Beck, R. Imwinkelried, S. Roggo, A. Wonnacott, *Helv. Chim. Acta* **1987**, 70, 954–974; c) K. Mikami, M. Terada, T. Nakai, *J. Am. Chem. Soc.* **1989**, 111, 1940–1941; K. Mikami, M. Terada, T. Nakai, *J. Am. Chem. Soc.* **1990**, 112, 3949–3954; K. Mikami, M. Terada, S. Narisawa, T. Nakai, *Synlett* **1992**, 255–266; K. Mikami, M. Terada, S. Narisawa, T. Nakai, *Org. Synth.* **1992**, 71, 14–21; d) A. Ketter, G. Glahsl, R. Herrmann, *J. Chem. Res. (M)* **1990**, 2118–2156; e) T. Mukaiyama, A. Inubushi, S.

- Suda, R. Hara, S. Kobayashi, *Chem. Lett.* **1990**, 1015–1018; f) A. L. Costa, M. G. Piazza, E. Tagliavini, C. Trombini, A. Umani-Ronchi, *J. Am. Chem. Soc.* **1993**, *115*, 7001–7002; g) G. E. Keck, K. H. Tarbet, L. S. Geraci, *J. Am. Chem. Soc.* **1993**, *115*, 8467–8468; h) K. Maruoka, N. Murase, H. Yamamoto, *J. Org. Chem.* **1993**, *58*, 2938–2939; i) D. R. Gauthier, Jr., E. M. Carreira, *Angew. Chem.* **1996**, *108*, 2521–2523; *Angew. Chem. Int. Ed. Engl.* **1996**, *35*, 2363–2365; j) S. Weigand, R. Brückner, *Chem. Eur. J.* **1996**, *2*, 1077–1084; k) T. Harada, M. Takeuchi, M. Hatsuda, S. Ueda, A. Oku, *Tetrahedron: Asymmetry* **1996**, *7*, 2479–2482; l) C.-M. Yu, H.-S. Choi, W.-H. Jung, S.-S. Lee, *Tetrahedron Lett.* **1996**, *37*, 7095–7098; m) S. Yamago, M. Furukawa, A. Azuma, J. Yoshida, *Tetrahedron Lett.* **1998**, *39*, 3783–3786; L. Pu, *Chem. Rev.* **1998**, *98*, 2405–2494.
- [100] a) S. Casolari, P. G. Cozzi, P. Orioli, E. Tagliavini, A. Umani-Ronchi, *Chem. Commun.* **1997**, 2123–2124; b) S. Kobayashi, H. Ishitani, M. Ueno, *J. Am. Chem. Soc.* **1998**, *120*, 431–432; c) S. Kobayashi, S. Komiyama, H. Ishitani, *Angew. Chem.* **1998**, *110*, 1026–1028; *Angew. Chem. Int. Ed.* **1998**, *37*, 979–981; d) T. Volk, T. Korenaga, S. Matsukawa, M. Terada, K. Mikami, *Chirality* **1998**, *10*, 717–721.
- [101] a) S. Kobayashi, H. Ishitani, *J. Am. Chem. Soc.* **1994**, *116*, 4083–4084; b) S. Kobayashi, *Synlett* **1994**, 689–701; c) H. Kitajima, T. Katsuki, *Synlett* **1997**, 568–570; d) I. E. Marko, G. R. Evans, P. Seres, I. Chelle, Z. Janousek, *Pure Appl. Chem.* **1996**, *68*, 113–122; e) M. Shibasaki, H. Sasai, T. Arai, *Angew. Chem.* **1997**, *109*, 1290–1310; *Angew. Chem. Int. Ed. Engl.* **1997**, *36*, 1236–1256, and references therein; f) K. Mikami, O. Kotera, Y. Motoyama, H. Sakaguchi, *Synlett.* **1995**, 975.
- [102] K. R. K. Prasad, N. N. Joshi, *Tetrahedron: Asymmetry* **1996**, *7*, 1957–1960.
- [103] a) H. Kitajima, K. Ito, T. Katsuki, *Chem. Lett.* **1996**, 343–344; H. Kitajima, K. Ito, Y. Aoki, T. Katsuki, *Bull. Chem. Soc. Jpn.* **1997**, *70*, 207–217; b) Q. S. Hu, W. S. Huang, D. Vitharana, X. F. Zhang, L. Pu, *J. Am. Chem. Soc.* **1997**, *119*, 12454–12464; W. S. Huang, Q. S. Hu, L. Pu, *J. Org. Chem.* **1998**, *63*, 1364–1365; Q. S. Hu, W. S. Huang, L. Pu, *J. Org. Chem.* **1998**, *63*, 2798–2799; W. S. Huang, L. Pu, *J. Org. Chem.* **1999**, *64*, 4222–4223.
- [104] S. E. Denmark, S. P. O'Connor, S. R. Wilson, *Angew. Chem.* **1998**, *110*, 1162–1165; *Angew. Chem. Int. Ed.* **1998**, *37*, 1149–1151.
- [105] P. G. Cozzi, A. Papa, A. Umani-Ronchi, *Tetrahedron Lett.* **1996**, *37*, 4613–4616.
- [106] R. Angelaud, Y. Matsumoto, T. Korenaga, K. Kudo, M. Senda, K. Mikami, *Chirality* **2000**, *12*, 544–547. (Special issue to honor the 1997 Chirality Medal for Professor Ryoji Noyori).
- [107] a) Review: M. Braun, *Angew. Chem.* **1996**, *108*, 565–568; *Angew. Chem. Int. Ed. Engl.* **1996**, *35*, 519–522; b) A. K. Beck, B. Bastani, D. A. Plattner, W. Petter, D. Seebach, H. Braunschweiger, P. Gysi, L. La Vecchia, *Chimia* **1991**, *45*, 238–244; c) D. Seebach, D. A. Plattner, A. K. Beck, Y. M. Yang, D. Hunziker, *Helv. Chim. Acta* **1992**, *75*, 2171–2209; d) K. Narasaka, N. Iwasawa, M. Inoue, T. Yamada, M. Nakashima, J. Sugimori, *J. Am. Chem. Soc.* **1989**, *111*, 5340–5344.
- [108] a) C. A. Martin, PhD thesis, Massachusetts Institute of Technology, USA, **1988**; b) J. T. Wang, X. Fan, X. Feng, Y. M. Qian, *Synthesis* **1989**, 291–292; c) G. E. Keck, K. H. Tarbet, L. S. Geraci, *J. Am. Chem. Soc.* **1993**, *115*, 8467–8468; d) S. Weigand, R. Brückner, *Chem. Eur. J.* **1996**, *2*, 1077–1084. See also: d) T. J. Boyle, D. L. Barnes, J. A. Heppert, L. Morales, F. Takusagawa, *Organometallics* **1992**, *11*, 1112–1126.
- [109] C. L. Hill, X. Zhang, *Nature* **1995**, *373*, 324–326.
- [110] H. B. Kagan, *J. Organomet. Chem.* **1998**, *567*, 3–6.
- [111] *Biochemistry of Signal Transduction and Regulation* (Ed.: G. Krauss), Wiley-VCH, Weinheim, **1999**.
- [112] Z. Guo, D. Zhou, P. G. Schultz, *Science*, **2000**, *288*, 2042–2045.



Enantioselective hetero-Diels–Alder reactions of carbonyl compounds and imines catalyzed by chiral Lewis acids. A painting by the Danish female artist Jo Dam Kærgaard provides the background for an overview of the described reactions and their catalysts.

Catalytic Asymmetric Hetero-Diels–Alder Reactions of Carbonyl Compounds and Imines

Karl Anker Jørgensen*

Asymmetric catalysis is a challenge for chemists: How can we design catalysts to achieve the goal of forming optically active compounds? This review provides the reader with an overview of the development of catalytic asymmetric hetero-Diels–Alder reactions of carbonyl compounds and imines. Since its discovery, the Diels–Alder reaction has undergone intensive development and is of fundamental importance for synthetic, physical, and theoretical chemists. The Diels–Alder reaction has been through different stages of development, and at the beginning of the 21st century catalytic Diels–Alder reactions are one of the main areas of focus. The preparation of numerous compounds of importance for our society is based on cycloaddition reac-

tions to carbonyl compounds and imines. There are several parallels between the reactions of carbonyl compounds and those of imines, which, however, begin to vanish on entering the field of catalytic reactions. Why? From a mechanistic point of view some similarities can be drawn, but the synthetic development of catalytic enantioselective hetero-Diels–Alder reactions of imines are several years behind those of the carbonyl compounds. For hetero-Diels–Alder reactions of carbonyl compounds there a number of different chiral catalysts, and great progress has been achieved in developing enantioselective reactions for unactivated and activated carbonyl compounds. In contrast the development of catalytic enantioselective

hetero-Diels–Alder reactions of imines is in its infancy and only few catalytic reactions have been published. This review will focus on the most important developments, and discuss the synthetic and mechanistic aspects of enantioselective hetero-Diels–Alder reactions of carbonyl compounds catalyzed by chiral Lewis acids. For the hetero-Diels–Alder reactions of imines, the diastereoselective reactions of optically substrates catalyzed by Lewis acids will be presented first, followed by the catalytic enantioselective reactions.

Keywords: asymmetric catalysis • carbonyl compounds • Diels–Alder reactions • imines • reaction mechanisms • synthetic methods

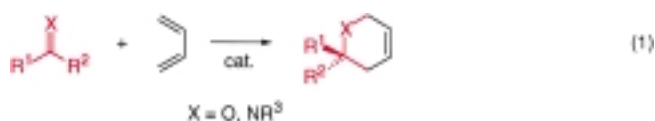
1. Introduction

The Diels–Alder (DA) reaction has, since its discovery in 1928 by Otto Diels and Karl Alder,^[1] been one of the cornerstone reactions in organic chemistry for the construction of six-membered rings. The various types of DA reactions have continued to further developed and their spectrum of application in chemistry is enormous. The use of DA reactions covers compounds of academic and industrial interest and several compounds of importance for our society are synthesized based on this approach.

Two major developments have taken place with regard to DA reactions over the last 50 years. With the introduction of the theory of conservation of orbital symmetry by Woodward

and Hoffmann, a lot of attention focused on the synthetic and mechanistic aspects of DA reactions—based on the Woodward–Hoffmann rules—in the 1960s and 1970s.^[2] In the last two decades the focus has changed to the development and application of DA reactions leading to optically active compounds. The reason for the interest in obtaining optically active compounds using the DA methodology is that the reactions normally are easy to perform and proceed generally in a highly regio- and diastereoselective manner. Furthermore, the DA reaction can give up to four new chiral centers. The enantioselective version, especially when promoted by chiral Lewis acid complexes has further enhanced its power in the synthesis of optically active compounds.^[3]

This review focuses on the development of catalytic asymmetric hetero-Diels–Alder (HDA) reactions of carbonyl compounds and imines with conjugated dienes [Eq. (1)].



[*] Prof. Dr. K. A. Jørgensen
Center for Metal Catalyzed Reactions
Department of Chemistry
Aarhus University
8000 Aarhus C (Denmark)
Fax: (+45) 86-19-61-88
E-mail: kaj@kemi.auu.dk

There are two basic strategies for asymmetric HDA reactions in order to control the absolute configuration of the product: 1) the use of a diene and/or a dienophile with a chiral auxiliary, and 2) the use of a chiral catalyst. The most efficient and economic way to effect an enantioselective reaction is probably the use of a chiral catalyst. This approach allows the direct formation of chiral compounds from achiral substrates under mild conditions and requires a substoichiometric amount of chiral material. To achieve catalytic enantioselective HDA reactions of carbonyl compounds and imines, coordination of a chiral Lewis acid to the carbonyl and imine functionalities is necessary. This coordination activates the substrate and provides the chiral environment that forces the approach of a diene to the substrate from the less sterically hindered face, introducing enantioselectivity in the reaction.

When a chiral Lewis acid catalyst is designed for a reaction, many parameters must be taken into account. The substrate should have a certain reactivity and be able to coordinate to a metal. The choice of the metal in combination with a chiral ligand is of particular importance. Furthermore, the Lewis acidity, the structural properties of the metal complex, and the electronic and structural properties of the chiral ligand all need to be considered.

The main group metals such as aluminum, boron, the hard early transition metals titanium and zirconium, and some lanthanide elements are all oxophilic metals which have been widely used in combination with chiral ligands containing oxygen as the coordinating atoms. Among the most commonly used chiral ligands of this type are the 1,1'-binaphthol (BINOL)- and $\alpha,\alpha,\alpha',\alpha'$ -tetraphenyl-2,2-dimethyl-1,3-dioxolan-4,5-dimethanol (TADDOL)-based ligands. However, problems such as aggregation may arise due to the high oxophilicity of these metals which can lead to a deactivation of the catalyst. Designing a ligand in such a way that catalyst aggregation is prevented has become a topic of current interest and includes the introduction of sterically demanding groups around the oxygen atoms, attachment of monomeric catalysts to a polymer, and synthesis of rigid polymeric chiral catalysts. Chiral ligands containing nitrogen as the coordinating atoms show a broad flexibility towards both hard and soft metals. Ligands containing phosphorus as the coordinating atoms, for example, the 2,2'-bis(diphenylphosphanyl)-1,1'-binaphthyl (BINAP) ligands, are soft ligands, and great

success has been achieved by applying these ligands in combination with soft metals, such as copper(I).

The discovery and development of a highly efficient catalyst system rely on the knowledge of the possible reactive intermediates and, not least, on extensive screening. The conformational preferences of the complex between the substrate and the Lewis acid are responsible for the stereochemical outcome of a given reaction. The understanding of asymmetric induction requires a knowledge of the structure and the relative reactivity of the substrate–Lewis acid complex(es) formed in the reaction solution. In some cases, solvents and/or additives may also play an important role in the stereochemical outcome since they can also coordinate to the Lewis acid leading to a change of the geometrical structure of the catalyst. All these factors must be kept in mind during the interpretation and prediction of the stereochemical outcome of a reaction promoted by a chiral Lewis acid catalyst.

Catalytic asymmetric HDA reactions have been intensively developed in recent years with the main focus on the synthetic aspects, while the number of mechanistic studies has been limited. In this review, the main attention will be on the development and understanding of HDA reactions in which Lewis acid catalysts are used for preparing optically active six-membered ring systems. For the HDA reactions of carbonyl compounds the focus will be on enantioselective reactions catalyzed by chiral Lewis acids. The section dealing with imines will be devoted to reactions leading to optically active HDA adducts obtained from Lewis acid catalyzed reactions starting from either optically active imines or dienes. Finally, catalytic enantioselective reactions of imines will be described. The reason for including the HDA reactions of optically active imines and dienes is that the use of these substrates has been intensively studied recently, while the development of catalytic enantioselective reactions is still in its infancy.

1.1. The Mechanistic Aspects and Concepts of Activation by Lewis Acids

One cannot discuss HDA reactions in the present context without trying to understand the reaction course from a mechanistic point of view. The majority of the reactions discussed can be classified into two types of $[\pi 2s + \pi 4s]$



Karl Anker Jørgensen, born 1955, is Professor at the Center for Metal Catalyzed Reactions at Aarhus University. Following a Ph.D. from Aarhus University in 1984 and a post-doctoral period with Roald Hoffmann at Cornell University, he joined the Aarhus University faculty. His main research interests focus on the development and understanding of metal-catalyzed reactions in organic chemistry.

cycloadditions, the normal and inverse electron demand HDA reactions, based on the relative energies of the frontier molecular orbitals (FMOs) of the diene and the dienophile (Figure 1).^[2, 4]

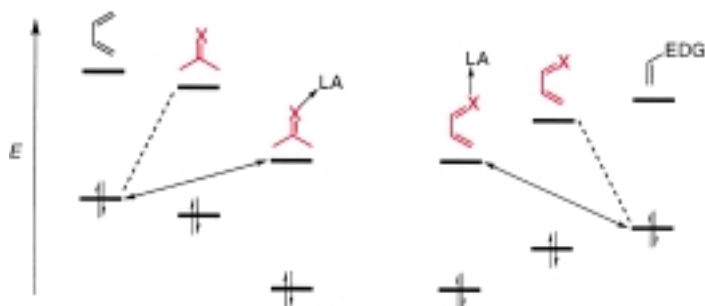


Figure 1. A FMO diagram of the normal (left; $\text{HOMO}_{\text{diene}}-\text{LUMO}_{\text{dienophile}}$ -controlled) and inverse electron demand HDA reaction (right; $\text{LUMO}_{\text{diene}}-\text{HOMO}_{\text{dienophile}}$ -controlled) in the absence and the presence of a Lewis acid. X = O, NR; LA = Lewis acid; EDG = electron-donating group.

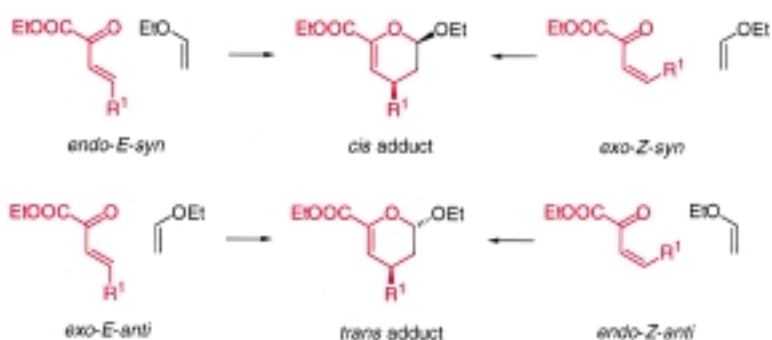
The normal electron demand reaction is a $\text{HOMO}_{\text{diene}}-\text{LUMO}_{\text{dienophile}}$ -controlled HDA reaction which predominantly occurs between electron-rich dienes and electron-deficient dienophiles (Figure 1, left, dashed line). The inverse electron demand HDA reaction is primarily controlled by a $\text{LUMO}_{\text{diene}}-\text{HOMO}_{\text{dienophile}}$ interaction which can be found, for example, in reactions of enones and heteroanalogues with alkenes having electron-donating groups (Figure 1, right, dashed line).

The basic concept of activation in HDA reactions is to utilize the lone pair of electrons of the carbonyl and imine functionality for coordination to the Lewis acid. The coordination of the dienophile to the Lewis acid changes the FMOs of the dienophile and for the normal electron demand reactions a decrease of the LUMO and HOMO energies is observed leading to a better interaction with the diene (Figure 1, left, solid line). The energy difference between the $\text{HOMO}_{\text{diene}}$ and the $\text{LUMO}_{\text{dienophile}}$ is thus reduced compared with that for the absence of a Lewis acid, and can therefore account for the activating effect of the Lewis acid. The catalytic properties of the Lewis acid for the inverse electron demand HDA reaction is due to the coordination of the Lewis acid to a heteroatom of the 1,3-diene, leading to a decrease of the $\text{LUMO}_{\text{diene}}$ and $\text{HOMO}_{\text{dienophile}}$ energies, and thus, based on a FMO way of reasoning, a more favorable interaction with the electron-rich alkene takes place (Figure 1, right, solid line). Furthermore, the coordination to the Lewis acid alters also, to some extent, the distribution of the atomic orbital coefficients of the dienophile and the 1,3-diene. For a carbonyl compound an increase in the magnitude of the LUMO atomic orbital coefficient at the carbonyl carbon atom is observed making it more susceptible to the diene. However, this polarization may also influence the reaction mechanism.

The stereochemistry of a product formed in the HDA reaction depends on the approach of the substrate; the HDA reaction can proceed *endo* or *exo*. For the HDA reaction of,

for example, an β,γ -unsaturated α -keto ester with ethyl vinyl ether there are four possible approaches leading to four diastereomers, as the β,γ -unsaturated α -keto ester can be both *E*- and *Z*-configured. These four possibilities are outlined in Scheme 1 and it appears that the *cis* adduct can be formed by either an *endo-E-syn* or *exo-Z-syn* orientation, whereas the *trans* adduct is obtained by either an *exo-E-anti* or *endo-Z-anti* orientation.

The diastereoselectivity of the HDA reaction of, for example, carbonyl compounds is affected by the presence of Lewis acids. The uncatalyzed reaction of aldehydes usually show *endo*-selectivity for the carbonyl substituent.^[5] In the presence of Lewis acids as catalysts, it has been proposed that the Lewis acid is oriented *trans* to the carbonyl substituent and that the modest *endo*-selectivity observed in most cases is due to a preference for the solvated Lewis acid being *exo* because of its size.^[6] However, when discussing the stereochemical course of HDA reactions, it is important to note that the configuration of the diene in the ground state does not necessarily have to be the same as that of the reacting diene.^[7]

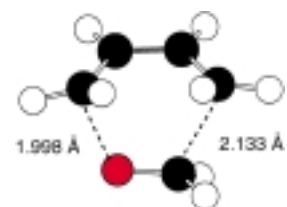


Scheme 1. The four different approaches for the HDA reaction of an β,γ -unsaturated α -keto ester with ethyl vinyl ether.

Compared to the numerous theoretical calculations on the normal DA reaction, only very few theoretical studies of HDA reactions have been performed,^[8] and even fewer on Lewis acid catalyzed HDA reactions. It has been pointed out that the HDA reaction can change from a concerted non-synchronous mechanism to a stepwise mechanism depending on the substituents on the reacting species and on the reaction conditions.

The transition state of the HDA reaction is generally found to be unsymmetrical. For the reaction of formaldehyde with 1,3-butadiene, Houk et al. have calculated the C–C and C–O bond lengths to be 2.133 and 1.998 Å, respectively, in the transition state **1** by using ab initio calculations (Scheme 2).^[8b] The reaction of formalimine follows the same trend for the transition-state structure.

An investigation of the HDA reaction of formaldehyde with 1,3-butadiene, in which the oxygen atom of the aldehyde was coordinated to BH_3 as a model for a Lewis acid,^[8b] gave two



Scheme 2. The transition state **1** (ab initio calculations) of the HDA reaction of formaldehyde with 1,3-butadiene is unsymmetrical.

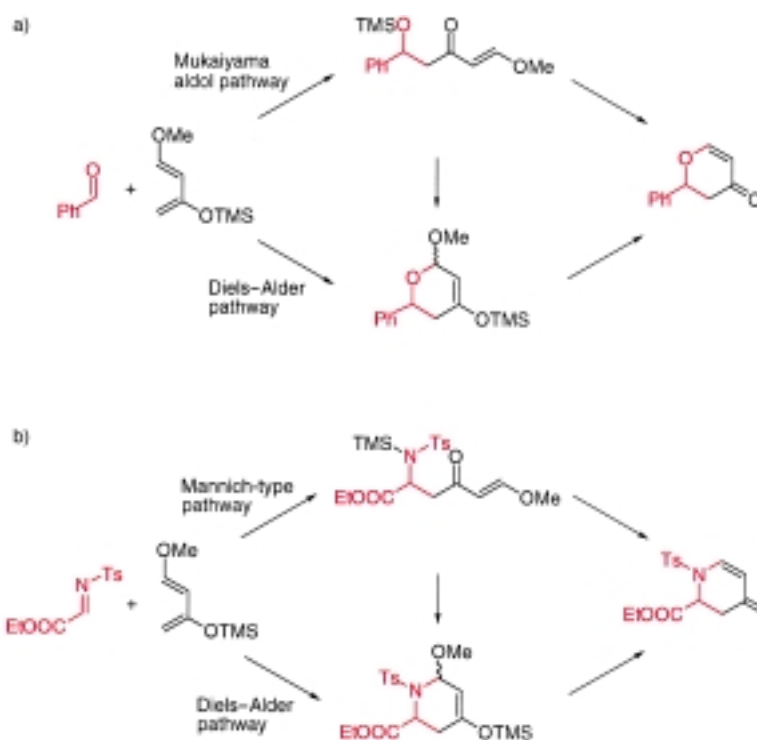
transition states, in which BH_3 adopts either an *exo* or an *endo* position relative to the diene. The transition state with the BH_3 in the *exo* position has the lowest energy and the calculated transition-state structure is much less symmetrical than **1**; the C–C bond length is calculated to be 0.42 Å longer, while the C–O bond length is 0.23 Å shorter than in **1**. The transition state of the Lewis acid catalyzed reaction has significant zwitterionic character, with a partial positive charge of 0.37 on the diene and a negative charge on the formaldehyde oxygen atom of -0.65 and -0.28 on BH_3 . The coordination of the carbonyl oxygen atom to BH_3 makes the carbonyl group an acceptor of negative charge, and the O–B bond length in the transition state is 0.12 Å shorter than that in the BH_3 –formaldehyde complex, indicating a tighter complexation in the transition state.

By coordination of the formaldehyde oxygen atom to BH_3 the activation energy of the reaction with 1,3-butadiene drops considerably. This is in agreement with the experimental results, since Lewis acid catalysis in general are required for reactions of carbonyl dienophiles to proceed^[9] and/or are found to enhance the reaction rate. Houk et al. have found that at the highest level of calculations (MP2/6-31G*), the activation energy is 8.9 kcal mol⁻¹, which is 12.0 kcal mol⁻¹ lower in energy than the uncatalyzed reaction.^[8b] The calculations indicate that the *exo* position is favored due to the greater electrostatic repulsion between BH_3 and the butadiene fragment in the *endo* transition-state structure.

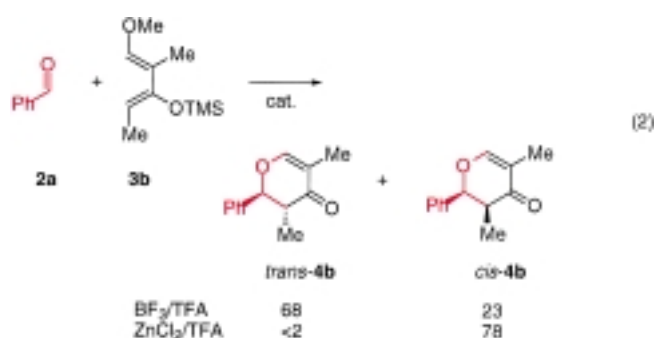
Two mechanistic pathways have generally been taken into account for the HDA reaction when Lewis acid catalyzed reactions are considered. The two pathways are formulated as 1) a traditional DA cycloaddition or 2) formation of the HDA adduct by a Mukaiyama–aldol reaction pathway in the case of a carbonyl compound, or a Mannich-type reaction for an imine (Scheme 3).

There are only few mechanistic studies of Lewis acid catalyzed HDA reactions with carbonyl compounds and imines. Danishefsky et al. concluded that the reaction of benzaldehyde **2** with *trans*-1-methoxy-3-(trimethylsilyloxy)-1,3-dimethyl-1,3-butadiene (**3b**) in the presence of BF_3 as the catalyst proceeds by a stepwise mechanism, whereas a concerted reaction takes place when ZnCl_2 or lanthanides are the catalysts.^[10] The evidence of a change in the diastereomeric outcome of the reaction is that *trans*-**4b** is the major HDA adduct in the BF_3 -catalyzed reaction, while *cis*-**4b** is the major adduct, for example, for the ZnCl_2 -catalyzed reaction—the latter resulting from an *exo* addition [Eq. (2)].

The influence of Lewis acids on the reaction pathway is also dependent on the reactant structure. The HDA reaction of monosubstituted dienes have shown that, for example, BF_3 catalysis can give the HDA adduct by a mechanism in which the Mukaiyama aldol and Michael cyclization pathway does not seem to operate.^[11]

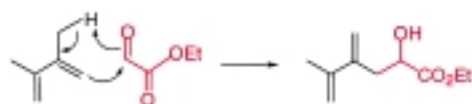
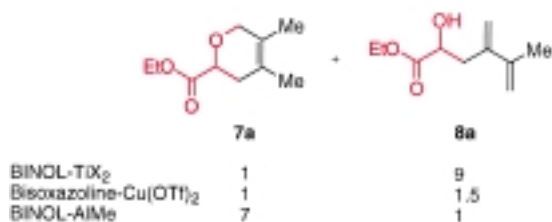


Scheme 3. The two different reactions pathways for the reaction of a) a carbonyl (benzaldehyde) and b) an imine (*N*-tosyl α -imino ester) with an activated diene (Danishefsky's diene). The HDA adduct can be formed by a traditional DA pathway as well as by a Mukaiyama–aldol reaction pathway in the case of the carbonyl compound and by a Mannich-type reaction for the imine. TMS = Me_3Si ; Ts = $\text{SO}_2\text{C}_6\text{H}_4\text{CH}_3$.



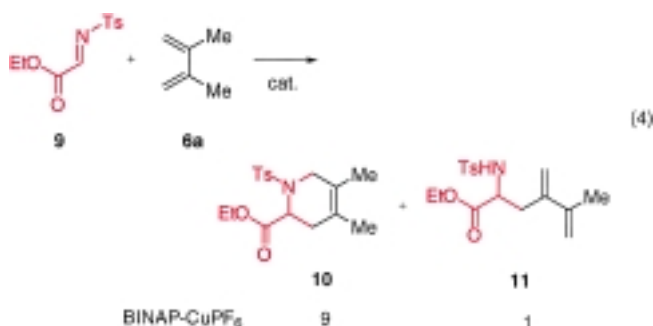
The reaction course of the HDA reaction can also be dependent on the Lewis acid complex used as the catalyst. When the substrate contains an allylic C–H bond, both a HDA and an ene reaction can take place. For the reaction of glyoxylate **5a** with 2,3-dimethyl-1,3-butadiene (**6a**) both the HDA adduct **7a** and ene adduct **8a** can be obtained [Eq. (3)]. In the presence of BINOL–titanium(IV) complexes as the catalyst, the ene adduct **8a** is the major product with a **7a**:**8a** ratio of up to 1:9,^[12] while using bisoxazoline–copper(II) as the catalyst, a nearly 1:1 ratio of **7a**:**8a**^[13] is obtained. However, the HDA adduct **7a** is the major product when a BINOL–aluminum(III) catalyst is applied.^[14] The mechanism of the reaction of **5a** with **6a** leading to the ene adduct **8** is outlined in Scheme 4.

For the HDA reaction of imines a similar observation has been made. The reaction of the *N*-tosyl α -imino ester **9** with



Scheme 4. The mechanism for the ene reaction of ethyl glyoxylate with a diene having an allylic C–H bond.

6a catalyzed by a BINAP–copper(I) complex gives the HDA and ene adducts **10** and **11**, respectively, in a 9:1 ratio [Eq. (4)].^[15]



The mechanistic picture of the HDA reactions which appears after this brief description of the aspects and concepts of activation of the substrate by Lewis acids indicates that many parameters have influence on reaction course.

2. Hetero-Diels–Alder Reactions of Carbonyl Compounds

The HDA [$\pi 2 + \pi 4$] cycloaddition reaction of aldehydes and ketones with 1,3-dienes is a well-established synthetic procedure for the preparation of dihydropyrans, which are attractive substrates for the synthesis of carbohydrates and other natural products.^[3] Carbonyl compounds are in general of limited reactivity in HDA reactions with dienes since only electron-deficient carbonyl groups as in glyoxylates, chloral, ketomalonate, 1,2,3-triketones, and related types of compounds, react with dienes having electron-donating groups. However, the use of Lewis acids or high-pressure conditions have led to a new era for HDA reactions. In particular, the application of chiral Lewis acid catalysts has provided new opportunities for enantioselective cycloadditions. The first

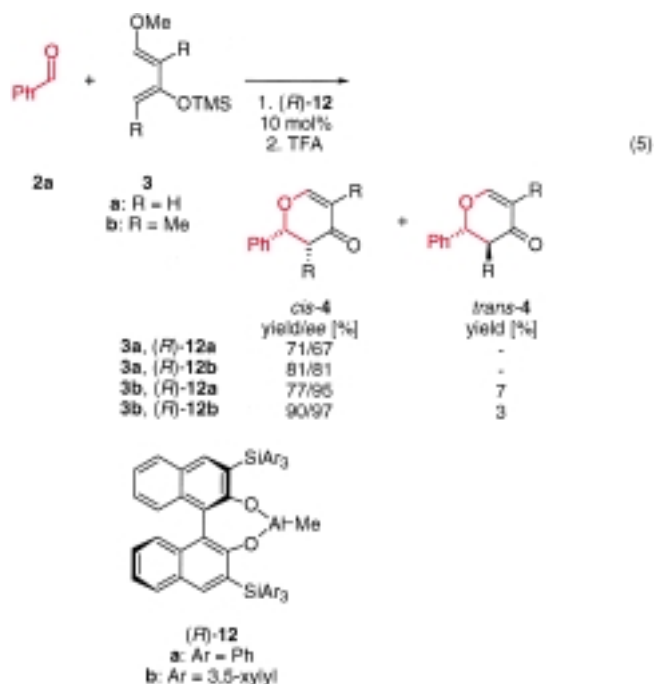
part of this section will be devoted exclusively to the development of enantioselective HDA reactions of carbonyl compounds catalyzed by chiral Lewis acids.

2.1. Reactions of Unactivated Aldehydes

Some of the developments of catalytic enantioselective HDA reactions have their origin in the DA chemistry where many of the catalysts have been applied. This is valid for catalysts which allow a monodentate coordination of the carbonyl functionality, such as the chiral aluminum and boron complexes. However, new chiral catalysts for HDA reactions have also been developed.

2.1.1. Chiral Aluminum and Boron Complexes

The first reliable and highly efficient chiral aluminum(III) catalyst for HDA reactions of aldehydes was reported by Yamamoto et al.^[16] The use of the chiral BINOL-AlMe complexes (*R*)-**12** was found to be highly effective for the HDA reaction of various aldehydes with activated Danishefsky-type dienes. For example, the reaction of benzaldehyde **2a** with *trans*-1-methoxy-3-(trimethylsilyloxy)-1,3-butadiene (Danishefsky's diene) and *trans*-1-methoxy-2-methyl-3-(trimethylsilyloxy)-1,3-pentadiene **3a** and **3b**, respectively, affords *cis*-dihydropyrones *cis*-**4** as the major product in high yield with up to 97% *ee* [Eq. (5)]. The reaction proceeds well



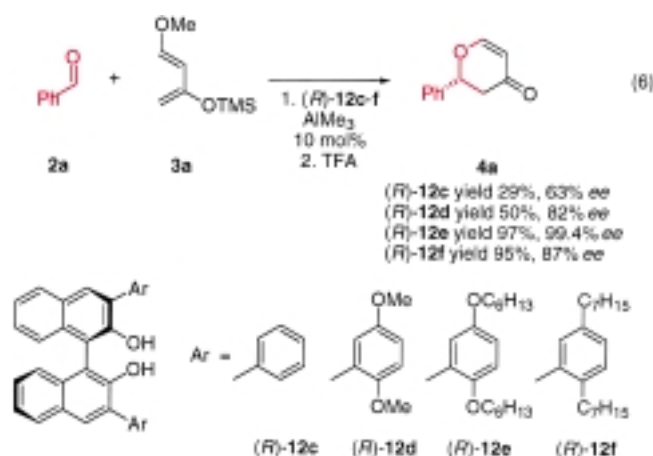
in nonpolar solvents such as toluene, where higher enantiofacial selectivity is observed compared to polar solvents such as CH₂Cl₂, where a significant retarded reaction rate is found.

The choice of the bulky triarylsilyl moiety in catalyst (*R*)-**12b** is crucial for the success of the reaction, and in contrast to this, the catalysts derived from AlMe₃ and (*R*)-3,3'-disubsti-

tuted binaphthol (substituent = H, Me, Ph) were only effective in stoichiometric amounts and gave fewer satisfactory results with regard to reactivity and enantioselectivity. The reason for this change might be that the catalyst bearing the sterically hindered auxiliary forms a complex with the aldehyde which is readily liberated from the catalyst after reaction with the diene to release steric repulsion, resulting in the regeneration of catalyst.

For the HDA reaction in Equation (5), it was found that chiral ketones such as 3-bromocamphor can bind selectively to one enantiomer of the complex.^[17] Thus, if the HDA reaction is performed in the presence of the racemic catalyst **12** and 3-bromocamphor (0.3 molar equivalents each), *cis*-**4** is isolated with up to 80% *ee* compared to 95% *ee* for the reaction catalyzed by (*R*)-**12b**.

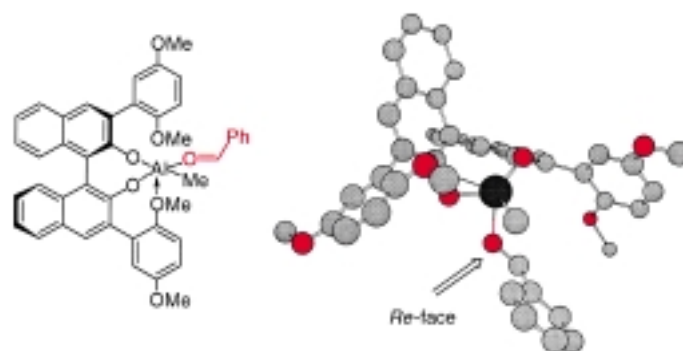
The use of the chiral BINOL–AlMe catalysts for the HDA reactions has also included ligands which have the possibility to form hypercoordinated aluminum complexes.^[18, 19] Performing the reaction of benzaldehyde **2a** with Danishefsky's diene **3a** leads to the formation of the HDA adduct **4a** in the presence (*R*)-**12c–f** in up to 97% yield and 99.4% *ee* using (*R*)-**12e** as the catalyst [Eq. (6)]. A clear trend appears: ligand (*R*)-**12c**, which has neither the steric bulk, nor the coordinating ether oxygen atoms characteristic of (*R*)-**12e**,



catalyzes the reaction, but only modest chemical and optical yields of **4a** are obtained. Ligand (*R*)-**12d**, having methoxy groups, is almost as efficient as (*R*)-**12e**, but with a modest chemical yield. Ligand (*R*)-**12f**, which should be expected to have steric properties similar to those of (*R*)-**12e**, proved to fall somewhere in between (*R*)-**12c** and (*R*)-**12e** with 87% *ee* for **4a**. The lack of the ether oxygen atoms in **12c**, which are capable of coordinating to the metal, significantly affects the enantioselectivity compared to (*R*)-**12e** and (*R*)-**12d**. These results indicate that hypercoordination can be an important factor for the design of HDA catalysts for carbonyl compounds.^[19]

Based on the absolute configuration of the HDA adduct **4a**, formed in the reaction which was catalyzed by (*R*)-**12e**, model calculations using (*R*)-**12d** show that the preferred geometry for the intermediate is one in which the two oxygen atoms from the BINOL ligand and the methyl substituent are

located in the equatorial plane with one of the ligand hypercoordinating ether oxygen atoms and the benzaldehyde oxygen atom as the two axial ligands (Scheme 5).^[19] The 2,5-dimethoxyphenyl substituent which is not coordinating to



Scheme 5. A model for the intermediate in the HDA reaction of benzaldehyde with activated dienes catalyzed by chiral BINOL–aluminum(III) complexes that are able to form hypercoordinating aluminum complexes.

aluminum is oriented perpendicular to the BINOL ligand, while the 2,5-dimethoxyphenyl substituent which hypercoordinates aluminum is twisted towards the metal. This twisting creates a chiral environment as the nonhypercoordinated 2,5-dimethoxyphenyl substituent shields the *Si* face of benzaldehyde, while the *Re* face is available for approach by the diene.

The mechanism for the HDA reaction of benzaldehyde **2a** with Danishefsky's diene **3a** catalyzed by aluminum complexes was investigated from a theoretical point of view using semiempirical calculations.^[20] The reaction was studied in the absence, and presence, of (MeO)₂AlMe as a model catalyst for the BINOL–AlMe system. The change in energy for the concerted HDA reaction, and formation of the HDA adduct by a Mukaiyama-aldol reaction, is shown in Figure 2. The conclusion of the study was that in the absence of a catalyst the concerted reaction is the most likely one with a transition-state energy of 27 kcal mol^{−1}, while for the reaction catalyzed by (MeO)₂AlMe, a two-step mechanism is found with a transition-state energy of 10 kcal mol^{−1} for the first step (the C–C bond being formed) leading to the Mukaiyama-aldol intermediate, followed by a 3 kcal mol^{−1} transition-state energy for the ring-closure step. The aldol intermediate seems to be stabilized by an interaction of the cation with the oxygen atom of the Lewis acid.

With regard to the asymmetric aluminum-catalyzed HDA reactions it should finally be mentioned that small *ee* values have been obtained in reactions with menthoxydichloroaluminum as the chiral catalyst.^[21]

Chiral boron(III) Lewis acid catalysts have been successfully applied for enantioselective HDA reactions of carbonyl compounds.^[22] The chiral acyloxylborane catalysts (CAB I) **13a–d**, were the first class of efficient chiral boron catalysts for asymmetric DA reactions.^[22, 23] The arylboron catalysts **13b** and **13c** which are air and moisture stable have been shown by Yamamoto et al. to induce excellent chiral induction in the HDA reaction between aldehydes such as **2a** and

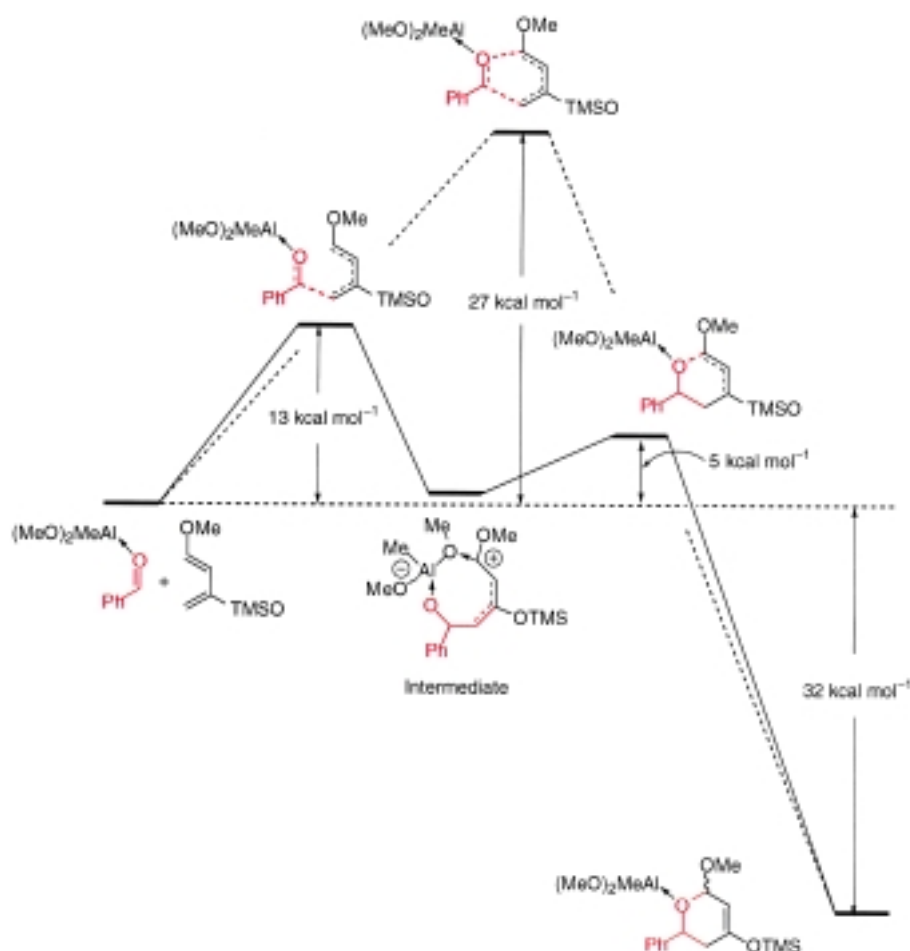
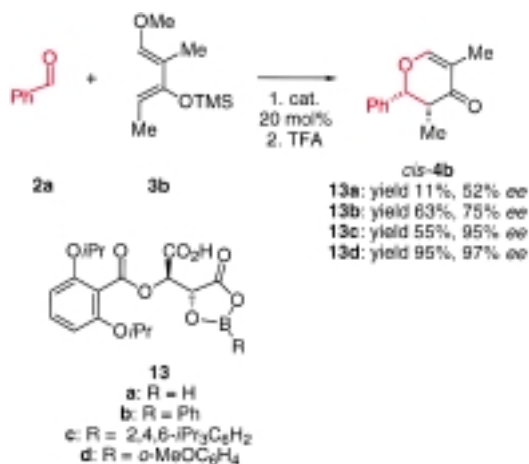


Figure 2. A schematic presentation of the energies of the transition states in the concerted reaction of benzaldehyde with Danishefsky's diene and the $(\text{MeO})_2\text{AlMe}$ catalyzed Mukaiyama-aldol like pathway.

Danishefsky's dienes such as **3a** with up to 95% yield and 97% *ee* of the HDA adduct *cis*-**4b** [Eq. (7)].^[22]



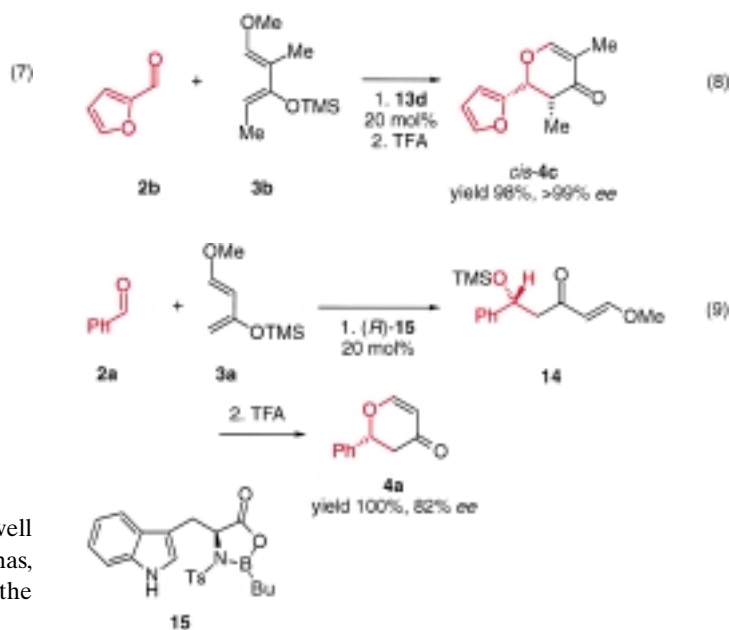
The HDA reaction catalyzed by complex **13d** proceeds well for several aromatic and α,β -unsaturated aldehydes and has, for example, been used for an enantioselective route to the carbon-branched pyranose derivative *cis*-**4c** [Eq. (8)].^[22]

The characteristic structural feature of the CAB I catalysts is a dioxaborolidinone formed with a tartaric acid derivative and a borane reagent. Following this concept, catalysts were prepared from, for example, *N*-sulfonyl α -amino acids.^[23] The chiral (*S*)-tryptophan-derived oxazaborolidine catalyst **15** developed by Corey et al. has been applied for the conversion of aldehydes to the HDA adduct **4a** by reaction with Danishefsky's diene **3a**.^[23b] The reaction of benzaldehyde **2a** affords mainly the Mukaiyama-aldol product **14** which after isolation was converted to **4a** by treatment with trifluoroacetic acid (TFA) [Eq. (9)]. It was observed that no HDA adduct was produced in the initial step providing evidence for the two-step process.

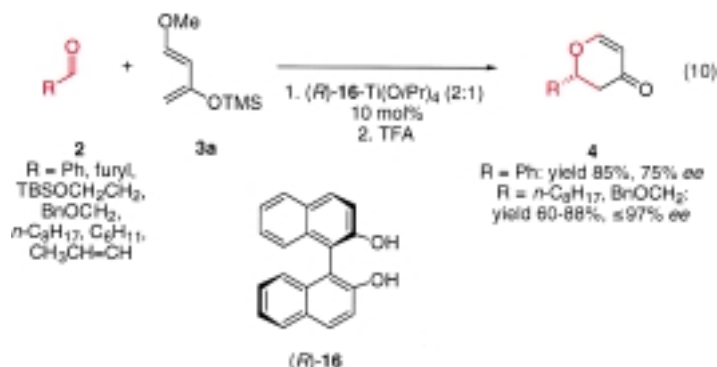
2.1.2. Chiral Transition and Lanthanide Metal Complexes

Different chiral transition- and lanthanide metal complexes can catalyze the HDA reaction of unactivated and activated (vide infra) aldehydes with especially activated dienes. For the chiral titanium catalysts the focus has been on the use of BINOL–titanium(IV) complexes for the HDA reactions. These catalysts have been widely used as chiral catalysts in enantioselective C–C bond-forming reactions of aldehydes.^[12, 24]

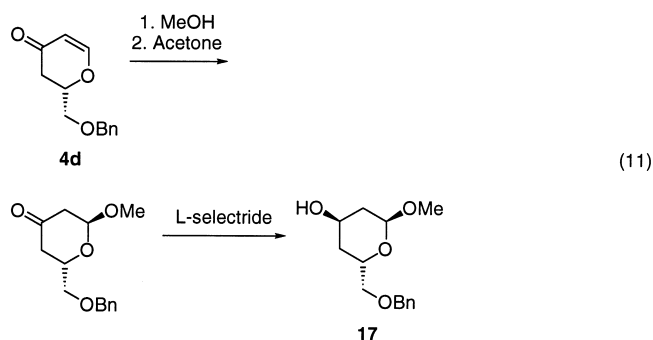
Keck et al. reported that a catalyst generated from (*S*)- or (*R*)-BINOL **16** and $\text{Ti}(\text{O}i\text{Pr})_4$ in a 2:1 ratio is more selective than the catalyst formed from a 1:1 mixture.^[24f] The former



catalyst was shown to catalyze the HDA reaction of aldehydes **2** with Danishefsky's diene **3a** affording the dihydropyrones **4** with moderate to excellent *ee* values (up to 97% *ee*) [Eq. (10)].

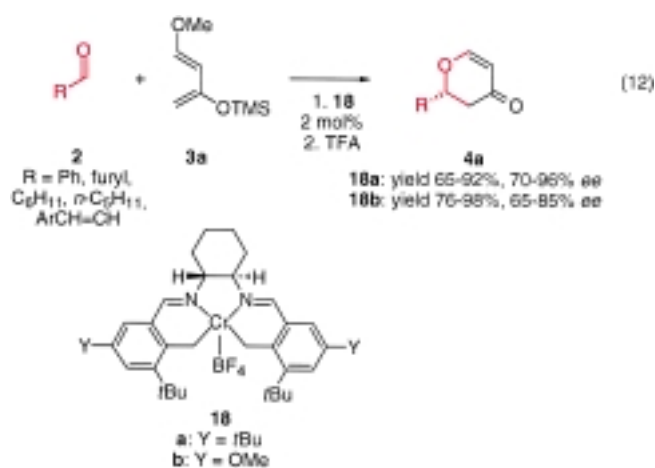


The dihydropyrones are not produced directly in the initial BINOL–titanium(IV) catalyzed reaction. The major product at this stage is the Mukaiyama–aldol product which subsequently was cyclized by treatment with TFA.^[24f] The formal HDA adduct **4d** (97% *ee*) obtained from α -(benzyloxy)acetaldehyde is an important intermediate for compactin and mevinolin (lovastatin), whose structural subunit **17** is available in three steps by applying the HDA approach [Eq. (11)].^[24f]



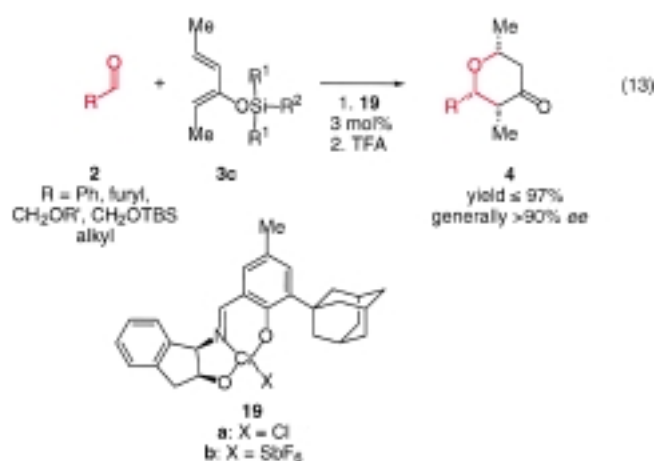
A bis[3-(heptafluorobutyl)camphorato]oxovanadium(IV) complex (5 mol %) was shown by Togni to catalyze the HDA reaction of mainly benzaldehyde with dienes of the Danishefsky type.^[25] Moderate to good enantioselectivities were observed if the reactions were carried out at low temperature. A thorough investigation was performed with benzaldehyde and various activated dienes, and reactions involving double stereodifferentiation using a chiral aldehyde.

The salen ligand has been used in catalytic enantioselective HDA reactions of carbonyl compounds with dienes in combination with metal salts such as chromium and cobalt (H_2 salen = bis(salicyliden)ethylenediamine). Jacobsen et al.^[26] have shown that the chiral salen–chromium(III) complexes **18a**, and **18b** can catalyze the HDA reaction of different aldehydes **2** containing aromatic, aliphatic, and conjugated substituents with Danishefsky's diene **3a** [Eq. (12)]. The reaction proceeds in good yield (up to 98%) and 62–93% *ee*. It was found that the presence of oven-dried powdered 4 Å



molecular sieves (MS) led to an increased yield and enantioselectivity. The lowest enantioselectivity (62% *ee*, catalyst **18b**) was obtained for hexanal, while the highest (93% *ee*, catalyst **18a**) was obtained for cyclohexylaldehyde. The mechanism of the HDA reaction was investigated in terms of a traditional HDA-type cycloaddition, or formation of the HDA-adduct by a Mukaiyama–aldol-reaction path (Scheme 3a). In the presence of the chiral salen–chromium(III) catalyst system, ¹H NMR spectroscopy of the crude reaction mixture of the reaction of benzaldehyde with **3a** revealed the exclusive presence of the HDA-pathway adduct. The Mukaiyama–aldol condensation adduct was prepared independently and subjected to the conditions of the chiral salen–chromium(III) catalyzed reactions. No detectable HDA adduct could be observed and these results point towards a [2+4] cycloaddition mechanism.

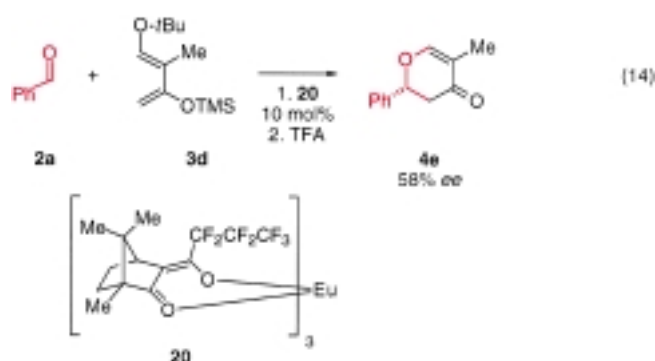
An important step in the development of a more general catalytic enantioselective HDA reaction has also been achieved by Jacobsen et al. by the introduction of chiral tridentate Schiff base chromium(III) complexes **19** [Eq. (13)].^[27] These complexes, which are highly diastereo- and enantioselective catalysts for the reaction of unactivated



aldehydes, can catalyze the reaction of less nucleophilic dienes bearing fewer than two oxygen substituents. The adamantyl-substituted catalysts **19a** and **19b** gave the best

results, and both aliphatic and aromatic aldehydes underwent HDA reactions. It was found that use of the hexafluoroantimonate chromium catalyst **19b** resulted in a faster and more enantioselective reaction and that the reaction can proceed without solvent. The reaction was tested for various dienes, for example 1-methoxy-1,3-butadiene reacts with $\text{TBSOCH}_2\text{-CHO}$ ($\text{TBS} = t\text{BuMe}_2\text{Si}$) in the presence of only 0.5 mol % catalyst **19a** to give the corresponding HDA adduct in >99% *ee*. This latter reaction provides, after hydrolysis and oxidation to the corresponding lactone, an efficient access to interesting natural product structures.

Danishefsky et al. were probably the first to observe that lanthanide complexes can catalyze the HDA reaction of aldehydes with activated dienes.^[28] The reaction of benzaldehyde **2a** with activated conjugated dienes such as **3d** was found to be catalyzed by $[\text{Eu}(\text{hfc})_3]$ (**20**) ($\text{hfc} = 3\text{-(heptafluoropropylhydroxymethylene)camphorate}$) giving up to 58% *ee* [Eq. (14)]. For other substrates the HDA adducts were



obtained with 20–40% *ee* when the reaction was performed in CHCl_3 at room temperature with 1 mol % of **20**. A significant improvement was obtained when the reaction was performed in the absence of a solvent and at reduced temperature. Catalyst **20** has also been applied for diastereoselective HDA reactions using chiral *O*-menthoxy-activated dienes, derived from (–)-menthol, giving up to 84% *de*^[28b,c] and has been used for the synthesis of optically pure saccharides.

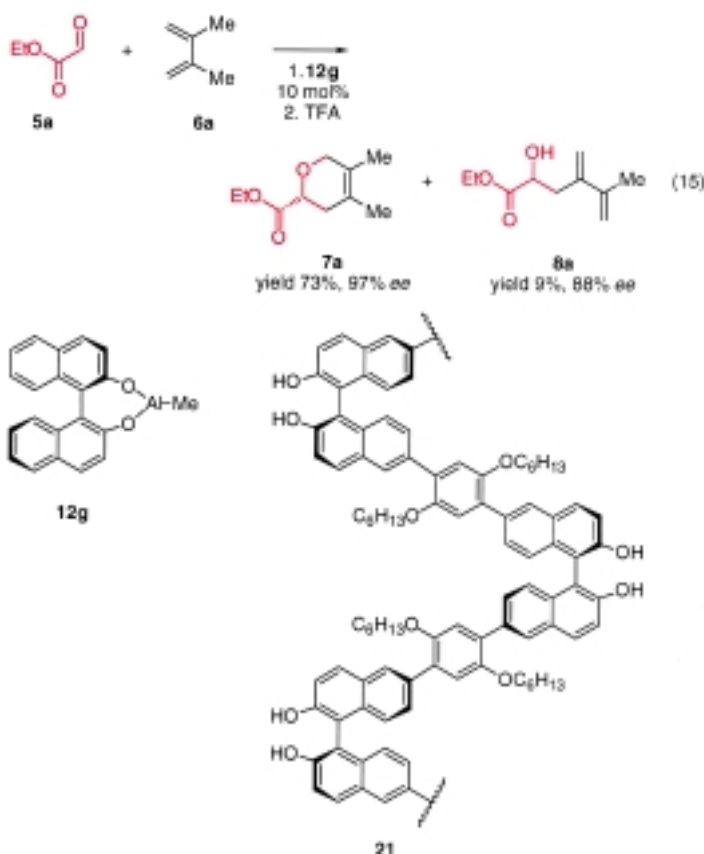
More recently, Inanaga et al. have shown that ytterbium tris[(*R*)-(–)-1,1'-binaphthyl-2,2'-diyl]phosphonate can catalyze the HDA reaction of aromatic aldehydes with Danishefsky's diene to give the HDA adduct in good yield and with up to 93% *ee* at room temperature.^[29] The addition of 2,6-lutidine improved the catalytic properties of the complex.

2.2. Reactions of Activated Aldehydes

Different main group, transition, and lanthanide metal complexes can catalyze the HDA reaction of activated aldehydes with activated and nonactivated dienes. The chiral metal complexes which can catalyze these reactions include complexes that allow substrates to coordinate in a mono- or bidentate fashion.

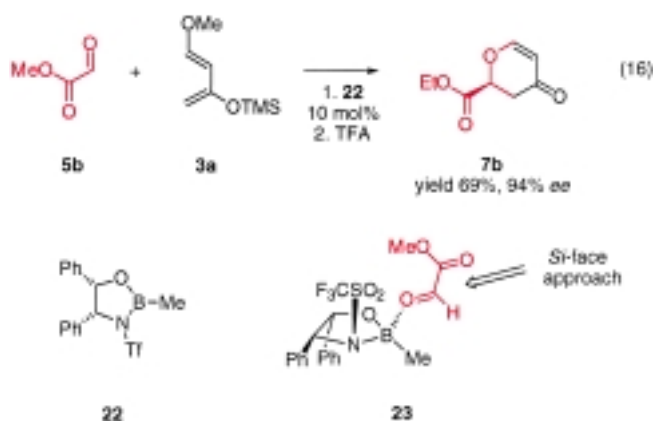
2.2.1. Chiral Aluminum and Boron Complexes

Chiral BINOL–AlMe complexes can catalyze a highly chemo- and enantioselective HDA reactions of activated aldehydes with conjugated dienes.^[14] The reaction of ethyl glyoxylate (**5a**) with simple dienes, such as 2,3-dimethyl-1,3-butadiene (**6a**), in the presence of (*R*)-BINOL–AlMe **12g** as the catalyst gives the HDA **7a** adduct as the major product in 73% yield with up to 97% *ee* and with only 7% of the ene adduct **8a** [Eq. (15)]. This is a significant change in chemoselectivity towards the HDA reaction pathway compared with the use of chiral titanium(IV) as well as chiral copper(II) and zinc(II) complexes, which give mainly the ene adduct, and a mixture of HDA and ene adducts, respectively (vide infra).



The reaction in Equation (15) was further developed to be the first catalytic enantioselective HDA reaction catalyzed by a chiral polymeric Lewis acid complex.^[30, 31] The use of the chiral polybinaphthyl polymer **21** in combination with AlMe_3 in the reaction of **5a** with **6a** gave the HDA adduct **7a** in 67% yield and up to 95% *ee*, and a **7a**:**8a** ratio of 5:1. The most important aspect of the using **21** is that it can easily be recovered by simple filtration with MeOH and reused without significant change in yield, chemo-, and enantioselectivity.

Mikami et al. have shown that chiral boron(III) complexes can catalyze the HDA reaction of glyoxylates with Danishefsky's diene [Eq. (16)].^[32] Two classes of chiral boron catalysts were tested, the β -amino alcohol derived complex **22** ($\text{Tf} = \text{SO}_2\text{CF}_3$) and bis-sulfonamide complexes. The former catalyst gave the best results for the reaction of methyl glyoxylate (**5b**)

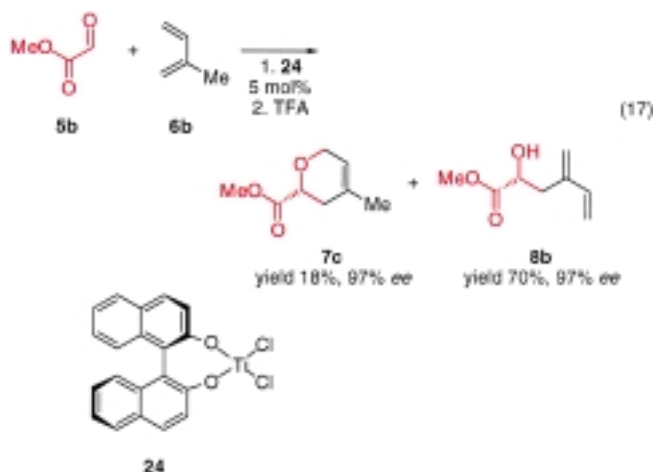


with diene **3a**, where the HDA adduct **7b** was isolated in 69 % yield and 94 % *ee*, while the chiral bis-sulfonamide boron complex gave only 62 % *ee*.

Based on the absolute configuration of **7b** [Eq. (16)], it was postulated that **5b** coordinates in a monodentate fashion to the chiral catalyst **22** as outlined in **23** by which the *Re*-face of the activated carbonyl functionality is shielded by the triflate group allowing the diene to approach in an *endo*-fashion to the *Si*-face of the carbonyl functionality.^[32]

2.2.2. Chiral Transition Metal and Lanthanide Complexes

The interest in chiral titanium(IV) complexes as catalysts for reactions of carbonyl compounds has, for example, been the application of BINOL–titanium(IV) complexes for ene reactions.^[12, 24] When isoprene **6b** was employed as the diene for reaction with methyl glyoxylate **5b** in the presence of catalyst **24** prepared in situ from [Ti(O*i*Pr)₂X₂] and an optically pure BINOL, both the HDA and ene products **7c** and **8b**, respectively, [**7c**:**8b** ratio 1:4] were obtained with excellent enantioselectivity (97 % *ee*) [Eq. (17)].^[33]



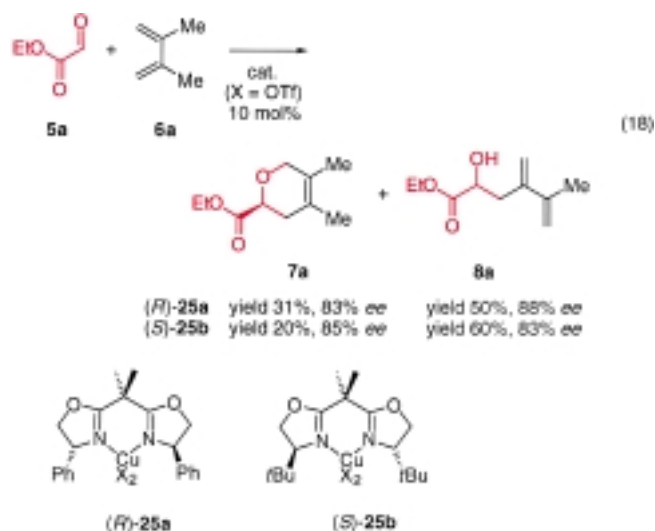
Mikami et al. have also shown that a BINOL–titanium(IV) complex in which the 6 and the 6'-position of the BINOL ligand is substituted with bromine catalyzes a selective HDA reaction of methyl glyoxylate with 1-methoxy-1,3-diene in up to 81 % yield and 97 % *ee*.^[33c]

The remarkable change in reaction course is notable when changing the metal from aluminum to titanium for HDA reactions using BINOL as the chiral ligand. When the chiral aluminum(III) catalyst is applied the HDA adduct is the major product, while for the chiral titanium(IV) catalyst, the ene adduct is the major product. The reason for this significant change in reaction course is not fully understood. Maybe the glyoxylate coordinates to the former Lewis acid complex in a monodentate fashion, while in the latter case, the glyoxylate coordinates in a bidentate fashion and these two coordination modes promote the two different reaction courses.

Chiral salen–cobalt(III) complexes can also catalyze the reaction of glyoxylates with activated dienes to give the HDA adduct in moderate yield and enantiomeric excess.^[34]

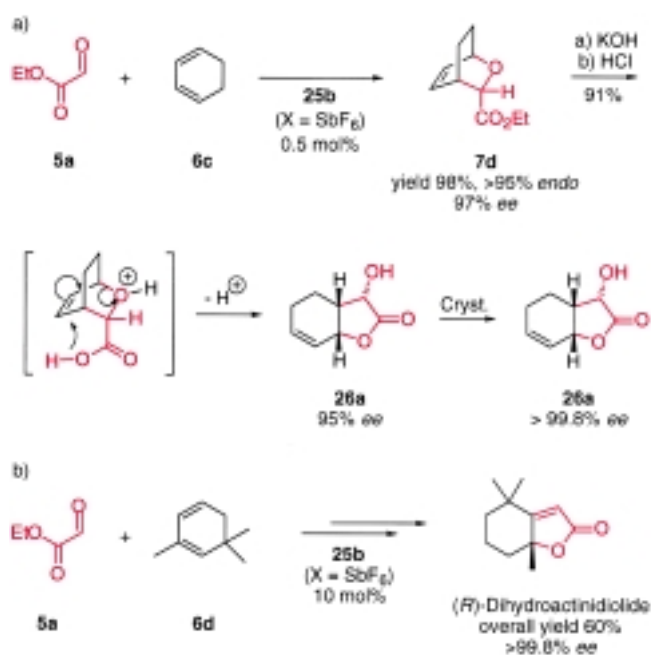
In 1995, it was demonstrated that chiral C₂-symmetric bisoxazoline–copper(II) complexes^[35–43] are efficient catalysts for HDA and ene reactions of glyoxylates with simple dienes^[13] leading to an intense activity in the use of these catalyst for different HDA reactions.

For the reaction of ethyl glyoxylate (**5a**) with, for example, 2,3-dimethyl-1,3-butadiene (**6a**) in the presence of Ph-BOX–CuX₂ (*R*)-**25a** or *t*Bu-BOX–CuX₂ (*S*)-**25b** (BOX = bisoxazoline) catalysts, ratios of 1:0.6 to 1:1.8 of the HDA adduct **7a** relative to the ene adduct **8a** were obtained [Eq. (18)]. These



results show that the chiral BOX–copper(II) system gives a higher ratio of HDA products than the chiral BINOL–titanium (IV) catalyst. The absolute configuration of the product in these HDA reactions catalyzed by the chiral BOX–copper(II) complexes led, according to the best of our knowledge, to the first report with the interesting observation that the 4-*tert*-butyl-BOX ligand and the 4-phenyl-BOX ligand in combination with copper(II) salts give opposite asymmetric induction in the product. Using the copper catalysts derived from the *R* enantiomer of the phenyl-BOX ligand and the *S* enantiomer of the *tert*-butyl-BOX ligand in combination with copper(II) afforded the same *S* enantiomer of the cycloaddition product.

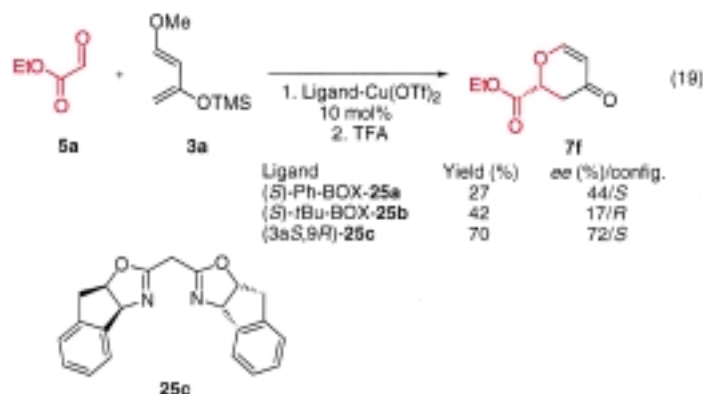
The enantioselective HDA reaction catalyzed by chiral BOX–copper(II) complexes can be used for conjugated cyclic dienes, such as 1,3-cyclohexadiene (**6c**) (Scheme 6a).^[13, 44]



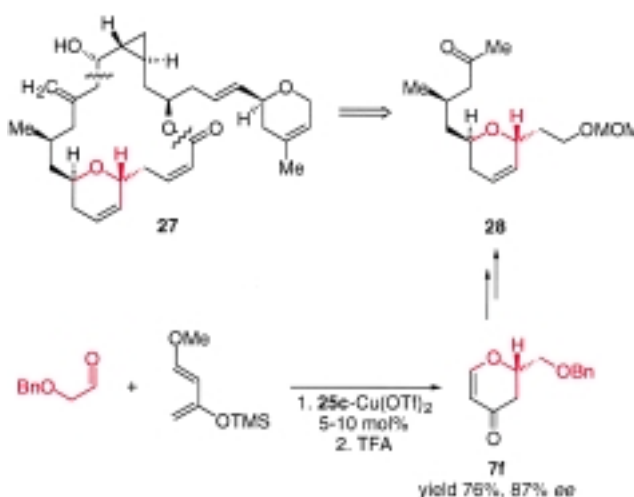
Scheme 6. a) Catalytic enantioselective HDA reaction of ethyl glyoxylate (**5b**) with 1,3-cyclohexadiene (**6c**) leading to a synthetic approach for the formation of the optically active bicyclic lactone **26a**. b) The catalytic enantioselective HDA approach for the formation of the optically active sex pheromone (*R*)-dihydroactinidiolide.

The HDA reaction of glyoxylates with conjugated dienes is dependent on solvent, and counterions have significant effects on the rate and enantioselectivity of this reaction.^[44] The reaction of **6c** was much faster when less coordinating SF_6^- was used instead of $\text{F}_3\text{CSO}_2\text{O}^-$ (OTf^- , triflate) as the counterion, and the reaction was carried out in a more polar solvent such as MeNO_2 instead of CH_2Cl_2 ; in this way the HDA adduct **7d** was isolated in 98% yield with >97% ee. It was rationalized that the reactive BOX–copper(II) catalyst is the dicationic species. Therefore, the dissociation of the two counterions from copper is important in order to activate the catalyst, and the more polar solvents will stabilize the dissociated ligand–copper cations. The potential of this reaction is illustrated by the enantioselective synthesis of a bicyclic lactone **26a** by treatment with base followed by a rearrangement reaction under acidic conditions (Scheme 6a). This approach has been used for the synthesis of (*R*)-dihydroactinidiolide (Scheme 6b),^[45] which is one of the main components of the pheromone for the queen recognition of the workers of the red fire ant, *Solenopsis invicta*. The total synthesis, which starts from ethyl glyoxylate (**5a**) and 2,6-trimethyl-1,3-cyclohexadiene (**6d**) shows for the HDA reaction the highly regio-, diastereo- and enantioselective catalytic properties of the (*S*)-*t*Bu-BOX– CuX_2 ($\text{X} = \text{SbF}_6$) complex **25b**. The catalytic enantioselective approach to the formation of the bicyclic lactones outlined in Scheme 6 seems to work only for 1,3-cyclohexadiene derivatives. However, the corresponding optically active bicyclic lactone containing a cyclopentene ring can easily be prepared by a catalytic enantioselective ene reaction catalyzed by chiral BOX–copper(II) complexes of glyoxylate with cyclopentene, followed by an iodolactonization reaction.^[43c]

Ghosh et al. have also investigated the HDA reaction catalyzed by chiral BOX–copper(II) complexes between ethyl glyoxylate (**5a**) and Danishefsky's diene **3a** by applying catalyst systems derived from $\text{Cu}(\text{OTf})_2$ and ligands (*S*)-Ph-BOX (*S*)-**25a**, (*S*)-*t*Bu-BOX (*S*)-**25b**, and the conformationally constrained BOX ligand **25c** in order to compare the properties of the latter ligand with the two others [Eq. (19)].^[46] The HDA adduct **7f** was obtained in 70% yield and 72% ee by using **25c** and $\text{Cu}(\text{OTf})_2$, which for this particular reaction was a significant improvement compared with the two other catalysts.



The methodology in Equation (19) has been used for the synthesis of the C_3 – C_{14} segment **28** of the antitumor agent laulimalide **27** (Scheme 7).^[47] The constrained chiral BOX ligand **25c** in combination with $\text{Cu}(\text{OTf})_2$ afforded dihydropyran **7f** by a HDA reaction in good yield and high enantiomeric excess, which was, converted to the C_3 – C_{14} segment **28** by a Ferrier type of rearrangement in several steps.



Scheme 7. The catalytic enantioselective HDA approach developed by Ghosh et al.^[47] for the formation of the optically active C_3 – C_{14} segment **28** of the antitumor agent laulimalide **27**. MOM = CH_2OMe .

Chiral BOX–zinc(II) complexes can also catalyze the HDA reaction of glyoxylates with conjugated dienes such as 2,3-dimethyl-1,3-butadiene and 1,3-cyclohexadiene.^[48] The reaction gave for the former diene a higher HDA:ene ratio than with the corresponding chiral copper(II) complexes, however,

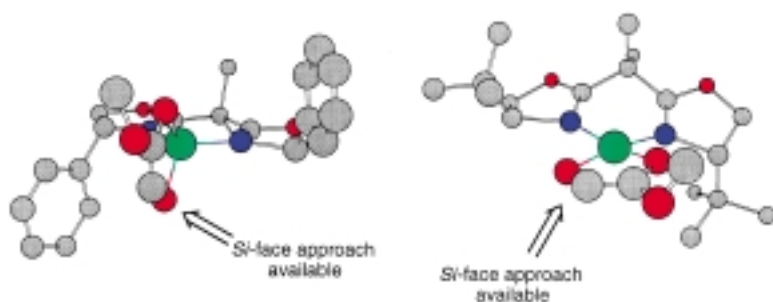
the enantiomeric excess was slightly reduced. For the reaction of 1,3-cyclohexadiene slightly lower yield and enantiomeric excess were also found.

Desimoni et al. have found that chiral BOX–manganese(II) complexes can catalyze intramolecular HDA and ene reactions with the latter as the major product.^[49]

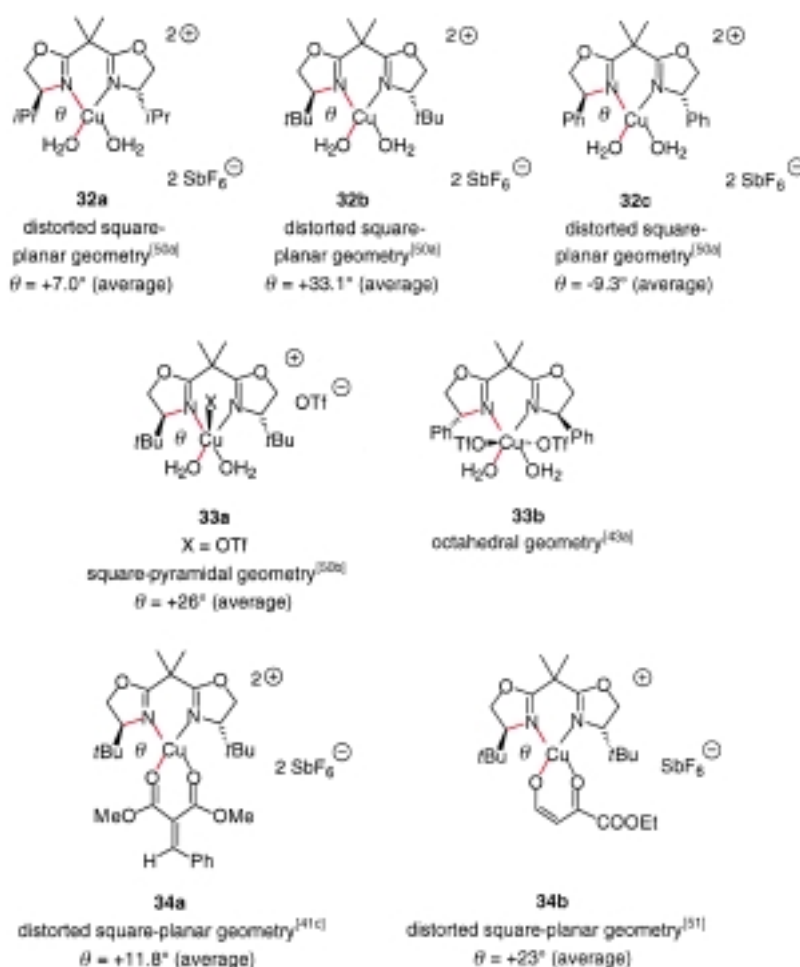
The mechanism and especially the intermediates of the HDA reactions catalyzed by the chiral BOX–copper(II) complexes deserve a separate discussion due to the peculiar ligand effect on the asymmetric induction. Based on the absolute configuration of the HDA adducts it was initially proposed that two different intermediates were operating in the reactions depending on the substituent attached to the chiral center in the BOX ligand.^[13] These two intermediates were a tetrahedral intermediate (**30**) for the reactions in which glyoxylate is coordinated to (*S*)-Ph-BOX-Cu^{II} in a bidentate fashion, while a square-planar intermediate (**31**) could account for the absolute configuration of the HDA adduct obtained in the reaction catalyzed by (*S*)-*t*Bu-BOX-Cu^{II}. The two different structural intermediates, **30** and **31**, allow the diene to approach the same face of the carbonyl functionality leading to the same absolute configuration in the product, although the absolute configuration of the chiral ligand is opposite (Scheme 8).

Several chiral BOX–copper(II) catalysts **32a–c**,^[50a] as well as **33a**^[50b] and **33b**,^[43a] and chiral BOX–copper(II) substrate/hydrolyzed enone complexes **34a, b**^[41c, 51] have been characterized by X-ray structure analysis (Scheme 9).

Chiral BOX–copper(II) coordinated complexes can have different coordination geometries. When the coordination number is four, copper(II) exhibits a distorted square-planar geometry with a dihedral angle θ in the range from $\theta = +7.0^\circ$ for the *i*Pr-BOX-Cu(OH)₂ complex **32a** to $\theta = +33.3^\circ$ for *t*Bu-BOX-Cu(OH)₂ **32b** and $\theta = -9.3^\circ$ for Ph-BOX-Cu(OH)₂ **32c**.^[50a] When the coordination number is five, the complex has a square-pyramidal geometry **33a** with the water molecules distorted 26° out of the plane.^[50b] For the (*S*)-Ph-BOX-Cu(OTf)₂(OH)₂ complex, an octahedral complex is



Scheme 8. Structures of intermediates **30** (left) and **31** (right).



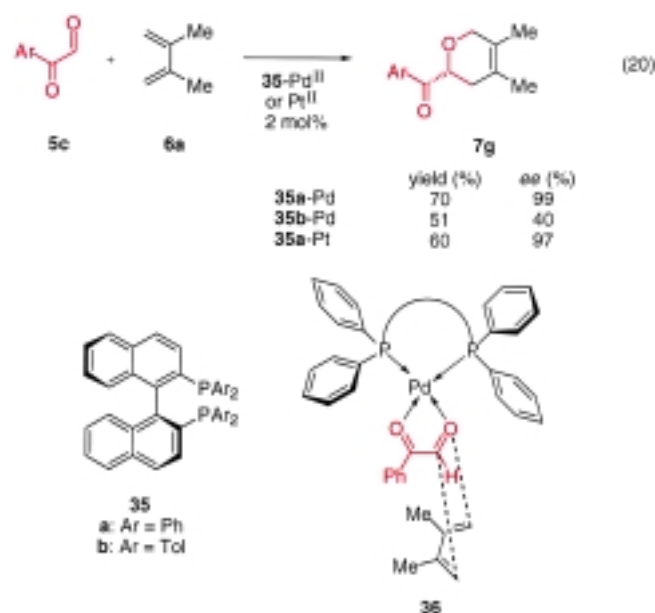
Scheme 9. The structures of some chiral BOX–copper(II)–ligand complexes characterized by X-ray crystallography. The bonds in red define the distortion angle θ .

found **33b**.^[43a] A chiral BOX–copper(II)–alkylidene malonate complex has a distorted square-planar geometry with an average distortion of 118° (**34a**).^[41c] In the inverse electron demand HDA reaction catalyzed by (*S*)-**25b** as the catalyst a failed reaction with an enone gave a crystal of the anion of the hydrolyzed enone bound to the chiral BOX–copper(II) **34b**, in which an average distortion of 23° of the two oxygen atoms was formed.^[51] If one assumes that glyoxylate replaces the two water molecules in **32b**, a chiral BOX–copper(II)–substrate intermediate **31** is formed which can account for the experimentally observed stereochemical outcome of the reactions catalyzed by the *t*Bu-BOX-Cu^{II} and *i*Pr-BOX-Cu^{II} complexes. Furthermore, the structure of the complexes **34a, b** supports also the distorted square-planar intermediate **31** for the reactions catalyzed by the *t*Bu-BOX-Cu^{II} complexes. However, the X-ray structure of the (*S*)-Ph-BOX-Cu(H₂O)₂·2SbF₆ complex **32c** can not account for the absolute configuration of the HDA adducts obtained by this catalyst, while the tetrahedral intermediate **31** does.

The above described X-ray structures were mainly obtained by Evans et al. However, they did not propose any model that rationalizes the asymmetric induction by the Ph-BOX-Cu^{II} catalyst

in the original paper dealing with DA reactions.^[52] Recently, a paper was published by the same group concerning the opposite asymmetric induction of the catalysts Ph-BOX-Cu^{II} and *t*Bu-BOX-Cu^{II}.^[50a] Although they could not offer an explanation for this phenomenon yet, it was indicated that a tetrahedral copper(II) center was unlikely. The major arguments for this conclusion were the high *endo*-selectivity observed from the HDA and ene reactions catalyzed by Ph-BOX-Cu^{II} and the lack of the obvious electronic effects from *para*-X-Ph-BOX ligands in combination with copper(II) salts. The enantiomeric excesses of the adduct obtained in HDA reactions using *para*-X-Ph-BOX ligands and copper(II) salts were 89 (X = Cl) 93 (X = H), 93 % (X = OMe). The unambiguous electronic effect of the *para*-substituents on X-Ph-BOX ligands can not exclude possible attractive catalyst–substrate (π -donor– π -acceptor) interactions.^[35c, 53] To account for the enantioselective induction in reactions catalyzed by *para*-X-Ph-BOX-Cu^{II} Evans et al. have proposed a square-pyramidal configuration.^[50a]

Cationic BINAP–palladium and –platinum complexes **35a, b** can catalyze highly enantioselective HDA reactions of arylglyoxals with acyclic and cyclic dienes [Eq. (20)].^[54] The HDA reaction proceeds well for reaction of phenylglyoxal **5c** with 2,3-dimethyl-1,3-butadiene (**6a**) in the presence of the



BINAP ligand and palladium(II) and platinum(II) salts giving 70 and 60 % yield, and 99 and 97 % *ee*, respectively, for the two Lewis acids. It is important that molecular sieves (3 Å) are added to the reaction to achieve the high enantiomeric excess, especially for the chiral palladium(II)-catalyzed reactions. The enantioselective reactions catalyzed by **35a, b** proceed with no ene adduct formation for *para*-substituted arylglyoxals and lead to good yields and high enantiomeric excesses for acyclic and cyclic dienes, such as 1,3-cyclohexadiene which gives 69 and 74 % yield and >99 % *ee* of the *endo* diastereomer as the only product for the two catalysts.

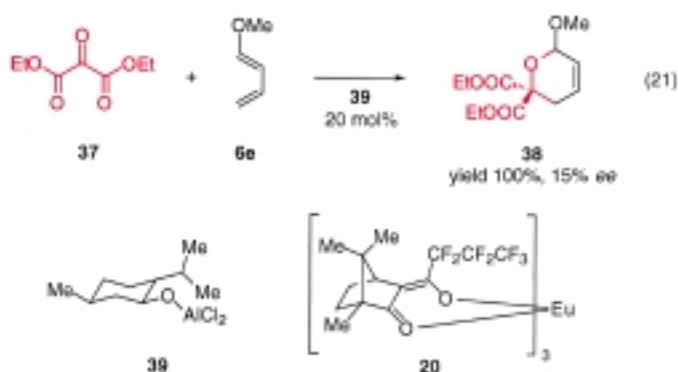
When glyoxylate esters are used as the dienophile, the reaction with, for example, 2,3-dimethyl-1,3-butadiene (**6a**) in the presence of **35a**–Pd^{II} as the catalyst gave an almost equal

amount of the HDA and ene adducts.^[54b] The enantioselectivity for the HDA adduct was excellent with up to 98 % *ee*. Based on the X-ray structure analysis of the cationic palladium species coordinated with an (*S*)-BINAP ligand having a slightly distorted square-planar geometry, it was proposed that the two carbonyl atoms of the phenyl glyoxal coordinate to the metal in a bidentate fashion as shown for **36**. Because the approach of the diene to the *Si*-face of the formyl group is blocked by the equatorial phenyl group of the ligand, the diene attacks the *Re*-face to favor the observed (*R*)-cycloadduct.^[54b]

Only few investigations have included chiral lanthanide complexes as catalysts for HDA reactions of activated aldehydes.^[55] The reaction of *tert*-butyl glyoxylate with Danishefsky's diene gave the expected HDA adduct in up to 88 % yield and 66 % *ee* when a chiral yttrium bis-trifluoromethanesulfonylamide complex was used as the catalyst.

2.3. Reactions of Ketones

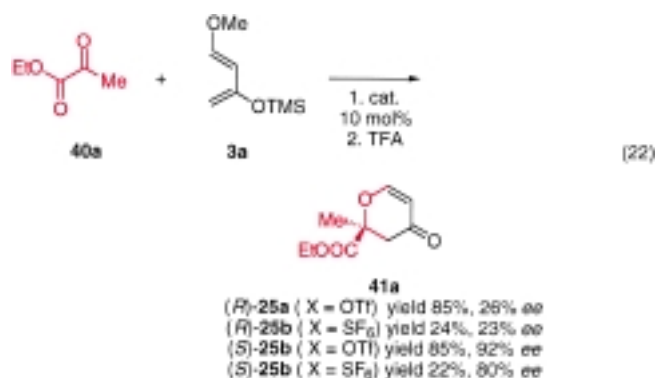
Ketones are generally less reactive than aldehydes. Therefore, the HDA reaction of ketones should be expected to be more difficult to achieve. This is well reflected in the few reported catalytic enantioselective HDA reactions of ketones compared with the many successful examples on the enantioselective reaction of aldehydes. Before we started our investigations of catalytic enantioselective HDA reactions of activated ketones^[56] there was, to the best of our knowledge, only one example reported of such a reaction by Jankowski et al. using the menthoxyaluminum catalyst **39** and chiral lanthanide catalysts **20**. The highest enantioselectivity of 15 % *ee* for the HDA adduct **38** was achieved for the reaction of ketomalonate **37** with 1-methoxy-1,3-butadiene (**6e**) using **39** as the catalyst [Eq. (21)].^[21]



The *C*₂-symmetric BOX–copper(II) complexes can also catalyze highly enantioselective HDA reactions of α -keto esters and α -diketones with conjugated dienes.^[56] These HDA reactions produce a chiral quaternary carbon center and the preparation of such a center is a demanding task in organic synthesis.^[57]

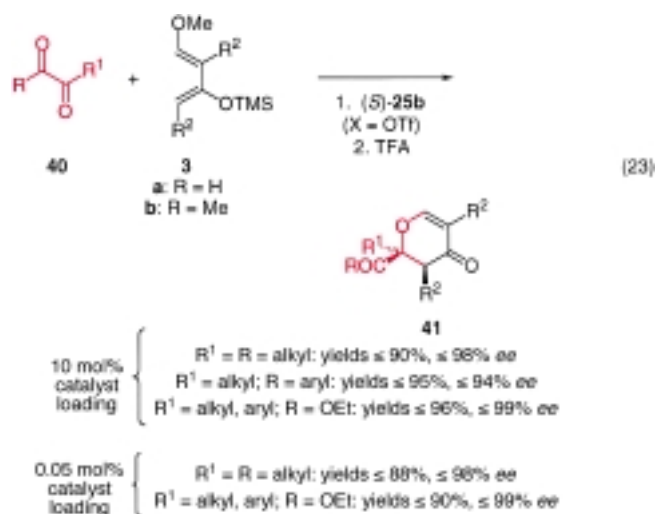
Simple dienes, such as 2,3-dimethyl butadiene or 1,3-cyclohexadiene, do not react in a HDA reaction with, for

example, ethyl pyruvate (**40a**) in the presence of chiral BOX–copper(II) complexes. However, the use of activated dienes, such as Danishefsky's diene **3a**, afforded the HDA reaction [Eq. (22)].^[56] Many different chiral BOX ligands



were tested and it was found that the *t*Bu-BOX–CuX₂ **25b** catalyst is the best for the reaction shown in Equation (22). The reaction is highly dependent on the counterions which have a significant effect on the yield and enantiomeric excess of the HDA adduct **41a**; the triflate ion is superior to the hexafluoroantimonate ion for this reaction as it led to higher yield and enantiomeric excess for all cases studied. This is opposite to the previous observations,^[44, 58] but the better results using triflate in the present reaction could be attributed to the fact that the triflate provides the suitable Lewis acidity for activating the present dienophile, and/or the fluoride atoms contained in the antimonate might destroy, or interfere, with the silyloxy-containing diene **3a**.

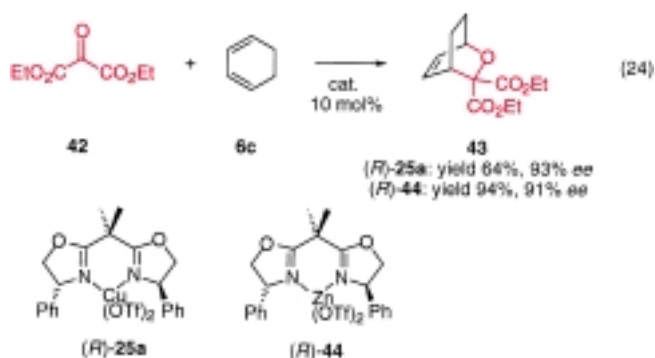
The HDA reaction of activated dienes catalyzed by *t*Bu-BOX–Cu^{II} (*S*)-**25b** is a reaction which can be used for different α -dicarbonyl compounds **40**. The results outlined in Equation (23) show the scope of the catalytic enantioselective reaction using 10 mol% of the catalyst. High yields and excellent enantiomeric excesses of the HDA adducts **41** were obtained in the reactions of **40** with the activated dienes **3a, b**. The results also show that the reaction proceeds well with good yield and very high enantiomeric excess for α -diketones and α -keto esters containing alkyl and phenyl



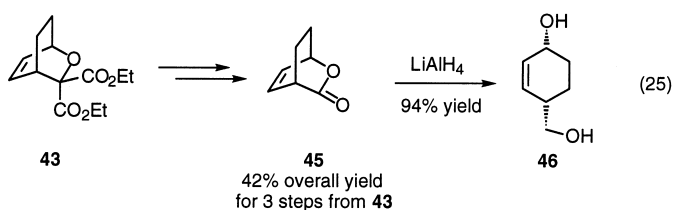
substituents. These HDA reactions of ketones can proceed to complete conversion using only 0.05 mol% of the catalyst (*S*)-**25b** (X = OTf) with only one enantiomer detected by chiral GC of the crude product.^[56b] The very low catalyst loading was found to be quite general for different α -dicarbonyl substrates and some representative results are also given in Equation (23). The turnover number for the reaction of methyl pyruvate with Danishefsky's diene is 1800 per mol catalyst (based on 90% yield using 0.05 mol% of the catalyst) for 20 h, or 90 mol^{−1} h^{−1}.^[56b] This is probably one of the lowest catalyst loadings, in addition to providing one of the highest turnover numbers in Lewis acid catalyzed asymmetric reactions. Wulff et al. have, for example, found a turnover number of 200 per mol catalyst in 4 h (50 mol^{−1} h^{−1}) reported by employing 0.5 mol% the VAPOL–aluminum(III) catalyst (VAPOL = vaulted biphenanthrol (2,2'-diphenyl-3,3'-biphenanthrene-4,4'-diol)) for enantioselective DA reactions,^[59] while Mikami et al. have reported the use of 0.2 mol% of a BINOL–titanium(IV) catalyst for glyoxylate–ene reactions^[33c] and Evans et al. have used 0.1 mol% BOX–copper(II) catalyst for the ene reaction of ethyl glyoxylate with methylenecyclohexane (0 °C, 24 h, = 90% yield, 94% ee).^[43b]

The absolute configuration of the HDA adduct obtained by the reaction of ketones with activated dienes catalyzed by (*S*)-**25b** points also to an intermediate in which the geometry around the central copper atom is square-planar similar to that in **31**, and that the diene approaches the carbonyl functionality in an *endo*-fashion.

The chiral BOX–metal(II) complexes can also catalyze HDA reactions of other ketonic substrates.^[60] The reaction of ethyl ketomalonate (**42**) with 1,3-cyclohexadiene (**6c**) can proceed with chiral BOX–copper(II) and –zinc(II) complexes, Ph-BOX–Cu(OTf)₂ (*R*)-**25a** and Ph-BOX–Zn(OTf)₂ (*R*)-**44**, respectively, as the catalysts [Eq. (24)]. The reaction proceeds with good yield and



enantioselectivity using (*R*)-**44** as the catalyst. Compared to the copper(II)-derived catalyst which affects a much faster reaction, the use of the zinc(II)-derived catalyst is more convenient as the reaction could be conducted at room temperature to achieve 94% yield and 94% ee of the HDA adduct **43**. The HDA adduct **43** formed in Equation (24) can be transformed into the optically active CO₂-synthon **45** which might have potential in organic synthesis as it can be converted into diol **46** [Eq. (25)],^[61] a key intermediate for

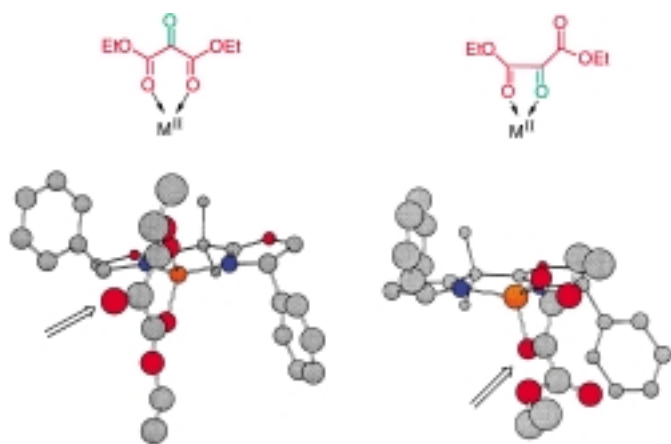


the synthesis of, for example, cyclohexenyl carbinols^[62] and anticapsin.^[63]

Notably the reaction of ketomalonate **42** with cyclopentadiene in the presence of *t*Bu-BOX-Cu(OTf)₂ between room temperature and -78°C showed some unexpected behavior.^[60] When the reaction was performed at room temperature no HDA adduct was observed. However, when the reaction temperature was lowered to -40 to -78°C ¹H NMR spectroscopy showed that the HDA adduct was formed with high conversion, but when the temperature was increased to above -30°C a retro-HDA took place.

Ketomalonate reacts also with other types of conjugated dienes with formation of HDA adducts in moderate to good enantioselectivity. For the Danishefsky-type dienes, good enantioselectivities and yield of the HDA adducts can also be achieved with chiral BOX-zinc(II) catalysts, while the copper(II)-derived catalysts gave the formal HDA and Mukaiyama-aldol products.^[60]

Calculations on the coordination of ketomalonate **42** to copper(II) and zinc(II) have revealed that the six-membered ring system is slightly more stable than the five-membered ring system (Scheme 10). The coordination of **42** to the Ph-BOX-Zn(OTf)₂ (*R*)-**44** catalyst shows that the six-membered



Scheme 10. The two different coordination modes, a five- and six-membered intermediate, for ethyl ketomalonate **42** to a Lewis acid (the reacting carbonyl functionality is green) and the proposed intermediate in which **42** is coordinated to the Ph-BOX-Zn^{II} (*R*)-**44** catalyst in the different coordination modes. In the *C*₂-symmetric intermediate (left) neither of the sides is protected, in the asymmetric intermediate (right) one of the sides is protected.

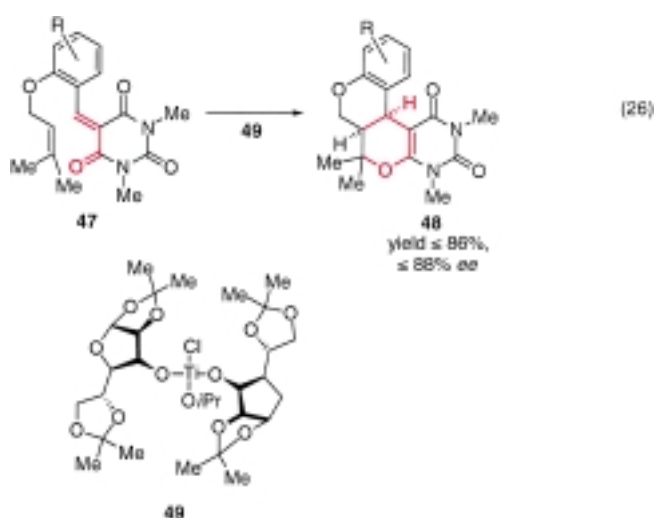
intermediate is *C*₂-symmetric with no obvious face-shielding of the carbonyl functionality (left), while for the five-membered intermediate (right) the carbonyl is shielded by the phenyl substituent. Calculations of the transition-state

energy for the reaction of the two intermediates with 1,3-cyclohexadiene leads to the lowest energy for the five-membered intermediate and this approach is in agreement with the experimental results.^[60]

2.4. Inverse Electron demand Reactions

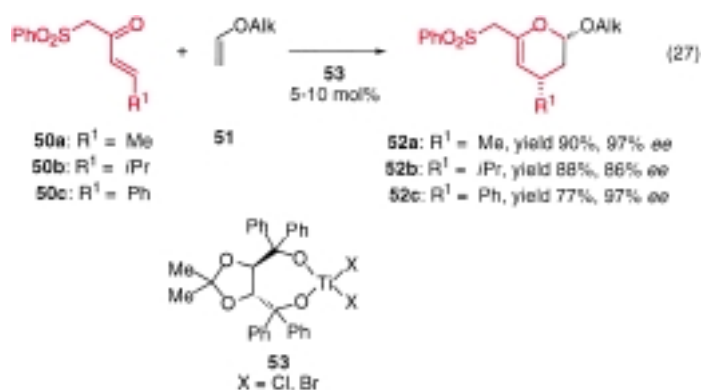
The catalytic enantioselective HDA reaction of α,β -unsaturated carbonyl compounds with electron-rich alkenes is a simple approach for the formation of 2-substituted 3,4-dihydro-2*H*-pyrans, which are useful precursors for natural products such as carbohydrates. This is an inverse electron demand controlled reaction with a dominant interaction between the LUMO of the 1-oxa-1,3-butadiene and the HOMO of the alkene (see Figure 1, right). This reaction is usually a concerted nonsynchronous transformation with retention of the configuration of the dienophile and shows normally high regioselectivity, which in the presence of Lewis acids is improved and, furthermore, also increases the reaction rate.

The inverse electron demand catalytic enantioselective HDA reaction has not been investigated to a very high extent. The first example of this class of reactions was published by Tietze et al. in 1992 where an intramolecular cycloaddition of the heterodiene **47** catalyzed by a diacetoneglucose-derived titanium(IV) Lewis acid **49** gave exclusively the *cis* product **48** in good yield and up to 88% *ee* [Eq. (26)].^[64] The reaction is



dependent on the solvent, and a racemate was obtained in CHCl₃, while the highest enantioselectivity was found in 1,2,3,5-tetramethylbenzene. The catalytic enantioselective intramolecular HDA reaction of **47** catalyzed by **49** shows an interesting temperature effect as **48** is formed in 88% *ee* at 25°C , while a racemic mixture is formed at 0°C and 100°C .

A chiral titanium(IV) complex was also applied by Wada et al. for the intermolecular HDA reaction of (*E*)-2-oxo-1-phenylsulfonyl-3-alkenes **50** with enol ethers **51** [Eq. (27)].^[65] The TADDOL-TiX₂ (X = Cl, Br) complexes **53** were found to catalyze an enantioselective reaction giving the dihydro-



pyrans **52**. The reaction is dependent on the anion of the catalyst; the best yield and enantioselectivity were found for the TADDOL–TiBr₂ complex. The dihydropyrans **52** were obtained in good yields and up to 97% ee.

The chiral BOX–copper(II) complexes are also effective catalysts for highly enantioselective HDA reactions of α,β -unsaturated acyl phosphonates^[66] and α,β -unsaturated keto esters.^[50b, 67]

The chiral BOX–copper(II) complexes, (*S*)-**25a** and (*R*)-**25b** (X = OTf, SbF₆), were found by Evans et al. to catalyze the enantioselective HDA reactions of the α,β -unsaturated acyl phosphonates **54** with ethyl vinyl ether **51a** or the cyclic enol ethers **55**, giving the HDA adducts **56** and **57**, respectively, in very high yields and enantioselectivities [Eq. (28)].^[66] Notably the acyclic and cyclic enol ethers react in a highly stereoselective manner and the same enantiomer of **56a** (R¹ = Me) is formed using (*S*)-**25a** and (*R*)-**25b** as the

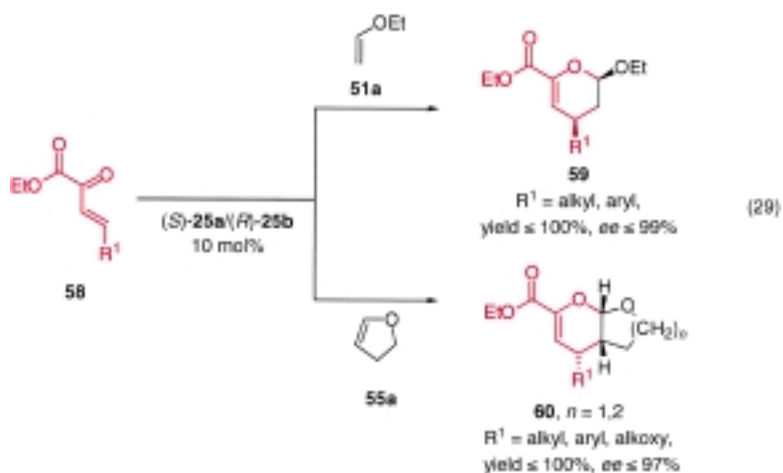


catalyst for the reaction in Equation (28). Furthermore, it is of practical importance that the HDA reaction can proceed in the presence of only 0.2 mol% of (*R*)-**25a** (X = SbF₆) with minimal reduction in the yield of the HDA adduct and no loss of enantioselectivity (93% ee).

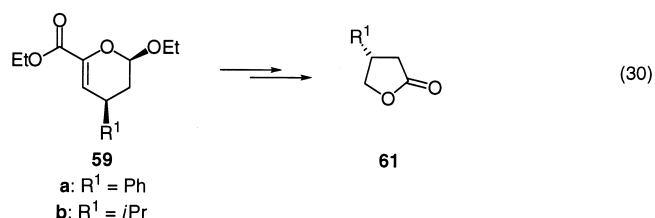
More recently, further developments have shown that the reaction outlined in Equation (28) can also proceed for other alkenes; for example, the reaction of the silyl enol ether of acetophenone^[66b] gives the *endo* diastereomer in up to 99% ee. Furthermore, it was shown that β -ethyl- β -methyl-

substituted acyl phosphonate also can undergo a diastereo- and enantioselective HDA reaction with ethyl vinyl ether catalyzed by the chiral Ph-BOX-copper(II) catalyst. The preparative use of the HDA reaction was demonstrated by performing reactions in gram scale and by showing that no special measures are required for the reaction and that the dihydropyrans can be obtained in high yield and with very high diastereo- and enantioselectivities.

Our development of the catalytic enantioselective inverse electron demand HDA reaction,^[67] which was followed by related papers by Evans et al.^[50b, 66b] focused in the initial phase on the reaction of mainly β,γ -unsaturated- α -keto esters **58** with ethyl vinyl ether (**51a**) and 2,3-dihydrofuran (**55a**) [Eq. (29)]. Under catalysis by **25b** (X = OTf₂) or the aqua complex **32b** (Scheme 9) this reaction proceeds in high yield, diastereo-, and enantioselectivity.^[50b, 66b, 67] The reaction toler-



ates a broad range of substituents at R¹, such as alkyl, aryl, alkoxy, and thiobenzyl. The reaction can proceed with only 0.5 mol% of catalyst **32b** with only a slight decrease in enantioselectivity and diastereoselectivity.^[50b, 66b] Furthermore, preliminary studies have indicated that the catalyst **32b** can be reused in multiple reaction cycles without significant loss in yield and stereoselectivity, and that the β,γ -unsaturated- α -keto esters were somewhat more reactive than α,β -unsaturated-acyl phosphonates in catalytic HDA reactions.^[50b, 66b] The absolute configuration of the HDA adducts **59a, b** was assigned by transformation to the lactones **61a, b** with known configuration [Eq. (30)].^[50b, 66b]

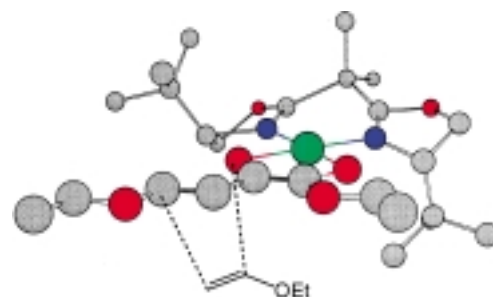


Further developments of this inverse electron demand catalytic enantioselective HDA reaction using β -substituted β,γ -unsaturated- α -keto esters **58** have resulted in simple

approaches for the synthesis of optically active carbohydrates^[51] including amino sugars^[68] (Scheme 11). The reaction can be used for the preparation of optically active spiro carbohydrates **62**, which is an important functionality found in natural products such as pheromones, steroidal compounds, antiparasitic agents, and polyether antibiotics.^[69] *cis*-Alkenes are also useful substrates for inverse electron demand catalytic enantioselective HDA reactions of β,γ -unsaturated α -keto esters, which lead to the HDA adduct in good yield and with very high diastereo- and enantioselectivities. This reaction has been used for the synthesis of the ethyl β -D-manonose tetraacetate (**63**). Interestingly, the β -glycoside linkage at C-1 of this monosaccharide is difficult to synthesize by standard carbohydrate chemistry, because it is neither possible to use the neighboring group effect at C-2, nor the anomeric effect. The HDA approach can also be used as a synthetic procedure for the preparation of the nonnaturally occurring acetal-protected C-2-branched carbohydrate **64**. The formation of amino sugars by this catalytic enantioselective reaction has shown that diastereomers **65** and **66** with different protecting groups can be formed in high yield, diastereo-, and enantioselectivities. Amino sugars can be applied as pharmaceuticals, for example, for the treatment of diabetes and as promising drugs against influenza.^[70]

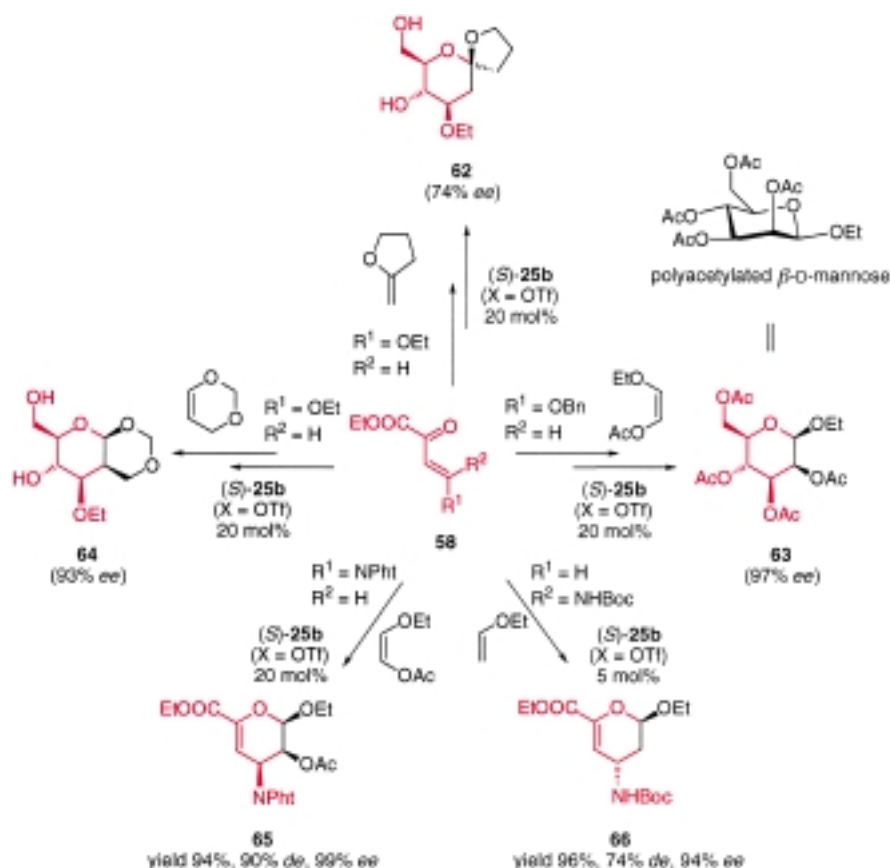
The absolute configuration of products obtained in the highly stereoselective HDA reactions with inverse electron demand catalyzed by the *t*Bu-BOX-Cu^{II} complex can also be

accounted for by a square-planar geometry at the copper(II) center. Support for a square-planar intermediate is provided by the X-ray structure analysis of the hydrolyzed enone bound to the chiral BOX-copper(II) catalyst (see **34b** in Scheme 9). It has been assumed that the γ -substituted β,γ -unsaturated α -keto ester **58** coordinates in a bidentate fashion through the carbonyl oxygen atoms to the (*S*)-*t*Bu-BOX-Cu^{II} catalyst leading to intermediate **67** (Scheme 12). The approach of, for



Scheme 12. Structure of the intermediate **67** formed in the reaction of **58** with **51a** in the presence of (*S*)-**25b**.

example, ethyl vinyl ether to the γ -substituted β,γ -unsaturated α -keto esters will thus take place from the *Si*-face of the reacting carbonyl functionality, as the *Re*-face is shielded by the *tert*-butyl substituent of the chiral ligand.



Scheme 11. The use of the BOX-copper(II) complex *t*Bu-BOX-Cu^{II} (*S*)-**25b** for the synthesis of optically active carbohydrates and amino sugars using catalytic inverse electron demand HDA reactions. NPht = phthalimidyl; Boc = *t*BuOCO.

3. Hetero-Diels–Alder Reactions of Imines

Nitrogen-containing compounds such as amino acids, peptides, and alkaloids are abundant in nature. They are of fundamental importance to our society and are, for example, particularly attractive for medicinal chemistry due to the pronounced biological and physiological properties of these compounds. The HDA, ene, and alkylation reactions of imines are powerful methodologies for the construction of nitrogen-containing compounds.^[3, 71, 72] With the increasing demands for producing optically active compounds in both enantiomeric forms, asymmetric synthesis of these compounds is a formidable challenge to the synthetic organic chemists. Not surprisingly, considerable attention has been paid to the development of asymmetric addition reactions to imines.

3.1. Diastereoselective Reactions

Great progress has been achieved in diastereoselective HDA and ene reactions, as well as the 1,2-nucleophilic

addition reactions of organometallic compounds to imines. However, many challenges remain and they need to be addressed, particularly with respect to the use of chiral Lewis acid catalysis for controlling the stereochemistry of reactions between achiral substrates.

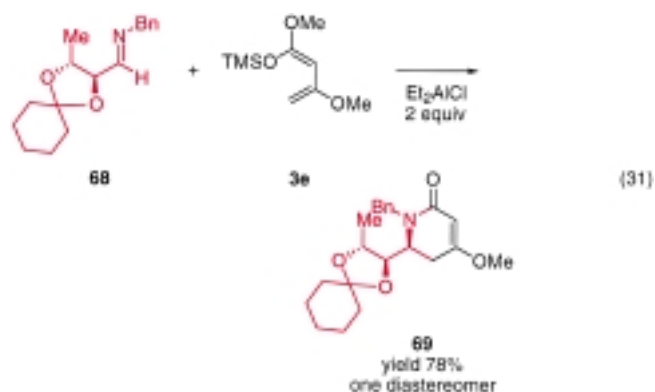
Compared to the great achievements during the last decade concerning enantioselective reactions of carbonyl compounds using chiral Lewis acid catalysts, the analogous enantioselective HDA reactions remained unavailable for a long time. Only very recently advances appeared for catalytic and catalytic enantioselective HDA reactions of imines. Some common problems related to the use of imines as substrates in catalytic enantioselective reactions can be summarized as follows: 1) the nitrogen atom of imines is more Lewis basic than the oxygen atom of carbonyl compounds. As a consequence, the coordination of the imine, or the product, to the chiral Lewis acid catalyst is stronger, leading to deactivation or inhibition of the catalyst. Therefore, stoichiometric amounts of chiral Lewis acids are often needed to achieve conversion and high asymmetric induction; 2) the flexible *E/Z* conformations of imines allow more possible structures to exist in solution; 3) the low reactivity and poor electrophilicity of the imine double bond; 4) the tendency towards deprotonation of the α -acidic proton of enolizable imines to form enamines; 5) some imines are unstable and difficult to isolate which can lead to additional difficulties.

The addition reactions of organometallic reagents, including the addition of allyl–metal reagents to C=N bonds, have been reviewed several times.^[73] In the present context an overview focusing on the catalyzed enantioselective HDA reactions of imines will be presented for the formation of optically active aza-DA compounds. First, the HDA reactions of chiral substrates catalyzed/mediated by Lewis acids will be discussed followed by catalytic enantioselective HDA reactions of achiral imines.

3.1.1. Reactions of Chiral Imines Derived from Chiral Carbonyl Compounds

Unactivated imines are normally not reactive enough to be used as dienophiles for HDA reactions. Exceptions are intramolecular additions^[74] or the use of iminium salts.^[75] In 1982, Danishefsky et al. reported the first cycloaddition involving imines with an activated diene in the presence of ZnCl_2 as the Lewis acid.^[76] It was later reported by Ojima et al. that TiCl_4 is an efficient catalyst for the reaction,^[77] and more recently, Kobayashi et al. described the use of only 10 mol % of lanthanide triflates as catalysts for an imino-DA reaction.^[78]

One of the first examples of an asymmetric cycloaddition of an unactivated imine was reported by Midland et al. in 1988.^[79] The cyclohexylidene-protected α,β -dialkoxy imine **68**, which is prepared from L-threonine, reacts with Brassard diene **3e** in the presence of a strong Lewis acid, such as Et_2AlCl , to afford a single isomer of lactam **69** in high yield [Eq. (31)]. The *syn*-configuration of the adduct was proposed to be in agreement with a “chelation-controlled” addition mechanism.

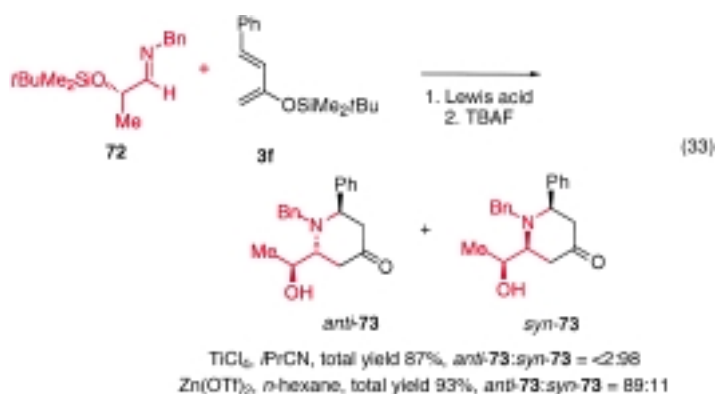


In order to investigate the effect of the nature of substrates and Lewis acids on the diastereoselectivity, Midland et al. prepared a series of α -alkoxy imines **70a–c** and studied the reaction with diene **3e** [Eq. (32)].^[80] The use of SnCl_4 gave the

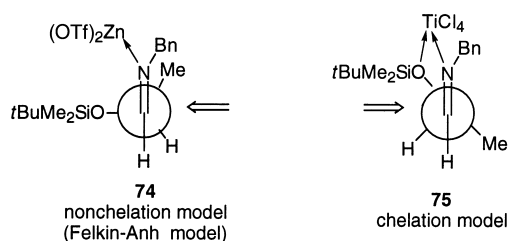


chelation-controlled diastereomers *syn*-**71** in low yields for all three substrates, while a higher *syn*-selectivity was observed when the steric bulk of the side chain was increased. When Et_2AlCl was used as the catalyst, both the “small” substrate **70a** and the “large” substrate **70c** led to a high degree of the “chelation-controlled” products *syn*-**71**, while for substrate **70b**, containing a medium-sized side chain, only poor diastereoselectivity was observed. The diastereoselectivity is also dependent on the stoichiometry of Et_2AlCl as an increase in the number of equivalents of Lewis acids from less than one equivalent to two equivalents resulted in an improvement of the *syn*-selectivity. It was concluded that in the case of Et_2AlCl as the catalyst, the mechanism may be more complicated than either a “chelation” or “nonchelation” rationale. In a real chelation-controlled process, a moderate diastereoselectivity should be expected in the case of a medium-sized substrate.

The HDA reaction of chiral α -silyloxy aldimines with activated 2-silyloxy-1,3-dienes has been investigated by Akiba et al.^[81] Only the diastereomers *anti*- and *syn*-**73** were obtained from the reaction of imine **72** with diene **3f** [Eq. (33)]. The diastereoselectivity is dependent on the Lewis acid, solvent, and temperature. Notably, using $\text{Zn}(\text{OTf})_2$ and TiCl_4 as the catalysts led to the formation of opposite diastereomers as the major products.

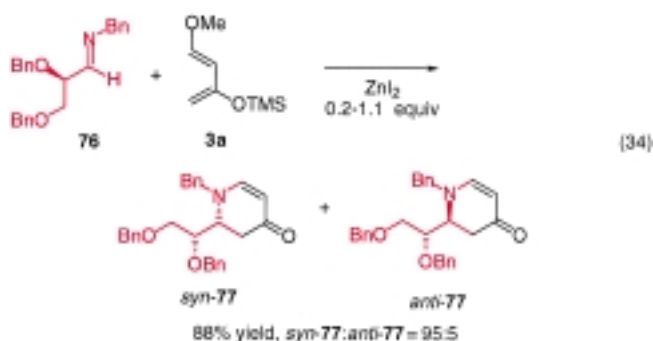


The nonchelation model **74** was proposed to account for the formation of *anti*-**73** as the major product using Zn(OTf)_2 as the catalyst, while chelation model **75** can account for the formation of *syn*-**73** using TiCl_4 as the catalyst (Scheme 13). The formation of the nonchelation product *anti*-**73** in the presence of Zn(OTf)_2 was explained by the insolubility of Zn(OTf)_2 in the solvent for the reaction (CH_2Cl_2). Thus, the reaction took place before the chelation complex of Zn(OTf)_2 –imine was formed.



Scheme 13. Chelation and nonchelation models proposed by Akiba et al.^[81] to account for the formation of the opposite induction in the presence of Zn(OTf)_2 and TiCl_4 .

Recently, Díaz-de-Villegas et al. reported an asymmetric reaction of imine **76**, derived from (*R*)-2,3-*di-O*-benzylglycerinaldehyde and benzylamine, with Danishefsky's diene **3a** [Eq. (34)].^[82] Among various Lewis acids such as MgBr_2 , ZnI_2 , $[\text{Eu}(\text{fod})_3]$ $\text{fod} = 7,7\text{-dimethyl-1,1,1,2,2,3,3-heptafluoro-}$



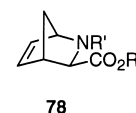
4,6-octaedioate), SnCl_4 , TiCl_4 , Et_2AlCl , and BF_3 , the catalyst ZnI_2 was the best in terms of yield and diastereoselectivity of the HDA adduct **77**. It was observed that in aprotic solvents, an increase in the solvent polarity led to an improvement of

the selectivity with *syn*-**77** as the major diastereomer (toluene: 50% *de*; CH_2Cl_2 : 82% *de*; CH_3CN or CH_3NO_2 : 90% *de*).

The stereochemical outcome of the reaction was not affected by the complexing properties of the Lewis acids as observed by Midland et al. Both the chelating Lewis acid and the aluminum or boron catalysts, which usually prefer tetracoordination, gave the same diastereomer *syn*-**77** (chelation product) in excess. A chelation model and an anti-Felkin–Anh model^[83] were proposed for the chelating Lewis acid ZnI_2 , and nonchelating Lewis acids, Et_2AlCl and BF_3 , respectively. The double asymmetric induction was investigated by employing imines bearing two chiral centers.^[82] The reaction of an imine derived from (*S*)- α -methylbenzylamine, with Danishefsky's diene gave only a single diastereomer, while the reaction of other imines afforded a mixture of enamionones with modest diastereoselectivity.

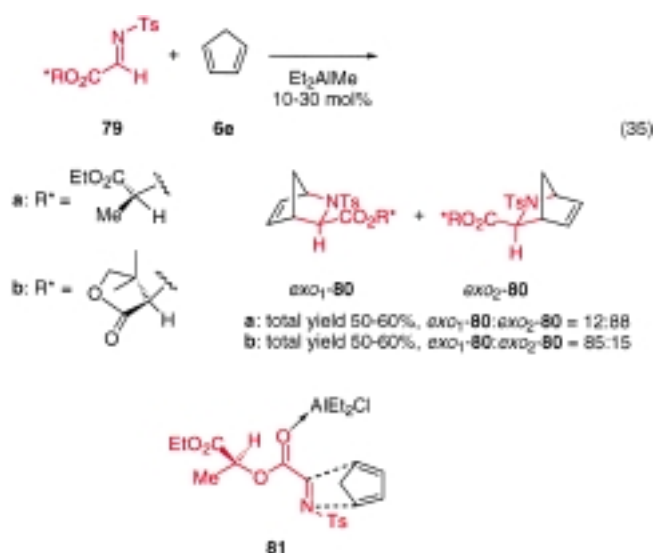
The Lewis acid catalyzed HDA reaction of chiral imines with dienes has been applied for the preparation of natural products. Herczegh et al. reported the synthesis of analogues of the natural product swainsonine by using an asymmetric HDA reaction of a Schiff base, formed in situ from the D- or L-arabinose aldehyde and benzylamine, with Danishefsky's diene in the presence of ZnCl_2 as the Lewis acid catalyst.^[84] Recently, Wang et al. reported the synthesis of azasugars by lanthanide-promoted HDA reactions in aqueous solution.^[85] In the presence of 10 mol % $[\text{Nd}(\text{OTf})_3]$ the reaction of a chiral aldehyde, prepared from D-glycosamine hydrochloride, and cyclopentadiene produced only one diastereomer in a moderate yield which could be converted into azasugars.

The HDA adduct azabicyclo[2.2.1]-heptene **78** might be a key compound for the synthesis of products of interest such as the pharmaceutically important compounds (–)-aristeromycin, carbosvir, 1592U89, and (1*R*,3*S*)-amidinomycin.^[86] Several examples are available for the synthesis of optically active **78** starting from chiral or achiral substrates in the absence^[86] and presence of a Lewis acid, as well as the presence of chiral Lewis acids, as catalysts.



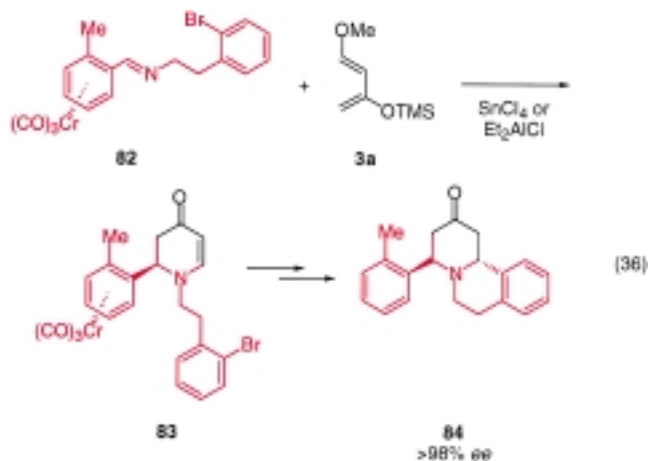
Holmes et al. have applied the (*S*)-lactate-derived *N*-tosyl imino acetate **79a** and (*R*)-panto-lactone derived imino acetate **79b** for reaction with cyclopentadiene **6e** [Eq. (35)]^[87] in various solvents, and in the absence and presence of different Lewis acids. In all cases, only the *exo*-diastereomers were obtained. The use of Et_2AlCl as catalyst resulted in 50–60% yield and 76% *de* for the lactate adduct *exo*-**80a**. In order to account for the formation of *exo*-**80a**, an approach of the cyclopentadiene to **79a** was proposed as outlined in **81**. In **81**, imine **79a** adopts an *E* conformation and the monodentate Et_2AlCl coordinates to the carbonyl oxygen atom *anti* to the bulky chiral auxiliary. This forces the approach of the cyclopentadiene to the less hindered face resulting in *Si*-attack.

The reaction outlined in Equation (35) has also been performed for imines with aromatic substituents on the nitrogen atom and the same chiral auxiliaries. This affords substituted tetrahydroquinolines in moderate to high yields with total regio- and stereoselectivity.^[88] However, high diastereoselectivity (up to 92%) was only obtained by using



an imine with 8-phenylmenthyl as the chiral auxiliary, while imines substituted with bornyl and menthyl auxiliaries gave almost no asymmetric induction (0–10% *de*).

Recently, tricarbonylchromium complexes have been introduced as novel chiral auxiliaries for HDA reactions.^[89] The reaction between the planar chiral *ortho*-substituted benzaldehyde imines **82** and Danishefsky's diene **3a** in the presence of 1.2 equivalents of Lewis acid, SnCl₄ or Et₂AlCl, gave single diastereomers, such as **83**, in most cases [Eq. (36)].^[89] The major diastereomer is presumably formed by the approach of a diene from the side opposite to the Cr(CO)₃ group and addition to the imine face of the preferred *E* conformation. Subsequent cyclization of the cycloadduct, and oxidative metal removal gave the quinolizidine derivative **84** with >98% *ee*.

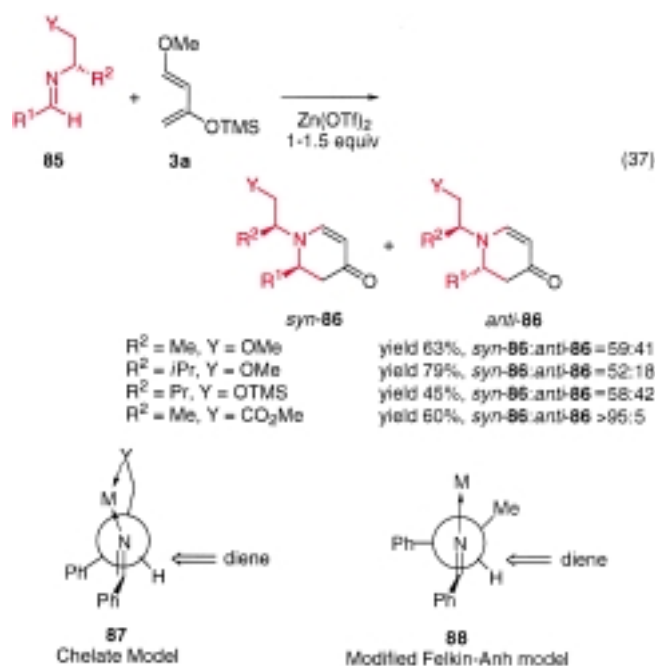


3.1.2. Chiral Imines Derived from Chiral Amines

Asymmetric HDA reactions employing chiral imines derived from chiral amines have been intensively investigated due to the easy access of both enantiomers. The most frequently used chiral amines are α -phenylethylamine, α -amino acids, β -amino alcohols, and their derivatives.^[90]

The use of camphoryl as the chiral auxiliary on the nitrogen atom of the *N*-sulfonyl glyoxylate imine (similar to **79**) was introduced by Whiting et al.^[91] This imine reacts with Danishefsky's diene **3a** affording up to 40% *de* in the presence of 0.25 equivalents of Ti(O*i*Pr)₄.

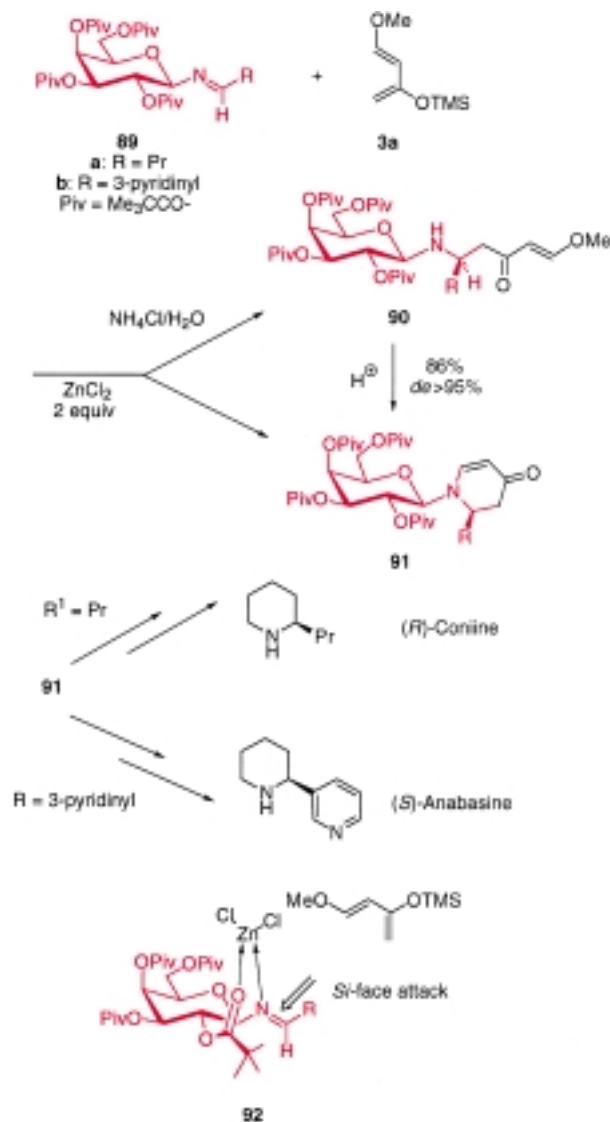
In 1993, Oh et al. reported excellent results using imines as the dienophiles for asymmetric HDA reactions which have the capacity to form a chelate.^[92] The imines **85**, synthesized from α -amino alcohols, react with Danishefsky's diene **3a** and show some distinctive and instructive trends [Eq. (37)]. The



size of the stereodirecting group R² directly influences the stereoselectivity. As the bulk of R² increased, the diastereoselectivity was enhanced. In contrast, the substituents on the aldehyde part had little influence, except that there was no reaction with the bulky *tert*-butyl group. Imines which can form a cyclic chelate gave almost similar diastereoselectivities for the HDA adduct *syn*-**86** as those which did not have a second chelating site. Furthermore, the imines with a more Lewis basic second chelating group (Y = CO₂Me, OH) gave higher diastereoselectivity than imines with a less Lewis basic site (Y = OTMS). When imines derived from α -amino esters and β -amino alcohols were used, only single diastereomers were formed. To account for the stereoselectivity, the cyclic chelate model **87** was used, and a modified Felkin–Anh model **88** for those which can only form a monodentate coordination to the Lewis acid.

The use of imines with a carbohydrate template as the dienophile in diastereoselective HDA reactions has been investigated by Kunz et al.^[93] The reaction of imines **89** with, for example, 2,3-dimethyl-1,3-butadiene or isoprene in the presence of ZnCl₂ as the catalyst proceeded well but afforded a mixture of three diastereomers (one from the α -anomer) with moderate diastereoselectivities. However, excellent selectivities could be achieved by reaction of **89** with Danishefsky's diene **3a** affording **91** in high yield and

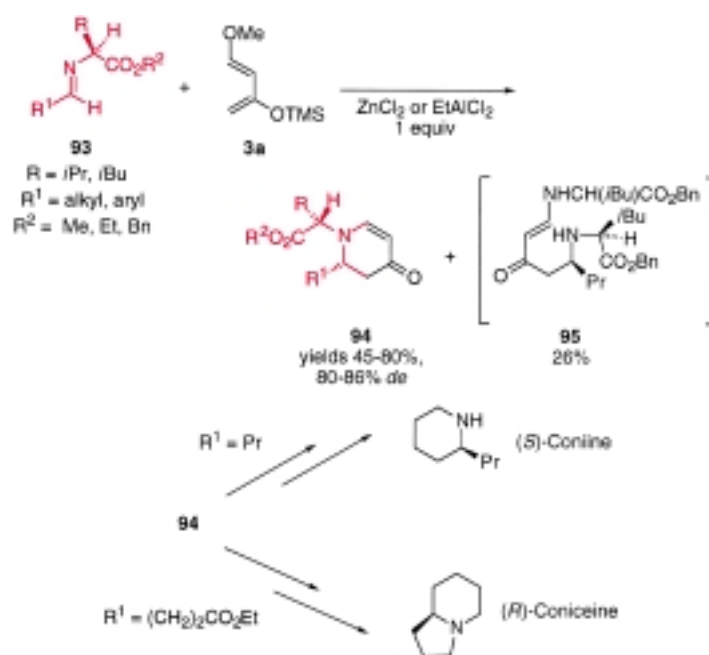
diastereoselectivity (Scheme 14). Compounds **91** were converted into (*R*)-coniine and (*S*)-anabasine, by subsequent reduction, decarbonylation, and removal of the carbohydrate template. It was believed that the reaction of **89** with isoprene was a concerted HDA process,^[93] whereas the reaction with Danishefsky's diene proceeded by a Mannich-type process as the corresponding Mannich-addition products **90** were isolated if the reaction was quenched with $\text{NH}_4\text{Cl}/\text{H}_2\text{O}$.



Scheme 14. Synthesis of (*R*)-coniine and (*S*)-anabasine by ZnCl_2 -catalyzed diastereoselective HDA reactions of carbohydrate-substituted imines as dienophile.^[93]

It has been proposed that Danishefsky's diene approach the sterically less shielded *Si*-face of the galactosyl imine-Lewis acid complex as outlined in **92** in Scheme 14.^[93b,c]

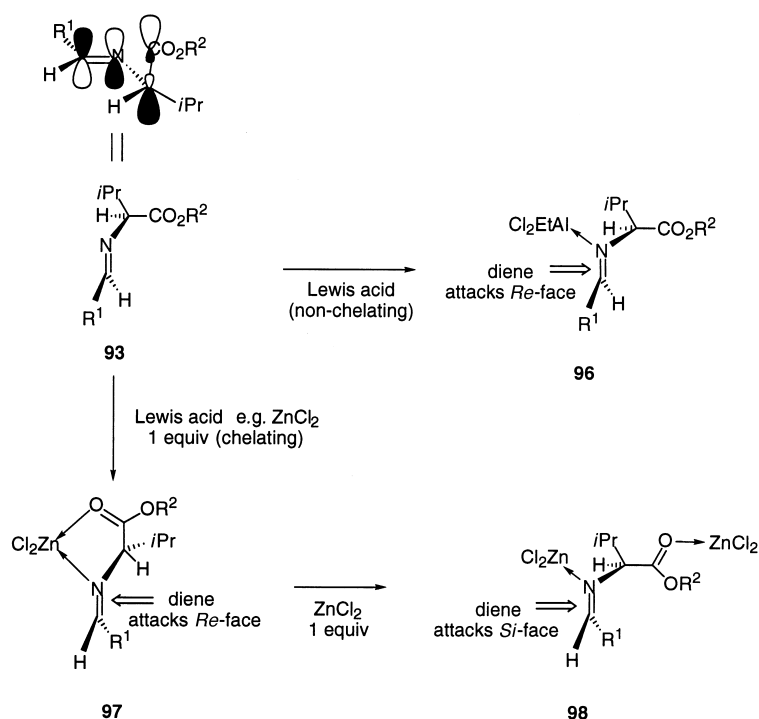
Asymmetric Mannich-type reactions between imines derived from α -amino acid esters with activated dienes, leading to the HDA adducts **94** have been reported by Waldmann et al.^[94] The reaction was found to be quite general as imines from aromatic and aliphatic aldehydes were good substrates. Excellent diastereoselectivities were obtained when valine and isoleucine esters were employed as the auxiliaries (Scheme 15). For the reactions of imines **93** with Danishef-



Scheme 15. Synthesis of (*S*)-coniine and (*R*)-coniceine by using catalytic diastereoselective HDA reactions of chiral imines with Danishefsky's diene.^[94]

sky's diene **3a**, neither the presumed HDA intermediate nor a stepwise Mannich-type intermediate were detected. The enaminone **94** was obtained directly after aqueous work-up, except in one case where compound **95** was isolated in 26 % yield as a by-product. The occurrence of **95** suggests that the reaction probably proceeds by a Mannich-type sequence. The removal of the chiral auxiliaries from the products required the cleavage of the chemically stable α -bond of the amino acid and the nitrogen atom. This was achieved for **94** and further reactions demonstrated that this HDA approach could be used for the synthesis of (*S*)-coniine and (*R*)-coniceine.

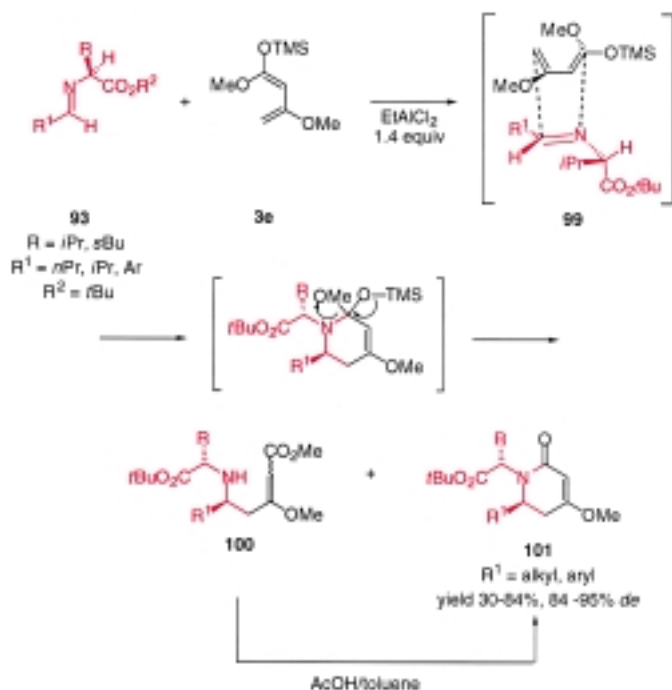
The sense of the stereoselectivity was found to be independent of the Lewis acids, as the same major isomer **94** was obtained by using either the chelating Lewis acids ZnCl_2 and TiCl_4 , or the nonchelating Lewis acids BF_3 and Et_2AlCl . The stereochemical outcome of the reaction with nonchelating Lewis acids can be explained by assuming the modified Felkin–Anh type of intermediate **96** in which the Lewis acid coordinates to the nitrogen atom of the imine, and where the α -C–COOR substituent at the nitrogen atom simultaneously is oriented perpendicular to the imine. From a FMO point of view this leads to a parallel orientation of the $\sigma^*(\alpha\text{-C-COOR})$ orbital and the $\pi^*(\text{C=N})$ orbital (Scheme 16). To account for the lack of reversal of the stereochemical outcome by changing from a nonchelating to a chelating Lewis acid, it was suggested that an equilibrium between the *cis*- and *trans*-imine in the presence of ZnCl_2 exists and that the *cis*-imine probably reacts faster. This explanation was also based on the observation of different ^1H NMR chemical shifts of the aldimine proton and the amino acid α -H with and without the presence of one equivalent of ZnCl_2 . The existence of the chelation intermediate **97** using one equivalent of ZnCl_2 was supported by the observation that the sense of the asymmetric induction was reversed by



Scheme 16. Models for the coordination of imine **93** to nonchelating and chelating Lewis acids.

using two equivalents of ZnCl_2 . The latter observation can be rationalized by the separate coordination of one equivalent of ZnCl_2 to the imine nitrogen atom and the second equivalent of ZnCl_2 to the ester carbonyl atom as outlined in **98**.

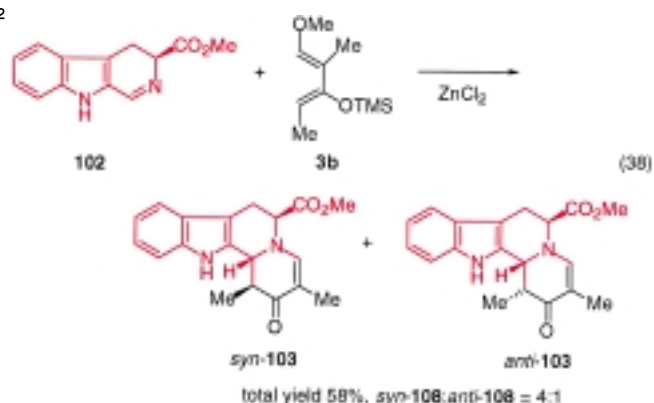
When the Brassard diene **3e** was treated with imine **93** in the presence of EtAlCl_2 as the catalyst, only the open-chain esters **100**, or a mixture of **100** and the HDA adduct **101** were isolated in high yields (Scheme 17).^[94c] Compound **100** can be



Scheme 17. The catalytic diastereoselective HDA reaction of imine **93** with diene **3e**.

transformed into **101** by heating in the presence of acetic acid. The steric course of the reaction between **93** and **3e** was rationalized by assuming an *anti*-Felkin–Anh transition state **99** in which the interaction between the bulky TMS group of the diene and the sterically demanding group of the amino acid side chain is minimized.

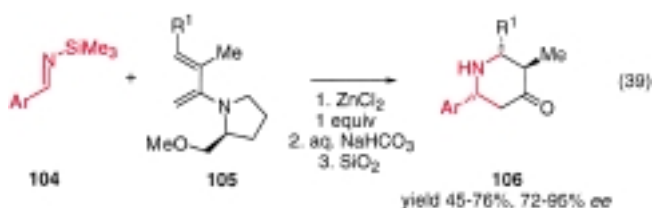
The principle that simple imines can participate in HDA reactions with activated dienes has been applied for the asymmetric synthesis of alkaloids. In 1985, Danishefsky et al. demonstrated the use of cycloadditions of chiral α -amino ester dienophiles for the synthesis of yohimbine congeners [Eq. (38)].^[95] The reaction of the optically active tricyclic imine **102** with diene **3b** catalyzed by ZnCl_2 gave *syn*-**103** and *anti*-**103** in 58 % combined yield and with a *syn*:*anti* ratio of 4:1.



As an extension and application of the reaction between amino acid ester imines and dienes outlined in Equation (38), Waldmann et al. demonstrated the asymmetric synthesis of indolo[2,3-*a*]quinolinizidin-2-ones using related imines.^[96] This diastereoselective synthesis of, for example, a tetracyclic amino ketone led to a new procedure for the preparation of optically active alkaloids of the yohimbine-type.

3.1.3. Chiral Dienes

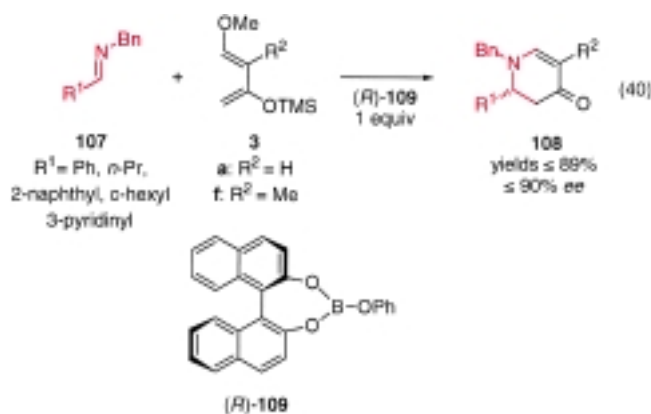
There are only very few examples dealing with the HDA reaction employing chiral dienes, and of these, the use of Lewis acid catalysis is even more limited. Barluenga et al. reported the synthesis and application of the chiral diene **105**, having a chiral pyrrolidine auxiliary. The reaction of the *N*-silylimines **104** with diene **105** catalyzed by ZnCl_2 afforded the piperidones **106** in moderate to good yields with good to excellent enantioselectivities [Eq. (39)].^[97] The application of



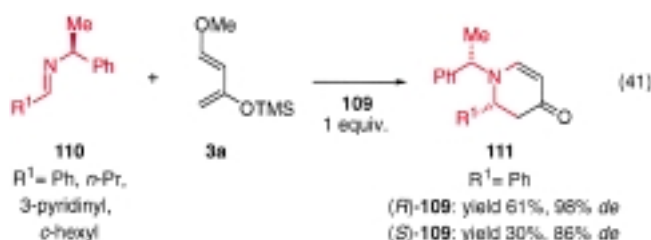
this methodology for the diastereo- and enantioselective synthesis of a pipeconic acid derivatives has also been described recently.^[97c]

3.2. Diastereoselective Reactions with Chiral Catalysts

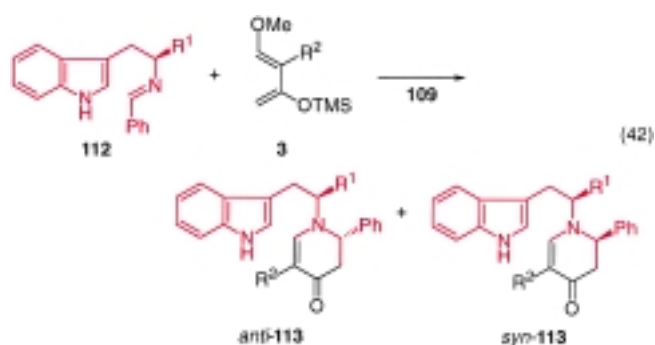
Lewis acid catalyzed diastereoselective HDA reactions using chiral imines and dienes have been investigated intensively. Excellent diastereoselectivities have been achieved in some cases, providing new synthetic procedures to optically active heterocycles. Despite the obvious advantages in the use of chiral catalysts, the development of chiral Lewis acid catalysts for the HDA reaction has only been carried out successfully over the last few years. In 1992, Yamamoto et al. showed that the chiral boron(III) reagent **109** could catalyze the HDA reaction of aldimines with Danishefsky-type dienes **3a** and **3f**.^[98] In the presence of stoichiometric amounts of **109**, imines **107** reacted smoothly with dienes **3a, f** affording the HDA adduct **108** in good yields and with up to 90% *ee* [Eq. (40)].



The chiral boron catalyst **109** has also been applied for the reaction of chiral imines leading to double asymmetric induction. The imines **110** derived from α -methylbenzylamine and aldehydes reacted faster with diene **3a** in the matching case and nearly complete diastereoselectivity was observed [Eq. (41)]. The methodology was used for the synthesis of enantiomerically pure (+)-coniine and (–)-anabesine.^[98b,c]

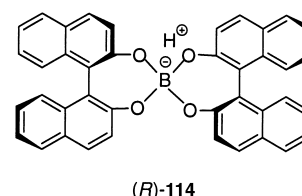


Waldmann et al. investigated the double asymmetric induction using catalyst **109** for the reaction of the chiral imines **112** with dienes **3** [Eq. (42)].^[99] When the reaction between **112** and **3** was performed in the presence of (R)-**109** (the matched pair), a much higher ratio of dihydropiperidinone



anti-113 to *syn-113* was obtained (*de* > 90%), compared to the use of B(OPh)₃ as the catalyst, while in the presence of (S)-**109** (mismatched case), only a slight enhancement was noted. The reaction of an achiral imine with an activated diene using the (R)-**109** as a catalyst gave the corresponding enaminones with low selectivity.

In a later investigation, Yamamoto et al. explored the use of another chiral boron catalyst, the Brønsted acid assisted Lewis acid **114**, for the HDA reactions in Equations (40) and (41).^[100] The catalyst **114** was shown to be an efficient catalyst

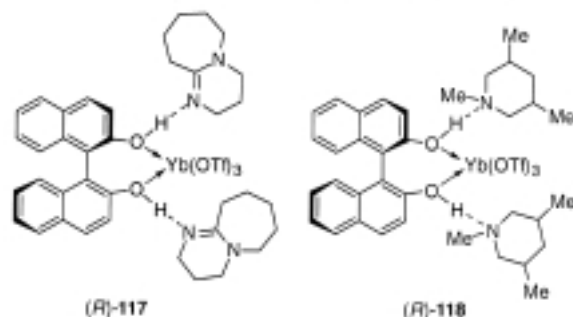
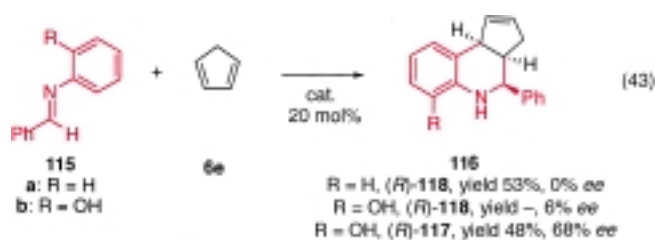


for the DA reaction between α -substituted α,β -enals and dienes.^[101] However, for the HDA reactions, the use of one equivalent of **114** is necessary in order to achieve high asymmetric induction.

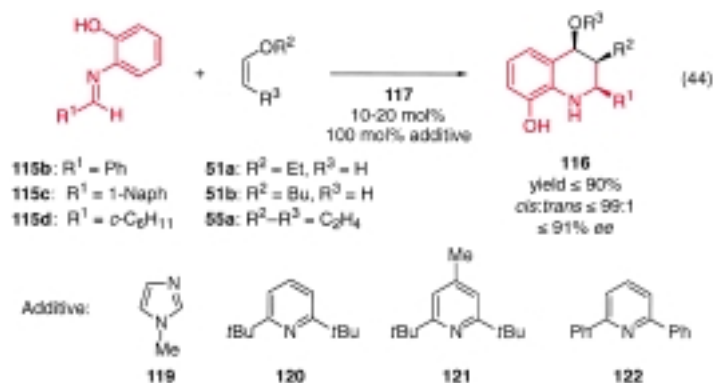
3.3. Catalytic Enantioselective Reactions

In 1996, Kobayashi et al. presented the first example of a catalytic enantioselective reaction of imines **115** (an azadiene) using chiral BINOL–ytterbium(III) complex **117** [Eq. (43)].^[102] A similar catalyst **118** containing 1,3,5-trimethylpiperidine (TMP) as the amine component, which was previously found to catalyze efficiently the DA reactions of 3-acryloyl-1,3-oxazolidin-2-one with dienes,^[103] catalyzed the reaction between **115a** and cyclopentadiene (**6e**). The tetrahydroquinoline derivative **116a** was isolated in 53% yield, but without chiral induction [Eq. (43)]. The use of imine **115b**, which is capable of coordinating in a bidentate fashion to the metal center, led to the formation of **116b** in high yield, but with only 6% *ee* in the presence of **118**. Changing TMP to diazabicyclo-[5.4.0]-undec-7-ene (DBU), however, led to an enantioselective reaction with 68% *ee*.

It was argued that the hydroxy group in **115b** could also interact with DBU to form a hydrogen bond with the hydroxy groups of the (R)-BINOL ligand, causing the decrease of the

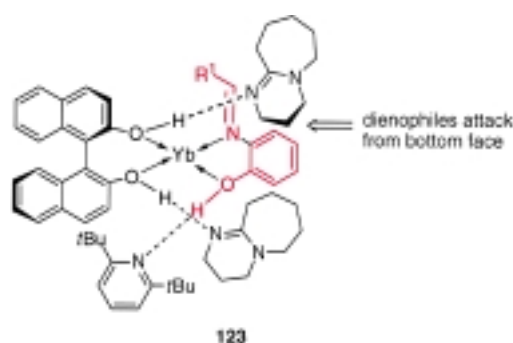


selectivity. Therefore, 20 mol % *N*-methylimidazole (NMI) **119** was added, and an improvement to 91 % *ee* was obtained, however, the yield was only 21 %. Different additives were then screened (**119**–**122**) and it was found that good yields and high enantioselectivities could be achieved if an appropriate additive was chosen for a particular substrate [Eq. (44)]. The reactions proceed in general with very high diastereoselectivity. The need for the different additives for different substrates in order to achieve the best results was explained by the slight difference in the asymmetric environment created by [Yb(OTf)₃], (*R*)-BINOL, and the additives. It should be noted that in the case of butyl vinyl ether **51b**, the *cis/trans* selectivity decreased significantly.

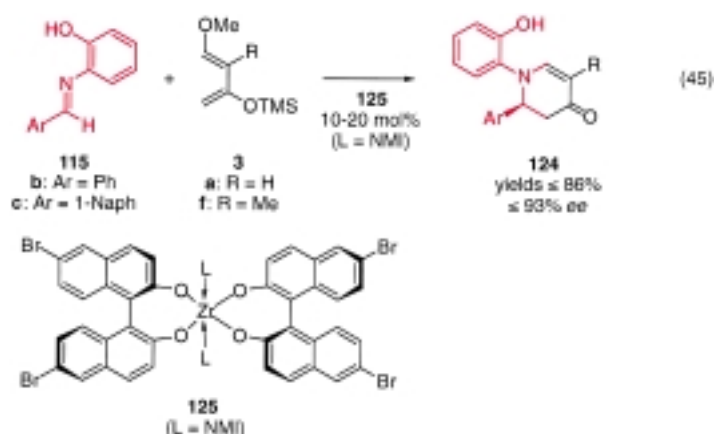


Kobayashi et al.^[102] proposed a transition-state model **123** for the reaction in which the imine coordinates in a bidentate fashion to the metal, and in which the axial chirality of the (*R*)-BINOL is transferred through hydrogen bonds to the amine parts. The additive interacts with the phenolic hydrogen atom of the imines, which is fixed by the bidentate coordination to the metal. Since the top face of the imine is shielded by the amine, the dienophiles approach from the bottom face.

In 1998, the same authors reported the catalytic enantioselective HDA reaction using imines **115** promoted by a chiral

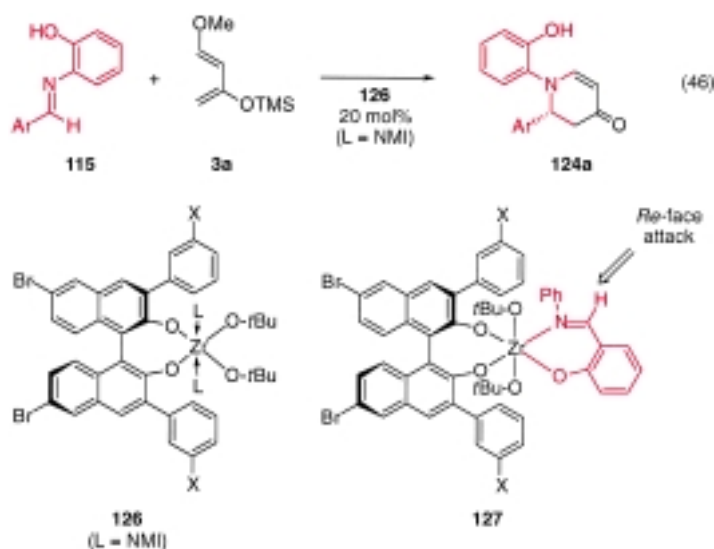


zirconium(IV) complex **125** [Eq. (45)].^[104] The catalyst was prepared from Zr(O*t*Bu)₄, (*R*)-Br-BINOL, and an amine ligand, for example NMI, in a ratio of 1:2:2–3. The reaction



between **115c** (Ar = 1-Naph = 1-naphthalinyl) and Danishefsky-type dienes **3** was found to be strongly influenced by both the ligands and the solvents. The best result (93 % yield and 93 % *ee*) was obtained from the reaction of **115c** and diene **3f** in toluene with NMI as the ligand in the presence of 10 mol % catalyst **125**. Furthermore, for a model reaction it was found that a chiral hafnium catalyst afforded slightly higher yield and enantioselectivity. Aldimines derived from aromatic and substituted aromatic aldehydes can be employed as the substrates for this reaction.

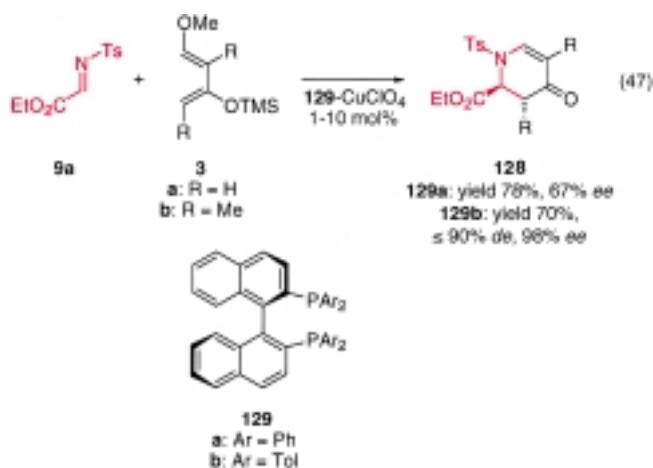
Generally, good enantioselectivities were achieved for *ortho*-substituted phenyl imines. However, for imine **115b** prepared from benzaldehyde, only 65 % *ee* was achieved. The *ortho*-hydroxy group in the imines is found to be essential to achieve a high level of enantioselectivity, since even the imine prepared from 2-methoxyaniline gave low enantioselectivity. The absolute configuration of the products was assigned as *S* using catalyst **125** derived from the (*R*)-Br-BINOL ligand. However, no mechanism for the absolute asymmetric induction was discussed. For the same type of chiral catalysts a switch of enantioselectivity for this HDA reaction has been found using catalyst **126** [Eq. (46)].^[105] The reaction of imine **115** with diene **3a** catalyzed by **126** (20 mol %) gave the corresponding piperidinone derivative in a slightly lower yield of 66 %, but with a similar high enantiomeric excess of 84 %. However, the absolute configuration of the product was found to be *R* which is opposite to the configuration obtained with



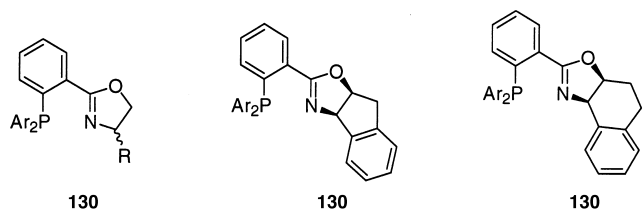
catalyst **125**. The results can be improved significantly by using molecular sieves. When the reaction was performed in the absence of molecular sieves at 0 °C, **124a** was isolated in only 45 % yield with 57 % *ee*; however, when molecular sieves (3 Å) were added the yield and enantioselectivity of **124a** improved to 80 % and 90 %, respectively.

The working model **127** was proposed^[105] to account for the observed induction of enantioselective. The two bulky *tert*-butoxy groups are expected to occupy the two axial positions. One of the 3,3'-phenyl groups would effectively shield one face of the imine, and consequently, the diene attacks from the opposite side which is the *Re*-face when (*R*)-**126** was applied as the catalyst.

Our contribution to the development of catalytic enantioselective HDA reactions^[106] of imines was initiated by the reaction of the *N*-tosyl α -imino ester **9a**^[107] with the Danishefsky-type dienes **3a, b** in the presence of the chiral BINAP–copper(I) complexes **129** [Eq. (47)]. For the reaction of **9a** with **3b** catalyzed by **129b** (1 mol %), the *S* configuration of the *endo* diastereomer of the dimethyl-substituted HDA adduct **128** was obtained in 70 % yield, and up to 90 % *de* and 98 % *ee*.

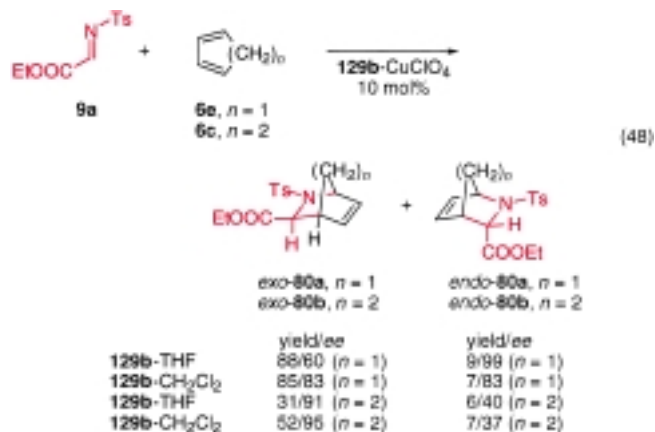


Further investigations of the reaction of the *N*-tosyl α -imino ester **9a** and other *N*-substituted α -imino esters **9b–e** have demonstrated that the metal complexes of the chiral phosphanyl-substituted oxazoline ligands **130a–j** are also good catalysts for especially the reaction of **9a** with Danishefsky's diene **3a**.^[108] A combination of the chiral ligands **130a–j** and CuClO₄ (10 mol %) leads to the formation of **128** in high yield (up to 97 %) and with up to 86 % *ee*. This reaction is very tolerant to various solvents and proceeds well for nearly all the ligands.



- a: Ar = Ph, R = Ph (*R*)
b: Ar = Ph, R = *i*Pr (*S*)
c: Ar = Ph, R = *t*Bu (*S*)
d: Ar = *p*-Tol, R = *t*Bu (*S*)
e: (3*aR*,9*bS*), Ar = Ph
f: (3*aR*,9*bS*), Ar = *p*-Tol
g: (3*aR*,9*bS*), Ar = 2,4-xylyl
h: (3*aR*,9*bS*), Ar = Ph
i: (3*aR*,9*bS*), Ar = *p*-Tol
j: (3*aR*,9*bS*), Ar = 2,4-xylyl

A significant improvement is that the reaction of the *N*-tosyl α -imino ester **9a** catalyzed by the chiral Tol-BINAP-Cu^I catalyst **129b** can proceed also with unactivated dienes.^[108] The reaction of the cyclic dienes, cyclopentadiene (**6e**) and 1,3-cyclohexadiene (**6c**), in the presence of **129b** gave the useful HDA adducts *exo*-**80a** and *exo*-**80b** in good yield and enantioselectivity [Eq. (48)]. It was found that *exo*-**80a** is



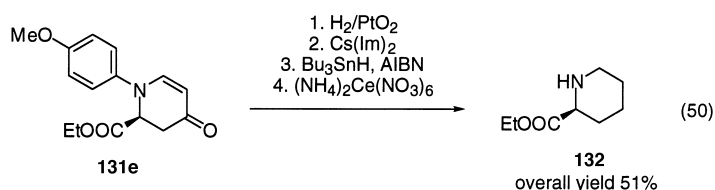
formed in 85 % yield and 83 % *ee*, while *exo*-**80b** is obtained by reaction with 1,3-cyclohexadiene in slightly lower yield, but with up to 95 % *ee*. This catalytic enantioselective approach opens up a new entry to the formation of the chiral fragment **78** which is a useful precursor for pharmaceutical important compounds (see Section 3.1.1.).

The catalytic enantioselective HDA reaction proceeds also for other types of dienes, and in several cases both HDA and ene adducts were formed. The catalytic ene reaction of the *N*-tosyl α -imino ester **9a** has been developed into a highly enantioselective reaction.^[15]

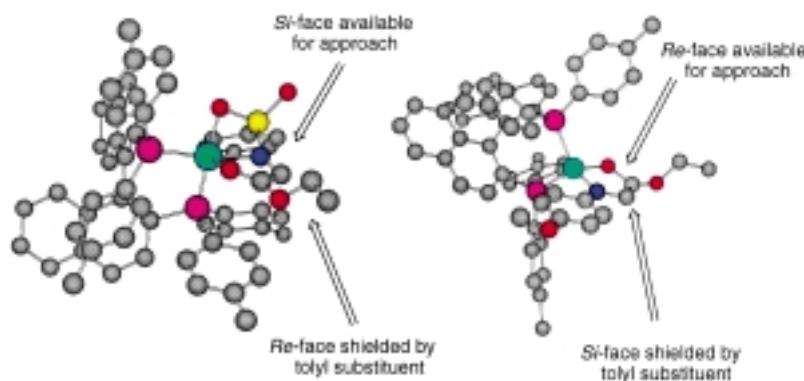
One of the drawbacks in using the *N*-tosyl α -imino ester **9a** is the removal of the *N*-tosyl substituent. This problem was solved by the introduction of other substituents which can be removed more easily.^[108] The imines **9b–e** are substrates which react with Danishefsky's diene **3a** in the presence of the Tol-BINAP-Cu^I catalyst **129b**-Cu^I leading to the HDA adducts **131b–e** in moderate to good yields and enantioselectivities [Eq. (49)]. The imines **9a–c**, allow coordination to the catalyst by the *N*-substituent, while this is not possible for the **9d, e**. A by-product observed in some of the reactions is the Mannich-type product.



The HDA adduct **131e**, formed by using (*R*)-Tol-BINAP-CuClO₄ **129b**-Cu^I as the catalyst, can be applied for the formation of (*R*)-ethyl pipercolic ester **132** without loss of optical activity [Eq. (50); Im = imidazolide, AIBN = azobisisobutyronitrile].^[108]



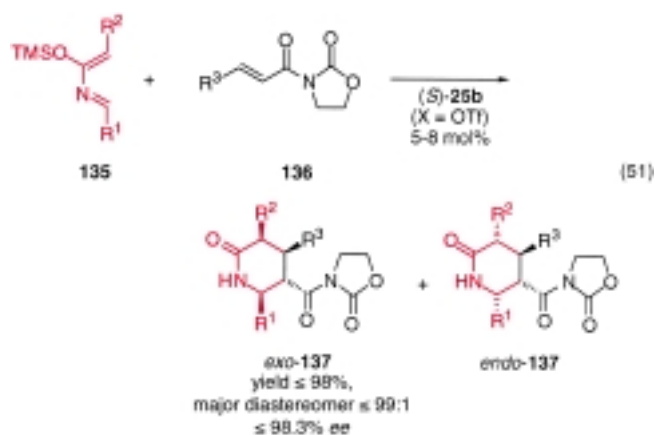
The HDA reaction of the imines **9a** and **9e** with the activated dienes catalyzed by the (*R*)-Tol-BINAP-CuClO₄ **129b**-Cu^I catalyst gave in the first case the *S* enantiomer and in the second case the *R* enantiomer, because the imines have two different binding modes to the catalyst. In the case of **9a**, the *N*-tosyl group can participate in the coordination to the chiral Lewis acid, while for **9e**, the *N*-*p*-methoxyphenyl substituent does not have this option. Based on the absolute configuration of the HDA adducts obtained in these reactions two different intermediates have been proposed.^[108] For imine **9a** the glyoxylate carbonyl oxygen atom, the sulfonyl oxygen atom, and the imine nitrogen atom can coordinate to the catalyst leading to intermediate **133** (Scheme 18). For imine **9e**, a tetrahedral intermediate, **134**, in which the glyoxylate



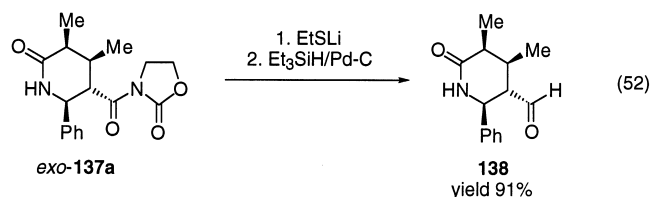
carbonyl oxygen atom and imine nitrogen atom coordinate to the catalyst, can account for the stereochemical outcome of the reaction.

It has also been demonstrated by Whiting et al.^[109] that a variety of different combinations of chiral ligands and Lewis acids can catalyze the enantioselective HDA reaction of an imine similar to **9e** (methyl rather than ethyl) with Danishefsky's diene to give the corresponding HDA adduct. The highest enantiomeric excess being 97% using a combination of (1*S*,2*S*)-1,2-diphenylethylenediamine and MgI₂ as the catalyst.

The final catalytic enantioselective reaction to be discussed is the application of the BOX-copper(II) complex *t*Bu-BOX-CuX₂ (*S*)-**25b** (X = OTf) for the HDA reaction between 2-azadienes **135** and the dienophile **136** [Eq. (51)].^[110] This



reaction, which was described by Jnoff and Ghosez, proceeds well for various substituted 2-azadienes to give **exo-137** as the major diastereomer in good yield and with up to 98.3% ee. This reaction affords a simple synthetic procedure for the formation of piperidones as the HDA adduct **exo-137a** can be converted to the piperidone **138** [Eq. (52)] in two steps (one-



pot process).^[110] Based on the absolute configuration of the product obtained it was proposed that the reaction proceeds by a square-planar intermediate (see **31** for a related intermediate), in which the 2-azadiene approaches the less hindered face of the dienophile in an *exo*-fashion.

4. Summary and Outlook

The major developments of catalytic asymmetric HDA reactions of carbonyl compounds and imines have been presented. Various chiral catalysts are available for the different types of carbonyl compounds; for unactivated aldehydes chiral catalysts such as BINOL–aluminum(III), BINOL–titanium(IV), acyloxyborane(III), and tridentate Schiff base chromium(III) complexes can catalyze highly diastereo- and enantioselective HDA reactions. The mechanism of these reactions can be a stepwise pathway via a Mukaiyama-aldol intermediate or a concerted-like mechanism. For α -dicarbonyl compounds, which can coordinate to the chiral catalyst in a bidentate fashion, the chiral BOX–copper(II) complexes have shown very promising results. These complexes can catalyze HDA reactions of glyoxylates, α -keto esters, α -diketones, and ketomalonate with conjugated dienes leading to the HDA adducts in high yields and with very high diastereo- and enantioselectivities. In some cases it was possible to perform the reactions with very low catalyst loading. These normal electron demand reactions proceed via different structural intermediates depending on the chiral ligand. The chiral BOX–copper(II) complexes can also be used as catalysts for inverse electron demand HDA reactions of α,β -unsaturated carbonyl compounds with electron-rich alkenes, leading to a simple procedure for the formation of 2-substituted 3,4-dihydro-2H-pyrans. These reactions proceed also in a highly selective manner and have been used for the synthesis of carbohydrates such as spiro carbohydrates, a β -D-manonose, and amino sugars.

For the corresponding HDA reactions of imines the main focus has been on diastereoselective reactions using imines derived from chiral carbonyl compounds, chiral amines, and chiral dienes. These reactions were catalyzed by different main group, transition, and lanthanide metal salts. In these reactions, the products are often formed in a highly diastereoselective manner and the use of these HDA reactions for the preparation of natural products has been presented. Furthermore, the mechanistic aspects of the reaction have been discussed, and diastereoselective reactions applying chiral catalysts have also been presented. A lot of effort has been devoted to the development of catalytic enantioselective HDA reactions of imines, but only a few successful reactions have been published. Chiral BINOL–ytterbium(III)-amine complexes can catalyze highly diastereo- and enantioselective reactions between *ortho*-hydroxy-substituted phenyl imines and activated dienes. BINAP- and phosphanyl-substituted oxazoline copper(I) complexes are useful as catalyst for an enantioselective HDA reaction of activated imines with activated and unactivated dienes. The chiral BOX–copper(II) complexes can also catalyze enantioselective HDA reactions of 2-azadienes.

What new developments will the beginning of this century bring us in the field of catalytic enantioselective HDA reactions of carbonyl compounds and imines? Hopefully, new catalysts leading to higher turnover numbers and higher selectivity. For the imines we are still in the beginning of the synthetic development and much work is required to reach the same level of selectivity as now available for carbonyl compounds.

We are only beginning to understand the fundamental role of the catalyst in these reactions—why are there such great differences in reaction course, selectivity, etc., when different metals containing the same chiral ligand are used for the same reaction? Mechanistic insight into these reactions will be of utmost importance in order to unveil the wonders and magic of catalysis that will allow us to take the next important steps in the fascinating world of the Diels–Alder chemistry.

The enthusiastic and dedicated contributions to our development and understanding of catalytic asymmetric HDA reactions by Mogens Johannsen, Sulan Yao, Rita G. Hazell, Hélène Audrain, Xiangming Fang, Anette Graven, Frank Reichel, Mark Roberson, Steen Saaby, Klaus B. Simonsen, Niels Svenstrup, Jacob Thorhauge, Wei Zhuang, Quio-Sheng Hu, Lin Pu, and Xiao-Fan Zheng are greatly acknowledged. Thanks are also expressed to Kurt V. Gothelf and Troels Skrydstrup for comments to the manuscript. This work was made possible by grants from The Danish National Research Foundation and The Carlsberg Foundation.

Received: December 21, 1999
March 31, 2000 [A 379]

- [1] O. Diels, K. Alder, *Liebigs Ann. Chem.* **1928**, 460, 98.
- [2] See for example: R. B. Woodward, R. Hoffmann, *The Conservation of Orbital Symmetry*, Verlag Chemie, Weinheim, **1970**.
- [3] See for example: a) W. Carruthers, *Cycloaddition Reactions in Organic Synthesis*, Pergamon, Elmsford, New York, **1990** (Tetrahedron Organic Chemistry Series Vol. 8); b) I. Ojima, *Catalytic Asymmetric Synthesis*, VCH publishers, New York, **1993**; c) R. Noyori, *Asymmetric Catalysis in Organic Synthesis*, Wiley, New York, **1994**; d) K. C. Nicolaou, E. J. Sorensen, *Classics in Total Synthesis: Targets, Strategies, Methods*, VCH, Weinheim, **1996**; e) D. L. Boger, S. H. Weinreb, *Hetero-Diels–Alder Methodology in Organic Synthesis*, Academic Press, New York, **1987**; f) H. Waldmann, *Synthesis* **1994**, 535; g) L. F. Tietze, G. Ketschau, *Top. Curr. Chem.* **1997**, 190, 1; h) L. F. Tietze, *Curr. Org. Chem.* **1998**, 2, 19.
- [4] See for example: L. Fleming, *Frontier Orbitals and Organic Chemical Reactions*, Wiley, London, **1977**.
- [5] See for example: J. Juracak, A. Golebiowski, A. Rahm, *Tetrahedron Lett.* **1986**, 27, 853.
- [6] S. J. Danishefsky, H. G. Selnick, R. E. Zelle, M. P. DeNinno, *J. Am. Chem. Soc.* **1988**, 110, 4368.
- [7] L. F. Tietze, T. Brumby, M. Pretor, G. Remberg, *J. Org. Chem.* **1988**, 53, 810.
- [8] See for example: a) L. F. Tietze, J. Fennen, E. Anders, *Angew. Chem.* **1989**, 101, 1420; *Angew. Chem. Int. Ed. Engl.* **1989**, 28, 1371; b) M. A. McCarrick, Y.-D. Wu, K. N. Houk, *J. Am. Chem. Soc.* **1992**, 114, 1499; *J. Org. Chem.* **1993**, 58, 3330; c) B. S. Jursic, Z. Zdravkovski, *J. Phys. Org. Chem.* **1994**, 7, 641; d) L. F. Tietze, A. Schuffenhauer, P. R. Achreiner, *J. Am. Chem. Soc.* **1999**, 120, 7952.
- [9] S. J. Danishefsky, D. C. Myles, D. F. Harrey, *J. Am. Chem. Soc.* **1987**, 109, 862.
- [10] See for example: S. J. Danishefsky, E. Larson, D. Ashkin, N. Kato, *J. Am. Chem. Soc.* **1985**, 107, 1246.

- [11] See also: M. T. Mujica, M. M. Afonso, A. Galindo, J. A. Palenzuela, *Tetrahedron* **1996**, 52, 2167.
- [12] See for example: a) K. Mikami, M. Terada, T. Nakai, *J. Am. Chem. Soc.* **1990**, 112, 3949; b) K. Mikami, M. Shimizu, *Chem. Rev.* **1992**, 92, 1021; c) D. J. Berrisford, C. Bolm, *Angew. Chem.* **1995**, 107, 1862; *Angew. Chem. Int. Ed. Engl.* **1995**, 34, 1717.
- [13] M. Johannsen, K. A. Jørgensen, *J. Org. Chem.* **1995**, 60, 5757.
- [14] A. Graven, M. Johannsen, K. A. Jørgensen, *Chem. Commun.* **1996**, 2373.
- [15] a) S. Yao, X. Fang, K. A. Jørgensen, *Chem. Commun.* **1998**, 2547; see also b) W. J. Drury III, D. Ferraris, C. Cox, B. Young, C. Lectka, *J. Am. Chem. Soc.* **1998**, 120, 11006.
- [16] a) K. Maruoka, T. Itoh, Y. Araki, T. Shirasaka, H. Yamamoto, *Bull. Chem. Soc. Jpn.* **1988**, 61, 2975; b) K. Maruoka, Y. Hoshino, T. Shirasaka, H. Yamamoto, *Tetrahedron Lett.* **1988**, 29, 3967; c) K. Maruoka, T. Itoh, T. Shirasaka, H. Yamamoto, *J. Am. Chem. Soc.* **1988**, 110, 310; d) K. Maruoka, A. B. Concepcion, H. Yamamoto, *Bull. Chem. Soc. Jpn.* **1992**, 65, 3501.
- [17] K. Maruoka, H. Yamamoto, *J. Am. Chem. Soc.* **1989**, 111, 789.
- [18] For hypercoordination see for example: a) K. Maruoka, T. Ooi, *Chem. Eur. J.* **1999**, 5, 829; b) T. Ooi, D. Uruguchi, N. Kagoshima, K. Maruoka, *J. Am. Chem. Soc.* **1998**, 120, 5327; c) D. P. Heller, D. R. Goldberg, W. D. Wulff, *J. Am. Chem. Soc.* **1997**, 119, 10551.
- [19] K. B. Simonsen, N. Svenstrup, M. Roberson, K. A. Jørgensen, *Chem. Eur. J.* **2000**, 6, 123.
- [20] M. Roberson, A. J. Jepsen, K. A. Jørgensen, *Tetrahedron* in press.
- [21] M. Quimpère, K. Jankowski, *J. Chem. Soc. Chem. Commun.* **1987**, 676.
- [22] a) Q. Gao, T. Maruyama, M. Mouri, H. Yamamoto, *J. Org. Chem.* **1992**, 57, 1951; b) Q. Gao, K. Ishihara, T. Maruyama, M. Mouri, H. Yamamoto, *Tetrahedron* **1994**, 50, 979.
- [23] a) M. Takasu, H. Yamamoto, *Synlett* **1990**, 194; b) D. Sartor, J. Saffrich, G. Helmchen, *Synlett* **1990**, 197; c) D. Sartor, J. Saffrich, G. Helmchen, C. J. Richards, H. Lambert, *Tetrahedron: Asymmetry* **1991**, 2, 639; d) E. J. Corey, T.-P. Loh, *J. Am. Chem. Soc.* **1991**, 113, 8966; e) E. J. Corey, T.-P. Loh, T. D. Roper, M. D. Azimioara, M. C. Noe, *J. Am. Chem. Soc.* **1992**, 114, 8290; f) E. J. Corey, A. Guzman-Perez, T.-P. Loh, *J. Am. Chem. Soc.* **1994**, 116, 3611; g) E. J. Corey, T.-P. Loh, *Tetrahedron Lett.* **1993**, 34, 3979; h) E. J. Corey, C. L. Cywin, T. D. Roper, *Tetrahedron Lett.* **1992**, 33, 6907.
- [24] See also for example: a) K. Mikami, S. Matsukawa, *J. Am. Chem. Soc.* **1993**, 115, 7039; b) K. Mikami, Y. Motoyama, M. Terada, *J. Am. Chem. Soc.* **1994**, 116, 2812; c) K. Mikami, S. Matsukawa, *Nature* **1997**, 385, 613; d) G. E. Keck, K. H. Tarbet, L. S. Geraci, *J. Am. Chem. Soc.* **1993**, 115, 8467; e) G. E. Keck, D. Krishnamurthy, *J. Am. Chem. Soc.* **1995**, 117, 2363; f) G. E. Keck, X.-Y. Li, D. Krishnamurthy, *J. Org. Chem.* **1995**, 60, 5998; g) K. Maruoka, N. Murase, H. Yamamoto, *J. Org. Chem.* **1993**, 58, 2938; h) A. L. Costa, M. G. Piazza, E. Tagliavini, C. Trombini, A. Umani-Ronchi, *J. Am. Chem. Soc.* **1993**, 115, 7001; i) R. O. Duthaler, A. Hafner, *Angew. Chem.* **1997**, 109, 43; *Angew. Chem. Int. Ed. Engl.* **1997**, 36, 43.
- [25] A. Togni, *Organometallics* **1990**, 9, 3106.
- [26] S. E. Schaus, J. Brånalt, E. N. Jacobsen, *J. Org. Chem.* **1998**, 63, 403.
- [27] A. G. Dossetter, T. F. Jamison, E. N. Jacobsen, *Angew. Chem.* **1999**, 111, 2549; *Angew. Chem. Int. Ed.* **1999**, 38, 2398.
- [28] a) M. Bednarski, C. Maring, S. Danishefsky, *Tetrahedron Lett.* **1983**, 24, 3451; b) M. Bednarski, S. Danishefsky, *J. Am. Chem. Soc.* **1983**, 105, 6968; c) *J. Am. Chem. Soc.* **1986**, 108, 7060.
- [29] T. Hanamoto, H. Furuno, Y. Sugimoto, J. Inanaga, *Synlett* **1997**, 79.
- [30] For an introduction to chiral binaphthyl polymers in asymmetric catalysis see for example: L. Pu, *Chem. Eur. J.* **1999**, 5, 2227.
- [31] M. Johannsen, K. A. Jørgensen, Z.-M. Lin, Q.-S. Hu, L. Pu, *J. Org. Chem.* **1999**, 64, 299.
- [32] Y. Motoyama, K. Mikami, *J. Chem. Soc. Chem. Commun.* **1994**, 1563.
- [33] a) K. Mikami, M. Terada, Y. Motoyama, T. Nakai, *Tetrahedron: Asymmetry* **1991**, 2, 643; see also: S. Matsukawa, K. Mikami, *Tetrahedron: Asymmetry* **1997**, 8, 815; c) Y. Motoyama, M. Terada, K. Mikami, *Synlett* **1995**, 967.
- [34] a) Y.-J. Hu, X.-D. Huang, Z.-J. Yao, Y.-L. Wu, *J. Org. Chem.* **1998**, 63, 2456; b) L.-S. Li, Y. Wu, Y.-J. Hu, L.-J. Xia, Y.-L. Wu, *Tetrahedron: Asymmetry* **1998**, 9, 2271.
- [35] See for example: a) A. Pfaltz, *Acc. Chem. Res.* **1993**, 26, 339; b) A. K. Ghosh, P. Mathivanan, J. Cappiello, *Tetrahedron: Asymmetry* **1998**, 9, 1; c) K. A. Jørgensen, M. Johannsen, S. Yao, H. Audrain, J. Thorhauge, *Acc. Chem. Res.* **1999**, 32, 605; J. S. Johnson, D. A. Evans, *Acc. Chem. Res.* **2000**, 33, in press.
- [36] For leading references to Mukaiyama-aldol reactions catalyzed by C₂-symmetric BOX complexes see for example: a) D. A. Evans, M. C. Kozlowski, J. A. Murry, C. S. Burgey, K. R. Campos, B. T. Connell, R. J. Staples, *J. Am. Chem. Soc.* **1999**, 121, 669, and references therein; b) D. A. Evans, C. S. Burgey, M. C. Kozlowski, S. W. Tregay, *J. Am. Chem. Soc.* **1999**, 121, 686, and references therein.
- [37] For a leading references to DA reactions catalyzed by C₂-symmetric BOX complexes see for example: a) D. A. Evans, D. M. Barnes, J. S. Johnson, T. Lectka, P. von Matt, S. J. Miller, R. D. Norcross, E. A. Shaughnessy, K. R. Campos, *J. Am. Chem. Soc.* **1999**, 121, 7582, and references therein; b) D. A. Evans, S. J. Miller, T. Lectka, P. von Matt, *J. Am. Chem. Soc.* **1999**, 121, 7559, and references therein.
- [38] 1,3-Dipolar cycloaddition reactions see for example: a) K. V. Gothelf, R. G. Hazell, K. A. Jørgensen, *J. Org. Chem.* **1996**, 61, 346; b) K. B. Jensen, R. G. Hazell, K. A. Jørgensen, *J. Org. Chem.* **1999**, 64, 2353.
- [39] Cyclopropanation reactions see for example: a) R. E. Lowenthal, S. Masamune, *Tetrahedron Lett.* **1991**, 32, 7373; b) D. A. Evans, K. A. Worpel, M. M. Hinman, M. M. Faul, *J. Am. Chem. Soc.* **1991**, 113, 726; c) D. A. Evans, K. A. Woerpel, M. J. Scott, *Angew. Chem.* **1992**, 104, 439; *Angew. Chem. Int. Ed. Engl.* **1992**, 31, 430; d) T. G. Gant, M. C. Noe, E. J. Corey, *Tetrahedron Lett.* **1995**, 36, 8745.
- [40] Allylic substitution reactions see for example: P. von Matt, G. C. Lloyd-Jones, A. B. E. Minidis, A. Pfaltz, L. Macko, M. Neuburger, M. Zehnder, H. Rüegger, P. S. Pregogin, *Helv. Chim. Acta* **1995**, 78, 265.
- [41] Allylation and addition reactions see for example: a) J. H. Wu, R. Radinov, N. A. Porter, *J. Am. Chem. Soc.* **1995**, 117, 11029; b) M. P. Sibi, J. Ji, J.-H. Wu, S. Gurtler, N. A. Porter, *J. Am. Chem. Soc.* **1996**, 118, 9200; c) D. A. Evans, T. Rovis, M. C. Kozlowski, J. S. Tedrow, *J. Am. Chem. Soc.* **1999**, 121, 1994.
- [42] Aziridination reactions see for example: a) D. A. Evans, M. M. Faul, M. T. Bilodeau, B. A. Anderson, D. M. Barnes, *J. Am. Chem. Soc.* **1993**, 115, 5328; b) K. B. Hansen, N. S. Finney, E. N. Jacobsen, *Angew. Chem.* **1995**, 107, 750; *Angew. Chem. Int. Ed. Engl.* **1995**, 34, 676.
- [43] Carbonyl-ene reactions see for example: a) D. A. Evans, C. S. Burgey, N. A. Paras, T. Vojtkovsky, S. W. Tregay, *J. Am. Chem. Soc.* **1998**, 120, 5824; b) F. Reichel, X. Fang, S. Yao, M. Ricci, K. A. Jørgensen, *Chem. Commun.* **1999**, 1505; c) N. Gathergood, K. A. Jørgensen, *Chem. Commun.* **1999**, 1869.
- [44] M. Johannsen, K. A. Jørgensen, *Tetrahedron* **1996**, 52, 7321; b) *J. Chem. Soc. Perkin Trans. 2* **1997**, 1183; c) M. Johannsen, S. Yao, A. Graven, K. A. Jørgensen, *Pure Appl. Chem.* **1997**, 70, 1117.
- [45] S. Yao, M. Johannsen, R. G. Hazell, K. A. Jørgensen, *J. Org. Chem.* **1998**, 63, 118.
- [46] A. K. Ghosh, P. Mathivanan, J. Cappiello, K. Krishnan, *Tetrahedron: Asymmetry* **1996**, 7, 2165.
- [47] A. K. Ghosh, P. Mathivanan, J. Cappiello, *Tetrahedron Lett.* **1997**, 38, 2427.
- [48] S. Yao, M. Johannsen, K. A. Jørgensen, *J. Chem. Soc. Perkin Trans. 1* **1997**, 2345.
- [49] G. Desimoni, G. Faita, P. P. Righetti, N. Sardone, *Tetrahedron* **1996**, 52, 12019.
- [50] a) D. A. Evans, J. S. Johnson, C. S. Burgey, K. R. Campos, *Tetrahedron Lett.* **1999**, 40, 2879; b) D. A. Evans, E. J. Olhava, J. S. Johnson, J. M. Janey, *Angew. Chem.* **1998**, 110, 3557; *Angew. Chem. Int. Ed.* **1998**, 37, 3373.
- [51] H. Audrain, J. Thorhauge, R. G. Hazell, K. A. Jørgensen, *J. Org. Chem.* **2000**, 65, 4487.
- [52] D. A. Evans, S. J. Miller, T. Lectka, *J. Am. Chem. Soc.* **1993**, 115, 6460.
- [53] R. W. Quan, Z. Li, E. N. Jacobsen, *J. Am. Chem. Soc.* **1996**, 118, 8156.
- [54] a) S. Oi, K. Kashiwagi, E. Terada, K. Ohuchi, Y. Inoue, *Tetrahedron Lett.* **1996**, 37, 6351; b) S. Oi, E. Terada, K. Ohuchi, T. Kato, Y. Tachibana, Y. Inoue, *J. Org. Chem.* **1999**, 64, 8660.
- [55] K. Mikami, O. Kotera, Y. Motoyama, H. Sakaguchi, *Synlett* **1995**, 975.
- [56] a) M. Johannsen, S. Yao, K. A. Jørgensen, *Chem. Commun.* **1997**, 2169; b) S. Yao, M. Johannsen, H. Audrain, R. G. Hazell, K. A. Jørgensen, *J. Am. Chem. Soc.* **1998**, 120, 8599.

- [57] E. J. Corey, A. Guzman-Perez, *Angew. Chem.* **1998**, *110*, 402; *Angew. Chem. Int. Ed.* **1998**, *37*, 388.
- [58] D. A. Evans, J. A. Murry, P. von Matt, R. D. Norcross, S. J. Miller, *Angew. Chem.* **1995**, *107*, 864; *Angew. Chem. Int. Ed. Engl.* **1995**, *34*, 798.
- [59] J. Bao, W. D. Wulff, A. L. Rheingold, *J. Am. Chem. Soc.* **1993**, *115*, 3814.
- [60] S. Yao, M. Roberson, F. Reichel, K. A. Jørgensen, *J. Org. Chem.* **1999**, *64*, 6677.
- [61] a) R. A. Ruden, R. Bonjouklian, *J. Am. Chem. Soc.* **1975**, *97*, 6892; b) R. Bonjouklian, R. A. Ruden, *J. Org. Chem.* **1977**, *42*, 4095; c) R. G. Salomon, S. Roy, M. F. Salomon, *Tetrahedron Lett.* **1988**, *29*, 769.
- [62] M. J. Konkel, R. Vince, *Tetrahedron* **1996**, *52*, 799.
- [63] J. E. Baldwin, R. M. Adlington, M. B. Mitchell, *J. Chem. Soc. Chem. Commun.* **1993**, 1332.
- [64] L. F. Tietze, P. Saling, *Synlett* **1992**, 281; L. F. Tietze, P. Saling, *Chirality* **1993**, *5*, 329.
- [65] a) E. Wada, H. Yasuoka, S. Kanamasa, *Chem. Lett.* **1994**, 1637; b) E. Wada, W. Pei, H. Yasuoka, U. Chin, S. Kanamasa, *Tetrahedron* **1996**, *52*, 1205.
- [66] a) D. A. Evans, J. S. Johnson, *J. Am. Chem. Soc.* **1998**, *120*, 4895; b) D. A. Evans, J. S. Johnson, E. J. Olhava, *J. Am. Chem. Soc.* **2000**, *122*, 1635.
- [67] J. Thorhauge, M. Johannsen, K. A. Jørgensen, *Angew. Chem. Int. Ed.* **1998**, *110*, 2543; *Angew. Chem. Int. Ed.* **1998**, *37*, 2404.
- [68] W. Zhuang, J. Thorhauge, K. A. Jørgensen, *Chem. Commun.* **2000**, 459.
- [69] See for example: F. Perron, K. F. Albizzati, *Chem. Rev.* **1989**, *89*, 1617.
- [70] See for example: a) S. P. Clissold, C. Edwards, *Drugs* **1988**, *35*, 214; b) J. A. Balfour, D. McTavish, *Drugs* **1993**, *46*, 1025; c) M. von Itzstein, W.-Y. Wu, G. B. Kok, M. S. Pegg, J. C. Dyason, B. Jin, T. V. Phan, M. L. Smythe, H. F. White, S. W. Oliver, P. M. Colman, J. N. Varghese, D. M. Ryan, J. M. Woods, R. C. Bethell, V. J. Hotham, J. M. Cameron, C. R. Penn, *Nature* **1993**, *363*, 418; d) C. U. Kim, W. Lew, M. A. Williams, H. Liu, L. Zhang, S. Swaminathan, N. Bischofberger, M. S. Chen, D. B. Mendel, C. Y. Tai, W. G. Laver, R. C. Stevens, *J. Am. Chem. Soc.* **1997**, *119*, 681; e) D. P. Calfee, F. G. Hayden, *Drugs* **1998**, *58*, 537.
- [71] a) H. Waldmann, *Synlett* **1995**, 133; b) R. M. Borzilleri, S. M. Weinreb, *Synthesis* **1995**, 347; c) D. L. Boger, *Chemtracts: Org. Chem.* **1996**, *9*, 149; d) “ α -Amino Acid Synthesis”: M. J. O'Donnell, *Tetrahedron* **1988**, *44*, 5253; e) “Recent Development in the Stereoselective Synthesis of α -Amino Acid”: R. O. Duthale, *Tetrahedron* **1994**, *50*, 1539.
- [72] For some elegant examples on the application of HDA and ene reactions of imines in the total synthesis of complex compounds, see for example: a) S. M. Weinreb, *Acc. Chem. Res.* **1985**, *18*, 16; b) T. R. Bailey, R. S. Garigipati, J. A. Morton, S. M. Weinreb, S. M. *J. Am. Chem. Soc.* **1984**, *106*, 3240; c) M. E. Kuehne, R. S. Muth, *J. Org. Chem.* **1991**, *56*, 2701; d) R. Lock, H. Waldmann, *Liebigs Ann. Chem.* **1994**, 511; e) A. B. Holmes, A. Kee, T. Ladduwahetty, D. Smith, *J. Chem. Soc. Chem. Commun.* **1990**, 1412; f) A. B. Holmes, J. Thompson, A. J. G. Baxter, J. Dixon, *J. Chem. Soc. Chem. Commun.* **1985**, 37; g) G. R. Heintzelman, S. M. Weinreb, *J. Org. Chem.* **1996**, *61*, 4594.
- [73] a) C. E. Masse, J. S. Panek, *Chem. Rev.* **1995**, *95*, 1293; b) Y. Yamamoto, N. Asao, *Chem. Rev.* **1993**, *93*, 2207; c) S. E. Denmark, O. J. Nicaise, *J. Chem. Soc., Chem. Commun.* **1996**, 999; d) D. Enders, U. Reinhold, *Tetrahedron: Asymmetry* **1997**, *8*, 1895; e) R. Bloch, *Chem. Rev.* **1998**, *98*, 1407; f) S. Kobayashi, H. Ishitani, *Chem. Rev.* **1999**, *99*, 1069.
- [74] a) B. Nader, R. W. Franck, S. M. Weinreb, *J. Am. Chem. Soc.* **1980**, *102*, 1153; b) B. Nader, T. R. Bailey, R. W. Franck, S. M. Weinreb, *J. Am. Chem. Soc.* **1981**, *103*, 7573.
- [75] S. D. Larsen, P. A. Grieco, *J. Am. Chem. Soc.* **1985**, *107*, 1768.
- [76] a) J. F. Kerwin, Jr., S. Danishefsky, *Tetrahedron Lett.* **1982**, *23*, 3739; b) S. Danishefsky, J. F. Kerwin, Jr., *J. Org. Chem.* **1982**, *47*, 3183.
- [77] S. M. Brandstadter, I. Ojima, *Tetrahedron Lett.* **1987**, *28*, 613.
- [78] S. Kobayashi, H. Ishitani, S. Nagayama, *Synthesis* **1995**, 1195.
- [79] M. M. Midland, J. I. McLoughlin, *Tetrahedron Lett.* **1988**, *29*, 4653.
- [80] M. M. Midland, R. W. Koops, *J. Org. Chem.* **1992**, *57*, 1158.
- [81] K. Ishimaru, Y. Yamamoto, K. Akiba, *Tetrahedron* **1997**, *53*, 5423.
- [82] R. Badorrey, C. Cativiela, M. D. Díaz-de-Villegas, J. A. Gálvez, *Tetrahedron Lett.* **1997**, *38*, 2547; R. Badorrey, C. Cativiela, M. D. Díaz-de-Villegas, J. A. Gálvez, *Tetrahedron* **1999**, *55*, 7601.
- [83] N. T. Anh, *Top. Curr. Chem.* **1980**, *88*, 145.
- [84] P. Herczegh, I. Kovács, L. Szilágyi, M. Zsély, F. Sztaricskai, *Tetrahedron Lett.* **1992**, *33*, 3133.
- [85] L. Yu, J. Li, J. Ramirez, D. Chen, P. G. Wang, *J. Org. Chem.* **1997**, *62*, 903.
- [86] See for example: a) M. Maggini, M. Prato, G. Scorrano, *Tetrahedron Lett.* **1990**, *31*, 6243; b) P. Pinho, P. G. Andersson, *Chem. Commun.* **1999**, 597; c) D. A. Alonso, S. K. Bertilsson, S. Y. Johnsson, S. J. M. Nordin, M. J. Södergren, P. G. Andersson, *J. Org. Chem.* **1999**, *64*, 2276; d) M. T. Crimmins, *Tetrahedron* **1998**, *54*, 9229; e) T. S. Mansour, R. Storer, *Curr. Pharm. Des.* **1997**, *3*, 227; f) M. T. Crimmins, B. W. King, *J. Org. Chem.* **1996**, *61*, 4192; g) H. Nagata, T. Taniguchi, K. Ogasawara, *Tetrahedron: Asymmetry* **1997**, *8*, 2679; h) S. M. Daluge, US-A 5,034,394, **1991**; i) V. E. Marquez, M.-I. Lim, *Med. Res. Rev.* **1986**, *6*, 1, and references therein; j) D. Zhang, M. J. Miller, *J. Org. Chem.* **1998**, *63*, 755; k) B. K. Chun, C. K. Chu, *Tetrahedron Lett.* **1999**, *40*, 3309; l) N. G. Ramesh, A. J. H. Klunder, B. Zwanzburg, *J. Org. Chem.* **1999**, *64*, 3635.
- [87] P. Hamley, G. Helmchen, A. B. Holmes, D. R. Marshall, J. W. M. MacKinnon, D. F. Smith, J. W. Ziller, *J. Chem. Soc. Chem. Commun.* **1992**, 786.
- [88] a) E. Borrione, M. Prato, G. Scorrano, M. Stivanello, V. Lucchini, G. Valle, *J. Chem. Soc. Perkin Trans. 1* **1989**, 2245; b) V. Lucchini, M. Prato, G. Scorrano, P. Tecilla, *J. Org. Chem.* **1988**, *53*, 2251.
- [89] a) E. P. Kündig, L. H. Xu, B. Schnell, *Synlett* **1994**, 413; b) E. P. Kündig, L. H. Xu, P. Romanens, G. Bernardinelli, *Synlett* **1996**, 270.
- [90] Some uncatalyzed examples are: a) H. Waldmann, M. Braun, *Liebigs Ann. Chem.* **1991**, 1045; b) E. Pombo-Villar, J. Boelsterli, M. M. Cid, J. France, B. Fuchs, M. Walkinshaw, H.-P. Weber, *Helv. Chim. Acta* **1993**, *76*, 1203; c) L. Stella, H. Abraham, *Tetrahedron Lett.* **1990**, *31*, 2603; d) P. D. Bailey, R. D. Wilson, G. R. Brown, *J. Chem. Soc. Perkin Trans. 1* **1991**, 1337; e) P. D. Bailey, G. R. Brown, F. Korber, A. Reed, R. D. Wilson, *Tetrahedron: Asymmetry* **1991**, *2*, 1263; f) P. D. Bailey, D. J. Londebrough, T. C. Hancox, J. Heffernan, A. B. Holmes, *J. Chem. Soc. Chem. Commun.* **1994**, 2543.
- [91] A. K. McFarlane, G. Thomas, A. Whiting, *Tetrahedron Lett.* **1993**, *34*, 2379; A. K. McFarlane, G. Thomas, A. Whiting, *J. Chem. Soc. Perkin Trans. 1* **1995**, 2803.
- [92] P. N. Devine, M. Reilly, T. Oh, *Tetrahedron Lett.* **1993**, *34*, 5827.
- [93] a) W. Pfrengle, H. Kunz, *J. Org. Chem.* **1989**, *54*, 4261; b) H. Kunz, W. Pfrengle, *Angew. Chem.* **1989**, *101*, 1041; *Angew. Chem. Int. Ed. Engl.* **1989**, *28*, 1067; c) M. Weymann, W. Pfrengle, D. Schollmeyer, H. Kunz, *Synthesis* **1997**, 1151; d) H. Kunz, W. Sager, W. Pfrengle, D. Schanzenbach, *Tetrahedron Lett.* **1988**, *29*, 4397; e) H. Kunz, W. Pfrengle, *J. Am. Chem. Soc.* **1988**, *110*, 651; f) S. Laschat, H. Kunz, *J. Org. Chem.* **1991**, *56*, 5883.
- [94] a) H. Waldmann, *Angew. Chem.* **1988**, *100*, 307; *Angew. Chem. Int. Ed. Engl.* **1988**, *27*, 274; b) H. Waldmann, *Liebigs Ann. Chem.* **1989**, 231; c) H. Waldmann, M. Braun, M. Dräger, *Angew. Chem.* **1990**, *102*, 1445; *Angew. Chem. Int. Ed. Engl.* **1990**, *29*, 1468; d) H. Waldmann, M. Braun, *J. Org. Chem.* **1992**, *57*, 4444.
- [95] S. Danishefsky, M. E. Langer, C. Vogel, *Tetrahedron Lett.* **1985**, *26*, 5983.
- [96] H. Waldmann, M. Braun, M. Weymann, M. Gewehr, *Tetrahedron* **1993**, *49*, 397.
- [97] a) J. Barluenga, F. Aznar, C. Valdés, A. Martín, S. García-Granda, E. Martín, *J. Am. Chem. Soc.* **1993**, *115*, 4403; b) J. Barluenga, F. Aznar, C. Ribas, C. Valdés, M. Fernández, M.-P. Cabal, J. Trujillo, *Chem. Eur. J.* **1996**, *2*, 805; c) J. Barluenga, F. Aznar, C. Valdés, C. Ribas, *J. Org. Chem.* **1998**, *63*, 3918.
- [98] a) K. Hattori, H. Yamamoto, *J. Org. Chem.* **1992**, *57*, 3264; b) K. Hattori, H. Yamamoto, *Tetrahedron* **1993**, *49*, 1749; c) K. Hattori, H. Yamamoto, *Synlett* **1993**, 129.
- [99] R. Lock, H. Waldmann, *Tetrahedron Lett.* **1996**, *37*, 2753.
- [100] K. Ishihara, M. Miyata, K. Hattori, T. Tada, H. Yamamoto, *J. Am. Chem. Soc.* **1994**, *116*, 10520.
- [101] K. Ishihara, H. Yamamoto, *J. Am. Chem. Soc.* **1994**, *116*, 1561.
- [102] H. Ishitani, S. Kobayashi, *Tetrahedron Lett.* **1996**, *37*, 7357.

- [103] S. Kobayashi, H. Ishitani, *J. Am. Chem. Soc.* **1994**, *116*, 4083.
 [104] S. Kobayashi, S. Komiyama, H. Ishitani, *Angew. Chem.* **1998**, *110*, 1026; *Angew. Chem. Int. Ed.* **1998**, *37*, 979.
 [105] S. Kobayashi, K. Kusakabe, S. Komiyama, H. Ishitani, *J. Org. Chem.* **1999**, *64*, 4220.
 [106] S. Yao, M. Johannsen, R. G. Hazell, K. A. Jørgensen, *Angew. Chem.* **1998**, *110*, 3318; *Angew. Chem. Int. Ed.* **1998**, *37*, 3121.
 [107] For the use of the *N*-tosyl α -imino ester in other reactions see for example: a) ref. [15], b) D. Ferraris, B. Young, T. Dudding, T. Lectka, *J. Am. Chem. Soc.* **1998**, *120*, 4548; c) D. Ferraris, B. Young, C. Cox, W. J. Drury III, T. Dudding, T. Lectka, *J. Org. Chem.* **1998**, *63*, 6090; d) X. Fang, M. Johannsen, S. Yao, N. Gathergood, R. G. Hazell, K. A. Jørgensen, *J. Org. Chem.* **1999**, *64*, 4888; e) K. Juhl, R. G. Hazell, K. A. Jørgensen, *J. Chem. Soc. Perkin Trans 1* **1999**, 2393.
 [108] S. Yao, S. Saaby, R. G. Hazell, K. A. Jørgensen, *Chem. Eur. J.* **2000**, *6*, 2435.
 [109] S. Bromidge, P. C. Wilson, A. Whiting, *Tetrahedron Lett.* **1998**, *39*, 8905.
 [110] E. Jnoff, L. Ghosez, *J. Am. Chem. Soc.* **1999**, *121*, 2617.

+++ THE LINK TO INTERNATIONAL CHEMISTRY +++

Reviews? Reviews!

...are indispensable for chemists wanting to keep up-to-date with all branches of chemistry. Reviews in *Angewandte Chemie* are written by leading experts. They summarize the important results of recent research on topical subjects in all branches of chemistry, point to unresolved problems, and discuss possible developments. Their informative approach is ideal for students and fast browsing.

Don't miss out on this important information. Order your personal copy of *Angewandte Chemie* (see the Order Form on the last page of this issue).

Here are the most cited Review articles from 1998:

- A. Kraft, A.C. Grimsdale, A.B. Holmes: Electro-luminescent Conjugated Polymers – Seeing Polymers in a New Light
- Y. Xia, G. Whitesides: Soft Lithography
- M. Dobson, A. Sali, M. Karplus: Protein Folding: A Perspective from Theory and Experiment
- J.F. Hartwig: Transition Metal Catalyzed Synthesis of Arylamines and Aryl Ethers from Aryl Halides and Triflates: Scope and Mechanism
- K.C. Nicolaou, et al.: Chemical Biology of Epithelones
- S.R. Batten, R. Robson: Interpenetrating Nets: Ordered, Periodic Entanglement
- E.J. Corey, A. Guzman-Perez: The Catalytic Enantioselective Construction of Molecules with Quaternary Carbon Stereocenters
- H. Waldmann et al.: Organic Synthesis and Biological Signal Transduction
- G.A. Ozin et al.: A New Model for Aluminophosphate Formation: Transformation of a Linear Chain Aluminophosphate to Chain, Layer, and Framework Structures
- L. Echegoyen et al.: Electrochemistry of Supramolecular Systems



WILEY-VCH, P.O. Box 10 11 61, 69451 Weinheim, Germany
 Phone +49 (6201) 606-328, Fax +49 (6201) 606-348
 e-mail: sales-journals@wiley-vch.de, http://www.wiley-vch.de

 WILEY-VCH

Hot Stones or Cold Soup? New Investigations on the Endogenous Origin of Organic Compounds on Earth

Kay Severin*

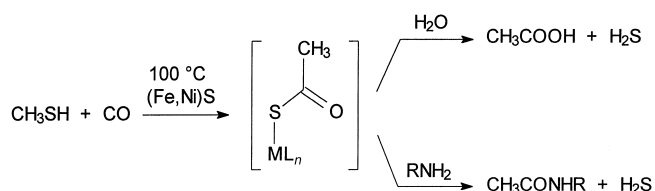
Understanding the origin of life is one of the big intellectual and experimental challenges of our time. Although there is no lack of hypotheses about this topic a generally accepted theory is presently not available. Agreement starts and stops with the fact that life on earth has existed for at least 3.5 billion years^[1] and that organic molecules were required for its emergence. But how did these molecules form? Important new investigations about the origin of the building blocks of life are presented in this highlight.

The most famous experiment in this context was carried out almost fifty years ago by Stanley L. Miller, at that time a PhD student in the group of Harold Urey in Chicago.^[2] Miller was able to show that electric discharges in an atmosphere of methane, ammonia, hydrogen, and water led to the formation of significant amounts of various amino acids. Experiments of this kind were repeated in numerous variants. If reducing gases were employed mixtures of organic compounds of low molecular weight could be detected in many cases. This has led to the popular idea that the primordial ocean resembled a nutritious soup.

But the possibility that earth once had a reducing atmosphere is questioned. A well known argument against it is the high photolability of methane and ammonia. Because a shielding layer of ozone was missing a high concentration of these gases is believed to be unlikely. Furthermore, several other results point to a neutral atmosphere of CO₂ and N₂. Given the fact that the atmosphere was based on an unproductive mixture of CO₂ and N₂ the nutritional value of the primordial ocean drops significantly.^[3]

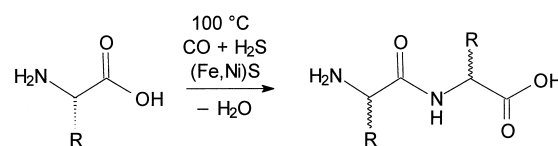
An alternative scenario has been propagated for several years by Wächterhäuser. Instead of a primordial soup he favors hot minerals as the place where organic molecules were initially built and life subsequently emerged. Especially sulfur-containing minerals like pyrite^[4] are proposed to have acted as an energy source and catalyst both under the extreme conditions found in hydrothermal or volcanic vents. Two new experimental studies by Huber and Wächterhäuser have attracted considerable interest, in which chemical model

reactions supporting the above hypothesis are described. First they were able to show that in an aqueous suspension of (Fe,Ni)S at 100 °C CH₃SH and CO react to form acetic acid.^[5] As an intermediate they postulate a metal-bonded thioacetate, which was detected by trapping reactions with amines (Scheme 1).



Scheme 1. Synthesis of activated acetic acid by carbon fixation of CO in the presence of (Fe,Ni)S. M = Fe, Ni.

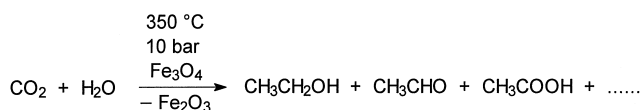
In a subsequent study it was reported that under similar conditions (100 °C, Fe/NiS, CO, H₂S or CH₃SH) amino acids are converted to (racemic) dipeptides (Scheme 2).^[6] This result is remarkable because the hydrolysis of peptides is thermodynamically strongly favored. Several exergonic reactions of CO are discussed which could provide the energy for the condensation.



Scheme 2. Condensation of amino acids at the surface of (Fe,Ni)S in the presence of CO and H₂S. R = H, CH₂Ph, CH₂C₆H₄OH.

After carbon fixation of CO under potentially prebiotic conditions had been realized in the laboratory, Chen and Bahnemann have recently shown that in the presence of magnetite CO₂ can be converted into organic substances.^[7] In a ternary mixture of CO₂, water, and Fe₃O₄ at 350 °C and 10 bar they were able to detect acetaldehyde, ethanol, and acetic acid (up to 4%) after a few hours (Scheme 3). The extreme conditions simulate the environment of the earth's crust. The reaction, which is inhibited by larger amounts of water, can even be performed in the presence of oxygen. Thus, the range of temperatures and redox conditions over which

[*] Dr. K. Severin
Department Chemie
Ludwig-Maximilians-Universität München
Butenandtstrasse 5–13, 81377 München (Germany)
Fax: (+49) 89-2180-7866
E-mail: kse@cup.uni-muenchen.de

Scheme 3. Carbon fixation of CO₂ in the presence of magnetite.

organic compounds can be produced from inorganic gases is significantly expanded. Given the fact that iron oxides are common in the crust, this could be a more important source for organic substances than was previously thought.

The work described above proves that a prebiotic organic chemistry with CO and CO₂ as C₁ building blocks could have occurred in hydrothermal or volcanic settings. Remarkably, even chemically inert N₂ can be converted under such conditions. This was shown by Brandes et al.^[8] Likewise with the help of magnetite the reduction of N₂, NO₂⁻, and NO₃⁻ to NH₃ is possible at elevated temperatures (300–800 °C) and pressures (0.1–0.4 GPa). In the presence of pyrite instead of magnetite the reduction of NO₂⁻ and NO₃⁻ is even faster. This shows that certain areas of the crust as well as hydrothermal vents represent a possible source for NH₃, a molecule with relevance for the production of amino acids as described above. Given that the ammonia produced this way finally makes its way into the atmosphere, a connection between the chemistry at hot minerals and the chemistry of a primordial soup begins to emerge.^[9]

Exogenous sources for organic molecules have also been discussed extensively.^[3, 10] Nevertheless, compounds with extraterrestrial origin have to have been produced sometime somewhere. Possibly, the underlying chemical reactions are the same as on earth. In this case, the model reactions described above are also important for a deeper understanding.

The prebiotic synthesis of organic molecules of low complexity was an important first step for the origin of life. In view

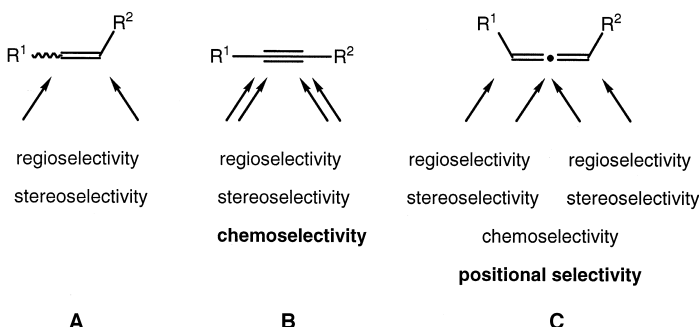
of the results presented the origin of these compounds appears to be less mysterious. But crucial further steps have not (or insufficiently) been simulated in the laboratory so far. How were long information-carrying biopolymers produced although the hydrolysis of such compounds is fast on the geological time scale? Did minerals^[11] or metal ions^[12] act as a catalyst? How and at which stage did the break of symmetry occur, which is manifested in the homochirality of present day biomolecules?^[10, 13] And what were the first molecules which were able to self-replicate^[14] and which were subsequently subjected to molecular evolution? There is plenty of room for new hypotheses and especially for new experiments.

- [1] There is experimental evidence that life on earth existed 3.8 billion years ago: S. J. Mojzsis, G. Arrhenius, K. D. McKeegan, T. M. Harrison, A. P. Nutman, C. R. L. Friend, *Nature* **1996**, 384, 55.
- [2] S. L. Miller, *Science* **1953**, 117, 528.
- [3] C. Chyba, C. Sagan, *Nature* **1992**, 355, 125.
- [4] E. Drobner, H. Huber, G. Wächtershäuser, D. Rose, K. O. Setter, *Nature* **1990**, 346, 742.
- [5] C. Huber, G. Wächtershäuser, *Science* **1997**, 276, 245.
- [6] C. Huber, G. Wächtershäuser, *Science* **1998**, 281, 670.
- [7] Q. W. Chen, D. W. Bahnemann, *J. Am. Chem. Soc.* **2000**, 122, 970.
- [8] J. A. Brandes, N. Z. Boctor, G. D. Cody, B. A. Cooper, R. M. Hazen, H. S. Yoder, Jr., *Nature* **1998**, 395, 365.
- [9] C. Chyba, *Nature* **1998**, 395, 329.
- [10] J. Podlech, *Angew. Chem.* **1999**, 111, 501; *Angew. Chem. Int. Ed.* **1999**, 38, 477.
- [11] a) G. von Kiedrowski, *Nature* **1996**, 381, 20; b) J. P. Ferris, A. R. Hill, Jr., R. Liu, L. E. Orgel, *Nature* **1996**, 381, 59.
- [12] B. M. Rode, Y. Suwannachot, *Coord. Chem. Rev.* **1999**, 190–192, 1085.
- [13] B. L. Feringa, R. A. van Delden, *Angew. Chem.* **1999**, 111, 3624; *Angew. Chem. Int. Ed.* **1999**, 38, 3418.
- [14] a) A. Robertson, A. J. Sinclair, D. Philip, *Chem. Soc. Rev.* **2000**, 29, 141; b) D. H. Lee, K. Severin, M. R. Ghadiri, *Curr. Opin. Chem. Biol.* **1997**, 37, 126; c) B. G. Brag, G. von Kiedrowski, *Pure Appl. Chem.* **1996**, 68, 2145.

New and Selective Transition Metal Catalyzed Reactions of Allenes

A. Stephen K. Hashmi*

Among the most popular organic substrates for transition metal catalyzed reactions are alkenes **A** and alkynes **B** (Scheme 1). Allenes **C** have received much less attention. This is easily explained by increasing selectivity problems when we proceed from **A** to **C**. While in **A** we face the question of regioselectivity (Markovnikov versus anti-Markovnikov ori-



[*] Priv.-Doz. Dr. A. S. K. Hashmi
 Institut für Organische Chemie
 Johann Wolfgang Goethe-Universität Frankfurt
 Marie-Curie-Strasse 11, 60439 Frankfurt am Main (Germany)
 Fax: (+49) 69-798-29464
 E-mail: hashmi@chemie.uni-frankfurt.de

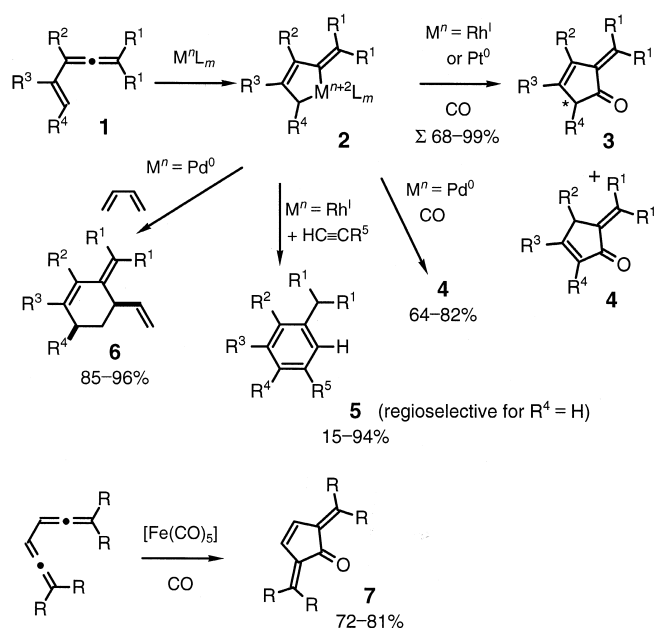
entation leading to constitutional isomers) and stereoselectivity of an addition reaction (*cis*- or *trans*-addition at possibly enantiotopic or diastereotopic faces of the double bond, leading to stereoisomers), in **B** we have to cope with the problem of chemoselectivity (single or double addition leading to different products) and for each addition the regio- and stereoselectivity problems apply as discussed for **A**. In **C** the situation is even more complicated: as with the alkynes chemo-, regio-, and stereoselectivity are significant, but furthermore we face the question of positional selectivity (which of the two orthogonal double bonds will react in the case of a single addition, thus again leading to constitutional isomers).

In early investigations of the reactions of allenes with transition metals the conversions proceeded quite unselectively, due to the *enhanced reactivity* of the allenes.^[1] This observation led to the neglect of allenes as substrates in such reactions for a long time. In the past decade allenes have reemerged as interesting compounds for scientists working in the field of transition metal catalysis. Three major principles were used to overcome the selectivity problem: 1) In intermolecular reactions, the positional selectivity was often controlled by steric hindrance, that is, by substituents on only one of the double bonds. 2) Intramolecularization of the reactions, usually by placing the groups at such a distance that five- or six-membered rings are formed, automatically solved the positional selectivity problem. 3) Allenes bearing functional groups on the carbon atom next to the allene unit allowed the control of the selectivity by both geometrical restrictions and electronic differentiation of the two cumulated double bonds of the allene, not only in intramolecular but also in intermolecular reactions.

While principle 1 has allowed some very interesting transformations and numerous mechanistic details could be investigated,^[2] the substituents used to provide steric hindrance also limited the synthetic potential. Principle 2 seems to have a higher potential for organic synthesis.^[3] Principle 3, in particular, seems to provide some interesting and truly new transformations, which shall be summarized here. The following section is organized in terms of the different types of substrates that all belong to the type of principle 3. If not otherwise stated, the reactions proceed with 0.5–5 mol % of catalyst.

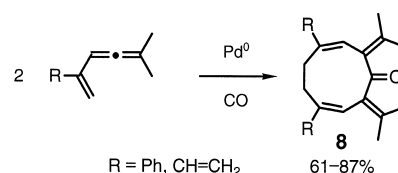
a) Vinyl Allenes

As mentioned in the introduction,^[1c] no selectivity was observed in early dimerization experiments of **1**. But when other partners were offered, the corresponding cross-dimerizations were quite selective. Probably methylene metallacyclopentenones **2**,^[4] which could be isolated, are intermediates that then react with the other partners (Scheme 2). Generally, the related 1,3-dienes are less reactive than **1** with its reactive allenic double bond and do not react in a similar manner.^[4a] Rh-catalyzed [4+1] cycloadditions with CO as a second reaction partner led to alkylidene cyclopentenones **3** and **4**,^[4, 5] while in Pd-catalyzed reactions where **1** was generated in situ and a base was present, only **4**^[6] was formed. When Pt⁰ was used instead of Rh^I in the carbonylation reaction, both in the



Scheme 2. Reactions of vinyl allenes **1**.

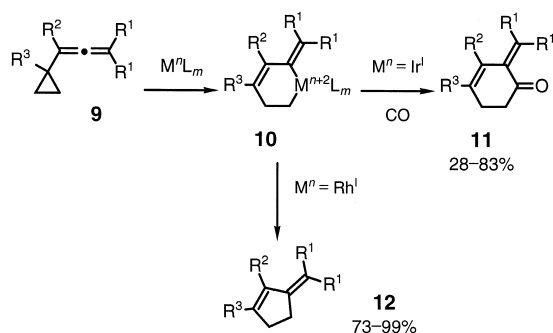
presence of the (*R,R*)-DuPHOS ligand, opposite enantiomers of **3** were obtained.^[5b] This observation still needs a precise explanation. [Fe(CO)₅]-mediated reactions of diallenes form dialkylidene cyclopentenones **7** (Scheme 2, here 10 mol % of catalyst are needed).^[7] Other partners like alkynes in Rh- or 1,3-dienes in Pd-catalyzed reactions led to arenes **5**^[8] or vinyl alkylidene cyclohexenes **6**.^[9] Since these [4+2] cycloadditions take place between two electronically quite similar partners, a direct Diels–Alder reaction is not feasible. With a certain substitution pattern even [4+4+1] cycloadditions that deliver nine-membered rings **8**^[10] could be achieved (Scheme 3). With Rh^I the same substrate delivers **3**.



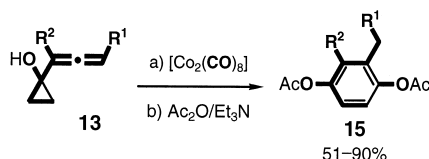
Scheme 3. Formation of nine-membered rings from vinyl allenes and CO.

b) Cyclopropyl Allenes

Substrates **9** can be regarded as homoolefinic derivatives of **1** (Scheme 4). Here also the analogous vinyl cyclopropanes do not react similarly to **9**; the allenic unit makes **9** more reactive.^[11] In Ir^I-catalyzed reactions with CO the six-membered analogues of **3**, the cyclohexenones **11**,^[11] were formed in a [5+1] cycloaddition (Scheme 4). On the other hand, Rh^I in the absence of CO leads to **12**^[12] formed by a vinyl cyclopropane/cyclopentene rearrangement. Such a rearrangement without a catalyst would require temperatures between 300 and 400 °C! Again one suspects metallacycles **10** as intermediates that either insert CO or undergo a reductive elimination immediately. With [Co₂Co₈] 1-hydroxycycloprop-

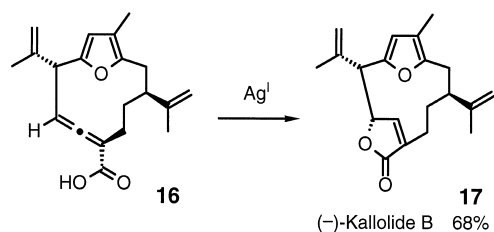
Scheme 4. Reactions of cyclopropyl allenes **9**.

yl allenes **13** can be transformed into hydroquinones **14** and the corresponding diacetates **15**, respectively, under mild conditions (Scheme 5).^[13] This methodology can be used in the synthesis of vitamin E and K analogues.

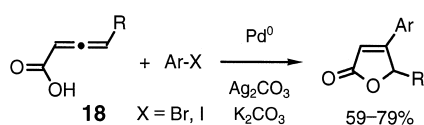
Scheme 5. Formation of dihydroquinones from cyclopropyl allenes **13**.

c) Allenes with Neighboring OH or NH Groups

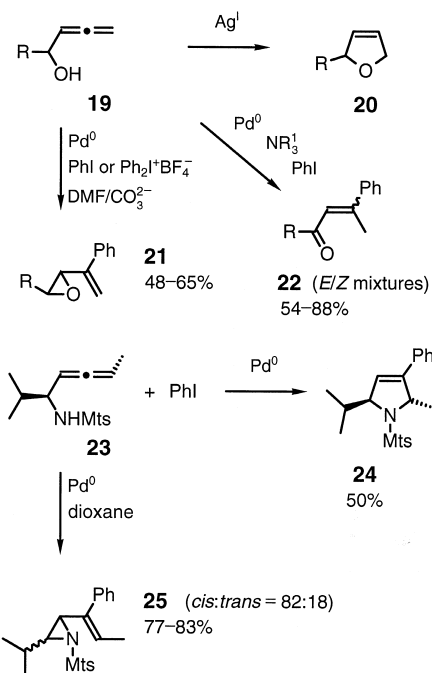
The addition of hydroxy groups to the distal double bond of the allene, mediated by Hg^{II} or Ag^I and leading to dihydrofurans, has been known for some time.^[14] Marshall very successfully applied this principle to the synthesis of natural products and extended it to allenyl carboxylic acids like **16**,^[15] which can lead to lactones like **17** (Scheme 6). With substrates

Scheme 6. Silver-catalyzed lactonization in Marshall's synthesis of (–)-kallolide B (**17**).

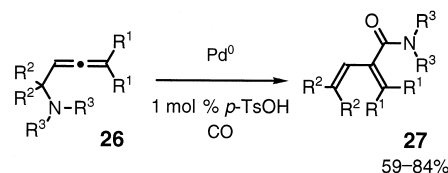
18 additional C–C bonds can be formed in Pd-catalyzed reactions with aryl halides as reaction partners (Scheme 7).^[16] In the case of Pd-catalyzed reactions of aryl halides with allenyl carbinols **19**, enones **22**^[17] were obtained (Scheme 8). Interestingly, in DMF as solvent and with CO_3^{2-} , for **19** a cyclization leading to the corresponding vinyl epoxides **21**^[18] could be achieved! Simple treatment of **19** with Ag^I delivers **20**. The silver(I) catalysts show significant lower reactivity, thus usually 20 mol % or even more are applied. Similar develop



Scheme 7. Combination of C–C bond formation and lactonization.

Scheme 8. Reactions of allenyl carbinols **19** and related amines **23**. Mts = 2,4,6-trimethylbenzenesulfonyl.

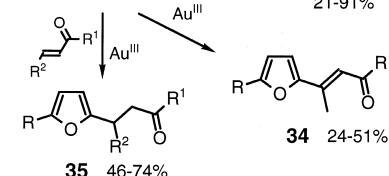
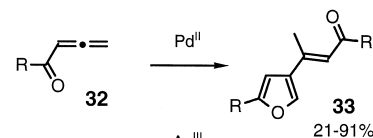
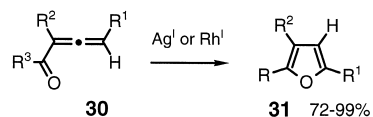
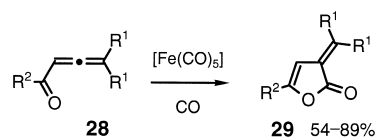
ments were possible for the amines **23**, which either formed dihydropyrroles **24** or vinyl aziridines **25** (Scheme 8).^[19] Here also the reaction heavily depends on the solvent, but no explanation has been provided so far. On the other hand in the presence of a Pd catalyst and CO, tertiary amines **26**, which cannot form another C–N bond, gave α -vinylacrylamides **27** (Scheme 9).^[20]

Scheme 9. Formation of vinylacrylamides **27**. $p-TsOH$ = *para*-toluenesulfonate.

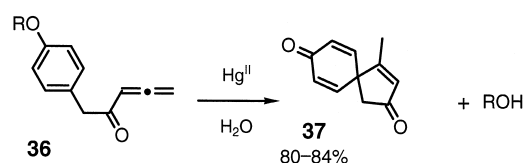
d) Allenyl Ketones

Here also a diversity of reactions was developed. With γ,γ -disubstituted derivatives **28** and $[Fe(CO)_5]$ (again 10 mol %), the lactones **29** were formed (Scheme 10).^[21] Rh^I or Ag^I cause the cycloisomerization of **30** to the corresponding furan **31**.^[22] Even greater is the diversity of substrates **32**. Pd^{II} leads to the formation of the dimer **33**,^[23] Au^{III} to a constitutional isomer of **33**, the dimer **34**. When the latter reaction was performed in the presence of Michael acceptors, the mixed dimers **35** were formed.^[24] Finally, in the case of alkoxy-substituted allenyl benzyl ketones **36**, the spirocycles **37** are obtained (Scheme 11).^[25]

Today many selective and synthetically interesting transformations of allenes are known but sometimes the unique chemoselectivity still lacks explanation. A deeper mechanistic understanding of these selectivities might be the key for the future development of even more exciting reactions.



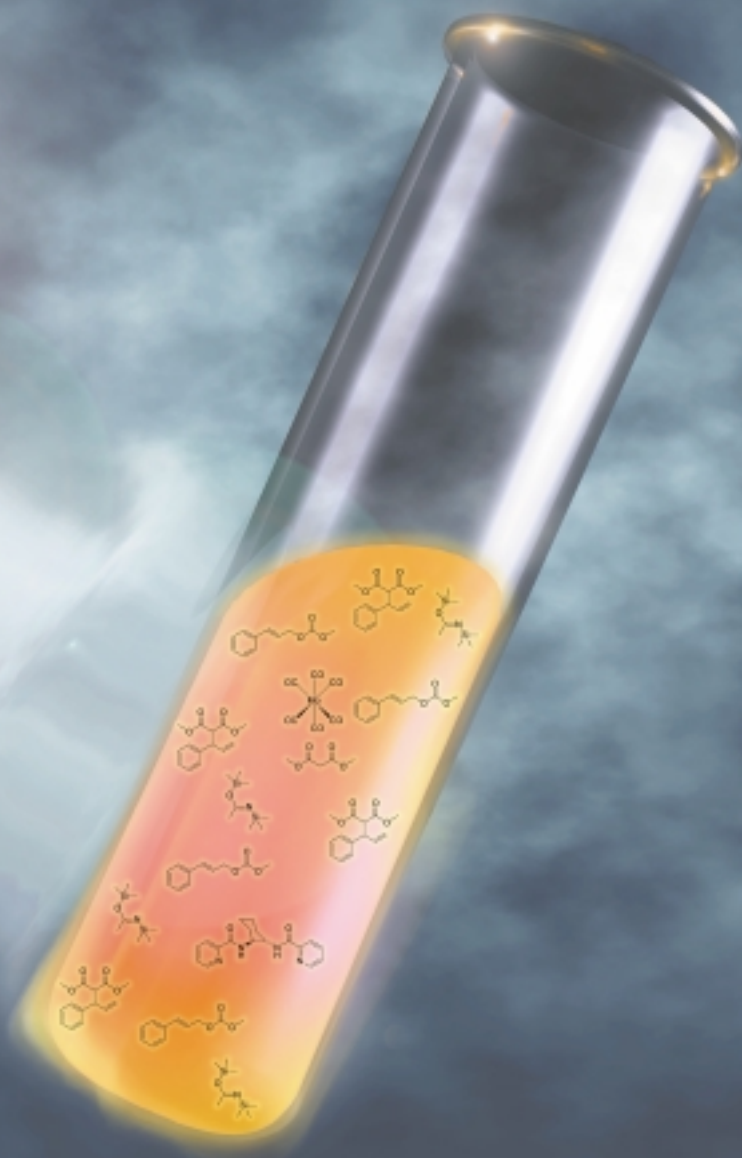
Scheme 10. Transition metal catalyzed reactions of allenyl ketones **28**, **30**, and **32**.



Scheme 11. Hg^{II} -catalyzed formation of spiro[4.5]decanes **37** from *p*-alkoxy allenyl ketones **36**.

- [1] a) B. L. Shaw, A. J. Stringer, *Inorg. Chem. Acta Rev.* **1973**, 7, 1–10; b) F. L. Bowden, R. Giles, *Coord. Chem. Rev.* **1976**, 20, 81–106; for further efforts, see: c) H. Siegel, H. Hopf, A. Germer, P. Binger, *Chem. Ber.* **1978**, 111, 3112–3118; d) G. Erker, *Methoden Org. Chem. (Houben-Weyl) 4th ed*, 1952–, Vol. E18, **1986**, pp. 870–873 and 882–883.
- [2] For selected examples and additional references, see: L. Besson, J. Goré, B. Cazes, *Tetrahedron Lett.* **1995**, 36, 3853–3856; W.-J. Xiao, G. Vasapollo, H. Alper, *J. Org. Chem.* **1998**, 63, 2609–2612; R. C. Larock, Y. He, W. W. Leong, X. Han, M. D. Refvik, J. M. Zenner, *J. Org. Chem.* **1998**, 63, 2154–2160; T. Sudo, N. Asao, V. Gevorgyan, Y. Yamamoto, *J. Org. Chem.* **1999**, 64, 2494–2499; S. Kacker, A. Sen, *J. Am. Chem. Soc.* **1997**, 119, 10028–10033; B. M. Trost, A. B. Pinkerton, *J. Am. Chem. Soc.* **1999**, 121, 10842–10843; D. Hideura, H. Urabe, F. Sato, *Chem. Commun.* **1998**, 271–272.
- [3] For selected examples and additional references, see: V. M. Arredondo, S. Tian, F. E. McDonald, T. J. Marks, *J. Am. Chem. Soc.* **1999**, 121, 3633–3639; R. D. Walkup, G. Park, *J. Am. Chem. Soc.* **1990**, 112, 1597–1603; R. Grigg, J. M. Sansano, *Tetrahedron* **1996**, 52, 13441–13454; C. Jonasson, J.-E. Bäckvall, *Tetrahedron Lett.* **1998**, 39, 3601–3604; D. N. A. Fox, D. Lathbury, M. F. Mahon, K. C. Molloy, G. Gallagher, *J. Am. Chem. Soc.* **1991**, 113, 2652–2656; M. Lautens, C. Meyer, A. van Oeveren, *Tetrahedron Lett.* **1997**, 38, 3833–3836; J. S. Prasad, L. S. Liebeskind, *Tetrahedron Lett.* **1988**, 29, 4253–4256; F. P. J. T. Rutjes, K. C. M. F. Tjen, L. B. Wolf, W. F. J. Karstens, H. E. Schoemaker, H. Hiemstra, *Org. Lett.* **1999**, 1, 717–720; K. M. Brummond, J. Lu, *J. Am. Chem. Soc.* **1999**, 121, 5087–5088; for an example of a diastereoselective reaction, see: P. A. Wender, M. Fuji, C. O. Husfeld, J. A. Love, *Org. Lett.* **1999**, 1, 137–139.
- [4] a) M. Murakami, K. Itami, Y. Ito, *Angew. Chem.* **1995**, 107, 2943–2946; *Angew. Chem. Int. Ed. Engl.* **1995**, 34, 2691; b) M. Murakami, K. Itami, Y. Ito, *J. Am. Chem. Soc.* **1996**, 118, 11672–11673.
- [5] a) M. Murakami, K. Itami, Y. Ito, *J. Am. Chem. Soc.* **1993**, 115, 5865–5866; b) M. Murakami, K. Itami, Y. Ito, *J. Am. Chem. Soc.* **1999**, 121, 4130–4135.
- [6] T. Mandai, J. Tsuji, Y. Tsujiguchi, S. Saito, *J. Am. Chem. Soc.* **1993**, 115, 5865–5866.
- [7] M. S. Sigman, B. E. Eaton, *J. Am. Chem. Soc.* **1996**, 118, 11783–11788.
- [8] M. Murakami, M. Ubukata, K. Itami, Y. Ito, *Angew. Chem.* **1998**, 110, 2362–2364; *Angew. Chem. Int. Ed.* **1998**, 37, 2248–2250.
- [9] M. Murakami, K. Itami, Y. Ito, *J. Am. Chem. Soc.* **1997**, 119, 7163–7164.
- [10] M. Murakami, K. Itami, Y. Ito, *Angew. Chem.* **1998**, 110, 3616–3619; *Angew. Chem. Int. Ed.* **1998**, 37, 3418–3420.
- [11] M. Murakami, K. Itami, M. Ubukata, I. Tsuji, Y. Ito, *J. Org. Chem.* **1998**, 63, 4–5.
- [12] M. Hayashi, T. Ohmatsu, Y.-P. Meng, K. Saigo, *Angew. Chem.* **1998**, 110, 877–879; *Angew. Chem. Int. Ed.* **1998**, 37, 837–839.
- [13] Y. Owada, T. Matsuo, N. Iwasawa, *Tetrahedron* **1997**, 53, 11069–11086.
- [14] L.-I. Olsson, A. Claesson, *Synthesis* **1979**, 743–745.
- [15] J. A. Marshall, K. G. Pinney, *J. Org. Chem.* **1993**, 58, 7180–7184; J. A. Marshall, G. S. Bartley, E. M. Wallace, *J. Org. Chem.* **1996**, 61, 5729–5735.
- [16] S. Ma, Z. Shi, *J. Org. Chem.* **1998**, 63, 6387–6389.
- [17] I. Shimizu, T. Sugiura, J. Tsuji, *J. Org. Chem.* **1985**, 50, 537–539.
- [18] S.-K. Kang, T. Yamaguchi, S.-J. Pyun, Y.-T. Lee, T.-G. Baik, *Tetrahedron Lett.* **1998**, 39, 2127–2130; S. Ma, S. Zhao, *J. Am. Chem. Soc.* **1999**, 121, 7943–7944.
- [19] H. Ohno, A. Toda, Y. Miwa, T. Taga, E. Osawa, Y. Yamaoka, N. Fujii, T. Ibuka, *J. Org. Chem.* **1999**, 64, 2992–2993; see also A. Claesson, C. Sahlberg, K. Luthman, *Acta Chem. Scand. B* **1979**, 33, 309–310.
- [20] Y. Imada, G. Vasapollo, H. Alper, *J. Org. Chem.* **1996**, 61, 7982–7983.
- [21] M. S. Sigman, C. E. Kerr, B. E. Eaton, *J. Am. Chem. Soc.* **1993**, 115, 7545–7546; M. S. Sigman, B. E. Eaton, J. D. Heise, C. P. Kubiak, *Organometallics* **1996**, 15, 2829–2832; for the analogous allenyl imines: M. S. Sigman, B. E. Eaton, *J. Org. Chem.* **1994**, 59, 7488–7491.
- [22] J. A. Marshall, E. D. Robinson, *J. Org. Chem.* **1990**, 55, 3450–3451; J. A. Marshall, G. S. Bartley, *J. Org. Chem.* **1994**, 59, 7169–7171.
- [23] A. S. K. Hashmi, *Angew. Chem.* **1995**, 107, 1749–1751; *Angew. Chem. Int. Ed. Engl.* **1995**, 34, 1581–1583; A. S. K. Hashmi, T. L. Ruppert, T. Knöfel, J. W. Bats, *J. Org. Chem.* **1997**, 62, 7295–7304.
- [24] A. S. K. Hashmi, L. Schwarz, J.-H. Choi, T. M. Frost, *Angew. Chem.* **2000**, 112, 2382–2385; *Angew. Chem. Int. Ed.* **2000**, 39, 2285–2288.
- [25] A. S. K. Hashmi, L. Schwarz, M. Bolte, *Tetrahedron Lett.* **1998**, 39, 8969–8972.

High-speed molybdenum-catalyzed asymmetric substitution can be performed with single-mode microwave heating. The reaction mixture is positioned inside the cavity and the microwave irradiation is released from the magnetron and strikes the sample from the top left.



Contrary to conventional conductive heating, microwave heat is generated inside the reaction mixture (in situ heating; no wall effects) and thus the sample is heated up evenly and very rapidly. This allows very selective organic reactions to be carried out in a highly reproducible fashion. More details are given on the following pages.

Fast, Convenient, and Efficient Molybdenum-Catalyzed Asymmetric Allylic Alkylation under Noninert Conditions: An Example of Microwave-Promoted Fast Chemistry**

Nils-Fredrik K. Kaiser, Ulf Bremberg, Mats Larhed,* Christina Moberg, and Anders Hallberg

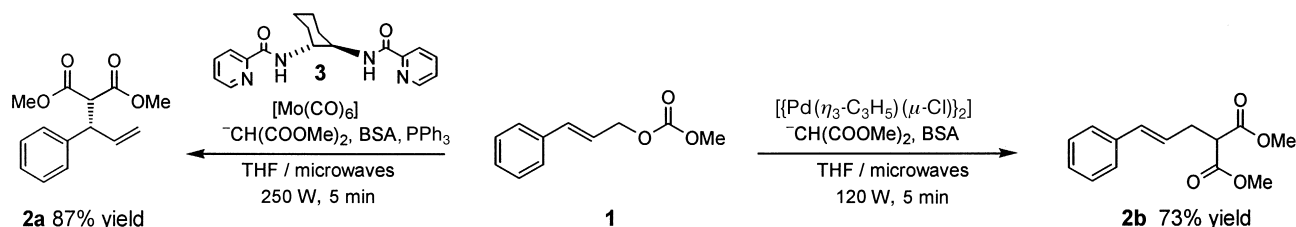
The delivery and distribution of energy has not yet attracted the attention it deserves among organic chemists. Modern focused microwave reactors are effective and reliable tools that could eliminate this neglect and become standard heating devices in chemical laboratories. Improved control of heating reactions opens new ways to achieve fast and selective synthesis, which is especially important in combinatorial processing.^[1]

While investigating the scope and limitations of the new focused microwave technique,^[2] we identified molybdenum(0)-catalyzed allylic malonate alkylation, innovatively developed by B. M. Trost et al., as a reaction suitable for study.^[3] The reported two-step alkylation of methyl (*E*)-3-phenyl-2-propenyl carbonate (**1**) allows isolation of the product with high regio- and stereopurity but requires an inert atmosphere, reaction times of 2–3 h, and 10 mol % of the molybdenum(0) catalyst.^[3c] Therefore, this reaction is a good subject for investigating the impact of microwave flash heating on product selectivity, shortening of reaction time, experimental convenience, and catalyst efficiency.

Previously, the molybdenum-catalyzed reactions were conducted with a preformed unstable $[(\text{EtCN})_3\text{Mo}(\text{CO})_3]$ precatalyst.^[3] We found it feasible to generate the catalyst system in situ from commercially available, stable $[\text{Mo}(\text{CO})_6]$ and ligand **3**. The allylic alkylations were conducted with micro-

wave flash heating under air in a one-pot mixture of 0.04 equivalents of $[\text{Mo}(\text{CO})_6]$, 0.05 equivalents of **3**, allylic carbonate **1**, a freshly prepared solution of dimethyl sodiomalonate/dimethyl malonate (1/11), and *N,O*-bis(trimethylsilyl)acetamide (BSA).^[4] Good reproducibility, complete conversion, high yields, and excellent *ee* values were achieved in only a few minutes (Scheme 1 and Table 1). In the standard solvent THF^[3], an irradiation power of 250 W was sufficient for obtaining a reaction time of 5 min, 87% yield, and high regioselectivity and enantiomeric excess (98%) of **2a** (Table 1, entry 4). Somewhat lower regioselectivities (**2a:2b** = 17–19:1) were obtained in the one-pot microwave reactions (entries 1–5) than in the previously reported two-step method (**2a:2b** = 32–49:1).^[3c] Using DME (entry 6) or 1,4-dioxane (entry 7) as solvent furnished higher yields and regioselectivities but lower reaction rates. Remarkably, the use of a nitrogen atmosphere did not improve the outcome of the reaction, while an oxygen atmosphere led to diminished catalyst activity (20% yield). Addition of small amounts of water (50 equivalents relative to catalyst) fully inhibited the catalysis. Triphenyl phosphite exhibited a similar but much weaker effect.^[5] All attempts to use acetate as leaving group, instead of carbonate, were unsuccessful. Efforts to increase the turnover number by using 0.006 equivalents of $[\text{Mo}(\text{CO})_6]$ also failed.

The low solubility of dimethyl sodiomalonate in THF prompted us to search for ways to generate the anionic nucleophile in situ, for example, by decomposition of the leaving methyl carbonate anion.^[6] Disappointingly, only very low yields of **2a** were obtained even at high temperatures. The use of BSA (probase) in conjunction with small amounts of anionic dimethyl malonate (9 mol%) gave a reaction as smooth as that with a saturated solution of the fully deprotonated nucleophile. Lowering the amount of anionic



Scheme 1. Molybdenum- and palladium-catalyzed allylic alkylation.

[*] Dr. M. Larhed, N.-F. K. Kaiser, Prof. A. Hallberg
Department of Organic Pharmaceutical Chemistry
Uppsala Biomedical Centre, Uppsala University
P.O. Box 574, 751 23 Uppsala (Sweden)
Fax: (+46) 18-471-4474
E-mail: mats.larhed@orgf3.bmc.uu.se

Dr. U. Bremberg, Prof. C. Moberg
Department of Chemistry, Organic Chemistry
Royal Institute of Technology
100 44 Stockholm (Sweden)

[**] We gratefully acknowledge financial support from Personal Chemistry, the Swedish Natural Science Research Council (C.M.), and the Swedish Research Council for Engineering Sciences (M.L., A.H.).

Supporting information for this article is available on the WWW under <http://www.wiley-vch.de/home/angewandte/> or from the author.

dimethyl malonate to 1% resulted in low yields even after prolonged irradiation.

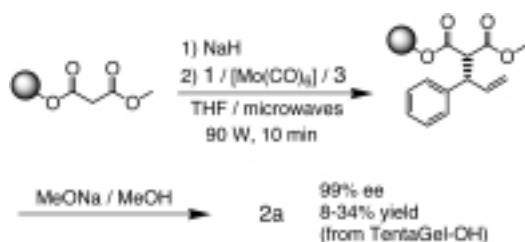
The molybdenum(0)-catalyzed alkylation also worked on a solid phase (TentaGel-OH, 99% *ee*, Scheme 2). Unfortunately, only low and variable overall yields were obtained (8–34% of **2a**).

Performing the microwave reaction with $[\text{Mo}(\text{CO})_6]$ in the absence of **3** resulted in a very low yield (<3%) of **2a** (major) along with **2b** (minor). The amount of product was too low to make an accurate estimate of the regioselectivity. Omitting $[\text{Mo}(\text{CO})_6]$ but otherwise using identical conditions provided no detectable quantities of the internally alkylated isomer **2a**. Instead, a very low yield of the terminally alkylated product

Table 1. Microwave-heated molybdenum(0)-catalyzed asymmetric allylic alkylation of **1** under air.^[a]

Entry	Power [W]	Time [min]	Solvent	Yield ^[b] (2a) [%]	Ratio ^[c] (2a : 2b)	ee ^[d] [%]	TOF ^[e] [h ⁻¹]
1	60	9	THF	86 ^[f]	18:1	98	160
2	90	6	THF	86 ^[f, g]	17:1	98	240
3	120	5	THF	86 ^[f]	19:1	98	280
4	250	5	THF	87 ^[f]	19:1	98	280
5	500	4	THF	85 ^[f, h]	19:1	95	350
6	120	6	DME	92	22:1	98	240
7	130	7	dioxane	94	28:1	98	220
8	22 °C	20 d	THF	< 1 ^[i]	n.d. ^[k]	n.d.	n.d.
9	80 °C	2 d	THF	11 ^[f, j]	17:1	n.d.	0.07
10	165 °C	6	THF	59 ^[f, i, j]	11:1	98	160
11	180 °C	6	THF	70 ^[f, i, j]	16:1	98	190
12	160 °C	7	dioxane	67 % ^[i, j]	28:1	98	160

[a] Reactions were performed in solvent (2.5 mL) with **1** (0.21 M; 0.53 mmol), nucleophile (110 mol %), [Mo(CO)₆] (4 mol %), **3** (5 mol %), and BSA (120 mol %). Selected combinations of power and irradiation time (Microwell 10). [b] Determined by GC-MS with 2,3-dimethylnaphthalene as internal standard. [c] Determined by GC-MS with individual response factors for **2a** and **2b**. [d] Values from 2–6 reactions measured by repeated chiral HPLC (Daicel Chiracel OD-H, isohexane/2-propanol 99/1; 0.5 mL min⁻¹). [e] TOF = turnover frequency (number of catalytic cycles per unit time). [f] Small amounts (~6%) of silylated cinnamyl alcohol were detected. [g] Yield of isolated product. [h] Noncontinuous heating; see Supporting Information. [i] Starting material remained. [j] Prolonged reaction time did not lead to higher yields. [k] n.d. = not determined.



Scheme 2. Solid-phase molybdenum(0)-catalyzed allylic alkylation.

2b was obtained, and this indicates a very slow, noncatalytic A·D (S_N2) path. The yield of **2b** in the latter experiment was much lower than that obtained with the Mo/**3** catalyst; hence, this implies an Mo/**3**-catalyzed route to **2b**.

Employing palladium(0)/PPh₃ as catalyst instead of Mo/**3** led to complete conversion of **1** into mainly the opposite regioisomer **2b** (Scheme 1; **2a**:**2b** = 1:13, 73 % yield of **2b**).^[2]

Despite the high temperatures attained by microwave heating (up to 220 °C, Figure 1) the excellent enantiomeric purity (98 % ee, Table 1) of product **2a** remained constant. Therefore, we assume that ligand **3** is strongly bound to molybdenum(0).^[7] The high temperatures are not only due to increased boiling points at elevated pressure, but also to a significant contribution from sustained superheating. Superheating phenomena have been well documented under microwave heating, even when open vessels are utilized, and constitute one of its main advantages.^[8] In the case of pure, microwave-transparent

1,4-dioxane,^[9] the microwave energy slowly heats the Duran tube, and this results in conductive heating of the solvent.

The microwave control experiments with pure THF and 1,4-dioxane furnished temperature profiles with lower temperature at every point relative to the reaction mixtures (Figure 1). The added substances, ionic or nonionic, must therefore contribute to the overall temperature profile when running the reaction.^[10] Also, as is apparent from Table 1, the yields from the oil-bath experiments are lower than those of the corresponding microwave-heated reactions, and they did not reach full conversion.^[11] This raises the question whether microwave-induced “hot-spots” exert an influence at the molecular level.^[10] It seems reasonable that when the substrate molecules act as “molecular radiators” in channeling energy from microwave radiation to bulk heat their

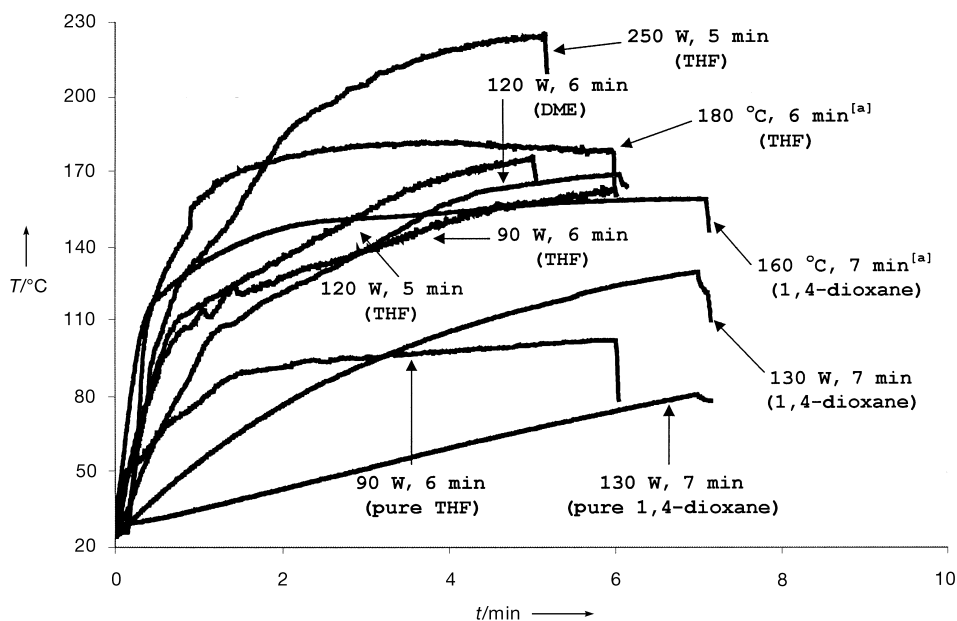


Figure 1. Selected temperature profiles for the microwave-heated, molybdenum(0)-catalyzed asymmetric allylic alkylations. Temperature profiles were recorded with a NoEMI-TS Reflex (Nortech Fibronic, Québec, Canada) equipped with a temperature-sensitive fluoroptic probe (TPP-01-M2.5-A, Nortech Fibronic). The probe was positioned at the bottom of the reaction tube. Sampling rate was 3 Hz. The reaction mixtures were efficiently cooled in water at room-temperature after completed irradiation. [a] Oil-bath heating.

reactivity might be enhanced.^[12] In addition, the beneficial impact of microwave irradiation can be attributed to the instant, internal heat-transfer mode, as opposed to conventional heat transfer from the walls that is characteristic of traditional heating devices.^[13] However, the origin of the increased efficiency in performing metal-catalyzed asymmetric high-temperature alkylations with focused microwave heating requires further investigation.

In conclusion, we have demonstrated a synthetically useful and easily handled microwave protocol for fast and selective molybdenum(0)-catalyzed allylic alkylation. The former sensitive reaction procedure has been transformed into a robust, air-stable, one-step procedure employing the inexpensive and stable precatalyst $[\text{Mo}(\text{CO})_6]$ in low concentration.

Received: March 31, 2000

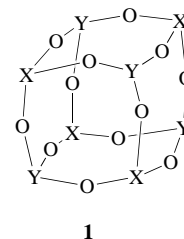
Revised: June 23, 2000 [Z14933]

- [1] a) R. E. Dolle, K. H. Nelson, Jr., *J. Comb. Chem.* **1999**, *1*, 235–271; b) M. Larhed, G. Lindeberg, A. Hallberg, *Tetrahedron Lett.* **1996**, *37*, 8219–8222.
- [2] a) U. Bremberg, S. Lutsenko, N.-F. K. Kaiser, M. Larhed, A. Hallberg, C. Moberg, *Synthesis* **2000**, in press; b) N.-F. K. Kaiser, U. Bremberg, M. Larhed, C. Moberg, A. Hallberg, *J. Organomet. Chem.* **2000**, in press; c) U. Bremberg, M. Larhed, C. Moberg, A. Hallberg, *J. Org. Chem.* **1999**, *64*, 1082–1083.
- [3] a) B. M. Trost, S. Hildbrand, K. Dogra, *J. Am. Chem. Soc.* **1999**, *121*, 10416–10417; b) F. Glorius, A. Pfaltz, *Org. Lett.* **1999**, *1*, 141–144; c) B. M. Trost, I. Hachiya, *J. Am. Chem. Soc.* **1998**, *120*, 1104–1105.
- [4] The order of addition did not influence the outcome of the reaction. J. Lehmann, G. C. Lloyd-Jones, *Tetrahedron* **1995**, *51*, 8863–8874.
- [5] $(\text{PhO})_3\text{P}$ is used as promoter in the synthesis of **3**.
- [6] J. Tsuji, I. Shimizu, I. Minami, Y. Ohashi, *Tetrahedron Lett.* **1982**, *23*, 4809–4812.
- [7] Ab initio calculations: S. P. Nolan, R. L. de la Vega, C. D. Hoff, *Organometallics* **1986**, *5*, 2529–2537.
- [8] D. M. P. Mingos, *Res. Chem. Intermed.* **1994**, *20*, 85–91.
- [9] C. R. Strauss, R. W. Trainor, *Aust. J. Chem.* **1995**, *48*, 1665–1692.
- [10] a) S. A. Galema, *Chem. Soc. Rev.* **1997**, *26*, 233–238; b) D. A. Lewis, J. D. Summers, T. C. Ward, J. E. McGrath, *J. Pol. Sci. A* **1992**, *30*, 1647–53.
- [11] Although the heating profiles for the oil-bath experiments with incomplete conversion (Table 1, entries 11 and 12) indicate higher reaction temperatures than were measured in the successful microwave reactions (entries 3 and 7), one should bear in mind that the measured temperatures might not be representative of the true reaction conditions.
- [12] A. Loupy, A. Petit, J. Hamelin, F. Texier-Boullet, P. Jacquault, D. Mathé, *Synthesis* **1998**, 1213–1234, and references therein.
- [13] C. Gabriel, S. Gabriel, E. H. Grant, B. S. J. Halstead, D. M. P. Mingos, *Chem. Soc. Rev.* **1998**, 213–223.

A Novel Borosilicate Cage Compound with an Incomplete B_4Si_4 Cube Structure: $[(t\text{BuSi})_4(\text{CH}_2=\text{CHC}_6\text{H}_4\text{B})_4\text{O}_{10}]^{**}$

Lorraine A. Neville, Trevor R. Spalding,* and George Ferguson

Recently there has been a proliferation of cube-based cages in which a variety of main group elements occupy corner sites and oxygen atoms bridge the main group atoms. Many “cubic” sections of the cages have the general formula $\text{X}_4\text{Y}_4\text{O}_{12}$ and adopt the double four-ring (D4R) (4-4) structure **1**. The positioning of the X and Y atoms at alternate corners is noteworthy and has been observed with various combinations of Group 13, 14, and 15 elements including those with $\text{X}=\text{Si}$ and $\text{Y}=\text{Al}$,^[1] Ga ,^[2] or In ,^[2b, 3] and those with $\text{X}=\text{P}$ and $\text{Y}=\text{B}$,^[4] Al ,^[5] or Ga .^[6] These compounds are related to silsesquioxanes ($\text{X}=\text{Y}=\text{Si}$ in **1**) which have been studied extensively.^[7] One aim in developing the chemistry of these compounds is to use them as building blocks



in the construction of more complex materials, possibly zeolites or catalyst supports. Another aim is to develop their applications in microelectronics as interlevel low k dielectrics. In the latter respect, silsesquioxanes have already attracted the attention of several industries including microelectronics manufacturers.^[8]

Relatively little work has been done on the chemistry of molecular borosilicates. Established borosilicate cages which have been reported are $[\text{tBuSi}\{\text{O}(\text{BC}_6\text{H}_4\text{Br})\text{O}\}_3\text{Si}t\text{Bu}]$ (**2**)^[9] with a $\{\text{B}_3\text{Si}_2\text{O}_6\}$ cage, $[\text{B}(\text{OSiPh}_2\text{OSiPh}_2\text{O})_3\text{B}]$ (**3**)^[10] with a $\{\text{B}_2\text{Si}_6\text{O}_9\}$ cage, and the silsesquioxane-based borosilicates $[\{(\text{cyclo-C}_6\text{H}_{11}\text{Si})_7\text{BO}_{12}\}_2]$ ^[11] and $[\{(\text{cyclo-C}_6\text{H}_{11}\text{Si})_8\text{O}_{13}(\text{Bn-Bu})\}]$,^[12] and anionic silsesquioxane-borato complexes of the types $[\text{R}_7\text{Si}_8\text{O}_{12}\{\text{OB}(\text{C}_6\text{F}_5)_3\}]^-$ and $[\text{R}_7\text{Si}_7\text{O}_9(\text{OH})_2\{\text{OB}(\text{C}_6\text{F}_5)_3\}]^-$.^[13] Whereas all the silsesquioxane-based compounds were synthesized from preformed silsesquioxane fragments and single boron-containing reagents, compounds **2** and **3** were synthesized from reagents containing only single silicon and boron. In the case of **2**, the reagents were $t\text{BuSi}(\text{OH})_3$ and a boronic acid, and for **3** the reagents were $\text{Ph}_2\text{Si}(\text{OH})_2$ and boric acid. We have now used single boron- and silicon-containing reagents to synthesize a new type of cube-based compound with both three- and four-coordinate corner sites. The compound $[(t\text{BuSi})_4(\text{CH}_2=\text{CHC}_6\text{H}_4\text{B})_4\text{O}_{10}]$

[*] Prof. T. R. Spalding, L. A. Neville
 Chemistry Department
 University College, Cork (Ireland)
 Fax: (+353)-21-274097

G. Ferguson^[+]
 School of Chemistry
 University of St. Andrews, Fife, KY16 9ST (UK)

[+] On leave from the Department of Chemistry and Biochemistry,
 University of Guelph, Guelph, ON, N1G 2W1 (Canada)

[**] The authors thank Dr. J. D. Kennedy, University of Leeds (UK) for many helpful discussions and the ¹¹B and ²⁹Si NMR spectra. Research grants to G.F. from NSERC Canada and to L.A.N. from Forbairt (Ireland) are gratefully acknowledged.

(**4**) (see Figure 1) has an incomplete cage with a pair of $B_2Si_2O_4$ faces held together by two Si-O-Si bridges. The construction of a cube-based cage with two X or two Y atoms at adjacent corners has not previously been realized.

Compound **4** was synthesized in 19% yield from the reaction between $tBuSiCl_3$, 4-vinylphenylboronic acid, aniline, and water in refluxing toluene. An alternative synthesis from the reaction between $tBuSi(OH)_3$ and 4-vinylphenylboronic acid in refluxing toluene also afforded **4** but in less reproducible yields. The constitution of **4** as a molecular borosilicate with a 1:1 ratio of B:Si was confirmed by IR and 1H , ^{11}B , and ^{29}Si NMR spectra. The former showed intense absorptions due to B-O-Si and Si-O-Si units. The 1H spectrum contained signals due to tBu and $C_6H_4CH=CH_2$ substituents in a 9:7 ratio. The single singlet resonance signals in the ^{11}B and ^{29}Si NMR spectra were typical of three-coordinate boron and $\{tBuSiO_3\}$ units, respectively. The exact configuration of the molecule in the solid state was determined by an X-ray crystal structure analysis (Figure 1). The molecule lies about a crystallographic inversion center and the borosilicate cage can be described as being formed from two inversion-related eight-membered {B-O-Si-O-B-O-Si-O} "rings" joined confacially through two Si-O-Si bridges. Since there is no bonding between opposite boron atoms, the cube structure is incomplete. In each $\{B_2Si_2O_4\}$ face, one silicon, both borons, and all oxygen atoms are essentially coplanar but the other silicon atom clearly lies out of this plane. Thus, the atoms Si1, B3, B7, O2, O4, O6, and O8 lie in a plane with a root mean square deviation of 0.053 and maximum deviations from the mean plane of -0.062 (0.001) Å (for Si1) and 0.081 (0.002) Å (for O8). However, one silicon atom, Si5, is 0.705 (0.002) Å from the mean plane. This contrasts with the configurations found

in the $\{B_2Si_2O_4\}$ rings in $(PhBO)_2(Ph_2SiO)_2$ ^[14] and $(PhBO)_2(tBu_2SiO)_2$.^[15] In the former compound the $\{B_2Si_2O_4\}$ ring is essentially planar with maximum deviations from the mean plane of 0.137 Å for O2 and -0.025 Å for B1.^[14] In the latter compound the $\{B_2Si_2O_4\}$ ring lies about an inversion center. Six of the atoms, that is both boron and all oxygen atoms, are essentially coplanar with deviations from the six-atom plane of ± 0.010 to 0.014 Å. The silicon atoms are ± 0.303 Å from the six-atom plane. These observations clearly illustrate the flexibility of borosilicate rings.

The mean B-O interatomic distance in the symmetry-related borosilicate rings in **4** is 1.366(3) Å, typical of distances between three-coordinate boron centers and oxygen atoms (compare mean values in **2**^[9] and **3**^[10] of 1.362 and 1.356 Å, respectively). The mean Si-O distance in **4** is 1.616(4) Å (compare mean values in **2** and **3** of 1.621 and 1.631 Å, respectively) and the Si-O distances in the Si-O-Si bridges average 1.607(4) Å. In **4**, the Si-O-Si angle is 154.14(14)°; large variations in Si-O-Si angles are well established with values from 89.4° to 180°.^[16] The individual B-O-Si angles vary significantly from 137.5(2)° to 154.4(2)°. This is not surprising, since B-O-Si angles show considerable flexibility in borosilicate rings containing trigonal-planar boron atoms; reported values range from 129.89(14)° in $(PhBO)(Ph_2SiO)_2$ ^[17] to 160.9(3)° in $(PhBO)_2(Ph_2SiO)_2$.^[14] This feature of borosilicate chemistry has been discussed in detail elsewhere.^[18] The mean values of the angles at boron and silicon are close to those expected for trigonal-planar boron and tetrahedral silicon centers at 120.8° and 109.10°, respectively, but it is noteworthy that the O-Si-O angles in the borosilicate rings of **4** are significantly larger (110.23 and 112.51°) than those involving the Si-O-Si bridging oxygen atoms (from 107.02 to 108.88°).

These values are typical of those reported in the structures of the cages of **2** and **3**.

A notable feature of **4** is the parallel nature of both the phenyl and vinyl units in the vinylphenyl groups (Figure 1). The torsion angles C12-C13-C14-C17 and C22-C23-C24-C27 are 178.6(4)° and 175.6(4)°, respectively. Values of the various C-C dimensions are in accord with accepted values, except for those of the terminal vinyl moieties whose atoms (C18, C28) show marked anisotropy; attempts to model this with slightly disordered vinyl groups led to no improvement in the *R* factor and had no effect at all on the Si cage geometry.

The formation of the $\{B_4Si_4O_{10}\}$ cage of **4** most probably proceeds through the condensation reaction of two cyclic borosilicate intermediates which have structure **5** with X = OH and which have

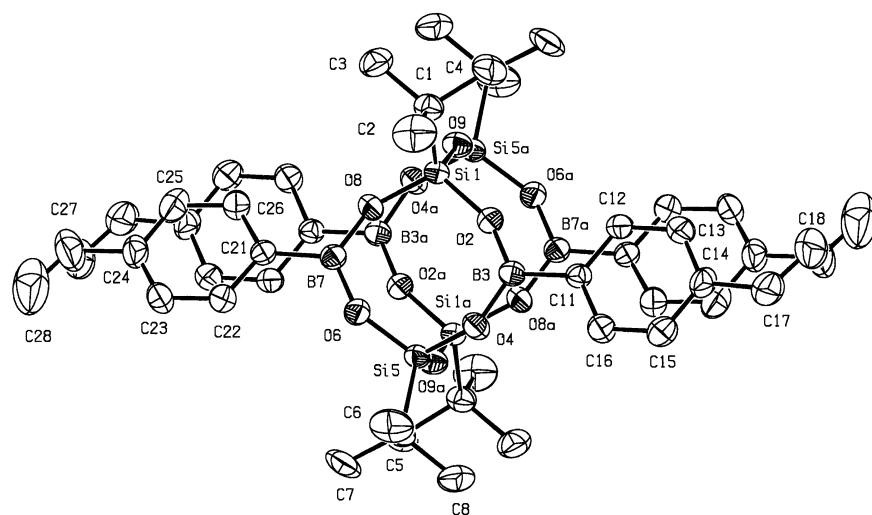
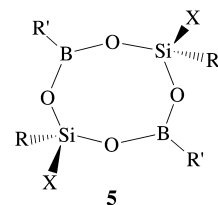
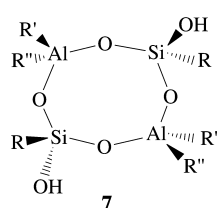


Figure 1. Molecular structure of **4** in the crystal (ORTEP plot). Thermal ellipsoids are drawn at the 30% probability level. Hydrogen atoms are omitted for clarity. Selected bond lengths [Å] and angles [°]: Si1-O2 1.609(2), Si1-O8 1.620(2), Si1-O9 1.603(2), Si1-C1 1.843(3), B3-O2 1.361(4), B3-O4 1.367(4), B3-C11 1.541(4), Si5-O4 1.619(2), Si5-O6 1.616(2), Si5-O9a 1.611(2) [atom O9a is at equivalent position $-x, -y, -z$], Si5-C5 1.847(3), B7-O6 1.369(4), B7-O8 1.366(4), B7-C21 1.536(5); O2-Si1-O8 112.51(12), O2-Si1-O9 107.02(12), O2-Si1-C1 110.08(15), O8-Si1-O9 107.42(12), O8-Si1-C1 109.85(14), O9-Si1-C1 109.87(13), Si1-O2-B3 154.4(2), O2-B3-O4 120.7(3), O2-B3-C11 120.6(3), O4-B3-C11 118.7(3), B3-O4-Si5 137.5(2), O4-Si5-O6 110.23(12), O4-Si5-C5 108.59(14), O6-Si5-C5 109.11(14), O4-Si5-O9 108.51(12), O6-Si5-O9 108.88(11), O9-Si5-C5 111.52(13), Si5-O6-B7 139.4(2), O6-B7-O8 120.9(3), O8-B7-C21 120.2(3), O6-B7-C21 118.9(3), Si1-O8-B7 147.9(2), Si1-O9-Si5a 154.14(14) [atom Si5a is at equivalent position $-x, -y, -z$].

the $\{t\text{BuSiX}\}$ moieties configured in a *cis* arrangement across the borosilicate ring. The condensation of two such rings would clearly lead to a structure with parallel “eclipsed” $\{\text{B}_2\text{Si}_2\text{O}_4\}$ faces. This intermediate could be formed from the chlorosilane precursor ($\text{X}=\text{Cl}$) by hydrolysis or, in the reaction with $t\text{BuSi}(\text{OH})_3$ directly. We have previously shown that, under the conditions used in the present study, that is in refluxing toluene, dehydration reactions of mixtures of $\text{B}-\text{OH}$ and $\text{Si}-\text{OH}$ reagents form $\text{B}-\text{O}-\text{Si}$ linkages in preference to either $\text{Si}-\text{O}-\text{Si}$ or $\text{B}-\text{O}-\text{B}$ linkages.^[18] Hence an alternating $\text{B}-\text{O}-\text{Si}$ motif shown in **5** would be expected initially. Furthermore, structural studies of silesquioxane-based polyhydroxy derivatives^[19] demonstrate the importance of intermolecular hydrogen bonding in stabilizing the solid-state structures of these compounds. The recently reported compound tetrahydroxy *cis,cis,cis*- $[\text{Ph}_4\text{Si}_4\text{O}_4(\text{OH})_4]$ (**6**) is of particular importance to the present study.^[19c] Compound **6** was isolated from the hydrolytic condensation of PhSiCl_3 in aqueous acetone. It was found to be a single isomer both in the solid state and in solution. The crystalline state contains pairs of molecules linked by intermolecular hydrogen bonds. When catalytic hydrogenation of **6** was attempted, the major product identified was the condensed cubic silesquioxane $[(\text{cyclo-hexyl})_8\text{Si}_8\text{O}_{12}]$ (15%).^[19c] It is also noteworthy that the more sterically hindered aluminosilicate $\{\text{Al}_2\text{Si}_2\text{O}_4\}$ ring compound which has tetrahedrally coordinated aluminum and



silicon atoms (**7**) with $\text{R}=(2,6\text{-}i\text{Pr}_2\text{C}_6\text{H}_3)\text{N}(\text{SiMe}_3)$, $\text{R}'=i\text{Bu}$, $\text{R}''=\text{thf}$, was only isolated as the all *trans* isomer.^[20] Moreover, no cubic cage compound with structure **1** was isolated during the study.

We have no direct evidence concerning the stereochemistry of the intermediates that lead to **4**, but it is possible that both *cis* and *trans* isomers of **5** could be formed. The low yield of **4** (19%) may be due in part to the inability of the *trans* isomer of **5** to produce the $\{\text{B}_4\text{Si}_4\text{O}_{10}\}$ cage. Although the construction of the $\{\text{B}_4\text{Si}_4\text{O}_{10}\}$ cage is understandable in the light of the foregoing comments, the possible role of the vinylphenyl groups in the formation of **4** is unclear and requires further work.

Experimental Section

The synthesis was carried out in an inert atmosphere: isolation of the product was in air.

4: A mixture of *tert*-butylsilane trichloride (0.6 g, 3.1 mmol) and 4-vinylphenylboronic acid (0.46 g, 3.1 mmol) was dissolved in toluene (50 mL). A mixture of aniline (0.87 g, 9.4 mmol) and water (0.06 g, 3.1 mmol) in toluene (10 mL) were added to this mixture through an addition funnel over a period of 10 min. The reaction mixture was heated at reflux temperature for 16 h. After cooling, a colorless precipitate of $[\text{PhNH}_3]\text{Cl}$ was filtered off. Removal of solvent from the filtrate and crystallization of the resulting residue from CH_2Cl_2 /heptane solution (1:2) afforded **4** (0.124 g, 18.6%). Compound **4** does not melt below 370°C. ^1H NMR (270 MHz, CDCl_3 , TMS): $\delta=7.46$ (d, 2H; C_6H_4), 7.11 (d, 2H; C_6H_4), 6.61 (m, 1H; CHCH_2), 5.74 (d, 1H; CHCH_2), 5.26 (d, 1H; CHCH_2), 1.22 (s, 9H; $\text{C}(\text{CH}_3)_3$); ^{13}C NMR (67.9 MHz, CDCl_3 , TMS): $\delta=140.76$, 136.93, 135.69, 133.77 (all C_6H_4), 125.47 (CHCH_2), 114.58 (CHCH_2), 25.52 ($\text{C}(\text{CH}_3)_3$), 17.07 ($\text{C}(\text{CH}_3)_3$); ^{11}B NMR (128 MHz, CDCl_3 , F_3BOEt_2): $\delta=25.5$ (s); ^{29}Si NMR (99 MHz, CDCl_3 , TMS): $\delta=-66.0$ (s); FTIR (KBr disc): $\tilde{\nu}_{\text{max}}=$

2959 m, 2862 w, 1608 m, 1307 vs ($\text{B}-\text{O}-\text{Si}$), 1262 w, 1097 s ($\text{Si}-\text{O}-\text{Si}$), 991 w, 908 w, 908 w, 665 m cm^{-1} ; elemental analysis calcd for $\text{C}_{48}\text{H}_{64}\text{B}_4\text{O}_{10}\text{Si}_4$ (%): C 60.3, H 6.7; found: C 60.3, H 6.5.

Crystal structure data for **4**: $\text{C}_{48}\text{H}_{64}\text{B}_4\text{O}_{10}\text{Si}_4$, $M_r=956.59$, monoclinic, space group $P2_1/n$, $a=10.4526(13)$, $b=18.6540(16)$, $c=14.6121(15)$ Å, $\beta=106.936(8)^\circ$, $V=2725.5(5)$ Å³, $Z=2$, $\rho_{\text{calcd}}=1.166$ g cm^{-3} , $F(000)=1016$, $\lambda=0.71073$ Å, $T=294(1)$ K, $\mu(\text{MoK}\alpha)=0.160$ mm⁻¹. Intensity data were measured on an Enraf-Nonius CAD4 diffractometer for a colorless needle crystal of dimensions $0.42 \times 0.24 \times 0.22$ mm³ in the range $4^\circ < 2\theta < 50^\circ$ using $\theta/2\theta$ scans and graphite-monochromated radiation. The data were corrected for Lorentz, polarization, and absorption effects (Gaussian correction,^[21] transmission coefficients 0.960–0.971). From the 5203 measured reflections, 4762 were independent ($R_{\text{int}}=0.016$) and 2113 had $I > 2\sigma(I)$. The structure was solved by direct methods (SHELXS-97)^[22] and refined by using all measured F^2 data using SHELXL-97.^[23] In the full-matrix least-squares refinement (299 parameters) all non-hydrogen atoms were refined anisotropically and hydrogen atoms were allowed for as riding atoms. Max./min. residual electron density $+0.342/-0.214$ e Å⁻³. $R1(F) > 4\sigma(F)=0.0461$ and $wR2=0.1266$ (all data) with $R1=\Sigma||F_o|-|F_c||/\Sigma|F_o|$ and $wR2=(\Sigma w(F_o^2-F_c^2)^2/\Sigma w(F_o^2)^2)^{0.5}$. Crystallographic data (excluding structure factors) for the structures reported in this paper have been deposited with the Cambridge Crystallographic Data Centre as supplementary publication no. CCDC-118471. Copies of the data can be obtained free of charge on application to CCDC, 12 Union Road, Cambridge CB2 1EZ, UK (fax: (+44) 1223-336-033; e-mail: deposit@ccdc.cam.ac.uk).

Received: May 8, 2000 [Z15098]

- a) M. L. Montero, A. Voigt, M. Teichert, I. Usón, H. W. Roesky, *Angew. Chem.* **1995**, *107*, 2761; *Angew. Chem. Int. Ed. Engl.* **1995**, *34*, 2504; b) V. Chandrasekhar, M. L. Montero, A. Voigt, H. W. Roesky, H.-G. Schmidt, M. Noltemeyer, *Organometallics* **1996**, *15*, 918; c) R. Murugavel, V. Chandrasekhar, H. W. Roesky, *Acc. Chem. Res.* **1996**, *29*, 183.
- a) A. Voigt, R. Murugavel, E. Parisini, H. W. Roesky, *Angew. Chem.* **1996**, *108*, 823; *Angew. Chem. Int. Ed. Engl.* **1996**, *35*, 748; b) R. Murugavel, A. Voigt, M. G. Walawalkar, H. W. Roesky, *Chem. Rev.* **1996**, *96*, 2205.
- a) A. Voigt, M. G. Walawalkar, R. Murugavel, H. W. Roesky, E. Parisini, P. Lubini, *Angew. Chem.* **1997**, *109*, 2313; *Angew. Chem. Int. Ed. Engl.* **1997**, *36*, 2203.
- a) M. G. Walawalkar, R. Murugavel, H. W. Roesky, H.-G. Schmidt, *Organometallics* **1997**, *16*, 516; b) K. Diemert, U. Englert, W. Kuchen, F. Sandt, *Angew. Chem.* **1997**, *109*, 251; *Angew. Chem. Int. Ed. Engl.* **1997**, *36*, 241.
- Y. Yang, M. G. Walawalkar, J. Pinkas, H. W. Roesky, H.-G. Schmidt, *Angew. Chem.* **1998**, *110*, 101; *Angew. Chem. Int. Ed.* **1998**, *37*, 96.
- a) M. R. Mason, M. S. Mashuta, J. F. Richardson, *Angew. Chem.* **1997**, *109*, 249; *Angew. Chem. Int. Ed. Engl.* **1997**, *36*, 239; b) M. R. Mason, A. M. Perkins, R. M. Matthews, J. D. Fisher, M. S. Mashuta, A. Vij, *Inorg. Chem.* **1998**, *37*, 3734.
- a) M. G. Voronkov, V. Lavrent'ev, *Top. Curr. Chem.* **1982**, *102*, 199; b) F. J. Feher, T. A. Budzichowski, *Polyhedron* **1995**, *14*, 3239; c) F. J. Feher, K. D. Wyndham, *Chem. Commun.* **1998**, 323.
- T. Batchelder, W. Cai, J. Bremmer, D. Gray, *Solid State Tech.* **1999**, 29.
- B. O'Leary, D. M. Murphy, T. R. Spalding, G. Ferguson, *J. Organomet. Chem.* **1996**, 526, 195.
- A. T. O'Dowd, T. R. Spalding, G. Ferguson, J. F. Gallagher, D. Reed, *J. Chem. Soc. Chem. Commun.* **1993**, 1816.
- F. J. Feher, T. A. Budzichowski, J. W. Ziller, *Inorg. Chem.* **1992**, *31*, 5100.
- F. J. Feher, D. Soulivong, F. Nguyen, J. W. Ziller, *Angew. Chem.* **1998**, *110*, 2808; *Angew. Chem. Int. Ed.* **1998**, *37*, 2663.
- R. Duchateau, R. A. van Santen, G. P. A. Yap, *Organometallics* **2000**, *19*, 809.
- B. J. Brisdon, M. F. Mahon, K. C. Molloy, P. J. Schofield, *J. Organomet. Chem.* **1992**, 436, 11.
- A. Mazzah, A. Haoudi-Mazzah, M. Noltemeyer, H. W. Roesky, *Z. Anorg. Allg. Chem.* **1991**, 604, 93.

- [16] R. West in *Tailor-made Silicon-Oxygen Compounds; from molecules to materials* (Eds.: R. Corriu, P. Jutzi), Vieweg, Braunschweig, **1996**, p. 3, and references therein.
- [17] D. A. Foucher, A. J. Lough, I. Manners, *Inorg. Chem.* **1992**, *31*, 3034.
- [18] a) D. Murphy, J. P. Sheehan, T. R. Spalding, G. Ferguson, A. J. Lough, J. F. Gallagher, *J. Mater. Chem.* **1993**, *3*, 1275; b) B. O'Leary, T. R. Spalding, G. Ferguson, *Polyhedron* **1999**, *18*, 3135.
- [19] a) F. J. Feher, T. A. Budzichowski, R. L. Blanski, K. J. Weller, J. W. Ziller, *Organometallics* **1991**, *10*, 2526; b) F. J. Feher, S. H. Phillips, J. W. Ziller, *Chem. Commun.* **1997**, 829; c) F. J. Feher, J. J. Schwab, D. Soulivong, J. W. Ziller, *Main Group Chem.* **1997**, *2*, 123.
- [20] M. L. Montero, I. Usón, H. W. Roesky, *Angew. Chem.* **1994**, *106*, 2198; *Angew. Chem. Int. Ed. Engl.* **1994**, *33*, 2103.
- [21] E. J. Gabe, Y. Le Page, J.-P. Charland, F. L. Lee, P. S. White, *J. Appl. Crystallogr.* **1989**, *22*, 384.
- [22] G. M. Sheldrick, SHELXS-97, program for the solution of crystal structures, University of Göttingen, **1997**.
- [23] G. M. Sheldrick, SHELXL-97, program for the refinement of crystal structures, University of Göttingen, **1997**.

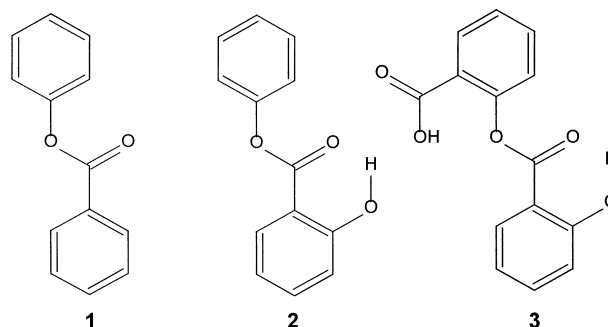
Hydrogen Bonding Interactions in Amorphous Salicyl Salicylate**

Bryan Greener,* Stephen J. Archibald, and Michael Hodgkinson

The macroscopic physical properties of a chemical substance are determined by the intra- and intermolecular interactions of each individual molecule comprising it. Presently, reliable prediction of the three-dimensional structure of a multiple-atom chemical species from only its structural formula is not possible,^[1] thus the *ab initio* prediction of bulk physical properties is likewise not currently attainable. To circumvent this obstacle, empirical studies of systematic chemical series have been pursued, and experimentally derived properties, such as crystal structure^[2] and melting point,^[3] have been correlated with structural formula.

Our research is concerned with the production of supramolecular materials, a field that has promised much.^[4] Recent work in the field of supramolecular materials assembly has focused upon the synthesis of molecules containing multiple hydrogen bonding motifs at chain termini^[5] and inner-chain sites.^[6] We wished to make a departure from this approach to understand the macroscopic physical effect of systematic changes in the chemical structure of simple species. We aimed to maximize the observed change in physical attributes while

minimizing the structural change at the molecular level. We studied the molecular series: phenyl benzoate (**1**), phenyl salicylate (**2**), and salicyl salicylate (**3**).



Each compound was melted and allowed to cool at ambient temperature. Compound **1** melted at 342 K and recrystallized at this temperature upon cooling; **2** melted at 317 K and undercooled to ambient temperature without crystallization, the low viscosity undercooled liquid could be maintained in this state for several weeks without difficulty; **3** melted over the range 412–424 K and undercooled to a high viscosity liquid that could be moulded and stress-fractured: a potentially useful material (crystallization in **3** could not be induced by any means, including crystal seeding and holding at the crystallization temperature for several hours. Recrystallization could be achieved only by dissolution and reprecipitation.). Thus we observed gross physical changes with small molecular alterations in the series **1–3**.

To elucidate the molecular interactions giving rise to these physical manifestations we reviewed the single-crystal structures of **1**^[7] and **2**,^[8] and determined the structure of **3**. In addition, **3** was studied extensively by NMR and IR spectroscopy.

The low viscosity of the amorphous **3** at temperatures in the range 373–423 K allowed study by ¹³C NMR spectroscopy. The spectrum recorded at 423 K is shown in Figure 1, and was assigned by 2D NMR experiments,^[9] and comparison with reference spectra.^[10] Multiple resonances were observed for many peaks, most notably those carbon atoms lying along the functional backbone: C14, C9, C1, C3, and C4. The acid carbonyl, C2, gave a single resonance signal. The ester carbonyl resonance, C1, was composed of at least five discrete signals, indicating that at least this many environments were stable on the NMR time scale. This multiple-resonance effect persisted, without diminution, across the observable temperature range. Peak shifting within the multiple-resonance sets was observed over the temperature range, in all cases peaks moved, at various rates, to lower field with cooling (increased hydrogen bonding^[11]).

To assess potential structural similarities between the amorphous and crystalline phases of **3**, solid-state ¹³C NMR spectra of both were recorded at ambient temperature (Figure 1).^[12] There was a good correlation between the liquid and solid-state NMR spectra of amorphous **3** and the solid-state NMR spectra of crystalline **3**. The lack of significant chemical shifting of resonances in any of the spectra suggests

[*] Dr. B. Greener
Smith & Nephew Group Research Centre
York Science Park, Heslington, York YO10 5DF (UK)
Fax: (+44)1904-824004
E-mail: bryan.greener@smith-nephew.com
Dr. S. J. Archibald, M. Hodgkinson
Department of Chemistry
University of York
Heslington, York YO10 5DD (UK)

[**] We thank the staff of the University of York NMR service for their time and care in running our samples.

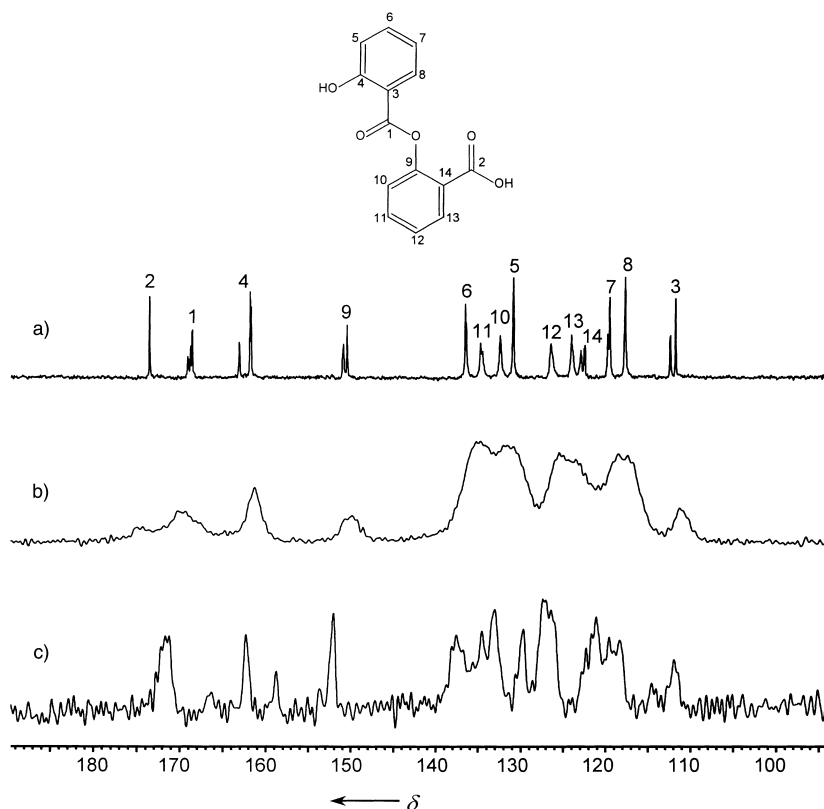


Figure 1. ^{13}C NMR spectra and assignment of amorphous **3** recorded at 373 K (liquid, 126 MHz) (a) and 273 K (solid, 101 MHz) (b),^[12] and crystalline **3** recorded at 273 K (solid, 101 MHz) (c).^[12]

close structural similarity in the amorphous and crystalline phases. Multiple resonances were not observed in solution ^{13}C NMR spectra of **3** recorded in $[\text{D}_6]\text{acetone}$ or CDCl_3 at ambient temperature but a large shifting of C1 did occur: from $\delta = 165.7$ in $[\text{D}_6]\text{acetone}$ to $\delta = 168.8$ in CDCl_3 , and all other resonances were shifted to a significant but lesser extent.^[13] Multiple resonances were not observed in neat **2** studied by this method.

In an attempt to elucidate the behavior of the hydrogen-bonded protons in the 373–423 K temperature range, ^1H NMR spectra of neat **3** were recorded at 10 K intervals (Figure 2). Integration confirmed that both “alcoholic” and

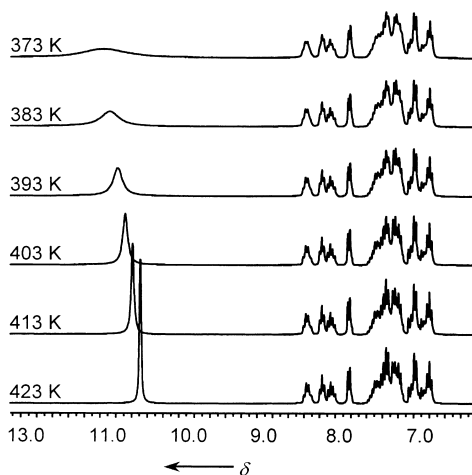


Figure 2. ^1H NMR spectra (liquid, 270 MHz) of amorphous **3** recorded at 373–423 K.

“acidic” protons were present as a single resonance, appearing sharp at 423 K and broadening significantly, with shifting to lower field, down to 373 K. Shifting occurred at a constant rate of $9.5 \times 10^{-3} \delta \text{K}^{-1}$ over this temperature range. Both alcohol and acid protons appear chemically equivalent by this analysis technique and the resonance broadening with decrease in temperature is indicative of an exchange phenomenon. The solution spectrum of **3** (CDCl_3 , 270 MHz), recorded at ambient temperature, contained discrete resonance signals for alcoholic (sharp, $\delta = 10.26$) and acidic (broad, $\delta = 11.24$) protons.^[14] Using this resonance separation, we calculated that the observed proton coalescence would occur at exchange rates exceeding 1700 s^{-1} . ^1H NMR spectra of neat **2** were recorded at 10 K intervals in the range 303–423 K. Alcoholic proton shifting occurred at a constant rate of $3.4 \times 10^{-3} \delta \text{K}^{-1}$ over this temperature range. The alcoholic proton resonance was composed of at least two environments that became less distinct as the temperature was lowered.

The IR spectra (293 K) of **3** recorded as KBr pressed pellet (crystalline) and film cast from CHCl_3 (amorphous) are shown in Figure 3. The amorphous spectrum contained a

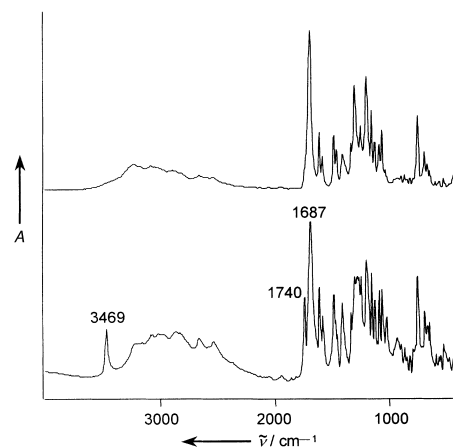


Figure 3. IR spectra of amorphous (top) and crystalline (bottom) **3** recorded at ambient temperature. A = absorbance.

multiple peak carbonyl resonance at $\sim 1685 \text{ cm}^{-1}$, indicating that all ester carbonyl groups were in hydrogen-bonded environments.^[11] The spectrum of the crystalline sample was identical to that of the amorphous sample with the exception of additional bands appearing at 3469 and 1740 cm^{-1} , consistent with the disruption of an intramolecular hydrogen bond between alcohol and ester carbonyl group. The IR spectrum (293 K) of crystalline **2** contained a broad carbonyl absorbance at 1679 cm^{-1} and a hydroxyl absorbance at 3191 cm^{-1} , these absorbances shifted to higher energy in the amorphous phase (1691 and 3229 cm^{-1} , respectively).

To further elucidate the intra- and intermolecular interactions present in the crystalline state, **3** was crystallized from acetone–water and its crystal structure determined by single-crystal X-ray diffraction.^[15] The disordered structure obtained is shown in Figure 4, labeled to show percentage structural

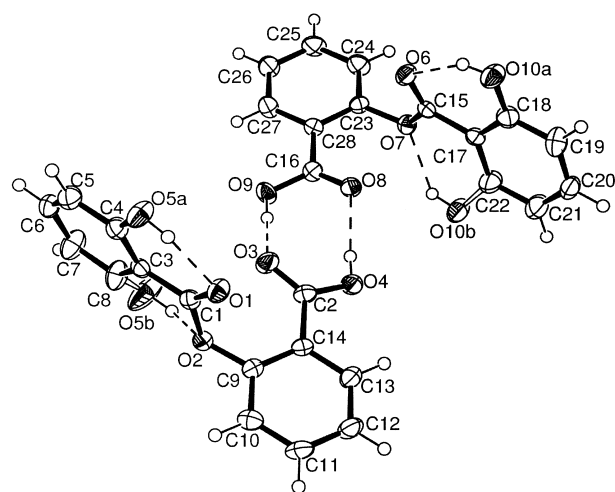


Figure 4. Structure of a dimer of **3** showing positional disorder in the salicylate moiety (ORTEP^[20] representation; 50% probability thermal ellipsoids, 150 K): O10a (60%), O10b (40%), O5a (80%), O5b (20%). Selected distances [Å] and angles [°]: O3–O9 2.635(4), O4–O8 2.649(4), O1–O5a 2.662(5), O2–O5b 2.613(2), O6–O10a 2.624(6), O7–O10b 2.661(8); C8–C3–C1–O1 170.7(4), C10–C9–O2–C1 101.0(4); molecular benzene ring dihedrals 86.1(2) and 78.0(2)°.

occupancy. Compound **3** crystallized as noncentrosymmetric hydrogen-bonded carboxylic acid dimers, disordered about the salicylate ring over two geometries with intramolecular hydroxyl hydrogen bond donation to both ester oxygen atoms. Hydroxyl oxygen occupancy varied on each side of the dimer: 80%/20% and 60%/40% in favor of the carbonyl oxygen interaction. The general dimeric structural geometry was consistent with those observed in similar species such as benzoic acid,^[16] salicylic acid,^[17] and gentisic acid,^[18] while the phenyl benzoate section of **3** was isomorphous with those observed in **1**^[7] and **2**.^[8] Intramolecular hydrogen bond disorder of the type seen in **3** was not observed in **2**.

Small-angle X-ray scattering (SAXS) was measured for amorphous **3** at 150 K.^[19] The scattering pattern observed was characteristic of an amorphous material and showed two scattering rings. The two were calculated to arise from close-contact spacings in the range of 4.7–5.9 Å and 8.2–11.2 Å, similar to intermolecular spacings observed in the crystal structure. The shorter spacing correlated well with the body-center separation of each molecule in the dimeric unit, and the longer spacing correlated well with the nearest-neighbor dimeric separation observed crystallographically. The density of the amorphous material was 1.35 g cm^{−3} (293 K) compared to 1.40 g cm^{−3} (293 K) for the crystalline solid.

X-ray analysis and IR and NMR spectroscopic analysis of **3** are consistent with structural disorder in both the crystalline state and the amorphous state. The ¹H NMR spectroscopic observations indicate that rapid acid–alcohol proton exchange is occurring in the amorphous phase, well below the

melting point of **3**. The observation of several distinct ¹³C NMR environments in **3** is consistent with structural conformers that are stable on the NMR time scale. We hypothesize that the amorphous behavior observed in **3** and the undercooling observed in **2** is a consequence of intermolecular hydrogen bond interactions in which protons are undergoing rapid intermolecular exchange. The absence of this structural arrangement in **1** precludes the facile undercooling of this material. We hope that molecules such as **3** will provide the basis for new, amorphous engineered materials, complementing the rapidly expanding field of crystal engineering.^[21]

Experimental Section

Compounds **1** and **2** (99%) were used as supplied by Aldrich Ltd. Compound **3** (99%) was used as supplied by Acros Organics. Instrumentation: IR spectra: Mattson Galaxy 5020 FTIR spectrometer; ¹³C NMR liquid spectra: Bruker 500 MHz NMR spectrometer; ¹³C NMR solid-state spectra: Bruker DSSX400 400 MHz NMR spectrometer; ¹H NMR spectra: Jeol 270 MHz NMR spectrometer.

Received: May 11, 2000 [Z15111]

- [1] J. C. MacDonald, G. M. Whitesides, *Chem. Rev.* **1994**, *94*, 2383.
- [2] J. D. Dunitz, A. Gavezzotti, *Acc. Chem. Res.* **1999**, *32*, 677.
- [3] V. R. Thalladi, R. Boese, H.-C. Weiss, *Angew. Chem.* **2000**, *112*, 942; *Angew. Chem. Int. Ed.* **2000**, *39*, 918.
- [4] J. S. Moore, *Curr. Opin. Coll. Interf. Sci.* **1999**, *4*, 108.
- [5] R. P. Sijbesma, F. H. Beijer, L. Brunsveld, B. J. B. Folmer, J. H. K. K. Hirschberg, R. F. M. Lange, J. K. L. Lowe, E. W. Meijer, *Science* **1997**, *278*, 1601.
- [6] B. Greener, J. Rose, *Chem. Commun.* **1999**, *23*, 2361.
- [7] M. Shibakami, A. Sekiya, *Acta Crystallogr. Sect. C* **1995**, *51*, 326.
- [8] J. H. Bilgram, U. Dürig, M. Wächter, *J. Cryst. Growth* **1982**, *57*, 1.
- [9] 2D Gradient COSY and 2D Gradient HMQC NMR spectra were recorded for CDCl₃ solutions of **3**.
- [10] C. J. Pouchert, J. Behnke, *The Aldrich Library of ¹³C and ¹H FT-NMR Spectra*, Vol. 2, 1st ed., Aldrich Chemical, Milwaukee, WI, **1993**: benzoic acid, *o*-anisic acid, methyl benzoate, salicylic acid, phenyl benzoate.
- [11] S. N. Vinogradov, R. H. Linnell, *Hydrogen Bonding*, Van Nostrand Reinhold, New York, **1971**.
- [12] Spectra recorded at 100.6 MHz (293 K) using a 2.5 mm CPMAS probe (12 kHz rotation).
- [13] **3**: ¹³C NMR (270 MHz, [D₆]acetone): δ = 165.7 (C1), 169.5 (C2), 113.3 (C3), 162.5 (C4), 131.8 (C5), 137.3 (C6), 120.5 (C7), 118.3 (C8), 151.1 (C9), 132.9 (C10), 135.1 (C11), 127.5 (C12), 125.0 (C13), 124.7 (C14); **3**: ¹³C NMR (270 MHz, CDCl₃): δ = 168.8 (C1), 169.9 (C2), 111.9 (C3), 162.0 (C4), 130.8 (C5), 136.5 (C6), 119.6 (C7), 117.7 (C8), 150.5 (C9), 132.8 (C10), 135.0 (C11), 126.7 (C12), 124.1 (C13), 122.5 (C14).
- [14] **3**: ¹H NMR (270 MHz, CDCl₃): δ = 11.24 (s br.; OH), 10.26 (s sh; COOH), 8.11 (dd, *J* = 7.8, 1.9 Hz; H10), 8.04 (dd, *J* = 7.8, 1.6 Hz; H5), 7.65 (dt, *J* = 8.1, 1.6 Hz; H11), 7.51 (ddd, *J* = 9.0, 7.5, 1.9 Hz; H6), 7.38 (dd, *J* = 7.8, 1.2 Hz; H12), 7.23 (dd, *J* = 8.1, 2.6 Hz; H13), 7.01 (dd, *J* = 8.4, 1.2 Hz; H8), 6.91 (ddd, *J* = 8.1, 7.8, 0.9 Hz; H7).
- [15] Crystal data for **3**: C₁₄H₁₀O₅, *M_r* = 258.22, monoclinic, space group *Cc* (no. 9), *a* = 12.965(4), *b* = 12.982(4), *c* = 15.530(3) Å, β = 114.039(15)°, *V* = 2387.2(11) Å³, *Z* = 4, ρ_{calcd} = 1.431 g cm^{−3}, μ(MoKα) = 0.7107 Å, *F*(000) = 1064, *T* = 150 K; colorless rhombs, 0.45 × 0.40 × 0.35 mm, Rigaku AFC6 four-circle diffractometer, Oxford Cryosystems N₂ cooler (150 K) 2105 independent reflections. The structure was solved by direct methods, all non-hydrogen atoms were refined anisotropically using full-matrix least-squares based on *F*² to give *R*₁ = 0.0341, *wR*₂ = 0.0913 for 1644 independently observed reflections (*I*₀ > 2σ(*I*₀)) and 366 parameters. Crystallographic data (excluding structure factors) for the structure reported in this paper have been

deposited with the Cambridge Crystallographic Data Centre as supplementary publication no. CCDC-143946. Copies of the data can be obtained free of charge on application to CCDC, 12 Union Road, Cambridge CB21EZ, UK (fax: (+44) 1223-336-033; e-mail: deposit@ccdc.cam.ac.uk).

- [16] G. Bruno, L. Randaccio, *Acta Crystallogr. Sect. B* **1980**, *36*, 1711.
 [17] M. Sundaralingham, L. H. Jensen, *Acta Crystallogr.* **1965**, *18*, 1053; W. Cochran, *Acta Crystallogr.* **1953**, *6*, 260.
 [18] M. Haisa, S. Kashino, S.-I. Hanada, K. Tanaka, S. Okazaki, M. Shibagaki, *Acta Crystallogr. Sect. B* **1982**, *38*, 1480.
 [19] SAXS: 0.7 mm diameter cylinder of **3**. Rigaku RU200 rotating anode, graphite-monochromated ($\mu(\text{Cu}_{K\alpha}) = 1.5418 \text{ cm}^{-1}$, 50 kV, 100 mA) and Marresearch Imaging Plate System, 300.0 mm sample to plate distance.
 [20] C. K. Johnson, ORTEP, Report ORNL-5138, Oak Ridge National Laboratory, Oak Ridge, TN, **1976**.
 [21] G. R. Desiraju, *Angew. Chem.* **1995**, *107*, 2541; *Angew. Chem. Int. Ed. Engl.* **1995**, *34*, 2311.

Cooperative Asymmetric Catalysis with Dendrimeric [Co(salen)] Complexes**

Rolf Breinbauer and Eric N. Jacobsen*

The synthesis of dendrimers with well-defined architectures has advanced at an accelerating pace since the first examples of cascade-like molecules were introduced in the late 1970s.^[1] Indeed, highly pure polyamidoamine (PAMAM) and poly-(propyleneimine) dendrimers are now commercially available at a moderate price, and good experimental procedures exist for the preparation of a variety of other dendrimeric compounds. Over the last several years, research in this area has extended from the synthesis and characterization of these compounds to the search for specific properties and functions that are a direct consequence of the dendritic architecture.^[1e] One area that has attracted particular interest is in the development of so-called dendrimeric catalysts, and recently several groups have demonstrated that dendrimers bearing catalytic units covalently linked to the terminal sites can combine the best features of homogeneous and heterogeneous catalysts.^[2, 3] Thus, a dendrimeric catalyst can present molecularly defined reactive sites in a macromolecule that can be reisolated easily by precipitation^[3e,i] or filtration through a membrane.^[3p-r]

The relative proximity of terminal sites may be controlled by the nature and generation number of the dendrimer.

Therefore, at least in principle, a dendritic framework may be used to enforce and control cooperative interactions between catalyst units. However, while there have been a number of reports of cooperative binding effects with dendrimers incorporating recognition elements such as amino acids or carbohydrates,^[4] no examples of enhanced catalytic activity due to cooperative effects have been reported in dendrimeric systems devised thus far.^[5, 6]

In our ongoing studies of asymmetric ring opening (ARO) of epoxides by metal–salen complexes (H_2salen = bis(salicylidene)ethylenediamine),^[7] substantial mechanistic evidence has been collected in support of a mechanism involving cooperative, bimetallic catalysis.^[7, 8] This has led to a proposed mechanism for ARO reactions involving simultaneous activation of both epoxide and nucleophile by different metal–salen units (Figure 1 a). Based on this hypothesis, we speculated whether dendrimeric analogues of these catalysts might reinforce cooperative catalytic activity in AROs (Figure 1 b).

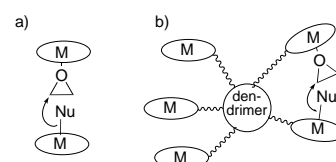
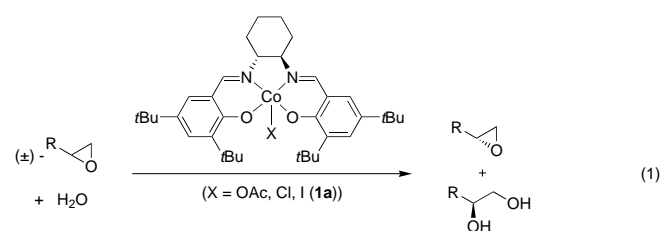


Figure 1. a) Proposed mechanism for cooperative catalysis in the asymmetric ring opening (ARO) of epoxides catalyzed by (salen)metal complexes. b) Cooperative catalytic ARO within a dendrimeric framework.

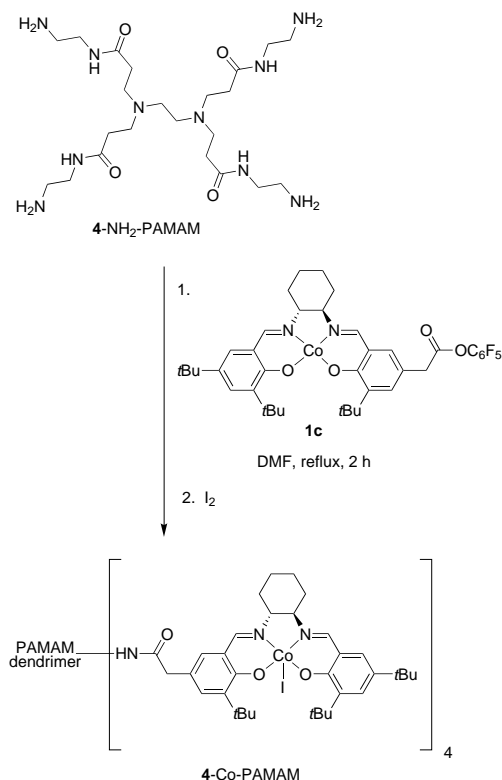
Herein we report the synthesis of dendrimer-bound $[\text{Co}^{\text{III}}(\text{salen})]$ complexes, and demonstrate that these catalysts indeed exhibit significantly enhanced catalytic activity in the hydrolytic kinetic resolution (HKR) of terminal epoxides [Eq. (1)].



We selected the commercially available NH_2 -terminated PAMAM dendrimers for the syntheses of the dendrimeric $[\text{Co}(\text{salen})]$ catalysts. For example, 4- NH_2 -PAMAM was derivatized by covalent attachment to chiral $[\text{Co}^{\text{II}}(\text{salen})]$ units through amide linkages by reaction with pentafluorophenyl ester derivative **1c** following standard peptide coupling methods (Scheme 1).^[9] The resulting dendrimeric complex was purified by precipitation of concentrated THF solutions with hexanes followed by size-exclusion chromatography with Sephadex, and was characterized by FAB MS ($[\text{M}+\text{Na}]^+$: 2888, calcd for $\text{C}_{158}\text{H}_{224}\text{Co}_4\text{N}_{18}\text{O}_{16}$: 2865). Oxidation of the $[\text{Co}^{\text{II}}(\text{salen})]$ sites with elemental iodine in THF proceeded in quantitative yield and afforded the catalytically

[*] Prof. E. N. Jacobsen, Dr. R. Breinbauer
 Department of Chemistry and Chemical Biology
 Harvard University
 Cambridge, MA 02138 (USA)
 Fax: (+1) 617-496-1880
 E-mail: jacobsen@chemistry.harvard.edu

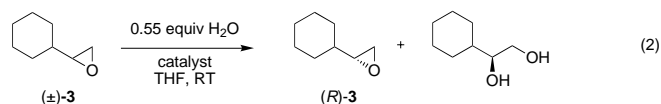
[**] Prof. M. T. Reetz (Max Planck-Institut für Kohlenforschung, Mülheim/Ruhr) and Mr. J. Hong (Harvard University) are gratefully acknowledged for stimulating discussions. This work was supported by the NIH (GM 43214). R.B. thanks Fonds zur Förderung der Wissenschaftlichen Forschung, Vienna (Erwin-Schrödinger-Fellowship) and Land Oberösterreich (Sonderförderung außerhalb des KIP-Programms) for postdoctoral fellowship support. H_2salen = bis(salicylidene)ethylenediamine.



Scheme 1. Synthesis of dendrimer catalyst **4-Co-PAMAM**.

active Co^{III} dendrimer (**4-Co-PAMAM**) as a dark brown solid.^[10, 11] In a similar manner, the higher generation **8-Co-PAMAM** and **16-Co-PAMAM** complexes were also prepared (Figure 2).

As a direct consequence of the second-order kinetic dependence of the HKR on the concentration of $[\text{Co}(\text{salen})]$ complex,^[7d, 8c] reduction of catalyst loadings using the monomeric catalyst **1a** leads to sharp decreases in overall reaction rate; as a practical matter, attainment of useful rates ($t_{1/2} < 10$ h) in the HKR of a representative substrate such as vinylcyclohexane oxide (**3**) requires catalyst concentrations of about 2.5×10^{-2} M (0.5 mol % relative to racemic epoxide in solvent-free reactions). In order to assess whether intramolecular cooperativity could occur within the dendrimeric $[\text{Co}(\text{salen})]$ catalyst, we investigated the HKR of (\pm) -**3** using **8-Co-PAMAM** at a concentration of 2.0×10^{-4} M [Eq. (2), Table 1]. This corre-



sponds to an overall loading of metal complex of 0.027 mol % relative to epoxide. As expected, reaction with the monomeric $[\text{Co}^{\text{III}}(\text{salen})]$ complex **1a** at the 0.025 mol % level led to no measurable conversion after 40 h. In contrast, the dendritic catalyst **8-Co-PAMAM** effected complete kinetic resolution of **3** under the same conditions, affording highly enantioenriched ($> 98\%$ ee) epoxide at 50% conversion.

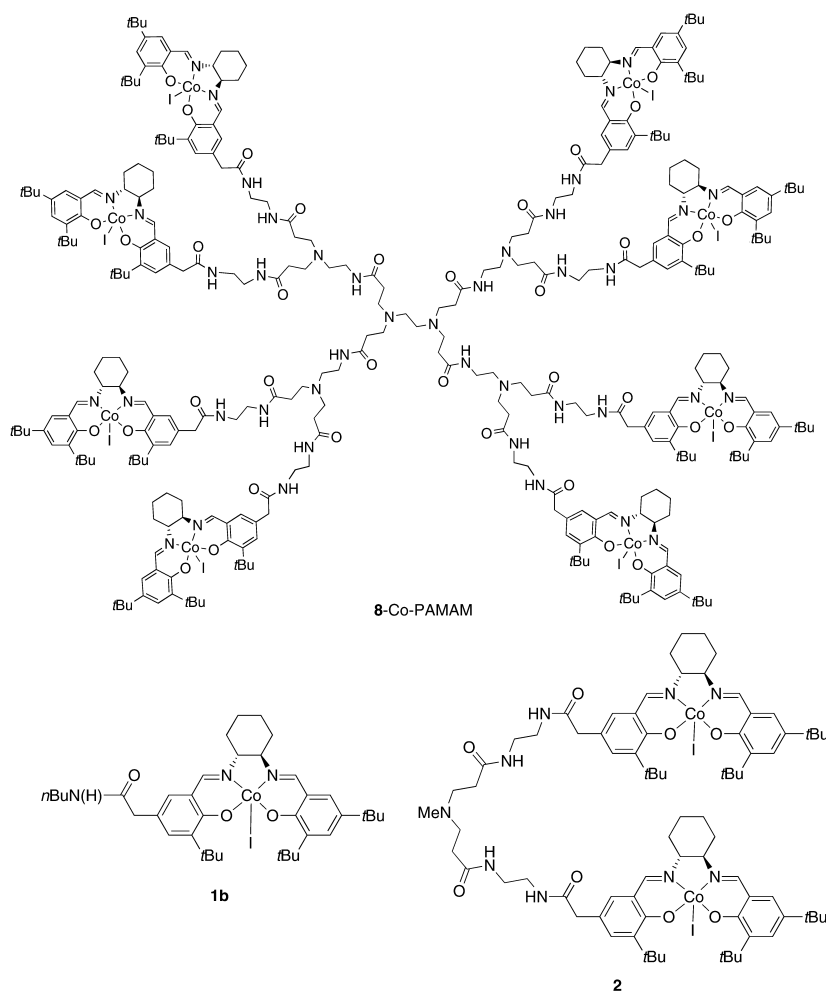


Figure 2. Structures of the dendrimeric catalyst **8-Co-PAMAM** and of model compounds **1b** and **2**. The dendrimeric catalyst **16-Co-PAMAM** (not shown) bears 16 $[\text{Co}(\text{salen})]$ units in a structure analogous to **8-Co-PAMAM**.

Table 1. Hydrolytic kinetic resolution of (rac) -vinylcyclohexane epoxide ((\pm) -**3**) at low catalyst loading.

Catalyst	Catalyst loading [mol %] ^[a]	Time [h]	Conversion [%] ^[b]	ee of recovered epoxide [%] ^[c]
(R,R) - 1a	0.025	40	< 1	n.d.
8-Co-PAMAM (R,R)	0.027	20	50	98

[a] Catalyst loadings are on a per-cobalt basis relative to racemic epoxide. Catalyst concentrations are given in the text. [b] Determined by GC by integration against an internal standard (bromobenzene). [c] Determined by GC analysis using a commercial chiral column (γ -TA). n.d. = not determined.

Having demonstrated dramatically enhanced reactivity of the dendrimeric catalyst **8-Co-PAMAM** relative to monomer **1a**, we sought to establish the precise origins of the observed rate acceleration. In this vein we prepared monomer **1b**, which bears the same salen ligand substituents as that of the dendrimeric catalysts, and the dimeric model compound **2**, which mimics the tethered relationship of two catalyst units within a branch of the PAMAM dendrimers (Figure 2).^[12] Kinetic studies of the HKR of (rac) -1,2-epoxyhexane ((\pm) -**4**) revealed that all of the dendrimeric catalysts were substan-

tially more reactive than the monomeric complex **1b**.^[13] More significantly, the dendrimeric catalysts also displayed significantly higher catalytic activity than the dimeric model compound **2** (Figure 3). It is possible that this positive

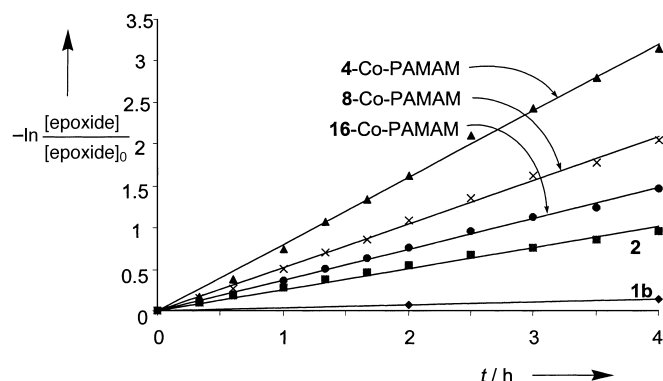


Figure 3. Rate plots for the HKR of (*rac*)-1,2-epoxyhexane ((\pm)-**4**) using 0.55 equivalents of H₂O in THF.

“dendrimer effect” arises from restricted conformations imposed by the dendrimer structure, thereby creating a greater effective molarity of [Co(salen)] units. Alternatively, the multimetric nature of the dendrimer may lead to higher order productive cooperative interactions between [Co(salen)] units.^[8b] While the reactivity of the dendrimers increased on a per-molecule basis with increasing generations (Table 2), on a per-cobalt basis maximum reactivity was attained with **4-Co-PAMAM**.

Table 2. Kinetic data for the HKR of (*rac*)-1,2-epoxyhexane ((\pm)-**4**) catalyzed by the monomeric, dimeric, and dendrimeric [Co(salen)] catalysts.

Catalyst	k [M ⁻¹ s ⁻¹] ^[a]	No. of (salen)CoI units	Relative rate per [Co(salen)] unit	Diol ee [%] (conv, [%]) ^[b]
1b	5.6×10^{-3}	1	1.0	98.2 (29.1)
2	7.9×10^{-2}	2	7.1	99.2 (37.0)
4-Co-PAMAM	5.4×10^{-1}	4	24	99.2 (42.8)
8-Co-PAMAM	6.7×10^{-1}	8	15	99.4 (40.1)
16-Co-PAMAM	9.4×10^{-1}	16	11	99.3 (39.8)

[a] Rate constants were obtained from plots of $\ln([epoxide]/[epoxide]_0)$ versus time (Figure 3) and calculated by dividing the slopes by the absolute concentration of catalyst. [b] ee values were determined at the indicated conversions of epoxide.

This work demonstrates for the first time enhanced reactivity in a dendrimeric catalyst resulting from cooperative reactivity between catalytic units. Further exploration and optimization of such multimetric catalysts in related asymmetric reactions appears warranted, and is the focus of our continuing efforts.

Received: May 17, 2000 [Z15138]

- [1] For leading reviews, see a) D. A. Tomalia, H. D. Durst, *Top. Curr. Chem.* **1993**, 165, 193–313; b) A. W. van der Made, P. W. N. M. van Leeuwen, J. C. de Wilde, R. A. C. Brands, *Adv. Mater.* **1993**, 5, 466–468; c) J. Issberner, R. Moors, F. Vögtle, *Angew. Chem.* **1994**, 106, 2507–2514; *Angew. Chem. Int. Ed. Engl.* **1994**, 33, 2413–2420;

- d) R. F. Service, *Science* **1995**, 267, 458–459; e) R. G. Newkome, C. Moorefield, F. Vögtle *Dendritic Macromolecules: Concepts, Syntheses, Perspectives*, VCH, Weinheim, **1996**; f) F. Zeng, S. C. Zimmerman, *Chem. Rev.* **1997**, 97, 1681–1712; g) H. W. I. Peerlings, E. W. Meijer, *Chem. Eur. J.* **1997**, 3, 1563–1570; h) D. K. Smith, F. Diederich, *Chem. Eur. J.* **1998**, 4, 1353–1361; i) H.-F. Chow, T. K.-K. Mong, M. F. Nongrum, C.-W. Wan, *Tetrahedron* **1998**, 54, 8543–8600; j) D. Seebach, P. B. Rheiner, G. Greiveldinger, T. Butz, H. Sellner, *Top. Curr. Chem.* **1998**, 197, 125–164; k) M. Fischer, F. Vögtle, *Angew. Chem.* **1999**, 111, 934–955; *Angew. Chem. Int. Ed.* **1999**, 38, 884–905; l) M. A. Hearshaw, J. R. Moss, *Chem. Commun.* **1999**, 1–8; m) G. R. Newkome, E. He, C. N. Moorefield, *Chem. Rev.* **1999**, 99, 1689–1746.
- [2] J. W. J. Knapen, A. W. van der Made, J. C. de Wilde, P. W. N. M. van Leeuwen, P. Wijkens, D. M. Grove, G. van Koten, *Nature* **1994**, 372, 659–663.
- [3] For selected examples of dendrimeric catalysts, see a) J.-L. Fillaut, J. Linares, D. Astruc, *Angew. Chem.* **1994**, 106, 2540–2542; *Angew. Chem. Int. Ed. Engl.* **1994**, 33, 2460–2462; b) A. Miedaner, C. J. Curtis, R. M. Barkley, D. L. DuBois, *Inorg. Chem.* **1994**, 33, 5482–5490; c) J.-J. Lee, W. T. Ford, J. A. Moore, Y. Li, *Macromolecules* **1994**, 27, 4632–4634; d) H. Brunner, *J. Organomet. Chem.* **1995**, 500, 39–46; e) D. Seebach, R. E. Marti, T. Hintermann, *Helv. Chim. Acta* **1996**, 79, 1710–1740; f) C. Bolm, N. Derrien, A. Seger, *Synlett* **1996**, 367–388; g) P. Bhyrappa, J. K. Young, J. S. Moore, K. S. Suslick, *J. Mol. Catal. A* **1996**, 113, 109–116; h) P. Bhyrappa, J. K. Young, J. S. Moore, K. S. Suslick, *J. Am. Chem. Soc.* **1996**, 118, 5708–5711; i) M. T. Reetz, G. Lohmer, R. Schwickardi, *Angew. Chem.* **1997**, 109, 1559–1562; *Angew. Chem. Int. Ed. Engl.* **1997**, 36, 1526–1529; j) T. Suzuki, Y. Hirokawa, K. Ohtake, T. Shibata, K. Soai, *Tetrahedron: Asymmetry* **1997**, 8, 4033–4040; k) C. C. Mak, H.-F. Chow, *Macromolecules* **1997**, 30, 1228–1230; l) H.-F. Chow, C. C. Mak, *J. Org. Chem.* **1997**, 62, 5116–5127; m) C. Köllner, B. Pugin, A. Togni, *J. Am. Chem. Soc.* **1998**, 120, 10274–10275; n) R. A. Gossage, J. T. B. H. Jastrzebski, J. van Ameijde, S. J. E. Mulders, A. J. Brouwer, R. M. J. Liskamp, G. van Koten, *Tetrahedron Lett.* **1999**, 40, 1413–1426; o) H. P. Dijkstra, P. Steenwinkel, D. M. Grove, M. Lutz, A. L. Spek, G. van Koten, *Angew. Chem.* **1999**, 111, 2322–2324; *Angew. Chem. Int. Ed.* **1999**, 38, 2186–2188; recently dendritic palladium catalysts have been used for the allylic substitution in a continuously operating membrane reactor: p) N. Brinkmann, D. Giebel, G. Lohmer, M. T. Reetz, U. Kragl, *J. Catal.* **1999**, 183, 163–168; other applications of dendritic catalysts in membrane reactors: q) N. J. Hovestad, E. B. Eggeling, H. J. Heidebüchel, J. T. B. H. Jastrzebski, U. Kragl, W. Keim, D. Vogt, G. van Koten, *Angew. Chem.* **1999**, 111, 1763–1765; *Angew. Chem. Int. Ed.* **1999**, 38, 1655–1658; r) D. de Groot, E. B. Eggeling, J. C. de Wilde, H. Kooijman, R. J. van Haaren, A. W. van der Made, A. L. Spek, D. Vogt, J. N. H. Reek, P. C. J. Kramer, P. W. N. M. van Leeuwen, *Chem. Commun.* **1999**, 1623–1624; s) P. B. Rheiner, D. Seebach, *Chem. Eur. J.* **1999**, 5, 3221–3236; t) H. Sellner, D. Seebach, *Angew. Chem.* **1999**, 111, 2039–2041; *Angew. Chem. Int. Ed.* **1999**, 38, 1918–1920.
- [4] For recent reviews see: a) M. Mammen, S.-K. Chio, G. M. Whitesides, *Angew. Chem.* **1998**, 110, 2908–2953; *Angew. Chem. Int. Ed.* **1998**, 37, 2755–2794; b) R. Roy, *Top. Curr. Chem.* **1997**, 187, 241–274; c) N. Jayaraman, S. A. Nepogodiev, J. F. Stoddart, *Chem. Eur. J.* **1997**, 3, 1193–1199.
- [5] Detty et al. reported increased activity per catalytic group in successive generations in the two-phase oxidation of bromide by hydrogen peroxide catalyzed by phenylseleno-containing dendrimers. The authors proposed that the “dendrimer effect” observed in these catalysis may be due to the micelle-like nature of the oxidized catalyst. C. Francavilla, F. V. Bright, M. R. Detty, *Org. Lett.* **1999**, 1, 1043–1046.
- [6] Recently, van Koten et al. reported an interesting inhibitory dendrimer effect in a catalytic system: A. W. Kleij, R. A. Gossage, J. T. B. H. Jastrzebski, J. Boersma, G. van Koten, *Angew. Chem.* **2000**, 112, 179–181; *Angew. Chem. Int. Ed.* **2000**, 39, 176–178.
- [7] For reviews, see a) E. N. Jacobsen, M. H. Wu in *Comprehensive Asymmetric Catalysis, Vol. III* (Eds.: E. N. Jacobsen, A. Pfaltz, H. Yamamoto), Springer, New York, **1999**, pp. 1309–1326; b) E. N. Jacobsen, *Acc. Chem. Res.* **2000**, 33, 421–431; for key primary reports, see: c) L. E. Martinez, J. L. Leighton, D. H. Carsten, E. N. Jacobsen, *J.*

- Am. Chem. Soc.* **1995**, *117*, 5897–5898; d) M. Tokunaga, J. F. Larrow, F. Kakiuchi, E. N. Jacobsen, *Science* **1997**, *277*, 936–938; e) J. M. Ready, E. N. Jacobsen, *J. Am. Chem. Soc.* **1999**, *121*, 6086–6087.
- [8] a) K. B. Hansen, J. L. Leighton, E. N. Jacobsen, *J. Am. Chem. Soc.* **1996**, *118*, 10924–10925; b) R. Konsler, J. Karl, E. N. Jacobsen, *J. Am. Chem. Soc.* **1998**, *120*, 10780–10781; c) J. Hong, D. G. Blackmond, E. N. Jacobsen, unpublished results.
- [9] J. Kovacs, L. Kisfaludy, M. Q. Ceprini *J. Am. Chem. Soc.* **1967**, *89*, 183–184. Pentafluorophenyl ester **1c** was prepared from commercially available 4-hydroxyphenylacetic acid in seven steps and 26% overall yield.
- [10] Although oxidation to the [(salen)Co^{III}(acetate)] complexes using HOAc/O₂ is the method of choice for the preparation of the monomeric catalysts (see ref. [7d]), this proved impractical with the PAMAM-Co complexes because of the basic amine sites in the dendrimer. The [(salen)Co^{III}(iodide)] complexes obtained by oxidation with I₂ have been found to display similar reactivity to the corresponding acetate complexes.^[8c]
- [11] **4-Co-PAMAM**: IR (KBr): $\tilde{\nu}_{\text{max}}$ = 3339, 2948, 2864, 1663 (br.), 1609, 1526, 1435, 1253, 1170, 1031, 783; ¹H NMR (400 MHz, [D₆]DMSO): δ = 8.1 (br., 8H), 7.83 (s, 4H), 7.79 (s, 4H), 7.47 (s, 4H), 7.43 (s, 4H), 7.33 (s, 4H), 7.29 (s, 4H), 3.62 (br. s, 16H), 3.38 (br. s, 12H), 3.10 (br. s, 16H), 2.6–2.2 (br., 16H), 1.98 (br., 4H), 1.89 (br., 4H), 1.76 (s, 36H), 1.72 (s, 36H), 1.60 (br. m, 8H), 1.28 (s, 36H); ¹³C NMR (100 MHz, [D₆]DMSO): δ = 170.7, 164.4, 163.7, 162.5, 161.6, 141.9, 141.4, 135.6, 133.0, 132.2, 129.0, 128.5, 121.2, 118.4, 118.2, 69.2, 69.1, 41.2, 38.2, 35.7, 35.5, 33.5, 31.4, 30.3, 30.2, 29.5, 29.4, 24.2.
- [12] **1b**: IR (KBr): $\tilde{\nu}_{\text{max}}$ = 3365, 2950, 2864, 1630, 1611, 1526, 1436, 1254, 1170, 783; ¹H NMR (400 MHz, [D₆]DMSO): δ = 8.00 (t, J = 5.6 Hz, 1H), 7.85 (s, 1H), 7.80 (s, 1H), 7.50 (d, J = 2.4 Hz, 1H), 7.43 (d, J = 2.4 Hz, 1H), 7.33 (s, 1H), 7.30 (s, 1H), 3.62 (br. s, 2H), 3.35 (s, 2H), 3.10 (br. s, 2H), 3.05 (m, J = 6.8 Hz, 2H), 2.00 (br., 2H), 1.91 (br., 2H), 1.76 (s, 9H), 1.60 (br. m, 2H), 1.40 (m, J = 7.2 Hz, 2H), 1.32 (s, 9H), 1.28 (m, J = 7.2 Hz, 2H), 0.85 (t, J = 7.2 Hz, 3H); ¹³C NMR (100 MHz, [D₆]DMSO): δ = 170.7, 164.6, 164.0, 162.8, 162.0, 142.2, 141.8, 135.9, 133.2, 132.3, 129.2, 128.7, 122.0, 118.8, 118.6, 69.3, 69.2, 41.4, 38.1, 35.7, 35.5, 33.5, 31.5, 31.2, 30.4, 30.3, 29.6, 29.4, 24.2, 19.5, 13.7. **2**: IR (KBr): $\tilde{\nu}_{\text{max}}$ = 3307, 2949, 2862, 1658, 1620, 1526, 1435, 1253, 1170, 1030, 783; ¹H NMR (400 MHz, [D₆]DMSO): δ = 8.1 (br., 4H), 7.82 (s, 2H), 7.78 (s, 2H), 7.47 (s, 2H), 7.43 (s, 2H), 7.31 (s, 2H), 7.27 (s, 2H), 3.62 (br. s, 8H), 3.35 (br. s, 7H), 3.10 (br. s, 8H), 2.6–2.2 (br., 8H), 1.98 (br., 4H), 1.89 (br., 4H), 1.76 (s, 18H), 1.72 (s, 18H), 1.60 (br. m, 4H), 1.28 (s, 18H); ¹³C NMR (100 MHz, [D₆]DMSO): δ = 171.7, 165.3, 164.7, 163.5, 162.6, 142.8, 142.4, 136.6, 133.9, 129.9, 129.5, 122.3, 119.4, 119.2, 70.1, 70.0, 42.0, 39.2, 36.6, 36.4, 34.3, 32.3, 31.2, 31.1, 30.4, 30.3, 25.1; MS (FAB) of the corresponding Co^{II} complex: 1456 [M+Na]⁺ (calcd exact mass: 1433.76).
- [13] Experimental procedure for the kinetic experiments: 10 mL vials were charged with a stir bar and 12.5 μ mol (referring to Co) catalyst **1b**, **2**, **4-Co-PAMAM**, **8-Co-PAMAM**, or **16-Co-PAMAM**. The catalysts were dissolved in THF (4.00 mL), then (*rac*)-1,2-epoxyhexane (3.00 mL, 25 mmol) and bromobenzene (200 μ L; as an internal standard) were added to the dark brown solution. After the mixture had been stirred for 1 h at 4 °C, water (250 μ L) was added. Reaction conversion was monitored by GC analysis (HP-5 column) of 20 μ L aliquots withdrawn periodically from the reaction mixture.

Structural Characterization of a Cyclohexameric *meta*-Phenyleneethynylene Made by Alkyne Metathesis with In Situ Catalysts**

Ping-Hua Ge, Wei Fu, Wolfgang A. Herrmann, Eberhardt Herdtweck, Charles Campana, Richard D. Adams,* and Uwe H. F. Bunz*

Cyclophenyleneethynylenes (CPEs) have recently made a spectacular appearance as a novel class of carbon-rich supramolecular materials.^[1, 2] Moore and co-workers have established *meta*-cyclophenyleneethynylenes (*m*-CPEs)^[1–3] as tubular discotic liquid crystals^[3d] and as porous, hydrogen-bonded, channel-forming organic solids.^[4] Channels in *m*-CPEs are formed through a combination of hydrogen bonds and the internal cavities of the hexagonally packed *m*-CPE. However only a low-quality single-crystal X-ray structure of this exciting CPE was obtained^[4] and to our surprise, no high-quality X-ray structures of *m*-CPE-derivatives are known.^[2b, 5]

In the past CPEs have been made by the Pd/Cu-catalyzed coupling of the Heck–Sonogashira type. Substrates were either a preformed linear oligomer,^[3] a half-cycle,^[5] or 1-ethynyl-3-halo-substituted benzenes.^[6] The latter compounds gave only very low yields of CPEs. Weiss et al.,^[7] Fürstner et al.,^[8] and our group^[9] have reported that alkyne metathesis either with defined carbyne complexes^[7, 8] or with in situ catalysts, which are obtained from [Mo(CO)₆] and 4-chlorophenol in off-the-shelf 1,2-dichlorobenzene,^[10, 11] is an excellent method for preparing saturated and unsaturated ring systems. Herein, we report the synthesis of the new hexameric *meta*-cyclophenyleneethynylenes **2a**, **b**, **d** from dipropynylated benzenes **1** by alkyne metathesis as well as the isolation of the corresponding polymers **3a–d** (Scheme 1).^[12] The isolated *m*-CPE **2a** and its triosmiumdicarbonyl complex **4a** have been characterized structurally by single-crystal X-ray diffraction analyses.

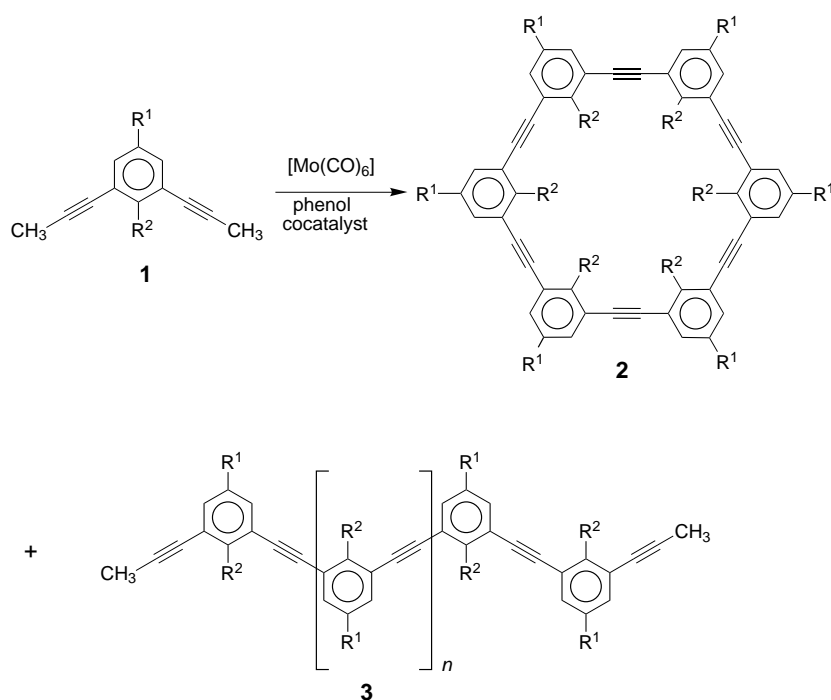
The monomers **1** were prepared from the corresponding diiodides^[12] by Pd-catalyzed propynylations.^[10] Heating **1a**, [Mo(CO)₆], and either 4-chlorophenol or 4-trifluoromethylphenol in off-the-shelf 1,2-dichlorobenzene under a slow stream of nitrogen furnishes a mixture of oligomers and

[*] Prof. U. H. F. Bunz, Prof. R. D. Adams, Dr. P.-H. Ge, W. Fu
Department of Chemistry and Biochemistry
The University of South Carolina
Columbia, SC 29208 (USA)
Fax: (+1) 803-777-9521
E-mail: bunz@mail.chem.sc.edu

Prof. W. A. Herrmann, Dr. E. Herdtweck
Institut für Anorganische Chemie
Technische Universität München
Lichtenbergstrasse 4, 85747 Garching (Germany)

Dr. C. Campana
Bruker AXS, Inc.
5465 East Cheryl Parkway, Madison, WI 53711-5373 (USA)

[**] U.H.F.B. and P.-H.G. thank the National Science Foundation (CHE 9814118), the Research Corporation, and the EPSCoR Office of the State of South Carolina for generous support. R.D.A. thanks the Alexander von Humboldt Foundation for an award which supported this work.



Scheme 1. Synthesis of **2** and **3**. Substituent pattern: **a**: $\text{R}^1 = \text{tert-butyl}$, $\text{R}^2 = \text{H}$; **b**: $\text{R}^1 = \text{hexyl}$, $\text{R}^2 = \text{H}$; **c**: $\text{R}^1 = \text{dodecyl}$, $\text{R}^2 = \text{H}$; **d**: $\text{R}^1 = \text{tert-butyl}$, $\text{R}^2 = \text{methyl}$.

polymers. Mass spectrometry of the reaction mixtures showed the occurrence of at least one significant peak, which could be assigned to the respective cyclohexamer (**2a–d**). A second molecular ion of considerably decreased intensity was assigned to the corresponding cycloheptamers. While it was easy to establish the presence of *m*-CPEs in the reaction mixture,^[7c] their separation was tedious, and the rings **2a** and **2b** could only be isolated after repeated thin-layer chromatography on silica gel by using hexane–dichloromethane mixtures. With this protocol **2a** (6%), **2b** (1.2%), and **2d** (0.5%) were obtained from the polymerization mixtures of **1a**, **1b**, and **1d**, respectively. The cycles **2** were unambiguously characterized by mass spectrometry, ^1H NMR and ^{13}C NMR spectroscopy, and in the case of **2a** by an X-ray single-crystal diffraction analysis. A suitable specimen of **2a** was grown from dichloromethane–hexane mixtures at room temperature.^[13] In the solid state the molecule **2a** contains a center of symmetry and is nearly planar (Figure 1a). The three independent C–C triple bond distances are 1.199(3), 1.203(3), and 1.205(3) Å. They are not significantly different from each other or the C–C triple bond length found in tolane.^[14] The crystal contains two equivalents of disordered hexane (not shown in Figure 1) per molecule, as supported by elemental analysis results. One of the hexane molecules passes through the center of each ring and a second one is located between stacks of rings. The rings in **2a** are aligned and stacked in columns^[15] to form channels (5 Å × 8 Å; see

Figure 1b). At the same time the molecules in these columns are tilted by approximately 60° with respect to the column axis (see Figure 1b). The stacks themselves are oriented to form a herringbone-type pattern, not unusual for large aromatic systems.^[16] Interspersed in these stacks and parallel to the *a* axis is the second molecule of hexane solvent, which separates the stacks. Thus despite the fact that we have formally extended channels in this structure (see Figure 1b), the material is not porous in a materials sense, and the hexane is retained in the crystal at ambient temperature. In this regard cycle **2a** resembles decaphenylanthracene prepared by Pascal, Jr., et al.^[17]

We have found that the alkyne groups in **2a** are active coordination sites for metal atoms. This was demonstrated by the preparation of the triosmiumdecacarbonyl complex **4a**, obtained in 11% yield by treatment of **2a** with $[(\text{MeCN})_2\text{Os}_3(\text{CO})_{10}]$. The molecular structure of **4a** shows an $[\text{Os}_3(\text{CO})_{10}]$ cluster coordinated, adopting the $\mu_3\text{-II}$ ($\text{C}\equiv\text{C}$ bond is parallel to an Os–Os

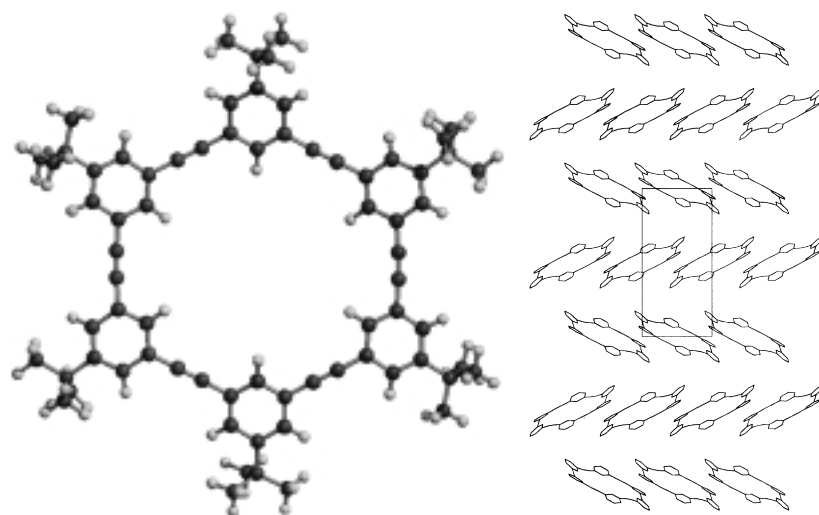


Figure 1. a) Molecular structure of **2a**. b) Packing of **2a** in the crystal; *tert*-butyl substituents and hydrogen atoms are omitted for clarity.

bond) coordination mode (Figure 2). Most interestingly, the attachment of the cluster to the CPE leads to a significant disruption of the planarity of the ring. This can be attributed to the induced nonlinearity at the atoms C1–C2–C13 (131(1)°) and C45–C1–C2 (117(1)°), as a consequence of the coordination of the metal atoms and the steric interaction of the CO ligands with the bulky *tert*-butyl groups.

Alkyne metathesis of *meta*-dipropynylated benzenes furnishes macrocycles of the type **2** and the corresponding *meta*-polymers **3**.^[12] The high-quality X-ray crystal structure of the hydrocarbon *m*-CPE reveals that **2a** forms a porous solid with infinite elliptical channels. The result demonstrates that nonfunctional but shape-persistent *m*-CPE **2a** does not

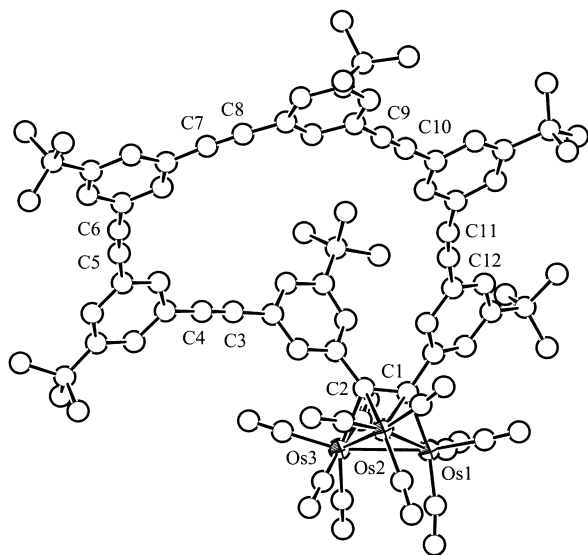


Figure 2. Molecular structure of **4a**.

require hydrogen-bonding or long alkyl chains to arrange into tubular solids with intrastack channels—van der Waals interactions are sufficient to perform this task.

Experimental Section

Monomer **1a** (2.00 g, 9.52 mmol), $[\text{Mo}(\text{CO})_6]$ (126 mg, 0.477 mmol), and 4-chlorophenol (1.23 g, 9.57 mmol) were dissolved in off-the shelf 1,2-dichlorobenzene (50 mL) and heated for 16 h to 150 °C under a light stream of N_2 . The reaction was worked-up by washing with water, dilute HCl, and dilute NaOH followed by precipitation into methanol to furnish a mixture (1.25 g, 84 %) of polymer **3a** and cycle **2a**. Of the product mixture, 500 mg were subjected to repeated thick-layer chromatography (1:6 CH_2Cl_2 /hexane) leading to the isolation of the cycle **2a** (30 mg, 6 %). M.p. > 250 °C; MS: m/z : $\text{C}_{72}\text{H}_{72}$: calcd: 936; found: 936 $[M^+]$; ^1H NMR (CDCl_3): δ = 7.58 (s, 1H), 7.55 (s, 2H), 1.33 (s, 9H); ^{13}C NMR (CDCl_3): δ = 152.73, 133.66, 129.64, 124.24, 90.37, 36.11, 32.49; IR (KBr): $\tilde{\nu}$ = 3060 (w), 2963, (s), 2904 (s), 2889 (s), 2210 (w), 1593 (s), 1475 (m), 1432 (s), 1364 (s), 1242 (s), 1000 (m), 877 (s), 693 (s) cm^{-1} ; UV/Vis: λ_{max} = 248 (sh), 280 (sh), 310 nm; elemental analysis calcd for **2a** · C_6H_{14} (%): C 91.53, H 8.47; found: C 91.37, H 8.02.

2b: Yield: 4.8 mg, 1 %. MS: m/z : $\text{C}_{84}\text{H}_{86}$: calcd: 1104; found: 1105 $[M^+ + 1]$; ^1H NMR (CDCl_3): δ = 7.52 (s, 1H), 7.33 (s, 2H), 2.59 (t, 2H), 1.63 (quint, 2H), 1.31 (bs, 6H), 0.88 (t, 3H); ^{13}C NMR (CDCl_3): δ = 144.30, 132.89, 132.64, 124.31, 90.12, 36.78, 32.94, 32.36, 30.16, 23.84, 15.38.

2d, 3d: Yield: 2.3 mg, 0.5 %, mixture of hexamer and heptamer: MS: m/z : $\text{C}_{78}\text{H}_{84}$: 1021 $[M^+ + 1]$; $\text{C}_{91}\text{H}_{98}$: 1191 $[M^+ + 1]$; ^1H NMR (CDCl_3): δ = 7.53 (s, 2H), 2.75 (s, 3H), 1.31 (s, 9H).

4a: $[\text{Os}_3(\text{CO})_{10}(\text{MeCN})_2]$ (10.1 mg, 0.011 mmol) and **2a** (9.3 mg, 0.010 mmol) were dissolved in CH_2Cl_2 (10 mL) and heated to reflux for 0.5 h. The product was separated by TLC (silica gel) using a 6:1 hexane/dichloromethane solvent mixture to yield **4a** (2.0 mg; 11 %) as a yellow product. Spectral data for **4a**: IR (hexane): $\tilde{\nu}_{\text{CO}}$ = 2100 (m), 2067 (s), 2046 (s), 2029 (s), 2010 (s), 2000 (m), 1993 (m), 1979 (w), 1961 (vw) cm^{-1} ; ^1H NMR (CDCl_3): δ = 7.62 (m, 4H), 7.52 (m, 8H), 7.28 (s, 2H), δ = 7.06 (s, 2H), 6.85 (s, 2H), 1.36 (s, 18H), 1.35 (s, 18H), 1.17 (s, 18H); MS (FAB): m/z : 1788.2 $[M^+]$; elemental analysis: calcd: C 55.07, H 4.02; found: C 55.04, H 4.09.

Received: May 17, 2000 [Z15133]

- [1] For excellent reviews see a) J. S. Moore, *Acc. Chem. Res.* **1997**, 30, 402; b) M. M. Haley, J. J. Pak, S. C. Brand, *Top. Curr. Chem.* **1999**, 201, 81.
[2] a) Y. Tobe, N. Utsumi, A. Nagano, K. Naemura, *Angew. Chem.* **1998**, 110, 1347; *Angew. Chem. Int. Ed.* **1998**, 37, 1285. b) For a strained *m*-

- CPE with four phenyleneethynylenes units and its X-ray crystal structure see T. Kawase, N. Ueda, H. R. Darabi, M. Oda, *Angew. Chem.* **1996**, 108, 1658; *Angew. Chem. Int. Ed. Engl.* **1996**, 35, 1556.
[3] a) O. Y. Mindyuk, M. R. Stetzer, D. Gidalevitz, P. A. Heiney, J. C. Nelson, J. S. Moore, *Langmuir* **1999**, 15, 6897, and references therein; b) J. K. Young, J. C. Nelson, J. S. Moore, *J. Am. Chem. Soc.* **1994**, 116, 10841; c) J. S. Zhang, D. J. Pesak, J. L. Ludewick, J. S. Moore, *J. Am. Chem. Soc.* **1994**, 116, 4227; d) O. Y. Mindyuk, M. R. Stetzer, P. A. Heiney, J. C. Nelson, J. S. Moore, *Adv. Mater.* **1998**, 10, 1363.
[4] D. Venkataraman, S. Lee, J. S. Zhang, J. S. Moore, *Nature* **1994**, 371, 591.
[5] Höger has recently published the structure determination of a related type of ring: S. Höger, V. Enkelmann, *Angew. Chem.* **1995**, 107, 2917; *Angew. Chem. Int. Ed. Engl.* **1995**, 34, 2713.
[6] H. Staab, K. Neunhöffer, *Synthesis* **1974**, 424.
[7] a) K. Weiss (Bayreuth) first reported the formation of the macrocycle **2b** in alkyne metathesis mixtures of **1b** by using $[(t\text{BuO})_3\text{W}=\text{CC-Me}_3]^{[9b]}$; b) K. Weiss, A. Michel, unpublished results, Bayreuth, **1997**; c) K. Weiss, A. Michel, E. M. Auth, U. H. F. Bunz, T. Mangel, K. Müllen, *Angew. Chem.* **1997**, 109, 522; *Angew. Chem. Int. Ed. Engl.* **1997**, 36, 506.
[8] A. Fürstner, O. Guth, A. Rumbo, G. Seidel, *J. Am. Chem. Soc.* **1999**, 121, 11108; A. Fürstner, C. Mathes, C. W. Lehmann, *J. Am. Chem. Soc.* **1999**, 121, 9453; A. Fürstner, G. Seidel, *Angew. Chem.* **1998**, 110, 1758; *Angew. Chem. Int. Ed.* **1998**, 37, 1734.
[9] a) L. Kloppenburg, D. Song, U. H. F. Bunz, *J. Am. Chem. Soc.* **1998**, 120, 7973; b) U. H. F. Bunz, L. Kloppenburg, *Angew. Chem.* **1999**, 111, 506; *Angew. Chem. Int. Ed.* **1999**, 38, 478.
[10] L. Kloppenburg, D. Jones, U. H. F. Bunz, *Macromolecules* **1999**, 32, 4194.
[11] N. G. Pschirer, W. Fu, R. D. Adams, U. H. F. Bunz, *Chem. Commun.* **2000**, 87.
[12] T. Mangel, A. Eberhardt, U. Scherf, U. H. F. Bunz, K. Müllen, *Macromol. Rapid Commun.* **1995**, 16, 571. The authors reported the synthesis of **3b** by Pd-catalyzed coupling of the Heck-type.
[13] a) X-ray structure analysis for **2a**: Suitable single crystals for the X-ray diffraction study were grown from *n*-hexane. $\text{C}_{72}\text{H}_{72}$: (937.30): monoclinic $P2_1/a$; a = 11.3607(3), b = 23.5383(6), c = 14.1410(3) Å, β = 106.661(1)°. V = 3622.7(2) Å³, Z = 2, ρ_{calcd} = 0.859 g cm⁻³; μ = 0.048 mm⁻¹. A clear colorless plate of **2a** (0.5 mm × 0.4 mm × 0.08 mm) was stored under perfluorinated ether, transferred in a Lindemann capillary, fixed, and sealed. Preliminary examination and data collection were carried out on a Kappa CCD area detector (Nonius; MACH3) equipped with a rotating anode and graphite-monochromated MoK_α radiation (Nonius; FR951, λ = 0.71073 Å, $2\theta_{\text{max}}$ = 50°). The unit cell parameters were obtained by full-matrix least-squares refinements of 11971 reflections. Data collection was performed at 123 K (exposure time: 100 s per frame; 9 sets, θ and ω scans, $\Delta\theta/\Delta\omega$: 1°; dx: 40.0 mm). A total of 12551 reflections were collected. Raw data were corrected for Lorentz and polarization effects, not corrected for absorption and decay effects, and scaled with the program DENZO-SMN. After merging (R_{int} = 0.0341), 6366 independent reflections remained and were used for all calculations. All "heavy atoms" of the asymmetric unit were refined anisotropically. All hydrogen atoms were located in the difference Fourier map and refined with individual isotropic temperature parameters. Full-matrix least-squares refinements were carried out by minimizing $\Sigma w(F_o^2 - F_c^2)^2$ by using the SHELXL-97 weighting scheme and stopped at shift/err < 0.001 with $R1(\text{all data})$ = 0.0829, $R_w(\text{all data})$ = 0.1587, and GOF 1.050. Neutral atom scattering factors for all atoms and anomalous dispersion corrections for the non-hydrogen atoms were taken from *International Tables for Crystallography*. All calculations were performed on a DEC 3000 AXP workstation and an Intel Pentium II PC, with the STRUX-V system, including the programs PLATON, SHELXS-86, and SHELXL-97. One solvent molecule (C_6H_{14}) is highly disordered in the crystal and could not be located and refined correctly. The problem was solved by using the SQUEZZE strategy (A. L. SPEK, PLATON, 1999); b) X-ray structure analysis for **4a**: A cube of **4a** (0.05 mm × 0.04 mm × 0.05 mm) was grown from dichloromethane. Data were obtained on a Bruker Smart 1000 CCD diffractometer at 298 K. The structure was solved and refined with the programs SHELXS86 and SHELXL97 and by using heavy-atom

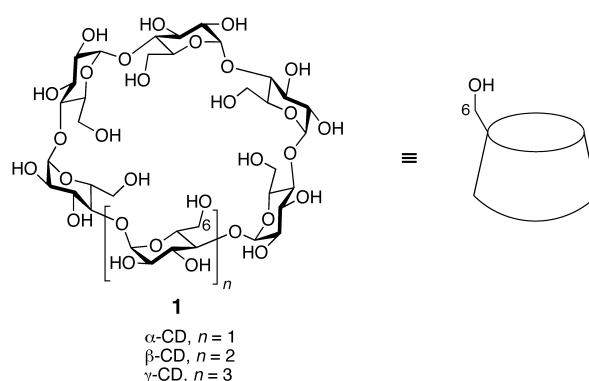
(Patterson) methods. Hydrogen atoms were localized and refined in the riding mode. The crystal was mounted on a glass fiber. $\text{Os}_3\text{O}_{10}\cdot\text{C}_{12}\text{H}_{22}$ ($M_r = 1788.00$); MoK_α radiation; $\lambda = 0.71073 \text{ \AA}$, graphite monochromator; $2\theta_{\text{max}} = 22.50^\circ$, monoclinic $C2/c$; $a = 54.641(5)$, $b = 11.7486(10)$, $c = 33.250(3) \text{ \AA}$, $\beta = 120.447(3)^\circ$, $V = 18401(3) \text{ \AA}^3$, $Z = 8$, $\rho_{\text{calcd}} = 1.291 \text{ g cm}^{-3}$, $\mu = 41.79 \text{ mm}^{-1}$, absorption correction: SADABS; 12021 reflections were measured and all reflections with $(I = 2\sigma(I))$ observed, $R = 0.0747$, $R_w = 0.1710$. Crystallographic data (excluding structure factors) for the structures reported in this paper have been deposited with the Cambridge Crystallographic Data Centre as supplementary publication nos. CCDC-143392 (**2a**) and CCDC-143393 (**4a**). Copies of the data can be obtained free of charge on application to CCDC, 12 Union Road, Cambridge CB2 1EZ, UK (fax: (+44) 1223-336-033; e-mail: deposit@ccdc.cam.ac.uk).

- [14] The C–C triple bond length in diphenylacetylene is 1.198 \AA . A. Mavridis, I. Moustakali-Mavridis, *Acta Crystallogr. Sect. B* **1977**, 33, 3612.
- [15] U. H. F. Bunz, V. Enkelmann, *Chem. Eur. J.* **1999**, 5, 263.
- [16] A. J. Berresheim, M. Müller, K. Müllen, *Chem. Rev.* **1999**, 99, 1747; M. Müller, C. Kübel, K. Müllen, *Chem. Eur. J.* **1998**, 4, 2099; R. Goddard, M. W. Haenel, W. C. Herndon, C. Krüger, M. Zander, *J. Am. Chem. Soc.* **1995**, 117, 30.
- [17] X. Qiao, M. A. Padula, D. M. Ho, N. J. Vogelaar, C. E. Schutt, R. A. Pascal, Jr., *J. Am. Chem. Soc.* **1996**, 118, 741.

Diisobutylaluminum-Promoted Regioselective De-*O*-benzylation of Perbenzylated Cyclodextrins: A Powerful New Strategy for the Preparation of Selectively Modified Cyclodextrins**

Alan J. Pearce and Pierre Sinaÿ*

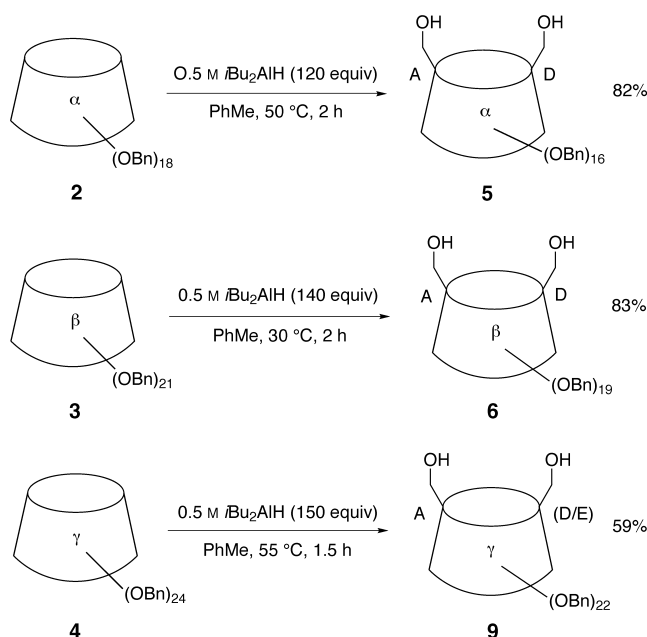
Cyclodextrins (CDs) **1** and their derivatives are of great importance in supramolecular chemistry,^[1] analytical chemistry,^[2] as artificial enzymes,^[3] drug delivery systems,^[4] and modifiers of chemical reactions (Scheme 1).^[5] The preparation of selectively modified cyclodextrins for these applications remains a crucial challenge in organic synthesis despite considerable effort and several well defined protocols.^[6] Traditional methods may be classified^[6a] as a) “long”, involving lengthy protection and deprotection steps; b) “clever”, where the chemistry of cyclodextrin is exploited to get the desired product by the shortest route; and c) “sledgehammer”, where indiscriminate reaction leads to complex product mixtures and lengthy separation. A far more elegant alternative approach is the regioselective deprotection of perfunctionalized cyclodextrins,^[7] thus combining the advantageous aspects of the first two methods mentioned above.



Scheme 1. Schematic structural representation of CDs.

We recently reported that triisobutylaluminum (TIBAL) led to highly regioselective mono-de-*O*-benzylation of perbenzylated mono- and disaccharide derivatives.^[8] Herein, we report the first regioselective de-*O*-benzylation of perbenzylated CDs by application of this methodology.

Perbenzylated CDs **2–4** were prepared by direct benzylation of CDs **1** in DMSO with benzyl chloride and NaH, in excellent yield using the method of Sato et al.^[9] When α -CD(OBn)₁₈ (**2**) was treated with excess diisobutylaluminum (DIBAL)^[10] in toluene at 50°C we observed formation of a single product **5** of di-*O*-debenzylation in 82% yield (Scheme 2). The structure of **5** was identified as the AD



Scheme 2. Highly regioselective DIBAL-promoted di-*O*-debenzylation affords AD diols in excellent yield.

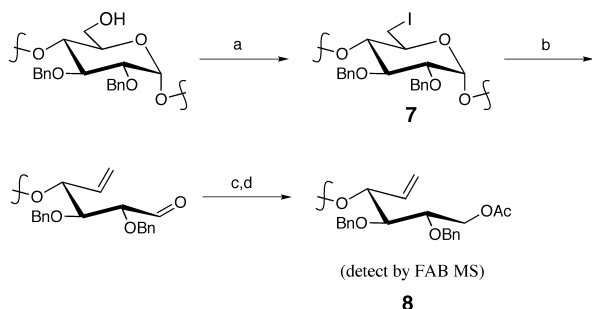
regioisomer by ^1H and ^{13}C NMR spectroscopy, which indicated high C_2 symmetry, and was further confirmed by chemical degradation using the “hex-5-enose method” as described below. The regioselectivity of this di-*O*-debenzylation is remarkable. Statistical calculations indicate that for di-*O*-deprotection of α -CD(OBn)₁₈ (**2**) 27 regioisomers are possible, of which, we obtain only one in excellent yield.

[*] Prof. P. Sinaÿ, Dr. A. J. Pearce
Département de Chimie, Associé au CNRS
Ecole Normale Supérieure
24 Rue Lhomond, 75231 Paris cedex 05 (France)
Fax: (+33) 1-44-32-33-97
E-mail: pierre.sinaÿ@ens.fr

[**] The authors thank the European Community for a TMR Marie Curie Research Training Grant (no. ERBFMBICT983225) to A.J.P.

Supporting information for this article is available on the WWW under <http://www.wiley-vch.de/home/angewandte/> or from the author.

Similarly, β -CD(OBn)₂₁ (**3**) underwent smooth di-*O*-debenzylation with excess DIBAL to give a single diol **6** in 83 % yield (Scheme 2). We obtain only one of 33 possible regioisomers as product, indicating the high regioselectivity of the di-*O*-debenzylation process. The regiochemistry of **6** was not assignable using a combination of TOCSY-ROESY NMR experiments^[11] as the low symmetry of **6** led to extensive overlapping in spectra. However, the structure of **6** was established using the “hex-5-enose method” (Scheme 3).^[12]



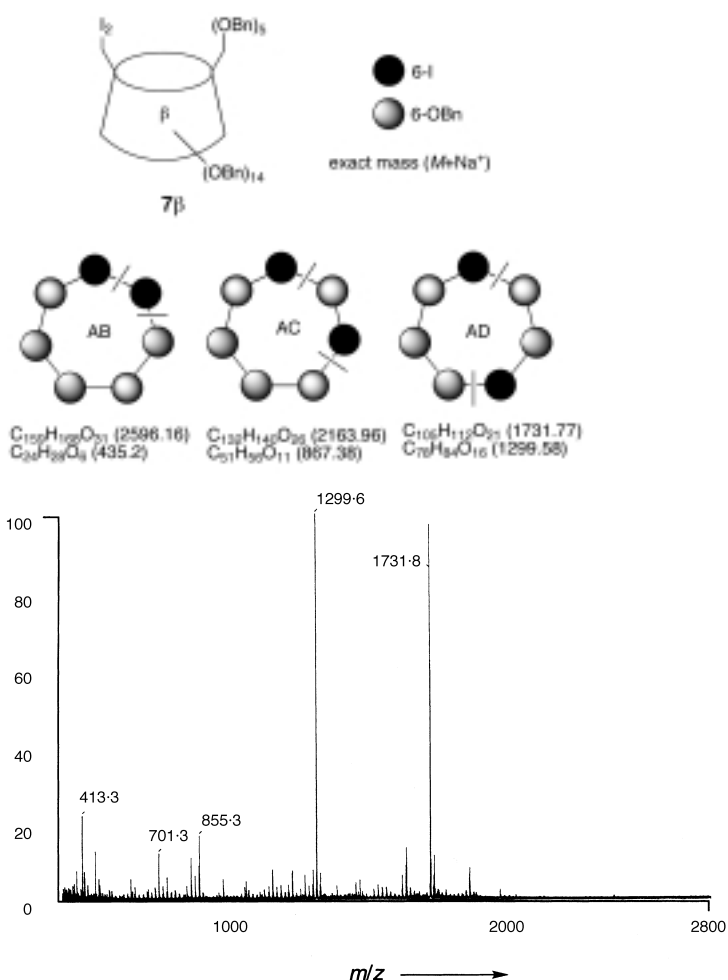
Scheme 3. The “hex-5-enose degradation” method. Reagents: a) I₂, PPh₃, imidazole, toluene, 62 % for **7a**, 85 % for **7β**, 81 % for **7γ**; b) Zn, *n*PrOH, H₂O, reflux, 1 h; c) NaBH₄, MeOH, H₂O; d) Ac₂O, pyridine.

Thus, **6** was converted to the (bis)iodide **7β** using Garegg's conditions^[13] and subsequently fragmented by using activated zinc, then reduced with NaBH₄, and acetylated. Analysis of the products **8** by FAB MS identified only the two fragments arising from the AD regioisomer **7β** and hence the diol **6** was assigned as the AD regioisomer accordingly (Scheme 4).

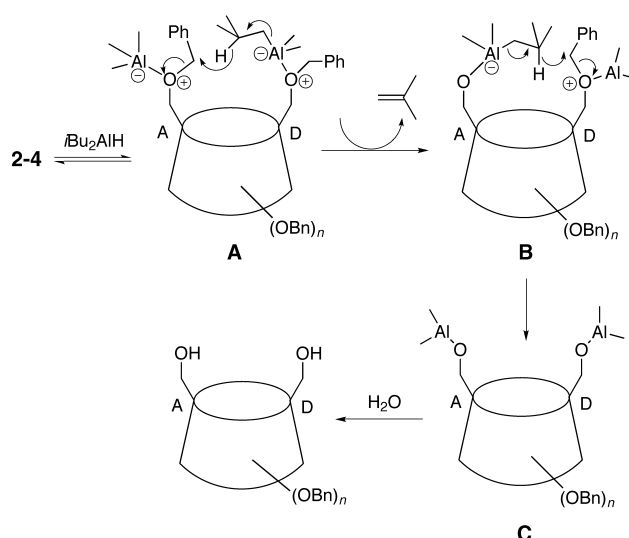
DIBAL-promoted di-*O*-debenzylation of γ -CD(OBn)₂₄ (**4**) gave a mixture of AD/AE diols **9** in 59 % yield (see Scheme 2) after analysis and assignment by the “hex-5-enose method”.

A proposed mechanism for this de-*O*-benzylation is shown in Scheme 5. In the presence of a large excess of the Lewis acidic DIBAL, coordination of the perbenzylated CD may lead to the product-productive intermediate **A**. Hydride transfer from the ate complex^[14] at position D to the proximal and activated benzyl at position A may then occur affording **B**. The aluminate complex at A remains an activated hydride donor and subsequently “directs” a second hydride transfer back to the correctly disposed and activated benzyl group at D. Hydrolysis of intermediate **C** on work-up affords the observed diol products.

This method is particularly powerful given that the derivatives obtained in preparative yield are selectively protected and therefore suitable for direct further functionalization. The synthetic utility of the selective protection in **5** is highlighted in Scheme 6. Allylation of **5**, followed by ring-closing metathesis^[15] using the Grubbs' initiator and hydrogenolysis gave the unusual rigidly AD-capped α -cyclodextrin **10** in 80 % yield from **5**. Methylation of **5** followed by hydrogenolysis gave the AD-bis-methylated α -cyclodextrin **11** in 82 % yield (from **5**). Derivatives **10** and **11** also maintained the high C₂ symmetry in NMR spectra.

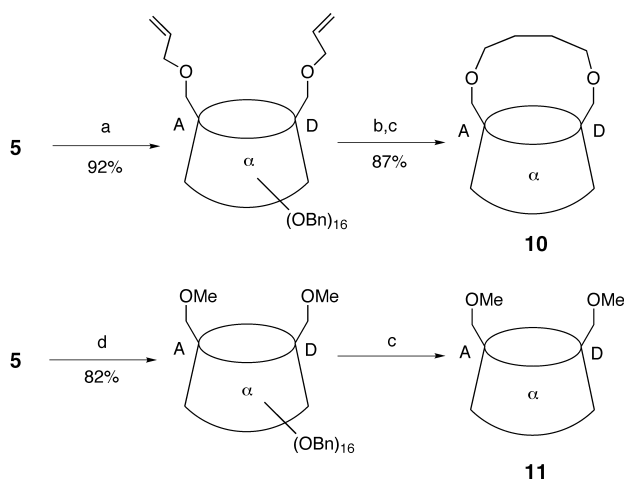


Scheme 4. Structural confirmation (by FAB MS) of **7β** (and **6**) by the “hex-5-enose degradation”.



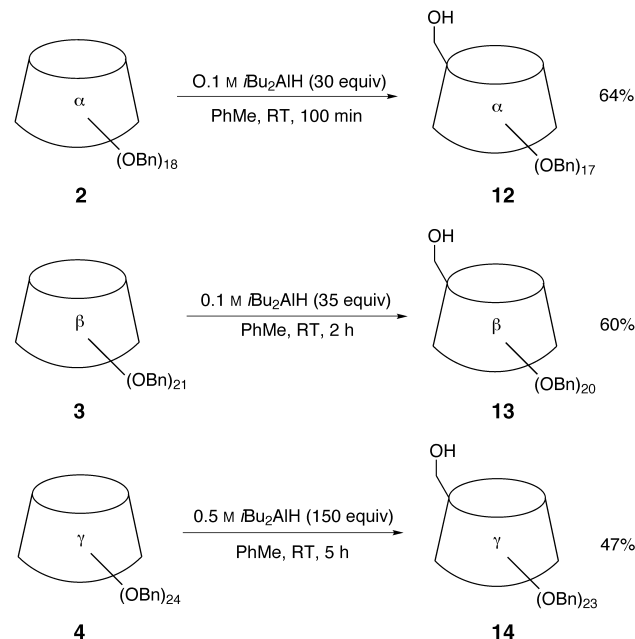
Scheme 5. Postulated mechanism of the DIBAL-promoted de-*O*-benzylation.

Careful modification of the reaction conditions also allowed access to products of mono-de-*O*-benzylation. Thus, when α -CD(OBn)₁₈ (**2**) was treated with excess DIBAL under



Scheme 6. AD-modified cyclodextrins. Reagents: a) NaH, allylBr, DMF, RT; b) 6 mol % $[\text{Cl}_2(\text{PCy}_3)_2\text{Ru}=\text{CHPh}]$, PhH, 60 °C, 4 h; c) Pd/C, EtOAc, MeOH, RT, 48 h, quant; d) NaH, MeI, DMF, RT.

dilute conditions at room temperature we isolated the mono-debenzylated product **12**^[16] in 64 % yield together with **5** (21 %) and recovered **2** (13 %) (Scheme 7). Using these



Scheme 7. DIBAL-promoted regioselective mono-de-O-benzoylation occurs exclusively at the primary torus of CDs.

conditions, the β -CD(OBn)₂₁ (**3**) gave the mono-debenzylated product **13** in 60 % yield together with diol **6** (27 %) and recovered starting material **3** (12 %). Finally, in the case of γ -CD(OBn)₂₄ (**4**), DIBAL-promoted debenzoylation gave the alcohol **14** in 47 % yield along with diol **9** (25 %) and recovered **4** (10 %).

In conclusion we have demonstrated that DIBAL-promoted de-O-benzoylation of perbenzylated cyclodextrins occurs with remarkably high regioselectivity, giving access to either mono-6-O-debenzylated or AD-di-O-debenzylated derivatives, which are selectively protected for direct further functionalization. This very simple method gives access to

large quantities of selectively modified cyclodextrins suitable for advanced applications. We are currently exploring further applications of this powerful de-O-alkylation process.

Experimental Section

DIBAL (62.0 mL, 93.0 mmol, 1.5 M in toluene) was added to a stirred solution of **3** (2.0 g, 0.7 mmol) in anhydrous toluene (140 mL) at room temperature under argon. The reaction mixture was heated at 30 °C for 2 h, after which time TLC (EtOAc/cyclohexane = 1/3) indicated no starting material (R_f = 0.5) but a major product (R_f = 0.3). The mixture was cooled to 0 °C, water (100 mL) was carefully added dropwise, and the mixture was stirred vigorously at room temperature for 15 min. The mixture was filtered (Celite) into a separating funnel washing thoroughly with hot EtOAc (3 × 200 mL). The organic layer was washed with brine (150 mL), dried (MgSO₄), filtered, and the solvent was removed in vacuo. The residue was purified by flash chromatography (eluent gradient, 20–25 % EtOAc in cyclohexane) to afford **6** as a colorless foam (1.6 g, 83 %), $[\alpha]_D^{25} = +34$ (c = 1.0 in CHCl₃); ¹H NMR (400 MHz, CDCl₃, 25 °C, TMS): δ = 5.61 (d, ³J(1,2) = 3.7 Hz, 1H; H-1), 5.56 (d, ³J(1,2) = 3.8 Hz, 1H; H-1), 5.04 (d, ³J(1,2) = 3.5 Hz, 1H; H-1), 5.02 (d, ³J(1,2) = 3.4 Hz, 1H; H-1), 5.00 (d, ³J(1,2) = 4.0 Hz, 1H; H-1), 4.98 (d, ³J(1,2) = 3.7 Hz, 1H; H-1), 4.89 (d, ³J(1,2) = 3.3 Hz, 1H; H-1), 2.78 (brs, 1H; OH), 2.69 (brs, 1H; OH); ¹³C NMR (100 MHz, CDCl₃, 25 °C, TMS): δ = 99.2, 99.1, 98.4, 98.2, 98.0, 97.6, 97.4 (7 × d, 7C; C-1A-G), 69.3, 69.15, 69.1, 69.0, 68.7 (5 × t, 5C; C-6BCEFG), 61.5 (2 × t, 2C; C-6AD); MS (FAB): m/z (%): 2868.1 (100) $[\text{MNa}^+]$.

Received: May 30, 2000 [Z15199]

- [1] G. Wenz, *Angew. Chem.* **1994**, *106*, 851; *Angew. Chem. Int. Ed. Engl.* **1994**, *33*, 803–822.
- [2] S. Li, W. C. Purdy, *Chem. Rev.* **1992**, *92*, 1457–1470.
- [3] R. Breslow, S. D. Dong, *Chem. Rev.* **1998**, *98*, 1997–2011.
- [4] K. Takahashi, *Chem. Rev.* **1998**, *98*, 2013–2033.
- [5] K. Uekama, F. Hirayama, T. Irie, *Chem. Rev.* **1998**, *98*, 2045–2076.
- [6] a) A. R. Khan, P. Forgo, K. J. Stine, V. T. D'Souza, *Chem. Rev.* **1998**, *98*, 1977–1996; b) A. P. Croft, R. A. Bartsch, *Tetrahedron* **1983**, *39*, 1417–1474; c) R. Breslow, J. W. Canary, M. Varney, S. T. Waddell, D. Yang, *J. Am. Chem. Soc.* **1990**, *112*, 5212–5219; d) I. Tabushi, K. Yamamura, T. Nabeshima, *J. Am. Chem. Soc.* **1984**, *106*, 5267–5270; e) I. Tabushi, K. Shimokawa, K. Fujita, *Tetrahedron Lett.* **1977**, 1527–1530.
- [7] The classical acetolysis of primary benzyl ethers has been applied to perbenzylated CDs, see: P. Angibeaud, J.-P. Utille, *Synthesis* **1991**, 737–738.
- [8] M. Sollogoub, S. K. Das, J.-M. Mallet, P. Sinaÿ, *C. R. Acad. Sci. Ser. 2* **1999**, 441–448.
- [9] T. Sato, H. Nakamura, Y. Ohno, T. Endo, *Carbohydr. Res.* **1990**, *199*, 31–35.
- [10] De-O-alkylation of ethers using TIBAL or DIBAL has been reported, see: E. Winterfeldt, *Synthesis* **1975**, 617–630. Indeed, when **2** was treated with TIBAL in toluene at 55 °C de-O-benzoylation to **5** also occurred but in only 52 % yield—hence all de-O-benzoylations have been performed with DIBAL.
- [11] H.-J. Schneider, F. Hacket, V. Rüdiger, *Chem. Rev.* **1998**, *98*, 1755–1785.
- [12] a) T. Tanimoto, M. Tanaka, T. Yuno, K. Koizumi, *Carbohydr. Res.* **1992**, *223*, 1–10; b) T. Tanimoto, T. Sakaki, K. Koizumi, *Chem. Pharm. Bull.* **1993**, *41*, 866–869; c) G. O. Aspinall, L. Khondo, J. A. Kinnear, *Carbohydr. Res.* **1988**, *179*, 211–221; d) G. O. Aspinall, R. C. Carpenter, L. Khondo, *Carbohydr. Res.* **1987**, *165*, 281–298.
- [13] P. Garegg, B. Samuelsson, *J. Chem. Soc. Perkin Trans. 1* **1980**, 2866–2869.
- [14] Initial hydride transfer is illustrated to occur from the *i*Bu group, consistent with the tentative observation of isobutene evolution when DIBAL is added to the reaction mixture.
- [15] R. H. Grubbs, S. Chang, *Tetrahedron* **1998**, *54*, 4413–4450.
- [16] Previously prepared by multistep synthesis during the de novo synthesis of α -CD: Y. Takahashi, T. Ogawa, *Carbohydr. Res.* **1987**, *169*, 127–149.

Experimental Charge Densities of Semiconducting Cage Structures Containing Alkaline Earth Guest Atoms**

Anders Bentien, Anders E. C. Palmqvist, J. Daniel Bryan, Susan Lattner, Galen D. Stucky, Lars Furenliid, and Bo B. Iversen*

Semiconducting clathrate structures (Figure 1) have recently stimulated much interest as potential thermoelectric energy converters.^[1] A large number of elemental compositions can form clathrate type I structures, and frameworks of most Group 3, 4, and 5 elements have been made with guests from groups 1, 2, and 7.^[2] Common to most of the compositions is the sum of the number of valence electrons of the elements present (184 e). Several studies have shown that the

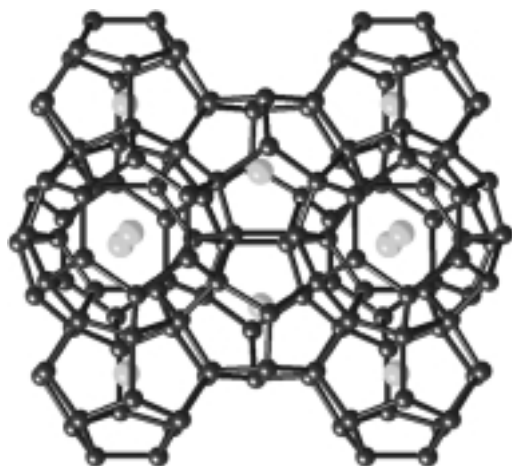


Figure 1. The clathrate type I structure. The two types of cages, the 20-atom dodecahedron and the 24-atom tetrakaidecahedron, are present in a 2:6 ratio in the unit cell. The guest atoms are located at (0,0,0) in the small cage, M(1), and at (1/4, 1/2, 0) in the large cage, M(2).

[*] Dr. B. B. Iversen, A. Bentien

Department of Chemistry
University of Aarhus
8000 Aarhus (Denmark)
Fax: (+45) 86196199
E-mail: bo@kemi.aau.dk

Dr. A. E. C. Palmqvist

Department of Applied Surface Chemistry
Chalmers University of Technology
412 96 Göteborg (Sweden)

J. D. Bryan, S. Lattner, Prof. G. D. Stucky
Department of Chemistry, University of California
Santa Barbara, CA 93106 (USA)

Dr. L. Furenliid

Department of Radiology and Optical Sciences Center
University of Arizona, Tucson, AZ 85724 (USA)

[**] Work at the X10c beamline at NSLS was supported by the Division of Materials Sciences of the US Department of Energy (DE-AC02-98CH10886). B.B.I. and A.E.C.P. gratefully acknowledge support from the Danish and Swedish Research Councils (SNF, TFR, STINT). This work was partially supported by the Office of Naval Research (G.D.S., J.D.B., S.L., A.E.C.P.), and it made use of MRL Central Facilities supported by the National Science Foundation under Award No. DMR96-32716. Dr. R. L. Paul of NIST is thanked for the Cold Neutron Prompt Gamma Ray Activation Analysis.

weakly bound guest atoms can exhibit extreme motion inside the oversized cavities.^[3] This motion contributes to the reduction of the thermal conductivity of the clathrate materials, which is important for obtaining a high thermoelectric figure of merit (ZT).^[4] Owing to the compositions of known clathrates there is a general belief that the guest atoms donate valence electrons to the framework atoms. Theoretical calculations surprisingly show that, contrary to common belief, the Sr guest atoms in $\text{Sr}_8\text{Ga}_{16}\text{Ge}_{30}$ appear neutral.^[5] Clearly, it is important that this intriguing theoretical suggestion is validated by experiment. It is the subtle features of the host–guest interactions in framework materials, which to a large extent determine their highly desirable properties. Herein, we examine the structures, oxidation states, and host–guest interactions in two promising clathrates, $\text{Sr}_8\text{Ga}_{16}\text{Ge}_{30}$ and $\text{Ba}_8\text{Ga}_{16}\text{Ge}_{30}$, based on analysis of the X-ray electron density by using the maximum entropy method (MEM-ED analysis), and X-ray absorption near-edge structure (XANES) studies.

Figures 2 and 3 show the Sr K and the Ba L_{III} X-ray absorption edges for $\text{Sr}_8\text{Ga}_{16}\text{Ge}_{30}$ and $\text{Ba}_8\text{Ga}_{16}\text{Ge}_{30}$, respectively. The Sr in $\text{Sr}_8\text{Ga}_{16}\text{Ge}_{30}$ has a broad absorption edge with an energy similar to that of elemental Sr, and about 7 eV lower in energy than that of Sr^{II} in $\text{Sr}(\text{OH})_2 \cdot 8\text{H}_2\text{O}$. The Ge K-edge energy in $\text{Sr}_8\text{Ga}_{16}\text{Ge}_{30}$ is equal to that of elemental Ge and 5 eV lower than in GeO_2 , whereas the Ga K-edge is 1 eV higher than for elemental Ga and 4 eV lower than for Ga_2O_3 . In contrast to Sr in $\text{Sr}_8\text{Ga}_{16}\text{Ge}_{30}$, the Ba in $\text{Ba}_8\text{Ga}_{16}\text{Ge}_{30}$ appears positively charged with an edge energy close to that of Ba^{II} in BaO. The Ge and Ga edges in $\text{Ba}_8\text{Ga}_{16}\text{Ge}_{30}$ have approximately the same values as in $\text{Sr}_8\text{Ga}_{16}\text{Ge}_{30}$. In summary the XANES data indicate that in $\text{Ba}_8\text{Ga}_{16}\text{Ge}_{30}$ the guest atoms donate electrons, whereas they appear more neutral in $\text{Sr}_8\text{Ga}_{16}\text{Ge}_{30}$. However, the different behavior of the guest atoms does not lead to appreciable differences in the framework absorption spectra within the resolution of the present experiments.

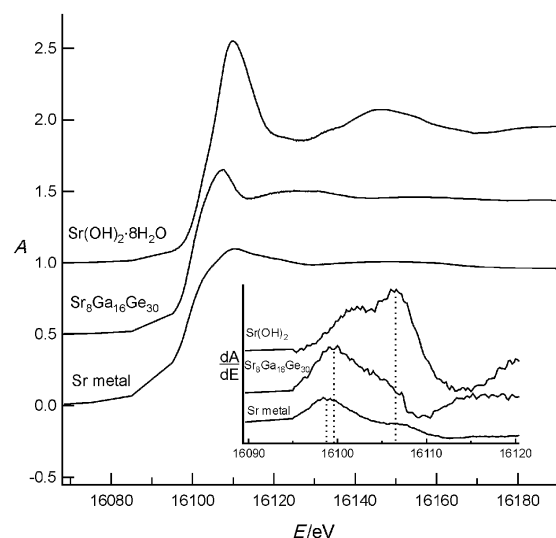


Figure 2. Sr K-edge XANES spectra of Sr metal, $\text{Sr}_8\text{Ga}_{16}\text{Ge}_{30}$, and $\text{Sr}(\text{OH})_2 \cdot 8\text{H}_2\text{O}$. The abscissa shows the normalized absorption (A). The insert shows the derivative curves used to determine the edge energies (16099, 16100, and 16107 eV).

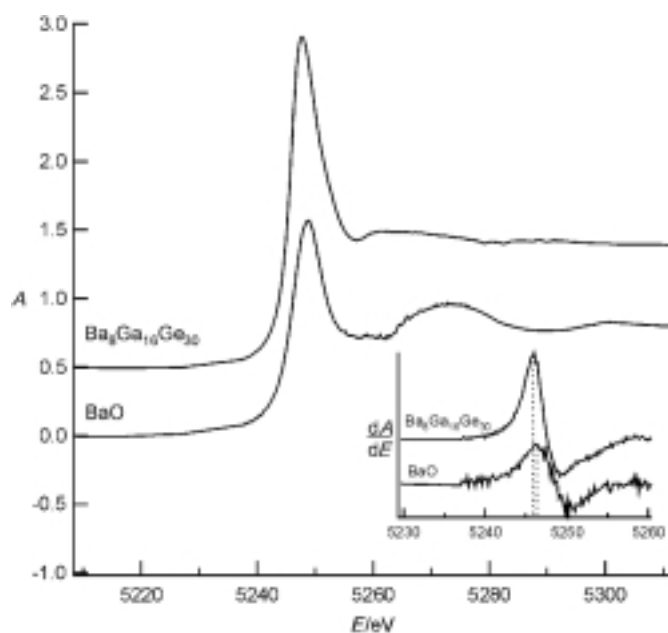


Figure 3. Ba L_{III} -edge XANES spectra of $Ba_8Ga_{16}Ge_{30}$ and BaO. The edge energy is 5246 eV for both samples.

The most conspicuous feature of the MEM-ED data of $Sr_8Ga_{16}Ge_{30}$ is the abnormally large smearing of the Sr(2) density. This feature must be due to large thermal motion or disorder of the Sr(2) guest atom, which is convoluted on the static density to give the smeared MEM density. In a single-crystal neutron diffraction study of $Sr_8Ga_{16}Ge_{30}$, Chakoumakos et al. found that the Sr(2) site is best modeled with four disordered sites.^[6] Figure 4a shows the MEM deformation density (DD) of $Sr_8Ga_{16}Ge_{30}$. The insert shows the DD in the (100) plane, and it clearly reveals the Sr(2) disorder in the form of a torus-shaped density. It appears that the four-site disorder model is too simple an approximation for Sr(2). The MEM DD also suggests that the Sr(1) site is disordered. Figure 4b shows the MEM DD of $Ba_8Ga_{16}Ge_{30}$. Even though the Ba(2) guest atom is also diffuse compared with the other atoms in the structure, it has not been possible with least-squares modeling to refine a disordered Ba(2) site. However, the DD shows that the Ba(2) atom is disordered over four sites. As for $Sr_8Ga_{16}Ge_{30}$ there is furthermore evidence for disorder on the Ba(1) site. It is a virtue of the MEM that disorder does not need to be modeled explicitly. This makes it a strong tool in many materials research applications.

Theoretical calculations by Blake et al. suggest that the Sr atoms in $Sr_8Ga_{16}Ge_{30}$ are close to neutral and thus presumably have limited electronic interaction with the framework.^[5] It is, however, very difficult to unambiguously define an atomic charge, and many definitions of atomic charge are in common use.^[7] Attempts to refine monopolar charges on the atoms were unsuccessful. On the other hand the MEM-ED may allow an experimental estimation of the atomic charges by comparing the MEM densities with the nonuniform prior densities. These densities were constructed from assemblies of harmonically vibrating, neutral atoms, and the differences between the nonuniform priors and the MEM densities therefore provide an indication of the charge flow upon

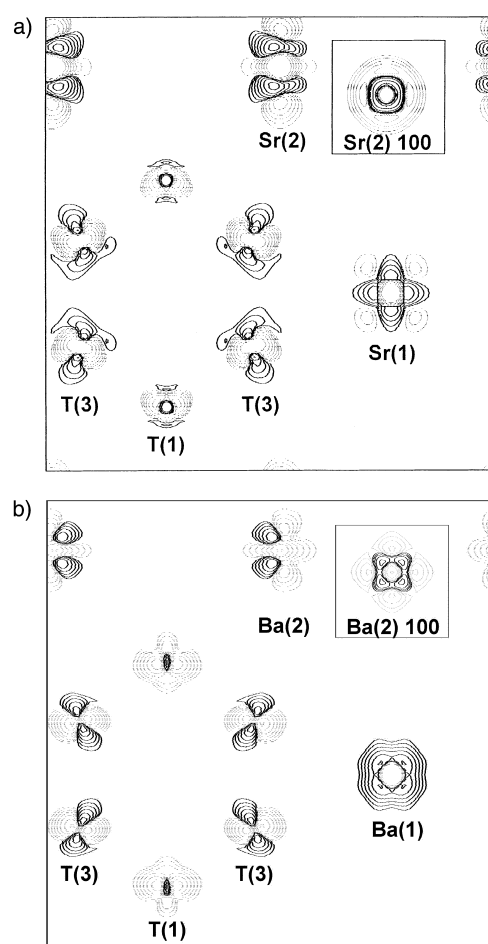


Figure 4. MEM deformation density, $\rho(\text{MEM}) - \rho(\text{reference})$, where the reference density is based on an independent atom model with ordered guest sites. a) $Sr_8Ga_{16}Ge_{30}$, and b) $Ba_8Ga_{16}Ge_{30}$ in the (001) plane through $z=0$. The origins have been shifted. The densities are plotted on logarithmic scales, 0.1×2^N . Solid contours are positive, dotted contours are negative. The inserts show the deformation densities in the (100) planes of the M(2) guest atoms.

formation of the solids. Figure 5 shows a plot of the integrated charges as a function of spherical integration radii for $Sr_8Ga_{16}Ge_{30}$. Unfortunately the Sr(1) charge estimate is strongly affected by the few low-order reflections which suffer from extinction, as well as by the exact site occupancy. We have tested a number of models with various degrees of occupancy on the guest sites. As for the extinction, it is mostly the Sr(1) charge estimate which is affected by changes in the occupancy.^[8] For comparison we have estimated atomic charges in NaF. It is notable that the method correctly retrieves positive Na and negative F, although the values are underestimated. In summary the MEM charge estimates support the XANES results with neutral Sr(2) atoms in $Sr_8Ga_{16}Ge_{30}$. However, owing to the combined effects of extinction and partial occupancy we have not been able to obtain reliable MEM charge estimates for Sr(1) and the Ba atoms in $Ba_8Ga_{16}Ge_{30}$.

The exact framework siting of the Ga and Ge atoms is known to be very important for the thermoelectric properties of clathrate materials.^[5] Refinement of framework occupancies results in random distributions for both compounds. This

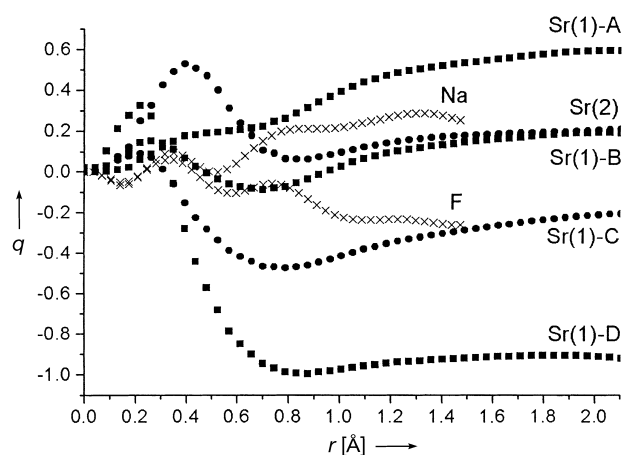


Figure 5. Spherical integration around the guest atom positions of the difference between the nonuniform prior density and the MEM density in $\text{Sr}_8\text{Ga}_{16}\text{Ge}_{30}$. For Sr(1) four charge estimates are shown. A) The five most extinction corrected data removed (006, 222, 035, 123, 004) and 100 % Sr(1) occupancy; B) as A) but refined Sr(1) occupancy (98.6 %); C) all data and refined Sr(1) occupancy; D) as A) but 95 % Sr(1) occupancy. For Sr(2) the charge estimate is nearly constant between models, and the plot is based on B). Results obtained from MEM analysis of literature data on NaF are also included.^[16] q = atomic charge; r = radius.

could be real, but it could also be because the difference between the Ga and Ge EDs in the clathrate is too small to distinguish. Differentiation between Ga and Ge may be further hindered if the Ga atoms receive electrons from the guest atoms. Figure 6 shows the integrated difference density for the three framework sites. The plot shows that relative to

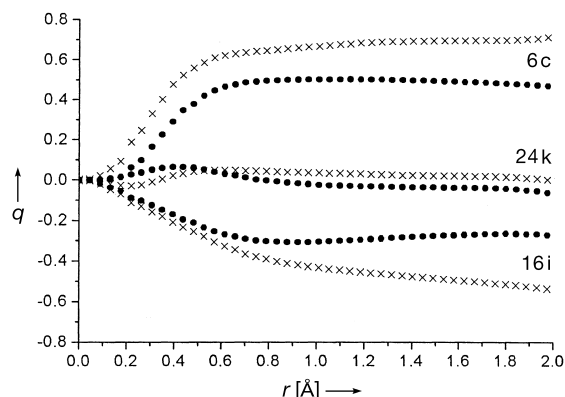


Figure 6. Spherical integration around the framework positions of the difference between nonuniform prior densities corresponding to random Ga/Ge distributions and the MEM densities. The crosses are $\text{Sr}_8\text{Ga}_{16}\text{Ge}_{30}$ and the circles $\text{Ba}_8\text{Ga}_{16}\text{Ge}_{30}$. For $\text{Sr}_8\text{Ga}_{16}\text{Ge}_{30}$ the framework atoms are located at 6c(0.25, 0, 0.5), 16i(0.18913, 0.18913, 0.18913), and 24k(0, 0.30914, 0.11731). q = atomic charge; r = radius.

the reference models having random distributions of neutral Ga and Ge atoms, the 6c sites are depleted of electrons and the 16i sites have a charge accumulation. This indicates that Ga preferentially occupies the non-tetrahedral 6c sites (6-rings), and avoids the tetrahedral 16i sites. This siting also leads to fewer Ga–Ga contacts, which have been shown by theory to be energetically unfavorable.^[5] The plot suggests that the difference from a random siting model is smaller for

$\text{Ba}_8\text{Ga}_{16}\text{Ge}_{30}$ than for $\text{Sr}_8\text{Ga}_{16}\text{Ge}_{30}$. This indirectly supports the XANES data, which show that Ba is more positively charged in the clathrates than Sr.

It is clear that the host–guest interactions in these clathrate materials are highly tunable and are a key ingredient for the understanding of thermoelectric and transport properties. The present study demonstrates the ability of framework structures to selectively modify the chemical behavior of guest species. Such abilities are widely used in, for example, zeolite catalysts, but it appears that the chemistry of guest species trapped in framework systems is richer than conventionally believed based on simple chemical arguments. The fact that the guest atoms are not fully ionized and may have partial occupancy also suggests that the framework can have a range of Ga/Ge compositions.

Experimental Section

Synthesis: In a high-purity Ar-filled dry box, stoichiometric amounts of alkaline earth element (Cerac, >99.7 % purity) and Ge (Cerac, >99.999 % purity) were placed in a quartz tube along with a large excess of Ga (Cerac, 99.99 % purity). The reaction mixtures were heated at 3.0 K min^{-1} to 1100°C and held at this temperature for one hour. The reactions were then cooled at 0.3 K min^{-1} to their respective melting points. Each reaction was then annealed for 100 h at 10°C below their melting point. After the annealing procedure each reaction was cooled at 1 K min^{-1} to room temperature. The air-stable crystal/gallium matrix was removed from the quartz tubes and placed in an evaporating dish on a hot plate to keep the gallium molten. The crystals were then plucked out of the liquid gallium with tweezers and placed into a bath of concentrated hydrochloric acid for several days to dissolve the remaining gallium.

The composition of single crystals of $\text{Sr}_8\text{Ga}_{16}\text{Ge}_{30}$ and $\text{Ba}_8\text{Ga}_{16}\text{Ge}_{30}$ was determined by electron microprobe analysis using a Cameca SX-50 with standard settings. Calibration was made by using geologic mineral standards of known composition and elemental gallium (Cerac 99.999 %). The compositions by weight: $\text{Sr}_8\text{Ga}_{16}\text{Ge}_{30}$: 17.13 % Sr, 27.33 % Ga, 56.01 % Ge; $\text{Ba}_8\text{Ga}_{16}\text{Ge}_{30}$: 25.25 % Ba, 24.55 % Ga, 49.64 % Ge. This correlates to $\text{Sr}_{7.73}\text{Ga}_{15.50}\text{Ge}_{30.50}$ and $\text{Ba}_{8.16}\text{Ga}_{15.63}\text{Ge}_{30.36}$, respectively. An error of no greater than 3.4 % from the ideal 8:16:30 stoichiometry is observed for the Sr clathrate and 2.3 % for the Ba clathrate. The observed error is a result of slight deviations in the take-off-angle of the emitted X-rays from the near orthogonal crystal faces sampled. This stoichiometry gives 183.96 and 184.65 valence electrons for the Sr and Ba clathrates, respectively, and thus the structures are believed to be free of defects.

Cold neutron gamma ray activation analysis provided by the National Institute of Standards and Technology (NIST) was used to monitor hydrogen absorption of the $\text{Sr}_8\text{Ga}_{16}\text{Ge}_{30}$ clathrate during the isolation procedure. Samples isolated by acid dissolution of the Ga flux were compared to a control sample isolated by sonication in the absence of acid. Emission of gamma rays, monitored by a high-purity germanium detector, allows the de-excitation of the complex nuclei formed from the neutron capture event. The control sample measured $0.018(5) \text{ counts s}^{-1}$, while the sample isolated from acid measured $0.013(3) \text{ counts s}^{-1}$. These results indicate that no hydrogen is present within any of the samples.

X-ray absorption spectroscopy: XANES measurements were carried out at beamline X10C at the NSLS, Brookhaven National Laboratory. The K-edges of Ga, Ge, and Sr, and the L_{III} edge of Ba, were studied in transmission mode on powdered samples evenly smeared on to scotch tapes, which were folded into eight layers to ensure even sample distributions without pinholes. Elemental as well as oxidized standards (Sr, $\text{Sr}(\text{OH})_2 \cdot 8\text{H}_2\text{O}$, BaO, Ga, Ga_2O_3 , Ge, and GeO_2) were used as references for the photon energy scales at the absorption edges, which were scanned by using 0.2 eV steps. The elemental Sr was sealed under argon in aluminized Mylar film. The data were analyzed by using the MacXAFS3.6 software package,^[9] and absorption edge energies were determined at the maximum values of the derivatives of the absorption curves.

X-ray diffraction: Tube measurements were done at room temperature on a Bruker SMART CCD diffractometer ($\text{MoK}\alpha$). Data collection and integration was carried out with the SMART software. Averaging and empirical absorption corrections were carried out with SADABS.^[10] Least-squares refinements were made with programs LINEX^[11] and XD^[12] in the space group $Pm\bar{3}n$. For both structures free refinement of framework atom occupancies resulted in random distributions of Ga and Ge atoms. Refinement of guest atoms occupancies showed all sites to be fully occupied except Sr(1), which refined to 98.6(4) % occupancy. In both refinements anisotropic thermal parameters were employed on all atoms as well as isotropic extinction parameters. For $\text{Sr}_8\text{Ga}_{16}\text{Ge}_{30}$ a split-atom model was used for Sr(2) as in reference [6] ($(x, y, z) = (0, 0.4784, 0.9784)$). $\text{Sr}_8\text{Ga}_{16}\text{Ge}_{30}$ [$\text{Ba}_8\text{Ga}_{16}\text{Ge}_{30}$]: $a = 10.740(2)$ [10.785(2)] Å, $V = 1238.7(1)$ [1254.4(1)] Å³, $V_{\text{crystal}} = 0.0004$ [0.0003] mm³, $\rho_{\text{calc}} = 5.354$ [5.791] g cm⁻³, $\lambda = 0.7107$ Å, $(\sin\theta/\lambda)_{\text{max}} = 0.923$ [0.836] Å⁻¹, $\mu_1 = 345$ [322] cm⁻¹, T_{max} , $T_{\text{min}} = 0.2060$, 0.0883 [0.2534, 0.1132], no. of measured reflections = 35927 [54576], no. of unique = 691 [558], $R_{\text{w}}(\text{int}) = 0.0451$ [0.0361], $N_{\text{obs}} = 691$ [558] ($I > 0\sigma(I)$), $N_{\text{par}} = 19$ [16], GOF = 0.40 [0.52], $R_{\text{F}} = 0.0256$ [0.0170], $R_{\text{wF}} = 0.0254$ [0.0169], $Y_{\text{min}}(\text{extinction}) = 0.79$ [0.81] (10 and 8 reflections have $Y < 0.95$). Further details on the crystal structure investigations may be obtained from the Fachinformationszentrum Karlsruhe, 76344 Eggenstein-Leopoldshafen, Germany (fax: (+49) 7247-808-666, on quoting the depository numbers CSD-411062 ($\text{Sr}_8\text{Ga}_{16}\text{Ge}_{30}$) and CSD-411063 ($\text{Ba}_8\text{Ga}_{16}\text{Ge}_{30}$)).

MEM calculations: Absorption, extinction, and anomalous dispersion-corrected observed structure factors phased and scaled with program XD were used for MEM calculations with the MEED program.^[13] The calculations employed nonuniform prior densities obtained by a structure factor aliasing procedure^[14] proposed by Roversi et al.^[15] This method is superior to straightforward Fourier transformation, which gives series termination ripples. In the present calculations 28 structure factor copies were used with a cut-off value of 10^{-9} . The nonuniform priors correspond to the EDs of assemblies of neutral atoms having anisotropic harmonic thermal motion. This means that the observed data are used to estimate the effects of chemical bonding, charge transfer, and disorder. For $\text{Sr}_8\text{Ga}_{16}\text{Ge}_{30}$ the MEM density was almost unchanged between calculations with nonuniform priors having ordered and disordered (i.e. split) Sr(2) sites. In all MEM calculations a $128 \times 128 \times 128$ pixel grid was used and iterations were stopped at $\chi^2 = 1$. Estimated standard uncertainties on the structure factors were obtained from the data averaging procedure.

Received: December 21, 1999

Revised: August 3, 2000 [Z14432]

- [1] F. J. DiSalvo, *Science* **1999**, 285, 703–706.
- [2] a) J. S. Kasper, P. Hagenmuller, M. Pouchard, *Science* **1965**, 150, 1713–1714; b) v. H. Menke, H. G. von Schnering, *Z. Anorg. Allg. Chem.* **1973**, 395, 223–238; c) B. Eisenmann, H. Schäfer, R. Zagler, *J. Less-Comm. Met.* **1986**, 118, 43–55.
- [3] B. C. Sales, B. C. Chakoumakos, D. Mandrus, J. W. Sharp, *J. Solid State. Chem.* **1999**, 146, 528–532.
- [4] The thermoelectric figure of merit is defined as $ZT = TS^2\sigma/\kappa$, where S is the Seebeck coefficient, σ the electrical conductivity, and κ the thermal conductivity.
- [5] N. P. Blake, L. Møllnitz, G. Kresse, H. Metiu, *J. Chem. Phys.* **1999**, 111, 3133–3144.
- [6] B. C. Chakoumakos, B. C. Sales, D. G. Mandrus, G. S. Nolas, *J. Alloys Compd.* **2000**, 296, 80–86.
- [7] P. Coppens, *X-ray charge densities and chemical bonding*, Oxford University Press, Oxford, **1997**.
- [8] The occupancy of the guest sites can only be less than 100%, and thus partial occupancy on Sr(2) can only make the charge estimate more negative. Changing the occupancy on Sr(2) has little effect on the charge estimate, but for Sr(1) it alters the estimate significantly. However, changes in the Sr(1) occupancy also degrades the crystallographic R factors (e.g. $R(F^2) = 0.0274$ (95%), $R(F^2) = 0.0256$ (98.6%)).
- [9] MacXAFS3.6 Software Package, C. E. Bouldin, W. T. Elam, L. Furenli, *Physica B* **1995**, 208, 190–192.

- [10] Owing to the enormous redundancy of the data, empirical absorption corrections were found to give much better results than corrections based on approximate analytical crystal shapes.
- [11] P. Coppens, Program LINEX, Department of Chemistry, State University of New York at Buffalo, New York 14260, **1974**.
- [12] T. Koritsanszky, S. T. Howard, P. R. Mallison, Z. Su, T. Richter, N. K. Hansen, Program XD, Institute of Crystallography, Freie Universität, Berlin, Germany, **1999**. The program was locally modified to handle atoms with $Z > 36$ by Dr. Piero Macchi.
- [13] S. Kumazawa, Y. Kubota, M. Takata, M. Sakata, Y. Ishibashi, *J. Appl. Crystallogr.* **1993**, 26, 453–457.
- [14] A. Bentien, Program ASF, Department of Chemistry, University of Aarhus, 8000 Aarhus C, Denmark, **2000**.
- [15] P. Roversi, J. J. Irwin, G. Bricogne, *Acta Crystallogr. Sect. A* **1998**, 54, 971–996.
- [16] C. J. Howard, R. D. G. Jones, *Acta Crystallogr. Sect. A* **1977**, 33, 776.

Self-Assembly of Pentameric Porphyrin Light-Harvesting Antennae Complexes**

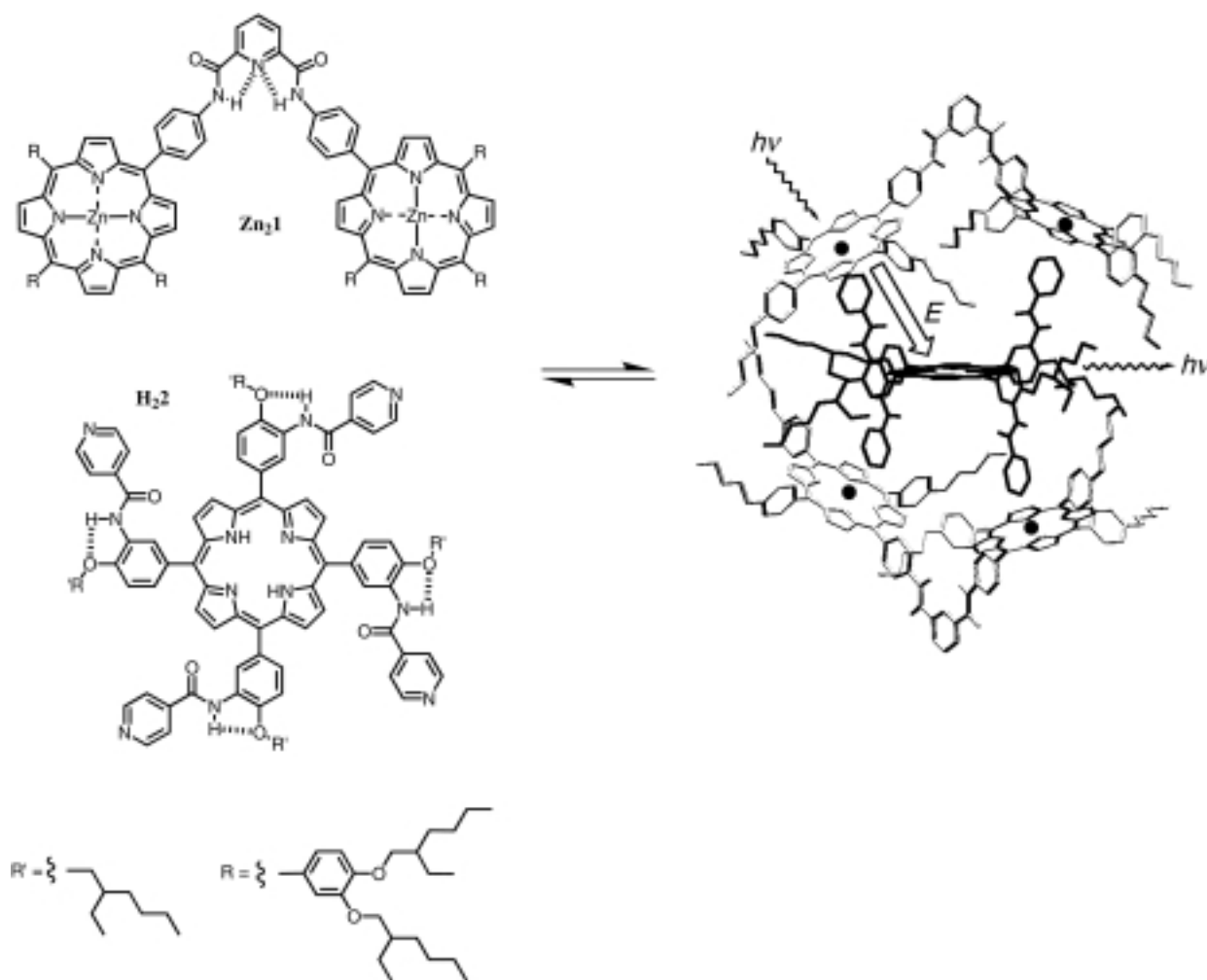
Richard A. Haycock, Arkady Yartsev, Ulrike Michelsen, Villy Sundström, and Christopher A. Hunter*

The reaction centers of natural photosynthetic systems are excited indirectly through their light-harvesting antennae complexes.^[1–3] These units contain a network of chromophores which absorb light energy and channel this very efficiently by singlet energy transfer to the photochemical reaction centres.^[4, 5] The photochemical properties of porphyrins lend themselves to the design of artificial organic antennae systems,^[6] and covalently linked arrays of five or more porphyrins have been constructed.^[7–10] We demonstrate here that cooperative self-assembly processes are ideally suited to the construction of stable structurally well-defined chromophore arrays for use as antennae systems.^[11, 12]

Zn₂1 and **H₂2** were designed to be perfectly complementary, preorganized partners for the self-assembly process shown in Scheme 1.^[13] Intramolecular hydrogen bonds constrain both molecules to essentially one conformation, thus minimizing the loss of rotational entropy upon binding. The spacing of the coordination sites ensures that **Zn₂1** will coordinate to the *trans-meso* ligands across the face of **H₂2** with no strain in the final complex.^[14] The central free-base porphyrin is encapsulated in a spherical array of four zinc

[*] Prof. C. A. Hunter, Dr. R. A. Haycock, Dr. U. Michelsen
 Krebs Institute for Biomolecular Science
 Department of Chemistry
 University of Sheffield
 Sheffield S3 7HF (UK)
 Fax: (+44) 114-273-8673
 E-mail: C.Hunter@shef.ac.uk
 Dr. A. Yartsev, Prof. V. Sundström
 Department of Chemistry
 University of Lund
 Lund (Sweden)

[**] We thank the EPSRC (R.A.H.) and the Lister Institute (C.A.H.) for funding. V.S. and A.Y. thank the Swedish NFR and the K&A Wallenberg Foundation for financial support.



Scheme 1. Self-assembly of a 2:1 complex from **Zn₂₁** and **H₂₂**. The molecular mechanics model of the complex shows the observed photoinduced energy transfer from the outer antennae zinc porphyrins to the central free-base porphyrin.

porphyrins, and this arrangement should funnel energy absorbed by the outer pigments into the center of the complex.

Both compounds were prepared on gram scales by using the procedures of Lindsey and Wagner for the synthesis of the corresponding nitroporphyrins,^[15] followed by reduction with SnCl_2 , amide coupling, and metalation.^[16] Mixing **Zn₂₁** and **H₂₂** in organic solvents resulted in the formation of a stable complex, which was characterized by using a range of spectroscopic techniques. The ^1H NMR spectrum of a 2:1 mixture of **Zn₂₁** and **H₂₂** shows large complexation-induced changes in the chemical shifts for the signals corresponding to the pyridyl protons of **H₂₂**: upfield shifts of 5.8 and 2.5 ppm for the signals corresponding to the α and β protons, respectively, are diagnostic of pyridine ligands fully coordinated to the face of a metalloporphyrin.^[12] A characteristic red-shift in the Soret band of the UV/Vis absorption spectrum of **Zn₂₁** on addition of half an equivalent of **H₂₂** indicates the formation of a fully-bound zinc porphyrin–pyridine complex at micromolar concentrations.^[12] UV/Vis absorption spectroscopy was used to monitor a titration of **H₂₂** into a solution of **Zn₂₁** (Figure 1). A stoichiometry of 2:1 with two identical

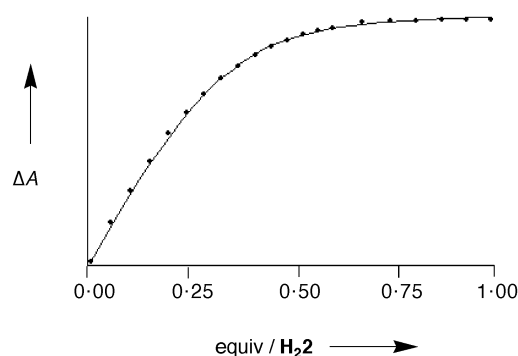


Figure 1. UV/Vis titration data for addition of **H₂₂** to **Zn₂₁** ($1.5 \times 10^{-6} \text{ M}$) in dichloromethane (arbitrary vertical scale). The calculated line is the best fit 2:1 binding isotherm used to determine the association constant.

binding sites is the only isotherm that will fit the data, and the microscopic association constant for each binding event is $2.0 \pm 0.5 \times 10^6 \text{ M}^{-1}$, which reflects the significant cooperativity in the formation of multiple binding interactions compared with a single zinc–pyridine coordination interaction ($K \sim 10^3 \text{ M}^{-1}$).^[12]

Mass spectrometric studies (ES-MS, FAB-MS, and matrix-assisted laser desorption/ionization (MALDI)) all failed to reveal the presence of complexes: only the free components could be detected in mixtures. However, vapour pressure osmometry (VPO) of a 2:1 mixture of **Zn₂1** and **H₂2** at millimolar concentrations in chloroform consistently gave a molecular weight of 7330 ± 700 , which confirmed the presence of a 2:1 complex (molecular weight = 7720). The pure components **Zn₂1** and **H₂2** do not self-associate in isolation, and give VPO molecular weights of 2890 ± 180 (**Zn₂1** = 3056) and 1640 ± 140 (**H₂2** = 1608), respectively, under the same conditions. The only structure that is consistent with all of this evidence is the porphyrin pentamer shown in Scheme 1.

The photochemical properties of the assembly were investigated using fluorescence titrations (Figure 2). **H₂2** can be selectively excited at 520 nm, but it is not possible to selectively excite **Zn₂1**. Emission from **H₂2** can be selectively

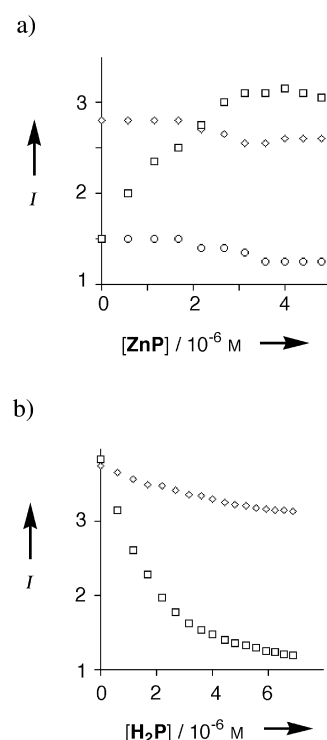
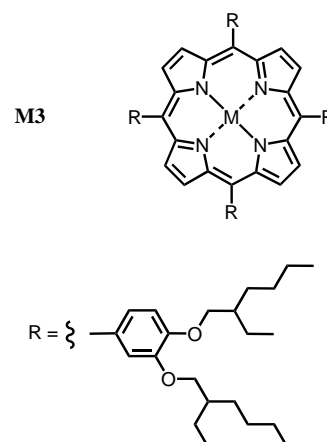


Figure 2. Fluorescence titration data in dichloromethane (fluorescence intensity *I* is an arbitrary scale): a) Addition of zinc porphyrins to **H₂2** (2.0×10^{-6} M). □: **ZnP** = **Zn₂1**: Simultaneous excitation of both chromophores at 560 nm and emission from **H₂2** at 720 nm. ◇: **ZnP** = **Zn₂1**: selective excitation of **H₂2** at 520 nm and emission from **H₂2** at 720 nm. ○: **ZnP** = **Zn₃**: Simultaneous excitation of both chromophores at 560 nm and emission from **H₂2** at 720 nm. b) Addition of free base porphyrins to **Zn₂1**. ◇: **H₂P** = **H₂3**: Simultaneous excitation of both chromophores at 560 nm and emission from **Zn₂1** at 600 nm. □: **H₂P** = **H₂2**: Simultaneous excitation of both chromophores at 560 nm and emission from **Zn₂1** at 600 nm.

detected at 720 nm, and emission from **Zn₂1** can be selectively detected at 600 nm. When **Zn₂1** was added to **H₂2** and both chromophores were simultaneously excited at 560 nm, the intensity of the **H₂2** emission at 720 nm increased until two equivalents of **Zn₂1** had been added (Figure 2a). However when **H₂2** was preferentially excited at 520 nm, there was no change in the fluorescence intensity at 720 nm on addition of

Zn₂1. To prove that this behavior is a property of the complex in Scheme 1 we also investigated the titration of a monomeric zinc porphyrin which does not form stable complexes at micromolar concentrations (**Zn3**) into **H₂2**. Addition of **Zn3** caused no change in the intensity of the **H₂2** emission at



720 nm when both chromophores were simultaneously excited at 560 nm (Figure 2a). The reverse titration data are shown in Figure 2b. Addition of **H₂2** to **Zn₂1** caused a 70 % decrease in the intensity of the **Zn₂1** emission at 600 nm when both chromophores were simultaneously excited at 560 nm. When an unfunctionalized free-base porphyrin, which can not form intermolecular complexes (**H₂3**) was used in place of **H₂2**, the decrease in the intensity of the **Zn₂1** emission arising from competitive absorption was very small. We conclude therefore that the formation of the 2:1 complex in Scheme 1 quenches the **Zn₂1** fluorescence and enhances the **H₂2** emission as a result of energy transfer from the antennae zinc porphyrins to the free-base core of the complex.

Time-resolved experiments using streak-camera fluorescence measurements were undertaken to determine the rate of energy transfer (Figure 3). In pure samples, the fluorescence decay time of **Zn₂1** is 1330 ± 20 ps, and the fluorescence

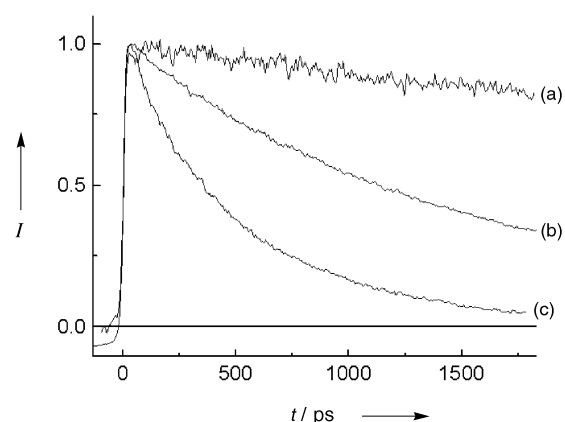


Figure 3. Fluorescence decay profiles (excitation at 562 nm) showing normalized fluorescence intensity (*I*) as a function of time (*t*): a) emission from **H₂2** at 650 nm; b) emission from **Zn₂1** at 650 nm; c) emission from a 2:1 mixture of **Zn₂1** and **H₂2**.

decay time for **H₂2** is 9500 ± 100 ps. For the 2:1 complex, the zinc porphyrin was preferentially excited at 562 nm, and the decay of the excited state monitored at 600 nm where only the zinc porphyrins emit was nonexponential. A simple model which assumes there are two independent processes for deactivation of the zinc porphyrin excited state, fluorescence (with a lifetime of 1330 ps as observed for **Zn₂1**) and energy transfer, fits the fast part of the decay well and gives an energy-transfer time of 490 ps. The intensity of the 720 nm emission from **H₂2** was too weak to extract reliable kinetic parameters for the increase in fluorescence.^[17] Thus the rate of the energy-transfer process illustrated in Scheme 1 is 2×10^9 s⁻¹. These rate constants give a quantum yield for energy transfer of 73 %, which is in good agreement with the steady-state experiments.^[18]

In conclusion, self-assembly offers a relatively straightforward method for the construction of large multi-chromophore arrays with extremely well-defined three-dimensional structures. The system described here functions as a simple light-harvesting antennae system which funnels incident excitation energy into the center of the complex, but other more sophisticated arrangements may be envisaged.

Received: May 12, 2000 [Z15118]

- [1] a) S. M. Prince, M. Z. Papiz, A. A. Freer, G. McDermott, A. M. Hawthornwaite-Lawless, R. J. Cogdell, N. W. Isaacs, *J. Mol. Biol.* **1997**, *268*, 412–423; b) G. McDermott, S. M. Prince, A. A. Freer, A. M. Hawthornwaite-Lawless, M. Z. Papiz, R. J. Cogdell, N. W. Isaacs, *Nature* **1995**, *374*, 517–521.
- [2] J. Dissenhofer, O. Epp, K. Miki, R. Huber, H. Michel, *Nature* **1985**, *318*, 618–624.
- [3] G. Feher, J. P. Allen, M. Y. Okamura, D. C. Rees, *Nature* **1989**, *339*, 111–116.
- [4] R. Van Grondelle, J. P. Dekker, T. Gillbro, V. Sundström, *Biochim. Biophys. Acta* **1994**, *1187*, 1–65.
- [5] T. Pullerits, V. Sundström, *Acc. Chem. Res.* **1996**, *29*, 381–389.
- [6] a) A. Harriman, *Supramolecular Photochemistry*, (Ed.: V. Balzani), Reidel, Dordrecht, **1987**, pp. 207–238; b) J. K. M. Sanders in *Comprehensive Supramolecular Chemistry*, Vol. 9 (Ed.: J. L. Atwood), Pergamon, Oxford, **1997**, pp. 131–164.
- [7] a) J. Seth, V. Palaniappan, T. E. Johnson, S. Prathapan, J. S. Lindsey, D. E. Bocian, *J. Am. Chem. Soc.* **1994**, *116*, 10578–10592; b) J. Z. Li, A. Ambroise, S. I. Yang, J. R. Diers, J. Seth, C. R. Wack, D. F. Bocian, D. Holten, J. S. Lindsey, *J. Am. Chem. Soc.* **1999**, *121*, 8927–8940; c) D. Kuciauskas, P. A. Liddell, S. Lin, T. E. Johnson, S. J. Weghorn, J. S. Lindsey, A. L. Moore, T. A. Moore, D. Gust, *J. Am. Chem. Soc.* **1999**, *121*, 8604–8614.
- [8] a) T. Nagata, A. Osuka, K. Marayuma, *J. Am. Chem. Soc.* **1990**, *112*, 3054–3059; b) A. Nakano, A. Osuka, I. Yamazaki, T. Yamazaki, Y. Nishimura, *Angew. Chem.* **1998**, *110*, 3172–3176; *Angew. Chem. Int. Ed.* **1998**, *37*, 3023–3027.
- [9] H. A. M. Biemans, A. E. Rowan, A. Verhoeven, P. Vanoppen, L. Latterini, J. Foekema, A. P. H. Schenning, E. W. Meijer, F. C. de Schryver, R. J. M. Nolte, *J. Am. Chem. Soc.* **1998**, *120*, 11054–11060.
- [10] P. N. Taylor, H. L. Anderson, *J. Am. Chem. Soc.* **1999**, *121*, 11538–11545.
- [11] a) S. Anderson, H. L. Anderson, J. K. M. Sanders, *Acc. Chem. Res.* **1993**, *26*, 469–475; b) S. Anderson, H. L. Anderson, A. Bashall, M. McPartlin, J. K. M. Sanders, *Angew. Chem.* **1995**, *107*, 1196; *Angew. Chem. Int. Ed. Engl.* **1995**, *34*, 1096–1099.
- [12] a) C. A. Hunter, L. D. Sarson, *Angew. Chem.* **1994**, *106*, 2424–2427; *Angew. Chem. Int. Ed. Engl.* **1994**, *33*, 2313–2316; b) X. Chi, A. J. Guerin, R. A. Haycock, C. A. Hunter, L. D. Sarson, *J. Chem. Soc. Chem. Commun.* **1995**, 2567–2569; c) C. A. Hunter, R. H. Hyde, *Angew. Chem.* **1996**, *108*, 2064–2067; *Angew. Chem. Int. Ed. Engl.* **1996**, *35*, 1936–1939.
- [13] A related architecture was reported by J. N. H. Reek, A. P. H. Schenning, A. W. Bosman, E. W. Maijer, M. J. Crossley, *Chem. Commun.* **1998**, 11–12.
- [14] The porphyrin *meso* substituents are depicted in an $\alpha\beta\alpha\beta$ conformation, but exchange between different atropisomers is fast (on the seconds timescale), and so they equilibrate rapidly to the most stable arrangement for complexation. Models suggest that while **Zn₂1** could coordinate across two *cis-meso* ligands, this arrangement is less favorable than the *trans* structure shown in Scheme 1.
- [15] J. S. Lindsey, R. W. Wagner, *J. Org. Chem.* **1989**, *54*, 828–836.
- [16] We used racemic 2-ethylhexyl substituents to solubilize **H₂2**, so the compound is actually a mixture of diastereoisomers. However, the chiral centers are sufficiently far away from the sites of interaction that no adverse consequences are observed, and the solubility of the porphyrin is dramatically improved. We have also prepared a diastereomeric mixture of the 2-ethylhexyl analogue of **Zn₂1**, and the behavior of this system is identical to the *n*-pentyl-solubilized compound. **Zn₂1**: ¹H NMR (250 MHz, CDCl₃): δ = 1.0 (102 H, m), 1.50 (132 H, m), 1.80 (6 H, quin), 1.90 (6 H, quin), 3.95 (12 H, d), 4.15 (12 H, d), 7.20 (6 H, d), 7.70 (6 H, d), 7.75 (6 H, s), 8.30 (8 H, m), 8.75 (3 H, d), 9.05 (16 H, m), 10.00 (2 H, s); MS (+ve FAB) *m/z* calcd for C₁₉₁H₂₅₁N₁₁O₁₄Zn: 3055.91; found: 3057 [MH⁺]; elemental analysis calculated for C₁₉₁H₂₅₁N₁₁O₁₄Zn: C 75.07, H 8.28, N 5.04%; found: C 75.03, H 8.26, N 4.84%; m.p. 235–237 °C; λ_{max} (ϵ): 425.6 (7.52×10^5), 550.4 (4.97×10^4), 590.4 nm (1.72×10^4). **H₂2**: ¹H NMR (250 MHz, CDCl₃): δ = 2.75 (2 H, s), 1.00 (36 H, m), 1.50 (44 H, m), 2.00 (4 H, quin), 4.25 (8 H, d), 7.35 (4 H, d), 7.8 (8 H, d), 7.90 (4 H, dd), 8.80 (8 H, d), 9.0 (12 H, s), 9.45 (4 H, m); MS (+ve FAB) *m/z* calcd for C₁₀₀H₁₁₀N₁₂O₈: 1608.04; found: 1608 [M⁺]; accurate mass (+ve FAB) calculated mass for C₁₀₀H₁₁₀N₁₂O₈: 1607.864785; found: 1607.857164 (+7.6 mDa, +4.7 ppm). Elemental analysis calcd for C₁₀₀H₁₁₀N₁₂O₈·H₂O: C 73.84, H 6.94, N 10.33%; found C 73.94, H 6.89, N 10.48%; m.p. > 298 °C; λ_{max} (ϵ): 424.5 (3.39×10^5), 519.0 (1.82×10^4), 556.0 (1.14×10^4), 593.0 (6.10×10^3), 649.0 nm (5.50×10^3). **Zn3**: ¹H NMR (250 MHz, CDCl₃): δ = 8.95 (8 H, s), 7.80 (4 H, s), 7.70 (4 H, d), 7.23 (4 H, d), 4.20 (8 H, d), 4.00 (8 H, d), 1.2–2.1 (64 H, m), 0.8–1.19 (48 H, m); MS (+ve FAB) *m/z* calcd for C₁₀₈H₁₅₆N₄O₈Zn: 1703.44; found: 1703 [M⁺]; m.p. 141.8 °C; λ_{max} (ϵ): 426.0 (2.30×10^5), 553.0 (2.20×10^4), 594.0 nm (7.05×10^4).
- [17] The emission from **H₂2** at 720 nm is complicated by the dynamics in the red wing of the decaying fluorescence of **Zn₂1**. Qualitatively, there was a rise component in the fluorescence at 720 nm, which is consistent with the 500 ps time scale determined from the decay in the signal at 600 nm, but the fluorescence of **H₂2** at 720 nm was too weak relative to the intense **Zn₂1** fluorescence to extract reliable kinetic parameters.
- [18] Quantum yield of energy transfer = $k(\text{energy transfer})/[k(\text{energy transfer}) + k(\text{fluorescence})]$.

A Refined Model for $[\text{Fe}_3\text{S}_4]^0$ Clusters in Proteins**

Detlef Bentrup, Ivano Bertini,* Marco Borsari, Grazia Cosenza, Claudio Luchinat, and Yohei Niikura

In 1987 Mössbauer spectra of the $[\text{Fe}_3\text{S}_4]^0$ center in *Desulfovibrio gigas* ferredoxin II (*Dg* Fd II) were interpreted in terms of a pair of $\text{Fe}^{2.5+}$ ions and a single Fe^{3+} ion. The two $\text{Fe}^{2.5+}$ ions were shown to possess a ground-state subspin $S_{12} = 9/2$, which is antiferromagnetically coupled to the $S_3 = 5/2$ of the Fe^{3+} ion. The overall ground-state spin is thus $S' = 2$.^[1] Similar results were obtained for the $[\text{Fe}_3\text{S}_4]^0$ cluster of *Azotobacter vinelandii* Fd (*Av* Fd) at high and low pH.^[2]

Analogous analyses were performed on $[\text{Fe}_4\text{S}_4]^{3+}$ and $[\text{Fe}_4\text{S}_4]^+$ clusters containing a pair of $\text{Fe}^{2.5+}$ ions and two Fe^{3+} ions or two Fe^{2+} ions, respectively.^[3, 4] The ^1H NMR resonance signals of the cysteine ligands bound to the cluster exhibit hyperfine shifts that were shown to be related to the oxidation state of the iron center to which the cysteine is bound.^[5, 6] By exploiting the high-resolution and sensitivity of NMR spectroscopy it was found that the various iron centers are not equivalent. This was attributed to equilibria between forms with different charge locations within the cluster.^[7]

Several attempts have been made to study $[\text{Fe}_3\text{S}_4]^0$ cluster containing proteins by ^1H NMR spectroscopy, but no resonance signals from the $\beta\text{-CH}_2$ protons of the cluster cysteine ligands could be detected.^[7–12] The Fe_7S_8 ferredoxin from *Bacillus schlegelii* (*Bs* Fd), containing one $[\text{Fe}_3\text{S}_4]$ and one $[\text{Fe}_4\text{S}_4]$ cluster, was labeled with deuterated cysteine groups.^[13] The ^2H nucleus has a magnetogyric ratio that is 6.5 times smaller than that of the ^1H nucleus and the resonance lines should be 42 times narrower. Therefore, if paramagnetism is responsible for proton line broadening beyond detection, then the narrower ^2H signals should be detected. This was not the case.^[13] Although based on only negative evidence, it was proposed that the line broadening beyond detection might be because of chemical exchange, that is that the exchange of valence between $\text{Fe}^{2.5+}$ and Fe^{3+} could occur with a rate constant of the order of the expected hyperfine shift difference (about 10^5 – 10^6 s $^{-1}$).

The $[\text{Fe}_3\text{S}_4]^0$ clusters are formally derived from the so-called “cubane” $[\text{Fe}_4\text{S}_4]^{2+}$ cluster by removal of one Fe^{2+} ion. As one

vertex of the cubane is deprived of an iron atom, only one of the four sulfide ions ($\mu_3\text{-S}$ ion) bridges three iron centers, while the other three sulfide ions ($\mu\text{-S}$ ions) each bridge two iron centers. Realizing that the reduction of the $[\text{Fe}_3\text{S}_4]^0$ cluster at physiological pH requires a proton,^[14–17] and following the idea that the proton could bind to any of the three $\mu\text{-S}$ ions,^[2, 16–19] we propose the hypothesis that the proton could jump among the $\mu\text{-S}$ ions at the above rate and provide the required exchange mechanism. To demonstrate this model, we planned an NMR experiment at pH > 9, that is, well above the pK_a for the release of H^+ ions. Under these conditions, the mechanism responsible for the proton exchange within the reduced $[\text{Fe}_3\text{S}_4]$ cluster is deactivated, and the ^1H NMR signals should appear. A relatively low magnetic field of 4.7 T (200 MHz proton resonance frequency) was chosen to minimize the adverse effect of Curie line broadening, which is predicted to be sizable for a high-spin ($S' = 2$) metal cluster.^[20]

The *Bs* ferredoxin was characterized during this work by electrochemical measurements. The potential for the one-electron reduction and reoxidation of the $[\text{Fe}_3\text{S}_4]^+$ cluster is -337 mV at pH 7.2. The pH dependence is very similar to that of the homologous *A. vinelandii* ferredoxin I (*Av* Fd I).^[15] The slope $\text{d}E^{\text{red}}_{\text{obs}}/\text{d}(\text{pH})$ in the linear part of the pH dependence curve is -51 mV (pH unit) $^{-1}$ (-53 mV (pH unit) $^{-1}$ for *Av* Fd I), close to the -59 mV (pH unit) $^{-1}$ predicted for the coupling of the one-electron transfer to the transfer of a single proton. Fitting^[15, 21] of the pH dependence data gave $E^{\text{red}}_{\text{alk}} = -390$ mV and $\text{pK}_a = 8.1$ at 293 K; the corresponding values for native *Av* Fd I at 273 K are -430 mV and 7.7, respectively.^[15]

The paramagnetic ^1D ^1H NMR spectrum of concentrated *Bs* Fd (ca. 8 mM), reduced at pH 9.7 with sodium dithionite shows, besides some resonance signals shifted downfield in the $\delta = 10$ – 50 region (Figure 1A), a broad signal at $\delta = 60$

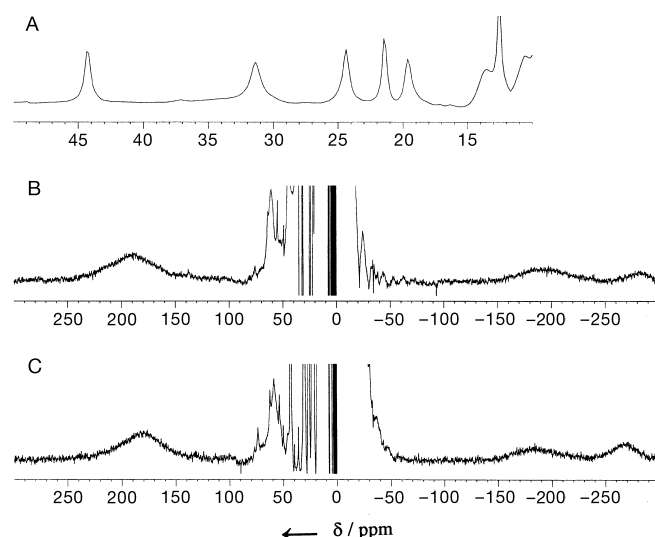


Figure 1. 200 MHz ^1H NMR spectra of dithionite-reduced *Bs* Fd at pH 9.7 (200 mM borate/NaOH buffer). A) spectrum at 297.3 K showing the $\delta = 10$ – 50 region containing the resonance signals of the cysteine ligands of the $[\text{Fe}_4\text{S}_4]^+$ cluster. B) Spectrum at 297.3 K showing the spectral window from $\delta = -310$ to 300 containing resonances from the cysteine ligands of the $[\text{Fe}_3\text{S}_4]^0$ cluster. C) The same sample and window as in B) but at 306.8 K.

[*] Prof. I. Bertini, Dr. D. Bentrup,^[+] G. Cosenza, Prof. C. Luchinat, Y. Niikura
Magnetic Resonance Center
University of Florence
Via L. Sacconi 6, 50019 Sesto Fiorentino (Italy)
Fax: (+39)055-4209271
E-mail: bertini@cerm.unifi.it

Prof. M. Borsari
Department of Chemistry, University of Modena
Via Campi 183, 41100, Modena (Italy)

[+] Present address: Physiologie II, Universität Tübingen
Ob dem Himmelreich 7, 72074 Tübingen (Germany)

[**] This work was supported by MURST (ex 40%) and by the European Union through the Large Scale Facility Parabio (ERBFM-GECT950033) and the HCM Network (ERBCHRXCT040626). We are grateful to Prof. S. Aono for the use of the expression system of the *B. schlegelii* ferredoxin.

and three extremely broad signals at $\delta = 190$, -192 , and -282 (Figure 1B). A search for further signals shifted beyond $\delta = 200$ or -300 gave negative results. The shifts of the four hyperfine shifted signals show a Curie-type temperature dependence (Figure 1C). The intensity ratio of the three most shifted signals is approximately 2:1:1. These signals must be attributed to the cysteine residues coordinated to the $[\text{Fe}_3\text{S}_4]^0$ cluster, which to the best of our knowledge have never been observed before.

From established models based on exchange coupling among the three iron centers,^[1, 2] the two upfield signals at $\delta = -192$ and -282 in Figure 1B correspond to the $\beta\text{-CH}_2$ protons of the cysteine residue coordinated to the Fe^{3+} ion. The signal shifted downfield at $\delta = 190$ has a relative intensity of 2, thus it could be assigned to the two $\beta\text{-CH}_2$ protons of one of the two cysteine units ligated to the mixed-valence pair of iron centers. The resonance signals of two more $\beta\text{-CH}_2$ protons are expected to be shifted even further and broadened, and therefore can not be observed.^[13] A modest inequivalence of the two mixed-valence iron centers may be present, as suggested by the NMR spectra^[8, 11, 22] of the oxidized form,^[8, 11, 22] which lacks the cluster-bound proton over the pH range of interest. If the four downfield-shifted signals are pairwise inequivalent, only the less shifted and less broadened pair would be observed. The resonance signal at $\delta = 60$ can be assigned tentatively to a $\text{H}\alpha$ proton of one the cysteine ligands bound to the mixed-valence pair of iron centers, presumably of the cysteine that gives rise to the most shifted resonance signal.

The present experiments are relevant to the biochemical behavior of the $[\text{Fe}_3\text{S}_4]^0$ cluster, and account for the Mössbauer and NMR spectroscopy data reported. The Mössbauer data indicate the presence of an Fe^{3+} ion and a pair of $\text{Fe}^{2.5+}$ ions.^[1, 2] The NMR data at neutral pH are consistent with the presence of a chemical exchange process with a rate constant of the order of $10^5\text{--}10^6\text{ s}^{-1}$ ^[13] which wipes out the NMR signals. Electrochemistry shows that at neutral pH the uptake of the electron is associated with the uptake of a proton. Consistent with results from magnetic circular dichroism (MCD) and circular dichroism (CD) experiments,^[15–17, 23] and following suggestions of Armstrong and co-workers that the protonation occurs at one of the three $\mu\text{-S}$ ions^[15] and that “wherever the proton is bound to the cluster, it can be moved easily...”,^[19] a reasonable model emerges (Figure 2) in which 1) each of the three $\mu\text{-S}$ ions is protonated for a fraction of time (including the $\mu\text{-S}_1$ that has been proposed to be the gateway for proton exchange^[18, 19, 24]); 2) the protonated $\mu\text{-S}$ ion determines the location of the mixed-valence pair as being the two iron centers that are bridged by that sulfide. The exchange of a proton among the three $\mu\text{-S}$ ions determines the interchange of the valences of each iron; 3) the NMR signals of the cysteine ligands coordinated to each iron jump by hundreds of ppm from upfield to downfield because of this valence interchange, and are exchange-broadened beyond detection if the exchange occurs with a rate constant of $10^5\text{--}10^6\text{ s}^{-1}$.

At a pH higher than the pK_a value the proton is released, and the ^1H NMR signals appear in the far-shifted regions. The signals are still broad and shifted strongly because of the

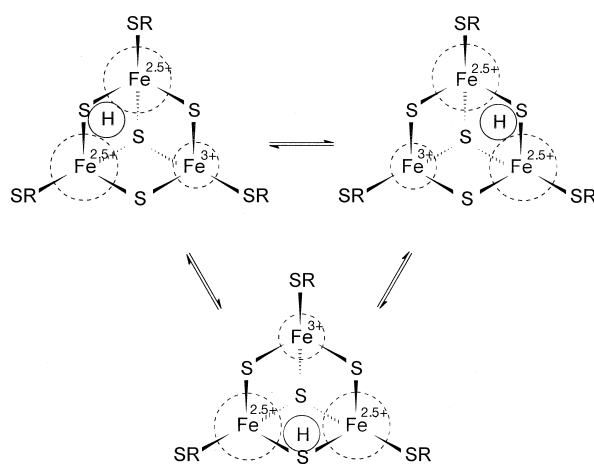


Figure 2. Schematic model of the proton–electron exchange in the low-pH form of the $[\text{Fe}_3\text{S}_4]^0$ cluster. According to this model, 1) the cluster is protonated at one of the three $\mu\text{-S}$ ions; 2) the mixed-valence pair is the one bridged by the protonated $\mu\text{-S}$ ion; 3) each of the three $\mu\text{-S}$ ions is protonated for a fraction of time; 4) the proton jumps from one $\mu\text{-S}$ ion to another at a rate of $10^5\text{--}10^6\text{ s}^{-1}$, thereby causing a “merry-go-round” of iron valences in the cluster.

high resulting total spin state $S' = 2$ and large hyperfine coupling constants. The resulting picture at high pH values is that of a cluster with a single valence distribution. This is in contrast to the $[\text{Fe}_4\text{S}_4]^{3+}$ clusters which show fast exchange equilibria on the NMR time scale.^[7]

Experimental Section

The Fe_7S_8 Fd from *Bs*^[25] was reduced with a small amount of solid sodium dithionite (Fluka) under an argon atmosphere at pH 9.7 in $\text{H}_3\text{BO}_3/\text{NaOH}$ buffer (200 mM) and 99% D_2O .

The ^1D ^1H NMR spectra of reduced *Bs* Fd were recorded at 297.3 and 306.8 K on a wide-bore Bruker MSL 200 spectrometer with a superWEFT pulse sequence (180-tau-pulse-acquisition).^[26] The maximum spectral window of 125 kHz was applied.

Voltammetric measurements were carried out at 293 K with solutions containing $100\text{ }\mu\text{M}$ of *Bs* Fd and 0.1 M NaCl in buffers of different pH values (5.9–10.1) using a standard three-electrode cell in a procedure already described.^[21]

Received: December 21, 1999

Revised: July 6, 2000 [Z 15020]

- [1] V. Papaefthymiou, J.-J. Girerd, I. Moura, J. J. G. Moura, E. Münck, *J. Am. Chem. Soc.* **1987**, *109*, 4703–4710.
- [2] Z. G. Hu, D. Jollie, B. K. Burgess, P. J. Stephen, E. Münck, *Biochemistry* **1994**, *33*, 14475–14485.
- [3] L. Noodleman, *Inorg. Chem.* **1988**, *27*, 3677–3679.
- [4] J. Jordanov, E. K. H. Roth, P. H. Fries, L. Noodleman, *Inorg. Chem.* **1990**, *29*, 4288–4292.
- [5] E. Babini, I. Bertini, M. Borsari, F. Capozzi, A. Dikiy, L. D. Eltis, C. Luchinat, *J. Am. Chem. Soc.* **1996**, *118*, 75–80.
- [6] I. Bertini, F. Briganti, C. Luchinat, L. Messori, R. Monnanni, A. Scozzafava, G. Vallini, *Eur. J. Biochem.* **1992**, *204*, 831–839.
- [7] L. Banci, I. Bertini, S. Ciurli, S. Ferretti, C. Luchinat, M. Piccioli, *Biochemistry* **1993**, *32*, 9387–9397.
- [8] A. L. Macedo, P. N. Palma, I. Moura, J. LeGall, V. Wray, J. J. G. Moura, *Magn. Reson. Chem.* **1993**, *31*, 59–67.
- [9] H. Cheng, K. Grohmann, W. V. Sweeney, *J. Biol. Chem.* **1992**, *267*, 8073–8080.

- [10] K. Nagayama, D. Ohmori, Y. Imai, T. Oshima, *FEBS Lett.* **1983**, *158*, 208–212.
- [11] A. L. Macedo, I. Moura, J. J. G. Moura, J. LeGall, B. H. Huynh, *Inorg. Chem.* **1993**, *32*, 1101–1105.
- [12] C. M. Gorst, Y.-H. Yeh, Q. Teng, L. Calzolari, Z.-H. Zhou, M. W. W. Adams, G. N. La Mar, *Biochemistry* **1995**, *34*, 600–610.
- [13] I. Bertini, C. Luchinat, G. Mincione, A. Soriano, *Inorg. Chem.* **1998**, *37*, 969–972.
- [14] J. L. C. Duff, J. L. J. Breton, J. N. Butt, F. A. Armstrong, A. J. Thomson, *J. Am. Chem. Soc.* **1996**, *118*, 8593–8603.
- [15] B. Shen, L. L. Martin, J. N. Butt, F. A. Armstrong, C. D. Stout, G. M. Jensen, P. J. Stephens, G. N. La Mar, C. M. Gorst, B. K. Burgess, *J. Biol. Chem.* **1993**, *268*, 25928–25939.
- [16] M. K. Johnson, D. E. Bennett, J. A. Fee, W. V. Sweeney, *Biochim. Biophys. Acta* **1987**, *911*, 81–94.
- [17] P. J. Stephen, G. M. Jensen, F. Delvin, T. V. Morgan, C. D. Stout, B. K. Burgess, *Biochemistry* **1991**, *30*, 3200–3209.
- [18] C. D. Stout, *J. Biol. Chem.* **1993**, *268*, 25920–25927.
- [19] J. Hirst, J. L. C. Duff, G. N. L. Jameson, M. A. Kemper, B. K. Burgess, F. A. Armstrong, *J. Am. Chem. Soc.* **1998**, *120*, 7085–7094.
- [20] M. Gueron, *J. Magn. Reson.* **1975**, *19*, 58–66.
- [21] H. A. Azab, L. Banci, M. Borsari, C. Luchinat, M. Sola, M. S. Viezzoli, *Inorg. Chem.* **1992**, *31*, 4649–4655.
- [22] I. Bertini, A. Dikiy, C. Luchinat, R. Macinai, M. S. Viezzoli, M. Vincenzini, *Biochemistry* **1997**, *36*, 3570–3579.
- [23] S. E. Iismaa, A. E. Vazquez, G. M. Jensen, P. J. Stephen, J. N. Butt, F. A. Armstrong, B. K. Burgess, *J. Biol. Chem.* **1991**, *266*, 21563–21571.
- [24] H. Cheng, K. Grohmann, W. V. Sweeney, *J. Biol. Chem.* **1990**, *265*, 12388–12392.
- [25] S. Aono, S. Nakamura, R. Aono, I. Okura, *Biochem. Biophys. Res. Commun.* **1994**, *201*, 938–942.
- [26] T. Inubushi, E. D. Becker, *J. Magn. Reson.* **1983**, *51*, 128–133.

The Total Synthesis of the Annonaceous Acetogenin, Muricatetrocin C**

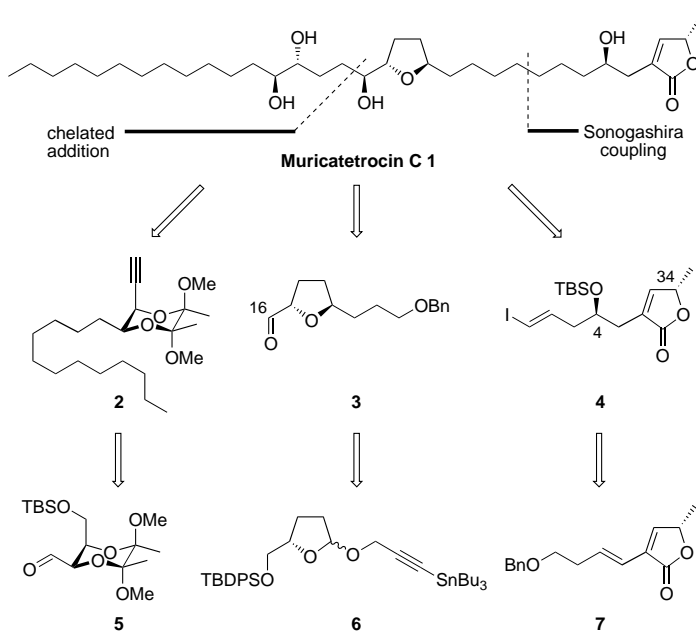
Darren J. Dixon, Steven V. Ley,* and Dominic J. Reynolds

The annonaceous acetogenins comprise a rapidly growing class of natural products exhibiting a broad spectrum of biological properties. These include antibacterial, antimalarial, in vivo antitumor, parasitocidal, and pesticidal effects.^[1] Perhaps most exciting is their novel and selective mode of action as inhibitors of oxidative phosphorylation, which offers a unique potential for these compounds as anticancer agents. The acetogenins are known to be powerful inhibitors of complex I (NADH:ubiquinone oxidoreductase) in mammalian and insect mitochondrial electron transport systems and

of NADH oxidase found in the plasma membranes of cancer cells.^[2,3] These actions lead to ATP deprivation and subsequent apoptosis.^[4] More recently the annonaceous acetogenins have also been shown to overcome resistance in multi-drug resistant (MDR) tumors.^[5] Thus, for the above reasons and by virtue of their limited availability from natural sources, these compounds have been targeted for total synthesis by a number of research groups.^[6]

In 1996 McLaughlin and co-workers reported the isolation of muricatetrocin C (**1**; see Scheme 1) from the leaves of *Rollinia mucosa*.^[7] The molecule exhibits potent inhibitory action against PC-3 prostatic adenocarcinoma, PACA-2 pancreatic carcinoma, and A-549 lung carcinoma. Herein we report the first total synthesis of **1**, which was achieved by using a highly convergent synthetic strategy.^[8]

The synthetic plan to **1** hinged on the enantioselective preparation of fragments **2**, **3**, and **4** and their subsequent coupling reactions (Scheme 1). It was believed that in

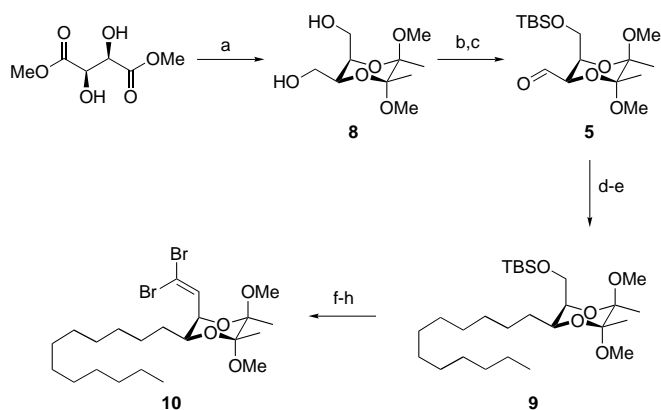


Scheme 1. Synthetic plan for **1**. Bn = benzyl, TBS = *tert*-butyldimethylsilyl, TBDPS = *tert*-butyldiphenylsilyl.

addition to allowing an efficient synthesis of **1**, these three components would provide an excellent platform for both the evolution of existing group methodology and the potential development of new synthetic tools. The key features of our approach are: the application of the recently reported (*R',R',R,S*)-2,3-butanediactal-protected butane tetrol **8** (see Scheme 2) as a building block for the *anti*-1,2-diol component **2** through selective chemical differentiation of the incongruous hydroxy termini;^[9] the use of the recently developed anomeric O–C rearrangement protocol for the stereoselective construction of the 2,5-*trans*-disubstituted THF ring component **3**;^[10] and finally the implementation of a new approach to the (*S*)-hydroxy-butenolide terminus **4**, using a hetero-Diels–Alder (HDA) reaction to simultaneously install the 1,5-stereochemical relationship and mask the butenolide double bond.

[*] Prof. Dr. S. V. Ley, Dr. D. J. Dixon, D. J. Reynolds
Department of Chemistry
University of Cambridge
Lensfield Road
Cambridge, CB2 1EW (UK)
Fax: (+44) 1223-336-442
E-mail: svl1000@cam.ac.uk

[**] We thank the EPSRC (D.J.D. and D.J.R.), the Novartis Research Fellowship (S.V.L.), and the BP Research Endowment (S.V.L.) for generous financial support for this work.



Scheme 2. Synthesis of fragment **10**, a fragment for **2**. a) Reference [9]; b) NaH, THF, 30 min, 20 °C then TBSCl, 1 h, 20 °C (72%); c) DMSO, (COCl)₂, CH₂Cl₂, -78 °C; NEt₃, -78 °C → 0 °C; d) CH₃(CH₂)₁₀PPh₃I, *n*BuLi, THF, 30 min, -78 °C (75%; two steps); e) RaNi, H₂, EtOH, 30 min, 20 °C; f) TBAF, THF, 2 h, 20 °C (93%, two steps); g) DMSO, (COCl)₂, CH₂Cl₂, -78 °C; NEt₃, -78 °C → 0 °C; h) PPh₃, CBr₄, CH₂Cl₂, 30 min, 0 °C (91%; two steps). TBSCl = *tert*-butyldimethylsilyl chloride, DMSO = dimethyl sulfoxide, RaNi = Raney nickel, TBAF = tetrabutylammonium fluoride.

With regard to the final steps of the synthesis, addition of the alkynyllithium reagent derived from **2** to the anomerically disposed aldehyde **3** was envisaged to introduce the remaining stereogenic center at C-16. Subsequent manipulation to unmask a terminal alkyne, would then allow a Sonogashira coupling with **4** to complete the carbon skeleton; upon selective hydrogenation and global deprotection this would afford the natural product **1**.

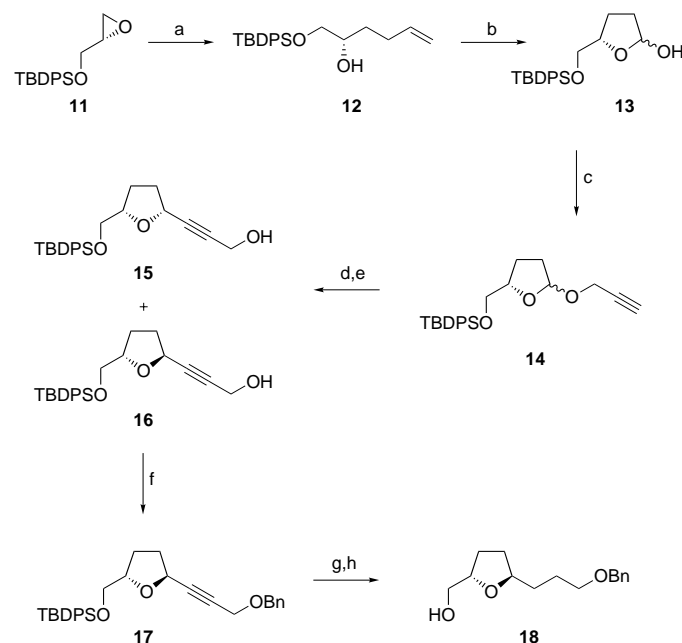
The synthesis of fragment **2** began with the easily accessible diol **8**, which was readily converted to the equatorial aldehyde **5** in two steps according to the previously established procedure (Scheme 2).^[9b] Subsequent Wittig reaction allowed introduction of an eleven-carbon side chain with moderate (1:4, *E/Z*) selectivity—for ease of characterization the unsaturation was removed at this stage by hydrogenation over Raney nickel to afford **9** in good yield (50%, four steps). Conversion to the vinyl dibromide required a further three steps; thus desilylation, Swern oxidation, then olefination according to the Corey–Fuchs procedure furnished **10** in 46% yield starting from **8**.^[11]

The 2,5-*trans*-disubstituted tetrahydrofuran unit **3** was then constructed by addition of allylmagnesium bromide to the least hindered end of *O*-silylated-(*R*)-glycidol **11**, which proceeded—in the presence of catalytic Li₂CuCl₄—in excellent yield (93%) (Scheme 3).^[12] Ozonolysis of the alkenol **12** to give the lactol **13**, followed by treatment of this crude material with an excess of propargyl alcohol and a catalytic amount of Amberlyst A15 in refluxing benzene afforded the rearrangement precursor **14** in 93% yield as a 1:1 mixture of anomers. With multigram quantities of the propargylic ether available, the anomeric O–C rearrangement was attempted following our original protocol.^[10a] Thus standard stannylation, followed by treatment of the resulting crude material with boron trifluoride diethyl etherate produced the rearranged species **16** and **15** in a combined yield of 85%, and in a 5.5:1 ratio favoring the *trans* product **16**. Subsequent benzy-

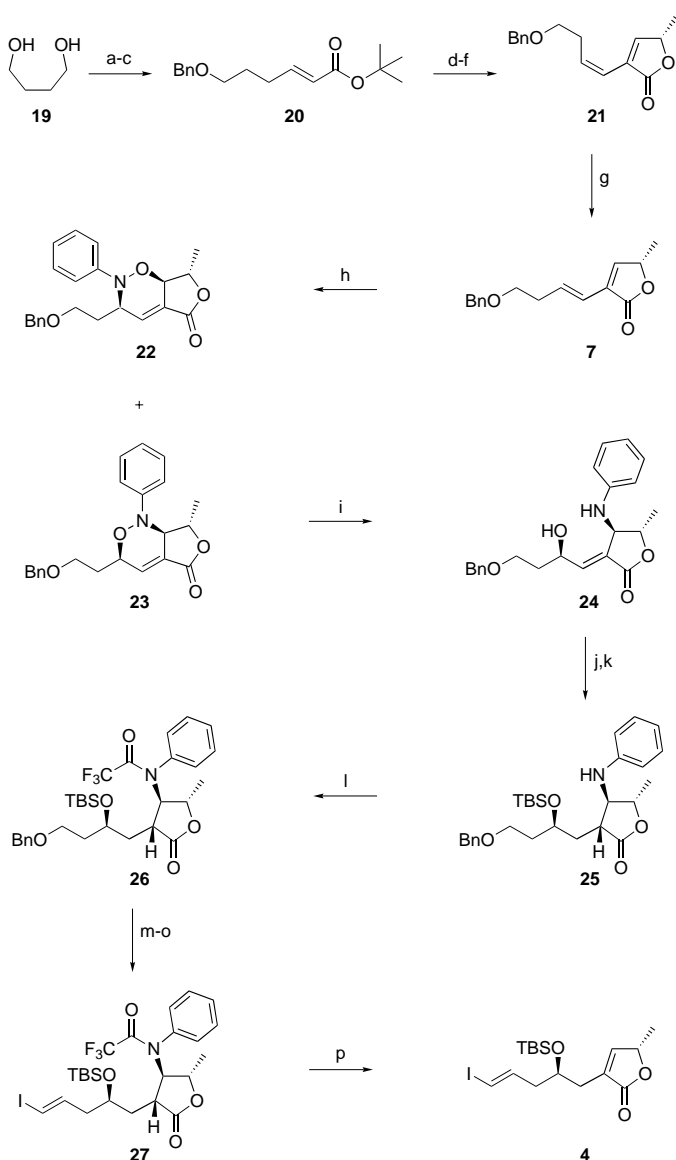
lation of the mixture allowed chromatographic separation to give diastereomerically pure material, **17** (80% yield) at this stage. Treatment of **17** with TBAF followed by selective hydrogenation of the alkyne over Raney nickel, gave **18**, a direct precursor to the desired coupling fragment **3**, in 89% yield.

With the two units **10** and **18** completed, the remaining butenolide fragment **4** was then investigated. It was envisaged that the 1,5-stereochemical relationship could be installed by a HDA reaction between diene **7** and nitrosobenzene. The required regioselectivity was predicted by frontier orbital calculations,^[13] whilst it was believed that unfavorable steric interaction between the aryl ring of the dienophile and the methyl substituent of **7** would deliver the necessary diastereoselectivity. Subsequent N–O bond cleavage followed by elimination of the aryl amine portion to reintroduce the butenolide unsaturation would permit elaboration to **4**.

Thus, starting with 1,4-butanediol **19**, monobenzylolation by trapping of the sodium anion precipitate of **19** with benzyl bromide, followed by tandem Swern–Wittig reaction afforded the α,β -unsaturated ester **20** in excellent yield (79%) over three steps (Scheme 4). Homo-enolate formation by deprotonation with LDA in the presence of HMPA,^[14] followed by quenching with (*S*)-(2)-(tert-butyldimethylsilyloxy)propanal,^[15] then subjection of the resulting crude oil to acidic methanol allowed cyclization to form a β -hydroxy- γ -lactone. Subsequent treatment with methanesulfonyl chloride and triethylamine afforded diene **21** in 60% yield, with a 6:1 (*Z/E*) selectivity at the external double bond. The desired *E* isomer



Scheme 3. Synthesis of fragment **18**, a precursor for **3**. a) allylMgBr, CuLi₂Cl₄, (10 mol %), THF, 2 h, -30 °C (93%); b) O₃, CH₂Cl₂, 15 min, -78 °C; PPh₃, 14 h, -78 °C → 20 °C (93%); c) propargyl alcohol, A15, benzene, 15 min, reflux (quant); d) *n*BuLi, THF, 30 min, -78 °C; Bu₃SnCl, 30 min, -78 °C → 20 °C; e) BF₃ · OEt₂, CH₂Cl₂, 5 min, -10 °C (85%; two steps (5.5:1, **16**:**15**)); f) KHMDs, 30 min, -78 °C, BnBr, THF, -78 °C → 20 °C (80%); g) TBAF, THF, 2 h, 20 °C; h) RaNi, H₂, EtOH, 30 min, 20 °C (89%; two steps). A15 = Amberlyst 15, KHMDs = potassium hexamethyldisilazide.



Scheme 4. Synthesis of fragment **4**. a) NaH, BnBr, DMF, 20 °C (82 %); b) DMSO, (COCl)₂, CH₂Cl₂, –78 °C; NEt₃, –78 °C → 0 °C; c) (*tert*-butoxycarbonylmethylene)triphenylphosphorane, CH₂Cl₂, 14 h, 0 °C → 20 °C (96 %; two steps); d) LDA/HMPA/THF, 30 min, –78 °C, then (*S*)-2-(*tert*-butyldimethylsilyloxy)propanal, –78 °C → 0 °C; e) MeOH/HCl (sat.), 5 min, (repeat), 20 °C; f) MsCl, NEt₃, CH₂Cl₂, 30 min, 0 °C; g) I₂ (5 mol %), 4 h, irradiation (60 %; four steps); h) PhNO, MeOH/CH₂Cl₂ (1/1), 14 h, 0 °C (89 % (7:3, **23**:**22**)); i) [Mo(CO)₆], MeCN, reflux 4 h; then **23**, H₂O, 15 min, 20 °C; j) TBSCl, imidazole, DMF, 14 h, 20 °C (80 %); k) PtO₂ (20 mol %), H₂, EtOH, 30 min, 20 °C (92 %); l) TFAA, Hünig's base, CH₂Cl₂, 30 min, 0 °C; m) Pd(OH)₂ (20 mol %), H₂, MeOH, 2 h, 20 °C (80 %; two steps); n) DMSO, (COCl)₂, CH₂Cl₂, –78 °C; NEt₃, –78 °C → 0 °C; o) CrCl₂, CH₃I, 14 h, THF 0 °C → 20 °C (80 %; two steps); p) DBU, CH₂Cl₂, 30 min, 0 °C (95 %). DMF = *N,N*-dimethylformamide, LDA = lithium diisopropylamide, HMPA = hexamethyl phosphoramide, MsCl = methanesulfonyl chloride, TFAA = trifluoroacetic anhydride, DBU = 1,8-diazabicyclo[5.4.0]undec-7-ene.

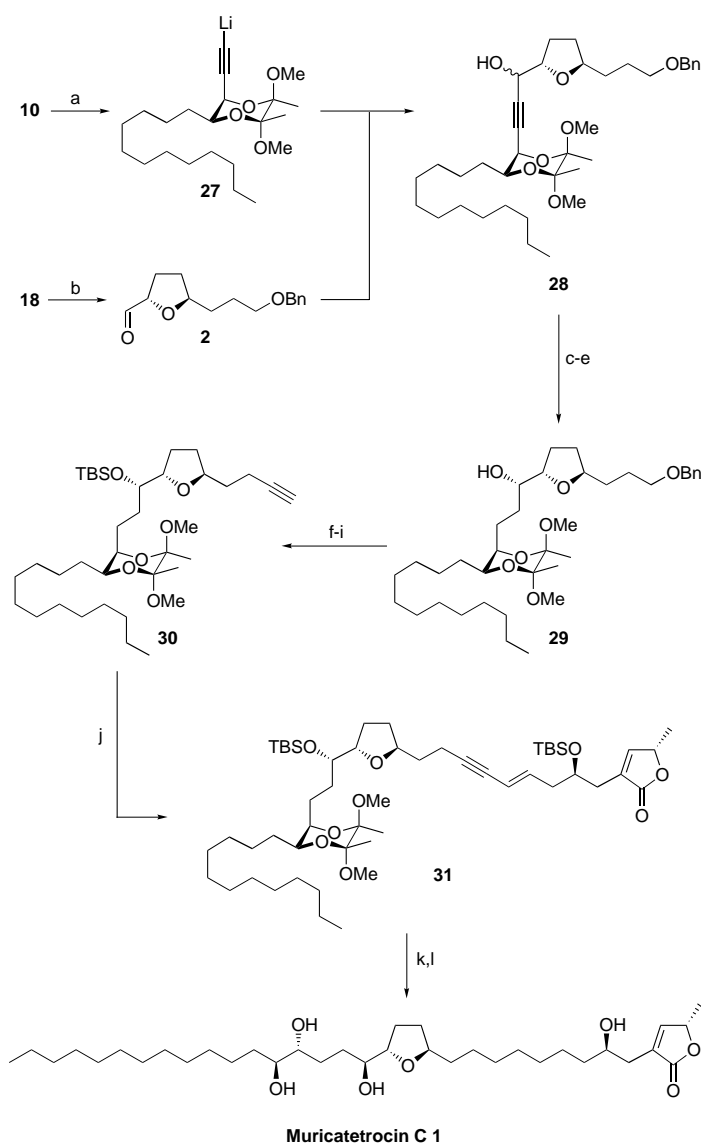
7 was then accessed with a ratio of greater than 20:1 by sunlamp irradiation of **21** in the presence of a catalytic quantity of iodine.^[16]

With **7** in hand, the key HDA reaction was then investigated. It was found that overnight stirring of a methanol/dichloromethane (1/1) solution of **7** with nitrosobenzene at

0 °C afforded a mixture of regioisomers (7:3, **23**:**22**), favoring the desired adduct **23** in overall 89 % yield. Pleasingly, inspection of the crude ¹H NMR spectrum showed that the major regioisomer **23** had been formed with a diastereomeric ratio of over 20:1—thus the observed diastereoselection appeared to be limited only by the original geometry of the external olefin in the diene precursor. The required diastereomerically pure regioisomer **23** was obtained in 55 % yield following separation by HPLC; the slightly diminished yield reflecting the propensity for retro-Diels–Alder reaction on silica that has been previously documented for these types of compounds.^[17]

The next synthetic challenge required selective cleavage of the N–O bond in the presence of the α,β -unsaturation. This was crucial in order to avoid transactonization to the other possible γ -lactone species.^[18] After screening a variety of reagents we found that freshly prepared [Mo(CO)₃(MeCN)₃] in the presence of water could effect this transformation at ambient temperature, affording **24** in 70 % yield.^[19] Subsequent silylation of the resultant secondary alcohol followed by hydrogenation of the α,β -unsaturation over platinum dioxide proceeded to give **25** as one diastereoisomer in 74 % yield over two steps. The aryl amine was activated as a suitable leaving group to unmask the butenolide double bond by treatment with trifluoroacetic anhydride and Hünig's base, leading to the formation the trifluoroacetamide **26**. Preparation of the vinyl iodide required a further three steps: hydrogenation of the benzyl ether over Pd(OH)₂, then Swern oxidation followed by one-carbon homologation according to the Takai procedure.^[20] This provided **27** as a 4:1 ratio of isomers in overall 64 % yield (four steps), favoring the *E* geometry. Subsequent elimination of the trifluoroacetamide group was effected by using DBU to afford **4** in 95 % yield with no epimerization of the C-34 methyl substituent.

With all three fragments successfully prepared, the initial coupling between **2** and **3** was investigated. Swern oxidation of **18** produced aldehyde **2**, which was found to be unstable and hence was not purified, but used crude in the subsequent coupling step (Scheme 5). Thus, treatment of **10** with butyllithium produced the lithiated alkyne species **27**, which was then quenched by the addition of crude **2** to afford propargylic alcohol **28** in good yield (72 %). However, the reaction proceeded with poor diastereoselection, which was subsequently shown to favor the undesired *R* epimer at the newly formed C-16 stereocenter. Attempts to optimize this coupling proved unsuccessful and ultimately an oxidation–reduction protocol was adopted. Consequently, hydrogenation of the alkyne **28** over Raney nickel allowed complete separation of the desired *S* epimer **29**. The remaining material was then recycled by TPAP oxidation,^[21] followed by reduction with L-Selectride; this route gave a 4:1 ratio of products favoring **29**, in 64 % yield over three steps. With the final stereogenic center installed, **29** was prepared for coupling with **4**. Thus silylation of the secondary alcohol then hydrogenation over Pd(OH)₂, allowed Dess–Martin oxidation to the aldehyde,^[22] followed by one-carbon homologation using the Colvin–Gilbert–Seyferth reagent to afford the terminal alkyne **30** in 62 % yield.^[23]



Muricatetrocin C 1

Scheme 5. Coupling reactions and synthesis of **1**. a) *n*BuLi, THF, 30 min, $-78^{\circ}\text{C} \rightarrow 0^{\circ}\text{C}$; -78°C then **2**; b) DMSO, $(\text{COCl})_2$, CH_2Cl_2 , -78°C ; NEt_3 , $-78^{\circ}\text{C} \rightarrow 0^{\circ}\text{C}$ (72%; two steps); c) RaNi , H_2 , EtOH, 30 min, 20°C (91%); d) TPAP (7 mol %), NMO, NEt_3 , CH_2Cl_2 , 45 min, 0°C ; e) L-Selectride, THF, -100°C (70%; two steps); f) TBSCl, DMF, imidazole, 14 h, 45°C ; g) $\text{Pd}(\text{OH})_2$ (20 mol %), H_2 , EtOH, 10 h, 20°C (87%; two steps); h) DMP, CH_2Cl_2 , 45 min, $0^{\circ}\text{C} \rightarrow 20^{\circ}\text{C}$; i) diethyl methylidiazophosphonate, *t*BuOK, THF, -78°C , 16 h; 20°C 4 h, (71%; two steps); j) $[\text{Pd}(\text{PPh}_3)_2\text{Cl}_2]$ (10 mol %), CuI (30 mol %), NEt_3 , 2 h, 20°C (86%); k) $[\text{Rh}(\text{PPh}_3)_3\text{Cl}]$, H_2 , THF, 10 h, 20°C (76%); l) TFA/ H_2O 9/1, 1 min; repeat (82%). TPAP = tetrapropyl ammonium perruthenate, NMO = 4-methyl-morpholine-*N*-oxide, DMP = Dess–Martin periodinane, TFA = trifluoroacetic acid.

Sonogashira cross coupling of **30** with the vinyl iodide **4** proceeded smoothly in the presence of catalytic $[\text{Pd}(\text{PPh}_3)_2\text{Cl}_2]$ and CuI in triethylamine, in 86% yield.^[24] Selective hydrogenation of the resultant enyne **31** was achieved in 76% yield by using Wilkinson's catalyst. Final desilylation and removal of the butane diacetal (BDA) group could be carried out in one step using aqueous trifluoroacetic acid. Purification by silica gel chromatography afforded **1** as a white amorphous solid in 82% yield. The spectroscopic data for synthetic **1** (^1H NMR, ^{13}C NMR, IR, MS, m.p. and specific

rotation)^[25] were in excellent agreement with those reported for naturally occurring Muricatetrocin C.^[7]

In summary the first stereoselective synthesis of **1** has been achieved by implementing new methods for each of the three coupling fragments. Thus our *anti*-diol building block, (*R'*,*R'*,*S*)-2,3-BDA-protected butane tetrol **8** has found further utility in total synthesis, the recently developed anomeric O–C rearrangement methodology has been used to install the 2,5-*trans*-disubstituted THF moiety **3** and a new approach to the (*S*)-hydroxy-butenolide terminus **4** that employs a highly diastereoselective HDA reaction has been developed. Further studies aimed at expanding our synthetic approach to other members of this family of bioactive natural products are currently underway.

Received: July 6, 2000 [Z15399]

- a) F. Q. Alali, X.-X. Liu, J. L. McLaughlin, *J. Nat. Prod.* **1999**, 62, 504; b) L. Zeng, Q. Ye, N. H. Oberlies, G. Shi, Z. Gu, K. He, J. L. McLaughlin, *Nat. Prod. Rep.* **1996**, 13, 275, and references therein.
- M. C. Gonzalez, J. R. Tormo, A. Bermejo, M. C. Zafra-polo, E. Estornell, D. Cortes, *Bioorg. Med. Chem. Lett.* **1997**, 7, 1113, and references therein.
- D. J. Morré, R. deCabo, C. Farley, N. H. Oberlies, J. L. McLaughlin, *Life Sci.* **1995**, 56, 343.
- D. Decaudin, I. Marzo, C. Brenner, G. Kroemer, *Int. J. Oncol.* **1998**, 12, 141.
- N. H. Oberlies, V. L. Croy, M. L. Harrison, J. L. McLaughlin, *Cancer Lett.* **1997**, 15, 73.
- For recent reviews see: a) G. Cassiraghi, F. Zanardi, L. Battistini, G. Rassu, G. Appendino, *Chemtracts: Org. Chem.* **1998**, 11, 803; b) R. Hoppe, H. D. Scharf, *Synthesis* **1995**, 1447; c) B. Figadère, *Acc. Chem. Res.* **1995**, 28, 359.
- G. Shi, Z. Gu, K. He, K. Wood, L. Zeng, Q. Ye, J. MacDougall, J. L. McLaughlin, *Biorg. Med. Chem.* **1996**, 4, 1281.
- Independently, Koert and co-workers recently adopted a similar disconnection strategy in their synthesis of the related compounds Muricatetrocin A and B and Mucocin. a) S. Bäurle, U. Peters, T. Friedrich, U. Koert, *Eur. J. Org. Chem.* **2000**, 2207; b) S. Bäurle, S. Hoppen, U. Koert, *Angew. Chem.* **1999**, 111, 1341; *Angew. Chem. Int. Ed.* **1999**, 38, 1263.
- a) D. J. Dixon, A. C. Foster, S. V. Ley, D. J. Reynolds, *J. Chem. Soc. Perkin Trans. 1* **1999**, 1631. b) D. J. Dixon, A. C. Foster, S. V. Ley, D. J. Reynolds, *J. Chem. Soc. Perkin Trans. 1* **1999**, 1635.
- a) M. F. Buffet, D. J. Dixon, S. V. Ley, E. W. Tate, *Synlett* **1998**, 1091; b) M. Chorghade, D. J. Dixon, S. V. Ley, D. J. Reynolds, *Synth. Commun.* **2000**, 30, 1955.
- E. J. Corey, P. L. Fuchs, *Tetrahedron Lett.* **1972**, 3769.
- The various applications of this useful reagent are reviewed by A. S. Thompson in *Encyclopedia of Reagents for Organic Synthesis*, Vol. 3 (Ed.: L. A. Paquette), Wiley, New York, **1995**, pp. 1957–1960. For a discussion of the reaction mechanism see J.-E. Backväll, M. Sellén, *J. Chem. Soc. Chem. Commun.* **1987**, 827.
- Geometries were obtained in MacroModel using MM2 forcefield. Calculations of eigenvalues carried out in CADPAC using 3-21++G basis set. Calculations kindly carried out by A. G. Leach.
- M. W. Rathke, D. Sullivan, *Tetrahedron Lett.* **1972**, 4249.
- Y. Ito, Y. Kobayashi, T. Kawabata, M. Takosa, S. Terashima, *Tetrahedron* **1980**, 36, 557.
- P. E. Sonnet, *Tetrahedron* **1980**, 36, 557, and references therein.
- E. R. Möller, K. A. Jørgensen, *J. Org. Chem.* **1996**, 61, 5770, and references therein.
- T. R. Hoye, P. R. Hanson, L. E. Hasenwinkel, E. A. Ramirez, Z. Zhaung, *Tetrahedron Lett.* **1994**, 35, 8525.
- a) M. Nitta, T. Kobayashi, *J. Chem. Soc. Perkin Trans. 1* **1985**, 1401. b) S. Cicchi, A. Goti, A. Brondi, A. Guarna, F. De Sarlo, *Tetrahedron Lett.* **1990**, 31, 3351.

- [20] K. Takai, K. Nitta, K. Utimoto, *J. Am. Chem. Soc.* **1986**, *108*, 7408.
 [21] S. V. Ley, J. Norman, W. P. Griffith, S. P. Marsden, *Synthesis* **1994**, 639.
 [22] a) D. B. Dess, J. C. Martin, *J. Org. Chem.* **1983**, *48*, 4155; b) D. B. Dess, J. C. Martin, *J. Am. Chem. Soc.* **1991**, *113*, 7277.
 [23] For preparation of the reagent see: R. T. Lewis, W. B. Motherwell, *Tetrahedron* **1992**, *48*, 1465; for a review see: F. Eymery, B. Iorga, P. Savignac, *Synthesis* **2000**, 185.
 [24] a) T. R. Hoye, P. R. Hanson, A. C. Kovelesky, T. D. Ocain, Z. P. Zhuang, *J. Am. Chem. Soc.* **1991**, *113*, 9369; b) K. Sonogashira, Y. Thoda, N. Magihara, *Tetrahedron Lett.* **1975**, *12*, 4467.
 [25] Spectroscopic data for synthetic **1**, a white amorphous solid: M.p. 65–67 °C (lit. [7] 65–66 °C); $[\alpha]_D^{25} = +5.8$ ($c = 0.38$ in CH_2Cl_2 , lit. [7] +6.3 in CH_2Cl_2); ^1H NMR (600 MHz; CDCl_3): $\delta = 7.18$ (d, 1H, $J = 1.1$ Hz; H-33), 5.06 (qd, 1H, $J = 6.8, 1.1$ Hz; H-34), 3.89–3.87 (m, 1H, H-12), 3.87–3.83 (m, 1H, H-4), 3.82 (q, 1H, $J = 7.2$ Hz, H-15), 3.63–3.60 (m, 2H; H-19, H-20), 3.47–3.43 (m, 1H; H-16), 2.90 (s (br), 2H; OH), 2.53 (dt, 1H, $J = 15.1, 1.6$ Hz; H-3), 2.40 (dd, 1H, $J = 15.1, 8.3$ Hz; H-3), 2.04–2.01 (m, 1H; H-13), 2.00–1.97 (m, 1H; H-14), 1.70–1.40 (m, 6H; H₂-21, H₂-18, H₂-17), 1.60–1.40 (m, 3H; H-13, H₂-11), 1.62–1.55 (m, 1H; H-14) 1.50–1.40 (m, 2H; H₂-5), 1.43 (d, 3H, $J = 6.8$ Hz; H₃-35), 1.40–1.20 (m, 32H; H₂-6 → H₂-10, H₂-22 → H₂-31, 2 × OH), 0.88 (t, 3H; $J = 6.9$ Hz, H₃-32); ^{13}C NMR (150 MHz; CDCl_3): $\delta = 174.5$ (C-1), 151.7 (C-33), 131.2 (C-2), 81.7 (C-15), 79.3 (C-12), 77.9 (C-34), 74.7, 74.4 (C-20, C-19), 74.3 (C-16), 70.0 (C-4), 37.4 (C-5), 33.5–22.7 (C-6 → C-11, C-17, C-18, C-21 → C-31), 33.4 (C-3), 32.4 (C-13), 28.4 (C-14), 19.1 (C-35), 14.1 (C-32); IR (CDCl_3): $\tilde{\nu}_{\text{max}} = 3422$ (br OH), 2928, 2855 (C–H), 1733 (C=O) and 1675 (C=C) cm^{-1} ; HRMS $[M+\text{Na}]^+$ found: m/z : 619.4522, $\text{C}_{35}\text{H}_{64}\text{O}_7\text{Na}$ required: m/z : 619.4544.

Development of a Diversity-Based Approach for the Discovery of Stereoselective Polymerization Catalysts: Identification of a Catalyst for the Synthesis of Syndiotactic Polypropylene**

Jun Tian and Geoffrey W. Coates*

The discovery of efficient and selective catalysts for organic and polymer synthesis will be a crucial requirement for the sustained growth of the chemical industry as economic and environmental constraints become more restrictive in the new millennium. Increasingly important will be the stereoselective catalysts that provide key enantiomerically pure building

blocks to the pharmaceutical industry^[1] as well as stereoregular macromolecules to the polymer industry.^[2] Due to the complicated mechanistic nature of many transition metal based catalysts, structure–activity relationships are often unpredictable leaving empirical exploration and serendipity the most common routes to discovery. Although impressive catalyst breakthroughs have been made, more efficient strategies clearly must be implemented to aid the pursuit of new catalysts. Perhaps the most widely heralded approach that is proposed to influence the discovery and optimization of new catalysts is combinatorial chemistry.^[3–5] Combinatorial methods have significantly hastened the discovery of new drugs through the rapid synthesis and efficient screening of diverse sets (libraries) of organic molecules.^[6–8] It seems reasonable that a similar strategy might impact catalyst discovery and optimization if metal complex libraries can be rapidly synthesized and their desired properties tested.^[9] Although the combinatorial approach is often viewed by some with skepticism, it should be stressed that the more rapidly new classes of highly selective catalysts are discovered, the faster traditional chemists can initiate studies to elucidate their detailed mechanisms of operation. Large collections of structure–activity data will not only provide a solid information base upon which mechanistic hypotheses can be proposed and supported, but will also facilitate the development of new catalyst systems. Herein we report a combinatorial approach for the discovery of stereoselective polymerization catalysts. Using this method, we identified a new catalyst system for the syndiospecific polymerization of propylene.

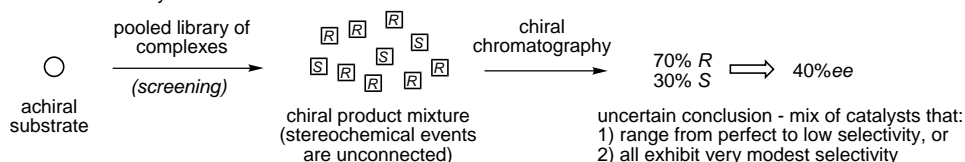
The development of new polymerization catalysts can be subdivided into three main steps: ligand preparation, complex synthesis, and screening of the behavior of these complexes for a specific reaction. Depending on the catalyst system under investigation, any one of these can be the rate-determining step that limits improvement. The synthesis and testing of catalyst libraries can occur primarily in two formats, parallel (spatially separate reaction vessels) and pooled (combined in one reaction vessel) libraries.^[10, 11] Although each format has its advantages, the use of combinatorial methods for developing enantioselective catalysts for small-molecule transformations has thus far relied on the parallel synthesis of ligands and complexes, followed by the serial screening for enantioselectivity using chiral chromatography.^[12, 13] Due to the time-consuming nature of sequentially screening the enantioselectivities of the products of a parallel library, one might wonder why the screening of a pooled, bead-bound stereoselective catalyst library has not been reported. Exchange of products between different beads and/or the reaction solution occurs, therefore only an average stereoselectivity of the library can be determined (Scheme 1).^[14]

Interestingly, the situation changes in the case of stereoselective polymerization catalysts (Scheme 1). Unlike the asymmetric transformation of small molecules where the stereochemical events of the reaction are unconnected, the polymer itself serves as a stereochemical recording of the events of the polymerization catalyst. Assuming that the catalyst species do not interact with one another, then a group of complexes for stereoselective polymerization can be

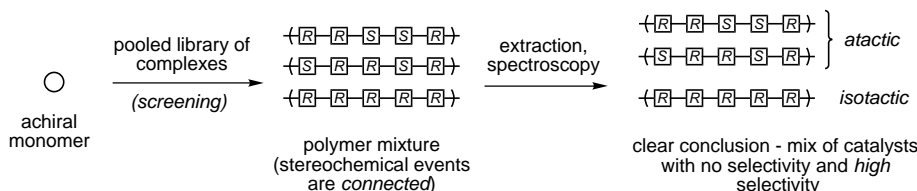
[*] Prof. G. W. Coates, Dr. J. Tian
 Department of Chemistry and Chemical Biology
 Baker Laboratory
 Cornell University
 Ithaca, NY 14853-1301 (USA)
 Fax: (+1) 607-255-4137
 E-mail: gc39@cornell.edu

[**] This work was supported by the Cornell Center for Materials Research (CCMR), a Materials Research Science and Engineering Center of the National Science Foundation (DMR-9632275), and the Exxon Chemical Corporation. G.W.C. gratefully acknowledges an NSF Career Award (CHE-9875261), a Camille and Henry Dreyfus New Faculty Award, a Research Corporation Research Innovation Award, an Alfred P. Sloan Research Fellowship, an Arnold and Mabel Beckman Foundation Young Investigator Award, a Camille Dreyfus Teacher-Scholar Award, a 3M Untenured Faculty Grant, an IBM Partnership Award, and a Union Carbide Innovation Recognition Award.

Small-Molecule Catalysis:



Polymerization Catalysis:



Scheme 1. Pooled screening of stereoselective catalysis: small-molecule catalysts and polymerization catalysts.

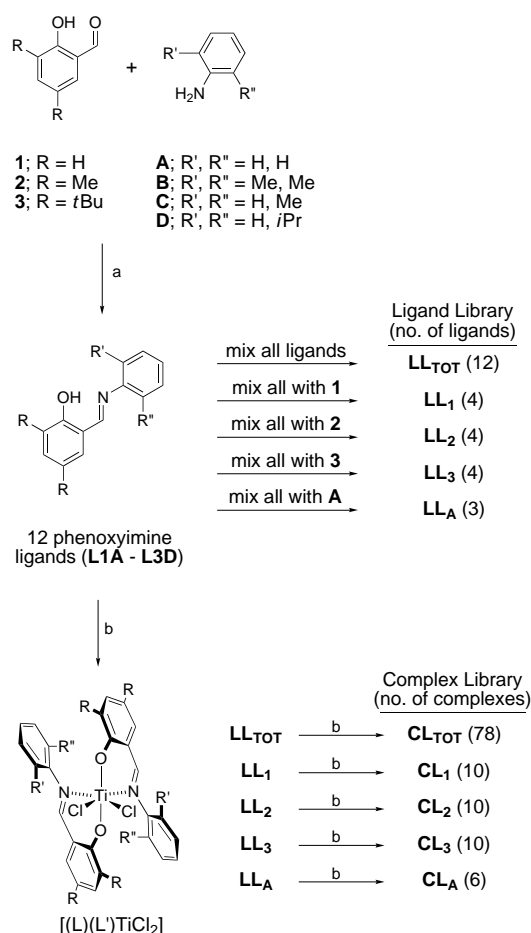
simultaneously screened. For example, a simple solvent extraction can identify the presence of a stereoregular polymer due to its lower solubility than the atactic form. Once a hit catalyst is detected, the library can be systematically narrowed and the new catalyst easily identified.^[15]

There are several additional benefits of this pooled polymerization catalyst discovery strategy. Since the catalysts all exist in the same reaction vessel, they can be simultaneously synthesized from a ligand library if high-yield complex preparations are available. Complex synthesis and storage often requires an inert atmosphere, therefore this feature saves considerable time and expense. The approach can also be used to detect catalysts which produce polymer of high molecular weight by analysis of the crude polymer product using gel permeation chromatography. If high molecular polymer is present, the catalyst responsible for it can in theory be ascertained from the catalyst library. Likewise, incorporation of unreactive comonomers can be screened if there is a spectroscopic method to reveal its incorporation into the polymer chain. Similarly, carefully constructed sub-libraries of the main catalyst collection can rapidly reveal the catalyst(s) that are capable of comonomer incorporation. Herein we demonstrate the feasibility of such a discovery process by identifying a new catalyst for the synthesis of syndiotactic polypropylene.^[16–19]

To demonstrate the feasibility of this pooled polymerization catalyst discovery strategy, we designed a catalyst system after consideration of the following criteria. First, we reasoned that the ligands should be efficiently synthesized from commercially available starting materials. Second, complex synthesis must also be high yielding; bis-ligated complexes are favored over mono-ligated complexes since the former increase the diversity of the library (n ligands will form n mono-ligated species while $(n^2 + n)/2$ bis-ligated complexes are formed). Third, ligand–metal bond strengths should be significant enough to ensure that a statistical library of the complexes is generated. Based on these considerations, we chose to investigate titanium complexes bearing salicylaldiminato ligands (Scheme 2). These ligands are readily synthesized by the condensation of a wide range of amines and salicylaldehydes. Although several recent reports have described the

polymerization of ethylene using these complexes,^[20–24] to our knowledge their behavior for propylene polymerization is unreported. Due to their C_2 symmetry, we anticipated that they might be isospecific catalysts for propylene polymerization.

To investigate a wide range of steric effects yet keep the library size manageable, we designed a 12-component ligand library made from three salicylaldehydes (**1–3**) and four anilines (**A–D**) (Scheme 2). The salicylaldi-



Scheme 2. Synthesis of the library of complexes. a) parallel synthesis; MeOH, reflux, 12 h, > 95%; b) pooled synthesis; *n*BuLi, -60°C to 20°C , 4 h (1 equiv); $TiCl_4$, -60°C to 20°C , 16 h (0.5 equiv), > 90%.

mines were separately made and extensively purified by recrystallization. Equimolar amounts of the ligands were combined to make a 12-ligand library (**LLTOT**). Deprotonation of **LLTOT** with *n*BuLi at -60°C followed by reaction with 0.5 equivalents of $TiCl_4$ yielded complex library **CLTOT** (78 possible species). To investigate whether a statistical mixture

of complexes is formed, we reacted equal amounts of deprotonated **L1A** and **L3A** with TiCl_4 . ^1H NMR spectroscopy of the product revealed the complexes $[(\text{L1A})_2\text{TiCl}_2]$, $[(\text{L1A})(\text{L3A})\text{TiCl}_2]$, and $[(\text{L3A})_2\text{TiCl}_2]$ in an approximate 1:2:1 ratio. Although we have not been able to collect acceptable mass spectrometry data on **CL_{TOT}**, we believe this experiment is strong evidence that at least an appreciable amount of each complex exists in the library.

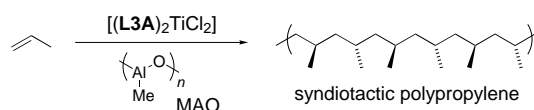
The complex library **CL_{TOT}** was activated with methylaluminoxane (MAO; $[\text{Al}]/[\text{Ti}] = 100$) in toluene and the resultant catalyst solution was exposed to propylene (2.7 atm) at 20 °C. Polypropylene (PP) was slowly formed with an activity of 480 g PP per mol Ti per hour. Although 90% of the resultant polymer was soluble in refluxing diethyl ether (atactic polypropylene), the remaining 10% was insoluble and unexpectedly was found to be *syndiotactic polypropylene* by ^{13}C NMR microstructural analysis.^[25] To ascertain the identity of the catalyst(s) responsible for the formation of this stereoregular polymer, we investigated the polymerization behavior of four sub-libraries of **CL_{TOT}** (see Table 1). **CL₁** and **CL₂** produced only atactic polymer. However **CL₃** and **CL_A**

Table 1. Propylene polymerization using MAO activated bis(salicylaldiminato)titanium complexes.

Complex/Library ^[a]	Activity ^[b]	% Et ₂ O soluble	% Et ₂ O insoluble
CL_{TOT}	0.480	90	10
CL₁	0.310	100	0
CL₂	0.610	100	0
CL₃	4.00	81	19
CL_A	3.10	68	32
$[(\text{L3A})_2\text{TiCl}_2]$	8.80	0	100

[a] Polymerization reactions were performed in toluene solution at 20 °C and 2.7 atm propylene for 6 h. [b] kg PP per mol Ti per h.

produced 19% and 32%, respectively, of polymer that was insoluble in diethyl ether. We have synthesized $[(\text{L3A})_2\text{TiCl}_2]$, the common species of **CL₃** and **CL_A**, and found that it forms monodisperse, highly syndiotactic polypropylene (Scheme 3).^[26] Microstructural analysis using ^{13}C NMR



Scheme 3. Polymerization of propylene using $[(\text{L3A})_2\text{TiCl}_2]/\text{MAO}$ yields syndiotactic polypropylene with errors consistent with a chain-end control mechanism.

spectroscopy reveals that a chain-end control mechanism appears to operate.^[25] Aside from the syndiotactic $[\text{rrrr}]$ pentad, only the $[\text{rrrm}]$, and $[\text{rmrr}]$ pentads are present (1:1 ratio). Analysis of the peak intensities using a Bernoullian statistical model reveals that the probability of an *r*-dyad placement in the polymer chain is 92%. To our knowledge, this is the highest reported degree of chain-end control in a propylene polymerization.^[27] When the polymerization is carried out at 0 °C, a polymer with 94% *r*-dyads is formed; Figure 1 shows the ^{13}C NMR spectrum of the methyl region of this polymer. This semicrystalline polymer exhibits a peak melting temperature of 108 °C.

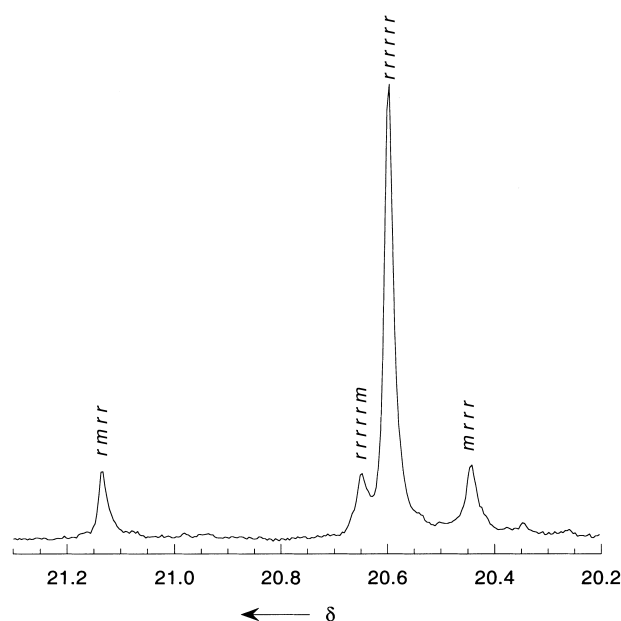


Figure 1. Quantitative proton-decoupled ^{13}C NMR spectrum of the methyl region of polypropylene prepared with $[(\text{L3A})_2\text{TiCl}_2]/\text{MAO}$ at 0 °C (100 MHz, C_6D_6).

At the current time, the detailed mechanism of polymerization is unknown. One unusual aspect of the reaction is that a chain-end mechanism apparently overrides the chiral C_2 symmetry of the catalyst precursor. Two intriguing mechanistic possibilities are currently being investigated. The first prospect is that the olefin is enchainned by a secondary (2,1) mechanism, placing the last stereogenic center of the polymer chain on the carbon bound to the titanium center. Second is a ligand isomerization pathway, in which the catalyst site undergoes site inversion between olefin insertions due to the chain-end geometry of the polymer.^[28]

In conclusion, we report a valuable strategy for the rapid screening of polymerization catalyst libraries. When a desired polymer product has distinguishing chemical or physical properties, techniques such as solubility, spectroscopy, or chromatography can be used to quickly probe the crude product of a pooled polymerization reaction to see if a noteworthy catalyst is present. Then the systematic synthesis of catalyst sub-libraries can be used to rapidly identify the desired catalyst. The viability of this strategy was successfully demonstrated by using a library of bis(salicylaldiminato)titanium complexes, where a syndiospecific catalyst for propylene polymerization was identified. To our knowledge, this is the first time that combinatorial methods have been reported to identify a new polymerization catalyst with unexpected, yet desirable properties.

Experimental Section

Complex library (CL_{TOT}**) synthesis:** Twelve ligands (**L1A**–**L3D**, 0.500 mmol each) were carefully weighed and then codissolved in diethyl ether (40 mL) in a predried Schlenk tube under nitrogen. At –60 °C, the ligand library solution was treated dropwise with *n*BuLi (3.75 mL, 1.6 M in hexanes, 6.00 mmol) by using a gas-tight syringe. After the temperature of the reaction mixture had been allowed to rise to room temperature, the reaction was stirred for another 4 h. Half of the ligand solution was

cannulated into a solution of TiCl_4 (0.569 g, 3.00 mmol) in Et_2O (20 mL) at -60°C ; after stirring at -60°C for 30 min, the other half of the ligand solution was added. The resultant solution was stirred while it was allowed to warm to room temperature. After 16 h, solvent was removed in vacuo and the complex was dissolved in dichloromethane. The mixture was filtered through Celite and was then dried in vacuo to yield a deep red powder.

Polymer synthesis: Polymerizations were conducted in a 6 ounce Lab-Crest pressure reaction vessel equipped with a magnetic stir bar. After drying in vacuo, the reactor was charged with dry MAO (1.80 g, 31 mmol) and toluene (150 mL) under N_2 . At this point the atmosphere of the reactor was exchanged with propylene gas three times, and then adjusted to the desired pressure and temperature. Complex library CL_{TOT} (200 mg, 0.31 mmol) was dissolved in toluene (6 mL) at room temperature under nitrogen. The solution was then added to the reactor by using a gas-tight syringe to initiate the polymerization. After the desired period of time, the reactor was vented. The polymer was precipitated from methanol/HCl, filtered, washed with methanol, and then dried to constant weight.

Received: June 13, 2000 [Z15268]

- [1] *Comprehensive Asymmetric Catalysis, Vol. 1–3* (Eds.: E. N. Jacobsen, A. Pfaltz, H. Yamamoto), Springer, Berlin, **1999**.
- [2] G. W. Coates, *Chem. Rev.* **2000**, *100*, 1223–1252.
- [3] B. Jandeleit, D. J. Schaefer, T. S. Powers, H. W. Turner, W. H. Weinberg, *Angew. Chem.* **1999**, *111*, 2648–2689; *Angew. Chem. Int. Ed.* **1999**, *38*, 2495–2532.
- [4] K. D. Shimizu, M. L. Snapper, A. H. Hoveyda, *Chem. Eur. J.* **1998**, *4*, 1885–1889.
- [5] J. M. Newsam, F. Schuth, *Biotechnol. Bioeng.* **1999**, *61*, 203–216.
- [6] S. L. Schreiber, *Science* **2000**, *287*, 1964–1969.
- [7] F. Balkenhohl, C. von dem Bussche-Hünnefeld, A. Lansky, C. Zechel, *Angew. Chem.* **1996**, *108*, 2436–2487; *Angew. Chem. Int. Ed. Engl.* **1996**, *35*, 2289–2337.
- [8] L. A. Thompson, J. A. Ellman, *Chem. Rev.* **1996**, *96*, 555–600.
- [9] J. M. J. Fréchet, *ACS Poly. Mater. Sci. Eng.* **1999**, *80*, 494.
- [10] For representative examples that demonstrate potential methods for the parallel synthesis of catalyst libraries and their pooled screening for polymerization activity, see: a) T. R. Boussie, C. Coutard, H. Turner, V. Murphy, T. S. Powers, *Angew. Chem.* **1998**, *110*, 3472–3475; *Angew. Chem. Int. Ed.* **1998**, *37*, 3272–3275; b) T. R. Boussie, V. Murphy, K. A. Hall, C. Coutard, C. Dales, M. Petro, E. Carlson, H. W. Turner, T. S. Powers, *Tetrahedron* **1999**, *55*, 11699–11710.
- [11] An elegant mass-spectrometry technique has recently been reported in which a pooled library of living polymerization catalysts was screened for the ability to form high molecular weight polymer: a) C. Hinderling, P. Chen, *Angew. Chem.* **1999**, *111*, 2393–2396; *Angew. Chem. Int. Ed.* **1999**, *38*, 2253–2256; b) C. Hinderling, C. Adlhart, P. Chen, *Chimia* **2000**, *54*, 232–235.
- [12] Some inventive, alternate high-throughput methods for screening asymmetric catalysts have recently been reported. For example, see: a) G. T. Copeland, S. J. Miller, *J. Am. Chem. Soc.* **1999**, *121*, 4306–4307 (a fluorescent sensor approach to identify highly active, and hence selective catalysts); b) M. T. Reetz, M. H. Becker, H. W. Klein, D. Stockigt, *Angew. Chem.* **1999**, *111*, 1872–1875; *Angew. Chem. Int. Ed.* **1999**, *38*, 1758–1761 (the use of mass spectrometry to determine the enantioselectivity of reactions involving *pseudo*-enantiomeric, -prochiral, and -*meso* substrates).
- [13] For some recent examples of catalytic, asymmetric methods developed by using combinatorial methods, see the following. Diethylzinc additions to aldehydes: a) G. Liu, J. A. Ellman, *J. Org. Chem.* **1995**, *60*, 7712–7713; b) C. Gennari, S. Ceccarelli, U. Piarulli, C. Montalbetti, R. F. W. Jackson, *J. Org. Chem.* **1998**, *63*, 5312–5313; c) K. L. Ding, A. Ishii, K. Mikami, *Angew. Chem.* **1999**, *111*, 519–523; *Angew. Chem. Int. Ed.* **1999**, *38*, 497–501; d) A. J. Brouwer, H. J. van der Linden, R. M. J. Liskamp, *J. Org. Chem.* **2000**, *65*, 1750–1757; enamide hydrogenation: e) S. R. Gilbertson, X. Wang, *Tetrahedron Lett.* **1996**, *37*, 6475–6478; aza-Diels–Alder: f) S. Bromidge, P. C. Wilson, A. Whiting, *Tetrahedron Lett.* **1998**, *39*, 8905–8908; alkene epoxidation: g) M. B. Francis, E. N. Jacobsen, *Angew. Chem.* **1999**, *111*, 987–991; *Angew. Chem. Int. Ed.* **1999**, *38*, 937–941; C–H insertion: h) K. Burgess, H. J. Lim, A. M. Porte, G. A. Sulikowski, *Angew. Chem.* **1996**, *108*, 192–194; *Angew. Chem. Int. Ed. Engl.* **1996**, *35*, 220–222; cyanide addition to epoxides: i) B. M. Cole, K. D. Shimizu, C. A. Krueger, J. P. A. Harrity, M. L. Snapper, A. H. Hoveyda, *Angew. Chem.* **1996**, *108*, 1776–1779; *Angew. Chem. Int. Ed. Engl.* **1996**, *35*, 1668–1671; j) K. D. Shimizu, B. M. Cole, C. A. Krueger, K. W. Kuntz, M. L. Snapper, A. H. Hoveyda, *Angew. Chem.* **1997**, *109*, 1781–1785; *Angew. Chem. Int. Ed. Engl.* **1997**, *36*, 1704–1707; Strecker reaction: k) M. S. Sigman, P. Vachal, E. N. Jacobsen, *Angew. Chem.* **2000**, *112*, 1336–1338; *Angew. Chem. Int. Ed.* **2000**, *39*, 1279–1281.
- [14] H. B. Kagan, *J. Organomet. Chem.* **1998**, *567*, 3–6.
- [15] Interestingly, two milestone discoveries concerning isospecific propylene polymerization foretell the feasibility of this strategy. In Natta's original report of the synthesis of isotactic polypropylene, a multitisted heterogeneous titanium-based catalyst produced a mixture of polymer chains. Solvent extraction was used to separate isotactic from atactic chains; later generations of these catalysts were empirically modified to produce only isotactic polypropylene (G. Natta, P. Pino, P. Corradini, F. Danusso, E. Mantica, G. Mazzanti, G. Moraglio, *J. Am. Chem. Soc.* **1955**, *77*, 1708–1710). Three decades later, Ewen reported that a mixture of Brintzinger's *meso* and *racemic* titanocenes (a "library" of two species) also produced a mixture of polymer chains. Solvent extraction revealed isotactic and atactic polymer, produced by the *racemic* and *meso* isomers, respectively (J. A. Ewen, *J. Am. Chem. Soc.* **1984**, *106*, 6355–6364).
- [16] G. Natta, I. Pasquon, A. Zambelli, *J. Am. Chem. Soc.* **1962**, *84*, 1488–1490.
- [17] J. A. Ewen, R. L. Jones, A. Razavi, J. D. Ferrara, *J. Am. Chem. Soc.* **1988**, *110*, 6255–6256.
- [18] T. A. Herzog, D. L. Zubris, J. E. Bercaw, *J. Am. Chem. Soc.* **1996**, *118*, 11988–11989.
- [19] D. Veghini, L. M. Henling, T. J. Burkhardt, J. E. Bercaw, *J. Am. Chem. Soc.* **1999**, *121*, 564–573.
- [20] P. G. Cozzi, E. Gallo, C. Floriani, A. Chiesi-Villa, C. Rizzoli, *Organometallics* **1995**, *14*, 4994–4996.
- [21] S. Matsui, Y. Tohi, M. Mitani, J. Saito, H. Makio, H. Tanaka, M. Nitabaru, T. Nakano, T. Fujita, *Chem. Lett.* **1999**, 1065–1066.
- [22] S. Matsui, M. Mitani, J. Saito, Y. Tohi, H. Makio, H. Tanaka, T. Fujita, *Chem. Lett.* **1999**, 1263–1263.
- [23] S. Matsui, M. Mitani, J. Saito, N. Matsukawa, H. Tanaka, T. Nakano, T. Fujita, *Chem. Lett.* **2000**, 554–555.
- [24] J. Strauch, T. H. Warren, G. Erker, R. Fröhlich, P. Saarenketo, *Inorg. Chem. Acta* **2000**, *300*, 810–821.
- [25] L. Resconi, L. Cavallo, A. Fait, F. Piemontesi, *Chem. Rev.* **2000**, *100*, 1253–1345.
- [26] Due to our sub-library searching routine, a stereoselective, mixed-ligand catalyst might have gone undetected. Given the high selectivity of $[(\text{L}3\text{A})_2\text{TiCl}_2]$, we have abandoned the search for such a hybrid species.
- [27] For representative examples of chain-end stereocontrol in alkene polymerization, see: a) Y. Doi, *Macromolecules* **1979**, *12*, 1012–1013 (polymerization of propene using $\text{VCl}_4/\text{AlEt}_2\text{Cl}$ at -78°C produces syndiotactic polymer with $[r]=0.87$); b) J. A. Ewen, *J. Am. Chem. Soc.* **1984**, *106*, 6355–6364 (polymerization of propene using Cp_2TiCl_2 at -45°C produces isotactic polymer with $[m]=0.85$); c) L. Resconi, L. Abis, G. Franciscano, *Macromolecules* **1992**, *25*, 6814–6817 (polymerization of butene using $[\text{Cp}^*\text{MCl}_2]$ ($\text{M}=\text{Zr}, \text{Hf}$) at -20°C produces syndiotactic polymer with $[r]=0.88$); d) C. Pellecchia, A. Zambelli, *Macromol. Rapid Commun.* **1996**, *17*, 333–338 (polymerization of propene using a nickel catalyst at -78°C produces syndiotactic polymer with $[r]=0.89$); e) B. L. Small, M. Brookhart, *Macromolecules* **1999**, *32*, 2120–2130 (polymerization of propene using an iron catalyst at -20°C produces isotactic polymer with $[m]=0.91$).
- [28] M. Brookhart, M. I. Wagner, *J. Am. Chem. Soc.* **1996**, *118*, 7219–7220.

Pentaatomic Tetracoordinate Planar Carbon, $[\text{CAI}_4]^{2-}$: A New Structural Unit and Its Salt Complexes**

Xi Li, Hai-Feng Zhang, Lai-Sheng Wang,*
Grant D. Geske, and Alexander I. Boldyrev*

Since the pioneering theoretical formulation of hypothetical tetracoordinate planar carbon (TPC) molecules by Hoffmann et al. thirty years ago,^[1] there have been substantial research efforts to design new molecules that may contain tetracoordinate planar carbon.^[2–13] Schleyer et al.^[2–4] computationally tested and predicted a wide variety of candidate molecules for TPC, many of which were reviewed recently.^[4] Keese et al.^[6, 7] performed calculations on promising candidates and synthesized many such molecules. Radom et al.^[8, 9] performed calculations on a class of polycyclic hydrocarbons, called alkaplans, in which TPC can be achieved by steric constraints. A divanadium complex, characterized structurally by Cotton and Millar,^[10] is probably the first compound with a TPC atom. A variety of organometallic compounds, mostly containing elements of Groups 4 and 5, have since been reported by Erker, Gleiter, and co-workers to contain TPC.^[11–13]

Our efforts to design new TPC molecules have concentrated on small five-atom species, the smallest molecules that can contain a TPC atom, in which the bonding of the central carbon atom to its four ligands can be easily traced. Furthermore, planarity in these species is not enforced by their molecular architecture, but rather by their intrinsic and unique electronic structure. On the basis of a simple molecular orbital picture, we found a general rule for achieving planarity in pentaatomic species composed of a first-row central atom and four second- or third-row ligand atoms: such species should possess 17 or 18 valence electrons.^[14–16] Planarity of these species is achieved through a four-center peripheral ligand–ligand bonding interaction in their highest occupied molecular orbital (HOMO).

Here we discuss the possibility of designing new materials containing such pentaatomic TPC species as building blocks for bulk solid materials. We previously established that the 17-valence-electron CAI_4^- is a TPC molecule^[16] in which the ligand–ligand bonding HOMO is singly occupied. When the extra electron is detached, the 16-valence-electron neutral CAI_4 becomes tetrahedral. The CAI_4^- ion, with its open electronic shell, is thus expected to be able to accept one more electron into its four-center ligand–ligand bonding HOMO to generate the closed-shell, 18-valence-electron dianion CAI_4^{2-} . However, this doubly charged anion is not expected to be stable towards electron autodetachment in its isolated state due to strong Coulomb repulsion between the two extra electrons, analogous to the sulfate dianion SO_4^{2-} , which is well known to be unstable in the gas phase.^[17] One strategy to stabilize such a dianion is to provide it with a counterion, as we observed recently in a series of stable $\text{M}^+[\text{SO}_4^{2-}]$ species.^[18] Here we report the first experimental realization of such a salt-stabilized TPC dianion, namely, $\text{Na}^+[\text{CAI}_4^{2-}]$, and a theoretical investigation of this anion and the neutral $(\text{Na}^+)_2[\text{CAI}_4^{2-}]$ species. We confirm that the TPC species CAI_4^{2-} can indeed maintain its structural integrity in the presence of one or two counterions. These findings represent the first step towards the realization of bulk materials based on crystal structural units containing the TPC dianion $[\text{CAI}_4^{2-}]$ as a novel building block.

The experiment was performed with a magnetic-bottle photoelectron spectroscopy apparatus equipped with a laser vaporization source.^[19] We made NaCAI_4^- by laser vaporization of an Al/C/Na composite target containing 75 % Al, 5 % C, and 20 % NaI by weight. Various Al_xC_y species and clusters containing Na and I were observed and analyzed by a time-of-flight mass spectrometer. The NaCAI_4^- ions were mass-selected and detached by a laser beam in the interaction zone of the magnetic-bottle photoelectron analyzer. Photoelectron spectra were measured at two detachment photon energies, 355 nm (3.496 eV) and 266 nm (4.661 eV), as shown in Figure 1. The electron energy resolution was better than 30 meV for 1 eV electrons.

In the theoretical investigation,^[20, 21] we studied extensively possible structures for $\text{Na}^+[\text{CAI}_4^{2-}]$ and $(\text{Na}^+)_2[\text{CAI}_4^{2-}]$. At the B3LYP/6-311 + G* level of theory, the most stable structure for $\text{Na}^+[\text{CAI}_4^{2-}]$ was found to be planar with coordination of Na^+ to an edge of CAI_4^{2-} (Figure 2a). Two other structures, in which Na^+ is coordinated to a corner Al atom or directly to the C atom to form a square pyramid are first- and second-order saddle points lying 14.5 and 12.1 kcal mol^{−1} higher in energy than the bidentate global-minimum structure, respectively. There is, however, another local minimum corresponding to a structure (Figure 2b), which can be viewed as exchanging the positions of Na^+ and one of the corner Al atoms in the ground-state structure. This isomer is 25.4 kcal mol^{−1} higher in energy. When we exchanged Na and one of the bridged Al atoms in the ground-state structure, the resulting species collapsed into the global minimum upon optimization. For $(\text{Na}^+)_2[\text{CAI}_4^{2-}]$, the most stable structure is also planar with coordination of the two Na^+ ions to opposite edges of CAI_4^{2-} (Figure 2c). We found another low-lying stable isomer, which is also planar, but in

[*] Prof. Dr. A. I. Boldyrev, G. D. Geske
Department of Chemistry and Biochemistry
Utah State University
Logan, UT 84322 (USA)
Fax: (+1) 435-797-3390
E-mail: boldyrev@cc.usu.edu

Prof. Dr. L.-S. Wang,^[+] X. Li,^[+] Dr. H.-F. Zhang^[+]
Department of Physics, Washington State University
2710 University Drive, Richland, WA 99352 (USA)
E-mail: ls.wang@pnl.gov

[+] W. R. Wiley Environmental Molecular Sciences Laboratory
Pacific Northwest National Laboratory
MS K8-88, P. O. Box 999, Richland, WA 99352 (USA)
Fax: (+1) 509-376-6066

[**] The theoretical work was done at Utah State University and supported by the donors of The Petroleum Research Fund (ACS-PRF no. 35255-AC6), administered by the American Chemical Society. The experimental work was supported by the National Science Foundation (DMR-9622733) and performed at the W. R. Wiley Environmental Molecular Sciences Laboratory, a national scientific user facility sponsored by DOE's Office of Biological and Environmental Research and located at Pacific Northwest National Laboratory, which is operated for DOE by Battelle. L.S.W. is an Alfred P. Sloan Foundation Research Fellow.

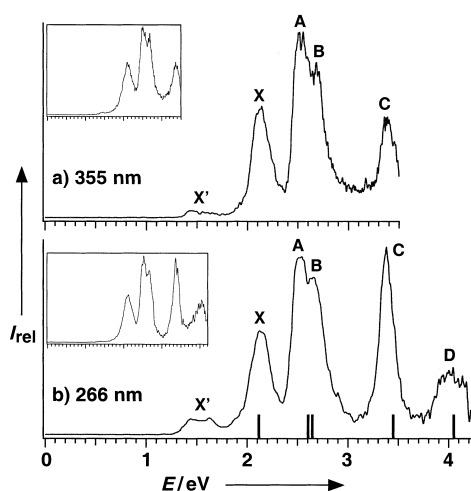


Figure 1. Photoelectron spectra of $\text{Na}^+[\text{CAI}_4]^{2-}$ at 355 nm (3.496 eV) and 266 nm (4.661 eV), plotted in increasing electron binding energy. The five major detachment channels observed are labeled (X, A, B, C, and D). The vertical bars in b) mark the calculated vertical electron detachment energies from the ground state of $\text{Na}^+[\text{CAI}_4]^{2-}$. The insets display spectra recorded with a slightly hotter source condition and show the disappearance of the X' feature, which was due to a higher energy isomer (see text). I_{rel} = relative electron intensity.

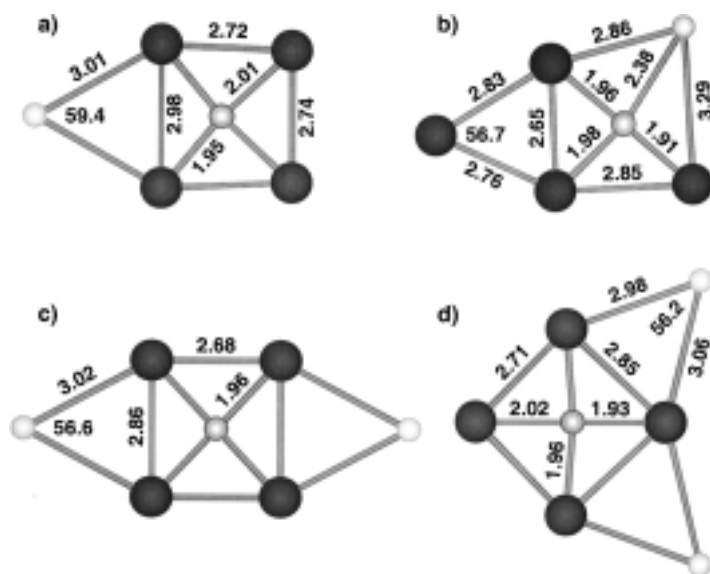


Figure 2. The global minima and low-lying isomers of $\text{Na}^+[\text{CAI}_4]^{2-}$ and $(\text{Na}^+)_2[\text{CAI}_4]^{2-}$ optimized at the B3LYP/6-311 + G* level of theory. a) and c) represent the global minimum structures for each species, whereas b) and d) are the corresponding low-lying isomers. The selected bond lengths are in Å and the bond angles in degrees.

which the two Na^+ ions are coordinated to adjoining edges of CAI_4^{2-} (Figure 2d). This isomer is 3.7 kcal mol⁻¹ higher in energy than the global minimum. The saddle point, corresponding to the transition state (barrier height –6.9 kcal mol⁻¹) on the intramolecular rearrangement from the structure of Figure 2d to that of Figure 2c, is a planar structure in which one Na^+ ion is coordinated to an edge and the other to a corner Al atom of CAI_4^{2-} . Two more structures with direct coordination of Na^+ to the carbon atom and to two Al atoms at opposite corners were also examined. Both structures are second-order saddle points and are 29.2 and 20.9 kcal mol⁻¹ higher in energy than the global minimum, respectively.

At the more sophisticated MP2/6-311 + G* level of theory, the structures shown in Figure 2 are slightly nonplanar, but the bond lengths and valence angles are essentially the same as those obtained at the B3LYP/6-311 + G* level. Moreover, the energy differences between the perfectly planar structures and the slightly nonplanar global-minimum structures were smaller than the differences in the zero-point energies. Therefore, the vibrationally averaged structures are all essentially planar. This slight nonplanarity is similar to that of the parent TPC anion CAI_4^- .^[16] In the interpretation of the experimental spectra, we used the planar C_{2v} structure of $\text{Na}^+[\text{CAI}_4]^{2-}$. At the highest level of theory (CCSD(T)/6-311 + G(2df)//MP2/6-311 + G*), the second isomer of $(\text{Na}^+)[\text{CAI}_4]^{2-}$ (Figure 2b) is 25.2 kcal mol⁻¹ higher in energy than the global-minimum structure (Figure 2a), and the second isomer of $(\text{Na}^+)_2[\text{CAI}_4]^{2-}$ (Figure 2d) is 4.0 kcal mol⁻¹ higher in energy than the global-minimum structure (Figure 2c).

The 355-nm spectrum of NaCAI_4^- revealed four major features (X, A–C) (Figure 1 a), whereby the A and B features are closely spaced. At 266 nm, an additional feature (D) was observed (Figure 1 b). The weak feature near 1.5 eV (X') was assigned to the second isomer of NaCAI_4^- . The insets in Figure 1 display a set of data recorded with a slightly hotter source; here the X' feature was almost completely eliminated. This observation is consistent with the isomer assignment, because the higher energy isomer may isomerize to the ground-state structure more readily under the slightly hotter conditions. The measured adiabatic and vertical electron binding energies (ADEs and VDEs, respectively) for the global minimum structure and the second isomer are given in Table 1. The theoretical results for the global minimum are in excellent agreement with the experimental ADEs and VDEs (Figure 1 b), and this confirms that we have indeed made the $\text{Na}^+[\text{CAI}_4]^{2-}$ charge-transfer salt containing the TPC dianion CAI_4^{2-} . The calculated VDE for the second isomer was 1.70 eV, which agrees well with the X' feature near 1.5 eV and confirms our assignment for the second isomer. The features of higher binding energy for the second isomers were probably buried in the spectral features of the ground-state anion (Figure 1).

Bonding in $\text{Na}^+[\text{CAI}_4]^{2-}$ can be understood by analyzing the molecular orbitals and calculated effective atomic charges. The interaction between Na^+ and CAI_4^{2-} is mostly ionic. The representative atomic charges (NPA) were calculated to be: $Q(\text{Na}) = +0.57 |e|$, $Q(\text{bridged Al}) = +0.15 |e|$, $Q(\text{corner Al}) = +0.32 |e|$, and $Q(\text{C}) = -2.51 |e|$ for the global minimum of $\text{Na}^+[\text{CAI}_4]^{2-}$ (Figure 2a). On the basis of these charge distributions, one might expect that the pyramidal structure should be the most stable, because the positively charged sodium atom is supposed to be favorably coordinated directly to the most electronegative carbon atom. However, the pyramidal structure is much less stable and is not even a local minimum. Insight into this paradox can be obtained by examining the molecular orbitals of $\text{Na}^+[\text{CAI}_4]^{2-}$. Figure 3 shows its four highest orbitals: the ligand–ligand bonding HOMO ($5a_1$) and three nonbonding ligand lone-pair orbitals ($3b_2$, $4a_1$, $2b_2$). The Na^+ ion is actually coordinated to the electron density that corresponds to the ligand–ligand

Table 1. Experimental and theoretical vertical (VDE) and adiabatic (ADE) electron detachment energies for the ground state and the low-lying isomer of $\text{Na}^+[\text{CaI}_4^{2-}]$.

State	Experimental VDE [eV]	Experimental ADE [eV]	Detachment channel ^[a]	Theoretical ^[b] VDE [eV]	Theoretical ^[c] ADE [eV]
Ground state of $\text{Na}^+[\text{CaI}_4^{2-}]$ (Figure 2a)					
X	2.12 (0.03)	2.02 (0.06)	$5a_1$ (2A_1)	2.11 (0.86)	2.00
A	2.54 (0.04)	2.65 (0.03)	$3b_2$ (2B_2)	2.62 (0.84)	–
B	2.67 (0.04)	–	$4a_1$ (2A_1)	2.63 (0.85)	–
C	3.38 (0.03)	3.28 (0.06)	$2b_2$ (2B_2)	3.47 (0.83)	–
D	4.04 (0.08)	3.88 (0.06)	$1b_1$ (2B_1)	4.07 (0.86)	–
Low-lying isomer of $\text{Na}^+[\text{CaI}_4^{2-}]$ (Figure 2b)					
X'	≈ 1.5	≈ 1.4	$8a'$ ($^2A'$)	1.70 (0.86)	–
A'	–	–	$7a'$ ($^2A'$)	2.26 (0.84)	–
B'	–	–	$6a'$ ($^2A'$)	2.89 (0.84)	–
C'	–	–	$1a''$ ($^2A''$)	3.71 (0.85)	–
D'	–	–	$5a'$ ($^2A'$)	3.87 (0.80)	–

[a] The final state of $\text{Na}^+[\text{CaI}_4^{2-}]$ is given in parentheses. See Figure 3 for pictures of the orbitals of the ground-state structure. [b] All data are at the OVGF/6-311 + G(2df)//MP2/6-311 + G* level of theory. The pole strength is given in parentheses. [c] At the CCSD(T)/6-311 + G(2df)//MP2/6-311 + G* level of theory.

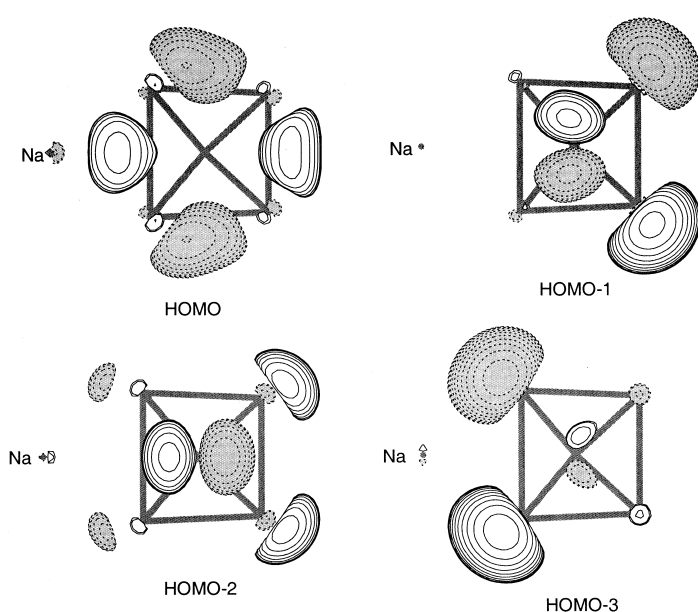


Figure 3. The four highest valence molecular orbitals^[22] of $\text{Na}^+[\text{CaI}_4^{2-}]$ (C_{2v} , 1A_1): HOMO ($5a_1$), HOMO-1 ($3b_2$), HOMO-2 ($4a_1$), HOMO-3 ($2b_2$).

peripheral bond with only minor perturbation to the TPC unit. Therefore, for this molecule we need to consider not only the effective atomic charges, but also peripheral electron density, which is not represented by the atomic charges. The fact that the four-center peripheral ligand–ligand bond and the TPC unit in both $\text{Na}^+[\text{CaI}_4^{2-}]$ and $(\text{Na}^+)_2[\text{CaI}_4^{2-}]$ can maintain their integrity is remarkable and suggests that there is considerable potential that bulk solid materials containing $[\text{CaI}_4^{2-}]$ as a new chemical structural unit may be prepared with the composition $(\text{M}^+)_2[\text{CaI}_4^{2-}]$.

Received: May 8, 2000 [Z15097]

- [1] R. Hoffmann, R. W. Alder, C. F. Wilcox, Jr., *J. Am. Chem. Soc.* **1970**, 92, 4992.
- [2] J. B. Collins, J. D. Dill, E. D. Jemmis, Y. Apeloig, P. von R. Schleyer, R. Seeger, J. A. Pople, *J. Am. Chem. Soc.* **1976**, 98, 5419.
- [3] A. Streitwieser, S. M. Bachrach, A. Dorigo, P. von R. Schleyer in *Lithium Chemistry: A Theoretical and Experimental Overview* (Eds.: A.-M. Sapse, P. von R. Schleyer), Wiley, New York, **1995**, p. 1.

- [4] K. Sorger, P. von R. Schleyer, *J. Mol. Struct.* **1995**, 338, 317.
- [5] D. Stahl, F. Maquin, T. Gaumann, H. Schwarz, P.-A. Carrupt, P. Vogel, *J. Am. Chem. Soc.* **1985**, 107, 5049.
- [6] R. Keese, *Nachr. Chem. Tech.* **1982**, 30, 844.
- [7] W. Luef, R. Keese, *Adv. Strain Org. Chem.* **1993**, 3, 229.
- [8] M. P. McGrath, L. Radom, *J. Am. Chem. Soc.* **1992**, 114, 8531.
- [9] D. R. Rasmussen, L. Radom, *Angew. Chem.* **1999**, 111, 3052; *Angew. Chem. Int. Ed.* **1999**, 38, 2876.
- [10] F. A. Cotton, M. Millar, *J. Am. Chem. Soc.* **1977**, 99, 7886.
- [11] G. Erker, J. Wicher, K. Engel, F. Resenfeldt, W. Dietrich, C. Kruger, *J. Am. Chem. Soc.* **1980**, 102, 6344.
- [12] D. Rottger, G. Erker, *Angew. Chem.* **1997**, 109, 840; *Angew. Chem. Int. Ed. Engl.* **1997**, 36, 812.
- [13] D. Rottger, G. Erker, R. Frohlich, M. Grehl, S. Silverio, I. Hyla-Kryspin, R. Gleiter, *J. Am. Chem. Soc.* **1995**, 117, 10503.
- [14] P. von R. Schleyer, A. I. Boldyrev, *J. Chem. Soc. Chem. Commun.* **1991**, 1536.
- [15] A. I. Boldyrev, J. Simons, *J. Am. Chem. Soc.* **1998**, 120, 7967.
- [16] X. Li, L. S. Wang, A. I. Boldyrev, J. Simons, *J. Am. Chem. Soc.* **1999**, 121, 6033.
- [17] A. I. Boldyrev, J. Simons, *J. Phys. Chem.* **1994**, 98, 2298.
- [18] X. B. Wang, C. F. Ding, J. B. Nicholas, D. A. Dixon, L. S. Wang, *J. Phys. Chem. A* **1999**, 103, 3423.
- [19] L. S. Wang, H. S. Cheng, J. Fan, *J. Chem. Phys.* **1995**, 102, 9480; L. S. Wang, H. Wu in *Advances in Metal and Semiconductor Clusters. IV. Cluster Materials* (Ed.: M. A. Duncan), JAI, Greenwich, **1998**, pp. 299–343.
- [20] We initially optimized geometries and calculated frequencies of $\text{Na}^+[\text{CaI}_4^{2-}]$ and $(\text{Na}^+)_2[\text{CaI}_4^{2-}]$ by using analytical gradients with polarized split-valence basis sets (6-311 + G*) and a hybrid method known in the literature as B3LYP. Then we refined geometries and calculated frequencies at the second-order Møller-Plesset perturbation theory (MP2) level. The energies of the lowest energy structures were refined by using the coupled-cluster (CCSD(T)) method and the more extended 6-311 + G(2df) basis sets. The first ADE of $\text{Na}^+[\text{CaI}_4^{2-}]$ were calculated by using the CCSD(T)/6-311 + G(2df) method. The VDEs were calculated by the outer valence green function method (OVGF) with 6-311 + G(2df) basis sets. All core electrons were kept frozen in treating the electron correlation at the MP2, CCSD(T), and OVGF levels of theory.
- [21] Gaussian 98 Revision A.7, M. J. Frisch, G. W. Trucks, H. B. Schlegel, G. E. Scuseria, M. A. Robb, J. R. Cheeseman, V. G. Zakrzewski, J. A. Montgomery, Jr., R. E. Stratmann, J. C. Burant, S. Dapprich, J. M. Millam, A. D. Daniels, K. N. Kudin, M. C. Strain, O. Farkas, J. Tomasi, V. Barone, M. Cossi, R. Cammi, B. Mennucci, C. Pomelli, C. Adamo, S. Clifford, J. Ochterski, G. A. Petersson, P. Y. Ayala, Q. Cui, K. Morokuma, D. K. Malick, A. D. Rabuck, K. Raghavachari, J. B. Foresman, J. Cioslowski, J. V. Ortiz, A. O. Baboul, B. B. Stefanov, G. Lui, A. Liashenko, P. Piskorz, I. Komaromi, R. Gomperts, R. L. Martin, D. J. Fox, T. Keith, M. A. Al-Laham, C. Y. Peng, A.

Nanayakkara, C. Gonzalez, M. Challacombe, P. M. W. Gill, B. G. Johnson, W. Chen, M. W. Wong, J. L. Andres, M. Head-Gordon, E. S. Replogle, J. A. Pople, Gaussian, Inc., Pittsburgh, PA. 1998.

- [22] The MO pictures were made with the MOLDEN3.4 program: G. Schaftenaar, MOLDEN3.4, CAOS/CAMM Center, The Netherlands, 1998.

Ferromagnetic Ordering in a Two-Dimensional Copper Complex with Dual End-to-End and End-On Azide Bridges**

Zhen Shen, Jing-Lin Zuo,* Song Gao, You Song, Chi-Ming Che, Hoong-Kun Fun, and Xiao-Zeng You*

The construction of multidimensional magnetic materials with ferromagnetic ordering is one of the major challenges in magneto chemistry.^[1] Azide-bridged metal complexes have attracted much attention because of the structural diversity of azide compounds and the electronic versatility of the two bridging modes, end-on (EO) and end-to-end (EE), which mediate ferro- and antiferromagnetic exchange interactions, respectively. The dinuclear azide-bridged copper(II) complexes with both kinds of bridging mode were the first to be studied and well-documented,^[2] then trinuclear,^[3] tetranuclear,^[4] one-dimensional (1D) (uniform^[5] and alternating^[6]), and even alternating two-dimensional (2D)^[7] polymeric complexes have also been characterized structurally and magnetically in recent years. Ferromagnetic interactions were found in EO-bridged dinuclear compounds.^[2a-d,g,h] The 1D and 2D compounds reported are antiferro-^[5a,b, 6a,b,d, 7a] or ferrimagnetic^[6c]. Herein, we report the synthesis, structure, and magnetic properties of the ferromagnetically coupled 2D Cu^{II} compound $[\{\text{Cu}(\text{L})(\text{N}_3)_2\}_n]$ (**1**) (L = benzylamine) (order at $T_c = 7$ K) with both EO and EE bridging modes. Two-dimensional systems that are ordered at low temperatures and contain

both azide coordination modes, have only been reported for Mn^[8] and Ni^[9] compounds, in which the ordering was attributed to canting phenomena. Noteworthy is that 2D Cu^{II}-azide compounds are much rarer than Ni and Mn-azide complexes.

The crystal structure of **1**^[10] shows it to be a neutral sheetlike molecule in which each Cu^{II} ion is five-coordinate in the form of a slightly distorted square-based pyramid, CuN₅ (Figure 1). The apical position is occupied by one nitrogen atom N(3A) of the azide bridge in the EE mode (Cu–N apical bond of 2.332 Å) and the equatorial plane is formed by nitrogen atoms from the amine ligand (N(7)), two EO azide

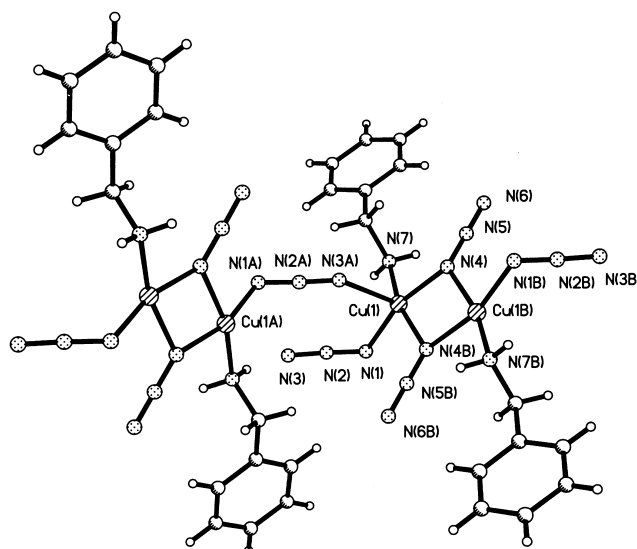


Figure 1. The molecular structure of **1** showing the atom-numbering scheme.

bridges (N(4), N(4B)) and a second EE azide bridge (N(1)). The average Cu–N bond length in the basal plane is 2.005 Å. The maximum deviation from the mean plane of N(1)–N(4)–N(4B)–N(7) is 0.017 Å and the copper atom lies 0.236 Å above this plane. Each Cu^{II} center is bonded to another Cu^{II} center by two EO azide bridges, giving an asymmetrical planar entity (Cu(1)–N(4)–Cu(1B)–N(4B)); the EO bridging azides, which are quasi-linear (N(4)–N(5)–N(6), 179.5(5)°), slightly deviate (up and down) from this plane. The two Cu^{II} ions are related by an inversion center. This feature has been found in several dinuclear Cu^{II} complexes in which the Cu^{II} ions are linked by two EO N₃[−] ions.^[2a,d] In **1** each dinuclear entity is further linked through EE azide bridges to four neighboring dimers, leading to a neutral network (Figure 2). The Cu⋯Cu separation through the EO azide bridges is 3.129 Å, and through the EE bridges is 5.751 Å. The Cu(1)–N(4)–Cu(1B) angle in the EO bridge is 102.0(2)°, which lies in the typical range for this type of bridge. For the EE bridges, the Cu(1)–N(1)–N(2) angle is 121.5(3)° and the Cu(1)–N(3A)–N(2A) is 144.6(3)°.

The IR spectrum of **1** shows two sharp bands at 2094 and 2056 cm^{−1}, consistent with the presence of both EO and EE bridging azides.^[6a] The X-band EPR spectra recorded at room temperature show a very broad feature centered at $g = 2.067$ and no signal at half-field. The spectra remain almost unchanged on lowering the temperature to 110 K, which

[*] Dr. J.-L. Zuo, Prof. X.-Z. You, Dr. Z. Shen, Dr. Y. Song
Coordination Chemistry Institute
State Key Laboratory of Coordination Chemistry
Nanjing University, Nanjing 210093 (China)
Fax: (+86)10-331-7761
E-mail: xyz@netra.nju.edu.cn

Prof. S. Gao
State Key Laboratory of Rare Earth Materials Chemistry and Applications, College of Chemistry and Molecular Engineering
Peking University, Beijing 100871 (China)

Prof. C.-M. Che
Department of Chemistry
The University of Hong Kong and Nanjing University (China)

Prof. H.-K. Fun
X-Ray Crystallography Unit, School of Physics
Universiti Sains Malaysia, 11800 USM, Penang (Malaysia)

[**] This work was supported by the National Natural Science Foundation of China (NSF 29631040 and 29929001), The Major State Basic Research Development Program (Grant No. G2000077500 and No. G1998061306), and the Malaysian Government research grant R&D No. 305/pfizik/622004.

Supporting information for this article is available on the WWW under <http://www.wiley-vch.de/home/angewandte/> or from the author.

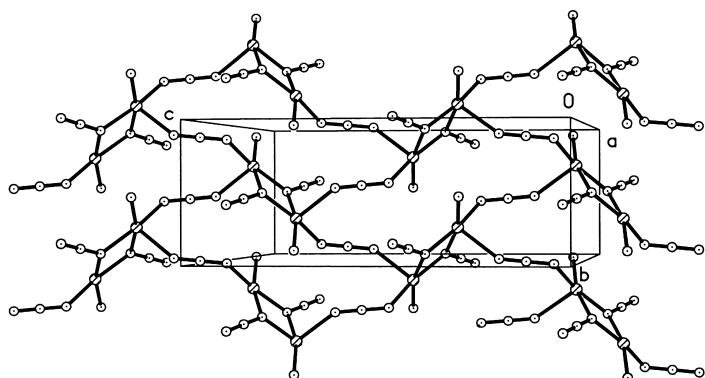


Figure 2. Arrangement of the 2D network of **1** in the *bc* plane (hydrogen and carbon atoms of the amine ligands have been omitted for clarity).

indicates that the square-pyramidal environment of the Cu^{II} ion does not alter to any great extent and the interaction between the Cu^{II} ions is rather weak, in the range of 300–110 K.

The $\chi_{\text{M}}T$ versus T plot of **1** is shown in Figure 3a (χ_{M} being the molar magnetic susceptibility per two Cu^{II} ions). At room temperature $\chi_{\text{M}}T$ is equal to $1.08 \text{ emu mol}^{-1} \text{ K}$, which is

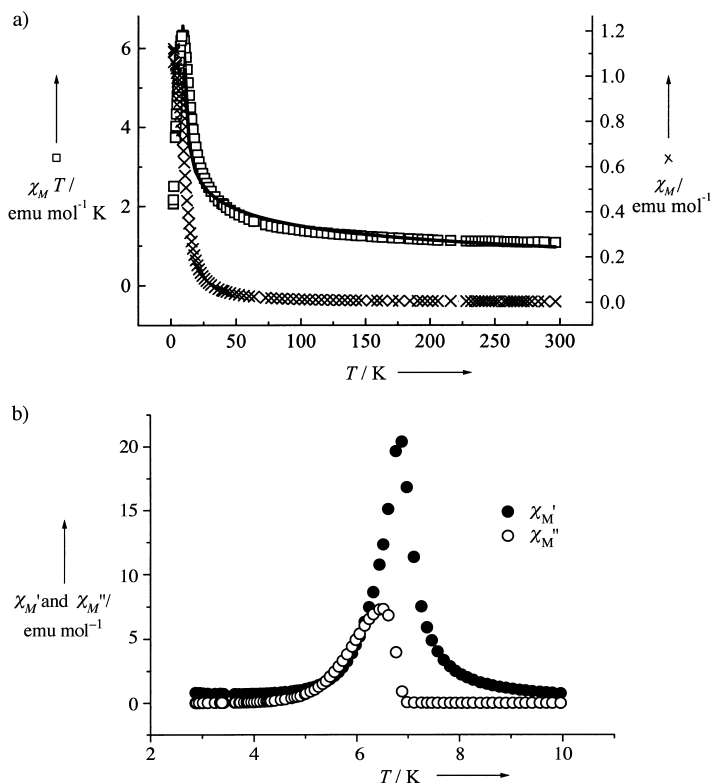


Figure 3. a) Plot of the temperature dependence of $\chi_{\text{M}}T$ (□) and χ_{M} (×) of **1** measured at 10 kOe field. The solid line corresponds to the best theoretical fit (see text); b) temperature dependence of AC susceptibility obtained at zero external magnetic field, $H_{\text{AC}} = 2 \text{ Oe}$, 111 Hz.

slightly higher than that expected for two uncoupled Cu^{II} ions. It increases upon cooling and reaches a maximum at 9 K ($\chi_{\text{M}}T = 6.33 \text{ emu mol}^{-1} \text{ K}$) and then decreases to $2.06 \text{ emu mol}^{-1} \text{ K}$ at 2 K. No maximum was observed in the χ_{M} versus T plot. Apparently, short-range ferromagnetic correlation is present in the system, and it develops into a

long range ordering state below 9 K. This is evidenced by zero field alternating current (AC) susceptibility shown in Figure 3b, from which $T_{\text{c}} = 7 \text{ K}$ was determined as the maximum of χ_{M}' . The plot also shows the appearance of nonzero χ_{M}'' . The magnetization at 1.9 K (Figure 4a) increases very rapidly in low field, as expected for a magnet, and reaches $2.07 \mu_{\text{B}}$

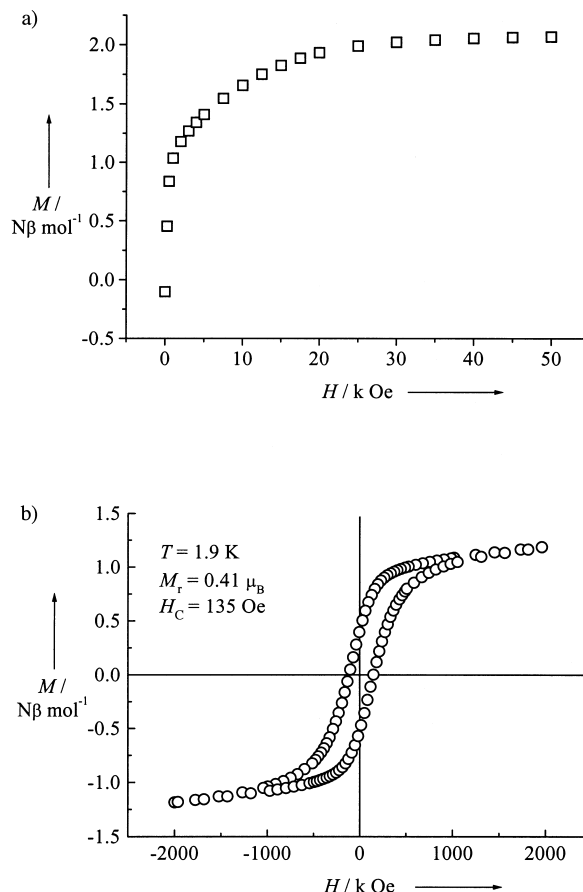


Figure 4. a) Magnetization versus field up to $H = 50 \text{ kOe}$ at 1.9 K for **1**; b) hysteresis loop in the $\pm 2 \text{ kOe}$ range at $T = 1.9 \text{ K}$.

at 50 kOe, which corresponds to the theoretical saturation value for two ferromagnetically ordered $S_{\text{Cu(dimer)}} = 1$, $g = 2.07$. Furthermore, a characteristic hysteresis loop is observed at 1.9 K with a remanent magnetization (M_{r}) of $0.41 \mu_{\text{B}}$ and a coercive field (H_{c}) of 135 Oe (Figure 4b). These results are all indicative of a long-range ordered ferromagnetic ground state. From a magnetic viewpoint, the double EO azide bridges should promote ferromagnetic interaction for angles between 100° – 105° , while asymmetric EE bridges with short equatorial Cu–N bonds and a long axial Cu–N bond could propagate negligible interaction for square-pyramidal geometry at the copper center.^[2a] Thus, ferromagnetic coupling is predominant in compound **1**. To evaluate the super-exchange coupling constants in such a magnetic system we tried to simplify it by treating it as an interacting dimer, μ -(1,1- N_3) $_2\text{Cu}_2$, with the exchange through the EE azide bridges as an inter-dimer molecular field^[6b] [Eq. (1)]. In this case J is the intra-dimer exchange constant through the double EO bridges, J' is the inter-dimer coupling constant transferred by the single EE azide group and z is 4.

$$\chi_{\text{dimer}} = N g^2 \mu_B^2 S(S+1) (1+u)/3kT \quad (1a)$$

$$u = \coth[JS(S+1)/kT] - kT/JS(S+1) \quad (1b)$$

$$\chi_M = \chi_{\text{dimer}}/[1 - \chi_{\text{dimer}}(2zJ/Ng^2\mu_B^2)] \quad (1c)$$

The best fit for $\chi_M T$ versus T in the range of 9–300 K (solid line shown in Figure 3a) leads to the following parameters: $J/k = 71.18$ K, $J'/k = 0.58$ K, $g = 2.07$ and $R = 2.0 \times 10^{-2}$ ($R = \Sigma[(\chi_M)_{\text{obs}} - (\chi_M)_{\text{calcd}}]^2 / \Sigma[(\chi_M)_{\text{obs}}]^2$). The small positive J' value implies that the exchange interaction through the axial asymmetrical EE bridging azide is very weakly ferromagnetic. This is mainly because of the strict orthogonality of σ_x and π_z azide orbitals.^[3b] The low temperature magnetic data (2–20 K) measured at different external fields between 200 Oe to 10 kOe indicate that the value of $\chi_M T$ increases greatly with decreasing magnetic field. This result suggest that the presence of field-saturation effects in addition to the possible weak inter-layer antiferromagnetic interaction may cause the decrease of $\chi_M T$ below 9 K.

Very recently, Monfort et al.^[11] reported a 2D molecular material with Ni^{II} centers and azide units that shows metamagnetic behavior. Our work supplies the first 2D metal–azide bridged compounds with long-range ferromagnetic ordering properties. Details of further magnetic measurements can be found in the Supporting Information.

Experimental Section

A solution of CuCl₂·6H₂O (1 mmol) in methanol (10 mL) was added to a solution of NaN₃ (2 mmol) and the hydrobromide salt of benzylamine (1 mmol) in H₂O (25 mL). A Black-brown precipitate formed over several minutes. The solid was collected by filtration and washed with methanol and diethyl ether (yield ca. 75 %). Elemental analysis calcd for C₇H₅CuN₇ (%): C 32.97, H 3.53, N 38.47, Cu, 24.93; found: C 32.78, H 3.70, N 38.56, Cu 25.00; IR: $\tilde{\nu}_{\text{max}} = 2094, 2056$ cm⁻¹(ν_{asym} N₃). Black needles suitable for single-crystal X-ray analysis were obtained by slow evaporation of the filtrate in air.

Received: April 17, 2000 [Z14999]

- [1] O. Kahn, *Molecular Magnetism*, VCH, Weinheim, 1993.
 [2] a) S. Sikorav, I. Bkouche-Waksman, O. Kahn, *Inorg. Chem.* **1984**, 23, 490; b) O. Kahn, S. Sikorav, J. Gouteron, S. Jeannin, Y. Jeannin, *Inorg. Chem.* **1983**, 22, 2877; c) J. Comarmond, P. Plumere, J. M. Lehn, Y. Agnus, R. Louis, R. Weiss, O. Kahn, I. Morgenstern-Badarau, *J. Am. Chem. Soc.* **1982**, 104, 6330; d) R. Cortes, M. Karnele Urtiaga, L. Lezama, J. R. Larramendi, M. Isabel Arriortua, T. Rojo, *J. Chem. Soc. Dalton Trans.* **1993**, 3685; e) Y. Agnus, R. Louis, R. Weiss, *J. Am. Chem. Soc.* **1979**, 3381; f) M. Charlot, O. Kahn, M. Chaillet, C. Larrieu, *J. Am. Chem. Soc.* **1986**, 108, 2574; g) K. D. Karlin, J. C. Hayes, J. P. Hutchinson, J. Zubieta, *J. Chem. Soc. Chem. Commun.* **1983**, 376; h) M. A. Aebersold, B. Gillon, O. Plantevin, L. Pardi, O. Kahn, P. Bergerat, I. Seggern, F. Tuzek, L. Ohrstrom, A. Grand, E. Lelievre-Berna, *J. Am. Chem. Soc.* **1998**, 120, 5238.
 [3] a) M. H. W. Lam, Y. Y. Tang, K. M. Fung, X. Z. You, W. T. Wong, *Chem. Commun.* **1997**, 957; b) J. C. Liu, D. G. Fu, J. Z. Zhuang, C. Y. Duan, X. Z. You, *J. Chem. Soc. Dalton Trans.* **1999**, 2337.
 [4] S. S. Tandon, L. K. Thompson, D. O. Miller, *Chem. Commun.* **1995**, 1907.
 [5] a) Z. N. Chen, H. X. Zhang, K. B. Yu, B. S. Kang, *Chem. Lett.* **1998**, 275; b) G. D. Munno, M. Julve, F. Lloret, J. Faus, M. Verdager, A. Caneschi, *Angew. Chem.* **1993**, 105, 1122; *Angew. Chem. Int. Ed. Engl.* **1993**, 32, 1046; c) L. K. Thompson, S. S. Tandon, F. Lloret, J. Cano, M. Julve, *Inorg. Chem.* **1997**, 36, 3301; d) G. W. Bushnell, M. A. Khan, *Can. J. Chem.* **1974**, 52, 3125; e) F. A. Mautner, M. A. S. Goher, *Polyhedron* **1994**, 13, 2141; f) M. A. S. Goher, F. A. Mautner, *Polyhedron* **1998**, 17, 1561.
 [6] a) G. D. Munno, M. G. Lombardi, M. Julve, F. Lloret, J. Faus, *Inorg. Chim. Acta* **1998**, 282, 82; b) Z. Shen, J. L. Zuo, Z. Yu, Y. Zhang, J. F.

- Bai, C. M. Che, H. K. Fun, J. J. Vittal, X. Z. You, *J. Chem. Soc. Dalton Trans.* **1999**, 3393; c) A. Escuer, R. Vicente, M. S. El Fallah, M. A. S. Goher, F. A. Mautner, *Inorg. Chem.* **1998**, 37, 4466; d) T. C. W. Mak, M. A. S. Goher, *Inorg. Chim. Acta* **1986**, 115, 17; e) F. A. Mautner, M. A. S. Goher, *Polyhedron* **1992**, 11, 2537; f) F. A. Mautner, M. A. S. Goher, *Polyhedron* **1993**, 12, 2823.
 [7] a) Z. N. Chen, J. Qiu, Z. K. Wu, D. G. Fu, K. B. Yu, W. X. Tang, *J. Chem. Soc. Dalton Trans.* **1994**, 1923; b) A. Escuer, R. Vicente, M. A. S. Goher, F. A. Mautner, *Inorg. Chem.* **1998**, 37, 782; c) G. De Munno, T. Poerio, G. Viau, M. Julve, F. Lloret, Y. Journaux, E. Riviere, *Chem. Commun.* **1996**, 2587; d) A. Escuer, R. Vicente, M. A. S. Goher, F. A. Mautner, *Inorg. Chem.* **1995**, 34, 5707.
 [8] A. Escuer, R. Vicente, M. A. S. Goher, F. A. Mautner, *Inorg. Chem.* **1997**, 36, 3440.
 [9] J. Ribas, M. Monfort, X. Solans, M. Drillon, *Inorg. Chem.* **1994**, 33, 742.
 [10] Crystal data (C₇H₅CuN₇): monoclinic, space group $P2_1/c$; $a = 13.664(1)$, $b = 5.4609(4)$, $c = 14.165(1)$ Å, $\beta = 96.395(1)^\circ$, $V = 1050.38(13)$ Å³, $Z = 4$, $\rho_{\text{calcd}} = 1.611$ g cm⁻³, $\mu = 2.058$ mm⁻¹, $F(000) = 516$, $\lambda = 0.71073$ Å, $T = 293$ K; 7132 reflections were measured on a Siemens SMART CCD area detector diffractometer and yielded 2586 unique data ($2\theta_{\text{max}} = 56.62^\circ$, $R_{\text{int}} = 0.0664$, semiempirical absorption corrections). The structure was solved by direct methods and refined by full-matrix least-squares methods using SHELXTL. $R(\text{on } F^2) = 0.0504$, $\omega R(\text{on } F^2) = 0.0827$, 136 parameters. Largest difference peak/hole $0.751/-0.730$ e Å⁻³. Crystallographic data (excluding structure factors) for the structure reported in this paper have been deposited with the Cambridge Crystallographic Data Centre as supplementary publication no. CCDC-142222. Copies of the data can be obtained free of charge on application to CCDC, 12 Union Road, Cambridge CB21EZ, UK (fax: (+44) 1223-336-033; e-mail: deposit@ccdc.cam.ac.uk).
 [11] M. Monfort, I. Resino, J. Ribas, H. Stoeckli-Evans, *Angew. Chem.* **2000**, 112, 197; *Angew. Chem. Int. Ed. Engl.* **2000**, 39, 191.

Asymmetric Conjugate Addition of Azide to α,β -Unsaturated Carbonyl Compounds Catalyzed by Simple Peptides**

Thomas E. Horstmann, David J. Guerin, and Scott J. Miller*

Stimulated by the efficiency exhibited by enzymes, chemists have sought not only to understand the mechanistic basis for enzymatic reactions, but also to reproduce and even surpass their capabilities. The complementary fields of enzymatic catalysis and transition metal based asymmetric catalysis have recorded many successes in the field of enantioselective reaction development. One question at the interface of these

[*] Prof. S. J. Miller, T. E. Horstmann, D. J. Guerin
 Department of Chemistry
 Boston College
 Chestnut Hill, MA 02467-3860 (USA)
 Fax: (+1) 617-552-3620
 E-mail: scott.miller.1@bc.edu

[**] This research was supported by the U.S. National Institutes of Health (GM-57595). We are also grateful to the U.S. National Science Foundation for generous support in the form of a CAREER Award (CHE-9874963). In addition, we thank DuPont, Eli Lilly, Glaxo-Wellcome, and the Merck Chemistry Council for research support. S.J.M. is a Fellow of the Alfred P. Sloan Foundation, a Cottrell Scholar of Research Corporation, and a Camille Dreyfus Teacher-Scholar.

Supporting information for this article is available on the WWW under <http://www.wiley-vch.de/home/angewandte/> or from the author.

crotonate are inert under the reaction conditions. The more conventional oxazolidinone **6** is somewhat less reactive than **4a**, and the product **7** shows also a reduced level of enantiomeric excess in comparison to product **5a** (85 % yield, 45 % *ee*, Table 1, entry 6).

Examination of a variety of other peptides reveals that, as in our studies of asymmetric acyl transfer, subtle changes in the β -turn structure have a substantial impact on reaction efficiency. Catalysts **8–11** provide representative results (Table 2). In general, all peptides containing the N-terminal

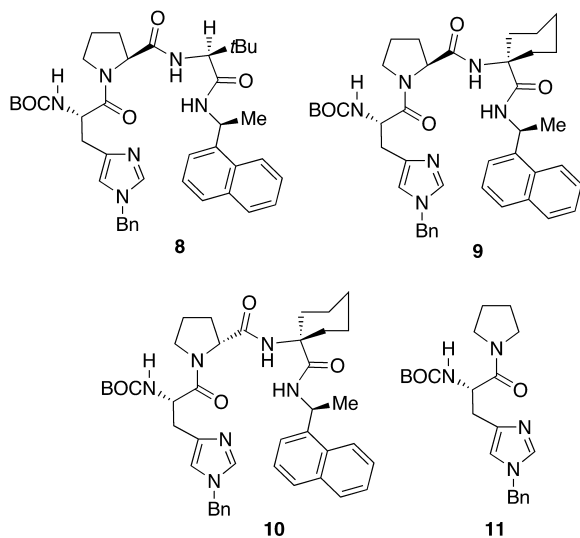


Table 2. Screen of selected catalysts for β -azidation of substrate **4a**.

Entry	Catalyst	Conversion [%] ^[a]	<i>ee</i> [%] ^[b]
1	3	100	63
2	8	74	14
3	9	82	63
4	10	75	–21
5	11	72	no Selectivity

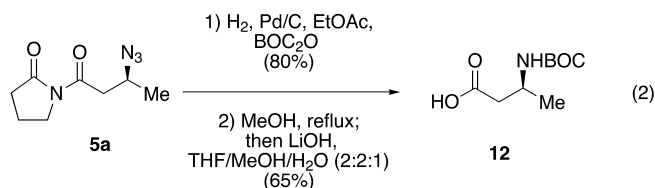
[a] Determined by 400 MHz ^1H NMR spectroscopy. [b] Determined by chiral HPLC. See Supporting Information for details.

τ -(benzyl)-histidine residue were found to be catalytically active. Systematic variation of the residues revealed that in the $i+2$ position, D-*t*-Leu was found to give rise to a more selective catalyst than L-*t*-Leu. As stated above, for the crotonyl-substituted substrate **4a**, catalyst **3** affords the product with quantitative conversion and 63 % *ee* (Table 2, entry 1). However, when catalyst **8** is employed (identical to **3** except for the exchange of L-*t*-Leu in place of the D-*t*-Leu), the product is obtained in only 14 % *ee* (74 % conversion, Table 2, entry 2). The effect of the proline stereogenic center was ascertained by comparing the performance of peptides **9** and **10**, with a spirocyclic amino acid in the $i+2$ position. In the case of catalyst **9**, with L-Pro in the $i+1$ position, the product is obtained in 63 % *ee* (82 % conversion, Table 2, entry 3). However, with D-Pro in this position (catalyst **10**, Table 2, entry 4), the product is delivered with only 21 % *ee*. Notably, this diastereomeric catalyst afforded opposite enantioselectivity in the conjugate addition. Control peptide **11**, devoid of

any secondary structure, resulted in nonselective reactions under all conditions employed (Table 2, entry 5).

The mechanistic basis for the reaction selectivities is under investigation. Certainly, the conformation of the peptide catalyst plays a role in dictating the enantioselectivity of a given catalyst, and studies to determine the reactive conformations are underway.^[13] In addition, “nonlinear” effects have achieved an important status in asymmetric catalysis as a tool for elucidating kinetically significant noncovalent interactions among chiral catalysts. We thus carried out a study to probe for such effects in reactions catalyzed by **3**. Indeed, a linear increase in product *ee* is observed with a linear increase in the *ee* value of the catalyst at the optimized dilution for the reaction conditions ($R^2 = 0.98$).^[14] While the interpretation of such probes for nonlinear behavior is a matter of some discussion,^[15] the results are consistent with the catalyst behaving in a monomeric form during the stereochemistry-determining step.

To demonstrate that the pyrrolidinone-derived products of these reactions are readily converted to the corresponding protected β -amino acid synthons, we carried out the following sequence [Eq. (2)]. Product **5a** was subjected to catalytic hydrogenation (Pd/C, EtOAc) in the presence of BOC₂O (80 % yield; BOC = butoxycarbonyl). The resulting protected amine was then hydrolyzed by employing a two-step sequence that affords the N-BOC amino acid **12** in 65 % yield.



In summary, we have shown that simple β -turn peptides armed with a τ -(benzyl)-His residue are enantioselective catalysts for the azidation of β -substituted acrylate derivatives. As in our previous studies of asymmetric acyl transfer, there appears to be a close connection between amino acid sequence in the peptides and the enantioselectivities that are observed. Future studies will involve a combination of catalyst screening and mechanistic studies targeted at improved catalyst selectivities and also a detailed understanding of how these systems work.

Received: June 5, 2000 [Z 15220]

- [1] a) M. S. Sigman, E. N. Jacobsen, *J. Am. Chem. Soc.* **1998**, *120*, 4901–4902; b) M. S. Iyer, K. M. Gigstad, N. D. Namdev, M. Lipton, *J. Am. Chem. Soc.* **1996**, *118*, 4910–4911.
- [2] a) S. J. Miller, G. T. Copeland, N. Papaioannou, T. E. Horstmann, E. M. Ruel, *J. Am. Chem. Soc.* **1998**, *120*, 1629–1630; b) G. T. Copeland, E. R. Jarvo, S. J. Miller, *J. Org. Chem.* **1998**, *63*, 6784–6785; c) E. R. Jarvo, G. T. Copeland, N. Papaioannou, P. J. Bonitatebus, Jr., S. J. Miller, *J. Am. Chem. Soc.* **1999**, *121*, 11638–11643.
- [3] B. List, R. A. Lerner, C. F. Barbas III, *J. Am. Chem. Soc.* **2000**, *122*, 2395–2396.
- [4] C. Agami, C. Puchot, H. Sevestre, *Tetrahedron Lett.* **1986**, 1501–1504.
- [5] K. A. Ahrendt, C. J. Borths, D. W. C. MacMillan, *J. Am. Chem. Soc.* **2000**, *122*, 4243–4244.

- [6] For other representative metal-free asymmetric catalysts that do not employ peptides, see: a) Y. Iwabuchi, M. Nakatani, N. Yokoyama, S. Hatakeyama, *J. Am. Chem. Soc.* **1999**, *121*, 10219–10220; b) E. J. Corey, M. J. Grogan, *Org. Lett.* **1999**, *1*, 157–160; c) H. Hemstra, H. Wynberg, *J. Am. Chem. Soc.* **1981**, *103*, 417–430. For examples involving peptide-based catalysts, see: d) K. Tanaka, A. Mori, S. Inoue, *J. Org. Chem.* **1990**, *55*, 181–185; e) S. Itsuno, M. Sakakura, K. Ito, *J. Org. Chem.* **1990**, *55*, 6047–6049.
- [7] D. J. Guerin, T. E. Horstmann, S. J. Miller, *Org. Lett.* **1999**, *1*, 1107–1109.
- [8] See also: a) P. Lakshminpathi, A. V. Rama Rao, *Tetrahedron Lett.* **1997**, *38*, 2551–2552; b) B. Y. Chung, Y. S. Park, I. S. Cho, B. C. Hyun, *Bull. Korean Chem. Soc.* **1988**, *9*, 269–270.
- [9] a) *Enantioselective Synthesis of β -Amino Acids* (Ed.: E. Juaristi), Wiley-VCH, New York, **1997**; b) D. C. Cole, *Tetrahedron* **1994**, *50*, 9517–9582.
- [10] For noteworthy recent advances, see: a) S. Kobayashi, S. Nagayama, *J. Am. Chem. Soc.* **1997**, *119*, 10049–10053; b) D. Ferraris, B. Young, T. Dudding, T. Lectka, *J. Am. Chem. Soc.* **1998**, *120*, 4548–4549; c) M. P. Sibi, J. J. Shay, M. Liu, C. P. Jasperse, *J. Am. Chem. Soc.* **1998**, *120*, 6615–6616; d) B. J. Kim, Y. S. Park, P. Beak, *J. Org. Chem.* **1999**, *64*, 1705–1708; e) D. A. Evans, L. D. Wu, J. J. M. Wiener, J. S. Johnson, D. H. B. Ripin, J. S. Tedrow, *J. Org. Chem.* **1999**, *64*, 6411–6417; f) T. P. Tang, J. A. Ellman, *J. Org. Chem.* **1999**, *64*, 12–13.
- [11] For representative studies in the field, see: a) D. H. Appella, J. J. Barchi, S. R. Durrell, S. H. Gellman, *J. Am. Chem. Soc.* **1999**, *121*, 2309–2310; b) K. Gademan, M. Ernst, D. Hoyer, D. Seebach, *Angew. Chem.* **1999**, *111*, 1302–1304; *Angew. Chem. Int. Ed.* **1999**, *38*, 1223–1226.
- [12] J. K. Myers, E. N. Jacobsen, *J. Am. Chem. Soc.* **1999**, *121*, 8959–8960.
- [13] For example, we have recently reported that β -turns with τ -(benzyl)-His in the N-terminal position can adopt Asx-Pro turnlike structures. See: J. T. Blank, D. J. Guerin, S. J. Miller, *Org. Lett.* **2000**, *2*, 1247–1249.
- [14] The plot documenting the absence of a nonlinear effect may be found in the Supporting Information.
- [15] a) D. G. Blackmond, *Acc. Chem. Res.* **2000**, *33*, 402–411; b) H. B. Kagan, T. O. Luukas in *Comprehensive Asymmetric Catalysis, Vol. 1* (Eds.: E. N. Jacobsen, A. Pfaltz, H. Yamamoto), **1999**, pp. 101–118.

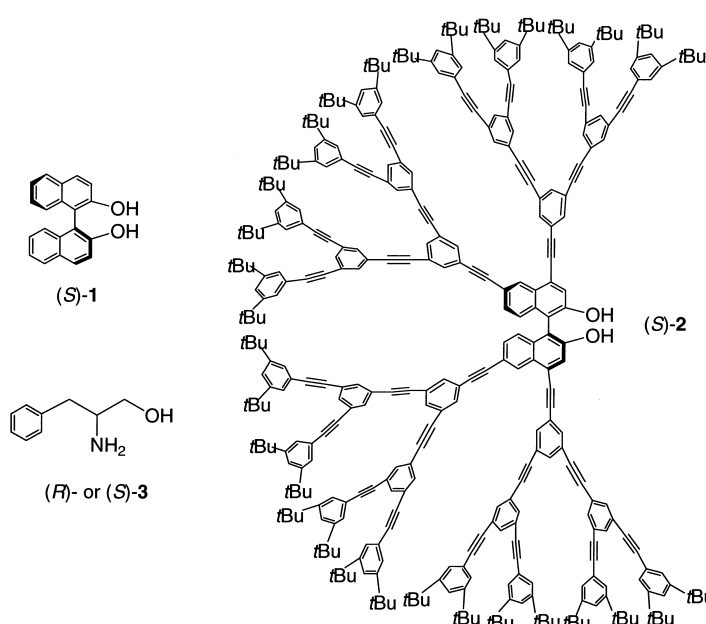
The First Dendrimer-Based Enantioselective Fluorescent Sensor for the Recognition of Chiral Amino Alcohols**

Vincent J. Pugh, Qiao-Sheng Hu, and Lin Pu*

The development of fluorescence-based molecular sensors has received broad attention in research in recent years.^[1–3] The use of fluorescence spectroscopic methods for molecular recognition has many advantages: fluorescence provides many more signaling modes for substrate detection, such as quenching, fluorescence enhancement, excimers, exciplexes,

and lifetimes, than electronic absorption. The high sensitivity of fluorescence techniques requires the use of only very small amounts of sensor molecules. Fluorescence spectrometers are also of low cost and widely available. Fluorescence sensors can be further applied to continuous monitoring and remote sensing by using optical fibers. A large number of fluorescent sensors have been designed for applications in the detection of metal ions, phosphates, and neutral molecules.^[1–3] Recently, a fluorescent sensor has also been used in the combinatorial search for catalysts.^[4a] If such fluorescent sensors could be made enantioselective, they would allow a rapid analysis of the enantiomeric composition of thousands of chiral molecules generated by the combinatorial synthesis. This process would greatly facilitate the combinatorial discovery of asymmetric catalysts or reagents since the current chromatographic analysis of enantiomers is inherently a slow process. An enzyme-catalyzed release of fluorophores has been used in the search for catalytic antibodies for the enantioselective hydrolysis of acetates.^[4b] Chiral discrimination by luminescence has also been studied in the past two decades.^[5–9] These studies involve a variety of luminescent materials including inorganic complexes,^[5] organic molecules,^[6–8] and enzymes.^[9] Enantioselective responses have been observed when chiral luminophores are treated with chiral quenchers or enhancers. The relationship between the fluorescence properties of the sensors and the enantiomeric purity of the substrates have been established in a few cases.^[5b, 6g, 7, 9b]

Recently, we carried out a program to incorporate chiral dendrimers^[10] into enantioselective fluorescent sensors as a real-time technique to quantitatively or semi-quantitatively determine the enantiomeric composition of chiral molecules. Properly designed dendritic materials have been found to show efficient migration of energy from the dendrons or periphery groups to the more conjugated units or core, which has led to greatly enhanced fluorescence intensity.^[11–17] The strong fluorescence signals of such dendrimers should be very useful in the development of fluorescent sensors. Based on the structure of chiral 1,1'-bi-2-naphthol ((*S*)-**1**)^[18] and the den-



[*] Prof. Dr. L. Pu, Dr. V. J. Pugh, Dr. Q.-S. Hu
Department of Chemistry
University of Virginia
Charlottesville, VA 22901
E-mail: lp6n@virginia.edu

[**] The support of this work by the National Institute of Health (1R01GM58454) is gratefully acknowledged. We also thank the partial support from the donors of the Petroleum Research Fund—administered by the American Chemical Society.

drons of Xu and Moore,^[11] we have synthesized optically active dendrimers such as (S)-2.^[19] We have found that there is very efficient migration of energy from the phenylacetylene dendrons of (S)-2 to the chiral binaphthyl core.^[19] Thus, the dendritic arms of (S)-2 serve as light-harvesting antenna. This result is similar to that observed by Xu and Moore in the optically inactive phenyleneacetylene dendrimer system.^[11] Herein we report that dendrimer (S)-2 can carry out enantioselective fluorescent sensing of chiral amino alcohols.

We have compared the fluorescence of dendrimer (S)-2 with that of the parent molecule (S)-1, and have found that the fluorescence intensity of the dendrimer is dramatically increased over that of (S)-1. This enhancement occurs because of the increased number of absorbing units as well as from the efficient intramolecular migration of energy in (S)-2.^[19] Dendrimer (S)-2 emits at $\lambda_{em}=422$ and 441 (sh) nm when excited at 310 nm. Figure 1 shows the fluorescence spectra of dendrimer (S)-2 (excited at 310 nm, the maximum in its

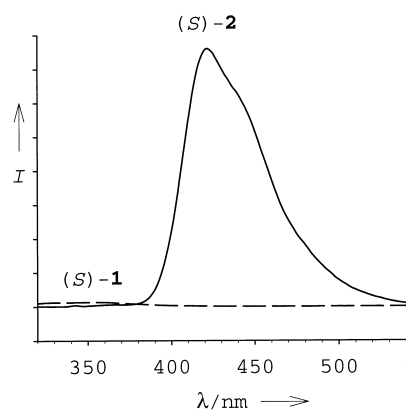


Figure 1. Comparison of the fluorescence spectrum of dendrimer (S)-2 with that of (S)-1 in benzene:hexane (20:80) (uncorrected).

excitation spectrum) and (S)-1 (excited at 280 nm, the maximum in its excitation spectrum) at the same concentration (4.0×10^{-8} M) in a mixed solvent of benzene and hexane (20:80). Only when the concentration of (S)-1 is increased over 170 times, does its fluorescence intensity become comparable with that of (S)-2. The greatly enhanced fluorescence of the dendrimer makes it potentially more useful as a fluorescent sensor than the weakly fluorescent 1,1'-bi-2-naphthol. (S)-2 is a second generation dendrimer. Its fluorescence is also much stronger than that of the lower generation ones.^[19]

We have studied the fluorescence of dendrimer (S)-2 in the presence of chiral amino alcohols and amines, such as 2-amino-1-propanol, 3-methyl-1-butanol, 2-amino-3-phenyl-1-propanol, 2-amino-4-methyl-1-pentanol (leucinol), and *trans*-1,2-diaminocyclohexane. We found that of the compounds studied the enantiomers of 2-amino-3-phenyl-1-propanol (phenylalaninol, (R)- and (S)-3) quench the fluorescence of (S)-2 very efficiently and also with a significantly different rate. Other chiral amino alcohols or amines also quench the fluorescence of (S)-2 efficiently, but with smaller enantioselective responses. Figure 2 shows the Stern–Völmer

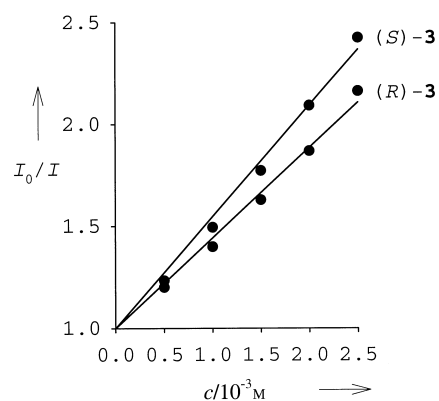


Figure 2. The Stern–Völmer plot of dendrimer (S)-2 in the presence of (R)- and (S)-3.

quenching plot of (S)-2 (4.0×10^{-8} M) in the presence of (R)- and (S)-3 in a mixed solvent of benzene and hexane (20:80).^[20] The amino alcohols were purchased from Aldrich with a purity of 98 % for both (R)- and (S)-3. These two compounds were dissolved in methanol and filtered through silica gel, and then recrystallized from EtOAc:hexane (2.5:1). As shown in Figure 2, the fluorescence quenching of the chiral dendrimer by the amino alcohol is enantioselective. The Stern–Völmer constant is $556 \text{ M}^{-1} \pm 2\%$ (K_{sv}^S) in the presence of (S)-3 and $473 \text{ M}^{-1} \pm 2\%$ (K_{sv}^R) in the presence of (R)-3. Thus, $K_{sv}^S - K_{sv}^R = 83 \text{ M}^{-1}$ and $K_{sv}^S/K_{sv}^R = 1.18$. The *S* enantiomer of 3 quenches the fluorescence of the chiral dendrimer more efficiently than the *R* enantiomer. The opposite enantiomer of the dendrimer shows the opposite trend in quenching efficiency for the amino alcohol enantiomers, which indicates there is a chirality-based luminescence-quenching selectivity.

In 1992, Iwanek and Mattay found certain enantioselectivity in the quenching of the luminescence of (R)- and (S)-1 by optically active amines and amino alcohols.^[6c] We have also studied the fluorescence of (S)-1 in the presence of (S)- and (R)-3 in the mixed solvent of benzene and hexane (20:80) and found the Stern–Völmer constants of 121 and 118 M^{-1} , respectively. Thus, $K_{sv}^S - K_{sv}^R = 3 \text{ M}^{-1}$ and $K_{sv}^S/K_{sv}^R = 1.03$. This indicates that dendrimer (S)-2 not only provides much stronger fluorescence signals than (S)-1 for observation, but also leads to higher enantioselectivity in chiral recognition. The much larger Stern–Völmer constants of the dendrimer demonstrate that the fluorescence of the dendrimer is much more sensitive to the amino alcohol quencher than that of the parent binaphthol.

The amine-induced fluorescence quenching of (R)- and (S)-1 were attributed to both ground-state hydrogen bonding as well as excited-state deprotonation of individual binaphthol molecules.^[6c] We found that the ground-state deprotonation of (S)-1 in benzene:hexane (20:80) by NaOH was accompanied by a large red-shift (45 nm) in the lowest energy absorption in the UV/Vis spectrum. A similar large red-shift (50 nm) of the lowest energy UV/Vis absorption of dendrimer (S)-2 was also observed in the presence of NaOH in the same mixed solvent. The deprotonated form showed very weak fluorescence. However, a red-shift of only 5 nm was observed for (S)-2 in the presence of 3 (2.0×10^{-3} M) in benzene/hexane (20/80). This indicates a hydrogen-bonding interaction be-

tween (*S*)-**2** and **3** rather than proton transfer in the ground state. It was found that the lowest singlet-excited-state pK_a^* value for β -naphthol is 2.8, whereas the ground-state pK_a value is 9.5.^[21] The acidity of β -naphthol is increased by over six orders of magnitude from the ground state to the excited state. A similarly small pK_a^* value is expected for (*S*)-**2** in its excited state. Thus, dendrimer (*S*)-**2** in the presence of **3** should be deprotonated in the excited state. Therefore, the possible pathways for the fluorescence quenching of (*S*)-**2** by **3** might include a radiationless decay of the hydrogen-bonded complex formed between (*S*)-**2** and **3** and the formation of a poorly emissive proton-transfer complex in the excited state.

We have also found that the hydroxyl groups of (*S*)-**2** are necessary for efficient quenching by amino alcohols as there was no significant quenching by (*S*)-**3** when the two hydroxyl groups of (*S*)-**2** were converted into two methoxy groups. The hydroxyl groups of (*S*)-**2** allow the fluorescence quenching to occur at the binaphthyl core, to where the light-harvesting dendrons funnel the energy.^[11, 19] This effect increases the sensitivity of the dendrimer toward the amino-alcohol quencher and explains the much larger Stern–Völmer constants of dendrimer (*S*)-**2** than those of the small molecule (*S*)-**1**.

The enantioselective quenching of the fluorescence of (*S*)-**2** by (*R*)- and (*S*)-**3** has led us to study the effect of the enantiomeric purity of **3** on the value of the Stern–Völmer quenching constant of the dendrimer. When (*S*)-**2** (4.0×10^{-8} M) was treated with **3** (2.0×10^{-3} M) in which the ratio of the *R* and *S* enantiomers were varied a linear plot of the K_{sv} value versus the percentage of the *S* enantiomer in the *R* and *S* mixture of **3** was obtained (Figure 3). The fluorescence signal

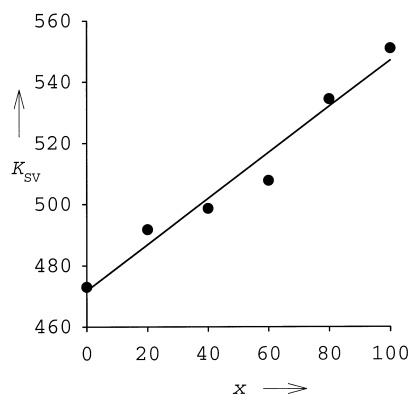


Figure 3. The relationship of the K_{sv} value of the dendrimer (*S*)-**2** with the enantiomeric composition of chiral amino alcohol **3**; x: percent of (*S*)-**3**.

of the dendrimer is quenched by about 48–53% at this concentration. As the percentage of the *S* enantiomer increases, there is a linear increase in the Stern–Völmer constant. This experiment demonstrates that the enantiomeric composition of a chiral molecule can be determined with the use of a fluorescent dendritic sensor. Thus, the K_{sv} value of the fluorescent dendrimer can be used to predict the enantiomeric excess (*ee*) of a chiral quencher.

In summary, we have discovered that there is a dramatic enhancement of fluorescence intensity from 1,1'-bi-2-naphthol to the corresponding dendrimer, as a result of the

exponentially increased number of absorbing units and an efficient intramolecular migration of energy. The fluorescence of the chiral binaphthol-based dendrimer can be enantioselectively quenched by a chiral amino alcohol. A linear relationship has been established between the Stern–Völmer constant of the dendrimer and the enantiomeric composition of the chiral amino alcohol. Such enantioselective fluorescent sensors may allow a rapid determination of the enantiomeric composition of chiral molecules, and are potentially useful in the high-throughput combinatorial search for asymmetric catalysts and reagents. The strong fluorescence of the dendrimer provides intense signals for detection and allows the use of very small amounts of the chiral materials. In addition, the light-harvesting antennas of the dendrimer funnel energy to the center where it is quenched by the amino alcohol. This allows the dendrimer sensor to have much more sensitive fluorescence responses than the corresponding small molecule sensor. We are currently working on extending the observed enantioselective fluorescence response of this class of chiral dendrimers to other chiral organic substrates in order to develop sensors for practical applications. The influence of the dendrimer generation on the enantioselectivity and sensitivity will also be studied.

Received: March 28, 2000
Revised: May 23, 2000 [Z14914]

- [1] "Fluorescent Chemosensors for Ion and Molecular Recognition": ACS Symp. Ser. **1993**, 538.
- [2] A. P. de Silva, H. Q. N. Gunaratne, T. Gunnlaugsson, A. J. M. Huxley, C. P. McCoy, J. T. Rademacher, T. E. Rice, *Chem. Rev.* **1997**, 97, 1515.
- [3] L. Fabbri, *Acc. Chem. Res.* **1999**, 32, 846.
- [4] a) G. T. Copeland, S. J. Miller, *J. Am. Chem. Soc.* **1999**, 121, 4306; b) G. Klein, J.-L. Reymond, *Helv. Chim. Acta* **1999**, 82, 400.
- [5] a) D. P. Glover-Fischer, D. H. Metcalf, J. P. Bolender, F. S. Richardson, *Chem. Phys.* **1995**, 198, 207; b) D. H. Metcalf, S. W. Snyder, J. N. Demas, F. S. Richardson, *J. Am. Chem. Soc.* **1990**, 112, 5681; c) D. H. Metcalf, J. M. M. Stewart, S. W. Snyder, C. M. Grisham, F. S. Richardson, *Inorg. Chem.* **1992**, 31, 2445; d) R. Corradini, G. Sartor, R. Marchelli, A. Dossena, A. Spisni, *J. Chem. Soc. Perkin Trans. 2* **1992**, 1979; e) R. B. Rexwinkel, S. C. J. Meskers, H. P. J. M. Dekkers, J. P. Riehl, *J. Phys. Chem.* **1992**, 96, 5725; f) S. C. J. Meskers, H. P. J. M. Dekkers, *J. Am. Chem. Soc.* **1998**, 120, 6413.
- [6] For references on chiral binaphthyl molecules used in enantioselective discrimination by fluorescence, see a) M. Irie, T. Yoroze, K. Hayashi, *J. Am. Chem. Soc.* **1978**, 100, 2236; b) T. Yoroze, K. Hayashi, M. Irie, *J. Am. Chem. Soc.* **1981**, 103, 5480; c) T. D. James, K. R. A. S. Sandanayake, S. Shinkai, *Nature* **1995**, 374, 345; d) T. D. James, K. R. A. S. Sandanayake, R. Iguchi, S. Shinkai, *J. Am. Chem. Soc.* **1995**, 117, 8982; e) W. Iwanek, J. Mattay, *J. Photochem. Photobiol. A* **1992**, 67, 209; f) D. Avnir, E. Wellner, M. Ottolenghi, *J. Am. Chem. Soc.* **1989**, 111, 2001; g) K. S. Parker, A. Townshend, S. J. Bale, *Anal. Proc. (London)* **1995**, 32, 329; h) for a review article on using binaphthyl-based molecules in colorimetric recognition of amines, see Y. Kubo, *Synlett* **1999**, 2, 161.
- [7] a) T. Grady, S. J. Harris, M. R. Smyth, D. Diamond, *Anal. Chem.* **1996**, 68, 3775; b) T. Grady, T. Joyce, M. R. Smyth, S. J. Harris, D. Diamond, *Anal. Commun.* **1998**, 35, 123.
- [8] a) M. A. Fox, N. J. Singletary, *Tetrahedron Lett.* **1979**, 35, 21892; b) P. Tundo, J. H. Fendler, *J. Am. Chem. Soc.* **1980**, 102, 1760; c) F. López-Arbeloa, M. V. D. Auweraer, F. Ruttens, F. C. De Schryver, *J. Photochem. Photobiol. A* **1988**, 44, 63; d) H. Yang, C. Bohne, *J. Photochem. Photobiol. A* **1995**, 86, 209.
- [9] a) A. Gafni, *J. Am. Chem. Soc.* **1980**, 102, 7367; b) Y. Yan, M. L. Myrick, *Anal. Chem.* **1999**, 71, 1958.

- [10] For selected references on chiral dendrimers, see a) D. Seebach, P. B. Rheiner, G. Greiveldinger, T. Butz, H. Sellner, *Top. Curr. Chem.* **1998**, *197*, 125; b) H. W. I. Peerlings, E. W. Meijer, *Chem. Eur. J.* **1997**, *3*, 1563; c) K. Aoi, K. Itoh, M. Okada, *Macromolecules* **1995**, *28*, 5391; d) J. Shao, J. P. Tam, *J. Am. Chem. Soc.* **1995**, *117*, 3894; e) H.-F. Chow, C.-C. Mak, *J. Chem. Soc. Perkin Trans. 1* **1994**, 2223; f) H.-T. Chang, C.-T. Chen, T. Kondo, G. Siuzdak, K. B. Sharpless, *Angew. Chem.* **1996**, *108*, 202; *Angew. Chem. Int. Ed. Engl.* **1996**, *35*, 182; g) J. R. McElhanon, D. V. McGrath, *J. Am. Chem. Soc.* **1998**, *120*, 1647; h) J. Issberner, H. Böhme, S. Grimme, M. Nieger, W. Paulus, F. Vögtle, *Tetrahedron: Asymmetry* **1996**, *7*, 2223.
- [11] a) J. S. Moore, *Acc. Chem. Res.* **1997**, *30*, 402; b) Z. Xu, J. S. Moore, *Angew. Chem.* **1993**, *105*, 1394; *Angew. Chem. Int. Ed. Engl.* **1993**, *32*, 1354–1357.
- [12] a) M. Kawa, J. M. J. Fréchet, *Chem. Mater.* **1998**, *10*, 286; b) S. L. Gilat, A. Adronov, J. M. J. Fréchet, *Angew. Chem.* **1999**, *111*, 1519; *Angew. Chem. Int. Ed.* **1999**, *38*, 1422.
- [13] a) M. A. Fox, W. E. Jones, Jr, D. M. Watkins, *Chem. Eng. News* **1993**, *71*(11), 38; b) G. M. Stewart, M. A. Fox, *J. Am. Chem. Soc.* **1996**, *118*, 4354.
- [14] V. Balzani, S. Campagna, G. Denti, A. Juris, S. Serroni, M. Venturi, *Acc. Chem. Res.* **1998**, *31*, 26.
- [15] a) A. Bar-Haim, J. Klafer, R. Kopelman, *J. Am. Chem. Soc.* **1997**, *119*, 6197; b) A. Bar-Haim, J. Klafer, *J. Phys. Chem. B* **1998**, *102*, 1662.
- [16] a) D.-L. Jiang, T. Aida, *J. Am. Chem. Soc.* **1998**, *120*, 10895; b) D.-L. Jiang, T. Aida, *Nature* **1997**, *388*, 454.
- [17] F. Li, S. I. Yang, Y. Ciringh, J. Seth, C. Martin III, D. L. Singh, D. Kim, R. R. Birge, D. F. Bocian, D. Holten, J. S. Lindsey, *J. Am. Chem. Soc.* **1998**, *120*, 10001.
- [18] For a review on binaphthyl-based materials, see L. Pu, *Chem. Rev.* **1998**, *98*, 2405.
- [19] Q.-S. Hu, V. Pugh, M. Sabat, L. Pu, *J. Org. Chem.* **1999**, *64*, 7528.
- [20] The Stern–Völmer equation: $I_0/I = 1 + K_{sv}[Q]$ where I_0 and I are the fluorescence intensity of the luminophore in the absence and presence of a quencher, respectively; $[Q]$ is the concentration of the quencher; K_{sv} is the Stern–Völmer constant. For an explanation of Stern–Völmer constants and plots, see J. R. Lakowicz, *Principles of Fluorescence Spectroscopy*, 2nd ed., Kluwer Academic, Plenum, New York, **1999**.
- [21] J. Stam, J.-E. Lofroth, *J. Chem. Educ.* **1986**, *63*, 181.

Catalyst for DNA Ligation: Towards a Two-Stage Replication Cycle**

Jingdong Ye, Yahaloma Gat, and David G. Lynn*

The chemical methods available for the ligation of complementary oligomers along a DNA template are complex, requiring transition metal and imidazole catalysis of the condensation reaction. We were interested in simplifying the required conditions by converting the DNA template itself into a better catalyst, and report a modified backbone linkage which greatly simplifies the reaction. As related backbone linkages have been prepared by chemically reading the DNA

sequence, this reaction completes a replication cycle, simplifying the ubiquitous three-stage replication cycle, the central dogma of biology,^[1] to a two-stage chemical process.

Several laboratories have contributed to optimizing the reaction conditions for template-directed phosphodiester formation.^[2] In the BrCN, imidazole, NiCl₂ cocktail, BrCN has a half-life of several minutes in the aqueous media. Premixing the cocktail generates *N*-cyanoimidazole, the reagent required to activate ligation.^[2d,e] While more stable than BrCN under the reaction conditions, displaying a half-life of several hours, *N*-cyanoimidazole will chemoselectivity ligate a nick site along a DNA template. Many aromatic drugs are known to bind tightly within the narrow minor groove of DNA, particularly A/T tracts,^[3] including netropsin, distamycin, Hoechst 33258, and the bis-amidine compounds benenil and pentamidine, and do so by displacing specific well-ordered H₂O molecules known to line this cavity.^[4] It is therefore possible that *N*-cyanoimidazole associates with the nick site better than BrCN to facilitate the activation and/or the ligation steps in the condensation.

In an attempt to replicate this effect by template modification, five synthetic templates, T_{N-H}, T_{N-pr}, T_{N-bu}, T_{N-im}, and T_{N-ea}, were compared with the native DNA (T_P) under ligation conditions (Figure 1). Each template was prepared

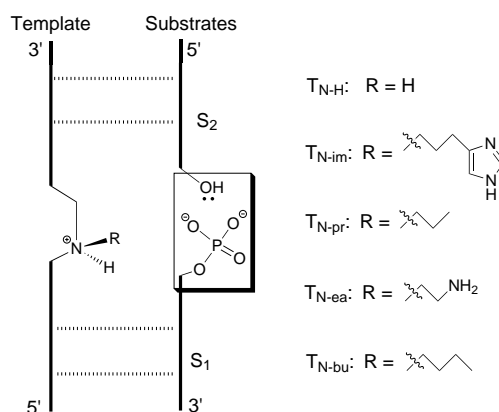


Figure 1. The ternary complex formed by template and complementary substrates, 8mer S₁ and 12mer S₂. The sequence of the template is HO-dCpCpGpTpTpCpGpTpTpTXXTpCpTpGpTpCpTpCpG-OH. S₁ is HO-dApCpGpApApCpGpGp-OH, and S₂ is HO-dCpGpApGpApCpApGpApApA-OH. X in the sequence represents the site of insertion of the various linkage structures. In Tp, X represents the native phosphodiester linkage of DNA.

with the appropriate synthetic amine thymidine dimer incorporated into standard solid-phase synthesis protocols.^[5d] The 20mer templates were designed such that the complementary DNA substrates, S₁ and S₂, displayed high binding affinity with the template. Thermal melting analyses indeed established that the melting temperature for all template–substrate duplexes T/S₁ (35 ± 2 °C) and T/S₂ (45 ± 2 °C) were very similar and > 10 °C above the reaction temperature. A 1:1:1 stoichiometry therefore generated significant and equivalent concentrations of the ternary complexes (T:S₁:S₂) for each reaction.

All modified templates and substrates were purified prior to reaction by reverse-phase chromatography, and purity was

[*] D. G. Lynn, J. Ye, Y. Gat
Departments of Chemistry and Biology, Emerson Hall
Emory University, Atlanta, GA 30322 (USA)
Department of Chemistry
University of Chicago
Chicago, IL 60637
Fax: (+1) 404-727-9348
E-mail: dlynn2@emory.edu

[**] We are grateful to Paul Gardner for assistance with solid-phase synthesis and the NIH (R21 RR12723) for support.

confirmed by denaturing PAGE. The 8mer S_1 was enzymatically 5'-phosphorylated by using T4 polynucleotide kinase and γ - ^{32}P -ATP. Figure 2a shows a typical phosphoimage analysis of the reaction after incubation for 24 h with three templates, T_P , T_{N-H} , and T_{N-pr} , using the full conditions optimized for DNA ligation (BrCN, imidazole, NiCl_2).^[2] The fastest running material is the 5'-phosphorylated 8mer substrate S_1 . In the presence of template, a single new higher molecular weight species grew in with time at the expense of S_1 intensity. The new band was assigned as the ligated product by electrophoretic comparison with synthetic 5'-phosphorylated 20mer.

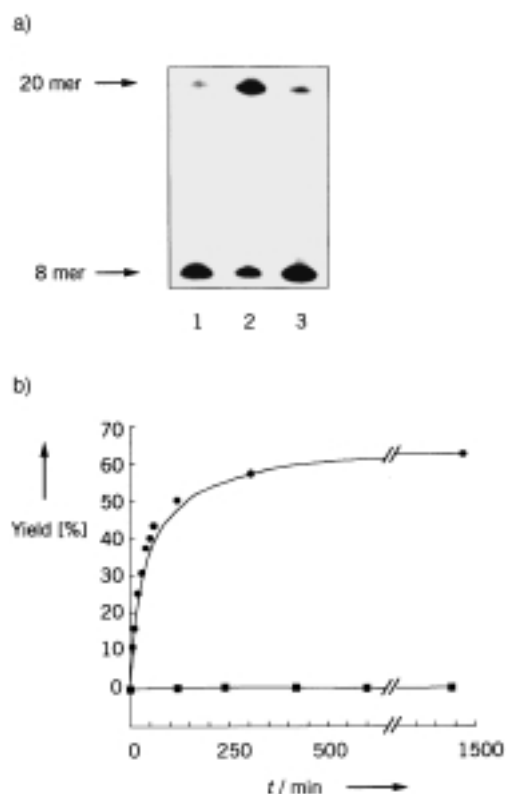


Figure 2. a) Autoradiograms of PAGE gels. Each coupling reaction was analyzed after 24 h under full DNA activation conditions (BrCN, imidazole, NiCl_2): Lane 1, T_P ; lane 2, T_{N-H} ; lane 3, T_{N-pr} . b) Time dependence of ligation reactions with templates T_P (■) and T_{N-pr} (●) using BrCN alone as the activating reagent.

Table 1 summarizes the initial rates of ligation obtained by catalysis with the different templates. Surprisingly, T_{N-H} was equally as good a catalyst as T_P . DNA strands containing a

Table 1. Initial rates of ligation.^[a]

Activation	T_P	T_{N-H}	T_{N-im}	T_{N-pr}	T_{N-ea}	T_{N-bu}
full conditions	1.1	1.2	15	22	1.6	21
without imidazole	n.d.	n.d.	23	34	n.d.	31
BrCN only	n.d.	n.d.	28	63	n.d.	76

[a] Ligation yields were determined from the percentage of radioactivity in the product band relative to that of the whole lane; initial rates are expressed as $10^{-1} \mu\text{M h}^{-1}$. The reaction conditions were full: 40 mM BrCN, 20 mM imidazole, 40 mM NiCl_2 ; without imidazole; and BrCN only. n.d. = not determined; the reaction yields in these cases were less than 4% after 24 h.

single amine linkage were previously shown to form less stable duplexes with complementary DNA,^[5d] and T_{N-H} was expected to be less preorganized for condensation at the nick site as a result of the flexibility of the amine linkage.^[3] While the template containing imidazole T_{N-im} was a better catalyst than T_P , giving a >10 -fold larger initial rate and significantly better yields under these activation conditions, both T_{N-pr} and T_{N-bu} were even better. Without imidazole added to the reaction, both T_P and T_{N-H} were inactive, while the catalytic activity of T_{N-im} , T_{N-pr} , and T_{N-bu} was further improved. Figure 2b compares the relative effectiveness of T_{N-pr} and T_P with BrCN alone. Under these conditions, T_{N-pr} and T_{N-bu} are exceptional catalysts, while DNA is inactive.

The data in Table 1 establish that the addition of *N*-alkyl substituents to the template dramatically increases the rate of ligation with BrCN alone. The ligation rates with *N*-cyanoimidazole were tested by premixing the cocktail for 5 h prior to addition of T and S. The T_P -catalyzed initial rate was elevated from 0.11 to $2.4 \mu\text{M h}^{-1}$, identical with the T_{N-pr} rate. Therefore, T_{N-pr} does not enhance the reaction of all dehydrating agents at the nick site, but opens the BrCN manifold.

The role of more polar groups in the R substituent was further explored through the preparation of the T_{N-ea} template. The *N*-ethylamine substituent is isosteric with the *N*-propyl, but likely contains a protonated primary amine in solution at pH 8.^[6] As shown in Table 1, the enhancement observed with this template was weak at best, the T_{N-ea} template giving a 14-fold lower initial rate than T_{N-pr} under the full activating conditions and inactive otherwise. In contrast, the more sterically demanding but neutral T_{N-bu} template showed catalytic activity equivalent with T_{N-pr} . The incorporation of more polar functional groups to aid in the catalytic steps may be possible, but minimally their placement must be carefully considered.

To test for the global effect of the backbone modification, the reaction site was shifted by a single base pair to either the 5' or 3' side of the modification by investigation of the 9mer+11mer and 7mer+13mer complementary substrate pairs. Under full activation conditions where observed initial rates could be compared and expressed relative to the DNA template, T_{N-pr}/T_P , both the 7 + 13 and 9 + 11 substrate pairs gave ratios of 1, while the 8 + 12 substrate pair was 20 (Table 1). Therefore, consistent with a B-DNA conformation found for related T_{N-H} templates,^[3d] the site of closest backbone-backbone approach in the duplex is offset by three base pairs in linear sequence, and a one base pair shift to either side eliminates the *N*-propyl enhancement. The effect of the *N*-propyl substituent is therefore local and site-specific, with no apparent global change in duplex structure contributing to catalysis.

While a greater understanding of the catalytic reactions of the $T_{N-alkyl}$ templates will require further structural and kinetic analyses, covalently anchoring the hydrophobic substituents to the backbone amine within the nick site opens the reaction manifold with BrCN. The alkyl substituent on the amine linker, as was seen with alkyl groups on the bases,^[7] should alter local groove solvation, minimally allowing BrCN access so as to open the new reaction manifold. Clearly such

backbone modifications can profoundly enhance ligation reactions and we suspect can be further extended by the appropriate placement of functional groups.

Our understanding of template-directed synthesis and sequence replication will benefit considerably from the discovery that such simple modifications to the backbone can open reaction manifolds inaccessible to DNA. DNA can be chemically translated into T_{N-H} backbones.^[5a, b] By exploiting features of the reading reaction, $>10^6$ fold amplification of the encoded sequence information has been achieved (Figure 3).^[5c, e] Here we complete the cycle, establishing that

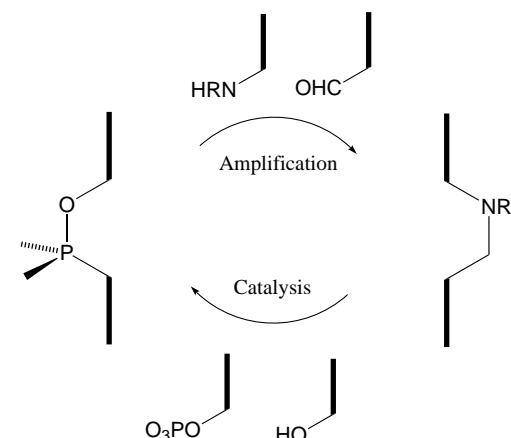


Figure 3. Proposed two-stage replication cycle showing both the amplification in the synthesis of the ethylamine-containing backbone and the use of that backbone to catalyze the synthesis of the original template.

the amplified product can catalyze the transfer of the encoded information back into DNA in an efficient, site-specific manner, and under conditions where DNA is inactive. For a single turn of this overall two-stage replication cycle, greater than the biological exponential growth limit could be achieved. Certainly, it is now possible to read the DNA-encoded information into different polymers that have unique catalytic properties, in this case to catalyze the synthesis of the initial DNA template. To the extent that these single ligation steps can be extended to multiple ligation or polymerization events, the design of strategies for molecular evolution and functional selection in materials other than natural biopolymers becomes possible.

Experimental Section

Thymidine dimers: The initial dimer was synthesized by a previously developed convergent approach.^[5c,d] Reductive amination of the 5'- and 3'-bis-silyl-protected dimer with the appropriate aldehyde gave the required tertiary alkylamines chemoselectively in 85% yield. Deprotection with $Et_3N \cdot 3HF$ followed by 5'-dimethoxytrityl and 3'-phosphorylation with 2-cyanoethyl *N,N*-diisopropylchlorophosphoramidite gave the activated thymidine dimer for solid-phase synthesis. Thymidine dimers containing primary and secondary amines were protected by trifluoroacetylation prior to activation and cleaved at the end of the solid-phase synthesis in concentrated ammonia.

5'-Phosphorylation: In a typical procedure, the oligonucleotide (900 pmol), T4 polynucleotide kinase (30 U), γ -³²P-ATP (10 pmol), ATP (1125 pmol,

1.25 equiv), $MgCl_2$ (10 mM), DTT (5 mM), and Tris-HCl (70 mM) at pH 7.6 were incubated in a total volume of 50 μ L at 37 °C for 30 min. The enzyme was heat inactivated at 65 °C for 20 min, and the oligonucleotide was purified by reverse-phase Sep-Pak filtration.

Ligation: Condensation reactions were initiated at 24 °C by the addition of a freshly prepared BrCN solution to give a mixture containing: both substrates and template (10 μ M), BrCN (40 mM), $NiCl_2$ (20 mM), imidazole (20 mM), and 0.5 M NaCl at pH 8 in Tris-HCl (20 mM) in a total volume of 30 μ L. Each reaction was quenched with urea (5 M) and analyzed by high-resolution denaturing 20% polyacrylamide gels. No product ($>1\%$) could be detected in the absence of template.

Received: February 17, 2000

Revised: June 10, 2000 [Z14726]

- [1] F. H. C. Crick, *Symp. Soc. Exp. Biol.* **1958**, 12, 138; D. Mazia in *Enzymes: Units of Biological Structure and Function* (Ed.: E. H. Gaebler), Academic Press, **1956**, pp. 261–278.
- [2] a) E. Kanaya, H. Yanagawa, *Biochemistry* **1986**, 25, 7423; b) K. J. Luebke, P. B. Dervan, *J. Am. Chem. Soc.* **1989**, 111, 8733; c) G. Zuber, C. Sirlin, J.-P. Behr, *J. Am. Chem. Soc.* **1993**, 115, 4939; d) N. G. Dolinnaya, N. I. Sokolova, D. T. Ashirbekova, Z. A. Shabarova, *Nucleic Acids Res.* **1991**, 19, 3067; e) J. Selvasekaran, K. D. Turnbull, *Nucleic Acids Res.* **1998**, 26, 1.
- [3] H. R. Drew, R. E. Dickerson, *J. Mol. Biol.* **1981**, 535; M. G. Kubinec, D. E. Wemmer, *J. Am. Chem. Soc.* **1992**, 114, 8739; E. Liepinsh, G. Otting, K. Wuthrich, *Nucleic Acids Res.* **1992**, 20, 6549; Y. Duan, P. Wilkosz, M. Crowley, J. M. Rosenberg, *J. Mol. Biol.* **1997**, 272, 553.
- [4] C. M. Nunn, S. Neidle, *J. Med. Chem.* **1995**, 38, 2317; T. C. Jenkins, A. N. Lane, *Biochim. Biophys. Acta* **1997**, 1350, 189; S. Neidle, *Biopolymers* **1997**, 44, 105; A. Guerri, I. J. Simpson, S. Neidle, *Nucleic Acids Res.* **1998**, 26, 2873; B. S. P. Reddy, S. M. Sondhi, J. W. Lown, *Pharmacol. Ther.* **1999**, 84, 1.
- [5] a) J. T. Goodwin, D. G. Lynn, *J. Am. Chem. Soc.* **1992**, 114, 9197; b) J. T. Goodwin, P. Z. Luo, J. C. Leitzel, D. G. Lynn in *Self-Production of Supramolecular Structures* (Eds.: G. R. Fleischaker, S. Colonna, P. L. Luisi), Kluwer, Dordrecht, **1994**, pp. 99–104; c) Z.-Y. J. Zhan, D. G. Lynn, *J. Am. Chem. Soc.* **1997**, 119, 12420; d) P. Z. Luo, J. C. Leitzel, D. G. Lynn, *J. Am. Chem. Soc.* **1998**, 120, 3019–3031; e) Y. Gat, D. G. Lynn, *Biopolymers* **1998**, 48, 19; f) “Template-Directed Ligation: Towards the synthesis of sequence specific polymers”, Y. Gat, D. G. Lynn in *Templated Organic Synthesis* (Eds.: P. J. Stang, F. Diederich), Wiley-VCH, Weinheim, **1999**.
- [6] D. D. Perrin, *Dissociation Constants of Organic Bases in Aqueous Solution*, Butterworths, London, **1965**.
- [7] a) L. E. Xodo, G. Manzini, F. Quadrifoglio, G. A. van der Marel, J. H. van Boom, *Nucleic Acids Res.* **1991**, 19, 5625; b) B. C. Froehler, S. Wadwani, T. J. Terhorst, S. R. Gerrard, *Tetrahedron Lett.* **1992**, 33, 5307; c) R. W. Wagner, M. D. Matteucci, J. G. Lewis, A. J. Gutierrez, C. Moulds, B. C. Froehler, *Science* **1993**, 260, 1510.

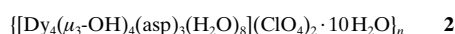
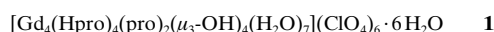
From Cubane to Supercubane: The Design, Synthesis, and Structure of a Three-Dimensional Open Framework Based on a Ln_4O_4 Cluster**

Bao-Qing Ma, Da-Shun Zhang, Song Gao,*
Tian-Zhu Jin, Chun-Hua Yan, and Guang-Xian Xu

High-nuclearity clusters are of great interest due to their fascinating structures and potential magnetic, optical, electronic, and catalytic applications, which may ultimately lead to new materials.^[1] Additionally, high-nuclearity clusters represent a mesoscopic state between the macro- and microphase in terms of dimension.^[2] As nanoparticles, they may exhibit unusual physical and chemical properties as exemplified by the well-known Mn_{12} cluster which displayed a quantum tunnel effect.^[3] On the other hand, the nanoparticles prepared by the cluster complex method have advantages such as being grain-homogeneous and the ability to control the size through modifying the dimension of the cluster core. The synthesis of the high-nuclearity clusters is still a great challenge. The commonly employed strategy is to control the hydrolysis or alcoholysis of metal ions with the aid of supporting ligands.^[4] In general, hydrophilic groups such as hydroxy, oxo, and carboxylate, lie within the core and induce the core aggregation, while hydrophobic groups form the periphery preventing the core from infinite aggregation. The choice of auxiliary ligands is critical to the cluster formation. Very recently, we have shown that amino acids, such as proline, valine, tyrosine, leucine, methionine, alanine, isoleucine, are an effective and promising family of ligands for the formation of lanthanide clusters at higher pH (6–6.5). Most of the clusters obtained display a Ln_4O_4 cubane structural motif. Even a pentadecanuclear lanthanide cluster with tyrosine comprises five corner-sharing Ln_4O_4 units.^[5] Thus, the cubane Ln_4O_4 core appears to be a common type^[6] and can serve as a building block for condensed clusters. The next logical step for us was to investigate whether the cubane units could be connected through bridging ligands to give multidimensional networks. In principle, the aqua position can be replaced by ligands capable of strong coordination such as 4,4'-bipyridine, and the partial monocarboxylate can be substituted by a dicarboxylate

such as 1,4-benzenedicarboxylic acid. Among the natural amino acids there are two dicarboxylates, namely L-aspartic acid (asp) and L-glutamic acid (glu); these not only retain the nature of amino acids but also possess bridging capability. Thus it should be feasible to link discrete Ln_4O_4 cubane units into an extended network and this assumption has been confirmed by the reaction of $\text{Dy}(\text{ClO}_4)_3$ and asp to give a three-dimensional supercubane open framework. Although metal–organic open frameworks have been extensively exploited because of their gas sorption, guest inclusion, and ion-exchange properties,^[7] the microporous networks containing lanthanide ions are still limited in spite of their special luminescence properties and catalytic activity.^[8] Herein we describe a lanthanide microporous framework, to the best of our knowledge, the first assembly of a discrete lanthanide cluster into a three-dimensional (3D) network.

As typical examples, we report the tetranuclear cluster **1** and the three-dimensional network **2**, which were prepared by mixing $\text{Ln}(\text{ClO}_4)_3$ ($\text{Ln} = \text{Gd}, \text{Dy}$) and L-proline or L-aspartic acid, respectively, in aqueous solution, and subsequently adjusting pH values to about 6.5 using aqueous NaOH solution.



X-ray structure analysis reveals that the compound **1** is composed of a discrete tetranuclear cation $[\text{Gd}_4(\text{Hpro})_4(\text{pro})_2(\mu_3\text{-OH})_4(\text{H}_2\text{O})_7]^{6+}$, perchlorate, and lattice water.^[9] The tetrameric cation (Figure 1) is based on a Gd_4 trigonal pyramid, in which Gd1 is located on a threefold axis, and

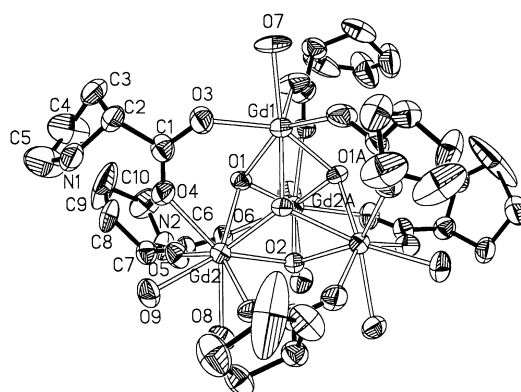


Figure 1. A perspective view of partial structure in compound **1**.

occupies the apical position, while the other three Gd2 ions lie in the basal plane. The $\text{Gd1} \cdots \text{Gd2}$ and $\text{Gd2} \cdots \text{Gd2A}$ separations are 3.8542(11) and 3.8629(8) Å, respectively; thus the Gd_4 unit is very close to a regular tetrahedron. Each triangular Gd_3 face is capped by a triply bridging hydroxy ligand with $\text{Gd} \cdots \text{O}$ bond lengths in the range between 2.367(3) and 2.482(3) Å. These may be compared to the $\text{Gd} \cdots \text{O}$ distances of 2.363(7)–2.412(7) Å in $[\text{Gd}_4(\mu_3\text{-OH})_4(\mu_2\text{-H}_2\text{O})_2(\text{H}_2\text{O})_4(\text{hfpd})_8]^{6+}$ ($\text{hfpd-H} = 1,1,1,5,5,5\text{-hexafluoropentane-2,4-dione}$),^[6b] which has a tetrahedral geometry with

[*] Prof. Dr. S. Gao, Dr. B.-Q. Ma, Prof. T.-Z. Jin, Prof. Dr C.-H. Yan, Prof. Dr. G.-X. Xu
State Key Laboratory of Rare Earth Materials Chemistry and Applications
PKU-HKU Joint Laboratory on Rare Earth Materials and Bioinorganic Chemistry
Peking University
Beijing 100871 (P. R. China)
Fax: (+86) 10-6275-1708
E-mail: gaosong@chemms.chem.pku.edu.cn
Prof. D.-S. Zhang
Changde Normal College, Changde 415000 (P. R. China)

[**] This work was supported by the National Natural Science Foundation of China (No. 29771001, 29831010), National Key Project for Fundamental Research (G1998061306), and the Excellent Young Teachers Fund of MOE, P.R. China

Supporting information for this article is available on the WWW under <http://www.wiley-vch.de/home/angewandte/> or from the author.

face-capping hydroxy groups. Each pair of adjacent Gd ions are also bridged by one carboxy group of a proline ligand in the *syn-syn* mode (mean Gd–O_{carboxyl} bond length, 2.367 Å). Alternatively, the structure may be regarded as a distorted cubane, in which the four bridging OH[−] groups are also considered as vertices of the polyhedron. The Gd1 ion is seven-coordinate, surrounded by three OH[−] groups, three carboxy oxygen atoms, and an aqua ligand O7 lying in the C₃ axis, yielding a monocapped trigonal antiprism. The Gd2 ion is eight-coordinate, surrounded by three OH[−] groups, three carboxy oxygen atoms, and two aqua ligands in a square antiprism, in which the top and bottom planes are defined by O1, O2, O5, O8 and O4, O9, O1B, O6B, respectively.

Compound **2** forms a three-dimensional network based on a Dy₄O₄ cubane core connected by bridging asp ligands.^[9] The Ln₄O₄ cubane core is similar to that observed in **1** (Figure 2). The Ln₄ tetrahedron is embedded in the Dy₄O₄ cubane core; the Dy⋯Dy separation ranges between 3.7211(5) and 3.8526(6) Å. Each triangular face is capped by a triply bridging hydroxy ligand (av Dy–O 2.357 Å, Dy–O–Dy 106.62°). Each Dy ion is eight-coordinate, surrounded by three OH[−] groups, three carboxy oxygen atoms (av Dy–O 2.342 Å), and two aqua ligands (av Dy–O 2.441 Å), yielding a distorted square antiprism.

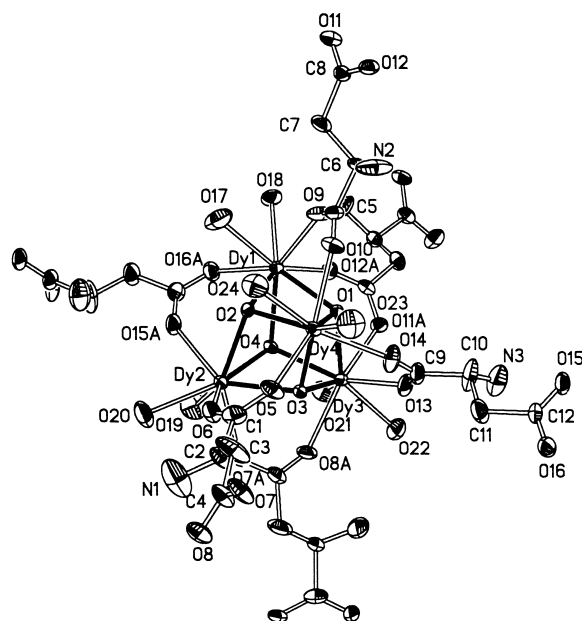


Figure 2. Structure of one of the units that forms the extended network of compound **2**.

Each edge of each Dy₄ tetragon is connected by dicarboxylate ligands to give a {Ln₄(OH)₄(COO)₆} cluster as a basic unit. These are then further extended to form a three-dimensional network with an intersecting parallelepiped-shaped pore (11.78 Å), which houses water molecules and ClO₄[−] ions. Allowing for the van der Waals radii, the free pore volume of the structure is 33.1 %, based on the calculation approach adopted by Yaghi et al.;^[10] this value is large among the known microporous networks (Figure 3). When the bound water molecules are removed, the volume increases up to

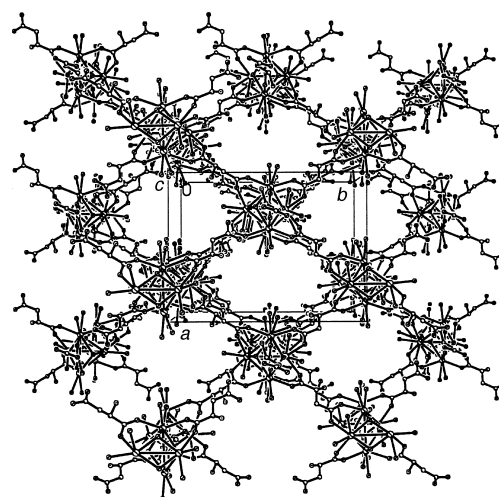


Figure 3. 3D network of compound **2** along [001] direction, exhibiting large channels.

50.1 %, close to that observed in [Zn₄O(bdc)₃(DMF)₈·(C₆H₅Cl)] (bdc = benzenedicarboxylate), which is regarded as the prototype for a third generation of open framework,^[7] in which a regular Zn₄O tetrahedron is linked by O₂–C–C₆H₄–C–O₂ struts to give an extended network with a three-dimensional intersecting channel with a spacing between the centers of adjacent clusters of 12.94 Å.

The variable-temperature magnetic susceptibility of both compounds was measured and $\chi_M T$ values for the [Ln]₄ unit at room temperature are 31.40 and 55.84 cm³ K mol^{−1} for **1** and **2**, respectively, very close to the expected values of 31.5 and 56.5 cm³ K mol^{−1} for four noninteracting Ln³⁺ free ions. The $\chi_M T$ value of **1** remains almost constant from room temperature to about 20 K, and then decreases rapidly on further cooling, reaching a minimum value of 25.82 cm³ K mol^{−1} at 5 K. The data in the range between 5 and 300 K can be well fitted to the Curie–Weiss law with $C = 31.37$ cm³ K mol^{−1}, and $\theta = -1.01$ K, indicating weak antiferromagnetic interactions between the Gd³⁺ ions. Compound **2** has a $\chi_M T$ versus T curve similar to that of **1**. However, the rapid drop of $\chi_M T$ at low temperature probably results primarily from the splitting of ligand field of the Dy³⁺ ion together with some contribution from the weak antiferromagnetic coupling between Dy³⁺ ions, as for the Gd₄O₄ unit.

In summary, a rational synthesis route from discrete cubane to supercubane has been designed and established. A three-dimensional framework has been obtained with intersecting channels of 11.78 Å. The large size of the cavities and access channels in **2** offer appreciable potential for guest molecule occupation and investigations in this direction are in progress.

Experimental Section

1: Gd(ClO₄)₃ and L-proline (pro) were mixed in a 2:1 molar ratio in water. The mixed solution was adjusted to pH 6.3 with 0.1 M aqueous NaOH under heating and stirring. The lanthanide ions were partially hydrolyzed to form a precipitate. The precipitate was filtered off and the filtrate was evaporated slowly at room temperature to afford colorless prismatic crystals. Yield: 45 %. Elemental analysis calcd for C₃₀H₈₂C₁₆Gd₄N₆O₅₃ (%): N 3.79, C 16.25, H 3.73; found: N 3.12, C 13.81, H 3.69.

2: L-Aspartic acid (asp) (1 mmol) was added to an aqueous solution of Dy(ClO₄)₃ under stirring and heating at 80 °C, then 0.1 M aqueous NaOH was added to adjust the pH to 6.5. The precipitate formed due to the partial hydrolysis of Ln³⁺ ions was filtered off and the filtrate was allowed to stand at room temperature. Colorless block-shaped crystals were obtained after one month. Yield: 34 % based on the aspartic acid. Elemental analysis calcd for C₁₂H₃₄Cl₂Dy₄N₃O₄₂ (%): N 2.57, C 8.82, H 3.31; found: N 2.16, C 7.49, H 3.22.

Received: June 5, 2000 [Z15222]

Remarkable Anionic Axial Ligand Effects of Iron(III) Porphyrin Complexes on the Catalytic Oxygenations of Hydrocarbons by H₂O₂ and the Formation of Oxoiron(IV) Porphyrin Intermediates by *m*-Chloroperoxybenzoic Acid**

Wonwoo Nam,* Mi H. Lim, So-Young Oh, Jung H. Lee, Ha J. Lee, Seung K. Woo, Cheal Kim, and Woonsup Shin

The reactions of iron(III) porphyrin complexes with various oxidants such as peroxy acids and hydroperoxides have been extensively studied for the past two decades, with the intention of elucidating the mechanisms of O–O bond activation and developing biomimetic oxygenation reactions.^[1] Since hydrogen peroxide (H₂O₂) is a biologically important and environmentally clean oxidant, use of the oxidant in catalytic oxygenation of hydrocarbons by iron porphyrin complexes has attracted much attention in the communities of bioinorganic and oxidation chemistry.^[1] Traylor et al. reported for the first time that the reactions of iron porphyrins with H₂O₂ in a protic solvent such as CH₃OH generate oxoiron(IV) porphyrin cation radical complexes [Fe^{IV}(porp)⁺⁺(O)] that epoxidize olefins to give the corresponding oxide products.^[2] We and Mansuy et al. also showed recently that highly electron-deficient iron porphyrin complexes react with H₂O₂ to form intermediates that are capable of oxygenating olefins and unactivated alkanes in aprotic solvent.^[3, 4]

Another oxidant that has been widely used in the mechanistic studies of O–O bond activation by iron(III) porphyrin complexes is peroxy acids such as *m*-chloroperoxybenzoic acid (*m*-CPBA).^[1] It is generally believed that iron porphyrins react with peroxy acids to form [Fe^{IV}(porp)⁺⁺(O)] by O–O bond heterolysis in polar solvents such as CH₂Cl₂.^[5] As far as we have been able to discern, there is no report that shows that both heterolysis and homolysis can occur concurrently in the *m*-CPBA reactions in polar solvent. Herein, we report two novel results that were obtained using an electron-deficient iron(III) porphyrin complex containing different anionic axial ligands: the remarkable anionic axial ligand effects on 1) the catalytic epoxidation and hydroxylation of hydrocarbons by

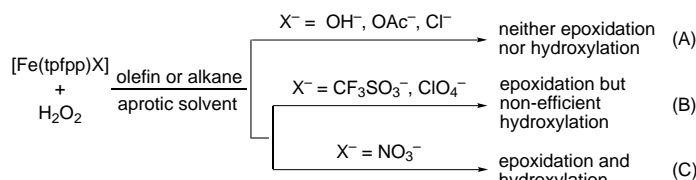
- [1] D. Gatteschi, *Adv. Mater.* **1994**, 6, 635.
- [2] D. Gatteschi, A. Caneschi, R. Sessoli, *Chem. Soc. Rev.* **1996**, 101.
- [3] a) R. Sessoli, D. Gatteschi, A. Caneschi, M. A. Novak, *Nature* **1993**, 365, 141; b) P. D. W. Boyd, Q. Li, J. B. Vincent, K. Folting, H. R. Chang, W. E. Streib, J. C. Huffman, G. Christou, D. N. Hendrickson, *J. Am. Chem. Soc.* **1988**, 110, 8537.
- [4] a) A. J. Blake, C. M. Grant, S. Parsons, J. M. Rawson, R. E. P. Winpenny, *J. Chem. Soc. Chem. Commun.* **1994**, 2363; b) S. P. Watton, P. Fuhrmann, L. E. Pence, A. Caneschi, A. Cornia, G. L. Abbati, S. J. Lippard, *Angew. Chem.* **1997**, 109, 2917; *Angew. Chem. Int. Ed. Engl.* **1997**, 36, 2774.
- [5] a) R. Y. Wang, Z. P. Zheng, T. Z. Jin, R. J. Staples, *Angew. Chem.* **1999**, 111, 1929; *Angew. Chem. Int. Ed. Engl.* **1999**, 38, 1813; b) R. Y. Wang, Z. M. Wang, S. Gao, T. Z. Jin, Z. D. Chen, C. H. Yan, G. X. Xu, C. H. He, *Chin. Chem. Lett.* **1998**, 9, 1141.
- [6] a) X. M. Chen, Y. L. Wu, Y. X. Tong, Z. Sun, D. N. Hendrickson, *Polyhedron* **1997**, 16, 4265; b) J. C. Plakatouras, I. Baxter, M. B. Hursthouse, K. M. Abdul Malik, J. McAleese, S. R. Drake, *J. Chem. Soc. Chem. Commun.* **1994**, 2455; c) W. J. Evans, M. A. Greci, J. W. Ziller, *Inorg. Chem.* **1998**, 37, 5221; d) D. Freedman, J. H. Melman, T. J. Emge, J. G. Brennan, *Inorg. Chem.* **1998**, 37, 4162; e) T. Dube, S. Gambarotta, G. Yap, *Organometallics* **1998**, 17, 3967.
- [7] a) H. Li, M. Eddaoudi, M. O'Keeffe, O. M. Yaghi, *Nature* **1999**, 402, 276; b) M. J. Zaworotko, *Nature* **1999**, 402, 242.
- [8] T. M. Reineke, M. Eddaoudi, M. Fehr, D. Kelley, O. M. Yaghi, *J. Am. Chem. Soc.* **1999**, 121, 1651.
- [9] Crystal structure analysis data: compound **1**: [Gd₄(Hpro)₄(pro)₂(μ₃-OH)₄(H₂O)](ClO₄)₆·6H₂O, *M_r* = 2216.72, rhombohedral, *R*₃, *a* = *b* = *c* = 12.8953(15) Å, *α* = *β* = *γ* = 100.663(17)°, *V* = 2016.8(4) Å³, *Z* = 1, *ρ*_{calcd} = 1.825 Mg m⁻³, *μ* = 3.545 mm⁻¹, *GOF* = 1.083, *F*(000) = 1086, *R*₁ = 0.0683, *wR*₂ = 0.1876, 317 parameters, 4130 reflections [*I* > 2σ(*I*)]. The intensity data was collected at 294 K on a Rigaku RAXIS IIC imaging-plate diffractometer using MoK_α radiation (*λ* = 0.71073 Å) from a rotating-anode generator operating at 50 kV and 90 mA (2θ_{min} = 3°, 2θ_{max} = 55°, 34 oscillation frames in the range of 0–180°, exposure 8 min per frame). A self-consistent semiempirical absorption correction based on Fourier coefficient fitting was applied using ABSCOR. Compound **2**: C₁₂H₃₄Cl₂Dy₄N₃O₄₂, *M_r* = 1633.48, orthorhombic, *P*₂₁2₁2₁, *a* = 14.011(3), *b* = 18.822(4), *c* = 23.421(5) Å, *V* = 6176(2) Å³, *Z* = 4, *ρ*_{calcd} = 1.757 Mg m⁻³, *μ* = 4.958 mm⁻¹, *F*(000) = 3124, *GOF* = 1.013. The data were collected on a Nonius Kappa CCD with MoK_α radiation (*λ* = 0.71073 Å) at 293 K. The structure was solved by direct methods and refined by full-matrix least-squares based on *F*² using the SHELXL 97 program. *R*₁ = 0.0497, *wR*₂ = 0.1354, 483 parameters, 12942 reflections [*I* > 2σ(*I*)]. Crystallographic data (excluding structure factors) for the structures reported in this paper have been deposited with the Cambridge Crystallographic Data Centre as supplementary publications no. CCDC-141086 (**1**) and CCDC-141085 (**2**). Copies of the data can be obtained free of charge on application to CCDC, 12 Union Road, Cambridge CB2 1EZ, UK (fax: (+44) 1223-336-033; e-mail: deposit@ccdc.cam.ac.uk).
- [10] O. M. Yaghi, C. E. Davis, G. Li, H. Li, *J. Am. Chem. Soc.* **1997**, 119, 2861.

- [*] Prof. Dr. W. Nam, M. H. Lim, S.-Y. Oh, J. H. Lee, H. J. Lee
Department of Chemistry and Division of Molecular Life Sciences
Ewha Womans University, Seoul 120-750 (Korea)
Fax: (+82) 2-3277-2384
E-mail: wwnam@mm.ewha.ac.kr
- Prof. Dr. C. Kim
Department of Fine Chemistry
Seoul National Polytechnic University
Seoul 139-743 (Korea)
- S. K. Woo, Prof. Dr. W. Shin
Department of Chemistry
Sogang University
Seoul 121-742 (Korea)

[**] This work was supported by Center for Cell Signaling Research (1999-2-122-002-4), the Korean Research Foundation (KRF-99-042-D00068), and the MOST through the Women's University Research Fund (99-N6-01-01-A-07).

aqueous 30 % H₂O₂ in aprotic solvent and 2) the formation of two distinct oxoiron(IV) porphyrin intermediates in *m*-CPBA reactions in polar solvent.

When the catalytic oxygenations of olefins and alkanes by H₂O₂ were carried out in the presence of [Fe(tpfpp)X] (tpfpp = *meso*-tetrakis(pentafluorophenyl)porphyrinato dianion) in a solvent mixture of CH₃CN and CH₂Cl₂, no or only trace amounts of oxygenated products such as epoxides and alcohols were formed in the reactions where X[−] in [Fe(tpfpp)X] was OH[−], CH₃CO₂[−], and Cl[−] (see Table 1 and Scheme 1, pathway A). However, when the identical reactions

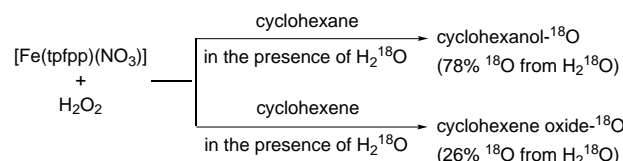


Scheme 1. A schematic diagram showing the anionic axial ligand effect on the epoxidation and hydroxylation of hydrocarbons by [Fe(tpfpp)X] and H₂O₂.

were carried out with [Fe(tpfpp)X] complexes containing different anionic axial ligands such as CF₃SO₃[−], ClO₄[−], and NO₃[−], the formation of epoxide and alcohol products was observed (see Table 1). In the epoxidation of cyclohexene, high yields of cyclohexene oxide were formed with trace amounts of allylic oxidation products (Table 1, entry 1). Also, *cis*-stilbene was predominantly oxidized to *cis*-stilbene oxide with trace amounts of *trans*-stilbene oxide and benzaldehyde formation (Table 1, entry 2). These results indicate that Fenton-type oxidation reactions were not involved in the olefin epoxidation reactions.^[6] More interestingly, in the hydroxylation of alkanes, the [Fe(tpfpp)(NO₃)] complex yielded alcohols as the major products with high alcohol to ketone ratios (Table 1, entries 3 and 4; also see Scheme 1, pathway C).^[7] The kinetic isotope effect (*k*_H/*k*_D) was deter-

mined to be 4.3 ± 0.3 in the competitive hydroxylation of cyclohexane and [D₁₂]cyclohexane by [Fe(tpfpp)(NO₃)] and H₂O₂ at 20 °C.^[3a]

We then studied the hydroxylation of cyclohexane and the epoxidation of cyclohexene by [Fe(tpfpp)(NO₃)] and H₂O₂ by using isotopically labeled water (H₂¹⁸O) to gain a better understanding of the nature of reactive intermediates responsible for the oxygenations of alkanes and olefins.^[8] The percentages of ¹⁸O incorporated from H₂¹⁸O into cyclohexanol (20 % yield based on H₂O₂ used) and cyclohexene oxide (55 % yield based on H₂O₂ used) were 78 ± 4 % and 26 ± 3 %, respectively (Scheme 2). These results demonstrate that the reactive



Scheme 2. Results of ¹⁸O-labeled water experiments in the oxygenation of cyclohexane and cyclohexene by [Fe(tpfpp)(NO₃)] and H₂O₂.

species, which was formed in the reaction of [Fe(tpfpp)(NO₃)] and H₂O₂ carried out in the presence of water, was an oxoiron(IV) porphyrin cation radical complex [Fe^{IV}(tpfpp)⁺•(O)] (1).^[8] We also suggest that the different amounts of ¹⁸O incorporation into the cyclohexanol and cyclohexene oxide is due to the fact that oxygen transfer from the intermediate to organic substrates competes with the oxygen exchange between the intermediate and labeled water.^[8b, 9] Thus, the reactivity of iron porphyrin catalysts in epoxidation and hydroxylation reactions is markedly influenced by the nature of anionic axial ligands, and the catalytic efficiency of the [Fe(tpfpp)X] complexes decreases in the order: X[−] = NO₃[−] > CF₃SO₃[−], ClO₄[−] ≫ OAc[−], Cl[−] ≥ OH[−].

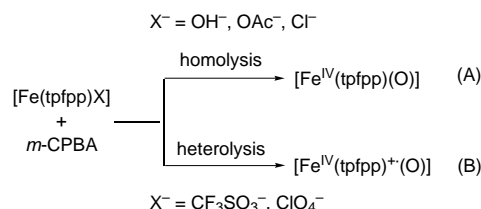
The anionic axial ligand effect was also observed in the reactions of [Fe(tpfpp)X] and *m*-CPBA carried out in polar

Table 1. Effect of anionic axial ligands of [Fe(tpfpp)X] on the catalytic epoxidation and hydroxylation of hydrocarbons by H₂O₂.^[a,b]

Entry	Substrate	Products	Yields of products ^[c] [%]					
			X [−] = OH [−]	OAc [−]	Cl [−]	CF ₃ SO ₃ [−]	ClO ₄ [−]	NO ₃ [−]
A. Epoxidation of olefins								
1	cyclohexene	cyclohexene oxide	< 2	< 2	< 2	65 ± 5	68 ± 5	78 ± 6
		cyclohexenol	0	3 ± 3	0	3 ± 2	4 ± 2	6 ± 4
		cyclohexenone	0	3 ± 3	0	2 ± 2	2 ± 2	5 ± 3
2	<i>cis</i> -stilbene	<i>cis</i> -stilbene oxide	< 2	9 ± 2	14 ± 2	78 ± 5	76 ± 5	74 ± 5
		<i>trans</i> -stilbene oxide	0	0	0	3 ± 1	3 ± 1	3 ± 1
		benzaldehyde	2 ± 1	2 ± 1	2 ± 1	3 ± 1	3 ± 1	3 ± 1
B. Hydroxylation of alkanes								
3	cyclohexane	cyclohexanol	< 1	< 1	< 1	6 ± 1	6 ± 1	30 ± 2
		cyclohexanone	0	0	0	1 ± 1	1 ± 1	1 ± 1
4	[D ₁₂]cyclohexane	[D ₁₂]cyclohexanol	< 1	< 1	< 1	3 ± 1	3 ± 1	17 ± 2
		[D ₁₀]cyclohexanone	0	0	0	0	0	0
C. Fe ^{III} /Fe ^{II} redox potential ^[d]								
5			− ^[e]	−0.44	−0.44	−0.12	−0.11	−0.15

[a] See Experimental Section for detailed reaction procedures. [b] All reactions were run at least in triplicate, and the data reported represent the average of these reactions. Although the yields and product distributions obtained in the oxygenation reactions were not affected by molecular oxygen, all the reactions were performed under argon atmosphere at room temperature. All iron porphyrin complexes used in this study were obtained from Mid-Century Chemicals and used without further purification. [c] Based on the amounts of H₂O₂ used. [d] In volts versus Fc/Fc⁺ couple. [e] No clear reversible cathodic and anodic peaks were obtained.

solvent. As mentioned above, it is generally believed that the reactions of iron(III) porphyrin complexes with *m*-CPBA in polar solvent generate $[\text{Fe}^{\text{IV}}(\text{porp})^+\cdot(\text{O})]$ by O–O bond heterolysis.^[5] However, when $[\text{Fe}(\text{tpfpp})\text{X}]$ complexes containing OH^- , OAc^- , and Cl^- as axial ligands were allowed to react with *m*-CPBA in a solvent mixture of CH_2Cl_2 and CH_3CN at -60°C , the formation of $[\text{Fe}^{\text{IV}}(\text{tpfpp})(\text{O})]$ (**2**) was observed (Scheme 3, pathway A; also see Figure 1 A for the



Scheme 3. Dependence of heterolytic versus homolytic O–O bond cleavage of *m*-CPBA on the anionic axial ligands of [Fe(tpfp)X] in polar solvent.

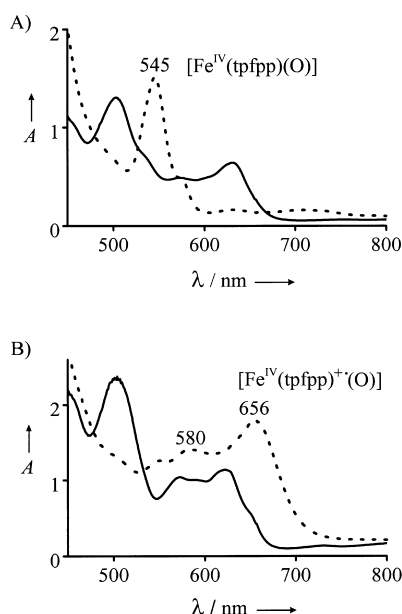


Figure 1. UV/Vis spectra of A) [Fe(tpfpp)Cl] (solid line) and **2**-Cl (dotted line) and B) [Fe(tpfpp)(CF₃SO₃)] (solid line) and **1**-CF₃SO₃ (dotted line).^[10a]

UV/Vis spectrum of 2-Cl (i.e. $[\text{Fe}^{\text{IV}}(\text{tpfp})\text{O}]$) generated from $[\text{Fe}(\text{tpfp})\text{Cl}]$) as a representative of the spectra of all other compounds).^[10] In contrast, when the identical reactions were carried out with $[\text{Fe}(\text{tpfp})\text{X}]$ ($\text{X}^- = \text{CF}_3\text{SO}_3^-$ and ClO_4^-) complexes, $[\text{Fe}^{\text{IV}}(\text{tpfp})^{+\cdot}(\text{O})]$ (**1**) was formed by O–O bond heterolysis (Scheme 3, pathway B; also see Figure 1 B, UV/Vis spectrum of **1**- CF_3SO_3 (i.e., $[\text{Fe}^{\text{IV}}(\text{tpfp})^{+\cdot}(\text{O})]$) generated from $[\text{Fe}(\text{tpfp})\text{CF}_3\text{SO}_3]$).^[11] On the basis of these results, we conclude that the mechanism of O–O bond cleavage of *m*-CPBA by electron-deficient iron porphyrin complexes is significantly affected by the nature of the anionic axial ligands and that both heterolysis and homolysis can occur in the reactions of iron porphyrin complexes with *m*-CPBA even in polar solvent.^[12]

Then, what is the effect of the anionic axial ligands on the activation of H_2O_2 and the mechanism of O–O bond cleavage of *m*-CPBA? It is well-known that the types and rates of O–O bond cleavage of $[(\text{porp})\text{Fe}^{\text{III}}-\text{OOR}]$ species are significantly affected by the electronic properties of axial ligands bound to the iron(III) ion in heme enzymes and iron porphyrin models.^[13] In addition, the reactivities of oxoiron(IV) porphyrin cation radical $[\text{Fe}^{\text{IV}}(\text{porp})^+(\text{O})]$ and iron(III) peroxo porphyrin intermediates $[\text{Fe}^{\text{III}}(\text{porp})(\text{O}_2^-)]$ are shown to be greatly influenced by the electronic nature of axial ligands bound to the iron porphyrin intermediates.^[13–15] Therefore, it may be suggested that the anionic axial ligand effect observed in this study is due to the difference of the electron-donating ability of the anionic axial ligands. In fact, the electron-donating ability of the anionic axial ligands has been determined from the NMR and resonance-Raman studies of $[\text{Fe}(\text{tmp})\text{X}]$ ($\text{X}^- = \text{Cl}^-$, OAc^- , CF_3SO_3^- , and ClO_4^- ; tmp = *meso*-tetramesitylporphinato dianion) complexes and their oxidized derivatives, $[(\text{tmp})^+\text{Fe}^{\text{IV}}=\text{O}(\text{X})]$.^[16] On the basis of the NMR and resonance-Raman spectral features, the axial ligands bound to the $[\text{Fe}(\text{tmp})\text{X}]$ complexes were grouped into two sets: one set with stronger electron donors such as Cl^- and OAc^- and another set with weaker electron donors such as CF_3SO_3^- and ClO_4^- . We also found in the present study that the anionic axial ligands of $[\text{Fe}(\text{tpfpp})\text{X}]$ are divided into two groups, on the basis of $\text{Fe}^{\text{III}}/\text{Fe}^{\text{II}}$ reduction potentials (Table 1, entry 5) and the reactivity patterns of the $[\text{Fe}(\text{tpfpp})\text{X}]$ complexes: one group with stronger electron donors such as Cl^- and OAc^- and another group with weaker electron donors such as CF_3SO_3^- , ClO_4^- , and NO_3^- . Interestingly, the $[\text{Fe}(\text{tpfpp})\text{X}]$ complexes with the axial ligands of weaker electron donors (i.e., CF_3SO_3^- , ClO_4^- , and NO_3^-) give high yields of oxygenated products in the H_2O_2 reactions and form **1** in the *m*-CPBA reactions, whereas the iron porphyrins with the axial ligands of stronger electron donors (i.e., Cl^- and OAc^-) yield low or no oxygenated products in the H_2O_2 reactions and form **2** in the reactions of *m*-CPBA.^[17] Although we propose at this moment that the electron-donating ability of the anionic axial ligands is a key factor in controlling the catalytic activity of $[\text{Fe}(\text{tpfpp})\text{X}]$ complexes in the H_2O_2 reactions and the formation of oxoiron(IV) porphyrin intermediates in the *m*-CPBA reactions, more detailed studies are in progress to gain a better understanding of the exact roles of the anionic axial ligands.

Experimental Section

Caution! Perchlorate salts of metal complexes with organic ligands are potentially explosive.

All reactions were carried out at room temperature under argon. Catalytic epoxidation of olefins: H_2O_2 (0.05 mmol, diluted in CH_3CN (0.3 mL)) was slowly added over a period of 20 min to a stirred solution containing $[\text{Fe}(\text{tpfp})\text{X}]$ (1×10^{-3} mmol) and olefin (2 mmol) in a solvent mixture (2.2 mL) of CH_3CN and CH_2Cl_2 (1:1). The reaction mixture was stirred for 10 min and directly analyzed by GC for cyclohexene and by HPLC for *cis*-stilbene. Product yields were determined by comparison with standard curves of known authentic samples.

Catalytic hydroxylation of alkanes: H_2O_2 (0.02 mmol, diluted in CH_3CN (0.5 mL)) was slowly added over a period of 1 h to a stirred solution containing $[\text{Fe}(\text{tpfp})\text{X}]$ (1×10^{-3} mmol) and alkane (1 mmol) in a solvent mixture (1 mL) of CH_3CN and CH_2Cl_2 (3:1). The reaction mixture was

further stirred for 5 min and directly analyzed by GC. The competitive hydroxylation of cyclohexane and [D₁₂]cyclohexane was performed with a mixture of cyclohexane (0.3 mmol) and [D₁₂]cyclohexane (1 mmol).

Labeled water (H₂¹⁸O) experiment: H₂O₂ (0.04 mmol, diluted in CH₃CN (0.5 mL)) was slowly added over a period of 1 h to a stirred solution containing [Fe(tpfp)(NO₃)] (1 × 10⁻³ mmol), substrate (1 mmol), and H₂¹⁸O (50 μL, 95% ¹⁸O enriched) in a solvent mixture (1 mL) of CH₃CN and CH₂Cl₂ (3:1). The reaction mixture was further stirred for 5 min and directly analyzed by GC/MS. The ¹⁶O and ¹⁸O compositions in cyclohexanol and cyclohexene oxide were determined by the relative abundances of mass peaks at *m/z* 57 and 59 for cyclohexanol and at *m/z* 83 and 85 for cyclohexene oxide. Control reactions, performed by stirring cyclohexanol-¹⁶O or cyclohexene oxide-¹⁶O in a solution containing [Fe(tpfp)(NO₃)] and H₂¹⁸O, showed that the oxygen of the products did not exchange with labeled water under the reaction conditions.

Electrochemical measurements: All electrochemical experiments were performed under an N₂ atmosphere in a glove box using a BAS 50W voltammetric analyzer. The cyclic voltammetric measurements were carried out in a solvent mixture of CH₃CN/CH₂Cl₂ (1:1) containing iron porphyrin (0.2 mM) and tBu₄NPF₆ (40 mM) as a supporting electrolyte in one compartment. The working electrode was a glassy carbon disk and the counter electrode was a platinum wire. The potential was measured by using a Ag/Ag⁺ (0.01 M) reference electrode and reported versus a Fc/Fc⁺ couple. The cyclic voltammograms were run at a scan rate of 50 mV s⁻¹.

Received: April 26, 2000

Revised: June 19, 2000 [Z15048]

- [1] a) J. L. McLain, J. Lee, J. T. Groves in *Biomimetic Oxidations Catalyzed by Transition Metal Complexes* (Ed.: B. Meunier), Imperial College Press, London, **2000**, pp. 91–169; b) P. R. Ortiz de Montellano, *Cytochrome P450: Structure, Mechanism, and Biochemistry*, 2nd ed., Plenum Press, New York, **1995**; c) T. G. Traylor, P. S. Traylor in *Active Oxygen in Biochemistry* (Eds.: J. S. Valentine, C. S. Foote, A. Greenberg, J. F. Liebman), Chapman & Hall, London, **1995**, pp. 84–187; d) B. Meunier in *Metalloporphyrins Catalyzed Oxidations* (Eds.: F. Montanari, L. Casella), Kluwer, Dordrecht, **1994**, pp. 1–47.
- [2] T. G. Traylor, C. Kim, J. L. Richards, F. Xu, C. L. Perrin, *J. Am. Chem. Soc.* **1995**, *117*, 3468–3474, and references therein.
- [3] a) W. Nam, Y. M. Goh, Y. J. Lee, M. H. Lim, C. Kim, *Inorg. Chem.* **1999**, *38*, 3238–3240; b) Y. J. Lee, Y. M. Goh, S.-Y. Han, C. Kim, W. Nam., *Chem. Lett.* **1998**, 837–838.
- [4] J. F. Bartoli, P. Battioni, W. R. De Foor, D. Mansuy, *J. Chem. Soc. Chem. Commun.* **1994**, 23–24.
- [5] J. T. Groves, Y. Watanabe, *J. Am. Chem. Soc.* **1988**, *110*, 8443–8452.
- [6] R. A. Sheldon, J. K. Kochi, *Metal-Catalyzed Oxidations of Organic Compounds*, Academic Press, New York, **1981**.
- [7] Hydroxylation of alkanes by hydroxyl or alkoxyl radicals by free radical pathways affords equal amounts of alcohol and ketone products.^[6] P. A. MacFaul, K. U. Ingold, D. D. M. Wayner, L. Que, Jr., *J. Am. Chem. Soc.* **1997**, *119*, 10594–10598.
- [8] a) J. Bernadou, B. Meunier, *Chem. Commun.* **1998**, 2167–2173; b) K. A. Lee, W. Nam, *J. Am. Chem. Soc.* **1997**, *119*, 1916–1922; c) J. T. Groves, J. Lee, S. S. Marla, *J. Am. Chem. Soc.* **1997**, *119*, 6269–6273.
- [9] Y. M. Goh, W. Nam, *Inorg. Chem.* **1999**, *38*, 914–920.
- [10] a) Reaction conditions: *m*-CPBA (1.5 × 10⁻³ mmol and 3 × 10⁻³ mmol for [Fe(tpfp)Cl] and [Fe(tpfp)(CF₃SO₃)] reactions, respectively, diluted in a solvent mixture (50 μL) of CH₃CN and CH₂Cl₂ (1:1)) was introduced into a 0.1-cm UV cell containing [Fe(tpfp)X] (5 × 10⁻⁴ mmol and 1 × 10⁻³ mmol for [Fe(tpfp)Cl] and [Fe(tpfp)-(CF₃SO₃)]), respectively in a solvent mixture (0.5 mL) of CH₃CN and CH₂Cl₂ (1:1) at –60 °C. Spectral changes were directly monitored by UV/Vis spectroscopy (Hewlett Packard 8453 spectrophotometer equipped with Optostat variable-temperature liquid-nitrogen cryostat (Oxford Instruments)). b) Further evidence that **2** was formed in the reaction of [Fe(tpfp)Cl] and *m*-CPBA was the silent EPR spectra and the appearance of a β-pyrrole hydrogen resonance signal at δ = 4.0 at –50 °C.

- [11] H. Fujii, *Chem. Lett.* **1994**, 1491–1494.
- [12] Solvent and axial ligand effects on the formation of **1** and iron(III) porphyrin *N*-oxide have been observed in the reaction of an electron-rich iron porphyrin complex, [Fe(tmp)X] (tmp = *meso*-tetramesitylporphinato dianion), with *m*-CPBA in toluene.^[5] E. Bill, X.-Q. Ding, E. L. Bominaar, A. X. Trautwein, H. Winkler, D. Mandon, R. Weiss, A. Gold, K. Jayaraj, W. E. Hatfield, M. L. Kirk, *Eur. J. Biochem.* **1990**, *188*, 665–672.
- [13] a) J. H. Dawson, *Science* **1988**, *240*, 433–439; b) N. Suzuki, T. Higuchi, Y. Urano, K. Kikuchi, H. Uekusa, Y. Ohashi, T. Uchida, T. Kitagawa, T. Nagano, *J. Am. Chem. Soc.* **1999**, *121*, 11571–11572, and references therein; c) T. L. Poulos, *J. Biol. Inorg. Chem.* **1996**, *1*, 356–359; d) K. Yamaguchi, Y. Watanabe, I. Morishima, *J. Am. Chem. Soc.* **1993**, *115*, 4058–4065.
- [14] a) H.-A. Wagenknecht, W.-D. Woggon, *Angew. Chem.* **1997**, *109*, 404–407; *Angew. Chem. Int. Ed. Engl.* **1997**, *36*, 390–392; b) Z. Gross, *J. Biol. Inorg. Chem.* **1996**, *1*, 368–371.
- [15] a) M. Selke, J. S. Valentine, *J. Am. Chem. Soc.* **1998**, *120*, 2652–2653; b) M. Selke, M. F. Sisemore, J. S. Valentine, *J. Am. Chem. Soc.* **1996**, *118*, 2008–2012.
- [16] K. Czarnecki, S. Nimri, Z. Gross, L. M. Proniewicz, J. R. Kincaid, *J. Am. Chem. Soc.* **1996**, *118*, 2929–2935.
- [17] We reported recently that electron-deficient iron(III) porphyrin complexes tend to cleave the O–O bond of hydroperoxides heterolytically in protic solvent systems, whereas O–O bond homolysis predominates in the reactions of electron-rich iron(III) porphyrins with the oxidants: W. Nam, H. J. Han, S.-Y. Oh, Y. J. Lee, J.-H. Choi, S.-Y. Han, C. Kim, S. K. Woo, W. Shin, *J. Am. Chem. Soc.*, in press.

Dynamics of Hole Trapping by G, GG, and GGG in DNA**

William B. Davis,* Izabela Naydenova,
Reinhard Haselsberger, Alexander Ogrodnik,
Bernd Giese,* and Maria E. Michel-Beyerle*

Oxidative damage to DNA by ionizing radiation, carcinogenic agents, and photosensitizers occurs predominately at guanine (G) bases,^[1,2] a result which can be rationalized by the hierarchy of in vitro oxidation potentials of the isolated nucleobases (G < A ≪ C, T).^[3] Strand cleavage reactions, induced, for instance, by piperidine treatment,^[4] have shown consistently that multiple guanine tracts in DNA are more susceptible to oxidative damage than isolated guanine bases.

[*] Dr. W. B. Davis, Prof. Dr. M. E. Michel-Beyerle, Dr. I. Naydenova, Dipl.-Phys. R. Haselsberger, Priv.-Doz. Dr. A. Ogrodnik
Institut für Physikalische und Theoretische Chemie
Technische Universität München
Lichtenbergstrasse 4, 85748 Garching (Germany)
Fax: (+49) 89-289-13026
E-mail: Bill.Davis@ch.tum.de
Michel-Beyerle@ch.tum.de

Prof. Dr. B. Giese
Institut für Organische Chemie der Universität
St.-Johanns-Ring 19, 4056 Basel (Switzerland)
Fax: (+41) 61-2671105
E-mail: giese@ubaclu.unibas.ch

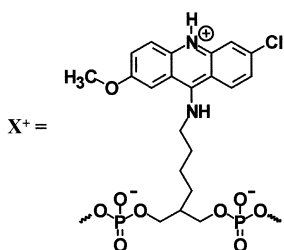
[**] We thank Joshua Jortner, Notker Rösch, and Alexander Voityuk for stimulating discussions and critical reading of the manuscript. W.B.D. greatly appreciates a postdoc fellowship from the Alexander von Humboldt Foundation. Financial support from the Volkswagenstiftung is gratefully acknowledged.

This feature has been utilized in long-range hole transport studies,^[5] which are based on GGG being a better trap than a single G base. In addition, an orientational dependence of the oxidation site, which leads to strand cleavage, is observed because the energetics of guanine are dependent upon their immediate environment. In a GG trap, the 5'-guanine is the preferred cleavage site,^[6, 7] and in GGG either the 5'- or central guanine is the preferred cleavage site depending upon the nucleobases immediately neighboring the trap.^[8, 9] This view of preferred sites of charge localization in GG and GGG traps is supported independently by the quantum mechanical calculations of Voityuk et al.^[10] The interesting question is now whether a distant hole donor populates the preferred cleavage site(s) in either GG or GGG in a direct unistep reaction or whether a sequential kinetic scheme must be envisioned, in which the nearest G is oxidized first and trapping of the charge at the preferred G occurs in a subsequent step (two-step mechanism).

To analyze the dynamics of hole trapping in multiple G tracts, we investigate here the kinetics of hole transfer (HT) from a photoexcited donor to either a G, GG, or GGG site. In order to optimize the sensitivity, we chose protonated 9-amino-6-chloro-2-methoxyacridine (X^+)^[11] which has been shown to undergo activated hole transfer to G in cases where one or more A:T base pair(s) serve as a bridge.^[12] The most interesting result from the present study is that hole transfer proceeds in all cases to the closest guanine base. Subsequently relaxation of the hole occurs, which in multiple guanine tracts

such as GG or GGG, leads to localization of the hole within the G tract. The site of localization may differ from initially oxidized state, and may be that responsible for strand cleavage.

The chemical structure of the X^+ oxidant and the DNA sequences studied are shown in Scheme 1. All samples were



characterized by their steady-state absorption and fluorescence spectra (Figure 1). Photoexcitation of X^+ in all seven duplexes with ~ 2 ns, 450 nm pump pulses^[13] results in two transient kinetic features (Figure 2). The first feature is the decay of the excited state absorption probed in the spectral region from 570 \rightarrow 800 nm, characteristic for the $S_1 \rightarrow S_n$ absorption of X^+ . The second feature is the ground state recovery probed at 420 nm. As a representative for all duplexes under study, the transient features of 3'- X^+ -A-GG are shown in Figure 2. The equivalence of the two kinetic traces indicates that the rate determining step in the kinetic Scheme (Scheme 2) is the forward hole-transfer rate and that charge recombination cannot be resolved. This phenomenon is a necessary consequence of the high thermal activation of the forward rate^[12] and a zero, or small, activation energy for the back transfer.^[14]

Monoexponential rates obtained from least-squares fitting of these data are compiled in Table 1. The monoexponentiality, together with the structural characterization by Tanaka et al.,^[11] points to the fact that the acridine must be intercalated in a well defined site.^[15]

Duplex	x	y	z
X^+ -(AT)	A	A	T
5'- X^+ -A-G	G	A	T
5'- X^+ -A-GG	G	G	T
5'- X^+ -A-GGG	G	G	G
3'- X^+ -A-G	T	A	G
3'- X^+ -A-GG	T	G	G
3'- X^+ -A-GGG	G	G	G

Duplexes X^+ -(AT) and 5'- X^+ -A
5'-GCG TTA TAT A(X^+)A xyz TAT GCG-3'
Duplexes 3'- X^+ -A
5'-GCG TTA xyz A(X^+)A TAA TAT GCG-3'

Scheme 1. Structure of the X^+ dye and the studied DNA sequences. An adenine base was placed opposite X^+ in all duplexes similar to those in the studies of Tanaka et al.^[11] and all other bases were paired with their normal Watson-Crick complements. DNA single strands were purchased from Eurogentec Köln (Germany) and delivered lysophilized after polyacrylamide gel electrophoresis (PAGE) purification. Stock solutions were made by dissolving the single strands in a buffer solution (10 mM Na_2HPO_4/NaH_2PO_4 , 100 mM NaCl, pH 7.2). X^+ -labeled strands were mixed with a 10% excess of counter-strand to help ensure that all X^+ molecules were incorporated into duplex DNA. Hybridization was performed by heating the mixtures of single strands to 80 °C, followed by slow cooling over 2 h to room temperature. All samples had an adenine base opposite to X^+ on the counter-strand, similar to the studies of Tanaka et al.^[11] All samples were placed in a quartz cuvette (1 mm pathlength) and had an optical density of ~ 0.3 at 450 nm.

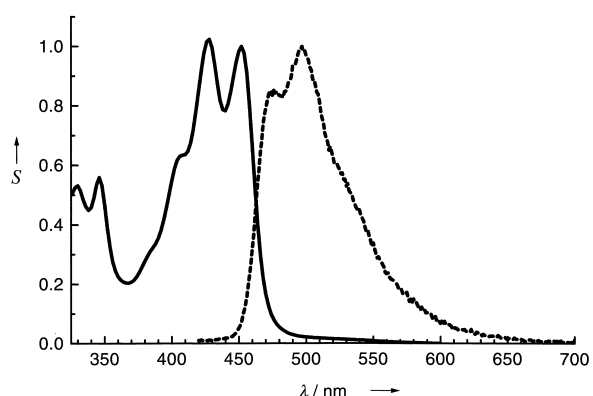


Figure 1. Ground state absorption (—) and static fluorescence spectra (---) of X^+ in duplex 5'- X^+ -A-G at 283 K. The absorption spectra shows $S_0 \rightarrow S_1$ absorption bands at 452 and 428 nm, and $S_0 \rightarrow S_2$ bands at 346 and 330 nm. The steady-state fluorescence has two bands at 474 nm and 497 nm.

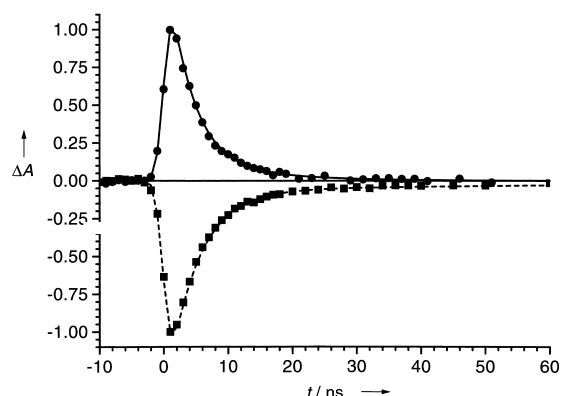
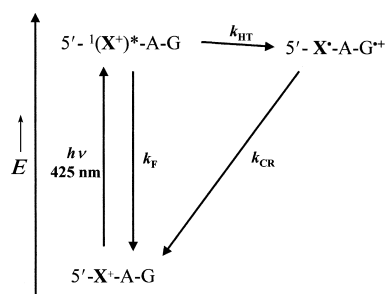


Figure 2. Transient absorption kinetics of duplex 3'- X^+ -A-GG (283 K) monitoring ground state recovery (425 nm, ---) and excited state decay (575 nm, —) after excitation of X^+ at 450 nm. Both states evolve on the same time scale and there is no evidence for a long-lived ground state recovery due to trapping by GG.



Scheme 2. Kinetic scheme for the photoinduced hole-transfer reaction in all six hole-transfer duplexes using 5'-X⁺-A-G as an illustrative example. k_{HT} is the rate of hole transfer, k_F is the fluorescence lifetime of $1(X^+)^*$, k_{CS} is the rate of the forward charge-shift reaction, and k_{CR} is the rate of charge recombination. k_{CS} is a highly activated reaction in this duplex leading to $k_{CR} > k_{CS}$; therefore there are no observable intermediate features in the transient absorption data (Figure 2).

Table 1. Measured excited-state decay lifetimes (τ_{ES})^[a] and the calculated hole-transfer lifetimes (τ_{HT})^[b] for all seven duplexes at 283 K.

Duplex	τ_{ES} [ns]	τ_{HT} [ns]
X ⁺ -(AT)	18.0	
5'-X ⁺ -A-G	12.0 (12.7)	36.0
5'-X ⁺ -A-GG	8.9 (9.6)	17.6
5'-X ⁺ -A-GGG	9.0 (9.4)	18.0
3'-X ⁺ -A-G	6.9 (7.4)	11.2
3'-X ⁺ -A-GG	4.5 (4.2)	6.0
3'-X ⁺ -A-GGG	5.7 (5.3)	8.3

[a] The numbers in parentheses are the measured rates of ground state recovery. [b] τ_{HT} was calculated from the formula $1/\tau_{HT} = 1/\tau_{ES} - 1/\tau_0$, where τ_0 is the excited state lifetime of the model duplex, X⁺-(AT).

If we compare the sequence 5'-X⁺-A-G with 5'-X⁺-A-GG and 5'-X⁺-A-GGG (Table 1), we observe that the oxidation rates in all cases are similar to within a factor of two. In fact, the oxidation of both GG and GGG occurs slightly faster. The small, factor of two variance in the rates is in line with recent calculations of the energetics of guanine bases in such combinations.^[10] Because we do not expect different electronic couplings between X⁺ and the closest guanine, this result indicates that it is this closest guanine which is in all cases the initially oxidized site.

If we change the directionality of the hole transfer, by comparison of the sequences 3'-X⁺-A-G, 3'-X⁺-A-GG, and 3'-X⁺-A-GGG (Table 1), we observe again that the hole transfer rates are similar, in which the oxidation rates of GG and GGG are slightly faster. The similarity of the hole-transfer rates points to the fact that, in this case also, the hole-accepting site is the proximate G.

As a final comparison, we look at the differences in rates between 5'-X⁺-A-G and 3'-X⁺-A-G and between their GG and GGG counterparts. What we conclude from the data compiled in Table 1 is a systematic factor of three difference in rates, with transfer in the 3'-X⁺-A sequences consistently faster. This result can be rationalized by the difference in electronic coupling between G and A in the two directions of the helix because 5'-G-A (valid for 3'-X⁺-A duplexes) coupling is predicted to be slightly stronger than 3'-G-A coupling (valid for 5'-X⁺-A duplexes).^[16] However, one caveat on the validity of the theoretical argument is that the difference in rates between the two helical directions could

also arise from asymmetrical electronic coupling of the acridine chromophore with the neighboring adenine bases.

Since the G proximal to a hole-injection site in GGG tracts is initially populated, there must be a subsequent process which leads to long-lived hole trapping in GGG. This process is expected to involve charge transfer as a consequence of structural and energetic relaxation. This entire process is what we refer to as the trapping reaction in GGG. The lifetime data reported in Table 1 are in excellent accord with the yield data of a reduced hole donor that we have described recently.^[17] In these experiments, the donor species is the enolether radical cation.

In recent experiments, Lewis et al.^[18] used delayed ground-state recovery dynamics of a photoexcited stilbene chromophore to measure the one-AT superexchange mediated, forward and back hole-transfer rates between G and GG in a hairpin DNA duplex. By fitting a simple kinetic model to their data, their published rate for forward transfer exceeds the one for back transfer by a factor of eight. The difference in rates was interpreted in a model, where GG is, a priori, a deeper hole trap than G and the asymmetry between the forward- and back-transfer rates is due to energetic differences. The results of our study may add an important detail to the understanding of this trapping reaction. We postulate that the lower energetics, characteristic of GG, are the result of an intraguanine tract-relaxation process subsequent to the primary oxidation kinetics. The order of magnitude similarity between the Lewis hopping rate to that extracted from a detailed model^[19] of the chemical yield experiments^[5] confirms the validity of the chemical yield approach to measuring charge transfer rates in DNA. In addition, it is rewarding to see that direct kinetic measurements and the dynamics modeled from chemical yield data support each other.

Received: July 31, 2000 [Z15563]

- [1] a) S. Steenken, *Biol. Chem.* **1997**, 378, 1293; b) U. Diederichsen, *Angew. Chem.* **1997**, 109, 2411; *Angew. Chem. Int. Ed. Engl.* **1997**, 36, 2317; c) C. J. Burrows, J. G. Muller, *Chem. Rev.* **1998**, 98, 1109; d) F. LePage, A. Guy, J. Cadet, A. Sarasin, A. Gentil, *Nucleic Acids Res.* **1998**, 26, 1276.
- [2] a) P. M. Cullis, J. D. McClymoun, M. C. R. Symons, *J. Chem. Soc. Faraday Trans.* **1990**, 86, 591; b) P. O'Neill, E. M. Fielden, *Adv. Radiat. Biol.* **1993**, 17, 53; c) S. Steenken, *Chem. Rev.* **1989**, 89, 503; d) C. von Sonntag, H.-P. Schuchmann, *Int. J. Radiat. Biol.* **1986**, 49, 1; e) A. P. Breen, J. A. Murphy, *Free Radical Biol. Med.* **1995**, 18, 1033.
- [3] a) C. A. M. Seidel, A. Schulz, H. M. Sauer, *J. Phys. Chem.* **1996**, 100, 5541; b) S. Steenken, S. V. Jovanovic, *J. Am. Chem. Soc.* **1997**, 119, 617; c) V. Y. Shafirovich, S. H. Courtney, N. Ya, N. E. Geacintov, *J. Am. Chem. Soc.* **1995**, 117, 4920.
- [4] a) A. Spassky, D. Angelov, *Biochemistry* **1997**, 36, 6571; b) P. M. Cullis, M. E. Malone, L. A. Merson-Davies, *J. Am. Chem. Soc.* **1996**, 118, 2775; c) K. Kino, I. Saito, H. Sugiyama, *J. Am. Chem. Soc.* **1998**, 120, 7373.
- [5] a) E. Meggers, M. E. Michel-Beyerle, B. Giese, *J. Am. Chem. Soc.* **1998**, 120, 12950; b) B. Giese, S. Wessley, M. Spormann, U. Lindemann, E. Meggers, M. E. Michel-Beyerle, *Angew. Chem.* **1999**, 111, 1050; *Angew. Chem. Int. Ed.* **1999**, 38, 996.
- [6] a) I. Saito, M. Takayama, H. Sugiyama, K. Nakatani, A. Tsuchida, M. Yamamoto, *J. Am. Chem. Soc.* **1995**, 117, 6406; b) K. Ito, S. Inoue, K. Yamamoto, S. Kawanishi, *J. Biol. Chem.* **1993**, 268, 13221; c) D. T. Breslin, G. B. Schuster, *J. Am. Chem. Soc.* **1996**, 118, 2311; d) K. Nakatani, C. Dohno, T. Nakamura, I. Saito, *Tetrahedron Lett.* **1998**, 39, 2779; e) T. Melvin, S. Cunniffe, D. Papworth, T. Roldan-Arjona, P.

- O'Neill, *Photochem. Photobiol.* **1997**, 65, 660; f) J. G. Muller, R. P. Hickerson, R. J. Perez, C. J. Burrows, *J. Am. Chem. Soc.* **1997**, 119, 1503; g) M. F. Sistare, S. J. Codden, G. Heimlich, H. H. Thorp, *J. Am. Chem. Soc.* **2000**, 122, 4742.
- [7] a) I. Saito, T. Nakamura, K. Nakatani, *J. Am. Chem. Soc.* **2000**, 122, 3001; b) H. Sugiyama, I. Saito, *J. Am. Chem. Soc.* **1996**, 118, 7063; c) F. Prat, K. N. Houk, C. S. Foote, *J. Am. Chem. Soc.* **1998**, 120, 845; d) M. Hutter, M. Clark, *J. Am. Chem. Soc.* **1996**, 118, 7574.
- [8] a) S. Kawanishi, S. Oikawa, M. Murata, H. Tsukitome, I. Saito, *Biochemistry* **1999**, 38, 16733; b) K. Ito, S. Inoue, K. Yamamoto, S. Kawanishi, *J. Biol. Chem.* **1993**, 268, 13221; c) K. Ito, S. Kawanishi, *Biochemistry* **1997**, 36, 1774; d) A. Spassky, D. Angelov, *Biochemistry* **1997**, 36, 6571; e) D. B. Hall, R. E. Holmlin, J. K. Barton, *Nature* **1996**, 382, 731; f) R. E. Holmlin, P. J. Dandliker, J. K. Barton, *Angew. Chem.* **1997**, 109, 2830; *Angew. Chem. Int. Ed. Engl.* **1997**, 36, 2714; g) D. B. Hall, S. O. Kelley, J. K. Barton, *Biochemistry* **1998**, 37, 15933.
- [9] a) I. Saito, T. Nakamura, K. Nakatani, Y. Yoshioka, K. Yamaguchi, H. Sugiyama, *J. Am. Chem. Soc.* **1998**, 120, 12686; b) Y. Yoshioka, Y. Kitagawa, Y. Takano, K. Yamaguchi, T. Nakamura, I. Saito, *J. Am. Chem. Soc.* **1999**, 121, 8712.
- [10] A. A. Voityuk, J. Jortner, M. Bixon, N. Rösch, *Chem. Phys. Lett.* **2000**, 324, 430.
- [11] For studies involving similar X^+ -DNA duplexes, see: a) K. Fukui, K. Tanaka, M. Fujitsuka, A. Watanabe, O. Ito, *J. Photochem. Photobiol. B* **1999**, 50, 18; b) K. Fukui, K. Tanaka, *Angew. Chem.* **1998**, 110, 167; *Angew. Chem. Int. Ed.* **1998**, 37, 158; c) K. Fukui, K. Tanaka, *Nucleic Acids Res.* **1996**, 24, 3962.
- [12] S. Hess, M. Götz, W. B. Davis, M. E. Michel-Beyerle, unpublished results. When intercalated in the DNA duplexes presented in this paper, X^+ displays a rapid excited-state relaxation (on the 50 ps time scale) which leads to energy loss. When a charge-shift reaction can compete with this relaxation, the forward-transfer rate has been shown to be (nearly) free of activation barriers and is faster than the back-transfer rate, which is deep in the Marcus-inverted region of the log (rate) versus energy plot. In this case, the intermediate X^+ is seen in absorption. Conversely, when charge transfer cannot compete with relaxation, there is excited-state energy loss and the activation energy of the forward transfer increases. This leads to kinetics where the rate of charge recombination is faster than that of the forward charge-shift reaction and, thus, the X^+ intermediate is not detectable.
- [13] The laser system used to obtain the data reported here has been described in detail previously (M. Volk, G. Aumeier, T. Häberle, A. Ogrodnik, M. E. Michel-Beyerle, *Biochim. Biophys. Acta* **1992**, 1102, 253) and is arranged for ultrahigh sensitivity probing, $\Delta OD > 10^{-4}$.
- [14] In the inverted region, electron-transfer reactions usually display small activation energies due to vibronic coupling. See, for instance: a) R. A. Marcus, N. Sutin, *Biochem. Biophys. Acta* **1985**, 811, 265; b) M. Bixon, J. Jortner, *Adv. Chem. Phys.* **1999**, 106, 35.
- [15] Structural characterization of the duplexes using 2D-NMR techniques is currently underway in collaboration with C. Griesinger, University of Frankfurt.
- [16] A. A. Voityuk, N. Rösch, M. Bixon, J. Jortner, *J. Phys. Chem. B* **2000**, in press.
- [17] E. Meggers, D. Kusch, M. Spichy, U. Willie, B. Giese, *Angew. Chem.* **1998**, 110, 474; *Angew. Chem. Int. Ed.* **1998**, 37, 460.
- [18] F. D. Lewis, X. Liu, J. Liu, S. E. Miller, R. T. Hayes, M. R. Wasielewski, *Nature* **2000**, 406, 51.
- [19] M. Bixon, B. Giese, S. Wessely, T. Langenbacher, M. E. Michel-Beyerle, J. Jortner, *Proc. Natl. Acad. Sci. USA* **1999**, 96, 11 713.

From Glycals to Glycopeptides: A Convergent and Stereoselective Total Synthesis of a High Mannose N-Linked Glycopeptide**

Zhi-Guang Wang, XuFang Zhang, David Live, and Samuel J. Danishefsky*

Given the elaborate machinery required for the biosynthesis of glycoproteins in cells, it seems likely that such systems perform significant biological functions.^[1, 2] Indeed, protein glycosylation has been implicated in mediating protein folding,^[3] in protecting against proteolysis,^[4] in cellular differentiation,^[5] and in cell–cell communication.^[6] Major breakthroughs in the detection, purification, sequencing, and spectroscopic analysis of glycans have enabled a growing appreciation of the role of glycobiology in vital life processes.^[7] Chemical synthesis^[8–10] can play an important role in our understanding of glycobiology by providing access to well-selected, homogeneous, but realistically complex, probe structures for elucidating the relationship of glycoarchitecture and function.^[11, 12]

Broadly speaking, glycoproteins are of two major types. In one motif, the terminal galNAc hexose of the saccharide domain is joined to the polypeptide through an α -O-glycosidic linkage to the hydroxyl group of a serine (or threonine).^[13] The target systems which prompted the research described herein are N-linked glycoproteins, wherein the two domains are joined through a β -N linkage of an asparagine group to a GlcNAc unit at the reducing end of the oligosaccharide.^[14]

Specifically, we focused on a target where the consensus core high mannose pentamer sequence (see below) would be joined to the peptide domain through a carboxyl group of an Asp side chain (**1**, Scheme 3). Our goals in reaching **1** by chemical synthesis included a concise and efficient assembly of the required oligosaccharide.^[15] Clearly, global deprotection of diversely protected functionalities would eventually be required. To this set of specifications we added another, namely, that the fashioning of the asparagine linkage be conducted in a maximally convergent sense with high stereocontrol by joining a fully mature high mannose saccharide to a fully mature peptide. In this way we hoped to pave the way for

[*] Prof. S. J. Danishefsky, Dr. Z.-G. Wang, X. Zhang
Laboratory for Bioorganic Chemistry
Sloan-Kettering Institute for Cancer Research
1275 York Avenue, New York, N.Y. 10021 (USA)
Fax: (+1) 212-772-8691
E-mail: s-danishefsky@ski.mskcc.org

Dr. D. Live
Department of Biochemistry
Molecular Biol. and Biophysics University of Minnesota Minneapolis,
MN 55455 (USA)

Prof. S. J. Danishefsky
Department of Chemistry
Columbia University, Havemeyer Hall
New York, N.Y. 10027 (USA)
E-mail: dshefsky@chem.columbia.edu

[**] This work was supported by the National Institutes of Health (Grant Numbers AI16943/CA28824). We thank Dr. George Sukenick of the MSKCC NMR Core Facility for NMR and mass spectral analyses (NIH Grant Number: CA08748).

addition of fully synthetic high mannose core structures to preselected aspartate-presenting polypeptides.

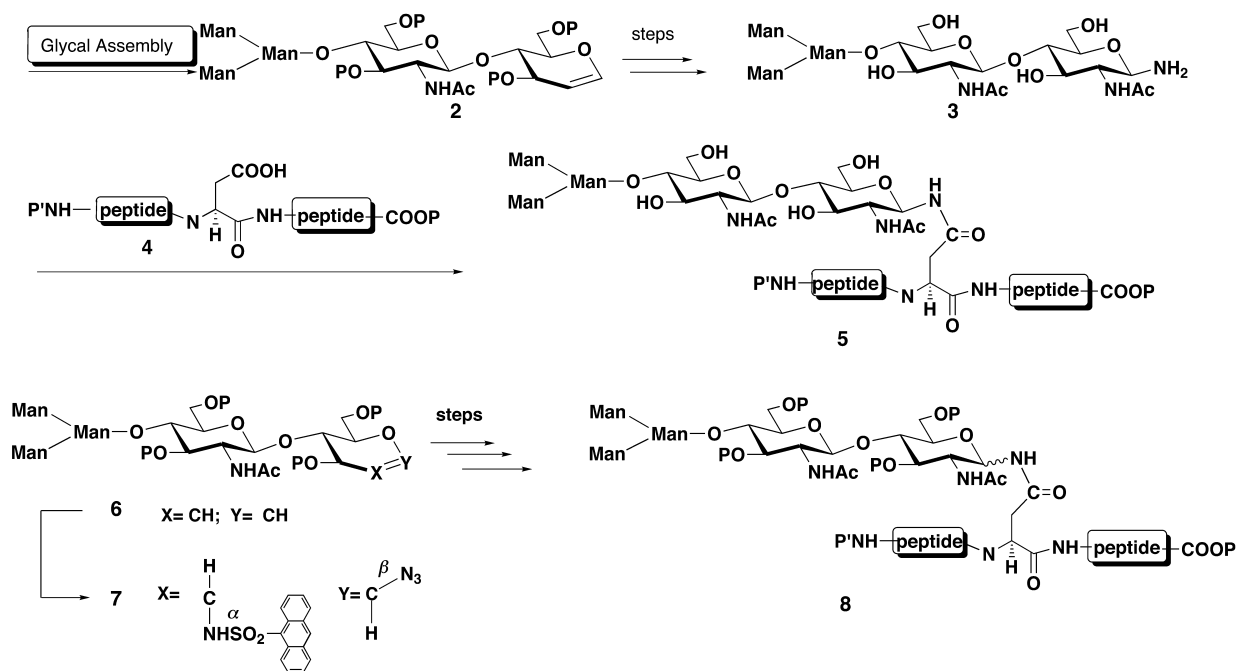
Toward this quest, the progression shown in Scheme 1 presented itself. The pertinent high mannose core oligosaccharide would be synthesized as a terminal glycal, thereby taking advantage of the economies of glycal assembly.^[16] The double bond would be transformed to the signature chitobiose subunit bearing the β -anomeric amine (**3**). The fully synthetically derived pentamer ensemble would be joined, in a maximally convergent acylation reaction, to the aspartate-presenting peptide, which contains an interior Asp residue and is equipped with a differentiated ω -carboxyl group (**4**). The two central challenges we faced were the conversion of **2** \rightarrow **3** and the acylation of the latter with **4**, all with tight stereochemical control, en route to **5**.

In a previously reported first generation protocol^[17] a fully protected glycal was converted after a complex sequence into a terminal 1- β -azido glcNAc residue (**6** and **7**). However, following reduction of the azido linkage and acylation of the resulting amine with an Asp-containing pentapeptide, the product glycopeptide was obtained as an approximate 1:1 mixture of anomers. During the reduction/acylation sequence, the β anomeric stereochemistry of the azide had been badly compromised en route to the glycopeptide (**8**). A productive solution to the problem of convergence and high stereochemical maintenance in a total synthesis setting is described herein.

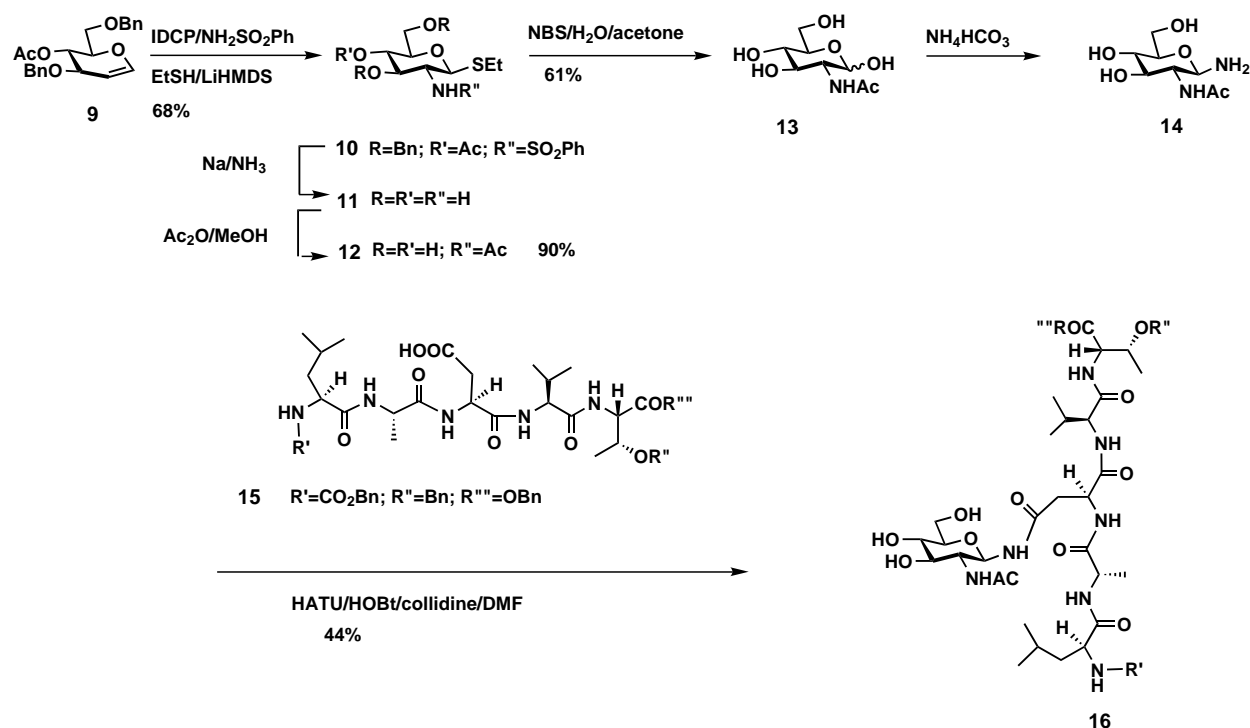
As a model for what had to be accomplished, we started with the simple differentiated glycal **9** (Scheme 2). Following implementation of a standard iodosulfonimidation/ethane thiolate rearrangement sequence,^[18] **10** was in hand. Conversion of **10** \rightarrow **11** was conducted as shown. The 2- α -amino group of the latter was selectively acetylated with acetic anhydride in methanol, containing no added base or acylation catalyst, to give **12**. A key step in the model series involved

oxidative hydrolytic cleavage of the anomeric β -thioethyl group through the use of *N*-bromosuccinimide (NBS)^[19] to produce the model free reducing sugar **13**. Treatment of **13** with ammonium bicarbonate afforded β -anomeric glycosylamine **14**.^[20, 21] The latter condensed with Asp-containing peptide **15**, under the conditions indicated, to afford **16**. Remarkably, as was implicit in earlier work of Cohen-Anisfeld and Lansbury,^[21, 22] the reaction is highly selective for producing the β -glycosylasparagine-linked glycopeptide. In fact, we did not detect any α -glycoside or aspartoylation through the α -carboxyl group.

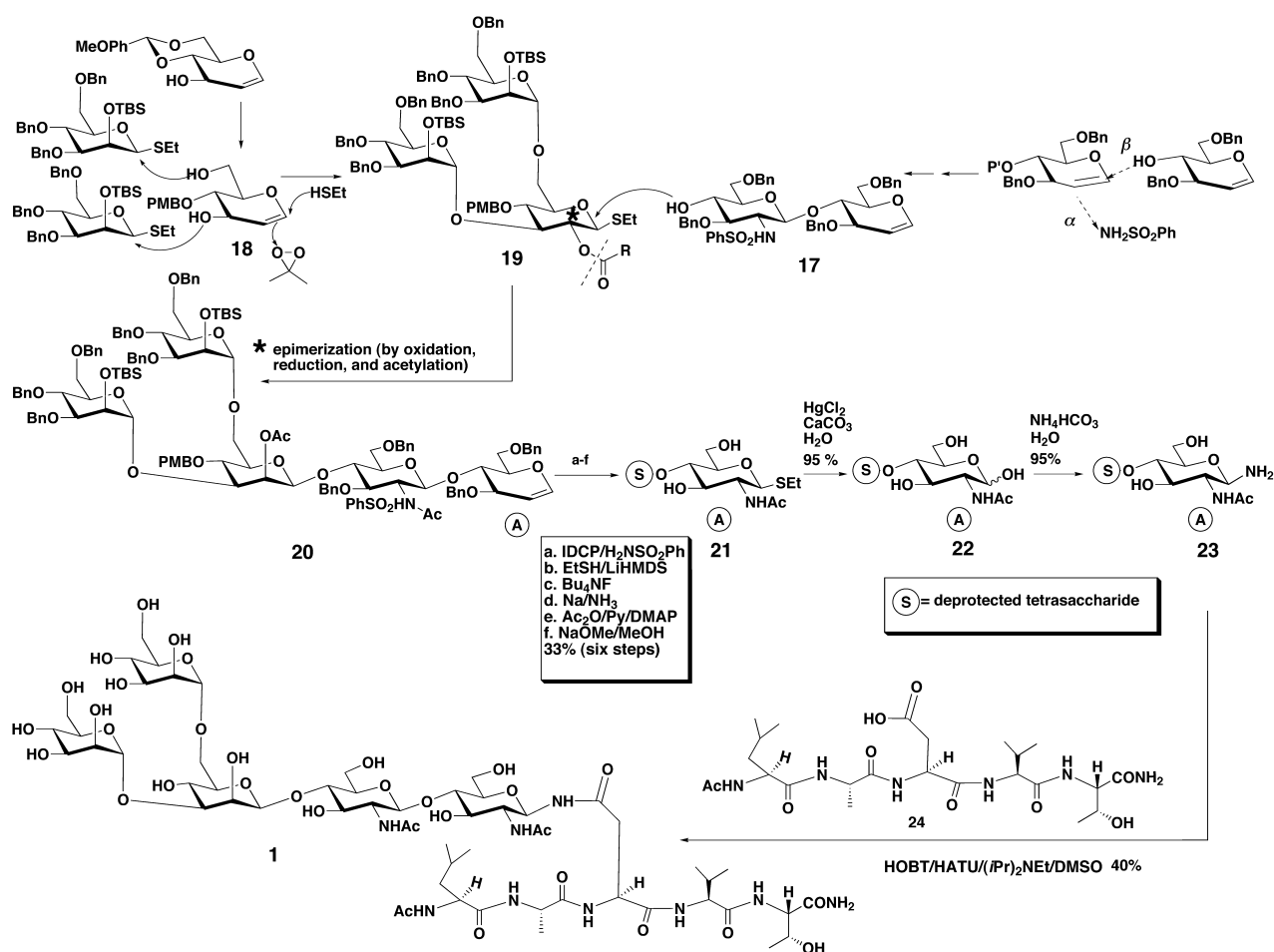
The issue to be faced now was whether the methodology used for the simple model could be transferred to a strategically protected high mannose glycal, itself obtained by total synthesis. The logic of the glycal assembly used here had already been charted, but the implementation was now modified and optimized. The "pre-chitobiose glycal" segment **17** was fashioned by the joining of glucal building blocks through azaglycosidation (Scheme 3).^[18] A dimannosylated glucosyl donor (**19**) was derived from glycal **18**, itself obtained from the corresponding 4,6-*p*-methoxybenzylidene glycal derivative. Coupling **19** (R = phenyl) with **17** produced the expected β -glucosyl attachment smoothly and stereospecifically. Epimerization at C2^[17] (see asterisk) was accomplished by an oxidation/reduction sequence, thereby leading to the protected high mannose glycal (**20**). In the first stage (steps a, b) of converting **20** into **23**, the terminal glycal was used to introduce the 1 β -thioethyl (and 2- α -sulfonamido) functions. In step c the silyl protecting groups were removed and in step d both C2 α -amino groups of the sulfonamidochitobiose were exposed. In this case, as opposed to the monosaccharide in Scheme 1, we resorted to peracetylation (all hydroxyl and the two amino groups) for purification. Concurrent deacetylation of all of the ester linkages led to compound **21**. The anomeric thioethyl function suffered cleavage under



Scheme 1. The current and past synthetic strategy from glycal to glycopeptide; P, P': protecting groups.



Scheme 2. Bn: benzyl; IDCP: bisdicollidine iodonium perchloride; LiHMDS = lithium hexamethyldisilazide; HATU: *N*-(dimethylamino)-1*H*-1,2,3-triazole[4,5-*b*]-pyridin-1-ylmethylene]-*N*-methylmethanaminium hexafluorophosphate; HOBT: 1-hydroxy-1*H*-benzotriazole hydrate; collidine = 2,4,6-trimethylpyridine.



Scheme 3. Synthesis of the high mannose glycopeptide; Py: pyridine; DMAP: 4-dimethylaminopyridine.

mediation by mercury(II) catalysis (anomers **22**).^[23] Once again, aminolysis, following the precedents of Cohen-Anisfeld and Lansbury,^[20, 21] led to the pure β -amino anomer **23**. The latter underwent acylation with peptide construct **24**,^[24] as shown, to provide the desired homogeneous target **1** (40% after purification by HPLC). The structure assignment of **1** is fully consistent with mass spectral analysis^[25] (calcd: m/z 1449 [M^+]; found: m/z 1472 [$M+Na^+$]).

Furthermore, the 1H NMR spectrum of **1** measured at 800 MHz (Figure 1) is fully supportive of the stereochemical assignment of the five anomeric linkages, including the β -Asn configuration ($\delta = 5.0$, $J = 10$ Hz). The eight NH signals of secondary amides within the glycopeptide were also found and assigned (see inserts). A full assessment of the spectroscopically derived conformation of this highly organized glycopeptide will be published separately.

With proof of principle demonstrated, focus is already directed to new avenues. These include building longer peptide constructs so that the effects of glycosylation on conformation can be probed in detail along a peptide chain. Also underway are experiments where the oligosaccharides

entering into the glycopolypeptides present determinants of established biological function. The concise, *totally synthetic* routes to homogeneous glycopeptides demonstrated here will prove to be valuable in furthering progress in glycobiology.

Received: June 5, 2000 [Z15221]

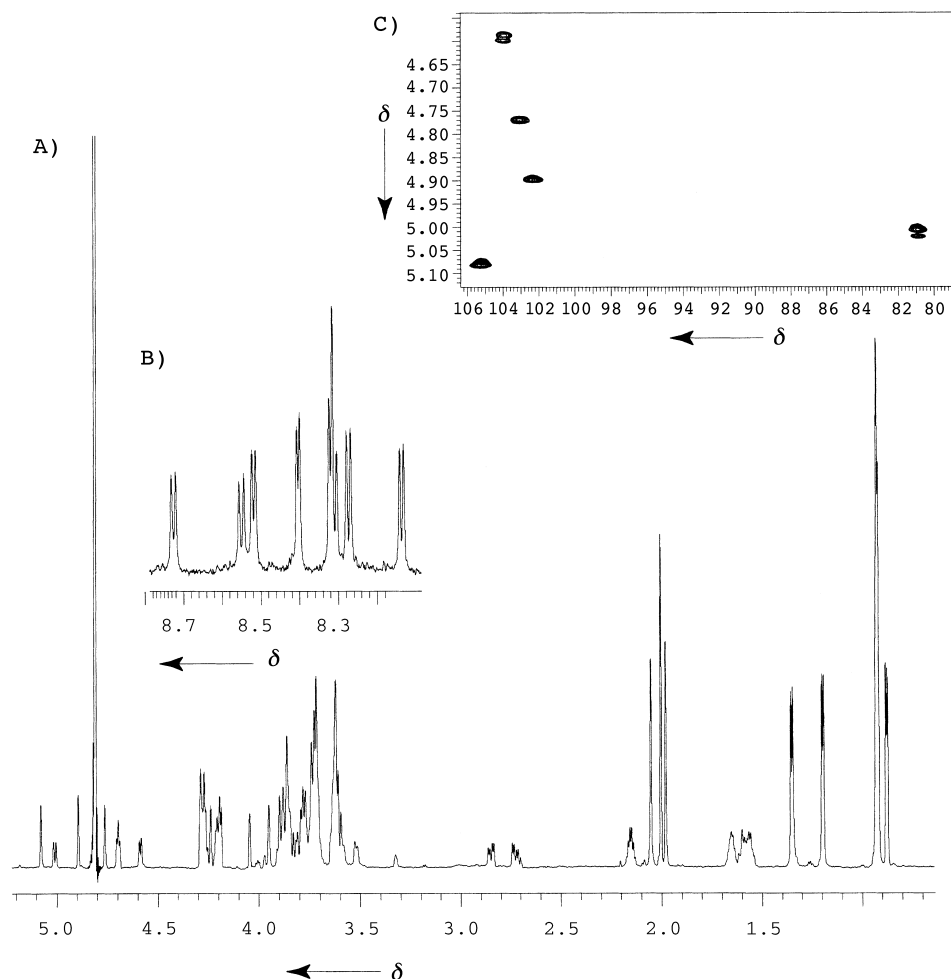


Figure 1. A) 1H NMR (800 MHz) spectrum of **1** in D_2O at 20°C and pH 3.7 (phosphate buffer). B) Section of the 1H spectrum of **1** in H_2O at 5°C and pH 3.5 (phosphate buffer) showing the secondary NH signals of amides from the peptide backbone, side chain, and GlcNAc sites. The protons of the terminal carboxamide (not shown) are observed slightly upfield of this region. C) The anomeric region of the 1H - ^{13}C HMQC spectrum at 800 MHz of **1** in D_2O at 20°C and pH 3.7 (phosphate buffer). The GlcNAc anomeric sites at $\delta = 4.58$ and 5.01 (1H) are clearly distinguished by their larger 1H couplings.

- [1] a) P. Burda, M. Aebi, *Biochem. Biophys. Acta* **1999**, 1426, 239; b) R. A. Dwek, *Chem. Rev.* **1996**, 96, 683; c) "Glycoproteins": *New Comprehensive Biochemistry*, Vol. 29a (Eds: A. Neuberger, L. L. M. Deener), Elsevier, New York, **1995**.
- [2] For critical insights into the chemistry and biology of the N-linked systems, see B. Imperiali, S. E. O'Connor, *Curr. Opin. Chem. Biol.* **1999**, 3, 643; B. Imperiali, *Acc. Chem. Res.* **1997**, 30, 452; D. F. Wyss, G. Wagner, *Curr. Opin. Biotechnol.* **1996**, 7, 409.
- [3] A. Varki, *Glycobiology* **1993**, 3, 97; A. Helenius, *Mol. Biol. Cell* **1994**, 5, 253; M. Ruderer, M. Hinnen, *J. Bacteriol.* **1991**, 173, 3539.
- [4] R. D. Klausner, R. Sitia, *Cell* **1990**, 62, 611.
- [5] L. H. Shevinsky, B. B. Knowles, I. Demjanov, D. Solter, *Cell* **1982**, 30, 697; P. W. Andrew, P. N. Goodfellow, L. H. Shevinsky, D. L. Bronson, B. B. Knowles, *Int. J. Cancer* **1982**, 29, 253.
- [6] G. Wagner, D. F. Wyss, *Curr. Opin. Struct. Biol.* **1994**, 4, 841.
- [7] R. A. Dwek, *Biochem. Soc. Trans.* **1995**, 23, 1.
- [8] For a review on the syntheses of O- and N-linked glycopeptides, see G. Arsequell, G. Valencia, *Tetrahedron: Asymmetry* **1997**, 8, 2839; G. Arsequell, G. Valencia, *Tetrahedron: Asymmetry* **1999**, 10, 3045.
- [9] For the all-chemical and chemoenzymatic synthesis of high mannose linked glycopeptides, see, for example, Matsuo, Y. Nakahara, Y. Ito, T. Nukuda, V. Nakara, T. Ogawa, *Bioorg. Med. Chem.* **1995**, 3, 1455; Y. Ito, T. Ogawa, *J. Am. Chem. Soc.* **1997**, 119, 5562; Z. W. Guo, Y. Nakahara, T. Ogawa, *Angew. Chem.* **1997**, 109, 1527; *Angew. Chem. Int. Ed. Engl.* **1997**, 36, 1464; C. Unverzagt, *Carbohydr. Res.* **1998**, 305, 423; C. Unverzagt, *Angew. Chem.* **1997**, 109, 2078; *Angew. Chem. Int. Ed. Engl.* **1997**, 36, 1989; C. Unverzagt, *Angew. Chem.* **1996**, 108, 2507; *Angew. Chem. Int. Ed. Engl.* **1996**, 35, 2350; C. Unverzagt, *Angew. Chem.* **1994**, 106, 1170; *Angew. Chem. Int. Ed. Engl.* **1994**, 33, 1102; M. Mizuno, K. Handa, R. Iguchi, I. Muramoto, T. Kawakami, S. Aimoto, K. Yamamoto, T. Inazu, *J. Am. Chem. Soc.* **1999**, 121, 284; R. R. Schmidt, R. R. Kinzy, *Adv. Carbohydr. Chem. Biochem.* **1994**, 50, 21.
- [10] W. Gunther, H. Kunz, *Carbohydr. Res.* **1992**, 228, 217; S. Weiler, R. R. Schmidt, *Tetrahedron Lett.* **1998**, 39, 2299; E. Meinjohanns, M. Meldal, H. Paulsen, R. A. Dwek, K. Bock, *J. Chem. Soc. Perkin Trans. 1* **1998**, 549; S. Cherif, J. M. Clavel, C. Monneret, *J. Carbohydr. Chem.* **1998**, 17, 1203.
- [11] T. J. Rutherford in *Glycopeptides and Related Compounds* (Eds.: D. C. Large, C. D. Warren), Marcel Dekker, New York **1997**, chap. 14, p. 661.
- [12] M. Fukuda in *Glycoconjugates* (Eds.: H. J. Allen, E. C. Kisailus), Marcel Dekker, New York, **1992**, chap. 12, p. 379.

- [13] For recent synthetic advances from our laboratory in the area of O-linked glycopeptides see W. Glunz, S. Hintermann, J. B. Schwarz, S. D. Kuduk, X.-T. Chen, L. J. Williams, D. Sames, S. J. Danishefsky, V. Kudryashov, K. O. Lloyd, *J. Am. Chem. Soc.* **1999**, *121*, 10636, and references therein.
- [14] R. D. Cummings in *Glycoconjugates* (Eds.: H. J. Allen, E. C. Kisailus), Marcel Dekker, New York, **1992**, chap. 10, p. 333.
- [15] For the general strategy we employ in reaching the "high mannose" core system, see P. H. Seeberger, P. F. Cirillo, S. Hu, X. Beebe, M. T. Bilodeau, S. J. Danishefsky, *Enantiomer J. Stereochem.* **1996**, *1*, 311.
- [16] S. J. Danishefsky, M. T. Bilodeau, *Angew. Chem.* **1996**, *108*, 1482; *Angew. Chem. Int. Ed. Engl.* **1996**, *35*, 1380.
- [17] S. J. Danishefsky, S. Hu, P. F. Cirillo, M. Eckhardt, P. H. Seeberger, *Chem. Eur. J.* **1997**, *3*, 1617.
- [18] see: D. A. Griffith, S. J. Danishefsky, *J. Am. Chem. Soc.* **1990**, *112*, 5811.
- [19] E. N. Cain, L. L. Welling, *Tetrahedron Lett.* **1975**, *16*, 1353.
- [20] L. M. Likhoshervostov, O. S. Novikova, V. A. Derevitskaja, N. K. Kochetkov, *Carb. Res.* **1986**, *146*, C1; S. T. Cohen-Anisfeld, P. T. Lansbury, Jr., *J. Org. Chem.* **1990**, *55*, 5560.
- [21] S. T. Cohen-Anisfeld, P. T. Lansbury, Jr., *J. Am. Chem. Soc.* **1993**, *115*, 10531.
- [22] Since our yield is far from quantitative, we cannot rule out the possibility of aspartimide formation, or even products arising from N-acylation by the α -carboxy group of the Asn residue via such an intermediate. This same issue, which can be raised with respect to the previous cases,^[21] requires further detailed study.
- [23] A. I. Meyers, D. L. Comins, D. M. Roland, R. Henning, K. Shimizu, *J. Am. Chem. Soc.* **1979**, *101*, 7104.
- [24] Prepared by San San Yi, Microchemistry Laboratory, Sloan-Kettering Institute for Cancer Research.
- [25] PE Sciex API-100.

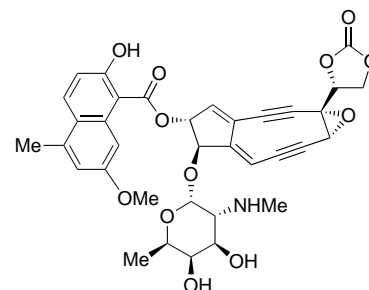
Chemical Synthesis and DNA Photocleavage of the Intercalator–Carbohydrate Hybrid Moiety of the Neocarzinostatin Chromophore**

Kazunobu Toshima,* Shigeki Takai, Yutaka Maeda, Ryusuke Takano, and Shuichi Matsumura

Dedicated to Professor Kuniaki Tatsuta on the occasion of his 60th birthday

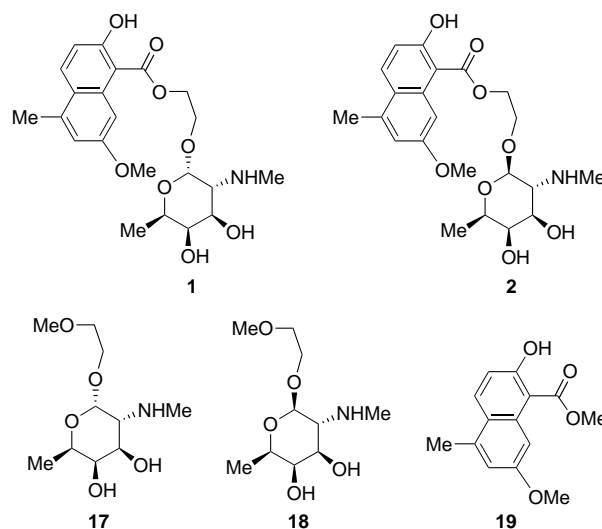
The development of photochemical DNA-cleaving agents, which effectively cleave DNA by irradiation at a specific wavelength under mild conditions and without any additives such as metals and reducing agents, is very interesting from a chemical and biological standpoint and offers considerable

potential in medicine.^[1] Indeed, photodynamic therapy using a photosensitizing drug has recently emerged as a promising modality against cancer and allied diseases.^[2] Sugiura et al.^[3] first demonstrated the light-induced DNA cleavage by the antitumor enediyne antibiotic neocarzinostatin^[4] and Hirama et al.^[5] reported the photoinduced cycloaromatization of the neocarzinostatin chromophore (Scheme 1), which is responsible for the DNA-cleavage activity of neocarzinostatin. In



Scheme 1. Neocarzinostatin chromophore.

this context, we anticipated that if the intercalator–carbohydrate hybrid moiety of the neocarzinostatin chromophore, without its enediyne moiety, interacts with DNA and if the C=O bond in the hybrid generates a photoexcited $^3(n-\pi^*)$ radical-like^[5] state by photoirradiation, then the intercalator–carbohydrate hybrid moiety of the enediyne-free neocarzinostatin chromophore could be capable of DNA cleavage. Herein, we report the chemical synthesis and DNA-photocleavage properties of the intercalator–carbohydrate hybrids^[6, 7] **1** and **2**, which correspond to the intercalator and the carbohydrate moieties of the enediyne antibiotic, neocarzinostatin (Scheme 2).



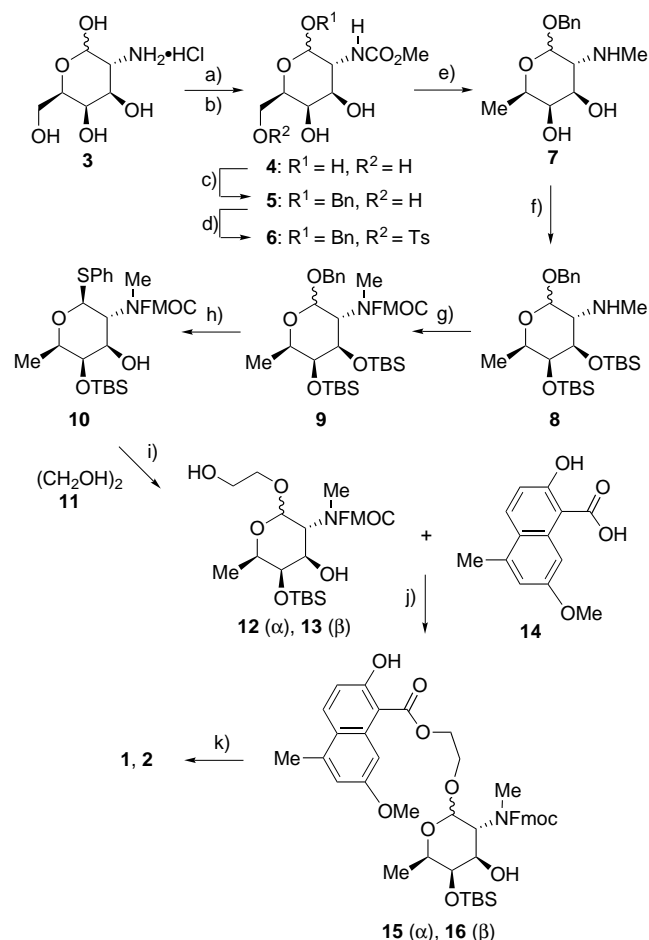
Scheme 2. The intercalator–carbohydrate hybrids and their components.

To confirm our hypothesis, we designed and synthesized **1** and **2**, in which the aromatic and sugar moiety of the neocarzinostatin chromophore were linked by only an ethylene glycol unit to each other. Compounds **1** and **2** are the anomers of each other. Their synthesis began with the

[*] Prof. Dr. K. Toshima, S. Takai, Y. Maeda, R. Takano, Prof. Dr. S. Matsumura
Department of Applied Chemistry
Faculty of Science and Technology
Keio University
3-14-1 Hiyoshi, Kohoku-ku, Yokohama 223-8522 (Japan)
Fax: (+81)45-566-1576
E-mail: toshima@apple.keio.ac.jp

[**] This research was partially supported by a Grant-in-Aid for Encouragement of Young Scientists from the Ministry of Education, Science, Sports, and Culture, Japan, and a research grant of Keio University Special Grant-in-Aid for Innovative Collaborative Research Projects.

conversion of D-galactosamine hydrochloride (**3**) into the benzyl glycoside **6** in four standard steps (Scheme 3). After separation of the pyranosides **6** and the corresponding furanosides by column chromatography at this stage, the lithium aluminum hydride (LAH) reduction of **6** gave **7**, which



was subjected to protection with *tert*-butyldimethylsilyl (TBS) and 9-fluorenylmethoxycarbonyl (Fmoc) groups to afford **9** in high overall yield. Conversion of the benzyl glycoside **9** into the phenylthio glycoside **10** accompanied by deprotection of the TBS group at the C-3 position was next carried out using PhSH and BF₃·OEt₂. The glycosidation of **10** (1.0 equiv) with ethylene glycol **11** (5.0 equiv) using *N*-bromosuccinimide (NBS)^[8] in the presence of molecular sieves (MS 4 Å) in MeCN gave both the α -glycoside **12** and the β -glycoside **13** in 97% yield in a ratio of 1:1.8. After their separation by column chromatography, **12** (1.0 equiv) and **13** (1.0 equiv) were esterified with the carboxylic acid **14**^[9] (2.0 equiv) using 1-ethyl-3-(3-dimethylaminopropyl)carbodiimide hydrochloride

(WSCD·HCl) in CH₂Cl₂ to give the hybrids **15** and **16** in 64% and 60% yields, respectively. Finally, the deprotection of the TBS and Fmoc groups in **15** and **16** using tetrabutylammonium fluoride (TBAF) in THF furnished the intercalator-carbohydrate hybrids **1** and **2**, respectively.

The photoinduced DNA-cleavage activities of the intercalator-carbohydrate hybrids **1** and **2**, along with the components of these hybrids **17–19**,^[10] were assayed using covalently closed supercoiled Φ X174 DNA (Form I). As noted in Figure 1, and, as expected, the intercalator-carbohydrate

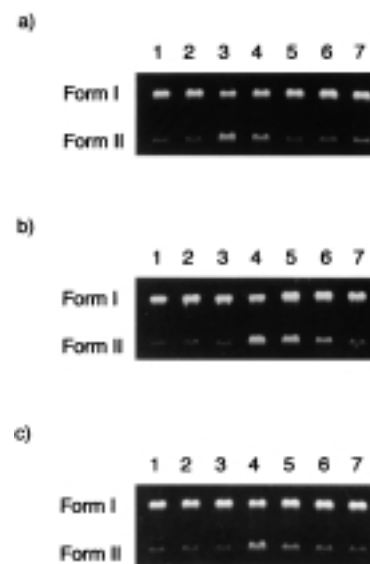


Figure 1. Photocleavage of supercoiled Φ X174DNA. Φ X174DNA (50 μ M per base pair) was incubated with various compounds in 19% acetonitrile and 1% dimethyl sulfoxide in Tris/HCl buffer (pH 7.5, 50 mM) at 25 °C for 2 h under UV irradiation (365 nm, 15 W) from a lamp placed at 10 cm from the mixture. The product was analyzed by gel electrophoresis (0.9% agarose gel, ethidium bromide stain): a) lane 1, DNA alone; lane 2, DNA with UV; lanes 3–7, compounds **1**, **2**, **17**, **18**, and **19** (500 μ M), respectively; b) lane 1, DNA alone; lane 2, DNA with UV; lane 3, DNA + **1** (500 μ M) without UV; lanes 4–7, **1** (500), **1** (100), **1** (20), and **1** (5 μ M), respectively; c) lane 1, DNA alone; lane 2, DNA with UV; lane 3, DNA + **2** (500 μ M) without UV; lanes 4–7, **2** (500), **2** (100), **2** (20), and **2** (5 μ M), respectively.

hybrids **1** and **2** (500 μ M) cleaved the DNA and caused a single strand break, leading to the nicked, open-circular DNA (Form II) by photoirradiation with long wavelength UV light (365 nm), while **17–19** did not show DNA cleavage activity under the same conditions. These results clearly indicate a new and interesting fact, that the intercalator-carbohydrate hybrid moiety of the neocarzinostatin chromophore, without its enediyne moiety, induced photocleavage of the DNA. The importance of the hybrid structure, as constructed from the intercalator and the carbohydrate, towards DNA cleavage was confirmed. It was also confirmed that no DNA cleavage by **1** and **2** was observed in the absence of light. Furthermore, the DNA photocleavage of **1** was stronger than that of its anomer **2**, as **1** cleaved the DNA in concentrations over 20 μ M at 25 °C. The cleavage site specificity of the **1** and **2** was also analyzed according to the Sanger protocol.^[11] These results, shown in Figure 2, clearly show the identical high guanine selectivity. Furthermore, these results also indicated that the

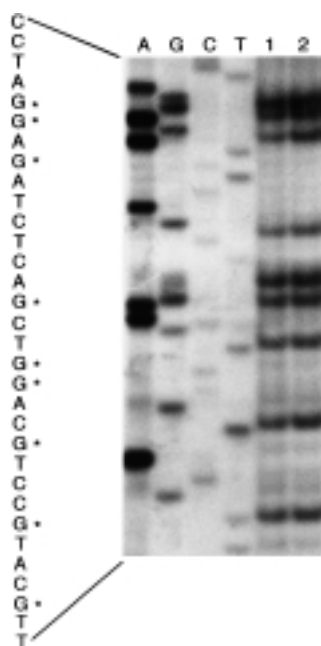


Figure 2. Autoradiogram of polyacrylamide/urea (12%/8M) slab gel electrophoresis for sequence analysis. The 5'-end-labeled M13mp18 DNA was cleaved by the hybrids at pH 7.5 and 25 °C for 2 h under irradiation, as described in Figure 1. Bases 48–79 are shown: lanes A, G, C, and T; Sanger A, G, C, and T reactions, respectively; lanes 1 and 2; **1** and **2** (500 μ M), respectively.

cleavage site selectivity of **1** and **2** was different from that of natural neocarzinostatin chromophore.^[3]

Received: December 14, 1999 [Z14390]

Revised: May 17, 2000

- [1] B. Armitage, *Chem. Rev.* **1998**, 98, 1171–1200.
- [2] A. R. Morgan, *Curr. Med. Chem.* **1995**, 2, 604–615; R. Bonnett, *Chem. Soc. Rev.* **1995**, 19–33; *Photodynamic Therapy: Basic Principles and Clinical Applications*, (Eds.: R. W. Henderson, T. J. Dougherty), Marcel Dekker, New York, **1992**.
- [3] Y. Uesawa, J. Kuwahara, Y. Sugiura, *Biochem. Biophys. Res. Commun.* **1989**, 164, 903–911.
- [4] For a review of neocarzinostatin, see: I. H. Goldberg, *Acc. Chem. Res.* **1991**, 24, 191–198.
- [5] T. Gomibuchi, M. Hirama, *J. Antibiot.* **1995**, 48, 738–740.
- [6] K. Takahashi, T. Tanaka, T. Suzuki, M. Hirama, *Tetrahedron* **1994**, 50, 1327–1340.
- [7] Total synthesis of the neocarzinostatin chromophore, see: A. G. Myers, J. Liang, M. Hammond, P. M. Harrington, Y. Wu, E. Y. Kuo, *J. Am. Chem. Soc.* **1998**, 120, 5319–5320.
- [8] K. C. Nicolaou, S. P. Seitz, D. P. Papahatjis, *J. Am. Chem. Soc.* **1983**, 105, 2430–2434.
- [9] M. Shibuya, K. Toyooka, S. Kubota, *Tetrahedron Lett.* **1984**, 25, 1171–1174; K. Shishido, A. Yamashita, K. Horoya, K. Fukumoto, T. Kametani, *Tetrahedron Lett.* **1989**, 30, 111–112; K. Takahashi, T. Suzuki, M. Hirama, *Tetrahedron Lett.* **1992**, 33, 4603–4604; A. G. Myers, V. Subramanian, M. Hammond, *Tetrahedron Lett.* **1996**, 37, 587–590.
- [10] These compounds were obtained by ways similar to that for the hybrids **1** and **2**.
- [11] F. Sanger, S. Nicklen, A. R. Coulson, *Proc. Natl. Acad. Sci. USA* **1977**, 74, 5463–5467. Since the Sanger sequencing reactions result in base incorporation, cleavage at nucleotide *N* (sequencing) represents cleavage site by the agent or the Maxam–Gilbert reaction at *N* + 1. See also: D. L. Boger, S. A. Munk, H. Zarrinmayeh, T. Ishizaki, J. Hought, M. Bina, *Tetrahedron* **1991**, 47, 2661–2682.

Alkane Carbonylation with Carbon Monoxide on Sulfated Zirconia: NMR Observation of Ketone and Carboxylic Acid Formation from Isobutane and CO**

Alexander G. Stepanov,* Mikhail V. Luzgin, Alexey V. Krasnoslobodtsev, Vera P. Shmachkova, and Nina S. Kotsarenko

Direct conversion of inert alkanes into carbonyl-containing organic compounds is an important goal for industrial organic chemistry. Alkanes can be carbonylated into carboxylic acids or aldehydes in superacidic HF/SbF₅ or CF₃SO₃H/SbF₅ systems.^[1] However, environmental concerns require the use of more environmentally friendly solid catalysts. The strong acidity and exceptionally high activity of sulfated zirconia^[2] (SZ) means it has received much attention as a potential catalyst for hydrocarbon conversion,^[3] and especially for overcoming the chemical inertness of alkanes. The direct carbonylation of benzene with CO using a pure SZ as the solid acid catalyst has been reported recently.^[4] However, saturated hydrocarbons were never reported to be involved in carbonylation reactions on SZ, only the inhibiting effect of carbon monoxide on linear alkane isomerization with SZ has been demonstrated.^[5] Herein we report direct ¹³C solid-state NMR spectroscopic measurements of the carbonylation of isobutane with CO, using a pure SZ as the solid acid catalyst.

Figure 1 displays the ¹³C cross-polarization magic-angle spinning (CP/MAS) NMR spectra obtained after coadsorption of isobutane and CO on SZ and subsequent heating of the sample at 70 °C for 1 h. We rationalize these spectra in terms of selective formation of methyl isopropyl ketone (**5**) by pathways a), d), g) and/or b), c), g) in Scheme 1. If 2-¹³C-labeled isobutane ([2-¹³C]iC₄H₁₀, that is, isobutane labeled at the quaternary carbon atom) and unlabeled CO are coadsorbed, the following spectral features are observed (Figure 1A): the intense signal at δ = 47.0 arises from the labeled CH group of the isopropyl fragment of **5**, the weak signal at δ = 19.6 is assigned to the unlabeled CH₃ group of the isopropyl fragment, while the signal at δ = 25.5 arises from residual isobutane. The resonance signal of the other unlabeled methyl group of **5** is not seen because of its very low intensity. If unlabeled isobutane and ¹³C-labeled carbon monoxide are coadsorbed (Figure 1B), the resonance signal

[*] Dr. A. G. Stepanov, Dr. M. V. Luzgin, Dr. V. P. Shmachkova, Dr. N. S. Kotsarenko
Group of NMR Spectroscopy for Catalytic Hydrocarbon Conversion and Laboratory for Zeolites and Acid-Base Catalysis
Boreskov Institute of Catalysis
Siberian Branch of the Russian Academy of Sciences
Prospekt Akademika Lavrentieva 5, Novosibirsk 630090 (Russia)
Fax: (+7) 3832-34-3056
E-mail: a.g.stepanov@catalysis.nsk.su
A. V. Krasnoslobodtsev
Natural Science Department, Novosibirsk State University
ul. Pirogova 2, Novosibirsk 630090 (Russia)

[**] This work was supported by grant No. 99-03-32454 from the Russian Foundation for Basic Research (RFBR) and in part by a joint RFBR-INTAS grant (No. 95-0194). The authors sincerely thank Dr. V. N. Sidelnikov for GC-MS analysis.

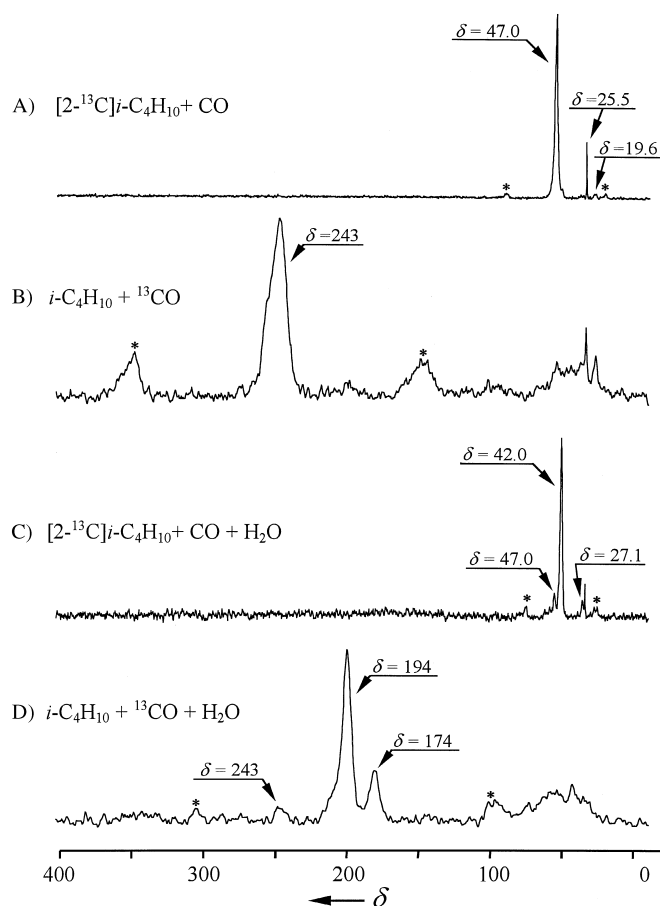
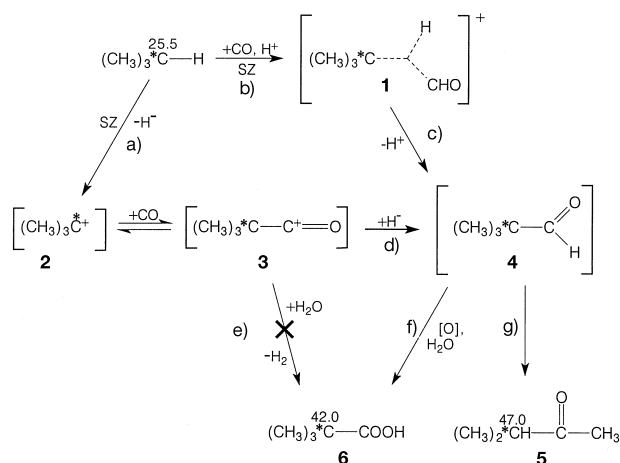


Figure 1. The ^{13}C CP/MAS NMR spectra of the products formed from isobutane and CO and water on SZ at 70 °C: a) coadsorption of the $[2\text{-}^{13}\text{C}]i\text{-C}_4\text{H}_{10}$ (82% ^{13}C enrichment) and unlabeled CO; b) coadsorption of ^{13}CO (90% ^{13}C enrichment) and unlabeled $i\text{-C}_4\text{H}_{10}$; c) coadsorption of $[2\text{-}^{13}\text{C}]i\text{-C}_4\text{H}_{10}$, (82% ^{13}C enrichment), CO, and H_2O ; d) coadsorption of ^{13}CO (90% ^{13}C enrichment), $i\text{-C}_4\text{H}_{10}$, and H_2O . * denotes spinning side band.



Scheme 1. Mechanism of isobutane carbonylation on SZ. *C denotes a ^{13}C -labeled carbon atom. Above each of the ^{13}C -labeled carbon atoms the corresponding ^{13}C NMR chemical shifts are given (δ).

of the carbonyl group of **5** becomes clearly visible at $\delta = 243$. We further confirmed the formation of **5** by both GC-MS and high-resolution ^{13}C NMR spectroscopy of the product extracted from the catalyst with Et_2O . The ^{13}C NMR spectrum of

the product in CDCl_3 exhibits resonance signals at $\delta = 18.1$ (CH_3), 41.65 (CH), 27.5 (CH_3), 212.6 ($\text{C}=\text{O}$), which are in good agreement with those reported for methyl isopropyl ketone.^[6] However, the resonance signal of the carbonyl group of **5** adsorbed on SZ is shifted downfield by $\Delta\delta = 30$ ppm relative to that in CDCl_3 . This may be related to the strong protonation^[7a] or complexation^[7b,c,8] of the ketone carbonyl group by the Brønsted acid sites.

We have not observed the formation of pivalic aldehyde (**4**), which is expected to be the most probable product of isobutane carbonylation. This observation is in a good agreement with earlier findings on the rearrangement of **4** into **5** in the presence of strong acids.^[1b,9]

When the reaction was carried out in the presence of water, the other carbonylation route was utilized (Scheme 1, pathways a), d), f) and/or b), c), f). Upon interaction with CO and H_2O , isobutane converts primarily into pivalic acid (**6**) (see Figures 1 C, D). Resonance signals at $\delta = 42.0$ and 27.1 arise from the ^{13}C -labeled quaternary carbon atom and unlabeled methyl groups of **6**,^[8] respectively. Upon reaction with ^{13}CO , we observe a signal at $\delta = 194$ from the COOH group of **6**^[8] (Figure 1 D). Low intensity signals at $\delta = 47.0$ and 243 in Figures 1 C and D, respectively, are from compound **5** and indicate that, in the presence of water, a conversion of the alkane into the acid **6** represents the main route of isobutane carbonylation, while in the absence of water **6** is formed only in a trace amount (see Figure 1 A, the low intensity signal at $\delta = 42.0$, which is seen as the shoulder to the intense signal at $\delta = 47.0$ from **5**, arises from **6**).

The conversion of isobutane was 36% at 70 °C in the absence of water, with **5** and **6** being formed with 97% and 3% selectivity, respectively. In the presence of water at 70 °C, only 21% of the isobutane was converted and the selectivity for **5** and **6** being 29 and 71%, respectively.

Noteworthy is the absence of molecular hydrogen (H_2) evolution in the carboxylic acid formation. Evolution of H_2 , readily detectable by in situ ^1H MAS NMR spectroscopy as a narrow signal, expected at $\delta \approx 4$,^[10] would provide evidence for a protolytic step in isobutane activation to form a pentacoordinate carbonium ion,^[11] which further evolves H_2 to give the *tert*-butyl carbenium ion **2** (Scheme 1). The cation **2** is trapped with CO and H_2O to form the carboxylic acid by pathway e) in Scheme 1. The absence of H_2 suggests another route for isobutane conversion into the acid. We conclude that oxidation of the intermediate aldehyde^[12] **4** by the SZ sulfate groups^[4] (noncatalytic pathway f)), rather than quenching of **3** with water (pathway e)), represents the main route for isobutane conversion into the acid in the presence of water.

It should be noted that for the reaction of ^{13}CO with isobutane in the presence of water (Figure 1 D), as well as for the interaction of only CO and H_2O at 70 °C, an additional signal is observed at $\delta = 174$ arising from a formate species.^[13] To date, we have no additional experimental data which could help us to show if a formate compound plays some role in the activation step of the alkane on SZ. One can suggest that the formyl cation $[\text{HC}^+\text{O}]$ is formed from formate as an equilibrated species, producing **4** by direct formylation of isobutane by pathways b) and c) with the formation of a three-center two-electron-bonded pentacoordinate carbonium ion

as the transition state, similar to superacidic solutions.^[1b] At the same time, according to literature data both parallel pathways a), d) and b), c) are possible for the formation of pivalic aldehyde (**4**) by the direct formylation of the C–H bond in isobutane with the [HC⁺O] cation^[1b] and by reduction of pivaloyl cation **3** with hydride ion.^[1b, 14] Thus, we are not able to demonstrate by which pathway (a) and d) or b) and c)) the intermediate pivalic aldehyde (**4**) preferentially forms.

The observed alkane carbonylation provides new insight into the negative influence of CO on the alkane isomerization over SZ. The data obtained imply that suppression of the alkane isomerization by CO may result not only from the blocking of Lewis acid sites with CO^[5] or from the reversible formation of **3** from **2**,^[15, 16] but that carbon monoxide can also change the reaction route from isomerization towards carbonylation, thus contributing to the inhibiting effect on the alkane isomerization rate.

In conclusion, the present work represents the first small-alkane carbonylation on a SZ catalyst. The valuable chemical products (carboxylic acids and ketones) have been shown to be selectively produced over SZ at low temperature. This finding opens up a new possibility for the use of SZ-based catalysts for direct carbonylation of alkanes with CO.

Experimental Section

A sample of SZ of the low-temperature tetragonal phase with a surface area of 60 m² g⁻¹ and 9.9 wt % SO₃ content was prepared by a procedure described earlier.^[17] The sample of SZ was calcined at 600 °C in air for 1 h and at 400 °C in vacuum (10⁻⁵ Torr) for 2 h. Equal amounts of isobutane (ca. 300 μmol g⁻¹) and CO (or isobutane, CO and H₂O) were frozen out on the SZ under vacuum at liquid nitrogen temperature. After sealing the SZ sample inside a glass tube (volume 0.2 cm³) it was heated at 70 °C for 1 h; the pressure of CO was 8 atm under these conditions. Reaction products were analyzed in situ in the sealed glass tubes by ¹³C CP/MAS NMR spectroscopy.

The ¹³C CP/MAS NMR and ¹³C high-resolution NMR spectra in CDCl₃ solution were recorded on a Bruker MSL-400 NMR spectrometer at room temperature (~23 °C). The conditions used for CP experiments are described in refs. [7c, 8], spinning rate was 3–10 kHz. A few thousand scans were collected for each spectrum. Chemical shifts (δ) of the organic compounds adsorbed and in CDCl₃ were measured with respect to TMS as external reference.

GC-MS analysis of the reaction products extracted with Et₂O from the SZ sample was made with VG 70–70 mass spectrometer. The fused silica capillary column of 35 m × 0.3 mm internal diameter with SE 30 as the active phase, forming a film of 0.3 μm thickness, was used for the separation of the organic products.

Received: March 17, 2000

Revised: July 17, 2000 [Z 14865]

- [1] a) R. Paatz, G. Weisberger, *Chem. Ber.* **1967**, *100*, 984–990; b) O. Farooq, M. Marcelli, G. K. S. Prakash, G. A. Olah, *J. Am. Chem. Soc.* **1988**, *110*, 864–867; c) S. Delavarenne, M. Simon, M. Fauconet, J. Sommer, *J. Am. Chem. Soc.* **1989**, *111*, 383–384.
- [2] M. Hino, S. Kobayashi, K. Arata, *J. Am. Chem. Soc.* **1979**, *101*, 6439.
- [3] X. Song, A. Sayari, *Catal. Rev. Sci. Eng.* **1996**, *38*, 329–412.
- [4] T. H. Clingenpeel, T. E. Wessel, A. I. Biaglow, *J. Am. Chem. Soc.* **1997**, *119*, 5469–5470.
- [5] F. Pinna, M. Signoretto, G. Strukul, G. Cerrato, C. Morterra, *Catal. Lett.* **1994**, *26*, 339–344.
- [6] C. G. Andrieu, D. Debruyne, D. Paquer, *Org. Magn. Reson.* **1978**, *11*, 528–532.

- [7] a) G. A. Olah, D. White, *J. Am. Chem. Soc.* **1969**, *91*, 5801–5810; b) T. Xu, E. J. Munson, J. F. Haw, *J. Am. Chem. Soc.* **1994**, *116*, 1962–1972; c) M. V. Luzgin, V. N. Romannikov, A. G. Stepanov, K. I. Zamaraev, *J. Am. Chem. Soc.* **1996**, *118*, 10890–10891.
- [8] A. G. Stepanov, M. V. Luzgin, V. N. Romannikov, V. N. Sidelnikov, K. I. Zamaraev, *J. Catal.* **1996**, *164*, 411–421.
- [9] a) S. Danilow, E. Vanus-Danilowa, *Ber. Dtsch. Chem. Ges. B* **1926**, *59*, 377; b) H. Hopff, C. D. Nenitzescu, D. A. Isacescu, I. P. Cantunari, *Ber. Dtsch. Chem. Ges. B* **1936**, *69*, 2244; c) G. A. Olah, D. H. O'Brien, M. Calin, *J. Am. Chem. Soc.* **1967**, *89*, 3582–3586.
- [10] M. V. Luzgin, A. G. Stepanov, A. Sassi, J. Sommer, *Chem. Eur. J.* **2000**, *6*, 2368–2376.
- [11] T.-K. Cheung, B. C. Gates, *Top. Catal.* **1998**, *6*, 41–47.
- [12] R. T. Morrison, R. N. Boyd, *Organic Chemistry*, Allyn & Bacon, Boston, **1970**.
- [13] a) T. M. Duncan, R. W. Vaughan, *J. Catal.* **1981**, *67*, 49–70; b) N. D. Lazo, D. K. Murray, M. L. Kieck, J. F. Haw, *J. Am. Chem. Soc.* **1992**, *114*, 8552–8559.
- [14] A. T. Balaban, C. D. Nenitzescu, *Tetrahedron* **1960**, *10*, 55–64.
- [15] V. Adeeva, H. Y. Liu, W. M. H. Sachtler, *Top. Catal.* **1998**, *6*, 61–76.
- [16] a) A. Goepfert, B. Louis, J. Sommer, *Catal. Lett.* **1998**, *56*, 43–48; b) J. Sommer, D. Habermacher, R. Jost, A. Sassi, A. G. Stepanov, M. V. Luzgin, D. Freude, H. Ernst, J. Martens, *J. Catal.* **1999**, *181*, 265–270.
- [17] V. M. Mastikhin, A. V. Nosov, S. V. Filimonova, V. V. Tersikh, N. S. Kotsarenko, V. P. Shmachkova, V. I. Kim, *J. Mol. Catal.* **1995**, *101*, 81–90.


Nucleoglycoconjugates: Design and Synthesis of a New Class of DNA–Carbohydrate Conjugates**

Terry L. Sheppard, Chi-Huey Wong, and Gerald F. Joyce*

Solid-phase DNA synthesis, based upon phosphorus(III) coupling chemistry,^[1] has revolutionized the study of nucleic acids. In addition to providing synthetic DNA for molecular biological investigations, these solid-phase strategies have facilitated the synthesis of chemically modified oligonucleotides,^[2] which have been used as probes of DNA structure and function^[3] and as tools for mechanistic studies in nucleic acid biochemistry.^[4] The synthesis of modified DNA also has fueled antisense therapeutics^[5] and provided insight into the chemical evolution of nucleic acid structure.^[6] The phosphoramidite method offers a general strategy for the conjugation of molecules such as biotin and fluorescein to DNA through

[*] Prof. G. F. Joyce, Dr. T. L. Sheppard, Prof. C.-H. Wong
Departments of Chemistry and Molecular Biology and
The Skaggs Institute for Chemical Biology
The Scripps Research Institute
10550 North Torrey Pines Road
La Jolla, CA 92037 (USA)
Fax: (+858)-784-2943
E-mail: gjoyce@scripps.edu

[**] This work was supported by NASA and The Skaggs Institute for Chemical Biology at The Scripps Research Institute. T.L.S. was supported by a postdoctoral fellowship from the NASA Specialized Center for Research and Training in Exobiology.

 Supporting information for this article is available on the WWW under <http://www.wiley-vch.de/home/angewandte/> or from the author.

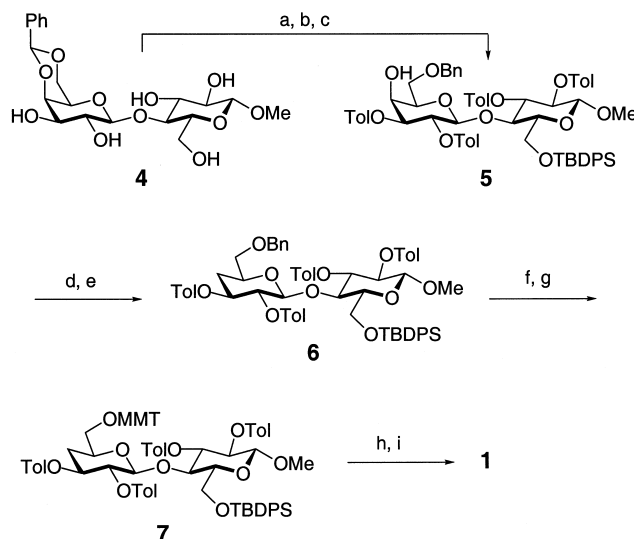
stable terminal or internal phosphodiester linkages.^[7] Phosphoramidite chemistry also has been used to prepare phosphorylated biomolecules including sugars,^[8] glycopeptides,^[9] carbohydrate–nucleoside drug hybrids,^[10] and phosphate-linked carbonucleotoid structures.^[11]

Herein we describe an efficient phosphoramidite-based method for the synthesis of a new class of DNA–carbohydrate conjugates, which we term nucleoglycoconjugates. Our strategy involves the preparation of mono- and disaccharide phosphoramidite derivatives and conjugation of these derivatives, by solid-phase chemistry, to terminal or internal positions of oligonucleotides. Our approach was motivated by the biological relevance and potential applications of carbohydrate–DNA conjugates. Carbohydrate modifications of DNA nucleobases have been observed in biological systems,^[12] and synthetic routes to these modified nucleotides have been demonstrated.^[13] Conjugation of carbohydrates to the 5'-end of DNA has been achieved previously by the direct glycosylation of the 5'-hydroxy group of oligonucleotides,^[14] and by the use of mannoside mono- and disaccharide phosphoramidite derivatives.^[15] However, no general method exists for the linkage of carbohydrates to internal sites of nucleic acids through phosphodiester bonds. Such carbohydrate-modified DNA molecules would be hydrolytically and thermally stable, and would possess the attractive features of both carbohydrates and nucleic acids. As such, nucleoglycoconjugates may have utility in oligonucleotide therapeutic strategies, as substrates for the *in vitro* evolution of new catalytic RNA and DNA molecules, and in the engineering of DNA-based materials.

We designed and synthesized three carbohydrate phosphoramidite derivatives **1–3** as nucleoglycoconjugate building blocks. Phosphoramidite **1**, based upon methyl 4'-deoxy-lactoside (Me-dLac), was designed to provide access to DNA containing an internal disaccharide linked through its primary hydroxy groups to adjacent DNA sequences. This deoxysugar

Thus, despite the increased synthetic challenge, the deoxy-sugar target **1** was chosen. Compounds **2** and **3** correspond to the reducing and nonreducing monosaccharide fragments, respectively, of the Me-dLac structure, and were designed to permit conjugation of these sugars to either the 5'- or 3'-end of DNA.

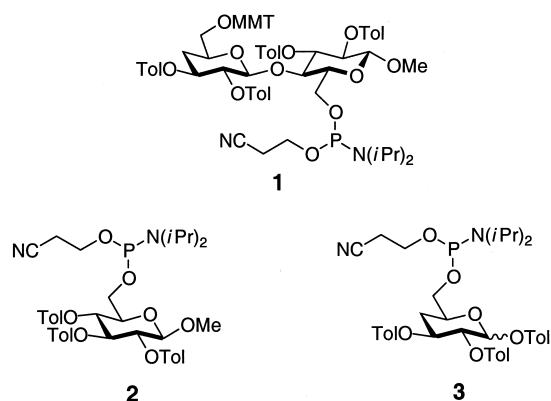
Phosphoramidite derivative **1** was prepared starting from the known^[16] 4',6'-benzylidene derivative of methyl- β -D-lactoside (**4**) (Scheme 1). Benzylidene **4** was silylated selectively at



Scheme 1. Synthetic route to **1**. a) TBDPSCl, pyr, DMAP (63%); b) *p*-MePhCOCl, pyr, DMAP (72%); c) NaCNBH₃, THF, HCl/Et₂O (94%); d) Im₂CS, CH₃CN (84%); e) *n*Bu₃SnH, AIBN, PhCH₃ (80%); f) H₂, Pd(OH)₂/C, EtOAc, EtOH (76%); g) MMTCl, pyr, DMAP (86%); h) TBAF, THF, HOAc (73%); i) [(*i*Pr)₂N]₂POCH₂CH₂CN, diisopropylammonium tetrazolide, CH₂Cl₂ (82%). AIBN = azobisisobutyronitrile, Im = imidazole, DMAP = 4,4-dimethylaminopyridine, pyr = pyridine.

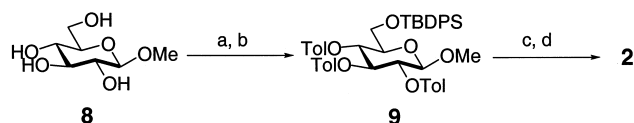
the 6-position of the glucopyranose ring using *tert*-butyldiphenylsilyl chloride (TBDPSCl). The remaining secondary alcohols were protected as *p*-toluoyl (Tol) esters. The 4'-hydroxy group was revealed by regioselective ring opening of the 4',6'-benzylidene derivative using sodium cyanoborohydride (NaCNBH₃) in HCl/diethyl ether^[17] to give the desired 6'-*O*-benzyl derivative **5**. Selective removal of the 4'-hydroxy group of lactose was accomplished by a two-step Barton oxygenation sequence to produce **6**.

With the Me-dLac skeleton in place, the synthesis of phosphoramidite **1** was completed by manipulation of protecting groups (Scheme 1). The 6'-*O*-benzyl group of **6** was removed by hydrogenolysis with Pd(OH)₂/C (Degussa) catalyst. The monomethoxytrityl (MMT) protecting group was introduced at the 6'-position by reaction with MMTCl in pyridine to afford compound **7**.^[18] Desilylation of **7** using tetrabutylammonium fluoride (TBAF) in THF^[19] liberated the 6-hydroxy group, which subsequently was converted to the 2-cyanoethyl diisopropylphosphoramidite derivative using the conditions employed by Caruthers and co-workers.^[20] Compound **1** was produced as a 1:1 mixture of diastereomers; ³¹P NMR revealed two signals with chemical shifts of δ = 151.2 and 151.4.



target was chosen over the fully hydroxylated lactose parent structure because, once incorporated into oligonucleotides, the 4'-hydroxy group in lactose could facilitate DNA strand scission at the carbohydrate site; intramolecular attack of the 4'-hydroxy group on the 6'-phosphate group would displace the upstream DNA sequence and form a cyclic phosphate.

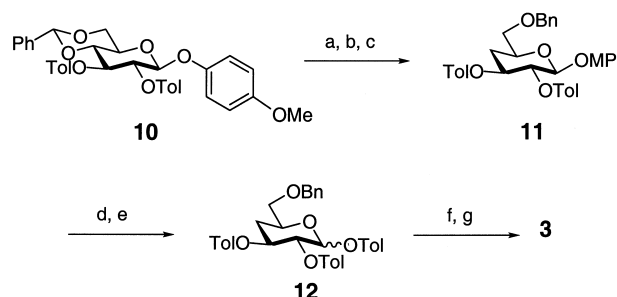
We next prepared phosphoramidite derivatives of the two monosaccharide components of the Me-dLac skeleton: the reducing-end methyl β -D-glucopyranoside (**2**) and the non-reducing-end 4-deoxy-D-glucose (**3**). Phosphoramidite **2** was synthesized in four steps starting from methyl β -D-glucopyranoside (**8**) (Scheme 2). Compound **9** was prepared by



Scheme 2. Synthetic route to **2**. a) TBDPSCl, imidazole, DMF (98 %); b) *p*-MePhCOCl, pyr, DMAP (75 %); c) CH_3COCl , MeOH, Et_2O (52 %); d) $[(i\text{Pr})_2\text{N}]_2\text{POCH}_2\text{CH}_2\text{CN}$, diisopropylammonium tetrazolide, CH_2Cl_2 (83 %).

silylation of **8** at the 6-position with TBDPSCl in DMF^[21] and subsequent esterification of the secondary hydroxy groups with *p*-toluoyl chloride. The TBDPS group of **9** was removed under acidic conditions, and the resulting primary hydroxy group was phosphitylated as described for **1** to produce monosaccharide phosphoramidite **2**.

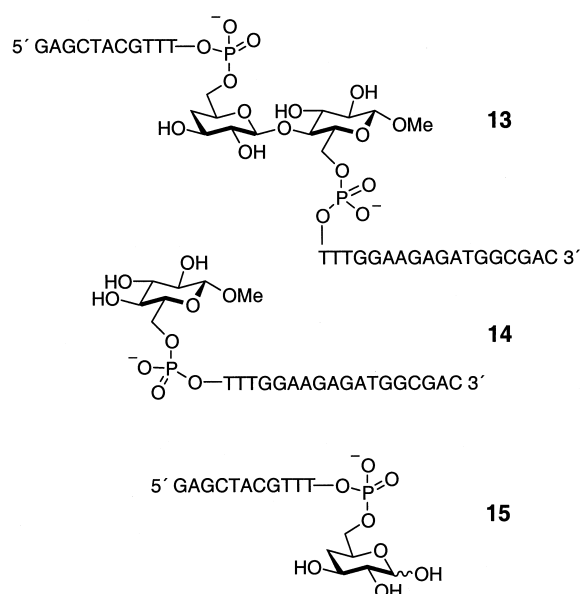
Phosphoramidite **3**, based upon 4-deoxyglucose, was synthesized in a manner similar to **1** (Scheme 3). The starting material, the known^[22] *p*-methoxyphenyl glycoside **10**, was



Scheme 3. Synthetic route to **3**. a) NaCNBH_3 , THF, $\text{HCl} \cdot \text{Et}_2\text{O}$ (69 %); b) Im_2CS , CH_3CN , reflux (87 %); c) $n\text{Bu}_3\text{SnH}$, AIBN, PhCH_3 (95 %); d) $\text{Ce}(\text{NH}_4)_2(\text{NO}_3)_6$, PhCH_3 , CH_3CN , H_2O (91 %); e) *p*-MePhCOCl, pyr, DMAP (96 %); f) H_2 , $\text{Pd}(\text{OH})_2/\text{C}$ cat., EtOAc, EtOH (85 %); g) $[(i\text{Pr})_2\text{N}]_2\text{POCH}_2\text{CH}_2\text{CN}$, diisopropylammonium tetrazolide, CH_2Cl_2 (80 %).

prepared in five steps from glucose pentaacetate. Regioselective ring opening of the 4,6-benzylidene **10** with NaCNBH_3 under acidic conditions afforded the 6-*O*-benzyl sugar. Barton deoxygenation of the revealed 4-hydroxy group yielded the 4-deoxyglucose derivative **11**. The anomeric center of **11** was deprotected by treatment with ceric ammonium nitrate to produce an equimolar mixture of three compounds: the desired α - and β -1-hydroxy anomers, and the α -anomer of the 1-*O*-*p*-toluoyl ester resulting from ester migration from the 2-position. This mixture was converted to the tri-*p*-toluoyl ester **12** by reaction with *p*-toluoyl chloride.^[23] The synthesis of amidite **3** was completed by debenzoylation of **12** and phosphitylation at the 6-position.

Phosphoramidites **1–3** coupled with high yields to DNA oligonucleotides to produce DNA–carbohydrate chimera containing internally embedded (**13**) and terminally conjugated (**14** and **15**) carbohydrates.^[24] Oligonucleotides **13** and



14 were prepared by using solid-phase DNA synthesis in the standard 3'-to-5' direction. Conjugate **15**, which required coupling of phosphoramidite derivative **3** to the 3'-end of the oligonucleotide, was synthesized in the 5'-to-3' direction using commercially available nucleoside 3'-*O*-DMT-5'-*O*-phosphoramidites.^[25] Nucleoglycoconjugates **13–15** were cleaved from the solid support and deprotected by treatment with concentrated aqueous ammonia. Subsequently, the modified oligonucleotides were purified by denaturing polyacrylamide gel electrophoresis and their identities were verified by matrix-assisted laser desorption ionization time-of-flight (MALDI-TOF) mass spectrometric analysis.

These DNA–carbohydrate conjugates behave like standard DNA oligonucleotides and are stable under conditions used in molecular biology experiments. Oligonucleotides **13–15** migrate normally in polyacrylamide gels, with each modified sugar-phosphate behaving like a nucleoside phosphate. No cleavage of the β -1,4-linkage of the deoxylactose disaccharide in oligonucleotide **13** was observed after 72 h over the pH range of 5.0–9.0 and the temperature range of 25–50 °C, as expected by recent measurements of glycoside stability.^[26] Thus, these carbohydrate-modified DNA molecules should be stable in buffered aqueous solutions and under thermal cycling conditions employed in the polymerase chain reaction (PCR).

The nucleoglycoconjugates form stable duplexes with complementary DNA oligonucleotides as demonstrated by UV-thermal denaturation analysis. Construct **13** was hybridized with a complementary 29mer DNA such that the Me-dLac moiety was unpaired and all of the flanking nucleotides were paired in a Watson–Crick fashion. The thermal stability of this duplex was compared to that of duplexes in which the Me-dLac residue was either replaced by an unpaired thymidylate or deleted to allow perfect complementarity. The fully complementary duplex had a T_m value of 74 °C. It was destabilized slightly by the presence of the unpaired thymidylate ($T_m = 70$ °C), and slightly more by the presence of the Me-dLac residue ($T_m = 66$ °C). A second set of

melting studies was performed by employing a 20mer rather than 29mer complementary DNA. These gave similar results, but with a T_m value that was 10–15 °C lower in all cases (see Supporting Information). Thus, despite the slight disruption of duplex structure, inclusion of the Me-dLac moiety within a DNA oligonucleotide does not significantly impair its ability to hybridize to a complementary template.

The nucleoglycoconjugates are substrates for common DNA-manipulating enzymes such as kinases and polymerases and can be utilized as primers in template-directed extension reactions. Nucleoglycoconjugates with a free 5'-hydroxy group (**13** and **15**) are efficiently labeled with radioactive [³²P]-phosphate by T4 polynucleotide kinase. Sugar-modified oligonucleotides with a free 3'-hydroxy group (**13** and **14**) are effective primers for enzymatic extension reactions,^[27] permitting the construction of large DNA molecules with specific internal (with **13**) or terminal (with **14**) carbohydrate modifications. PCR amplification of an 85-nucleotide insert also was possible using either **13** or **14** in concert with a second DNA primer and a thermostable DNA polymerase.

In summary, we have described the design, construction, and preliminary analysis of a new class of carbohydrate–DNA conjugates, which we term nucleoglycoconjugates. These DNA–saccharide hybrids are efficiently synthesized, chemically stable, and serve as substrates for standard DNA-modifying enzymes. We believe that these conjugates will provide a platform for the development of a new form of hybrid biomaterials. These materials could, in principle, be assembled from carbohydrate-modified DNA primers by the enzymes of carbohydrate and nucleic acid metabolism. They would possess the unique coding properties of nucleic acids and the recognition abilities of carbohydrates. In view of the prevalence of cell surface proteins (lectins) that recognize carbohydrate epitopes, these DNA-glycoconjugates may also be useful for increasing the specificity and efficiency of cellular uptake of therapeutic oligonucleotides.

Experimental Section

Oligonucleotides were synthesized using a Pharmacia Gene Assembler Special employing standard methods. Sugar phosphoramidites **1**–**3** were dissolved in absolute CH₃CN to a concentration of 0.1 M. Coupling yields for **1**–**3** were calculated by quantitation of DMT and MMT cation effluents. Syntheses employing phosphoramidites **1** and **2** were conducted in the standard 3'-to-5' direction using 3'-solid-supported nucleosides and nucleoside phosphoramidites containing labile base protecting groups (Glen Research, "Ultramild"). Syntheses employing phosphoramidite **3** were conducted in the reverse 5'-to-3' direction using 5'-solid-supported nucleosides and "reverse" 3'-O-DMT-5'-O-β-cyanoethyl phosphoramidites (Glen Research). Oligonucleotides were cleaved from the support and deprotected by using concentrated aqueous ammonia (normal synthesis: 8 h, 37 °C; reverse synthesis: 15 h, 55 °C), and were purified by denaturing polyacrylamide gel electrophoresis.

MALDI-TOF mass spectrometric analysis of **13**–**15** was performed on a PerSeptive Biosystems Voyager-STR mass spectrometer. The matrix was 2,4,6-trihydroxyacetophenone for **13** and 3-hydroxypicolinic acid for **14** and **15**. Conjugate **13**: m/z : calcd 9414.9; found M_{av} = 9409; conjugate **14**: m/z : calcd 5858.6; found M_{av} = 5859; conjugate **15**: m/z : calcd 3572.3; found M_{av} = 3572.

Received: February 28, 2000 [Z14779]

- [1] a) R. L. Letsinger, J. L. Finan, G. A. Heavner, W. B. Lunsford, *J. Am. Chem. Soc.* **1975**, *97*, 3278–3279; b) S. L. Beaucage, R. P. Iyer, *Tetrahedron* **1992**, *48*, 2223–2311.
- [2] S. L. Beaucage, R. P. Iyer, *Tetrahedron* **1993**, *49*, 6123–6194.
- [3] a) K. M. Guckian, T. R. Krugh, E. T. Kool, *Nat. Struct. Biol.* **1998**, *5*, 954–959; b) S. A. Wolfe, A. E. Ferentz, V. Grantcharova, M. Churchill, G. L. Verdine, *Chem. Biol.* **1995**, *2*, 213–222.
- [4] For example, in DNA damage and repair: J. Butenandt, L. T. Burgdorf, T. Carell, *Synthesis* **1999**, 1085–1105.
- [5] E. Uhlmann, A. Peyman, *Chem. Rev.* **1990**, *90*, 544–584.
- [6] M. Beier, F. Reck, T. Wagner, R. Krishnamurthy, A. Eschenmoser, *Science* **1999**, *283*, 699–703.
- [7] a) S. L. Beaucage, R. P. Iyer, *Tetrahedron* **1993**, *49*, 1925–1963; b) S. L. Beaucage, R. P. Iyer, *Tetrahedron* **1993**, *49*, 10441–10488.
- [8] a) H. Kondo, Y. Ichikawa, C.-H. Wong, *J. Am. Chem. Soc.* **1992**, *114*, 8748–8750; b) A. H. Haines, D. J. R. Massy, *Synthesis* **1996**, 1422–1424; c) P. Westerduin, P. Veeneman, G. A. van der Marel, J. H. van Boom, *Tetrahedron Lett.* **1986**, *27*, 6271–6274.
- [9] a) G. J. P. H. Boons, P. Hoogerhout, J. T. Poolman, G. A. van der Marel, J. H. van Boom, *Bioorg. Med. Chem. Lett.* **1991**, *1*, 303–308; b) R. Verduyn, J. J. A. Belén, C. M. Dreef-Tromp, G. A. van der Marel, J. H. van Boom, *Tetrahedron Lett.* **1991**, *32*, 6637–6640.
- [10] a) C. Le Bec, T. Huynh-Dinh, *Tetrahedron Lett.* **1991**, *32*, 6553–6556; b) T.-W. Cai, J.-M. Min, L.-H. Zhang, *Carbohydr. Res.* **1997**, *303*, 113–117.
- [11] K. C. Nicolaou, H. Flörke, M. G. Egan, T. Barth, V. A. Estevez, *Tetrahedron Lett.* **1995**, *36*, 1775–1778.
- [12] a) J. H. Gommers-Ampt, F. Van Leeuwen, A. L. de Beer, J. F. Vliegthart, M. Dizdaroglu, J. A. Kowalak, P. F. Crain, P. Borst, *Cell* **1993**, *75*, 1129–1136; b) I. R. Lehman, E. A. Pratt, *J. Biol. Chem.* **1960**, *235*, 3254–3259.
- [13] M. de Kort, E. Ebrahimi, E. R. Wijsman, G. A. van der Marel, J. H. van Boom, *Eur. J. Org. Chem.* **1999**, 2337–2343.
- [14] M. Adinolfi, G. Barone, L. De Napoli, L. Guariniello, A. Iadonisi, G. Piccialli, *Tetrahedron Lett.* **1999**, *40*, 2607–6610.
- [15] S. Akhtar, A. Routledge, R. Patel, J. M. Gardiner, *Tetrahedron Lett.* **1995**, *36*, 7333–7336.
- [16] R. S. Bhatt, L. Hough, A. C. Richardson, *Carbohydr. Res.* **1975**, *43*, 57–67.
- [17] A. Rivera-Sagredo, J. Jiménez-Barbero, M. Martín-Lomas, D. Solís, T. Díaz-Mauriño, *Carbohydr. Res.* **1992**, *232*, 207–226.
- [18] The standard dimethoxytrityl (DMT) protecting group used in DNA synthesis proved too labile at the 6-position of the disaccharide. Thus, the more stable MMT group was employed.
- [19] The reaction must be buffered to pH 7 with acetic acid to prevent ester migration to the revealed primary 6-hydroxy group.
- [20] M. H. Caruthers, A. D. Barone, S. L. Beaucage, D. R. Dodds, E. F. Fisher, L. J. McBride, M. D. Matteucci, Z. Stabinsky, J.-Y. Tang, *Methods Enzymol.* **1987**, *154*, 287–313.
- [21] E. M. Nashed, C. P. J. Glaudemans, *J. Org. Chem.* **1987**, *52*, 5255–5260.
- [22] T. M. Slaghek, Y. Nakahara, T. Ogawa, J. P. Kamerling, J. F. G. Vliegthart, *Carbohydr. Res.* **1994**, *255*, 61–85.
- [23] Product **12** was obtained as a 4:1 mixture of α/β -anomers.
- [24] Compound **1** coupled to DNA in >95 % yield. Extension of DNA after removal of the MMT group proceeded with a coupling yield of >70 %. Phosphoramidites **2** and **3** coupled to the termini of DNA in >90 % yield to provide **14** and **15**, respectively.
- [25] Reverse syntheses using commercially available nucleoside 5'-phosphoramidite derivatives proceeded with stepwise coupling yields of >90 %.
- [26] R. Wolfenden, X. Lu, G. Young, *J. Am. Chem. Soc.* **1998**, *120*, 6814–6815.
- [27] Polymerases that were tested included three reverse transcriptases (AMV, MMLV, and SuperScript II) and three thermostable DNA polymerases (*Taq*, *Pfu*, and *Tth*).

Aligned Coaxial Nanowires of Carbon Nanotubes Sheathed with Conducting Polymers**

Mei Gao, Shaoming Huang, Liming Dai,*
Gordon Wallace,* Ruiping Gao, and Zhonglin Wang

The discovery of carbon nanotubes by Iijima in 1991^[1] has generated enormous interest in carbon materials and nanotechnology. Since then, carbon nanotubes have been demonstrated to possess exceptional electrical, mechanical, and thermal properties, which are attractive for diverse potential applications ranging from nanoelectronics to biomedical devices.^[2–4] On the other hand, it is known that one-dimensional quantum nanowires play important roles, both as interconnecting and active components, in optoelectronic nanodevices and that their orientation has a significant impact on the performance of these devices.^[5] The scope for using carbon nanotubes in practical applications, however, has been largely limited by their poor processability (namely, they are insoluble and infusible).^[2, 6] Apart from possible improvements in the mechanical and electrical properties of polymers, the formation of nanotube/polymer composites has been and is still being explored as a promising approach for an effective incorporation of carbon nanotubes into devices.^[7–11] All studies on the carbon nanotube/polymer composites reported so far are based on randomly entangled nanotubes. The use of perpendicularly aligned carbon nanotubes^[2] should offer additional advantages to many applications, which includes electron-emitting flat-panel displays and electromechanical actuators.^[12]

We have recently developed simple but effective methods both for producing aligned carbon nanotubes normal to a quartz glass plate, by pyrolyzing iron(II) phthalocyanine ($\text{FeC}_{32}\text{N}_8\text{H}_{16}$, designated FePc) under Ar/H_2 at 800–1100 °C, and for (patterned) transfer of the aligned nanotubes onto other substrates.^[13] Herein, we describe that the aligned conducting nanotubes can be used to make novel conducting polymer–carbon nanotube (CP–NT) coaxial nanowires by electrochemically depositing a concentric layer of an appropriate conducting polymer uniformly onto each of the constituent aligned nanotubes. The coaxial structure allows the nanotube framework to provide mechanical stability^[3] and efficient thermal and electrical conduction^[4, 10] to and from

the conducting polymer layer. The large surface and interface area obtained for the nanotube-supported conducting polymer layer is an additional advantage for using them in many optoelectronic applications, for example in organic light-emitting diodes and photovoltaic cells, where the charge injection and separation are strongly limited by the interfacial area available in more conventional devices.^[14]

As seen in the scanning electron microscopic (SEM) images shown in Figure 1, we can not only produce homogeneous films of aligned carbon nanotubes by pyrolysis of FePc but

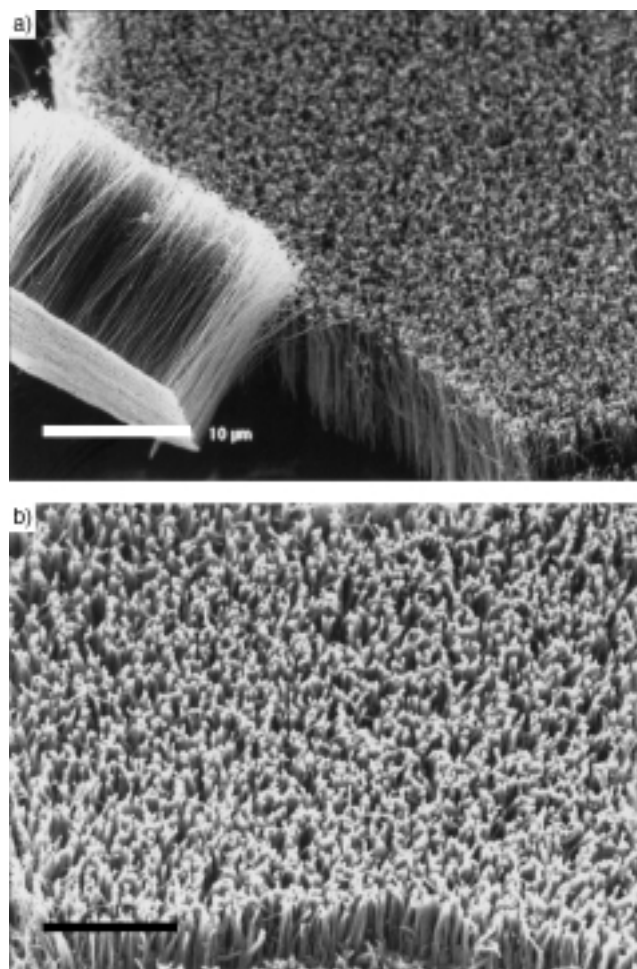


Figure 1. Typical SEM images of: a) aligned nanotubes after transfer onto a gold foil (a small piece of the as-synthesized aligned-nanotube film is included at the bottom-left corner to show the amorphous carbon layer as well; see the Experimental Section); and b) the CP–NT coaxial nanowires produced by cyclic voltammetry (scan rate 25 mVs^{-1}) on the aligned carbon nanotube electrode in an aqueous solution of NaClO_4 (0.1M) containing pyrrole (0.1M). Scale bar is 10 μm .

also transfer the as-synthesized aligned-nanotube film to a gold substrate with full integrity (Figure 1a) so that electrochemistry can be carried out (see the Experimental Section). The SEM image for the CP–NT coaxial nanowires given in Figure 1b shows the same features as the aligned nanotube array of Figure 1a but with a larger diameter due to the presence of the newly electropolymerized polypyrrole coating in this particular case.

[*] Dr. L. Dai, M. Gao, Dr. S. Huang
CSIRO Molecular Science
Bag 10, Clayton South, VIC 3169 (Australia)
E-mail: L.Dai@molsi.csiro.au
Fax: (+61) 39545-2553

Prof. G. Wallace, M. Gao
University of Wollongong, IPRI
Wollongong, NSW 2522, Australia

Dr. R. Gao, Prof. Z. Wang
School of Materials Science and Engineering
Georgia Institute of Technology
Atlanta, GA 30332-0245 (USA)

[**] M.G. is grateful for a joint scholarship from Wollongong University and CSIRO; S.H. and L.D. thank the support from the Department of Industry, Science, and Technology (DIST), Australia; R.P.G. and Z.L.W. thank the support of US NSF grants (DMR-9733160), and the NSF of China.

In a typical experiment on the electropolymerization of polyaniline by the cyclic voltammetric method, a current peak at approximately 1.0 V, attributable to aniline oxidation, was observed at the first cycle (Figure 2a). This was followed by

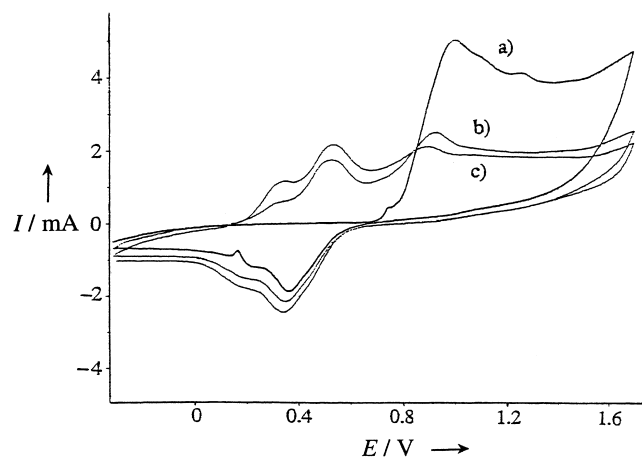


Figure 2. Electropolymerization of aniline (0.1M) in H_2SO_4 (0.2M) onto the aligned nanotube electrode. a) First cycle; b) second cycle; c) third cycle. Scan rate is 25 mV s^{-1} .

the appearance of two new peaks around 0.33 and 0.52 V at a cost of the peak at 1.0 V (Figure 2b). These new peaks can be assigned to the oxidation of polyaniline^[15] and the increase in their peak intensity over further cycles indicates a continuous deposition of polyaniline on the nanotube array. Evidence for the formation of the polyaniline layer was also given by the appearance of a greenish color characteristic of polyaniline emeraldine salt in solution around the nanotube electrode. By limiting the number of voltage sweeps, a thin polyaniline layer coating can be deposited along the length of individual nanotubes. Figure 3 shows representative transmission electron microscopic (TEM) images taken at the tip (left) and on the wall (right) of a CP–NT coaxial nanowire, which shows an homogenous polymer coating. The thickness of the polymer layer was determined from these TEM images to be about 40–50 nm.

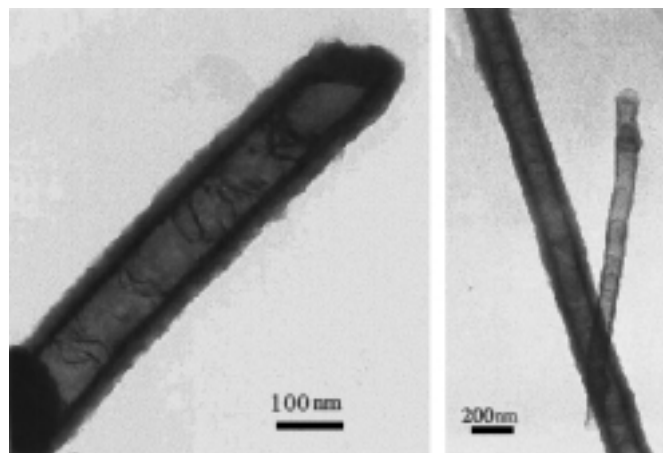


Figure 3. Typical TEM images of the CP–NT coaxial nanowires formed from the cyclic voltammetric method, the images are in the tip region (left) and on the wall (right).

Apart from an even growth of the polymer film, characteristic of electropolymerization of conducting polymers on conventional electrodes (such as on gold or platinum foil),^[15] Figure 4a shows a slower growth process around the air–electrolyte interface on a nanotube electrode that was partially immersed into the electrolyte solution. While Figure 4b reveals electrodeposition of a thin conducting polymer

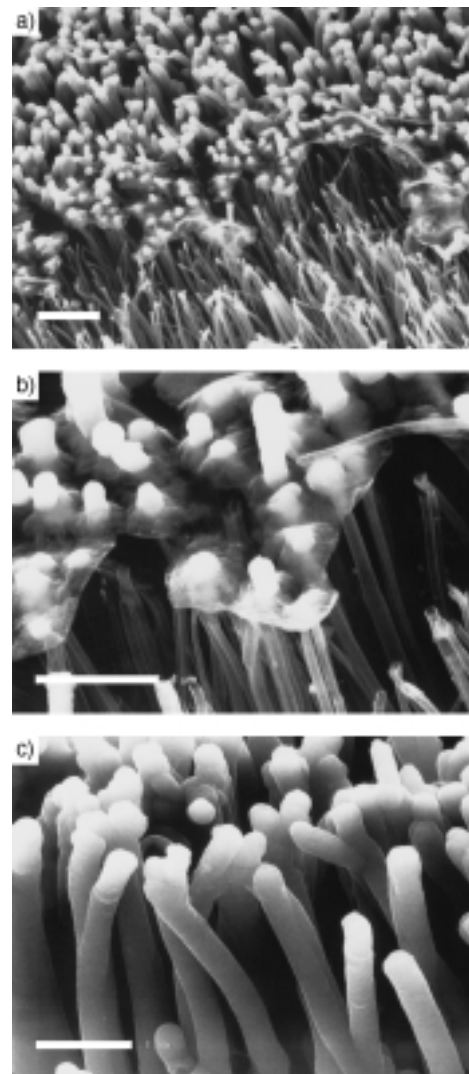


Figure 4. SEM micrographs taken from a nanotube electrode, which was partially inserted into an aqueous solution of NaClO_4 (0.1M) containing pyrrole (0.1M) after three cycles between -0.6 and 0.6 V (scan rate 25 mV s^{-1}). The images were taken at a) the air/electrolyte solution interface, b) the same position as a) at a higher magnification, and c) immersed in the electrolyte solution. Scale bars are 2 (a) and 1 μm (b, c).

layer onto the tips of those nanotubes located near the interfacial region, Figure 4c shows a full encapsulation of individual nanotubes immersed in the electrolyte solution. The observed partial polymer coverage is probably due to a relatively inefficient charge transfer in the interfacial region, coupled with an enhanced local field at the nanotube tips^[9] to facilitate the electrodeposition of the conducting polymer layer on top of the nanotube array. The newly formed conducting polymer film then results in a large depletion of the charge at the tip of the nanotubes, which leads to a

diffusive growth front towards the nanotube base. Under certain conditions, which depend on the nanotube density and monomer and electrolyte concentrations, the non-uniform growth could, therefore, allow the formation of CP–NT coaxial nanowires with only a predetermined portion of the nanotube length being covered by the conducting polymer layer.

To elucidate the chemical structure of the polymer layer, we carried out diffuse-reflectance Fourier-transform infrared and X-ray photoelectron spectroscopic measurements (FTIR, XPS).^[16] The electrochemical performance of the aligned CP–NT coaxial nanowires was evaluated by carrying out cyclic voltammetry measurements. As for polyaniline films electrochemically deposited on conventional electrodes, the cyclic voltammetric response of the polyaniline-coated nanotube array in an aqueous solution of H₂SO₄ (1M; Figure 5a) shows oxidation peaks at 0.33 and 0.52 V (with similar current

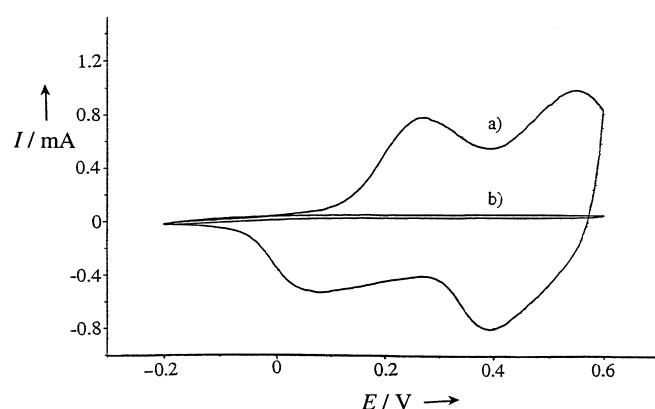


Figure 5. Cyclic voltammograms of a) the polyaniline-coated CP–NT coaxial nanowires and b) the bare aligned carbon nanotubes. Measured in an aqueous solution of 1M H₂SO₄ with a scan rate of 50 mV s^{−1}.

densities but much higher peak intensities due to the increased effective surface of the nanotube electrode).^[15] As a control, the cyclic voltammetry measurement was also carried out on bare, aligned nanotubes under the same conditions (Figure 5b). In the control experiment, only capacitive current was observed with no peak attributable to the presence of any redox-active species. Therefore, the polyaniline-coated nanotube composites prepared in this study are highly electroactive. DC conductivity of the polyaniline-coated nanotube film was measured by the standard van der Pauwe four-probe method^[19] to be in the order of 10 Scm^{−1}. This value of conductivity is one order of magnitude higher than the polyaniline film electrochemically deposited on a gold plate under the same conditions, possibly due to the “doping” effect associated with carbon nanotubes.^[10] Work on the detailed elucidation of charge transport in single CP–NT coaxial nanowires is currently in progress.

The newly prepared polymer–nanotube coaxial nanowire is expected to exhibit a high mechanical strength due to the existence of the graphitic framework. This measurement is possible using the electromechanical resonance technique developed recently.^[3] For a nanofiber-like structure, a TEM specimen holder was especially built for applying a voltage across the nanotube and its counter electrode. Each single

nanotube can be clearly observed in the TEM and the measurements can be done on a specific nanotube whose microstructure is determined by TEM. If a tunable alternating voltage is applied to the nanotube, resonance can be induced. When the frequency of the applied voltage equals the natural frequency of the nanotube, resonance is achieved and the Young’s modulus of the nanotube can be obtained from the resonance frequency.^[20] For a conducting-polymer sheathed nanotube with an outer diameter of 221 nm, inner diameter of 94.7 nm, and length 9.3 μm, the Young’s modulus was determined to be 13.6 GPa, a value which is slightly smaller than that of the nanotube^[21] but much higher than the polymer.^[22]

The well defined coaxial structure of these highly electroactive aligned CP–NT nanowires, together with the ease with which the conducting polymer coating could be transformed into an *n*- or a *p*-type semiconductor by doping with appropriate electron donors or acceptors,^[14] suggests a wide range of potential applications for the CP–NT nanowires, especially in optoelectronic nanodevices and sensors.

Experimental Section

Synthesis: The aligned carbon nanotube films were prepared by pyrolyzing iron(II) phthalocyanine under Ar/H₂ at 800–1100 °C and have been well characterized elsewhere.^[13] To construct a gold-supported nanotube electrode for electrochemical generation of the CP–NT coaxial nanowires, we sputter coated a thin film of gold (about 5 μm) onto the amorphous carbon layer covering an as-synthesized aligned nanotube film that was then separated from the quartz glass plate used in the preparation of the nanotube film with an aqueous solution of HF (30% w/w).^[13] In this study, we have used a cyclic voltammetric technique for electropolymerization of aniline (0.1M aniline/0.2M sulfuric acid/Milli-Q water) or pyrrole (0.1M pyrrole/0.1M NaClO₄/H₂O) onto a working electrode of the gold-supported nanotubes (2 × 3 mm², MacLab/4E analyser) in a three-compartment cell separated by porous glass. A platinum wire was used as a counter electrode and Ag/AgCl (3M KCl) as a reference.

Characterization: SEM images were obtained using a Philips XL-30 FEG SEM unit at 5 kV and TEM images were made on a JEOL 100C microscope at 100 kV. FTIR spectra were measured on a Perkin Elmer 2000 spectrometer. Raman scattering measurements were performed on a Renishaw Raman spectrometer using an excitation wavelength of 613 nm. XPS analyses were performed on a Kratos Analytical spectrometer using monochromatic AlK_α radiation at a power of 200 W.

Received: April 7, 2000 [Z14959]

- [1] S. Iijima, *Nature* **1991**, 354, 56.
- [2] See, for example: M. S. Dresselhaus, G. Dresselhaus, P. Eklund, *Science of Fullerenes and Carbon Nanotubes*, Academic Press, New York, **1996**; M. Terrones, W. K. Hsu, J. P. Hare, H. W. Kroto, H. Terrones, D. R. M. Walton, *Phil. Trans. R. Soc. London A* **1996**, 354, 2025; B. I. Yakobson, R. E. Smalley, *Am. Sci.* **1997**, 85, 325; W. A. de Heer, J.-M. Bonard, K. Fauth, A. Châtelain, L. Forró, D. Ugarte, *Adv. Mater.* **1997**, 9, 87; P. M. Ajayan, *Chem. Rev.* **1999**, 99, 1787; H. Dai, J. Kong, C. Zhou, N. Franklin, T. Tombler, A. Cassell, S. Fan, M. Chapline, *J. Phys. Chem. B* **1999**, 103, 11 246; L. Dai, A. W. H. Mau, *J. Phys. Chem. B* **2000**, 104, 1891.
- [3] P. Poncharal, Z. L. Wang, D. Ugarte, W. A. de Heer, *Science* **1999**, 283, 1513.
- [4] See, for example: S. Frank, P. Poncharal, Z. L. Wang, W. A. de Heer, *Science* **1998**, 280, 1744; T. W. Odom, J.-L. Huang, P. Kim, C. M. Lieber, *J. Phys. Chem. B* **2000**, 104, 2794, and references therein.
- [5] J. D. Holmes, K. P. Johnston, R. C. Doty, B. A. Korgel, *Science* **2000**, 287, 1471; Y. Zhang, K. Suenaga, C. Colliex, S. Iijima, *Science* **1998**, 281, 973.

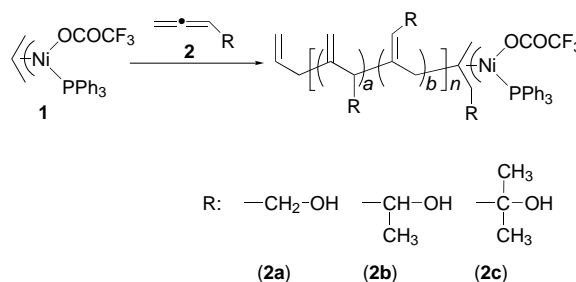
- [6] M. A. Hamon, J. Chen, H. Hu, Y. Chen, M. E. Itkis, A. M. Rao, P. C. Eklund, R. C. Haddon, *Adv. Mater.* **1999**, *11*, 834, and references therein.
- [7] See, for example: L. Dai, *Polym. Adv. Technol.* **1999**, *10*, 357, and references therein; M. S. P. Shaffer, A. H. Windle, *Adv. Mater.* **1999**, *11*, 937; J. Sandler, M. S. P. Shaffer, T. Prasse, W. Bauhofer, K. Schulte, A. H. Windle, *Polymer* **1999**, *40*, 5967.
- [8] See, for example: B. Z. Tang, H. Y. Xu, *Macromolecules* **1999**, *32*, 2569; J. Fan, M. Wan, D. Zhu, B. Chang, Z. Pan, S. Xie, *J. Appl. Polym. Sci.* **1999**, *74*, 2605; C. Downs, J. Nugent, P. M. Ajayan, D. J. Duquette, K. S. V. Santhanam, *Adv. Mater.* **1999**, *11*, 1028; G. Z. Chen, M. S. P. Shaffer, D. Coleby, G. Dixon, W. Zhou, D. J. Fray, A. H. Windle, *Adv. Mater.* **2000**, *12*, 522.
- [9] D. B. Romero, M. Carrard, W. A. de Heer, L. Zuppiroli, *Adv. Mater.* **1996**, *8*, 899; Y. Saito, S. Uemura, K. Hamaguchi, *Jpn. J. Appl. Phys.* **1998**, *37*, L346.
- [10] S. A. Curran, P. M. Ajayan, W. J. Blau, D. L. Carroll, J. N. Coleman, A. B. Dalton, A. P. Davey, A. Drury, B. McCarthy, S. Maier, A. Strevens, *Adv. Mater.* **1998**, *10*, 1091.
- [11] H. Ago, K. Petritsch, M. S. P. Shaffer, A. H. Windle, R. H. Friend, *Adv. Mater.* **1999**, *11*, 1281.
- [12] R. H. Baughman, C. Changxing, A. A. Zakhidov, Z. Iqbal, J. N. Barisci, G. M. Spinks, G. G. Wallace, A. Mazzoldi, D. de Rossi, A. G. Rinzler, O. Jaszinski, S. Roth, M. Kertesz, *Science* **1999**, *284*, 1340; M. Gao, L. Dai, R. H. Baughman, G. M. Spinks, G. G. Wallace, *SPIE*, in press.
- [13] S. Huang, L. Dai, A. W. H. Mau, *J. Phys. Chem. B* **1999**, *103*, 4223; Y. Yang, S. Huang, H. He, A. W. H. Mau, L. Dai, *J. Am. Chem. Soc.* **1999**, *121*, 10832; S. Huang, A. W. H. Mau, T. Turney, P. White, L. Dai, *J. Phys. Chem. B* **2000**, *104*, 2193; Q. Chen, L. Dai, *Appl. Phys. Lett.* **2000**, *76*, 2719; D. Li, L. Dai, S. Huang, A. W. H. Mau, Z. L. Wang, *Chem. Phys. Lett.* **2000**, *316*, 349.
- [14] L. Dai, *J. Macromol. Sci. Rev. Macromol. Chem. Phys.* **1999**, *39*, 237, and references therein.
- [15] D. Sazou, C. Georgolios, *J. Electroanal. Chem.* **1997**, *429*, 81; P. M. McManus, R. J. Cushman, S. C. Yang, *J. Phys. Chem.* **1987**, *91*, 744; A. G. MacDiarmid, J. C. Chiang, W. S. Huang, B. D. Humphrey, N. D. Somasiri, *Mol. Cryst. Liq. Cryst.* **1985**, *125*, 309.
- [16] The polyaniline-encapsulated nanotubes gave IR absorption peaks at 1514 (C=C stretching of the benzenoid rings), 1622 (C=C stretching of the quinoid rings), 1359 (C–N stretching), and 1197 cm⁻¹ (electronic-like absorption of N=Q=N, where Q represents the quinoid ring), consistent with reported data.^[14] XPS measurements indicated a decrease in the carbon content to 71.08% and concomitant increases to 12.11, 5.81, and 11.00% for nitrogen, sulfur, and oxygen, respectively, after the electrodeposition of polyaniline. The calculated C:N atomic ratio of 6.7 is close to that of aniline (C:N=6), suggesting the formation of a continuous polyaniline coating with a thickness greater than the XPS detection depth (typically, 10 nm; see Figure 3). The corresponding atomic ratios of 3.8 for O:S and 4.7 for N:S indicated a high doping level of the polymer coating by H₂SO₄.^[17] Further evidence for the electrodeposition of polyaniline on the nanotube surface comes from Raman scattering measurements. Whilst the Raman spectrum of the bare nanotubes shows an intense peak at 1584 cm⁻¹, attributable to the E_{2g} mode of the multiwall nanotubes, with a shoulder centered at 1322 cm⁻¹ associated with the amorphous graphite,^[2] the corresponding Raman spectrum for the polyaniline-coated nanotubes reveals broad bands around 1600, 1495, and 1390 cm⁻¹, typical for polyaniline.^[18] An additional peak at 1330 cm⁻¹ is associated with the stretching vibration of the -C-N⁺-polaron groups, indicating the conducting nature of the polymer coating.
- [17] L. Dai, J. Lu, B. Matthews, A. W. H. Mau, *J. Phys. Chem. B* **1998**, *102*, 4049.
- [18] A. H.-L. Goff, M. C. Bernard, *Synth. Met.* **1993**, *60*, 115.
- [19] L. Dai, White, J. W. *Polymer* **1997**, *38*, 775, and references therein.
- [20] Z. L. Wang, P. Poncharal, W. A. de Heer, *Microsc. Microanal.* **2000**, *6*, 224.
- [21] R. P. Gao, Z. L. Wang, Z. G. Bai, W. A. de Heer, L. Dai, M. Gao, *Phys. Rev. Lett.* **2000**, *85*, 622.
- [22] G. Shi, S. Jin, G. Xue, C. Li, *Science* **1995**, *267*, 994.

Living Coordination Polymerization of Allene Derivatives Bearing Hydroxy Groups by π -Allylnickel Catalyst

Masanori Taguchi, Ikuyoshi Tomita,* and Takeshi Endo*

Synthetic polymers such as poly(vinyl alcohol) and poly(2-hydroxyethyl methacrylate) bearing hydroxy groups in their repeating units are, because of their unique polar character and reactivities, useful starting materials for the preparation of many functional compounds.^[1] Nevertheless, with the exception of methods that involve the protection and deprotection of hydroxy groups, their use in well-defined synthesis has been limited.^[2]

Living polymerization, a technique which is insensitive to polar functional groups on the monomers, is thus a suitable method to prepare well-defined polymers directly from monomers bearing hydroxy groups. The living coordination polymerization of allene derivatives by $[(\pi\text{-allyl})\text{Ni}(\text{OCOCF}_3)_2]$ (**1**) is therefore attractive because this complex is able to polymerize monomers having a variety of functional groups, such as alkoxy,^[3a-c] aryl,^[3d] alkyl,^[3e-f] amide,^[3g] and carboalkoxy^[3h] moieties. Herein we investigate the coordination polymerization of allenes bearing hydroxy groups (**2a–2c**) mediated by **1** (Scheme 1).



Scheme 1. Living coordination polymerization of allene derivatives that contain hydroxy moieties (**2a–2c**).

The polymerization of 2,3-butadiene-1-ol (**2a**)^[4a] by **1** (**[2a]/[1]** = 60) was carried out in the presence of PPh₃ (**[PPh₃]/[1]** = 1.0) in EtOH at 50 °C (Table 1, entry 1). The polymerization was complete within 3 h and a white powdery polymer (poly(**2a**)) was obtained in 96% yield. The ¹H NMR spectrum of poly(**2a**) indicated that it consists of both the 1,2- and the 2,3-polymerized units (labeled *a* and *b* in Scheme 1) in a ratio

[*] Dr. I. Tomita
Department of Electronic Chemistry
Interdisciplinary Graduate School of Science and Engineering
Tokyo Institute of Technology
Nagatsuta 4259, Midori-ku, Yokohama 226-8502, (Japan)
Fax: (+81) 45-924-5489
E-mail: tomita@echem.titech.ac.jp
Prof. Dr. T. Endo, M. Taguchi
Research Laboratory of Resources Utilization
Tokyo Institute of Technology
Nagatsuta 4259, Midori-ku, Yokohama 226-8503, (Japan)
Fax: (+81) 45-924-5276
E-mail: tendo@res.titech.ac.jp

Table 1. Living coordination polymerization of **2** by **1**.

Entry	Monomer	[2]/[1]	<i>a</i> : <i>b</i> ^[a]	Yield [%] ^[b]	<i>M_n</i> (× 10 ³) ^[c]	<i>M_w</i> / <i>M_n</i> ^[c]
1	2a	60	40:60	96	9.6 ^[d]	1.13 ^[d]
2	2b	60	50:50	98	4.6	1.13
3	2c	50	35:65	94	6.4	1.08

[a] The ratio of 1,2- and 2,3-polymerized units, determined by ¹H NMR spectroscopy. [b] Yields after precipitation with hexane. [c] GPC (THF, polystyrene standard). [d] Determined by GPC measurement performed after the reaction with ethyl vinyl ether.

of about 40:60. Poly(**2a**) is soluble in polar organic solvents such as MeOH, EtOH, DMSO, and DMF but insoluble in hexane, benzene, CH₂Cl₂, THF, and water. In the reaction with ethyl vinyl ether, the hydroxy group attached to the polymer was converted quantitatively to acetal moieties and the resulting polymer was soluble in MeOH, THF, benzene, hexane, and CH₂Cl₂.^[5] Gel permeation chromatographic (GPC) analysis of the acetal-containing polymer revealed that the number-average molecular weight (*M_n*) and the molecular weight distribution (*M_w*/*M_n*) are 9.6 × 10³ and 1.13, respectively (THF, polystyrene standard; see Table 1). The living nature of the present system was confirmed by polymerization reactions with different ratios of [**2a**]/[**1**] (Figure 1). That is, the molecular weight of the polymers obtained after conversion of the hydroxy groups to the acetal moieties increased linearly as the ratio of [**2a**]/[**1**] increased, and *M_w*/*M_n* remained narrow (≈ 1.13).

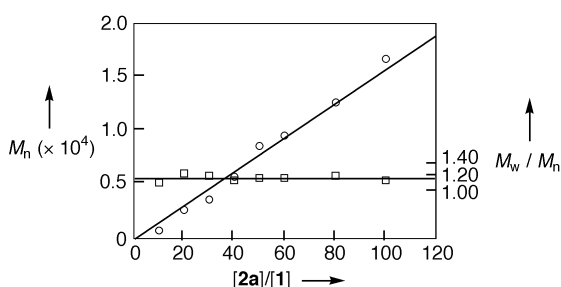


Figure 1. Dependence of *M_n* (○) and *M_w*/*M_n* (□) of poly(**2a**) on the ratio of monomer to initiator ([**2a**]/[**1**]).

The coordination polymerization of allenes bearing secondary and tertiary hydroxy groups (**2b**^[4b] and **2c**^[4b] respectively) also proceeds smoothly to give narrowly dispersed polymers in high yields (Table 1, entries 2 and 3).^[6]

The block copolymerization of **2a** with 1,2-heptadiene ((**3**) *n*-butylallene)^[4c] by the sequential addition of the monomers to **1** further confirmed the living nature of the polymerization. That is, after the polymerization of **2a** ([**2a**]/[**1**] = 40), **3** was added to the polymer solution ([**3**]/[**1**] = 50) and the postpolymerization was conducted at 50 °C for 3 h; a block copolymer was obtained quite effectively, as confirmed by GPC measurements (Figure 2).^[7]

These results show that well-defined poly(alcohol)s can be prepared without a multiple-step protection–deprotection process, and that the polymerization of allene derivatives by **1** can yield polymers bearing a variety of functional groups. This suggests that the designed synthesis of macromolecules, such as block copolymers with a versatile combination of func-

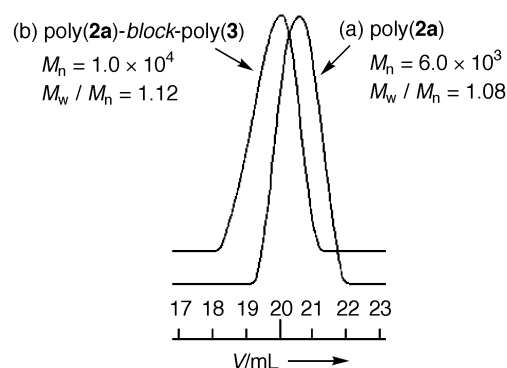


Figure 2. GPC traces a) before, and b) after postpolymerization with **3**.

tional blocks, should be possible. To the best of our knowledge, this is the first example of a living polymerization reaction capable of the polymerization of a wide variety of functionalized monomers.

Experimental Section

Typical living polymerization reaction: EtOH (2.0 mL), a solution of **1** (0.10 M, 0.2 mL, 0.020 mmol) in toluene, a solution of PPh₃ (1.0 M, 20 μL, 0.020 mmol) in toluene, and **2a** (0.084 g, 1.2 mmol, [**2a**]/[**1**] = 60) at 0 °C were placed under a nitrogen atmosphere in a test tube equipped with a three way tap and a magnetic stirrer bar. The mixture was stirred at 50 °C for 3 h. After the complete conversion of **2a** (monitored by gas chromatography), the solution was precipitated with hexane and dried in vacuo to give poly(**2a**) (0.081 g; 96%). ¹H NMR (300 MHz, [D₆]DMSO, 25 °C): δ = 1.96 (br, 2H × *b*; =C–CH₂–C=), 2.75 (br, 1H × *a*; –CH<), 3.34 (br, 2H × *a*; >C–CH₂–O–), 3.48 (br, 2H × *b*; =C–CH₂–O–), 4.03 (br, 1H; OH), 4.80 (br, 2H × *a*; >C=CH₂), 5.42 (br, 1H × *b*; >C=CH–O–); *a* and *b* are shown in Scheme 1; *a*:*b* = 0.40:0.60; ¹³C NMR (100 MHz, [D₆]DMSO, 25 °C): δ = 24.0, 24.9 (–CH₂–), 30.1, 31.6 (>CH–), 60.0 (>CH₂–CH₂–OH), 69.1 (=CH–CH₂–OH), 129.5, 129.8, 130.0 (=CH₂), 132.4, 133.0, 133.1, 134.6, 134.8, 139.4 (=CH–CH₂–OH, >C=CH₂, and >C=CH–CH₂–OH); IR (CHCl₃): ν̄ = 3389 (O–H), 2966, 2928, 1452, 1369 (C–H), 1682, 1633 (C=C), 1053 cm^{–1} (C–O).

Block copolymerization reaction: EtOH (2.0 mL), a solution of **1** (0.10 M, 0.2 mL, 0.020 mmol) in toluene, a solution of PPh₃ (1.0 M, 20 μL, 0.020 mmol) in toluene, and **2a** (0.056 g, 0.80 mmol, [**2a**]/[**1**] = 40) at 0 °C, were placed under a nitrogen atmosphere in a test tube equipped with a three way tap and a magnetic stirrer bar. The mixture was stirred at 50 °C for 3 h. After the complete conversion of **2a** (monitored by gas chromatography), a portion of the solution (ca. 50 μL) was removed, and **3** (0.096 g, 1.0 mmol, [**3**]/[**1**] = 50) was added to the remaining solution. After postpolymerization at 50 °C for 3 h, the product was precipitated with water and dried in vacuo to give the block copolymer (0.137 g, 90%). GPC measurements of both poly(**2a**) sampled before the addition of **3** and the block copolymer were performed after the treatment with ethyl vinyl ether. ¹H NMR (300 MHz, CDCl₃, 25 °C, TMS): δ = 0.82 (br, 3H × *n*; –CH₃), 1.12 (br, 4H × *n* + 2H × *m* × *c* + 2H × *n* × *d*; –CH₂–, >C–CH₂–, and =C–CH₂–), 1.96 (br, 2H × *m* × *b* + 2H × *n* × *d*, =C–CH₂–C=), 2.55 (br, 1H × *m* × *a* + 1H × *n* × *c*; –CH<), 3.40 (br, 2H × *m* × *a*; >C–CH₂–O–), 3.53 (br, 2H × *m* × *b*; =C–CH₂–O–), 4.07 (br, 1H × *m*; OH), 4.76 (br, 2H × *m* × *a* + 2H × *n* × *c*; >C=CH₂), 5.18 (br, 2H × *m* × *b* + 2H × *n* × *d*; >C=CH–O–); *a* and *b* are shown in Scheme 1; *a*:*b* = 0.43:0.57, *c* and *d* represent the 2,3- and the 1,2-polymerized units, respectively, in poly (**3**) segment *c*:*d* = 0.10:0.90, *m* and *n* represent the ratio of poly (**2a**) and poly (**3**), respectively, in the block copolymer *m*:*n* = 0.39:0.61; ¹³C NMR (100 MHz, CDCl₃, 25 °C, TMS): δ = 14.0 (–CH₃), 22.5, 24.0, 27.5 (–CH₂–), 30.1, 31.6, 35.6 (>CH–), 60.0 (>CH₂–CH₂–OH), 69.1 (=CH–CH₂–OH), 110.3, 128.4, 128.6, 130.0 (–CH₂–), 132.2, 132.1, 134.6, 134.8 (=CH–CH₂–OH, >C=CH₂, and >C=CH–CH₂–OH); IR (CHCl₃): ν̄ = 3395 (O–H), 2957, 2928, 2858, 1464, 1379 (C–H), 1674, 1637 (C=C), 1095 cm^{–1} (C–O).

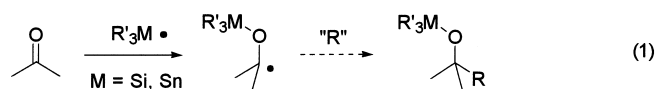
Received: March 7, 2000 [Z14816]

- [1] a) *Polyvinyl Alcohol Developments* (Ed.: C. A. Finch), Wiley, New York, **1992**; b) "Hydrogels for Medical and Related Applications" (Ed.: J. D. Andrade), *ACS Symp. Ser.*, Vol. 31 Washington, **1976**.
- [2] See, for example: A. Hirao, H. Kato, K. Yamaguchi, S. Nakahama, *Macromolecules* **1986**, 19, 1294–1299.
- [3] a) I. Tomita, Y. Kondo, K. Takagi, T. Endo, *Macromolecules* **1994**, 27, 4413–4414; b) I. Tomita, Y. Kondo, K. Takagi, T. Endo, *Acta Polym.* **1995**, 46, 432–436; c) I. Tomita, M. Ubukata, T. Endo, *React. Funct. Polym.* **1998**, 37, 27–32; d) K. Takagi, I. Tomita, T. Endo, *Macromolecules* **1997**, 30, 7386–7390; e) K. Takagi, I. Tomita, T. Endo, *Chem. Lett.* **1997**, 1187–1188; f) T. Endo, K. Takagi, I. Tomita, *Tetrahedron* **1997**, 53, 15187–15196; g) K. Takagi, I. Tomita, T. Endo, *Macromolecules* **1998**, 31, 6741–6747; h) K. Takagi, I. Tomita, T. Endo, *Chem. Commun.* submitted.
- [4] Allene monomers (**2a**, **2b**, **2c**, and **3**) were prepared by reported methods. See: a) L. Brandsma, H. D. Verkruijsse, *Synthesis of Acetylenes, Allenes and Cumulenes*, Elsevier, New York, **1981**, pp. 188–189; b) M. Kimura, S. Tanaka, Y. Tamaru, *Bull. Chem. Soc. Jpn.* **1995**, 68, 1689–1705; c) L. Brandsma, H. D. Verkruijsse, *Synthesis of Acetylenes, Allenes and Cumulenes*, Elsevier, New York, **1981**, pp. 157.
- [5] The reaction of poly(**2a**) with ethyl vinyl ether (twofold excess with respect to the hydroxy moieties) was carried out in the presence of *p*-toluenesulfonic acid (1.0 mol %) in DMSO at 50 °C for 10 min. Addition to water precipitated a polymer in 98 % yield whose acetal content was confirmed to be quantitative by ¹H NMR spectroscopy. The polymer thus obtained is soluble in various organic solvents including MeOH, THF, benzene, hexane, and CH₂Cl₂.
- [6] Both poly(**2b**) and poly(**2c**) have high solubility in THF, a poor solvent for poly(**2a**). Thus, the GPC measurements were performed without treatment with ethyl vinyl ether.
- [7] Since the block copolymer is soluble in THF, benzene, and CH₂Cl₂ which reflects the solubility of poly(**3**) segment, the GPC measurement was also performed directly without treatment with ethyl vinyl ether, and gave a unimodal elution peak (*M_n* = 8.3 × 10³, *M_w*/*M_n* = 1.12).

Novel Group-Transfer Three-Component Coupling of Silyltellurides, Carbonyl Compounds, and Isocyanides**

Hiroshi Miyazoe, Shigeru Yamago,* and Jun-ichi Yoshida*

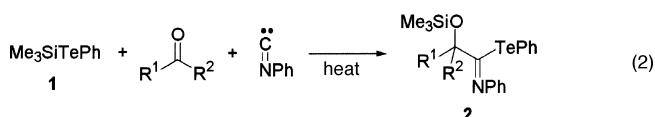
Silyl and stannyl radicals add to the carbonyl oxygen atom to generate α -alkoxy radicals, and this is an elemental step in the radical-mediated reduction of carbonyl compounds with silyl and stannyl hydride reagents.^[1,2] Addition of the α -alkoxy radicals to radical acceptors would form a new C–C bond [Eq. (1)].^[3] Indeed, α -stannyloxy radicals thus



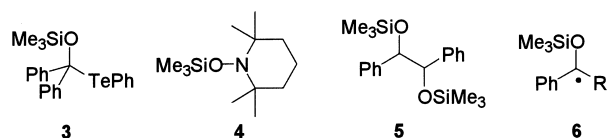
[*] Prof. S. Yamago, Prof. J.-i. Yoshida, H. Miyazoe
Department of Synthetic Chemistry and Biological Chemistry
Graduate School of Engineering, Kyoto University
Kyoto 606-8501 (Japan)
Fax: (+81) 75-753-5661
E-mail: yamago@sbchem.kyoto-u.ac.jp,
yoshida@sbchem.kyoto-u.ac.jp

[**] This work was partly supported by a Grant-in-Aid for Scientific Research from the Ministry of Education, Science, Sports, and Culture, Japan. We thank Professor S. Okazaki, Professor M. Oyama, and T. Morikawa of the Department of Material Chemistry of Kyoto University for the ESR measurement and valuable discussions.

formed have been utilized for intramolecular C–C bond formation,^[4] but there is no report on the intermolecular version, probably because reduction of the α -alkoxy radical by the metal hydride competes with C–C bond formation. Since organotellurium compounds are excellent precursors for carbon-centered radicals,^[5,6] we envisaged that silyl tellurides would act as silyl radical precursors which do not contain reducing hydrido groups.^[7] We examined reactions of silyl tellurides in the presence of several radical acceptors and found a new coupling reaction of phenyl trimethylsilyl telluride (**1**), carbonyl compounds, and phenyl isocyanide [Eq. (2)]. Here we report on this new three-component coupling reaction, which is of both mechanistic and synthetic interest.



The coupling reaction of **1**,^[8] benzophenone, and phenyl isocyanide proceeded under mild thermal conditions, and the group-transfer product **2a** (*R*¹ = *R*² = Ph) was formed in 82 % yield after heating at 100 °C for 12 h in propionitrile. The tellurium atom plays a crucial role in this reaction, and the use of the corresponding silyl selenide or sulfide led to complete recovery of the starting materials. In addition, various silyl and stannyl hydrides did not promote C–C bond formation, and either the recovery of the starting materials or the reduction of the carbonyl group was observed. Monitoring the reaction in CD₃CN by ¹H NMR spectroscopy indicated that the formation of the α -silyloxytelluride **3** competed with that of **2a** and that the amount of **3** gradually decreased with the progress of the reaction. Indeed, isolated **3** reacted with



phenyl isocyanide at 100 °C to give **2a** in 92 % yield. The coupling reaction was inhibited by the addition of 2,2,6,6-tetramethylpiperidine-*N*-oxyl (TEMPO) radical (1.0 equiv) and mainly afforded silylated TEMPO **4** (63 %); this suggests the intermediacy of trimethylsilyl radicals. The reaction proceeded faster in polar solvents such as propionitrile, DMF, and pyridine than in nonpolar solvents such as toluene, and the smooth reaction in basic media also ruled out the involvement of carbocation intermediates.^[9]

The present reaction is generally applicable to a variety of ketones and aldehydes, and its scope and efficiency are summarized in Table 1. Aromatic ketones reacted smoothly and gave the desired adducts in high yields when almost equimolar quantities of each reagent were used (entries 1–6). Aliphatic ketones and aldehydes also gave the desired adducts in good yields (entries 7 and 8), but they were slightly less reactive than aromatic ketones. The reaction of benzaldehyde

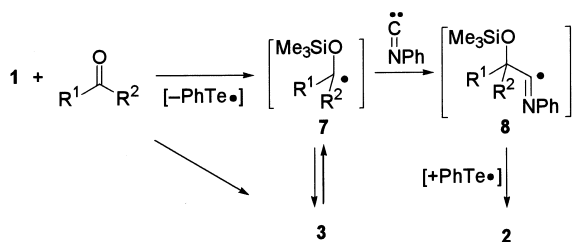
Table 1. Three-component coupling reactions.^[a]

Entry	Carbonyl compound	t [h]	Product	Yield [%]
1		12		82
2	R = OMe	24		73
3	R = NMe ₂	12		84
4	R = Cl	12		39 (63) ^[b]
5		24		48 ^[c] (81) ^[b]
6		24		56 ^[d] (73) ^[b]
7		12		61 ^[e]
8	<i>n</i> -C ₆ H ₁₃ CHO	12		55 ^[e]
9	PhCHO	12		46 ^[f, g]
10		12		93

[a] The reaction was carried out by heating a solution of **1** (1.1 equiv), carbonyl compound (1.0 equiv), and phenyl isocyanide (1.1 equiv) at 100 °C in propionitrile. [b] Yield based on converted carbonyl compound. [c] Two equivalents of phenyl isocyanide were used. [d] A 55:45 mixture of diastereomers was obtained. [e] Reaction was carried out at 120 °C with two equivalents of phenyl isocyanide. [f] Reaction was carried out in toluene. [g] The dimer **5** was formed in 54% yield.

gave the desired coupling product in moderate yield together with the dimer **5** (entry 9), which was probably formed by homocoupling of the α -siloxy radical **6a** (R = H). The generation of the α -siloxy radical species was further confirmed by the reaction of cyclopropyl phenyl ketone, and the ring-opened alkyl telluride, formed by the cyclopropylmethyl radical rearrangement of **6b** (R = cyclopropyl),^[10] was obtained as the sole product (entry 10).

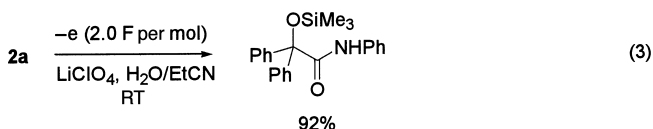
The formation of **3** and **5** suggests the most probable reaction pathway involves the generation of the silyl radical from **1** and its addition to the carbonyl compound (Scheme 1).^[11] Subsequent reaction of the resulting radical **7** with isocyanide gives the imido radical **8**, which undergoes a group-transfer reaction, presumably with **1**, to form **2**. The radical **7** also undergoes a group-transfer reaction to give **3**. However, **3** acts as a dormant species that regenerates **7** under



Scheme 1. Probable reaction pathway for the formation of **2**.

the reaction conditions. At present, however, other possibilities, including the ionic reaction of **1** and carbonyl compounds to generate **3**, cannot be rigorously ruled out.

Besides the novelty of the reaction type, the synthetic utility of the present reaction is noteworthy. The product **2** could be transformed into a variety of α -hydroxy carbonyl compounds by exploiting the reactive C–Te bond.^[12] For example, oxidative hydrolysis of **2a** afforded the corresponding α -silyloxy amides [Eq. (3)].^[6c] Experiments to ascertain the precise mechanism as well as the further synthetic explorations are currently under investigation.^[13]



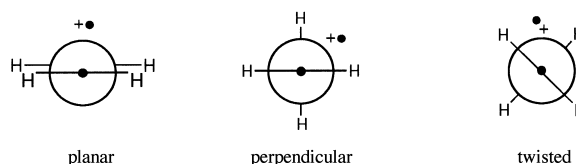
Experimental Section

2a: A mixture of **1** (151.2 mg, 0.55 mmol), benzophenone (91.1 mg, 0.50 mmol), and phenyl isocyanide (56.2 mg, 0.55 mmol) in propionitrile (0.5 mL) in a sealed tube was heated at 100 °C for 12 h. Removal of the solvent followed by purification on silica gel afforded **2a** as light orange oil (232.5 mg, 0.41 mmol, 82%). IR (neat): $\tilde{\nu}$ = 1660, 1595, 1485, 1445, 1250, 1210, 1170, 1100, 1070, 925, 885, 840, 800, 760, 730, 690, 640 cm⁻¹; ¹H NMR (300 MHz, CDCl₃): δ = –0.01 (s, 9H), 6.47–6.50 (m, 2H), 6.69–6.74 (m, 3H), 6.80–6.86 (m, 2H), 6.90–6.96 (m, 1H), 7.01–7.04 (m, 2H), 7.36–7.44 (m, 6H), 7.61–7.65 (m, 4H); ¹³C NMR (75 MHz, CDCl₃): δ = 1.6, 88.3, 114.7, 118.0, 123.4, 126.8, 127.7, 127.8, 128.1, 128.2, 130.0, 140.4, 142.9, 149.0, 169.5; FAB-MS (3-nitrobenzyl alcohol): *m/z*: 566 [M+H]⁺; elemental analysis calcd for C₂₉H₂₉NOSiTe (%): C 61.84, H 5.19, N 2.49; found: C 61.81, H 5.28, N 2.47.

Received: May 10, 2000
Revised: June 19, 2000 [Z15108]

- [1] a) C. Chatgililoglu, *Chem. Rev.* **1995**, 95, 1229; b) H. Gilman, D. Wittenberg, *J. Org. Chem.* **1958**, 23, 501; c) H. Sakurai, A. Hosomi, M. Kumada, *Bull. Chem. Soc. Jpn.* **1967**, 40, 1551; d) A. Hudson, R. A. Jackson, *J. Chem. Soc. Chem. Commun.* **1969**, 1323; e) C. Chatgililoglu, K. U. Ingold, J. C. Scaiano, *J. Am. Chem. Soc.* **1982**, 104, 5119; f) A. Algel, C. Chatgililoglu, *Tetrahedron* **1990**, 46, 3963.
- [2] M. Pereyre, J.-P. Quintard, A. Rahm, *Tin in Organic Synthesis*, Butterworths, London, **1987**, Chap. 4.
- [3] For reviews on the addition of radicals to C–C multiple bond, see: a) D. Curran, N. A. Porter, B. Giese, *Stereochemistry of Radical Reactions*, VCH, Weinheim, **1995**; b) D. Curran in *Comprehensive Organic Synthesis*, Vol. 4 (Eds.: B. M. Trost, I. Fleming), Pergamon, Oxford, **1991**, p. 715; c) B. Giese, *Radicals in Organic Synthesis: Formation of Carbon–Carbon Bonds*, Pergamon, Oxford, **1986**; d) I. Ryu, N. Sonoda, *Angew. Chem.* **1996**, 108, 1140; *Angew. Chem. Int. Ed. Engl.* **1996**, 35, 1050; e) I. Ryu, N. Sonoda, D. P. Curran, *Chem. Rev.* **1996**, 96, 177.
- [4] a) A. L. J. Beckwith, D. H. Roberts, *J. Am. Chem. Soc.* **1986**, 108, 5893; b) J. Ardisson, J. P. F  r  zou, M. Julia, A. Pancrazi, *Tetrahedron Lett.* **1987**, 28, 2001; c) T. Sugawara, B. A. Otter, T. Ueda, *Tetrahedron Lett.* **1988**, 29, 75; d) E. J. Enholm, G. Prasad, *Tetrahedron Lett.* **1989**, 30, 4939; e) E. J. Enholm, K. S. Kinter, *J. Am. Chem. Soc.* **1991**, 113, 7784; f) E. Lee, J. S. Tae, Y. H. Chong, Y. C. Park, *Tetrahedron Lett.* **1994**, 35, 129; g) T. Naito, K. Tajiri, T. Harimoto, I. Ninomiya, T. Kiguchi, *Tetrahedron Lett.* **1994**, 35, 2205; h) D. Hays, G. C. Fu, *J. Am. Chem. Soc.* **1995**, 117, 7283; i) D. Hays, G. C. Fu, *J. Org. Chem.* **1998**, 63, 6375.

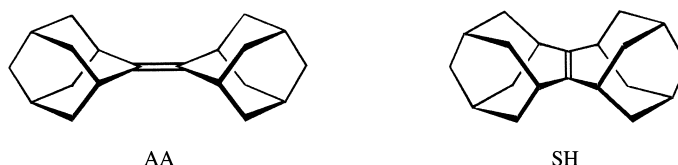
- [5] a) D. H. R. Barton, M. Ramesh, *J. Am. Chem. Soc.* **1990**, *112*, 891; b) L.-B. Han, K. Ishihara, N. Kambe, A. Ogawa, I. Ryu, N. Sonoda, *J. Am. Chem. Soc.* **1992**, *114*, 7591; c) D. Crich, C. Chen, J.-T. Hwang, H. Yuan, A. Papadatos, R. I. Walter, *J. Am. Chem. Soc.* **1994**, *116*, 8937; d) L. Engman, V. Gupta, *J. Org. Chem.* **1997**, *62*, 157; e) M. A. Lucas, C. H. Schiesser, *J. Org. Chem.* **1998**, *63*, 3032.
- [6] Free radical reactions with organotellurium compounds: a) S. Yamago, H. Miyazoe, J. Yoshida, *Tetrahedron Lett.* **1999**, *40*, 2339; b) S. Yamago, H. Miyazoe, J. Yoshida, *Tetrahedron Lett.* **1999**, *40*, 2343; c) S. Yamago, H. Miyazoe, R. Goto, J. Yoshida, *Tetrahedron Lett.* **1999**, *40*, 2347.
- [7] Reactivity of silyl telluride under radical conditions was reported recently: C. H. Schiesser, M. Skidmore, *J. Organomet. Chem.* **1998**, *552*, 145.
- [8] a) J. E. Drake, R. T. Hemmings, *Inorg. Chem.* **1980**, *19*, 1879; b) K. Sasaki, Y. Aso, T. Otsubo, F. Ogura, *Tetrahedron Lett.* **1985**, *26*, 453.
- [9] a) I. Ugi, U. Fetzer, *Chem. Ber.* **1961**, *94*, 1116; b) L. Capuano, C. Wamprecht, W. Hell, *Liebigs Ann. Chem.* **1986**, 132; c) M. Westling, R. Smith, T. Livinghouse, *J. Org. Chem.* **1986**, *51*, 1163.
- [10] D. C. Nonhebel, *Chem. Soc. Rev.* **1993**, 347.
- [11] While the direct observation of silyl radicals by ESR spectroscopy failed, a spin-trapping experiment with **1** and *N*-tert-butyl- α -phenylnitron (1 equiv) in benzene at 50 °C resulted in detection of the corresponding nitroxyl radical at $g = 2.0059$ with $a_N = 1.41$ mT and $a_H = 0.21$ mT. For spin trapping of trimethylsilyl radicals, see: a) B. B. Adeleke, S.-K. Wong, J. K. S. Wan, *Can. J. Chem.* **1974**, *52*, 2901; b) H. Chandra, I. M. T. Davidson, M. C. R. Symons, *J. Chem. Soc. Perkin Trans. 2* **1982**, 1353.
- [12] a) D. J. Ager in *Unpoled Synthons* (Ed.: T. A. Hase), Wiley, New York, **1987**, Chap. 2; b) M. Kolb in *Unpoled Synthons* (Ed.: T. A. Hase), Wiley, New York, **1987**, Chap. 3; c) Y. Ito, M. Murakami, *J. Synth. Org. Chem. Jpn.* **1991**, *41*, 184.
- [13] Synthetic transformations of C–Te bonds: N. Petragnani, *Tellurium in Organic Synthesis*, Academic Press, London, **1994**.



Scheme 1. Predicted structures of the parent ethylene cation radical.

Owing to the importance of ethylene as a precursor in polyethylene production, its cation radical has been subject to scrutiny in great detail using highly sophisticated theoretical methods including extended basis sets.^[5] Experimentally, vacuum ultraviolet studies^[6] and photoelectron spectroscopy^[7] in the gas phase support a nonplanar structure of ethylene cation radical with a twist of 25°. On the other hand, more recent EPR studies^[8] in frozen matrices at 4 K conclude that it can be almost planar (8°). In the last two decades, a number of sterically rigid olefinic cation radicals such as those from adamantylideneadamantane, and pagodadiene have been characterized in solution by using a variety of spectroscopic techniques.^[9–11] However, despite enormous theoretical and experimental effort,^[12] there is a singular lack of definitive X-ray crystallographic information on the structure of any alkyl-substituted olefinic cation radical.^[13]

Herein, we report the successful isolation of the novel cation radical derived from the olefinic donor sesquihomoadamantene (SH), an isomer of the well-known adamantylideneadamantane (AA). Sesquihomoadamantene was originally prepared by Wynberg et al.^[14] and it contains a



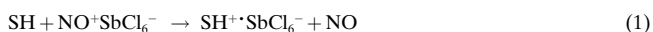
Structural Characterization of Novel Olefinic Cation Radicals: X-ray Crystallographic Evidence of σ – π Hyperconjugation**

Jay K. Kochi*, Rajendra Rathore, Chengjian Zhu, and Sergey V. Lindeman

Alkyl-substituted ethylene cation radicals are highly reactive intermediates that occur when a variety of electrophilic addition reactions such as epoxidation, hydroxylation, ozonation, oxidative cleavage, dimerization, and cationic polymerization^[1–3] proceed by prior electron transfer. As early as 1947, Mulliken and Roothaane^[4] predicted the structure of the parent ethylene cation radical to be twisted by 30° due to the contributions from both the planar structure (normal π bonding) and the perpendicular structure (hyperconjugative bonding) (Scheme 1).

tetrasubstituted double bond with rigid cyclic (cage) substituents.^[15] Most importantly, sesquihomoadamantene is planar and singularly nonstrained. Therefore its conversion to the cation radical could reveal the typical structural changes that can be expected upon the oxidative conversion of an olefinic donor.

The one-electron oxidation of sesquihomoadamantene (SH) in dichloromethane at –78 °C either electrochemically^[16] or chemically (using the well-known one-electron oxidant nitrosonium hexachloroantimonate)^[17] yielded a dark purple solution of the corresponding cation radical, the quantitative formation of which was established spectrophotometrically [Eq. (1)].^[18]



The purple salt was isolated as a microcrystalline powder by slow diffusion of toluene into the solution of $\text{SH}^{+\bullet}\text{SbCl}_6^-$ in dichloromethane at –78 °C; and the purity of the highly colored precipitate was determined to be greater than 98 % by iodometric titration.^[17] The identity of the isolated cation

[*] J. K. Kochi, R. Rathore, C. Zhu, S. V. Lindeman
Department of Chemistry
University of Houston
Houston, TX 77204-5641 (USA)
Fax: (+1) 713-743-2709
E-mail: jkochi@pop.uh.edu

[**] We thank the National Science Foundation and the Robert A. Welch Foundation for financial support.

radical $\text{SH}^{+\bullet}$ was further confirmed by its ready ability to quantitatively oxidize a variety of electron-rich organic donors^[19] to the corresponding cation radicals. For example, if a solution of $\text{SH}^{+\bullet}$ cation radical in dichloromethane ($\lambda_{\text{max}} = 360$ and 485 nm, $\epsilon_{360} = 4000 \pm 200 \text{ M}^{-1} \text{ cm}^{-1}$)^[20] was treated with incremental amounts of neutral CRET,^[17] the resulting (UV/Vis) spectral changes (with well-defined isosbestic points at $\lambda_{\text{max}} = 335$, 449 , and 538 nm, see Figure 1) clearly estab-

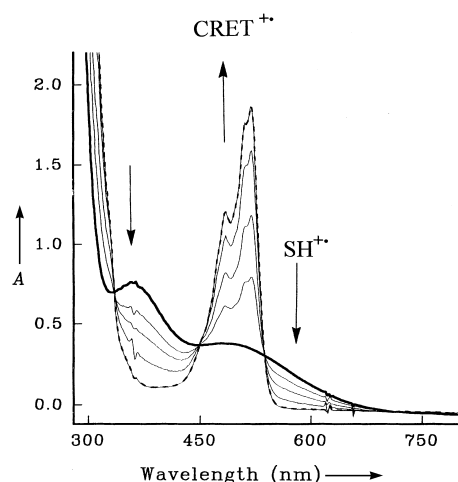
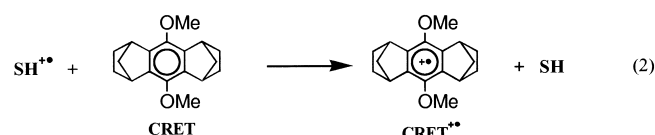


Figure 1. Spectral titration of $0.2 \text{ mM } \text{SH}^{+\bullet}\text{SbCl}_6^-$ ($7.3 \times 10^{-4} \text{ mmol}$) by incremental additions of neutral CRET ($7.3 \times 10^{-4} \text{ mmol}$) in dichloromethane at -78°C . Note that the $\text{CRET}^{+\bullet}$ spectrum (---) remains unchanged upon addition of excess CRET. A = absorbance.

lished the concomitant reduction of sesquihomoadamantene cation radical and oxidation of neutral CRET [Eq. (2)]. It should be noted that the highly robust cation radical $\text{CRET}^{+\bullet}$ has been well characterized by UV/Vis spectroscopy ($\lambda_{\text{max}} = 486$ and 518 nm, $\epsilon_{518} = 7300 \text{ M}^{-1} \text{ cm}^{-1}$) as well as by X-ray crystallography.^[17]



After repeated attempts to crystallize the powdered salt (especially by varying the solvent and temperature), we have now successfully isolated dark purple (single) crystals by the slow diffusion of hexane into a solution of pure $\text{SH}^{+\bullet}\text{SbCl}_6^-$ in dichloromethane at -50°C . Single-crystal analysis by X-ray crystallography at -150°C establishes its molecular structure, which clearly shows the central olefinic bond in the $\text{SH}^{+\bullet}$ cation radical to be twisted by 29° ,^[13] as shown by the sideways ORTEP diagrams in Figure 2 of both $\text{SH}^{+\bullet}$ (left) and SH (right). Moreover, a careful comparison of the precise X-ray structures of both neutral SH and its cation radical under identical conditions (see Experimental Section) demonstrates that the pronounced twist cannot be due to relief of steric strain, and thus provides us with the unique opportunity to

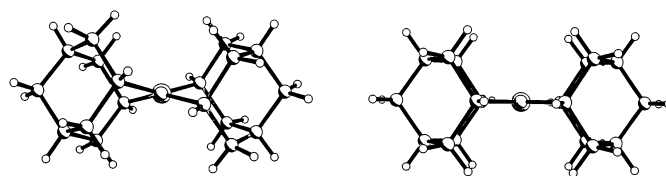


Figure 2. Left) Molecular structure of the cation radical salt $\text{SH}^{+\bullet}\text{SbCl}_6^-$ showing the twist around the central C–C bond. Hexachloroantimonate anion and the solvent molecule omitted for clarity. Right) In comparison, the molecular structure of the neutral SH donor is completely planar.

examine other more subtle structural changes that occur when a single electron is removed from the neutral olefinic donor.

Table 1 summarizes the systematic changes in the bond lengths as well as angular reorganization in sesquihomoadamantene cation radical ($\text{SH}^{+\bullet}$) as compared to the neutral olefin. Thus, the central C–C double bond expectedly lengthens by 5 pm. Most notably, however, the four C–C single bonds (α bonds denoted by a) directly attached to the olefinic

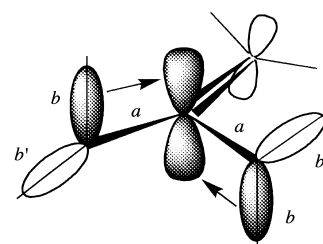
Table 1. Comparison of the principal geometrical parameters of the neutral SH and its cation radical $\text{SH}^{+\bullet}$.

Parameter	SH	$\text{SH}^{+\bullet}$	$\Delta (\text{SH} \rightarrow \text{SH}^{+\bullet})$
d [Å]	1.345(1)	1.397(3)	+0.052
a [Å]	1.526(1)	1.491(3)	−0.035
b [Å]	1.542(1)	1.558(3)	+0.016
b' [Å]	1.542(1)	1.541(3)	−0.001
α [°]	113.3(1)	108.1(2)	−5.2
α' [°]	113.3(1)	115.2(2)	+1.9
ϕ [°]	0.5(1)	29.0(2)	+28.5
τ [°] ^[a]	63.7(1)	82.3(2)	+18.6
τ' [°] ^[a]	−63.7(1)	−43.1(2)	+20.6

[a] τ and τ' are dihedral angles between planes determined by bonds $dalab$ and $da'ab'$ respectively.

carbon atoms *shorten* by 3 pm each, and only one of the two C–C bonds (β bonds denoted by b) attached to each allylic carbon atom is elongated by 1.5 pm. (Note that the other C–C bond (denoted by b') remains unchanged.) Moreover, the angles at the allylic carbon atoms undergo significant changes which are accompanied by an increase in the twist ($\sim 18^\circ\text{C}$) around the a bonds. As a result, the lengthened b bonds position themselves approximately *periplanar* to the (partially occupied) olefinic p orbitals, in a way different from those in the neutral olefin (Scheme 2).^[21]

The latter observation of distinct changes in the bond lengths of the remote β bonds (which lie *periplanar* to the cationic p orbi-



Scheme 2. Arrangement of the olefinic p orbitals in the sesquihomoadamantene cation radical ($\text{SH}^{+\bullet}$).

tals), coupled with the substantial shortening of the α bonds represents the first direct experimental evidence for the (classical) hyperconjugative stabilization of cationic charges.^[22] We believe that these definitive structural changes in SH^{+} will also be generally applicable to the characterization of cation radical structures of other olefin donors. As such, we are currently inquiring into the origin and generality of the structural twist and hyperconjugative stabilization in various olefinic cation radicals and carbocations using high-level theoretical calculations.^[23]

Experimental Section

A mixture of adamantlylideneadamantane (AA) and isomeric sesquihomoadamantene (SH) was prepared according to literature procedures^[14] and subjected to the standard conditions of epoxidation using *m*-chloroperbenzoic acid in dichloromethane for 1 h at 0 °C. Aqueous workup followed by chromatographic purification yielded pure sesquihomoadamantene SH (24 %) and adamantlylidene–adamantane oxide^[14] (51 %). Recrystallization from anhydrous diethyl ether at –20 °C afforded analytically pure SH, m.p. 202–203 °C (lit.^[14a] m.p. 199–201 °C).

X-ray crystallography: The intensity data were collected at –150 °C on a Siemens SMART diffractometer equipped with a CCD detector using $\text{MoK}\alpha$ radiation ($\lambda = 0.71073$ Å). The structures were solved by direct methods^[24] and refined by full-matrix least-squares procedures.

Crystal data for sesquihomoadamantene cation radical ($\text{SH}^{+}\text{SbCl}_6^{-}$): Brutto formula: $\text{C}_{20}\text{H}_{28}\text{O}_4 \cdot \text{SbCl}_6 \cdot \text{CH}_2\text{Cl}_2$, $M_r = 687.80$, monoclinic $P2_1/n$, $a = 10.4473(4)$, $b = 15.9754(6)$, $c = 15.6397(6)$ Å, $\beta = 93.396(1)^\circ$, $\rho_{\text{calcd}} = 1.753 \text{ g cm}^{-3}$, $V = 2605.7(2) \text{ Å}^3$, $Z = 4$. The total number of reflections measured was 37186, of which 11429 reflections were symmetrically nonequivalent. Final residuals were $R1 = 0.0339$ and $wR2 = 0.0625$ for 7397 reflections with $I > 2\sigma(I)$.

Crystal data for neutral sesquihomoadamantene (SH): Brutto formula: $\text{C}_{20}\text{H}_{28}$, $M_r = 268.42$, monoclinic, $P2_1/n$, $a = 6.4547(3)$, $b = 11.9580(6)$, $c = 9.6301(5)$ Å, $\beta = 91.772(1)^\circ$, $\rho_{\text{calcd}} = 1.200 \text{ g cm}^{-3}$, $V = 742.95(6) \text{ Å}^3$, $Z = 2$. The total number of reflections measured was 10380, of which 3266 reflections were symmetrically nonequivalent. Final residuals were $R1 = 0.0421$ and $wR2 = 0.1203$ for 2926 reflections with $I > 2\sigma(I)$. Crystallographic data (excluding structure factors) for the structures reported in this paper have been deposited with the Cambridge Crystallographic Data Centre as supplementary publication no. CCDC-143380 (neutral SH) and CCDC-143381 (SH^{+} cation radical). Copies of the data can be obtained free of charge on application to CCDC, 12 Union Road, Cambridge CB2 1EZ, UK (fax: (+44) 1223-336-033; e-mail: deposit@ccdc.cam.ac.uk).

Received: April 19, 2000 [Z15014]

- [1] a) S. F. Nelsen, *Acc. Chem. Res.* **1987**, *20*, 269, and references therein; b) T. Kim, G. A. Mirafzal, J. Liu, N. L. Bauld, *J. Am. Chem. Soc.* **1993**, *115*, 7653; c) S. F. Nelsen, R. Akaba, *J. Am. Chem. Soc.* **1981**, *103*, 2096; d) E. L. Clennan, W. Simmons, C. W. Almgren, *J. Am. Chem. Soc.* **1981**, *103*, 2098; e) C. M. Jefford, A. F. Boschung, *Tetrahedron Lett.* **1976**, 4771; f) R. Akaba, H. Sakuragi, K. Tokumaru, *Tetrahedron Lett.* **1984**, *25*, 665; g) E. Bosch, J. K. Kochi, *J. Am. Chem. Soc.* **1996**, *118*, 1319.
- [2] a) N. L. Bauld, *Tetrahedron* **1989**, *45*, 5307; b) N. L. Bauld, *J. Am. Chem. Soc.* **1992**, *114*, 5800; c) J. P. Dinnocenzo, D. A. Conlon, *J. Am. Chem. Soc.* **1988**, *110*, 2324; d) M. Schmittel, C. Wohlr, *J. Org. Chem.* **1995**, *60*, 8223, and references therein.
- [3] a) M. Tabata, A. Lund, P. O. Samskog, S. Lunell, M. B. Huang, *J. Polym. Sci. A* **1988**, *26*, 2725, and references therein; b) see also: N. Salhi-Benachenhou, J. R. Alvarez-Idaboy, S. Lunell, L. A. Eriksson, *Theor. Chem. Acc.* **1997**, *97*, 282; c) H. Zipse, *J. Am. Chem. Soc.* **1995**, *117*, 11798; d) S. S. Shaik, A. Pross, *J. Am. Chem. Soc.* **1989**, *111*, 4306; e) M. S. Workentin, N. P. Schepp, L. J. Johnston, D. D. Wayner, *J. Am. Chem. Soc.* **1994**, *116*, 1142.
- [4] a) R. S. Mulliken, C. C. Roothaane, *J. Chem. Rev.* **1947**, *41*, 219; b) R. S. Mulliken, C. C. Roothaane, *Tetrahedron* **1959**, *5*, 253.
- [5] a) S. Lunell, M.-B. Huang, *Chem. Phys. Lett.* **1990**, *168*, 63; b) N. Salhi-Benachenhou, B. Engels, M.-B. Huang, S. Lunell, *Chem. Phys.* **1998**, *236*, 53, and references therein; c) L. A. Eriksson, S. Lunell, R. J. Boyd, *J. Am. Chem. Soc.* **1993**, *115*, 6896; c) O. Takahashi, O. Kikuchi, *J. Chem. Phys.* **1994**, *100*, 1350.
- [6] a) A. J. Merer, L. Schoonveld, *J. Chem. Phys.* **1968**, *48*, 522; b) A. J. Merer, L. Schoonveld, *Can. J. Phys.* **1969**, *47*, 1731.
- [7] H. Koppel, W. Domcke, L. S. Cederbaum, W. V. Niessen, *J. Chem. Phys.* **1978**, *69*, 4252.
- [8] a) K. Toriyama, M. Okazaki, *Appl. Magn. Reson.* **1996**, *11*, 47, and references therein; b) M. Shiotani, Y. Nagata, J. Sohma, *J. Am. Chem. Soc.* **1984**, *106*, 4640; however, see: F. Gerson, G. Gescheidt, S. F. Nelsen, L. A. Paquette, M. F. Teasley, L. Waykole, *J. Am. Chem. Soc.* **1989**, *111*, 5518.
- [9] a) F. Gerson, J. Lopez, R. Akaba, S. F. Nelsen, *J. Am. Chem. Soc.* **1981**, *103*, 6716; b) T. Clark, M. F. Teasley, S. F. Nelsen, H. Wynberg, *J. Am. Chem. Soc.* **1987**, *109*, 5719; c) T. Clark, S. F. Nelsen, *J. Am. Chem. Soc.* **1988**, *110*, 868; d) S. F. Nelsen, M. F. Teasley, D. L. Kapp, C. R. Kessel, L. A. Grezzo, *J. Am. Chem. Soc.* **1984**, *106*, 791; e) S. F. Nelsen, C. R. Kessel, *J. Am. Chem. Soc.* **1979**, *101*, 2503.
- [10] a) H. Prinzbach, G. Gescheidt, H.-D. Martin, R. Herges, J. Heinze, G. K. S. Prakash, G. A. Olah, *Pure Appl. Chem.* **1995**, *67*, 673, and references therein; b) H. Prinzbach, B. A. R. C. Murty, W.-D. Fessner, J. Mortensen, J. Heinze, G. Gescheidt, F. Gerson, *Angew. Chem.* **1987**, *99*, 488; *Angew. Chem. Int. Ed. Engl.* **1987**, *26*, 457; c) G. Gescheidt, R. Herges, H. Neumann, J. Heinze, M. Wollenweber, M. Etkorn, H. Prinzbach, *Angew. Chem.* **1995**, *107*, 1109; *Angew. Chem. Int. Ed. Engl.* **1995**, *34*, 1016; d) M. Etkorn, F. Wahl, M. Keller, H. Prinzbach, F. Barbosa, V. Peron, G. Gescheidt, J. Heinze, R. Herges, *J. Org. Chem.* **1998**, *63*, 6080, and references therein.
- [11] a) T. Shida, Y. Egawa, A. Kubodera, T. Kato, *J. Chem. Phys.* **1980**, *73*, 5963; b) M. Kira, H. Nakazawa, H. Sakurai, *J. Am. Chem. Soc.* **1983**, *105*, 6983; c) Y. Itagaki, M. Shiotani, A. Hasegawa, H. Kawazoe, *Bull. Chem. Soc. Jpn.* **1998**, *71*, 2547; d) O. West, *J. Am. Chem. Soc.* **1997**, *119*, 5713; e) A. D. Trifunac, D. W. Werst, *J. Am. Chem. Soc.* **1996**, *118*, 9444; f) H. D. Roth, *Top. Curr. Chem.* **1992**, *163*, 131, and references therein.
- [12] a) D. J. Bellville, N. L. Bauld, *J. Am. Chem. Soc.* **1982**, *104*, 294; b) M. J. Shephard, M. N. Paddon-Row, *J. Phys. Chem.* **1995**, *99*, 3101; c) S. D. Chemerisov, D. W. Werst, A. D. Trifunac, *Chem. Phys. Lett.* **1998**, *291*, 262; d) F. Gerson, P. Felder, R. Schmidlin, H. N. C. Wong, *J. Chem. Soc. Chem. Commun.* **1994**, 1659; e) T. Nishinaga, K. Komatsu, N. Sugita, H. J. Lindner, J. Richter, *J. Am. Chem. Soc.* **1993**, *115*, 11642.
- [13] Tetraanisylethylene cation radical is the only known example which has been characterized crystallographically and it also shows a twist of 30° around the central C–C bond, see: R. Rathore, S. V. Lindeman, A. S. Kumar, J. K. Kochi, *J. Am. Chem. Soc.* **1998**, *120*, 6931.
- [14] a) H. Wynberg, E. Boelema, J. H. Wieringa, J. Strating, *Tetrahedron Lett.* **1970**, 3613; b) E. Boelema, H. Wynberg, J. Strating, *Tetrahedron Lett.* **1971**, 4029.
- [15] X-ray structure of sesquihomoadamantene has been determined at room temperature, see: W. H. Watson, A. Nagl, *Acta Crystallogr. Sect. C* **1987**, *43*, 2465.
- [16] The one-electron oxidation of SH to its purple cation radical can also be carried out electrochemically at $E_{\text{ox}}^0 = 1.36 \text{ V}$ versus SCE in anhydrous dichloromethane (containing tetra-*n*-butylammonium hexafluorophosphate as the supporting electrolyte) at –78 °C.
- [17] For a general procedure for the oxidation of organic donors using $\text{NO}^+\text{SbCl}_6^-$, see: R. Rathore, J. K. Kochi, *J. Org. Chem.* **1994**, *60*, 4399.
- [18] The identity of liberated NO was confirmed by UV/Vis and IR spectroscopy (W. G. Fateley, H. A. Bent, B. Crawford, Jr., *J. Chem. Phys.* **1959**, *31*, 204).
- [19] For a list of donors which afford stable cation radical salts, see: R. Rathore, A. S. Kumar, S. V. Lindeman, J. K. Kochi, *J. Org. Chem.* **1998**, *63*, 5847.
- [20] In addition, a very weak absorption at $\lambda > 750 \text{ nm}$ (see Figure 1) accounts for the purple color of the cation radical salt. The ESR spectrum of $\text{SH}^{+}\text{SbCl}_6^-$ in dichloromethane at –70 °C was the same as that obtained by Nelsen and co-workers in a mixture of trifluoro-

acetic acid and trifluoroacetic anhydride using the electrochemical method.^[9b,c]

- [21] Note that the remote *b'* bonds which remain unchanged in the cation radical lie almost orthogonal to the p orbitals and thus do not participate in stabilizing the cationic charge, compare: J. F. King, R. Rathore, *J. Am. Chem. Soc.* **1990**, *112*, 2001.
- [22] a) J. Rosenbaum, M. C. R. Symons, *Proc. Chem. Soc.* **1959**, 92; b) see also: S. F. Nelsen, M. F. Teasley, D. L. Kapp, C. R. Kessel, L. A. Grezzo, *J. Am. Chem. Soc.* **1984**, *106*, 791.
- [23] Theoretical calculations of olefinic cation radicals are in progress with Professor P. von R. Schleyer.
- [24] G. M. Sheldrick, SHELXS-86, program for structure solution, University of Göttingen, Germany, **1986**.

The First Templated Borogermanate (C₂N₂H₁₀)₂[(BO_{2.5})₂(GeO₂)₃]: Linkage of Tetrahedra of Significantly Different Sizes**

Mike S. Dadachov,* Kai Sun, Tony Conradsson, and Xiaodong Zou*

The classes of microporous materials—tetrahedral- and mixed-framework compounds—with open structures continue to expand in terms of framework-forming elements.^[1] The most accomplished and also largest classes of tetrahedral-framework compounds are aluminosilicates (Al-Si-O),^[2] aluminophosphates (Al-P-O)^[3] as well as their isomorphic substituted forms. Attempts to synthesize frameworks with elements other than Al, Si, and P, especially with transition metals, have resulted in many new classes, such as gallophosphates,^[4] titanosilicates,^[5] beryllium,^[6] zinc,^[7] cobalt,^[8] iron,^[9] vanadium,^[10] nickel,^[11] and molybdenum^[12] phosphates. Since most transition metal atoms are too large to fit comfortably into the hole formed by a van der Waals oxygen tetrahedron, they are often coordinated by additional terminal OH and F groups, forming trigonal bipyramids, square bipyramids, or octahedra in open framework structures. As a consequence, the Me–O bonds become weaker and thus most of these compounds are thermally unstable. Besides the framework compounds containing oxygen, other compounds such as sulfides^[13] and a phosphonitride^[14] have been reported.

During recent years, attempts have been made to include boron atoms into the ZSM-*n* frameworks. However, very little aluminum/silicon could be replaced by boron.^[15] Furthermore, a few templated metal borophosphates were reported.^[16]

Open framework germanates are an interesting and expanding class of microporous materials. Germanium forms oxygen polyhedra with 4-, 5-, and 6-coordination, and

germanates consisting of both purely tetrahedrally coordinated frameworks^[17] and mixed polyhedral frameworks^[18] have been reported.

Herein we report the synthesis and structure determination of the first templated borogermanate (C₂N₂H₁₀)₂[(BO_{2.5})₂(GeO₂)₃]. The hydrothermal reaction of ethylenediamine, boric acid, germanium dioxide, hydrofluoric acid, and pyridine gave transparent platelike crystals of (C₂N₂H₁₀)₂[(BO_{2.5})₂(GeO₂)₃] in high yield. X-ray analysis of these crystals^[19] revealed a layered structure with large openings in the layers and organic templates between the layers.

There are three unique Ge and two unique B atoms in the structure, all of them tetrahedrally coordinated by oxygen atoms (Figure 1). The structure can be described as undulating borogermanate layers, each one constructed of isolated

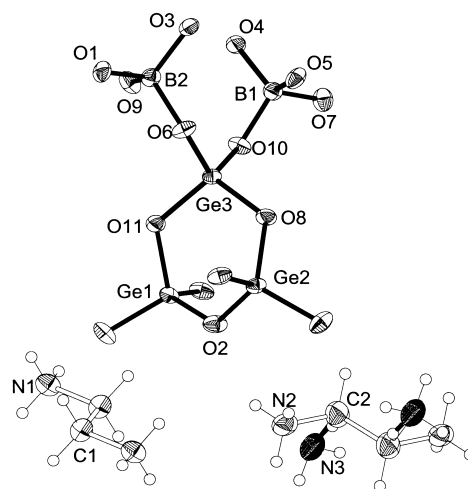


Figure 1. Atom-labeling scheme for all the non-hydrogen atoms of the asymmetric unit of (C₂N₂H₁₀)₂[(BO_{2.5})₂(GeO₂)₃] (ORTEP plot; 50% probability ellipsoids). The NH₃ terminal groups (N2 and N3) bonded to C2 are the two different conformations of the diprotonated ethylenediamine.

3-rings of germanium tetrahedra, [GeO₂]₃, connected by pairs of boron tetrahedra, [BO_{2.5}]₂ (Figure 2). The borogermanate layers can also be described in terms of large 9-rings formed by alternating two-corner-linked germanium tetrahedra (six in total) and one pair of boron tetrahedra (three pairs in total) (Figure 2). The layers are connected by hydrogen bonding through the two unique charge-compensating diprotonated ethylenediamine cations. One of those cations was found to have two different conformations (Figure 1). Such behavior is not uncommon in this type of structure, since the cations reside in large cavities and possess a considerable freedom of motion.

The bond lengths and angles for both the framework atoms and the guests are unexceptional. All Ge–O distances are between 1.719 and 1.768 Å and the O–Ge–O angles are between 104.27 and 115.18°. All oxygen atoms of the germanium coordination polyhedra are shared either between Ge and Ge or between Ge and B atoms. Three of the four oxygen atoms of each BO₄ tetrahedron are shared between boron and germanium, and one acts as a terminal oxygen atom pointing towards the interlayer. As a consequence, the B–O distances fall into two categories. The three bridging

[*] Dr. M. S. Dadachov, Dr. X. D. Zou, Dr. K. Sun, T. Conradsson
Structural Chemistry, Stockholm University
S-106 91 Stockholm (Sweden)
Fax: (+46) 8-16-31-18
E-mail: zou@struc.su.se

[**] This work was supported by the Swedish Natural Science Research Council (NFR).

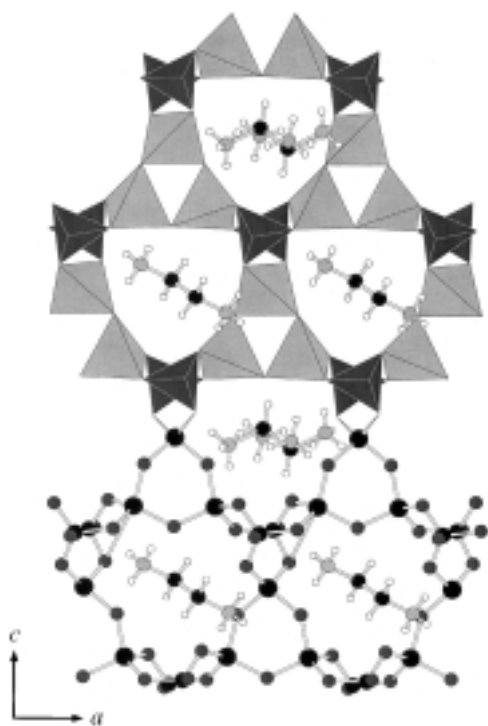


Figure 2. Polyhedral and ball-and-stick representations of the structure viewed along the b axis. Three GeO_4 3-rings are connected by three pairs of BO_4 tetrahedra, leading to 9-ring channels in the $[010]$ direction. Ethylenediamine molecules are located at the center of each channel.

B–O (–Ge) distances are practically the same (1.475(5) Å). The B–O distances to the terminal oxygen atoms are somewhat shorter (1.435(4) Å).

The radius of boron is much smaller than that of germanium. Though boron could fit into tetrahedral polyhedra, it is most commonly found to be in trigonal-planar coordination, and germanium is octahedrally coordinated by oxygen atoms. The cation-to-anion radius ratio for both B and Ge is somewhat outside the commonly observed range for tetrahedral oxygen environment. It is remarkable that they are found together in the same structure. This is probably the templated inorganic framework with the largest size difference between different tetrahedral units.

The most intriguing feature of the $(\text{C}_2\text{N}_2\text{H}_{10})_2[(\text{BO}_{2.5})_2(\text{GeO}_2)_3]$ structure is its resemblance to that of $(\text{X})_4[(\text{GeO}_2)_3(\text{GeO}_{1.5}\text{F}_3)_2] \cdot y\text{H}_2\text{O}$ ($\text{X} = \text{NH}_4$ or K , $y = 0.67 - 1.0$).^[20–21] The structure topology within the layers is the same in both structures, except that the $[\text{GeO}_{1.5}\text{F}_3]$ octahedra are replaced by $[\text{BO}_{2.5}]$ tetrahedra (Figures 3 and 4). This replacement is nontrivial in terms of crystal chemistry, since B and Ge differ widely in valence and size. Although the $[\text{BO}_{2.5}]$ tetrahedra and the $[\text{GeO}_{1.5}\text{F}_3]$ octahedra are very different polyhedra with different sizes, they play the same structural role in the framework. The match of these very different polyhedra to the same framework can be seen by the similarity of the unit cell parameters (a and c) of these two compounds in the layer plane: $a = 7.0065$ and $c = 11.7976$ Å for $(\text{NH}_4)_4[(\text{GeO}_2)_3(\text{GeO}_{1.5}\text{F}_3)_2] \cdot (\text{H}_2\text{O})_{0.67}$ and $a = 6.9765$ and $c = 11.6943$ Å for $(\text{C}_2\text{N}_2\text{H}_{10})_2[(\text{BO}_{2.5})_2(\text{GeO}_2)_3]$. The relative position of the two adjacent layers is very similar in both structures (Figure 4),

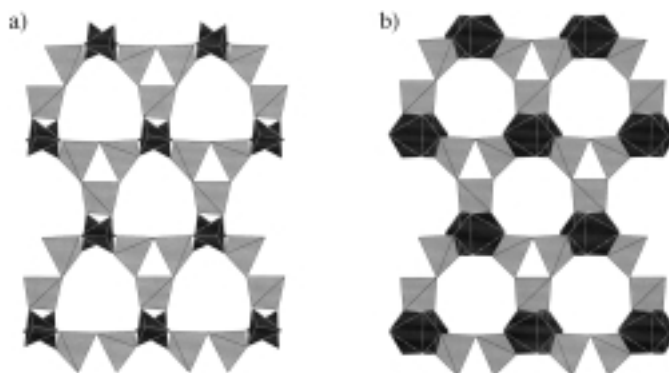


Figure 3. Comparison of the connections of the polyhedra within the layer between a) $(\text{C}_2\text{N}_2\text{H}_{10})_2[(\text{BO}_{2.5})_2(\text{GeO}_2)_3]$ and b) $(\text{NH}_4)_4[(\text{GeO}_2)_3(\text{GeO}_{1.5}\text{F}_3)_2] \cdot (\text{H}_2\text{O})_{0.67}$. GeO_4 tetrahedra are shown in light gray and BO_4 tetrahedra and GeO_6 octahedra in dark gray. The GeO_4 tetrahedra are arranged in a similar way in both structures. The only difference is that the BO_4 tetrahedral pairs in a) are replaced by GeO_6 octahedral pairs in b). Both structures contain 3- and 9-rings.

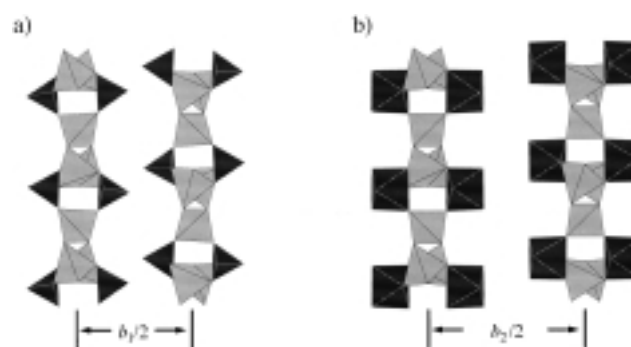


Figure 4. Comparison of the geometrical relationship between the layers. a) $(\text{C}_2\text{N}_2\text{H}_{10})_2[(\text{BO}_{2.5})_2(\text{GeO}_2)_3]$ and b) $(\text{NH}_4)_4[(\text{GeO}_2)_3(\text{GeO}_{1.5}\text{F}_3)_2] \cdot (\text{H}_2\text{O})_{0.67}$. GeO_4 tetrahedra are shown in light gray and BO_4 tetrahedra and GeO_6 octahedra in dark gray. The relative layer positions in the two structures are very similar, except that the distance between the layers in $(\text{C}_2\text{N}_2\text{H}_{10})_2[(\text{BO}_{2.5})_2(\text{GeO}_2)_3]$ ($= b_1/2$) is shorter than in $(\text{NH}_4)_4[(\text{GeO}_2)_3(\text{GeO}_{1.5}\text{F}_3)_2] \cdot (\text{H}_2\text{O})_{0.67}$ ($= b_2/2$). This is due to the size difference between the BO_4 tetrahedra and GeO_6 octahedra and the locations of the guest molecules in the interlayers.

even though different molecular and ionic species are present in the interlayers. The interlayer distances are different in the two structures, however, due to the size differences of the $[\text{BO}_{2.5}]$ tetrahedra and $[\text{GeO}_{1.5}\text{F}_3]$ octahedra, and the different locations of the intercalated species of ethylenediamine and ammonium cations and water. The $[\text{BO}_{2.5}]^{2-}$ and $[\text{GeO}_{1.5}\text{F}_3]^{2-}$ units, which are the only negatively charged parts of the framework layers, are compensated by the diprotonated ethylenediamines and ammonium cations in $(\text{C}_2\text{N}_2\text{H}_{10})_2[(\text{BO}_{2.5})_2(\text{GeO}_2)_3]$ and $(\text{NH}_4)_4[(\text{GeO}_2)_3(\text{GeO}_{1.5}\text{F}_3)_2] \cdot (\text{H}_2\text{O})_{0.67}$, respectively.

We have shown for the first time that boron can be incorporated into templated germanate frameworks. This opens possibilities for synthesizing other templated borogermanates with novel structure topologies.

Experimental Section

Crystals of $(\text{C}_2\text{N}_2\text{H}_{10})_2[(\text{BO}_{2.5})_2(\text{GeO}_2)_3]$ were synthesized from an organic-rich solution consisting of ethylenediamine, H_3BO_3 , GeO_2 , HF, pyridine, and H_2O in a molar ratio of 12:2:1:2:40:5. GeO_2 (0.15 mg) was added to a

mixture of pyridine (4.55 g) and water (0.147 g). Then ethylenediamine (1.038 g) was added and stirred until the mixture became a clear solution. Finally boric acid (0.18 g) and 40% HF (0.062 g) were added to the obtained solution (pH 11.12), which was then heated at 170°C for 10 days in a 23 mL Teflon-lined Parr autoclave. The product (yield 0.206 g), consisting of a white powder and thin platelike single crystals, was collected, washed with deionized water and ethanol, and dried at room temperature. The Ge content was confirmed by energy-dispersive spectroscopy (EDS).

Received: May 11, 2000 [Z15112]

- [1] A. K. Cheetham, G. Férey, T. Loiseau, *Angew. Chem.* **1999**, *111*, 3466; *Angew. Chem. Int. Ed.* **1999**, *38*, 3268.
- [2] a) R. M. Barrer, *Hydrothermal Chemistry of Zeolites*, Academic Press, New York, **1989**; b) W. M. Meier, D. H. Olson, *Atlas of Zeolite Structure Types*, Elsevier, London, **1996**.
- [3] S. T. Wilson, B. M. Lok, C. A. Messina, T. R. Cannon, E. M. Flanigen, *J. Am. Chem. Soc.* **1982**, *104*, 1146.
- [4] a) J. B. Parise, *Inorg. Chem.* **1985**, *24*, 4312; b) J. B. Parise, *Acta Crystallogr. Sect. C* **1984**, *40*, 1641; c) G. Yang, S. Feng, R. Xu, *J. Chem. Soc. Chem. Commun.* **1987**, 1254; d) G. Férey, *J. Fluorine Chem.* **1995**, *72*, 187; e) G. Férey, *C. R. Acad. Sci. Ser. C* **1988**, *1*, 1.
- [5] D. M. Chapman, A. L. Rol, *Zeolites* **1990**, *10*, 730.
- [6] a) G. Harvey, W. M. Meier, *Stud. Surf. Sci. Catal. A* **1989**, *49*, 411; b) T. E. Gier, G. D. Stucky, *Nature* **1991**, *349*, 508.
- [7] a) T. E. Gier, G. D. Stucky, *Nature* **1991**, *349*, 508; b) G. Y. Yang, S. C. Sevov, *J. Am. Chem. Soc.* **1999**, *121*, 8389.
- [8] P. Feng, X. Bu, G. D. Stucky, *Nature* **1997**, *388*, 735.
- [9] D. R. Corbin, J. F. Whitney, W. C. Fulz, G. D. Stucky, M. M. Eddy, A. K. Cheetham, *Inorg. Chem.* **1986**, *25*, 2280; b) M. Cavellac, D. Riou, C. Ninctaus, J. M. Greneche, G. Férey, *Zeolites* **1996**, *17*, 260; c) K.-H. Li, Y.-F. Huang, V. Zima, C.-Y. Huang, H.-M. Lin, Y.-C. Jiang, F.-L. Liao, S.-L. Wang, *Chem. Mater.* **1998**, *10*, 2599, and references therein.
- [10] a) V. Soghomonian, Q. Chen, R. C. Haushalter, J. Zubieta, *Angew. Chem.* **1995**, *107*, 229; *Angew. Chem. Int. Ed. Engl.* **1995**, *34*, 223; b) V. Soghomonian, Q. Chen, R. C. Haushalter, J. Zubieta, J. O'Connor, *Science* **1993**, *259*, 1596.
- [11] N. Guillo, Q. Gao, M. Nogues, R. E. Morris, M. Hervieu, G. Férey, A. K. Cheetham, *C. R. Acad. Sci. Paris Ser. 2* **1999**, 387.
- [12] R. C. Haushalter, L. A. Mundi, *Chem. Mater.* **1992**, *4*, 31, and references therein.
- [13] a) R. L. Bedard, S. T. Wilson, L. D. Vail, J. M. Bennet, E. M. Flanigen, *Stud. Surf. Sci. Catal. A* **1989**, *49*, 375; b) J. B. Parise, *J. Chem. Soc. Chem. Commun.* **1990**, 1553; c) C. L. Chahill, Y. Ko, J. B. Parsie, *Chem. Mater.* **1998**, *10*, 19.
- [14] W. Schnick, J. Lucke, *Angew. Chem.* **1992**, *104*, 208; *Angew. Chem. Int. Ed. Engl.* **1992**, *31*, 213.
- [15] a) E. Unnerberg, S. Kolboe, *Appl. Catal. A* **1995**, *124*, 345, and references therein; b) F. DiRenzo, M. Derewinski, G. Chiari, *Microporous Mater.* **1996**, *6*, 151; c) M. Shibata, Z. Gabelica, *Appl. Catal. A* **1997**, *162*, 93.
- [16] a) R. P. Bontchev, J. Do, A. J. Jacobson, *Angew. Chem.* **1999**, *111*, 2063; *Angew. Chem. Int. Ed.* **1999**, *38*, 1937, and references therein; b) R. Knip, G. Schäfer, H. Engelhardt, I. Boy, *Angew. Chem.* **1999**, *111*, 3858; *Angew. Chem. Int. Ed.* **1999**, *38*, 3642; c) S. C. Sevov, *Angew. Chem.* **1996**, *108*, 2814; *Angew. Chem. Int. Ed. Engl.* **1996**, *35*, 2630; d) C. J. Warren, R. C. Haushalter, D. J. Rose, J. Zubieta, *Chem. Mater.* **1997**, *9*, 2694.
- [17] a) H. Li, O. M. Yaghi, *J. Am. Chem. Soc.* **1998**, *120*, 10569; b) M. O'Keefe, O. M. Yaghi, *Chem. Eur. J.* **1999**, *5*, 2796, and references therein.
- [18] a) J. Cheng, R. Xu, G. Yang, *J. Chem. Soc. Dalton Trans.* **1991**, 1537; b) R. H. Jones, J. Chen, J. M. Thomas, A. George, M. B. Hursthouse, R. Xu, S. Li, Y. Li, G. Yang, *Chem. Mater.* **1992**, *4*, 808.
- [19] X-ray structure analysis: STOE IPDS system with image plate; graphite monochromator; $\lambda(\text{MoK}\alpha) = 0.71073 \text{ \AA}$; $T = 293 \text{ K}$; the structure was solved by using the direct-method routine of SIR-97^[22] and refined by full-matrix least-squares methods using SHELXL-97^[23] numerical absorption correction by X-RED^[24], $T_{\text{min}} = 0.4281$, $T_{\text{max}} = 0.8850$. Crystal data for $(\text{C}_2\text{N}_2\text{H}_{10})_2[(\text{BO}_{2.5})_2(\text{GeO}_2)_3]$: crystal dimen-

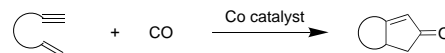
sions $0.10 \times 0.10 \times 0.02 \text{ mm}$, monoclinic, space group $P2_1/n$, $a = 6.9765(9)$, $b = 14.4103(12)$, $c = 11.6943(14) \text{ \AA}$, $\beta = 91.093(15)^\circ$, $V = 1175.46(23) \text{ \AA}^3$, $Z = 4$, $\rho_{\text{calcd}} = 2.69 \text{ g cm}^{-3}$, $\mu(\text{MoK}\alpha) = 76.833 \text{ cm}^{-1}$, $2\theta_{\text{min}} = 6.4^\circ$, $2\theta_{\text{max}} = 47^\circ$, $R_1 = 0.034$ for 1525 reflections with $F_o > 4\sigma(F_o)$ and 0.039 for all 1729 reflections, $wR_2(F^2) = 0.095$, GOF = 1.136, 194 parameters were refined, max/min. residual electron density $-0.79/0.86 \text{ e \AA}^{-3}$. One of the $(\text{H}_3\text{NCH}_2\text{CH}_2\text{NH}_3)^{2+}$ ions was found to have two different conformations (Figure 1). This was refined as the N-population parameters of the N2 atom at two sites as 0.73 and 0.27. All other parameters are unexceptional. Most of the hydrogen atom positions could be located on the final difference Fourier maps, and they were introduced by the rigid-group riding mode, allowing refinement of their isotropic thermal parameters. Crystallographic data (excluding structure factors) for the structure reported in this paper have been deposited with the Cambridge Crystallographic Data Centre as supplementary publication no. CCDC-143794. Copies of the data can be obtained free of charge on application to CCDC, 12 Union Road, Cambridge CB2 1EZ, UK (fax: (+44) 1223-336-033; e-mail: deposit@ccdc.cam.ac.uk).

- [20] T. Conradsson, X. D. Zou, M. S. Dadachov, *Inorg. Chem.* **2000**, *39*, 1716.
- [21] X. Bu, P. Feng, G. D. Stucky, *Chem. Mater.* **1999**, *11*, 3423.
- [22] A. Altomare, G. Cascarano, C. Giacovazzo, A. Guagliardi, A. G. G. Moliterni, M. C. Burla, G. Polidori, C. Camalli, R. Spagna, SIR97, a package for structure solution by direct methods and refinement, User's Manual, **1997**.
- [23] G. M. Sheldrick, SHELXL97, program for refinement of crystal structures, University of Göttingen, Germany, **1997**.
- [24] STOE and CIE, X-RED 1.07, program for data reduction for STADI4 and IPDS, Darmstadt, Germany, **1996**.

Dodecacarbonyltetracobalt Catalysis in the Thermal Pauson–Khand Reaction**

Marie E. Krafft* and Llorente V. R. Boñaga

Dicobaltoctacarbonyl, $[\text{Co}_2(\text{CO})_8]$, has always been the metal complex of choice in the widely used Pauson–Khand reaction for the formation of bicyclo[3.3.0]octenones by the cyclocarbonylation of an alkene and an alkyne (Scheme 1).^[1] Alternative sources of zero valent cobalt, namely [(indenyl)Co(cod)] and $[\text{Co}(\text{acac})_2]/\text{NaBH}_4$, and cobalt carbonyl clusters, such as $[\text{Co}_4(\text{CO})_{12}]$, $[\text{Co}_3(\text{CO})_9(\mu_3\text{-CH})]$, and $[\text{Co}_4(\text{CO})_{11}\text{P}(\text{O}^i\text{Pr})_3]$, have also been developed but are less



Scheme 1. Cobalt catalysis in the Pauson–Khand reaction. Co catalyst: $[\text{Co}_2(\text{CO})_8]$ with or without additive (phosphite, phosphane, cyclohexylamine (CyNH₂), phosphane sulfide, 1,2-dimethoxyethane (DME), water), $[\text{Co}_4(\text{CO})_{12}]$, $[\text{Co}_4(\text{CO})_{11}\text{P}(\text{O}^i\text{Pr})_3]$, $[\text{Co}_3(\text{CO})_9(\mu_3\text{-CH})]$, [(indenyl)Co(cod)], $[\text{Co}(\text{acac})_2]/\text{NaBH}_4$. cod = cycloocta-1,4-diene; acac = acetylacetonate.

[*] Prof. M. E. Krafft, L. V. R. Boñaga
Department of Chemistry
The Florida State University
Tallahassee, FL 32306-4390 (USA)
Fax: (+1) 850-644-8281
E-mail: mek@chem.fsu.edu

[**] This work was supported by the National Science Foundation and the donors to the Krafft Research Fund.

frequently employed. Of particular interest is the congeneric tetranuclear carbonyl cluster $[\text{Co}_4(\text{CO})_{12}]$, which has seen very limited practical utility in this cyclization under one atmosphere of CO at moderate temperatures (such as 70°C).^[2, 7a, 8b] In fact, the advent of many protocols in the cobalt-catalyzed reactions stems from the common belief that $[\text{Co}_4(\text{CO})_{12}]$ formation deters $[\text{Co}_2(\text{CO})_8]$ catalysis and is generally regarded as a dead end route in this reaction.^[1i, 3] Presumably derived from dimerization of “ $[\text{Co}_2(\text{CO})_n]$ ” upon release of the cyclopentenone product, $[\text{Co}_4(\text{CO})_{12}]$ was suggested to be one of the cobalt species or clusters, which were believed to be nonviable for the reaction.^[1i, 4] Consequently, development of methods involving $[\text{Co}_2(\text{CO})_8]$ catalysis was based on preserving the catalytic species and preventing the formation of inactive cobalt species. Successful catalytic cyclizations using $[\text{Co}_2(\text{CO})_8]$ were carried out with additives^[5] or ultraviolet light,^[6] under high operating temperatures and CO pressures,^[7] or in supercritical fluids.^[8] In addition to providing low valent cobalt species, the role of NaBH_4 in the $[\text{Co}(\text{acac})_2]/\text{NaBH}_4$ catalyst system for the Pauson–Khand reaction was also based on these premises.^[9]

The formation of $[\text{Co}_4(\text{CO})_{12}]$ from the thermal decomposition of $[\text{Co}_2(\text{CO})_8]$ in hexane, heptane, or toluene was extensively studied by several groups.^[10] Isolation of this cobalt cluster was also reported by Pauson and co-workers in their seminal studies on the thermal cyclizations of $[(\text{HC}\equiv\text{CH})\text{Co}_2(\text{CO})_6]$ complexes with norbornene and its derivatives under a nitrogen atmosphere.^[11a] Generation of $[\text{Co}_4(\text{CO})_{12}]$ under these cyclization conditions in aromatic solvents, such as toluene and benzene, was also indicated by the isolation of $[(\text{arene})\text{Co}_4(\text{CO})_9]$ complexes.^[11b,c]

In our continuing studies on the Pauson–Khand reaction, we observed that cyclizations can be effected using catalytic quantities of commercially available $[\text{Co}_2(\text{CO})_8]$ under one atmosphere of CO. The efficiency of this process was further enhanced by the addition of cyclohexylamine (CyNH_2).^[5b] It was later discovered that, in the presence of added cyclohexylamine, substoichiometric amounts of $[\text{Co}_2(\text{CO})_8]$ were sufficient to catalyze the Pauson–Khand reaction under an N_2 atmosphere.^[12] In these studies, we speculated an additive-derived stabilization of reaction intermediates originating from its

coordination, by virtue of its Lewis basicity,^[13] to coordinatively unsaturated organocobalt species. We also proposed that cyclohexylamine preserved the active cobalt species under the catalytic conditions and an iterative disproportionation of residual cobalt species, “ $[\text{Co}_2(\text{CO})_n\text{L}_{8-n}]$ ”, where $\text{L} = \text{CO}$, CyNH_2 , or DME, to provide active species under the substoichiometric conditions. Kinetic studies on the disproportionation of $[\text{Co}_2(\text{CO})_8]$ by nitrogen-containing bases, such as cyclohexylamine, have been reported.^[14c] Lewis bases, such as ammonia, pyridine, methanol, and ethanol are also well documented to induce disproportionation of $[\text{Co}_4(\text{CO})_{12}]$.^[14]

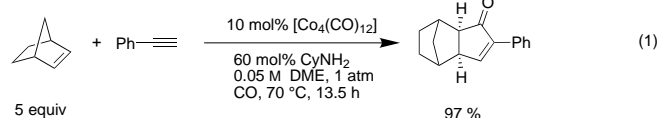
We conducted Pauson–Khand cyclization studies with the $[\text{Co}_4(\text{CO})_{12}]$ cluster in an attempt to understand the efficiency enhancement provided by the amine ligand and to verify our hypothesis that cyclohexylamine preserves the active catalyst and induces its formation via disproportionation of $[\text{Co}_4(\text{CO})_{12}]$, which may possibly be formed during catalytic reactions using $[\text{Co}_2(\text{CO})_8]$. As anticipated, we observed that catalytic amounts of $[\text{Co}_4(\text{CO})_{12}]$ could be used in conjunction with CyNH_2 to catalyze thermal Pauson–Khand reactions under practical reaction conditions. We then verified the extent of these observations in a series of catalytic cyclizations of a variety of substrates employing the $[\text{Co}_4(\text{CO})_{12}]/\text{CyNH}_2$ system (Table 1).^[15, 16] As was observed with the $[\text{Co}_2(\text{CO})_8]/$

Table 1. $[\text{Co}_4(\text{CO})_{12}]/\text{CyNH}_2$ as catalyst system for a practical thermal Pauson–Khand reaction.^[a]

Entry	Substrate	Product ^[16] [diastereomeric ratio, dr]	Yield [%]
1			92, 94 ^[b]
2			64
3			92, 70, ^[c] 89, ^[d] 55 ^[e]
4			88 ^[b]
5			81
6			85, 70, ^[d] 65 ^[e]
7			91
8			80
9			56, ^[f] 61 ^[c]
10			44, ^[f] 30 ^[c]

[a] Reactions were carried out at substrate concentrations of 0.05 M in DME using 10 mol % $[\text{Co}_4(\text{CO})_{12}]$ and 60 mol % CyNH_2 under a CO atmosphere at 70°C . Reactions lasted typically 13–18 h. [b] 5 mol % $[\text{Co}_4(\text{CO})_{12}]$, 30 mol % CyNH_2 . [c] With pyridine. [d] In dichloroethane. [e] In isooctane. [f] 30 mol % $[\text{Co}_4(\text{CO})_{12}]$, 60 mol % CyNH_2 . TBS = *tert*-butyldimethylsilyl.

CyNH₂ system,^[5b] good to excellent yields were obtained from enynes with significant Thorpe–Ingold properties (entries 1, 3–5, 8), although a lower yield was obtained from an enyne bearing a disubstituted olefin (entry 2). With the present catalyst system, a complete cyclization of enyne **7** was achieved using only a 10/60 ratio of [Co₄(CO)₁₂]/CyNH₂ whereas, with the [Co₂(CO)₈]/CyNH₂ system, a 30/60 ratio of [Co₂(CO)₈]/CyNH₂ was necessary. Similarly, enynes bearing internal alkynes and lacking significant Thorpe–Ingold assistance (entry 9) or which are sterically hindered (entry 10) needed higher catalyst loading (for example 30 mol%) for complete reactions, albeit still in modest yields. In our efforts to improve the cyclizations depicted in entries 9 and 10, pyridine was substituted for cyclohexylamine^[12] but essentially identical results were obtained. Pyridine is one of the Lewis bases known to induce disproportionation of [Co₂(CO)₈] and [Co₄(CO)₁₂].^[14] In contrast, cyclization of enyne **3** with pyridine as the additive was found to be inferior to cyclohexylamine (entry 3). An intermolecular version of this [Co₄(CO)₁₂]/CyNH₂-catalyzed cyclization was also demonstrated by the reaction of phenylacetylene and the reactive alkene norbornene to give the cycloadduct in 97% yield [Eq. (1)].



We have therefore shown that efficient cycloadditions of enynes could be attained using catalytic amounts of [Co₄(CO)₁₂], with cyclohexylamine enhancing the reaction efficiency. These findings further exemplified the utility of additives, such as amines, in improving the catalytic efficiency of cobalt carbonyls in Pauson–Khand reactions. In the early studies on the thermal decomposition of [Co₂(CO)₈] (in toluene), Ungvary and Marko showed that coordinatively unsaturated [Co₂(CO)₆] fragments are necessary for the formation of [Co₄(CO)₁₂].^[10d] Hence, an atmosphere of CO or the presence of coordinating ligands, such as CyNH₂ would be expected to inhibit the formation of these fragments and, consequently, the dimerization to the tetranuclear cluster. On the contrary, it had been suggested that *only* at high CO pressures would formation of the dinuclear cobalt carbonyl be effectively favored from [Co₄(CO)₁₂].^[3b]

To further elucidate this observed reactivity, we examined the cyclizations of enyne **1** using [Co₄(CO)₁₂] in the absence of additives in solvents commonly used in Pauson–Khand reactions (Table 2). Although we intended to confirm its lack of reactivity under our reaction conditions, we discovered otherwise that [Co₄(CO)₁₂] catalyzes the cycloaddition in a number of solvents under normal laboratory conditions, in which the highest catalytic efficiency was observed in 1,2-dichloroethane (DCE) and isooctane. Interestingly, Pauson and co-workers isolated [Co₄(CO)₁₂] from stoichiometric Pauson–Khand reactions in isooctane as the solvent.^[11a] For comparison, cyclization efficiencies in DCE and DME under

Table 2. [Co₄(CO)₁₂] and [Co₂(CO)₈] catalyses in different solvents.^[a]

Entry	Solvent	[Co ₄ (CO) ₁₂]			[Co ₂ (CO) ₈]		
		Yield [%]	TON ^[b]		Yield [%]	TON ^[b]	
		1	11		1	11	
1	dimethyl sulfoxide	93	–	0	94	–	0
2	acetonitrile	61	35	6.9	76	9	1.7
3	dichloromethane	47	–	0			
4	dichloroethane	–	68	14.3	29	26	5.0
5					–	37 ^[c]	3.7
6					–	50 ^[d]	2.4
7	tetrahydrofuran	–	21	4.4			
8	1,2-dimethoxyethane	–	23	4.4	9	41	7.8
9			59 ^[e]	6.0	–	82 ^[c]	8.3
10	toluene	86	9	1.9			
11	<i>n</i> -hexane	24	37	6.2			
12	<i>n</i> -heptane	30	41	8.7			
13	isooctane	–	59	12.5	31	19	3.3
14		–	61 ^[e]	6.5	–	57 ^[d]	2.6

[a] In [Eq. (2)], E = CO₂Et, catalyst = [Co₄(CO)₁₂] or [Co₂(CO)₈]. [b] Turnover number (TON) is the mole ratio of product to catalyst. [c] 10 mol%. [d] 20 mol%.

the reaction conditions described in Table 1 are comparable (see entries 3 and 6). However, under these catalytic conditions, no cyclization was evident in dimethyl sulfoxide (DMSO), presumably due to the formation of inactive DMSO–cobalt complexes.^[17] Owing to its strong coordinating ability, DMSO possibly formed complexes with [Co₄(CO)₁₂] or its degradation products which were inert toward catalysis in the Pauson–Khand reaction. On the contrary, DMSO has been widely used as an additive to promote Pauson–Khand reactions in benzene of [(alkyne)Co₂(CO)₆] complexes (40 °C, air)^[17c] and of [(allylpropargylsulfide)Co₂(CO)₆] complexes (60 °C, O₂) in the presence of dimethylsulfide as a coligand.^[17d] These suggest that DMSO is beneficial to [(alkyne)Co₂(CO)₆] complexes, which renders them more reactive towards alkene coordination, but is detrimental to [Co₂(CO)₈] and [Co₄(CO)₁₂] complexes. As was already demonstrated by Kim and Chung, [Co₄(CO)₁₂] did not exhibit any catalytic activity in dichloromethane under one atmosphere of CO and optimal catalysis was only achieved at 150 °C and 10 atm of CO.^[7] In contrast, [Co₂(CO)₈] exhibited its highest catalytic activity in DME.^[18] A subsequent increase in yield was noted for cyclizations in DME when higher amounts of [Co₂(CO)₈] were used (entries 8 versus 9), although less notably in dichloroethane (entries 4–6) and isooctane (entries 13–14).

The observed reactivity of [Co₄(CO)₁₂] at 70 °C and one atmosphere of CO suggested that, under our conditions, it probably underwent disproportionation into [Co₂(CO)₈] or a similar catalytically active cobalt species.^[19] Although generation of [Co₄(CO)₁₂] under the [Co₂(CO)₈]-catalyzed conditions has been only assumed, we have discounted the assumption that [Co₄(CO)₁₂] is inactive toward the Pauson–Khand cyclizations under mild conditions, such as a normal pressure of CO and a lower temperature. Thus, [Co₄(CO)₁₂] can now serve as an alternative for [Co₂(CO)₈], which is more

prone to air oxidation,^[20] and possibly $[\text{Co}_3(\text{CO})_9(\mu_3\text{-CH})]$.^[21] It is also noteworthy that commercially available samples of $[\text{Co}_4(\text{CO})_{12}]$ were used without purification and found to be catalytically efficient.^[22]

In conclusion, we demonstrated that, contrary to common belief, $[\text{Co}_4(\text{CO})_{12}]$ catalyzes the Pauson–Khand reaction under very practical laboratory conditions (70 °C, 1 atm CO). Its catalytic efficiency was further enhanced by the utility of an additive, such as cyclohexylamine, which possibly facilitated its disproportionation into and promoted preservation of the catalytically active cobalt species. Finally, we have provided the first practical procedures using the commercially available and more stable $[\text{Co}_4(\text{CO})_{12}]$ cluster as a catalyst precursor. Studies on reactions using this cluster are underway.

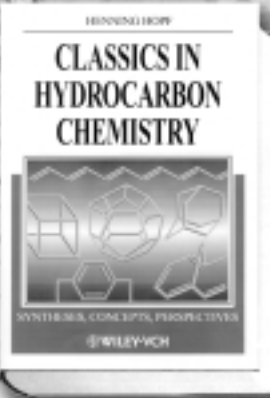
Received: May 18, 2000

Revised: July 24, 2000 [Z15144]

- [1] For reviews, see: a) P. L. Pauson, *Tetrahedron* **1985**, *41*, 5855; b) P. L. Pauson in *Organometallics in Organic Synthesis, Aspects of a Modern Interdisciplinary Field* (Eds.: A. de Meijere, H. tom Dieck), Springer, Berlin, **1988**, p. 233; c) N. E. Schore, *Chem. Rev.* **1988**, *88*, 1081; d) N. E. Schore, *Org. React. (N.Y.)* **1991**, *40*, 1; e) N. E. Schore in *Comprehensive Organic Synthesis, Vol. 5* (Eds.: B. M. Trost, I. Fleming), Pergamon, Oxford, **1991**, p. 1037; f) N. E. Schore in *Comprehensive Organometallic Chemistry II, Vol. 12* (Eds.: E. W. Abel, F. A. Stone, G. Wilkinson), Elsevier, New York, **1995**, p. 703; g) O. Geis, H. G. Schmalz, *Angew. Chem.* **1998**, *110*, 955; *Angew. Chem. Int. Ed.* **1998**, *37*, 911; h) S. T. Ingate, J. Marco-Contellas, *Org. Prep. Proced. Int.* **1998**, *30*, 123; i) N. Jeong in *Transition Metals in Organic Synthesis, Vol. 1* (Eds.: M. Beller, C. Bolm), Wiley-VCH, Weinheim, **1998**, p. 560; j) Y. K. Chung, *Coord. Chem. Rev.* **1999**, *188*, 297; k) K. M. Brummond, J. L. Kent, *Tetrahedron*, **2000**, *56*, 3263.
- [2] A general review on tetranuclear clusters contains many references to $[\text{Co}_4(\text{CO})_{12}]$: a) P. Chini, B. T. Heaton, *Top. Curr. Chem.* **1977**, *71*, 3; see also: b) R. D. W. Kemmitt, D. R. Russell in *Comprehensive Organometallic Chemistry, Vol. 5* (Eds.: E. W. Abel, F. A. Stone, G. Wilkinson), Pergamon, Oxford, **1982**, p. 7.
- [3] a) P. Magnus, L. M. Principe, M. J. Slater, *J. Org. Chem.* **1987**, *52*, 1483; b) V. Rautenstrauch, P. Megard, J. Conesa, W. Kuster, *Angew. Chem.*, **1990**, *102*, 1441; *Angew. Chem. Int. Ed. Engl.* **1990**, *29*, 1413.
- [4] $[\text{Co}_4(\text{CO})_{12}]$ was claimed to be inert toward enynes, thus, in the Pauson–Khand reaction. However, its reactivity with alkynes was previously documented. $[\text{Co}_4(\text{CO})_{12}]$ react with alkynes to yield $[(\text{alkyne})\text{Co}_4(\text{CO})_{10}]$ complexes. Under the normal Pauson–Khand reaction conditions, this complex might be expected to decompose to an $[(\text{alkyne})\text{Co}_2(\text{CO})_6]$ complex, a requisite initial complex for the Pauson–Khand reaction, and cobalt carbonyl fragments: a) R. S. Dickson, G. R. Tailby, *Aust. J. Chem.* **1970**, *23*, 229; b) R. S. Dickson, P. J. Fraser, *Adv. Organomet. Chem.* **1974**, *12*, 323; c) For a review on alkyne cobalt complexes, see ref. [2b], p. 192; d) V. Cadierno, M. P. Gamasa, J. Gimeno, J. M. Moreto, S. Ricart, A. Roig, E. Molins, *Organometallics* **1998**, *17*, 697.
- [5] Additives were used as co-ligands to presumably stabilize the working intermediates throughout the reaction and prevent dimerization of the active cobalt species: a) phosphite and phosphane: N. Jeong, S. H. Hwang, Y. Lee, Y. K. Chung, *J. Am. Chem. Soc.* **1994**, *116*, 3159; b) cyclohexylamine: M. E. Krafft, L. V. R. Boñaga, C. Hirose, *Tetrahedron Lett.* **1999**, *40*, 9171; see also: c) M. E. Krafft, C. Hirose, L. V. R. Boñaga, *Tetrahedron Lett.* **1999**, *40*, 9177; d) D. B. Belanger, T. Livinghouse, *Tetrahedron Lett.* **1998**, *39*, 7641; e) T. Sugihara, M. Yamada, H. Ban, M. Yamaguchi, C. Kaneko, *Angew. Chem.* **1997**, *109*, 2884; *Angew. Chem. Int. Ed. Engl.* **1997**, *36*, 2801; f) phosphane sulfide: M. Hayashi, Y. Hashimoto, Y. Yamamoto, J. Usuki, K. Saigo, *Angew. Chem.* **2000**, *112*, 645; *Angew. Chem. Int. Ed.* **2000**, *39*, 631; g) DME and water: T. Sugihara, M. Yamaguchi, *Synlett* **1998**, 1384; h) For a chiral bisphosphine, see: K. Hiroi, T. Watanabe, R. Kawagishi, I. Abe, *Tetrahedron Lett.* **2000**, *41*, 891.
- [6] B. L. Pagenkopf, T. Livinghouse, *J. Am. Chem. Soc.* **1996**, *118*, 2285.
- [7] High operating temperatures and CO pressures were envisioned to prevent the formation of inactive cobalt species or clusters and favor the regeneration of $[\text{Co}_2(\text{CO})_8]$ or active cobalt catalyst. a) No reaction proceeded under five atmosphere of CO. J. W. Kim, Y. K. Chung, *Synthesis* **1998**, 142. See also ref. [3b].
- [8] Under supercritical fluids, it was believed that the catalytic metals would be well dispersed and the chances of their aggregation would be substantially reduced: a) supercritical CO_2 : N. Jeong, S. H. Hwang, Y. W. Lee, J. S. Lim, *J. Am. Chem. Soc.* **1997**, *119*, 10 549; b) supercritical ethylene: N. Jeong, S. H. Hwang, *Angew. Chem.* **2000**, *112*, 650; *Angew. Chem. Int. Ed.* **2000**, *39*, 636.
- [9] a) N. Y. Lee, Y. K. Chung, *Tetrahedron Lett.* **1996**, *37*, 3145; see also: b) T. Rajesh, M. Periasamy, *Tetrahedron Lett.* **1998**, *39*, 117; T. Rajesh, M. Periasamy, *Organometallics* **1999**, *18*, 5709.
- [10] a) G. Bor, U. K. Dietler, *J. Organomet. Chem.* **1980**, *191*, 295; b) G. Bor, U. K. Dietler, P. Pino, A. Poe, *J. Organomet. Chem.* **1978**, *154*, 301; c) F. Ungvary, L. Marko, *J. Organomet. Chem.* **1974**, *71*, 283; d) F. Ungvary, L. Marko, *Inorg. Chim. Acta* **1970**, *4*, 324; e) M. F. Mirbach, A. Saus, A. M. Krings, M. J. Mirbach, *J. Organomet. Chem.* **1981**, *205*, 229.
- [11] a) I. U. Khand, G. R. Knox, P. L. Pauson, W. E. Watts, M. I. Foreman, *J. Chem. Soc. Perkin Trans. 1* **1973**, 977; b) I. U. Khand, G. R. Knox, P. L. Pauson, W. E. Watts, *J. Chem. Soc. Chem. Commun.* **1971**, 36; c) I. U. Khand, G. R. Knox, P. L. Pauson, W. E. Watts, *J. Chem. Soc. Perkin Trans. 1* **1973**, 975.
- [12] M. E. Krafft, L. V. R. Boñaga, *Synlett* **2000**, 959.
- [13] For a review on the utility of Lewis bases in the Pauson–Khand reaction, see: a) T. Sugihara, M. Yamaguchi, M. Nishizawa, *Rec. Res. Devel. Organomet. Chem.* **1999**, *2*, 13, and references therein; b) T. Sugihara, M. Yamaguchi, M. Nishizawa, *Rev. Heteroatom Chem.* **1999**, *21*, 179. The Lewis base character of amines is also believed to facilitate the decarbonylation step to generate a vacant site on the cobalt center and thereby speeding up the reaction. See ref. [5e].
- [14] Both $[\text{Co}_2(\text{CO})_8]$ and $[\text{Co}_4(\text{CO})_{12}]$ are known to undergo disproportionation upon reaction with Lewis bases. $[\text{Co}_2(\text{CO})_8]$: a) F. Calderazzo, R. Ercoli, G. Natta in *Organic Syntheses via Metal Carbonyls, Vol. 1* (Eds.: I. Wender, P. Pino), Interscience-Wiley, New York, **1968**, Chapter 1; b) I. Wender, H. W. Sternberg, M. Orchin, *J. Am. Chem. Soc.* **1952**, *74*, 1216; $[\text{Co}_4(\text{CO})_{12}]$: ref. [2a], p. 56. Kinetic studies on the disproportionation of $[\text{Co}_2(\text{CO})_8]$ induced by nitrogen-containing bases, such as cyclohexylamine, was also reported: c) E. Mentasti, E. Pelizzetti, R. Rossetti, P. L. Stanghellini, *Inorg. Chim. Acta* **1977**, *25*, 7; for a review on Lewis-base–metal-carbonyl complexes see: d) T. Manuel, *Adv. Organomet. Chem.* **1965**, *3*, 181.
- [15] Representative experimental procedure: In a vessel equipped with a three-way stopper and a balloon of CO, a mixture of enyne **1** (31 mg, 0.11 mmol) and $[\text{Co}_4(\text{CO})_{12}]$ (3 mg, 0.05 mmol, 5 mol %) was pumped briefly and purged three times with CO. DME (1.2 mL) and CyNH_2 (3.6 μL , 0.03 mmol, 30 mol %) in DME (1.0 mL) were added successively and the resulting deep purple solution was heated at 70 °C for 13 h. Upon completion of the reaction, the brown mixture was cooled to room temperature, diluted with 3 mL of 10 % ethyl acetate in hexanes and filtered under reduced pressure through a pad of silica gel. Subsequent removal of the solvent and purification by flash chromatography (SiO_2 , 20 % ethyl acetate in hexanes) afforded 32 mg of bicyclopentenone **11** (94 % yield) as a colorless oil. DME was purified by refluxing over sodium in a continuous still and was freshly distilled prior to use. Precautions were also taken to avoid introduction of air into the system. $[\text{Co}_2(\text{CO})_8]$ and $[\text{Co}_4(\text{CO})_{12}]$ were purchased from Strem Chemicals Boston, MA, USA and were used without purification. All reactions were performed in base-washed glassware.
- [16] References for enynes and their corresponding cycloadducts: entry 1: T. Kondo, N. Suzuki, T. Okada, T. Mitsudo, *J. Am. Chem. Soc.* **1997**, *119*, 6187; entry 2: ref. [18a]; entries 3 and 4: ref. [6]; entries 5 and 7: M. E. Krafft, A. M. Wilson, O. A. Dasse, B. Shao, Y. Y. Cheung, Z. Fu, L. V. R. Boñaga, M. K. Mollman, *J. Am. Chem. Soc.* **1996**, *118*, 6080; entry 8: S. Shambayati, W. E. Crowe, S. L. Schreiber, *Tetrahedron Lett.* **1990**, *31*, 5289; entry 9: ref. [12]; entries 6 and 10: ref. [5b]; entry 10:

- see also: P. Magnus, C. Exon, P. Albaugh-Robertson, *Tetrahedron* **1985**, *41*, 5861.
- [17] A rate-decelerating effect of DMSO was evident in the amine oxide-promoted stoichiometric Pauson–Khand reaction, presumably due to the strong coordinating ability of DMSO as a ligand: a) M. E. Krafft, I. L. Scott, R. H. Romero, S. Feibelman, C. E. Van Pelt, *J. Am. Chem. Soc.* **1993**, *115*, 7199; see also: b) K. M. Brummond, H. Wan, J. Kent, *J. Org. Chem.* **1998**, *63*, 6535. For DMSO as additive, see: c) Y. K. Chung, B. Y. Lee, N. Jeong, M. Hudecek, P. L. Pauson, *Organometallics* **1993**, *12*, 220; d) A. Stumpf, N. Jeong, H. Sunghee, *Synlett* **1997**, 205; e) N. Jeong, S. J. Lee, B. Y. Lee, Y. K. Chung, *Tetrahedron Lett.* **1993**, *34*, 4027.
- [18] Cobalt-catalyzed Pauson–Khand reactions are usually performed in DME. See refs. [5a–d, 7]. See also: a) D. B. Belanger, D. J. R. O'Mahony, T. Livinghouse, *Tetrahedron Lett.* **1998**, *39*, 7637; b) B. Y. Lee, Y. K. Chung, Y. K. Jeong, Y. Lee, S. H. Hwang, *J. Am. Chem. Soc.* **1994**, *116*, 8793. For reactions in toluene, DME is a better additive than cyclohexylamine. See: T. Sugihara, M. Yamaguchi, *Synlett* **1998**, 1384.
- [19] It was reported that under 1 atm of CO, at 53 °C a hexane solution of $[\text{Co}_4(\text{CO})_{12}]$ would be converted to a solution in which 50% of the cobalt content is present as $[\text{Co}_2(\text{CO})_8]$ ($t_{1/2} = 160$ days).^[10b]
- [20] Upon exposure to air, $[\text{Co}_4(\text{CO})_{12}]$ oxidizes to a purple Co^{II} species but this proceeds at an appreciably slower rate than $[\text{Co}_2(\text{CO})_8]$: a) ref. [2b]; b) R. B. King in *Organometallic Syntheses, Vol. 1* (Eds.: J. J. Eisch, R. B. King), Academic Press, New York, **1965**, p. 103.
- [21] T. Sugihara, M. Yamaguchi, *J. Am. Chem. Soc.* **1998**, *120*, 10782. Optimal catalysis of the methylidenetricobalt nonacarbonyl cluster was achieved in toluene at 120 °C under 7 atm of CO. It is of interest that the use of the parent cobalt cluster, $[\text{Co}_4(\text{CO})_{12}]$, was not reported in these studies.
- [22] Highly purified $[\text{Co}_2(\text{CO})_8]$ and $[\text{Co}_4(\text{CO})_{12}]$ were reported by Jeong et al. to undergo spontaneous ignition upon exposure to air; ref. [8b]. See also ref. [5b].

CLASSICS FROM WILEY-VCH



BRUNNEN TRUPP
**CLASSICS IN
HYDROCARBON
CHEMISTRY**
SYNTHESE, CONCEPTS, PERSPECTIVES
WILEY-VCH

Hopf, H.
Technical University Braunschweig, Germany
CLASSICS IN HYDROCARBON CHEMISTRY
Syntheses, Concepts, Perspectives
1999. IX, Approx 530 pages with approx 300 figures.
Softcover.
Approx DM 98.-/ £ 34.95
ISBN 3-527-29606-9
Publication date: December 1999


Carbon and Hydrogen: the two basic building blocks can be combined in a million different ways to create a plethora of fascinating organic compounds. H. Hopf presents not only the most remarkable structures and properties of hydrocarbon compounds but also illustrates how molecules such as Pagodane or Dehydrobenzene challenge the synthetic skills of every organic chemist. Graduate students and researchers alike will find this book a gold mine of useful information essential for their daily work.

Nicolaou, K. C. / Sorensen, E. J.
University of California, San Diego, USA
CLASSICS IN TOTAL SYNTHESIS
Targets, Strategies, Methods
1996. XXIII, 798 pages with 444 figures. Softcover.
DM 98.-/ £ 34.95
ISBN 3-527-29231-4

This book is a must for every synthetic chemist. With didactic skill and clarity, K. C. Nicolaou and E. Sorensen present the most remarkable and ingenious total syntheses from outstanding synthetic organic chemists.

John Wiley & Sons, Ltd. • Baffins Lane
Chichester, West Sussex
PO 19 1UD, UK
Fax: +44 (0)1243-775878

WILEY-VCH • P.O. Box 10 11 61
69451 Weinheim, Germany
Fax: +49 (0) 62 01 - 60 61 84
e-mail: sales-books@wiley-vch.de

 **WILEY-VCH**

The First Stable Diazonium Ion on Solid Support—Investigations on Stability and Usage as Linker and Scavenger in Solid-Phase Organic Synthesis**

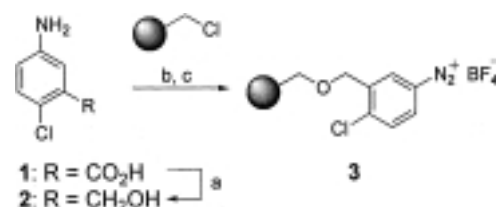
Stefan Dahmen and Stefan Bräse*

Diazonium ions represent one of the most versatile functional groups in organic chemistry.^[1, 2] The most important reactions of aromatic diazonium ions are the Sandmeyer, Schiemann, Meerwein, Pschorr, and Gomberg-Bachmann reactions, but also the Heck reaction^[3] and the formation of triazenes^[4] and azo compounds^[5] represent important processes. Diazonium ions are also of interest in theoretical chemistry. In more recent theoretical works they are considered as electron donor/acceptor complexes between a phenyl cation and a dinitrogen molecule.^[6, 7]

The property that limits the application of diazonium ions most is their lability. Aromatic diazonium ions undergo fragmentation to nitrogen and reactive phenyl intermediates. Ionic and radical pathways, initiated by single-electron transfer reactions, are known. Also our linker for secondary amines (T2)^[8] was only synthesized as an intermediate and had to be stored and handled below 0 °C to avoid decomposition. Thus, one of our aims was to develop a stable diazonium ion on solid support, to combine the broad chemical usage of diazo chemistry with the simple handling of solid-phase organic chemistry.

Most important for the stability of aromatic diazonium ions is, besides the choice of the counterion,^[9] the substitution pattern of the arene. Furthermore, the chosen arene had to be highly tolerant towards as many chemical reactions as possible. In the already mentioned theoretical studies of Glaser,^[10] and from experimental data^[11] it was shown that *p*-chloro-substituted diazonium ions are very stable. For that reason we chose 2-chloro-5-aminobenzyl alcohol (**2**) as starting material for the formation of a stable diazonium ion on solid support (Scheme 1).

The aminobenzyl alcohol **2** was synthesized in two steps from commercially available 2-chloro-5-aminobenzoic acid (**1**). Esterification with trimethylchlorosilane in methanol gave the methyl ester, which was reduced with lithium aluminum hydride (LiAlH₄) in THF to the corresponding benzyl alcohol **2**. Coupling to Merrifield resin and subsequent diazotization led to the polymer-bound diazonium ion **3**.



Scheme 1. Synthesis of the T2* linker **3**: a) 1. TMSCl in MeOH; 2. LiAlH₄, THF, 0 °C → reflux, 2 h; b) sodium hydride in DMF, 40 °C, 4 h; c) *t*BuONO, BF₃ · OEt₂ in THF, 0 °C.

The stability of diazonium ions can be increased by complexation with crown ethers;^[12] complexes with [21]crown-7 show the highest thermal stability. Therefore the polymer-bound diazonium ion **3** was treated with [18]crown-6 as well as [21]crown-7 and the resulting resins (**3** · [18]c-6 and **3** · [21]c-7, respectively) were examined by IR spectroscopy (Figure 1). The complexation by [18]crown-6 shifts the N≡N stretching vibration clearly to higher frequencies (shifts of 20–29 cm⁻¹ are mentioned in literature^[12]), whereas for complexes from [21]crown-7 only small shifts are observed (about +5 cm⁻¹ compared to the uncomplexed diazonium ion).

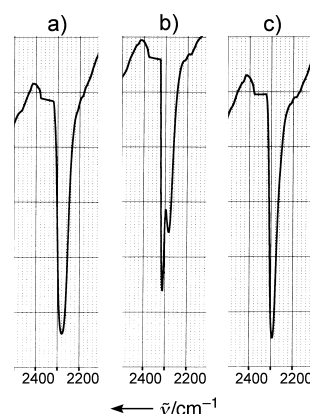


Figure 1. Part of the IR spectra of polymer-bound diazonium ions; the $\nu(\text{N}\equiv\text{N})$ bands of the uncomplexed diazonium ion (a), as well as that of partly [18]crown-6 complexed (b), and that in the [21]crown-7 complex (c) are displayed.

The stability of these resins (**3** · [18]c-6, **3** · [21]c-7) was investigated by differential scanning calorimetry (DSC) measurements (Figure 2). The corresponding diazonium ions show a high thermal stability. The rate of decomposition is only significant at temperatures higher than 90 °C. Analysis of the DSC data gave a reaction enthalpy of $\Delta_{\text{R}}H = -120 \text{ kJ mol}^{-1}$ for the fragmentation reaction, which is independent of complexation. Kinetic analysis based on DSC measurements at different heating rates gave an activation energy for the thermal decomposition of **3** of $E_{\text{a}} = 114 \text{ kJ mol}^{-1}$. The decomposition rates are consistent with a first-order reaction, which was expected by comparison with the literature.^[13]

To gain insights into the shelf life of resin **3** during normal laboratory use, decomposition studies were carried out at 60 °C, and the conversion was examined by elemental analysis

[*] Dr. S. Bräse, Dipl.-Chem. S. Dahmen
Institut für Organische Chemie der Technischen Hochschule Aachen
Professor-Pirlet-Strasse 1, 52074 Aachen (Germany)
Fax: (+49)241-8888 127
E-mail: Braese@oc.RWTH-Aachen.de

[**] Nitrogen-Based Linkers, Part 8. This work was supported by the Fonds der Chemischen Industrie (Liebig-Stipend to S.B.) and the Deutsche Forschungsgemeinschaft (BR1750-1). We thank Prof. Dr. D. Enders for the generous support of our work. The companies BASF AG, Bayer AG, Degussa-Hüls AG, and Calbiochem-Novabiochem AG are acknowledged for donations of chemicals and Grünenthal GmbH for financial support. For DSC measurements we also thank Prof. Dr. Franz-Josef Wortmann and Dr. Numan Özgün at the Deutsches Wollforschungsinstitut (DWI) at the RWTH Aachen. Part 7: M. Lormann, S. Dahmen, S. Bräse, *Tetrahedron Lett.* **2000**, 41, 3813–3816.

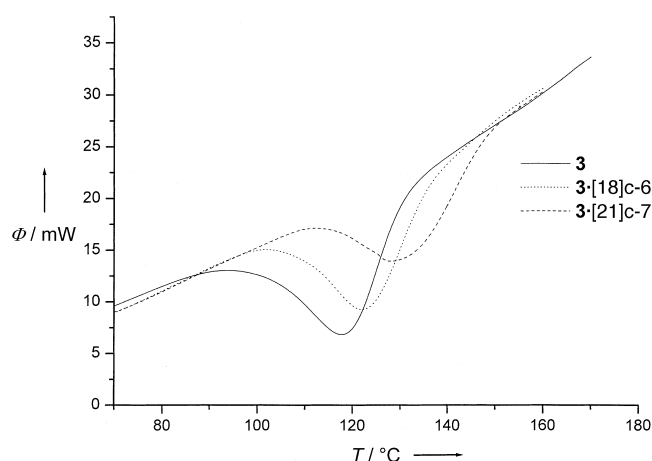
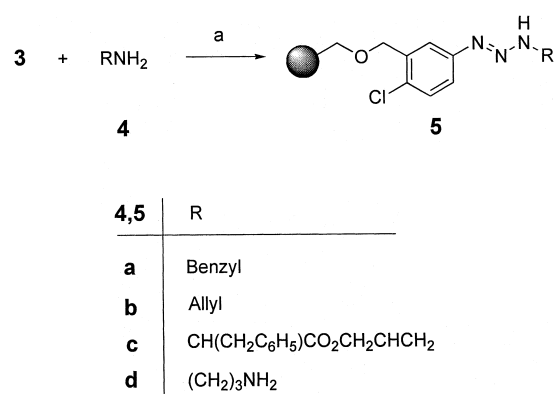


Figure 2. DSC measurements on the polymer-bound diazonium ions **3**, **3·[18]c-6**, and **3·[21]c-7**; measurements were performed with 8–12 mg resin and heating rates of 10.0 K min⁻¹.

(C₆H₅N).^[14] The experimentally determined half-life of resin **3** was eleven hours at 60 °C, which leads to a calculated half-life of 130 days at room temperature (20 °C) or 10 years for storage at 0 °C. Thus resin **3** is, to the best of our knowledge, the first, storable polymer-bound diazonium ion.

This so-called T2* linker represents an improvement of the T2 linker and can be used to immobilize and modify secondary amines on solid support.^[8] In addition it is possible to couple primary amines **4** with the diazonium resin **3** to give the corresponding polymer-bound triazenes, which can be used in further transformations (Scheme 2). In this case the use of a polymer-bound system enables the clean synthesis of 1,3-disubstituted triazenes **5**, while suppressing the formation of pentazenes, which is a competing reaction in the analogous liquid-phase synthesis.^[1]

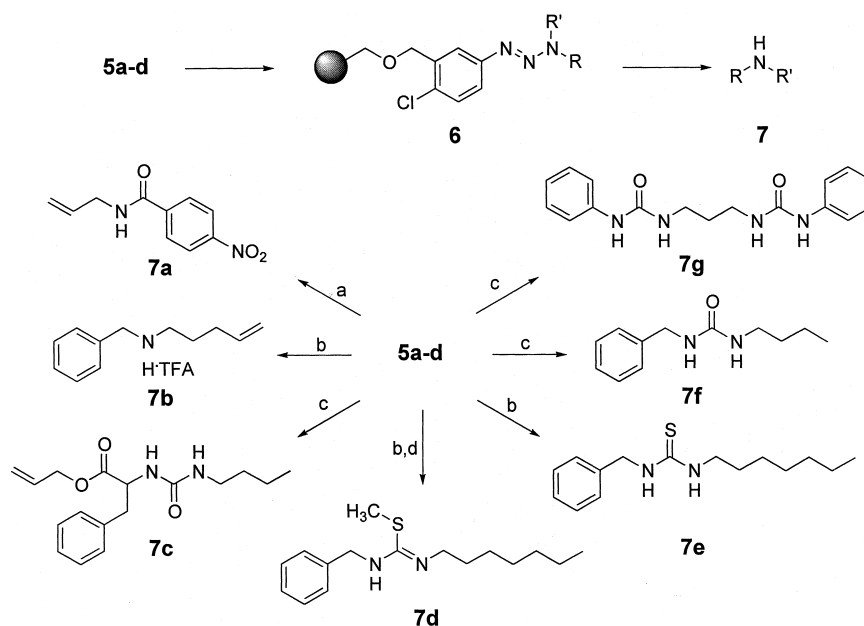
The synthesized 1,3-disubstituted triazenes **5** have successfully been applied in various reactions. Alkylation with alkyl bromides or acylation of the triazenes **5a–d** with carboxylic acid chlorides, isocyanates, and isothiocyanates were successfully carried out under mild conditions, and gave rise to the trisubstituted triazenes **6** in quantitative yields. The reaction is regioselective at the N3-nitrogen atom of the triazene group. The alkylation of the polymer-bound thiourea **6e** was performed, without affecting the triazene group. Cleavage of the products was conducted by using a solution of trifluoroacetic acid (TFA; 5%) in dichloromethane. In Scheme 3 some of the possible functionalizations of the T2* linker are summarized. With the possibility of attachment and subsequent acylation of primary amines, this linker represents a new BAL concept (backbone amide linker).^[15]



Scheme 2. Attachment of amines to the T2* linker. a) Amine **4** (2–5 equiv) in THF, 30 min, 0 °C.

Owing to the constantly increasing application of combinatorial chemistry in liquid phase, the use of scavenger resins has become more and more important.^[16, 17] In many cases the application of scavenger resins avoids complicated workup procedures to remove by-products or excess reagents and makes an efficient high-throughput synthesis possible. The temperature stability of the T2* linker should enable its application as a scavenger for the removal of amines, anilines, and phenols under formation of triazenes or azo compounds.

The ionic nature of diazonium ions requires the addition of bases to remove tetrafluoroboric acid from the reaction equilibrium, which is generated by reaction with nucleophiles. Tertiary amines are not suitable, because they may cause a spontaneous decomposition of diazonium ions. On the other



Scheme 3. The T2* resin as a linker in the synthesis of amine derivatives. a) Carboxylic acid chloride (1.5–2 equiv), pyridine, DMF, room temperature, 2 h; b) sodium hydride, DMF, electrophile (2–5 equiv), room temperature, 2 h; c) isocyanate (1.5–2 equiv), DMF, room temperature, 2 h; d) MeI, THF, room temperature, 30 min. Cleavage was conducted with 5% TFA in dichloromethane, room temperature, 5 min. The overall yield for attachment, modification, and cleavage of the amines was between 20 and 100%, generally greater than 80%, where the yields refer to the theoretically possible loading of the resin given by the starting material. Attachment of the linker and diazotation are considered as quantitative reactions, which was also confirmed by elemental analysis. After cleavage all products were obtained in > 95% purity, as determined by integration of the ¹H NMR signals and by HPLC analysis.

hand addition of insoluble bases (e.g. K_2CO_3 or KOH) or polymer-bound tertiary amines appears appropriate as these reagents undergo no side reactions with diazonium ions and are easily separated from the reaction mixture by filtration.

Scheme 4 shows that primary and secondary amines can be removed quantitatively from solution. Anilines and phenols are removed in high yields, as long as they are not too electron poor and therefore are not sufficiently nucleophilic. Nevertheless nearly all phenols could be removed by using the T2* resin upon deprotonation of the phenol, but this procedure requires strong bases like KOH or NaH, and therefore makes aqueous workup necessary. However phenols, which react only with very electrophilic diazonium ions (e.g. 2,6-di-*tert*-butylphenol) could not be removed.

In summary, immobilized diazonium ions can have a high stability, which enables their application as linkers and scavengers in solid-phase organic chemistry. They could, for example, be used as backbone amide linkers in peptide chemistry, or for the immobilization of carbon nucleophiles such as malonic acid esters or silylenol ethers. Furthermore they are easy to handle, both in terms of stability and toxicity of the compounds. Thus triazenes, which are formed upon reaction with amines and which are considered as carcinogens, can be easily and safely handled.

Experimental Section

All resins were characterized by IR spectroscopy, and loadings and conversions were evaluated by elemental analysis (C,H,N). Typical loadings of the used chloromethylpolystyrene were between 0.6 and 1.4 mmol g⁻¹. Chloromethylpolystyrene (Merrifield resin) was obtained from Calbiochem-Novabiochem or Polymer Laboratories. The T2* resin is

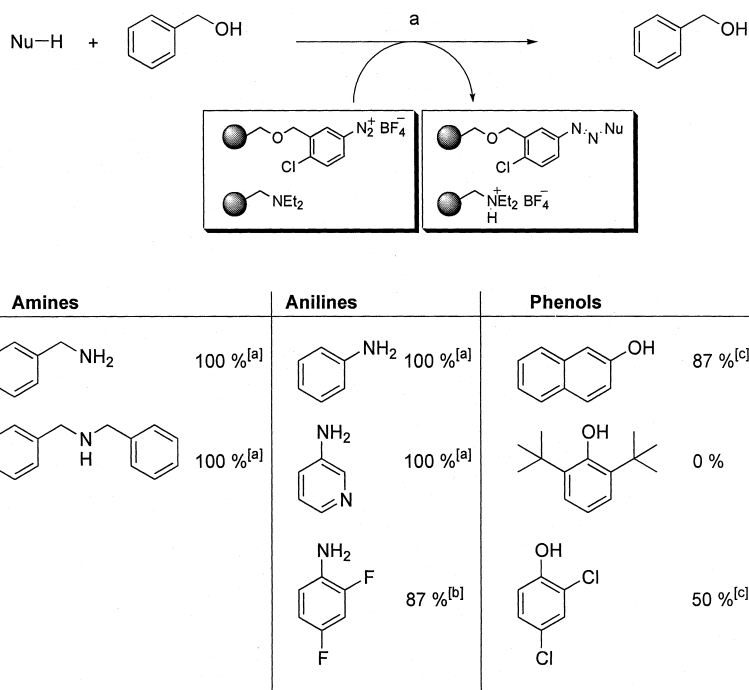
available from Calbiochem-Novabiochem. All new compounds were fully characterized or compared to known substances.

The DSC measurements were carried out on a Perkin Elmer DSC 7 with a polymer-bound diazonium ion with a loading of 1.0 mmol g⁻¹. The DSC analysis of the used chloromethylpolystyrene starting material resulted in an endothermic melting enthalpy of 2.6 J per gram resin at the melting point of 118 °C. The melting point lies in the region of the exothermal decomposition of the diazonium ions, but the melting enthalpy is about 50 times smaller. As the tolerance of the method is about 10%, the melting enthalpy was not taken into account for the examination of the reaction enthalpy.

Typical procedure for the attachment of amines to the T2* resin: Resin **3** (5.0 g, 5.5 mmol, loading 1.1 mmol g⁻¹) was suspended in THF (50 mL) and cooled to 0 °C. Benzylamine (3.0 mL, 5 equiv, 27.5 mmol) was added slowly under careful stirring. After 1 h, the resin was filtered, washed alternately with THF and MeOH, and dried in high vacuum.

Typical procedure to remove nucleophiles with the T2* resin and diethylaminomethylpolystyrene: Resin **3** (100 mg, 0.11 mmol, loading 1.1 mmol g⁻¹) and diethylaminomethylpolystyrene (50 mg, 0.116 mmol, loading 2.33 mmol g⁻¹) were weighed into a reaction vessel. Then, 2 mL of an equimolar solution of nucleophile (0.05 mmol) and benzyl alcohol (0.05 mmol) as an internal reference in THF were added, the reaction vessel was closed and agitated for 1 h using a shaker. The resin was filtered off and the eluate was analyzed by gas chromatography.

Received: May 3, 2000 [Z15072]



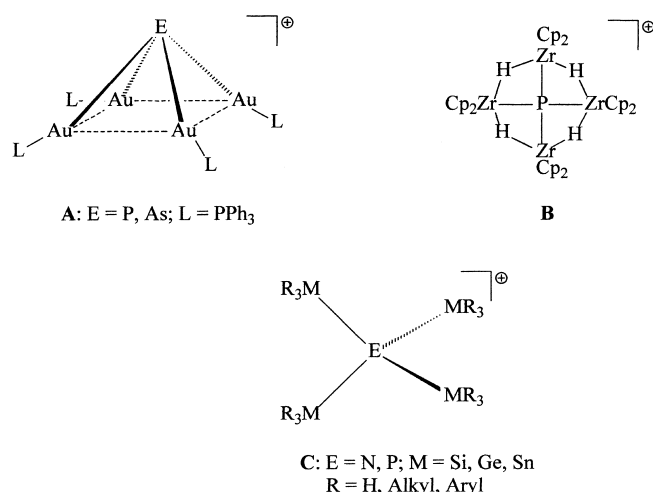
Scheme 4. The T2* resin as a scavenger for amines, anilines, and phenols. The percentage of removed nucleophile is given. Benzyl alcohol was used as an internal standard. a) Resin **3** (2 equiv), base in THF, 1 h. Filtration of the resin and analysis of the filtrate by gas chromatography. [a] Base: diethylaminomethylpolystyrene (2 equiv, loading 2.33 mmol g⁻¹). [b] Base: a basic ion-exchange resin (Merck Lewatit MP 5080). [c] Base: finely powdered potassium hydroxide (4–5 equiv).

- [1] H. Zollinger, *Diazo Chemistry*, Vol. 1, VCH, Weinheim **1994**.
- [2] D. S. Wulfman in *The Chemistry of Diazonium and Diazo Groups*, Vol. 1 (Ed.: S. Patai), Wiley, New York **1978**, pp. 247–339.
- [3] S. Bräse, A. de Meijere in *Metal-catalyzed Cross-coupling Reactions* (Eds.: F. Diederich, P. J. Stang), Wiley-VCH, Weinheim, **1998**, p. 112.
- [4] A. Engel, *Methoden Org. Chem. (Houben-Weyl)* 4th ed. 1952–, Vol. E 16a/2, **1990**, pp. 1182–1226.
- [5] *The chemistry of the hydrazo, azo and azoxy groups*, Vol. 1 + 2 (Ed.: S. Patai), Wiley, New York, **1975**.
- [6] R. Glaser, J. Horan, *J. Org. Chem.* **1995**, 60, 7518–7528.
- [7] R. Glaser, J. Horan, H. Zollinger, *Angew. Chem.* **1997**, 109, 2324–2328; *Angew. Chem. Int. Ed. Engl.* **1997**, 36, 2210–2213.
- [8] S. Bräse, J. Köbberling, D. Enders, M. Wang, R. Lazny, S. Brandtner, *Tetrahedron Lett.* **1999**, 40, 2105–2108.
- [9] C. Colas, M. Goeldner, *Eur. J. Org. Chem.* **1999**, 1357–1366.
- [10] R. Glaser, C. J. Horan, M. Lewis, H. Zollinger, *J. Org. Chem.* **1999**, 64, 902–913.
- [11] C. G. Swain, J. E. Sheats, K. G. Harbison, *J. Am. Chem. Soc.* **1975**, 97, 783–790.
- [12] R. A. Bartsch in *Crown ethers and analogs* (Eds.: S. Patai, Z. Rappoport), Wiley, Chichester, **1989**, p. 505–517. Although a high excess of the crown ether was used, the polymer-bound diazonium salts could not be transformed into their [18]crown-6 complexes quantitatively, because the complexation constants are smaller than in the case of the corresponding [21]crown-7 complexes. Therefore it is possible that [18]crown-6 was partly washed off the resin during workup.
- [13] M. L. Crossley, R. H. Kienle, C. H. Benbrook, *J. Am. Chem. Soc.* **1940**, 62, 1400–1403. Usually an S_N1-type mechanism is considered, although there are indications for an S_NAr-type mechanism in the presence of nucleophiles.
- [14] Experimentally examined loading of the resins correlate well with the results from CHN combustion analysis.
- [15] K. J. Jensen, J. Alsina, M. F. Songster, J. Vagner, F. Albericio, G. Barany, *J. Am. Chem. Soc.* **1998**, 120, 5441–5452.
- [16] D. L. Flynn, R. V. Devraj, J. J. Parlow in *Solid-Phase Organic Synthesis* (Ed.: K. Burgess), Wiley, New York, **2000**, pp. 149–194.
- [17] V. Austel in *Combinatorial Chemistry* (Ed.: G. Jung), Wiley-VCH, Weinheim, **1999**, pp. 77–123.

Perstannylated Ammonium and Phosphonium Ions: Organometallic Onium Ions That Are also Base-Stabilized Stannylum Ions**

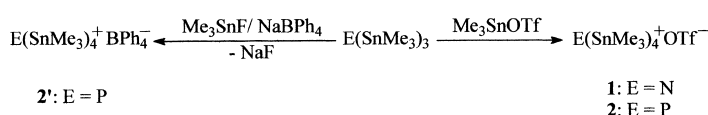
Matthias Driess,* Christian Monsé, Klaus Merz und Christoph van Wüllen

Among the four-coordinate onium ions of Group 15 elements (N, P, As, Sb, and Bi) the derivatives with organometallic substituents are a special case.^[1] In fact, only a few discrete tetra-metal ammonium, phosphonium, and arsonium ions of the form $[EL_4]^+$ (L = metal or metalloid; E = N, P, As) have been described. For transition metal derivatives the initial work of Schmidbaur et al. on the tetrahedral tetraaurated ammonium ion $[(Ph_3P)Au]_4N^+$ and the phosphorus and the arsenic analogues $[(Ph_3P)Au]_4E^+$ (E = P, As) **A** that have a nonclassical quadratic-pyramidal structure, in which the P and As atoms are found at the apex of the pyramid, have attracted considerable attention.^[2] Recently we reported the first planar tetracoordinate phosphonium ion $[(C_5H_5)_2(H)Zr]_4P^+$ **B** (Cp = C₅H₅), which has an “anti-van’t-Hoff-Le-Be” configuration caused mainly by the strong π -acceptor character of the Zr center.^[3]



In contrast permetalated ammonium and phosphonium ions with main group element substituents are so far unknown. Noteworthy is that even the apparently simple tetrasilyl, tetragermyl, or tetrastannyl derivatives of the form $[(R_3M)_4E]^+$ (R = H, alkyl, aryl; M = Si, Ge, Sn; E = N, P) **C**

have eluded unequivocal characterization.^[4,5] Herein we demonstrate that the high lability of these onium ions is based on a tug-of-war between $(R_3M)_3E$, the anion, and solvent molecules as Lewis bases on one side and the Me_3M^+ ion on the other, in which the presence of sufficient weakly coordinating anions and solvent molecules favors the formation of the onium ion. With the synthesis of the partially silylated ammonium ion $[(Me_3Si)_2NH_2]^+$, the unusual solid-state polymer $BaYbSi_4N_7$, which contains linked Si₄N tetrahedra, and other related partially stannylated complexes Schnick et al. and Dehnicke et al. have made exceptional advances;^[6–8] in this context the recently synthesized cubic Si₃N₄ species is also worth mentioning.^[7b] Herein we report the surprisingly simple synthesis of the first tetrakis(trimethylstannyl)ammonium and -phosphonium cations **1** and **2**, respectively, that dissociate slightly in solution and thus represent masked Me_3Sn^+ ions. The triflate salts of **1** and **2** are isolated as colorless crystals from the reaction of $(Me_3Sn)_3E$ (E = N, P) with the strong Lewis acid Me_3SnOTf (OTf = OSO₂CF₃) in toluene in 50 and 82 % yield, respectively.



The ammonium salt **1** crystallized in the trigonal space group R3; only three of the Me_3Sn groups per cation interact weakly with an oxygen atom from one of three OTf anions (Figure 1).^[9] The Sn...O interaction (3.07 Å)^[10] results in a

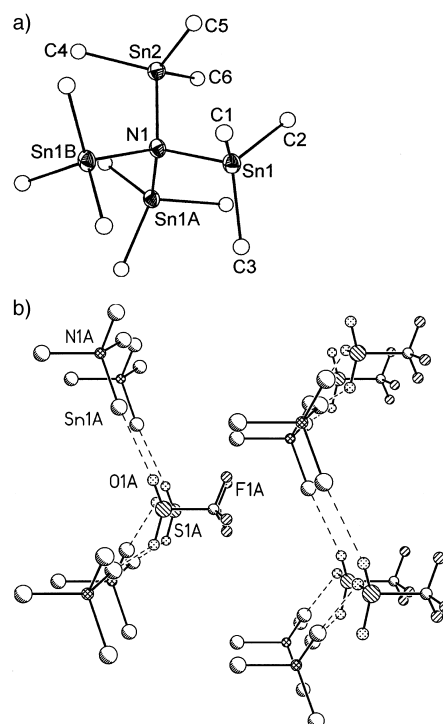


Figure 1. a) Molecular structure of the $[N(SnMe_3)_4]^+$ ion in **1**. Selected bond lengths [Å] and angles [°]: Sn1–N1 2.178(5), Sn2–N1 2.177(5), Sn1–C1 2.120(11), Sn1–C2 2.137(11), Sn1–C3 2.159(12); C1–Sn1–C2 113.1(5), Sn1–N1–Sn2 108.6(4), Sn1A–N1–Sn1 110.3(4), $\Sigma(C-Sn1-C)$ 340.1. b) Crystal packing diagram of **1**. For clarity the Me groups of the Sn atoms are not shown.

[*] Prof. Dr. M. Driess, Dr. C. Monsé, Dr. K. Merz
Lehrstuhl für Anorganische Chemie I
Molekül- und Koordinationschemie
Ruhr-Universität Bochum
Universitätsstrasse 150, 44801 Bochum (Germany)
Fax: (+49)234-32-14378
E-mail: Matthias.Driess@AC1.ruhr-uni-bochum.de

Priv.-Doz. Dr. C. van Wüllen
Lehrstuhl für Theoretische Chemie der Ruhr-Universität Bochum
Universitätsstrasse 150, 44801 Bochum (Germany)

[**] This work was supported by the Deutsche Forschungsgemeinschaft, the Ministerium für Schule, Weiterbildung und Forschung des Landes Nordrhein-Westfalen und by the Fonds der Chemischen Industrie.

strongly distorted trigonal-bipyramidal coordination at the Sn center (sum of the C–Sn–C bond angles 340.1°), whereas the Sn atom normally has a perfect tetrahedral coordination geometry.

The N atom has an almost perfect tetrahedral coordination sphere (108.6 and 110.3(4)°, respectively); however, the average Sn–N bond length (2.178(5) Å) is about 7% longer than the Sn–N bond in (Me₃Sn)₃N (2.038 Å).^[11] Similar Sn–N bond lengths are found in the ions [(Me₃Sn)₂NH₂]⁺ (av. 2.171(9) Å) and [(Me₃Sn)₃NH]⁺ (2.168(3) Å),^[8] which clearly indicates that steric effects play only a subordinate role. This idea is supported by density functional calculations (DFT) on EL₃ and [EL₄]⁺ (E = N, P; L = silyl, stannyl) which show that in going from NL₃ to [NL₄]⁺ the M–N bonds (M = Si, Sn) become significantly longer than the corresponding M–P bonds in the phosphorus analogues (Table 1).^[12]

Table 1. DFT-calculated N–L and P–L bond lengths [Å] (experimental values in parentheses).^[12]

L	<i>r</i> (NL ₃)	<i>r</i> ([NL ₄] ⁺)	<i>r</i> (PL ₃)	<i>r</i> ([PL ₄] ⁺)
SiH ₃	1.769	1.891	2.280	2.318
SiMe ₃	1.794	1.948	2.293 (2.244) ^[c]	2.357
SnH ₃	2.065	2.200	2.559	2.600
SnMe ₃	2.083 (2.036) ^[a]	2.232 (2.178) ^[b]	2.567	2.623 (2.547) ^[d]

[a] See reference [11]. [b] See Figure 1. [c] See reference [15]. [d] See Figure 2.

The increase in the M–N bond lengths in the ammonium system (M = Si 7–8%, M = Sn 6–7%) can be explained most simply in ionic models through electrostatic repulsion between the four strongly electropositive R₃M groups. This repulsion arises through the electronegativity differences in the Si/N and Sn/N pairs. In agreement with this explanation the natural bond orbital (NBO) analysis of [E(MMe₃)₄]⁺ (E = N, P; M = Si and Sn) shows that the Si and Sn atoms in the ammonium ions have an approximately 20% greater partial charge than in the phosphonium ions.^[11] As a result of its significantly less polar Sn–P bonds the [P(SnMe₃)₄]⁺ ion in **2** has an Sn–P bond length (2.547(1) Å) similar to that in stannylphosphanes (ca. 2.52 Å).^[13] Compound **2** crystallizes in the tetragonal space group *P4/nmm*, which implies that there is one Sn...O interaction per Me₃Sn group of the cation (Figure 2).^[9] Thus as in **1** the Sn atoms have a strongly distorted trigonal-bipyramidal coordination (Sn...O 3.12 Å, sum of the C–Sn–C bond angles 342°). The perfectly tetrahedral Sn₄P framework is not disordered, unlike the methyl groups attached to the Sn atoms and also the O and F atoms of the OTf anions.

Like **1**, compound **2** is only soluble enough for room-temperature multinuclear NMR experiments in polar solvents such as THF. The ¹H and ³¹P NMR spectra of **1** and **2** each show only one broad signal, without Sn satellites, at δ = 0.43 and –325, respectively. Correspondingly the ¹¹⁹Sn NMR spectra does not show the expected doublets but a broad signal at δ = 37.6 (ν_{1/2} = 430 Hz); the position of this signal indicates a five-coordinate base-stabilized stannylum ion.^[14]

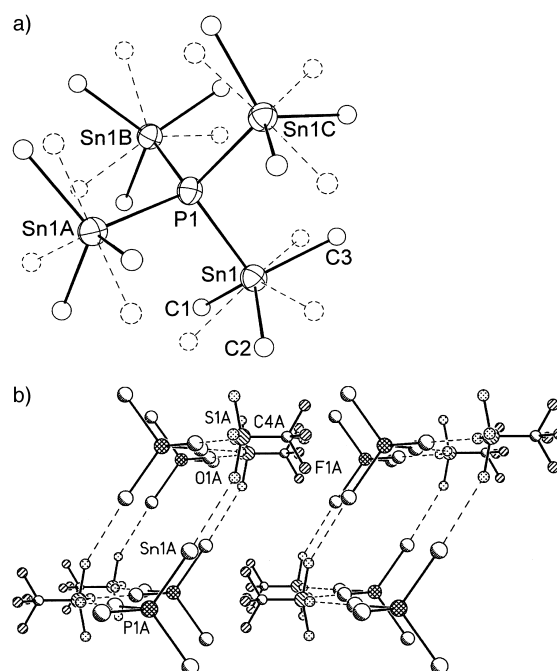


Figure 2. a) Molecular structure of the [P(SnMe₃)₄]⁺ ion in **2**. The Me groups are to 50% disordered. Selected bond lengths [Å] and angles [°]: Sn1–P1 2.547(1), Sn1–C1 2.11(2), Sn1–C2 2.13(2), Sn1–C3 2.13(2); Sn1–P1–Sn2 108.80(2), Sn1B–P1–Sn1 110.81(5), Σ(C–Sn1–C) 342(2). b) Crystal packing diagram of **2**. For clarity the Me groups of the Sn atoms are not shown. In contrast to the cation the CF₃ and SO₃ groups of the OTf anion are rotation disordered about a fourfold axis.

When “free” (Me₃Sn)₃P (³¹P NMR (25 °C): δ = –328.0) is added to the THF solution there is no change in the multinuclear NMR spectra. This observation can only be explained by dissociation and a rapid exchange of Me₃Sn⁺ on the NMR time scale. The BPh₄ salt **2'**, is more soluble in THF (to –25 °C) and can be prepared from the reaction of (Me₃Sn)₃P with Me₃SnF in the presence of NaBPh₄ in THF. The salt **2'**, shows the same NMR behavior as **2**, which implies that the influence of the anion on the dynamics is low. However, below –10 °C an additional sharp singlet appears at δ = –314.0 and has a complicated Sn satellite multiplet. This singlet is not assigned to the intact [(Me₃Sn)₄P]⁺ ion but to a “frozen” cation–THF complex of a Me₃Sn⁺ ion that is simultaneously base stabilized from (Me₃Sn)₃P and THF. Noteworthy is that the nucleophilicity of E(SiMe₃)₃ (E = N, P) in hexane is not sufficient compared to that of Me₃SiOTf to form the corresponding onium salts. In contrast the reaction of E(SnMe₃)₃ (E = N, P) with Me₃SiOTf leads by metathesis reactions (depending upon molar ratios) to mixed amines and phosphanes, respectively, or to **1** and **2**. By using electrophilic silylation reagents that are stronger than Me₃SiOTf^[16] in nonpolar solvents it should be possible to isolate discrete tetrasilyl-substituted ammonium and phosphonium ions.

Experimental Section

1: A solution of Me₃SnOTf (0.71 g, 2.27 mmol) in toluene (20 mL) was added to a solution of (Me₃Sn)₃N (1.16 g, 2.29 mmol) at room temperature. The precipitate was recrystallized from THF and afforded cubic crystals that were insoluble in nonpolar solvents, and were sensitive to air and hydrolysis (0.93 g, 1.14 mmol, 50%). Elemental analysis calcd for

$C_{13}H_{36}F_3O_3PSSn_4$ (817.8) (%): C 19.1, H 4.4, N 1.7; found: C 19.2, H 4.2, N 1.4. The mass spectrum showed only signals from fragments of the Me_3Sn group; 1H NMR ($[D_8]THF$, 28 °C): $\delta = 0.36$ (s, $w_{1/2} = 75$ Hz); $^{13}C\{^1H\}$ NMR ($[D_8]THF$, 28 °C): $\delta = -1.3$ (s, $w_{1/2} = 40$ Hz); $^{119}Sn\{^1H\}$ NMR ($[D_8]THF$, 25 °C): $\delta = 88.5$ (s, $w_{1/2} = 430$ Hz); ^{19}F NMR ($[D_8]THF$, 28 °C): $\delta = -79.6$ (s).

2: (Me_3Sn)₃P (1.29 g, 2.47 mmol) was slowly added dropwise to a solution of Me_3SnOTf (0.77 g, 2.46 mmol) in toluene (ca. 20 mL) at room temperature. A colorless precipitate formed immediately and was crystallized from THF (ca. 10 mL) by cooling. This afforded cubic colorless crystals of **2** which were sparingly soluble in THF, insoluble in nonpolar solvents, and completely stable in air and towards hydrolysis (1.69 g, 2.02 mmol, 82 %). Elemental analysis calcd for $C_{13}H_{36}F_3O_3PSSn_4$ (834.8) (%): C 18.7, H 4.3; found: C 18.7, H 4.2. The mass spectrometric investigations (EI) gave signals corresponding to the cleavage of (Me_3Sn)₃P and (Me_3Sn)₂PH; 1H NMR: $\delta = 0.43$ (s, $w_{1/2} = 7$ Hz); ^{31}P NMR: $\delta = -325.5$ (s, $w_{1/2} = 50$ Hz); $^{13}C\{^1H\}$ NMR: $\delta = -3.3$ (s), CF_3 signal not observed; $^{119}Sn\{^1H\}$ NMR: $\delta = 37.6$ (s, $w_{1/2} = 430$ Hz); ^{19}F NMR: $\delta = -79.5$ (s).

2': A solution of $NaBPh_4$ (2.01 g, 5.88 mmol) in THF (ca. 10 mL) was added to a suspension of Me_3SnF (1.16 g, 6.35 mmol) and (Me_3Sn)₃P (3.37 g, 6.45 mmol) in THF (ca. 20 mL) at room temperature. The mixture was stirred for 24 h at 45 °C. The solution was separated by centrifugation from the NaF formed and the solvent removed under vacuum. The resulting powder was crystallized from a small amount of THF to give compound **2** which is very soluble in THF and only slightly air and moisture sensitive (3.29 g, 3.27 mmol, 56 %). Elemental analysis calcd for $C_{36}H_{56}BPSn_4$ (1004.6) (%): C 43.0, H 5.6; found: C 42.8, H 5.3; 1H NMR ($[D_8]THF$): $\delta = 7.35$ (m, 8H, *o*-CH), 6.94 (pseudo-t, $^3J(H,H) = 7.2$ Hz, 8H, *m*-CH), 6.80 (m, 4H, *p*-CH), 0.40 (s, $w_{1/2} = 4$ Hz, 36H); ^{31}P NMR ($[D_8]THF$): $\delta = -323.6$ (s, $w_{1/2} = 90$ Hz); $^{13}C\{^1H\}$ NMR ($[D_8]THF$): $\delta = 164.3$ (q, C(1), $^1J(C,B) = 49.4$ Hz), 136.6 (q, C(3), $^3J(C,B) = 1.2$ Hz), 125.1 (q, C(2), $^2J(C,B) = 3.0$ Hz), 121.3 (s, C(4)), -4.2 (s, $w_{1/2} = 11$ Hz); $^{119}Sn\{^1H\}$ NMR ($[D_8]THF$): $\delta = 38.4$ (s, $w_{1/2} = 180$ Hz).

Received June 2, 2000 [Z15207]

- [1] G. A. Olah, K. K. Laali, Q. Wang, G. K. S. Prakash, *Onium Ions*, Wiley, New York, 1998.
- [2] a) E. Zeller, H. Beruda, A. Kolb, P. Bissinger, J. Riede, H. Schmidbaur, *Nature* **1991**, 352, 141; b) A. Schier, A. Grohmann, J. M. López-de-Luzuriaga, H. Schmidbaur, *Inorg. Chem.* **2000**, 39, 547.
- [3] M. Driess, J. Aust, K. Merz, C. van Wüllen, *Angew. Chem.* **1999**, 111, 3967; *Angew. Chem. Int. Ed.* **1999**, 38, 3677.
- [4] The $[(H_3Si)_4P]^+$ ion was reported but definitive proof of its structure has not yet been made: B. J. Aylett, H. J. Emeléus, A. G. Maddock, *J. Inorg. Nucl. Chem.* **1955**, 1, 187.
- [5] N. Wiberg, K. H. Schmid, *Z. Anorg. Allg. Chem.* **1966**, 345, 93; U. Wannagat, *Fortschr. Chem. Forsch.* **1967**, 9, 102; *Gmelin Handbuch der Anorganischen Chemie*, Vol. B4, Springer, Berlin, **1989**, p. 78.
- [6] R. Bettenhausen, W. Milius, W. Schnick, *Chem. Eur. J.* **1997**, 3, 1337.
- [7] a) H. Huppertz, W. Schnick, *Angew. Chem.* **1996**, 108, 2115; *Angew. Chem. Int. Ed. Engl.* **1996**, 35, 1983; b) A. Zerr, G. Miehe, G. Serghiou, M. Schwarz, E. Kroke, R. Riedel, H. Fueb, P. Kroll, R. Boehler, *Nature* **1999**, 400, 340.
- [8] R. Hillwig, K. Harms, K. Dehnicke, U. Müller, *Z. Anorg. Allg. Chem.* **1997**, 623, 676.
- [9] **1:** Trigonal, space group $R\bar{3}$, $a = b = 10.0939(1)$, $c = 21.655(4)$ Å, $Z = 3$, $V = 1910.7(5)$ Å³, 1064 independent reflections ($I > 2\sigma(I)$), $R1 = 0.0332$ (observed reflections), $wR2 = 0.0895$ (all data). **2:** Tetragonal, space group $P4/nmm$, $a = b = 12.4613(19)$, $c = 8.885(2)$ Å, $Z = 2$, $V = 1379.7(4)$ Å³, 658 independent reflections ($I > 2\sigma(I)$), $R1 = 0.0631$ (observed reflections), $wR2 = 0.1693$ (all data). Intensity data was collected with a Bruker-AXS-SMART diffractometer (MoK_{α} radiation, $\lambda = 0.71073$ Å, ω -Scan, $T = 203$ K). The structure was solved by direct methods (SHELXL97), the refinement against F^2 was with all the measured reflections (SHELXL97). The non-hydrogen atoms were refined anisotropically and the H atoms isotropically. The methyl groups in the $[P(SnMe_3)_4]^+$ ion of **2** are disordered, with an occupancy of 0.5, while the triflate anion is rotation disordered about a fourfold axis. Crystallographic data (excluding structure factors) for the structures reported in this paper have been deposited with the

Cambridge Crystallographic Data Centre as supplementary publication nos. CCDC-145133 (**1**) and CCDC-145132 (**2**). Copies of the data can be obtained free of charge on application to CCDC, 12 Union Road, Cambridge CB21EZ, UK (fax: (+44) 1223-336-033; e-mail: deposit@ccdc.cam.ac.uk).

- [10] The Sn–O bond lengths in Me_3SnOTf , which forms a polymer chain with trigonal-bipyramidal coordinated Sn atoms, are 2.34–2.37 Å: M. Driess, C. Monsé, K. Merz, unpublished results; synthesis of Me_3SnOTf : H. W. Roesky, H. Wier, *Chem. Ber.* **1971**, 104, 2258.
- [11] A. Appel, C. Kober, C. Neumann, H. Nöth, M. Schmidt, W. Storch, *Chem. Ber.* **1996**, 129, 175.
- [12] a) DFT calculations with the BP86-functional: A. B. Becke, *Phys. Rev. A* **1988**, 38, 3098; J. P. Perdew, *J. Chem. Phys.* **1994**, 100, 5829; quasi relativistic pseudo-potential at Sn with TZVP basis sets: A. Schäfer, C. Huber, R. Ahlrichs, *J. Chem. Phys.* **1994**, 100, 5829; Program system TURBOMOLE; b) NBO analysis (same functional, same basis set) with the program suit Gaussian 98.
- [13] D. Bongert, H. D. Hausen, W. Schwarz, G. Heckmann, H. Binder, *Z. Anorg. Allg. Chem.* **1996**, 622, 1167, and references therein.
- [14] J. B. Lambert, B. Kuhlmann, *J. Chem. Soc. Chem. Commun.* **1992**, 931, and references therein.
- [15] G. A. Forsyth, D. W. H. Rankin, H. E. Robertson, *J. Mol. Struct.* **1990**, 239, 209.
- [16] J. B. Lambert, L. Kania, S. Zhang, *Chem. Rev.* **1995**, 95, 1191.

New and Facile Entry to Nitrilium Phosphane Ylide Complex Chemistry by Using 7-Phosphanorbornadiene Complexes**

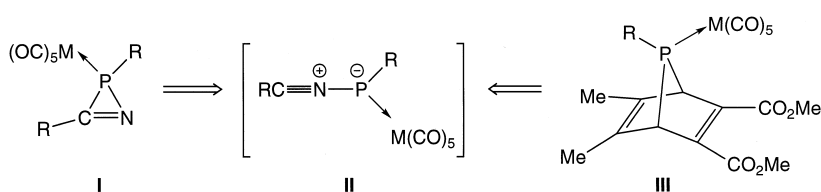
Rainer Streubel,* Udo Schiemann, Peter G. Jones, Ngoc Hoa Tran Huy, and François Mathey*

Dedicated to Professor Heinrich Vahrenkamp on the occasion of his 60th birthday

It is known that nitrilium phosphane ylide complexes **II** can be efficiently generated by thermally^[1] or photochemically^[2] induced ring opening of 2*H*-azaphosphirene complexes **I** (Scheme 1) and subsequently trapped by electronically activated π systems such as alkynes,^[3] nitriles,^[4] or phosphalkynes,^[5] thus providing access to a variety of new unsaturated N,P-heterocyclic ring systems. To develop the synthetic potential of this methodology, it was necessary to find a novel access to nitrilium phosphane ylide complexes **II**, thus providing N,P-heterocycles with more ubiquitous substituents

- [*] Priv.-Doz. Dr. R. Streubel, Dipl.-Chem. U. Schiemann, Prof. Dr. P. G. Jones
Institut für Anorganische und Analytische Chemie der Technischen Universität Braunschweig
Postfach 3329, 38023 Braunschweig (Germany)
Fax: (+49) 531-391-5387
E-mail: r.streubel@tu-bs.de
- Prof. Dr. F. Mathey, Dr. N. H. Tran Huy
Laboratoire Hétéroéléments et Coordination
UMR 7653 CNRS, DCPH, Ecole Polytechnique
91128 Palaiseau Cedex (France)
Fax: (+33) 169-33-39-90
E-mail: francoismathey@polytechnique.fr

[**] This work was supported by the Deutsche Forschungsgemeinschaft and the Fonds der Chemischen Industrie. We are grateful to Andreas Weinkauff for the X-ray structure data measurement.



Scheme 1. 2H-azaphosphirene **I** and 7-phosphanorbornadiene complexes **III** as synthons for the generation of transient nitrilium phosphane ylide complexes **II** (R = alkyl, aryl; [M] = metal complex fragment).

at phosphorus such as methyl, phenyl, or even functional groups. Although it is now well established that 7-phosphanorbornadiene complexes **III** serve as efficient precursors for transient terminal phosphanediyl complexes and react with a wide variety of π systems,^[6] giving cycloaddition products in most cases, no reactions of derivatives of **III** with nitriles have been reported. Nevertheless, there is also evidence for the transient formation of 1,3-dipole systems such as phosphacarbonyl ylide complexes in reactions of complexes of type **III** with carbonyl compounds.^[7–9]

Here we report the synthesis of *P*-methyl- and *P*-phenyl-substituted 2H-1,2-azaphosphole complexes using three-component reaction conditions and 7-phosphanorbornadiene complexes, 1-piperidinonitrile, and dimethylacetylenedicarboxylate (DMAD) as components, as well as the structure of a *P*-methyl-substituted 2H-1,2-azaphosphole complex.

The thermal decomposition of 7-phosphanorbornadiene complexes **1a,b**,^[10] 1-piperidinonitrile, and DMAD in toluene at 120 °C yielded selectively the 2H-1,2-azaphosphole complexes **5a,b** as main products (crude product yields > 80 %) (Scheme 2); two by-products ($\leq 5\%$) were detected by ^{31}P NMR spectroscopy (reaction to give **5a**: $\delta = 124.4$, $|J(^{31}\text{P},^{183}\text{W})| = 262.6$ Hz; reaction to give **5b**: $\delta = 125.3$, $|J(^{31}\text{P},^{183}\text{W})| = 270.1$ Hz), but could not be isolated. The 2H-1,2-azaphosphole complexes **5a,b** are isolated by low-temperature chromatography and crystallization from *n*-pentane/toluene. The suggested structures of the complexes **5a,b** are based on solution NMR-spectroscopic and MS data^[11] and are confirmed in the case of **5a** by a single-crystal X-ray structure analysis.^[12]

The product formation is readily explained by assuming that nitrilium phosphane ylide complexes **4a,b** are transiently

formed, by reaction of the terminal phosphanediyl complexes **2a,b** with 1-piperidinonitrile, and undergo [3+2] cycloaddition reactions with DMAD to yield complexes **5a,b**. This interpretation is strongly supported by observations, made earlier, on nitrile/nitrile exchange processes of nitrilium phosphane ylide complexes.^[4b] Interestingly, cycloaddition reactions of **4a,b** to the C–O π system of DMAD, which would give Δ^3 -1,3,2-oxazaphospholene complexes, were not observed.^[4b] The complexes **5a,b** display ^{31}P NMR signals in the range of $\delta = 75$ –80 with $|J(^{31}\text{P},^{183}\text{W})|$ values of about 250 Hz and characteristic ^{13}C chemical shifts of the carbon atoms of the five-membered rings in the range $\delta = 140$ –160.^[11, 3]

As also observed for pentacarbonyl[2-bis(trimethylsilyl)-methyl-3,4-bis(methoxycarbonyl)-5-dimethylamino-2H-1,2-azaphosphole- κ P]tungsten(o) (**6**),^[13] the molecular structure of complex **5a** (Figure 1) shows a planar five-membered ring (mean deviation 3 pm) with N1–C8 and C7–C6 bond lengths of 131.9(2) and of 135.0(2) pm, respectively, which are similar to those of complex **6** (N–C: 131.2(5); C–C: 133.8(6)^[13]). The different steric situation in the $(OC)_5\text{WPR}$ structural units of

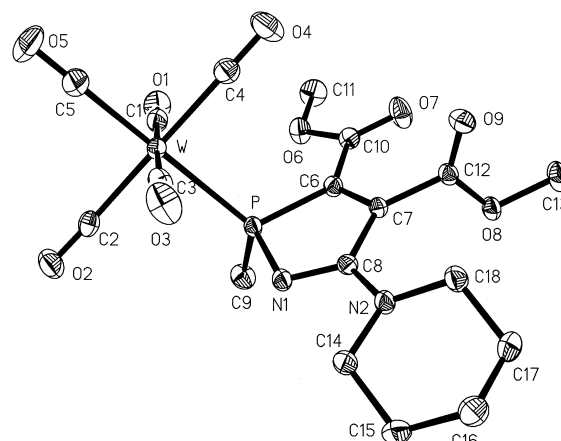
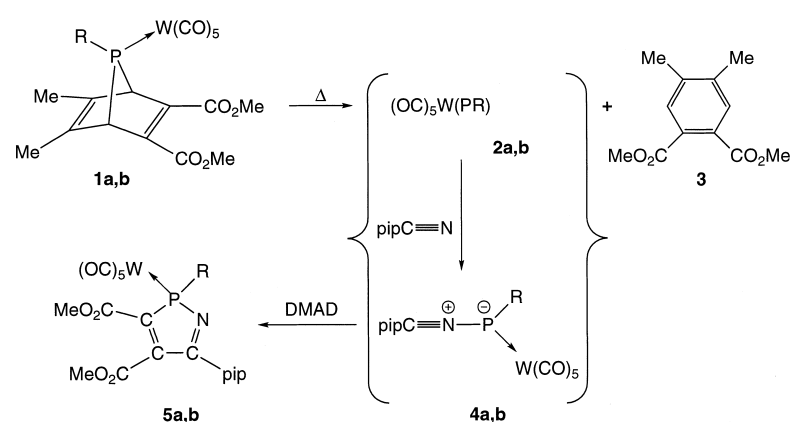


Figure 1. Molecular structure of complex **5a** in the crystal (ellipsoids represent 30% probability levels; H atoms are omitted for clarity). Selected bond lengths [pm] and angles [°]: W–P 249.96(5), P–N1 168.22(15), N1–C8 131.9(2), C8–C7 151.3(2), C7–C6 135.0(2), C6–P 181.51(17), C9–P 181.4(2); N1–P–C6 93.6(2), P–C6–C7 108.36(12), C6–C7–C8 111.10(14), C7–C8–N1 114.74(15), C8–N1–P 111.60(12).

5a (R = Me) and **6** (R = CH(SiMe₃)₂) correlates with shortened bond lengths in **5a** (W–P 249.96(5) and C9–P 181.4(2) pm; **6**: W–P 252.37(11) and C–P 183.6(4) pm^[13]) and a narrowing of the W–P–C6 bond angle in **5a** (114.97(6)° vs 119.26(14)° in **6**^[13]).

Experimental Section

5a, b: DMAD (0.5 mL, 3 mmol) and 1-piperidinonitrile (0.5 mL, 4.7 mmol) were added to a solution of **1a** (0.80 g, 1.3 mmol) or **1b** (0.90 g, 1.3 mmol) in toluene (10 mL) and the reaction mixture was stirred for 3.5–4 h at 120 °C. When the reaction was complete (as monitored by ^{31}P NMR), the solution was evaporated to dryness in vacuo (ca. 0.1 mbar), and the residue subjected to low-temperature column chromatography on silica (–32 °C, *n*-hexane/diethyl ether



Scheme 2. Proposed reaction course for the formation of 2H-1,2-azaphosphole complexes **5a, b**. R = Me (**a**), Ph (**b**); pip = 1-piperidino; DMAD = MeO₂CC≡CCO₂Me.

9/1). The eluates were evaporated to dryness in vacuo (ca. 0.1 mbar), and the residues recrystallized from *n*-pentane/toluene (9/1). Selected physical and NMR spectroscopic data for **5a**, **b** (the deuterated solvents were used as internal and 85 % H₃PO₄ as external standards). **5a**: yellow powder, yield: 180 mg (34 %), m.p. 113 °C (decomp). **5a**: ¹³C{¹H} NMR (50.3 MHz, C₆D₆, 25 °C): δ = 20.3 (d, ¹J(P,C) = 27.1 Hz; PCH₃), 24.2 (s; NCCCH₂), 25.7 (s; NCCCH₂), 48.5 (s; NCCCH₂), 52.3 (s; OMe), 52.8 (s; OMe), 141.6 (d, ²⁺³J(P,C) = 21.1 Hz; PCC), 159.7 (d, ¹⁺⁴J(P,C) = 8.4 Hz; PCC), 160.2 (d, ²⁺³J(P,C) = 5.4 Hz; PNC), 161.4 (d, ¹J(P,C) = 11.1 Hz; CO₂Me), 165.6 (d, ¹J(P,C) = 15.4 Hz; CO₂Me), 196.5 (d, ²J(P,C) = 7.6 Hz; *cis*-CO), 199.8 (d, ²J(P,C) = 21.7 Hz; *trans*-CO); ³¹P{¹H} NMR (81.0 MHz, C₆D₆, 25 °C): δ = 76.0 (s, ¹J(P,¹⁸³W) = 248.7 Hz). **5b**: yellow powder, yield: 80 mg (13 %), m.p. 124 °C (decomp). ¹³C{¹H} NMR (50.3 MHz, C₆D₆, 25 °C): δ = 24.3 (s; NCCCH₂), 25.9 (s; NCCCH₂), 48.9 (s; NCCCH₂), 52.8 (s; OMe), 53.4 (s; OMe), 128.7 (d, ²J(P,C) = 10.6 Hz; *o*-Ph), 130.8 (d, ³J(P,C) = 14.1 Hz; *m*-Ph), 131.2 (d, ⁴J(P,C) = 2.9 Hz; *p*-Ph), 131.9 (d, ¹J(P,C) = 42.1 Hz; *i*-Ph), 140.0 (d, ²⁺³J(P,C) = 20.4 Hz; PCC), 159.3 (d, ¹⁺⁴J(P,C) = 7.6 Hz; PCC), 160.9 (d, ²⁺³J(P,C) = 5.4 Hz; PNC), 161.4 (d, ¹J(P,C) = 10.8 Hz; CO₂Me), 165.6 (d, ¹J(P,C) = 15.3 Hz; CO₂Me), 196.0 (d, ²J(P,C) = 6.4 Hz; *cis*-CO), 199.0 (d, ²J(P,C) = 22.8 Hz; *trans*-CO); ³¹P{¹H} NMR (81.0 MHz, C₆D₆, 25 °C): δ = 78.8 (s, ¹J(P,¹⁸³W) = 254.0 Hz).

Received: April 14, 2000 [Z14994]

- [1] R. Streubel, H. Wilkens, A. Ostrowski, C. Neumann, F. Ruthe, P. G. Jones, *Angew. Chem.* **1997**, *109*, 1549–1550; *Angew. Chem. Int. Ed. Engl.* **1997**, *36*, 1492–1493.
- [2] R. Streubel, H. Wilkens, F. Ruthe, P. G. Jones, *Chem. Commun.* **1999**, 2127–2128.
- [3] a) U. Rohde, F. Ruthe, P. G. Jones, R. Streubel, *Angew. Chem.* **1999**, *111*, 158–160; *Angew. Chem. Int. Ed.* **1999**, *38*, 215–217; b) H. Wilkens, A. Ostrowski, J. Jeske, F. Ruthe, P. G. Jones, R. Streubel, *Organometallics* **1999**, *18*, 5627–5642.
- [4] a) H. Wilkens, J. Jeske, P. G. Jones, R. Streubel, *Chem. Commun.* **1997**, 2317–2318; b) H. Wilkens, F. Ruthe, P. G. Jones, R. Streubel, *Chem. Eur. J.* **1998**, *4*, 1542–1553; c) R. Streubel, U. Schiemann, N. Hoffmann, Y. Schiemann, P. G. Jones, D. Gudat, *Organometallics* **2000**, *19*, 475–481.
- [5] G. N. Cloke, P. B. Hitchcock, U. Schiemann, R. Streubel, J. F. Nixon, D. J. Wilson, unpublished results.
- [6] Reviews: a) F. Mathey, *Angew. Chem.* **1987**, *99*, 285–296; *Angew. Chem. Int. Ed. Engl.* **1987**, *26*, 275–286; b) K. B. Dillon, F. Mathey, J. F. Nixon, *Phosphorus: The Carbon Copy*, Wiley, Chichester, **1998**, p. 14–39.
- [7] a) Y. Inubushi, N. H. Tran Huy, F. Mathey, *Chem. Commun.* **1996**, 1903–1904; b) Y. Inubushi, N. H. Tran Huy, L. Ricard, F. Mathey, *J. Organomet. Chem.* **1997**, *533*, 83–86.
- [8] R. Streubel, A. Ostrowski, H. Wilkens, F. Ruthe, J. Jeske, P. G. Jones, *Angew. Chem.* **1997**, *109*, 409–413; *Angew. Chem. Int. Ed. Engl.* **1997**, *36*, 378–381.
- [9] A. Marinetti, F. Mathey, J. Fischer, A. Mitschler, *J. Chem. Soc. Chem. Commun.* **1982**, 667–668.
- [10] Selected MS and IR spectroscopic data of **5a**, **b**: **5a**: MS (EI, 70 eV, ¹⁸⁴W): *m/z*: 622 [*M*⁺]; **5b**: MS (EI, 70 eV, ¹⁸⁴W): *m/z*: 684 [*M*⁺]; satisfactory C,H elemental analyses for **5a**, **b**.
- [11] Crystal structure analysis of complex **5a**: C₁₈H₁₉N₂O₉PW, *M*_r = 622.17; monoclinic, space group *P*2₁/*c*: *a* = 1046.17(10), *b* = 993.21(10), *c* = 2167.5(2) pm, β = 97.627(3)°, *V* = 2.2322(4) nm³; *Z* = 4, ρ_{calcd} = 1.851 Mg m⁻³, λ = 0.71073 pm, *T* = 143 K. A crystal (0.27 × 0.20 × 0.17 mm) was mounted in perfluoropolyether at –130 °C on a Bruker SMART 1000 CCD. Intensities were registered to 2θ = 60°. Of 40 121 reflections, 6787 were independent (*R*_{int} = 0.0524). An absorption correction was based on multiple scans. The structure was solved by direct methods and refined against *F*² (SHELXL-97) (SHELXL-97: G. M. Sheldrick, Universität Göttingen, **1997**). Methyl H atoms were included using rigid groups, all other H atoms with a riding model. Final *wR*₂ = 0.0461 based on *F*² for all data, conventional *R*(*F*) = 0.0206, for 283 parameters; max. Δρ = 722 e nm⁻³. Crystallographic data (excluding structure factors) for the structure reported in this paper have been deposited with the Cambridge Crystallographic Data Centre as supplementary publication no. CCDC-143302. Copies of the

data can be obtained free of charge on application to CCDC, 12 Union Road, Cambridge CB21EZ, UK (fax: (+44) 1223-336-033; e-mail: deposit@ccdc.cam.ac.uk).

- [12] H. Wilkens, F. Ruthe, P. G. Jones, R. Streubel, *Chem. Commun.* **1998**, 1529–1530.
- [13] R. Streubel, H. Wilkens, U. Rohde, A. Ostrowski, J. Jeske, F. Ruthe, P. G. Jones, *Eur. J. Inorg. Chem.* **1999**, 1567–1579.

Spin Frustration in a Dimeric Mn^{II} Complex with a Metallocene-Substituted α-Nitronyl Nitroxide Radical**

Daniel Ruiz-Molina, Christian Sporer, Klaus Wurst, Peter Jaitner,* and Jaume Veciana*

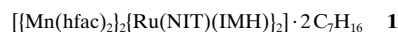
The synthesis of new molecular magnetic materials that combine paramagnetic metal ions and pure organic radicals as ligating sites has attracted much more attention in the last few years.^[1] Such systems enhance the diversity and/or dimensionality of magnetic systems made up from paramagnetic metal ions and diamagnetic coordinating ligands. So far, different types of stable organic radicals have been studied although one of the families most extensively used is that of α-nitronyl nitroxides (NIT). Since the nitroxyl groups are only weakly coordinating, α-nitronyl nitroxides bearing different coordinating functionalities have been reported.^[2, 3] Variation of the coordination ability provided access to new complexes, whose diversity ranged from discrete molecules^[4] to high-spin clusters^[5] and to extended two- or three-dimensional systems.^[6] Another approach successfully used to expand the dimensionality of the systems, ensuring the presence of large exchange interactions, has been the use of multicoordinating polyradical ligands. For instance, Iwamura et al. reported complexes with such polyradicals and manganese(II) hexa-

- [*] Prof. J. Veciana, Dr. D. Ruiz-Molina
Institut de Ciencia de Materials de Barcelona (CSIC)
Campus Universitari de Bellaterra 08193, Cerdanyola (Spain)
Fax: (34) 93-580-5729
E-mail: vecianaj@icmab.es
- Prof. P. Jaitner, C. Sporer, Dr. K. Wurst
Institut für Allgemeine, Anorganische und Theoretische Chemie,
Universität Innsbruck
Innrain 52a, 6020 Innsbruck (Austria)
Fax: (43) 512-507-2934
E-mail: Peter.Jaitner@uibk.ac.at

[**] This work was supported by grants from DGES (project PB96-0802-CO2-01), CIRIT (project SGR 96-00106), Fonds zur Förderung der Wissenschaftlichen Forschung, Vienna (Project P 13128), Austrian Federal Ministry of Science (BMWV), Acción Integrada Hispano-Austríaca (HU-1999-0015), and the 3MD Network of the TMR program of the E.U. (contract ERBFMRX CT980181). C.S. thanks the Austrian Federal Ministry of Science for the award of a research scholarship. D.R.-M. thanks the Generalitat de Catalunya for a postdoctoral grant. The authors acknowledge the suggestions given by one of the referees.

fluoroacetylacetonate, $[\text{Mn}(\text{hfac})_2]$, showing two- or three-dimensional networks that exhibited ferrimagnetic behavior.^[7] Herein we propose the use of the ruthenocene-substituted α -nitronyl nitroxide diradical $[\text{Ru}(\text{NIT})_2]$ (see Scheme 1), previously reported by us,^[8] as a new multicoordinating ligand to obtain complexes that combine paramagnetic metal ions and organic radicals and show nonconventional magnetic behaviors.

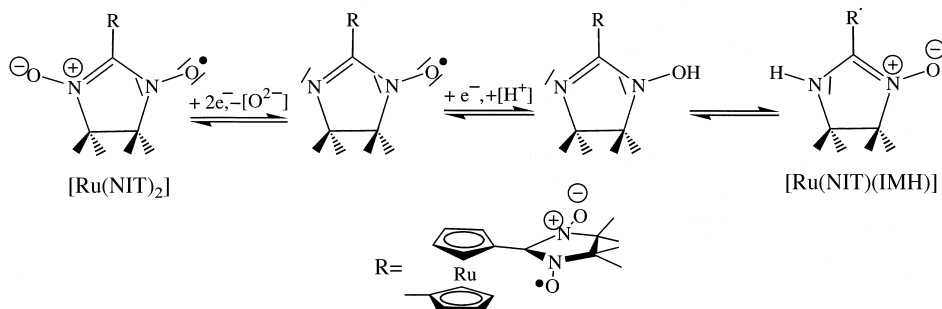
Complex **1** (hfac = hexafluoroacetylacetonate; IMH = reduced form of the imino nitroxide) was obtained from $[\text{Mn}(\text{hfac})_2] \cdot 2\text{H}_2\text{O}$ and $[\text{Ru}(\text{NIT})_2]$. During the complexation



reaction a partial reduction of the $[\text{Ru}(\text{NIT})_2]$ diradical to the monoradical $[\text{Ru}(\text{NIT})(\text{IMH})]$ takes place (Scheme 1). This fact was confirmed by X-ray structure analysis^[9] and the IR spectrum of complex **1**, which exhibited an absorption peak at 3350 cm^{-1} characteristic of the stretching vibration of the N–H group.

The reduction of α -nitronyl nitroxide radicals in the presence of $[\text{Mn}(\text{hfac})_2]$ has already been described.^[10] In all the examples so far reported, the reduced radicals bind to the manganese ions through the O(1) atom of the amidino-oxide group to generate a dimeric structure, which seems to be the structure thermodynamically favored. This is also the case for complex **1** as shown by the ORTEP views of the $[\{\text{Mn}(\text{hfac})_2\}(\text{Ru}(\text{NIT})(\text{IMH}))]$ asymmetric unit and complex **1** in Figure 1.

The asymmetric unit comprises one Mn^{II} center and one $[\text{Ru}(\text{NIT})(\text{IMH})]$ unit coordinated to the Mn^{II} center through the O(1) atom of the amidino-oxide group. The N(1)–O(1) bond length of $1.376(3)\text{ \AA}$ is in agreement with those reported in analogous reduced radicals, which range from 1.37 to 1.39 \AA . Moreover, the substituents on the cyclopentadienyl rings adopt a *cisoid* conformation resulting from an intramolecular $\text{H}(2n) \cdots \text{O}(4)$ hydrogen bond of 2.00 \AA . This hydrogen bond is expected to play an active role in enhancing the magnetic exchange interactions between the Mn^{II} ions and the organic radicals. The uniqueness of the system becomes clearly apparent when the complete structure of complex **1** is considered. As shown in Figure 1, complex **1** adopts a butterfly arrangement in which the two Mn^{II} atoms occupy the central or body positions of the core and the nonreduced NIT radicals occupy the external or wing-tip positions. This



Scheme 1. Mechanism proposed for the partial reduction of the $[\text{Ru}(\text{NIT})_2]$ diradical to the monoradical $[\text{Ru}(\text{NIT})(\text{IMH})]$.

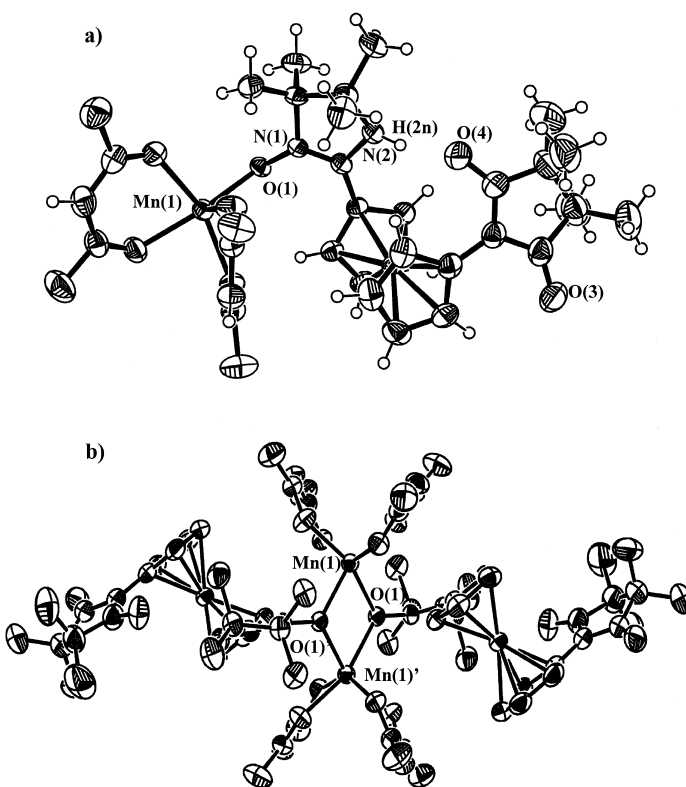


Figure 1. ORTEP views of a) the $[\{\text{Mn}(\text{hfac})_2\}(\text{Ru}(\text{NIT})(\text{IMH}))]$ asymmetric unit and b) complex **1**. The fluorine atoms have been omitted for clarity. The central $\text{Mn} \cdots \text{Mn}$ distance is $3.546(1)\text{ \AA}$ with $\text{Mn}(1)\text{--O}(1)\text{--Mn}(1')$ and $\text{Mn}(1)\text{--O}(1')\text{--Mn}(1')$ bridging angles of 108.8° . The bond lengths $\text{Mn--O}(1)$ and $\text{Mn--O}(1')$ are $2.164(2)$ and $2.198(2)\text{ \AA}$, respectively.

type of arrangement has already been shown to induce spin frustration in polynuclear transition metal complexes consisting of four interacting metal ions.^[11]

Variable-temperature magnetic susceptibility data for a crystalline sample of complex **1** was measured on a SQUID susceptometer over the temperature range of $2\text{--}300\text{ K}$ with an applied external field of 1 kG . A plot of χT versus T is depicted in Figure 2. The value of χT gradually decreases from $7.8\text{ emu K mol}^{-1}$ at 300 K to $0.4\text{ emu K mol}^{-1}$ at 2 K . Attempts to fit the data in Figure 2 to the equation defined for a pair of interacting $S_1 = S_2 = 5/2$ systems with an isotropic exchange interaction and two noninteracting $S = 1/2$ radicals were unsuccessful. By contrast, the data was nicely fitted to a

magnetic model based on a butterfly arrangement of the metal ions and organic radicals, consistent with the structure shown in Figure 1. The spin Hamiltonian, \hat{H} , for this butterfly system is given by Equation (1),^[12] where J is the wing-tip/body exchange interaction between the manganese(II) ions and the organic radicals and J_{13} is the body/body interaction between the two manganese(II) ions (Scheme 2).

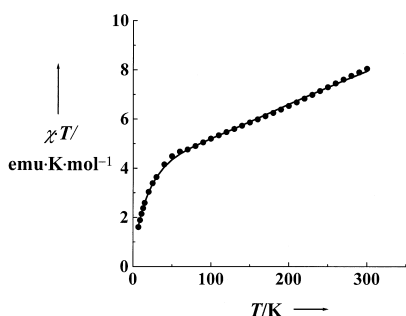
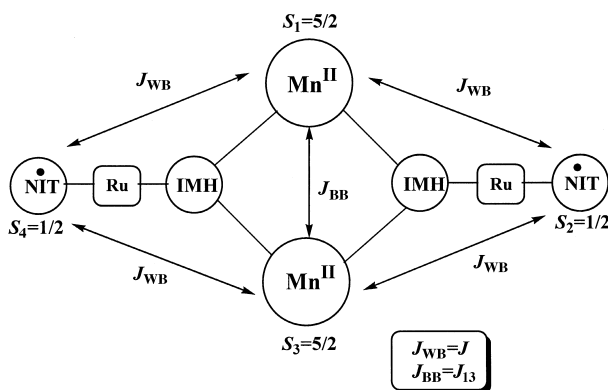


Figure 2. Temperature dependence of the magnetic susceptibilities for complex **1** in the form χT versus T . The solid line was calculated with the described equation and parameters.



Scheme 2. Butterfly-like arrangement of the metal ions and organic radicals in the structure of complex **1** and magnetic exchange coupling constants involved.

Equation (1) can be transformed to Equation (2) with $\hat{S}_{13} = \hat{S}_1 + \hat{S}_3$, $\hat{S}_{24} = \hat{S}_2 + \hat{S}_4$, $\hat{S}_T = \hat{S}_{13} + \hat{S}_{24}$. The eigenvalues E deduced from Equation (2) using the Kambe method^[13] are shown in Equation (3), where $S_{13} = S_1 + S_3$, $S_{24} = S_2 + S_4$, and $S_T = S_{13} + S_{24}$.

$$\hat{H} = -2J(\hat{S}_1\hat{S}_2 + \hat{S}_2\hat{S}_3 + \hat{S}_3\hat{S}_4 + \hat{S}_4\hat{S}_1) - 2J_{13}\hat{S}_1\hat{S}_3 \quad (1)$$

$$\hat{H} = -2J(\hat{S}_T^2 - \hat{S}_{13}^2 - \hat{S}_{24}^2) - 2J_{13}\hat{S}_{13}^2 \quad (2)$$

$$E = -J[S_T(S_T + 1) - S_{13}(S_{13} + 1) - S_{24}(S_{24} + 1)] - J_{13}[S_{13}(S_{13} + 1)] \quad (3)$$

A theoretical expression for the χT versus T behavior of complex **1** was derived from Equation (3) and the Van Vleck equation, and the resulting expression, modified to take into account intermolecular interactions (θ) in the molecular field approximation, was then used to least-squares fit the experimental data.^[14] The best fit was obtained for $J = -31.8 \text{ cm}^{-1}$, $J_{13} = -9.8 \text{ cm}^{-1}$, $\theta = -6.4 \text{ K}$, and $g = 1.91$. The value of the body/body interaction, $J_{13} = -9.8 \text{ cm}^{-1}$, is within the range of those previously reported for the same kind of interaction in other butterfly-like tetranuclear manganese clusters, as it is also the case for the g values (1.70–2.00).^[15] However, the value of $J = -31.8 \text{ cm}^{-1}$, associated to the magnetic exchange coupling between the manganese(II) ions and the NIT radicals, is considerably smaller than those previously reported for other mono- and polynuclear complexes with the radicals directly coordinated to Mn^{II} ions through the O atom of the N–O group.^[16] This fact is not surprising if we consider that in

the latter complexes there is a direct overlap between the d orbitals of the manganese ions and the π orbitals of the radicals, whereas in the complex described herein, the exchange interaction occurs mediated by the diamagnetic IMH ligand. A plausible explanation of the magnetic exchange interactions could be that the IMH part of the $[\text{Ru}(\text{NIT})(\text{IMH})]$ group promotes an antiferromagnetic exchange interaction between the Mn^{II} centers as well as an antiferromagnetic exchange between the Mn^{II} atoms and the peripheral NIT radical groups. The latter may be due either to a delocalization of spin density over the ruthenocene unit or to a spin polarization mechanism. Such a spin polarization mechanism may take place through the σ skeleton of the ruthenocene unit and, most likely, through the O–N–C–N–H group of the reduced IMH unit.^[17] That both exchange coupling parameters, J and J_{13} , are negative indicates that any two neighboring spins tend to align antiferromagnetically. However, the topological arrangement of metal ions and organic radicals in the butterfly structure results in a spin frustration due to the presence of competing interactions. The ground state of complex **1** is, in the format (S_T, S_{13}, S_{24}) , the quintet state (2,3,1) with a first triplet excited state (1,2,1) and a second septet excited state (3,4,1) at energies above the ground state of 4 and 14 cm^{-1} , respectively. This is one of the rare examples of a spin-frustrated system composed of organic radicals and metal ions. As far as we know, there is only another example described by Iwamura et al.^[18] with the main difference that in the latter case the body/body interaction J_{13} corresponded to the interaction between the two radicals, which are covalently linked, whereas in the complex described herein such an interaction corresponds to the interaction between the two manganese ions.

In summary, we have shown that metallocene-substituted α -nitronyl nitroxides are good multicoordinating ligands for obtaining new complexes following the metal–radical approach. In addition, we have reported a new dimeric Mn^{II} complex with a butterfly structure and competing magnetic exchange interactions between the manganese ions and the organic radicals. Efforts are currently underway to obtain new complexes derived from $[\text{Ru}(\text{NIT})_2]$, or related metallocene diradicals, with two- or three-dimensional extended structures.

Experimental Section

1: A solution of $[\text{Mn}(\text{hfac})_2] \cdot 2\text{H}_2\text{O}$ (0.370 mmol) in dry *n*-heptane (20 mL) was refluxed until the solution acquired a light yellow color. After stabilization at 60°C , a solution of diradical $[\text{Ru}(\text{NIT})_2]$ (0.185 mmol) in dry chloroform (2 mL) was added under vigorous stirring. The resulting mixture was filtered under argon and allowed to stand at room temperature for one day giving a blue precipitate. Single crystals of **1** were grown from an *n*-heptane/chloroform solution by means of a crystallization box equipped with a heating block described by Hulliger.^[19]

Received: April 6, 2000 [Z14947]

- [1] A. Caneschi, D. Gatteschi, P. Rey, *Prog. Inorg. Chem.* **1991**, 39, 331; H. Iwamura, K. Inoue, T. Hayamizu, *Pure Appl. Chem.* **1996**, 68, 243.
- [2] H. Oshio, T. Watanabe, A. Ohto, T. Ito, H. Masuda, *Inorg. Chem.* **1996**, 35, 472.
- [3] C. Rancurel, J.-P. Sutter, T. Le Hoerff, L. Ouahab, O. Kahn, *New. J. Chem.* **1999**, 1333.

- [4] C. Benelli, A. Caneschi, D. Gatteschi, L. Pardi, *Inorg. Chem.* **1992**, *31*, 741.
- [5] A. Marvilliers, Y. Pei, J. Cano, K. E. Vostrikova, C. Paulsen, E. Rivière, J.-P. Audière, T. Mallah, *Chem. Commun.* **1999**, 1951; A. Caneschi, D. Gatteschi, J. Laugier, P. Rey, R. Sessoli, C. Zanchini, *J. Am. Chem. Soc.* **1988**, *110*, 2795; T. Mallah, C. Auberger, M. Verdaguer, P. Veillet, *J. Chem. Soc. Chem. Commun.* **1995**, 61.
- [6] M. G. F. Vaz, L. M. M. Pinehiro, H. O. Stumpf, A. F. C. Alcantara, S. Goleen, L. Ouahab, O. Cador, C. Mathonière, O. Kahn, *Chem. Eur. J.* **1999**, *5*, 1486; K. Fey, D. Luneau, T. Ohm, C. Paulsen, P. Rey, *Angew. Chem.* **1998**, *110*, 1331; *Angew. Chem. Int. Ed.* **1998**, *37*, 1270.
- [7] K. Inoue, H. Iwamura, *Adv. Mater.* **1996**, *8*, 73.
- [8] O. Jürgens, J. Vidal-Gancedo, C. Rovira, K. Wurst, C. Sporer, B. Bildstein, H. Schottenberger, P. Jaitner, J. Veciana, *Inorg. Chem.* **1998**, *37*, 4547.
- [9] X-ray structure analysis of $C_{68}H_{70}F_{24}Mn_2N_8O_{14}Ru_2 \cdot 2C_7H_{16}$, $M_r = 2191.7$; blue prism with the dimensions $0.8 \times 0.4 \times 0.3$ mm; triclinic, space group $P\bar{1}$ (no. 2), $a = 12.883(5)$, $b = 14.113(5)$, $c = 15.274(5)$ Å, $\alpha = 101.63(2)$, $\beta = 113.55(2)$, $\gamma = 91.78(2)^\circ$, $V = 2474.2(15)$ Å³, $\rho_{\text{calc}} = 1.471$ g cm⁻³, $Z = 1$, $T = 218(2)$ K, $\mu(\text{MoK}\alpha) = 0.71703$. Bruker P4 diffractometer, corrected for Lorentz, polarization, and absorption (ψ scans); 7937 measured reflections, of which 6747 with $I > 2\sigma(I)$ were included in the structure refinement against F^2 (SHELXL 93). The structure was solved by direct methods (SHELXS 93); heavy atoms with anisotropic temperature factors; the hydrogen atom at N(2) was found and refined isotropically; the other hydrogen atoms were calculated. Three CF₃ groups display an orientation disorder of the fluorine atoms. Refinement with 681 variables with a GOF of 1.033, $R_1 = 0.0349$ (against $|F^2|$) and $R_2 = 0.0864$ (against $|F|$). Crystallographic data (excluding structure factors) for the structure reported in this paper have been deposited with the Cambridge Crystallographic Data Centre as supplementary publication no. CCDC-142644. Copies of the data can be obtained free of charge on application to CCDC, 12 Union Road, Cambridge CB21EZ, UK (fax: (+44) 1223-336-033; e-mail: deposit@ccdc.cam.ac.uk).
- [10] Z.-H. Jiang, B.-W. Sun, D.-Z. Liao, G.-L. Wang, B. Donnadieu, J.-P. Tuchages, *Inorg. Chim. Acta* **1998**, *279*, 76; M. D. Carducci, R. J. Doedens, *Inorg. Chem.* **1989**, *28*, 2492; A. Caneschi, D. Gatteschi, J. Launier, P. Rey, C. Zanchini, *Inorg. Chem.* **1989**, *28*, 1969.
- [11] S. L. Castro, Z. Sun, C. M. Grant, J. C. Bollinger, D. N. Hendrickson, G. Christou, *J. Am. Chem. Soc.* **1998**, *120*, 2365, and references therein.
- [12] J. B. Vincent, C. Christmas, H.-R. Chang, Q. Li, P. D. Boyd, J. C. Huffman, D. N. Hendrickson, G. Christou, *J. Am. Chem. Soc.* **1989**, *111*, 2086.
- [13] K. Kambe, *J. Phys. Soc. Jpn.* **1950**, *5*, 48.
- [14] Experimental magnetization data of complex **1** at 2 K follow the theoretical expression derived from the Van Vleck equation and Equation (3) using the reported J , J_{13} , θ , and g values and therefore, supporting the proposed magnetic interaction for **1**.
- [15] a) D. N. Hendrickson, *Research Frontiers in Magnetochemistry* (Ed.: C. J. O'Connor), World Scientific, Singapore, **1993**, p. 87; b) E. Libby, J. K. McCusker, E. A. Schmitt, K. Folting, D. N. Hendrickson, G. Christou, *Inorg. Chem.* **1991**, *30*, 3486; c) J. B. Vincent, C. Christmas, H.-R. Chang, Q. Li, P. D. Boyd, J. C. Huffman, D. N. Hendrickson, G. Christou, *J. Am. Chem. Soc.* **1989**, *111*, 2086.
- [16] A. Caneschi, D. Gatteschi, J. P. Renard, P. Rey, R. Sessoli, *Inorg. Chem.* **1989**, *28*, 3314.
- [17] The observed magnetic exchange couplings, J , between two α -nitronyl nitroxides in metallocene diradicals of the type $[M(\text{NIT})_2]$ in the solid state range from -2.2 to -6.1 cm⁻¹ (see reference [8]). These values are considerably smaller than the magnetic exchange coupling $J = -31.8$ cm⁻¹ here reported for the interaction between the Mn^{II} ions and the NIT radicals of complex **1**. This fact supports the critical role of the reduced IMH unit and the strong intramolecular H(2n) ... O(4) hydrogen bond in transmitting the magnetic exchange interactions by a spin polarization mechanism.
- [18] M. Tanaka, K. Matsuda, T. Itoh, H. Iwamura, *Angew. Chem.* **1998**, *110*, 866; *Angew. Chem. Int. Ed.* **1998**, *37*, 810.
- [19] J. Hulliger, *Angew. Chem.* **1994**, *106*, 151; *Angew. Chem. Int. Ed. Engl.* **1994**, *33*, 143.

Al₅Br₇ · 5 THF—The First Saltlike Aluminum Subhalide

Christoph Klemp, Gregor Stöber, Ingo Krossing, and Hansgeorg Schnöckel*

In memory of Josef Goubeau

Al^{III} halides have been studied intensively in the solid state, in solution, and in the gas phase,^[1, 2] whereas for aluminum subhalides for a long time only the monomeric AlX high-temperature molecules had been characterized by gas-phase IR spectroscopy.^[3, 4] With the development of matrix isolation spectroscopy, subsequently dimeric Al₂X₂ species were also investigated.^[4, 5] A further development of this technique for preparative applications was presented by the cocondensation technique, which provided access to a donor-stabilized metastable AlX solution.^[5] From these solutions, Al^{II} and Al^I halides, in the form of Al₂Br₄ · 2 anisole and Al₄Br₄ · 4 NEt₃, respectively, were structurally characterized for the first time in 1994,^[6] and additional isomers of the type Al₂X₄ · 2 D and E₄X₄ · 4 D (D = Donor) have since been found.^[7] The first polyhedral subhalide Al₂₂X₂₀ · 12 D, which we reported on recently in this journal,^[8] represented a new compound type. Herein we report on the first example for the mixed-valent compound type Al₅X₇ · 5 D.

Cocondensation of the high-temperature molecule AlX (X = Cl, Br, I) with a toluene/THF mixture according to the method described in reference [5] gave dark red-brown, metastable AlX · THF/toluene solutions. The Al^{II} solution decolorized at room temperature, without the deposition of aluminum, and colorless crystals of Al₅I₄ · 2 THF (**1**) were isolated after cooling of the concentrated solution.^[9] Compound **1** displays the typical D · X₂Al–AlX₂ · D structure.^[10] In contrast, in addition to aluminum, among others, the well-known AlCl₃ · THF^[2b] precipitated from the AlCl solution at room temperature.

Besides aluminum and Al₂₂Br₂₀ · 12 THF^[8] the AlBr · THF/toluene solution afforded a colorless, brittle compound (**2**) of the composition “Al₅Br₇ · 5 THF”, which crystallizes in the triclinic crystal system. An X-ray crystal structure analysis revealed that **2** is a salt comprising [Al₅Br₈ · 4 THF]⁻ ions and [Al₅Br₆ · 6 THF]⁺ ions (**2a** and **2b**, respectively; Figure 1).^[9] The Al₅ framework of both ions consists of a central Al atom, which is tetrahedrally surrounded by four Al atoms. In the case of the (approximately S₄-symmetric) anion, these four Al atoms each bear two Br atoms and a coordinated THF molecule. In contrast, in the (approximately C₂-symmetric) cation only two AlBr₂ · THF groups as well as two AlBr · 2 THF groups are arranged about the central Al atom. Thus the formula [Al(AlBr₂ · 2 THF)₂(AlBr₂ · THF)₂]⁺[Al(AlBr₂ · THF)₄]⁻ provides a better description of the bonding situation. This ion pair possesses two Al atoms with the formal

[*] Prof. Dr. H. Schnöckel, C. Klemp, G. Stöber, Dr. I. Krossing
Institut für Anorganische Chemie der Universität Karlsruhe (TH)
Engesserstrasse, Gebäude 30.45
76128 Karlsruhe (Germany)
Fax: (+49) 721-608-4854
E-mail: hg@achpc9.chemie.uni-karlsruhe.de

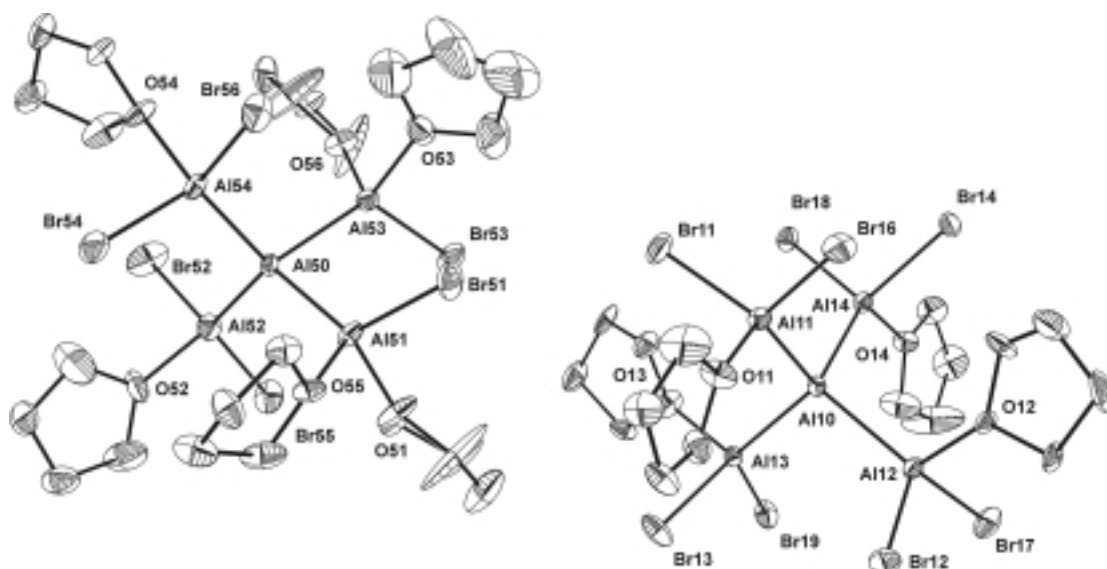


Figure 1. Molecular structure (without H atoms) of $[\text{Al}_5\text{Br}_6 \cdot 6 \text{THF}]^+ \mathbf{2b}$ (left) and $[\text{Al}_5\text{Br}_8 \cdot 4 \text{THF}]^- \mathbf{2a}$ (right) in the solid state (triclinic distorted CsCl structure). Distances are given in Table 1. Anion and cation have very similar molecular structures, since $\mathbf{2b}$ can be converted into $\mathbf{2a}$ by substitution of the O55 and O56 atoms (THF) for Br atoms. In the crystal all Br atoms with the exception of Br55 and Br56 lie in layers, which are arranged tilted to the molecular layers.

oxidation state 0, two with +1, and six with +2; thus, the average oxidation state is +1.4.

The measured distances and those calculated by density functional theory (DFT) methods^[11] in $\mathbf{2a}$ and $\mathbf{2b}$ are given in Table 1 together with those of comparable compounds. As expected the average measured bond lengths in the anion are slightly longer than those in the cation, and the calculated distances prove to be slightly longer owing to the consider-

reaction of a $\text{AlCl} \cdot \text{OEt}_2$ /toluene solution with SiCl_4 or GeCl_4 led to the compounds $\text{Si}(\text{AlCl}_2 \cdot \text{OEt}_2)_4$ and $\text{Ge}(\text{AlCl}_2 \cdot \text{OEt}_2)_4$, respectively, which are isoelectronic to the anion $\mathbf{2a}$.^[13] The cocondensation of GaCl with toluene/ OEt_2 gave the neutral compound $\text{Ga}_5\text{Cl}_7 \cdot 5 \text{OEt}_2$ ($\mathbf{3}$), which is analogous to $\mathbf{2}$, with only one $\text{Ga}^{\text{I}}\text{Cl} \cdot 2 \text{OEt}_2$ group.^[14, 15] With $\mathbf{1}$ and these compounds a mechanism for the formation of $\mathbf{2}$ can be deduced, which is presented in Scheme 1.

Starting from $\text{E}^{\text{III}}\text{X}_3 \cdot \text{D}$ ($\text{E} = \text{Al, Ga}$; $\text{X} = \text{Cl, Br, I}$), the (comproportionation) products $\text{E}_2\text{X}_4 \cdot 2 \text{D}$, $\text{E}_3\text{X}_5 \cdot 3 \text{D}$, ($\text{E}_4\text{X}_6 \cdot 4 \text{D}$), and $\text{E}_5\text{X}_7 \cdot 5 \text{D}$ can be formed by successive addition (insertion) of $\text{E}^{\text{I}}\text{X} \cdot \text{D}$. For the first product of the (oxidative) insertion of $\text{E}^{\text{I}}\text{X} \cdot \text{D}$ in a $\text{E}^{\text{III}}\text{—X}$ bond there are numerous examples in the chemistry of aluminum and gallium^[16, 17] besides the $\text{Al}_2\text{I}_4 \cdot 2 \text{THF}$ compound presented here. The intermediate of a second insertion has been structurally characterized in the form of $\text{Ga}_3\text{I}_5 \cdot 3 \text{PET}_3$.^[17] The

third intermediate, $\text{E}_4\text{X}_6 \cdot 4 \text{D}$ or better $\text{E}(\text{EX}_2 \cdot \text{D})_3 \cdot \text{D}$, has so far not been trapped, since evidently an additional $\text{E}(\text{I})\text{X} \cdot \text{D}$ molecule coordinates readily so that $\text{E}_5\text{X}_7 \cdot 5 \text{D}$ (cf. $\mathbf{3}$) forms directly.^[18]

Two of these $\text{E}_5\text{X}_7 \cdot 5 \text{D}$ molecules can be converted into the ionic compound $[\text{E}_5\text{X}_6 \cdot 6 \text{D}]^+[\text{E}_5\text{X}_8 \cdot 4 \text{D}]^-$, thus $\mathbf{2b} \cdot \mathbf{2a}$, by mutual exchange of a halide ion for a donor. The experimental findings that in the case of gallium the neutral compound $\text{Ga}_5\text{Cl}_7 \cdot 5 \text{OEt}_2$ forms, however, in the case of aluminum, the ionic compound $[\text{Al}_5\text{Br}_6 \cdot 6 \text{THF}]^+[\text{Al}_5\text{Br}_8 \cdot 4 \text{THF}]^-$ is obtained^[19] can be supported by quantum-chemical calculations: According to DFT calculations the energies ΔE_{R} necessary for the halide transfer in the gas phase are +170 kJ mol^{-1} for reaction (1) and +190 kJ mol^{-1} for reaction (2).

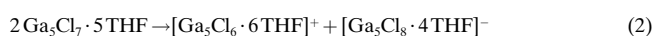
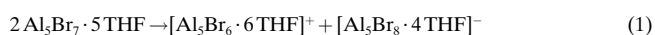


Table 1. Average measured and (in parentheses) calculated^[11] bond lengths [pm] of $\mathbf{2b}$, $\mathbf{2a}$, and two related compounds.

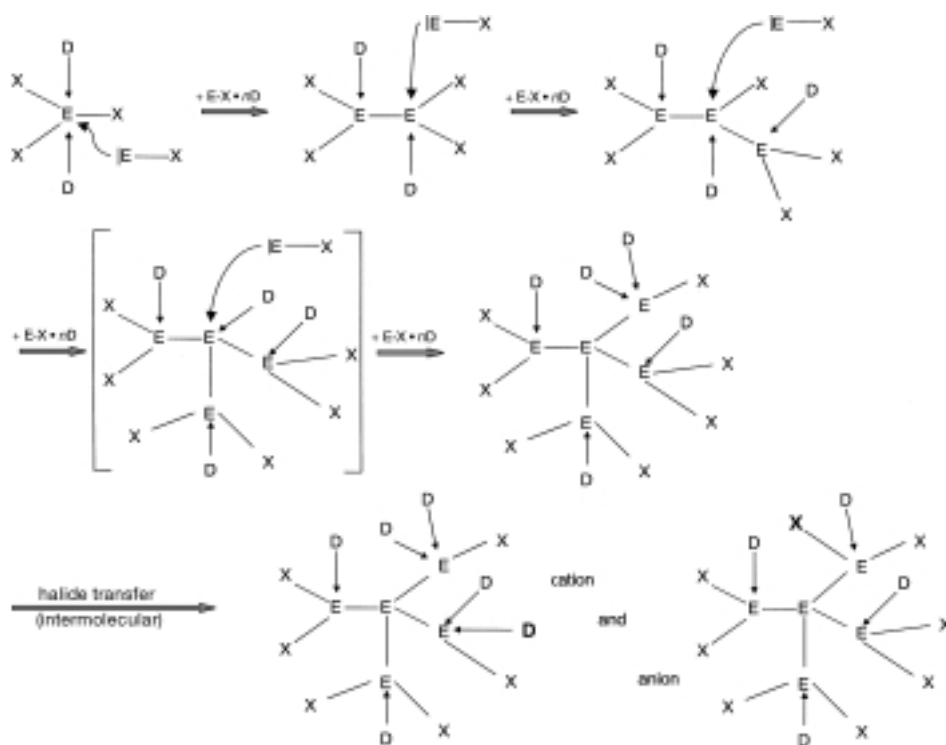
	$\mathbf{2b}$	$\mathbf{2a}$	$\text{Al}_2\text{Br}_4 \cdot 2 \text{anisole}$	$\text{Al}_{22}\text{Br}_{20} \cdot 12 \text{THF}$ ^[a]
Al—Al	253.2 (255.3)	254.3 (258.3)	252.7 (254.7)	252.6 (254.1)
Al—Br	234.6/238.0 (236.4/239.3)	236.8 (236.7)	230.6 (233.8)	229.9 (—)
Al—O	188.4 (197.1)	190.5 (197.8)	193.0 (202.6)	189.2 (193.7)

[a] $(\text{Al—AlX}_2 \cdot \text{D} \text{ group})$, calcd: $\text{X} = \text{Cl}$, $\text{D} = \text{H}_2\text{O}$.

ation of the compounds in the gas phase. In the AlBr_2 groups of the cation one of the two $\text{Al}^{\text{II}}\text{—Br}$ distances is lengthened (Br52 and Br54 in Figure 1), whereas the other resembles $\text{Al}^{\text{I}}\text{—Br}$ distances. Accordingly, the small differences in the lengths of the bonds to the Al atom (e.g. Al—Br) are not so dependent on the oxidation state but rather on the Coulombic repulsion and steric effects within each of the molecules, since these relationships are also confirmed by ab initio calculations of the molecules in the gas phase.^[12]

Compound $\mathbf{2}$ decomposes on warming above 100 °C, leading to the deposition of small amounts of aluminum. The mass spectrum of $\mathbf{2}$ does not show a peak for the molecular ion. Instead a peak is detected for $[\text{AlBr}_3 \cdot \text{THF}]^+$ (m/z 238.9) (direct ionization at 90 °C); however, dominant fragments are $[\text{AlBr}_2 \cdot \text{THF}]^+$ (m/z 258.9) and $[\text{AlBr}_2 \cdot \text{THF}]^+ - \text{C}_3\text{H}_7$ (m/z 215.8).

Whereas a chloro compound analogous to $\mathbf{2}$ has not been obtained to date under similar experimental conditions, the



Scheme 1. Potential mechanism for the formation of **2-cha;-/cha;**, postulated on the basis of the characterization of trapped analogous intermediates.

The solvation enthalpies, which need to be considered in solution particularly for the ionic products, are almost identical for the Al and Ga compound and can hardly reach the order of magnitude of ΔE_R .^[20] Therefore the significant difference in energies for the above-mentioned reactions is attributed to the different (gas-phase) reaction energies ΔE_R , whereby ΔE_R is larger for the gallium compound on the basis of the stronger M–X bond. Thus the formation of **2a** and **2b** should be favored over that of the hypothetical ionic Ga compound, which is confirmed by the crystal structures of **2a**, **2b**, and **3**.

Compound **2** is the first compound that contains binary aluminum subhalide ions with Al–Al bonds,^[21] and through its Al^0 central atom (calculated partial charge ca. -0.8) **2** represents the smallest Al-centered cluster; it could possibly play a key role in metal formation. In the chemical deposition of Al by disproportionation of Al^I compounds the intermediary character of Al subhalides is confirmed by the formation of numerous trapping products: The metalloid clusters $Al_7R_6^-$, $Al_{12}R_8^-$, $Al_{14}R_6I_6^{2-}$, and $Al_{77}R_{20}^{2-}$ ($R = N[SiMe_3]_2$)^[22–24] are already indicative of sections from the α -Al lattice. In contrast, for the electrolytic deposition of Al the question still remains, whether—and if yes, at what stage—subhalides formed such as Al_2X_4 , Al_3X_5 , Al_5X_7 , or even larger subhalides (or their ionic form) can be considered as intermediates that contribute to the metal deposition by disproportionation.^[25]

Experimental Section

1: AlI (40 mmol) was cocondensed with toluene (85 mL) and THF (15 mL), and 10 mL of the resulting 0.4 M AlI solution was concentrated to a quarter

of the volume at room temperature; the solution slowly decolorized but without deposition of aluminum. Compound **1** crystallized overnight at -30°C in the form of large colorless needles (m.p. $\approx 0^\circ\text{C}$). Yield: 380 mg (12%).

2: In analogy to the preparation of **1**, AlBr (40 mmol) was cocondensed with toluene (85 mL) and THF (15 mL), and 10 mL of the resulting 0.4 M AlBr solution (4 mmol AlBr) was concentrated to half the volume at room temperature. After one day amorphous aluminum deposited. After two further days colorless, brittle platelets of **2** (in addition to yellow $Al_{22}Br_{20}$ crystals) crystallized from the concentrated filtrate, which could be recrystallized from THF. Yield: 78.1 mg (0.037 mmol, 9.25%).

Mass spectrometry: Varian-MAT-711 and Finnigan-MAT-MS8223 spectrometers; EI: 70 eV; DI at $50-150^\circ\text{C}$. Measured and calculated masses as well as isotope patterns are in agreement.

Received: April 25, 2000 [Z15037]

[1] $AlX_3 \cdot nD$: a) D. M. Gruen, R. L. McBeth, *Inorg. Chem.* **1969**, *8*, 2625; b) R. Kniep, P. Blees, W. Poll,

Angew. Chem. **1982**, *94*, 370; *Angew. Chem. Int. Ed. Engl.* **1982**, *21*, 386.

[2] $AlX_3 \cdot nD$: a) H. Nöth, R. Rurländer, P. Wolfgang, *Z. Naturforsch. B* **1982**, *37*, 29; b) L. M. Engelhardt, P. C. Junk, C. L. Raston, B. W. Skelton, A. H. White, *J. Chem. Soc. Dalton Trans.* **1996**, 3297; c) L. Jakobsmeier, I. Krossing, H. Nöth, M. J. H. Schmidt, *Z. Naturforsch. B* **1996**, *51*, 1117.

[3] $AlCl_3$: W. Klemm, E. Voss, K. Geiersberger, *Z. Anorg. Allg. Chem.* **1948**, 256, 15.

[4] a) K. P. Huber, G. Herzberg, *Molecular Structure IV, Constants of Diatomic Molecules*, Van Nostrand Reinhold, New York, **1979**; b) H. Schnöckel, S. Schunk, *Chem. Unserer Zeit* **1987**, *21*, 73; c) M. Tacke, H. Schnöckel, *Inorg. Chem.* **1989**, *28*, 2895.

[5] C. Dohmeier, D. Loos, H. Schnöckel, *Angew. Chem.* **1996**, *108*, 141; *Angew. Chem. Int. Ed. Engl.* **1996**, *35*, 129.

[6] a) $Al_2Br_4 \cdot 2\text{anisole}$: M. Mocker, C. Robl, H. Schnöckel, *Angew. Chem.* **1994**, *106*, 946; *Angew. Chem. Int. Ed. Engl.* **1994**, *33*, 862; b) $Al_4Br_4 \cdot 4NEt_3$: M. Mocker, C. Robl, H. Schnöckel, *Angew. Chem.* **1994**, *106*, 1860; *Angew. Chem. Int. Ed. Engl.* **1994**, *33*, 1754.

[7] a) $Al_2X_4 \cdot 2D$: A. Ecker, M. A. Friesen, M. A. Junker, C. Üffing, R. Köppe, H. Schnöckel, *Z. Anorg. Allg. Chem.* **1998**, *624*, 513; b) $Al_4I_4 \cdot 4D$: A. Ecker, H. Schnöckel, *Z. Anorg. Allg. Chem.* **1996**, *622*, 149.

[8] $Al_{22}Br_{20} \cdot 12THF$: C. Klemp, R. Köppe, E. Weckert, H. Schnöckel, *Angew. Chem.* **1999**, *111*, 1851; *Angew. Chem. Int. Ed.* **1999**, *38*, 1739.

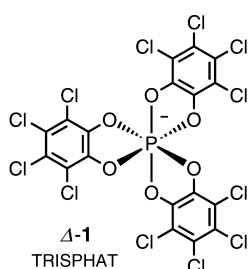
[9] X-ray structure analyses of **1** and **2**: The data were collected on a STOE-IPDS diffractometer with MoK_{α} radiation ($\lambda = 0.71073$) and graphite monochromator. The structures were solved by direct methods and refined anisotropically against F^2 for all observed reflections. Hydrogen atoms were refined in calculated positions according to a riding model. Programs used: SHELXS and SHELXT(L) (G. M. Sheldrick, Universität Göttingen), Resview, Diamond. Crystallographic data (excluding structure factors) for the structures reported in this paper have been deposited with the Cambridge Crystallographic Data Centre as supplementary publication nos. CCDC-143867 (**1**) and CCDC-143868 (**2**). Copies of the data can be obtained free of charge on application to CCDC, 12 Union Road, Cambridge CB21EZ, UK (fax: (+44) 1223-336-033; e-mail: deposit@ccdc.cam.ac.uk). **1**: Colorless needle, $0.3 \times 0.1 \times 0.1 \text{ mm}^3$, measurement temperature 180 K, orthorhombic, space group $Pca2_1$.

- (no. 29), $a = 30.060(3)$, $b = 9.0121(6)$, $c = 16.0246(11)$ Å, $V = 4341.1(6)$ Å³, $Z = 4$, $\rho_{\text{calc}} = 1.644$ Mg m⁻³, $\mu_{\text{Mo}} = 2.938$ mm⁻¹, $\theta_{\text{min}} = 2.26^\circ$, $\theta_{\text{max}} = 20.81^\circ$, reflections: 16026 measured, 4302 independent, 3400 observed, 350 parameters, numerical absorption correction, $R_{\text{int}} = 0.0544$, $R_1 = 0.0428$, $wR_2 = 0.1089$, GOF = 1.046, 1 restraint, max./min. residual electron density 0.501/−0.462 e Å⁻³. The THF molecules in **1** are slightly disordered. This disorder was incorporated in the structure refinement by increased anisotropic temperature factors and H atoms (at calculated positions). Four toluene molecules (likewise disordered) per Al₂I₄ unit are housed in the crystal, which evidently contribute to the low melting point (ca. 0 °C). **2**: Colorless platelets, $0.3 \times 0.2 \times 0.05$ mm³, measurement temperature 200 K, triclinic, space group $P\bar{1}$ (no. 2), $a = 10.980(4)$, $b = 19.075(5)$, $c = 21.080(7)$ Å, $\alpha = 109.88(4)^\circ$, $\beta = 102.07(4)^\circ$, $\gamma = 103.97(2)^\circ$, $V = 3818(2)$ Å³, $Z = 2$, $\rho_{\text{calc}} = 1.835$ Mg m⁻³, $\mu_{\text{Mo}} = 7.496$ mm⁻¹, $\theta_{\text{min}} = 1.93^\circ$, $\theta_{\text{max}} = 24.01^\circ$, reflections: 23476 measured, 11262 independent, 6457 observed, 964 parameters, numerical absorption correction, $R_{\text{int}} = 0.0947$, $R_1 = 0.0546$, $wR_2 = 0.1366$, GOF = 0.879, 100 restraints (for THF in the disordered portion), max./min. residual electron density 0.884/−1.049 e Å⁻³ (localized around Br atoms). Several crystals of **2** from different solutions were investigated by X-ray crystallography. The structure refinement repeatedly revealed a disorder, in particular, of the ligand-bearing Al atoms, in the molecules **2a** and **2b**, which was described by two completely isomeric molecules for **2a** and for **2b**, whereby the one isomer (83%) can be converted into the other isomer (17%) by reflection at the respective central atom (two local inversion centers at Al10 and Al50 in Figure 1). The four ligand-bearing Al atoms of the S_4 -symmetric Al frameworks are thus the only atoms that are not inversion-symmetric, in contrast to the ligand shell (bromide and THF), which, however, determines the packing in the crystal. For a 1:1 disorder and only one type of molecule (thus only one inversion center), this problem could have been solved through the choice of an appropriate space group, as an analogous problem has shown.[8] Here the detailed description using two complete molecules (with $R_1 = 0.0546$ for a reflection/parameter ratio of 6.7) was favored over a description using only disordered Al atoms (with $R_1 \approx 0.09$ for a reflection/parameter ratio of 10). The superposition of these disorders can falsify bond lengths; thus, especially the distances to the central Al atoms (in particular in **2b**) should not be considered and quoted for an exact discussion.
- [10] The bond lengths in **1** lie in the expected range and are similar to those of Al₂I₄·2OEt₂, which were compared with calculated distances in ref. [7a].
- [11] All quantum-chemical calculations were carried out with the RIDFT module (B-P86/SVP functional) of the TURBOMOLE program^[26] with SV(P) basis set on the following systems: [Al₃Br₆·6THF]⁺ in C₁, [Al₃Br₈·4THF][−] in S₄, Al₃Br₇·5THF in C₁ (and analogously for Ga), Al₃Br₄·2H₂O in C_{2h}, Al₂Cl₂₀·12H₂O in C₁.
- [12] The population analysis^[27] of **2a** shows a partial charge of −0.76 for the central Al⁰ atom and +0.12 for the surrounding Al^{II} atoms. In **2b** these values are −0.81 for Al⁰, +0.07 for Al^{II}, and +0.19 for Al^I atoms. The partial charge of the Br atom bound to Al^I (−0.17) is less negative than those for the Br atoms bound to Al^{II}. For these the value is −0.20 and for Br52 as well as Br54 (longer Al–Br bond) −0.24.
- [13] A. Purath, C. Dohmeier, E. Baum, R. Köppe, H. Schnöckel, *Z. Anorg. Allg. Chem.* **1999**, 625, 2214.
- [14] D. Loos, H. Schnöckel, D. Fenske, *Angew. Chem.* **1993**, 105, 1124; *Angew. Chem. Int. Ed. Engl.* **1993**, 32, 1059.
- [15] The smaller spatial requirement of chloride over bromide ligands is evidently well balanced by the smaller radius of Ga, Si, and Ge compared to that of Al.
- [16] Ga₂X₄·2D: J. C. Beamish, A. Boardman, R. W. H. Small, I. J. Worrall, *Polyhedron* **1985**, 4, 983; J. C. Beamish, R. W. H. Small, I. J. Worrall, *Inorg. Chem.* **1979**, 18, 220; R. W. H. Small, I. J. Worrall, *Acta Crystallogr. Sec. B* **1982**, 38, 250.
- [17] Ga₂I₄·2PEt₃, Ga₂I₄·2PPh₃, Ga₃I₅·3PEt₃: A. Schnepf, C. Doriati, E. Möllhausen, H. Schnöckel, *Chem. Commun.* **1997**, 2111.
- [18] An overview of other follow-up products of such insertion reactions with subsequent AlX₃ cleavage revealed compound Si(AlCl₂·OEt₂)₄ which is isoelectronic to **2a**. In the presence of AlCl and AlR this finally leads to a remarkable SiAl₁₄R₆ cluster.^[28]
- [19] An analogous case in the third and fourth periods of Group 15 is PCl₅, which exists in the ionic components PCl₄⁺ and PCl₆[−], whereas AsCl₅ is unstable in the ionic form.
- [20] Calculated reaction energies and free reaction enthalpies do not differ in this reaction, because no entropy is produced. The solvation enthalpy liberated in the reaction in solution is almost identical for the ionic Al and Ga compounds and can here amount to maximal 185 kJ mol^{−1} (dielectric constant $\epsilon_r \rightarrow \infty$) according to the Born equation.^[29] For decreasing polarity it sinks for a THF solution ($\epsilon_r = 7.52$) to 160 kJ mol^{−1}, for diethyl ether ($\epsilon_r = 4.27$) to 142 kJ mol^{−1}, and for toluene ($\epsilon_r = 2.2$) to 101 kJ mol^{−1}. The solvation enthalpy of the uncharged starting materials is neglected in this approximation. Whether the halide transfer favored for **2** already occurs in solution or first in connection with the crystallization, has yet to be verified.
- [21] The organometallic contact ion pair Cp₃⁺Al₃I₆[−] is to date the only example for Al–Al bonds in a cationic component (Cp₂⁺Al₃I₂⁺).^[30]
- [22] A. Purath, R. Köppe, H. Schnöckel, *Angew. Chem.* **1999**, 111, 3114; *Angew. Chem. Int. Ed.* **1999**, 38, 2926.
- [23] A. Ecker, E. Weckert, H. Schnöckel, *Nature* **1997**, 387, 379.
- [24] a) Al₁₂R₈[−]: A. Purath, H. Schnöckel, *Chem. Commun.* **1999**, 1933; b) Al₁₄R₆I₆^{2−}: H. Köhnlein, G. Stößer, E. Baum, E. Möllhausen, U. Huniar, H. Schnöckel, *Angew. Chem.* **2000**, 112, 828; *Angew. Chem. Int. Ed.* **2000**, 39, 799.
- [25] As a low-valent halide, **2** provides a potential reaction channel in the electrolytic deposition of Al, by which initially formed AlX species can immediately react further with AlX₃ present in excess to give Al₂X₄. Further follow-up reactions such as our observed formation of **2**, however, presumably proceed only for large local AlX concentrations. The formation of low-valent aluminum compounds in the anodic oxidation of aluminum under high current density is already known.^[31]
- [26] a) TURBOMOLE: O. Treutler, R. Ahlrichs, *J. Chem. Phys.* **1995**, 102, 346; b) B–P86 functional: A. D. Becke, *Phys. Rev. A* **1998**, 38, 3098, J. P. Perdew, *Phys. B* **1996**, 33, 8822; c) RIDFT: K. Eichkorn, O. Treutler, H. Öhm, M. Häser, R. Ahlrichs, *Chem. Phys. Lett.* **1995**, 242, 652; K. Eichkorn, F. Weigend, O. Treutler, R. Ahlrichs, *Theor. Chem. Acc.* **1997**, 97, 119.
- [27] R. Heinzmann, R. Ahlrichs, *Theor. Chim. Acta* **1985**, 68, 231.
- [28] SiAl₁₄R₆: A. Purath, C. Dohmeier, A. Ecker, R. Köppe, H. Krautscheid, H. Schnöckel, R. Ahlrichs, C. Stoermer, J. Friedrich, P. Jutzi, *J. Am. Chem. Soc.* **2000**, 122, 6955.
- [29] P. W. Atkins, *Physical Chemistry*, 4th ed., Oxford University Press, Oxford, **1990**, p. 248; *Physikalische Chemie*, 2nd ed., VCH, Weinheim, **1996**, S. 298.
- [30] C. Üffing, E. Baum, R. Köppe, H. Schnöckel, *Angew. Chem.* **1998**, 110, 2488; *Angew. Chem. Int. Ed.* **1998**, 37, 2397.
- [31] *Chemistry of Aluminium, Gallium, Indium and Thallium*, (Ed.: A. J. Downs), Blackie Academic & Professional, London, **1993**, S. 198.

Efficient Enantioselective Extraction of Tris(diimine)ruthenium(II) Complexes by Chiral, Lipophilic TRISPHAT Anions**

Jérôme Lacour,* Catherine Goujon-Ginglinger, Sonya Torche-Halldimann, and Jonathan J. Jodry

Chiral tris(diimine)ruthenium(II) complexes have been extensively studied because of their photochemical, photo-physical, and biological properties.^[1] The complexes are commonly synthesized in racemic form and obtained enantiopure by resolution procedures that separate the Δ and Λ enantiomers. Traditionally, resolution of the chiral cationic complexes is realized by the formation of diastereomeric ion pairs with anionic chiral-resolving agents. Selective crystallization^[2] or ion-pair chromatography^[3] may then result in the separation of the diastereomeric salts. We now report a novel enantioselective method of resolution based on the asymmetric extraction of racemic, water-soluble $[\text{Ru}(\text{diimine})_3]\text{Cl}_2$



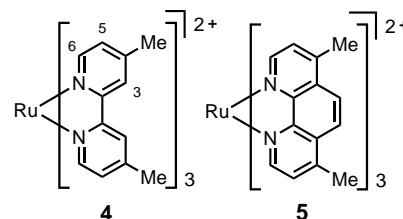
complexes with lipophilic, tris-(tetrachlorobenzenediolato)phosphate(v) (TRISPHAT) salts. Phase separation allows the isolation of the Δ and Λ enantiomers of the ruthenium complexes with selectivity ratios up to 49:1.

The resolution of racemic substrates by preferential extraction of one enantiomer from water into immiscible organic solvents has been well studied.^[4] The extraction and the subsequent selectivity arise from the preferential binding in the organic phase of one enantiomer of the substrate to a chiral lipophilic selector. The racemic substrates are traditionally ammonium salts or zwitterionic amino acids.^[5] Crown ethers with chiral elements in or around the backbone are usually used to ensure the asymmetric discrimination. Selectivity ratios as high as 99:1 have been obtained.^[5g] Recent studies have described the use of novel selectors, such as, lanthanide tris(β -diketonates) and polymeric columnar aggregates of deoxyguanosine.^[6] Of most relevance to our current work is the observation by Lindoy, Everett, and co-workers that chiral Co^{III} amine complexes can be extracted from aqueous layers into CHCl_3 using Lasalocid A as the chiral host with a diastereomeric ratio (d.r.) of up to 2.6:1.^[7]

We recently reported the synthesis and resolution of TRISPHAT anion **1**^[8] which has D_3 symmetry. This anion is an efficient NMR chiral shift reagent and a chiral inducer onto

iron(II) tris(diimine) complexes.^[8] The Λ enantiomer of **1** is isolated as the tri(*n*-butyl)ammonium (**2**) salt (**[2][Λ -1]**) and is soluble in pure CHCl_3 . The Δ enantiomer of **1** is prepared as the cinchonidinium (**3**) salt (**[3][Δ -1]**) and is soluble in more polar solvent mixtures (>7.5% DMSO in CHCl_3). More importantly, we observed that the lipophilic^[9] TRISPHAT anion confers an affinity for organic solvents on these salts and, once dissolved, **[2][Λ -1]** and **[3][Δ -1]** do not partition in aqueous layers. We thus considered using the anions **1** as chiral selectors in asymmetric extraction procedures of chiral cations.

We selected the complexes $[\text{Ru}(4,4'\text{-Me}_2\text{bpy})_3]^{2+}$ (**4**) and $[\text{Ru}(4,7\text{-Me}_2\text{phen})_3]^{2+}$ (**5**) (4,4'-Me₂bpy = 4,4'-dimethylbipyridine; 4,7-Me₂phen = 4,7-dimethylphenanthroline) as chiral substrates because of their solubility in water as dichloride salts. The racemic salts **[4][PF₆]₂** and **[5][PF₆]₂** were prepared



in a single step from $[\text{Ru}(\text{dmsO})_4]\text{Cl}_2$ and three equivalents of the respective ligand.^[10] The solubilization of **[4][PF₆]₂** and **[5][PF₆]₂** in water in the presence of Dowex 1X8 afforded the dichloride salts **[4]Cl₂** and **[5]Cl₂**, respectively, in quantitative yield. The simple and efficient extraction of the cations **4** and **5** by the TRISPHAT anion **1** was then demonstrated. Solutions of the salts **[2][Λ -1]** in CHCl_3 or **[3][Δ -1]** in 7.5–10% DMSO/ CHCl_3 were prepared (10^{-3} M , 1 equiv) and added to the orange solutions of racemic **[4]Cl₂** or **[5]Cl₂** in water (1 equiv). Upon vigorous stirring of the biphasic mixtures, a partial transfer of color from the aqueous to the organic layer occurred.^[11] Several experiments demonstrated that stirring for 10 min is sufficient to complete the extraction.

The organic and aqueous phases were separated, concentrated in vacuo and the resulting orange solid residues analyzed by ^1H NMR spectroscopy. The residue from the aqueous layer contained the chloride complexes that had not been extracted and the cations **2** or **3** that had been transferred from the organic layer during the extraction; no trace of **1** (^{31}P NMR) was observed in the aqueous layer. The residue from the organic layer contained the extracted ruthenium complexes **4** and **5** with two equivalents of the counterion **1** (**[4][1]₂** or **[5][1]₂**). In the experiments performed with the salt **[2][Λ -1]**, we often observed traces of the cation **2** (0–15%) in the organic layer. Cation **2** is associated with a chloride anion and could be removed by washing the organic layer several times with water.

The selectivity of the extraction was readily determined by ^1H NMR spectroscopy. In the organic phases, the enantiopure anions Δ -**1** or Λ -**1**, associated with the cations **4** or **5**, behave as efficient NMR chiral shift reagents.^[8a] With cation **4**, two sets of signals are observed, which correspond to the Δ and Λ enantiomers (Figure 1); the d.r. of $\geq 8.7:1$ was measured by

[*] Dr. J. Lacour, C. Goujon-Ginglinger, S. Torche-Halldimann, J. J. Jodry
Département de Chimie Organique
Université de Genève
quai Ernest Ansermet 30, 1211 Genève 4 (Switzerland)
Fax: (+41)22-328-73-96
E-mail: lacour@sc2a.unige.ch

[**] This work was supported by the Swiss National Science Foundation. We thank A. Pinto, J.-P. Saulnier, W. Kloeti, and E. Sandmeyer for NMR and MS measurements. TRISPHAT = tris(tetrachlorobenzenediolato)phosphate(v).

Supporting information for this article is available on the WWW under <http://www.wiley-vch.de/home/angewandte/> or from the author.

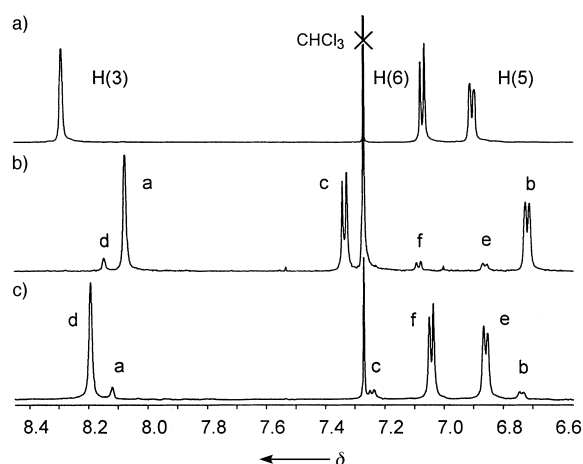


Figure 1. Extraction of $[rac-4]Cl_2$ with $[2][A-1]$. 1H NMR spectra ($\delta = 8.45-6.6$; $[D_6]DMSO/CDCl_3$ (20/80)) of a) $rac-4-Cl_2$, b) the organic layer (d.r. = 8.7:1), and c) the aqueous layer + 2.7 equiv of $[2][A-1]$ (e.r. = 8.4:1). Signals a–c and d–f correspond to the hydrogens H(3), H(5), and H(6) in $[A-4][A-1]_2$ and $[A-4][A-1]_2$, respectively.

integration of the respective signals (Table 1, entries 1 and 2). When the cation **5** was used we could detect the signals of a single diastereomer by 1H NMR spectroscopy. This result indicates that the diastereoselectivity of the extraction of **5** is excellent (d.r. $\geq 49:1$). In both examples with the cations **4** and **5** the diastereoselectivity is largely independent of the source of the TRISPHAT anion.

Table 1. Results of the asymmetric extraction of complexes $[4]Cl_2$ or $[5]Cl_2$ by $[2][A-1]$ or $[3][A-1]$.

Entry	Cation	$S^{[a]}$	EY $^{[b]}$ [%]	OLC $^{[c]}$	d.r. $^{[d]}$	ALC $^{[e]}$	e.r. $^{[f]}$
1 $^{[g]}$	4	Δ	48	Δ	8.7:1	Δ	8.4:1
2 $^{[h]}$	4	Δ	46	Δ	12.3:1	Δ	–
3 $^{[i]}$	5	Δ	45	Δ	> 49:1	Δ	35:1
4 $^{[j]}$	5	Δ	48	Δ	49:1	Δ	–

[a] S is the configuration of the anion **1** in the chiral selector used. [b] EY is the extraction yield. [c] OLC is the configuration of the most abundant enantiomer of the cation in the organic layer. [d] d.r. $^{[d]}$ the diastereomeric ratio. [e] ALC is the configuration of the most abundant enantiomer of the cation in the aqueous layer. [f] e.r. $^{[f]}$ the enantiomeric ratio. [g] Organic layer: $CHCl_3$. [h] Organic layer: 7.5% DMSO in $CHCl_3$. [i] Organic layer: 10% DMSO in $CHCl_3$.

The absolute configurations of the complexes **4** or **5** extracted in the organic layers— Δ and Δ for the experiments with $[2][A-1]$ and $[3][A-1]$, respectively—were assigned by circular dichroism (CD) in 1% DMSO in CH_2Cl_2 . $^{[3a, 12]}$ Homochiral diastereomers ($[A^+][A^-]_2$ and $[A^+][A^-]_2$) are thus preferentially extracted. $^{[13]}$ The CD spectra of the salts $[4]Cl_2$ and $[5]Cl_2$ which remained in the aqueous layer after the extraction and phase separation showed, as expected, opposite Cotton effects.

In the extraction experiments performed with the salt $[2][A-1]$, we also determined the enantiomeric purity of the complexes $[4]Cl_2$ and $[5]Cl_2$, that remained in the aqueous layer after the phase separation (Table 1). $^{[8a, 14]}$ Enantiomeric ratios of 8.4:1 and 35:1 were measured for complexes $[4]Cl_2$ (Figure 1) and $[5]Cl_2$, respectively. The diastereomeric and

enantiomeric ratios—in the organic layer and aqueous layer—are thus quasi identical. This is an important feature of this extraction procedure. In many examples of asymmetric extraction, an excess of the racemic substrate (5- to 35-fold) is used in the presence of the chiral selector. The enantiomeric purity of the substrate that remains in the aqueous layer is then low, even if the diastereoselectivity of the extraction is very high.

Experimental Section

Full details of the experimental and extraction procedures can be found in the Supporting Information.

In a flask (25 mL) equipped with a magnetic stirrer, a solution of either $[4]Cl_2$ or $[5]Cl_2$ (10 μ mol) in water (10 mL) was added to a solution of $[nBu_3NH][A-1]$ (10 μ mol) in $CHCl_3$ (10 mL) or $[cinchonidinium][A-1]$ (10 μ mol) in 7.5–10% DMSO in $CHCl_3$. $^{[15]}$ After 10 min of vigorous stirring the reaction mixture was left to stand for 5 min. The two phases were separated and the organic layer was washed with water. The organic phase was dried (Na_2SO_4), filtered, and concentrated in vacuo to afford an orange solid. The diastereomeric purity of this extracted adduct was measured directly by 1H NMR analysis. The aqueous layer was concentrated in vacuo and dried at 50 °C for 12 h to afford an orange solid. In the experiments performed with $[nBu_3NH][A-1]$, the enantiomeric purity of the complexes $[4]Cl_2$ and $[5]Cl_2$ that remained in the aqueous phases was determined by 1H NMR analysis after the addition of 2–3 equiv of the NMR chiral shift reagent $[nBu_3NH][A-1]$.

Received: February 3, 2000

Revised: May 12, 2000 [Z14645]

- a) A. von Zelewsky, P. Belser, P. Hayoz, R. Dux, X. Hua, A. Suckling, H. Stoeckli-Evans, *Coord. Chem. Rev.* **1994**, 132, 75–85; b) J. K. Barton, *Science* **1986**, 233, 727–734; c) J. K. Barton, *Pure Appl. Chem.* **1989**, 61, 563–564; d) I. Ortmans, C. Moucheron, A. Kirsch-De Mesmaeker, *Coord. Chem. Rev.* **1998**, 168, 233–271.
- a) F. P. Dwyer, E. C. Gyarfas, *J. Proc. R. Soc. N.S.W.* **1949**, 83, 174–176; b) F. P. Dwyer, E. C. Gyarfas, *J. Proc. R. Soc. N.S.W.* **1949**, 83, 170–173; c) R. D. Gillard, R. E. E. Hill, *J. Chem. Soc. Dalton Trans.* **1974**, 1217–1236; d) G. B. Porter, R. H. Sparks, *J. Photochem.* **1980**, 13, 123–131.
- a) T. J. Rutherford, P. A. Pellegrini, J. Aldrich-Wright, P. C. Junk, F. R. Keene, *Eur. J. Inorg. Chem.* **1998**, 1677–1688; b) B. T. Patterson, F. R. Keene, *Inorg. Chem.* **1998**, 37, 645–650; c) N. C. Fletcher, P. C. Junk, D. A. Reitsma, F. R. Keene, *J. Chem. Soc. Dalton Trans.* **1998**, 133–138; d) T. J. Rutherford, M. G. Quagliotto, F. R. Keene, *Inorg. Chem.* **1995**, 34, 3857–3858; e) F. R. Keene, *Coord. Chem. Rev.* **1997**, 166, 121–159; f) J. Lacour, S. Torche-Halldimann, J. J. Jodry, C. Ginglinger, F. Favarger, *Chem. Commun.* **1998**, 1733–1734.
- E. L. Eliel, S. H. Wilen, *Stereochemistry of Organic Compounds*, Wiley, New York, **1994**, pp. 416–421.
- a) E. B. Kyba, K. Koga, L. R. Sousa, M. G. Siegel, D. J. Cram, *J. Am. Chem. Soc.* **1973**, 95, 2692–2693; b) R. C. Helgeson, J. M. Timko, P. Moreau, S. C. Peacock, J. M. Mayer, D. J. Cram, *J. Am. Chem. Soc.* **1974**, 96, 6762–6763; c) S. M. Peacock, D. J. Cram, *J. Chem. Soc. Chem. Commun.* **1976**, 282–285; d) J.-M. Lehn, J. Simon, A. Moradpour, *Helv. Chim. Acta* **1978**, 61, 2407–2418; e) D. S. Lingenfelter, R. C. Helgeson, D. J. Cram, *J. Org. Chem.* **1981**, 46, 393–406; f) V. Prelog, Z. Stojanac, K. Kovacevic, *Helv. Chim. Acta* **1982**, 65, 377–384; g) A. Galán, D. Andreu, A. M. Echavarren, P. Prados, J. de Mendoza, *J. Am. Chem. Soc.* **1992**, 114, 1511–1512; h) K. Maruyama, H. Sohmiya, H. Tsukube, *Tetrahedron* **1992**, 48, 805–818; i) M. V. Martínez-Díaz, J. de Mendoza, T. Torres, *Tetrahedron Lett.* **1994**, 35, 7669–7672; j) Y. Abe, Q. Wang, T. Shoji, S. Fukui, M. Suzuki, T. Kamiyama, M. Kobayashi, H. Nishizawa, *Chem. Pharm. Bull.* **1996**, 44, 1250–1251; k) A. Metzger, K. Gloe, H. Stephan, F. P. Schmidtchen, *J. Org. Chem.* **1996**, 61, 2051–2055; l) H. Tsukube, J. Uenishi, T. Kanatani, H. Itoh, O. Yonemitsu, *Chem. Commun.* **1996**,

- 477–478; m) M. Nazhaoui, J. P. Joly, S. Kitane, M. Berrada, *J. Chem. Soc. Perkin Trans. 1* **1998**, 3845–3850.
- [6] a) H. Tsukube, S. Shinoda, J. Uenishi, T. Kanatani, H. Itoh, M. Shiode, T. Iwachido, O. Yonemitsu, *Inorg. Chem.* **1998**, *37*, 1585–1591; b) V. Andrisano, G. Gottarelli, S. Masiero, E. H. Heijne, S. Pieraccini, G. P. Spada, *Angew. Chem.* **1999**, *111*, 2543–2544; *Angew. Chem. Int. Ed.* **1999**, *38*, 2386–2388.
- [7] a) P. S. K. Chia, L. F. Lindoy, G. W. Walker, G. W. Everett, *J. Am. Chem. Soc.* **1991**, *113*, 2533–2537; b) P. S. K. Chia, L. F. Lindoy, G. W. Walker, G. W. Everett, *Pure Appl. Chem.* **1993**, *65*, 521–526.
- [8] a) J. Lacour, C. Ginglinger, F. Favarger, S. Torche-Halldimann, *Chem. Commun.* **1997**, 2285–2286; b) C. Ginglinger, D. Jeannerat, J. Lacour, S. Jugé, J. Uziel, *Tetrahedron Lett.* **1998**, *39*, 7495–7498; c) J. Lacour, J. J. Jodry, C. Ginglinger, S. Torche-Halldimann, *Angew. Chem.* **1998**, *110*, 2522–2524; *Angew. Chem. Int. Ed.* **1998**, *37*, 2379–2380.
- [9] J. Lacour, S. Barchéath, J. J. Jodry, C. Ginglinger, *Tetrahedron Lett.* **1998**, *39*, 567–570.
- [10] a) I. P. Evans, A. Spencer, G. Wilkinson, *J. Chem. Soc. Dalton Trans.* **1973**, 204–209; b) L. F. Cooley, C. E. L. Headford, C. M. Elliot, D. F. Kelley, *J. Am. Chem. Soc.* **1988**, *110*, 6673–6682.
- [11] In the absence of TRISPHAT salts, no transfer of color from the aqueous to the organic layer is observed.
- [12] a) A. J. McCaffery, S. F. Mason, B. J. Norman, *J. Chem. Soc. (A)* **1969**, 1428–1441; b) M. Ziegler, A. von Zelewsky, *Coord. Chem. Rev.* **1998**, *177*, 257–300.
- [13] Chiral discriminations occur among three-bladed propellers. For leading references see: a) J. Breu, K. J. Range, *Monatsh. Chem.* **1994**, *125*, 141–151; b) J. Breu, C. R. A. Catlow, *Inorg. Chem.* **1995**, *34*, 4504–4510; c) H. Sato, A. Yamagishi, S. Kato, *J. Am. Chem. Soc.* **1992**, *114*, 10933–10940; d) A. Yamagishi, Y. Goto, M. Taniguchi, *J. Phys. Chem.* **1996**, *100*, 1827–1832; e) I. Dance, M. Scudder, *J. Chem. Soc. Dalton Trans.* **1998**, 1341–1350; f) J. Breu, A. J. Stoll, *Acta Crystallogr. Sect. C* **1996**, *52*, 1174–1177; g) J. Breu, P. Belser, H. Yersin, *Acta Crystallogr. Sect. C* **1996**, *52*, 858–861.
- [14] In the experiments performed with [3][4-1], the signals for the aromatic protons of cation 3 overlap with the signals of the [Ru(diimine)₃]²⁺ ions. Our protocol of NMR enantiomeric determination by addition of [2][4-1]^[8a] cannot be used.
- [15] The solutions of [3][4-1] are prepared by dissolution of the salt in DMSO and then dilution with CHCl₃.

Pb₂²⁻ as Ligand in [Ph₄P]₂[(W(CO)₅)₄Pb₂]^{**}

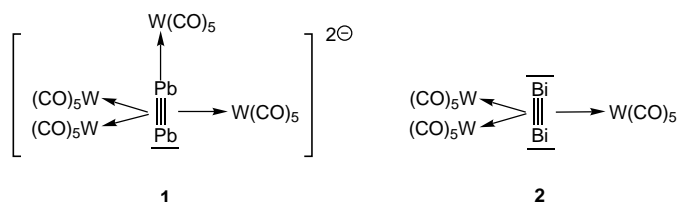
Peter Rutsch and Gottfried Huttner*

*Dedicated to Professor Hans Brintzinger
on the occasion of his 65th birthday*

The heavy element homologues of dinitrogen are only stable at high temperature in the gas phase.^[1] In the condensed phase such compounds can be stabilized by coordination to organometallic building blocks.^[2,3] For the element dimers As₂, Sb₂, and Bi₂ the coordination of the diatomic molecules to three side-on-bound 16-valence-electron complex fragments has proven to be particularly appropriate as a method for stabilizing such units.^[3] In the

cartwheel-shaped compounds [(W(CO)₅)₃X₂] (X = As, Sb, Bi (2)) the distances between the main group elements X are only slightly longer than in the free particles X₂ (cf. d(Bi–Bi) 2.66 Å in Bi_{2(g)}^[1] and 2.82 Å in [(W(CO)₅)₃Bi₂]^[3d]). The three W(CO)₅ building blocks, which symmetrically surround the X₂ unit in the axis of the molecule, can therefore be considered as an organometallic matrix, within which these units are trapped.

As an isoelectronic analogue of Bi₂ it should also be possible to stabilize Pb₂²⁻ in this way.^[4] All attempts, however, to construct this fragment, which is also isoelectronic to C₂²⁻, and to integrate it in a stabilizing matrix have thus far been unsuccessful. We report here on **1**, which was synthesized from [K₂W₂(CO)₁₀] and Pb(NO₃)₂ and was obtained as the tetraphenylphosphonium salt in the form of black, metallic shiny crystals. [(Ph₄P)⁺]₂-**1** dissolves in THF to give an intense violet solution, the IR and ¹³C NMR spectrum of this solution confirm the presence of two types of W(CO)₅ units in **1**. Thus, the known compound [(W(CO)₅)₃Bi₂] (**2**) was prepared for comparison.^[3d]



Compound **2** displays, as expected for a complex with three equivalent W(CO)₅ units, the spectroscopic signature of equivalent, coordinatively bound W(CO)₅ groups with a sharp band at 2054 cm⁻¹ and a broad, intense absorption at 1963 cm⁻¹. The ν_{CO} band pattern in **1** is considerably more complex and its overall appearance and, in particular, the two shortwave bands at 2057 and 2034 cm⁻¹ which display a ratio of intensities of 1:3, indicates that two different sets of W(CO)₅ groups are present in **1**. The anionic character of **1** is evident in a shift of the center of the ν_{CO} bands from 1980 cm⁻¹ in the neutral compound **2** to 1928 cm⁻¹ in **1**. The ¹³C NMR spectrum of **1** shows an intense signal at δ = 202.9 that has both ²⁰⁷Pb and ¹⁸³W satellites (²J_{Pb,C} = 34, ¹J_{W,C} = 124 Hz). This signal is assigned to the equatorial carbonyl groups. The signal for the axial carbonyl groups of the side-on-coordinated W(CO)₅ units (²J_{Pb,C} = 26 Hz) appears at δ = 206.5. The weaker signal of the axial carbonyl group of the terminal W(CO)₅ unit occurs at δ = 208.4 (²J_{Pb,C} = 20, ¹J_{W,C} = 126 Hz). The ratio of intensities and the positions of the signals support the given assignments. The fundamental similarity between the bonding in **1** and **2** mirrors itself in the UV/Vis spectra. The longwave absorption of **2** (570 nm, ε = 11 700 M⁻¹cm⁻¹) corresponds to an absorption of **1** at 583 nm (ε = 4500 M⁻¹cm⁻¹); the prominent absorptions at shorter wavelengths (428 nm (ε = 12 200 M⁻¹cm⁻¹) in **2**; 415 nm (ε = 6600 M⁻¹cm⁻¹) in **1**) as well as the shoulders (340 nm (ε = 13 000 M⁻¹cm⁻¹) in **2**; 320 nm (ε = 21 000 M⁻¹cm⁻¹) in **1**) also correspond. These bands lie in a region, which is characteristic for Bi₂ or the isoelectronic PbTe in the gas phase.^[1] The

[*] Prof. Dr. G. Huttner, Dipl.-Chem. P. Rutsch
Anorganisch-chemisches Institut der Universität Heidelberg
Im Neuenheimer Feld 270, 69120 Heidelberg (Germany)
Fax: (+49) 6221-545-707
E-mail: g.huttner@indi.aci.uni-heidelberg.de

[**] This work was supported by the Fonds der Chemischen Industrie and by the Deutsche Forschungsgemeinschaft (SFB 247).

structure of **1** was determined for crystals of the salt $[(\text{Ph}_4\text{P})^+]_2\text{-1}$ at 233 K.^[5]

Compound **1** contains a dumbbell-shaped Pb_2 unit, which is surrounded in a cartwheel-like fashion by three $\text{W}(\text{CO})_5$ units (W_b , Figure 1) and which carries a further $\text{W}(\text{CO})_5$ group on one end (Pb1 , W_a). The Pb–W distance to the terminally bound $\text{W}(\text{CO})_5$ group is 287 pm, the Pb–W distances to the

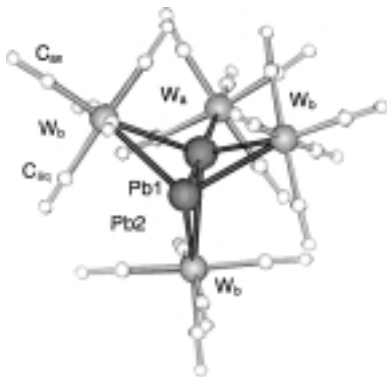


Figure 1. Structure of **1** in the crystal of $[(\text{Ph}_4\text{P})^+]_2\text{-1}$.^[6] Selected bond lengths [pm] and angles [°]: Pb1–Pb2 280.6(8), Pb1– W_a 287.1(8), Pb1– W_b 333.9(1), 326.3(9), 325.1(1), Pb2– W_b 320.2(1), 322.1(5), 322.0(1), W_b – C_{eq} 194.2(1)–204.1(3), W_a – C_{eq} 201.2(1)–205.3(1), W_b – C_{ax} 193.6(1)–195.6(1), W_a – C_{ax} 198.1(1); W_a –Pb1–Pb2 178.1(9), Pb1– W_b –Pb2 50.8(2)–51.4(2), W_b –Pb1–Pb2 62.1(2)–63.7(2), W_b –Pb2–Pb1 64.9(2)–67.1(2), W_a –Pb1– W_b 114.8(3)–117.9(3), W_b –Pb1– W_b 99.1(3)–103.4(3), W_b –Pb2– W_b 100.7(2)–107.3(3).

tungsten centers of the side-on-bound units are significantly longer (325 pm).^[7] These unusually long bond lengths correspond to the likewise unusually long Bi–W distances in **2** (311 pm). The distance between the two lead centers in the axis of the molecule of **1** is only 281 pm. It is the shortest known Pb–Pb distance.^[6] This finding is consistent with the interpretation of the Pb_2 unit in **1** as Pb_2^{2-} , which is stabilized by coordination to $\text{W}(\text{CO})_5$ units. The Bi–Bi distances in $\text{Bi}_{2(g)}$ (266 pm)^[1] and in **2** (282 pm)^[3d] can be considered as a basis for the Pb–Pb distance expected in Pb_2^{2-} . In view of the lower nuclear charge of Pb in comparison to that of Bi, and in view of the two negative charges in **1**, the Pb–Pb distance in Pb_2^{2-} should be longer than the Bi–Bi distance in the isoelectronic $\text{Bi}_{2(g)}$. The observed value of 281 pm for **1** meets this expectation and shows in comparison with the corresponding value of **2** the electronic similarity between Pb_2^{2-} and Bi_2 in the complexes **1** and **2**, respectively. The terminal coordination of an additional $\text{W}(\text{CO})_5$ group in **1** reveals that Pb_2^{2-} can function as an end-on-coordinating Lewis base.

Experimental Section

Synthesis of $[(\text{Ph}_4\text{P})_2][\text{W}(\text{CO})_5]_4\text{Pb}_2$ $[(\text{Ph}_4\text{P})^+]_2\text{-1}$ (experimental conditions see ref. [8]; C,H analyses: Mikroanalytisches Laboratorium, Organisch-chemisches Institut der Universität Heidelberg): $[\text{W}(\text{CO})_6]$ (1755 mg, 5 mmol) was added to a suspension of KC_8 (1350 mg, 10 mmol) in THF (200 mL).^[8, 9] The colorless mixture was stirred for 6 h at room temperature. It changed color progressively from yellow to yellow-brown to brown; the initially strong evolution of CO ceased with time. Filtration through Kieselgur gave a brown solution, from which $[\text{K}_2\text{W}_2(\text{CO})_{10}]$ (760 mg, 1.04 mmol; 42%) precipitated as a yellow-orange powder, after concentration to 10 mL and addition of diethyl ether (100 mL). The

identity of the product was deduced from a comparison of its IR spectrum with that of pure $[\text{Na}_2\text{W}_2(\text{CO})_{10}]$.^[10] For the preparation of **1**, $[\text{K}_2\text{W}_2(\text{CO})_{10}]$ was not isolated, but the suspension was used directly, which according to the stoichiometry and yield still contained unconverted KC_8 . $\text{Pb}(\text{NO}_3)_2$ (2 g, 6 mmol) was added to the reaction mixture, which was then stirred for a further 36 h under exclusion of light. Filtration of the black suspension through Kieselgur (5 cm) and concentration to 3 mL afforded a violet oil, which was purified by chromatography on silica gel (15 cm). After separation of $[\text{W}(\text{CO})_6]$ and other $\text{W}(\text{CO})_5$ -containing compounds with THF, the dipotassium salt of **1** was eluted with ethanol as a deep violet band. After concentration to 5 mL, a solution of Ph_4PCl (1110 mg, 3 mmol) in EtOH (5 mL) was added, which led to the precipitation of $[(\text{Ph}_4\text{P})^+]_2\text{-1}$ in the form of black crystal flakes. After careful decanting the residue was dissolved in THF (≈ 3 mL), layered with ethanol, and left to crystallize. After 5 d $[(\text{Ph}_4\text{P})^+]_2\text{-1}$ (450 mg, 0.19 mmol; 38% yield, based on $[\text{K}_2\text{W}_2(\text{CO})_{10}]$) was obtained in the form of black, metallic shiny crystals. ^1H NMR: $\delta = 7.97$ – 7.79 (m, 40H; H_{arom}); ^{13}C NMR: $\delta = 208.4$ (m, $^2J_{\text{C,Pb}} = 20$ Hz, $^1J_{\text{C,W}} = 126$ Hz, 1C; C_{ax}), 206.5 (t, $^2J_{\text{C,Pb}} = 26$ Hz, 3C; C_{ax}), 202.9 (m, $^2J_{\text{C,Pb}} = 34$, $^1J_{\text{C,W}} = 124$ Hz, 16C; C_{eq}), 135.8–118.4 (m, 48C; C_{arom}); ^{31}P NMR: $\delta = 24.1$ (s, 2P; Ph_4P); IR (THF): $\tilde{\nu}(\text{CO}) = 2057$ (w), 2034 (s), 2013 (vs), 1997 (vs), 1915 (br), 1869 (sh), 1858 cm^{-1} (sh); UV/Vis (THF): $\lambda_{\text{max}}(\epsilon) = 320$ (21000), 415 (6600), 583 nm ($4500\text{ M}^{-1}\text{cm}^{-1}$); elemental analysis (%): calcd: C 34.19, H 1.68; found: C 33.88, H 2.08.

Received: March 22, 2000 [Z14880]

- [1] K. P. Huber, G. Herzberg in *Molecular Spectra and Molecular Structure, IV. Constants of Diatomic Molecules*, Vol. 4, Van Nostrand Reinhold Company, New York, 1979.
- [2] C. F. Campana, A. Vizi-Orosz, G. Palyi, L. Markó, L. F. Dahl, *Inorg. Chem.* **1979**, 18, 3054–3059.
- [3] a) B. Sigwarth, L. Zsolnai, H. Berke, G. Huttner, *J. Organomet. Chem.* **1982**, 226, C5–C8; b) B. Sigwarth, O. Scheidsteger, L. Zsolnai, O. Orama, G. Huttner, *Organometallics* **1985**, 4, 326–332; c) O. Scheidsteger, B. Sigwarth, U. Weber, G. Huttner, *Angew. Chem.* **1982**, 94, 210–211; *Angew. Chem. Int. Ed. Engl.* **1982**, 21, 411; d) U. Weber, L. Zsolnai, G. Huttner, *Z. Naturforsch. B* **1982**, 37, 707–710.
- [4] The bond dissociation energy of Pb_2^{2-} is not known. The experimentally determined sequence of dissociation energies of Pb_2 (8 valence electrons, 0.8 eV), PbBi (9 valence electrons, 1.4 eV), and BiBi (10 valence electrons, 2.0 eV) suggests that Pb_2^{2-} with 10 valence electrons should be comparably stable. For details on the properties of diatomic molecules see ref. [1].
- [5] At lower temperatures the crystals of $[(\text{Ph}_4\text{P})^+]_2\text{-1}$ decompose with retention of their habitus to give an X-ray amorphous powder (for the structure of $[(\text{Ph}_4\text{P})^+]_2\text{-1}$ see ref. [6]).
- [6] Crystal structure data: The X-ray structure analysis was carried out on a Nonius-Kappa-CCD diffractometer with $\text{MoK}\alpha$ radiation ($\lambda_{\text{Mo}} = 0.71074$ Å). Data collection and reduction was performed with the Nonius Software COLLECT.^[11] The SHELXTL-PLUS software package was used for the structure solution and refinement. The structures were solved by direct methods with SHELXS-86 and refined with SHELXL-93.^[12] The program XPM was used for the graphical workup of the data.^[13] The figure was generated with WINRAY-32.^[14] The refinement was carried out anisotropically against F^2 , hydrogen atoms were included in calculated positions. Structure data for **1**: space group $P\bar{1}$, $a = 12.343(3)$, $b = 12.806(3)$, $c = 24.605(5)$ Å, $\alpha = 96.69(3)$, $\beta = 96.94(3)$, $\gamma = 110.85(3)^\circ$, $V = 3554 \times 10^6$ pm³, $\rho_{\text{calcd}} = 2.232$ g cm^{−3}, $2\theta_{\text{max}} = 61.8^\circ$, $Z = 2$, 41 927 measured reflections, 21 593 independent reflections, of which 12 537 were observed ($I > 2\sigma(I)$), 868 refined parameters, $R = 0.051$, $R_w = 0.113$, residual electron density $\leq 4.39 \times 10^{-6}$ e pm^{−3}. (An overview of more than 250 X-ray crystallographically determined Pb–Pb distances is found in the database of the Cambridge Crystallographic Data Centre (status 1999): F. H. Allen, J. E. Davis, J. J. Galloy, O. Johnson, O. Kennard, C. F. Macrae, E. M. Mitchell, G. F. Mitchell, J. M. Smith, D. G. Watson, *J. Chem. Inf. Comput. Sci.* **1991**, 31, 187–204.) Crystallographic data (excluding structure factors) for the structure reported in this paper have been deposited with the Cambridge Crystallographic Data Centre as supplementary publication no. CCDC-141592. Copies of the data can be obtained free of charge on

- application to CCDC, 12 Union Road, Cambridge CB21EZ, UK (fax: (+44) 1223-336-033; e-mail: deposit@ccdc.cam.ac.uk).
- [7] The distances to Pb1, which bears the terminal $W(CO)_5$ group, are all slightly longer than the W_5 –Pb2 distances to the non-terminally coordinated Pb center (see Figure 1).
- [8] P. Kircher, G. Huttner, K. Heinze, *J. Organomet. Chem.* **1998**, 562, 217–227.
- [9] a) M. A. Schwindt, T. Lejon, L. S. Hegedus, *Organometallics* **1990**, 9, 2814–2819; b) J. Maher, R. Beatty, R. Cooper, *Organometallics* **1985**, 4, 1354–1361; c) J. Ellis, S. Hentges, D. Kalina, G. Hagen, *J. Organomet. Chem.* **1975**, 97, 79–93.
- [10] E. Lindner, H. Behrens, S. Birkel, *J. Organomet. Chem.* **1968**, 15, 165–175.
- [11] COLLECT, software for data collection, Nonius, **1998**; <http://www.nonius.com>.
- [12] a) G. M. Sheldrick, SHELXS-86, Program for Crystal Structure Solution, Universität Göttingen, **1986**; b) G. M. Sheldrick, SHELXL-93, Program for Crystal Structure Refinement, Universität Göttingen, **1993**; <http://www.shelx.uni-ac.gwdg.de/shelx/index.html>; c) *International Tables for X-Ray Crystallography*, Vol. 4, Kynoch, Birmingham, **1974**.
- [13] L. Zsolnai, G. Huttner, XPM, Universität Heidelberg, **1998**; <http://www.rzuser.uni-heidelberg.de/~v54/xpm.html>.
- [14] R. Soltek, G. Huttner, WINRAY-32, Universität Heidelberg, **1998**; <http://www.rzuser.uni-heidelberg.de/~v54>.

Strong Field Iron(II) Complex Converted by Light into a Long-Lived High-Spin State**

Franz Renz,* Hiroki Oshio, Vadim Ksenofontov, Markus Waldeck, Hartmut Spiering, and Philipp Gülich*

Octahedral coordination compounds of transition metal ions with a d^4 to d^7 electronic configuration can be classified according to the ligand-field strength (LFS) into three groups: 1) low-spin (LS) state (strong LFS); 2) high-spin (HS) state (weak LFS), and 3) thermal spin crossover between $HS \leftrightarrow LS$ (intermediate LFS), for example in the case of iron(II) complexes with a $HS(^5T_{2g}) \leftrightarrow LS(^1A_{1g})$ transition.^[1]

More than ten years ago, the surprising observation was made that thermally switchable Fe^{II} spin-crossover complexes can also be optically switched from the LS to the HS state (LIESST=light-induced excited spin-state trapping^[(2), (1a)]) and from the HS to the LS state (reverse LIESST^[(1a)]).

Usually, LS Fe^{II} complexes decay after photoexcitation within nanoseconds from the metastable HS state back to the

LS state.^[3] Herein, we report on an entirely unexpected observation: Complex molecules of $[Fe(tpy)_2]^{2+}$ ($tpy = 2,2':6',2''$ -terpyridine) embedded at a 2% concentration in the host matrix of the corresponding manganese compound $[Fe_{0.02}Mn_{0.98}(tpy)_2](ClO_4)_2$ (**1**) exhibit LS behaviour at room temperature, yet may be converted by light to the HS state with an effectively infinite lifetime (low-temperature tunneling lifetime $t_{HL}^0 > 10^5$ s) at 10 K (LIESST effect).

The compounds **1** and $[Fe(tpy)_2](ClO_4)_2$ (**2**) were prepared by literature methods.^[4a, 5] The Mössbauer spectra^[4b] of **1** (Figure 1) and **2** exhibit LS behavior at ambient and lower temperatures ($^1A_{1g}$ ground state). The spectra of **1** at 300, 170, and 10 K each exhibits a quadrupole doublet of isomer shift values ($\delta = 0.13, 0.20, 0.22$ mm s⁻¹) and quadrupole splitting values ($\Delta E_Q = 0.98, 0.95, 0.98$ mm s⁻¹), respectively. These values are typical for LS Fe^{II} .^[6]

Figure 2 shows the Mössbauer spectrum of **1** recorded after 30 min irradiation with green light at 10 and 80 K. At 10 K the spectrum now contains two quadrupole doublets: one ($\delta = 0.22$ mm s⁻¹, $\Delta E_Q = 0.97$ mm s⁻¹) originates from the original LS ground state; the other ($\delta = 0.95$ mm s⁻¹, $\Delta E_Q = 2.08$ mm s⁻¹) is indicative of Fe^{II} in the HS state (LIESST).^[6] Presuming the Lamb–Mössbauer factors for the LS and HS states are equal, the fraction of $[Fe(tpy)_2]^{2+}$ complex molecules converted by light to the long-lived LIESST state is 66%, as estimated from the area fraction of the HS doublet. The spectrum recorded at 80 K (Figure 2) shows only the quadrupole doublet ($\delta = 0.21$ mm s⁻¹, $\Delta E_Q = 0.94$ mm s⁻¹) of the original LS ground state. This observation—which shows that the light-induced metastable HS state has relaxed back to the LS state—was fully reproducible. No light-induced spin-state conversion was observed for compound **2**, the pure iron compound.

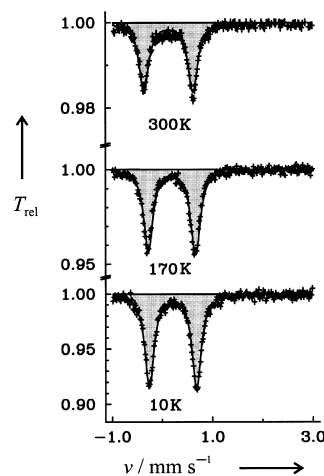


Figure 1. Mössbauer spectra of **1** at 300, 170, and 10 K. The spectra indicate only one quadrupole doublet, which is typical for Fe^{II} in the LS state.

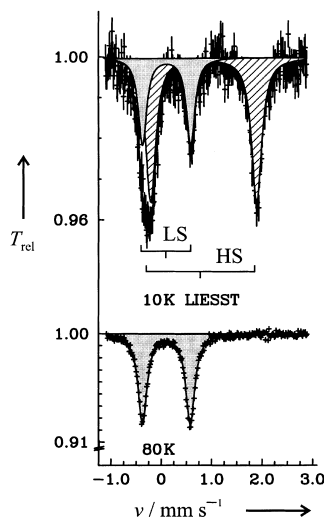


Figure 2. Mössbauer spectrum of compound **1** after irradiation with green light at 10 K. Comparison with Figure 1 shows that the major fraction has been converted to the HS state. After heating to 80 K, the Mössbauer spectrum indicated only the LS state remained.

[*] Dr. F. Renz, Prof. Dr. P. Gülich, Dr. V. Ksenofontov, M. Waldeck, Dr. habil. H. Spiering
Institut für Anorganische Chemie und Analytische Chemie
Universität Mainz, Staudinger Weg 9, 55099 Mainz (Germany)
Fax: (+49) 6131-39-22990
E-mail: Franz.Renz@uni-mainz.de
P.Guelich@uni-mainz.de

Prof. Dr. H. Oshio
Department of Chemistry
Graduate School of Science
Tohoku University, Sendai 980-8578 (Japan)

[**] We are grateful for financial support from the TMR Research Network No. ERB-FMRX-CT98-0199, the Fonds der chemischen Industrie, and the University of Mainz (MWFZ).

Compounds **1** and **2** contain aromatic ligands with energetically low lying π^* orbitals, which favour the appearance of metal-to-ligand charge-transfer (MLCT) transitions. The population of the metastable HS states of Fe^{II} occurs essentially through MLCT transitions (as recognized by the intense color of the LS complexes), which cover the weaker d–d transitions. Excitation at 514 nm excites primarily the $^1A_1 \rightarrow ^1MLCT_1$ transition (Figure 3).

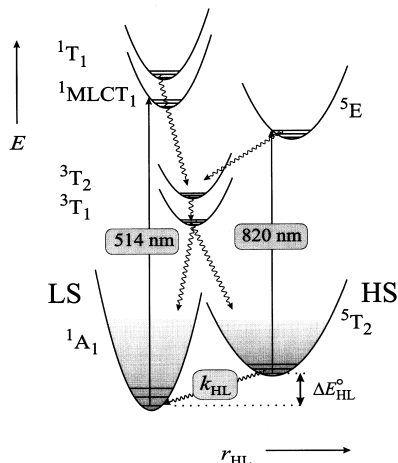


Figure 3. Mechanism of the “light-induced excited spin-state trapping” (LIESST) and reverse LIESST.

The relaxation kinetics of the decaying LIESST state was examined experimentally by Hauser^[3] and described with a nonadiabatic multiphonon relaxation model based on an earlier theory proposed by Buhks et al.^[7] One of the essential features of the model is that t_{HL}^0 (namely, the low temperature tunneling relaxation rate $k_{HL}^0 = (t_{HL}^0)^{-1}$) of the LIESST state is strongly correlated with the energy difference ΔE_{HL}^0 between the lowest vibronic levels of the HS and LS states involved (inverse energy-gap law; Figure 3). The energy gap ΔE_{HL}^0 increases with increasing LFS. Since ΔE_{HL}^0 is not experimentally accessible, Hauser^[3] instead presented the logarithm of k_{HL}^0 versus the transition temperature $T_{1/2}$ (the temperature at which 50% of the Fe^{II} centers are in the HS state during the thermal spin transition) for a series of spin-crossover compounds (Figure 4).

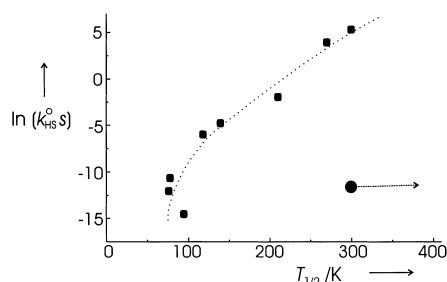


Figure 4. Experimental low-temperature tunneling rates $\ln k_{HL}^0$ plotted against $T_{1/2}$ for some Fe^{II} spin-crossover complexes^[3] (square). The dashed line indicates the trend of the inverse energy-gap law. Complex **1** deviates unexpectedly from this law (circle; with $T_{1/2} \gg 300$ K). The data are from reference [3] ($T_{1/2}$ values in K): [Fe/Zn(ptz)₆](BF₄)₂ (95), [Fe/Mn(pic)₃]Cl₂·EtOH (76), [Fe/Zn(pic)₃]Cl₂·EtOH (78), [Fe/Mn(pic)₃]Cl₂·MeOH (118), [Fe/Zn(pic)₃]Cl₂·MeOH (140), [Fe/Zn(mepy)₃(tren)](PF₆)₂ (210), [Fe(mepy)₂(py)(tren)]²⁺ in PMMA (270). ptz = 1-*n*-propyltetrazole, pic = α -picoline, mepy = 2-methylpyridine, tren = tris(2-aminoethyl)amine.

The idea behind this approximation is that $T_{1/2}$, given by the Boltzmann population of the HS manifold, is essentially proportional to ΔE_{HL}^0 . Hauser^[3] therefore collected data of highly diluted compounds and complexes of similar type (with six nitrogen donor atoms around the metal), such that the vibrational partition functions are similar. From the dependence of $T_{1/2}$ on t_{HL}^0 , short t_{HL}^0 are expected for strong-field complexes of Fe^{II} with LS behaviour at room temperature, that is, $T_{1/2}$ is well above room temperature. For example, t_{HL}^0 is on the order of microseconds for tris(bipyridine) iron(II) complexes^[3] (15 μ s for [Fe/Zn(bipy)₃](PF₆)₂ at 10 K) and of nanoseconds for tris(phenanthroline) iron(II) complexes^[8] (<6 ns for [Fe/Zn(phen)₃](PF₆)₂ at 10 K). Experimentally, we found a lifetime for the metastable HS state of complex **1** of the order of several days at ≤ 20 K. The observed lifetime of the LIESST state in **1** is more than eight orders of magnitude larger than expected on the basis of the inverse energy-gap law. We therefore name this new phenomenon the strong-field LIESST effect (SF-LIESST).

In conclusion, we have found that metal-diluted LS Fe^{II} complexes also show a LIESST effect; so far the LIESST effect has appeared to be restricted to thermal spin-crossover complexes of Fe^{II} with a $T_{1/2}$ below about 200 K. These results introduce a new class of optically switchable Fe^{II} complexes with possible device applications. While we are not yet able to explain the unexpectedly long lifetime of the optically induced LIESST state in an Fe^{II} complex, which is in the LS state at room temperature, low temperature X-ray diffraction and EXAFS studies before and after irradiation are underway to explore this aspect further.

Received: March 21, 2000 [Z14874]

- [1] a) P. Gütllich, A. Hauser, H. Spiering, *Angew. Chem.* **1994**, *106*, 2109–2141; *Angew. Chem. Int. Ed. Engl.* **1994**, *33*, 2024–2054; b) P. Gütllich, *Struct. Bonding (Berlin)* **1981**, *44*, 83–195; c) E. König, *Struct. Bonding (Berlin)* **1991**, *76*, 53–150.
- [2] S. Decurtins, P. Gütllich, K. M. Hasselbach, A. Hauser, H. Spiering, *Inorg. Chem.* **1985**, *24*, 2174–2178.
- [3] a) A. Hauser, *Comments Inorg. Chem.* **1995**, *17*, 17–40, and references therein; b) A. Hauser, *Habilitationsschrift*, Universität Mainz, **1991**, and references therein.
- [4] a) As per literature procedures,^[5] a methanolic terpyridine solution was added slowly to a methanolic, mixed-metal chloride solution. Precipitation occurred after addition of NaClO₄. The salts FeCl₂, MnCl₂, and the tpy ligand were used as supplied by Aldrich Company. For ⁵⁷Fe Mössbauer measurements on the diluted system with only 2% iron, it was necessary to synthesize **1** with ⁵⁷Fe-enriched (about 90%) salts which were prepared from metallic ⁵⁷Fe with HCl. The purity of the complexes was checked by elemental analysis and the iron content by AAS. b) For Mössbauer measurements, about 30 mg of the polycrystalline ⁵⁷Fe-enriched samples were placed in a disc-shaped, polished PMMA container (approximately 4 cm² surface) and mounted in a helium cryostat for temperature variation between 10 K and 300 K. ⁵⁷Fe Mössbauer spectra were recorded with a conventional spectrometer (measuring time typically 60 minutes per spectrum) and the isomer shift values are relative to α -iron. The samples were irradiated at 10 K with an argon-ion laser (514 nm, 25 mW cm⁻²).
- [5] R. Hogg, R. G. Wilkins, *J. Chem. Soc.* **1962**, 341–350.
- [6] P. Gütllich, R. Link, A. Trautwein, *Mössbauer Spectroscopy and Transition Metal Chemistry*, Springer, Berlin, **1978**.
- [7] E. Buhks, G. Navon, M. Bixon, J. Jortner, *J. Am. Chem. Soc.* **1980**, *102*, 2918–2923.
- [8] A. Hauser, *Chem. Phys. Lett.* **1990**, *173*, 507–512.

In situ Transfer of Parahydrogen-Induced Nuclear Spin Polarization—Structural Characterization of Hydrogenation Intermediates**

Patrick Hübler and Joachim Bargon*

Recently, we reported the in situ detection of hydrogenation products intermediately attached to cationic Rh^{I} -diphosphane catalysts during the homogeneous hydrogenation of styrene derivatives.^[1, 2] The detection of these hydrogenation intermediates present in very low concentrations was possible using PHIP NMR spectroscopy (PHIP = *para*hydrogen-induced polarization), which takes advantage of the large signal enhancement produced by the (pairwise) transfer of para-enriched hydrogen.^[3, 4] The intermediate product–catalyst complexes have a life time of a few seconds at room temperature.^[2] Several facts indirectly lead to the conclusion that the arene ring of the product molecule, for a short time, remains η^6 -coordinated to the Rh^{I} center.^[1] However, no direct proof for the intermediate bonding between the catalyst and the product molecule could so far be obtained. Based on the PHIP effect, we present the first NMR experiments that detect intra- and intermolecular cross relaxation (NOE)^[5] within the life time of a hydrogenation intermediate. To that end, we used two NMR pulse sequences that, in one of many possible applications, detect a polarization transfer from the methylene proton of hydrogenated $[\text{D}_8]\text{styrene}$ to the *o*-phenyl protons of the active catalyst species $[\text{Rh}(\text{dppb})]^+$.^[6] In this class of catalysts, the four phenyl groups form an “edge-face” array that, in the analogous case of chiral diphosphane ligands, represents the template for enantio-recognition of prochiral substrates.^[7] In future work, polarization transfer from suitable auxiliary molecules to the surrounding will be used to investigate enantioselective hydrogenation, molecular recognition, and the structure of protein cavities with improved sensitivity.

The NOE is most frequently used for structural investigations with NMR spectroscopy,^[8, 9] even though cross correlation effects recently have been exploited for this purpose.^[10, 11] In contrast to conventional NMR spectroscopy, the initial density operator of PHIP is described by longitudinal two-spin order, $I_{1z}I_{2z}$ (with the two former parahydrogen nuclei numbered by 1 and 2).^[4] However, bilinear operators can hardly be used to investigate intermolecular^[12] interactions because the correlation of two spins is lost if the interaction is not pairwise.^[13] Hence, the first step of the pulse sequences presented below is to convert two-spin order into longitudinal

magnetization, I_{1z} (or into I_{1y} if an ROE^[15] is used). Subsequently, the polarization is transferred to nuclei in the surrounding by cross relaxation by either an NOE or an ROE. We propose the reduction of two-dimensional to one-dimensional experiments in order to minimize the number of scans for in situ investigations under nonstationary conditions. The one-dimensional DPGSE-NOE and GOESY^[14] experiments developed by Shaka et al.^[15, 16] form the basis for the development of pulse sequences for an NOE transfer in PHIP experiments. We chose the DPGSE-NOE principle instead of GOESY because diffusion processes in low-viscosity solvents dramatically reduce the signal intensity in longer periods of spatial dephasing by pulsed-field-gradients.^[15] To detect an in situ transfer of polarization, we developed the pulse sequences PH-1D-NOESY and PH-1D-ROESY outlined in Figure 1.

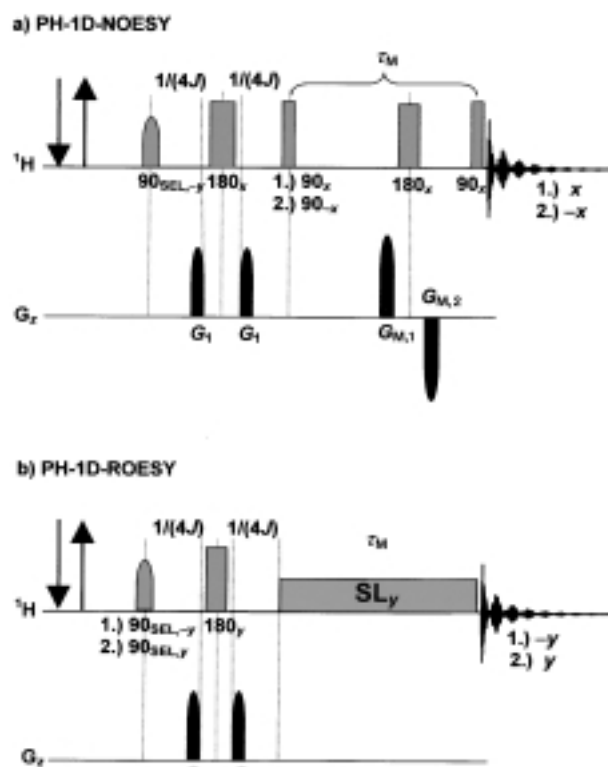


Figure 1. a) PH-1D-NOESY pulse sequence. The gray half ellipse represents the selective (SEL) pulse; the black half ellipses represent pulsed field gradients. The arrows indicate the up and down motion of the capillary providing a constant stream of parahydrogen. b) PH-1D-ROESY pulse sequence. SL_y represents a ROESY spinlock period with phase y .

By means of the excitation sequence $90_y(1)-1/(4J)-G_1-180_x-G_1-1/(4J)-90_x$, the operator $2I_{1z}I_{2z}$ is transformed into I_{1z} .^[17, 18] This preparation sandwich is superior to the excitation by nonselective 45° pulses normally used,^[3] because zero- (and double-) quantum coherence generated in the latter case produces artifacts in NOESY spectra. Furthermore, when using a selective excitation sandwich, the spectra represent rows of two-dimensional experiments.^[19]

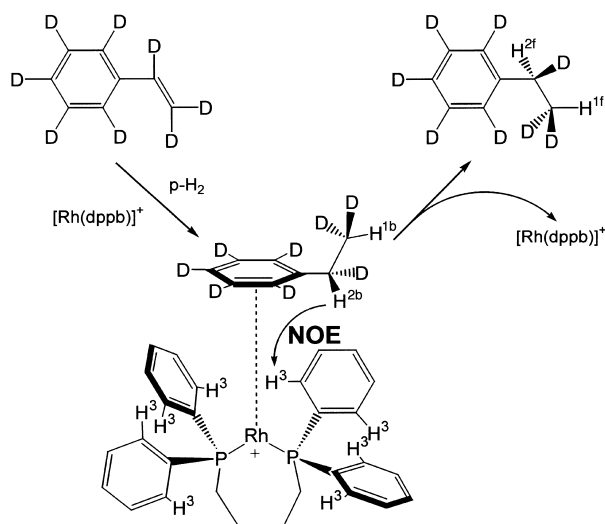
Imperfections of the pulses are eliminated by the pulsed field gradients. During the mixing time, τ_M , of the PH-1D-

[*] Prof. Dr. J. Bargon, Dr. P. Hübler
Institut für Physikalische und Theoretische Chemie der Universität
Wegelerstrasse 12, 53115 Bonn (Germany)
Fax: (+49)228-739-424
E-mail: bargon@uni-bonn.de

[**] This work was supported by the Deutsche Forschungsgemeinschaft and the Fonds der Chemischen Industrie. P. Hübler thanks the Fonds der Chemischen Industrie for a graduate fellowship. We thank Prof. Dr. S. J. Glaser (Technische Universität München, Germany) for valuable discussions.

NOESY sequence (Figure 1a), I_{1z} is transferred to other nuclei by means of either cross relaxation or chemical reactions. Longitudinal magnetization produced by the thermal equilibrium and flipped by the 90_x pulse is eliminated by the pulsed field gradients during τ_M . Observable magnetization not created by means of the selective excitation is subtracted in every second scan. Additionally, T_1 recovery of thermally induced magnetization is reduced by the 180_x pulse during the mixing period τ_M . In contrast to conventional NMR experiments, $\langle I_{1z} \rangle$ and $-\langle I_{1z} \rangle$ both relax to zero because the density operator of the thermal equilibrium can be neglected. Therefore, in-phase magnetization is transferred during the entire mixing time and is accumulated by the phase cycling. Relayed production of two-spin order due to the hydrogenation is not observable.

The pulse sequence PH-1D-NOESY was applied to the reaction depicted in Scheme 1. For our experiments, we chose $[D_8]$ styrene as the substrate to approximately establish the



Scheme 1. Observable steps of the hydrogenation of $[D_8]$ styrene with $[Rh(dppb)]^+$.

simple condition of an AX spin system in the product. To observe small effects under real catalytic conditions, we used $[Rh(dppb)(cod)]BF_4$ as the catalyst precursor in D_2O/CD_3OD (2:3; $c = 0.5$ mm). The resulting PH-1D-NOESY spectra are shown in Figure 2.

As can be seen in Figure 2b, in situ polarization transfer from attached $[D_8]$ ethylbenzene to the *o*-phenyl protons H^3 of the catalyst occurs when proton H^{2b} is excited selectively. This proves that H^{2b} and H^3 are connected through a time-modulated dipolar interaction causing the cross relaxation rate σ^{NOE} .^[20] According to Figure 2a, no cross relaxation occurs if the corresponding proton H^{2f} of free $[D_8]$ ethylbenzene is excited. The signals between $\delta = 0.9$ and 2.7 stem from a superposition of the detachment process of $[D_8]$ ethylbenzene (leading to a peak with positive intensity) and the dipolar interactions between H^{1b} and H^{2b} and H^{1f} and H^{2f} (leading to a peak with negative intensity). Compared to the excitation of H^{2b} , a smaller signal is detected at the resonance of the catalyst if the methyl proton H^{1b} is excited (Figure 2c).

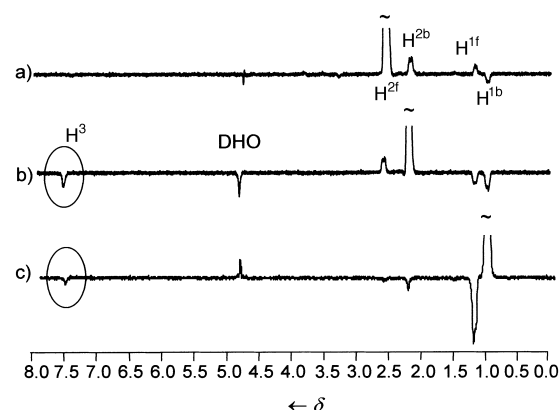


Figure 2. Experimental results of applying the PH-1D-NOESY sequence to the reaction depicted in Scheme 1. The resonance excited by the selective pulse is cut off. Each spectrum was recorded with four scans.

This corresponds to the larger (time-averaged) distance to the catalyst. The negative signal for H^{1f} in Figure 2c is a consequence of partially exciting this proton. For all experiments, Gaussian-shaped selective pulses with a duration of 35 ms were used.

An intramolecular NOE transfer from dihydride ligands to *o*-phenyl protons based on the PHIP effect has already been observed in the case of a steady-state formation of stable Ir^I di- and trihydride complexes.^[21, 22] The spectra in Figures 2 and 3, however, represent the first direct proof of a dipolar interaction between a hydrogenated molecule and a catalyst within an intermediate state. PH-1D-NOESY experiments are restricted to cases where this intermediate lives for a period of time (at least half a second) that is long enough for an in situ detection.

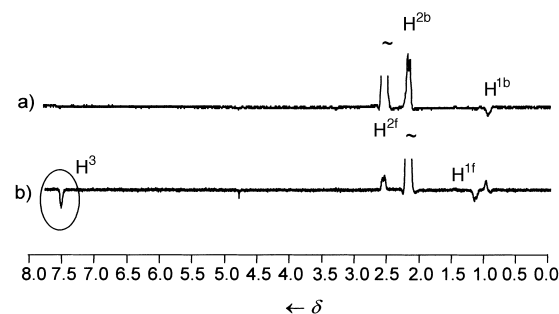


Figure 3. Experimental results of applying the PH-1D-ROESY sequence to the reaction depicted in Scheme 1. Each spectrum was recorded with four scans.

In medium-sized molecules where the spectral density function for cross relaxation is small or even zero, the ROESY technique usually is applied which detects cross relaxation in the rotating frame.^[23] During a spinlock-period, (in-phase) y -magnetization is transferred to the neighboring protons. The corresponding pulse sequence PH-1D-ROESY is outlined in Figure 1b. Again, phase cycling is used to eliminate all magnetization that has not been produced by the selective excitation sequence. Under the same experimental conditions as chosen for the experiments in Figure 2 but using the pulse sequence PH-1D-ROESY, very similar spectra are obtained

(Figure 3). Again, excitation of the proton H^{2b} yields a cross relaxation signal at the resonance of the catalyst proton H^3 , whereas excitation of the proton H^{2f} does not.

Experimental Section

All NMR experiments were conducted at 298 K using a Bruker DRX200 spectrometer. The chemicals were used as obtained by Aldrich. The enrichment of parahydrogen was performed at 77 K catalyzed by activated charcoal. For the PHIP experiments, the resulting 50:50 mixture of ortho- and parahydrogen was bubbled through the reactive solution inside of the magnetic field for 3 s.

Received: March 30, 2000
Revised: June 13, 2000 [Z14922]

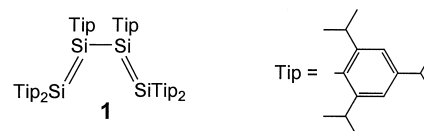
- [1] R. Giernoth, P. Hübler, J. Bargon, *Angew. Chem.* **1998**, *110*, 2649–2651; *Angew. Chem. Int. Ed.* **1998**, *37*, 2473–2475.
- [2] P. Hübler, R. Giernoth, G. Kümmerle, J. Bargon, *J. Am. Chem. Soc.* **1999**, *121*, 5311–5318.
- [3] S. B. Duckett, C. J. Sleight, *Prog. NMR Spectrosc.* **1999**, *34*, 71–92.
- [4] J. Natterer, J. Bargon, *Prog. NMR Spectrosc.* **1997**, *31*, 293–315.
- [5] NOE = nuclear Overhauser effect; ROE = rotating frame nuclear Overhauser effect.
- [6] dppb = diphenylphosphanylbutane; cod = cycloocta-1,5-diene.
- [7] J. Halpern, *Science* **1982**, *217*, 401–407.
- [8] J. Cavanagh, W. J. Fairbrother, A. G. Palmer III, N. J. Skelton, *Protein NMR Spectroscopy. Principles and Practice*, 1st ed., Academic Press, San Diego, **1996**.
- [9] D. Williamson, M. P. Neuhaus, *The Nuclear Overhauser Effect in Structural and Conformational Analysis*, VCH, New York, **1989**.
- [10] B. Reif, M. Hennig, C. Griesinger, *Science* **1997**, *276*, 1230–1233.
- [11] B. Reif, H. Steinhausen, B. Junker, M. Reggelin, C. Griesinger, *Angew. Chem.* **1998**, *110*, 2006–2009; *Angew. Chem. Int. Ed.* **1998**, *37*, 1903–1906.
- [12] The term “intermolecular” in this case means: short-time contact between the molecules and no J coupling between the two interacting nuclei.
- [13] N. R. Skrynnikov, R. R. Ernst, *J. Magn. Reson.* **1999**, *137*, 276–280.
- [14] NOESY = nuclear Overhauser spectroscopy; GOESY = gradient-enhanced nuclear Overhauser spectroscopy; DPGSE = double pulsed-field-gradient spin-echo.
- [15] K. Stott, J. Keeler, Q. N. Van, A. J. Shaka, *J. Magn. Reson.* **1997**, *125*, 302–324.
- [16] K. Stott, J. Stonehouse, T. L. Hwang, J. Keeler, A. J. Shaka, *J. Am. Chem. Soc.* **1995**, *117*, 4199–4200.
- [17] J. Barkemeyer, J. Bargon, H. Sengstschmidt, R. Freeman, *J. Magn. Reson. A* **1996**, *120*, 129–132.
- [18] H. Sengstschmidt, R. Freeman, J. Barkemeyer, J. Bargon, *J. Magn. Reson. A* **1996**, *120*, 249–257.
- [19] H. Kessler, S. Mronga, G. Gemmecker, *Magn. Reson. Chem.* **1991**, *29*, 527–557.
- [20] Semiempirical structure calculations indicate that the *o*-phenyl protons H^3 and the proton H^{2b} have a short distance in the intermediate complex.
- [21] C. J. Sleight, S. B. Duckett, B. A. Messerle, *Chem. Commun.* **1996**, 2395–2396.
- [22] S. Hasnip, S. B. Duckett, D. R. Taylor, M. J. Taylor, *Chem. Commun.* **1998**, 923–924.
- [23] A. A. Bothner-By, R. L. Stephens, J.-M. Lee, C. D. Warren, R. W. Jeanloz, *J. Am. Chem. Soc.* **1984**, *106*, 811–813.

Hexaaryltetragermabuta-1,3-diene: A Molecule with Conjugated Ge–Ge Double Bonds**

Helmut Schäfer, Wolfgang Saak, and
Manfred Weidenbruch*

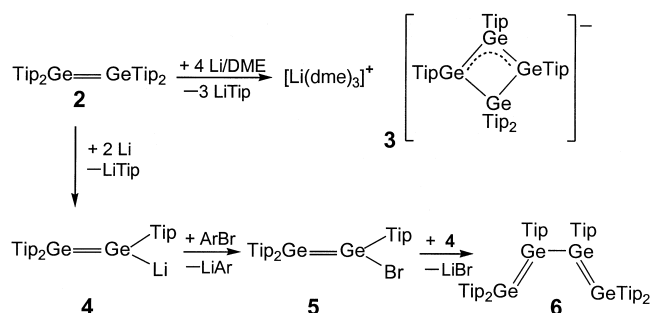
With the recent isolation of the first diplumbenes,^[1, 2] molecules containing a short lead–lead double bond, homo-nuclear double bonds of the type $R_2E=ER_2$ ($E = C, Si, Ge, Sn, Pb$) are now known between all elements of Group 14.^[3] The strong decrease in bond dissociation energies of these double bonds from silicon to lead is reflected in the distinctly different behavior in the crystalline state and in solution. Under exclusion of air and moisture all compounds are stable in the solid state. This is also true for solutions of most disilenes, whereas digermenes tend to dissociate partly into germylenes $R_2Ge\cdot$. Distannenes and diplumbenes, on the other hand, exist almost exclusively as stannylenes $R_2Sn\cdot$ and plumbylens $R_2Pb\cdot$ in solution.^[3]

Recently, we obtained the tetrasilabuta-1,3-diene **1**, the first and to date only molecule containing conjugated Si–Si double bonds. The most remarkable feature of this brownish-red



substance **1** is that it adopts the *s-cis* conformation in the solid state,^[4] which is also the favored form in solution. We have now examined if the germanium compound **6** analogous to **1** is accessible by following a similar synthetic approach (Scheme 1).

As a starting compound we chose the tetraaryldigermene **2** whose structural integrity, according to previous investiga-



Scheme 1. Ar = 2,4,6-Me₃C₆H₂ (Mes), 2,4,6-*i*Pr₃C₆H₂ (Tip).

[*] Prof. Dr. M. Weidenbruch, Dipl.-Chem. H. Schäfer, Dipl.-Chem. W. Saak
Fachbereich Chemie der Universität
Carl-von-Ossietzky-Strasse 9–11, 26111 Oldenburg (Germany)
Fax: (+49) 441-798-3352
E-mail: Manfred.Weidenbruch@Univ.Oldenburg.de

[**] Compounds of Germanium, Tin, and Lead, Part 37. This work was supported by the Deutsche Forschungsgemeinschaft and the Fonds der Chemischen Industrie. Part 36: F. Meiners, W. Saak, M. Weidenbruch, *Organometallics* **2000**, *19*, 2835–2836.

tions, is also retained in solution,^[5, 6] and for which we recently found a synthetic approach that yields acceptable quantities.^[7] In contrast to a previous report,^[5] treatment of **2** with an excess of lithium did not afford the digermenyllithium compound **4**, but instead we obtained a dark-red solid, which, owing to its insolubility and low volatility, could only be characterized by an X-ray structure analysis (Figure 1).^[8]

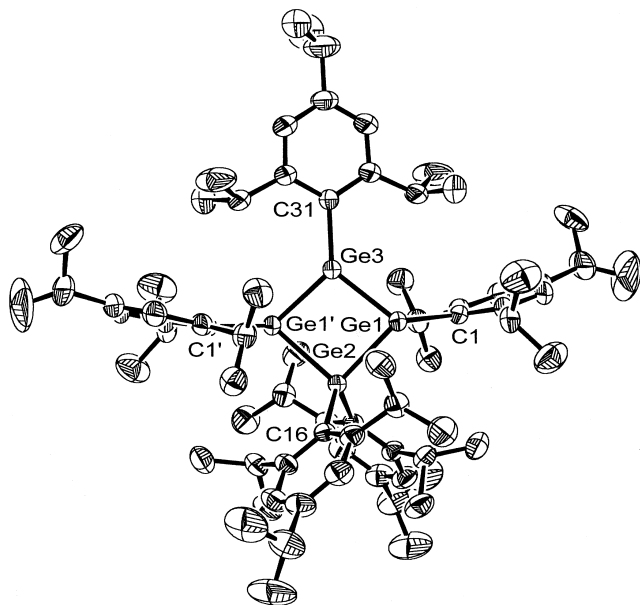


Figure 1. Structure of the anion of **3** in the crystal (hydrogen atoms omitted, ellipsoids at the 50% probability level). Selected bond lengths [pm] and angles [°]: Ge1–Ge2 251.16(6), Ge1–Ge3 236.79(6), Ge1–C1 202.2(5), Ge2–C16 203.2(4), Ge3–C31 200.3(6); Ge1–Ge3–Ge1' 97.71(3), Ge3–Ge1–Ge2 85.93(2), Ge1–Ge2–Ge1' 90.44(3)

In accordance with the observed properties we found an ionic compound (**3**) containing an allyl-like Ge₃ ion as part of a four-membered ring. Within this planar ring (sum of angles 360°) the Ge–Ge multiple bonds differ substantially in length from the Ge–Ge single bonds. This bond type in the anion of **3**, unusual to germanium chemistry, can best be compared to the acyclic, allyl-like Ge₃ anion, obtained by Power et al. from the cleavage of a cyclotrigermeryl radical with KC₈.^[10]

Precisely how **3** is formed remains unclear, since it not only involves the cleavage of Ge–C bonds in **2**, but also the formation of Ge–Ge bonds. In order to eliminate all subsequent reactions of the primarily expected compound **4**, we shortened the reaction time of **2** with lithium to such an extent, that most of the digermene **2** had reacted before the formation of **3** could become the main reaction. This approach did indeed lead to compound **4**, which by subsequent reaction with an aryl bromide presumably resulted in the bromine derivative **5**, from which compound **6** was formed by intermolecular coupling under elimination of LiBr.

The X-ray structure analysis^[8] of the resulting greenish-black crystals did not only confirm the constitution of the tetragermabutadiene **6**, it also revealed some remarkable details (Figure 2). Similar to **1**, compound **6** does adopt the *s-cis* form. The dihedral angle of the Ge₄ framework (22.5°) is notably smaller than in the corresponding Si₄ unit (51°). With

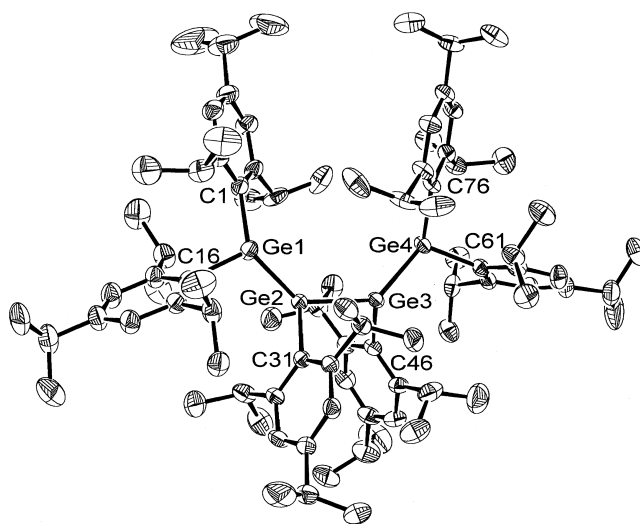


Figure 2. Structure of **6** in the crystal (hydrogen atoms omitted, ellipsoids at the 50% probability level). Selected bond lengths [pm] and angles [°]: Ge1–Ge2 235.68(6), Ge2–Ge3 245.81(5), Ge3–Ge4 234.39(5), Ge1–C1 198.5(4), Ge1–C16 199.6(4), Ge2–C31 200.3(3), Ge3–C46 199.7(4), Ge4–C61 193.3(4), Ge4–C76 198.6(3); Ge1–Ge2–Ge3 136.18(2), Ge2–Ge3–Ge4 134.99(2), Ge2–Ge1–C1 126.0(1), Ge2–Ge1–C16 109.8(1), Ge1–Ge2–C13 108.9(1), Ge4–Ge3–C46 101.25(10), Ge3–Ge4–C61 112.56(10), Ge3–Ge4–C76 126.2(1)

an average value of 235 pm the Ge–Ge double bonds are considerably elongated in comparison to those in the digermene **2** (221.3(1) pm), although they are still in the range of typical digermenes.^[3, 11] The length of the formal Ge–Ge single bond (245.81(5) pm) in **6** is in good agreement with the normal bond length. Compared to the analogous bonds in **3**, a considerable shortening is observed. In analogy to the angles in **1** the Ge–Ge–Ge bond angles in **6** are also widened significantly with a mean value of 135.5°.

Both Ge–Ge double bonds display a considerable *trans* bending of the substituents away from the respective Ge=Ge vector. The values of 35.4 and 31.1° for the Ge1–Ge2 bond and 33.3 and 31.1° for the Ge3–Ge4 bond are among the largest *trans* pyramidalization so far observed in digermenes.^[3, 11] In addition, both double bonds show a small but noticeable torsion, with values of 22.4° (Ge1–Ge2) and 21.3° (Ge3–Ge4).

Even though the crystal structure of **6** reveals the existence of two Ge–Ge double bonds, it does not give any information about a possible conjugation between these bonds. The electronic spectrum is more revealing: The dark blue solution of **6** in *n*-hexane shows a longest wavelength absorption at 560 nm, which compared to the yellow or orange digermenes,^[11] corresponds to a bathochromic shift of about 140 nm and even exceeds the absorptions of tetrasilyldigermenes^[12] by almost 100 nm.

With compound **6**, we have succeeded for the first time in the isolation, albeit in a low yield, of a thermally stable, yet extremely air-sensitive molecule with conjugated Ge–Ge double bonds. Owing to the nearly complete dissociation of distannenes and diplumbenes in solution into stannylenes and plumbynes, it seems doubtful whether this result may be applied to the heavier homologues tin and lead.

Experimental Section

Lithium powder (0.100 g, 14.4 mmol) was added to a solution of **2** (1.23 g, 1.28 mmol) in DME (70 mL). The initially black mixture turned red and was stirred for five hours at room temperature. Insoluble compounds were filtered off and the solution was treated with 1-bromo-2,4,6-triisopropylbenzene (0.220 g, 0.78 mmol) at -18°C . Over a period of ten hours the solution was slowly warmed to room temperature. DME was removed and the precipitate was dissolved in *n*-hexane (10 mL). Renewed filtration, concentration to a volume of 3 mL, and cooling to -30°C afforded greenish-black crystals of **6** (0.103 g; 11% yield). M.p. $175-182^{\circ}\text{C}$. ^1H NMR (500 MHz, $[\text{D}_8]\text{THF}$, 25°C): $\delta = 0.02-0.10$ (m, 6H), 0.19 (d, 6H, $J = 6.6$ Hz), 0.29 (d, 6H, $J = 6.6$ Hz), 0.35 (d, 6H, $J = 6.6$ Hz), 1.05–1.17 (m, 48H), 1.21 (d, 12H, $J = 6.6$ Hz), 1.42 (d, 6H, $J = 6.6$ Hz), 1.51 (d, 6H, $J = 6.6$ Hz), 1.56 (d, 6H, $J = 6.6$ Hz), 1.60 (d, 6H, $J = 6.6$ Hz), 2.70 (sept, 4H), 2.75 (sept, 2H), 2.84 (sept, 2H), 3.09 (sept, 2H), 3.24 (sept, 2H), 3.35 (sept, 2H), 4.11 (sept, 2H), 4.27 (sept, 2H), 6.55 (s, 2H), 6.76 (s, 2H), 6.78 (s, 2H), 6.80 (s, 2H), 6.94 (s, 2H), 7.11 (s, 2H); ^{13}C NMR (125 MHz, $[\text{D}_8]\text{THF}$, 25°C): $\delta = 14.39, 23.49, 23.93, 24.11, 24.20, 24.28, 24.36, 24.51, 27.07, 32.51, 32.51, 34.99, 35.04, 35.27, 35.39, 37.99, 39.93, 122.14, 122.33, 122.64, 122.76, 123.52, 123.69, 142.00, 144.52, 148.05, 149.41, 150.47, 151.21, 152.45, 153.58, 154.12, 154.59$; UV/Vis (*n*-hexane): $\lambda_{\text{max}}(\epsilon) = 405$ (10450), 560 (12750) nm; C,H analysis: calcd: C 71.56, H 9.21; found: C 71.30, H 9.03.

Received: June 13, 2000 [Z15259]

Functionalized Tellurium(II) Thiolates: Tellurium Bis(2-hydroxyethanethiolate) Hydrate, the First $\text{H}_2\text{O}-\text{Te}^{\text{II}}$ Complex**

Holger Fleischer* and Dieter Schollmeyer

Tellurium(II) thiolates, $\text{Te}(\text{SR})_2$ ($\text{R} = \text{alkyl, aryl}$) are of both chemical^[1–5] and biochemical^[6] interest. Thiolates $\text{Te}(\text{SR})_2$, in which R contains a functional group, have not yet been described, despite their potential interest for synthetic and structural chemistry, for example the synthesis of precursors for the production of HgTe or CdTe semiconductors by chemical vapor deposition (CVD). We report here the synthesis of the first representative of this class of compounds and the crystal structure of its monohydrate.

Reaction of TeO_2 with $\text{HOCH}_2\text{CH}_2\text{SH}$ yields $\text{Te}(\text{SCH}_2\text{CH}_2\text{OH})_2$ by a reductive elimination according to Equation (1).^[7] With exclusion of light, solutions of $\text{Te}(\text{SCH}_2\text{CH}_2\text{OH})_2$ in CDCl_3 are stable at room temperature for several days. On the other hand, ^1H NMR spectroscopy reveals rapid decomposition and the formation of Te and $(\text{SCH}_2\text{CH}_2\text{OH})_2$, when such a solution is irradiated with UV light ($\lambda = 254$ nm). The decomposition obeys first-order kinetics, suggesting a monomolecular mechanism for the photolysis. Preliminary results show that the OH groups of $\text{Te}(\text{SCH}_2\text{CH}_2\text{OH})_2$ can be acetylated, and a more comprehensive account of its chemistry will be published in due course.



The complex $\text{Te}(\text{SCH}_2\text{CH}_2\text{OH})_2 \cdot \text{H}_2\text{O}$ was obtained at -45°C from an ethanolic solution of $\text{Te}(\text{SCH}_2\text{CH}_2\text{OH})_2$ containing traces of water.^[8] The $\text{Te} \cdots \text{O}$ distance (249.5(10) pm) is in the range of known intramolecular dative $\text{O} \rightarrow \text{Te}$ interactions, for example 223.7(8) pm in 2-benzamidyldibromotellurium,^[11] and 324.4(2) pm in 4-methoxyphenyl-(*O*-methylxanthogenato)tellurium.^[12] The sum of the bond angles at the tellurium center is approximately 310° ; thus, the configuration of the three-coordinate Te atom can be described as distorted trigonal pyramidal. In the solid state, $\text{Te}(\text{SCH}_2\text{CH}_2\text{OH})_2$ molecules form chains through $\text{O}3-\text{H}3 \cdots \text{O}6'$ hydrogen bonds (Figure 1); the structural parameters of the hydrogen bond are similar to those in ice.^[13] Adjacent chains are linked through short $\text{O}-\text{H} \cdots \text{S}$ hydrogen bonds (cf reference [13]).

The strong intermolecular interactions lead to significant differences between the molecular structure of $\text{Te}(\text{SCH}_2\text{CH}_2\text{OH})_2 \cdot \text{H}_2\text{O}$ optimized by ab initio methods and its structure in the crystal. In particular, the $\text{Te}-\text{O}$ bond

The strong intermolecular interactions lead to significant differences between the molecular structure of $\text{Te}(\text{SCH}_2\text{CH}_2\text{OH})_2 \cdot \text{H}_2\text{O}$ optimized by ab initio methods and its structure in the crystal. In particular, the $\text{Te}-\text{O}$ bond

- [1] M. Stürmann, W. Saak, H. Marsmann, M. Weidenbruch, *Angew. Chem.* **1999**, *111*, 145–147; *Angew. Chem. Int. Ed.* **1999**, *38*, 187–189.
- [2] M. Stürmann, W. Saak, M. Weidenbruch, K. W. Klinkhammer, *Eur. J. Inorg. Chem.* **1999**, 579–582.
- [3] For recent reviews see a) P. P. Power, *Chem. Rev.* **1999**, *99*, 3463–3502; b) M. Weidenbruch, *Eur. J. Inorg. Chem.* **1999**, 373–381.
- [4] M. Weidenbruch, S. Willms, W. Saak, G. Henkel, *Angew. Chem.* **1997**, *106*, 2612–2613; *Angew. Chem. Int. Ed. Engl.* **1997**, *36*, 2503–2504.
- [5] J. Park, S. A. Batcheller, S. Masamune, *J. Organomet. Chem.* **1989**, *367*, 39–45.
- [6] W. Ando, H. Itoh, T. Tsumuraya, *Organometallics* **1989**, *8*, 2759–2766.
- [7] H. Schäfer, W. Saak, M. Weidenbruch, *Organometallics* **1999**, *18*, 3159–3163.
- [8] Crystal structure analyses: Stoe-IPDS area detector, MoK_α radiation, graphite-monochromator; $T = 193(2)$ K. The structures were solved by direct methods and refined by full-matrix least-squares techniques against F^2 .^[9] Hydrogen atoms were placed in calculated positions and refined with isotropic temperature factors; all other atoms were refined anisotropically. **6**: $\text{C}_{90}\text{H}_{138}\text{Ge}_4 \cdot \text{DME}$, triclinic, space group $P\bar{1}$, $a = 1576.46(7)$, $b = 1579.47(5)$, $c = 1991.89(6)$ pm, $\alpha = 78.570(4)$, $\beta = 72.713(4)$, $\gamma = 79.400(5)^{\circ}$, $Z = 2$, $V = 4600.2(3) \times 10^6$ pm³, $\rho_{\text{calcd}} = 1.155$ g cm⁻³, $2\theta_{\text{max}} = 52^{\circ}$. Of 56147 measured reflections, 16544 were independent, and 10596 observed for $I > 2\sigma(I)$. $R1 = 0.0460$, $wR2 = 0.1007$ (all data) for 901 parameters. **3**: $\text{C}_{87}\text{H}_{145}\text{Ge}_4\text{LiO}_6$, monoclinic, space group $C2/c$, $a = 2116.74(5)$, $b = 1800.15(7)$, $c = 2537.82(6)$ pm, $\beta = 113.395(2)^{\circ}$, $Z = 4$, $V = 8875.2(5) \times 10^6$ pm³, $\rho_{\text{calcd}} = 1.186$ g cm⁻³, $2\theta_{\text{max}} = 52^{\circ}$. Of 32739 measured reflections, 8135 were independent, and 4949 observed for $I > 2\sigma(I)$. $R1 = 0.0538$, $wR2 = 0.1553$ (all data) for 429 parameters. Crystallographic data (excluding structure factors) for the structures reported in this paper have been deposited with the Cambridge Crystallographic Data Centre as supplementary publication no. CCDC-145476 (**6**) and CCDC-145477 (**3**). Copies of the data can be obtained free of charge on application to CCDC, 12 Union Road, Cambridge CB21EZ, UK (fax: (+44) 1223-336-033; e-mail: deposit@ccdc.cam.ac.uk).
- [9] G. M. Sheldrick, SHELXL-97, program for crystal structure refinement, Universität Göttingen, **1997**.
- [10] M. M. Olmstead, L. Pu, R. S. Simons, P. P. Power, *Chem. Commun.* **1997**, 1595–1595.
- [11] Review: K. M. Baines, W. G. Stibbs, *Adv. Organomet. Chem.* **1996**, *39*, 275–324.
- [12] M. Kira, T. Iwamoto, T. Maruyama, C. Kabuto, H. Sakurai, *Organometallics* **1996**, *15*, 3767–3769.

[*] Dr. H. Fleischer
Institut für Anorganische Chemie und Analytische Chemie
Johannes-Gutenberg-Universität Mainz
Duesbergweg 10–14, 55099 Mainz (Germany)
Fax: (+49) 6131-3923351
E-mail: fleische@mail.zdv.uni-mainz.de
Dr. D. Schollmeyer
Institut für Organische Chemie
Johannes-Gutenberg-Universität (Germany)

[**] This work was supported by the Fonds der Chemischen Industrie.

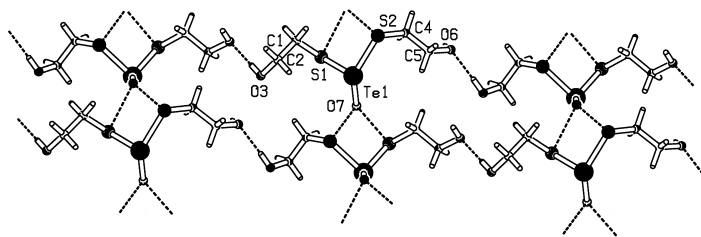


Figure 1. Packing diagram of $\text{Te}(\text{SCH}_2\text{CH}_2\text{OH})_2 \cdot \text{H}_2\text{O}$ in the crystal. Selected distances [pm] and angles [°]: Te1-S1 239.4(3), Te1-S2 240.1(3), Te1-O7 249.5(10), S1-C1 179.9(12), S2-C4 181.5(12), C1-C2 149.9(17), C4-C5 149.2(18), C2-O3 143.4(17), C5-O6 142.8(14), O3-O6' 276.2(12), O7-S1' 277.4(14), O7-S2' 252.2(15); S1-Te1-S2 101.3(1), S1-Te1-O7 75.2(3), S2-Te1-O7 133.0(3), Te1-S1-C1 103.8(4), Te1-S2-C4 104.5(4), S1-C1-C2 114.6(8), S2-C4-C5 111.3(8), C1-C2-O3 113.6(10), C4-C5-O6 113.0(10), O3-H3-O6' 174.6; O7-Te1-S1-C1 152.9(5), O7-Te1-S2-C4 -8.6(6), C1-S1-Te1-S2 -75.4(4), C4-S2-Te1-S1 -88.8(4), C2-C1-S1-Te1 -72.2(8), C5-C4-S2-Te1 -81.6(8), O3-C2-C1-S1 -63.9(12), O6-C5-C4-S2 178.9(8).

(249.5(10) pm), which arises mainly from an $n(\text{O})-\sigma^*(\text{Te}-\text{S})$ interaction (32.8 kJ mol⁻¹), is significantly longer in the isolated molecule (296.4 pm) than in the solid state structure. The ¹H NMR chemical shifts of the OCH₂ and SCH₂ groups of $\text{Te}(\text{SCH}_2\text{CH}_2\text{OH})_2 \cdot \text{H}_2\text{O}$ correspond to those of $\text{Te}(\text{SCH}_2\text{CH}_2\text{OH})_2$, which suggests complete dissociation of the adduct in CDCl₃ solution. The absolute values of the S-Te-S-C torsion angles are close to 90° (calculated: 75.1 and 81.1°), as was found for other $\text{Te}(\text{SR})_2$ compounds;^[4] this may be attributed to strong hyperconjugative (n_p)S¹-σ(Te-S²) interactions (69.3 kJ mol⁻¹).

Experimental Section and Computational Methods

NMR: Bruker DRX 400, 25 °C, $B_1(^1\text{H}) = 400.0$, $B_1(^{125}\text{Te}) = 126.387$ MHz; standards: TMS (¹H) and Te(CH₃)₂ (¹²⁵Te). IR: Mattson Galaxy 2030 FTIR, resolution 4 cm⁻¹, CsI pellet, 4000–200 cm⁻¹.

$\text{Te}(\text{SCH}_2\text{CH}_2\text{OH})_2$: HSCH₂CH₂OH (10.24 g, 131.1 mmol) and TeO₂ (5.00 g, 31.4 mmol) were suspended in methanol (40 mL) and concentrated HCl (0.2 mL) was added. The suspension was stirred in the dark for 60 h at room temperature and then filtered. The solid residue was washed several times with methanol, and the combined filtrates were concentrated and kept for two days at -45 °C. $\text{Te}(\text{SCH}_2\text{CH}_2\text{OH})_2$ precipitated as a yellow-orange solid. Yield: 5.32 g (60.1 %). M.p. 58–60 °C (decomp). Elemental analysis (%): C₄H₁₀O₂S₂Te, $M = 281.84$ g mol⁻¹; calcd: C 17.05, H 3.58; S 22.75; found: C 17.06, H 3.48, S 22.41; ¹H NMR (CDCl₃): δ = 3.84 (t, ³J(H,H) = 5.6 Hz, 2H; OCH₂); 3.33 (t, ³J(H,H) = 5.6 Hz, 2H; SCH₂); 2.30 (br., 1H; OH); ¹²⁵Te NMR (CDCl₃): δ = 1234.2; IR: $\tilde{\nu} = 3275$ vs (ν(O-H)), 2909 s (ν(C-H)), 2858 s (ν(C-H)), 1465 s (δ(CH₂)), 1403 s (δ(CH₂)), 1013 vs (ν(C-O)), 726 (ν(S-C)), 417 m (ν(Te-S)), 335 s (ν(TeS₂)).

The ab initio calculations were performed on various servers of the Zentrum für Datenverarbeitung, Universität Mainz, using the GAUSSIAN94 software package.^[15, 16]

Received: April 11, 2000 [Z14973]

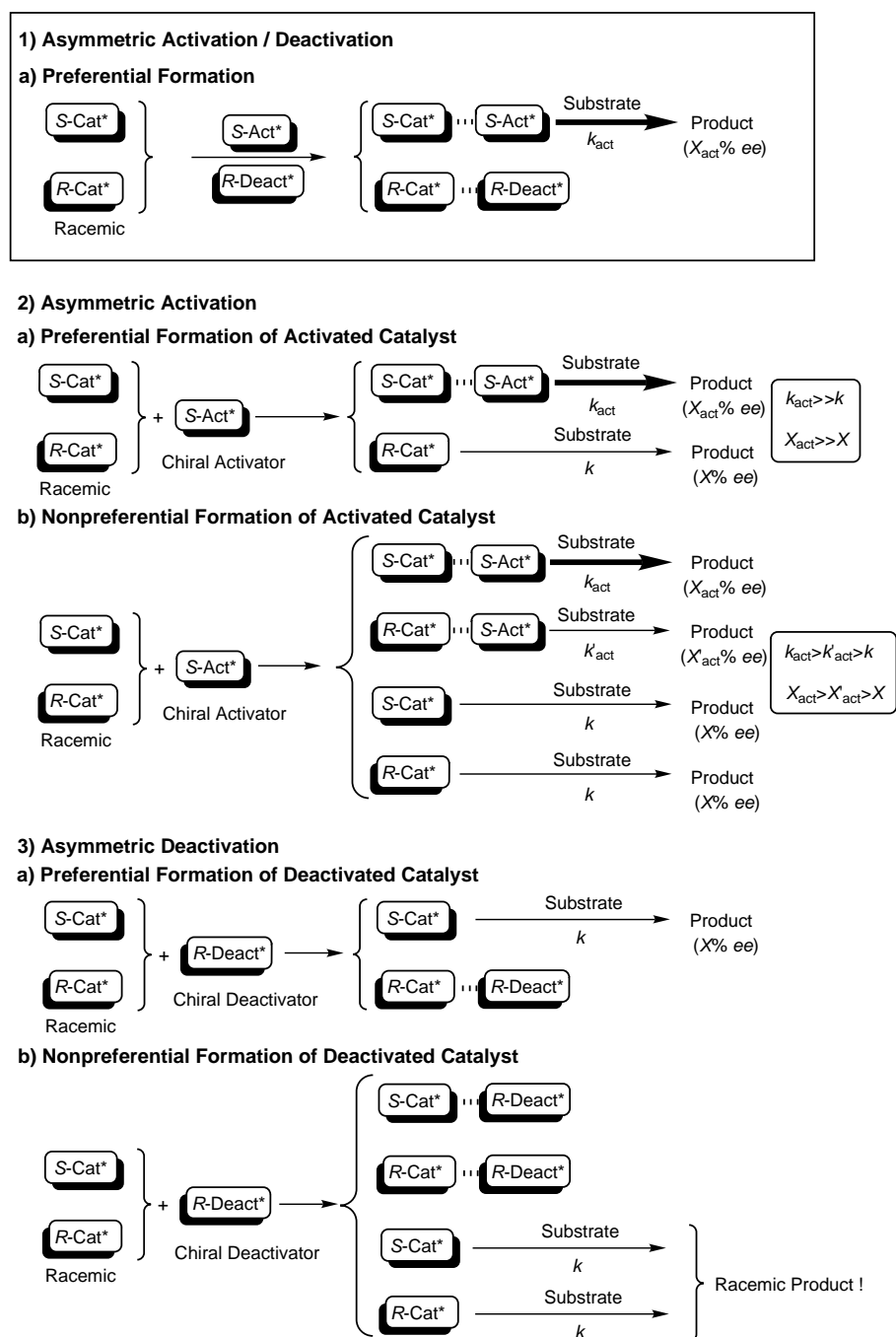
- [1] W. Mazurek, A. G. Moritz, M. J. O'Connor, *Inorg. Chim. Acta* **1986**, 113, 143–146.
- [2] E. A. Stukalo, E. M. Yur'eva, L. N. Markovskii, *Zh. Org. Khim.* **1983**, 19, 343–346.
- [3] T. Chivers, *J. Chem. Soc. Dalton Trans.* **1996**, 1185–1194.
- [4] H. Fleischer, S. Stauf, D. Schollmeyer, *Inorg. Chem.* **1999**, 38, 3725–3729.

- [5] R. E. Allan, H. Gornitzka, J. Kärcher, M. A. Paver, M.-A. Rennie, C. A. Russell, P. R. Raithby, D. Stalke, A. Steiner, D. S. Wright, *J. Chem. Soc. Dalton Trans.* **1996**, 1727–1730.
- [6] A. Albeck, H. Weitman, B. Sredni, M. Albeck, *Inorg. Chem.* **1998**, 37, 1704–1712.
- [7] The reactivity of monothio glycol hence differs from that of *o*-sulfanyphenol, which does not reduce Te^{IV} to Te^{II}: a) Werner Schnabel, PhD Thesis, Universität Hamburg, **1980**; b) K. von Deuten, W. Schnabel, G. Klar, *Cryst. Struct. Commun.* **1980**, 9, 161–165.
- [8] $\text{Te}(\text{SCH}_2\text{CH}_2\text{OH})_2 \cdot \text{H}_2\text{O}$, $M_r = 299.86$, m.p. 45–47 °C, monoclinic, space group *Pc*, $a = 1104.1(4)$, $b = 480.5(2)$, $c = 870.7(3)$ pm, $\beta = 103.769(5)^\circ$, $V = 0.4486(5)\text{nm}^3$; $Z = 2$; $\rho_{\text{calc}} = 2.220\text{Mg m}^{-3}$, $\lambda = 0.71073\text{pm}$, $T = 187\text{K}$, crystal dimensions $0.125 \times 0.145 \times 0.228\text{mm}^3$; Siemens-P4 diffractometer, $2\theta_{\text{max}} = 56^\circ$, 4166 reflections, 2115 independent ($R_{\text{int}} = 0.055$), observed 1692, $R = 0.0525$ ($|F| > 4\sigma(F)$), $wR2 = 0.1291$, max./min. residual electron density $2.51/-1.65\text{e}\text{\AA}^{-3}$. Structure solution by direct methods (SIR92),^[9] refinement against F^2 (SHELXL-97).^[10] Hydrogen atoms were refined with a riding model. The hydrogen atoms of the water molecule were not found in the analysis of the single-crystal X-ray structure. Their presence could be established by the signal intensity of the H atoms attached to O atoms relative to that of the H atoms attached to C atoms in a ¹H NMR spectrum of other crystals from the same sample. Crystallographic data (excluding structure factors) for the structure reported in this paper have been deposited with the Cambridge Crystallographic Data Centre as supplementary publication no. CCDC-143980. Copies of the data can be obtained free of charge on application to CCDC, 12 Union Road, Cambridge CB21EZ, UK (fax: (+44) 1223-336-033; e-mail: deposit@ccdc.cam.ac.uk).
- [9] SIR—a program for the automatic solution of crystal structures by direct methods: A. Altomare, G. Casciaro, C. Giacovazzo, A. Guagliardi, M. C. Burla, G. Polidori, M. Camalli, *J. Appl. Crystallogr.* **1994**, 27, 435–436.
- [10] G. M. Sheldrick, SHELXL-97, Program for crystal structure refinement, Universität Göttingen, **1997**.
- [11] L. Dupont, O. Dideberg, J. Lamotte, L.-J. Piette, *Acta Crystallogr. Sect. B* **1979**, 35, 849.
- [12] S. Husebye, K. Maarthmann-Moe, O. Mikalsen, *Acta Chem. Scand.* **1989**, 43, 754–756.
- [13] L. Pauling, *The Nature of the Chemical Bond and the Structure of Molecules and Crystals*, 3rd ed., Cornell University Press, Cornell, **1960**.
- [14] K. Mereiter, A. Preisinger, A. Zellner, W. Mikenda, H. Steidl, *J. Chem. Soc. Dalton Trans.* **1984**, 1275–1277.
- [15] Gaussian 94, Revision E.1, M. J. Frisch, G. W. Trucks, H. B. Schlegel, P. M. W. Gill, B. G. Johnson, M. A. Robb, J. R. Cheeseman, T. Keith, G. A. Petersson, J. A. Montgomery, K. Raghavachari, M. A. Al-Laham, V. G. Zakrzewski, J. V. Ortiz, J. B. Foresman, J. Cioslowski, B. B. Stefanov, A. Nanayakkara, M. Challacombe, C. Y. Peng, P. Y. Ayala, W. Chen, M. W. Wong, J. L. Andres, E. S. Replogle, R. Gomperts, R. L. Martin, D. J. Fox, J. S. Binkley, D. J. Defrees, J. Baker, J. P. Stewart, M. Head-Gordon, C. Gonzalez, J. A. Pople, Gaussian, Inc., Pittsburgh, PA, **1995**.
- [16] Geometry optimization and single-point energy calculation of $\text{Te}(\text{SCH}_2\text{CH}_2\text{OH})_2 \cdot \text{H}_2\text{O}$ (*C*₁-Symmetry) was performed at the MP2 level by using a double-zeta effective core potential basis set, according to Hay and Wadt,^[17] augmented by polarization functions for Te, S, O, and C determined by Höllwarth et al. (MP2/LANL2DZP).^[18] The hyperconjugative interaction in the natural bond orbital (NBO) basis was calculated by using the method developed by Reed et al.^[19]
- [17] W. R. Wadt, P. J. Hay, *J. Chem. Phys.* **1985**, 82, 284–298.
- [18] A. Höllwarth, M. Böhme, S. Dapprich, A. W. Ehlers, A. Gobbi, V. Jonas, K. F. Köhler, R. Stegmann, A. Veldkamp, G. Frenking, *Chem. Phys. Lett.* **1993**, 208, 237–240.
- [19] A. E. Reed, L. A. Curtiss, F. Weinhold, *Chem. Rev.* **1988**, 88, 899–926.

Asymmetric Activation/Deactivation of Racemic Ru Catalysts for Highly Enantioselective Hydrogenation of Ketonic Substrates**

Koichi Mikami,*
Toshinobu Korenaga,
Takeshi Ohkuma, and
Ryoji Noyori

In asymmetric catalytic reactions^[1] racemic catalysts give only racemic products, whereas nonracemic catalysts generate nonracemic products. Recently, an enantiomer-selective deactivation strategy for racemic catalysis was reported to provide a level of asymmetric induction that does not exceed that attained by enantiopure catalysts. In this system, the selective complexation and deactivation with a “chiral poison” is indispensable (Scheme 1; 3a versus 3b).^[2] In contrast, a “chiral activator” may selectively complex but activate rather than deactivate one enantiomer of a racemic catalyst; an enantioselectivity higher than that achieved with enantiopure catalysts ($x_{\text{act}} \gg x$), as well as a higher level of catalyst efficiency ($k_{\text{act}} \gg k$; Scheme 1; 2a), can be obtained.^[3] Asymmetric activation can also be achieved by nonpreferential complexation (Scheme 1; 2b), which utilizes the difference in the turnover frequencies (catalytic activities) between the activated diastereomers ($k_{\text{act}} > k'_{\text{act}}$); these differences depend on the substrates employed.^[3d] We report here an asymmetric acti-



Scheme 1. Asymmetric activation/deactivation.

[*] Prof. Dr. K. Mikami, Dr. T. Korenaga
Department of Chemical Technology
Tokyo Institute of Technology
Ookayama, Meguro-ku, Tokyo 152-8552 (Japan)
Fax: (+81)3-5734-2776
E-mail: kmikami@o.cc.titech.ac.jp

Prof. Dr. T. Ohkuma, Prof. Dr. R. Noyori
Department of Chemistry and Molecular Chirality
Research Unit, Nagoya University
Chikusa, Nagoya 464-8602 (Japan)

[**] We are grateful to Drs. H. Kumobayashi and N. Sayo of the Takasago International Corp. for providing the BINAP ligands. We also thank Dr. Kenji Yoza of the Nippon Bruker Co. for X-ray analysis of the $[\text{RuCl}_2(\text{dm-dabn})(\text{binap})]$ complex. This work was financially supported by the Ministry of Education, Science, Sports, and Culture of Japan (Nos. 07CE2004, 09238209, and 10208204) and the Research Fellowships of the Japan Society for the Promotion of Science.

vation/deactivation protocol for achieving higher enantioselectivity irrespective of the substrates employed (Scheme 1; 1) by maximizing the difference in the catalytic activity between the catalyst enantiomers.

The preferential complexation of $[\text{RuCl}_2((R)\text{-binap})]$ (BINAP = 2,2'-bis(diphenylphosphanyl)-1,1'-binaphthyl)^[4] with (R) -3,3'-dimethyl-1,1'-binaphthyl-2,2'-diamine (DM-DABN)^[5] was readily explained from a modeling study (Figure 1a). As expected, the addition of a racemic $[\text{RuCl}_2(\text{binap})]$ species to 0.5 molar equivalents of (R) -DM-DABN resulted in a preferential complexation to form the single diastereomeric complex $[\text{RuCl}_2((R)\text{-dm-dabn})((R)\text{-binap})]$. Only the $[\text{RuCl}_2((R)\text{-dm-}$

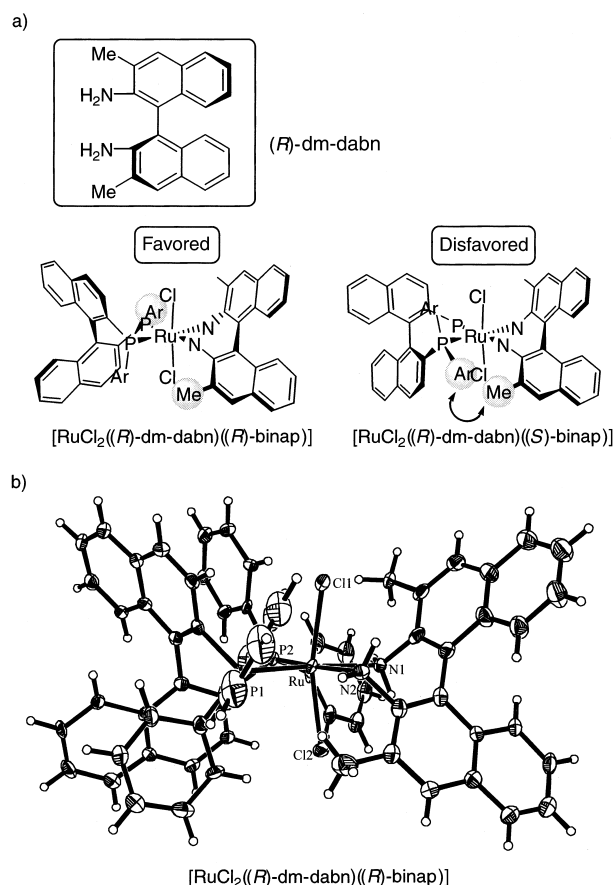


Figure 1. a) Model study of the [RuCl₂(dm-dabn)((*R*)-binap)] complex. b) X-ray analysis of [RuCl₂((*R*)-dm-dabn)((*R*)-binap)]. Selective bond lengths [Å] and bond angles [°]: Ru-Cl1 2.418(4), Ru-Cl2 2.401(3), Ru-P1 2.273(3), Ru-P2 2.270(4), Ru-N1 2.228(9), Ru-N2 2.263(10); Cl1-Ru-Cl2 165.34(11), P1-Ru-P2 89.80(12), N1-Ru-N2 80.1(4).

dabn)((*R*)-binap)] complex formed even when a racemic complex of [RuCl₂(binap)] was treated with an excess of (*R*)-DM-DABN in CDCl₃ at room temperature. No [RuCl₂((*R*)-dm-dabn)((*S*)-binap)] complex was evident in the ¹H NMR (CDCl₃) spectrum, which showed only one set of amino protons corresponding to the [RuCl₂((*R*)-dm-dabn)((*R*)-binap)] complex (δ = 3.80, 4.69). The (*R*)/(*R*) configuration of the [RuCl₂(dm-dabn)(binap)] diastereomer was confirmed by X-ray analysis^[6] of the single crystal obtained from a mixture of dichloromethane/diethyl ether/hexane (Figure 1b). This structure showed that the reason why no complex was formed from a mixture of [RuCl₂((*S*)-binap)] and (*R*)-DM-DABN was because of the severe steric repulsion that would result between the aryl group of (*S*)-binap and the methyl group of (*R*)-DM-DABN, as exemplified in the modeling study (Figure 1a). However, the [RuCl₂((*S*)-binap)] complex gave a different complex with enantiopure (*S,S*)- or (*R,R*)-diphenylethylenediamine (DPEN).^[7, 8] The two different dichlororuthenium complexes formed with DM-DABN and DPEN may be further converted into mono- or dihydridoruthenium species under hydrogenation conditions,^[9, 10] although the dm-dabn complex is far less catalytically active under such conditions (Table 1).

Table 1. Hydrogenation of 1'-acetonaphthone **4** by [RuCl₂((*R*)-dm-binap)] with diamines.

4 + H₂ (8 atm) → **5**

[RuCl₂((*R*)-dm-binap)(dmf)_{*n*}] (**1**) (0.4 mol%)
diamine (0.4 mol%)
KOH (0.8 mol%)
(CH₃)₂CHOH
RT

(*R*)-DM-DABN **2**

(*R,R*)-dpn **3**

(*S,S*)-dpn **3**

Diamines	Time [h]	ee [%] of 5	Yield [%] of 5
none	14	4 (<i>R</i>)	4
(<i>R</i>)-DM-DABN (2)	14	7 (<i>R</i>)	6
(<i>R,R</i>)-DPEN (3)	4	> 99 (<i>S</i>) ^[a]	> 99
(<i>S,S</i>)-DPEN (3)	4	56 (<i>S</i>)	> 99

[a] The enantiomeric pair (*S*)-**1**/(*S,S*)-**3** afforded the enantiomeric product of (*R*)-**5**.

Thus, a racemic [Ru(dm-binap)]^[9f, 11] catalyst achieves higher enantioselectivity in carbonyl hydrogenation after activation/deactivation by the sequential addition of two different types of chiral diamines than that attained by simple activation.^[3d] The mixture of [RuCl₂((±)-dm-binap)(dmf)_{*n*}] and 0.6 molar equivalents of (*R*)-DM-DABN was stirred for 30 minutes at room temperature in dichloromethane. After removal of the dichloromethane under reduced pressure, 0.5 molar equivalents of (*S,S*)-DPEN in 2-propanol was added to give [RuCl₂((*R*)-dm-dabn)((*R*)-dm-binap)] and [RuCl₂((*S,S*)-dpn)((*S*)-dm-binap)], selectively. Enantioselective hydrogenation was performed after the addition of KOH and ketones **4**, and **6–8** to a mixture of [RuCl₂(dm-binap)(dmf)_{*n*}] (**1**), (*R*)-DM-DABN (**2**), and (*S,S*)-DPEN (**3**). The efficiency of this asymmetric activation/deactivation protocol was reflected in the higher enantioselectivity in the hydrogenation irrespective of the ketonic substrates was used relative to the enantioselectivity obtained using the [RuCl₂((*S,S*)-dpn)((±)-dm-binap)] complex at the same temperature and pressure (Table 2). Thus, (*R*)-1-(1-naphthyl)-ethanol^[12] (**5**) was obtained with 96 % ee in quantitative yield. 2,4,4-Trimethyl-2-cyclohexenone^[3d, 9d, 13] (**9**) was also hydrogenated in high enantioselectivity by changing the chirality of DPEN from *S* to *R*.

In summary, we have developed an “asymmetric activation/deactivation” strategy for highly enantioselective hydrogenation irrespective of the ketonic substrates used by maximizing the difference in the catalytic activity between the enantiomeric catalysts. Thus, the present “asymmetric activation/deactivation protocol” can be regarded as a paradigm shift in racemic catalysis.

Experimental Section

5: [RuCl₂((±)-dm-binap)(dmf)_{*n*}] (**1**; 10.5 mg, 10 μmol) and (*R*)-DM-DABN (**2**; 1.9 mg, 6 μmol) were placed in an autoclave, and the air replaced with argon. Dichloromethane (3.3 mL) was added to the autoclave under a

Table 2. Hydrogenation of ketones by the racemic [RuCl₂(dm-binap)] complex through asymmetric activation/deactivation.

$$\begin{array}{c}
 \text{Ar-C(=O)-R} + \text{H}_2 \xrightarrow[\text{KOH (0.8 mol\%), 2-propanol, RT}]{\text{[RuCl}_2\text{((}\pm\text{)-dm-binap)(dmf)}_n\text{)] (1) (0.4 mol\%), (R)-DM-DABN (2) (0.22 mol\%), dpn (3) (0.2 mol\%)}} \\
 \text{Ar-CH(OH)-R}
 \end{array}$$

ketones

4: 1-(1-naphthyl)ethanone
6: 1-(2-naphthyl)ethanone
7: R = H
8a: R = o-Me
8b: R = m-Me
8c: R = p-Me
9: 1-(cyclohex-1-en-1-yl)ethanone

Ketones	(R)-2 ^[a]	3	Time [h]	ee [%]	Yield [%]
4	++	(S,S)	4	96 (R)	> 99
4	–	(S,S)	4	80 (R)	> 99
6	++	(S,S)	4	91 (R)	> 99
6	–	(S,S)	4	45 (R)	> 99
7	++	(S,S)	4	95 (R)	> 99
7	–	(S,S)	4	70 (R)	> 99
8a	++	(S,S)	4	95 (R)	> 99
8a	–	(S,S)	4	82 (R)	> 99
8b	++	(S,S)	6	95 (R)	> 99
8b	–	(S,S)	4	60 (R)	> 99
8c	++	(S,S)	4	93 (R)	> 99
8c	–	(S,S)	4	60 (R)	> 99
9	++	(R,R)	4	92 (R)	> 99 ^[b]
9	–	(R,R)	4	84 (R)	> 99 ^[b]

[a] ++ denotes the presence of (R)-2. [b] Racemic [RuCl₂(Tol-binap)] was used; Tol-BINAP = (2,2'-bis(di-4-tolylphosphanyl)-1,1'-binaphthyl).

stream of argon. After the mixture had been stirred at room temperature for 30 min, the dichloromethane was removed under reduced pressure. The autoclave was again purged with argon after the addition of (S,S)-DPEN (3; 1.0 mg, 4.5 μmol). 2-Propanol (2.8 mL) was added to the autoclave under a stream of argon, followed by the addition of KOH/2-propanol (0.5 M, 40 μL, 20 μmol) with stirring at room temperature for 30 min. 1'-Acetonaphthone (4; 0.38 mL, 2.5 mmol) was added to the autoclave at room temperature under a stream of argon, and then hydrogen was introduced at a pressure of 8 atm. After vigorously stirring the mixture for 4 h at room temperature, the solvent was removed under reduced pressure. The residue was filtered through a short column of silica gel. The chemical yield and enantiomeric ratio of 1-(1-naphthyl)ethanol (5) were calculated by gas chromatography on a column with a chiral stationary phase (> 99%, 96% ee (R)). The product could also be isolated by column chromatography on silica gel (eluent, hexane/EtOAc 5/1) to give 426 mg (99%) of 5. [α]_D²⁵ = +75.5 (c = 1.0, CHCl₃) (Ref. [12]) [α]_D²⁵ = +78.9 (c = 1, CHCl₃), R isomer; ¹H NMR (300 MHz, CDCl₃): δ = 1.59 (d, J = 6.6 Hz, 3H, CH₃), 1.90 (d, J = 3.6 Hz, 1H, OH), 5.59 (dq, J = 3.6, 6.6 Hz, 1H, CH), 7.37–7.51 (m, 3H, aromatic CH), 7.60 (d, J = 6.6 Hz, 1H, aromatic CH), 7.70 (d, J = 8.1 Hz, 1H, aromatic CH), 7.78–7.81 (m, 1H, aromatic CH), 8.02–8.05 (m, 1H, aromatic CH); GC (column CP-Cyclodextrin-β-2,3,6-M-19, i.d. 0.25 mm × 25 m, CHROMPACK; carrier gas, nitrogen (75 KPa); column temp. 160 °C; injection temp. 190 °C; split ratio 100/1), retention time (t_R); (R)-(+)-5: 32.7 min (98.1%), (S)-(–)-5: 31.6 min (1.9%), 4: 21.3 min (0%).

Received: April 13, 2000 [Z14986]

- [1] a) R. Noyori, *Asymmetric Catalysis in Organic Synthesis*, Wiley, New York, 1994; b) H. Brunner, W. Zettlmeier, *Handbook of Enantioselective Catalysis*, VCH, Weinheim, 1993; c) *Catalytic Asymmetric*

- Synthesis*, Vol. I and II (Ed.: I. Ojima), VCH, New York, 1993 and 2000; d) H. B. Kagan, *Comprehensive Organic Chemistry*, Vol. 8, Pergamon, Oxford, 1992; e) *Asymmetric Catalysis* (Ed.: B. Bosnich), Martinus Nijhoff Publishers, Dordrecht, 1986.
- [2] a) N. W. Alcock, J. M. Brown, P. J. Maddox, *J. Chem. Soc. Chem. Commun.* 1986, 1532–1534; b) J. M. Brown, P. J. Maddox, *Chirality* 1991, 3, 345–354; c) K. Maruoka, H. Yamamoto, *J. Am. Chem. Soc.* 1989, 111, 789–790; d) J. W. Faller, J. Parr, *J. Am. Chem. Soc.* 1993, 115, 804–805; e) J. W. Faller, M. Tokunaga, *Tetrahedron Lett.* 1993, 34, 7359–7362; f) J. W. Faller, D. W. I. Sams, X. Liu, *J. Am. Chem. Soc.* 1996, 118, 1217–1218; g) R. Sablong, J. A. Osborn, J. W. Faller, *J. Organomet. Chem.* 1997, 527, 65–70.
- [3] a) S. Matsukawa, K. Mikami, *Enantiomer* 1996, 1, 69–73; b) K. Mikami, S. Matsukawa, *Nature* 1997, 385, 613–615; c) S. Matsukawa, K. Mikami, *Tetrahedron: Asymmetry* 1997, 8, 815–816; d) T. Ohkuma, H. Doucet, T. Pham, K. Mikami, T. Korenaga, M. Terada, R. Noyori, *J. Am. Chem. Soc.* 1998, 120, 1086–1087; e) K. Mikami, T. Korenaga, M. Terada, T. Ohkuma, T. Pham, R. Noyori, *Angew. Chem.* 1999, 111, 517–519; *Angew. Chem. Int. Ed.* 1999, 38, 495–497.
- [4] M. Kitamura, M. Tokunaga, T. Ohkuma, R. Noyori, *Org. Synth.* 1993, 71, 1–13.
- [5] DM-DABN was named after 1,1'-binaphthyl-2,2'-diamine (DABN): K. J. Brown, M. S. Berry, J. R. Murdoch, *J. Org. Chem.* 1985, 50, 4345–4349.
- [6] The single crystal was grown from a dichloromethane/diethyl ether/hexane mixed solvent at room temperature. X-ray crystallographic analysis was performed with a Bruker SMART 1000 diffractometer (graphite monochromator, MoK_α radiation, λ = 0.71073 Å). Crystal data for [RuCl₂((R)-dm-dabn)((R)-binap)]: C₆₆H₅₂Cl₂N₂P₂Ru, reddish-orange, crystal dimensions 0.07 × 0.17 × 0.22 mm, orthorhombic, space group P2₁2₁2 (No. 18), a = 20.822(3), b = 22.130(3), c = 13.1320(18) Å, V = 6051.2(14) Å³, Z = 4, ρ_{calcd} = 1.215 g cm^{–3}, μ(MoK_α) = 1.43 cm^{–1}, T = 103 K, 10304 reflections were independent and unique, and 6256 with I > 2σ(I) (2θ_{max} = 24.7°) were used. The structure was solved by direct methods and expanded using Fourier techniques. The non-hydrogen atoms were refined anisotropically. Hydrogen atoms were included but not refined. R = 0.095, wR2 = 0.2116. Crystallographic data (excluding structure factors) for the structure reported in this paper have been deposited with the Cambridge Crystallographic Data Centre as supplementary publication no. CCDC-144099. Copies of the data can be obtained free of charge on application to CCDC, 12 Union Road, Cambridge CB2 1EZ, UK (fax: (+44) 1223-336-033; e-mail: deposit@ccdc.cam.ac.uk).
- [7] a) P. Mangeney, T. Tejero, A. Alexakis, F. Grosjean, J. Normant, *Synthesis* 1988, 255–257; b) S. Pikul, E. J. Corey, *Org. Synth.* 1993, 71, 22–29.
- [8] The ¹H NMR spectrum of the mixture of [RuCl₂((S,S)-dpn)((S)-binap)] and [RuCl₂((R)-dm-dabn)((R)-binap)] shows: δ = 2.92 (m, 2H, NH₂ of DPEN), 3.19 (m, 2H, NH₂ of DPEN), 3.80 (d, J = 9.6 Hz, 2H, NH₂ of DM-DABN), 4.20 (m, 2H, CH-NH₂ of DPEN), 4.69 (d, J = 9.6 Hz, 2H, NH₂ of DM-DABN).
- [9] For the hydrogenation of ketones by [RuCl₂(dpn)(binap)], see: a) T. Ohkuma, H. Ooka, S. Hashiguchi, T. Ikariya, R. Noyori, *J. Am. Chem. Soc.* 1995, 117, 2675–2676; b) T. Ohkuma, H. Ooka, T. Ikariya, R. Noyori, *J. Am. Chem. Soc.* 1995, 117, 10417–10418; c) T. Ohkuma, H. Ooka, M. Yamakawa, T. Ikariya, R. Noyori, *J. Org. Chem.* 1996, 61, 4872–4873; d) T. Ohkuma, H. Ikehira, T. Ikariya, R. Noyori, *Synlett* 1997, 467–468; e) H. Doucet, T. Ohkuma, K. Murata, T. Yokozawa, M. Kozawa, E. Katayama, A. F. England, T. Ikariya, R. Noyori, *Angew. Chem.* 1998, 110, 1792–1796; *Angew. Chem. Int. Ed.* 1998, 37, 1703–1707; f) T. Ohkuma, M. Koizumi, H. Doucet, T. Pham, M. Kozawa, K. Murata, E. Katayama, T. Yokozawa, T. Ikariya, R. Noyori, *J. Am. Chem. Soc.* 1998, 120, 13529–13530.
- [10] For the six-membered cyclic transition state, see: a) M. Yamakawa, H. Ito, R. Noyori, *J. Am. Chem. Soc.* 2000, 122, 1466–1478; b) K. Murata, T. Ikariya, *J. Org. Chem.* 1999, 64, 2186–2187; c) K.-J. Haack, S. Hashiguchi, A. Fujii, T. Ikariya, R. Noyori, *Angew. Chem.* 1997, 109, 297–300; *Angew. Chem. Int. Ed. Engl.* 1997, 36, 285–288; d) R. Noyori, S. Hashiguchi, *Acc. Chem. Res.* 1997, 30, 97–102; for the dihydridoruthenium species, see: e) A. Aranyos, G. Csirnyik, K. J. Szabó, J.-E. Bäckvall, *Chem. Commun.* 1999, 351–352, and references

- therein; for the monohydridoruthenium species, see: f) H. Kawano, T. Ikariya, Y. Ishii, M. Saburi, S. Yoshikawa, Y. Uchida, H. Kumobayashi, *J. Chem. Soc. Perkin Trans. 1* **1989**, 1571–1575, and references therein.
- [11] dm-binap = Xylbinap (2,2'-bis(di-3,5-xylylphosphanyl)-1,1'-binaphthyl): a) K. Mashima, Y. Matsumura, K. Kusano, H. Kumobayashi, N. Sayo, Y. Hori, T. Ishizaki, S. Akutagawa, H. Takaya, *J. Chem. Soc. Chem. Commun.* **1991**, 609–610; b) K. Mashima, K. Kusano, N. Sato, Y. Matsumura, K. Nozaki, H. Kumobayashi, N. Sayo, Y. Hori, T. Ishizaki, S. Akutagawa, H. Takaya, *J. Org. Chem.* **1994**, 59, 3064–3076.

- [12] P. D. Theisen, C. H. Heathcock, *J. Org. Chem.* **1988**, 53, 2374–2378; W. H. Pirkle, S. D. Beare, *J. Am. Chem. Soc.* **1967**, 89, 5485–5487.
- [13] K. Mori, P. Puapoomchareon, *Liebigs Ann. Chem.* **1991**, 1053–1056.

Become an expert in the field of carbohydrate chemistry

T. K. Lindhorst,
University of Hamburg, Germany

Essentials of Carbohydrate Chemistry and Biochemistry

2000. XIV, 218 pages with 244 figures and 11 tables. Softcover. DM 98.-/ £ 32.50
ISBN 3-527-29643-7

Carbohydrates are probably nature's most common product. Plants and algae biosynthesize millions of tons of them every year. Carbohydrates are stores of energy and structural building blocks; they are versatile enough to serve as encoders of biological information and, last but not least, they are involved in recognition processes at a molecular level. Research into carbohydrate and glycoconjugate functions in cell-to-cell communication processes has even created a new and rapidly developing field of study: glycobiology.


Thisbe K. Lindhorst is one of the leading "next generation" scientists in the area of carbohydrate research. Within her current book she presents a comprehensive introduction to the fascinating world of carbohydrates. In a lucid, explicit language she explains carbohydrate structures and the basic concepts of saccharide chemistry and saccharide biochemistry. With the same clarity she spans the gap to the glycobiological aspects of modern "glycoscience". Sample descriptions of research methods supplement the vital teaching text and open an experienced scientist's bag of tricks required to synthesize and analyze sugar derivatives easily and successfully.

This book offers valuable guidance for students as well as for researchers working in chemistry, biochemistry and biomedicine.

WILEY-VCH

Thisbe K. Lindhorst


Essentials of Carbohydrate Chemistry and Biochemistry



From the Contents:

- Introduction
- Structure of saccharides
- Protecting groups for carbohydrates
- Glycoside synthesis
- Important modifications and functionalizations of the sugar ring
- Structure and biosynthesis of glycoconjugates
- Glycobiology
- Analysis of carbohydrates
- The literature of carbohydrate chemistry


Become an expert in the field of carbohydrate chemistry



WILEY

John Wiley & Sons, Ltd., Baffins Lane
Chichester, West Sussex, PO 19 1UD, UK

WILEY-VCH, P.O., Box 10 11 61
69451 Weinheim, Germany



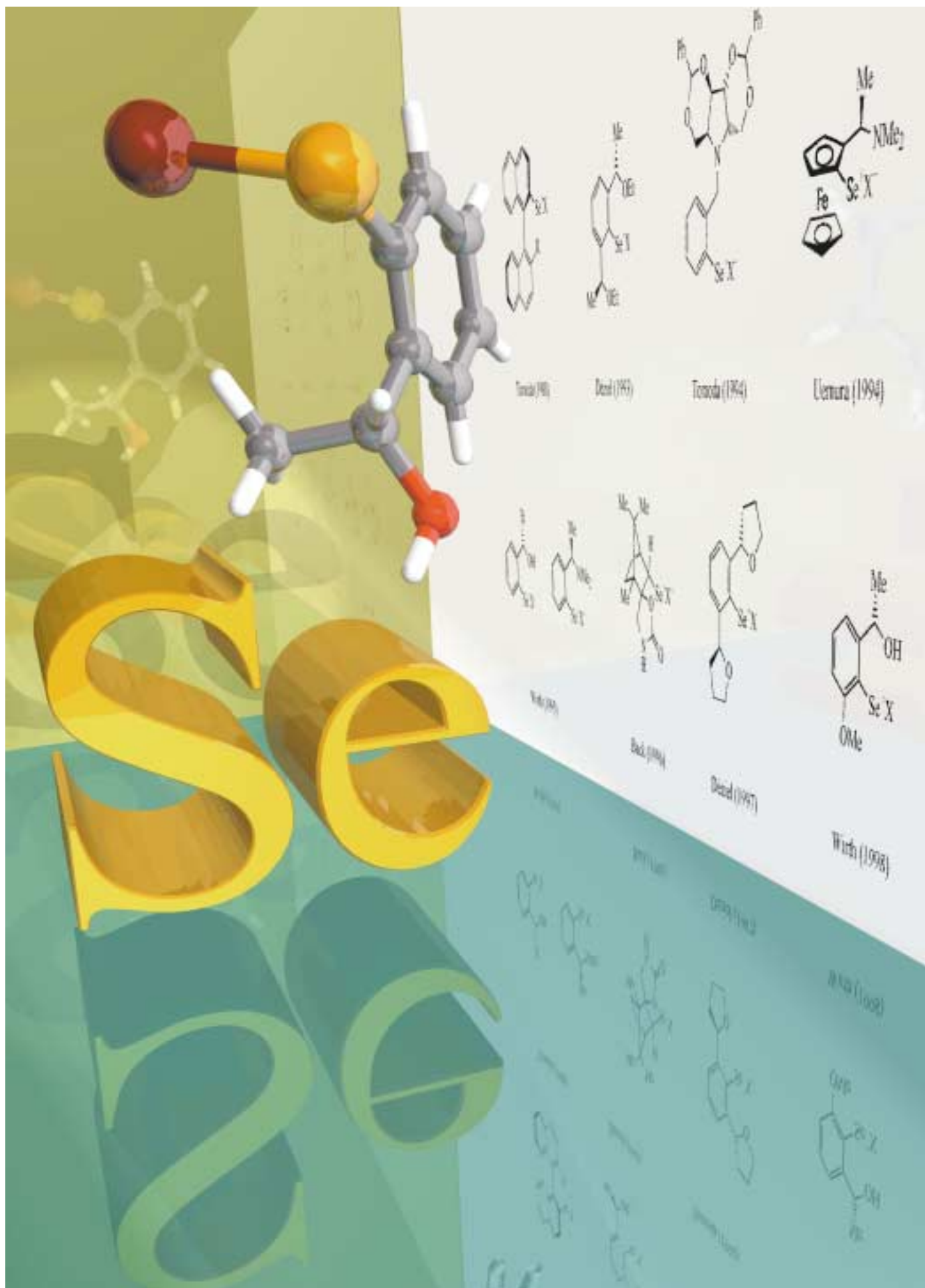
WILEY-VCH

Cover Picture

Lars T. Burgdorf, and Thomas Carell

The cover picture shows the sun together with a damaged (back) and repaired (front) DNA strand. The emitted sun energy is the basis for all life on earth. The UV part of the electromagnetic spectrum, however, causes the formation of a variety of mutagenic DNA lesions, which endanger the integrity of the genetic material. These lesions are repaired by a class of photolyases which utilize long-wavelength sunlight and a flavin coenzyme to initiate a critical electron transfer from the enzyme to the UV lesion. Carell and co-workers describe on p. 3918 ff the synthesis of lesion-containing DNA strands in which the flavin coenzyme was integrated. These DNA strands show a sunlight-driven self-repair process based on a surplus electron transfer through the base stack. (The sun picture is courtesy of the SOHO consortium; SOHO – Solar and Heliospheric Observatory—is a project of international cooperation between ESA and NASA.)





Selenium—a multitalented element: Selenium reagents offer numerous possibilities in organic synthesis—particularly in stereoselective reactions.

ANGEWANDTE
CHEMIE © WILEY-VCH

Organoselenium Chemistry in Stereoselective Reactions

Thomas Wirth*

Dedicated to Professor Bernd Giese on the occasion of his 60th birthday

Selenium-based methods have developed rapidly over the past few years and organoselenium chemistry has become a very useful tool in the hands of synthetic chemists. The different reactivity of selenium-containing compounds in contrast to the sulfur analogues has led to versatile and new synthetic methods in organic chemis-

try. Various functionalities can be selectively introduced into complex molecules under very mild reaction conditions. In this review, the principles of organoselenium chemistry are traced back to their origins and are highlighted with respect to stereoselective synthesis. The unique properties of selenium allow the development of

new and highly selective transformations, which can be employed subsequently in new routes for the synthesis of versatile chiral building blocks and for natural product synthesis.

Keywords: organoselenium chemistry
• selenium • stereoselective synthesis
• synthetic methods

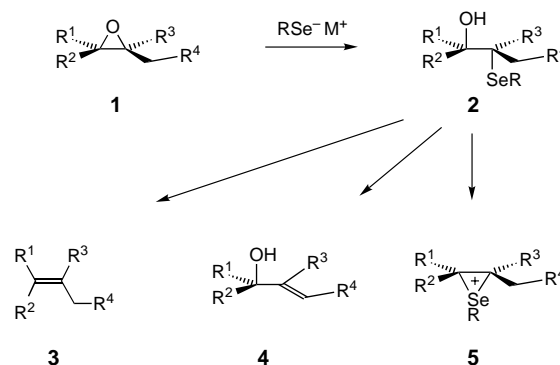
1. Introduction

The discovery of the selenoxide elimination in the early 1970s is believed to have been the major breakthrough for the subsequent developments of organoselenium chemistry.^[1] Since that time, a variety of organoselenium reagents has been developed and several are now commercially available. Two recently published books cover the broad range of organoselenium chemistry from practical aspects to synthetic applications,^[2] older books or book chapters^[3] as well as review articles^[4] describe different aspects. There is still a need for efficient stereoselective transformations in organic chemistry, and certain features of selenium-containing compounds make these reagents particularly valuable for those reactions. Within the scope of this review nucleophilic and electrophilic reagents for the introduction of selenium into organic molecules are discussed as well as stereoselective reactions with selenium-containing compounds for the synthesis of valuable building blocks.

2. Nucleophilic Reagents

Nucleophilic selenium reagents are easily formed from various precursors; for example, by reduction of either

elemental selenium or diselenides or by insertion of selenium into organometallic reagents.^[5] Selenolates are highly reactive, soft nucleophiles that can be introduced into a variety of organic compounds. Their chemistry began with the nucleophilic ring opening of epoxides **1**, which proceeds in an *anti* stereospecific fashion (Scheme 1).^[6] The β -hydroxyselenides **2** can be used for various subsequent transformations. For



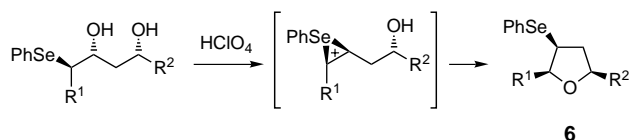
Scheme 1. Ring opening of epoxides with selenolates and subsequent reactions.

instance, *trans* elimination from compounds **2** gives alkenes of type **3**.^[7] The overall reaction sequence is a deoxygenation of epoxides to alkenes with retention of configuration.^[8] The *syn* elimination of the corresponding selenoxides affords allylic alcohols **4** with high selectivities.^[6] This reaction sequence has been utilized in various natural product syntheses.^[9] Treatment of β -hydroxyselenides **2** with acids results in an

[*] Prof. T. Wirth
Department of Chemistry, Cardiff University
Cardiff CF10 3TB (UK)
Fax: (+44) 29-2087-4030
E-mail: wirth@cf.ac.uk

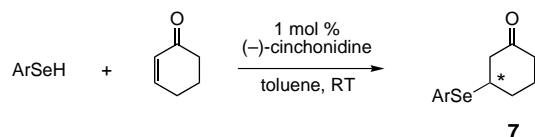
activation of the hydroxy group and in formation of seleniranium^[10] ions **5**, which can be opened in an inter- or intramolecular fashion to yield further functionalized compounds.

Seleniranium ions are usually generated by reaction of alkenes with selenium electrophiles (see Section 3). A stereoselective synthesis of substituted cyclic ethers such as tetrahydrofuran derivatives **6** is possible by using such a reaction sequence (Scheme 2).^[11]



Scheme 2. Synthesis of tetrahydrofuran derivatives via seleniranium intermediates.

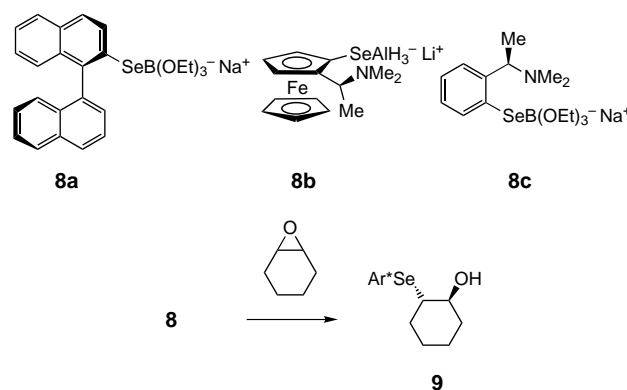
The chemistry of nucleophilic selenium reagents with respect to asymmetric synthesis began with the addition of selenols to α,β -unsaturated carbonyl compounds catalyzed by chinchona alkaloids (Scheme 3).^[12] Products of type **7** were obtained in up to 43 % *ee*.



Scheme 3. First asymmetric synthesis with selenium reagents.

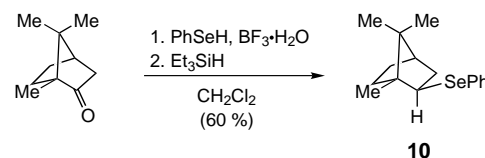
The nucleophilic ring opening of epoxides was the first reaction, in which chiral selenium reagents were used. Binaphthyl selenolates such as **8a** can react with *meso* epoxides yielding products **9** with up to 50 % *de*.^[13] New developments include the ferrocenyl selenolates **8b** which can open cyclohexenoxide with up to 69 % *de* (Scheme 4).^[14] Chiral selenolates such as **8c** without an axial chiral element are much less efficient, the product **9** is formed with only 11 % *de*.^[15] Interestingly, the counterion of the selenolates and the reaction conditions seem to have a dramatic influence on the yields and selectivities of the epoxide-opening reactions. The origin of these effects is not yet fully understood.

Selenolates can also be used for addition reactions to activated carbonyl groups. If chiral ketones like camphor



Scheme 4. Stereoselective ring opening of cyclohexene oxide.

are employed, the Lewis acid catalyzed hemiselenoacetal formation and the subsequent reduction of the selenonium ion yields enantiomerically pure selenides of type **10** (Scheme 5).^[16]



Scheme 5. Selenolate addition to carbonyl groups.

Other versatile reactions with selenium nucleophiles such as substitution reactions with aryl or alkyl halides, Michael reactions, or ester and lactone cleavages are not discussed herein, because these reactions have not been used in stereoselective synthesis. Also polymer-bound selenium nucleophiles have not yet been employed to perform the above-mentioned reactions.^[5]

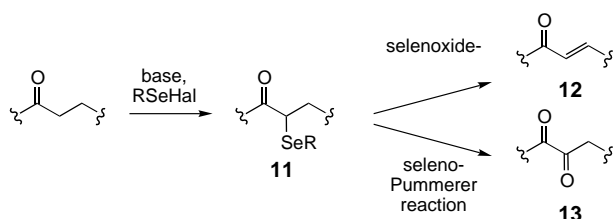
3. Electrophilic Reagents

Very versatile precursors for the preparation of various electrophilic selenium reagents are the corresponding diselenides. They can be transferred easily into selenenyl halides or into selenenyl compounds with non-halide counterions. These electrophilic reagents can react with a variety of carbon or



Thomas Wirth, born in 1964, studied Chemistry in Bonn, Germany, and stayed there to carry out his diploma work with Prof. S. Blechert. He then moved along with his supervisor to the Technical University of Berlin, where he received his Ph.D. in 1992. After a postdoctoral stay with Prof. K. Fuji at Kyoto University, Japan, as a JSPS fellow, he started 1994 his independent research at the Universität of Basel, Switzerland, obtaining his habilitation on stereoselective oxidation reactions in 1999. In the fall of 1999 he was a guest lecturer at the University of Toronto, Canada, and in spring 2000 he was a visiting scientist at the Chuo University in Tokyo, Japan. In September 2000 he was appointed as a Professor of Organic Chemistry at Cardiff University, Wales, UK. He was awarded the Werner-Prize from the New Swiss Chemical Society (NSCG) in October 2000.

heteroatom nucleophiles to produce a wide range of different selenenylated compounds. The α -selenenylation of carbonyl compounds leads to products **11**. Although a stereogenic center is formed in this reaction, no asymmetric versions have been reported up to now—probably, because this reaction usually is followed by a selenoxide elimination and allows the conversion to synthetically important, achiral α,β -unsaturated carbonyl compounds **12**.^[4d] From conformationally flexible ketones only *E*-configured enones **12** were obtained. The reaction sequence, shown in Scheme 6, was independently

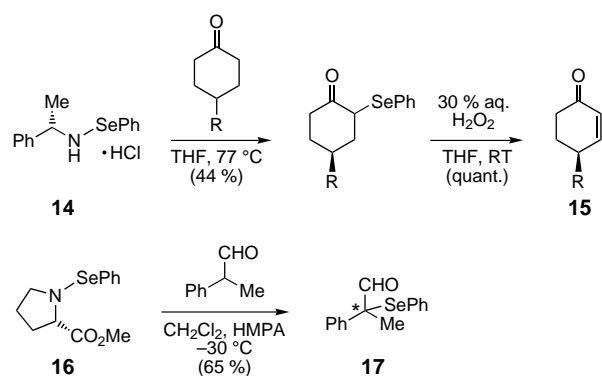


Scheme 6. α -Selenenylation of ketones and subsequent reactions.

reported by several research groups in the early 1970s.^[17] The introduction of α,β -unsaturation in carbonyl compounds with organoselenium chemistry is very important and frequently applied in total syntheses.^[4d, 18] The α -selenenylation of carbonyl compounds can also be followed by a seleno-Pummerer reaction to give 1,2-bisketones **13**.^[19] Silylenol ethers can also be α -selenenylated in high yields^[20] and the products of type **11** have been used recently in diastereoselective reductions.^[21]

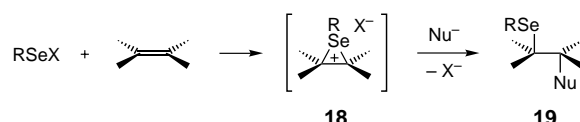
The reactions of selenium electrophiles with heteroatom nucleophiles are synthetically less important, but this reaction has been used for the preparation of the first chiral electrophilic organoselenium compounds. Phenylselenenyl bromide reacts with chiral amines to give selenenamides such as **14**. These reagents have been used in stereoselective α -selenenylations of cyclohexanones. After selenoxide elimination the cyclohexenones **15** were obtained in up to 26% *ee* (Scheme 7).^[22] Similar reagents such as **16** seem to be more efficient as shown in the α -selenenylation of 2-phenylpropanal, which leads to **17** in up to 60% *ee*.^[23]

Selenium electrophiles are quite powerful and able to react with double bonds to generate, after addition of a nucleophile,



Scheme 7. Stereoselective α -selenenylation of ketones. HMPA = hexamethylphosphoric acid amide.

the corresponding addition products.^[24] The two steps of the addition reaction involve the formation of seleniranium intermediates **18**, followed by a nucleophilic attack to yield the addition products **19** (Scheme 8). These reactions exhibit *anti* stereoselectivity with the nucleophile attacking usually at the higher substituted carbon atom (Markownikoff regioselectivity). Some mechanistic investigations have been performed earlier.^[25] Reactions with hindered alkenes led to the isolation and structural determination of seleniranium species.^[26] The products **19** of these selenenylations are very useful, because a wide range of alkenes as well as nucleophiles can be employed in these transformations and many different subsequent reactions are possible.^[27]



Scheme 8. Electrophilic selenenylation of alkenes.

It was recognized early that apart from the *anti* stereoselectivity and the Markownikoff regioselectivity the electrophilic attack could be favored upon one of the two faces of the π system. The facial selectivity is dependent on the alkene, which is usually attacked by the selenium electrophiles from the sterically less hindered side.^[28] Even reactions with alkenes having sterically equally accessible faces can be performed stereoselectively. For this purpose chiral electrophilic selenium reagents are of particular interest, which have been developed recently and applied to stereoselective synthesis. A common feature of these reagents is a heteroatom that coordinates to the positively charged selenium atom. Such an intramolecular interaction between the heteroatom and the selenium atom has been proven in different ways. X-ray structural data of suitably substituted compounds,^[29] NMR spectral data of such reagents,^[30] and *ab initio* calculations^[30a, 31] all indicate the interaction of a lone pair of electrons of the heteroatom with the σ^* orbital of the selenium atom. This induces a conformational rigidity into these molecules as shown in **20** (Figure 1). This interaction can

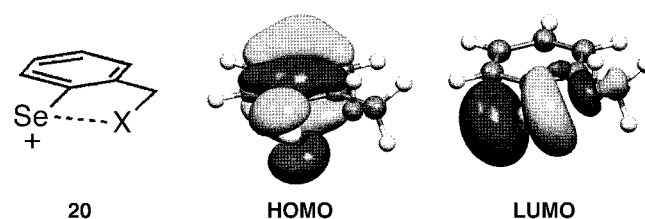
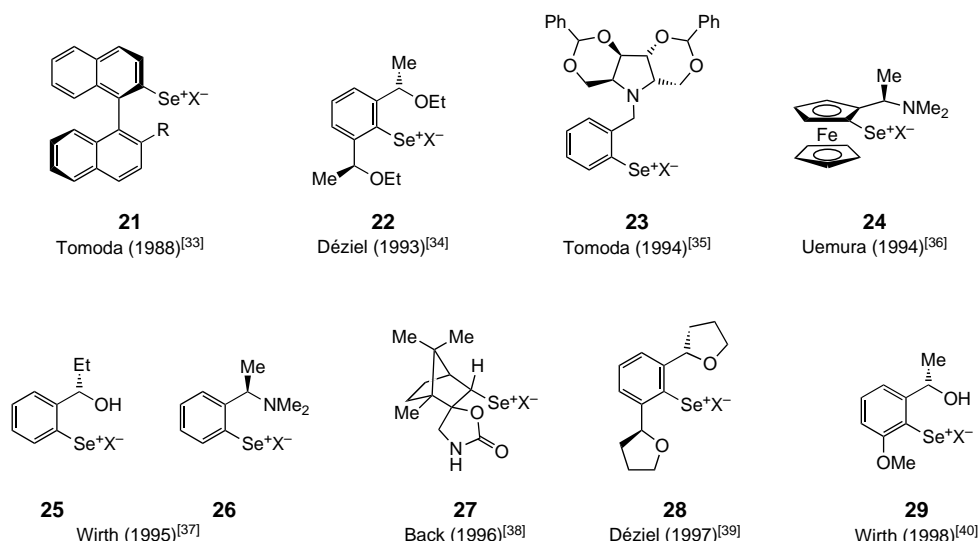


Figure 1. HOMO and LUMO of selenium electrophiles of type **20** ($X = OH$).

also be seen in the LUMO ($X = OH$).^[32] The LUMOs of the selenium electrophiles are relatively low in energy and their interaction with the HOMOs of the alkenes should play the predominant role in the electrophilic addition reactions.

The introduction of chiral elements into molecules of type **20** leads to chiral selenium electrophiles. They are usually prepared from the corresponding diselenides. Scheme 9 shows



Scheme 9. Chiral selenium electrophiles.

chiral selenium electrophiles **21–29**, which have been employed in stereoselective addition reactions.^[33–40]

Different chiral motifs can be found in these reagents. Depending on the complexity, the synthetic route to these reagents sometimes consists of many steps. All the reagents in Scheme 9 have been extensively employed in the stereoselective oxyseleenylation of alkenes. As already pointed out in Scheme 8, these reactions typically proceed via seleniranium ion intermediates of type **18** resulting in an *anti* addition of the moieties ArSe and Nu. The formation of the seleniranium ions is reversible, but at low temperatures the reaction is under kinetic control. The mechanistic course of the oxyseleenylation reaction with the chiral reagents **22** and **25** has been investigated in detail.^[31, 41] The presence of a chiral moiety in these reagents results in a differentiation between the two faces of unsymmetrically substituted alkenes. The attack of the alkene double bond from either the *Re*- or the *Si*-side is different from the steric and electronic point of view, and the resulting seleniranium ions **18a**⁺ and **18b**⁺ are diastereomers (Scheme 10). On the other hand, symmetrical (*Z*)-alkenes lead to identical seleniranium ions and the stereoselectivity is determined by the nucleophilic attack in the product-forming step.^[33a, 38e]



Scheme 10. Formation of diastereoselective seleniranium ions.

The stereoselectivities observed with the reagents **22** and **25** can be rationalized by the relative stability of the transition states for the attack of nucleophiles on the seleniranium intermediates of type **18**. The reaction pathways have been calculated at an *ab initio* level. It was found that the cationic species involved in the reaction are stabilized by solvent

molecules, although the solvent–selenium interaction is relatively weak and reversible.^[41] Furthermore, alkenes with aromatic substituents can π -stack with the aryl surface of the reagents, leading to seleniranium ions with higher stabilities than alkenes with alkyl substituents. The independent synthesis of the diastereomeric seleniranium ions allowed a detail study of the different stabilities of these intermediates.^[31] Up to now little effort has been made to understand the role of the counterion in asymmetric selenenylation reactions; for instance in the above-mentioned

calculations the nature of the counterion was not considered. However, the counterion has an influence on the stereochemical outcome of the reaction. In Table 1 the results of the methoxyselenenylation of (*E*)-1-phenylpropene **30** with various selenium electrophiles are summarized. These reactions lead to addition products **31**; the absolute configuration of the elimination product **32** is also indicated. The addition reactions of various selenium electrophiles to styrene have also been compared and similar results have been obtained.^[24]

However, these trends can unfortunately not be generalized. Applying other reaction conditions or using different alkenes can result in different stereoselectivities and sometimes even in a reverse face selection. Less nucleophilic counterions lead to more electrophilic selenium reagents, and the results of various experiments reveal that more electrophilic reagents yield higher stereoselectivities in these addition reactions.^[35d, 42]

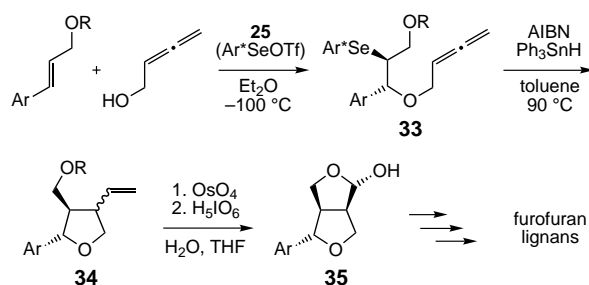
A variety of different nucleophiles have been investigated in selenenylation reactions. It was found that even functionalized nucleophiles could be used in these reactions, which

 Table 1. Stereoselective methoxyselenenylation of (*E*)-1-phenylpropene.

		30	31	32			
Ar ⁺ Se ⁺ X [−]	X [−]	Conditions solvent T [°C]	de 31 [%]	Yield of 31 [%]	Yield of 32	Config.	Ref.
21 ^[a]	Br [−]	MeOH 25	24	49		[c]	[33d]
21 ^[b]	Br [−]	MeOH 25	79	87		<i>R</i>	[33d,f]
22	TfO [−]	Et ₂ O −78	86	82		<i>S</i>	[34a]
23	Br [−]	CH ₂ Cl ₂ −78	52	85		<i>R</i>	[35d]
23	PF ₆ [−]	CH ₂ Cl ₂ −78	95	58		<i>R</i>	[35d]
24	TfO [−]	CH ₂ Cl ₂ −78	96	99		<i>S</i>	[36d]
25	TfO [−]	Et ₂ O −100	80	45		<i>S</i>	[37c]
28	TfO [−]	Et ₂ O −78	98	81		<i>S</i>	[39]
29	TfO [−]	Et ₂ O −100	85	51		<i>S</i>	[40]

[a] R = H. [b] R = 1-(2,4-Dinitrophenyl)-pyrrolidin-2-yl-carboxamide.
[c] Configuration not determined.

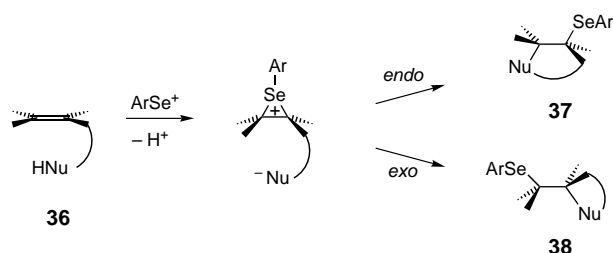
allowed a subsequent radical cyclization. This reaction sequence was applied to the synthesis of furofuran lignans as shown in Scheme 11. Stereoselective selenenylation using selenium electrophile **25** and an allenyl alcohol as nucleophile gave addition products of type **33** in good yields and diastereoselectivities. After the radical cyclization reaction the vinylic side chain of the tetrahydrofuran derivative **34** is oxidized, providing a fast access to furofurans of type **35**, versatile building blocks for the synthesis of various lignans.^[43]



Scheme 11. Total synthesis of furofuran lignans by a sequence of selenenylation and subsequent radical cyclization. AIBN = 2,2'-azobisisobutyronitrile; Tf = CF₃SO₂.

Other external nucleophiles such as carbamates or azides (Nu⁻ in Scheme 8) can be employed in these addition reactions as well. Although these reactions are also *anti* additions and sometimes proceed with high regioselectivity, chiral selenium electrophiles have not been investigated yet.

Internal nucleophiles in selenenylations lead to cyclization reactions, which have been employed in various syntheses for a long time.^[44] Depending on the chain length and on the substitution pattern of the alkene **36**, the addition reaction can occur by an *endo* or by an *exo* pathway leading to cyclic products of type **37** or **38**, respectively. As shown in Scheme 12, the cyclization reactions are stereospecific *anti* additions like their intermolecular counterparts, and calcu-

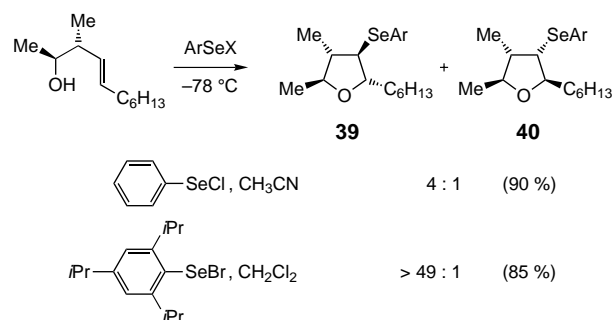


Scheme 12. Selenium-mediated cyclization reactions.

lations on the course of this reaction have been performed recently.^[45] This reaction type has been used widely for the synthesis of different cyclic compounds and recently it was found that stereoselective ring-closing reactions are possible using chiral electrophilic selenium reagents.

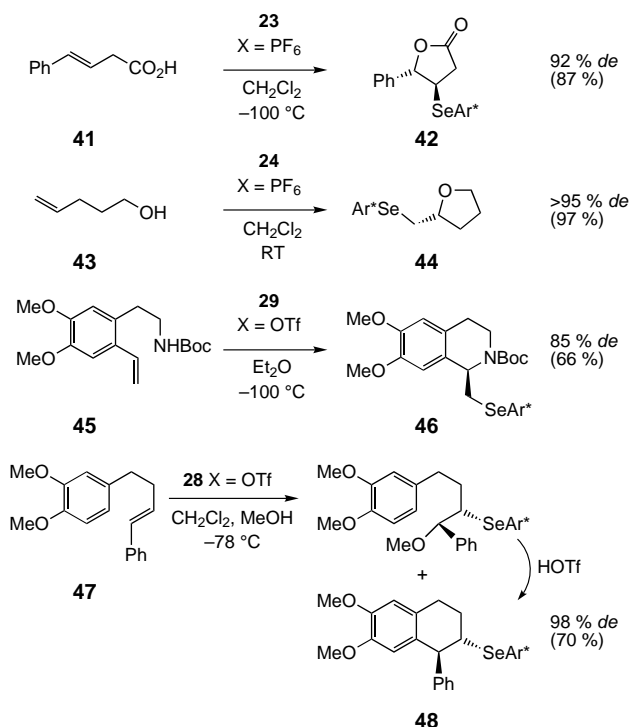
The seleniranium intermediates can be generated from the corresponding β -hydroxyselenides, as shown in Scheme 2, or from suitably substituted alkenes. Depending on the alkene and on the selenium electrophile, cyclizations can be performed with high selectivities. The size of the electrophilic

reagent has a large influence on the diastereomeric ratio of the **39** and **40**, which varies from 4:1^[46] to >49:1 (Scheme 13).^[47]



Scheme 13. Stereoselective cyclizations with achiral selenium electrophiles.

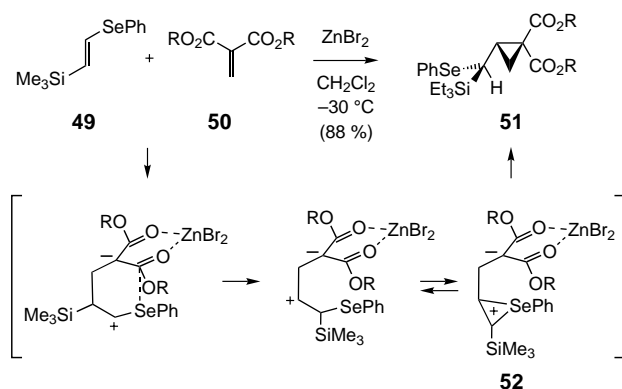
Almost all chiral selenium electrophiles shown in Scheme 9 have been employed in stereoselective cyclization reactions. Oxygen, nitrogen, and carbon nucleophiles have been used to construct different cyclic systems by intramolecular cyclizations. Depending on the alkene and on the nature of the electrophilic reagent, different selectivities have been observed. First applications of stereoselective selenocyclization reactions have also been reported in natural product synthesis. Some selected examples are shown in Scheme 14. The unsaturated carboxylic acid **41** has been used as a substrate for stereoselective selenolactonizations to give **42**, for which the selenium electrophiles **23**^[35b] and **28**^[39] were found to be quite efficient. Substituted tetrahydrofuran derivatives like **44** can be synthesized from the corresponding unsaturated alcohols



Scheme 14. Stereoselective cyclizations with chiral selenium electrophiles. Boc = *tert*-butoxycarbonyl.

43, in the series of aliphatic alkenes only a few selenium electrophiles like **24** lead to high selectivities.^[48] The intramolecular amidoselenenylation was found to be a versatile reaction for the preparation of **46**, a precursor in the synthesis of the tetrahydroisoquinoline alkaloid salsolidine.^[49] Also carbocycles can be formed by this methodology as shown in the cyclization of **47**. Methanol as external nucleophile competes, but the subsequent treatment with trifluoromethanesulfonic acid allows the synthesis of **48** in very high selectivities.^[50]

The Lewis acid promoted stereoselective [2+1] cycloaddition reaction of 1-seleno-2-silyl ethene **49** to dicarboxylates **50** ($R = t\text{Bu}$) proceeds probably also via seleniranium intermediates **52**. After a selenium-assisted 1,2-silicon migration process a stabilized seleniranium intermediate can be formed which is opened under formation of the cyclopropane derivative **51**.^[51] The use of chiral dicarboxylates **50** ($R = (-)$ -menthyl) allows the synthesis of cyclopropanes **51** with up to 86 % *de* (Scheme 15).^[52]

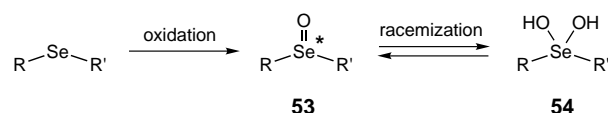


Scheme 15. Synthesis of cyclopropanes from vinylselenides.

4. Rearrangements

Selenoxide eliminations and [2,3] sigmatropic rearrangements of various selenium-containing compounds are useful tools in the hand of synthetic organic chemists.^[53] The application of these transformations in stereoselective synthesis was developed only recently. The use of optically active organoselenium compounds with a chiral center at the selenium atom is the prerequisite for the stereoselective synthesis. In contrast to the analogous sulfur-based chemistry, the activation energies for rearrangements with organoselenium compounds are much lower making them ideal for use in stereoselective synthesis. The selenoxide elimination reaction has not only brought organoselenium chemistry into the focus of organic chemists, but because of the extremely mild reaction conditions this rearrangement has also been applied in many syntheses since its discovery.

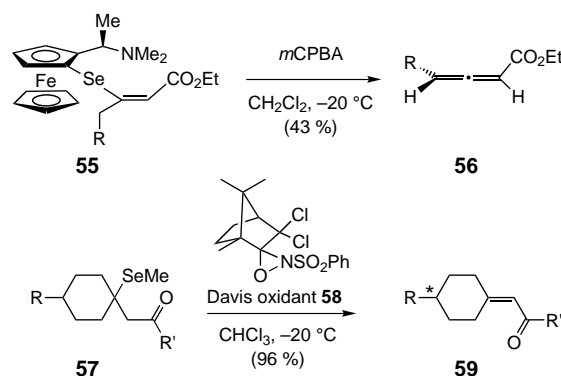
Chiral selenoxides **53** can be obtained either by enantioselective oxidation^[54] of the corresponding selenides ($R \neq R'$) or by diastereoselective oxidation^[55] of selenides bearing a chiral moiety (R or R' : chiral) (Scheme 16). It had been shown that the formation of an achiral hydrate **54** accounts for the fast



Scheme 16. Synthesis and racemization of selenoxides via achiral hydrates.

racemization of selenoxides in the presence of acid and water.^[56] Bulky substituents can prevent racemization^[57] but in the presence of a β -hydrogen atom the subsequent selenoxide elimination leads to more stable products.

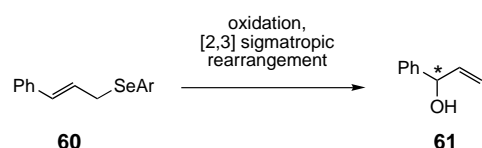
The asymmetric version of the selenoxide elimination after diastereoselective oxidation was first applied to the synthesis of chiral allenes (Scheme 17). Ferrocenyl-substituted vinyl selenides of type **55** are employed in the oxidation–elimination sequence to yield the chiral allenes **56** in up to 89 % *ee*.^[58] Enantioselective oxidation of selenide **57** is possible with the Davis oxidant **58**, and the cyclohexylidene ketone **59** is obtained in up to 83 % *ee*.^[59]



Scheme 17. Stereoselective selenoxide eliminations. mCPBA = *meta*-chloroperoxybenzoic acid.

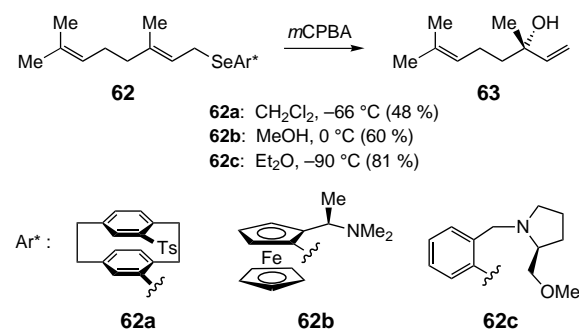
The [2,3] sigmatropic rearrangements via allylic selenoxides involve an oxygen transfer from selenium to carbon and after hydrolysis of the allylic selenenates the allylic alcohols are obtained. It was proven that these rearrangements proceed predominantly via an *endo* transition state.^[55] The rearrangement of the allylic selenoxides proceeds much faster than that of the corresponding sulfoxides, and detailed kinetic and thermodynamic studies have been carried out.^[60] The stereoselective version of these rearrangements can again be performed either by enantioselective oxidation of achiral allylic selenides or by diastereoselective oxidation of allylic selenides bearing a chiral substituent. Several stereoselective syntheses of allylic alcohols have been reported recently. For instance, oxidation of aryl cinnamyl selenides **60** with the Davis oxidant **58** and subsequent rearrangement gave the allylic alcohol **61** with only modest stereoselectivity (up to 60 % *ee*).^[54] By the use of the Sharpless oxidant $\{\text{Ti}(\text{O}i\text{Pr})_4, (+)\text{-diisopropyltartrate/tert-butyl hydroperoxide}\}$, however, the allylic alcohol **61** can be obtained in up to 92 % *ee* (Scheme 18).^[61]

Several examples are also known for the diastereoselective oxidation of chiral allylic selenides. One of the test reactions for several chiral compounds is the synthesis of (*S*)-linalool **63**



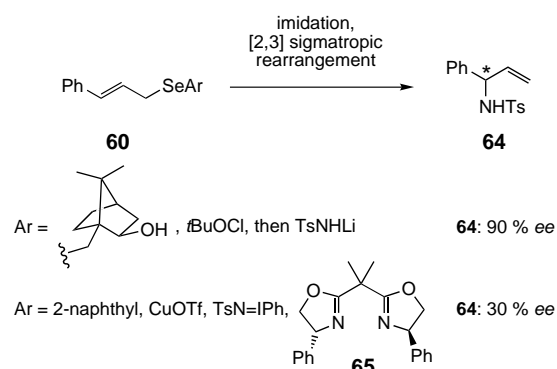
Scheme 18. Stereoselective [2,3] sigmatropic rearrangement of allylic selenides.

from precursors of type **62**. Depending on the chiral moiety, good stereoselectivities can be obtained (**62a**: 67 % *ee*, **62b**: 83 % *ee*, **62c**: 61 % *ee*) as shown in Scheme 19.^[55, 58b, 62]



Scheme 19. Synthesis of linalool **63** by [2,3] sigmatropic rearrangements. Ts = *para*-toluenesulfonyl.

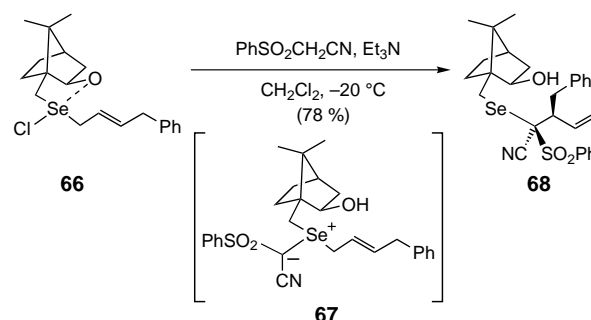
In principle, the [2,3] sigmatropic rearrangements via allylic selenoxides mentioned above can also be performed with selenimides as nitrogen-analogous intermediates.^[63] Chiral allylic amines are therefore accessible by this route. Chloramine T (TsNCINa) or *N*-(*p*-tolylsulfonyl)imino(phenyl)iodinane (TsN=IPh) can be used as imidation reagents of either chiral allylic selenides^[63a,b] or, with the help of chiral ligands such as the bis(oxazoline) **65**, also for the imidation of achiral allylic selenides.^[63c] The rapid selenimide–selenoxide equilibrium must be suppressed by using water-free reaction conditions. Although the stereoselectivities are still low, these reactions open a promising route to chiral allylic amines such as **64** (Scheme 20).



Scheme 20. Stereoselective [2,3] sigmatropic rearrangements leading to chiral allylic amides **64**.

Although selenonium ylides have been known for a long time, it was shown recently that chiral selenonium ylides can be prepared. They can also be quite versatile precursors for [2,3] sigmatropic rearrangements. The reaction of the allylic

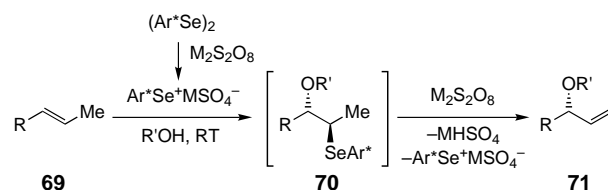
chloroselenuranes **66** with (phenylsulfonyl)acetonitrile generates the corresponding selenonium ylides **67**, and after the [2,3] sigmatropic rearrangement homoallylselenides **68** are obtained with high stereoselectivities (up to 88 % *de*) (Scheme 21).^[64]



Scheme 21. Stereoselective [2,3] sigmatropic rearrangement via selenonium ylides.

5. Catalytic Reactions

Selenium-containing reagents can be used as catalysts or as ligands in various stereoselective reactions. For instance, it is possible to perform selenenylation–deselenenylation sequences with only catalytic amounts of selenium species. This reaction sequence provides double bond transpositioned allylic ethers or allylic alcohols from the corresponding alkenes (Scheme 22). This sequence can be performed electrochemically,^[65] but stereoselective versions using chiral

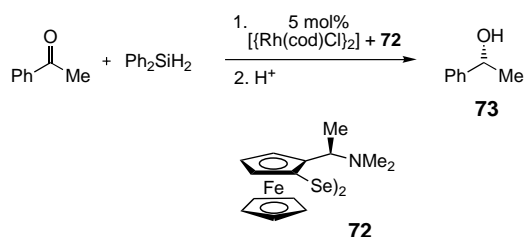


Scheme 22. Selenenylation–elimination sequence with catalytic amounts of diselenides.

diselenides rely on the formation of the selenenyl sulfates from diselenides with peroxodisulfates^[66] as electrophilic reagents for the initial addition reaction to the alkene **69**. The resulting selenide **70** is then oxidized by an excess peroxodisulfate and the subsequent elimination reaction yields allylic compounds of type **71**. Different chiral diselenides have been employed in this reaction and after careful optimization of the reaction conditions enantioselectivities up to 75 % (*R* = Ph, *R'* = Me in **71**) have been obtained.^[67] However, the turnover numbers are still small and further work is needed to improve the catalytic oxyselenenylation–elimination sequence.

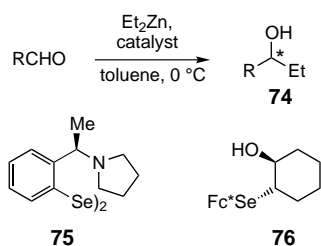
Chiral ferrocenyl diselenides like **72** have been found to serve as efficient ligands for transition metal catalyzed stereoselective reactions such as asymmetric hydrosilylations or transfer hydrogenations of various ketones. Diselenide **72** was found to be the most efficient ligand for the rhodium(i)-

catalyzed hydrosilylation of acetophenone leading to the product **73** with 85 % *ee* (Scheme 23).^[68] Other ferrocenyl diselenides with variations in the chiral side chain as well as the analogous disulfide and ditelluride afforded the product with much lower enantioselectivity. The same ferrocenyl diselenide **72** has been investigated in rhodium(i)- as well as in iridium(i)- and in ruthenium(ii)-catalyzed stereoselective transfer-hydrogenations of ketones. However, the stereoselectivities obtained are low in most of the examples reported (up to 48 % *ee*).^[69]



Scheme 23. Enantioselective hydrosilylation using chiral diselenide ligands. cod = cycloocta-1,5-diene.

Nitrogen-containing diselenides like **75** are very efficient procatalysts for the addition of diethylzinc to aldehydes. The secondary alcohols **74** are obtained in up to 98 % yield and with up to 98 % *ee* (Scheme 24). It has been shown that the selenium–selenium bond of the diselenides is cleaved rapidly and that catalytically active zinc selenolates are formed. A positive nonlinear relationship (asymmetric amplification)



Scheme 24. Catalytic addition of diethylzinc to aldehydes.

between the optical purities of the catalyst and the product was observed.^[70] Other selenium-containing catalysts such as **76** (Fc* = ferrocenyl moiety **62b**) leading to enantioselectivities up to 94 % in the products **74** have been investigated as well in this addition reaction.^[71]

Palladium-catalyzed allylic substitutions can be performed with catalysts containing a selenium atom, but the selectivities obtained are lower than with the chiral phosphorus-containing ligands usually employed in these reactions.^[72]

6. Summary and Outlook

Recent advances using selenium compounds in stereoselective reactions are described in this review. Various aspects using chiral selenium reagents in stoichiometric and in catalytic reactions are summarized. Although high stereoselectivities can be obtained for several reaction types such as electrophilic additions to alkenes, low or only modest stereoselectivities are found in other reactions and further work is needed in these areas. Improved and new selenium-containing reagents will surely be developed in the future to gain further benefit from the usually very mild conditions in these

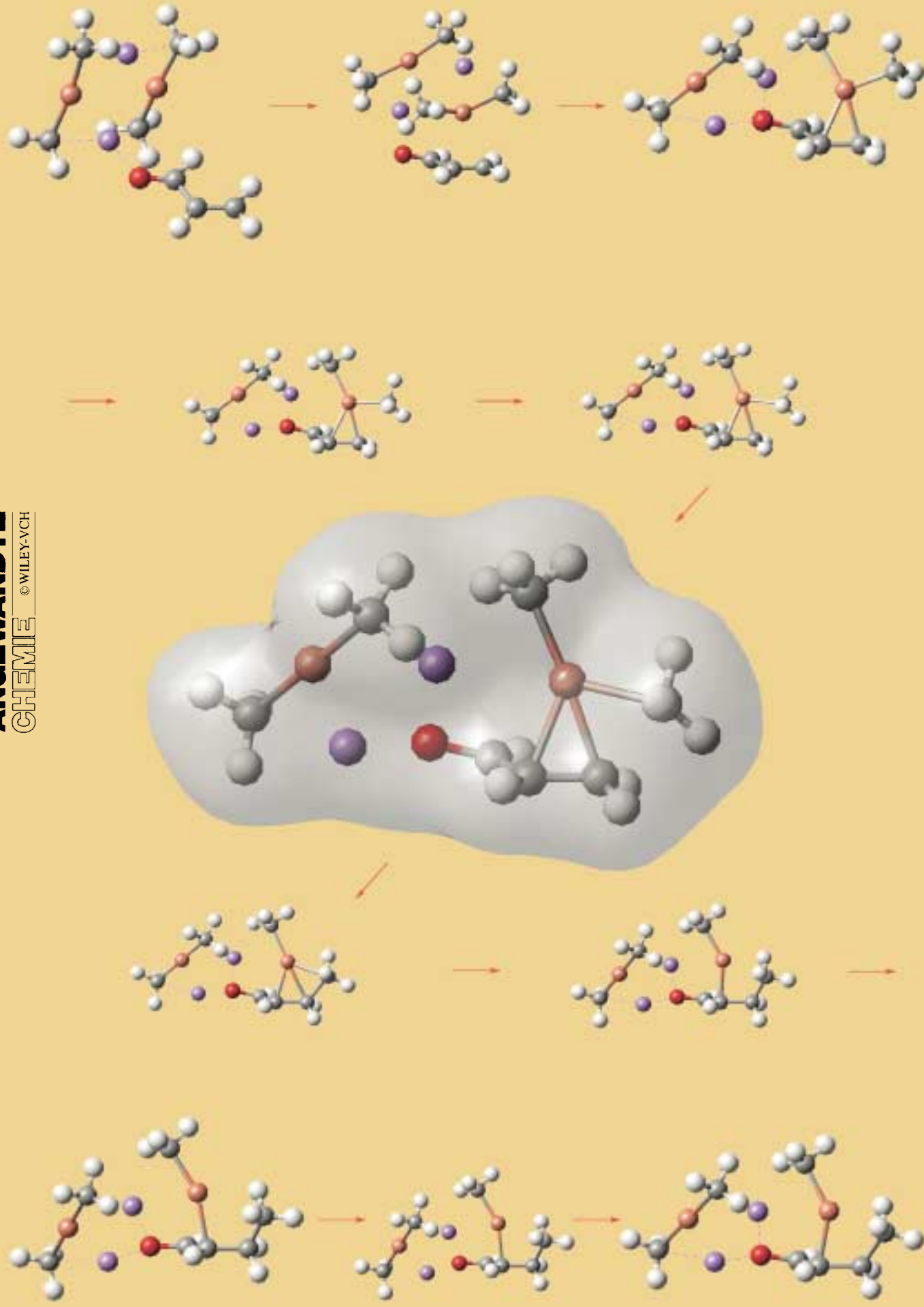
reactions. This will lead to enhanced stereoselectivities in known reactions, to new selenium-based transformations and methods, and to new applications of this chemistry.

I would like to thank my co-workers Gianfranco Fragale, Jürgen Haas, Urs Hirt, Martin Spichty, and Lars Uehlin for their outstanding contributions. Financial support by the Schweizer Nationalfonds is gratefully acknowledged.

Received: February 16, 2000 [A397]

- [1] a) J. L. Huguet, *Adv. Chem. Ser.* **1967**, 76, 345–351; b) D. N. Jones, D. Mundy, R. D. Whitehouse, *J. Chem. Soc. Chem. Commun.* **1970**, 86–87; c) R. Walter, J. Roy, *J. Org. Chem.* **1971**, 36, 2561–2563.
- [2] a) *Organoselenium Chemistry* (Ed.: T. G. Back), Oxford University Press, Oxford, **1999**; b) *Top. Curr. Chem.* **2000**, 208.
- [3] a) *Organic Selenium Compounds: Their Chemistry and Biology* (Eds.: D. L. Klayman, W. H. H. Günther), Wiley, New York, **1973**; b) K. C. Nicolaou, N. A. Petasis, *Selenium in Natural Products Synthesis*, CIS, Philadelphia, **1984**; c) C. Paulmier, *Selenium Reagents and Intermediates in Organic Synthesis*, Pergamon, Oxford, **1986**; d) *The chemistry of organic selenium and tellurium compounds* (Eds.: S. Patai, Z. Rappoport), Wiley, New York, **1986**; e) *Organoselenium Chemistry* (Ed.: D. Liotta), Wiley, New York, **1987**; f) A. Krief, L. Hevesi, *Organoselenium Chemistry I*, Springer, Berlin, **1988**.
- [4] a) J. Gosselek, *Angew. Chem.* **1963**, 75, 831–840; *Angew. Chem. Int. Ed. Engl.* **1963**, 2, 660–669; b) K. B. Sharpless, K. M. Gordon, R. F. Lauer, D. W. Patrick, S. P. Sinder, M. W. Young, *Chem. Scr.* **1975**, 8A, 9–13; c) H. J. Reich, *Acc. Chem. Res.* **1979**, 12, 22–30; d) H. J. Reich, S. Wollowitz, *Org. React.* **1993**, 44, 1–296; e) M. Tiecco, L. Testaferri, M. Tingoli, L. Bagnoli, F. Marini, C. Santi, A. Temperini, *Gazz. Chim. Ital.* **1996**, 126, 635–643; f) L. A. Wessjohann, U. Sinks, *J. Prakt. Chem.* **1998**, 340, 189–203.
- [5] M. Iwaoka, S. Tomoda, *Top. Curr. Chem.* **2000**, 208, 55–80.
- [6] K. B. Sharpless, R. F. Lauer, *J. Am. Chem. Soc.* **1973**, 95, 2697–2699.
- [7] a) H. J. Reich, F. Chow, *J. Chem. Soc. Chem. Commun.* **1975**, 790–791; b) J. Réunion, W. Dumont, A. Krief, *Tetrahedron Lett.* **1976**, 1385–1388; c) D. L. J. Clive, V. N. Kalè, *J. Org. Chem.* **1981**, 46, 231–234.
- [8] a) D. L. J. Clive, C. V. Denyer, *J. Chem. Soc. Chem. Commun.* **1973**, 253; b) P. E. Sonnet, *Tetrahedron* **1980**, 36, 557–604.
- [9] a) R. H. Schlessinger, A. Lopes, *J. Org. Chem.* **1981**, 46, 5252–5253; b) M. Miyashita, T. Suzuki, A. Yoshikoshi, *J. Am. Chem. Soc.* **1989**, 111, 3728–3734.
- [10] The intermediates **5** have been sometimes called episelenonium ions, but the IUPAC name is preferable today: G. H. Schmid, *Phosphorus Sulfur* **1988**, 36, 197–200.
- [11] a) E. D. Mihelich, *J. Am. Chem. Soc.* **1990**, 112, 8995–8997; b) M. Gruttadauria, P. Lo Meo, R. Noto, *Tetrahedron* **1999**, 55, 4769–4782.
- [12] H. Pluim, H. Wynberg, *Tetrahedron Lett.* **1979**, 1251–1254.
- [13] S. Tomoda, M. Iwaoka, *J. Chem. Soc. Chem. Commun.* **1988**, 1283–1284.
- [14] Y. Nishibayashi, J. D. Singh, S. Fukuzawa, S. Uemura, *J. Chem. Soc. Perkin Trans. I* **1995**, 2871–2876.
- [15] T. Wirth, *Tetrahedron* **1999**, 55, 1–28.
- [16] D. J. Procter, N. J. Archer, R. A. Needham, D. Bell, A. P. Marchington, C. M. Rayner, *Tetrahedron* **1999**, 55, 9611–9622.
- [17] a) H. J. Reich, I. L. Reich, J. M. Renga, *J. Am. Chem. Soc.* **1973**, 95, 5813–5815; b) K. B. Sharpless, R. F. Lauer, A. Y. Teranishi, *J. Am. Chem. Soc.* **1973**, 95, 6137–6139; c) D. L. J. Clive, *J. Chem. Soc. Chem. Commun.* **1973**, 695–696; d) H. J. Reich, J. M. Renga, I. L. Reich, *J. Am. Chem. Soc.* **1975**, 97, 5434–5447.
- [18] a) P. A. Grieco, T. Oguri, S. Burke, E. Rodriguez, G. T. DeTitta, S. Fortier, *J. Org. Chem.* **1978**, 43, 4552–4554; b) W. C. Still, *J. Am. Chem. Soc.* **1979**, 101, 2493–2495; c) S. Danishefsky, K. Vaughan, R. Gadwood, K. Tsuzuki, *J. Am. Chem. Soc.* **1981**, 103, 4136–4141; d) G. Han, M. G. LaPorte, J. J. Folmer, K. M. Werner, S. M. Weinreb, *Angew. Chem.* **2000**, 112, 243–246; *Angew. Chem. Int. Ed.* **2000**, 39, 237–240.

- [19] a) J. A. Marshall, R. D. Royce, *J. Org. Chem.* **1982**, *47*, 693–698; b) S. L. Schreiber, C. Santini, *J. Am. Chem. Soc.* **1984**, *106*, 4038–4039.
- [20] I. Ryu, S. Murai, I. Niwa, N. Sonoda, *Synthesis* **1977**, 874–876.
- [21] M. Shirahata, H. Yamazaki, S. Fukuzawa, *Chem. Lett.* **1999**, 245–246.
- [22] K. Hiroi, S. Sato, *Synthesis* **1985**, 635–638.
- [23] C. Paulmier, F. Outurquin, J. Plaquevent, *Tetrahedron Lett.* **1988**, *29*, 5889–5892.
- [24] M. Tiecco, *Top. Curr. Chem.* **2000**, *208*, 7–54.
- [25] G. H. Schmid, D. G. Garratt, *J. Org. Chem.* **1983**, *48*, 4169–4172.
- [26] G. I. Borodkin, Y. V. Gatilov, T. V. Rybalova, E. I. Chernyak, V. G. Shubin, *Izv. Akad. Nauk SSSR Ser. Khim.* **1986**, 2832.
- [27] S. R. Harring, E. D. Edstrom, T. Livinghouse in *Advances in Heterocyclic Natural Product Synthesis*, Vol. 2 (Ed.: W. H. Pearson), JAI, Greenwich, **1992**, 299–376.
- [28] a) D. G. Garratt, A. Kabo, *Can. J. Chem.* **1980**, *58*, 1030–1041; b) D. G. Garratt, M. D. Ryan, A. Kabo, *Can. J. Chem.* **1980**, *58*, 2329–2339.
- [29] a) R. Eriksen, S. Hauge, *Acta Chem. Scand.* **1972**, *26*, 3153–3164; b) D. H. R. Barton, M. B. Hall, Z. Lin, S. I. Parekh, R. Reibenspies, *J. Am. Chem. Soc.* **1993**, *115*, 5056–5059; c) H. Fujihara, H. Mima, N. Furukawa, *J. Am. Chem. Soc.* **1995**, *117*, 10153–10154; d) R. Kaur, H. B. Singh, R. P. Patel, *J. Chem. Soc. Dalton Trans.* **1996**, 2719–2726; e) G. Mugesh, H. B. Singh, R. J. Butcher, *Tetrahedron: Asymmetry* **1999**, *10*, 237–242; f) A. Panda, G. Mugesh, H. B. Singh, R. J. Butcher, *Organometallics* **1999**, *18*, 1986–1993.
- [30] a) M. Iwaoka, S. Tomoda, *J. Am. Chem. Soc.* **1996**, *118*, 8077–8084; b) M. Iwaoka, H. Komatsu, S. Tomoda, *Chem. Lett.* **1998**, 969–970; c) H. Komatsu, M. Iwaoka, S. Tomoda, *Chem. Commun.* **1999**, 205–206; d) G. Mugesh, A. Panda, H. B. Singh, R. J. Butcher, *Chem. Eur. J.* **1999**, *5*, 1411–1421.
- [31] T. Wirth, G. Fragale, M. Spichly, *J. Am. Chem. Soc.* **1998**, *120*, 3376–3381.
- [32] The calculations have been performed by Martin Spichly, University of Basel, with the Gaussian98 program on the HF/6-31G* level of theory. The results are similar with X=OH (shown in Figure 1) and X=NH₂.
- [33] a) S. Tomoda, M. Iwaoka, *Chem. Lett.* **1988**, 1895–1898; b) S. Tomoda, M. Iwaoka, K. Yakushi, A. Kawamoto, J. Tanaka, *J. Phys. Org. Chem.* **1988**, *1*, 179–184; c) S. Tomoda, M. Iwaoka, *J. Chem. Soc. Chem. Commun.* **1988**, 1283–1284; d) S. Tomoda, K. Fujita, M. Iwaoka, *J. Chem. Soc. Chem. Commun.* **1990**, 129–131; e) S. Tomoda, K. Fujita, M. Iwaoka, *Chem. Lett.* **1992**, 1123–1124; f) S. Tomoda, K. Fujita, M. Iwaoka, *Phosphorus Sulfur* **1992**, *67*, 247–252.
- [34] a) R. Déziel, S. Goulet, L. Grenier, J. Bordeleau, J. Bernier, *J. Org. Chem.* **1993**, *58*, 3619–3621; b) R. Déziel, E. Malenfant, *J. Org. Chem.* **1995**, *60*, 4660–4662; c) R. Déziel, E. Malenfant, G. Bélanger, *J. Org. Chem.* **1996**, *61*, 1875–1876.
- [35] a) K. Fujita, M. Iwaoka, S. Tomoda, *Chem. Lett.* **1994**, 923–926; b) K. Fujita, K. Murata, M. Iwaoka, S. Tomoda, *J. Chem. Soc. Chem. Commun.* **1995**, 1641–1642; c) K. Fujita, K. Murata, M. Iwaoka, S. Tomoda, *Tetrahedron Lett.* **1995**, *36*, 5219–5222; d) K. Fujita, K. Murata, M. Iwaoka, S. Tomoda, *Tetrahedron* **1997**, *53*, 2029–2048.
- [36] a) Y. Nishibayashi, J. D. Singh, S. Uemura, S. Fukuzawa, *Tetrahedron Lett.* **1994**, *35*, 3115–3118; b) Y. Nishibayashi, S. K. Srivastava, H. Takada, S. Fukuzawa, S. Uemura, *J. Chem. Soc. Chem. Commun.* **1995**, 2321–2322; c) Y. Nishibayashi, J. D. Singh, S. Fukuzawa, S. Uemura, *J. Org. Chem.* **1995**, *60*, 4114–4120; d) S. Fukuzawa, K. Takahashi, H. Kato, H. Yamazaki, *J. Org. Chem.* **1997**, *62*, 7711–7716; e) S. Uemura, *Phosphorus Sulfur* **1998**, *136*–138, 219–234.
- [37] a) T. Wirth, *Angew. Chem.* **1995**, *107*, 1872–1873; *Angew. Chem. Int. Ed. Engl.* **1995**, *34*, 1726–1728; b) T. Wirth, G. Fragale, *Chem. Eur. J.* **1997**, *3*, 1894–1902; c) T. Wirth, *Liebigs Ann.* **1997**, 2189–2196.
- [38] a) T. G. Back, B. P. Dyck, M. Parvez, *J. Chem. Soc. Chem. Commun.* **1994**, 515–516; b) T. G. Back, B. P. Dyck, M. Parvez, *J. Org. Chem.* **1995**, *60*, 703–710; c) T. G. Back, B. P. Dyck, *Chem. Commun.* **1996**, 2567–2568; d) T. G. Back, S. Nan, *J. Chem. Soc. Perkin Trans. 1* **1998**, 3123–3124; e) T. G. Back, B. P. Dyck, S. Nan, *Tetrahedron* **1999**, *55*, 3191–3208.
- [39] R. Déziel, E. Malenfant, C. Thibault, S. Fréchette, M. Gravel, *Tetrahedron Lett.* **1997**, *38*, 4753–4756.
- [40] G. Fragale, M. Neuburger, T. Wirth, *Chem. Commun.* **1998**, 1867–1868.
- [41] X. Wang, K. N. Houk, M. Spichly, T. Wirth, *J. Am. Chem. Soc.* **1999**, *121*, 8567–8576.
- [42] M. Tiecco, L. Testaferri, C. Santi, F. Marini, L. Bagnoli, A. Temperini, *Tetrahedron Lett.* **1998**, *39*, 2809–2812.
- [43] a) T. Wirth, K. J. Kulicke, G. Fragale, *J. Org. Chem.* **1996**, *61*, 2686–2689; b) T. Wirth, *Liebigs Ann.* **1997**, 1155–1158.
- [44] a) D. J. L. Clive, G. Chittattu, N. J. Curtis, W. A. Kiel, C. K. Wong, *J. Chem. Soc. Chem. Commun.* **1977**, 725–727; b) K. C. Nicolaou, Z. Lysenko, *Tetrahedron Lett.* **1977**, 1257–1260.
- [45] Z. Markovic, S. Konstantinovic, I. Juranic, L. Dosen-Micovic, *Gazz. Chim. Ital.* **1997**, *127*, 429–434.
- [46] E. D. Mihelich, G. A. Hite, *J. Am. Chem. Soc.* **1992**, *114*, 7318–7319.
- [47] B. H. Lipshutz, T. Gross, *J. Org. Chem.* **1995**, *60*, 3572–3573.
- [48] H. Takada, Y. Nishibayashi, S. K. Srivastava, K. Ohe, S. Uemura, *Proc. 24th Symp. Heteroatom Chem.* **1997**, S. 124–126.
- [49] T. Wirth, G. Fragale, *Synthesis* **1998**, 162–166.
- [50] R. Déziel, E. Malenfant, C. Thibault, *Tetrahedron Lett.* **1998**, *39*, 5493–5496.
- [51] S. Yamazaki, T. Inoue, T. Hamada, T. Takada, K. Yamamoto, *J. Org. Chem.* **1999**, *64*, 282–286, and references therein.
- [52] S. Yamazaki, H. Kataoka, S. Yamabe, *J. Org. Chem.* **1999**, *64*, 2367–2374.
- [53] Y. Nishibayashi, S. Uemura, *Top. Curr. Chem.* **2000**, *208*, 201–233.
- [54] F. A. Davis, R. T. Reddy, *J. Org. Chem.* **1992**, *57*, 2599–2606.
- [55] H. J. Reich, K. E. Yelm, *J. Org. Chem.* **1991**, *56*, 5672–5679.
- [56] F. A. Davis, O. D. Stringer, J. P. McCauley, *Tetrahedron* **1985**, *41*, 4747–4757.
- [57] T. Shimizu, M. Kobayashi, *J. Org. Chem.* **1987**, *52*, 3399–3403.
- [58] a) N. Komatsu, Y. Nishibayashi, T. Sugita, S. Uemura, *J. Chem. Soc. Chem. Commun.* **1992**, 46–47; b) Y. Nishibayashi, J. D. Singh, S. Fukuzawa, S. Uemura, *J. Org. Chem.* **1995**, *60*, 4114–4120.
- [59] N. Komatsu, S. Matsunaga, T. Sugita, S. Uemura, *J. Am. Chem. Soc.* **1993**, *115*, 5847–5848.
- [60] H. J. Reich, K. E. Yelm, S. Wollowitz, *J. Am. Chem. Soc.* **1983**, *105*, 2503–2504.
- [61] N. Komatsu, Y. Nishibayashi, S. Uemura, *Tetrahedron Lett.* **1993**, *34*, 2339–2342.
- [62] K. Fujita, M. Kanakubo, H. Ushijima, A. Oishi, Y. Ikeda, Y. Taguchi, *Synlett* **1998**, 987–988.
- [63] a) Y. Nishibayashi, T. Chiba, K. Ohe, S. Uemura, *J. Chem. Soc. Chem. Commun.* **1995**, 1243–1244; b) N. Kurose, T. Takahashi, T. Koizumi, *J. Org. Chem.* **1996**, *61*, 2932–2933; c) H. Takada, M. Oda, Y. Miyake, K. Ohe, S. Uemura, *Chem. Commun.* **1998**, 1557–1558.
- [64] N. Kurose, T. Takahashi, T. Koizumi, *J. Org. Chem.* **1997**, *62*, 4562–4563.
- [65] a) S. Torii, K. Uneyama, M. Ono, *Tetrahedron Lett.* **1980**, *21*, 2653–2654; b) S. Torii, K. Uneyama, M. Ono, T. Bannou, *J. Am. Chem. Soc.* **1981**, *103*, 4606–4608.
- [66] M. Tiecco, L. Testaferri, M. Tingoli, D. Chianelli, D. Bartoli, *Tetrahedron Lett.* **1989**, *30*, 1417–1420.
- [67] a) K. Fujita, M. Iwaoka, S. Tomoda, *Chem. Lett.* **1994**, 923–926; b) S. Fukuzawa, K. Takahashi, H. Kato, H. Yamazaki, *J. Org. Chem.* **1997**, *62*, 7711–7716; c) M. Tiecco, L. Testaferri, C. Santi, F. Marini, L. Bagnoli, A. Temperini, *Tetrahedron Lett.* **1998**, *39*, 2809–2812; d) T. Wirth, S. Häuptli, M. Leuenberger, *Tetrahedron: Asymmetry* **1998**, *9*, 547–550.
- [68] a) Y. Nishibayashi, J. D. Singh, K. Segawa, S. Fukuzawa, S. Uemura, *J. Chem. Soc. Chem. Commun.* **1994**, 1375–1376; b) Y. Nishibayashi, K. Segawa, J. D. Singh, S. Fukuzawa, K. Ohe, S. Uemura, *Organometallics* **1996**, *15*, 370–379.
- [69] Y. Nishibayashi, J. D. Singh, Y. Arikawa, S. Uemura, M. Hidai, *J. Organomet. Chem.* **1997**, *531*, 13–18.
- [70] a) T. Wirth, *Tetrahedron Lett.* **1995**, *36*, 7849–7852; b) T. Wirth, K. J. Kulicke, G. Fragale, *Helv. Chim. Acta* **1996**, *79*, 1957–1966; c) C. Santi, T. Wirth, *Tetrahedron: Asymmetry* **1999**, *10*, 1019–1023.
- [71] S. Fukuzawa, K. Tsudzuki, *Tetrahedron: Asymmetry* **1995**, *6*, 1039–1042.
- [72] a) J. Sprinz, M. Kiefer, G. Helmchen, M. Reggelin, G. Huttner, O. Walter, L. Zsolnai, *Tetrahedron Lett.* **1994**, *35*, 1523–1526; b) K. Hiroi, Y. Suzuki, I. Abe, *Tetrahedron: Asymmetry* **1999**, *10*, 1173–1188.



Wherefore Art Thou Copper? Structures and Reaction Mechanisms of Organocuprate Clusters in Organic Chemistry

Eiichi Nakamura* and Seiji Mori

Organocopper reagents provide the most general synthetic tools in organic chemistry for nucleophilic delivery of hard carbanions to electrophilic carbon centers. A number of structural and mechanistic studies have been reported and have led to a wide variety of mechanistic proposals, some of which might even be contradictory to others. With the recent advent of physical and theoretical methodologies, the accumulated knowledge on organocopper chemistry is being put together into a few major mechanistic

principles. This review will summarize first the general structural features of organocopper compounds and the previous mechanistic arguments, and then describe the most recent mechanistic pictures obtained through high-level quantum mechanical calculations for three typical organocuprate reactions, carbocupration, conjugate addition, and S_N2 alkylation. The unified view on the nucleophilic reactivities of metal organocuprate clusters thus obtained has indicated that organocuprate chemistry represents an intricate

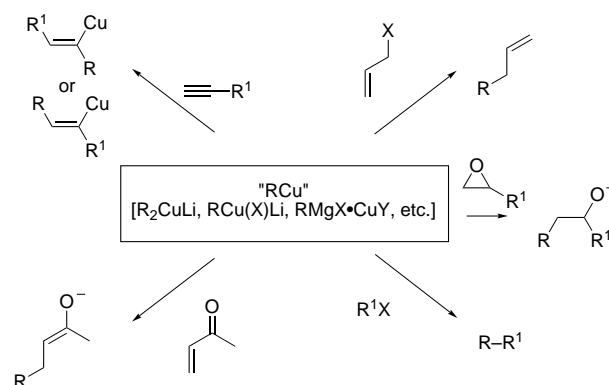
example of molecular recognition and supramolecular chemistry, which chemists have long exploited without knowing it. Reasoning about the uniqueness of the copper atom among neighboring metal elements in the periodic table will be presented.

Keywords: catalysis • conjugate additions • copper • density functional calculations • supramolecular chemistry

1. Introduction

The desire to learn about the nature of elements has been and will remain a main concern of chemists. In this review, we will consider what properties of copper make organocopper chemistry so useful in organic chemistry.

Lying on the border between the transition metals and the main group elements, copper occupies a unique position in the periodic table. The key roles of copper have been widely recognized in various areas including superconductivity,^[1] biological oxygenation,^[2] and organic synthesis.^[3–6] The most important utility of copper in organic chemistry is in the form of nucleophilic organocopper(II) reagents, which are used either in a catalytic or a stoichiometric manner. Generally formulated as R_2CuM with a variety of metal and organic groups (M and R, respectively), metal organocuprates and related species are uniquely effective synthetic reagents for nucleophilic delivery of hard anionic nucleophiles such as alkyl, vinyl, and aryl anions (Scheme 1). Conjugate addition,^[7] carbocupration,^[8] alkylation,^[9] and allylation^[10] represent the

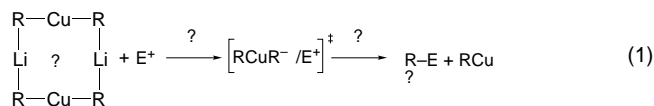


Scheme 1. Nucleophilic reactivities of organocopper reagents RCu . $R = sp^2, sp^3$ carbon anionic centers; $X, Y = \text{halogen, etc.}$

reactions that can be achieved readily with organocuprate reagents but not with other organometallics (Scheme 1). Half a century after Kharasch and Tawney's initial discovery,^[11] organocopper reagents are still the most useful synthetic reagents among transition metal organometallics.^[12] The chemistry of organocopper reagents has been reviewed many times with emphasis on synthetic utility and sometimes on structural properties,^[13] but rarely on reaction mechanisms.^[14]

[*] Prof. Dr. E. Nakamura, Dr. S. Mori
Department of Chemistry
The University of Tokyo
Bunkyo-ku, Tokyo 113-0033 (Japan)
Fax: (+81) 3-5800-6889
E-mail: nakamura@chem.s.u-tokyo.ac.jp

In spite of the long history and popularity of copper, there remains the fundamental question: what properties of copper make organocopper reagents so useful? In a similar manner to Juliet on the balcony, we may say to ourselves “O Copper, O Copper, wherefore art thou Copper?” Information on the nature of reactive species in solution and their reactivities has been fragmentary and incomplete. The most widely accepted “resting state” of the metal organocuprate(i) species in solution is represented by the eight-centered dimer $(R_2CuLi)_2$ shown in Equation (1), but there has been little consensus on

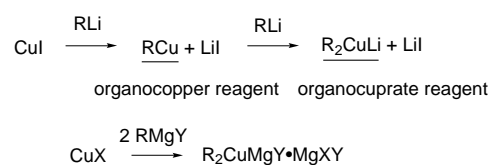


the “reactive conformation of a true reactive species”. To make matters worse, the structures of the final copper-containing products are generally unknown. Those exploring the frontiers of organocopper chemistry in industry and academia have desperately required a better mechanistic understanding.

Two sources of mechanistic information have surfaced in the past several years, new analytical and theoretical methods. As recently demonstrated by Nakamura, Morokuma, and co-workers, theoretical analysis of the reactions of large lithium organocuprate clusters with realistic electrophiles has become possible with explicit consideration of solvent molecules and bulk solvent polarity.^[15–23] In this review, the current status of understanding of organocuprate mechanisms will be summarized by focusing on lithium dialkylcuprate(i) clusters in the context of the following topics: (1) structures of the clusters in crystals, in solution, and as studied by theoretical methods, (2) conventional mechanistic schemes for organocuprate reactions, and (3) reaction pathways of large lithium dialkylcuprate(i) clusters as analyzed through a combination of theoretical and experimental data. We will suggest an answer to part of the question “Wherefore art thou copper?”

1.1. Historical Background and Recent Progress

The initial implication of the forthcoming golden age of organocopper chemistry was in 1941, when Kharasch and Tawney^[11] reported the 1,4-addition reaction of a Grignard reagent to an α,β -unsaturated ketone in the presence of a small amount of a Cu^I salt.^[24] Gilman et al. reported in 1952 that addition of one equivalent of MeLi to a Cu^I salt results in the formation of yellow precipitates, which then afford a colorless solution upon addition of another equivalent of MeLi (Scheme 2).^[25] In 1966 Costa et al. isolated a complex between phenylcopper(i) and magnesium, as well as crystals of a lithium diphenylcuprate(i) complex.^[26] Although the organocopper reagents derived from Grignard reagents are widely used and may be described as R_2CuMgX , it is still uncertain to what extent this reflects the reality in solution.



Scheme 2. Preparation of organocopper reagents.

The organic chemistry of organocuprates started its rapid development in 1966, when House et al. showed that the reactive species of conjugate addition is the lithium diorganocuprate(i) called the “Gilman reagent”.^[27] Foundations for subsequent vigorous synthetic development were laid by Corey and Posner,^[28] and other important initial developments, such as substitution reactions on sp^2 carbons or in an allylic system^[10, 29–31] and the carbocupration of acetylene^[32] were reported before the mid 1970s.

The nature of the Gilman reagent now needs some careful definition. While numerous reports (in particular, old ones) describe the Gilman reagent as R_2CuLi , a vast majority of

Eiichi Nakamura received his PhD in Chemistry from Tokyo Institute of Technology in 1978. Following postdoctoral study in the Department of Chemistry at Columbia University, he joined the faculty of his alma mater in 1980 and was promoted to the rank of full professor in 1993. In 1995, he moved to the Department of Chemistry of the University of Tokyo. His interest in the dynamism of action of organic molecules forms the basis for his research activities which range through organic synthesis, chemical theory, and biology.

Seiji Mori was born in 1968 in Tokyo. He studied at the Tokyo Institute of Technology, and was awarded his BSc in 1993 and MSc in 1995. In 1998, he received his PhD degree at the University of Tokyo under the guidance of Professor Eiichi Nakamura. He became a fellow of Japan Society for the Promotion of Science in 1997, worked at Emory University in USA, and is currently an assistant professor at Ibaraki University in Japan. His research interests center on the theoretical studies of organic and organometallic reactions.



E. Nakamura



S. Mori

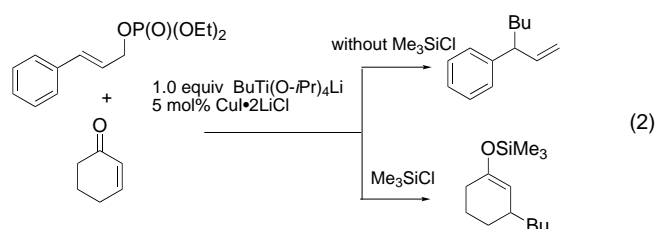
them actually used an LiX cluster $R_2CuLi \cdot LiX$, prepared by an in situ reaction between RLi and CuX (X = Br, I, or CN, sometimes with a ligand such as Me_2S and PR_3). Although R_2CuLi and $R_2CuLi \cdot LiX$ may show largely the same reactivities, Lipshutz et al.^[33] showed by analyses of reactivities and spectroscopic properties that they are indeed different species. Even a small difference of solvent may affect the composition of the reagent and hence the reactivities. Due to such complexity, it is now customary to show all ingredients upon describing a reagent (for example, $R_2CuLi \cdot LiI \cdot Me_2S/BF_3 \cdot Et_2O$ in THF/hexane).

Shortly after the opening of the “Lewis acid age” with the discovery of the Mukaiyama aldol reaction in 1973,^[34] Yamamoto and Maruyama’s reports on the “ $RCu \cdot BF_3$ ” reagent^[35] introduced the new concept of Lewis acid assistance in organocopper chemistry.^[36] Although the identity of $RCu \cdot BF_3$ is still elusive,^[37] the BF_3 activation was applied to numerous synthetic works, as illustrated in Scheme 3 by a diastereoselective addition of a homoenolate species in a total synthesis.^[38]

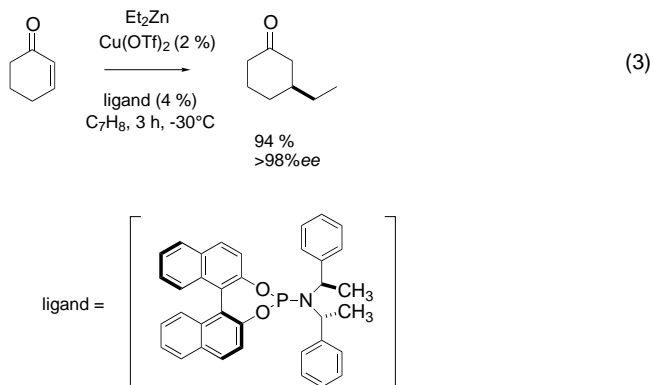
Since the initial discovery by Nakamura and Kuwajima in 1984,^[39] Me_3SiCl has become a standard reagent for acceleration of conjugate addition. This effect was reported first for the copper-catalyzed conjugate addition of the zinc homoenolate of propionic acid esters, as shown in Scheme 3, then for Grignard-based catalytic reagents^[40, 41] and stoichiometric lithium diorganocuprate(s).^[42–46]

The zinc homoenolate started the chemistry of metal homoenolates.^[47–49] The synthetic scope of such a “nucleophile-bearing electrophile” was further exploited by Tamaru, Yoshida, and co-workers first,^[50] and then extensively by Knochel et al., and others.^[51–53] Dominated by lithium- and magnesium-based systems until the mid 1980s, organocopper chemistry now routinely utilizes much milder organometallic nucleophiles, such as organozinc, -titanium,^[54] -zirconium,^[55, 56] and -aluminum reagents.^[57] With the aid of proper activators, these mildly reactive reagents show selectivities unavailable with the conventional reagents, as illustrated in Equation (2) for Me_3SiCl -dependent chemoselectivity.^[58]

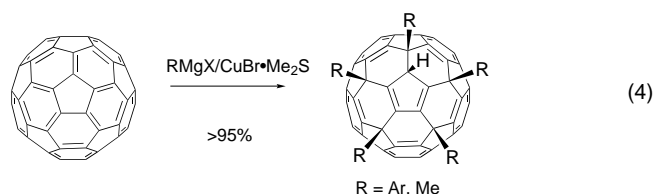
Organocopper chemistry is still rapidly expanding its synthetic scope. The scope of carbocupration, previously limited to acetylenes, has been extended to olefins.^[59–62] Enantioselective conjugate addition^[63] has become truly useful through the use of dialkylzinc, a cationic copper



catalyst, and a chiral ligand [Eq. (3)].^[64] Magnesium-based reagents have found use in quantitative fivefold arylation of

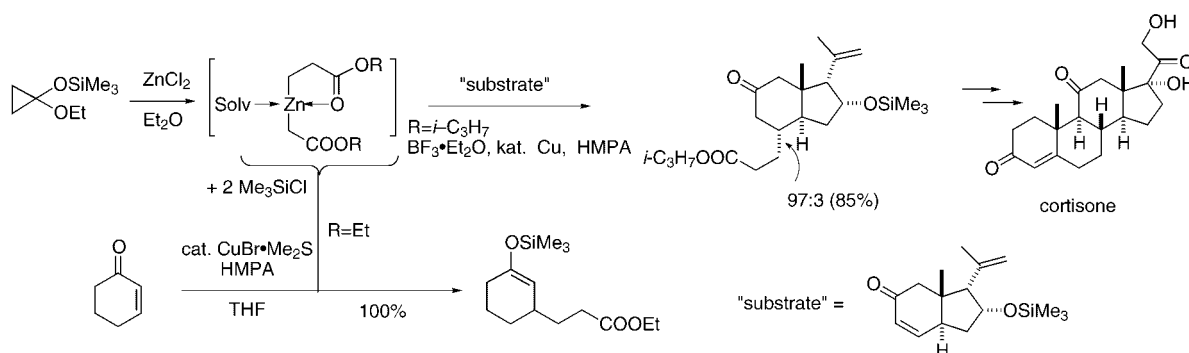


C_{60} ^[65] [Eq. (4)] and threefold arylation of C_{70} ,^[66] this paves the way to new classes of cyclopentadienyl and indenyl ligands with unusual chemical properties.^[67]



1.2. Controversial Mechanistic Issues

With the lack of detailed mechanistic information, various fundamental mechanistic issues have remained the subject of controversy. They are outlined in this section and some will be discussed later in more detail.



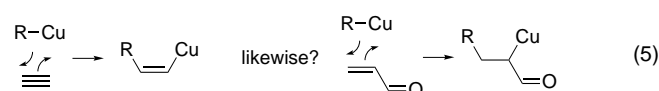
Scheme 3. An Me_3SiCl - and BF_3 -accelerated catalytic conjugate addition reaction and cortisone synthesis. HMPA = hexamethyl phosphoramide.

1.2.1. The Single Electron Transfer Controversy

House proposed in the 1970s^[68] that conjugate addition of organocuprate starts with single-electron transfer (SET) from the reagent to the enone substrate, and this hypothesis became widely believed for some time. After many years of studies, however, the evidence obtained for SET has proven to be too weak to substantiate this once-favored mechanism.

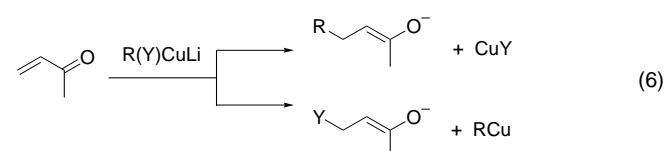
1.2.2. The 1,2-Addition Mechanism in Conjugate Addition

Conjugate addition and carbocupration were once suggested to take place through direct 1,2-addition of R–Cu across a C–C multiple bond [Eq. (5)].^[69] As detailed in Section 4, recent theoretical studies have shown that the two reactions do take place in the same manner but not through this mechanism.



1.2.3. The Dummy Ligand

A synthetic problem associated with the use of homoorganocuprates $[\text{R}_2\text{Cu}]^-$ is that the reagent can transfer only one of the two precious R ligands to the target electrophile (E^+ , for example, an α,β -unsaturated carbonyl compound) and one R ligand is lost as an unreactive RCu species. The introduction, in 1972, of mixed organocuprates $[\text{R}(\text{Y})\text{Cu}]^-$,^[70] in which the Y group acts as a nontransferable dummy ligand, provided the first general solution to this problem [Eq. (6)]. Typical

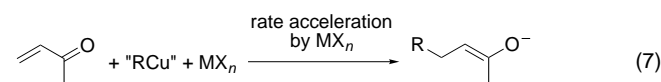


dummy ligands include alkynyl,^[71] cyano,^[72] phenylsulfanyl,^[73] dialkylamino, and phosphanyl groups.^[73, 74] The selectivity of ligand transfer has been thought to arise during the process of ligand–ligand coupling in an intermediate bearing three ligands, R, Y, and E. A widely accepted hypothesis has been that a Y group forming a stronger Cu–Y bond acts as a better dummy ligand (because it resists transfer). While this hypothesis has been successfully applied to the design of dummy ligands, recent theoretical studies by Nakamura and Yamanaka revealed an entirely different controlling factor in the dummy ligand chemistry (see Section 4.2).^[22]

1.2.4. Lewis Acid Effects of the Counteraction

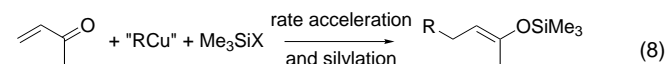
It has been shown for all major categories of lithium organocuprate reactions^[15, 17, 75] that addition of a crown ether significantly retards the desired reactions. In addition, sodium organocuprates are much inferior to lithium organocuprates

for conjugate addition.^[76] On the other hand, $\text{BF}_3 \cdot \text{Et}_2\text{O}$ accelerates conjugate addition^[35] and alkylation of epoxides.^[77] In the allylation chemistry, zinc-,^[49] titanium-,^[54] and aluminum-^[78] based organocuprate reagents show much higher $\text{S}_{\text{N}}2'$ selectivity than lithium organocuprate. The Lewis acidity of the counteraction to the organocuprate is undoubtedly important, but the mechanistic role still needs further studies [Eq. (7)].^[18, 23]



1.2.5. Me_3SiCl Acceleration

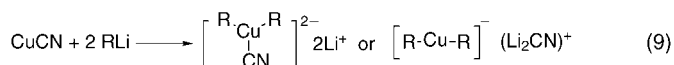
Acceleration and change of selectivity of conjugate additions by a silylating agent are now well established [Eq. (8)].^[46] Me_3SiCl also affects the stereoselectivity of carbonyl 1,2-addition.^[79] Considerable mechanistic discussions have occurred in the literature.^[80] One argument



assumes simple Lewis acid activation of the starting enone with Me_3SiCl ,^[81] which is supported neither by experiments nor by theory.^[82] To the contrary, the lithium cation in the organocuprate reagent has been shown to coordinate to Me_3SiCl (on the chlorine atom).^[80a] Chloride coordination to copper was suggested by theory^[80b] on the basis of seemingly erroneous experimental data.^[83] Another theorem, combined with an inner-sphere electron-transfer hypothesis, assumes in situ trapping of an enolate-like intermediate by the silylating agent, which makes the process irreversible.^[42] The positive correlation between the silylation power of the reagent and the magnitude of rate acceleration^[83, 84] suggests that the rate-determining step of the reaction is the silylation step rather than the C–C bond-forming step. Mechanistic data such as reaction rate, stereochemistry, and theoretical analysis are still lacking, however.

1.2.6. The Higher Order Organocuprate Controversy

Organocuprate(i) species bearing three anionic groups, $[\text{R}_3\text{Cu}]^{2-}$, are called “higher order” organocuprates.^[27] To allow differentiation, conventional organocuprate(i) species $[\text{R}_2\text{Cu}]^-$ may be called “lower order organocuprates”. It has been the subject of controversy whether or not there exists, as a stable species, a higher order lithium cyanocuprate “ $\text{R}_2\text{Cu}(\text{CN})\text{Li}_2$ ” that bears two carbanionic residues and a cyanide anion on the copper [Eq. (9)]. The controversy generated numerous mechanistic and structural studies on organocuprates in general.



It was reported in the 1970s that a higher order organocuprate reagent, which was prepared by the use of more than two equivalents of an alkyllithium reagent for a copper(I) salt, is more reactive^[27, 85, 86] and more selective than ordinary organocuprates.^[87] Ashby and Watkins showed by NMR spectroscopy and cryoscopy that species form which may be considered as higher order organocuprates.^[88] Bertz and Dabbagh demonstrated for the first time the presence of a tricoordinated Cu^I complex ($[\text{R}_3\text{Cu}_2]^-$) by solution NMR spectroscopic studies,^[89] and Olmstead and Power^[90] demonstrated the existence of a tricoordinated organocuprate $[\text{Li}_3\text{Cu}_2\text{Ph}_5(\text{SMe}_2)_4]$ in crystals.^[91]

Lipshutz et al. reported that reagents formed by addition of two equivalents of RLi to CuCN are higher yielding than the corresponding Gilman organocuprates (R_2CuLi) or lower order cyanocuprates ($\text{RCu}(\text{CN})\text{Li}$), and described it as $\text{R}_2\text{Cu}(\text{CN})\text{Li}_2$ to imply a tricoordinated structure.^[72b, 92] With the aid of ^{13}C , ^6Li , and ^{15}N NMR data,^[93, 94] Bertz et al. pointed out that cyanide is not attached to copper(I) in the Lipshutz mix, and started the controversy.^[95] Physical measurements by Penner-Hahn and co-workers^[96, 97] and Lipshutz et al.,^[98] and theoretical studies by the groups of Snyder,^[99] and Penner-Hahn and Frenking^[97] contributed much to the discussion. All of the recent crystallographic data for the cyanocuprates of “higher order stoichiometry” reported by Boche et al.^[100] and van Koten and co-workers^[101] indicated that the cyanide anion is coordinated to lithium and not to copper. Consensus after many years of studies is therefore that three-coordinated $[\text{R}_2\text{Cu}(\text{CN})]^{2-}$ is not a stable structure in ethereal solution.^[94, 102–104] In spite of this conclusion, the Lipshutz mix still remains as the reagent of choice in many synthetic transformations,^[105] and the presence of a tricoordinated cuprate(I) dianion was indicated by ^{13}C – ^{13}CN carbon coupling for the cyanostannylvinylcuprate(I) dianion in a mixture of THF/HMPA.^[106] In addition, the cyanide anion finds its way to copper at the end of the reaction and forms $\text{RCu}(\text{CN})\text{Li}$, although it is not known when the cyanide–copper coordination starts. The true role of the cyano group in the reactions of higher order cyanocuprates still remains obscure.^[103]

1.2.7. Other Issues

While a large number of studies have reported on conjugate addition and $\text{S}_{\text{N}}2$ alkylation reactions, mechanisms of many important organocopper reactions have not been discussed. These reactions involve substitution on sp^2 carbons,^[28] acylation with acyl halide,^[107] carbonyl addition, oxidative coupling,^[108] nucleophilic opening of electrophilic cyclopropanes,^[109] and the Kocienski reaction.^[110] The chemistry of organocopper(II) species has rarely been studied experimentally^[111–113] or theoretically.

2. Structures of Organocopper Compounds

Organocopper compounds can be classified into four basic types, RCu^{I} , $\text{R}_2\text{Cu}^{\text{I}}\text{Li}$, $\text{R}_3\text{Cu}^{\text{I}}\text{Li}_2$, and $\text{R}_3\text{Cu}^{\text{III}}$. As represented by polymeric MeCu, the RCu reagents are unreactive and not very useful synthetic reagents. R_2CuM ($\text{M} = \text{Li}, \text{MgX}$, etc.)

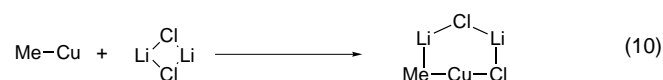
and $\text{R}_3\text{Cu}^{\text{I}}\text{Li}_2$ generated in situ are the most useful sources of carbon nucleophiles and hence have been studied most extensively. The structure of the $\text{R}_3\text{Cu}^{\text{III}}$ species, which has long been discussed in the literature without rigorous proof of its existence, was recently determined. A summary of the structures of organocopper reagents will be given below. Discussions will be limited to those pertinent to the understanding of organocuprate reaction mechanisms, as more extensive structural reviews^[13] have already been published. Several representative crystal structures are shown in Figure 1, and will be discussed in the following sections.

2.1. Mono- and Dicoordinated Organocopper(I) Compounds

2.1.1. Neutral Organocopper(I) Compounds: RCu

Though MeCu itself is polymeric in ethereal solution, RCu may form a monomeric cluster such as $[\text{MeCu}(\text{PPh}_3)_3]$ in the presence of a ligand having high affinity to copper (such as phosphane; Figure 1a).^[114] A strong neutral donor ligand (like PPh_3) may increase the reactivity of a neutral organocopper reagent.^[115] Neutral organocopper(I) compounds have also been characterized as eight-centered cyclic tetramers, for example, $[(2\text{-Me}_2\text{NC}_6\text{H}_4)\text{Cu}]_4$,^[116] $[(\text{Me}_3\text{SiCH}_2)\text{Cu}]_4$,^[117] and $[\text{PhCu}]_4 \cdot 2\text{Me}_2\text{S}$ ^[118] (Figure 1b). We see here that a copper atom in a neutral RCu compound may accept a solvent molecule as a ligand. It is a general characteristic of neutral RCu aggregates that we find a three-center two-electron bonding pattern and the copper atoms solvated with a heteroatom ligand.

Since the method commonly used for generation of RCu species produces an extra alkali metal salt in solution (Scheme 2), the reagent commonly described as a neutral RCu reagent may react as a halocuprate complex. In fact, density functional calculations indicate that conversion of free monomeric MeCu into a six-centered cluster $\text{MeCu} \cdot 2\text{LiCl}$ is an energetically favorable process [Eq. (10)].^[117] In addition,



the crystal structure of a mixed alkylhalocuprate bearing an R-Cu-X moiety was reported recently (Figure 1c).^[119] The particular compound reported was isolated as a monomeric species owing to the bulkiness of the organic group.

2.1.2. Linear Free Organocuprates: $[\text{R}_2\text{Cu}]^-$

The most basic structural property of diorganocuprate(I) is their linear R-Cu-R arrangement. It is clearly seen in $[\text{Li}([12]\text{-crown-4})_2][\text{CuPh}_2] \cdot \text{THF}$, prepared by mixing Ph_2CuLi and the crown ether (Figure 1d).^[120] A linear organocuprate structure of $[\text{Me}_2\text{Cu}]^-$ ^[120] was also identified in crystals. Note that these solvent-separated ion pairs are unreactive in many standard organocopper reactions, the

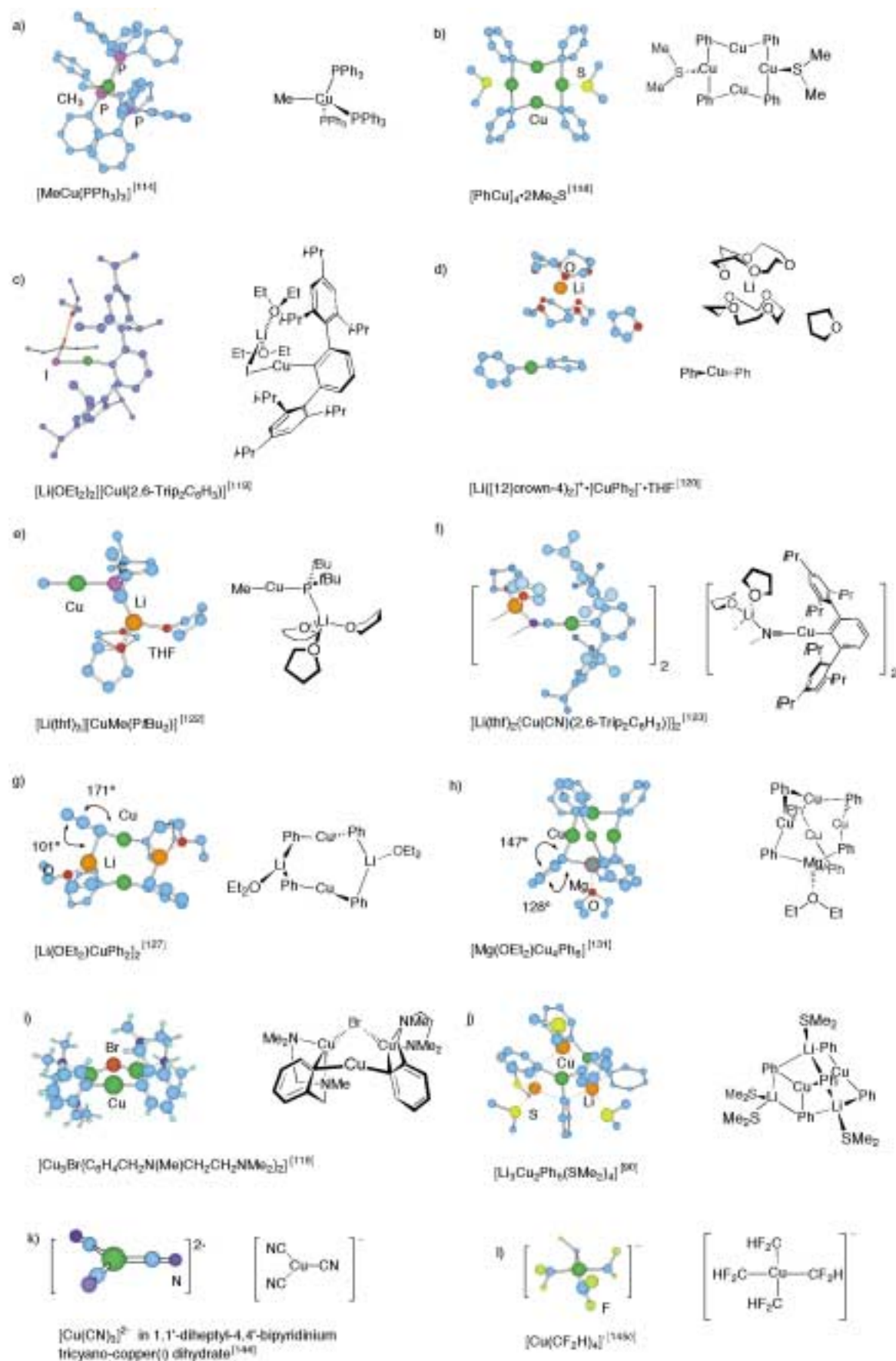


Figure 1. Crystal structures of representative organocopper compounds. Hydrogen atoms are omitted for clarity. In (g) and (h) the dihedral angles are given. Trip = 2,4,6-*i*-Pr₃C₆H₂.

reasons for which have recently been elucidated by the studies of Nakamura, Morokuma and co-workers.^[15]

2.1.3. Minimum Lithium Organocuprate Clusters: R_2CuLi

Coordination of a lithium cation to the linear $R-Cu-R$ anion creates $R-Cu-R-Li$, which may be called a minimum lithium diorganocuprate(i) cluster. For the partial charges on the two ends to be neutralized, the minimum cluster dimerizes, polymerizes, or attracts an ambiphilic LiX unit to form a closed cluster, $R_2CuLi \cdot LiX$.^[121] Due to the high energy cost of bending the $R-Cu-R$ bond,^[21] the four-centered cyclic structure (often found for alkyl lithium compounds) does not form.

Monomeric $[Li(thf)_3][CuMe(PtBu_2)]$ (Figure 1e)^[122] has been observed in crystals obtained from a reagent mixture that shows the typical reactivity of an organocuprate bearing a dummy ligand. In the structure of linear dimers of lower order cyanocuprates $ArCu(CN)Li$ (Figure 1f),^[123] we also see strong $Li-N$ association. Such a dimeric unit structure may be found in a polymeric complex.^[100]

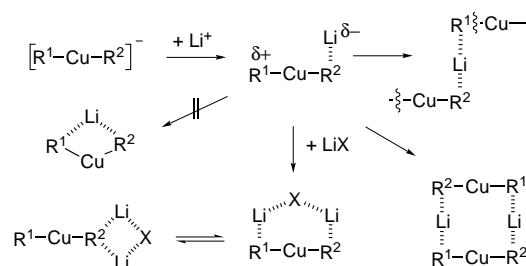
2.1.4. Closed Clusters: $R_2CuLi \cdot LiX$ and $(R_2CuLi)_2$

The neutral closed cluster is widely detected in crystals and in solution, and accepted as the typical resting state of lithium organocuprates in ethereal solution. Eight-centered dimers of R_2CuLi were suggested first by van Koten and Noltes on the basis of NMR spectroscopic and cryoscopic analyses of lithium diarylcuprate(i) compounds in benzene.^[124] The dimeric structure was further indicated in NMR spectroscopy, cryoscopic, and X-ray scattering experiments by Pearson and Gregory.^[125] Following the first crystal structure determination of a R_2CuLi by van Koten et al.,^[126] Weiss and Lorenzen, and Olmstead and Power determined various dimeric structures $[[Li(OEt_2)]CuPh_2]_2$ (Figure 1g),^[127] $[Li_2(SMe_2)_3-Cu_2Ph_4]$,^[118] and $[[Li(SMe_2)]Cu(Me_3SiCH_2)_2]_2$.^[128] These structures have their lithium cation tricoordinated (two R groups and one solvent molecule). The R groups (aryl and alkyl) are pentacoordinated with a stronger bond to copper and a weaker electrostatic bond to lithium. As seen from the metal- $C_{ipso}-C_{ortho}-C_{meta}$ angles in lithium diphenylcuprate (Figure 1g), the copper atom is σ -bonded and the lithium atom is π -coordinated to the *ipso* phenyl carbon atom. In a dialkylcuprate(i), the copper atom is covalently bound to a nearly tetrahedral sp^3 carbon, which is electrostatically associated with a lithium atom. Unlike the copper atom in neutral RCu complexes (see Section 2.1.1.), the negatively charged copper atom is not Lewis acidic and does not accept an extra ligand (solvent).^[129, 130]

A structure of an organomagnesium-based organocopper(i) compound is known and has a magnesium-bridged structure (Figure 1h).^[131] As seen from the dihedral angle in Figure 1h, the Lewis acidic magnesium atom is more tightly bound to the phenyl group than than the lithium in the lithium organocuprate. Organocuprates bearing more Lewis acidic metals such as zinc(II) and titanium(IV) cations have not yet been characterized.^[132]

While no crystal structures have been determined for $R_2CuLi \cdot LiX$ (X = halogen), the presence of $(Li_nX_{n+1})^-$ units in organocuprate clusters has been suggested through studies using electrospray ionization mass spectrometry.^[133] The six-centered structure of a neutral arylcopper complex (Figure 1i)^[116] offers a good model, and is similar to the structure of $Me_2CuLi \cdot LiCl$ or $Me_2CuLi \cdot LiI$ determined by calculations.

In the hypothetical structural conversion shown in Scheme 4, we may start with a free dialkylcuprate(i) anion $[R^1R^2Cu]^-$ and go through a minimum cluster R^1R^2CuLi to either polymers, eight-centered dimers, or mixed cyclic clusters. The linear R^1-Cu-R^2 structure will be retained throughout the conversion. The stable linear $C-Cu-C$ geometry is due to bonding participation of the copper d_{z^2} orbital.^[21]



Scheme 4. Various structural possibilities of cuprates. Solid lines indicate (largely) covalent bonds and dashed lines indicate (largely) electrostatic bonds between a metal cation and an organic or heteroatomic anion. (Such distinctions will not be generally made in the remaining schemes in this review.) $X = RCuR$, halogen, CN, etc.

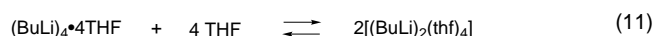
2.1.5. Dynamic Equilibria in Solution

Although the crystal structures offer important reference points, they do not reflect the reactive conformations of these species in solution. Recent experimental studies revealed a wealth of information on the time-averaged, as well as dynamic, structures in solution.

The Me_2CuLi dimer is the species studied most carefully. Its molecular weight indicates a (time-averaged) dimeric structure in diethyl ether and Me_2S , and X-ray scattering studies support this conclusion by showing the $Cu-Cu$ distance in solution as 2.6–2.8 Å,^[125, 130] which is close to the value in crystals. The extended X-ray absorption fine structure (EXAFS) spectra in solution indicate dicoordination of the copper atom with a $C-Cu$ bond length of 1.94–1.96 Å.^[130, 134] All these data are consistent with the persistence of the eight-centered structure both in crystals and in solution.

Cryoscopic measurement of the reagent $Me_2CuLi \cdot LiI$ in THF indicated persistence of this stoichiometry,^[135] whose stable structure was shown by theory to be the six-centered structure shown in Scheme 4. Supporting such a structure, EXAFS spectroscopic studies on $Me_2CuLi \cdot LiCN$ and $Me_2CuLi \cdot LiI$ in THF indicated a single Cu atom in a cluster.^[96a, 130, 136] According to NMR spectroscopy studies in diethyl ether,^[137] the cuprate may exist as an equilibrium mixture of the Me_2CuLi dimer and the LiX cluster.

Recent NMR studies by Berger and co-workers on the cuprates Me_2CuLi , $\text{Me}_2\text{CuLi} \cdot \text{LiMe}$, and $\text{Me}_2\text{CuLi} \cdot \text{LiCN}$ in THF revealed the dynamic properties of the clusters in solution.^[104] The lithium atom exists in the time-averaged vicinity of the methyl group in the $[\text{Me}_2\text{Cu}]^-$ moiety, but rapidly exchanges with other lithium atoms. Hence, a predominant and thermodynamically stable cyclic cluster undergoes fast and reversible cleavage of the Me–Li electrostatic bond (Scheme 5). The spectroscopic observations are consistent with the experimental and theoretical thermodynamic considerations. Dissociation of the $(\text{Me}_2\text{CuLi})_2$ dimer to the monomer is enthalpically highly disfavored by gas-phase calculations,^[138] and must also be entropically disfavored due to solvent participation,^[139, 140] as is known experimentally for alkyl lithium oligomers (see Equation (11)); the dissociation process is accompanied by a loss of $18.8 \text{ cal mol}^{-1} \text{ K}^{-1}$ ^[140].



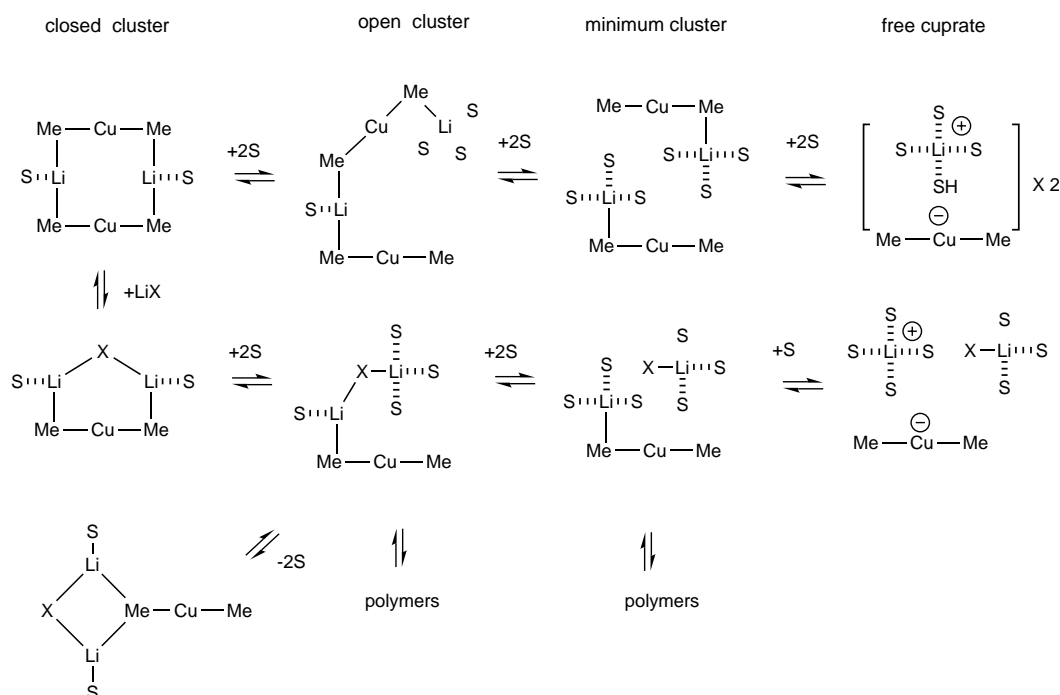
The presence of lithium halide is known to affect reactivities and selectivities,^[33] but only to an energy scale of a few kcal mol^{-1} of activation energy. This may be partly due to accelerated cluster reorganization or to coordination of lithium halide to a Cu^{III} intermediate, which is formed during nucleophilic reactions. In the light of contrasting reports (one reports slower conjugate addition in THF than in diethyl ether,^[141] another reports a faster reaction in toluene,^[142] and the further one reports that 1,4-addition in toluene can be promoted over 1,2-addition in the presence of Me_2S ^[143]), solvent effects are a difficult subject to deal with.

Putting together the body of current data, one can draw a series of mobile equilibria, as shown in Scheme 5, for $(\text{Me}_2\text{CuLi})_2$ and $\text{Me}_2\text{CuLi} \cdot \text{LiX}$; they will dissociate sequentially into free $[\text{Me}_2\text{Cu}]^-$ with Gibbs free energy loss in ethereal solution. $\text{Me}_2\text{CuLi} \cdot \text{LiX}$ equilibrates with the dimer through exchange of an Me_2CuLi unit with LiX . Oligomers and polymers may also form. As will be discussed in Section 4, the “open cluster” (among other clusters) serves as a gateway channel to organocuprate reactions.

2.2. Tricoordinated Copper Compounds: $[\text{R}_3\text{Cu}^{\text{I}}]^{2-}$ and $\text{R}_3\text{Cu}^{\text{III}}$

2.2.1. Higher Order Organocuprates

$[\text{Li}_3\text{Cu}_2\text{Ph}_5(\text{SMe}_2)_4]$ (shown in Figure 1j)^[90, 91] is the only crystal structure known for the controversial^[89] nucleophilic higher order organocuprates. This complex forms only from a dimethylsulfide solution, and not from diethyl ether or THF. Therefore it is not clear if the higher order organocuprates can also exist in ethereal solution. Solution NMR studies^[104] indicated that Me_3CuLi_2 dissociates into Me_2CuLi and MeLi through rapid exchange of lithium atoms. As to the controversial higher order cyanocuprates, no such tricoordinated copper(I) species have been experimentally or theoretically identified, except a case reported for $[\text{Cu}(\text{CN})_3]^{2-}$ (Figure 1k),^[144] where the two negative charges are stabilized by the presence of three cyano groups. Other than this tricyano structure, all known organocuprates of a higher order cyanocuprate stoichiometry have usual dicoordinated copper centers.^[100, 101, 123]



Scheme 5. Rapid cluster equilibration for $(\text{Me}_2\text{CuLi})_2$ and $\text{Me}_2\text{CuLi} \cdot \text{LiX}$. Dashed lines indicate coordination between a metal cation and a neutral solvent molecule or ligand; S = solvent; X = halogen, CN, RO, etc.

2.2.2. Organocopper(III) Species

Although trialkylcopper(III) species have appeared in numerous mechanistic discussions since the 1970s, it is only since the late 1980s that crystal structures substantiated the presence of such species. We now have three crystal structures of discrete organocopper(III) species.^[145] As illustrated for $[\text{Cu}(\text{CF}_2\text{H})_4]^-$ in Figure 11,^[145c] all of them are nearly square planar in geometry in consonance with the formal d^8 electronic system of the copper atom, and they can be regarded as T-shaped neutral Cu^{III} species bearing a fourth ligand. Recent theoretical analysis on the stability of $\text{Me}_3\text{Cu}^{\text{III}}$ ^[146–149] supported the stabilizing effects of a donor ligand.

2.3. Theoretical Analysis of Organocopper Structures

Although a variety of structural data were already accumulated by the beginning of the 1990s, connecting this mass of structural data into molecular level mechanisms has been a difficult task. With the advent of theory and computers, quantum mechanical calculations are now playing the key role. The development of post Hartree–Fock (HF) and density functional calculations, which was honored by the 1998 Nobel Prize, has made a strong impact on the study of organocopper chemistry.

Pioneering theoretical works by Poirier et al.,^[150] Ziegler et al.,^[151] Morokuma et al.,^[152, 153] Bauschlicher et al.,^[154] Frenking et al.,^[155] and Baerends et al.^[156] often used monomeric MeCu . Studies by Hwang and Power, Snyder et al., Sosa et al., and Frenking and co-workers demonstrated the importance of electron-correlated calculations in the structural studies of organocuprate clusters.^[119, 121a, 157, 158] The electron-correlated methods (MP2, B3LYP, and higher levels) are mandatory for description of the intermediates and transition states in the reactions of lithium organocuprate clusters. Good description of the high-lying copper 3d orbitals is necessary. The HF calculations give very low-lying d_{xz} orbitals, and understandably fail in adequate description of π -backdonation ability of the cuprates.^[19] As is the case for R_2Zn , neutral RCu has 3d orbitals that are too low-lying to be nucleophilic, and it behaves rather as a Lewis acid.^[19] Relativistic effects on copper are small on structures and energetics.^[15] The high activation energies of MeCu addition reactions obtained in earlier studies^[115, 156, 157] are due to lack of d-orbital participation.

3. Experimental Studies on Organocuprate Reaction Mechanisms

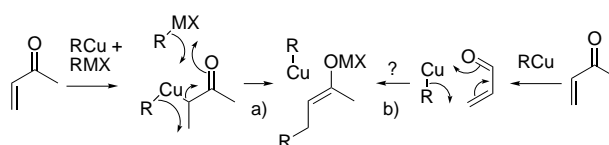
Mechanistic studies on organocuprate reactions have been hampered by the complexity of the cluster structures. Crystallographic and spectroscopic structural analyses have provided information only for discrete data points. Various contradicting mechanistic proposals have made obscure the mechanistic pictures of organocuprate chemistry. Nonetheless, a certain mechanistic consensus has been achieved, and is summarized in the following sections. Three important

categories of organocuprate reactions, conjugate addition, carbocupration reactions, and alkylation reactions, have been most extensively studied.

3.1. Conjugate Addition

3.1.1. The Four- and Six-Centered Mechanisms

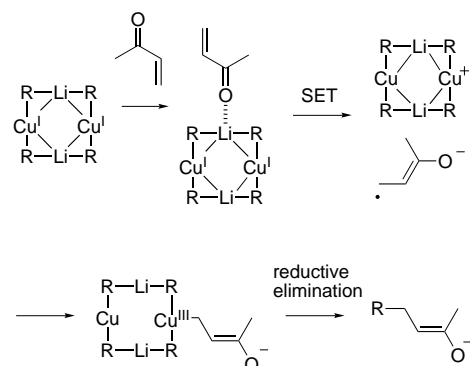
Four-centered addition of RCu to an enone was discussed in the 1960s.^[162] There have been discussions about a six-centered transition state until recently,^[152] but this does not explain however the formation of an *E/Z* mixture of enolate stereoisomers.^[159, 160] These mechanisms (Scheme 6) must now be considered obsolete.



Scheme 6. a) 1,2-Addition and b) 1,4-addition mechanisms.

3.1.2. The Single Electron Transfer Theorem

House and co-workers pioneered the synthetic and mechanistic studies of organocuprate reactions in the 1970s. In their papers a mechanism was proposed that assumes a single electron transfer (SET) from the dimer which would lead to a Cu^{III} intermediate (Scheme 7).^[68, 161] The SET/ Cu^{III} theo-

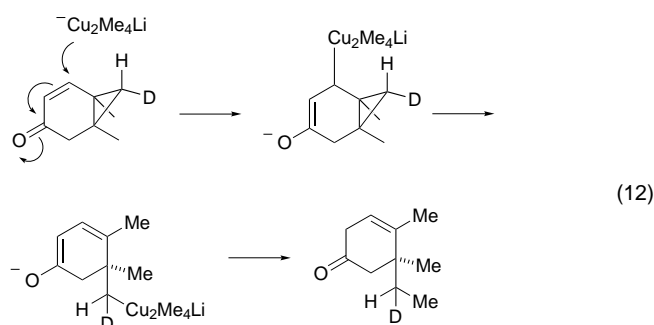


Scheme 7. The House mechanism of 1,4-addition.

rem had a strong impact for many years. However, most of the experimental facts, once considered to support the SET process, are not accepted as evidence of SET now. Only the Cu^{III} hypothesis has survived the test of the time.

1) *E/Z* Isomerization of the olefinic part in an enone was once taken as evidence for reversible electron transfer. It was later reported that the isomerization takes place even in the presence of LiI , a usual component of the Gilman cluster reagent (that is, $\text{Me}_2\text{CuLi} \cdot \text{LiI}$).^[163] Such isomerization is also possible by reversible generation of an advanced $d \rightarrow \pi^*$ copper/enone complex along the reaction pathway,^[42, 164] and, thus, does not represent strong evidence of SET.

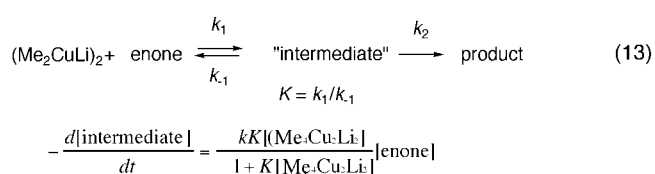
- 2) Qualitative correlation of the apparent rate of 1,4-addition with the reduction potential of the enone^[161] was later proven by quantitative kinetic studies by Krauss and Smith to be only superficial.^[165]
- 3) β -Cyclopropyl α,β -unsaturated ketones, such as the one shown in Equation (12), often give a ring-opened product, which was taken as strong evidence for radical anion formation by SET.^[166] An elegant study by Casey and Cesa with deuterium-labeled substrate indicated stereospecificity of the cyclopropane ring opening that denies the radical mechanism [Eq. (12)].^[167] On the basis of a series of control experiments, Bertz et al. reinterpreted the results in terms of Cu^{III} intermediates formed by two-electron transfer.^[168]



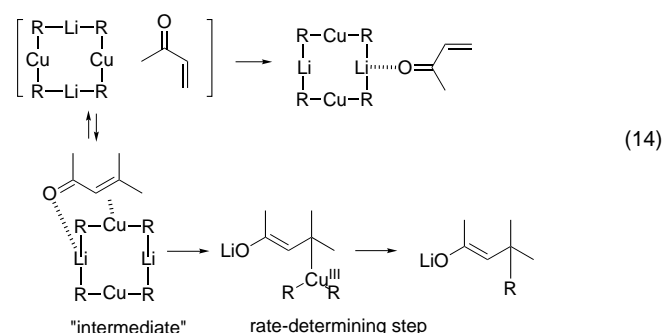
- 4) Electron spin resonance (ESR) and chemically induced dynamic nuclear polarization (CIDNP) spectroscopic studies for detecting the radical intermediates failed.^[169] Conjugate addition of a vinylcuprate reagent to enone takes place with retention of the vinyl geometry, indicating that a vinyl radical intermediate is not involved.^[170, 171] Kinetic isotope effects and substituent effects on organocuprate addition to benzophenone indicate that the C–C bond formation is rate-determining, which is not consistent with the involvement of a radical ion pair intermediate.^[172]
- The SET processes do not occur among moderately electrophilic olefinic acceptors, but are likely to be involved with highly electrophilic substrates. A recent example is the polyaddition of an organocuprate to fullerenes (see Section 1.1; [Eq. (4)]). A fluorenone ketyl radical has been detected in an organocuprate reaction of fluorenone.^[159] Doubly activated olefins^[173, 174] and bromonaphthoquinone^[175, 176] are also likely to react by SET.

3.1.3. Kinetics and the Spectroscopic Analysis of Intermediates

Conjugate addition to α,β -unsaturated ketones and esters are the most important organocuprate reactions. Important kinetic studies by Krauss and Smith for Me_2CuLi and a variety of ketones revealed the kinetic expressions shown in Equation (13), which are first order for both the organocuprate dimer and the enone.^[165]

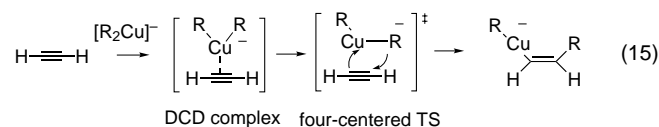


This rate expression is consistent with the reaction scheme shown in Equation (14) which was prepared on the basis of the Krauss and Smith paper. Thus, the first-formed organocuprate dimer/enone complex with lithium–carbonyl and



copper–olefin coordinations^[177] forms the product via the intermediate(s). A lithium–carbonyl complex also forms but is a dead-end intermediate. Although the detailed structures of the intermediates remained obscure for a long time, the essence of this scheme has been supported by subsequent NMR spectroscopic studies and recent theoretical studies. The key “intermediate” is now considered to be an organocupper(III) species formed by two-electron inner-sphere electron transfer [Eq. (14)].^[16, 20]

Corey and Boaz proposed explicitly a Dewar–Chatt–Duncanson (DCD) complex for such a Cu^{III} /olefin complex (see [Eq. (15)]).^[42] X-ray absorption near-edge structure



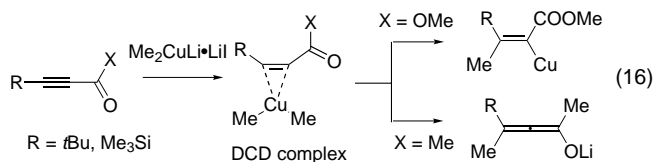
(XANES) investigation of a complex between a *trans*-cinnamate and $\text{Me}_2\text{CuLi} \cdot \text{LiI}$ in THF indicated elongation of the C–Cu bond and increase of the coordination number of the copper atom. NMR spectroscopic studies on the organic part of the complexes by Ullenius and co-workers,^[178] Krause et al.,^[179] and others^[180] indicated loosening of the olefinic bond. Very recently, Krause et al. determined, for the first time, the kinetic activation energies ($E_a = 17–18 \text{ kcal mol}^{-1}$) of some conjugate addition reactions.^[181]

3.2. Carbocupration of Acetylenes and Olefins

Carbocupration of acetylene smoothly takes place in a *cis* fashion to provide a reliable synthetic route to vinyl copper

species [Eq. (15)].^[32] Magnesium and zinc, which are more Lewis acidic than lithium, are better counteranions for this reaction, and strong coordination of a lithium dialkylcuprate(i) with a crown ether dramatically slows down the reaction.^[15] This reaction was generally considered to proceed through a four-centered mechanism, and, hence, to be mechanistically different from the conjugate addition.

In the addition of Me_2CuLi reagents to electron-deficient acetylenes,^[182–184] DCD-type complexes have been identified by NMR spectroscopy.^[185] As shown in Equation (16), ynoates

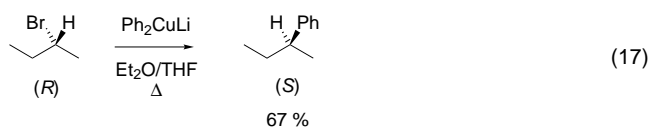


afford vinylcopper intermediates, and ynones instead afford allenolates.^[186] The origin of this diversity remains unclear. A related carbocupration mechanism was also proposed for the reaction with allenylphosphane oxide.^[69] Carbocupration of olefins is known for dienes^[187] and cyclopropenes^[60] but the mechanisms also remain unknown.

3.3. The $\text{S}_{\text{N}}2$ Substitution Reaction on sp^3 Carbons

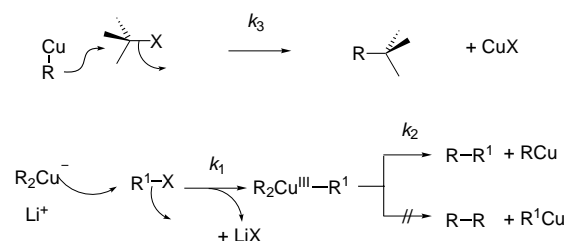
The $\text{S}_{\text{N}}2$ substitution reaction of an alkyl halide with a hard nucleophile such as an alkyl anion can be most readily achieved with the aid of organocopper chemistry.^[188] The $\text{S}_{\text{N}}2$ reaction with epoxides and aziridines is also synthetically useful.^[189] The accelerating effects of $\text{BF}_3 \cdot \text{Et}_2\text{O}$ in the latter reaction imply the importance of substrate activation.^[190]

The alkylation of an alkyl bromide, tosylate, or epoxide with organocuprates takes place with 100% inversion of the configuration at the electrophilic carbon as shown in Equation (17).^[29, 191] The magnitudes of primary and secondary



kinetic isotope effects in the reaction of $\text{Me}_2\text{CuLi} \cdot \text{LiI} \cdot \text{PBU}_3$ with CH_3I strongly suggested that the rate-determining step of the reaction is the $\text{S}_{\text{N}}2$ -displacement stage.^[192] The reaction with alkyl halide, aryl halide, and alkyl tosylate of R_2CuLi has been shown to be first order to the concentration of the $(\text{R}_2\text{CuLi})_2$ dimer and the alkylating reagent.^[125, 197] RCu and $\text{RCu}(\text{PBU}_3)$ do not react with epoxides,^[189] and alkylation reactions of R_2CuLi do not take place in the presence of a crown ether, indicating the importance of a Lewis acidic LiX compound associated with the organocuprate moiety.

Two mechanistic possibilities have been suggested for the substitution reactions (Scheme 8).^[5] The first assumes simple $\text{S}_{\text{N}}2$ substitution by the R anion group. The second one



Scheme 8. Two proposed mechanisms for alkylation reactions.

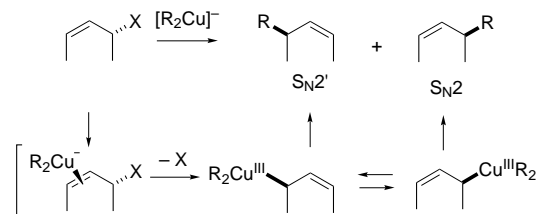
assumes rate-determining displacement of the leaving group with copper bearing a formal negative charge, and subsequent formation of a trialkylcopper(III) intermediate.^[146] The latter then undergoes reductive elimination to give the cross-coupling product. Although the second mechanism may look pleasing enough for a copper specialist, it leaves unanswered a few important questions, namely: the role of the lithium cation, the relative magnitude of k_1 and k_2 , and, among others, the reason why exclusive production of a cross-coupled product $\text{R}-\text{R}'$ is always observed from the symmetrical $\text{R}_2(\text{R}')\text{Cu}^{\text{III}}$ intermediate.

The proposed participation of a Cu^{III} intermediate is based on analogy to the chemistry of lithium diorganocuprate(i) compounds, $\text{R}_2\text{Au}^{\text{I}}\text{Li}$.^[193–196] Crystallographic data of Cu^{III} species^[145] further supported the similarity between Au^{III} and Cu^{III} .^[197]

The SET mechanism has also been discussed for the alkylation of secondary alkyl iodides, where the substitution reaction takes place stereorandomly.^[29, 191b] The reaction of triphenylmethylbromide and Me_2CuLi generated an ESR-active triphenylmethyl radical; this may, however, be regarded as a special case.^[198] Intramolecular cyclization of an olefinic iodide in the presence of an organocopper reagent has been taken as possible but not conclusive evidence of SET.^[199]

3.4. The $\text{S}_{\text{N}}2'$ -Allylation Reaction

Organocuprates react rapidly with allylic halides (or acetates),^[31, 200] propargyl halides (or acetates),^[201] and vinyl-oxiranes,^[30] often with $\text{S}_{\text{N}}2'$ regioselectivity (Scheme 9). The reaction takes place with *anti* stereochemistry with respect to



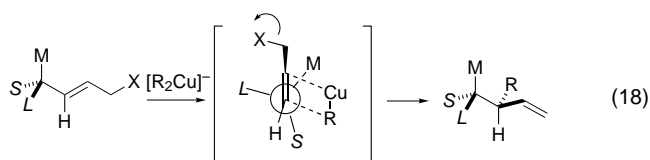
Scheme 9. An *anti*- $\text{S}_{\text{N}}2'$ allylation reaction with a competing $\text{S}_{\text{N}}2$ reaction pathway. $\text{X} = \text{OAc}$, halogen, $\text{OP}(\text{O})\text{Y}_2$.

the leaving group, while *syn* substitution occurs when an allylic carbamate is employed as the substrate.^[202]

The reaction of R_2CuLi tends to give a mixture of $\text{S}_{\text{N}}2$ and $\text{S}_{\text{N}}2'$ products, which has been suggested to be due to the

involvement of the regioisomeric σ -allylic Cu^{III} species shown in brackets in Scheme 9.^[200] Studies on substituent effects in competitive reactions suggested that the rate-determining stage might involve a two-electron transfer from copper to the allylic substrate.^[214] The $\text{S}_{\text{N}}2$ selectivity of the reaction of $\text{Bu}_2\text{Cu}(\text{X}) \cdot 2\text{MgBr}$ is higher with $\text{X} = \text{I}$, OTs than with $\text{X} = \text{Cl}$, Br, and is also higher in ether than in THF.^[203] A combination of an organocopper compound and a Lewis acid, such as $\text{RCu} \cdot \text{BF}_3$, $\text{R}_2\text{CuLi} \cdot \text{ZnCl}_2$,^[49] $\text{R}_2\text{CuLi} \cdot \text{Ti}^{\text{IV}}$,^[54] or $\text{R}_2\text{CuLi} \cdot \text{AlCl}_3$,^[78] greatly enhances the $\text{S}_{\text{N}}2'$ selectivity. NMR spectroscopic studies on $\text{R}_2\text{CuLi} \cdot \text{ZnCl}_2$ and $\text{R}_2\text{CuLi} \cdot \text{Ti}^{\text{IV}}$ only showed rapid transmetalation from Cu to Zn or Ti, giving us little information on a putative Cu/Zn or Cu/Ti mixed reagent.^[53, 57]

Scant information is available for the transition state. The stereoselectivity of the $\text{S}_{\text{N}}2'$ reaction of δ -substituted allylic halides suggested that the transition state for the delivery of an R group from copper has a four-centered character, as shown in Equation (18) (S, M, L = small, medium, and large substituents, respectively).^[54, 129, 204] This conjecture was supported by theoretical comparison of the transition state geometries of olefin carbolithiation with acetylene carbocupration (compare with Scheme 10).^[16, 205]



4. Theory-Based Molecular Pictures of Organocuprate Reactions

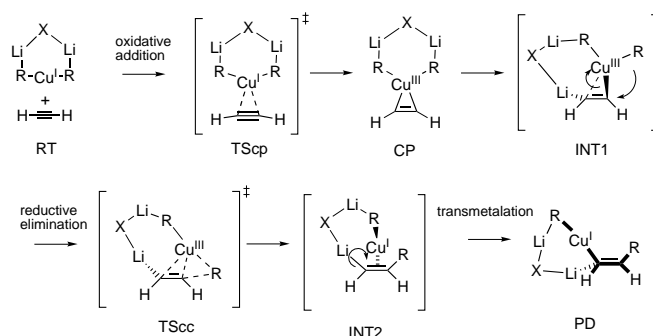
As summarized in the foregoing sections, numerous experimental studies indicated active participation of large organocopper clusters. They typically bear nucleophilic alkyl residues, copper(I) atoms, and counteranions (typically lithium). The Nakamura–Morokuma theoretical analysis has provided answers to a fair number of questions among the numerous problems in organocuprate chemistry. Three representative reactions, carbocupration, conjugate addition, and $\text{S}_{\text{N}}2$ alkylation reaction, have been examined so far in detail to obtain molecular pictures on the cluster participation and the $\text{Cu}^{\text{I}}/\text{Cu}^{\text{III}}$ redox chemistry in these reactions.

4.1. The Reaction Pathway of Acetylene Carbocupration

Carbocupration of acetylene was studied systematically for five model species, MeCu , $[\text{Me}_2\text{Cu}]^-$, Me_2CuLi , $\text{Me}_2\text{CuLi} \cdot \text{LiCl}$, and $(\text{Me}_2\text{CuLi})_2$,^[15] all of which were invoked once in a while in the discussions of organocuprate mechanisms. A few general conclusions have been made for the reactivities of these reagents with π acceptors. (1) As its d orbital is very low lying (and hence not available for redox chemistry),^[21] MeCu can only undergo addition by a four-centered mechanism [Eq. (5)]. (2) This four-centered path requires high energy,

since the covalent $\text{Me}-\text{Cu}$ bond with an energy of 55 kcal mol^{-1} ^[206] must be cleaved. The neutral RCu species is, therefore, not a reactive nucleophile. (An ancillary result of this analysis suggests that the conventional “ RCu ” reagent must be a certain kind of $\text{RCu} \cdot \text{X}^-$ cluster, where X^- may be a halide anion.) (3) Being electron-rich (and having high-lying d orbitals), lithium organocuprates, such as $(\text{R}_2\text{CuLi})_2$, bind tightly to acetylene through two-electron donation from the copper atom (see CP in Scheme 10 and Figure 2). (4) In such complex formation, a cluster structure larger than the parent species R_2CuLi is certainly necessary to achieve cooperation of lithium and copper.

The reaction pathway may be viewed as a “trap-and-bite” mechanism: The structures are shown in Scheme 10 and Figure 2, and the approximate energetics in Figure 3. The cluster opens up and traps the acetylene (INT1), transfers electrons, and then “bites” the substrate to form a C–C bond (TScc). The important events include: formation of a DCD complex CP via a low energy transition state TS_{sc},^[21] inner-



Scheme 10. The “trap and bite” pathway of carbocupration. $\text{X} = \text{RCuR}$, halogen, etc.

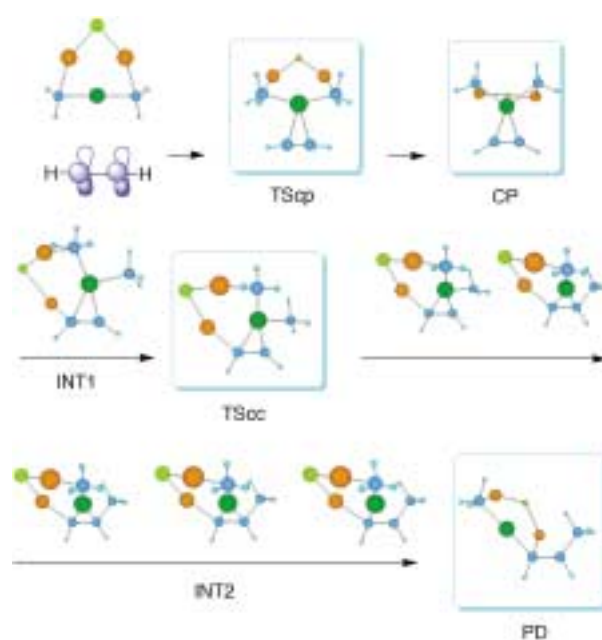


Figure 2. “Snapshots” of intermediates on the potential surface of acetylene carbocupration with $\text{Me}_2\text{CuLi} \cdot \text{LiCl}$. Color code: Cu = dark green, Li = orange, Cl = light green, C = large blue, H = small blue spheres.

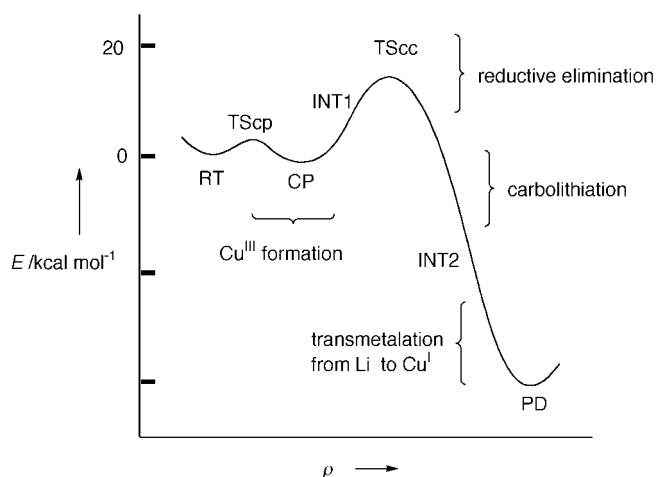


Figure 3. Approximate energy profile of acetylene carbocupration. The energies are relative to the energies of the reactants. E = relative energies, ρ = reaction coordinates. (In physical and theoretical chemistry all species on the potential surface are termed intermediates.)

sphere electron transfer to form a transient intermediate INT1, C–C bond formation through the rate-determining stage (TS_{CC}), and intra-cluster transmetalation from lithium to copper(i) (INT2). The DCD character of CP is shown by the localized molecular orbitals (LMOs, Figure 4) and was also

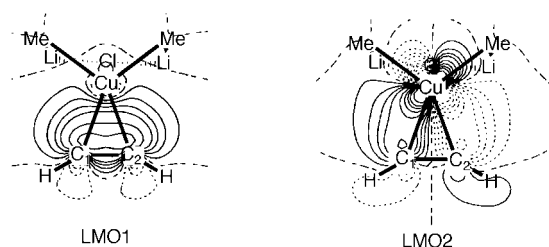


Figure 4. Localized molecular orbitals between $\text{Me}_2\text{CuLi} \cdot \text{LiCl}$ and acetylene in complex CP.

found in the conjugate addition to enals and enones.^[16] Since the C–Cu^{III} bond is very unstable, the activation energy for the C–C bond formation via TS_{CC} becomes small ($<20 \text{ kcal mol}^{-1}$). In solution, the reaction may directly go to INT1 or related species through an open cluster, as depicted in Scheme 5.

Note that drawing the “organic” arrows and indicating the valence of the metal, as in Scheme 10 (and other schemes in the following paragraphs), are necessarily inaccurate from a purely inorganic or theoretical viewpoint. Nonetheless, we have indicated them to put the theoretical results into the framework of conventional organic chemistry, and to facilitate understanding of the chemistry by organic chemists who are using the reagents in their everyday research life.

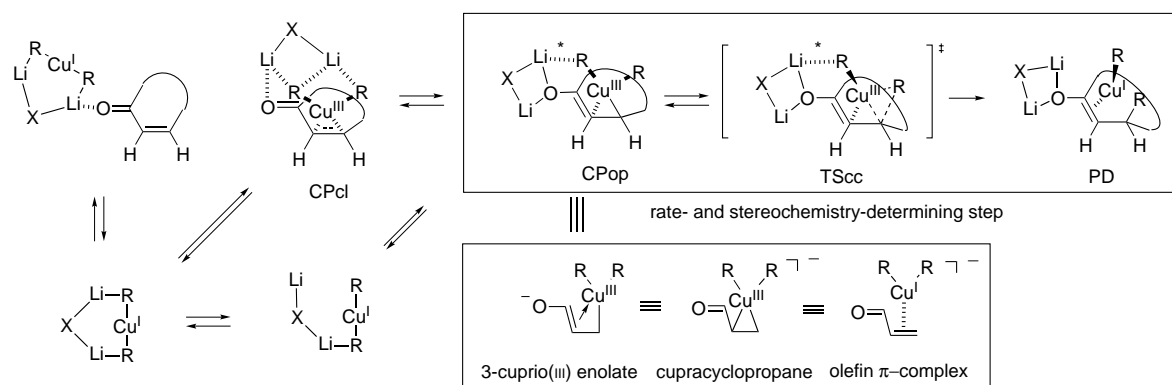
In Figure 2, snapshots of intermediary species on the potential surface of carbocupration are depicted to illustrate the metamorphosis of the reacting complex. The formation of the transient carbolithiated intermediate INT2 is the most striking because recognition of this intermediate provides the key to understanding the kinship of carbocupration, $\text{S}_{\text{N}}2'$ -allylation,^[15] and conjugate addition.^[16]

4.2. The Reaction Pathway of Conjugate Addition

The reaction pathway of the conjugate addition of Me_2CuLi and $\text{Me}_2\text{CuLi} \cdot \text{LiCl}$ has been studied for acrolein^[16] and cyclohexenone,^[20] and favorably compared for the ^{13}C NMR properties of intermediates, kinetic isotope effects,^[207] and the diastereofacial selectivity. The trap-and-bite mechanism also operates in this reaction, as summarized in Scheme 11. As illustrated in Figure 5, the rate-determining step of the reaction (to form TS_{CC}) is the C–C bond formation caused by reductive elimination from Cu^{III} to Cu^I.

Formation of TS_{CC} is also the stage where the enantioface selectivity of the reaction is determined.^[20] This statement stands in contrast to the conventional assumption that the face selectivity is achieved in the initial π complexation, which is now shown to represent an equilibrium preceding TS_{CC} formation.^[208] The calculated activation energy ($E_a = 10.6 \text{ kcal mol}^{-1}$), taking into consideration the recently determined solvation of the lithium atoms, shows reasonable agreement with the experimental data ($E_a = 17\text{--}18 \text{ kcal mol}^{-1}$).^[181]

The central feature of the mechanism is the 3-cuprio(III) enolate which is of open dimeric nature. As shown by theory/experiment comparison for ^{13}C NMR spectroscopic results



Scheme 11. Possible pathways for conjugate addition of $(\text{R}_2\text{CuLi})_2$ to an enone. Solvent molecules are omitted for clarity. The lithium atoms are fully solvated. The R–Li association is indicated with a starred broken line in CPop and TS_{CC} but may be extremely small or nonexistent in solution. $\text{X} = \text{RCuR}$, halogen, etc.

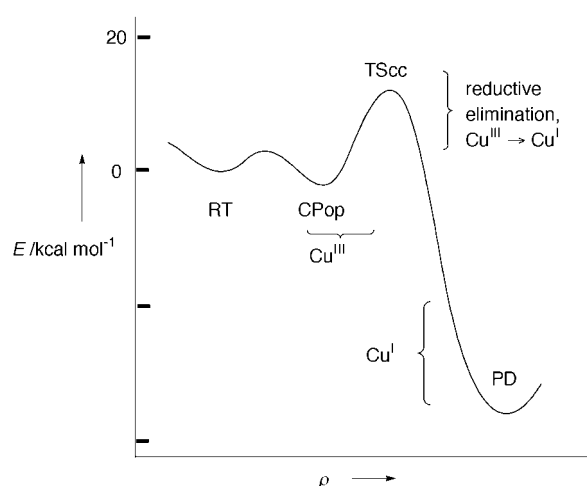


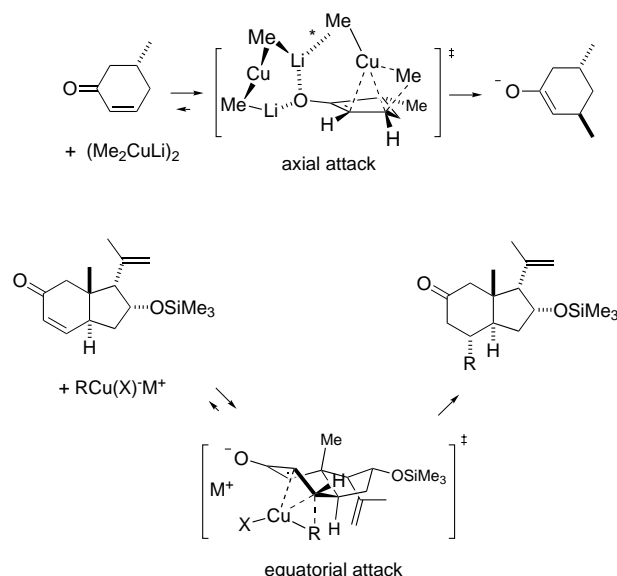
Figure 5. Approximate energy profile of conjugate addition of $(R_2CuLi)_2$ to an enone.

and kinetic isotope effects,^[20, 207] this species serves as a direct precursor to the product (PD in Scheme 11, upper box). In this critical complex CPop, there is achieved a copper/olefin (soft/soft) interaction and a lithium/carbonyl (hard/hard) interaction. The open complex may be directly formed through an open cluster (bottom left of Scheme 11) or by complexation of a closed cluster with the enone (to form Cpcl). Experiments have shown that the enone/lithium complex (top left of Scheme 11) is a dead-end species.^[165, 179]

The intermediate CPop is the “ β -cuprio ketone” intermediate that has been widely debated in the mechanistic discussions of conjugate addition (compare with Equations (13) and (16)). On the basis of the Nakamura–Morokuma theoretical analysis, one can now consider three limiting structures for CPop that are shown in the lower box in Scheme 11. The reason for the exceptional stability of CPop as a trialkylcopper(III) species can be readily understood with the “3-cuprio(III) enolate” structure where the internal enolate anion acts as a strong stabilizing ligand of the Cu^{III} state.^[23]

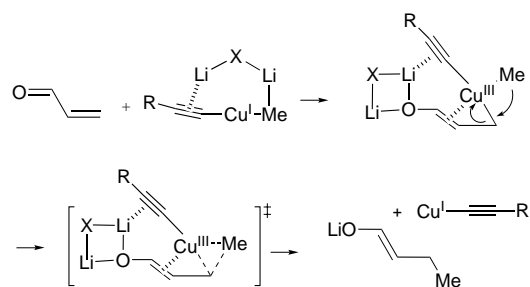
In spite of the apparent difference between conjugate addition and carbocupration reactions (Schemes 8 and 9), the similarity of the key organometallic feature in the two reactions is now evident. In both reactions, inner-sphere electron transfer converts the stable $C-Cu^I$ bond to an unstable $C-Cu^{III}$ bond, and the cluster opening generates a nucleophilic tetracoordinated alkyl group. The difference is that the product PD of conjugate addition remains as a lithium enolate complexed with RCu^I (Scheme 11), while the initial product of carbocupration (INT2) undergoes further reaction (Li/Cu transmetalation) and generates a new organocuprate compound (Scheme 10). (Note however that this difference could become more subtle since the product of conjugate addition could behave more like an α -cuprio(II) ketone complexed with a lithium cation than a lithium enolate complexed with copper(II)). In both reactions, no evidence of radical intermediates (that is, from SET) was found by theoretical calculations.^[15, 16, 20]

Synthetic chemists can now work with three-dimensional pictures of conjugate addition which are available on a web site^[*, 20]. In the absence of steric hindrance (for example, with 5-methylcyclohexenone), “axial attack” through a half-chair conformation is favored (Scheme 12), while “equatorial attack” through a half-boat conformation is favored under the constraint of bicyclic rings (for example, in the cortisone synthesis in Scheme 3).



Scheme 12. Transition states for diastereoselective conjugate additions. In solution, the lithium and metal (M) cations are fully solvated with solvent molecules. The Me–Li association (*) may be extremely weak or nonexistent in solution. X = $RCuR$, halogen, etc.

Recognition of the importance of cluster structure led to a new understanding of the role of a dummy ligand (Y) in the chemistry of mixed cuprates $MeCu(Y)Li$.^[22] As shown in Scheme 13 for the case of Y = alkynyl, the transfer of the



Scheme 13. Dummy ligands: selective transfer of the methyl (or alkyl, alkenyl, aryl) group in preference to transfer of the alkynyl group. X = $RCuR$, halogen, etc.

[*] <http://www.chem.s.u-tokyo.ac.jp/~common/HTML/3D.structure.html> for retrieval of the theoretical 3D pictures and coordinates

methyl group is overwhelmingly favored over the transfer of the alkynyl group. This is because the alkynyl group acts as a tight bridge between Cu^{III} and Li^+ (Figure 6). Namely, the

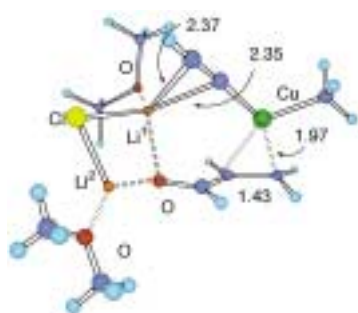


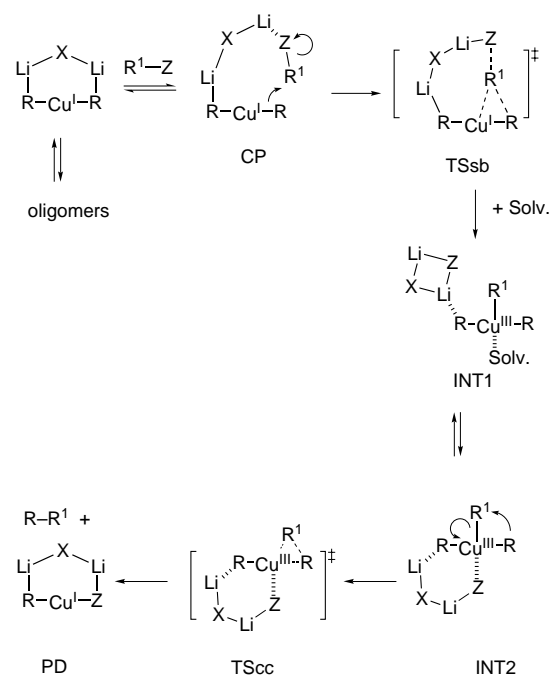
Figure 6. Three dimensional structure of the open complex between acrolein and $\text{Me}(\text{C}_2\text{H})\text{CuLi} \cdot \text{LiCl}$, which bears an Me_2O group on each lithium atom (B3LYP/631A). Bond lengths are given in angstroms. Color code: Cu = dark green, Li = orange, Cl = light green, O = red, C = dark blue, H = light blue spheres.

alkynyl dummy group simultaneously binds to Cu and Li atoms (that is, there is a strong electrostatic interaction between the Li atom and alkynyl group), and hence stays on the copper atom. By default, the much less effective bridging organic ligand is transferred to the enone substrate. This is different to the conventional hypothesis that the Y group forming a stronger Cu–Y bond acts as a better dummy ligand (because it resists transfer), providing an additional illustration of the critical roles of cluster structures in organocopper chemistry.

4.3. The Reaction Pathway of the $\text{S}_{\text{N}}2$ Alkylation Reaction

The alkylation reaction revealed a different mechanistic aspect of the organocuprate reaction. Theoretical analyses of the reactions of alkyl halides (MeI and MeBr)^[17] and epoxides (ethylene oxide and cyclohexene oxide)^[18] with lithium organocuprate clusters ($(\text{Me}_2\text{CuLi})_2$ dimer or $\text{Me}_2\text{CuLi} \cdot \text{LiCl}$, Scheme 14 and Figure 7) resolved the long-standing questions on the mechanism of the alkylation reaction. The density functional calculations showed that the rate-determining step of the alkylation reaction (through TSsb) is the substitution of the C–Z bond with an incoming R–Cu σ bond. The linear $3d_{z^2}$ orbital of copper acts here as the nucleophile, as shown by the LMO illustrated in Figure 8. The computed and the experimental kinetic isotope effects for the reaction of methyl iodide showed good agreement with each other, supporting this conclusion.^[209]

Note that one can identify again an open-cluster structure in TSsb where the lithium atom electrophilically activates the leaving group. A trialkylcopper(III) intermediate may form after the rate-determining, halide-displacement step but only as an unstable transient species INT1 or INT2 (Scheme 14). These are trialkylcopper(III) complexes of T-shape geometry with the fourth ligand (solvent or halide) making a square planar structure.^[23] The *trans* relationship for the two alkyl



Scheme 14. Reaction of $\text{R}_2\text{CuLi} \cdot \text{LiX}$ with $\text{R}'\text{Z}$. The solvent molecules coordinated to the lithium atoms are omitted for clarity. Z = halogen; X = RCuR , halogen, etc.

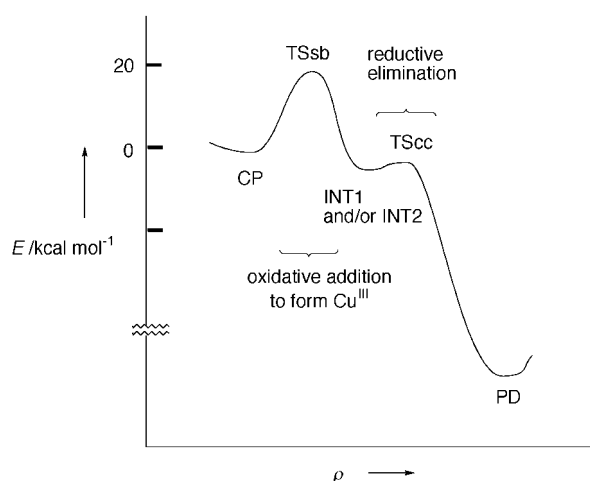


Figure 7. Approximate energy profile of the $\text{S}_{\text{N}}2$ -substitution reaction between $\text{R}_2\text{CuLi} \cdot \text{LiX}$ and $\text{R}'\text{Z}$.

groups R is secured by the linear geometry of the organocuprate moiety in the transition state TSsb, which warrants cross-coupling between R and R' in TScc. Interestingly, this mechanism is a hybrid of the two previous proposals (shown in Figure 8).

A similar reaction pathway was found for the $\text{S}_{\text{N}}2$ substitution of an epoxide with a lithium organocuprate cluster.^[18] In contrast to the MeBr reaction, the configuration of the electrophilic carbon center is already inverted in the transition state, providing the reasoning for the preferred “*trans* diaxial epoxide

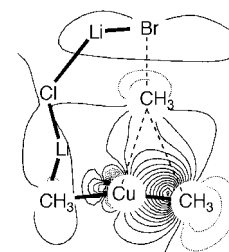
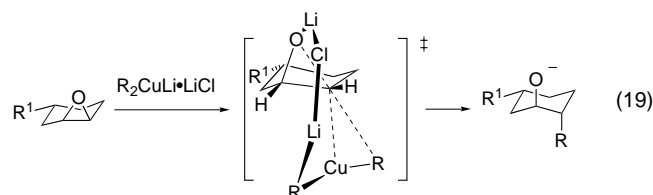


Figure 8. Localized molecular orbitals in the transition state of the $\text{S}_{\text{N}}2$ reaction between $\text{Me}_2\text{CuLi} \cdot \text{LiCl}$ and MeBr .

opening” that has been widely observed in synthetic studies. The transition state of the S_N2 reaction of cyclohexene oxide is shown in Equation (19).



4.4. Orbital Interactions in Organocuprate Reactions

The Nakamura–Morokuma theoretical analysis revealed an intriguing difference between the addition reactions and the S_N2 alkylation reaction for the geometry of the nucleophilic C–Cu–C moiety. As summarized in Section 2, the C–Cu–C fragment in dicoordinated organocuprate(i) anions found in stable structures is always linear. As the highest occupied molecular orbital (HOMO) of a linear $[R_2Cu]^-$ molecule is largely the $3d_{z^2}$ copper orbital,^[19, 21] the linear C–Cu–C group is suitable for interaction with the σ^* orbital of MeBr, as illustrated in Figure 9a.^[21]

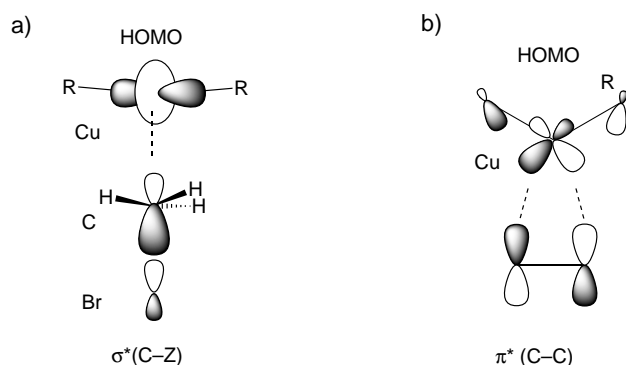


Figure 9. Orbital interactions between $[R_2Cu]^-$ and substrates in: a) an early stage of the reaction with methyl bromide, and b) π -complexation to an acetylene or olefin.

Bending the C–Cu–C moiety to less than 150° causes mixing of the $3d_{xz}$ copper orbital with the $2p$ methyl orbital to make it the HOMO of the organocuprate (Figure 9b), which is now suitable for interaction with the π^* orbitals of enones and acetylenes. Energy gain through back-donation largely compensates the energy loss associated with the bending (approximately 20 kcal mol^{-1} to achieve a 120° angle).

The above analysis for copper also applies to the same class of compounds for gold, which, however, forms much more stable C–Au^I bonds^[156] and hence is unreactive. On the other hand, the d orbitals of zinc(II), a main group neighbor, are too low lying to make organozinc compounds as nucleophilic as organocopper compounds.^[19]

4.5. The Roles of Cluster Structure in Organocuprate Reactions

The previous experimental and theoretical data point out several important characteristics of organocuprate structures and their reaction mechanisms.

- 1) The C–Cu–C angle in a covalently bonded $[R_2Cu]^-$ fragment in stationary states is always nearly 180° .^[21] In ethereal solution, R_2CuLi exists as higher aggregates, whose Li–R bonds are fractional.^[127, 136] One can invariably identify a neutral fragment, R–Cu–R–Li, in crystals of cyclic oligomers and higher polymers (see Scheme 4). Depending on the nature of the reacting electrophiles (σ^* or π^*), either a linear or a bent conformation of the C–Cu–C moiety becomes important for nucleophilic reactions (Figure 9).^[21]
- 2) Due to the fractional R–Li bonds,^[140] clusters and polymers can reversibly form open clusters, which trap the unsaturated substrate through multiple-point binding (see Schemes 10 and 11). Lithium cations assist electron flow from the organocuprate to the electrophile, and to achieve such cooperative action, a cluster of appropriate size may be necessary. Lewis acidic metals other than lithium (for example, Zn^{II}) will also play similar roles. One may appreciate the elegance in the molecular arrangement in the reactions of Me_2CuLi clusters, as illustrated in Figure 10.

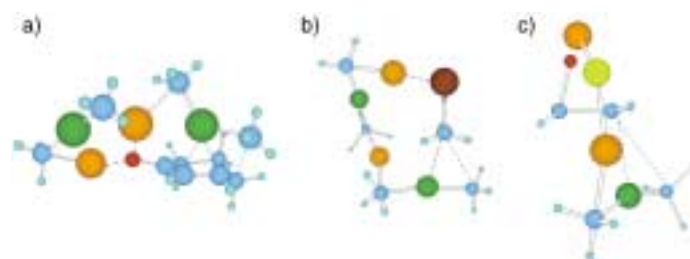


Figure 10. Three-dimensional views of the transition state (B3LYP) of: a) $(Me_2CuLi)_2$ with cyclohexenone, b) $(Me_2CuLi)_2$ with methyl bromide, and c) $Me_2CuLi \cdot LiCl$ with ethylene oxide. Color code: Cu = dark green, Li = orange, Cl = light green, O = red, Br = red with black stripes, C = large blue, H = small blue spheres.

- 3) A C–Cu^I bond is a stable covalent bond, and is difficult to cleave by itself.^[213] After charge transfer from organocuprate(i) to substrate, however, the cleavage of the resulting R–Cu^{III} bond becomes an easy task. The reductive elimination reaction regenerates RCu^I , which may take part in further catalytic cycles. Thus, in copper-catalyzed reactions, excess R^- anion will react with RCu to regenerate the necessary organocuprate species.
- 4) Although acetylene carbocupration and conjugate addition have previously been considered to be two separate reactions, they have been shown to share essentially the same reaction mechanism. The kinship among carbocupration, conjugate addition, S_N2' allylation,^[15] and S_N2 alkylation has now been established, through the Nakamura–Morokuma theoretical studies.

5) Demonstration of the critical role of the open conformation of the polymetallic clusters highlights the theoretical analysis of the organocuprate chemistry. Polymetallic clusters in various synthetic reactions are currently attracting the attention of synthetic and mechanistic chemists alike.^[210–216]

5. Summary and Outlook

Wherefore art thou copper? The uniqueness of the organocopper chemistry stems primarily from the fact that copper lies on the border line between main group and transition metal elements. Comparison may be made for the neighboring elements, Ni⁰, Cu^I, Ag^I, Au^I, and Zn^{II}, all of which are in the d¹⁰ configuration. The energy levels of the 3d orbitals in copper(I) compounds are much higher than in zinc(II), and become even higher upon mixing with the 2p orbital of the alkyl ligand through [R₂Cu][−] formation.^[15, 21] A redox system such as the Cu^I/Cu^{III} system is unavailable for zinc(II). Organonickel and organosilver species are not as stable and are hence much less synthetically viable than organocopper(I) reagents. Organogold(I) species are too stable to be synthetically useful. The C–Cu–C angle is intimately connected to the reactivities of the diorganocuprate(I), and the Lewis acid (often Li⁺) in organocuprate clusters provides a push–pull electronic assistance for charge transfer from Cu^I to the electrophile. The diversity of the coordination structures revealed by calculations indicates that organocopper chemistry represents an ultimate “supramolecular chemistry” that chemists have exploited for a long time without knowing it. Numerous other aspects of organocopper chemistry await further mechanistic studies. The importance of R₃Cu^{III} species is now fully recognized,^[23] and needs more careful attention in the future studies of mechanistic and synthetic organocopper chemistry.

We thank Prof. Keiji Morokuma for fruitful collaboration on the theoretical analysis of copper chemistry, and Monbusho (The Ministry of Education, Science, Culture, and Sport), Japan for financial support in the form of a Grant-in-Aid for Scientific Research on a Priority Area (No. 283, Innovative Synthetic Reactions). A part of the work was carried out under the JSPS/NSF Cooperative Research Program. E.N. thanks the Colorado State University for the Syntex Distinguished Lectureship, which stimulated the idea of writing this review. S.M. is grateful for a JSPS postdoctoral fellowship.

Received: August 18, 1999

Revised: February 14, 2000 [A 358]

- [1] a) J. G. Bednorz, K. A. Müller, *Z. Phys. B* **1986**, *64*, 189–193; b) L. Gao, Y. Y. Xue, F. Chen, Q. Xiong, R. L. Meng, D. Ramirez, C. W. Chu, J. H. Eggert, H. K. Mao, *Phys. Rev. B* **1994**, *50*, 4260.
- [2] a) S. J. Lippard, *Science* **1995**, *268*, 996–997; b) N. Kitajima, Y. Morokuma, *Chem. Rev.* **1994**, *94*, 737–757; c) M. J. Henson, P. Mukherjee, D. E. Root, T. D. P. Stack, E. I. Solomon, *J. Am. Chem. Soc.* **1999**, *121*, 10332–10345, and references therein.
- [3] J. F. Normant, *Synthesis* **1972**, 63–80; G. H. Posner, *An Introduction to Synthesis Using Organocopper Reagents*, Wiley, New York, **1980**;

- Y. Yamamoto, *Angew. Chem.* **1986**, *98*, 945–957; *Angew. Chem. Int. Ed. Engl.* **1986**, *25*, 947–959.
- [4] E. Nakamura, *Synlett* **1991**, 539–547.
- [5] B. H. Lipshutz, S. Sengupta, *Org. React.* **1992**, *41*, 135–631.
- [6] a) *Organocopper Reagents* (Ed.: R. J. K. Taylor), Oxford University Press, Oxford, **1994**; b) B. H. Lipshutz in *Comprehensive Organometallic Chemistry II*, Vol. 12 (Eds.: E. W. Abel, F. G. A. Stone, G. Wilkinson), Pergamon, Oxford, **1995**, pp. 59–130; c) N. Krause, A. Gerold, *Angew. Chem.* **1997**, *109*, 194–213; *Angew. Chem. Int. Ed. Engl.* **1997**, *36*, 186–204; d) Y. Ibuka, Y. Yamamoto, *Synlett* **1992**, 769–777.
- [7] a) G. H. Posner, *Org. React.* **1972**, *19*, 1–113; b) J. A. Kozlowski in *Comprehensive Organic Synthesis*, Vol. 4 (Eds.: B. M. Trost, I. Fleming), Pergamon, Oxford, **1991**, p. 169–198; c) P. Perlmutter, *Conjugate Addition Reactions in Organic Synthesis*, Pergamon, Oxford, **1992**.
- [8] J. F. Normant, A. Alexakis, *Synthesis* **1981**, 841–870.
- [9] a) G. H. Posner, *Org. React.* **1975**, *22*, 253–400; b) J. M. Klunder, G. H. Posner in *Comprehensive Organic Synthesis*, Vol. 3 (Eds.: B. M. Trost, I. Fleming), Pergamon, Oxford, **1991**, pp. 207–239.
- [10] J. A. Marshall, *Chem. Rev.* **1989**, *89*, 1503–1511.
- [11] M. S. Kharasch, P. O. Tawney, *J. Am. Chem. Soc.* **1941**, *63*, 2308–2315.
- [12] J. P. Collman, L. S. Hegedus, J. R. Norton, R. G. Finke, *Principles and Applications of Organotransition Metal Chemistry*, 2nd ed., University Science Books, Mill Valley, CA, **1987**, Chap. 14.
- [13] a) A. E. Jukes, *Adv. Organomet. Chem.* **1974**, *12*, 215–322; G. van Koten, J. G. Noltes in *Comprehensive Organometallic Chemistry*, Vol. 2 (Eds.: G. Wilkinson, F. G. A. Stone), Pergamon, Oxford, **1982**, pp. 709–763; b) G. van Koten, S. L. James, J. T. B. H. Jastrzebski in *Comprehensive Organometallic Chemistry II*, Vol. 3 (Eds.: E. W. Abel, F. G. A. Stone, G. Wilkinson), Pergamon, Oxford, **1995**, pp. 57–133; c) P. P. Power, *Prog. Inorg. Chem.* **1991**, *39*, 75–111.
- [14] R. A. J. Smith, A. S. Vellekoop in *Advances in Detailed Reaction Mechanisms*, Vol. 3 (Ed.: J. M. Coxon), JAI, Greenville, CT, **1994**, pp. 79–130.
- [15] E. Nakamura, S. Mori, M. Nakamura, K. Morokuma, *J. Am. Chem. Soc.* **1997**, *119*, 4887–4899.
- [16] E. Nakamura, S. Mori, K. Morokuma, *J. Am. Chem. Soc.* **1997**, *119*, 4900–4910.
- [17] E. Nakamura, S. Mori, K. Morokuma, *J. Am. Chem. Soc.* **1998**, *120*, 8273–8274.
- [18] S. Mori, E. Nakamura, K. Morokuma, *J. Am. Chem. Soc.* **2000**, *122*, 7294–7307.
- [19] S. Mori, E. Nakamura, *J. Mol. Struct. (Theochem)* **1999**, *461*–462, 167–175.
- [20] S. Mori, E. Nakamura, *Chem. Eur. J.* **1999**, *5*, 1534–1543.
- [21] S. Mori, E. Nakamura, *Tetrahedron Lett.* **1999**, *40*, 5319–5322; S. Mori, A. Hirai, M. Nakamura, E. Nakamura, *Tetrahedron* **2000**, *56*, 2805–2807.
- [22] E. Nakamura, M. Yamanaka, *J. Am. Chem. Soc.* **1999**, *121*, 8941–8942.
- [23] E. Nakamura, M. Yamanaka, S. Mori, *J. Am. Chem. Soc.* **2000**, *122*, 1826–1827.
- [24] J. Munch-Petersen, *J. Org. Chem.* **1957**, *22*, 170–176.
- [25] H. Gilman, R. G. Jones, L. A. Woods, *J. Org. Chem.* **1952**, *17*, 1630–1634.
- [26] G. Costa, A. Camus, L. Gatti, N. Marsich, *J. Organomet. Chem.* **1966**, *5*, 568–572.
- [27] H. O. House, W. L. Respess, G. M. Whitesides, *J. Org. Chem.* **1966**, *31*, 3128–3141.
- [28] E. J. Corey, G. H. Posner, *J. Am. Chem. Soc.* **1967**, *89*, 3911–3912; E. J. Corey, G. H. Posner, *J. Am. Chem. Soc.* **1968**, *90*, 5615–5616.
- [29] G. M. Whitesides, W. F. Fischer, Jr., J. San Filippo, Jr., R. W. Bashe, H. O. House, *J. Am. Chem. Soc.* **1969**, *91*, 4871–4882.
- [30] R. Anderson, C. A. Henrick, J. B. J. Siddall, *J. Am. Chem. Soc.* **1970**, *92*, 735–737; R. J. Anderson, *J. Am. Chem. Soc.* **1970**, *92*, 4978–4980; R. W. Herr, C. R. Johnson, *J. Am. Chem. Soc.* **1970**, *92*, 4980–4981; J. Staroscik, B. Rickborn, *J. Am. Chem. Soc.* **1971**, *93*, 3046–3047; D. M. Wieland, C. R. Johnson, *J. Am. Chem. Soc.* **1971**, *93*, 3047–3049.
- [31] Compare with: H. L. Goering, S. Kantner, *J. Org. Chem.* **1981**, *46*, 2144–2148.

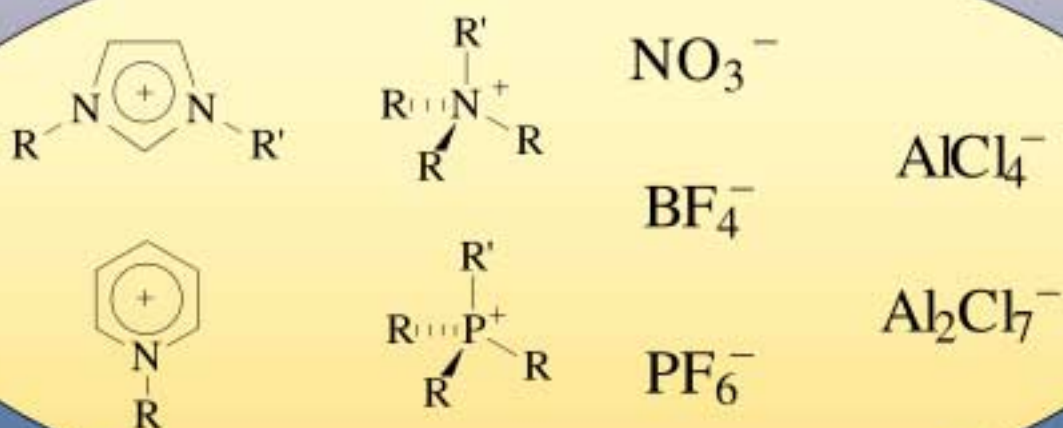
- [32] A. Alexakis, J. Normant, J. Villiéras, *Tetrahedron Lett.* **1976**, 3461–3462.
- [33] B. H. Lipshutz, J. A. Kozlowski, C. M. Breneman, *J. Am. Chem. Soc.* **1985**, *107*, 3197–3204.
- [34] a) T. Mukaiyama, K. Narasaka, K. Banno, *Chem. Lett.* **1973**, 1011–1014; b) T. Mukaiyama, K. Banno, K. Narasaka, *J. Am. Chem. Soc.* **1974**, *96*, 7503–7509.
- [35] a) K. Maruyama, Y. Yamamoto, *J. Am. Chem. Soc.* **1977**, *99*, 8068–8070; b) Y. Yamamoto, K. Maruyama, *J. Am. Chem. Soc.* **1978**, *100*, 3240–3241.
- [36] A. B. Smith III, P. J. Jerris, *J. Am. Chem. Soc.* **1981**, *103*, 194–195.
- [37] B. H. Lipshutz, E. L. Ellsworth, S. H. Dimock, *J. Am. Chem. Soc.* **1990**, *112*, 5869–5871.
- [38] Y. Horiguchi, E. Nakamura, I. Kuwajima, *J. Am. Chem. Soc.* **1989**, *111*, 6257–6265.
- [39] E. Nakamura, I. Kuwajima, *J. Am. Chem. Soc.* **1984**, *106*, 3368–337.
- [40] J. Enda, I. Kuwajima, *J. Am. Chem. Soc.* **1985**, *107*, 5495–550.
- [41] E. Nakamura, S. Matsuzawa, Y. Horiguchi, I. Kuwajima, *Tetrahedron Lett.* **1986**, *27*, 4029–4032.
- [42] E. J. Corey, N. W. Boaz, *Tetrahedron Lett.*, **1985**, *26*, 6015–6018; E. J. Corey, N. W. Boaz, *Tetrahedron Lett.*, **1985**, *26*, 6019–6022.
- [43] A. Alexakis, J. Berlan, Y. Besace, *Tetrahedron Lett.* **1986**, *27*, 1047–1050.
- [44] Y. Horiguchi, S. Matsuzawa, E. Nakamura, I. Kuwajima, *Tetrahedron Lett.* **1986**, *27*, 4025–4028; S. Matsuzawa, Y. Horiguchi, E. Nakamura, I. Kuwajima, *Tetrahedron* **1989**, *45*, 349–362.
- [45] R. J. Linderman, A. Godfrey, *Tetrahedron Lett.* **1986**, *27*, 4553.
- [46] E. Nakamura in *Organocopper Reagents* (Ed.: R. J. K. Taylor), Oxford University Press, Oxford, **1994**, Chap. 6, pp. 129–142.
- [47] E. Nakamura, S. Aoki, H. Oshino, I. Kuwajima, *J. Am. Chem. Soc.* **1985**, *109*, 8056–8066.
- [48] Reviews: a) E. Nakamura, *J. Synth. Org. Chem. Jpn.* **1989**, *47*, 931–938; b) “Metal Homoenoates”: I. Kuwajima, E. Nakamura in *Comprehensive Organic Synthesis*, Vol. 2 (Eds.: B. M. Trost, I. Fleming), Pergamon, Oxford, **1991**, Chap. 1.14; c) M. Nakamura, E. Nakamura, *J. Synth. Org. Chem. Jpn.* **1998**, *56*, 632–644.
- [49] E. Nakamura, I. Kuwajima, *J. Am. Chem. Soc.* **1977**, *99*, 7360–7361; E. Nakamura, H. Oshino, I. Kuwajima, *J. Am. Chem. Soc.* **1986**, *108*, 3745–3755.
- [50] a) Y. Tamaru, H. Ochiai, T. Nakamura, Z. Yoshida, *Angew. Chem.* **1987**, *99*, 1193–1195; *Angew. Chem. Int. Ed. Engl.* **1987**, *26*, 1157–1159; b) Y. Tamaru, H. Ochiai, F. Sanda, Z.-i. Yoshida, *Tetrahedron Lett.* **1985**, *26*, 5529–5532; c) Y. Tamaru, H. Ochiai, T. Nakamura, K. Tsubaki, Z. Yoshida, *Tetrahedron Lett.* **1985**, *26*, 5559–5562.
- [51] a) P. Knochel, M. C. P. Yeh, S. C. Berk, J. Talbert, *J. Org. Chem.* **1988**, *53*, 2390; b) P. Knochel, *Synlett* **1995**, 393–403.
- [52] P. Knochel, R. D. Singer, *Chem. Rev.* **1993**, *93*, 2117–2188.
- [53] E. Nakamura in *Organometallic Chemistry, A Manual*, 2nd ed. (Ed.: M. Schlosser), Wiley, New York, in preparation.
- [54] M. Arai, E. Nakamura, B. H. Lipshutz, *J. Org. Chem.* **1991**, *56*, 5489–5491.
- [55] B. H. Lipshutz, E. L. Ellsworth, *J. Am. Chem. Soc.* **1990**, *112*, 7440–7441.
- [56] B. H. Lipshutz, E. L. Ellsworth, S. H. Dimock, *J. Am. Chem. Soc.* **1990**, *112*, 5869–5871.
- [57] T. Ibuka, H. Minakata, *Synth. Commun.* **1980**, *10*, 119–125.
- [58] M. Arai, B. H. Lipshutz, E. Nakamura, *Tetrahedron* **1992**, *48*, 5709–5718.
- [59] A. Alexakis, J. F. Normant, *Isr. J. Chem.* **1984**, *24*, 113–117.
- [60] A. T. Stoll, E.-i. Negishi, *Tetrahedron Lett.* **1985**, *26*, 5671–5674.
- [61] J. Berlan, J. Besace, E. Stephan, P. Cresson, *Tetrahedron Lett.* **1985**, *26*, 5765–5768.
- [62] E. Nakamura, M. Isaka, S. Matsuzawa, *J. Am. Chem. Soc.* **1988**, *110*, 1297–1298.
- [63] a) B. E. Rossiter, N. M. Swingle, *Chem. Rev.* **1992**, *92*, 771–806; b) T. Kanai, Y. Nakagawa, K. Tomioka, *J. Syn. Org. Chem. Jpn.* **1996**, *35*, 474–480; c) G. van Koten, *Pure Appl. Chem.* **1994**, *66*, 1455–1462; d) A. Alexakis, J. C. Frutos, P. Mangeney, *Tetrahedron: Asymmetry* **1993**, *4*, 2427–2430; e) A. Alexakis in *Transition Metal Catalysed Reactions* (Eds.: S.-I. Murahashi, S. G. Davies), Blackwell Science, Oxford, UK, **1999**, pp. 303.
- [64] a) B. L. Feringa, M. Pineschi, L. A. Arnold, R. Imbos, A. H. M. de Vries, *Angew. Chem.* **1997**, *109*, 2733–2736; *Angew. Chem. Int. Ed. Engl.* **1997**, *36*, 2620–2623; b) A. K. H. Knöbel, I. H. Escher, A. Pfaltz, *Synlett* **1997**, 1429–1431; c) R. Naasz, L. A. Arnold, M. Pineschi, E. Keller, B. L. Feringa, *J. Am. Chem. Soc.* **1999**, *121*, 1104–1105.
- [65] M. Sawamura, H. Iikura, E. Nakamura, *J. Am. Chem. Soc.* **1996**, *118*, 12850–12851.
- [66] M. Sawamura, H. Iikura, A. Hirai, E. Nakamura, *J. Am. Chem. Soc.* **1998**, *120*, 8285–8286.
- [67] H. Iikura, S. Mori, M. Sawamura, E. Nakamura, *J. Org. Chem.* **1997**, *62*, 7912–7913.
- [68] H. O. House, *Acc. Chem. Res.* **1976**, *9*, 59–67.
- [69] J. Berlan, J.-P. Battioni, K. Koosha, *Tetrahedron Lett.* **1976**, 3351–3354; K. Koosha, J. Berlan, M.-L. Capmau, W. Chodkiewicz, *Bull. Chim. Soc. Fr. II* **1975**, 1284–1291; K. Koosha, J. Berlan, M.-L. Capmau, W. Chodkiewicz, *Bull. Chim. Soc. Fr.* **1975**, 1291–1294; J. Berlan, J.-P. Battioni, K. Koosha, *Bull. Chim. Soc. Fr.* **1978**, II 183–190; J. Berlan, J.-P. Battioni, K. Koosha, *J. Organomet. Chem.* **1978**, *152*, 359–365; J. Berlan, K. Koosha, *J. Organomet. Chem.* **1978**, *153*, 99–106; J. Berlan, K. Koosha, *J. Organomet. Chem.* **1978**, *153*, 107–113.
- [70] E. J. Corey, D. J. Beames, *J. Am. Chem. Soc.* **1972**, *94*, 7210–7211.
- [71] a) E. J. Corey, D. M. Floyd, B. H. Lipshutz, *J. Org. Chem.* **1978**, *43*, 3418–3420; b) H. O. House, M. J. Umen, *J. Org. Chem.* **1973**, *38*, 3893–3901; c) W. H. Mandeville, G. M. Whitesides, *J. Org. Chem.* **1974**, *39*, 400–405.
- [72] a) J. P. Gorlier, L. Hamon, J. Levisalles, J. Wagnon, *J. Chem. Soc. Chem. Commun.* **1973**, 88; b) B. H. Lipshutz, R. S. Wilhelm, J. A. Kozlowski, *Tetrahedron* **1984**, *40*, 5005–5038.
- [73] S. H. Bertz, G. Dabbagh, G. M. Villacorta, *J. Am. Chem. Soc.* **1982**, *104*, 5824–5826; compare with: G. H. Posner, C. E. Whiten, *Tetrahedron Lett.* **1973**, 1815–1818; G. H. Posner, C. E. Whiten, J. J. Sterling, *J. Am. Chem. Soc.* **1973**, *95*, 7788–7800.
- [74] Magnesium mixed organocuprates: J. Drouin, F. Leyendecker, J.-M. Conia, *New J. Chem.* **1978**, *2*, 267–270; F. Leyendecker, J. Drouin, J.-M. Conia, *New J. Chem.* **1978**, *2*, 271–274.
- [75] C. Ouannes, G. Dressaire, Y. Langlois, *Tetrahedron Lett.* **1977**, 815–818.
- [76] S. H. Bertz, C. P. Gibson, G. Dabbagh, *Organometallics* **1988**, *7*, 227–232.
- [77] A. Alexakis, D. Jachiet, J. F. Normant, *Tetrahedron* **1986**, *42*, 5607–5619; A. Ghribi, A. Alexakis, J. F. Normant, *Tetrahedron Lett.* **1984**, *25*, 3075–3078; A. Ghribi, A. Alexakis, J. F. Normant, *Tetrahedron Lett.* **1984**, *25*, 3079–3082.
- [78] S. Flemming, J. Kabbara, K. Nickisch, J. Westermann, J. Mohr, *Synlett* **1995**, 183–185.
- [79] S. Matsuzawa, M. Isaka, E. Nakamura, I. Kuwajima, *Tetrahedron Lett.* **1989**, *30*, 1975–1978; M. Arai, T. Nemoto, Y. Ohashi, E. Nakamura, *Synlett* **1992**, 309–310.
- [80] For some mechanistic proposals, see: a) B. H. Lipshutz, S. H. Dimock, B. James, *J. Am. Chem. Soc.* **1993**, *115*, 9283–9284; b) S. H. Bertz, G. Miao, B. E. Rossiter, J. P. Snyder, *J. Am. Chem. Soc.* **1995**, *117*, 11023–11024; c) S. H. Bertz, A. Chopra, M. Eriksson, C. A. Ogle, P. Seagle, *Chem. Eur. J.* **1999**, *5*, 2680–2691.
- [81] Y. Horiguchi, M. Komatsu, I. Kuwajima, *Tetrahedron Lett.* **1989**, *30*, 7087–7090.
- [82] B. H. Lipshutz, D. H. Aue, B. James, *Tetrahedron Lett.* **1996**, *37*, 8471–8474.
- [83] M. Eriksson, A. Johansson, M. Nilsson, T. Olsson, *J. Am. Chem. Soc.* **1996**, *118*, 10904–10905.
- [84] M. Bergdahl, E.-L. Lindstedt, M. Nilsson, T. Olsson, *Tetrahedron* **1988**, *44*, 2055–2062.
- [85] a) E. C. Ashby, J. Lin, J. J. J. Watkins, *J. Org. Chem.* **1977**, *42*, 1099–1102; b) E. C. Ashby, J. J. Lin, *J. Org. Chem.* **1977**, *42*, 2805–2808.
- [86] a) H. Westmijze, H. Kleijn, J. Meijer, P. Vermeer, *Recl. Trav. Chim. Pays-Bas* **1981**, *100*, 98–102; b) D. L. J. Clive, V. Farina, P. L. Beaulieu, *J. Org. Chem.* **1982**, *47*, 2572–2582.
- [87] T. L. Macdonald, W. C. Still, *J. Am. Chem. Soc.* **1975**, *97*, 5280–5281; W. C. Still, T. L. Macdonald, *Tetrahedron Lett.* **1976**, *31*, 2659–2662.
- [88] E. C. Ashby, J. J. Watkins, *J. Am. Chem. Soc.* **1977**, *99*, 5312–5317.

- [89] S. H. Bertz, G. Dabbagh, *J. Am. Chem. Soc.* **1988**, *110*, 3668–3670.
- [90] M. M. Olmstead, P. P. Power, *J. Am. Chem. Soc.* **1989**, *111*, 4135–4136.
- [91] F. Olbrich, J. Kopf, E. Weiss, *Angew. Chem.* **1993**, *105*, 1136; *Angew. Chem. Int. Ed. Engl.* **1993**, *32*, 1077–1079.
- [92] B. H. Lipshutz, R. S. Wilhelm, J. A. Kozlowski, *Synthesis* **1987**, 325–341; B. H. Lipshutz, R. S. Wilhelm, D. M. Floyd, *J. Am. Chem. Soc.* **1981**, *103*, 7672–7674; B. H. Lipshutz, J. Kozlowski, R. S. Wilhelm, *J. Am. Chem. Soc.* **1982**, *104*, 2305–2307; B. H. Lipshutz, *Tetrahedron Lett.* **1983**, *24*, 127–130; B. H. Lipshutz, K. Siegmann, E. Garcia, F. Kayser, *J. Am. Chem. Soc.* **1993**, *115*, 9276–9282.
- [93] S. H. Bertz, *J. Am. Chem. Soc.* **1990**, *112*, 4031–4032; S. H. Bertz, *J. Am. Chem. Soc.* **1991**, *113*, 5470–5471; S. H. Bertz, *Chem. Eng. News* **1997**, 75(15), 4.
- [94] S. H. Bertz, K. Nilsson, Ö. Davidson, J. P. Snyder, *Angew. Chem.* **1998**, *110*, 327–331; *Angew. Chem. Int. Ed.* **1998**, *37*, 314–317.
- [95] B. H. Lipshutz, S. Sharma, E. L. Ellsworth, *J. Am. Chem. Soc.* **1990**, *112*, 4032–4034; B. H. Lipshutz, B. James, *J. Org. Chem.* **1994**, *59*, 7585–7587.
- [96] a) T. Stemmler, J. E. Penner-Hahn, P. Knochel, *J. Am. Chem. Soc.* **1993**, *115*, 348–350; b) T. M. Barnhart, H. Huang, J. E. Penner-Hahn, *J. Org. Chem.* **1995**, *60*, 4310–4311.
- [97] T. L. Stemmler, T. M. Barnhart, J. E. Penner-Hahn, C. E. Tucker, P. Knochel, M. Böhme, G. Frenking, *J. Am. Chem. Soc.* **1995**, *117*, 12489–12497.
- [98] B. H. Lipshutz, K. L. Stevens, B. James, J. G. Pavlovich, J. P. Snyder, *J. Am. Chem. Soc.* **1996**, *118*, 6796–6797; B. H. Lipshutz, J. Keith, D. J. Buzard, *Organometallics* **1999**, *18*, 1571–1574.
- [99] a) J. P. Snyder, D. P. Spangler, J. R. Behling, B. E. Rossiter, *J. Org. Chem.* **1994**, *59*, 2665–2667; b) J. P. Snyder, S. H. Bertz, *J. Org. Chem.* **1995**, *60*, 4312–4313; c) H. Huang, K. Alvarez, Q. Cui, T. M. Barnhart, J. P. Snyder, J. E. Penner-Hahn, *J. Am. Chem. Soc.* **1996**, *118*, 8808–8816; erratum: H. Huang, K. Alvarez, Q. Cui, T. M. Barnhart, J. P. Snyder, J. E. Penner-Hahn, *J. Am. Chem. Soc.* **1996**, *118*, 12252.
- [100] G. Boche, F. Bosold, M. Marsch, K. Harms, *Angew. Chem.* **1998**, *110*, 1779–1781; *Angew. Chem. Int. Ed.* **1998**, *37*, 1684–1686.
- [101] C. M. P. Kronenburg, J. T. B. H. Jastrzebski, A. L. Spek, G. van Koten, *J. Am. Chem. Soc.* **1998**, *120*, 9688–9689.
- [102] S. H. Bertz, G. Dabbagh, *J. Chem. Soc. Chem. Commun.* **1982**, 1030–1032.
- [103] S. H. Bertz, G. Miao, M. Eriksson, *Chem. Commun.* **1996**, 815–816.
- [104] T. A. Mobley, F. Müller, S. Berger, *J. Am. Chem. Soc.* **1998**, *120*, 1333–1334.
- [105] N. Krause, *Angew. Chem.* **1999**, *111*, 83–85; *Angew. Chem. Int. Ed.* **1999**, *38*, 79–81.
- [106] J. A. Cabezas, A. C. Oehlschlager, *J. Am. Chem. Soc.* **1997**, *119*, 3878–3886.
- [107] W. C. Still, J. A. Schneider, *Tetrahedron Lett.* **1980**, *21*, 1035–1038.
- [108] G. M. Whitesides, J. SanFilippo, Jr., C. P. Casey, E. J. Panek, *J. Am. Chem. Soc.* **1967**, *89*, 5302–5303.
- [109] G. H. Posner, J.-S. Ting, C. M. Lentz, *Tetrahedron* **1976**, *32*, 2281–2287.
- [110] P. Kocienski, S. Wadman, K. Cooper, *J. Am. Chem. Soc.* **1989**, *111*, 2363–2365.
- [111] G. V. Buxton, J. C. Green, *J. Chem. Soc. Faraday Trans.* **1978**, *74*, 697–714.
- [112] J. K. Kochi, *Acc. Chem. Res.* **1974**, *7*, 351–360; compare with: I. Ryu, M. Ando, A. Ogawa, S. Murai, N. Sonoda, *J. Am. Chem. Soc.* **1983**, *105*, 7192–7194.
- [113] Metastable dimethylgold(II) clusters were recently trapped. See: D. Zhu, S. V. Lindeman, J. K. Kochi, *Organometallics* **1999**, *18*, 2241–2248.
- [114] P. S. Coan, K. Folting, J. C. Huffman, G. Caulton, *Organometallics* **1989**, *8*, 2724–2728; R. Lingnau, J. Strähle, *Angew. Chem.* **1988**, *100*, 409; *Angew. Chem. Int. Ed. Engl.* **1988**, *27*, 436.
- [115] S. Sakaki, Y. Musashi, *Inorg. Chem.* **1995**, *34*, 1914–1923.
- [116] M. D. Janssen, M. A. Corsten, A. L. Spek, D. M. Grove, G. van Koten, *Organometallics* **1996**, *15*, 2810–2820.
- [117] M. F. Lappert, R. Pearce, *J. Chem. Soc. Chem. Commun.* **1973**, 24–25; J. A. J. Jarvis, R. Pearce, M. F. Lappert, *J. Chem. Soc. Dalton Trans.* **1977**, 999–1003.
- [118] M. M. Olmstead, P. P. Power, *J. Am. Chem. Soc.* **1990**, *112*, 8008–8014.
- [119] C.-S. Hwang, P. P. Power, *Organometallics* **1999**, *18*, 697–700.
- [120] H. Hope, M. M. Olmstead, P. P. Power, J. Sandell, X. Xu, *J. Am. Chem. Soc.* **1985**, *107*, 4337–4338.
- [121] a) J. P. Snyder, G. E. Tipword, D. J. Spangler, *J. Am. Chem. Soc.* **1992**, *114*, 1507–1510; b) See also Ref. [99a].
- [122] S. F. Martin, J. R. Fishpaugh, J. M. Power, D. M. Giolando, R. A. Jones, C. M. Nunn, A. H. Cowley, *J. Am. Chem. Soc.* **1988**, *110*, 7226–7228.
- [123] C.-S. Hwang, P. P. Power, *J. Am. Chem. Soc.* **1998**, *120*, 6409–6410.
- [124] G. van Koten, J. G. Noltes, *J. Chem. Soc. Chem. Commun.* **1972**, 940–941.
- [125] R. G. Pearson, C. D. Gregory, *J. Am. Chem. Soc.* **1976**, *98*, 4098–4104.
- [126] G. van Koten, J. T. B. H. Jastrzebski, F. Muller, C. H. Stam, *J. Am. Chem. Soc.* **1985**, *107*, 697–698.
- [127] N. P. Lorenzen, E. Weiss, *Angew. Chem.* **1990**, *102*, 322–324; *Angew. Chem. Int. Ed. Engl.* **1990**, *29*, 300–302.
- [128] M. M. Olmstead, P. P. Power, *Organometallics* **1990**, *9*, 1720–1722.
- [129] 3D structures searched by Cambridge Structural Database System in April, 1999.
- [130] H. Huang, C. H. Liang, J. E. Penner-Hahn, *Angew. Chem.* **1998**, *110*, 1628–1630; *Angew. Chem. Int. Ed.* **1998**, *37*, 1564–1566.
- [131] S. I. Khan, P. G. Edwards, H. S. H. Yuan, R. Bau, *J. Am. Chem. Soc.* **1985**, *107*, 1682–1684.
- [132] E. Nakamura, *J. Synth. Org. Chem. Jpn.* **1993**, *51*, 985–994.
- [133] B. H. Lipshutz, J. Keith, D. J. Buzard, *Organometallics* **1999**, *18*, 1571–1574.
- [134] T. M. Barnhart, H. Huang, J. E. Penner-Hahn, *J. Org. Chem.* **1995**, *60*, 4310–4311.
- [135] A. Gerold, J. T. B. H. Jastrzebski, C. M. P. Kronenburg, N. Krause, G. van Koten, *Angew. Chem.* **1997**, *109*, 778–780; *Angew. Chem. Int. Ed. Engl.* **1997**, *36*, 755–757.
- [136] T. Stemmler, J. E. Penner-Hahn, P. Knochel, *J. Am. Chem. Soc.* **1993**, *115*, 348–350.
- [137] S. H. Bertz, A. S. Vellekoop, R. A. J. Smith, J. P. Snyder, *Organometallics* **1995**, *14*, 1213–1220.
- [138] M. Böhme, G. Frenking, M. T. Reetz, *Organometallics* **1994**, *13*, 4237–4245.
- [139] G. Fraenkel, M. Henrichs, J. M. Hewitt, B. M. Su, M. J. Geckele, *J. Am. Chem. Soc.* **1980**, *102*, 3345–3350.
- [140] J. Heinzer, J. F. M. Oth, D. Seebach, *Helv. Chim. Acta* **1985**, *68*, 1848–1862.
- [141] G. Hallenmo, C. Ullenius, *Tetrahedron* **1983**, *39*, 1621–1625.
- [142] C. L. Kingsbury, R. A. J. Smith, *J. Org. Chem.* **1997**, *62*, 4629–4634; C. L. Kingsbury, R. A. J. Smith, *J. Org. Chem.* **1997**, *62*, 7637–7643.
- [143] C. L. Kingsbury, K. S. Sharp, R. A. J. Smith, *Tetrahedron* **1999**, *55*, 14693–14700.
- [144] C. Kappenstein, R. P. Hugel, *Inorg. Chem.* **1978**, *17*, 1945–1949; P. Chaudhuri, K. Oder, K. Wiegardt, J. Weiss, J. Reedijk, V. Hinrichs, J. Wood, A. Ozarowski, H. Stratemaier, D. Reinen, *Inorg. Chem.* **1986**, *25*, 2951–2958; J. Cernak, J. Chomic, C. Kappenstein, M. Dunaj-Jurco, *Z. Kristallogr.* **1994**, *209*, 43.
- [145] a) M. A. Willert-Porada, D. J. Burton, N. C. Baenziger, *J. Chem. Soc. Chem. Commun.* **1989**, 1633–1634; b) D. Naumann, T. Roy, K.-F. Tebbe, W. Crump, *Angew. Chem.* **1993**, *105*, 1555–1556; *Angew. Chem. Int. Ed. Engl.* **1993**, *32*, 1482–1483; c) R. Eujen, B. Hoge, D. J. Brauer, *J. Organomet. Chem.* **1996**, *519*, 7–20.
- [146] a) A. E. Dorigo, J. Wanner, P. von R. Schleyer, *Angew. Chem.* **1995**, *107*, 492–494; *Angew. Chem. Int. Ed. Engl.* **1995**, *34*, 476–478; b) J. P. Snyder, *J. Am. Chem. Soc.* **1995**, *117*, 11025–11026.
- [147] J. P. Snyder, *Angew. Chem.* **1995**, *107*, 112–113; *Angew. Chem. Int. Ed. Engl.* **1995**, *34*, 80–81.
- [148] M. Kaupp, H. G. von Schnering, *Angew. Chem.* **1995**, *107*, 1076; *Angew. Chem. Int. Ed. Engl.* **1995**, *34*, 986.
- [149] J. P. Snyder, *Angew. Chem.* **1995**, *107*, 1076–1077; *Angew. Chem. Int. Ed. Engl.* **1995**, *34*, 986–987; compare with: J. K. Bera, A. G. Samuelson, J. Chandrasekhar, *Organometallics* **1998**, *17*, 4136–4145.
- [150] R. A. Poirier, G. A. Ozin, D. F. McIntosh, G. Csizmadia, R. Daudel, *Chem. Phys. Lett.* **1983**, *191*, 221–229.

- [151] T. Ziegler, V. Tschinke, A. Becke, *J. Am. Chem. Soc.* **1987**, *109*, 1351–1358.
- [152] A. E. Dorigo, K. Morokuma, *J. Am. Chem. Soc.* **1989**, *111*, 4635–4643; A. E. Dorigo, K. Morokuma, *J. Am. Chem. Soc.* **1989**, *111*, 6524–6536.
- [153] E. Nakamura, Y. Miyachi, N. Koga, K. Morokuma, *J. Am. Chem. Soc.* **1992**, *114*, 6686–6692; E. Nakamura, M. Nakamura, Y. Miyachi, N. Koga, K. Morokuma, *J. Am. Chem. Soc.* **1993**, *115*, 99–106.
- [154] C. W. Bauschlicher, Jr., S. R. Langhoff, H. Partridge, L. A. Barnes, *J. Chem. Phys.* **1989**, *91*, 2399–2411.
- [155] I. Antes, G. Frenking, *Organometallics* **1995**, *14*, 4263–4268; compare with: M. Böhme, G. Frenking, *Chem. Phys. Lett.* **1994**, *224*, 195–199.
- [156] P. Belanzoni, M. Rosi, A. Sgamellotti, E. J. Baerends, C. Floriani, *Chem. Phys. Lett.* **1996**, *257*, 41–48.
- [157] C. Sosa, J. Andzelm, B. C. Elkin, E. Wimmer, K. D. Dobbs, D. A. Dixon, *J. Phys. Chem.* **1992**, *96*, 6630–6636.
- [158] M. Böhme, G. Frenking, M. T. Reetz, *Organometallics* **1994**, *13*, 4237–4245.
- [159] H. O. House, W. L. Respess, G. M. Whitesides, *J. Org. Chem.* **1966**, *31*, 3128–3141.
- [160] K. Yamamoto, H. Ogura, J.-i. Jukuta, H. Inoue, K. Hamada, Y. Sugiyama, S. Yamada, *J. Org. Chem.* **1998**, *63*, 4449–4458.
- [161] H. O. House, M. J. Umen, *J. Am. Chem. Soc.* **1972**, *94*, 5495–5497.
- [162] J. Munch-Petersen, C. Bretting, P. M. Jørgensen, S. Refu, V. K. Andersen, *Acta Chem. Scand.* **1961**, *15*, 277–292; see also: Y. Yamamoto, J. Yamada, T. Ueyehara, *J. Am. Chem. Soc.* **1987**, *109*, 5820–5822.
- [163] E. J. Corey, F. J. Hannon, N. W. Boaz, *Tetrahedron* **1989**, *45*, 545–555.
- [164] A. S. Vellekoop, R. A. J. Smith, *J. Am. Chem. Soc.* **1994**, *116*, 2902–2913.
- [165] S. R. Krauss, S. G. Smith, *J. Am. Chem. Soc.* **1981**, *103*, 141–148.
- [166] H. O. House, K. A. J. Snoble, *J. Org. Chem.* **1976**, *41*, 3076–3083.
- [167] C. P. Casey, M. C. Cesa, *J. Am. Chem. Soc.* **1979**, *101*, 4236–4244.
- [168] S. H. Bertz, G. Dabbagh, J. M. Cook, V. Honkan, *J. Org. Chem.* **1984**, *49*, 1739–1743.
- [169] D. J. Hannah, R. A. J. Smith, *Tetrahedron Lett.* **1975**, 187–190; R. A. J. Smith, D. J. Hannah, *Tetrahedron* **1979**, *35*, 1183–1189.
- [170] C. P. Casey, R. A. Boggs, *Tetrahedron Lett.* **1971**, *27*, 2455–2458.
- [171] G. M. Whitesides, P. E. Kendall, *J. Org. Chem.* **1972**, *37*, 3718–3725; F. Näf, P. Degen, *Helv. Chim. Acta* **1971**, *54*, 1939–1949.
- [172] H. Yamataka, N. Fujimura, Y. Kawafuji, T. Hanafusa, *J. Am. Chem. Soc.* **1987**, *109*, 4305–4308.
- [173] Y. Chounan, T. Ibuka, Y. Yamamoto, *J. Chem. Soc. Chem. Commun.* **1994**, 2003–2004.
- [174] Y. Yamamoto, S. Nishii, T. Ibuka, *J. Am. Chem. Soc.* **1988**, *110*, 617–618.
- [175] Y. Chounan, H. Horino, T. Ibuka, Y. Yamamoto, *Bull. Chem. Soc. Jpn.* **1997**, *50*, 1953–1959.
- [176] C. T. Wigal, J. R. Grunwell, J. Hersherberger, *J. Org. Chem.* **1991**, *56*, 3759–3761; S. J. Anderson, W. T. Hopkins, C. T. Wigal, *J. Org. Chem.* **1992**, *57*, 4304–4305.
- [177] J. Berlan, J.-P. Battioni, K. Koosha, *Bull. Chim. Soc. Fr.* **1979**, II183–190.
- [178] G. Hallnemo, T. Olsson, C. Ullenius, *J. Organomet. Chem.* **1984**, *265*, C22–C24; G. Hallnemo, T. Olsson, C. Ullenius, *J. Organomet. Chem.* **1985**, *282*, 133–144; B. Christenson, G. Hallnemo, C. Ullenius, *Chem. Scr.* **1987**, *27*, 511–512; C. Ullenius, B. Christenson, *Pure Appl. Chem.* **1988**, *60*, 57–64.
- [179] N. Krause, R. Wagner, A. Gerold, *J. Am. Chem. Soc.* **1994**, *116*, 381–382.
- [180] S. Sharma, A. C. Oehlschlager, *Tetrahedron* **1991**, *47*, 1177–1184; S. H. Bertz, R. A. J. Smith, *J. Am. Chem. Soc.* **1989**, *111*, 8276–8277; B.-S. Lou, G. Li, F.-D. Lung, V. J. Hruby, *J. Org. Chem.* **1995**, *60*, 5509–5514.
- [181] J. Canisius, A. Gerold, N. Krause, *Angew. Chem.* **1999**, *111*, 1727–1730; *Angew. Chem. Int. Ed.* **1999**, *38*, 1644–1646.
- [182] J. Klein, R. Levene, *J. Chem. Soc. Perkin Trans. 2* **1973**, 1971–1979.
- [183] N. Krause, *Tetrahedron Lett.* **1989**, *30*, 5219–5222.
- [184] E. J. Corey, J. A. Katzenellenbogen, *J. Am. Chem. Soc.* **1969**, *91*, 1851–1852; J. B. Siddall, M. Biskup, J. H. Fried, *J. Am. Chem. Soc.* **1969**, *91*, 1852–1854; J. Klein, R. M. Turckel, *J. Am. Chem. Soc.* **1969**, *91*, 6186–6187; J. Klein, N. Aminadav, *J. Chem. Soc. C* **1970**, 1380–1385; Y. Yamamoto, H. Yatagai, K. Maruyama, *J. Org. Chem.* **1979**, *44*, 1744–1746; J. P. Marino, R. J. Linderman, *J. Org. Chem.* **1981**, *46*, 3696–3702; I. Fleming, D. A. Perry, *Tetrahedron* **1981**, *37*, 4027–4034.
- [185] K. Nilsson, C. Ullenius, N. Krause, *J. Am. Chem. Soc.* **1996**, *118*, 4194–4195.
- [186] K. Nilsson, T. Andersson, C. Ullenius, *J. Organomet. Chem.* **1997**, *546*, 591–595; K. Nilsson, T. Andersson, C. Ullenius, A. Gerold, N. Krause, *Chem. Eur. J.* **1998**, *4*, 2051–2508.
- [187] J. Normant, G. Cahiez, J. Villieras, *J. Organomet. Chem.* **1975**, *92*, C28–C30.
- [188] Reviews: J. M. Klunder, G. H. Posner in *Comprehensive Organic Synthesis*, Vol. 3 (Eds.: B. M. Trost, I. Fleming), Pergamon, Oxford, **1991**, pp. 207–239.
- [189] R. W. Herr, D. M. Wieland, C. R. Johnson, *J. Am. Chem. Soc.* **1970**, *92*, 3813–3814; C. R. Johnson, R. W. Herr, D. M. Wieland, *J. Org. Chem.* **1973**, *38*, 4263–4268; compare with: M. Aratani, L. V. Dunkerton, T. Fukuyama, Y. Kishi, H. Kakoi, S. Sugiura, S. Inoue, *J. Org. Chem.* **1975**, *40*, 2009–2011.
- [190] M. J. Eis, B. Ganem, *Tetrahedron Lett.* **1985**, *26*, 1153–1156.
- [191] a) C. R. Johnson, G. A. Dutra, *J. Am. Chem. Soc.* **1973**, *95*, 7783–7787; b) B. H. Lipshutz, R. S. Wilhelm, *J. Am. Chem. Soc.* **1982**, *104*, 4696–4698.
- [192] C.-y. Guo, M. L. Brownawell, J. San Filippo, Jr., *J. Am. Chem. Soc.* **1985**, *107*, 6028–6030.
- [193] S. Komiya, T. A. Albright, R. Hoffmann, J. K. Kochi, *J. Am. Chem. Soc.* **1976**, *98*, 7255–7265.
- [194] S. Komiya, T. A. Albright, R. Hoffmann, J. K. Kochi, *J. Am. Chem. Soc.* **1976**, *98*, 8440–8447.
- [195] A. Tamaki, J. K. Kochi, *J. Organomet. Chem.* **1973**, *51*, C39–C42.
- [196] J. Stein, J. P. Fackler, Jr., C. Paparizos, H.-W. Chen, *J. Am. Chem. Soc.* **1981**, *103*, 2192–2198.
- [197] J. P. Collman, *Acc. Chem. Res.* **1968**, *1*, 136–143.
- [198] E. C. Ashby, R. N. DePriest, A. Tuncay, S. Srivastava, *Tetrahedron Lett.* **1982**, *23*, 5251–5254.
- [199] E. C. Ashby, D. Coleman, *J. Org. Chem.* **1987**, *52*, 4554–4565; S. H. Bertz, G. Dabbagh, A. M. Majsce, *J. Am. Chem. Soc.* **1991**, *113*, 631–636.
- [200] H. L. Goering, C. C. Tseng, *J. Org. Chem.* **1983**, *48*, 3986–3990; H. L. Goering, S. S. Kantner, *J. Org. Chem.* **1984**, *49*, 422–426; H. L. Goering, S. S. Kantner, E. P. Seitz, Jr., *J. Org. Chem.* **1985**, *50*, 5495–5499.
- [201] a) M. A. Sevin, W. Chodkiewicz, P. Cadiot, *Tetrahedron Lett.* **1965**, 1953–1959; b) P. Rona, P. Crabbé, *J. Am. Chem. Soc.* **1968**, *90*, 4733–4734; P. Rona, P. Crabbé, *J. Am. Chem. Soc.* **1969**, *91*, 3289–3292; J. L. Luche, E. Barreiro, J. M. Dollat, P. Crabbé, *Tetrahedron Lett.* **1975**, 4615–4618; J.-M. Dollat, J.-L. Luche, P. Crabbé, *J. Chem. Soc. Chem. Commun.* **1977**, 761–762; c) P. Vermeer, J. Meijer, L. Brandsma, *Rec. Trav. Chim. Pays-Bas* **1975**, *94*, 112–114; A. Alexakis, I. Marek, P. Mangeney, J. F. Normant, *J. Am. Chem. Soc.* **1990**, *112*, 8042–8047.
- [202] C. Gallina, P. G. Ciattini, *J. Am. Chem. Soc.* **1979**, *101*, 1035–1036; H. L. Goering, S. S. Kantner, C. C. Tseng, *J. Org. Chem.* **1983**, *48*, 715–721.
- [203] J.-E. Bäckvall, M. Sellén, B. Grant, *J. Am. Chem. Soc.* **1990**, *112*, 6615–6621; E. S. M. Persson, J.-E. Bäckvall, *Acta. Chem. Scand.* **1995**, *49*, 899–906.
- [204] E. Nakamura, K. Sekiya, M. Arai, S. Aoki, *J. Am. Chem. Soc.* **1989**, *111*, 3091–3093.
- [205] M. Nakamura, E. Nakamura, N. Koga, K. Morokuma, *J. Chem. Soc. Faraday Trans.* **1994**, *90*, 1789–1798; K. Kubota, S. Mori, M. Nakamura, E. Nakamura, *J. Am. Chem. Soc.* **1998**, *120*, 13334–13341.
- [206] P. B. Armentrout, R. Georgiadis, *Polyhedron* **1988**, *7*, 1573–1581.
- [207] D. E. Frantz, D. A. Singleton, J. P. Snyder, *J. Am. Chem. Soc.* **1997**, *119*, 3383–3384.
- [208] B. E. Rossiter, N. M. Swingle, *Chem. Rev.* **1992**, *92*, 771–806.
- [209] Note that, in contrast to MeI, secondary iodides do not react in an S_N2 manner. See Ref. [18].

- [210] M. Nakamura, E. Nakamura, N. Koga, K. Morokuma, *J. Am. Chem. Soc.* **1993**, *115*, 11016–11017.
- [211] S. Mori, B.-H. Kim, M. Nakamura, E. Nakamura, *Chem. Lett.* **1997**, 1079–1080.
- [212] E. Kaufmann, P. von R. Schleyer, K. N. Houk, Y.-D. Wu, *J. Am. Chem. Soc.* **1985**, *107*, 5560–5562.
- [213] M. P. Bernstein, D. B. Collum, *J. Am. Chem. Soc.* **1993**, *115*, 789–790; P. G. Willard, Q.-Y. Liu, *J. Am. Chem. Soc.* **1993**, *115*, 3380–3381; F. E. Romesberg, D. B. Collum, *J. Am. Chem. Soc.* **1995**, *117*, 2166–2178; K. W. Henderson, A. E. Dorigo, Q.-Y. Liu, P. G. Willard, P. von R. Schleyer, P. R. Bernstein, *J. Am. Chem. Soc.* **1996**, *118*, 1339–1347; compare with: E. L. Coitiño, E. Ciuffarin, F. M. Floris, J. Tomasi, *J. Phys. Chem. A* **1998**, *102*, 8369–8376.
- [214] M. Schlosser, G. Jan, E. Byrne, J. Sicher, *Helv. Chim. Acta* **1973**, *56*, 1630–1637; M. Schlosser, T. D. An, *Angew. Chem.* **1981**, *93*, 1114; *Angew. Chem. Int. Ed. Engl.* **1981**, *20*, 1039–1041; M. G. Stanton, C. B. Allen, R. M. Kissling, A. L. Lincoln, M. R. Gagné, *J. Am. Chem. Soc.* **1998**, *120*, 5981–5989; E. K. van den Beuken, B. L. Feringa, *Tetrahedron* **1998**, 12985–13011.
- [215] See: H. Suzuki, H. Omori, Y. Moro-oka, *Organometallics* **1988**, *7*, 2579–2581; H. Suzuki, H. Omori, D. H. Lee, Y. Yoshida, M. Fukushima, M. Tanaka, Y. Moro-oka, *Organometallics* **1994**, *13*, 1129–1146; M. Shibasaki, H. Sasai, T. Arai, *Angew. Chem.* **1997**, *109*, 1290–1310; *Angew. Chem. Int. Ed. Engl.* **1997**, *36*, 1236–1256; see also: T. Iida, N. Yamamoto, H. Sasai, M. Shibasaki, *J. Am. Chem. Soc.* **1997**, *119*, 4783–4784; I. Ojima, M. Okabe, K. Kato, H. B. Kwon, I. T. Horváth, *J. Am. Chem. Soc.* **1988**, *110*, 150–157; H. Steinhagen, G. Helmchen, *Angew. Chem.* **1996**, *108*, 2489–2492; *Angew. Chem. Int. Ed. Engl.* **1996**, *35*, 2339–2342; S. J. Lippard, *Science* **1995**, *268*, 996–997.
- [216] E. Nakamura, A. Hirai, M. Nakamura, *J. Am. Chem. Soc.* **1998**, *120*, 5844–5845; A. Hirai, M. Nakamura, E. Nakamura, *J. Am. Chem. Soc.* **1999**, *121*, 8665–8666.

Ionic Liquid



Ionic Liquids—New “Solutions” for Transition Metal Catalysis

Peter Wasserscheid* and Wilhelm Keim

Ionic liquids are salts that are liquid at low temperature ($< 100^\circ\text{C}$) which represent a new class of solvents with nonmolecular, ionic character. Even though the first representative has been known since 1914, ionic liquids have only been investigated as solvents for transition metal catalysis in the past ten years. Publications to date show that replacing an organic solvent by an ionic liquid can lead to remarkable

improvements in well-known processes. Ionic liquids form biphasic systems with many organic product mixtures. This gives rise to the possibility of a multiphase reaction procedure with easy isolation and recovery of homogeneous catalysts. In addition, ionic liquids have practically no vapor pressure which facilitates product separation by distillation. There are also indications that switching from a nor-

mal organic solvent to an ionic liquid can lead to novel and unusual chemical reactivity. This opens up a wide field for future investigations into this new class of solvents in catalytic applications.

Keywords: biphasic catalysis • homogeneous catalysis • ionic liquids • solvent effects

1. Introduction

In general, an ionic liquid is a liquid that consists only of ions. However, this term includes an additional special definition to distinguish it from the classical definition of a molten salt.^[1] While a molten salt is generally thought to refer to a high-melting, highly viscous and very corrosive medium, ionic liquids are already liquid at low temperatures ($< 100^\circ\text{C}$) and have relatively low viscosity. The apparently somewhat arbitrary line drawn between molten salts and ionic liquids at a melt temperature of 100°C can be justified by the abrupt improvement in the range of applications for liquid salts below this temperature. Even though some examples are known in which high-temperature salt melts have been successfully used as reaction media for synthetic applications,^[2] only a liquid range below 100°C can enable the versatile substitution of conventional, organic solvents by ionic liquids.

The development of ionic liquids goes back to 1914. First research efforts dealt with the synthesis of ethylammonium nitrate.^[3] This salt is liquid at room temperature but usually contains a small amount of water (200–600 ppm).^[4]

The first ionic liquids with chloroaluminate ions were developed in 1948 by Hurley and Wier at the Rice Institute in

Texas as bath solutions for electroplating aluminum.^[5] However, these systems were not studied further until the late 1970s when the groups of Osteryoung and Wilkes rediscovered them. For the first time, they succeeded in preparing room-temperature liquid chloroaluminate melts.^[6] Research and development concentrated mainly on electrochemical applications at this time.

As early as 1967, a publication by Swain et al described the use of tetra-*n*-hexylammonium benzoate as a solvent for kinetic and electrochemical investigations.^[7] Even though the liquid salt was a hemihydrate at room temperature, this research work had a pioneering significance because it already contained a quantitative determination of the ionization strength of the ionic medium.

In the early 1980s the groups of Seddon and Hussey began to use chloroaluminate melts as nonaqueous, polar solvents for the investigation of transition metal complexes. The investigations generally started with the electrochemical aspects of the relevant transition metal complexes;^[8] spectroscopic and complex chemistry experiments followed.^[9] It is specially thanks to Seddon's work that ionic liquids became more familiar to a broad public.

The first publications in which ionic liquids were described as new reaction media and catalysts for organic synthesis appeared at the end of the 1980s. Acidic ionic liquids with chloroaluminate ions proved to be effective Friedel–Crafts catalysts;^[10] phosphonium halide melts were used successfully in nucleophilic aromatic substitution reactions.^[11]

The use of ionic liquids as solvents for homogeneous transition metal catalysts was described for the first time in

[*] Dr. P. Wasserscheid, Prof. W. Keim
Institut für Technische Chemie und
Makromolekulare Chemie der RWTH Aachen
Worringer Weg 1, 52074 Aachen (Germany)
Fax: (+49) 241-8888177
E-mail: Wasserscheidp@itc.rwth-aachen.de

1990 by Chauvin et al. and by Wilkes et al. Chauvin's group dissolved nickel catalysts in weakly acidic chloroaluminate melts and investigated the resulting ionic catalyst solutions for the dimerization of propene.^[12] Wilkes et al. used also weakly acidic chloroaluminate melts and studied therein the ethylene polymerization with Ziegler–Natta catalysts.^[13]

The concept of ionic liquids received a substantial boost by the work of Wilkes's group when they described in 1992 the synthesis of systems with significantly enhanced stability against hydrolysis, for example low melting tetrafluoroborate melts.^[14] In contrast to chloroaluminate ionic liquids, these systems offer high tolerance versus functional groups which opens up a much larger range of applications especially for transition metal catalysis. Ionic liquids with tetrafluoroborate ions have been successfully used, for example, in the rhodium-catalyzed hydroformylation of olefins.^[15]

Based on Wilkes's work, it became clearly apparent that ionic liquids were by no means limited to chloroaluminate melts, quite to the contrary, a whole range of cation/anion combinations can form low-melting salts.

The most recent publications are concerned with the synthesis of new ionic liquids,^[16] with the systematic investigation of their physical and chemical properties,^[17] and with further applications as solvents and catalysts.^[18]

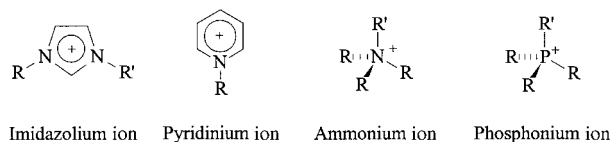
Two excellent reviews by Welton^[19] and by Seddon and Holbrey^[20] have been already published describing in special detail the use of chloroaluminate ionic liquids in synthetic and catalytic applications. Electrochemical^[21] and complex chemistry^[22] investigations in ionic liquids have already been reviewed, too.

The aim of our review is to describe the synthesis, properties, and potential of ionic liquids with respect to their

application as solvent in transition metal catalysis. In this context, we would like to offer especially to the chemist working in the field of homogeneous catalysis a set of criteria to identify suitable candidates out of the large number of ionic liquids (some authors speak about 10^{18} possible cation/anion combinations^[20]). This section will be followed by a selection of examples which demonstrate that ionic liquids can be successful alternative “solutions” for many applications. Hereby, we will focus our attention on recently published work describing transition metal catalysis in “non-chloroaluminate” systems.

2. Ionic Liquid Synthesis

The initial step in the synthesis of ionic liquids is the quaternization, of an amine or phosphane for example, to form the cation.^[6c, 22] The most important, reported cation types are shown in Scheme 1. Salts with different anions are



Scheme 1. Important types of cations in ionic liquids.

obtained by the quaternization reaction depending on the alkylation reagent. Interestingly, melting points under 100°C can be obtained for a series of cation/anion combinations in this way (Table 1).

Peter Wasserscheid, born in 1970 in Würzburg, studied chemistry at the RWTH Aachen and received his PhD in 1998 in the group of Professor Keim with a dissertation on Ni-catalyzed C–C linkage reactions in ionic liquids. At present he is carrying out his Habilitation at the Institut für Technische Chemie und Makromolekulare Chemie at the RWTH Aachen and is working on further applications of ionic liquids in synthetic and catalytic reactions. His scientific abilities were recognized at an early stage when he was awarded 1st prize in a German National competition “Jugend Forscht”. He received the DECHEMA Student prize for excellent performance in study and diploma work and the Friedrich-Wilhelm prize from the RWTH Aachen.



P. Wasserscheid



W. Keim

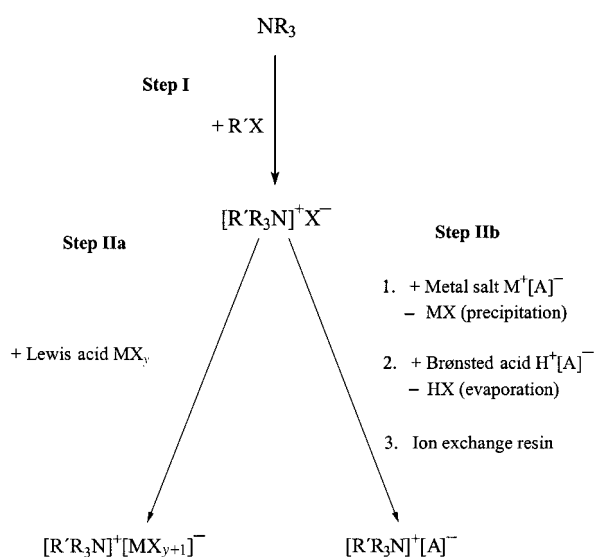
Wilhelm Keim, born in 1934 in Oberhausen, studied chemistry and received his PhD in 1963 under the guidance of Professor G. Wilke at the Max-Planck-Institut für Kohleforschung. After a year as a Postdoc with T. Kalz at Columbia University, New York, he began work at the Shell Development Company in Emeryville, CA. By 1972 he had advanced to Head of Fundamental Research. In 1973 he accepted the position of Professor and Institute Director at the Institut für Technische Chemie und Petrolchemie at the RWTH Aachen. His research activities include homogeneous and heterogeneous catalysis, carbonylation and functionalization of olefins, and selective C–C bonding. In this connection, Professor Keim is investigating aspects of the heterogenization of homogeneous catalysts and biphasic catalysis. He is the author of around 200 publications and 40 patents. His scientific achievements have recently been recognized with the award of the “Alwin-Mittasch” medal and the “Karl-Engler” medal.

Table 1. Examples of ionic liquids that can be formed by direct quaternization.

Ionic liquid	Alkylation reagent	M. p. [°C]	Ref.
[EMIM]CF ₃ SO ₃ ^[a]	methyl triflate	−9	[16a]
[BMIM]CF ₃ SO ₃ ^[b]	methyl triflate	16	[16a]
[Ph ₃ POc]OTs ^[c]	OcOTs	70–71	[24]
[Bu ₃ NMe]OTs	MeOTs	62	[25]
[BMIM]Cl	chlorobutane	65–69	[6c]

[a] EMIM = 1-ethyl-3-methylimidazolium; CF₃SO₃ = triflate anion. [b] BMIM = 1-*n*-butyl-3-methylimidazolium. [c] Oc = octyl; Ts = H₃CC₆H₄-SO₂ (tosyl).

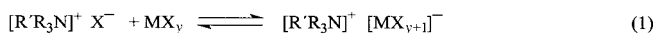
In cases where it is not possible to form the desired anion directly by the quaternization reaction, a further step follows (synthesis steps IIa or IIb in Scheme 2). For example, starting from an ammonium halide [R'R₃N]⁺X[−], two different paths to vary the anion are possible. First, the halide [R'R₃N]⁺X[−] can be treated with a Lewis acid MX_y. This leads to an ionic liquid of the type [R'R₃N]⁺[MX_{y+1}][−] (synthesis step IIa, Scheme 2).



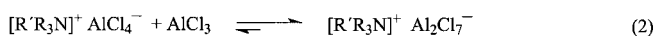
Scheme 2. Synthesis paths for the preparation of ionic liquids exemplified for an ammonium salt.

Alternatively it is possible to exchange the halide ion X[−] for the desired anion. This can be done by the addition of a metal salt M⁺[A][−] (with precipitation of M⁺X[−]) over an ion exchanger or by displacement of the halide ion by a strong acid H⁺[A][−] (with the release of H⁺X[−]) (synthesis step IIb, Scheme 2).

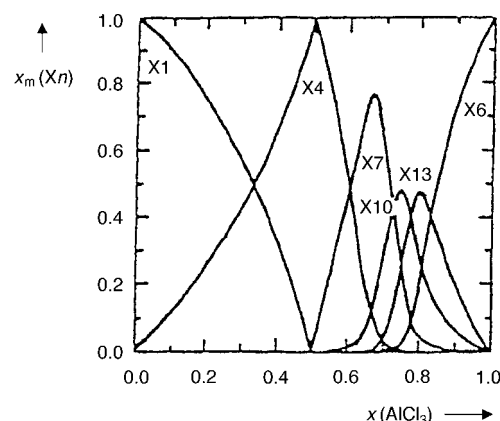
In the first case, several anion species are often present in equilibrium, which depends on the ratio of the two components [R'R₃N]⁺X[−] and MX_y [Eq. (1)].



With an excess of the Lewis acid MX_y additional anion species can be formed from further acid–base reactions with the already present anion. Such behavior is displayed by chloroaluminate melts, for example [Eq. (2) and (3)].^[26] The



formation of different anions occurs as a function of the chloride/AlCl₃ ratio. From Figure 1 it can be seen that addition of aluminum trichloride to the chloride initially results in the formation of the AlCl₄[−] ion. With an aluminum trichloride mole fraction of exactly 0.5, this is essentially the only anion present. In systems with *x*(AlCl₃) > 0.5 multi-nuclear chloroaluminate anions are formed which are in equilibrium with each other, the AlCl₄[−] ion and, at very high AlCl₃ contents, with dimeric aluminum trichloride.^[26]

Figure 1. Mole fraction *x_m* of different anion species *X_n* in chloroaluminate melts (X1 = Cl[−]; X4 = AlCl₄[−]; X7 = Al₂Cl₇[−]; X10 = Al₃Cl₁₀[−]; X13 = Al₄Cl₁₃[−]; X6 = Al₂Cl₆).

Chloroaluminates are the best known but not the only ionic liquids that can be prepared by the reaction of a halide with a Lewis acid. Further examples are shown in Table 2.

Table 2. Examples of ionic liquids that can be generated by the reaction of a halide with a Lewis acid.

Ionic liquid ^[a]	Established anion	Ref.
[cation]Cl/AlCl ₃	Cl [−] , AlCl ₄ [−] , Al ₂ Cl ₇ [−] , Al ₃ Cl ₁₀ [−]	[27]
[cation]Cl/AlEtCl ₂	AlEtCl ₃ [−] , Al ₂ Et ₂ Cl ₅ [−]	[28]
[cation]Cl/BCl ₃	Cl [−] , BCl ₄ [−]	[29]
[cation]Cl/CuCl	CuCl ₂ [−] , Cu ₂ Cl ₃ [−] , Cu ₃ Cl ₄ [−]	[30]
[cation]Cl/SnCl ₂	SnCl ₃ [−] , Sn ₂ Cl ₅ [−]	[31]

[a] cation = pyridinium, imidazolium ion.

When the anion is varied by anion exchange ionic liquids of the type [cation]⁺[A][−] are formed (synthesis step IIb, Scheme 2), which contain only one anion species when the exchange reaction has proceeded to completion (Table 3).

At this point it should be noted that the synthesis of highly pure, binary ionic liquids places particular demands on the

Table 3. Examples of ionic liquids that can be prepared by anion exchange.

Ionic liquid ^[a]	Ref.
[cation]BF ₄	[14, 32]
[cation]PF ₆	[32, 33]
[cation]SbF ₆	[30]
[cation]NO ₃	[14]
[cation]CH ₃ CO ₂	[14]
[cation]HSO ₄	[16f]
[cation]B(Et ₃ Hex)	[34]

[a] cation = pyridinium, imidazolium, ammonium ion.

preparative work. The purity of the system is essential for many solvent applications and for the characterization of their physical and chemical properties. Whereas organic solvents are usually purified by distillation before use, this method is not suitable to clean up ionic liquids due to their nonvolatile character. For this reason, the highest purity possible must be attained during the synthesis itself. For example, during the exchange of chloride ions for the desired anions, it must be ensured that no halide ions remain in the system. Also traces of the acid used in the synthesis can lead to unwanted chemical reactivity. High purity in the synthesis of binary ionic liquids is usually achieved by anion exchange over an ion exchanger.

The described methods can, of course, also be used to prepare previously unknown combinations of cations and anions which could also result in low-melting salts. In addition there is the possibility to obtain ionic liquids with new properties by the mixture of several different salts.^[35]

3. Characteristic Properties of Ionic Liquids

The physical and chemical properties of ionic liquids can be specifically varied over a wide range by the selection of suitable cations and anions. The possibility arises to optimize the ionic reaction medium for a specific application by stepwise tuning the relevant solvent properties. For this reason ionic liquids have been referred to as “designer solvents” in several publications.^[36]

In the following section, we attempt to illustrate the relationships between the structural features of an ionic liquid and its important physical and chemical properties, on the basis of a few selected examples.

3.1. Melting Point

The key criterion for the evaluation of an ionic liquid is, by definition, its melting point. Of particular significance is therefore the question of the relationship between the structure and chemical composition of an ionic liquid and its melting point.

Comparison of the melting points of different chloride salts illustrates the influence of the cation clearly: High melting points are characteristic for alkali metal chlorides, whereas chlorides with suitable organic cations melt at temperatures below 150 °C (Table 4).^[6c, 37]

In the literature, the following features are discussed for cations of low-melting salts: low symmetry,^[1] weak intermo-

lecular interactions (such as the avoidance of hydrogen bonding),^[16a, 38] and a good distribution of charge in the cation.^[39]

Besides the cation, the anion influences the melting point, too. Comparison of the melting points of different salts with the 1-ethyl-3-methylimidazolium (EMIM) ion emphasizes that, in most cases, an increasing size of the anion with the same charge leads to a further decrease in the melting point (Table 5).

Table 5. Influence of different anions on the melting point of imidazolium salts.

Imidazolium salt	M. p. [°C]	Ref.
[EMIM]Cl	87	[6c]
[EMIM]NO ₂	55	[14]
[EMIM]NO ₃	38	[14]
[EMIM]AlCl ₄	7	[40]
[EMIM]BF ₄	6 ^[a]	[17d]
[EMIM]CF ₃ SO ₃	−9	[16a]
[EMIM]CF ₃ CO ₂	−14	[16a]

[a] Glass transition.

For ionic liquids prepared by reaction of a halide [cation]⁺X[−] with a Lewis acid MX_y, the molar ratio of the two reactants influences the melting points (Figure 2).^[40] As already shown in Figure 1, a quasi-binary system with the AlCl₄[−] ion only exists for exact 1:1 mixtures in the system [EMIM]Cl/AlCl₃. The fact that a local maximum in melting temperature is observed at exactly this composition indicates that the presence of several anions in the ionic liquid has the effect of decreasing the melting point.

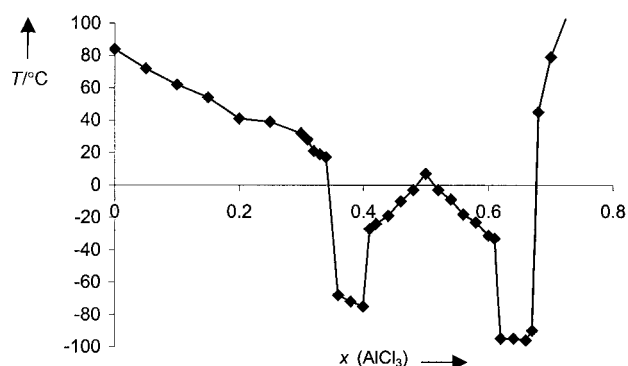


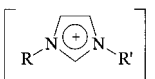
Figure 2. Experimental phase diagram in the system [EMIM]Cl/AlCl₃ (EMIM = 1-ethyl-3-methylimidazolium ion).

3.2. Vapor Pressure and Thermal Stability

Ionic liquids have no measurable vapor pressure. This is a great advantage from a process engineering viewpoint, since separation by distillation of a reaction mixture becomes more effective as a method of product isolation. The well-known problem of azeotrope formation between the solvent and the products does not arise.

The thermal stability of ionic liquids is limited by the strength of their heteroatom–carbon and their heteroatom–hydrogen bonds, respectively. Ionic liquids synthesized by direct protonation of an amine or phosphane show, for

Table 4. Melting points of various chlorides.

Salt	M. p. [°C]
NaCl	803
KCl	772
 Cl [−]	<div> R = R' = methyl ([MMIM]Cl)^[a] 125 R = methyl, R' = ethyl ([EMIM]Cl) 87 R = methyl, R' = <i>n</i>-butyl ([BMIM]Cl) 65 </div>

[a] MMIM = 1,3-dimethylimidazolium.

example, significantly restricted thermal stability. Many melts with trialkylammonium ions already decompose at a temperature below 80 °C in vacuo (depending on the boiling point of the related amine or acid). For ionic liquids obtained by alkylation of an amine or phosphane the tendency to undergo thermally induced transalkylation or dealkylation reactions (retro-quaternization reaction) is strongly related to the nature of their anion. While 150 °C has to be considered as maximum working temperature for most of the quaternary ammonium chloride salts, 1-ethyl-3-methylimidazolium (EMIM) tetrafluoroborate, for example, has been reported to be stable to about 300 °C^[41] and [EMIM][(CF₃SO₂)₂N] (m.p. −3 °C) is stable up to even more than 400 °C.^[16a] Consequently, some ionic liquids have, in contrast to water and most organic solvents, a liquid range of up to more than 400 °C.

3.3. Density

The dependence of the density of an ionic liquid on the type of cation and anion can be illustrated clearly by the example of chloroaluminate and bromoaluminate melts. A comparison of chloroaluminate melts with different cations reveals an almost linear relationship between the density and the length of the *N*-alkyl chain on the imidazolium cation (Figure 3).^[40]

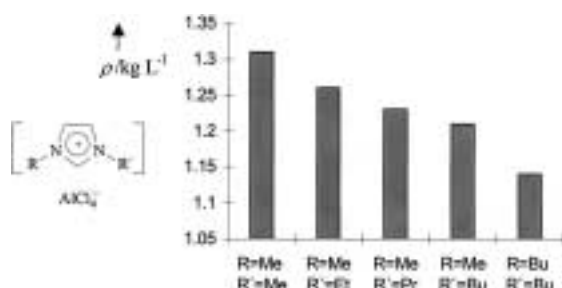


Figure 3. Dependence of the density ρ of 1,3-dialkylimidazolium tetrachloroaluminate melts on the type of both alkyl groups; measurement temperature at 60 °C, $x(\text{AlCl}_3) = 0.5$.

More generally, it can be concluded that the density of comparable ionic liquids decreases as the bulkiness of the organic cation increases. Slight structural changes in the cation allow a fine adjustment of the density.

Varying the anion results in more obvious effects in several cases. With bromoaluminate melts for example, it was possible to achieve densities unusual for normal organic solvents (Figure 4).^[42] Density measurements of ionic liquids with triflate or trifluoroacetate ions confirmed the more general result that a certain density range is established by the choice of anion, within which a fine adjustment is possible by careful choice of the cation.^[16a]

3.4. Viscosity

The viscosity of ionic liquids is essentially determined by their tendency to form hydrogen bonding and by the strength of their van der Waals interactions.^[16a]

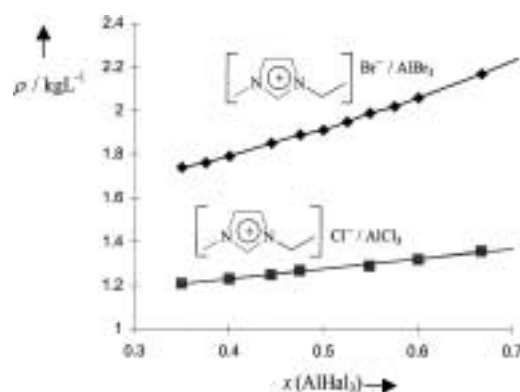


Figure 4. Dependence of the density ρ of two 1-ethyl-3-methylimidazolium tetrahaloaluminate melts on the mole fraction of aluminum trihalide at 60 °C.

The effect of hydrogen bonding becomes clear when, for example, the viscosities of chloroaluminate melts of different compositions are compared (Figure 5).^[40] The increase in viscosity of more than a factor of ten in ionic liquids with

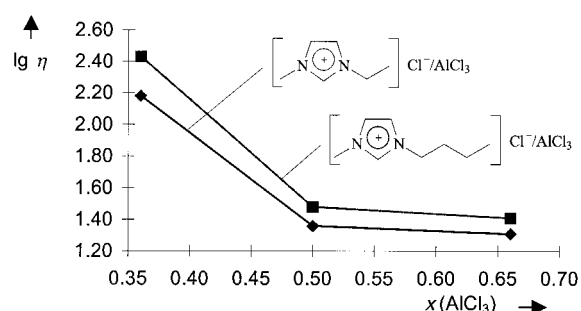


Figure 5. Dependence of the dynamic viscosity η [cP] of two 1,3-dialkylimidazolium tetrachloroaluminate melts on the mole fraction of aluminum trichloride at 25 °C.

$x(\text{AlCl}_3) < 0.5$ is a result of the formation of hydrogen bonds between the hydrogen atoms of the imidazolium cation and the basic chloride ion. This statement is supported by IR^[43] and X-ray spectroscopy,^[44] ROESY-NMR, and theoretical calculations.^[45] In acidic mixtures, however, the anions AlCl_4^- and Al_2Cl_7^- are present, in which the negative charge is much better distributed. This leads to the formation of weaker hydrogen bonds and a much lower viscosity.

Comparison of the viscosity of different, hydrophobic ionic liquids with 1-*n*-butyl-3-methylimidazolium (BMIM) ions emphasizes, in addition, the interplay between van der Waals interactions and hydrogen bonding (Table 6).^[16a] The transition from the triflate ion to the $n\text{-C}_4\text{F}_9\text{SO}_3^-$ ion, and from the trifluoroacetate ion to the $n\text{-C}_3\text{F}_7\text{COO}^-$ ion reveals an

Table 6. Dynamic viscosities η of various 1-*n*-butyl-3-methylimidazolium (BMIM) salts at 20 °C.

	Anion [A] [−]	η [cP]
	CF_3SO_3^-	90
	$n\text{-C}_4\text{F}_9\text{SO}_3^-$	373
	CF_3COO^-	73
	$n\text{-C}_3\text{F}_7\text{COO}^-$	182
	$(\text{CF}_3\text{SO}_2)_2\text{N}^-$	52

obvious increase in viscosity. It is apparent that the stronger van der Waals interactions in the case of the $n\text{-C}_4\text{F}_9\text{SO}_3^-$ and $n\text{-C}_7\text{F}_7\text{COO}^-$ ions result in a higher viscosity of the ionic liquid. Comparison of the viscosities of $[\text{BMIM}]\text{CF}_3\text{SO}_3$ with $[\text{BMIM}](\text{CF}_3\text{SO}_2)_2\text{N}$, reveals a lower viscosity despite stronger van der Waals interactions for ionic liquids with the $(\text{CF}_3\text{SO}_2)_2\text{N}^-$ ion. In this case, the almost complete suppression of hydrogen bonding overcompensates for the expected increase in viscosity.^[16a]

The structure of the cation also influences the viscosity of the ionic liquid. The lowest viscosities are usually obtained for melts with the 1-ethyl-3-methylimidazolium (EMIM) ion, in which a side chain with sufficient mobility is combined with a low molar mass. Longer or fluorinated alkyl chains result in higher viscosities because of stronger van der Waals interactions.^[16a]

The viscosity of ionic liquids can be lowered, drastically in some cases, by only slight increases in temperature^[40, 46] or by the addition of small amounts of organic cosolvents.^[47]

3.5. Solvation Strength and Solubility Characteristics

The tuning of solubility properties of an ionic liquid by the careful choice of cation and anion deserves particular attention.

The influence of the cation, for example, is shown by investigations of the solubility of 1-octene in different tosylate melts (Figure 6).^[25] It can be seen that with increasing nonpolar character of the cation, the solubility of 1-octene in the melt increases markedly. In methyl-tri- n -octylammonium tosylate a single-phase reaction mixture is obtained.

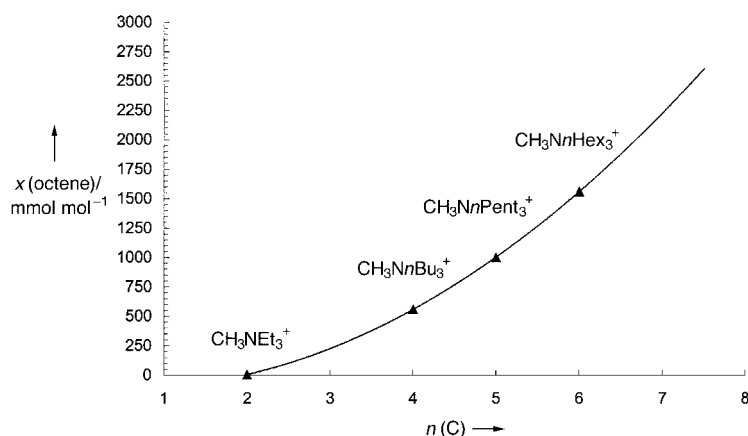


Figure 6. Solubility of 1-octene in four different tri- n -alkylmethylammonium tosylate melts at 80 °C. $n(\text{C})$ = number of C atoms of the alkyl residue.

This example shows that stepwise variation of the solubility properties can be achieved by variation of the alkyl group on the cation.

The influence of the anion on the solubility characteristics of ionic liquids can be demonstrated in an impressive fashion by the example of the water solubility of different melts containing the BMIM ion. While $[\text{BMIM}]\text{Br}$, $[\text{BMIM}]\text{CF}_3\text{COO}$, and $[\text{BMIM}]\text{CF}_3\text{SO}_3$ are highly water-soluble, ionic liquids with the same cation but with a PF_6^- or $(\text{CF}_3\text{SO}_2)_2\text{N}^-$ ion form biphasic mixtures with water. The water content of the ionic liquid $[\text{BMIM}](\text{CF}_3\text{SO}_2)_2\text{N}$ at 20 °C is only 1.4 weight percent.^[16a]

Several ionic liquids showing a miscibility gap with water have been considered as interesting candidates for separation processes by liquid–liquid extraction. Rogers et al. investigated, for example, the solubility of different acids and bases in water/ $[\text{BMIM}]\text{PF}_6$ at different pH values of the aqueous phase.^[48] Interestingly, their results reveal a higher solubility of neutral substrates in the ionic liquid, while ionic species dissolve preferentially in the aqueous layer. The authors conclude that the solubility properties of $[\text{BMIM}]\text{PF}_6$ versus water show high similarity to organic solvents. The substitution of volatile organic solvents by ionic liquids in extractive separation processes may therefore be an interesting option.

Many ionic liquids are completely miscible with organic solvents if their dielectric constants exceed a characteristic limit. This limit appears to be specific for each cation/anion combination (Table 7).^[16a]

The solubility of supercritical CO_2 in $[\text{BMIM}]\text{PF}_6$ that has recently been investigated by Brennecke's group is remarkable, too.^[49] In the biphasic system $\text{scCO}_2/[\text{BMIM}]\text{PF}_6$ 60 mol % of CO_2 dissolve in the ionic liquid at 80 bar CO_2 pressure. Hereby, the volume of the ionic liquid increases only by 10–20%, however. As a first application of this interesting biphasic system, the authors investigated the extraction of naphthalene from the ionic liquid. They succeeded in recovering the naphthalene quantitatively without any detectable contamination of the extract by the ionic liquid.

Without doubt, the key to the successful use of ionic liquids lies in the skillful exploitation of their exceptional solubility characteristics. Further systematic investigations are necessary, however, to take full advantage of this huge potential.

One very promising possibility is, for example, the investigation of the polarity of ionic liquids. The polarity of a solvent is usually determined in a purely empirical fashion. A well-understood, easily measurable and strongly solvent-dependent process is deter-

Table 7. Miscibility of various ionic liquids with the 1-ethyl-3-methylimidazolium (EMIM) ion in organic solvents with the dielectric constant ϵ .^[a]

Solvent	ϵ	$[\text{EMIM}]\text{CF}_3\text{SO}_3$	$[\text{EMIM}]\text{CF}_3\text{COO}$	$[\text{EMIM}]n\text{-C}_3\text{F}_7\text{COO}$	$[\text{BMIM}]\text{CF}_3\text{COO}^{[b]}$	$[\text{BMIM}]n\text{-C}_3\text{F}_7\text{COO}$
CH_2Cl_2	8.93	m	m	m	m	m
THF	7.58	m	m	m	m	m
ethyl acetate	6.02	m	pm	pm	m	m
toluene	2.38	im	im	im	im	im
1,4-dioxane	2.01	im	im	im	im	im

[a] m: miscible; pm: partially miscible; im: immiscible.

mined in a large number of different solvents, for example the spectral absorption of a solvatochromic dye. Empirical solvent polarity parameters are derived from the measured absorption maxima, which reflect the solvating ability of a solvent much more comprehensively than the individual physical constants.^[50] Amongst the many empirical polarity scales, the $E_{\text{T}}(30)$ scale introduced by Dimroth et al. in 1963^[51] and further developed by Reichardt et al. in 1971 has proven successful, and is based on the solvatochromism of a pyridinium-*N*-phenolate betaine dye.^[52] This method has also been used successfully to determine the polarity of a small number of ionic liquids. The results obtained confirm the considerable width of variation of solvent polarity of ionic liquids. While, for example, tetra-*n*-hexylammonium benzoate with an $E_{\text{T}}(30)$ value of 0.41 lies within the polarity range of DMF,^[53] an $E_{\text{T}}(30)$ value of 0.95 was determined for ethylammonium nitrate corresponding to a polarity between $\text{CF}_3\text{CH}_2\text{OH}$ and water.^[4, 54] [BMIM]PF₆ was investigated by using the same method and its $E_{\text{T}}(30)$ value was found to correspond to a polarity in the range of methanol.^[55]

However, recent work by Armstrong et al. gave rise to the question whether the chemical nature of the solvatochromic dye influences the result of the polarity determination of an ionic liquid. These authors coated GC columns with several ionic liquids and compared the retention times of a large number of substances.^[56] The results of their study indicate different polarity of ionic liquids depending on the nature of the tested compounds.

While [BMIM]PF₆, for example, acts like an unpolar stationary phase versus unpolar molecules (like *n*-octane), very long retention times are observed with proton-donor compounds. The authors attribute a dual polarity behavior to the ionic liquids under investigation.

Unfortunately the number of systematic investigations concerning the polarity of ionic liquids is still very limited. More research in this field should be encouraged in order to establish efficient criteria to determine the right ionic liquid candidate for a given solvent application.

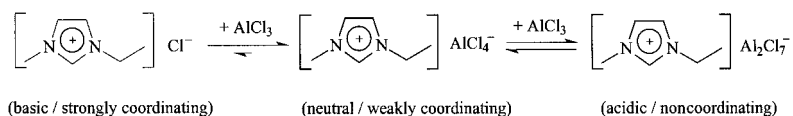
3.6. Acidity and Coordination Ability

The acidity and coordination properties of an ionic liquid are essentially determined by the nature of its anion. Many intermediate levels between “strongly basic/strongly coordinating” and “strongly acidic/practically noncoordinating” can be realized by careful choice of the anion (Table 8).^[30]

Table 8. Coordinative characteristics of various anions.

basic/strongly coordinating		Acidity/coordination neutral/weakly coordinating		acidic/non-coordinating
Cl [−]		AlCl ₄ [−]		Al ₂ Cl ₇ [−]
Ac [−]		CuCl ₂ [−]		Al ₃ Cl ₁₀ [−]
NO ₃ [−]		SbF ₆ [−]		
	SO ₄ ^{2−}	BF ₄ [−]	Cu ₂ Cl ₃ [−]	
		PF ₆ [−]		Cu ₃ Cl ₄ [−]

In this context, those ionic liquids have to be mentioned which form a neutral anion (e.g. AlCl₄[−]) or an acidic anion (e.g. Al₂Cl₇[−]) from a basic anion (e.g. Cl[−]) by addition of a Lewis acid (e.g. AlCl₃). In Scheme 3 this behavior is illustrated by the example of a EMIM chloroaluminate melt.

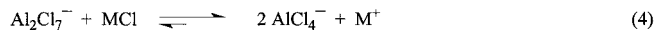


Scheme 3. Control of the acidity of ionic liquids by the ratio of halide to Lewis acid exemplified for 1-ethyl-3-methylimidazolium (EMIM) chloroaluminate melt.

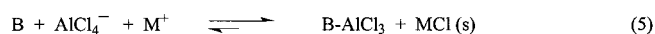
Chloroaluminate melts are designated as basic when the molar ratio of AlCl₃ is smaller than 0.5. A neutral melt is referred to at an AlCl₃ ratio of exactly 0.5, where essentially only the anion AlCl₄[−] is present.^[22a] Finally, an acidic chloroaluminate melt is one in which the AlCl₃ ratio is larger than 0.5. In such acidic melts, the anions Al₂Cl₇[−] and Al₃Cl₁₀[−] exist, which act as very strong Lewis acids.^[27]

Two further phenomena in the field of acid/base chemistry of ionic liquids deserve to be mentioned. These are the so-called “latent acidity” and “superacidity” of protons in ionic liquids.

The latent acidity of ionic liquids arises when weak bases are added to buffered neutral chloroaluminate melts. Such melts are formed when, for example, excess alkali metal chloride (MCl) is added to an acidic chloroaluminate melt.^[57] The alkali metal chloride MCl reacts according to Equation (4) with the acidic chloroaluminate dimers until the melt



becomes neutral. A buffered melt is one in which the neutrality of the melt is maintained by reaction of excess alkali metal chloride when acid AlCl₃ is added. The latent acidity of this neutral system becomes noticeable when a weak base (B) such as *N,N*-dimethylaniline, pyrrole, or acetylferrocene is added.^[58] An adduct is formed between the added base and AlCl₃ with precipitation of the alkali chloride MCl [Eq. (5)].



This reaction is not observed in the absence of excess alkali metal cations. The latent acidity of different ionic liquids has already been quantitatively measured.^[59] In our group, ionic liquids with latent acidity have been successfully used as solvents in the Ni-catalyzed oligomerization of 1-butene (see Section 4.8).^[60]

The superacidity of protons in several ionic liquids is also worth mentioning. It has been observed when strong mineral acids were dissolved in acidic chloroaluminate ionic liquids.^[61] Smith and co-workers investigated the acidity of such protons in ionic liquids by the protonation of aryl compounds with a solution of HCl gas in acidic [EMIM]Cl/AlCl₃ melts. The acidity of the protons in the melt were measured quantita-

tively by UV spectroscopy.^[61a] Acid strengths were obtained as a function of the melt's acidity which were clearly above the one of 100 % sulfuric acid (Figure 7).^[62]

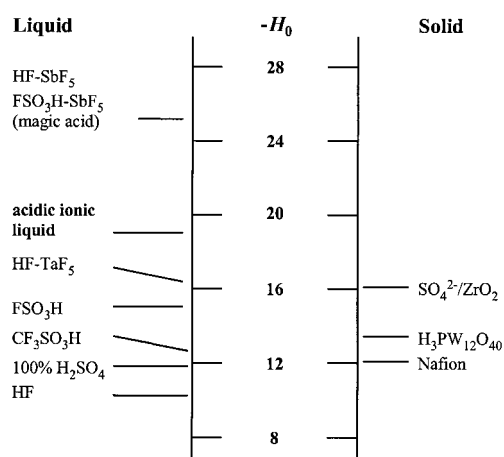


Figure 7. Comparison of the acid strength of superacid ionic liquids with those of conventional superacids.

The superacid properties of protons in acidic chloroaluminate melts have been explained by the reaction between the dissolved HCl and the acidic species in the melt, which releases protons with extremely low solvation and therefore very high reactivity [Eq (6)].



In contrast to normal superacid systems, superacid ionic liquids are much easier and safer to handle.^[61a] They could, therefore, represent very promising alternatives to the superacids normally used.

Finally we should note that the cation of an ionic liquid also has an influence on the acidity of the system. A weak Lewis acidity is, for example, attributed to the imidazolium ion itself. The catalytic effect of imidazolium bromide melts in Diels–Alder reactions is reported to be related to this weak acidity of the imidazolium ion.^[63] Moreover, the H atom in the 2-position of an imidazolium ion possesses significant Brønsted acidity.^[64] This is of special importance for reactions with transition metal complexes, since in the presence of bases in situ carbene complexes can be formed.^[65]

3.7. Handling and Availability

The handling of ionic liquids depends essentially on the stability of the anion towards hydrolysis. Whereas ionic liquids with nitrate, benzenesulfonate, and [bis(trifluoromethylsulfonyl)amide] ions, for example, are air and water stable and can even be synthesized in water, systems with chloroaluminate anions must be classified as extremely hygroscopic and labile towards hydrolysis. More difficulties arise when traces of water in chloroaluminate melts react with the anions of the melt to release superacid protons. These cause unwanted side reactions and possess a considerable potential

for corrosion. Since the preparation of a completely water-free chloroaluminate melt is difficult (for a detailed description of protic and oxidic impurities in chloroaluminate melts we recommend Welton's review^[19]) the level of tolerable impurities has to be determined for each planned application. To sum up: the handling and stability of ionic liquids cannot be easily assessed, but it is mainly dependent on the nature of the anion.

The commercial availability of ionic liquids was very limited until recently. Only a small number of systems could be purchased from chemical distributors in small quantities (up to 25 g).^[66] Since the end of 1999, a large variety of ionic liquids is now commercially available in up to 5 liter scale.^[67] If demand for ionic liquids grows further, we suppose that in the near future particularly producers of ionic liquid precursor compounds (such as amines) will enter the market. In this case we expect drastically decreasing prices for ionic liquids.

In this context it should be mentioned that after most applications the used ionic liquid can be easily recovered, cleaned up—if necessary—and reused repeatedly. In an ideal case the cost for the ionic liquid can be therefore regarded as an one-time investment.

3.8. Environmental Aspects

Recently ionic liquids have often been discussed as promising solvents for “clean processes” and “green chemistry”.^[36, 68] These two catchwords represent current efforts to reduce drastically the amounts of side and coupling products and also the solvent and catalyst consumption in chemical processes. The use of ionic liquids could make a contribution in this area, particularly with regard to solvent and catalyst usage.

In contrast to volatile organic solvents and extraction media, ionic liquids have no measurable vapor pressure. Therefore there is no loss of solvent through evaporation. Environmental and safety problems arising through the use of volatile organic solvents can also be avoided by the use of a nonvolatile ionic reaction medium.

With respect to efforts to reduce catalyst consumption, two aspects arise with the use of ionic liquids: First, the special solubility characteristics of an ionic reaction medium enables a biphasic reaction procedure in many cases. Exploitation of the miscibility gap between the ionic catalyst phase and the products allows, in this case, the catalyst to be isolated effectively from the product and reused many times. Second, the nonvolatile nature of ionic liquids enables a more effective product isolation by distillation. The possibility also exists here to reuse the isolated ionic catalyst phase. In both cases, the total reactivity of the applied catalysts is increased and catalyst consumption relative to generated product is reduced.

For environmental and safety reasons the use of ionic liquids could gain in significance particularly in processes with superacid catalysts. Substitution of HF by nonvolatile superacid ionic liquids presents a promising alternative in this context.

In the meantime, many examples have shown (see Section 4) that the application of ionic liquid solvents can result in

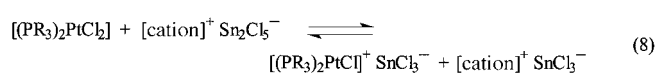
significantly reduced environmental impact. Therefore we fully agree with the classification of ionic liquids as “green solvents”. However, in this context it should be mentioned that aspects of their toxicity and their disposal have not been fully explored yet.

4. Ionic Liquids as Solvents for Transition Metal Catalyzed Reactions

Ionic liquids are able to dissolve organometallic compounds and are therefore possible solvents for reactions with homogeneous catalysts. Depending on the coordinative properties of the anion (see Section 3.6), the ionic liquid can be regarded as an “innocent” solvent or as a cocatalyst.

Ionic liquids with tetrafluoroborate or hexafluorophosphate ions, for example, have to be considered as inert solvents in most reactions (for exceptions see, for example, Section 4.5). In these cases the role of the ionic liquid is solely to provide a polar, weakly coordinating medium for the transition metal catalyst that additionally offers special solubility for feedstock and products. The use of ionic liquids often allows a combination of solvent properties which can not be realized with water or common organic solvents.

Ionic liquids formed by the reaction of a halide with a Lewis acid (e.g. chloroaluminate or chlorostannate melts) generally act as a cocatalyst. The reason for this is the Lewis acidity or basicity which is always present (at least latent), and which results in strong interactions with the catalyst complex. In many cases, the Lewis acidity of an ionic liquid is used to convert the neutral catalyst precursor into the corresponding cationic active form. The activation of $[\text{Cp}_2\text{TiCl}_2]$ in acidic chloroaluminate melts and the activation of $[(\text{PR}_3)_2\text{PtCl}_2]$ in chlorostannate melts are examples for this kind of activation [Eq. (7) and (8)].^[31c]

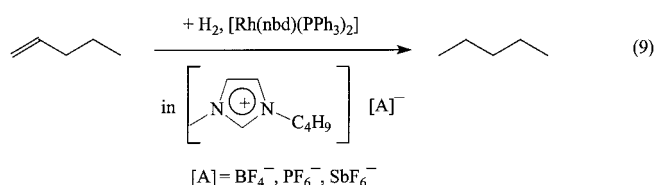


There are many good reasons to study ionic liquids as alternative solvents in well-known transition metal catalyzed reactions. Besides the engineering advantage of their non-volatile nature, the investigation of new biphasic reactions with an ionic catalyst phase is of special interest. Here, the possibility to adjust solubility properties by different cation/anion combinations allows a systematical optimization of the biphasic reaction, for example, with regard to product selectivity. Attractive options to improve selectivity in multiphase reactions derive from the preferential solubility of only one reactant in the catalyst solvent or from the in situ extraction of reaction intermediates out of the catalyst layer. Finally, the ionic liquid may be in many cases a superior solvent for transition metal catalysis in comparison to water and common organic solvents especially when ionic complexes are used as catalysts. In these cases, significant enhancement of catalyst activity and stability is possible.

In our group we have been investigating the reactivity of ionic transition metal catalyst solutions since 1995 and are currently working on the hydrogenation, hydroformylation, oxidation, and oligomerization of functionalized and non-functionalized alkenes. In the following section an overview of recent developments in the field of transition metal catalysis in ionic liquids is presented.

4.1. Hydrogenations

The first successful hydrogenation reactions in ionic liquids were studied by the groups of de Souza^[32] and Chauvin^[15] in 1995. De Souza et al. investigated the Rh-catalyzed hydrogenation of cyclohexene in BMIM tetrafluoroborate. Chauvin et al. dissolved the cationic “Osborn complex” $[\text{Rh}(\text{nbd})(\text{PPh}_3)_2]\text{PF}_6$ (nbd = norbornadiene) in ionic liquids with weakly coordinating anions (e.g. PF_6^- , BF_4^- , and SbF_6^-) and used the ionic catalyst solutions thus obtained according to Equation (9) for the biphasic hydrogenation of 1-pentene.

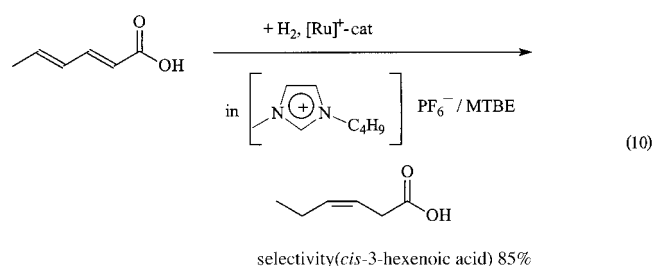


Although the reactants have only limited solubility in the catalyst phase, the rates of hydrogenation in $[\text{BMIM}]\text{SbF}_6$ are almost five times faster than for the comparable reaction in acetone. All ionic catalyst solutions tested could be reused repeatedly. The loss of rhodium through leaching into the organic phase lay below the detection limit of 0.02%. These results are of general importance for the field of biphasic catalysis since this was the first time that a rhodium catalyst could be “immobilized” in a polar solution without the use of specially designed ligands.

Moreover, Chauvin et al. described the selective hydrogenation of cyclohexadiene to cyclohexene by making use of the biphasic reaction system.^[15] Since the solubility of cyclohexadiene in $[\text{BMIM}]\text{SbF}_6$ is about five times higher than the solubility of cyclohexene in the ionic liquid, the latter was obtained in 98% selectivity at 96% conversion. The authors observed complete suppression of the hydrogenation activity however, if the used ionic liquid contained some Cl^- impurities.

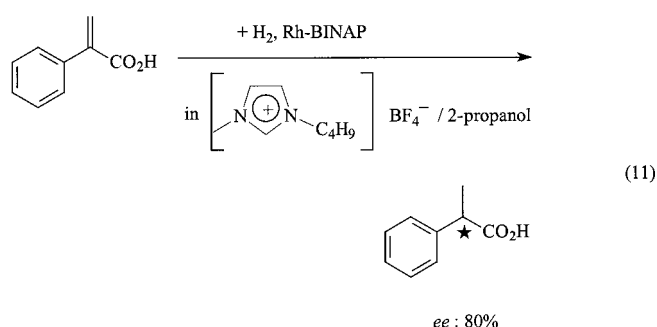
Rhodium- and cobalt-catalyzed hydrogenation of butadiene and 1-hexene,^[69, 32] and the Ru-catalyzed hydrogenation of aromatic compounds^[18c] and acrylonitrile–butadiene copolymers^[70] have also been reported to be successful in ionic liquids.

A stereoselective hydrogenation in ionic liquids was recently successfully carried out in our institute. Based on investigations in the biphasic system water/*n*-heptane,^[71] the ruthenium-catalyzed hydrogenation of sorbic acid to *cis*-3-hexenoic acid according to Equation (10) in the system $[\text{BMIM}]\text{PF}_6/\text{MTBE}$ (MTBE = methyl *tert*-butyl ether) was



studied.^[72] In comparison to other polar solvents (e.g. glycol) a more than threefold increase in activity with comparable selectivity to *cis*-3-hexenoic acid was observed in the ionic liquid. After reaction, the ionic catalyst solution could be recovered by phase separation and reused repeatedly.

Enantioselective hydrogenation in ionic liquids is also possible. Chauvin et al. hydrogenated α -acetamidocinnamic acid in the presence of a [Rh(cod)((-)-diop)] catalyst (cod = cycloocta-1,3-diene; diop = 4,5-bis[(diphenylphosphanyl)methyl]-2,2-dimethyl-1,3-dioxolan-4,5-diol) in a [BMIM]SbF₆ melt with 64 % *ee* to (*S*)-phenylalanine.^[15] Dupont et al. were able to obtain up to 80 % *ee* in the reaction of 2-arylacrylic acid to (*S*)-2-phenylpropionic acid with Ru-BINAP catalysts (BINAP = 2,2'-bis(diphenylphosphanyl)-1,1'-binaphthyl)^[73] in [BMIM]BF₄ melts [Eq. (11)]. Both reactions were carried out in two phases with the help of an additional organic solvent (e.g. *i*PrOH). The catalyst could be reused with the same activity and enantioselectivity after decanting the hydrogenation products.

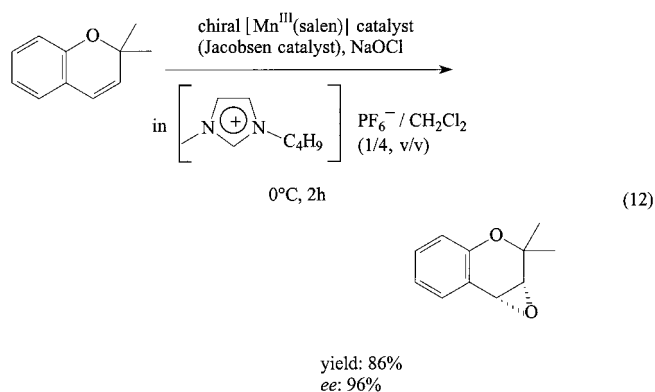


In general, transition metal catalyzed hydrogenation reactions in ionic liquids are judged to be particularly promising: On the one hand, a large number of known hydrogenation catalysts exist.^[74] On the other hand, the solubility of hydrogen and many alkenes in the ionic liquid appears to be sufficiently high to achieve good reaction rates. At the same time, the miscibility gap between the saturated reaction products and the ionic liquid is large so that, in the majority of cases, a biphasic procedure is possible.

4.2. Oxidations

Recently published results by Song and Roh indicate that the use of ionic liquids is also of advantage in selective oxidation reactions.^[75] They investigated the epoxidation of, for example, 2,2-dimethylchromene with a chiral Mn^{III}(salen) complex

([*N,N'*-bis(3,5-di-*tert*-butylsalicylidene)-1,2-cyclohexanediamine]manganese(III) chloride) in a mixture of [BMIM]PF₆ and CH₂Cl₂ (1:4 v/v) [Eq. 12]. The authors describe a clear enhancement of the catalyst activity by the



addition of the ionic liquid to the organic solvent. In the presence of the ionic liquid an 86 % conversion of 2,2-dimethylchromene was observed after 2 h. Without the ionic liquid the same conversion was obtained only after 6 h. In both cases the enantiomeric excess was as high as 96 %.

Moreover, the use of the ionic liquid solvent allows an easy catalyst recycle without the need of any catalyst modification. By washing the organic phase with water followed by extraction of the product with hexane, the ionic catalyst solution is recovered after reaction and can be reused. Though, after five recycles the conversion drops from 83 % to 53 % under identical reaction conditions. The authors explain this loss in activity by a slow degradation of the [Mn^{III}(salen)] complex.

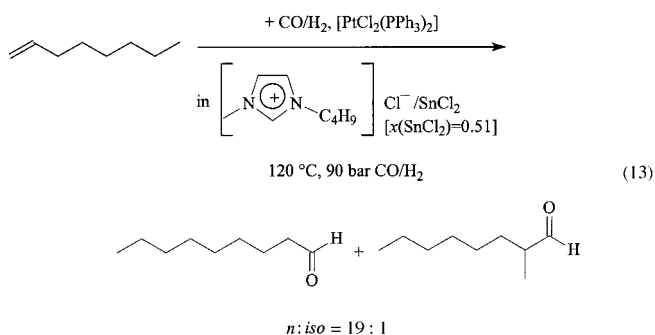
To our best knowledge the publication of Song and Roh is the first published example of a transition metal catalyzed oxidation reaction in an ionic liquid. This is quite surprising taking in account that the ionic liquid concept appears particularly suitable for oxidation reactions. It is known from electrochemical studies that some ionic liquids show high oxidation stability.^[16a] Moreover, recent studies in our laboratory showed that low melting imidazolium and pyridinium salts are stable even versus highly oxidizing media such as fuming sulfuric acid (30 % SO₃) if short alkyl chains are chosen at the cation.^[76] The investigation of further oxidation reactions in ionic liquids looks therefore quite promising.

4.3. Hydroformylations

As early as 1972 Parshall described the platinum-catalyzed hydroformylation of ethene in tetraethylammonium trichlorostannate melts.^[31a] The ionic liquid used in this case has, however, a rather high melting point of 78 °C. In addition, the publication does not contain details of the catalytic activity of the platinum catalyst dissolved in the melt.

In our group, we have therefore studied the platinum-catalyzed hydroformylation in chlorostannate melts anew. In BMIM trichlorostannate, which is liquid at room temperature,

the hydroformylation of 1-octene, according to Equation (13), succeeded with remarkable *n/iso* selectivities.^[31c] Despite the

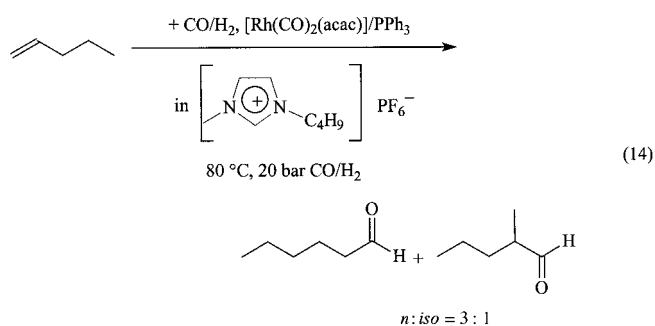


limited solubility of 1-octene in the ionic catalyst phase, a remarkable activity of the platinum catalyst was achieved (turnover frequency (TOF) = 126 h⁻¹). The biphasic nature of the reaction enabled a very simple product isolation, leaching of the platinum catalyst into the product phase was not observed.

Ruthenium- and cobalt-catalyzed hydroformylation of internal and terminal alkenes in molten tetra-*n*-butylphosphonium bromide was investigated by Knifton.^[23c] The author described a stabilization of the active ruthenium–carbonyl complex by the ionic medium. An increased catalyst lifetime at low synthesis gas pressures and higher temperatures was observed.

Recently the rhodium-catalyzed hydroformylation of 1-hexene was performed in higher melting (>70 °C) phosphonium salts, too.^[24] The authors made use of the higher melting point of the salt to “pour off” the organic product from the solid catalyst medium at room temperature. After renewed heating above the salt’s melting point, the catalyst could be reused with the same reactivity.

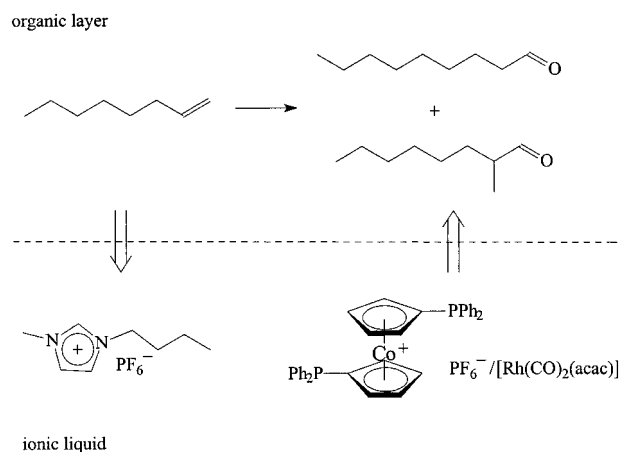
Investigations of the rhodium-catalyzed hydroformylation in room temperature liquid molten salts were published by Chauvin et al. in 1995.^[15, 77] The hydroformylation of 1-pentene with [Rh(CO)₂(acac)]/PPh₃ (acac = acetylacetonate) succeeded, for example, in a [BMIM]PF₆ melt [Eq. (14)].



Compared with the reaction in toluene (TOF = 297 h⁻¹) a slightly improved activity (TOF = 333 h⁻¹) was achieved. In addition the biphasic procedure allows a simple product isolation. However, a slight leaching of the catalyst into the organic phase was observed. The use of a monosulfonated triphenylphosphane (tppms) ligand was able to suppress this

completely but the activity of the system was significantly reduced (TOF = 59 h⁻¹).

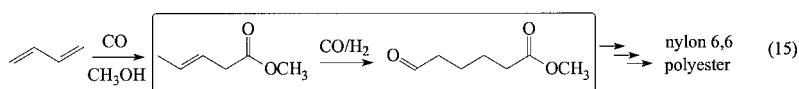
This result gives rise to the question whether the observed deactivation with the tppms ligand is a result of the ionic liquid solvent or an effect of the sulfonated ligand. We have therefore investigated in our laboratories the application of other ionic ligands for the hydroformylation in ionic liquids. Cationic cobaltocenium diphosphane ligands proved to be particularly successful in the biphasic hydroformylation of 1-octene in [BMIM]PF₆ (Scheme 4).^[78] The ligands used for



Scheme 4. Biphasic, Rh-catalyzed hydroformylation of 1-octene in 1-*n*-butyl-3-methylimidazolium (BMIM) hexafluorophosphate using a cationic cobaltoceniumdiphosphane ligand.

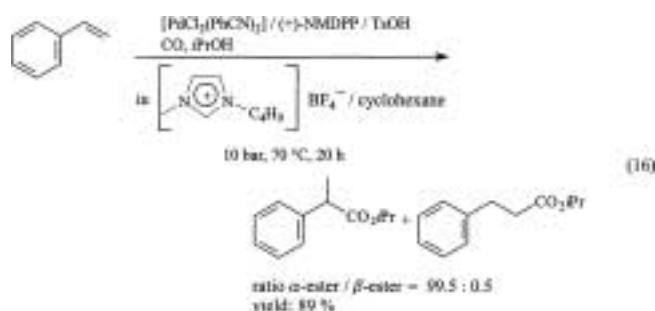
our studies have been developed and synthesized by Salzer and Brasse.^[79] Especially with the ligand 1,1'-bis(diphenylphosphanyl)cobaltocenium hexafluorophosphate the system shows activities that are at least remarkable for the biphasic hydroformylation of 1-octene (TOF = 810 h⁻¹). The selectivity for the linear aldehyde (*n*:*iso*: 16.2:1) was found to be in a technically interesting range, too. The catalyst leaching into the organic layer was less than 0.5 % and the recyclability of the ionic liquid catalyst solution could be proved in principle. Evidently, the Rh-catalyzed, biphasic hydroformylation of long-chain α -olefins in ionic liquids is possible in a highly active and selective manner if suitable (cationic) ligands are used.

Interestingly not only biphasic hydroformylation reactions result in process engineering advantages if ionic liquids are applied. In the monophasic hydroformylation of methyl-3-pentenoate our group succeeded, by the use of [BMIM]PF₆ as the solvent, to stabilize the rhodium catalyst under the harsh product distillation conditions (0.2 mbar vacuum, 110 °C) in the reactor. The ionic catalyst phase was recycled ten times without significant loss in activity.^[80] The total productivity of the rhodium catalyst used in this case could be increased tenfold in this way. The reaction has industrial significance as a step of an alternative synthesis route to produce adipic acid from butadiene [Eq. (15)].



4.4. Alkoxy-carbonylations

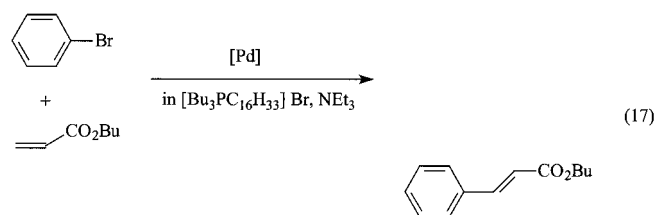
An interesting biphasic example of the palladium-catalyzed alkoxy-carbonylation of styrene and styrene derivatives was published by Monteiro et al.^[18a] In the system BMIM tetrafluoroborate/cyclohexane, styrene, isopropyl alcohol, and carbon monoxide to react to form 2-isopropyl phenylpropionate, for example. With (+)-neomenthylphosphine ((+)-NMDPP) as the ligand, the product was obtained in high yield and very good regioselectivity. Despite the chiral phosphine ligands, the observed asymmetric induction was, however, very low (*ee* < 5%) [Eq. (16)]. The



ionic liquid allowed simplified product isolation due to the biphasic reaction procedure. Reuse of the ionic catalyst solution obtained by phase separation only succeeded if the conversion was previously restricted to <35%. With complete conversion of the substrate, the authors observed the partial or complete decomposition of the active palladium catalyst.

4.5. Heck Reactions

The use of ionic liquids as reaction media for the palladium-catalyzed Heck reaction was first described by Kaufmann et al. in 1996.^[81] The reaction of bromobenzene with butyl acrylate to butyl *trans*-cinnamate succeeded in high yield in molten tetraalkylammonium and tetraalkylphosphonium bromide salts [Eq. (17)]. The authors describe a stabilizing effect



of the ionic liquid on the palladium catalyst. In almost all reactions no precipitation of elemental palladium was observed even at complete conversion of the aromatic halide. The reaction products were isolated by distillation from the nonvolatile ionic liquid.

Extensive studies on the Heck reaction in low melting salts have been recently presented by Hermann and Böhm.^[82] Their results indicate that the application of ionic solvents

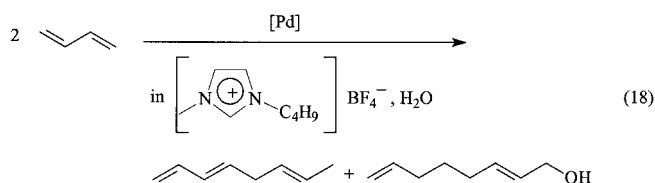
show clear advantages over commonly used organic solvents (such as DMF) especially for the conversion of the industrially interesting chloroarenes. With almost all tested catalyst systems an additional activation and stabilization was observed. Molten [NBu₄]Br (m.p. 103 °C) proved to be a particularly suitable reaction medium among the ionic solvent systems under investigation. In the reaction of bromobenzene with styrene using diiodobis(1,3-dimethylimidazolin-2-ylidene)palladium(II) as catalyst the yield of stilbene could be increased from 20% (DMF) to over 99% ([NBu₄]Br) under otherwise identical conditions. Again, a distillative product separation from the nonvolatile ionic catalyst solution was possible. The latter could be reused up to thirteen times without significant drop in activity. Additional advantages of the new solvent concept arise from the excellent solubility of all reacting molecules in the ionic solvent and the possibility to use cheap inorganic bases. The authors conclude that the application of ionic solvents could represent a standard procedure for Heck reactions in the future.

Other examples of the Heck reaction in ionic solvents were investigated by Seddon's group.^[83] They described the option of a work-up procedure in the three-phase system [BMIM]PF₆/water/hexane. While the used catalyst [(BMIM)₂PdCl₄] remains in the ionic liquid, the products dissolve in the organic layer. The salt formed as a by-product of the reaction ([Hbase]⁺X⁻) is extracted into the aqueous phase. Interestingly, the authors observed significant differences in reactivity between the application of either imidazolium salts or pyridinium salts in the Heck reaction. They assume the abstraction of the 2-H-hydrogen atom at the imidazolium cation by the base of the Heck reaction and the formation of palladium-carbene complexes.

The in situ formation of palladium-carbene complexes in imidazolium melts under the reaction conditions of the Heck reaction was recently confirmed by a publication of Xiao et al.^[65] They described a significantly enhanced reactivity of the Heck reaction in [BMIM]Br in comparison to the same reaction in [BMIM]BF₄ and explained this difference with the fact that only in the bromide melt the formation of palladium-carbenes was observed. From the bromide ionic liquid they could isolate and characterize the carbene complexes. The isolated complexes proved to be active catalysts in the Heck reaction when redissolved in [BMIM]Br.

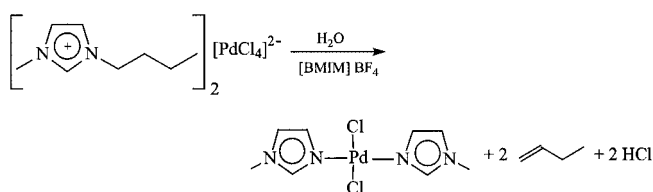
4.6. Hydrodimerizations/Telomerizations

Dupont et al. investigated the hydrodimerization/telomerization of 1,3-butadiene with palladium(II) compounds in [BMIM]BF₄ melts.^[84] In addition to 1,3,6-octatriene, the telomer octa-2,7-dien-1-ol was obtained [Eq. (18)]. The



activity of the catalyst was given with a turnover frequency (TOF) of 118 h^{-1} and could be increased to 204 h^{-1} by operating under CO_2 pressure. Interestingly, the reaction takes place in a monophasic reaction system at 70°C ; cooling to 5°C induces the formation of an ionic catalyst phase and a product phase. In this way, simple product isolation becomes possible and the ionic catalyst phase can be recovered.

One of the catalyst precursors used for this reaction, the complex $[(\text{BMIM})_2\text{PdCl}_4]$, was analyzed by X-ray spectroscopy. The authors describe the activation of this catalyst complex via a palladium(IV) compound, which is formed by oxidative addition of the imidazolium nitrogen atom and the alkyl group with cleavage of the C–N bond of the [BMIM] ion leading to a bis(methylimidazole)dichloropalladate (Scheme 5). This reaction was only observed in the presence of water, however.

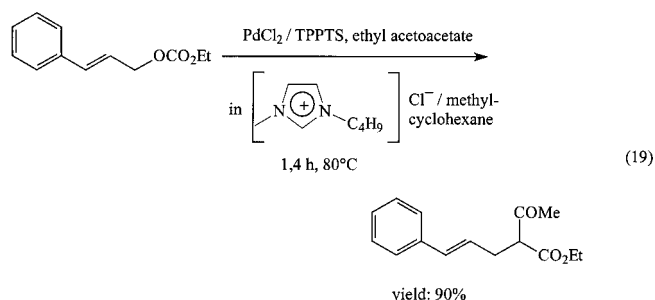


Scheme 5. Formation of the active catalyst from $[(\text{BMIM})_2\text{PdCl}_4]$ for the hydrodimerization of 1,3-butadiene.

4.7. Trost–Tsuji Couplings

The nucleophilic, allylic substitution catalyzed by palladium(0) complexes is an attractive way to form C–C bonds in organic synthesis. The reaction could be successfully carried out in ionic liquids as well. Xiao et al. described the monophasic reaction of 3-acetoxy-1,3-diphenylprop-1-ene with dimethyl malonate in $[\text{BMIM}]\text{BF}_4$.^[85] The reaction proceeded in 5 h (80°C) to complete conversion with $\text{Pd}(\text{OAc})_2/\text{PPh}_3$ (1/4) as catalyst system and K_2CO_3 as base. The desired coupling product could be isolated in 91 % yield. The possibility of generating the nucleophile in situ is regarded as a special advantage of the use of the ionic liquid solvent.

de Bellefon et al. investigated biphasic Trost–Tsuji coupling reactions.^[86] They converted ethyl cinnamyl carbonate with ethyl acetoacetate in $[\text{BMIM}]\text{Cl}$ /methylcyclohexane and compared the results to the identical reaction in the system butyronitrile/water [Eq. (19)]. Evidently, the reaction in the ionic catalyst solvent shows clear advantage over the reaction in the aqueous biphasic system. An enhancement of the



catalytic activity by a factor of ten is observed in the ionic liquid mainly due to the much better solubility of the substrate molecules in the ionic liquid. Furthermore, the reaction in $[\text{BMIM}]\text{Cl}$ /methylcyclohexane shows significantly improved selectivity since the formation of cinnamyl alcohol (by reaction of water as nucleophile) and the formation of phosphonium salts (by reaction of the Pd-allyl complex with trisulfonated triphenylphosphane (tppts) as ligand) is suppressed and very much decreased, respectively, in the ionic liquid.

4.8. Oligomerizations

Many cationic transition metal complexes are known to be excellent oligomerization catalysts.^[87] However, these complexes are often poorly soluble in unpolar solvents. With common organic solvents this situation usually requires a compromise between the solvation and the coordination properties of the solvent used. In order to achieve sufficient solubility of the metal complex a solvent of higher polarity is requested that may compete with the substrate for the coordination sites at the catalytic center. In this context some ionic liquids—especially those with chloroaluminate, hexafluorophosphate, and tetrafluoroborate ions—offer a new perspective due to their ability to combine a certain solvent polarity with weak coordination to the metal centre in a unique way.

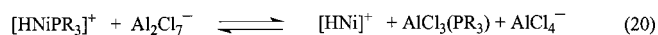
In our group we investigated, for example, the ethylene oligomerization with $(\eta^3\text{-methallyl})[\text{bis}(\text{diphenylphosphanyl})\text{-methane-monoxide-}\kappa^2\text{-P,O}]\text{nickel(II) hexafluoroantimonate}$ $[(\eta^3\text{-methallyl})\text{Ni}(\text{dppmO})]\text{SbF}_6$ as catalyst in different solvents. CH_2Cl_2 proved thereby to be the best choice among the organic solvents studied.^[88] By using the ionic liquid $[\text{BMIM}]\text{PF}_6$ the activity of the cationic Ni complex could be increased by about a factor seven.^[85] The overall selectivity of the biphasic reaction to linear α -olefins was as high as 88 % which is even slightly higher than found in the monophasic reaction in CH_2Cl_2 .

In tetrafluoroborate and hexafluorophosphate melts, the Pd-catalyzed dimerization of butadiene, for example, was performed as well.^[18b] Again, the use of the ionic liquid enabled a biphasic reaction procedure. In addition, the authors observed a substantial increase in activity of the catalyst in comparison to the reaction in tetrahydrofuran.

The nickel-catalyzed oligomerization of short-chain alkenes in chloroaluminate melts is one of the best investigated applications of transition metal catalysts in ionic liquids up to the present. As early as 1990, Chauvin et al. published the first investigations of the dimerization of propene in ionic liquids of the type $[\text{BMIM}]\text{Cl}/\text{AlCl}_3/\text{AlEtCl}_2$.^[12] Related systems have been used later for the oligomerization of ethene^[90] and butenes.^[91]

In general, the Ni-catalyzed oligomerization in chloroaluminate melts deserves particular attention since it is proposed for commercialization under the name “Difasol process” by the Institut Français du Pétrole (IFP).^[36, 92] The first industrial application of ionic liquids is therefore in sight.

Some detailed aspects of this reaction are introduced in the following example of the dimerization of propene (Table 9).^[12, 28a, 93] In basic melts (Table 9, entry a) no dimerization activity is observed. Presumably the basic chloride ions prevent the formation of free coordination sites on the nickel catalyst. In acidic chloroaluminate melts, an oligomerization reaction takes place even in the absence of a nickel catalyst (Table 9, entry b). However, not the desired dimers but a mix of different oligomers formed by cationic oligomerization reactions is obtained. Superacid protons and the reactivity of the acidic anions Al_2Cl_7^- and $\text{Al}_3\text{Cl}_{10}^-$ are discussed as cause for this reactivity.^[12, 60] The addition of alkylaluminum compounds suppresses this unwanted cationic oligomerization activity completely. In the presence of NiCl_2 as catalytic precursor, the ionic catalyst solution formed shows good activity in the dimerization of propene (Table 9, entry c). Without additional phosphane ligands however, a product distribution is obtained with no particular selectivity to the valuable highly branched products. With additional phosphane ligands, the product distribution depends on the steric demands of the ligand in question (Table 9, entry d). This corresponds well to results of earlier investigations by Wilke and Bogdanović in organic solvents.^[94] Selectivities to the valuable highly branched dimer, 2,3-dimethylbutene, of up to 83% are achieved. At longer reaction times, however, a decrease in the selectivity to highly branched products is observed. It has been postulated that a competing reaction of the basic phosphane ligand with the hard Lewis acid AlCl_3 takes place [Eq. (20)]. This assumption is supported by the observation that the addition of a soft competing base such as tetramethylbenzene can prevent the loss in selectivity.



Unfortunately, investigations with ionic liquids containing high amounts of AlEt_2Cl_2 reveal several limitations: The reductive effect of the alkylaluminum compound affects the temperature stability of the nickel catalyst. At very high alkylaluminum concentrations a precipitation of black metallic nickel is observed even at room temperature. In addition it has been observed with longer reaction times that small amounts of the alkylaluminum compound leach into the organic phase. This changes the composition and the chemical properties of the ionic liquid. At the border between the two phases the Equilibria (21) and (22) have been assumed.^[28]

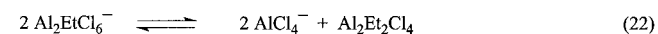
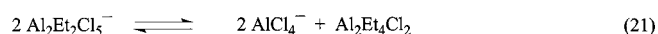


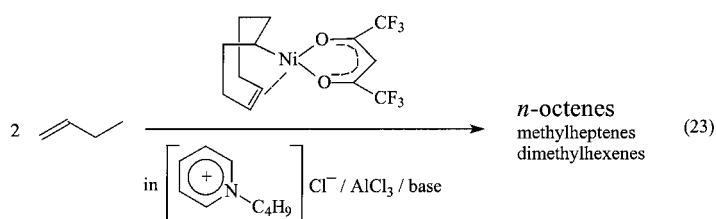
Table 9. Results for the dimerization of propene in ionic liquids at -15°C .

Entry	Ionic liquid	Composition	Ni complex	Aktivität [$\text{kg g}(\text{Ni})^{-1} \text{h}^{-1}$]	Product ratio DMB/M2P/nHex ^[a]
a)	[BMIM]Cl/ AlCl_3	1/0.8	$[\text{NiBr}_2\text{L}_2]^{\text{[b]}}$	0	
b)	[BMIM]Cl/ AlCl_3	1/1.5	–	– ^[c]	
c)	[BMIM]Cl/ AlEt_2Cl_2	1/1.2	NiCl_2	2.5	5/74/21
d)	[BMIM]Cl/ AlEt_2Cl_2	1/1.2	$[\text{NiCl}_2(\text{iPr}_3\text{P})_2]$	2.5	74/24/2
e)	[BMIM]Cl/ $\text{AlCl}_3/\text{AlEt}_2\text{Cl}_2$	1/1.2/0.1	$[\text{NiCl}_2(\text{iPr}_3\text{P})_2]$	12.5	83/15/2

$T = -15^\circ\text{C}$. [a] DMB = dimethylbutene, M2P = methylpentene, nHex = n-hexene. [b] L = 2-methylallyl. [c] Highly viscous cationic oligomers were obtained.

Despite this, the biphasic IFP “Difasol” process, which uses chloroaluminate ionic liquids with small amounts of alkylaluminum compounds as catalyst, offers significant advantages over the industrially realized, homogeneous one-phase Dimersol process (25 Dimersol units are currently in operation producing octane booster for gasoline with a total processing capacity of 3.4 million tons per year).^[92b] According to IFP, the novel ionic liquid process reduces drastically the consumption of Ni catalyst and alkylaluminum compounds. Additional advantages arise from the good performance obtained with highly diluted feedstocks and the significantly improved dimer selectivity of the biphasic ionic liquid process.^[92]

In our group we have investigated the applicability of chloroaluminate ionic liquids as solvents for the linear dimerization of 1-butene with the catalyst (η -4-cycloocten-1-yl)(1,1,1,5,5,5-hexafluoro-2,4-pentanedionato-*O,O'*)nickel [(Hcod)Ni(hfacac)] according to [Eq. (23)] (Hcod = cyclooct-4-ene-1-yl). Hereby ionic liquids containing alkylaluminum



compounds proved to be not suitable due to their strong isomerization activity.^[91] Since only the α -olefin can be linked to form linear octenes, isomerization activity of the solvent inhibits the formation of the desired product.

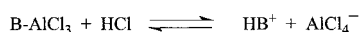
We have therefore developed chloroaluminate melts that enable selective nickel-catalyzed C–C linkage in ionic liquids without the addition of alkylaluminum compounds.^[60, 95] When weak organic bases such as quinoline or pyrrole are added to an acidic chloroaluminate melt, a reaction medium is obtained in which the Ni catalyst is much more active than in toluene, with only slightly lower linear selectivity (Table 10). The function of the added base is to buffer all the acid species in the ionic liquid that could catalyze the unselective, cationic oligomerization reaction (Scheme 6).

In addition to activation of [(Hcod)Ni(hfacac)] in the ionic liquid, we were principally interested in aspects of lifetime and overall activity of the ionic catalyst system. A continuous flow loop reactor was constructed for this purpose in our laboratories (Figure 8).^[96] The ionic catalyst solution is placed in the loop at the start of reaction and the loop is filled with reactant. During the experiment, reactant is continuously

Table 10. Comparison of the linear dimerization of 1-butene with the [(Hcod)Ni(hfacac)] in toluene and in chloroaluminate melts.

Reaction in toluene	Reaction in [4-MBP]Cl/AlCl ₃ /quinoline (0.43/0.53/0.04) ^[a]
<ul style="list-style-type: none"> ● single phase ● no activity of the catalyst at < 50 °C ● results at 90 °C^[b] TOF = 500 h⁻¹ dimer selectivity 85 % linear selectivity 75 % 	<ul style="list-style-type: none"> ● biphasic, no detectable leaching of the catalyst ● obvious activity even at -10 °C ● results at 25 °C^[b] TOF = 1240 h⁻¹ dimer selectivity 98 % linear selectivity 64 %

[a] 4-MBP = 1-*n*-butyl-4-methylpyridinium ion. [b] At 20 % conversion.



Scheme 6. Suppression of cationic side reactions in acidic chloroaluminate melts by addition of a weak organic base B.

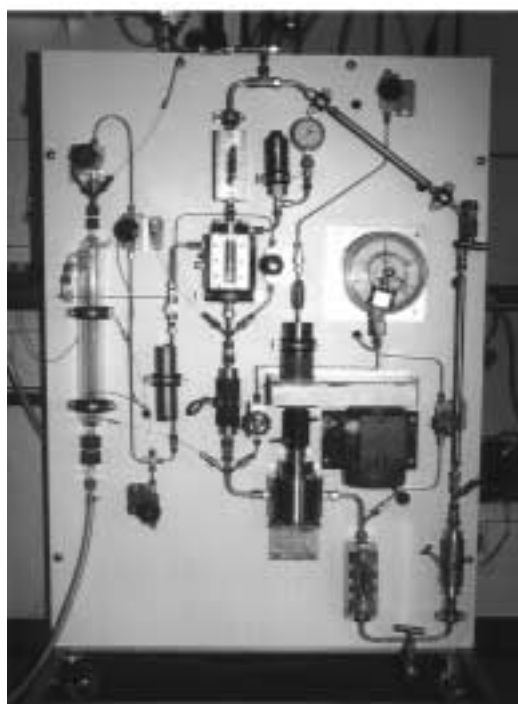
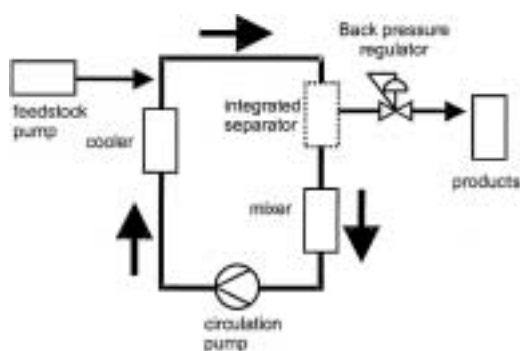


Figure 8. Schematic representation and view of a loop reactor for the investigation of the lifetime of ionic transition metal catalyst solutions.

refilled. The ionic catalyst solution and the organic product phase are separated in an integrated separator within the reactor loop. Since the ionic catalyst solution is present in the

reactor loop at all times, any changes in the system can be registered by means of the collected products without time delay. Continuous experiments on linear dimerization of 1-butene resulted in an overall activity (turnover number) of over 18000 for the [(Hcod)Ni(hfacac)] catalyst.^[97]

5. Summary and Outlook

Ionic liquids represent a unique class of new reaction media for transition metal catalysis. Their nonvolatile nature enables significant engineering advantages for distillative product separation and prevents uncontrolled evaporation. The possibility to specifically vary their physical and chemical properties make them ideal candidates for applications in biphasic catalysis.

The advantages mentioned above can be used in many applications to minimize solvent and catalyst consumption. Therefore it is highly justified to discuss ionic liquids as “green solvents”.^[36, 68] In this respect, ionic liquids complete in a very attractive manner alternative „green solvent“ concepts like water or supercritical CO₂. While supercritical CO₂ covers applications commonly using unpolar solvents, ionic liquids can be considered as replacements for polar organic solvents. First results showing that both concepts can be combined successfully have already been published.^[49]

Compared to water, ionic liquids will be—even in a long-term view—significantly more expensive. Therefore, they will be mainly used in those applications where aqueous systems are not possible or show serious drawbacks. In this context, the reactivity of water with many active catalyst complexes has to be considered as a limiting factor. Additionally, many substrates show low solubility in water.

In many applications ionic liquids with weakly coordinating anions and suitable substituted cations are attractive alternative „solutions“ to commonly used solvents. Switching from an organic solvent to an ionic reaction medium often results in an altered chemical reactivity of the dissolved catalyst. The examples presented show that well-known reactions can be accelerated in suitable ionic solutions and can proceed with improved selectivities. In some cases an increased stability of the catalyst is observed in the ionic liquid. In addition, the unusual properties of ionic liquids appear to possess enormous potential for transition metal catalysis: The formation of liquid crystal phases in some ionic liquids is, for example, well-known^[1, 17a,d] and recently indications for an ordered surface structure of ionic liquids have been reported.^[98] Will this enable new possibilities for the investigation of transition metal catalysts in highly ordered solvents? Is it possible to use the electrochemical properties of ionic liquids to actively maintain transition metal catalysts in certain unusual oxidation states? The use of ionic liquids as solvents for transition metal catalysis opens up a wide field for future investigations.

Investigations cited here from our working group were supported by BP Amoco Chemicals, the European Community under the BRITE 96-3745 project, the Max-Buchner Foundation, and the Ministerium für Schule und Weiterbildung, Wissenschaft und Forschung des Landes Nordrhein-Westfalen within the framework of the Katalyseverbundes Nordrhein-Westfalen. The authors also thank Dr. M. Eichmann, Dr. H. Waffenschmidt, M. Sesing, and H. Wolff for their contributions to the manuscript. Fruitful advice from Prof. Ken Seddon, especially at the beginning of our work with ionic liquids, is gratefully acknowledged.

Received: March 15, 1999 [A 333]

- [1] a) K. R. Seddon, *J. Chem. Tech. Biotechnol.* **1997**, 68, 351–356; b) K. R. Seddon, *Kinet. Catal. Engl. Transl.* **1996**, 37, 693–697.
- [2] a) W. Sundermeyer, *Angew. Chem.* **1965**, 77, 241–258; *Angew. Chem. Int. Ed. Engl.* **1965**, 4, 222–239; b) W. Sundermeyer, *Chem. Unserer Zeit* **1967**, 1, 150–157; c) S. V. Volkov, *Chem. Soc. Rev.* **1990**, 19, 21–28.
- [3] S. Sugden, H. Wilkins, *J. Chem. Soc.* **1929**, 1291–1298, and references therein.
- [4] I.-M. Herford, H. Schneider, *Liebigs Ann. Chem.* **1991**, 27–31.
- [5] a) F. H. Hurley, U.S. Patent 2,446,331, **1948** [*Chem. Abstr.* **1949**, 43, P7645b]; b) F. H. Hurley, T. P. Wier, Jr., *J. Electrochem. Soc.* **1951**, 98, 207–212.
- [6] a) H. L. Chum, V. R. Koch, L. L. Miller, R. A. Osteryoung, *J. Am. Chem. Soc.* **1975**, 97, 3264–3265; b) J. Robinson, R. A. Osteryoung, *J. Am. Chem. Soc.* **1979**, 101, 323–327; c) J. S. Wilkes, J. A. Levisky, R. A. Wilson, C. L. Hussey, *Inorg. Chem.* **1982**, 21, 1263–1264.
- [7] C. G. Swain, A. Ohno, D. K. Roe, R. Brown, T. Maugh II, *J. Am. Chem. Soc.* **1967**, 89, 2648–2649.
- [8] a) T. B. Scheffler, C. L. Hussey, K. R. Seddon, C. M. Kear, P. D. Armitage, *Inorg. Chem.* **1983**, 22, 2099–2100; b) T. M. Laher, C. L. Hussey, *Inorg. Chem.* **1983**, 22, 3247–3251; c) T. B. Scheffler, C. L. Hussey, *Inorg. Chem.* **1984**, 23, 1926–1932; d) P. B. Hitchcock, T. J. Mohammed, K. R. Seddon, J. A. Zora, C. L. Hussey, E. H. Ward, *Inorg. Chim. Acta* **1986**, 113, L25–L26.
- [9] a) D. Appleby, C. L. Hussey, K. R. Seddon, J. E. Turp, *Nature* **1986**, 323, 614–616; b) A. J. Dent, K. R. Seddon, T. Welton, *J. Chem. Soc. Chem. Commun.* **1990**, 315–316.
- [10] J. A. Boon, J. A. Levisky, J. L. Pflug, J. S. Wilkes, *J. Org. Chem.* **1986**, 51, 480–483.
- [11] S. E. Fry, N. J. Pienta, *J. Am. Chem. Soc.* **1985**, 107, 6399–6400.
- [12] Y. Chauvin, B. Gilbert, I. Guibard, *J. Chem. Soc. Chem. Commun.* **1990**, 1715–1716.
- [13] R. T. Carlin, R. A. Osteryoung, *J. Mol. Catal.* **1990**, 63, 125–129.
- [14] J. S. Wilkes, M. J. Zaworotko, *J. Chem. Soc. Chem. Commun.* **1992**, 965–967.
- [15] Y. Chauvin, L. Mußmann, H. Olivier, *Angew. Chem.* **1995**, 107, 2941–2943; *Angew. Chem. Int. Ed. Engl.* **1995**, 34, 2698–2700.
- [16] a) P. Bonhôte, A.-P. Dias, N. Papageorgiou, K. Kalyanasundaram, M. Grätzel, *Inorg. Chem.* **1996**, 35, 1168–1178; b) J. H. Davis, Jr., K. J. Forrester, *Tetrahedron Lett.* **1999**, 40, 1621–1622; c) J. H. Davis, Jr., K. J. Forrester, T. Merrigan, *Tetrahedron Lett.* **1998**, 39, 8955–8958; d) R. Hagiwara, T. Hirashige, T. Tsuda, Y. Ito, *J. Fluorine Chem.* **1999**, 99, 1–3; e) M. Hasan, I. V. Kozhevnikov, M. R. H. Siddiqui, A. Steiner, N. Winterton, *Inorg. Chem.* **1999**, 38, 5637–5641; f) W. Keim, W. Korth, P. Wasserscheid, WO 2000016902, **2000** [*Chem. Abstr.* **2000**, 132, P238691].
- [17] a) C. M. Gordon, J. D. Holbrey, A. R. Kennedy, K. R. Seddon, *J. Mater. Chem.* **1998**, 8, 2627–2636; b) P. A. Z. Suarez, S. Einloft, J. E. L. Dullius, R. F. de Souza, J. Dupont, *J. Chim. Phys.* **1998**, 95, 1626–1639; c) A. J. Carmichael, C. Hardacre, J. D. Holbrey, M. Nieuwenhuyzen, K. R. Seddon, *Anal. Chem.* **1999**, 71, 4572–4574; d) J. D. Holbrey, K. R. Seddon, *J. Chem. Soc. Dalton Trans.* **1999**, 2133–2140.
- [18] a) D. Zim, R. F. de Souza, J. Dupont, A. L. Monteiro, *Tetrahedron Lett.* **1998**, 39, 7071–7074; b) S. M. Silva, P. A. Z. Suarez, R. F. de Souza, J. Dupont, *Polymer Bull.* **1998**, 40, 401–405; c) P. J. Dyson, D. J. Ellis, D. G. Parker, T. Welton, *Chem. Commun.* **1999**, 25–26; d) C. M. Gordon, A. McCluskey, *Chem. Comm.* **1999**, 1431–1432; e) M. J. Earle, P. B. McCormac, K. R. Seddon, *Green Chemistry* **1999**, 1, 23–25; f) C. W. Lee, *Tetrahedron Lett.* **1999**, 40, 2461–2464; g) D. Crofts, P. J. Dyson, K. M. Sanderson, N. Srinivasan, T. Welton, *J. Organomet. Chem.* **1999**, 573, 292–298; h) T. Fischer, A. Sethi, T. Welton, J. Woolf, *Tetrahedron Lett.* **1999**, 40, 793–796; i) R. Y. Saleh, WO 2000015594, **2000** [*Chem. Abstr.* **2000**, 132, P222341]; j) C. J. Adams, M. J. Earle, K. R. Seddon, *Green Chemistry* **2000**, 2, 21–23; k) L. Green, I. Hemeon, R. D. Singer, *Tetrahedron Lett.* **2000**, 41, 1343–1346.
- [19] T. Welton, *Chem. Rev.* **1999**, 99, 2071–2083.
- [20] J. D. Holbrey, K. R. Seddon, *Clean Products and Processes* **1999**, 1, 223–226.
- [21] R. L. Hussey in *Chemistry of Nonaqueous solutions* (Eds.: G. Mamantov, A. I. Popov), VCH, Weinheim, **1994**, pp. 227–276.
- [22] a) R. T. Carlin, J. S. Wilkes in *Chemistry of Nonaqueous Solutions* (Eds.: G. Mamantov, A. I. Popov), VCH, Weinheim, **1994**, pp. 277–306; b) C. L. Hussey, *Pure Appl. Chem.* **1988**, 60, 1763–1772.
- [23] a) Imidazolium salts with longer alkyl chains: A. A. K. Abdul-Sada, P. W. Ambler, P. K. G. Hodgson, K. R. Seddon, N. J. Steward, WO 95/21871, **1995** [*Chem. Abstr.* **1995**, 123, P341298k]; b) ammonium salts: R. H. Dubois, M. J. Zaworotko, P. S. White, *Inorg. Chem.* **1989**, 28, 2019–2020; c) phosphonium salts: J. F. Knifton, *J. Mol. Catal.* **1987**, 43, 65–78; d) trialkylammonium salts: C. P. M. Lacroix, F. H. M. Dekker, A. G. Talma, J. W. F. Seetz, EP 989134, **1998** [*Chem. Abstr.* **2000**, 132, 237092].
- [24] N. Karodia, S. Guise, C. Newlands, J.-A. Andersen, *Chem. Commun.* **1998**, 2341–2342.
- [25] H. Waffenschmidt, Dissertation, RWTH Aachen, Germany, **2000**.
- [26] H. A. Øye, M. Jagtoyen, T. Oksefjell, J. S. Wilkes, *Mater. Sci. Forum* **1991**, 73–75, 183–189.
- [27] a) Z. J. Karpinski, R. A. Osteryoung, *Inorg. Chem.* **1984**, 23, 1491–1494; b) A. A. K. Abdul-Sada, A. M. Greenway, K. R. Seddon, T. Welton, *Org. Mass Spectrom.* **1993**, 28, 759–765.
- [28] a) Y. Chauvin, S. Einloft, H. Olivier, *Ind. Eng. Chem. Res.* **1995**, 34, 1149–1155; b) B. Gilbert, Y. Chauvin, H. Olivier, F. Di Marco—Van Tiggelen, *J. Chem. Soc. Dalton Trans.* **1995**, 3867–3871.
- [29] S. D. Williams, J. P. Schoebrechts, J. C. Selkirk, G. Mamantov, *J. Am. Chem. Soc.* **1987**, 109, 2218–2219.
- [30] Y. Chauvin, H. Olivier-Bourbigou, *CHEMTECH* **1995**, 25, 26–30.
- [31] a) G. W. Parshall, *J. Am. Chem. Soc.* **1972**, 94, 8716–8719; b) G. Ling, N. Koura, *Denki Kagaku oyobi Kogyo Butsuri Kagaku* **1997**, 65, 149–153; c) H. Waffenschmidt, P. Wasserscheid, *J. Mol. Catal.* accepted.
- [32] P. A. Z. Suarez, J. E. L. Dullius, S. Einloft, R. F. de Souza, J. Dupont, *Polyhedron*, **1996**, 15, 1217–1219.
- [33] J. Fuller, R. T. Carlin, H. C. de Long, D. Haworth, *J. Chem. Soc. Chem. Commun.* **1994**, 299–300.
- [34] W. T. Ford, R. J. Hauri, D. J. Hart, *J. Org. Chem.* **1973**, 38, 3916–3918.
- [35] S. P. Zingg, A. S. Dworkin, M. Sorlie, D. M. Chapman, A. C. Buchanan, G. P. Smith, *J. Electrochem. Soc.* **1984**, 131, 1602–1608.
- [36] M. Freemantle, *Chem. Eng. News* **1998**, 76, 32–37.
- [37] *CRC Handbook of Chemistry and Physics*, 73th ed. (Ed.: D. R. Lide), CRC Press, Boca Raton, **1992**.
- [38] A. Elaiwi, P. B. Hitchcock, K. R. Seddon, N. Srinivasan, Y.-M. Tan, T. Welton, J. A. Zora, *J. Chem. Soc. Dalton Trans.* **1995**, 3467–3472.
- [39] H. Stegemann, A. Rhode, A. Reiche, A. Schnittke, H. Füllbier, *Electrochim. Acta* **1992**, 37, 379–383.
- [40] A. A. Fannin, Jr., D. A. Floreani, L. A. King, J. S. Landers, B. J. Piersma, D. J. Stech, R. L. Vaughn, J. S. Wilkes, J. L. Williams, *J. Phys. Chem.* **1984**, 88, 2614–2621.
- [41] M. L. Mutch, J. S. Wilkes, *Proc. Electrochem. Soc.* **1998**, 98, 254–260.
- [42] J. R. Sanders, E. H. Ward, C. L. Hussey, *J. Electrochem. Soc.* **1986**, 133, 325–330.
- [43] S. Tait, R. A. Osteryoung, *Inorg. Chem.* **1984**, 23, 4352–4360.
- [44] C. J. Dymek, D. A. Grossie, A. V. Fratini, W. W. Adams, *J. Mol. Struct.* **1989**, 213, 25–34.
- [45] R. A. Mantz, P. C. Trulove, R. T. Carlin, R. A. Osteryoung, *Inorg. Chem.* **1995**, 34, 3846–3847.
- [46] J. Fuller, R. T. Carlin, R. A. Osteryoung, *J. Electrochem. Soc.* **1997**, 144, 3881–3886.

- [47] a) R. L. Perry, K. M. Jones, W. D. Scott, Q. Liao, C. L. Hussey, *J. Chem. Eng. Data* **1995**, *40*, 615–619; b) Q. Liao, C. L. Hussey, *J. Chem. Eng. Data* **1996**, *41*, 1126–1130; c) P. Wasserscheid, Dissertation, RWTH Aachen, Germany, **1998**.
- [48] a) J. G. Huddleston, H. D. Willauer, R. P. Swatloski, A. E. Visser, R. D. Rogers, *Chem. Commun.* **1998**, 1765–1766; b) A. E. Visser, R. P. Swatloski, R. D. Rogers, *Green Chemistry* **2000**, *2*, 1–4.
- [49] L. A. Blanchard, D. Hancu, E. J. Beckman, J. F. Brennecke, *Nature* **1999**, *399*, 28–29.
- [50] C. Reichardt, *Nachr. Chem. Tech. Lab.* **1997**, *45*, 759–763.
- [51] K. Dimroth, C. Reichardt, T. Siepmann, F. Bohlmann, *Liebigs Ann. Chem.* **1963**, *661*, 1–37.
- [52] C. Reichardt, *Chem. Rev.* **1994**, *94*, 2319–2358.
- [53] C. Reichardt, E. Harbusch-Görnert, *Liebigs Ann. Chem.* **1983**, 721–743.
- [54] S. K. Poole, P. H. Shetty, C. F. Poole, *Anal. Chim. Acta* **1989**, *218*, 241–263.
- [55] C. Gordon, personal communication.
- [56] D. W. Armstrong, L. He, Y.-S. Liu, *Anal. Chem.* **1999**, *71*, 3873–3876.
- [57] a) T. J. Melton, J. Joyce, J. T. Meloy, J. A. Boon, J. S. Wilkes, *J. Electrochem. Soc.* **1990**, *137*, 3865–3869; b) C. Scordilis-Kelley, J. Fuller, R. T. Carlin, J. S. Wilkes, *J. Electrochem. Soc.* **1992**, *139*, 694–699.
- [58] a) I. C. Quarmby, R. A. Mantz, L. M. Goldenberg, R. A. Osteryoung, *Anal. Chem.* **1994**, *66*, 3558–3561; b) I. C. Quarmby, R. A. Osteryoung, *J. Am. Chem. Soc.* **1994**, *116*, 2649–2650.
- [59] P. Koronaios, D. King, R. A. Osteryoung, *Inorg. Chem.* **1998**, *37*, 2028–2032.
- [60] B. Ellis, W. Keim, P. Wasserscheid, *Chem. Commun.* **1999**, 337–338.
- [61] a) G. P. Smith, A. S. Dworkin, R. M. Pagni, S. P. Zingg, *J. Am. Chem. Soc.* **1989**, *111*, 525–530; b) M. Ma, K. E. Johnson, *J. Am. Chem. Soc.* **1995**, *117*, 1508–1513.
- [62] C. L. Hussey, *Adv. Molten Salt Chem.* **1983**, *5*, 185–230.
- [63] J. Howarth, K. Hanlon, D. Fayne, P. McCormac, *Tetrahedron Lett.* **1997**, *38*, 3097–3100.
- [64] a) A. J. Arduengo, R. L. Harlow, M. Kline, *J. Am. Chem. Soc.* **1991**, *113*, 361–363; b) A. J. Arduengo, H. V. R. Dias, R. L. Harlow, M. Kline, *J. Am. Chem. Soc.* **1992**, *114*, 5530–5534; c) G. T. Cheek, J. A. Spencer in *9th Int. Symp. on Molten Salts* (Eds.: C. L. Hussey, D. S. Newman, G. Mamantov, Y. Ito), The Electrochem. Soc., New York, **1994**, pp. 426–432.
- [65] L. Xu, W. Chen, J. Xiao, *Organometallics* **2000**, *19*, 1123–1127.
- [66] M. Tinkl, *Chem. Rundsch.* **1999**, *2*, 59.
- [67] Solvent Innovation GmbH: <http://www.solvent-innovation.com>.
- [68] a) M. Freemantle, *Chem. Eng. News* **1999**, *77*, 23–24; b) D. Bradley, *Chem. Ind.* **1999**, 86; c) M. Freemantle, *Chem. Eng. News* **2000**, *78*, 37–50.
- [69] P. A. Z. Suarez, J. E. L. Dullius, S. Einloft, R. F. de Souza, J. Dupont, *Inorg. Chim. Acta* **1997**, *255*, 207–209.
- [70] L. A. Müller, J. Dupont, R. F. de Souza, *Makromol. Chem. Rapid Commun.* **1998**, *19*, 409–411.
- [71] a) B. Drießen-Hölscher, J. Heinen, *J. Organomet. Chem.* **1998**, *570*, 141–146; b) J. Heinen, M. S. Tupayachi, B. Drießen-Hölscher, *Catalysis Today* **1999**, *48*, 273–278.
- [72] S. Steines, B. Drießen-Hölscher, P. Wasserscheid, *J. Prakt. Chem.* **2000**, *342*, 348–354.
- [73] A. L. Monteiro, F. K. Zinn, R. F. de Souza, J. Dupont, *Tetrahedron: Asymmetry* **1997**, *2*, 177–179.
- [74] P. A. Chaloner, M. A. Esteruelas, F. Joó, L. A. Oro, *Homogeneous Hydrogenation*, Kluwer, Dordrecht, **1994**.
- [75] C. E. Song, E. J. Roh, *Chem. Commun.* **2000**, 837–838.
- [76] P. Wasserscheid, W. Müller, C. Werth, A. Jess, unpublished results.
- [77] Y. Chauvin, H. Olivier, L. Mußmann, FR 95/14,147, **1995** [*Chem. Abstr.* **1997**, *127*, P341298k].
- [78] C. C. Brasse, U. Englert, A. Salzer, H. Waffenschmidt, P. Wasserscheid, *Organometallics*, accepted.
- [79] A. Salzer, C. C. Brasse, WO99/16776 **1999** [*Chem. Abstr.* **1999**, *130*, 267580x].
- [80] W. Keim, D. Vogt, H. Waffenschmidt, P. Wasserscheid, *J. Catal.* **1999**, *186*, 481–484.
- [81] D. E. Kaufmann, M. Nouroozian, H. Henze, *Synlett* **1996**, 1091–1092.
- [82] a) W. A. Herrmann, V. P. W. Böhm, *J. Organomet. Chem.* **1999**, *572*, 141–145; b) V. P. W. Böhm, W. A. Herrmann, *Chem. Eur. J.* **2000**, *6*, 1017–1025.
- [83] A. J. Carmichael, M. J. Earle, J. D. Holbrey, P. B. McCormac, K. R. Seddon, *Org. Lett.* **1999**, *1*, 997–1000.
- [84] J. E. L. Dullius, P. A. Z. Suarez, S. Einloft, R. F. de Souza, J. Dupont, J. Fischer, A. D. Cian, *Organometallics* **1998**, *17*, 815–819.
- [85] W. Chen, L. Xu, C. Chatterton, J. Xiao, *Chem. Commun.* **1999**, 1247–1248.
- [86] C. de Bellefon, E. Pollet, P. Grenouillet, *J. Mol. Catal.* **1999**, *145*, 121–126.
- [87] a) R. B. A. Pardy, I. Tkatschenko, *J. Chem. Soc. Chem. Commun.* **1981**, 49–50; b) J. R. Ascenso, M. A. A. F. De C. T. Carrando, A. R. Dias, P. T. Gomes, M. F. M. Piadade, C. C. Romao, A. Revillon, I. Tkatschenko, *Polyhedron* **1989**, *8*, 2449–2457; c) P. Grenouillet, D. Neibecker, I. Tkatschenko, *J. Organomet. Chem.* **1983**, *243*, 213–222; d) J.-P. Gehrke, R. Taube, E. Balbolov, K. Kurtev, *J. Organomet. Chem.* **1986**, *304*, C4–C6.
- [88] a) I. Brassat, Dissertation, RWTH Aachen (Germany) **1998**; b) I. Brassat, U. Englert, W. Keim, D. P. Keitel, S. Killat, G.-P. Suranna, R. Wang, *Inorg. Chim. Acta*, **1998**, *280*, 150–162.
- [89] P. Wasserscheid, C. Hilgers, W. Keim, unpublished results.
- [90] S. Einloft, F. K. Dietrich, R. F. de Souza, J. Dupont, *Polyhedron* **1996**, *15*, 3257–3259.
- [91] a) Y. Chauvin, H. Olivier, C. N. Wyrvalski, L. C. Simon, R. F. de Souza, *J. Catal.* **1997**, *165*, 275–278; b) L. C. Simon, J. Dupont, R. F. de Souza, *J. Mol. Catal.* **1998**, *175*, 215–220.
- [92] a) E. Burridge, *ECN Chemscape* **1999**, 27–28; b) H. Olivier, *J. Mol. Catal.* **1999**, *146*, 285–289.
- [93] Y. Chauvin, S. Einloft, H. Olivier, FR 93/11,381, **1996** [*Chem. Abstr.* **1995**, *123*, 144896c].
- [94] G. Wilke, B. Bogdanović, P. Hardt, P. Heimbach, W. Keim, M. Kröner, W. Oberkirch, K. Tanaka, E. Steinrück, D. Walter, H. Zimmermann, *Angew. Chem.* **1966**, *78*, 157–172; *Angew. Chem. Int. Ed. Engl.* **1966**, *5*, 151–164.
- [95] P. Wasserscheid, W. Keim, WO 9847616, **1997** [*Chem. Abstr.* **1998**, *129*, 332457h].
- [96] M. Eichmann, Dissertation, RWTH-Aachen, Germany, **1999**.
- [97] a) P. Wasserscheid, M. Eichmann, *Proc. 3rd. Int. Symp. Catal. in Multiphase Reactors*, Naples, **2000**, 249–261; b) M. Eichmann, P. Wasserscheid, *Catal. Today*, submitted; c) M. Eichmann, P. Wasserscheid, unpublished results.
- [98] T. J. Gannon, G. Law, P. R. Watson, A. J. Carmichael, K. R. Seddon, *Langmuir* **1999**, *15*, 8429–8434.

On Closed-Shell Interactions, Polar Covalences, d Shell Holes, and Direct Images of Orbitals: The Case of Cuprite

Response to the Essay by S. G. Wang and W. H. E. Schwarz

J. M. Zuo,* M. O'Keeffe, M. Kim, and J. C. H. Spence

In their critical Essay on the charge distribution in cuprite,^[1] Wang and Schwarz concluded that there is no proof of significant Cu⁺–Cu⁺ closed shell binding and disagreed with our interpretation of the nature of the Cu^I–O bonds. These conclusions are drawn from their approximate theoretical calculations and their purported agreement with the previous X-ray measurements, rather than from a careful reexamination of the experimental and theoretical evidence presented in our original report.^[2]

Much of the criticism of Wang and Schwarz is directed to statements made in the interpretation of our report.^[1] By quoting sentences which were not in the original text and commenting on them together with our original report, the authors confuse the scientific content of our original report with media chatter for which we cannot be held responsible. Putting these aspects aside, there are two main points worthy of serious discussion. Before we look into these in detail, it is helpful to recall the basic approximations in all electronic structure calculations: 1) the use of an approximate treatment for the exchange and correlation energy,^[3] and 2) the assumption of a static crystal that ignores the thermal motion of atoms. The limitation of the first approximation is well-known, a highly relevant example is its failure in predicting the correct antiferromagnetic ground states of Cu-based high-temperature superconductors.^[4] In addition to these two approximations, the calculations of Wang and Schwarz used a 25-atom cluster to approximate the three-dimensional infinite crystal.

Most crystals contain defects. The treatment of X-ray diffraction in a real crystal with defects is based on the mosaic

model, first introduced by Darwin in 1922.^[5] In this model, an ideal imperfect crystal is defined as one comprised of very small mosaic blocks with slightly different orientations. This is opposite to the ideal perfect crystal free of defects. Real crystals are often in between the ideally perfect and ideally imperfect models, and the measured X-ray integrated intensity is often less than predicted by the theory for ideally imperfect crystals (extinction) but larger than predicted by the theory for an ideal perfect crystal. An improved treatment of real crystals introduces a statistical distribution for the mosaic block orientations and also the size of mosaic blocks, and derives a formula for the averaged integrated intensities of diffracted beams.^[6, 7] The accuracy of such an averaged treatment ultimately depends on the defect distribution in the crystal, and is fundamentally limited in accuracy by the statistical fluctuations in the distribution of defects and by the oversimplification of the complex strain field introduced by defects with mosaic blocks.

By comparison, our electron diffraction measurements use the convergent beam electron diffraction (CBED) technique with a focused probe a few nanometers in diameter on a crystal of thickness from 100 to 200 nanometers. The crystal under the probe is selected free from defects by using electron imaging. Thus, electron diffraction within the probed volume can be described by the perfect crystal theory. The refinement procedure that we used for measuring electron structure factors compares experimental intensities with the Bloch wave theory of electron diffraction which takes the full account of primary extinction (multiple scattering) and absorption.^[8] As a result, the measured electron structure factors are free from extinction and absorption, and can be used directly in charge density analysis without corrections. It also allows us to assess the errors due to extinction in conventional X-ray data. The method has proved its accuracy, as demonstrated, for example, in Ref. [9].

Figure 1 shows the ratio R ($R = F_x/F_{fit}$) of as-measured X-ray data by Restori and Schwarzenbach^[10] and the structure factors obtained from our best multipole model fit as a function of Q [Eq. (1)]. For ideal imperfect crystals, the ratio should be a constant one. For strong low order reflections with

$$Q = \left| \frac{e^2 F}{m_e c^2 V} \right|^2 \frac{\lambda^3}{\sin 2\theta} \quad (1)$$

[*] Prof. J. M. Zuo,^[+] M. Kim, J. C. H. Spence

Department of Physics and Astronomy
Arizona State University
Tempe, AZ 85287 (USA)
E-mail: jianzuo@uiuc.edu

M. O'Keeffe
Department of Chemistry
Arizona State University
Tempe, AZ 85287 (USA)

[+] Present address:

Department of Materials Science and Engineering
University of Illinois at Urbana-Champaign
1304 West Green Street, Urbana, IL 61801 (USA)
Fax: (+1)217-333-2736

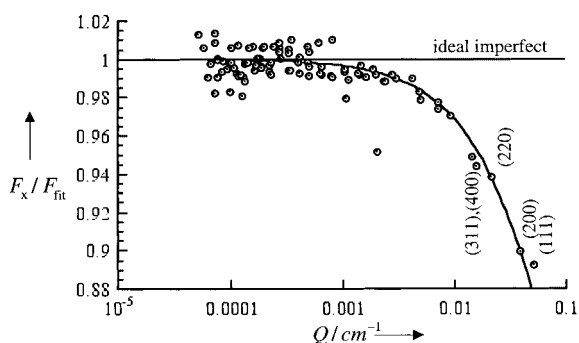


Figure 1. The ratio of as-measured X-ray data (F_x) [10] and the structure factors obtained from our best multipole model fit (F_{fit}) as a function of the scattering strength Q . The curved solid line is the best fit using the Zachariasen extinction model. The standard deviation from Zachariasen's model is about 0.8%, which is generally larger than the measurement error. The error comes from the random distribution of crystalline defects and the limitation of an averaging model such as Zachariasen's model, and it is the main source of error in charge densities determined by X-ray.

a large Q , the ratios are much lower than one, as we expected from the extinction effect. Using the Zachariasen's two-beam model for correcting extinction effects, we have obtained a best fit to extinction with this data. For strong reflections with $Q > 0.001$, we estimated the standard deviation of R from Zachariasen's model to be about 0.008 and the associated error in the structure factor of strong reflections to be $0.008 \cdot F(h,k,l)/R$. This amounts to about 1% for the (111) and (200) reflections. The error is larger than the measurement error, which is about 0.4%. In comparison, the error in the extinction-free electron diffraction measurements is less than 0.3% for the same reflections.

The error due to extinction significantly reduces the amount of information about the charge distribution that we can obtain from the measured X-ray data. Figure 2a and b plot the contributions to the total structure factor from each term in the multipole model for O and Cu, respectively. For O, contributions significantly above the experimental error are limited to three reflections: (110), (111), and (200). Individually, the charge transfer term dominates (110) and the octopole of charge deformation only affects (111). For Cu, the charge transfer term is too small to be detected. Conversely, the effect of the nonspherical modulation of Cu extends to many reflections over a wide scattering angle, with the largest contribution from the quadrupole ($l=2, m=0$). As a result, the determination of charge transfer and bond charge distribution depends critically on the first three low-order reflections. Among these, both the (111) and (200) are strong and have large extinction errors in the X-ray measurement. The estimated X-ray structure factor errors for the (111) and (200) reflections are approximately twice the expected changes from bonding. This is the reason for the observed extreme model dependence of the charge transfer and the oxygen charge deformation in the previous X-ray refinements.^[10, 11]

The definition of partial charges of ions in crystals, while it is often found to be useful as a simple number in chemistry, is problematic in practice. Fundamentally, it is impossible to define a unique partial charge based on a single charge density measurement or calculation.^[12] The partial charges obtained

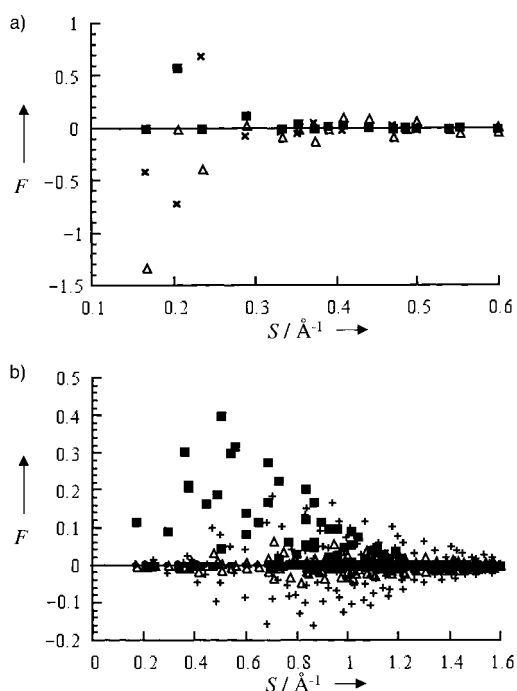


Figure 2. Contributions to the total structure factor (in units of e/cell) from each term in the multipole model for: a) oxygen with charge (triangles), octopole charge transfer (black squares), and hexapole charge transfer (crosses); and b) copper for each of three nonspherical terms with $(lm) = \{20, 40, 43\}$ (represented as black squares, crosses, and triangles, respectively). The charge transfer term (black circles) is significant only for oxygen.

by different definitions often differ significantly in scale (sometimes by a factor of 10, according to Ref. [13]). In their calculations, Wang and Schwarz used the wave function based Mulliken partial charges, which give $\text{Cu}^{0.5+}\text{O}^{1-}$. Our definition of charge transfer is based on the multipole model for the experimental deformation density, from which we obtain $\text{Cu}^{1+}\text{O}^{2-}$. When we apply the same multipole model to the theoretical charge density calculated with the full potential linearized augmented plane wave (LAPW) method which uses the same density functional theory (DFT) approximation, we obtain $q=0.9$, which compares favorably with our "experimental" value of 1.0. Given the widely different definitions for the partial charges used, the disagreement between the Mulliken charges of Wang and Schwarz and our multipole model charge transfer is not surprising. What is surprising is the purported agreement between previous experiments and the calculation of Wang and Schwarz. In fact, the charge transfer term in the quoted refinement of Restori and Schwarzenbach depends so much on the model and the treatment of experimental data, it was deemed experimentally meaningless by the original authors.^[10] The synchrotron measurement^[11] improves upon the data set of Restori and Schwarzenbach by an additional measurement of 21 very weak reflections, which are dominated by the anisotropic thermal vibration of Cu, and thus does not fundamentally alter the conclusions reached by Restori and Schwarzenbach. Their reported difference charge density map (Figure 8a of ref. [11]) differs from theoretical calculations in basic features around Cu.

Our experimental map shows a significant amount of charge between Cu⁺ ions. This is due to the observed differences in low-order structure factors between experiment and theory, not because of the model deficiency as suggested by Wang and Schwarz. We have applied the same charge density reconstruction procedure to the theoretical map we obtained from LAPW calculations to test the flexibility of our model and check for possible systematic errors. Figure 3 shows the reconstructed theoretical map using the same set of reflections as the experiment. Compared to the original theoretical map, the model recovers most of the features.

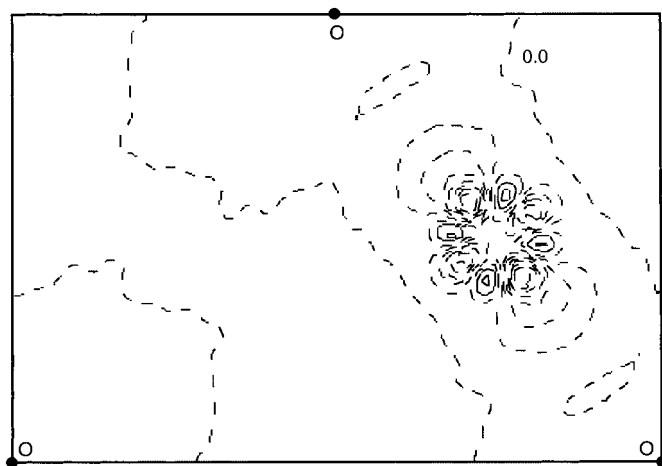


Figure 3. Theoretical difference map in a (110) plane with a contour increment of $0.2 \text{ e } \text{\AA}^{-3}$ obtained by fitting the same multipole model used in our experiment to the theoretical structure factors obtained from the LAPW calculation. This map recovers most features of the original theoretical map and demonstrates the flexibility of the model for charge density analysis.

The calculation of Wang and Schwarz differs significantly from our LAPW calculations and our experimental map in the oxygen charge distribution. Their difference map (Figure 4 in ref. [1]) between the crystal charge density and the superimposed spherical Cu⁺ and O²⁻ ions shows a large surplus electron density around oxygen, which is absent in our experiment and the LAPW calculations.^[2, 14] The calculation of Wang and Schwarz also differs significantly from our LAPW calculations regarding the charge distribution between Cu ions. The LAPW calculations show a broad surplus charge distribution of $0.17 \text{ e } \text{\AA}^{-3}$ near Cu slowly reducing to about $0.06 \text{ e } \text{\AA}^{-3}$ at the center of the empty tetrahedral site, this is in contrary to the maximum of $0.045 \text{ e } \text{\AA}^{-3}$ estimated by Wang and Schwarz for this region.

It is also important to recall that the reference atoms used in the difference map, that is, the charges of spherical O²⁻ and Cu⁺ ions, are different in theory and in the experiment. The experimental map uses the atomic charge density obtained by multiconfigurational Dirac–Fock calculations. Our theoretical map uses the atomic charge density calculated with the same DFT approximations used in the LAPW calculations. The references used by Wang and Schwarz are presumably different too.

We wish also to comment on the question of whether the Cu–Cu distance precludes any bonding in cuprite as suggested

by Wang and Schwarz. It has been known for many years that bond lengths vary significantly with bond strength, and chemists often use the interatomic distance as a guide to the strength of a bond. Many years ago Pauling suggested^[17] an exponential dependence of bond strength or valence (v) on length (d): $d = R + b \ln v$ where R is the single bond length ($v = 1$). It follows that for a given pair of atoms, the difference in bond length for a difference in bond valence is as shown in Equation (2). Brown and Altermatt^[18] proposed that $b = -0.37 \text{ \AA}$ could be taken as a universal parameter, and it was subsequently shown^[19] that this applied to a wide range of materials including covalent molecules, ionic crystals, and metals.

$$d_1 - d_2 = b \ln \left(\frac{v_1}{v_2} \right) \quad (2)$$

It is well documented^[20] that in the case of compounds of metals, one cannot always use metal–metal distances as diagnostic of bonding; but the question at hand is whether the Cu–Cu distance (3.02 \AA) in Cu₂O precludes significant bonding. Our benchmark is elemental copper which has the same Cu atom arrangement, and in which the Cu–Cu distance is 2.55 \AA . Equation (2) shows that this difference in interatomic distance would correspond to $(v_1/v_2) = 0.28$; so that if the Cu–Cu distance in Cu₂O were determined just by Cu–Cu bonding, there would be very considerable bonding. Actually the Cu–Cu distance in that material is determined very largely by the Cu–O bond length, but the important conclusion remains that the Cu–Cu distance does not preclude significant Cu–Cu bonding.

In questioning experiments based on the findings of approximate theoretical calculations, Wang and Schwarz raise an interesting question about the relative accuracy of experimental and theoretical charge densities. In the case of silicon, where both accurate experimental and theoretical structure factors are available, we have shown that the difference between experiment and theory is due to the approximate treatment of core electrons in the density functional approximation.^[21] Theoretically, the remarkable agreement between experiment and the DFT-based calculations reported in our paper is due to the nearly closed-shell configuration of Cu⁺ ions. In the case of Cu²⁺ with an open-shell configuration, the current DFT approximations are known to be insufficient due to the neglect of strong electron–electron interactions. In cuprite, both experiment and theory reveal that a d hole exists and that the Cu configuration is in between Cu⁺ and Cu²⁺. Thus, it is an open question as to how well current theories agree with the experiment. Understanding this will go a long way toward our understanding of high-temperature superconductivity.

In conclusion, we would like to emphasize that our results were built upon the accumulated experience of past decades about experimental measurements of charge density.^[15, 16] Significant results about charge states and bonding in various crystals have been obtained by X-ray diffraction, especially, for organic crystals with light elements where the proportion of bonding electrons is much higher and thus much easier to measure. For inorganic crystals with a relatively small unit

cell, experimental measurement of charge density requires very great accuracy for the few low order reflections that contain critical bonding information. This is where electron diffraction can play an important role.

- [1] S. G. Wang, W. H. E. Schwarz, *Angew. Chem.* **2000**, *112*, 1827; *Angew. Chem. Int. Ed.* **2000**, *39*, 1757.
- [2] J. M. Zuo, M. Kim, M. O'Keeffe, J. C. H. Spence, *Nature* **1999**, *401*, 49.
- [3] For example, see: *Electronic Structure, Dynamics, and Quantum Structural Properties of Condensed Matter* (Eds.: J. T. Devreese, P. Van Camp), Plenum, New York, **1984**.
- [4] W. E. Pickett, *Rev. Mod. Phys.* **1989**, *61*, 433.
- [5] C. G. Darwin, *Philos. Mag.* **1922**, *43*, 800.
- [6] W. H. Zachariasen, *Acta Crystallogr.* **1967**, *23*, 558.
- [7] P. J. Becker, P. Coppens, *Acta Crystallogr. Sect. A* **1974**, *30*, 129.
- [8] J. M. Zuo, *Microsc. Res. Tech.* **1999**, *46*, 220.
- [9] J. M. Zuo, M. O'Keeffe, P. Rez, J. C. H. Spence, *Phys. Rev. Lett.* **1997**, *78*, 4777.
- [10] R. Restori, D. Schwarzenbach, *Acta Crystallogr. Sect. B* **1986**, *42*, 201.
- [11] A. Kirfel, K. Eichhorn, *Acta Crystallogr. Sect. A* **1990**, *46*, 271.
- [12] C. R. A. Catlow, A. M. Stoneham, *J. Phys. C* **1983**, *16*, 4321; K. Jug, Z. B. Maksic in *The Meaning and Distribution of Atomic Charges in Molecules, Part 3: Molecular Spectroscopy, Electronic Structure and Intermolecular Interactions* (Ed.: Z. B. Maksic), Springer, Berlin, **1991**.
- [13] J. Meister, W. H. E. Schwarz, *J. Phys. Chem.* **1994**, *98*, 8245.
- [14] P. Marksteiner, P. Blaha, K. Schwarz, *Z. Phys. B: Condens. Matter* **1986**, *64*, 119.
- [15] P. Coppens, *X-ray Charge Densities and Chemical Bonding*, Oxford University Press, Oxford, **1997**.
- [16] V. G. Tsirelson, R. P. Ozerov, *Electron Density and Bonding in Crystals*, Institute of Physics, Bristol, **1996**.
- [17] L. Pauling, *J. Am. Chem. Soc.* **1947**, *69*, 542.
- [18] I. D. Brown, D. Altermatt, *Acta Crystallogr. Sect. B* **1985**, *41*, 244.
- [19] M. O'Keeffe, N. E. Brese, *J. Am. Chem. Soc.* **1991**, *113*, 3226.
- [20] M. O'Keeffe, B. G. Hyde, *Nature* **1984**, *309*, 411.
- [21] J. M. Zuo, P. Blaha, K. Schwarz, *J. Phys. C: Condens. Matter* **1997**, *9*, 7541.

Final Comment on the Discussions of "The Case of Cuprite"***

Shu Guang Wang and W. H. Eugen Schwarz*

Introduction

During recent years (1) closed-shell interactions, (2) polar covalences, (3) d-shell holes, and (4) direct images of orbitals^[1] have been the subject of many investigations. The discussions in the literature had culminated in the "direct observation of d-orbital holes and Cu–Cu bonding in Cu₂O",^[2] accompanied by "electrons seen in orbit", in *Nature*.^[3] Since this journal declined further discussion of questionable statements, comments had to be published elsewhere (see Refs. [1, 4–6]; see also Refs. [7, 8] and Refs. [6a–h] in [1]). Focussing on topics (1) to (4) listed above, our Essay^[1] touched a dozen specific points. About one half of them (concerning the other points, see, for instance: Refs. [4–6]) became the subject of the preceding letter of Zuo et al.,^[9] namely:

- 1) the correct values of the *experimental structure factors* of defectless cuprite (Cu₂O) crystals;
- 2) the validity of the *derived electron density distributions* around oxygen and around copper, and the existence or

nonexistence of a local electronic charge accumulation in the center of the "empty" Cu₄ tetrahedra of the cuprite structure;

- 3) the *effective partial charges* on O and on Cu; and
- 4) the *differences* between, and the reliability and accuracy of, the different diffraction experiments and quantum calculations.

The aim of our Essay,^[1] and especially of the four respective sections of the present Correspondence, is to formulate some open scientific questions as clearly as possible. Possible answers, and suggestions of how to corroborate them by scientific procedures, shall be given. In the concluding Section 5 we will address the following more general issues: a) What are the forces that hold cuprite together; b) how strongly deformed are the copper and oxygen units in cuprite; and c) how ionic is this transition metal oxide?

1. Experimental Structure Factors

The most accurate experimental structure factors of Cu₂O are, most probably, those from the Arizona (Zuo et al.^[2, 9]) and Hamburg groups (Lippmann and Schneider: Refs. [11a, b] in Ref. [1]; and Ref. [10]). The latter works, however, were not considered by Zuo et al. The statement by Zuo et al.^[9] that the differences in the published electron density maps are "due to observed differences in low order structure factors" has still to be substantiated. We suggest here once more that the two experimental groups perform a cross-analysis of their multipole refinement procedures for the other group's data sets. So far it is an open question whether, and how much, the experimental structure factors really differ.

[*] Prof. Dr. W. H. E. Schwarz, Prof. Dr. S. G. Wang
Theoretische Chemie
Universität Siegen
57068 Siegen (Germany)
Fax: (+49)271-740-2851
E-mail: schwarz@chemie.uni-siegen.de
and
School of Chemistry
Jiao Tong University
Shanghai
P.R. China

*** We acknowledge discussions with P. Coppens (SUNY, Buffalo), A. Kirfel (Bonn), T. Lippmann (DESY, Hamburg), P. Pykkö (Helsinki), and E. Scerri (Los Angeles).

2. Electron Density Distributions Derived Therefrom

The different densities, derived from data obtained by different experimental procedures on different specimens by different mathematical procedures differ, without doubt. The densities were determined by fitting *single* zeta multipole basis functions to the measured structure factors, assuming the vibrating rigid atom model. The single zeta restriction, for instance, can result in unphysical correlations of the calculated “experimental” densities at different positions in the crystal.

- 1) A most stirring proposition is that of an electron difference density maximum of $0.2 \text{ e } \text{\AA}^{-3}$ in the center of the otherwise *empty* Cu_4 tetrahedra (note that $D(\text{Cu} \cdots \text{Cu}) = 3 \text{\AA}$, while the effective radius of Cu^+ is 0.5\AA). That is a position of high potential energy,^[1] because it is surrounded by six O^{2-} ions at distances of 2.1 and 3.0\AA , where the tails of the oxygen single zeta model functions^[2] overlay significantly. We suggest to add a Gaussian function at the center of Cu_4 and to refine it in order to generate a less biased “experimental” density at that position. Anyhow there are needed more arguments than just the statement^[9] that this density is not an artifact of the applied multipole model. Zuo’s reference to Figure 3 of Ref. [9] is not relevant, because the increment of the contour lines is large, namely $0.2 \text{ e } \text{\AA}^{-3}$, and because this figure just does not show any maximum at the position of the center of Cu_4 . We reiterate that no “bond density” between the copper ions is needed for van der Waals attraction between them.
- 2) Concerning the *oxygen region*, there is quite good agreement between the densities of Zuo et al. and our’s. We cannot explain why Zuo et al.^[9] insist on the respective opposite statement. There is *no* “large surplus electron density around oxygen” in our calculated map (see Figure 4 of Ref. [1]) “which is [also] absent in [Zuo et al.’s]^[2] experiment and calculations”.
- 3) Concerning *copper*, we find, by density functional theory (DFT), as well as by ab initio MP2 cluster-calculations, just as Zuo et al. do in their experimental and DFT crystal electron density maps (Figure 3 of Ref. [9]), very localized charge accumulations in the not fully occupied 3d shell near the Cu nucleus. Furthermore, we find a belt of weak 3d–4s hybrid density at distances $\geq 1 \text{\AA}$ in the equatorial plane around Cu, which is absent in the maps of Zuo et al. (compare Figures 5a, b in Ref. [1]). Note, however, that our two lowest contour lines correspond to 0.025 and $0.05 \text{ e } \text{\AA}^{-3}$, while Zuo et al.’s lines correspond to 0.2 and $0.4 \text{ e } \text{\AA}^{-3}$. We suggest to refer to contour lines of comparable order of magnitude when comparing contour maps.

3. Effective Atomic Charges

Despite the inherent basic problems with the definitions of atomic effective charges in compounds,^[11] those charges have a meaning to the practicing chemist. The sense of communicating charges is to transfer that chemically useful informa-

tion. The formulas $\text{A}^{1.0+}\text{B}^{1.0-}$ or $\text{Cu}_2^{1.0+}\text{O}^{2.0-}$ (Zuo et al.^[2]) mean to the chemist that these compounds are highly ionic compounds like NaCl or K_2O . We, however, find only a polar, partially ionic bond in Cu_2O , in addition to some covalent overlap population.^[1] We suggest to investigate what the “chemical” meaning of the charge values calculated by Zuo et al.^[2] might be.

4. Agreement and Differences

4.1. Experiments

One of the problems with density determinations, mentioned by Zuo et al.^[9], is the zero-point and thermal motion of the atoms in the crystal. One tries to eliminate this motion by different recipes in the experimental and theoretical static density maps. Ample experiences, with experimental X-ray scattering^[12] as well as with theoretical investigations (for example, Ref. [13]), demonstrate that liquid nitrogen temperatures, not to speak of room temperatures, often principally rule out the extraction of the more subtle details of the bond densities from X-ray or from electron-scattering experiments or from vibrationally smeared calculations. When discussing bond densities, low-temperature experiments are recommended (“He temperatures” of the order of 10 to 20 K). In addition we suggest to the experimentalists to include higher order anharmonic terms in the atomic Debye–Waller factors of the multipole refinement.

4.2. Calculations

In principle there are also specific problems with the quantum chemical calculations. Zuo et al. note problems of DFT with open-shell transition metal systems. They mention that the Cu units carry a fractional hole in the 3d shell and interpret this as an intermediate state of Cu in cuprite between Cu^+ and Cu^{2+} . This is faulty, the “3d shell” of Cu is closed, but polarized, that is, 3d–4sp hybridized. Zuo also mentions possible differences between a crystal and a cluster embedded in the crystal field. However, Zuo et al.’s^[2, 9] self consistent field (SCF) DFT calculations of the crystal, our SCF-DFT calculation of an embedded cluster, and our respective non-DFT ab initio correlated MP2 calculation, all agree very well; they are, for instance, within only $0.02 \text{ e } \text{\AA}^{-3}$ (!) at the saddle point of the difference density in the center of the heavily discussed Cu_4 units. The same density value, within this small error range, was experimentally found by the Lippmann and Schneider group.^[10] Only Zuo et al.’s “experimental” map^[2] shows really more electron density (0.2 instead of $0.05 \text{ e } \text{\AA}^{-3}$ difference density) in this very region.

5. Conclusions

The Madelung energy of a point charge lattice of cuprite is weakly repulsive in the sense of $[\text{Cu}_4\text{O}_2] \rightarrow 2[\text{Cu}_2\text{O}]$.^[14] The multipole interaction contributions, the polarization contributions, and the dispersion contributions to the energy seem

sufficient to explain the stability.^[1] Experimental and theoretical investigations on Cu–O cluster molecules and similar systems (see, for example, Refs. [15, 16]) are consistent with our picture of cuprite. The isolated evidence^[2] of a localized charge accumulation at a high potential energy saddle point^[1] in the middle between Cu⁺ ions at 3 Å distance, interpreted as covalent Cu⁺–Cu⁺ bonding, is so unexpected and unusual that it deserves further investigation and checking. Above we have given some suggestions.

There is astonishingly good agreement between different experiments and different calculations concerning the following points: (1) the oxygen anions are only weakly deformed, and (2) the copper cations are closed-shell subunits with a deficit of 3d population along the O–Cu–O *z* axis and in the *xy* plane (mainly due to d–s hybridization, which leads to slight density increase in the *xy* plane at larger distances), and localized deformation density maxima between those d–s orbital holes (density minima) near the Cu nucleus. This density difference looks topologically similar to an f atomic orbital. Furthermore it is to be stressed that the Cu–O covalent interaction corresponds to electron deficit on the bond line, with respect to Cu⁺ and O^{2–}.

There exists disagreement concerning the following points: (1) the electron density inside the “empty” Cu₄ tetrahedra—most investigations show very little density; and (2) how strongly ionic Cu₂O is—we find covalent back-donation of electronic charge from oxygen, which is only a formally charged O^{2–}, into the (only partially positively charged) copper 4sp shell.

- [1] S. G. Wang, W. H. E. Schwarz, *Angew. Chem.* **2000**, *112*, 1827; *Angew. Chem. Int. Ed.* **2000**, *39*, 1757.
- [2] J. M. Zuo, M. Kim, M. O’Keeffe, J. C. H. Spence, *Nature* **1999**, *401*, 49.
- [3] C. J. Humphreys, *Nature* **1999**, *401*, 21.
- [4] M. A. Spackman, J. A. K. Howard, R. Destro, *Int. Union Crystallogr. Newslett.* **2000**, *8*(1), 2.
- [5] E. Scerri, *J. Chem. Educ.* **2000**, *77*(11), in press.
- [6] E. Scerri, *Foundat. Chem.* **2000**, *2*, 1; *Proceedings of PSA 2000*, Philosophy of Science Association, East Lansing, MI, USA, **2000**, in press.
- [7] J. I. Pascual, J. Gómez-Herrero, C. Rogero, A. M. Baró, D. Sánchez-Portal, E. Artacho, P. Ordejón, J. M. Soler, *Chem. Phys. Lett.* **2000**, *321*, 78.
- [8] M. Jacoby, *Chem. Eng. News* **1999**, *77*(36), 8.
- [9] J. M. Zuo, M. O’Keeffe, M. Kim, J. C. H. Spence, *Angew. Chem.* **2000**, *112*, 3947; *Angew. Chem. Int. Ed.* **2000**, *39*, 3791. (There, these authors criticise their own “media chatter, for which [they] can not be held responsible”.)
- [10] T. Lippmann, J. R. Schneider, *Acta Crystallogr. Sect. B* **2000**, *56*, in press.
- [11] J. Meister, W. H. E. Schwarz, *J. Phys. Chem.* **1994**, *98*, 8245.
- [12] P. Coppens, *X-ray Charge Densities and Chemical Bonding*, Oxford University Press, Oxford, **1997**; V. G. Tsirelson, R. P. Ozerov, *Electron Density and Bonding in Crystals*, Institute of Physics, Bristol, **1996**.
- [13] H. Bruning, W. H. E. Schwarz, unpublished results.
- [14] M. O’Keeffe, *J. Chem. Phys.* **1963**, *38*, 3035.
- [15] C. Kölmel, R. Ahlrichs, *J. Phys. Chem.* **1990**, *94*, 5536; P. Reis, F. Weigend, D. Fenske, R. Ahlrichs, *Angew. Chem.* **2000**, *112*, 4085; *Angew. Chem. Int. Ed.* **2000**, *39*, 3925; L. S. Wang, H. B. Wu, S. R. Desai, L. Lou, *Phys. Rev. B* **1996**, *53*, 8028.
- [16] P. Pykkö, *Chem. Rev.* **1997**, *97*, 597; P. Pykkö, N. Runeberg, F. Mendizabal, *Chem. Eur. J.* **1997**, *3*, 1451; K. Doll, P. Pykkö, H. Stoll, *J. Chem. Phys.* **1998**, *109*, 2339.

Stable Systems with a Triple Bond to Silicon or Its Homologues: Another Challenge

Peter Jutzi*

Already early in the last century scientists observed that rules developed for the organic chemistry of carbon were not applicable for the element silicon. According to F. S. Kipping it was not possible to generate stable compounds comparable to olefins or ketones bearing a Si=C or a Si=O double bond.^[1] E. Wiberg mentioned the nonexistence of the disilene $\text{H}_2\text{Si}=\text{SiH}_2$, which is comparable to ethylene. He pointed out that in general the elements of the second row show no tendency to form double bonds as found for their first-row counterparts. They achieve the noble gas configuration by polymerization generating larger structures.^[2] In that context E. Wiberg referred to the “not well-known double-bond rule”, which strictly speaking still holds for basic systems.^[3]

However, the introduction of substituents that were capable of kinetic and/or thermodynamic stabilization led already in the 1970s to many exceptions to this rule.^[4] By the end of the century one had, through the use of well chosen substituents (by actual “design” of the substituents) and from the results of high level calculations, a comprehensive understanding of both the double-bond systems incorporating elements of Groups 13, 14, and 15 and of their often energetically preferred isomeric counterparts. Excellent reviews are available which describe this subject very extensively.^[5]

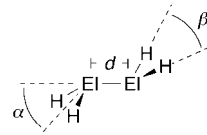
Besides the double-bond systems, the triple-bond systems have recently become—as a final challenge—the focus of interest.^[6] Herein a short report is given on the latest results on the triple-bond systems R_2El_2 and $[\text{L}_n\text{MEIR}]$ ($\text{El} = \text{Si}, \text{Ge}$), which can be regarded as compounds analogous to alkynes and carbyne complexes, respectively. For a better awareness of the recent developments, the current understanding in the field of double-bond systems is summarized by using the compounds R_4El_2 and $[\text{L}_n\text{MEIR}_2]$, which are analogous to alkenes and carbene complexes, respectively, as examples.

Disilenes, -germenes, -stannenes, and -plumbenes R_4El_2

Theoretical papers have discussed the geometric changes in the ground state between the stable ethene molecule and the

highly reactive homologues H_4El_2 ($\text{El} = \text{Si}, \text{Ge}, \text{Sn}, \text{Pb}$), which are unknown or experimentally difficult to prepare.^[7, 8] Density functional theory (DFT) calculations revealed the expected planar configuration for the ethene molecule, whereas for all the other molecules a *trans* bent configuration with pyramidalization at the element center was calculated (Table 1).^[9] The angle α increases and the angle H-El-H decreases with increasing atomic number. The ratio of double-bond length to single-bond length (d/δ) also increases with increasing atomic number. The factor d/δ results from the calculated distances for single ($\delta(\text{El}-\text{El})$) and double bonds ($d(\text{El}=\text{El})$).

Table 1. Structural data for H_4El_2 molecules from DFT calculations.^[9]



El	C	Si	Ge	Sn	Pb
α [°]	0	36.1	47.3	51.0	53.6
β [°]	116.5	112.4	109.5	105.8	107.7
$d_{\text{El}=\text{El}}$ [(Å)]	1.323	2.150	2.245	2.569	2.819
$\delta_{\text{El}-\text{El}}$ [(Å)]	1.511	2.322	2.413	2.721	2.931
d/δ	0.876	0.926	0.930	0.944	0.962

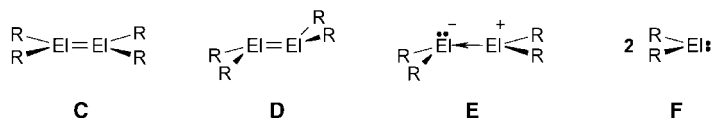
There are several models to explain the different bonding.^[5, 8, 9] A simple approach predicts a distortion from the planar geometry when the corresponding fragment ElR_2 has a singlet ground state. The formation of *trans* bent double-bond systems can then be described by two donor–acceptor interactions between the filled s orbitals and the empty p orbitals of two singlet ElR_2 units (**A** in Scheme 1). Classic planar double-bond systems are formed by the interaction of two ElR_2 units in the triplet ground state (**B**).



Scheme 1. Construction of R_4El_2 structures from singlet (**A**) and triplet R_2El fragments (**B**).

[*] Prof. Dr. P. Jutzi
Fakultät für Chemie
Universität Bielefeld
33615 Bielefeld (Germany)
Fax: (+49) 521-1066026
E-mail: peter.jutzi@uni-bielefeld.de

Through the design of the substituent R, today a large number of compounds of the type R_4El_2 are known, which are kinetically or thermodynamically stabilized.^[5] These compounds are stable under normal conditions and their structures are known in solution and in the solid state. The different types of structure **C–F** are shown in Scheme 2. All the tin and lead compounds, which are known so far,^[10] along



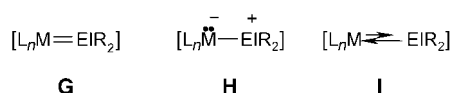
Scheme 2. Structural types of R_4El_2 compounds.

with some silicon and germanium compounds, dissociate in solution forming species of the type **F**. This behavior expresses clearly the “inert pair effect” of the involved s electron pair. The energetic differences between the structures **C** and **D** are often very small, particularly for silicon, where the variation of the substituents causes interesting effects.^[5b] In general, for structures with extremely bulky substituents a discrepancy is noted between the experimentally observed and the theoretically predicted structures.

Silylene, Germylene, Stannylenes, and Plumbylene Transition Metal Complexes

About ten years after the discovery of the Fischer carbene complexes of the type $[L_nMCR_2]$, the first complexes with GeR_2 , SnR_2 , and PbR_2 ligands were described.^[11] In contrast to the situation in carbene complex chemistry, one had the advantage of the existence of stable ElR_2 units, which could be used for successful ligand exchange reactions. After the discovery of stable silylenes, this strategy was then applied for the preparation of silylene complexes $[L_nMSiR_2]$ (the same was true for carbene complexes). Cationic silylene complexes of the type $[L_nMSiR_2]^+$ can be prepared by removing an anionic substituent X^- from the corresponding silyl complex $[L_nMSiR_2X]$.^[12] Variation of substituents at the Group 14 element as well as variations of the metal unit meanwhile have led to a huge number of stable complexes with ligands which are analogous to carbenes.^[13]

As for the Fischer carbene complexes, the Dewar–Chatt–Duncanson model can be applied to explain the bonding (Scheme 3).^[14] The strength of the π -back bond expressed by the mesomeric structure **G** determines the double-bond character of the $M-El$ bond. For example, high double-bond

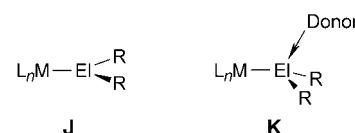


Scheme 3. Description of the bonding in $[L_nMElR_2]$ complexes.

character has been found in cationic silylene complexes. In many other complexes, in particular those with SnR_2 or PbR_2 ligands, the donor–acceptor bond is clearly preferred (mesomeric structure **H**). It is easier to formulate double bonds than to establish them; thus, cautious authors describe the bonding

in the form of **I**! The controversial discussion about multiple bonds in gallium chemistry shows that caution is appropriate.^[15]

In the case of the carbon homologues, besides complexes with a planar arrangement at the Group 14 element (**J** in Scheme 4), several complexes are known that show a distorted tetrahedral arrangement (**K**); this is caused by the coordination of an additional donor group. The apparent acidic character of the ElR_2 fragment in **K** confirms the importance of the resonance structure **H** in describing the bonding.



Scheme 4. Donor-free and donor-stabilized complexes.

A special type of germylene complex is represented by the compounds $[RH_4C_5(CO)_2Mn=Ge=Mn(CO)_2C_5H_4R]$ ($R = Me, H$).^[16] Here, two carbenoid metal centers are bound to one germanium atom; calculations reveal even a partial triple-bond character for the $Mn-Ge$ bonds.^[17]

The Problem of the $Si\equiv Si$ Triple Bond

In 1991 an experiment that postulated a different structure for disilyne (H_2Si_2) than for acetylene, generated considerable interest: the microwave spectrum of a SiH_4 plasma at $-196^\circ C$ indicated a bridged structure.^[18] The bonding parameters of H_2Si_2 are shown in Figure 1; the $Si-H$ distance is approximately 12 % longer than normal and typical for a three-center–two-electron bond. Thus, older calculations were confirmed which showed that H_2Si_2 has a double-bridged structure in the ground state and that a compound with a structure analogous to acetylene does not even correspond to a minimum on the potential surface!^[9, 19]

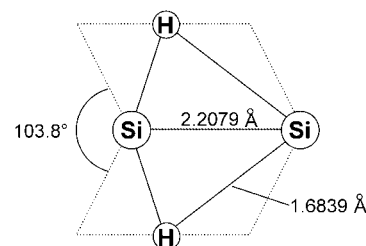


Figure 1. Structure of H_2Si_2 .

The energetic array of the calculated structures for the H_2Si_2 molecule along with those for the H_2Ge_2 molecule is shown in Figure 2.^[8] These structures can be explained through the different orientation of the HEl fragments in the doublet state ($^2\pi$) which lead to different interactions and structures. The $ns^2np^1np^1$ configuration expresses the low tendency for hybridization.^[20]

Larger structural changes can be expected by the introduction of other substituents. Calculations predict a stabilization of a bent triple-bond structure for bulky σ -donor

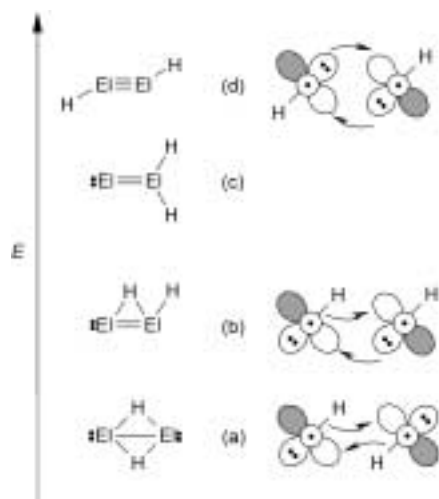
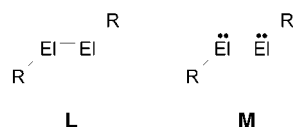


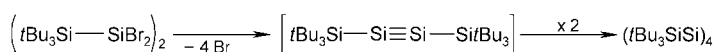
Figure 2. Energetic array of H_2El_2 structures ($\text{El} = \text{Si}, \text{Ge}$) and their construction from HEI units.

substituents such as $t\text{Bu}_3\text{Si}$ (**L** in Scheme 5) (see below for experiments on this topic).^[21] In contrast, π -donor substituents should lead to a single-bond structure **M**.^[8] The latter is undoubtedly preferred for the heavier homologues tin and lead, if the steric demand of the substituents doesn't cause a different structure.



Scheme 5. Structural possibilities for R_2El_2 compounds.

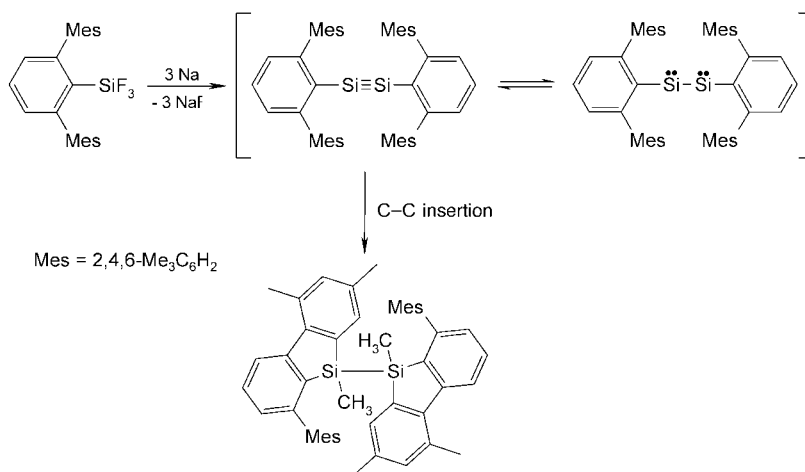
Preparative work with the thrilling aim of stabilizing $\text{Si}\equiv\text{Si}$ triple bonds under normal conditions is perhaps close to a breakthrough. Currently, the research group of N. Wiberg is dealing with the question of whether it is possible to stabilize a disilyne, which is discussed as an intermediate in the tetrasilatetrahedran synthesis (Scheme 6), by using bulkier silyl groups.^[22]



Scheme 6. Tetrasilatetrahedrane synthesis.

Experiments in the research group of R. West on the reduction of special aryltrifluorosilanes showed that the generated disilyne (or its structural isomer), which is formed as intermediate, is such a reactive molecule that it even inserts into C–C bonds (Scheme 7).^[23] The attempt for future work is to prevent this “interfering” reaction by designing special substituents.

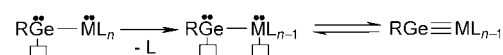
At this point the experimental evidence of formal triple bonds to silicon by matrix isolation spectroscopy ($\text{HSi}\equiv\text{N}$,^[24] $\text{HN}\equiv\text{Si}$,^[25] and $\text{C}_6\text{H}_5\text{N}\equiv\text{Si}$,^[26]), by neutralization reionization (NR) mass spectrometry ($\text{HC}\equiv\text{SiX}$ ($\text{X} = \text{F}, \text{Cl}$)^[27]), as well as by photoelectron spectroscopy ($\text{C}_6\text{H}_5\text{N}\equiv\text{Si}$,^[28]) should be mentioned.



Scheme 7. C–C insertion of an intermediary disilyne.

The First Stable Gernmylene Transition Metal Complexes

After the successful synthesis of metallogermynes,^[29] there was at least an obvious strategy for the preparation of gernmylene complexes: it was necessary to create a situation at the transition metal comparable to that at the germanium center; through the neighborhood of the two centers, which both possess a lone pair of electrons as well as a free coordination site, the electronic interactions should be such so as to allow the formation of up to a triple bond (Scheme 8).



Scheme 8. Strategy for the preparation of transition metal gernmylene complexes.

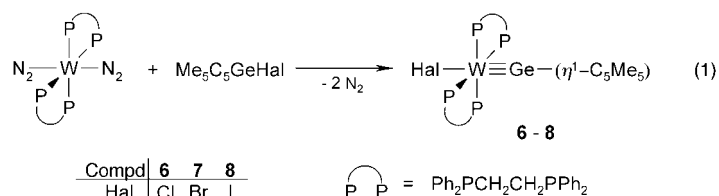
However, in the case of the ferriogernmylene [(2,4,6- $t\text{Bu}_3\text{C}_6\text{H}_2$) $\text{GeFe}(\text{CO})_2\text{C}_5\text{Me}_5$] one observes an insertion of the gernmylene unit into one of the C–H bonds of the aryl ligand instead of the desired CO loss.^[29] In contrast, the experiments in the research group of P. P. Power are leading in the right direction: treatment of extremely bulky aryl-(chloro)germylenes with cyclopentadienyl(tricarbonyl)metallates of chromium, molybdenum, and tungsten gave the first stable gernmylene complexes **1–5**, which could be isolated as red crystals (Table 2).^[30] In the case of the synthesis of **1**, **2**, and **4** there is a spontaneous loss of CO, while in the course of the preparation of **3** and **5** it was possible to isolate and characterize the metallogermynes as stable intermediates; CO loss is then observed on thermal or photochemical treatment.

Table 2. Data of **1–5**.

		$\text{ArGeCl} + \text{Na}[\text{M}(\text{CO})_3\text{Cp}] \xrightarrow[-\text{NaCl}]{-\text{CO}}$		$[\text{ArGe}\equiv\text{M}(\text{CO})_2\text{Cp}]$	
				1–5	
Compd.	M	Aryl	$d_{\text{Ge-M}}$ [Å]	$\angle \text{M-Ge-C}$ [°]	
1	Mo	2,6-(2,4,6- $\text{Me}_3\text{C}_6\text{H}_2$) $_2\text{C}_6\text{H}_3$	2.271(1)	172.2(2)	
2	W	2,6-(2,4,6- $\text{Me}_3\text{C}_6\text{H}_2$) $_2\text{C}_6\text{H}_3$	2.2767(14)	170.9(3)	
3	Cr	2,6-(2,4,6- $i\text{Pr}_3\text{C}_6\text{H}_2$) $_2\text{C}_6\text{H}_3$	2.1666(4)	175.99(6)	
4	Mo	2,6-(2,4,6- $i\text{Pr}_3\text{C}_6\text{H}_2$) $_2\text{C}_6\text{H}_3$	2.272(8)	174.25(14)	
5	W	2,6-(2,4,6- $i\text{Pr}_3\text{C}_6\text{H}_2$) $_2\text{C}_6\text{H}_3$	–	–	

Compounds **1–5** were characterized by NMR, UV/Vis, and IR spectroscopy and except for **5** by X-ray diffraction. The Ge≡M bonds are usually about 0.4 Å shorter than the corresponding Ge–M single bonds. As expected, the Ge≡M–C(aryl) arrangements are almost linear (Table 2). Apparently, in these complexes the triple bond is shielded in an excellent way by these tailor-made aryl ligands.

A completely different approach to stable germylyne complexes was recently presented by the research group of A. C. Filippou.^[31] Here the synthetic strategy was based on the easy loss of dinitrogen molecules from a double dinitrogen-substituted metal complex, on the formal oxidative addition of a RGeHal unit at the corresponding metal center, and on the concomitant reorganization of the electronic system leading to the formation of a triple bond. Treatment of the tungsten complex *trans*-[W(dppe)₂(N₂)₂] (dppe = 1,2-bis(diphenylphosphanyl)ethane) with germanium(II) compounds of the type Me₅C₅GeHal gave the stable germylyne complexes **6–8** as orange or red-brown powders [Eq. (1)]. These



compounds are also fully characterized by spectroscopic means. The X-ray structure analysis of crystalline **6**·toluene confirms the existence of a distorted octahedral complex with *trans* configuration of the chlorine and the germylyne ligand; the Ge≡W distance is 2.302(1) Å, and the C–Ge≡W arrangement is again almost linear with an angle of 172.2°.

Density functional calculations show that the triple bond should be described in a classical way. The germylyne ligand is a weaker σ donor than a carbyne ligand, but a comparable π acceptor. The synthetic route used by Filippou et al. is very promising because of the existence of many dinitrogen complexes that could be used as starting compounds to prepare germylyne complexes. In addition the Me₅C₅ substituent is generally accepted as a good leaving group in main group chemistry,^[32] which will also be beneficial for reactivity studies on substitutions at the germanium center.

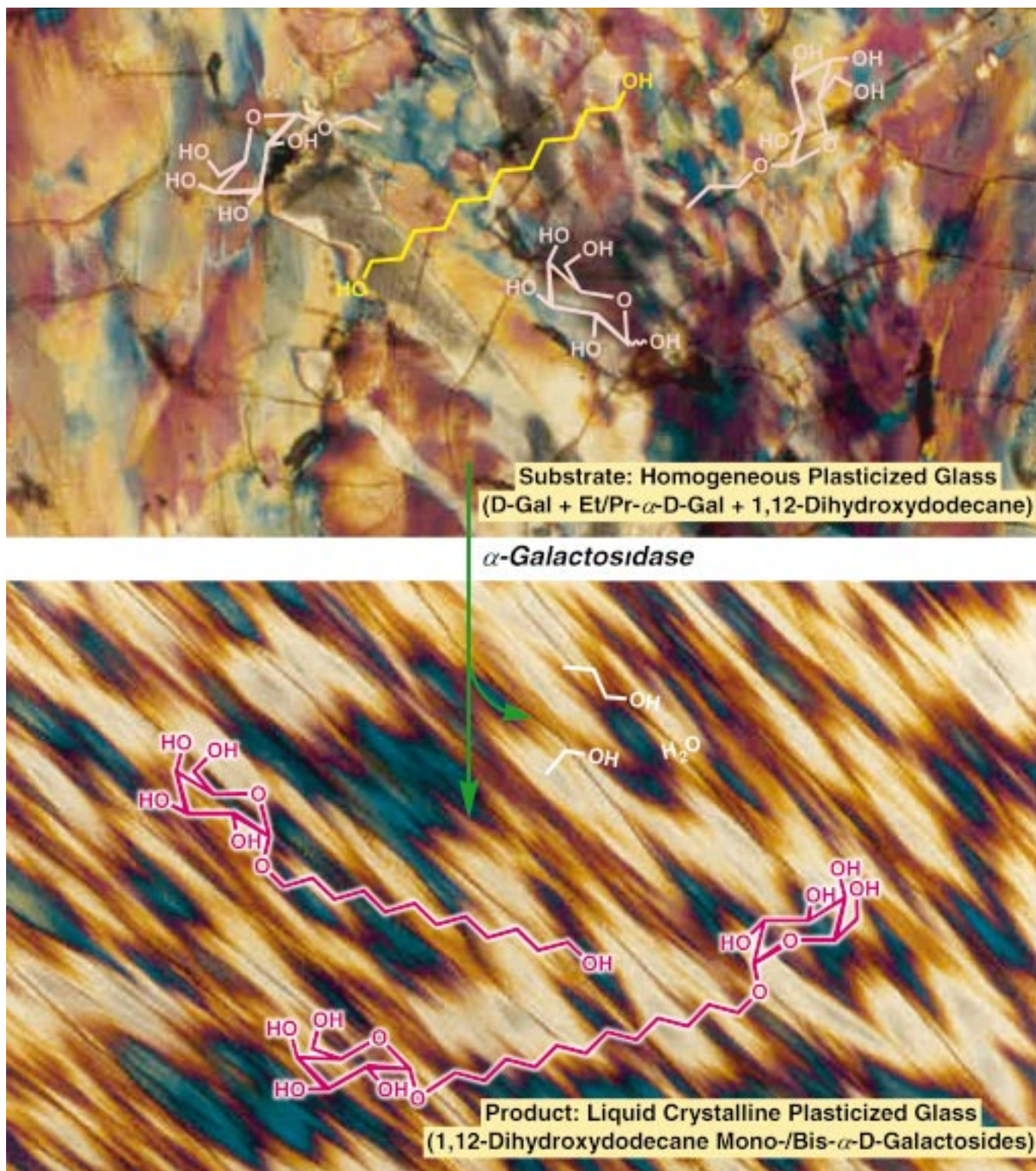
The most recent results in the area of compounds with real or formal triple bonds to silicon or its homologues illustrate that one can expect extremely interesting results in the near future.

[1] F. S. Kipping, *Proc. R. Soc. London A* **1937**, 159, 139.

[2] O. Stecher, E. Wiberg, *Chem. Ber.* **1942**, 75, 2003.

- [3] Holleman-Wiberg, *Lehrbuch der Anorganischen Chemie*, 22nd and 23rd ed., **1943**, p. 207, 291, 292, 346.
- [4] a) P. Jutzi, *Angew. Chem.* **1975**, 87, 269; *Angew. Chem. Int. Ed. Engl.* **1975**, 14, 232; b) P. Jutzi, *Chem. Unserer Zeit* **1981**, 15, 149.
- [5] a) P. P. Power, *Chem. Rev.* **1999**, 99, 3463; b) M. Driess, H. Grützmacher, *Angew. Chem.* **1996**, 108, 900; *Angew. Chem. Int. Ed. Engl.* **1996**, 35, 828; c) J. Escudie, H. Ranaivonjatovo, *Adv. Organomet. Chem.* **1999**, 44, 113.
- [6] A different type of triple bond is well established and can be formed in π complexes of the type R₃C₃El⁺ (El = Ge, Sn, Pb): P. Jutzi, N. Burford, *Chem. Rev.* **1999**, 99, 969.
- [7] Mass spectrometric evidence for Si₂H₄: K. Tonokura, T. Murasaki, M. Koshi, *Chem. Phys. Lett.* **2000**, 319, 507.
- [8] R. S. Grev, *Adv. Organomet. Chem.* **1991**, 33, 125.
- [9] H. Jacobsen, T. Ziegler, *J. Am. Chem. Soc.* **1994**, 116, 3667.
- [10] M. Stürmann, W. Saak, H. Marsmann, M. Weidenbruch, *Angew. Chem.* **1999**, 111, 145; *Angew. Chem. Int. Ed.* **1999**, 38, 187.
- [11] a) W. Petz, *Chem. Rev.* **1986**, 86, 1019; b) M. F. Lappert, R. S. Rove, *Coord. Chem. Rev.* **1990**, 100, 267; c) T. D. Tilley, *Comm. Inorg. Chem.* **1990**, 10, 37; d) P. D. Lickiss, *Chem. Soc. Rev.* **1992**, 271.
- [12] S. K. Grumbine, G. P. Mitchell, D. A. Straus, T. Don Tilley, A. L. Rheingold, *Organometallics* **1998**, 17, 5607.
- [13] Recent work: silylene complexes;^[12] germylene complexes: K. Ueno, K. Yamaguchi, H. Ogino, *Organometallics* **1999**, 18, 4468; J. E. Bender IV, A. J. Shusterman, M. M. Banaszak Holl, J. W. Kampf, *Organometallics* **1999**, 18, 1547; stannylenes complexes: M. Weidenbruch, A. Stilter, W. Saak, K. Peters, H. G. von Schnering, *J. Organomet. Chem.* **1998**, 560, 125; J. J. Schneider, N. Czap, D. Bläser, R. Boese, J. Ensling, P. Gütllich, C. Janiak, *Chem. Eur. J.* **2000**, 6, 468.
- [14] C. Boehme, G. Frenking, *Organometallics* **1998**, 17, 5801.
- [15] a) R. Dagani, *Chem. Eng. News* **1998**, 76(11), 31; b) R. Köppe, H. Schnöckel, *Z. Anorg. Allg. Chem.* **2000**, 626, 1095.
- [16] a) W. Gäde, E. Weiss, *J. Organomet. Chem.* **1981**, 213, 451; b) J. D. Korb, I. Bernal, R. Hörlein, R. Serrano, W. A. Herrmann, *Chem. Ber.* **1985**, 118, 340.
- [17] N. M. Kostic, R. F. Fenske, *J. Organomet. Chem.* **1982**, 233, 337.
- [18] M. Bogey, H. Bolvin, C. Demynck, J. L. Destombes, *Phys. Rev. Lett.* **1991**, 66, 413.
- [19] H. Lischka, H. J. Kohler, *J. Am. Chem. Soc.* **1983**, 105, 6646.
- [20] W. Kutzelnigg, *Angew. Chem.* **1984**, 96, 262; *Angew. Chem. Int. Ed. Engl.* **1984**, 23, 272.
- [21] K. Kobayashi, S. Nagase, *Organometallics* **1997**, 16, 2489.
- [22] N. Wiberg, *Coord. Chem. Rev.* **1997**, 163, 217.
- [23] a) R. Pietschnig, R. West, D. R. Powell, *Organometallics* **2000**, 19, 2724; b) R. Pietschnig, R. West, *Abstr. Pap. 33rd Organosilicon Symposium* (Saginaw, Michigan, USA) **2000**, pp. B5.
- [24] G. Maier, J. Glatthaar, *Angew. Chem.* **1994**, 106, 486; *Angew. Chem. Int. Ed. Engl.* **1994**, 33, 473.
- [25] J. F. Ogilvie, S. Craddock, *J. Chem. Soc. Chem. Commun.* **1966**, 364.
- [26] J. G. Radziszewski, D. Littmann, V. Balaji, L. Fabry, G. Gross, J. Michl, *Organometallics* **1993**, 12, 4816.
- [27] M. Karni, Y. Apeloig, D. Schröder, W. Zummack, R. Rabezzana, H. Schwarz, *Angew. Chem.* **1999**, 111, 344; *Angew. Chem. Int. Ed.* **1999**, 38, 332.
- [28] H. Bock, R. Dammel, *Angew. Chem.* **1985**, 97, 128; *Angew. Chem. Int. Ed. Engl.* **1985**, 24, 111.
- [29] a) R. S. Simmons, P. P. Power, *J. Am. Chem. Soc.* **1996**, 118, 1196; b) P. Jutzi, C. Leue, *Organometallics* **1994**, 13, 2898.
- [30] L. Pu, B. Twamley, S. T. Haubrich, M. M. Olmstead, B. V. Mork, R. S. Simons, P. P. Power, *J. Am. Chem. Soc.* **2000**, 122, 650.
- [31] A. C. Filippou, A. I. Philippopoulos, P. Portius, D. U. Neumann, *Angew. Chem.* **2000**, 112, 2281; *Angew. Chem. Int. Ed.* **2000**, 39, 2778.
- [32] P. Jutzi, G. Reumann, *J. Chem. Soc. Dalton Trans.* **2000**, 2237.

Monosaccharide-Alkyl Glycoside Glasses



Doping of monosaccharides with alkyl glycosides results in glasses with depressed glass transition temperatures and greatly increased hydrophobicities. These can be liquified (plasticized) by alcohols and are capable of dissolving a variety of hydrophobic compounds to form

homogeneous or heterogeneous liquid phases. Glycosidase enzymes are active in these media and catalyze the O-glycosylation of a wide range of acceptors in good yields. Find out more on the following pages.

Monosaccharide–Alkyl Glycoside Glass Phases: Plasticization with Hydrophilic and Hydrophobic Molecules

Iqbal Gill* and Rao Valivety

The ability of carbohydrates to form amorphous glassy solids is a well-known phenomenon, which has assumed great importance in the fields of cryobiology, room-temperature stabilization of biologicals, microbiology, and food technology.^[1] In particular, the ability to engineer the glass transition temperature (T_g) of carbohydrate glasses and the facile encapsulation and stabilization of proteins, nucleic acids, lipids, and volatiles into glass matrices have found uses in areas as diverse as the production of shelf-stable enzymes, therapeutics, biomembranes, and other biologicals,^[2, 3] the encapsulation of flavours and aromas, and the production of low moisture foods.^[1]

Although such glasses are efficient matrices for hydrophilic substances, problems arise with the incorporation of hydrophobic molecules, which invariably lead to the formation of biphasic sugar–dopant glasses. As part of our efforts to develop new reaction media for the glycosidase-mediated synthesis of O-glycosides, we undertook a study of mixtures of monosaccharides, alkyl glycosides, and various dopants. We now report that admixtures of lower alkyl glycosides with their parent monosaccharides form glasses akin to those of pure sugars. The T_g values of the glasses can be lowered by the inclusion of water and/or hydrophilic or hydrophobic molecules to form monophasic liquids (plasticized glasses) that are stable to phase separation. To our knowledge, this is the first report of sugar–alkyl glycoside glasses, and of the solubilization of hydrophobic species, including alkyl and arylalkyl alcohols, phenols, terpenols, and lipids, therein.

Starting with glucose, galactose, mannose, or 2-acetamido-2-deoxyglucose, mixtures containing 72–87% (all percentages quoted are the weight to weight ratio (w:w)) of ethyl, propyl, butyl, and/or but-3'-enyl glycoside and 13–28% of monosaccharide were synthesized by the addition of excess alcohol to a supersaturated solution of the sugar containing the requisite enzyme. Thus, a glass with a T_g value of 23–26 °C and composed of D-glucose (11%), ethyl β -D-glucopyranoside (39%), propyl β -D-glucopyranoside (45%), water (3%), and propan-1-ol (2%) was obtained by the almond β -D-glucosidase mediated condensation of a solution of D-glucose with ethanol:propan-1-ol (1:1), followed by evaporation.

As with conventional sugar glasses, the addition of water or lower alcohols resulted in the dramatic depression of the T_g value (Figure 1).^[1] More importantly, we found that the glass

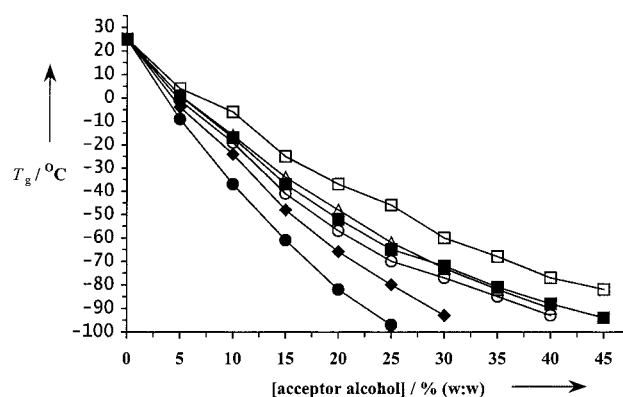


Figure 1. Plasticization of a D-glucose:ethyl β -D-glucoside:propyl β -D-glucoside:water:propanol glass (11:39:45:3:2) by various compounds. □ = Benzyl alcohol, △ = pent-4-en-1-ol, ■ = 2-hydroxyethyl methacrylate, ○ = glycidol, ◆ = ethanol, and ● = water.

could also be plasticized by other alcohols such as glycidol, 2-hydroxyethyl methacrylate (HEMA), pent-4-en-1-ol, and benzyl alcohol (Figure 1), with the depression in the T_g value being more pronounced for the more hydrophilic plasticizers. Further experiments showed that 41–68% of these plasticizers could be doped into the glasses without phase separation (Table 1). The resultant plasticized glasses were viscous, free-flowing isotropic liquids that were stable to phase separation and/or crystallization for over one week under ambient conditions, and displayed T_g values well below room temperature.

Differential scanning calorimetry (DSC) and microscopic studies of the system benzyl alcohol:(glucose:ethyl β -D-glucoside:propyl β -D-glucoside (12:41:47)):buffer uncovered six distinct regions in the phase diagram (Figure 2): (A) *monophasic glass*: a stable/metastable isotropic plasticized glass region for benzyl alcohol concentrations up to 53% and buffer contents up to 72%, with T_g values extending from below –70 °C up to 44 °C; (B) *microemulsion–glass*: a solution of alkyl glucoside in buffer-saturated benzyl alcohol, dispersed as a microemulsion in a plasticized glass phase; (C) *macroemulsion–glass*: a two-phase system of benzyl alcohol:buffer:alkyl glucoside solution together with a plasticized glass phase; (D) *monophasic solution*: a saturated solution of alkyl glucoside in buffer-saturated benzyl alcohol; (E) *biphasic solution*: a biphasic system of alkyl glucoside in water-saturated benzyl alcohol, together with benzyl alcohol in a buffer/alkyl glucoside solution; (F) *monophasic solution*: a homogeneous, isotropic ternary solution of alkyl glucoside and benzyl alcohol in buffer.

Encouraged by these results, we examined the plasticization of sugar–alkyl glycoside glasses of α - and β -D-glucose and galactose, β -D-mannose, and *N*-acetyl- β -D-glucosamine by a variety of dopants including long-chain alcohols, phenols, amino acid derivatives, hydroxyacids, glycerolipids, sphingolipids, and cardenolides (Table 1). The T_g values of the anhydrous glasses ranged over 38–50 °C, with the inclusion of 5–8% of water:propanol (w:w) depressing these to 18–25 °C. Importantly, these glasses could be plasticized with 13–35% of hydrophobic dopants before phase separation was observed. Even hydrophobic compounds such as digi-

[*] Dr. I. Gill, Dr. R. Valivety
Biotransformation Department
Biotechnology Center of Excellence
Roche Vitamins Inc., Building 102
340 Kingsland Street, Nutley, NJ 07110-1199 (USA)
Fax: (+1) 973-284-5979
E-mail: iqbalgill@hotmail.com
E-mail: iqbal_s.gill@roche.com

Supporting information for this article is available on the WWW under <http://www.wiley-vch.de/home/angewandte/> or from the author.

Table 1. Plasticization of monosaccharide – alkyl glycoside glasses by various dopants (plasticizers).^[a]

Composition of pure glass phase ^[b] [%]	H ₂ O [%]	PrOH [%]	T _g ^[c] [°C]	Dopant	[Dop] _{sat} ^[d] [%]	T _g ^[e] [°C]
D-Glc:Et-β-D-Glcp:Pr-β-D-Glcp (12:41:47)	3	2	25 (44)	glycidol	68	< –100
	3	2	25 (44)	2-hydroxyethyl methacrylate	61	< –100
	3	2	25 (44)	pent-4-en-1-ol	56	< –100
	3	2	25 (44)	benzyl alcohol	41	–82
	3	2	25 (44)	hydroquinone	18	–28
	3	2	25 (44)	(R)-rhododendrol	32	–46
	3	2	25 (44)	(S)-N-Aloc-Ser-OMe	35	–50
	3	2	25 (44)	(R,S)-1-O-oleoylglycerol	19	–43
	3	2	25 (44)	sphingosine	23	–49
	3	2	25 (44)	digitoxigenin	11	–23
D-Glc:Et-α-D-Glcp:Pr-α-D-Glcp (19:37:44)	5	10	–24 (44)	(R,S)-1-O-oleoylglycerol	28	–61
	5	10	–24 (44)	digitoxigenin	17	–60
D-Gal:Et-α-D-Galp:Pr-α-D-Galp (18:39:43)	3	1	27 (47)	geraniol	29	–77
D-Gal:Et-β-D-Galp:Pr-β-D-Galp (16:36:48)	4	1	22 (41)	nerol	24	–74
D-Man:Et-β-D-Manp:Pr-β-D-Manp (17:46:37)	5	2	25 (50)	ricinoleic acid	14	–28
D-Man:Et-β-D-Manp:Pr-β-D-Manp (17:46:37)	6	2	18 (38)	vanillin	13	–45
D-GlcNAc:Et-β-D-GlcNAcp:Pr-β-D-GlcNAcp (15:59:26)	5	5	28 (54)	α-ionone	9	–37

[a] All percentages quoted are the weight to weight ratio. [b] Composition of the anhydrous sugar – alkyl glycoside glass. [c] T_g value of the anhydrous sugar – alkyl glycoside glass (in parenthesis) and the given monosaccharide:alkyl glycoside:water:propanol glass (without parenthesis). [d] Maximum amount of dopant possible without phase separation. [e] T_g value of the sugar:alkyl glycoside:water:propanol:dopant composition. The plasticized glasses were formed by heating the mixtures to above the T_g value of the pure sugar glasses, followed by cooling to room temperature.

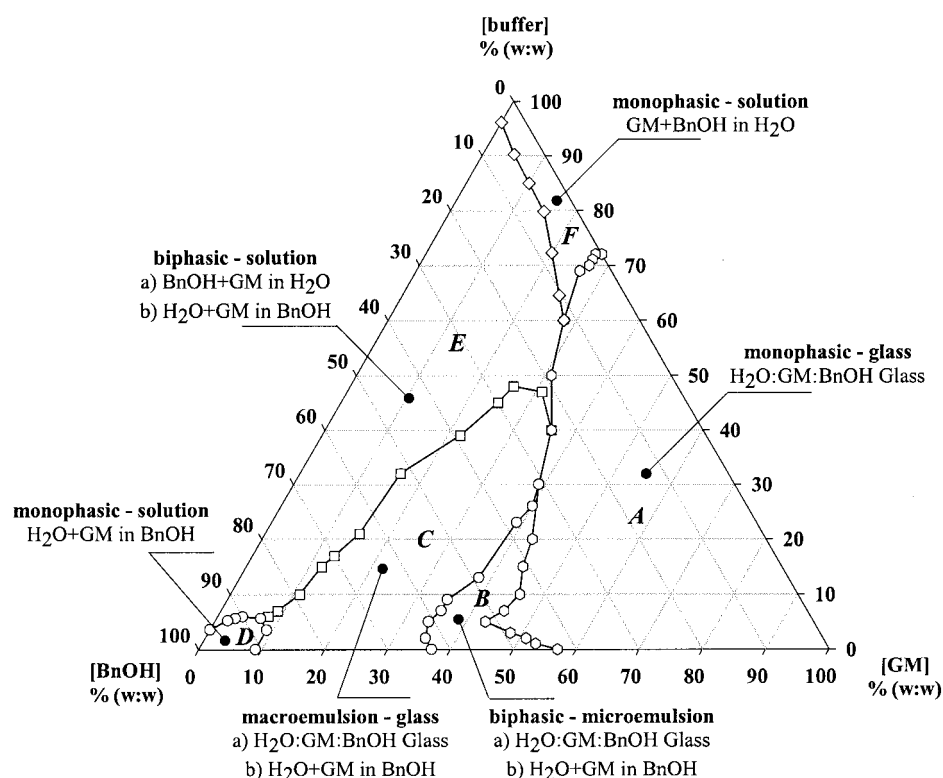


Figure 2. Ternary phase diagram for a system containing benzyl alcohol/glucose:(ethyl β-D-glucoside: (propyl β-D-glucoside (12:41:47))), and acetate buffer (50 mM, pH 6). The compositions were formed by heating the sugar – glucoside glass to 40 °C, followed by dilution with benzyl alcohol and/or buffer. The mixtures were allowed to equilibrate at room temperature for 24 h prior to examination by DSC and microscopy. Gm = glucose-glucoside mixture

toxigenin and ricinoleic acid could be incorporated at levels of 11–14% into the glasses, contrasting with their very low solubilities in pure monosaccharide glasses or aqueous solutions. Furthermore, the judicious elevation of the water: propanol contents of the glasses enabled significant increases in dopant concentrations, and also allowed the effective

solubilization of highly hydrophobic and nonhydroxylated molecules, such as α- and β-ionone (Table 1).

On examination of various amino acid, peptide, aromatic, lipid, and terpenoid acceptors, we discovered that above their saturating concentrations the plasticizers gave rise to a variety of microheterogeneous systems. In the simplest cases, these consisted of micro- and macroemulsions (higher alkyl alcohols, arylalkyl alcohols, ricinoleic acid) or solid suspensions (hydroquinones, cardenolides) of the excess dopant dispersed in the dopant-saturated plasticized glass (Figure 3b). However, in the cases of diols, diamides, and peptides, two-phase plasticized glass – eutectoid systems were readily formed (Figure 3c). Meanwhile, bicontinuous plasticized glass – liquid crystal phases were observed for glycerolipid and sphingolipid dopants (Figure 3d).

The results demonstrate the existence of a novel class of glasses derived from mixtures of monosaccharides and their alkyl glycosides, which are capable of solubilizing a variety of hydrophilic and hydrophobic compounds to form isotropic liquids. Preliminary results indicate the possibility of engineering the T_g values and plasticization profiles of the glasses by varying the alkyl glycosides used for glass formation, the ratios of the glass-forming components, and the amounts of modifiers such

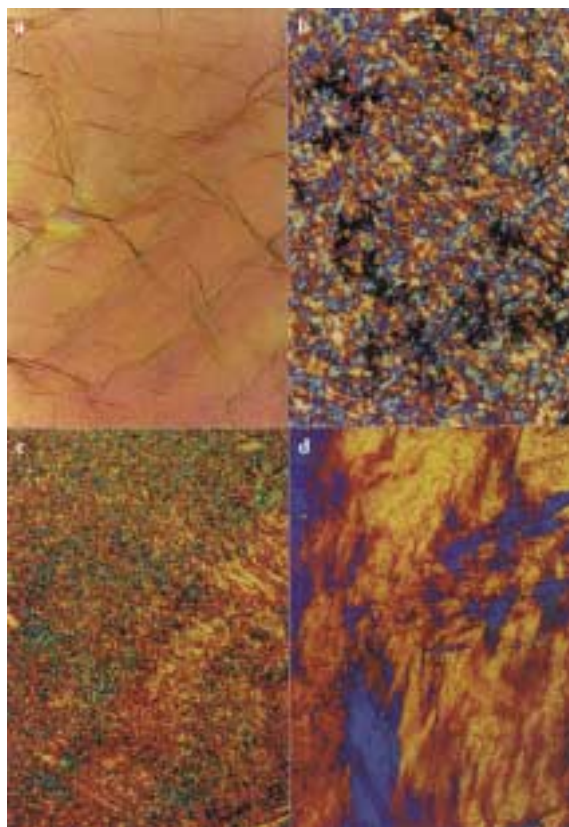


Figure 3. Examples of homogeneous and heterogeneous plasticized glass phases. a) Homogeneous glass: benzyl alcohol:(β -D-Glc:Et- β -D-Glcp:Pr- β -D-Glcp (12:41:47)):buffer:ethanol (4:4:1:1), -60°C . b) Heterogeneous suspension of a solid acceptor in a plasticized glass: hydroquinone:(β -D-Glc:Et- β -D-Glcp:Pr- β -D-Glcp (11:42)):buffer:ethanol (40:45:10:5), 30°C . c) Liquid eutectoid in plasticized glass: (*S,S*)-*N*¹-Aloc:serinylalanine methyl ester:(β -Gal:Et- β -D-Gal:Pr- β -D-Gal (16:36:48)):buffer:ethanol (25:55:10:10), 30°C . d) Liquid crystal in plasticized glass: (*R,S*)-1-oleoylglycerol:(β -Gal:Et- β -D-Galp:Pr- β -D-Galp (16:36:48)):buffer:ethanol (60:25:5:10), 30°C .

as water and lower alcohols. In addition to applications in the encapsulation/stabilization of hydrophobic bioactives and biological samples, such plasticized glasses are promising media for glycosidase-catalyzed glycosylations.

Experimental Section

Representative synthesis of glass-forming 12:41:47 β -D-Glc:Et- β -D-Glcp:Pr- β -D-Glcp mix. β -D-Glucose (100 g) was dissolved in hot acetate buffer (40 mL, 15 mM, pH 6, containing 5 mM of calcium and magnesium acetates), and the solution was cooled to 65°C . Ethanol (20 mL), then almond β -D-glucosidase (0.5 g in 5 mL of buffer containing 10 mM of 1,4-dithiothreitol), were added to the solution at 65°C , and ethanol:1-propanol (2:3, 500 mL) was added over 4 h. Further portions of the enzyme (1×0.5 g in 5 mL of buffer) and alcohol mixture (500 mL, over 6 h) were added, and reaction continued for 52 h. Filtration through silica gel, then rotary evaporation at 60°C gave the product as a pale yellow glass containing 3% of water and 2% of propanol (117 g, 88% of β -D-glucosides, $T_g = 23$ – 26°C). The other monosaccharide–glycoside glasses were synthesized in a similar manner, as described in the Supporting Information.

Received: May 23, 2000 [Z15159]

- [1] a) E. Y. Shalaev, F. Franks, *J. Chem. Soc. Faraday Trans.* **1995**, *91*, 1511–1517; b) Y. Roos, *Carbohydr. Res.* **1993**, *238*, 39–48; c) Y. Roos, M. Karel, *J. Food Sci.* **1991**, *56*, 1676–1681; d) L. Finegold, F. Franks,

R. H. M. Hatley, *J. Chem. Soc. Faraday Trans. 1* **1989**, *85*, 2945–2951; e) F. Franks, *Pure Appl. Chem.* **1993**, *12*, 2527–2537.

- [2] a) F. Franks, *Biotechnology* **1994**, *12*, 253–256; b) T. Moreira, J. Pendas, A. Gutierrez, R. Pomes, J. Duque, F. Franks, *Cryo-Lett.* **1998**, *19*, 115–122; c) S. P. Duddu, P. R. DalMonte, *Pharm. Res.* **1997**, *14*, 591–595; d) W. Q. Sun, A. C. Leopold, L. M. Crowe, J. H. Crowe, *Biophys. J.* **1996**, *70*, 1769–1776; e) K. L. Koster, Y. P. Lei, M. Anderson, S. Martin, G. Bryant, *Biophys. J.* **2000**, *78*, 1932–1946.
- [3] a) J. H. Crowe, A. E. Oliver, F. A. Hoekstra, L. M. Crowe, *Cryobiology* **1997**, *35*, 20–30; b) F. A. Hoekstra, W. F. Wolters, J. Buitinik, E. A. Golovina, J. H. Crowe, L. M. Crowe, *Comp. Biochem. Physiol.* **1997**, *117*, 335–341.

Enzymatic Glycosylation in Plasticized Glass Phases: A Novel and Efficient Route to O-Glycosides**

Iqbal Gill* and Rao Valivety

Glycosidation is widely encountered in nature where it serves to modulate the biological activity, solubility, transport, bioavailability, and chemical/biological stability of aglycones.^[1,2] Major efforts have been invested into developing strategies for glycosidation,^[3] with enzymatic methods attracting especial interest, by virtue of their mildness, high selectivity, and acceptance of unprotected sugars as substrates.^[3b,4] The ability of glycosidases to use nonactivated sugars, their broad specificity for aglycones, and their wide availability, has made these enzymes attractive for synthetic applications.^[4] Thus, glycosidases have been used for the glycosylation of sugars and aza-sugars,^[5] aliphatic and aromatic alcohols,^[6,7] peptides,^[8] glycerides and sphingolipids,^[9] terpenoids,^[10] phenolics,^[11] alkaloids,^[12] and antibiotics.^[13]

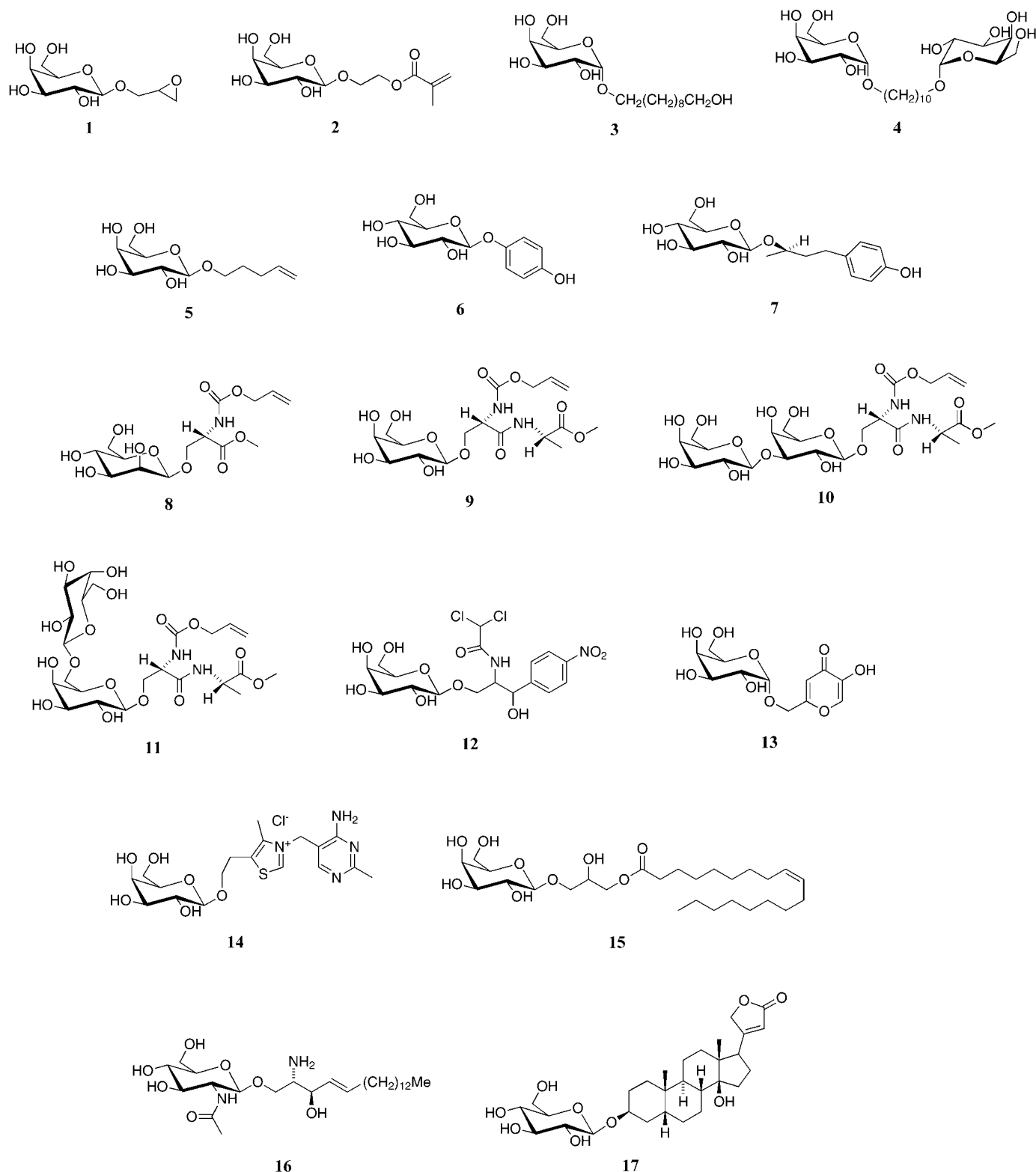
In the preceding communication we disclosed the formation of plasticized glasses by mixtures of monosaccharides, alkyl glycosides and various hydrophilic and hydrophobic compounds. We now describe the application of these liquids as media for glycosidase-catalyzed reactions. Plasticized glasses support high concentrations of both acceptor and sugar donor and enable the synthesis of a variety of glycosides (Scheme 1) in good yields and with unprecedented productivities.

Despite extensive synthetic applications of glycosidases, the difficulties encountered in accommodating solvent requirements of the substrates, thermodynamic considerations, and prerequisites for efficient biocatalyst function have limited

[*] Dr. I. Gill, Dr. R. Valivety
Biotransformation Department
Biotechnology Center of Excellence
Roche Vitamins Inc., Building 102
340 Kingsland Street, Nutley, NJ 07110-1199 (USA)
Fax: (+1) 973-284-5979
E-mail: iqbalgill@hotmail.com
E-mail: iqbal_s.gill@roche.com

[**] We thank J. Eagles and Dr. M. A. Masood for NMR spectroscopy and mass spectrometry analyses.

Supporting information for this article is available on the WWW under <http://www.wiley-vch.de/home/angewandte/> or from the author.



Scheme 1.

the synthetic efficiencies, notably with hydrophobic acceptors. The problems are: (1) The native enzymes perform poorly in aqueous or organic media with water contents below 5–10 % (all percentages are weight to weight ratios (w/w) unless otherwise stated); (2) the thermodynamic considerations require the water content to be minimized for maximal

yields; (3) it is difficult to satisfy the divergent solvent requirements of hydrophilic sugar donors and hydrophobic acceptors; and (4) glycosidases do not tolerate high levels of solvents such as DMF, DMSO, and pyridine, which have been employed for overcoming solubility issues in other hydrolase-catalyzed syntheses.^[4d]

To circumvent these issues, we examined whether sugar/alkyl glycoside/dopant plasticized glasses could be applied as reaction media. First, we examined the performance of almond β -glucosidase in liquids formed by plasticizing a 12/41/47 D-glucose/ethyl β -D-glucoside/propyl β -D-glucoside glass with glycidol, 2-hydroxyethyl methacrylate (HEMA), pent-4-en-1-ol, or benzyl alcohol. In all cases, the enzyme was found to readily catalyze glycosylation, providing that the initial water content was approximately 10% or higher. In Figure 1, the benzyl β -D-glucoside formation profiles are compared for a plasticized glass, the devitrified glass (obtained by freeze–thaw cycling), a biphasic system, and a solution in acetonitrile. The best performance was attained

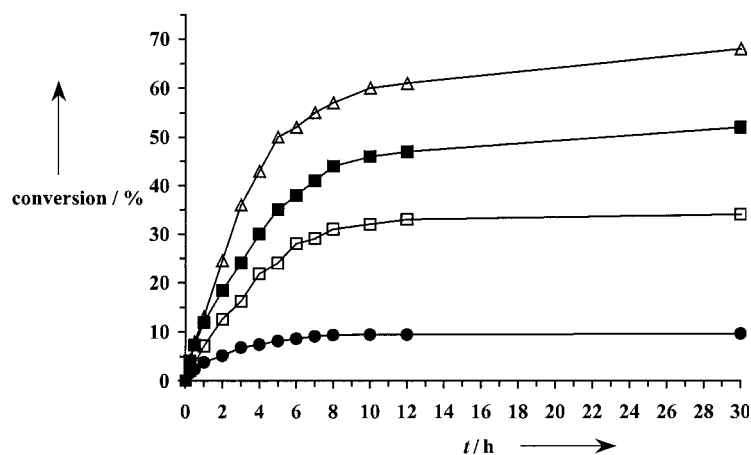


Figure 1. Almond β -glucosidase mediated formation of benzyl β -D-glucopyranoside in conventional media and plasticized glass phases. Δ = Plasticized glass ($T_g < -50^\circ\text{C}$), with 40% glucose–glucoside (1.91M), 40% benzyl alcohol (3.74M), 10% acetate buffer (50mM, pH 6, with 10mM of calcium and magnesium acetates and DTT), and 10% ethanol. \blacksquare = Biphasic medium, with 10% (v/v) glucose–glucoside solution (2.0M in buffer, 0.2M sugar) and 90% (v/v) benzyl alcohol (8.33M). \square = Devitrified glass, consisting of glucose–glycoside saturated buffer, a benzyl alcohol rich phase, and solid glucose–glycoside. \bullet = Organic solvent medium, with 10% (v/v) aqueous glucose–glucoside solution (2.0M), and 90% (v/v) of acetonitrile containing 1.1M benzyl alcohol. A 12/41/47 mix of D-Glc/Et- β -D-Glcp/Pr- β -D-Glcp was used as the sugar donor. All reactions were run at 60°C using enzyme (100 mg mL^{-1} in buffer) at 100 U g^{-1} . Sealed, stirred vials were used for the conventional reactions, and static vials, closed for 2 h and open thereafter, for the glass-phase reactions.

with the plasticized glass, which gave a final yield of 67%, corresponding to a benzyl β -D-glucoside concentration of 1.3M (0.35 g per gram of reaction mixture). This compares very well with the yields of 53% (0.11M) and 12% (0.024M) and productivities of 0.03 and 0.007 g per gram of reaction mixture that were observed for the biphasic and acetonitrile media, respectively.

In addition to almond β -glucosidase, β -galactosidases from *K. fragilis*, *E. coli*, *A. niger*, and *A. oryzae*, and the α -galactosidases of *A. niger* and *C. arabica*, also catalyzed the glycosylation of glycidol, HEMA, pent-4-en-1-ol, and long-chain diols capable of forming plasticized glasses, providing that sufficient water (8–13%) was present to activate the biocatalyst (Table 1). Plasticized glasses doped with 20–60% of the acceptors furnished yields of 63–71%, corresponding to productivities of 0.31–0.65 g per gram of reaction mixture. Homogeneous liquids were not essential, with reactions also readily proceeding in micro- and macroemul-

sions, which comprised of excess acceptor dispersed in acceptor-saturated plasticized glass, albeit with lower rates and yields.

Analysis of reaction mixtures during the course of benzyl β -D-glucoside formation in a system with starting composition D-Glc (4.8), Et- β -D-Glcp (16.4), Pr- β -D-Glcp (18.8), BnOH (40), EtOH (10), and H_2O (10%) indicated that most of the conversion occurred by transglycosylation rather than by reverse hydrolysis. Thus, after 4 h, the conversion of 41% of glucose/glycoside substrates into benzyl β -D-glucoside was largely at the expense of Et- β -D-Glcp and Pr- β -D-Glcp, the amounts of which decreased by 42 and 51% respectively, while the amount of glucose decreased by only 9%. Analysis

of rate data indicated that the rate of transglycosylation exceeded that of reverse hydrolysis by a factor of 6.7–9.1. After 42 h, 67% of the substrates had been transformed into benzyl β -D-glucoside, with net corresponding decreases of 23, 81, and 93% in D-Glc, Et- β -D-Glcp, and Pr- β -D-Glcp, respectively. The final, dry reaction mixture had the composition D-Glc (4.7), Et- β -D-Glcp (5.6), Pr- β -D-Glcp (3.3), BnOH (35.1), Bn- β -D-Glcp (46.2), and oligosaccharides (5.1%).

We then examined systems where the acceptor was solid and only partially soluble in the glass phase. A 40/45/10/5 mix of hydroquinone/glucose–alkyl glycoside/buffer/ethanol, which contained the majority of the acceptor as crystalline solid, was used as the test system. Despite the heterogeneous medium, β -D-glucosidases from *P. dulcis* and *T. reesei* and bovine liver β -D-glucuronidase mediated glycosylation to afford hydroquinone β -D-glucoside with respective yields of 26, 19, and 65% and productivities of 0.18, 0.13, and 0.46 gram per gram of reaction mixture. Encouraged by these results, we attempted the glycosylation of other partially miscible/soluble acceptors which furnished heterogeneous mixtures with sugar–glycoside glasses (Table 1). As before, upon including approximately 5–10% of water and by operating at 40 – 60°C above T_g in order to ensure a low-viscosity plasticized glass, biocatalysis proceeded smoothly to furnish the required glycosides in good

yields. Yields of 39–58% were obtained, with resulting productivities of 0.25–0.49 g per gram of reaction mixture, the latter exceeding those of conventional systems described to date by one order of magnitude or more.

In conclusion, glycosidases are catalytically active in plasticized glasses and mediate the glycosylation of a variety of acceptors. The high substrate concentrations enabled in these media can result in synthesis rates of up to one magnitude higher than for dilute systems, and can furnish product concentrations of 0.13–0.65 g per gram of reaction mixture.

Experimental Section

Representative synthesis of a glycoside in a plasticized glass phase. **15:** A D-Gal/Et- β -D-Galp/Pr- β -D-Galp mixture (16/36/48, 0.42 g) was mixed with metaphosphate buffer (40 μL , 50 mM, pH 7, with 10 mM each of calcium and magnesium acetates) and ethanol (0.21 mL) in a vial. The vial was then sealed and the mixture heated until a homogeneous liquid was formed. After cooling, (*R,S*)-1-*O*-oleoylglycerol (1.0 g) was added, the mix incu-

Table 1. Examples of glycosidation catalysed by glycosidases in plasticized glass phases.

Product	Reaction mixture components (concentration [%])	Scale [mmol]	System ^[a] (T_i [°C])	Enzyme	T [°C]	t [h]	Yield ^[b] [%]	Y [g g ⁻¹]
1	D-Gal (8), Et- β -D-Gal (18)	47.8	type I	<i>K. fragilis</i> β -D-galactosidase	40	26	71 (64) ^[c]	0.48
	Pr- β -D-Gal (24), H ₂ O (10) (<i>R,S</i>)-glycidol (40)	4.78	$T_g < -80$	<i>E. coli</i> β -D-galactosidase	40	26	67	0.44
2	D-Gal (7), Et- β -D-Gal (16)	17.5	type I	<i>E. coli</i> β -D-galactosidase	35	40	67 (58) ^[d]	0.50
	Pr- β -D-Gal (22), H ₂ O (10), HEMA (45)	17.5	$T_g < -80$	<i>A. niger</i> β -D-galactosidase	35	40	43	0.32
3	D-Gal (3), Et- α -D-Gal (7)	9.50	type I	<i>A. niger</i> α -D-galactosidase	40	26	74 (71) ^[e]	0.31
	Pr- α -D-Gal (10), H ₂ O (10), EtOH (10) 1,10-dihydroxydecane (60)	0.95	$T_g = -34$	<i>C. arabica</i> α -D-galactosidase	40	50	31	0.13
4	D-Gal (9), Et- α -D-Gal (22)	17.2	type I	<i>A. niger</i> α -D-galactosidase	40	30	63 (58) ^[f]	0.65
	Pr- α -D-Gal (29), H ₂ O (10), EtOH (10) 1,10-dihydroxydecane (20)		$T_g = -34$					
5	D-Gal (6), Pr- β -D-Gal (34)	18.6	type I	<i>A. oryzae</i> β -D-galactosidase	40	50	64 (60) ^[g]	0.47
	H ₂ O (10), EtOH (10), pent-4-en-1-ol (40)	9.30	$T_g = -63$	<i>E. coli</i> β -D-galactosidase	40	50	39	0.30
6	D-Glc (5), Et- β -D-Glc (19)	21.1	type II	bovine β -D-glucuronidase	40	30	65 (59) ^[h]	0.46
	Pr- β -D-Glc (21), H ₂ O (10), EtOH (5)	21.1	$T_g = -47$	almond β -D-glucosidase	60	36	26	0.18
7	hydroquinone (40)	21.1		<i>T. reesei</i> β -D-glucosidase	40	62	19	0.13
	D-Glc (4), Et- β -D-Glc (14), Pr- β -D-Glc (17), H ₂ O (10), EtOH (5)	6.64 1.66	type II $T_g = -61$	almond β -D-glucosidase bovine β -D-glucuronidase	70 35	20 52	58 (54) ^[i] 38	0.49 0.31
8	D-Man (4), Et- β -D-Man (9)	3.03	type III	<i>H. aspersa</i> β -D-mannosidase	40	60	52 (48) ^[j]	0.26
	Pr- β -D-Man (7), H ₂ O (10), EtOH (10) (<i>S</i>)- <i>N</i> -Aloc-Ser-OMe (60)		$T_e = 27$ $T_g = -68$					
9	D-Gal (3), Et- β -D-Gal (7)	6.37	type IV	<i>E. coli</i> β -D-galactosidase	45	44	45 (41) ^[k]	0.25
	Pr- β -D-Gal (10), H ₂ O (10), EtOH (10)	1.90	$T_e = 21$	<i>K. fragilis</i> β -D-galactosidase	40	52	28	0.15
10	(<i>S,S</i>)- <i>N</i> ¹ -Aloc-Ser-Ala-OMe (60)	1.90	$T_g = -64$	<i>A. oryzae</i> β -D-galactosidase	40	52	37	0.21
	D-Gal (9), Et- β -D-Gal (20)	7.28	type V	<i>E. coli</i> β -D-galactosidase	45	38	46 (41) ^[l]	0.31
11	Pr- β -D-Gal (26), H ₂ O (10), EtOH (10)		$T_e = 16$				24 (21) ^[l]	0.16
	(<i>S,S</i>)- <i>N</i> ¹ -Aloc-Ser-Ala-OMe (25)		$T_g = -57$					
12	D-Gal (5), Et- β -D-Gal (11)	7.20	type II	<i>A. oryzae</i> β -D-galactosidase	35	36	41 (37) ^[m]	0.35
	Pr- β -D-Gal (14), H ₂ O (10), EtOH (5)	1.44	$T_g = -73$	<i>E. coli</i> β -D-galactosidase	35	36	26	0.21
13	chloramphenicol (50), <i>n</i> PrOH (5)	1.44		<i>K. fragilis</i> β -D-galactosidase	40	36	32	0.28
	D-Glc (5), Et- α -D-Glc (11)	3.60	type II	<i>S. cerevisiae</i> α -D-glucosidase	40	60	43 (38) ^[n]	0.29
14	Pr- α -D-Glc (14), H ₂ O (10), EtOH (5)		$T_g = -59$					
	kojic acid (50 %), <i>n</i> PrOH (5)							
15	D-Gal (5), Et- β -D-Gal (11)	7.15	type II	<i>A. oryzae</i> β -D-galactosidase	40	48	45 (41) ^[o]	0.38
	Pr- β -D-Gal (14), H ₂ O (10), EtOH (10) thiamine chloride (50)	1.43	$T_g = -62$	<i>K. fragilis</i> β -D-galactosidase	40	48	27	0.21
16	D-Gal (4), Et- β -D-Gal (9)	1.98	type VI	<i>E. coli</i> β -D-galactosidase	40	36	42 (38) ^[p]	0.31
	Pr- β -D-Gal (12), H ₂ O (5), EtOH (10)		$T_g = -51$	<i>A. oryzae</i> β -D-galactosidase	40	36	21	0.14
17	(<i>R,S</i>)-1- <i>O</i> -oleoylglycerol (60)			<i>K. fragilis</i> β -D-galactosidase	40	36	37	0.28
	D-GlcNAc (4), Et- β -D-GlcNAc (8)	1.23	type VI	<i>A. oryzae</i> β -D- <i>N</i> -acetylhexosaminidase	42	35	48 (44) ^[q]	0.36
18	Pr- β -D-GlcNAc (18), H ₂ O (10), EtOH (5)		$T_g = -62$					
	sphingosine (50), <i>n</i> PrOH (5)							
19	D-Glc (3), Et- β -D-Glc (8)	1.34	type II	bovine β -D-glucuronidase	40	43	39 (36) ^[r]	0.28
	Pr- β -D-Glc (9), H ₂ O (10), EtOH (10)	0.54	$T_g = -75$	almond β -D-glucosidase	60	46	21	0.16
20	digitoxigenin (50), <i>n</i> PrOH (10)	0.54		<i>T. reesei</i> β -D-glucosidase	40	69	35	0.24

[a] Phase types determined by microscopy and differential scanning calorimetry (DSC): I, homogeneous plasticized glass; II, solid acceptor suspended in plasticized glass; III, microemulsion of acceptor in plasticized glass; IV, plasticized glass in liquid eutectoid of acceptor; V, liquid eutectoid of acceptor in plasticized glass; VI, liquid crystal of acceptor in plasticized glass. T_i = transition temperature, T_g = glass transition temperature, T_e = eutectic temperature.
 [b] The first figure is the conversion as determined by HPLC analysis, the figure in parentheses is the isolated yield (based on the limiting substrate), and the third figure is the quantity obtained, in grams, per gram of reaction mixture; Higher glycosides were also formed. [c] 10 % of diglycosides formed. [d] 8 % of diglycosides and 5 % of triglycosides formed. [e] 11 % of **4** formed. [f] 13 % of tri- and tetraglycosides formed. [g] 11 % of di- and triglycosides formed. [h] 9 % of di- and triglycosides formed. [i] 15 % of diglycosides formed. [j] 14 % of diglycosides formed. [k] 16 % of a mixture of **10** and **11** formed. [l] 11 % of triglycosides formed. [m] 23 % of diglycosides formed. [n] 16 % of di- and triglycosides formed. [o] 19 % of diglycosides formed. [p] 10 % of 2-*O*-glycosides and 7 % of diglycosides formed. [q] 18 % of diglycosides and 12 % of triglycosides formed. [r] 24 % of di- and triglycosides formed. T_e , eutectic temperature.

bated at 40 °C, and *E. coli* β -D-galactosidase (5 mg in 40 μ L of 100 mM buffer containing 10 mM DTT) added with thorough mixing. The vial was sealed, placed in a heating block (40 °C) for 3 h, and then opened, and the reaction was allowed to continue for 33 h. The mix was extracted with methanol (3 \times 3 mL), and the extract was concentrated by rotary evaporation, then purified by medium pressure chromatography to give the product as a pale yellow oil (0.40 g, 38 % yield, 95 % purity). This and the other glycosides were fully characterized as detailed in the Supporting Information.

Received: May 23, 2000 [Z15160]

- [1] R. Ikan, *Naturally Occurring Glycosides*, Wiley, New York, 1999.
- [2] a) L. L. Hench, J. K. West, *Chem. Rev.* **1990**, *90*, 33; b) P. Sears, C.-H. Wong, *Angew. Chem.* **1999**, *111*, 2446–2471; *Angew. Chem. Int. Ed.* **1999**, *38*, 2300–2324; c) H. Lis, N. Sharon, *Eur. J. Biochem.* **1993**, *218*, 1–27; d) A. Varki, *Glycobiology* **1993**, *3*, 97–130.
- [3] a) K. Toshima, K. Tatsuta, *Chem. Rev.* **1993**, *93*, 1503–1531; b) B. G. Davies, *J. Chem. Soc. Perkin Trans. 1* **1999**, 3215–3237.
- [4] a) F. van Rantwijk, M. Woudenberg-van Oosterom, R. A. Sheldon, *J. Mol. Catal. B* **1999**, *6*, 511–532; b) M. Scigelova, S. Singh, D. H. G. Crout, *J. Mol. Catal. B* **1999**, *6*, 483–494; c) P. Sears, C.-H. Wong,

- Chem. Commun.* **1998**, 1161–1171; d) S. Takayama, G. J. McGarvey, C.-H. Wong, *Chem. Soc. Rev.* **1997**, 26, 407–416; e) V. Kren, J. Thiem, *Chem. Rev.* **1997**, 26, 463–474; f) K. Drauz, H. Waldmann, *Enzyme Catalysis in Organic Synthesis*, VCH, Weinheim, **1995**.
- [5] a) C. H. Tran, P. Critchley, D. H. G. Crout, C. J. Britten, S. J. Witham, M. I. Bird, *J. Chem. Soc. Perkin Trans. 1* **1998**, 2295–2300; b) H. Kono, M. R. Waelchli, M. Fujiwara, T. Erata, M. Takai, *Carbohydr. Res.* **1999**, 321, 67–74; c) R. L. Lio, J. Thiem, *Carbohydr. Res.* **1999**, 317, 180–190; d) S. Singh, M. Scigelova, D. H. G. Crout, *Chem. Commun.* **1999**, 2065–2066.
- [6] a) H. Shinoyama, Y. Kamiyama, T. Yasui, *Agric. Biol. Chem.* **1988**, 52, 2197–2202; b) A. Trincone, B. Nicolaus, L. Lama, A. Gambacora, *J. Chem. Soc. Perkin Trans. 1* **1991**, 2841–2844; c) M. Gelo-Pujic, E. Guibe-Jampel, A. Loupy, A. Trincone, *J. Chem. Soc. Perkin Trans. 1* **1997**, 1001–1002; d) G. Vic, J. Biton, D. L. Beller, J.-M. Michel, D. Thomas, *Biotechnol. Bioeng.* **1995**, 46, 109–116.
- [7] a) S. Matsumura, H. Kubokawa, K. Toshima, *Makromol. Chem. Rapid Commun.* **1993**, 14, 55–58; b) M. Santin, F. Rosso, A. Sada, G. Peluso, R. Improta, A. Trincone, *Biotechnol. Bioeng.* **1996**, 49, 217–222; c) A. M. Blinkovsky, J. S. Dordick, *Tetrahedron: Asymmetry* **1993**, 4, 1221–1228.
- [8] a) K. G. I. Nilsson, M. Scigelova, *Biotechnol. Lett.* **1994**, 16, 677–682; b) K. Suzuki, H. Fujimoto, Y. Ito, T. Sasaki, K. Ajisaka, *Tetrahedron Lett.* **1997**, 38, 1211–1214; c) K. Haneda, T. Inazu, M. Mizuno, R. Iguchi, K. Yamamoto, H. Kumagai, S. Aimoto, H. Suzuki, T. Noda, *Biorg. Med. Chem. Lett.* **1998**, 8, 1303–1312; d) K. G. I. Nilsson, *Biotechnol. Lett.* **1996**, 18, 791–794.
- [9] a) Y. Okahata, T. Mori, *J. Chem. Soc. Perkin Trans. 1* **1996**, 2861–2866; b) B. Guilbert, S. L. Flitsch, *J. Chem. Soc. Perkin Trans. 1* **1994**, 1181–1186; c) T. Morimoto, A. Nagatsu, N. Murakami, J. Sakakibara, *Tetrahedron* **1995**, 51, 6443–6450.
- [10] a) H. Nakagawa, M. Yoshiyama, S. Shimura, K. Kirimura, S. Usami, *Biosci. Biotechnol. Biochem.* **1996**, 60, 1914–1915; b) Z. Gunata, M. J. Vallier, J. C. Sapis, R. Baumes, C. Bayonove, *Enzyme Microbial Technol.* **1994**, 16, 1055–1058; c) A. Cheriti, A. Babadjanian, G. Balansard, *Nat. Prod. Lett.* **1994**, 4, 81–84.
- [11] a) M. A. Hassan, F. Ismail, S. Yamamoto, H. Yamada, K. Nakanishi, *Biosci. Biotechnol. Biochem.* **1995**, 59, 543–545; b) P. Wang, B. D. Martin, S. Parida, D. G. Rethwisch, J. S. Dordick, *J. Am. Chem. Soc.* **1995**, 117, 12885–12886; c) T. Yasukochi, K. Fukase, Y. Suda, K. Takagaki, M. Endo, S. Kusumoto, *Bull. Chem. Soc. Jpn.* **1997**, 70, 2719–2725; d) G. Vic, D. Thomas, D. H. G. Crout, *Enzyme Microb. Technol.* **1997**, 20, 597–603;
- [12] a) V. Kren, C. Auge, P. Sedmera, V. Havlicek, *J. Chem. Soc. Perkin Trans. 1* **1994**, 2481–2484; b) M. Scigelova, V. Kren, K. G. I. Nilsson, *Biotechnol. Lett.* **1994**, 16, 683–688.
- [13] a) Y. Susuki, K. Uchida, *Biosci. Biotechnol. Biochem.* **1994**, 58, 1273–1276; b) C. Scheckermann, F. Wagner, L. Fischer, *Enzyme Microb. Technol.* **1997**, 20, 629–634; c) M. Pozo, V. Gotor, *J. Chem. Soc. Perkin Trans. 1* **1993**, 1001–1002.

(CN₃H₆)₄[Zn₃(SeO₃)₅]: The First Organically Templated Selenite**

William T. A. Harrison,* Mark L. F. Phillips,
Jesse Stanchfield, and Tina M. Nenoff

An astonishing variety of inorganic networks templated by organic species have been reported over the last 10 years.^[1] A great deal of attention has been paid to the structure-directing role of the organic species,^[2] and the structural effect of variously coordinated cations, for example distorted octahedral vanadium^[3] and pyramidal tin(II).^[4] Less exploratory work has been carried out on the “anionic” part of the inorganic network, and most groups reported so far (phosphate,^[5] germanate,^[6] etc.) invariably adopt tetrahedral coordination. The possibilities of incorporating the pyramidal [HPO₃]^{2−} hydrogen phosphite group into extended structures templated by *inorganic*, alkaline earth cations was explored a few years ago.^[7] Herein we report the synthesis, crystal structure, and some properties of (CN₃H₆)₄[Zn₃(SeO₃)₅], the first organically templated phase to contain the pyramidal selenite [SeO₃]^{2−} ion.

(CN₃H₆)₄[Zn₃(SeO₃)₅], which is built up from 13 framework atoms, consists of layers of distorted ZnO₄ tetrahedra and SeO₃ groups, sharing vertices. The two distinct zinc atoms both form four Zn–O–Se bonds to selenium atom neighbors resulting in average Zn1–O and Zn2–O bond lengths of 1.950(4) and 1.972(4) Å, respectively. Zn2 has twofold rotational symmetry. The three crystallographically distinct selenium(IV) atoms adopt their characteristic pyramidal coordination, with the lone pair of electrons presumably directed towards the fourth tetrahedral vertex. Average Se–O bond lengths of 1.679(4), 1.682(4), and 1.691(4) Å result for Se1, Se2, and Se3, respectively, in good agreement with previous studies.^[8] The terminal Se1–O7 and Se3–O8 bonds are short (*d* = 1.648(4) and 1.648(5) Å, respectively), indicating that the oxygen atoms are not protonated.^[8] Se3 occupies a crystallographic mirror plane. The average Zn–O–Se bond angle of the six bridging O atoms is 124.9° (spread of values: 119.3(2)–127.7(2)°).

The connectivity of the ZnO₄ and SeO₃ units in (CN₃H₆)₄[Zn₃(SeO₃)₅] results in infinite, anionic layers of stoichiometry [Zn₃(SeO₃)₅]^{4−} which propagate normal to [010]. A novel grouping of three adjacent ZnO₄ tetrahedra

[*] Dr. W. T. A. Harrison
Department of Chemistry
University of Aberdeen
Aberdeen, AB24 3UE (UK)
Fax: (+44) 1224-272921
E-mail: w.harrison@abdn.ac.uk
Dr. M. L. F. Phillips
27468 Hayward Boulevard, Hayward, CA 94542 (USA)
J. Stanchfield, Dr. T. M. Nenoff
Catalysis and Chemical Technologies Department, PO Box 5800, MS
0710, Sandia National Laboratories, Albuquerque, NM 87185-0710
(USA)

[**] This work was supported by the U.S. Department of Energy (DOE) under contract DE-AC04-94AL85000. Sandia is a multiprogram laboratory operated by Sandia Corporation, a Lockheed Martin Company, for the U.S. DOE.

doubly capped by a pair of Se2 atoms (as selenite groups) is present (Figure 1). This results in an exceedingly large O5–Zn2–O5 bond angle of $130.4(2)^\circ$, where O5 forms the Zn2–O–Se2 bridge. The layers are completed by nominal (Se1–O7)

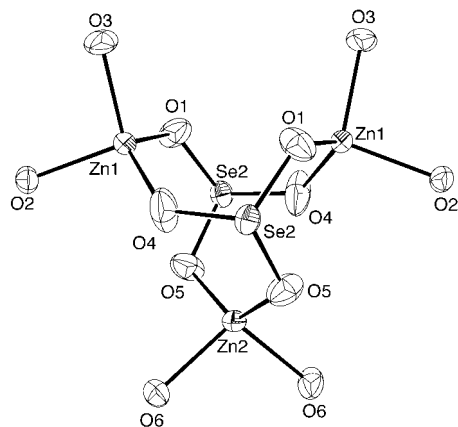


Figure 1. Structure of the $[\text{Zn}_3\text{Se}_2\text{O}_{12}]^{10-}$ fragment in $(\text{CN}_3\text{H}_6)_4[\text{Zn}_3(\text{SeO}_3)_5]$, showing the top-and-bottom capping of three adjacent ZnO_4 groups by Se2 (50% thermal ellipsoids).

groups which link the $\text{Zn}_3\text{Se}_2\text{O}_{12}$ moieties in the [100] direction, and nominal (Se3–O8) pairs which fuse these groupings in the [001] direction (Figure 2). This connectivity results in bifurcated 12-ring windows (i.e., windows built up from 12 polyhedral building blocks, six ZnO_4 and six SeO_3 groups) in the (101) plane. The maximum dimensions of this slightly squashed 12-ring, measured from O atom to O atom, are approximately $8.4 \times 8.9 \text{ \AA}$. The Se3 lone pairs point into this 12-ring.

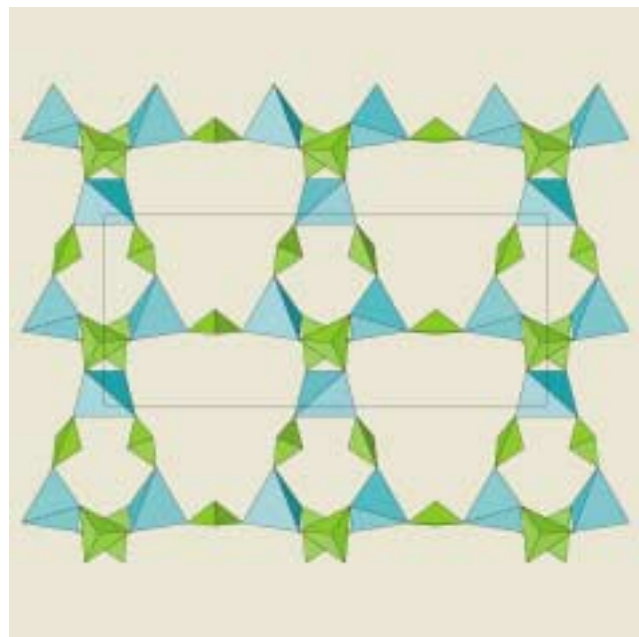


Figure 2. Polyhedral view down [010] of the sheet topology of $(\text{CN}_3\text{H}_6)_4[\text{Zn}_3(\text{SeO}_3)_5]$. The ZnO_4 groups are light blue, and the SeO_3 lone pair of electrons is represented by the fourth vertex of the flattened, light green, pseudo-tetrahedron.

The C–N distances for the propeller-shaped $[\text{CN}_3\text{H}_6]^+$ ions are typical.^[9] The C2-centered guanidinium cation displays a striking templating effect in occupying the 12-ring window of the Zn/Se/O layer and bonding to it by way of N–H \cdots O hydrogen bonds (Figure 3). The C1- and C3-centered guanidinium cations serve to bridge the inorganic layers in the [010] direction (Figure 4). Eleven of the twelve symmetry-independent guanidinium hydrogen atoms are involved in

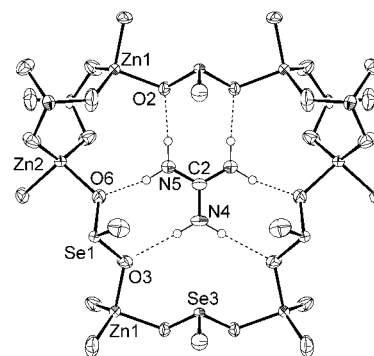


Figure 3. View approximately down [010] of a 12-ring window in $(\text{CN}_3\text{H}_6)_4[\text{Zn}_3(\text{SeO}_3)_5]$ showing the templating effect of the guanidinium cation, with the proposed N–H \cdots O hydrogen bonds indicated by dotted lines. Note the Se3 lone pair of electrons projecting into the 12-ring window.

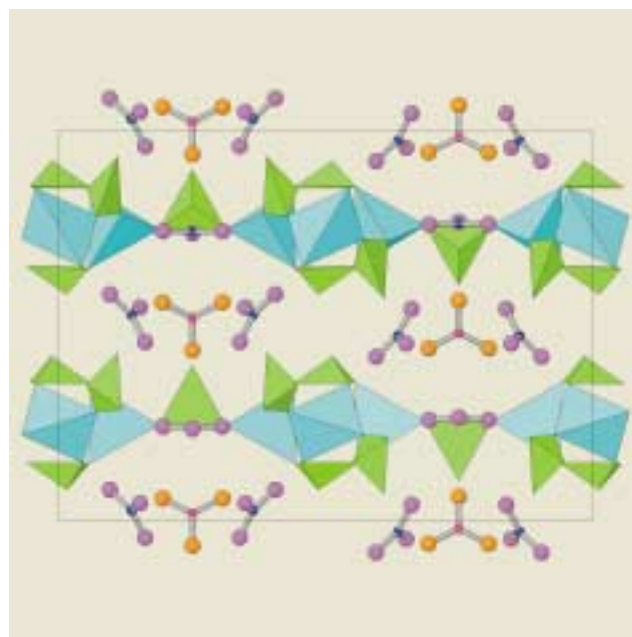


Figure 4. View down [100] of the $(\text{CN}_3\text{H}_6)_4[\text{Zn}_3(\text{SeO}_3)_5]$ structure showing the sandwich-motif of alternating inorganic and organic layers (inorganic color scheme as for Figure 2). For clarity, the C1-centered guanidinium cation is colored (C: blue; N: purple) as is the C3-centered species (C: red; N: orange).

N–H \cdots O hydrogen bonds, assuming a maximum H \cdots O bond length of 2.3 \AA . Based on geometrical positioning of the H atoms [$d(\text{N–H}) = 1.00 \text{ \AA}$], these H \cdots O contacts vary in length from 1.91 to 2.29 \AA . Seven of the acceptor oxygen atoms form parts of Zn–O–Se bridges and the two terminal Se–O groups accept two hydrogen bonds each.

The $(\text{CN}_3\text{H}_6)_4[\text{Zn}_3(\text{SeO}_3)_5]$ structure is completely different to those of previously characterized “inorganic” zinc selenites, all of which contain a dense network of ZnO_6 octahedra and $(\text{H})\text{SeO}_3$ pyramids.^[10] The 12-ring templating effect of the C2-centered guanidinium cation may be likened to its effect in templating polyhedral 12-rings (six ZnO_4 and six PO_4 tetrahedra) in zincophosphate (ZnPO) frameworks,^[11] although the overall structures of the ZnPO materials are completely different to that of the title compound. $(\text{CN}_3\text{H}_6)_4[\text{Zn}_3(\text{SeO}_3)_5]$ is the first member of a family of organically templated selenites which we will describe in more detail in the near future.

Experimental Section

Synthesis: Guanidinium carbonate (1.80 g, 10 mmol), ZnO (0.81 g, 10 mmol), SeO_2 (2.22 g, 20 mmol), and H_2O (20 mL) were added to a PTFE bottle, shaken well, and placed in a 95 °C oven. The bottle was vented and recapped after 1 h. An essentially quantitative yield of intergrown transparent slabs (longest dimension up to 1 mm) of $(\text{CN}_3\text{H}_6)_4[\text{Zn}_3(\text{SeO}_3)_5]$ was recovered by vacuum filtration after 7 days.

Properties: A simulation based on the $(\text{CN}_3\text{H}_6)_4[\text{Zn}_3(\text{SeO}_3)_5]$ single-crystal structure was in excellent agreement with X-ray powder data, indicating phase purity and high crystallinity. Thermogravimetric analysis/differential thermal analysis (TGA/DTA) (ramp at 10 °K min⁻¹ to 900 °C in air) for $(\text{CN}_3\text{H}_6)_4[\text{Zn}_3(\text{SeO}_3)_5]$ revealed the onset of a multistage 72 % weight loss at ~200 °C, which was complete by ~580 °C. Strong endothermic transitions at ~205, ~270, and ~570 °C were apparent. The weight loss of ~23 % occurring between ~200 °C and ~280 °C probably corresponds to loss of the guanidine template molecules (calcd 22.0 %). The overall weight loss is in fair agreement with a scheme involving the loss of all the organic species and selenium (as SeO_2) to result in a residue of $3 \times \text{ZnO}$ (calcd 77 %). The FTIR spectrum for $(\text{CN}_3\text{H}_6)_4[\text{Zn}_3(\text{SeO}_3)_5]$ revealed strong peaks at 3344 and 1671 cm⁻¹, corresponding to guanidinium N–H stretches and C–N/C=N stretches, respectively. Elemental analysis was satisfactory (%): calcd: C 4.48, H 2.26, N 15.69; found: C 4.11, H 2.23, N 14.59.

Structure determination: A crystal of $(\text{CN}_3\text{H}_6)_4[\text{Zn}_3(\text{SeO}_3)_5]$ (broken fragment, dimensions ~0.27 × 0.12 × 0.11 mm) was selected for data collection on a Bruker SMART 1000 CCD diffractometer (graphite-monochromated MoK_α radiation, $\lambda = 0.71073$ Å, $T = 300$ K): orthorhombic cell parameters from 4753 reflections ($4.6^\circ < 2\theta < 50^\circ$), 16466 reflections scanned ($2^\circ < 2\theta < 50^\circ$). After merging ($R_{\text{int}} = 0.055$), 1830 of the 2429 unique reflections were considered observed [$I > \sigma(I)$]. An absorption correction was applied with SADABS^[12] (min., max. equivalent transmission factors = 0.496, 0.862). The structure was solved by direct methods using SHELXS,^[13] refined by full-matrix least squares using CRYSTALS,^[14] and illustrated using ORTEP^[15] and ATOMS.^[16] Hydrogen atoms associated with the guanidinium cations were placed geometrically and refined by riding. Final residuals: $R(F) = 0.026$, $R_w(F) = 0.028$.

Crystal data: $(\text{CN}_3\text{H}_6)_4[\text{Zn}_3(\text{SeO}_3)_5]$, $M_r = 1071.25$, orthorhombic, space group $Pbcm$ (no. 57), $a = 8.9007(4)$, $b = 15.0771(7)$, $c = 20.5096(9)$ Å, $V = 2752.3(4)$ Å³, $Z = 4$, $\mu = 92.9$ cm⁻¹, $\rho_{\text{calcd}} = 2.586$ g cm⁻³, $F(000) = 2048$. Further details on the crystal structure investigation may be obtained from the Fachinformationszentrum Karlsruhe, 76344 Eggenstein-Leopoldshafen, Germany (fax: (+49) 7247-808-666; e-mail: crysdata@fiz-karlsruhe.de), on quoting the depository number CSD-411298.

Received: May 15, 2000 [Z15124]

- [1] A. K. Cheetham, G. Férey, T. Loiseau, *Angew. Chem.* **1999**, *111*, 3466; *Angew. Chem. Int. Ed.* **1999**, *38*, 3268.
- [2] M. E. Davis, R. F. Lobo, *Chem. Mater.* **1992**, *4*, 756.
- [3] M. I. Khan, L. M. Meyer, R. C. Haushalter, A. L. Schweizer, J. Zubietta, J. L. Dye, *Chem. Mater.* **1996**, *8*, 43.
- [4] S. Natarajan, A. K. Cheetham, *J. Solid State Chem.* **1998**, *140*, 435.
- [5] R. J. Francis, M. J. Drewhitt, P. S. Halasyamani, C. Ranganathachar, D. O'Hare, W. Clegg, S. J. Teat, *Chem. Commun.* **1998**, 279.

- [6] X. Bu, P. Feng, G. D. Stucky, *J. Am. Chem. Soc.* **1998**, *120*, 11204.
- [7] M. Shieh, K. J. Martin, P. J. Squattrito, A. Clearfield, *Inorg. Chem.* **1990**, *29*, 958.
- [8] G. Geister, *Z. Kristallogr.* **1998**, *213*, 266.
- [9] Z. Bircsak, W. T. A. Harrison, *Inorg. Chem.* **1998**, *37*, 5387.
- [10] W. T. A. Harrison, *Acta Crystallogr. Sect. C* **1999**, *55*, 1980.
- [11] W. T. A. Harrison, M. L. F. Phillips, *Chem. Mater.* **1997**, *9*, 1837.
- [12] Program SADABS, Bruker AXS Inc., Madison, Wisconsin, USA, **1999**.
- [13] G. M. Sheldrick, SHELXS86 user guide, University of Göttingen, Germany, **1986**.
- [14] D. J. Watkin, J. R. Carruthers, P. W. Betteridge, CRYSTALS user guide, Chemical Crystallography Laboratory, University of Oxford, UK, **1999**.
- [15] L. J. Farrugia, *J. Appl. Crystallogr.* **1997**, *30*, 565.
- [16] Program ATOMS, Shape Software Inc., Kingsport, Tennessee, USA, **1999**.

Correlation of the Topology of the Electron Density of Pyrite-Type Transition Metal Sulfides with Their Catalytic Activity in Hydrodesulfurization**

Yosslen Aray,* Jesus Rodriguez, David Vega, and Eloy Nouel Rodriguez-Arias

Transition metal sulfides (TMSs) are an important class of catalysts that are stable under the severe conditions of sulfuro-reductive hydroprocessing of petroleum-based feedstocks.^[1, 2] Systematic experimental^[2, 3] and theoretical^[2–5] studies on the hydrodesulfurization (HDS) activity towards dibenzothio-phene (DBT) of various metal sulfide catalysts have shown that the strength of the metal–sulfur bonding plays an important role in the HDS process. Two different models for assessing the M–S bond strength have been developed.^[2, 5] In the model developed by Topsøe et al.,^[2] the M–S bond energy is obtained from the bulk modulus of the metal and the degree of filling of the TMS d band (calculated by ab initio methods). This model predicts that HDS activity is inversely correlated with M–S bond strength. Hence, the highest activity is

[*] Y. Aray
Centro de Quimica
IVIC, Apartado 21827
Caracas 1020 A (Venezuela)
Fax: (+58) 2-504-1350
E-mail: yaray@quimica.ivic.ve

J. Rodriguez
Centro de Quimica
IVIC, Caracas (Venezuela)
D. Vega
FACYT, Universidad de Carabobo, Valencia (Venezuela)
E. N. Rodriguez-Arias
Laboratorio de Modelaje en Catalisis
Departamento de Química, Universidad Simón Bolívar
Caracas (Venezuela)

[**] The authors acknowledge CONICIT of Venezuela (Projects S1-95001616 and S1-2673) for providing funding for the SGI ORIGIN 2000 and SGI O2 workstations used in this work.

observed for TMSs that possess the most weakly bound sulfur atoms at the surface. In the model developed by Toulhoat et al.,^[5] the M–S bond strength is estimated as the bulk cohesive energy (experimental or calculated by ab initio methods) per formula unit divided by the number of TM–S bonds. Using this model gives a typical “volcano” plot for the correlation between HDS activity and the metal–sulfur bond strength. This suggests the existence of an optimum M–S bond strength. This result was interpreted in the spirit of the Sabatier principle:^[6] solids whose heats of formation and hence whose metal–sulfur bond strengths are too large or too small are practically inactive, while those with intermediate M–S bond strengths are active. Pyrite-type sulfides of the second- and third-row transition metals (RuS₂, OsS₂ and IrS₂) with intermediate bulk M–S bond strengths were found to be the most active catalysts.

The topological theory of Bader et al. provides a rigorous definition of chemical bonds for all classes of molecules and solids.^[7–9] This theory uses the total electron density $\rho(\mathbf{r})$ of a molecule or solid to determine its topology. This topology is characterized by its critical points (CPs): maxima, minima, and saddle points. These are points where the gradient vector field $\nabla\rho(\mathbf{r})$ vanishes, and they are classified by the $\rho(\mathbf{r})$ curvatures or three eigenvalues λ_i ($i=1, 2, 3$) of the Hessian matrix ($H_{ij} = \partial^2\rho(\mathbf{r})/\partial x_i\partial x_j$).^[7] In general, $\rho(\mathbf{r})$ exhibits local maxima only at the nuclear positions and a saddle point between each pair of bonded nuclei. The latter is called a bond critical point, and its presence is a necessary condition for the existence of a chemical bond.^[7, 8] A unique pair of trajectories of the vector field $\nabla\rho(\mathbf{r})$ that originate at the bond critical point define a line that links the nuclei, along which the electron density is a maximum with respect to any other neighboring line. This is a bond path, and its presence is a necessary and sufficient condition for the existence of a bond.^[8] Bond paths determine and characterize all atomic interactions in a given system. The connection between the topology of the electron density and the chemical and structural stability of isolated molecules is well established.^[7] In particular, the strength of the bonding between a given pair of atoms in a molecule correlates with the values of the electron density at the bond critical point ρ_b .^[7] A simple relationship between the binding energy and ρ_b in periodic solids was also reported.^[10–12]

We carried out a systematic determination of the topology of $\rho(\mathbf{r})$ for pyrite-type TMSs (RuS₂, OsS₂, IrS₂, FeS₂, and NiS₂) in order to examine the connection between the topologically defined M–S bond and HDS activity. The electron densities were calculated with the WIEN-97^[13] program by using a Kohn–Sham Hamiltonian, which includes the generalized gradient approximation developed by Perdew et al.^[14] and an unrestricted scheme for obtaining spin-polarized wave functions. The topology of $\rho(\mathbf{r})$ was analyzed with a local version of the EXTREM program,^[15] incorporated in the EXCUBO^[16] program and adapted to WIEN-97. The TMS experimental cell parameters were used.^[17] We located all CPs in the cells, and Figure 1 shows the three-dimensional CP positions in the pyrite-type crystals. There are four M nuclei per primitive cell, eight S nuclei, twenty-four

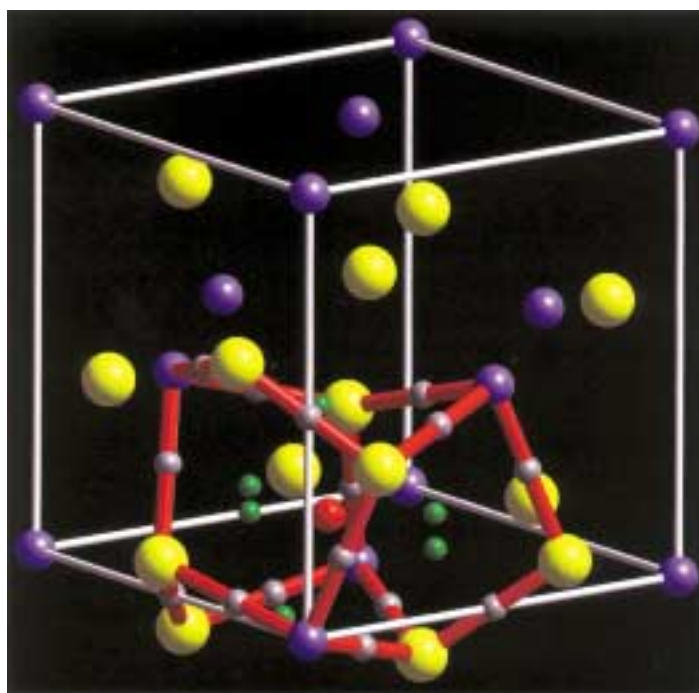


Figure 1. $\rho(\mathbf{r})$ critical points in the unit cell (white cube) of RuS₂. Blue and yellow spheres represent Ru and S atoms, respectively. Red rods denote the bond paths defined by the bond critical points (gray spheres). Only one cage critical point (red sphere), defined by a six-face polyhedron, is shown. Green spheres denote the five-membered ring CPs.

M–S bond CPs (b_{MS}), four S–S bond CPs (b_{SS}), twenty-four ring CPs, and eight cage CPs. The $\nabla\rho(\mathbf{r})$ trajectories that originate at each of the four cages and terminate at a b CP, define an interatomic surface (Figure 2). The M and S atoms are bonded by sets of six and four such surfaces, respectively. In the middle of each surface, there is a b CP, and the parameters that characterize these CPs are listed in Table 1. The $\rho(b_{MS})$ values allow us to predict that the trend in M–S bond strength is Os > Ir > Ru > Fe > Ni. Note that exactly the inverse trend is observed for the $\rho(b_{SS})$ values, that is, the S–S bond strength increases as the M–S bond strength decreases. Additionally, the curvatures of $\rho(\mathbf{r})$ at b are intimately related to the nature of the chemical bond.^[18] The two negative curvatures λ_1 and λ_2 are connected to the perpendicular contraction of $\rho(\mathbf{r})$, which leads to a contraction of charge towards b . The positive curvature λ_3 is related to the parallel expansion of $\rho(\mathbf{r})$ and cause its depletion away from b . In a covalent bond^[18] the negative curvatures dominate ($|\lambda_1 + \lambda_2| > \lambda_3$), so the electronic charge is concentrated in the internuclear region, and $\rho_b > 0.1$. In ionic bonds^[18] the positive curvature dominates ($|\lambda_1 + \lambda_2| < \lambda_3$), so the electronic charge is depleted away from the internuclear region, and $\rho_b < 0.1$. The data listed in Table 1 show that the S–S bonds exhibit characteristics associated with a covalent nature, while the M–S bonds possess values typical of ionic or polar covalent bonds. A contour map of the Laplacian distribution^[19] (Figure 3) corroborates that the M–S bonds correspond to the interaction of a relatively hard core of density on M with a softer, more polarizable region of charge concentration dominated by contractions of $\rho(\mathbf{r})$ towards the b_{SS} CP. Examination of Figures 2 and 3 reveals that sulfur atoms

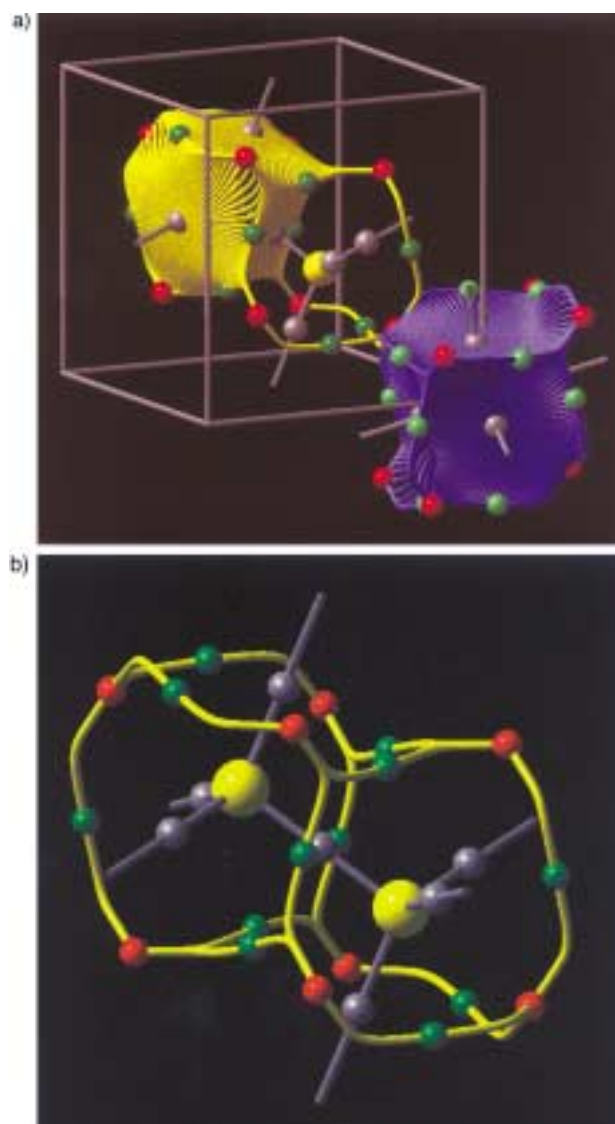


Figure 2. a) Representation of the region of space bounded by the six and four interatomic surfaces that define a Ru atom (blue zone) and an S atom (yellow zone), respectively. b) An S_2 group is defined by eight cage CPs (red spheres) and the surface perimeter is formed by the trajectories of the vector field $\nabla\rho(r)$ (yellow lines) originating at the cage points and ending at the ring points (green spheres). Bond paths (gray rods) to six metal atoms link each S_2 group.

Table 1. Topological properties (a.u.) of $\rho(r)$ at the critical points for bulk pyrite-type transition metal sulfides.

Critical point	$\rho(r_c)$	λ_1	λ_2	λ_3
		RuS ₂		
b_{MS}	0.09030	-0.07197	-0.06931	0.32877
b_{SS}	0.12498	-0.14805	-0.14805	0.22292
		OsS ₂		
b_{MS}	0.09905	-0.07180	-0.06771	0.32877
b_{SS}	0.11680	-0.13738	-0.13738	0.22292
		IrS ₂		
b_{MS}	0.09580	-0.07745	-0.07748	0.28627
b_{SS}	0.11901	-0.13768	-0.13768	0.23730
		FeS ₂		
b_{MS}	0.07903	-0.04604	-0.04372	0.27775
b_{SS}	0.13251	-0.15756	-0.15756	0.20880
		NiS ₂		
b_{MS}	0.06574	-0.04715	-0.04679	0.20889
b_{SS}	0.14745	-0.16544	-0.16544	0.17789

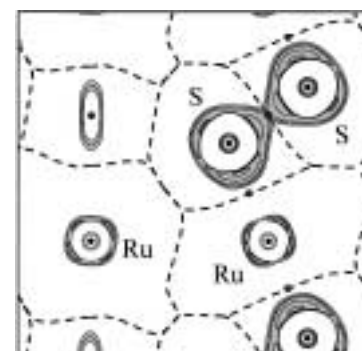


Figure 3. Contour map of $\nabla^2\rho$ on the (110) plane for bulk RuS₂. The contours denote negative values of $\nabla^2\rho$, that is, concentration of electronic charge (shaded zones). The outermost contour is 0.0 and indicates the surface that separates the charge-concentration zone from the outer, charge-depletion zone. Dotted lines mark the intersection of the interatomic surfaces with the plane of the figure. The map shows that S_2 dimers are linked to the metal atoms.

form covalently bonded S–S groups which assemble about a metal atom. Thus, the pyrite-type TMS crystal packing results from the interaction of each metal atom with six such S_2 groups.

The HDS activity of TMSs has been related to the ability of the catalyst to form and regenerate sulfur vacancies,^[2, 3] that is, to the breaking of M–S bonds. The model developed by Topsøe et al.^[2] suggests that the highest HDS activities correspond to the TMSs with the lowest M–S bond strength (RuS₂, OsS₂, and IrS₂), that is with the lowest $\rho(b_{MS})$ value. However, sulfides of second- and third-row transition metals show $\rho(b_{MS})$ values greater than those of sulfides of first-row metals (Table 1). This result is in contrast with the above model. To further study the HDS behavior of TMSs, we also calculated $\rho(b_{MS})$ for the less active compounds VS, FeS, MnS, and PtS.^[20] We observed that $\rho(b_{MS})$ shows exactly the same trend (Pt > Ir > Os > Ru > V > Fe > Mn) of the M–S bond strength as was reported by Toulhoat et al.^[5] The variation of the HDS activity with $\rho(b_{MS})$ is shown in Figure 4. Like

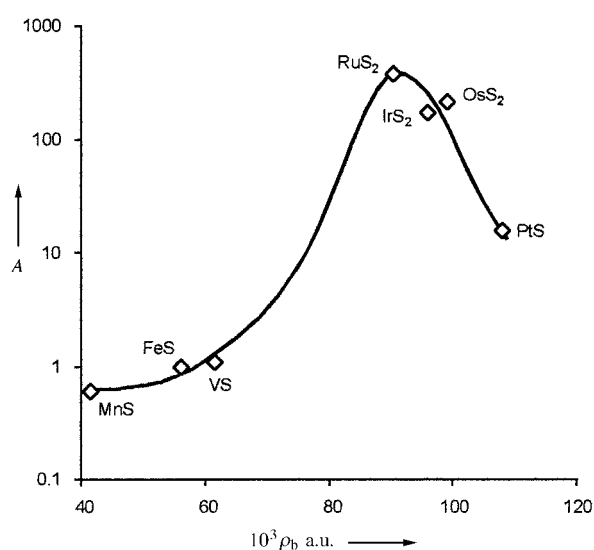


Figure 4. HDS activity A (10^{16} molecules of DBT converted per mmole metal per second)^[3] of the TMS catalysts as a function of the electron density at the metal–sulfur bond critical point.

Toulhoat et al., we found the typical volcano plot. It is evident that TMSs with either too high or too low $\rho(b_{\text{MS}})$ values possess only low HDS activity. The most active catalysts are characterized by intermediate values of the electronic density at the M–S bond critical point. This result corroborates, by means of a bond concept that is rigorously defined by the topological theory of $\rho(r)$, the consistency of TMS-catalyzed HDS with the Sabatier principle.

Received: April 13, 2000
Revised: June 13, 2000 [Z14987]

- [1] O. Weisser, S. Landa, *Sulfide Catalysts: Their Properties and Applications*, Pergamon, Oxford, 1973.
- [2] H. Topsøe, B. S. Clausen, F. Massoth, *Hydrotreating Catalysis in Catalysis, Science and Technology, Vol. 11*, Springer, Berlin, 1996.
- [3] T. A. Pecoraro, R. R. Chianelli, *J. Catal.* **1981**, 67, 430.
- [4] J. K. Norskov, B. S. Clausen, H. Topsøe, *Catal. Lett.* **1992**, 13, 1.
- [5] P. Raybaud, G. Kresse, J. Hafner, H. Toulhoat, *J. Phys. Condens. Matter* **1997**, 9, 11085; H. Toulhoat, G. Kresse, *Abstr. Pap. Symp. on Advances and Applications of Computational Chemical Modeling to Heterogeneous Catalysis* (New York: American Chemical Society) **1997**, p. 114.
- [6] P. Sabatier, *Ber. Dtsch. Chem. Ges.* **1911**, 44; M. Boudart, *Chem. Eng. Prog.* **1961**, 57, 33.
- [7] R. F. W. Bader, *Atoms in Molecules—A Quantum Theory*, Clarendon, Oxford, UK, 1990.
- [8] R. F. W. Bader, *J. Phys. Chem.* **1998**, 102, 7314.
- [9] R. F. W. Bader, P. L. A. Popelier, T. A. Keith, *Angew. Chem.* **1994**, 106, 647; *Angew. Chem. Int. Ed. Engl.* **1994**, 33, 620.
- [10] P. Zou, R. F. W. Bader, *Acta Crystallogr. Sect. A* **1994**, 50, 714.
- [11] V. Luaña, M. A. Pendás, A. Costales, *Phys. Rev. B* **1997**, 55, 4285.
- [12] Y. Aray, J. Rodriguez, D. Vega, *J. Phys. Chem. B* **2000**, 104, 4608.
- [13] P. Blaha, K. Schwarz, J. Luitz, *WIEN 97*, Vienna University of Technology **1997** (Improved and updated Unix version of the original copyrighted WIEN code: P. Blaha, K. Schwarz, P. Sorantin, S. B. Trickey, *Compt. Phys. Commun.* **1990**, 59, 399.)
- [14] J. P. Perdew, S. Burke, M. Ernzerhof, *Phys. Rev. Lett.* **1996**, 77, 3865.
- [15] R. F. W. Bader, P. Krugg, Department of Chemistry, McMaster University, Hamilton, Ontario, Canada, 1990, personal communication.
- [16] Y. Aray, J. Rodriguez, J. Rivero, *J. Phys. Chem.* **1997**, 101, 6976.
- [17] RuS₂: H. D. Lutz, B. Mueller, T. Schmidt, T. Sting, *Acta Crystallogr. Sect. C* **1990**, 46, 2003; OsS₂: T. Sting, B. Mueller, H. D. Lutz, *Z. Kristallogr.* **1992**, 202, 161; IrS₂: E. Parthé, D. Hohnke, F. Hulliger, *Acta Crystallogr.* **1967**, 23, 832; FeS₂: S. Finklea, C. Leconte, E. Amma, *Acta Crystallogr. Sect. B* **1976**, 32, 529; NiS₂: T. Fuji, K. Tanaka, F. Marumo, Y. Noda, *Mineral. J. Jpn.* **1987**, 13, 448.
- [18] R. F. W. Bader, H. J. Essen, *J. Chem. Phys.* **1984**, 80, 1943; S. Grimme, *J. Am. Chem. Soc.* **1996**, 118, 1529.
- [19] A contour map of the Laplacian $\nabla^2\rho$ (the sum of the three curvatures at each point in space) allows us to see the extent and relative position of the regions where electronic density is concentrated ($\nabla^2\rho < 0$) or depleted ($\nabla^2\rho > 0$). In a covalent bond, the electron density is concentrated between the nuclei, around the bond critical point (ref. [7]) and “The Laplacian of the Electronic Charge Distribution”: P. J. MacDougall, PhD Thesis, McMaster University, Hamilton, Ontario, Canada, 1989).
- [20] Cell parameters: VS: W. Biltz, A. Koecher, *Z. Anorg. Allg. Chem.* **1939**, 241, 324; FeS: J. M. D. Coey, H. Roux-Buisson, *Mater. Res. Bull.* **1979**, 14, 711; MnS: T. Chattopadhyay, H. G. von Schnering, R. F. D. Stansfield, G. J. McIntyre, *Z. Kristallogr.* **1992**, 199, 13; PtS: F. A. Bannister, M. H. Hey, *Miner. Mag. J. Mineral. Soc.* **1932**, 23, 188.

Higher Adducts of C₆₀ by Tether-Directed Remote Functionalization: X-Ray Crystal Structure and Reactivity of a Chiral Hexakis-Cyclopropanated Fullerene with all Addends Located along an Equatorial Belt**

Craig R. Woods, Jean-Pascal Bourgeois, Paul Seiler, and François Diederich*

Hexakis adducts of C₆₀ are increasingly attracting interest as three-dimensional building blocks for advanced materials applications.^[1, 2] Among those, derivatives with a pseudooctahedral (*T_h*) addition pattern have been the earliest and most widely investigated ones.^[3–7] Recently, Rubin and co-workers reported the synthesis of a hexakis adduct with a novel, *D₃*-symmetric addition pattern, which features unusually strong fluorescence and electroluminescence properties.^[1] Both types of hexakis adducts are accessible by stepwise additions and their addends are evenly distributed over the entire carbon sphere. In recent years, regio- and stereoselective tether-directed remote functionalization techniques^[8] have provided access to a great variety of higher adducts of C₆₀, which either cannot be synthesized by stepwise additions or are obtained only in small yield from complex isomeric mixtures. Using such a methodology,^[9] we became interested in preparing hexakis adducts with completely novel addition patterns, that feature the location of all addends along an equatorial belt rather than evenly distributed over the entire carbon sphere. In the chiral *D₂*-symmetric structure **A** (Figure 1) the addition sites are aligned in a distinct helical array,

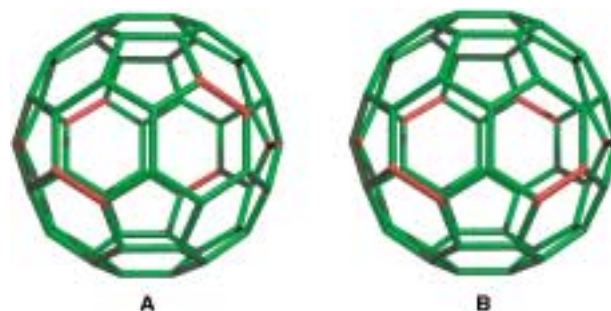


Figure 1. Novel hexakis addition patterns of C₆₀ with the addend sites located along an equatorial belt.

whereas structure **B**, with a *D_{3d}*-symmetric addition pattern, features a circumferential (“Saturn”-like) functionalization about the equator which dissects the residual π -electron chromophore of the fullerene into two polar halves with no direct π -electron conjugation. Here, we report the synthesis,

[*] Prof. Dr. F. Diederich, Dr. C. R. Woods, Dipl.-Chem. J.-P. Bourgeois, P. Seiler
Laboratorium für Organische Chemie
ETH-Zentrum
Universitätstrasse 16, 8092 Zürich (Switzerland)
Fax: (+41)1-632-1109
E-mail: diderich@org.chem.ethz.ch

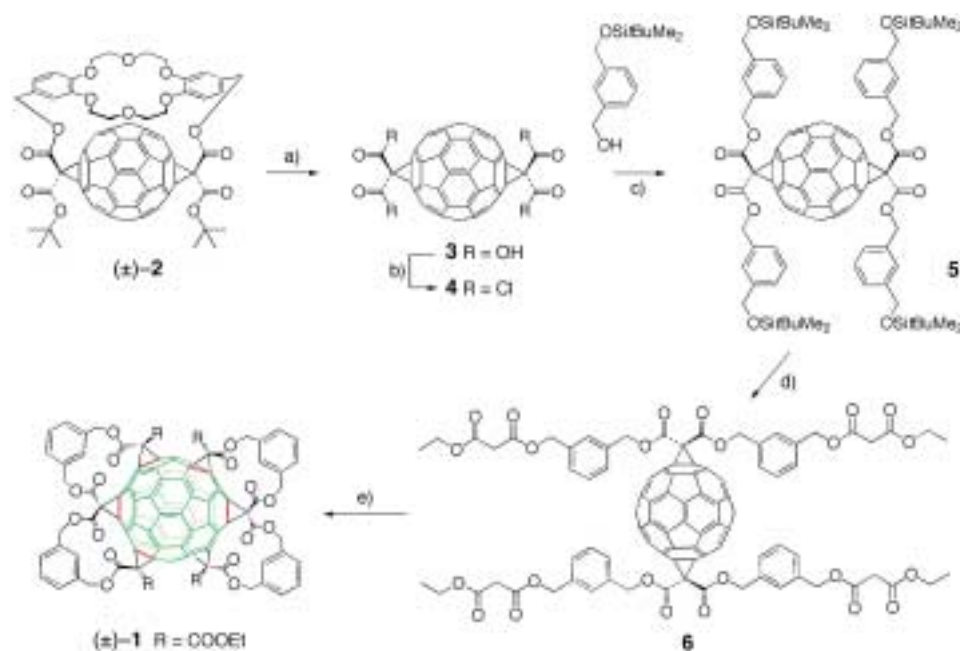
[**] This work was supported by the Swiss National Science Foundation and the German Fonds der Chemischen Industrie

crystal structure, and chemical reactivity of the D_2 -symmetric hexakis adduct (\pm)-**1**, which features addition pattern **A**.

Target compound (\pm)-**1** was synthesized by a short route that involves two sequential tether-directed remote functionalization steps. The first consisted in the preparation of *trans*-1 bis-adduct (\pm)-**2** by Bingel macrocyclization of C_{60} with dibenzo[18]crown-6 appended with two bis-malonate moieties. The reaction is templated by K^+ ions and gives the product in a 50% yield, as previously described.^[10] Cleavage of the crown ether template and the *tert*-butyl ester groups with 4-toluenesulfonic acid monohydrate (*p*-TsOH·H₂O) in toluene afforded tetraacid **3**,^[10b] which was transformed into tetrakis(acyl chloride) **4** (Scheme 1). Coupling with mono-*t*BuMe₂Si-protected 1,3-benzenedimethanol^[11] yielded **5**, which was then deprotected with HF/pyridine and converted with ethyl malonyl chloride into **6**.^[12] Fourfold intramolecular Bingel addition^[13] of **6** under high dilution conditions, flash-chromatographic workup (SiO₂-H; CH₂Cl₂/AcOEt (99/1)), and further chromatographic separation of the middle fraction (SiO₂-H; CH₂Cl₂/AcOEt (99.5/0.5)) gave (\pm)-**1** as a single hexakis adduct in 10% yield.

The molecular formula of the hexakis adduct was unambiguously revealed by high-resolution matrix-assisted laser desorption-ionization mass spectrometry (MALDI-TOF MS) which showed the sodium complex of the molecular ion as parent ion at $m/z = 1875.275$ (100%, $[M+Na]^+$, $C_{118}H_{52}NaO_{24}^+$; calcd: 1875.275). 1,3-Benzenedimethanol-tethered bis-malonates are well known to yield regioselectively *cis*-2 addition patterns on the fullerene.^[8, 9, 14] Fourfold intramolecular Bingel addition of **6** with *cis*-2 selectivity can only give (with equiprobability) two hexakis adducts, D_2 -symmetric (\pm)-**1** with addition pattern **A**, or a C_{2h} -symmetric compound with addition pattern **B** (Figure 1). Whereas the symmetry of the two regioisomers does not allow differentiation using ¹H NMR, this can, in principle, be performed by ¹³C NMR spectroscopy. In the C_{2h} -symmetric compound, the mirror plane cuts through four sp²-hybridized carbon atoms, to give 22 ¹³C_{sp²} (three C=O, six benzene, and 13 fullerene) resonances. On the other hand, the C_2 axes in D_2 -symmetric (\pm)-**1** do not pass through any carbon atoms and therefore 21 ¹³C_{sp²} (three C=O, six benzene, and 12 fullerene) resonances were expected. Unfortunately, the ¹³C NMR spectrum (125.8 MHz, CDCl₃) of the isolated compound displayed only 20 distinguishable ¹³C_{sp²} resonances due to accidental isochrony; hence, it was not useful for assigning symmetry and molecular constitution.

Fortunately, one small red-black crystal, suitable for an X-ray analysis, was successfully grown from a solution of



Scheme 1. Synthesis of the hexakis adduct (\pm)-**1**. a) *p*-TsOH·H₂O, PhMe, reflux, 16 h; b) (COCl)₂, CH₂Cl₂, reflux, 48 h; c) Py, CH₂Cl₂, 20 °C, 12 h, 21% (from (\pm)-**2**); d) 1) HF/Py, CH₂Cl₂, 0 °C, 1 h; 2) ClCOCH₂CO₂Et, DMA, CH₂Cl₂, 20 °C, 80%; e) I₂, DBU, PhMe/Me₂SO, 20 °C, 12 h, 10%. DMA = *N,N*-dimethylaniline; DBU = 1,8-diazabicyclo[5.4.0]undec-7-ene.

CH₂Cl₂, hexane, and benzene. The molecular structure (Figures 2 and 3) nicely reveals the distinct helical nature of addition pattern **A** and allows an unambiguous assignment of structure (\pm)-**1** to the isolated hexakis adduct.^[15] Distortion of the C_{60} sphere in (\pm)-**1** due to the belt of six fused cyclopropane rings is small and its overall shape closely resembles that determined for the bis-adduct (\pm)-**2**.^[10]

π -Electron conjugation between the two unsubstituted poles in (\pm)-**1** is maintained through two *trans*-stilbene-like bridges (Figure 4). As a result of this retained, extended conjugation, the compound is red in solution with an end

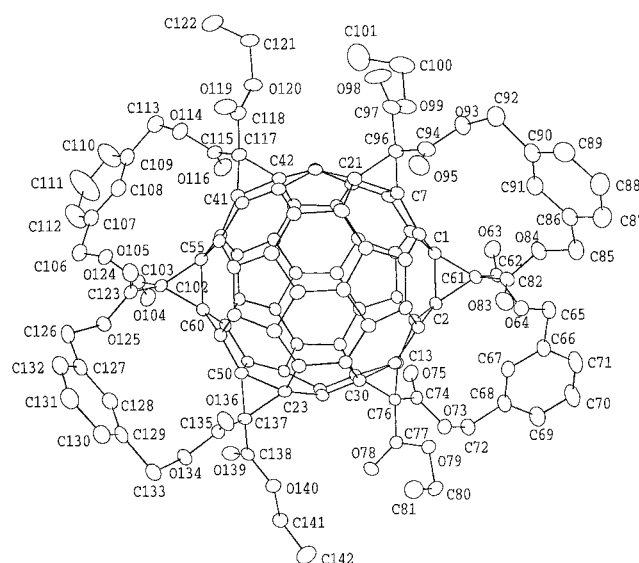


Figure 2. X-ray crystal structure of (\pm)-**1**. Atomic displacement parameters obtained at 228 K are drawn at the 20% probability level.

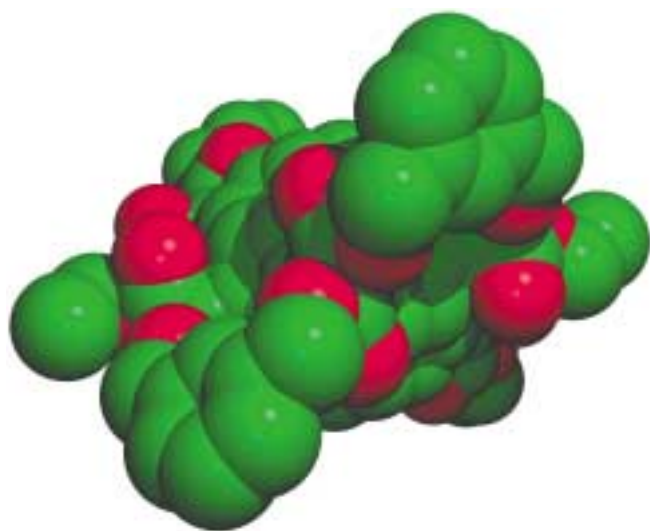


Figure 3. Space-filling representation of the X-ray crystal structure of (±)-1, which shows the distinct helical nature of the addition pattern.

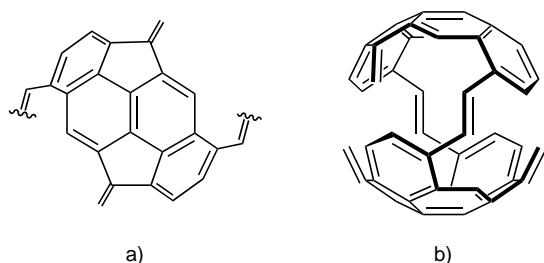
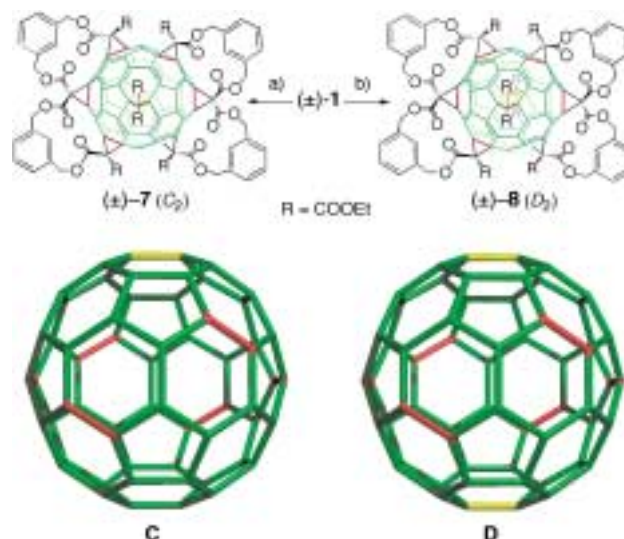


Figure 4. Residual π -electron chromophore in (±)-1: a) view atop one of the two unfunctionalized poles and b) side view onto the *trans*-stilbene-like moiety, which maintains electronic communication between the two polar regions.

absorption extending to 600 nm. This contrasts with the light-yellow color (end absorption around 450 nm) of the hexakis adducts with pseudooctahedral addition patterns, in which the residual π -electron chromophore is reduced to a benzenoid “cubic cyclophane”-type substructure.^[1–7]

The novel hexakis-adduct (±)-1 undergoes further functionalization at the central 6–6 bond of each pole. A Bingel reaction with diethyl 2-bromomalonate (2 equiv) in toluene/DMSO (1/1) in the presence of DBU afforded the heptakis-adduct (±)-7 as a single new product together with some starting material. Addition of a 20-fold excess of the same 2-bromomalonate to (±)-1 produced another unique compound, the octakis-adduct (±)-8, along with traces of (±)-7 (Scheme 2). The high-resolution MALDI-TOF mass spectra showed the sodium complexes of the molecular ions as parent ions, which correspond to the heptakis and octakis adducts from a single and double Bingel addition, respectively ((±)-7: $m/z = 2033.331$ (100%, $[M+Na]^+$, $C_{125}H_{62}NaO_{28}^+$; calcd: 2033.332); (±)-8: $m/z = 2191.388$ (100%, $[M+Na]^+$, $C_{132}H_{72}NaO_{32}^+$; calcd: 2191.390)). Unambiguous proof for the proposed addition patterns was provided by the 1H NMR spectra (300 MHz, $CHCl_3$). The spectrum of (±)-7 corresponds to a C_2 -symmetric compound, with four AB systems for four different benzylic CH_2 groups, whereas the spectrum of (±)-8 displays only two such AB systems, in agreement with



Scheme 2. Synthesis of the heptakis and octakis adducts (±)-7 and (±)-8 with addition patterns **C** and **D**, respectively. a) (EtOOC) $_2$ CHBr (2 equiv), DBU (6.6 equiv), PhMe/Me $_2$ SO, 20°C, 12 h; \approx 40%; b) (EtOOC) $_2$ CHBr (20 equiv), DBU (66 equiv), PhMe/Me $_2$ SO, 20°C, 12 h, \approx 80%. The indicated yields have high uncertainty due to the small quantities of materials used.

a higher, D_2 symmetry. Addition patterns of this symmetry can only be obtained starting from (±)-1 by mono- and bis-cyclopropanation at the central polar 6–6 bonds. Attack at these specific 6–6 bonds is favored since they are sterically the least hindered ones and are in an equatorial (*e*) relationship with respect to the two malonate addends with *trans*-1 relationship introduced in the first tether-directed remote functionalization step.^[4a] Since the *trans*-stilbene type conjugation between the two polar chromophoric regions is still maintained, the hypsochromic shift upon passing from (±)-1 (longest wavelength absorption maximum at $\lambda_{max} = 576$ nm), to (±)-7 ($\lambda_{max} = 556$ nm, sh), and to (±)-8 ($\lambda_{max} = 551$ nm) is not large and solutions of the latter still display an orange-yellow color.

We were unable to isolate the regioisomer of (±)-1 with addition pattern **B**, although molecular modeling calculations^[16] predicted only little energetic differences between the two compounds. There may, however, exist differential steric interactions between adjacent EtOOC groups in the transition states of the two final cyclopropanation steps. The geometric relationship between two adjacent ethyl malonate addends in (±)-1 is *cis*-3, whereas it is *cis*-2 in the regioisomer (Figure 1), and the closer proximity of adjacent EtOOC groups in the latter could render its formation unfavorable. We intend to test this hypothesis with an analog of **6** that contains four smaller, terminal methyl malonate moieties, which we expect to yield hexakis adducts with both **A** and **B** addition patterns. The pronounced helical nature of the inherently chiral addition pattern of (±)-1 promises interesting chiroptical properties.^[17] Therefore, we are now introducing chiral tethers instead of the 1,3-benzenedimethanol moieties in **6** to prepare optically active derivatives of (±)-1 in a diastereoselective way.^[18, 9]

Received: June 23, 2000 [Z15317]

- [1] a) G. Schick, M. Levitus, L. Kvetko, B. A. Johnson, I. Lamparth, R. Lunkwitz, B. Ma, S. I. Khan, M. Garcia-Garibay, Y. Rubin, *J. Am. Chem. Soc.* **1999**, *121*, 3246–3247; b) K. Hutchison, J. Gao, G. Schick, Y. Rubin, F. Wudl, *J. Am. Chem. Soc.* **1999**, *121*, 5611–5612.
- [2] a) M. Hetzer, H. Clausen-Schaumann, S. Bayerl, T. M. Bayerl, X. Camps, O. Vostrowsky, A. Hirsch, *Angew. Chem.* **1999**, *111*, 2103–2106; *Angew. Chem. Int. Ed.* **1999**, *38*, 1962–1965; b) M. Brettreich, S. Burghardt, C. Böttcher, T. Bayerl, S. Bayerl, A. Hirsch, *Angew. Chem.* **2000**, *112*, 1915–1918; *Angew. Chem. Int. Ed.* **2000**, *39*, 1845–1848.
- [3] P. J. Fagan, J. C. Calabrese, B. Malone, *J. Am. Chem. Soc.* **1991**, *113*, 9408–9409.
- [4] a) A. Hirsch, I. Lamparth, T. Grösser, *J. Am. Chem. Soc.* **1994**, *116*, 9385–9386; b) I. Lamparth, C. Maichle-Mössmer, A. Hirsch, *Angew. Chem.* **1995**, *107*, 1755–1757; *Angew. Chem. Int. Ed. Engl.* **1995**, *34*, 1607–1609; c) I. Lamparth, A. Herzog, A. Hirsch, *Tetrahedron*, **1996**, *52*, 5065–5075; d) X. Camps, A. Hirsch, *J. Chem. Soc. Perkin Trans. 1* **1997**, 1595–1596.
- [5] a) B. Kräutler, J. Maynollo, *Angew. Chem.* **1995**, *107*, 69–70; *Angew. Chem. Int. Ed. Engl.* **1995**, *34*, 87–88; b) B. Kräutler, J. Maynollo, *Tetrahedron*, **1996**, *52*, 5033–5042; c) R. Schwenniger, T. Müller, B. Kräutler, *J. Am. Chem. Soc.* **1997**, *119*, 9317–9318.
- [6] a) L. Isaacs, R. F. Haldimann, F. Diederich, *Angew. Chem.* **1994**, *106*, 2434–2437; *Angew. Chem. Int. Ed.* **1994**, *33*, 2339–2342; b) L. Isaacs, P. Seiler, F. Diederich, *Angew. Chem.* **1995**, *107*, 1636–1639; *Angew. Chem. Int. Ed. Engl.* **1995**, *34*, 1466–1469; c) P. Timmerman, L. E. Witschel, F. Diederich, C. Boudon, J.-P. Gisselbrecht, M. Gross, *Helv. Chim. Acta*, **1996**, *79*, 6–20; d) P. Seiler, L. Isaacs, F. Diederich, *Helv. Chim. Acta*, **1996**, *79*, 1047–1058; e) R. F. Haldimann, F.-G. Klärner, F. Diederich, *Chem. Commun.* **1997**, 237–238; f) L. Isaacs, F. Diederich, R. F. Haldimann, *Helv. Chim. Acta*, **1997**, *80*, 317–342.
- [7] W. Qian, Y. Rubin, *Angew. Chem.* **1999**, *111*, 2505–2508; *Angew. Chem. Int. Ed.* **1999**, *38*, 2356–2360.
- [8] a) F. Diederich, R. Kessinger, *Acc. Chem. Res.* **1999**, *32*, 537–545; b) F. Diederich, R. Kessinger in *Templated Organic Synthesis* (Eds.: F. Diederich, P. J. Stang), Wiley-VCH, Weinheim, **1999**, pp. 189–218.
- [9] a) J.-F. Nierengarten, V. Gramlich, F. Cardullo, F. Diederich, *Angew. Chem.* **1996**, *108*, 2242–2244; *Angew. Chem. Int. Ed. Engl.* **1996**, *35*, 2101–2103; b) J.-F. Nierengarten, T. Habicher, R. Kessinger, F. Cardullo, F. Diederich, V. Gramlich, J.-P. Gisselbrecht, C. Boudon, M. Gross, *Helv. Chim. Acta*, **1997**, *80*, 2238–2276.
- [10] a) J.-P. Bourgeois, L. Echegoyen, M. Fibbioli, E. Pretsch, F. Diederich, *Angew. Chem.* **1998**, *110*, 2203–2207; *Angew. Chem. Int. Ed.* **1998**, *37*, 2118–2121; b) J.-P. Bourgeois, L. Echegoyen, M. Fibbioli, E. Pretsch, F. Diederich, *Helv. Chim. Acta* **1999**, *82*, 1572–1595.
- [11] A. G. Myers, P. S. Dragovich, E. L. Kuo, *J. Am. Chem. Soc.* **1992**, *114*, 9369–9386.
- [12] New compounds were fully characterized by ¹H and ¹³C NMR, FT-IR, UV/Vis, and high resolution MALDI-TOF MS.
- [13] C. Bingel, *Chem. Ber.* **1993**, *126*, 1957–1959.
- [14] a) J.-F. Nierengarten, D. Felder, J.-F. Nicoud, *Tetrahedron Lett.* **1999**, *40*, 273–276; b) J.-F. Nierengarten, C. Schall, J.-F. Nicoud, *Angew. Chem.* **1998**, *110*, 2037–2040; *Angew. Chem. Int. Ed.* **1998**, *37*, 1934–1936.
- [15] X-ray crystal data of (±)-**1** (C₁₁₈H₅₂O₂₄·≈3.5CH₂Cl₂, M_r=2150.8): monoclinic, space group P2₁/c (no. 14), ρ=1.495 g cm⁻³, Z=4, a=20.332(3), b=19.860(3), c=23.696(3) Å, β=93.02(1)°, V=9555(2) Å³, T=228 K. Nonius-CAD4 diffractometer, CuK_α radiation, λ=1.5418 Å. One red-black, slightly twinned crystal (linear dimensions approximately 0.3 × 0.2 × 0.1 mm) was obtained by liquid–liquid diffusion of hexane into a CH₂Cl₂/C₆H₆ solution of (±)-**1**. The crystal was mounted at low temperature to prevent evaporation of the enclosed solvents. The twinning led to asymmetric reflection profiles for many reflections; an appropriate background correction was made to compensate for this effect. In addition, a semiempirical absorption correction, based on psi-scans, was applied to the data (T_{max}=0.99, T_{min}=0.61). The structure was solved by direct methods (SIR92: A. Altomare, G. Cascarano, C. Giacovazzo, A. Guagliardi, M. C. Burla, G. Polidori, M. Camalli, *J. Appl. Crystallogr.* **1994**, *27*, 435) and refined by full-matrix least-squares analysis (SHELXL-97, G. M. Sheldrick, University of Göttingen, Germany, **1997**) with the use of an isotropic extinction correction and w=1/[σ²(F_o²) + (0.125 P)² + 25.85 P], where P=(F_o² + 2 F_c²)/3. It consists of one ordered molecule of (±)-**1** and five

disordered CH₂Cl₂ molecules with population parameters between about 0.5 and 0.75. All heavy atoms were refined anisotropically (hydrogen atoms of the ordered fullerene isotropically, in which hydrogen atomic positions are based on stereochemical considerations). Final R(F)=0.085, wR(F²)=0.235 for 1365 parameters and 8593 reflections with I>2σ(I) and 2.2<θ<57.0° (corresponding R values based on all 12832 reflections are 0.125 and 0.274, respectively). Crystallographic data (excluding structure factors) for the structure reported in this paper have been deposited with the Cambridge Crystallographic Data Centre as supplementary publication no. CCDC-145416. Copies of the data can be obtained free of charge on application to CCDC, 12 Union Road, Cambridge CB21EZ, UK (fax: (+44) 1223-336-033; e-mail: deposit@ccdc.cam.ac.uk).

- [16] Sybyl force field from Spartan V.5.0 (Wavefunction, Irvine, CA, **1997**).
- [17] C. Thilgen, I. Hosse, F. Diederich, *Top. Stereochem.*, in press.

High-Throughput Structure Verification of a Substituted 4-Phenylbenzopyran Library by Using 2D NMR Techniques**

Harald Schröder,* Peter Neidig, and Gérard Rossé

Innovative technologies for combinatorial chemistry and automated synthesis make possible the synthesis of large collections of compounds as potential sources of lead structures in medicinal chemistry. While the synthesis, purification, and biological screening of combinatorial libraries can be performed automatically, purity control and structure verification remain bottlenecks. Insufficient purity or ambiguous structures of screened samples hinder the exploitation of structure–activity relationships, which are critical elements for the further design of libraries. The HPLC, MS, and liquid chromatography mass spectrometry (LC-MS) techniques are generally accepted as the most appropriate means of characterization.^[1] These analytical methods are fast and easy to automate, but they do not provide sufficient structural and quantitative data on the desired product. The existing automated methods based on ¹³C and ¹H NMR spectroscopy^[2] are not routinely applied due to the intrinsic low sensitivity of ¹³C NMR spectroscopy and the lack of reliable proton-based automated structure verification methods. We report here a novel approach for the automated structure verification of compound libraries by using the experimental data from 2D

[*] Dr. H. Schröder, Dr. G. Rossé^[+]
Pharma Division, Preclinical Research
F. Hoffmann-La Roche Ltd., 4070 Basel (Switzerland)
Fax: (+41) 61-688-7408
E-mail: harald.schroeder@roche.com

Dr. P. Neidig
Bruker Analytik GmbH
Silberstreifen, 76287 Rheinstetten (Germany)

[+] Present Address:
Selectide Corporation, A subsidiary of Aventis Pharmaceuticals, Inc.
1580 E. Hanley Blvd., Tucson, AZ 85737 (USA)

[**] We thank W. Meister for the electrospray-ionization mass spectrometry (ESIMS) and Dr. H. Senn for fruitful discussions and critical reading of the manuscript.

^1H , ^{13}C -correlated (HSQC) NMR spectra. The method is designated as the automated definition and recognition of patterns (AutoDROP).^[3] AutoDROP was applied to the rapid structure verification of all members of a library of ninety-six substituted 4-phenylbenzopyrans **1**. The automated analysis of the 2D HSQC NMR spectra gave the structural classification true, false, or unclear.

Structures from a library of compounds can be formally decomposed into a central core common to all compounds and a few variable modules (A_x , B_y , C_z , ...), which are varied systematically with a limited number of structural fragments within the library (Figure 1). Molecules are thus regarded as a

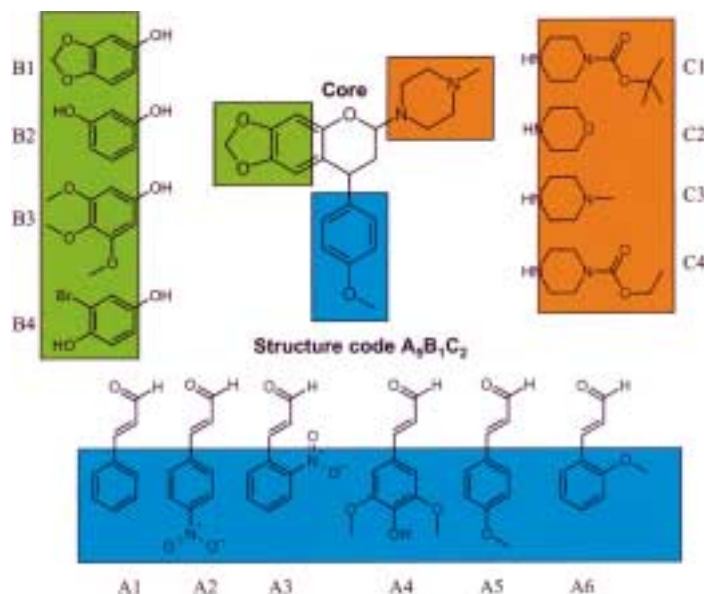
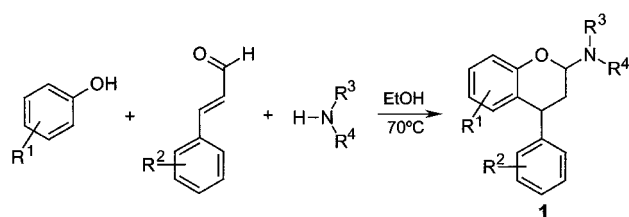


Figure 1. Redundant information in compounds array $A_x B_y C_z$. For $x=6$, $y=4$, and $z=4$, $x \times y \times z=96$ different compounds with the structure codes $A_x B_y C_z$ are obtained. This library is characterized by $x+y+z+\text{core}=15$ different structural fragments, and six of the ninety-six compounds contain all structural fragments (i.e., $A_1 B_1 C_1$, $A_2 B_2 C_2$, $A_3 B_3 C_3$, $A_4 B_4 C_4$, $A_5 B_1 C_3$, and $A_6 B_2 C_4$).

combination of different substructures, and a structure code $A_x B_y C_z$, defined by its synthesis, is assigned to each. Correspondingly, 2D HSQC NMR spectra can be regarded as a sum of spectra of substructures. A 4-phenylbenzopyran^[4] library **1** was used to validate the automated structure-verification procedure (Scheme 1). The ^1H and 2D HSQC NMR spectra were acquired for each of the ninety-six substituted 4-phenylbenzopyrans and interpreted by using AutoDROP. In addition, compounds were analyzed by ESIMS (electrospray-ionization mass spectrometry) and HPLC.



Scheme 1. Synthesis of 4-phenylbenzopyran library **1**.

The key idea of AutoDROP is to systematically examine representative 2D HSQC NMR spectra and to derive from them individual subspectra of the individual substructures A_x , B_y , C_z . The subspectra are managed as spectral patterns in AutoDROP. Once the spectral patterns of all individual substructures have been defined, all available spectra can be tested for the presence of particular substructures in the synthesized compounds.

In the first step, an automated procedure was applied to define spectral patterns. The 2D HSQC spectra are peak-picked, and all peaks are given a normalized intensity of unity. Linear combinations of spectra were applied in a systematic way to automatically isolate and define the spectral patterns of specific substructures (Table 1). An addition and subtrac-

Table 1. Linear combination of spectra to obtain the patterns for the substructure A_1 .^[a]

	A1	A2	B1	B2	C1	C2	C3	C4
+ A1B1C1	1	0	1	0	1	0	0	0
+ A1B1C2	1	0	1	0	0	1	0	0
+ A1B2C3	1	0	0	1	0	0	1	0
+ A1B2C4	1	0	0	1	0	0	0	1
– A2B1C1	0	1	1	0	1	0	0	0
– A2B1C2	0	1	1	0	0	1	0	0
– A2B2C3	0	1	0	1	0	0	1	0
– A2B2C4	0	1	0	1	0	0	0	1
sum:	4	–4	0	0	0	0	0	0

[a] The threshold is adjusted so that only peak areas of the substructure remain. A threshold of two would discriminate between A_1 and all other substructures. Integral boxes are then defined for the remaining peak areas.

tion procedure affected thereby all peaks within a given search radius. Peak areas were finally obtained by an unsupervised direct cluster analysis, which detects groups of peaks. Rectangular envelopes around such groups were then compiled into spectral patterns (Figure 2). Alternatively, the spectral patterns could be obtained by manual interpretation of the representative 2D HSQC spectra.

In the second step of AutoDROP, the compound structures were validated by applying the defined spectral patterns to the NMR spectra. This automated operation was based on the integration of spectral patterns. The peak integral of the central core shared by all members of library **1** was used as an internal reference integral. Suitable reference spectra for each structural fragment were selected, and the ratio of each integral to the reference integral (ratio of core integral to single integral) was calculated for all spectra. This ratio was set to 100 % for the reference spectra, and integral values for all other spectra were rescaled accordingly. Comparison of the ratio of the spectrum to be analyzed with the ratio of the corresponding reference spectrum allowed discrimination between correct and incorrect structures. A given structural fragment was verified when the threshold was above a predetermined value. For library **1** a threshold of 35 % was selected. The proposed structure was assigned the attribute true when the patterns of all expected structural fragments of the compound were found in the 2D HSQC spectra (Table 2). The ratio of core integral to single integral or the signal-to-noise ratio was used to identify samples containing very small

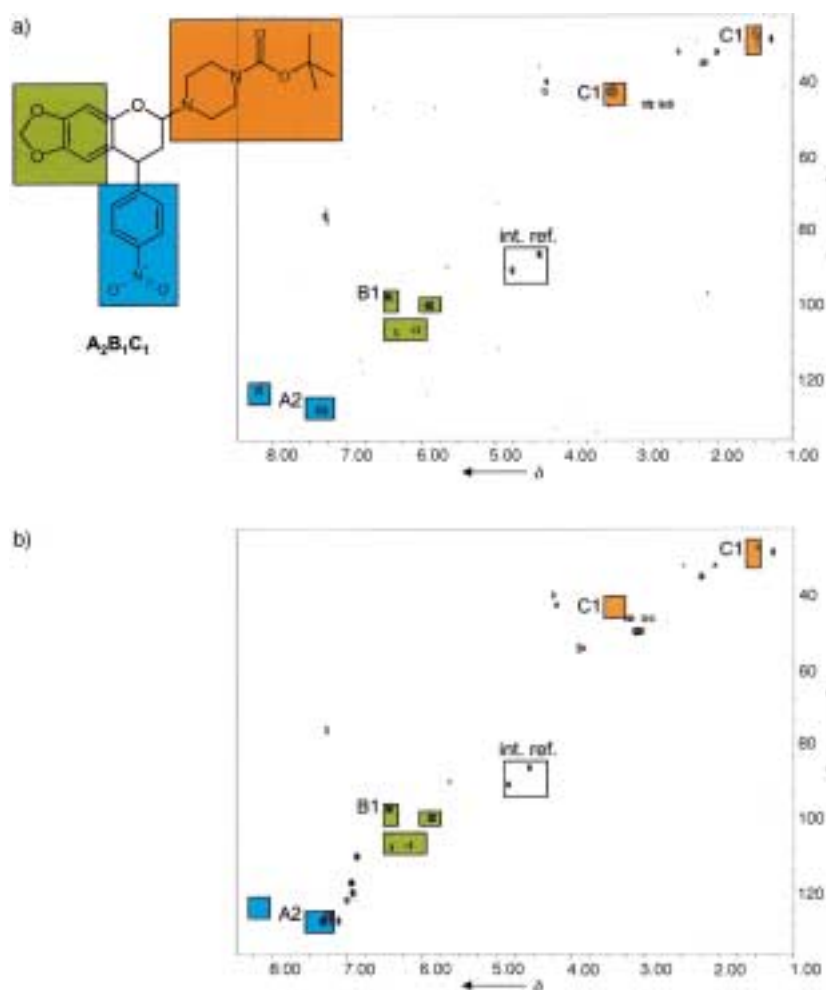
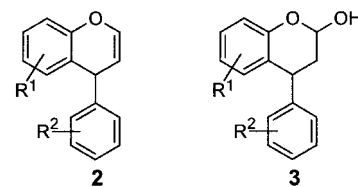


Figure 2. Decomposition of a 2D HSQC spectrum of a compound into the spectral patterns (color-coded). For example, the spectral pattern of B1 is composed of three signal regions (rectangular envelopes). a) The spectral patterns of each A₂, B₁, C₁ were found, and the structure of the expected compound A₂B₁C₁ is therefore validated. b) Structure of compound A₂B₁C₁ was not verified because the spectral patterns of both A2 and C1 are missing.

amounts of compound, as well as samples with large contents of impurities. The attribute “unclear” was assigned to these particular samples.

The ¹H NMR and 2D HSQC experiments established that the 4-phenylbenzopyrans were obtained as mixtures of diastereomers in an approximately 1.8:1 (*syn:anti*) ratio.

Signals of two side products **2** and **3** overlap with signals of the compound in the spectrum. The spectra of the ninety-six 4-phenylbenzopyrans were measured in 16 h. The automated calculation steps to interpret all spectra were performed in less than 5 min.



Of the ninety-six compounds analyzed with AutoDROP, sixty-eight proposed structures were found to be true (one false positive), eleven were proved false (one false negative), and seventeen designated “unclear”. Subsequent manual analysis of the ¹H NMR spectra of these seventeen unclear structures found nine to be true (A6, C4, C10, D2, E6, E10, G5, G6, G10; see Figure 3) and eight false (B10, C12, D1, D8, D9, F12, H7, H8). These analyses showed that eighteen compounds were not obtained by the synthetic procedure. Comparison of the results of the NMR method with those of an automated ESIMS analysis (Figure 3) showed that the structures of four samples out of the ninety-six were not validated by either NMR or ESIMS analysis, and four analyses were in contradiction. These four samples were classified by interpretation of the ¹H NMR spectra. Erroneous automated NMR results were obtained for compounds in wells A12 (true structure) and

D04 (false structure) but were easily corrected by means of the ¹H NMR spectra.

A novel procedure based on 2D NMR experiments was used for the rapid automated structure validation of all members of a 4-phenylbenzopyran library. The throughput of the AutoDROP NMR method is comparable to that of

Table 2. Graphical output of the NMR automated structure verification.^[a]

	Result	A1	A2	A3	A4	A5	A6	B1	B2	B3	B4	C1	C2	C3	C4
A1B1C1	+	+	–	–	–	–	–	+	–	–	–	+	–	–	–
A1B2C1	+	+	–	–	–	–	–	–	+	–	–	+	–	–	–
A1B3C1	–	+	–	–	–	–	–	–	–	–	–	+	–	–	–
A1B4C1	?	+	–	–	–	–	–	–	–	–	+	–	–	–	–
A1B1C2	+	+	–	–	–	–	–	+	–	–	–	–	+	–	–
A1B2C2	+	+	–	–	–	–	–	–	+	–	–	–	+	–	–
A1B3C2	–	+	–	–	–	–	–	–	+	–	–	–	+	–	–
A1B4C2	–	+	–	–	–	–	–	–	–	–	+	–	–	–	–
A2B1C1	+	–	+	–	–	–	–	+	–	–	–	+	–	–	–
A2B2C1	+	–	+	–	–	–	–	–	+	–	–	+	–	–	–

[a] All 2D HSQC spectra were tested for the presence of each of the possible substructures by using the integration procedure. The substructure was considered to be present in the molecule (+) when all integrals of one substructure exceeded a defined threshold. When all substructures of the sample were present, the structure was assigned the category true (+). When some of the expected substructures were not found, the structure was given the category false (–). If the signal-to-noise ratio or the ratio of the core integral to the single integral was below a certain limit, the category unclear (?) was assigned.

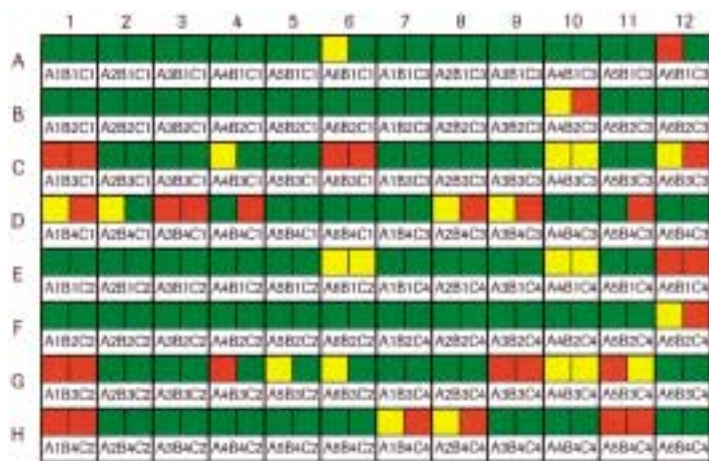


Figure 3. Combined results of the automated NMR and ESIMS analysis are summarized. Each cell contains the expected structure code and the data for NMR (top left), ESIMS (top right). Green means that the proposed structure is true in NMR spectroscopy and gives the expected molecular ion in ESIMS. Yellow indicates unclear results in both NMR spectroscopy and ESIMS. Red means that the proposed structure is false by NMR spectroscopy or does not give a diagnostic molecular ion in ESIMS.

current LC-MS methods. An automated qualitative and relative quantitative analysis of the compounds by using AutoDROP would be possible if the exact amount of sample were known. AutoDROP can be used in combination with ESIMS to analyze compound arrays from combinatorial chemistry and automated synthesis programs, and a wide application of this method is expected.

Experimental Section

The samples (from <1 to 5 mg) were dissolved in [D₆]DMSO (600 µL). NMR spectra were acquired in standard NMR tubes (5 mm) on a 400 MHz Bruker DRX 400 spectrometer equipped with a 120-sample changer. Tetramethylsilane was used as internal standard. For ¹H NMR 16 experiments were performed; two scans per increment and 128 experiments were performed for 2D HSQC. Cycle time to acquire ¹H and 2D HSQC NMR spectra and change the sample was 10 min per sample. AutoDROP is implemented in AMIX software (Bruker) and can be applied to 1D or 2D NMR spectra. ESIMS spectra were acquired on a PE Sciex API 300. Gradient of acetonitrile and H₂O/0.05 % trifluoroacetic acid were used for HPLC. Analytical HPLC was performed on a YMC Pack Pro C₁₈ column (5 µm, 75 × 4.6 mm), flow rate 2.5 mL min⁻¹, detection at 254 nm.

Library 1^[4] was synthesized by a multicomponent reaction^[5]. A 0.5 M stock solution of all reagents was prepared in ethanol. A solution of a phenol (400 µL, 0.2 mmol) was added to the reactor, and a solution of the corresponding unsaturated aldehyde (400 µL, 0.2 mmol) followed by a solution of the appropriate secondary amine (400 µL, 0.2 mmol) were dispensed. The reactors were closed and heated to 70 °C for 3 h. After cooling to room temperature, twenty-four compounds were collected by decantation, and the remaining seventy-two compounds were purified by preparative HPLC on a YMC Pack Pro C₁₈ column (5 µm, 120 Å, 50 × 20 mm).

Received: May 26, 2000 [Z15177]

- [1] a) *Combinatorial Chemistry* (Ed.: G. Jung), Wiley-VCH, Weinheim, 1999 and references therein; b) N. Sepetov, O. Issakova, *Comb. Chem. Technol.* 1999, 169–203.
[2] a) A. Pretsch, *Nachr. Chem. Tech. Lab.* 1998, 46, 71–73, Suppl. 4; b) R. Bürgin Schaller, M. E. Munk, E. Pretsch, *J. Chem. Inf. Comput. Sci.* 1996, 36, 239–243; c) A. Williams, D. Mityushev, V. Shilay, M. Kvasha, Presentation at Eastern Analytical Symposium, Somerset, NJ, 1999;

d) M. Will, W. Fachinger, J. R. Richert, *J. Chem. Inf. Comput. Sci.* 1996, 32, 221–227.

- [3] a) H. Schröder, P. Neidig, DE-19849231-C2, 1998; b) H. Schröder, G. Rossé, P. Neidig, *Automated Structure Verification of Combinatorial Library Members using 2D NMR Techniques*, 37th IUPAC Congress/27th GDCh General Meeting, Berlin, 1999; c) Technical components of AutoDROP are described in: H. Schröder, P. Neidig, *Bruker Report* 1999, 147, 18–21.
[4] L. Jurd, *J. Heterocycl. Chem.* 1991, 28, 983–986.
[5] a) I. Ugi, A. Dömling, B. Ebert in *Combinatorial Chemistry* (Ed.: G. Jung), Wiley-VCH, Weinheim, 1999, pp. 125–165; b) L. Weber, K. Illgen, M. Alsmstter, *Synlett* 1999, 3, 366–374.

Molecular Topology: Easy Self-Assembly of an Organometallic Doubly Braided [2]Catenane**

Christopher P. McArdle, Jagadees J. Vittal, and
Richard J. Puddephatt*

Molecular topology^[1–5] is in a period of remarkable growth as the advent of new synthetic strategies, based on ideas such as metal-ion templating^[6–8] and self-assembly through non-covalent interactions,^[9–15] has allowed the design and isolation of supermolecules such as catenanes, rotaxanes, and knots.^[16–18] Today, with the synthesis of increasingly intricate molecular topologies,^[19–22] these supermolecules attract continued attention for their potential application in the development of molecular devices.^[23] In this context, we report the discovery of an elegant example of molecular self-assembly which has led to the isolation and first structural characterization of a doubly braided [2]catenane. This complex organometallic structure, assembled in one step from eight components, exhibits evidence of a fast “rocking” motion of the two 50-membered rings. Fine tuning the organic backbone results in the formation of topologically distinct complexes; a simple ring and a single braid [2]catenane.

In a system comprising two rings, the formation of mechanical bonds (nonbonded interconnections) can lead to topologically isomeric molecules (Figure 1). While simple rings (A) and [2]catenanes (B) are both well recognized at the molecular level, the doubly braided [2]catenane (C) has

[*] Prof. R. J. Puddephatt, Dr. C. P. McArdle

Department of Chemistry
University of Western Ontario
London, ON, N6A 5B7 (Canada)
Fax: (+1) 519-661-3022
E-mail: pudd@uwo.ca

Prof. J. J. Vittal
Department of Chemistry
National University of Singapore
3 Science Drive 3, Singapore 117543 (Singapore)

[**] We thank Dr. C. Kirby for assistance with low-temperature NMR studies, Dr. M. C. Jennings for the X-ray structure determination of 3, and the NSERC (Canada) for financial support. Funding from the National University of Singapore for the purchase of a Bruker AXS CCD diffractometer is also gratefully acknowledged.

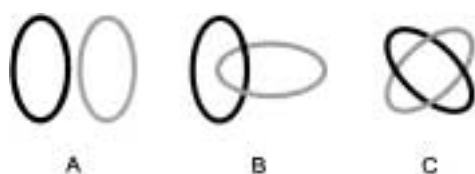
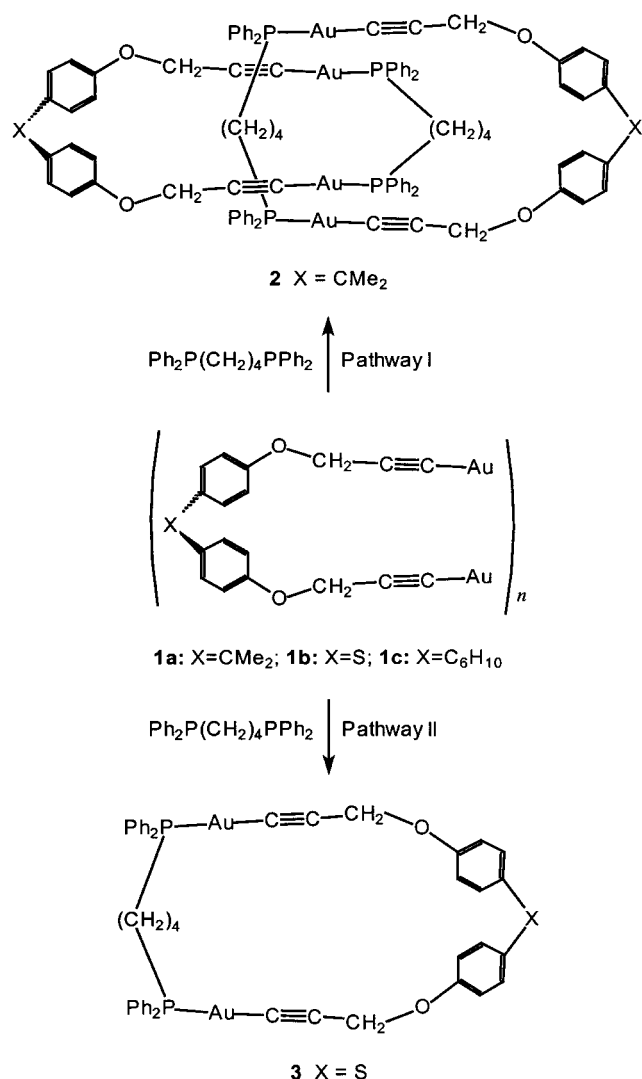


Figure 1. Schematic representation of topological isomers.

remained a serious synthetic challenge, since it requires two rings to be interlocked not once but twice. The doubly braided catenanes **C** have been synthesized by metal-templating strategies,^[24, 25] but no X-ray structural characterization has been reported.

Scheme 1 shows how large organogold rings can be formed by self-assembly on reaction of a complex digold(ii) diacetylide with a diphosphane ligand, $\text{Ph}_2\text{P}(\text{CH}_2)_4\text{PPh}_2$ (dppb). The singly braided [2]catenane **2** was reported to be formed by combination of four components (2+2) when $\text{X}=\text{CMe}_2$ (pathway I).^[26] The following question naturally arises: can different forms of self-assembly be induced by subtle molec-



Scheme 1. Formation of the [2]catenane complex **2** (pathway I) and the simple ring complex **3** (pathway II).

ular tailoring, such as changing the “hinge” group X ? The answer is a dramatic yes, as shown below.

Scheme 1 shows that when the hinge group X is a sulfur atom ($\text{X} = \text{S}$), the reaction of **1b** with dppb gave only the simple 25-membered ring (complex **3**) by pathway II, in a reaction which involves the simplest possible combination of two components (1+1). Compound **3** was characterized by both NMR spectroscopy (^1H , ^{31}P , ^{13}C , and 2D experiments) and by X-ray structure determination. The cavity sizes of individual 25-membered rings in **2** and **3** are similar, but the minor conformational changes induced by the different hinge groups clearly affect the secondary aryl–aryl attractive forces that control catenation.^[27]

The most exciting development occurred in the case with the hinge group $\text{X} = \text{cyclohexylidene}$, C_6H_{10} . The reaction of **1c** with dppb led to the self-assembly of the doubly braided [2]catenane **4** (Figure 2), isolated in pure form in 72 % yield. X-ray structure determination (Figure 2b) showed that **4** contains two 50-membered rings, and the cavity formed by each giant ring is large enough to allow the double braid to form. Figure 2c shows the complete structure, illustrating the exquisite way in which the double braiding occurs. The structure contains multiple aryl–aryl secondary bonds (four phenyl–phenyl and four phenyl–aryl) as well as two strong inter-ring aurophilic attractions.^[27, 28] Figure 2d shows in a space-filling representation of how the phenyl substituents (along with two solvent dichloromethane molecules that are not shown) pack the remaining cavity. It is truly remarkable that such a complex structure, requiring self-assembly of eight components (4+4), could occur so easily and selectively to give an octagold complex with molecular weight of 4651. This first X-ray structure of any doubly braided catenane (Figure 2) illustrates the inherent chiral nature of such compounds arising from clockwise or anticlockwise braiding.

How rigid is the doubly braided catenane **4**? This is an important question if catenanes are to act as molecular devices. The structure shown in Figure 2, contains no crystallographically imposed symmetry but there are two chemically distinct environments for the phosphorus atoms which may be bound to gold atoms that are or are not engaged in close inter-ring aurophilic attractions. The ^{31}P NMR spectrum (Figure 3) recorded at -90°C contained two resonances, as expected for the structure shown in Figure 2, but at room temperature only one resonance was observed, indicating that rapid exchange between the two environments is possible. The activation energy at the coalescence temperature of -70°C was $\Delta G^\ddagger = 41(\pm 1) \text{ kJ mol}^{-1}$. Similar coalescence of inequivalent resonances occurred for the phenol group resonances in the ^1H NMR spectra (Figure 3). The least motion that can cause such coalescence is a back-and-forth rocking motion, indicated schematically in Figure 3, that is well suited to molecular switching. More extensive snaking of the two rings^[24] is likely to be prevented by eclipsing of bulky diphenylphosphanyl substituents.

In conclusion, all possible combinations of the simple ring, singly, and doubly braided [2]catenanes of Figure 1 can be synthesized easily by judicious choice of the hinge group X in the precursor molecules **1**. The first structure of a doubly braided catenane is reported and it is shown that it undergoes

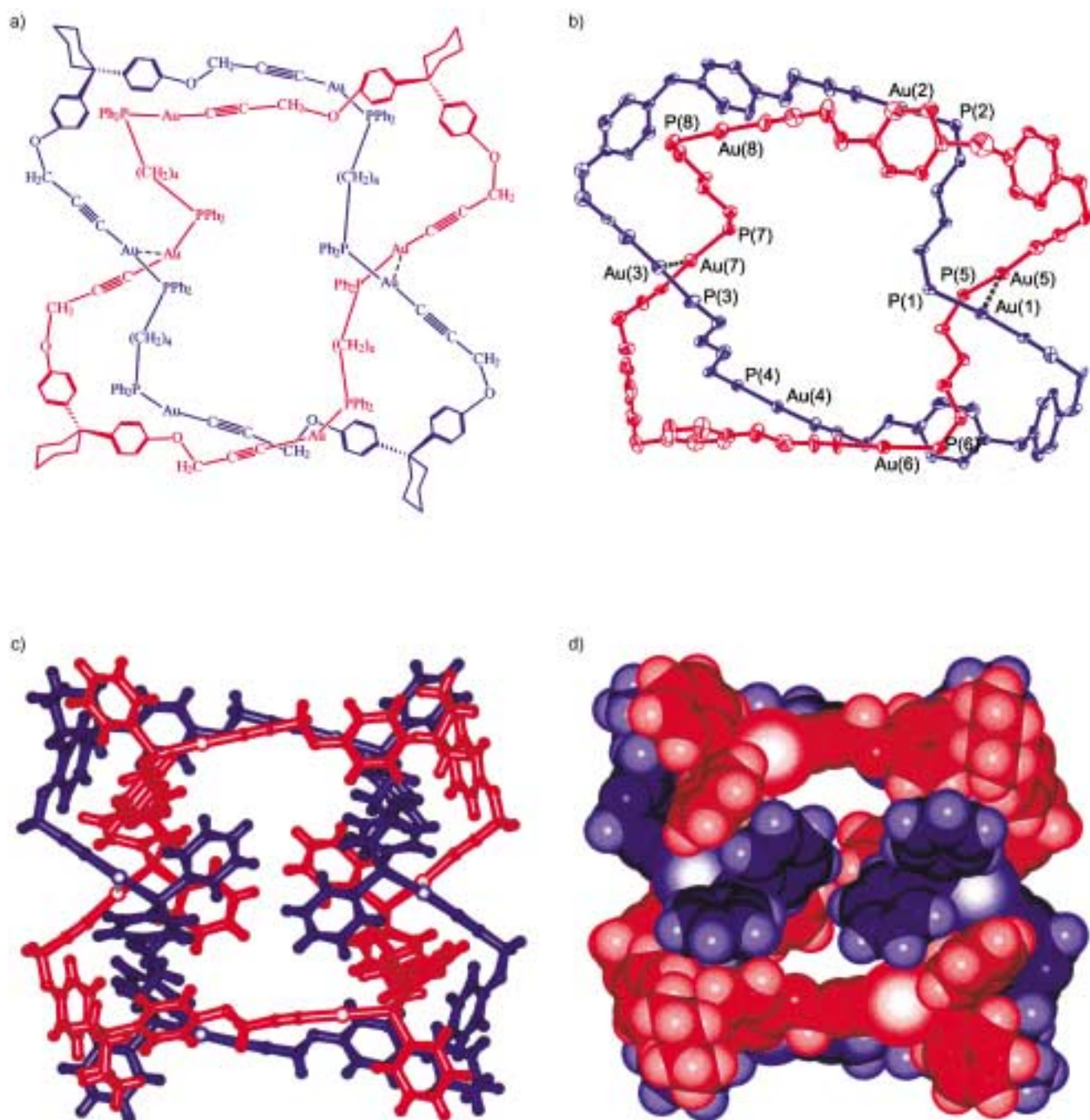


Figure 2. Structure of the doubly braided [2]catenane, complex **4**. a) Structural formula. b) X-ray structure showing core ring atoms only. c) Ball-and-stick representation of the complete structure. d) Space-filling representation of the X-ray structure.

an easy molecular switching motion. Simple extensions to yield yet more intricate molecular topologies are readily envisioned.

Experimental Section

3: A mixture of **1b** (0.100 g, 0.146 mmol) and $\text{Ph}_2\text{P}(\text{CH}_2)_4\text{PPh}_2$ (0.056 g, 0.131 mmol) in CH_2Cl_2 (50 mL) was stirred for 3 h at room temperature. Activated charcoal was added to the solution, which was stirred for a further 0.5 h then filtered. The filtrate was concentrated (ca. 1–2 mL) and addition of pentane (100 mL) precipitated **3** as a white solid. The powder was collected by filtration, washed with diethyl ether and pentane, and dried. Yield 0.087 g, 60%. IR (CH_2Cl_2): $\tilde{\nu} = 2135$ (w, $\text{C}\equiv\text{C}$) cm^{-1} ; ^1H NMR

(CD_2Cl_2 , 25 °C): $\delta = 1.73$ (m, 4H; CH_2), 2.34 (m, 4H; CH_2), 4.78 (s, 4H; OCH_2), 7.04 (m, 4H; C_6H_4), 7.35 (m, 4H; C_6H_4), 7.41–7.64 (m, 20H; Ph); ^{31}P NMR (CD_2Cl_2 , 25 °C): $\delta = 38.89$; ^{13}C NMR (CD_2Cl_2 , 25 °C): $\delta = 27.7$ (CH_2), 28.0 (CH_2), 56.9 (OCH_2), 97.0 (d, $^3J_{\text{PC}} = 26$ Hz; $\text{C}\equiv\text{C}$), 116.2 (C_6H_4), 127.6 (Ph), 129.3 (C_6H_4), 129.4 (Ph), 130.4 (d, $^2J_{\text{PC}} = 54$ Hz; $\text{C}\equiv\text{C}$), 131.8 (Ph), 133.3 (C_6H_4), 133.4, 133.5 (both Ph), 157.8 (C_6H_4); elemental analysis calcd for $\text{C}_{46}\text{H}_{40}\text{Au}_2\text{P}_2\text{O}_2\text{S}$ (%): C 49.65, H 3.62; found: C 49.96, H 3.66. X-ray quality crystals were grown from $\text{Et}_2\text{O}/\text{CH}_2\text{Cl}_2$ solution at 0 °C.

4: This was prepared similarly from **1c** (0.100 g, 0.136 mmol) and $\text{Ph}_2\text{P}(\text{CH}_2)_4\text{PPh}_2$ (0.052 g, 0.122 mmol) in CH_2Cl_2 (50 mL), and isolated as a white solid. Yield 0.103 g, 72%. IR (CH_2Cl_2): $\tilde{\nu} = 2134$ (w, $\text{C}\equiv\text{C}$) cm^{-1} ; ^1H NMR (CD_2Cl_2 , 25 °C): $\delta = 1.51$ (m, 24H; C_6H_{10}), 1.73 (m, 16H; CH_2), 2.23 (m, 16H; C_6H_{10}), 2.34 (m, 16H; CH_2), 4.76 (s, 16H; 2 OCH_2), 6.99 (m,

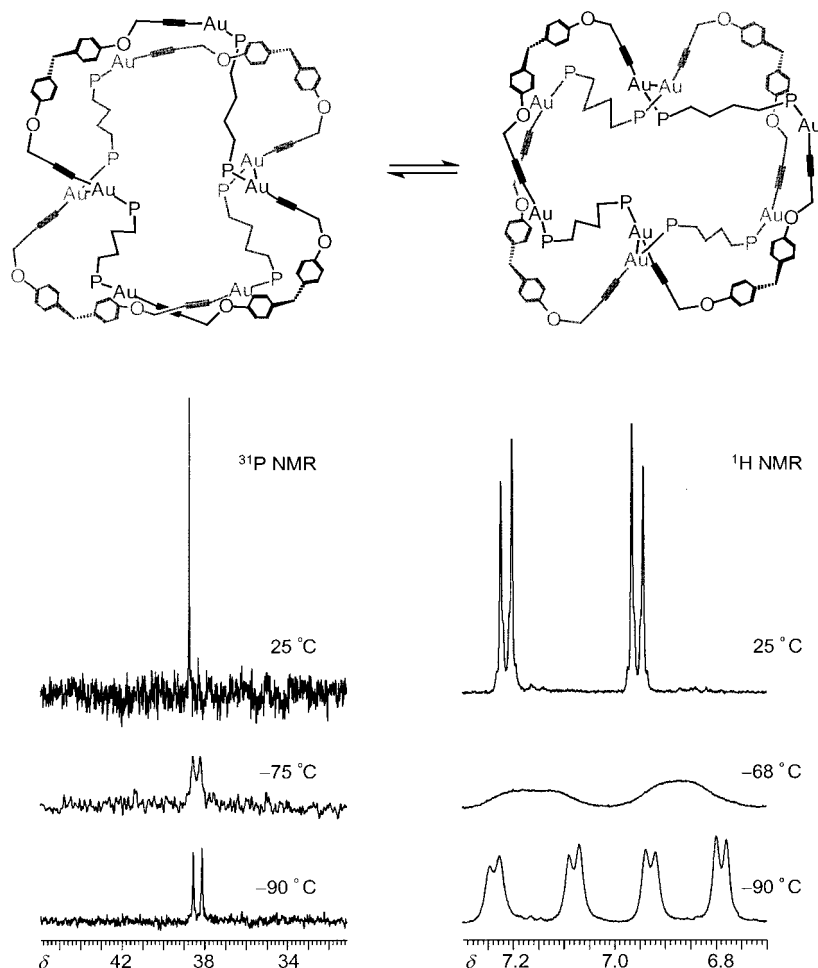


Figure 3. Variable-temperature NMR observations of complex **4**, and the proposed molecular switching motion (cyclohexylidene and phenyl groups are omitted for clarity).

16H; C_6H_4), 7.25 (m, 16H; C_6H_4), 7.43–7.63 (m, 80H; Ph); ^{31}P NMR (CD_2Cl_2 , 25 °C): δ = 38.75; ^{13}C NMR (CD_2Cl_2 , 25 °C): δ = 23.1 (C_6H_{10}), 27.8 (CH_2), 28.1 (CH_2), 37.6 (C_6H_{10}), 44.8 (C_6H_{10}), 56.4 (OCH_2), 97.5 (d, $^3J_{PC}$ = 26 Hz; $C\equiv C$), 114.7, 128.0 (both C_6H_4), 129.3, 129.4 (both Ph), 130.5 (d, $^3J_{PC}$ = 54 Hz; $C\equiv C$), 131.7 (C_6H_4), 133.4, 133.5 (both Ph), 155.7 (C_6H_4); elemental analysis calcd for $C_{208}H_{200}Au_8P_8O_8$ (%): C 53.71, H 4.33; found: C 53.59, H 4.38.

Crystallographic study of complex **4**: X-ray quality crystals were grown by slow diffusion of Et_2O into a CH_2Cl_2 solution of complex **4**, at 0 °C. A crystal was sealed in a glass capillary and data were collected at 20 °C. Crystal data: monoclinic, $P2_1/n$; a = 27.1682(3), b = 27.9905(4), c = 31.9272 Å, β = 91.280(1)°, V = 24273(1) Å³, Z = 4, λ = 0.71073 Å, $R1$ = 0.1295, $wR2$ = 0.2643 for 19347 reflections with $F_o > 4\sigma(F_o)$. In this refinement, disordered CH_2Cl_2 molecules were located in seven places in the asymmetric unit and totalled three molecules, and partial occupation by water molecules of solvation was also indicated. The agreement factor is poor as a result of the crystal quality, by the presence of large cavities in the lattice occupied by disordered solvents, and by disorder in some cyclohexyl and phenyl substituents. However, all heavy atoms were clearly identified, and the connectivity of the organometallic rings is proved beyond any doubt. Crystallographic data (excluding structure factors) for the structure reported in this paper have been deposited with the Cambridge Crystallographic Data Centre as supplementary publication no. CCDC-145603. Copies of the data can be obtained free of charge on application to CCDC, 12 Union Road, Cambridge CB21EZ, UK (fax: (+44)1223-336-033; e-mail: deposit@ccdc.cam.ac.uk).

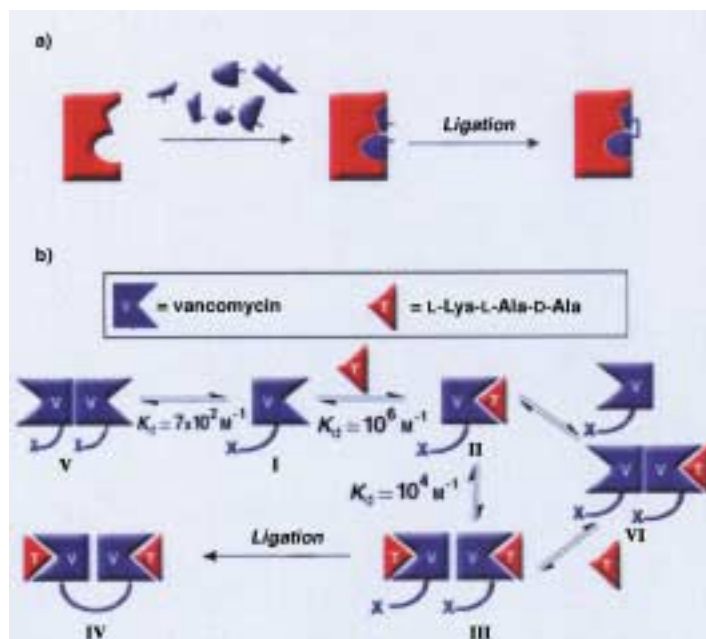
- [1] D. M. Walba, *Tetrahedron* **1985**, *41*, 3161–3212.
- [2] H. Dodzuik, K. S. Nowinski, *Tetrahedron* **1998**, *54*, 2917–2930.
- [3] G. A. Breault, C. A. Hunter, P. C. Mayers, *Tetrahedron* **1999**, *55*, 5265–5293.
- [4] E. Wasserman, *J. Am. Chem. Soc.* **1960**, *82*, 4433–4434.
- [5] H. L. Frisch, E. Wasserman, *J. Am. Chem. Soc.* **1961**, *83*, 3789–3795.
- [6] J.-P. Sauvage, C. O. Dietrich-Buchecker, J.-C. Chambron in *Comprehensive Supramolecular Chemistry*, Vol. 2 (Eds.: J.-P. Sauvage, M. W. Hosseini), Pergamon, Oxford, **1995**, chap. 2, pp. 43–83.
- [7] J.-C. Chambron, C. O. Dietrich-Buchecker, V. Heitz, J.-F. Nierengarten, J.-P. Sauvage, C. Pascard, J. Guilhem, *Pure Appl. Chem.* **1995**, *67*, 233–240.
- [8] R. Hoss, F. Vögtle, *Angew. Chem.* **1994**, *106*, 389–398; *Angew. Chem. Int. Ed. Engl.* **1994**, *33*, 375–384.
- [9] C. Seel, F. Vögtle, *Chem. Eur. J.* **2000**, *6*, 21–24.
- [10] M. Fujita, *Acc. Chem. Res.* **1999**, *32*, 53–61.
- [11] T. J. Kidd, D. A. Leigh, A. J. Wilson, *J. Am. Chem. Soc.* **1999**, *121*, 1599–1600.
- [12] K. N. Houk, S. Menzer, S. P. Newton, F. M. Raymo, J. F. Stoddart, D. J. Williams, *J. Am. Chem. Soc.* **1999**, *121*, 1479–1487.
- [13] D. G. Hamilton, J. E. Davies, L. Prodi, J. K. M. Sanders, *Chem. Eur. J.* **1998**, *4*, 608–620.
- [14] F. Vögtle, T. Dönnwald, T. Schmidt, *Acc. Chem. Res.* **1996**, *29*, 451–460.
- [15] C. A. Hunter, *J. Am. Chem. Soc.* **1992**, *114*, 5303–5311.
- [16] G. Schill, *Catenanes, Rotaxanes and Knots*, Academic Press, New York, **1971**.
- [17] J.-P. Sauvage, C. O. Dietrich-Buchecker in *Molecular Catenanes, Rotaxanes and Knots* (Eds.: J.-P. Sauvage, C. O. Dietrich-Buchecker), Wiley-VCH, Weinheim, **1999**.
- [18] D. B. Amabilino, J. F. Stoddart, *Chem. Rev.* **1995**, *95*, 2725–2828.
- [19] S. Leininger, B. Olenyuk, P. J. Stang, *Chem. Rev.* **2000**, *100*, 853–908.
- [20] M. Fujita, N. Fujita, K. Ogura, K. Yamaguchi, *Nature* **1999**, *400*, 52–55.
- [21] S.-G. Roh, K.-M. Park, G.-J. Park, S. Sakamoto, K. Yamaguchi, K. Kim, *Angew. Chem.* **1999**, *111*, 672–675; *Angew. Chem. Int. Ed.* **1999**, *38*, 638–640.
- [22] S. R. Batten, R. Robson, *Angew. Chem.* **1998**, *110*, 1558–1595; *Angew. Chem. Int. Ed.* **1998**, *37*, 1460–1494.
- [23] C. P. Collier, E. W. Wong, M. Belohradsky, F. M. Raymo, J. F. Stoddart, P. J. Kuekes, R. S. Williams, J. R. Heath, *Science* **1999**, *285*, 391–394.
- [24] C. O. Dietrich-Buchecker, J.-P. Sauvage, *Chem. Commun.* **1999**, 615–616; J.-F. Nierengarten, C. O. Dietrich-Buchecker, J.-P. Sauvage, *New J. Chem.* **1996**, *20*, 685–693.
- [25] F. Ibukuro, M. Fujita, K. Yamaguchi, J.-P. Sauvage, *J. Am. Chem. Soc.* **1999**, *121*, 11014–11015.
- [26] C. P. McArdle, M. J. Irwin, M. C. Jennings, R. J. Puddephatt, *Angew. Chem.* **1999**, *111*, 3571–3573; *Angew. Chem. Int. Ed.* **1999**, *38*, 3376–3378.
- [27] C. A. Hunter, J. K. M. Sanders, *J. Am. Chem. Soc.* **1990**, *112*, 5525–5534.
- [28] H. Schmidbaur, A. Grohmann, M. E. Olmos in *Gold: Progress in Chemistry, Biochemistry and Technology* (Ed.: H. Schmidbaur), Wiley, Chichester, **1999**, chap. 18.

Received: June 19, 2000 [Z15286]

Target-Accelerated Combinatorial Synthesis and Discovery of Highly Potent Antibiotics Effective Against Vancomycin-Resistant Bacteria**

K. C. Nicolaou,* Robert Hughes, Suk Young Cho, Nicolas Winssinger, Christian Smethurst, Harald Labischinski, and Rainer Endermann

In the past decade combinatorial chemistry has evolved into a powerful tool for chemical biology and the drug discovery process.^[1] The complete sequencing of the human genome will inevitably increase the demand for libraries of small organic molecules and create a strong evolutionary pressure on methods to rapidly generate such molecules. Lehn and co-workers have recently proposed and demonstrated^[2, 3] the feasibility of “dynamic target-driven combinatorial synthesis” wherein the building blocks of a combinatorial library are allowed to assemble and react in the presence of a target (Scheme 1 a). This synthetic approach should, thus, selectively deliver the product with the highest affinity for the target out of a virtual library of all possible reaction products.^[4] In a related approach, Fesik and co-workers have developed a technique whereby the building blocks of potential combinatorial libraries are screened for binding to their target by NMR spectroscopy.^[5] The building blocks with the highest affinity for the target are then covalently tethered in a separate experiment. More recently, Ellman and co-workers reported a similar approach in which an initial combinatorial library was screened for binding to a target by an enzyme-linked immunosorbent assay (ELISA) in order to narrow down the selection of building blocks^[6] for eventual, separately performed, covalent tethering. Herein we report the application of direct target-accelerated combinatorial synthesis (TACS) of vancomycin dimers for the identification of ligands with the highest affinity for vancomycin’s receptor, D-Ala-D-Ala. Among the dimers synthesized are a number



Scheme 1. a) Schematic representation of target-accelerated combinatorial synthesis. A target (red shape) is incubated with a library of building blocks (blue shapes). The building blocks that show affinity for the target will assemble onto the target. Upon a ligation reaction, the selectively preorganized assembly will ligate preferentially. b) Schematic representation of dynamic target-accelerated combinatorial synthesis of vancomycin dimers. A library of vancomycin analogues (V, blue shape) are incubated with their target, Ac₂-L-Lys-D-Ala-D-Ala (T, red shape). Since the formation constant of the vancomycin dimer ($K_d \approx 7 \times 10^2 \text{ M}^{-1}$) is greater in the presence of its target ($K_d \approx 10^4 \text{ M}^{-1}$), it is expected that the target-bound dimeric assembly (III) should ligate faster than its nontarget-bound counterpart (V).

possessing potent activities against vancomycin-resistant *enterococci* (VRE) and vancomycin intermediate susceptible *Staphylococcus aureus* (VISA) that rival or exceed the most active compounds known today^[7] for these bacterial strains.

Vancomycin (**1**, Scheme 2a),^[8, 9] a prominent member of the glycopeptide class of antibiotics, has been used clinically for the past 40 years to treat infections caused by Gram-positive bacteria. Its renowned action against methicillin-resistant *Staphylococcus aureus* (MRSA) bacteria has made it an antibiotic of last resort. However, the emergence of vancomycin-resistant *enterococci* (VRE)^[10] and, more recently, vancomycin intermediate susceptible *Staphylococcus aureus* (VISA)^[11] are raising serious health concerns and has prompted renewed and vigorous research activities targeting modified vancomycin analogues with restored activity against VRE or VISA.^[12, 13] Vancomycin’s antibacterial activity arises from its ability to inhibit peptidoglycan biosynthesis within the bacterial cell wall. Specifically, vancomycin binds to the terminal Lys-D-Ala-D-Ala fragment of the growing peptidoglycan biosynthetic precursor through an intricate network of five hydrogen bonds (Scheme 2a),^[14] thereby inhibiting cell-wall growth and cross-linking. While the resistance mechanism of VISA is not yet understood in detail,^[15, 16] the molecular mechanism of VRE (types A and B) defense against vancomycin relies on a modified peptidoglycan biosynthesis in which the terminal D-Ala residue is substituted

[*] Prof. Dr. K. C. Nicolaou, R. Hughes, Dr. S. Y. Cho, Dr. N. Winssinger, Dr. C. Smethurst

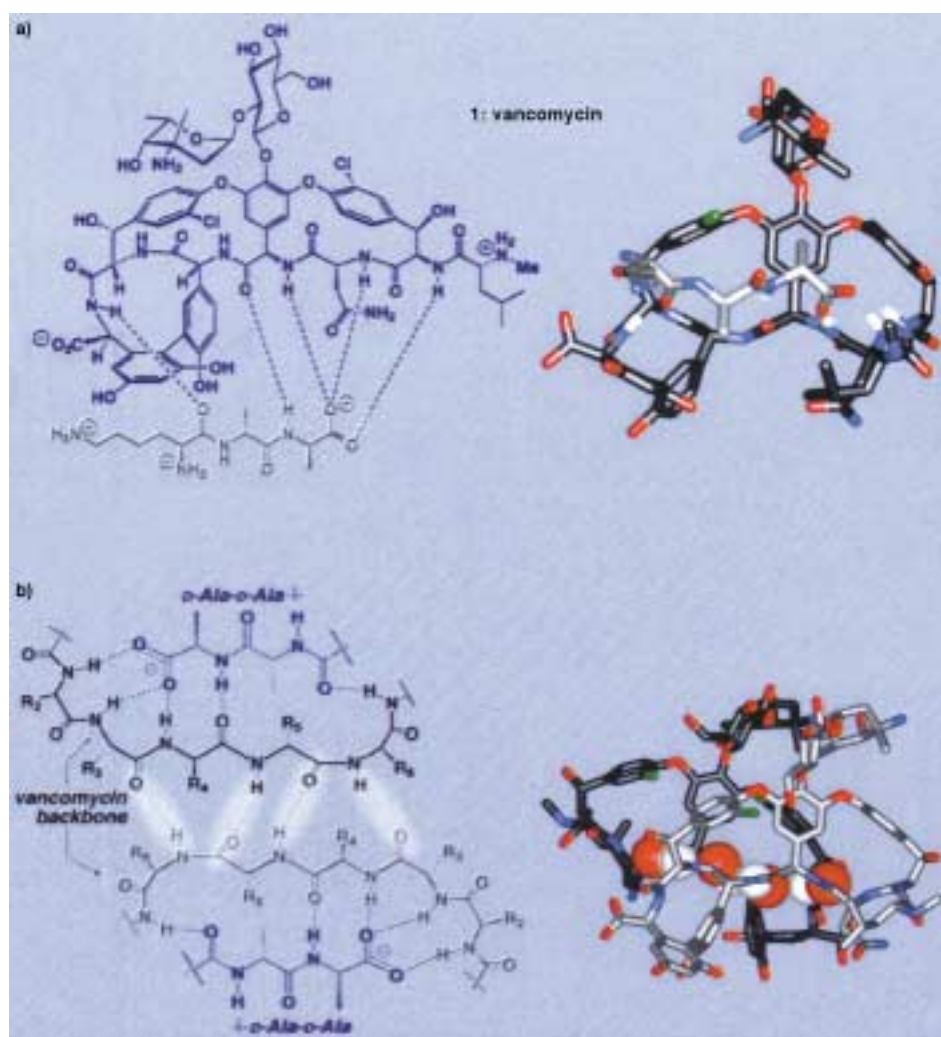
Department of Chemistry
and The Skaggs Institute for Chemical Biology
The Scripps Research Institute
10550 North Torrey Pines Road, La Jolla, CA 92037 (USA)
Fax: (+1) 858-784-2469

and
Department of Chemistry and Biochemistry
University of California San Diego
9500 Gilman Drive, La Jolla, CA 92093 (USA)
E-mail: kcn@scripps.edu

Dr. H. Labischinski, Dr. R. Endermann
Bayer AG, PH-R-Anti-infectives, Wuppertal (Germany)

[**] We thank Dr. Gary Siuzdak for mass spectrometric assistance and Prof. Dr. Gunter Benz and Drs. Rudolf Hanks and Joachim Krueger of Bayer AG for helpful discussions. This work was financially supported by the National Institutes of Health (USA), The Skaggs Institute for Chemical Biology, and Bayer AG, as well as by fellowships from the Division of Organic Chemistry of the American Chemical Society (sponsored by Hoescht Marion Roussel, to R.H.) and the George Hewitt Foundation (to N.W.).

Supporting information for this article is available on the WWW under <http://www.wiley-vch.de/home/angewandte/> or from the author.



Scheme 2. a) Hydrogen-bond network between vancomycin (dark structure) and the L-Lys-D-Ala-D-Ala tripeptide (light structure) as a ChemDraw (left) and as a wire-frame model (right). b) Hydrogen-bonding network of the vancomycin back-to-back dimer as a ChemDraw (left) and as a wire-frame model (right, one vancomycin molecule is shown in light gray whereas the other is shown in black) with the hydrogen bonds in the latter highlighted by space-filling atoms (oxygen = red; hydrogen = white).^[18]

by a D-Lac moiety.^[17] This substitution results in the loss of one hydrogen bond with the consequence that the reduced affinity of vancomycin for D-Ala-D-Lac is no longer sufficient to inhibit the peptidoglycan biosynthesis.

A number of glycopeptide antibiotics form dimers^[18, 19] and, significantly, their propensity to dimerize has been correlated to their biological activity.^[20] Vancomycin has been shown to form a weak back-to-back dimer with a dimerization constant^[21] of approximately $7 \times 10^2 \text{ M}^{-1}$. In addition to the benefit of multivalency,^[22] an important feature of this back-to-back dimerization is the strengthening of the hydrogen-bonding interaction between the vancomycin framework and its target (Scheme 2b). Thus, back-to-back dimerization is mediated by a network of hydrogen bonds which involve the same amide linkages as those involved in binding to the D-Ala-D-Ala moiety. The net result of this cooperative, back-to-back binding is that the dimer has greater affinity for its target than the monomer; likewise, vancomycin bound to its target has a greater dimerization constant (ca. 10^4 M^{-1}) than vanco-

mycin alone.^[23] Griffin and co-workers have prepared covalent dimers^[24] linked through the C-terminus of vancomycin which exhibit moderate activity against VRE. Interestingly, the biological activity of these dimers varied significantly with the nature of the tether. Several other covalent vancomycin dimers,^[25–27] a trimer,^[28] and a polymer^[29] have also been reported. Most recently, surface plasmon resonance was used to investigate the self-association of several covalent vancomycin dimers. The study indicated that the biological activity of such covalent dimers is correlated to their ability to self-assemble (that is, to adopt the back-to-back conformation).^[30]

On the basis of the structure of the back-to-back dimer (Scheme 2b) we reasoned that the most appropriate means by which to form such a stable dimer would be to construct a bridge across the saccharide domains of two vancomycin molecules. However, selecting the appropriate tether so as to permit the full cooperation of the two monomers in forming the desired back-to-back arrangement was the more demanding challenge. We postulated that a dynamic target-accelerated combinatorial synthesis of such a dimer (Scheme 1b) would be

particularly attractive for the case of vancomycin dimers (Scheme 1b), with the ones with the strongest affinity for the target being favored. As such, a library of vancomycin analogues (monomers) would be allowed to self-assemble in the presence of their target while a latent reactive functionality could later be utilized to covalently dimerize the product of the most stable and longest-lived supramolecular assembly.^[31] Since the vancomycin template has a higher formation constant for the dimer when bound to its target, we hypothesized that the selection should function for both the adequacy of the tether and the binding affinity of the vancomycin analogue to its target. Such a strategy would also enable the formation of covalent hetero-vancomycin dimers.^[32] The final task was to choose an appropriate ligation method which could operate efficiently at biologically relevant temperatures and in aqueous media, be compatible with vancomycin's polyfunctional structure, and, most importantly, operate reversibly so as to allow equilibration. Towards this end we selected two processes, the olefin metathesis reac-

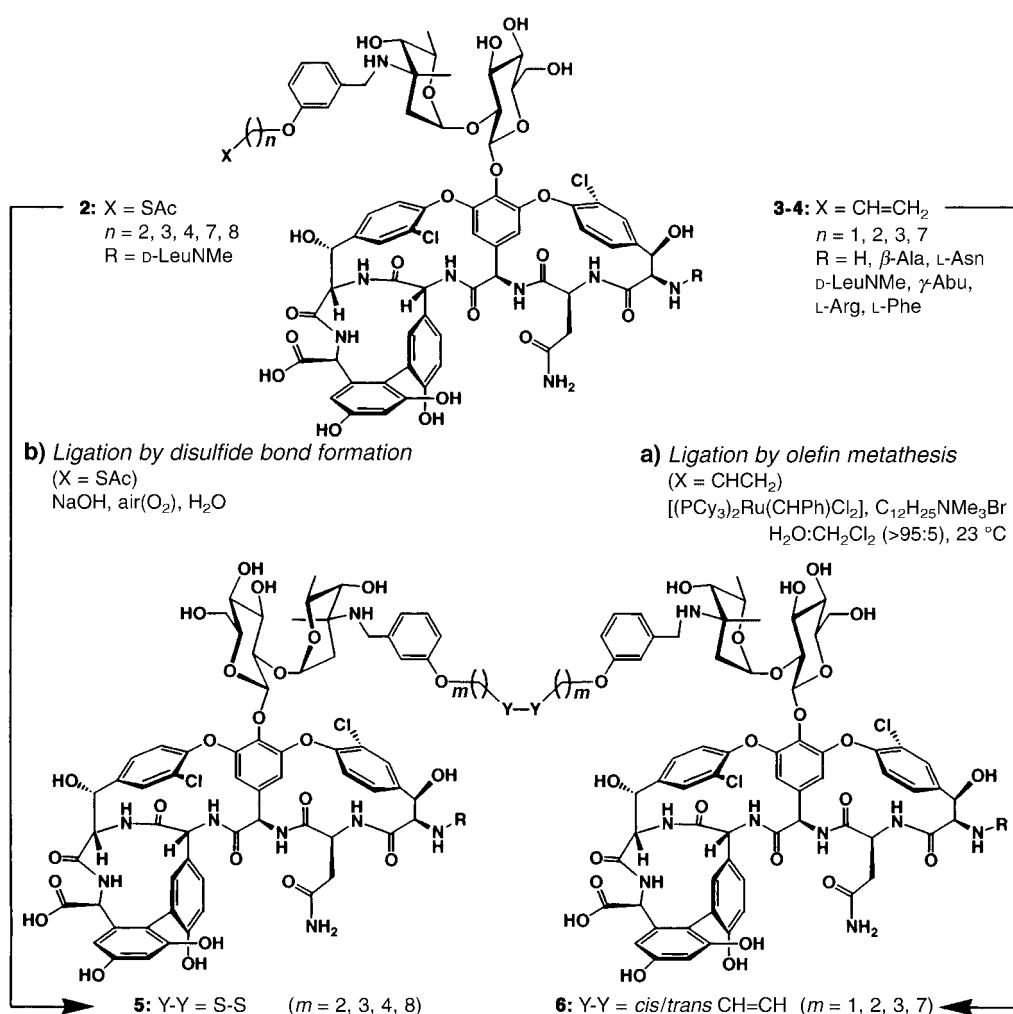
tion^[33] and the formation of a disulfide bond, which could meet these stringent requirements.

We employed both solid- and solution-phase combinatorial chemistry (see Supporting Information) to synthesize the required substrates for the target-accelerated dimerization studies. All synthesized vancomycin libraries were then subjected to biological screening for antibacterial properties, and a representative set of the library members were chosen for the proposed dimerization studies.

As an initial experiment to validate the target-accelerated dimerization hypothesis we subjected vancomycin derivatives **2** and **3** to disulfide formation and to olefin metathesis, respectively, in both the absence and presence of vancomycin's targets Ac-D-Ala-D-Ala and Ac₂-L-Lys-D-Ala-D-Ala for which vancomycin has the greatest affinity (Scheme 3). To achieve olefin metathesis, [(PCy₃)₂Ru(CHPh)Cl₂] was used as a catalyst in conjunction with the phase-transfer catalyst C₁₂H₂₅NMe₃Br, with the reactions carried out in water at 23 °C. The reactions proceeded at reasonable rates under these conditions and were conveniently monitored by

both HPLC and mass spectrometry. A significant rate acceleration for this reaction was observed in the presence of either ligand relative to the control experiment as measured by product formation by HPLC (Figure 1). As expected, Ac₂-L-Lys-D-Ala-D-Ala induced the highest rate acceleration by virtue of its higher affinity for vancomycin. The positive correlation between the observed target-induced rate acceleration and the target binding affinity to vancomycin is in accord with the postulated target-induced rate-acceleration mechanism. Likewise, the series of vancomycin thioacetate analogues **2** were saponified with NaOH and induced to dimerize by air oxidation in aqueous solution at ambient temperature in the absence and presence of Ac₂-L-Lys-D-Ala-D-Ala. Again, a strong target-induced rate acceleration was observed in the presence of these vancomycin targets (data not shown).

Having established the validity of the target-accelerated synthesis of vancomycin dimers from individual monomers,



Scheme 3. Dimerization of monomeric vancomycin thioacetates (**2**) and vancomycin derivatives with terminal olefins (**3**, **4**) to form disulfides (**5**) and olefinic dimers (**6**), respectively. Reagents and conditions: a) [(PCy₃)₂Ru(CHPh)Cl₂] (0.2 equiv), C₁₂H₂₅NMe₃Br (2.2 equiv), H₂O:CH₂Cl₂ (>95:5), 23 °C; b) NaOH (10.0 equiv), H₂O, 23 °C. Individual compounds (homo-dimers) were most conveniently prepared as single compounds from the corresponding monomers and were isolated in pure form by HPLC. Isolated compounds were characterized by NMR spectroscopy and mass spectrometry. In this report, we use the convention **xx**-(**R**)C_n to designate library members with the following designations: **xx** = compound number; (**R**) = the first amino acid residue; C_n = number of carbon atoms between the phenolic oxygen atom and the dimerization moiety X. Thus, **3**-(LeuNMe)C₄ designates a monomer and **6**-(LeuNMe)C₄-(LeuNMe)C₄ designates its corresponding dimer. Cy = cyclohexyl.

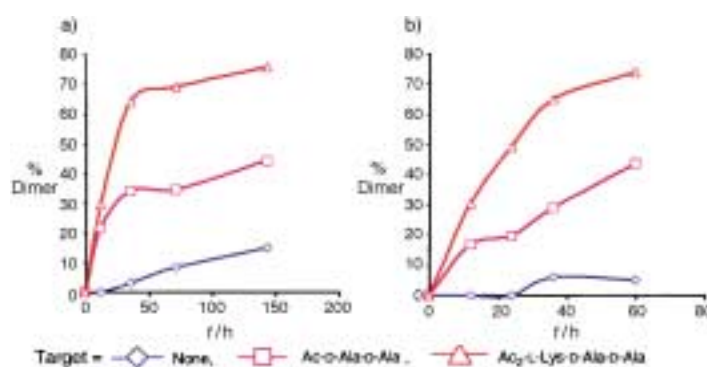


Figure 1. Proof of principle of target-accelerated synthesis of covalently linked vancomycin dimers through the olefin metathesis reaction in the absence and in the presence of the target. Formation of a) **6**-(LeuNMe)C₂-(LeuNMe)C₂ and b) **6**-(LeuNMe)C₄-(LeuNMe)C₄. Reagents and conditions: vancomycin analogue (550 μM), C₁₂H₂₅NMe₃Br (2.75 mM), target (110 μM), [(PCy₃)₂Ru(CHPh)Cl₂] (110 μM), H₂O:CH₂Cl₂ (>95:5), 23 °C (see Scheme 3 for reaction and structures).

we then investigated a combinatorial version of this reaction. Therefore, three vancomycin analogues **3-(LeuNMe)C₂**, **3-(LeuNMe)C₃**, and **3-(LeuNMe)C₄** (see Scheme 3 and Supporting Information) bearing tethers of differing length were mixed and subjected to target-accelerated covalent dimerization under combinatorial conditions. In the absence of the target, the expected statistical mixture (1:2:3:2:1; two permutations are degenerate) of all possible (six) dimers (**6-(LeuNMe)C₂-(LeuNMe)C₂**, **6-(LeuNMe)C₂-(LeuNMe)C₃**, **6-(LeuNMe)C₂-(LeuNMe)C₄**, **6-(LeuNMe)C₃-(LeuNMe)C₃**, **6-(LeuNMe)C₃-(LeuNMe)C₄**, and **6-(LeuNMe)C₄-(LeuNMe)C₄**) was observed, whereas in the presence of the target (**Ac₂-L-Lys-D-Ala-D-Ala**) a clear bias for dimers with shorter tethers was observed ($n = 1$ and 2 ; Figure 2). The individual olefinic dimers (homodimers only) were tested for their biological activity and a good agreement between the target-induced rate acceleration and their potency was observed (Figure 3a). The same correlation between length and activity was also observed for the disulfide dimers (Figure 3b). Most signifi-

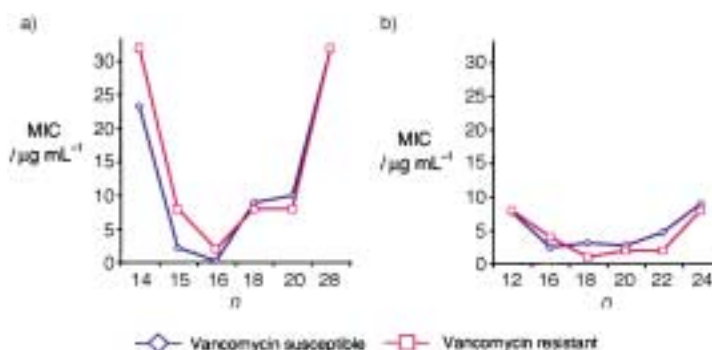


Figure 3. Correlation between the tether length n and antibacterial activity of vancomycin dimers. The number corresponding to the tether length represents the total number of atoms between the two nitrogen atoms of the olefinic (a) and disulfide dimers (b). The data for the vancomycin-susceptible bacteria represent the average of nine vancomycin-susceptible strains (*Streptococcus pneumoniae* (Sa8250 and Sp670), *Enterococcus faecalis* (27266, 4002, 27261), *Staphylococcus aureus* (48N, 25701, LO3, 133); see Scheme 3 for structures).

cantly, dimers from both the olefinic and the disulfide categories with optimal tether length (16–18 atoms between the two nitrogen atoms) exhibited strong activities, particularly against VRE. In comparing the results for these two sets of compounds it is noteworthy recalling that olefinic bonds have been used as disulfide bond mimics. As a consequence of the expected superiority of the olefinic compounds over their disulfide counterparts as potential drug candidates, because of their greater metabolic stability, we focused the remainder of our studies on the mediation of the dimerization process by olefin metathesis.

With the optimum length of the tethering bridge established, we then turned our attention to the influence of the binding affinity between the target (**Ac₂-L-Lys-D-Ala-D-Ala**) and the ligand (vancomycin residue) on the rate of dimerization. A convenient and potentially productive way of modulating this affinity is to vary the first amino acid residue of vancomycin (see Supporting Information). Thus, a combination of two vancomycin analogues (**3-(LeuNMe)C₂** and **4-(β-ala)C₂**; for definitions of abbreviations, see the legend in Scheme 3) were treated under the above-described olefin metathesis conditions in both the absence and presence of their target (**Ac₂-L-Lys-D-Ala-D-Ala**; see Supporting Information). Interestingly, in the absence of the target, the homodimer of the β-Ala-substituted vancomycin (**6-(β-Ala)C₂-(β-Ala)C₂**) was formed preferentially over the vancomycin homo-dimer (**6-(LeuNMe)C₂-(LeuNMe)C₂**; Figure 4a). This result may be attributed to a higher tendency of the β-Ala-substituted vancomycin monomer to dimerize in the absence of the target. In the presence of the target, however, the vancomycin homo-dimer **6-(LeuNMe)C₂-(LeuNMe)C₂** was formed preferentially as expected (Figure 4b). The results of this experiment are again consistent with the biological activities exhibited by these compounds (Table 1), and that the stronger affinity for the target translates into higher dimerization rates by monomer selection. The observed enhancement results also demonstrate that the background reaction is relatively inconsequential.

Having established that the target-accelerated dimerization of vancomycin analogues selects for both the adequacy of the tether and the affinity for the target, we performed an eight-

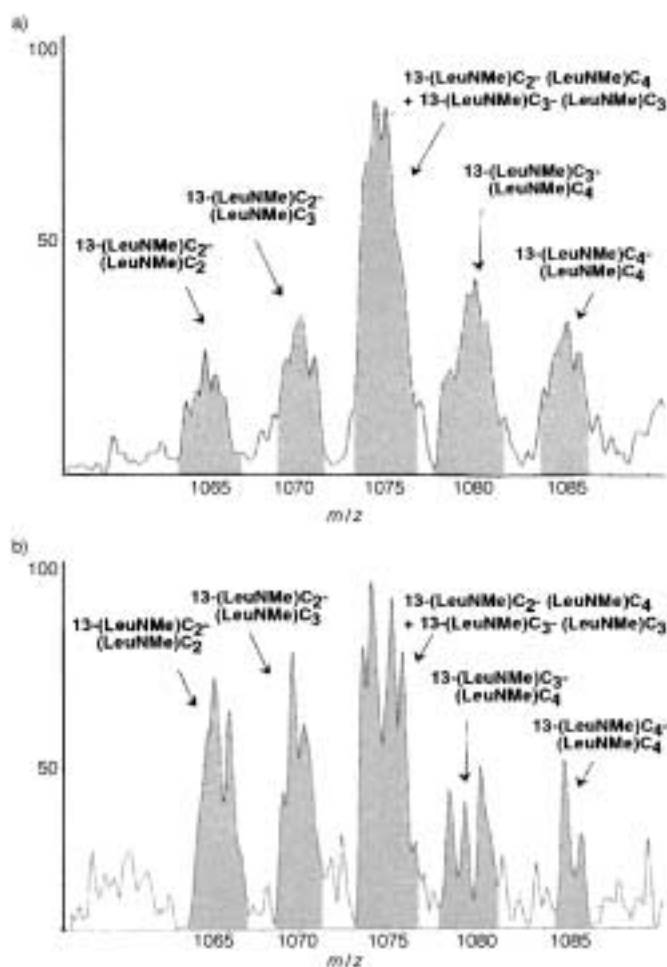


Figure 2. Mass spectrometric analysis of the vancomycin dimer mixture formed from **3-(LeuNMe)C₂**, **3-(LeuNMe)C₃**, and **3-(LeuNMe)C₄** (see Supporting Information). In the absence (a) of the target a statistical mixture (1:2:3:2:1) of products is observed whereas in the presence (b) of the target (**Ac₂-L-Lys-D-Ala-D-Ala**) shorter tethered dimers (**6-(LeuNMe)C₂-(LeuNMe)C₂** and **6-(LeuNMe)C₂-(LeuNMe)C₃**) are formed preferentially (see Scheme 3 for structures).

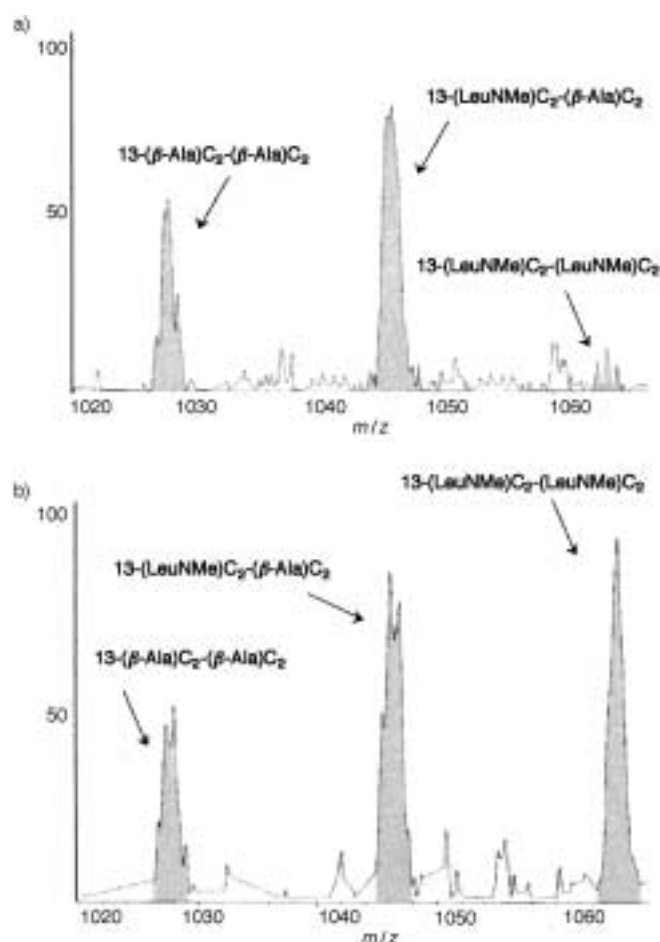


Figure 4. Mass spectrometric analysis of the vancomycin dimer mixture formed from **3-(LeuNMe)C₂** and **4-(β-Ala)C₂**. Note that in the absence of the target (a), the dimer containing D-LeuNMe (**6-(LeuNMe)C₂-(LeuNMe)C₂**) is formed at a slower rate than the ones containing β-Ala. In the presence (b) of the target (Ac₂-L-Lys-D-Ala-D-Ala) the dimers containing D-LeuNMe (**6-(LeuNMe)C₂-(LeuNMe)C₂**) rather than β-Ala are formed preferentially.

component (**3-(LeuNMe)C₂**, **3-(LeuNMe)C₄**, **4-(β-Ala)C₂**, **4-(β-Ala)C₄**, **4-(Asn)C₂**, **4-(Asn)C₄**, **4-(H)C₂**, **4-(H)C₄**) target-accelerated (Ac₂-L-Lys-D-Ala-D-Ala) combinatorial synthesis experiment employing the olefin metathesis reaction (Figure 5). Thirty-six library members were expected, but only thirty could be observed separately by mass spectrometry as a consequence of the degeneracy of six of the dimers. The vertical bars in Figure 5 reflect the observed relative abundance of each of the thirty distinct (with regard to their mass) vancomycin dimers after adjustment to account for the expected statistical occurrence (average values for three experiments). The eleven compounds indicated by letters (a–j; all homo-dimers, except for d) were individually synthesized from their respective monomers through separate reactions and purified by HPLC for biological evaluation. Figure 6 and Table 1 show a selection of the antibacterial activities of these discrete compounds (a–j) against a number of vancomycin-susceptible and vancomycin-resistant bacterial strains. Gratifyingly, the target-accelerated dimerization experiments predicted quite reliably the overall trend of the observed biological activity of the library members, with only relatively small deviations. The identification and correct ranking of compounds a: **6-(LeuNMe)C₂-(LeuNMe)C₂**, b: **6-(LeuNMe)C₂-(β-Ala)C₂**, and c: **6-(LeuNMe)C₂-(LeuNMe)C₄** as highly potent antibacterial agents effective against both vancomycin-susceptible and vancomycin-resistant strains is highly significant. Since six out of the seven most abundant compounds contain LeuNMe, the results also underscore the importance of the natural first amino acid residue (LeuNMe) for strong binding and presumed (observed in some cases) biological activity. Table 1 lists further examples of highly potent vancomycin dimers from the disulfide family.

In conclusion, we have demonstrated the power of the target-accelerated combinatorial synthesis concept and applied it to the discovery of a number of highly potent antibiotics active against both vancomycin-susceptible and

Table 1. Antibacterial activity (MIC: μg mL⁻¹) of selected vancomycin dimers against vancomycin susceptible strains, a vancomycin intermediate resistant strain, and a vancomycin-resistant strain.

[Rank]Compound	Sa8250 ^[a]	Sp670 ^[a]	27266 ^[a]	Strain L4002 ^[a]	48Na ^[a]	Mu50 ^[b]	L4001 ^[c]
tetracycline	3.13	50	100	100	> 100	50	50
vancomycin	0.4	0.4	3.13	0.8	0.8	3.1	> 100
<i>olefinic dimers</i>							
[a] 6-(LeuNMe)C₂-(LeuNMe)C₂	< 0.03	< 0.03	0.125	0.25	0.25	1	2
[b] 6-(LeuNMe)C₂-(β-Ala)C₂	< 0.03	0.125	0.25	0.25	1	4	8
[c] 6-(LeuNMe)C₃-(LeuNMe)C₃	< 0.03	< 0.03	1	1	4	8	4
[d] 6-(β-Ala)C₄-(β-Ala)C₄	1	0.5	4	2	2	4	8
[e] 6-(LeuNMe)C₄-(LeuNMe)C₄	4	8	> 16	16	16	> 16	> 16
[f] 6-(β-Ala)C₂-(β-Ala)C₂	0.25	0.25	1	0.25	2	4	> 16
[g] 6-(Asn)C₄-(Asn)C₄	4	8	16	8	16	> 16	> 16
[h] 6-(H)C₂-(H)C₂	2	4	16	16	> 16	> 16	> 16
[i] 6-(Asn)C₂-(Asn)C₂	8	> 16	> 16	> 16	> 16	> 16	> 16
[j] 6-(H)C₄-(H)C₄	8	4	16	8	16	> 16	> 16
<i>disulfide dimers</i>							
5-(LeuNMe)C₂-(LeuNMe)C₂	< 0.03	< 0.03	1	1	8	8	1
5-(LeuNMe)C₂-(LeuNMe)C₂	< 0.03	< 0.03	2	1	4	8	2
5-(LeuNMe)C₃-(LeuNMe)C₃	0.125	0.06	4	2	8	8	2

[a] Vancomycin-susceptible strains (Sa8250 and Sp670 are *Streptococcus pneumoniae* strains; 27266 and L4002 are *Enterococcus faecalis* strains; 48N is a multiresistant *Staphylococcus aureus* strain (MRSA)). [b] Vancomycin intermediate resistant strain (MU50 is a *Staphylococcus aureus* strain). [c] Vancomycin-resistant strain (L4001 is a *Enterococcus faecium* strain).

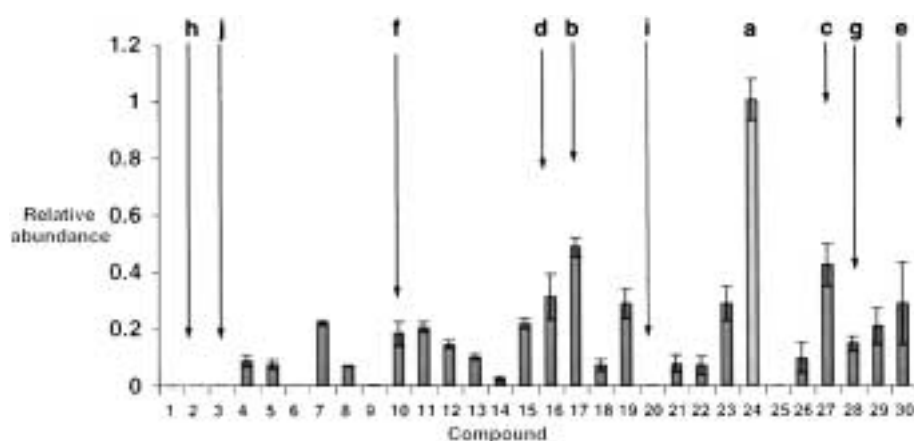


Figure 5. Target-accelerated combinatorial synthesis of a 36-member library of vancomycin dimers. The vertical bars represent the relative abundance of the vancomycin dimers relative to that of **6-(LeuNMe)C₂-(LeuNMe)C₂** (**a**) after the appropriate statistical adjustment. The error bars represent the range over three experiments. Compounds are labeled as follows: 1: **6-(H)C₂-(H)C₂**, 2: **6-(H)C₂-(H)C₄**, 3: **6-(H)C₄-(H)C₄**, 4: **6-(H)C₂-(β-Ala)C₂**, 5: **6-(β-Ala)C₂-(H)C₄**, 6: **6-(H)C₂-(Asn)C₂**, 7: **6-(H)C₂-(LeuNMe)C₂**, 8: **6-(H)C₄-(β-Ala)C₄**, 9: **6-(Asn)C₂-(H)C₄**, 10: **6-(β-Ala)C₂-(β-Ala)C₂**, 11: **6-(LeuNMe)C₂-(H)C₄**, 12: **6-(β-Ala)C₂-(β-Ala)C₄**, 13: **6-(Asn)C₄-(H)C₄**, 14: **6-(β-Ala)C₂-(Asn)C₂**, 15: **6-(LeuNMe)C₄-(H)C₄**, 16: **6-(β-Ala)C₄-(β-Ala)C₄**, 17: **6-(LeuNMe)C₂-(β-Ala)C₂**, 18: **6-(β-Ala)C₂-(Asn)C₄**, 19: **6-(β-Ala)C₂-(LeuNMe)C₄**, 20: **6-(Asn)C₂-(Asn)C₂**, 21: **6-(Asn)C₂-(β-Ala)C₄**, 22: **6-(LeuNMe)C₂-(Asn)C₂**, 23: **6-(β-Ala)C₄-(LeuNMe)C₄**, 24: **6-(LeuNMe)C₂-(LeuNMe)C₂**, 25: **6-(Asn)C₂-(Asn)C₄**, 26: **6-(Asn)C₂-(LeuNMe)C₄**, 27: **6-(LeuNMe)C₂-(LeuNMe)C₄**, 28: **6-(Asn)C₄-(Asn)C₄**, 29: **6-(Asn)C₄-(LeuNMe)C₄**, and 30: **6-(LeuNMe)C₄-(LeuNMe)C₄** (see Scheme 3 for structures).

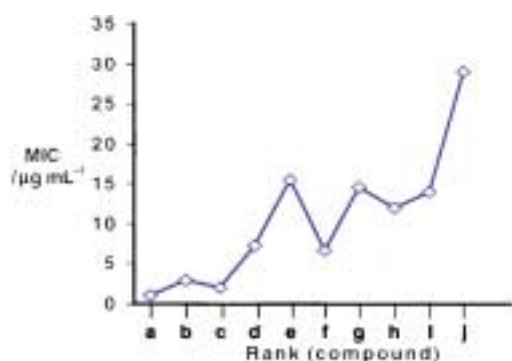


Figure 6. Correlation of the relative abundance of vancomycin dimers (**a–j**, Figure 5 and Table 1) with antibacterial activity (minimum inhibition concentration MIC, average of values against the nine vancomycin susceptible strains listed in Figure 3).

vancomycin-resistant bacteria (VRE or VISA). A strong correlation between rate enhancement and antibiotic activity has confirmed the usefulness of this strategy in predicting biological properties at a pre-screening stage. While the acute need for new antibiotics dictates further development of these compounds, the described combinatorial synthesis strategy may be applied to other biological targets.

Received: August 7, 2000 [Z15590]

- [6] D. J. Maly, I. C. Choong, J. A. Ellman, *Proc. Natl. Acad. Sci. USA* **2000**, *97*, 2419–2424.
- [7] J. Zhu, *Exp. Opin. Ther. Patents* **1999**, *9*, 1005–1019.
- [8] D. H. Williams, B. Bardsley, *Angew. Chem.* **1999**, *111*, 1264–1286; *Angew. Chem. Int. Ed.* **1999**, *38*, 1173–1193.
- [9] K. C. Nicolaou, C. N. C. Boddy, S. Bräse, N. Winssinger, *Angew. Chem.* **1999**, *111*, 2230–2287; *Angew. Chem. Int. Ed.* **1999**, *38*, 2096–2152.
- [10] R. Leclercq, E. Derlot, J. Duval, P. Courvalin, *N. Engl. J. Med.* **1988**, *319*, 157–161.
- [11] K. Hiramatsu, *Drug Resist. Updates* **1998**, *1*, 135–150.
- [12] R. Xu, G. Greiveldinger, L. Marenus, A. Cooper, J. A. Ellman, *J. Am. Chem. Soc.* **1999**, *121*, 4898–4899.
- [13] M. Ge, Z. Chen, H. R. Onishi, J. Kohler, L. L. Silver, R. Kerns, S. Fukuzawa, C. Thompson, D. Kahne, *Science* **1999**, *284*, 507–511.
- [14] W. H. Williams, M. P. Williamson, D. W. Butcher, S. J. Hammond, *J. Am. Chem. Soc.* **1983**, *105*, 1332–1339.
- [15] H. Hanaki, K. Kuwahara-Arai, S. Boyle-Vavra, R. S. Daum, H. Labischinski, K. Hiramatsu, *J. Antimicrob. Chemother.* **1998**, *42*, 199–209.
- [16] H. Hanakai, H. Labischinski, Y. Inaba, K. Hiramatsu, *Jpn. J. Antibiot.* **1998**, *51*, 272–280.
- [17] C. T. Walsh, S. L. Fisher, I.-S. Park, M. Prahalad, Z. Wu, *Chem. Biol.* **1996**, *3*, 21–28.
- [18] J. P. Mackay, U. Gerhard, D. A. Beauregard, R. A. Maplestone, D. H. Williams, *J. Am. Chem. Soc.* **1994**, *116*, 4573–4580.
- [19] P. J. Loll, A. E. Bevivino, B. D. Korty, P. H. Axelsen, *J. Am. Chem. Soc.* **1997**, *119*, 1516–1522.
- [20] D. A. Beauregard, D. H. Williams, M. N. Gwynn, D. J. C. Knowles, *Antimicrob. Agents Chemother.* **1994**, *116*, 781–785.
- [21] U. Gerhard, J. P. Mackay, R. A. Maplestone, D. H. Williams, *J. Am. Chem. Soc.* **1993**, *115*, 232–241.
- [22] M. Mammen, S.-K. Choi, G. M. Whitesides, *Angew. Chem.* **1998**, *110*, 2908–2953; *Angew. Chem. Int. Ed.* **1998**, *37*, 2754–2794.
- [23] D. H. Williams, A. J. Maguire, W. Tsuzuki, M. S. Westwell, *Science* **1998**, *280*, 711–714.
- [24] U. N. Sundram, J. H. Griffin, T. I. Nicas, *J. Am. Chem. Soc.* **1996**, *118*, 13107–13108.
- [25] J. Rao, G. M. Whitesides, *J. Am. Chem. Soc.* **1997**, *119*, 10286–10287.
- [26] T. Staroske, D. H. Williams, *Tetrahedron Lett.* **1998**, *39*, 4917–4920.
- [27] D. R. Stack, R. G. Thompson, EP 0801075 A1, **1997**.
- [28] J. Rao, J. Lahiri, L. Isaacs, R. M. Weis, G. M. Whitesides, *Science* **1998**, *280*, 708–711.
- [29] H. Arimoto, K. Nishimura, T. Kinumi, I. Hayakawa, D. Uemura, *Chem. Commun.* **1999**, 1361–1362.
- [30] M. Adamczyk, J. A. Moore, D. R. Sushil, Y. Zhiguang, *Bioorg. Med. Chem. Lett.* **1999**, *9*, 2437–2440.
- [31] T. D. Clark, M. R. Ghadiri, *J. Am. Chem. Soc.* **1995**, *117*, 12364–12365.
- [32] T. Staroske, D. P. O'Brien, T. J. D. Jorgensen, P. Roepstorff, D. H. Williams, A. J. R. Heck, *Chem. Eur. J.* **2000**, *6*, 504–509.
- [33] R. H. Grubbs, S. Chang, *Tetrahedron* **1998**, *54*, 4413–4450.

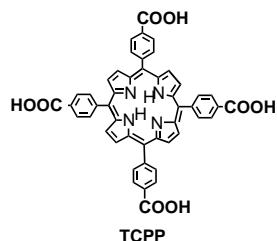
- [1] Special issue, “Combinatorial Chemistry”: *Curr. Opin. Chem. Biol.* **2000**, *4*, 243–355.
- [2] I. Huc, J.-M. Lehn, *Proc. Natl. Acad. Sci. USA* **1997**, *94*, 2106–2110.
- [3] J.-M. Lehn, *Chem. Eur. J.* **1999**, *5*, 2455–2463.
- [4] D. H. Lee, K. Severin, Y. Yokobayashi, M. R. Ghadiri, *Nature* **1997**, *390*, 591–594.
- [5] S. B. Shuker, P. J. Hajduk, R. P. Meadows, S. W. Fesik, *Science* **1996**, *274*, 1531–1534.

Photoinduced Electron Transfer from a Porphyrin to an Electron Acceptor in an Antibody-Combining Site

Hiroyasu Yamaguchi, Mikiharu Kamachi, and Akira Harada*

Much effort has been directed toward mimicking the electron transfer of natural photosynthetic systems.^[1] Electron transfer in covalently linked donor–acceptor systems has been extensively studied.^[2] Recently, attention has been focused on the design of noncovalently assembled donor–acceptor arrays^[3, 4] because the chromophores of the in vivo photosynthetic reaction center are not linked covalently through spacer groups but simply held in space by the protein environment. In order to incorporate both artificial porphyrins (electron donors) and electron acceptors into the protein domain, it seemed most appropriate to make monoclonal antibodies for porphyrin–acceptor systems.

Previously, we reported preparation of monoclonal antibodies against *meso*-tetrakis(4-carboxyphenyl)porphyrin (TCPP)^[5] and found that one of these antibodies binds not only TCPP but also a TCPP–metal complex (metal = Cu, Zn, Fe).^[6] We also found that the monoclonal antibody showed catalytic activities^[7] and could control photoinduced electron transfer from a zinc porphyrin to electron

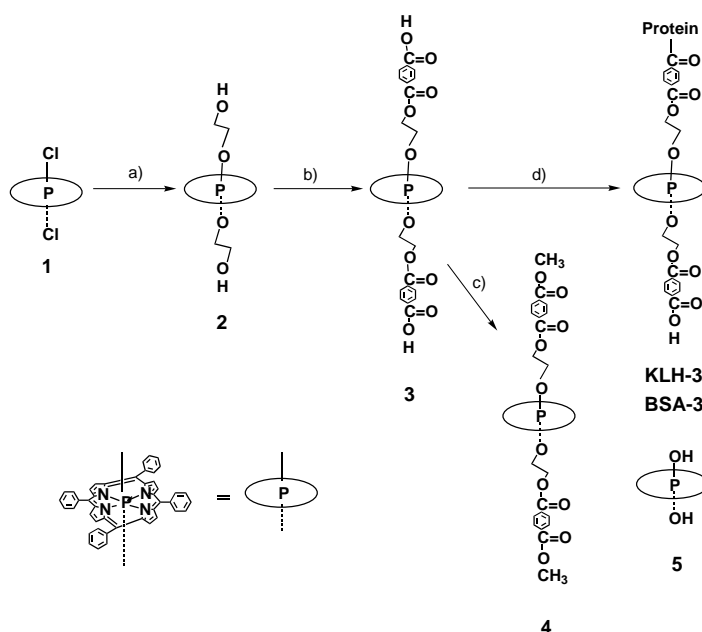


acceptor molecules by the formation of the complexes between the antibodies and the zinc porphyrin.^[8]

It is more important to design an antibody combining site that can accommodate not only metalloporphyrins but also organic substrates^[9] or electron acceptors. Herein, we report the first example of the design and preparation of such an antibody-combining site for both a porphyrin and an electron acceptor. Monoclonal antibodies are raised against an porphyrin which is linked to an electron acceptor by a spacer. A monoclonal antibody was then used to bind the porphyrin and the acceptor without a formal covalent linkage. The complementary combining sites for the porphyrin and acceptor, when linked, were found to have sufficient binding strength to bind the separate moieties with high selectivity. We also found that the antibody binds both porphyrin and an acceptor simultaneously and thereby the antibody facilitates the electron transfer from the porphyrin to an acceptor.

Phosphorus(v) porphyrin was used as a hapten because these complexes are able to form stable axial bonds from the

central phosphorus atom.^[10] Water-stable, axial dialkoxy hypervalent phosphorus(v) porphyrins were synthesized by efficient substitution of the axial chloride ligands in dichlorophosphorus(v) tetraphenylporphyrin **1**^[11] (Scheme 1).



Scheme 1. Synthesis of the antigen. a) Ethylene glycol, b) terephthaloyl chloride/pyridine, c) methanol/pyridine, d) 1) EDC/DMF, 2) protein/phosphate buffer (pH 7). EDC = 1-ethyl-3-(3-dimethylaminopropyl)carbodiimide; Protein = keyhole limpet hemocyanin (KLH) or bovine serum albumin (BSA).

Five monoclonal antibodies have been obtained by immunization of KLH-conjugated porphyrin **3** (KLH-3)^[12] to Balb/c mice. One of these antibodies, 74D7A, binds the antigen strongly (dissociation constant $K_d = 2.2 \times 10^{-7}$ M). The antibody also shows a high selectivity. Antibody 74D7A binds **BSA-3** but not TCPP, as shown by an enzyme-linked immunosorbent assay (ELISA) as well as by the absorption and emission spectra. Although antibody 74D7A does not bind TCPP, it binds **2**, **3**, and **5** with K_d values of 7.5×10^{-7} , 2.2×10^{-7} , and 2.1×10^{-6} M, respectively. The differences of dissociation constants for the complexes between antibody 74D7A and these porphyrins indicate that the antibody recognizes not only the porphyrin moiety but also the axial ligands.

The antibody was found to bind terephthalic acid. Figure 1 shows Klotz plots for benzoic acid and phthalic acid derivatives. Table 1 shows the dissociation constants of the complexes between antibody 74D7A and various substrates. Although the dissociation constant of the antibody with benzoic acid is 1.1×10^{-2} M, that of the antibody with terephthalic acid is 1.2×10^{-5} M; the affinity of the antibody for terephthalic acid is about 1000 fold greater than that for benzoic acid. The antibody shows an excellent specificity to the part of the axial ligands.

Terephthalic acid and its derivatives act as an electron acceptor^[13] for porphyrins. Fixation of terephthalic acid to the

[*] Prof. A. Harada, H. Yamaguchi
Department of Macromolecular Science
Graduate School of Science, Osaka University
Toyonaka, Osaka 560–0043 (Japan)
Fax: (+81) 6-6850-5446
E-mail: harada@chem.sci.osaka-u.ac.jp
Prof. M. Kamachi
Fukui University of Technology
Fukui 910-8505 (Japan)

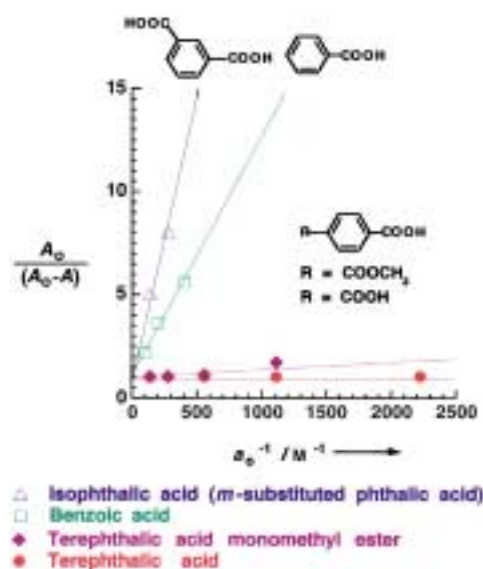


Figure 1. Binding of benzoic acid and phthalic acid derivatives as shown by a Klotz plot. Klotz equation: $A_0/(A_0 - A) = 1 + K_d/a_0$, where A_0 or A are the ELISA absorbances at 405 nm in the absence or presence of substrates, a_0 is the total substrate concentration, and K_d is the dissociation constant.

Table 1. Dissociation constants of the complexes between antibody 74D7A and benzoic acid or phthalic acid derivatives.

Substrate	Dissociation constant K_d [M]
<chem>HOOC-C6H4-COOH</chem>	1.1×10^{-2}
<chem>HOOC-C6H3(COOH)-COOH</chem>	$< 10^{-1}$
<chem>HOOC-C6H4(COOCH3)-COOH</chem>	3.0×10^{-2}
<chem>HOOC-C6H4(COOCH3)-COOCH3</chem>	1.2×10^{-5}
	4.5×10^{-5}

axis of porphyrin induces the changes of photochemical properties of phosphorus(v) porphyrin. For example, the lifetime of the singlet excited state of **KLH-3** is shorter than that of porphyrin **2** (**KLH-3**: 0.4 ns; **2**: 4.4 ns; in phosphate borate buffer/ CH_3CN). The fluorescence quenching and the shortened excited state lifetime of **KLH-3** are considered to be due to an intramolecular electron transfer between the porphyrin and the terephthaloyl moiety. When the complex between porphyrin **2** and antibody 74D7A is formed, it is expected that the antibody may provide a space where acceptor molecules may enter. Table 2 shows the degree of fluorescence quenching of porphyrins on addition of terephthalic acid or isophthalic acid in the presence of the

Table 2. Fluorescent quenching of porphyrins on addition of terephthalic acid or isophthalic acid in the presence of antibody 74D7A.

Porphyrin	Substrate	Quenching ^[a] [%]
2	<chem>HOOC-C6H4-COOH</chem>	20
2	<chem>HOOC-C6H3(COOH)-COOH</chem>	2
TCCP	<chem>HOOC-C6H4(COOH)-COOH</chem>	5

[a] Fluorescent quenching = $(1 - I/I_0) \times 100$. I_0 = fluorescent intensity of the porphyrin in the presence of antibody 74D7A; I = as I_0 but with substrate present.

antibody. A 20% fluorescence quenching of **2** in the presence of antibody 74D7A was observed on addition of terephthalic acid. This degree of quenching on addition of terephthalic acid is ten-fold greater than that of added isophthalic acid. Under the same conditions (**2** (8.0×10^{-7} M) and terephthalic acid (1.6×10^{-6} M)), the quenching behavior was not observed in the absence of the antibody. The titration experiments of fluorescence quenching of **2** with terephthalic acid showed that terephthalic acid – antibody binding is at a 1:1 molecular ratio.

The fluorescence decay of porphyrin **2** in the presence of the antibody was expressed by a monoexponential curve with a lifetime of 4.5 ns. Addition of terephthalic acid shortened the lifetime to 0.3 ns.^[14] On the other hand, the lifetime of **2** with terephthalic acid was 4.5 ns in the absence of antibody 74D7A. These results show that the electron transfer from porphyrin to an electron-accepting molecule occurred in the antibody combining site. The rate constant for the electron transfer from the porphyrin to terephthalic acid in the combining site was estimated to be $3.1 \times 10^9 \text{ s}^{-1}$. Figure 2 shows a schematic representation of donor – acceptor system in the antibody combining site.

In conclusion, one of the antibodies elicited by an antigen containing both phosphorus(v) porphyrin and terephthalic acid positioned axially shows high selectivity for both porphyrins and axial parts. Moreover, the antibody was found to bind both the porphyrin and terephthalic acid simultaneously and that the specific insertion of terephthalic acid as an electron acceptor into the antibody combining site makes it possible to facilitate the electron transfer from the porphyrin to the acceptor molecule. Detailed investigation of the mechanism is underway.



Figure 2. Representation of the donor – acceptor system in the antibody combining site.

Received: May 2, 2000
Revised: July 14, 2000 [Z15066]

- a) J. Deisenhofer, O. Epp, K. Miki, R. Huber, H. Michel, *J. Mol. Biol.* **1984**, *180*, 385 – 398; b) J. Deisenhofer, H. Michel, *Angew. Chem.* **1989**, *101*, 872 – 892; *Angew. Chem. Int. Ed. Engl.* **1989**, *28*, 829 – 847; c) D. Gust, T. A. Moore, *Science* **1989**, *244*, 35 – 41; d) R. Huber, *Angew. Chem.* **1989**, *101*, 849 – 871; *Angew. Chem. Int. Ed. Engl.* **1989**, *28*, 848 – 869.
- a) A. Osuka, K. Maruyama, N. Mataga, T. Asahi, I. Yamazaki, N. Tamai, *J. Am. Chem. Soc.* **1990**, *112*, 4958 – 4959; b) M. R. Wasielewski, *Chem. Rev.* **1992**, *92*, 435 – 461; c) A. Giraudeau, L. Ruhlmann, L. El Kahef, M. Gross, *J. Am. Chem. Soc.* **1996**, *118*, 2969 – 2979; d) A. Osuka, S. Marumo, N. Mataga, S. Taniguchi, T. Okada, I. Yamazaki, Y. Nishimura, T. Ohno, K. Nozaki, *J. Am. Chem. Soc.* **1996**, *118*, 155 – 168; e) K. Uosaki, T. Kondo, X.-Q. Zhang, M. Yanagida, *J. Am. Chem. Soc.* **1997**, *119*, 8367 – 8368; f) K. Tsukahara, N. Sawai, S. Hamada, K. Koji, Y. Onoue, T. Nakazawa, R. Nakagaki, N. Nozaki, T. Ohno, *J.*

- Phys. Chem. B* **1999**, *103*, 2867–2877; g) S. Tsuchiya, *J. Am. Chem. Soc.* **1999**, *121*, 48–53; h) H. Tsue, H. Imahori, T. Kaneda, Y. Tanaka, T. Okada, K. Tamaki, Y. Sakata, *J. Am. Chem. Soc.* **2000**, *122*, 2279–2288.
- [3] a) A. M. Brun, A. Harriman, V. Heitz, J. P. Sauvage, *J. Am. Chem. Soc.* **1991**, *113*, 8657–8663; b) A. M. Brun, S. J. Atherton, A. Harriman, V. Heitz, J. P. Sauvage, *J. Am. Chem. Soc.* **1992**, *114*, 4632–4639; c) J. L. Sessler, B. Wang, A. Harriman, *J. Am. Chem. Soc.* **1993**, *115*, 10418–10419; d) J. L. Sessler, B. Wang, A. Harriman, *J. Am. Chem. Soc.* **1995**, *117*, 704–714; e) A. Berman, E. S. Izraeli, H. Levanon, B. Wang, J. L. Sessler, *J. Am. Chem. Soc.* **1995**, *117*, 8252–8257; f) M. Linke, J.-C. Chambron, V. Heitz, J.-P. Sauvage, *J. Am. Chem. Soc.* **1997**, *119*, 11329–11330; g) M. D. Ward, *Chem. Soc. Rev.* **1997**, *26*, 365–375; h) T. D. Ros, M. Prato, D. Galdi, E. Alessio, M. Ruzzi, L. Pasimeni, *Chem. Commun.* **1999**, 635–636; i) A. Berg, Z. Shuali, M. Someda, H. Levanon, M. Fuhs, K. Möbius, R. Wang, C. Brown, J. L. Sessler, *J. Am. Chem. Soc.* **1999**, *121*, 7433–7434; j) D. J. Fermín, H. D. Duong, Z. Ding, P.-F. Brevet, H. H. Girault, *J. Am. Chem. Soc.* **1999**, *121*, 10203–10210; k) M. Andersson, M. Linke, J.-C. Chambron, J. Davidsson, V. Heitz, J.-P. Sauvage, L. Hammarström, *J. Am. Chem. Soc.* **2000**, *122*, 3526–3527.
- [4] a) T. Hayashi, T. Takimura, H. Ogoshi, *J. Am. Chem. Soc.* **1995**, *117*, 11606–11607; b) K. Shreder, A. Harriman, B. L. Iverson, *J. Am. Chem. Soc.* **1995**, *117*, 2673–2674; c) K. Shreder, A. Harriman, B. L. Iverson, *J. Am. Chem. Soc.* **1996**, *118*, 3192–3201; d) R. Sadamoto, N. Tomioka, T. Aida, *J. Am. Chem. Soc.* **1996**, *118*, 3978–3979.
- [5] A. Harada, K. Okamoto, M. Kamachi, T. Honda, T. Miwatani, *Chem. Lett.* **1990**, 917–918.
- [6] a) A. Harada, K. Okamoto, M. Kamachi, *Chem. Lett.* **1991**, 953–956; b) A. Harada, H. Fukushima, K. Shiotsuki, M. Kamachi, *Supramol. Chem.* **1993**, *2*, 153–156; c) A. Harada, K. Shiotsuki, H. Fukushima, H. Yamaguchi, M. Kamachi, *Inorg. Chem.* **1995**, *34*, 1070–1076; d) A. Harada, H. Yamaguchi, F. Oka, M. Kamachi, *Proc. SPIE Int. Soc. Opt. Eng.* **1999**, *3607*, 126–135.
- [7] A. Harada, H. Fukushima, K. Shiotsuki, H. Yamaguchi, F. Oka, M. Kamachi, *Inorg. Chem.* **1997**, *36*, 6099–6102.
- [8] A. Harada, H. Yamaguchi, K. Okamoto, H. Fukushima, K. Shiotsuki, M. Kamachi, *Photochem. Photobiol.* **1999**, *70*, 298–302.
- [9] S. Nimri, E. Keinan, *J. Am. Chem. Soc.* **1999**, *121*, 8978–8982.
- [10] a) C. J. Carrano, M. Tsutsui, *J. Coord. Chem.* **1977**, *7*, 79–83; b) P. Sayer, M. Gouterman, C. R. Connell, *J. Am. Chem. Soc.* **1977**, *99*, 1082–1087; c) C. A. Marrese, C. J. Carrano, *Inorg. Chem.* **1983**, *22*, 1858–1862; d) H. Segawa, K. Kunimoto, A. Nakamoto, T. Shimidzu, *J. Chem. Soc. Perkin Trans. 1* **1992**, 939–940; e) H. Segawa, A. Nakamoto, T. Shimidzu, *J. Chem. Soc. Chem. Commun.* **1992**, 1066–1067; f) H. Segawa, K. Kunimoto, K. Susumu, M. Taniguchi, T. Shimidzu, *J. Am. Chem. Soc.* **1994**, *116*, 11193–11194.
- [11] Characterization of porphyrin **3** was carried out by exchanging of the end groups (acid chlorides) in the product to methyl ester **4**. **4**: ¹H NMR (CDCl₃): δ = –2.17 (m, 4H), 0.78 (dt, 4H), 1.38 (s, 6H), 7.75–8.01 (m, 28H), 9.06 (s, 8H). UV/Vis: λ_{max} = 428, 520, 559, 599 nm. Elemental analysis calcd for C₆₆H₅₀N₄O₁₀·PCL: C 70.43, H 4.48, N 4.98; found: C 70.45, H 4.70, N 5.11.
- [12] KLH-3 was used as immunogen and bovine serum albumin conjugate (BSA-3) was prepared as the antigen of the ELISA procedure.
- [13] N. Ichinose, N. Kitamura, H. Masuhara, *Macromolecules* **1993**, *26*, 2331–2339.
- [14] Fluorescence lifetimes were measured using a Horiba NAES-550 time-correlated single-photon counting instrument. A solution of terephthalic acid was added to the solution of porphyrin **2**–antibody complex. The concentrations of **2**, terephthalic acid, and antibody 74-D7A combining site were set at 1.6, 3.2, and 3.2 μM, respectively. The error values are less than 0.1 ns.

Hexagonal Layered Materials Composed of [M₂(O₂CCF₃)₄] (M = Ru and Rh) Donors and TCNQ Acceptors**

Hitoshi Miyasaka, Cristian S. Campos-Fernández, Rodolphe Clérac, and Kim R. Dunbar*

Multidimensional assemblies consisting of paramagnetic metal ions and polycyano organic acceptor molecules are being prepared in an effort to access molecule-based magnetic/conducting materials based on dπ–pπ electronic interactions.^[1–4] Achieving high conductivity through the backbone of a metalloorganic polymer is one of the most challenging goals, and one that has been realized in only one case, namely in the [Cu(DCNQI)₂]_∞ family of compounds (DCNQI = *N,N'*-dicyanoquinonediimine).^[5] These materials consist of a three-dimensional skeleton containing tetrahedral mixed-valence Cu^I/Cu^{II} ions connected by partially reduced DCNQI radicals arranged in π-stacked columns throughout the three-dimensional network. Although the latter structural feature is a main contributor to the conducting pathway, it has been demonstrated that delocalization through the Cu–DCNQI skeleton is crucial for stabilizing the metallic state of these materials.

The use of electron-rich dimetal complexes to prepare dπ–pπ delocalized systems began in our laboratories with the isolation of the “dimer-of-dimers” [(Re₂Cl₄(dppm)₂)(μ-TCNQ)] (dppm = 1,2-bis(diphenylphosphanyl)methane, TCNQ = 7,7,8,8-tetracyanoquinodimethane). This compound is the first example of a charge transfer complex of TCNQ with a metal–metal-bonded donor. The presence of the oxidized Re–Re species (σ²π⁴δ²δ*¹) and reduced TCNQ^{•–} was confirmed by spectroscopic and magnetic studies.^[6] In this 2:1 donor–acceptor system, electronic delocalization is favored through good metal dπ/organic pπ overlap; this can be represented by the resonance structures: [Re₂^{II,III}–(TCNQ^{•–})–Re₂^{II,II}] (1) ⇌ Re₂^{II,II}–(TCNQ)–Re₂^{II,II}] (2) ⇌ [Re₂^{II,III}–(TCNQ^{•–})–Re₂^{II,III}] (3), with forms 1 and 3 being the main contributors.

A logical extension of the aforementioned chemistry is the construction of networks based on electron-rich Ru^{II}/Ru^{III} complexes. This idea is predicated on the notion that the dπ orbitals on Ru^{II}/Ru^{III} and the pπ orbitals of the TCNQ ligands will be energetically compatible; indeed there is ample

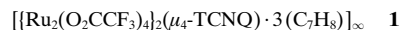
[*] Prof. K. R. Dunbar, Dr. H. Miyasaka,^[+] C. S. Campos-Fernández, Dr. R. Clérac^[++]
Department of Chemistry
Texas A&M University
PO Box 30012, College Station, TX 77842-3012 (USA)
Fax: (+1) 979-845-7177
E-mail: dunbar@chem.mail.tamu.edu

[+] Current address:
Department of Chemistry, Faculty of Science
Tokyo Metropolitan University
Minami-Ohsawa 1-1, Hachioji, Tokyo 192-0397 (Japan)

[++] Current address:
Centre de Recherche Paul Pascal, CNRS UPR 8641
Avenue du Dr. Schweitzer, 33600 Pessac (France)

[**] TCNQ = 7,7,8,8-tetracyanoquinodimethane. H.M. is a recipient of a JSPS Research Fellowship for Young Scientists.

precedence for electronic delocalization in Ru/nitrogen donor ligand complexes.^[7] In this work, we report the assembly of $[\text{Ru}_2(\text{O}_2\text{CCF}_3)_4]$ and $[\text{Rh}_2(\text{O}_2\text{CCF}_3)_4]$ with TCNQ to yield the two-dimensional compounds **1** and **2**, respectively ($\text{C}_7\text{H}_8 = \text{toluene}$). X-ray structural data support the conclusion that electronic delocalization is occurring within the two-dimensional (2D) network.



Compounds **1** and **2** were synthesized from solutions of TCNQ treated with an excess of the dimetal precursor. The reaction between $[\text{Ru}_2(\text{O}_2\text{CCF}_3)_4]$ and TCNQ proceeds under refluxing conditions to afford a dark green powder. Slow cooling of the filtrate from the reaction leads to dark green crystals of **1** (yield < 10%). Infrared spectra reveal that the powder and crystals are essentially identical; the yield of the bulk powder is ~80%. There is no evidence for product formation at lower temperatures, a fact that appears to be related to a lack of lability of the axial THF ligands in $[\text{Ru}_2(\text{O}_2\text{CCF}_3)_4(\text{thf})_2]$. In contrast, **2** was obtained directly as purplish-brown crystals by a slow diffusion of *n*-hexanes into a solution containing $[\text{Rh}_2(\text{O}_2\text{CCF}_3)_4]$ and TCNQ in toluene (yield > 80%).

Infrared spectra are useful for assigning the oxidation state of TCNQ in its compounds.^[2, 8] The $\nu(\text{C}\equiv\text{N})$ modes are strongly affected by the nature of the metal binding interaction as well as the redox state, but the $\delta(\text{C}-\text{H})$ mode is sensitive mainly to the oxidation state. The infrared spectrum of **1** contains three $\nu(\text{C}\equiv\text{N})$ stretches at 2203, 2155, and 2117 cm^{-1} (for **1b**; see Experimental Section) at lower energies than free TCNQ (2222 cm^{-1}), whereas compound **2** exhibits a single feature at 2237 cm^{-1} . The shift to lower energies in **1** is in accord with increased $\text{M}_2\text{-TCNQ}$ π -backbonding for the Ru derivative. The $\delta(\text{C}-\text{H})$ modes of TCNQ^0 and TCNQ^- occur at ~860 cm^{-1} and between 820–825 cm^{-1} , respectively. The corresponding values for partially reduced TCNQ are known to occur at about 840 cm^{-1} .^[8a,b] The new compounds exhibit $\delta(\text{C}-\text{H})$ bending modes at 842 cm^{-1} for **1** and 844 cm^{-1} for **2**, which suggests that the TCNQ unit is partially reduced. The colors of **1** and **2** are dark green and dark purplish-brown, respectively, which is in accord with a TCNQ chromophore that is not neutral. The electronic spectral features of reduced TCNQ in the visible region typically give rise to green or dark blue colors due to an intense $\pi-\pi^*$ transition, the exact energy of which is determined by the degree of charge transfer.

Compound **1** crystallizes in the monoclinic space group $\text{C}2/m$ with an inversion center at the midpoint of the M–M bond. The TCNQ ligands are bisected by a C_2 axis and a mirror plane which leads to only one unique Ru(1)–N(1) bond.^[9] A view of one TCNQ unit surrounded by four Ru_2 units in **1** is depicted in Figure 1. All four cyano groups of TCNQ are coordinated to independent Ru_2 molecules, the result of which is a distorted hexagonal 2D network. Figure 2 shows one of the 2D sheets in **1**. The Ru–Ru distance of 2.2875(7) Å is slightly longer than the corresponding distances in

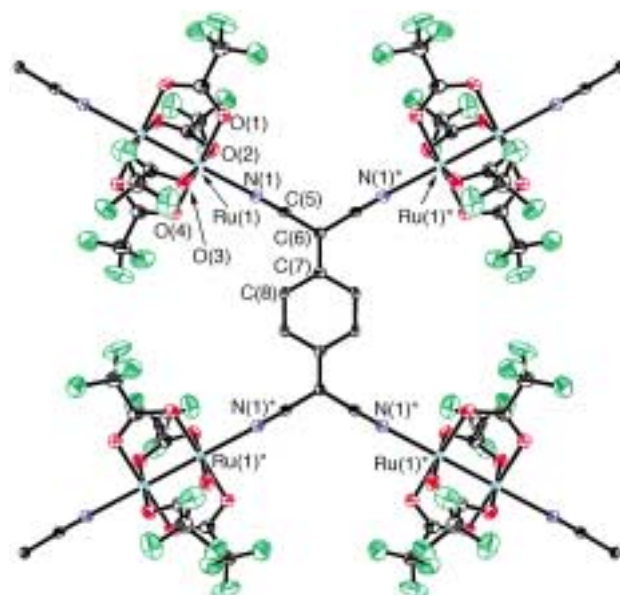


Figure 1. Structure of one TCNQ ligand coordinated to four independent $[\text{Ru}_2(\text{O}_2\text{CCF}_3)_4]$ units in **1** (ORTEP representation) with atom-numbering scheme.

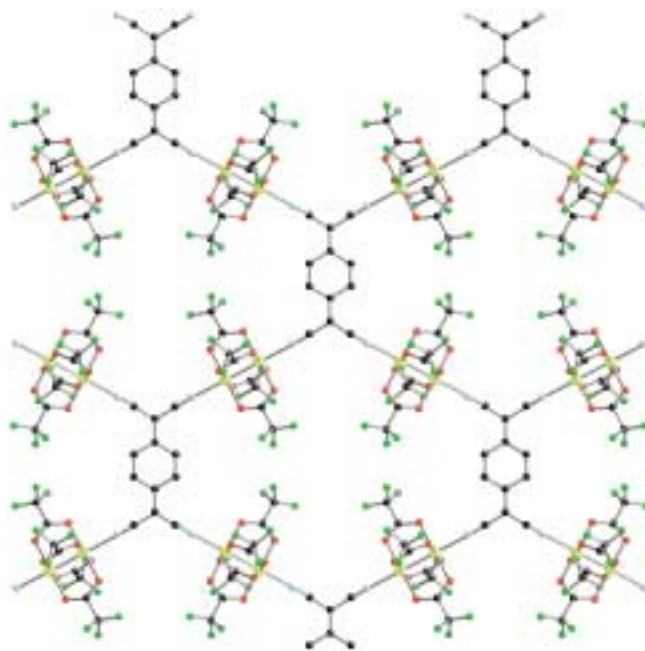


Figure 2. Perspective view of the two-dimensional network of **1**.

$[\text{Ru}_2^{\text{II,III}}(\text{O}_2\text{CCF}_3)_4(\text{thf})_2]^{[10]}$ (2.276(3) Å) or $[\text{Ru}_2^{\text{II,III}}(\text{O}_2\text{CCF}_3)_5]$ (2.278(1) Å).^[11] The Ru–N_{axial} distance is 2.277(3) Å, which is typical of such interactions.

Compound **2** is isostructural to **1**. The Rh–Rh bond length of 2.4053(8) Å is comparable to the single bond lengths found in $[\text{Rh}_2^{\text{II,III}}(\text{O}_2\text{CCF}_3)_4\text{L}_2]$ adducts (~2.40 Å).^[12] The Rh–N(nitrile) distance is 2.174(4) Å, which is essentially identical to the corresponding distance in $[\{\text{Rh}_2(\text{O}_2\text{CCF}_3)_4\}_2(\mu_4\text{-TCNE})]_\infty$ (av 2.175 Å),^[13] but slightly shorter than the axial interactions in $[\text{Rh}_2(\text{O}_2\text{CCF}_3)_4(\text{MeCN})_2]$ (2.201(5) Å)^[13] and $[\text{Rh}_2(\text{O}_2\text{CCF}_3)_4(\text{L})]_\infty$ (L = 2,5-dimethyl-*N,N'*-dicyanoquinonediimine (DMDCNQI), 2.189(7) Å; *N,N'*-dicyanonaphthoquinone diimine (DCNNQI), 2.212(2) Å).^[14] These differences can be ex-

plained by the fact that the nitrile ligands in $[\text{Rh}_2(\text{O}_2\text{CCF}_3)_4(\text{CH}_3\text{CN})_2]$ and $[\text{Rh}_2(\text{O}_2\text{CCF}_3)_4(\text{L})]_\infty$ ($\text{L} = \text{DM-DCNQI}$, DCNNQI) behave as σ donors, whereas in **2** and $[\text{Rh}_2(\text{O}_2\text{CCF}_3)_4(\mu_4\text{-TCNE})]_\infty$, M-L π -back-donation is occurring.

In the context of electronic issues, the most important structural features in TCNQ complexes are the bond lengths within the TCNQ ligand. These are listed in Table 1 for **1** and **2** along with data for previously reported compounds. The $\text{C}\equiv\text{N}$ bond length is affected mainly by M-N coordination, but the C-C distances within the TCNQ ring are good

indicators of the oxidation state. The bond lengths for “free” TCNQ^0 and TCNQ^- were determined by averaging the data for a number of compounds. The bond lengths within the TCNQ units are nearly the same in **1** and **2** (Table 1). Interestingly they are intermediate between the values for TCNQ^0 and TCNQ^- , which is an indication of partially reduced TCNQ. The degree of charge transfer from a donor to TCNQ has been estimated by Kistenmacher et al., from the relationship $\rho = A[c/(b+d)] + B$ ($A = -41.667$ and $B = 19.833$ are determined from neutral $\text{TCNQ}^{[15]}$ ($\rho = 0$) and $\text{RbTCNQ}^{[16]}$ ($\rho = -1$)).^[17] The values of c , b , and d are TCNQ

Table 1. Important structural features in TCNQ complexes.

Compound	Charge	a	b	c	d	e	b + d	c/(b + d)	$\rho^{[a]}$	Ref.
Noncoordinated TCNQ										
TCNQ	0	1.140(1)	1.441(4)	1.374(3)	1.448(4)	1.346(3)	2.889	0.476	0	[15]
CsTCNQ ₃	0	1.140(4)	1.428(4)	1.371(5)	1.444(4)	1.341(5)	2.872	0.477	−0.04	[16]
	−1	1.152(3)	1.419(3)	1.410(4)	1.427(3)	1.355(4)	2.846	0.495	−0.81	
RbTCNQ	−1	1.153(7)	1.416(8)	1.420(1)	1.423(3)	1.373(1)	2.839	0.500	−1	[18]
(TMPD)(TCNQ) ₂	−1/2	1.17(1)	1.427(3)	1.395(2)	1.434(2)	1.354(2)	2.861	0.488	−0.50	[19]
(TPP)(TCNQ) ₂	−1/2	1.17(1)	1.428(3)	1.396(2)	1.434(2)	1.354(2)	2.862	0.488	−0.50	[20]
[Pd(MeCN) ₄](TCNQ) ₄]										
	−1/2	1.138(2)	1.428(2)	1.388(4)	1.428(2)	1.356(5)	2.856	0.486	−0.42	[21]
	−1/2	1.138(2)	1.428(4)	1.393(8)	1.426(3)	1.358(11)	2.854	0.488	−0.50	
	−1/2	1.139(3)	1.428(2)	1.384(1)	1.430(1)	1.355(5)	2.858	0.484	−0.33	
Coordinated TCNQ										
<i>cis</i> -μ ₂ -[TCNQ]										
	−1	1.147(9)	1.401(10)	1.404(8)	1.43(2)	1.365(8)				
		1.129(8)	1.407(10)	1.421(7)	1.43(1)					
		[1.138]	[1.404]	[1.4125]	[1.43]	[1.365] ^[b]	2.834	0.498	−0.93 ^[c]	[1a]
	−1	1.160(4)	1.421(4)	1.431(4)	1.419(4)	1.365(4)				
		1.151(4)	1.416(4)	1.425(4)	1.423(4)					
		[1.1555]	[1.4185]	[1.428]	[1.421]	[1.365] ^[b]	2.840	0.503	−1.13 ^[c]	[1a]
<i>syn</i> -μ ₂ -[TCNQ]										
	−1	1.147(2)	1.415(2)	1.419(2)	1.429(2)	1.365(2)				
		1.147(2)	1.417(2)	1.419(2)	1.430(2)					
		[1.147]	[1.416]	[1.419]	[1.4295]	[1.365] ^[b]	2.846	0.499	−0.96 ^[c]	[1a]
μ ₄ -[TCNQ]										
	−1	1.141(9)	1.412(8)	1.389(11)	1.341(8)	1.378(10)				
		1.138(11)	1.411(8)	1.414(11)	1.424(8)					
		[1.1395]	[1.4115]	[1.4015]	[1.3825]	[1.378] ^[b]	2.794	0.502	−1.08 ^[c]	[2]
	−1	1.138(9)	1.405(13)		1.424(9)	1.358(13)				
		1.146(9)	1.47(8)	1.422(8)	1.431(9)					
		[1.142]	[1.4375]	[1.422]	[1.4275]	[1.358] ^[b]	2.865	0.496	−0.83 ^[c]	[22]
	0	1.126(8)	1.453(8)	1.361(9)	1.451(8)	1.337(9)				
		1.148(8)	1.431(9)							
		[1.137]	[1.442]	[1.361]	[1.451]	[1.337] ^[b]	2.893	0.470	0.25 ^[c]	[23]
1		1.132(4)	1.431(4)	1.393(6)	1.435(4)	1.349(6)	2.866	0.486	−0.42	this work
2		1.131(6)	1.436(5)	1.409(9)	1.432(5)	1.358(8)	2.868	0.491	−0.63	this work

[a] $\rho = A[c/(b+d)] + B$ with $A = -41.667$ and $B = 19.833$.^[17, 24] [b] Average value. [c] Estimated from the average values.

bond lengths defined in Table 1.^[18–24] The charges for **1** and **2** estimated from the Kistenmacher relation are -0.42 and -0.63 , respectively. These values point to partially reduced TCNQ bridges in these compounds, which agrees with the aforementioned IR data in the $\delta(\text{C-H})$ region.

A packing diagram for **1** is shown in Figure 3. Each two-dimensional sheet is separated by 6.6 \AA , which allows for toluene molecules to reside between the layers. One type of C_7H_8 molecule π -stacks with TCNQ ligands in one-dimensional columns along the c axis (phenyl–phenyl distance is about 4.2 \AA and the nitrile–phenyl distance is about 3.3 \AA). The remaining two independent toluene molecules occupy the one-dimensional channels that run throughout the crystal.

Magnetic measurements performed on powder samples of **1** and **2** were measured between 1.8 and 300 K. As expected, **2**

was found to be diamagnetic, but **1** possesses a moment of $0.678 \text{ cm}^3 \text{ K mol}^{-1}$ at 300 K (expressed as $\chi_M T$) which continuously decreases with cooling. A large zero-field splitting arising from the $S = 1 \text{ Ru}_2^{\text{II,II}}$ units ($D \sim 300 \text{ cm}^{-1}$) contributes to the reduced moments observed at low temperatures,^[25] but the moment at room temperature is already significantly less than the expected value of $\chi_M T = 2.0 \text{ cm}^3 \text{ K mol}^{-1}$ for two isolated $S = 1$ spin centers. These data are in accord with a relatively strong antiferromagnetic interaction through the TCNQ bridges, which is an indication of electronic communication. Attempts are underway to grow sufficiently large crystals so that single-crystal conductivity and magnetic measurements can be performed.

In summary, two-dimensional networks that consist of $[\text{M}_2(\text{O}_2\text{CCF}_3)_4]$ molecules connected to each other by μ_4 -TCNQ ligands exhibit appreciable M–L π -backbonding. This situation can be described by the resonance structures depicted in Figure 4.

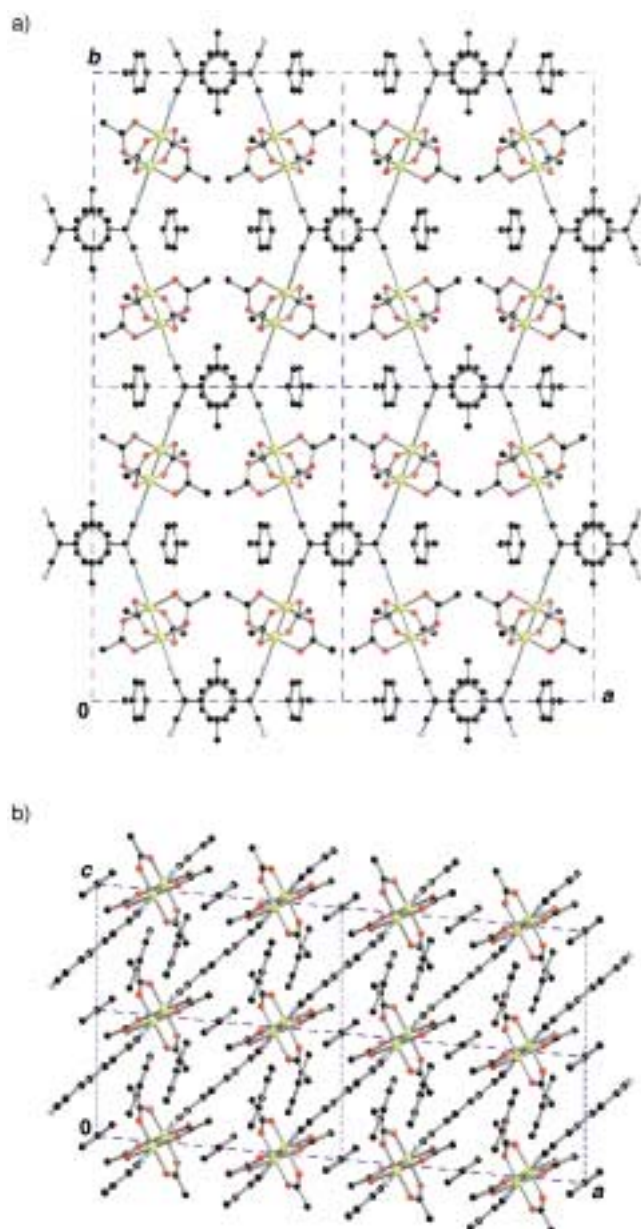


Figure 3. Packing diagram view of a) **1** along the c axis and b) along the b axis, showing the alternating π – π stacked columns and the one-dimensional channels along the c axis. The fluorine atoms were omitted for the sake of clarity.

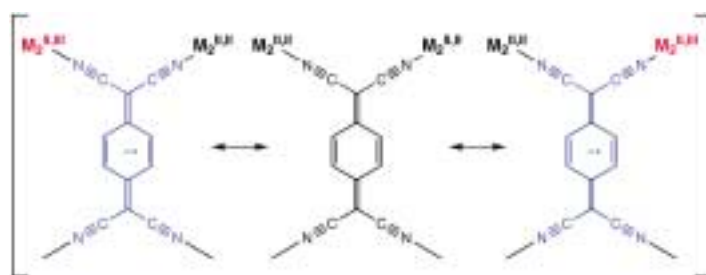


Figure 4. Resonance structures of a one-electron delocalized system for the (2:1) donor–acceptor assemblies.

Experimental Section

1: All synthetic procedures were performed anaerobically. TCNQ (20 mg, 0.1 mmol) was added to a solution of $[\text{Ru}_2(\text{O}_2\text{CCF}_3)_4(\text{thf})_2]$ (160 mg, 0.2 mmol) in toluene (40 mL), and the brown suspension was refluxed for 1 h at 120°C . The resulting dark green precipitate was separated from the hot solution, washed with toluene (20 mL), and dried in vacuo (**1a**, yield > 80%). The hot filtrate was cooled to room temperature and allowed to stand undisturbed for two days during which time a crop of X-ray quality, dark green crystals was obtained (**1b**, yield < 10%). IR (Nujol): for **1a**: $\tilde{\nu} = 2207$ (sh), 2159 (m), 2120 (sh) $\nu(\text{C}\equiv\text{N})$; 842 cm^{-1} (w) $\delta(\text{C-H})$; for **1b**: $\tilde{\nu} = 2203$ (sh), 2155 (m), 2117 (sh) $\nu(\text{C}\equiv\text{N})$; 842 cm^{-1} (w) $\delta(\text{C-H})$.

2: TCNQ (20 mg, 0.1 mmol) was added to a solution of $[\text{Rh}_2(\text{O}_2\text{CCF}_3)_4]$ (132 mg, 0.2 mmol) in toluene (30 mL) to give a light green suspension which was heated at 80°C for 2 h. During this time, the solution color changed from green to reddish brown. The resulting solution was cooled to room temperature, reduced in volume to 20 mL and treated with dichloromethane (30 mL). After filtration, the solution was layered in a narrow Schlenk tube with n -hexanes (30 mL), which led to the formation of dark purplish-brown single crystals after one week. IR (Nujol): $\tilde{\nu} = 2237$ (m, br) $\nu(\text{C}\equiv\text{N})$, 1539 (m) $\nu(\text{C-O})$, 844 cm^{-1} (w) $\delta(\text{C-H})$.

Received: June 20, 2000 [Z15297]

- [1] a) H. Zhao, R. A. Heintz, X. Ouyang, K. R. Dunbar, *Chem. Mater.* **1999**, *11*, 736; b) R. A. Heintz, H. Zhao, X. Ouyang, G. Grandinetti, J. Cowen, K. R. Dunbar, *Inorg. Chem.* **1999**, *38*, 144; c) H. Zhao, R. A. Heintz, X. Ouyang, G. Grandinetti, J. Cowen, K. R. Dunbar in *Supramolecular Engineering of Synthetic Metallic Materials* (Eds.: J. Veciana, C. Rovira, D. B. Amabilino), Kluwer Academic, Netherlands, **1999**, pp. 353.

- [2] S. A. O'Kane, R. Clérac, H. Zhao, X. Ouyang, J. R. Galán-Mascarós, R. Heintz, K. R. Dunbar, *J. Solid State Chem.* **2000**, *152*, 159, and references therein.
- [3] a) J. M. Manriquez, G. T. Yee, R. S. McLean, A. J. Epstein, J. S. Miller, *Science* **1991**, *252*, 1415; b) "Conjugated Polymers and Related Materials: The International Journal of Chemical and Electronic Structure": J. S. Miller, G. T. Yee, J. M. Manriquez, A. J. Epstein, *Proceedings of Nobel Symposium NS-81*, Oxford University Press, New York, **1993**, p. 461; c) "Conjugated Polymers and Related Materials: The International Journal of Chemical and Electronic Structure": A. J. Epstein, J. S. Miller, *Proceedings of Nobel Symposium NS-81*, Oxford University Press, New York, **1993**, p. 475; d) D. C. Gordon, L. Deakin, A. M. Arif, J. S. Miller, *J. Am. Chem. Soc.* **2000**, *122*, 290, and references therein.
- [4] a) J. S. Miller, J. C. Calabrese, R. S. McLean, A. J. Epstein, *Adv. Mater.* **1992**, *4*, 498; b) A. Böhm, C. Vazquez, R. S. McLean, J. C. Calabrese, S. E. Kalm, J. L. Manson, A. J. Epstein, J. S. Miller, *Inorg. Chem.* **1996**, *35*, 3083; c) E. J. Brandon, A. M. Arif, B. M. Burkhart, J. S. Miller, *Inorg. Chem.* **1998**, *37*, 2792; d) E. J. Brandon, D. K. Rittenberg, A. M. Arif, J. S. Miller, *Inorg. Chem.* **1998**, *37*, 3376.
- [5] a) A. Aumüller, P. Erk, S. Hünig, G. Klebe, J. U. von Schütz, H. P. Werner, *Angew. Chem.* **1986**, *98*, 760; *Angew. Chem. Int. Ed. Engl.* **1986**, *25*, 740; b) A. Aumüller, P. Erk, S. Hünig, *Mol. Cryst. Liq. Cryst.* **1988**, *156*, 215; c) P. Erk, H.-J. Gross, U. L. Hünig, H. Meixner, H.-P. Werner, J. U. von Schütz, H. C. Wolf, *Angew. Chem.* **1989**, *101*, 1297; *Angew. Chem. Int. Ed. Engl.* **1989**, *28*, 1245; d) R. Kato, H. Kobayashi, A. Kobayashi, *J. Am. Chem. Soc.* **1989**, *111*, 5224; e) A. Aumüller, P. Erk, S. Hünig, E. Hädicke, K. Peters, H. G. von Schnering, *Chem. Ber.* **1991**, *124*, 2001; f) K. Sinzger, S. Hünig, M. Jopp, D. Bauer, W. Beitsch, J. U. von Schütz, H. C. Wolf, R. K. Kremer, T. Metzenthin, R. Bau, S. I. Khan, A. Lindbaum, C. L. Lengauer, E. Tillmanns, *J. Am. Chem. Soc.* **1989**, *115*, 7696.
- [6] S. L. Bartley, K. R. Dunbar, *Angew. Chem.* **1991**, *103*, 447; *Angew. Chem. Int. Ed. Engl.* **1991**, *30*, 448.
- [7] a) C. Creutz, H. Taube, *J. Am. Chem. Soc.* **1973**, *95*, 1086; b) C. Creutz, *Prog. Inorg. Chem.* **1983**, *30*, 1; c) M. A. S. Aquino, F. L. Lee, E. J. Gabe, C. Bensimon, J. E. Greedan, R. J. Crutchley, *J. Am. Chem. Soc.* **1992**, *114*, 5130; d) C. E. B. Evans, M. L. Naklicki, A. R. Rezvani, C. A. White, V. V. Kondratiev, R. J. Crutchley, *J. Am. Chem. Soc.* **1998**, *120*, 13096, and references therein.
- [8] a) S. L. Schiavo, G. Tresoldi, A. M. Mezzasalma, *Inorg. Chim. Acta* **1997**, *254*, 251; b) W. Pukacki, M. Pawlak, A. Graja, M. Lequan, R. M. Lequan, *Inorg. Chem.* **1987**, *26*, 1328; c) L. Ballester, A. Gutiérrez, M. F. Perpiñán, M. T. Azcond, *Coord. Chem. Rev.* **1999**, *190–192*, 447, and references therein.
- [9] Crystal data for $[\text{Ru}_2(\text{O}_2\text{CCF}_3)_4](\text{TCNQ}) \cdot 3(\text{C}_7\text{H}_8)_\infty$ (**1**): $\text{C}_{49}\text{H}_{28}\text{N}_4\text{O}_{16}\text{F}_{12}\text{Ru}_4$, monoclinic, space group $C2/m$, $a = 16.682(3)$, $b = 20.881(4)$, $c = 8.6120(17)$ Å, $\beta = 95.47(3)^\circ$, $V = 2986.2(10)$ Å³, $Z = 2$, $\rho_{\text{calcd}} = 1.736$ g cm⁻³, $\mu = 1.10$ mm⁻¹, $F(000) = 1524.00$, $R1$ ($wR2$) = 0.0350 (0.0843) ($I > 2\sigma(I)$), $R1$ ($wR2$) = 0.1536 (0.0961) (all data), GOF = 0.940. Crystal data for $[\text{Rh}_2(\text{O}_2\text{CCF}_3)_4](\text{TCNQ}) \cdot 3(\text{C}_7\text{H}_8)_\infty$ (**2**): $\text{C}_{49}\text{H}_{28}\text{N}_4\text{O}_{16}\text{F}_{12}\text{Rh}_4$, monoclinic, space group $C2/m$, $a = 16.793(3)$, $b = 20.806(4)$, $c = 8.4450(17)$ Å, $\beta = 95.54(3)^\circ$, $V = 2936.9(10)$ Å³, $Z = 2$, $\rho_{\text{calcd}} = 1.774$ g cm⁻³, $\mu = 1.21$ mm⁻¹, $F(000) = 1532.00$, $R1$ ($wR2$) = 0.0471 (0.1202) ($I > 2\sigma(I)$), $R1$ ($wR2$) = 0.0689 (0.1360) (all data), GOF = 0.997. Data were collected on a Bruker SMART CCD diffractometer in the range $1.57 < 2\theta < 28.32$ for **1** and $1.56 < 2\theta < 28.26$ for **2** at 110(2) K with graphite-monochromated MoK_α radiation ($\lambda = 0.71069$ Å). Of the 18164 and 9188 unique reflections, 3747 and 3548 were unique for **1** and **2**, respectively. The structures were solved by direct methods (SHELXS-97)^[26] and refined by full-matrix least-squares calculations on F^2 (SHELXL-97).^[27] The non-hydrogen atoms were refined anisotropically, while hydrogen atoms were refined isotropically. Full-matrix least-squares refinement was based on 3747 reflections ($I > 2.00\sigma(I)$) for **1** and 3548 reflections ($I > 2.00\sigma(I)$) for **2**. The highest peaks in the final difference map were 1.272 and 1.546 e⁻ Å⁻³ for **1** and **2**, respectively. Crystallographic data (excluding structure factors) for the structures reported in this paper have been deposited with the Cambridge Crystallographic Data Centre as supplementary publication no. CCDC-145608 (**1**) and CCDC-145609 (**2**). Copies of the data can be obtained free of charge on application to CCDC, 12 Union Road, Cambridge CB21EZ, UK (fax: (+44) 1223-336-033; e-mail: deposit@ccdc.cam.ac.uk).
- [10] A. J. Lindsay, G. Wilkinson, *J. Chem. Soc. Dalton Trans.* **1987**, 2723.
- [11] F. A. Cotton, M. Matusz, B. Zhong, *Inorg. Chem.* **1988**, *27*, 4368.
- [12] F. A. Cotton, R. A. Walton, *Multiple Bonds Between Metal Atoms*, 2nd ed., Oxford University Press, Oxford, **1993**.
- [13] F. A. Cotton, Y. Kim, *J. Am. Chem. Soc.* **1993**, *115*, 8511.
- [14] H. Miyasaka, C. Campos, J.-R. Galán-Mascarós, K. R. Dunbar, *Inorg. Chem.* submitted.
- [15] R. E. Long, R. A. Sparks, K. N. Trueblood, *Acta Crystallogr.* **1965**, *18*, 932.
- [16] A. Hoekstra, T. Spoelder, A. Vos, *Acta Crystallogr. Sect. B* **1972**, *28*, 14.
- [17] T. J. Kistenmacher, T. J. Emge, A. N. Bloch, D. O. Cowan, *Acta Crystallogr. Sect. B* **1982**, *38*, 1193.
- [18] C. J. Fritchie, Jr., P. Arthur, Jr., *Acta Crystallogr.* **1966**, *21*, 139.
- [19] A. W. Hanson, *Acta Crystallogr. Sect. B* **1968**, *24*, 768.
- [20] P. Goldstein, K. Seff, K. N. Trueblood, *Acta Crystallogr. Sect. B* **1968**, *24*, 778.
- [21] S. Z. Goldberg, R. Eisenberg, J. S. Miller, A. J. Epstein, *J. Am. Chem. Soc.* **1976**, *98*, 5173.
- [22] L. Shields, *J. Chem. Soc. Faraday Trans. 2* **1985**, *81*, 1.
- [23] C. Campana, K. R. Dunbar, X. Ouyang, *Chem. Commun.* **1996**, 2427.
- [24] S. L. Stang, F. Conan, J. S. Pala, Y. L. Mest, M. T. Garland, R. Baggio, E. Faulquest, A. Leblanc, P. Molinier, L. Toupet, *J. Chem. Soc. Dalton Trans.* **1998**, 489.
- [25] A. Cogne, E. Belorizky, J. Laugier, P. Rey, *Inorg. Chem.* **1994**, *33*, 3364.
- [26] G. M. Sheldrick, SHELXS-97, Program for Crystal Structure Determination, University of Göttingen, Göttingen, Germany, **1997**.
- [27] G. M. Sheldrick, SHELXL-97, Program for Refinement of Crystal Structure, University of Göttingen, Göttingen, Germany, **1997**.

Supramolecular Chemistry of Anionic Cobalt(III) Bis(dicarbollide) and Cyclotrimeratrylene in the Solid State and the Gas Phase**

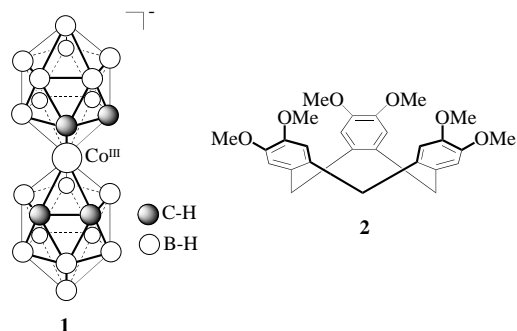
Michaele J. Hardie and Colin L. Raston*

Despite the fundamental role played by anionic species in many natural processes the supramolecular chemistry of anions has been one of the least explored aspects of supramolecular chemistry.^[1] While the neutral, isomeric icosahedral carboranes *o*, *m*, *p*-C₂B₁₀H₁₂, for instance, are emerging as versatile components in supramolecular systems, forming hydrogen-bonded complexes^[2] and host–guest species with a range of host molecules and assemblies,^[3–9] studies on the supramolecular chemistry of anionic carboranes, or indeed anionic boranes, are limited. The most significant example of the binding of a borane anion in a supramolecular system is that of the divalent anion [B₁₀H₁₀]²⁻ which forms a host–guest

[*] Prof. C. L. Raston, Dr. M. J. Hardie
Department of Chemistry
Monash University
Clayton, Melbourne, Victoria 3800 (Australia)
Fax: (+613) 9905-4597
E-mail: c.raston@sci.monash.edu.au

[**] This work was supported by the Australian Research Council. We thank Sally Duck for collecting mass spectrometry data.

complex with a trimeric mercury–carborane macrocycle.^[10] As part of our studies on the binding of large molecules with convex surfaces, including spherical molecules such as carboranes and fullerenes, by curved host molecules we have investigated the host–guest chemistry of the aspherical carborane anion cobalt(III) bis(dicarbollide) $[\text{Co}(\text{C}_2\text{B}_9\text{H}_{11})_2]^-$ (**1**) with the rigid bowl-shaped cyclic molecule cyclotrimeratrylene (**2**; CTV). The 23 vertex complex **1** is known to be a



weakly coordinating anion^[11] and herein its use in supramolecular chemistry is established for the first time. CTV forms intracavity host–guest complexes with large spherical main group cage molecules such as fullerenes^[8, 12] and *o*-carborane,^[7, 8] as well as with cationic organometallic complexes such as $[\text{FeCp}(\text{C}_6\text{H}_5\text{R})]^+$ (Cp = cyclopentadiene).^[13] However, small organic molecules are not usually bound as intracavity guests in the solid state, rather they form channel-type structures with intercalated organic molecules situated in spaces created by the homo-assembled CTV packing motif.^[14] Recently we demonstrated that CTV can act as a ligand towards Group 1 metals in complexes such as $[\text{Na}(\text{CTV})_2(\text{OH})(\text{H}_2\text{O})](\text{H}_2\text{O})(\text{DMF})_2(o\text{-carborane})$,^[9] where the Na^+ , CTV, water, and hydroxide form a coordinate and hydrogen-bonded infinite two-dimensional (2D) array. The normal inclusion properties of CTV within the array are altered with *N,N'*-dimethylformamide (DMF) being complexed as an intracavity guest molecule; DMF does not usually form any type of complex with CTV.^[15]

Mixing equimolar quantities of Na-**1** and CTV in polar organic solvents such as acetonitrile, DMF, or 2,2,2-trifluoroethanol yields a yellow powder, the microanalysis of which is consistent with the formula $[\text{Na}(\text{CTV})][\text{Co}(\text{C}_2\text{B}_9\text{H}_{11})_2]$. The powder can be recrystallized from very dilute 2,2,2-trifluoroethanol solutions or from more concentrated 2,2,2-trifluoroethanol solutions with a trace of DMF to give orange crystals of $[\text{Na}(\text{CTV})][\text{Co}(\text{C}_2\text{B}_9\text{H}_{11})_2](\text{CF}_3\text{CH}_2\text{OH})_{0.25}$ (**3**). The crystals rapidly lose solvent when removed from their mother liquor; their composition and structure were determined from X-ray diffraction data collected at 123(1) K.^[16] The structure has several interesting features: a novel two-dimensional sodium–CTV coordination polymer, intracavity host–guest complexation of $\text{CF}_3\text{CH}_2\text{OH}$ molecules by CTV, and the presence of the large organometallic anion **1** within the channels created by the packing of the coordination polymers.

The sodium–cyclotrimeratrylene coordination polymer of **3** is shown in Figure 1 a. All the sodium ions and CTV molecules

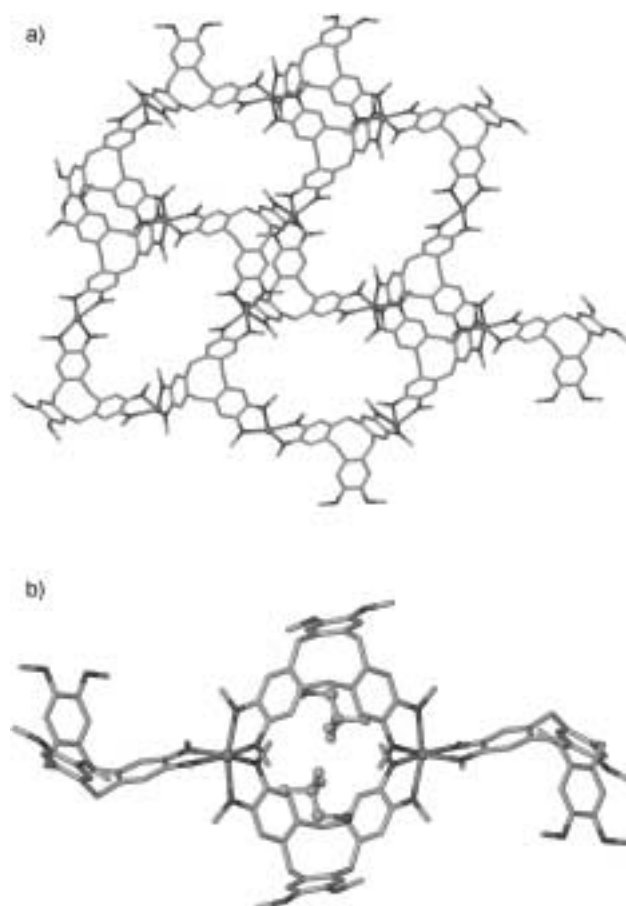


Figure 1. a) Section of the 2D network formed by Na^+ ions and CTV ligands in the complex **3**. The network topology is that of a three-connected 4:8 plane net. b) CTV– $\text{CF}_3\text{CH}_2\text{OH}$ host–guest cavity (see text). Closest $\text{F}\cdots\text{F}$ contact is 2.69 Å, however, each $\text{CF}_3\text{CH}_2\text{OH}$ molecule is estimated to have a 25 % occupancy, giving an approximately 6 % probability of two $\text{CF}_3\text{CH}_2\text{OH}$ guests inhabiting one cavity as shown here and about a 56 % chance of the cavity being empty.

within the polymer are crystallographically equivalent. The Na^+ ion is six coordinate with three chelating CTV ligands having Na–O bond lengths between 2.310(2) and 2.369(2) Å, and is in a highly distorted octahedral environment (*cis* angles range from 67.13(6) (chelate ring) to 110.00(7)°, *trans* angles 152.66(8), 155.81(7), and 160.16(7)°). Adjacent Na^+ centers within the network have opposite configurations, hence the network is not chiral (Figure 1 b). The orientation of the CTV bowls around each Na^+ ion alternates between two up, one down and one up, two down throughout the network. The previous example of CTV acting as a chelating ligand has two CTV molecules around the Na^+ or K^+ centers and in the latter case a coordinate chain is formed.^[9] Each CTV molecule is a μ_3 bridging ligand coordinating to three Na^+ ions, thus creating a two-dimensional infinite network where both Na^+ and CTV act as three-connectors. The network topology is described according to classification by Wells as a three-connected 4:8 plane net,^[17] which means every node within the net, in this case sodium cations and the centers of the CTV molecules, connects to three others creating tetra-gons and octa-gons as the shortest loops. To the best of our knowledge this is the first time such a network topology has been

observed in a coordination polymer; three-connected 2D networks more commonly adopt the (6,3) net which features hexa-gons as the only type of shortest loop.^[18] The 4:8 topology is known for the hydrogen-bonded network of caprolactam and the layer structures of LnB_2C_2 (Ln = lanthanide), $\text{BaFeSi}_4\text{O}_{10}$, and $\text{CaCuSi}_4\text{O}_{10}$.^[17]

The network is not planar, it has two tiers of Na centers and the connections between them are the topological tetra-gons. These tetra-gons form host–guest cavities within the network by virtue of the curved, bowl-like nature of CTV, and because the bowls are in opposite and inward orientations (Figure 1 b). The distance across the cavity, defined by the distance between the centroids of the methylene planes of the CTV molecules, is 11.2 Å. For each CTV molecule there is a guest molecule of $\text{CF}_3\text{CH}_2\text{OH}$ situated with its CH_2 group directly over the center of the CTV bowl ($\text{C}\cdots\text{center of CTV methylene plane}$ 4.33 Å), however the occupancy of the $\text{CF}_3\text{CH}_2\text{OH}$ molecule is estimated at only 25 %^[16] and hence the cavities are largely empty. Nevertheless this is a distinctly different host–guest behavior to that usually associated with CTV.

The $[\text{Na}(\text{CTV})]_\infty$ network has large holes, which are apparent in Figure 1 a, with an approximate cross section of 3.5×10.9 Å (measured as the closest $\text{H}\cdots\text{H}$ distances between OMe groups). In the overall crystal lattice, the $[\text{Na}(\text{CTV})]_\infty$ networks pack so that these holes are more or less aligned, thus creating methyl-lined channels of roughly circular cross section. One of the three arene faces of each CTV shows a π – π stacking interaction at a separation of 3.6 Å to the centroid of CTV from its adjacent network. This manner of network packing is contrary to close-packing considerations and is therefore likely to arise from templation by the large organometallic ion $[\text{Co}(\text{C}_2\text{B}_9\text{H}_{11})_2]^-$ (**1**) which occupies the channels (Figure 2 a). There are two crystallographically distinct types of **1** both of which have their Co core positioned on a center of symmetry and have different staggered arrangements of carborane ligands with C–C \cdots C–C torsion angles of -41° and 0° . Reported X-ray structures of **1** are either disordered or have a staggered arrangement.^[19] The $[\text{Co}(\text{C}_2\text{B}_9\text{H}_{11})_2]^-$ ions within the circular channels, shown in purple in Figures 2 a b, are positioned 4.34 Å apart ($\text{B}\cdots\text{B}$ distance, the corresponding $\text{B–H}\cdots\text{H–B}$ distance is 2.90 Å) and stack in a slightly offset manner. The second type of **1**, shown in orange, run in zigzag chains perpendicular to the first with a closest $\text{B}\cdots\text{B}$ separation of 5.00 Å (the corresponding $\text{B–H}\cdots\text{H–B}$ distance is 3.48 Å). These anions also occupy channels of diamond-like cross section created by the packing of the $[\text{Na}(\text{CTV})]_\infty$ networks as is evident in the complete crystal packing diagram of **3** shown in Figure 2 b. The two types of **1** are quite close to one another with a closest C \cdots B distance of 3.75 Å (the corresponding C–H \cdots H–B distance is 2.40 Å).

Crystals of **3** are soluble in $\text{CF}_3\text{CH}_2\text{OH}$ and thus the coordination polymer breaks up in solution. The electrospray ionization (ESI) mass spectrum of **3** in $\text{CF}_3\text{CH}_2\text{OH}$ reveals a number of singly charged species present in the gas phase. Peaks at m/z 1373, 923, and 473 correspond to $[\text{Na}(\text{CTV})_3]^+$, $[\text{Na}(\text{CTV})_2]^+$, and $[\text{Na}(\text{CTV})]^+$ ions, respectively. These species are also present in the mass spectrum obtained from

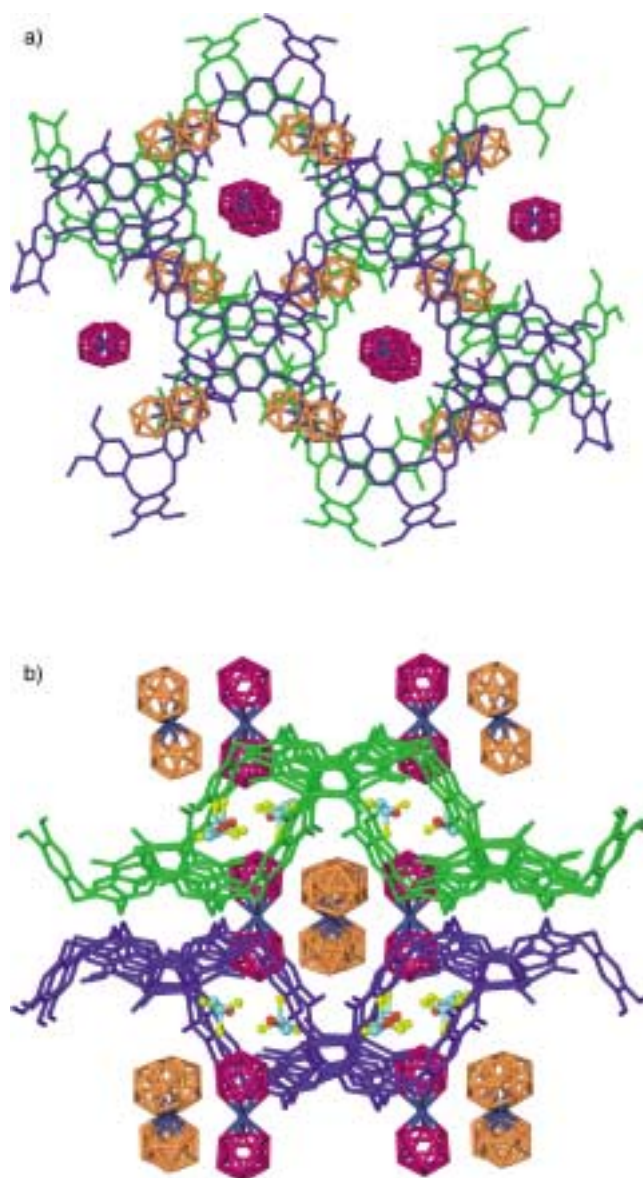


Figure 2. Crystal packing in **3**. a) Packing of two $[\text{Na}(\text{CTV})]_\infty$ networks shown in blue and green. The two types of $[\text{Co}(\text{C}_2\text{B}_9\text{H}_{11})_2]^-$ ions are highlighted in purple or orange, the C/B positions are not distinguished. Guest $\text{CF}_3\text{CH}_2\text{OH}$ molecules are omitted for clarity; b) crystal packing showing a side-on view of the $[\text{Na}(\text{CTV})]_\infty$ networks, highlighting the $\text{CF}_3\text{CH}_2\text{OH}$ -containing cavities within each network and the diamond-like channels created by network packing and occupied by the $[\text{Co}(\text{C}_2\text{B}_9\text{H}_{11})_2]^-$ ions shown in orange.

CTV treated with an equimolar amount of NaCl, and run under similar conditions, along with a number of doubly charged clusters including the $[\text{Na}_2(\text{CTV})_3]^{2+}$ ion at m/z 698. The $[\text{Na}(\text{CTV})_3]^+$ ion is only present in trace amounts with $[\text{Na}(\text{CTV})_2]^+$ being the predominant species in the gas phase. The ESI mass spectrum of **3** also contains a series of peaks with a different isotope pattern that shows the formation of host–guest complexes in the gas-phase between the sodium–CTV clusters and the ionic **1**. The complexes $[\{\text{Na}_2(\text{CTV})_3\}\{\text{Co}(\text{C}_2\text{B}_9\text{H}_{11})_2\}]^+$, $[\{\text{Na}_2(\text{CTV})_2\}\{\text{Co}(\text{C}_2\text{B}_9\text{H}_{11})_2\}]^+$, and $[\{\text{Na}_2(\text{CTV})\}\{\text{Co}(\text{C}_2\text{B}_9\text{H}_{11})_2\}]^+$ are present at m/z 1721, 1270, and 820, respectively, which is consistent with the observation of $[\text{Na}_2(\text{CTV})_3]^{2+}$ ions in the spectrum of CTV

and NaCl. The observed and the calculated isotope pattern for the complex $[\text{Na}_2(\text{CTV})][\text{Co}(\text{C}_2\text{B}_9\text{H}_{11})_2]^+$ are shown in Figure 3, and are a convincing match with the observed (820.4687) and calculated (820.4692) m/z values for the major peak. Two cobalt(III) bis(dicarbollide) anions may also be

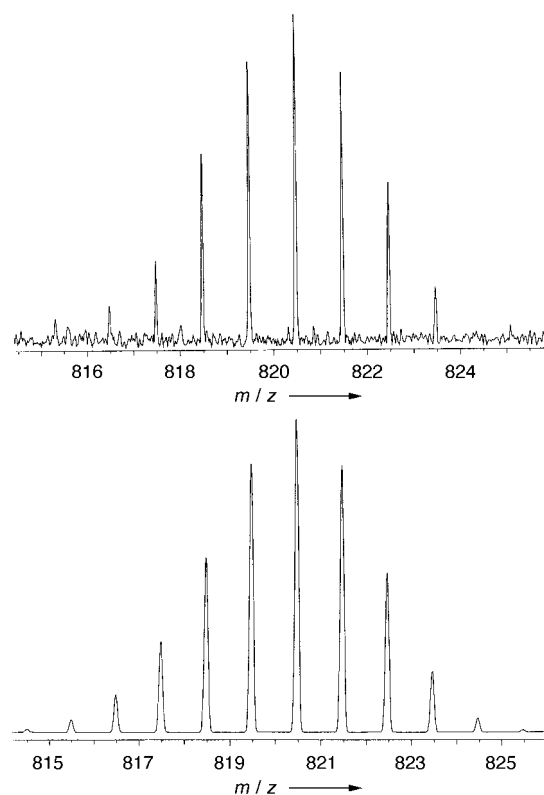


Figure 3. The observed (upper) and calculated (lower) isotope pattern for the host-guest species $[\text{Na}_2(\text{CTV})][\text{Co}(\text{C}_2\text{B}_9\text{H}_{11})_2]^+$ from the ESI mass spectrum of **3** in $\text{CF}_3\text{CH}_2\text{OH}$. The spectrum was run on a Bruker FT mass spectrometer at 65 V.

complexed, as evidenced by the small peak at m/z 1617 which corresponds to the complex $[\text{Na}_3(\text{CTV})_2][\text{Co}(\text{C}_2\text{B}_9\text{H}_{11})_2]_2^+$. The negative mode ESI mass spectrum of **3** shows only the presence of $[\text{Co}(\text{C}_2\text{B}_9\text{H}_{11})_2]^-$ at m/z 324. The use of soft-ionization mass spectrometry to study supramolecular systems has become more prominent in recent years^[20] and, while smaller, weakly coordinating anions such as BF_4^- and PF_6^- or small organic anions have been shown to be complexed in the gas phase,^[21] the complexation of such a large organometallic anion is particularly noteworthy.

The solid-state and gas-phase supramolecular behaviors of Na-**1** and CTV are quite distinct. The crystalline complex $[\text{Na}(\text{CTV})][\text{Co}(\text{C}_2\text{B}_9\text{H}_{11})_2](\text{CF}_3\text{CH}_2\text{OH})_{0.25}$ features a 2D $[\text{Na}(\text{CTV})]_\infty$ coordination polymer with novel topology and layers templated around the counterion **1**. Unusually for CTV, host molecules within the polymer can complex guest solvent molecules, which further supports the argument that the inclusion properties of a known host molecule can be altered by incorporating it into an extended hydrogen-bonded or coordinate network.^[8,9] The $[\text{Na}(\text{CTV})]_\infty$ coordination polymer breaks up in solution and $[\text{Na}_n(\text{CTV})_m]^{n+}$ clusters are present in the gas phase and can complex one or two

molecules of **1**. These findings may prove to form the basis of a general approach to the supramolecular chemistry of metal ion salts of large anions, including reduced fullerenes, in the presence of CTV or indeed related types of rigid, curved receptor molecules.

Experimental Section

Cyclotrimeratrylene (20.1 mg, 0.045 mmol) and $\text{Na}[\text{Co}(\text{C}_2\text{B}_9\text{H}_{11})_2]$ (15.5 mg, 0.045 mmol) were dissolved separately in $\text{CF}_3\text{CH}_2\text{OH}$ and mixed at room temperature to yield $[\text{Na}(\text{CTV})][\text{Co}(\text{C}_2\text{B}_9\text{H}_{11})_2]$ as a yellow amorphous powder (29.8 mg, 83 %). Elemental analysis calcd for $\text{C}_{31}\text{H}_{52}\text{B}_{18}\text{CoNaO}_6$ (%): C 46.70, H 6.57; found: C 46.75, H 6.31. Orange prismatic crystals of **3** were grown overnight from dilute solutions of $[\text{Na}(\text{CTV})][\text{Co}(\text{C}_2\text{B}_9\text{H}_{11})_2]$ in $\text{CF}_3\text{CH}_2\text{OH}$.

Received: May 29, 2000 [Z15185]

- [1] *Supramolecular Chemistry of Anions* (Eds.: A. Bianchi, K. Bowman-James, E. Garcia-España), Wiley-VCH, New York, **1997**.
- [2] a) M. G. Davidson, T. G. Hibbert, J. A. K. Howard, A. Mackinnon, K. Wade, *Chem. Commun.* **1996**, 2285; b) G. Harakas, T. Vu, C. B. Knobler, M. F. Hawthorne, *J. Am. Chem. Soc.* **1998**, *120*, 6405.
- [3] A. Harada, S. Takahashi, *J. Chem. Soc. Chem. Commun.* **1988**, 1352.
- [4] T. Kusakawa, M. Fujita, *Angew. Chem.* **1998**, *110*, 3327; *Angew. Chem. Int. Ed.* **1998**, *37*, 3142.
- [5] P. D. Godfrey, W. J. Grigsby, P. J. Nichols, C. L. Raston, *J. Am. Chem. Soc.* **1997**, *119*, 9283.
- [6] M. J. Hardie, C. L. Raston, *Eur. J. Inorg. Chem.* **1999**, 195.
- [7] R. J. Blanch, M. Williams, G. D. Fallon, M. G. Gardiner, R. Kaddour, C. L. Raston, *Angew. Chem.* **1997**, *109*, 520; *Angew. Chem. Int. Ed. Engl.* **1997**, *36*, 504.
- [8] M. J. Hardie, P. D. Godfrey, C. L. Raston, *Chem. Eur. J.* **1999**, *5*, 1828.
- [9] M. J. Hardie, C. L. Raston, B. Wells, *Chem. Eur. J.* **2000**, *6*, 3293.
- [10] X. Yang, C. B. Knobler, M. F. Hawthorne, *J. Am. Chem. Soc.* **1993**, *115*, 4904.
- [11] a) M. F. Hawthorne, D. C. Young, T. D. Andrews, D. V. Howe, R. L. Pilling, A. D. Pitts, M. Reintjes, L. F. Warren, Jr., *J. Am. Chem. Soc.* **1968**, *90*, 879; b) Z. Xie, T. Jelinek, R. Bau, C. A. Reed, *J. Am. Chem. Soc.* **1994**, *116*, 1907.
- [12] a) J. L. Atwood, M. J. Barnes, M. G. Gardiner, C. L. Raston, *Chem. Commun.* **1996**, 1449; b) J. L. Atwood, M. J. Barnes, R. S. Burkhalt, P. C. Junk, J. W. Steed, C. L. Raston, *J. Am. Chem. Soc.* **1994**, *116*, 10346; c) A. M. Bond, W. Miao, C. L. Raston, T. J. Ness, M. J. Barnes, J. L. Atwood, *J. Phys. Chem.*, submitted.
- [13] K. T. Holman, J. W. Steed, J. L. Atwood, *Angew. Chem.* **1997**, *109*, 1840; *Angew. Chem. Int. Ed. Engl.* **1997**, *36*, 1736.
- [14] J. W. Steed, Z. Zhang, J. L. Atwood, *Supramolec. Chem.* **1996**, *7*, 37.
- [15] J. A. Hyatt, E. N. Duesler, D. Y. Curtin, I. C. Paul, *J. Org. Chem.* **1980**, *45*, 5074.
- [16] Crystal data for **3**. Data were collected on a yellow crystal of dimensions $0.38 \times 0.18 \times 0.10$ mm at 123(1) K on an Enraf-Nonius Kappa CCD diffractometer with MoK_α radiation. $\text{C}_{31}\text{H}_{52}\text{B}_{18}\text{CoF}_{0.75}\text{NaO}_{6.25}$; $M_r = 822.49$, monoclinic, $C2/c$, $a = 29.9709(4)$, $b = 19.7021(3)$, $c = 19.2700(3)$ Å, $\beta = 129.505(1)^\circ$, $V = 8779.5(2)$ Å³, $Z = 8$, $\rho_{\text{calcd}} = 1.245$ g mol⁻¹, $\mu = 0.445$ mm⁻¹ (no correction), $\theta_{\text{max}} = 28.3^\circ$, 66 129 data collected, 10 811 unique ($R_{\text{int}} = 0.087$), 546 parameters, no restraints, $R_1 = 0.0558$ (7236 data $I > 2\sigma(I)$), $wR_2 = 0.1333$ (all data), $S = 1.040$. The structure was solved by Patterson map and partial structure expansion (SHELXS-97) and refined with a full-matrix least-squares refinement on F^2 (SHELXL-97). Occupancy of the $\text{CF}_3\text{CH}_2\text{OH}$ guest molecule was estimated at 0.25, a more accurate analysis through microanalysis was not possible because the crystals rapidly lost solvent when removed from the mother liquor. The carbon atom positions within the $[\text{Co}(\text{C}_2\text{B}_9\text{H}_{11})_2]^-$ ions were assigned by an analysis of anisotropic displacement factors, however, without a neutron diffraction study they should be regarded as tentative. The $\text{CF}_3\text{CH}_2\text{OH}$ guest was refined isotropically otherwise all non-hydrogen atoms were refined anisotropically and all C-H and B-H hydrogen atoms included at calculated positions with a riding refinement. Crystallo-

graphic data (excluding structure factors) for the structure reported in this paper have been deposited with the Cambridge Crystallographic Data Centre as supplementary publication no. CCDC-144465. Copies of the data can be obtained free of charge on application to CCDC, 12 Union Road, Cambridge CB21EZ, UK (fax: (+44)1223-336-033; e-mail: deposit@ccdc.cam.ac.uk).

- [17] A. F. Wells, *Structural Inorganic Chemistry*, 4th ed., Clarendon Press, Oxford, **1975**.
- [18] S. R. Batten, R. Robson, *Angew. Chem.* **1998**, *110*, 1558; *Angew. Chem. Int. Ed.* **1998**, *37*, 1461.
- [19] a) A. Zalkin, T. E. Hopkins, D. H. Templeton, *Inorg. Chem.* **1967**, *6*, 1911; b) L. Borodinsky, E. Sinn, R. N. Grimes, *Inorg. Chem.* **1982**, *21*, 1686.
- [20] for recent examples, see a) C. A. Schalley, *Int. J. Mass Spectrom.* **2000**, *194*, 11; b) C. A. Schalley, R. K. Castellano, M. S. Brody, D. M. Rudkevich, G. Siuzdak, J. Rebek, Jr., *J. Am. Chem. Soc.* **1999**, *121*, 4586; c) P. A. Brady, J. K. M. Sanders, *New J. Chem.* **1998**, 411; d) D. L. Caulder, R. E. Powers, T. N. Parac, K. N. Raymond, *Angew. Chem.* **1998**, *110*, 1940; *Angew. Chem. Int. Ed.* **1998**, *37*, 1840; e) K. A. Jolliffe, M. C. Calama, R. Fokkens, N. M. M. Nibbering, P. Timmerman, D. N. Reinhoudt, *Angew. Chem.* **1998**, *110*, 1294; *Angew. Chem. Int. Ed.* **1998**, *37*, 1247; f) E. Ishow, A. Gourdon, J.-P. Launay, *Chem. Commun.* **1998**, 1909; g) M. Przybylski, M. O. Glocker, *Angew. Chem.* **1996**, *108*, 878; *Angew. Chem. Int. Ed. Engl.* **1996**, *35*, 806.
- [21] see, for example a) S. J. Cantrill, M. C. T. Fyfe, A. M. Heiss, J. F. Stoddart, A. J. P. White, D. J. Williams, *Chem. Commun.* **1999**, 1251; b) P. R. Ashton, M. C. T. Fyfe, M.-V. Martínez-Díaz, S. Menzer, C. Schiavo, J. F. Stoddart, A. J. P. White, D. J. Williams, *Chem. Eur. J.* **1998**, *4*, 1523; c) J. S. Fleming, K. L. V. Mann, C.-A. Carraz, E. Psillakis, J. C. Jeffery, J. A. McCleverty, M. D. Ward, *Angew. Chem.* **1998**, *110*, 1315; *Angew. Chem. Int. Ed.* **1998**, *37*, 1279; d) R. Bakhtiar, H. Chen, S. Ogo, R. H. Fish, *Chem. Commun.* **1997**, 2135; e) B. Hasenknoph, J.-M. Lehn, N. Boumediene, E. Leize, A. Van Dorsselaer, *Angew. Chem.* **1998**, *110*, 3458; *Angew. Chem. Int. Ed.* **1998**, *37*, 3265.

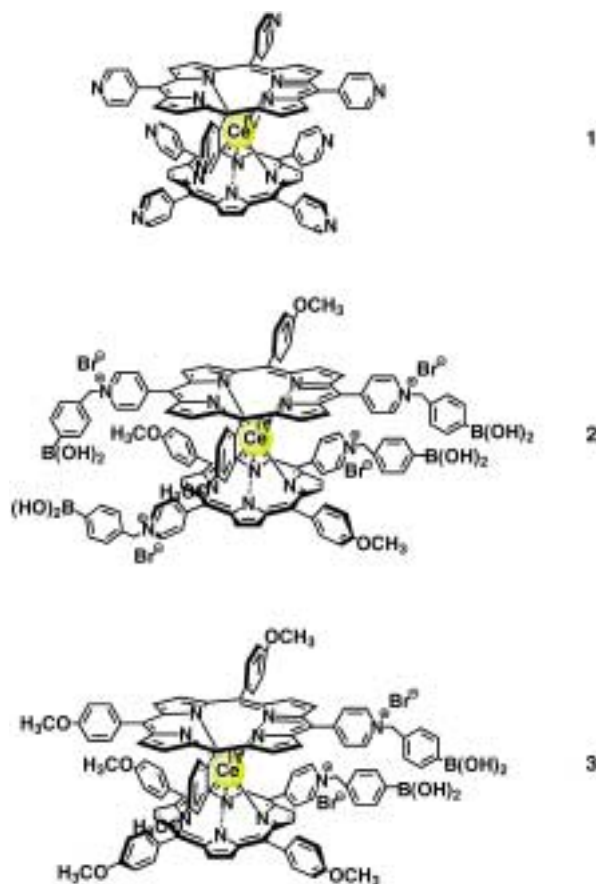
Novel Oligosaccharide Binding to the Cerium(IV) Bis(porphyrinate) Double Decker: Effective Amplification of a Binding Signal through Positive Homotropic Allostery

Atsushi Sugasaki, Masato Ikeda, Masayuki Takeuchi, and Seiji Shinkai*

The biomimetic design of allosteric systems is of great significance because they are readily applicable to the efficient regulation of drug release, catalytic reactions, and information transduction.^[1] In particular, the positive homotropic allosteric system is useful as a unique tool for amplifying and transforming weak chemical or physical signals into other forms and for constructing novel sensory systems with higher affinity and/or greater selectivity towards

analytes. Although there are several examples of artificial heterotropic allostery in which a substrate and an effector communicate (either positively or negatively) with each other,^[1, 2] successful examples of artificial positive homotropic allostery, however, are very limited.^[3–6]

Undoubtedly, the allosteric binding of saccharides that can take place even in aqueous media is essential as a research target in molecular recognition and influential in many related systems: for example, many water-soluble drugs such as vancomycin, ramoplanin, and teicoplanin have a saccharide moiety and the allosteric capture and release of these drugs are of great significance. Previously, we demonstrated that the cerium(IV) bis[tetrakis(4-pyridyl)porphyrinate] double decker (**1**) binds certain dicarboxylic acids in a positive allosteric



manner (Hill coefficient 4.0) through hydrogen-bonding interactions to form only the 1:4 complex.^[5] In this system the binding of the first dicarboxylic acid to a pair of pyridyl groups through the hydrogen-bonding interaction, although very weak, can suppress the rotation of the two porphyrin planes; as a result, the subsequent binding of the three dicarboxylic acids to the three pairs of aligned pyridyl groups can occur cooperatively. This characteristic double-decker architecture can be used as a scaffold in a system showing positive allosteric binding^[6a–c] of saccharides by introducing boronic acid groups, which are known to act as excellent saccharide receptors in aqueous media.^[7, 8] By taking these factors into consideration, we designed compound **2** which bears two pairs

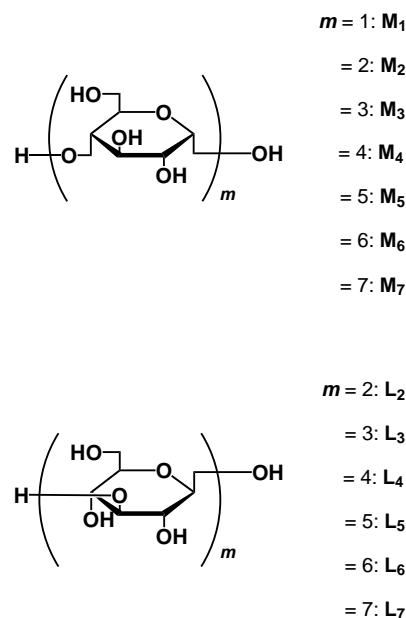
[*] Prof. S. Shinkai, A. Sugasaki, M. Ikeda, Dr. M. Takeuchi
Department of Chemistry & Biochemistry
Graduate School of Engineering
Kyushu University, Fukuoka 812-8581 (Japan)
Fax: (+81)92-642-3611
E-mail: seijitcm@mbx.nc.kyushu-u.ac.jp

Supporting information for this article is available on the WWW under <http://www.wiley-vch.de/home/angewandte/> or from the author.

of boronic acid groups. Very surprisingly, we found that **2** can bind oligosaccharides (maltooligosaccharides and laminarioligosaccharides) with the large association constants ($K = 10^5 - 10^6 \text{ M}^{-2}$) typical for a positive homotropic allostereism in aqueous media to form 1:2 **2**:saccharide complexes. This positive homotropic allostereism is indispensable for the highly efficient binding of oligosaccharides which had until now not been achieved,^[9] and the amplification of the chemical or physical signal by host–guest interactions.

Compound **2**^[6c, 10] has previously been synthesized by treatment of bis[5,15-bis(4-methoxyphenyl)-10,20-di(4-pyridyl)porphyrinato]cerium(IV) with 2-(4-bromomethylphenyl)-1,3-dioxaborane in DMF. 1,3-Propanediol-protected **2** was characterized by IR and ¹H NMR spectroscopy and elemental analysis. This product was used for further spectral measurements without deprotection of the propanediol groups.^[11]

We evaluated the binding affinities of **2** toward oligosaccharides such as maltooligosaccharides (**M_m**: α-1,4-linked oligomers of D-glucose) and laminarioligosaccharides (**L_m**: β-1,3-linked oligomers of D-glucose). The addition of oligosaccharide to a solution of **2** ($1.00 \times 10^{-5} \text{ M}$) in a mixture of 50 mM carbonate buffer and MeOH (1:1, v:v) at pH 10.5, resulted in



virtually no change in the absorption spectra ($\lambda_{\text{max}} = 409 \text{ nm}$) of **2**. In contrast, exciton-coupling-type CD bands, which have a spectral pattern inherent to each oligosaccharide, were clearly observed upon addition of oligosaccharides (Figure 1). The saturated CD_{max} values at 405 nm plotted against *m* reveal that a) in the **M_m** series, maltose (**M₂**) and maltopentaose (**M₅**) give a particularly strong peak at 405 nm whereas D-glucose (**M₁**) and the other maltooligosaccharides give a relatively weak peak at 405 nm, b) the complexes with **M₁** and **M₅–M₇** give a positive peak at 405 nm whereas **M₂–M₄** all give a negative peak at 405 nm, and c) in the **L_m** series, **L₁–L₇** all give a positive peak at 405 nm (see Supporting Information). The results suggest that 1) **M₂** and **M₅** can form stable complexes with **2**, 2) two porphyrin planes are oriented into opposite

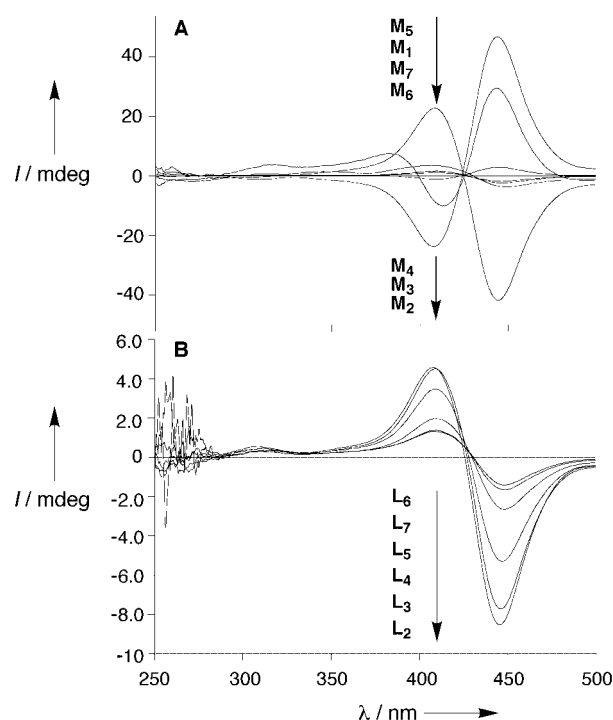


Figure 1. CD spectra of **2** ($1.00 \times 10^{-5} \text{ M}$) in the presence of **M_m** (A) or **L_m** (B); *I* denotes the CD intensity; [**M_m**] = $3.00 \times 10^{-3} \text{ M}$; [**L_m**] = $2.00 \times 10^{-2} \text{ M}$ at 25 °C in a mixture of 50 mM carbonate buffer and MeOH (1:1, v:v) at pH 10.5.

directions in the **L_m**, **M₁**, and **M₅–M₇** complexes than in the other complexes. In addition, *n*-dodecyl-β-maltoside and *p*-nitrophenyl-α-maltopentaoside, which have only one available diol moiety for binding to boronic acid, do not yield any perceptible CD bands.^[12] These findings consistently support the view that two diol moieties in the two terminal glucose units of the saccharides are bound to two boronic acid groups in **2** and bridge two porphyrin planes. This bridging effect suppresses the rotation of the two porphyrin planes and is regarded as the origin of the strong CD band.^[2i]

Detailed spectral studies were carried out on the **M_m** series to obtain further insights into the binding mode. The CD spectra measured as a function of the saccharide concentration provided several isosbestic points, which indicated that the reaction consists of only two species in a single equilibrium (see Supporting Information). Figure 2 shows plots of the CD intensity at 405 nm versus [**M_m**]. Very interestingly, compound **2** shows a sigmoidal binding isotherm for **M₁–M₅**, which indicates that the binding of the guests to **2** is “cooperative”. This cooperative guest-binding profile can be analyzed with the Hill equation: $\log(y/(1-y)) = n \log[\text{guest}] + \log K$, where *K* and *n* are the association constant and Hill coefficient, respectively, and $y = K/([\text{guest}]^{-n} + K)$.^[13] We obtained *K* (M^{-2}) and *n* for maltooligosaccharides from the intercept and the slope of the linear plots, respectively (Table 1 and see Supporting Information). It is seen from Table 1 that a) the association constants for oligosaccharides are greater than that of the monosaccharide **M₁** (D-glucose), b) Hill coefficients *n* of 1.6–2.0 for **M_m** are consistent with a highly cooperative binding mechanism, and c) the saturated CD_{max} values increase with an increase in the *K* values. These

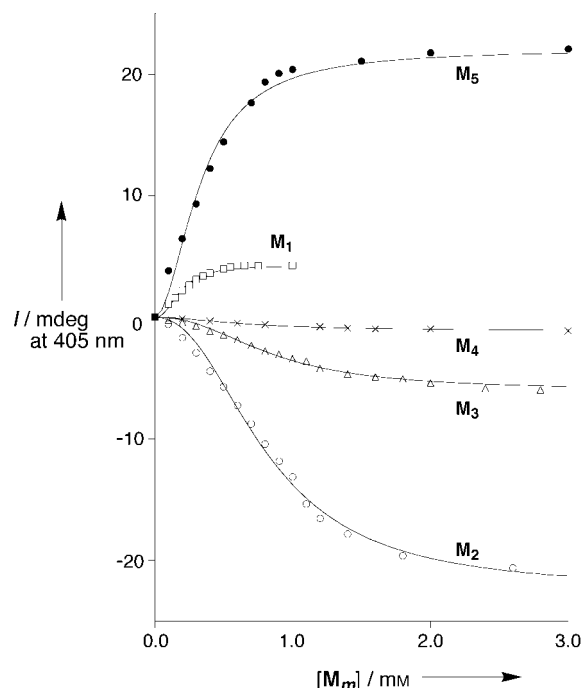


Figure 2. Plots of the CD intensity of **2** (1.00×10^{-5} M) at 405 nm versus $[M_m]$. The solid lines represent the theoretical curves for the formation of the $[2 \cdot (M_m)_2]$ complex. The measurement conditions are given in the caption to Figure 1.

Table 1. Binding parameters obtained from the Hill plot and the Job plot.

M_m	$K [M^{-2}]$	n	Stoichiometry
M_1 (D-glucose)	9.6×10^5	1.6	1:2
M_2	2.9×10^6	2.0	1:2
M_3	1.5×10^6	2.0	1:2
M_4	5.7×10^5	1.8	1:2
M_5	2.9×10^6	1.8	1:2
M_6	—[a]	—[a]	—[a]
M_7	—[a]	—[a]	—[a]

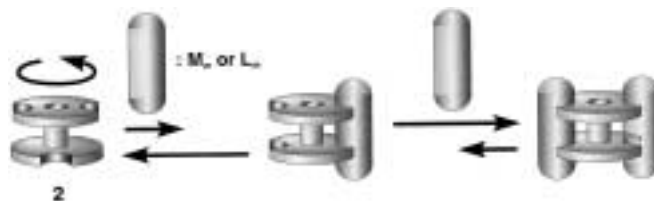
[a] The CD spectral changes were too small to determine K and n .

results mean that the saccharide giving the largest CD intensity has the largest affinity to **2**.

The stoichiometry of the CD-active complexes was further confirmed by a Job plot.^[14] A plot of the CD intensity at 405 nm against $[2]/([2] + [M_m])$ has a maximum at 0.33 (see Supporting Information). This observation supports the view that the complex consists of one host (**2**) and two guests (M_m). In the Scatchard plots in which Hill coefficients (n) are correlated with the maximum values (y_{\max}) by $n = 1/(1 - y_{\max})$,^[15] the positive and negative allosterisms are expressed by the upward and downward curvatures, respectively. Scatchard plots of the M_m series result in the upward curvature, which supports the positive allosterism (see Supporting Information).

The findings consistently indicate that the binding of the first saccharide guest suppressed the rotational freedom of the two porphyrin planes and that the remote second binding site is aligned for the highly cooperative binding of the second guest. As a result, two pairs of boronic acid groups in **2** can cooperatively bind the oligosaccharide guest molecules with high association constants and give CD-active species. The

binding of the saccharide is conceptually illustrated in Scheme 1. The most stable conformations of the $[2 \cdot (M_2)_2]$ and $[2 \cdot (M_5)_2]$ complexes as calculated by computational



Scheme 1.

methods (Discover 3/Insight II 98.0) are shown in Figure 3.^[16] It is seen from Figure 3 that the $[2 \cdot (M_2)_2]$ complex has a right-handed helical twist whereas the $[2 \cdot (M_5)_2]$ complex with the longer oligosaccharide chain length, has a left-handed helical twist. This result undoubtedly shows that the difference in the length of the oligosaccharide is the origin of the opposite CD signs for the two complexes.

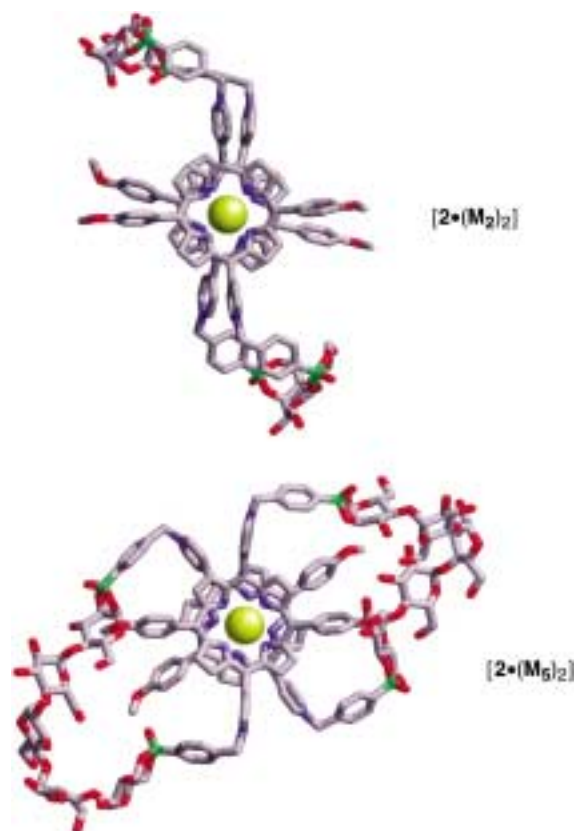


Figure 3. Energy-minimized structures of the $[2 \cdot (M_2)_2]$ (top) and $[2 \cdot (M_5)_2]$ (bottom) complexes.

To clarify the role of the positive homotropic allosterism in **2** we studied the binding of maltose (M_2) to **3**, which has only one pair of boronic acids. Analysis of the titration curve for **3** with M_2 gave an association constant of $154 M^{-1}$ for the formation of the 1:1 complex $[3 \cdot M_2]$ (see Supporting Information). The saturated CD_{\max} value at 446 nm of the $[3 \cdot M_2]$ complex was 18 times smaller than that of the

$[2 \cdot (M_2)_2]$ complex. These results clearly support the view that positive homotropic allostereism is indispensable for the highly efficient binding of the oligosaccharide and the amplification of the CD signal from the $[2 \cdot (M_m)_2]$ complex.

Finally, we measured the ^1H NMR chemical shifts of $[2 \cdot (M_2)_2]$ in CD_3OD to obtain structural information (see Supporting Information). The *endo-m*-proton of the 4-methoxyphenyl groups and *endo-m*-proton of the pyridinium groups shifted to higher magnetic fields than in **2**. This observation indicates that the peripheral *meso*-aryl moieties overlap each other in the $[2 \cdot (M_2)_2]$ complex as illustrated in Figure 3.^[17]

There are many biologically important oligosaccharides to which this receptor may be applied. As a preliminary experiment, we have found that Sialyl Lewis^x, which is a trigger saccharide for cell adhesion, can be also bound to **2** as a result of positive homotropic allostereism ($K = 3.2 \times 10^6 \text{ M}^{-2}$, $n = 2.0$; see Supporting Information).

In conclusion, we have demonstrated that **2** is a scaffold for the effective binding of oligosaccharides in aqueous media, and shows positive, homotropic allostereism with Hill coefficients of 1.6–2.0. Significant binding of oligosaccharides is nearly impossible without the aid of positive homotropic allostereism. With this saccharide receptor it becomes possible for the first time to catch and release various saccharide-containing materials in an allosteric manner. We believe that this system should be widely applicable, for example, to sensing biologically important oligosaccharides, the regulation of the function of saccharide-containing drugs and glycolipid membranes, and the monitoring of enzyme activities.

Experimental Section

CD Spectroscopy: A stock solution of oligosaccharide prepared in water was added to a solution of **2** ($1.00 \times 10^{-5} \text{ M}$) in a mixture of carbonate buffer and MeOH (1:1, 50 mM) at pH 10.5. The CD spectra were recorded from 250 to 500 nm with a JASCO J-720WI spectrophotometer at 15 different concentrations of each guest molecule at 25 °C.

Absorption, CD, and ^1H NMR spectra were measured with a Shimadzu UV 2500-PC, JASCO J-720WI, and Bruker DMX 600 spectrometers, respectively.

Received: June 26, 2000 [Z15329]

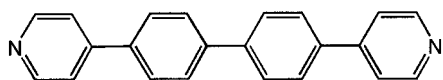
- [1] a) T. Nabeshima, *Cood. Chem. Rev.* **1996**, *148*, 151; b) G. H. Czerlinski, *Biophys. Chem.* **1989**, *34*, 169; c) J. Rebek, Jr., *Acc. Chem. Res.* **1984**, *17*, 258; d) I. Tabushi, *Pure Appl. Chem.* **1988**, *60*, 581.
- [2] a) T. G. Traylor, M. J. Mitchell, J. P. Ciconene, S. Nelson, *J. Am. Chem. Soc.* **1982**, *104*, 4986; b) J. Rebek, Jr., T. Costello, L. Marshall, R. Wattle, R. C. Gadwood, K. Onan, *J. Am. Chem. Soc.* **1985**, *107*, 7481; c) I. Tabushi, S. Kugimiya, M. G. Kinnaird, T. Sasaki, *J. Am. Chem. Soc.* **1985**, *107*, 4129; I. Tabushi, S. Kugimiya, *J. Am. Chem. Soc.* **1986**, *108*, 6926; d) P. D. Beer, A. S. Rothin, *J. Chem. Soc. Chem. Commun.* **1988**, 52; e) R. C. Petter, J. S. Salek, C. T. Sikorski, G. Kumaravel, F.-T. Lin, *J. Am. Chem. Soc.* **1990**, *112*, 3860; f) H.-J. Schneider, D. Ruf, *Angew. Chem.* **1990**, *102*, 1192; *Angew. Chem. Int. Ed. Engl.* **1990**, *29*, 1159; g) R. P. Sijbesma, R. J. Nolte, *J. Am. Chem. Soc.* **1991**, *113*, 6695; h) Y. Kobuke, Y. Satoh, *J. Am. Chem. Soc.* **1992**, *114*, 789; i) M. Takeuchi, T. Imada, S. Shinkai, *J. Am. Chem. Soc.* **1996**, *118*, 10658.
- [3] a) S. Blanc, P. Yakirevitch, E. Leize, M. Meyer, J. Libman, A. Van Dorsselaer, A. M. Albrecht-Gray, A. Shanzer, *J. Am. Chem. Soc.* **1997**, *119*, 4934; b) K. Kobayashi, Y. Asakawa, Y. Kato, Y. Aoyama, *J. Am. Chem. Soc.* **1992**, *114*, 10307; c) F. Ebmeyer, J. Rebek, Jr., *Angew. Chem.* **1990**, *102*, 1191; *Angew. Chem. Int. Ed. Engl.* **1990**, *29*, 1148.
- [4] T. E. Glass, *J. Am. Chem. Soc.* **2000**, *122*, 4522.
- [5] a) M. Takeuchi, T. Imada, S. Shinkai, *Angew. Chem.* **1998**, *110*, 2242; *Angew. Chem. Int. Ed.* **1998**, *37*, 2096; b) M. Ikeda, M. Takeuchi, A. Sugasaki, A. Robertson, T. Imada, S. Shinkai, *Supramol. Chem.*, in press. It is known that the rate of rotation of the porphyrin ring in the cerium(IV) bis(porphyrinate) double decker is comparable with or slower than the NMR time scale. However, the allosteric behavior is basically observable for the present “static” equilibrium system as long as the porphyrin rings are able to rotate, see M. Takeuchi, T. Imada, M. Ikeda, S. Shinkai, *Tetrahedron Lett.* **1998**, *39*, 7897; K. Tashiro, K. Konishi, T. Aida, *Angew. Chem.* **1997**, *109*, 882; *Angew. Chem. Int. Ed. Engl.* **1997**, *36*, 856.
- [6] a) A. Sugasaki, M. Ikeda, M. Takeuchi, A. Robertson, S. Shinkai, *J. Chem. Soc. Perkin Trans 1* **1999**, 3259; b) M. Ikeda, T. Tanida, M. Takeuchi, S. Shinkai, *Org. Lett.* **2000**, *2*, 1803; c) A. Sugasaki, M. Ikeda, K. Koumoto, M. Takeuchi, S. Shinkai, *Tetrahedron* **2000**, *56*, 4717; d) M. Ikeda, S. Shinkai, A. Osuka, *Chem. Commun.* **2000**, 1047.
- [7] For recent comprehensive reviews, see a) T. D. James, K. R. A. Sandanayake, S. Shinkai, *Supramol. Chem.* **1995**, *6*, 141; b) T. D. James, P. Linnane, S. Shinkai, *Chem. Commun.* **1996**, 281; c) T. D. James, K. R. A. Sandanayake, S. Shinkai, *Angew. Chem.* **1996**, *108*, 2038; *Angew. Chem. Int. Ed. Engl.* **1996**, *35*, 1910, and references therein.
- [8] J. C. Norrild, H. Eggert, *J. Am. Chem. Soc.* **1995**, *117*, 1479.
- [9] Several disaccharide binding receptors have been reported but the molecular design has not been extended in depth to the binding of oligosaccharides, see reference [7].
- [10] J. W. Buchler, M. Nawra, *Inorg. Chem.* **1994**, *33*, 2830, and references therein.
- [11] ^1H NMR spectral measurements have established that the protecting groups are readily eliminated in aqueous media. In fact, the addition of 1,3-propanediol ($\sim 10^{-4} \text{ M}$) scarcely affected the plots of the CD intensity versus [saccharide] (Figure 2). Hence, this compound can be used without needing any special treatment to deprotect it.
- [12] $[n\text{-dodecyl-}\beta\text{-maltoside}] = [p\text{-nitrophenyl-}\alpha\text{-maltopentaoside}] = 2.00 \times 10^{-2} \text{ M}$.
- [13] K. A. Connors, *Binding Constants*, Wiley, New York, **1987**.
- [14] A. Job, *Ann. Chim.* **1928**, *9*, 113.
- [15] B. Permuter-Hyman, *Acc. Chem. Res.* **1986**, *19*, 90.
- [16] Conformations with low potential energies located during a 100 ps MD simulation at 300 K were selected. The system was minimized using the conjugate gradient and Newton–Raphson methods until convergence was attained for a gradient of $0.01 \text{ kcal mol}^{-1} \text{ \AA}^{-1}$. The force field used in this study was ESFF.
- [17] An alternative possible explanation is that the complex-induced chemical shifts arise from the twist of the *meso*-aryl groups to an outer side (against the Ce^{IV} ion).

- [1] a) T. Nabeshima, *Cood. Chem. Rev.* **1996**, *148*, 151; b) G. H. Czerlinski, *Biophys. Chem.* **1989**, *34*, 169; c) J. Rebek, Jr., *Acc. Chem. Res.* **1984**, *17*, 258; d) I. Tabushi, *Pure Appl. Chem.* **1988**, *60*, 581.
- [2] a) T. G. Traylor, M. J. Mitchell, J. P. Ciconene, S. Nelson, *J. Am. Chem. Soc.* **1982**, *104*, 4986; b) J. Rebek, Jr., T. Costello, L. Marshall, R. Wattle, R. C. Gadwood, K. Onan, *J. Am. Chem. Soc.* **1985**, *107*, 7481; c) I. Tabushi, S. Kugimiya, M. G. Kinnaird, T. Sasaki, *J. Am. Chem. Soc.* **1985**, *107*, 4129; I. Tabushi, S. Kugimiya, *J. Am. Chem. Soc.* **1986**, *108*, 6926; d) P. D. Beer, A. S. Rothin, *J. Chem. Soc. Chem. Commun.* **1988**, 52; e) R. C. Petter, J. S. Salek, C. T. Sikorski, G. Kumaravel, F.-T. Lin, *J. Am. Chem. Soc.* **1990**, *112*, 3860; f) H.-J. Schneider, D. Ruf, *Angew. Chem.* **1990**, *102*, 1192; *Angew. Chem. Int. Ed. Engl.* **1990**, *29*, 1159; g) R. P. Sijbesma, R. J. Nolte, *J. Am. Chem. Soc.* **1991**, *113*, 6695; h) Y. Kobuke, Y. Satoh, *J. Am. Chem. Soc.* **1992**, *114*, 789; i) M. Takeuchi, T. Imada, S. Shinkai, *J. Am. Chem. Soc.* **1996**, *118*, 10658.
- [3] a) S. Blanc, P. Yakirevitch, E. Leize, M. Meyer, J. Libman, A. Van Dorsselaer, A. M. Albrecht-Gray, A. Shanzer, *J. Am. Chem. Soc.*

Open Square-Grid Coordination Polymers of the Dimensions $20 \times 20 \text{ \AA}$: Remarkably Stable and Crystalline Solids Even after Guest Removal**

Kumar Biradha, Yoshito Hongo, and Makoto Fujita*

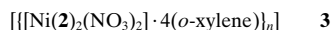
The synthesis of coordination polymers using 4,4'-bipyridine (4,4'-bpy, **1**) and transition metal ions has thus far produced several novel networks with a high degree of porosity.^[1,2] Among all the networks, square-grid polymers are of particular importance due to their predictable pore sizes and selective inclusion of guest molecules. The first square-grid complex $[\{\text{Zn}(\mathbf{1})_2(\text{PF}_6)_2\}_n]$ was reported by Robson et al. in 1990; it is interpenetrated and thus nonporous.^[3] In 1994 we prepared the noninterpenetrated square-grid complex $[\{\{\text{Cd}(\mathbf{1})_2(\text{H}_2\text{O})_2\}(\text{NO}_3)_2\}_n]$.^[4] Despite the simple structural design, however, **1** has not been replaced by analogous structural units that are significantly longer. A few structures with a longer ligand Py-X-Py (Py = 4-pyridyl, X = CH_2CH_2 , $\text{CH}=\text{CH}$, or $\text{C}\equiv\text{C}$) have been reported; however, these ligands are longer than **1** by only 2 Å.^[5] Herein we show that noninterpenetrated square-grid networks can be obtained with the larger ligand **2**, which is 8.5 Å longer than **1**.



2

Treatment of **2** with $\text{Ni}(\text{NO}_3)_2$ (1:2 ratio) gives an extraordinarily big square-grid polymer with dimensions of about $20 \times 20 \text{ \AA}$. Surprisingly, the grid framework thus obtained is so stable that the crystals *after removal of the guest* were analyzed by single-crystal X-ray diffraction.^[6]

The single crystals of the complex of **2** were grown by layering a solution of $\text{Ni}(\text{NO}_3)_2$ in MeOH over a solution of **2** in *o*-xylene and isolated in 80 % yield. The crystal structure of this complex revealed the formation of a noninterpenetrated square-grid polymer **3**. The Ni atom resides in a distorted



octahedral environment with four pyridyl groups at the equatorial positions and two nitrate groups at the apical positions. The guest molecules occupy 58 % of the crystal volume. The square cavity has dimensions of $19.9 \times 20.0 \text{ \AA}$. Each cavity is occupied by six *o*-xylene molecules: two of them that are parallel to the grid plane lie within the cavity, while the other four that are perpendicular to the grid plane exist partly outside the cavity (Figure 1 a).

[*] Prof. Dr. M. Fujita, Dr. K. Biradha, Y. Hongo
Department of Applied Chemistry, Graduate School of Engineering
Nagoya University and CREST, Japan Science and Technology
Corporation (JST)
Chikusa-ku, Nagoya 464-8603 (Japan)
Fax: (+81)52-789-3199
E-mail: mfujita@apchem.nagoya-u.ac.jp

[**] K.B. thanks Japan Society for the Promotion of Science (JSPS) for postdoctoral fellowship.

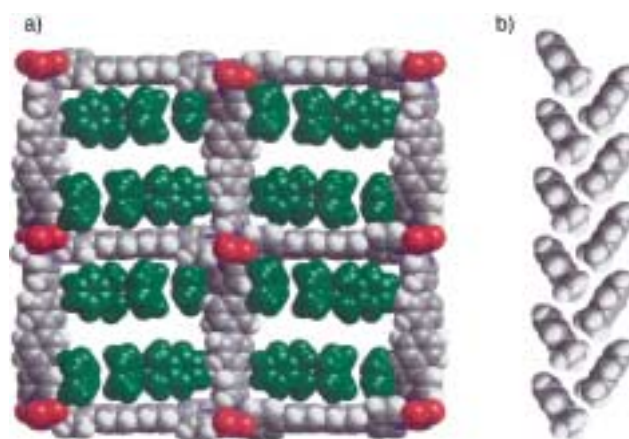


Figure 1. Square-grid network (a) and one-dimensional column of *o*-xylene in complex **3** (b).

Besides the formation of big square cavities, another important feature of this structure is the packing of the grids that creates big rectangular channels (ca. $10 \times 20 \text{ \AA}$; Figure 2), which are occupied by a one-dimensional (1D) column of guest molecules (Figure 1 b). The two-dimensional (2D) layers in **3**, unlike those in metal-(4,4'-bipyridine) square

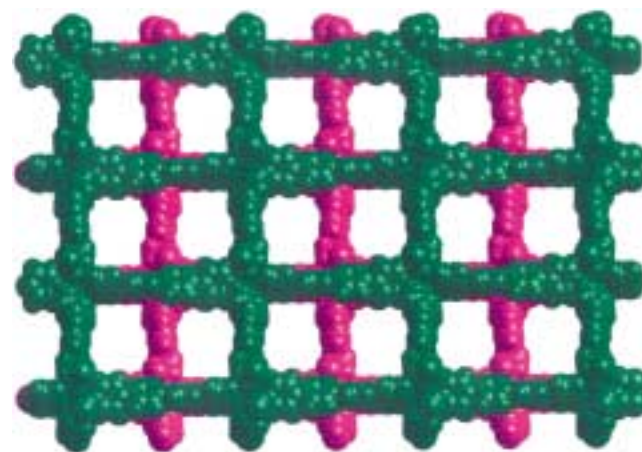


Figure 2. The packing of the grids showing the formation of rectangular channels (ca. $20 \times 10 \text{ \AA}$) in **3**. Alternate layers are represented by identical colors.

grids that have a large interlayer separation (6–8 Å), display a very short interlayer separation of 4.5 Å, and the ligands of adjacent grids interact with each other through edge-to-face aromatic interactions. For instance, the distance between the plane of the C_6 ring of the ligand of one layer and the edge of the C_5N ring of the ligand of a neighboring layer is as short as 3.4 Å. The guest molecules interact with each other through $\text{Me} \cdots \text{Me}$ ($\text{C} \cdots \text{C}$ 3.940 Å) interactions and $\text{Me} \cdots \pi$ interactions (distance from C of Me group to plane of C_6 ring of neighboring molecule: 3.631 Å). The aromatic moieties of the guest also interact with the host through edge-to-face aromatic interactions.

The existence of uniform channels and the short interlayer separation prompted us to study the stability of the structure after removal of guest molecules. Thermogravimetric analysis

of **3** indicated that the framework maintains its integrity up to 300 °C, while the guest is liberated between 70 and 150 °C. Most surprisingly, the stability of the framework *after guest removal* was confirmed by single-crystal and powder X-ray diffraction studies. The single-crystal X-ray analysis of a sample of **3** from which the guest had been removed, which was prepared by heating the crystals at 150 °C under reduced pressure (100 mmHg) for 3 h, resulted in a sample with very similar cell constants and the same space group as **3**.^[7] The crystal structure of the guest-free grid complex was essentially identical with that of **3** except for the loss of the guest. The powder X-ray diffraction spectra of the sample without the guest was also identical with that of **3** except for the absence of two peaks at 2θ values of 10.9° and 22.37° (Figure 3).

The ligand **2** formed a similar noninterpenetrated square-grid complex **4** when benzene was used in place of *o*-xylene.



Although the packing of the grids is identical in both complexes, the square grids in **4** are much less symmetrical than those in **3**.^[8] Interestingly, the 2D layer in complex **4** was built up of two crystallographically independent squares **A** and **B**. The square cavities of **A** are occupied by five benzene molecules, while those of **B** are occupied by five benzene and two MeOH molecules (Figure 4a).^[9] Both **A** and **B** are slightly distorted and have dimensions of about 19.85×19.87 Å and 19.94×19.87 Å, respectively. The big rectangular channels are occupied by a 1D column of guest molecules (Figure 4b). The 1D column is formed by the combination of benzene and MeOH molecules through the layers of the grid sheets. All the benzene molecules in the column interact with each other and also interact with the walls of the channels through edge-to-face aromatic interactions (3.5–4.5 Å). The length of the repeating unit of the 1D column is equivalent to that of the long axis of the unit cell (49.646 Å). The lower symmetry of

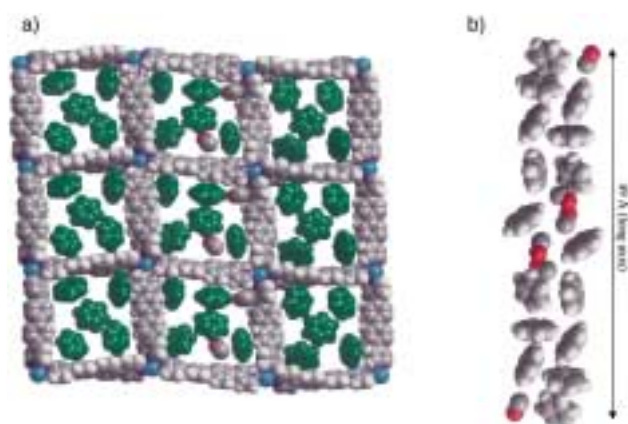


Figure 4. a) The square grid network in complex **4**. The square cavities in consecutive columns display different arrangements of guest molecules. There are two types of distorted squares: One includes five benzene molecules (square **A**), while the other includes five benzene molecules and two methanol molecules (square **B**). b) Representation of the one-dimensional column of benzene and MeOH molecules.

the grid compared to **3** can be attributed to the lower symmetry in guest–guest interactions: benzene, being a symmetrical molecule, shows less selectivity in guest–guest interactions and forms a more unsymmetrical 1D column with inclusion of MeOH, whereas *o*-xylene, being an unsymmetrical molecule, shows more selectivity in guest–guest interactions and forms a very symmetrical 1D column (Figure 2b). The asymmetric unit of the crystal contains three MeOH molecules: two of them interact with each other ($\text{O} \cdots \text{O}$ 2.68 Å), while the other interacts with nitrate ion ($\text{O} \cdots \text{O}$ 2.77 Å).

Experimental Section

2: 2-(4-Pyridyl)-4,4,5,5-tetramethyl-1,3-dioxaborolone: 4-Bromopyridine (38 mmol, 6 g) in dry Et_2O (300 mL) was slowly added to *n*BuLi (1.5 M in hexane, 46 mmol, 30 mL) at -78°C . After 30 min $\text{B}(\text{O}i\text{Pr})_3$ (46 mmol, 10.6 g) was added and the temperature was raised slowly over two hours to room temperature. Pinacol was added to this solution, and then after 10 min AcOH was added. The resulting crude ester was crystallized from cyclohexane (yield: 5.0 g, 64%). A mixture of the above ester (0.8 g, 3.9 mmol), 4,4'-dibromobiphenyl (0.4 g, 1.3 mmol), K_3PO_4 (1.7 g, 7.8 mmol), and $[\text{Pd}(\text{PPh}_3)_4]$ (0.15 g, 0.13 mmol) in dioxane (40 mL) was refluxed under an Ar atmosphere for three days. After removal of the dioxane, the resulting mass was worked-up with CHCl_3 – H_2O and crystallized from CHCl_3 –methanol (yield: 0.27 g, 67%).

3: The single crystals of **3** were prepared by layering a solution of $\text{Ni}(\text{NO}_3)_2 \cdot 6\text{H}_2\text{O}$ (6 mg) in MeOH (5 mL) onto a solution of **2** (12.6 mg) in *o*-xylene (15 mL). After the solution had been allowed to stand for seven days, the crystals formed were isolated in 80% yield by filtration. Monoclinic, $C2/c$, $a = 27.187(3)$, $b = 19.963(2)$, $c = 12.685(4)$ Å, $\beta = 106.923(2)^\circ$, $V = 6585.9(12)$ Å³, $Z = 4$, $\rho_{\text{calcd}} = 1.235$ g cm^{−3}, 5932 unique reflections out of 7770 with $I > 2\sigma(I)$, $1.29 < \theta < 27.98^\circ$, final R factors $R_1 = 0.067$, $wR_2 = 0.2054$. Elemental analysis: calcd: C

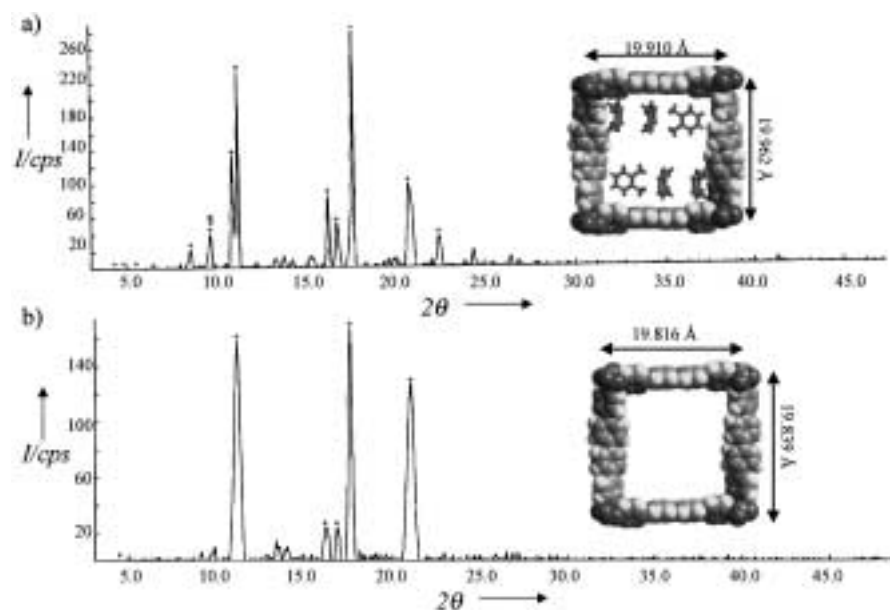


Figure 3. Powder X-ray diffraction spectra and single-crystal X-ray structures for **3** with guest (a) and without guest (b). The grids from the corresponding single-crystal X-ray diffraction analysis are also shown. The differences in grid dimensions are minimal after guest removal.

74.57, H 5.93, N 6.87; found: C 73.58, H 5.69, N 7.06. These results indicate the loss of 0.5 *o*-xylene per metal: calculated values for $[\text{Ni}(\text{2})_2(\text{NO}_3)_2 \cdot 3.5(\text{o-xylene})]$: C 73.85, H 5.77, N 7.18.

Crystal data for **4**: The crystals were prepared in the same way as above but benzene was used instead of *o*-xylene. However few crystals were obtained with some powdery material (in 15% yield). Monoclinic, $P2_1/n$, $a = 13.570(2)$, $b = 19.874(3)$, $c = 49.646(7)$ Å, $\beta = 96.815(3)^\circ$, $V = 13294(3)$ Å³, $Z = 8$, $\rho_{\text{calcd}} = 1.237 \text{ g cm}^{-3}$, 23360 unique reflections out of 68329 with $I > 2\sigma(I)$, $1.32 < \theta < 25^\circ$, final R factors $R_1 = 0.1561$; $wR_2 = 0.3795$. The data for both **3** and **4** were measured on a Siemens SMART/CCD diffractometer ($\text{Mo K}\alpha$ radiation $\lambda = 0.71073$ Å) at 193 K. An empirical absorption correction was applied by using the SADABS program. Non-hydrogen atoms were refined anisotropically and hydrogen atoms were fixed at calculated positions and refined using a riding model. Crystallographic data (excluding structure factors) for the structures reported in this paper have been deposited with the Cambridge Crystallographic Data Centre as supplementary publication nos. CCDC-141218 (**3**), and CCDC-141217 (**4**). Copies of the data can be obtained free of charge on application to CCDC, 12 Union Road, Cambridge CB21EZ, UK (fax: (+44) 1223-336-033; e-mail: deposit@ccdc.cam.ac.uk).

Received: March 6, 2000

Revised: August 14, 2000 [Z14813]

- [1] Only eight polymeric structures were published before 1990 for reactions of **1** with transition metals, while from 1990 to 1998 about 70 polymeric structures were published. Statistics were taken from Cambridge Structural Database: Version 5.17 (197481 Structures, April, 1999 release): F. H. Allen, O. Kennard, *Chemical Des. Autom. News* **1993**, 8, 31.
- [2] Recent references on coordination polymers with **1** and transition metals: a) K. Biradha, C. Seward, M. J. Zaworotko, *Angew. Chem.* **1999**, 111, 584; *Angew. Chem. Int. Ed.* **1999**, 38, 492; b) K. Biradha, K. V. Domasevitch, B. Moulton, C. Seward, M. J. Zaworotko, *Chem. Commun.* **1999**, 1327; c) H. Gudbjartson, K. Biradha, K. M. Poirier, M. J. Zaworotko, *J. Am. Chem. Soc.* **1999**, 121, 2599; d) O. Wang, X. Wu, W. Zhang, T. Sheng, P. Lin, J. Li, *Inorg. Chem.* **1999**, 38, 2223; e) M.-L. Tong, B.-H. Ye, J.-W. Cai, X.-M. Chen, S. W. Ng, *Inorg. Chem.* **1998**, 37, 2645; f) L. R. MacGillivray, R. H. Groeneman, J. L. Atwood, *J. Am. Chem. Soc.* **1998**, 120, 2676; g) C.-Y. Su, B.-S. Kang, H.-Q. Liu, Q.-G. Wang, T. C. W. Mak, *Chem. Commun.* **1998**, 1551; h) D. Hargman, R. P. Hammond, R. Haushalter, J. Zubietta, *Chem. Mater.* **1998**, 10, 2091; i) J. Lu, C. Yu, T. Niu, T. Paliwala, G. Crisci, F. Somosa, A. J. Jacobson, *Inorg. Chem.* **1998**, 37, 4637; j) M. Kondo, T. Yoshitomi, K. Seki, H. Matsuzaka, S. Kitagawa, *Angew. Chem.* **1997**, 109, 1844; *Angew. Chem. Int. Ed. Engl.* **1997**, 36, 1725; k) O. M. Yaghi, H. Li, T. L. Groy, *Inorg. Chem.* **1997**, 36, 4292.
- [3] R. W. Gable, B. F. Hoskins, R. Robson, *J. Chem. Soc. Chem. Commun.* **1990**, 1677.
- [4] M. Fujita, Y. J. Kwon, S. Washizu, K. Ogura, *J. Am. Chem. Soc.* **1994**, 116, 1151.
- [5] a) M. Fujita, Y.-J. Kwon, M. Miyazawa, K. Ogura, *Chem. Commun.* **1994**, 1977; b) J. A. Real, E. Andrés, M. C. Muñoz, M. Julve, T. Granier, A. Bousseksou, F. Varret, *Science* **1995**, 268, 265; c) T. L. Hennigar, D. C. MacQuarrie, P. Losier, R. D. Rogers, M. J. Zaworotko, *Angew. Chem.* **1997**, 109, 1044; *Angew. Chem. Int. Ed. Engl.* **1997**, 36, 972; d) Y.-B. Dong, R. C. Layland, M. D. Smith, N. G. Pschirer, U. H. F. Bunz, H.-C. zur Loye, *Inorg. Chem.* **1999**, 38, 3056.
- [6] a) Quite recently a three-dimensional coordination polymer was characterized following removal of guest molecule by single-crystal X-ray diffraction: H. Li, M. Eddaoudi, M. O'Keeffe, O. M. Yaghi, *Nature* **1999**, 402, 276; b) for zeolite analogues see: D. W. Breck in *Zeolite Molecular Sieves*, Wiley, New York, **1974**.
- [7] Crystal data for **3** after removal of guest molecule: monoclinic, $C2/c$, $a = 26.234(5)$, $b = 19.839(3)$, $c = 13.236(2)$ Å, $\beta = 109.514(4)^\circ$, $V = 6493(2)$ Å³, $Z = 4$, $\rho_{\text{calcd}} = 0.818 \text{ g cm}^{-3}$, 2541 unique reflections out of 7718 with $I > 2\sigma(I)$, final R factors $R_1 = 0.1943$, $wR_2 = 0.4494$, largest difference peak and hole 2.126 and -0.764 e Å^{-3} . Elemental analysis suggests that the crystal absorbed water from atmosphere: calcd for $[\text{Ni}(\text{2})_2(\text{NO}_3)_2] \cdot 1.5(\text{H}_2\text{O})$: C 63.94, H 4.27, N 10.17; found: C 64.17, H 3.90, N 9.96.

- [8] The data collection for **4** at room temperature resulted in different cell constants and space group as well as disordered ligands and nitrates. All the benzene molecules were located with relatively high thermal motions in comparison to those found for the low-temperature structure, but the MeOH molecules could not be located at this temperature. Monoclinic, Cm , $a = 12.731(7)$, $b = 19.912(9)$, $c = 13.902(7)$ Å, $\beta = 96.544(1)^\circ$, $V = 3501(3)$ Å³, $Z = 2$, $\rho_{\text{calcd}} = 1.129 \text{ g cm}^{-3}$, 3846 unique reflections out of 5211 with $I > 2\sigma(I)$, final R factors $R_1 = 0.0887$; $wR_2 = 0.2166$.
- [9] One of the MeOH molecules which is close to the corner of a square interacts with benzene through a C-H...O hydrogen bond (H...O, 2.522 Å; C...O 3.441 Å; C-H...O 169.8°). The square **B** (diagonal–diagonal distances: 26.067 and 30.099 Å) is more distorted than square **A** (diagonal–diagonal distances: 27.911 and 28.270 Å).

The Electrical Properties of Gold Nanoparticle Assemblies Linked by DNA**

So-Jung Park, Anne A. Lazarides, Chad A. Mirkin,* Paul W. Brazis, Carl R. Kannewurf,* and Robert L. Letsinger

Electron transport through DNA has been one of the most intensely debated subjects in chemistry over the past five years.^[1] Some scientists claim that DNA is able to transport electrons efficiently, while others believe it to be an insulator. In a seemingly disparate field of study, a great deal of effort has been devoted to examining the electrical properties of nanoparticle-based materials.^[2–5] Indeed, many research groups have explored ways to assemble nanoparticles into two- and three-dimensional networks and have investigated the electronic properties of such structures. However, virtually nothing is known about the electrical properties of nanoparticle-based materials linked with DNA.

- [*] Prof. C. A. Mirkin, S.-J. Park, Dr. A. A. Lazarides
Department of Chemistry and Center for Nanofabrication and Molecular Self Assembly
Northwestern University
2145 Sheridan Road, Evanston, IL 60208-3113 (USA)
Fax: (+1) 847-467-5123
E-mail: camirkin@chem.nwu.edu
- Prof. C. R. Kannewurf, P. W. Brazis
Department of Electrical and Computer Engineering
Northwestern University
2145 Sheridan Road, Evanston, IL 60208-3118 (USA)
Fax: (+1) 847-491-4455
E-mail: c.kannewurf@ece.nwu.edu
- Prof. R. L. Letsinger
Department of Chemistry, Northwestern University
2145 Sheridan Road, Evanston, IL 60208-3113 (USA)

[**] C.A.M. acknowledges the NSF, the ARO, and NIH for support of this research. R.L.L. acknowledges the NIH. C.R.K. and C.A.M. acknowledge support by the NSF through the Northwestern University MRC (Grant DMR 96-32472). The DND-CAT Synchrotron Research Center is supported by E.I. DuPont de Nemours & Co., The Dow Chemical Company, the U.S. National Science Foundation (Grant DMR-9304725), and the State of Illinois through the Department of Commerce and the Board of Higher Education (Grant IBHE HECA NWU 96). Use of the Advanced Photon Source was supported by the U.S. Department of Energy, Basic Energy Sciences, Office of Energy Research (Contract No. W-31-102-Eng-38).

In 1996 we reported a new approach to materials synthesis which utilized inorganic nanoparticles as building blocks and chemically modified synthetic duplex DNA as the molecules interconnecting the particles.^[6] Since that report, a great deal of effort has been devoted to studying the optical properties of such structures. Importantly, an understanding of those optical properties has led to the development of a series of highly sensitive and selective colorimetric detection methods for DNA.^[7] Moreover, this programmed assembly methodology, by virtue of the oligonucleotide sequence, has provided an excellent opportunity to tailor the architectural parameters of nanoparticle-based structures assembled with DNA.^[8] Such parameters include nanoparticle size and composition, particle periodicity, and interparticle distance. One of the intriguing outstanding issues in this new field pertains to the use of such materials in electronic applications. At the heart of this issue is the following question: can nanoparticles assembled by DNA still conduct electricity or will the DNA interconnects, which are heavily loaded on each particle,^[9] act as insulating shells? Herein, we examine the electrical conductivities of these materials as a function of temperature, oligonucleotide length, and relative humidity. The DNA-linked nanoparticle structures have been characterized by field-emission scanning electron microscopy (FE-SEM), synchrotron small angle X-ray scattering (SAXS) experiments, thermal denaturation profiles, and UV/Vis spectroscopy.

In a typical experiment citrate-stabilized 13-nm gold nanoparticles were modified with 3' and 5' alkanethiol-capped 12-mer oligonucleotides (**1** and **2**, respectively). DNA strands with lengths of 24, 48, and 72 bases (**3**–**5**) were used as linkers (Scheme 1). Nanoparticle assemblies were constructed by adding **1**-modified gold nanoparticles (652 μ L, 9.7 nm) and **2**-modified gold nanoparticles (652 μ L, 9.7 nm) to linker DNA **3**, **4**, or **5** (30 μ L, 10 μ M). After full precipitation, the aggregates were washed with 0.3 M $\text{CH}_3\text{COONH}_4$ solution to remove excess linker DNA and NaCl. Lyophilization (10^{-3} – 10^{-2} torr) of the aggregate to dryness resulted in pellets and removal of the volatile salt, $\text{CH}_3\text{COONH}_4$. Unfunctionalized, citrate-

stabilized particles, prepared by the Frens method,^[10] were dried as a film and used for comparison purposes.

The resulting dried aggregates had a color resembling tarnished brass and were very brittle. FE-SEM images demonstrate that oligonucleotide-modified nanoparticles remain intact upon drying (Figure 1 a) while citrate-stabilized

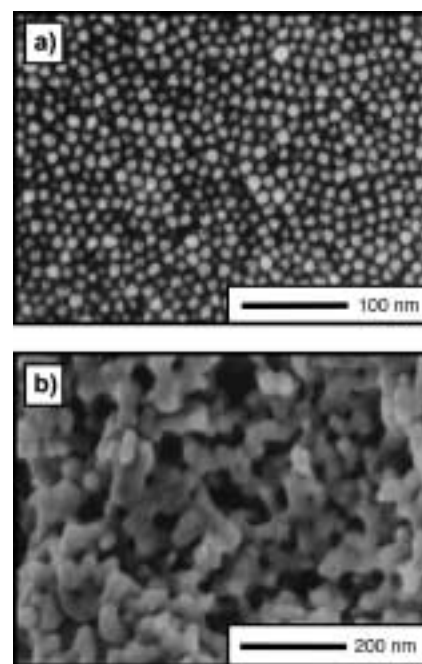
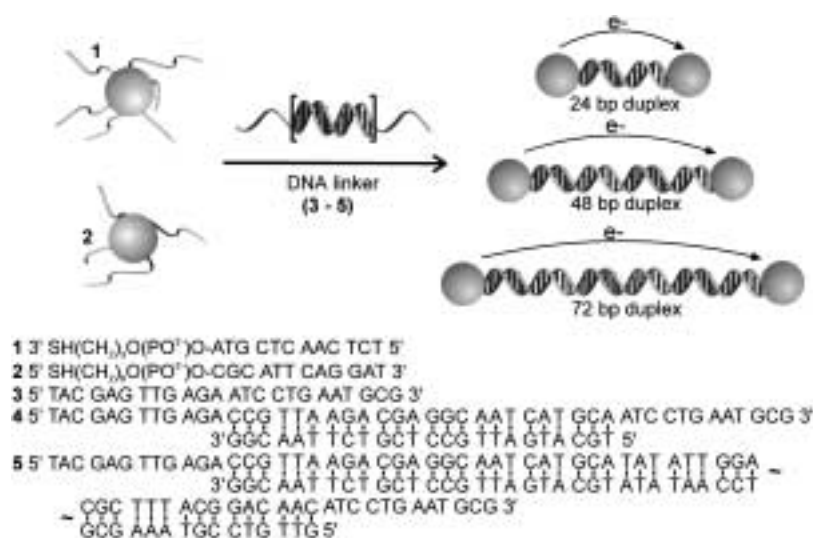


Figure 1. Scanning electron microscopy images of: a) DNA-modified gold nanoparticles, and b) citrate-stabilized gold nanoparticles dried on indium tin oxide.

nanoparticles fuse to one another (Figure 1 b). Significantly, the dried DNA-linked aggregates could be redispersed in 0.3 M PBS buffer (1 mL) and exhibit excellent melting properties; heating such a dispersion to 60 °C results in dehybridization of the DNA interconnects to yield a red solution of dispersed nanoparticles (Figure 2). This observation com-



Scheme 1. Schematic representation showing Au nanoparticle assembly with different length DNA linkers.

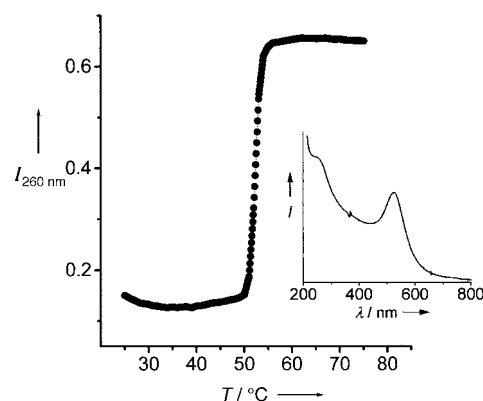


Figure 2. Thermal dissociation curve for dried aggregates linked by **3** and redispersed in 0.3 M PBS buffer. The extinction at 260 nm was obtained at 1° intervals as the temperature was increased from 25 to 75 °C with a holding time of 1 min per degree. Inset: UV/Vis spectrum of the redispersed dried aggregates measured at 62 °C.

bined with the FE-SEM data conclusively demonstrates that DNA-modified gold nanoparticles are not irreversibly aggregated upon drying.

The electrical conductivities of the three samples (dried aggregates linked by **3**, **4**, and **5**) were measured by the four-probe method. Surprisingly, the conductivities of the aggregates formed from all three linkers ranged from 10^{-5} to 10^{-4} S cm $^{-1}$ at room temperature, and they showed similar temperature-dependent behavior (Figure 3). The conductivities of the DNA-linked aggregates showed Arrhenius behavior up to about 190 K, which is characteristic of a nonmetallic

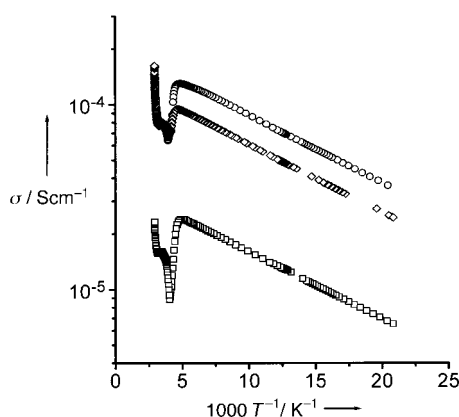


Figure 3. Plot of the conductivity as a function of temperature for gold nanoparticle assemblies linked by 24-, 48-, and 72-mer DNA (**3–5**). \circ = 24-mer-linked; \diamond = 48-mer-linked; \square = 72-mer-linked assemblies.

material. Activation energies of charge transport (E_a) can be obtained from a plot of $\ln \sigma$ versus $1/T$ using Equation (1), where σ is the electrical conductivity, σ_0 is a constant, k is the Boltzmann constant, and T is the temperature.

$$\sigma = \sigma_0 \exp[-E_a/(kT)] \quad (1)$$

The average activation energies calculated from three measurements are 7.4 ± 0.2 meV, 7.5 ± 0.3 meV, and 7.6 ± 0.4 meV for the 24-, 48-, and 72-mer-linked aggregates, respectively. Conductivity data obtained between 50 and 150 K were used for these calculations.

Since the electrical properties of these types of materials should depend on the distance between the particles, synchrotron SAXS experiments were used to determine interparticle distances of the dispersed and dried aggregates. Scattered intensities (I) as a function of $s = 2 \sin(\theta)/\lambda$, where 2θ is the scattering angle and λ is the wavelength of the incident radiation, are presented in Figure 4. The s values of the first peaks indicate characteristic distances of $d = 1/s$. The position of the first peaks drastically changes from s values of 0.063 nm^{-1} , 0.048 nm^{-1} , and 0.037 nm^{-1} for the 24-, 48-, and 72-mer-linked aggregates, respectively, to an s value of 0.087 nm^{-1} for all three aggregate structures upon drying. This result indicates that upon drying the aggregates, the interparticle distances decrease significantly to the point where the particles are almost touching. In other words, dried aggregates have interparticle distances that are virtually

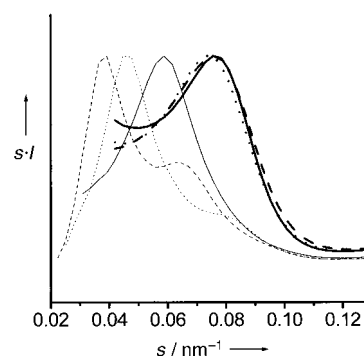


Figure 4. SAXS of gold nanoparticle aggregates linked by **3–5**. Thin lines: SAXS of aggregates in 0.3 M PBS buffer. The first peak of the DNA-linked aggregates shifts to smaller values of s as the length of the oligonucleotide linker is increased. Thick lines: SAXS of dried aggregates. The first peaks shift to larger values of s upon drying and are not dependent on the length of the DNA linker. —: 24-mer-linked; \cdots : 48-mer-linked; ---: 72-mer-linked aggregates.

independent of the length of the linker, while wet aggregates exhibit interparticle distances that are directly dependent on the length of the linker. This finding explains why similar activation energies are observed for the three different linker systems in the conductivity experiments involving dried pellets. Moreover, it also explains why relatively high conductivities are observed, regardless of how one views the electronic properties of DNA. Indeed, these results suggest that conductivity in these systems is a result of capacitive charging, much like aggregates formed from particles with short alkanethiol ligands.^[2,3] Finally, unlike the DNA-linked materials, the dried film of citrate-stabilized gold nanoparticles showed metallic behavior. This is consistent with the SEM data, which show that particles within such films fuse together (Figure 1 b).

Above 190 K the conductivities of the DNA-linked samples showed an anomalous dipping behavior. For all the samples the conductivity starts to decrease abruptly at approximately 190 K and continues to decrease until approximately 250 K, at which point it increases again (Figure 3). To investigate this unusual behavior in detail the electrical conductivity was measured as the sample was cooled and warmed repeatedly (Figure 5). Interestingly, the dip in conductivity only occurred in the direction of increasing temperature. Since DNA is hydrophilic and water could potentially affect the electrical properties of the hybrid structures, the effect of relative humidity on the conductivity of the gold aggregates was examined. The resistance increased by a factor of ten when the humidity was increased from 1 to 100%. It should be noted that the characteristic dip was very weak when the sample was kept in a vacuum (10^{-6} Torr) for 48 h prior to the conductivity measurement. From these observations we conclude that the unusual dip and then rise in conductivity above 190 K is associated with water melting and the hygroscopic nature of the DNA, which temporarily increases the interparticle distance (until evaporation takes place). SAXS measurements on a dried aggregate that was wetted with 0.3 M PBS buffer showed an approximately twofold increase in interparticle distance, which is consistent with the above hypothesis.

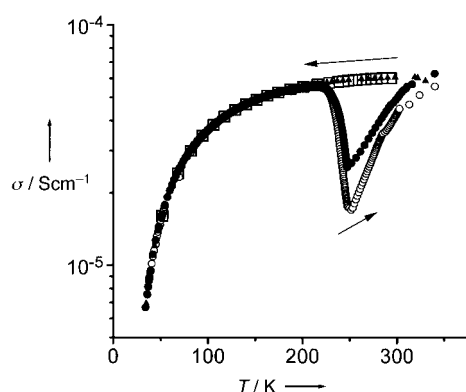


Figure 5. Electrical conductivity of gold nanoparticle assemblies linked by **3** as a function of temperature cycling. The first data collection was cycled between 294 and 4.2 K, and the second data collection was cycled between 340 and 4.2 K. The arrows indicate the direction of the temperature change. □ = first cooling; ○ = first warming; ▲ = second cooling; ● = second warming.

These studies are important for the following reasons. First, they show that one can use the molecular recognition properties of DNA to assemble nanoparticle-based materials without passivating them or destroying their discrete structural or electrical properties. If these DNA-functionalized particles are to be used to study electrical transport in three-dimensional macroscopic assemblies or even lithographically patterned structures,^[11] it is imperative that their electrical transport properties be delineated. Second, it shows that the conductivities of the dried assemblies formed with linkers of 24 to 72 base pairs are virtually independent of the length of the linker. This observation is likely a result of the removal of water and the use of a volatile salt in these experiments; indeed, the free volume created by the removal of solvent and salt allows the DNA to be compressed on the surface and the close approach of the particles within the aggregates. Third, the aggregates with the DNA-protected nanoparticles behave as semiconductors, while films formed from citrate-stabilized particles exhibit irreversible particle fusion and metallic behavior. Finally, these results point toward the intriguing possibility of using these materials in DNA diagnostic applications where sequence-specific binding events between nanoparticles functionalized with oligonucleotides and target DNA effect the closing of a circuit and a dramatic increase in conductivity (that is, from an insulator to a semiconductor).

Experimental Section

Preparation of DNA-modified gold nanoparticles and linker DNA strands: Synthesis of alkanethiol-capped oligonucleotides (**1** and **2**) and immobilization of them on gold nanoparticles are described elsewhere.^[7b] Linker DNA strands (**3–5**) were synthesized and purified by literature methods.^[7b, 8c] The DNA-modified nanoparticles and DNA linkers were stored in 0.3 M NaCl, 10 mM phosphate (pH 7) buffer (referred to as 0.3 M PBS) prior to use.

Conductivity measurements: The electrical conductivity was measured by the four-probe technique.^[12] Electrical contacts consisted of fine gold wires (25 and 60 μm diameter) attached to pellets with gold paste (Ted Pella). The sample dimensions were 0.185 × 0.370 × 0.056 mm, 0.352 × 0.722 × 0.017 mm, and 0.278 × 0.463 × 0.035 mm for the 24-mer-linked, 48-mer-linked, and 72-mer-linked aggregates, respectively. Samples were cooled in a moderate vacuum (10^{−3} to 10^{−2} torr), and conductivity was measured as

the temperature was increased under a dry, low pressure of helium gas unless otherwise specified. The sample chamber was insulated from light in order to eliminate possible optoelectronic effects. Excitation currents were kept at or below 100 nA, and the voltage across the entire sample was limited to a maximum of 20 V.

SAXS measurements: The SAXS experiments^[13] were performed at the Dupont-Northwestern-Dow Collaborative Access Team (DND-CAT) Sector 5 of the Advanced Photon Source, Argonne National Laboratory with X-rays of wavelength 1.54 Å. Aqueous samples were placed in 0.8-mm flat cells between Kapton windows. Dried samples were adhered to Kapton tape and supported by flat cells. Two sets of slits were used to define and collimate the X-ray beam and a pinhole was used to remove parasitic scattering. Samples were irradiated with a 0.3 × 0.3 mm beam and scattered radiation was detected with a CCD area detector. The 2D-scattering data were azimuthally averaged, and the radial coordinate of the resulting 1D profiles of scattered intensity was transformed into a scattering angle. All data were corrected for background scattering and sample absorption. Buffer scattering was subtracted from the solution samples.

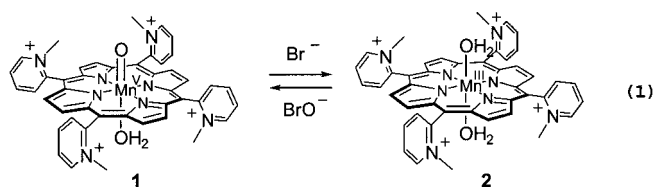
Received: July 10, 2000 [Z15427]

- [1] a) S. O. Kelley, J. K. Barton, *Science* **1999**, *283*, 375–381; b) N. J. Turro, J. K. Barton, *J. Biol. Inorg. Chem.* **1998**, *3*, 201–209; c) F. D. Lewis, R. L. Letsinger, *J. Biol. Inorg. Chem.* **1998**, *3*, 215–221; d) M. Ratner, *Nature* **1999**, *397*, 480–481; e) Y. Okahata, T. Kabayashi, K. Tanaka, M. Shimomura, *J. Am. Chem. Soc.* **1998**, *120*, 6165–6166.
- [2] R. H. Terrill, T. A. Postlethwaite, C.-H. Chen, C.-D. Poon, A. Terzis, A. Chen, J. E. Hutchison, M. R. Clark, G. Wignall, J. D. Londono, R. Superfine, M. Falvo, C. S. Johnson, Jr., E. T. Samulski, R. W. Murray, *J. Am. Chem. Soc.* **1995**, *117*, 12537–12548.
- [3] a) M. Brust, D. Bethell, D. J. Schiffrin, C. Kiely, *Adv. Mater.* **1996**, *7*, 795–797; b) D. Bethell, M. Brust, D. J. Schiffrin, C. Kiely, *J. Electroanal. Chem.* **1996**, *409*, 137–143; c) M. Brust, D. Bethell, C. Kiely, D. J. Schiffrin, *Langmuir* **1998**, *14*, 5425–5429.
- [4] M. D. Musick, C. D. Keating, M. H. Keefe, M. J. Natan, *Chem. Mater.* **1997**, *9*, 1499–1501.
- [5] C. P. Collier, R. J. Saykally, J. J. Shiang, S. E. Henrichs, J. R. Heath, *Science* **1997**, *277*, 1978–1981.
- [6] C. A. Mirkin, R. L. Letsinger, R. C. Mucic, J. J. Storhoff, *Nature* **1996**, *382*, 607–609.
- [7] a) R. Elghanian, J. J. Storhoff, R. C. Mucic, R. L. Letsinger, C. A. Mirkin, *Science* **1997**, *277*, 1078–1081; b) J. J. Storhoff, R. Elghanian, R. C. Mucic, C. A. Mirkin, R. L. Letsinger, *J. Am. Chem. Soc.* **1998**, *120*, 1959–1964; c) T. A. Taton, C. A. Mirkin, R. L. Letsinger, *Science* **2000**, *289*, 1757–1760.
- [8] a) R. C. Mucic, J. J. Storhoff, C. A. Mirkin, R. L. Letsinger, *J. Am. Chem. Soc.* **1998**, *120*, 12674–12675; b) G. P. Mitchell, C. A. Mirkin, R. L. Letsinger, *J. Am. Chem. Soc.* **1999**, *121*, 8122–8123; c) J. J. Storhoff, A. A. Lazarides, C. A. Mirkin, R. L. Letsinger, R. C. Mucic, G. C. Schatz, *J. Am. Chem. Soc.* **2000**, *122*, 4640–4650.
- [9] R. C. Mucic, PhD thesis, Northwestern University, IL, USA, **1999**.
- [10] G. Frens, *Nat. Phys. Sci.* **1973**, *241*, 20–22.
- [11] R. D. Piner, J. Zhu, F. Xu, S. Hong, C. A. Mirkin, *Science* **1999**, *283*, 661–663; S. Hong, J. Zhu, C. A. Mirkin, *Science* **1999**, *286*, 523–525; S. Hong, C. A. Mirkin, *Science* **2000**, *288*, 1808–1811.
- [12] J. W. Lyding, H. O. Morey, T. J. Marks, C. R. K. Kannerwurf, *IEEE Trans. Instrum. Meas.* **1998**, *37*, 76–80.
- [13] A. Guinier, G. Fournet, *Small angle scattering of X-rays*, Wiley, New York, **1955**.

Rapid, Reversible Oxygen Atom Transfer between an Oxomanganese(V) Porphyrin and Bromide: A Haloperoxidase Mimic with Enzymatic Rates**

Ning Jin, James L. Bourassa, Steven C. Tizio, and John T. Groves*

Synthetic manganese porphyrins and related systems have been used extensively in chemical modeling of biological monooxygenation reactions catalyzed by heme proteins.^[1] They are also versatile catalysts for the oxygenation of alkanes, alkenes, and nitrogen- and sulfur-containing compounds using oxygen donors such as iodosylbenzene, sodium hypochlorite, alkyl, aryl, and hydrogen peroxide, amine *N*-oxides, and molecular oxygen.^[2] Only recently has the key oxomanganese(V) intermediate been well characterized.^[3] Here we report that the oxomanganese(V)-5,10,15,20-tetrakis(*N*-methyl-2-pyridyl)porphyrin (**1**) can efficiently transfer its oxo ligand to bromide ion, and that this oxo transfer is rapid and reversible. [Eq. (1)]



The forward reaction mimics the halide oxidation reaction catalyzed by haloperoxidases,^[4] while the reverse reaction is the catalyst activation step in substrate oxygenation by manganese porphyrins. This well-behaved equilibrium allows the assignment of a free energy change for the reaction depicted in Equation (1).

OxoMn^VTM-2-PyP (**1**) has unusual stability in aqueous solution compared to other oxoMn^V porphyrin intermediates.^[3b] It can be generated by the stoichiometric reaction of Mn^{III}TM-2-PyP^[5] (**2**) with oxidants such as HSO₅⁻, *m*-CPBA (chloroperoxybenzoic acid), and OCl⁻. We have found that hypobromite, a weaker oxidant,^[6] is also able to generate **1** smoothly. Figure 1a shows the reaction between 5 μM **2** and 50 μM HOBr/OBr⁻^[7] at pH 8.5 monitored by stopped-flow spectrophotometry.^[3a,b] Clear isosbestic points were observed at 392, 444, and 558 nm. Remarkably, the identical isosbestic behavior was also found for the reverse reaction, oxoMn^V+Br⁻ at higher bromide concentration. Typical spectral changes observed for the oxo-transfer reaction from

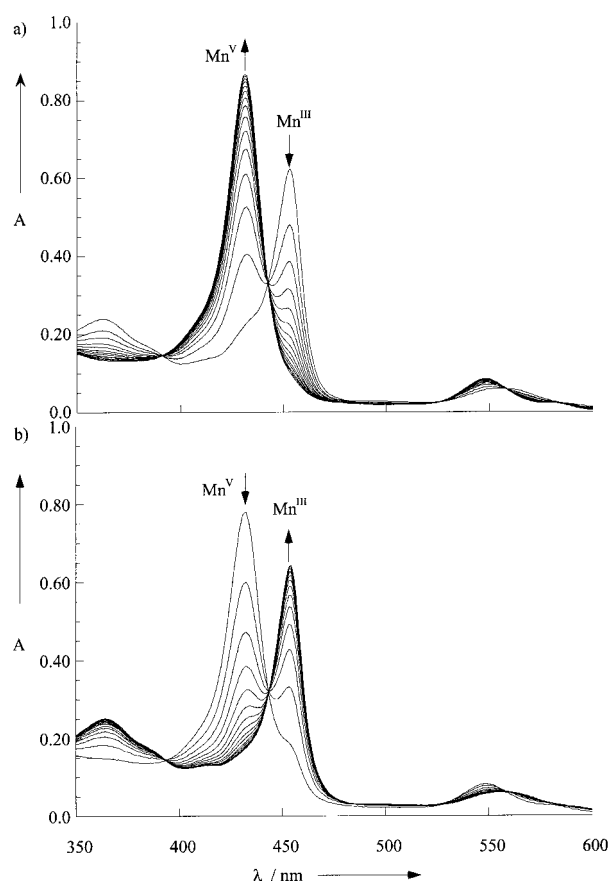


Figure 1. Time-resolved UV/Vis spectra for the reaction of a) 5 μM Mn^{III}TM-2-PyP (**2**) and 50 μM HOBr/OBr⁻; b) 5 μM Mn^VTM-2-PyP (**1**) and 50 mM Br⁻ at pH 8.5 (10 mM Na₂B₄O₇/H₂SO₄ buffer). For both reactions there were 60 scans in 120 ms. Every fourth scan is shown.

1 to Br⁻ are shown in Figure 1b. The generation of hypobromite, which is favored by excess bromide and lower pH, was confirmed by observing the diagnostic bromination reaction of phenol red.^[8]

The pH dependence of the rate of oxo transfer to bromide was examined between pH 5.2 and 9.0 (I = 0.25 M NaClO₄). The reaction was found to be first-order in both oxoMn^V and Br⁻, and independent of the buffer concentration. Kinetic profiles were obtained by monitoring oxoMn^V (**1**) at 433 nm. Pseudo-first-order fitting of the kinetic data to a single exponential was carried out with at least six concentrations of Br⁻ at each pH value. The apparent second-order rate constant *k*_{app} was calculated from the slope of the linear plot of *k*_{obs} versus *C*_{Br⁻}. Our results show that **1** was nearly as effective an oxygen donor to Br⁻ (3.8 × 10⁵ M⁻¹ s⁻¹ at pH 7.0) as myeloperoxidase compound I (1.1 × 10⁶ M⁻¹ s⁻¹ at pH 7.0),^[9] and much more effective than vanadium bromoperoxidase (estimated to be 2.78 × 10³ M⁻¹ s⁻¹ at pH 7.9 and 1.75 × 10⁵ M⁻¹ s⁻¹ at pH 4.0) and related functional mimics.^[10] The pH dependence of *k*_{app}, spanning five orders of magnitude, is plotted in Figure 2.

To explain this profound pH dependence, *two* proton transfers must be involved. We propose that **1** exists as a dioxo species [O=Mn^V=O] at high pH,^[11] which is inert to the nucleophilic attack of Br⁻. Two fast acid–base equilibria

[*] Prof. J. T. Groves, N. Jin, Dr. J. L. Bourassa, S. C. Tizio
Department of Chemistry
Princeton University
Princeton, NJ 08544 (USA)
Fax: (+1) 609-258-0348
E-mail: jtgroves@princeton.edu

[**] This work is supported by the National Science Foundation (CHE-9814301), the National Institutes of Health (GM36928), and Bayer AG.

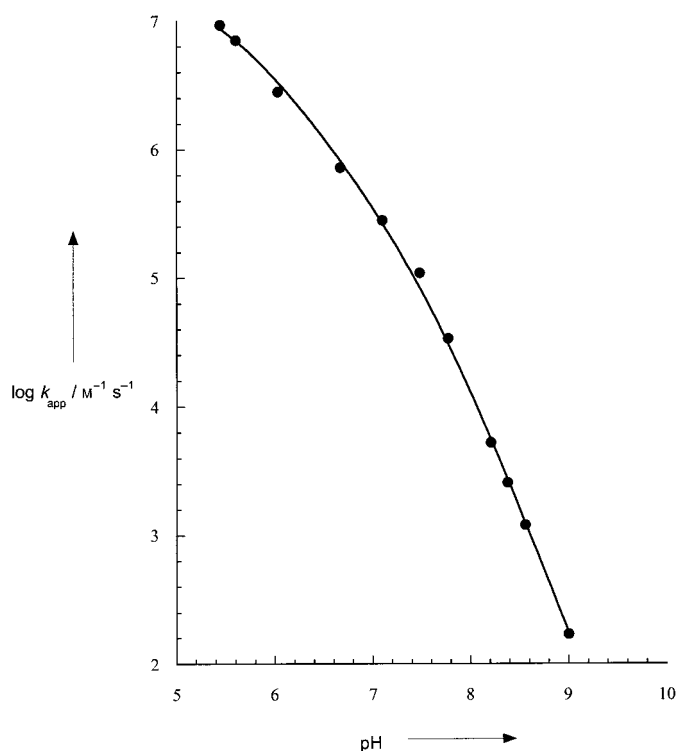


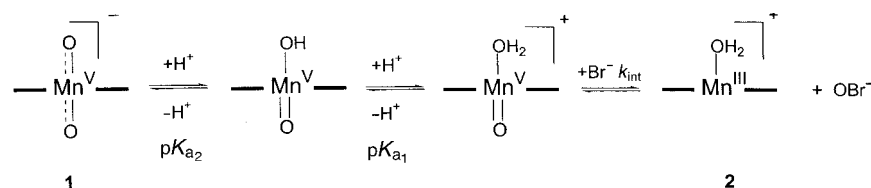
Figure 2. Plot of the second-order rate constants ($\log k_{\text{app}}$) as a function of pH for the reaction between oxoMn^VTM-2-PyP (**1**) and Br[−] (25°C, $I = 0.25 \text{ M NaClO}_4$). Compound **1** was generated by the reaction of 5 μM Mn^{III}TM-2-PyP (**2**) and 5 μM potassium peroxymonosulfate (see ref. [3b]). Bromide concentrations ranged from 100 μM to 50 mM depending on pH. The plotted curve was computed on the basis of best-fit parameters obtained from nonlinear least-squares analysis of the data points using Equation (2).

between the dioxo Mn^V [O=Mn^V–O[−]], oxo–hydroxo Mn^V [O=Mn^V–OH], and oxo–aqua Mn^V [O=Mn^V–OH₂] species must be required to fully activate the oxoMn^V species prior to oxo-transfer reaction.^[12] The experimental points fit well to Equation (2) ($R = 0.9993$) which was deduced from this reaction model (Scheme 1).

$$k_{\text{app}} = \frac{k_{\text{int}} a_{\text{H}}^2}{a_{\text{H}}^2 + a_{\text{H}} k_{\text{a1}} + k_{\text{a1}} k_{\text{a2}}} \quad (2)$$

From the data in Figure 2, we determined the $\text{p}K_{\text{a2}}$ of the oxo–aqua Mn^V species to be 7.7 ± 0.1 . The $\text{p}K_{\text{a1}}$ must be less than 5 and beyond the range of the data. The intrinsic or pH-independent rate constant for the reaction between the doubly protonated oxo–aqua Mn^V species and bromide ion, k_{int} , could be estimated to be around $10^8 \text{ M}^{-1} \text{ s}^{-1}$.

This fast, reversible oxo-transfer reaction provides an unusual opportunity to determine the equilibrium constant K_{oxo} for Equation (1) and to define the free energy of the high-



Scheme 1. Reaction model for the oxo-transfer reaction.

valent oxoMn^V intermediate. K_{oxo} was calculated from the ratio of the forward and reverse rate constants,^[13] k_f/k_r , at a given pH. Alternatively, K_{oxo} was determined directly by finding the concentration ratio $C_{\text{BrO}^-}/C_{\text{Br}^-}$ that caused no UV/Vis spectral changes in a Mn^V–Mn^{III} solution (2.5 μM in each) upon stopped-flow mixing with a BrO[−]–Br[−] solution. K_{oxo} was found to vary from 3.5 at pH 7.3 to 2.9×10^{-5} at pH 9.6. The data could be extrapolated to other pH regions with the Nernst equation from the known Mn^V and Mn^{III} $\text{p}K_{\text{a}}$ values.^[11] Figure 3 shows a potential versus pH diagram for the oxoMn^V/Mn^{III}TM-2-PyP system and those for the BrO[−]/Br[−] and ClO[−]/Cl[−] redox pairs. Interestingly, this relationship predicts that

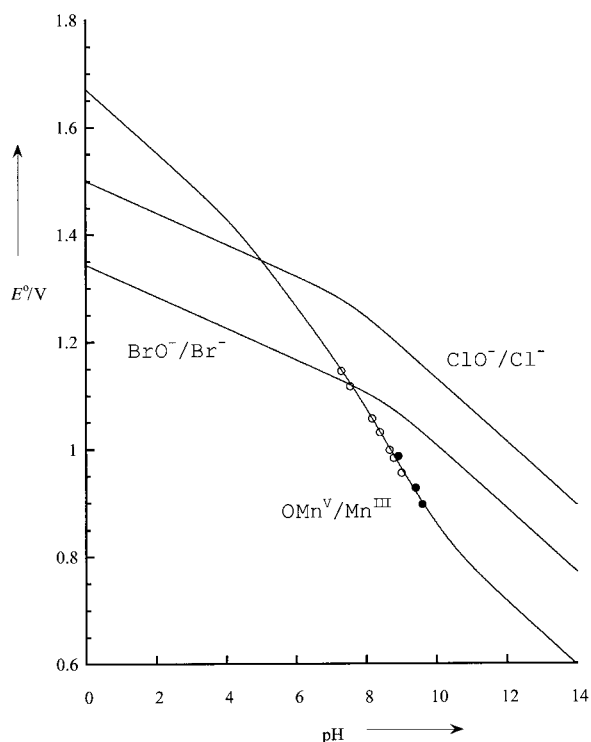


Figure 3. Standard electrode potential (E°) versus pH diagram for the oxoMn^V/Mn^{III}TM-2-PyP system along with BrO[−]/Br[−], ClO[−]/Cl[−] redox pairs. Equilibrium constants were either measured directly (solid circles), or calculated from the ratio of forward and reverse reaction rate constants k_f/k_r (empty circles). E° was then calculated from equilibrium constants and known BrO[−]/Br[−] potentials.^[6] The oxoMn^V/Mn^{III} curve was extrapolated to other pH regions with the Nernst equation using the experimental data and the following $\text{p}K_{\text{a}}$ values: Mn^{III}(OH)₂, $\text{p}K_{\text{a1}} = 9.6$, $\text{p}K_{\text{a2}} = 10.7$; oxoMn^V(OH)₂, $\text{p}K_{\text{a1}} < 5$, $\text{p}K_{\text{a2}} = 7.7$, (see ref. [11]). Crossings of the BrO[−]/Br[−] and ClO[−]/Cl[−] lines are at pH 5.1 and 7.6, respectively.

chloride oxidation should become accessible near pH 5. Indeed, the reaction of Cl[−] with oxoMn^VTM-2-PyP (**1**) to afford hypochlorite, as monitored by the chlorination of methyl orange, was found to occur efficiently at pH < 5. The chlorination yields were significantly lower at higher pH^[14] in good agreement with the predicted behavior.

These results show that bromide and chloride are readily oxidized to the corresponding hypohalite by an oxoMn^V porphyrin (**1**). The reversibility of this process has placed this oxoMn^V intermediate on a

thermochemical energy scale.^[15] The more reactive oxoiron porphyrin systems^[16] are under current investigation.

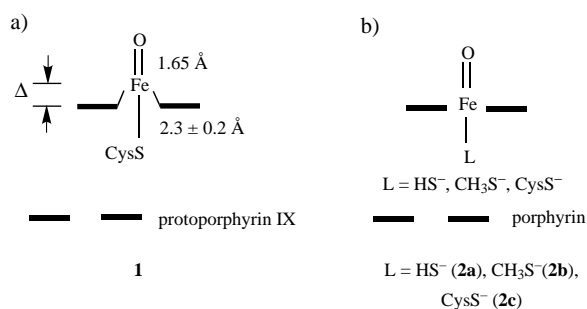
Received: June 8, 2000 [Z15242]

- [1] a) B. Meunier in *Biomimetic Oxidations Catalyzed by Transition Metal Complexes* (Ed.: B. Meunier), Imperial College Press, London, **2000**, pp. 171–214; b) J. L. McLain, J. Lee, J. T. Groves in *Biomimetic Oxidations Catalyzed by Transition Metal Complexes* (Ed.: B. Meunier), Imperial College Press, London, **2000**, pp. 91–170.
- [2] a) B. Meunier, *Chem. Rev.* **1992**, 92, 1411–1456; b) J. T. Groves, K. Shalyaev, J. Lee in *The Porphyrin Handbook, Vol. 4* (Eds.: K. M. Kadish, K. M. Smith, R. Guilard), Academic Press, San Diego, **2000**, pp. 17–40.
- [3] a) J. T. Groves, J. Lee, S. S. Marla, *J. Am. Chem. Soc.* **1997**, 119, 6269–6273; b) N. Jin, J. T. Groves, *J. Am. Chem. Soc.* **1999**, 121, 2923–2924; c) C. G. Miller, S. W. Gordon-Wylie, C. P. Horwitz, S. A. Strazisar, D. K. Peraino, G. R. Clark, S. T. Weintraub, T. J. Collins, *J. Am. Chem. Soc.* **1998**, 120, 11540–11541; d) F. M. MacDonnell, N. L. P. Fackler, C. Stern, T. V. O'Halloran, *J. Am. Chem. Soc.* **1994**, 116, 7431–7432.
- [4] a) B. W. Griffin in *Peroxidases in Chemistry and Biology, Vol. 2* (Eds.: J. Everse, K. E. Everse, M. B. Grisham), CRC Press, Boca Raton, FL, **1991**, pp. 85–138; b) A. Butler, J. V. Walker, *Chem. Rev.* **1993**, 93, 1937–1944; c) G. Labat, B. Meunier, *J. Chem. Soc. Chem. Commun.* **1990**, 1414–1416; d) H.-A. Wagenknecht, C. Claude, W. D. Woggon, *Helv. Chim. Acta.* **1998**, 81, 1506–1520.
- [5] Mn^{III}TM-2-PyP was purchased from Mid-century, Posen, IL, and was further purified. Its concentration was standardized spectrophotometrically using $\epsilon = 129\,000\text{ cm}^{-1}\text{M}^{-1}$; I. Batinic-Haberle, L. Benov, I. F. Spasojevic, I. Fridovich, *J. Biol. Chem.* **1998**, 273, 24521–24528.
- [6] T. Mussini, G. Faita in *Encyclopedia of Electro-chemistry of the Elements, Vol. 1* (Ed.: A. J. Bard), Marcel Dekker, New York, **1973**, p. 11 and p. 64.
- [7] Solutions of HOBr[−]/OBr[−] that were free of Br[−] were prepared by mixing equimolar amounts of OCl[−] and Br[−]; M. Gazda, D. W. Margerum, *Inorg. Chem.* **1994**, 33, 118–123.
- [8] A buffered (pH 7.0, 25 mM phosphate buffer) solution of 10 μM (**2**), 5 mM NaBr, and 50 μM phenol red had 100 μM HSO₅[−] added, resulting in production of bromophenol blue (yield 30%, $\lambda_{\text{abs}} = 592\text{ nm}$) within 1 s. In the absence of catalyst, control experiments showed less than 1% production of bromophenol blue within 1 min.
- [9] P. G. Furtmüller, U. Burner, C. Obinger, *Biochemistry* **1998**, 37, 17923–17930.
- [10] A. Butler, A. H. Baldwin, *Struct. Bonding (Berlin)* **1997**, 89, 109–132, and references therein.
- [11] The dioxo nature of **1** at pH 12–14 was first suggested by Su et al. F. C. Chen, S. H. Cheng, C. H. Yu, M. H. Liu, Y. O. Su, *J. Electroanal. Chem.* **1999**, 474, 52–59.
- [12] The second protonation can occur either on the hydroxo ligand affording an oxo-aqua species (shown in Scheme 1) or on the oxo ligand giving a dihydroxo species. Our results support the oxo-hydroxo tautomerism mechanism proposed by Meunier to explain the solvent oxygen incorporation to substrate in manganese porphyrin catalyzed processes. J. Bernadou, B. Meunier, *Chem. Commun.* **1998**, 20, 2167–2173.
- [13] In the pH region investigated, the reverse reaction rate constant, k_r , was found to be first order in both $c_{\text{Mn}^{\text{III}}}$ and $c_{\text{OBr}^{\text{−}}+\text{HOBr}^{\text{−}}}$.
- [14] In a typical experiment, 1 M NaCl (1 mL), **2** (1 mL), 50 mM pH 5 phosphate buffer solution (2 mL), 1 mM methyl orange (1 mL) were mixed prior to the addition of a 10 mM oxone (HSO₅[−]: 100 μL) solution. After two minutes, this was extracted with *n*-heptane. GC-MS analysis revealed monochlorodimethylaniline (m/z 154) and dichlorodimethylaniline (m/z 188), matching with calibration experiments using methyl orange and authentic hypochlorite. The estimated yields of OCl[−] per mole of oxone were 85% at pH 5, 5.5% at pH 7.6, and 0.3% at pH 9.0.
- [15] R. H. Holm, J. P. Donahue, *Polyhedron* **1993**, 12, 571–589.
- [16] J. Lee, J. A. Hunt, J. T. Groves, *J. Am. Chem. Soc.* **1998**, 120, 7493–7501.

The High-Valent Compound of Cytochrome P450: The Nature of the Fe–S Bond and the Role of the Thiolate Ligand as an Internal Electron Donor**

François Ogliaro, Shimrit Cohen, Michael Filatov, Nathan Harris, and Sason Shaik*

Recently, Schlichting et al.^[1] have used time-lapse X-ray crystallography to “photograph” the hydroxylation pathway of camphor by cytochrome P450_{cam}, which includes the elusive, high-valent iron-oxene species (**1** in Scheme 1 a). In response to this exciting work, we present here an extensive density functional theoretical (DFT) investigation of iron



Scheme 1. Selected X-ray diffraction data for a) the high-valent P450 iron oxene species **1**. Δ indicates the protrusion of the iron center from the porphyrin plane. b) Model systems **2a–c**.

oxene (**2a–c**, Scheme 1b) with emphasis on geometry, electronic structure, and unusual features of the Fe–S bonding. Thus, while the X-ray diffracting species^[1] qualitatively fits iron oxene, its precise geometric data are less certain. For example, the distance between the iron and the proximal ligand, $r_{\text{Fe-S}}$, appears quite short but the value $2.3 \pm 0.2\text{ Å}$ has a significant uncertainty. Another uncertainty, discussed by the authors,^[1] is the possible contamination by an additional species. Theory^[2] itself has not as yet settled on a value for this distance, which appears to vary between $2.37\text{–}2.69\text{ Å}$ for different models systems and computational levels.^[2] An associated issue is the theoretical characterization of the flexibility of the Fe–S linkage in **1** and the role of the thiolate ligand as an internal electron donor.^[3] A still uncertain feature of P450 iron oxene is whether it involves a porphyrin cation radical, as in the analogous Compound I species of horseradish peroxidase^[4a] and synthetic models,^[4b] or, rather, does it possess a sulfur radical situation,^[2a,e] or perhaps a resonance hybrid of these forms.^[3,5] A related question concerns the spin-state identity; high-spin as in some Compound I species,^[4a,b] or low

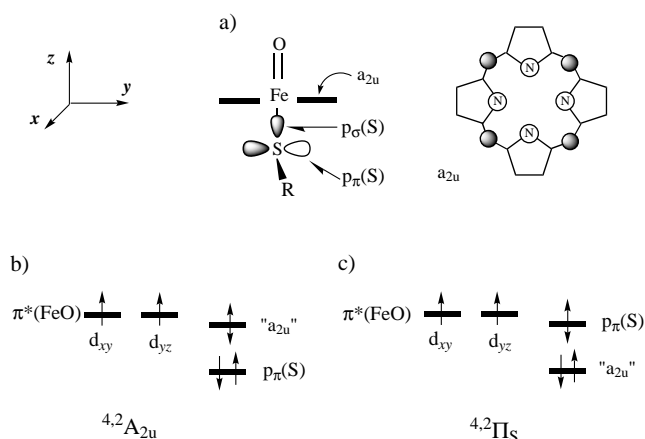
[*] Prof. S. Shaik, Dr. F. Ogliaro, S. Cohen, Dr. M. Filatov, Dr. N. Harris
Department of Organic Chemistry and
The Lise Meitner-Minerva Center for
Computational Quantum Chemistry
Hebrew University, 91904 Jerusalem (Israel)
Fax: (+972) 2-6584680
E-mail: sason@yfaat.ch.huji.ac.il

[**] This research was sponsored in part by the Israeli Science Foundation (ISF) and the Binational German–Israeli Foundation (GIF). F.O. thanks the EU for a Marie Curie Fellowship.

spin as in chloro peroxidase.^[4a] These issues, and the great interest in P450 iron oxene as a potent oxidizing agent,^[5] call for a theoretical treatment focused on these points.

This paper presents a DFT study of the four lower-most states of Compound I for three different thiolate ligands (**2a–c** in Scheme 1b), as isolated molecules and in a polarizing medium. Calculations were done with the GAUSSIAN98 package,^[6] using the unrestricted hybrid-functional UB3LYP^[7] with full geometry optimization. Four basis sets were used, labeled as B1–B4.^[8, 9] The least extensive, B1, uses an effective core potential and the double-zeta quality LACVP basis set.^[8] The most extensive, B4, uses the all electron 6-311 + G* basis set.^[6] Solvent calculations were carried out with the IEF-CPM model^[10] implemented in GAUSSIAN,^[6] which used a dielectric constant for water of $\epsilon = 78$. The effect of a low dielectric constant was tested with the solvation with JAGUAR using $\epsilon = 5.7$ (for C_6Cl_6).^[11] The electric field and hydrogen bonding in the protein pocket are very important.^[12] Our solvent calculation represents a simple way to approach the problem and we must emphasize that the calculations are intended only to reveal trends induced by medium polarization. As will be shown later, the trends for $\epsilon = 5.7$ and $\epsilon = 78$ are identical.

P450 iron oxene has four low-lying states, each of which is a tri-radicaloid, as depicted in Scheme 2. Two of the unpaired electrons occupy the π^* orbitals of the ferryl group with a triplet overall spin. The third electron is coupled to the triplet



Scheme 2. Key orbitals and tri-radicaloid states of P450 iron oxene.

pair in either a ferromagnetic or antiferromagnetic manner, to give a quartet and doublet spin states.^[2, 4] The $4,2A_{2u}$ states (Scheme 2b) arise from a single occupation of the “ a_{2u} ” orbital, which is composed of the corresponding a_{2u} orbital of the free porphyrin mixed with the $p_{\sigma}(S)$ orbital (see Scheme 3a). The $4,2\Pi_s$ states involve single occupation of the sulfur $p_{\pi}(S)$ orbital (Scheme 2c) mixed with the $d_{yz}(\pi^*(FeO))$ orbital. State characterization was achieved by a detailed inspection of the unrestricted Kohn–Sham orbitals and by transformation of these orbitals to the corresponding delocalized natural orbitals.^[13] In C_1 symmetry, there is interstate mixing but the A_{2u} or Π_s parenthood is still recognizable by the natural orbital analysis.

The relative ordering of the four states derives from the relative π - versus σ -donor capability of the thiolate ligand with respect to the porphyrin (through its a_{2u} orbital) and, therefore, depends on the thiolate ligand, the porphyrin substituents, and the polarization due to electric field or hydrogen bonding in the protein pocket (which also possesses a water population^[1, 12]). The three ligands of choice (**2a–c**) and the solvent calculations can reveal insight regarding these factors.

Table 1 shows the relative energies of the A_{2u} and Π_s state types for the different ligands at the optimized geometries.^[8, 9] The energy spacing within the state types is much smaller (see Figure 1). It is seen that, while for $L = HS^-$ (**2a**) and $CysS^-$

Table 1. $A_{2u} - \Pi_s$ energy gaps^[a] for the model systems in different basis sets (Bi). In parentheses are values obtained for a fixed geometry of the corresponding ground state.

Basis set	L =		
	HS^- (2a)	CH_3S^- (2b)	$CysS^-$ (2c)
B1	5.46 (6.17)	0.31 (1.68)	7.75 (7.86)
B2	4.86 (5.34)	0.20 (1.29)	– (6.81)
B3	5.33 (6.32)	0.66 (–)	– (–)

[a] In $kcal\ mol^{-1}$.

(**2c**), the $A_{2u} - \Pi_s$ energy difference is appreciable; in the case of $L = CH_3S^-$ (**2b**), the four states are jammed into a space of about $1\ kcal\ mol^{-1}$. The CH_3S^- ligand, the best π -donor among the three ligands, over stabilizes the Π_s states relative to the A_{2u} states. Single-point values using the optimized $4A_{2u}$ geometry for all the four states, are given in parentheses in Table 1 and show that the trend is independent of the precise geometric details of the different states. This trend persists even if the B3P86 functional is used instead of B3LYP. Thus, HS^- appears to be a more faithful mimic of the full $CysS^-$ ligand. This is apparent also from the Fe–S bond dissociation energies (see below). Thus, HS^- is the choice model ligand for $CysS^-$. As recently pointed out,^[2c] an alternative model is one which uses $L = CH_3S^-$ but with the full protoporphyrin IX moiety. In this case, the porphyrin substituents level the relative donor abilities of the proximal ligand with respect to the porphyrin ring.

Figure 1 shows the two lowest states for the three ligands, in different basis sets and with a solvation effects included ($\epsilon = 78$). In agreement with others,^[2a,c,d] for **2b**, better basis sets and medium polarization favor the doublet state for all three ligands. Using the low dielectric constant ($\epsilon = 5.7$) for **2a** gave precisely the same trend, preferring slightly the doublet state. This conclusion is in accord with EPR assignment^[4] of the ground state in Compound I of chloro peroxidase. The J value^[14] for **2a** in a solvent is $-42\ cm^{-1}$, in accord with the EPR data^[2e] ($-37\ cm^{-1}$). Considering experimental uncertainties^[2e] and the accuracy limits of the DFT method, this

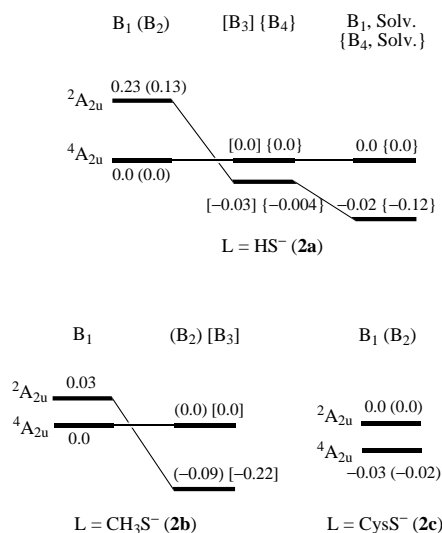


Figure 1. ${}^4A_{2u}$ – ${}^2A_{2u}$ energy gaps for the model systems for different basis sets and with solvent polarization.

agreement must be taken with caution. A prudent conclusion, at this point, is that the two states are predicted by theory to be virtually degenerate. The factors involved in the choice of the ground state will be discussed later.

Figure 2 shows the geometries of A_{2u} states in different basis sets; in C_s symmetry for the first two ligands and in C_1 for the full cysteinato ligand. C_1 results for **2a** show that the C_1 and C_s geometries and energies are very close.^[15] The geometric parameters of the FeO porphyrin moieties are almost invariant and agree with experimental estimates,^[1] **1** in Scheme 1. Also in agreement is the protrusion of the Fe atom above the porphyrin plane, which itself undergoes a modest ruffling of a few degrees. The Fe–S bond (for the choice ligands HS^- and $CysS^-$) is about 0.3–0.4 Å longer than the experimental estimate. However, the discrepancy may not be all that large considering the experimental error bar (± 0.2 Å).^[1] The Fe–S distance varies with the donor capability of the ligand; it is the longest for **2b**^[2d] and shortest for

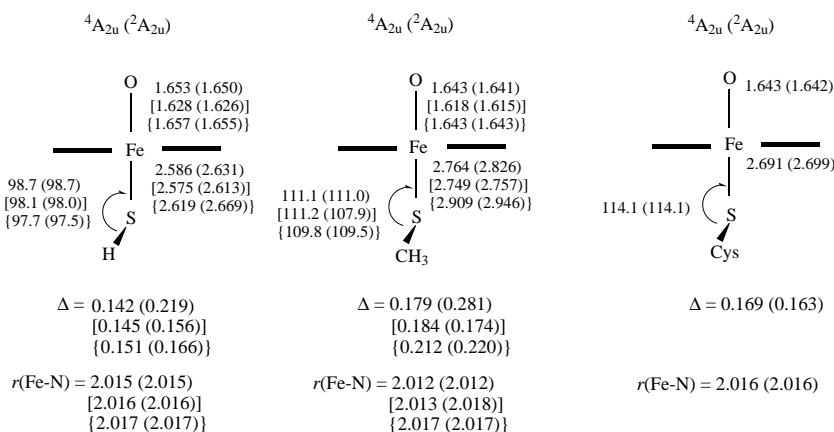


Figure 2. Optimized geometries for the ${}^4A_{2u}$ and ${}^2A_{2u}$ states of the model systems (C_s ^[15] for HS^- and CH_3S^- , and C_1 for $CysS^-$). Unbracketed values correspond to B1; those in square brackets to B2, and those in curly brackets to B3. The Δ values [Å] correspond to the protrusion of the Fe atom above the porphyrin plane; $r(Fe-N)$ is the average bond length.

2a. The doublet state, as a rule, has a longer bond than the quartet state.^[2c,d]

Figure 3a shows the state ordering as a function of the Fe–S distance for **2a**. At longer Fe–S distances (>2.7 Å), the ground state is ${}^2A_{2u}$, while at shorter distances the ground state is ${}^4A_{2u}$. Based on approaches for diradicaloids,^[16, 4b] the

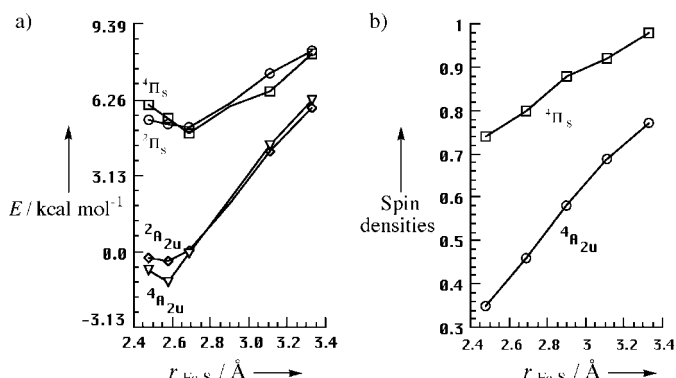
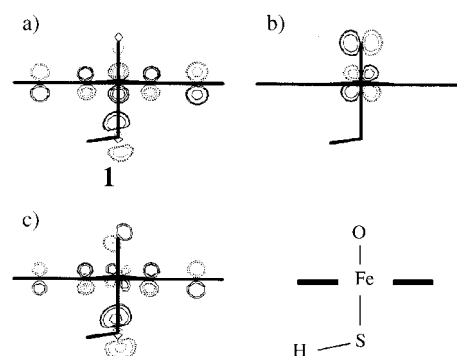


Figure 3. a) States energies (for **2a**; B1 level) as a function of the Fe–S distance. b) SH spin densities for ${}^4A_{2u}$ and ${}^4\Pi_S$ as a function of the Fe–S distance. The corresponding spin densities for the low-spin states are negative and have a mirror image behavior to the high-spin states.

major factor is the exchange integral, K_{ij} , of orbitals i and j which accommodate the unpaired electrons. High-spin states are favored by a large K_{ij} , as conferred when the two orbitals share common atoms. When the orbitals are disjoint, K_{ij} is small and the low-spin state will be favored by virtue of superior Coulomb correlation. By reference to Scheme 2, the two orbitals which will determine the ground state spin are the “ a_{2u} ” and d_{yz} orbitals (the in plane π_{FeO}^*). These orbitals are virtually disjoint and have a small exchange integral (Scheme 3a,b). However, since the two orbitals are of the

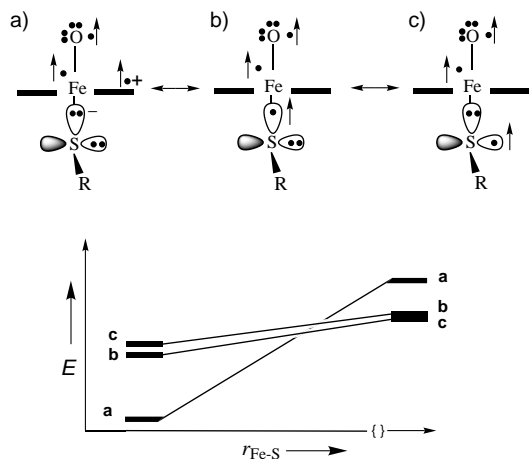


Scheme 3. Contour plots of a) the “ a_{2u} ” and b) π_{FeO}^* Kohn–Sham orbitals, and c) the natural “ a_{2u} ” orbital.

same symmetry species, one expects some mixing, which is readily apparent by inspection of the natural “ a_{2u} ”-type orbital (Scheme 3c). The shorter the Fe–S distance, the stronger this admixture and the corresponding exchange integral $K_{a_{2u}-\pi^*}$ increasingly favors the high-spin ${}^4A_{2u}$ state. Thus, at short Fe–S distances, the ${}^4A_{2u}$ high-spin state is the ground state while at longer distances the low-spin ${}^2A_{2u}$ state is preferentially stabilized and becomes the ground state.^[17a]

Since the spin identity of the ground state depends on the Fe–S bond distance, one wonders how variable is the bond length. As seen in Figure 3 a, a displacement of the Fe–S bond over 1 Å, costs about 6 kcal mol^{−1} (at most, since we did not allow for geometric relaxation during stretching). Especially soft is the direction of bond shortening from 2.8 → 2.4 Å which requires about 1 kcal mol^{−1}. Clearly, thiolate enzymes, with different constraints on Fe–S distance and differing proximal pocket polarities which attenuate the donor ability of the thiolate^[12] will possess slightly different Fe–S bond distances and have either ⁴A_{2u} or ²A_{2u} as ground states. A spin state equilibrium^[3c] or mixed-spin state situations are likely.

The fluxionality of the Fe–S bond is rooted in the thiolate spin-density variation in Figure 3 b, which shows that the A_{2u} spin density starts as approximately 0.5e at short distances and increases with Fe–S elongation. Thus, the Fe–S bond elongation is attended by internal charge transfer from the thiolate toward the porphyrin “hole”. In fact, iron oxene dissociates into the neutral (porphyrin)FeO and the thiyl radical, with effectively a very small bond dissociation energy *D* of 6.3 (**2c**), 6.9 (**2a**), and 3.0 kcal mol^{−1} (**2b**). As shown in Scheme 4, the bond dissociation involves a crossing of



Scheme 4. Resonance contributors to the electronic structure of P450 iron oxene and their relative energies as a function of the Fe–S distance.

resonance structures;^[3a,d, 5b,c] one (a) involves a thiolate anionic state and the other (b) involves a σ -thiyl radical situation. At shorter distances (<2.6 Å) both (a) and (b) mix and contribute to the electronic structure. As the Fe–S bond becomes longer, the thiyl radical structure (b) is stabilized and eventually crosses below (a). Another form, (c), nascent with (b) at the dissociation limit. The three forms mix, avoid the crossing, and thereby induce a flat potential and an effectively weak bond energy. The role of such resonance forms, termed also “redox tautomerism”,^[3d] has been postulated based on experimental findings^[3a,d, 5b,c] and is supported here by theoretical calculations. The imprint of this mechanism should be tractable, as demonstrated by vibrational spectroscopy of the high-spin ferric form of P450_{cam}.^[3b]

In summary, the Fe–S bond of Compound I has a small bond dissociation energy (6–7 kcal mol^{−1}) and is flexible, due

to internal charge transfer from the thiolate to the porphyrin ring. Our solvent calculations show that, irrespective of dielectric constant, the polarization of the medium reduces the thiolate spin density. Should the same effect be exerted within the protein pocket,^[3c] then, based on the relation in Figure 3 b, some shortening of the Fe–S bond would be expected. Such an effect, imparted by hydrogen bonding, has been demonstrated recently in model compounds.^[12f] It follows also that isoforms of P450 and related thiolate enzymes (like CPO, NOS, and so forth), which differ in their pocket polarities^[12b,c] and acidities may possess different Fe–S characters and spin situations. This prediction merits appropriate computational tests.

As pointed out, the C₁ symmetry will cause some Π_s –A_{2u} state mixing, due to rehybridization of the p _{π} (S) and p_o(S) orbitals. This mixing will increase as the Fe–S bond stretches and tilts off axis in the C_s plane (Scheme 4).^[17b] Significant spin-orbit coupling conferred by the sulfur atom will further enhance the rate of spin-state transitions through ^{2,4} Π_s –^{4,2}A_{2u} mixing.^[5b, 17c] This latter feature, as well as the bond flexibility, are likely to have an impact on the oxidative reactions of Compound I.^[2d, 18]

Received: April 13, 2000
Revised: August 2, 2000 [Z14990]

- [1] I. Schlichting, J. Berendzen, K. Chu, A. M. Stock, S. A. Maves, D. A. Benson, R. M. Sweet, D. Ringe, G. A. Petsko, S. G. Sligar, *Science* **2000**, 287, 1615.
- [2] a) M. T. Green, *J. Am. Chem. Soc.* **1999**, 121, 7939; b) D. L. Harris, G. H. Loew, *J. Am. Chem. Soc.* **1998**, 120, 8941; c) D. L. Harris, G. H. Loew, *Chem. Rev.* **2000**, 100, 407; d) M. Filatov, N. Harris, S. Shaik, *J. Chem. Soc. Perkin Trans. 2* **1999**, 399; e) J. Antony, M. Grodzicki, A. X. Trautwein, *J. Phys. Chem. A* **1997**, 101, 2692.
- [3] a) J. H. Dawson, M. Sono, *Chem. Rev.* **1987**, 1255; b) P. M. Champion, *J. Am. Chem. Soc.* **1989**, 111, 3433; O. Bangcharoenpaupong, P. M. Champion, S. A. Martinis, S. G. Sligar, *J. Chem. Phys.* **1987**, 87, 4273; c) M. Unno, J. F. Christian, D. E. Benson, N. C. Gerber, S. G. Sligar, P. M. Champion, *J. Am. Chem. Soc.* **1997**, 119, 6614; d) J. Bernadou, A.-S. Fabiano, A. Robert, B. Meunier, *J. Am. Chem. Soc.* **1994**, 116, 9375.
- [4] a) C. E. Schulz, R. Rutter, J. T. Sage, P. G. Debrunner, L. P. Hager, *Biochemistry* **1984**, 23, 4734; b) E. Bill, X.-Q. Ding, A. X. Trautwein, H. Winkler, D. Mandon, R. Weiss, A. Gold, K. Jayaraj, W. E. Hatfield, M. L. Kirk, *Eur. J. Biochem.* **1990**, 188, 665.
- [5] a) J. T. Groves, Y.-Z. Hang in *Cytochrome P450: Structure, Mechanisms and Biochemistry*, 2nd ed. (Ed.: P. R. Ortiz de Montellano), Plenum, New York, **1995**, chap. 1; b) W.-D. Woggon, *Top. Curr. Chem.* **1996**, 184, 40; c) M. Sono, M. P. Roach, E. D. Coulter, J. H. Dawson, *Chem. Rev.* **1996**, 96, 2841.
- [6] GAUSSIAN98, Gaussian, Inc., Pittsburgh PA, **1998**.
- [7] P. J. Stevens, F. J. Devlin, C. F. Chabrowski, M. J. Frisch, *J. Phys. Chem.* **1994**, 98, 11623.
- [8] LACVP: J. P. Hay, W. R. Wadt, *J. Chem. Phys.* **1985**, 82, 299.
- [9] a) B2 is generated from LACVP by adding polarization functions on the heavy atoms, LACVP*; b) B3 is 6-311 + G.
- [10] E. Canes, B. Mennucci, J. Tomasi, *J. Chem. Phys.* **1997**, 107, 3032.
- [11] JAGUAR 3.5, Schrödinger, Inc, Portland, Oregon. This is an improved solvent model, analogous to PCM but with a different implementation than in GAUSSIAN. See its performance in: B. Marten, K. Kim, C. Cortis, R. A. Friesner, R. B. Murphy, M. N. Ringnalda, D. Sitkoff, B. Honig, *J. Phys. Chem.* **1996**, 100, 11775. See also its application to bacteriochlorophyll and bacteriopheophytin in: L. Y. Zhang, R. A. Friesner, *J. Phys. Chem.* **1995**, 99, 16479.
- [12] a) The proximal pocket involves hydrogen bonds to the cysteinato sulfur and the positive ends of the local dipoles are oriented toward it

(T. L. Poulos, J. C. Vickery, H. Li in *Cytochrome P450: Structure, Mechanisms and Biochemistry*, 2nd ed. (Ed.: P. R. Ortiz de Montellano), Plenum, New York, **1995**, chap. 6). This will further make the donor ability of the cysteinato ligand similar to HS⁻; b) both CPO and iNOS are known to possess more extensive hydrogen bonding to the cysteinato ligand and thereby weaken its interaction with the iron (D. L. Wang, D. J. Stuer, D. L. Rousseau, *Biochemistry* **1997**, *36*, 4595). In iNOS there is aromatic stacking which may stabilize the A_{2u} states with a prominent porphyrin hole (B. R. Crane, A. S. Arvai, R. Gacuchhui, C. Wu, D. Ghosh, E. D. Getzhoff, D. J. Stuehr, J. A. Tainer, *Science* **1997**, *278*, 425); c) for related discussions, see: H. Aissaoui, R. Bachmann, A. Schweiger, W.-D. Woggon, *Angew. Chem.* **1998**, *110*, 3191; *Angew. Chem. Int. Ed.* **1998**, *37*, 2998; D. Harris, G. H. Loew, *J. Am. Chem. Soc.* **1993**, *115*, 8775; d) to mimic the electric potential at the thiolate site, one needs electropositive moieties in model systems. See: H.-A. Wagenknecht, C. Claude, W.-D. Woggon, *Helv. Chim. Acta* **1998**, *81*, 1506; e) for recent mutation that probe the distal and proximal pockets, see: M. P. Roach, A. E. Pond, M. R. Thomas, S. G. Boxer, J. H. Dawson, *J. Am. Chem. Soc.* **1999**, *121*, 12088; f) NH-S hydrogen bonding shortens the Fe-S bond in a synthetic model. See: N. Suzuki, T. Higuchi, Y. Urano, K. Kikuchi, H. Uekusa, Y. Ohashi, T. Uchida, T. Kitagawa, T. Nagano, *J. Am. Chem. Soc.* **1999**, *121*, 11571.

- [13] E. D. Glendening, J. Badenhoop, A. E. Reed, J. E. Carpenter, F. Weinhold, Theoretical Chemistry Institute, University of Wisconsin, Madison, USA (NBO v.4.0). The natural orbital analysis identifies the three singly occupied orbitals (Scheme 2) and facilitates the states identification relative to the more tedious analysis of the UKS orbitals.
- [14] J is evaluated using the formulae ($H_{\text{spin}} = -JS_1S_2$), given in L. Noodleman, D. A. Case, *Adv. Inorg. Chem.* **1992**, *38*, 423.
- [15] For example, with basis set B1, the C_1 geometric parameters of the $^4A_{2u}$ ($^2A_{2u}$) states for **2a** are $r_{\text{FeO}} = 1.651$ (1.648), $r_{\text{FeS}} = 2.581$ (2.600), and $\Delta = 0.143$ (0.154) Å. The $^4A_{2u}$ ($^2A_{2u}$) energy difference is $+0.09$ kcal mol⁻¹. The main deviation from C_s symmetry is a tilt of the Fe-S axis off the C_s plane of symmetry and the energy stabilization of C_1 relative to C_s is small < 1 kcal mol⁻¹.
- [16] W. T. Borden in *Encyclopedia of Computational Chemistry*, Vol. 1 (Eds.: P. von R. Schleyer, N. L. Allinger, T. Clark, J. Gasteiger, P. A. Kollman, H. F. Schaefer III, P. R. Schreiner), Wiley, Chichester, **1998**, p. 708.
- [17] a) In the low-spin situation, the two natural orbitals form bonding and antibonding combinations; b) In C_1 some A_{2u} - A_{1u} admixture is also expected. The A_{2u} parenthood is still apparent though in the calculation and the corresponding A_{1u} states are slightly higher in energy than the Π_s states; c) The perpendicular relation of the $p_o(S)$ and $p_x(S)$ orbitals provides significant one center contribution to spin orbit coupling (SOC). A simple perturbation treatment of SOC ($\zeta_s = 388$ cm⁻¹ and an energy gap taken from Figure 1) leads to a mixing coefficient of 0.14–0.18 from the quartet into the doublet state.
- [18] N. Harris, S. Cohen, M. Filatov, F. Ogliaro, S. Shaik, *Angew. Chem.* **2000**, *112*, 2070; *Angew. Chem. Int. Ed.* **2000**, *39*, 2003.

Formation of Novel Ordered Mesoporous Silicas with Square Channels and Their Direct Observation by Transmission Electron Microscopy**

Tatsuo Kimura, Takayuki Kamata, Minekazu Fuziwara, Yuri Takano, Mizue Kaneda, Yasuhiro Sakamoto, Osamu Terasaki, Yoshiyuki Sugahara, and Kazuyuki Kuroda*

Since the discovery of an ordered mesoporous silica,^[1] the preparation of various mesoporous silicas by using surfactant assemblies has been developed.^[2–4] These mesoporous silicas have proved to be highly applicable as catalysts, catalyst supports, and adsorbents for relatively large molecules,^[5] which has stimulated a number of studies including both morphological control^[6, 7] and compositional variations.^[3, 8, 9] However, all the structures reported so far have been governed by the geometrical packing of surfactants^[4, 10] because the formation of the mesostructured precursors relies on the cooperative organization of inorganic species and surfactants.^[11] Herein, we report on the formation of novel mesoporous silicas (denoted as KSW-2) with rectangular arrangements of square or lozenge one-dimensional (1D) channels by mild acid treatment of a layered alkyltrimethylammonium (C_n TMA)–kanemite complex. Mesostructured precursors of KSW-2 formed through the bending of individual silicate sheets of kanemite. The square or lozenge shape of the relatively ordered pores has not previously been found among the reported mesoporous and mesostructured inorganic oxides.

Kanemite ($\text{NaHSi}_2\text{O}_5 \cdot 3\text{H}_2\text{O}$), a mineral, is made up of layered polysilicates composed of SiO_4 tetrahedral units,^[12] and the crystal structure was recently determined by Gies et al.^[13] Kanemite is a layered silicate composed of single sheets such as $\delta\text{-Na}_2\text{Si}_2\text{O}_5$ and KHSi_2O_5 ; the sheets are constructed by connecting 6-rings of SiO_4 tetrahedra wrinkled

[*] Prof. Dr. K. Kuroda,^[+] Dr. T. Kimura, T. Kamata, Y. Takano, Prof. Dr. Y. Sugahara
Department of Applied Chemistry, Waseda University
Ohkubo 3-4-1, Shinjuku-ku, Tokyo 169-8555 (Japan)
Fax: (+81) 3-5286-3199
E-mail: kuroda@mn.waseda.ac.jp


[+] Kagami Memorial Laboratory for Materials Science and Technology
Waseda University, Nishiwaseda 2-8-26, Shinjuku-ku, Tokyo 169-0051 (Japan)

M. Fuziwara
Materials Characterization Central Laboratory, Waseda University
Ohkubo 3-4-1, Shinjuku-ku, Tokyo 169-8555 (Japan)

M. Kaneda, Dr. Y. Sakamoto, Prof. Dr. O. Terasaki
Department of Physics, Graduate School of Science
Tohoku University, Sendai, 980-8578 (Japan)

Prof. Dr. O. Terasaki
CREST, JST and Center for Interdisciplinary Research
Tohoku University, Sendai, 980-8578 (Japan)

[**] This work was supported by CREST, Japan Science and Technology Corporation, and Grant-in-Aid for the Scientific Research from the Ministry of Education, Science, Sports, and Culture of the Japanese Government.

 Supporting information for this article is available on the WWW under <http://www.wiley-vch.de/home/angewandte/> or from the author.

regularly with interlayer hydrated Na^+ ions.^[13, 14] Following the report on the synthesis and reactivity of kanemite by Beneke and Lagaly,^[15] Yanagisawa et al. discovered a mesoporous silica (named as KSW-1 hereafter) by the reaction of kanemite and C_{16}TMA surfactants.^[1]

A mesostructured precursor of KSW-2 was obtained from a layered C_{16}TMA –kanemite complex by adjusting the pH value below 6.0. The preparation of the layered complex without altering the structure of the silicate framework is the most important step in obtaining the mesostructured precursor. Therefore, the synthesis procedure for KSW-2 is quite different from those reported for KSW-1 and FSM-16 derived from kanemite.^[1, 16]

A typical transmission electron microscopy (TEM) image and the corresponding electron diffraction (ED) pattern of the calcined KSW-2 obtained under the adjusted pH value of 4.0 are shown in Figure 1a. The TEM image of the calcined

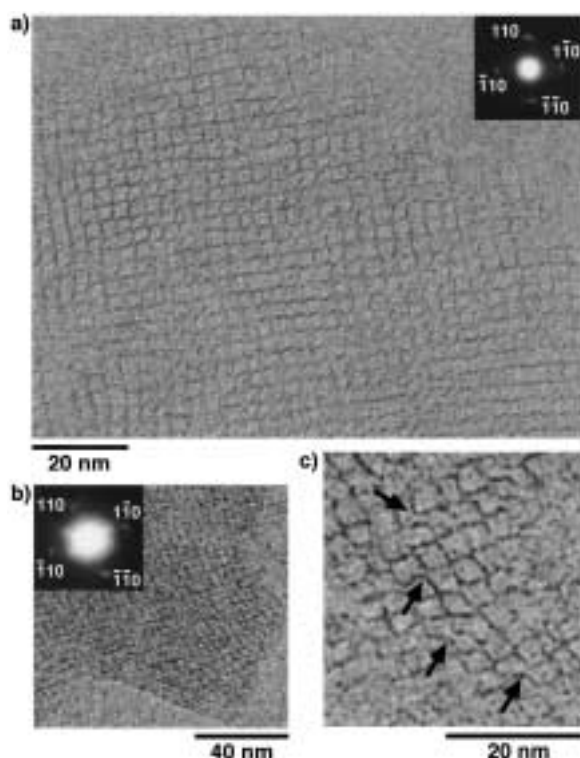


Figure 1. a) Typical TEM of calcined KSW-2 (pH 4.0) and the corresponding ED pattern indexed as $hk0$ projection. These were obtained by a JEM-3010 transmission electron microscope operated at 300 kV. b) Typical TEM and the corresponding ED pattern of as-synthesized KSW-2 (pH 6.0). c) Another TEM of the as-synthesized KSW-2 (pH 6.0). Arrows imply the observed place of the bending of silicate sheets derived from kanemite.

KSW-2 exhibits relatively ordered square arrangements that display a periodic distance of adjacent pores of about 3.3 nm. Striped patterns with the same periodic distance were also observed, strongly supporting the presence of one-dimensional (1D) mesopores. The ED pattern showed the angle of diagonal lines connecting the $[110]$ spots was close to 90° .

On the basis of the TEM results, all the powder X-ray diffraction (XRD) peaks of the as-synthesized and calcined KSW-2 are assigned to an orthorhombic structure ($C2mm$)

(as-synthesized: $a = 5.34$ nm, $b = 5.05$ nm, $c = \infty$; calcined: $a = 4.84$ nm, $b = 4.26$ nm, $c = \infty$; Figure 2).^[*] After calcination, the d_{110} value changed from 3.67 nm to 3.26 nm, which is in agreement with the periodic distance of adjacent pores observed by TEM (ca. 3.3 nm). On the basis of the N_2 adsorption isotherm of the calcined KSW-2, the BET surface area, the pore volume, and the average pore diameter were determined to be $1100 \text{ m}^2 \text{ g}^{-1}$, $0.46 \text{ cm}^3 \text{ g}^{-1}$, and 2.1 nm, respectively.^[17]

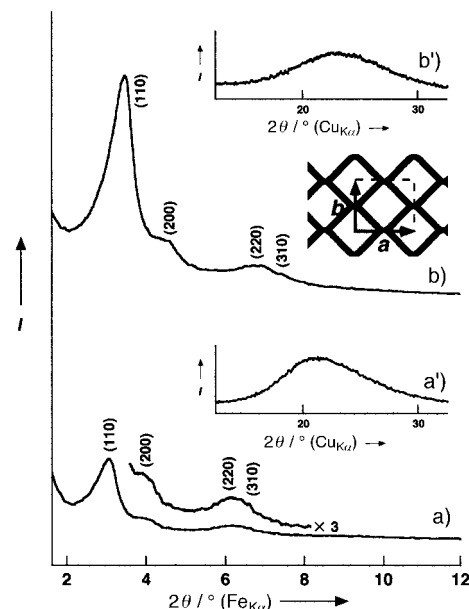


Figure 2. Powder XRD patterns of KSW-2 materials prepared at pH 4.0 a) before and b) after calcination. These were recorded by a Mac Science M03XHF²² diffractometer with monochromated $\text{FeK}\alpha$ radiation. a'), b') XRD patterns in higher 2θ regions were obtained by a Mac Science MXP³ diffractometer with monochromated $\text{CuK}\alpha$ radiation.

The mesopores are surrounded by relatively flat silicate walls (Figure 1a). Typical scanning electron micrographs showed that all the products have not morphologically changed; all the images are similar to that of kanemite (see Supporting Information, Figure A). This indicates that kanemite did not dissolve during the syntheses of both the layered C_{16}TMA –kanemite complex and the as-synthesized KSW-2, because the reactions were conducted at relatively low pH values at which silica does not dissolve.^[12]

Square-shaped mesopores have not been found among the reported ordered mesoporous materials^[1-11, 16] because those mesostructures were constructed by using supramolecular assemblies and were thus governed by their geometries.^[4, 10] Although the transformation of lamellar mesophase silicates has been conducted by hydrothermal post treatment^[18] or acid treatment,^[19] these types of transformation occur through the rearrangement of silicate frameworks and lead to the formation of hexagonal and cubic mesophase silicates, in which the silicate walls are formed along the curved surface of organic assemblies such as rodlike micelles. Even for KSW-1 and FSM-16, which were prepared by the direct reactions of

[*] We observed that the structural units of kanemite are partly retained, as discussed later, and therefore chose a 3D representation rather than a 2D one.

kanemite and C_{16} TMA surfactants,^[1, 15] the resulting meso-structure is hexagonal or less ordered.

The samples were prepared at various adjusted pH values above 4.0 in order to investigate the formation mechanism of the as-synthesized KSW-2. The ^{29}Si MAS NMR spectra of kanemite, the layered C_{16} TMA–kanemite complex, and the acid-treated products are shown in Figure 3. The spectrum of kanemite exhibited only one peak at $\delta = -97$, indicating that

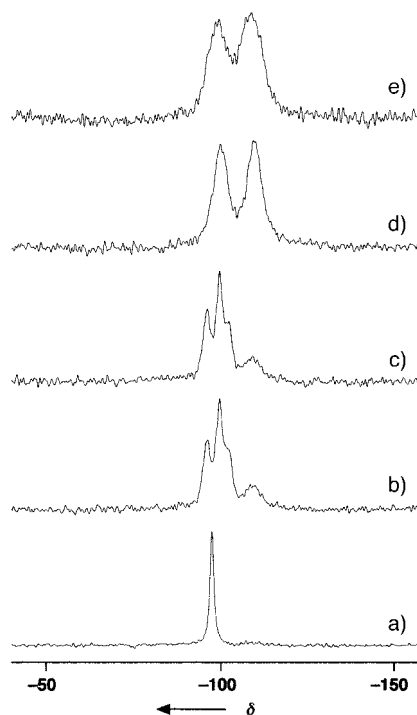


Figure 3. ^{29}Si MAS NMR spectra of a) kanemite, b) layered C_{16} TMA–kanemite complex, and c)–e) the products treated with acetic acid to give pH values of 8 (c), 6 (d), and 4 (e). These were obtained by a JEOL GSX-400 spectrometer with a spinning rate of 5 kHz and a resonance frequency of 79.30 MHz with a 45° pulse length of 4.1 μs and a recycle time of 60 s. The chemical shifts were expressed with respect to tetramethylsilane.

kanemite is composed of single-layered silicate sheets (Figure 3a).^[13, 14] In the spectrum of the layered C_{16} TMA–kanemite complex several peaks due to different Q^3 environments ($(\text{SiO})_3\text{SiO}$) were mainly observed in the range from $\delta = -95$ to -105 ,^[12] whereas a broad peak centered at $\delta = -110$ due to a Q^4 environment ($(\text{SiO})_3\text{SiOSi}$) was detected as a minor component (Figure 3b). This result reveals that the single silicate sheet structure in kanemite was essentially retained during the synthesis of the layered C_{16} TMA–kanemite complex. At a pH value of 8.0, the spectrum of the product hardly changed and the peak intensity at $\delta = -110$ increased slightly (Figure 3c). In contrast, the profiles of the acid-treated products obtained at pH values below 6.0 varied dramatically (Figure 3d, e); both the Q^3 and Q^4 peaks centered at $\delta = -101$ and -110 , respectively, were observed, which is in accordance with the structural change from the layered C_{16} TMA–kanemite complex to the as-synthesized KSW-2.

The as-synthesized product was thoroughly investigated by high-resolution TEM (HRTEM) at the point at which the

structural change occurs (pH 6.0). As well as the TEM images observed for calcined KSW-2 (pH 4.0), similar images were observed and the periodic distance between adjacent pores was about 4.0 nm (Figure 1b); the angle of diagonal lines connecting the $[110]$ spots was variable, ranging from nearly 90° to about 70° in the ED patterns. It was not possible to superimpose the striped patterns because the angle of the diagonal lines falls in a limited range (70° – 90°) and the images were observed at thin parts of the sample.

The bending of individual silicate sheets, which are not fully linked between adjacent layers, was partly observed (see Figure 1c). This observation is reproducible; the bending was directly observed by HRTEM for KSW-2 synthesized in another batch (see Supporting Information, Figure B). In addition, the range of pH values during the acid treatment did not lead to dissolution of silicate species, but led to their condensation.^[12] The observed wall thicknesses of the products during the acid treatment were almost constant (0.6–0.7 nm), and were consistent with the thickness of the silicate sheet in kanemite.^[13, 14] These findings strongly suggest that as-synthesized KSW-2 can be obtained from the layered C_{16} TMA–kanemite by bending the individual silicate sheets. Even in the TEM image of calcined KSW-2 (pH 4.0), bent silicate sheets were observed to a certain extent (Figure 1a).

The variations in C,H,N analysis (C_{16} TMA/Si ratio) and ^{29}Si MAS NMR spectra ($Q^4/(Q^3 + Q^4)$ ratio) of the products during the acid treatment are shown in Figure 4. On the basis of this data, the transformation steps of the layered complex into as-synthesized KSW-2 are schematically shown in Figure 5 and can be categorized as follows. 1) The $Q^4/(Q^3 + Q^4)$ ratio increases in the range of pH 9.6–7.0, and C_{16} TMA/Si ratio decreases slightly. This observation suggests that the beginning of the structural change is manifested by the formation of Q^4 silicate species. The formation of Q^4 species

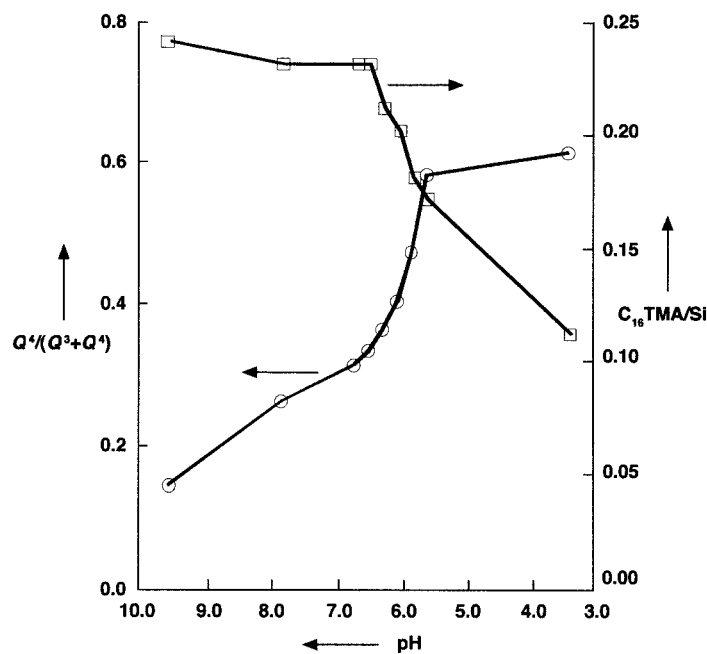


Figure 4. Variation in the amounts of C_{16} TMA ions and the $Q^4/(Q^3 + Q^4)$ ratios during acid treatment. The organic contents for calculation of C_{16} TMA/Si ratios of the acid-treated products were obtained with a Perkin Elmer PE-2400II.

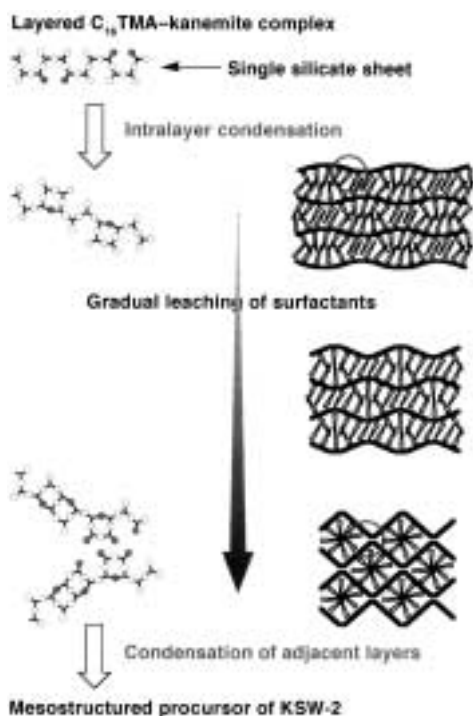


Figure 5. Schematic model for the formation of as-synthesized KSW-2 from a layered C_{16} TMA-kanemite complex. Oxygen atoms are denoted by open circles; those involved in the structural change are filled. On the basis of the schematic structure of kanemite, adjacent Si-OH groups are in very close proximity. Although the reaction steps are distinguished for convenience, these steps progress cooperatively.

occurs at the intralayers, since the structural change at pH 8.0 was hardly visible by XRD (see Supporting Information, Figure C). 2) In the range of pH 7.0–6.0, the transformation of the layered complex into as-synthesized KSW-2 is caused by partial removal of C_{16} TMA ions. The $Q^4/(Q^3 + Q^4)$ ratio increases further, indicating the condensation between adjacent layers as well as progressive intralayer condensation. 3) In the structural change at pH values below 6.0, additional condensation among Q^3 silicate species occurs between the adjacent layers. KSW-2 with a square 1D arrangement is thought to be formed through these processes (Figure 5).

The layered silicate network originating from the structure of kanemite connects two-dimensionally and is not destroyed under the conditions used. Thus, the bending of individual silicate sheets may be attributed to the limited structural changes that result from partial intralayer condensation and the accompanying structural change in C_{16} TMA assemblies during the gradual leaching. The crystal structure of kanemite,^[13, 14] reveals the intralayer condensation of Si-OH groups is possible only in the limiting direction. Indeed, the angles between the silicate sheets (after bending) and the edge of kanemite particles, observed by TEM, were often been around 45° (Figure 1 a; see also Supporting Information, Figure B).

The XRD patterns of the as-synthesized and the calcined products (pH 6.0) are shown in Figure 6. As in the case with the products obtained at pH 4.0, all the peaks at low 2θ angles are assigned to an orthorhombic structure (as-synthesized: $a = 6.34$ nm, $b = 5.58$ nm, $c = \infty$; calcined: $a = 5.16$ nm, $b =$

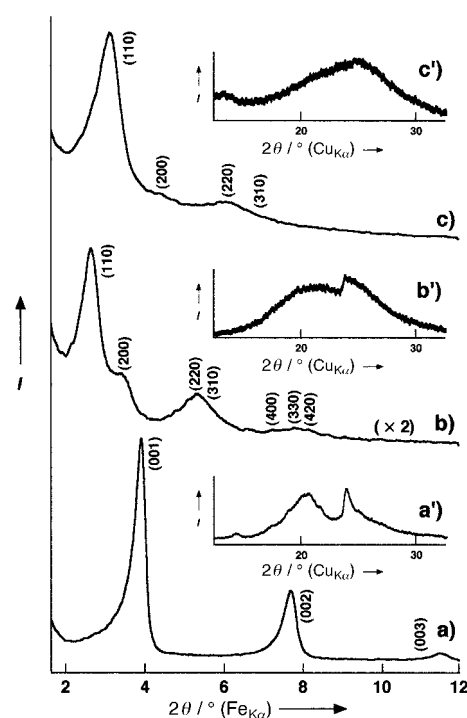


Figure 6. Powder XRD patterns of a layered C_{16} TMA-kanemite complex (a) and KSW-2 materials prepared at pH 6.0 before (b) and after calcination (c). These patterns including a')–c') were recorded by the same procedure as in Figure 2. For the layered C_{16} TMA-kanemite complex, the broad peak centered at $2\theta = 21.1^\circ$ seems to be overlapped by several peaks.

4.92 nm, $c = \infty$). Interestingly, the XRD profiles in the range 15° to 30° are somewhat different from those observed for the mesoporous materials reported up to date.^[1–11, 16, 18, 19] Though halo XRD peaks were observed for the KSW-2 materials obtained at pH 4.0 (see Figures 2 a' and b'), the XRD patterns of the KSW-2 materials prepared at pH 6.0 showed somewhat unusual peaks in the range 15° to 30° . The XRD pattern of the layered C_{16} TMA-kanemite complex (Figure 6 a') at higher angles showed a broad peak centered at $2\theta = 21.1^\circ$ and a sharp one at 24.3° , suggesting that the structural units of kanemite are at least partly retained in the layered C_{16} TMA-kanemite complex. Even in as-synthesized KSW-2, these peaks remained with some broadening (Figure 6 b). Although further broadening of such peaks was observed after calcination at 550°C for 6 h, the profile in the range of 15° to 30° was somewhat different from those observed for the mesoporous materials reported so far.^[1–11, 16, 18, 19] Further characterization of the structural features is currently in progress. On the basis of the N_2 adsorption isotherm, the BET surface area, the pore volume, and the average pore diameter of the calcined product were determined to be $1192\text{ m}^2\text{ g}^{-1}$, $0.56\text{ cm}^3\text{ g}^{-1}$, and 2.8 nm, respectively. The material has a high hydrocarbon sorption capacity on the basis of an adsorbed amount of benzene (0.74 g g^{-1} at $P/P_0 = 0.65$).

We utilized a layered C_{16} TMA-kanemite complex as the starting material, in which the basic structural framework was retained at least partly after the formation of the layered complex. The formation mechanism of KSW-2 proposed here is based on the bending of intralayer-condensed silicate sheets

of kanemite. The resulting square pore system has not been observed among reported mesoporous materials^[1–11, 16, 18, 19] and is not defined by the geometrical packing of surfactant molecules.^[4, 10] Although the frameworks are not fully retained after calcination, this approach provides a way to incorporate inorganic structural units into mesostructured materials, which will lead to the development of novel mesoporous materials with crystalline inorganic frameworks.

Experimental Section

A layered C₁₆TMA–kanemite complex was prepared by mixing a layered polysilicate kanemite (NaHSi₂O₅·3H₂O (1.05 g) derived from δ-Na₂Si₂O₅ (1.00 g)) and a 0.1M C₁₆TMACl aqueous solution (200 mL) at room temperature; the C₁₆TMA/Si ratio was 2. The resulting C₁₆TMA–kanemite complex is a layered material, which was confirmed by the powder XRD pattern of the product (Figure 6a). The peak at a *d* spacing of 2.9 nm and the higher ordered diffraction peaks were observed, and the spacings increased when *n*-decyl alcohol was further intercalated into the product. The resulting layered complex (1.01 g) was dispersed in distilled water (150 mL; pH ca. 9.6). The pH value of this suspension was decreased by the addition of acetic acid (1M); the addition procedure was conducted slowly over 30 min. The as-synthesized KSW-2 powders were air-dried and calcined at 550 °C with a heating rate of 10 K min^{–1} in ambient air for 6 h to remove organic fractions. Although the acid species are not significant for the synthesis of KSW-2, the concentration of acids must be carefully chosen, depending on the acid species used. The amount of distilled water and the adjusted pH value are also important because the solubility of C_nTMA ions is one of the key conditions for the formation of KSW-2.

Received: March 2, 2000

Revised: June 17, 2000 [Z14796]

- [1] T. Yanagisawa, T. Shimizu, K. Kuroda, C. Kato, *Bull. Chem. Soc. Jpn.* **1990**, 63, 988–992.
- [2] C. T. Kresge, M. E. Leonowicz, W. J. Roth, J. C. Vartuli, J. S. Beck, *Nature* **1992**, 359, 710–712.
- [3] Q. Huo, D. I. Margolese, U. Ciesla, P. Feng, T. E. Gler, P. Sieger, R. Leon, P. M. Petroff, F. Schüth, G. D. Stucky, *Nature* **1994**, 368, 317–321.
- [4] Q. Huo, R. Leon, P. M. Petroff, G. D. Stucky, *Science* **1995**, 268, 1324–1327.
- [5] A. Corma, *Chem. Rev.* **1997**, 97, 2373–2419.
- [6] H. Yang, A. Kuperman, N. Coombs, S. Mamiche-Afara, G. A. Ozin, *Nature* **1996**, 379, 703–705; H. Yang, N. Coombs, I. Sokolov, G. A. Ozin, *Nature* **1996**, 381, 589–592.
- [7] Y. Lu, R. Ganguli, C. A. Drewien, M. T. Anderson, C. J. Brinker, W. Gong, Y. Guo, H. Soyez, B. Dunn, M. H. Huang, J. I. Zink, *Nature* **1997**, 389, 364–368.
- [8] A. Sayari, P. Liu, *Microporous Mater.* **1997**, 12, 149–177.
- [9] T. Kimura, Y. Sugahara, K. Kuroda, *Chem. Lett.* **1997**, 983–984; T. Kimura, Y. Sugahara, K. Kuroda, *Chem. Commun.* **1998**, 559–550; T. Kimura, Y. Sugahara, K. Kuroda, *Microporous Mesoporous Mater.* **1998**, 22, 115–126; T. Kimura, Y. Sugahara, K. Kuroda, *Chem. Mater.* **1999**, 11, 508–518.
- [10] Q. Huo, D. I. Margolese, G. D. Stucky, *Chem. Mater.* **1996**, 8, 1147–1160.
- [11] A. Firouzi, D. Kumar, L. M. Bull, T. Besier, P. Sieger, Q. Huo, S. A. Walker, J. A. Zasadzinski, C. Glinka, J. Nicol, D. Margolese, G. D. Stucky, B. F. Chmelka, *Science* **1995**, 267, 1138–1143.
- [12] F. Liebau, *Structural Chemistry of Silicates*, Springer, Heidelberg, **1985**, and the references therein. The variation in the chemical shifts is probably due to the changes in the various bond angles among SiO₄ tetrahedra in the single layered silicate sheets owing to the difference in the ionic radii between Na⁺ and the head group of C₁₆TMA⁺.
- [13] H. Gies, B. Marler, S. Vortmann, U. Oberhagemann, P. Bayat, K. Krink, J. Rius, I. Wolf, C. Fyfe, *Microporous Mesoporous Mater.* **1998**, 21, 183–197; S. Vortmann, J. Rius, B. Marler, H. Gies, *Eur. J. Mineral.* **1999**, 11, 125–134.

- [14] L. A. J. Garvie, B. Devouard, T. L. Groy, F. Camara, P. R. Buseck, *Am. Mineral.* **1999**, 84, 1170–1175.
- [15] K. Beneke, G. Lagaly, *Am. Mineral.* **1977**, 62, 763–771.
- [16] S. Inagaki, A. Koiwai, N. Suzuki, Y. Fukushima, K. Kuroda, *Bull. Chem. Soc. Jpn.* **1996**, 69, 1449–1457. The obtained mesoporous silica in the paper was denoted as FSM-16.
- [17] G. Horváth, K. Kawazoe, *J. Chem. Eng. Jpn.* **1983**, 16, 470–475. The pore size was calculated from the adsorption branch by the Horváth–Kawazoe method.
- [18] A. Monnier, F. Schüth, Q. Huo, D. Kumar, D. Margolese, R. S. Maxwell, G. D. Stucky, M. Krishnamurty, P. Petroff, A. Firouzi, M. Janicke, B. F. Chmelka, *Science* **1993**, 261, 1299–1303.
- [19] C. A. Fyfe, G. Fu, *J. Am. Chem. Soc.* **1995**, 117, 9709–9714.

Second-Order Nonlinear Optical Properties of Functionalized Ionophores: Cation-Steered Modulation of the First Hyperpolarizability**

Stephan Houbrechts,* Yuji Kubo, Tomokazu Tozawa, Sumio Tokita, Tatsuo Wada,* and Hiroyuki Sasabe

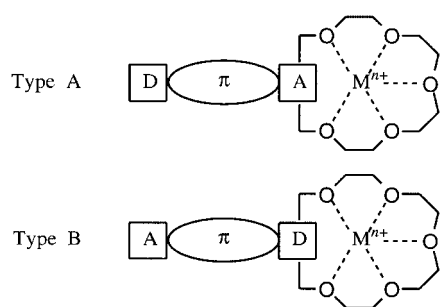
Functionalized ionophores are of major interest for their ability to complex various ionic species. As complex formation generally induces severe changes in their photophysical properties, they are widely used as a tool for ion recognition. Accordingly, the influence of cation binding on the intramolecular charge-transfer (ICT) transition has been studied intensively, mostly on donor–acceptor substituted aromatic chromoionophores.^[1–3] Among them, two classes of ionophores can be distinguished (Scheme 1): type A chromophores that interact with the ion through the acceptor site of the chromophore, which enhances the ICT and induces a bathochromic shift of the charge transfer band; and type B chromophores that interact via the donor site and reduce the ICT (hypsochromic shift).

[*] Dr. S. Houbrechts,^[+] Dr. T. Wada, Dr. H. Sasabe
Frontier Research Program
The Institute of Physical and Chemical Research (RIKEN)
2-1 Hirosawa, Wako, Saitama 351-01 (Japan)
Fax: (+49)48-462-4695
E-mail: stephan.houbrechts@fys.kuleuven.ac.be,
tatsuow@postman.riken.go.jp

Prof. Dr. Y. Kubo
Form and Function, PRESTO
Japan Science and Technology Corporation (JST)
Department of Applied Chemistry
Saitama University
255 Shimo-ohkubo, Urawa, Saitama 338-8570 (Japan)
Prof. Dr. Y. Kubo, T. Tozawa, Prof. Dr. S. Tokita
Department of Applied Chemistry
Saitama University
255 Shimo-ohkubo, Urawa, Saitama 338-8570 (Japan)

[+] Present address:
Laboratory of Chemical and Biological Dynamics
Catholic University of Leuven
Celestijnenlaan 200D, 3001 Heverlee (Belgium)
Fax: (+32)16-327982

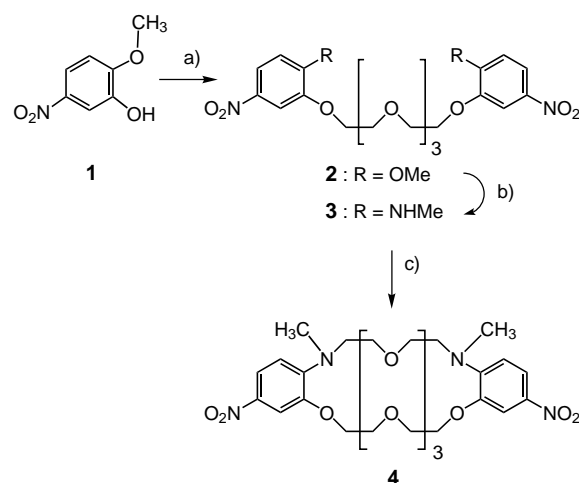
[**] This work was supported by the Frontier Research Program and the Japan Science and Technology Corporation. S.H. is a postdoctoral researcher of the FWO (Flanders).



Scheme 1. Types of interaction between chromoionophores (composed of a donor D, acceptor A, and bridging moiety) and ions.

Nonlinear optics (NLO) have received attention for its applications in the domain of optoelectronics and photonics. Organic and, more recently, organometallic materials have been the subject of elaborate studies. Their versatile synthesis, combined with large and rapid NLO properties, makes them preeminent materials of choice.^[4–6] Until recently, the optimization of their second-order NLO properties has merely focused on the synthesis of compounds with improved donor, acceptor, or bridging moieties in typical D- π -A derivatives and octopoles (noncentrosymmetry is a prerequisite for second-order NLO). Parallel to this “synthetic” approach, a new route to tailor the molecular NLO response is now being explored, namely the modification of the optical nonlinearity “after synthesis”, using the photo- or electrochemical properties of the NLO compound.^[7–9] As for the chromoionophores, the changes induced by these processes on the ICT properties are in fact responsible for the modulation of the second-order NLO efficiencies.^[10] In this regard, the influence of cation binding on the molecular hyperpolarizability of a NLO functionalized crown ether (**4**; Scheme 2) is examined.

The functionalized crown shows an intense absorption band in the visible region attributed to ICT from the amine donor to the nitro acceptor moieties. Addition of alkaline(earth) ions induces antiauxochromic (hypsochromic and hypochromic effect) shifts in the absorption spectra (Table 1), as



Scheme 2. Synthesis of NLO functionalized crown ether. a) 3,6,9-trioxaundecane-1,11-diyl bistosylate, K_2CO_3 , dry acetone, reflux, quant.; b) methanolic MeNH_2 solution (40% v/v), in a sealed tube, 100 °C, quant.; c) 3,6,9-trioxaundecane-1,11-diyl bistosylate, NaH, dry DMF, 80 °C, 22%.

Table 1. Experimental results for the crown ether.

	$\Delta\lambda^{[a]}$ [nm]	$\beta_{\text{excess}}^{[b]}$ [10^{-30} esu]	$\beta_{\text{titr}}^{[c]}$ [10^{-30} esu]	$\log K_{\text{HRS}}^{[d]}$	$\log K_A^{[d]}$
Crown		38			
+ Na^+	– 12	32	28	1.6 ± 0.1	1.20 ± 0.02
+ K^+	– 14	27	28	2.5 ± 0.1	2.23 ± 0.02
+ Ba^{2+}	– 13	24	26	$3 \pm 2^{[e]}$	$6 \pm 3^{[e]}$

[a] λ_{max} of the crown ether is 406 nm. [b] Hyperpolarizability obtained using an excess of cation. [c] Hyperpolarizability obtained by titration. [b,c] *p*-nitroaniline was used as an external reference (29×10^{-30} esu), relative error on $\beta = 5\%$, except for $\text{Ba}^{2+} = 10\%$. [d] Stability constant K obtained by hyper-Rayleigh scattering (HRS) or absorption (A) measurements. [e] A slight increase of the signal at high concentrations prohibits a more accurate determination of K . This increment most likely originates from a weak type A interaction.

expected for type B interactions. Moreover, upon gradual addition of the cation, the spectra show a well defined isosbestic point (Figure 1), which suggests a 1:1 stoichiometry for the crown ether–ion complex formed. Although the observed blue shift is rather small, it does indicate that the interaction between the nitrogen lone pair and the alkaline(earth) ion hinders the ICT from the amine donor to the nitro acceptor within the conjugated NLO-phore. In other words, interaction with the cation reduces the electron donor strength of the amine. As such, a reduction of the nonlinear response may be expected.

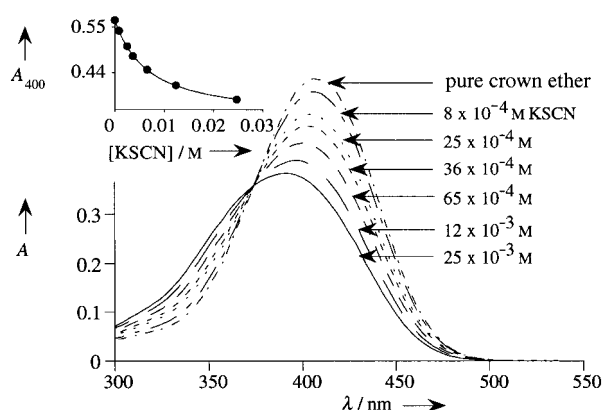


Figure 1. Effect of KSCN addition upon the absorption spectra of the crown ether **4**. Inset: Absorption at 400 nm versus the concentration of KSCN.

The molecular hyperpolarizability β of crown ether and complexes are determined by hyper-Rayleigh scattering (HRS).^[11, 12] As the induced hypsochromic shifts are rather modest and as the CT band is far from the second-harmonic wavelength (532 nm), variations in resonance enhancement are kept to a minimum. Therefore, the differences in β can be entirely attributed to the effect of the ion on the electronic structure of the NLO-active functionality.

HRS reveals a reduction of β by 25–35% upon addition of an excess amounts of cation (β_{excess} in Table 1). The largest reduction is obtained for Ba^{2+} , affirming that the bivalent ion is more efficient in attenuating the electron-donor character of the crown nitrogen atom. Further, both alkaline metal ions diminish the NLO response evenly. Hence, whereas both

diameter and charge of alkaline(earth) ions are known to influence the extent of complexation with crown ethers,^[1–3] the hyperpolarizability seems to be modulated only by their charge. Next, the NLO response has been monitored while gradually increasing the ion concentration. A progressive decrease of the HRS signal was observed (Figure 2). Utilizing

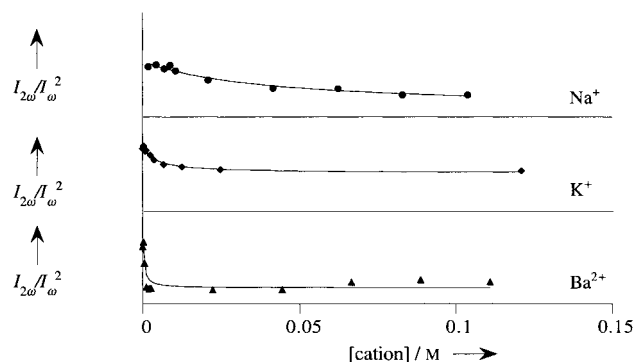


Figure 2. HRS signal ($I_{2\omega}/I_{\omega}^2$) as a function of the cation concentration. Solid lines represent the best fits according to Equation (4).

a modified HRS equation [Eq. (4)], we were able to describe this HRS signal as a function of the concentration of the added cation. The hyperpolarizabilities, as determined in the titration experiment, confirm the values found with an excess of cation. Again, the largest decrease is observed for complexation with the bivalent alkaline-earth ion. In addition, the modified HRS equation not only allowed for the assessment of β but also of the stability constant K (Table 1). The latter is shown to be in good agreement with the stability constant obtained with absorption titrimetry. In contrast to the NLO parameter, the stability constant does depend on both charge ($K_{\text{Ba}^{2+}} > K_{\text{K}^+}, K_{\text{Na}^+}$) and diameter of the cation ($K_{\text{Na}^+} < K_{\text{K}^+}$). This indicates that the match between the ionophore topology and the cation characteristics (for example, crown cavity versus ion radius) acts upon the ion affinity.^[1–3]

The results presented above demonstrate that the first hyperpolarizability of a NLO-functionalized ionophore can be reduced through cation binding. Correspondingly, they suggest that tuning can also be accomplished using type A interactions (that is, with the acceptor). To examine this route, we have studied the effect of binding K^+ on a 1,3-*cone* functionalized calixarene (**5**).^[13] For this system, the ICT band displays a significant bathochromic shift (40 nm) with an enhanced extinction coefficient upon cation binding (Figure 3), in accordance with type A interactions. As such, cation binding improves the ICT and the nonlinear response may be enhanced. The latter is again verified by HRS. In contrast to what was observed for the crown ether, the resonant enhanced hyperpolarizability of the calixarene indeed increases upon binding of the cation (Figure 4). However, no well defined isosbestic point was observed in the spectra

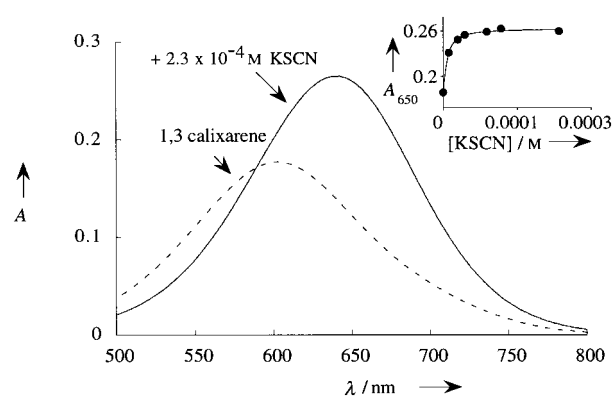
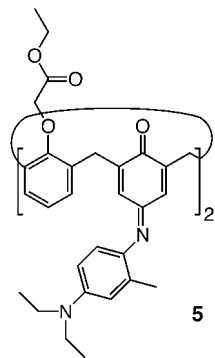


Figure 3. Effect of KSCN addition upon the absorption spectra of the indole calixarene **5**. Inset: Absorption at 650 nm versus the concentration of KSCN.

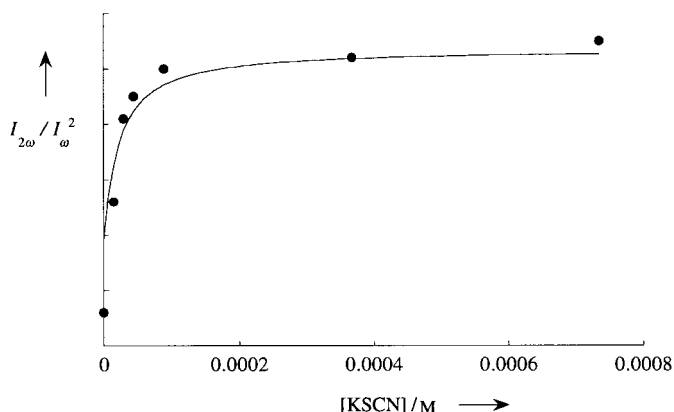


Figure 4. HRS signal of the calixarene in function of the added KSCN concentration. Solid lines represent the best fit with Equation (4).

during complex formation (no 1:1 complex), which precludes a correct determination of K , and β in the case of HRS, by titration. The study of the limiting structures revealed an increase in β of 70 % ($\beta_{\text{free calixarene}} = (170 \pm 10) \times 10^{-30}$ esu).

In conclusion, we have demonstrated that the molecular first hyperpolarizability of NLO-functionalized ionophores can be modulated through direct interaction of cations with the ionophore donor and acceptor moieties. Unprecedented, the difference in NLO response of crown ether and complex allowed us to monitor the cation binding and to determine the stability constant using hyper-Rayleigh scattering. As such, this technique offers a good alternative to study cation binding.

Experimental Section

Compound **1** was treated with 3,6,9-trioxaundecane-1,11-diyl bistosylate in the presence of K_2CO_3 to produce podand **2**, then a nucleophilic reaction with MeNH_2 afforded **3** in a quantitative yield (Scheme 2). Again, the Williamson synthesis with 3,6,9-trioxaundecane-1,11-diyl bistosylate was performed to give dibenzo-diaza[30]crown-10 derivative **4** in 22% yield after column chromatography. The synthesis of **5** has been reported elsewhere.^[13]

For the NLO experiments, acetonitrile was used as a solvent. Alkaline and alkaline-earth thiocyanides were of the highest quality available. HRS has

been discussed in detail previously.^[11, 12] Here, only the current analysis method used to monitor a titration will be elucidated:

The following considerations apply to 1:1 complexes with a stability constant K defined by [Eq. (1)], in which $[C]$, $[M]$, $[MC]$ represent the concentrations of crown ether, metal ion and complex, respectively.

$$K = \frac{[MC]}{[C][M]} \quad (1)$$

In our experiment, as well as the solvent and the crown ether as in a common HRS experiment (binary systems), the complex and the thiocyanide salt have also to be taken into account. Fortunately, no contribution of the salt could be observed; so the new HRS equation simplifies to [Eq. (2)], in which $I_{2\omega}$ (I_ω) is the harmonic (fundamental) intensity, g is a calibration constant, and $[i](\beta_i)$ are the actual concentrations (hyperpolarizability) of solvent ($i = S$) crown ($i = C$) and complex ($i = MC$).

$$\left(\frac{I_{2\omega}}{I_\omega^2}\right) = g[S]\beta_S^2 + g[C]\beta_C^2 + g[MC]\beta_{MC}^2 \quad (2)$$

Further, if we could assume that $[M] \approx [M]_0$, we can derive [Eq. (3)].

$$\left(\frac{I_{2\omega}}{I_\omega^2}\right) = g[S]\beta_S^2 + g[C]_0 \left\{ \frac{\beta_C^2 + K\beta_{MC}^2}{1 + K[M]_0} \right\} \quad (3)$$

Here, the HRS signal is represented as a function of the initial concentrations of crown ether $[C]_0$ and salt $[M]_0$. Therefore, if the hyperpolarizability of the crown ether is known, one can obtain the hyperpolarizability of the complex and the stability constant by plotting the HRS signal as a function of the initial concentration of added metal ion.

However, as the efficiency of complexation of the studied crown ether is too high, $[M]$ cannot be approximated by $[M]_0$. Consequently, the full HRS equation is given by [Eq. (4)].

$$\left(\frac{I_{2\omega}}{I_\omega^2}\right) = g[S]\beta_S^2 + g[C]_0\beta_C^2 + g(\beta_{MC}^2 - \beta_C^2) \frac{[C]_0 + [M]_0 + 1/K - \sqrt{([C]_0 + [M]_0 + 1/K)^2 - 4[C]_0[M]_0}}{2} \quad (4)$$

Again, a nonlinear least-squares analysis of the HRS signal versus $[M]_0$ delivers K and β_{MC} . A similar relation can be derived for the spectrophotometric analysis.^[14]

Received: January 31, 2000
Revised: June 5, 2000 [Z14620]

- [1] H. G. Löhner, F. Vögtle, *Acc. Chem. Res.* **1985**, *18*, 65.
- [2] B. Valeur in *Topics in Fluorescence Spectroscopy: Probe Design and Chemical Sensing*, Vol. 4 (Eds.: J. R. Lakowicz), Plenum, New York, **1994**, p. 21.
- [3] T. Hayashita, M. Takagi in *Molecular Recognition: Receptors for Cationic Guests*, Vol. 1 (Eds.: J. L. Atwood, J. E. D. Davies, D. D. MacNicol, F. Vögtle, G. W. Gokel), Elsevier Science, Oxford, **1996**, p. 635.
- [4] P. N. Prasad, D. J. Williams, *Introduction to Nonlinear Optical Effects in Molecules and Polymers*, Wiley-Interscience, New York, **1991**.
- [5] T. Verbiest, S. Houbrechts, M. Kauranen, K. Clays, A. Persoons, *J. Mater. Chem.* **1997**, *7*, 2175.
- [6] I. R. Whittall, A. M. McDonagh, M. G. Humphrey, M. Samoc, *Adv. Organomet. Chem.* **1998**, *42*, 291.
- [7] P. C. Ray, P. K. Das, *Chem. Phys. Lett.* **1997**, *281*, 243.
- [8] B. J. Coe, *Chem. Eur. J.* **1999**, *5*, 2464.
- [9] S. Yitzchaik, T. J. Marks, *Acc. Chem. Res.* **1996**, *29*, 197.
- [10] J. L. Oudar, D. S. Chemla, *J. Chem. Phys.* **1977**, *66*, 2664.
- [11] K. Clays, A. Persoons, *Rev. Sci. Instrum.* **1992**, *63*, 3285.
- [12] I. D. Morrison, R. G. Denning, W. M. Laidlaw, M. A. Stammers, *Rev. Sci. Instrum.* **1996**, *67*, 1445.
- [13] Y. Kubo, S. Tokita, Y. Kojima, Y. T. Osano, T. Matsuzaki, *J. Org. Chem.* **1996**, *61*, 3758.
- [14] J. Bourson, J. Pouget, B. Valeur, *J. Phys. Chem.* **1993**, *97*, 4552.

Self-Assembled Organometallic Block Copolymer Nanotubes**

Jose Ruez, Raluca Barjovanu, Jason A. Massey, Mitchell A. Winnik,* and Ian Manners*

Nanostructured materials offer exciting new possibilities in science and technology because of their unique characteristics.^[1] Since the discovery of carbon-based nanotubes,^[2] the prospect of using such structures as components in nanotechnology has led researchers to explore the design and fabrication of nanotubules using various other materials.^[3] The self-assembly of amphiphilic block copolymers in block-selective solvents has been shown to result in a myriad of nanoscale morphologies including spheres, cylinders, vesicles, and layers.^[4] In addition, bilayer tubule formation was recently reported for crew-cut polystyrene-*b*-poly(ethylene oxide) in water by Yu and Eisenberg,^[5] while Stewart and Liu^[6] have constructed monolayer nanotubes from a triblock copolymer which forms cylindrical micelles by sequential corona cross-linking and selective core degradation. Jenekhe and Chen have also formed monolayer tubules from rod-coil block copolymers and have examined the encapsulation of fullerenes.^[7]

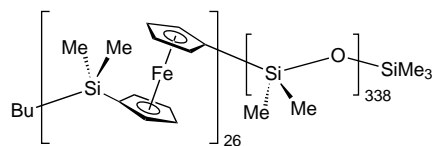
The self-assembly of block copolymers clearly offers a potentially powerful route for the generation of nanostructured materials however, to date, virtually all the studies have focussed on organic block polymers. As a result of the discovery of the living anionic ring-opening polymerization (ROP) of strained silicon-bridged [1]ferrocenophanes, it has become possible to access polyferrocene block copolymers which combine organometallic segments with inorganic or organic coblocks.^[8, 9] The incorporation of the polyferrocene block offers the opportunity to access self-assembled materials with redox-active, semiconducting or preceramic nano-domains, or with large periodic variations in the refractive index suitable for optical and photonic applications.^[10, 11] We have previously reported the self-assembly of poly(ferrocenyldimethylsilane-*b*-dimethylsiloxane) (PFS-*b*-PDMS, block ratio of 1:6) to form PFS cylinders within a PDMS matrix in the solid state and novel “wormlike” micelles with a PFS core and a PDMS corona in hexane. As a result of the presence of a PFS core such phase separated structures are of interest as

[*] Prof. M. A. Winnik, Prof. I. Manners, J. Ruez, R. Barjovanu, Dr. J. A. Massey
Department of Chemistry
University of Toronto
80 St. George Street, Toronto, ON, M5S 3H6 (Canada)
Fax: (1)416-978-6157
E-mail: mwinnik@chem.utoronto.ca
imanners@chem.utoronto.ca

[**] This research was supported by the Natural Science and Engineering Research Council of Canada (NSERC). In addition, I.M. is grateful to the NSERC for a Steacie Fellowship (1997–99), the University of Toronto for a McLean Fellowship (1997–2003), and the Ontario Government for a PREA Award (1999–2004). M.A.W. expresses his gratitude to the Canada Council for a Killam Fellowship. The authors thank Batista Calvieri and Steve Doyle of the Microscopy and Imaging Laboratory (Faculty of Medicine, University of Toronto) for their assistance in obtaining TEM images. We also thank Dr. Matthew Moffitt and Lan Cao for the enlightening discussions.

possible semiconductive or magnetic nanowires.^[12] Herein, we report the surprising and facile formation of the first organo-metallic nanotubes using a PFS-*b*-PDMS block copolymer with a different block ratio of 1:13.

The synthesis of PFS₂₆-*b*-PDMS₃₃₈ (**1**) was accomplished by using a sequential anionic ROP procedure analogous to that described previously.^[12] In a block selective solvent for PDMS such a block ratio would be expected to promote the



PFS-*b*-PDMS, **1**

formation of spherical “starlike” micelles with a PFS core. However, a remarkable self-assembly process to form tubules was achieved simply by the direct dissolution of block copolymer **1** in hexanes, a good solvent for PDMS and a precipitant for PFS. Micellar solutions with various initial concentrations of polymer **1** were prepared and the formation of the tubes was confirmed by transmission electron microscopy (TEM) after solvent evaporation. As the ferrocene units are electron rich and TEM relies on differences in electron density for contrast, the poly(ferrocene) regions were imaged selectively without staining. The PDMS corona is not apparent in the TEM images unless the entire micelle is shadowed with Pt atoms (see below).

Figure 1 illustrates the network of nanotubes produced at a polymer concentration of 2.1 mg mL^{−1} (in hexanes). The width of the tubules is 29 nm, and remains constant along the entire length. The width of the PFS shell is about 9 nm, which

of the nanotubes. As discussed below, these spheres appear to fuse over time.

At a lower concentration of 0.55 mg mL^{−1} (Figure 1b), hollow spheres and tubes of various lengths form, which provided further interesting data. The tubes are 40 nm wide, with a cavity of 22 nm width and lengths ranging from 50 to 500 nm. Hollow spheres are also observed in the image, with a diameter that is close to the thickness of the tubes. Even though the width of the tubes is larger than that formed at higher concentration, the width of the PFS layer remains constant at approximately 9 nm.

Based on the crystal structure of a linear pentameric oligo(ferrocenyldimethylsilane), the distance between monomers in a fully extended chain would be 6.91 Å.^[13, 14] Thus, the theoretical length of a fully stretched block with 26 PFS units in the shell is 18 nm, twice as long as the measured thickness of the PFS layer. Therefore, the PFS block does not appear to be fully extended. A similar result has been observed in PFS-*b*-PDMS wormlike micelles, where the PFS core has a diameter of 20 nm, which represents a maximum PFS block length of 10 nm.^[9] As 33 ferrocene units are present in the PFS block of that particular block copolymer, the theoretical fully stretched length is 22 nm, which is also twice the actual length. This observation suggests that the packing of the PFS chains in the cylindrical micelles is similar to that in the nanotubes.

Valuable information can also be extracted from Figure 1b to suggest how the organometallic tubules may form. Nanotube assembly appears to arise from the fusion of smaller “subunits”, such as spherical aggregates and shorter tubes. Although no intermediate has been trapped thus far and no vesicles have been found to pinch together as Yu and Eisenberg have observed,^[5] the increase of tubule length as a function of concentration suggests the fusion of smaller structures to form longer ones. A detailed time-dependence study is desirable, and we have performed some preliminary experiments. Figure 2a shows a sample taken from the 2.1 mg mL^{−1} micellar solution in hexanes after three weeks, where the length of the tubes reaches 1.50 μm, and the number of spheres has dramatically decreased. Figure 2b shows a sample taken from the 0.55 mg mL^{−1} solution after six weeks, where the spherical aggregates are also no longer present and the tubes have increased in length. These results imply that the hollow spheres are precursors of the tubules.

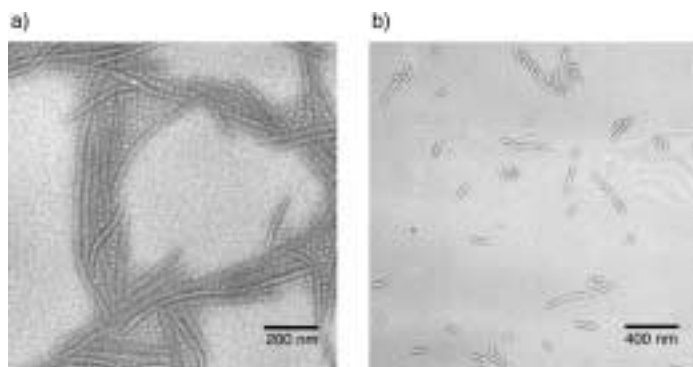


Figure 1. TEM micrographs of PFS-*b*-PDMS micelles in hexanes taken after three days of self-assembly at concentrations of: a) 2.1 mg mL^{−1} and b) 0.55 mg mL^{−1}.

corresponds to the average PFS block length in a distribution of lengths, and thus leaves a cavity width of 11 nm. Tubules formed at a concentration of 1 mg mL^{−1} or greater have the same width. The length of these nanotubes ranges from 360 to 930 nm. One can also observe the presence of monodisperse spherical aggregates or hollow spheres, among the tubules. These spheres have a diameter of 29 nm, the same as the width

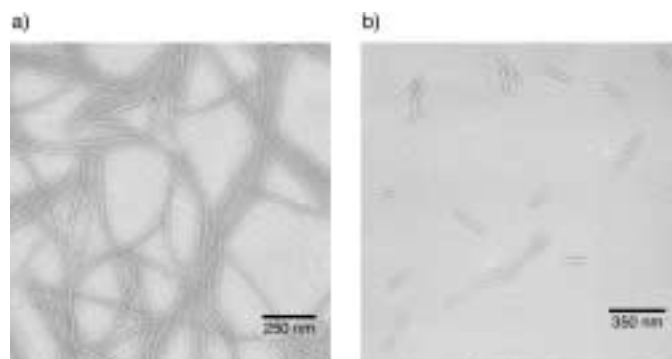


Figure 2. TEM micrographs of PFS-*b*-PDMS micelles in hexanes: a) 2.1 mg mL^{−1} taken after three weeks, b) 0.55 mg mL^{−1} taken after six weeks.

Although there is no theory explaining the formation of cavities in systems such as ours, de Gennes predicted the formation of bilayer tubules from vesicles for a rod-coil system.^[15, 16]

Noteworthy is that optical effects can make it difficult to distinguish between hollow tubes and solid cylinders by TEM a result of misfocussing. To address this issue we deposited the aggregates derived from **1** in hexanes onto a TEM grid already covered with solid cylindrical micelles of PFS₄₂-*b*-PI₁₈₈ (PI = polyisoprene). Reexamination of the grid showed the presence of both nanotubes and cylinders.

Based on the analysis of the TEM micrographs we propose the structure for these tubules shown schematically in Figure 3a. Although we have shown evidence to indicate that these structures are single walled, it is possible that some of

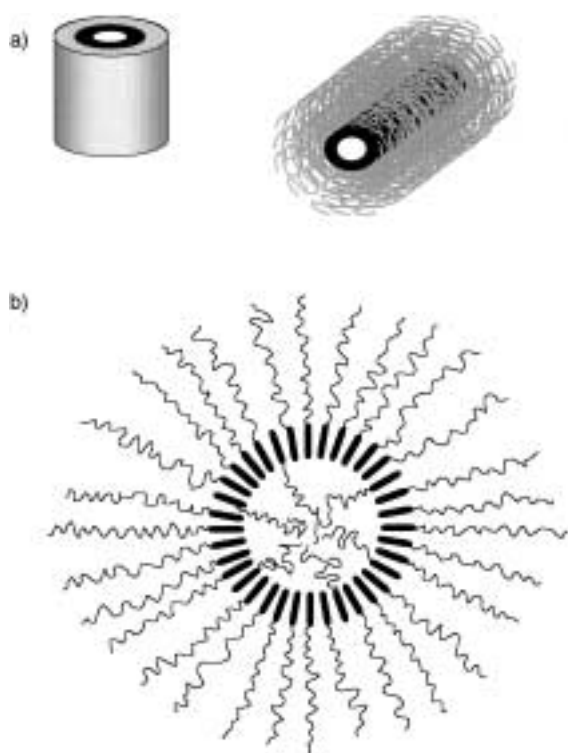


Figure 3. a) Schematic representation of a PFS-*b*-PDMS tubule. The PDMS block is the corona (gray region or coils), and the PFS block is the shell in the tube (black). The cavity is located in the middle (white). The schematic tubule is not drawn to scale. b) Schematic cross section of a tubule. PFS blocks are represented by rods and the PDMS blocks are represented by coils.

the PDMS chains are inverted, pointing towards the tubular cavity (Figure 3b). Thus some PDMS blocks may be trapped within the cavities during the self-assembly process. Because of the curvature, which leads to the formation of spherical and, eventually, tubular morphologies, we imagine that the number of PDMS chains in the exterior corona is much larger than the number inside the cavity.

Although the images in Figure 1 and 2 indicate that the micelles formed are hollow, we attempted to obtain additional evidence to support this proposition by trying to fill the cavity with a substance that could be detected in TEM experiments. This encapsulant chosen was *n*-butylferrocene (BuFc) as this

species is sufficiently volatile that material not encapsulated by the tubes would evaporate under the vacuum present in the TEM sample chamber. At the same time we hoped that loss of material by leakage through the tube ends would be relatively slow. Encapsulation was achieved by dissolving **1** in a solution of BuFc in hexanes. This procedure caused the tubules to assemble while trapping BuFc within their cavities (Figure 4).

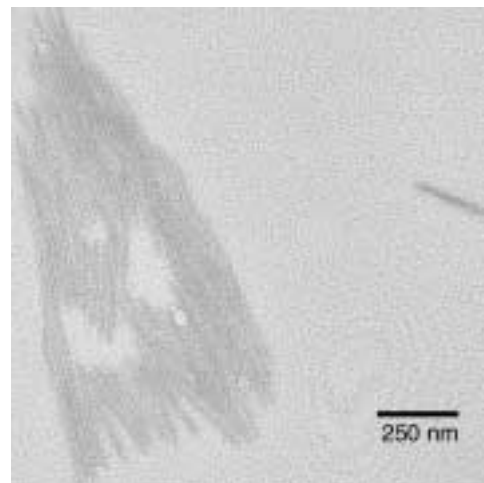


Figure 4. TEM micrograph of PFS-*b*-PDMS tubules with *n*-butylferrocene encapsulated within the cavities.

Two important pieces of information can be extracted from the Figure. First, since BuFc is electron rich it is dark under TEM relative to the background. Such contrast can be seen in the middle region of the tube, which appears clear in tubules without added BuFc, and supports the premise that these tubules are indeed hollow and that they have been “filled” with BuFc. Second, encapsulation of BuFc did not distort the morphology or dimensions (still 29 nm in width) of the self-assembled tubules.^[17] As shown previously, the PFS blocks can crystallize (melting temperature (T_m) ca. 122–143 °C) and lock a structure in place.^[11, 14] It would then be unlikely that facile distortion of the nanotubes would occur, and it appears that these structures are indeed stable to the addition of small molecules.

We attempted to take advantage of the hydrophobicity of the PDMS corona and added water to see if the tubules would fuse together. Four weeks after the self-assembly of tubules in a 1 mg mL⁻¹ micellar solution in hexanes twice the volume of water was added, and the mixture was agitated. TEM images showed that this treatment resulted in the organization of tubules into bundles (Figure 5). This process also increased the tubule length to 7 μm whereas the tubule width was unaffected. The fusion of these tubes in the presence of water provides further evidence for the formation of long tubes from smaller tubes and hollow spheres.

As TEM selectively images the PFS regions, the TEM-derived dimensions exclude the width of the PDMS corona. We therefore performed Pt shadow-casting TEM on the 1 mg mL⁻¹ sample to estimate the width of the corona in the solid state. Figure 6 reveals the nanostructure with a Pt coating; the hollow cavity of the tube is no longer apparent as

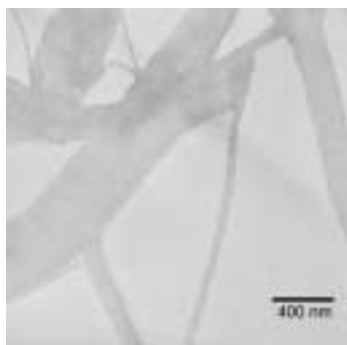


Figure 5. TEM micrograph of PFS-*b*-PDMS tubules after the addition of water.

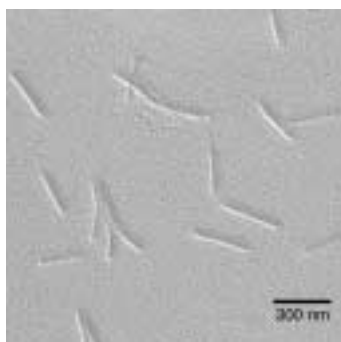


Figure 6. Platinum shadow-casting TEM micrograph of PFS-*b*-PDMS tubules performed at a 20° angle.

the dense Pt atoms cover the entire micelle. By performing some basic geometric calculations based on the angle at which this procedure was carried out (20°) and the length of the shadow, we determined the height of the tube to be between about 10–20 nm and the overall width to be around 40–50 nm. It appears that the Pt coating used partially buried the tubes, thus leading to a smaller apparent height than expected, and the geometry of the cross section therefore cannot be confirmed to be a perfect circle.

In summary, we have demonstrated the facile and unexpected formation of novel organometallic nanotubes by the self-assembly of PFS-*b*-PDMS block copolymer **1** in hexanes. Encapsulation of BuFc also showed the presence of a cavity within the tubes and the ability to insert small molecules inside the structures.

Experimental Section

The synthesis of polymer **1** was performed by a published procedure,^[9,12] the only difference was the amount of monomer used so as to obtain a 1:13 PFS:PDMS ratio. A solution of the block copolymer **1** in THF was analyzed by gel permeation chromatography (GPC) versus polystyrene standards, which revealed an estimated M_n of 36300 g mol⁻¹, polydispersity index (PDI) = 1.04. ¹H NMR spectroscopic analysis was used to determine the ratio of PFS to PDMS (1:13). The number of repeat units for the PFS block was determined by GPC (M_n = 6360 g mol⁻¹) for a homopolymer sample which was removed prior to block copolymer formation. ¹H NMR (200 MHz, C₆D₆): δ = 0.28 (s, 78H, SiO(CH₃)₂), 0.55 (s, 6H, FcSi(CH₃)₂), 4.10 (s, 4H, C₃H₄), 4.26 (s, 4H, C₃H₄). The sample of PFS₄₂-*b*-PI₁₈₈ was prepared as part of a separate study.^[17]

Encapsulation of *n*-butylferrocene (BuFc) was performed by diluting BuFc (100 mg; purchased from Aldrich Co.) with hexanes (10 mL), followed by

the addition of PFS-*b*-PDMS (10 mg) to the mixture. Excess BuFc spontaneously evaporated inside the microscope.

Samples for TEM were prepared by aerosol spraying a micellar solution (ca. 50 μL) with a specific polymer concentration onto a carbon film (ca. 10 Å) grown on mica and then floated off the mica and placed on 300-mesh gilder copper TEM grids. For the samples mixed with water, a micellar solution (20 μL of a 1 mg mL⁻¹ solution) was mixed with water (40 μL). The mixture was briefly agitated and then the two-phase mixture (15 μL) was placed on a 300-mesh gilder copper grid for 2 min. The excess fluid was removed by touching the droplet with a piece of filter paper. Transmission electron micrographs were obtained on a Hitachi model 600 electron microscope.

For platinum shadow casting, a micellar solution (1 mg mL⁻¹) was sprayed on a carbon-coated mica and then placed in a high vacuum chamber coater (Edwards, model E12E4) above a 5 mm spherical platinum source at a 20° angle. Pt atoms were sprayed onto the mica by inducing high voltage at 10⁻⁵ Torr. The sample was then floated onto a 300-mesh copper grid.

Received: April 26, 2000 [Z15045]

Publication delayed at authors' request

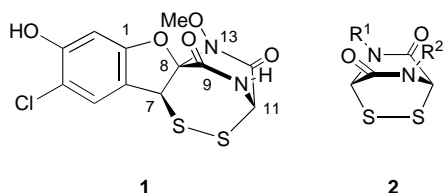
- [1] G. A. Ozin, *Adv. Mater.* **1992**, *4*, 612.
- [2] P. M. Ajayan, *Chem. Rev.* **1999**, *99*, 1787, and references therein.
- [3] a) F. Krumeich, H. J. Muhr, M. Niederberger, F. Bieri, B. Schnyder, R. Nesper, *J. Am. Chem. Soc.* **1999**, *121*, 8324; b) M. Adachi, T. Harada, M. Harada, *Langmuir* **2000**, *16*, 2376; c) K. B. Shelimov, M. Moskovits, *Chem. Mater.* **2000**, *12*, 250; d) J. C. Hulteen, K. B. Jirage, C. R. Martin, *J. Am. Chem. Soc.* **1998**, *120*, 6603; e) C. M. Zelenski, P. K. Dorhout, *J. Am. Chem. Soc.* **1998**, *120*, 734; f) C. R. Marti, *Chem. Mater.* **1998**, *10*, 1738; g) M. Remsak, Z. Skraba, M. Regula, C. Ballif, R. Sanjinés, F. Lévy, *Adv. Mater.* **1998**, *10*, 246.
- [4] a) C. Price, *Pure Appl. Chem.* **1983**, *55*, 1563; b) M. Antonietti, S. Heinz, M. Schmidt, C. Rosenauer, *Macromolecules* **1994**, *27*, 3276; c) L. Zhang, A. Eisenberg, *Science* **1995**, *268*, 1728; d) L. Zhang, A. Eisenberg, *J. Am. Chem. Soc.* **1996**, *118*, 3168; e) A. Singh, P. Schoen, J. Schnur, *J. Chem. Soc. Chem. Commun.* **1988**, 1222; f) K. Yu, C. Bartels, A. Eisenberg, *Langmuir* **1999**, *15*, 7157; g) G. Liu, *Adv. Mater.* **1997**, *9*, 437; h) J. Ding, G. Liu, *Chem. Mater.* **1998**, *10*, 537; i) J. P. Spatz, S. Mößmer, M. Möller, *Angew. Chem.* **1996**, *108*, 1673; *Angew. Chem. Int. Ed. Engl.* **1996**, *35*, 1510.
- [5] K. Yu, A. Eisenberg, *Macromolecules* **1998**, *31*, 3509.
- [6] S. Stewart, G. Liu, *Angew. Chem.* **2000**, *112*, 348; *Angew. Chem. Int. Ed.* **2000**, *39*, 340.
- [7] S. Jenekhe, L. Chen, *Science* **1998**, *279*, 1903.
- [8] R. Rulkens, Y. Ni, I. Mannes, *J. Am. Chem. Soc.* **1994**, *116*, 12121.
- [9] Y. Ni, R. Rulkens, I. Mannes, *J. Am. Chem. Soc.* **1996**, *118*, 4102.
- [10] J. A. Massey, K. N. Power, M. Winnik, I. Mannes, *Adv. Mater.* **1998**, *10*, 1559.
- [11] a) I. Mannes, *Chem. Commun.* **1999**, 857; b) I. Mannes, *Pure Appl. Chem.* **1999**, *71*, 1471.
- [12] J. Massey, K. N. Power, I. Mannes, M. Winnik, *J. Am. Chem. Soc.* **1998**, *120*, 9533.
- [13] R. Rulkens, A. J. Lough, I. Mannes, *J. Am. Chem. Soc.* **1994**, *116*, 797.
- [14] R. Rulkens, A. J. Lough, I. Mannes, S. R. Lovelace, C. Grant, W. E. Geiger, *J. Am. Chem. Soc.* **1996**, *118*, 12683.
- [15] A rod-coil system refers to block copolymers in which one of the blocks is rigid and aggregates spontaneously in certain solvents, while the other block is a coil. a) M. Müller, M. Schick, *Macromolecules* **1996**, *29*, 8900; b) A. Halperin, *Macromolecules* **1990**, *23*, 2724.
- [16] P. G. de Gennes, *C. R. Acad. Sci. Ser. 2*, **1987**, *304*, 259.
- [17] One might expect some *n*-butylferrocene (BuFc) to be solubilized into the PFS domains but this was not observed. We believe that this is a consequence of the crystalline nature of the PFS block. For recent work addressing the effects of crystallinity of the PFS core in cylindrical micelles of PFS-*b*-PDMS, see J. A. Massey, K. Temple, L. Cao, Y. Rharbi, J. Racz, M. A. Winnik, I. Mannes, *J. Am. Chem. Soc.* **2000**, *122*, in press.

A Three-Step Entry to the Spirochlorine Family of Antifungal Agents**

Zhicai Wu, Lawrence J. Williams, and Samuel J. Danishefsky*

Dedicated to Professor Yoshito Kishi

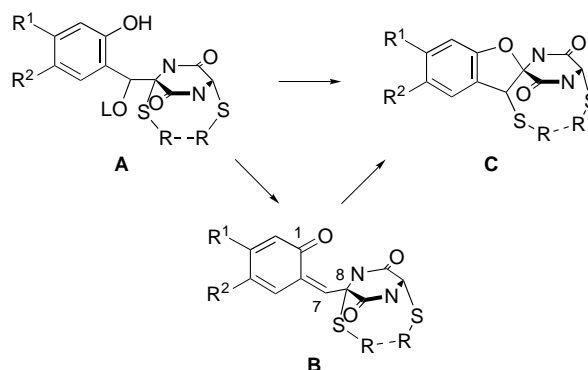
Our laboratory has been studying a variety of natural products containing diketopiperazines (DKP) in the setting of indole alkaloid structures.^[1] It was in this context that aspirochlorine (**1**), a bacterially derived metabolite isolated from various *Aspergillus* species, first caught our attention.^[2] While initial reports on the biological properties of aspirochlorine had not been particularly encouraging, a recent disclosure from the Lepetit Research Center^[3] indicated that this compound is a rather selective and potent inhibitor of fungal protein synthesis.



In addition to its increasingly attractive biological profile, aspirochlorine exhibits several structural features of particular interest. The epidithiodiketopiperazine (EDKP) moiety **2** is certainly well known in other natural products.^[4] However, in the case of aspirochlorine one of the sulfur atoms is anchored not to the piperazine, but to the C(7) position of a spiro-fused dihydrobenzofuran substructure. Moreover, the two nitrogens of the DKP present novel structural characteristics as well. One of these nitrogens, N(13), bears a most unusual *N*-methoxy substituent, which is rarely present in DKP natural products. The other nitrogen atom is present in the form of a free NH linkage bearing a geminal sulfur atom. As such, there could well be concern over the possibility of a low energy, but destabilizing, pathway leading to acyl iminium character at C(11).^[5]

These structural complexities notwithstanding, a total synthesis of aspirochlorine was accomplished by Williams and Miknis.^[6] Our interest in revisiting the aspirochlorine prob-

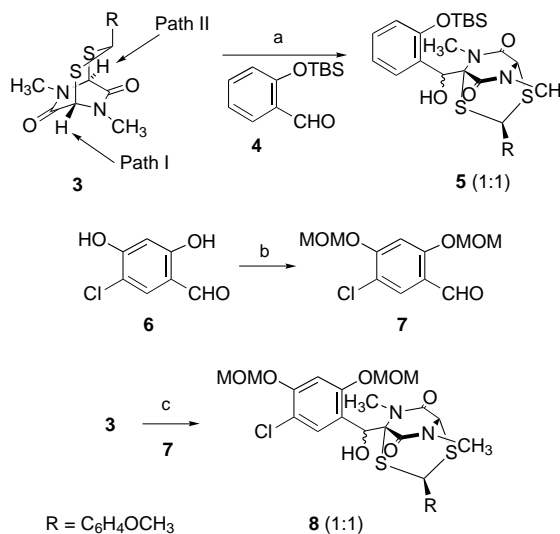
lem, by a route quite different than that used in the previous synthesis, arose from a provocative, albeit unsupported, conjecture (Scheme 1). The thought was that the ring-enlarged dithio system present in **1** could arise from the rearrangement^[7] of a more typical type of EDKP precursor **A**.^[8] The electrophilic character that promotes rearrangement to **C** might arise directly upon heterolysis of the leaving group (OL) in **A**. Alternatively, loss of HOL from **A** might give rise to quinomethide **B**, which could serve as the active electro-



Scheme 1. Proposed sulfur rearrangement.

phile.^[9] The ultimate hope in this case was that the sulfur migration step, though in principle reversible, might be followed by attack of the oxygen attached at position C(1) upon the now electrophilic C(8) bridgehead, thereby giving rise to the dihydrobenzofuran core of our target, **C**. While direct rearrangement of **A** to **C**, or rearrangement of **A** to **C** via **B**, implicitly raises issues of stereoselectivity at the migration terminus C(7), we postpone consideration of this interesting question until the results of the research are presented.

To evaluate the feasibility of such a functional group reorganization in a model system, we synthesized the known bicyclic thioacetal **3** (Scheme 2).^[10] We were well aware of the



Scheme 2. Preparation of alcohols **5** and **8**. Conditions: a) BuLi, THF, then **4**, -78°C , 40%; b) MOMCl, $i\text{Pr}_2\text{NEt}$, DMF, $0^{\circ}\text{C} \rightarrow \text{RT}$, 95%; c) BuLi, THF, then **7**, -78°C , 67%. MOM = methoxymethyl, TBS = *tert*-butyldimethylsilyl, RT = room temperature.

[*] Prof. S. J. Danishefsky, Dr. L. J. Williams
Laboratory for Bioorganic Chemistry
Sloan-Kettering Institute for Cancer Research
1275 York Avenue, New York, NY 10021 (USA)
Fax: (+1) 212-772-8691
E-mail: s-danishefsky@ski.mskcc.org

Prof. S. J. Danishefsky, Dr. Z. Wu
Department of Chemistry, Columbia University
Havemeyer Hall, 3000 Broadway, New York, NY 10024 (USA)

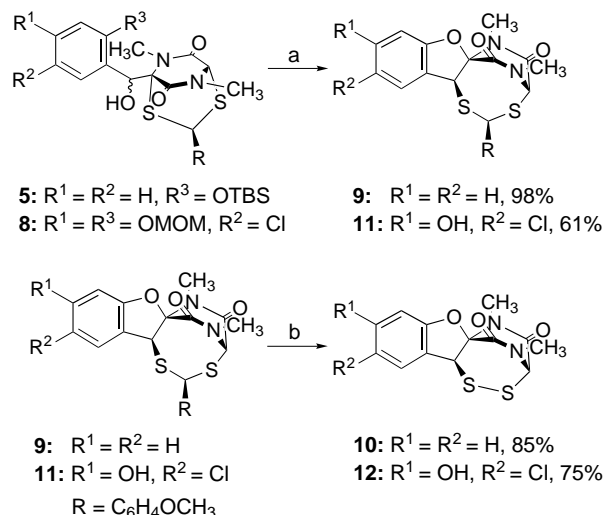
[**] This work was supported by the National Institutes of Health (grant numbers: AI16943/CA28824/HL25848). L.J.W. gratefully acknowledges the NIH for a Postdoctoral Fellowship Grant (grant number: NIHF32CA79120). Prof. Gerard Parkin and Mr. Brian M. Bridgewater of Columbia University are gratefully acknowledged for the X-ray analysis.

Supporting information for this article is available on the WWW under <http://www.wiley-vch.de/home/angewandte/> or from the author.

penetrating studies of Kishi and co-workers^[11] which served to demonstrate that, in a system of this sort, deprotonation of the seemingly similar bridgehead protons may well occur with high diastereotopic selectivity. Indeed, based on the precedents of Kishi et al., it might be expected that deprotonation would follow the course suggested by Path I in preference to Path II. For our purposes it would be necessary to extend such findings to aldol-like reactions of such anions.^[12]

Accordingly, we wondered about base-induced condensation of **3** with substituted benzaldehydes, such as **4**, with the expectation of reaching precursors of type **A**. Indeed, exposure of **3** to butyl lithium, at low temperature, followed by addition of **4** gave the corresponding alcohols **5** (Scheme 2). In a similar vein, a more realistic aldehyde **7** was prepared by protection of **6**^[13] as the bis methoxymethyl ether. The condensation procedure was then executed to combine the anion of **3** with **7** and give the expected alcohols **8**. In each of these cases, NMR analysis indicated the formation of a two-component (1:1) mixture of products. At the time, we could not be certain whether the components of the mixture reflected stereochemical randomness in the deprotonation or in the C–C bond formation process. Nonetheless, we moved to the next phase of the synthesis.

We chose to start with simple acidolysis of the benzylic alcohol (Scheme 3). Remarkably, the action of anhydrous trifluoromethanesulfonic acid in acetonitrile on **5** furnished



Scheme 3. Rearrangement of EDKPs **9** and **11**. Conditions: a) CF_3SO_3H , CH_3CN , RT; b) *m*CPBA, CH_2Cl_2 , $0^\circ C$; then Me_2S , then $HClO_4$ in $MeOH$, $0^\circ C \rightarrow RT$. *m*CPBA = *meta*-chloroperoxybenzoic acid.

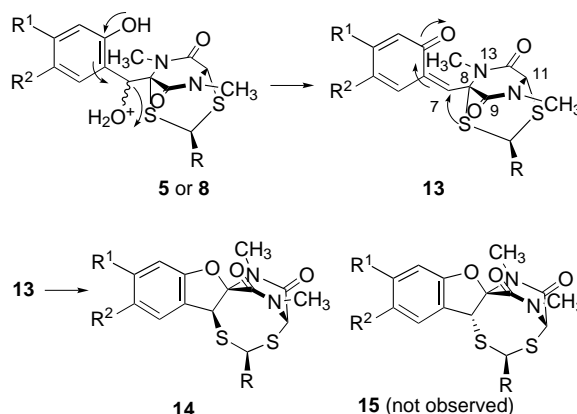
exclusively a dehydration product as a single diastereomer and in near quantitative yield. We concluded that **5** was indeed a 1:1 mixture of hydroxy epimers. These had converged to a single product by sulfur migration and associated formation of the spiro linkage. That this product was in fact the desired compound **9** with the relative stereochemistry required for aspirochlorine was unequivocally established by crystallographic analysis.^[14]

Having effected the desired rearrangement there remained the issue of removing the thioacetal and forming the disulfide bridge, as it is present in the natural product. Following the precedent of Kishi and co-workers^[11] it might be expected that

disulfide formation in a protected EDKP could be effected from a *p*-methoxybenzylidene dithioacetal by oxidation of one of the sulfur atoms to a sulfoxide. The conversion of a non-EDKP thioacetal of type **9** however, was not precedent. Happily, the action of *meta*-chloroperoxybenzoic acid followed by treatment of the monosulfoxide with perchloric acid cleanly converted **9** into the corresponding disulfide **10**.

It was important to test the applicability of this chemistry in a more realistic scenario. Upon applying anhydrous acid conditions to benzylic alcohols **8**, the rearranged product **11** was obtained as a single diastereomer. Moreover, application of the thioacetal deprotection sequence to produce **12** also proceeded smoothly, to give an advanced model of the natural product, which differs from aspirochlorine only in the substituents on the nitrogen atoms.^[15]

Clearly the stereochemical outcomes at position C(7) in the rearrangements are independent of the configurations at this center in the starting alcohols **5** and **8** (Scheme 4). This finding rules out obligatory inversion at the migration terminus in the



Scheme 4. Mechanistic rationalization of the stereoselective rearrangement of **5** and **8**.

rearrangement but does not go into the question of the intermediacy of quinomethide (see **13**). We also note that the preference for sulfur migration to the β -face^[16] of position C(7) (that is, *syn* to C(9)) cannot easily be interpreted as a consequence of least-motion considerations,^[17] since the plane containing the bridgehead carbons C(8) and C(11), as well as the two sulfur atoms, appears to bisect the median plane of the DKP ring. Hence, the observed stereospecificity reflects an inherent preference of the sulfur to migrate *syn* to position C(9) rather than N(13). A possible, though certainly unproven, interpretation is that in the operative β -face pathway leading to **14**, the sulfur atom can maintain a favorable long-range interaction with the C(9) carbonyl center.^[18] By contrast, movement from the α -face (leading to unobserved product **15**) might incur relatively unfavorable electronic or steric interactions with the N(13) methyl function.^[19] Thus, it will be of interest, and of importance to the total synthesis, to learn whether this face selectivity is responsive to the nature of the substituent at position N(13).^[20]

In summary, we have demonstrated an unprecedented sulfur migration in a protected EDKP. This rearrangement occurs in a highly stereoselective manner and in high yield. The amenability of this chemistry to produce structural

diversity in a quest for superior antifungal agents is apparent on inspection. Efforts to implement this rearrangement as a key simplifying transformation in the total synthesis of the fully elaborated aspirochlorine system will be reported in due course.

Received: July 4, 2000 [Z15385]

- [1] Spirotryprostatin A: S. Edmondson, S. J. Danishefsky, L. Sepp-Lorenzino, N. Rosen, *J. Am. Chem. Soc.* **1999**, *121*, 2147; himastatin: T. M. Kamenecka, S. J. Danishefsky, *Angew. Chem.* **1998**, *110*, 3166; *Angew. Chem. Int. Ed.* **1998**, *37*, 2995; 5-*N*-acetylardeemin and amaumine: K. M. Depew, S. P. Marsden, D. Zatorska, A. Zatorski, W. G. Bornmann, S. J. Danishefsky, *J. Am. Chem. Soc.* **1999**, *121*, 11953; gypsetin, deoxybrevianamide E, brevianamide E, and tryprostatin: J. M. Schkeryantz, J. C. G. Woo, P. Siliphaivanh, K. M. Depew, S. J. Danishefsky, *J. Am. Chem. Soc.* **1999**, *121*, 11964; spirotryprostatin B: F. von Nussbaum, S. J. Danishefsky, *Angew. Chem.* **2000**, *112*, 2259; *Angew. Chem. Int. Ed.* **2000**, *39*, 2175.
- [2] A. Kato, T. Saeki, S. Suzuki, K. Ando, G. Tamura, *J. Antibiot.* **1969**, *22*, 322; D. H. Berg, R. P. Massing, M. M. Hoehn, L. D. Boeck, R. L. Hamill, *J. Antibiot.* **1976**, *29*, 394; K. Sakata, A. Masago, A. Sakurai, N. Takahashi, *Tetrahedron Lett.* **1982**, *23*, 2095; K. Sakata, T. Kuwatsuka, A. Sakurai, N. Takahashi, G. Tamura, *Agric. Biol. Chem.* **1983**, *47*, 2673; K. Sakata, M. Maruyama, J. Uzawa, A. Sakurai, H. S. M. Lu, J. Clardy, *Tetrahedron Lett.* **1987**, *28*, 5607; for structurally related gliovirin and FA-2097, see: R. D. Stipanovic, C. R. Howell, *J. Antibiot.* **1982**, *35*, 1326 (gliovirin); C. Miyamoto, K. Yokose, T. Furumai, H. B. Maruyama, *J. Antibiot.* **1982**, *35*, 376 and K. Yokose, N. Nakayama, C. Miyamoto, T. Furumai, H. B. Maruyama, R. D. Stipanovic, C. R. Howell, *J. Antibiot.* **1984**, *37*, 667 (FA-2097).
- [3] F. Moonti, F. Ripamonti, S. P. Hawser, I. Khalid, *J. Antibiot.* **1999**, *52*, 311.
- [4] A. W. Braithwaite, R. D. Eichner, P. Waring, A. Mullbacher, *Mol. Immunol.* **1987**, *24*, 47; P. Waring, R. D. Eichner, A. Mullbacher, *Med. Res. Rev.* **1988**, *8*, 499; R. D. Eichner, P. Waring, A. M. Geue, A. W. Braithwaite, A. Mullbacher, *Med. Res. Rev.* **1988**, *8*, 499.
- [5] H. Hiemstra, W. N. Speckamp in *Comprehensive Organic Synthesis*, Vol. 2 (Eds: B. M. Trost, I. Fleming), Pergamon, Oxford, **1991**, pp. 1047–1082; H. De Koning, W. N. Speckamp, *Methods Org. Chem. (Houben-Weyl) 4th ed.*, 1952–, Vol. E21, **1995**, p. 1953; W. N. Speckamp, M. J. Moolenaar, *Tetrahedron* **2000**, *56*, 3817.
- [6] a) R. M. Williams, G. F. Miknis, *Tetrahedron Lett.* **1990**, *30*, 42997; b) G. F. Miknis, R. M. Williams, *J. Am. Chem. Soc.* **1993**, *115*, 536.
- [7] For recent examples of sulfanyl migrations, see: L. Djakovitch, J. Eames, D. J. Fox, F. H. Sansbury, S. Warren, *J. Chem. Soc. Perkin Trans. 1* **1999**, 2771; J. Eames, S. Warren, *J. Chem. Soc. Perkin Trans. 1* **1999**, 2783; J. Eames, D. J. Fox, M. A. D. L. Haras, S. Warren, *J. Chem. Soc. Perkin Trans. 1* **2000**, 1903; and references therein.
- [8] At this stage we leave unspecified the nature of the R---R insert in structures **A**–**C**. The sulfur groups may be separated, directly connected, or connected through a linker.
- [9] It is recognized that the species produced from protonation of the ketonic oxygen of quinomethide **B** formally converges with the product of **A** upon acid-induced heterolysis of OL.
- [10] For the preparation of **3**, see Ref. [11a], and references therein.
- [11] a) Y. Kishi, T. Fukuyama, S. Natatsuka, *J. Am. Chem. Soc.* **1973**, *95*, 6490; b) T. Fukuyama, S. Natatsuka, Y. Kishi, *Tetrahedron* **1981**, *37*, 2045.
- [12] Refs. [11a] and [11b] include the addition of nucleophiles derived from **3** to primary halides and acid chlorides.
- [13] Several preparations of **6** exist; see, for example, Ref. [6b], and references therein.
- [14] All new compounds display satisfactory spectroscopic and analytical data consistent with the assigned structures. Crystallographic data (excluding structure factors) for compound **9** reported in this paper have been deposited with the Cambridge Crystallographic Data Centre as supplementary publication no. CCDC-147018. Copies of the data can be obtained free of charge on application to CCDC, 12 Union Road, Cambridge CB2 1EZ, UK (fax: (+44) 1223-336-033; e-mail: deposit@ccdc.cam.ac.uk).

- [15] Stereochemical assignments of compounds **11** and **12** were based upon similarity of spectroscopic data in comparison to compounds **9** and **10**, respectively. See the Supporting Information.
- [16] We use the expression β -face migration as referring to establishment of the S–C(7) bond *syn* to position C(9) of the spiro diketopiperazine substructure.
- [17] J. Hine, *Adv. Phys. Org. Chem.* **1977**, *15*, 1; see also: K. B. Carpenter, *J. Am. Chem. Soc.* **1985**, *107*, 5730; R. H. Newman-Evans, R. J. Simon, B. K. Carpenter, *J. Org. Chem.* **1990**, *55*, 695.
- [18] A similar stabilizing interaction between a sulfur atom and a carbonyl group was invoked in Ref. [11b].
- [19] The arguments advanced above focus on the migrating sulfur atom wherein the sense of rotation around the C(7)–C(8) bond accommodates the preferred modality of sulfur migration. Alternatively, it could be that a preferred sense to the C–C rotation itself serves to determine the face of the sulfur migration.
- [20] We note that the observed rearrangement process is suggestive of a possible biosynthesis of aspirochlorine.

Ion-Specific Aggregation in Conjugated Polymers: Highly Sensitive and Selective Fluorescent Ion Chemosensors**

Jinsang Kim, D. Tyler McQuade, Sean K. McHugh, and Timothy M. Swager*

Conjugated polymers are emerging as versatile elements for the design of chemical sensors.^[1, 2] An expansive range of structures is known, and thus the facile tuning of properties by modification of the polymer backbone or the introduction of side groups is possible. A variety of transduction methods that modify the emission and conductivity of a conjugated polymer is available, these include photochemically induced electron transfer, doping, conformational changes, and metal ligation.^[1–3] Interchain interactions play a decisive role in controlling the conductive and emissive properties of conjugated polymers in the bulk material.^[4] Nevertheless, no sensory system which directly exploits interchain interactions in conjugated polymers has been reported. Herein, we report a new transduction mechanism based on the aggregation of

[*] Prof. T. M. Swager


Department of Chemistry and Center for Materials Science and Engineering
Massachusetts Institute of Technology
Cambridge, MA 02139 (USA)
Fax: (+1) 617-253-7929
E-mail: tswager@mit.edu

J. Kim

Department of Materials Science and Engineering
Department of Chemistry and Center for Materials Science and Engineering

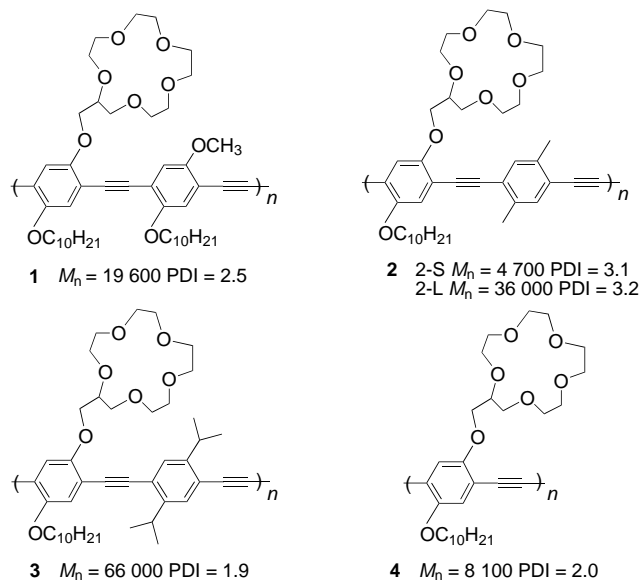
Dr. D. T. McQuade, S. K. McHugh
Department of Chemistry

[**] The authors thank the Office of Naval Research, the Defense Advanced Research Projects Agency, and the Draper Laboratory for generous financial support. D.T.M. thanks the National Institute of Health for a post-doctoral fellowship through NIGMS.

 Supporting information for this article is available on the WWW under <http://www.wiley-vch.de/home/angewandte/> or from the author.

conjugated sensory polymers induced by K^+ ions; this new system displays enhanced sensitivity because of energy migration processes and has a high selectivity for K^+ over Na^+ ions.

We synthesized the poly(*p*-phenylene ethynylene)s **1–4** with the molecular weight (M_n) and polydispersity index (PDI) shown (2-S and 2-L designate short and long polymers, respectively) by the Sonogashira–Hagihara coupling reac-



tion.^[5] We endeavored to design a system in which potassium ions will induce polymer aggregation whereas sodium ions will not so that a selective ion sensor would be produced. To accomplish this we have exploited the well known 2:1 sandwich complex formed between K^+ ions and [15]crown-5.^[6] Potassium ions cause the polymers to aggregate, thus creating low-energy traps in the electronic structure of the polymer. Energy migration to these traps can result in a large response even at a dilute analyte concentration. Recently several research groups have reported K^+ ion sensors based on [15]crown-5 groups in which the response to K^+ ions is seen by changes in either the absorbance or the fluorescence spectra of the ionophore.^[7] Our new poly(*p*-phenylene ethynylene) systems also have a high sensitivity and offer the advantage of dual detection methods, both UV/Vis and fluorescence spectroscopy can be employed.

Li^+ or Na^+ ions form 1:1 complexes with [15]crown-5, and exert no observable effect on any of the spectroscopic properties of the polymer. The absorbance and fluorescence spectra of polymer **1** in solution are essentially unchanged even after the addition of a 1500-fold excess of Li^+ or Na^+ ions. In contrast, addition of K^+ ions to a solution of **1** produced a new red-shifted peak at 457 nm in the absorption spectra and also fluorescence quenching was evident (Figure 1). Previous studies in our group and in others provide substantial evidence that the new peak and quenching are the result of interpolymer π -stacking aggregation^[4, 8] which, in this case, is induced by K^+ ion bridges between two [15]crown-5 units on different polymer chains (Scheme 1).

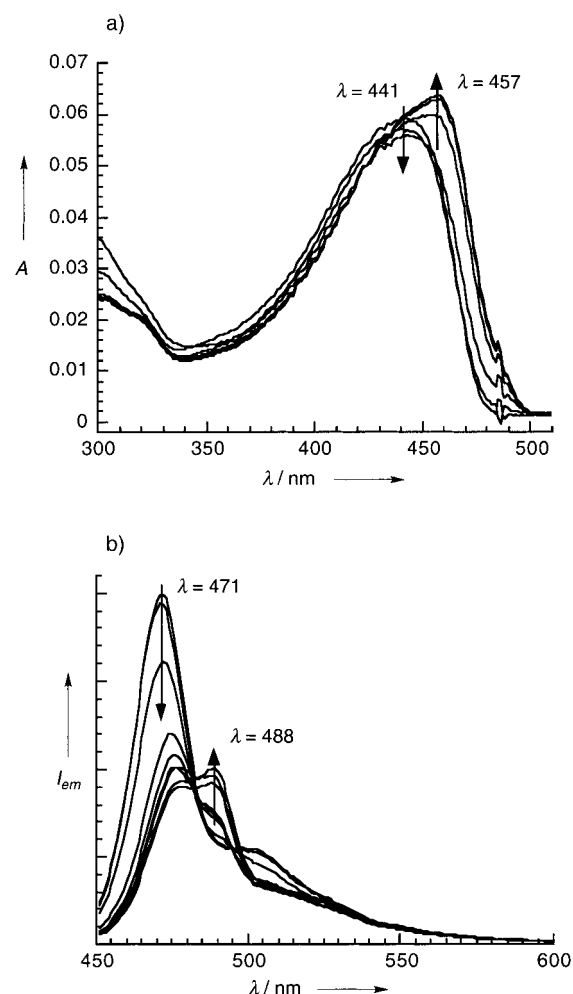
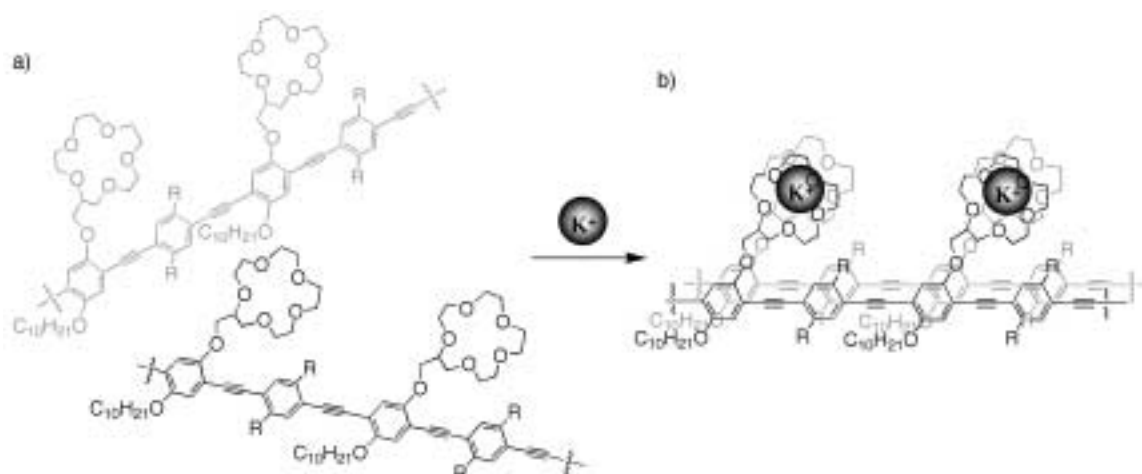


Figure 1. a) Absorbance and b) fluorescence spectra of polymer **1** with various mole ratios of K^+ ions. A solution of KPF_6 (18 mm) in acetonitrile was added gradually to a solution of the polymer (5 μ M, 3.6 mL) in THF. The arrows indicate the changes that result from progressively increasing the concentration ratio of K^+ ions to [15]crown-5: [15]crown-5: K^+ = 1:0, 1:0.5, 1:1, 1:2.5, 1:5, 1:10, and additionally, for the fluorescence spectra, at 1:20, 1:50, 1:100. The polymer was excited with radiation of $\lambda = 343$ nm.

The effectiveness of the interpolymer π -stacking aggregation can be governed by the bulk of the side groups attached to the polymer.^[8] Polymer **2** with two methyl groups in every second repeating unit offers the least resistance to the formation of interpolymer π -stacking aggregates, and thus displays the most pronounced aggregation which is noticeable by visual inspection. Of the polymers studied the fluorescent quenching of polymer **2** (2-L) is most sensitive and an 82% decrease in intensity at 452 nm is observed with a 1:0.5 (5.0 μ M:2.5 μ M) crown ether:potassium mole ratio (Figure 2). This ion-specific aggregation and consequent fluorescent quenching are stable for extended periods. There was no precipitation and the spectroscopic properties remained unchanged for three weeks at ambient temperature. In the presence of K^+ ions polymer **2** is only weakly emissive, with a broad aggregate band centered at 540 nm. The complete disappearance of the peak corresponding to the nonaggregated polymer indicates that much more effective aggregation occurs than in polymer **1** (Figure 2b). One explanation for the



Scheme 1. Schematic representation of the K^+ ion induced aggregation. a) Randomly orientated state; b) π -aggregated state induced by ([15]crown-5)– K^+ –([15]crown-5) bridges.

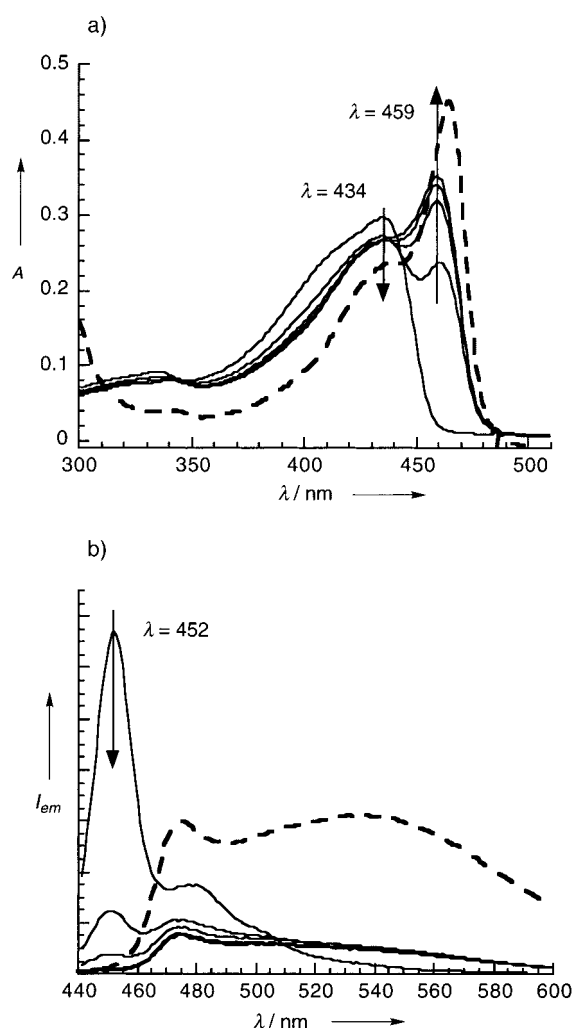


Figure 2. a) Absorbance and b) fluorescence spectra of polymer 2(2-L) with various mole ratios of K^+ ions. A solution of KPF_6 (18 mM) in acetonitrile was added gradually to a solution of the polymer (5 μ M, 3.6 mL) in THF. The arrows indicate the changes that result from progressively increasing the concentration ratio of K^+ to [15]crown-5: [15]crown-5: K^+ = 1:0, 1:0.5, 1:1, 1:2.5, 1:5 and the dashed lines are data from a monolayer Langmuir–Blodgett (LB) film. The intensities of the spectra of the LB films are adjusted for clarity. For the K^+ ion dependent fluorescence spectra the polymer was excited at the pseudo isosbestic point, 343 nm.

lower response of polymer **1** is its ability to form a lariat ether type complexation between [15]crown-5 and the methoxy oxygen atom bound to the phenyl unit of the next repeating unit. This binding competes with the formation of the 2:1 sandwich complex and thereby results in less effective aggregation.

To prove that the sensory response is a result of the interpolymer π -stacking aggregations, we prepared a completely aggregated film of polymer **2**(2-L) by utilizing its surfactant properties and the Langmuir–Blodgett method.^[4f, g] Polymer **2** has hydrophobic decyloxy groups *para* to the hydrophilic [15]crown-5 units, and based upon previously established studies and the extrapolated area per repeating unit (37 \AA^2 per phenylene ethynylene unit) we determined that polymer **2**(2-L) forms an edge-on structure at the air–water interface (Figure 3).^[4f, g] Therefore, the conjugated π planes face each other to form π -stacked aggregates. The absorption and fluorescence spectra of a monolayer Langmuir–Blodgett film of polymer **2** on a hydrophobic substrate (the dashed lines in Figure 2) are essentially the same as solutions in which aggregation is induced by K^+ ions.

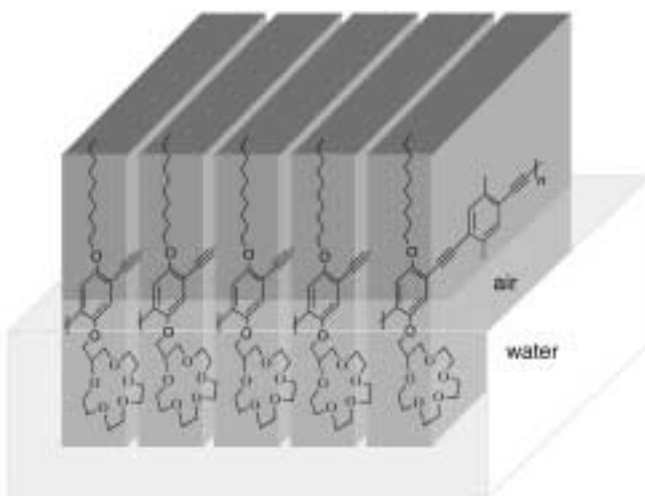


Figure 3. Schematic representation of the edge-on structure of polymer 2(2-L) at the air–water interface.

The exciton transport properties of conjugated polymers have been shown to produce amplification of a sensory signal.^[1, 10] In this system a longer polymer should have higher sensitivity at low analyte concentration than a shorter polymer. This assertion does require that the excitons are able to sample the entire polymer chain. The lifetime of an exciton and its mobility in polymers, similar to those presented here allows the exciton to sample up to 108 phenylene ethynylene repeating units.^[10] In good agreement with these concepts, the higher molecular weight polymer **2** (2-L) revealed a higher sensitivity than the shorter polymer **2** (2-S; Figure 4). However, the amplification effect is less than we

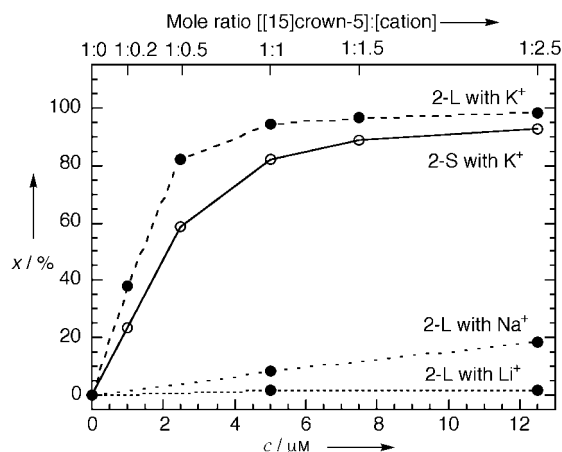


Figure 4. Fluorescence quenching of polymers **2**(2-L) and **2**(2-S) by various concentrations of cations. The ordinate shows the fluorescence quenching $X\%$ $[(I_0 - I)/I_0 \times 100]$; I_0 = fluorescence intensity at 452 nm of a solution of polymer **2** (5 μM) without cations; I = fluorescence intensity at 452 nm of a polymer **2** solution (5 μM) in the presence of cations.

expected. The increase in the peaks in the UV/Vis spectra arising from aggregation and the fluorescence quenching both indicate a cooperative response to K^+ ions. We postulate that the initial K^+ ion bridging brings two polymers closer together, thus providing preorganized sites for K^+ ion bridges. Therefore, the formation of further bridges between the two polymers is preferred over aggregation with other isolated polymer chains. Since just a few aggregated sites are needed to quench two polymers, an unnecessary abundance of K^+ ion bridges makes the amplification effect less than in the ideal case in which only the optimum (minimum) number of potassium bridges are formed among polymer chains.

Increasing interchain bulk should stifle interpolymer aggregation and lower the response to potassium ions. To test this hypothesis we synthesized polymer **3** which contains isopropyl groups. Accordingly, the spectra of polymer **3** show no significant changes upon adding Li^+ , Na^+ , or K^+ ions which indicates that the isopropyl groups are sufficiently bulky to prevent π -stacking aggregation with any ion.^[8]

The distance between [15]crown-5 groups in a single polymer chain is also a key design parameter. Surprisingly, polymer **4** with [15]crown-5 groups on every repeating unit is not responsive to K^+ , Na^+ , or Li^+ ions. An explanation is that the distance between the [15]crown-5 groups in polymer **4** favors, based on entropic considerations, the formation of

intrapolymer bridges. The formation of the intrapolymer ([15]crown-5)– K^+ –([15]crown-5) bridge is favorable according to molecular modeling studies.^[11] Polymer **4**, which is not regioregular, can form three isomeric K^+ ion complexes (Figure 5). Polymers **1**, **2**, and **3** with [15]crown-5 groups on

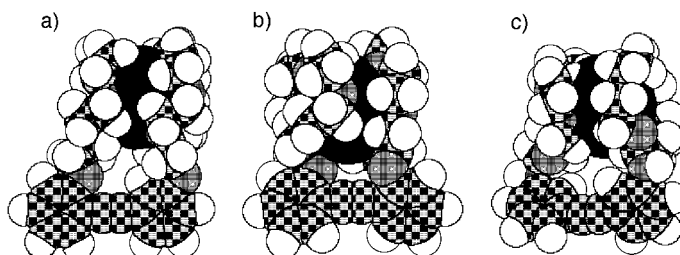


Figure 5. Space-filling models of the potassium complexes of model compounds that represent different regio isomeric dyads in polymer **4**: a) 2,3'-di(oxyethylene [15]crown-5) diphenylethyne; b) 2,2'-di(oxyethylene [15]crown-5) diphenylethyne; c) 3,3'-di(oxyethylene [15]crown-5) diphenylethyne. Hatched circles = oxygen atoms; large black circles = potassium ions.

every second repeating unit can only form intrapolymer bridges by severe twisting and bending of the polymer backbone. Therefore, intrapolymer binding is unlikely, thus K^+ ions form interpolymer bridges as illustrated in Scheme 1.

In summary, we report a highly specific and sensitive transduction mechanism that utilizes ion-mediated interpolymer aggregation. This new system illustrates a general principle that is applicable to multivalent recognition events often found in biological systems.^[12]

Detailed experimental conditions and material preparations are available in the Supporting Information.

Received: April 13, 2000 [Z14989]

- [1] T. M. Swager, *Acc. Chem. Res.* **1998**, *31*, 201.
- [2] M. Leclerc, *Adv. Mater.* **1999**, *11*, 1491.
- [3] a) M. J. Marsella, R. J. Newland, P. J. Carroll, T. M. Swager, *J. Am. Chem. Soc.* **1995**, *117*, 9842; b) K. B. Crawford, M. B. Goldfinger, T. M. Swager, *J. Am. Chem. Soc.* **1998**, *120*, 5187; c) J.-S. Yang, T. M. Swager, *J. Am. Chem. Soc.* **1998**, *120*, 5321; d) J.-S. Yang, T. M. Swager, *J. Am. Chem. Soc.* **1998**, *120*, 11864.
- [4] a) S. A. Jenekhe, J. A. Osaheni, *Science* **1994**, *265*, 765; b) E. Conwell, *Trends Polym. Sci.* **1997**, *5*, 218; c) H. Li, D. R. Powell, R. K. Hayashi, R. West, *Macromolecules* **1998**, *31*, 52; d) C. E. Halkyard, M. E. Rampey, L. Kloppenburg, S. L. Studer-Martinez, U. H. F. Bunz, *Macromolecules* **1998**, *31*, 8655; e) C. Weder, M. S. Wrighton, *Macromolecules* **1996**, *29*, 5157; f) J. Kim, S. K. McHugh, D. T. McQuade, T. M. Swager *Polym. Prepr. Am. Chem. Soc. Div. Polym. Chem.* **1999**, *40*, 748, and unpublished results.
- [5] K. Sonogashira, Y. Tohda, N. Hagihara, *Tetrahedron Lett.* **1975**, 4467. Molecular weights were determined by gel permeation chromatography (GPC) relative to monodispersed polystyrene standards.
- [6] G. W. Gokel, *Crown Ethers and Cryptands*, The Royal Society of Chemistry, Cambridge, UK, **1991**, pp. 99–128.
- [7] a) A. Yamauchi, T. Hayashita, S. Nishizawa, M. Watanabe, N. Teramae, *J. Am. Chem. Soc.* **1999**, *121*, 2319; b) W.-S. Xia, R. H. Schmehl, C.-J. Li, *J. Am. Chem. Soc.* **1999**, *121*, 5599; c) A. Boldea, I. Lévesque, M. Leclerc, *J. Mater. Chem.* **1999**, *9*, 2133.
- [8] D. T. McQuade, J. Kim, T. M. Swager, *J. Am. Chem. Soc.* **2000**, *122*, 5885.
- [9] J. Kim, S. K. McHugh, T. M. Swager, *Macromolecules* **1999**, *32*, 1500.

- [10] Q. Zhou, T. M. Swager, *J. Am. Chem. Soc.* **1995**, *117*, 7017.
 [11] All calculations were performed by using the Spartan 5.0 molecular modeling program running on a SGI O2 (R12000) workstation.^[11a] Geometry optimizations were performed by using molecular mechanics with MMFF94 force field without constraints.^[11b] a) Wavefunction, Inc.: 18401 Von Karmann, No. 210, Irvine, CA; b) T. A. Halgren, *J. Comput. Chem.* **1996**, *17*, 490.
 [12] M. Mammen, S.-K. Choi, G. M. Whitesides, *Angew. Chem.* **1998**, *110*, 2908; *Angew. Chem. Int. Ed.* **1998**, *37*, 2754.

$[\{\text{Ir}(\eta^5\text{-C}_5\text{Me}_5)(\text{CO})\}_6\text{Hg}_8][\text{CF}_3\text{CO}_2]_6$, a Mixed-Metal Cluster with an Ir_6Hg_6 Twelve-Membered Ring and Additional Hg Centers and Metal–Metal Bonds**

Giuseppina Chiaradonna, Giovanni Ingrosso,* and Fabio Marchetti*

In 1995 one of us reported that benzene can be directly aminated by diethylamine in the presence of $[\text{Ir}(\eta^5\text{-C}_5\text{Me}_5)(\text{CO})_2]$ (**1**) and a mercury(II) salt, typically HgSO_4 ; one of the roles played by the latter is most probably that of making the carbonyl ligands more susceptible to nucleophilic attack.^[1] Accordingly, the literature^[2] documents that the interaction of the metal–base^[3] **1** with HgCl_2 results in a marked shift of the CO stretching frequencies to higher wavenumbers as a consequence of the formation of the adduct $[(\eta^5\text{-C}_5\text{Me}_5)(\text{CO})_2\text{IrHgCl}][\text{HgCl}_3]$ (**2**). These preliminary remarks prompted us to start an extensive investigation of the reaction of **1** with various mercury(II) salts with the aim of exploring further the chemistry of such a reaction. Hereby, we have discovered a quite complex reactivity which varies markedly on varying the nature of the salt. Herein, we report on the reaction of **1** with $\text{Hg}(\text{CF}_3\text{CO}_2)_2$ in CH_2Cl_2 which yields the unexpected compound $[\{\text{Ir}(\eta^5\text{-C}_5\text{Me}_5)(\text{CO})\}_6\text{Hg}_8][\text{CF}_3\text{CO}_2]_6$ (**3**) as a red crystalline diamagnetic solid. The course of the reaction is still unclear; however, the definite nature of **3** clearly indicates an oxidative role played by the Hg^{2+} ion. Although transition metal compounds containing bonds with mercury have been known for a long time, mercury clusters

are relatively rare^[4] and the structure of **3** is unique in this field.

The ^1H NMR spectrum of compound **3** exhibits two sharp singlets at $\delta = 2.28$ and 2.53 ([D]chloroform) in a 2:1 ratio for two sets of magnetically equivalent $\eta^5\text{-C}_5\text{Me}_5$ methyl groups, both being downfield from the value for **1** ($\delta = 2.18$, [D]chloroform).^[5] The IR spectrum of **3** shows four CO stretching frequencies at 1972, 1957, 1948, and 1935 cm^{-1} (nujol) that are lower than those for **1** (2000 and 1925 cm^{-1}).^[5] Thus, a comparison of the ^1H NMR and IR data for **3** with those reported for **2** (i.e. $\delta = 2.31$, and $\nu(\text{CO}) = 2085$ and 2045 cm^{-1})^[2] provides evidence in favor of increased electron density at the iridium centers in **3**. Thus, the nature of the Ir–Hg bonds in **3** is significantly different from that in **2**. In fact in **2**, the metal–metal bond causes a withdrawal of electron density from the iridium center.^[2]

The molecular geometry of **3** was determined by single-crystal X-ray analysis at 293 K (Figure 1). The cationic component of **3**, that is $[\{\text{Ir}(\eta^5\text{-C}_5\text{Me}_5)(\text{CO})\}_6\text{Hg}_8]^{6+}$, contains a novel ring system with an Ir_6Hg_6 twelve-membered ring with

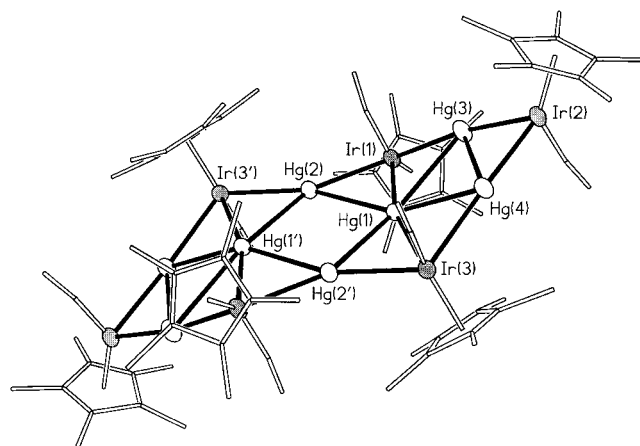


Figure 1. The molecular structure of the cation in **3**. The CF_3CO_2^- ions and H atoms are omitted for clarity. The metals are represented by thermal ellipsoids at 30 % probability. The superscript ' denotes the atoms generated by the symmetry operation $1 - x, 1 - y, -z$. Metal–metal bond lengths [Å] (standard deviations are given in parentheses): Hg(1)–Ir(1) 2.739(2), Hg(1)–Ir(3) 2.749(2), Hg(1)–Hg(2') 2.982(2), Hg(1)–Hg(2) 3.0278(18), Hg(1)–Hg(3) 3.070(2), Hg(1)–Hg(4) 3.078(2), Hg(2)–Ir(1) 2.675(2), Hg(2)–Ir(3') 2.679(2), Hg(2)–Hg(1') 2.982(2), Hg(3)–Ir(2) 2.599(2), Hg(3)–Ir(1) 2.685(2), Hg(3)–Hg(4) 2.962(2), Hg(4)–Ir(2) 2.604(2), Hg(4)–Ir(3) 2.701(2).

additional Hg centers; Hg–Hg and Hg–Ir bonds give rise to a network within the Ir_6Hg_6 ring. The whole metal network appears roughly disposed on three different planes bent in a way which is reminiscent of the chair conformation of cyclohexane. The core moiety of $[\{\text{Ir}(\eta^5\text{-C}_5\text{Me}_5)(\text{CO})\}_6\text{Hg}_8]^{6+}$ (Figure 2), formed by the Hg(1), Hg(2), Ir(1), Ir(3), Hg(1'), Hg(2'), Ir(1'), and Ir(3') metal centers, is almost exactly planar with a maximum deviation of 0.04 Å . Interestingly, the same fascinating arrangement^[6] has al-

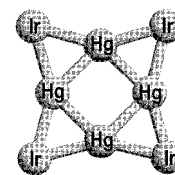


Figure 2. The Hg_4Ir_4 core moiety of $[\{\text{Ir}(\eta^5\text{-C}_5\text{Me}_5)(\text{CO})\}_6\text{Hg}_8]^{6+}$.

[*] Prof. Dr. G. Ingrosso, Dr. G. Chiaradonna
 Dipartimento di Chimica e Chimica Industriale
 Università di Pisa
 Via Risorgimento 35, 56126 Pisa (Italy)
 Fax: (+39)050-918410
 E-mail: vanni@dccl.unipi.it

Prof. Dr. F. Marchetti
 Dipartimento di Ingegneria Chimica, dei Materiali, delle Materie
 Prime e Metallurgia
 Università La Sapienza
 Via del Castro Laurenziano 7, 00161 Roma (Italy)
 Fax: (+39)050-918260
 E-mail: fama@dst.unipi.it

[**] This work was supported by MURST (Rome, Italy) (Programmi di Rilevante Interesse Nazionale).

ready been found in two structurally characterized compounds, namely $[\{\text{Mn}(\eta^5\text{-C}_5\text{H}_4\text{Me})(\text{CO})_2\text{Hg}\}_4]^{[7]}$ and $[\{\text{Re}(\eta^5\text{-C}_5\text{H}_5)(\text{CO})_2\text{Hg}\}_4]^{[8]}$.

$[\{\text{Ir}(\eta^5\text{-C}_5\text{Me}_5)(\text{CO})\}_6\text{Hg}_8]^{6+}$ allows a crystallographic inversion operation; its local symmetry is higher and may approximately be considered as $2/m$ (C_{2h}), with the twofold axis passing through the Hg(2) and Hg(2') atoms. According to the ^1H NMR spectrum, this is probably the symmetry that **3** has in solution.

Interestingly, either the Hg–Ir or the Hg–Hg bond lengths show a significant increase on increasing the coordination number of the metal centers (see caption to Figure 1).

Two of the six trifluoroacetate anions in **3** (not shown in Figure 1) point their oxygen atoms towards Hg(1) and towards Hg(1'), respectively, both at a Hg...O distance of 2.95 Å on opposite sides of the cluster; each is located where the corresponding mercury centers are less sterically shielded by the bulky $\eta^5\text{-C}_5\text{Me}_5$ ligands. The other four anions are distributed around the cation with different orientations.

Looking at the metal arrangements observed to date in mixed-metal mercury clusters,^[4] the Hg centers in **3** show quite surprising structural environments. Indeed, according to their coordination, the eight Hg centers can be subdivided into three categories: the six-coordinate Hg(1) centers, the four-coordinate Hg(3) and Hg(4) centers, and the four-coordinate Hg(2) centers. Moreover, two types of iridium centers may be distinguished: one is represented by Ir(1) and Ir(3) (Figure 1) that are bonded to a $\eta^5\text{-C}_5\text{Me}_5$ ligand, a terminal CO ligand, and three Hg centers, and the other one is represented by Ir(2) centers that are bonded to a $\eta^5\text{-C}_5\text{Me}_5$ ligand, a terminal CO ligand, and two Hg centers. All the iridium atoms are located on the cluster edges. Probably due to steric reasons, the $\eta^5\text{-C}_5\text{Me}_5$ and CO ligands are alternately placed on opposite sides of the metal cluster. Remarkably, while the Ir(2) centers exhibit the well-known “three-legged piano stool geometry”, the Ir(1) and Ir(3) centers exhibit unprecedented coordination number and coordination geometry which can be described as a highly distorted square pyramid; the square is defined by three Hg and one C (CO) atoms, and the apex by the centroid of the $\eta^5\text{-C}_5\text{Me}_5$ group.

In conclusion, **3** is a highly unusual mixed-metal cluster whose bonding properties cannot be explained readily by standard electron counting. Therefore, further work is necessary to throw light on the complex metal–metal bonding situation exhibited by this compound.

Experimental Section

A mixture of $\text{Hg}(\text{CF}_3\text{CO}_2)_2$ (61 mg, 0.14 mmol) and $[\text{Ir}(\eta^5\text{-C}_5\text{Me}_5)(\text{CO})_2]$ (55 mg, 0.14 mmol) in dichloromethane (10 mL) was stirred for 30 min at room temperature under a pure argon atmosphere. Slow diffusion of diethyl ether (10 mL) into the above solution caused the precipitation of analytically pure **3** (53 mg) as red, well-shaped crystals in the course of ten days. Elemental analysis calcd for $\text{C}_{78}\text{H}_{90}\text{F}_{18}\text{O}_{18}\text{Hg}_8\text{Ir}_6$ (4415.57) (%): C 21.22, H 2.05; found: C 20.82, H 2.11.

X-ray structure analysis for **3**: a deep red prism of approximate dimensions $0.45 \times 0.22 \times 0.014$ mm³ was glued at the end of a glass fiber, and the intensity data were collected on a Siemens P4 diffractometer using the MoK_α graphite-monochromated radiation ($\lambda = 0.71073$ Å). Cell parameters

were calculated on the accurately centered setting angles of 35 strong reflections with $5.2^\circ < \theta < 11.2^\circ$. Crystal data: $\text{C}_{78}\text{H}_{90}\text{F}_{18}\text{Hg}_8\text{Ir}_6\text{O}_{18}$, $M_r = 4415.57$, $T = 293(2)$ K, space group $P2_1/n$ (no. 14), $a = 12.2292(13)$, $b = 19.681(2)$, $c = 21.304(2)$ Å, $\beta = 101.869(9)^\circ$, $V = 5018(1)$ Å³, $Z = 2$, $\rho_{\text{calcd}} = 2.922$ g cm⁻³, $\mu(\text{MoK}_\alpha) = 20.194$ mm⁻¹, $F(000) = 3932$. The intensities of 7695 reflections with $2^\circ \leq \theta \leq 22^\circ$ were collected. After merging the equivalent ones and after correction for Lorentz, polarization, and absorption effects with an integration method,^[9] an internal R value $[\Sigma |F_o^2 - F_o^2(\text{mean})| / \Sigma(F_o^2)]$ of 0.0686 was obtained. The structure was solved by standard direct and Fourier methods and refined by full-matrix least-squares procedures. Rotational disorder was present in the three independent anions and two of them had to be refined as rigid groups. Some degree of disorder also extended to the $\eta^5\text{-Cp}^*$ ligands. The disorder could not be accounted for through a simple model characterized by two distinct positions. In the final refinement cycle anisotropic thermal parameters were used for Ir, Hg, and some of the C and O atoms, giving a conventional R factor (F_o) of 0.0767, calculated for 312 parameters on 4096 observed reflections, and a value of 0.1185 for all 6140 data. Thirteen residual peaks of $2\text{--}5$ e Å⁻³ were present in the final difference Fourier map at distances between 1.0 and 1.6 Å from Hg and Ir atoms. Crystallographic data (excluding structure factors) for the structure reported in this paper have been deposited with the Cambridge Crystallographic Data Centre as supplementary publication no. CCDC-145995. Copies of the data can be obtained free of charge on application to CCDC, 12 Union Road, Cambridge CB2 1EZ, UK (fax: (+44) 1223-336-033; e-mail: deposit@ccdc.cam.ac.uk).

Received: June 23, 2000 [Z15322]

- [1] P. Diversi, L. Ermini, G. Ingrosso, A. Lucherini, C. Pinzino, L. Sagromora, *J. Organomet. Chem.* **1995**, 494, C1–C2.
- [2] F. W. B. Einstein, X. Yan, X. Zhang, D. Sutton, *J. Organomet. Chem.* **1992**, 439, 221–230.
- [3] H. Werner, *Angew. Chem.* **1983**, 95, 932–954; *Angew. Chem. Int. Ed. Engl.* **1983**, 22, 927–949.
- [4] L. H. Gade, *Angew. Chem.* **1993**, 105, 25–41; *Angew. Chem. Int. Ed. Engl.* **1993**, 32, 24–40; E. Rosenberg, K. I. Hardcastle in *Comprehensive Organometallic Chemistry*, Vol. 10 (Eds.: E. W. Abel, F. G. A. Stone, G. Wilkinson), Pergamon, Oxford, **1995**, pp. 323–350.
- [5] J. W. Kang, K. Moseley, P. M. Maitlis, *J. Am. Chem. Soc.* **1969**, 91, 5971–5977.
- [6] H. J. Deiseroth, *Prog. Solid State Chem.* **1997**, 25, 73–123.
- [7] W. Gäde, W. Weiss, *Angew. Chem.* **1981**, 93, 796–797; *Angew. Chem. Int. Ed. Engl.* **1981**, 20, 803–804.
- [8] N. E. Kobolova, Z. Valueva, E. I. Kazimirschuk, V. G. Adrianov, Y. T. Struchov, *Izv. Akad. Nauk SSSR Ser. Khim.* **1984**, 920–922.
- [9] G. M. Sheldrick, SHELXTL-Plus, Rel. 5.03, Siemens Analytical X-ray Instruments Inc., Madison, Wisconsin, **1995**.

Synthesis of Thymine Glycol Containing Oligonucleotides from a Building Block with the Oxidized Base**

Shigenori Iwai*

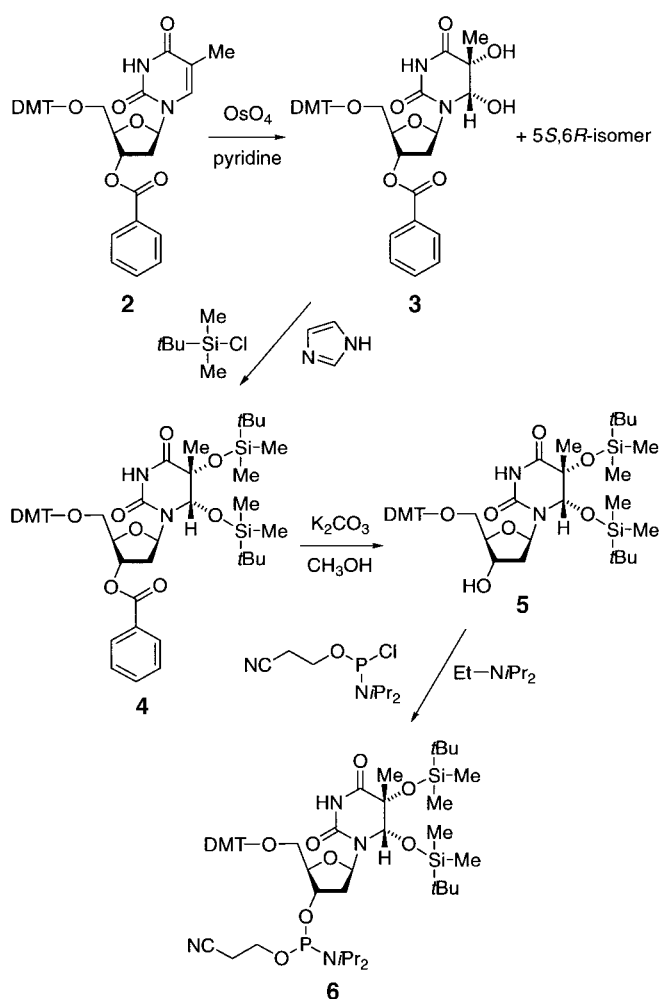
Thymine glycol (5,6-dihydro-5,6-dihydroxythymine) is a major form of DNA base damage generated by oxidation with a hydroxyl radical^[1] or by ionizing radiation.^[2] The *cis*-5*R*,6*S* form (shown as part of an oligonucleotide in **1**) is produced preferentially by the oxidation of thymidine or oligonucleotides,^[3] while it was reported that γ irradiation of DNA resulted in the formation of the two *cis* isomers (5*R*,6*S* and 5*S*,6*R*) in equal amounts.^[4] The *cis* forms are in equilibrium with the *trans* isomers in solution.^[5] Although mutation frequency is low,^[6] this damage can block

DNA replication.^[7] Thymine glycol is excised by enzymes such as endonuclease III^[8] and endonuclease VIII^[9] in cells, and in vitro experiments showed that this damage is also repaired by the human nucleotide excision repair system.^[10]

In spite of the biological significance of thymine glycol, chemical synthesis of oligonucleotides containing this damage has not been reported hitherto. Such oligonucleotides have been prepared by the oxidation of short oligomers, which contain thymine at a single site, with KMnO_4 or OsO_4 . However, oxidation with KMnO_4 gives various products, which make identification and isolation of the desired product extremely difficult.^[3b, 6b, 11] When OsO_4 is used as an oxidizing agent, thymine glycol is produced almost exclusively, but its yield is very low.^[6b, 12] Furthermore, the chain length and sequence are limited in these postsynthetic oxidation methods.

In this study, I tried to develop a method for the direct incorporation of a thymine glycol building block into oligonucleotides. The problem was that this oxidized base is labile under the alkaline conditions normally used for the deprotection of the other nucleobases after coupling.^[5] This problem might be solved, to some extent, by the use of a (4-*tert*-butylphenoxy)acetyl (tBPA) protecting group on the nucleobases; this group can be removed by a short ammonia treatment at room temperature.^[13] It was also expected that protection of the hydroxyl functions of thymine glycol might improve the stability of this base moiety.

The design and the synthesis of the building block are shown in Scheme 1. The *tert*-butyldimethylsilyl (TBDMS) group, which is commonly used for RNA synthesis,^[14] was chosen for the protection of the hydroxyl functions at the C5



Scheme 1. Synthesis of the thymine glycol building block **6**.

and C6 positions, because the groups at these positions should be removed at the final step, after the deprotection with ammonium hydroxide.

First, thymidine protected with the 4,4'-dimethoxytriphenylmethyl (DMT) and benzoyl groups at the 5' and 3' positions, respectively, was oxidized with OsO_4 .^[15] Barvian and Greenberg stated that they used a catalytic amount of OsO_4 to prepare thymidine glycol,^[16] but an equimolar amount was required in my case. Two products were obtained, and ^1H NMR analysis revealed that they were the two isomers of *cis*-thymine glycol. The ratio of the major and minor products was 6:1, as determined by ^1H NMR spectroscopy. The configuration of each isomer was assigned by comparison of the NOESY spectra of the products. For both isomers, a crosspeak was found between H6 and the methyl proton, but no NOE effect was detected between H6 and H1'. These observations indicated that the two hydroxyl groups were in the *cis* orientation and that the base moiety was in the *anti* conformation around the glycosyl bond. For the minor isomer, a strong NOE was detected between H6 and H2', whereas the corresponding crosspeak was too weak to be discriminated from the noise for the major product. As suggested by Vaishnav et al.,^[3a] it can be concluded from this difference that the configuration of the thymine glycol used in this study was 5*R*,6*S*.

[*] Dr. S. Iwai
Biomolecular Engineering Research Institute
6-2-3 Furuedai, Suita, Osaka 565-0874 (Japan)
Fax: (+81) 6-6872-8219
E-mail: iwai@bioorg.beri.co.jp

[**] I am grateful to Ms. R. Yuuji and Dr. K. Hirayama, Ajinomoto Company Inc., and Dr. H. Urata, Osaka University of Pharmaceutical Sciences, for obtaining the high-resolution mass data.

Supporting information for this article is available on the WWW under <http://www.wiley-vch.de/home/angewandte/> or from the author.

The next step was the protection of the hydroxyl functions at C5 and C6. Although the C5 hydroxyl is tertiary, it was silylated without difficulty. Detection of the imino proton in the NMR analysis demonstrated that the second silylation did not occur at the oxygen atom at the C2 or C4 positions. The benzoyl group of **4** was removed with potassium carbonate in methanol,^[17] and the 3'-hydroxyl function of **5** was phosphitylated with (2-cyanoethyl)-*N,N*-diisopropylchlorophosphoramidite.^[18]

Using the building block **6** and the tBPA-protected phosphoramidites of the other nucleosides, a 6-mer, d(GCTgAGC), a 13-mer, d(ACGCGATgACGCCA), and a 30-mer, d(CTCGTCAGCATCTTgCATCATACAGTCAGTG), were synthesized on a solid support (Tg represents thymine glycol). Since the coupling yield of **6** was low (74–78%) when the standard cycle was used, the reaction time was prolonged to 5 min when coupling **6**, to obtain a nearly 100% yield. After the chain assembly, the oligonucleotides were cleaved from the support, simultaneously deprotected with 28% aqueous ammonium hydroxide at room temperature for

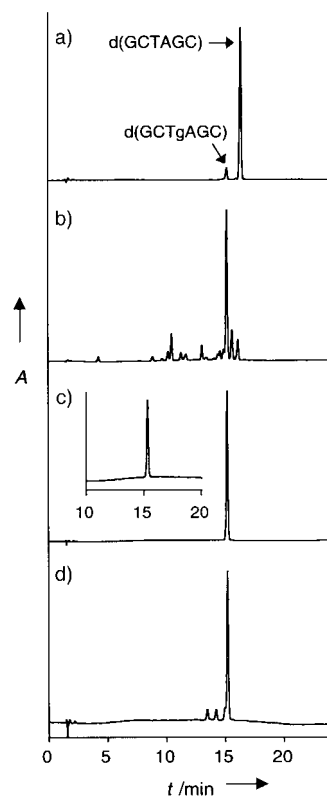


Figure 1. HPLC analysis of the 6-mer with an acetonitrile gradient of 2.5–10% during 20 min. Elution profiles monitored at 254 nm are shown. a) A mixture after the OsO_4 oxidation of d(GCTAGC). b) A crude mixture after deprotection of d(GCTgAGC) synthesized using the building block **6**. c) The 6-mer purified from the mixture shown in (b). The inset is the trace obtained from coinjection with the authentic 6-mer. d) Treatment of the purified 6-mer with ammonium hydroxide at room temperature for 2 h.

2 h, and then treated with 1.0M tetrabutylammonium fluoride in tetrahydrofuran for 16 h to remove the TBDMS group. Following the method described previously,^[6b] d(GCTgAGC) was prepared by oxidation of d(GCTAGC) with OsO_4 and was used as the authentic 6-mer for comparison. The authentic 13-mer was also prepared in the same way.

Figure 1 shows the results of the HPLC analysis of the 6-mer. As shown in trace (b), a large peak was detected at the same retention time as that of the OsO_4 -oxidized product in trace (a). The product giving the main peak was purified by HPLC, and its identity with the authentic 6-mer was demonstrated by coinjection, as shown by trace (c). Treatment of the purified 6-mer with ammonium hydroxide at room temperature for 2 h resulted in degradation of approximately 18% of this oligonucleotide (trace (d)). Since the peaks corresponding to the degraded products were not found in the crude mixture, it is concluded that the protec-

tion of the hydroxyl groups of thymine glycol increased the stability of this oxidized base under alkaline conditions. However, after cleavage from the support, treatment with ammonia at 55 °C for 12 h resulted in complete degradation of the thymine glycol containing oligonucleotide, even if ethanol was added to prevent the removal of the TBDMS group (data not shown).^[19] The HPLC elution profiles of the crude 13- and 30-mers are shown in Figure 2, and the identity of the 13-mer with the authentic one was demonstrated by coinjection.

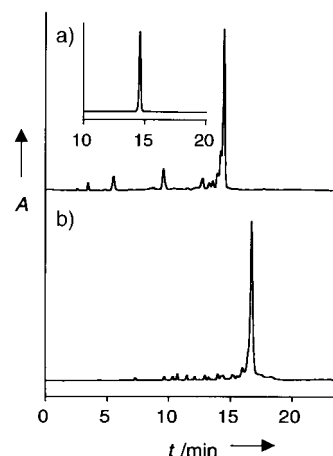


Figure 2. HPLC analysis of the 13-mer (a) and the 30-mer (b). The inset is the trace obtained from a coinjection of the purified 13-mer with the authentic one. The acetonitrile gradients were 5–13% and 5–15% for the 13- and 30-mers, respectively.

After purification with HPLC, the oligonucleotides were analyzed by matrix-assisted laser desorption/ionization time of flight (MALDI-TOF) mass spectrometry. Although characterization of the 30-mer was not successful because of broad peaks, the difference between the undamaged and thymine glycol containing oligonucleotides was equal to the mass of two hydroxyl groups, as shown in Figure 3.

As described above, a method for the synthesis of oligonucleotides containing thymine glycol at any site within defined sequences has been developed. In my previous studies, oligonucleotides containing the [6–4] photoproduct, which is one of the major forms of DNA damage caused by ultraviolet light, were synthesized,^[20] and these oligonucleotides,^[21] as well as those containing other DNA lesions,^[22] have been used in various studies. Similarly, thymine glycol containing oligonucleotides synthesized by this method will contribute significantly to studies of the molecular biology of DNA repair.

Received: April 20, 2000 [Z 15022]

- [1] R. Adelman, R. L. Saul, B. N. Ames, *Proc. Natl. Acad. Sci. USA* **1988**, *85*, 2706–2708.
- [2] a) R. Teoule, C. Bert, A. Bonicel, *Radiat. Res.* **1977**, *72*, 190–200; b) K. Frenkel, M. S. Goldstein, G. W. Teebor, *Biochemistry* **1981**, *20*, 7566–7571.
- [3] a) Y. Vaishnav, E. Holwitt, C. Swenberg, H.-C. Lee, L.-S. Kan, *J. Biomol. Struct. Dyn.* **1991**, *8*, 935–951; b) H. C. Kung, P. H. Bolton, *J. Biol. Chem.* **1997**, *272*, 9227–9236.
- [4] G. Teebor, A. Cummings, K. Frenkel, A. Shaw, L. Voituriez, J. Cadet, *Free Radical Res. Commun.* **1987**, *2*, 303–309.

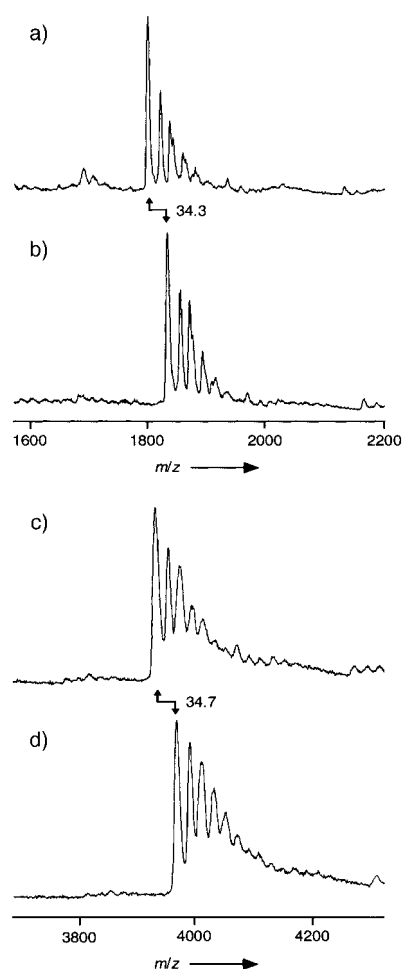


Figure 3. MALDI-TOF MS analysis of: a) d(GCTAGC); b) d(GCTgAG C); c) d(ACGCGATACGCCA); and d) d(ACGCGATgACGCCA).

- [5] M. J. Lustig, J. Cadet, R. J. Boorstein, G. W. Teebor, *Nucleic Acids Res.* **1992**, *20*, 4839–4845.
- [6] a) R. C. Hayes, L. A. Petrucci, H. Huang, S. S. Wallace, J. E. LeClerc, *J. Mol. Biol.* **1988**, *201*, 239–246; b) A. K. Basu, E. L. Loechler, S. A. Leadon, J. M. Essigmann, *Proc. Natl. Acad. Sci. USA* **1989**, *86*, 7677–7681.
- [7] a) H. Ide, Y. W. Kow, S. S. Wallace, *Nucleic Acids Res.* **1985**, *13*, 8035–8052; b) J. M. Clark, G. P. Beardsley, *Nucleic Acids Res.* **1986**, *14*, 737–749; c) R. C. Hayes, J. E. LeClerc, *Nucleic Acids Res.* **1986**, *14*, 1045–1061; d) J. M. McNulty, B. Jerkovic, P. H. Bolton, A. K. Basu, *Chem. Res. Toxicol.* **1998**, *11*, 666–673.
- [8] a) B. Dimple, S. Linn, *Nature* **1980**, *287*, 203–208; b) M. Dizdaroglu, J. Laval, S. Boiteux, *Biochemistry* **1993**, *32*, 12105–12111; c) S. Ikeda, T. Biswas, R. Roy, T. Izumi, I. Boldogh, A. Kurosky, A. H. Sarker, S. Seki, S. Mitra, *J. Biol. Chem.* **1998**, *273*, 21585–21593.
- [9] R. J. Melamede, Z. Hatahet, Y. W. Kow, H. Ide, S. S. Wallace, *Biochemistry* **1994**, *33*, 1255–1264.
- [10] J. T. Reardon, T. Bessho, H. C. Kung, P. H. Bolton, A. Sancar, *Proc. Natl. Acad. Sci. USA* **1997**, *94*, 9463–9468.
- [11] C. D'Ham, A. Romieu, M. Jaquinod, D. Gasparutto, J. Cadet, *Biochemistry* **1999**, *38*, 3335–3344.
- [12] J. Y. Kao, I. Goljer, T. A. Phan, P. H. Bolton, *J. Biol. Chem.* **1993**, *268*, 17787–17793.
- [13] N. D. Sinha, P. Davis, N. Usman, J. Pérez, R. Hodge, J. Kremsky, R. Casale, *Biochimie* **1993**, *75*, 13–23.
- [14] N. Usman, K. K. Ogilvie, M.-Y. Jiang, R. J. Cedergren, *J. Am. Chem. Soc.* **1987**, *109*, 7845–7854.
- [15] J. S. Baran, *J. Org. Chem.* **1960**, *25*, 257.
- [16] M. R. Barvian, M. M. Greenberg, *J. Org. Chem.* **1993**, *58*, 6151–6154.

- [17] W. H. A. Kuijpers, J. Huskens, L. H. Koole, C. A. A. van Boeckel, *Nucleic Acids Res.* **1990**, *18*, 5197–5205.
- [18] N. D. Sinha, J. Biernat, J. McManus, H. Köster, *Nucleic Acids Res.* **1984**, *12*, 4539–4557.
- [19] J. Stawinski, R. Strömberg, M. Thelin, E. Westman, *Nucleic Acids Res.* **1988**, *16*, 9285–9298.
- [20] a) S. Iwai, M. Shimizu, H. Kamiya, E. Ohtsuka, *J. Am. Chem. Soc.* **1996**, *118*, 7642–7643; b) T. Mizukoshi, K. Hitomi, T. Todo, S. Iwai, *J. Am. Chem. Soc.* **1998**, *120*, 10634–10642.
- [21] a) Y. Fujiwara, S. Iwai, *Biochemistry* **1997**, *36*, 1544–1550; b) K. Hitomi, S.-T. Kim, S. Iwai, N. Harima, E. Otsu, M. Ikenaga, T. Todo, *J. Biol. Chem.* **1997**, *272*, 32591–32598; c) H. Kamiya, S. Iwai, H. Kasai, *Nucleic Acids Res.* **1998**, *26*, 2611–2617; d) K. Sugawara, J. M. Y. Ng, C. Masutani, S. Iwai, P. J. van der Spek, A. P. M. Eker, F. Hanaoka, D. Bootsma, J. H. J. Hoeijmakers, *Mol. Cell* **1998**, *2*, 223–232; e) Y. Fujiwara, C. Masutani, T. Mizukoshi, J. Kondo, F. Hanaoka, S. Iwai, *J. Biol. Chem.* **1999**, *274*, 20 027–20 033.
- [22] J. Butenandt, L. T. Burgdorf, T. Carell, *Synthesis* **1999**, 1085–1105.

A Concise Stereoselective Route to the Pentacyclic Frameworks of Arisugacin A and Territrem B**

Luke R. Zehnder, Richard P. Hsung,* Jiashi Wang, and Geoffrey M. Golding

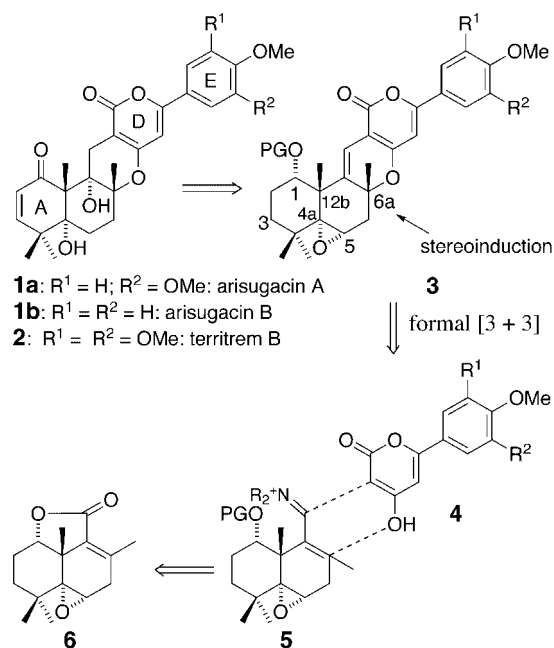
Arisugacin A (**1a**, Scheme 1) was first isolated from *Penicillium* sp. Fo-4259 as a potent and selective inhibitor of acetylcholinesterase (AChE) with an IC_{50} value of 1 nM.^[1] Because of the potential therapeutic value of **1a** in the treatment of Alzheimer's disease,^[2] and the structural similarity of **1a** to important natural products such as territrem (for example, territrem B (**2**))^[3] and pyripyropenes,^[4] we have been exploring a number of different synthetic routes that may be suitable for an efficient and stereoselective synthesis of arisugacins or territrem.^[5, 6] Our recent work involving a formal [3+3] cycloaddition reaction using α,β -unsaturated iminiums and diketo systems^[7–9] allowed us to envision a highly concise entry to these natural products. We report here our success in using a stereoselective variant of this formal cycloaddition reaction to construct the pentacyclic frameworks of arisugacin A (**1a**) and territrem B (**2**).

An advanced pentacyclic intermediate such as **3** that is suitable for the syntheses of arisugacins and territrem can be obtained readily by a stereoselective formal [3+3] cycloaddition reaction using the 4-hydroxy-2-pyrone **4**^[10] and α,β -unsaturated iminium **5** (Scheme 1). The critical stereoinduction to be achieved in this key reaction is the stereochemistry

[*] Prof. R. P. Hsung, L. R. Zehnder, J. Wang, G. M. Golding
Department of Chemistry
University of Minnesota
Minneapolis, MN 55455 (USA)
Fax: (+1) 612-626-7541
E-mail: hsung@chem.umn.edu

[**] This work was supported by the University of Minnesota.

Supporting information for this article is available on the WWW under <http://www.wiley-vch.de/home/angewandte/> or from the author.

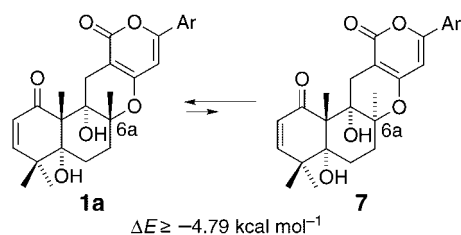


Scheme 1. PG = protecting group.

of the angular methyl group at C6a. The formation of iminium **5** from the epoxy lactone **6** may be envisioned and this should give the required stereochemistry at C12b and C4a in the AB ring.

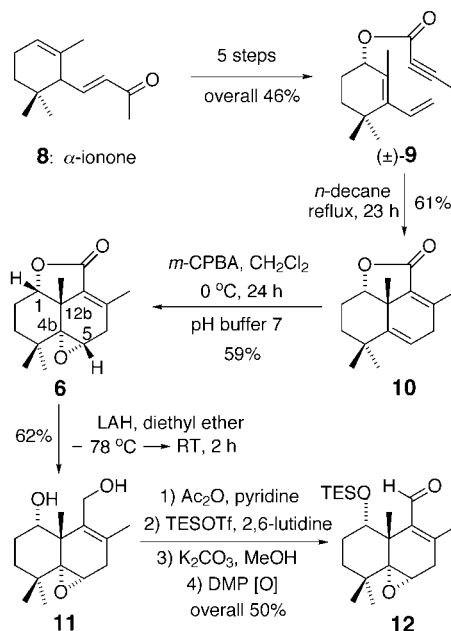
Although this proposed route appears to be feasible on the basis of the existing understanding of the key formal [3+3] cycloaddition,^[6a, 9a] there are two major uncertainties that could cause this attempt to fail. First, we have demonstrated that α,β -unsaturated iminium groups containing steric encumbrance comparable to that in **5** can effectively shut down the reaction.^[9a, 11] Second, and more significantly, there have been no successful stereoselective examples of this particular formal cycloaddition using chiral α,β -unsaturated iminium groups.^[6a, 9a, 11] Hence, the ability to control the stereochemistry at C6a through this reaction was highly speculative.

Recent work, however, suggested that the 6π -electron electrocyclic ring closure, the third mechanistic step in these formal [3+3] cycloaddition reactions, is reversible, and leads to the thermodynamically more-stable isomer with high diastereoselectivity.^[8] Our calculations (PM3 using the Spartan package) suggested that the diastereomer **7**, in which the angular methyl group at C6a is β (Scheme 2), is 4.79 kcal mol⁻¹ more stable than the α -epimer. This result suggests that a favorable diastereoselective control could be achieved in a thermodynamic manner by using α,β -unsaturated iminium compounds such as **5**.



Scheme 2. Ar = 3,4-dimethoxyphenyl.

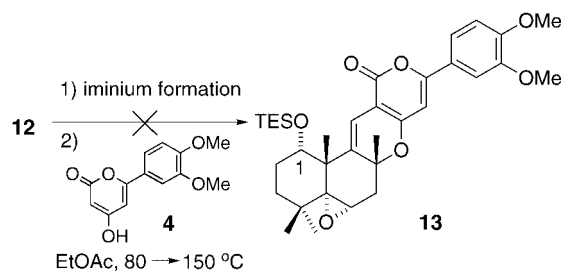
Encouraged by this calculation we pursued the synthesis of α,β -unsaturated aldehydes that would serve as precursors to **5**. The racemic ester **9** (Scheme 3) could be obtained readily in five steps from α -ionone (**8**) in 46% overall yield by a sequence previously used in the synthesis of forskolin.^[12] A subsequent intramolecular Diels–Alder reaction of **9**^[13] followed by epoxidation led to the α -epoxy lactone **6**^[14] in



Scheme 3. *m*-CPBA = *meta*-chloroperbenzoic acid; LAH = lithium aluminum hydride; TESOTf = triethylsilyl trifluoromethanesulfonate; DMP[O] = Dess–Martin oxidation.

59% yield. The corresponding β -epoxy isomer was also isolated in 10–20% yield. The stereochemistry of **6** was assigned using global NOE experiments, and it was thereby established that the relative stereochemistry required at C4a and C12b for arisugacins and territrems was present. Compound **6** was reduced to the diol **11** in 62% yield using LAH, with the epoxide remaining unopened. Appropriate functional group manipulations provided the aldehyde **12** in 50% overall yield from **11** (see Supporting Information).

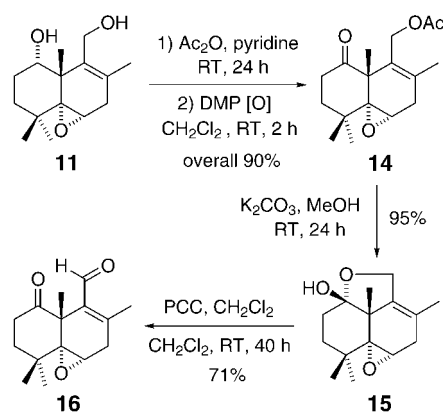
Under our standard conditions,^[9a] as well as a under a variety of other conditions known to generate iminium groups, formal [3+3] cycloaddition reactions of **12** with the pyrone **4** failed to provide the desired pentacycle **13** (Scheme 4). This failure prompted us to speculate that the



Scheme 4.

aldehyde **12** may be too sterically hindered, thereby effectively shutting down the cycloaddition reaction pathway.^[9] Inspection of molecular models revealed that this steric congestion could be alleviated if the C1 carbon atom was sp² hybridized.

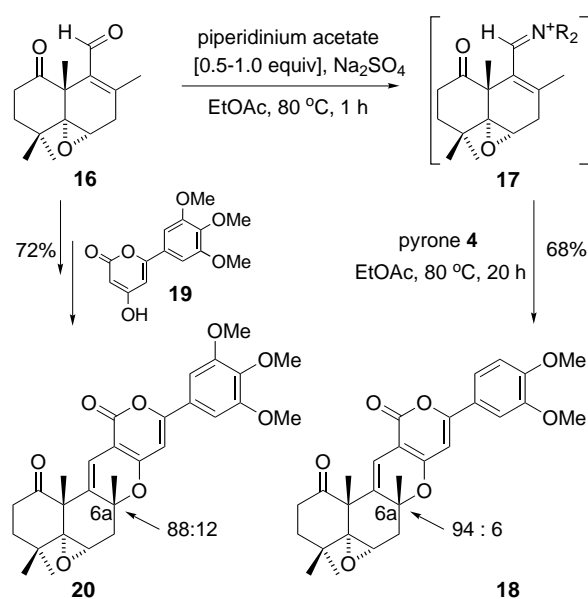
Acetylation of the diol **11**, followed by Dess–Martin oxidation, afforded the ketone **14** in 90% overall yield (Scheme 5). Deacetylation of **14** led to the formation of the lactol **15**, and only oxidation with PCC was successful in giving



Scheme 5. PCC = pyridinium chlorochromate.

the ketoaldehyde **16** (71% yield, 75% conversion). The ketoaldehyde **16** proved to be suitable for the construction of pentacycles. The iminium intermediate **17** was generated from **16** using 0.5–1.0 equivalents of piperidinium acetate in the presence of Na₂SO₄ at 80°C for 1 h (Scheme 6).^[15] A subsequent formal [3+3] cycloaddition reaction with pyrone **4** in EtOAc at 80°C for 20 h enabled the pentacycle **18** to be isolated in 68% yield with a diastereomeric ratio of 94:6.

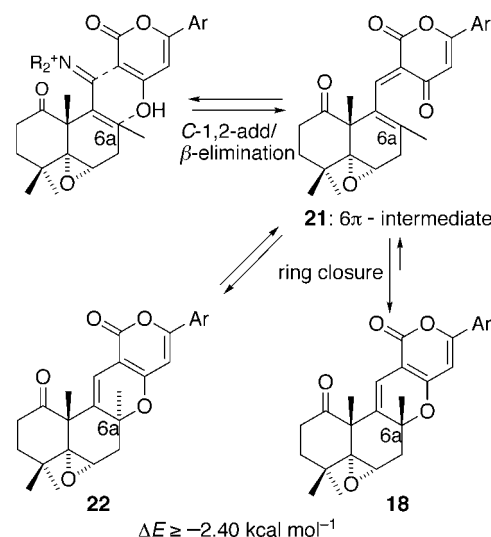
The angular methyl group at C6a was established as β for the major isomer of **18** and α for the minor isomer by using NOE experiments. The pentacycle **18** should prove to be



Scheme 6.

useful for the synthesis of arisugacin A (**1a**). By using 6-(3,4,5-trimethoxyphenyl)-4-hydroxy-2-pyrone (**19**) under the same reaction conditions the pentacycle **20** was obtained in 72% yield with a diastereomeric ratio of 88:12, with the β -epimer again being the major product. Compound **20** contains the desired E-ring necessary for the synthesis of territrems B (**2**).

The high diastereoselectivity obtained in these reactions here can be explained as a result of the reversible 6 π -electron electrocyclic ring closure^[7,16] via the 6 π intermediate (**21** in Scheme 7), which leads to the thermodynamically more stable isomer **18**. Our PM3 calculations again support that compound **18** is more stable than **22** by about 2.40 kcal mol⁻¹.



Scheme 7. Ar = 3,4-dimethoxyphenyl.

We have described here a concise route to the pentacyclic frameworks of arisugacin A and territrems B using a stereoselective formal [3+3] cycloaddition reaction. Efforts to complete the total syntheses of arisugacins and territrems using this synthetic approach are still underway.

Received: April 27, 2000 [Z15050]

- [1] K. Otaguro, F. Kuno, S. Ōmura, *Pharmacol. Ther.* **1997**, 76, 45.
- [2] V. John, I. Lieberburg, E. D. Thorsett, *Annu. Rep. Med. Chem.* **1993**, 28, 197.
- [3] a) K. H. Ling, C.-K. Yang, F.-T. Peng, *Appl. Environ. Microbiol.* **1979**, 37, 355; b) T. H. Hseu, C.-K. Yang, K. H. Ling, C. J. Wang, C. P. Tang, *Cryst. Struct. Commun.* **1982**, 11, 199; c) S.-S. Lee, F.-C. Peng, C.-M. Chiou, K. H. Ling, *J. Nat. Prod.* **1992**, 55, 251.
- [4] a) H. Tomoda, N. Tabata, D. J. Yang, I. Namatame, H. Tanaka, S. Ōmura, T. Kaneko, *J. Antibiotics* **1996**, 49, 292; b) A. B. Smith III, T. Kinsho, T. Sunazuka, S. Ōmura, *Tetrahedron Lett.* **1996**, 6461; c) T. Nagamitsu, T. Sunazuka, R. Obata, H. Tomoda, H. Tanaka, Y. Harigaya, S. Ōmura, A. B. Smith III, *J. Org. Chem.* **1995**, 60, 8126; d) K. A. Parker, L. Resnick, *J. Org. Chem.* **1995**, 60, 5726.
- [5] a) R. P. Hsung, *J. Org. Chem.* **1997**, 62, 7904; b) K. G. Granum, G. Merkel, J. A. Mulder, S. A. Debbins, R. P. Hsung, *Tetrahedron Lett.* **1998**, 9597.
- [6] For other related studies, see a) D. H. Hua, Y. Chen, H.-S. Sin, M. J. Maroto, P. D. Robinson, S. W. Newell, E. M. Perchellet, J. B. Ladesich, J. A. Freeman, J.-P. Perchellet, P. K. Chiang, *J. Org. Chem.* **1997**, 62, 6888; b) R. Obata, T. Sunazuka, Z. Tian, H. Tomoda, Y. Harigaya, S. Ōmura, A. B. Smith III, *Chemistry Lett.* **1997**, 935.

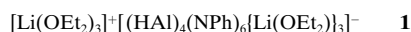
- [7] a) H. M. Sklenicka, R. P. Hsung, L.-L. Wei, M. J. McLaughlin, A. I. Gerasuto, S. J. Degen, J. A. Mulder, *Organic Lett.* **2000**, 2, 1161; b) R. P. Hsung, L.-L. Wei, H. M. Sklenicka, H. C. Shen, M. J. McLaughlin, L. R. Zehnder in *Advances in Cycloaddition* (Ed.: M. Harmata), JAI, Greenwich, **2000**, in press.
- [8] R. P. Hsung, L.-L. Wei, H. H. Sklenicka, C. J. Douglas, M. J. McLaughlin, J. A. Mulder, L. J. Yao, *Organic Lett.* **1999**, 1, 509.
- [9] a) R. P. Hsung, H. C. Shen, C. J. Douglas, C. D. Morgan, S. J. Degen, L. J. Yao, *J. Org. Chem.* **1999**, 64, 690; b) L. R. Zehnder, J. W. Dahl, R. P. Hsung, *Tetrahedron Lett.* **2000**, 1901.
- [10] C. J. Douglas, H. M. Sklenicka, H. C. Shen, G. M. Golding, D. S. Mathias, S. J. Degen, C. D. Morgan, R. A. Shih, K. L. Mueller, L. H. Seurer, E. W. Johnson, R. P. Hsung, *Tetrahedron* **1999**, 55, 13683.
- [11] M. Jonassohn, O. Sterner, H. Anke, *Tetrahedron* **1996**, 52, 1473.
- [12] a) K. C. Nicolaou, W. S. Li, *J. Chem. Soc. Chem. Commun.* **1985**, 421; For related approaches, see b) E. J. Corey, P. D. S. Jardine, J. C. Rohloff, *J. Am. Chem. Soc.* **1988**, 110, 3672; c) F. E. Ziegler, B. H. Jaynes, M. T. Saindane, *J. Am. Chem. Soc.* **1987**, 109, 8115; d) P. R. Jenkins, K. A. Menear, P. Barraclough, M. S. Nobbs, *J. Chem. Soc. Chem. Commun.* **1984**, 1423.
- [13] B. Delpech, D. Calvo, R. Lett, *Tetrahedron Lett.* **1996**, 1015.
- [14] All new compounds are characterized by ^1H NMR, ^{13}C NMR, and FT-IR spectroscopy, as well as mass spectrometry.
- [15] a) L. E. Overman, M. H. Rabinowitz, *J. Org. Chem.* **1993**, 58, 3235; b) L. E. Overman, M. H. Rabinowitz, P. A. Renhowe, *J. Am. Chem. Soc.* **1995**, 117, 2657.
- [16] For leading references on electrocyclic ring closures involving 1-oxa- or 1-azatrienes, see a) T. Kametani, M. Kajiura, K. Fukumoto, *Tetrahedron* **1974**, 30, 1053; b) K. Shishido, M. Ito, S.-I. Shimada, K. Fukumoto, T. Kametani, *Chem. Lett.* **1984**, 1943; c) D. F. Maynard, W. H. Okamura, *J. Org. Chem.* **1995**, 60, 1763; d) W. H. Okamura, A. R. de Lera, W. Reischl, *J. Am. Chem. Soc.* **1988**, 110, 4462.

Formation of the Unprecedented Trilithio-Capped Heteroadamantanyl Iminoalane Anion $[(\text{HAl})_4(\text{NPh})_6\{\text{Li}(\text{OEt}_2)\}_3]^-$: An Open Cage Derived from a Rhombododecahedron**

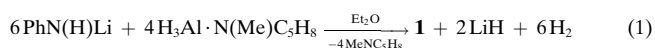
Kenneth W. Henderson,* Alan R. Kennedy, Arlene E. McKeown, and Robert E. Mulvey

There is a great deal of current interest in the preparation of organometallic compounds containing combinations of p-block elements due to their uses in the electronics industry,^[1] in catalysis,^[2] and in the search for new types of π bonding.^[3] As a result, a wide variety of heterodimetallic species that adopt polyhedral cage frameworks have been characterized, and structural patterns within their mixed-metal cores are now emerging. A notable example exists for the isovalent series of compounds with general formulas $\text{M}_4\text{E}_6\text{Li}_4$ (where $\text{M} = \text{Al}, \text{Ga}, \text{In}, \text{Sn}$; $\text{E} = \text{AsSiPr}_3$, $\text{E} = \text{AlMe}$ or Sn , $\text{E} = \text{PC}_6\text{H}_{11}$)^[4] or $\text{M}_2\text{E}_6\text{Li}_6$ (where $\text{M} = \text{Sb}$, $\text{E} = \text{NCH}_2\text{CH}_2\text{Ph}$,

NC_6H_{11} , NtBu , $\text{NC}_6\text{H}_3(\text{OMe})_2$, or PC_6H_{11} ;^[5] $\text{M} = \text{Ge}, \text{tBu}$, $\text{E} = \text{AsSiPr}_3$;^[6] $\text{M} = \text{SiR}$, $\text{E} = \text{NR}'$;^[7] where $\text{R} = \text{H}$, $\text{R}' = \text{Me}_3\text{Si}$; $\text{R} = \text{Me}$, tBu or Ph , $\text{R}' = \text{Me}_3\text{Si}$; $\text{R} = \text{Me}$ or Ph , $\text{R}' = \text{tBu}$; $\text{R} = \text{Me}$ or tBu , $\text{R}' = \text{Me}$; $\text{M} = \text{SiEt}$, $\text{E} = \text{PSiPr}_3$), which all adopt structures containing very similar 14-membered rhombododecahedral cage cores (Lewis base complexants within the compounds are ignored for simplicity). In contrast, we now report the synthesis of the novel, charge-separated complex **1**, which though isovalent with the above compounds adopts a unique molecular geometry.



Complex **1** was originally prepared from the equimolar reaction between the primary amidolithium $\text{PhN}(\text{H})\text{Li}$ and the alane adduct $\text{H}_3\text{Al} \cdot \text{N}(\text{Me})\text{C}_5\text{H}_8$ (where $\text{N}(\text{Me})\text{C}_5\text{H}_8 = 1$ -methyl-1,2,3,6-tetrahydropyridine)^[8] in diethyl ether solution. However, measurement of H_2 evolution from the reaction has established that the ideal stoichiometry for the preparation of **1** is that shown in Equation (1). Crystallographic analysis of **1**



revealed a remarkable structure consisting of a cage anion (**1a**; Figure 1) and a solvent-separated counteranion, with no discernible close contacts between the two.^[9]

Solution NMR data (^{27}Al and low-temperature ^7Li) appear to be consistent with the solid-state structure of **1**, indicating the presence of two distinct signals (apical/equatorial Al, and cation/anion Li). However, a full understanding of the

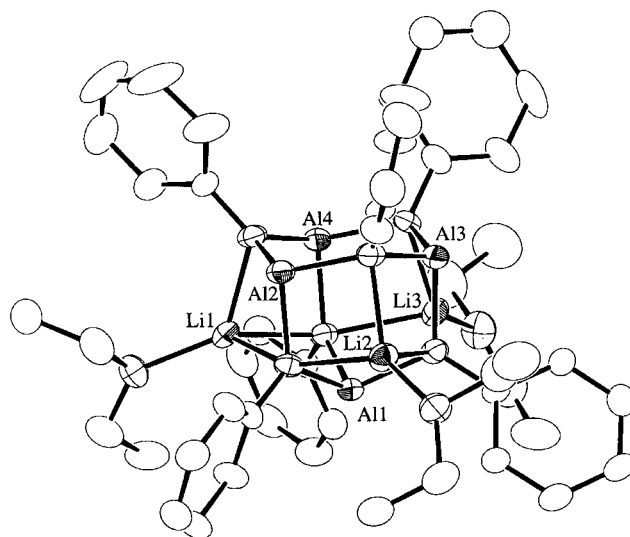


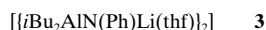
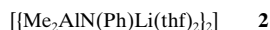
Figure 1. Molecular structure of **1a** with hydrogen atoms omitted for clarity. Selected bond lengths [Å] and angles [°]: Al1-N1 1.882(6), Al1-N3 1.901(7), Al1-N4 1.895(6), Al2-N1 1.914(6), Al2-N2 1.873(7), Al2-N5 1.881(7), Al3-N2 1.860(7), Al3-N3 1.918(6), Al3-N6 1.890(7), Al4-N4 1.924(6), Al4-N5 1.881(7), Al4-N6 1.868(7), Li1-O1 1.929(14), Li2-O2 1.950(14), Li3-O3 1.930(13), Li1-N1 2.205(15), Li1-N4 2.227(15), Li1-N5 2.106(14), Li2-N1 2.218(15), Li2-N2 2.059(14), Li2-N3 2.227(15), Li3-N3 2.225(14), Li3-N4 2.221(14), Li3-N6 2.069(13); N-Li-N 84.97 (mean), N-Al1-N 104.17 (mean), N-Al2-N 105.40 (mean), N-Al3-N 105.40 (mean), N-Al4-N 105.73 (mean).

[*] Dr. K. W. Henderson, Dr. A. R. Kennedy, A. E. McKeown, Prof. R. E. Mulvey
Department of Pure and Applied Chemistry
University of Strathclyde
Glasgow, G1 1XL (UK)
Fax: (+44)141-552-0876
E-mail: k.w.henderson@strath.ac.uk

[**] We thank the Royal Society for a University Research Fellowship (K.W.H.) and BP Amoco for funding (A.E.M.).

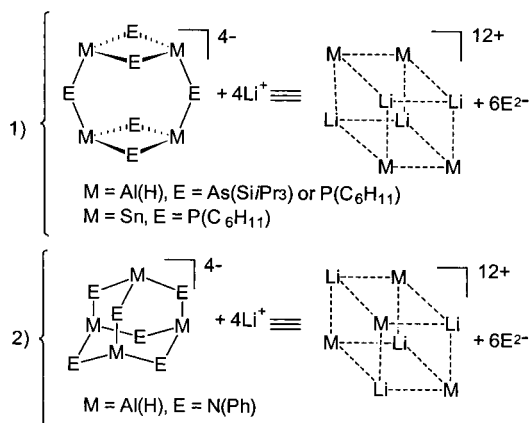
complex dynamic processes occurring in solution has yet to be determined.

The fascinating feature of the “missing” vertex of the cage can be explained in terms of the cavity size of the Al_3N_3 rings. Analysis of the bond lengths within **1a** indicate only small differences for the Al–N distances (range from 1.860(7) to 1.924(6) Å; mean 1.890 Å). These are consistent with the distance of 1.888(5) Å found in both of the related Li/Al amide dimers **2** and **3**.^[10] Significantly, the Li–N distances



show much greater variance, ranging from 2.059(14) to 2.227(15) Å, and the mean distance of 2.173 Å is much longer than those found in **2** and **3** (2.023(12) and 1.980(17) Å, respectively). Each Li center in **1a** asymmetrically caps a Al_3N_3 ring, with one relatively short contact to the nitrogen atom on the open face of the cage (mean 2.078 Å), and two long contacts, to the remaining nitrogen atoms (mean 2.220 Å). The overall effect is that the uncapped Al_3N_3 face of the cage is more open (less puckered) than the three Li-capped Al_3N_3 faces. Further evidence for this distortion is the differences in the transannular N...N distances, which are 2.94 Å (mean) for the capped faces and 3.18 Å (mean) for the open face. The widening of the fourth Al_3N_3 ring results in a larger cavity, which can no longer accommodate (or trap) a Li center, leading to the preferential formation of a charge-separated complex.

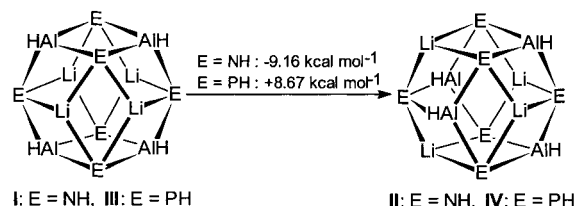
Further examination of **1a** reveals a surprising difference in the arrangement of the atoms within the cage skeleton compared to the previously mentioned isovalent 14-membered cage compounds.^[4–7] These complexes, with the general core formula $\text{M}_4\text{E}_6\text{Li}_4$ (M = Al, E = As or P; M = Sn, E = P), have almost identical frameworks. They consist of a pair of dimeric M_2E_2 rings connected through two additional bridging E ligands, leading to a tetraanionic polycycle (Scheme 1). Another view is to consider the structures composed of two orthogonal rectangular planes of metals, M_4/Li_4 . This view can be extended to include the compounds with the general core formula $\text{M}_2\text{E}_6\text{Li}_6$ (M = Sb or Si, E = N and M = Ge, E = As),



Scheme 1. Simplified view of the alternative cores in the dimetallic cages, 1) bridged dimers and 2) heteroadamantanyl.

where one rectangular plane of metals is composed of a dimetallic M_2Li_2 ring. In contrast, **1a** breaks with this structural pattern by adopting a unique $(\text{HAl})_4(\text{NPh})_6$ heteroadamantanyl tetraanionic core, which has three of the four six-membered Al_3N_3 rings capped by $\mu_3\text{-Li}$ centers. In theory, placement of a fourth Li atom to make a closed cage structure would result in two interpenetrating tetrahedra of metals, that is an isomer of the related heterodimetallic complexes (Scheme 1).

Ab initio molecular orbital calculations (HF/6-31G*) were carried out for two isomers of the model complex $[(\text{HAl})_4(\text{NH})_6\text{Li}_4]$: 1) bisecting planes of metals (**I**) and 2) interpenetrating tetrahedra of metals (**II**) (Scheme 2).^[11]



Scheme 2. Generalized view of the calculated molecules.

Interestingly, **II** was found to be more stable than **I** by 9.16 kcal mol^{−1}, in agreement with the heteroadamantanyl core found for **1a**. This preference is due to an alleviation of metal–metal repulsions in the heteroadamantanyl isomer. In **I** there are two short Al...Al and Li...Li distances of 2.656 and 2.345 Å (mean), respectively (transannular repulsions in the M_2N_2 rings); however, in **II** the metals are separated by 3.357 and 3.889 Å (mean), respectively. Other distances in **I** and **II** are similar (Li–N 2.063 and 2.074 Å (mean), respectively, and Al–N 1.920 and 1.909 Å (mean), respectively).

Calculations on the related P-bridged model complexes $[(\text{HAl})_4(\text{PH})_6\text{Li}_4]$ (**III** and **IV**) indicate that all the metal–metal separations are > 3 Å for both isomers as a consequence of the larger bridging anion. Moreover, and consistent with experimental data,^[4b] the bridged dimers isomer **III** was found to be favored over the heteroadamantanyl isomer **IV** by 8.67 kcal mol^{−1}.

Therefore, the formation of the heteroadamantanyl core in **1a** is driven principally by minimizing the metal–metal repulsions, while maintaining strong metal–N interactions. Furthermore, the factors governing the generation of the charge-separated species are complex and include the aromatic nature of the phenyl groups attached to the imido nitrogen atoms, the effect of solvation by Et_2O , and the cavity size of the Al_3N_3 rings.

Experimental Section

1: $n\text{BuLi}$ (10 mmol, 5.9 mL of a 1.7 M solution in hexanes) was added to a Schlenk tube by syringe, and all solvent was removed in vacuo. The resulting yellow oil was dissolved in Et_2O (10 mL), the solution was cooled to -78°C , and aniline (10 mmol, 0.91 mL) was then added dropwise by syringe. This solution was stirred at -78°C for 30 min, then allowed to warm to ambient temperature and stirred for a further 2 h. After dilution with Et_2O (30 mL), the solution was recooled to -78°C . $\text{H}_3\text{Al}\cdot\text{N}(\text{Me})\text{C}_5\text{H}_8$ (10 mmol, 1.27 g; where $\text{N}(\text{Me})\text{C}_5\text{H}_8 = 1\text{-methyl-1,2,3,6-tetrahydropyridine}$ ^[8]) was added to the solution through a solids addition tube, and the

reaction mixture was stirred for 1 h before it was allowed to warm to ambient temperature. After the mixture had been stirred for a further 24 h, a cloudy yellow/brown solution was produced. The mixture was filtered through Celite, cooled to -20°C , and left to stand for 12 h, resulting in the precipitation of small, colorless crystals of **1**. Yield 60.5%; m.p. $> 300^{\circ}\text{C}$; IR (Nujol): $\tilde{\nu} = 1775\text{ cm}^{-1}$ (Al–H); elemental analysis calcd for $\text{C}_{60}\text{H}_{94}\text{Al}_4\text{Li}_4\text{N}_6\text{O}_6$ (%): C 63.72, H 8.32, N 7.43; found: C 63.45, H 7.55, N 8.70; ^1H NMR (variable-temperature studies showed only one set of resonances (with broadening) in the range 300–193 K; 400.13 MHz, C_6D_6 , 300 K): $\delta = 7.76$ (d, 2H; *o*-H, Ph), 7.16 (t, 2H; *m*-H, Ph), 6.74 (t, 1H; *p*-H, Ph), 5.40 (v br., 1H; AlH), 2.88 (q, 4H; OCH_2), 0.60 (t, 6H; CH_3); ^{13}C NMR (100.62 MHz, C_6D_6 , 300 K): $\delta = 156.70$ (*i*-C; Ph), 129.21 (*m*-C; Ph), 124.88 (*o*-C; Ph), 117.58 (*p*-C; Ph), 65.33 (OCH_2), 13.66 (CH_3); ^7Li NMR (variable-temperature studies showed only a single resonance in the range 300–213 K but the appearance of a second resonance at 193 K; 155.51 MHz, referenced to LiCl in D_2O , $[\text{D}_8]\text{toluene}$, 193 K): $\delta = 6.75$, $\delta = 6.58$; ^{27}Al NMR (C_6D_6 , 298 K, 52.12 MHz, referenced to AlCl_3 in D_2O): $\delta = 131.30$, 69.91.

Received: April 25, 2000 [Z15042]

- [1] A. C. Jones, *Chem. Soc. Rev.* **1997**, 101.
- [2] a) H. Yamamoto in *Organometallics in Synthesis* (Ed.: M. Schlosser), Wiley, Chichester, UK, **1994**, chap. 7; b) Y. Koide, S. G. Bott, A. R. Barron, *J. Am. Chem. Soc.* **1993**, 115, 4971.
- [3] M. A. Petrie, S. C. Shoner, H. V. R. Dias, P. P. Power, *Angew. Chem.* **1990**, 102, 1061; *Angew. Chem. Int. Ed. Engl.* **1990**, 29, 1033.
- [4] a) M. Driess, S. Kuntz, K. Merz, H. Pritzkow, *Chem. Eur. J.* **1998**, 4, 1628; b) R. E. Allan, M. A. Beswick, P. R. Raithby, A. Steiner, D. S. Wright, *J. Chem. Soc. Dalton Trans.* **1996**, 4153; c) R. E. Allan, M. A. Beswick, N. L. Cromhout, M. A. Paver, P. R. Raithby, A. Steiner, M. Trevithick, D. S. Wright, *Chem. Commun.* **1996**, 1501.
- [5] a) A. J. Edwards, M. A. Paver, P. R. Raithby, M.-A. Rennie, C. A. Russell, D. S. Wright, *Angew. Chem.* **1994**, 106, 1334; *Angew. Chem. Int. Ed. Engl.* **1994**, 33, 1277; b) M. A. Beswick, N. Choi, C. N. Harmer, A. D. Hopkins, M. McPartlin, M. A. Paver, P. R. Raithby, A. Steiner, M. Tombul, D. S. Wright, *Inorg. Chem.* **1998**, 37, 2177; c) M. A. Beswick, J. M. Goodman, C. N. Harmer, A. D. Hopkins, M. A. Paver, P. R. Raithby, A. E. H. Wheatley, D. S. Wright, *Chem. Commun.* **1997**, 1879.
- [6] L. Zsolnai, G. Huttner, M. Driess, *Angew. Chem.* **1993**, 105, 1549; *Angew. Chem. Int. Ed. Engl.* **1993**, 32, 1439.
- [7] a) P. Kosse, E. Popowski, M. Veith, V. Huch, *Chem. Ber.* **1994**, 127, 2103; b) D. J. Brauer, H. Bürger, G. R. Liewald, J. Wilke, *J. Organomet. Chem.* **1985**, 287, 305; c) D. J. Brauer, H. Bürger, G. R. Liewald, *J. Organomet. Chem.* **1986**, 308, 119; d) G. Huber, A. Jockisch, H. Schmidbaur, *Z. Naturforsch. B* **1999**, 54, 8; e) M. Veith, A. Spaniol, J. Pöhlmann, F. Gross, V. Huch, *Chem. Ber.* **1993**, 126, 2625; f) M. Driess, G. Huttner, N. Knopf, H. Pritzkow, L. Zsolnai, *Angew. Chem.* **1995**, 107, 354; *Angew. Chem. Int. Ed. Engl.* **1995**, 34, 316.
- [8] J. L. Atwood, F. R. Bennett, F. M. Elms, C. Jones, C. L. Raston, K. D. Robinson, *J. Am. Chem. Soc.* **1991**, 113, 8183.
- [9] Crystal structure data for **1**: $\text{C}_{60}\text{H}_{94}\text{Al}_4\text{Li}_4\text{N}_6\text{O}_6$, $M_r = 1131.1$, colorless plates, cut to approximately $0.60 \times 0.40 \times 0.20\text{ mm}$. $\text{MoK}\alpha$ graphite-monochromated radiation ($\lambda = 0.71069\text{ \AA}$), $T = 123\text{ K}$; monoclinic, space group $C2/c$; $a = 22.035(6)$, $b = 12.818(3)$, $c = 46.487(6)\text{ \AA}$; $\beta = 90.581(15)^{\circ}$; $V = 13129(5)\text{ \AA}^3$, $Z = 8$, $\mu = 0.121\text{ mm}^{-1}$, $\rho_{\text{calcd}} = 1.144\text{ Mg m}^{-3}$, $2\theta_{\text{max}} = 46^{\circ}$, 8786 reflections collected, 8509 unique used ($R_m = 0.0650$). The structure was solved and refined on F^2 using published programs and techniques (a) A. Altomare, M. C. Burla, M. Camalli, G. Cascarano, C. Giacovazzo, A. Guagliardi, G. Polidori, *J. Appl. Crystallogr.* **1994**, 27, 435; b) G. M. Sheldrick, SHELXL-97. University of Göttingen, Germany, **1997** to convergence at $R1 = 0.0917$ (for 4592 reflections with $I > 2\sigma(I)$), $wR2 = 0.2271$ and $S = 1.064$ for 777 parameters. Maximum residual electron density 0.505 e \AA^{-3} . Several factors combined to adversely affect the quality of the solution. The crystals reacted with the oil used to mount them and the large c axis gave overlapping reflections. Additionally the ether groups of the cation were severely disordered over two sites each. There was also some movement in the phenyl ring bonded to N6. Crystallographic data (excluding structure factors) for the structure reported in this paper have been deposited with the Cambridge

Crystallographic Data Centre as supplementary publication no. CCDC-142922. Copies of the data can be obtained free of charge on application to CCDC, 12 Union Road, Cambridge CB2 1EZ, UK (fax: (+44) 1223-336-033; e-mail: deposit@ccdc.cam.ac.uk).

- [10] a) D. A. Atwood, D. Rutherford, *Organometallics* **1996**, 15, 436; b) D. A. Atwood, D. Rutherford, *J. Am. Chem. Soc.* **1996**, 118, 11535.
- [11] Gaussian 94, revision E. 2. No constraints were used in any of the calculations. M. J. Frisch, G. W. Trucks, H. B. Schlegel, P. M. W. Gill, B. G. Johnson, M. A. Robb, J. R. Cheeseman, T. Keith, G. A. Petersson, J. A. Montgomery, K. Raghavachari, M. A. Al-Laham, V. G. Zakrzewski, J. V. Ortiz, J. B. Foresman, J. Cioslowski, B. B. Stefanov, A. Nanayakkara, M. Challacombe, C. Y. Peng, P. Y. Ayala, W. Chen, M. W. Wong, J. L. Andres, E. S. Replogle, R. Gomperts, R. L. Martin, D. J. Fox, J. S. Binkley, D. J. Defrees, J. Baker, J. P. Stewart, M. Head-Gordon, C. Gonzalez, J. A. Pople, Gaussian Inc., Pittsburgh PA, **1995**.

New Fused Bicyclic Cyclotrigermanes from Cycloaddition Reactions of Cyclotrigermene**

Norihisa Fukaya, Masaaki Ichinohe, and Akira Sekiguchi*

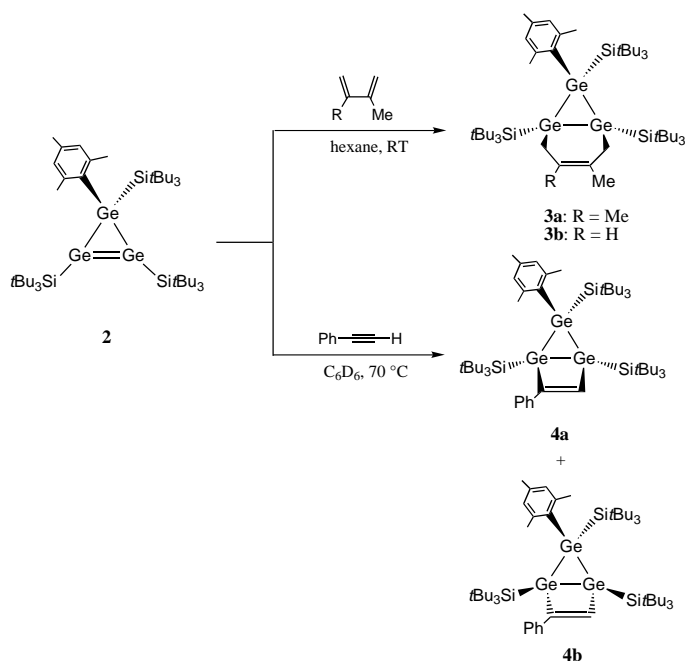
The chemistry of three- and four-membered ring systems consisting of Group 14 elements heavier than carbon is a subject of considerable interest.^[1] The thermal and photochemical conversion of cyclotrigermanes into digermenes and germylenes is well established and has been used for the synthesis of a variety of novel germanium compounds.^[2] However, cyclotrigermene derivatives incorporating a bicyclic system are completely unknown for synthetic reasons.^[3, 4] Most of the cyclotrigermene derivatives were synthesized by the simple reductive coupling reaction of the corresponding diorganodihalogermene with the appropriate reducing agents.^[1, 2] Recently, we succeeded in synthesizing a variety of cyclotrigermene analogues of cyclopropene by reaction of the cyclotrigermanium ion with nucleophiles.^[5] The reactivity of the cyclotrigermenes is of special interest, since cycloaddition to the endocyclic Ge=Ge bond could provide access to new bicyclic compounds. We now report the synthesis of the first bicyclic cyclotrigermene derivatives by the reaction of a mesityl-substituted cyclotrigermene with isoprene, 2,3-dimethyl-1,3-butadiene, and phenylacetylene.

After the successful synthesis of tetrakis(tri-*tert*-butylsilyl)-cyclotrigermene ($t\text{Bu}_3\text{Si})_4\text{Ge}_3$ (**1a**)^[6] and tetrakis(tri-*tert*-butylgermyl)cyclotrigermene ($t\text{Bu}_3\text{Ge})_4\text{Ge}_3$ (**1b**)^[6] by reaction of GeCl_2 (dioxane) with $t\text{Bu}_3\text{SiNa}$ or $t\text{Bu}_3\text{GeLi}$, we presumed that the cyclotrigermenes should be suitable as precursors of

[*] Prof. Dr. A. Sekiguchi, Dipl.-Chem. N. Fukaya, Dr. M. Ichinohe
Department of Chemistry, University of Tsukuba
Tsukuba, Ibaraki 305-8571 (Japan)
Fax: (+81) 298-53-4314
E-mail: sekiguch@staff.chem.tsukuba.ac.jp

[**] This work was supported by a Grant-in-Aid for Scientific Research (Nos. 10304051, 12020209, 12042213) from the Ministry of Education, Science and Culture of Japan, and TARA (Tsukuba Advanced Research Alliance) Fund.

bicyclic cyclotrigermanes. Nevertheless, all attempted reactions of **1a,b** with various dienes or acetylenes failed due to the steric overcrowding of **1a,b**. However, we found that 1,2,3-tris(tri-*tert*-butylsilyl)-3-mesitylcyclotrigermene (**2**)^[5] shows relatively high reactivity at the Ge=Ge bond due to the decrease in steric crowding on replacing one *t*Bu₃Si group at the saturated germanium atom with a mesityl group. The reaction of **2** with 2,3-dimethyl-1,3-butadiene in hexane at room temperature produced the Diels–Alder adduct **3a** as a yellow, air-stable crystalline compound in 63 % yield (Scheme 1). The reaction of **2** with isoprene gave **3b** in 78 % yield. These [2+4] cycloadducts were isolated by chromatography on silica gel without any decomposition. The NMR spectral data and X-ray crystal structure suggest the formation of just one of the two possible stereoisomers.



Scheme 1. Synthesis of **3** and **4**.

The molecular structure of **3b** was determined by X-ray diffraction (Figure 1).^[7] It reveals that isoprene attacked the Ge=Ge bond from the mesityl side of the three-membered ring to give only one stereoisomer. The difference in the steric bulk of the substituents on the sp³ Ge atom of **2** (Mes < *t*Bu₃Si) apparently can control the facial selectivity in the [2+4] cycloaddition. The three *t*Bu₃Si groups in **3b** are arranged in the same direction relative to the three-membered cyclotrigermane skeleton. Due to the large steric bulk of the *t*Bu₃Si group, the three *t*Bu₃Si groups occupy the less hindered pseudoequatorial positions, whereas the mesityl group and the CH₂C(Me)=CHCH₂ moiety occupy the pseudoaxial positions, as determined by the angles between the three-membered ring plane and the Ge–R bond (R = *t*Bu₃Si, CH₂C(Me)=CHCH₂, and Mes): 29.6° for *t*Bu₃Si, 100.8° for CH₂C(Me)=CHCH₂, and 106.6° for Mes. The Ge1–Ge2 (2.5938(3) Å) and Ge1–Ge3 (2.6068(3) Å) bond lengths lie in the upper range of known values for cyclotrigermanes

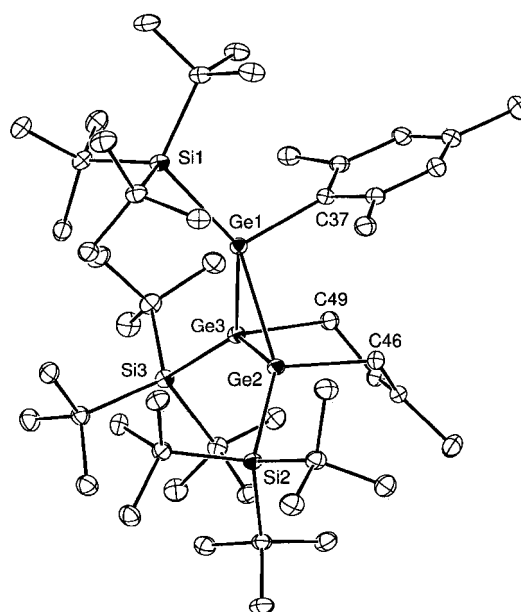


Figure 1. Structure of **3b** (ORTEP plot; hydrogen atoms omitted for clarity). Selected bond lengths [Å] and angles [°]: Ge1–Ge2 2.5938(3), Ge1–Ge3 2.6068(3), Ge2–Ge3 2.4705(3), Ge1–Si1 2.5529(7), Ge2–Si2 2.4873(6), Ge3–Si3 2.5314(7), Ge1–C37 2.029(2), Ge2–C46 2.048(2), Ge3–C49 2.050(2); Ge2–Ge1–Ge3 56.724(9), Ge3–Ge2–Ge1 61.903(9), Ge2–Ge3–Ge1 61.374(9).

(typically 2.460–2.590 Å).^[1, 2] In contrast, the Ge2–Ge3 bond is appreciably shorter (2.4705(3) Å), probably due to the effect of the fused ring system.

The [2+2] cycloaddition of **2** with phenylacetylene at 70 °C smoothly proceeded to give the more strained molecule **4** (Scheme 1), which was isolated as orange crystals of the two isomers **4a** (57 %) and **4b** (22 % yield).

The molecular structure of the favored isomer **4a** was determined by X-ray crystallography (Figure 2).^[7] The three

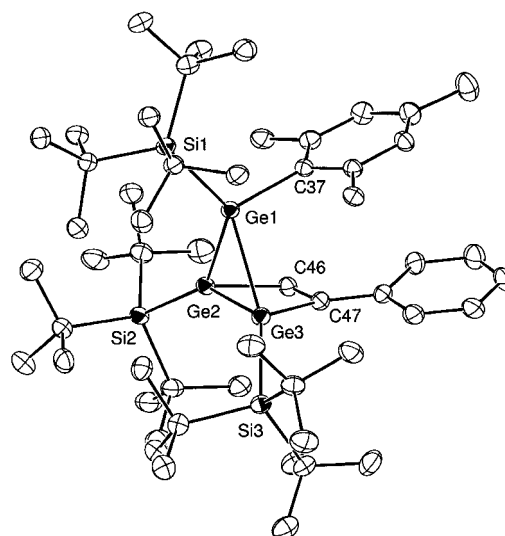
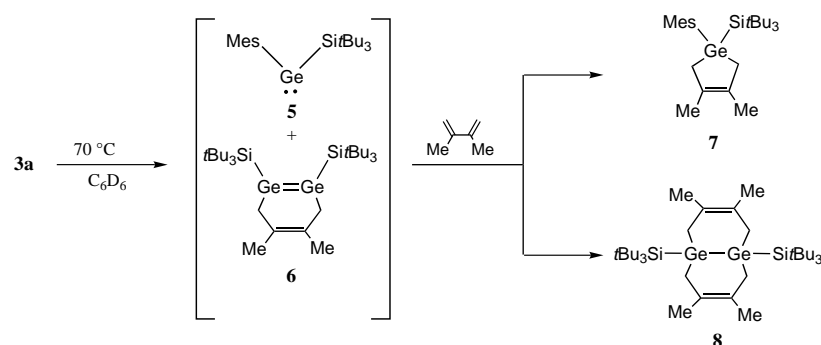


Figure 2. Structure of **4a** (ORTEP plot; hydrogen atoms omitted for clarity). Selected bond lengths [Å] and angles [°]: Ge1–Ge2 2.5958(5), Ge1–Ge3 2.5592(4), Ge2–Ge3 2.4857(4), Ge1–Si1 2.5248(9), Ge2–Si2 2.4780(9), Ge3–Si3 2.4797(9), Ge1–C37 2.032(3), Ge2–C46 1.963(3), Ge3–C47 2.021(3), C46–C47 1.357(4); Ge3–Ge1–Ge2 57.65(1), Ge3–Ge2–Ge1 60.44(1), Ge2–Ge3–Ge1 61.91(1), C46–Ge2–Ge3 73.36(9), C47–Ge3–Ge2 73.66(9), C47–C46–Ge2 109.1(2), C46–C47–Ge3 103.8(2).

*t*Bu₃Si groups are situated in *cis,cis* positions, as in **3b**, and the bicyclo[2.1.0] skeleton is highly folded to relieve steric repulsion, as shown by the dihedral angle between the planes of the three- and four-membered rings (97.4°).

It is noteworthy that **3** is a good precursor of germylene and digermene under mild conditions. Thermolysis of cyclotrimer-germane **3a** at 70 °C in dry C₆D₆ for 3 h in the presence of an excess of 2,3-dimethyl-1,3-butadiene cleanly yielded germacyclopent-3-ene **7** (80%) and digermabicyclo[4.4.0]deca-3,8-diene **8** (86%), clear evidence for the trapping of the germylene **5** and the digermene **6**, respectively (Scheme 2). However, heating of **3** in the solid state at 180 °C in vacuo led to the quantitative formation of **2** by retro-Diels–Alder reaction.



Scheme 2. Thermolysis of **3a** and trapping of the thermolysis products.

The present [2+4] and [2+2] cycloaddition reactions of cyclotrimer-germanes cleanly afford fused bicyclic cyclotrimer-germane derivatives and thus provide a new route to small ring systems of Group 14 elements heavier than carbon.

Experimental Section

3a: Orange crystals of **2** (60 mg, 0.064 mmol) were placed in a reaction vessel with a magnetic stirrer. Dry, degassed hexane (1.5 mL) and 2,3-dimethyl-1,3-butadiene (70 mg, 0.85 mmol) were introduced by vacuum transfer, and the mixture was stirred for 6 h at room temperature. The solvent and excess 2,3-dimethyl-1,3-butadiene were removed in vacuo, and the resulting residue was separated by column chromatography on silica gel with hexane as eluent to give **3a** (41 mg, 63%) as yellow crystals; m.p. 123–126 °C (decomp); ¹H NMR ([D₆]benzene, TMS): δ = 1.30 (s, 27H), 1.37 (s, 54H), 1.70 (s, 6H), 1.90 (s, 3H), 2.60 (s, 2H), 2.64 (s, 2H), 2.80 (s, 6H), 6.78 (s, 2H); ¹³C{¹H} NMR ([D₆]benzene, TMS): δ = 14.3, 23.0, 25.6, 26.8, 28.4, 29.9, 32.9, 33.5, 126.6, 128.8, 129.1, 137.0, 144.8; ²⁹Si{¹H} NMR ([D₆]benzene, TMS): δ = 45.9, 49.4; UV/Vis (*n*-hexane): λ_{max} (ε) = 277 (18950), 388 nm (1740); elemental analysis calcd for C₃₁H₁₀₂Ge₃Si₃ (%): C 60.21, H 10.10; found: C 60.14, H 10.17.

3b: Compound **3b** was prepared in 78% yield as yellow crystals; m.p. 130–132 °C (decomp); ¹H NMR ([D₆]benzene, TMS): δ = 1.30 (s, 27H), 1.35 (s, 27H), 1.37 (s, 27H), 1.84 (s, 3H), 1.97 (s, 3H), 2.57–2.61 (m, 2H), 2.70–2.73 (m, 1H), 2.79 (s, 3H), 2.80 (s, 3H), 2.95–3.00 (m, 1H), 5.51–5.53 (m, 1H), 6.78 (s, 2H); ¹³C{¹H} NMR ([D₆]benzene, TMS): δ = 20.9, 22.7, 25.6, 25.8, 26.8, 26.9, 27.0, 28.0, 28.6, 32.8, 32.9, 33.4, 123.3, 129.0, 129.1, 132.0, 137.0, 143.7, 144.5, 144.8; ²⁹Si{¹H} NMR ([D₆]benzene, TMS): δ = 45.3, 45.4, 47.9; UV/Vis (*n*-hexane): λ_{max} (ε) = 277 (16860), 388 nm (1520); elemental analysis calcd for C₅₀H₁₀₀Ge₃Si₃ (%): C 59.85, H 10.04; found: C 59.74, H 10.06.

4a and **4b:** Orange crystals of **2** (60 mg, 0.064 mmol) were placed in a reaction tube. Dry, degassed benzene (0.5 mL) and phenylacetylene (90 mg, 0.88 mmol) were introduced by vacuum transfer, and the mixture was heated for 6 h at 70 °C. The solvent and the excess phenylacetylene

were removed in vacuo, and the resulting residue was separated by column chromatography on silica gel with hexane as eluent to give **4a** (57 mg, 57%) and **4b** (22 mg, 22%). **4a:** orange crystals; m.p. 178–180 °C; ¹H NMR ([D₆]benzene, TMS): δ = 1.30 (s, 27H), 1.37 (s, 27H), 1.40 (s, 27H), 1.89 (s, 3H), 2.67 (s, 3H), 3.11 (s, 3H), 6.59 (s, 1H), 6.61 (s, 1H), 6.82–6.99 (m, 5H), 7.24 (s, 1H); ¹³C{¹H} NMR ([D₆]benzene, TMS): δ = 20.9, 25.5, 26.0, 26.4, 29.3, 30.8, 32.3, 32.7, 33.2, 125.7, 126.1, 127.3, 128.5, 128.7, 129.8, 130.0, 136.1, 143.1, 143.5, 144.7, 145.5, 155.9, 170.8; ²⁹Si{¹H} NMR ([D₆]benzene, TMS): δ = 38.5, 44.7, 50.0; UV/Vis (*n*-hexane): λ_{max} (ε) = 250 (46700), 303 (21930), 410 nm (2410); **4b:** orange crystals; m.p. 90–93 °C; ¹H NMR ([D₆]benzene, TMS): δ = 1.19 (s, 27H), 1.27 (s, 27H), 1.38 (s, 27H), 2.11 (s, 3H), 2.99 (s, 3H), 3.18 (s, 3H), 6.81 (s, 2H), 7.06 (t, *J* = 7.8 Hz, 1H), 7.22 (t, *J* = 7.8 Hz, 2H), 7.45 (d, *J* = 7.8 Hz, 2H), 7.52 (s, 1H); ¹³C{¹H} NMR ([D₆]benzene, TMS): δ = 21.2, 25.8, 26.0, 26.5, 30.3, 31.0, 32.3, 32.4, 33.6, 126.5, 127.2, 128.0, 128.1, 129.1, 137.3, 140.7, 143.6 (2C), 145.7, 153.0, 167.4; ²⁹Si{¹H} NMR ([D₆]benzene, TMS): δ = 39.6, 45.5, 49.4; UV/Vis (*n*-hexane): λ_{max} (ε) = 240 (41200), 302 (20900), 400 nm (2500).

Received: May 16, 2000 [Z15130]

- [1] For general reviews on the chemistry of Si, Ge, Sn, and Pb, see: a) *The Chemistry of Organic Germanium, Tin and Lead Compounds* (Ed.: S. Patai), Wiley, Chichester, **1995**; b) *The Chemistry of Organic Silicon Compounds*, Vol. 2 (Eds.: Z. Rappaport, Y. Apeloig), Wiley, New York, **1998**.
- [2] Reviews: a) T. Tsumuraya, S. A. Batcheller, S. Masamune, *Angew. Chem.* **1991**, *103*, 916; *Angew. Chem. Int. Ed. Engl.* **1991**, *30*, 902; b) J. Escudié, C. Couret, H. Ranaivonjatovo, J. Satgé, *Coord. Chem. Rev.* **1994**, *130*, 427; c) M. Weidenbruch, *Chem. Rev.* **1995**, *95*, 1479; d) M. Driess, H. Grützmacher, *Angew. Chem.* **1996**, *108*, 900; *Angew. Chem. Int. Ed. Engl.* **1996**, *35*, 828; e) K. M. Baines, W. G. Stibbs, *Adv. Organomet. Chem.* **1996**, *39*, 275; f) M. Weidenbruch, *Eur. J. Inorg. Chem.* **1999**, 373.
- [3] Related three- and four-membered ring systems of Si, Ge, and Sn: Cyclotrisilenes: a) T. Iwamoto, C. Kabuto, M. Kira, *J. Am. Chem. Soc.* **1999**, *121*, 886; b) M. Ichinohe, T. Matsuno, A. Sekiguchi, *Angew. Chem.* **1999**, *111*, 2331; *Angew. Chem. Int. Ed.* **1999**, *38*, 2194; cyclotrimer-germanes: see refs. [5] and [6]; Cyclotrisilene-germanium ions: c) A. Sekiguchi, M. Tsukamoto, M. Ichinohe, *Science* **1997**, *275*, 60; d) M. Ichinohe, N. Fukaya, A. Sekiguchi, *Chem. Lett.* **1998**, 1045; e) A. Sekiguchi, N. Fukaya, M. Ichinohe, Y. Ishida, *Eur. J. Inorg. Chem.* **2000**, 1155; cyclotrimer-germyl radical: f) M. M. Olmsted, L. Pu, R. S. Simons, P. P. Power, *Chem. Commun.* **1997**, 1595; cyclotrisilene: g) N. Wiberg, H.-W. Lerner, S.-K. Vasisht, S. Wagner, K. Karaghiosoff, H. Nöth, W. Ponikwar, *Eur. J. Inorg. Chem.* **1999**, 1211; cyclotetrasilenes: h) M. Kira, T. Iwamoto, C. Kabuto, *J. Am. Chem. Soc.* **1996**, *118*, 10303; i) T. Iwamoto, M. Kira, *Chem. Lett.* **1998**, 277; j) N. Wiberg, H. Auer, H. Nöth, J. Knizek, K. Polborn, *Angew. Chem.* **1998**, *110*, 3030; *Angew. Chem. Int. Ed.* **1998**, *36*, 2869.
- [4] For polyhedral germanium compounds containing three-membered rings, see: a) A. Sekiguchi, C. Kabuto, H. Sakurai, *Angew. Chem.* **1989**, *101*, 97; *Angew. Chem. Int. Ed. Engl.* **1989**, *28*, 55; b) A. Sekiguchi, T. Yatabe, C. Kabuto, H. Sakurai, *J. Am. Chem. Soc.* **1993**, *115*, 5853; c) N. Wiberg, W. Hochmuth, H. Nöth, A. Appel, M. Schmidt-Amelunxen, *Angew. Chem.* **1996**, *108*, 1437; *Angew. Chem. Int. Ed. Engl.* **1996**, *35*, 1333.
- [5] A. Sekiguchi, N. Fukaya, M. Ichinohe, N. Takagi, S. Nagase, *J. Am. Chem. Soc.* **1999**, *121*, 11587.
- [6] A. Sekiguchi, H. Yamazaki, C. Kabuto, H. Sakurai, S. Nagase, *J. Am. Chem. Soc.* **1995**, *117*, 8025.
- [7] Diffraction data were collected at 120 K for **3b** and 150 K for **4a** on a Mac Science DIP2030 Image Plate Diffractometer with a rotating anode (50 kV, 90 mA) and graphite-monochromated MoK_α radiation (λ = 0.71070 Å). The structures were solved by direct methods and refined by full-matrix least-squares method with the SHELXL-97 program. Crystal data for **3b**·C₇H₈: C₅₇H₁₀₈Ge₃Si₃, *M*_r = 1095.47, monoclinic, space group *P*2₁/*n*, *a* = 15.2160(3), *b* = 13.6410(3), *c* = 29.2430(5) Å, β = 99.810(1)°, *V* = 5981.0(2) Å³, *Z* = 4, ρ_{calcd} =

1.217 g cm⁻³. The final *R* factor was 0.0461 (*R*_w = 0.1328) for 12902 reflections with *I* > 2σ(*I*). Crystal data for **4a** · 0.5 C₆H₁₄: C₅₆H₁₀₈Ge₃Si₃, *M*_r = 1080.47, triclinic, space group = *P* $\bar{1}$, *a* = 13.7810(7), *b* = 14.485(1), *c* = 15.339(1) Å, α = 100.917(3), β = 91.953(4), γ = 95.408(4)°, *V* = 2988.9(3) Å³, *Z* = 2, ρ_{calcd} = 1.201 g cm⁻³. The final *R* factor was 0.0496 (*R*_w = 0.1408) for 10780 reflections with *I* > 2σ(*I*). Crystallographic data (excluding structure factors) for the structures reported in this paper have been deposited with the Cambridge Crystallographic Data Centre as supplementary publication nos. CCDC-144512 and CCDC-144513. Copies of the data can be obtained free of charge on application to CCDC, 12 Union Road, Cambridge CB21EZ, UK (fax: (+44) 1223-336-033; e-mail: deposit@ccdc.cam.ac.uk).

Direct Bromination of Keggin Fragments To Give [PW₉O₂₈Br₆]³⁻: A Polyoxotungstate with a Hexabrominated Face*

R. John Errington,* Richard L. Wingad, William Clegg, and Mark R. J. Elsegood

The design and synthesis of polyoxometalates with specific structures and properties requires synthetic methodologies that enable framework morphology and surface functionality to be manipulated in a rational fashion and, although some progress has been made in recent years, there is still enormous scope for new, systematic chemistry in this area. Since the initial work by Knoth,^[1] a particularly fruitful approach has been the attachment of organometal or organometalloid groups to lacunary species such as the tungstate Keggin fragments [PW₁₁O₃₉]⁷⁻, [SiW₁₁O₃₉]⁸⁻, [SiW₁₀O₃₆]⁸⁻, [PW₉O₃₄]⁹⁻, and [SiW₉O₃₄]¹⁰⁻, and derivatives resulting from this strategy have been reviewed recently.^[2] However, reactions involving the metathesis of labile halides, a ubiquitous method for ligand manipulation in synthetic organometallic and metal-organic chemistry, are not generally available for the surface functionalization of polyoxometalates because of the paucity of suitable halogenated derivatives. Although several fluoropolyxoanions have been characterized,^[2] and polyoxometalates containing heterometal-halide bonds have been prepared from reactions between lacunary anions and heterometal halides,^[3] previously reported attempts to halogenate a polyoxometalate surface to produce reactive M-X sites resulted instead in degradation of the polyoxometalate framework and the production of low-nuclearity oxohalide complexes.^[4] Herein we report the first successful halogenation of Keggin derivatives [PW₉O₃₄]⁹⁻ and [NaPW₁₁O₃₉]⁶⁻

and the structure of the resulting unique polyoxometalate with multiple terminal halide ligands.

The bromoanion [PW₉O₂₈Br₆]³⁻ (**1**) was initially obtained as one of the products from the reaction between (nBu₄N)₆[NaPW₁₁O₃₉]^[5] and C₂O₂Br₂ in an attempt to attach oxalate groups to the surface of the PW₁₁ Keggin fragment. The acetonitrile solvate of (nBu₄N)₃-**1** crystallized as yellow crystals along with colorless crystals of (nBu₄N)₂[W₂O₄Br₄(μ-C₂O₄)] and both compounds were structurally characterized by single-crystal X-ray diffraction.^[6] The bromoanion **1** has the β, A-PW₉ structure (Figure 1), and is formally

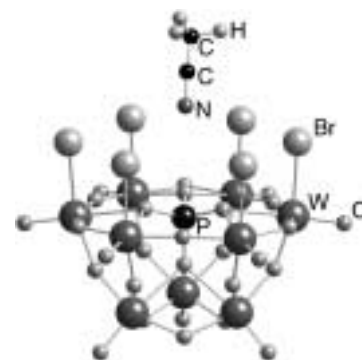


Figure 1. Structure of **1** showing also the position of the acetonitrile solvate molecule. Selected bond lengths [Å] and angles [°] (mean values within W₆ ring, values in parentheses are ranges of esds for individual measurements): W-Br 2.500(2–3), W-O_{term} 1.698(10–13), W-O(P) 2.399(10–11), W-O(W) (edge-sharing) 1.902(11–12), W-O(W) (corner-sharing) 1.881(10–12), W-O-W (edge-sharing) 125.3(5–6), W-O-W (corner-sharing) 159.9(6–7). Mean values between W₆ and W₃ rings: (Br)W-O(W) 1.875(11–13), (Br)W-O-W 1.928(11–14), W-O-W 147.8(6).

derived from the triply vacant lacunary Keggin anion β, A-[PW₉O₃₄]⁹⁻ by replacement of six terminal oxo ligands with six bromo ligands, giving a molecular oxide with a fully brominated face. The structure of the dinuclear anion [W₂O₄Br₄(μ-C₂O₄)]²⁻ (**2**) is analogous to that of the molybdenum chloro analogue [Mo₂O₄Cl₄(μ-C₂O₄)]²⁻^[7] and will be reported separately.

The mean W-Br bond length of 2.50 Å in **1** is similar to that in **2** (2.52 Å) and, although no discrete β, A-[PW₉O₂₈X₆] structures have previously been reported, W-O bond lengths in **1** are similar to those in α, A-[PW₉O₃₄{Si(*t*Bu)OH}₃]³⁻^[8] and in [(PhSnOH)₃(β, A-PW₉O₃₄)₂]¹²⁻.^[9]

Another feature of this crystal structure also shown in Figure 1 is the acetonitrile solvate molecule situated with the N atom 1.19 Å above the mean plane of the six bromo ligands, with N...Br distances of 3.773–4.053 Å. Partial occupancy of a second acetonitrile molecule position is correlated with disorder in some cation alkyl chains. The formation of **1** from [NaPW₁₁O₃₉]⁶⁻ and C₂O₂Br₂ is consistent with a degradation process in which initial electrophilic attack at the basic oxide surface is followed by excision of two WO₂Br₂ fragments as the oxalato-bridged dinuclear complex **2**.

Bands for ν(P-O), ν(W=O), and ν(W-O-W) in the IR spectrum of (nBu₄N)₃-**1** are at higher wavenumbers than those for Na₈H[PW₉O₃₄], as previously observed for α, A-[PW₉O₃₄(RPO)₂]⁵⁻ ions.^[10] A band at 928 cm⁻¹ is low for terminal W=O, and may reflect stronger bonding in the

[*] Dr. R. J. Errington, R. L. Wingad, Prof. Dr. W. Clegg, Dr. M. R. J. Elsegood
Department of Chemistry
Bedson Building
University of Newcastle upon Tyne
NE1 7RU (UK)
Fax: (+44) 191-222-6929
E-mail: John.Errington@ncl.ac.uk

[**] This work was supported by the UK Engineering and Physical Sciences Research Council.

asymmetric W-O-W bridges between the W_6 and W_3 rings due to the presence of *trans*-bromo ligands.

^{31}P and ^{183}W NMR spectra showed that **1** was produced in good yield from this reaction. The ^{31}P NMR peak for **1** occurs at $\delta_{\text{P}} = -11.6$, and in the ^{183}W NMR spectrum the brominated tungsten atoms WBr of **1** and WBr_2 of **2** have characteristic low-field chemical shifts with peaks at $\delta_{\text{W}} = 189.1$ and 281.6 , respectively. The tungsten atoms in the W_3 cap of **1** give rise to a peak at $\delta_{\text{W}} = -123.1$, and the $^2J_{\text{W,W}}$ value of 25 Hz is consistent with previously reported values of $^2J_{\text{W,W}} > 10$ Hz for A-type EW_9 fragments.^[8–11] The effect of bromination on δ_{W} can be seen by comparison with the ^{183}W NMR spectrum of $[(\text{PhSnOH})_3(\text{PW}_9\text{O}_{34})_2]^{12-}$, the only other structurally characterized example of a functionalized polyoxometalate containing the $\beta, \text{A-PW}_9$ fragment.^[9] In this “sandwich” anion, the tungsten atoms in the W_6 “belt” appear at $\delta_{\text{W}} = -202$, while the W_3 “cap” tungsten atoms appear at $\delta_{\text{W}} = -123$. Hence, replacement of terminal oxo by bromo ligands causes a downfield shift of about 390 ppm for the belt tungsten atoms, whereas δ_{W} for tungsten atoms in the W_3 cap is remarkably unaffected. This is consistent with the previously reported downfield shift of δ_{W} upon replacement of oxo by a chloro ligand,^[4] although replacement of oxo by a fluoro ligand has been shown to result in an upfield shift.^[12]

Bromination of $(n\text{Bu}_4\text{N})_6[\text{NaPW}_{11}\text{O}_{39}]$ with SOBr_2 also resulted in excision of two tungsten atoms and formation of $(n\text{Bu}_4\text{N})_3\text{-1}$ as the major phosphotungstate product (67% of the total integrated intensity in the ^{31}P NMR spectrum). In an effort to avoid framework degradation reactions and concomitant generation of tungsten oxobromide by-products, we treated $\text{Na}_8\text{H}[\text{PW}_9\text{O}_{34}] \cdot 23\text{H}_2\text{O}$ ^[13] (after partial dehydration in vacuo at room temperature) with SOBr_2 in the presence of $(n\text{Bu}_4\text{N})\text{Br}$ and obtained 70–85% yields of $(n\text{Bu}_4\text{N})_3\text{-1}$, as determined by ^{31}P NMR spectroscopy. Similar reactions were also carried out in the presence of the bases Et_3N and K_2CO_3 to minimize any structural rearrangements that might be caused by the presence of HBr generated from SOBr_2 and water of crystallization. In all cases **1** was formed in high yield, and the few phosphotungstate impurities present varied in number and amounts with the reaction conditions. The series of species $\beta, \text{A-PW}_9\text{O}_{34-x}\text{Br}_x]^{(9-x)-}$ ($x = 0-6$) would give rise to seventeen ^{31}P NMR peaks (as would the α -isomeric series) and a much larger number of ^{183}W NMR peaks due to the reduced symmetry of the partially brominated oxoanions. Bromination in the presence of K_2CO_3 appeared to be significantly cleaner by ^{31}P NMR spectroscopy (Figure 2), but samples of $(n\text{Bu}_4\text{N})_3\text{-1}$ in this case were contaminated with small amounts of acetamide hemihydrobromide,

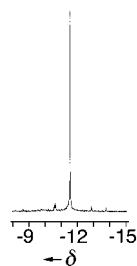


Figure 2. ^{31}P NMR spectrum (121.5 MHz, CH_3CN) of $(n\text{Bu}_4\text{N})_3\text{-1}$ obtained by treatment of $\text{Na}_8\text{H}[\text{PW}_9\text{O}_{34}] \cdot 7\text{H}_2\text{O}$ with SOBr_2 and $(n\text{Bu}_4\text{N})\text{Br}$ in the presence of K_2CO_3 .

$[(\text{CH}_3\text{CONH}_2)_2\text{H}]^+\text{Br}^-$, formed by hydrolysis of the MeCN solvent. Very few impurity peaks are observed in ^{183}W NMR spectra of $(n\text{Bu}_4\text{N})_3\text{-1}$ samples, as shown in Figure 3, and the small peak at $\delta_{\text{W}} = -96.9$ can be assigned to $[\text{PW}_{12}\text{O}_{40}]^{3-}$.

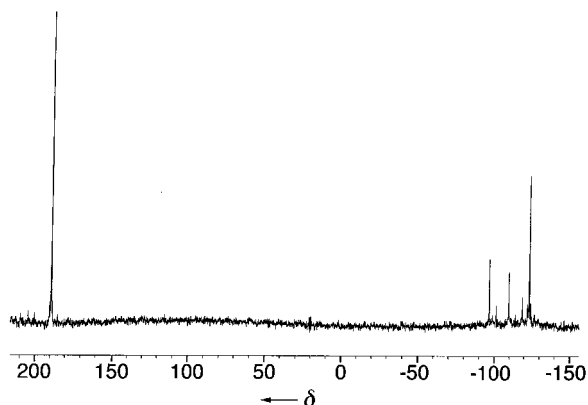


Figure 3. ^{183}W NMR spectrum (12.5 MHz, CH_3CN) of $(n\text{Bu}_4\text{N})_3\text{-1}$ obtained by treatment of $\text{Na}_8\text{H}[\text{PW}_9\text{O}_{34}] \cdot 7\text{H}_2\text{O}$ with SOBr_2 and $(n\text{Bu}_4\text{N})\text{Br}$ in the presence of K_2CO_3 .

Solutions of $(n\text{Bu}_4\text{N})_3\text{-1}$ are stable in the absence of air, and the ^{31}P NMR spectrum of a sample in a screw-top NMR tube showed only a small amount of decomposition after one year at ambient conditions.

The reaction between $(n\text{Bu}_4\text{N})_3\text{-1}$ and six equivalents of NaOMe has been monitored by ^{31}P NMR spectroscopy, and the number of peaks in the spectrum of the product suggested that the reaction had not gone to completion and that isomers of $[\text{PW}_9\text{O}_{28}\text{Br}_x(\text{OMe})_{6-x}]$ were present. However, X-ray diffraction data on single crystals obtained from this reaction, although not of high quality, revealed a $\alpha, \text{A-PW}_9$ structure,^[14] demonstrating that structural rearrangement of the oxide framework occurs readily during metathesis of the bromo ligands in **1**.

In conclusion, we have achieved, for the first time, direct halogenation of polyoxometalate structures. The methodology used to prepare the hexabromoanion **1** from PW_9 or PW_{11} lacunary Keggin anions should be applicable to other polyoxometalates with basic surfaces, providing a range of halide derivatives for systematic studies of surface reactivity. Further studies on controlled halogenation of polyoxometalates, the optimization of reaction conditions and on the reactivity of **1** are in progress.

Experimental Section

All operations were carried out under dry dinitrogen using Schlenk and dry-box techniques.^[15] Recrystallized $(n\text{Bu}_4\text{N})_3\text{-1}$ was invariably contaminated with traces of other salts and consistent microanalytical results were not obtained.

$(n\text{Bu}_4\text{N})_3\text{-1}$: Method 1: A solution of SOBr_2 (0.37 mL, 4.68 mmol) in MeCN (10 mL) was added to a stirred mixture of $\text{Na}_8\text{H}[\text{PW}_9\text{O}_{34}] \cdot 7\text{H}_2\text{O}$ (2.00 g, 0.78 mmol) and $n\text{Bu}_4\text{NBr}$ (0.75 g, 2.34 mmol) in MeCN (20 mL) at -70°C . The mixture was allowed to warm to room temperature and was then stirred overnight to give a yellow solution and a white precipitate. Volatiles were removed from the filtered solution and a yellow powder was obtained after trituration with diethyl ether (2.59 g).

Method 2: A solution of $n\text{Bu}_4\text{NBr}$ (7.85 g, 24.36 mmol) and SOBr_2 (8.3 mL, 105.56 mmol) in MeCN (10 mL) was added dropwise to a stirred suspension of $\text{Na}_8\text{H}[\text{PW}_9\text{O}_{34}] \cdot 7\text{H}_2\text{O}$ (20.81 g, 8.12 mmol) and K_2CO_3 (8.00 g, 57.88 mmol) in MeCN (200 mL) at -70°C . After 1 h, the solution was filtered and the volatiles removed under reduced pressure. The resulting solid was redissolved in MeCN (40 mL) and filtered. Removal of the solvent and trituration with diethyl ether gave an orange powder (26.13 g). IR: $\tilde{\nu}$: 1064 (s), 1022 (w), 998 (w), 989 (w), 974 (s), 928 (s), 868 (m), 787 (s, br), 737 (w), 580 (w), 519 (m) cm^{-1} .

Received: January 20, 2000

Revised: August 7, 2000 [Z14574]

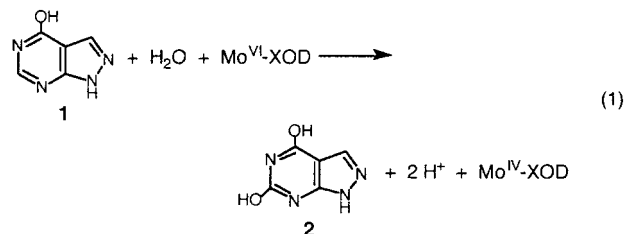
Control of Xanthine Oxidase Activity by Light**

Lin Ai Tai and Kuo Chu Hwang*

Photocontrol of enzyme activities has been a subject of active research.^[1–8] Natural photoenzymes are very rare. To date, only three natural photoenzymes have been reported, namely, DNA photolyase,^[9] [6–4] photoproduct lyase,^[10] and protochlorophyllide reductase.^[11] With their ability of transforming optical signals into chemical motion, photoenzymes might have important future applications in molecular-scale electronics in the areas of signal transformation, amplification, integration, and information storage.

Previously, photoinduced release of a light-active antigen from an antibody was reported.^[12] Photochemical inhibition of nicotinic acetylcholine receptors by a photoisomerizable inhibitor was also reported.^[13] Enzymes can also be chemically modified by covalently bonding a “gating molecule” to the neighborhood of the enzyme active site^[3–5] or at the enzyme cofactor^[6–8] to control the entry of substrates. Common gating molecules of choice are photoisomerizable olefins and photochromic compounds. Chemical modification of natural enzymes often results in partial loss of enzyme activity. Moreover, the location of the gating molecule is limited to the availability of chemically modifiable amino acids around the active site, and is quite difficult to control at will. Herein, we report a simple, novel xanthine oxidase (XOD) photoenzyme system, with allopurinol as a substrate, in which the activity can be switched on or off by light. A photoinduced intra-enzyme electron-transfer model is proposed to rationalize the photoregulation of XOD activity.

XOD is a 300 kDa homodimer protein, with each unit containing a molybdenum(vi), two Fe/S clusters, and one flavin adenine dinucleotide (FAD) moiety.^[14] The Mo^{VI} ion at the active site can activate a water molecule and oxidize a C–H bond in various substrates to C–OH. After gaining two electrons from the substrate, Mo^{IV} passes two electrons sequentially, by way of the Fe/S clusters, to the FAD cofactor which then reduces molecular oxygen to generate superoxide (or hydrogen peroxide in acidic conditions).^[15] As an XOD substrate, allopurinol (**1**) is oxidized and converted to alloxanthine (**2**) [Equation (1)], which is a potent, slow-



[*] K. C. Hwang, L. A. Tai
Department of Chemistry
National Tsing Hua University
Hsinchu (Taiwan)
Fax: (+886)3-571-1082
E-mail: kchwang@mx.nthu.edu.tw

[**] The authors are grateful for financial support from the National Science Council, Taiwan (NSC 88-2113-M-007-016).

- [1] W. H. Knoch, *J. Am. Chem. Soc.* **1979**, *101*, 759.
- [2] P. Gouzerh, A. Proust, *Chem. Rev.* **1998**, *98*, 77.
- [3] W. H. Knoch, P. J. Domaille, D. C. Roe, *Inorg. Chem.* **1983**, *22*, 198.
- [4] Y-J Lu, R. H. Beer, *Polyhedron* **1996**, *15*, 1667.
- [5] We have shown by X-ray crystallography that this compound has the α -PW₁₁ structure.
- [6] Crystal data for $(n\text{Bu}_4\text{N})_3 \cdot 1.56\text{MeCN}$: C_{51.08}H_{112.62}Br₆N_{4.56}O₂₈PW₉, $M_r = 3403.9$, monoclinic, space group $P2_1/n$, $a = 15.0129(10)$, $b = 25.831(2)$, $c = 22.8859(15)$ Å, $\beta = 93.452(2)^\circ$, $V = 8859.0(10)$ Å³, $Z = 4$, $\rho_{\text{calcd}} = 2.552$ gcm⁻³, MoK α radiation, $\lambda = 0.71073$ Å, $\mu = 14.43$ mm⁻¹, $T = 160$ K; of 37732 measured reflections corrected for absorption, 14773 were unique, $R_{\text{int}} = 0.0668$; $R = 0.0600$ ($I > 2\sigma$), $R_w = 0.1345$ (F^2 , all data), GOF = 1.147, 968 parameters, final difference map extremes +2.38 and -1.20 e Å⁻³. Disorder was refined for some alkyl chains and one partially occupied acetonitrile position with the aid of restraints. Crystallographic data (excluding structure factors) for the structure reported in this paper have been deposited with the Cambridge Crystallographic Data Centre as supplementary publication no. CCDC-139046. Copies of the data can be obtained free of charge on application to CCDC, 12 Union Road, Cambridge CB2 1EZ, UK (fax: (+44) 1223-336-033; e-mail: deposit@ccdc.cam.ac.uk).
- [7] S. Liu, S. N. Shaikh, J. Zubietta, *Inorg. Chem.* **1988**, *27*, 3064.
- [8] A. Mazeaud, N. Ammari, F. Robert, R. Thouvenot, *Angew. Chem.* **1996**, *108*, 2089; *Angew. Chem. Int. Ed. Engl.* **1996**, *35*, 1961.
- [9] F. Xin, M. T. Pope, *Organometallics* **1994**, *13*, 4881.
- [10] C. R. Mayer, R. Thouvenot, *J. Chem. Soc. Dalton Trans.* **1998**, *7*.
- [11] J. Lefebvre, F. Chauveau, P. Doppelt, C. Brevard, *J. Am. Chem. Soc.* **1981**, *103*, 4589.
- [12] W. McFarlane, A. M. Noble, J. M. Whitfield, *J. Chem. Soc. (A)* **1971**, 948.
- [13] P. J. Domaille, *Inorg. Synth.* **1990**, *27*, 100.
- [14] R. J. Errington, R. L. Wingad, W. Clegg, R. A. Coxall, unpublished results.
- [15] R. J. Errington, *Advanced Practical Inorganic and Metalorganic Chemistry*, Blackie Academic and Professional, London, **1997**.

binding XOD inhibitor capable of binding to the reduced form $\text{Mo}^{\text{IV}}\text{-XOD}$, but not to the oxidized $\text{Mo}^{\text{VI}}\text{-XOD}$.^[16]

The enzymatic conversion of allopurinol into alloxanthine can be monitored by UV/Vis absorbance at 277 nm, the absorption maximum of alloxanthine. During the enzymatic reaction, the increase of absorption at 277 nm slowly levels off, due to the slow inhibition of XOD by alloxanthine (see Figure 1 a, trace 1). Upon exposure to the output from a high-pressure Hg lamp, the enzyme activity was recovered, as

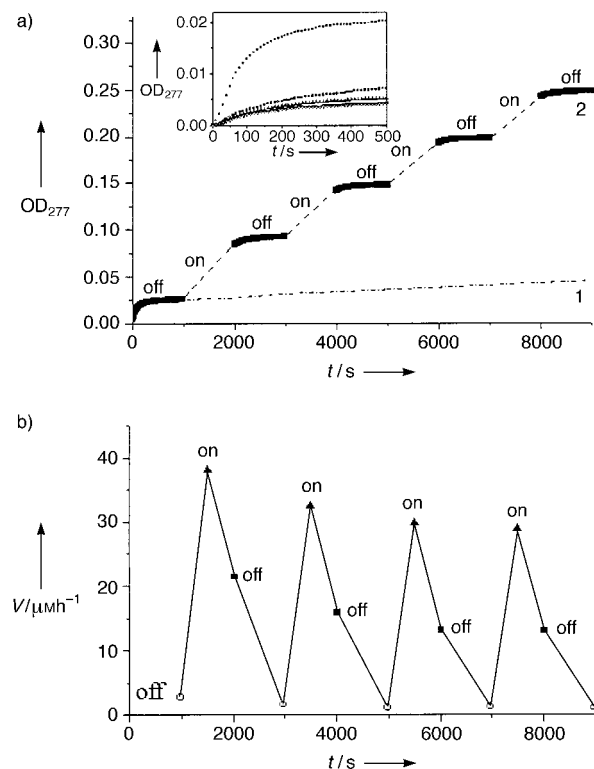


Figure 1. a) The optical density (OD) at 277 nm from a solution of allopurinol and XOD (200 μM and 0.15 μM , respectively) as a function of the reaction time. Trace 1: The solution was maintained in the dark. Trace 2: The solution was put through many dark–light cycles. In each light cycle, the solution was irradiated for 900 s (power density at the sample $\approx 0.01 \text{ W cm}^{-2}$; $\lambda \geq 320 \text{ nm}$). Inset: The OD changes (from top to bottom) of the first, second, third, and fourth dark cycles from trace 2 as a function of the reaction time. b) The enzyme catalysis rate (V) obtained from trace 2 in (a) at different reaction times: 50 s before irradiation (open circle), during irradiation (solid triangles), and 50 s after irradiation (solid squares).

evidenced by the dramatic increase in the absorption at 277 nm (see Figure 1 a, trace 2). When the enzyme solution was removed from the light, the XOD activity was inhibited again by the alloxanthine (see Figure 1 a, the dark sections of trace 2). The XOD activity can be turned on or off by many dark–light cycles without noticeable deterioration of the enzyme activity. The absorbance change (that is, the amount of alloxanthine produced) during the “light” cycles is clearly far more than that in the “dark” cycles, indicating the dramatic photoeffect on increasing the XOD activity.

The inset of Figure 1 a shows the alloxanthine formation rate during the first 500 s of the first, second, third, and fourth dark cycles (from top to bottom). Each trace in the inset shows the typical slow-binding inhibition behavior of allo-

xanthine. The formation rate becomes smaller in later dark cycles, which is due to the higher concentration of alloxanthine (the inhibitor) present during later cycles. Figure 1 b shows the variation of the alloxanthine formation rates (or catalysis velocity) during the dark–light cycles. In the dark, the catalysis velocity is approximately $2 \mu\text{M h}^{-1}$, before the onset of the subsequent light cycle. Upon irradiation, the catalysis velocity is increased to about $40 \mu\text{M h}^{-1}$. Irradiation increases the enzyme activity by a factor of approximately 2000%! Upon switching the light off, the catalysis velocity soon decays back to its initial low values. The data in Figure 1 clearly shows that the XOD activity can be regulated on or off photochemically.

Before irradiation, most of the XOD was inhibited by alloxanthine. To recover the enzyme activity, the inhibitor has to be released from the active site. It seems that exposure to light triggers the release of inhibitor (that is, the alloxanthine) from the XOD active site. How does light initiate the dissociation of the alloxanthine–XOD complex? It is known that alloxanthine can only bind the reduced $\text{Mo}^{\text{IV}}\text{-XOD}$.^[16] Photoexcitation probably converts the Mo^{IV} ion into other forms, such as Mo^{V} or Mo^{VI} . The change in the electron density at the Mo ion then leads to the dissociation of alloxanthine from the active site.^[17] The Mo^{VI} species does not exhibit an ESR signal, but Mo^{V} does. To examine this possibility, alloxanthine–XOD complexes were prepared by mixing XOD with excess allopurinol for 10 min. The solution was then frozen at 180 K in the presence of air, and irradiated by the output of a high-pressure Hg lamp for 3 min. Figure 2 a shows the difference spectrum obtained by subtracting the ESR spectrum after irradiation from the one obtained before irradiation. The left ESR band ($g = 2.0047$, linewidth $\Delta H_{\text{pp}} = 19.3 \text{ Gauss}$) has the same g value and linewidth as that reported in the literature for FADH^{\bullet} .^[18] The two smaller ESR bands ($g = 1.9716, 1.9636$; $\Delta H_{\text{pp}} = 8.5, 9.0 \text{ G}$, respectively) resemble the “alloxanthine signal”^[16, 18, 19] and are designated to the Mo^{V} species.^[20] Figure 2 b shows the computer-simulated FADH^{\bullet} and Mo^{V} signals.

The results in Figure 2 support the hypothesis that irradiation causes electron transfer from Mo^{IV} to the other two cofactors, Fe/S and FAD, to generate Mo^{V} , $(\text{Fe/S})_{\text{red}}$, and FADH^{\bullet} intermediate states. Subsequent electron transfer of the second electron from the Mo center to the other cofactors and release of the alloxanthine from the active site leads to recovery of free, active XOD. Therefore, the overall XOD activity is recovered by light. The ESR signal of Fe/S was not observed at the experimental conditions used ($T = 180 \text{ K}$). It has been reported that the ESR signal of Fe/S has never been observed at temperatures above 42 K because of its very short relaxation time and, thus, very broad ESR linewidth.^[21]

We have reported a novel XOD system in which the enzyme activity can be regulated on or off by light. This system represents a prototype of natural biological photo-switches/integrators. For example, as shown in trace 2 of Figure 1 a, the amount of alloxanthine product is continuously being integrated (or accumulated) upon stimulation by the incoming light signals. We believe that this system might have future applications as a photoswitch/integrator in molecular-scale optoelectronics.

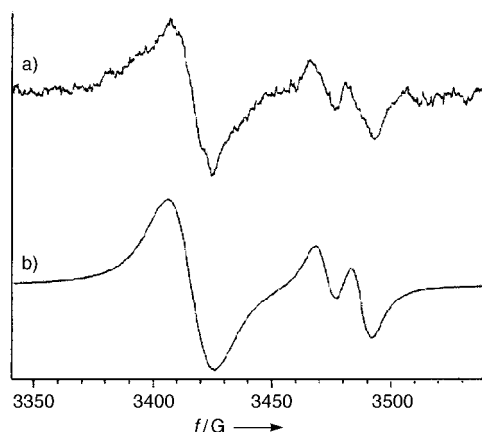


Figure 2. a) The ESR spectrum obtained by subtracting the spectrum after irradiation from the spectrum obtained before irradiation for an aqueous solution of XOD (20 μM) in the presence of excess allopurinol in air. The enzyme solution was frozen at 180 K, and the first spectrum was recorded. Then the frozen enzyme solution was irradiated (power density at the sample $\approx 0.13 \text{ W cm}^{-2}$) for 3 min, and the second spectrum was obtained. The microwave power was 10 mW, the modulation was 5 Gauss, and the frequency was 9.5819 GHz. b) Computer-simulated spectra of the FADH^\bullet ($g = 2.0047$, $\Delta H_{\text{pp}} = 19.3 \text{ G}$) and Mo^{V} ($g = 1.9716, 1.9636$; $\Delta H_{\text{pp}} = 8.5, 9.0 \text{ G}$) signals.

Experimental Section

XOD (0.08 unit mg^{-1} , Sigma) and allopurinol (TCI) were used as received. The enzyme solution was adjusted to pH 7.5 in Na_2HPO_4 buffer (0.1 M). The pH value and buffer concentration are the same in all experiments. The concentration of XOD was determined by its absorption at 450 nm, with the absorption coefficient $\epsilon_{450} = 37800 \text{ M}^{-1} \text{ cm}^{-1}$.^[22] In general, allopurinol (2 mM) in NaOH solution (0.01 N) was prepared first, then aliquots of the solution were added to the enzyme solution to reach the required final concentration. The enzyme catalysis rate was monitored at the absorption maximum of the product, 277 nm for alloxanthine.

All experiments were performed in the presence of air. The light source is the output from a high-pressure Hg lamp (Oriol) fitted with a CuSO_4 filter solution ($\lambda \geq 320 \text{ nm}$). ESR spectra were taken on a Bruker EMX-12 spectrometer. A 1,1-diphenyl-2-picrylhydrazyl (DPPH) sample in a second resonator chamber was used as the reference for the g value measurements. The temperature was controlled by a Bruker B-VT 2000 variable temperature control unit.

Received: February 29, 2000 [Z14789]

- [1] For excellent reviews of photocontrol of enzyme activities, see: a) I. Willner, S. Rubin, *Angew. Chem.* **1996**, *108*, 419–439; *Angew. Chem. Int. Ed. Engl.* **1996**, *35*, 367–385; b) I. Willner, *Acc. Chem. Res.* **1997**, *30*, 347–356; c) T. P. Begley, *Acc. Chem. Res.* **1994**, *27*, 394–401, and references therein.

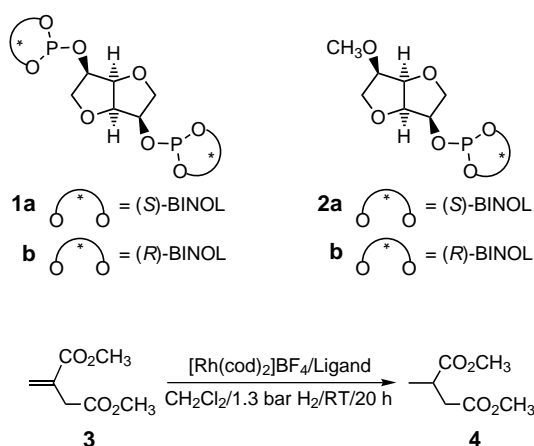
- [2] P. R. Westmark, J. P. Kelly, B. D. Smith, *J. Am. Chem. Soc.* **1993**, *115*, 3416–3419.
 [3] I. Willner, E. Zahavy, *Angew. Chem.* **1994**, *106*, 594–595; *Angew. Chem. Int. Ed. Engl.* **1994**, *33*, 581–583.
 [4] S. Monti, G. Montagnoli, L. Nannicini, *J. Am. Chem. Soc.* **1977**, *99*, 3808–3811.
 [5] S. Martinek, I. V. Berezin, *Photochem. Photobiol.* **1979**, *29*, 637–645.
 [6] R. Blonder, E. Katz, I. Willner, V. Wray, A. F. Bückmann, *J. Am. Chem. Soc.* **1997**, *119*, 11747–11757.
 [7] E. Zahavy, I. Willner, *J. Am. Chem. Soc.* **1996**, *118*, 12499–12514.
 [8] A. Riklin, E. Katz, I. Willner, A. Stocker, A. F. Bückmann, *Nature* **1995**, *376*, 672–675.
 [9] a) D. B. Sanders, O. Wiest, *J. Am. Chem. Soc.* **1999**, *121*, 5127–5134; b) D. Burdi, T. P. Begley, *J. Am. Chem. Soc.* **1991**, *113*, 7768–7770.
 [10] a) S. T. Kim, K. Malhatra, C. A. Smith, J. S. Taylor, A. Sancar, *J. Biol. Chem.* **1994**, *269*, 8535–8540; b) T. Todo, H. Takamon, H. Ryo, M. Ihara, T. Matsunaga, O. Nikaido, K. Sato, T. Nomura, *Nature* **1993**, *361*, 371–374.
 [11] T. P. Begley, H. Young, *J. Am. Chem. Soc.* **1989**, *111*, 3095–3096.
 [12] a) M. Harada, M. Sisido, J. Hirose, M. Nakanishi, *FEBS* **1991**, *286*, 6–8; b) R. Blonder, S. Levi, G. Tao, I. Ben-Dov, I. Willner, *J. Am. Chem. Soc.* **1997**, *119*, 10467–10478.
 [13] a) J. M. Nerbonne, R. E. Sheridan, L. D. Chabala, H. A. Lester, *Mol. Pharmacol.* **1983**, *23*, 344–349; b) L. D. Chabala, H. A. Lester, *Biophys. J.* **1985**, *48*, 241–246.
 [14] a) R. C. Bray, *Q. Rev. Biophys.* **1988**, *21*, 299–329; b) R. Hille, *Biochem. Biophys. Acta* **1994**, *1184*, 143–169.
 [15] R. Hille, *Chem. Rev.* **1996**, *96*, 2757–2816.
 [16] J. W. Williams, R. C. Bray, *Biochem. J.* **1981**, *195*, 753–760.
 [17] Photooxidation of alloxanthine by the excited Mo^{IV} center is also one of the possible pathways. We isolated the alloxanthine–XOD complex and split it into two portions. One portion was maintained in the dark, waiting for dissociation into alloxanthine and the free enzyme; the other portion was photolyzed to force dissociation of the complex. The UV spectra of these samples were then compared. No clear difference was observed in the absorption of the dissociated alloxanthine. In addition, irradiation of the alloxanthine–XOD complex did not show any detectable ESR signal corresponding to an alloxanthine cation radical. Therefore, it seems that majority of alloxanthine molecules leave the enzyme's active site without being oxidized. However, the current data can certainly not exclude the possibility of photooxidation of alloxanthine as a minor process.
 [18] V. Massey, H. Komai, G. Palmer, G. B. Elion, *J. Biol. Chem.* **1970**, *245*, 2837–2844.
 [19] T. R. Hawkes, G. N. George, R. C. Bray, *Biochem. J.* **1984**, *218*, 961–968.
 [20] The ESR data shown in Figure 2 resemble very closely the FADH^\bullet and Mo^{V} signals of Figure 6 in Ref. [18] except that the phase of the ESR spectrometer is reversed.
 [21] a) R. Hille, W. R. Hagen, W. R. Dunham, *J. Biol. Chem.* **1985**, *260*, 10569–10575; b) D. J. Lowe, R. C. Bray, *Biochem. J.* **1978**, *169*, 471–479.
 [22] V. Massey, R. E. Brumby, H. Komai, G. Palmer, *J. Biol. Chem.* **1969**, *244*, 1682–1691.

Highly Enantioselective Rh-Catalyzed Hydrogenation Reactions Based on Chiral Monophosphite Ligands

Manfred T. Reetz* and Gerlinde Mehler

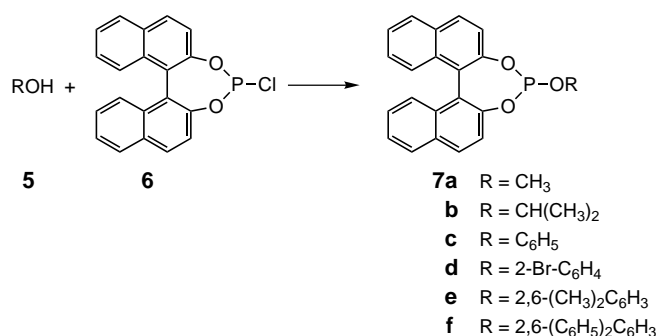
The first examples of asymmetric transition metal catalyzed hydrogenation reactions of prochiral olefins were described in 1968 independently by Horner et al.^[1] and Knowles and Sabacky.^[2] The ligands were chiral monophosphanes (e.g., methyl-*n*-propylphenylphosphane). However, the Rh-complexes derived thereof gave low enantioselectivities (*ee* = 3–15%). Other ligands possessing only one donor function were also rather ineffective in hydrogenation reactions.^[3] It was Kagan's group who in 1971 showed for the first time that a Rh-complex of a chelating diphosphane (diop) with chiral information in the backbone gives enantioselectivities of 70–80% *ee*.^[4] Shortly thereafter Knowles et al. demonstrated that in hydrogenation reactions the Rh-complex of a chelating diphosphane having stereogenic centers at phosphorus (dipamp) is also consistently superior than the corresponding monophosphane (*ee* > 90%).^[5] Likewise, Takaya and Noyori described highly efficient catalysts based on the chelating ligand 2,2'-bis(diphenylphosphino)-1,1'-binaphthyl (BINAP).^[6] To explain the high degrees of enantioselectivity resulting from these and other chiral diphosphanes, conformational control as a result of decreased rotational freedom around the donor-atom–metal bond in the metallacycle was postulated.^[3] Herein we now show that this long-standing rule is not as general as usually assumed.^[7]

Recently we described the first highly enantioselective Rh-catalyzed hydrogenation reactions using chiral chelating diphosphites **1a**, **b**.^[8] In the hydrogenation of itaconic acid dimethyl ester **3** *ee* values of 88% and 95% were observed in favor of (*S*)-**4** and (*R*)-**4**, respectively, an indication that the chiral information in the P heterocycle is decisive and that the combination of (*R*)-BINOL and dianhydro-D-mannite in the form of **1a** represents the matched case.



[*] Prof. Dr. M. T. Reetz, G. Mehler
Max-Planck-Institut für Kohlenforschung
Kaiser-Wilhelm-Platz 1, 45470 Mülheim/Ruhr (Germany)
Fax: (+49) 208-306-2985
E-mail: reetz@mpi-muelheim.mpg.de

Surprisingly, the monophosphite units **2a** and **2b** give similar stereoselectivities. The precatalysts were prepared as usual^[3, 8] by the reaction of the ligands with [Rh(cod)₂]BF₄. By using a Rh:ligand ratio of 1:1, a Rh:substrate ratio of 1:1000, and otherwise identical conditions the hydrogenation of substrate **3** led to enantioselectivities of 97.8% (100% conversion) and 95.2% (73% conversion) in favor of the products (*S*)-**4** and (*R*)-**4**, respectively. Although the matched case (**2a**) results in a much more active Rh-catalyst than the mismatched combination (**2b**), the additional increase in enantioselectivity is not pronounced. This could be because one of the three ether moieties behaves as a hemilabile ligand, and thus reduces the conformational freedom. To test this hypothesis the very simple monophosphites **7a–7f**, some of



which have been described already,^[9, 10] were prepared and tested as ligands in the Rh-catalyzed hydrogenation of **3**. All the hydrogenation reactions were carried out at room temperature, under a slight positive pressure of H₂, and with a Rh:ligand ratio of 1:1. Although a standard reaction time of 20 h was chosen,^[8] most of the reactions were complete within 3 h.

The results of the Rh-catalyzed hydrogenation reactions are summarized in Table 1 and show that simple BINOL-based monophosphites are excellent ligands provided that in the ligand synthesis the appropriate achiral alcohol **5** is chosen, for example, isopropanol (**5b**) in the case of **7b** (97.6% *ee* in the hydrogenation product **4**). Upon incorporating a sterically smaller alcohol such as methanol (**7a**), the *ee* value drops to 89.2%. Although the phenol-based ligand leads to a high *ee* value (96.6%) and is therefore comparable to the isopropanol derivative **7b**, the introduction of ortho-substituents reduces enantioselectivity (Table 1, entries 4–6). Dichloro-

Table 1. Enantioselective Rh-catalyzed hydrogenation of itaconic acid dimethyl ester (**3**) using ligands **7a–7f**.^[a]

Entry	Ligand	Conversion [%]	<i>ee</i> [%] ^[b]
1	(<i>S</i>)- 7a	100	89.2
2	(<i>S</i>)- 7b	100	97.6
3	(<i>S</i>)- 7c	100	96.6
4	(<i>S</i>)- 7d	100	89.8
5	(<i>S</i>)- 7e	78	39.2
6	(<i>S</i>)- 7f	8	28.6

[a] In all cases the Rh:ligand ratio is 1:1 and the Rh:substrate ratio is 1:1000. Solvent: CH₂Cl₂; *p*(H₂) = 1.3 bar; *T* = 20°C; reaction time: 20 h.
[b] *S* configuration of **4** in each case.

methane was usually chosen as the solvent. In pure isopropanol inferior results were obtained.

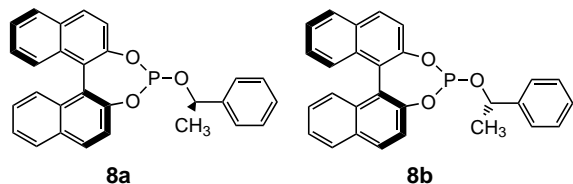
To see if BINOL in combination with simple *chiral* alcohols lacking additional functional groups also leads to efficient ligands, the two phosphites **8a**, **b**,^[11] prepared from (*S*)-**6** and (*R*)- and (*S*)-1-phenylethanol (76% and 80% yield, respectively), were tested in the Rh-catalyzed hydrogenation of **3**. Under otherwise identical conditions *ee* values of 99.2% and 98.2% were observed in favor of (*S*)-**4** (100% conversion) (Table 2). Thus, it is clear that 1-phenylethanol is a better component than isopropanol, however, the additional stereogenic center appears to play a minor role. Indeed, upon

Table 2. Enantioselective Rh-catalyzed hydrogenation of itaconic acid dimethyl ester (**3**) using ligands **8a**, **b**.^[a]

Entry	Ligand	Rh:ligand	Rh:substrate	Conversion [%]	<i>ee</i> [%] ^[b]
1	8a	1:1	1:1000	100	99.2
2	8b	1:1	1:1000	100	98.2
3	8a	1:1	1:2500	100	99.4
4	8a	1:1	1:5000	100	99.4
5	8a	1:1	1:10000	49	96.2
6	8a	1:2	1:1000	100	99.6
7	8a	1:4	1:1000	100	99.5

[a] Solvent: CH₂Cl₂; *p*(H₂) = 1.3 bar; *T* = 20 °C; reaction time: 20 h. [b] *S*-Configuration of **4** in each case.

employing an approximately 1:1 mixture of diastereomeric ligands **8a** and **8b** in the hydrogenation of **3** (Rh:ligand = 1:1; Rh:substrate = 1:1000), the *ee* value of the product (*S*)-**4** was found to be 98.8% (100% conversion). A practical consequence of this result is that the synthesis of the ligand **8** does



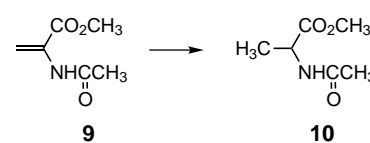
not require enantiomerically pure 1-phenylethanol. However, the possible role of nonlinear effects^[12] upon using diastereomeric mixtures^[8b] cannot be assessed at this time. In the case of pure **8a** the catalyst/substrate ratio was reduced to 1/5000 without any loss in yield or enantioselectivity (Table 2, entry 4). That the Rh:ligand ratio has no influence on enantioselectivity is synthetically significant and constitutes an important starting point for future mechanistic studies (Table 3, entries 1, 6 and 7). A 1:2 ratio appears to be optimal.

Table 3. Enantioselective Rh-catalyzed hydrogenation of 2-acetamido acrylic acid methyl ester (**9**).^[a]

Entry	Ligand	Conversion [%]	<i>ee</i> [%]
1	(<i>S</i>)- 7a	100	72.8
2	(<i>S</i>)- 7b	100	94.8
3	(<i>S</i>)- 7c	100	80.6
4	(<i>S</i>)- 7d	67	70.0
5	8a	100	95.5
6	8b	100	93.3

[a] Reaction conditions as in Table 1. [b] *R* configuration of **10** in each case.

Finally, the Rh-catalyzed hydrogenation of 2-acetamido acrylic acid ester (**9**) to the alanine derivative **10** was investi-



gated. Here again a strong dependence of enantioselectivity upon the nature of the alcohol **5** used in the preparation of the ligands was observed (Table 3). The methanol- and phenol-derived ligands **7a** and **7c** give *ee* values of only 72.8% and 80.6%, respectively, whereas the isopropanol-based ligand **7b** gives an enantioselectivity of 94.8%. Ligand **8a** is even more selective (*ee* = 95.5%). In all cases the monophosphite ligands contain (*S*)-BINOL, which results in preferential formation of the *R*-configured product **10**.

This study disproves the long-standing notion that chelating ligands are necessary for high enantioselectivities to be observed in hydrogenation reactions. This is not only of theoretical, but also of practical interest. For example, phosphites are less sensitive to oxidation than phosphanes. Moreover, because of the modular construction of the monophosphites, structural diversity is easily possible so that enantioselectivity can be maximized for each new substrate as necessary. Studies of this kind as well as mechanistic investigations are underway in our laboratories.

Received: May 31, 2000 [Z 15200]

- [1] L. Horner, H. Siegel, H. Büthe, *Angew. Chem.* **1968**, *80*, 1034–1035; *Angew. Chem. Int. Ed. Engl.* **1968**, *7*, 942–943.
- [2] W. S. Knowles, M. J. Sabacky, *Chem. Commun.* **1968**, 1445–1446.
- [3] K. E. Koenig in *Chiral Catalysis (Asymmetric Synthesis, Vol. 5)* (Ed.: J. D. Morrison), Academic Press, Orlando, **1985**, pp. 71–101; b) J. Halpern in *Chiral Catalysis (Asymmetric Synthesis, Vol. 5)* (Ed.: J. D. Morrison), Academic Press, Orlando, **1985**, pp. 41–69; c) H. Brunner, W. Zettlmeier, *Handbook of Enantioselective Catalysis with Transition Metal Compounds, Vol. I–II*, VCH, Weinheim, **1993**; d) R. Noyori, *Asymmetric Catalysis in Organic Synthesis*, Wiley, New York, **1994**; e) *Comprehensive Asymmetric Catalysis, Vol. I–III* (Eds.: E. N. Jacobsen, A. Pfaltz, H. Yamamoto), Springer, Berlin, **1999**.
- [4] T. P. Dang, H. B. Kagan, *J. Chem. Soc. D* **1971**, 481.
- [5] W. S. Knowles, M. J. Sabacky, B. D. Vineyard, D. J. Weinkauff, *J. Am. Chem. Soc.* **1975**, *97*, 2567–2568.
- [6] A. Miyashita, A. Yasuda, H. Takaya, K. Toriumi, T. Ito, T. Souchi, R. Noyori, *J. Am. Chem. Soc.* **1980**, *102*, 7932–7934.
- [7] Isolated cases of *ee* values up to 90% have been reported; see review by F. Lagasse, H. B. Kagan, *Chem. Pharm. Bull.* **2000**, *48*, 315–324.
- [8] a) M. T. Reetz, T. Neugebauer, *Angew. Chem.* **1999**, *111*, 134–137; *Angew. Chem. Int. Ed.* **1999**, *38*, 179–181; b) D. G. Blackmond, T. Rosner, T. Neugebauer, M. T. Reetz, *Angew. Chem.* **1999**, *111*, 2333–2335; *Angew. Chem. Int. Ed.* **1999**, *38*, 2196–2199.
- [9] Synthesis of **7c**: P. H. Dussault, K. R. Woller, *J. Org. Chem.* **1997**, *62*, 1556–1559.
- [10] We thank M. Pastó (MPI für Kohlenforschung) for the synthesis of the phosphite **7d**.
- [11] The synthesis of **8** as a diastereomeric mixture starting from racemic 1-phenylethanol is known: A. A. Bredikhin, Z. A. Bredikhina, F. F. Nigmatzyanov, *Russ. Chem. Bull.* **1998**, *47*, 411–416.
- [12] a) C. Girard, H. B. Kagan, *Angew. Chem.* **1998**, *110*, 3088–3127; *Angew. Chem. Int. Ed.* **1998**, *37*, 2922–2959; b) monophosphoramidite ligands in conjugate additions: B. L. Feringa, *Acc. Chem. Res.* **2000**, *33*, 346–353.
- [13] Whereas nonlinear effects in enantiomeric catalysts are well known,^[12] related phenomena in the case of diastereomeric catalysts have only recently been described: a) S. Y. Zhang, C. Girard, H. B. Kagan, *Tetrahedron: Asymmetry* **1995**, *6*, 2637–2640; b) C. Bolm, K. Muñoz, J. P. Hildebrand, *Org. Lett.* **1999**, *1*, 491–493; c) see reference [8b].

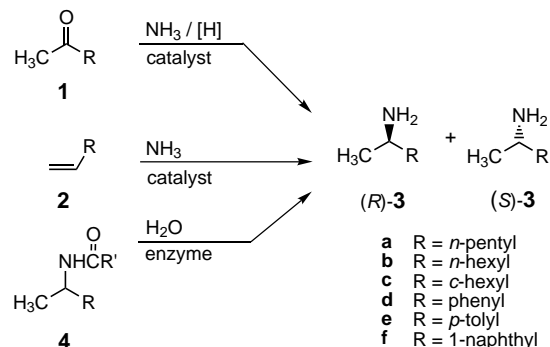
Super-High-Throughput Screening of Enantioselective Catalysts by Using Capillary Array Electrophoresis**

Manfred T. Reetz,* Klaus M. Kühling, Alfred Deege, Heike Hinrichs, and Detlev Belder*

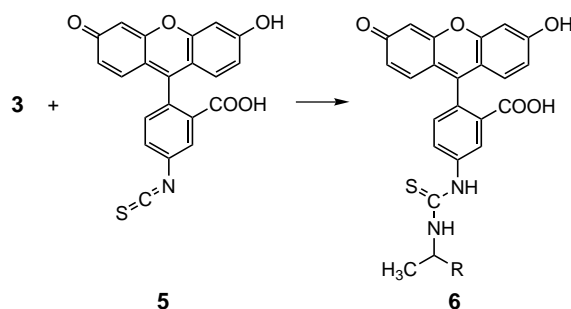
The enantiomeric purity of a product resulting from an asymmetric reaction is usually determined by direct chromatographic separation of the enantiomers by using conventional gas chromatography (GC),^[1] high pressure liquid chromatography HPLC^[2] or capillary electrophoresis (CE)^[3] in conjunction with chiral stationary phases. However, throughput in these sequentially run assays is generally restricted to less than a few dozen determinations of the enantiomeric excess (% *ee*) per day. As a part of our investigations concerning directed evolution as a method to create enantioselective enzymes, we have been engaged in the development of high-throughput *ee*-screening systems.^[4] Such assays are also crucial to the success of combinatorial methods in the development of enantioselective transition metal catalysts.^[5] The currently available *ee*-screening systems developed by us^[4] and other groups^[6] are based on UV/Vis and fluorescence spectroscopy, circular dichroism or mass spectrometry, and all have limitations with respect to the type of substrate or reaction, throughput being limited to 300–1000 samples per day. Herein we describe a new screening system which allows for thousands of *ee* determinations per day.

The starting point of our considerations was conventional CE in which the electrophoretic separation of enantiomers is possible by the use of appropriate chiral selectors as part of the electrolyte.^[3] Accordingly, soluble cyclodextrins (CDs) were employed as so-called pseudo-stationary phases. An important field of application of CE is DNA analysis and sequencing. In particular for the human-genome project various technical versions have emerged to increase throughput drastically.^[7, 8] Among them is capillary array electrophoresis (CAE) in which a high number of capillaries are operated in a parallel manner so that DNA separations and sequencing can be performed automatically with high-throughput.^[7] Special instruments of this kind, specifically designed for DNA analysis, are commercially available, for example, the MegaBACE system^[9] consisting of 6 bundles of 16 capillaries which spatially address standard 96-well microtiter plates. Our approach to high-throughput screening of enantioselective catalysts was based on the adaptation of this technology by using chirally modified electrolytes.^[10] As a specific goal we chose the *ee* determination of chiral amines.

Chiral amines of the type **3** constitute important intermediates in the synthesis of pharmaceuticals and plant protecting agents.^[11] They can be prepared by various methods including the catalytic reductive amination of ketones **1**, Markovnikov addition of NH₃ to olefin **2**, or hydrolytic enzyme-catalyzed kinetic resolution of amides **4** (or reverse reaction).



In exploratory experiments we first varied the electrophoretic conditions of a conventional, single-capillary CE system for the enantiomeric separation of the chiral amines **3**. To make parallel detection possible by laser-induced fluorescence (LIF) in a capillary array system, the amines **3** were treated with the standard fluorescein isothiocyanate^[12] (FITC) **5**, which results in the formation of the derivatives **6**.



Although complete optimization of the electrolyte composition was not carried out for all the compounds, the experiments do show that the use of various commercially available cyclodextrin derivatives as chiral selectors does lead to an acceptable antipode separation of the substrates (Table 1).

As part of a model study we attempted the antipode separation of the amine derivative **6c** with the help of CAE. To this end the parameters obtained in the conventional single-capillary system had to be adapted for application in the multi-capillary MegaBase system. As a result of the special characteristics of this system which was developed for DNA analyses (only electrokinetic injection and detection solely at the anode), the electrolyte system had to be adapted for our purposes. Electrolytes which led to excellent results in single-capillary CE systems provided very unstable electrophoretic runs with large fluctuations in the electric current. The results obtained, which are not very reproducible, can be

[*] Prof. M. T. Reetz, Dr. D. Belder, Dr. K. M. Kühling, A. Deege, H. Hinrichs
Max-Planck-Institut für Kohlenforschung
Kaiser-Wilhelm-Platz 1, 45470 Mülheim an der Ruhr (Germany)
Fax: (+49)208-306-2985
E-mail: reetz@mpi-muelheim.mpg.de

[**] We thank Amersham Pharmacia Biotech Europe GmbH (Freiburg, Germany) and particularly Dr. Gönne Spierings for advice in carrying out the experiments involving the MegaBACE system.

Table 1. Results of chiral CE separations of the amine derivatives **6** at various electrolyte compositions.^[a]

Buffer ^[b]	6a	6b	6c	6d	6e	6f
40 mmol CHES, 40 mmol γ -CD+15% CH ₃ CN	B	B	–	n.m.	–	–
20 mmol borate, 20 mmol DM- β -CD	–	–	–	–	–	–
40 mmol CHES, 20 mmol DM- β -CD	–	–	–	–	–	–
40 mmol CHES, 5 mmol DM- β -CD	–	–	–	P	–	–
40 mmol CHES, 40 mmol HE- β -CD	–	–	–	–	–	–
40 mmol CHES, 20 mmol HE- β -CD	P	–	–	P	–	–
40 mmol CHES, 10 mmol HE- β -CD	P	–	–	P	P	–
40 mmol CHES, 5 mmol HE- β -CD	aB	P	P	aB	aB	–
40 mmol CHES, 2.5 mmol HE- β -CD	aB	P	P	P	aB	–
40 mmol CHES, 5 mmol HP- α -CD	–	–	–	–	–	–
40 mmol CHES, 20 mmol HP- β -CD	–	–	–	P	–	–
40 mmol CHES, 5 mmol HP- β -CD	P	–	P	aB	P	–
40 mmol CHES, 20 mmol HP- β -CD+15% CH ₃ CN	P	–	–	P	–	P
40 mmol CHES, 25 mmol HP- γ -CD	–	–	P	–	–	–
40 mmol CHES, 6.25 mmol HP- γ -CD	–	–	B	–	P	aB
40 mmol CHES, 25 mmol HP- γ -CD+15% CH ₃ CN	–	–	B	–	–	–
40 mmol CHES, 10 mmol NH ₂ - β -CD	–	–	–	–	–	–
40 mmol CHES, 10 mmol β -CD	–	–	–	–	–	–

[a] P: partial separation; B: base-line separation; aB: almost base-line separation; –: no separation; n.m.: not measured. [b] DM: heptakis(2,6-di-*O*-methyl); HE: hydroxyethyl; HP: hydroxypropyl; NH₂: 6^A-amino-6^A-desoxy; CHES: 2-(*N*-cyclohexylamino)ethanesulfonic acid.

explained in part by the conjecture that the electrokinetic injection of the anionic analytes, even at only weak cathodic electroosmotic flow (EOF), as found in the polyacrylamide coated capillaries used, is problematic. In contrast, reproducible results of higher quality were obtained by using a viscous electrolyte containing a linear polyacrylamide (LPA) as an electrolyte additive which reduces the EOF. The electrolyte consists of γ -CD (6.25 mM) dissolved in CHES buffer (40 mM) at pH 9.1, in ratio 5:1 with the highly viscous LPA buffer (from Amersham Pharmacia). The voltage per capillary was adjusted to –10 kV at 8 μ A at a sampling voltage of –2 kV for 9 s.

Initially, 12 solutions of (+)/(–) mixtures of **6c** were analyzed by the adapted MegaBACE system.^[9] Figure 1

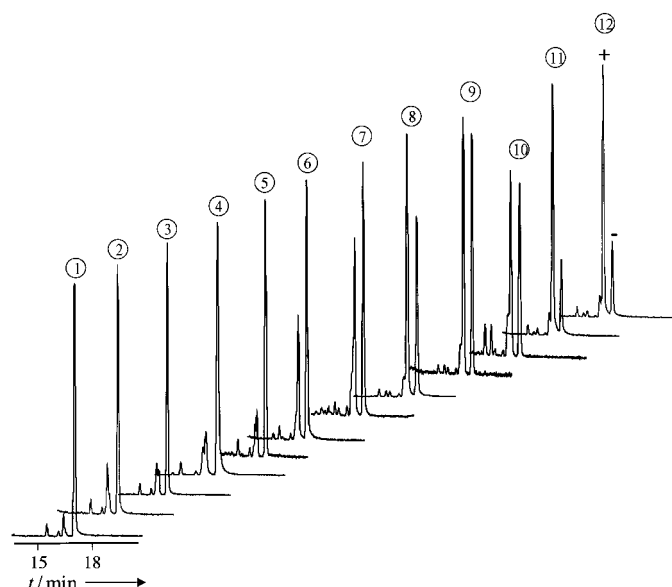


Figure 1. CAE separation of representative samples of the amine derivatives **6c**.

shows the electropherograms obtained in parallel and Table 2 the *ee* values determined by CAE. As a control, the enantiomeric purities of the corresponding non-derivatized amines (+)/(–)-**3c** were checked by using GC with a chiral stationary phase (Ivadex-1/PS086 *d_f*: 0.15 μ m, i.d.: 0.25, *l*: 25 m). The agreement is very good, although integration of the signal corresponding to the (+)-isomer in the CAE experiments was made difficult by an impurity, especially at low (+)/(–) ratios (Table 2, entry 1).

Table 2. Comparison of the experimentally determined enantiomeric excess of samples of (+)/(–)-**3c** by GC and the corresponding enantiomeric excess of (+)/(–)-**6c** determined by CAE.

Sample	<i>ee</i> 3c (GC) [%]	<i>ee</i> 6c (CAE) [%]
1	98	> 95
2	88	90
3	84	82
4	74	70
5	74	70
6	38	38
7	18	16
8	18	16
9	0	0
10	0	2
11	54	52
12	54	52

This unoptimized antipode separation requires about 19 minutes. Upon using the automated 96-array system at least 7000 *ee* determinations are possible per day. By optimizing the experimental parameters, such as increasing the electric field strength and/or control of the electroosmotic flow by the use of special capillaries,^[3g] considerably shorter analysis times can be reached so that a daily throughput of 15000 to 30000 *ee* determinations is realistic. Such super-high-throughput screening of enantioselectivity is not possible using any other system currently available. As CAE has many advantages, including the use of very small amounts of sample, practically no utilization of solvents, absence of high-pressure pumps and valves as well as variable use of different and relatively cheap chiral phases, the present assay appears particularly attractive.

Another possibility to increase throughput of CE makes use of chip technology in which photolithographic techniques are preferably applied to create one or more capillaries on microchips.^[8] Such CE microchips are made of plastic or glass and have been used in the analysis of oligonucleotides, DNA-sequence fragments, amino acids, DNA restriction fragments as well as PCR products. These highly miniaturized systems allow for extremely rapid separations within seconds or minutes. We have therefore started to study separations of enantiomers on CE microchips.^[13] Whereas in the separation of biomolecules in aqueous electrolytes plastic or glass chips can be utilized (as in the case of amino acids)^[14] we observed that in the separation of conventional organic compounds, in electrolytes that contain organic solvents, on plastic (poly-methyl methacrylate (PMMA)) based microchips the system is not chemically stable enough. We have therefore concentrated on glass chips.

Since appropriate CE instruments based on microchips are not yet commercially available, we first built our own

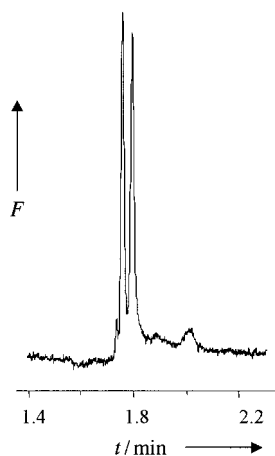


Figure 2. Chiral electrophoretic separation of the racemic amine derivative **6c** on a CE microchip; F = fluorescence intensity.

configuration equipped with two high-voltage sources, high-voltage switches, and an LIF-detector (argon-ion laser). In initial experiments, by using CE glass chips from Micralyne (Edmonton, Canada), we obtained very promising results concerning chiral separations of FITC-derivatized amines. In the case of **6c** practically complete basis-line separation of the antipodes was achieved within two minutes (Figure 2). In doing so we used the same electrolyte as before (Figure 1), but without LPA. For sample injection a voltage of 1 kV was applied at the electrodes, at the buffer inlet, buffer outlet, as well as

the sample inlet, whereas the sample outlet was kept at the ground-level potential. For separation the voltage was switched so that the voltage at the four electrodes was as follows: buffer inlet 1 kV, sample inlet 0.6 kV, sample outlet 0.6 kV, buffer outlet 0 V.

Further development of this analytical instrument with the capability of higher electric-field strength leading to the possibility of chiral separation within seconds is in progress. Thus, a second CE-based method for super-high-throughput screening of enantioselective catalysts can be anticipated. Another goal is to carry out the actual catalytic reactions on microchips and to couple this process directly with such a CE-screening system.

Our study shows that the development of capillary electrophoresis in the form of CAE for the determination of enantiomeric purity can be used in a truly high-throughput manner (> 7000 ee determinations per day). This result as well as the optimization of the methods described herein are of great significance for the further development of combinatorial asymmetric transition metal catalysis^[5] and directed evolution of enantioselective enzymes.^[4, 15]

Received: June 28, 2000 [Z15352]

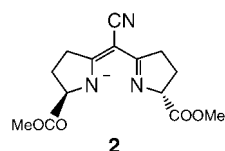
- [1] W. A. König, *Gas Chromatographic Enantiomer Separation with Modified Cyclodextrins*, Hüthig, Heidelberg, **1992**.
- [2] *Chiral Separation by HPLC* (Ed.: A. M. Krstulovic), Ellis Horwood, Chichester, **1989**.
- [3] a) B. Chankvetadze, *Capillary Electrophoresis in Chiral Analysis*, Wiley, Chichester, **1997**; b) E. Gassmann, J. E. Kuo, R. N. Zare, *Science* **1985**, *230*, 813–814; c) L. G. Blomberg, H. Wan, *Electrophoresis* **2000**, *21*, 1940–1952; d) H. Nishi, T. Fukuyama, S. Terabe, *J. Chromatogr.* **1991**, *553*, 503–516; e) S. Fanali, *J. Chromatogr.* **1989**, *474*, 441–446; f) A. Guttman, A. Paulus, A. S. Cohen, N. Grinberg, B. L. Karger, *J. Chromatogr.* **1988**, *448*, 51–53; g) D. Belder, G. Schomburg, *J. Chromatogr. A* **1994**, *666*, 351–365; h) D. Wistuba, V. Schurig, *J. Chromatogr. A* **2000**, *875*, 255–276; i) G. Blaschke, B. Chankvetadze, *J. Chromatogr. A* **2000**, *875*, 3–25.
- [4] a) M. T. Reetz, A. Zonta, K. Schimossek, K. Liebeton, K.-E. Jaeger, *Angew. Chem.* **1997**, *109*, 2961–2963; *Angew. Chem. Int. Ed. Engl.* **1997**, *36*, 2830–2832; b) M. T. Reetz, K.-E. Jaeger, *Chem. Eur. J.* **2000**, *6*, 407–412.

- [5] a) B. Jandeleit, D. J. Schaefer, T. S. Powers, H. W. Turner, W. H. Weinberg, *Angew. Chem.* **1999**, *111*, 2648–2689; *Angew. Chem. Int. Ed.* **1999**, *38*, 2494–2532; b) G. Liu, J. A. Ellman, *J. Org. Chem.* **1995**, *60*, 7712–7713; c) S. R. Gilbertson, X. Wang, *Tetrahedron* **1999**, *55*, 11609–11618; d) K. D. Shimizu, B. M. Cole, C. A. Krueger, K. W. Kuntz, M. L. Snapper, A. H. Hoveyda, *Angew. Chem.* **1997**, *109*, 1782–1785; *Angew. Chem. Int. Ed. Engl.* **1997**, *36*, 1704–1707; e) M. B. Francis, E. N. Jacobsen, *Angew. Chem.* **1999**, *111*, 987–991; *Angew. Chem. Int. Ed.* **1999**, *38*, 937–941; f) A. M. Porte, J. Reibenspies, K. Burgess, *J. Am. Chem. Soc.* **1998**, *120*, 9180–9187; g) C. Gennari, S. Ceccarelli, U. Piarulli, C. A. G. N. Montalbetti, R. F. W. Jackson, *J. Org. Chem.* **1998**, *63*, 5312–5313; h) P. P. Pescarmona, J. C. van der Waal, I. E. Maxwell, T. Maschmeyer, *Catal. Lett.* **1999**, *63*, 1–11.
- [6] a) L. E. Janes, A. C. Löwendahl, R. J. Kazlauskas, *Chem. Eur. J.* **1998**, *4*, 2324–2331; b) U. T. Bornscheuer, J. Altenbuchner, H. H. Meyer, *Bioorg. Med. Chem.* **1999**, *7*, 2169–2173; c) G. Klein, J.-L. Reymond, *Helv. Chim. Acta* **1999**, *82*, 400–406; d) see also: G. T. Copeland, S. J. Miller, *J. Am. Chem. Soc.* **1999**, *121*, 4306–4397; e) K. Ding, A. Ishii, K. Mikami, *Angew. Chem.* **1999**, *111*, 519–523; *Angew. Chem. Int. Ed.* **1999**, *38*, 497–501; f) M. T. Reetz, M. H. Becker, H.-W. Klein, D. Stöckigt, *Angew. Chem.* **1999**, *111*, 1872–1875; *Angew. Chem. Int. Ed.* **1999**, *38*, 1758–1761; g) see also: J. Guo, J. Wu, G. Siuzdak, M. G. Finn, *Angew. Chem.* **1999**, *111*, 1868–1871; *Angew. Chem. Int. Ed.* **1999**, *38*, 1755–1758.
- [7] a) X. C. Huang, M. A. Quesada, R. A. Mathies, *Anal. Chem.* **1992**, *64*, 2149–2154; b) H. Kambahara, S. Takahashi, *Nature* **1993**, *361*, 565–566; c) N. J. Dovichi, *Electrophoresis* **1997**, *18*, 2393–2399; d) G. Xue, H. Pang, E. S. Yeung, *Anal. Chem.* **1999**, *71*, 2642–2649; e) S. Behr, M. Mätzig, A. Levin, H. Eickhoff, C. Heller, *Electrophoresis* **1999**, *20*, 1492–1507.
- [8] a) D. J. Harrison, K. Fluri, K. Seiler, Z. Fan, C. S. Effenhauser, A. Manz, *Science* **1993**, *261*, 895–897; b) S. C. Jacobson, R. Hergenroder, L. B. Koutny, R. J. Warmack, J. M. Ramsey, *Anal. Chem.* **1994**, *66*, 1107–1113; c) L. D. Hutt, D. P. Glavin, J. L. Bada, R. A. Mathies, *Anal. Chem.* **1999**, *71*, 4000–4006; d) D. Schmalzing, L. Koutny, A. Adourian, P. Belgrader, P. Matsudaira, D. Ehrlich, *Proc. Natl. Acad. Sci. USA* **1997**, *94*, 10273–10278; e) S. C. Jacobson, C. T. Culbertson, J. E. Daler, J. M. Ramsey, *Anal. Chem.* **1998**, *70*, 3476–3480; f) S. Liu, H. Ren, Q. Gao, D. J. Roach, R. T. Loder, Jr., T. M. Armstrong, Q. Mao, I. Blaga, D. L. Barker, S. B. Jovanovich, *Proc. Natl. Acad. Sci. USA* **2000**, *97*, 5369–5374; g) S. R. Wallenborg, C. G. Bailey, *Anal. Chem.* **2000**, *72*, 1872–1878; h) I. Rodriguez, L. J. Jin, S. F. Y. Li, *Electrophoresis* **2000**, *21*, 211–219.
- [9] The MegaBACE instrument is commercially available from Amersham Pharmacia Biotech Europe GmbH (Freiburg, Germany).
- [10] M. T. Reetz, K. M. Kühling, A. Deege, H. Hinrichs, D. Belder (Studiengesellschaft Kohle mbH), patent application **2000**.
- [11] a) *Chirality in Industry: The Commercial Manufacture and Applications of Optically Active Compounds* (Eds.: A. N. Collins, G. N. Sheldrake, J. Crosby), Wiley, Chichester, **1992**; b) *Chirality in Industry II: Developments in the Commercial Manufacture and Applications of Optically Active Compounds* (Eds.: A. N. Collins, G. N. Sheldrake, J. Crosby), Wiley, Chichester, **1997**; c) R. A. Sheldon, *Chirotechnology: Industrial Synthesis of Optically Active Compounds*, Marcel Dekker, New York, **1993**; d) F. Balkenhohl, K. Dittrich, B. Hauer, W. Ladner, *J. Prakt. Chem./Chem.-Ztg* **1997**, *339*, 381–384.
- [12] a) L. Hernandez, R. Marquina, J. Escalona, N. A. Guzman, *J. Chromatogr.* **1990**, *502*, 247–255; b) S. P. D. Lalljie, P. Sandra, *Chromatographia* **1995**, *40*, 519–526; c) A. Ramseier, F. von Heeren, W. Thormann, *Electrophoresis* **1998**, *19*, 2967–2975.
- [13] M. T. Reetz, K.-E. Jaeger, A. Zonta, K. Schimossek, K. Liebeton (Studiengesellschaft Kohle mbH), DE-A 197 319 90.4, **1997**.
- [14] Hutt et al.^[8c] and Li et al.^[8h] have recently described chiral CE separations of amino acids on a glass chip. It should be possible to develop a high-throughput screening system for this class of compounds by using robotics.
- [15] a) K. Liebeton, A. Zonta, K. Schimossek, M. Nardini, D. Lang, B. W. Dijkstra, M. T. Reetz, K.-E. Jaeger, *Chem. Biol.*, in press; b) O. May, P. T. Nguyen, F. H. Arnold, *Nat. Biotechnol.* **2000**, *18*, 317–320; c) E. Henke, U. T. Bornscheuer, *Biol. Chem.* **1999**, *380*, 1029–1033.

Novel Nickel(II) Complexes for the Catalytic Copolymerization of Ethylene and Carbon Monoxide: Polyketone Synthesis in Supercritical Carbon Dioxide**

Wolfgang Kläui,* Jochen Bongards, and Guido J. Reiß

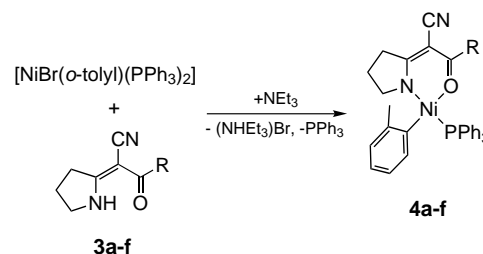
Polyketone: Suddenly the rush is on.^[1] Since 1996 polyketones have been produced industrially as a new class of synthetic materials with superior properties. This was made possible with the discovery of a palladium(II)–phosphane complex that catalyses the formation of perfectly alternating copolymers of CO and olefins at low pressures and temperatures.^[2] Since the precious metal remains in the polymer, attempts have been made to use the less expensive nickel as the catalyst metal. So far only a few nickel(II) complexes are known to catalyze the formation of polyketones from CO and ethylene.^[3] These systems usually start with the formation of polyethylene; in fact, carbon monoxide initially acts as an inhibitor for the catalysis.^[4] Recently, we synthesized the first nickel(II) complex that catalyses the formation of a strictly alternating polyketone of CO and ethylene.^[5] This complex was identified by X-ray structure analysis to be [Ni(*o*-tolyl)(PPh₃)Tp^{Ph}] (**1**), an aryl–nickel(II) complex with the sterically demanding tris(pyrazolyl)borate ligand Tp^{Ph},^[6] which coordinates as a bidentate N,N-chelating ligand to the nickel atom. The mechanism of the catalysis is unknown to date. The crystal structure shows that the hydrogen atom of the borane moiety lies within close proximity of the nickel center. This has led us to hypothesize that a nickel hydride species might initiate the catalytic cycle. However, we were only able to synthesize the closely related compound [Ni(*o*-tolyl)(PPh₃)Tp^{Tol}] but none with the ligands Tp, Tp^{Me,Me}, Tp^{tBu}, or Tp^{Tol,Me}. It seemed as if compound **1** was a unique case. We could not determine whether the boron–hydrogen moiety plays a role for the catalytic activity. Now we have discovered that the tripodal ligand Tp^{Ph} can be exchanged for



a bidentate N,N-chelating ligand of the semicorrine-type (shown as the anion **2**).^[7]

The aryl–nickel(II) complex [Ni(*o*-tolyl)(PPh₃)(**2**)] is about twice as active a catalyst as compound **1** for the polyketone formation from ethylene and carbon monoxide. Evidently neither the borane–hydrogen atom nor the tridenticity of the Tp^{Ph} ligand is of any importance for the catalysis. In the development of complexes with the semicorrine ligand, we have

discovered a class of N,O-chelating ligands (**3**) that also form aryl–nickel(II) complexes. These new compounds (**4**), which are reported here, catalyze the formation of strictly alternating copolymers from CO and ethylene at low pressures and temperatures with an efficiency that lies orders of magnitude beyond that of all currently known nickel complexes. The novel complexes **4** can be prepared in high yields as shown in Scheme 1.



Scheme 1. Synthesis of the complexes **4**.

The complexes **4** are air-stable, bright yellow solids that give stable aryl complexes upon reaction with carbon monoxide. In the ³¹P NMR spectrum of **4d** only one phosphorus peak is detected for the aryl complex resulting from the insertion of CO into the Ni^{II}–C bond, even after a long period of time and CO pressures of up to 40 bar; no signal for the degradation of the complex to a carbonyl–phosphane–Ni⁰ species occurs (the formation of phosphane–Ni⁰ complexes is the main termination reaction for the catalysis).

Figure 1 shows the crystal structure of **4d**. The nickel atom is coordinated in a square-planar fashion with the triphenylphosphane ligand in the *trans*-position to the N atom of the

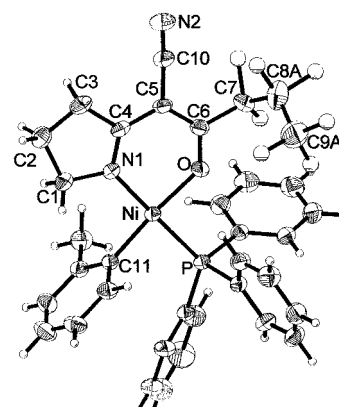


Figure 1. Structure of **4d** in the crystal. For clarity, only one variant of the 1:1 disordered C₃F₇ group is shown as a ball-and-stick model; thermal ellipsoids correspond to 50% probability. Selected bond lengths [Å] and angles [°]: Ni–N1 1.926(2), Ni–O 1.918(2), Ni–P 2.1935(10), Ni–C11 1.893(2), N1–C4 1.299(3), C4–C5 1.438(4), C5–C6 1.387(4), O–C6 1.268(3), C6–C7 1.535(4); O–Ni–N1 91.13(8), O–Ni–P 87.42(6), C11–Ni–P 87.82(8), C11–Ni–N1 93.59(10), N1–Ni–P 177.46(7), C11–Ni–O 175.07(9).

chelating ligand.^[8] Some of the complexes described here copolymerize ethylene and carbon monoxide with very high efficiencies. While efficiencies for catalysts of type **1** lie at about 170, compounds **4d** and **4e** show efficiencies of up to about 11 000 gram polyketone per gram nickel^[9] (Table 1).

[*] Prof. Dr. W. Kläui, J. Bongards, Dr. G. J. Reiß
Institut für Anorganische Chemie und Strukturchemie der Heinrich-Heine-Universität Düsseldorf
Universitätsstrasse 1, 40225 Düsseldorf (Germany)
Fax: (+49)211-81-12287
E-mail: klaui@uni-duesseldorf.de

[**] This work was supported by the Fonds der Chemischen Industrie. We thank Prof. Dr. W. Keim, Aachen, for many helpful discussions and Dr. W. Leitner and Dr. A. Wegner at the Max-Planck-Institut für Kohlenforschung at Mülheim an der Ruhr for their kind support and their help in performing the reactions in supercritical carbon dioxide.

Table 1. Polymerization efficiencies of **4a–f**.

R	Ligand	Nickel complex	Efficiency ^[a]
Me	3a	4a	2000
Ph	3b	4b	2000
CF ₃	3c	4c	4000
C ₃ F ₇	3d	4d	11 000
C ₇ F ₁₅	3e	4e	11 000
OMe	3f	4f	0

[a] In gram polyketone per gram nickel.

The catalysis can be performed in dichloromethane, THF, or toluene with approximately the same efficiency, which makes a possible participation of the solvent, for example, by stabilizing a coordinatively unsaturated transition state, improbable.

A striking feature of the catalysis is the great dependency of the efficiency on the substituent R. As shown in Table 1, the best results can be achieved by the introduction of electron-withdrawing groups. In contrast, no polyketone was obtained with compound **4f**. Why perfluorinated side chains have such a positive impact on the catalysis remains the subject for further investigations. It may be possible that the catalyst's ability to stay on the surface of the growing polymer is enhanced with the presence of perfluorinated side chains, thus ensuring the diffusion of ethylene and carbon monoxide. Compounds **4d** and **4e** show almost identical efficiencies. We did not try to further optimize the reaction conditions. Notably, the longer the side chain the more soluble the complexes **4c–e** become in nonpolar solvents. The C₇F₁₅ side chain enables complex **4e** to dissolve even in supercritical carbon dioxide (scCO₂). First attempts have shown that **4e** catalyses the formation of a strictly alternating copolymer with ethylene and carbon monoxide in scCO₂. Numerous polymerization reactions in scCO₂ are known to date^[10], but to our knowledge the synthesis of polyketones in supercritical carbon dioxide has never been achieved.

The novel nickel(II) complexes reported here show a significantly higher efficiency than all previously reported nickel(II) systems and display a remarkable stability towards carbon monoxide. Thus these catalysts are not dependent on a start of the catalysis by ethylene or low carbon monoxide pressures. Also, for the first time it was possible to perform a copolymerization reaction in supercritical carbon dioxide, which is viewed as one of the solvents of the future for the polymer industry, due to its good dissolving qualities and overall environmental friendliness.^[10]

Experimental Section

Ligands 3a–e: (E/Z)-(Pyrrolidine-2-ylidene)acetonitrile (1.1 g, 10 mmol)^[11] in toluene (100 mL) was treated with NEt₃ (1.0 g, 10 mmol) under an atmosphere of dry nitrogen. After the solution had been cooled to 0 °C, the corresponding acid chloride (10 mmol) was added slowly. The mixture was stirred overnight and the resulting (NHET₃)Cl filtered off. The filtrate was washed with NaHCO₃ solution, separated from the aqueous layer, evaporated, and recrystallized from either diethyl ether or a mixture of diethyl ether/pentane. For example, **3e**: ¹H NMR (200 MHz, CDCl₃, 25 °C): δ = 2.28 (m, ³J(H,H) = 7.5 Hz, 2H; CH₂), 3.19 (t, ³J(H,H) = 8.0 Hz, 2H; CH₂), (t, ³J(H,H) = 7.7 Hz, 2H; CH₂), 10.80 (s, 1H; NH); IR (KBr): $\tilde{\nu}$ = 3273 (NH), 2218 (CN), 1628 (C=O), 1581 (C=C); MS(70 eV): *m/z*: 504 [*M*⁺], 485 [*M*⁺ – F], 135 [*M*⁺ – C₇F₁₅]; elemental analysis (%): calcd for

C₁₄H₇N₂F₁₅O: C 33.35, H 1.40, N 5.56; found: C 33.50, H 1.35, N 5.61; yield 3.5 g (70 %).

Ligand **3f** was prepared as reported in reference [11].

Complexes 4a–f: Under N₂ a suspension of [NiBr(*o*-tolyl)(PPh₃)₂] (2.0 g, 2.7 mmol)^[12] and **3a–f** (2.7 mmol) in THF (50 mL) was treated with NEt₃ (2.7 mmol) and stirred for 16 h at room temperature. The suspension was evaporated to 10 mL and the resulting (NHET₃)Br was separated. The filtrate was evaporated and the resulting solid taken up in small amounts of dichloromethane. The solution was treated with hexanes or methanol, and the complexes **4a–f** precipitated upon evaporation of CH₂Cl₂. Yields 60–85 %. For example, **4e**: ¹H NMR (300 MHz, CD₂Cl₂, 25 °C): δ = 1.65 (m, ³J(H,H) = 7.9 Hz, 2H; CH₂), 2.85 (s, 3H; CH₃-tolyl), 2.86 (m, 4H; 2 × CH₂), 6.39 (d, ³J(H,H) = 6.7 Hz, 1H; tolyl), 6.49 (t, ³J(H,H) = 7.1 Hz, 1H; tolyl), 6.56 (t, ³J(H,H) = 7.2 Hz, 1H; tolyl), 7.30 (m, 15H; PPh₃, 1H; tolyl); ³¹P{¹H} NMR (121 MHz, CD₂Cl₂, 25 °C): δ = 26.8 (s); IR (KBr): $\tilde{\nu}$ = 2214 cm^{–1} (CN), 1587 (C=O), 1435 (PPh₃); MS(FAB): *m/z*: 915 [*M*⁺ + H], 823 [*M*⁺ + tolyl], 652 [*M*⁺ – PPh₃], 562 [*M*⁺ – PPh₃ – tolyl]; elemental analysis (%): calcd for C₃₉H₂₈N₂F₁₅NiOP: C 51.18, H 3.08, N 3.06; found: C 51.10, H 2.92, N 2.90.

General preparation for the synthesis of polyketones: Compounds **4a–e** (0.007 mmol, 4.0–6.5 mg) in 10 mL solvent were transferred into a 100-mL autoclave. The solution was pressurized with 40 bar ethylene and 10 bar of carbon monoxide and stirred with a magnetic stirrer at 60 °C for 16 h. The white solid was filtered off, washed with methanol, and dried. Yields: 0.8–4.5 g; m.p. 260–265 °C; IR (KBr): $\tilde{\nu}$ = 1693 cm^{–1} (C=O); elemental analysis (%): calcd for (C₃H₄O)_n: C 64.3, H 7.2; found: C 64.1, H 7.1.

To monitor the time-dependence of the polyketone formation, the catalysis with **4d** was stopped after 1, 2, and 3 h. The turnover number (TON) was 2300 after 1 h, 2000 after 2 h, and 1800 g polyketone per g nickel per hour after 3 h, corresponding to efficiencies of 2300, 4000, and 5400 g polyketone per g nickel, respectively.

Preparation for the synthesis of polyketones in scCO₂: Compound **4e** (5.5 mg, 0.006 mmol) was transferred to a 20-mL autoclave under N₂. The solution was pressurized with ethylene (2.0 g; 40 bar), carbon monoxide (0.4 g; 10 bar) and carbon dioxide (15.6 g), heated to 70 °C, and stirred overnight. The resulting white solid was washed with methanol and dried. Yield: 0.78; m.p. 255–262 °C; IR (KBr): $\tilde{\nu}$ = 1692 cm^{–1} (C=O); elemental analysis (%): calcd for (C₃H₄O)_n: C 64.3, H 7.2; found: C 64.4, H 7.1.

Received: May 9, 2000 [Z15101]

- [1] J. Murphy, *High Perform. Plastics* **1995**, 5, 2.
- [2] E. Drent, P. H. M. Budzelaar, *Chem. Rev.* **1996**, 96, 663–681.
- [3] a) U. Klabunde, T. H. Tulip, D. C. Roe, S. D. Ittel, *J. Organomet. Chem.* **1987**, 334, 141–156; b) U. Klabunde, S. D. Ittel, *J. Mol. Catal.* **1987**, 41, 123–134; c) S. Y. Desjardins, K. J. Cavell, J. L. Hoare, B. W. Skelton, A. N. Sobolev, A. H. White, W. Keim, *J. Organomet. Chem.* **1997**, 544, 163–174.
- [4] Keim et al. have reported an in situ catalytic system from thiol carboxylic acids and nickel compounds that can start the catalysis even in the presence of carbon monoxide: B. Driessen, M. J. Green, W. Keim (BP), US-A 5214126 **1993**, B. Driessen, M. J. Green, W. Keim (BP), EP-B 470759 **1992** [*Chem. Abstr.* **1992**, 116, 152623g].
- [5] B. Dommhöver, W. Kläui, A. Kremer-Aach, R. Bell, D. Mootz, *Angew. Chem.* **1998**, 110, 3218–3220; *Angew. Chem. Int. Ed.* **1998**, 37, 3050–3052.
- [6] The abbreviation is used here according to the nomenclature introduced by Trofimenko: S. Trofimenko, *Chem. Rev.* **1993**, 93, 943–980.
- [7] H. Fritsch, U. Leutenegger, K. Siegmann, A. Pfaltz, *Helv. Chim. Acta* **1988**, 71, 1541–1552.
- [8] Crystal structure analysis of **4d**: C₃₅H₂₈F₇N₂NiOP, *M*_r = 715.27; crystal dimensions: 0.6 × 0.7 × 0.8 mm³, *a* = 11.410(2), *b* = 12.500(2), *c* = 13.950(3) Å, *α* = 113.30(3), *β* = 93.90(3), *γ* = 111.30(3)°, *V* = 1649.6(5) Å³, *Z* = 2, *ρ*_{calcd} = 1.440 Mg m^{–3}, triclinic, P₁. Siemens P₂₁, MoK_α radiation (λ = 0.71073 Å), graphite monochromator, *T* = 25 °C, *θ*_{max} = 28.5°, –1 < *h* < 15, –16 < *k* < 16, –18 < *l* < 18, 9496 reflections were detected, 8311 independent (*R*_{int} = 0.022), 5779 were classified as observed with *I* > 2σ(*I*), *μ* = 0.71 mm^{–1}, direct methods (SHELXS97), and difference Fourier syntheses (SHELXL97), min-

imizing of $\Sigma w(F_o^2 - F_c^2)$ with $w = 1/[\sigma^2(F_o^2) + 0.02P^2 + 1.1P]$ and $P = (F_o^2 + 2F_c^2)/3$, 483 refined parameter, $R_1 = 0.0442$, $wR_2 = 0.0953$, $\Delta\rho_{\max}/\Delta\rho_{\min}$: 0.405 / -0.338 e Å⁻³. Crystallographic data (excluding structure factors) for the structure reported in this paper have been deposited with the Cambridge Crystallographic Data Centre as supplementary publication no. CCDC-144043. Copies of the data can be obtained free of charge on application to CCDC, 12 Union Road, Cambridge CB21EZ, UK (fax: (+44)1223-336-033; e-mail: deposit@ccdc.cam.ac.uk).

- [9] The highest possible efficiency may exceed the one described here. Our 100-mL autoclaves are clogged by a solid plug of polyketone which may prevent further formation of polymer.
- [10] J. L. Kendall, D. A. Canelas, J. L. Young, J. M. DeSimone, *Chem. Rev.* **1999**, 99, 543–563.
- [11] M. Misun, A. Pfaltz, *Helv. Chim. Acta* **1996**, 79, 961–972.
- [12] M. Hidai, T. Kashiwagi, T. Ikeuchi, Y. Uchida, *J. Organomet. Chem.* **1971**, 30, 279–284.

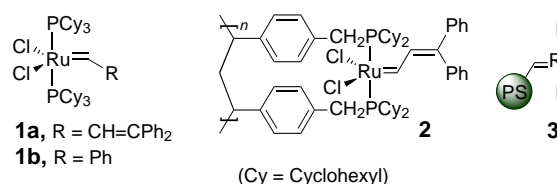
A Soluble Polymer-Bound Ruthenium Carbene Complex: A Robust and Reusable Catalyst for Ring-Closing Olefin Metathesis**

Qingwei Yao*

Facile catalyst separation and subsequent reuse are of prime importance in both industrial and academic settings. From the viewpoint of atom economy,^[1] a catalyst should ideally be completely recoverable and reusable. In this respect, immobilized or heterogeneous catalysts offer inherent operational and economical advantages over their homogeneous counterparts. Herein we report the first soluble polymer-bound olefin-metathesis catalyst derived from Grubbs' ruthenium carbene complex and poly(ethylene glycol) (PEG). The new PEG-bound catalyst exhibits remarkable chemical stability and can be repeatedly used and recycled in the ring-closing metathesis (RCM) of a variety of α,ω -dienes.

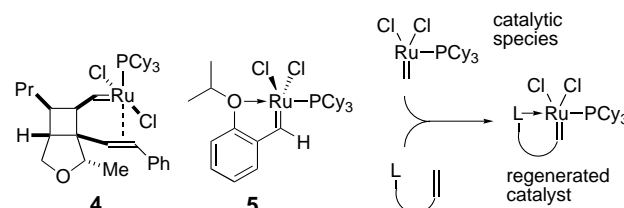
The enormous recent success of olefin metathesis^[2] catalyzed by metal carbene complexes stems from the availability of several well-defined catalysts,^[2a] which include the Schrock molybdenum alkylidene^[3] and the Grubbs-type ruthenium alkylidenes **1a**^[4] and **1b**.^[5, 6] Earlier attempts by Grubbs and Nguyen^[7] to prepare polystyrene-supported catalysts based on **1a** met with only limited success and the resulting polymer-supported Ru carbene (for example, **2**) was found to be about two orders of magnitude less reactive than the homogeneous analogue **1a**. Moreover, recovery and reuse led to losses in activity (20 % after each cycle). To the best of our knowledge,

no further application of this catalyst has been reported in the literature. Very recently, Barrett and co-workers^[8] have reported the immobilization of **1b** on vinyl polystyrene. Unfortunately, attempted recycling and reuse of the immobilized catalyst **3** led to a dramatic decrease in activity. The



catalyst survives only a limited number of recyclings and completely loses its activity after the third cycle. Therefore, despite the obvious and much desired advantage, development of immobilized ruthenium carbene complexes as active, truly recyclable and reusable catalysts for olefin metathesis remains a challenging task.^[9]

In contemplating a novel approach to the immobilization of metathesis catalysts, we were attracted by two serendipitous findings from the groups of Snapper^[10] and Hoveyda.^[11] Thus, ruthenium carbenes **4**^[10] and **5**^[11] (Scheme 1), each bearing one phosphane ligand bound to the metal, were found to be



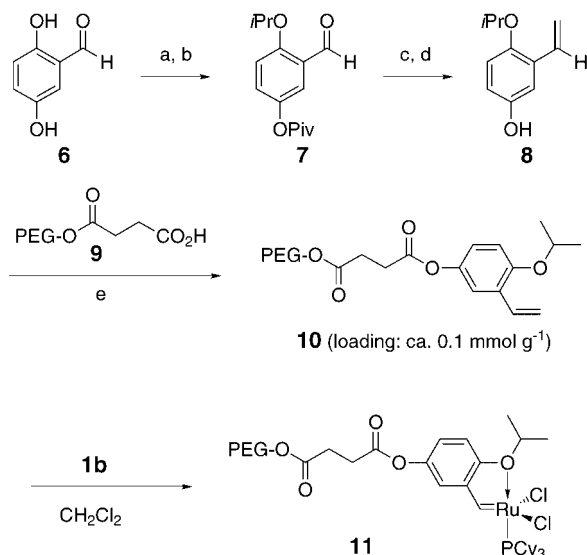
Scheme 1. Monophosphane-based metathesis catalysts^[10, 11] and their regeneration at the end of the reaction.

remarkably stable and could be isolated and purified by silica-gel column chromatography. Hoveyda and co-workers also demonstrated^[11] that **5** could be recycled by column chromatography and reused in olefin metathesis. Moreover, these complexes catalyze olefin metathesis with greater propagating rates than **1**. The bidentate nature of the non-phosphane ligands is particularly attractive in terms of catalyst regeneration since this should be entropically favored. We expected that attaching **5** to a polymeric support would give a recyclable and reusable olefin metathesis catalyst. We envisioned that it would be advantageous to use a soluble polymer^[12] such as poly(ethylene glycol) as the support since this would allow the catalysis reaction to be carried out under standard homogeneous conditions and would enable the simple recovery of the catalyst by precipitation and filtration. However, it was not clear whether the backbone of the polymer would compete with substrate binding by chelating through its multiple ether functionalities.^[13]

Starting from the aldehyde **6**, the functionalized styrene **8** was prepared in a straightforward manner (Scheme 2). This material was then coupled to poly(ethylene glycol) monomethyl ether (MeO-PEG) derivatized with a succinate ester

[*] Prof. Dr. Q. Yao
 Department of Chemistry and Biochemistry
 The Michael Faraday Laboratories
 Northern Illinois University
 DeKalb, IL 60115-2862 (USA)
 Fax: (+1) 815-753-4802
 E-mail: qyao@niu.edu

[**] Financial support by Northern Illinois University is acknowledged.
 Supporting information for this article is available on the WWW under <http://www.wiley-vch.de/home/angewandte/> or from the author.



Scheme 2. Preparation of a soluble polymer PEG-bound ruthenium carbene complex: a) Et_3N , Piv-Cl, DMF, 0°C then RT, 6 h, H_2O , 65%; b) $i\text{PrI}$, Cs_2CO_3 (cat.)/ K_2CO_3 , DMF, RT, 10 h, H_2O , 93%; c) $\text{Ph}_3(\text{CH}_3)\text{P}^+\text{Br}^-$, LHMDS, THF, 0°C then RT, 12 h, Et_2O , 75%; d) $t\text{BuO}^-\text{Na}^+$, MeOH, RT, 4 h, NH_4Cl , 99%; e) DCC, DMAP, CH_2Cl_2 reflux 12 h, 0°C Et_2O . Piv-Cl = trimethylacetyl chloride, LHMDS = lithium bis(trimethylsilyl)amide, DCC = 1,3-dicyclohexylcarbodiimide, DMAP = 4-dimethylaminopyridine, Cy = cyclohexyl. Full experimental details are available in the Supporting Information.

linker **9**^[14] to give **10** (Scheme 2). The loading of the styrene moiety in **10** was estimated by 500 MHz ^1H NMR spectroscopy to be about 0.1 mmol g^{-1} .^[15] Following Hoveyda's method^[11] for the synthesis of **5** from **1b**, the polymer-bound catalyst **11** (Scheme 2) was prepared as a brownish powder by stirring an equimolar mixture of **10** and **1b** in refluxing CH_2Cl_2 followed by precipitation with dry diethyl ether.

When a solution of the diene **12** in CH_2Cl_2 was treated with 5 mol % of **11** for 2 h at reflux, **12** was converted cleanly to the cyclic olefin **13** in greater than 98 % conversion, as determined by 500 MHz ^1H NMR spectroscopy (Table 1). Importantly,

Table 1. Recycling and reuse of polymer-bound Ru complex **11** in the ring-closing metathesis of diene **12**.

cycle	1	2	3	4	5	6	7	8
conversion [%]	98	97.5	96.5	95	95	93	93	92

the catalyst is readily recovered^[16] by precipitation with diethyl ether and, as shown in Table 1, the recycled material was used for the next cycle of metathesis, and gave a similarly high conversion. After up to eight runs of recycling and reuse, the catalyst remains active with only very slight loss of activity.

Table 2 lists the results of experiments with other substrates leading to the formation of different carbo- and heterocycles. Ring-closing metathesis of **14** goes cleanly, with high conversion, under conditions similar to those for the metathesis of **12** (cycles 1–3). Use of a reduced amount (2.5 mol %) of

Table 2. Ring-closing metathesis catalyzed by polymer-bound Ru complex **11** in CH_2Cl_2 .

Cycle	Substrate [conc]	Product	Catalyst [mol %]	Conditions	Conversion [%]
		14			
		15			
1	(0.05 M)		5	reflux, 2 h	96
2	(0.05 M)		5	reflux, 2 h	94
3	(0.05 M)		5	reflux, 2 h	92
4	(0.1 M)		2.5	reflux, 3.5 h	96.5
5	(0.1 M)		2.5	RT, 12 h	> 99
		16			
		17			
6	(0.1 M)		2.5	reflux, 2 h	90
		18			
		19			
1	(0.1 M)		2.5	reflux, 2 h	96
		20			
		21			
2	(0.1 M)		2.5	reflux, 3 h	> 98

catalyst relative to the substrate in CH_2Cl_2 led to high conversion at elevated or room temperatures (cycles 4 and 5, respectively). The recycled catalyst from the reaction of **14** was subsequently used for the metathesis of a second substrate **16** (cycle 6). The crude product from **16** consists of only the cyclized product **17** and unreacted **16**, devoid of any contamination from the previous reaction. It should be noted that sequential use of the same batch of a catalyst in two different reactions is rarely possible, thus being able to do this represents a great practical advantage. The same strategy was applied to the metatheses of **18** and **20**. After the catalyst was used for the reaction of substrate **18**, the recycled catalyst was employed to catalyze the metathesis of the silicon-tethered^[17] diene **20**. With 2.5 mol % of the recycled catalyst, **20** was converted to the cyclic silyl ether **21** in 98 % conversion and 94 % yield.

While the data presented in Tables 1 and 2 show that the PEG-bound ruthenium carbene complex exhibits remarkable recyclability and can be repeatedly reused in the metathesis of various diene substrates, a slight decrease in catalytic activity is also evident. We attribute this to the slow but competing decomposition of the propagating species, presumably a monophosphane-based Ru carbene,^[11] $[\text{Cy}_3\text{PCL}_2\text{Ru}=\text{CHR}]$ ($\text{R}=\text{H}$ or Me). A mechanistic study conducted by Grubbs and Ulman^[18] has established that decomposition of ruthenium carbene based metathesis catalysts follows a bimolecular pathway involving a monophosphane ruthenium species, formed after the dissociation of one phosphane ligand.

In summary, we have developed a stable and readily recyclable, soluble, polymer-bound catalyst for olefin meta-

thesis. In addition to the advantages discussed above, it is envisaged that this catalyst will find application in cases where the limited solubility of a substrate in organic solvents necessitates that the metathesis be carried out in aqueous media, a topic of current interest.^[19] Full experimental details can be found in the Supporting Information.

Received: February 16, 2000

Revised: May 17, 2000 [Z14719]

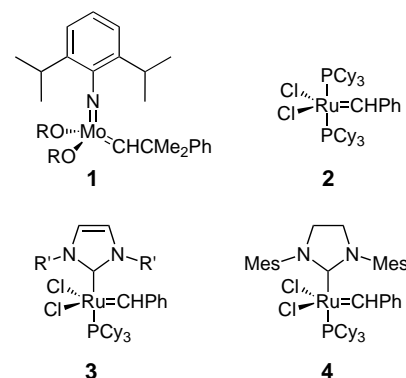
- [1] B. M. Trost, *Angew. Chem.* **1995**, *107*, 285–307; *Angew. Chem. Int. Ed. Engl.* **1995**, *34*, 259–281.
- [2] Selected recent reviews: a) R. H. Grubbs, S. J. Miller, G. C. Fu, *Acc. Chem. Res.* **1995**, *28*, 446–452; b) M. Schuster, S. Blechert, *Angew. Chem.* **1997**, *109*, 2124–2145; *Angew. Chem. Int. Ed. Engl.* **1997**, *36*, 2036–2056; c) S. K. Armstrong, *J. Chem. Soc. Perkin Trans. 1* **1998**, 371–388; d) R. H. Grubbs, S. Chang, *Tetrahedron* **1998**, *54*, 4413–4445; e) A. F. Noels, A. Demonceau, *J. Phys. Org. Chem.* **1998**, *11*, 602–609; f) U. K. Pandit, H. S. Overleef, B. C. Borer, H. Bieräugel, *Eur. J. Org. Chem.* **1999**, 959–968; g) A. J. Phillips, A. D. Abell, *Aldrichimica Acta* **1999**, *32*, 75–90; h) A. Fürstner, *Angew. Chem.* **2000**, *112*, 3140–3172; *Angew. Chem. Int. Ed.* **2000**, *39*, 3012–3043.
- [3] R. R. Schrock, J. S. Murdzek, G. C. Bazan, J. Robbins, M. DiMare, M. O'Regan, *J. Am. Chem. Soc.* **1990**, *112*, 3875–3886.
- [4] S. T. Nguyen, R. H. Grubbs, J. W. Ziller, *J. Am. Chem. Soc.* **1993**, *115*, 9858–9859.
- [5] a) P. Schwab, M. B. France, J. W. Ziller, R. H. Grubbs, *Angew. Chem.* **1995**, *107*, 2179–2181; *Angew. Chem. Int. Ed. Engl.* **1995**, *34*, 2039–2041; b) P. Schwab, R. H. Grubbs, J. W. Ziller, *J. Am. Chem. Soc.* **1996**, *118*, 100–110.
- [6] For latest additions to well-defined Ru-based alkylidene catalysts, see: a) M. Scholl, T. M. Trnka, J. P. Morgan, R. H. Grubbs, *Tetrahedron Lett.* **1999**, *40*, 2247–2250; b) M. Scholl, S. Ding, C. W. Lee, R. H. Grubbs, *Org. Lett.* **1999**, *1*, 953–956; c) J. Huang, E. D. Stevens, S. P. Nolan, J. L. Petersen, *J. Am. Chem. Soc.* **1999**, *121*, 2674–2678; d) L. Jafarpour, J. Huang, E. D. Stevens, S. P. Nolan, *Organometallics* **1999**, *18*, 3760–3763; e) L. Jafarpour, H.-J. Schanz, E. D. Stevens, S. P. Nolan, *Organometallics* **1999**, *18*, 5416–5419; f) T. Weskamp, W. C. Schattenmann, M. Spiegler, W. A. Herrmann, *Angew. Chem.* **1998**, *110*, 2631–2633; *Angew. Chem. Int. Ed.* **1998**, *37*, 2490–2493; see also a corrigendum: *Angew. Chem.* **1999**, *111*, 277; *Angew. Chem. Int. Ed.* **1999**, *38*, 262; g) T. Weskamp, F. J. Kohl, W. Hieringer, D. Gleich, W. A. Herrmann, *Angew. Chem.* **1999**, *111*, 2573–2576; *Angew. Chem. Int. Ed.* **1999**, *38*, 2416–2419; h) S. M. Hansen, M. A. Q. Volland, F. Rominger, F. Eisenträger, P. Hofmann, *Angew. Chem.* **1999**, *111*, 1360–1364; *Angew. Chem. Int. Ed.* **1999**, *38*, 1273–1276; i) A. Fürstner, M. Picquet, C. Bruneau, P. H. Dixneuf, *Chem. Commun.* **1998**, 1315–1316.
- [7] S. T. Nguyen, R. H. Grubbs, *J. Organomet. Chem.* **1995**, *497*, 195–200.
- [8] M. Ahmed, A. G. M. Barrett, D. C. Braddock, S. M. Cramp, P. A. Procopiou, *Tetrahedron Lett.* **1999**, *40*, 8657–8662.
- [9] The use of supercritical CO₂ as reaction media for olefin metathesis may have the potential to facilitate catalyst separation and reuse. See: A. Fürstner, D. Koch, K. Langemann, W. Leitner, C. Six, *Angew. Chem.* **1997**, *109*, 2562–2565; *Angew. Chem. Int. Ed. Engl.* **1997**, *36*, 2466–2469.
- [10] J. A. Tallarico, P. J. Bonitatebus, M. L. Snapper, *J. Am. Chem. Soc.* **1997**, *119*, 7157–7158.
- [11] J. S. Kingsbury, J. P. A. Harrity, P. J. Bonitatebus, A. H. Hoveyda, *J. Am. Chem. Soc.* **1999**, *121*, 791–799.
- [12] For leading reviews on the use of soluble polymer-supported reagents and catalysts, see: a) D. J. Gravert, K. Janda, *Chem. Rev.* **1997**, *97*, 489–510; b) C. W. Harwig, D. J. Gravert, K. Janda, *Chemtracts: Org. Chem.* **1999**, *12*, 1–26; c) P. Wentworth, K. Janda, *Chem. Commun.* **1999**, 1917–1924.
- [13] Coordinating solvents such as diethyl ether, dioxane, or THF are rarely used in olefin metathesis reactions, and catalyst **1b** is inactive in polar, aprotic solvents such as DMSO and DMF, which also hints at this potentially detrimental effect.

- [14] S. P. Douglas, D. M. Whitfield, J. J. Krepinsky, *J. Am. Chem. Soc.* **1991**, *113*, 5095–5096.
- [15] In contrast to the many reported couplings of amines and alcohols with an acid functionality on PEG, coupling of phenol **8** with the succinic acid linker of **9** was found to be quite slow. Under optimized conditions with eight equivalents of DCC four equivalents of **8** and 0.4 equivalents of DMAP in refluxing CH₂Cl₂, **10** was obtained with 0.1 mmol g⁻¹ loading, corresponding to 50% conversion of the free acid groups in **9**.
- [16] All operations including evaporation of the reaction mixture, precipitation, filtration and washing with reagent grade diethyl ether were carried out in vessels open to the air.
- [17] For examples of silicon-tethered ring-closing metathesis, see: a) S. Chang, R. H. Grubbs, *Tetrahedron Lett.* **1997**, *38*, 4757–4760; b) J. H. Cassidy, S. P. Marsden, G. Stemp, *Synlett* **1997**, 1411–1413; c) P. A. Evans, V. S. Murthy, *J. Org. Chem.* **1998**, *63*, 6768–6769.
- [18] M. Ulman, R. H. Grubbs, *J. Org. Chem.* **1999**, *64*, 7202–7207.
- [19] T. A. Kirkland, D. M. Lynn, R. H. Grubbs, *J. Org. Chem.* **1998**, *63*, 9904–9909.

Synthesis and Application of a Permanently Immobilized Olefin-Metathesis Catalyst**

Stephan C. Schürer, Simon Gessler, Nicole Buschmann, and Siegfried Blechert*

Olefin metathesis has made a tremendous impact in synthetic organic chemistry^[1] as a result of the availability of well-defined catalysts like **1**^[2] and **2**^[3] (Scheme 1). The potential of ring-closing metathesis (RCM) for the construction of small, medium, and large rings has fully been recognized^[1] and



Scheme 1. Metathesis catalysts. R = CMe(CF₃)₂; R' = *i*Pr, Cy, Mes; Cy = cyclohexyl; Mes = 2,4,6-Me₃C₆H₂.

[*] Prof. S. Blechert, S. C. Schürer, S. Gessler, N. Buschmann
Institut für Organische Chemie
Technische Universität Berlin
Sekt. C3, Strasse des 17. Juni 135, 10623 Berlin (Germany)
Fax: (+49) 30-314-23619
E-mail: Blechert@chem.tu-berlin.de

[**] This work was supported by the Fonds der Chemische Industrie. S.G. and N.B. would like to thank the Graduiertenkolleg "Synthetische, mechanistische und reaktionstechnische Aspekte von Metallkatalysatoren" for their Ph.D. grants.

several applications of catalysts **1** and **2** to cross metathesis,^[4] ring-opening metathesis,^[5] and rearrangement reactions^[6] have been published.

Catalyst **2** in particular enjoys high popularity because of its stability and tolerance towards functional groups. Nevertheless disadvantages remain associated with the use of homogeneous catalysts. After completion of a metathesis reaction the removal of the colored ruthenium complexes from the reaction products is often problematic and residual ruthenium may cause problems such as olefin isomerization, decomposition of the products over time, and increased toxicity of the final material. In addition to the separation of products and catalyst,^[7] the recovery of the ruthenium catalyst has become a subject of interest.^[8] Immobilization of a metathesis catalyst on a solid support would allow the catalyst to be separated from the reaction products simply and efficiently by filtration. Grubbs and Nguyen introduced phosphane ligands to attach ruthenium catalysts onto a polystyrene matrix, these systems have been used in living polymerization.^[9] Barrett and co-workers have reported a “boomerang” catalyst, which was obtained by the reaction of **2** with vinyl polystyrene.^[10] This precatalyst becomes soluble during the course of the reaction and can be recaptured by the polymer.

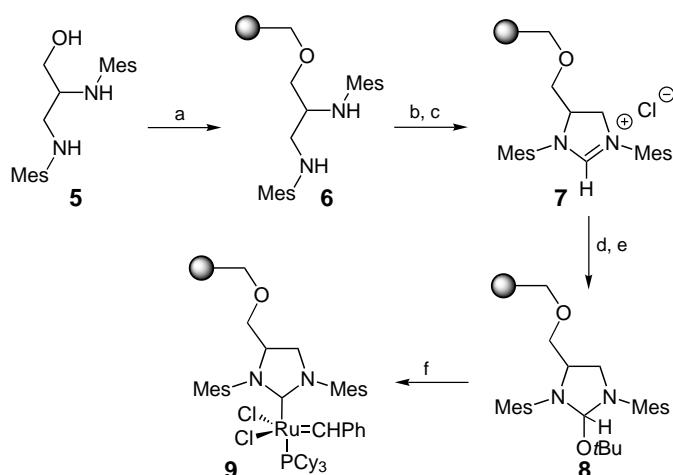
The need for further developments in this area led us to try an alternative approach to efficiently immobilize a metathesis catalyst, which is described herein. The potential of this catalyst is demonstrated by its application to different types of metathesis reactions.

Recently, new ruthenium-based alkylidene catalysts **3**^[11] and **4**^[12] bearing N-heterocyclic carbene (NHC) ligands have been reported (Scheme 1). These catalysts show an increased metathesis activity similar to that of **1** but have also retained the remarkable air and water stability of **2**.^[12, 13]

The N-heterocyclic carbene ligands are stronger Lewis bases than the phosphane ligands, thus, the dissociation of a phosphane ligand in **3** or **4** has been proposed as initial step in the mechanism of olefin metathesis, which leaves the NHC ligand bound to the ruthenium center.^[11a] The saturated 4,5-dihydroimidazole carbene (in complex **4**) shows even higher Lewis basicity than the imidazole carbene (in complex **3**). Therefore a permanently immobilized and highly active metathesis catalyst should result if **4** was attached to a polymeric support by its N-heterocyclic carbene ligand.

Such a support-bound ruthenium complex should be accessible from **2** by ligand exchange, similar to the synthesis of the soluble catalyst **4**.^[12a] This approach requires the synthesis of a suitably immobilized ligand precursor, which could be obtained from the diamine **5** (see Scheme 2). Compound **5** can be prepared from 2,3-dibromo-1-propanol and 2,4,6-trimethylaniline.^[14] After deprotonation of the hydroxy group compound **5** was attached to Merrifield polystyrene (1% divinyl benzene (DVB)) by an ether linkage to quantitatively yield **6** (Scheme 2) as confirmed by elemental analysis. Compound **6** was then cyclized under acidic conditions, and anion exchange yielded the support-bound 3,4-dimesityl-4,5-dihydroimidazolium chloride **7**.

After treatment with TMSOTf/lutidine (TMSOTf = Me₃-SiOSO₂CF₃) **7** was converted into the corresponding 2-*tert*-



Scheme 2. Synthesis of support-bound catalyst **9**. a) 1.0 equiv KO^tBu, DMF, RT, 20 min, then 0.5 equiv Merrifield-polystyrene (1% DVB), TBAI, DMF, 60 °C, 12 h; b) HC(OMe)₃, HCO₂H, toluene, 100 °C, 100 mbar, 15 h; c) 0.1 M HCl in THF, RT, 5 min; d) TMSOTf, 2,6-lutidine, CH₂Cl₂, RT, 30 min; e) KO^tBu, THF, RT, 60 min; f) 1.5 equiv **2**, toluene, 70–80 °C, 1 h. TBAI = tetrabutylammonium iodide.

butoxy-4,5-dihydroimidazoline **8** (Scheme 2), obtained as an orange resin. 2-Alkoxy-imidazolidines undergo α -elimination at elevated temperatures and can thus be regarded as protected carbenes.^[15] Therefore, in analogy to the synthesis of the soluble complex **4**,^[12a] **8** was deprotected in situ in the presence of **2**, yielding the desired support-bound 1,3-dimesityl-4,5-dihydroimidazolin-2-ylidene ruthenium complex **9** as a pinkish brown material. This four-step synthesis from **5** is particularly simple, because all the steps are performed on the solid support. Polymer-bound catalyst **9** is obtained with a loading level between 0.14 and 0.40 mmol g⁻¹ (determined by elemental analysis and mass increase) depending on the initial loading level of the Merrifield resin employed (0.50 to 0.90 mmol g⁻¹).

As a first test diallyl malonic acid diethyl ester was cyclized using 5 mol% of catalyst **9**. At 45 °C in CD₂Cl₂ the RCM product was quantitatively formed after 40 min and could be isolated as a colorless oil after filtration and concentration. With the soluble catalyst **4** this reaction is complete in less than 5 min, which clearly suggests that fast metathesis reactions are diffusion controlled when the immobilized catalyst **9** is employed.

Various metathesis reactions have then been performed by using 5 mol% of support-bound catalyst **9** (Table 1). Substrate **10** was cleanly cyclized to give **11** as a colorless oil and accordingly the pyrroline derivative **13** was obtained from **12**. The RCM of **14** yielded the seven-membered heterocycle **15** as colorless crystals without need for further purification and the macrolactone **17** was obtained in 80% yield from acyclic ester **16**. Apart from RCM we tested the capability of **9** to catalyze other types of metathesis. For example, triolefin **18** could be converted cleanly into **19** by double ring-closure using 5 mol% of catalyst **9** (entry 5). The enantiomerically pure diene **20** rearranged quantitatively in the presence of **9** and ethylene into **21**; upon concentration of the crude filtrate **21** crystallized immediately as a colorless solid.

Table 1. Results of metathesis reactions utilizing the immobilized catalyst **9**^[a].

Entry	Substrate	Product	Yield [%]
1			100
2			90
3			100
4			80
5			100
6 ^[b]			100
7			100
8			80

[a] All reactions have been performed under standard conditions employing 5 mol % of **9** at 45 °C in CH₂Cl₂ for 12–18 h. [b] Reaction has been performed in the presence of ethylene. E = ester group, Tr = triphenylmethyl, Ts = *p*-toluenesulfonyl, Ns = *p*-nitrobenzylsulfonyl, TBS = *tert*-butyldimethylsilyl.

The catalyst **9** also catalyzes cross-metathesis reactions as demonstrated by the atom economical yne–ene metathesis^[16] of the acetylene **22** with the allyl trimethylsilane (**23**) to yield the 1,3-disubstituted butadiene **24** (entry 7). After complete consumption of **22** compound **24** was isolated as a mixture of isomers (¹H NMR spectroscopy) by filtration and removal of the excess volatile allyl silane **23** under vacuum. The increased activity of catalyst **9** compared to **2** is demonstrated by the yne–ene cross metathesis of the sterically hindered cyclohexyl acetylene **25** and the allyl silane **23** (entry 8). In this reaction no products are obtained with **2**, whereas using **9**, the diene **26** was obtained in high yield as a colorless oil after removal of the excess starting material under vacuum.

The practical simplicity of product isolation when the polymer-supported catalyst **9** is used is clearly evident. Products of high purity (as determined by NMR spectroscopy) were obtained after filtration as the only purification step. This ease of isolation should allow automatization and

makes catalyst **9** particularly suited to combinatorial applications.

As well as studying different types of metathesis reactions we were also interested in the potential recycling of catalyst **9**. For this purpose we varied the reaction conditions (reaction time, concentration, temperature) and the loading level. As a first substrate we chose **14** and obtained varying results. In the best case catalyst **9**, with a loading level of 0.14 mmol g^{−1}, gave the complete cyclization of **14** in four runs. The substrate (**14**; 0.025 M, CH₂Cl₂ solution) was refluxed together with 5 mol % of **9**, which was recovered by filtration under inert conditions. The reaction times for complete cyclization increased from 1.5 h in the first run, to 4 h in the second, 12 h in the third and two days in the fourth run. Investigations of the structure of the catalyst **9** (benzylidene or methylidene complex) are in progress. Detailed studies regarding further optimization of the recycling potential and stability of **9** and similar catalysts are also in progress.

Experimental Section

9: Polymer **6** (2.0 g; loading level 0.50–0.70 mmol g^{−1}) in a mixture of toluene (40 mL), trimethylorthoformate (10 mL, 91 mmol), and formic acid (0.5 mL, 13 mmol) was heated to 100 °C under vacuum (100 mbar) for 15 h and shaken. The polymer was isolated by filtration, washed (2 × CH₂Cl₂, MeOH, THF, 3 × 0.1 M HCl in THF, 3 × THF, 3 × MeOH, 3 × CH₂Cl₂, 2 × MeOH, 2 × CH₂Cl₂, 2 × pentane), and dried. The IR spectrum indicated complete cyclization. The resulting polymer **7** was then shaken for 30 min in a solution containing TMSOTf (0.2 M) and 2,6-lutidine (0.3 M) in CH₂Cl₂ (30 mL) followed by filtration and washing (3 × CH₂Cl₂, 2 × pentane, 3 × CH₂Cl₂, 2 × pentane). The above capping step was repeated. The polymer was then suspended in THF (1 mL for 150 mg of support) and KO^tBu (3 mL; 1 M in THF (for 150 mg of support)) was added and the mixture slowly shaken for 1 h under exclusion of moisture and air. After filtration and washing (3 × THF) toluene (1 mL) and **2** (1.5 equivalents with respect to polymer **7**) were added and the suspension was then heated to 70–80 °C for 1 h. The polymer was then collected by filtration, washed (5 × toluene, 3 × CH₂Cl₂, 2 × MeOH, 2 × CH₂Cl₂, 2 × MeOH, 2 × CH₂Cl₂, 3 × pentane), and dried to yield **9** as a pinkish brown resin.

³¹P NMR (202.5 MHz, CH₂Cl₂/C₆D₆): δ = 28.4 (br); IR (KBr pellet): ν̄ = 1264 (br, m) cm^{−1}.

Metathesis reactions utilizing **9**: The substrate was dissolved in CH₂Cl₂ and 5 mol % of catalyst **9** was added. The suspension was heated to 45 °C for 12–18 h. The product was obtained as a colorless oil or solid after filtration and concentration. New compounds have been fully characterized (¹H and ¹³C NMR, IR spectroscopy and high-resolution MS).

Received: April 6, 2000
Revised: July 7, 2000 [Z14946]

- [1] For recent reviews see: a) R. H. Grubbs, S. Chang, *Tetrahedron* **1998**, 54, 4413–4450; b) A. Fürstner, *Top. Organomet. Chem.* **1998**, 1, 37–72; c) M. Schuster, S. Blechert, *Angew. Chem.* **1997**, 109, 2124–2144; *Angew. Chem. Int. Ed. Engl.* **1997**, 36, 2036–2056; d) A. Fürstner, *Angew. Chem.* **2000**, 112, 3140–3172; *Angew. Chem. Int. Ed.* **2000**, 39, 3012–3043.
- [2] Selected reference: G. C. Baznan, J. H. Oskam, H. N. Cho, L. Y. Park, R. R. Schrock, *J. Am. Chem. Soc.* **1991**, 113, 6899–6907.
- [3] Selected reference: P. Schwab, R. H. Grubbs, J. W. Ziller, *J. Am. Chem. Soc.* **1996**, 118, 100–110.
- [4] For recent examples see: a) O. Brümmer, A. Rückert, S. Blechert, *Chem. Eur. J.* **1997**, 3, 441–446; b) R. Roy, R. Dominique, S. K. Das, *J. Org. Chem.* **1999**, 64, 5408–5412; c) H. E. Blackwell, D. J. O'Leary, A. K. Chatterjee, R. A. Washenfelder, D. A. Bussmann, R. H. Grubbs, *J. Am. Chem. Soc.* **2000**, 122, 58–71.

- [5] For recent examples see: a) M. F. Schneider, N. Lucas, J. Velder, *Angew. Chem.* **1997**, *109*, 257–259; *Angew. Chem. Int. Ed. Engl.* **1997**, *36*, 257–259; b) J. A. Tallarico, P. J. Bonitatebus, Jr., M. L. Snapper, *J. Am. Chem. Soc.* **1997**, *119*, 7157–7158; c) R. Stragies, S. Blechert, *Synlett* **1998**, 169–170.
- [6] For recent references see: a) R. Stragies, S. Blechert, *Tetrahedron* **1999**, *55*, 8179–8188; b) J. A. Adams, J. G. Ford, P. J. Stamatou, A. H. Hoveyda, *J. Org. Chem.* **1999**, *64*, 9690–9696.
- [7] a) H. D. Maynard, R. H. Grubbs, *Tetrahedron Lett.* **1999**, *40*, 4137–4140; b) L. A. Paquette, J. D. Schloss, I. Efremov, F. Fabris, F. Gallou, J. Méndez-Andino, J. Yang, *Org. Lett.* **2000**, *2*, 1259–1261.
- [8] J. S. Kingsbury, J. P. Harrity, P. J. Bonitatebus, Jr., A. H. Hoveyda, *J. Am. Chem. Soc.* **1999**, *121*, 791–799.
- [9] S. T. Nguyen, R. H. Grubbs, *J. Organomet. Chem.* **1995**, *497*, 195–200.
- [10] M. Ahmed, A. G. M. Barrett, D. C. Braddock, S. M. Cramp, P. A. Procopiou, *Tetrahedron Lett.* **1999**, *40*, 8657–8662.
- [11] a) T. Weskamp, F. J. Kohl, W. Hieringer, D. Gleich, W. A. Herrmann, *Angew. Chem.* **1999**, *111*, 2573–2576; *Angew. Chem. Int. Ed.* **1999**, *38*, 2416–2419; b) J. Huang, E. D. Stevens, S. P. Nolan, J. L. Peterson, *J. Am. Chem. Soc.* **1999**, *121*, 2674–2678.
- [12] a) M. Scholl, S. Ding, C. Woo Lee, R. H. Grubbs, *Org. Lett.* **1999**, *1*, 953–956; b) A. K. Chatterjee, R. H. Grubbs, *Org. Lett.* **1999**, *1*, 1751–1753.
- [13] a) M. Scholl, T. M. Trnka, J. P. Morgan, R. H. Grubbs, *Tetrahedron Lett.* **1999**, *40*, 2247–2250; b) L. Ackermann, A. Fürstner, T. Weskamp, F. J. Kohl, W. A. Herrmann, *Tetrahedron Lett.* **1999**, *40*, 4787–4790; c) A. Fürstner, O. R. Thiel, L. Ackermann, H.-J. Schanz, S. P. Nolan, *J. Org. Chem.* **2000**, *65*, 2204–2207.
- [14] L. Lajos, Z. Zubovics, M. Kurti, I. Schafer (Egyt Gyo. Gyar), DE-B 2916140, **1979** [*Chem. Abstr.* **1980**, *92*, 181226w].
- [15] B. Lachmann, H.-W. Wanzlick, *Justus Liebigs Ann. Chem.* **1969**, 729, 27–32.
- [16] R. Stragies, M. Schuster, S. Blechert, *Angew. Chem.* **1997**, *109*, 2628–2630; *Angew. Chem. Int. Ed. Engl.* **1997**, *36*, 2518–2520.

Speciation in Solution: Silicate Oligomers in Aqueous Solutions Detected by Mass Spectrometry**

Patrick Bussian, Frank Sobott, Bernhard Brutschy, Wolfgang Schrader, and Ferdi Schüth*

Nucleation of solids from solution is one of the most challenging problems in solid-state chemistry. For a better understanding of processes taking place during crystallization, detailed knowledge about the species present in solution, such as particle size distribution and morphology, is mandatory to control the final properties of the solid.^[1] However, only very

few techniques are suited for such analyses, such as NMR spectroscopy for selected nuclei. Mass spectrometry could be a very versatile technique, since there are in principle no limitations with respect to the elements which can be analyzed. However, surprisingly only a few publications are available, in which mass spectrometry has been used for the analysis of speciation of crystallite precursors in solution. Most of the work reported to date has been limited to the investigation of partially hydrolyzed alkoxide solutions with predominantly alcohol as the solvent.^[2] Herein we present for the first time data which show that oligomeric species in aqueous solutions can be reliably analyzed by using mass spectrometry. Electrospray ionization mass spectrometry (ESI-MS) has been used to study oligomer distribution in silicate solutions, since in this system the species can be independently analyzed with ²⁹Si NMR spectroscopy. However, in addition ESI-MS allows one to obtain information on oligomers and to address questions such as charge and degrees of hydrolysis of the species present in solution. Besides the availability of ²⁹Si NMR spectroscopy as an independent technique for analysis, the silicate system was chosen because of the importance of oligomeric species in zeolite synthesis,^[3] sol–gel chemistry,^[4] and silsesquioxane chemistry.^[2c, 5]

Earlier studies showed the distribution of silicate oligomers depends on the alkyl chain length of the added tetraalkylammonium counterion.^[3] Silicate solutions containing tetramethylammonium hydroxide (TMAOH) stabilize the cubooctameric double-four-membered ring (D4R), whereas in the presence of tetraethylammonium hydroxide (TEAOH) the formation of the double–three-membered ring (D3R) is preferred. Figure 1 depicts a typical ²⁹Si NMR spectrum and the corresponding negative-ion ESI mass spectrum for an aqueous/methanolic TMAOH solution containing dissolved silica. The ²⁹Si NMR spectrum indicates the high amount of D4R species (88.3%), but there are also D3R (3.8%), monomeric (3.0%), dimeric (1.2%), linear and cyclic trimeric (1.6%), and different tetrameric (1.5%) species present. The species detected in the ²⁹Si NMR are found in the ESI mass spectrum as well. The relative intensities of the peaks attributable to these species are in qualitative agreement for the two techniques. However, the intensity distribution in ESI-MS is somewhat dependent on the cone voltage and type of mass spectrometer used (see below), thus, full quantification is difficult. From the simple singly charged D4R oligomer at *m/z* 551 a series of peaks with a spacing of $\Delta(m/z)$ 73 to higher masses is observed. These can be assigned to species of higher charged cubic octamers that are clustered to TMA⁺ ions. The series of peaks extends up to *m/z* 770, corresponding to a fourfold negatively charged D4R silicate clustered with three TMA⁺ ions, while the doubly charged species clustered with one TMA⁺ ion and the triply charged species clustered with two tetramethylammonium cations can be seen at *m/z* 624 and 697, respectively.

A second series of peaks starts at *m/z* 551. The following peaks at *m/z* 565, 579, and 593 shows a mass spacing of $\Delta(m/z)$ 14, which indicates a substitution of up to three hydroxyl groups at the silicon atoms by methoxy groups, which would be expected for highly alkaline solutions containing relatively large amounts of methanol. However, it can not be excluded

[*] Prof. Dr. F. Schüth, Dipl.-Chem. P. Bussian, Dr. W. Schrader
Max-Planck-Institut für Kohlenforschung
Kaiser-Wilhelm-Platz 1, 45470 Mülheim/Ruhr (Germany)
Fax: (+49) 208-306-2995
E-mail: schueth@mpi-muelheim.mpg.de
Dipl.-Chem. F. Sobott, Prof. Dr. B. Brutschy
Institut für Physikalische und Theoretische Chemie
Marie-Curie-Strasse 11, 60439 Frankfurt am Main (Germany)

[**] We thank I. Prieß (Frankfurt) and H. W. Klein (Mülheim) for recording the mass spectra, M. T. Reetz for access to his electrospray ionization (ESI) mass spectrometer, and P. Philipps for recording the NMR spectra.

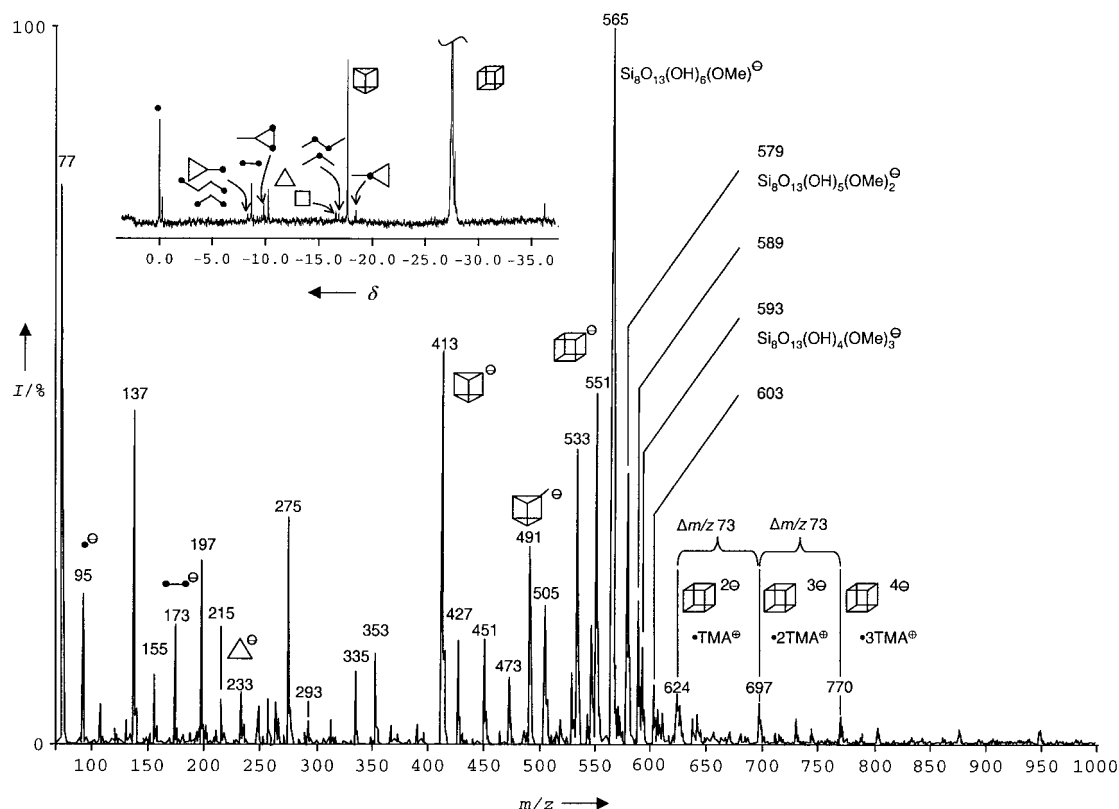


Figure 1. Negative-ion ESI mass spectrum and ^{29}Si NMR spectrum of a silicate solution containing tetramethylammonium (TMA) ions in which the cubic octamer is the predominant species. In the ^{29}Si NMR spectrum, the full intensity of the signal for the cubic octamer is much higher and the scale has been changed to show the peaks of the other oligomers.

that these methoxylated species are generated during the desorption process or by ligand exchange in the gas phase. The D3R species is also detectable. The signal at m/z 413 belongs to the singly charged species, whereas the signal at m/z 491 would appear to belong to a singly charged D3R species that has another $\text{Si}(\text{OH})_3$ unit linked to its framework. Again, the analogous species in which a hydroxy group is substituted by a methoxy group are present (m/z 427 and 505). In contrast to the ^{29}Si NMR spectrum, only the dimer at m/z 173 can be detected as a fully hydroxylated linear species. The trimer and the tetramer do not appear in the mass spectrum. Instead, signals are detected that on first inspection would not seem to belong to siliceous species. The appearance of these peaks can be explained by the dehydroxylation of these species in the mass spectrometer (Scheme 1). The condensation of two hydroxy groups with the elimination of water leads to the formation of the oxo species. The tendency of these species not to appear as the fully hydroxylated moieties increases with increasing silicate chain length.

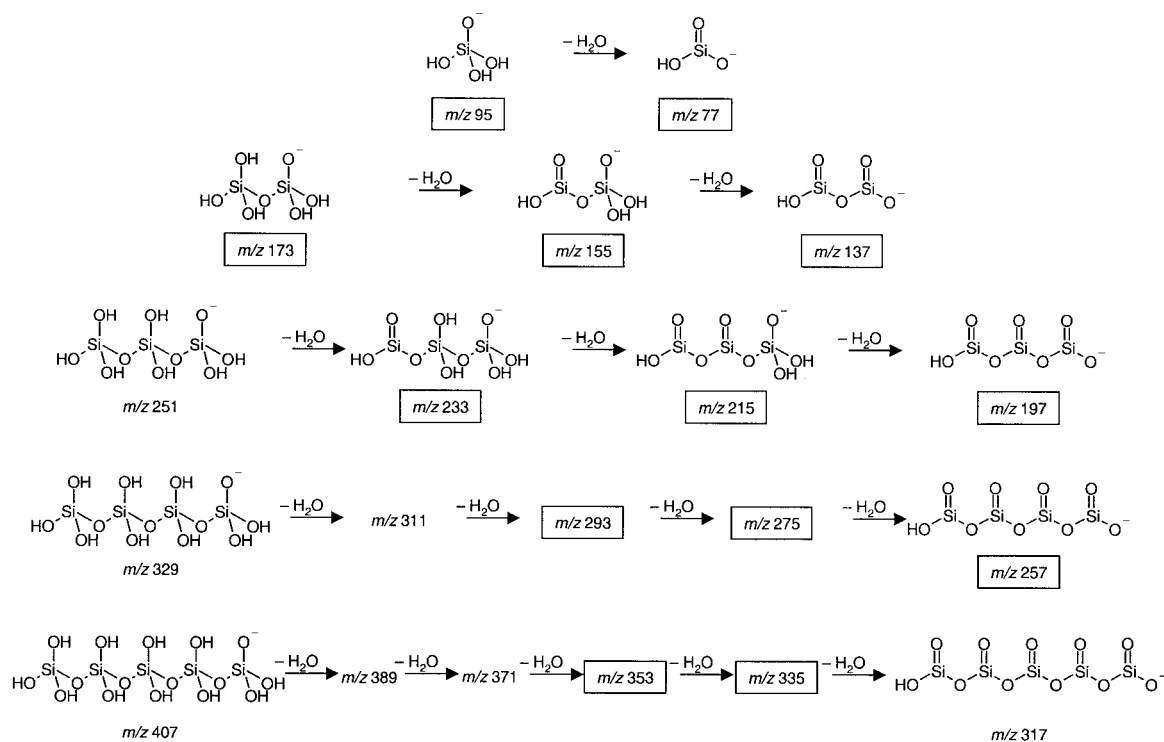
For comparison, Figure 2 shows the mass spectrum and ^{29}Si NMR spectrum of an ethanolic/aqueous silicate solution containing tetraethylammonium ions. The ^{29}Si NMR spectrum confirms the distribution of anions evident in the mass spectrum. As expected, no signals at $m/z > 500$ were detected, proving the absence of D4R ions. Again most of the partially dehydroxylated linear moieties are present.

Finally, Figure 3 shows the same system with a silicate concentration which is 5.6-fold lower. This results in the disappearance of the higher condensed species like the D3R

ion, as can easily be seen in the ^{29}Si NMR spectrum. Only the monomeric, dimeric, and cyclic trimeric species are stable in this diluted silicate solution. In the corresponding mass spectrum only the monomer (m/z 95 and 77) and the dimer (m/z 173) can be reliably identified. All other species present seem to be unstable intermediates, whose detection is dependent upon the cone-skimmer (declustering) potential.

In order to check the influence of sample injection and ion source geometry, spectra were also recorded in a second ESI-MS system (HP 5989B) which is rather optimized for the detection of higher masses. In this system, species with $m/z < 400$ can be less reliably detected. Figure 4 shows the spectrum which corresponds to the one in Figure 1 measured with the other spectrometer. The signal-to-noise ratio is much lower than in the mass spectrum shown in Figure 1. Thus, only the main species such as the singly charged D4R (m/z 551) and the following series of peaks with a spacing of $\Delta(m/z)$ 14 to higher mass is observed, indicating the exchange of hydroxy by methoxy groups. The reasons for these differences will be discussed in a forthcoming paper, in which the performance of several different mass spectrometers will be compared.

The results presented show that ESI-MS is a powerful tool for the analysis of species in solution, for example, for silicate oligomers low fragmentation is observed during the desorption process especially at high mass-to-charge ratios. If this approach can be extended to other systems, ESI-MS would be ideally suited for the analysis of higher oligomers, which are the crucial species responsible for nucleation of solids in



Scheme 1. Silicate oligomers that are partly dehydroxylated. Only those m/z values written in boxes were observed in the ESI-MS experiments.

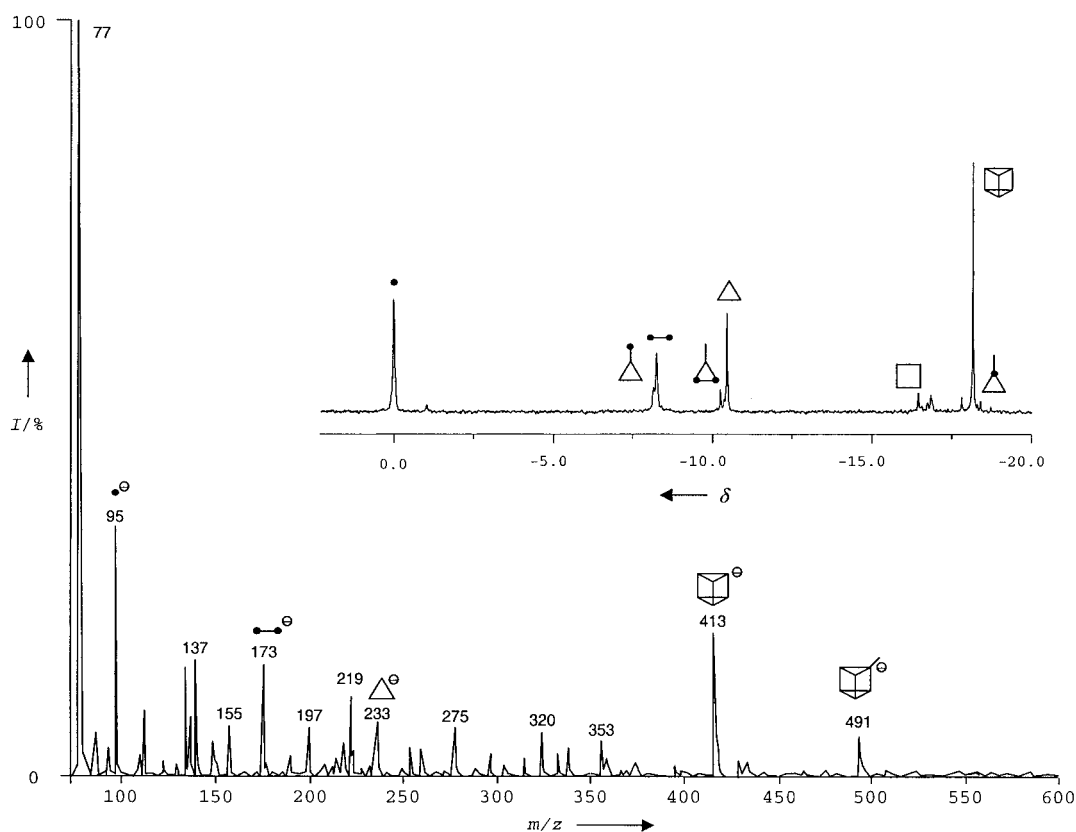


Figure 2. Negative-ion ESI mass spectrum and ^{29}Si NMR spectrum of a silicate solution containing tetraethylammonium ions in which the prismatic hexamer is the predominant species.

solutions. Even for highly alkaline and concentrated (0.5–1.0 M) solutions, which have a high ionic strength, ESI-MS allows the determination of species without strong interfer-

ence in the system. D4R units with a charge of up to -4 and as a mixture with different degrees of hydroxylation and methoxylation could be detected; such information cannot

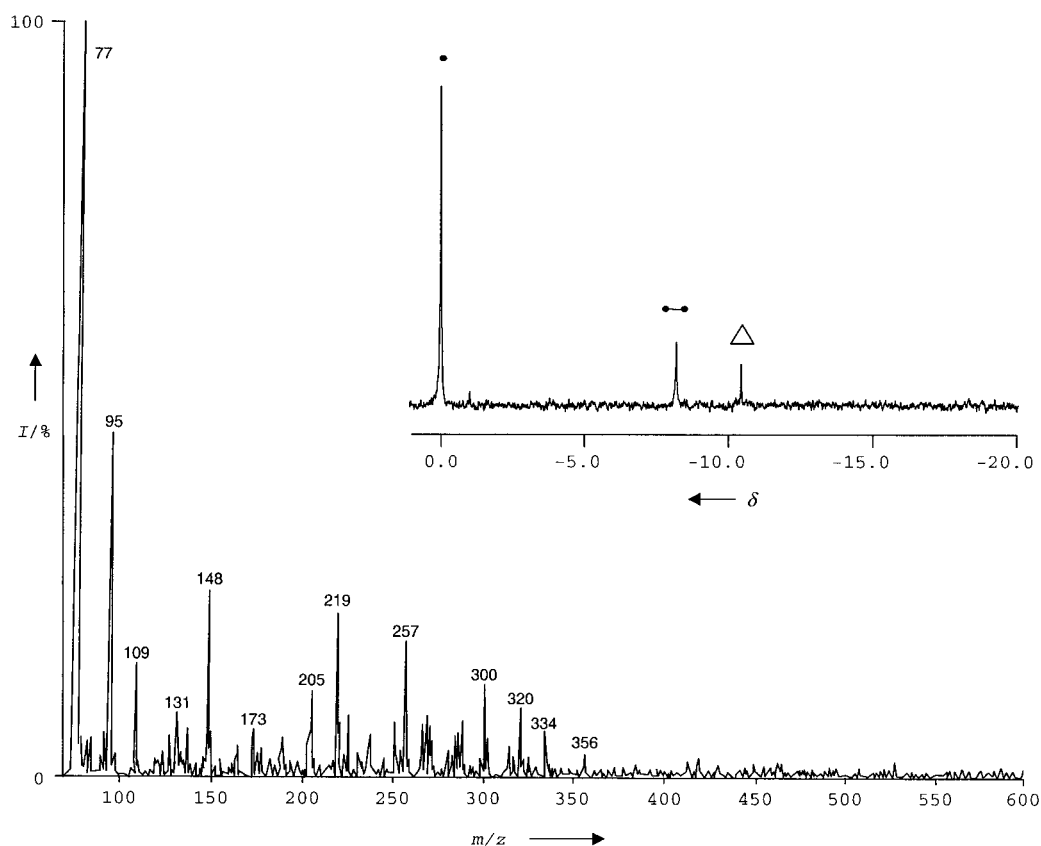


Figure 3. Negative-ion ESI mass spectrum and ^{29}Si NMR spectrum of a silicate solution of lower concentration containing only smaller oligomers.

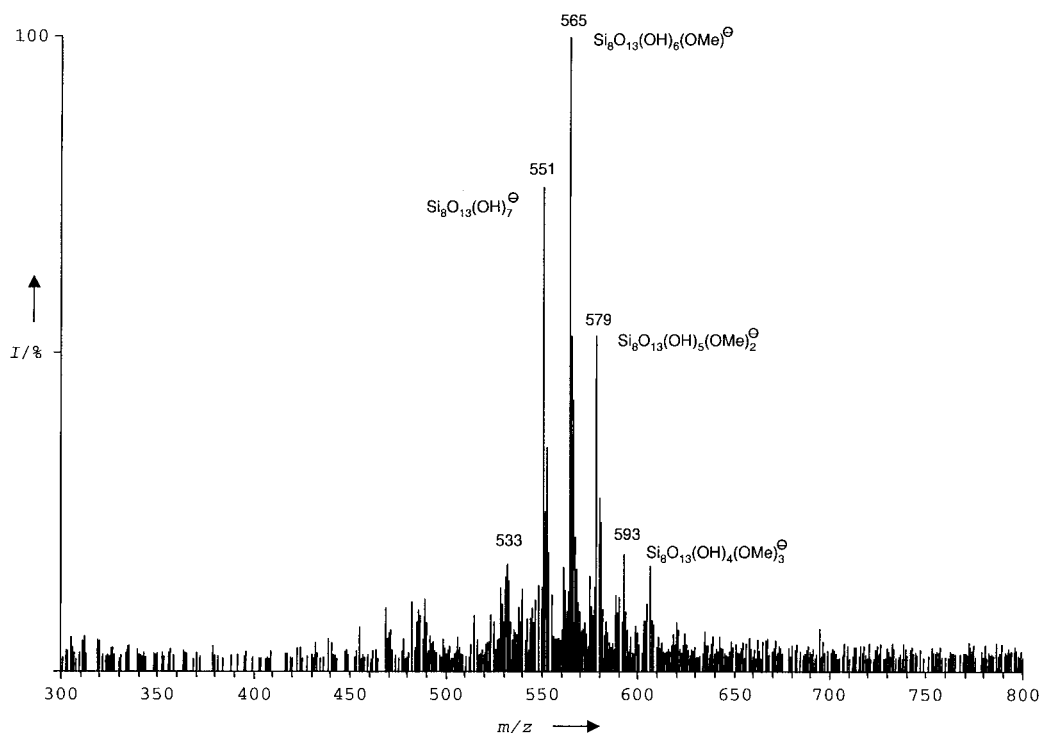


Figure 4. Negative-ion ESI mass spectrum of a silicate solution stabilizing the double-four-membered ring, recorded on a Hewlett Packard HP 5989B mass spectrometer.

be obtained by NMR spectroscopy. However, the power of mass spectrometry will become even more obvious in systems in which NMR spectroscopy fails due to the lack of suitable nuclei.

Experimental Section

The solution in which double-four ring (D4R) silicate oligomers are stabilized was prepared by dissolving Aerosil 130 (Degussa) (0.75 g, 12.45 mmol) in aqueous tetramethylammonium hydroxide (TMAOH)

solution (5.0 g; 25 wt %; Aldrich), ultra-purified water (4.67 g; Millipore), and methanol (5.625 g, 175.55 mmol; Fluka, p.a.). Double-three ring (D3R) containing solutions were prepared by dissolving Aerosil 130 (0.193 g, 3.21 mmol) in aqueous tetraethylammonium hydroxide (5.0 g; 35 wt %; Aldrich), ultra-purified water (0.146 g; Millipore), and ethanol (1.817 g, 39.5 mmol; Fischer & Rintelen, puriss.). All solutions were stirred for 30 min and then heated at 70 °C for 18 h. The clear solutions were then filtered through a polyether sulfone membrane (Nalgene) with a pore width of 0.2 µm before being injected into the mass spectrometer.

The mass spectra were recorded with a Fisons VG Platform II instrument with a quadrupole analyzer. The sample was injected directly through a Rheodyne valve. Skimmer cone voltages were varied between 30 and 100 V. In order to obtain an independent verification of the findings, a second series of experiments was carried out on a quadrupole mass spectrometer (Hewlett Packard HP MS-Engine 5989B), fitted with an Analytica of Brandford ESI-source. The solutions were injected by direct infusion and measured with an ESI voltage of 3640 V, a flow rate of 40 µL min⁻¹, a desolvation temperature of 150 °C, a CapEx voltage of -133 V, and a skimmer voltage of -31.5 V.

²⁹Si NMR spectra were recorded with an AMX 400 Bruker spectrometer operating at 79.483 MHz. Samples containing D₂O for the deuterium locking frequency were placed in a 10-mm PTFE NMR tube liner without a glass sample tube to minimize the silicon background from the glass. The pulse sequence used to acquire the spectra was a ²⁹Si{¹H} inverse-gated experiment with a waltz16 composite pulse program for proton decoupling. Generally for the ²⁹Si determination a 13.6 µs pulse with a 8 s relaxation delay was used between each acquisition. The number of acquisitions ranged from 15000 to 30000 depending on the concentration of the solutions.

Received: May 8, 2000 [Z15088]

- [1] a) J. A. Dirksen, T. A. Ring, *Chem. Eng. Sci.* **1991**, *46*, 2389–2427; b) E. Matijevic, *Chem. Mater.* **1993**, *5*, 412–426.
- [2] a) T. Løver, W. Henderson, G. A. Bowmaker, J. M. Seakins, R. P. Cooney, *J. Mater. Chem.* **1997**, *8*, 1553–1558; b) F. Sobott, S. A. Schunk, F. Schüth, B. Brutschy, *Chem. Eur. J.* **1998**, *4*, 2353–2359; c) D. A. Loy, J. P. Carpenter, S. A. Yamanaka, M. D. McClain, J. Greaves, S. Hobson, K. J. Shea, *Chem. Mater.* **1998**, *10*, 4129–4140; d) S. Cristoni, L. Armelao, S. Gross, E. Tondello, P. Traldi, *Rapid Commun. Mass Spectrom.* **2000**, *14*, 662–668.
- [3] A. V. McCormick, A. T. Bell, *Catal. Rev. Sci. Eng.* **1989**, *31*, 97–127.
- [4] C. J. Brinker, G. W. Scherer, *Sol-Gel Science*, Academic Press, Boston, **1990**.
- [5] a) R. Murugavel, A. Voigt, M. G. Walawalkar, H. W. Roesky, *Chem. Rev.* **1996**, *96*, 2205–2236; b) F. J. Feher, D. A. Newman, J. F. Walzer, *J. Am. Chem. Soc.* **1989**, *111*, 1741–1748.

Stepwise Assembled Photoactive Films Containing Donor-Linked Fullerenes**

Chuping Luo, Dirk M. Guldi,* Michele Maggini, Enzo Menna, Simonetta Mondini, Nicholas A. Kotov, and Maurizio Prato

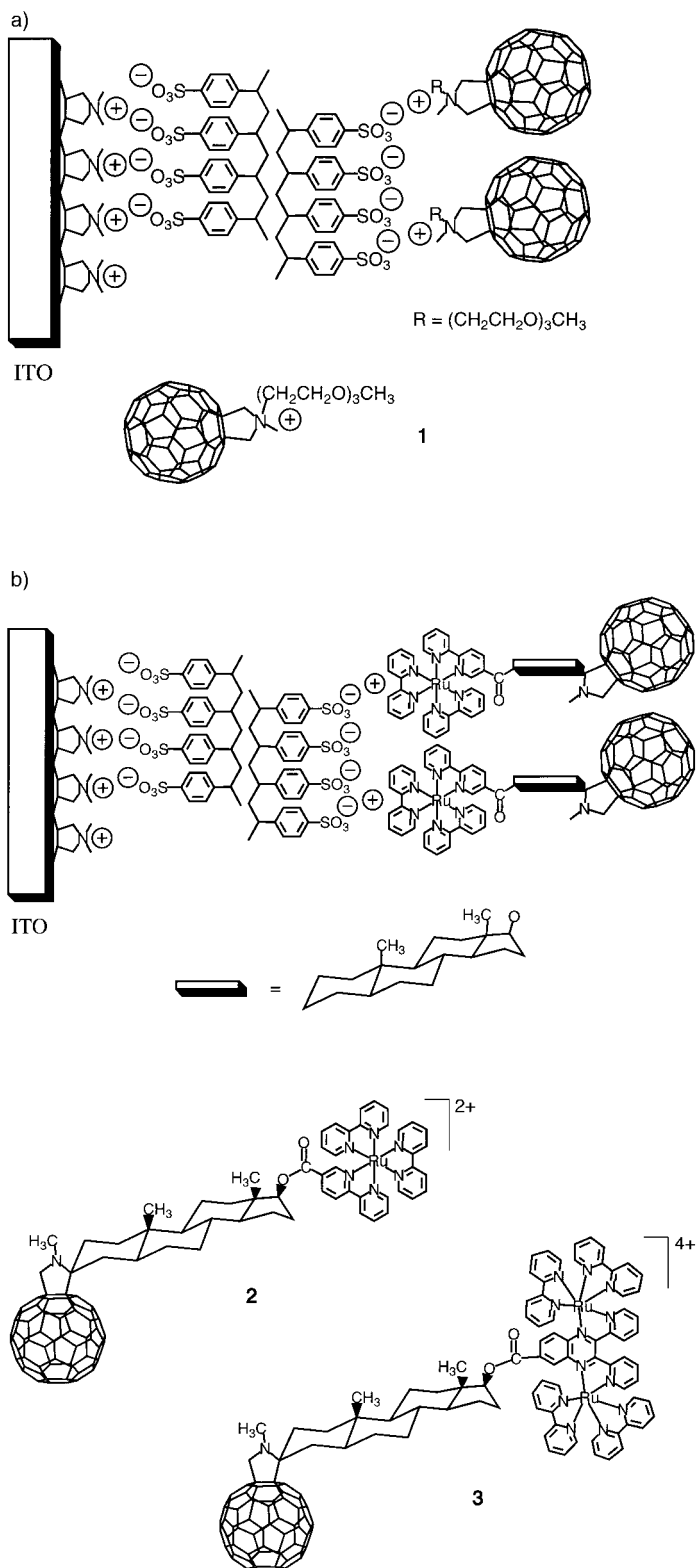
The construction of molecular devices such as photoelectrochemical cells for use in solar energy conversion is a very useful but challenging task.^[1] Most common problems relate to the interfacial diffusion of the donor and acceptor molecules or the lack of semiconductor materials with large band gaps that give an efficient light response in the visible region.^[2, 3]

Herein we present the supramolecular organization of donor-linked fullerenes as a viable alternative for the assembly of photoactive indium tin oxide (ITO) electrodes which exhibit an efficient generation of photocurrent.^[4] The fundamental advantage of the fabrication of these tailored architectures is the control that can be exerted at a molecular level over the thickness and composition of the assembled films.^[5] Equally important is the specific alignment and the orientation of the incorporated donor–acceptor systems so as to facilitate the electron transfer among adjacent layers.^[6] Thus, the efficiency of the generated photocurrents is expected to depend on the cooperative interaction of these individual parameters (film thickness, alignment, and orientation).

In the following we describe the layer-by-layer deposition of a positively charged fulleropyrrolidinium ion (**1**) and a series of positively charged ruthenium(II)–polypyridyl–fullerene donor–acceptor dyads (**2** and **3**, the counterion is PF₆⁻ in both cases, Scheme 1) on solid substrates (quartz or semiconducting ITO electrodes). The ruthenium(II)–polypyridyl complexes employed show a marked red-shift in their absorption maxima while maintaining a high photopotential.^[7, 8] Both parameters are essential in order to guarantee an elevated monochromatic photon-to-current conversion efficiency at longer wavelength. More importantly, the use of

- [*] Dr. habil. D. M. Guldi, Dr. C. Luo
Radiation Laboratory, University of Notre Dame
Notre Dame, IN 46556 (USA)
Fax: (+1) 219-631-8068
E-mail: guldi.1@nd.edu
- Prof. M. Maggini, Dr. E. Menna, Dr. S. Mondini
Dipartimento di Chimica Organica, Università di Padova
Via Marzolo 1, 35131 Padova (Italy)
- Prof. N. A. Kotov
Chemistry Department, Oklahoma State University
Stillwater, OK, 74078 (USA)
- Prof. M. Prato
Dipartimento di Scienze Farmaceutiche
Università di Trieste
Piazzale Europa, 1, 34127 Trieste (Italy)

[**] This work was supported by the Office of Basic Energy Sciences of the Department of Energy and by MURST (no. 9803194198). This publication is document NDRL-4166 from the Notre Dame Radiation Laboratory. We thank Prof. Janos H. Fendler and Dr. T. Cassagneau (Clarkson University) for helpful discussions during the initial phase of the experiments. N.A.K. acknowledges the NSF for a CAREER award (CHE-9876265).



Scheme 1. Schematic representation of the spontaneous self-assembly of composite nanostructured films, with a) fulleropyrrolidinium ion **1** and b) the ruthenium(II)–polypyridyl–fullerene donor–acceptor dyads **2** and **3**.

covalently attached donor–acceptor systems (such as in dyads **2** and **3**) is sought to avoid the commonly encountered phase separation and, thereby, ensure stable donor–acceptor interfaces.

The synthesis of pyrrolidinium salt **1**-PF₆^[9] and the tris(2,2'-bipyridine)ruthenium(II)-C₆₀ dyad (**2**)^[7] have already been reported. Dyad **3** was prepared by following a similar synthetic protocol^[8] as for dyad **2**, but with a 2,3-bis(2-pyridyl)quinoxaline moiety used as the bridging ligand to coordinate the two metal centers.

The key step in the deposition of the C₆₀-based materials involves the coverage of the substrate surface with a negatively charged material. This was achieved in two separate steps, namely, by anchoring a poly(diallyldimethylammonium) chloride (PDDA chloride) layer to the hydrophilic surface, followed by the adsorption of a sodium poly(styrene-4-sulfonate) (PSS) coating. The subsequent deposition of the fullerene derivatives became possible through uniformly directed Coulombic forces and short-range van der Waals forces that govern the physisorption process between opposite charged ions.^[5] For example, charge attraction is operative between the negative sulfonate groups and the pyrrolidinium cation in **1** and the ruthenium(II) complexes in **2** and **3**. After this modification, the hydrophobic fullerene core covers the surface of the modified electrode and this can then be coated with another dyad layer by making use of the hydrophobic interactions.^[12]

The regularities of the stepwise deposition procedure were monitored by recording the UV/Vis absorption spectra of the resulting films after each deposition step. It should be noted that neither the PDDA layer nor the PSS layers exhibit strong absorption characteristics in the range monitored. The pyrrolidinium ion, on the other hand, was unequivocally identified in the monolayer from a set of maxima at 226, 260, and 336 nm. A solution of the same pyrrolidinium salt in dichloromethane exhibits transitions at 218, 257, and 330 nm, which is in excellent agreement with the monolayered films. Up to 20 individual coating runs were performed to obtain a sufficiently absorbing electrode. Repeated absorption patterns were evident in the absorption spectra of the deposited films on quartz. The linear dependence noted here is a meaningful criterion that indicates the satisfactory and uniform stacking of individually deposited films.

The linearity of the multilayer growth has also been confirmed by monitoring the ellipsometric thickness of the films (Figure 1). The increment of the deposition cycle of PSS and **1** is equal to 4.3 nm, which corresponds to the adsorption of 2–3 monolayers of **1** and a layer of PSS, whose thickness is typically 0.5–1 nm. The layer-by-layer pattern of the film growth can be clearly seen in the images (not shown) obtained by atomic force microscopy (AFM). The morphologies of PDDA/PSS and PDDA/PSS/**1** layers as observed in the AFM images are significantly different. PDDA/PSS forms a fairly flat surface with occasional pores. After adsorption of the pyrrolidinium salt **1**, the roughness of the surface decreases, while the fine-grained structure of the fullerene layer appears. Importantly, the surface becomes uniformly covered with characteristic 20–50-nm large 2D aggregates assembled in a continuous uniform film. No troughs can be observed in the entire area surveyed. A similar regularity and quality of the surface are expected for those formed with the other fullerene derivatives discussed below.

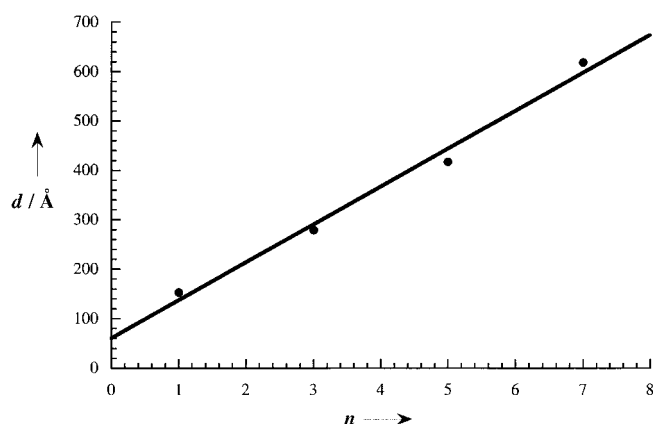


Figure 1. Ellipsometric thickness d of layers of **1** assembled on a silicon wafer.

The deposition of **1** onto a hydrophilic ITO electrode instead of quartz was carried out through the same sequence of steps and its progression was monitored by means of absorption spectroscopy. The low transparency of ITO in the UV region limited the film analysis to the wavelength region greater than 350 nm. All films (that is, on quartz and ITO) were found to be mechanically and chemically stable in air, but were kept in the dark prior to their photochemical investigation. It is worth noting that most films deposited by the Langmuir–Blodgett technique have a high environmental instability, especially those that contain fullerenes.^[10]

In the next step the photoactivity spectra of one, five, and ten self-assembled monolayers of **1** on ITO were measured. The most important observation is that the photocurrent responded linearly at most wavelengths to the number of monolayers (Figure 2). This result is of extreme importance since it underlines the benefit of the supramolecular organization, rather than the adsorption of the photosensitizer (that is, the fulleropyrrolidinium ion) on mesoporous substrates, such as nanostructured TiO_2 or SnO_2 .^[3, 11] In addition, the photoactivity spectrum follows unequivocally the absorption spectrum of the pyrrolidinium salt.

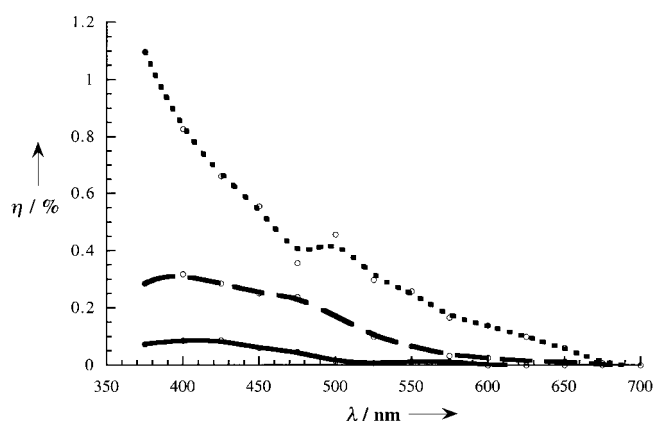


Figure 2. Photon-to-current conversion efficiency η of one (—), five (---), and ten (····) self-assembled monolayers of the pyrrolidinium ion **1** on an ITO electrode; the efficiency was determined from the following expression $\eta[\%] = I_{\text{SC}}/I_{\text{inc}} \times 1240/\lambda [\text{nm}] \times 100$ (I_{SC} = short-circuit photocurrent; I_{inc} = light intensity incident on the electrode).

To probe the direction of the photocurrent observed (hole or electron transport) we added various concentrations first of an electron acceptor (methylviologen) and second of a sacrificial electron donor (ascorbic acid) to the electrolyte solution. In the case of methylviologen, a concentration-dependent decrease in the photocurrent was noted (Table 1).

Table 1. Photocurrent I (measured at 400 nm) of a modified ITO electrode covered with ten layers of fulleropyrrolidinium ion **1** upon adding various concentrations c of an electron donor (ascorbic acid) and electron acceptor (methylviologen).

Quencher	c [mM]	I [nA]
methylviologen	0	9.0
	5.8	5.2
	10.3	4.0
ascorbic acid	0	10
	6.6	58
	13.4	65

This relationship suggests that the electron acceptor competes efficiently with the modified ITO electrode to accept an electron from the photoexcited fullerene moiety. This proposal leads to the assumption that the addition of a sacrificial electron donor, such as ascorbic acid, should result in a net increase in the photocurrent. In fact, a significant enhancement (Table 1) was observed relative to the methylviologen case and also to that when there was no additive. We can conclude from these trends that the electron transfer into the ITO conduction band evolves from the fullerene excited state.

The promising features of the above-described system stimulated us to extend our investigation to the ruthenium–fullerene dyads **2** and **3**. The substantially red-shifted absorption maxima, which extend far into the visible region, in these dyads are expected to improve the light-harvesting properties of the modified electrodes. The maxima of the metal-to-ligand charge transfer (MLCT) transitions of dyad **2** and **3** lie at 460 and 640 nm, respectively. The strongest absorption of the fullerene moiety, on the other hand, is in the near visible region (around 335 nm).

The successive layer-by-layer deposition of **2** and **3** either onto quartz or ITO was monitored by absorption spectroscopy by using procedures similar to that used for **1**. Now, both absorption patterns, namely, that of the fullerene core (220, 260, and 335 nm) and that of the ruthenium(II)–polypyridyl complex fragments (**2**: 290 and 460 nm; **3**: 286, 408, 520, and 640 nm), were useful probes. Figure 3a displays the UV/Vis absorption spectrum of a quartz substrate covered with two to ten monolayers of **3**. Regardless of the origin, the absorption of both moieties (fullerene and ruthenium(II)–polypyridyl complex fragments) increased linearly with the number of layers. Figure 3b displays plots of the absorbance at 284 and 641 nm as a function of the number of monolayers of **3**.

Various attempts to use just the ruthenium complexes without the fullerene unit failed. Although noticeable amounts of the ruthenium complexes were assembled, subsequent immersion of the ruthenium-covered electrode into the PSS solutions led to a nearly quantitative dissolution

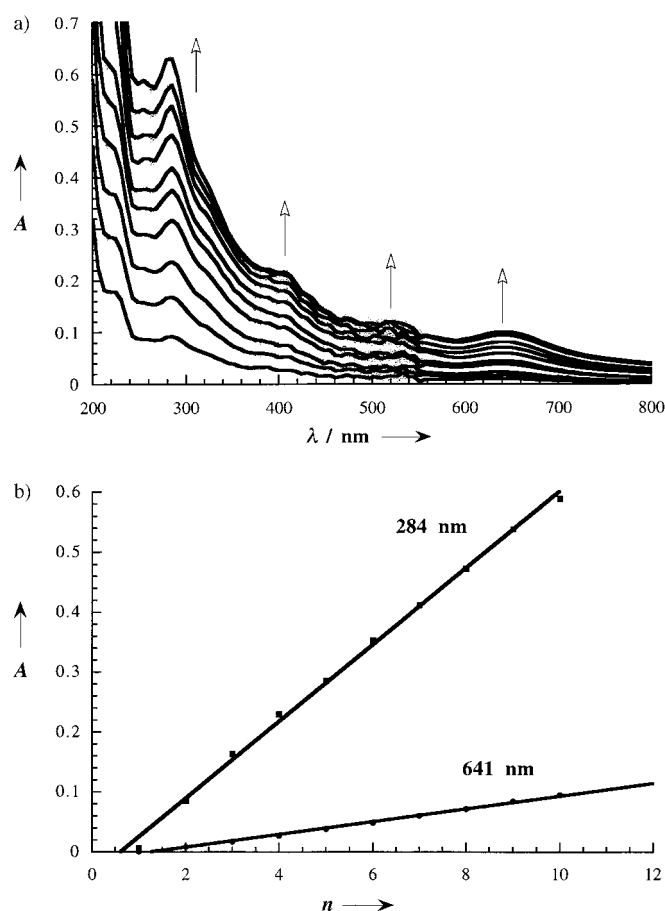


Figure 3. a) UV/Vis absorption spectra of a quartz substrate covered with two to ten monolayer films of the ruthenium(II)-polypyridyl-fullerene donor-acceptor dyad **3**. b) Plots of the absorbance at 284 and 641 nm as a function of the number of monolayers of **3**.

of the water-soluble complexes. Also, placement of a reference fulleropyrrolidine (that is, a compound with no positive charge on the nitrogen atom) was unsuccessful. Therefore, in **2** and **3** only the presence of the positive charges in combination with the adequate balance between the hydrophobic (fullerene) and the hydrophilic part (ruthenium complex fragment), opens the opportunity for the described assembly approach.^[12]

It is noteworthy that the photocurrent followed exactly the trend established for the pyrrolidinium salt **1**. In particular, the photoactivity spectra are in good agreement with the ground-state absorption features of both ruthenium(II)-polypyridyl complexes. For example, the photocurrent of dyad **2** reaches a maximum at around 475 nm, while electrodes covered with dyad **3** showed a maximum between 600 and 625 nm, as well as another much stronger maximum at 400 nm.^[13] The photocurrent ratio ($I_{400\text{nm}}/I_{600\text{nm}}$) of **3** is a good reflection of the ground-state absorption ($A_{400\text{nm}}/A_{600\text{nm}}$) both in solution and in the deposited film. Besides the observation that **3** is photoactive over practically the entire UV/Vis region, the response between 300 and 400 nm is enhanced by a factor of three relative to **2**.

The efficiency of these electrodes was studied as a function of the number of layers. In particular, modified ITO electro-

des with a coverage of 1, 5, 10, and 20 layers of **2** or **3** were investigated. From these experiments a tendency was observed which is analogous to that summarized for the fulleropyrrolidinium salt namely, a progressive intensification of the photocurrent occurs with increasing numbers of layers. Furthermore, measurements over a time interval of 200 seconds gave rise to a repeatable and almost stable photocurrent in the case of **3**. For **2**, on the other hand, we found an exponential decay of about 25 % during the first 20 seconds, followed then by a nearly steady-state current. All the films investigated responded uniformly to the repeatedly applied "light on/light off" intervals.

In summary, layer-by-layer deposition can be used as a viable alternative for the fabrication of photoactive films containing covalently linked donor-acceptor systems by using simple electrostatic attraction between oppositely charged moieties. Not only is the stability of the film remarkable, as a consequence of the strong adhesion of adjacent layers, but the layer-by-layer deposition technique can be performed in a systematic and controlled manner as monitored by the ground-state absorption and ellipsometry data on the modified electrode. Most significantly, the photocurrent response of the chemically modified electrodes increases with increasing film thickness (that is, with increasing number of assembled monolayers). No doubt, these characteristics point to the potential of these modified electrodes for materials and devices that have practical applications, such as solar energy conversion. Thus, this work provides a significant improvement over alternative approaches in which a single self-assembled monolayer on, for example, a gold electrode is employed.

Currently, we are intensifying our efforts to obtain a picture at molecular resolution, by means of AFM, of the modified fullerene ITO electrodes after each deposition step, that is, of the PDDA, PDDA/PSS, and PDDA/PSS/fullerene dyad. We are also pursuing ways to vary the polymeric PSS matrix with a view for improving the conductance between the aqueous environment and the ITO electrode and thereby obtaining higher efficiencies of the modified ITO electrodes.

Received: 10 February, 2000 [Z14679]

- [1] V. Balzani, *Supramolecular Photochemistry*, D. Reidel, Dordrecht, **1987**; F. L. Carter, *Molecular Electronic Devices*, Dekker, New York, **1987**; M. A. Fox, M. Channon, *Photoinduced Electron Transfer*, Elsevier, Amsterdam, **1988**; E. Pelizzetti, M. Schiavello, *Photochemical Conversion and Storage of Solar Energy*, Kluwer, Dordrecht, **1997**.
- [2] J. H. Fendler, I. Dekany, *Nanoparticles in Solids and Solutions*, Kluwer, Dordrecht, **1996**; P. V. Kamat, D. Meisel, *Semiconductor Nanoclusters*, Elsevier, Amsterdam, **1997**; J. H. Fendler, *Nanoparticle and Nanostructured Films*, WILEY-VCH, Weinheim, **1998**.
- [3] P. V. Kamat, *Chem. Rev.* **1993**, 93, 267; A. Hagfeldt, M. Grätzel, *Chem. Rev.* **1995**, 95, 49.
- [4] For other examples of fullerene photovoltaics, see N. S. Sariciftci, L. Smilowitz, A. J. Heeger, F. Wudl, *Science* **1992**, 258, 1474; L. Ouali, V. V. Krasnikov, U. Stalmach, G. Hadzioannou, *Adv. Mater.* **1999**, 11, 1515; H.-L. Wang, D. W. McBranch, V. I. Klimov, R. Helgeson, F. Wudl, *Chem. Phys. Lett.* **1999**, 315, 173; J. F. Nierengarten, J. F. Eckert, J. F. Nicoud, L. Ouali, V. Krasnikov, G. Hadzioannou, *Chem. Commun.* **1999**, 617; H. Imahori, H. Yamada, Y. Nishimura, I. Yamazaki, Y. Sakata, *J. Phys. Chem. B* **2000**, 104, 2099; for a review, see H. Imahori, Y. Sakata, *Eur. J. Org. Chem.* **1999**, 2445.

- [5] For leading references on layer-by-layer assembly, see M. Ahlers, W. Müller, A. Reichert, H. Ringsdorf, J. Venzmer, *Angew. Chem.* **1990**, *102*, 1310; *Angew. Chem. Int. Ed. Engl.* **1990**, *29*, 1269; J. H. Fendler, F. C. Meldrum, *Adv. Mater.* **1995**, *7*, 607; S. W. Keller, S. A. Johnson, E. S. Brigham, E. H. Yonemoto, T. E. Mallouk, *J. Am. Chem. Soc.* **1995**, *117*, 12879; G. Decher, *Science* **1997**, *277*, 1232; X. Zhang, J. Shen, *Adv. Mater.* **1999**, *11*, 1139; N. A. Kotov, T. Haraszti, L. Turi, G. Zavala, R. E. Geer, I. Dékány, J. H. Fendler, *J. Am. Chem. Soc.* **1997**, *119*, 6821.
- [6] For previous reports on self-assembled fullerene layers using electrostatic interactions, see G. Decher, *Nachr. Chem. Tech. Lab.* **1993**, *41*, 793; H. Hong, D. Davidov, C. Kallinger, U. Lemmer, J. Feldmann, E. Harth, A. Gügel, K. Müllen, *Synth. Met.* **1999**, *102*, 1487.
- [7] M. Maggini, D. M. Guldi, S. Mondini, G. Scorrano, F. Paolucci, P. Ceroni, S. Roffia, *Chem. Eur. J.* **1998**, *4*, 1992.
- [8] D. M. Guldi, M. Maggini, E. Menna, G. Scorrano, F. Paolucci, M. Marcaccio, P. Ceroni, S. Roffia, *Chem. Eur. J.* submitted; M. Maggini, D. M. Guldi in *Molecular and Supramolecular Photochemistry Vol. 4* (Eds.: V. Ramamurthy, K. S. Schanze), Marcel Dekker, New York, **2000**, p. 149.
- [9] T. Da Ros, M. Prato, M. Carano, P. Ceroni, F. Paolucci, S. Roffia, *J. Am. Chem. Soc.* **1998**, *120*, 11645.
- [10] C. A. Mirkin, W. B. Caldwell, *Tetrahedron* **1996**, *52*, 5113; L. Leo, G. Mele, L. Valli, G. Vasapollo, D. M. Guldi, G. Mascolo, *Langmuir* **2000**, *4599*.
- [11] C. P. Luo, C. H. Huang, L. B. Gan, D. J. Zhou, W. S. Xia, Q. K. Zhuang, Y. L. Zhao, Y. Y. Huang, *J. Phys. Chem.* **1996**, *100*, 16685; P. V. Kamat, M. Gevaert, K. Vinodgopal, *J. Phys. Chem. B* **1997**, *101*, 4422; M. Kocher, T. K. Daubler, E. Harth, E. Harth, U. Scherf, A. Gügel, D. Neher, *Appl. Phys. Lett.* **1998**, *72*, 650; P. V. Kamat, S. Barazzouk, K. G. Thomas, S. Hotchandani, *J. Phys. Chem.* **2000**, *104*, 4014.
- [12] N. A. Kotov, *Nanostruct. Mater.* **1999**, *12*, 789.
- [13] The photon-to-current conversion efficiency at 475 nm of a single monolayer of dyads **2** and **3** in the absence of any sacrificial electron donor are 0.0784 and 0.0833 %, respectively.

Breaking the Rule: Synthesis and Molecular Structure of Dinuclear Rhodium Complexes with Bridging and Semibridging Trialkylphosphane Ligands**

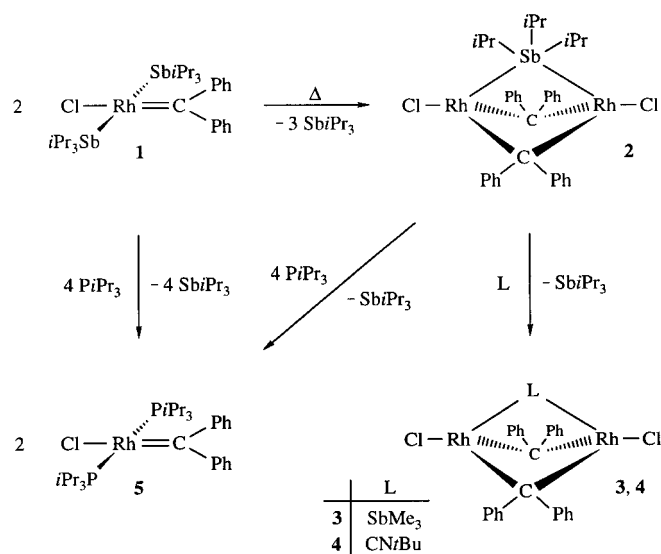
Thomas Pechmann, Carsten D. Brandt, and Helmut Werner*

In memory of John Osborn

Tertiary phosphanes PR_3 with $\text{R} = \text{alkyl or aryl}$ belong like CO to the most well-known ligands in coordination chemistry.^[1] While with regard to CO not only numerous metal complexes with *terminal* but also with *bridging* carbonyl

ligands have been reported, the same is not true for tertiary phosphanes. Textbooks on Inorganic Chemistry^[2] as well as corresponding monographs and reviews^[3] mention without exception that tertiary phosphanes (and tertiary arsanes AsR_3 and stibanes SbR_3 as well) behave exclusively as terminal coordinated ligands.

Recently, we have begun to illustrate that this postulate may need to be modified by showing that the thermal reaction of the square-planar precursor **1** leads to the dinuclear complex **2** from which the related compounds **3** and **4** were obtained by exchange of the bridging SbiPr_3 ligand for SbMe_3 and CNrBu (Scheme 1).^[4] However, attempts to substitute the stibane by a tertiary phosphane failed. Treatment of **2** with PiPr_3 did not afford $[\text{Rh}_2\text{Cl}_2(\mu\text{-PiPr}_3)(\mu\text{-CPh}_2)_2]$ but gave the mononuclear complex **5** by displacement of the stibane and cleavage of the carbene bridges. Now we have found that



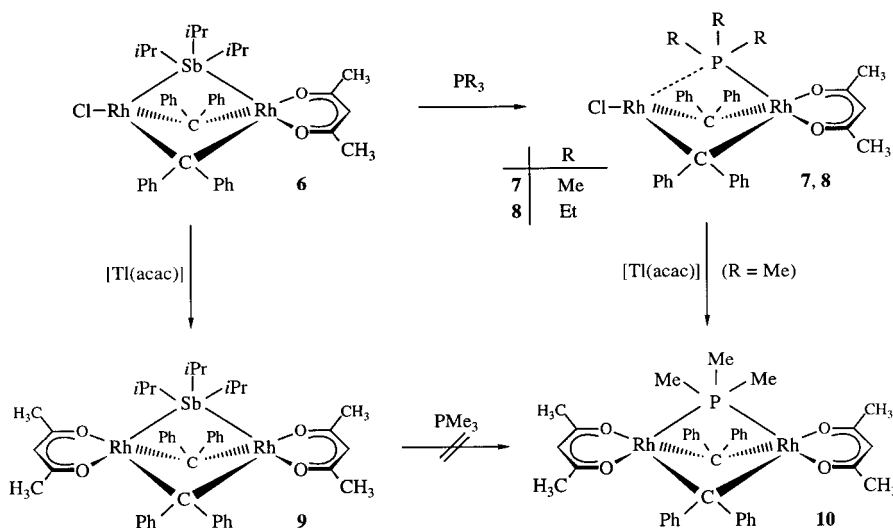
Scheme 1.

replacing one of the chloro ligands in **2** by acetylacetonate (acac) changes the reactivity of the stibane-bridged dinuclear compound dramatically and turns the dream of the isolation of a transition metal complex with $\text{M}(\mu\text{-PR}_3)_3\text{M}$ as a molecular unit into reality.

The dinuclear compound **6**, obtained from **2** and an equimolar amount of $[\text{Ti}(\text{acac})_3]$, reacts with PMe_3 in the molar ratio of 1:1 in pentane/diethyl ether to give the substitution product **7** (Scheme 2). After recrystallization from acetone, red-brown crystals of **7** were isolated in 82 % yield. The ^{31}P NMR spectrum of **7** (in C_6D_6) displays a doublet of doublets at $\delta = -36.4$ with $^{31}\text{P} - ^{103}\text{Rh}$ coupling constants of 147.5 and 81.4 Hz, indicating that the PMe_3 ligand is not linked to one of the metal centers in a terminal fashion. For the dirhodium compound $[(\text{acac})\text{Rh}(\mu\text{-CO})\{\mu\text{-C}(p\text{-Tol})_2\}_2\text{Rh}(\text{acac})(\text{PMe}_3)]$, which is formed by stepwise reaction of $[(\text{acac})\text{Rh}(\mu\text{-SbiPr}_3)\{\mu\text{-C}(p\text{-Tol})_2\}_2\text{Rh}(\text{acac})]$ with PMe_3 and CO and which contains a *terminal* $\text{Rh}-\text{PMe}_3$ bond,^[5] the $^{31}\text{P} - ^{103}\text{Rh}$ coupling constants of the signal observed in the ^{31}P NMR spectrum at $\delta = -5.2$ are 129.7 and 7.6 Hz, respectively. The ^{31}P NMR resonance signals for the PMe_3 ligand of other

[*] Prof. Dr. H. Werner, Dipl.-Chem. T. Pechmann, Dipl.-Chem. C. D. Brandt
Institut für Anorganische Chemie der Universität Würzburg
Am Hubland, 97074 Würzburg (Germany)
Fax: (+49) 931-888-4605
E-mail: helmut.werner@mail.uni-wuerzburg.de

[**] This work was supported by the Deutsche Forschungsgemeinschaft (SFB 347) and the Fonds der Chemischen Industrie. We thank in particular Dr. J. Wolf and Dr. U. Herber, Universität Würzburg, for valuable advice and discussions.



Scheme 2.

dinuclear complexes of the general composition $[(\text{L})_x\text{Rh}(\mu\text{-X})_n\text{Rh}(\text{PMe}_3)(\text{L}')_y]$ show differences for $^1J(^{31}\text{P},^{103}\text{Rh})$ and $^3J(^{31}\text{P},^{103}\text{Rh})$ also of this magnitude.^[6] The reaction of **6** with PET_3 takes a similar course to that with PMe_3 and affords compound **8** in 81 % yield.

The X-ray crystal structure analysis of **7** (Figure 1) confirms^[7] that the phosphane ligand occupies a *semibridging* position rather than a terminal position.^[8] Apart from the distances Rh1-P and Rh2-P , characteristic features are in particular the bond angles in the Rh_2P triangle, which are significantly smaller than 90° . In the case of a nonbridging arrangement, the angle Rh1-Rh2-P should be considerably larger than 90° .^[9] Owing to the higher coordination number of Rh1 compared to Rh2 , not only the phosphane but also the two diphenylcarbene ligands are linked to the metal centers in

an unsymmetrical fashion. The distances Rh2-C1 and Rh2-C2 are about 0.11 \AA shorter than those from Rh1 to C1 and C2 , quite similar to the situation found for compound **6**.^[10] The bond length Rh1-Rh2 ($2.5318(8) \text{ \AA}$) in **7** is rather short and comparable with that in the dinuclear complex **2** ($2.5349(5) \text{ \AA}$).^[4a]

Compound **7** reacts with $[\text{Ti}(\text{acac})]$ in the molar ratio of 1:1.2 in acetone at room temperature by substitution of the chloro for the acetylacetonato ligand to give the dinuclear complex **10** (Scheme 2). The light-brown, only moderately air-sensitive solid is obtained in 98 % yield. In contrast to **7**, the ^{31}P NMR spectrum of **10** does not display a doublet of doublets but a

triplet, illustrating that the trimethylphosphane ligand is coordinated to both rhodium centers in a *bridging* (and not in a *semibridging*) mode. The X-ray crystal structure analysis confirms this proposal (Figure 2).^[7] Although the two Rh-P bond lengths are not exactly the same, the difference of about 0.3 \AA is only half of that in **7**. Since neither the ^{31}P nor the ^1H NMR spectrum of **10** is temperature-dependent, it is conceivable that the small deviation of the ideal symmetry for the sterically hindered molecule found in the crystal is due to packing effects. In our opinion the more important fact is that the bond angles Rh1-Rh2-P , Rh2-Rh1-P , and Rh1-P-Rh2 deviate only by a maximum of 7.1° from the value of 60° required for an isosceles triangle. It should be mentioned that we failed to prepare **10** from **9** by treatment with an equimolar amount of PMe_3 . In this case a dinuclear compound of

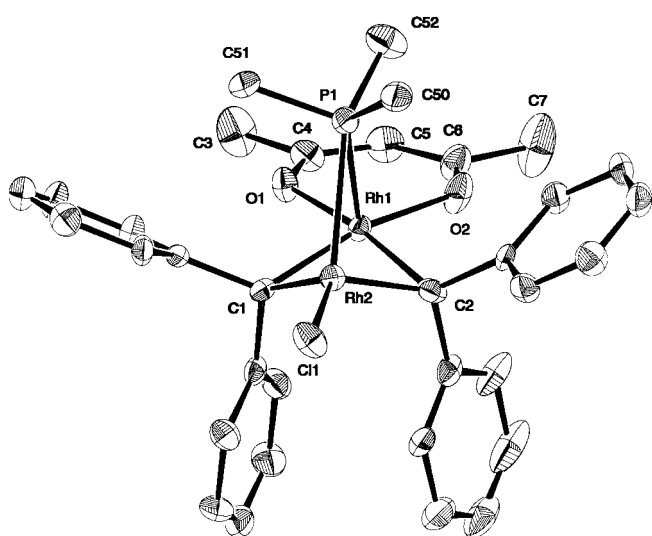


Figure 1. Molecular structure of **7** (ORTEP plot) in the crystal. Selected bond lengths [\AA] and angles [$^\circ$]: Rh1-Rh2 $2.5318(8)$, Rh1-P1 $2.2406(15)$, Rh2-P1 $2.8410(14)$, Rh1-C1 $2.060(5)$, Rh1-C2 $2.057(5)$, Rh2-C1 $1.939(5)$, Rh2-C2 $1.949(5)$, Rh1-O1 $2.115(3)$, Rh1-O2 $2.116(4)$, Rh2-Cl1 $2.3072(15)$; Rh1-P1-Rh2 $58.34(4)$, P1-Rh1-Rh2 $72.78(4)$, P1-Rh2-Rh1 $48.88(4)$, Rh1-Rh2-Cl1 $172.30(4)$, Rh1-Cl1-Rh2 $78.49(16)$, Rh1-C2-Rh2 $78.36(18)$, C1-Rh1-C2 $86.77(19)$, C1-Rh2-C2 $93.3(2)$, O1-Rh1-O2 $85.42(13)$.

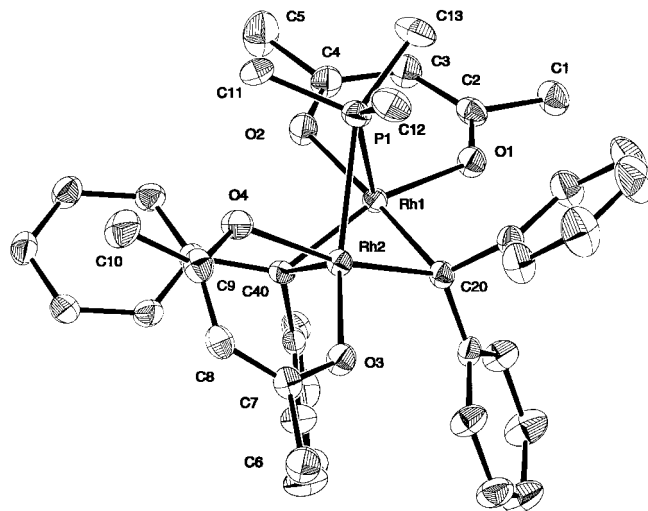


Figure 2. Molecular structure of **10** (ORTEP plot) in the crystal. Selected bond lengths [\AA] and angles [$^\circ$]: Rh1-Rh2 $2.5281(5)$, Rh1-P1 $2.2707(7)$, Rh2-P1 $2.5700(8)$, Rh1-C20 $2.069(3)$, Rh1-C40 $2.038(2)$, Rh2-C20 $1.995(2)$, Rh2-C40 $1.974(3)$, Rh1-O1 $2.1138(18)$, Rh1-O2 $2.1596(19)$, Rh2-O3 $2.0760(19)$, Rh2-O4 $2.2097(19)$; Rh1-P1-Rh2 $62.61(2)$, P1-Rh1-Rh2 $64.50(2)$, P1-Rh2-Rh1 $52.890(19)$, Rh1-C20-Rh2 $76.90(9)$, Rh1-C40-Rh2 $78.09(9)$, C20-Rh1-C40 $84.55(10)$, C20-Rh2-C40 $88.23(10)$, O1-Rh1-O2 $84.11(7)$, O3-Rh2-O4 $83.67(7)$.

unknown structure is formed which presumably contains a terminal phosphane ligand.

The presented compounds **7**, **8**, and **10** are the first dinuclear complexes with bridging or semibridging trialkylphosphane ligands. As far as we know, the capability of phosphanes (in particular of Ph_2PH) to possibly behave as bridging units was first discussed in a speculative way by Braunstein et al.^[11] Shortly thereafter, van Leeuwen and co-workers described a dinuclear palladium(II) dication containing two chelated 1,3-bis(diphenylphosphanyl)propane ligands, in which two of the four PPh_2 groups occupy an unsymmetrical bridging position with respect to the palladium atoms.^[12] A nearly symmetrical triply bridging position of PF_3 has been found in a Pd_3 complex,^[13] which appears not so unusual regarding the analogy in the bonding mode of CO and PF_3 in coordination compounds.^[14]

Experimental Section

7: A solution of **6** (77 mg, 0.08 mmol) in pentane/diethyl ether (30 mL, 2/1) was treated at -78°C with PMe_3 (8.6 μL , 0.08 mmol) and, after warming, stirred for 30 min at room temperature. A change of color from dark red to yellow accompanied by the formation of a red-brown solid occurred. The mother liquor was decanted and the remaining residue washed three times with 5 mL portions of pentane/diethyl ether (2/1). After recrystallization from acetone (15 mL) at 5°C red-brown crystals were isolated and dried in vacuo; yield 51 mg (82%); m.p. 204°C (decomp); ^1H NMR (200 MHz, C_6D_6): $\delta = 5.45$ (s, 1H; CH of acac), 1.89 (s, 6H; CH_3 of acac), 0.74 (d, $^2J(\text{P,H}) = 10.6$ Hz, 9H, PCH_3); $^{13}\text{C}\{^1\text{H}\}$ NMR (100.6 MHz, CD_2Cl_2): $\delta = 189.3$ (s; CO of acac), 174.8 (ddd, $^1J(\text{Rh,C}) = 30.5$, $^1J(\text{Rh',C}) = 20.7$, $^2J(\text{P,C}) = 3.6$ Hz; CPh_2), 100.9 (d, $^3J(\text{Rh,C}) = 1.5$ Hz; CH of acac), 28.2 (s; CH_3 of acac), 22.4 (d, $^1J(\text{P,C}) = 40.7$ Hz, PCH_3); ^{31}P NMR (81.0 MHz, C_6D_6): $\delta = -36.4$ (dd, $^1J(\text{Rh,P}) = 147.5$, $^1J(\text{Rh',P}) = 81.4$ Hz); ^{31}P NMR (162.0 MHz, CD_2Cl_2): $\delta = -29.0$ (dd, $^1J(\text{Rh,P}) = 154.6$, $^1J(\text{Rh',P}) = 70.3$ Hz).

8: Preparation analogous to that for **7**. Dark brown crystals; yield 81%; m.p. 146°C (decomp); ^1H NMR (200 MHz, C_6D_6): $\delta = 5.54$ (s, 1H; CH of acac), 1.94 (s, 6H; CH_3 of acac), 1.13 (m, 6H; PCH_2), 0.69 (m, 9H; PCH_2CH_3); $^{13}\text{C}\{^1\text{H}\}$ NMR (75.5 MHz, CD_2Cl_2): $\delta = 189.4$ (s; CO of acac), 171.7 (ddd, $^1J(\text{Rh,C}) = 31.6$, $^1J(\text{Rh',C}) = 21.5$, $^2J(\text{P,C}) = 4.0$ Hz; CPh_2), 101.2 (d, $^3J(\text{Rh,C}) = 1.8$ Hz; CH of acac), 28.6 (d, $^3J(\text{Rh,C}) = 1.1$ Hz; CH_3 of acac), 21.6 (d, $^1J(\text{P,C}) = 34.5$ Hz; PCH_2), 8.5 (d, $^2J(\text{P,C}) = 5.1$ Hz; PCH_2CH_3); ^{31}P NMR (81.0 MHz, C_6D_6): $\delta = -2.7$ (dd, $^1J(\text{Rh,P}) = 144.9$, $^1J(\text{Rh',P}) = 68.7$ Hz).

10: A solution of **7** (119 mg, 0.13 mmol) in acetone (20 mL) was treated with $[\text{Ti}(\text{acac})_3]$ (47 mg, 0.15 mmol) and stirred for 1 h at room temperature. The solvent was removed in vacuo and the remaining residue was extracted three times with pentane/diethyl ether (2/1; 30 mL each). The combined extracts were brought to dryness in vacuo and the residue was washed three times with 3 mL portions of pentane (-30°C). After recrystallization from acetone (10 mL) at 5°C light-brown crystals were isolated and dried in vacuo; yield 103 mg (98%); m.p. 62°C (decomp); ^1H NMR (300 MHz, C_6D_6): $\delta = 5.54$ (s, 2H; CH of acac), 1.96 (s, 12H; CH_3 of acac), 1.06 (d, $^2J(\text{P,H}) = 11.0$ Hz, 9H; PCH_3); $^{13}\text{C}\{^1\text{H}\}$ NMR (75.5 MHz, C_6D_6): $\delta = 188.7$ (s; CO of acac), 170.7 (dt, $^1J(\text{Rh,C}) = 24.7$, $^2J(\text{P,C}) = 4.4$ Hz; CPh_2), 100.8 (s; CH of acac), 28.4 (s; CH_3 of acac), 22.1 (d, $^1J(\text{P,C}) = 39.6$ Hz; PCH_3); ^{31}P NMR (81.0 MHz, C_6D_6): $\delta = -30.4$ (t, $^1J(\text{Rh,P}) = 110.6$ Hz).

Received: June 23, 2000 [Z15316]

- [1] a) L. H. Gade, *Koordinationschemie*, WILEY-VCH, Weinheim, **1998**;
b) R. Demuth, F. Kober, *Grundlagen der Komplexchemie*, 2nd ed., Salle und Sauerländer, Frankfurt, **1992**.
- [2] a) A. F. Holleman, E. Wiberg, *Lehrbuch der Anorganischen Chemie*, 101st ed, de Gruyter, Berlin, **1995**, chap. XIV; b) F. A. Cotton, G. Wilkinson, C. A. Murillo, M. Bochmann, *Advanced Inorganic Chem-*

istry, 6th ed., Wiley, New York, **1999**, chap. 16.4; c) E. Riedel, *Moderne Anorganische Chemie*, de Gruyter, Berlin, **1999**, chap. 4.3.

- [3] a) G. Booth in *Organic Phosphorus Compounds*, Vol. 1 (Eds.: G. M. Kosolapoff, L. Maier), Wiley, New York, **1972**, chap. 3A; b) O. Stelzer, *Top. Phosphorus Chem.* **1977**, 9, 1–229; c) W. Levason, C. A. McAuliffe, *Phosphine, Arsine and Stibine Complexes of the Transition Elements*, Elsevier, Amsterdam, **1979**; d) W. Levason, C. A. McAuliffe, *Acc. Chem. Res.* **1978**, 11, 363–368; e) C. A. McAuliffe in *Comprehensive Coordination Chemistry*, Vol. 2 (Eds.: G. Wilkinson, R. D. Gillard, J. A. McCleverty), Pergamon, Oxford, **1987**, pp. 989–1066.
- [4] a) P. Schwab, N. Mahr, J. Wolf, H. Werner, *Angew. Chem.* **1994**, 106, 82–84; *Angew. Chem. Int. Ed. Engl.* **1994**, 33, 97–99; b) P. Schwab, Dissertation, Universität Würzburg, **1994**; c) H. Werner, *J. Organomet. Chem.* **1995**, 500, 331–336.
- [5] U. Herber, Dissertation, Universität Würzburg, **2000**.
- [6] a) H. Werner, B. Klingert, R. Zolk, P. Thometzek, *J. Organomet. Chem.* **1984**, 266, 97–107; b) B. Klingert, H. Werner, *J. Organomet. Chem.* **1987**, 333, 119–128.
- [7] Data for the X-ray structure analyses: **7**: Crystals from acetone, $\text{C}_{34}\text{H}_{36}\text{ClO}_2\text{PRh}_2$ ($M_r = 748.90$); crystal size $0.20 \times 0.20 \times 0.30$ mm³; monoclinic, space group $C2/c$ (no. 15), $a = 33.925(7)$, $b = 10.279(2)$, $c = 18.109(4)$ Å, $\beta = 98.15(3)^\circ$, $Z = 8$, $V = 6251(2)$ Å³, $\rho_{\text{calcd}} = 1.591$ g cm⁻³; $T = 173(2)$ K; $2\theta = 50.00^\circ$; 12940 reflections measured, 5450 were unique ($R_{\text{int}} = 0.0663$), and 3183 observed ($I > 2\sigma(I)$); IPDS (Stoe), $\text{MoK}\alpha$ radiation ($\lambda = 0.71073$ Å), graphite-monochromated; Lp correction. The structure was solved by direct methods and refined with the full-matrix, least-squares method; $R_1 = 0.0354$, $wR_2 = 0.0575$ (for 3183 reflections with $I > 2\sigma(I)$), $R_1 = 0.0814$, $wR_2 = 0.0632$ (for all 5450 data); data-to-parameter ratio 14.93; residual electron density $+0.537/-1.091$ e Å⁻³. **10**: Crystals from acetone, $\text{C}_{39}\text{H}_{43}\text{O}_4\text{PRh}_2$ ($M_r = 812.52$); crystal size $0.40 \times 0.40 \times 0.40$ mm³; monoclinic, space group $P2_1/c$ (no. 14), $a = 10.436(2)$, $b = 21.5125(10)$, $c = 16.678(4)$ Å, $\beta = 107.843(10)^\circ$, $Z = 4$, $V = 3564.2(11)$ Å³, $\rho_{\text{calcd}} = 1.514$ g cm⁻³; $T = 193(2)$ K; $2\theta = 53.92^\circ$; 9426 reflections measured, 7753 were unique ($R_{\text{int}} = 0.0216$) and 6642 observed ($I > 2\sigma(I)$); CAD4 (Enraf-Nonius), $\text{MoK}\alpha$ radiation ($\lambda = 0.71073$ Å), graphite-monochromated, Zr filter (faktor 15.20); Lp correction. The structure was solved by direct methods and refined with the full-matrix, least-squares method; $R_1 = 0.0292$, $wR_2 = 0.0662$ (for 6642 reflections with $I > 2\sigma(I)$), $R_1 = 0.0375$, $wR_2 = 0.0713$ (for all 7753 data); data-to-parameter ratio 18.37; residual electron density $+0.355/-0.856$ e Å⁻³. Crystallographic data (excluding structure factors) for the structures reported in this paper have been deposited with the Cambridge Crystallographic Data Centre as supplementary publication nos. CCDC-146302 (**7**) and CCDC-146303 (**10**). Copies of the data can be obtained free of charge on application to CCDC, 12 Union Road, Cambridge CB21EZ, UK (fax: (+44) 1223-336-033; e-mail: deposit@ccdc.cam.ac.uk).
- [8] For definition of “semibridging” see: C. Elschenbroich, A. Salzer, *Organometallics*, 2nd ed., VCH, Weinheim, **1992**, p. 225.
- [9] In the dinuclear compound $[(\text{acac})\text{Rh}(\mu\text{-CO})[\mu\text{-C}(\text{p-Tol})_2\text{Rh}(\text{acac})(\text{PMe}_3)]]$ the bond angle Rh–Rh–P is $132.89(4)^\circ$.^[5]
- [10] U. Herber, B. Weberndörfer, H. Werner, *Angew. Chem.* **1999**, 111, 1707–1710, *Angew. Chem. Int. Ed.* **1999**, 38, 1609–1613.
- [11] R. Bender, P. Braunstein, A. Dedieu, Y. Dusauroy, *Angew. Chem.* **1989**, 101, 931–934; *Angew. Chem. Int. Ed. Engl.* **1989**, 28, 923–925.
- [12] P. H. M. Budzelaar, P. W. N. M. van Leeuwen, C. F. Roobeek, *Organometallics* **1992**, 11, 23–25.
- [13] A. L. Balch, B. J. Davis, M. M. Olmstead, *Inorg. Chem.* **1993**, 32, 3937–3942.
- [14] a) T. Kruck, *Angew. Chem.* **1967**, 79, 27–43; *Angew. Chem. Int. Ed. Engl.* **1967**, 6, 53–69; b) J. F. Nixon, *Adv. Inorg. Chem. Radiochem.* **1970**, 13, 363–469.
- [15] The ^1H and ^{13}C NMR data of the phenyl groups were omitted for simplicity.

Cisplatin Changes the Mechanics of Single DNA Molecules**

Rupert Krautbauer, Hauke Clausen-Schaumann, and Hermann E. Gaub*

Recent experiments have revealed that on a molecular scale not only the energies, but also the forces involved in biological and chemical processes are important structural and functional parameters;^[1] for example, enzymes involved in gene regulation and gene expression exert piconewton (pN) forces on DNA to fulfill their biological function.^[2] Stretching experiments with individual molecules have shown that double-stranded DNA (dsDNA) can be overstretched to almost twice its contour length without rupturing.^[3–5] The force versus distance curves (see Figure 1 A) show a distinct plateau around 70 pN where the molecule is forced into a structural transition from its native B conformation to an overstretched state, called S-DNA. This transition is highly cooperative in native DNA. If the molecule is stretched beyond the B-S transition a second structural transition can be

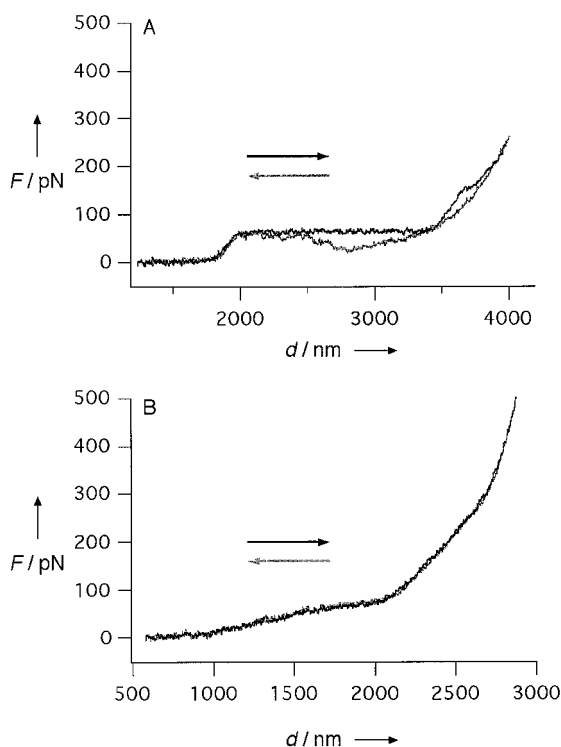


Figure 1. The force versus distance curves obtained on untreated λ -digest DNA (A) and after reaction with cisplatin (B). Here and in the following figures the black curve shows the extension and the gray curve the relaxation traces.

[*] Prof. Dr. H. E. Gaub, Dipl. Phys. R. Krautbauer, Dr. H. Clausen-Schaumann
Lehrstuhl für Angewandte Physik
Amalienstrasse 54, 80799 Munich (Germany)
Fax: (+49) 89-2180-2050
E-mail: gaub@physik.uni-muenchen.de

[**] Helpful discussions and support from Dipl. Phys. Jan Richter, Prof. Dr. Matthias Rief, Dipl. Phys. Ralf Seidel, and Dipl. Phys. Stefan Wild are gratefully acknowledged. This work was supported by the Deutsche Forschungsgemeinschaft.

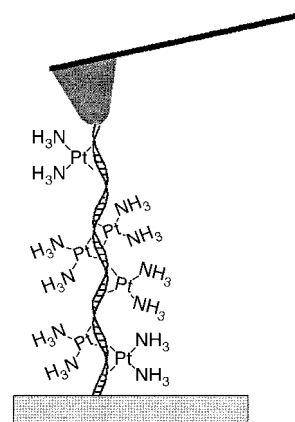
observed during which the double helix is split into two single strands. The flattening of the force curves in this melting transition also indicates that a certain degree of cooperativity is involved in the process. The molecule may recombine to its double helical conformation upon relaxation.^[6, 7] The extent of hysteresis (see Figure 1 A) between stretching and relaxation depends on the experimental parameters such as the pulling velocity.

Cisplatin is one of the most common anticancer drugs, and its interactions with DNA have been studied intensively for many years.^[8] Cisplatin is known to form cross-links in DNA, where it preferentially binds to the N7 atoms of guanine bases. The most common bifunctional products with dsDNA are the intrastrand cross-links between two guanine bases, which can either be neighboring or separated by any other base (G*G* or G*XG*, respectively), and the intrastrand cross-links between a guanine base and an adenine base (5'-A*G*-3'). Cisplatin can also form interstrand cross-links between two guanine bases at a GC sequence.

Here we report the direct observation of structural changes induced by cisplatin as measured by single-molecule force spectroscopy.^[9] Individual molecules with different base composition attached between an atomic force microscopy (AFM) tip and a gold substrate were stretched (Scheme 1) and the force versus distance curves were recorded. The experiments revealed significant changes in the mechanical properties of the DNA molecules after platination as compared to untreated molecules. These changes strongly depend on the sequence of the stretched molecules and we attribute them to the formation of bifunctional products between cisplatin and DNA, namely inter-strand and intrastrand cross-links.

The force versus distance curve taken on a single molecule of λ -digest DNA after reaction with an excess of cisplatin is shown in Figure 1 B. Here all of the adducts described above may have formed. The B-S transition is significantly less cooperative than in native DNA: instead of a flat plateau, a steady rise in force up to (73 ± 5) pN is observed. At forces of (318 ± 22) pN a second kink appears, but there is almost no flattening of the curve as is observed in the melting transition of untreated molecules.^[6, 7] The forces at which these features occur are independent of the pulling velocity within the experimentally accessible range (200 nm s^{-1} to $4 \mu\text{m s}^{-1}$). Moreover, the relaxation traces are virtually indistinguishable from the extension traces, even if the molecules are stretched up to forces of more than 500 pN. This observation shows that cisplatin inhibits a permanent mechanical separation of the double helix.

The same kind of stretching experiments were also carried out on synthetic dsDNA molecules of specific



Scheme 1. An individual platinated DNA molecule is stretched between an AFM tip and the substrate.

base composition in order to correlate the changes in the mechanics to certain adducts. Cisplatin can form only two different adducts in p(dGdC)-p(dGdC): the intrastrand cross-link G*CG* and the interstrand cross-link between two guanine bases at any two neighboring base pairs. The untreated molecules exhibit the well known B-S transition around 70 pN and a melting transition at higher forces (Figure 2A). As both strands in p(dGdC)-p(dGdC) are also complementary to themselves, they fold back onto themselves

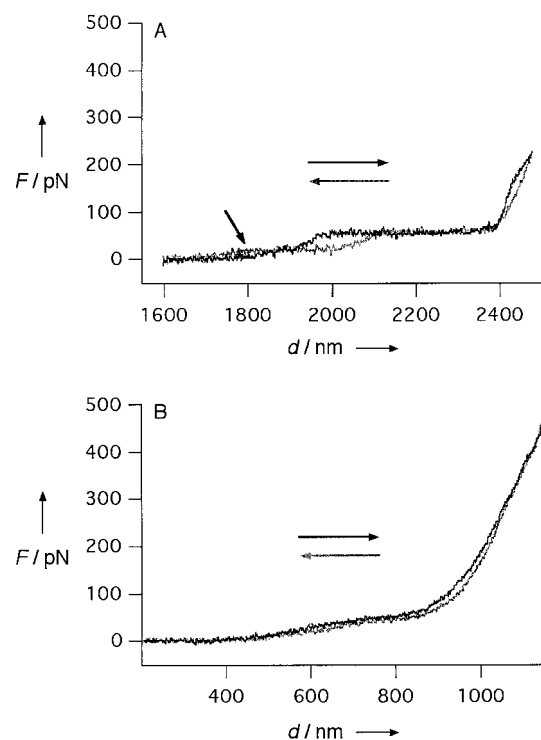


Figure 2. A) The force versus distance curves of untreated p(dGdC)-p(dGdC) shows the formation of hairpins (indicated by the arrow) after partial denaturation of the molecule. B) After reaction with cisplatin the melting is inhibited and no formation of hairpins is observed.

after initial strand separation. As reported previously, the formation of these hairpins can be observed in the force curves as plateaus at 20 pN (see arrow in Figure 2A). After platination (Figure 2B) the B-S transition loses its cooperativity and the force increases only slowly as the molecule is overstretched. The distinct melting transition has almost disappeared—there is no flattening in the curves above 80 pN. Almost no hysteresis between the stretching and relaxation traces can be found and no formation or unfolding of hairpins can be detected, even after stretching the molecules with forces of some hundred pN and keeping them stretched for a few minutes. Hence, all the structural changes that are induced in the molecules upon the application of mechanical tension are reversible on the time scale of the experiment.

Pure p(dAdT)-p(dAdT) molecules show far less mechanical stability in their native state (Figure 3A). The B-S transition starts at approximately 35 pN in the stretching curves. There is distinct hysteresis between stretching and relaxation, which shows that a force-induced melting of the duplex can already occur during the B-S transition (see also

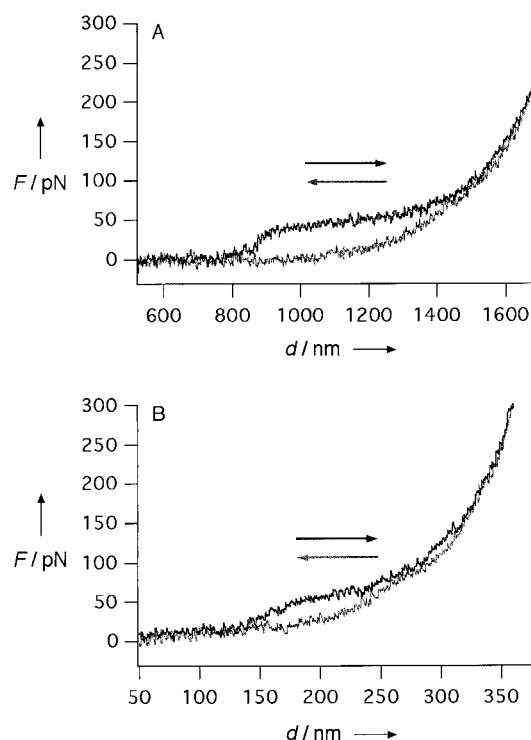


Figure 3. Force versus distance curves obtained on untreated (A) p(dAdT)-p(dAdT) and after treatment with cisplatin (B). After reaction with cisplatin the molecules can still be mechanically denatured.

[7]). No changes in the mechanical properties could be observed when p(dAdT)-p(dAdT) is stretched after incubation with cisplatin (Figure 3B). This result is not unexpected since no formation of bifunctional products of cisplatin with adenine and thymine bases has ever been reported. Hysteresis between the stretching and relaxation traces is seen, which indicates that the double helix can still be denatured by mechanical tension.

The stretching of p(dAdC)-p(dGdT), in which cisplatin can only form intrastrand cross-links between guanine bases (G*TG*), reveals more aspects of the sequence specificity of the drug. The stretching behavior of untreated molecules (Figure 4A) is very similar to that of λ -phage DNA with a cooperative B-S transition at forces of around 70 pN and melting at higher forces. In the stretching curves of the platinated molecules (Figure 4B), the B-S transition has again lost some of its cooperativity, which indicates a perturbation of the B-DNA conformation in the relaxed molecule. A second transition occurs at forces of around 300 pN which appears to be identical to the melting transition in the untreated molecules. However, upon relaxation the trace resembles the shape of the extension curve. The lack of hysteresis in the force curves, even after stretching the molecules beyond the melting transition, shows that the two strands must be able to recombine faster than the relaxation of the molecules occurs.

Cisplatin can only form intrastrand cross-links of the types G*G* or G*XG* on the p(dG) strand in p(dG)-p(dC). The stretching behavior of the native molecules (Figure 5A) is in good agreement with that of other B-DNA molecules with a cooperative B-S transition around 70 pN and a melting

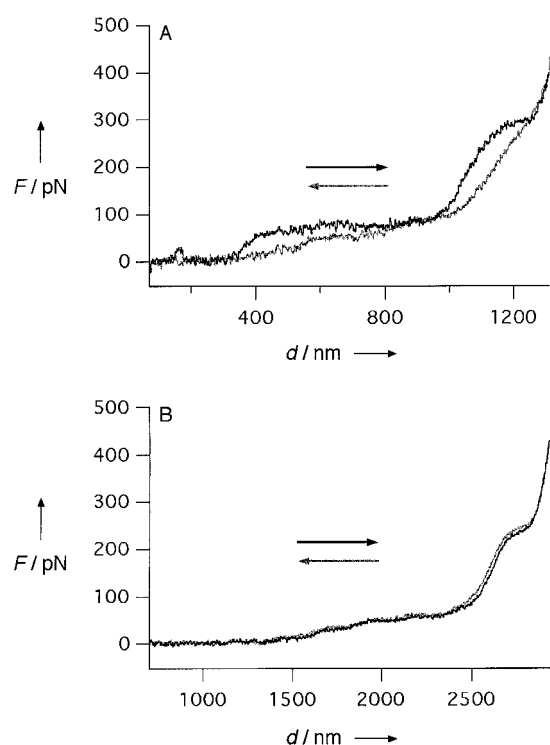


Figure 4. Force versus distance curves obtained on untreated p(dAdC)-p(dGdT) (A) and after reaction with cisplatin (B).

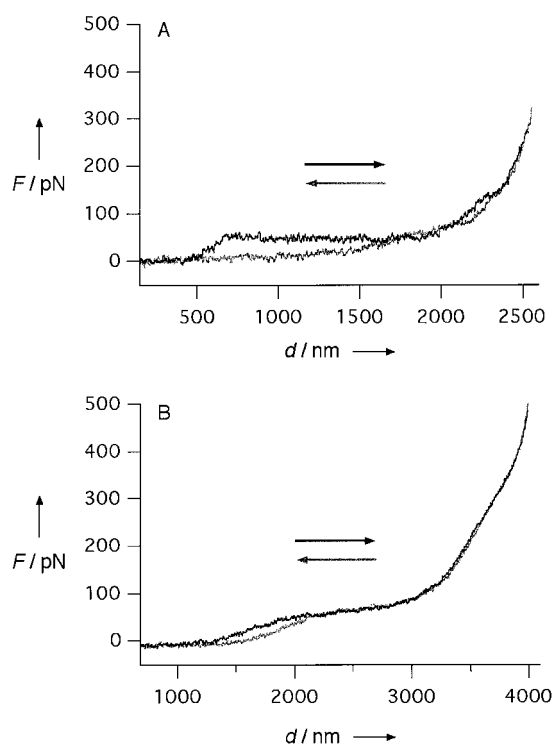


Figure 5. Force versus distance curves obtained on untreated p(dG)-p(dC) (A) and after platination (B).

transition at higher forces. The reaction with cisplatin again disrupts the B-S transition (Figure 5B), and makes it less cooperative. The melting transition has almost vanished in the stretching curves and only a slight kink above 300 pN can be seen. Compared to the untreated molecules there is only very

small hysteresis between the stretching and relaxation traces. Hysteresis only occurs if the molecules are stretched with forces above 80 pN and are subsequently relaxed to about 0.7 times their contour length. This result implies the existence of a mechanically induced structural reorganization in the molecule which occurs at forces above 80 pN. However, the double helix cannot be separated permanently.

Our results show that the B-S transition is very sensitive to the binding of cisplatin, which we attribute to deviations of the molecule from the native B-DNA conformation. In all molecules in which bifunctional adducts can be formed there is a loss of cooperativity in the B-S transition, which may indicate a disruption of the cooperative units of this process. Since new theoretical models predict a strong dependence of the cooperativity of the B-S transition on the base-stacking interaction,^[10] we attribute a change in the slope of the B-S plateau mainly to a change in the stacking interaction of DNA bases. Spectroscopic and calorimetric studies report lowered melting temperatures for DNA complexed with cisplatin. The reduced thermal stability is of enthalpic origin, which also suggests that the base-stacking interaction is disturbed.^[8] There is no distinct melting transition in all the molecules with possible G*G* adducts or interstrand cross-links, which indicates that a loss of cooperativity occurs in the melting process too. This proposal is in agreement with the reported broader temperature range for the melting of various types of DNA after complexation with cisplatin, which also suggests a lowered cooperativity.^[8] The strongly reduced hysteresis in all curves obtained for guanine containing molecules, however, suggests that—if there is strand separation in the first place—reannealing can occur much faster than in unplatinated molecules. We assume that the two strands in λ -DNA and p(dGdC)-p(dGdC) are kept in proximity to each other by the interstrand cross-links and this gives rise to a drastically accelerated reannealing of the denatured parts of the double helix which are not affected directly by the binding of the drug. The data also show that a permanent mechanical separation of the double helix is inhibited by interstrand cross-links. The intrastrand cross-links also seem to stabilize the double-stranded structure, as seen in the p(dAdC)-p(dGdT) molecules. This observation can be explained by the formation of two new hydrogen bonds in the G*TG* products. Molecular dynamics simulations show that these hydrogen bonds stabilize the double-stranded structure and keep the two strands in proximity.^[11]

However, the high force transition in the platinated p(dAdC)-p(dGdT) curves shows that the intrastrand cross-links do not disrupt the force-induced melting process itself. It is likely that the undisturbed Watson–Crick base pairs in this adduct can be separated mechanically at forces similar to those in untreated molecules, which leads to the melting transition in the force versus distance curves. As there appears to be a force-induced structural change in p(dG)-p(dC) which is not observed in p(dAdC)-p(dGdT), it seems unlikely that it is caused by products of the type G*GG*. In this case further studies are needed to reveal more details about the origin of this behavior and its possible consequences.

This study demonstrates the unique potential of single-molecule force spectroscopy as an analytical tool for obtain-

ing new structural information about DNA and its interaction with binding agents. It highlights the close correlation between structure and force and points out the particular role of force as a parameter controlling biological function, for example, in preventing mechanical strand separation in DNA.

Experimental Section

λ -BstE II digested DNA and cisplatin (*cis*-diammine(dichloro)platinum(II)) were purchased from Sigma (Deisenhofen, Germany). All other DNA molecules were purchased from Pharmacia (Freiburg, Germany). For the reaction, a saturated cisplatin stock solution (50 μ L) was added to a DNA-containing solution (150 μ L; 100 μ g mL⁻¹, 130 mM NaCl, 10 mM Tris, 1 mM EDTA, pH 8.0) and allowed to react for 24 h at 37 °C in darkness to give an excess of cisplatin per base pair. The sample preparation and the details of the force experiments are described elsewhere.^[6, 7] All experiments were carried out in Tris buffer (10 mM, pH 8.0) containing NaCl (150 mM) and EDTA (1 mM). The spring constants of all cantilevers (Microlevers, Park Scientific Instruments, Sunnyvale, CA) were determined using the thermal noise method.^[12] All force curves shown consist of 4096 points and were smoothed using an 11-point box integrator.

Received: February 4, 2000 [Z14648]

- [1] a) J. F. Allemand, D. Bensimon, R. Lavery, V. Croquette, *Proc. Natl. Acad. Sci. USA* **1998**, 95, 14152–14157; b) M. Grandbois, M. Beyer, M. Rief, H. Clausen-Schaumann, H. E. Gaub, *Science* **1999**, 283, 1727–1730; c) J. F. Léger, G. Romano, A. Sarkar, J. Robert, L. Bourdieu, D. Chatenay, J. F. Marko, *Phys. Rev. Lett.* **1999**, 83, 1066–1069.
- [2] a) M. Hegner, S. B. Smith, C. Bustamante, *Proc. Natl. Acad. Sci. USA* **1999**, 96, 10109–10114; b) J. F. Léger, J. Robert, L. Bourdieu, D. Chatenay, J. F. Marko, *Proc. Natl. Acad. Sci. USA* **1998**, 95, 12295–12299; c) M. D. Wang, M. J. Schnitzer, H. Yin, R. Landick, J. Gelles, S. M. Block, *Science* **1998**, 282, 902–907; d) H. Yin, M. D. Wang, K. Svoboda, R. Landick, S. M. Block, J. Gelles, *Science* **1995**, 270, 1653–1657.
- [3] P. Cluzel, A. Lebrun, C. Heller, R. Lavery, J.-L. Viovy, D. Chatenay, F. Caron, *Science* **1996**, 271, 792–794.
- [4] S. B. Smith, L. Finzi, C. Bustamante, *Science* **1992**, 258, 1122–1126.
- [5] S. B. Smith, Y. Cui, C. Bustamante, *Science* **1996**, 271, 795–798.
- [6] H. Clausen-Schaumann, M. Rief, C. Tolksdorf, H. E. Gaub, *Biophys. J.* **2000**, 78, 1997–2007.
- [7] M. Rief, H. Clausen-Schaumann, H. E. Gaub, *Nat. Struct. Biol.* **1999**, 6, 346–349.
- [8] a) S. E. Sherman, S. J. Lippard, *Chem. Rev.* **1987**, 87, 1153–1181; b) N. P. Johnson, J.-L. Butour, G. Villani, F. L. Wimmer, M. Defais, V. Pierson, V. Brabec, *Prog. Clin. Biochem. Med.* **1989**, 10, 1–24; c) C. A. Lepre, S. J. Lippard, *Nucleic Acids Molec. Biol.* **1990**, 4, 9–38; d) M. J. Bloemink, J. Reedijk, *Met. Ions Biol. Syst.* **1996**, 32, 641–685; e) D. Yang, A. H.-J. Wang, *Prog. Biophys. Molec. Biol.* **1996**, 66, 81–111; f) N. Poklar, D. S. Pilch, S. J. Lippard, E. A. Redding, S. U. Dunham, K. J. Breslauer, *Proc. Natl. Acad. Sci. USA* **1996**, 93, 7606–7611.
- [9] A. Janshoff, M. Neitzert, Y. Oberdörfer, H. Fuchs, *Angew. Chem.* **2000**, 112, 3346–3374; *Angew. Chem. Int. Ed.* **2000**, 38, 3212–3237.
- [10] Z. Haijun, Z. Yang, O.-Y. Zhong-can, *Phys. Rev. Lett.* **1999**, 82, 4560–4563.
- [11] Y. Z. Chen, Y.-I. Zhang, E. W. Prohofsky, *Phys. Rev. E* **1997**, 55, 5843–5848.
- [12] H. J. Butt, M. Jaschke, *Nanotechnology* **1995**, 6, 1–7.

Spherical Aromaticity in I_h Symmetrical Fullerenes: The $2(N+1)^2$ Rule**

Andreas Hirsch,* Zhongfang Chen, and Haijun Jiao

*Dedicated to Professor Fred Wudl
on the occasion of his 60th birthday*

Aromatic compounds exhibit a significantly raised diamagnetic susceptibility.^[1] The aromaticity of annulenes follows the Hückel rule. Due to their closed-shell structures, annulenes with $4N+2$ π electrons are not distorted (D_{nh} symmetry) and show strong diamagnetic ring currents, while $4N$ π annulenes are often distorted and have paratropic character. Although there is no such comparable rule for hetero- and polycyclic π systems, substructures with $4N+2$ π electrons frequently possess pronounced diamagnetic ring currents. Spherical fullerenes represent a special group of polycyclic π systems. In neutral C_{60} , an encapsulated ^3He nucleus is only subject to weak diamagnetic shielding.^[2] The 20 six-membered rings in C_{60} show diamagnetic ring currents,^[3] as indicated by the negative nucleus-independent chemical shifts (NICS)^[4] in the center^[5] as well as above and under the six-membered rings,^[6] but this effect is roughly compensated by the 12 paratropic five-membered rings^[3] (positive NICS values),^[5] therefore the ^3He chemical shift of $\text{He}@C_{60}$ is only $\delta = -6.3$.^[2] Other neutral fullerenes,^[7] such as $\text{He}@C_{70}$, $\text{He}@C_{76}$, $\text{He}@C_{78}$, $\text{He}@C_{82}$, and $\text{He}@C_{84}$, behave similarly^[5] and the highest diamagnetic endohedral chemical shift of $\delta = -28.8$ is observed for $\text{He}@C_{70}$.^[2] For the other cases, the chemical shifts are in the range between these two values.^[5] Dramatic effects are found upon reduction to hexaanions.^[8] While adding six electrons to C_{60} leads to an extreme shielding effect ($\delta(\text{He}@C_{60}^{6-}) = -48.7$), the opposite effect is observed for C_{70} ($\delta(\text{He}@C_{70}^{6-}) = 8.3$). Significantly, the five-membered rings in both cases become diatropic but the diatropy of the six-membered rings in C_{60} increases, whereas, to a large extent, it decreases in C_{70} . The experimentally determined ^3He NMR chemical shifts of fullerenes can be well reproduced computationally.^[3, 5, 7, 9–13] No correlation between magnetism and cluster size or charge of fullerenes has been found as yet. Herein, we demonstrate that the total diatropy of icosahedral fullerenes such as C_{20} ,^[14] C_{60} , and C_{80} ,^[15] (Figure 1) and their cluster distortion depend on the degree of the electron occupation in the valence shell. The resulting $2(N+1)^2$ rule represents the spherical analog to the $4N+2$ rule for the cyclic annulenes.

The π -electron system of an icosahedral fullerene can be approximately considered as a spherical electron gas, which surrounds the surface of a sphere. The wave functions of this electron gas can be characterized by the angular momentum quantum numbers ($l=0, 1, 2, 3, \dots$). The s shell ($l=0$) is

[*] Prof. Dr. A. Hirsch, Dr. Z. Chen, Dr. H. Jiao
Institut für Organische Chemie der Universität Erlangen–Nürnberg
Henkestrasse 42, 91054 Erlangen (Germany)
Fax: (+49) 9131-85-26864
E-mail: hirsch@organik.uni-erlangen.de

[**] This work was supported by the Alexander von Humboldt Stiftung and the Fonds der Chemischen Industrie. We thank Prof. Dr. Paul von Ragué Schleyer for valuable discussions and suggestions.

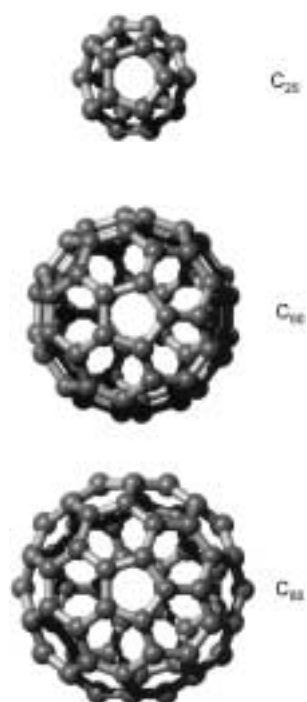


Figure 1. Models of the fullerenes C_{20} , C_{60} , and C_{80} .

(the g shell), are fully filled. The analogous shape of the calculated molecular s, p, d, f, and g orbitals of the π electron systems of C_{60}^{10+} and the hydrogen atomic orbitals is obvious (Figure 2). The B3LYP/6-31G*^[18] computed lengths of the [6,6] and [5,6] bonds of C_{60}^{10+} are 1.43 and 1.46 Å, while their alternation (0.03 Å) is smaller than that of C_{60} (0.06 Å) but comparable with that of the T_h -symmetrical hexakis adducts with benzenoid substructures such as $C_{66}(\text{COOEt})_{12}$.^[19] We have shown recently that the characteristic bond length alternation in C_{60} is due to the incomplete filling of the h shell ($l=5$).^[20] No distortion of the π electron system is expected for fully filled shells, since the angular momenta are symmetrically distributed. In C_{60} , only the h_u orbitals of the h shell are filled. The h_u orbitals display bonding interactions within the [6,6] bonds and antibonding interactions within the [5,6] bonds.^[20] Therefore, the molecule stabilizes itself by shortening the [6,6] bonds relative to the [5,6] bonds. In C_{60}^{6-} and C_{60}^{12-} , this effect is suppressed,^[21] since the next higher t_{1g} and t_{1u} orbitals^[22] are filled and display bonding interactions within the [5,6] bonds and antibonding interactions within the [6,6] bonds.

The correlation of aromatic character with the electronic level filling of C_{60} is shown in Table 2. The computed He chemical shift for the closed-shell $\text{He}@C_{60}^{10+}$ molecule is $\delta = -81.4$ and this is the largest theoretically estimated diamagnetic shielding up to now. The same behavior is found for the next smaller and larger icosahedral fullerenes C_{20} and C_{80} . The wave functions for $l=0, 1, 2, \dots$ also show a formal analogy to the atomic s, p, and d orbitals, and so forth. The diatropic character of C_{20} is smaller than that of C_{20}^{2+} , which has a closed-shell system fully filled with $n_c = 18$ electrons ($N=2$) (Table 1). As expected, the incomplete filling of the $l=3$ shell in C_{20} leads to an asymmetrical distribution of the angular

comparable to an atomic s orbital. The major difference is that the surface of the sphere represents a nodal plane and the electron density in the center should approach zero (Figure 2).^[16] The wave functions characterized by $l=1, 2, 3, \dots$ are analogous to the atomic p, d, and f orbitals, and so forth (Figure 1). The irreducible representations of the icosahedral symmetry can be deduced by lowering the symmetry using group theory (Table 1).^[17] Considering the Pauli principle, all π shells are fully filled with $2(N+1)^2$ electrons and show therefore a spherical charge distribution (Figure 2).

For example, the charged fullerene C_{60}^{10+} represents a closed-shell system, in which all π orbitals, including $l=4$

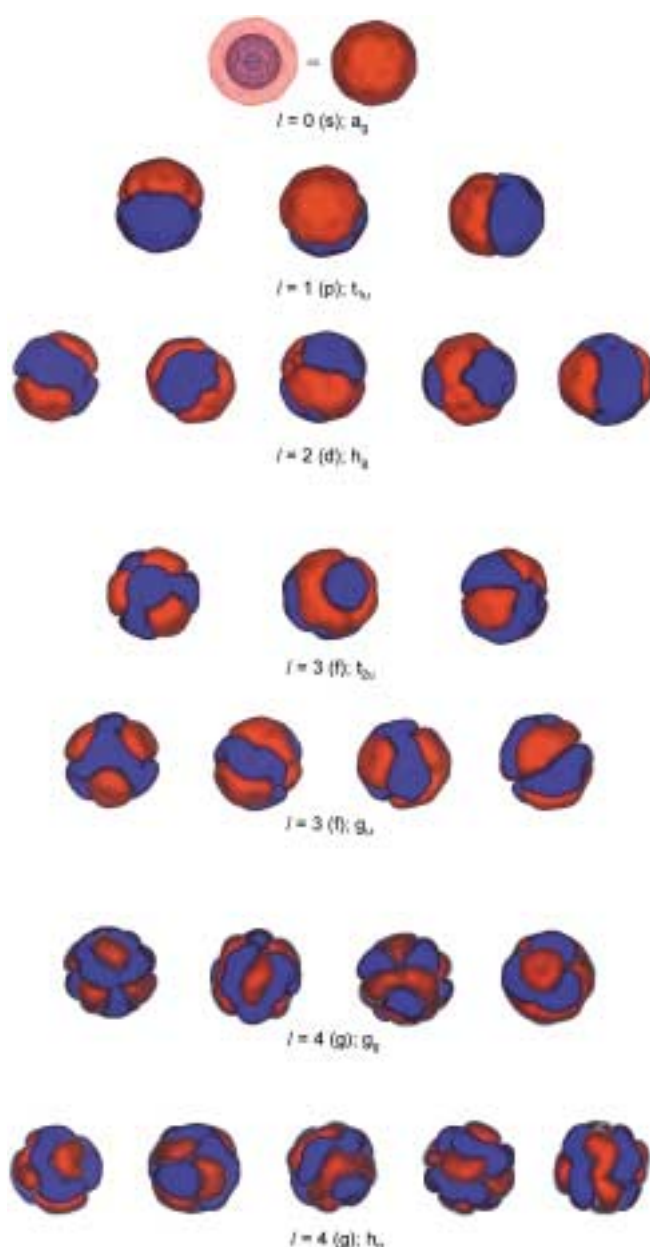


Figure 2. The π orbitals of C_{60}^{10+} calculated at the PM3/MNDO level.^[16] The position of the C_{60} skeleton is the same in all orbital presentations. The "s" orbital is also shown in a wire mesh presentation to make the nodal plane visible, which is otherwise hidden in the other representations.

momenta. Therefore, C_{20} is distorted (C_2 symmetry), while C_{20}^{2+} has I_h symmetry (Table 3). With the cluster size of 80, the octacation C_{80}^{8+} ($n_c = 72$) forms a closed-shell structure of I_h symmetry (Table 3). With increasing energetic order, the t_{1u} , t_{2u} , and h_u orbitals of the $l=5$ shell are completely filled. Therefore, the octacation exhibits the largest diamagnetic ring currents (in both the five- and six-membered rings) within this series. The stepwise filling up of the $l=6$ shell leads first to the decrease of the diamagnetic behavior and then, especially within C_{80}^{2-} , to the highly antiaromatic character. In C_{80}^{6-} , diamagnetic shielding appears again in the cluster center. Apart from the closed-shell C_{80}^{8+} with I_h symmetry, all other systems with partially filled shells are distorted to D_{5d} symmetry, most pronounced within paratropic C_{80}^{2-} .

Table 1. Electron ground-state configurations^[17] of the fully (bold) and partially filled π shells of icosahedral fullerenes.

$l^{[a]}$	Shell	Electrons per shell	$n_c^{[b]}$	HOMO (I_h symmetry ^[c])
0	s	2	2	a_g^2
1	p	6	8	t_{1u}^6
2	d	10	18	h_g^{10}
3	f	14	24	t_{2u}^6
			26	g_u^8
			32	$t_{2u}^6 g_u^8$
4	g	18	40	g_g^8
			42	h_u^{10}
			50	$g_g^8 h_g^{10}$
5	h	22	56	t_{1u}^6 or t_{2u}^6
			60	h_u^{10}
			62	$t_{1u}^6 t_{2u}^6$
			66	$t_{1u}^6 h_u^{10}$ or $t_{2u}^6 h_u^{10}$
			72	$t_{1u}^6 t_{2u}^6 h_u^{10}$

[a] Angular momentum quantum number for a spherical shell of π electrons. [b] Number of π electrons for the ground state configurations with closed shell or inner shell. [c] HOMO symmetries for all levels at a given l ; the superscripted digit shows the number of electrons for complete occupation of the shell.

Table 2. Calculated and experimental endohedral ^3He chemical shifts and symmetries of $\text{He}@C_{60}$ species with different degrees of π -electron filling.

Species	Symmetry	$\delta(^3\text{He})_{\text{calcd}}^{[b]}$	$\delta(^3\text{He})_{\text{expt}}$
C_{60}^{10+} (closed $l = 4$ shell)	$I_h^{[a]}$	− 81.4	−
C_{60}	$I_h^{[c]}$	− 8.0	− 6.3 ^[1]
C_{60}^{6-}	$I_h^{[a]}$	− 55.6	− 48.7 ^[8]

[a] Weak bond length alternation between the [6,6] and [5,6] bonds of 0.03 Å for C_{60}^{10+} and 0.02 Å for C_{60}^{6-} (B3LYP/6-31G*). [b] GIAO-SCF/3-21G//B3LYP/6-31G*. [c] Strong bond length alternation between [6,6] and [5,6] bonds of 0.06 Å (B3LYP/6-31G*).

Table 3. Calculated endohedral ^3He chemical shifts and symmetry of $\text{He}@C_{20}$ and $\text{He}@C_{80}$ species with different degrees of π -electron filling.

Species	Symmetry	$\delta(^3\text{He})^{[a]}$	NICS(5) ^[b]	NICS(6) ^[c]
C_{20}^{2+} (closed $l = 2$ shell)	I_h	− 66.2	− 25.1	−
C_{20}	C_2	− 31.7	− 1.1, − 12.7	−
C_{80}^{8+} (closed $l = 5$ shell)	I_h	− 82.9	− 29.1	− 30.3
C_{80}^{6+}	D_{5d}	− 70.0	− 25.1	− 26.6
C_{80}^{2+}	D_{5d}	− 54.5	− 17.2	− 20.2
C_{80} (triplet)	D_{5d}	− 8.4	− 17.2	− 4.2
C_{80}^{2-}	D_{5d}	+ 78.6	− 3.7	+ 29.8
C_{80}^{6-}	D_{5d}	− 32.8	− 18.9	− 13.4

[a] GIAO-SCH/3-21G//HF/6-31G*. [b] Nucleus-independent chemical shifts in the center of the five-membered rings. [c] Nucleus-independent chemical shifts in the center of the six-membered rings.

Compared to the cyclic annulenes, which follow the $4N+2$ rule, the spherical fullerenes show the maximum diatropy more rarely, and there are numerous intermediate situations, including molecules with both aromatic and antiaromatic regions. One key conclusion is that the entire molecule must be taken into account, in order to understand the aromatic properties of icosahedral fullerenes. The applicability of this introduced concept to less symmetrical fullerenes must be examined. It is assumed that local substructures, for example,

the graphite-like equatorial belt of C_{70} , also determines the magnetic behavior. This $2(N+1)^2$ rule should be universally applicable for all conjugated π systems, including inorganic compounds, in which the nuclei are distributed symmetrically over the spherical surface.

Received: April 7, 2000 [Z14955]

- [1] a) V. I. Minkin, M. N. Glukhovtsev, B. Y. Simkin, *Aromaticity and Antiaromaticity*, Wiley, New York, **1994**; b) P. von R. Schleyer, H. Jiao, *Pure Appl. Chem.* **1996**, 68, 209–218.
- [2] M. Saunders, H. A. Jimenez-Vazquez, R. J. Cross, S. Mroczkowski, D. I. Freedberg, F. A. L. Anet, *Nature* **1994**, 367, 256–258.
- [3] A. Pasquarello, M. Schluter, R. C. Haddon, *Science* **1992**, 257, 1660–1661.
- [4] P. von R. Schleyer, C. Maerker, A. Dransfeld, H. Jiao, N. J. R. van Eikema Hommes, *J. Am. Chem. Soc.* **1996**, 118, 6317–6318.
- [5] M. Bühl, *Chem. Eur. J.* **1998**, 4, 734–739.
- [6] P. von R. Schleyer, personal communication.
- [7] M. Saunders, H. A. Jimenez-Vazquez, R. J. Cross, W. E. Billups, C. Gesenberg, A. Gonzalez, W. Luo, R. C. Haddon, F. Diederich, A. Hermann, *J. Am. Chem. Soc.* **1995**, 117, 9305–9308.
- [8] E. Shabtai, A. Weitz, R. C. Haddon, R. E. Hoffman, M. Rabinovitz, A. Khong, R. J. Cross, M. Saunders, P.-C. Cheng, L. T. Scott, *J. Am. Chem. Soc.* **1998**, 120, 6389–6393.
- [9] M. Pasquarello, M. Schluter, R. C. Haddon, *Phys. Rev. A* **1993**, 47, 1783–1789.
- [10] V. Elser, R. C. Haddon, *Nature* **1987**, 325, 792–794.
- [11] M. Bühl, W. Thiel, H. Jiao, P. von R. Schleyer, M. Saunders, F. A. L. Anet, *J. Am. Chem. Soc.* **1994**, 116, 6005–6006.
- [12] M. Bühl, W. Thiel, *Chem. Phys. Lett.* **1995**, 233, 585–589.
- [13] J. Cioslowski, *Chem. Phys. Lett.* **1994**, 227, 361–364.
- [14] Recently, C_{20} in variable charged states were undoubtedly proved; H. Prinzbach, A. Weiler, P. Landenberger, F. Wahl, J. Wörth, L. T. Scott, M. Gelmont, D. Olevano, B. v. Issendorff, *Nature*, in press.
- [15] Presumably due to its unstable triplet character, the empty $I_h C_{80}$ was not isolated. In contrast, the endohedral derivative as $\text{Sc}_3\text{N}@C_{80}$, in which the I_h -symmetrical C_{80} cluster appears as a hexaanion, was recently isolated and fully characterized: S. Stevenson, G. Rice, T. Glass, K. Harloh, F. Cromer, M. R. Jordan, J. Craft, E. Nadj, R. Bible, M. M. Olmstead, K. Maltra, A. J. Fisher, A. L. Balch, H. C. Dorn, *Nature* **1999**, 401, 55–57.
- [16] Hyperchem 5.0, Hypercube, Waterloo, ON, **1997**.
- [17] M. S. Dresselhaus, G. Dresselhaus, P. C. Eklund, *Science of Fullerenes and Carbon Nanotubes*, Academic Press, San Diego, **1996**.
- [18] Gaussian 98, Revision A.5, M. J. Frisch, G. W. Trucks, H. B. Schlegel, G. E. Scuseria, M. A. Robb, J. R. Cheeseman, V. G. Zakrzewski, J. A. Montgomery, Jr., R. E. Stratmann, J. C. Burant, S. Dapprich, J. M. Millam, A. D. Daniels, K. N. Kudin, M. C. Strain, O. Farkas, J. Tomasi, V. Barone, M. Cossi, R. Cammi, B. Mennucci, C. Pomelli, C. Adamo, S. Clifford, J. Ochterski, G. A. Petersson, P. Y. Ayala, Q. Cui, K. Morokuma, D. K. Malick, A. D. Rabuck, K. Raghavachari, J. B. Foresman, J. Cioslowski, J. V. Ortiz, B. B. Stefanov, G. Liu, A. Liashenko, P. Piskorz, I. Komaromi, R. Gomperts, R. L. Martin, D. J. Fox, T. Keith, M. A. Al-Laham, C. Y. Peng, A. Nanayakkara, C. Gonzalez, M. Challacombe, P. M. W. Gill, B. Johnson, W. Chen, M. W. Wong, J. L. Andres, C. Gonzalez, M. Head-Gordon, E. S. Replogle, J. A. Pople, Gaussian Inc., Pittsburgh, PA, **1998**.
- [19] I. Lamparth, C. Maichle-Mössmer, A. Hirsch, *Angew. Chem.* **1995**, 107, 1755–1757; *Angew. Chem. Int. Ed. Engl.* **1995**, 34, 1607–1609.
- [20] A. Hirsch, *Top. Curr. Chem.* **1999**, 199, 1–65.
- [21] a) W. Andreoni, F. Gygi, M. Parinello, *Phys. Rev. Lett.* **1992**, 68, 823; b) J. Kohanoff, W. Andreoni, M. Parinello, *Chem. Phys. Lett.* **1992**, 198, 472.
- [22] In C_{60} , the t_{1g} orbitals of the $l = 6$ shell are filled prior to the t_{2u} orbitals of the $l = 5$ shell, see ref. [21] and R. C. Haddon, L. E. Brus, K. Raghavachari, *Chem. Phys. Lett.* **1986**, 125, 459–464.

Self-Repairing DNA Based on a Reductive Electron Transfer through the Base Stack**

Anja Schwögler, Lars T. Burgdorf, and Thomas Carell*

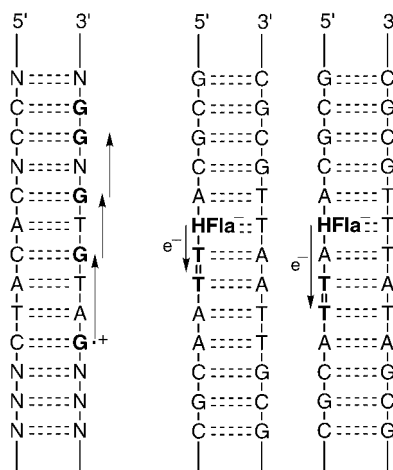
DNA photolyases utilize light energy to initiate the repair of highly mutagenic UV-induced cyclobutane pyrimidine dimers that form the major photolesions in DNA.^[1, 2] The basis of the repair reaction, which rescues many insects, fish, amphibians, and plants from UV-induced cell death and mutagenesis,^[3] is a light-induced electron transfer from a reduced and deprotonated flavin coenzyme to the DNA lesion.^[4] The lesion undergoes a spontaneous cycloreversion as its radical anion to the corresponding monomers.^[5] Although the general mechanism of the light-driven repair process is known, no information is currently available about the critical electron-donation process from the flavin donor to the dimer acceptor in the DNA strand.^[6] In particular, the question as to what extent the DNA double strand is able to mediate the transport of the electron in the base stack is still under debate (Scheme 1).^[7] This question is directly linked to

one basis for the seemingly “distance independent” hole transfer.^[11–15]

A deeper understanding of oxidative damage to DNA and the design of DNA-based bioanalytical devices is crucially dependent upon the elucidation of the electron- and hole-transfer properties of double-stranded DNA.^[16, 17] Herein we report the preparation of DNA strands containing a flavin building block and a cyclobutane thymidine dimer lesion.^[18, 19] These doubly modified DNA strands show light-induced self-repairing properties and allowed insight to be gained into the ability of DNA to mediate a reductive (“surplus”) electron-transfer reaction.^[20–22]

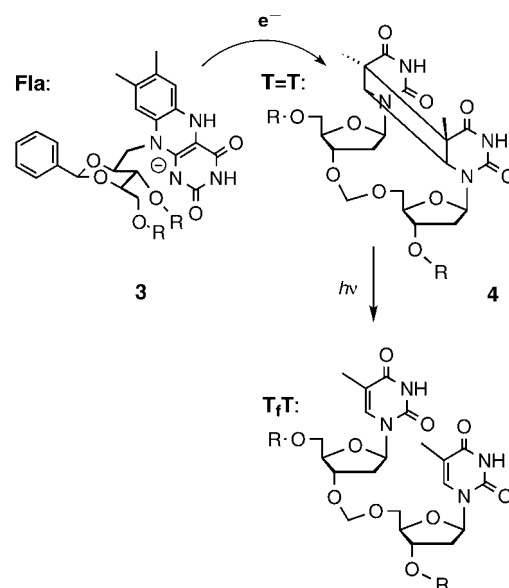
The oligonucleotides **1** and **2** were synthesized for studying the reductive self-repairing electron transfer and the repair process (Scheme 2). All the DNA double strands investigated contain the riboflavin coenzyme nucleobase **3** and the thymidine dimer DNA lesion **4** as central units. The synthesis and the incorporation of both building blocks into DNA was performed as recently described.^[18, 19, 23] The melting temperatures and fluorescence spectra of the double strands were measured to investigate whether the flavin and dimer

Oxidative Hole Transfer Reductive Electron Transfer



Scheme 1. Schematic depiction of the hole-transfer process (oxidative electron transfer) via guanine bases and of the proposed reductive electron-transfer event leading to the self-repair of the DNA.

investigations of the electron hole transport properties of DNA.^[8] Hole transfer was recently shown to proceed over relatively large distances in an undisturbed DNA double strand.^[9, 10] Experiments carried out recently provided compelling evidence that a hopping process in which guanine bases (which react to form guanine radical cations) act as stepping stones in the DNA double helix (Scheme 1) could be



1T	5' -d(GCGCA- Fla - T = T AACGC) -3' 3' -d(CGCGT-T - A-ATTGCG) -5'
1C	5' -d(GCGCA- Fla - T = T AACGC) -3' 3' -d(CGCGT - C - A-ATTGCG) -5'
1G	5' -d(GCGCA- Fla - T = T AACGC) -3' 3' -d(CGCGT - G - A-ATTGCG) -5'
1A	5' -d(GCGCA- Fla - T = T AACGC) -3' 3' -d(CGCGT - A - A-ATTGCG) -5'
2T	5' -d(GCGCA- Fla - AT = T ACGC) -3' 3' -d(CGCGT - T - TA-ATTGCG) -5'
2C	5' -d(GCGCA- Fla - AT = T ACGC) -3' 3' -d(CGCGT - C - TA-ATTGCG) -5'

Scheme 2. Electron-transfer initiated cycloreversion of an analogue of the thymidine dimer lesion in DNA. The six flavin- and dimer-modified DNA double strands are also indicated. R shows the continuation of the DNA strands.

[*] T. Carell, A. Schwögler, L. T. Burgdorf
Fachbereich Chemie
Philipps-Universität Marburg
Hans-Meerwein-Strasse, 35032 Marburg (Germany)
Fax: (+49) 6421-2822189
E-mail: carell@mail.uni-marburg.de

[**] We thank the University of Marburg and the Volkswagenstiftung for financial support. The Boehringer Ingelheim Fonds is gratefully acknowledged for a scholarship to L.T.B.

containing oligonucleotides^[24] form stable double-stranded DNA, which was found to be crucial for the transfer of a hole through DNA. Figure 1A shows as an example the melting curves determined at 275 nm for the flavin- and dimer-containing double strand **2T**. The normal melting behavior

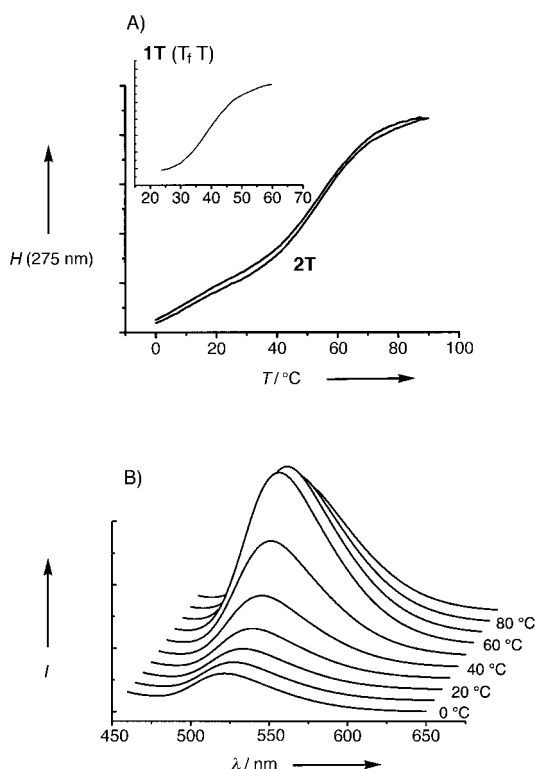


Figure 1. A) Melting curve of **2T** showing both the heating and the cooling curve measured at 275 nm ($c_{\text{DNA}} = 3 \mu\text{M}$, 150 mM NaCl, 0.01 M Tris pH 7.5). The inset depicts the melting curve of **1T** at 460 nm. This double strand has a Fla-T "base pair" and a formacetal-linked thymidyl and thymidine bases (T_fT ; $c_{\text{DNA}} = 30 \mu\text{M}$, 0.01 M Tris, pH 7.5, 150 mM NaCl). B) Dependence of the fluorescence of strand **1T** on temperature

of the doubly modified DNA double strands is clearly evident; no hysteresis between the heating and the cooling curve is observed. Double-strand melting was also detectable at 460 nm, where only the flavin coenzyme absorbs light (Figure 1A inset). This hypochromicity effect of the flavin base supports our assumption that the coenzyme is positioned inside the DNA double helix.^[18] The melting points of all flavin-containing DNA strands were found to depend on the flavin counterbase chosen; for example, the following melting points were measured for strand **1** with the various counterbases: **1T**: 58 °C, **1C**: 56 °C, **1G**: 51 °C, and **1A**: 53 °C ($c_{\text{DNA}} = 3 \mu\text{M}$, 150 mM NaCl, 0.01 M Tris pH 7.5). The highest melting points were measured when thymidine and cytidine were used, and hence were consequently chosen as the flavin counterbases in this study.

Further evidence for the presence of the flavin in the DNA-base stack was obtained from fluorescence studies. The fluorescence of the flavin in a double strand is strongly quenched if a guanosine acts as the counterbase (**1G**). The reason for the decreased fluorescence is that a light-induced electron transfer occurs from the guanosine to the flavin, which yields a transient $G^{+\cdot} \cdots \text{Fla}^-$ zwitterion. The reduced

fluorescence is consistent with the hypothesis that both heterocycles are in contact, which is only possible if the flavin is positioned in the DNA stack. Furthermore, studies of the temperature dependence of the fluorescence of the DNA double strand **1G** show a strong increase in the flavin fluorescence upon melting the double strand (Figure 1B). The hypochromicity observed in the UV-melting experiments and the temperature-dependence of the fluorescence data provide evidence for our assumption that the flavin coenzyme is positioned inside the DNA double helix.

In order to investigate the reductive electron transfer from the flavin to the dimer in the DNA base stack the DNA strands **1T**, **1C**, **2T**, and **2C** were dissolved in Tris buffer (pH 7.5, 150 mM NaCl) and transferred into fluorescence cuvettes and stoppered with a rubber septum. After purging the cuvettes with nitrogen for 10 min, sodium dithionite solution was added to reduce and deprotonate ($pK_a = 6.8$) the flavin coenzyme. The fluorescence arising from the flavin disappeared after reduction. This was monitored during irradiation to ensure complete reduction of the flavin during the whole experiment.^[25] The fluorescence cuvettes were finally exposed to monochromatic light in a fluorimeter at 360 nm or to daylight. Nitrogen was slowly bubbled through the DNA solution during its exposure to light to ensure the irradiation conditions were homogenous. Small aliquots were removed from the assay solution with a microsyringe and immediately reoxidized by shaking the samples in the presence of air. Analysis of the samples by reversed-phase HPLC (Figure 2) showed that the dimer lesions in the DNA

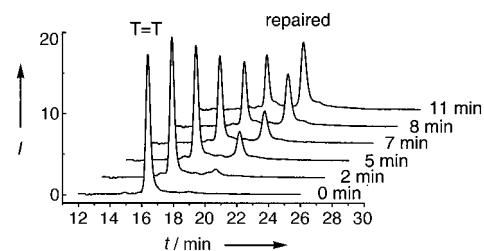


Figure 2. HPLC traces of the aliquots taken during an irradiation experiment with strand **2C** showing the clean conversion of the damage-containing DNA strand into the repaired strand.

double strands were cleanly repaired. The appearance of only one new oligonucleotide was detected, which was proved to be the repaired DNA strand by co-injection. It is clear from Figure 2 that the photo reaction induces a self-repair of the lesion-containing DNA strand into the repaired strand. No other oligonucleotides are formed, which means that side reactions causing DNA degradation do not occur. In fact, complete self-repair of the lesion-containing oligonucleotides under our conditions was accomplished after just 30 min of irradiation. No repair was observable in the absence of light.^[26–28] Further experiments, in which a flavin-containing DNA strand was reduced and irradiated in the presence of a DNA strand containing a noncomplementary thymine dimer showed no repair either. Both control experiments prove that the self-repair process is a light-driven reaction that proceeds intramolecularly inside the DNA double strand.

To obtain insight into the ability of DNA to mediate the reductive electron-transfer process all four DNA double strands **1T**, **1C**, **2T**, and **2C**, which contain either a Fla-T or a Fla-C base pair and two different flavin–dimer distances, were investigated for their self-repairing capabilities. The data (Table 1) show that the double strands **1T** and **2T** having a Fla-T base pair (highest melting points) show a faster self-repair than **1C** and **2C**, possibly because they form the most undisturbed double helices.

Table 1. Repair yield data ($\pm 10\%$) and quantum yields ($\pm 50\%$) of the photo process in the DNA strands **1T**, **1C**, **2T**, and **2C**.^[a]

DNA double strand	Repair yield (5 min) [%]	Quantum Yield Φ
1T 5'-d(GCGCA-Fla-T=TAACGCG)-3' 3'-d(CGCGT-T-A ATTGCGC)-5'	35	0.004
1C 5'-d(GCGCA-Fla-T=TAACGCG)-3' 3'-d(CGCGT-C-A ATTGCGC)-5'	35	0.004
2T 5'-d(GCGCA-Fla-AT=TACGCG)-3' 3'-d(CGCGT-T-TA ATGCGC)-5'	20	0.003
2C 5'-d(GCGCA-Fla-AT=TACGCG)-3' 3'-d(CGCGT-C-TA ATGCGC)-5'	15	0.002

[a] $c_{\text{DNA}} = 40 \mu\text{M}$, 360 nm, 150 mM NaCl, 0.01M Tris, pH 7.5, the photon flux was measured with a United Detector Technology Dual Channel Optometer, $\epsilon_{\text{flavinH}^+} = 4900 \text{ L M}^{-1} \text{ cm}^{-1}$.

In addition, the repair of the double strands **1T** and **1C** were found to proceed to about 35 % completion after 5 min. This is just a factor of two more efficient than **2T** and **2C** (20 and 15 %, respectively), in which an additional A-T base pair separates the electron-transfer partners. This small difference is a very surprising result to us, because the distance between the flavin and the dimer unit increases from 11 (in **1T** and **1C**) to 17 (in **2T** and **2C**) single bonds. In the case of the oxidative hole transfer in DNA such an additional A-T base pair between the electron hole and the next donating guanosine base would result in an approximately tenfold decrease in the reaction yield.^[11]

The data show that a reductive electron transfer through the base stack from a flavin electron donor to a UV dimer lesion, as performed by the enzyme DNA photolyase, is possible.^[22, 29] The light-driven electron transfer leads exclusively to the cycloreversion of the dimer lesion. This process is effective even when the DNA lesion and the flavin donor are separated by an intervening base pair. The results open a new avenue for the development of the therapeutic repair of thymine dimers and shows that the arming of DNA with flavin coenzymes allows functional oligonucleotides with, in our case, self repairing properties to be created.

Received: July 31, 2000 [Z15558]

- [1] A. Sancar, *Biochemistry* **1994**, 33, 2–9.
- [2] T. Carell, *Angew. Chem.* **1995**, 107, 2697–2700; *Angew. Chem. Int. Ed. Engl.* **1995**, 34, 2491–2494.
- [3] J.-S. Taylor, *Acc. Chem. Res.* **1994**, 27, 76–82.
- [4] P. F. Heelis, R. F. Hartman, S. D. Rose, *Chem. Soc. Rev.* **1995**, 289–297.
- [5] T. Carell, R. Epple, *Eur. J. Org. Chem.* **1998**, 1245–1258.
- [6] F. D. Lewis, X. Liu, Y. Wu, S. E. Miller, M. R. Wasielewski, R. L. Letsinger, R. Sanishvili, A. Joachimiak, V. Tereshko, M. Egli, *J. Am. Chem. Soc.* **1999**, 121, 9905–9906.

- [7] J. Jortner, M. Bixon, T. Langenbacher, M. E. Michel-Beyerle, *Proc. Natl. Acad. Sci. USA* **1998**, 95, 12759–12765.
- [8] F. D. Lewis, T. Wu, Y. Zhang, R. L. Letsinger, S. R. Greenfield, M. R. Wasielewski, *Science* **1997**, 277, 673–676.
- [9] D. B. Hall, R. E. Holmlin, J. K. Barton, *Nature* **1996**, 382, 731–735.
- [10] R. E. Holmlin, P. J. Dandliker, J. K. Barton, *Angew. Chem.* **1997**, 109, 2830–2848; *Angew. Chem. Int. Ed. Engl.* **1997**, 36, 2715–2730.
- [11] E. Meggers, M. E. Michel-Beyerle, B. Giese, *J. Am. Chem. Soc.* **1998**, 120, 12950–12955.
- [12] B. Giese, S. Wessely, M. Sporman, U. Lindemann, E. Meggers, M. E. Michel-Beyerle, *Angew. Chem.* **1999**, 111, 1050–1052; *Angew. Chem. Int. Ed.* **1999**, 38, 996–998. Since the nucleobases T and C possess a similar reduction potential, which is more positive than A and G, these authors postulate a sequence-independent electron-hopping process from a donor to an acceptor attached to the DNA strand. For such a system see ref. [20].
- [13] A phonon-assisted polaron-hopping model to explain charge transport through DNA has been forwarded by: D. Ly, L. Sanii, G. B. Schuster, *J. Am. Chem. Soc.* **1999**, 121, 9400–9410; P. T. Henderson, D. Jones, G. Hampikian, Y. Kan, G. B. Schuster, *Proc. Natl. Acad. Sci. USA* **1999**, 96, 8353–8358; see also G. B. Schuster, *Acc. Chem. Res.* **2000**, 33, 253–260.
- [14] F. D. Lewis, X. Liu, J. Liu, S. E. Miller, R. T. Hayes, M. R. Wasielewski, *Nature* **2000**, 406, 51–53.
- [15] S. O. Kelley, J. K. Barton, *Science* **1999**, 283, 375–381.
- [16] W. K. Pogozelski, T. D. Tullius, *Chem. Rev.* **1998**, 98, 1089–1107.
- [17] D. J. Caruana, A. Heller, *J. Am. Chem. Soc.* **1999**, 121, 769–774.
- [18] A. Schwögler, T. Carell, *Org. Lett.* **2000**, 2, 1415–1418.
- [19] J. Butenandt, A. P. M. Eker, T. Carell, *Chem. Eur. J.* **1998**, 4, 642–653.
- [20] T. J. Meade, J. F. Kayyem, *Angew. Chem.* **1995**, 107, 358–360; *Angew. Chem. Int. Ed.* **1999**, 34, 352–354.
- [21] M. G. Debijs, M. T. Milano, W. A. Bernhard, *Angew. Chem.* **1999**, 111, 2926–1231; *Angew. Chem. Int. Ed.* **1999**, 38, 2752–2755.
- [22] S. Steenken, *Biol. Chem.* **1997**, 378, 1293–1297.
- [23] J. Butenandt, L. T. Burgdorf, T. Carell, *Synthesis* **1999**, 1085–1105.
- [24] Several detailed NMR studies prove that the dimer lesion is positioned inside the DNA double helix. See for example: J. Kemmick, R. Boelens, T. Koning, G. A. van der Marel, G. A. van Boom, R. Kaptein, *Nucleic Acids Res.* **1987**, 15, 4645–4653; K. McAteer, Y. Jing, J. Koa, J.-S. Taylor, M. A. Kennedy, *J. Mol. Biol.* **1998**, 282, 1013–1032; J.-K. Kim, D. Patel, B.-S. Choi, *Photochem. Photobiol.* **1995**, 62, 44–50.
- [25] Reduction of the flavin in the DNA environment is fully reversible. Shaking the assay solution in the presence of air caused complete reoxidation accompanied by the reoccurrence of the flavin fluorescence.
- [26] The repair of a thymine dimer as its radical cations with a rhodium intercalator or a naphthalenediimide, which both remove light-induced an electron from the DNA strand has been reported by P. J. Dandliker, R. E. Holmlin, J. K. Barton, *Science* **1997**, 275, 1465–1468; D. A. Vicić, D. T. Odom, M. E. Núñez, D. A. Gianolio, L. W. McMaughlin, J. K. Barton, *J. Am. Chem. Soc.* **2000**, 122, 8603–8611, and ref. [27]. Most recent studies question oxidative dimer repair in DNA.^[28] Our own results show that irradiation of DNA strands containing the nonreduced flavin, which also abstracts an electron from the DNA, gives no detectable dimer repair.
- [27] P. J. Dandliker, M. E. Núñez, J. K. Barton, *Biochemistry* **1998**, 37, 6491–6502.
- [28] A. K. Dotse, E. K. Boone, G. B. Schuster, *J. Am. Chem. Soc.* **2000**, 122, 6825–6833.
- [29] Radiolysis studies show that thymidine and cytidine radical anions are most likely formed after the addition of an electron since they are the nucleobases with the most positive reduction potentials. Rapid protonation of the cytidine radical anion ($pK_a > 13$) is a highly favorable reaction and should strongly compete with a potential electron-hopping process. See for example ref. [22] and S. Steenken, J. P. Telo, H. M. Novais, L. P. Candeias, *J. Am. Chem. Soc.* **1992**, 114, 4701–4709. Electron transfer from a thymidine or cytidine radical anion to the dimer should be an endergonic reaction because of the more negative reduction potential of the dimer unit: S.-R. Yeh, D. E. Falvey, *J. Am. Chem. Soc.* **1992**, 114, 7313–7314. Further studies are now needed to explain the basis for the self-repair process.

Room Temperature Oxidation of Carbon Monoxide Catalyzed by Hydrous Ruthenium Dioxide**

Ling Zang and Horst Kisch*

The catalytic oxidation of carbon monoxide to carbon dioxide at room temperature and atmospheric pressure is a key process for respiratory protection and industrial air purification. Examples where it is used include safety devices for mining industry, space technology, and deep sea diving; removal of CO in flue gases; the stabilization of carbon dioxide lasers; and fuel cells.^[1] Numerous studies were therefore performed to improve the catalytic oxidation of carbon monoxide at low temperatures, typically less than 100 °C. It was found that noble metals such as Au, Ag, Pd, Pt, and Ru supported on various metal oxides can catalyze the oxidation of CO in the range of 30–75 °C.^[2] Similar results were reported for gold catalysts supported on MnO_x, Fe₂O₃, Co₃O₄, NiO, and CuO.^[3] However, most of these metal catalysts can not be applied practically in humid air since the presence of water induces anodic corrosion. For this reason many attempts have been made to use mixed metal oxides as possible substitutes for the precious metals. One of the best known is hopcalite^[4] (CuMn₂O₄), which is the active component of various technical devices. Further examples are SnO₂/CuO gels^[5], Mn/Ag composite oxides,^[6] Cu/Zn oxides,^[7] and supported PdCl₂/CuCl₂ catalysts.^[8] Herein we report that a simple binary oxide, hydrous ruthenium(IV) oxide, is an efficient catalyst for the low-temperature oxidation of carbon monoxide by humid air. Although this oxide has been widely used as a catalyst for the photo and thermal oxidation of water to O₂,^[9, 10] no report on CO oxidation under the corresponding mild reaction conditions could be found in the literature. These experimental conditions differ significantly from very recent findings in which CO is oxidized at the RuO₂ (110) crystal surface at about 600 K. Heating to a higher temperature reconstitutes the surface.^[11]

Figure 1 displays conversion versus time curves for the room-temperature oxidation of CO (0.8 vol %) in undried air catalyzed by RuO₂·*x*H₂O powder spread onto a glass plate carrier. Almost 40% of the CO was converted into CO₂ after 20 min. The stability of the catalyst is demonstrated by the negligible change in activity upon multiple use. In situ IR spectroscopy on the reaction revealed the presence of an isosbestic point, which suggests a clean oxidation reaction occurs.

To investigate the dependence of activity on the heating treatment, a series of RuO₂·*x*H₂O samples were dried at various temperatures and their catalytic activity was tested at 21 ± 1 °C in a CO/O₂ mixture with a partial pressure ratio (*p*(CO)/*p*(O₂)) of 1/1 (Table 1). The untreated sample con-

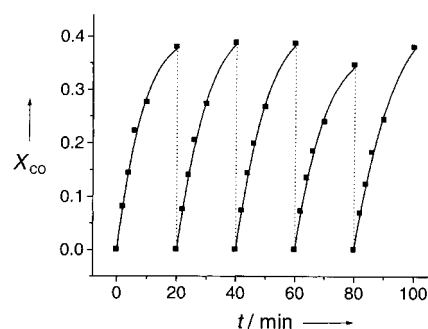


Figure 1. Five successive cycles for the room temperature oxidation of CO in the presence of RuO₂·*x*H₂O (dried at 150 °C) in undried air. The dotted lines correspond to the readjustment of the CO concentration (0.8 vol % in air) after the previous run.

Table 1. Dependence of the initial rate of reaction (*v*₀ [mL min⁻¹]) and CO conversion (*X*_{CO} [%]) after 10 min^[a] on the water content (*x*_{H₂O} [wt %]), after various drying times *t* and different temperatures *T*; *p*(CO)/*p*(O₂) = 1/1.

<i>T</i> [°C]	<i>t</i> [h]	<i>x</i> _{H₂O} [wt %]	<i>v</i> ₀ mL min ⁻¹	<i>X</i> _{CO} [%]
RT ^[b]	1.5	82	0.1	0.1
21	15 ^[c]	33	5.3	2.9
60	12	16	75	36
150	4	10	82	46
250	10	9	90	42
450	0.5	2	1.1	0.7
600	2	0.6	0.9	0.6

[a] Based on the amount of CO₂ produced. [b] Highly hydrous sample, 1.5 h of exposure to ambient air after filtering off. [c] Dried in air.

tained 82 wt % of water and exhibited almost negligible activity. When it was dried in ambient air, its initial rate increased from 0.1 to 5.3 mL min⁻¹. The highest initial rates of 80–90 mL min⁻¹ and conversions of 42–46% (after 10 min) were observed when the samples were dried at 150–250 °C; in these cases the powders contained 9–10 wt % of H₂O. When the samples were dried at 450 or 600 °C the water content decreased sharply to 0.6% and the activity was almost as low as for the highly hydrous sample. This large decrease in the activity may arise from partial decomposition or a decrease in the specific surface area caused by the process of sintering and crystallization.^[9] The initial rate of 71 mL min⁻¹ for a sample loaded on silica gel at low coverage (RuO₂·*x*H₂O/SiO₂ = 3/10 (wt/wt)) almost matches that of the unsupported catalyst dried at 150 °C. This result may be attributed to the large surface area of silica gel (340 m² g⁻¹), which provides a higher concentration of catalytic sites.

TiO₂ powder, which consists mainly of the anatase and to a lesser extent of the rutile modification, was chosen as another support because of its nontoxicity and the fact that RuO₂ has a rutile structure. A further advantage of TiO₂ is that it adheres firmly to the surface of the glass plate carrier. It is thus possible to use the catalyst repeatedly under exactly the same conditions. We therefore investigated in this system the oxidation of CO in the temperature range of 22–79 °C using a mixture of CO and O₂ with a partial pressure ratio of 1/1 (Figure 2a). The activation energy (*E*_a) was determined as 8.6 kcal mol⁻¹ from the temperature dependence of the initial

[*] Prof. Dr. H. Kisch, Dr. L. Zang
Institut für Anorganische Chemie der Universität Erlangen-Nürnberg
91058 Erlangen (Germany)
Fax: (+49) 9131-857363
E-mail: horst.kisch@chemie.uni-erlangen.de

[**] L.Z. is indebted to the Alexander-von-Humboldt-Stiftung for a fellowship.

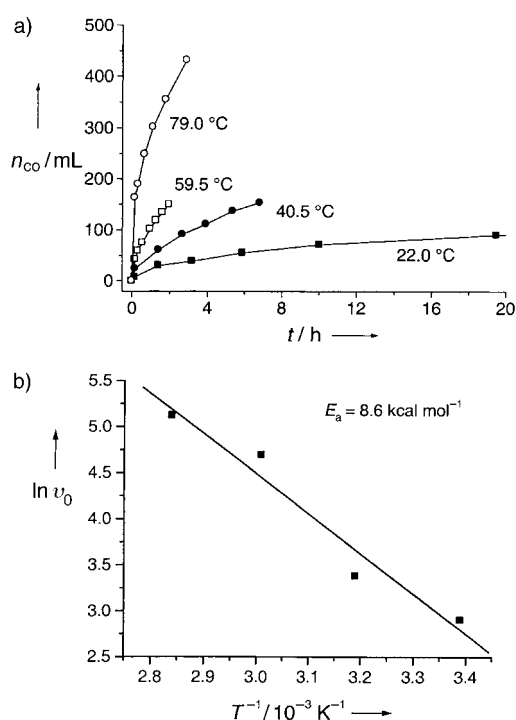


Figure 2. Temperature-dependence of the CO oxidation when catalyzed by TiO_2 -supported $\text{RuO}_2 \cdot x\text{H}_2\text{O}$ (dried at 200°C); $p(\text{CO})/p(\text{O}_2) = 1/1$. a) The turnover–time curve, $n_{\text{CO}} = \text{CO consumption}$; b) The Arrhenius plot, where v_0 is the initial rate of the reaction.

rate (Figure 2b). This value is much lower than the ones reported for other metal oxides such as Cu_2O ($13.9 \text{ kcal mol}^{-1}$), CuO ($16.7 \text{ kcal mol}^{-1}$), and Fe_2O_3 ($26.4 \text{ kcal mol}^{-1}$).^[12, 13] This lower value may explain the higher activity of the hydrous ruthenium oxide at room temperature.

Table 2 presents the effect of the composition of the CO/O_2 mixture on the rate of CO oxidation at room temperature with a catalyst dried at 150°C . It is evident that the initial reaction rate increases steadily with increasing partial pressure of CO.

Table 2. CO oxidation rates v_0 and conversion $X^{[a]}$ at different CO/O_2 partial pressure ratios.

CO/O_2	1/11.5	1/4	1/1.5	1/0.89	1/0.56	1/0.16
$v_0 [\text{mL min}^{-1}]^{[b]}$	5.4	12	56	84	113	150
$X [\%]^{[c]}$	18	19	29	33	36	20

[a] From the disappearance of CO. [b] Initial rate. [c] After 6 min.

The catalyst is quite active with respect to CO conversion over the whole range of CO/O_2 ratios with an optimum value at a partial pressure ratio ($p(\text{CO})/p(\text{O}_2)$) of 1/0.56. In the three experiments where CO is in excess of O_2 the reaction proceeded violently, accompanied by red fire flashing at the surface of the catalyst powder. However, at the highest CO partial pressure ratio of 1/0.16 the activity decreased within several minutes, possibly as a consequence of the reduction of the Ru^{IV} species to lower oxidation states by CO. This proposal might explain the decrease in the conversion of CO into CO_2 observed at this high CO partial pressure. Generally, the high activity, good stability at low CO partial pressures,

and tolerance towards humidity makes this material a promising catalyst for CO removal. Examples for practical applications are fuel cells, air filters, antipollution paints, and various environmental safety devices.

Experimental Section

Triply distilled water (30 mL) was added to $\text{RuCl}_3 \cdot n\text{H}_2\text{O}$ (439 mg, 41 % Ru) with stirring. The solution was kept for 30 min before the pH value was adjusted 4.5–5.0 by the slow addition of 2 M NaOH. Subsequent stirring of the mixture for another 30 min was followed by the addition of further 2 M NaOH until pH 6 was reached and precipitation of $\text{RuO}_2 \cdot x\text{H}_2\text{O}$ occurred. After stirring the mixture for a further 60 min the solution was finally adjusted to pH 7.0 to complete the process. Thereafter stirring was continued for another 60 min and the solution was refluxed at 100°C for 2 h. The black precipitate was filtered off and washed 10 times with water. Water contents were calculated from the weight loss after annealing. SiO_2 - or TiO_2 -supported catalysts were prepared by sonication of the corresponding suspension containing hydrous RuO_2 . After drying the samples for more than 2 days at 60°C , $\text{RuO}_2 \cdot x\text{H}_2\text{O}/\text{SiO}_2$ (3/10 (wt/wt)) was heated for 4 h at 150°C , and $\text{RuO}_2 \cdot x\text{H}_2\text{O}/\text{TiO}_2$ (3/10 (wt/wt)), coated on the glass plate, was heated for 20 min at 200°C in an air stream. Oxidation of CO was carried out in a closed reaction system (total volume of 2435 mL) containing the catalyst powder cast onto a heatable glass plate ($4 \times 4 \text{ cm}$) and fitted with a membrane pump for gas circulation and a gas cell with KBr windows for IR measurement. A total pressure of 1 atm of the reactant gases (CO/O_2 or CO/air) was maintained in all experiments. The production of CO_2 and the decrease of CO were monitored from the changes in the IR absorption, after calibration with the pure gases.

Received: April 11, 2000 [Z14969]

- [1] D. L. Shawn, T.-Ch. Hsiao, J.-R. Chang, A. S. Lin, *J. Phys. Chem. B* **1999**, 103, 97.
- [2] S. D. Gardner, G. B. Hoflund, D. R. Schryer, J. Schryer, B. T. Upchurch, E. J. Kielin, *Langmuir* **1991**, 7, 2135.
- [3] M. Haruta, N. Yamada, T. Kobayashi, S. Iijima, *J. Catal.* **1989**, 115, 301.
- [4] a) T. H. Rogers, C. S. Piggot, W. H. Bahlke, J. M. Jennings, *J. Am. Chem. Soc.* **1921**, 43, 1973. b) H. A. Jones, H. S. Taylor, *J. Phys. Chem.* **1923**, 27, 623.
- [5] M. J. Fuller, M. E. Warwick, *J. Catal.* **1974**, 34, 445.
- [6] S. Imamura, H. Sawada, K. Uemura, S. Ishida, *J. Catal.* **1988**, 109, 198.
- [7] S. H. Taylor, G. J. Hutchings, A. A. Mirzai, *Chem. Commun.* **1999**, 1373.
- [8] J. S. Lee, E. D. Park, B. J. Song, *Catal. Today* **1999**, 54, 57.
- [9] A. Mills, *Chem. Soc. Rev.* **1989**, 18, 285.
- [10] A. Harriman, *Platinum Met. Rev.* **1983**, 27, 102.
- [11] a) H. Over, Y. D. Kim, A. P. Seitsonen, S. Wendt, E. Lundgren, M. Schmid, P. Varga, A. Morgante, G. Ertl, *Science* **2000**, 287, 1474 (we thank one of the referees for communicating this reference); b) A. Böttcher, M. Rogozia, A. Niehus, H. Over, G. Ertl, *J. Phys. Chem. B* **1999**, 103, 6267.
- [12] J. S. Walker, G. I. Straguzzi, W. H. Manogue, G. C. A. Schuit, *J. Catal.* **1988**, 110, 298.
- [13] G. G. Jernigan, G. A. Somorjai, *J. Catal.* **1994**, 147, 567.

The Cl₄⁺ Ion**

Stefan Seidel and Konrad Seppelt*

The first oxidation product of the chlorine molecule, Cl₂⁺, stubbornly refuses to be prepared in a chemical system. In the diluted gas phase it can be detected by UV spectroscopy.^[1] The shortened Cl–Cl distance of 189 pm and the increased valence frequency of 645.3 cm^{−1} of Cl₂⁺ with respect to molecular Cl₂ (199 pm and 558 cm^{−1}, respectively) are indicative of a bond order of one and half. In comparison, cherry red Br₂^{+[2–7]} and light blue I₂⁺ have been known for a long time and have been investigated intensively.^[8, 9] I₂⁺ was observed on the grounds of its color as early as 1882 on dissolution of I₂ in oleum,^[10–12] but only in 1966 was it identified as such.^[8]

Recently we showed that oxidation of Cl₂ with O₂⁺SbF₆[−] yields the remarkable trapezoid-shaped Cl₂O₂⁺ ion, which can be described as a *side-on* π complex of (singlet) O₂ to Cl₂^{+[13]} Since the binding between O₂ and Cl₂⁺ is reversible, as has been shown by isotopic substitution, Cl₂⁺ might also be obtainable, if one works under oxygen-free conditions. Therefore we chose iridium hexafluoride with an electron affinity (EA) of approximately 6.5 eV as oxidizing agent, which should just be able to oxidize Cl₂ which has a first ionization potential (IP) of 11.5 eV, if these numbers are compared with those of PtF₆ (EA 7.0 eV) and xenon (first IP 12.12 eV).^[14, 15] The reaction of the latter afforded the first xenon compound “XePtF₆”, whose exact composition still remains unknown.^[16] The above calculation is based on the assumption that lattice energies of Cl₂⁺IrF₆[−] and Xe⁺PtF₆[−] should be quite similar.

The reaction, however, proceeds under formation of the Cl₄⁺ ion [Eq. (1)]. Cl₄⁺IrF₆[−] is obtained as a blue solid that



decomposes at −78 °C to salts of the Cl₃⁺ ion, which are well known with various anions.^[13] Elemental chlorine can also be replaced by chlorine-containing compounds, for example, CF₂Cl₂. In spite of its instability the new compound has been characterized by a single-crystal structure determination as well as by Raman and EPR spectroscopy, and has been simulated by calculations.

According to the crystal structure determination, the compound contains a rectangular Cl₄⁺ ion that shows no significant contacts to the fluorine atoms of the octahedral IrF₆[−] ion

(Figure 1). The short Cl–Cl distance is significantly shorter than in Cl₂, but somewhat longer than in gaseous Cl₂⁺. This is in accord with the oxidation state Cl₂^{+1/2}. The association of both parts can be explained, similarly to Cl₂O₂⁺, in terms of

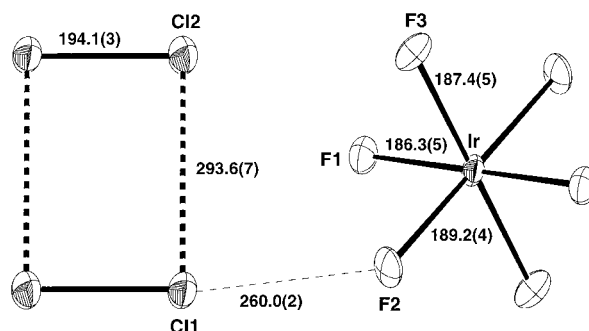


Figure 1. Structure of Cl₄⁺IrF₆[−] in the crystal (ORTEP plot, 50% probability ellipsoids). One molecular unit with the shortest interionic distance is shown. Atoms not indexed are generated by the center of symmetry. Values in pm.

π*–π* interactions, as has been shown by ab initio and density functional theory (DFT) calculations (Table 1). A reliable prediction for the weak interaction is only possible with fairly large basis sets. The bond energy between the two parts of the cations is calculated to be approximately 100 kJ mol^{−1} with respect to Cl₂ + Cl₂⁺ (see Table 1). This bond energy represents a very simple case of resonance energy of a system that is exclusively π-bonded.

The Raman spectrum (see Figure 2 and Experimental Section) shows the bands of the octahedral IrF₆[−] ion and the Cl–Cl valence vibrations. The high intensity of the band at 175 cm^{−1}, which is possibly due to a Raman resonance, is striking, since the first and second overtone can be seen, although the excitation frequency of 1064 nm is far from the absorption in the visible region. This vibration is assigned to the symmetric stretch of the Cl₄⁺ ion along the long bonds, which has also been shown by the calculations. Owing to the

Table 1. Parameters for the Cl₄⁺ ion determined experimentally and by ab initio and DFT calculations.

	Experiment	MP2/6-311++G(3df,3pd) ^[a]	Becke3LYP/6-311++G(3df,3pd) ^[a]
Cl–Cl [pm]	194.1(3)	194.0	195.6
Cl⋯Cl [pm]	293.7(3)	297.5	334.3
ΔH(Cl ₂ + Cl ₂ ⁺ → Cl ₄ ⁺) [kJ mol ^{−1}]		−101.5	−104.5
ν(Cl–Cl), A _g [cm ^{−1}]	578		588.8(46)
ν(Cl–Cl), B _{1u} [cm ^{−1}]			562.9(0)
δ(Cl⋯Cl), B _{3g} [cm ^{−1}]	241		115.5(19)
ν(Cl⋯Cl), A _g [cm ^{−1}]	175		103.5(100)
ν(Cl⋯Cl), B _{2u} [cm ^{−1}]			77.7(0)
τ, A _u [cm ^{−1}]			57.0(0)

[a] See ref. [22].

[*] Prof. K. Seppelt, Dipl.-Chem. S. Seidel
Institut für Chemie der Freien Universität Berlin
Fabeckstrasse 34–36, 14195 Berlin (Germany)
Fax: (+49)30-8384289
E-mail: seppelt@chemie.fu-berlin.de

[**] This work was supported by the Deutsche Forschungsgemeinschaft and the Fonds der Chemischen Industrie.

large amount of computing time and space needed these frequency calculations could only be done with a smaller basis set and the DFT method. This results in an elongated Cl⋯Cl distance and consequently in systematically lowered frequencies except for the two Cl–Cl stretching vibrations.

The EPR spectrum shows only a noncharacteristic broad resonance. We could show with H₂F⁺IrF₆[−], prepared by

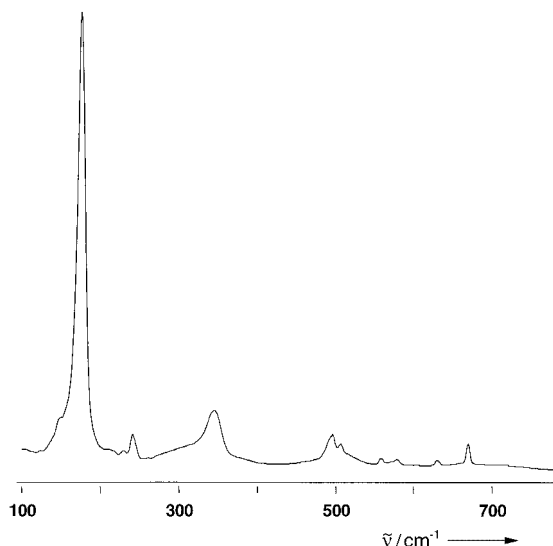


Figure 2. Raman spectrum of $\text{Cl}_4^+\text{IrF}_6^-$ at -80°C . For the frequency values see Experimental Section.

reaction of IrF_6 with SO_2 in HF , that IrF_6^- gives no EPR signal. This agrees with the finding that K^+IrF_6^- and $\text{Cs}^+\text{IrF}_6^-$ display temperature-independent paramagnetism.^[17]

It is possible that the blue and very unstable product of chlorine with the dioxygenyl cation (under excess of Cl_2) also contains the Cl_4^+ ion.^[13] A solid-state EPR spectrum of a product from Cl_2 and SbF_5 at 4.2 K is also assigned to the Cl_4^+ ion, but has fine structure.^[18]

The Cl_4^+ ion is related to the I_4^{2+} ion, the dimerization product of I_2^+ in the solid state.^[19, 20] This also has a rectangular structure with short (258.6(3) pm) and long bonds (324.7(3) pm).

Other parallels are the dimer of O_2 at high pressures or the diamagnetic dimer of ClO_2 below -108°C .^[21, 22] A difference between the latter dimers and Cl_4^+ and Cl_2O_2^+ is, however, that in all previous cases two electrons exist for the two (long) bonds, in the latter ones only one electron.

Cl_4^+ reacts with oxygen that diffuses slowly through the perfluoroethylene-propylene (FEP) reaction vessel to form black crystals, which are similarly sensitive and consist of $\text{Cl}_2\text{O}_2^+\text{Hir}_2\text{F}_{12}^-$ (Figure 3). The Cl_2O_2^+ ion present herein is identical with the cation in $\text{Cl}_2\text{O}_2^+\text{SbF}_6^-$ and $\text{Cl}_2\text{O}_2^+\text{Sb}_2\text{F}_{11}^-$ that we published recently.^[13] The anion is also of interest and has a very short F-H-F bridge. It can be described either as protonated IrF_6^- ($\text{F}_5\text{Ir}-\text{F}\cdots\text{H}^+\cdots\text{F}-\text{IrF}_5^-$) or as HF_2^- , solvated by IrF_5 ($\text{F}_5\text{Ir}\cdots\text{F}-\text{H}-\text{F}\cdots\text{IrF}_5$).

Experimental Section

Method 1: IrF_6 (240 mg, 0.8 mmol) and Cl_2 (50 mg, 0.7 mmol) were condensed with help of a stainless steel vacuum line into a perfluoroethylene-propylene (FEP) reaction vessel (inner diameter 6 mm) cooled to -196°C . The reaction mixture turned blue immediately. Anhydrous HF (500 mg) was condensed into the vessel, and the tube was sealed. Upon warming to -80°C a black, almost HF -insoluble solid was formed. The FEP ampule was briefly warmed, shaken, and cooled to -90°C . Above the frozen solution black, needle-shaped crystals were formed. Above -78°C $\text{Cl}_4^+\text{IrF}_6^-$ decomposed.

Method 2: Similarly IrF_6 (170 mg, 0.6 mmol) and CF_2Cl_2 (800 mg, 6.7 mmol) were condensed together. Upon warming to -90°C a red

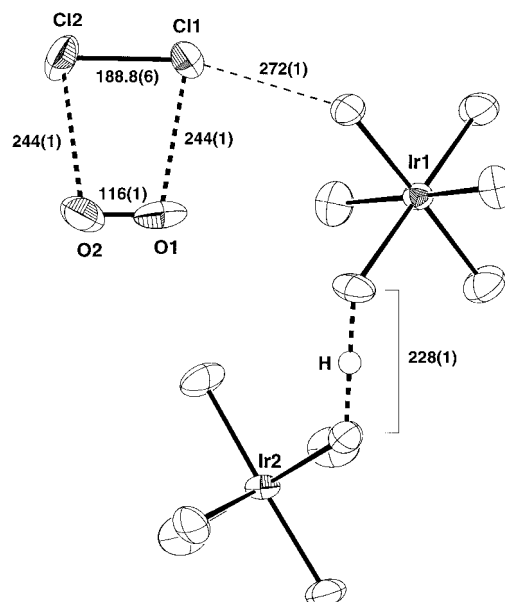


Figure 3. Structure of $\text{Cl}_2\text{O}_2^+\text{Hir}_2\text{F}_{12}^-$ in the crystal (ORTEP plot, 50% probability ellipsoids). One molecular unit with the shortest interionic distance is shown. Values in pm.

solution was formed. After a few minutes a blue coloration was observed above the liquid. The solution was kept for 12 h at -78°C . Within this period black, needle-shaped crystals were formed at the ampule wall above the solution.

Ab initio and DFT calculations have been done with the program GAUSSIAN 98.^[23]

Raman spectrum (1064 nm, -80°C , solid, cm^{-1}): $\tilde{\nu} = 669$ (8, $\nu_{\text{A}_{1g}}(\text{IrF}_6)$), 630 (1, $\nu_{\text{E}_g}(\text{IrF}_6)$), 578 (1, $\nu_{\text{A}_g}(\text{Cl}-\text{Cl})$), 558 (1, $\nu_{\text{B}_{1u}}(\text{Cl}-\text{Cl})$), 525 (shoulder, $3 \times \nu_{\text{A}_g}(\text{Cl}\cdots\text{Cl})$), 506 (7), 496 (11), 345 (15, $2 \times \nu_{\text{A}_g}(\text{Cl}\cdots\text{Cl})$), 241 (10, $\delta_{\text{F}_{2g}}(\text{IrF}_6)$), 229 (1), 175 (100, $\nu_{\text{A}_g}(\text{Cl}\cdots\text{Cl})$), 155 (shoulder); EPR spectrum (-83°C , X-band): $\delta = 2.00823$, half width 300 Gauss.

Crystal structure analysis: With a special apparatus^[24] a suitable crystal was mounted and measured on a Bruker-SMART-CCD-1000 TM diffractometer. Monoclinic, space group $P2_1/c$, $a = 512.2(1)$, $b = 1038.7(2)$, $c = 739.4(1)$ pm, $\beta = 93.668(3)^\circ$, $V = 392.6 \times 10^6 \text{ pm}^3$, $T = -120^\circ\text{C}$, $Z = 2$, $\text{MoK}\alpha$ radiation, graphite monochromator, scan width $0-3\omega$, measurement time 10 s per frame, 3345 measured, 770 unique reflections, 53 parameters, $R(F \geq 4\sigma(F)) = 0.038$, $wR_2 = 0.102$. After a semiempirical absorption correction by equalizing symmetry-equivalent reflections (SADABS), structure solution and refinement were carried out with the SHELX programs.^[25, 26]

$\text{Cl}_2\text{O}_2^+\text{Hir}_2\text{F}_{12}^-$: A sample prepared as described under Method 1 was kept in cold ethanol at -90°C for about seven days. Above the frozen solution black, needle-shaped crystals were formed on the wall of the ampule. Crystal structure analysis: Measurement as described above. Monoclinic, space group $P2_1/c$, $a = 540.24(4)$, $b = 1818.6(1)$, $c = 1191.4(1)$ pm, $\beta = 100.705(5)^\circ$, $V = 1150.1 \times 10^6 \text{ pm}^3$, $T = -120^\circ\text{C}$, $Z = 4$, 9218 measured, 2031 unique reflections, 164 parameters, $R(F \geq 4\sigma(F)) = 0.037$, $wR_2 = 0.081$. The position of the hydrogen atom was assumed exactly between the F16 and F21 atoms because of their short distance. Other bond lengths [pm]: Ir1-F11 182.0(9), Ir1-F12 184.5(9), Ir1-F13 185.4(8), Ir1-F14 184.0(8), Ir1-F15 184.9(8), Ir1-F16 196.6(8), Ir2-F21 197.1(9), Ir2-F22 185.9(8), Ir2-F23 185.0(7), Ir2-F24 184.5(8), Ir2-F25 181.8(9), Ir2-F26 184.9(8).

Further details on the crystal structure investigations may be obtained from the Fachinformationszentrum Karlsruhe, 76344 Eggenstein-Leopoldshafen, Germany (fax: (+49) 7247-808-666, on quoting the depository numbers CSD-411351 ($\text{Cl}_4^+\text{IrF}_6^-$) and CSD-411358 ($\text{Cl}_2\text{O}_2^+\text{Hir}_2\text{F}_{12}^-$).

Received: June 29, 2000 [Z15359]

- [1] G. Herzberg, *Molecular Spectra and Molecular Structure*, Vol. 1., Von Nostrand, Princeton, NJ, USA, **1960**, p. 520.
- [2] R. J. Gillespie, M. J. Morton, *Chem. Commun.* **1968**, 24, 1565–1567.
- [3] A. J. Edwards, G. R. Jones, R. J. C. Sills, *Chem. Commun.* **1968**, 1527–1528.
- [4] A. J. Edwards, G. R. Jones, *J. Chem. Soc. (A)* **1971**, 2318–2320.
- [5] R. J. Gillespie, M. J. Morton, *Inorg. Chem.* **1972**, 3(11), 586–593.
- [6] W. W. Wilson, R. C. Thompson, F. Aubke, *Inorg. Chem.* **1980**, 19, 1489–1493.
- [7] D. K. Padma, R. D. Peacock, *J. Fluorine Chem.* **1981**, 17, 539–541.
- [8] R. J. Gillespie, J. B. Milne, *Inorg. Chem.* **1966**, 5, 1577–1582.
- [9] R. D. W. Kemmitt, M. Murray, V. M. McRae, R. D. Peacock, M. C. R. Symons, T. A. O'Donnell, *J. Chem. Soc. (A)* **1968**, 862–866.
- [10] R. Weber, *J. Prakt. Chem.* **1882**, 25, 224–231.
- [11] G. Oddo, A. Sconzo, *Gazz. Chim. Ital.* **1927**, 57, 83–103.
- [12] O. Ruff, H. Graf, W. Heller, Knoch, *Ber. Dtsch. Chem. Ges.* **1906**, 39, 4310–4327.
- [13] T. Drews, W. Koch, K. Seppelt, *J. Am. Chem. Soc.* **1999**, 121, 4379–4384.
- [14] *Handbook of Chemistry and Physics* 76th ed., CRC, Boca Raton, FL, **1995–1996**, chap. 10, pp. 187–188.
- [15] N. Bartlett, *Angew. Chem.* **1968**, 80, 453–460; *Angew. Chem. Int. Ed. Engl.* **1968**, 7, 433–439.
- [16] N. Bartlett, *Proc. Chem. Soc.* **1962**, 218; L. Graham, O. Graudejus, N. K. Jha, N. Bartlett, *Coord. Chem. Rev.* **2000**, 197, 321–324.
- [17] A. Earnshaw, B. N. Figgis, J. Lewis, R. D. Peacock, *J. Chem. Soc.* **1961**, 3132–3138.
- [18] R. S. Eachus, M. C. R. Symons, *J. Chem. Soc. Dalton* **1976**, 431–434.
- [19] R. J. Gillespie, R. Kapoor, R. Faggiani, C. J. L. Lock, M. Murchie, J. Passmore, *J. Chem. Soc. Chem. Commun.* **1983**, 8–9.
- [20] R. Faggiani, R. J. Gillespie, R. Kapoor, C. J. L. Lock, J. E. Vekris, *Inorg. Chem.* **1988**, 27, 4350–4355.
- [21] F. A. Gorelli, L. Ulivi, M. Santoro, R. Bini, *Phys. Rev. Lett.* **1999**, 83, 4093–4096.
- [22] A. Rehr, M. Jansen, *Angew. Chem.* **1991**, 103, 1506–1508; *Angew. Chem. Int. Ed. Engl.* **1991**, 30, 1510–1512; A. Rehr, M. Jansen, *Inorg. Chem.* **1992**, 31, 4240–4242.
- [23] Gaussian 94, Revision E.2: M. J. Risch, G. W. Trucks, H. B. Schlegel, P. M. W. Gill, B. G. Johnson, M. A. Robb, J. R. Cheeseman, T. Keith, G. A. Peterson, J. A. Montgomery, K. Raghavachari, M. A. Al-Laham, V. G. Zakrzewski, J. V. Ortiz, J. B. Foresman, J. Cioslowski, B. B. Stefanov, N. Nanayakkara, M. Challacombe, C. Y. Peng, P. Y. Ayala, W. Chen, M. W. Wong, J. L. Andres, E. S. Replogle, R. Gomperts, R. L. Martin, D. J. Fox, J. S. Brinkley, D. J. Defrees, J. Baker, J. P. Stewart, M. Head-Gordon, C. Gonzalez, J. A. Pople, Gaussian, Inc., Pittsburgh, PA, USA, **1995**.
- [24] H. Schumann, W. Genthe, E. Hahn, M.-B. Hossein, D. van der Helm, *J. Organomet. Chem.* **1986**, 28, 2561–2567.
- [25] G. Sheldrick, Program for Crystal Structure Solution, Göttingen, **1986**.
- [26] G. Sheldrick, SHELXS-93, Göttingen, **1993**.

[[Ag(*t*BuNH₂)₂]₄][{Ag(*t*BuNH₂)-(*t*BuN=CHCH₃)₂][Ag₁₂(CF₃CO₂)₁₄]: A Compound with an Ag₁₂⁸⁺ Cluster Core**

Peter Reiß, Florian Weigend, Reinhart Ahlrichs, and Dieter Fenske*

Dedicated to Professor Herbert W. Roesky on the occasion of his 65th birthday

The tendency of silver to form subvalent compounds has been observed in the structures of, for example, Ag₃O,^[1] Ag₅GeO₄,^[2] Ag₅SiO₄,^[3] and Ag₆Ge₁₀P₁₂.^[4] These compounds contain octahedral Ag₆⁴⁺ cluster units in which two electrons of a 6-center 2-electron (6c2e) bond occupy the lowest bonding molecular orbital (a_{1g}). Furthermore, the influence of d¹⁰–d¹⁰ interactions is invoked to explain the existence of these silver clusters.^[2, 3, 5]

The reaction of silver trifluoroacetate with LiNH*t*Bu leads to the formation of **1**, a molecular compound which contains two similar Ag₆⁴⁺ units connected to give an Ag₁₂⁸⁺ cluster.



Herein, in addition to the X-ray structure analysis of **1**^[6] we present quantum chemical calculations to elucidate the electronic structure in the metal cluster.

Complex **1** features a central Ag₁₂ cluster clamped by μ₂ bridging trifluoroacetate ligands. This core is surrounded by six silver diamine units (Figure 1). In four of them, the silver atoms (Ag(13) to Ag(16)) are linearly coordinated by two *t*BuNH₂ ligands which are formed by the protonation of the (*t*BuNH)[–] units. Additionally, two [Ag(*t*BuNH₂)-(*t*BuN=CHCH₃)]⁺ ions (Ag(17) and Ag(18)) are present, the structure for Ag(17) is presented in Figure 2. A *tert*-butylamine ligand and a *tert*-butylacetateimine ligand both bind to a silver atom in this fragment. The atom N(10) has a trigonal planar coordination sphere and the N–C bond length (N(10)–C(63) = 123(3) pm) is significantly shorter than a N–C single bond.

The existence of [Ag(*t*BuNH₂)(*t*BuN=CHCH₃)]⁺ ions could be demonstrated conclusively by electrospray ionization mass spectroscopy, however, the reaction pathway that yields these unexpected units is not yet clear. The C₂H₄ group bound to N(10) is probably generated by the cleavage of the solvent diethyl ether. In this case the resulting ethanal would react with dissolved amido or amine ligands to form imine groups which then coordinate to an Ag⁺ ion or to a [Ag(*t*BuNH₂)]⁺ unit.

The Ag–N bond lengths in the six complex ligands (average 214 pm) are in agreement with the values reported for

[*] Prof. Dr. D. Fenske, Dr. P. Reiß, Dr. F. Weigend, Prof. Dr. R. Ahlrichs
Institut für Anorganische Chemie der Universität
Engesserstrasse, Geb. 30.45
76128 Karlsruhe (Germany)
Fax: (+49) 721-661-921
E-mail: dieter.fenske@chemie.uni-karlsruhe.de

[**] This work was supported by the Deutsche Forschungsgemeinschaft. We thank Dr. Oliver Hampe for the recording of an electrospray ionization mass spectrum of the title compound.

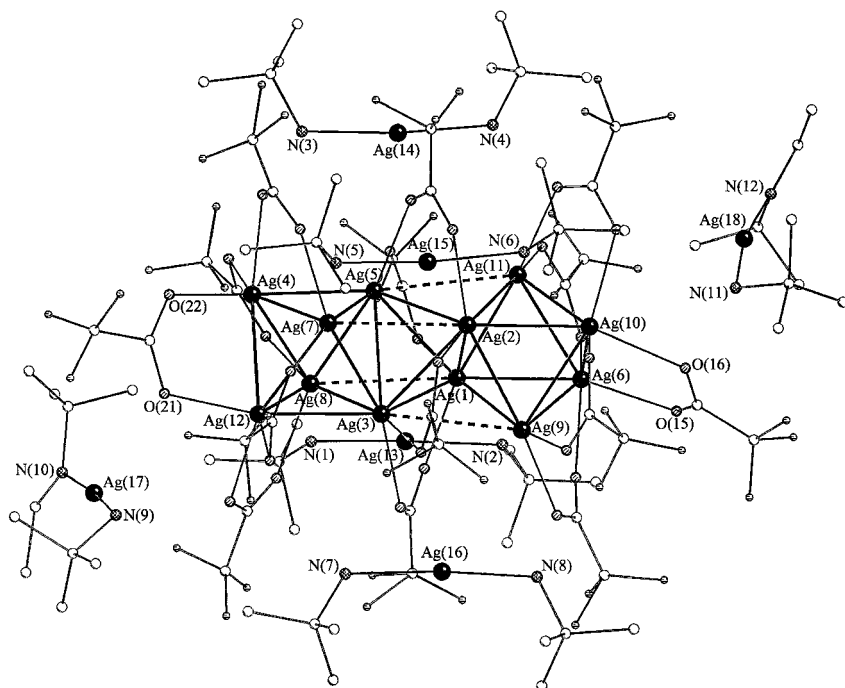


Figure 1. Molecular structure of **1** (hydrogen atoms are omitted for clarity).

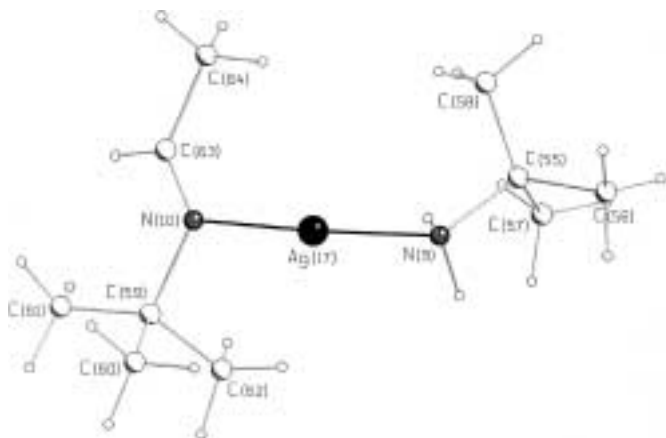


Figure 2. Structure of the $[\text{Ag}(\text{tBuNH}_2)(\text{tBuN}=\text{CHCH}_3)]^+$ ions in **1**.

linear silver diamine and silver diimine cations.^[7] The $[\text{Ag}(\text{tBuNH}_2)_2]^+$ ligands as well as the $[\text{Ag}(\text{tBuNH}_2)(\text{tBuN}=\text{CHCH}_3)]^+$ groups are connected to the cluster core by N–H \cdots O and C–H \cdots F hydrogen bonds.

If the charge of the outer complex ligands (6+) and the charge of the fourteen trifluoroacetate ligands (14–) is taken into account, a net charge of 8+ results for the Ag_{12} cluster unit. This polyhedral framework with 20 triangular faces and a total length of 760 pm can be described as two octahedrons rotated by 90° away from one another, both octahedrons share one edge with a central tetrahedron. These two shared edges are the longest Ag–Ag bonds within the

polyhedron; all the other metal–metal bonds are significantly shorter than those found in silver metal (289 pm).

These short metal–metal bond cannot be caused solely by the constraining effect of the chelate ligands since in each octahedral unit six of twelve edges are not bridged by ligands (Figure 3). In fact, the shortest Ag–Ag bonds (average 275.9(3) pm) are observed for these nonbridged edges which indicates the existence of additional attractive interactions. This interaction could be described by a 12c4e bond for the metal framework, giving an average formal oxidation number of 2/3 for the silver atoms.

The topology of the Ag_6^{4+} units in the silver suboxides^[1–3] agrees well with that of **1** even when the oxygen coordination sphere is considered (this is naturally not true for the edges Ag(1)–Ag(2) and Ag(3)–Ag(5), which belong to the central tetrahedron). The centers Ag(6), Ag(10), Ag(4), and Ag(12) have a trigonal pyramidal coordination environment while the other silver atoms show a bent coordination.

Both these coordination modes are found in the silver suboxide species however the O–Ag–O angles do not deviate from 90° as much as those found in **1**. The trifluoroacetate ligands bound to Ag(4)/Ag(12) or Ag(6)/Ag(10), show an average out-of-plane angle of 8.0(7)° with respect to the surface of the octahedron. Therefore, the almost ideal D_{2d} symmetry of the Ag_{12} cluster core is perturbed and thus the cluster anion as a whole is chiral with approximate D_2 symmetry.

The Ag_{12} framework in **1** shows a remarkable similarity to the In_{12} framework in $[\text{In}_{12}(\text{tBu}_3\text{Si})_8]^{[8]}$ and the Al_{12} framework in $[\text{Al}_{12}[\text{N}(\text{SiMe}_3)_2]_8]^-$.^[9] All three metal polyhedrons can be regarded as small fragments of a cubic closed packed array of metal atoms. Further examples of subvalent coinage-metal clusters include the compound $[\text{Ag}_{13}\text{Fe}_8(\text{CO})_{32}]^{4-}$ ^[10]

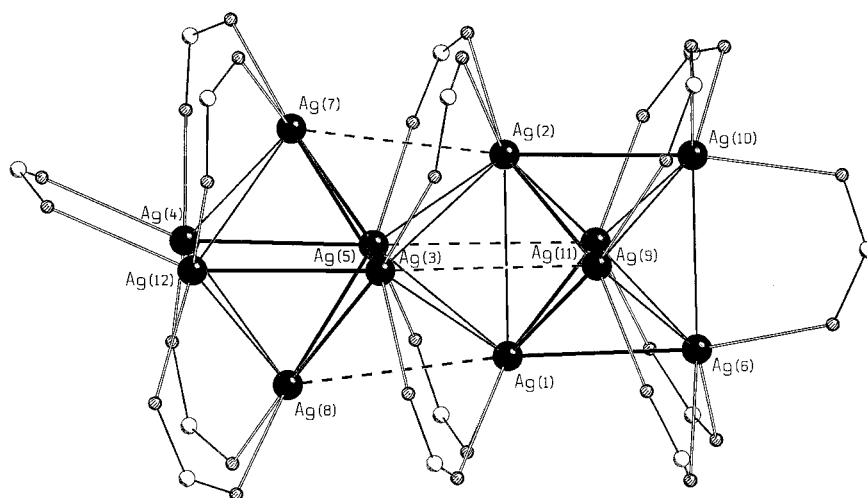
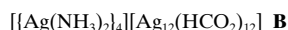


Figure 3. Representation of the Ag_{12}^{8+} cluster in **1** with bridging ligands (CF_3 groups are omitted for clarity).

and also the dimetallic Ag/Au clusters synthesized by Teo et al.^[11]

To check the structure geometry and to investigate the electronic structure Ab initio calculations were carried out for two model compounds. To identify the physical effects relevant for the structure the results of several different Ab initio treatments were compared. All the calculations were performed with the TURBOMOLE program package.^[12] For the density functional theory (DFT) calculations^[13] the Becke–Perdew (BP) functional was used,^[14, 15] for all the elements (auxiliary) basis sets of the SV(P) type^[16] were chosen; the inner 28 electrons of the silver atoms were represented by effective core potentials (ECPs) which include a treatment of scalar relativistic effects.^[17] The Coulomb part was calculated within the RI (resolution of the identity) approximation.^[16c] The MP2 calculations were carried out using the RI-MP2 method.^[18] For these and the HF calculations the following basis sets (and corresponding auxiliary basis sets) were used:^[16] TZVPP basis for Ag centers, TZVP basis (triple zeta valence with one polarization function) for N and O centers, SV(P) basis (split valence plus polarization) for C and H centers. The 1s(C,N,O) and the 4s(Ag) orbitals were neglected in all MP2 calculations (“frozen core” approximation).

We considered two model compounds; **A** derived from **1** by the substitution of the CF₃ groups by H atoms and the *t*Bu groups by Me groups; the smaller model compound **B** differs



from **A** in that the $[\text{Ag}(\text{MeNH}_2)(\text{MeN}=\text{CHCH}_3)]^+$ units are missing, and the Ag atoms Ag(6) and Ag(10) as well as Ag(4) and Ag(12) are no longer bridged by chelate ligands. In this way charge neutrality is preserved and D_{2d} symmetry is obtained.

The model **B** was calculated at the levels DFT, HF, and MP2, **A** only with the efficient DFT method.^[16c] The relevant parameters for the optimized geometric structures are collected in Table 1. The parameters for DFT(**A**), DFT(**B**), and MP2(**B**) agree well with the experimental values and thus justify the choice of methods and the model system **B**; the deviations are usually smaller than 15 pm. An exception is the Ag(4)–Ag(12) edge of the octahedron which is bridged in **A**, but not in **B**; the calculated bond length is 35 pm too long for DFT(**B**).

The comparison of MP2(**B**) and HF(**B**) allows an investigation of the physical effects that are relevant for the geometric structure. Compared to MP2, the HF structure shows a pronounced increase in the length of the bridged Ag–Ag bonds in the tetrahedron and in the octahedron ($d_{\text{HF}} - d_{\text{MP2}} \approx +65$ pm) as well as for the nonbridged edges of the octahedron (+20 to +50 pm). The edge Ag(4)–Ag(12), which is nonbridged in **B**, is opened completely. Clearly these bonds are “soft” as small deviations in the potential hyper-surface lead to large changes in the bond lengths.

These investigations show that the geometric structure of the cluster core is determined mainly by electron-correlation effects (the HF method neglects the dynamic electronic

Table 1. Selected bond lengths [pm] for the calculated structures and for the experimental structure.

Ag–Ag ^[a]	B			A	
	DFT	MP2	HF	DFT	1 Experimental
1	320	305	309	306–307	297–305
2	285	275	296	278–281	273–279
3	279	275	330	284–289	275–278
4	278	275	338	278–283	277–282
5	281	271	338	286–295	282–287
6	320	295	546	293–296	284–285
Ag–O	230–234	225–227	224–242	231–246	229–241
Ag–N	216–217	211	234–239	215–218	208–216

[a] The Ag–Ag bonds are numbered as follows: 1) Common edge of octahedron and tetrahedron (1–2 and 3–5). 2) Octahedral edge, non-bridged (1–9, 1–11, 2–9, 2–11, 3–7, 3–8, 5–7, 5–8). 3) Octahedral edge, non-bridged (1–6, 2–10, 3–12, 4–5). 4) Octahedral edge, bridged (4–7, 4–8, 12–7, 12–8, 6–9, 6–11, 10–9, 10–11). 5) Tetrahedral edge, bridged (1–3, 1–5, 2–3, 2–5). 6) Octahedral edge, bridged in **A**, non-bridged in **B** (4–12 and 6–10).

correlation which MP2 accounts for by means of perturbation theory). To investigate whether particular electrons are in any way responsible for the correlation effects we calculated correlation energies regarding only an, energetically well separated, subset of orbitals. The density of states, $D(\epsilon)$, which results from the HF wave function^[19] in the DFT geometry is shown in Figure 4; its shape implies a partition of the MOs, also shown in Figure 4. Furthermore, the contributions to the Mulliken electron gross population are listed (separately for each atom type) which arise from the particular groups of MOs.

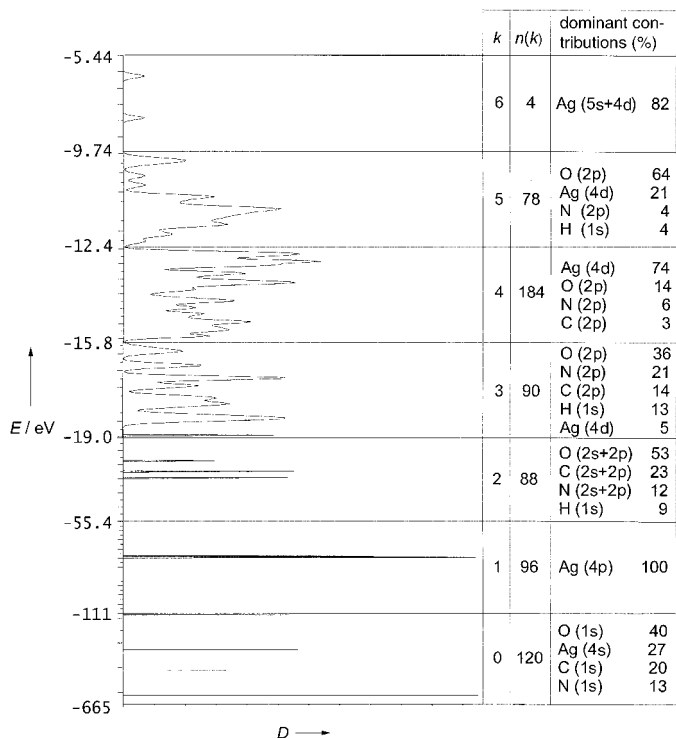


Figure 4. Density of states D (in arbitrary units) resulting from the HF wave function in the DFT equilibrium geometry for model **B** and partitioning of the different energy states into groups k . At the right hand side Mulliken electron gross populations $n(k)$ are listed separately for each atom type and shell. The HF orbital energies are superimposed as Gauss functions of width 0.2 eV to aid comprehension and to reflect the situation to the solid state.

Next an interpolation (characterized by a parameter I) was performed between the DFT equilibrium geometry ($I=0$) and the HF geometry ($I=1$). For several values of I the following energies were calculated:

- $E_0 = E_{\text{HF}}$
- $E_1 = E_{\text{HF}} + E_{\text{MP2}}$ (partitions 1–6, “full” MP2 energy)
- $E_2 = E_{\text{HF}} + E_{\text{MP2}}$ (partition 4, mainly 4d-electrons of the Ag-atoms, “4d(Ag)”))
- $E_3 = E_{\text{HF}} + E_{\text{MP2}}$ (partitions 1–3, 5, 6)
- $E_4 = E_{\text{DFT}}$

The differences from the corresponding value for $I=0$ (DFT geometry) for all the calculated energies are shown in Figure 5. As expected, the DFT and the “full” MP2 energy (partition 1–6) increase from the DFT equilibrium geometry to the HF equilibrium geometry, whereas the HF energy decreases. Remarkably, both E_3 (E_{HF} +correlation contributions mainly from 4d(Ag)) and E_4 (E_{HF} +correlation contributions of all electrons except for 4d(Ag)) display a shape very similar to that of the HF energy. The cluster geometry is

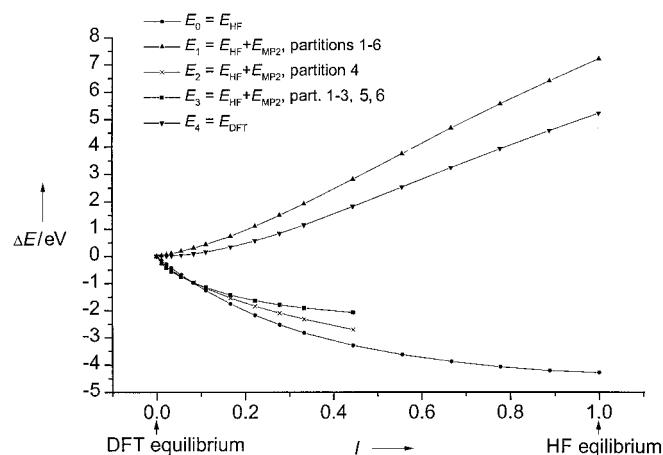


Figure 5. Dependency of calculated total energies on the geometric structure (interpolation parameter I , see text). Changes Δ compared to the corresponding energy in the DFT structure are plotted for DFT, HF, and (HF + MP2). In the MP2 calculations, electrons from different groups of orbitals are correlated. E_1 accounts for correlation of all (relevant) electrons, E_2 mainly contains correlation contributions of the 4d(Ag) electrons, E_3 contains contributions of all the other electrons.

therefore predominantly determined by the effects of electron correlation between the 4d(Ag) electrons and the other electrons and not by correlation effects between the 4d(Ag) electrons alone, that is, not by $d^{10}-d^{10}$ interactions between the silver atoms.

For a more detailed investigation a series of MP2 calculations at $I=0.11$ was carried out, where only the electrons from partition 4 (4d(Ag)) and those of one or more other partitions were considered (Table 2). It is evident that mainly electrons from orbitals with an energy similar to that of the 4d(Ag) electrons are relevant for correlation effects; but only when all the valence electrons are included (as in the “full” MP2 calculation and the DFT calculation), does one get a higher energy for $I=0.11$ than for $I=0$. Thus the cluster core geometry is determined by correlation of the 4d(Ag) electrons with the majority of the valence electrons of the other atoms.

Further insight in the electronic structure is obtained by investigating the energetic and spatial orientation of the frontier orbitals of the HF wave function in the DFT equilibrium structure for **A** and **B**. The orbital energy and the contribution of the Ag_{12} cluster core to the Mulliken gross population, $n_i(\text{Ag}_{12})$, for the 20 highest occupied MOs $|i\rangle$ are shown in Figure 6. The two highest occupied MOs are energetically well separated from the others and mainly localized in the Ag_{12} cluster core: $n_i(\text{Ag}_{12}) = 1.5$ and 1.7 (for a complete localization on the cluster core $n_i(\text{Ag}_{12}) = 2$). The MOs below these ($n_i(\text{Ag}_{12}) = 0-0.9$) are either more delocalized ($n_i(\text{Ag}_{12}) \cong 1$) or localized somewhat outside the cluster core ($n_i(\text{Ag}_{12}) \cong 0$).

Experimental Section

All experimental steps were carried out in a dry nitrogen atmosphere using standard Schlenk techniques and avoiding exposure to light. LiNHtBu (0.13 g 1.72 mmol) was added to a stirred suspension of AgCF_3CO_2 (0.38 g, 1.72 mmol) in absolute diethyl ether (25 mL), reaction time 5 min. The resulting dark solution was kept at 0°C for 5 days and then filtered to remove a brown precipitate. Storing the resulting yellow solution at -40°C for 4 weeks afforded clumps of yellow crystals of **1** in 35 % yield. The C, H, and N analyses of **1** correspond to the formula specified.

Received: May 15, 2000 [Z15121]

Table 2. Energy differences ΔE_i of a structure that is interpolated between DFT and HF equilibrium geometry (interpolation parameter $I=0.11$, see text) and of the DFT equilibrium structure ($I=0$) for HF and DFT energy as well as for different MP2 energies in which electrons from different energy partitions were considered (see Figure 4).

i	Correlated energy partitions k							Number of correlated electrons	$\Delta E_i = E_i(I=0.11) - E_i(I=0)$ [eV]
	0	1	2	3	4	5	6		
0	HF							0	-1.2662
1	–	×	×	×	×	×	×	540	+0.4325
2	–	–	–	–	×	–	–	184	-1.1793
3	–	×	×	×	–	×	×	356	-1.1501
4	–	×	–	–	×	–	–	280	-1.1643
5	–	–	×	–	×	–	–	272	-0.9099
6	–	–	–	×	×	–	–	274	-0.5173
7	–	–	–	–	×	×	–	262	-0.7887
8	–	–	–	–	×	–	×	188	-1.1165
9	–	–	–	–	×	×	×	266	-0.6738
10	–	–	–	×	×	×	–	352	-0.1591
11	–	–	–	×	×	×	×	356	+0.0009
12	–	–	×	×	×	×	×	444	+0.2658
13	DFT							(660)	+0.1548

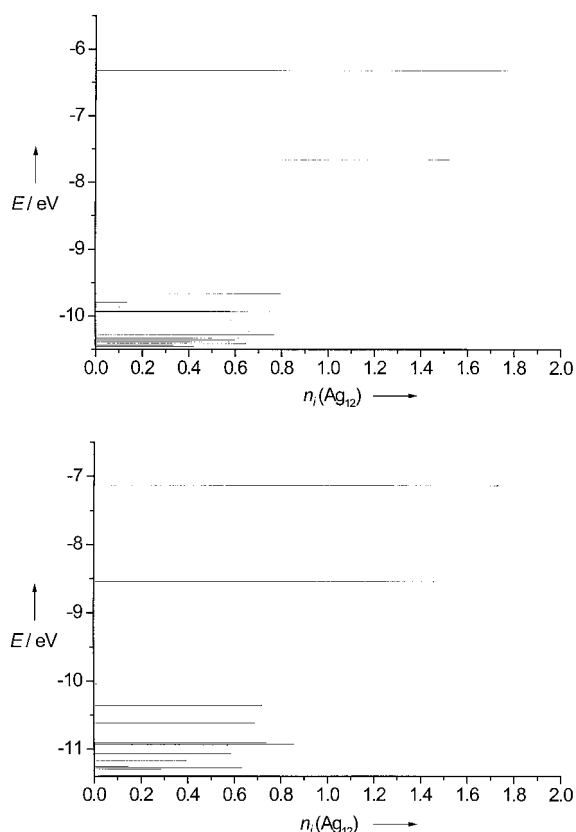


Figure 6. Orbital energy E and contribution of the cluster core to the Mulliken population, $n_i(\text{Ag}_{12})$, for the 20 highest lying molecular orbitals for model **A** (top) and model **B** (bottom). The data are based on the HF wave function in the DFT equilibrium geometry.

- [1] W. Beesk, P. G. Jones, H. Rumpel, E. Schwarzmann, G. M. Sheldrick, *J. Chem. Soc. Chem. Commun.* **1981**, 664–665.
- [2] C. Linke, M. Jansen, *Angew. Chem.* **1992**, *104*, 618–619; *Angew. Chem. Int. Ed. Engl.* **1992**, *31*, 653–654.
- [3] C. Linke, M. Jansen, *Inorg. Chem.* **1994**, *33*, 2614–2616.
- [4] H. G. von Schnering, K. G. Häusler, *Rev. Chim. Miner.* **1976**, *13*, 71–81.
- [5] M. Jansen, *Angew. Chem.* **1987**, *99*, 1136–1149; *Angew. Chem. Int. Ed. Engl.* **1987**, *26*, 1098–1111.
- [6] X-ray structure analysis of **1**: STOE-IPDS ($\text{MoK}\alpha$ -radiation), data collection and refinement (SHELXS-86, SHELXL-93). Monoclinic, space group $P2_1$ (No. 4), $Z=2$, unit cell dimensions (190 K): $a=1539.5(4)$, $b=3180.0(6)$, $c=1553.7(4)$ pm, $\beta=105.23(2)^\circ$, $V=7339(3) \times 10^6 \text{ pm}^3$; $\mu(\text{MoK}\alpha)=24.55 \text{ cm}^{-1}$; $2\theta_{\text{max}}=50.2^\circ$; 26208 reflections, 20871 independent reflections ($R_{\text{int}}=0.104$), 14349 reflections with $I>2\sigma(I)$, 1637 parameters; largest differential peak and hole = $1.46/-1.13 \text{ e}(\times 10^6 \text{ pm})^{-3}$; absolute structure parameter = $-0.03(5)$; $R_1=0.061$; $wR_2=0.157$. Coordinates of the hydrogen atoms were calculated for idealised positions, all other atomic coordinates (except for these of the disordered fluorine atoms) were refined using anisotropic displacement parameters. Crystallographic data (excluding structure factors) for the structures reported in this paper have been deposited with the Cambridge Crystallographic Data Centre as supplementary publication no. CCDC-144150. Copies of the data can be obtained free of charge on application to CCDC, 12 Union Road, Cambridge CB21EZ, UK (fax: (+44) 1223-336-033; e-mail: deposit@ccdc.cam.ac.uk).
- [7] a) H. M. Mauer, A. Weiss, *Z. Kristallogr.* **1977**, *146*, 227–240; b) A. Pajunen, S. Pajunen, *Acta Crystallogr. Sect. C* **1994**, *50*, 1884–1885; c) E. Bang, *Acta Chem. Scand. Sect. B* **1978**, *32*, 555–557; d) P. J. Bailey, K. J. Grant, S. Pace, S. Parsons, L. J. Stewart, *J. Chem. Soc. Dalton Trans.* **1997**, 4263–4266; e) W. Schneider, A. Bauer, H. Schmidbaur, *J. Chem. Soc. Dalton Trans.* **1997**, 415–420; f) J. F.

- Modder, J.-M. Ernsting, K. Vrieze, M. de Wit, C. H. Stam, G. van Koten, *Inorg. Chem.* **1991**, *30*, 1208–1214.
- [8] N. Wiberg, T. Blank, H. Nöth, W. Ponikwar, *Angew. Chem.* **1999**, *111*, 887–890; *Angew. Chem. Int. Ed.* **1999**, *38*, 839–842.
- [9] A. Purath, R. Köppe, H. Schnöckel, *Chem. Commun.* **1999**, 1933–1934.
- [10] V. G. Albano, L. Grossi, G. Longoni, M. Monari, S. Mullay, A. Sironi, *J. Am. Chem. Soc.* **1992**, *114*, 5708–5713.
- [11] B. K. Teo, H. Zhang, *Coord. Chem. Rev.* **1995**, *143*, 611–636.
- [12] R. Ahlrichs, M. Bär, M. Häser, H. Horn, C. Kölmel, *Chem. Phys. Lett.* **1989**, *162*, 165–169.
- [13] O. Treutler, R. Ahlrichs, *J. Chem. Phys.* **1995**, *102*, 346–354.
- [14] A. D. Becke, *J. Chem. Phys.* **1993**, *98*, 5648–5652.
- [15] J. P. Perdew, *Phys. Rev. Sect. B* **1986**, *33*, 8822–8824.
- [16] TURBOMOLE (auxiliary) basis sets can be retrieved from <http://www.chemie.uni-karlsruhe.de/PC/TheoChem/turbomole/index.html> as cited in: a) A. Schäfer, H. Horn, R. Ahlrichs, *J. Chem. Phys.* **1992**, *97*, 2571–2577; b) A. Schäfer, C. Huber, R. Ahlrichs, *J. Chem. Phys.* **1994**, *100*, 5829–5835; c) K. Eichkorn, O. Treutler, H. Öhm, M. Häser, R. Ahlrichs, *Chem. Phys. Lett.* **1995**, *240*, 283–290; d) K. Eichkorn, F. Weigend, O. Treutler, R. Ahlrichs, *Theor. Chim. Acc.* **1997**, *97*, 119–124; e) F. Weigend, M. Häser, H. Patzelt, R. Ahlrichs, *Chem. Phys. Lett.* **1998**, *294*, 143–152.
- [17] D. Andrae, U. Häußermann, H. Stoll, H. Preuß, *Theor. Chim. Acta* **1990**, *77*, 123–141.
- [18] F. Weigend, M. Häser, *Theor. Chim. Acc.* **1997**, *97*, 331–340.
- [19] The HF wave function was used because it represents the reference wave function of the MP2 calculations.

Synthesis, Crystal Structure, and Binding Properties of the Mixed Valence Clusters $[\text{Cu}_{32}\text{As}_{30}(\text{dppm})_8]$ and $[\text{Cu}_{26}\text{Te}_{12}(\text{PET}_2\text{Ph})_{12}]^{**}$

Reinhart Ahlrichs, Jörn Besinger, Andreas Eichhöfer, Dieter Fenske,* and Axel Gbureck

Dedicated to Professor Dieter Sellmann on the occasion of his 60th birthday

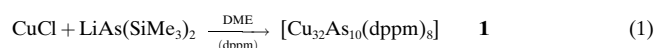
A possible way to synthesize transition metal clusters bridged by main group elements is the reaction of a transition metal salt MX_n (M = metal, X = halide, acetate) with silylated derivatives of the heavier main Group 5 and 6 elements.^[1] In this way, not only chalcogen bridged coinage-metal clusters were prepared, for example, $[\text{Cu}_{146}\text{Se}_{73}(\text{PPh}_3)_{30}]^{[2]}$ or $[\text{Ag}_{172}$

- [*] Prof. Dr. D. Fenske, Dipl.-Chem. J. Besinger
Institut für Anorganische Chemie der Universität
Engesserstrasse 15
76131 Karlsruhe (Germany)
Fax: (+49) 721-661-921
E-mail: dieter.fenske@chemie.uni-karlsruhe.de
- Prof. Dr. R. Ahlrichs
Institut für Physikalische Chemie der Universität
Engesserstrasse 15, 76131 Karlsruhe (Germany)
- Dr. A. Eichhöfer, Dr. A. Gbureck
Institut für Nanotechnologie (INT)
Forschungszentrum Karlsruhe
76344 Eggenstein-Leopoldshafen (Germany)

[**] We thank the Deutsche Forschungsgemeinschaft (SFB 195) and the Fonds der Chemische Industrie for their support of this work. dppm = Bis(diphenylphosphanyl)methane.

$\text{Se}_{40}(\text{SenBu})_{92}(\text{dppp})_4$],^[3] (dppp = bis(diphenylphosphanyl)propane) but also phosphorus bridged clusters of copper and silver, such as $[\text{Cu}_{96}\text{P}_{30}\{\text{P}(\text{SiMe}_3)_2\}_6(\text{PET}_3)_{18}]$ and $[\text{Ag}_{50}(\text{PPh})_{20}\text{Cl}_7\text{P}(\text{PnPr}_3)_{13}]$,^[4, 5] could be obtained. Up to now, arsinidene bridged clusters of the coinage metals are known only for silver and gold, for example $[\text{Ag}_{14}(\text{AsPh})_6\text{Cl}_2(\text{PET}_3)_8]$ and $[\text{Au}_{10}(\text{AsPh})_4(\text{PhAsSiMe}_3)_2(\text{PnPr}_3)_6]$.^[6] In contrast, polynuclear complexes of these metals with arsenic as a bridging ligand are unknown. Recently, by reactions of CuX ($\text{X} = \text{SCN}, \text{Cl}, \text{OAc}$) with tertiary phosphanes and $\text{AsR}(\text{SiMe}_3)_2$ ($\text{R} = \text{Ph}, \text{SiMe}_3$), we were successful in synthesizing the first arsinidene bridged copper cluster compounds, such as $[\text{Cu}_8(\text{AsSiMe}_3)_4(\text{PrBu}_3)_4]$, $[\text{Cu}_{10}(\text{AsPh})_4\text{Cl}_2(\text{PMe}_3)_8]$, $[\text{Cu}_{12}(\text{AsPh})_6(\text{PPh}_3)_6]$, and $[\text{Cu}_{14}(\text{AsPh})_6\text{Cl}_2(\text{PET}_3)_8]$.^[7] Herein we report the synthesis, single crystal X-ray analysis and the electronic structure of $[\text{Cu}_{32}\text{As}_{10}(\text{dppm})_8]$ (**1**).

During the reaction of copper(I) chloride with the bidentate ligand bis(diphenylphosphanyl)methane (dppm) and $\text{LiAs}(\text{SiMe}_3)_2$ in dimethoxyethane (DME), a brilliant red solution is formed at -20°C . With increasing temperature, the color of this solution becomes more intensive until at room temperature it turns black [Eq. (1)]. After reducing the volume of the solution, one obtains black needles of the arsenido bridged copper cluster $[\text{Cu}_{32}\text{As}_{10}(\text{dppm})_8]$ (**1**) within a few days at room temperature.



Cluster **1** crystallizes in the monoclinic space group $P2_1/c$ with four formula units and twenty molecules of DME per unit cell.^[8] The molecular structure of **1** is shown in Figure 1. The molecule itself displays no crystallographic symmetry. The most noticeable structural element of **1** is a nearly regular Cu_6 octahedron, which is formed by the atoms Cu27 to Cu32, and is situated in the cluster core. This central Cu_6 octahedron

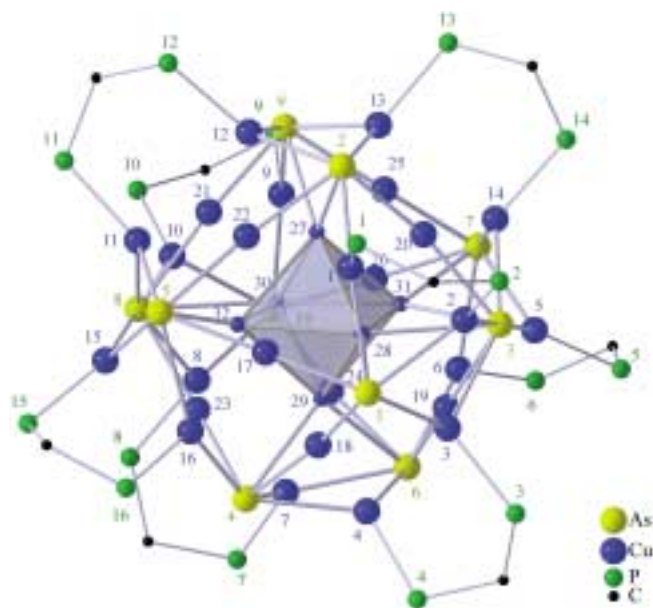


Figure 1. The molecular structure of **1** (phenyl groups are omitted for clarity). The Cu, As, and P atoms are indicated by blue, yellow, or green numbers respectively.

is enclosed by a complex network of 26 copper and ten arsenic atoms. At the surface, the cluster is completely protected by eight molecules of the bidentate phosphane ligand dppm.

The shell-like structure of **1** can also be described in the following way: the core consists of a Cu_6 octahedron (first shell) surrounded by eight further copper atoms (Cu18 to Cu25) that are arranged like a distorted square antiprism (second shell). The edge lengths of the octahedron are 251.8(3)–267.5(3) pm, those of the square antiprism vary from 347.4(3) to 489.5(3) pm. The shortest bond between two copper atoms of the first and the second shell is 239.9(3) pm which is considerably shorter than in copper metal (256 pm).^[9] The residual 18 copper atoms form the third shell of **1** (Cu1 to Cu17, and Cu26), however, its structure can not be described in terms of a regular polyhedron. Cu1, Cu9, Cu11, and Cu14, and Cu3, Cu6, Cu8, and Cu16 lie roughly in the same plane as the faces of the square antiprism and bridge its edges. Cu4 and Cu7, and Cu12 and Cu13 are situated above or below the faces, respectively, and also bridge one edge each. The residual six copper atoms (Cu2, Cu5, Cu10, Cu15, Cu17, and Cu26) form a six-membered ring in boat conformation and occupy about six of the eight edges between the two basic planes of the square antiprism. The shortest bond between two copper atoms of the second and the third shell is 246.9(3) pm.

The arsenic atoms of **1** are embedded in the third shell of the cluster. Two pairs of arsenic atoms (As2 and As9, As6 and As4) are situated above and below the basic planes of the square antiprism of the second shell, bridging the remaining unoccupied edges (Cu20–Cu22, Cu21–Cu25, Cu18–Cu19, Cu23–Cu24). The remaining arsenic atoms (As1, As3, As5, As7, As8, As10) are arranged like a six-membered ring, in boat conformation, between the two square faces of the antiprism. All the arsenic atoms together form a distorted polyhedron similar to that of the boron atoms in the *closo*-borane $\text{B}_{10}\text{H}_{10}^{2-}$.^[10] The Cu–As bond lengths, for the copper atoms of the second and third shell, vary from 234.8(1) to 265.3(3) pm. The copper atoms in **1** show three different coordination geometries. The centers Cu1 to Cu16 have a distorted trigonal planar geometry and are coordinated by two arsenic atoms and by a phosphorus atom from a dppm ligand. In contrast, the centers Cu17 to Cu26 are coordinated by two arsenic atoms in a nearly linear manner, and finally, the octahedrally arranged atoms, Cu27 to Cu32, interact only weakly with the arsenic atoms (260.6(1)–292.8(2) pm).

In an alternative description, the outer cluster shell is constructed by six Cu_2As_2 four-membered rings, that are linked together by copper atoms (Cu17 to Cu26) that are linearly coordinated by two arsenic ligands. The phosphorus bound copper atoms Cu1 to Cu16 are localized within these Cu_2As_2 rings. Thereby, the centers of the Cu_2As_2 rings point towards the copper atoms of the central Cu_6 octahedron.

Assuming that the ten μ_5 -As ligands in **1** have the formal charge of 3^- , then the Cu_{32} cluster has a total charge of 30^+ . Thus, the cluster must be a mixed valence compound that consists of 30 Cu^{1+} and two Cu^0 centers. However, in light of the molecular structure this localized distribution of charges is not possible. It is noteworthy that even in **1** a tendency for the formation of nonstoichiometric compounds occurs, as also

observed for β -Cu₃As, which possesses a substantial phase range.^[11]

We found a similar situation in PR₃ stabilized copper chalcogenide clusters. Noteworthy is that in the Cu₂S and Cu₂Se clusters, examples being [Cu₂₈S₁₄(PrBu₂Me)₁₂] and [Cu₇₂Se₃₆(PPh₃)₂₀], a well-defined assignment of charges is possible.^[12] In both cases, Cu¹⁺ coexists with S²⁻ or Se²⁻ centers, respectively. In contrast, in the similar copper telluride clusters a definite tendency towards nonstoichiometric compositions is observed; for example compounds such as [Cu₄₄Te₂₃(PPh₃)₁₅] and [Cu₁₆Te₉(PPh₃)₈] contain copper atoms in the formal oxidation states 1+ and 2+.^[13] In these cases, charge transfer bands of low intensity are observed in the 600–2000 nm range.

Compounds that contain copper atoms in the oxidation states 0 and 1+ side by side are rarer. In these compounds the charge transfer bands mentioned above are absent from the UV/Vis spectra. An example of this type of compound is the recently synthesized and characterized cluster [Cu₂₆Te₁₂(PEt₂Ph)₁₂] (**2**), formally containing 24 Cu¹⁺ and two Cu⁰ centers.^[13] A detailed description of the structure of **2** is given in ref [13]. As in **1**, a central Cu₆ octahedron (Figure 2)

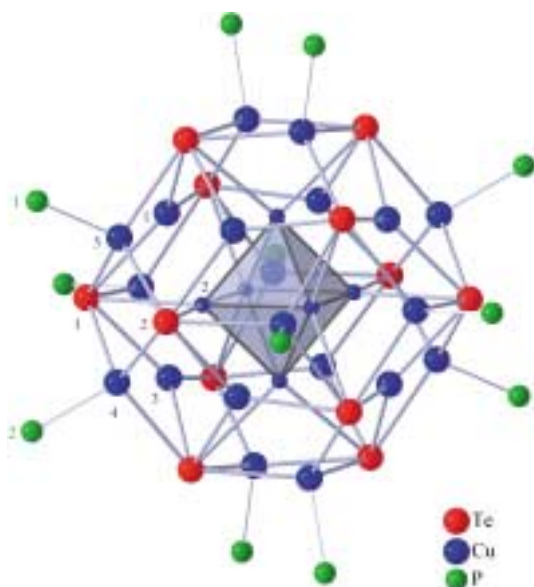


Figure 2. The molecular structure of **2** (organic groups are omitted for clarity. The Cu, Te, and P atoms are indicated by blue, red, or green numbers respectively.

exists, formed by Cu1 and Cu2 and their symmetry equivalents. In contrast to **1**, this octahedron is surrounded by a shell of 20 Cu and 12 Te²⁻ centers forming a distorted icosahedron (Te...Te 431.1–459.3(3) pm); 12 Cu atoms (Cu4, Cu5 and symmetry equivalent sites) occupy 12 Te₃ triangular faces. Binding to one further phosphorus atom (from the PEt₂Ph ligand) each, these copper atoms obtain a distorted tetrahedral coordination sphere (Cu–Te 266.1–271(1) pm; Cu–P 223.0–225.6(2) pm). The remaining eight Te₃ faces of the Te₁₂ icosahedron are μ_3 -bridged by Cu1 and Cu3 (and symmetry equivalent sites; Cu–Te 259.5–265.2(1) pm). These copper atoms lie below the Te₃ faces. The bond lengths within the aforementioned Cu₆ octahedron

are relatively short (259.2–260.7(2) pm) so that the situation is similar to that in **1**. This also applies to the orientation of the Cu centers of the Cu₆ octahedron which are equally directed towards six four-membered Cu₂Te₂ rings at the cluster periphery.

Formally, one can assign the charge 4+ to the central octahedron in **1** and **2**. This corresponds to the situation in the cluster anion [Ag₁₂(CF₃CO₂)₁₄]⁶⁻, recently prepared by us, where two Ag₆⁴⁺ clusters are connected to each other.^[14] A similar situation was observed in Ag₃O, Ag₃SiO₄, and Ag₃GeO₄. In these compounds, d¹⁰–d¹⁰ interactions between the silver centers were discussed.^[15] However, Ab initio calculations show that in the case of the Ag₁₂ cluster, the d¹⁰–d¹⁰ interactions between the silver atoms are not important.^[14]

To understand the electronic structures of the mixed valence compounds **1** and **2** Ab initio calculations for various model systems have been carried out.^[16] The calculations also enable the geometrical structures of **1** and **2** to be checked. In the theoretical treatment the substituents of the phosphane ligands were, in each case, replaced by methyl groups to give the model compounds [Cu₃₂As₁₀{P(CH₃)₂CH₂P(CH₃)₂}] (**1a**) from **1** and [Cu₂₆Te₁₂{P(CH₃)₃}] (**2a**) from **2**. An even greater simplification, the use of H atoms instead of methyl groups, leads to the compounds [Cu₃₂As₁₀(PH₂CH₂PH₂)₈] (**1b**) and [Cu₂₆Te₁₂(PH₃)₁₂] (**2b**).

The calculated structural parameters of both the model compounds **1a** and **1b** agree very well with the experimental results from **1** (Table 1). The Cu–Cu bond lengths within the slightly compressed Cu₆ octahedron deviate by less than 4 pm from the experimental values. The calculated separations

Table 1. Selected interatomic distances for **1** and **1a**.

Separation ^[a]	1 (experimental)	1a (DFT)
Cu(Oct)–Cu(Oct)	252.0–264.3	249.7–263.7
Cu(Oct)–Cu(Oct) (non bonding)	350.9, 370.4, 372.0	351.5, 370.1, 370.2
Cu(Oct)–Cu(Rem)	239.9–263.4	244.0–264.5
Cu–Cu (bridged by dppm)	256.1–259.1	251.5–252.1
Cu(P)–As	239.0–265.5	241.7–269.4
Cu(Rem)–As	233.6–247.5	238.8–255.5
Cu–P	221.3–230.5	225.6–231.8

[a] Cu(Oct) = Cu atoms in the octahedron (cluster core); Cu(P) = Cu atoms bonded to P atoms; Cu(Rem) = remaining Cu atoms.

between the atoms of the octahedral core and the remaining Cu atoms also deviate only slightly from the experimental values. Only the calculated value of the surprisingly short Cu–Cu bond (239.9 pm) in **1** is too long (by 4.1 pm in **1a**). The influence of the smaller model ligand compared to dppm is seen in the separations between the Cu atoms bridged by this ligand. In **1a**, these distances are 4–7 pm shorter than in **1**; in **1b** they are calculated to be even shorter. In both experiment and theory the Cu–As bond lengths cover a broad range, from 238.8–296.5 in **1a** compared to 233.6–293.0 pm in **1**, but overall the range in theory and experiment agree very well. The results of the calculations for the model compounds **1a** and **1b** confirm the unusual structure of **1**.

The crystal structure of **2** exhibits an inversion center within the cluster and a C₃ axis running through two of the atoms of

the octahedron. Without phosphane ligands the cluster has higher symmetry, namely T_h .^[17] In **2a** and **2b**, the model ligands are adjusted according to this symmetry. This higher symmetry enabled us, for comparison, to carry out a complete geometrical optimization for **2b** at the Hatree–Fock (HF) level. In the following discussion, for a better comparison to the calculated values, the experimental separations were averaged to T_h symmetry. The density functional theory (DFT) equilibrium geometries of **2a** and **2b** reproduce very well the important structure parameters of **2**; for example, calculated Cu–Cu bond lengths within the cluster core deviate by less than 1% from the experimentally determined. Only the μ_3 -bridging Cu atoms are moved slightly away from the Te centers towards the Cu atoms which are directly bound to the phosphane ligands. Thus the corresponding calculated Cu–Cu bonds are about 10 pm too short, while the calculated bonds of the μ_3 -bridging Cu atoms to the Te atoms are about 10 pm too long. The remaining Cu–Te bond lengths of **2a** and **2b** again deviate by less than 1% from those of **2**. The structure calculated at the HF/SV(P) level of theory gives, in contrast to the DFT calculations, large deviations from the experimental values. The absence of the of electron correlation effects (in the HF/SV(P) treatment) elongates the bonds, especially the Cu–Cu bonds which are up to 45 pm longer than in **2**.

The aforementioned investigations on the cluster anion $[\text{Ag}_{12}(\text{CF}_3\text{CO}_2)_{14}]^{6-}$ showed energetic and spatial separation of the two highest occupied molecular orbitals, which are predominantly centered on two Ag_6 substructures and thus formally correspond to a model double Ag_6^{4+} cluster.^[14] For **1** and **2**, analogous results would lead to Cu_6^{4+} fragments in the cluster core. To explain the electronic structure the orbital energies were investigated. The results of the DFT calculations were supplemented with the HF calculations in the DFT equilibrium geometry for the two more simplified clusters **1b** and **2b**.^[16] Population analyses were performed, where the known basis-set dependence can be more or less avoided by combining only those atomic orbitals that are situated at the Cu atoms in the central octahedron. This yields a population $n_i(\text{Oct})$ that describes to which extent a MO is localized at the octahedron.^[18] The independence from the chosen basis set

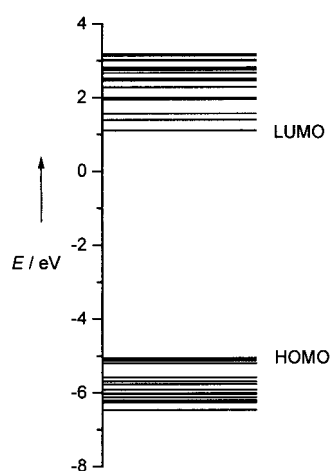


Figure 3. HF[SV(P)] orbital energies E for **1b**.

was verified by a calculation with a modified SV(P) basis.^[16]

However, the results for the model clusters **1b** and **2b** differ from the silver cluster ion $[\text{Ag}_{12}(\text{CF}_3\text{CO}_2)_{14}]^{6-}$.^[14] Neither DFT nor HF calculations exhibit a clear energetic separation of the frontier orbitals in **1b** and **2b** (Figure 3 and Figure 4 show the results of the HF calculations in the DFT equilibrium geometry). In both cases the HOMO is embedded in the almost bandlike

structure of the remaining orbitals. Only the LUMO in **2b** is separated (by 2.1 eV) from the remaining unoccupied orbitals.

Furthermore, in contrast to $[\text{Ag}_{12}(\text{CF}_3\text{CO}_2)_{14}]^{6-}$, the frontier molecular orbitals in **1b** are located only to a small extent at the octahedron in the cluster core: for the HOMO in **1b**, $n_i(\text{Oct}) = 0.7$ (Figure 5); for the HOMO in **2b** $n_i(\text{Oct}) = 0.08$ (Figure 6). Orbitals with $n_i(\text{Oct}) > 1$ are found only for much lower lying energies: at 6.8 eV (**1b**) and 8.7 eV (**2b**) below the energy of the corresponding HOMO.

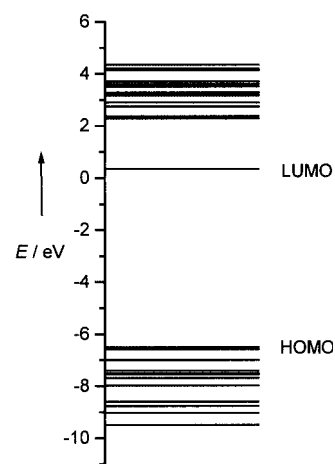


Figure 4. HF[SV(P)] orbital energies E for **2b**.

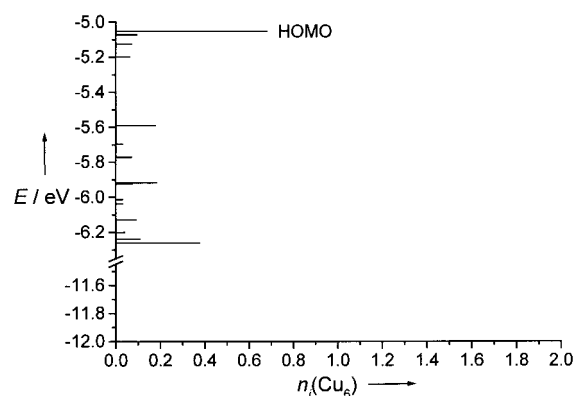


Figure 5. Contribution $n_i(\text{Oct})$ of the basis functions centered at the Cu_6 octahedron to the population of the MO ϕ_i for **1b**; $E = \text{HF[SV(P)]}$ orbital energy.

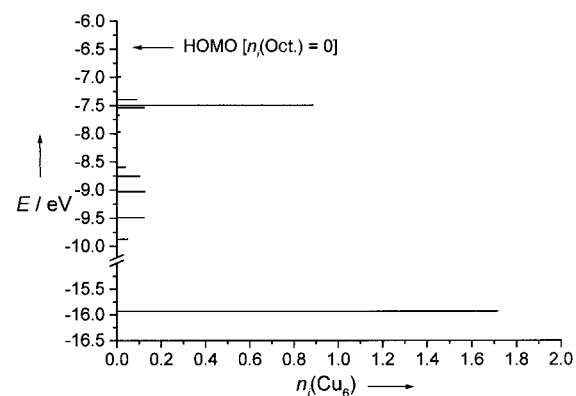


Figure 6. Contribution $n_i(\text{Oct})$ of the basis functions centered at the Cu_6 octahedron to the population of the MO ϕ_i for **2b**; $E = \text{HF[SV(P)]}$ orbital energy.

These results—as well as the aforementioned tendency to form mixed valence compounds, which is in contrast to Cu_2S and Cu_2Se clusters—can be explained by the differences in ionization potentials (IP), electron affinities (EA), and

electronegativities (EN), which are too small between Cu and As or Te for a discrete separation into Cu^{1+} and $\text{As}^{3-}/\text{Te}^{2-}$ ions; IP: 745.4(Cu), 946.5(As), 869.2(Te); EA: 118.5(Cu), 78.2(As), 190.2(Te); EN(Pauling): 1.9(Cu), 2.0(As), 2.1(Te). In other words, the formal charge assignment to give Cu^{1+} and $\text{As}^{3-}/\text{Te}^{2-}$ centers produces an “additional” electron pair which is described by an MO that is embedded in the valence band formed by the arsenic 4p orbitals or the tellurium 5p orbitals, and the 4s orbitals of copper.

Experimental Section

$\text{LiAs}(\text{SiMe}_3)_2 \cdot 1.2\text{THF}$ (0.77 g, 2.4 mmol) was added to a suspension of CuCl (0.2 g, 2 mmol) and dppm (0.5 g, 1.3 mmol) in DME (50 mL) at -20°C . A clear yellow solution was formed which as the temperature increased towards room temperature gradually turned a brilliant red, and was nearly black at room temperature. After reducing the volume of the solution by about half, black needlelike crystals of **1** were obtained in under two weeks (yield, based on CuCl , 0.12 g, 30%). The C and H analyses of **1** fit the given formula.

Received: June 21, 2000 [Z15307]

- [1] D. Fenske, J. Ohmer, J. Hachgenei, K. Merzweiler, *Angew. Chem.* **1988**, 100, 1300–1320; *Angew. Chem. Int. Ed. Engl.* **1988**, 27, 1277–1296.
- [2] H. Krautscheid, D. Fenske, G. Baum, M. Semmelmann, *Angew. Chem.* **1993**, 105, 1364–1367; *Angew. Chem. Int. Ed. Engl.* **1993**, 32, 1303–1305.
- [3] D. Fenske, N. Zhu, T. Langetepe, *Angew. Chem.* **1998**, 110, 2784–2788; *Angew. Chem. Int. Ed.* **1998**, 37, 2640–2644.
- [4] D. Fenske, W. Holstein, *Angew. Chem.* **1994**, 106, 1311–1312; *Angew. Chem. Int. Ed. Engl.* **1994**, 33, 1290–1292.
- [5] D. Fenske, F. Simon, *Angew. Chem.* **1997**, 109, 240–243; *Angew. Chem. Int. Ed. Engl.* **1997**, 36, 230–233.
- [6] D. Fenske, F. Simon, *Z. Anorg. Allg. Chem.* **1996**, 622, 45–52.
- [7] D. Fenske, J. Besinger, unpublished results.
- [8] X-ray structural analysis of **1**: STOE-IPDS (MoK_α irradiation), data collection and refinement (SHELXS-86, SHELXL-93). Monoclinic, space group $P2_1/c$ (no. 14), $Z=4$, cell (203 K): $a=3088.0(6)$, $b=2261.0(5)$, $c=3303.0(7)$ pm, $\beta=105.83(3)^\circ$, $V=22187(8) \cdot 10^6$ pm³, $\mu(\text{MoK}_\alpha)=46.43$ cm⁻¹; $2\theta_{\text{max}}=48^\circ$; 105 964 reflections, of which 33 395 are independent ($R_{\text{int}}=0.1163$), 24 809 reflections with $I>2\sigma(I)$, 2443 parameters; maximum / minimum electron density = 1.19 / -1.12 e⁻ · (10⁶ pm)⁻³; $R_1=0.05$; $wR_2=0.131$. The positions of the H atoms were calculated, all other atoms were refined anisotropically except those of the DME molecules. Crystallographic data (excluding structure factors) for the structures reported in this paper have been deposited with the Cambridge Crystallographic Data Centre as supplementary publication no. CCDC-145570. Copies of the data can be obtained free of charge on application to CCDC, 12 Union Road, Cambridge CB2 1EZ, UK (fax: (+44) 1223-336-033; e-mail: deposit@ccdc.cam.ac.uk).
- [9] A. F. Holleman, E. Wiberg, *Lehrbuch der Anorganischen Chemie*, 91st–100th ed., de Gruyter, Berlin, **1985**, p. 1032.
- [10] C. Elschenbroich, A. Salzer, *Organometallchemie*, 3rd ed., Teubner, Stuttgart, **1993**, p. 87.
- [11] *Gmelins Handbuch der Anorganischen Chemie, Kupfer Teil B, Lieferung 2*, 8th ed., Verlag Chemie, Weinheim, **1961**, p. 934.
- [12] S. Dehnen, D. Fenske, *Chem. Eur. J.* **1996**, 2, 1407–1416; A. Eichhöfer, D. Fenske, *J. Chem. Soc. Dalton Trans.* **1998**, 2969–2972.
- [13] A. Eichhöfer, J. F. Corrigan, D. Fenske, E. Tröster, *Z. Anorg. Allg. Chem.* **2000**, 626, 338–348.
- [14] P. Reis, F. Weigend, R. Ahlrichs, D. Fenske, *Angew. Chem.* **2000**, 112, 4085–4089; *Angew. Chem. Int. Ed.* **2000**, 39, 3925–3929.
- [15] W. Beesk, P. G. Jones, H. Rumpel, E. Schwarzmann, G. M. Sheldrick, *J. Chem. Soc. Chem. Commun.* **1981**, 664; C. Linke, M. Jansen, *Angew. Chem.* **1992**, 104, 618–619; *Angew. Chem. Int. Ed. Engl.* **1992**, 31, 653–654; C. Linke, M. Jansen, *Inorg. Chem.* **1994**, 33, 2614–2616;

H. G. von Schnering, K. G. Häusler, *Rev. Chim. Miner.* **1976**, 13, 71; M. Jansen, *Angew. Chem.* **1987**, 99, 1136–1138; *Angew. Chem. Int. Ed. Engl.* **1987**, 26, 1098–1110.

- [16] All calculations were carried out with the program package TURBOMOLE. a) R. Ahlrichs, M. Bär, M. Häser, H. Horn, C. Kölmel, *Chem. Phys. Lett.* **1989**, 162, 165–169. The DFT calculations were made with the Becke–Perdew 86 functional (BP) within the RI approximation (RI = resolution of the identity). b) A. D. Becke, *Phys. Rev. A* **1988**, 38, 3098–3100; c) S. J. Vosko, L. Wilk, M. Nusair, *Can. J. Phys.* **1980**, 58, 1200–1211; d) J. P. Perdew, *Phys. Rev. B* **1986**, 33, 8822–8824; erratum: J. P. Perdew, *Phys. Rev. B* **1986**, 34, 7406; e) K. Eichkorn, O. Treutler, H. Öhm, M. Häser, R. Ahlrichs, *Chem. Phys. Lett.* **1995**, 242, 652. The basis sets used in the DFT calculations were SV(P) (split-valence plus polarization for all non-hydrogen atoms) and TZVP (triple zeta valence plus one polarization function); f) A. Schäfer, H. Horn, R. Ahlrichs, *J. Chem. Phys.* **1992**, 97, 2571–2577; g) A. Schäfer, C. Huber, R. Ahlrichs, *J. Chem. Phys.* **1994**, 100, 5829–5835. The core electrons of Te atoms were described by an effective core potential (ECP); h) A. Bergner, M. Dolg, W. Kuechle, H. Stoll, H. Preuss, *Mol. Phys.* **1993**, 80, 1431. The basis set dependency within population analyses was checked for HF calculations with a modified SV(P) basis set for the Cu atoms which was developed by an optimization of valence s functions for a small model cluster (Cu_4Cl_2).
- [17] If the symmetry threshold is lowered, S_6 , a subgroup of T_h is found. Therefore, a geometry optimization in S_6 symmetry was performed in which the energy as well as in the calculated structure converged to the results of T_h symmetry.
- [18] The combination of all basis functions would give for doubly occupied MOs $n_i=2$; for the population n_i , however, only those basis functions are combined which are centered at the cluster core, that is, the Cu atoms of the octahedra in **1b** and **2b**. Thus, the closer the value of n_i is to 2, the more this orbital is localized at the cluster core.

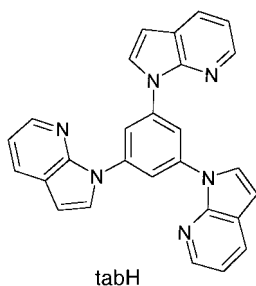
A Blue Luminescent Starburst Molecule and Its Orange Luminescent Trinuclear Pd^{II} Complex: 1,3,5-tris(7-azaindol-1-yl)benzene (tabH) and $[\text{Pd}^{\text{II}}(\text{tab})_2\text{Cl}_4]**$

Qingguo Wu, Andrea Hook, and Suning Wang*

Luminescent organic and organometallic compounds have attracted much attention recently, mostly because of their potential applications in organic light-emitting devices (OLEDs).^[1,2] We have demonstrated previously that Al^{III} and B^{III} complexes of 7-azaindolyl (deprotonated 7-azaindole) are bright blue emitters^[3] and capable of producing a bright blue light when in OLEDs.^[4] Our recent efforts have focused on the modification of the 7-azaindolyl ligand to improve the stability and performance of compounds based on 7-azaindole. One of the modifications we carried out was to replace the proton on the indole nitrogen atom by an

[*] Prof. Dr. S. Wang, Q. Wu, A. Hook
Department of Chemistry
Queen's University
Kingston, Ontario, K7L 3N6 (Canada)
Fax: (+1) 613-533-6669
E-mail: wangs@chem.queensu.ca

[**] This work was financially supported by the Natural Sciences and Engineering Research Council of Canada and the Xerox Research Foundation.



aromatic group so that the new ligand can bind to a metal ion as a neutral chelate ligand.^[5] An example of the modified 7-azaindolyl ligands obtained by our group is the novel starburst molecule, 1,3,5-tris(7-azaindol-1-yl)benzene (tabH).

tabH was synthesized by the reaction of 1,3,5-tribromobenzene with 7-azaindole using Ullmann condensation methods,^[6] in which Cu^{II} and K₂CO₃ were used as the catalyst and bromide scavenger. tabH has a melting point of 220 °C and emits a bright blue color in solution and in the solid state when irradiated by UV light. The emission maxima of tabH in solution (5 mg mL⁻¹, CH₂Cl₂) and the solid state are at 409 nm and 413 nm, respectively (Figure 1). The luminescence of tabH is believed

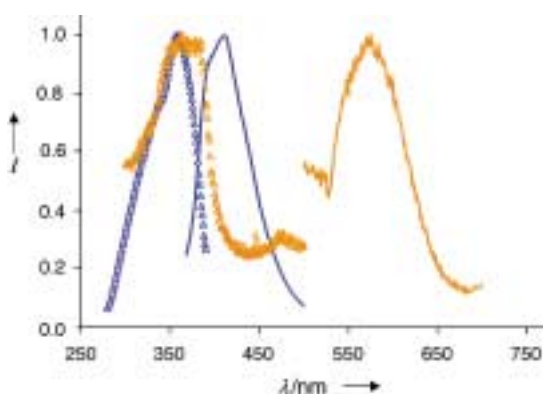


Figure 1. Excitation and emission spectra of solid tabH (blue) at ambient temperature and **1** (orange) at 77 K. Excitation = triangles, emission = solid line.

to be of fluorescent origin, based upon our previous studies on related molecules.^[3, 4] The blue luminescence of tabH is in sharp contrast to 7-azaindole, which has an emission band in the $\lambda_{\text{max}} < 400$ nm region. The attachment of the benzene moiety to 7-azaindole is clearly responsible for the red shift of emission energy by tabH. A similar red shift in the emission energy, on account of the replacement of the indole proton in 7-azaindole by an aromatic group, has been observed previously.^[5] The photoluminescent efficiency of tabH in solution was determined to be ~0.40 relative to that of 9,10-diphenylanthracene, which indicates that it is a bright blue emitter. Examples of luminescent and electroluminescent starburst organic molecules are previously known.^[7] However, stable and blue luminescent starburst molecules are still rare. Our preliminary investigation showed that tabH is promising as a blue emitter in OLEDs. Further details will be published in due course.

Recently, several examples of luminescent transition metal complexes have been reported to be promising emitters in light-emitting devices.^[8] However, luminescent transition metal complexes that are useful in OLEDs are still scarce. We therefore investigated the potential of the tabH molecule as a ligand to form luminescent transition metal complexes. We have found that the tabH molecule complexes readily with

Pd^{II} and Pt^{II} ions to form a variety of novel compounds, an example of which is [Pd₃(tab)₂Cl₄] (**1**), obtained from the treatment of K₂PdCl₄ with tabH in a 3:2 ratio using a procedure similar to that reported recently by Cadenas et al.^[9] The structure of **1** was determined by a single-crystal X-ray diffraction analysis.^[10] As shown in Figures 2 and 3, **1** has three Pd^{II} ions in two different environments: Pd(2) is situated at the crystallographically imposed inversion center and coordinated by two nitrogen and two chlorine atoms in a *trans* fashion while Pd(1) and Pd(1A) are related by the inversion

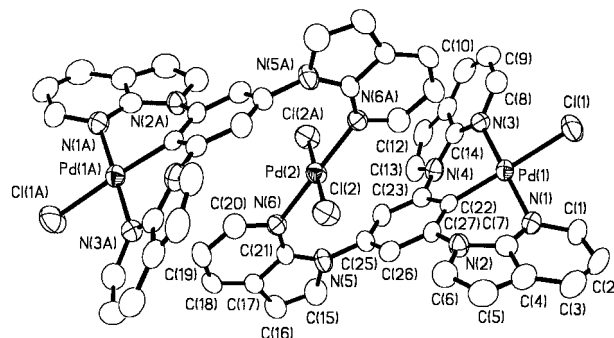


Figure 2. ORTEP representation of the molecular structure of **1** with labeling schemes and 50 % thermal ellipsoids. Hydrogen atoms are omitted for clarity. Selected bond lengths [Å] and angles [°]: Pd(1)–C(22) 1.989(5), Pd(1)–N(1) 2.019(5), Pd(1)–N(3) 2.047(4), Pd(1)–Cl(1) 2.3946(15), Pd(2)–N(6) 2.045(4), Pd(2)–Cl(2) 2.3031(14); N(1)–Pd(1)–N(3) 176.22(18), C(22)–Pd(1)–Cl(1) 172.96(15), N(6)–Pd(2)–Cl(2) 89.07(12), N(6)–Pd(2)–Cl(2A) 90.93(12).

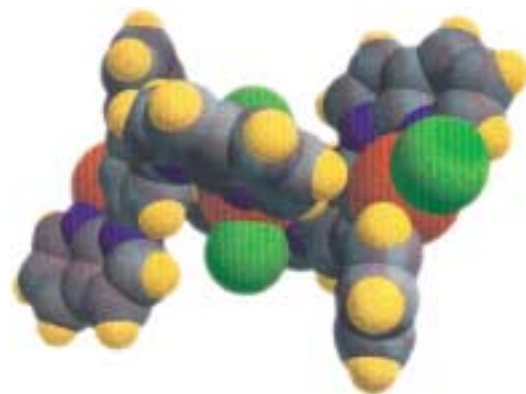


Figure 3. A space-filling diagram showing the orientation of the tab⁻ ligands in **1**.

center of symmetry and coordinated by two nitrogen, one chlorine and one carbon atom. Owing to the presence of the inversion center, the three Pd^{II} ions are in a rigorous linear arrangement with the Pd(1)–Pd(2) separation being 5.866(1) Å. The Pd(1) and Pd(2) centers have a square-planar geometry with a dihedral angle of 30.0° between the Pd(1) and Pd(2) square planes. The tab ligand acts both as a chelating and a bridging ligand. The formation of the Pd(1)–C(22) bond is a consequence of cyclometalation of tabH, favored by the geometry of the ligand and the chelating effect—a common phenomenon in organopalladium and organoplatinum compounds.^[9, 11] The palladium–ligand bonds in **1** are typical.^[9, 11] The three 7-azaindolyl groups of the tab ligand are not coplanar with the benzene moiety. The dihedral angles between the benzene ring and the N(2), N(4), and N(6) rings

are 23.4°, 35.1°, and 68.4°, respectively, attributable to steric interactions between hydrogen atoms and the geometric constraint of the ligand.

The coordination of the tabH ligand to the Pd^{II} centers leads to a drastic change of luminescence. At ambient temperature, in contrast to the free tabH ligand, **1** has no luminescence. At 77 K, upon excitation at $\lambda = 370$ nm, an orange emission band at $\lambda_{\text{max}} = 575$ nm from **1** was observed, as shown in Figure 1. The excitation band of **1** is similar to that of tabH. The ~160 nm red shift of the emission energy cannot be attributed to the abstraction of one proton from the benzene ring of tabH, based on the fact that Li⁺tab[−] does not have an orange emission. Luminescence observed in previously reported Pd^{II} complexes has often been attributed to metal-to-ligand charge transfer (MLCT) or metal-metal-to-ligand charge transfer (MMLCT) bands.^[11] The Pd–Pd separation distance of 5.866 Å in **1** is too large to allow any significant Pd–Pd interactions or MMLCT. The participation of 4d orbitals from the Pd^{II} ion in the luminescent transition of **1** appears to be very likely, based on the results of our preliminary ab initio molecular orbital calculations. However, a complete understanding of the luminescence displayed by **1** awaits further theoretical and experimental study.

Although **1** is not suitable as an emitter for electroluminescent devices because of the absence of luminescence at ambient temperature, it demonstrates that the tab[−] ligand can bind readily to a transition metal center to form luminescent complexes, thus providing a new avenue for luminescent transition metal compounds. It is conceivable, that with the appropriate choice of the central metal ion and the non-emitting ligands (for example, chloride in **1**), bright luminescent transition metal complexes based on tab ligands could be obtained.

Experimental Section

tabH: 1,3,5-Tribromobenzene (4.00 mmol, 1.259 g), 7-azaindole (16.00 mmol, 1.890 g), K₂CO₃ (16.00 mmol, 2.211 g), and CuSO₄ (0.100 mmol, 0.025 g) were mixed and heated at 205°C for 9 h under N₂. After being cooled to ambient temperature, the reaction mixture was dissolved in CH₂Cl₂ (300 mL) and washed with water. The organic layer was separated, dried over sodium sulfate, and evaporated to dryness by vacuum. The residue was passed through a silica gel column using hexanes/ethyl acetate (3/1) as the eluent. The first fraction collected was 1-bromo-3,5-bis(7-azaindol-1-yl)benzene, the second was tabH. Recrystallization from CH₂Cl₂/hexanes yielded a colorless solid of tabH (0.92 g, 54% yield). M.p. 220°C. ¹H NMR (CDCl₃, 25°C): δ = 8.36 (d, ³J = 5.1 Hz, 3H; 7-azain), 8.34 (s, 3H; benzene), 7.97 (dd, ³J₁ = 7.5, ³J₂ = 1.8 Hz, 3H; 7-azain), 7.70 (d, ³J = 4.2 Hz, 3H; 7-azain), 7.14 (dd, ³J₁ = 7.5, ³J₂ = 4.5 Hz, 3H; 7-azain), 6.67 (d, ³J = 3.6 Hz, 3H; 7-azain); ¹³C NMR (CDCl₃, 25°C): δ = 143.72 (7-azain), 129.20 (7-azain), 127.77 (7-azain), 117.05 (benzene), 116.12 (7-azain), 102.36 (7-azain); elemental analysis for C₂₇H₁₈N₆ · 0.3 CH₂Cl₂: calcd: C 72.55, H 4.08, N 18.59; found: C 72.35, H 3.99, N 18.41; MS: *m/z*: 426.3 [*M*⁺].

[Pd₃(tab)₂Cl₄] (**1**): tabH (0.20 mmol, 0.0853 g) and K₂PdCl₄ (0.30 mmol, 0.0979 g) were added to acetate acid (10 mL). The mixture was heated at 110–120°C and refluxed for 6 h under N₂. After the reaction mixture was cooled to ambient temperature, the off-white solid was collected by filtration and washed by acetic acid, CH₃OH, and diethylether (each 5 mL). Recrystallization of the crude product from DMF and ethanol yielded light yellow crystals of **1** in a 76% yield. M.p. 196°C. ¹H NMR ([D₆]DMSO, 25°C): δ = 9.08 (d, ³J = 5.7 Hz, 2H; 7-azain), 8.58 (d, ³J = 3.9 Hz, 2H; 7-azain), 8.36–8.30 (m, 3H; 7-azain), 8.09 (d, ³J = 7.5 Hz, 1H; 7-azain), 8.03 (d, ³J = 3.6 Hz, 1H; 7-azain) 7.93(s, 2H; benzene), 7.33 (dd, ³J₁ = 7.2, ³J₂ =

6.3 Hz, 2H; 7-azain), 7.22 (dd, ³J₁ = 7.5, ³J₂ = 4.5 Hz, 1H; 7-azain), 7.02 (d, ³J = 3.6 Hz, 2H; 7-azain), 6.69 (d, ³J = 3.6 Hz, 1H; 7-azain); ¹³C NMR ([D₆]DMSO, 25°C): δ = 156.69 (benzene), 148.18 (7-azain), 146.96 (7-azain), 143.10 (7-azain), 141.35 (7-azain), 137.26 (benzene), 136.27 (benzene), 132.47 (7-azain), 129.39 (7-azain), 128.62 (7-azain), 128.09 (7-azain), 123.07 (benzene), 121.44 (7-azain), 116.94 (7-azain), 113.96 (7-azain), 109.99 (7-azain), 105.49 (7-azain), 101.64 (7-azain); elemental analysis for C₃₄H₃₄N₁₂Cl₄Pd₃ · 2(CH₃)₂NCHO · H₂O: calcd: C 48.77, H 3.38, N13.27; found: C 48.33, H 3.50, N 13.22.

Received: May 18, 2000 [Z15141]

- [1] a) C. W. Tang, S. A. VanSlyke, *Appl. Phys. Lett.* **1987**, *51*, 913; b) C. W. Tang, S. A. VanSlyke, C. H. Chen, *J. Appl. Phys.* **1989**, *65*, 3611; c) Y. Shirota, Y. Kuwabara, H. Inada, T. Wakimoto, H. Nakada, Y. Yonemoto, S. Kawami, K. Imai, *Appl. Phys. Lett.* **1994**, *65*, 807; d) Y. Hamada, T. Sano, M. Fujita, T. Fujii, Y. Nishio, K. Shibata, *Jpn. J. Appl. Phys.* **1993**, *32*, L514; e) V. Bulovic, G. Gu, P. E. Burrows, S. R. Forrest, *Nature* **1996**, *380*, 29.
- [2] a) N.-X. Hu, M. Esteghamatian, S. Xie, Z. Popovic, B. Ong, A. M. Hor, S. Wang, *Adv. Mater.* **1999**, *11*, 1460; b) C. Adachi, T. Tsutsui, S. Saito, *Appl. Phys. Lett.* **1990**, *56*, 799; c) X. T. Tao, H. Suzuki, T. Wada, H. Sasabe, S. Miyata, *Appl. Phys. Lett.* **1999**, *75*, 1655; d) Z. Shen, P. E. Burrows, V. Bulovic, S. R. Forrest, M. E. Thompson, *Science* **1997**, *276*, 2009; e) H. Aziz, Z. Popovic, N. X. Hu, A. M. Hor, G. Xu, *Science* **1999**, *283*, 1900; f) Y. Hamada, T. Sano, H. Fujii, Y. Nishio, H. Takahashi, K. Shibata, *Appl. Phys. Lett.* **1997**, *71*, 3338; g) Q. Wu, M. Esteghamatian, N. X. Hu, Z. Popovic, G. Enright, Y. Tao, M. D'Iorio, S. Wang, *Chem. Mater.* **2000**, *12*, 79.
- [3] a) W. Liu, A. Hassan, S. Wang, Q. Wu, *Organometallics* **1997**, *16*, 4257; b) J. Ashenhurst, L. Brancaloni, A. Hassan, W. Liu, H. Schmider, S. Wang, Q. G. Wu, *Organometallics* **1998**, *17*, 3186; c) J. Ashenhurst, G. Wu, S. Wang, *J. Am. Chem. Soc.* **2000**, *122*, 2541; d) S. Gao, Q. G. Wu, G. Wu, S. Wang, *Organometallics* **1998**, *17*, 4666; e) A. Hassan, S. Wang, *Commun. Chem.* **1998**, 211.
- [4] Q. Wu, M. Esteghamatian, N. X. Hu, Z. Popovic, G. Enright, S. R. Breeze, S. Wang, *Angew. Chem.* **1999**, *111*, 1039; *Angew. Chem. Int. Ed.* **1999**, *38*, 985.
- [5] a) S. F. Liu, Q. Wu, H. L. Schmider, H. Aziz, N. X. Hu, Z. Popovic, S. Wang, *J. Am. Chem. Soc.* **2000**, *122*, 3671; b) Q. Wu, J. Lavigne, S. Wang, *Inorg. Chem.* **2000**, in press.
- [6] a) H. B. Goodbrand, N. X. Hu, *J. Org. Chem.* **1999**, *64*, 670; b) J. Lindley, *Tetrahedron* **1984**, *40*, 1433; c) P. E. Fanta, *Synthesis* **1974**, 1.
- [7] N. Tamoto, C. Adachi, K. Nagai, *Chem. Mater.* **1997**, *9*, 1077.
- [8] a) M. A. Baldo, S. Lamansky, P. Burrows, M. E. Thompson, S. R. Forrest, *Appl. Phys. Lett.* **1999**, *75*, 5; b) M. A. Baldo, D. F. O'Brien, Y. You, A. Shoustikov, S. Sibley, M. E. Thompson, S. R. Forrest, *Nature* **1998**, *395*, 151; c) X. Gong, P. K. Ng, W. K. Chan, *Adv. Mater.* **1998**, *10*, 1337; d) D. F. O'Brien, M. A. Baldo, M. E. Thompson, S. R. Forrest, *Appl. Phys. Lett.* **1999**, *74*, 442; e) R. C. Kwong, S. Sibley, T. Dubovoy, M. Baldo, S. R. Forrest, M. E. Thompson, *Chem. Mater.* **1999**, *11*, 3709.
- [9] D. J. Cárdenas, A. M. Echavarren, *Organometallics* **1999**, *18*, 3337.
- [10] The crystals of **1** were obtained from a DMF/ethanol solution. Crystal data for **1**: C₃₄H₃₄N₁₂Cl₄Pd₃ · 2(CH₃)₂NCHO, monoclinic, space group P2₁/c, *a* = 9.1343(6), *b* = 15.6271(10), *c* = 20.3907(15) Å, β = 102.1530(10)°, *V* = 2845.4(3) Å³, *Z* = 2, GOF(*F*²) = 0.881, *R*₁ = 0.0356 (*I* > 2 σ (*I*)), *wR*₂ = 0.0719; *R*₁ = 0.0621 (all data), *wR*₂ = 0.0779. Data were collected on a Siemens Smart CCD 1000 X-ray diffractometer operated at 50 kV and 35 mA at ambient temperature. The structural solution and refinement were performed on a PC using Bruker AXS SHELXTL software package (Version 5.10). Crystallographic data (excluding structure factors) for the structure reported in this paper have been deposited with the Cambridge Crystallographic Data Centre as supplementary publication no. CCDC-144749. Copies of the data can be obtained free of charge on application to CCDC, 12 Union Road, Cambridge CB21EZ, UK (fax: (+44) 1223-336-033; e-mail: deposit@ccdc.cam.ac.uk).
- [11] a) K. A. Van Houten, D. C. Heath, C. A. Barringer, A. L. Rheingold, R. S. Pilato, *Inorg. Chem.* **1998**, *37*, 4647; b) F. Neve, A. Crispini, S. Campagna, *Inorg. Chem.* **1997**, *36*, 6150; c) S. W. Lai, T. C. Cheung, M. C. W. Chan, K. K. Cheung, S. M. Peng, C. M. Che, *Inorg. Chem.* **2000**, *39*, 255.